XENOBIOTICA, 2002, VOL. 32, NO. 1, 1–17

Taylor & Francis
healthsciences

CYP3A4-mediated hepatic metabolism of the HIV-1 protease inhibitor saquinavir *in vitro*

V. A. EAGLING†§, H. WILTSHIRE‡, I. W. A. WHITCOMBE‡ and D. J. BACK†*

† Department of Pharmacology and Therapeutics, University of Liverpool, Liverpool, L69 3GE, UK
‡ Roche Discovery Welwyn, Welwyn Garden City, AL7 3AY, UK
§ Present address: Quintiles Scotland Ltd, Research Avenue South, Heriot Watt Research Park, Riccarton, Edinburgh EH14 4AP, UK.

Received 4 May 2001

1. The aim was to identify the major metabolites of saquinavir (SQV) from human hepatic microsomal incubations and the CYP isoform(s) responsible.

2. Ten fractions containing various metabolites were separated by isocratic reversed-phase HPLC and characterized by HPLC, mass spectrometry and NMR.

3. Metabolites were either mono- or di-hydroxylated derivatives of SQV. Fast-atom bombardment and electrospray MS showed that hydroxylation was predominantly situated on the decahydroisoquinoline ring. A major metabolite (M4) was rigorously identified as 6-equatorial-hydroxy SQV.

4. Metabolism of saquinavir to all metabolites was inhibited by the CYP3A4-selective inhibitor ketoconazole ($IC_{50} = 0.55 \pm 0.12\,\mu M$). Other isoform-selective inhibitors were non-inhibitory. The protease inhibitors ritonavir, indinavir and nelfinavir potently inhibited SQV metabolism in hepatic microsomes with $IC_{50} = 0.025 \pm 0.004$, 0.82 ± 0.26 and $0.58 \pm 0.14\,\mu M$, respectively.

5. Saquinavir metabolism correlated with immunochemically determined CYP3A4 levels and testosterone 6β-hydroxylation, but it failed to correlate with either immunochemically determined CYP1A2 levels or marker activities for CYP1A2, 2C9 or 2E1.

6. Heterologously expressed CYP3A4 metabolized saquinavir with a similar metabolic profile to that of human liver microsomes.

7. K_m and V_{max} for total SQV metabolism were $0.61 \pm 0.19\,\mu M$ and 1.82 ± 1.13 nmol mg^{-1} min^{-1}, respectively.

8. The extensive involvement of hepatic CYP3A4 in the metabolism of saquinavir predicts high intrinsic clearance of saquinavir. Inhibitors of CYP3A4 such as other protease inhibitors will substantially increase the bioavailability of saquinavir.

Introduction

Saquinavir (Ro 31-8959) was the first protease inhibitor licenced for the treatment of human immunodeficiency virus (HIV) infection. It is highly active and selective against HIV-1 and HIV-2 *in vitro*, exerting antiretroviral activity at low nanomolar concentrations (Craig *et al.* 1991). The hard gelatine capsule formulation of saquinavir, Invirase, exhibits low oral bioavailablity, measured as 4% in healthy volunteers after a single dose and estimated to be approximately 10%

* Author for correspondence; e-mail: daveback@liv.ac.uk

Xenobiotica ISSN 0049–8254 print/ISSN 1366–5928 online © 2002 Taylor & Francis Ltd
http://www.tandf.co.uk/journals
DOI: 10.1080/00498250110085845

at steady-state in HIV-positive patients (Steimer *et al.* 1998). To increase drug exposure, a new soft gel formulation of saquinavir, Fortovase, has been introduced with a bioavailability of approximately three times that of Invirase. Elimination of saquinavir is predominantly non-renal, with about 1% of the drug excreted unchanged in the urine and 88% eliminated in the faeces as unchanged drug and metabolites (Perry and Noble 1998).

Low oral bioavailability is often attributed to extensive hepatic metabolism, but the human intestinal mucosa also expresses a variety of drug-metabolizing enzymes, with CYP3A4 being identified as the predominant P450 isoform in human small intestinal enterocytes (Kolars *et al.* 1992, Prueksaritanont *et al.* 1996). In addition, the P-glycoprotein efflux pump can reduce absorption and increase gut wall metabolism by causing drugs such as the HIV-protease inhibitors (Kim *et al.* 1998) to cycle through the enterocytes, so raising their chance of presystemic biotransformation. The Fortovase formulation is thought to be well absorbed and the resultant higher concentrations, compared with those of Invirase, partially saturate the processes which reduce the oral bioavailability of saquinavir (Steimer *et al.* 1998).

Fitzsimmons and Collins (1997) demonstrated the *in vitro* metabolism of saquinavir by both human intestinal and hepatic microsomes and showed that the major metabolites of saquinavir were hydroxylated derivatives. They also proposed a potential contribution for intestinal CYP3A4 in the first-pass metabolism of saquinavir.

CYP3A4 is also involved in the metabolism of the protease inhibitors, indinavir (Chiba *et al.* 1997), ritonavir (Kumar *et al.* 1996) and amprenavir (Decker *et al.* 1998). Other isoforms (CYP2C9, CYP2D6) have also been implicated in the biotransformation of ritonavir, and ritonavir is a potent inhibitor of these CYP isoforms (Eagling *et al.* 1998).

The aim of the current study was to identify the major metabolites of saquinavir (SQV) from human hepatic microsomal incubations and identify the CYP isoform(s) involved. A battery of approaches was employed, including correlation analyses with immunoquantified CYP levels and marker substrates, the use of isoform-selective chemical inhibitor probes, heterologously expressed CYP isoforms, mass spectrometry and NMR spectroscopy.

Materials and methods

Chemicals

Sulphaphenazole, quinidine, diethyldithiocarbamate and β-NADPH (reduced form) were purchased from Sigma Chemical Co. (Poole, UK). Furafylline was purchased from Ultrafine Chemicals (Manchester, UK). Ketoconazole, ritonavir, nelfinavir and indinavir were gifts from Janssen (Beerse, Belgium), Abbott Laboratories (Chicago, IL, USA), Agouron Pharmaceuticals, Inc. (La Jolla, CA, USA) and Merck (Westpoint, CT, USA) respectively. Saquinavir (^{3}H- and ^{14}C-) was synthesized by Roche Products Ltd (Wiltshire *et al.* 1998). Radiochemical purity was >99% for both. Flow Scint A was obtained from Packard (Groningen, The Netherlands). HPLC-grade far-UV acetonitrile (AcN) and methanol (MeOH) were purchased from Fisons Plc (Loughborough, UK). All other reagents were of the highest grade possible.

Human liver microsomes

Histologically normal human livers were obtained from kidney transplant donors (two male, two female, average age 27.5 years). Consent for their removal was obtained from the donor's relatives and

Ethics Committee approval was granted for their use in the study. Liver tissue (10–20 g portions) was frozen in liquid nitrogen and stored at −80 °C until required. Washed microsomes (105 000*g* pellets) were prepared by the differential centrifugation technique as follows. Liver portions (10–20 g) were chopped and homogenized using a Polytron ultraturax (Philip Harris, Ashby de la Zouch, UK) device (2 × 10-s bursts) in phosphate buffer (0.067 M, pH 7.4) containing KCl (1.15% w/v). Homogenates were then centrifuged at 10 000*g* (20 min, 4 °C) in an MSE Prepspin centrifuge (Santo Gallenkamp Plc, Loughborough, UK). The resultant supernatant was centrifuged at 100 000*g* (65 min, 4 °C). Microsomal pellets were washed by resuspending in phosphate buffer (0.067 M, pH 7.4, 1.15% KCl) and recentrifuged at 100 000*g*. Pellets were resuspended in phosphate buffer (without KcL) and stored at −80 °C before use. Microsomal protein yield was determined by the method of Lowry *et al.* (1951).

Human intestinal microsomes

Microsomes prepared from human small intestine were kindly provided by Dr J. M. Collins (FDA, USA). Microsomal samples were prepared as detailed by Fitzsimmons and Collins (1997).

Human lymphoblastoid cell line microsomes

Microsomes prepared from human lymphoblastoid cell lines (AHH-1TK±) transfected with cDNAs for NADPH-cytochrome P450 reductase and for CYP1A2 (162 pmol CYP mg protein^{-1}), CYP2C9 (66 pmol CYP mg protein^{-1}), 2E1 (98 pmol CYP mg protein $^{-1}$) and 3A4 (56 pmol CYP mg protein^{-1}) were purchased from the Gentest Corporation (Woburn, MA, USA) along with control cell line microsomes, cHol (undetectable CYP content).

Identification of saquinavir metabolites

Isolation of metabolites. Large quantities of SQV metabolites were prepared from incubations (20 × 5 ml) containing 10 sequential additions of ^{14}C-SQV (3 μM; 0.03 μCi) in the presence of 1.0 mg ml^{-1} microsomal protein, $MgCl_2$ (10 mM) and NADPH (5 mM) in phosphate buffer (0.67 M, pH 7.4). Incubations were terminated with the addition of MeOH (5 ml) to precipitate microsomal protein followed by centrifugation to remove precipitated protein. Samples were then evaporated to dryness. The residue was redissolved in 35% acetonitrile in 0.075 M aqueous ammonium acetate containing 0.25% acetic acid (5 ml) and passed through a primed Bond-Elut cartridge. The metabolites were extracted from the cartridge with methanol (2 × 1 ml), evaporated, redissolved in 35% acetonitrile on 0.075 M aqueous ammonium acetate containing 0.25% acetic acid (5 ml) and filtered through a Nalgene GF 25-mm filter. The efficiency of the purification was measured by liquid scintillation counting of small samples, dissolving the aliquots in NE260 scintillation fluid (10 ml, Nuclear Enterprises) and measuring the radioactivity with an LKB Rack-Beta scintillation counter. Chromatographic purification of the large-scale reaction was carried out on a 'phenyl' Radial-Pak cartridge (8 × 100mm, 4 μm particle size) in a Radial Compression Module fitted with a 'phenyl' Guard-Pak (Waters) using an isocratic system with 35% acetonitrile in 0.075 M aqueous ammonium acetate containing 0.25% acetic acid. The samples were reconstituted in eluent and injected in 0.5–1.5 ml aliquots using a rheodyne injector with a 2 ml loop. The effluent was monitored at 235 nm (LKB 2141 variable wavelength detector) and fractions were collected manually. Further purification of individual fractions was accomplished using methanol-containing (55–65%) mobile phases and 0.075 M ammonium acetate (pH 6.9). After evaporation of the methanol, the individual metabolites were extracted with dichloromethane (3 × 5 ml), which was evaporated to dryness. The residues were dissolved in methanol, evaporated and then freeze dried from deuterium oxide.

Spectroscopic analysis of saquinavir metabolites. NMR spectra were obtained in deuterated methanol (Aldrich Chemical Co., 99.9%D) using Bruker DRX500 or DRX400 instruments. The NMR spectra were acquired in 16 K data points and zero-filled to 32 K using 512–1024 scans with a pulse angle of 30°. Solvent presaturation of the residual water signal was used when necessary. Two-dimensional correlation spectroscopy (COSY) spectra were obtained using a double-quantum filter with or without water presaturation with 80 scans per increment (2 K × 256, zero-filled to 2 K × 1 k).

Mass spectra were acquired after reversed-phase HPLC with a Finnigan MAT 4500 instrument, fitted with a MAT TSP-1 thermospray interface and with a Finnigan MAT TSQ-7000 instrument fitted with an electrospray interface. The chromatographic conditions used 70 or 80% methanol in aqueous ammoniun acetate (pH 6.9), but were otherwise the same as above. Fast-atom bombardment spectra (FAB) were obtained for some of the purified metabolites on a VG 7070E instrument equipped with an Ion Tech FAB gun operated at 8 keV and using xenon as the ionization gas. An aliquot of each purified metabolite (~10 μg) was applied to the target using 4:1 glycerol:trifluroacetic acid as matrix.

Identification of CYP isoforms responsible for the metabolism of saquinavir

Linearity studies. Saquinavir (^{14}C-SQV, 3 μM, 0.03 μCi) was incubated in a 500 μl incubation volume containing $MgCl_2$ (10 mM), NADPH (1 mM) in phosphate buffer (0.067 M, pH 7.4). Studies were performed over a range of incubation periods (at 0.2 mg ml^{-1} microsomal protein) or with a range of protein concentrations (incubation time 7 min). Incubations were terminated by the addition of methanol (500 μl) to precipitate microsomal protein, followed by centrifugation to remove precipitated protein. Supernatants were evaporated to dryness and reconstituted in mobile phase (120 μl) before analysis of an aliquot (90 μl). SQV metabolism was assessed by HPLC with on-line radiometric detection.

Correlation studies. The metabolism of ^{14}C-SQV (3 μM, 0.03 μCi) was assessed in a panel of human liver microsomes ($n = 13$). Incubations were performed with a 0.2 mg ml^{-1} protein concentration and a 7-min incubation. The extent of SQV metabolism was determined by HPLC with on-line radiometric detection. Correlation analysis was performed between SQV metabolism and immunochemically determined levels of CYP1A2 and CYP3A4 (as described by Gentile *et al.* 1996) and against activities of marker substrates of individual CYP isoforms: namely phenacetin *O*-deethylation, tolbutamide 4-hydroxylation, chlorzoxazone 6-hydroxylation and testosterone 6β-hydroxylation as markers for CYP1A2, CYP2C9, CYP2E1 and CYP3A4 respectively ($n = 13$). Assays for CYP probe substrates were as detailed by Eagling *et al.* (1997).

Inhibition studies. Studies were performed under standard incubation conditions. SQV (3 μM, 0.03 μCi) was incubated with a range of inhibitor concentrations and 0.1 mg microsomal protein for 10 min. Initial concentrations of inhibitors were chosen as follows: furafylline, sulphaphenazole, quinidine and diethyldithiocarbamate, 10 and 50 μM. Concentrations of ketoconazole were 0.1 and 1 μM. Mechanism-based inhibitors (furafylline and diethyldithiocarbamate) were incubated with microsomal protein and NADPH (1 mM) for 30 min before the addition of substrate. Ketoconazole (0.1–5.0 μM), ritonavir (0.01–0.1 μM), indinavir (0.5–10.0 μM) and nelfinavir (0.5–10.0 μM) were then screened over a more comprehensive range of concentrations and IC_{50} were determined by GraFit (Version 3.01).

In addition to IC_{50}, K_i for ketoconazole and ritonavir was determined using a range of substrate and inhibitor concentrations as follows: ^{3}H-SQV (0.1 μCi): 0.25, 0.50, 0.75, 1.00, 2.00, 5.00 μM, ketoconazole: 0.10, 0.40, 0.60 μM and ritonavir: 0.01, 0.02, 0.04 μM. For K_i determinations, 0.05 mg microsomal protein and 1-min incubation were employed to ensure linear conditions at low substrate concentrations. SQV metabolism was assessed by HPLC with on-line radiometric detection of ^{3}H-SQV. K_i was determined by substituting K_m and V_{max} into the appropriate equations.

K_m and V_{max} determination

K_m and K_{max} were determined in four human livers over a range of SQV concentrations (0.25–20 μM). SQV was incubated in a 500-μl incubation volume containing $MgCl_2$ (10 mM), NADPH (1 mM) in phosphate buffer (0.067 M, pH 7.4). A microsomal protein concentration of 0.05 mg ml^{-1} and an incubation of 1 min was employed to ensure linearity at low substrate concentrations. Total metabolism was determined by HPLC with UV detection and was quantified as percentage metabolism from the area under SQV and metabolite peaks. K_m and V_{max} parameters were calculated by fitting the Michaelis–Menten equation for a one-enzyme site to the data using the iterative non-linear regression program Grafit (Version 3.01). K_m and V_{max} were also determined in a single human small intestinal microsomal sample (0.05 mg protein, 1-min incubation).

Metabolism by cDNA expressed CYP isoforms

A 500-μl reaction mixture containing ^{14}C-SQV (3 μM, 0.03 μCi) was incubated in the presence of $MgCl_2$ (10 mM), NADPH (1 mM) and Gentest cell line microsomes (0.05 mg) expressing CYP1A2, 2C9, 2E1, 3A4 and control (no detectable CYP) in phosphate buffer (0.067 M, pH 7.4) for 20 min. Reactions were terminated as previously described and assayed by HPLC with on-line radiometric detection.

HPLC analysis of saquinavir and metabolites

SQV and metabolites were resolved on a Prodigy column (15 cm × 4 mm; Phenomenex, Macclesfield, UK) using a gradient mobile-phase system, flow rate 1.5 ml min^{-1}. Mobile phase comprised ammonium acetate (75 mM, pH 6.8) and AcN (far UV). Initial run conditions were 72% ammonium acetate:28% AcN. Between 25 and 35 min, there was a linear increase to 40% AcN. At 42 min there was a further linear increase to 50% AcN over 8 min, which remained constant for 5 min. This was followed by a return to initial run conditions over 5 min and a 5-min re-equilibration.

Results

Identification of the microsomal metabolites of saquinavir

Ten fractions containing the various metabolites were separated by isocratic reversed-phase HPLC using an acidic, acetonitrile-containing mobile phase (figure 1). These fractions were then characterized by isocratic reverse-phase HPLC using a neutral, methanolic mobile phase and mass spectral and UV detection. Further HPLC purification and solvent-extraction gave samples sufficiently pure for NMR analysis.

The diagnostic ions, modification of the parent structure and metabolite identification numbers are included in table 1 and figure 2. The mass spectra, obtained with a thermospray interface, of the metabolites of saquinavir showed

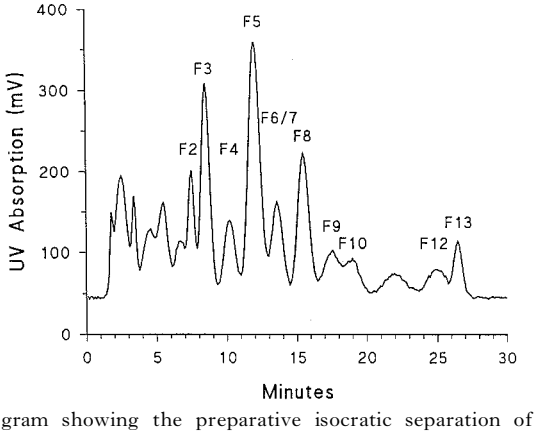
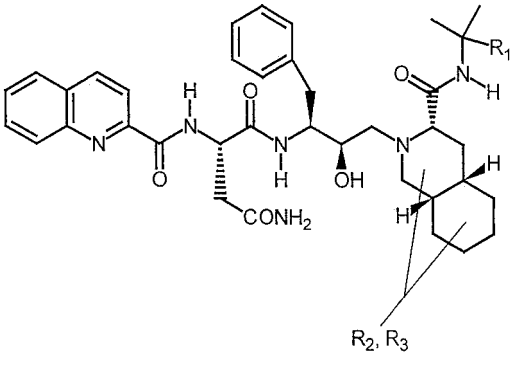


Figure 1. UV chromatogram showing the preparative isocratic separation of the main human microsomal metabolites of saquinavir. Parent compound is not shown as it elutes at 60 min under these chromatographic conditions. Peaks eluting before F2 are not compound related.



Metabolite no.	R1	R2	R3
M1, 2a, 3, 5	CH_3	OH	OH
M2	CH_2OH	OH	H
M4, 6, 7/8	CH_3	OH	H
M11, 12	CH_3	=O	–
M10	CH_2OH	H	H

Figure 2. Diagnostic fragmentation pattern of saquinavir.

Table 1. Mass spectral (thermospray interface) characterization of the microsomal metabolites of saquinavir.

Fraction no. and relative amount (%)	Metabolite no.	Mass spectral ions (m/z) and (relative intensities)	Transformation
SQV		173 (95), 270 (34), 402 (100), 482 (13), 499 (53), 654 (8), 671 (63)	
F2 (8%)	M1	173 (100), 270 (6), 434 (50), 514 (10), 531 (5), 686 (0.5), 703 (1)	dihydroxy
F3a (10%)	M2	270 (30), 434 (100), 514 (20), 531 (14), 703 (5)	dihydroxy
F3b (5%)	M2a	270 (12), 434 (100), 514 (8), 685 (1), 703 (2)	dihydroxy
F4 (6%)	M3	270 (20), 434 (100), 514 (13), 531 (8), 686 (0.5), 703 (0.5)	dihydroxy
F5 (21%)	M4	173 (48), 270 (5), 418 (100), 498 (20), 670 (4)	monohydroxy
F6/7 (9%)	M5	173 (100), 270 (12), 434 (87), 514 (12), 531 (6), 703 (5)	dihydroxy
F8 (24%)	M6	270 (2), 418 (100), 498 (12), 515 (14), 670 (1), 687 (0.5)	monohydroxy
F9 (5%)	M7/8*	270 (1), 418 (100), 498 (6), 515 (14), 687 (1)	monohydroxy
F10 (2%)	M11	173 (100), 270 (25), 416 (80), 496 (10), 513 (10), 668 (1), 685 (11)	'ketone'
F12 (2%)	M12	173 (66), 270 (30), 416 (100), 496 (10), 513 (28), 668 (3), 685 (10)	'ketone'
F13 (6%)	M10	173 (36), 270 (6). 418 (100), 498 (10), 515 (12), 670 (1), 687 (11)	monohydroxy

*M7/8 were identified as two compounds in animals, but only one has been characterized in man.

generally weak protonated molecular ions and strong fragments corresponding to cleavage of the asparaginyl-phenylalanyl peptide bond (figure 3a). A second fragment of intermediate intensity resulted from loss of quinaldamide.

The structure of M4, M6, M7/M8 and M10 were shown by their protonated molecular ions to be mono-hydroxylated derivatives of saquinavir whereas M1, M2, M2a, M3 and M5 were dihydroxylated compounds. The fragmentation pattern showed that the oxidation occurred in the 'right-hand side' of the molecule (figure 3a), but the thermospray spectra did not definitively place the oxygen atoms in the decahydroisoquinoline ring. This was, however, accomplished with both FAB and electrospray mass spectral techniques that generated fragments due to cleavage on either side of the decahydroisoquinoline ring (figure 3b and c). Thus, M4, M6 and M7 all exhibited ions at m/z 586 and 138 in their FAB spectra showing that it was the decahydroisoquinoline ring that bore the hydroxyl group (figure 3b and table 2). Although the electrospray spectra fragmented similarly, the complementary ion to that at m/z 138 (m/z 433) was observed (figure 3c). Thus, M4 had ions at m/z 586 and 433 showing that the hydroxyl group was in the decahydroisoquinoline ring system. M6 lost water readily under electrospray conditions to give dehydro-SQV (m/z 669) and then fragmented in a similar manner to SQV (m/z 568 and 433). The spectrum of M10, however, was similar to that of SQV with ions at m/z 570 and 433, showing that it had been hydroxylated on the tertiary butyl group. M2 dehydrated in a similar way to M6 to give hydroxydehydro-SQV with m/z 685 and then fragmented further like M10 and SQV (m/z 584 and 433). Thus, it appeared that one of its hydroxyl groups was in the decahydroisoquinolyl ring and the other on the tertiarybutyl moiety. The diagnostic ions and modification of parent structure are presented in table 3.

Two minor metaboldites (M11, M12) had molecular weights 14 Daltons greater than that of saquinavir (table 1). These are assumed to be ketones resulting

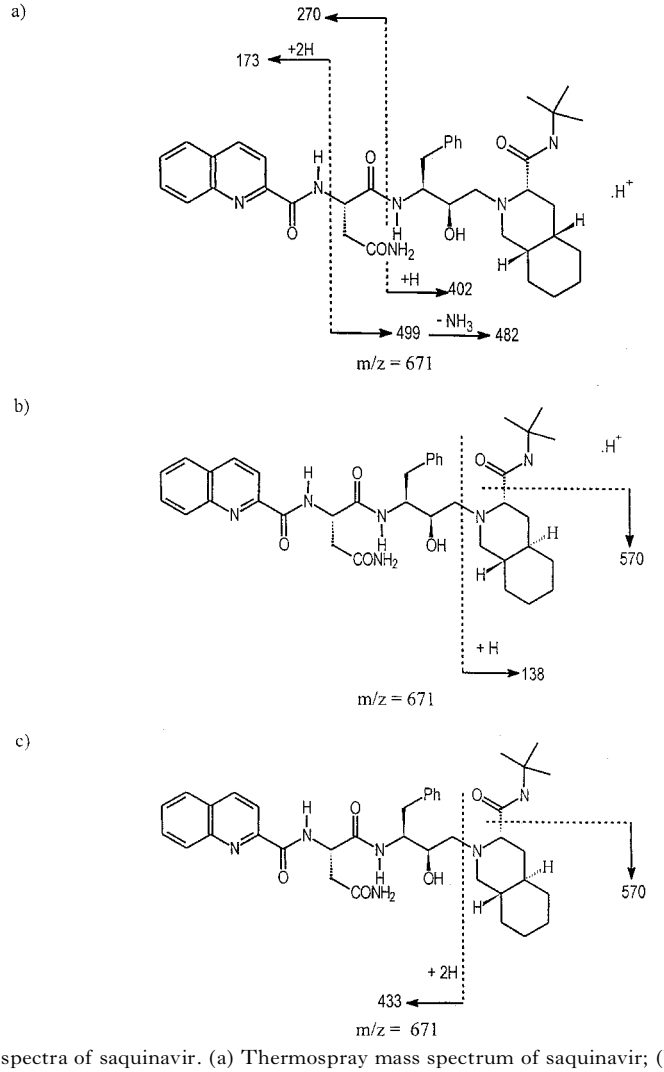


Figure 3. Mass spectra of saquinavir. (a) Thermospray mass spectrum of saquinavir; (b) FAB mass spectrum of saquinavir; (c) electrospray mass spectrum of saquinavir.

Table 2. Mass spectral (FAB) characterization of the microsomal metabolites of saquinavir.

Metabolite no.	Mass spectral ions (m/z) and (relative intensities)	Transformation
SQV	671 (100), 570 (17), 138 (80)	
M4	687 (56), 586 (16), 154 (100)	monohydroxy
M6	687 (100), 586 (18), 154 (80)	monohydroxy
M7/8*	687 (85), 586 (15), 154 (90)	monohydroxy

*M7/8 were identified as two compounds in animals, but only one has been characterized in man.

from further oxidation of mono-hydroxylated metabolites, but could also have arisen by partial dehydration (possibly during isolation) of vicinal diols.

M4 was formed in the greatest amount and was isolated in sufficient purity for a definitive NMR spectrum (figure 4). The proton α to the hydroxyl group

Table 3. Mass sapectral (electrospray interface) characterization of the microsomal metabolites of saquinavir.

Metabolite no.	Mass spectral ions (m/z) and (relative intensities)*	Transformation
SQV	671 (100), 570 (18), 433 (20)	
M2	703 (100), 685 (40), 602 (6), 584 (35), 433 (10)	dihydroxy
M4	687 (100), 586 (62), 433 (10)	monohydroxy
M6	687 (100), 669 (32), 568 (70), 433 (11)	monohydroxy
M10	687 (100), 570 (48), 433 (84)	monohydroxy

* Instrument operated in collision-induced dissociation mode.

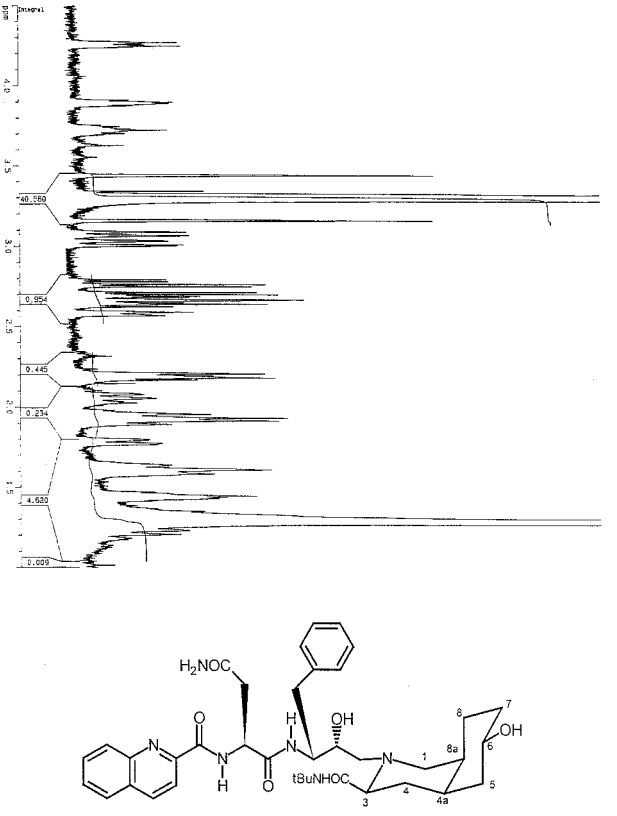


Figure 4. NMR spectrum of M4.

($\delta = 3.7$ ppm) was coupled to four other protons ($\delta = 1.25$, 1.45, 1.8, 1.95 ppm, see COSY spectrum; figure 5) and was therefore at the '6' or '7' position. Its relatively large coupling constants ($\mathcal{J} = \sim 7$–8 Hz) showed that the proton was axial and hence the alcohol group was equatorial. The low field, '1 equatorial' proton ($\delta = 3.1$ ppm) was coupled to the '1 axial' proton ($\delta = 2.2$ ppm) and both were coupled to the '8a' proton ($\delta = 1.65$ ppm). The '3 axial' proton ($\delta = 2.6$ ppm) was coupled to the '4 axial and equatorial' protons ($\delta = 1.95$ and 1.45 ppm, respectively). The '8 axial' proton ($\delta = 2.1$ ppm) was readily identified because of its large coupling constants. It was coupled both to the above-mentioned '8a' proton and to the '7 axial' proton

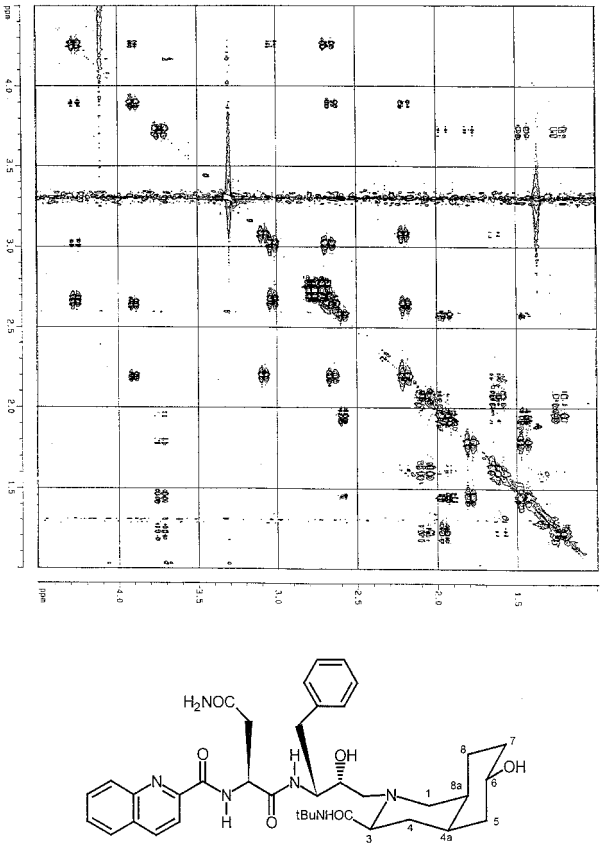


Figure 5. COSY spectrum of M4.

($\delta = 1.25$ ppm) with a typical axial–axial coupling constant of 5 Hz. Since the '7' carbon atom was joined to a proton with a chemical shift at this high field, it could not be hydroxylated. Hence, M4 was 6-equatorial-hydroxysaquinavir (figure 5).

Identification of the CYP isoforms responsible for saquinavir metabolism

Linearity studies. The overall metabolism of SQV was linear at protein concentrations up to 0.3 mg ml^{-1} (at an incubation of 7 min) and an incubation up to 10 min (at a protein concentration of 0.4 mg ml^{-1}). For further studies, an incubation of 7 min at a protein concentration of 0.2 mg ml^{-1} (0.1 mg/incubation) was employed, unless otherwise stated. Under these conditions, SQV was metabolized to multiple products (figure 6).

Correlation studies. A four-fold variability in total SQV metabolism was observed in the microsomal samples screened. To summarize this data (original data not shown), total SQV metabolism correlated with immunochemically determined CYP3A4 levels ($r = 0.92$, $p < 0.001$) and testosterone 6β-hydroxylation ($r = 0.78$,

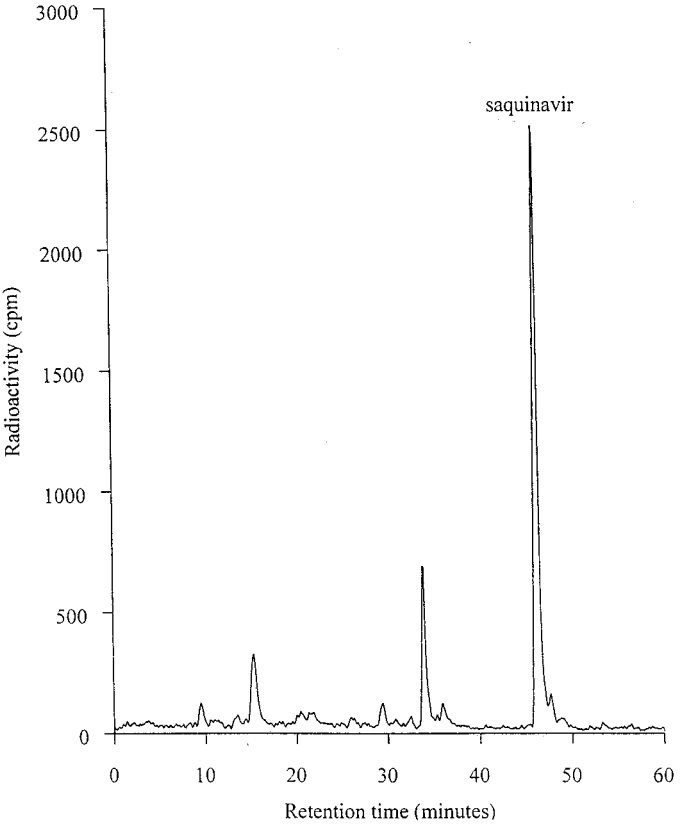


Figure 6. Representative radiochromatograph showing the metabolism of saquinavir (3 μM, 0.03 μCi) by human liver microsomes (0.1 mg, 7-min incubation).

$p < 0.005$). No significant correlations were observed between total SQV metabolism and immunochemically determined levels of CYP1A2 ($r = 0.48$) or metabolism of marker substrates phenacetin ($r = 0.39$), tolbutamide ($r = -0.06$) or chlorzoxazone ($r = 0.12$) as probes for CYP1A2, CYP2C9 and CYP2E1 respectively.

Inhibition studies. An initial screen of CYP-isoform selective inhibitors demonstrated that furafylline, sulphaphenazole (figure 7) and quinidine failed to inhibit SQV metabolism. Diethyldithiocarbamate, an alleged CYP2E1-selective inhibitor, caused some inhibition of SQV metabolism, with $47.5 \pm 10.5\%$ (mean $\pm$ SD) activity remaining at 50 μM. Ketoconazole caused the most potent inhibition of SQV metabolism, with $31.7 \pm 7.5\%$ activity remaining, at a concentration of 1 μM (figure 7). $IC_{50} = 0.55 \pm 0.12$ μM was determined for ketoconazole (figure 8).

Of the protease inhibitors, ritonavir was the most potent inhibitor of SQV metabolism, with an $IC_{50} = 0.025 \pm 0.004$ μM, Indinavir and nelfinavir had roughly equal orders of potency to ketoconazole, with $IC_{50} = 0.82 \pm 0.26$ and 0.58 ± 0.14 μM, respectively (figure 8).

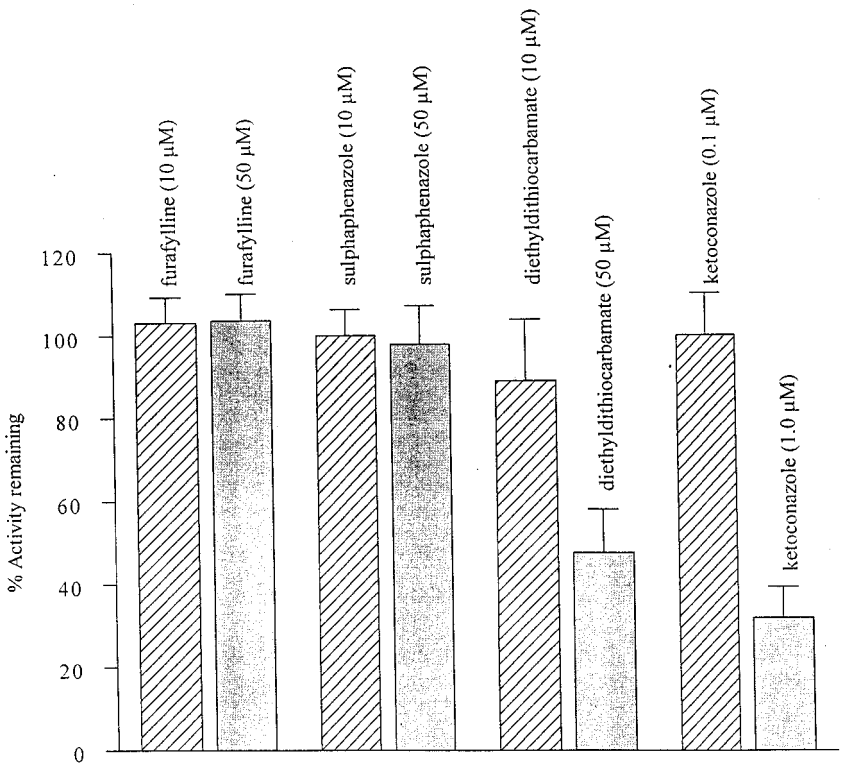


Figure 7. Inhibition of saquinavir metabolism (3 μM; 0.03 μCi) by CYP isoform-selective probe inhibitors. Data are the mean ± SD of determinations in four individual human liver microsomal preparations.

$K_i = 0.22 \pm 0.05$ and 0.021 ± 0.005 μM were determined for ketoconazole and ritonavir, respectively.

Metabolism by cDNA expressed CYP isoforms

Gentest cell-line microsomes expressing CYP3A4 (co-expressing NADPH-cytochrome P450 reductase) catalysed the biotransformation of SQV with a similar metabolic profile to human liver microsomes. No metabolism was observed when control cell line microsomes or cell line microsomes expressing CYP1A2, CYP2C9 or CYP2E1 were incubated with SQV under identical conditions (data not shown).

K_m *and* V_{max} *determinations*

The total metabolism of SQV followed Michaelis–Menten kinetics for a single enzyme (as evidenced by linear Eadie–Hofstee plots). A representative kinetic plot for a single human liver is presented in figure 9. SQV was metabolized with apparent K_m and V_{max} of 0.61 ± 0.19 μM and 1.82 ± 1.13 nmol mg^{-1} min^{-1} respectively. SQV metabolism by human small intestinal microsomes was also catalysed by a single enzyme, apparent K_m and V_{max} of 1.08 μM and 0.67 nmol mg^{-1} min^{-1}

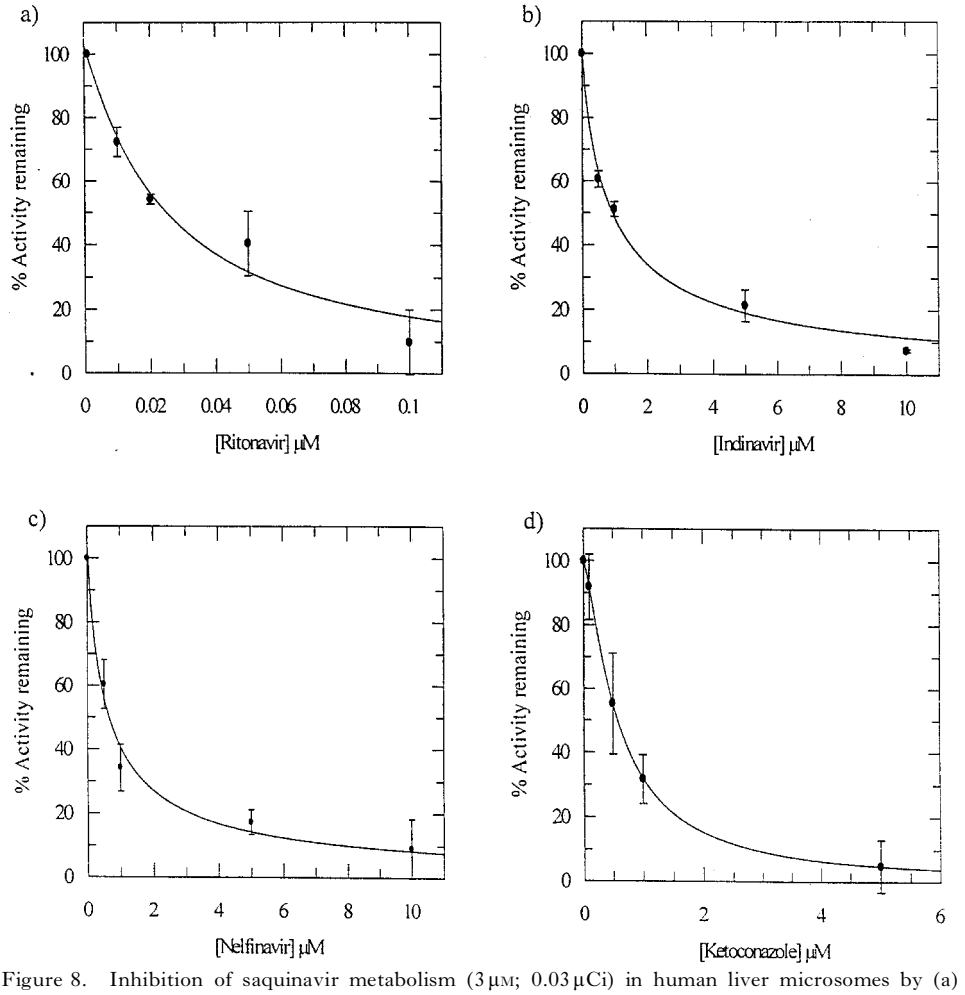


Figure 8. Inhibition of saquinavir metabolism (3 μM; 0.03 μCi) in human liver microsomes by (a) ritonavir, (b) indinavir, (c) nelfinavir and (d) ketoconazole. Data are the mean ± SD of determinations in four individual human liver microsomal preparations.

were determined in a single human intestinal sample (figure 9). Intrinsic clearance was $2.80 \pm 0.84\,ml\,min^{-1}\,mg^{-1}$ for human hepatic microsomes and $0.62\,ml\,min^{-1}\,mg^{-1}$ in human intestinal microsomes.

Discussion

The systemic bioavailability of orally administered saquinavir is reduced by a combination of P-glycoprotein efflux and cytochrome P450-mediated metabolism in the gut wall and liver (Aungst 1999). Since these three processes are potentially saturable, relatively small increases in absorption can be magnified. Thus, an estimated increase in absorption of 2.4-fold from the Fortovase (1200 mg), as opposed to the Invirase (600 mg), formulation leads to a 3.3-fold increase in bioavailability (Steimer *et al.* 1998).

The metabolic profile of saquinavir in microsomal incubations appears to be dependent on the conditions of the reaction. The formation of certain metabolites

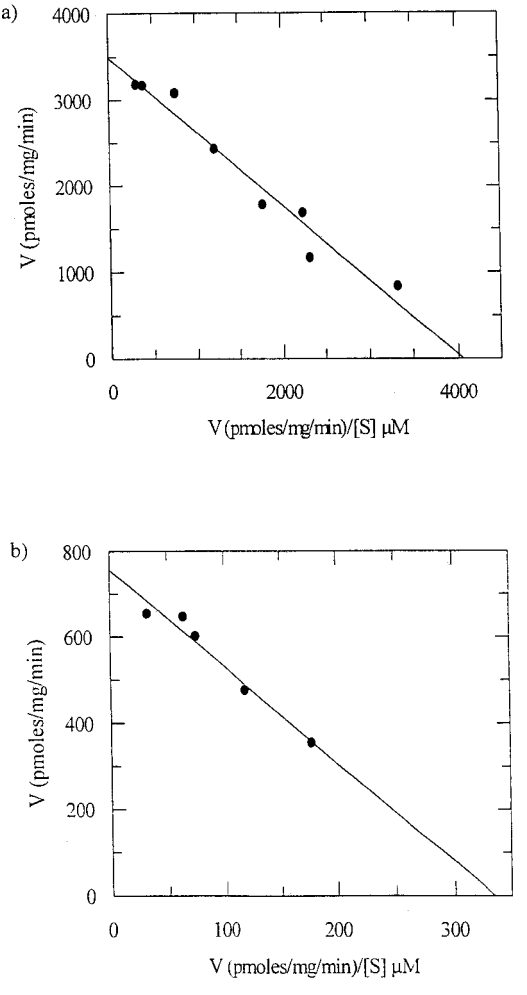


Figure 9. Representative Eadie–Hofstee plots illustrating K_m and V_{max} determination for saquinavir metabolism by (a) human hepatic microsomes and (b) human intestinal microsomes. Data are the mean of duplicate incubations.

is probably saturable and some, at least, of the initially formed monohydroxy derivatives are further hydroxylated. Although the biotransformation of saquinavir appears complicated, it seems to be limited to the decahydroisoquinoline part of the molecule. Fitzsimmons and Collins (1997) have identified three monohydroxy metabolites (M2, M3, M7), which probably correspond to M4, M6 and M10 in our nomenclature. A major metabolite, M4, has been unambiguously identified as 6-equatorial-hydroxysaquinavir by a combination of mass spectrometry and NMR.

The range of *in vitro* techniques used in the present study collectively indicate that CYP3A4 is the sole isoform involved in the hydroxylation of saquinavir to its multiple metabolites. Total saquinavir metabolism was shown to correlate significantly with immunoquantified CYP3A4 levels in a panel of human liver microsomal preparations ($r = 0.92$, $p < 0.001$) and with the 6β-hydroxylation of testosterone a known marker substrate for CYP3A4 activity ($r = 0.72$, $p < 0.005$) (Waxman *et al.* 1988, Waxman *et al.* 1991).

The CYP-isoform selective inhibitor probes furafylline (CYP1A2; Sesardic *et al.* 1990, Birkett *et al.* 1993, Kunze and Trager 1993, Halpert *et al.* 1994), sulphaphenazole (CYP2C9; Birkett *et al.* 1993, Halpert *et al.* 1994, Baldwin *et al.* 1995) and quinidine (CYP2D6; Birkett *et al.* 1993, Halpert *et al.* 1994) all failed to inhibit the metabolism of saquinavir to any of its products. Diethyldithiocarbamate, an alleged specific inhibitor of CYP2E1 (Guengerich *et al.* 1991, Halpert *et al.* 1994) demonstrated some inhibition of saquinavir metabolism, causing around 50% inhibition at 50 μM concentrations. We have previously shown that at this concentration diethyldithiocarbamate caused inhibition of CYP3A4-mediated testosterone 6β-hydroxylation (Eagling *et al.* 1998). Other groups have also demonstrated some non-selectivity of this compound as a probe inhibitor of CYP2E1 (Chang *et al.* 1994). Ketoconazole, a selective CYP3A4 inhibitor at low concentrations (Baldwin *et al.* 1995), potently inhibited the hydroxylation of saquinavir ($IC_{50} = 0.55 \pm 0.12\,\mu M$), providing additional evidence for the involvement of CYP3A4 in the biotransformation of saquinavir.

Only lymphoblastoid cell line microsomes expressing CYP3A4 (co-expressing NADPH-cytochrome P450 reductase) were capable of catalysing the metabolism of saquinavir. There was no evidence for metabolism by cell line microsomes expressing CYP1A2, 2C9, 2E1 or control cell line microsomes; CYP2D6 microsomes were not tested for activity. The metabolite profile for saquinavir in these CYP3A4 expressing microsomes was qualitatively very similar to that of human liver microsomal preparations.

Human hepatic microsomes metabolized saquinavir, with a single enzyme being implicated (monophasic Eadie–Hofstee plot, figure 9). Apparent K_m and V_{max} were $0.61 \pm 0.19\,\mu M$ and $1.82 \pm 1.13\,nmol\,mg^{-1}\,min^{-1}$ respectively. The calculated intrinsic clearance of $2.8 \pm 0.84\,mg^{-1}\,min^{-1}$ is extremely high (Houston 1994) and is consistent with the high first-pass metabolism of the compound. The kinetic parameters for saquinavir metabolism by human intestinal microsomes were comparable with those of human liver preparations, catalysing total saquinavir metabolism with a $K_m = 1.08\,\mu M$ and $V_{max} = 0.67\,nmol\,mg^{-1}\,min^{-1}$. Previous studies comparing the 6β-hydroxylation of testosterone as a marker for CYP3A4 activity in both human hepatic and intestinal microsomal preparations yielded two identical K_m (Preuksaritanont *et al.* 1996). This is in keeping with recent reports indicating that intestinal and hepatic cDNAs are identical to each other (Lown *et al.* 1998). Fitzsimmons and Collins (1997) demonstrated that human intestinal microsomes catalyse the hydroxylation of saquinavir and implicated CYP3A4 in this biotransformation, with a $K_m = \sim 0.5\,\mu M$. They suggested a role for intestinal CYP3A4 in the first-pass metabolism of saquinavir and, hence, the low oral bioavailability of this compound.

Ritonavir, another protease inhibitor, demonstrated extensive inhibition of saquinavir metabolism with an $IC_{50} = 0.025 \pm 0.004\,\mu M$, appearing to be an even more potent inhibitor than ketoconazole. Ritonavir has been shown to inhibit strongly CYP3A4-mediated metabolism of other substrates (Eagling *et al.* 1997, von Moltke *et al.* 1998). Indinavir and nelfinavir also inhibited saquinavir biotransformation with $IC_{50} = 0.82 \pm 0.26$ and $0.55 \pm 0.14\,\mu M$ respectively. CYP3A4 has been implicated in the metabolism of ritonavir and indinavir (Chiba *et al.* 1996, Kumar *et al.* 1996).

Ritonavir, indinavir and nelfinavir have been reported to undergo clinical interactions with saquinavir. Ritonavir demonstrates the most exaggerated effects

causing > 20-fold increase in saquinavir area under the plasma concentration–time curve (AUC) (Merry *et al*. 1997a). Nelfinavir has been demonstrated to cause around a 4-fold increase in saquinavir AUC (Merry *et al*. 1997b). These differences in the observed effects of the protease inhibitors on saquinavir plasma levels can largely be explained by their *in vitro* potency against CYP3A4-mediated metabolism (ritonavir > indinavir ≈ nelfinavir).

We previously reported that ritonavir and ketoconazole were equipotent at inhibiting CYP3A4-mediated testosterone 6β-hydroxylation, with $IC_{50} = 0.04$ and 0.03 μM respectively (Eagling *et al*. 1997, Eagling *et al*. 1998). However, when saquinavir is studied as a substrate, ritonavir is an order of magnitude more potent than ketoconazole. This is reflected in the clinical situation where ketoconazole has been shown to increase saquinavir AUC by only around 3-fold (Noble and Faulds 1996) compared with a 20-fold increase with ritonavir (Merry *et al*. 1997a). The different relative potencies of ritonavir and ketoconazole as inhibitors of CYP3A4-catalysed metabolism of testosterone and saquinavir indicate that this isoform, with its large active site (Lewis *et al*. 1996), binds these two substrates in a different manner. As a result, ketoconazole inhibits testosterone metabolism more effectively than it does saquinavir metabolism. Ritonavir, on the other hand, is equipotent against both compounds. This demonstrates the necessity of studying more than one substrate of CYP3A4 when investigating drug–drug interactions.

Extensive metabolism in both the liver and intestine may play a role in the systemic bioavailability of saquinavir. The basis for the interaction between saquinavir and ritonavir (and other protease inhibitors) is likely to involve inhibition of CYP3A4-mediated first-pass metabolism at both these sites. However, as reported for cyclosporin A (Lown *et al*. 1997), intestinal P-glycoprotein may also play a critical role in the interpatient variability in the systemic availability and pharmacokinetics of protese inhibitors. Lee *et al*. (1998), Kim *et al*. (1998) and Profit *et al*. (1999) reported that saquinavir, ritonavir and indinavir are all substrates for P-glycoprotein.

In conclusion, a combination of factors including hepatic and intestinal CYP3A4 levels and the multidrug efflux pump, P-glycoprotein, will affect the oral bioavailability of saquinavir *in vivo*. In addition to the inhibition of intestinal and hepatic CYP3A4-mediated metabolism of saquinavir, the interaction observed between protease inhibitors may also arise as a consequence of inhibition of P-glycoprotein-mediated drug efflux.

Acknowledgements

The authors are grateful to Dr J. L. Maggs and Mr A. J. Moore for the LC/MS analysis, and to Dr G. Williams for the NMR of saquinavir metabolites. Financial support for the studies was provided by the Medical Research Council and Roche Products Ltd.

References

Aungst, B. J., 1999, P-glycoprotein, secretory transport, and other barriers to the oral delivery of anti-HIV drugs. *Advances in Drug Delivery Review*, **39**, 105–116.

Baldwin, S. J., Bloomer, J. C., Smith, G. J., Ayrton, A. D., Clarke, S. E. and Chenery, R. J., 1995, Ketoconazole and sulphaphenazole as the respective selective inhibitors of P4503A and 2C9. *Xenobiotica*, **25**, 261–270.

Birkett, D. J., Mackenzie, P. I., Veronese, M. E. and Miners, J. O., 1993, *In vitro* approaches can predict human drug metabolism. *TIPS*, **4**, 292–294.

Chang, T. K. H., Gonzalez, F. J. and Waxman, D. J., 1994, Evaluation of triacetyloleandomycin, α-naphthoflavone and diethyldithiocarbamate as selective chemical probes for inhibition of human cytochrome P450. *Archives of Biochemical Biophysics*, **311**, 437–442.

Chiba, M., Hensleigh, M. and Lin, J. L., 1997, Hepatic and intestinal metabolism of indinavir, an HIV protease inhibitor, in rat and human microsomes. Major role of CYP3A. *Biochemical Pharmacology*, **53**, 1187–1195.

Craig, J. C., Duncan, I. B., Hockley, D., Grief, C., Roberts, N. A. and Mills, J. S., 1991, Antiviral properties of Ro 31-8959, an inhibitor of human immunodeficiency virus (HIV) proteinase. *Antiviral Research*, **16**, 295–305.

Decker, C. J., Laitiner, L. M., Bridson, G. W., Raybuck, S. A., Tung, R. D. and Chaturredi, P. R., 1998, Metabolism of amprenavir in liver microsomes: role of CYP3A4 inhibition for drug interactions. *Journal of Pharmaceutical Science*, **87**, 803–807.

Eagling, V. A., Back, D. J. and Barry, M. G., 1997, Differential inhibition of cytochrome P450 isoforms by the protease inhibitors, ritonavir, saquinavir and indinavir. *British Journal of Clinical Pharmacology*, **44**, 190–194.

Eagling, V. A., Tjia, J. T. and Back, D. J., 1998, Differential selectivity of cytochrome P450 inhibitors against probe substrates in human and rat liver microsomes. *British Journal of Clinical Pharmacology*, **45**, 107–114.

Fitzsimmons, M. E. and Collins, J. M., 1997, Selective biotransformation of the human immunodeficiency virus protease inhibitor saquinavir by human small intestinal cytochrome P450. *Drug Metabolism and Disposition*, **25**, 256–267.

Gentile, D. M., Tomlinson, E. S., Maggs, J. L., Park, B. K. and Back, D. J., 1996, Dexamethasone metabolism by human liver *in vitro*. Metabolite identification and inhibition of 6-hydroxylation. *Journal of Pharmacology and Experimental Therapeutics*, **277**, 105–112.

Guengerich, F. P., Kim, D. H. and Iwasaki, M., 1991, Role of human cytochrome P450 IIE1 in the oxidation of many low molecular weight cancer suspects. *Chemical Research in Toxicology*, **4**, 168–179.

Halpert, J. R., Guengerich, F. P., Bend, J. R. and Correia, M. A., 1994, Selective inhibitors of cytochromes P450. *Toxicology and Applied Pharmacology*, **125**, 163–175.

Houston, J. B., 1994, Utility of *in vitro* drug metabolism data in predicting *in vivo* metabolic clearance. *Biochemical Pharmacology*, **47**, 1469–1479.

Kim, R. B., Fromm, M. F., Wandel, C., Leake, B., Wood, A. J. J., Roden, D. M. and Wilkinson, G. R., 1998, The drug transporter P-glycoprotein limits oral absorption and brain entry of HIV-1 protease inhibitors. *Journal of Clinical Investigation*, **101**, 289–294.

Kolars, J. C., Schmiedlin-Ren, P., Schuetz, J. D., Fang, C. and Watkins, P. B., 1992, Identification of rifampicin-inducible P4503A4 in human small bowel enterocytes. *Journal of Clinical Investigation*, **90**, 1871–1878.

Kumar, G. N., Rodrigues, A. D., Buko, A. M. and Denissen, J. F., 1996, Cytochrome P450 mediated metabolism of the HIV-1 protease inhibitor Ritonavir (ABT-538) in human liver microsomes. *Journal of Pharmacology and Experimental Therapeutics*, **277**, 23–31.

Kunze, K. L. and Trager, W. F., 1993, Isoform-selective mechanism-based inhibition of human cytochrome P450 1A2 by furafylline. *Chemical Research in Toxicology*, **6**, 649–656.

Lee, C. G. L., Gottesman, M. M., Cardarelli, C. O., Ramachandra, M., Jeang, K.-T., Ambudcar, S. V., Pastan, I. and Dey, S., 1998, HIV-1 protease inhibitors are substrates for the *MDR*1 multidrug transporter. *Biochemistry*, **37**, 3594–3601.

Lewis, D. V. F., Eddershaw, P. J., Glodfarb, P. S. and Tarbit, M. H., 1996, Molecular modelling of CYP3A4 from an alignment with CYP102: identification of key interactions between putative active site residues and CYP3A-specific chemicals. *Xenobiotica*, **26**, 1067–1086.

Lown, K. S., Ghosh, M. and Watkins, P. B., 1998, Sequences of intestinal and hepatic cytochrome P450 3A4 cDNAs are identical. *Drug Metabolism and Disposition*, **26**, 185–187.

Lown, K. S., Mayo, R. R., Leichtman, A. B., Hsiao, H., Turgeon, K., Schmeidlin-Ren, P., Brown, M. B., Guo, W., Rossi, S. J. Benet, L. Z. and Watkins, P. B., 1997, Role of intestinal P-glycoprotein (mdr1) in interpatient variation in the oral bioavailability of cyclosporine. *Clinical and Pharmacology and Therapeutics*, **62**, 248–260.

Lowry, O. H., Rosebrough, N. J., Farr, A. L. and Randall, R. J., 1951, Protein determination with the Folin phenol reagent. *Journal of Biological Chemistry*, **193**, 265–275.

Merry, C., Barry, M. G., Mulcahy, F., Halifax, K. L. and Back, D. J., 1997b, Saquinavir pharmacokinetics alone and in combination with nelfinavir in HIV-infected patients. *AIDS*, **11**, F117–F120.

Merry, C., Barry, M. G., Mulcahy, F., Ryan, M., Heavey, J., Tjia, J. F., Gibbons, S. E., Breckenridge, A. M. and Back, D. J., 1997a, Saquinavir pharmacokinetics alone and in combination with ritonavir in HIV infected patients. *AIDS*, **11**, F29–F33.

Noble, S. and Faulds, D., 1996, Saquinavir. A review of its pharmacology and clinical potential in the management of HIV infection. *Drugs*, **52**, 93–112.

Perry, C. M. and Noble, S., 1998, Saquinavir soft-gel capsule formulation. A review of its use in patients with HIV infection. *Drugs*, **55**, 461–486.

Profit, L., Eagling, V. A. and Back, D. J., 1999, Modulation of P-glycoprotein function in human lymphocytes and Caco-2 cell monolayers by HIV-1 protease inhibitors. *AIDS*, **13**, 1623–1627.

Prueksaritanont, T., Gorham, L. M., Hochman, J. H., Tran, L. O. and Vyas, K. P., 1996, Comparative studies of drug metabolizing enzymes in dog, monkey, and human small intestines, and in Caco-2-cells. *Drug Metabolism and Disposition*, **24**, 634–642.

Sesardic, D., Boobis, A. R., Murray, B. P., Segura, J., De La Torre, R. and Davies, D. S., 1990, Furafylline is a potent and selective inhibitor of cytochrome P4501A2 in man. *British Journal of Clinical Pharmacology*, **29**, 651–663.

Steimer, J. L., Fotteler, B., Gieschke, R., Wiltshire, H. and Buss, N., 1998, Predicting the optimal dose of saquinavir via modelling of dose–exposure and exposure–effect relationships. In M. Danhof and J. L. Steimer (eds), *Measurement and Kinetics of In Vivo Drug Effects: Advances in Simultaneous Pharmacokinetic/Pharmacodynamic Modelling* (Leiden: Amsterdam Center for Drug Research), pp. 79–86.

Von Moltke, L. L., Greenblatt, D. J., Grassi, J. M., Granda, B. W., Duan, S. X., Fogelman, S. M., Daily, J. P., Harmatz, J. S. and Shader, R. I., 1998, Protease inhibitors as inhibitors of human cytochromes P450: high risk associated with ritonavir. *Journal of Clinical Pharmacology*, **38**, 106-111.

Waxman, D. J., Attisano, C., Guengerich, F. P. and Lapenson, D. P., 1988, Human liver microsomal steroid metabolism. Identification of the major microsomal steroid 6β hydroxylase cytochrome P450 enzyme. *Archives in Biochemistry and Biophysics*, **290**, 160–166.

Waxman, D. J., Lapenson, D. P., Aoyama, T., Gelboin, H. V., Gonzalez, F. J. and Korzekwa, K., 1991, Steroid hormone hydroxylase specificities of eleven cDNA-expressed human cytochrome P450s. *Archives in Biochemistry and Biophysics*, **290**, 160–166.

Wiltshire, H. R., Prior, K. J., Dhesi, J., Trach, F., Schlageter, M. and Schönenberger, H., 1998, The synthesis of labelled forms of saquinavir. *Journal of Labelled Compounds and Radiopharmacology*, **41**, 1103–1126.

XENOBIOTICA, 2002, VOL. 32, NO. 1, 19–27

Taylor & Francis
healthsciences

Pharmacokinetics of a benzodithiin (RD3-0028) following aerosol treatment in rat

K. SUDO†§*, K. YOSHIDA‡, K. KONNO†, S. NINOMIYA‡, M. HIBINO‡, S. SHIGETA§ and T. YOKOTA†

† Rational Drug Design Laboratories, 4-1-1, Misato, Matsukawa-Machi, Fukushima 960-1242, Japan
‡ Tokai Research Laboratories, Daiichi Pure Chemicals Co. Ltd, 2117 Muramatsu, Tokai, Ibaraki, 319-1182, Japan
§ Department of Microbiology, Fukushima Medical College, Fukushima, 960-1295 Japan

Received 14 May 2001

1. RD3-0028, a benzodithiin compound, has potent antiviral activity against respiratory syncytial virus (RSV) in cell culture. The compound also inhibits growth of RSV and improves pathologic changes of interstitial pneumonia in the immunosuppressed mouse when delivered by small-particle aerosol.

2. In the present study, the absorption, distribution and excretion of ^{14}C-RD3-0028 were compared in rat following either a single aerosol treatment or oral administration.

3. The plasma concentration was maintained at the same level from 5 min to 1 h, and decreased with a half-life of 2.2 ± 0.1 h for 1–8 h.

4. The excretion of radioactivity in the urine and faeces at 24 h after aerosol treatment was 89.3 and 4.5%, respectively, indicating that almost all the radioactivity was rapidly excreted in the urine. The excretion of total radioactivity was 98.9% within 168 h.

5. The concentrations of radioactivity in the lung and trachea following aerosol treatment were higher than those in other tissues, and were detected even at 72 h.

6. These results suggest that the aerosol treatment might be useful for delivering RD3-0028 to the respiratory tract of RSV-infected patients.

Introduction

Human respiratory syncytial virus (RSV), a member of the family Paramyxoviridae, is the most prevalent infectious agent of acute lower respiratory illness in infants and young children (Henderson *et al.* 1979) and is associated with a significant morbidity in children with underlying cardiopulmonary disease (MacDonald *et al.* 1982). One therapy for RSV infection, intravenous administration of immunoglobulin, has not been effective (Groothuis *et al.* 1988, 1991, Prince *et al.* 1990). 1-β-D-ribofuranosyl-1,2,4-triazole-3-carboxamide (ribavirin), a broad-spectrum antiviral agent, is administered only as chemotherapy for severe RSV-induced illness in patients with bronchopulmonary dysplasia (Hall *et al.* 1985, Shuto *et al.* 1992). Gilbert *et al.* (1988, 1991) reported the pharmacokinetics of ribavirin when administered as aerosol to mouse. Its utility is questionable, however, because of its controversial efficacy and high cost (Ohmit *et al.* 1996).

* Author for correspondence; Metabolic Diseases Research, Pharmacology Laboratories, Institute for Drug Discovery Research, Yamanouchi Pharmaceutical Co. Ltd, 21 Miyukigaoka, Tsukuba-shi, Ibaraki 305-8585, Japan; e-mail: sudou.kenji@yamanouchi.co.jp

Xenobiotica ISSN 0049–8254 print/ISSN 1366–5928 online © 2002 Taylor & Francis Ltd
http://www.tandf.co.uk/journals
DOI: 10.1080/00498250110079158

RD3-0028, 1,4-dihydro-2,3-benzodithiin, is a potent inhibitor of RSV replication. Its action is specific and no activity is seen against other viruses (Watanabe *et al.* 1998). RD3-0028 is effective in the immunosuppressed RSV-infected mouse model and has been shown to inhibit growth of pulmonary RSV in infected mice when delivered by small particle aerosol using a head-exposure chamber (Sudo *et al.* 1999). The minimal effective dose for RD3-0028 against RSV-induced infection in mice is significantly less than that observed with ribavirin. Sections of lung from RSV-infected mice show histologic evidence of interstitial pneumonia, monocyte and eosinophil infiltration in peribronchiolar and perivascular spaces, thickening of alveolar walls, and arteritis followed by monocyte infiltration in the artery (Sudo *et al.* 1999). In contrast, mice treated with RD3-0028 aerosol improved to the level of uninfected controls (Sudo *et al.* 1999). No toxic effects were noted in mice from an effective dose administered for 10 consecutive days (Sudo *et al.* 1999).

The present study used a rat model to study the disposition of the aerosol treatment of RD3-0028 compared with oral administration in more detail and to relate the efficacy to pharmacokinetics and distribution of ^{14}C-RD3-0028 in rat.

Materials and methods

Labelled compound

^{14}C-benzodithiin (^{14}C-RD3-0028) was synthesized by Daiichi Pure Chemicals Co., Ltd (Ibaraki, Japan) and the labelled position of ^{14}C-RD3-0028 is shown in figure 1. The specific radioactivity of the labelled compounds was 10.4 MBq mg^{-1}, and the radiochemical purity of the labelled compounds was >99% during the experimental period.

Experimental animals

Sprague–Dawley strain SPF rats (Charles River Japan, Inc., Yokohama, Japan) consisting of 7-week-old males weighing 270 g were used. Rats were allowed water and pellet food (MF, Oriental Yeast Co., Ltd, Nagahama, Japan) *ad libitum*, and were acclimatized for >1 week to a room temperature of 23 ± 2°C and a relative humidity of 55 ± 10% on a 12-h light/dark cycle.

Dose label and administration

^{14}C-RD3-0028 was dissolved in 10% dimethyl sulphoxide (DMSO)/saline containing 1% Tween 80 for administration by the aerosol route. The aerosol was generated using a head-exposure chamber, mono-position, with a mist generator (Sibata Scientific Technology Ltd, Tokyo, Japan). The mass median aerodynamic diameter of the aerosol particle was 2.1 μm, with a geometric SD = 1.86 (Sudo *et al.* 1999). Rats were exposed to the ^{14}C-RD3-0028 aerosol for 15 min and killed at indicated times after the end of exposure. Because the aerosol treatment with ^{14}C-RD3-0028 exposed the rat to 8.8 μg (91.5 kBq)/animal, the solution of this compound was orally administered at a dose of 8.8 μg/body.

Measurement of radioactivity

Radioactivity in each test sample was counted using a liquid scintillation counter (LSC-903 or LSC-3600, ALOKA) for 2 min, the efficiency of the count being corrected by the channel ratio method with

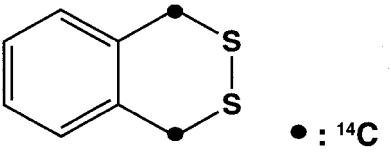


Figure 1. Chemical structure of ^{14}C-RD3-0028. The position of the radiolabel is indicated by the closed circles.

external standard sources. Concentrations of radioactivity in plasma and tissues were expressed as ng-equivalents of RD3-0028 ml^{-1} or g^{-1}.

Determination of radioactivity concentration in plasma

After aerosol treatment of ^{14}C-RD3-0028, the rats were housed in cages, and 250 µl sample of blood was withdrawn from the caudal vein of each animal at 5, 15, 30 min, 1, 2, 4, 6, 8, 24, 48 and 72 h after treatment and immediately centrifuged (4°C, 1800*g*, 15 min) to obtain plasma. Plasma samples were dissolved in 2 ml tissue solubilizer SOLUENE-350 (Packard Instrument Co., Meriden, CT, USA) and the radioactivity in each sample was counted after the addition of 13 ml scintillator HIONICFLUOR (Packard Instrument Co., Meriden, CT, USA).

Determination of excretion of radioactivity in urine and faeces

After aerosol treatment with ^{14}C-RD3-0028, the rats were housed in glass metabolic cages with a trap for expired air. Urine and faeces were collected at 0–4, 4–8, 8–24, 24–48, 48–72, 72–96, 96–120, 120–144 and 144–168 h after treatment. Each urinary sample was diluted with water and the radioactivity in each 1 ml diluent was counted after the addition of 10 ml scintillator HIONICFLUOR. All faecal samples were homogenized in water and the radioactivity in each 1 ml homogenate was counted after the addition of 10 ml scintillator HIONICFLUOR. After collection of urine and faeces at the final determination time, rats were killed by ether inhalation, and each carcass was dissolved by reflux heating in a mixture of 0.5 N sodium hydroxide and toluene for 72 h. The solution from each carcass was then homogenized in water and the radioactivity in each 1 ml homogenate was counted after the addition of 10 ml scintillator HIONICFLUOR.

Whole-body autoradiography

After aerosol treatment with ^{14}C-RD3-0028, rats were housed in cages and killed by ether inhalation at 5 min, 2, 6, 24 and 72 h after treatment. The nasal cavity and anus were filled with 5% carboxymethyl cellulose (CMC), and each carcass was frozen in a dry ice–acetone mixture at −70°C. The frozen carcass was then embedded in 5% CMC on a microtome stage, held in a CRYOMICROTOME (PMV 450 MP, LKB) and cut into ~35-µm slices at −25°C. Frozen slices were stripped off with adhesive tape (No. 810, Sumitomo 3M) and freeze-dried at −25°C. The surface of the slices was covered with a protective film (4 µm, Dia Foil) and placed in contact with X-ray film (BIOMAX-MR, Eastman Kodak), which were exposed at 4°C for 35 days and then developed for whole-body autoradiography. A focus was made only on the lung autoradiograms.

Determination of radioactivity in tissue

After aerosol treatment with ^{14}C-RD3-0028, rats were housed in cages and exsanguinated from the abdominal aorta under ether anaesthesia at 5 min, 2, 6, 24 and 72 h after treatment. The following tissues were collected for examination: plasma, trachea, lung, liver and kidney. Except for the kidney, the whole tissues or part of the selected tissues were weighed and the radioactivity was determined by the method used for plasma described above. Cerebrum and kidney were dissolved in 10 ml tissue solubilizer SOLUENE-350, diluted with toluene and the radioactivity in each 2 ml of diluent was counted after the addition of 10 ml scintillator HIONICFLUOR.

Calculation of pharmacokinetic parameters

The pharmacokinetic parameters were calculated from the individual plasma concentration–time curve of radioactivity. The areas under the concentration–time curve (AUC) were calculated using the trapezoidal method. Apparent half-lives ($T_{1/2}$) were estimated using the least square method from the original data.

Results

Radioactivity in plasma

The radioactivity determinations (equivalent to RD3-0028) after aerosol treatment and oral administration of ^{14}C-RD3-0028 are shown in figure 2. Five minutes after termination of a 15-min exposure to 8.8 µg/body RD3-0028, the plasma concentration of the compound was determined to be 21.7 ± 6.4 ng ml^{-1}. The peak plasma concentrations (C_{max}) of RD3-0028 were observed within 5 min of the termination of administration. Following oral administration of ^{14}C-RD3-

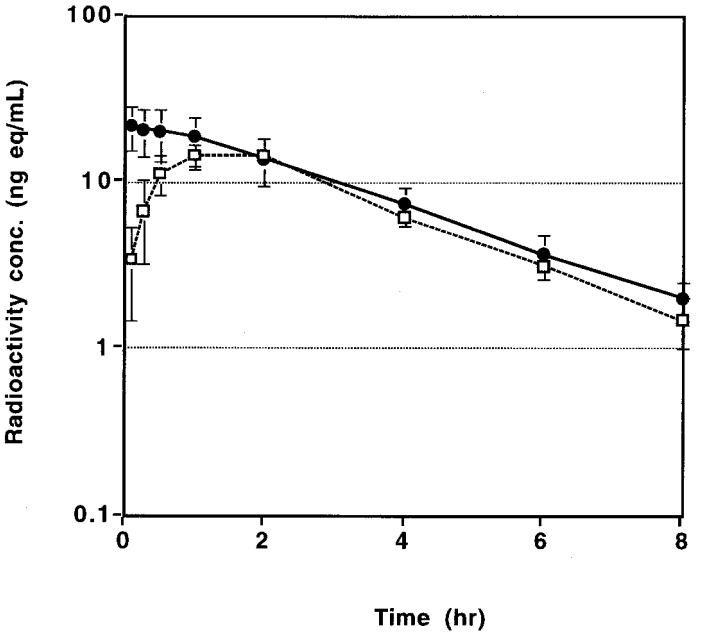


Figure 2. Plasma concentrations of radioactivity following aerosol treatment and oral administration of ^{14}C-RD3-0028 (8.8 μg/body) to rat. (solid circle) Aerosol treatment, (white square) oral administration. Data are expressed as the mean ± SD for three rats.

0028 (8.8 μg/body), C_{max} was observed at 1.5 h. The plasma concentrations of radioactivity declined with a half-life of 2.2 ± 0.1 h from 1 to 8 h and was below the limit of detection at 24 h when RD3-0028 was administered by aerosol treatment. Aerosol-delivered RD3-0028, as well as orally administered RD3-0028, was eliminated from plasma. The mean half-life of radioactivity after oral administration was 1.8 ± 0.2 h from 1 to 8 h. The AUC (0–8) was 74.3 ± 22.2 ng-eq. h ml^{-1} after aerosol treatment. On the other hand, the AUC (0–8) after oral administration was 58.4 ± 8.3 ng-eq. h ml^{-1}.

Excretion of radioactivity in urine and faeces

Table 1 shows the cumulative radioactivity excretion in the urine and faeces in rats after aerosol treatment of ^{14}C-RD3-0028. After aerosol exposure to a dose of 8.8 μg/body RD3-0028, the excretion of radioactivity in the urine was 56.5% of the dose within 4 h, 89.3% of the dose within 24 h, and 94.1% within 168 h. The excretion in the faeces was 4.5% of the dose within 24 h, and 4.8% within 168 h after treatment and the residual radioactivity in the carcass was 1.1% of the dose at 168 h. There was no excretion of radioactivity in the expired air within 168 h after aerosol treatment in the preliminary study (data not shown). The excretion of total radioactivity was 93.8% of the dose within 24 h, and 98.9% within 168 h. After oral administration, the radioactivity in the urine was 91.5% of total excretion. These results indicate that RD3-0028 is mostly excreted from urine after both aerosol treatment and oral administration. The contents in the urine following oral administration were analysed by high-performance liquid chromatography.

Table 1. Cumulative excretion of radioactivity in urine and faeces following aerosol treatment of ^{14}C-RD3-0028 (8.8 μg/body) to rat.

	Excretion of radioactivity (% of calculated dose)		
Time (h)	Urine	Faeces	Total
0–4	56.5 ± 8.0	–	–
8	76.7 ± 5.2	–	–
24	89.3 ± 2.5	4.5 ± 2.1	93.8 ± 2.3
48	91.5 ± 2.3	4.8 ± 2.3	96.3 ± 1.1
72	92.3 ± 2.2	4.8 ± 2.3	97.1 ± 0.6
96	92.8 ± 2.2	4.8 ± 2.3	97.6 ± 0.4
120	93.3 ± 2.3	4.8 ± 2.3	98.1 ± 0.3
144	93.7 ± 2.3	4.8 ± 2.3	98.5 ± 0.2
168	94.1 ± 2.3	4.8 ± 2.3	98.9 ± 0.2

Data are the mean ± SD for three rats.

Water-soluble metabolites of RD3-0028, as opposed to unchanged RD3-0028, were found in urine (data not shown).

Tissue distribution of radioactivity

Radioactivity levels in tissues directly demonstrate the fate of ^{14}C-RD3-0028 in the body. The lung autoradiograms of rats after aerosol treatment and oral administration of ^{14}C-RD3-0028 are shown in figure 3. High levels of radioactivity were found in the lung at 5 min after aerosol treatment, then the concentrations gradually decreased, but radioactivity was still present at 24 and 72 h. On the other hand, the radioactivity levels in the lung were highest at 2 h after oral administration. The residual levels in the trachea and lung after aerosol treatment were 5.0 and 16.8 times higher than those after oral administration (table 1). Concentrations versus time curves for selected tissues following aerosol treatment are shown in figure 4. The highest concentration of radioactivity was found in the trachea at 5 min, followed by the lung. The concentration gradually decreased in all tissues. Whereas the radioactivity was not detected at 72 h in the other tissues including the liver and kidney, it was still detected in the trachea and lung at 24–72 h.

Discussion

Nebulization of drugs is an alternative route of administration for direct delivery of a drug to the pulmonary surface. The administration of compounds as a small-particle aerosol is effective in the treatment of respiratory infectious disease (Hruska *et al.* 1982, Wyde *et al.* 1986). Gilbert *et al.* (1991) reported ribavirin triacetate and ribavirin administered by aerosol in an influenza virus encephalitis mouse model was superior to intraperioneal injection for increasing survival time and rates. Aerosols are also an effective way to deliver ribavirin, not only to the lungs and the systemic circulation, but also non-invasively to the brain. The pharmacokinetics of ribavirin aerosol have also been described (Gilbert and Wyde 1988). A general exposure apparatus, not nasal exposure, was used for aerosol treatment. Recently, there were reports of antiviral effects in an *in vivo* infection model following aerosol exposure using a head-exposure chamber, mono-

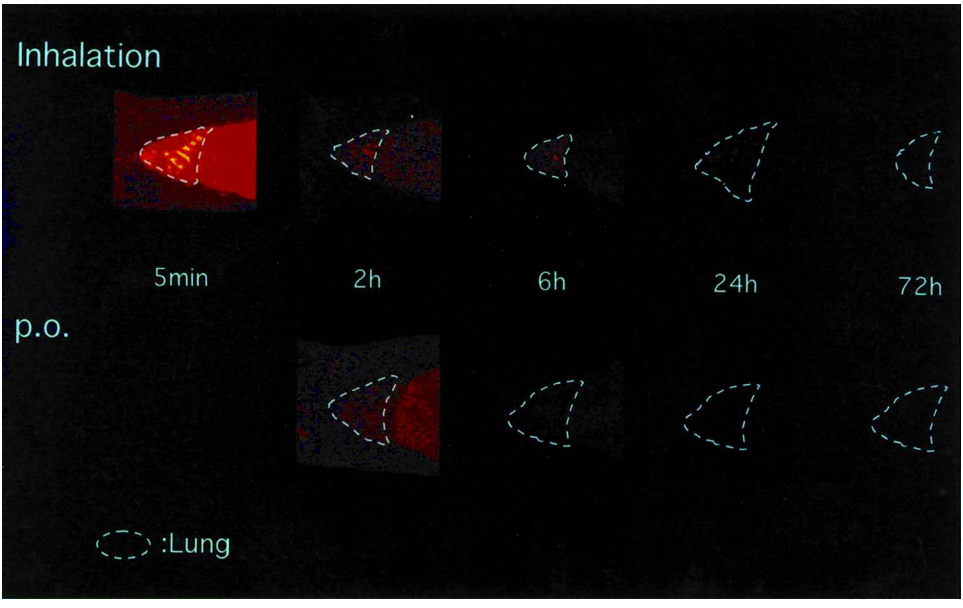


Figure 3. Autoradiograms showing the distribution of radioactivity in the lung following aerosol treatment and oral administration of ^{14}C-RD3-0028 (8.8 μg/body) to rat.

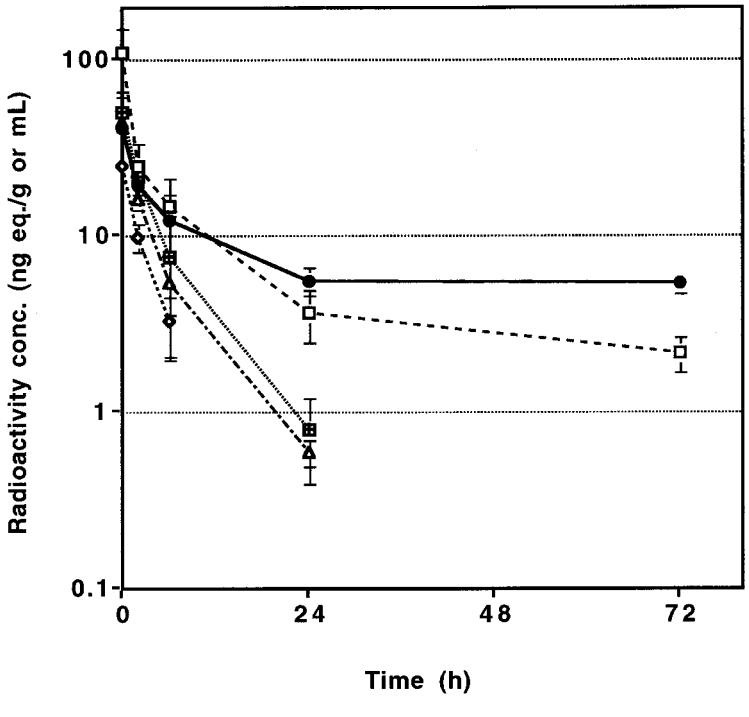


Figure 4. Tissue concentrations of radioactivity following aerosol treatment of ^{14}C-RD3-0028 (8.8 μg/body) to rat. (white diamond) plasma, (white square) trachea, (closed circle) lung, (white triangle) liver, (crossed square) kidney. Data are expressed as the mean ± SD for three rats.

position, with a mist generator (Shigeta *et al.* 1997, Sudo *et al.* 1999). The aim of the current study was to determine the pharmacokinetics and disposition of RD3-0028 in the rat after aerosol treatment using a head-exposure chamber. We studied the absorption, distribution, and excretion of ^{14}C-RD3-0028 after single inhalation and oral administration. RD3-0028 is rapidly cleared from the circulation. Excretion into the urine is the major route of elimination, however radioactivity remained in the lung and trachea for 72 h following inhalation.

Plasma concentration after aerosol treatment was maintained at the same level from 5 min to 1 h. Moreover, whole-body autoradiograms indicated that high levels of radioactivity in the gastric contents 5 min after aerosol treatment and in the intestinal contents at 2 h. These results indicate that RD3-0028 aerosol treatment is absorbed intestinally as well as intratracheally. In the case of amiloride given by aerosol, double plasma concentration peaks (C_{max1}, C_{max2}) occurred in most patients, probably the result of pulmonary and extrapulmonary absorption of the nebulized solution (Jones *et al.* 1997). C_{max1} might be due to direct pulmonary absorption of amiloride, because T_{max1} occurred much earlier than T_{max} after oral dosing. C_{max2} might result from extrapulmonary absorption of the nebulized amiloride solution by gastrointestinal, buccal and/or oropharyngeal routes because patients tend to swallow nebulized drug (Borgstrom and Nilsson 1990, Sly and LeSouef 1991) and because T_{max2} corresponds with the T_{max} after oral dosing. Kobayashi *et al.* (1985) also described a biphasic pattern of the blood level following inhalation of ^{3}H-fenoterol hydrobromide in rat; the peak time in the second phase resembled that after oral administration. It was found that the plasma concentrations of radioactivity following aerosol administration of RD3-0028 were maintained at the same level from 15 min to 1 h, and then decreased with a half-life of 2.2 ± 0.1 h from 1 to 8 h. Considering that the plasma concentration after oral administration reached a maximum at 1.5 h, RD3-0028 is also absorbed by the gastrointestinal route.

Proteins of high molecular weight and low lipophilicity must be administered parenterally to achieve the desired therapeutic blood level. The absorption of peptide and protein agents by rat lung following their intratracheal administration has been investigated (Okumura *et al.* 1992, Komada *et al.* 1994). These studies demonstrated that the intratracheal route was useful for delivery of the agents. Adjei and Garren (1990) demonstrated the importance of particle size in the pulmonary delivery of leuprolide to humans. In the present study, the mass median aerodynamic diameter of aerosol particle was determined to be 2.10 μm with a geometric SD = 1.86 (Sudo *et al.* 1999). Schanker and Hemberger (1983) suggested that there are at least three different populations of pore size in the rat lung that are permeable to hydrophilic compounds. The absorption of hydrophilic compounds of molecular weights ranging from 60 to 75 000 is inversely related to molecular weight. Numerous small pores are permeable to compounds of molecular weights >122, whereas their pores exclude compounds with a molecular weight of ≥ 5250, and very few large pores are permeable to compounds with molecular weight >5250 (Taylor 1990). High molecular weight and hydrophilic peptides are thought to be absorbed via junctions between the cells and/or via pinocytosis. The permeability of RD3-0028 appears to be dependent on small pores.

In the present study, ^{14}C-RD3-0028 is rapidly cleared from the circulation following aerosol treatment and excretion into the urine is the major route of

Table 2. Distribution of radioactivity in the trachea and lung at 72 h following aerosol treatment and oral administration of ^{14}C-RD3-0028 to rat.

	Radioactivity conc. (ng eq g^{-1})		Ratio (B)/(A)
	p.o. (A)	inhalation (B)	
Trachea	0.44 ± 0.14	2.20 ± 0.52	5.04
Lung	0.32 ± 0.15	5.43 ± 0.70	16.77

Data are the mean ± SD for three rats.

elimination. Following aerosol treatment with ^{14}C-RD3-0028, radioactivity was largely excreted in the urine, with >90% excreted within 48 h. Whole-body autoradiograms indicated high levels of radioactivity in gastric contents 5 min after aerosol treatment and in intestinal contents at 2 h (data not shown). The metabolites excreted in urine within 24 h were more water-soluble than RD3-0028. It is possible that these metabolites are conjugated. It was found that a high concentration of RD3-0028 reached the trachea and the lung 5 min after treatment and the level of radioactivity was maintained throughout the observation period. Distribution of radioactivity in the tissues after inhalation of ^{3}H-fenoterol, was observed in the lung, stomach and small intestine (Kobayashi *et al.* 1985).

Following aerosol treatment of ^{14}C-RD3-0028 to the rat, the dose was rapidly absorbed from lung and gastrointestinal tract, and almost all the radioactivity was excreted in the urine. Whereas RD3-0028 was rapidly eliminated from the circulation, the level of radioactivity persisted in the lung and trachea. The concentrations of radioactivity in the lung following aerosol treatment with a solution of ^{14}C-RD3-0028 at 2.5 mg ml^{-1} was equivalent to ~1 μg g^{-1} tissue. This concentration exceeds the EC_{50} (0.7 μg ml^{-1}) determined in an *in vitro* study (Watanabe *et al.* 1998). The results of the present study suggest that aerosol administration of RD3-0028 is an effective route for topical target or systemic delivery that merits further evaluation.

References

Adjei, A. and Garren, J., 1990, Pulmonary delivery of peptide drugs: Effect of particle size on bioavailability of leuprolide acetate in healthy male volunteers. *Pharmaceutical Research*, **7**, 565–569.

Borgstrom, L. and Nilsson, M., 1990, A method for determination of the absolute pulmonary bioavailability of inhaled drugs: Terbutaline. *Pharmaceutical Research*, **7**, 1068–1070.

Gilbert, B. E. and Wyde, P. R., 1988, Pharmacokinetics of ribavirin aerosol in mice. *Antimicrobial Agents and Chemotherapy*, **32**, 117–121.

Gilbert, B. E., Wyde, P. R., Wilson, S. Z. and Robins, R. K., 1991, Aerosol and intraperitoneal administration of ribavirin and ribavirin triacetate: Pharmacokinetics and protection of mice against intracerebral infection with influenza A/WSN virus. *Antimicrobial Agents and Chemotherapy*, **35**, 1448–1453.

Groothuis, J. R., Gutierrez, K. M. and Lauer, B. A., 1988, Respiratory syncytial virus infection in children with bronchopulmonary dysplasia. *Pediatrics*, **82**, 199–203.

Groothuis, J. R., Levin, M. J., Rodriguez, W., Hall, C. B., Long, C. E., Kim, H. W., Lauer, B. A. and Hemming, V. G., 1991, Use of intravenous gamma globulin to passively immunize high-risk children against respiratory syncytial virus: safety and pharmacokinetics. The RSVIG Study Group. *Antimicrobial Agents and Chemotherapy*, **35**, 1469–1473.

Hall, C. B., McBride, J. T., Gala, C. T., Hildreth, S. W. and Schnabel, K. C., 1985, Ribavirin treatment of respiratory syncytial viral infection in infants with underlying cardiopulmonary disease. *Journal of the American Medical Association*, **254**, 3047–3051.

Henderson, F. W., Collier, A. M., Clyde, W. A., Jr and Denny, F. W., 1979, Respiratory syncytial virus infections, reinfections and immunity: a prospective longitudinal study in young children. *New England Journal of Medicine*, **300**, 530–534.

Hruska, J. F., Morrow, P. E., Suffin, S. C. and Douglas, R. G., Jr, 1982, *In vivo* inhibition of respiratory syncytial virus by ribavirin. *Antimicrobial Agents and Chemotherapy*, **21**, 125–130.

Jones, K. M., Liao, E., Hohneker, K., Turpin, S. M., Henry, M., Selinger, K., Hsyu, P. H., Boucher, R. C., Knowles, M. R and Dukes, G. E, 1997, Pharmacokinetics of amiloride after inhalation and oral administration in adolescents and adults with cystic fibrosis. *Pharmacotherapy*, **17**, 263–270.

Kobayashi, S., Yoshida, T., Matsumura, R. and Kohei, H., 1985, Disposition of ^{3}H-fenoterol after inhalation in rats. *Drug Research*, **35**, 360–363.

Komada, F., Iwakawa, S., Yamamoto, N., Sakakibara, H. and Okumura, K., 1994, Intratracheal delivery of peptide and protein agents: absorption from solution and dry powder by rat lung. *Journal of Pharmaceutical Sciences*, **83**, 863–867.

MacDonald, N. E., Hall, C. B., Suffin, S. C., Alexson, C., Harris, P. J. and Manning, J. A., 1982, Respiratory syncytial viral infection in infants with congenital heart disease. *New England Journal of Medicine*, **307**, 397–400.

Ohmit, S. E., Moler, F. W., Monto, A. S. and Khan, A. S., 1996, Ribavirin utilization and clinical effectiveness in children hospitalized with respiratory syncytial virus infection. *Journal of Clinical Epidemiology*, **49**, 963–967.

Okumura, K., Iwakawa, S., Yoshida, T., Seki, T. and Komada, F., 1992, Intracheal delivery of insulin absorption from solution and aerosol by rat lung. *International Journal of Pharmaceutics*, **88**, 63–73.

Prince, G. A., Hemming, V. G., Horswood, R. L., Baron, P. A., Murphy, B. R. and Chanock, R. M., 1990, Mechanism of antibody-mediated viral clearance in immunotherapy of respiratory syncytial virus infection of cotton rats. *Journal of Virology*, **64**, 3091–3092.

Schanker, L. S. and Hemberger, J. A., 1983, Relation between molecular weight and pulmonary absorption rate of lipid-insoluble compounds in neonatal and adult rats. *Biochemical Pharmacology*, **32**, 2599–2601.

Shigeta, S., Mori, S., Watanabe, J., Soeda, S., Takahashi, K. and Yamase, T., 1997, Synergistic anti-influenza virus A (H1N1) activities of PM-523 (polyoxometalate) and ribavirin *in vitro* and *in vivo*. *Antimicrobial Agents and Chemotherapy*, **41**, 1423–1427.

Shuto, S., Obara, T., Toriya, M., Hosoya, M., Snoeck, R., Andrei, G., Balzarini, J. and De Clercq, E., 1992, New neplanocin analogues. 1. Synthesis of 6′-modified neplanocin A derivatives as broad-spectrum antiviral agents. *Journal of Medicinal Chemistry*, **35**, 324–331.

Sly, P. and Le Souef, P., 1991, Inhaled therapy in paediatrics. *Journal of Paediatrics and Child Health*, **27**, 7–10.

Sudo, K., Watanabe, W., Konno, K., Sato, R., Kajiyashiki, T., Shigeta, S. and Yokota., T., 1999, Efficacy of RD3-0028 aerosol treatment against respiratory syncytial virus infection in immunosuppressed mice. *Antimicrobial Agents and Chemotherapy*, **43**, 752–757.

Taylor, G., 1990, The absorption and metabolism of xenobiotics in the lung. *Advanced Drug Delivery Reviews*, **5**, 37–61.

Watanabe, W., Sudo, K., Sato, R., Kajiyashiki, T., Konno, K., Shigeta, S. and Yokota, T., 1998, Novel anti-respiratory syncytial (*RS*) viral compounds: Benzodithiin derivatives. *Biochemical and Biophysical Research Communications*, **249**, 922–926.

Wyde, P. R., Wilson, S. Z., Gilbert, B. E. and Smith, R. H. A., 1986, Protection of mice from lethal influenza virus infection with high dose-short duration ribavirin aerosol. *Antimicrobial Agents and Chemotherapy*, **30**, 942–944.

XENOBIOTICA, 2002, VOL. 32, NO. 1, 29–43

Taylor & Francis
healthsciences

N-O glucuronidation: a major human metabolic pathway in the elimination of two novel anti-convulsant drug candidates

I. M. ISMAIL†*, G. J. DEAR†, A. D. ROBERTS†, R. S. PLUMB†, J. AYRTON†, B. C. SWEATMAN† and G. D. BOWERS‡

† Structural Identification Group, GlaxoSmithKline Research and Development, Park Road, Ware SG12 0DP, UK
‡ Structural Identification Group, GlaxoSmithKline, Inc., 3030 Cornwallis Road, RTP, NC 27709, USA

Received 11 April 2001

1. The urinary metabolites of the anti-convulsant compound 4-amino-1-(2,6-difluorobenzyl)-1*H*-1,2,3-triazolo[4,5-*c*]-pyridine hydrochloride (GI265080) obtained following a single oral dose to man have been detected and quantified relative to each other using ^{19}F-NMR spectroscopy.

2. The human urinary metabolites of GI265080 were isolated using semipreparative HPLC and unequivocally characterized using ^{1}H-NMR spectroscopy, two-dimensional heteronuclear NMR spectroscopy and mass spectrometry. The assignments of the *N*-(5)-oxide and the *N*-(5)-*O*-glucuronide metabolites of GI265080 were further confirmed by independent synthesis. The urinary metabolites obtained following single oral doses to dog and rat have also been isolated and characterized.

3. The human urinary metabolites of GI265080 comprise the *N*-(5)-oxide, the quaternary N^{+}-(5)-glucuronide, the 7-hydroxy glucuronide and a glucuronide conjugate of the *N*-(5)-oxide. The *N*-(5)-*O*-glucuronide conjugate is a novel species in human metabolism and is a significant route of elimination of GI265080 in man.

4. The urinary metabolites of the potential anti-convulsant GW273293 (6-amino-3-(2,3,5-trichlorophenyl)pyrazin-2-ylamine) obtained following a single oral dose to man have also been isolated and characterized. The formation of a novel *N*-*O*-glucuronide was also observed and was shown to constitute a significant route of elimination of GW273293 in man.

Introduction

GI265080 (4-amino-1-(2,6-difluorobenzyl)-1*H*-1,2,3-triazolo[4,5-*c*]-pyridine hydrochloride) (figure 1) is a novel anti-convulsant recently in development for the treatment of partial and generalized tonic–clonic seizures. Its pattern of activity in animal models is similar to that shown by other anti-convulsant drugs that prevent the spread of seizures such as carbamazepine, phenytoin and lamotrigine. The mechanism of action has not been completely characterized but appears to be different from that of currently marketed anti-epileptic drugs. GI265080 is metabolized extensively in man and animal species *in vivo*, the majority of drug-related material being eliminated via the urine. The isolation and characterization of its major metabolites following administration of a single oral dose to man, dog and rat is described here.

* Author for correspondence; e-mail: imi2682@glaxowellcome.co.uk

Xenobiotica ISSN 0049–8254 print/ISSN 1366–5928 online © 2002 Taylor & Francis Ltd
http://www.tandf.co.uk/journals
DOI: 10.1080/00498250110081623

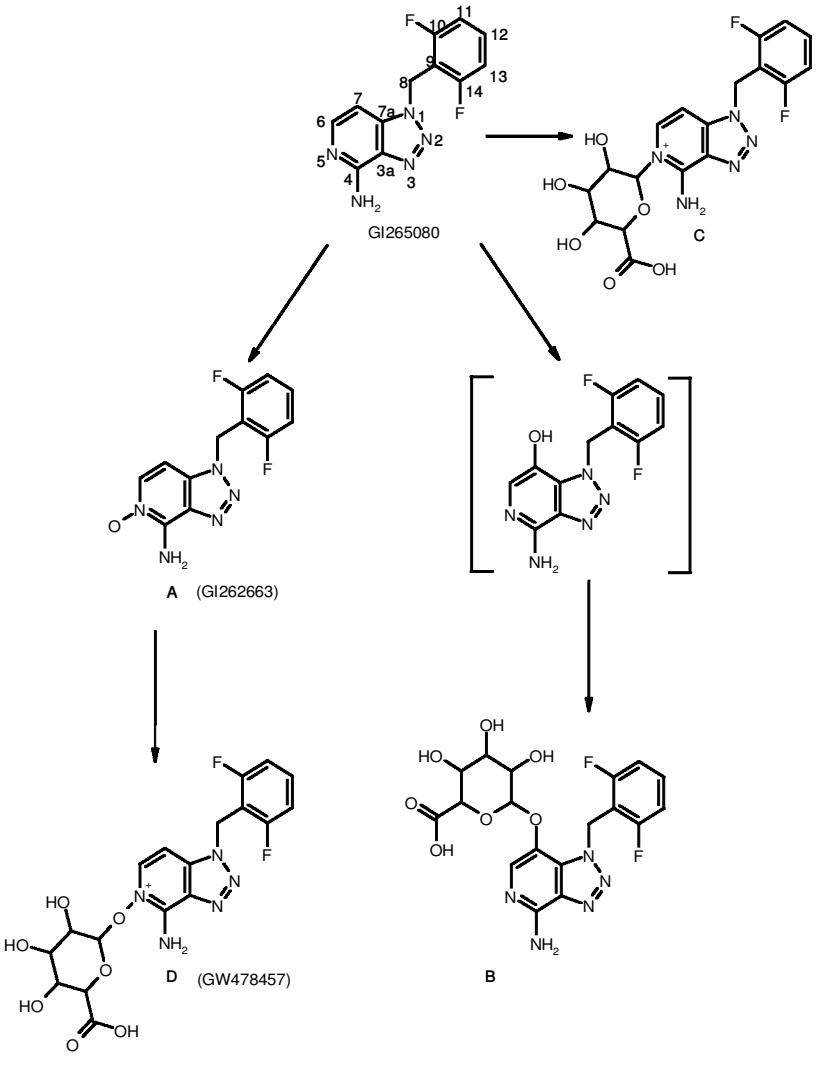


Figure 1. Metabolism of GI265080 in man.

The use of ^{19}F-NMR has long been suggested as a viable alternative to the use of radiolabelled drug material in human clinical studies (Wade *et al*. 1988, Malet-Martino and Martino 1989) and has recently been used in animal studies for this purpose (Scarfe *et al*. 1998, Ismail *et al*. 1999, Dear *et al*. 2000). The present study shows its utility in readily tracing the urinary elimination of fluorinated compounds in human clinical trials without the use of radiolabelled drug material. Additionally, the determination of the number of metabolites formed over the course of the study may be possible, although the potential for overlapping signals must be recognized if ^{19}F-NMR is to be used without any isolation procedures.

The complete and unambiguous characterization of the metabolites described here required the use of semipreparative HPLC, NMR spectroscopy, mass spectrometry (MS) and the synthesis of authentic materials. Of particular sig-

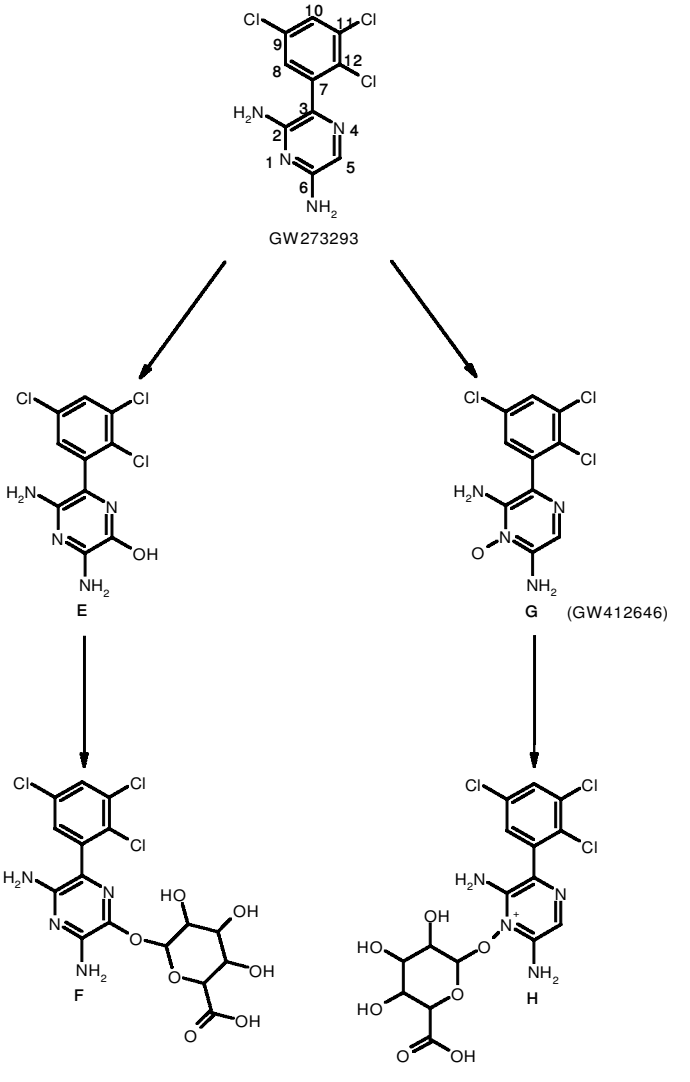


Figure 2. Metabolism of GW273293 in man.

nificance were the long-range heteronuclear-correlated NMR experiments such as heteronuclear multiple-bond correlation (HMBC), which normally requires substantial amounts of material (in the order of hundreds of micrograms). Conventionally, this would have required laborious and time-consuming isolation. However, the use of automated semipreparative HPLC to isolate large amounts of drug-related material (Dear *et al*. 1999, Plumb *et al*. 1999) permits the use of these information-rich NMR experiments and allows the rapid characterization of the metabolites. This methodology has also been used here to investigate the metabolism of a second anti-convulsant, GW273293 (6-amino-3-(2,3,5-trichlorophenyl)pyrazin-2-ylamine) (figure 2).

The metabolism of xenobiotics often involves oxidation and/or conjugation reactions and with heterocyclic nitrogen-containing molecules a nitrogen atom may be the centre of metabolic activity.

Doig and Clare (1991) demonstrated that both direct conjugation with glucuronic acid and formation of *N*-oxides at reactive nitrogen sites can contribute significantly to the metabolic clearance of aminoazaheterocyclic molecules such as lamotrigine. They noted considerable interspecies variation in metabolic profile, but the major metabolite in humans was the *N*-2-glucuronide. The direct conjugation of glucuronic acid with an *N*-oxide to form an *N*-*O*-glucuronide metabolite has been proposed for the amino heteroaromatic *N*-oxide compound minoxidil (2,4-diamino-6-piperidinopyrimidine 3-*N*-oxide) in dog (Thomas and Harpootlian 1975). Further assignments of similar metabolites have been reported in guinea pig and rabbit urine following administration of mianserin (Delbressine *et al.* 1992) and pinacidil (Sakamoto and Nakamura 1993). In the few literature examples where *N*-*O*-glucuronide metabolites have been reported, they were detected only in animal species, not in humans and the precise structures were not unequivocally assigned.

We report here the formation of *N*-*O*-glucuronide conjugates as major human metabolites following administration of GI265080 and GW273293. We also present the first unequivocal structural characterization of these conjugates through the use of both one- and two-dimensional NMR experiments as well as mass spectrometry.

Materials and methods

Reagents

The acetonitrile used for NMR analysis was Fluka Residue Analysis grade (Sigma-Aldrich Ltd, Poole, UK), all other organic solvents were of HPLC grade (Rathburn Chemicals Ltd, Walkerburn, UK) and deuterium oxide (99.9%) was obtained from Fluorochem Ltd (Old Glossop, UK). The experimental compounds GI265080, its *N*-(5)-oxide (GI262663) and GW478457 the *N*-*O*-glucuronide (figure 1) together with GW273293 and (GW412646) its *N*(1)-oxide (figure 2) were synthesized at GlaxoWellcome Research and Development (Stevenage, UK).

Urine collection

Human. A single oral dose of GI265080 (200 mg) was administered in capsule form to informed healthy male volunteers. Urine samples were collected predose and over the following periods post-dose: 0–4, 4–12, 12–24 h and then daily until 240 h.

A single oral dose of GW273293 (200 mg) was administered in capsule form to informed healthy male volunteers. Urine samples were collected predose and over the following periods post-dose: 0–6, 6–24 h and then daily until 120 h.

All samples were kept stored frozen at –20 °C before analysis.

Dog. Single doses of GI265080 (20 mg kg^{-1} body weight) were administered by gastric intubation, as solutions in 10^{-2} M HCl, to one male and two female adult beagle dogs. The dogs were housed individually in metal metabolism cages with free access to food (Harland Tekland 9682 dog maintenance diet, Harland Tekland, UK) and water; urine was collected predose and at 0–8, 8–24 and 24–48 h post-dose. All samples were kept stored frozen at –20 °C before analysis.

Rat. Single doses of GI265080 (10 mg kg^{-1} body weight) were administered by gastric intubation, as solutions in 10^{-2} M HCl, to male and female adult Sprague–Dawley rats. The rats were housed individually in glass metabolism cages with free access to food (R&M1, SDS, Witham, UK) and water; urine was collected predose and up to 24 h post-dose. All samples were kept stored frozen at –20 °C before analysis.

Sample preparation

Pooled urine samples collected following oral administration of GI265080 to man (100 ml), dog (50 ml) and rat (10 ml) were freeze-dried and reconstituted in distilled water, 2 ml for the rat and 10 ml for the dog and human samples. Pooled urine samples collected following oral administration of GW273293 to man (100 ml) were freeze-dried and reconstituted in 10 ml distilled water. The resulting concentrated urine samples were centrifuged at 16249*g* for 5 min and the supernatants removed and stored at 0–8 °C before isolation by preparative HPLC as described below.

Preparative HPLC

For GI265080 samples preparative chromatography was performed on a Magellen C18 60 × 10 mm 5 µm column (Phenomenex, UK) using a Gilson 233-XL autosampler, two Gilson 307 pumps (Gilson, France) controlled by Unipoint (v.1.6) software. The sample eluent was monitored by UV absorbance using a LDC Spectro-Monitor 3100 (Thermoseparations, USA). Injections of the concentrated urine samples (2 or 10 ml) were made onto the preparative column. The column effluent was collected into 96-well microtitre plates under the control of the Unipoint software, using 15 s fractions (corresponding to 1 ml column effluent). Separations were achieved at 4 ml min^{-1} using a mobile phase of 0.1% formic acid in an aqueous/acetonitrile gradient. The proportion of acetonitrile was held at 0% for an initial 3 min, and then programmed to increase linearly from 0 to 25% over 35 min. The column effluent was monitored at 254 nm.

The pooled and concentrated GW273293 human urine (10 ml) was fractionated as described above using an Intersil ODS3 100 × 10 mm 5 µm column (Capital HPLC, Edinburgh, UK). The proportion of acetonitrile was programmed to increase linearly from 0 to 25% over 35 min. All other conditions are as described for GI265080 samples.

Collected fractions were evaporated to dryness under a constant flow of nitrogen at 25 °C, redissolved in 600 µl Residue Analysis grade acetonitrile/deuterium oxide (50/50 v/v) and transferred individually to 5 mm NMR tubes for analysis.

NMR

NMR experiments were performed on a Bruker DRX-600 spectrometer (Bruker, Rheinstetten, Germany) equipped with a 5 mm dual ^{1}H-^{19}F-NMR probe operating at 600.13 MHz for ^{1}H and 564.4 MHz for ^{19}F. ^{19}F-NMR spectra of unprocessed GI265080 human urine were acquired using urine (0.4 ml) mixed with 20% (0.1 ml) deuterium oxide (D_2O) to provide a field frequency lock and placed in 5 mm NMR tubes. The NMR spectra were recorded at 25 °C using the conditions described below.

Isolated HPLC fractions were also analysed by ^{1}H- and ^{19}F-NMR spectroscopy for the presence of drug-related material for GI265080 samples, and by ^{1}H-NMR spectroscopy alone for GW273293 samples. The ^{19}F-NMR measurements were obtained using a single 90° pulse observed with broadband proton decoupling using the Waltz-16 sequence. Typically, 1024 transients were acquired into 128 K data points over a spectral width of 28 248 Hz (50 ppm) producing a total pulse repetition time of 5 s. The data were line broadened by 2 Hz before Fourier transformation and the chemical shifts referenced externally to $CFCl_3$ (δ0.0 ppm).

The ^{1}H-NMR experiments were performed at 600.13 MHz using a nOesy sequence to achieve dual presaturation of the residual HOD and acetonitrile signals. Typically, 64 transients were acquired into 32 K data points over a spectral width of 12 019 Hz (20 ppm) and a pulse repetition time of 3.2 s. The nOesy mix time was 74 ms and either single or double presaturation of solvent signals was employed depending upon whether the sample was in water alone or an acetonitrile/D_2O-H_2O mixture obtained from semipreparative HPLC.

The gradient enhanced selective nOe's experiments (GOESY) employed the double-pulsed field method of Stonehouse *et al.* (1994). Typically, 4 K transients were acquired as above but with a mix time of 500 ms and a 180° gaussian-shaped selective inversion pulse. The gradient percent ratios were 11, 17, 40 and –40 in order to select and observe the enhancements.

The inverse heteronuclear multiple quantum correlation (HMQC) and inverse heteronuclear multiple bond correlation (HMBC) experiments were performed for ^{1}H-^{13}C and ^{1}H-^{15}N on a Varian Inova 750, operating at 750.29 MHz for ^{1}H, 188.68 MHz for ^{13}C and 76.06 MHz for ^{15}N observation. Reference 1D ^{1}H nOesy presat experiments were acquired into 98 304 data points over a spectral width of 15 009 Hz (20 ppm). A varying number of transients, 32–64 (depending upon concentration of metabolites), was acquired with a mix time of 100 ms and a total pulse repetition of 6.4 s. All proton chemical shifts were referenced to acetonitrile at 2.0 ppm.

The 2D experiments were gradient selected to reduce artefacts. They typically involved 32 transients for ^{13}C or 1024 transients for ^{15}N acquired into 4 or 8 K data points over a spectral width of 6948 Hz in the acquisition domain (F2). A total of 128 complex increments was acquired to define the second heteronuclear dimension (F1), 200 ppm for ^{13}C and 300 ppm for ^{15}N. The data were processed by applying a non-shifted cosine window apodization function before Fourier transformation in both

dimensions. The ^{13}C shifts were referenced to acetonitrile methyl carbon at 1.4 ppm and the ^{15}N shifts to the acetonitrile nitrogen at –145 ppm.

LC/MS

LC/MS and LC/MS/MS experiments were performed on either one of two systems:

- A Hewlett-Packard Model 1100 liquid chromatograph (Hewlett Packard, Waldbronn, Germany) coupled in series to a Finnigan MAT LCQ ion-trap mass spectrometer (Thermoquest, CA, USA) fitted with an atmospheric pressure ionization source (API). The instrument was operated with positive ion electrospray using either full scan, product ion or MS^3 scan modes. Separations were performed on a 150 × 2.1 mm Waters Symmetry C18 analytical column (Waters, MA, USA) operated at 25 °C, using a mobile phase consisting of 0.1% formic acid in water/acetonitrile. The proportion of acetonitrile was maintained at 0% for 0–5 min, then programmed to increase linearly from 0 to 40% in 25 min and maintained at 40% for a further 10 min. The flow rate through the analytical column was 0.2 ml min^{-1}, directed unsplit to the electrospray interface.
- A Hewlett-Packard Model 1100 liquid chromatograph coupled in series to a Bruker Esquire ion trap mass spectrometer (Bruker Daltonics, Bremen, Germany) fitted with an API source. The instrument was operated with positive-ion electrospray using either full scan or data-dependent MS/MS modes. Separations were performed on a 250 × 4.6 mm Zorbax RxC8 column (Hewlett Packard, Little Falls, USA) operated at 25 °C, using a mobile phase consisting of 0.1% formic acid in water/acetonitrile. The proportion of acetonitrile was programmed to increase linearly from 0% (v/v) to 50% in 30 min. The flow rate through the analytical column was 1.0 ml min^{-1}, split ~1 in 10 to the electrospray interface.

In both systems, nitrogen was used as the nebulizer gas and helium was used as the buffer gas. Product ion formation was induced through resonant excitation.

Results

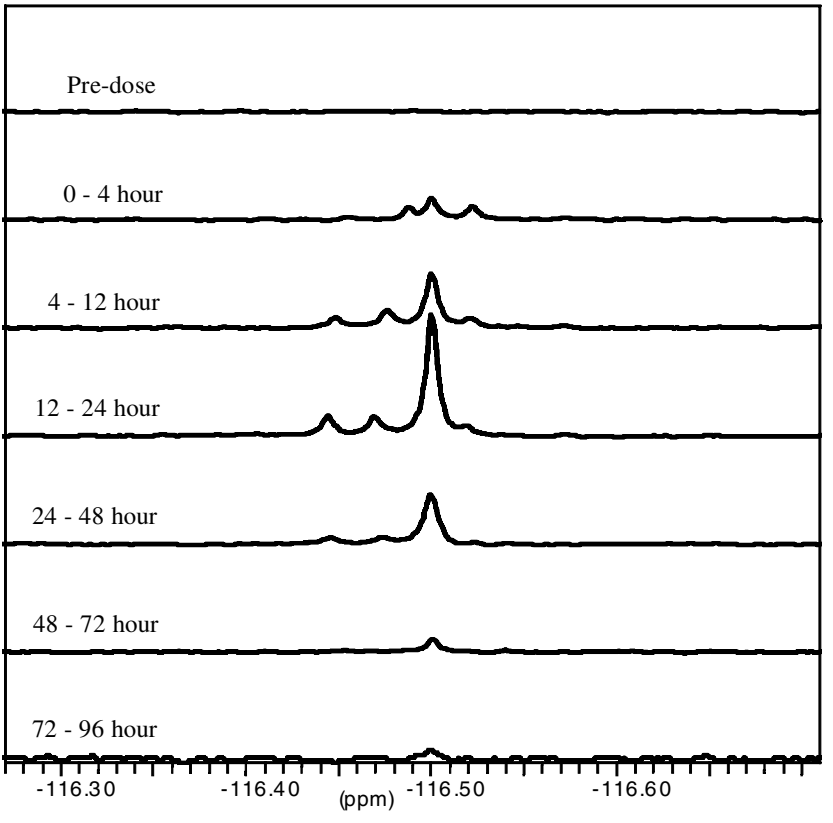
Identification of human urinary metabolites of GI265080

^{19}F-NMR spectroscopy demonstrated the presence of four major metabolites of GI265080 in untreated human urine following oral administration, which were designated as metabolites A–D (figure 3b). Elimination of these metabolites was essentially complete 96 h after dosing (figure 3a), with the maximum amount of drug-related material being eliminated in the 4–24-h period. The relative quantities of metabolites A–D for the 4–12-h collection period on the basis of the ^{19}F-NMR integrals were 11, 10, 17 and 62%, respectively (figure 3b).

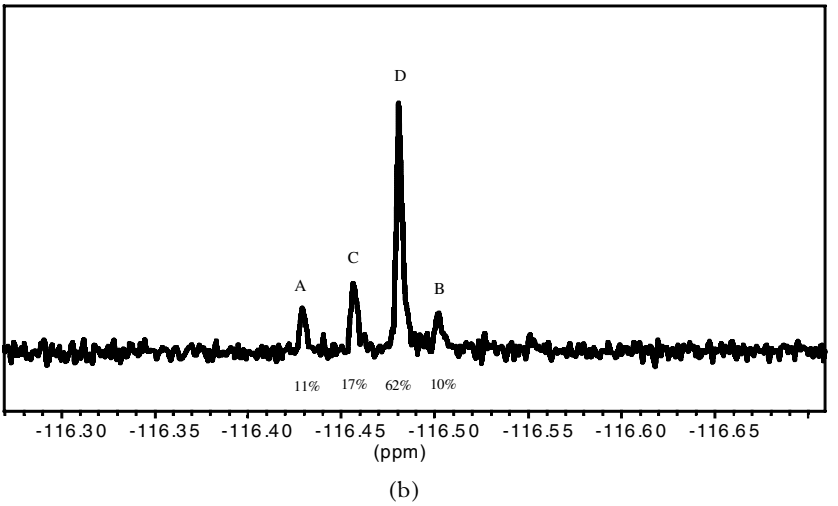
The structures of the metabolites isolated by semipreparative HPLC were determined using a combination of NMR spectroscopy and mass spectrometry and by comparison with authentic standards. The chemical shift assignments for GI265080 and its metabolites are summarized in table 1.

Inspection of the ^1H-NMR spectrum of metabolite A indicated that no aromatic substitution had occurred and the H6 aromatic proton adjacent to the pyridine nitrogen was deshielded by δ 0.24 compared with GI265080. Metabolite A had a molecular mass of 16 daltons greater than GI265080 and this served to identify it as the *N*-(5)-oxide (figure 1). Final confirmation was provided by comparison of the ^1H-NMR spectra with that of GI262663, the authentic standard of GI265080 *N*-(5)-oxide (table 1).

Inspection of the NMR spectrum of metabolite B indicated the loss of the aromatic doublets observed at δ 7.69 and δ 7.19 for the H6 and H7 protons of GI265080. The appearance of a new aromatic signal at δ 7.62 suggested that aromatic hydroxylation had occurred. Additional signals at δ 5.05 and between δ 3.54 and δ 3.80 attributable to the protons of a glucuronide conjugate suggested



(a)



(b)

Figure 3. (a) ^{19}F-NMR stacked plots of whole urine showing excretion profile 0–96 h following administration of GI265080 to man. (b). Integrated ^{19}F-NMR of 4–12-h sample following administration of GI265080 to man showing relative percentages of metabolites A–D.

Table 1. ^{1}H- ^{13}C- and ^{15}N-NMR chemical shift assignments for GI265080 and its human metabolites, A–D.

		Human urine metabolites			
Proton	GI265080	A	B	C	D
6(CH)	7.69 (d)	7.93 (d)	7.62 (s)	7.99 (d)	8.21 (d)
7(CH)	7.19 (d)	7.05 (d)	–	7.31 (d)	7.27 (d)
8(CH_2)	5.90 (s)	5.86 (s)	6.14 (s)	5.91 (s)	5.93 (s)
11,13(CH)	7.07 (t)	7.06 (t)	7.06 (t)	7.07 (t)	7.07 (t)
12(CH)	7.47 (m)	7.46 (m)	7.45 (m)	7.47 (m)	7.47 (m)
1′(CH)	–	–	5.05 (d)	5.68 (d)	5.18 (d)
2′(CH)	–	–	~3.66 (m)	3.83 (m)	3.64 (m)
3′(CH)	–	–	~3.64 (m)	3.66 (m)	3.53 (m)
4′(CH)	–	–	~3.54 (m)	3.66 (m)	3.52 (m)
5′(CH)	–	–	3.80 (d)	3.94 (m)	3.65 (d)
Nitrogen*					
1(N)	NM	NM	−146	−144	−143
4(NH_2)	NM	NM	−301	−299	−298
5(N)	NM	NM	−231	−224	−179
Carbon*					
3a	NM	NM	NM	133.1	NM
4	NM	NM	NM	150.6	NM
6	NM	NM	NM	135.0	135.1
7	NM	NM	NM	99.4	97.0
7a	NM	NM	NM	138.8	NM
8	NM	NM	NM	41.3	40.9
9	NM	NM	NM	111.0	NM
10,14	NM	NM	NM	162.1	NM
11,13	NM	NM	NM	113.0	112.4
12	NM	NM	NM	133.5	132.6
1′	NM	NM	NM	89.7	108.9
2′	NM	NM	NM	72.6	71.5
3′	NM	NM	NM	72.4	71.7
4′	NM	NM	NM	77.1	75.8
5′	NM	NM	NM	80.6	77.0
6′	NM	NM	NM	174.8	NM

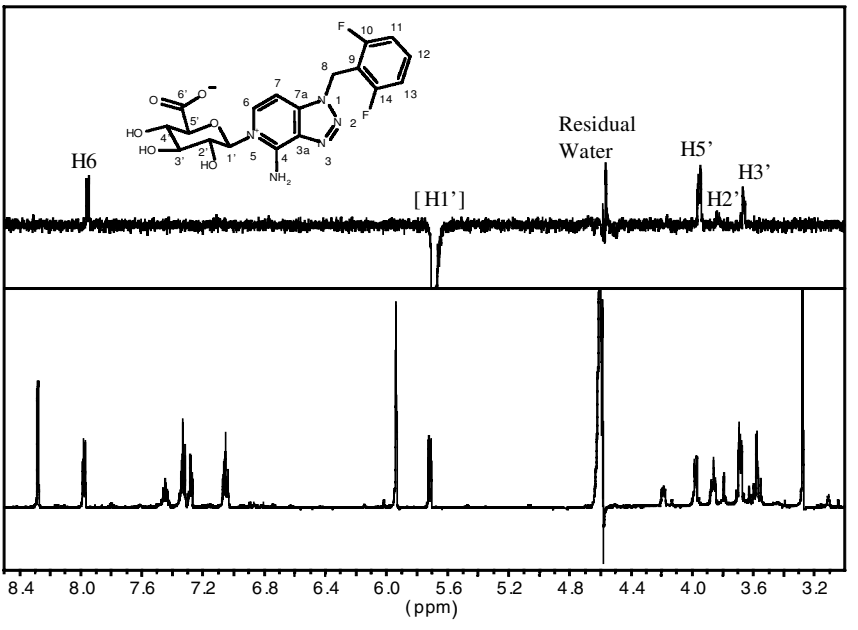
*Values were obtained from HMBC and HMQC experiments. The N2 and N3 shifts were not observed owing to lack of proton-coupling partners.

NM, not measured.

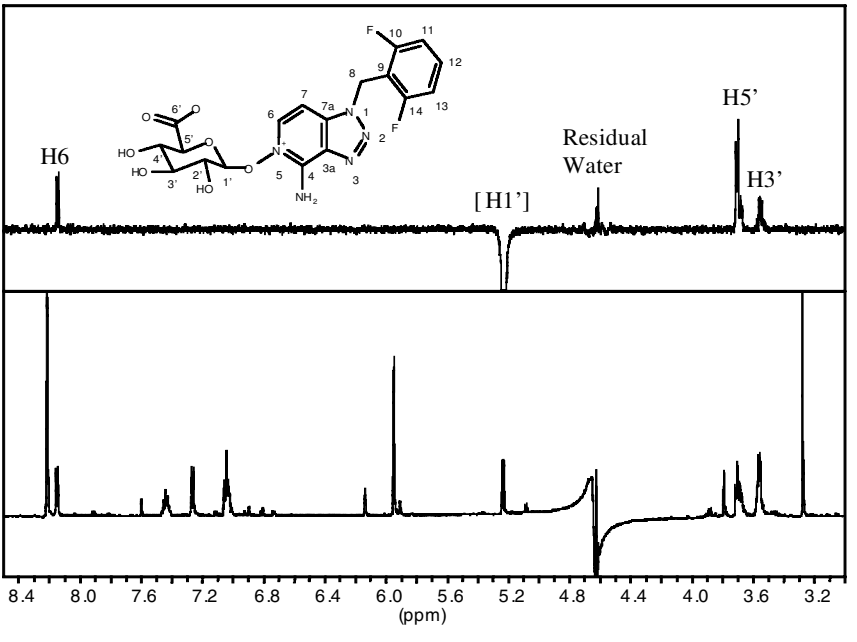
that hydroxylation was followed by conjugation to form the glucuronide. The base peak in the electrospray mass spectrum of metabolite B, m/z 454, assigned as the MH^+ ion, indicated a molecular weight of 453. This is consistent with mono-oxidation and subsequent conjugation with glucuronic acid. The MS/MS and MS^3 data obtained from products of m/z 454 and 454 → 278, respectively, provide additional confirmation of the structure proposed from the NMR data.

The NMR spectra of metabolites C and D indicated that both were unsubstituted as they contained all the aromatic and aliphatic protons observed in GI265080. In addition, both were conjugated with glucuronic acid with the anomeric proton of the glucuronic acid moiety at δ5.7 and δ5.2 for metabolites C and D, respectively.

Selective excitation 1D nOe experiments from the anomeric protons of the glucuronic acid conjugates of metabolites C and D both gave positive enhancements to the aromatic proton doublet (H6) adjacent to the pyridine nitrogen (figure 4a, b). This clearly demonstrated that the point of conjugation for both metabolites C and D was through the pyridine nitrogen.



(a)



(b)

Figure 4. (a) Gradient-selected nOe on metabolite C. The upper trace shows the anomeric proton selectively inverted; the lower trace the reference ^{1}H spectrum. Annotations indicate observed nOe's. (b) Gradient-selected nOe on metabolite D. The upper trace shows the anomeric proton selectively inverted; the lower trace the reference ^{1}H spectrum. Annotations indicate observed nOe's (note the 2′ may be obscured by the 5′ that overlaps it).

Analysis of the ^{1}H-^{13}C one bond and long range 2D NMR spectra of metabolite C showed correlation from the anomeric glucuronic acid proton to the C6 carbon in the aromatic ring adjacent to the pyridine nitrogen, as well as the expected 3′ and 5′ carbons of the glucuronic acid moiety. This indicated conjugation through the pyridine nitrogen to form a quaternary N^{+}-glucuronide. An ^{1}H-^{15}N NMR HMBC spectrum for metabolite C showed no correlation of the anomeric glucuronide proton with the pyridine nitrogen (figure 5a). The latter was assigned through the correlation observed to it from the aromatic protons of the pyridine ring (H7 and H6). This is not unexpected considering the small size of 2 bond ^{1}H-^{15}N couplings from protons on sp^{3} hybridized carbons.

In contrast, the ^{1}H-^{15}N NMR HMBC for metabolite D (figure 5b) clearly showed a correlation from the anomeric H1′ proton of the glucuronide to the same pyridine nitrogen at δ–179 as the H7 of the pyridine ring. This would be expected from a proposed *N*-*O*-glucuronide, which would have a larger 3 bond ^{1}H-^{15}N coupling from the anomeric proton to the pyridine nitrogen. The 2D NMR experiments together with the nOe results confirmed the proposed structures of metabolites C and D as the quaternary N^{+}-glucuronide and the N^{+}-*O*-glucuronide conjugates respectively

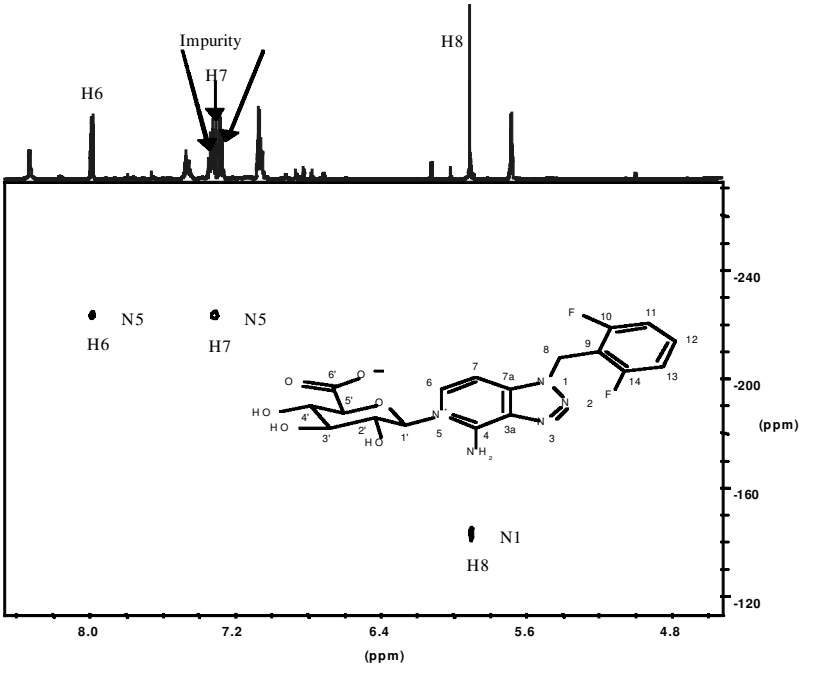
Mass spectral data obtained for metabolites C and D showed MH^{+} ions at m/z 438 and 454, which are equivalent to an increase in molecular weight of 176 and 192 daltons, relative to GI265080, and are consistent with the structures proposed from the NMR data. The mass spectrum obtained from product ion analysis of the molecular ion m/z 438 for metabolite C showed an ion at m/z 262 assigned as loss of the glucuronyl moiety. Data obtained for the MS^{3} experiment for metabolite C (m/z 438 → 262 → products) suggest that following the loss of the glucuronic acid group, the product remaining is GI265080. These findings support the structure proposed by NMR for metabolite C.

The mass spectrum of metabolite D obtained from product ion analysis of m/z 454, showed an ion at m/z 278 again assigned as the loss of the glucuronyl moiety. Data obtained from the MS^{3} experiment for metabolite D (m/z 454 → 278 → products) shows an ion at m/z 261 that is assigned as [m/z 278-OH]. The loss of 17 daltons is also observed in the MS/MS spectrum of the *N*(5)-oxide metabolite of GI265080. An additional product ion at m/z 127 was assigned as the 2,5-fluoro-substituted benzyl cation, and is further indication that oxidation has not occurred on this particular phenyl ring system. These data support the structure proposed from the NMR data, which indicate glucuronic acid conjugation at the oxygen atom of a pyridine *N*-oxide.

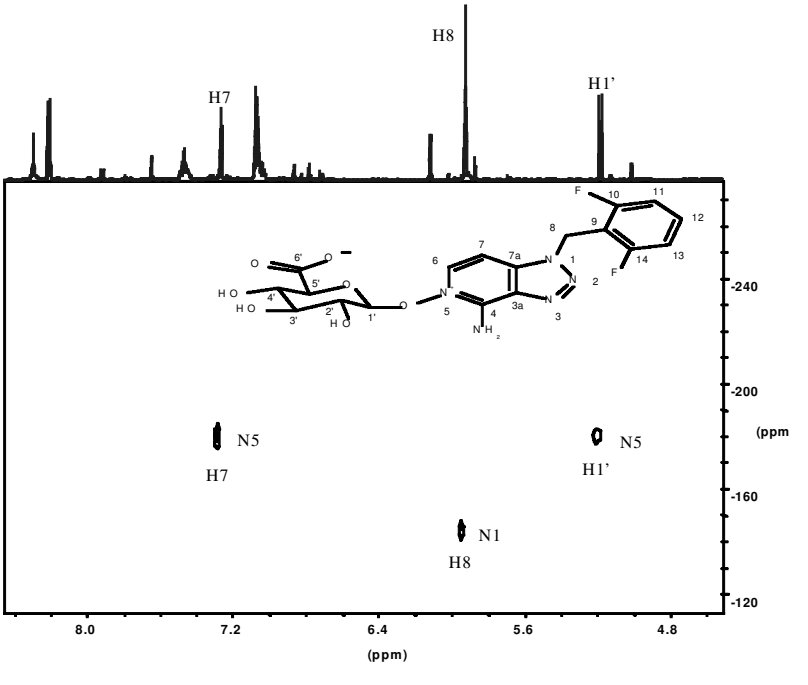
Final confirmation of the structure of metabolite D as the *N*-*O*-glucuronide was obtained by comparison of the NMR spectrum of metabolite D with that of authentic standard obtained through the independent synthesis of compound.

Identification of rat and dog urinary metabolites of GI265080

Metabolites present in dog and rat urine were similarly identified. Dog urine contained three major metabolites of GI265080, all of which were seen in human urine. These were the *N*(5)-oxide of GI265080 (GI265663, A), the hydroxyglucuronide (B) and the quaternary N^{+}-glucuronide of GI265080 (C); quantitatively the first and the third of these metabolites were the most important. Rat urine contained two major metabolites of GI265080, although only one of these,



(a)



(b)

Figure 5. (a) Gradient-selected ^{1}H-^{15}N HMBC of metabolite C. (b) Gradient-selected ^{1}H-^{15}N HMBC of metabolite D.

GI265663, was identified. The *N-O-glucuronide* conjugate (D) of GI265663, identified in human urine, was not detected in either dog or rat urine. There were no obvious major sex-related differences in the urinary profiles of drug-related material in either species.

Identification of human urinary metabolites of GW273293

^{1}H-NMR of isolated fractions indicated the presence of four human urinary metabolites of GW273293, assigned as E–H (figure 2). The minor metabolite E was assigned as the C5 hydroxyl metabolite, based on the disappearance of the C5 proton resonance at δ7.22 in comparison with authentic GW273293. The aromatic protons of the trichloro-substituted phenyl ring, at δ7.69 and 7.44 (C8 and C10), remained largely unperturbed. This assignment was supported by MS data, in which metabolite E was detected as its MH^+ ion at m/z 305. MS detection was aided by the appearance of a characteristic chlorine isotope pattern. In a similar manner, metabolite F was confirmed as the *O*-glucuronide of the C5 hydroxyl metabolite, giving rise to glucuronyl proton resonances at δ5.52, 3.85 and 3.4–3.6. LC/MS/MS of metabolite F gave rise to an MH^+ ion at m/z 481 and a fragment ion at m/z 305, corresponding to loss of the glucuronyl moiety.

Metabolite G was assigned as the *N*-(1)-oxide of GW273293, through a comparison of its ^{1}H-NMR shifts and chromatographic retention time with authentic standard.

Metabolite H, was shown to be unsubstituted in the trichloro-substituted phenyl ring through detection of the proton signals at δ 7.72 and δ 7.39. The shift of the C5 proton downfield to δ7.8 from δ7.22, relative to GW273293, was consistent with a substitution within the pyrazine ring. An H1′ anomeric glucuronyl proton was visible at δ5.5, together with the additional H2–H5 protons in the range δ3.4–3.9. A selective gradient nOe (GOESY) experiment from the H1′ anomeric proton at δ5.5 of the glucuronide moiety showed an enhancement of the pyrazine C5 proton signal (figure 6). Nitrogen chemical shifts were obtained for

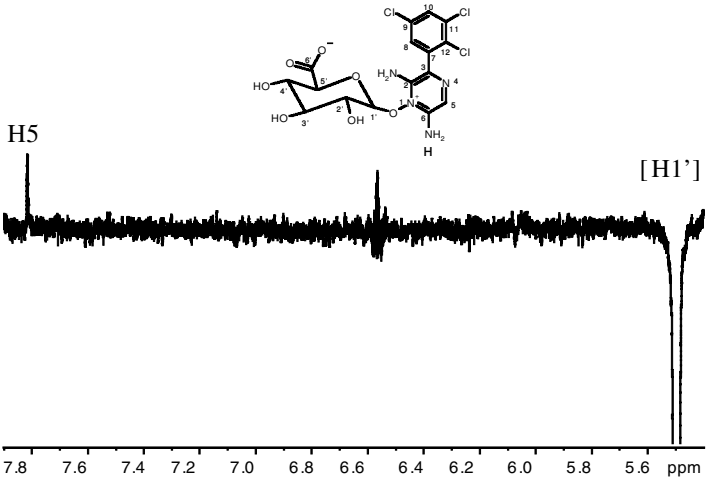


Figure 6. Gradient-selected nOe on metabolite H showing correlation from the H1 anomeric proton to the pyrazine C5 proton of GW273293.

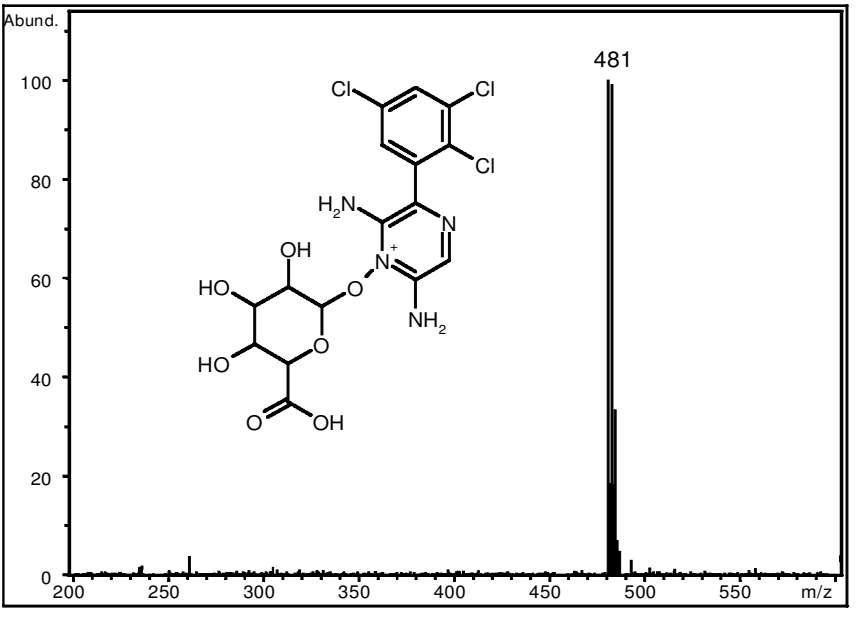


Figure 7. Electrospray MS spectrum of metabolite H.

authentic parent drug (GW273293), the *N*-(1)-oxide (G) and the isolated glucuronide metabolite (H) via ^{15}N-gradient HMBC experiments. The ^{1}H-^{15}N HMBC for metabolite H showed a correlation from the anomeric glucuronide proton at δ5.5 to a nitrogen atom at –224 ppm.

Literature data suggests that there can be a downfield shift of up to 72 ppm in the ^{15}N chemical shift in going from pyridine to the *N*-hydroxyl pyridinium salt (Levy and Lichter 1979, Martin *et al*. 1981) and this supports the conclusion that the metabolite must be a *N*-(1)-*O*-glucuronide, since a 72 ppm substituent effect to the –143 ppm chemical shift for the *N*1 ^{15}N signal in GW273293 gives a value close to that observed. MS confirmed the molecular weight of the *N-O-glucuronide*, through the detection of the ion at *m*/*z* 481 (figure 7). A summary of the chemical shifts for GW273293 and its human urine metabolites is shown in table 2. A comparison of the proton integrals for the isolated metabolites, E–H, indicated that formation of the *N*-(1)-*O*-glucuronide of GW273293 in man is a significant route of elimination.

Discussion

During the course of the present study, the metabolites of GI265080 have been investigated in human, dog and rat urine. The four major urinary metabolites in man have been isolated and characterized, including one that represents a new and significant secondary conjugation pathway in man. The formation of *N*-oxides and charged quaternary N^+-glucuronides are common metabolic pathways in nitrogen-containing xenobiotics, as is the formation of aromatic ring-hydroxylated glucuronic acid conjugates; and these pathways represent significant metabolic clearance routes for GI265080 in both man and animal species.

Table 2. ^{1}H and ^{15}N-NMR chemical shift assignments for GW273293 and its human metabolites, E–H.

		Human urine metabolites			
Proton	GW273293	E	F	G	H
5(CH)	7.22 (s)	–	–	7.56 (s)	7.80 (s)
8(CH)	7.65 (d)	7.69 (d)	7.65 (d)	7.72 (d)	7.72 (d)
10 (CH)	7.35 (d)	7.44 (d)	7.41 (d)	7.38 (d)	7.39 (d)
1′(CH)	–	–	5.52 (d)	–	5.54 (d)
2′(CH)	–	–	3.4–3.6 (m)	–	~3.85 (m)
3′(CH)	–	–	3.4–3.6 (m)	–	~3.57 (m)
4′(CH)	–	–	3.4–3.6 (m)	–	~3.42 (m)
5′(CH)	–	–	3.85 (d)	–	3.77 (d)
Nitrogen*					
1(N)	−143	NM	NM	−147	−224
4(N)	−47	NM	NM	−49	NM

*Values were obtained from HMBC and HMQC experiments.
NM, not measured.

The formation of glucuronic acid conjugates of *N*-oxides, however, is not as well known and has not been extensively reported in animal species or man. The formation of an *N*-*O*-glucuronide metabolite of minoxidil, a drug administered as an *N*-(3)-oxide, was postulated as being formed in man (Thomas and Harpootlian 1975). The formation of this novel secondary conjugation has also been reported in the metabolism of pinacidil in rabbit and monkey (Sakamoto and Nakamura 1993) and in guinea pig urine following administration of mianserin (Delbressine *et al.* 1992).

The formation of a sulphate conjugate of minoxidil in man has also been reported (Thomas and Harpootlian 1975) and provides further evidence for the potential *N*-oxides to undergo further conjugation. The present study has demonstrated that the formation of *N*-*O*-glucuronide is not only possible, but also can be a major route of renal clearance in man accounting for between 40 and 60% of the observed urinary metabolites in the case of GI265080. The differences in relative amounts of the respective metabolites may represent subject to subject variation but are of significant proportions in each case. It is interesting to note that formation of the *N*-oxide species (GI262663) is the major metabolic route in rat and dog; and further conjugation with glucuronic acid to form the *N*-*O*-glucuronide does not occur to any significant degree in these species. The structure of the *N*-*O*-glucuronide has been proven unequivocally by use of extensive NMR and mass spectrometry studies. In addition, the presence of an *N*-*O*-glucuronide metabolite of a related compound, GW273293, was also confirmed in human urine, in a separate study.

The formation of *N*-*O*-glucuronide conjugates may well be more common than is appreciated since their characterization is difficult and may be confused with the more common hydroxyglucuronic acid conjugates, a mistake easily made if mass spectrometry is the only technique used for their characterization. This may be the case particularly if the *N*-*O*-glucuronide is unstable and reverts to the *N*-oxide under the conditions used for the analysis (Sakamoto and Nakamura 1993).

The mechanism of *N*-*O*-glucuronide formation is unclear and it is possible that it will proceed via a transient *N*-OH (*N*-hydroxy) species in the case of quaternary

N-oxides rather than the *N*-oxide species acting directly as a substrate for glucuronyl transferase. The mechanism of formation of *N*-*O*-glucuronide species from the oxidation of primary, secondary and quaternary amines is worthy of further investigation.

It has been shown here that NMR and mass spectrometry need to be used in a complementary fashion to effectively and unequivocally characterize drug metabolites. The use of mass spectrometry alone may lead to the incorrect assignments of structures if MS/MS is not used.

Acknowledgements

The authors thank Bill Gristwood and Richard Churchus for provision of samples, and Ian Waterhouse for synthesis of authentic standards.

References

Doig, M. V. and Clare, R. A., 1991, Use of thermospray liquid chromatography-mass spectrometry to aid in the identification of urinary metabolites of a novel antiepileptic drug, Lamotrigine. *Journal of Chromatography*, **554**, 181–189.

Dear, G. J., Ayrton, J., Plumb, R., Sweatman, B. C. and Ismail, I. M., 1999, Tandem mass spectrometry linked fraction collection for the isolation of drug metabolites from biological matrices. *Rapid Communications in Mass Spectrometry*, **13**, 886–894.

Dear, G. J., Ismail, I., Mutch, P. J., Davies, L. H., Plumb, R. and Sweatman, B. C., 2000, Urinary metabolites of a novel non-nucleoside reverse transcriptase inhibitor in rabbit, mouse and human: identification of fluorine NIH shift metabolites using NMR and tandem MS. *Xenobiotica*, **30**, 407–426.

Delbressine, L. P. C., Moonen, M. E. G., Kaspersen, F. M., Jacobs, P. L. and Wagenaars, G. L., 1992, Biotransformations of mianserin in laboratory animals and man. *Xenobiotica*, **22**, 227–236.

Ismail, I., Dear, G. J., Mutch, P. J., Davies, L. H., Plumb R. and Sweatman, B. C., 1999, The urinary metabolism of the novel non-nucleoside reverse transcriptase inhibitor GW420867X in dog, Cynomolgus monkey and mini-pig. *Xenobiotica*, **29**, 957–967.

Levy, G. C. and Lichter, R. L., 1979, *Nitrogen-15 Nuclear Magnetic Resonance Spectroscopy* (Chichester: Wiley-Interscience).

Martin, G. J., Martin, M. V. and Gouesnard, J. P., 1981, *^{15}N-NMR Spectroscopy* (Berlin: Springer-Verlag).

Malet-Martino, M. C. and Martino, R., 1989, The application of nuclear magnetic resonance spectroscopy to drug metabolism studies. *Xenobiotica*, **19**, 583–607.

Plumb, R., Dear, G. J., Ayrton, J., Sweatman, B. C. and Ismail, I. M., 1999, The use of preparative HPLC with tandem mass spectrometric directed fraction collection for the isolation and characterisation of drug metabolites in urine by NMR and LC/MS^{n}. *Rapid Communications in Mass Spectrometry*, **13**, 845–854.

Sakamoto, K. and Nakamura, Y., 1993, Urinary metabolites of pinacidil. II. Species differences in the metabolism of pinacidil. *Xenobiotica*, **23**, 649–656.

Scarfe, G. B., Wright, B., Clayton, E., Taylor, S., Wilson, I. D., Lindon, J. C. and Nicholson, J. K., 1998, ^{19}F-NMR and directly coupled HPLC-NMR-MS investigations into the metabolism of 2-bromo-4-trifluoromethylaniline in rat: urinary excretion balance study without the use of radiolabelling. *Xenobiotica*, **28**, 373–388.

Stonehouse, J., Adell, P., Keeler, J. and Shaka, A. J., 1994, Ultra high-quality NOE Spectra, *Journal of the American Chemical Society*, **116**, 6037.

Thomas, R. C. and Harpootlian, H., 1975, Metabolism of minoxidil, a new hypotensive agent II: Biotransformation following oral administration to rats, dogs and monkeys. *Journal of Pharmaceutical Sciences*, **64**, 1366–1371.

Wade, K. E., Troke, J., Macdonald, C. M., Wilson, I. D. and Nicholson J. K., 1988, 19F studies of the metabolism of trifluoro-methylaniline. In E. Reid, J. D. Robinson and I. D. Wilson (eds), *Bioanalysis of Drugs and Metabolites* (London: Plenum), pp. 383–387.

XENOBIOTICA, 2002, VOL. 32, NO. 1, 45–62

Taylor & Francis
healthsciences

Comparative metabolism of genistin by human and rat gut microflora: detection and identification of the end-products of metabolism

N. G. COLDHAM†*, C. DARBY‡, M. HOWS†, L. J. KING‡, A.-Q. ZHANG† and M. J. SAUER†

†Department of Risk Research, Veterinary Laboratories Agency, Addlestone, Surrey KT15 3NB, UK
‡School of Biomedical and Life Sciences, University of Surrey, Guildford, Surrey GU2 5XH, UK

Received 14 May 2001

1. Biotransformations by gut microflora play a pivotal role in determining the biological activity of isoflavones that occur in soya-based foods predominantly as β-glycosyl conjugates. Microflora prepared from rat caecae and human faeces were used to investigate the metabolic fate of genistein β-glycosides extracted from soya flour. The end-products of such metabolism were determined by parallel incubations of microflora with [2′,3′,5′,6′-^{3}H] and [4-^{14}C]-labelled genistein.

2. Quantitative analysis by LC-MS/MS indicated very rapid and complete degradation of genistin, which was associated with a transient increase in genistein. Qualitative studies indicated that the malonyl and acetyl glycosides of genistein were also degraded by the microflora.

3. Incubation of caecal and faecal microflora with [^{3}H] and [^{14}C]genistein yielded similar radiolabelled metabolites, which were identified by radio-LC-MS^{n} as the intermediates dihydrogenistein and 6′-hydroxy-*O*-desmethylangolensin and end-product 4-hydroxyphenyl-2-propionic acid. This profile of genistein metabolites indicated selective hydrolysis of 6′-hydroxy-*O*-desmethylangolensin between carbon atoms 1′ and 1 to yield the end-products 4-hydroxyphenyl-2-propionic acid and 1,3,5-trihydroxybenzene.

4. The biological significance of the products of genistein metabolism warrant further investigation since they may play an important role in mediating the beneficial antioxidant health effects associated with the consumption of isoflavones in food.

Introduction

Estimation of the benefit or risk that natural dietary constituents in food present to the consumer is dependent on a range of factors including the extent of dietary exposure and the biological activity of parent compound and metabolites. The isoflavones genistein, daidzein and glycitein occur in most soya-based foods as *β*-glycosides, which include glycosyl (genistin, daidzin and glycitin), malonyl glycosyl and acetyl glycosyl conjugates (Barnes *et al.* 1998, Setchell 1998). Their consumption has been associated with a wide range of beneficial health effects including the prevention of certain cancers (Messina *et al.* 1994, Setchell 1998). Such effects may be a consequence of exposure to either parent isoflavone or metabolites (Setchell and Adlercreutz 1988). Mass balance studies (Xu *et al.* 1994) suggest extensive biotransformation in man since the recovery of parent isofla-

* Author for correspondence; e-mail: n.g.coldham@vla.defra.gsi.gov.uk

Xenobiotica ISSN 0049–8254 print/ISSN 1366–5928 online © 2002 Crown Copyright
http://www.tandf.co.uk/journals
DOI: 10.1080/00498250110085809

vones in excreta is typically < 20% of an oral dose. Similar investigations in rats following oral administration of [4-^{14}C]-labelled genistein have yielded essentially complete recovery of radioactivity in excreta (Coldham and Sauer 2000) but indicated extensive biotransformation by conjugation with glucuronic and sulphuric acids in the liver and reduction followed by heterocyclic ring fission by microbes of the gut (Coldham *et al.* 1999). The range of genistein metabolites identified in plasma and excreta from man, laboratory and farm animals now include dihydrogenistein, 6′-hydroxy-*O*-desmethylangolensin (6′-OH-ODMA), 4-ethylphenol, glucuronide and sulphate conjugates of these products and parent compound and 4-hydroxyphenyl-2-propionic acid (4-HP-2-PA) (Batterham *et al.* 1971, Joannou *et al.* 1995, Barnes *et al.* 1998, Setchell 1998, Cimino *et al.* 1999, Coldham *et al.* 1999). Biotransformation of genistein (figure 1) by gut microflora proceeds via reduction of the C-ring double bond to form dihydrogenistein and is followed by further reduction with opening of the ether bridge to generate 6′-OH-ODMA (Joannou *et al.* 1995, Coldham *et al.* 1999). Thereafter, several end-products of 6′-OH-ODMA metabolism have been reported. In sheep, [4-^{14}C]genistein is biotransformed by microbes in the rumen to the unlabelled end-product 4-ethylphenol (Batterham *et al.* 1971, Braden *et al.* 1967); this metabolite has also been found in the urine and plasma of rats (Barnes *et al.* 1998, King 1998) and man (Setchell 1998) after administration of food containing soya or pure genistein. In contrast, recent studies in rat have reported metabolism of [4-^{14}C]genistein by caecal microflora to the terminal metabolite 4-HP-2-PA (Coldham *et al.* 1999), no evidence was found, from either mass balance or *in vitro* metabolism studies for further decarboxylation with loss of the radiolabel to 4-ethylphenol (Coldham and Sauer 2000). The biological significance of 4-HP-2-PA, which accumulated in the prostate gland of rats, has not been determined. 4-HP-2-PA has not yet been reported as a metabolite of genistein in humans.

In vitro tissue preparations, derived from different compartments of the body, such as precision-cut liver slices or faecal microflora, provide a means of identifying the principal sites and pathways of metabolism (Coldham *et al.* 1999, Schneider *et al.* 1999). While Phase II conjugation reactions with the free hydroxyl groups predominate in liver and intestinal cells (Barnes *et al.* 1996, Coldham *et al.* 1999), biotransformation by microbes in the gut play a pivotal role in the bioactivation of certain isoflavones. For example, demethylation of biochanin A and formononetin to genistein and daidzein respectively (Braden *et al.* 1967, Batterham *et al.* 1971) and production of equol, a potent oestrogen, from daidzein (Setchell *et al.* 1988) are established metabolic activation processes mediated by gut microflora. Microbes are also thought to play an important role in the hydrolysis of flavonone glycosides to the unconjugated aglycone since following oral administration of naringin, hesperidin and rutin to germ free rats, they were found unchanged in urine and faeces but not in those from normal animals (Griffiths and Barrow 1972). Use of cultures of faecal or caecal microflora facilitate the investigation of pure test chemicals or specific food extracts and enable periodic sampling for detection of intermediates and end-products of flavonoid or lignan metabolism under defined and controlled conditions (Borriello *et al.* 1985, Schneider *et al.* 1999).

Radiochemicals labelled with carbon-14 or tritium are widely used to investigate pathways of xenobiotic metabolism since they enable the selective detection of metabolites derived exclusively from the labelled parent compound. For most

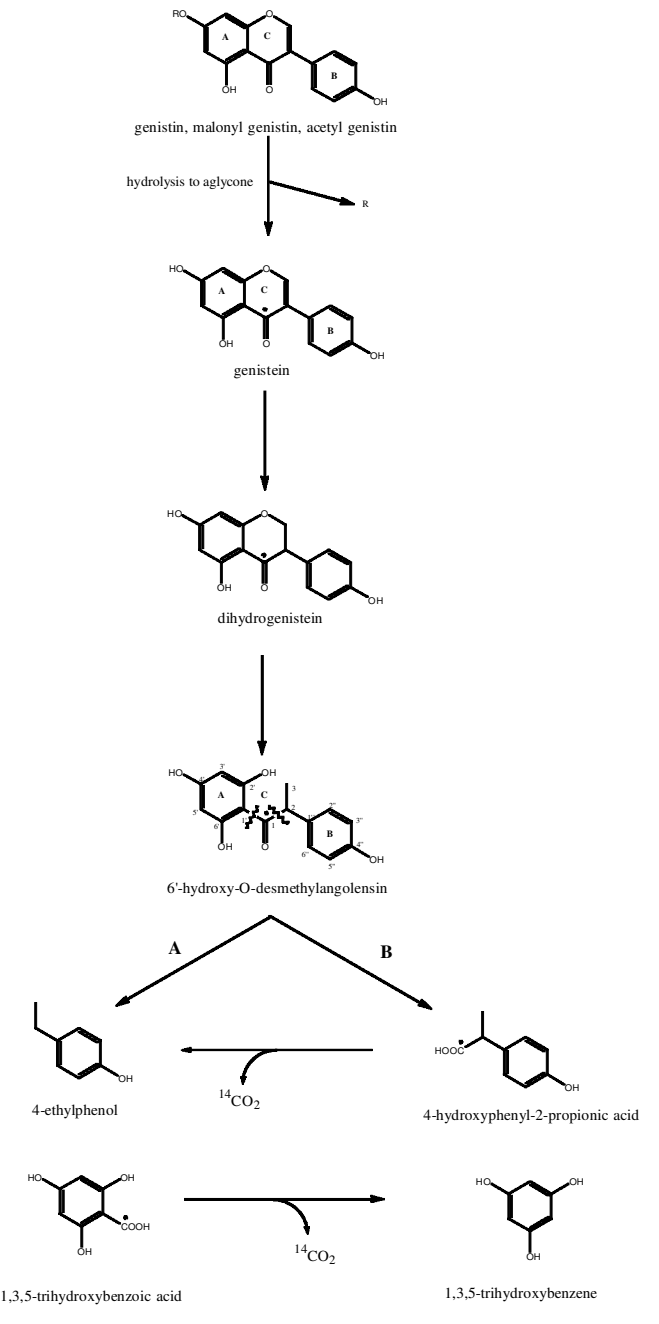


Figure 1. Metabolic scheme for the biotransformation of genistein glycosides and genistein. Hypothetical pathways A and B are presented for hydrolysis of 6′-hydroxy-*O*-desmethylangolensin between carbon atoms 1′ and 1 or 1 and 2 respectively. The proposed products of such metabolism are 4-ethylphenol and 1,3,5-trihydroxybenzoic acid from pathway A and 4-hydroxyphenyl-2-propionic acid and trihydroxybenzene from B. Further potential biotransformation of 1,3,5-trihydroxybenzoic acid and 4-hydroxyphenyl-2-propionic acid by decarboxylation to trihydroxybenzene and 4-ethylphenol respectively with loss of the ^{14}C are also indicated. R represents glucose for genistin, acetylglucose for acetylgenistin or malonylglucose for malonylgenistin. *Position of the ^{14}C-label derived from [4-^{14}C]genistein. The A, B and C (opened) rings are indicated within the structure of 6′-hydroxy-*O*-desmethylangolensin.

applications, carbon-14 is the radioisotope of first choice since incorporation of the label into the molecular skeleton avoids issues of facile loss or dehydrogenation reactions associated with tritium-labelled compounds. However, the utility of any single label is compromised where metabolic molecular fission occurs releasing an unlabelled metabolite. This problem is particularly evident during the biotransformation of [4-^{14}C]genistein since hydrolysis of the intermediate metabolite 6′-OH-ODMA may, at least in theory, occur between carbon atoms 1′ and 1 or 1 and 2 (figure 1). Such hydrolysis would yield the products 4-ethylphenol and 1,3,5-trihydroxybenzoic acid or 4-HP-2-PA and 1,3,5-trihydroxybenzene (THB) from pathways A or B respectively. Further decarboxylation of these products may convert the labelled metabolite from each pathway (1,3,5-trihydroxybenzoic acid or 4-HP-2-PA) to an unlabelled product (4-ethylphenol or 1,3,5-trihydroxybenzene). Similar heterologous sites for hydrolysis around the C-ring of quercetin have been described (Winter *et al.* 1989) and support the hypothesis made herein for two potential pathways for hydrolysis of 6′-OH-ODMA presented in figure 1. Given the limitations discussed above and difficulties associated with synthesis of isoflavones labelled in both aromatic rings, radiochemicals catalytically labelled by tritium exchange, offer an alternative approach to single [^{14}C]-labelling and provide the potential to detect both fission products of 6′-OH-ODMA, corroborate existing metabolite identification, establish functional pathways of biotransformation and end-products of metabolism.

The objective of the present study was to evaluate and compare the role of gut microflora, derived from rat caecae and human faeces, in the biotransformation of genistein through to end-products. These studies also examined the fate of genistein glycosides since these are the predominant forms in which isoflavones occur in most soya-based foods. The effect of genistein glycoside treatment with HCl (1 M) was also investigated as representative of conditions in the human stomach since this represents a potential source of significant chemical transformation. The functional pathways for hydrolysis of 6′-OH-ODMA by microflora were studied by the use of 4-^{14}C- and multiply ^{3}H-labelled genistein to determine the end metabolites likely to be produced in rats and man.

Materials and methods

Chemicals

[4-^{14}C]genistein (2.07 GBq mmol^{-1}; Amersham International, Little Chalfont, UK) was synthesized from a deoxybenzoin intermediate (Coldham *et al.* 1999) to a purity of 99%. [^{3}H]genistein (629 GBq mmol^{-1}) was produced from unlabelled genistein (Sigma, Poole, UK) by tritium exchange in the presence of a platinum catalyst to a purity of 98% (Amersham). The location of the tritium atoms in [^{3}H]genistein was determined by nanospray product ion mass spectrometry as described below. The purity of both radiochemicals was confirmed before use by radio-HPLC using the conditions described below for analysis of genistein metabolites. Genistein, genistin, 1,3,5-trihydroxybenzene (phloroglucinol), 1,3,5-trihydroxybenzoic acid (gallic acid) and 4-ethylphenol were obtained at purities of >99% from Sigma. Dihydrogenistein and 6′-OH-ODMA were obtained from Plantech (Reading University, Reading, UK) and 4-HP-2PA from Acros Organics (Fisher Scientific, Loughborough, UK).

Structural analysis [^{3}H]genistein

Product ion nanospray mass spectrometry was used to determine the molecular location of tritium introduced into genistein by platinum catalysis. Stock [^{3}H]genistein (2 µl;37 kBq µl^{-1}) was diluted with an equal volume of 70% methanol containing 1% formic acid and introduced into a Picotip^{TM} (1 µm orifice diameter, New Objectives, Inc., Cambridge, MA, USA) nanospray needle. The Picotip was

mounted onto a nanospray probe (Protana, Odense, Denmark) and the sample electrosprayed directly into the heated capillary orifice of an LCQ mass spectrometer. The ion (MS^1) and product ion (MS^2) mass spectra of [^{3}H]genistein were collected over the mass ranges m/z 265–285 and 75–300 respectively. The product ion mass spectrum of [^{3}H]genistein was collected in the positive-ion mode to enable comparison with previous structural elucidation data (Coldham *et al.* 1999) and location of the tritium atoms. The mass spectrometer settings for nanospray analysis were similar to those described below with the exception of the source voltage, which was reduced to −1 kV.

Preparation of microflora

Rat caecal and human faecal microflora were prepared and incubated under anaerobic conditions to preserve the potential biotransformation capacity of oxygen-sensitive microbes (Worrell *et al.* 1989). Male and female Wistar rats (250 g; Central Toxicology Laboratory, Zeneca, Alderley, Macclesfield, UK) were euthanized by CO_2 asphyxiation and immediately transferred to an anaerobic cabinet (Forma Scientific, OH, USA) containing an atmosphere of H_2(5–10% w/v), CO_2(10% v/v) and N_2(80% v/v). Intestinal tracts were excised and the caecal contents removed, diluted to 2.5–10% w/v in potassium phosphate buffer (0.1 M, pH 7.4) and cellular debris removed from the microflora suspension by centrifugation (500*g* for 2 min). Human faecal microflora were prepared from freshly voided stools and processed in a similar manner to that described above for caecal contents. These cultures were used to investigate the hydrolysis of genistein glycosides and metabolism of radiolabelled genistein.

Preparation of genistein glycosides

Glycosyl (genistin), malonyl glycosyl and acetyl glycosyl conjugates of genistein were prepared from soya flour by extraction with solvent since analytical reference standards of the latter two β-glycoside esters were not commercially available. Soya flour (30–100 mg) was transferred to volumetric flasks, suspended with 80% methanol (v/v; 10 ml) and isoflavones extracted by probe sonication (2 × 30 s). Extracts (1 ml) were passed through polytetrafluoroethane filters (1 μm), the filters were washed with methanol (9 ml) and the combined filtrates taken to dryness under reduced pressure at 55°C in a centrifugal evaporator (Gyrovap GT, Howe, Banbury, UK). Residues were dissolved in water (1 ml) and the isoflavones were back-extracted into ethylacetate (2 × 5 ml). The two phases were separated by centrifugation (2000*g* for 5 min) and the pooled ethyl acetate extracts taken to dryness under nitrogen at 55°C. These extracts containing genistein glycosides and a trace of unconjugated genistein were dissolved in phosphate buffer and used as substrates for hydrolysis studies by microflora or HCl. The acetyl and malonyl glycosides in these extracts were identified by HPLC-MS/MS (solvent system 1; see below) using precursor (m/z 271 genistein) and neutral loss (m/z 204 acetyl glycoside; m/z 248 malonyl glycoside) scanning experiments as described by Barnes *et al.* (1994).

Hydrolysis of genistein glycosides by HCl

The potential for hydrolysis of genistein glycosides by acid in the human stomach was investigated by incubation of the soya flour extract (1 ml) with either HCl (1 M final concentration; 4 ml) or phosphate buffer (0.1 M; pH 7.4) controls for up to 4 h at 37°C. Aliquots of the incubation mixture (2 ml) were collected after incubations of 15, 30, 60 and 240 min, snap-frozen on Cardice and stored at −20°C before extraction and analysis by LC-MS/MS.

Hydrolysis of genistein glycosides by gut microflora

The potential for hydrolysis of genistein glycosides by rat caecal and human faecal microflora was investigated by incubation of the soya flour extract (1 ml) with either active cultures (10 ml) or parallel heat-inactivated control preparations (100°C for 30 min) in tightly capped tubes for up to 4 h at 37°C. Aliquots of the cultures (2 ml) were collected after incubations of 15, 30, 60 and 240 min, centrifuged at 10 000*g*, the supernatants retained, snap-frozen on Cardice and stored at −20°C before extraction and analysis by LC-MS/MS.

Analysis of genistein glycoside hydrolysis by LC-MS/MS

Genistein glycosides (substrate) and genistein (product) were extracted from cultures of microflora or HCl incubated with the soya flour extract into ethyl acetate (2 × 5 ml). The aqueous and organic phases were separated by centrifugation (2000*g*; 2 min) and the ethyl acetate fraction taken to dryness under nitrogen at 55°C. The extracts were dissolved in HPLC mobile phase and the concentration of genistin and genistein determined by HPLC-MS/MS. Analytes were chromatographed using the conditions described below (solvent system 1) and detected with a Sciex API 2000 triple quadrupole mass spectrometer equipped with a Turbo-ion electrospray probe in the positive-ion mode. The mass transition m/z 271 (Q1) to 153 (Q3) facilitated detection of genistein and of all the β-glycoside conjugates since the latter readily fragmented with the loss of the sugar moiety to the aglycone ion (m/z 271) in the ion-focussing quadrupole (Q0). Chromatographic peaks corresponding to genistein and

genistin were automatically detected and the mass of analyte calculated after interpolation from calibration curves prepared over the working range 10–10 000 ng ml^{-1} using the TurboQuan^{TM} (PE Biosystems) software package. Without reference standards, only a qualitative evaluation of the malonyl and acetyl glycosyl esters of genistein could be made.

Biotransformation of radiolabelled genistein

Biotransformation of radiolabelled genistein was investigated by incubation with cultures of rat caecal or human faecal microflora. Aliquots (10 ml) of caecal or faecal microflora and parallel heat-inactivated control preparations (100°C for 30 min) were incubated in tightly capped tubes with 100 μM genistein containing 2.2 kBq [^{14}C or ^{3}H]genistein ml^{-1} at 37°C. Aliquots of the cultures (2 ml) were collected after incubations of 15, 30, 60 and 240 min, centrifuged at 10 000*g*, the supernatants retained, snap-frozen on Cardice and stored at −20°C before extraction and analysis by radio-HPLC-MS^{n}.

Detection and MS^{n} analysis of radiolabelled genistein metabolites

Metabolites derived from [^{14}C or ^{3}H]genistein were extracted from cultures of microflora with C_{18} Bond Elut cartridges (1 g; Varian, Harbor City, CA, USA). Incubation mixtures (1 ml) were diluted with an equal volume of 0.2% (v/v) formic acid, applied to conditioned cartridges (methanol followed by 0.2% formic acid, v/v, 10 ml), washed with 0.2% (v/v) formic acid (3 × 10 ml) and the radiolabelled components eluted with methanol (5 ml). The extracts were taken to dryness under nitrogen at 55°C and the residue dissolved in mobile phase for metabolite analysis by radio-HPLC-MS^{n}. Metabolites derived from [^{14}C or ^{3}H]genistein and reference standards were chromatographed using either a HP 1050 or HP 1100 HPLC system (Hewlett Packard, Bracknell, UK) using a 2.1 × 150 mm Hypersil Elite (Hypersil, Runcorn, UK; 5 μ particle size) C_{18} column. Analytes were eluted at a flow rate of 0.3 ml min^{-1} with linear gradient binary mobile phase solvent systems ranging from 85:15 0.1% formic acid (v/v; system 1) or 15 mM ammonium acetate (pH 5.0; system 2):acetonitrile (both systems) to 45% acetonitrile over 20 min. The effluent from the column was split (∼50:50) with a Y-shaped tee (Upchurch Scientific, Anachem Ltd, Luton, UK) and connected in parallel to an A525 radiodetector (Canberra Packard, Pangbourne, UK) and LCQ mass spectrometer (see below). The radiodetector was equipped for narrow-bore chromatography with a low-volume scintillation cocktail/HPLC effluent mixing tee (10 μl) and a 35-μl liquid scintillation cell. The structure of genistein metabolites was determined using an ion-trap mass spectrometer (LCQ, Finnigan, Hemel Hempstead, UK), with negative-ion APCI providing greatest sensitivity for the analysis of single phenolic ring metabolites. Spectra were collected over the ranges m/z 50–300 and parent ions of genistein metabolites selected for MS^2 analysis by matching peaks of $[M - H]^-$ with those from radio-HPLC chromatograms. MS^{n} experiments on genistein metabolites were performed with a CID energy of 35% and a mass isolation width of 2 atomic mass units. APCI was performed using the following settings: vaporizer and heated capillary temperatures of 450 and 150°C respectively, source voltage and current 4 kV and 100 μA respectively, sheath gas and auxiliary gas flow rates 80 and 20 ml min^{-1} and a capillary voltage of −26 V. The maximum automatic gain control (AGC) ion storage time was 200 ms and three microscans were collected per spectrum.

Identification of genistein metabolites

Radiolabelled metabolites of genistein were identified by comparison of mass spectral and chromatographic characteristics with authentic standards using HPLC solvent systems 1 and 2. Peaks in the radio-HPLC chromatograms corresponding to metabolites of genistein are denoted as Gm 1, Gm 5 and Gm 6 to provide consistency with previous reports (Coldham *et al.* 1999, Coldham and Sauer 2000).

Results

Structural analysis [^{3}H]genistein

The MS^1 and MS^2 spectra of genistein and [^{3}H]genistein are summarized in table 1. The MS^1 spectrum of [^{3}H]genistein contained an ion at m/z 279 (M + H + 8) consistent with introduction of four tritium atoms into the molecule. The product ion MS^2 mass spectrum of [^{3}H]genistein contained ions at m/z 261, 251, 233, 223 and 195 consistent with introduction of four tritium atoms into the A-, B- or C-rings. A further product ion at m/z 167 indicated labelling in the B- or C-rings, whereas those at m/z 153 and 149 were unchanged from unlabelled genistein and demonstrated the absence of tritium from the A-ring. A product ion

Table 1. Summary of chromatographic and mass spectral data obtained from reference standards of potential genistein metabolites.

Metabolite/reference standard	Metabolite abbreviation	HPLC retention time (min) system 1	HPLC retention time (min) system 2	+/− Ionization mode and m/z molecular ion	Major product ions (m/z)
Genistein	G	17.1	17.1	−269	241, 225, 201*, 197, 183, 133, 107.
Genistein	G	17.1	17.1	+271	253, 243, 225, 215*, 187, 159, 153, 149, 119.
[^{3}H]genistein		17.1	17.1	+271	261, 251, 233, 223*, 195, 167, 153, 149, 127.
Genistin		6.9		+433	271*
Dihydrogenistein	Gm 5	16.2	16.3	−271	206, 165*, 151, 137, 119, 107.
6-OH-*O*-desmethyl angolensin	Gm 6	17.3	17.3	−273	255, 229*, 214, 187, 125.
4-Hydroxyphenyl-2-propionic acid	Gm 1	3.5	7.5	−165	121*, 119, 93.
4-Ethylphenol		18.3	18.3	−121	93, 59*.
Trihydroxybenzene		1.9	1.9	−125	83, 81, 57*
Trihydroxybenzoic acid		1.8	1.9	−169	125*

Genistein metabolite (Gm) abbreviations are provided in column 2 as assigned previously (Coldham *et al.* 1999). The retention times of the metabolites were determined with two separate solvent systems (1 and 2) using an identical C_{18} Hypersil Elite HPLC column. The ionization mode (+ve or −ve) and m/z ratio of metabolite protonated/deprotonated molecular ions are provided with major product ions derived from these using a collision energy of 35%.

*Base product-ion. Product-ion mass spectra for genistein and [^{3}H]genistein were collected in the positive-ion mode to enable qualitative structural analysis and location of the tritium atoms as described by Coldham *et al.* (1999). The positive-ion mode also offered greatest sensitivity for quantitative analysis of genistein and genistin by LC-MS/MS. The product-ion mass spectra of genistein is also provided in the negative-ion mode for comparison with the metabolites that resisted formation of positive ions.

at m/z 127 indicated that the four tritium atoms were located within the B-ring at the available 2′-, 3′-, 5′- and 6′-positions.

Hydrolysis of genistein glycosides by HCl

The concentration of genistin and genistein (trace) were not significantly changed compared with control preparations following incubation of soya flour extract with HCl (1M) for up to 4 h at 37°C (data not shown). Qualitative analysis suggested that the concentration of the acetyl and malonyl glycosides were also unchanged.

Hydrolysis of genistein glucosides by rat caecal and human faecal microflora

The concentration of genistin and genistein in cultures of rat caecal and human faecal microflora incubated with soya flour extract for up to 4 h are shown in figure 2. The concentration of genistin was reduced to baseline levels within the first 15 min of incubation with active caecal and faecal microflora. Degradation of genistin was closely associated with production of genistein, which reached a maxima after 15–30-min incubation with active caecal and faecal microflora

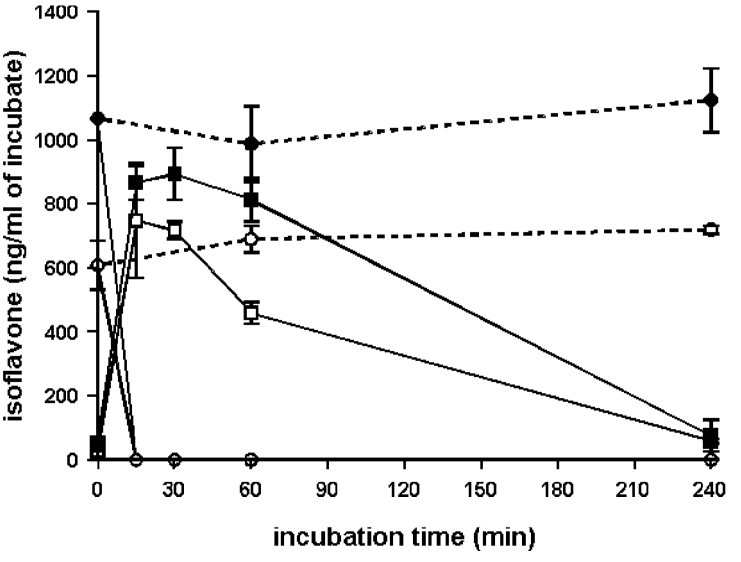


Figure 2. Biotransformation of genistin by cultures of microflora derived from rat caecae (open symbols) and human faeces (closed symbols). Cultures were prepared with either active (solid line) or heat-inactivated (broken line) microflora and incubated with genistin extracted from soya flour for up to 4 h under anaerobic conditions at 37°C. The concentrations of genistin (circles) and genistein (squares) were determined in extracts of microflora cultures by LC-MS/MS. Genistein appeared in the cultures of faecal and caecal microflora following hydrolysis of genistin. Data are the mean ±1 SD of three replicates per time point.

cultures. Thereafter, the concentration of genistein decreased in a time-dependent manner in cultures of both microflora due to biotransformation to other metabolites, which were further investigated using radiolabelled genistein. The concentration of genistin was unchanged in the control heat-inactivated microflora incubates throughout 4 h. Representative HPLC-MS/MS chromatograms of the soya flour extract incubated with active and heat-inactivated faecal microflora preparation for 15 min are shown in figure 3 and provided qualitative evidence for associated degradation of the acetyl and malonyl glucosides.

Biotransformation of [^{14}C] *and* [^{3}H]*genistein by rat caecal microflora*

Biotransformation by rat caecal microflora was evaluated with both [^{14}C] and [3H]-labelled genistein to provide comparison with previous studies (Coldham *et al.* 1999), which employed only the former radiolabel. Representative radio-HPLC chromatograms (solvent system 1) of extracts of caecal microflora (5% w/v) derived from female rats following incubation with [^{14}C] or [^{3}H]-labelled genistein for 15 min are presented in figure 4. Both chromatograms showed a similar range of [^{14}C] and [^{3}H]-labelled metabolites of genistein at retention times of 7.6 (Gm 1), 16.3 (Gm 5) and 17.1 min (Gm 6). A minor metabolite (Gm x) was also observed at a retention time of 6.8 min in radio-HPLC chromatograms of extracts following incubation of caecal microflora with [^{3}H]genistein. A time-course study for the biotransformation of [^{3}H]genistein by caecal microflora cultures (5% w/v) derived from a male rat, which produced a similar metabolite profile to females, is shown in figure 5 and revealed rapid conversion of parent compound to Gm 5, Gm 6 and

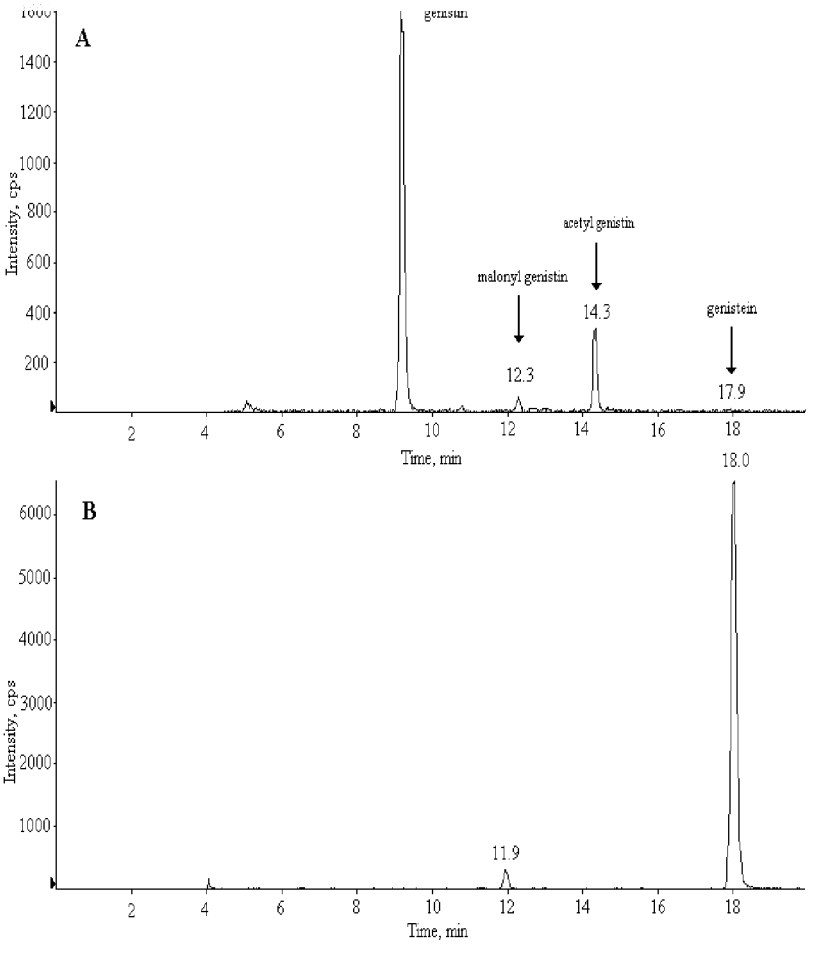


Figure 3. Representative HPLC-MS/MS total-ion current chromatograms of a soya flour extract incubated with heat-inactivated (top) or active human faecal microflora (bottom) for 15 min at 37°C. Genistein and genistein glycosides were detected by monitoring the mass transition m/z 271.1 (Q1) to 215.1 (Q3), which facilitated detection of aglycone and conjugates due to loss of the sugar moiety in the ion-focusing region (Q0) of the mass spectrometer. Genistin and genistein were identified by comparison of their HPLC retention times with that of reference standards. The retention times of genistin and genistein differ slightly from those presented in table 1 due to the use of a different HPLC system. Malonyl and acetyl genistin were identified from precursor-ion and neutral-loss scanning experiments as described (Barnes *et al.* 1994).

Gm x, which were all transient intermediates in the metabolism to the final product Gm 1. Further studies using 10% w/v rat caecal microflora preparations demonstrated complete metabolism of [^{3}H]genistein to Gm 1 within 60 min and again no evidence for further biotransformation up to 4 h incubation (data not shown).

Biotransformation of [^3H]genistein by human faecal microflora

Biotransformation by human faecal microflora was evaluated with only [^{3}H]-labelled genistein since the radiolabel provides a similar profile of metabolites as

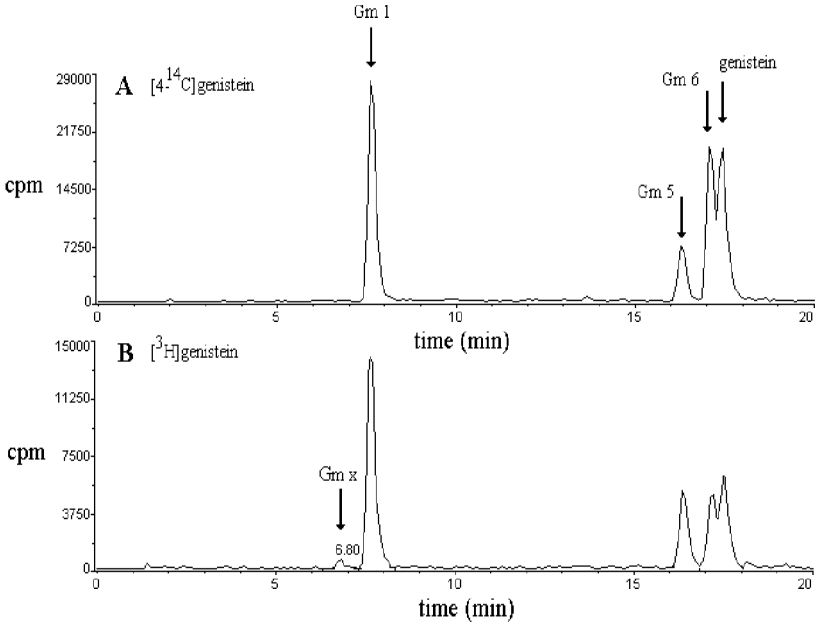


Figure 4. Representative radio-HPLC chromatograms illustrating the profiles of genistein metabolites found in extracts of rat caecal microflora (2.5% w/v) following incubation for 15 min with [4-^{14}C]genistein (A) and [^{3}H]genistein (B). Metabolites were separated by reverse-phase HPLC and identified by retention time and product-ion spectra using the chromatographic and mass spectral data presented in table 1. Metabolites are indicated by their abbreviations used in the text.

the [^{14}C]tracer in the studies with rat caecal microflora described above and additionally afforded detection of B-ring metabolites. Faecal microflora prepared from volunteer 1 (V1; male) produced metabolite Gm 1 only, whereas volunteer 2 (V2; female) also produced the intermediate Gm 5. The genistein metabolite Gm 6 was not evident in cultures derived from either subject. The 24-h time-course for the biotransformation of [^{3}H]genistein by faecal microflora (10% w/v) cultures derived from volunteers 1 and 2 is shown in figure 6.

Identification of genistein metabolites

The identities of genistein metabolites Gm 1, Gm 5 and Gm 6 produced by rat caecal and human faecal microflora were confirmed as 4-HP-2-PA, dihydrogenistein and 6′-OH-ODMA, respectively. The chromatographic and mass spectral properties of these and other potential metabolites of genistein are summarized in table 1. There was no evidence for production of 4-ethylphenol as a transient metabolite or end-product of genistein metabolism in any experiment.

Discussion

The β-glycosides of genistein extracted from a sample of soya flour were subjected to extensive biotransformation by gut microflora prepared from rat caecal contents and human faeces. The time-course studies using radiolabelled

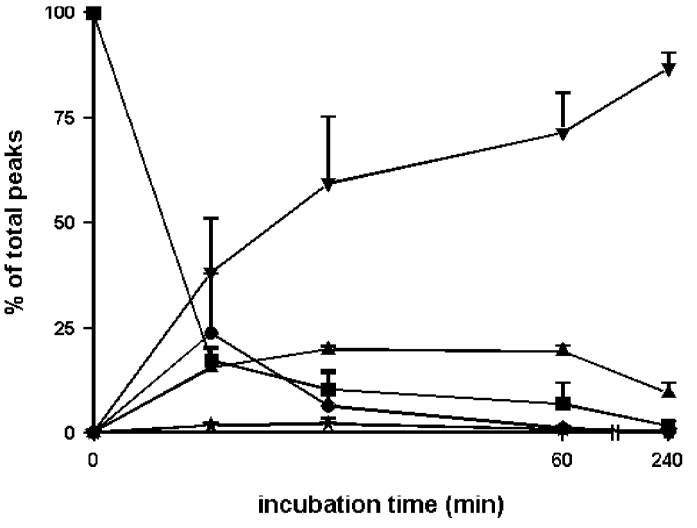


Figure 5. Biotransformation of [^{3}H]genistein by caecal microflora (5% w/v) derived from a male rat. Parent compound and metabolites were separated by reverse-phase HPLC and detected with an on-line radiochemical monitor. Transformation of genistein (squares) to the metabolites Gm × (stars), Gm 1 (inverted triangles), Gm 5 (triangles) and Gm 6 (circles) with increasing incubation time is shown. Data are the mean ±1 SD of three replicates per time point.

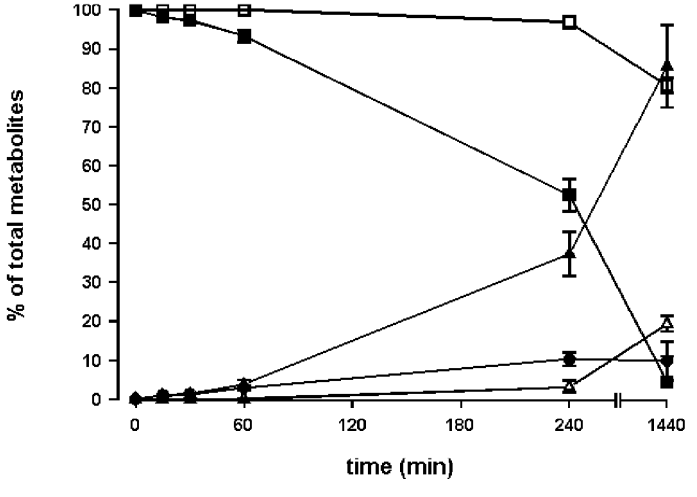


Figure 6. Biotransformation of [^{3}H]genistein by faecal microflora (10% w/v) derived from two human volunteers, V1 (open symbols) and V2 (solid symbols). Transformation of genistein (squares), to the metabolites Gm 1 (triangles) and Gm 5 (solid circle; V2 only) with increasing incubation time is shown. Data are the mean ±1 SD of three replicates per time point.

genistein facilitated the detection of both transient intermediates and an end-product of metabolism.

Initial studies demonstrated that the β-glycosides of genistein were resistant to treatment with HCl (1 M) at 37°C for up to 4 h. These findings indicate that these conjugates would be available for absorption from relatively sterile areas of the gut such as the stomach and duodenum. Acidic conditions in the stomach are also

likely to influence determinants of absorption such as solubility and binding to the proteinaceous component of food by promoting protonation of the weakly basic phenolic groups of genistein (Barnes *et al.* 1996). Hydrolysis of isoflavone acetyl and malonyl glycosides to the glucoside conjugate has been reported following treatment with HCl at 80°C (Barnes *et al.* 1994). Complete hydrolysis of all glycosides to the isoflavone aglycone may be achieved by treatment with HCl (1 M) for 2 h at the increased temperature of 100°C, and this procedure has been utilized for quantitative analysis of the total isoflavone content of food (Wang *et al.* 1990). In contrast, hydrolysis of genistein glycosides by the microflora was very rapid and accompanied by production of the unconjugated aglycone. Degradation of the aglycone was much slower, which suggested that hydrolysis of the glycosides is likely to precede metabolism within the isoflavone C-ring. Thus, in accord with the abundance of microbes in the intestines, it is suggested that genistein will become the predominant bioavailable form. Continued passage down the gut will enable further degradation of the aglycone by the microflora and absorption of intermediates and end-products of metabolism. Studies with rodents (Barnes *et al.* 1996, Coldham and Sauer 2000) have revealed extensive enterohepatic circulation of genistein, which will provide repeated opportunity for further bacterial metabolism. Several mammalian β-glucosidases have been reported (Day *et al.* 1998), which may play an active role in the hydrolysis of flavonoid glycosides. These include a broad specificity enzyme found in the intestine, liver and kidney, which is capable of hydrolysing certain flavonoid sugar conjugates including the 7β-glycosides of genistein and daidzein. However, the detection of unchanged glycosides in the urine and faeces of germ-free rats following oral administration of naringin, hesperidin and rutin argues for the prime importance of gut microflora in the hydrolysis of flavonoid conjugates over mammalian β-glucosidases. Having established essentially quantitative production of the aglycone by microfloral hydrolysis, the role of gut microflora biotransformation of the aglycone was evaluated by incubation with radiolabelled genistein to establish the definitive pathway between the substrate and the products of metabolism.

Metabolism studies with different microflora and radiolabelled genistein revealed variable rates of genistein biotransformation to 4-HP-2-PA; microflora prepared from rat caecae (2.5% w/v) achieved complete degradation to 4-HP-2-PA within 4 h, whereas at least 24 h was required by those derived from human faeces (10% w/v). This may reflect both inherent quantitative and qualitative differences between the microflora derived from the rat caecum and human faeces. Nevertheless, gut microflora from man and rat both produced 4-HP-2-PA as the only detectable end-product of genistein metabolism. The observation of similarities in biotransformation pathways is important since disparity between species would reduce the utility of the rats as a model for investigating the likely biological effects of genistein in man. 6′-OH-ODMA was rapidly degraded and only detected in significant quantities in incubations with rat caecal microflora at the highest dilution of 2.5% w/v, whereas the other intermediate dihydrogenistein was evident in all chromatograms from both species in which biotransformation of genistein had occurred. This would suggest that the rate-limiting step in the biotransformation of genistein by caecal microflora is hydrolysis of the C-ring ether bond of dihydrogenistein to yield 6′-OH-ODMA. The exclusive production of 4-HP-2-PA from both [^{14}C]- and [^{3}H]-labelled genisteins by rat caecal and human faecal microflora indicated selective hydrolysis of 6′-OH-ODMA between carbon atoms

1 and 1′ (figure 1). Further metabolism of 4-HP-2-PA by the microflora preparations was not evident from time-course studies and this was consistent with mass balance studies in rats that indicated essentially complete recovery of radioactivity following oral administration of [4-^{14}C]genistein (Coldham and Sauer 2000). The flavonoids quercetin and (+)-catechin are both cleaved at multiple sites in the C-ring to yield a range of straight alkyl chain phenyl carboxylic acids, such as 3-hydroxyphenylpropionoic acid, which may be degraded further by β-oxidation to benzoic acid (Hollman and Katan 1997). The apparent resistance of 4-HP-2-PA to such β-oxidation may be due to the location and steric hindrance of the 4-hydroyxphenyl substituent at the 2-position of propionic acid. Decarboxylation presents another potential biotransformation that would facilitate the production of 4-ethylphenol from 4-HP-2-PA, but was not evident in the present studies using [2′,3′,5′,6-^{3}H]genistein or others which have investigated the metabolism of similar flavonoid phenylcarboxylic acid metabolites (Hollman and Katan 1997).

There are several reports describing the biotransformation of genistein and biochanin A to 4-ethylphenol by ruminants and monogastric animals, including man, following administration of pure compounds or foods containing isoflavones. The ability unambiguously to detect 4-ethylphenol as a metabolite derived from genistein will depend upon the experimental approach and detection methods employed; use of appropriately labelled parent compound can be crucial in minimizing problems of interpretation. Genistein and biochanin A are both reported to be extensively metabolized in sheep to 4-ethylphenol, which was identified in urine extracts by means of gas chromatography and gas-density balance detection (Braden *et al.* 1967). Subsequent investigations in this species using [4-^{14}C]biochanin A (Batterham *et al.* 1971) supported these findings. However, it must be appreciated that in using ^{14}C in the 4-position any 4-ethylphenol produced will not be labelled and this can detract from the strength of evidence that this metabolite is indeed derived from the isoflavone in question. Studies of biotransformation of biochanin A by microflora derived from the rumen of cattle demonstrated only degradation to genistein (Dickinson *et al.* 1969). In contrast, cultures of rumen microflora prepared from sheep were capable of more extensive biotransformation of [^{3}H]biochanin A with demethylation to genistein followed by metabolism to other simple phenolic compounds which were not identified (Nilsson *et al.* 1967).

A number of studies have identified 4-ethylphenol in urine and plasma following administration of unlabelled genistein. 4-Ethylphenol was detected in the urine of rats following administration of either genistein or a soy extract by the relatively sensitive and specific technique of HPLC equipped with electrochemical detection (King 1998). Other studies (Setchell 1998), using similar analytical methods, have reported 4-ethylphenol in plasma and brain tissue following administration of genistein to a premenopausal woman and rat respectively. Tandem mass spectrometry (MS/MS) is another highly specific and sensitive technique for metabolite detection and identification and has been used to identify glucuronide and sulphate conjugates of 4-ethylphenol in the urine of rats following provision of feed containing isoflavones (Barnes *et al.* 1998). However, such studies cannot support the unequivocal assertion that the 4-ethylphenol was derived from genistein since the definitive link between radiolabelled parent and radiolabelled metabolites was not established. In the present investigation, mass

analysis was combined with on-line radiochemical detection to provide the definitive link between substrate and the products of metabolism.

The identification of [^{14}C]-labelled genistein metabolites, following selective solid-phase extraction procedures and radio-HPLC-MS^n, has been described in detail (Coldham *et al.* 1999). The chromatographic properties of the [^{3}H]-labelled genistein metabolites were further assessed with two different HPLC solvent systems to provide an additional level of confirmation to the identification of Gm 1 as 4-HP-2-PA. The HPLC retention time of reference 4-HP-2-PA was significantly reduced in solvent system 2 and consistent with that of Gm 1. Both HPLC solvent systems provided adequate separation between reference standards; indeed base line resolution was obtained between the peak for 4-ethylphenol (18.3 min) and the nearest adjacent peak which was that of genistein (17.1 min). Although the present studies demonstrated exclusive metabolism to 4-HP-2-PA, the production of 4-ethylphenol from genistein cannot be discounted without evaluation of microflora prepared from a wider population sample of both humans and rats. Excretion of equol in urine exhibits a high level of individual variation (Kelly *et al.* 1995) and was negatively correlated with *O*-desmethylangolensin and suggested disparity in preferred metabolic pathways of daidzein metabolism by different populations of gut microflora. In a similar manner, it may be argued that variability in the biotransformation of 6′-OH-ODMA to 4-HP-2-PA or 4-ethylphenol may also occur and this would provide a plausible explanation for the absence of 4-ethylphenol production observed in the present report. Alternatively, 4-ethylphenol may be produced by decarboxylation of 4-HP-2PA in other metabolically active organs such as the liver.

Detection and identification of the A-ring metabolite following hydrolysis of 6′-OH-ODMA, presumably THB, was not possible following application of [4-^{14}C] and [2′,3′,5′,6′-^{3}H]genistein since this product would be unlabelled due to migration of both radiolabels with the B-ring metabolite. In all probability, genistein labelled with tritium in the A-ring will also prove ineffective for metabolite detection due to resonance between the keto and enol isomers of 6′-OH-ODMA and exchange of the label with protons of the solvent. Thus, labelling with carbon-14 in the A-ring presents the only viable means of radiodetection of THB. Trihydroxybenzene has been identified as a transient metabolite in the degradation of quercitin-3-glucoside by *Eubacterium ramulus* (Schneider *et al.* 1999) and due to its abundance (10^7–10^9 organisms g^{-1} dry mass) is considered to be a key organism in flavonoid degradation in the human intestinal tract (Schneider and Blaut 1999). However, THB may evade detection due to formation of residues with culture medium components and further catabolism via dihydrophloroglucinol to acetate and butyrate (Winter *et al.* 1989). Indeed, many anaerobic bacteria have a substantial capacity for catabolism of such aromatic compounds (Heider and Fuchs 1997) via ring-opening reactions ultimately yielding acetate. The unidentified genistein metabolite (Gm x) may be a product of such aromatic ring metabolism. Flavonoids are readily metabolized by *Rhizobia* bacteria to a wide range of monocyclic phenolic products which have been identified by GC-MS (Rao and Cooper 1994). The first step in the metabolism of genistein and daidzein by these microbes was an aryl shift of the B-ring from carbon 3 to 2 followed by C-ring fission to yield a range of products which included gallic, 4-coumaric and 4-hydroxybenzoic acids.

Identification of the end-products of metabolism is an important element in the investigation of the likely biological effects of natural constituents in food such as isoflavones. Daidzein may be metabolized by gut microflora to equol, which, possibly due to its oestrogenic properties, is considered as an important end-product since reduced urinary excretion of the metabolite has been associated with breast cancer (Adlercreutz *et al.* 1982). The biological activity of 4-HP-2-PA has not been investigated but was found to accumulate in the prostate of rats following oral administration of [4-^{14}C]genistein (Coldham and Sauer 2000). Other bioflavonoid metabolites such as methyl-4-hydroxyphenyllactate have been shown to bind with high affinity to type II anti-oestrogen binding sites of ER ($K_d = 1\text{–}5$ nM) and inhibit oestradiol-stimulated growth in rat uterus and human breast cancer cells (Markaverich *et al.* 1988). In contrast, the toxicity of THB has been investigated and a safety assessment made (Andersen 1995) since this chemical has been used in cosmetics as an antioxidant and a hair colorant. The antioxidant properties of THB will act to reduce the concentration of potentially harmful free radicals in the gut contents and thus reduce exposure of the host cells to these damaging and potentially carcinogenic entities. Such antioxidant properties of THB warrant further investigation since this represents an important mechanism through which genistein, and other flavonoids which are also degraded to this metabolite, may contribute to reduced incidence of cancers in the gut.

The present metabolism studies with microflora derived from rat caecae and human faeces indicate hydrolysis of 6′-OH-ODMA between carbon atoms 1 and 1′ to yield 4-HP-2-PA and THB. No evidence was found to support production of 4-ethylphenol despite the use of sophisticated and sensitive methods of metabolite detection and identification. Clearly, pathways of isoflavone metabolism will be influenced by the presence and position of key chemical substituents. Genistein and daidzein both have carbonyl functions in the C-ring at the 4-position but suffer different fates since that of the former is protected by hydrogen bonding with the adjacent 5-hydroxyl group whereas that of the latter may be readily metabolized by reduction and dehydration to form equol. The 6′-hydroxy group of 6′-OH-ODMA, which is derived from that at the 5-position of genistein, may also influence the molecular site of C-ring hydrolysis. A potential chemical mechanism, which illustrates the role of the A-ring hydroxyl groups of 6′-OH-ODMA in directing the site of hydrolysis, is presented in figure 7 in support of the experimental evidence derived from incubation of [^{3}H]genistein with cultures of microflora. Hydrolysis of 6′-OH-ODMA is initiated under alkaline conditions by deprotonation of the 4′ hydroxyl group and followed by relocation of electron pairs around the A-ring to yield a negative charge on carbon 1′. The hydroxyl groups at the 2′ and 6′ positions play a key role in stabilizing the unpaired electron to carbon 1′, which directs the site of hydrolysis to between carbon atoms 1′ and 1 with consequent production of 4-OH-2-PA and THB. In contrast, an analogous mechanism for hydrolysis *O*-desmethylangolensin is less plausible since this molecule lacks the 6′-hydroxyl group adjacent to carbon atom 1′ for direction of the unpaired electron to this specific site. Thus, when considered in solely chemical mechanistic terms, 4-ethylphenol is a more plausible metabolite of daidzein than genistein which may provide an explanation for the origin of this metabolite. Other studies (Booth *et al.* 1958) have also implicated the location of surrounding aromatic hydroxyl groups in directing the molecular site of flavonoid C-ring hydrolysis.

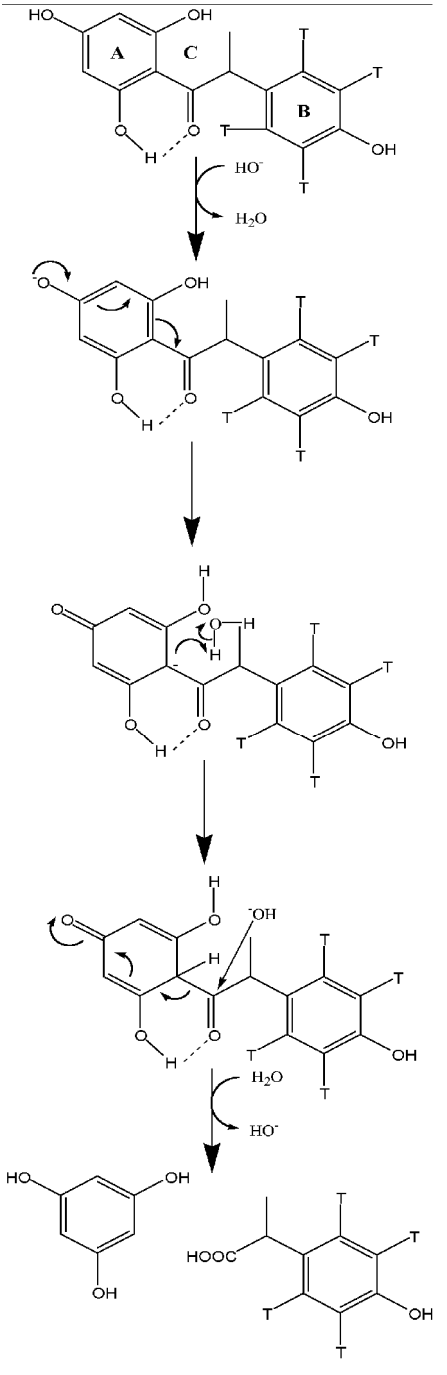


Figure 7. Proposed mechanism for the chemical hydrolysis of 6′-hydroxy-*O*-desmethylangolensin to trihydroxybenzene and 4-hydroxyphenyl-2-propionic acid. The mechanism is initiated by deprotonation of the 4′ hydroxyl group under alkaline conditions followed by movement of electron pairs (curved arrows) through the A-ring to leave a negative charge (–) on carbon 1′. Location of the negative charge on carbon 1′ directs hydrolysis to between carbon atoms 1′ and 1. T, location of tritium atoms as determined by product ion mass spectrometry. The numbering of the carbon atoms of 6′-hydroxy-*O*-desmethylangolensin is provided in figure 1.

Clearly, the present studies argue for a fresh evaluation of the likely end-products of genistein metabolism, favouring 4-HP-2-PA and THB rather than 4-ethylphenol. Further studies are required to determine the biological activity associated with these metabolites and their health implications.

Acknowledgements

The study was financially supported by the Food Standards Agency, UK.

References

Adlercreutz, H., Fotsis, T., Heikkinen, R., Dwyer, J. T., Woods, M., Goldin, B. R. and Gorbach, S. L., 1982, Excretion of the lignans enterolactone and enterodiol and of equol in omnivorous and vegetarian women and in women with breast cancer. *Lancet*, **ii**, 1295–1299.

Andersen, F. A., 1995, Final report on the safety assessment of phloroglucinol. *Journal of the American College of Toxicology*, **14**, 468–475.

Barnes, S., Coward, L., Kirk, M. and Sfakianos, J., 1998, HPLC-mass spectrometry analysis of isoflavones. *Proceedings of the Society for Experimental Biology and Medicine*, **217**, 254–262.

Barnes, S., Kirk, M. and Coward, L., 1994, Isoflavones and their conjugates in soy foods: Extraction conditions and analysis by HPLC-mass spectrometry. *Journal of Agricultural Food Chemistry*, **42**, 2466–2474.

Barnes, S., Sfakianos, J., Coward, L. and Kirk, M., 1996, Soy isoflavonoids and cancer prevention. *Advances in Experimental Medical Biology*, **401**, 87–100.

Batterham, T. J., Shutt, D. A., Hart, N. K., Braden, A. W. H. and Tweeddale, H. J., 1971, Metabolism of the intraruminally administered [4-^{14}C]formononetin and [4-^{14}C]biochanin A in sheep. *Australian Journal of Agricultural Research*, **22**, 131–138.

Booth, A. N., Jones, F. T. and DeEds, F., 1958, Metabolic fate of hesperidin, eriodictyol, homoeriodicytol and diosmin. *Journal of Biological Chemistry*, **230**, 661–668.

Borriello, S. P., Setchell, K. D. R., Axelson, M. and Lawson, A. M., 1985, Production and metabolism of lignans by the human faecal flora. *Journal of Applied Bacteriology*, **58**, 37–43.

Braden, A. W. H., Hart, N. K. and Lamberton, J. A., 1967, The oestrogenic activity and metabolism of certain isoflavones in sheep. *Australian Journal of Agricultural Research*, **18**, 335–348.

Coldham, N. G., Howells, L. C., Santi, A., Montesissa, C., Langlais, C., King, L. and Sauer, M. J., 1999, Biotransformation of genistein in the rat: Elucidation of metabolite structure by product ion mass fragmentology^{n}. *Journal of Steroid Biochemistry and Molecular Biology*, **70**, 169–184.

Coldham, N. G. and Sauer, M. J., 2000, Pharmacokinetics of [^{14}C]genistein in the rat; gender related differences, potential mechanisms of action and implications for human health. *Toxicology and Applied. Pharmacology*, **164**, 206–215.

Cimino, C. O., Shelnutt, S. R., Ronis, M. J. J. and Badger, T. M., 1999, An LC-MS method to determine concentrations of isoflavones and their sulfate and glucuronide conjugates in urine. *Clinica et Chimica Acta*, **287**, 69–82.

Day, A. J., DuPont, M. S., Ridley, S., Rhodes, M., Rhodes, M. J. C., Morgan, M. R. A. and Williamson, G., 1998, Deglycosylation of flavonoid and isoflavonoid glycosides by human small intestine and liver β-glucosidase activity. *Federation of European Biochemical Societies Letters*, **436**, 71–75.

Dickinson, J. M., Smith, G. R., Randel, R. D. and Pemberton, I. J., 1969, *In vitro* metabolism of formononetin and biochanin A in bovine rumen fluid. *Journal of Animal Science*, **66**, 1969–1973.

Griths, L. A. and Barrow, A., 1972, Metabolism of flavonoid compounds in germ-free rats. *Biochemical Journal*, **130**, 1161–1162.

Heider, J. and Fuchs, G., 1997, Anaerobic metabolism of aromatic compounds. *European Journal of Biochemistry*, **243**, 577–596.

Hollman, P. C. H. and Katan, M. B., 1997, Absorption, metabolism, and bioavailability of flavonoids. In C. A. Rice-Evans and L. Packer (eds), *Flavonoids in health and disease* (Boston: Marcel Dekker), pp. 483–522.

Joannou, G. E., Kelly, G. E., Reeder, A. Y., Waring, M. and Nelson, C., 1995, A urinary profile study of dietary phytoestrogens. The identification and mode of metabolism of new isoflavonoids. *Journal of Steroid Biochemistry and Molecular Biology*, **54**, 167–184.

Kelly, G. E., Joannou, G. E., Reeder, A. Y., Nelson, C. and Waring, M. A., 1995, The variable metabolic response to dietary isoflavones in humans. *Proceedings of the Society for Experimental Biology and Medicine*, **208**, 40–43.

King, R. A., 1998, Daidzein conjugates are more bioavailable than genistein conjugates in rats. *American Journal of Clinical Nutrition*, **68s**, 1496s–1499s.

Markaverich, B. M., Gregory, R. R., Alejandro, M. A., Clark, J. H., Johnson, G. A. and Middleditch, B. S., 1988, Methyl *p*-hydroxyphenyllactate an inhibitor of cell growth and proliferation and an endogenous ligand for nuclear type II binding sites. *Journal of Biological Chemistry*, **263**, 7203–7210.

Messina, M. J., Persky, V., Setchell, K. D. R. and Barnes, S., 1994, Soy intake and cancer risk: a review of the *in vivo* and *in vitro* data. *Nutrition and Cancer*, **21**, 113–131.

Nilsson, A., Hill, J. L. and Davies, H. L., 1967, An *in vitro* study of formononetin and biochanin A metabolism in rumen fluid from sheep. *Biochimica et Biophysica Acta*, **148**, 92–98.

Rao, J. R. and Cooper, J. E., 1994, Rhizobia catabolize nod gene-inducing flavonoids via C-ring fission mechanisms. *Journal of Bacteriology*, **176**, 5409–5413.

Schneider, H. and Blaut, M., 1999, Anaerobic degradation of flavonoids by *Eubacterium ramulus*. *Archives of Microbiology*, **173**, 71–75.

Schneider, H., Schwiertz, A., Collins, M. D. and Blaut, M., 1999, Anaerobic transformation of quercetin-3-glucoside by bacteria from the human intestinal tract. *Archives of Microbiology*, **171**, 81–91.

Setchell, K. D. R., 1998, Phytoestrogens: the biochemistry, physiology and implications for human health of soy isoflavones. *American Journal of Clinical Nutrition*, **46s**, 1333s–1346s.

Setchell, K. D. R. and Adlercreutz, H., 1988, Mammalian lignans and phyto-oestrogens. Recent studies on their formation, metabolism and biological role in health and disease. In I. A. Rowland (ed.), *Role of the Gut Flora in Toxicity and Cancer* (New York: Academic Press), pp. 315–345.

Setchell, K. D., Borriello, S. P., Hulme, P., Kirk, D. N. and Axelson, M., 1984, Nonsteroidal estrogens of dietary origin: possible roles in hormone-dependent disease. *American Journal of Clinical Nutrition*, **40**, 569–578.

Wang, G., Kuan, S. S., Francis, O. J., Ware, G. M. and Carman, A. S., 1990, A simplified HPLC method for the determination of phytoestrogens in soybean and its processed products. *Journal of Agricultural Food Chemistry*, **38**, 185–190.

Winter, J., Moore, L. H., Dowell, V. R. and Bokkenheuser, V. D., 1989, C-ring cleavage of flavonoids by human intestinal bacteria. *Applied Environmental Microbiology*, **55**, 1203–1208.

Worrell, N. R., Mallet, A. K., Cook, W. M., Baldwin, N. C. P. and Shepherd, M. J., 1989, The role of gut micro-organisms in the metabolism of deoxynivalenol. *Xenobiotica*, **19**, 25–32.

Xu, X., Wang, H.J., Murphy, P. A., Cook, L. and Hendrich, S., 1994, Daidzein is a more bioavailable soymilk isoflavone than is genistein in adult women. *Journal of Nutrition*, **124**, 825–832.

XENOBIOTICA, 2002, VOL. 32, NO. 1, 63–72

Taylor & Francis
healthsciences

Metabolism and urinary excretion of a new quinoline anticancer drug, TAS-103, in humans

R. AZUMA†*, M. SAEKI†, Y. YAMAMOTO†, Y. HAGIWARA‡, L. B. GROCHOW§¶ and R. C. DONEHOWER§

† Pharmacokinetics Research Laboratory, Taiho Pharmaceutical Co., Ltd., 224-2, Ebisuno, Hiraishi, Kawauchi-cho, Tokushima, 771-0194, Japan
‡ Chemistry Laboratory, Taiho Pharmaceutical Co., Ltd., 1-27, Misugidai, Hanno, Siatama 357-8527, Japan
§ Johns Hopkins Oncology Center, 1650 Orleans Street, Baltimore, MD 21231-1000, USA

Received 14 May 2001

1. TAS-103, a novel condensed quinoline derivative, has been developed as an anticancer drug targeting topoisomerases I and II.

2. The purpose of the present study was to characterize the metabolism and urinary excretion of TAS-103 after the intravenous infusion of a single dose to patients in Phase I clinical trials.

3. Five metabolites were detected using high-performance liquid chromatography (HPLC) photodiode array and a precursor scan by liquid chromatography mass spectrometry mass spectrometry (LC/MS/MS).

4. Structures of the five metabolites were determined using the results of enzymatic hydrolysis and the analysis of production mass spectra obtained by LC/MS/MS, and by comparing HPLC retention times and UV, mass and production mass spectra of authentic standards.

5. The metabolites were identified as demethyl-TAS-103 glucuronide (DM-TAS-103-G), TAS-103 glucuronide (TAS-103-G), TAS-103 glucuronide *N*-oxide (NO-TAS-103-G), demethyl-TAS-103 (DM-TAS-103) and TAS-103 *N*-oxide (NO-TAS-103).

6. The mean total amount of TAS-103 and TAS-103-G in urine was only 6.03% of the dose, suggesting that urine is not the main elimination route. TAS-103 was extensively metabolized, and a small percentage of the parent drug (0.41%) was found in urine.

Introduction

TAS-103, 6-[[2-(dimethylamino)ethyl]amino]-3-hydroxy-7*H*-indeno[2,1-*c*]-quinolin-7-one dihydrochloride, has been developed as an anticancer drug targeting topoisomerases I and II (Aoyagi *et al*. 1999). TAS-103 has marked efficacy against various lung metastatic tumors, and a broad antitumor spectrum in human xenografts (Utsugi *et al*. 1997). The concomitant use of TAS-103 and cisplatin has a greater cytotoxic effect on cancer cells than single drug use (Sunami *et al*. 1999), and a Phase I clinical study was performed in the USA (Donehower *et al*. 1998). TAS-103 is expected to be useful for treating lung, colon, stomach and prostate cancers.

The purpose of the present study was to characterize the metabolism and urinary excretion of TAS-103 after the intravenous infusion of a single dose to patients in Phase I clinical trials. The metabolite fractions from urine were purified

* Author for correspondence; e-mail: ryu-azuma@taiho.co.jp
¶ Present address: MPI, 54943, North Main Street, Mattawan, MI 49071, USA.

Xenobiotica ISSN 0049–8254 print/ISSN 1366–5928 online © 2002 Taylor & Francis Ltd
http://www.tandf.co.uk/journals
DOI: 10.1080/00498250110085818

by solid-phase extraction. The metabolites were detected by high-performance liquid chromatography (HPLC)-photodiode array, and liquid chromatography mass spectrometry mass spectrometry (LC/MS/MS). The structures of the metabolites were characterized by mass spectral analysis and enzymatic hydrolysis, and confirmed by comparisons of HPLC retention times and UV spectra, and by MS spectrometric techniques.

Materials and methods

Chemicals and reagents

TAS-103 (99.6% purity by HPLC analysis), DM-TAS-103 {6-[[2-(methylamino)ethyl]amino]-3-hydroxy-7*H*-indeno[2,1-*c*]-quinolin-7-one dihydrochloride, 99.7% purity}, NO-TAS-103 {6-[[2-(dimethylamino)ethyl]amino]-3-hydroxy-7*H*-indeno[2,1-*c*]-quinolin-7-one *N*-oxide dihydrochloride, 98.4% purity}, TAS-103-G {[6-[[2-(dimethylamino)ethyl]amino]-7-oxo-indeno[2,1-*c*]quinolin-3-yl]-β-D-glucopyranosiduronic acid, 95.9% purity}, and the internal standard, TAS-1-018 (99.6% purity; Azuma and Urakawa 1997), were synthesized at Chemistry Laboratory, Taiho Pharmaceutical Co., Ltd (Hanno, Japan).

HPLC-grade reagents, acetonitrile and methanol were purchased from Kanto Chemicals (Tokyo, Japan) or Nakalai Tesque (Kyoto, Japan). Trifluoroacetic acid, for protein sequencing, was purchased from Merck (Darmstadt, Germany). β-Glucuronidase from *E. coli*. (type IX-A, 125 000 units, sulfatase free) was purchased from Sigma (St Louis, MO, USA). The other reagents were of special grade. Water was purified with the Milli-Q system (Millipore, Tokyo, Japan).

Dosage and urine collection

TAS-103 for injection was a red-brown lyophilized powder. It was placed in 20-ml vials containing 100 mg TAS-103, 10 mg polysorbate 80 and 0.5 N sodium hydroxide in a quantity sufficient to adjust the pH to 3.0 and was dissolved in 500 ml saline. Six patients were treated via intravenous infusion over 90 min at a dose of 350 mg m^{-2} TAS-103. Three patients were treated at 430 mg m^{-2} and a single patient was treated at 540 mg m^{-2}. All patients were monitored for 3 weeks. Urine was collected during pretreatment, as well as at 0–12 and 12–24 h. Patients were instructed to void completely before infusion. The volume of collected urine was recorded and the samples kept refrigerated at $<4°C$. Aliquots of each sample (10 ml) were retained at $-80°C$ until transfer to Taiho Pharmaceutical Co., Ltd, where they were carried frozen on dry ice and kept at $-80°C$ until analysis.

Sample preparation for identification of metabolites

Following an established method (Azuma and Urakawa 1997), urine samples (1 ml) were purified and condensed with Sep-Pak Vac PS-2 cartridges (500 mg/3 ml; Nihon Waters, Tokyo, Japan). The internal standard was not added to the urine samples. The reconstituted solution was subjected to HPLC-photodiode array (10 µl) or LC/MS/MS (60 µl). To hydrolyse conjugates, the urine (1 ml) was incubated with β-glucuronidase (0.2–0.4 mg) at 37°C for 40 min and then extracted with Sep-Pak Vac PS-2 cartridges.

HPLC-photodiode array

The HPLC-photodiode array system was comprized of two Shimadzu LC-10AD pumps, an SIL-10A auto-injector, a CTO-10AC$_{VP}$ column oven, an SPD-10AV detector and an SPD-M10AV$_{VP}$ photodiode array detector (Kyoto, Japan). The photodiode array detector was connected with the UV detector in tandem. The data system was equipped with a CLASS LC-10 (v.1.62).

HPLC conditions were as follows: analytical column, J'sphere ODS-L80 (150 × 4.6 mm i.d.; YMC, Kyoto, Japan); column oven temperature, 40°C; mobile phase, 0.07% trifluoroacetic acid and acetonitrile, gradient from 17 to 35% over 18 min; flow rate, 1.0 ml min; photodiode array wavelength range, 220–600 nm; photodiode array time constant, 0.64 s; UV detector wavelength, 460 nm; autoinjector rinse solution, acetic acid/water/acetonitrile (2/48/50).

LC/MS/MS

LC/MS/MS was conducted with a Thermoquest TSQ 7000 triple-stage quadrupole mass spectrometer (Tokyo, Japan) equipped with a data system ICIS (v.3.1). For HPLC, a Hewlett Packard HP-1050 (Tokyo, Japan) was used. HPLC conditions were the same as for the HPLC-photodiode array system. Conditions for mass spectral analysis were as follows: ionization, positive electrospray; ion-spray voltage, 4.5 kV; heating capillary temperature, 230°C; sheath gas, 75 psi; auxually gas, 20 unit;

ion-multiple voltage, 1200 V (Q1MS) and 1600 V (MS/MS); collision-induced dissociation gas, argon, 2.0–2.5 mTorr; collision-induced dissociation energy, −30 eV.

Quantification of TAS-103 and the main metabolite, TAS-103-G

TAS-103 and TAS-1-018 (internal standard) were resolved in 50 mM glycine/perchloric acid buffer (pH 2.0). TAS-103-G was resolved in water. Their standard solutions (10, 5, 1, 0.2 and 0.1 μg ml^{-1}) were kept at room temperature to avoid deposition. Sample preparation (50 μl urine) and HPLC conditions were as described in Azuma and Urakawa (1997).

Intra- and interassays, extraction recovery and stability in the autoinjector (29 h) on freeze/thawing (two cycles at −20°C, then three cycles at −80°C), and in storage (−20°C for 15 days, −80°C for 185 days) were examined using three quality-control samples. The accuracy and precizion were evaluated as %bias and %CV, respectively (Causon 1997). %Bias ranged from −2.4 to 10.4%. %CV was <7.5% (Bressolle *et al.* 1996). Extraction recoveries of both compounds were >93%.

Results

Detection of metabolites by HPLC-photodiode array and LC/MS/MS

Representative HPLC-UV chromatograms for human urine after solid-phase extraction are shown in figure 1. Comparing figure 1A and C, four metabolites, M1, M2, M4 and M5, were detected. The peak at 8.0 min represents TAS-103. A chromatogram of urine purified after hydrolysis by β-glucuronidase is shown in figure 1B. The two peaks, M1 and M2, disappeared, and three peaks, M4, TAS-103 and M5, increased, indicating that M1 and M2 were glucuronide conjugates. The large amount of M2 in figure 1A and TAS-103 in figure 1B indicated that M2 was TAS-103-G. Moreover, another glucuronide peak was present although its retention time (t_R) was not clear.

TAS-103 is a novel condensed quinoline derivative and has a characteristic UV spectrum (figure 2), which shows maximum absorption at 243, 263, 296, 331 and 442 nm. To detect metabolites of TAS-103, we developed three-dimensional HPLC chromatograms as shown in figure 3. The UV spectra for peaks of 17–18 min in figure 1 differed from that for TAS-103, indicating that they are not

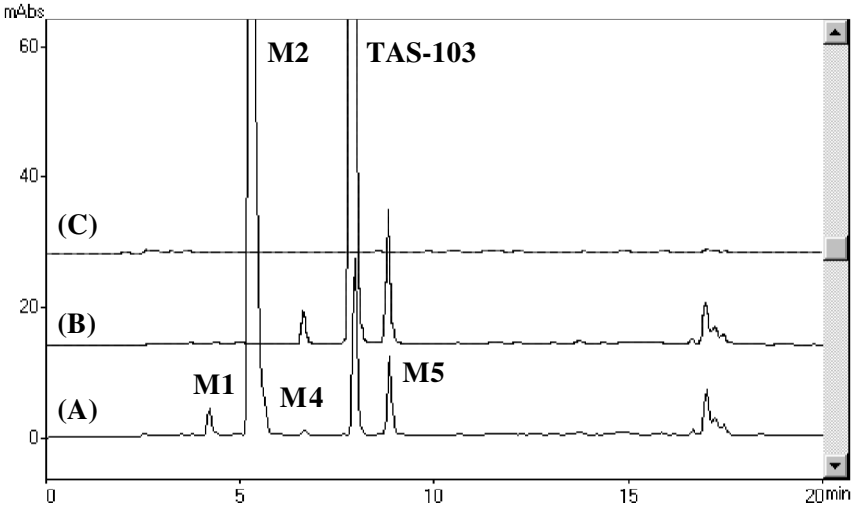


Figure 1. Representative HPLC chromatograms of human urine after intravenous infusion of TAS-103. (A) 0–12 h post-dose, (B) 0–12 h post-dose after hydrolysis by β-glucuronidase, (C) predose. The peak of M3 overlaps with that of M2.

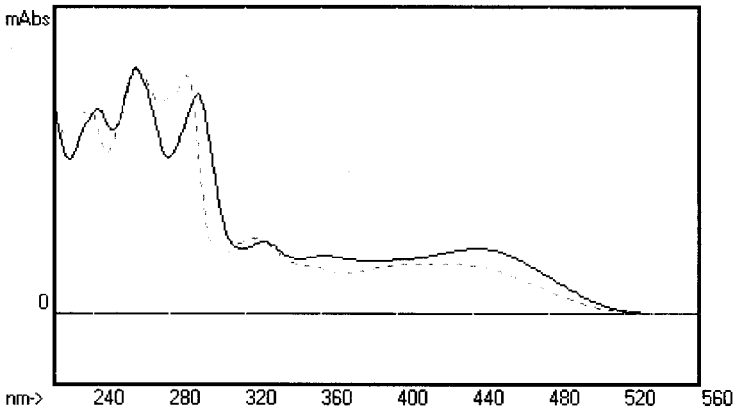


Figure 2. UV spectra of TAS-103 (solid line) and TAS-103-G (dotted line) analysed by HPLC-photodiode array. Scan ranged from 220 to 600 nm.

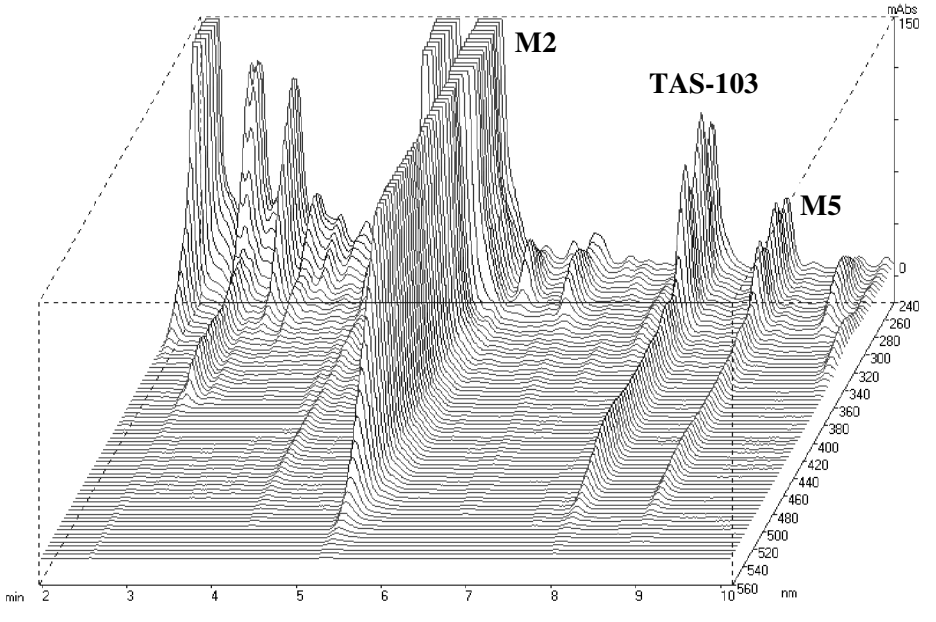


Figure 3. Three-dimensional HPLC chromatogram of human urine (0–12 h) after intravenous infusion of TAS-103. The magnified chromatogram was derived from the same urine sample in figure 1. The UV spectrum of M2 ($t_R = 5.3$ min) was consistent with that of the authentic standard of TAS-103-G.

metabolites of TAS-103 (data not shown). The UV spectrum of M2 ($t_R = 5.3$ min) was consistent with that of the authentic standard of TAS-103-G. The UV spectrum of M5 ($t_R = 8.9$ min) was similar to that of the authentic standards of TAS-103 and NO-TAS-103, implying M5 was a metabolite of TAS-103. Moreover, the UV spectra of M1 and M4 in visible regions resembled that of TAS-103, but the spectra in UV regions of M1 and M4 were not consistent with that of TAS-103 due to interference by endogenous compounds.

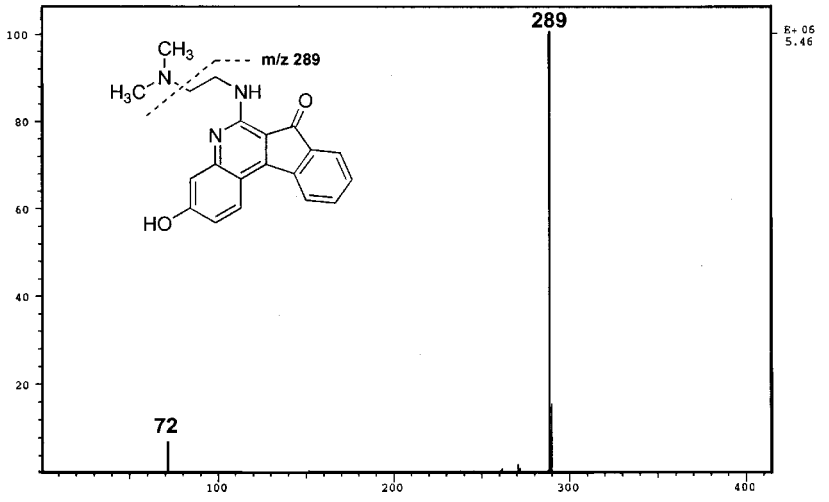


Figure 4. Production mass spectrum of $[M+H]^+$ ion at m/z 334 for TAS-103 (authentic standard).

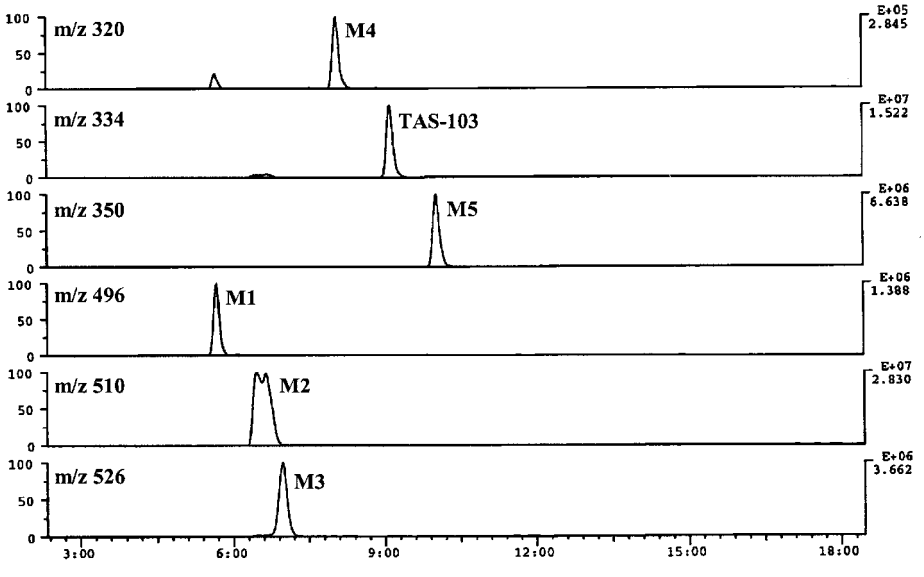


Figure 5. Mass chromatograms of precursor scan of m/z 289 from human urine after intravenous infusion of TAS-103. The peak of M2 was divided due to overloading of samples. The retention times of M1, M2, M3, M4, TAS-103 and M5 were 6.4, 6.8, 7.1, 8.4, 9.5 and 10.5 min, respectively.

The production mass spectrum obtained from precursor ion m/z 334, a protonated molecular ion of TAS-103, is shown in figure 4. Two fragment ions are observed at m/z 289 and 72, based on the loss of the *N*-dimethyl moiety and $(CH_3)_2NCH_2CH_2$, respectively. By precursor ion scanning of m/z 289, five metabolites, M1 (m/z 496), M2 (510), M3 (526), M4 (320) and M5 (350), were detected (figure 5). Although the separation of M2 and M3 on the UV chromatogram was poor, M3 separated from M2 completely on mass chromatograms obtained by precursor ion scan.

Determination of the structure of the metabolites of TAS-103

In precursor ion mass spectra scanned from m/z 289, the protonated molecular ion $[M+H]^+$ of M4 was observed at m/z 320, which is 14 mass units smaller than that of TAS-103. This suggests that M4 is an *N*-demethylated metabolite. The retention time on HPLC and UV, mass (Q1MS) and production mass spectra of M4 were completely consistent with those of the authentic standard of DM-TAS-103.

The protonated molecular ion $[M+H]^+$ of M5 was observed at m/z 336, which is 16 mass units larger than that of TAS-103. The retention time of M5 on HPLC was slightly longer than that of TAS-103. This suggests that M5 is not hydroxy-TAS-103, but TAS-103 *N*-oxide with an *N*-dimethyl moiety or aromatic nitrogen.

The protonated molecular ions $[M+H]^+$ of M1, M2 and M3 were observed at m/z 496, 510 and 526, which are 176 mass units larger than those of M4, TAS-103 and M5, respectively. This suggests that they are glucuronides of M4, TAS-103 and M5, respectively, consistent with the results of enzymatic hydrolysis.

The production mass spectrum of M2 scanned from the protonated molecular ion (m/z 510) is shown in figure 6A. The fragment ion m/z 334 indicates loss of glucuronic acid (176 mass units). Similar to TAS-103, the fragment ions m/z 289 and 72 were observed. The binding position of glucuronic acid was more likely to be the phenolic hydroxy group than the aromatic nitrogen. The retention time on HPLC, and UV, mass (Q1MS) and production mass spectra of M2 were completely consistent with those of the authentic standard of TAS-103-G.

The production mass spectrum of M1 scanned from the protonated molecular ion (m/z 496) revealed the fragment ions m/z 320 and 289 (data not shown). The m/z 320 would indicate loss of glucuronic acid. The binding position of glucuronic acid was presumed to be phenolic hydroxy group as in TAS-103-G. Consequently, M1 was presumed to be the glucuronide of M4, namely DM-TAS-103-G.

The production mass spectrum of M3 scanned from the protonated molecular ion (m/z 526) is shown in figure 6B. The fragment ion m/z 465 $[M-60]^+$ would indicate that *N*-oxide is located at the *N*-dimethyl moiety, and not the aromatic nitrogen. The binding position of glucuronic acid was presumed to be the phenolic hydroxy group as in TAS-103-G. Consequently, the position of *N*-oxide for M5 was determined. The retention time on HPLC, and UV, mass (Q1MS) and production mass spectra of M5 were completely consistent with those of the authentic standard of NO-TAS-103. Moreover, M3 was presumed to be glucuronide of M5, namely, NO-TAS-103-G.

Consequently, M2, M4 and M5 were identified as TAS-103-G, DM-TAS-103 and NO-TAS-103, respectively. M1 and M3 were presumed to be DM-TAS-103-G and NO-TAS-103-G, respectively.

Urinary excretion of TAS-103 and TAS-103-G

Urinary excretion of TAS-103 and TAS-103-G up until 24 h after a single intravenous infusion of TAS-103 at 350–540 mg m^{-2} (10 patients) is presented in table 1. The urinary excretion of the main metabolite, TAS-103-G, was 2.32–10.0% of the dose. The excretion of TAS-103 was minimal, namely 0.10–0.75% of the dose (mean 0.41%). Total excretion of both compounds ranged from 2.42 to 10.8% (mean 6.03%). Most of the metabolites were excreted within 12 h after dosing.

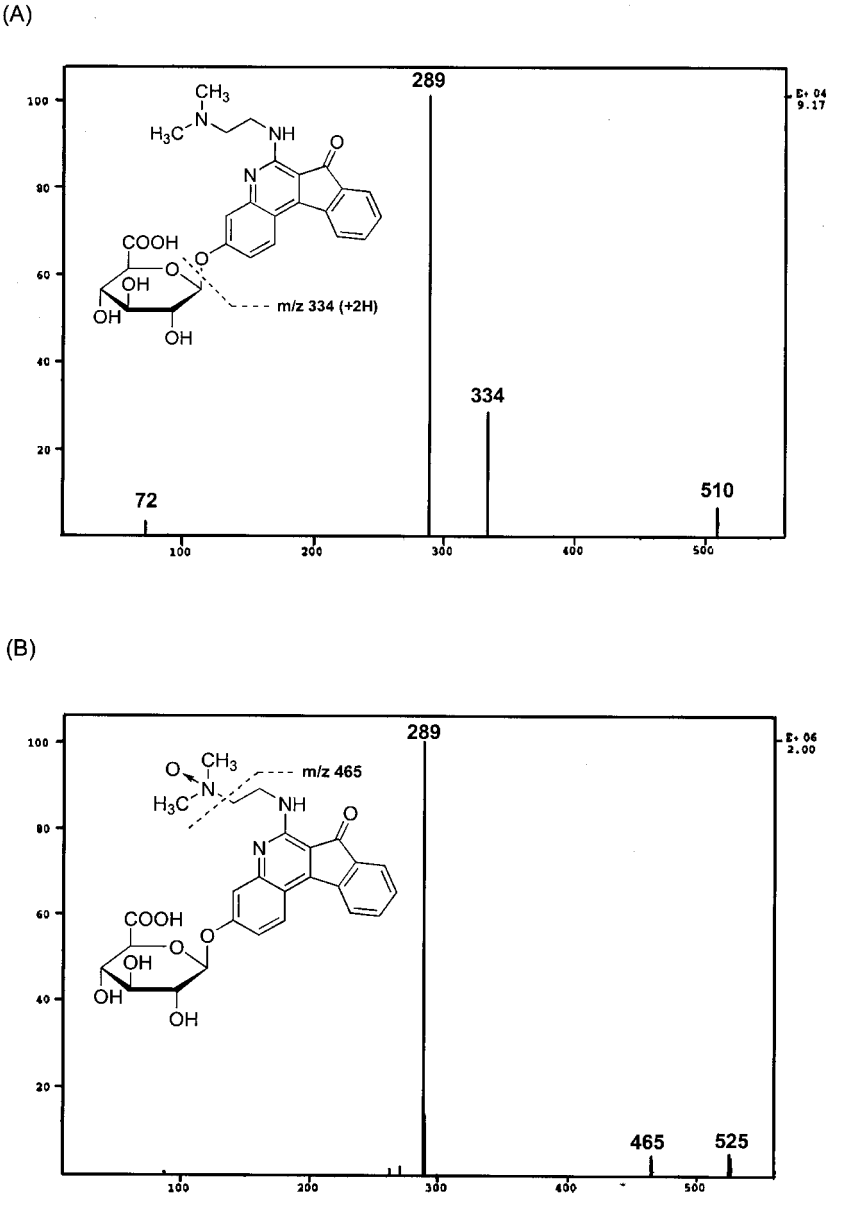


Figure 6. Production mass spectra of $[M+H]^+$ for M2 at m/z 510 (A) and M3 at m/z 526 (B) in the chromatogram depicted in figure 5.

Discussion

The focus of the present study was to elucidate the structure of metabolites of TAS-103 in human urine after intravenous infusion. Comparing UV chromatograms monitored at 460 nm of predose urine with those of post-dose urine (figure 1), a peak of the parent drug and four metabolite peaks were detected. Simultaneously, we developed three-dimensional chromatograms using a photodiode array detector. Photodiode array detection is a powerful tool with which to identify metabolites that have the UV properties of a chromophore (Law and

Table 1. Urinary excretion of TAS-103 and TAS-103-G after intravenous infusion of TAS-103 in humans.

	Dosage		TAS-103-G		TAS-103		
Patients	($mg\,m^{-2}$)	($mg\,kg^{-1}$)	0–12 h	12–24 h	0–12 h	12–24 h	Total
1	350	8.40	2.42	0.65	0.36	0.04	3.47
2	350	8.33	8.41	0.36	0.60	0.00	9.37
3	350	7.86	3.58	0.10	0.16	0.00	3.84
4	350	8.35	7.42	0.43	0.55	0.00	8.40
5	350	9.04	7.86	0.30	0.60	0.00	8.76
6	350	8.99	3.05	0.03	0.11	0.00	3.19
7	430	10.87	2.16	0.16	0.10	0.00	2.42
8	430	9.58	4.23	0.14	0.47	0.00	4.84
9	430	11.77	4.63	0.19	0.39	0.00	5.21
10	540	14.09	8.78	1.26	0.75	0.00	10.79

Results are given with the percentage of the administered dose.

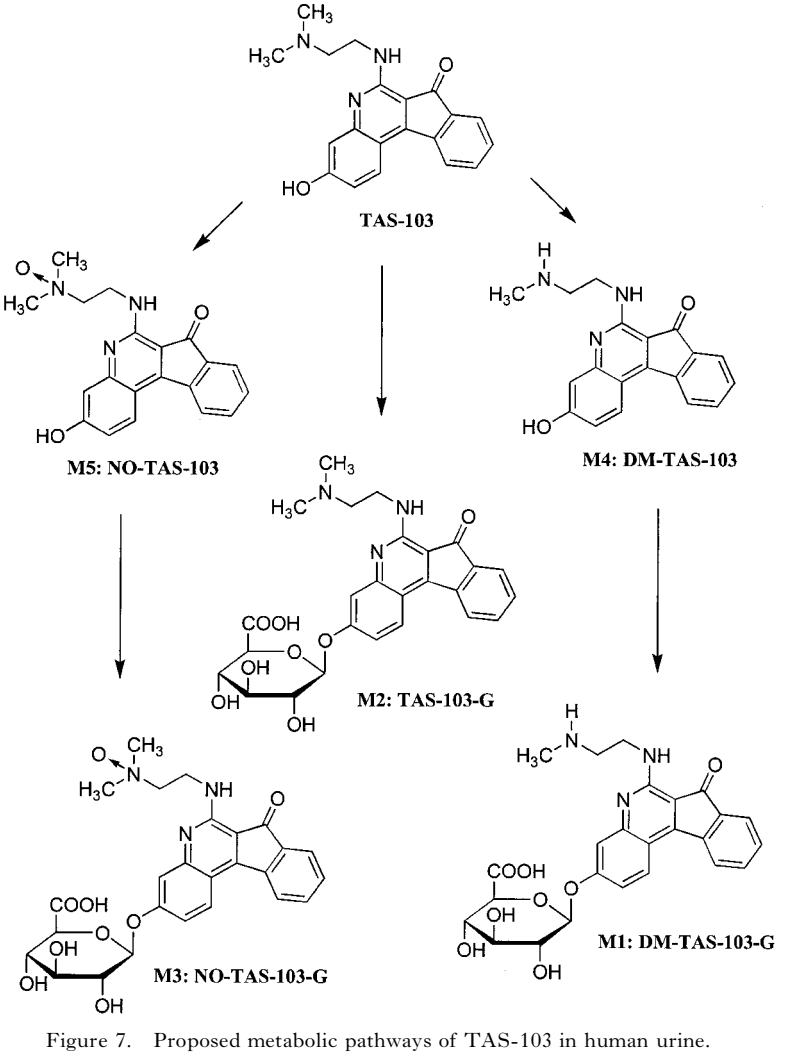


Figure 7. Proposed metabolic pathways of TAS-103 in human urine.

Stafford 1993, Vickers *et al*. 1998). Therefore, the peaks at 17–18 min in figure 1 were excluded because their UV spectra differed from that for TAS-103. The peaks of M1 and M2 disappeared after enzymatic hydrolysis, but the other three peaks increased in magnitude. We could not detect M3 in UV chromatograms using the photodiode array detector. The peak of M3 was masked by that of M2 under the HPLC conditions. By precursor ion scan of m/z 486 by LC/MS/MS, we detected one more peak (M3). The precursor ion scan mode is useful for detecting metabolites that have a common skeleton (Davis and Baillie 1995, Kondo *et al*. 1996, Kassahun *et al*. 1997). This technique facilitates detection of trace levels of metabolite, which have been insufficiently separated from other metabolites on HPLC. Consequently, we detected five metabolites and the parent drug.

The structures of the five metabolites were determined using the results of enzymatic hydrolysis and the production mass spectra obtained by LC/MS/MS, and by comparison with the HPLC retention times and UV, mass and production mass spectra of the authentic standards.

The mean total amount excreted in urine was only 6.03% of the dose, suggesting that urine is not the main elimination route. TAS-103 was extensively metabolized, and only a small percentage of the parent drug (0.41%) was found in urine. Based on the structures of metabolites, a plausible scheme of the metabolic pathways of TAS-103 in human is shown in figure 7. The major route of metabolism involved direct *O*-glucuronidation following phenolic hydroxylation (M2). The minor routes of metabolism involved *N*-oxidation of the terminal *N*-alkyl side chain (M5), and *N*-demethylation of the same terminal moiety (M4). These metabolites also underwent subsequent conjugation with glucuronic acid (M1, M2).

References

Aoyagi, Y., Kobunai, T., Utsugi, T., Oh-hara, T. and Yamada, Y., 1999, *In vitro* antitumor activity of TAS-103, a novel quinoline derivative that targets topoisomerases I and II. *Japanese Journal of Cancer Research*, **90**, 578–587.

Azuma, R. and Urakawa, A., 1997, Simultaneous determination of a novel anticancer drug, TAS-103, and its *N*-demethylated metabolite in monkey plasma by high-performance liquid chromatography using solid-phase extraction. *Journal of Chromatography B*, **691**, 179–185.

Bressolle, F., Bromet-Petit, M. and Audran, M., 1996, Validation of liquid chromatographic and gas chromatographic methods. Applications to pharmacokinetics. *Journal of Chromatography B*, **686**, 3–10.

Causon, R., 1997, Validation of chromatographic methods in biomedical analysis. Viewpoint and discussion. *Journal of Chromatography B*, **689**, 175–180.

Davis, M. R. and Baillie, T. A., 1995, Studies on the formation of reactive intermediates from the antineoplastic agent *N*,*N*′-bis(2-chloroethyl)-*N*-nitrosourea (BCNU) *in vitro* and *in vivo*. Characterization of novel glutathione adducts by ionspray tandem mass spectrometry. *Journal of Mass Spectrometry*, **30**, 57–68.

Donehower, R., Elza-Brown, K., O'Reilly, S., Israel, B. and Grochow, L., 1998, A phase I dose escalation, safety, tolerability, and pharmacokinetic study of TAS-103 in patients with refractory solid tumors. *Proceedings of the American Society of Clinical Oncology*, **17**, 209a.

Kassahun, K., Davis, M., Hu, P., Martin, B. and Baillie, T., 1997, Biotransformation of the naturally occurring isothiocyanate sulforaphane in the rat: identification of phase I metabolites and glutathione conjugates. *Chemical Research in Toxicology*, **10**, 1228–1233.

Kondo, T., Yoshida, K., Yoshimura, Y., Motohashi, M. and Tanayama, S., 1996, Characterization of conjugated metabolites of a new angiotensin II receptor antagonist, candesartan cilexetil, in rats by liquid chromatography/electrospray tandem mass spectrometry following chemical derivatization. *Journal of Mass Spectrometry*, **31**, 873–878.

Law, B. and Stafford, L. E., 1993, The use of ultraviolet spectra and chromatographic retention data as an aid to metabolite identification. *Journal of Pharmaceutical and Biomedical Analysis*, **11**, 729–736.

Sunami, T., Nishio, K., Kanzawa, F., Fukuoka, K., Kudoh, S., Yoshikawa, J. and Saijo, N., 1999, Combination effects of TAS-103, a novel dual topoisomerase I and II inhibitor, with other anticancer agents on human small cell lung cancer cells. *Cancer Chemotherapy and Pharmacology*, **43**, 394–401.

Utsugi, T., Aoyagi, K., Asao, T., Okazaki, S., Aoyagi, Y., Sano, M., Wierzba, K. and Yamada, Y., 1997, Antitumor activity of a novel quinoline derivative, TAS-103, with inhibitory effects on topoisomerases I and II. *Japanese Journal of Cancer Research*, **88**, 992–1002.

Vickers, S., Duncan, C. A., Slaughter, D. E., Arison, B. H., Greber, T., Olah, T. V. and Vyas, K. P., 1998, Metabolism of MK-499, a class III antiarrhythmic agent, in rats and dogs. *Drug Metabolism and Disposition*, **26**, 388–395.

XENOBIOTICA, 2002, VOL. 32, NO. 1, 73–86

Taylor & Francis
healthsciences

Biotransformation of benzydamine by microsomes and precision-cut slices prepared from cattle liver

A. SANTI†, P. ANFOSSI‡*, N. G. COLDHAM§, F. CAPOLONGO†, M. J. SAUER§ and C. MONTESISSA†

† Istituto di Patologia e Igiene veterinaria, Università di Padova, Agripolis, I-35020 Legnaro (PD), Italy
‡ Dipartimento di Sanità Pubblica Veterinaria e Patologia Animale, Università di Bologna, Ozzano Emilia, Bologna, Italy
§ Department of Risk Research, Veterinary Laboratories Agency, New Haw, Addlestone, Surrey KT15 3NB, UK

Received 14 May 2001

1. Benzydamine (BZ), a non-steroidal anti-inflammatory drug used in human and veterinary medicine, is not licensed for use in food-producing species. Biotransformation of BZ in cattle has not been reported previously and is investigated here using liver microsomes and precision-cut liver slices.

2. BZ was metabolized by cattle liver microsomes to benzydamine *N*-oxide (BZ-NO) and monodesmethyl-BZ (Nor-BZ). Both reactions followed Michaelis–Menten kinetics ($K_m = 76.4 \pm 16.0$ and $58.9 \pm 6.4\,\mu M$, $V_{max} = 6.5 \pm 0.8$ and $7.4 \pm 0.5\,nmol\,mg^{-1}\,min^{-1}$, respectively); sensitivity to heat and pH suggested that the *N*-oxidation is catalysed by the flavin-containing monooxygenases.

3. BZ-NO and Nor-BZ were the most abundant products derived from liver slice incubations, and nine other BZ metabolites were found and tentatively identified by LC-MS. Desbenzylated and hydroxylated BZ-NO analogues and a hydroxylated product of BZ were detected, which have been reported in other species. Product ion mass spectra of other metabolites, which are described here for the first time, indicated the formation of a BZ N^+-glucuronide and five hydroxylated and N^+-glucuronidated derivatives of BZ, BZ-NO and Nor-BZ.

4. The results indicate that BZ is extensively metabolized in cattle. Clearly, differences in metabolism compared with, for example, rat and human, will need to be considered in the event of submission for marketing authorization for use in food animals.

Introduction

Benzydamine (1-benzyl-3-[3-(dimethylamino)propoxy]-1*H*-indazole; BZ) is a non-steroidal analgesic anti-inflammatory drug used in humans by topical application. Although BZ has been used in veterinary medicine in cattle and pig (intramuscular administration) for the treatment of inflammatory conditions of the respiratory, gastrointestinal, genital and urinary systems and in horse by topical application for soft tissue injuries, it is not currently licensed in the EU for applications in food-producing species.

A wide range of BZ metabolites has been identified in rat, rabbit and man (Kataoka *et al.* 1971, 1973, Koppel and Tenczer 1985, Baldock *et al.* 1991). In rat, benzydamine *N*-oxide (BZ-NO) and glucuronide metabolites were found in urine

* Author for correspondence; e-mail: anfossi@vet.unibo.it

Xenobiotica ISSN 0049–8254 print/ISSN 1366–5928 online © 2002 Taylor & Francis Ltd
http://www.tandf.co.uk/journals
DOI: 10.1080/00498250110085827

and bile, whereas in rabbit the major metabolites were BZ-NO, a hydroxylbenzydamine derivative (BZ-OH) and its acetyl-, glucuronide and sulphate conjugates. In man, the major metabolites excreted in urine were BZ-NO, monodesmethyl-BZ (Nor-BZ), BZ-OH, the dedimethylaminopropyl-BZ, the desbenzyl-BZ and several glucuronides. Despite the use of BZ in food animals in the past and the knowledge that the drug undergoes a very complex metabolic fate in laboratory animals and man, there are no published data describing the metabolism of BZ in food species such as cattle. Establishing the extent to which the metabolite profile of the target species is representative of that evaluated in previous studies in laboratory animals provides the basis for determining whether further toxicity assessment is required for extension of licensing to a new food species. Furthermore, this provides an indication of the potential target residues for requisite pharmacokinetic and residues studies, etc.

Several *in vitro* models, including isolated hepatocytes and microsomes, are available for the assessment of xenobiotic metabolism. Recently, precision-cut liver slices have been utilized as an alternative method since the approach maintains tissue architecture and functional heterogeneity and provides a pathway for drug metabolism that is more consistent with *in vivo* metabolism than other models (Smith *et al*. 1987, Barr *et al*. 1991, Dogterom 1993, Miller *et al*. 1993, Saylers *et al*. 1994, George *et al*. 1999).

In vitro studies using rat liver and brain microsomes and hepatocytes from several species have demonstrated that the *N*-oxidation of BZ to BZ-NO is catalysed by the flavin-containing monooxygenases (FMO), whereas the *N*-demethylation of BZ to Nor-BZ involves cytochrome P450 monooxygenases (Kawaji *et al*. 1993, 1994, Ubeaud *et al*. 1999).

In vitro metabolism studies can be viewed as a means of readily enabling the generation of valuable qualitative comparative data as a basis for the initial assessment of equivalence with other target species and with model species used in toxicity studies, such as the rat. In addition, such preliminary data may better enable more effective planning of essential *in vivo* studies.

The biotransformation of BZ was investigated in the present study by using microsomes and precision-cut slices prepared from cattle liver to provide enzyme kinetic details on the production of BZ-NO and Nor-BZ as well as preliminary information on the likely pathways of BZ metabolism in the species. Metabolites were analysed by high-performance liquid chromatography (HPLC) with fluorimetric detection, and the structural identity of metabolites was investigated by mass spectrometry (MS).

Material and methods

Chemicals

Benzydamine hydrochloride (purity 99.8%), benzydamine *N*-oxide hydrochloride (97.3%) and norbenzydamine hydrochloride (99.7%) were supplied by Angelini Ricerche S.p.A. (Società per Azioni). NADPH and bovine serum albumin (BSA) were from Boehringer Mannheim Italia S.p.A. (Milan, Italy). Earl's balanced salt solution (EBSS) without phenol red, RPMI 1640 w/GLUTAMAX II with 25 mm HEPES and glutamine were supplied by Gibco BRL (Life Technologies, Paisley, UK). Methionine, hydrocortisone, insulin, foetal calf serum, gentamycin and amphoteracin B were supplied by Sigma Chemical Co. (St Louis, MO, USA). All other reagents, salts (analytical grade) and solvents (hplc grade) were purchased from Mallinchrodt Baker S.p.A. (Deventer, The Netherlands) and Carlo Erba (Milan, Italy).

Metabolism of BZ by liver microsomes

Samples of liver tissue (caudate lobe) from four healthy steers (550–600 kg b.w.) were collected at the slaughterhouse immediately *post mortem*. Samples of liver (~50 g) were cut into small pieces and washed three times with ice-cold 1.15% (w/v) KCl, suspended in 2 vols 0.1 M phosphate buffer (pH 7.4) and 1.15% (w/v) KCl solution (1:1 v/v) and homogenized in a Potter apparatus with a Teflon pestle (Heavy Stirrer, Apparecchi per Laboratori Chimici s.r.l., Milan, Italy). The homogenate was centrifuged at 9000*g* at 4°C for 20 min and the supernatant retained and further centrifuged at 105 000*g* for 60 min to obtain the microsomal fraction. The microsomes were suspended in 0.1 M phosphate buffer (pH 7.4):glycerol 80:20 (v/v) containing 0.1 M EDTA and stored under liquid N_2 pending biotransformation studies. Immediately before use, the microsomal fraction was thawed at 37°C and suspended in 0.1 M phosphate buffer (pH 7.4) or 0.1 M Tris-HCl buffer (pH 8.5) for evaluation of CYP- and FMO-catalysed reactions, respectively. The protein concentration of the microsomal preparation was determined using bovine serum albumin (BSA) as a calibration standard (Lowry *et al.* 1951). Total microsomal cytochrome P450 was determined by measuring the CO spectra of dithionite reduced P450 (Omura and Sato 1964).

Biotransformation was studied in triplicate by incubating 0.2 mg ml^{-1} microsomal protein, 1 mM NADPH, 2.5 mM $MgCl_2$, and substrate (BZ; concentrations from 2.5 to 1000 μM) in a final volume of 0.4 ml, with either 0.1 M phosphate buffer (pH 7.4) or 0.1 M Tris-HCl (pH 8.5) for 10 min at 37°C. Blank samples without NADPH or BZ were used to control for non-enzymatic transformations.

The effects of microsomal protein concentration and of incubation time on the formation of metabolites was evaluated as above over the range 0.1–1 mg ml^{-1} microsomal protein and from 5 to 30 min of incubation. The reactions were stopped by addition of acetonitrile (0.8 ml). After vortexing for 1 min, samples were centrifuged at 13 000*g* for 5 min (Microfuge E, Beckman, San Ramon, CA, USA), and the supernatant diluted from 1:1 to 1:20 v/v with the HPLC mobile phase.

To evaluate the contribution of CYP- and FMO-catalysed reactions, further assays were performed with substrate concentrations of 1.0 and 2.5 μM in a similar manner ± heat treatment (47°C for 3 min) to inactivate FMO (Ziegler 1988).

Metabolism of BZ by precision-cut liver slices

Samples of liver tissue were obtained from three healthy calves Angus/Friesian (cross steer, 7–10 months old) slaughtered by captive bolt and exsanguination. Livers were perfused within 10 min of slaughter with ice-cold Earl's balanced salt solution (EBSS, previously equilibrated with 95% O_2/5% CO_2) and transported to the laboratory on ice.

Cylindrical tissue cores were prepared using a 10-mm diameter motor-driven tissue-coring tool. Tissue slices (200–300 μm thick) were cut from the cylinders with a Krumdieck tissue slicer (Alabama Research and Development Corp., Munford, AL, USA) in oxygenated EBSS containing 25 mM glucose at 4°C. Liver slices were floated into 12-well plates (one slice per well) and incubated with culture medium (1 ml) employing a continuously submerged incubation system. The culture medium was prepared from RPMI 1640 medium containing 5% (v/v) foetal calf serum, 1 μM insulin, 0.5 mM L-methionine, 0.1 mM hydrocortisone-21-hemisuccinate and 50 μg ml^{-1} gentamycin (Coldham *et al.* 1995).

Culture plates were incubated at 37°C in a humidified atmosphere of 95% O_2/5% CO_2. After 30-min incubation, treatment was commenced by replacing the culture medium with fresh medium and a range of BZ concentrations (0, 100, 500, 1000 μM) was added to the appropriate wells.

Following incubations of 0, 2, 4, 6, 8 and 24 h, the medium was removed for analysis of metabolites. Liver slices were washed in 1.15% KCl, containing 50 mm Tris-HCl (1 ml), homogenized in this medium with a IKA-Labotechnic Ultra Turrax 25 and sonicated with an MSE Soniprep 150 Ultrasonic Disintegrator (MSE Scientific Instruments, Crawley, UK).

The liver slice homogenates and samples of culture medium were stored at −80°C before analysis. Whole homogenates of liver slices were assayed for protein content with BSA as calibration standard (Lowry *et al.* 1951). Samples of culture medium were diluted and analysed by HPLC and HPLC-MS.

HPLC analysis

HPLC consisted of a Jasco Pump PU 980 equipped with an LG 980 02 Ternary Gradient Unit and a GASSTORR GT-103 degasser, a Jasco Autosampler AS 950, and a Jasco fluorometric detector FP 920 (Japan Spectroscopic, Tokyo, Japan) set at 303 nm excitation and 350 nm emission.

Samples of microsomal supernatant and culture medium (20 μl) were chromatographed on a Prodigy ODS(3) column (5 μm; 250 × 4.6 mm i.d.) (Phenomenex, Torrance, CA, USA) using an isocratic binary mobile phase consisting of water 0.1% trifluoracetic acid (TFA):acetonitrile 0.082%TFA 65:35 (v/v) at a flow rate of 0.8 ml min^{-1}. Under these chromatographic conditions reference compounds eluted (retention time ± SD, min) in the order: Nor-BZ (11.8 ± 0.3), BZ (13.1 ± 0.3) and BZ-NO (15.7 ± 0.3).

Calibration curves of BZ, BZ-NO and Nor-BZ in the range 0.01−1 μm were prepared in the mobile phase starting from aqueous standard solutions (1 mM). The concentration of analyte in unknown samples was determined by interpolating from the appropriate calibration curve.

LC-MS analysis

Culture medium (20 µl) from precision-cut liver slices was analysed by LC-MS using an HP1050 HPLC system (Hewlett Packard, Bracknell, UK) and an ion-trap mass spectrometer (LCQ, Finnigan, Hemel Hempstead, UK) in series with a Shimatzu RF-535 fluorescence detector set at 303 nm excitation and 350 nm emission.

BZ metabolites were chromatographed on the same Prodigy RP column and eluted using a binary mixture of (A) water 2% formic acid:(B) acetonitrile 2% formic acid. Metabolites were eluted at flow rate of 0.8 ml min^{-1} with a linear gradient from 90% A to 65% A over 10 min, followed by an isocratic period at 65% A for 15 min.

Under these chromatographic conditions, the reference compounds were resolved (retention time ± SD, min) in the order Nor-BZ (16.4 ± 0.2), BZ (17.1 ± 0.3) and BZ-NO (18.2 ± 0.4).

MS was optimized by infusion of a BZ standard (1 µg ml^{-1}). Positive-ion electrospray provided the greatest sensitivity. The probe settings included a heated capillary temperature of 271.5°C and voltage of 23.6 V.

Mass spectra were collected in either full scan (m/z 100–550) or product ion modes, the latter being derived from the molecular ion $[M + H]^+$. MS experiments on BZ and metabolites were performed with CID energies of 30% and mass isolation width of 2 amu.

Analysis of BZ, Nor-BZ and BZ-NO fragmentation by MS was determined by direct infusion of 10 µM solutions into mobile phase at a flow rate of 10 µl min^{-1}.

Potential metabolites were investigated by selecting masses at m/z 236, 326, 342, 486, 488, 502 and 518 for further MS experiments (taking account of published literature and fragmentation pathways of BZ, Nor-BZ and BZ-NO), at elution times corresponding with peaks detected by fluorescence.

Results

Metabolism of BZ by liver microsomes

The content of cytochrome P450 in bovine microsomes was 0.61 ± 0.05 nmol mg^{-1} protein (mean ± SD, $n = 4$). After incubation of BZ with microsomes, three metabolites were observed in the supernatant (figure 1), the first unidentified product eluting at an earlier retention time (~9.9 min) than BZ (12.8 min) and two further metabolites co-eluting at retention times corresponding with

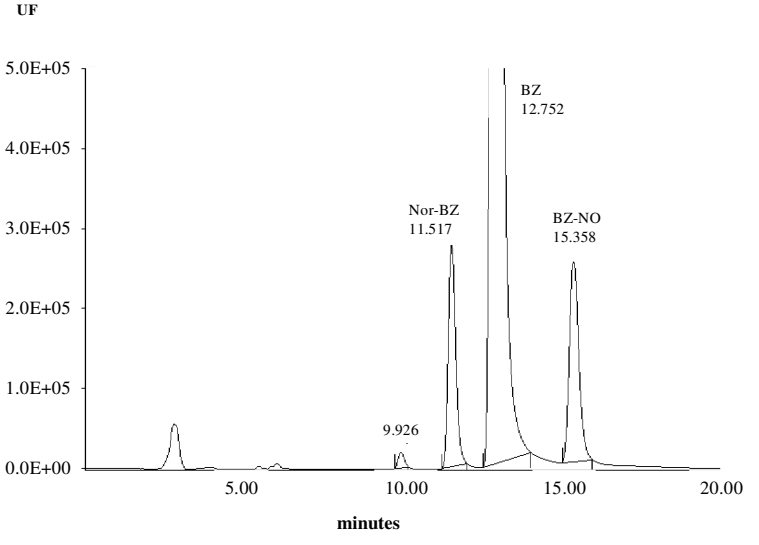


Figure 1. HPLC chromatogram obtained from cattle liver microsomes incubated with BZ (100 µm). The HPLC conditions were: Prodigy ODS(3) column (5 µm; 250 × 4.6 mm i.d.) (Phenomenex, Torrance, CA, USA); isocratic binary mobile phase consisting of water 0.1%TFA:acetonitrile 0.082%TFA 65:35 (v/v); flow rate 0.8 ml min^{-1}; fluorometric detection (303 nm excitation, 350 nm emission). UF, units of fluorescence.

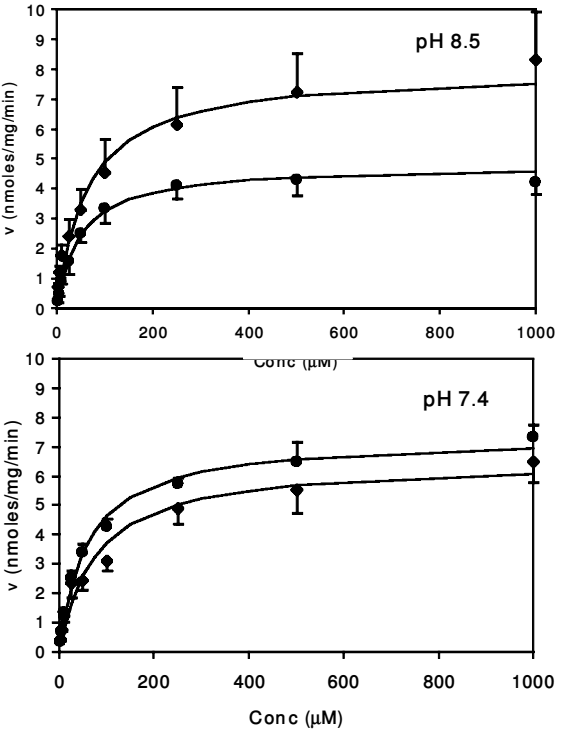


Figure 2. Production of Nor-BZ (●) and BZ-NO (◆) as a function of substrate concentration in cattle liver microsomes. Values are the mean ± SD of data derived from samples from four animals. A non-linear regression software (Fig.P 2.0, Biosoft, Cambridge, UK) was used to provide curves of best fit to data derived from the Michaelis–Menten equation.

Table 1. Kinetic parameters derived from the Michaelis–Menten equation for Nor-BZ and BZ-NO formation from BZ by cattle liver microsomes.

Product	K_m(μM)	V_{max} (nmol mg^{-1} min^{-1})
Nor-BZ		
pH 7.4	58.9 ± 6.4 (52.7–67.5)	7.4 ± 0.5 (6.9–7.9)
pH 8.5	46.7 ± 4.2 (41.2–51.4)	4.8 ± 0.5 (4.1–5.2)
BZ-NO		
pH 7.4	76.4 ± 16.0 (64.6–100.0)	6.5 ± 0.8 (5.6–7.5)
pH 8.5	63.6 ± 14.0 (46.8–79.6)	8.0 ± 1.6 (6.4–10.3)

Values are mean ± SD ($n = 4$) (range).

authentic Nor-BZ (11.5 min) and BZ-NO (15.4 min). The production of metabolites was linear up to 0.5 mg ml^{-1} of microsomal protein and for incubation times up to 15 min (data not shown).

The formation of Nor-BZ and BZ-NO followed Michaelis–Menten kinetics either when the incubations were performed at pH 8.5 or at pH 7.4 (figure 2). K_m and V_{max} (mean ± SD and ranges) are provided in table 1. The production of Nor-BZ and BZ-NO was greatest at pH 7.4 and 8.5, respectively, although the small number of animals weakened the statistical analysis.

The formation of Nor-BZ was not reduced by heat treatment of the microsomal protein, whereas that of BZ-NO decreased to 29–33% of the control samples.

Metabolism of BZ by precision-cut liver slices

Figure 3 shows HPLC chromatograms obtained from medium after incubation of precision-cut liver slices with BZ for 2, 6 and 24 h compared with a blank sample (liver slices incubated for 24 h). After 2 h of incubation, the main component was parent compound (95%), with only traces of Nor-BZ (1%) and BZ-NO (4%) evident. The percentage abundance of BZ-NO increased between 6 and 24 h

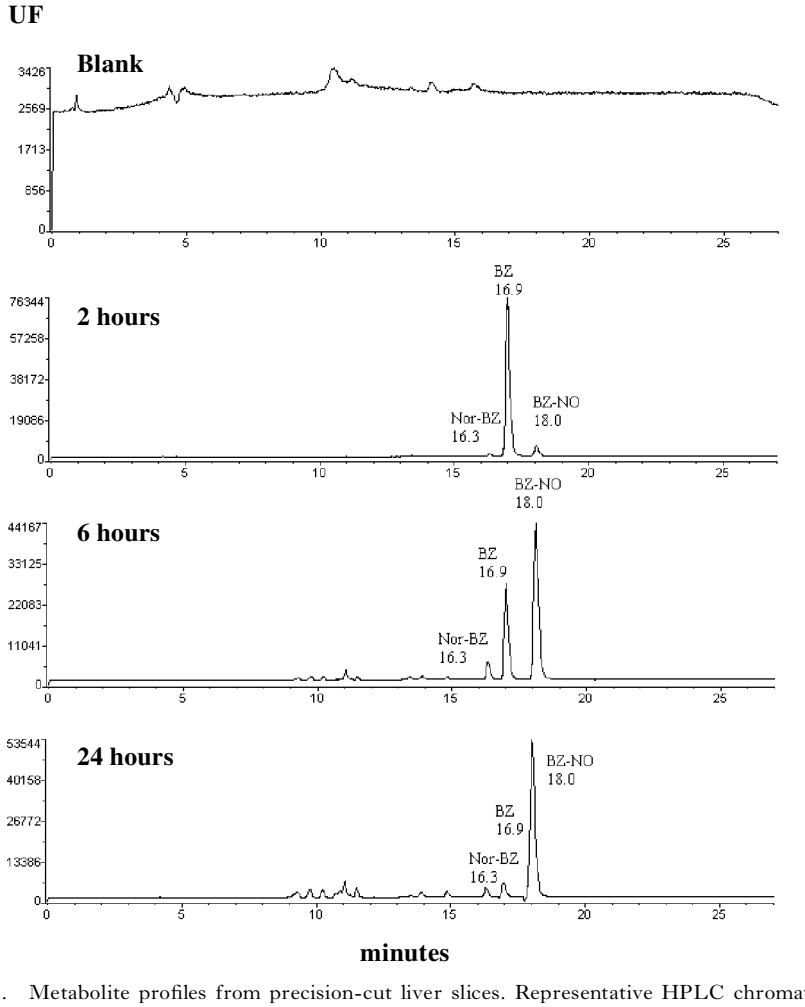


Figure 3. Metabolite profiles from precision-cut liver slices. Representative HPLC chromatograms have been selected to illustrate metabolites present in extracts of medium following incubation of precision-cut liver slices with BZ for 2, 6 and 24 h. The HPLC conditions were: Prodigy ODS(3) column (5 μm; 250 × 4.6 mm i.d.) (Phenomenex); elution by binary mixture of (A) water 2% formic acid; (B) acetonitrile 2% formic acid with a gradient from 90% A to 65% A over 10 min, followed by an isocratic period at 65% A for 15 min; flow rate of 0.8 ml min^{-1}; fluorometric detection (303 nm excitation, 350 nm emission). UF, units of fluorescence.

Table 2. Summary of major product ions formed following mass spectral analysis of BZ, Nor-BZ and BZ-NO $[M + H]^+$ parent ions (m/z 310, 296 and 326, respectively).

Compound	MS^n n	[Molecular ion], precursor ion (m/z)	Product ions (m/z)
BZ	2	[310]	265
	3	[310], 265	237, 187, 174*, 91
	4	[310], 265, 174	146*
	4	[310], 265, 237	209
Nor-BZ	2	[296]	265*, 225
	3	[296], 265	237, 209, 187, 174*
BZ-NO	2	[326]	265, 209, 102*
	3	[326], 265	237, 174*

* Base product ion in the spectra.

from 33 to 56%. In contrast, Nor-BZ production was maximal (5%) by 6 h. At 24 h several other peaks eluting before Nor-BZ were also evident.

LC-MS analysis of metabolites

Product ions generated from the molecular ions ($[M + H]^+$) of BZ (m/z 310), Nor-BZ (m/z 296) and BZ-NO (m/z 326) are summarized in table 2. A product ion of m/z 265 was evident in the spectrum of BZ, Nor-BZ and BZ-NO, whereas those at m/z 225 and 102 were only evident in the spectrum of Nor-BZ and BZ-NO, respectively.

Further LC-MS experiments were performed on ions that co-chromatographed with unidentified fluorescent entities found in the medium at 6- and 24-h incubations. Figure 4 shows selected ion chromatograms corresponding to the $[M + H]^+$ of eight putative metabolites (labelled M1–8 in order of elution) obtained from a representative 24-h medium sample; retention times, molecular and product ions for each are provided in table 3.

Two metabolites eluting at 13.3 and 17.9 min (M9 and BZ-NO respectively) were evident from the total ion current trace for the parent ion of m/z 326. The retention time and product ion spectrum of the latter were consistent with BZ-NO. The former metabolite was not detected by fluorescence but generated a single product ion of m/z 281, which was also evident as a product ion of other metabolites (table 3).

Discussion

The different roles of FMO and cytochrome P450 in the *N*-oxidation of BZ and *N*-demethylation of BZ, respectively, were previously established by Kawaji *et al.* (1993, 1994) using rat liver microsomes. From that model, K_m and V_{max} for the formation of Nor-BZ were produced that were ~50 times greater and 2000 times lower, respectively, than those for BZ-NO.

In the present study using liver microsomes from cattle, BZ-NO production increased at pH 8.5 and was sensitive to heat treatment, suggesting that FMOs may be largely responsible for catalysing this reaction. However, the closeness of

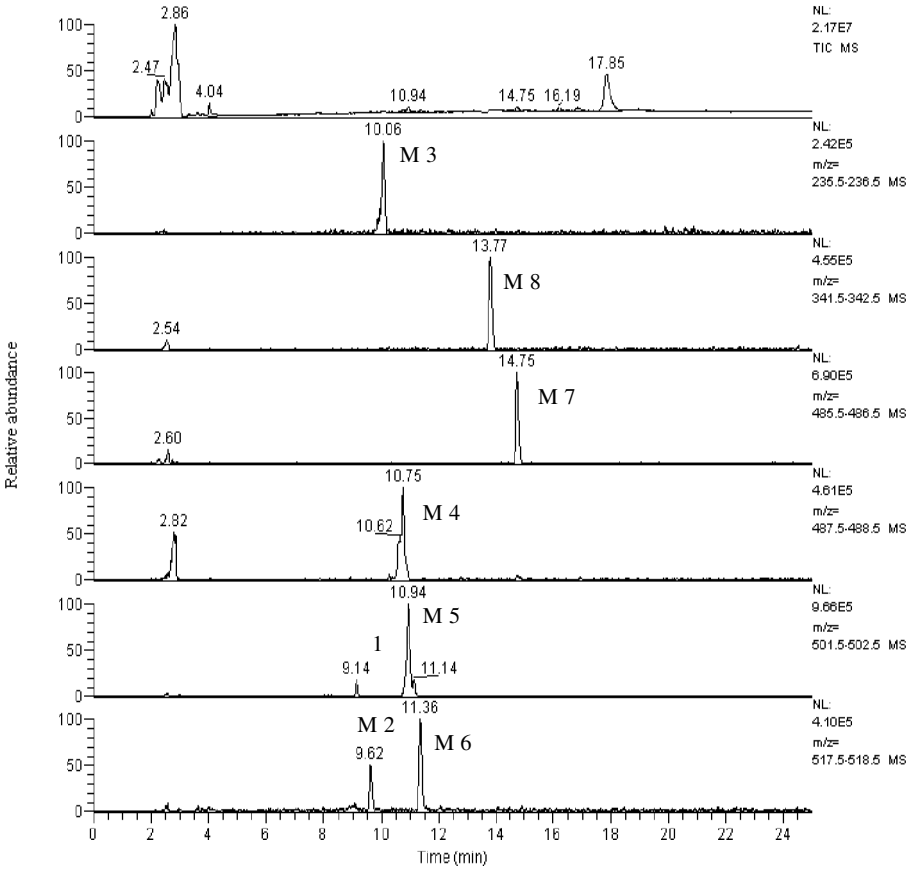


Figure 4. Identification of potential [M + H^+] molecular ions (*m/z* 236, 342, 486, 488, 502 and 518) of metabolites from precision-cut liver slices by LC-MS by extraction of ions from full-scan data. Precision-cut liver slices were incubated with BZ for 24 h and the incubation medium extracted and subjected to analysis by full scan (*m/z* 200–600) HPLC-MS.

Table 3. Fragmentation of precursor ions of metabolites found in the medium following incubation of precision-cut liver slices for 24 h.

Metabolite	Retention time (min)	Precursor ions (*m/z*)	MS^n *n*	Product ions (*m/z*)
M1	9.1	502 ($M + H^+$)	2	457*, 326, 281
		502, 457	3	281*, 191
M2	9.6	518 ($M + H^+$)	2	457*, 281
M3	10.1	236 ($M + H^+$)	2	175, 102*
M4	10.8	488 ($M + H^+$)	2	457, 312*, 281
		488, 312	3	281*, 175
M5	10.9	502 ($M + H^+$)	2	457, 326*, 281
		502, 457	3	281*, 175
M6	11.4	518 ($M + H^+$)	2	457, 342*, 281
M7	13.8	342 ($M + H^+$)	2	281, 102*
M8	14.7	486 ($M + H^+$)	2	441, 310, 265*
M9	13.3	326 ($M + H^+$)	2	281

* Base product ion in the MS spectra.

K_m and V_{max} of Nor-BZ and BZ-NO formation indicated the involvement of either the same enzyme or different enzymes with similar substrate affinity.

In addition to BZ, Nor-BZ and BZ-NO, only one further minor peak was evident in the HPLC chromatograms of microsomal incubations (figure 1). In contrast, chromatograms from the media of liver slices gave rise to several peaks that eluted before reference standards for BZ, Nor-BZ and BZ-NO (figure 3); these were present in sufficient quantity to enable direct identification by LC-MS analysis.

The concentration of BZ-NO in liver slice culture medium exhibited a striking increase from 2 to 24 h compared with the other metabolites, and this feature of BZ biotransformation could modify BZ residue kinetics. Back reduction to the parent compound is a mechanism already described for *N*-oxides and hydroxylamines in biological fluids (Bickel 1969, Kaibaf *et al*. 1992, Blake *et al*. 1995, Montesissa *et al*. 1998). Previous studies have demonstrated that BZ-NO can also form a reservoir of the parent compound, since it can be *N*-deoxygenated back to BZ, both *in vitro* by rat liver microsomes and *in vivo* after oral administration of BZ to rat (Kataoka *et al*. 1979a, b). *In vivo*, the reduction of *N*-oxidated metabolites is often related to the inability to detect these labile derivatives in biological fluids and to the increased half-life of their parent compounds.

The previously undetected BZ metabolites produced in cattle liver slices were tentatively identified as follows (figure 5): M1 (m/z 502), 1-benzyl-3-[3-(dimethylamino)propoxy]-1H-hydroxy-indazole N^+-glucuronide; M2 (m/z 518), 1-benzyl-3-[3-(dimethylamino)propoxy]-1H-hydroxy-indazole *N*-oxide N^+-glucuronide; M3 (m/z 236), 3-[3-(dimethylamino)propoxy]-1H-indazole *N*-oxide; M4 (m/z 488), 1-hydroxy-benzyl-3-[3-(methylamino)propoxy]-1H-indazole N^+-glucuronide; M5 (m/z 502), 1-hydroxy-benzyl-3-[3-(dimethylamino)propoxy]-1H-indazole N^+-glucuronide; M6 (m/z 518), 1-hydroxy-benzyl-3-[3-(dimethylamino)propoxy]-1H-indazole *N*-oxide N^+-glucuronide; M7 (m/z 342), hydroxylated analogue of BZ-NO; M8 (m/z 486), benzydamine N^+-glucuronide; and M9 (m/z 326), hydroxylated analogue of BZ. These products are presented in a proposed hepatic biotransformation pathway in figure 6.

Only three of the previously unidentified metabolites (M3, M7 and M9) (figures 5a and 6) found in the incubation medium of cattle liver slices were unconjugated compounds. The metabolite M3 (m/z 236) could be produced by either the loss of the benzyl group from BZ-NO or by debenzylation of BZ followed by an oxidation. Desbenzyl-BZ was first identified in rabbit urine by Kataoka *et al*. (1971) and subsequently in human urine by Koppel and Tenczer (1985).

The exact position of the hydroxyl group for the metabolites M7 (m/z 342) (figure 5a) and M9 (m/z 326) (figure 6) can not be assigned from the product ion spectra. However, Kataoka *et al*. (1971) described a hydroxy-benzyl derivative in rabbit urine with the site of hydroxylation at the 4-position of the benzyl ring, whereas Koppel and Tenczer (1985) suggested the 5-position of the indazole ring for a hydroxylated metabolite found in human urine.

The fragmentation patterns of the other metabolites (M1, M2, M4–6 and M8) were consistent with fragments formed from N^+-glucuronides. The peak for M8 (m/z 486) (table 3, figure 5b) gave rise to a product ion at m/z 441, which correspond to the sum of the major fragment of BZ (m/z 265, table 2) and glucuronic acid (m/z 176). This suggests that M8 is a novel N^+-glucuronide of

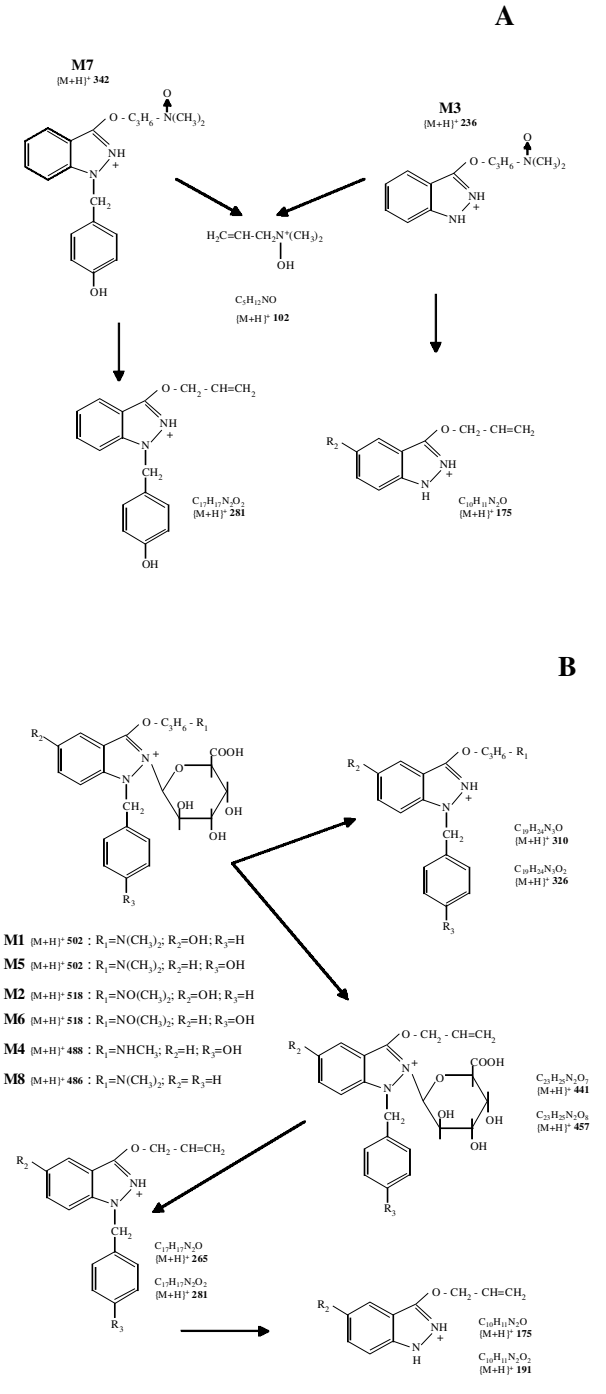


Figure 5. Proposed structures of precursor and product ions of BZ metabolites. Part A shows the unconjugated derivatives M3 (m/z 236, debenzyl BZ-NO) and M7 (m/z 342, hydroxylated BZ-NO). Part B shows the N^+-glucuronated derivatives M1 and M5 (m/z 502, hydroxylated BZ N^+-glucuronide), M2 and M6 (m/z 518, hydroxylated BZ-NO N^+-glucuronide), M4 (m/z 488, hydroxylated Nor-benzydamine N^+-glucuronide) and M8 (m/z 486, benzydamine N^+-glucuronide). The position of the hydroxyl group is suggested in every metabolite, but cannot be definitely stated based on product ion spectra.

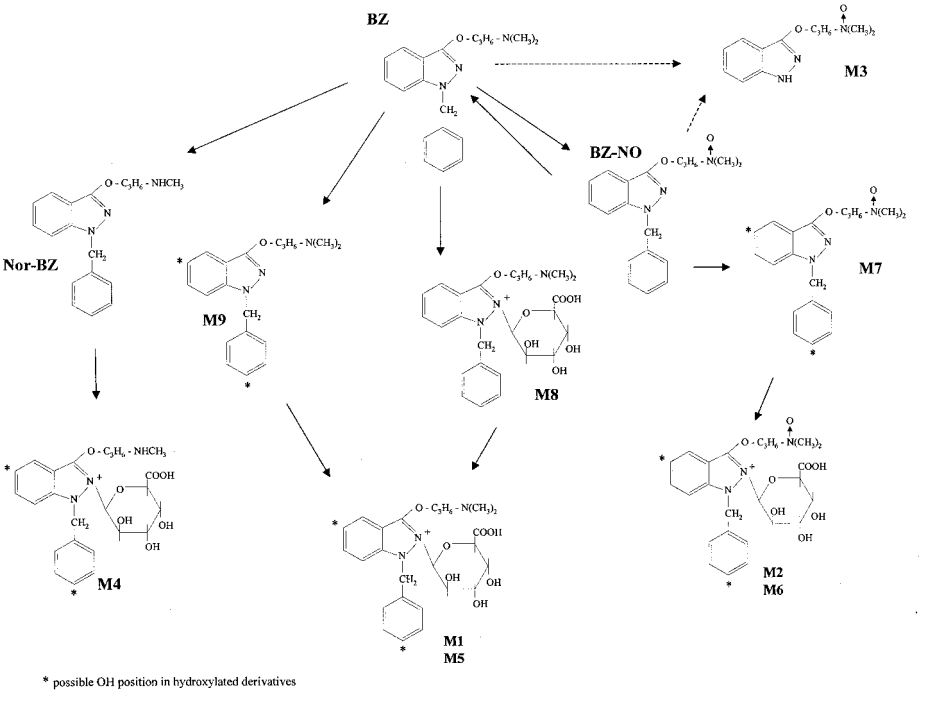


Figure 6. Proposed pathways for hepatic BZ metabolism in cattle.

BZ which to date has not been described in the literature. M4 (m/z 488), M1 and M5 (both m/z 502), M2 and M6 (both m/z 518) (table 3, figure 5b) generated a common fragment at m/z 457 which is an oxidated (+16 amu) fragment analogous to the one at m/z 441 originated from M8. The mass for the putative $[M + H]^+$ ion of M8 is consistent with benzydamine N^+-glucuronide; thus it is reasonable to propose analogous N^+-glucuronide structures for metabolites M1, M2 and M4–6 (figures 5b and 6). Maggs *et al*. (1997) reported that the *in vivo* glucuronidation of OH-carbamazepine (the main derivative of carbamazepine, an analgesic and anticonvulsant agent) gave rise to both *O*- and *N*-glucuronides. Their mass spectra have been compared and the product ion found to differ: the *O*-glucuronides (m/z 429) yielded only the aglycone fragment (m/z 253), whereas the *N*-glucuronide conjugate produced a fragment still bearing the glucuronic acid moiety (m/z 411). Thus, the ion at m/z 457 in the spectra of BZ metabolites M1, M2 and M4–6 is evidence of the *N*-conjugated moiety still bearing the glucuronic acid. This is confirmed in their MS spectra by the presence of a main fragment at m/z 281 corresponding to the loss of the glucuronic group. Further evidence for the N^+-glucuronide structural assignment was provided by metabolites such as M1/5 and M2/M6, which have identical masses but not HPLC retention times due to different molecular sites of hydroxylation and their polarities.

The unsaturated nitrogen of the imidazole moiety of BZ and BZ-OH is the most likely site for conjugation with glucuronic acid. In ring systems of aromatic tertiary amines, such as imidazole (where one ring nitrogen is substituted), pyridine, 1,2,4-triazine and polycyclic heterocycles, where N^+-glucuronidation

can occur at more than one site, conjugation has been observed to occur at the nitrogen with the less bulky substituent(s) (Hawes 1998).

The exact structures of the metabolites of BZ produced by precision-cut slices from cattle liver cannot be definitely stated without other analysis by NMR or synthesis of reference compounds. Nevertheless, the assignment of N^+-glucuronides at both the parent compound and its hydroxylated derivatives is strongly supported by the mass spectra and chromatographic data.

N^+-glucuronidation has been widely observed in man as a pathway in the Phase II metabolism of tricyclic drugs with an aliphatic tertiary amine group. Examples include imipramine, clomipramine, clozapine, chlorpromazine, trazodone, loxapine and trimipramine (Luo *et al.* 1995, Dain *et al.* 1997), but there are no reports in the literature describing N^+-glucuronidated products from hydroxylated BZ or reports on the ability of cattle to perform N^+-glucuronidation. Until now, only the rabbit, unlike the other laboratory species (dog, rat, cat) is reported to share this metabolic pathway with humans. In both species, N^+-glucuronides of ketotifen and cyproheptadine were produced during *in vivo* and *in vitro* studies, and N^+-glucuronides of tioconazole and croconazole were found in both rabbit and human urine (Hawes 1998).

As expected from published studies carried out in other animals and in man, the findings of the present study indicate that the metabolism of BZ is very complex in cattle. In the case of drugs adopted both for human and veterinary therapy, liver slices are an appropriate *in vitro* model to elucidate the metabolites to which humans can be re-exposed following consumption of animal tissues. To support the process of licensing of BZ in the bovine, and in food species in general, it is essential to define the composition of tissue residues after administration of the compound and to know whether the metabolites found in the target species are representative of those 'tested' in laboratory animals (as part of toxicity testing) and those found in humans. Glucuronidation is generally regarded as a means of detoxification and the clinical importance of N^+-glucuronides has not been thoroughly investigated. Nevertheless, a few studies described their effects on histamine release, as well as the competition for glucuronic substrate between tertiary amines and testosterone (Chiu and Huskey 1998).

The results of this study suggest that BZ metabolites in cattle are qualitatively different from those described in humans and laboratory animals, and further toxicity tests on metabolites in laboratory species should be required to enable marketing authorization of BZ for food species.

In view of the understanding of the mass balance of BZ in cattle and to highlight a pathway of detoxification that has never been reported in the bovine, the metabolism of BZ in cattle is worthy of further investigation.

Acknowledgements

The authors are grateful to Giancarlo Biancotto (Istituto Zooprofilattico Sperimentale delle Venezie di Padova) for his scientific contribution to the discussion of metabolite structure and to Professor Luigi Morganti (Director of the Dipartimento di Sanità Pubblica Veterinaria e Patologia Animale) for his support of the study. The work was supported by a MURST (Ministero dell'Università e della Ricerca Scientifica) grant (*ex*-40% 1998).

References

Baldock, G. A., Brodie, R. R., Chasseaud, L. F., Taylor, T., Walmsley, L. M. and Catanese, B., 1991, Pharmacokinetics of benzydamine after intravenous, oral, and topical doses to human subjects. *Biopharmaceutics and Drug Disposition*, **12**, 481–492.

Barr, J., Weir, A. J., Brendel, K. and Sipes, I. G., 1991, Liver slices in dynamic organ culture, an alternative *in vitro* technique for the study of rat hepatic drug metabolism. *Xenobiotica*, **21**, 331–339.

Bickel, M. H., 1969, The pharmacology and biochemistry of *N*-oxides. *Pharmacological Review*, **21**, 325–355.

Blake B. L., Rose, L. R., Mailman, R. B., Levi, P. E. and Hodgson, E., 1995, Metabolism of thioridazine by microsomal monooxygenases: relative roles of P450 and flavin-countering monooxygenases. *Xenobiotica*, **25**, 377–393.

Chiu, S. L. and Huskey, S. W., 1998, Species differences in *N*-glucuronidation. *Drug Metabolism and Disposition*, **26**, 838–847.

Coldham, N., Moore, A. S., Dave, M., Graham, P. J., Sivapathasundaram, S., Lake, B. G. and Sauer, M. J., 1995, Imidocarb residues in edible bovine tissues and *in vitro* assessment of imidocarb metabolism and cytotoxicity. *Drug Metabolism and Disposition*, **23**, 501–505.

Dain, J. G., Nicoletti, J. and Ballard, F., 1997, Biotransformation of clozapine in humans. *Drug Metabolism and Disposition*, **25**, 603–609.

Dogterom, P., 1993, Development of a simple incubation system for metabolism studies with precision-cut liver slices. *Drug Metabolism and Disposition*, **21**, 699–704.

George, E., Murdock, J., Aylott, M. and Westmoreland, C., 1999, Comparison of hepatocyte cultures and liver slices *in vitro* toxicity testing. *Alternatives to Laboratory Animals*, **27**, 769–781.

Hawes, E. M., 1998, N^+-glucuronidation, a common pathway in human metabolism of drugs with a tertiary amine group. *Drug Metabolism and Disposition*, **26**, 830–837.

Kaibaf, M., Sepai, O. and Lamb, J. H., 1992, Identification of metabolites of 4,4′-diaminodiphenylmethane (methylene dianiline) using liquid chromatographic and mass spectrometric techniques. *Journal of Chromatography Biomedical Application*, **583**, 63–76.

Kataoka, S., Naito, T., Nishimura, K. and Taira, K., 1979b, Effect of carrageenin treatment on the metabolism of benzydamine and its *N*-oxide in rat organ preparations. *Chemical and Pharmaceutical Bulletin*, **27**, 2904–2912.

Kataoka, S., Nishimura, K. and Naito T., 1979a, *In vivo* metabolism and anti-inflammatory activity of benzydamine hydrochloride in rats treated with carrageenin. *Chemical and Pharmaceutical Bulletin*, **27**, 2890–2903.

Kataoka, S., Taira, K., Ariyoshi, T. and Takabatake, E., 1973, Metabolism of benzydamine hydrochloride: species differences and the identification of unconjugated metabolites in rabbit urine. *Chemical and Pharmaceutical Bulletin*, **21**, 358–365.

Kataoka, S., Taira, K. and Takabatake, E., 1971, Metabolism of benzydamine hydrochloride. *Chemical and Pharmaceutical Bulletin*, **19**, 1511–1513.

Kawaji, A., Ohara, K. and Takabatake, E., 1993, An assay of flavin-containing monooxygenase activity with benzydamine *N*-oxidation. *Analytical Biochemistry*, **214**, 409–412.

Kawaji, A., Ohara, K. and Takabatake, E., 1994, Determination of flavin-containing monooxygenase activity in rat brain microsomes with benzydamine *N*-oxidation. *Biological and Pharmaceutical Bulletin*, **17**, 603–606.

Koppel, C. and Tenczer, J., 1985, Metabolism of benzydamine. *Arzneimittel-Forschung/Drug Research*, **35**, 634–635.

Lowry, O. H., Rosebrough, N. J., Farr, A. L. and Randall, R. J., 1951, Protein measurement with the Folin phenol reagent. *Journal of Biological Chemistry*, **293**, 265–275.

Luo, H., Hawes, E. M., McKay, G., Korchinski, E. D. and Midha, K. K., 1995, N^+ glucuronidation of aliphatic tertiary amines in human: antidepressant versus antipsychotic drugs. *Xenobiotica*, **25**, 291–301.

Maggs, J. L., Pirmohamed, M., Kitteringham, N. R. and Park, B. K., 1997, Characterization of the metabolites of carbamazepine in patient urine by liquid chromatography/mass spectrometry. *Drug Metabolism and Disposition*, **25**, 275–280.

Miller, M. G., Beyer, J., Hall, G. L., Degraffenried, L. and Adams, P. E., 1993, Predictive value of liver slices for metabolism and toxicity *in vivo*: use of acetaminophen as a model hepatotoxicant. *Toxicology and Applied Pharmacology*, **122**, 108–116.

Montesissa, C., Anfossi, P., Biancotto, G. and Angeletti, R., 1998, *In vitro* metabolism of clenbuterol and bromobuterol by pig liver microsomes. *Xenobiotica*, **28**, 1049–1060.

Omura, T. and Sato, R., 1964, The carbon monoxide binding pigment of liver microsomes. *Journal of Biological Chemistry*, **239**, 2370–2378.

Saylers, K. L., Barr, J. and Sipes, I. G., 1994, *In vitro* metabolism of theophylline by rat and human liver tissue. *Xenobiotica*, **24**, 389–399.

Smith, P. F., Fisher, R., Shubat, P. J., Gandol, V. J., Krumdieck, C. L. and Brendel, K., 1987, *In vitro* cytotoxicity of allyl alcohol and bromobenzenes in novel organ culture system. *Toxicology and Applied Pharmacology*, **87**, 509–522.

Ubeaud, G., Schiller, C. L., Hurbin, F., Jaeck, D. and Coassolo, P., 1999, Estimation of flavin-containing monooxygenase activity in intact hepatocyte monolayers of rat, hamster, rabbit, dog and human by using *N*-oxidation of benzydamine. *European Journal of Pharmaceutical Sciences*, **8**, 255–260.

Ziegler, D. M., 1988, Flavin-containing monooxygenases: catalytic mechanism and substrate specificities. *Drug Metabolism Review*, **19**, 1–32.

XENOBIOTICA, 2002, VOL. 32, NO. 2, 87–107

Taylor & Francis
healthsciences

Species differences in the metabolism of the antitumour agent 5,6-dimethylxanthenone-4-acetic acid *in vitro*: implications for prediction of metabolic interactions *in vivo*

S. F. ZHOU†*, M. D. TINGLE†, P. KESTELL‡ and J. W. PAXTON†

†Division of Pharmacology and Clinical Pharmacology, ‡Auckland Cancer Society Research Centre, Faculty of Medical and Health Sciences, University of Auckland, Auckland, New Zealand

Received 25 May 2001

1. Mouse studies have indicated that the antitumour effects of 5,6-dimethylxanthenone-4-acetic acid (DMXAA) are dramatically potentiated in combination with other drugs, and it has been proposed that optimization of the therapeutic potential of DMXAA would exploit combination therapy. The aim was to identify the most appropriate animal model for further investigations of the pharmacokinetics of possible DMXAA–drug combinations and their extrapolation to patients.

2. Qualitatively, the metabolic profile for DMXAA in liver microsomes was similar in mouse, rat, rabbit and humans, with glucuronidation and 6-methylhydroxylation the two major metabolic pathways. In all species, the intrinsic clearance by glucuronidation was at least 2-fold that due to hydroxylation. There was significant variability in the *in vitro* kinetic parameters (K_m, V_{max}), with the mouse being the least efficient DMXAA metabolizer compared with the other species.

3. Mouse, rat and rabbit renal microsomes exhibited DMXAA glucuronidation activity, but only the rabbit showed 6-methylhydroxylation. For the total *in vitro* CL_{int} (V_{max}/K_m) by glucuronidation and 6-methylhydroxylation, the ratio of kidney:liver was 0.67, 0.03 and 0.34 in the mouse, rat and rabbit respectively. However, taking into account the liver and kidney weight difference, it is apparent that the *in vivo* renal metabolism would not be a major contributor to the overall elimination of DMXAA.

4. The inhibitory profile for liver DMXAA glucuronidation was similar across species, but there was remarkable interspecies variability in the inhibition of liver DMXAA 6-methylhydroxylation.

5. Extrapolation of *in vitro* intrinsic clearance to *in vivo* gave a significant underestimation of plasma clearance for all species. However, there was a significant allometric relationship for plasma clearance and volume of distribution, but not for maximum tolerated dose across species.

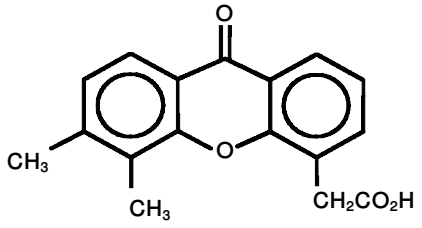
6. The results indicate that animal models may have a limited role in the extrapolation to patients of drug interactions with agents such as DMXAA that have immunomodulating activity that may vary widely between species.

Introduction

The results from recent preclinical and clinical studies involving the antitumour agent and biological response modifier 5,6-dimethylxanthenone-4-acetic acid (DMXAA; figure 1) have demonstrated that significant pharmacokinetic and pharmacodynamic differences exist between species (Kestell *et al.* 1999). As with many anticancer agents, most of the preclinical evaluation was performed in the mouse. The antitumour activity of DMXAA is thought to result from the

* Author for correspondence; e-mail: shufeng.zhou@auckland.ac.nz

Xenobiotica ISSN 0049–8254 print/ISSN 1366–5928 online © 2002 Taylor & Francis Ltd
http://www.tandf.co.uk/journals
DOI: 10.1080/00498250110092423



5,6-dimethylxanthenone-4-acetic acid

Figure 1. Chemical structure DMXAA.

combination of immunomodulating effects, such as cytokine induction (particularly tumour necrosis factor-α) (Philpott *et al.* 1995), and antivascular effects arising from increases in the production of serotonin (Baguley *et al.* 1997) and nitric oxide (Thomsen *et al.* 1990, 1991). Using the mouse model, the therapeutic antitumour properties of DMXAA were significantly potentiated when used in combination with other agents, and the utility of co-treatments involving cytotoxic drugs such as melphalan (Pruijn *et al.* 1997), radiotherapy (Wilson *et al.* 1998), bioreductive agents such as tirapazamine (Lash *et al.* 1998), thalidomide (Ching *et al.* 1995, Kestell *et al.* 2000) and cyproheptadine (Zhao *et al.* 2001) has been demonstrated. Indeed, the results so far, support the proposal that the optimization of the therapeutic potential of DMXAA in the clinic would exploit combination therapy. However, in the light of the significant species differences in the mode of action, drug tolerance and pharmacokinetics, extra caution must be taken when the effects of such combinations are examined in, or extrapolated to, humans. For example, interspecies differences are highlighted by the combination of DMXAA with thalidomide or cyproheptadine (Zhou *et al.* 2001a, b), and the contrasting toxicological and pharmacokinetic outcome in the mouse and rat (Kestell *et al.* 1999). Combinations with these compounds (thalidomide, a TNF-α synthesis inhibitor and cyproheptadine, a serotonin receptor antagonist) significantly increased the DMXAA plasma area under the concentration–time curve (AUC) in the mouse (Kestell *et al.* 2000, Zhou *et al.* 2001a), but had little or no effect on DMXAA pharmacokinetics in the rat (Zhou *et al.* 2001b). In the light of this, there is a need to understand the nature of the pharmacokinetic and pharmacodynamic differences between species to evaluate and explore potential antitumour DMXAA–drug combinations, which may have clinical application.

As part of an overall approach to understand why such significant species differences exist, we have studied the metabolism and disposition of DMXAA *in vivo* in laboratory animals. Whilst these studies have determined that toxicity and drug tolerance were not related to exposure as measured by AUC, very little insight was gained as to why plasma drug clearance on a weight related basis should be greatest in the larger bodied animals such as humans and slowest in the smallest such as the mouse. This is in contrast to most drugs, where the larger the animal, the smaller the capacity to metabolize xenobiotics on a per kg basis (Boxenbaum 1982, Davidson *et al.* 1986, Modenti 1986, Mahmood 1999). Similar atypical results were observed for DMXAA's clinical predecessor flavone acetic acid (FAA), where the mouse was less efficient in its ability to clear the drug compared with patients (Zaharko *et al.* 1986, Cummings *et al.* 1989).

Studies have also indicated that qualitatively the metabolism of DMXAA is similar in laboratory animals and humans, with glucuronidation of its acetic acid side-chain and 6-methylhydroxylation of the xanthenone ring the major pathways (Webster *et al.* 1995, Kestell *et al.* 1999). This results in the formation of DMXAA acyl glucuronide (DMXAA-G), and 6-hydroxymethyl-5-methylxanthenone-4-acetic acid (6-OH-MXAA), which are excreted in bile and urine (Webster *et al.* 1995, Kestell *et al.* 1999). Recent *in vitro* studies have demonstrated that these metabolic pathways are catalysed in human microsomes by uridine diphosphate glucuronosyltransferase (UGT) 1A9 and 2B7 (Miners *et al.* 1997), and by cytochrome P450 (CYP) 1A2 (Zhou *et al.* 2000), respectively. Therefore, to assess whether variations in drug clearance are associated with species differences in drug metabolism, we have undertaken a comprehensive study *in vitro* of the kinetics and inhibition of DMXAA glucuronidation and 6-methylhydroxylation using liver and kidney microsomes prepared from the mouse, rat and rabbit, and compared the results to those obtained from human microsomes.

In addition, and in view of the unusual species differences exhibited by DMXAA and its analogue FAA, the opportunity was taken using the data obtained from this and previous studies to ascertain whether any interspecies relationships could be established between physiological or toxicological parameters such as body weight (BW) or maximum tolerated dose (MTD) and the pharmacokinetic parameters. A similar exercise was also performed to establish whether any *in vitro–in vivo* correlations could be determined across the species using a variety of scaling techniques.

The aims of the studies were to identify the most appropriate animal model for the further evaluation of pharmacokinetic and pharmacodynamic interactions arising from DMXAA–drug combination therapy, and the extrapolation to patients.

Materials and methods

Drugs and reagents

DMXAA and the HPLC internal standard, 2,5-dimethylxanthenone-4-acetic acid (SN24350) were synthesized in the ACSRC (Auckland Cancer Society Research Centre) (Rewcastle *et al.* 1989) and were $>99\%$ pure when analysed by thin-layer chromatography. DMXAA was protected from light exposure to avoid degradation (Rewcastle *et al.* 1990). Authentic DMXAA-G and 6-OH-MXAA were isolated from rat bile and urine respectively by previously published methods, and their structures were identified by liquid chromatography-mass spectrometry (LC-MS) and nuclear magnetic resonance spectrometry (Kestell *et al.* 1999). Amitriptyline, bicinchoninic acid (BCA) reagent, Brij 58, chlorzoxazone, cimetidine, cyproheptadine, diclofenac, diethyldithiocarbamate (DDC), diflunizal, erythromycin, fenclofenac, fenoprofen, indomethacin, medazepam, a-naphthoflavone (ANF), oxazepam, paracetamol, phenacetin, quinidine, D-saccharic acid 1,4-lactone, testosterone, tolbutamide and troleandomycin (TAO) were purchased from Sigma-Aldrich Chemical Co. (Auckland, New Zealand). Furafylline was obtained from UFC Ltd (Manchester, UK). NADPH and UDPGA were purchased from Roche Diagnostics NZ Ltd (Auckland, New Zealand). Other reagents were obtained from the following sources: SKF525A (SmithKline Beecham Pharmaceuticals, Philadelphia, PA, USA); sulphaphenazole (Ciba Geigy, East Hanover, NJ, USA); ketoconazole (ICN Biomedicals, Costa Mesa, CA, USA). 1-Naphthol was from Merck AG (Darmstadt, Germany). All other reagents were of analytical or HPLC grade as appropriate.

Preparation of liver and kidney microsomes from various species

Male Wistar Kyoto rats (185–245 g, $n = 6$), male C57B1 mice (25–32 g, $n = 15$) and male white New Zealand rabbits (3–3.4 kg, $n = 3$) were housed under constant temperature ($23 \pm 1\,^{\circ}C$), relative humidity ($55 \pm 5\%$), and lighting (12-h light/dark cycle) according to institutional guidelines. Sterile food and water was available *ad libitum*. All animal procedures were approved by the Animal Ethics

Committee of the University of Auckland. Hepatic and renal microsomes from various species were prepared by differential centrifugation, as described (Robson *et al.* 1987). Human liver samples were donated by 14 individuals who either underwent liver resection for metastasis of colon cancer or hydatid disease, and one from a transplant donor (Zhou *et al.* 2000). Histological examination of the resected livers ensured the use of healthy liver tissue. Ethical approval was obtained from the Northern New Zealand Research Ethics Committee, and all donors gave written informed consent for liver tissues to be used for research. Livers and microsomes were stored at −80 °C until used. The yields of microsomes per g liver or kidney tissues were determined. Microsomal protein concentration was determined by the bicinchoninic acid binding method (Smith *et al.* 1985) and the P450 contents were determined as described (Omura and Sato 1964).

In vitro *kinetic and inhibition studies*

The *in vitro* kinetic and inhibition studies of DMXAA glucuronidation and 6-methylhydroxylation with mouse, rat, rabbit and human liver microsomes, and the metabolism of DMXAA in renal microsomes from animal species were performed using optimized incubation conditions with respect to microsomal protein concentration, incubation time and substrate concentration for each species (Zhou *et al.* 1999, 2000). For glucuronidation, Brij 58 (0.1–0.25:1, ratio of Brij 58 to microsomal protein, w/w) was incubated with microsomes at pH 6.8, along with D-saccharic acid 1,4-lactone to inhibit the activity of β-glucuronidase. All incubations were performed in triplicate, were initiated by the addition of UDPGA or NADPH, and conducted at 37 °C in a shaking water bath. The inhibition of liver DMXAA acyl glucuronidation and 6-methylhydroxylation *in vitro* by various UGT substrates and CYP inhibitors/substrates (tables 3 and 4) with pooled mouse, rat, rabbit, and various sources of human liver microsomes were investigated. Pooled human liver microsomes (from HL6, HL7 and HL8) were used for DMXAA glucuronidation as this pathway is catalysed by multiple UGT enzymes (UGT1A9/UGT2B7) (Miners *et al.* 1997), and the glucuronidation activity for DMXAA was similar in these human livers; whereas for DMXAA 6-methylhydroxylation, CYP1A2 is responsible for this pathway (Zhou *et al.* 2000), and significant interindividual variation in the inhibition of this pathway may occur, thus three sources of human livers (HL12, HL13, HL14) were used. The concentrations of DMXAA were 140, 120, 150 and 140 μM for glucuronidation, and 240, 160, 40 and 20 μM for 6-methylhydroxylation, the apparent K_m for each metabolism pathway in mouse, rat, rabbit and human respectively. The inhibitors and/or substrates for CYPs were tested initially at 0.5–500 μM. UGT substrate concentrations of 100 and 500 μM were initially used to screen for DMXAA glucuronidation inhibition, as these concentrations have shown potent inhibition for DMXAA glucuronidation in human liver microsomes (Miners *et al.* 1997). These data were then used for initial estimates of the IC_{50} (Moody *et al.* 1999). If significant inhibition was observed, the latter were then used to determine the inhibitor concentration range for K_i determination. The mechanism-based CYP inhibitors, DDC, TAO and furafylline (Halpert *et al.* 1994), were pre-incubated in the presence of NADPH at 37 °C for 15 min before the addition of DMXAA. When significant inhibition (> 35% at 100 μM inhibitor) was observed, further studies were undertaken to determine the inhibition constant (K_i).

Unbound fraction of DMXAA and blood:plasma concentration ratio (C_B/C_P) of DMXAA

The determination of unbound fraction (f_u) in plasma, blood and liver microsomes and the blood:plasma concentration ratio (R_B, C_B/C_P) for DMXAA in mouse, rat, rabbit and humans has been described (Zhou *et al.* 2001c). Briefly, bound and unbound DMXAA were separated by ultrafiltration and the concentration of DMXAA in ultrafiltrate and plasma, blood, or liver microsomes (0.2 and 1 mg ml^{-1}) was determined by HPLC.

HPLC and LC-MS

The methods for the determination and structural identification of DMXAA-G and 6-OH-MXAA have been described (Zhou *et al.* 1999, 2000). Briefly, the HPLC system consisted of a solvent delivery system, a Model SF250 fluorescence detector (excitation and emission wavelengths 345 and 409 nm, respectively), a Model 460 autosampler, and a Model D450 data-processing system (Kontron Instrument Co., Milan, Italy). A Luna C18 guard column and a 5 μm Spherex analytical column (150 × 4.6 mm; Phenomenex Co., Torrance, CA, USA) were used. The mobile phase (flow rate 2.5 ml min^{-1}) was acetonitrile: 10 mM ammonium acetate buffer (24:76 v/v, pH 5.0). All HPLC methods had acceptable accuracy (85–115% of true values) and precision (intra- and interassay coefficient variations < 15%). Assay specificity was indicated by the absence of interfering chromatographic peaks in microsomal samples and in incubations with potential inhibitors. The LC-MS system was fitted with either an atmospheric pressure chemical ionization or electrospray interface (Hewlett Packard, Avondale, PA, USA).

In vitro–in vivo *scaling*

To scale up the *in vitro* CL_{int} (ml min^{-1} mg^{-1}) determined in liver microsomal incubations from all species to *in vivo* CL_{int} (ml min^{-1} kg^{-1}) requires the microsomal protein content per gram liver (mg g^{-1} liver) as well as liver weight (g kg^{-1} body weight). Liver weight was estimated from the allometric relationship:

$$L = 0.037\,BW^{0.85}, \tag{1}$$

where L and BW are the liver weight (kg) and body weight (kg) respectively (Boxenbaum 1980). The liver weights (normalized by kg body weight) used in the calculations were 50 g kg^{-1} for mouse, 45 g kg^{-1} for rat, 40 g kg^{-1} for rabbit and 20 g kg^{-1} for human. Assuming that: (1) the rate of distribution of DMXAA into liver is only perfusion rate limited; (2) only the unbound DMXAA in blood is involved in metabolism; (3) there is good mixing of hepatic arterial blood and hepatic portal blood prior to transport down the sinusoids of the liver; and (4) there is a homogenous distribution of enzymes responsible for DMXAA metabolism within the liver; then the hepatic clearance of DMXAA can be described by the three liver models described below.

For the dispersion model (Roberts and Rowland 1986), the hepatic clearance ($CL_{h\text{-}pre}$) can be calculated from:

$$CL_{h\text{-}pre} = Q_h \times (1 - F_h) \tag{2}$$

$$F_h = \frac{4a}{(1+a)^2 \times e\{(a-1)/2D_N\} - (1-a)^2 \times e\{-(a+1)/2D_N\}} \tag{3}$$

$$a = \left[1 + \frac{4 \times f_B \times CL_{int} \times D_N}{Q_h}\right]^{1/2}, \tag{4}$$

where Q_h is the hepatic blood flow with 90, 60, 60 and 20 ml min^{-1} kg^{-1} for mouse, rat, rabbit and human respectively (Boxenbaum 1980); D_N is the dispersion number (= 0.17) (Roberts and Rowland 1986); F_h is the hepatic availability, f_B is the unbound fraction in blood and is estimated from the unbound fraction of plasma (f_u), and $C_B/C_P(R_B)$ by:

$$f_B = f_u/R_B. \tag{5}$$

For the well-stirred model (Rowland *et al.* 1973, Wilkinson 1975), $CL_{h\text{-}pre}$ is calculated using:

$$CL_{h\text{-}pre} = F_h \times f_B \times CL_{int} \tag{6}$$

$$F_h = \frac{Q_h}{Q_h + f_B \times CL_{int}} \tag{7}$$

For the parallel-tube model (Wilkinson 1975), $CL_{h\text{-}pre}$ is calculated using:

$$CL_{h\text{-}pre} = Q_h \times (1 - F_h) \tag{8}$$

$$F_h = e\{-f_B \times CL_{int}/Q_h\}. \tag{9}$$

In vivo *pharmacokinetic and toxicity data*

Pharmacokinetic data and MTD were obtained from mouse, rat, rabbit and human (Kestell *et al.* 1999, Jameson *et al.* 2000). As DMXAA exhibited dose-dependent pharmacokinetics, its pharmacokinetic parameters at low doses were used for interspecies scaling. All animal procedures were approved by the Animal Ethics Committee of the University of Auckland, and the clinical trial was approved by the Cancer Research Campaign's Phase I/II Clinical Trials Committee of the UK. The MTD of DMXAA in animals was defined as the non-lethal dose that animals can maximally tolerate (Kestell *et al.* 1999). The MTD of DMXAA in cancer patients was the MTD that causes dose-limiting toxicities, which was defined as two or more patients with treatment delay or grade 3 toxicity (National Cancer Institute common toxicity criteria) at the same dose level (WHO 1979). Full details of the Phase I trial of DMXAA will be published later this year. Plasma DMXAA concentrations were determined by HPLC (Kestell *et al.* 1999). The pharmacokinetic parameters, plasma clearance (CL) and volume of distribution at steady state (V_{dss}) were calculated using standard model-independent pharmacokinetic formulae. $AUC_{(0-t)}$ was calculated by the trapezoidal rule using a Prism 3.0 package (Graphpad Software Co., CA, USA) and $AUC_{(0-\infty)}$ was calculated by:

$$AUC_{(0-\infty)} = AUC_{(0-t)} + \frac{C_t \times t_{1/2\beta}}{\ln 2}, \tag{10}$$

where C_t is the plasma DMXAA concentration at last time point. The residual area was extrapolated from t using the elimination constant estimated by linear regression analysis of the terminal slope of log plasma concentration–time curve. The terminal elimination half-life ($t_{1/2\beta}$) was calculated as ln 2 divided by the elimination rate constant (β). The plasma clearance of DMXAA (CL) was calculated by

dividing DMXAA dose by $AUC_{(0-\infty)}$. Mean residence time (MRT) was calculated as AUMC/$AUC_{(0-\infty)}$, where AUMC is the area under the first moment curve. V_{dss} was estimated as CL × MRT (Gibaldi and Perrier 1982). The unbound CL (CL_u) and V_{dss} ($V_{dss/fu}$) were calculated as CL or V_{dss} divided by f_u. Blood clearance of DMXAA (CLB) was calculated by CL divided by R_B (Gibaldi and Perrier 1982).

Interspecies allometric scaling

For interspecies scaling, CL, CL_B, V_{dss} and MTD for each animal species were correlated with body weight (kg) on a log–log scale using the following equation (Boxenbaum 1980, Lin 1998):

$$Y = a \times BW^b, \tag{11}$$

where Y and BW are the specific parameter and the body weight respectively, and b is the allometric exponent. By plotting a specific parameter as a function of body weight on a log–log plot, a regression line can be obtained and an equation generated using Prism 3.0.

Data analysis

Data are presented as mean ± SD. Several models to describe the *in vitro* kinetics of DMXAA glucuronidation and 6-methylhydroxylation (single and two binding site, substrate–activator and substrate–inhibitor complex formation, and the sigmoid models) were fitted and compared using Prism 3.0. The choice of model was confirmed by comparing and reviewing the relative residuals and the standard error of the parameter estimates from the non-linear regression analysis. The single-enzyme model,

$$v = \frac{V_{max} \times [S]}{K_m + [S]} \tag{12}$$

gave the best fit, where v is the rate of hydroxylation, V_{max}, is the maximum velocity, K_m is the Michaelis–Menten constant and $[S]$ is the substrate concentration. The initial statistical analysis to evaluate the differences in the mean kinetic parameters among the different species, or within one species, was performed by a two-way analysis of variance with a Tukey–Kramer test. Dixon plots were used to identify the nature of the inhibition and the apparent K_i. For mechanism-based inhibitors, the inhibition kinetic parameters for enzyme inactivation were determined as described (Zhou *et al.* 2000). The apparent inactivation rate constant (k_{obs}) was obtained by the non-linear least-squares method (Prism 3.0) using:

$$k_{obs} = \frac{k_{inact} \times [I_0]}{K'_{app} + [I_0]}, \tag{13}$$

where k_{obs}, k_{inact} and K'_{app} are the apparent inactivation rate constant of the enzyme at the initial concentration of inhibitor (I_0), the maximum inactivation rate constant and the apparent dissociation constant between the enzyme and inhibitor, respectively.

Results

In vitro *DMXAA metabolism in various species*

Using the above optimized incubation conditions, both hepatic and renal microsomes from all species examined catalysed DMXAA acyl glucuronidation, but only hepatic microsomes from all species and renal microsomes from rabbit-catalysed 6-methylhydroxylation of DMXAA with time-, and cofactor (NADPH or UDPGA)-dependence (data not shown). Under the HPLC conditions used, the major peaks from the glucuronidation and oxidation incubations had retention times identical to those of authentic DMXAA-G and 6-OH-MXAA respectively. Further investigations using LC-MS showed that the molecular ions $[M+H]^+$ of these metabolites were m/z 459 or 299, which is consistent with the molecular weights of protonated DMXAA-G or 6-OH-MXAA.

In all species studied, hepatic and renal DMXAA metabolism followed Michaelis–Menten kinetics (figure 2). The comparison of kinetic parameters for DMXAA metabolism in liver and kidney microsomes from various species indicated significant species and tissue differences (table 1). All species supported

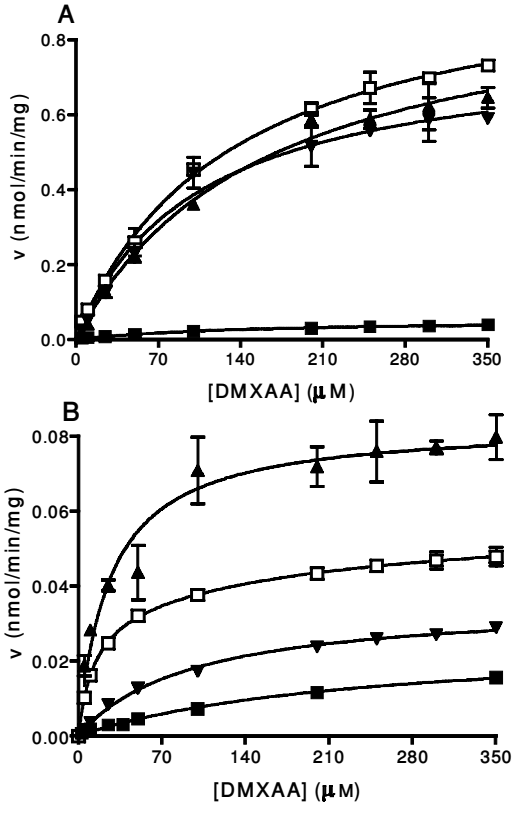


Figure 2. Typical Michaelis–Menten plots for DMXAA glucuronidation (A) and 6-methylhydroxylation (B) in mouse (■), rat (▼), rabbit (▲) and human (HL13, □) liver microsomes. Each point represents the mean ± SD of three determinations. The curves represent the fit of one-site enzyme model.

Table 1. Kinetic parameters for DMXAA glucuronidation and 6-methylhydroxylation in liver and kidney microsomes from various species[#].

	Liver			Kidney		
Metabolic pathway/species	K_m(μM)	V_{max} (nmol min^{-1} mg^{-1})	CL_{int} (m/min^{-1} g^{-1})	K_m(μM)	V_{max} (nmol min^{-1} mg^{-1})	CL_{int} (m/min^{-1} g^{-1})
Glucuronidation[#]						
Mouse, (pooled, $n = 15$)	144 ± 18	0.05 ± 0.00	0.35 ± 0.04	53 ± 11	0.016 ± 0.001	0.30 ± 0.08
Rat (pooled, $n = 6$)	118 ± 11	0.75 ± 0.03	6.36 ± 0.65	108 ± 10	0.019 ± 0.001	0.18 ± 0.03
Rabbit ($n = 2$)	149 ± 35	0.49 ± 0.09	6.31 ± 1.60	21 ± 3	0.091 ± 0.002	4.33 ± 0.72
Human ($n = 14$)	138 ± 79	0.74 ± 0.51	5.36 ± 6.76			
Hydroxylation						
Mouse (pooled, $n = 15$)	236 ± 44	0.026 ± 0.002	0.11 ± 0.02	nd	nd	nd
Rat (pooled, $n = 6$)	158 ± 21	0.036 ± 0.002	0.23 ± 0.04	nd	nd	nd
Rabbit ($n = 2$)	42 ± 16	0.097 ± 0.001	2.31 ± 0.88	24 ± 3	0.006 ± 0.000	0.25 ± 0.03
Human ($n = 14$)	21 ± 5	0.043 ± 0.019	2.05 ± 1.03			

[#] Kinetic parameters (mean ± SD) were obtained from detergent-activated liver microsomes. nd: Not determined due to undetectable formation of metabolite.

hepatic and renal glucuronidation of DMXAA, with a liver: kidney ratio of 1.2, 35 and 1.5 for the CL_{int} in mouse, rat and rabbit respectively. For liver glucuronidation, all species had similar apparent K_m (118–149 μM), but the mouse had a 15-fold lower V_{max} (0.05 ± 0.00 nmol min^{-1} mg^{-1}) compared with rat, rabbit and human (0.74–0.94 nmol $min\ mg^{-1}$), resulting in a 15-fold lower intrinsic clearance (V_{max}/K_m, i.e. CL_{int}) for mouse. In contrast, a large interspecies variation in apparent K_m was observed for liver 6-methylhydroxylation, with human (21 ± 5 μM) and rabbit (42 ± 16 μM) having similar values, but rat (158 ± 21 μM) and mouse (236 ± 44 μM) having much lower affinity. V_{max} for liver 6-methylhydroxylation showed a 4-fold variation with rabbit exhibiting the highest rate (0.097 ± 0.001 nmol min^{-1} mg^{-1}) and mouse the lowest (0.026 ± 0.002 nmol min^{-1} mg^{-1}), with human and rat intermediate. Comparison of liver CL_{int} for 6-methylhydroxylation indicated that mouse and rat were 20- and 10-fold lower than the values for rabbit and human. The liver CL_{int} ratio of glucuronidation 6-methylhydroxylation was 3.2, 25, 2.7 and 2.6 in mouse, rat, rabbit and humans, respectively.

For renal DMXAA glucuronidation, K_m were 53 ± 11, 108 ± 10 and 21 ± 3 μM in mouse, rat and rabbit respectively, with a rank order for CL_{int} of rabbit (4.33 ± 0.72 ml min^{-1} g^{-1}) > mouse (0.30 ± 0.08 ml min^{-1} g^{-1}) > rat (0.18 ± 0.03 ml min^{-1} g^{-1}). 6-Methyhydroxylation activity toward DMXAA was observed only with rabbit renal microsomes, with a $CL_{int} = 0.25 \pm 0.03$ ml min^{-1} g^{-1}. Consideration of overall CL_{int} by renal metabolism (glucuronidation and 6-methylhydroxylation) indicated a 25-fold difference across these species, with a rank order of rabbit (4.58 ml min^{-1} g^{-1}) > mouse (0.30 ml min^{-1} g^{-1}) > rat (0.18 ml min^{-1} g^{-1}). Quantitatively, the *in vitro* CL_{int} for renal DMXAA glucuronidation was comparable with hepatic CL_{int} in mouse (0.30 ± 0.03 versus 0.35 ± 0.04 ml min^{-1} g^{-1}) and rabbit (4.33 ± 0.72 versus 6.31 ± 1.60 ml min^{-1} g^{-1}), but not rat (0.18 ± 0.03 versus 6.36 ± 0.65 ml min^{-1} g^{-1}). Combining these *in vitro* renal CL_{int} (i.e. glucuronidation + hydroxylation) with hepatic CL_{int} (glucuronidation + hydroxylation) gave total $CL_{int} = 0.65$, 6.54 and 10.89 ml min^{-1} g^{-1} in mouse, rat and rabbit, indicating that rabbit remains the most efficient metabolizer for DMXAA. For the total *in vitro* CL_{int} (V_{max}/K_m) by glucuronidation and 6-methylhydroxylation, the ratio of kidney:liver was 0.67, 0.03 and 0.34 in mouse, rat and rabbit respectively.

The total *in vitro* liver and kidney CL_{int} for both glucuronidation and 6-methylhydroxylation of DMXAA in different species, plasma clearance, AUC at MTD, and MTD are shown in table 2. Although the rank order was preserved, there was no significant relationship ($r = 0.81$, $p > 0.05$) between total *in vitro* CL_{int} and the *in vivo* plasma clearance at a DMXAA dose of 99 μmol kg^{-1}.

Species differences in the inhibition of DMXAA acyl glucuronidation

The inhibitory profile of DMXAA glucuronidation *in vitro* by a range of UGT substrates was similar across species (table 3), although to some extent there were species differences in K_i for an individual inhibitor (table 4). K_i for a single potential inhibitor spanned variable ranges from 2-fold for medazepam to 15-fold for diclofenac across species (table 5). Fenclofenac was the most potent inhibitor with the rabbit ($K_i = 11$ μM), but increased to 37–88 μM for other species.

Table 2. *In vitro* total intrinsic clearance (CL_{int}) nad *in vivo* plasma clearance and MTD for DMXAA across species.

Species	$CL_{int}^{\#}$ ($ml\,min^{-1}\,g^{-1}$)	Plasma clearance* ($l\,h^{-1}\,kg^{-1}$)	MTD§ ($mg\,kg^{-1}$)	AUC at MTD§ ($\mu M\,h$)
Mouse	0.65 ± 0.08 ($n = 15$ pooled)	0.041 ($n = 3$ for each time point)	30	2400 ($n = 3$)
Rat	6.77 ± 0.71 ($n = 6$, pooled)	0.074 ± 0.005 ($n = 5$)	330	$19\,000 \pm 12$ ($n = 2$)
Rabbit	10.89 ± 3.12 ($n = 2$)	0.154 ± 0.003 ($n = 3$)	99	2400 ± 5 ($n = 3$)
Human	7.41 ± 7.79 ($n = 14$)	0.069 ± 0.015 ($n = 3$)	99	$12\,336 \pm 3382$ ($n = 2$)

CL_{int} is the sum of microsomal glucuronidation and 6-methylhydroxylation from liver and kidney, except for the human data, which consists only of liver microsomal preparations from 14 individual human livers.

* Total plasma clearances were determined at $30\,mg\,kg^{-1}$ ($99\,\mu mol\,kg^{-1}$) DMXAA in all species. Data for animals were obtained from Kestell *et al.* (1999), and human data were obtained from three patients who received $30\,mg\,kg^{-1}$ in the DMXAA Phase I clinical trial (Jameson *et al.* 2000).

§ Rodent MTD and AUC at MTD data were obtained from Kestell *et al.* (1999), and the human data were obtained from two patients in the DMXAA Phase I clinical trial (Jameson *et al.* 2000).

Table 3. Inhibitory effects of drugs on the DMXAA glucuronidation in mouse, rat, rabbit and human liver microsomes#.

Potential inhibitor	% glucuronidation activity compared with controls			
	Mouse	Rat	Rabbit	Human
Amitriptyline	94.7 ± 0.5	78.8 ± 1.0	$57.2 \pm 7.4^*$	$68.8 \pm 3.1^*$
	$(57.3 \pm 1.4)^*$	$(42.2 \pm 0.0)^*$	$(34.7 \pm 3.3)^*$	$(20.1 \pm 0.5)^*$
Cyproheptadine	75.5 ± 7.2	$69.0 \pm 2.0^*$	75.4 ± 3.9	$47.4 \pm 0.7^*$
	$(38.3 \pm 5.3)^*$	$(40.8 \pm 1.5)^*$	$(32.5 \pm 2.4)^*$	$(17.7 \pm 0.8)^*$
Diclofenac	$27.7 \pm 2.7^*$	$31.6 \pm 3.4^*$	$12.6 \pm 1.5^*$	$14.4 \pm 0.9^*$
	$(13.6 \pm 0.2)^*$	$(10.0 \pm 0.8)^*$	$(2.4 \pm 0.0)^*$	$(8.4 \pm 0.9)^*$
Diflunisal	$28.7 \pm 1.7^*$	$57.9 \pm 1.1^*$	$45.3 \pm 2.5^*$	$70.3 \pm 8.6^*$
	$(18.4 \pm 4.8)^*$	$(24.4 \pm 0.7)^*$	$(43.6 \pm 4.7)^*$	$(26.2 \pm 1.2)^*$
Fenclofenac	$30.4 \pm 1.1^*$	$46.4 \pm 1.7^*$	$12.0 \pm 0.3^*$	$29.6 \pm 3.2^*$
	$(15.0 \pm 1.1)^*$	$(31.8 \pm 2.0)^*$	$(5.5 \pm 0.4)^*$	$(13.4 \pm 0.7)^*$
Fenoprofen	$70.8 \pm 5.7^*$	$23.9 \pm 2.0^*$	$20.6 \pm 0.0^*$	$21.5 \pm 1.9^*$
	$(33.0 \pm 0.6)^*$	$(15.4 \pm 3.3)^*$	$(7.7 \pm 0.6)^*$	$(10.8 \pm 0.1)^*$
Indomethacin	$51.8 \pm 3.4^*$	$51.6 \pm 1.1^*$	$28.4 \pm 1.6^*$	$52.3 \pm 0.7^*$
	$(15.3 \pm 1.1)^*$	$(19.5 \pm 0.4)^*$	$(8.8 \pm 1.1)^*$	$(9.7 \pm 1.0)^*$
Medazepam	$67.3 \pm 11.3^*$	$57.5 \pm 0.8^*$	86.7 ± 0.4	$56.0 \pm 1.5^*$
	$(43.7 \pm 1.1)^*$	$(29.7 \pm 0.6)^*$	$(36.4 \pm 3.6)^*$	$(39.3 \pm 2.2)^*$
1-Naphthol	92.4 ± 3.6	98.2 ± 1.5	92.8 ± 8.8	99.1 ± 4.5
	$(52.1 \pm 0.9)^*$	$(69.1 \pm 1.9)^*$	$(49.3 \pm 0.9)^*$	$(67.3 \pm 1.7)^*$
Oxazepam	72.8 ± 4.9	71.7 ± 0.2	$62.1 \pm 0.2^*$	71.6 ± 1.9
	$(35.0 \pm 7.3)^*$	$(58.3 \pm 4.3)^*$	$(43.9 \pm 2.3)^*$	$(64.8 \pm 3.0)^*$
Paracetamol	100.2 ± 5.9	99.5 ± 2.8	101.6 ± 5.7	100.3 ± 4.2
	(86.8 ± 10.0)	(101.9 ± 3.5)	(95.3 ± 6.1)	(96.1 ± 5.2)

Data are the mean $\pm$ SD ($n = 3$) percentage of glucuronidation activity remaining in Brij 58-activated pooled microsomes from humans (HL6, 7, 8), rat ($n = 6$), mouse ($n = 15$) and rabbit ($n = 2$) at 100 or $500\,\mu M$ (data in parentheses) inhibitor concentration.

Table 4. Inhibitory effects of various inhibitors on the DMXAA 6-methylhydroxylation in mouse, rat, rabbit and human liver microsomes[#].

Potential inhibitor	Related human CYP	Concentrated (μM)	% hydroxylation activity compared with controls			
			Mouse	Rat	Rabbit	Human
SKF525A		100	60.8 ± 3.2*	61.4 ± 8.6*	62.3 ± 7.5*	66.2 ± 7.9*
		500	40.5 ± 8.5*	43.7 ± 9.8*	41.3 ± 5.3*	29.8 ± 0.3*
ANF	1A	0.5	19.5 ± 3.1*	35.6 ± 0.3*	70.5 ± 2.0*	20.1 ± 1.9*
		5	11.5 ± 0.9*	12.7 ± 0.9*	53.2 ± 0.1*	13.8 ± 0.8*
Furafylline	1A	20	88.7 ± 0.9	31.3 ± 0.5*	105.3 ± 21.6	29.3 ± 1.8*
		100	69.7 ± 1.7*	7.0 ± 0.3*	94.6 ± 4.7	23.8 ± 2.1*
Phenacetin	1A	100	97.5 ± 8.4	10.6 ± 1.6*	60.4 ± 2.0*	41.2 ± 2.2*
		500	52.2 ± 6.0*	2.9 ± 0*	32.1 ± 0.8*	13.1 ± 0.2*
Sulphaphenazole	2C	100	89.2 ± 9.1	101.5 ± 13.9	93.7 ± 2.8	99.2 ± 9.1
		500	92.4 ± 7.1	105.0 ± 9.1	83.0 ± 6.3	90.8 ± 5.9
Tobutamide	2C	100	59.4 ± 3.4*	80.6 ± 3.2	104.2 ± 4.6	107.7 ± 6.7
		500	39.2 ± 1.3*	77.0 ± 11.8	71.2 ± 0.1	102.1 ± 7.5
Diclofenac	2C	100	35.4 ± 4.8*	43.2 ± 0.0*	12.7 ± 1.6*	45.9 ± 0.9*
		500	19.9 ± 0.9*	27.9 ± 2.0*	12.7 ± 0.1*	33.9 ± 1.1*
Quinidine	2D	100	101.1 ± 10.2	91.8 ± 7.2	56.2 ± 2.3*	92.1 ± 8.2
		500	77.3 ± 2	79.2 ± 3.8	31.2 ± 0.5*	72.5 ± 3.5
Chlorzoxazone	2E	100	97.3 ± 22.8	101.6 ± 4.9	60.2 ± 2.4*	98.0 ± 1.0
		500	101.9 ± 12.5	70.3 ± 20.0	43.1 ± 0.1*	101.0 ± 3.7
DDC	2E	100	93.2 ± 5.8	44.8 ± 0.4*	102.2 ± 5.6	91.1 ± 2.8
		500	70.9 ± 6.3	4.0 ± 0.5*	77.5 ± 2.9	90.2 ± 11.6
Testosterone	3A	100	40.2 ± 2.0*	32.1 ± 1.2*	77.4 ± 0.7	63.7 ± 2.6*
		500	24.2 ± 2.0*	15.2 ± 3.2*	41.5 ± 0.7*	48.5 ± 0.6*
Erythromycin	3A	100	66.2 ± 3.1*	90.7 ± 8.9	86.8 ± 1.4	89.1 ± 13.8
		500	61.1 ± 1.6*	50.9 ± 1.2*	61.8 ± 1.5*	62.1 ± 4.6*
Ketoconazole	3A	0.5	97.6 ± 11.7	97.1 ± 5.5	87.0 ± 12.4	98.9 ± 7.8
		5	88.5 ± 86	97.7 ± 2.3	97.2 ± 9.4	95.1 ± 3.8
Cimetidine	3A	100	44.4 ± 6.1*	80.8 ± 0.7	65.7 ± 3.6*	99.2 ± 6.6
		500	43.6 ± 7.8*	72.8 ± 11.1	52.7 ± 2.0*	101.0 ± 2.2
TAO	3A	0.5	101.5 ± 7.1	85.4 ± 10.4	95.4 ± 2.1	98.9 ± 10.9
		5	99.8 ± 9.3	81.5 ± 9.2	93.7 ± 10.8	92.8 ± 7.0

[#] Data are the mean ± SD from three determinations using three sources of human liver microsomes from HL12, HL13 and HL14, pooled mouse, rat, and rabbit liver microsomes at various inhibitor concentration.

*$p < 0.05$.

Table 5. Inhibitory constants for DMXAA metabolism by various compounds.

Metabolic pathway/compounds	K_i(μM)			
	Mouse	Rat	Rabbit	Human
Glucuronidation				
Cyproheptadine	241	154	114	53
Diclofenac	54	55	3.7	10
Fenclofenac	50	88	11	37
Fenoprofen	260	50	18	30
Indomethacin	109	117	22	110
Medazepam	217	125	320	164
6-Methylhydroxylation				
SKF525A	127	165	130	83
ANF	0.11	0.38	12.7	0.036
Phenacetin	n.d.	4	129	23
Testosterone	21	22	n.d.	n.d.

n.d. Not determined.

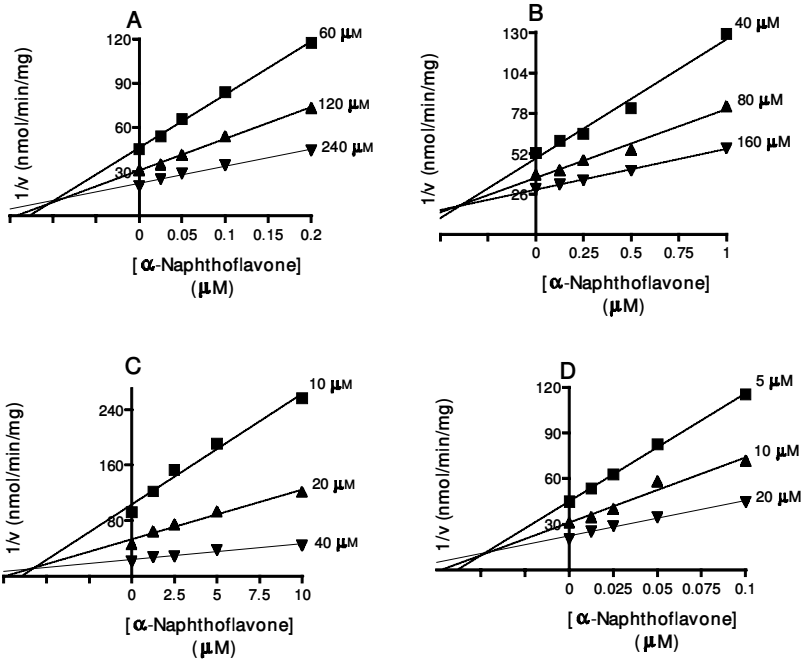


Figure 3. Dixon plots for the inhibition of DMXAA 6-methylhydroxylation by α-naphthoflavone in mouse (A), rat (B), rabbit (C) and human (D) liver microsomes. Data are derived from three determinations.

Species differences in the inhibition of DMXAA 6-methylhydroxylation

Significant species differences in the inhibition profile and K_i of DMXAA 6-methylhydroxylation by various CYP inhibitors and/or substrates in mouse, rat, rabbit and human liver microsomes were observed (tables 4 and 5). SKF525A inhibited 6-methyl hydroxylation in all species investigated, with similar K_i (83–165 μM). Although ANF demonstrated similar inhibition at 0.5 or 5 μM inhibitor concentration in all species, the difference in K_i was 353-fold between the lowest (0.036 μM) in human and the highest (12.7 μM) in rabbit, with mouse and rat being intermediate (0.11 and 0.38 μM respectively) (figure 3). Furafylline, a mechanism-based CYP1A inhibitor, showed negligible inhibition for DMXAA 6-methylhydroxylation in mouse and rabbit, but had significant ($p < 0.05$) inhibition in human ($k_{inact} = 0.23 \pm 0.04\,min^{-1}$, $K'_{app} = 15.6 \pm 6.7\,\mu M$) and rat ($k_{inact} = 0.21 \pm 0.03\,min^{-1}$, $K'_{app} = 19.2 \pm 7.3\,\mu M$) microsomes. Phenacetin caused significant ($p < 0.05$) inhibition in rat ($K_i = 4\,\mu M$), rabbit (129 μM) and human (23 μM) but not in mouse microsomes. Significant inhibition for DMXAA 6-methylhydroxylation was observed with testosterone in mouse ($K_i = 21\,\mu M$) and rat (33 μM), but much less inhibition was observed in human and rabbit.

Non-specific binding of DMXAA in liver microsomes

DMXAA was bound to liver microsomes from various species to a small extent with unbound fractions ($f_{u(mic)}$) mostly > 0.85. There were no significant differences ($p > 0.05$) in the binding of DMXAA to liver microsomal protein across

species. At 0.2 mg ml^{-1} microsomal protein (a concentration typically used in incubations for DMXAA acyl glucuronidation studies), $f_{u(mic)} = 0.952 \pm 0.023$, 0.961 ± 0.032, 0.961 ± 0.042 and 0.948 ± 0.022 for mouse, rat, rabbit and human respectively, whereas $f_{u(mic)}$ decreased to 0.885 ± 0.034, 0.894 ± 0.028, 0.910 ± 0.033 and 0.892 ± 0.031 respectively when the microsomal protein concentration was increased to 1 mg ml^{-1} (a concentration typically used in incubations for DMXAA methylhydroxylation studies). $f_{u(mic)}$ progressively decreased as the protein concentration increased and DMXAA concentration decreased.

In vitro–in vivo *correlation*

The *in vitro* DMXAA metabolism data obtained from liver microsomes were scaled up to enable direct comparison with the observed clearance *in vivo* (table 6). There was no significant difference between the predicted clearances using the three liver models ($p > 0.05$, two-way ANOVA). The hepatic availability was > 0.97 for all models used. The use of well-stirred or parallel-tube model, but not a dispersion model, resulted in a rank order of human > rabbit ≈ rat > mouse for $CL_{h\text{-}pre}$, which was similar to that of plasma clearance observed *in vivo*. There was a significant underestimation of hepatic clearance for all species with a ratio of 2.4–31 for the observed:predicted values. Quantitatively, the dispersion model was the best of three models used for the prediction of hepatic clearance of DMXAA as less underestimation of hepatic clearance was observed compared with other two models.

The impact of microsomal binding on the kinetics of DMXAA glucuronidation and 6-methylhydroxylation in liver microsomal preparations from mouse, rat, rabbit and human was evaluated. The unbound K_m for glucuronidation and 6-methylhydroxylation were ~10–30% lower than the bound apparent K_m in all

Table 6. *In vitro–in vivo* scaling for the hepatic clearance of DMXAA.

Parameter	Mouse	Rat	Rabbit	Human
CL_{int} (ml min^{-1} g^{-1} protein)	0.46 ± 0.06	6.59 ± 0.69	8.62 ± 2.48	7.41 ± 7.79
mg protein g $liver^{-1}$	41.5 ± 6.8	49.8 ± 7.9	42.5 ± 5.1	45.5 ± 14.3
g liver kg body $weight^{-1}$	50	45	40	20
CL_{int} (ml min^{-1} kg^{-1})	0.95 ± 0.12	14.77 ± 1.55	14.65 ± 4.22	6.74 ± 7.09
Q_h^* (ml min^{-1} kg^{-1}	90	60	60	20
f_u	0.046	0.026	0.020	0.046
C_B/C_P	0.581	0.667	0.637	0.673
f_B	0.079	0.039	0.031	0.068
$CL_{h\text{-}pre}$ (ml min^{-1} kg^{-1})				
Well-stirred model	0.035 ± 0.004	0.266 ± 0.028	0.261 ± 0.075	0.492 ± 0.518
Dispersion model	0.079 ± 0.010	0.520 ± 0.056	0.481 ± 0.134	0.450 ± 0.472
Parallel-tube model	0.035 ± 0.004	0.266 ± 0.028	0.261 ± 0.075	0.498 ± 0.523
CL (ml min^{-1} kg^{-1})[#]	1.115	1.232	2.574	3.650
$CL/CL_{h\text{-}pre}$ ratio				
Well-stirred model	31.9	4.6	9.7	7.4
Dispersion model	14.1	2.4	5.4	8.1
Parallel-tube model	31.9	4.6	9.7	7.3

[#] Data are obtained at low DMXAA doses (Kestell *et al.* 1999, Jameson *et al.* 2000).

[*] Q_h, hepatic blood flow; C_B/C_P, ratio of blood:plasma concentration; f_u, free plasma concentration; f_B, free blood concentration.

Table 7. Physiological and pharmacokinetic parameters plus toxicity data in various species.[#]

Parameters	Mouse	Rat	Rabbit	Human
Body weight (kg)	0.021	0.230	3.5	70.000
f_u	0.046	0.026	0.020	0.046
C_B/C_P	0.581	0.667	0.637	0.673
Dose (mg kg^{-1})	3	30	30	0.15–4.2
V_{dss} (l kg^{-1})	0.34	0.45	0.45	0.49
CL (l h^{-1} kg^{-1})	0.067	0.074	0.154	0.219
CL_B (l h^{-1} kg^{-1})	0.115	0.111	0.242	0.325
$t_{1/2}$ (h)	3.5	4.2	2.0	1.6
MTD (mg kg^{-1})	30	330	99	99

[#] Animal data of V_{dss}, CL and MTD were from Kestell *et al.* (1999). Human data for V_{dss} and CL were obtained from the first 18 patients enrolled in a Phase I clinical trial of DMXAA (Jameson *et al.* 2000).

species, with the V_{max} being unchanged, resulting in a slight increase in the unbound V_{max}/K_m.

Interspecies allometric scaling

All physiological, pharmacokinetic parameters and toxicity data are shown in table 7. Pharmacokinetic data at low DMXAA doses were used. All species had similar V_{dss}, but a 2- and 3-fold ranges in CL and $t_{1/2}$ were observed across species, with the human having the largest CL and shortest $t_{1/2}$. Rat tolerated DMXAA best with a MTD = 330 mg kg^{-1}, being 3-fold that for human and rabbit, and 10-fold that for mouse. Without correction, there were significant linear relationships between the log BW (kg) and log CL (l h^{-1}), log CL_B (l h^{-1}), and log V_{dss} (litres) (figure 4 and table 7), resulting in the allometric equations as follows:

$$CL = 1.316\ BW^{1.103} \tag{14}$$

$$CL_B = 0.003\ BW^{1.122} \tag{15}$$

$$V_{dss} = 0.428\ BW^{1.040}. \tag{16}$$

Similar allometric relationships were obtained between body weight and pharmacokinetic parameters based on the unbound DMXAA plasma concentration. There were no significant relationships between body weight and either MTD or $t_{1/2}$.

Discussion

Based upon their chemical structure, drugs such as DMXAA may generally be classified as belonging to the aryl acetic acid group. The metabolism and disposition of these compounds has been studied in a variety of species and the results reported in some depth over 30 years (Dixon *et al.* 1977, Emudianughe *et al.* 1987, Brunelle and Verbeeck 1996, Burchell *et al.* 1998). Thus, from this wealth of knowledge, it is possible to predict that a compound from this group, whose aryl moiety is not complex, would undergo metabolism principally by acyl glucuroni-

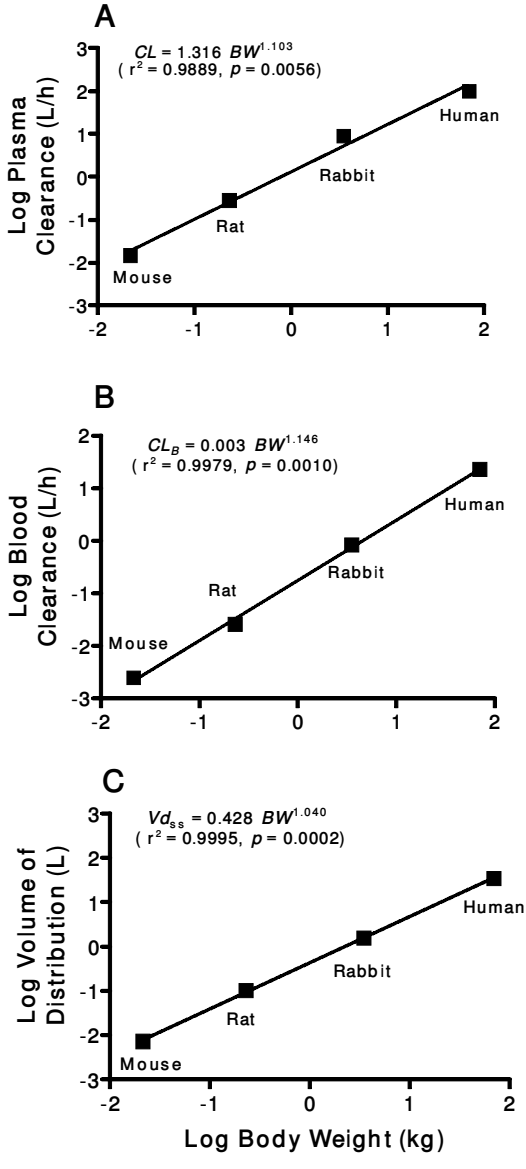


Figure 4. Allometric scaling plots for DMXAA of (A) CL versus species body weight, (B) CL_B versus body weight, and (C) V_{dss} versus body weight. Line represents least-square regression analysis of all the data points. Data are derived from at least three determinations.

dation and by hydroxylation to a minor extent. Previous *in vivo* studies using laboratory animals substantiate this (Schillings and Sisenwine 1986, Kestell *et al.* 1999).

The current study demonstrates that liver microsomes from mouse, rat, rabbit and humans could metabolize DMXAA to DMXAA-G and 6-OH-MXAA, reflecting the metabolite profile observed *in vivo*. Thus, from a qualitative view, one may conclude that mouse, rat and rabbit are an appropriate species for

conducting preclinical *in vitro* metabolism and drug interaction studies. However, significant species differences in the kinetic parameters of DMXAA metabolism *in vitro* were observed. Comparison of the total CL_{int}, i.e. glucuronidation plus 6-methylhydroxylation, indicated that rabbit is the most efficient at metabolizing DMXAA, but is in the same order of magnitude as human and rat. The rank order of total CL_{int}, i.e. rabbit > human > rat > mouse, is in agreement with the rank order of *in vivo* 'plasma clearance' (i.e. dose/AUC ratio at 99 μmol kg^{-1} DMXAA). However, this rank order was not conserved for MTD, where mouse was the most sensitive, indicating that both pharmacokinetic and pharmacodynamic mechanisms should be sought to explain the significant species differences in MTD. Indeed, our results highlight the mouse as a species somewhat different to the others, particularly with regard to its ability to glucuronidate DMXAA. It appears that although the mouse can metabolize this drug by acyl glucurination, it does so rather poorly. These findings are consistent with other studies involving structurally related compounds such as flavone-8-acetic acid (Cummings *et al.* 1989), 1-napthyl acetic acid (Dixon *et al.* 1977, Emudianughe *et al.* 1987) and Wy-41,770 (Schillings and Sisenwine 1986). Although these studies were carried out *in vivo* and may be complicated by factors associated with the enterohepatic recirculation of these drugs, a trend emerges which reinforces the finding that the mouse is not very efficient at acyl glucuronidation.

It is generally accepted that the liver is the major organ for drug metabolism (Woodhouse 1992), but a number of studies have indicated that extrahepatic tissues such as kidney, lung, brain and gastrointestinal tract have metabolic activity toward numerous drugs (Gram *et al.* 1986, Krishna and Klotz 1994, Lohr *et al.* 1998). Molecular techniques, such as Western blotting analysis, have indicated that most forms of CYP and UGT present in the liver also exist in the kidney (Burchell *et al.* 1998, Radominska-Pandya *et al.* 1999). Given that the kidney receives ~25% of the total cardiac output (Guyton 1981), and that all drugs excreted in the urine must pass through the kidney, it has been suggested that the kidney may play a role in the metabolism of some drugs. The present study has demonstrated that DMXAA may be metabolized by the kidney in mouse, rat and rabbit. As with the liver, glucuronidation was the major metabolism pathway compared with 6-methylhydroxylation, which was not detected in mouse and rat renal microsomes. This is in agreement with reports that phase I metabolism by kidney is insignificant, but phase II (especially glucuronidation) may contribute to the overall elimination of certain drugs such as diphenylacetic acid and nalidixic acid (Sallustio *et al.* 1989). For total *in vitro* CL_{int} by glucuronidation and 6-methylhydroxylation, the ratio of kidney:liver was 0.67, 0.03 and 0.34 in mouse, rat and rabbit respectively, suggesting that perhaps in mouse and rabbit, the kidney may play an important part in metabolism of DMXAA. However, taking into account that liver weight is ~5-fold that of two kidneys (Davidson *et al.* 1986), it would be predicted that *in vivo* the kidneys would at most contribute 13 and 7% to the total metabolic clearance of DMXAA in mouse and rabbit respectively. Thus, it would appear unlikely that renal dysfunction would have a significant impact on the overall metabolism and elimination of DMXAA.

The species-related variation in the apparent K_i for DMXAA glucuronidation and 6-methylhydroxylation may reflect involvement of different UGT and CYP isoforms across species, or variation in the contributions by multiple isoforms. The significant inhibition of DMXAA 6-methylhydroxylation in all species by

SKF525A, a non-selective inhibitor of CYP (Gorrod and Damani 1979), indicates the involvement of CYP. The CYP1A inhibitor ANF significantly inhibited DMXAA 6-methylhydroxylation, but there were significant differences in K_i across species, indicating the involvement of CYP1A and perhaps other forms, which varied across species. However, the mechanism-based CYP1A inhibitor furafylline (Sesardic *et al.* 1990) exhibited significant inhibition in human and rat, but not in mouse and rabbit, indicating that selective CYP1A inhibitors do not exhibit the same selectivity in all species. Eagling *et al.* (1998) observed a 40-fold difference in the inhibitory potency of furafylline against phenacetin *O*-deethylation in rat and human liver microsomes. Both CYP and UGT are superfamilies consisting of a number of forms with similarities in their amino acid sequences and significant variation across species (de Montellano 1999, Radominska-Pandya *et al.* 1999). Small alterations in the amino acid sequences can give rise to significant differences in substrate specificity and enzyme activity (Lewis *et al.* 1998), and it is not surprising that DMXAA metabolism *in vitro* showed species similarities and differences. The species differences in the effects of inhibitors and/or substrates on DMXAA metabolism may be due to a number of factors. Amino acid residues of UGT and CYP may vary, leading to differences in the active site of UGT and CYP (Halpert *et al.* 1994, Lewis *et al.* 1998). A metabolic pathway may be catalysed by different enzyme forms in different species. Thus, Veronese *et al.* (1990) reported that tolbutamide was metabolized by CYP2C9 in human, but by other CYP forms in the rat, leading to altered inhibition potency by sulphaphenazole. Different inhibitory sites have also been observed between species, even if the same enzyme subfamily is responsible for the metabolism. In addition, species differences in enzyme-specific ratios may lead to inhibition variation (Boobis *et al.* 1990). For example, the ratio of CYP1A2 to CYP1A1 is usually 4–20:1 in most mammalian species, but in rat it is 0.14–0.67:1 (Nedelcheva and Gut 1994). Therefore, it is not surprising that Bogaards *et al.* (2000) concluded in their recent comprehensive study of CYPs in different species that *in vitro* data derived from CYP subfamilies requires caution if used for extrapolation purposes. Thus, the differential inhibition of DMXAA metabolism by inhibitors causes complications in the choice of animal model for further DMXAA metabolism and drug interaction studies.

During drug development, attempts are made to extrapolate *in vitro* and *in vivo* pharmacokinetic and toxicological data from animals to humans. In particular, the clearance and MTD (Lin 1998). Interspecies scaling may use physiologically based models or allometric techniques (Boxenbaum 1980, Balant and Gex-Fabry 1990, Lin 1998). The former offers a mechanistic approach to extrapolate from one species to another by examining individual components, which interrelate to produce the characteristics of the whole system. This process requires the integration of various factors, such as tissue binding, hepatic intrinsic clearance and blood flow (Balant and Gex-Fabry 1990). However, the difficulty in collecting tissue data and the sophisticated numerical techniques are limiting factors in the use of such comprehensive physiological models. In contrast, the allometric technique is a simpler process to predict pharmacokinetics and toxicity of drugs in humans based on animal data (Lin 1998).

Since the microsomal clearances of DMXAA for the mouse, rat, rabbit and human were 0.46, 6.59, 8.62 and 7.41 ml min^{-1} g^{-1} microsomal protein respectively, it seemed likely that the prediction would be successful, as previous studies

have indicated this to be a reasonable exercise for drugs with low microsomal clearances, i.e. < 10 ml min^{-1} g^{-1} microsomal protein (Houston 1994). Although this approach has achieved acceptable results with other drugs (Ubeaud *et al*. 1995, Ito *et al*. 1998), this was not successful for DMXAA using either direct *in vitro–in vivo* regression analysis or incorporation of three liver models. This underestimation of DMXAA clearance by these methods was not due to non-specific binding of DMXAA to microsomal proteins which was small with a free fraction > 0.85, which is remarkably different from its extensive binding to plasma proteins (Zhou *et al*. 2001c). The small amount of binding of DMXAA to liver microsomes will result in a slight overestimation of K_m, without affecting the metabolic rate at saturating substrate concentrations. Thus, it can be concluded that the non-specific binding of DMXAA to liver microsomes has little impact on the estimation of *in vitro* kinetic parameters and correction for the unbound fraction in the *in vitro* incubation matrix is unlikely to improve significantly the prediction of pharmacokinetic clearance. In contrast, in several other studies, the clearance predictions have been successfully improved by correction for non-specific binding to liver microsomes (Obach 1997, Carlile *et al*. 1999, Obach 1999). Other factors that may contribute to the underestimation of DMXAA clearance include: (1) extrahepatic clearance (e.g. renal metabolism has been observed for DMXAA in the mouse, rat and rabbit); (2) a loss of enzyme activity during microsomal preparation (DMXAA is extensively glucuronidated, and UGT activity is subject to a number of influences such as enzyme latency, enzyme heterogeneity and multiplicity, with variable susceptibility to activity losses (Radominska-Pandya *et al*. 1999); (3) rate-limiting uptake of the drug into hepatocytes, leading to overestimation of *in vivo* clearance; and (4) active transport processes for drugs (which is not taken into account by the *in vitro* models).

Despite the lack of success in extrapolating DMXAA data from *in vitro* to *in vivo*, attempts were made to use allometric scaling for the prediction of pharmacokinetic parameters across species. With volume of distribution, the exponent was close to unity, indicating that this pharmacokinetic parameter increased proportionally to body weight across species. Indeed, the volume of distribution is the only pharmacokinetic parameter that has consistently exhibited statistically significant allometric relationships for drugs of differing classes (Lin 1998). An unusual feature was the highly significant relationship between body weight and clearance with an allometric exponent > 1, indicating that DMXAA is cleared more slowly in the smaller animal, which is in contrast to the majority of drugs (Paxton 1995, Lin 1998). Similar results have been observed with FAA (Zaharko *et al*. 1986). It is unknown whether this is related to the mouse having a low capacity to glucuronidate, or the influence of biliary excretion, or perhaps the changes in blood flow associated with the vascular effects of these drugs (Zwi *et al*. 1989, 1994). However, there was no significant linear relationship between MTD of DMXAA and body weight across species, suggesting that the allometric extrapolation of toxicity data from animals to humans is unlikely.

In summary, these results indicate qualitative similarities in DMXAA metabolism across species but significant quantitative differences. Of the species examined, mouse was the most different from human with regard to the *in vitro* kinetics of the metabolism of DMXAA. Although the *in vitro* extrapolation of hepatic clearance of DMXAA was less successful, it appears possible to extrapolate animal pharmacokinetic parameters to patients using allometric techniques, but

interspecies scaling of MTD appears unlikely. Significant interspecies variability in the inhibitory profile for a number of compounds was observed. Although possible inhibitors of DMXAA metabolism can be identified, it is apparent that prediction of the extent of their inhibitory action on DMXAA elimination in patients is not possible from animal studies. Additional complicating factors in the extrapolation of DMXAA–drug interactions from animals to humans may arise from indirect effects on metabolism due to the immunomodulating effects of DMXAA that may vary dramatically from species to species.

Acknowledgement

The authors appreciate the support of the Maurice and Phyllis Paykel Trust and the University of Auckland Research Fund. S. F. Zhou was a holder of the Auckland Medical Research Foundation Senior Scholarship and now has received an AMRF postdoctoral fellowship.

References

Baguley, B. C., Zhuang, L. and Kestell, P., 1997, Increased plasma serotonin following treatment with flavone-8-acetic acid, 5,6-dimethylxanthenone-4-acetic acid, vinblastine, and colchicine: relation to vascular effects. *Oncology Research*, **9**, 55–60.

Balant, L. P. and Gex-Fabry, M., 1990, Physiological pharmacokinetic modelling. *Xenobiotica*, **20**, 1241–1257.

Bogaards, J. J. P., Bertrand, M., Jackson, P., Oudshoorn, M. J., Weaver, R. J., Van Blanderen, P. J. and Walther, B., 2000, Determining the best animal model for human cytochrome P450 activities: a comparison of mouse, rat, rabbit, dog, micropig, monkey and man. *Xenobiotica*, **30**, 1131–1152.

Boobis, A. R., Sesardic, D., Murray, B. P., Edwards, R. J., Singleton, A. M., Rich, K. J., Murray, S., de la Torre, R., Segura, J., Pelkonen, O., Pasanen, M., Kobayashi, S., Zhi-Guang, T. and Davies, D. S., 1990, Species variation in the response of the cytochrome P450-dependent monooxygenase system to inducers and inhibitors. *Xenobiotica*, **20**, 1139–1161.

Boxenbaum, H., 1980, Interspecies variation in liver weight, hepatic weight, hepatic flow and antipyrine intrinsic clearance in extrapolation of data to benzodiazepines and phenytoin. *Journal of Pharmacokinetics and Biophamaceutics*, **8**, 165–176.

Boxenbaum, H., 1982, Interspecies scaling, allometry, physiological time, and the ground plan of pharmacokinetics. *Journal of Pharmacokinetics and Biopharmaceutics*, **10**, 201–227.

Brunelle, F. M. and Verbeeck, R. K., 1996, Glucuronidation of diflunisal in liver and kidney microsomes of rat and man. *Xenobiotica*, **26**, 123–131.

Burchell, B., Brieley, C. H., Monaghan, G. and Clarke, D. J., 1998, The structure and function of the UDP-glucuronosyltransferase gene family. *Advances in Pharmacology*, **42**, 335–338.

Carlile, D. J., Hakooz, N., Bayliss, M. K. and Houston, J. B., 1999, Microsomal prediction of *in vivo* clearance of CYP2C9 substrates in humans. *British Journal of Clinical Pharmacology*, **47**, 625–635.

Ching, L.-M., Xu, Z.-F., Gummer, B. H., Palmer, B. D., Joseph, W. R. and Baguley, B. C., 1995, Effect of thalidomide on tumour necrosis factor production and anti-tumour activity induced by 5,6-dimethylxanthenone-4-acetic acid. *British Journal of Cancer*, **72**, 339–343.

Cummings, J., Double, J. A., Bibby, M. C., Farmer, P., Evens, S., Kerr, D. J., Kaye, S. B. and Smyth, J. F., 1989, Characterization of the major metabolites of flavone acetic acid and comparison of their disposition in humans and mice. *Cancer Research*, **49**, 3587–3593.

Davidson, I. W. F., Parker, J. C. and Beliles, R. P., 1986, Biological basis for extrapolation across mammalian species. *Regulatory Toxicology and Pharmacology*, **6**, 211–237.

De Montellano, P. R. O., 1999, The cytochrome P450 oxidative system. In T. F. Woolf (ed.), *Handbook of Drug Metabolism* (New York: Marcel Dekker), pp. 203–227.

Dixon, P. A., Caldwell, J. and Smith, R. L., 1977, Metabolism of arylacetic acids. 1. The fate of 1-naphthylacetic acid and its variation with species and dose. *Xenobiotica*, **7**, 695–706.

Eagling, V. A., Tjia, J. F. and Back, D. J., 1998, Differential selectivity of cytochrome P450 inhibitors against probes substrates in human and rat liver microsomes. *British Journal of Clinical Pharmacology*, **45**, 107–114.

Emudianughe, T. S., Caldwell, J. and Smith, R. L., 1987, Studies on the metabolism of arylacetic acids. 6. Comparative metabolic conjugation of 1- and 2-naphthylacetic acids in the guinea pig, mouse, hamster and gerbil. *Xenobiotica*, **17**, 815–821.

Gibaldi, M. and Perrier, D., 1982, *Pharmacokinetics* (New York: Marcel Dekker).

Gorrod, J. W. and Damani, L. A., 1979, The effect of various potential inhibitors, activators and inducers on the N-oxidation of 3-substituted pyridines *in vitro*. *Xenobiotica*, **9**, 219–226.

Gram, T. E., Okine, L. K. and Gram, R. A., 1986, The metabolism of xenobiotics by certain extrahepatic organs and its relation to toxicity. *Annual Review in Pharmacology and Toxicology*, **26**, 259–292.

Guyton, A. C., 1981, *Textbook of medical Physiology* (London: W. B. Saunders).

Halpert, J. R., Guengerich, F. P., Bend, J. R. and Correia, M. A., 1994, Selective inhibitors of cytochromes P450. *Toxicology and Applied Pharmacology*, **125**, 163–175.

Houston, J. B., 1994, Utility of *in vitro* drug metabolism data in predicting *in vivo* metabolic clearance. *Biochemical Pharmacology*, **47**, 1469–1479.

Ito, K., Iwatsubo, T., Kanamitsu, S., Nukajima, Y. and Sugiyama, Y., 1998, Quantitative prediction of *in vivo* drug clearance and drug interactions from *in vitro* data on metabolism, together with binding and transport. *Annual Review of Pharmacology and Toxicology*, **38**, 461–499.

Jameson, M. B., Thomson, P. I., Baguley, B. C., Evans, B. D., Harvey, V. J., McCrystal, M. R. and Kestell, P., 2000. Phase I pharmacokinetic and pharmacodynamic study of 5,6-dimethylxanthenone-4-acetic acid (DMXAA), a novel antivascular agent. In *Proceeding of the Annual Meeting of American Society of Clinical Oncologists*, pp. 705.

Kestell, P., Paxton, J. W., Rewcastle, G. W., Dunlop, I. and Baguley, B. C., 1999, Plasma disposition, metabolism and excretion of the experimental antitumour agent 5,6-dimethylxanthenone-4-acetic acid in the mouse, rat and rabbit. *Cancer Chemotherapy and Pharmacology*, **43**, 323–330.

Kestell, P., Zhao, L., Ching, L.-M., Baguley, B. C. and Paxton, J. W., 2000, Modulation of the plasma pharmacokinetics of 5,6-dimethylxanthenone-4-acetic acid by thalidomide in mice. *Cancer Chemotherapy and Pharmacology*, **46**, 135–141.

Krishna, D. R. and Klotz, U., 1994, Extrahepatic metabolism of drugs in humans. *Clinical Pharmacokinetics*, **26**, 144–160.

Lash, C. J., Li, A. E., Rutland, M., Baguley, B. C., Zwi, L. J. and Wilson, W. R., 1998, Enhancement of the anti-tumour effects of the antivascular agent 5,6-dimethylxanthenone-4-acetic acid (DMXAA) by combination with 5-hydroxytryptamine and bioreductive drugs. *British Journal of Cancer*, **78**, 439–445.

Lewis, D. F., Ionnides, C. and Parke, D. V., 1998, Cytochrome P450 and species differences in xenobiotic metabolism and activation of carcinogen. *Environmental and Health Perspectives*, **106**, 633–641.

Lin, J. H., 1998, Applications and limitations of interspecies scaling and *in vitro* extrapolation in pharmacokinetics. *Drug Metabolism and Disposition*, **26**, 1202–1212.

Lohr, J. W., Willsky, G. R. and Acara, M. A., 1998, Renal drug metabolism. *Pharmacological Review*, **50**, 107–141.

Mahmood, I., 1999, Allometric issues in drug development. *Journal of Pharmaceutical Science*, **88**, 1101–1106.

Miners, J. O., Valente, L., Lillywhite, K. J., Mackenzie, P. I., Burchell, B., Baguley, B. C. and Kestell, P., 1997, Preclinical prediction of factors influencing the elimination of 5,6-dimethylxanthenone-4-acetic acid, a new anticancer drug. *Cancer Research*, **57**, 284–289.

Modenti, J., 1986, Dosage regimen design for pharmaceutical studies conducted in animals. *Journal of Pharmaceutical Science*, **75**, 852–856.

Moody, G. C., Griffin, S. J., Mather, A. N., McGinnity, D. F. and Riley, R. J., 1999, Fully automated analysis of activities catalysed by the major human liver cytochrome P450(CYP) enzymes: assessment of human CYP inhibition potential. *Xenobiotica*, **29**, 53–75.

Nedelcheva, D. and Gut, I., 1994, P450 in the rat and man: methods of investigation, substrate specificities and relevance to cancer. *Xenobiotica*, **24**, 1151–1175.

Obach, R. S., 1997, Nonspecific binding to microsomes: impact on scale-up of *in vitro* intrinsic clearance to hepatic clearance as assessed through examination of warfarin, imipramine, and propranolol. *Drug Metabolism and Disposition*, **25**, 1359–1369.

Obach, R. S., 1999, Prediction of human clearance of twenty-nine drugs from hepatic microsomal intrinsic clearance data: an examination of *in vitro* half-life approach and nonspecific binding to microsomes. *Drug Metabolism and Disposition*, **27**, 1350–1359.

Omura, T. and Sato, R., 1964, The carbon monoxide binding pigment of liver microsomes. I. Evidence for its hemoprotein nature. *Journal of Biological Chemistry*, **23**, 2370–2378.

Paxton, J. W., 1995, The allometric approach for interspecies scaling of pharmacokinetics and toxicity of anticancer drugs. *Clinical and Experimental Pharmacology and Physiology*, **22**, 851–854.

Philpott, M., Baguley, B. C. and Ching, L.-M., 1995, Induction of tumour necrosis factor-alpha by single and repeated doses of the antitumour agent 5,6-dimethylxanthenone-4-acetic acid. *Cancer Chemotherapy and Pharmacology*, **36**, 143–148.

Pruijn, F. B., Vandaalen, M., Holford, N. H. G. and Wilson, W. R., 1997, Mechanisms of enhancement of the antitumour activity of melphalan by the tumour-blood-flow inhibitor 5,6-dimethylxanthenone-4-acetic acid. *Cancer Chemotherapy and Pharmacology*, **39**, 541–546.

Radominska-Pandya, A., Czernik, P. J., Little, J. M., Battaglia, E. and Mackenzie, P. I., 1999, Structural and functional studies of UDP-glucuronosyltransferases. *Drug Metabolism Reviews*, **31**, 817–899.

Rewcastle, G. W., Atwell, G. J., Baguley, B. C., Calveley, S. B. and Denny, W. A., 1989, Potential antitumour agents. 58. Synthesis and structure–activity relationships of substituted xanthenone-4-acetic acids active against the colon 38 tumour *in vivo*. *Journal of Medicinal Chemistry*, **32**, 793–799.

Rewcastle, G. W., Kestell, P., Baguley, B. C. and Denny, W. A., 1990, Light-induced breakdown of flavone acetic acid and xanthenone analogues in solution. *Journal of the National Cancer Institute*, **82**, 528–529.

Roberts, M. S. and Rowland, M., 1986, A dispersion model of hepatic elimination: 1. Formulation of the model and bolus considerations. *Journal of Pharmacokinetics and Biopharmaceutics*, **14**, 227–260.

Robson, R. A., Matthews, A. P., Miners, J. O., McManus, M. E., Meyer, U. A., Hall, P. D. and Birkett, D. J., 1987, Characterisation of theophylline metabolism by human liver microsomes. *British Journal of Clinical Pharmacology*, **24**, 293–300.

Rowland, M., Benet, L. Z. and Graham, G. G., 1973, Clearance concepts in pharmacokinetics. *Journal of Pharmacokinetics and Biopharmaceutics*, **1**, 123–136.

Sallustio, B. C., Purdie, Y. J., Birkett, D. J. and Meffin, P. J., 1989, Effect of renal dysfunction on the individual components of the acyl-glucuronide futile cycle. *Journal of Pharmacology and Experimental Therapeutics*, **251**, 288–294.

Schillings, R. T. and Sisenwine, S. F., 1986, Disposition of (5H-dibenzo [a,d]cyclohepten-5-ylidene)acetic acid in laboratory animals. *Drug Metabolism and Disposition*, **14**, 405–412.

Sesardic, D., Boobis, A. R., Murray, B. P., Murray, S., Segura, J., De la Torre, R. and Davies, D. S., 1990, Furafylline is a potent and selective inhibitor of cytochrome P450IA2 in man. *British Journal of Clinical Pharmacology*, **29**, 651–663.

Smith, P. K., Krohn, R. I., Hermanson, G. T., Mallia, A. K., Garter, F. H., Provenzano, M. D., Fujimoto, E. K., Goeke, N. M., Olson, B. J. and Klenk, D. C., 1985, Measurement of protein using bicinchoninic acid. *Analytical Biochemistry*, **150**, 76–85.

Thomsen, L. L., Ching, L.-M. and Baguley, B. C., 1990, Evidence for the production of nitric oxide by activated macrophages treated with the antitumor agents flavone-8-acetic acid and xanthenone-4-acetic acid. *Cancer Research*, **50**, 6966–6970.

Thomsen, L. L., Ching, L.-M., Zhuang, L., Gavin, J. B. and Baguley, B. C., 1991, Tumor-dependent increased plasma nitrate concentrations as an indication of the antitumor effect of flavone-8-acetic acid and analogues in mice. *Cancer Research*, **51**, 77–81.

Ubeaud, G., Schmitt, C., Jaeck, D., Lave, T. and Coassolo, P. H. H., 1995, Bosentan, a new endothelin receptor antagonist: prediction of the systemic plasma clearance in man from combined *in vivo* and *in vitro* data. *Xenobiotica*, **25**, 1381–1390.

Veronese, M. E., McManus, M. E., Laupattarakasem, P., Miners, J. O. and Birkett, D. J., 1990, Tolbutamide hydroxylation by human, rabbit and rat liver microsomes and by purified forms of cytochrome P-450. *Drug Metabolism and Disposition*, **18**, 356–361.

Webster, L. K., Ellis, A. G., Kestell, P. and Rewcastle, G. W., 1995, Metabolism and elimination of 5,6-dimethylxanthenone-4-acetic acid in the isolated perfused rat liver. *Drug Metabolism and Disposition*, **23**, 363–368.

Wilkinson, G. R., 1975, A physiological approach to hepatic drug clearance. *Clinical Pharmacology and Therapeutics*, **18**, 377–390.

Wilson, W. R., Li, A. E., Cowan, D. S. M. and Siim, B. G., 1998, Enhancement of tumor radiation response by the antivascular agent 5,6-dimethylxanthenone-4-acetic acid. *International Journal of Radiation Oncology Biology Physics*, **42**, 905–908.

Woodhouse, K., 1992, Drugs and the liver. Part III: Ageing of the liver and the metabolism of drugs. *Biopharmaceutics and Drug Disposition*, **13**, 311–320.

World Health Organization, 1979, *WHO Handbook for Reporting Results of Cancer Treatment*. WHO Offset Publication No. 48 (Geneva: WHO).

Zaharko, D. S., Grieshaber, C. K., Plowman, J. and Cradock, J. C., 1986, Therapeutic and pharmacokinetic relationships of flavone acetic acid: an agent with activity against solid tumors. *Cancer Treatment Reports*, **70**, 1415–1421.

Zhao, L., Ketsell, P., Zhuang, L. and Baguley, B. C., 2001, Effects of the serotonin receptor antagonist cyproheptadine on the activity and pharmacokinetic of 5,6-dimethylxanthenone-4-acetic (DMXAA). *Cancer Chemotherapy and Pharmacology*, **47**, 491–497.

ZHOU, S. F., PAXTON, J. W., TINGLE, M. D., MCCALL, J. and KESTELL, P., 1999, Determination of two major metabolites of the novel anti-tumour agent 5,6-dimethylxanthenone-4-acetic acid in hepatic microsomal incubations by high-performance liquid chromatography with fluorescence detection. *Journal of Chromatography (B)*, **734**, 129–136.

ZHOU, S. F., PAXTON, J. W., TINGLE, M. D. and KESTELL, P., 2000, Identification of the human liver cytochrome P450 isozyme responsible for the 6-methylhydroxylation of the novel anticancer drug 5,6-dimethylxanthenone-4-acetic acid. *Drug Metabolism and Disposition*, **28**, 1449–1456.

ZHOU, S. F., PAXTON, J. W., TINGLE, M. D., KESTELL, P. and CHING, L.M., 2001a, In vitro and *in vivo* kinetic interactions of the anti-tumour agent 5,6-dimethylxanthenone-4-acetic acid with thalidomide and diclofenac. *Cancer Chemotherapy and Pharmacology*, **47**, 319–326.

ZHOU, S. F., KESTELL, P., TINGLE, M. D., CHING, L.-M. and PAXTON, J. W., 2001b, A difference between the rat and mouse in the pharmacokinetic interaction of 5,6-dimethylxanthenone-4-acetic acid with thalidomide. *Cancer Chemotherapy and Pharmacology*, **47**, 541–544.

ZHOU, S. F., PAXTON, J. W., KESTELL, P. and TINGLE, M. D., 2001c, Reversible binding of the novel anti-tumour agent 5,6-dimethylxanthenone-4-acetic acid to plasma proteins and blood cells in various species. *Journal of Pharmacy and Pharmacology*, **53**, 463–471.

ZWI, L. J., BAGULEY, B. C., GAVIN, J. B. and WILSON, W. R., 1989, Blood flow failure as a major determinant in the antitumor action of flavone acetic acid (NSC 347512). *Journal of the National Cancer Institute*, **81**, 1005–1013.

ZWI, L. J., BAGULEY, B. C., GAVIN, J. B. and WILSON, W. R., 1994, Correlation between immune and vascular activities of xanthenone acetic acid on tumour agents. *Oncology Research*, **6**, 79–85.

XENOBIOTICA, 2002, VOL. 32, NO. 2, 109–118

Taylor & Francis
healthsciences

Identification of the human P450 enzymes involved in the *in vitro* metabolism of the synthetic steroidal hormones Org 4060 and Org 30659

C. H. J. VERHOEVEN†*, T. T. M. VAN MUNSTER†, G. M. M. GROOTHUIS‡, R. M. E. VOS† and I. M. C. M. RIETJENS§

† Department of Toxicology & Drug Disposition, PO Box 20, 5340 BH Oss, The Netherlands
‡ Department of Pharmacokinetics and Drug Delivery, Groningen University Institute for Drug Explorations, University Centre for Pharmacy, Groningen, The Netherlands
§ Laboratories of Biochemistry and Division of Toxicology, University of Wageningen, Wageningen, The Netherlands

Received 14 May 2001

1. The type of human P450 enzymes involved in the *in vitro* metabolism of Org 4060 and Org 30659, two synthetic steroidal hormones currently under clinical development by NV Organon for use in oral contraceptive and hormone replacement therapy, was investigated.

2. Both steroids were mainly hydroxylated at the 6β-position in incubations with human liver microsomes.

3. The results from experiments with supersomes, correlation studies as well as inhibition studies with ketoconazole, a selective inhibitor of CYP3A, strongly suggest that the CYP3A family plays a significant role in the 6β-hydroxylation of both steroids.

4. Measurements of kinetic parameters of P450 enzymes that could metabolize both steroids, combined with the fact that CYP3A4 is known to be the most abundant P450 enzyme in the human liver, indicate that CYP3A4 will be of major importance for the *in vivo* human metabolism of Org 4060 and Org 30659.

Introduction

Knowledge on the P450 enzymes involved in the metabolism of new chemical entities is relevant in predicting drug interactions and explaining interindividual variation of drug metabolism. Large interindividual variability in the expression of the P450 enzymes and the related differences in metabolic clearance may be caused by genetic differences (genetic polymorphism) or differences in exposure to xenobiotics, which may induce or inhibit P450s. Disease states, diet and hormonal influences may also change the levels of P450 expression (Wrighton *et al.* 1996). The P450 enzymes are known to catalyse a large number of Phase I reactions in steroid metabolism. CYP3A4, for example, is the major P450 enzyme involved in the 6β-hydroxylation of testosterone, androstenedione and progesterone in human liver microsomes (Waxman *et al.* 1988), whereas the CYP2C family seems to have an important role in the 3-hydroxylation of desogestrel (Gentile *et al.* 1998). A

* Author for correspondence at: Clinical Development Department, NV Organon, PO Box 20, 5340 BH, Oss, The Netherlands; e-mail: carole.verhoeven@organon.com

Xenobiotica ISSN 0049–8254 print/ISSN 1366–5928 online © 2002 Taylor & Francis Ltd
http://www.tandf.co.uk/journals
DOI: 10.1080/00498250110093026

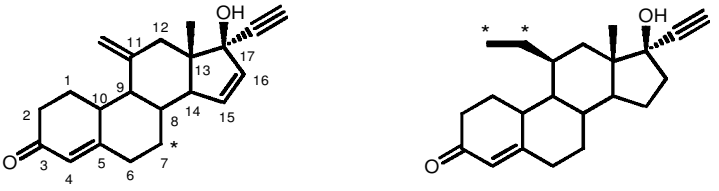


Figure 1. Structures of Org 30659 (left) and Org 4060 (right).

major contribution of CYP2C9 is suggested for the transformation of the prodrug mestranol to ethinylestradiol (Schmider *et al.* 1997). This enzyme also has progesterone 21-hydroxylation activity, although to a lower extent than CYP2C19. In addition, the oxidation of testosterone at the 17-position to form androstenedione is catalysed by the CYP2C19 enzyme (Yamazaki and Shimada 1997).

Org 30659 ((17α)-17-hydroxy-11-methylene-19-norpregna-4,15-dien-20-yn-3-one) and Org 4060 ((11β, 17α)-11-ethyl-17-hydroxy-19-norpregn-4-en-20-yn-3-one) (figure 1) are both synthetic steroidal hormones currently under clinical development by NV Organon for use in oral contraceptive and hormone replacement therapy. Org 30659 shows a very high progestagenic activity in pharmacological studies in rat and rabbit. In addition, a lack of androgenic activity (according to the Hershberger test) distinguishes Org 30659 from other frequently used synthetic progestagens. Except for some weak oestrogenic activity in rat, Org 30659 is devoid of other hormonal activities, including glucocorticoid and anti-glucocorticoid activity (Deckers *et al.* 1992). Org 4060 is strongly oestrogenic and progestagenic in rat and rabbit. In rat, Org 4060 displays minimal androgenic activity and only at a high dose, very weak glucocorticoid activity.

The present investigation was performed to identify the specific human P450 enzymes involved in the Phase I metabolism of both steroids. In addition, kinetic parameters of P450 enzymes capable of the conversion of Org 4060 and Org 30659 were determined.

Materials and methods

Chemicals

[^{3}H]-Org 4060 and [^{3}H]-Org 30659 labelled at the C11 ethyl and the C7, respectively, with radiochemical purities $\geq$ 98% were prepared by the Organic Isotope Section of the Department of Process Chemistry, NV Organon. The specific activities of Org 4060 and Org 30659 were 560 and 888 GBq mmol^{-1}, respectively. Unlabeled Org 4060, Org 30659, the 6β-OH metabolite of Org 4060, the 6β-OH metabolite of Org 30659 and ketoconazole (chemical purity $\geq$ 95%) were synthesized by the Department of Process Chemistry, NV Organon. All other chemicals were obtained from commercial sources and were of analytical grade.

In vitro *incubations*

Metabolites of Org 4060 and Org 30659 in human liver microsomal incubations. Human liver microsomes were prepared from surgical waste liver tissue, after consent from legal authorities and patients was obtained, in cooperation with the Human Liver Group Groningen (Dr G. M. M. Groothuis). Liver samples were homogenized using a Potter-Elvehjem homogenizer at 0°C in a 50 mm Tris-HCl buffer (pH 7.4) containing 0.25 M sucrose. Microsomes were prepared by centrifugation (20 min, 100 000*g*; supernatant 2 $\times$ 75 min, 1.000 000*g*). The microsomal pellet was resuspended in 100 mm potassium phosphate (pH 7.4) containing 20% (v/v) glycerol. The microsomal suspensions were stored at –80 °C, until used. The microsomal suspensions were characterized by the determination of P450 and protein contents. The concentration of P450 was calculated from the CO-reduced difference spectrum according to Omura and Sato (1964). The concentration of protein was measured by the method of Lowry *et al.* (1951) using bovine serum albumin as a standard.

Incubations were performed with a pool of four human liver microsomes. Human liver microsomes were incubated (final volume of 0.2 ml) at 37 °C in 100 mM potassium phosphate (pH 7.4), containing

(final concentration) 3 mM NADPH (the pre-incubation mixture) and an appropriate concentration of test compound. [^{3}H]-Org 4060 was incubated with human liver microsomes (final protein concentration range: 0.03–1 mg ml^{-1}) at a final concentration of 1.3 or 10 μM (170 kBq ml^{-1}). [^{3}H]-Org 30659 was incubated with human liver microsomes (final protein range 0.1–1 mg ml^{-1}) at a concentration of 1 or 10 μM (90 kBq ml^{-1}). After a pre-incubation of 2 min, incubations were started by the addition of the pre-incubation mixture to the test compound. Incubations were carried out in a shaking Eppendorf Thermomixer 5436 and were stopped after 5, 10 and 15 min by the addition of 20% ice-cold acetonitrile. After centrifugation, supernatants were subjected to HPLC analysis. All incubations were performed in duplicate. In addition, an incubation (final protein concentration 1 mg ml^{-1}) without NADPH was performed to determine the non-NADPH-dependent reactions.

In vitro *incubation studies with supersomes*. Incubations were performed using commercially available supersomes (CYP1A2, CYP2A6, CYP2D6, CYP2E1, CYP2C9, CYP2C19, CYP3A4 or CYP3A5) (Gentest Corporation). Supersomes were derived from baculovirus-insect cells with a specific human P450 enzyme expressed, co-expressed with human NADPH-cytochrome P450 reductase. The insect host cell line has been demonstrated not to contain a detectable P450 activity (in accordance with the Catalogue of Gentest Corporation). The conversion of suitable substrates by these P450 enzymes has been done by the supplier and is specified in their catalogue (Catalogue of Gentest Corporation).

Supersomes (final protein concentration 250 μg ml^{-1}) were incubated at 37 °C in 200 μl potassium phosphate (pH 7.4) containing 3 mM NADPH (final concentration) and the test compound in a final incubation volume of 0.2 ml. The final concentrations of [^{3}H]-Org 4060 and [^{3}H]-Org 30659 were 10 μM (170 kBq ml^{-1}) and 10 μM (90 kBq ml^{-1}), respectively. Incubations with CYP2A6 and CYP2C9 were performed using Tris buffer (100 mM, pH 7.4). After a pre-incubation of 2 min, incubations were started by the addition of the pre-incubation mixture to the test compound. Incubations were carried out in a shaking Eppendorf Thermomixer 5436 (Eppendorf, Germany) and were stopped after 15 min by the addition of 20% ice-cold acetonitrile. After centrifugation, supernatants were subjected to HPLC analysis. All incubations were performed in duplicate.

Kinetic studies with CYP3A4, CYP3A5 and CYP2C19 supersomes. Studies with CYP3A4, CYP3A5 and CYP2C19 (only Org 30659) supersomes were performed to determine apparent K_m and V_{max} for the 6β-hydroxylation of Org 4060 and Org 30659. Supersomes (final protein concentration 100–250 μg ml^{-1}) were incubated at 37 °C for 15 min in 100 mM potassium phosphate (pH 7.4) containing (final concentration) 3 mM NADPH and the test compound at various concentrations (0.3–100 μM) in a total volume of 200 μl. All incubations were performed in duplicate. Apparent K_m and V_{max} were determined by fitting the data to the standard Michaelis–Menten equation: $v = V_{max} * [S]/(K_m + [S])$, where $[S]$ is the substrate concentration, using the program of EZ-FIT (v.1.1, Medical Products Department, E. I. Dupont de Nemours & Co., 1988).

Correlation studies. A set of ten human liver microsomes with specified activities for selected P450 substrates (testosterone for CYP3A activity and *S*-mephenytoin for CYP2C19 activity) was obtained from the International Institute for the Advancement of Medicine (IIAM). Tissues were obtained by IIAM as a result of a medical/surgical procedure, recovery for transplantation (of non-transplantable organs or tissues) or *post mortem* recovery of tissues for research. All tissues were procured with the appropriate legal consent of the donor or the donor's next of kin. Human liver microsomes (final protein concentrations 100 μg ml^{-1} (Org 4060) and 250 μg ml^{-1} (Org 30659)) were incubated at 37 °C in 100 mm potassium phosphate (pH 7.4), containing 3 mM NADPH (final concentration) in a total volume of 200 μl. After a pre-incubation of 2 min, incubations were started by the addition of the pre-incubation mixture to the test compound (two different concentrations). The final concentrations of [^{3}H]-Org 4060 were 1.3 and 10 μM (170 kBq ml^{-1}) and the final concentrations of [^{3}H]-Org 30659 were 1 and 10 μM (90 kBq ml^{-1}). Incubations were carried out in a shaking Eppendorf Thermomixer 5436 (Eppendorf) and were stopped at 10 min (Org 4060) or 15 min (Org 30659) by the addition of 20% ice-cold acetonitrile. After centrifugation, supernatants were subjected to HPLC analysis.

Inhibitor studies with human liver microsomes. Inhibitor studies were performed with the human liver microsomes as described above. A pool of four different preparations of human liver microsomes was used. Microsomal incubations with [^{3}H]-Org 4060 and [^{3}H]-Org 30659 were performed in the presence of ketoconazole, a selective inhibitor for CYP3A (Baldwin *et al.* 1995). Incubations were performed at four inhibitor concentrations (0.01, 0.1, 1, 10 μM). Incubations containing ketoconazole were pre-incubated for 5 min before addition of the substrate. The incubation conditions were as described for the microsomal incubations in the correlation studies. All incubations were performed in duplicate. An additional incubation was performed under the conditions described above in the absence of inhibitor.

Sample analysis

Determination of radioactivity. The concentration of radioactivity in incubation samples was determined by liquid scintillation counting (LSC) (Tri-Carb 2500 TR/2, Canberra Packard, Germany).

HPLC analysis of the metabolite profiles of Org 4060 and Org 30659. Supernatants of the incubation samples, obtained after precipitation of microsomal protein with acetonitrile, were analysed by HPLC. HPLC analysis was performed using a μ-Bondapak C18 (internal length 300 mm, internal diameter 7.8 mm) column and a gradient of 0.1 M ammonium acetate buffer (pH 4.2) (solvent A) and methanol (solvent B). Elution was performed with a linear gradient from 10–90% (v/v) solvent B in 35 min at 500 °C. The flow rate was 2.5 ml min^{-1}. HPLC analysis was performed with a HP1090 liquid chromatograph equipped with a HP1040 diode array detector (Hewlett Packard, Germany) and a Flo-one/Beta model A525 on-line radioactivity detector (Canberra Packard). Samples were spiked with unlabeled Org 4060 and the 6β-OH metabolite of Org 4060 or Org 30659 and the 6β-OH metabolite of Org 30659 as references for retention times (UV signal at 254 nm).

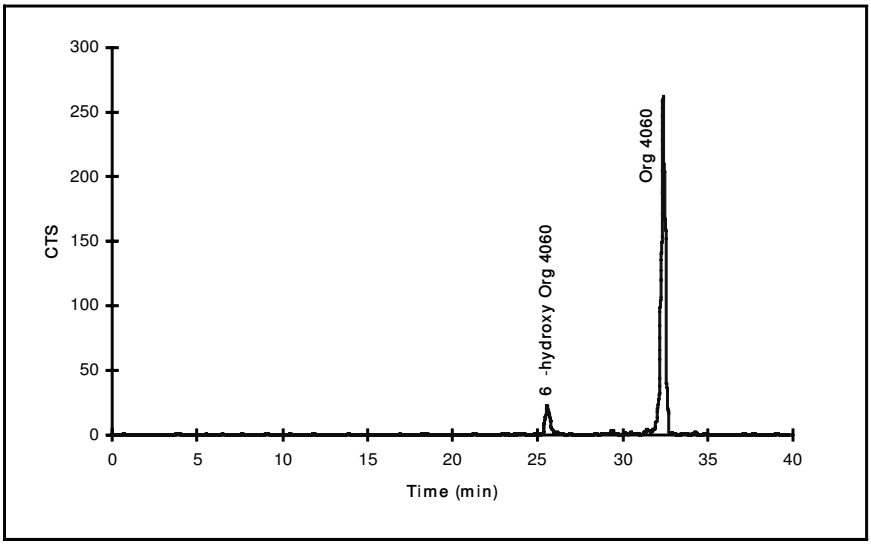
Spearman Rank correlation test. The correlation between the rates of formation of the metabolites of Org 4060 and Org 30659 and the activity of microsomes with selective P450 substrates (testosterone for CYP3A activity and *S*-mephenytoin for CYP2C19 activity) as specified by the supplier (IIAM) was calculated using the Spearman-Rank correlation test.

Results

In vitro *incubations*

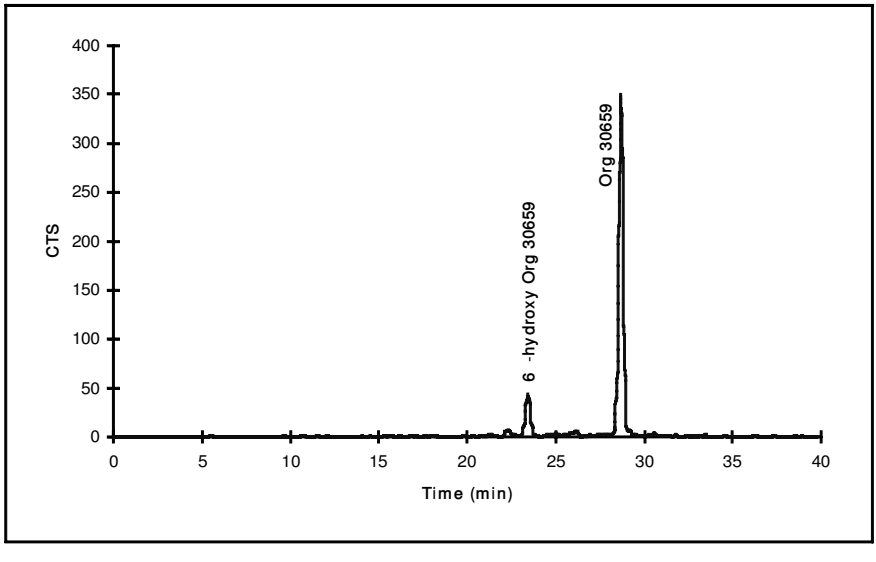
In the present study, the specific P450 enzymes involved in the Phase I metabolism of Org 4060 and Org 30659 were investigated. Three different *in vitro* experiments, namely incubations with supersomes, correlation analysis and incubations with ketoconazole (a selective inhibitor of CYP3A), were done to identify the P450 enzymes involved in the Phase I metabolism of the two synthetic steroidal hormones. It has been shown that the involvement of a particular enzyme can only be reliably established if multiple approaches are used (Guengerich 1996).

Metabolites of Org 4060 and Org 30659 in human liver microsomal incubations. The HPLC metabolite profile of the incubation of Org 4060 with pooled human liver microsomes in the presence of NADPH, shows the formation of one major metabolite (figure 2) under the conditions used. By co-chromatographic analysis with the 6β-OH Org 4060 reference compound, the presence of the 6β-OH metabolite of Org 4060 was confirmed. The initial rate of the formation of the 6β-OH metabolite of Org 4060 was linear with the microsomal protein concentrations between 0.03 and 0.1 mg ml^{-1} over a 10-min incubation (data not shown). To avoid the possibility of secondary metabolism, the final concentration of microsomal protein in further incubations was set at 0.1 mg ml^{-1} and incubation was set at 10 min. HPLC analysis of incubations with Org 30659 in human liver microsomes also shows the presence of one major metabolite (figure 3) under the conditions used. The formation of the 6β-OH metabolite was also confirmed for Org 30659 on the basis of co-chromatography with the authentic reference compound. For Org 30659, the initial rate of the formation of the 6β-OH metabolite was linear with the microsomal protein concentrations between 0.1 and 1 mg ml^{-1} over a 15 min incubation (data not shown). Based on these results, the final concentration of microsomal protein in further incubations with Org 30659 was set at 0.25 mg ml^{-1} and the incubation at 15 min to avoid possible secondary metabolism. For both test compounds, no metabolites were formed in incubations in the absence of NADPH (data not shown).



CTS: counts/8.5 sec

Figure 2. Typical chromatogram derived from incubations of Org 4060 for 10 min with human liver microsomes.



CTS: counts/8.5 sec

Figure 3. Typical chromatogram derived from incubations of Org 30659 for 15 min with human liver microsomes.

In vitro *incubation studies with supersomes*. In a first approach to identify the human P450 enzymes involved in the 6β-hydroxylation of Org 4060 and Org 30659, the formation of the 6β-OH metabolite of Org 4060 and Org 30659 was determined in incubations of Org 4060 and Org 30659 with supersomes (CYP1A2,

CYP2A6, CYP2D6, CYP2E1, CYP2C9, CYP2C19, CYP3A4 or CYP3A5). The formation of the 6β-OH metabolite of Org 4060 and Org 30659 by the individual supersomes, expressed as min^{-1}, is given in table 1. Formation of the 6β-OH metabolite of Org 4060 was only observed in incubations with CYP3A4 and CYP3A5, with CYP3A4 being the most active. The other enzymes showed no activity in the formation of the 6β-OH metabolite of Org 4060. The CYP3A4 and CYP3A5 supersomes also metabolized Org 30659 to its 6β-OH metabolite. However, the conversion rate for Org 30659 with CYP3A5 supersomes was ~10-fold lower than with CYP3A4 supersomes. In addition, the CYP2C19 microsomes could form the 6β-OH metabolite of Org 30659, although at a rate that was ~8-fold lower than observed with CYP3A4 supersomes. All the other microsomes failed to metabolize Org 30659 to a detectable level.

Kinetic studies with CYP3A4, CYP3A5 and CYP2C19 supersomes. Kinetic data for the 6β-hydroxylation of Org 4060 and Org 30659 by the three types of supersomes which could metabolize Org 4060 and Org 30659 are shown in table 2. The apparent K_m for the 6β-hydroxylation of Org 4060 in CYP3A4 was 2.0 μM. For Org 30659 an ~20 times higher apparent K_m = 41μM was observed in CYP3A4 supersomes, whereas the V_{max} = Org 4060 was three times lower as compared with the V_{max} determined for Org 30659 converted by CYP3A4. Both steroids were converted by CYP3A5 with relatively high K_m of 141 μM (Org 4060) and 390 μM (Org 30659) and also high V_{max}. The apparent K_m of CYP2C19 for Org 30659 (17 μM) was approximately two times lower than the apparent K_m for CYP3A4 conversion of Org 30659. The V_{max} determined for the conversion of Org 30659 by CYP2C19 was relatively low; 0.26 min^{-1}. Org 4060 was not converted by CYP2C19 to a detectable extent.

Correlation studies. To investigate further the enzyme involvement in the 6β-hydroxylation of both steroids, a correlation study between the formation of the 6β-OH metabolite of Org 4060 or Org 30659 (expressed as pmol min^{-1} mg $protein^{-1}$) and the 4-hydroxylation of *S*-mephenytoin (marker substrate for

Table 1. Formation of the 6β-OH metabolite of Org 4060 and Org 30659 by supersomes at a substrate concentration of 10 μM.

Supersomes	6β-OH Org 4060 (min^{-1})	6β-OH Org 30659 (min^{-1})
CYP1A2	n.a.	n.a.
CYP2A6	n.a.	n.a.
CYP2D6	n.a.	n.a.
CYP2C9	n.a.	n.a.
CYP2C19	n.a.	0.17
CYP2E1	n.a.	n.a.
CYP3A4	1.44	1.34
CYP3A5	0.50	0.13

Radioactive peaks in the HPLC metabolite profiles were characterized as a metabolite if the peak area was least the average area of five times 1−min integrated background noise (cpm) + 3*SD (standard deviation), the peak height was at least three times the average peak height (cpm) of five times 1−min integrated background noise and the peak duration was at least 0.5 min.

n.a. No detectable activity.

Table 2. Kinetic parameters for the formation of the 6β-OH metabolite by CYP3A4, CYP3A5 and CYP2C19 supersomes.

	CYP3A4		CYP3A5		CYP2C19	
	Org 4060	Org 30659	Org 4060	Org 30659	Org 4060	Org 30659
V_{max} [a]	1.74 ± 0.16	5.27 ± 0.29	8.39 ± 2.11	4.70 ± 0.64	–	0.26 ± 0.02
K_m [a]	2.0 ± 0.9	41 ± 5	141 ± 46	390 ± 64	–	17 ± 3
V_{max}/K_m	0.87	0.13	0.06	0.01	–	0.02

[a] Values are the mean $\pm$ SD of the fit, where individual data points are the mean of two replicates. V_{max} (min^{-1}); K_m (μM); V_{max}/K_m (min^{-1} μM^{-1}).

CYP2C19, expressed as pmol min^{-1} mg $protein^{-1}$) and the 6β-hydroxylation of testosterone (marker substrate for CYP3A, expressed as pmol min^{-1} mg $protein^{-1}$) was performed. The Spearman-Rank correlation data obtained from these experiments are given in table 3. The activities of the marker substrates were used as specified by the supplier. When Org 4060 and Org 30659 were incubated with a set of ten human liver microsomes, a significant correlation was observed between the formation of the 6β-OH metabolite of Org 4060 and Org 30659 and the activity of these microsomes in the selective assay for CYP3A activity, testosterone 6β-hydroxylation. No significant correlation was observed between the formation of the 6β-OH metabolite of Org 4060 and Org 30659 and the metabolism of *S*-mephenytoin, a substrate selective for CYP2C19.

Inhibitor study with human liver microsomes. Finally, the effect of the selective P4503A inhibitor ketoconazole (Baldwin *et al.* 1995) was investigated to corroborate the conclusion that CYP3A4 is the P450 enzyme preferentially involved. Ketoconazole showed a potent inhibitory effect on the formation of 6β-OH metabolite of Org 4060 and Org 30659 in a concentration-dependent manner (figure 4a and b respectively). From these results, it follows that the IC_{50} for the inhibition of the conversion of both steroids by ketoconazole is $< 0.1\,\mu M$.

Discussion

In the present study, the type of human P450 enzymes involved in the *in vitro* metabolism of Org 30659 and Org 4060 was investigated. Both steroids were mainly hydroxylated at the 6β-position. The 6β-hydroxy metabolite was previously identified in human liver microsomes for Org 30659 (Verhoeven *et al.*

Table 3. Spearman-Rank correlations (r) between the formation of the 6β-OH metabolite of Org 4060 and Org 30659 and the metabolism of the marker substrates for CYP2C19 and CYP3A activity.

P450	Marker substrate	Org 4060		Org 30659	
		1.3 μM	10 μM	1 μM	10 μM
CYP2C19	*S*-mephenytoin	0.22	0.35	0.35	0.26
CYP3A	testosterone	0.87^{***}	0.88^{***}	0.92^{***}	0.95^{***}

Statistical significance: *** $p < 0.001$.

1998) and Org 4060 (unpublished data). The 6β-hydroxylation is also the major metabolic pathway for testosterone, progesterone and androstenedione in human liver microsomes (Waxman *et al*. 1988). The results from the experiments with supersomes, correlation studies as well as the inhibition studies with ketoconazole, a selective inhibitor of CYP3A, strongly suggest that the CYP3A family plays a significant role in the 6β-hydroxylation of both steroids. The human CYP3A family, accounting for ~50% of total P450 in human liver, is clinically very important because the members of this family have been shown to metabolize a large number of drugs (Wrighton *et al*. 1989, Shimada *et al*. 1994, Wrighton *et al*. 1996). The human CYP3A subfamily includes family members CYP3A4, CYP3A5 and CYP3A7 (Hunt *et al*. 1992, Li *et al*. 1995). CYP3A4 is the major

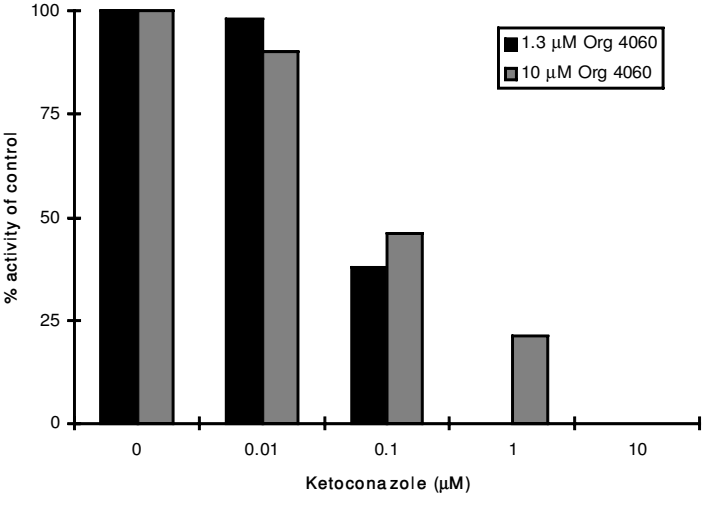


Figure 4a. Inhibition of the 6β-hydroxylation of Org 4060 by ketoconazole. (i) Absolute values of 100% control activities; (ii) data are the mean of duplicate incubations.

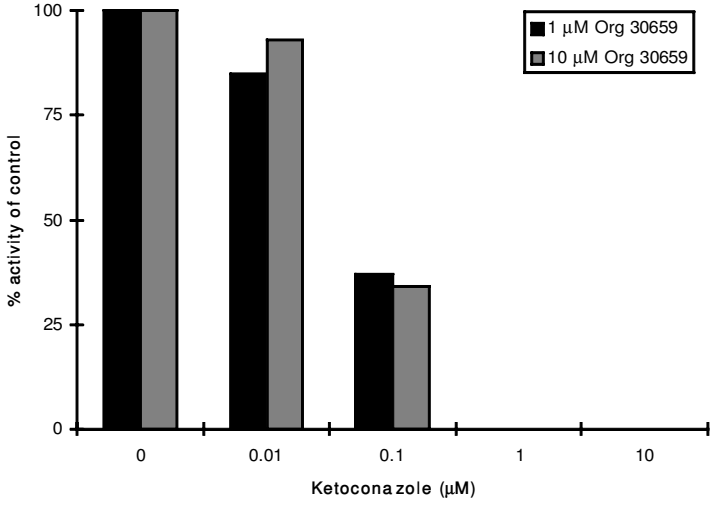


Figure 4b. Inhibition of the 6β-hydroxylation of Org 30659 by ketoconazole. (i) Absolute values of 100% control activities; (ii) data are the mean of duplicate incubations.

human liver CYP3A enzymes, whereas CYP3A5 is present in only ~10–30% of the human livers (Aoyama *et al*. 1989, Li *et al*. 1995, Wilkinson 1996). CYP3A7 is a major P450 enzyme present in foetal liver, but this enzyme appears not to be important in adults (Wilkinson 1996). Enzymes of the CYP3A superfamily are not only present in human liver, but also CYP3A-related P450 enzymes have been detected immunohistochemically in human kidneys, small intestine, pancreas, gall bladder, skin, testes and ovaries (Hunt *et al*. 1992).

Measurements of kinetic parameters of P450 enzymes able to metabolize Org 4060 and Org 30659, combined with the fact that CYP3A4 is known to be the most abundant P450 enzyme in human liver (Li *et al*. 1995), indicates CYP3A4 to be of major importance for the metabolism of both steroids *in vivo*. Kinetics of Org 4060 and Org 30659 metabolism revealed the relative differences in V_{max} and K_m for the conversion of Org 4060 and Org 30659 by CYP3A4, CYP3A5 and CYP2C19 (only Org 30659). The apparent K_m obtained for CYP2C19 for the 6β-hydroxylation of Org 30659 was ~2-fold lower than the K_m obtained for CYP3A4. The maximum human plasma concentration of Org 30659 after an oral administration of 250 µg/subject was ~7 nM (2.5 ng ml^{-1}) (unpublished data), which is several orders of magnitude below the K_m obtained. At very low substrate concentration, when $[S] < K_m$, the ratio of the enzymatic rate of CYP3A4 to CYP2C19 is given by the ratio V_{max}/K_m (enzyme efficiency) of both enzymes. This ratio of enzyme efficiency of both enzymes is 6.5, indicating that the formation of the 6β-OH metabolite by CYP3A4 is ~6–7 times higher than the formation by the CYP2C19 enzyme even at very low substrate concentrations. Furthermore, CYP3A4 appears to be the most abundant P450 enzyme in human liver (Li *et al*. 1995). Based on these findings, it may be predicted that the CYP3A4 enzyme is likely to play a major role in the 6β-hydroxylation of Org 30659 *in vivo*.

In conclusion, in this study, the involvement of the CYP3A family in the 6β-hydroxylation of the synthetic steroidal hormones Org 4060 and Org 30659 has been demonstrated by means of three different *in vitro* approaches.

References

Aoyama, T., Yamano, S., Waxman, D. J., Lapenson, D. P., Meyer, U. A., Fischer, V., Tyndale, R., Inaba, T., Kalow, W., Gelboin, H. V. and Gonzalez, F. J., 1989, Cytochrome P450 hPCN3, a novel cytochrome P-450 IIIa gene product that is differentially expressed in adult human liver. *Journal of Biological Chemistry*, **264**, 10388–10395.

Baldwin, S. J., Bloomer, J. C., Smith, G. J., Ayrton, A. D., Clarke, S. E. and Chenery, R. J., 1995, Ketoconazole and sulphaphenazole as the respective selective inhibitors of P4503A and 2C9. *Xenobiotica*, **25**, 261–270.

Deckers, G. H., Schoonen, W. G. and Kloosterboer, H. J., 1992, Receptor binding and biological studies with norethisterone derivatives. In *Proceedings of the 74th Annual Meeting of the Endocrine Society* (Bethesda: Endocrine Society), p. 234.

Gentile, D. M., Verhoeven, C. H. J., Shimada, T. and Back, D. J., 1998, The role of CYP2C in the *in vitro* bioactivation of the contraceptive steroid desogestrel. *Journal of Pharmacology and Experimental Therapeutics*, **287**, 975–982.

Guengerich, F. P., 1996, *In vitro* techniques for studying drug metabolism. *Journal of Pharmacokinetics and Biopharmacology*, **24**, 521–533.

Hunt, C. M., Watkins, P. B., Saenger, P., Stave, G. M., Barlascini, N., Watlington, C. O., Wright, J. T. and Guzelian, P. S., 1992, Heterogeneity of CYP3A isoforms metabolizing erythomycin and cortisol. *Clinical Pharmacology and Therapeutics*, **51**, 18–23.

Li, A. P., Kaminski, D. L. and Rasmusssen, A, 1995, Substrates of human hepatic cytochrome P450 3A4. *Toxicology*, **104**, 1–8.

Lowry, O. H., Rosebrough, N. J., Farr, A. L. and Randall, R. J., 1951, Protein measurement with the Folin phenol reagent. *Journal of Biological Chemistry*, **193**, 265–275.

Omura, T. and Sato, R., 1964, The carbon monoxide-binding pigment of liver microsomes. I. Evidence for its hemoprotein nature. *Journal of Biological Chemistry*, **239**, 2370–2378.

Schmider, J., Greenblatt, D. J., Moltke, L. L. v, Karsov, D., Vena, R., Friedman, H. L. and Shader, R. I., 1997, Biotransformation of mestranol to ethinyl oestradiol *in vitro*: the role of Cytochrome P-450 2C9 and metabolic inhibitors. *Journal of Clinical Pharmacology*, **37**, 193–200.

Shimada, T., Yamazaki, H., Mimura, M., Inui, Y. and Guengerich, F. P., 1994, Interindividual variation in human liver cytochrome P450 enzymes involved in the oxidation of drugs, carcinogens and toxic chemicals: studies with liver microsomes of 30 Japanese and 30 Caucasians. *Journal of Pharmacology and Experimental Therapeutics*, **270**, 414–423.

Verhoeven, C. H. J., Krebbers, S. F. M., Wagenaars, G. N., Booy, C. J., Groothuis, G. M. M., Olinga, P. and Vos, R. M. E., 1998, The *in vitro* and *in vivo* metabolism of the progestagen Org 30659 in several species. *Drug Metabolism and Disposition*, **26**, 1102–1112.

Waxman, D. J., Attisano, C., Guengerich, F. P. and Lapenson, D. P., 1988, Human liver microsomal steroid metabolism: Identification of the major microsomal steroid hormone 6β-hydroxylase cytochrome P450 enzyme. *Archives of Biochemistry and Biophysics*, **263**, 424–436.

Wilkinson, G. R., 1996, Cytochrome P4503A (CYP3A) metabolism: prediction of the *in vivo* activity in humans. *Journal of Pharmacokinetics and Biopharmacology*, **24**, 475–490.

Wrighton, S. A., Ring, B. J., Watkins, P. B. and VandenBranden, M., 1989, Identification of a polymorphically expressed member of the human cytochrome P450III Family. *Molecular Pharmacology*, **36**, 97–105.

Wrighton, S. A., VandenBranden, M. and Ring, B. J., 1996, The human drug metabolizing cytochromes P450. *Journal of Pharmacokinetics and Biopharmacology*, **24**, 461–473.

Yamazaki, H. and Shimada, T., 1997, Progesterone and testosterone hydroxylation by cytochromes P450 2C19, 2C9 and 3A4 in human liver microsomes. *Archives of Biochemistry and Biophysics*, **346**, 161–169.

XENOBIOTICA, 2002, VOL. 32, NO. 2, 131–140

Taylor & Francis
healthsciences

Metabolism of 10,11-dihydro-10-hydroxyimino-5*H*-dibenz/*b*, *f*/azepine-5-carboxamide, a potent anti-epileptic drug

D. HAINZL, A. I. LOUREIRO, A. PARADA and P. SOARES-DA-SILVA*

Department of Research & Development, Laboratórios Bial, Á Av. da Siderurgia Nacional, Apartado 19, 4745-457 S. Mamede do Coronado, Portugal

Received 20 February 2001

1. 10,11-Dihydro-10-hydroxyimino-5*H*-dibenzo/*b*, *f*/azepine-5-carboxamide (BIA 2-024) is a new anti-epileptic drug similar to oxcarbazepine (OXC) in structure and efficacy, but with a preferred pharmacodynamic profile. It possesses high *in vitro* activity, but since oximes are usually metabolized to their corresponding ketones, it is important to know whether its *in vivo* potency is a result of acting as a prodrug of OXC or if it is acting on its own.

2. The drug was given orally to rats, mice and rabbits, the metabolites identified and pharmacokinetic profiles compared between those species. Furthermore, the pharmacokinetic profile of the main metabolite was established in the rat. The results were compared to *in vitro* metabolism studies with liver microsomes from different mammalian species and humans.

3. In an atypical reaction for oximes, BIA 2-024 in rats was rapidly ($t_{max} = 2$ h) metabolized to the non-active 10-nitro-derivative (BIA 2-254), whereas rabbits and particularly mice oxidized the oxime moiety to a much lower extent. BIA 2-254 was then transformed to OXC and subsequently to the 10-hydroxy derivative and other minor metabolites.

4. *In vitro* data showed a very similar cross-species behaviour as the *in vivo* results; human liver microsomes catalysed the oxidation of BIA 2-024 to the nitro metabolite only at a low rate, and the same was observed for the subsequent metabolism to OXC.

5. The results allow prediction of the *in vivo* metabolism of BIA 2-024 in humans, where this drug is most likely absorbed efficiently and excreted mainly as the parent compound with a relatively low hepatic clearance. With the exception of rat, BIA 2-024 does not act as a prodrug of OXC.

Introduction

Carbamazepine (5*H*-dibenz/*b*,*f*/azepine-5-carboxamide, CBZ) was introduced in the early 1960s and since then has been the most frequently prescribed first-line drug for the treatment of partial and generalized tonic-clonic epileptic seizures (Loiseau and Duché 1995). Although it is very effective in the majority of cases, ~30–40% of patients with chronic epilepsy are not well controlled or are largely unresponsive to treatment (Shorvon 1996), and between 33 and 50% suffer from unwanted side-effects of the medication (Pellock 1987). Potent induction of hepatic microsomal enzymes (Eichelbaum *et al.* 1985) that cause self-induction of its own metabolism (Bertilsson and Tomson 1986) together with slow and

* Author for correspondence; e-mail: psoares.silva@bial.com

Xenobiotica ISSN 0049–8254 print/ISSN 1366–5928 online © 2002 Taylor & Francis Ltd
http://www.tandf.co.uk/journals
DOI: 10.1080/00498250110087960

erratic absorption makes medication and especially polymedication with CBZ complicated (Faigle and Feldmann 1995).

It was not until the introduction of oxcarbazepine (OXC) in 1990 that another dibenz/*b*, *f*/azepine derivative with some improved anti-epileptic properties appeared. This derivative seems to be equally effective as CBZ in the treatment of seizures and is generally accepted as a better tolerated drug (Grant and Faulds 1992, Gram 1994). Differences in biotransformation were suggested as an explanation for differences in toxicity and adverse effects seen between these two drugs (Faigle and Menge 1990).

General and neuronal toxicity of CBZ has been ascribed in part to the *in vivo* formation of the epoxide as the active main metabolite, which is further converted by a microsomal epoxide hydrolase into a pharmacologically inactive racemic mixture of the *trans*-diol metabolite. In comparison, OXC is rapidly and extensively metabolized in man to a mixture of the (10*S*)-alcohol and its (10*R*)-enantiomer, both appearing in human plasma (Flesch *et al.* 1992) and urine (Schutz *et al.* 1986) in the proportion of ~4/1, respectively. Further oxidation to a *trans*-diol of undetermined absolute configuration and enantiomeric purity presents only a minor (3.6% of the dose) metabolic pathway in humans (Schutz *et al.* 1986).

BIA 2-024 differs from OXC by bearing an oxime moiety instead of a keto-group in the 10-position (Learmonth *et al.* 2001). This leads not only to different pharmacological properties (Ambrosio *et al.* 2001a, b, Learmonth *et al.* 2001), but also to a rather uncommon metabolic pathway. In the current study, the *in vivo* metabolism in rat has been studied and compared with that in mouse and rabbit. Furthermore, *in vitro* studies have been used to predict the metabolism in humans.

Materials and methods

Animals

Male Wistar rats (190–330 g) were obtained from the animal house of Interfauna Ibérica (Barcelona, Spain). Rats were kept four per cage, under controlled environmental conditions (12 h light/dark cycle and room temperature 22 ± 1 °C). Rat maintenance diet (cat. no. 9609, Harlan-Teklad, Oxon., UK) and tap water were allowed *ad libitum* and experiments were all carried out during daylight hours. Male CD1 mice (Charles River, 25–30 g) obtained from the animal house of the Instituto Gulbenkian de Ciência (Oeiras, Portugal) and female New Zealand rabbits (3.5–4 kg) from Criffa, S.A. (Barcelona, Spain) were kept under the same conditions as the rats. All animals were fasted the night before treatment.

Chemicals

BIA 2-024 [10,11-dihydro-10-hydroxyimino-5*H*-dibenzo/*b*, *f*/azepine-5-carboxamide], the Z-isomer of BIA 2-024, BIA 2-254 [10,11-dihydro-10-nitro-5*H*-dibenzo/*b*, *f*/azepine-5-carboxamide], BIA 2-256 [10-nitro-5*H*-dibenzo/*b*, *f*/azepine-5-carboxamide], (±)-10,11-dihydro-10-hydroxy-5*H*-dibenzo/*b*, *f*/azepine-5-carboxamide (10-OH-CBZ) and 10,11-dihydrocarbamazepine (used as internal standard) were all synthesized in the Laboratory of Chemistry, BIAL, with purities >99.5%. The synthesis and chemical characterization of these compounds (NMR, MS, UV and IR spectra) have been described by Learmonth *et al.* (2001). OXC was provided by Farchemia (Italy) and pentobarbital was obtained from Sigma Chemical Co. (St Louis, MO, USA) and dissolved in saline (3% w/v) for interperitoneal (i.p.) administrations. Ultra pure (Milli-Q) water was used in all steps and solvents were of HPLC grade.

Animal treatment

Rats were administered orally with the test compound suspended in 4 ml kg^{-1} carboxymethylcellulose (0.5% w/v) as carrier vehicle. BIA 2-024 was administered at 80 mg kg^{-1} and blood, liver and brain samples were taken at 0.25, 0.5, 1, 2, 4 and 24 h post-dose from four animals. BIA 2-254 was administered orally and i.p. at 30 mg kg^{-1} and samples were taken as for BIA 2-024. Mice were treated

with 50 and 200 mg kg^{-1} BIA 2-024 and blood, liver and brain samples collected after 0.5, 1 and 4 h ($n = 4$). Only blood samples were collected from treated rabbits (80 mg kg^{-1}) at 1 and 4 h after oral administration ($n = 3$).

Blood sample processing

Blood was taken from the vena cava of rats and mice and from the ear vein of rabbits, respectively, stabilized with one drop of heparin in the syringe and kept on ice until centrifuged at ~3000*g* for 15 min (4 °C). Of the supernatant plasma phase, 1 ml was added to 1 ml 0.1 M sodium phosphate buffer (pH 4.6) containing 2 μg ml^{-1} 10,11-dihydrocarbamazepine as internal standard.

These samples were loaded on LiChrolut RP-18 SPE columns (3 ml, 200 mg, Merck), which were conditioned with 2 ml 5% aqueous acetonitrile and 2 × 2 ml water. After eluting the sample, the columns were allowed to equilibrate for 2 min and then washed with 2 ml water and 2 ml 5% aqueous acetonitrile. After drying the sorbent under airflow for 5 min, the remaining was eluted with 2 × 250 μl acetone, the solvent evaporated at 35–40 °C (Centrivac, Heraeus Instruments) and the residue reconstituted in 1 ml HPLC mobile phase, i.e. water/acetonitrile (73:27).

Processing of liver and brain samples

Liver and brain were dissected after taking the blood and stored in 20-ml plastic scintillation vials at –100 °C until use. After thawing and weighting the organs, 0.1 M sodium phosphate buffer (pH 4.6) was added (10 ml to liver, 5 ml to brain) and the samples homogenized using a Heidolph DIAX 900 mixer. The homogenates were transferred to 10-ml centrifugation tubes, i.e. the complete homogenate in the case of brains (~7 ml) and 10 ml of the brain suspension. Centrifugation at 15000*g* for 20 min at 4 °C gave clear supernatants of which 1 ml (2 ml in the case of brain samples) was added to 1 ml 0.1 M sodium phosphate buffer (pH 4.6) containing 2 μg ml^{-1} internal standard (2 μg ml^{-1} 10,11-dihydrocarbamazepine) and then proceeded as described for plasma samples.

In vitro *assays*

BIA 2-024 and BIA 2-254 were incubated with microsome preparations from rat, mouse, rabbit, dog and human liver. Pooled human liver microsomes as well as preparations from seven individual donors with defined cytochrome P450 activities were obtained from Gentest (Woburn, MA, USA), dog microsomes were provided by Quintiles (UK) and rat, mouse and rabbit microsomes were prepared by differential centrifugation.

Protein concentration was determined by the method of Lowry *et al.* (1951) for the dog preparations and by the method of Bradford (1976) for rat, mouse and rabbit. Final concentration of the test compound was 100 μm in 50 mM potassium phosphate buffer (pH 7.4) and incubations were carried out at 37°C in the presence and absence of metabolic cofactors. The cofactors consisted of 25 mM glucose 6-phosphate, 2 mM $NADP^+$ and 6 units ml^{-1} glucose 6-phosphate dehydrogenase, Type VII from Bakers yeast, dissolved in 1 ml 2% $NaHCO_3$ (0.04 ml per 2 ml incubation when added). The total volume was 1.5 ml and the protein content of the final incubation solution was 1 mg ml^{-1} in all cases. After a pre-incubation of 3 min at 37 °C, reactions were initiated with the addition of the test compound. Samples of 100 μl were removed at various time points (1, 2, 5, 10, 30 min) and transferred into 2-ml plastic tubes containing the same volume of ice-cold acetonitrile to stop the reaction. After centrifugation for 5 min at 16000*g* (Biofuge, Heraeus Instruments), 20 μl of the supernatant was directly injected onto the HPLC system.

HPLC analysis

Sample analysis was performed using LC-(AP-ESI)MS (HP 1100 Series, Agilent Technologies) with positive-ion detection. At the same time, UV spectra were recorded with a diode array detector (monitoring wavelength was set to 210 nm). The separation was performed on a Superspher 100 RP-18 column (LiChroCART 125-4, 5 μm, Merck) with a 4 × 4 mm guard column of the same stationary phase. The mobile phase was an isocratic mixture of water/acetonitrile (73:27), freshly prepared for each analysis, filtered (0.22 μm, NL 16, Schleicher & Schuell) and degassed, with a flow of 1 ml min^{-1}. Injection volume was 20 μl.

Selected-ion monitoring (SIM) with the detection of the sodium adducts of each compound of interest (except for the internal standard) was used for quantification: namely, m/z 277 (10-OH-CBZ), 275 (OXC), 290 (BIA 2-024 and its Z-isomer), 306 (BIA 2-254), 304 (BIA 2-256) and 239 (internal standard). Whenever high sensitivity was required, a time-programmed detection of these ions was used: namely, group 1 = 10-OH-CBZ, group 2 = BIA 2-024 and OXC, group 3 = BIA 2-254, and group 4 = BIA 2-256 and ISTD. The limit of quantification for the latter method was 10 ng ml^{-1} for BIA 2-024 and ranged between 7 (10-OH-CBZ) and 15 ng ml^{-1} (OXC) for the other compounds. For maximal sensitivity, the fragmentor energy was set to 100 V and further settings were 3500 eV for the capillary

voltage, 350 °C (nebulizer gas temperature) and 40 psi (nebulizer pressure). Retention times ranged from 3 min for 10-OH-CBZ to 12 min for the internal standard.

Data analysis

Apparent elimination half-lives were estimated by using appropriate terminal data (at least three data points) of the concentration–time curve and assuming first-order kinetics. AUC were calculated by trapezoidal integration of the concentration–time curve using GraphPad Prism (v.1.03, GraphPad Software).

All pharmacokinetic parameters were determined by non-compartmental models. Peak concentrations (c_{max}) and the time to peak (t_{max}) were read directly from the observed data.

Results

Metabolism and elimination of BIA 2-024 in rat

Plasma. The metabolic profile and the elimination rate of BIA 2-024 in plasma over the 24 h post-treatment is shown in figure 1 for the oral dose 80 mg kg^{-1}. The parent compound was rapidly metabolized mainly to BIA 2-254 and to a minor extent to OXC. The formation of BIA 2-256 and of the hydrolysis product 10-OH-CBZ was less important. The AUC versus time curve between 0 and 24 h ($AUC_{0\text{-}24h}$) is shown in table 1. The apparent elimination half-life for BIA 2-024 is ~6–7 h.

Brain and liver. OXC crossed the blood–brain barrier to a higher degree than the other compounds and accumulated to levels even exceeding those in plasma (figure 1). In liver, however, the picture was similar to the one found in plasma with BIA 2-254 as the predominant metabolite. The $AUC_{0\text{-}24h}$(metabolite)/$AUC_{0\text{-}24h}$(BIA 2-024) ratios are all higher in liver when compared with plasma

Table 1. Area under the concentration–time curve ($AUC_{0\text{-}24h}$ for rat and rabbit, $AUC_{0\text{-}8h}$ for mouse).

Sample	10-OH-CBA	Z-isomer	BIA 2-024 (μg h ml^{-1})	BIA 2-254	OXC	BIA 2-256
Rat						
BIA 2-024 (80 mg kg^{-1}, oral)						
Plasma	4.7	2.0	26.0	30.0	17.8	2.8
Brain	0.5	0.1	13.3	16.1	25.5	0.2
Liver	64.1	8.1	50.6	93.4	28.5	2.4
BIA 2-254 (30 mg kg^{-1}, oral)						
Plasma	0.4	0.0	0.4	42.9	43.5	0.2
BIA 2-254 (30 mg kg^{-1}, i.p.)						
Plasma	0.9	0.0	0.6	166.9	78.5	0.5
Mouse						
BIA 2-024 (200 mg kg^{-1}, oral)						
Plasma	0.2	0.0	45.8	0.7	1.4	0.0
BIA 2-024 (50 mg kg^{-1}, oral)						
Plasma	0.4	0.0	16.3	0.03	0.2	0.0
Rabbit						
BIA 2-024 (80 mg kg^{-1}, oral)						
Plasma	23.8	1.7	28.9	1.2	11.2	0.0

$n = 4$ in all cases except for rabbit, where $n = 3$ (mean ± SEM).

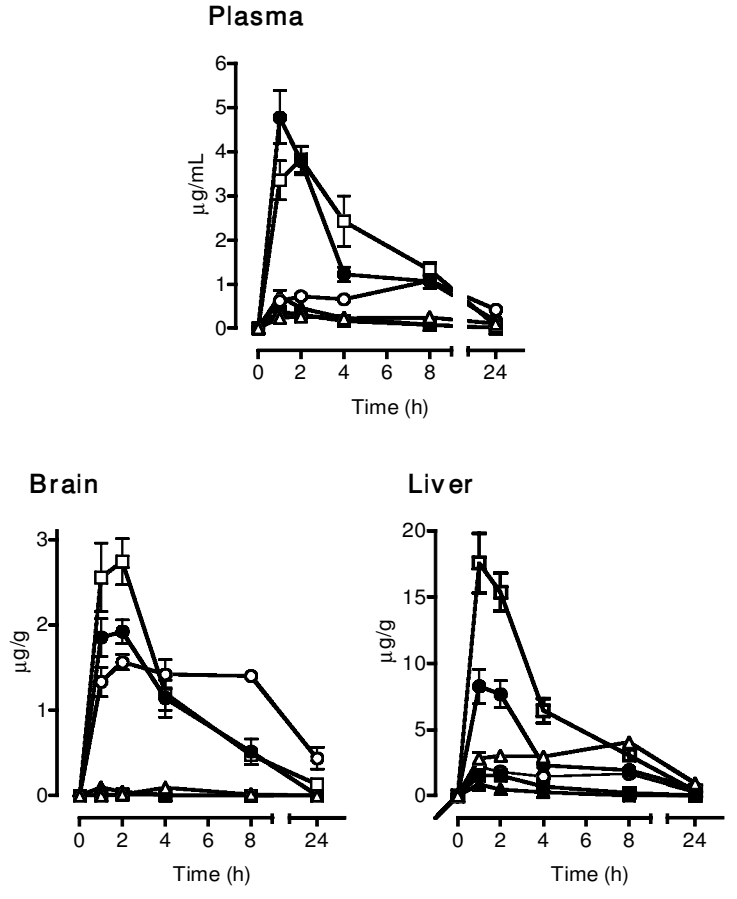


Figure 1. Rat plasma levels of metabolites after a single oral dose of 80 mg kg^{-1} BIA 2-024 ($n = 4$, mean ± SEM): BIA 2-024 (●), OXC (○), BIA 2-254 (□), 10-OH-CBZ (△), BIA 2-256 (▲) and the Z-isomer of BIA 2-024 (■).

levels, except for OXC and BIA 2-256. For 10-OH-CBZ, this ratio is ~7-fold higher than in plasma (table 1). For the parent drug BIA 2-024, the resulting c_{max} for plasma, liver and brain are 4.8, 8.2 and 1.9 µg g^{-1}, respectively.

Metabolism of BIA 2-024 in mice and rabbits

In mouse, BIA 2-024 was much more stable than in rat, and even 8 h after treatment the parent drug was with the predominant compound (85 and 91% after the 50 and 200 mg kg^{-1} doses, respectively) in plasma (figure 2A and table 1). Neither BIA 2-254 nor OXC was formed in significant amounts. In fact, the levels of both were below that of 10-OH-CBZ. The apparent half-life of BIA 2-024 in mouse is 13–14 h, which is twice as long as that in rat.

The metabolic profile of BIA 2-024 in rabbit was different to that found in the other species. The estimated half-life of BIA 2-024 is ~3 h the shortest of all three species and concerning the metabolites formed, the relative abundance's differed

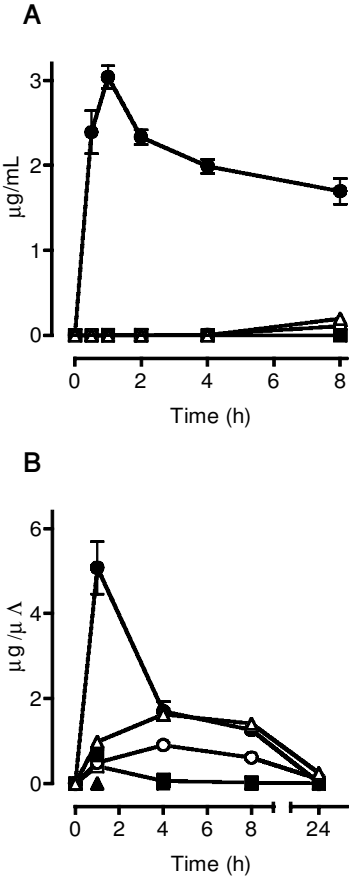


Figure 2. Plasma levels of BIA 2-024 and its metabolites in the mouse (A) and rabbit (B) after a single oral dose of 50 and 80 mg kg^{-1} BIA 2-024, respectively ($n = 4$ for mice, $n = 3$ for rabbits, mean ± SEM). BIA 2-024 (●), OXC (○), BIA 2-254 (□), 10-OH-CBZ (△), BIA 2-256 (▲) and the Z-isomer of BIA 2-024 (■).

greatly from the ones found in rat (figure 2B and table 1). The main metabolite in rabbit was 10-OH CBZ with an $AUC_{0\text{-}8h} = 23.8\,\mu g\,h\,ml^{-1}$, more than twice that for OXC. BIA 2-254 appeared here only as a minor metabolite, whereas the Z-isomer of the parent drug was formed in quantifiable amounts.

Metabolism of BIA 2-254 in rats

BIA 2-254 was metabolized in rat mainly to OXC and only to a very small extent to BIA 2-024 and 10-OH-CBZ (table 1), after both oral and i.p. administration of the parent compound. BIA 2-254 exhibited a higher c_{max} after i.p. administration and $AUC_{0\text{-}24h}$ was ~4-fold, indicating a relatively low absorption from the intestinal tract. Furthermore, oxidation to OXC was more efficient after oral treatment, reflected in the $AUC_{0\text{-}24h}$ ratios of parent compound to OXC, which are 2.13 and 0.99 after i.p. and oral administration, respectively.

In vitro *metabolism*

Human liver microsomes. Incubation of BIA 2-024 with pooled human liver microsomes resulted in a very slow rate of metabolism and the only detectable products after 1 h were BIA 2-254 (initial formation rate of 6 nmol mg protein^{-1} h^{-1}), and OXC (below limit of quantification). Under identical conditions, BIA 2-254 was transformed to OXC at a much higher rate (50 nmol mg^{-1} h^{-1}).

Other species. Reflecting the *in vivo* findings, incubation of BIA 2-024 with rat liver microsomes resulted in the formation of several metabolites, mainly BIA 2-254 and OXC, at much higher rates than with human liver microsomes (186 and 115 nmol mg^{-1} h^{-1}, respectively). The nitro metabolite BIA 2-254 was oxidized to OXC three times faster than BIA 2-024. BIA 2-256 underwent both oxidation to OXC and reduction to BIA 2-024 and its Z-isomer (ratio ~5:1). BIA 2-024 incubations with mouse and dog liver microsomes exhibited a very similar picture to the one obtained with human liver microsomes, i.e. no metabolism beyond the initial slow oxidation to BIA 2-254. The formation of 10-OH-CBZ could only be detected in the rabbit.

Discussion

The proposed metabolic pathway for BIA 2-024 in the rat is summarized in figure 3. The major metabolite is the inactive BIA 2-254 (Learmonth *et al.* 2001), an unusual oxidation of an oxime derivative to the corresponding nitro compound. Instead of being metabolized extensively, oximes rather seem to be quite stable products during the metabolism of many structurally different amines (e.g. Lin and Cashman 1997). Aliphatic oximes are usually oxidized to their corresponding ketones (Parmar and Burka 1991) and the same has been reported for α,β-unsaturated oximes (Li 1994). Therefore, in the case of BIA 2-024, OXC should be by far the major metabolite. But instead of C-10 (the carbon bearing the oxime moiety), it is the nitrogen that was oxidized by all investigated species, although an oxidation directly to OXC as a minor pathway can not be excluded.

Metabolism of the nitro derivative is only a minor pathway in mouse and is not apparent in the New Zealand rabbit. In the latter species, the BIA 2-254 formed is rapidly further oxidized to OXC and then extensively transformed to 10-OH-CBZ, which is consistent with the results reported after the administration of OXC itself (Feldmann *et al.* 1978, Hainzl *et al.* 1999, 2001). Mouse metabolized BIA 2-024 to an even lesser amount and both the major transformations in rat (BIA 2-024 to BIA 2-254) and rabbit (BIA 2-024 to 10-OH-CBZ via OXC) were not important in this species.

Rat brain contained BIA 2-024 and its metabolites in concentrations approximately half of those in plasma, with the exception of OXC, which accumulated in brain. According to the $AUC_{0\text{-}24h}$, OXC was the major compound in rat brain (1.9- and 1.6-times the values of BIA 2-024 and BIA 2-254, respectively). In liver, however, the picture was quite different from plasma and brain. Here, 10-OH-CBZ (only a minor product in plasma and not present in brain) was the major metabolite besides BIA 2-254. When considering the $AUC_{0\text{-}24h}$, the amount of 10-OH-CBZ relative to the total amount of all detected compounds was 25.9

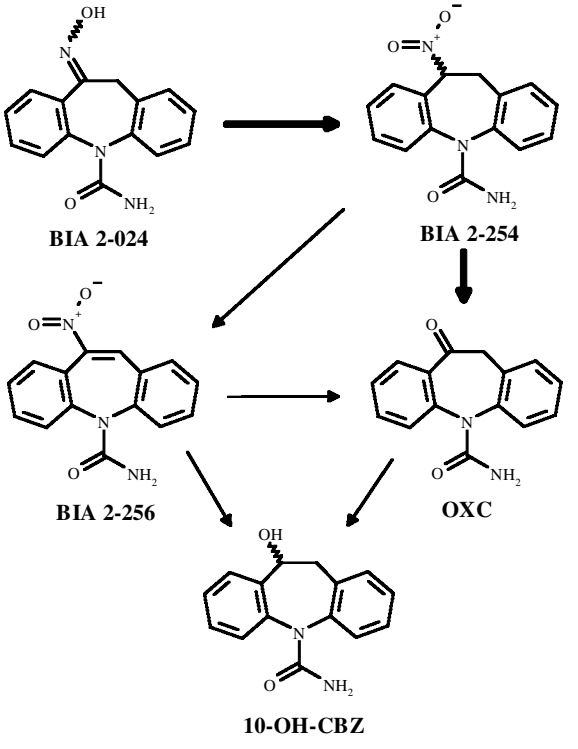


Figure 3. Proposed metabolism of BIA 2-024 in rat. The role of BIA 2-256 as possible intermediate has not yet been established.

compared with 5.6 (plasma) and 0.9% (brain). For BIA 2-254, these are 37.8 (liver), 36.1 (plasma) and 28.9% (brain) and, therefore, indicate a more equal distribution of this compound in rat.

To determine whether BIA 2-254 is an intermediate in the formation of OXC and 10-OH-CBZ (possibly via BIA 2-256) or whether it is formed independently, it was administered to rat both orally and i.p. Plasma analysis showed a very similar metabolic profile for both routes with OXC as the only significant metabolite, but the $AUC_{0\text{-}24h}$ for the parent compound differed greatly due to a low oral availability of the nitro compound. Since BIA 2-256 could not be detected, it is assumed that it is not an intermediate in the formation of OXC, at least with origin in BIA 2-254. The $AUC_{0\text{-}24h}$(OXC):$AUC_{0\text{-}24h}$(BIA 2-254) ratio after oral administration was more than twice that after i.p. treatment (1.01 versus 0.47), suggesting some additional oxidation already in the intestinal tract during absorption. After treating rats orally with BIA 2-024, this ratio was 0.59.

In vitro studies correlate with the *in vivo* findings in terms of metabolite formation and differences between species. Furthermore, the results show that hepatic metabolism in humans seems to be less extensive than in rat and most similar to that in mouse. BIA 2-024 was slowly metabolized to the nitro compound ($6\,nmol\,mg^{-1}\,h^{-1}$), which in turn is transformed to OXC.

These results allow prediction of the *in vivo* metabolism of BIA 2-024 in humans. It is most likely that the drug is absorbed efficiently and excreted mainly as the parent compound with a low clearance. It can also be expected that BIA 2-

024 effectively crosses the blood–brain barrier to ensure pharmacologically relevant concentrations in the brain. The inactive metabolite BIA 2-254 will be formed slowly and almost exclusively with very low levels of OXC as its main degradation product. Therefore, BIA 2-024 is expected to act on its own in humans and other species with a similar metabolic profile (e.g. mouse), whereas in rat the activity against seizures is most likely also due to the formation of OXC.

References

Ambrosio, A. F., Silva, A. P., Araujo, I., Malva, J. O., Soares-da-Silva, P., Carvalho, A. P. and Carvalho, C. M., 2001b, Neurotoxic/neuroprotective profile of carbamazepine, oxcarbazepine and two new putative antiepileptic drugs, BIA 2-093 and BIA 2-024. *European Journal of Pharmacology*, **406**, 191–201.

Ambrosio, A. F., Silva, A. P., Malva, J. O., Soares-da-Silva, P., Carvalho, A. P. and Carvalho, C. M., 2001a, Inhibition of glutamate release by BIA 2-093 and BIA 2-024, two novel derivatives of carbamazepine, due to blockade of sodium but not calcium channels. *Biochemical Pharmacology*, **61**, 1271–1275.

Bertilsson, L. and Tomson, T., 1986, Clinical pharmacokinetics and pharmacological effects of carbamazepine and carbamazepine-10,11-epoxide: an update. *Clinical Pharmacokinetics*, **11**, 177–198.

Bradford, M. M., 1976, A rapid sensitive method for the quantification of microgram quantities of protein utilizing the principle of protein–dye binding. *Analytical Biochemistry*, **72**, 248–254.

Eichelbaum, M., Tomson, T., Tybring, G. and Bertilsson, L., 1985, Carbamazepine metabolism in man: induction and pharmacogenetic aspects. *Clinical Pharmacokinetics*, **10**, 80–90.

Faigle, J. W. and Feldmann, K. F., 1995, Carbamazepine: chemistry and biotransformation. In R. H. Levy, R. H. Mattson and M. S. Meldrum (eds), *Antiepileptic Drugs* (New York: Raven), pp. 499–513.

Faigle, J. W. and Menge, G. P., 1990, Metabolic characteristics of oxcarbazepine and their clinical significance: comparison with carbamazepine. *Behavioural Neurology*, **3 (suppl. 1)**, 21–30.

Feldmann, K. F., Brechbühler, S., Faigle, J. W. and Imhof, P., 1978, Pharmacokinetics and metabolism of GP 47 680, a compound related to carbamazepine, in animals and rats. In H Meinardi and A. J. Rowan (eds), *Advances in Epileptology* (Amsterdam: Swets & Zeitlinger), pp. 290–294.

Flesch, G., Francotte, E., Hell, F. and Degen, P. H., 1992, Determination of the *R*-(–) and *S*-(+) enantiomers of the monohydroxylated metabolite of oxcarbazepine in human plasma by enantioselective high-performance liquid chromatography. *Journal of Chromatography*, **581**, 147–151.

Gram, L., 1994, Clinical experience with oxcarbazepine. *Epilepsia*, **35 (suppl. 3)**, 21–22.

Grant, S. M. and Faulds, D., 1992, Oxcarbazepine: a review of its pharmacology and therapeutic potential in epilepsy, trigeminal neuralgia and affective disorders. *Drugs*, **43**, 873–888.

Hainzl, D., Parada, A. and Soares-da-Silva, P., 1999, Enantioselective oxidation of 10,11-dihydro-10-hydroxy-dibenz/*b*,*f*/azepine-5-carboxamide, an active metabolite of oxcarbazepine, in the rat. *British Journal of Pharmacology*, **126**, 42.

Hainzl, D., Parada, A. and Soares-da-Silva, P., 2001, Metabolism of two new antiepileptic drugs and their principal metabolites *S*(+)- and *R*(–)-10,11-dihydro-10-hydroxy carbamazepine. *Epilepsy Research*, **44**, 197–206.

Learmonth, D. A., Benes, J., Parada, A., Hainzl, D., Beliaev, A., Bonifácio, M. J., Matias, P., Carrondo, M. A., Garrett, J. and Soares-da-Silva, P., 2001, Synthesis, anticonvulsant properties and pharmacokinetic profile of novel 10,11-dihydro-10-oxo-5*H*-dibenz/*b*,*f*/azepine-5-carboxamide derivatives. *European Journal of Medicinal Chemistry*, **36**, 227–236.

Li, Q., 1994, Aromatization and hydrolysis of norethisterone-3-oxime in rabbit. *Journal of Steroid Biochemistry and Molecular Biology*, **49**, 227–231.

Lin, J. and Cashman, J. R., 1997, Detoxication of tyramine by the flavin-containing monooxygenase: stereoselective formation of the *trans*-oxime. *Chemical Research in Toxicology*, **10**, 842–852.

Loiseau, P. and Duché, P., 1995, Carmazepine: clinical use. In R. H. Levy, R. H. Mattson and M. S. Meldrum (eds), *Antiepileptic Drugs* (New York: Raven), pp. 555–566.

Lowry, O. H., Rosebrough, N. J., Farr, A. L. and Randall, R. J., 1951, Protein measurement with the Folin phenol reagent. *Journal of Biological Chemistry*, **193**, 265–275.

Parmar, D. and Burka, L. T., 1991, Metabolism and disposition of cyclohexanone oxime in male F-344 rats. *Drug Metabolism and Disposition*, **19**, 1101–1107.

Pellock, J. M., 1987, Carbamazepine side effects in children and adults. *Epilepsia*, **28 (suppl. 3)**, 64–70.
Schutz, H., Feldmann, K. F., Faigle, J. W., Kriemler, H. P. and Winkler, T., 1986, The metabolism of ^{14}C-oxcarbazepine in man. *Xenobiotica*, **16**, 769–778.
Shorvon, S. D., 1996, The epidemiology and treatment of chronic and refractory epilepsy. *Epilepsia*, **37 (suppl. 2)**, 1–3.

XENOBIOTICA, 2002, VOL. 32, NO. 2, 141–151

Taylor & Francis
healthsciences

LC-MS-MS analysis of hydromorphone and hydromorphone metabolites with application to a pharmacokinetic study in the male Sprague–Dawley rat

M. ZHENG§, K. M. MCERLANE†* and M. C. ONG‡

† Faculty of Pharmaceutical Sciences, University of British Columbia, 2146 East Mall, Vancouver, BC, V6T 1Z3 Canada
‡ Chronic Pain Day Program, St Paul's Hospital, Vancouver, BC, V6Z 1Y6 Canada

Received 12 July 2001

1. A high performance liquid chromatography-mass spectrometry-mass spectrometry (LC-MS-MS) assay was developed for the analysis of hydromorphone and its metabolites, namely dihydromorphine, dihydroisomorphine, hydromorphone-3-glucuronide, dihydromorphine-3-glucuronide and dihydroisomorphine-3-glucuronide, in rat plasma samples.

2. Analytes were extracted by solid-phase extraction using C_2 cartridges. The extraction recoveries were $>76\%$ for all analytes. Both intra- and interassay variabilities were $\leq 12\%$. Using a plasma sample size of 100 µl, the limits of detection were 7.0 nmol l^{-1} (2.0 ng ml^{-1}) for hydromorphone, dihydromorphine and dihydroisomorphine and 11 nmol l^{-1} (5.0 ng ml^{-1}) for hydromorphone-3-glucuronide, dihydromorphine-3-glucuronide and dihydroisomorhine-3-glucuronide at a signal-to-noise ratio = 3.

3. The present assay was applied to a pharmacokinetic study in rat after intraperitoneal administration of hydromorphone.

Introduction

Hydromorphone is a strong analgesic used for the management of cancer pain (Bruera *et al.* 1996) and postoperative pain after thoracotomy (Gaeta *et al.* 1995), Caesarean section (Halpern *et al.* 1996), bone marrow transplant (Dunbar *et al.* 1995), coronary artery bypass surgery (Searle *et al.* 1994) and abdominal surgery (Rapp *et al.* 1996). Hydromorphone is about eight times as potent as morphine (Houde 1986), although recently a lower potency ratio of 5:1 has been reported (Coda *et al.* 1997, Lawlor *et al.* 1997). The higher water solubility of hydromorphone hydrochloride over morphine sulphate (five times more soluble) (Budavari *et al.* 1989) is a desirable feature for subcutaneous infusion that requires concentrated opioid solutions to be administered in small volumes (Bruera *et al.* 1993). Subcutaneous infusion of hydromorphone has been widely accepted for the management of chronic cancer pain because of the advantages of safety, simplicity, effectiveness and cost-efficiency (Bruera *et al.* 1996).

Radio-immunoassay (RIA) of hydromorphone (Honigberg and Stewart 1980, Lee *et al.* 1991) and modified RIA of morphine (Vallner *et al.* 1981) have been developed and applied to pharmacokinetic studies of hydromorphone (Vallner *et*

* Author for correspondence; e-mail: tuit@uinxg.ubc.ca
§ Present address: Metabolism and Pharmacokinetics, Pharmaceutical Research Institute, Bristol-Myers Squibb Co., Wallingford, CT 06492, USA.

Xenobiotica ISSN 0049–8254 print/ISSN 1366–5928 online © 2002 Taylor & Francis Ltd
http://www.tandf.co.uk/journals
DOI: 10.1080/00498250110091767

al. 1981, Ritschel *et al*. 1987, Parab *et al*. 1988, Babul *et al*. 1995, Hagen *et al*. 1995). Although the cross-reaction with hydromorphone-3-glucuronide may be minimized by incorporation of an extraction step (Lee *et al*. 1991), the interference by Phase I metabolites such as dihydromorphine (6α-hydroxy-hydromorphone) and dihydroisomorphine (6β-hydroxy-hydromorphone) still exists. More specific high-performance liquid chromatographic (HPLC) methods have been developed for the determination of hydromorphone in plasma (Wetzelsberger *et al*. 1986, Chang *et al*. 1988, Hill *et al*. 1991, Bouquillon *et al*. 1992) and dosage forms (Menon *et al*. 1989, Venkateshwaran and Stewart 1995) with either electrochemical (EC) detection (Wetzelsberger *et al*. 1986, Hill *et al*. 1991, Bouquillon *et al*. 1992) or ultraviolet (UV) detection (Chang *et al*. 1988, Menon *et al*. 1989, Venkateshwaran and Stewart 1995). The plasma samples were extracted by liquid–liquid extraction (Wetzelsberger *et al*. 1986, Chang *et al*. 1988) or by using solid-phase extraction cartridges (Hill *et al*. 1991, Bouquillon *et al*. 1992). The analysis of hydromorphone by gas chromatography-mass spectrometry (GC-MS) requires prior derivatization of hydromorphone with *N*-methyl-*bis*-trifluoroacetamide (MBTFA) (Saady *et al*. 1982) or propionic anhydride (Smith *et al*. 1995).

GC and GC-MS methods have also been developed for the determination of free and conjugated hydromorphone and its 6-hydroxy metabolites in urine samples from various species (Cone *et al*. 1977) and the analytes were derivatized with trifluoroacetic anhydride. The amount of conjugated analyte was estimated by subtracting its amount in untreated urine samples from its total amount in acid-hydrolysed urine samples.

Recently, conjugated hydromorphone and its 6-hydroxy metabolites were further identified as hydromorphone-3-glucuronide, dihydromorphine-3-glucuronide and dihydroisomorphine-3-glucuronide, respectively, by using a LC-MS-MS assay in a urine sample of a cancer patient (Zheng *et al*. 2001). The objectives of the current study were to improve the sensitivities of the LC-MS-MS assay reported in Zheng *et al*. (2001), to develop a solid-phase extraction method for the simultaneous determination of hydromorphone and both its Phase I and II metabolites in rat plasma and to apply this assay to a pharmacokinetic study in the male Sprague–Dawey rat after intraperitoneal (i.p.) administration of hydromorphone.

Material and methods

Materials

Hydromorphone hydrochloride (USP standard) was a generous gift from Knoll Pharma, Inc. (Mississauga, Ont., Canada). Dihydromorphine hydrochloride, dihydroisomorphine hydrochloride, hydromorphone-3-glucuronide, dihydromorphine-3-glucuronide and dihydroisomorphine-3-glucuronide were synthesized as described in Zheng *et al*. (2001) and were considered in-house standards. Nalorphine hydrochloride was obtained from the Health Protection Branch of Canada (Ottawa, Ont., Canada). Formic acid was obtained from BDH, Inc. (Toronto, Ont., Canada). Ammonium bicarbonate and ammonium hydroxide (30%) were obtained from Fisher (Fair Lawn, NJ, USA). All solvents were of HPLC grade and all chemicals were of reagent grade except where noted.

Stock solutions

A stock solution containing hydromorphone, dihydromorphine, dihydroisomorphine, hydromorphone-3-glucuronide, dihydromorphine-3-glucuronide and dihydroisomorphine-3-glucuronide was prepared in water at $100\,\mu g\,ml^{-1}$ (base or anhydrous equivalent) for each of the compounds. This

stock solution was further diluted with water to give working stock solutions at 50, 1000 and 10 000 ng ml^{-1}. The nalorphine internal solution was prepared by dissolving 457 μg nalorphine hydrochloride in 100 ml water (15 μmol l^{-1}).

Ammonium bicarbonate buffer (0.01 M, pH 9.3) was freshly prepared by dissolving 0.4 g ammonium bicarbonate in 470 ml water, adjusting pH to 9.3 with ammonium hydroxide and diluting with water to 500 ml.

LC-MS-MS conditions

The LC system consisted of a HP series II 1090 Liquid Chromatograph (Hewlett Packard, Avondale, PA, USA), a Zorbax SB-phenyl column (5 μm, 25 cm × 4.6 mm) (Rockland Technologies, Inc., Newport, DE, USA), a guard column equipped with a Brownlee phenyl cartridge (7 μm, 15 × 3.2 mm) (Santa Clara, CA, USA). The mobile phase was formic acid (0.1% v/v) in methanol:water (18:82 v/v), which was delivered at a flow rate of 0.7 ml min^{-1} with 10% of the effluent introduced into the MS-MS via a splitter.

The MS-MS system was a VG Quatro triple quadrupole mass spectrometer equipped with an electrospray interface (Fisons, Altrincham, UK). The electrospray source was operated with a capillary voltage of 3.4 kV, a HV lens of 0.50 kV, a cone voltage of 40 V and a source temperature of 130 °C. Nitrogen was used as both nebulizer gas and drying gas at flow rates of 15 and 250 l h^{-1}, respectively. The MS-MS analyses was performed in the mulitple reaction monitoring (MRM) mode. The first MS (MS1) was static at preselected protonated parent ion masses. The selected parent ions were introduced into the collision cell and the fragmentation occurred at a collision energy of −80 eV. Argon was used as a collision gas at a pressure $\sim 3 \times 10^{-4}$ mbar. The second MS (MS2) was static at predetermined daughter ion masses produced from the fragmentation in the collision cell. The low mass (LM) and high mass (HM) resolution of both MS were set at 7.0. A dwell time of 0.3 s was used for scanning.

The operation of the LC/MS/MS system was controlled by computer software MassLynx 2.1 (Fisons PLC).

Procedures of solid-phase extraction

The samples were extracted according to the procedures developed for morphine and morphine glucuronides (Pacifici *et al.* 1995) with modification. To 100 μl plasma in a 0.6 ml polypropylene microcentrifuge tube (Fisher, Pittsburgh, PA, USA) was added 10 μl nalorphine internal standard solution and 0.1 ml ammonium bicarbonate buffer. After mixing, the mixture was loaded onto a C_2 solid-phase extraction cartridge (3 ml/200 mg, Bond Elut, Varian, Harbor City, CA, USA) preconditioned with 3 ml methanol, 3 ml water and 2 ml ammonium bicarbonate buffer. The C_2 cartridge was connected to a Baker spe-10 vacuum manifold (J. T. Baker, Inc., Toronto, Canada), which allows the processing of ten samples at the same time. The cartridge was vacuum-dried for 30 s, washed with 1 ml ammonium bicarbonate buffer and again vacuum-dried for 2 min. The analytes were eluted with 2 ml methanol which was evaporated to dryness under a gentle stream of nitrogen. The residues were reconstituted in 100 μl of the HPLC mobile phase by vortex-mixing at high speed for 1 min followed by centrifugation at 2800 g for 5 min. An aliquot of 10 μl supernatant was injected for LC-MS-MS analyses.

Calibration curves

The calibration curves were determined in a series of blank 100 μl plasma samples to which were added 10 μl nalorphine internal standard solution 0, 0.20, 0.50, 1.0, 2.0, 8.0, 30, 60, 100 and 200 ng of each of the standards. The samples were extracted as described above. The calibration curves were constructed by plotting the peak area ratios of each analyte to the internal standard against the concentrations of that analyte in the samples.

Assay precision

The intra-assay variabilities for each of the standards were determined by the analyses of two sets of six 100-μl plasma samples to which 2.0 and 30 ng of each of the standards were added. After the addition of 10 μl internal standard solution, the samples were extracted and analysed, as described above, on the same day.

The interassay variabilities for each of the standards were determined by the analyses of two sets of four 100- μl plasma samples to which 2.0 and 30 ng of each of the standards were added. One sample at each concentration was extracted and analysed every day over a consecutive 4-day period.

Extraction recoveries

The extraction recoveries for each of the standards were determined by the analyses of two sets of six 100-μl plasma samples to which 2.0 and 30 ng of each of the standards were added, respectively. The samples were extracted and analysed as described above, except that the internal standard was added

during the final reconstitution. Standard solutions at the same concentrations along with the internal standard were prepared in parallel at the same time. The extraction recoveries were determined by comparison of the peak area ratios of each of the standards to the internal standard from extracted samples with the peak area ratios from the unextracted standard solutions.

Pharmacokinetic study in rat

The experimental protocol was approved by the Committee on Animal Care of the University of British Columbia (UBC). Male Sprague–Dawley rats were obtained from the Animal Care Center of UBC 6 days before the experiment. Rats were provided standard laboratory food (Laboratory Rodent Diet, PMI Feeds, Inc., Richmond, IN, USA) and water *ad libitum*. The animal housing room was maintained at 24 °C, with a 12-h light/dark cycle (lights on at 06:00 hours). The rats weighed 299 ± 2 g at the time of the experiment. Six animals were used for each of the compounds tested.

Hydromorphone hydrochloride was dissolved in 0.9% sodium chloride solution at 7 μmol ml^{-1} (2 mg ml^{-1}, base equivalent) and administered i.p. at a dose of 7 μmol kg^{-1} to rats. Blood samples of ~200 μl were obtained by transection of the tail, ~1–2 mm from the tip, at 5, 10, 15, 20, 30, 40, 80, 120 and 240 min after administration. Plasma was separated, collected in 0.6-ml polypropylene microcentrifuge tubes and kept at −20 °C until analyses.

Calculation of pharmacokinetic parameters

The area under the curve (AUC) was calculated by using the trapezoidal method (Gibaldi and Perrier 1982: 445). The maximum plasma concentrations (C_{max}) and the time for achieving C_{max} (T_{max}) were observed values. The elimination rate constant of hydromorphone (K_e) was calculated from the equation: $K_e = -2.3a$, where a is the slope deduced by linear regression analysis of the last four data points using SigmaPlot (Jandel Scientific, San Rafael, CA, USA). The apparent elimination half-life of hydromorphone ($t_{1/2}$) was thus calculated from: $t_{1/2} = 0.693/K_e$. Similarly, the slope of the elimination phase for hydromorphone-3-glucuronide was calculated by linear regression analysis of the last three data points.

Statistical analyses

Statistical analyses were performed by the two-tailed t-test at the significance level of $p = 0.05$ using a statistical software package prepared by the Departments of Botany and Zoology, Faculty of Science, the University of British Columbia.

Results and discussion

To avoid the contamination of the MS components by non-volatile buffers in most MS interfaces, volatile organic salts such as ammonium acetate, ammonium formate, trifluorocetic acid (TFA) and formic acid are used in the preparation of mobile phase for LC separation. Compared with our results in Zheng *et al.* (2001), formic acid used at 0.1% in the present mobile phase improved assay sensitivities by 19–46 fold, depending on the analyte (table 1). In addition, the current mobile phase was operated under the simpler isocratic mode which, in combination with a Zorbax phenyl column, provided good separation among the analytes and the internal standard nalorphine (figure 1B).

The solid-phase extraction using C_2 cartridges gave >80% of the extraction recoveries for each of the analytes (table 2). The recoveries were not significantly different at the two different concentrations evaluated for each analyte ($p > 0.05$). The extraction recoveries were also compared between two different sizes of cartridges. The cartridges containing more C_2 sorbent (200 mg) offered higher recoveries for the three glucuronides ($p < 0.05$; table 2). Both intra- and interassay variabilities were ≤12% (table 3).

The calibration curves were linear over the concentration ranges determined (table 4). The limits of detection were 7.0 nmol l^{-1} (2.0 ng ml^{-1}) for hydromorphone, dihydromorphine and dihydroisomorphine and 11 nmol l^{-1} (5.0 ng ml^{-1}) for hydromorphone-3-glucuronide, dihydromorphine-3-glucuronide and dihy-

Table 1. Peak areas of hydromorphone and its metabolites as determined by using TFA and formic acid as mobile phase modifiers.

Compound	Peak areas[a]		
	0.05% (v/v) TFA (Zheng *et al.* 2001)	0.1% (v/v) Formic acid (present study)	Peak areas ratios of formic acid/TFA
Dihydromorphine	5.8×10^4	1.3×10^6	22
Hydromorphone	2.5×10^4	8.0×10^5	32
Dihydroisomorphine	6.0×10^4	1.1×10^6	19
Dihydromorphine-3-gucuronide	1.9×10^4	6.6×10^5	34
Hydromorphone-3-glucuronide	1.4×10^4	6.4×10^5	46
Dihydroisomorphine-3-glucuronide	2.1×10^4	6.2×10^5	30

[a] Peak areas were determined at $5.0\,\mu g\,ml^{-1}$ for each of the compounds in the present study or corrected to $5.0\,\mu g\,ml^{-1}$ for some of the compounds as reported by Zheng *et al.* (2001).

droisomorphine-3-glucuronide (signal-to-noise ratio = 3), using a sample size of 100 µl.

The present LC-MS-MS assay was applied to a pharmacokinetic study in the male Sprague–Dawley rat after i.p. administration of hydromorphone at a dose of $7\,\mu mol\,kg^{-1}$ ($2\,mg\,kg^{-1}$). Figure 1C shows a mass chromatogram from a rat plasma sample collected at 80 min after the administration. Hydromorphone-3-glucuronide, dihydroisomorphine-3-glucuronide and dihydromorphine-3-glucuronide were detected as metabolites of hydromorphone. The peak appearing at 6.11 min in the 286 > 185 ion transition was due to the ionization of hydromorphone-3-glucuronide in MS1. The difference between the ion monitoring channels for the analysis of hydromorphone-3-glucuronide and dihydromorphine-3-glucuronide and dihydroisomorphine-3-glucuronide was only two mass units apart (462 > 286 and 464 > 288), thus there was cross-detection between the two channels, which was demonstrated by a peak present at 6.11 min in 464 > 288. While this was not evident when all analytes were present at similar concentrations, as seen with the plasma with the standards added (figure 1B) it was more problematic when the concentration of hydromorphone-3-glucuronide in the sample was >40-fold higher than the concentration of dihydroisomorphone-3-glucuronide (figure 1C). However, the near baseline separation by HPLC allowed a reliable measurement of dihydroisomormorphone-3-glucuronide concentration.

Representative plasma concentration profiles of hydromorphone and its metabolites in a rat following i.p. administration are shown in figure 2. Hydromorphone was not detected after 120 min in any of the rats. T_{max} was observed at 9.2 min (table 5) and the apparent elimination half-life was calculated as 34 min. Hydromorphone-3-glucurnide was detected as the predominant metabolite of hydromorphone. $AUC_{0\text{-}120\,min}$ for hydromorphone was 16% of the $AUC_{0\text{-}240\,min}$ for hydromorphone-3-glucuronide. The slopes of the elimination phases for hydromorphone and hydromorphone-3-glucuronide were not significantly different ($p > 0.05$) (table 5), which suggests that the formation of hydromorphone-3-glucuronide is the rate-limiting step for the hydromorphone-3-glucuronide following the administration of hydromorphone. Similar results have been shown for the elimination of morphine-3-glucuronide after the administration of morphine (Gibaldi and Perrier, 1982b: 18, Roland and Topaz 1995, Zheng *et al.* 1998). Thus, the true elimination rate constant of hydromorphone-3-glucuronide cannot

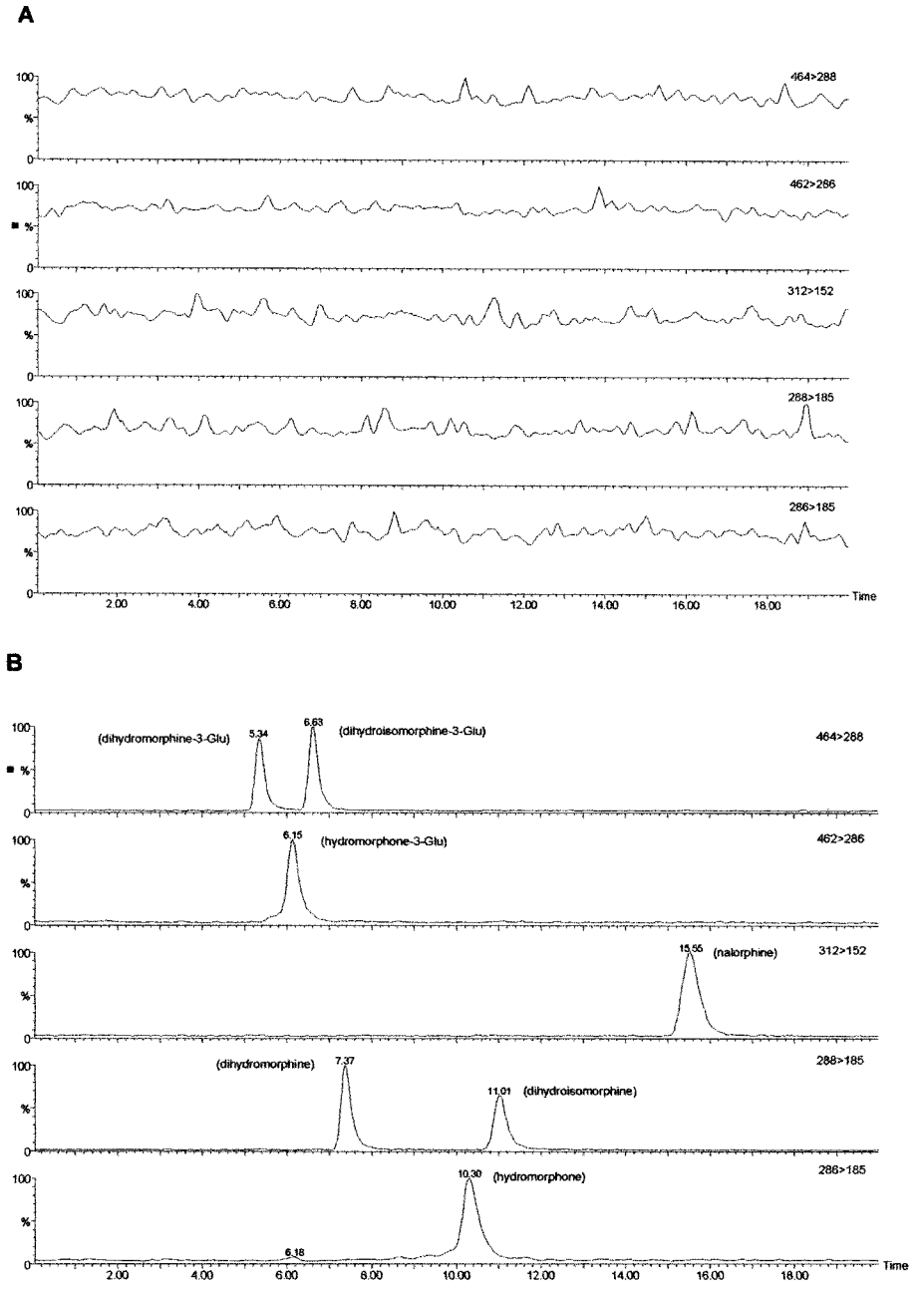


Figure 1. LC-MS-MS chromatograms of (A) blank rat plasma sample; (B) control rat plasma containing added standards of dihydromorphine-3-glucuronide and dihydroisomorphine-3-glucuronide, hydromorphone-3-glucuronide, nalorphine internal standard, dihydromorphine and dihydroisomorphine, and hydromorphone. The right corner of each chromatogram, e.g. 464 > 288, lists the parent-to-daughter ion transition that was used for MRM analysis. The number on the top of each peak is the retention time for that compound. The *y*-axis indicates relative intensity. Glu, glucuronide.

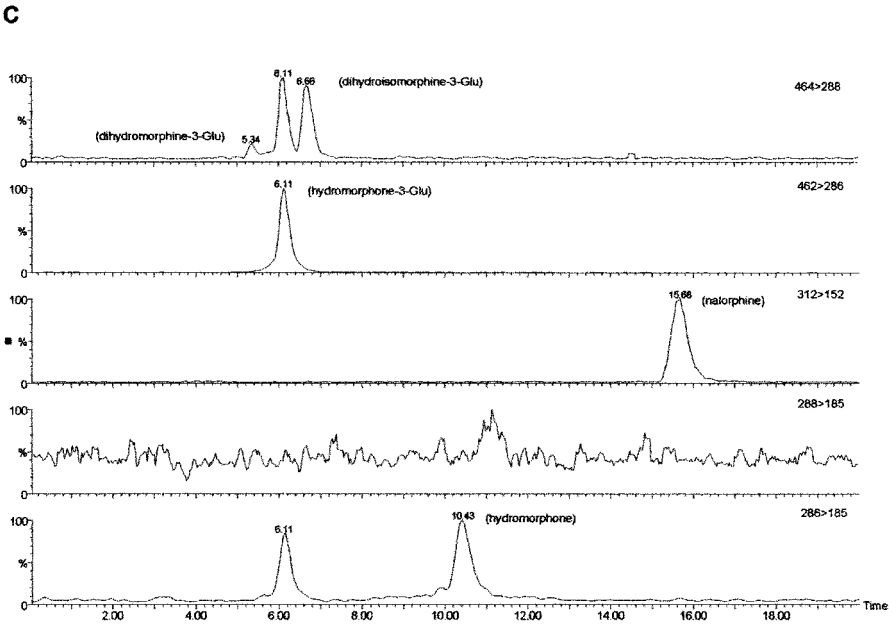


Figure 1. *(continued)* LC-MS-MS chromatograms of (C) plasma sample collected from a rat at 80 min following i.p. administration of hydromorphone hydrochloride at a dose of 7.0 μmole kg^{-1} (2.0 mg kg^{-1}). The peak at 6.11 min in 286 > 185 in (C) was due to the ionization of hydromorphone-3-glucuronide in MS1. The right corner of each chromatogram, e.g. 464 > 288, lists the parent-to-daughter ion transition that was used for MRM analysis. The number on the top of each peak is the retention time for that compound. The *y*-axis indicates relative intensity. Glu, glucuronide.

Table 2. Solid-phase extraction recoveries of hydromorphone and its metabolites from rat plasma samples.

Compound	Concentration (nmol l^{-1})	Recovery (%)[a] (C_2 200 mg)	Recovery (%)[a] (C_2 100 mg)
Hydromorphone	70	82 ± 3.5	
	1053	80 ± 2.3	80 ± 2.0
Dihydromorphine	70	84 ± 4.8	
	1045	80 ± 2.0	77 ± 1.8
Dihydroisomorphine	70	88 ± 4.4	
	1045	82 ± 1.9	78 ± 1.9
Hydromorphone-3-glucuronide	43	84 ± 2.4	
	651	82 ± 1.5[b]	70 ± 1.2[b]
Dihydromorphine-3-glucuronide	43	78 ± 5.1	
	648	80 ± 1.8[b]	68 ± 1.5[b]
Dihydroisomorphine-3-glucuronide	43	76 ± 2.7	
	648	82 ± 2.2[b]	73 ± 1.6[b]

[a] Results are mean ± SEM ($n = 6$).
[b] Recoveries are significantly different between the two types of cartridges ($p < 0.05$).

be determined using the slope of the elimination for hydromorphone-3-glucuronide (table 5), which reflects the elimination rate constant of hydromorphone. For these reasons, the elimination rate constant and the apparent elimination half-life of hydromorphone-3-glucuronide were not calculated. The elimination rate con-

Table 3. Intra- and interassay variabilities of hydromorphone and its metabolites in rat plasma samples.

Compound	Concentration ($nmol\,l^{-1}$)	Intra-assay variability (%)[a]	Interassay variability (%)[b]
Hydromorphone	70	11	6.6
	1053	3.8	12
Dihydromorphine	70	5.9	5.6
	1045	3.4	12
Dihydroisomorphine	70	7.7	4.8
	1045	4.7	12
Hydromorphone-3-glucuronide	43	5.8	6.8
	651	6.7	5.4
Dihydromorphine-3-glucuronide	43	9.0	5.9
	648	4.7	7.1
Dihydroisomorphine-3-glucuronide	43	7.3	12
	648	5.2	5.3

[a] Six samples were analysed at each concentration.
[b] Four samples were analysed at each concentration for each analyte over 4 days.

Table 4. Calibration curves of hydromorphone and its metabolites in the LC-MS-MS assay.

Compound	Concentration range ($nmol\,l^{-1}$)	Calibration curve
Hydromorphone	7.0–3509	$y = 2.4 \times 10^{-3}x + 0.022, r^2 = 0.9991$
Dihydromorphine	7.0–2090	$y = 4.9 \times 10^{-3}x + 0.023, r^2 = 0.9999$
Dihydroisomorphine	7.0–2090	$y = 4.0 \times 10^{-3}x + 0.036, r^2 = 0.9997$
Hydromorphone-3-glucuronide	11–4338	$y = 3.1 \times 10^{-3}x + 0.010, r^2 = 0.9999$
Dihydromorphine-3-glucuronide	11–2160	$y = 3.2 \times 10^{-3}x - 0.019, r^2 = 0.9998$
Dihydroisomorphine-3-glucuronide	11–2160	$y = 3.1 \times 10^{-3}x + 0.029, r^2 = 0.9996$

stant of hydromorphone-3-glucuronide should be determined following direct administration of hydromorphone-3-glucuronide.

Dihydroisomorphine-3-glucuronide was detected as a minor metabolite of hydromorphone, whose $AUC_{0\text{-}120\,min}$ was only 8.6% of the $AUC_{0\text{-}120\,min}$ for hydromorphone (table 5) and 1.4% of the $AUC_{0\text{-}240\,min}$ for hydromorphone-3-glucuronide. Another minor metabolite, dihydromorphine-3-glucuronide (figure 1C), was only detected at limited sampling points and at the concentrations close to the limit of detection. Other minor metabolites detected included dihydromorphine and dihydroisomorphine (data not shown). These minor metabolites were only detected in half of the rats at limited early time points and at concentrations close to the limits of detection of the assay.

In summary, a highly selective and sensitive LC-MS-MS assay was developed for the analyses of hydromorphone and its metabolites in rat plasma samples. This assay was successfully applied to a pharmacokinetic study of hydromorphone in rat which demonstrated that hydromorphone-3-glucuronide is the major metabolite of hydromorphone.

Acknowledgements

The authors thank Mr Roland Burton for technical assistance in the LC-MS-MS experiments and the financial support of Knoll Pharma, Inc.

Table 5. Pharmacokinetic parameters of hydromorphone and its metabolites in rat plasma after i.p. administration of hydromorphone at 7 μmol kg^{-1} (2 mg kg^{-1}).[a]

Compound	AUC[b] (nmol l^{-1} min)	C_{max} (nmol)	T_{max} (min)	$t_{1/2}$ (min)	K_e (min^{-1})	Slope[c]
Hydromorphone	$3.7 \times 10^4 \pm 9717$	621 ± 161	9.2 ± 2.4	34 ± 4.1	$0.022 \pm 2.4 \times 10^{-3}$	$9.5 \times 10^{-3} \pm 1.0 \times 10^{-3}$
Hydromorphone-3-glucuronide	$2.3 \times 10^5 \pm 1.3 \times 10^4$	2463 ± 188	38 ± 1.7	n.d.[d]	n.d.	$7.7 \times 10^{-3} \pm 6.0 \times 10^{-4}$
Dihydroisomorphine-3-glucuronide	$3.2 \times 10^3 \pm 491$	43 ± 7.5	47 ± 6.7	n.d.	n.d.	n.d.

[a] Results are the mean ± SE from six rats for each compound tested.

[b] AUC were calculated for 0–120, 0–240 and 0–120 min for hydromorphone, hydromorphone-3-glucuronide and dihydroisomorphine-3-glucuronide, respectively.

[c] Slopes were calculated by linear regression analyses of the last four data points for hydromorphone and the last three data points for hydromorphone-3-glucuronide.

[d] n.d. Not determined.

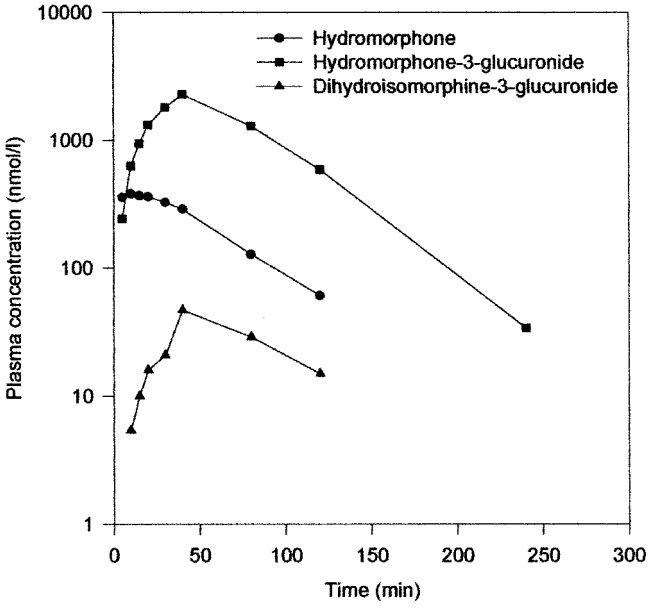


Figure 2. Representtive plasma concentraton–time curves of hydromorphone-3-glucuronide, hydromorphone and dihydroisomorphine-3-glucuronide in a rat following i.p. administration of hydromorphone hydrochloride at a dose of 7.0 μmole kg^{-1} (2.0 mg kg^{-1}).

References

Babul, N., Darke, A. C. and Hagen, N., 1995, Hydromorphone metabolite accumulation in renal failure. *Journal of Pain Symptoms and Management*, **10**, 184–186.

Bouquillon, A. I., Freeman, D. and Moulin, D. E., 1992, Simultaneous solid-phase extraction and chromatographic analysis of morphine and hydromorphone in plasma by high-performance liquid chromatography with electrochemical detection. *Journal of Chromatography*, **577**, 354–357.

Bruera, E., Maceachern, T., Macmillan, K., Miller, M. J. and Hanson, J., 1993, Local tolerance to subcutaneous infusions of high concentrations of hydromorphone: a prospective study. *Journal of Pain Symptoms and Management*, **8**, 201–204.

Bruera, E., Sloan, P., Mount, B., Scott, J. and Suarez-Almazor, M., 1996, A randomized, double-blind, double-dummy, crossover trial comparing the safety and efficacy of oral sustained-release hydromorphone with immediate-release hydromorphone in patient with cancer pain. *Journal of Clinical Oncology*, **14**, 1713–1717.

Budavari, S., O'Neil, M. J., Smith, A., Heckelman, P. E. and Kinneary, J. F. (eds), 1996, *The Merck Index*, 12th edn (Whitehouse Station: Merck), pp. 824, 1074.

Chang, S. F., Moore, L. and Chien, Y. W., 1988, Pharmacokinetics and bioavailability of hydromorphone: effect of various routes of administration. *Pharmaceutical Research*, **5**, 718–721.

Coda, B., Tanaka, A., Jacobson, R. C., Donaldson, G. and Chapman, C. R., 1997, Comparative efficacy of patient-controlled administration of morphine, hydromorphone, or sufentanil for the treatment of oral mucositis pain following bone marrow transplantation. *Pain*, **72**, 333–346.

Cone, E. J., Phelps, B. A. and Gorodetzky, C. W., 1977, Urinary extraction of hydromorphone and metabolites in humans, rats, dogs, guinea pigs and rabbits. *Journal of Pharmaceutical Sciences*, **66**, 1709–1713.

Dunbar, P. J., Buckley, P., Gavrin, J. R., Sanders, J. E. and Chapman, C. R., 1995, Use of patient-controlled analgesia for pain control for children receiving bone marrow transplant. *Journal of Pain Symptoms and Management*, **10**, 604–611.

Gaeta, R. R., Macario, A., Brodsky, J. B., Brock-Utne, J. G. and Mark, J. B. D., 1995, Pain outcomes after thoracotomy lumber epidural hydromorphone versus intrapleural bupivacaine. *Journal of Cardiothoracic and Vascular Anesthesia*, **9**, 534–537.

Gibaldi, M. and Perrier, D., 1982, *Pharmacokinetics* (New York: Marcel Dekker).

Hagen, N., Thirlwell, M. P., Dhaliwal, H. S., Babul, N., Harsanyi, Z. and Darke, A. C., 1995, Steady-state pharmacokinetics of hydromorphone and hydromorphone-3-glucuronide in cancer patients after immediate and controlled-release hydromorphone. *Journal of Clinical Pharmacology*, **35**, 37–44.

Halpern, S. H., Arellano, R., Preston, R., Carstoniu, J., O'Leary, G., Roger, S. and Sandler, A., 1996, Epidural morphine vs hydromorphone in post-caesarean section patients. *Canadian Journal of Anaesthesia*, **43**, 595–598.

Hill, H. F., Coda, B. A., Tanaka, A. and Schaffer, R., 1991, Multiple-dose evaluation of intravenous hydromorphone pharmacokinetics in normal human subjects. *Anesthesia and Analgesia*, **72**, 330–336.

Honigberg, I. L. and Stewart, J. T., 1980, Radioummunoassay of hydromorphone and hydrocodone in human plasma. *Journal of Pharmaceutical Sciences*, **69**, 1171–1173.

Houde, R. W., 1986, Clinical analgesic studies of hydromorphone. *Advances in Pain Research Therapy*, **8**, 129–135.

Lawlor, P., Turner, K., Hanson, J. and Bruera, E., 1997, Dose ratio between morphine and hydromorphone in patients with cancer pain: a retrospective study. *Pain*, **72**, 79–85.

Lee, J. W., Pedersen, J. E., Moravetz, T. L., Dzerk, A. M., Mundt, A. D. and Shepard, K. V., 1991, Sensitive and specific radioimmunoassays for opiates using commercially available materials. I: Methods for the determinations of morphine and hydromorphone. *Journal of Pharmaceutical Science*, **80**, 284–288.

Menon, S. K., Burchett, M. K. and Joseph, J. C., 1989, High performance liquid chromatography assay of hydromorphone hydrochloride injection. *Journal of Liquid Chromatography*, **12**, 657–671.

Pacifici, R., Pichini, S., Altieri, I., Caronna, A., Passa, A. R. and Zuccaro, P., 1995, High-performance liquid chromatographic-electrospray mass spectrometric determination of morphine and its 3- and 6-glucuronides: application to pharmacokinetic studies. *Journal of Chromatography B*, **664**, 329–334.

Parab, P. V., Ritschel, W. A., Coyle, D. E., Gregg, R. V. and Denson, D. D., 1988, Pharmacokinetics of hydromorphone after intravenous, peroral and rectal administraton to human subjects. *Biopharmaceutics and Drug Disposition*, **9**, 187–199.

Rapp, S. E., Egan, K. J., Ross, B. K., Wild, L. M., Terman, G. W. and Ching, J. M., 1996, A multidimensional comparison of morphine and hydromorphone patient-controlled analgesia. *Anesthesia and Analgesia*, **82**, 1043–1048.

Ritschel, W. A., Parab, P. V., Denson, D. D., Coyle, D. E. and Gregg, R. V., 1987, Absolute bioavailability of hydromorphone after peroral and rectal administration in humans: saliva/plasma ratio and clinical effects. *Journal of Clinical Pharmacology*, **27**, 647–653.

Roland, M. and Topaz, T. N., 1995, *Clinical Pharmacokinetics: Concepts and Applications* (Media: Williams & Wilkins), pp. 367.

Saady, J. J., Narasimhachari, N. and Blanke, R. V., 1982, Rapid, simultaneous quantification of morphine, codeine and hydromorphone by GC/MS. *Journal of Analytical Toxicology*, **6**, 235–237.

Searle, N. R., Roy, M., Bergeron, G., Perrault, J., Roof, J., Heermans, C., Courtemanche, M., Demers, C. and Cartier, R., 1994, Hydromorphone patient-controlled analgesia (PCA) after coronary artery bypass surgery. *Canadian Journal of Anaesthesia*, **41**, 198–205.

Smith, M. L., Hughes, R. O., Levine, B., Dickerson, S., Darwin, W. D. and Cone, E. J., 1995, Forensic drug testing for opiates. VI. Urine testing for hydromorphone, hydrocodone, oxymorphone and oxycodone with commercial opiate immunoassays and gas chromatography-mass spectrometry. *Journal of Analytical Toxicology*, **19**, 18–26.

Vallner, J. J., Stewart, J. T., Kotzan, J. A., Kirsten, E. B. and Honigberg, I. L., 1981, Pharmacokinetics and bioavailability of hydromorphone following intravenous and oral administration to human subjects. *Journal of Clinical Pharmacology*, **21**, 152–156.

Venkateshwaran, T. G. and Stewart, J. T., 1995, HPLC determination of morphine-hydromorphone-bupivacaine and morphine-hydromorphone-tetracaine mixtures in 0.9% sodium chloride injection. *Journal of Liquid Chromatography*, **18**, 565–578.

Wetzelsberger, N., Lücker, P. W. and Erking, W., 1986, High-pressure liquid chromatographic method for the determination of hydromorphone in human plasma with electrochemical detection. *Drug Research*, **36**, 1707–1710.

Zheng, M., McErlane, K. M. and Ong, M., 1998, High-performance liquid chromatography-mass spectrometry-mass spectrometry analysis of morphine and morphine metabolites and its application to a pharmacokinetic study in male Sprague–Dawley rats. *Journal of Pharmaceutical and Biomedical Analysis*, **16**, 971–980.

Zheng, M., McErlane, K. M. and Ong, M., 2002, Hydromorphone metabolites: isolation and identification from pooled urine samples of a cancer patient. *Xenobiotica* (in press).

XENOBIOTICA, 2002, VOL. 32, NO. 2, 153–163

Taylor & Francis
healthsciences

Absorption, metabolism and excretion of 4-chloro-2-methylphenoxyacetic acid (MCPA) in rat and dog

G. J. LAPPIN†*, T. D. HARDWICK†, R. STOW†, G. H. PIGOTT‡ and B. VAN RAVENZWAAY§

† Covance Laboratories Ltd, Otley Road, Harrogate HG3 1PY, UK
‡ A. H. Marks & Co. Ltd, Wyke, Bradford BD12 9EJ, UK
§ BASF Aktiengesellschaft, Z 470, 67056 Ludwigshafen, Germany

Received 10 July 2001

1. The oral no overall adverse effect level (NOAEL) for chronic toxicity of 4-chloro-2-methylphenoxyacetic acid (MCPA) in rat is ~1.3 mg kg^{-1} and in dog is 0.2 mg kg^{-1}. In an attempt to explain the difference in toxicology between these species, rats and dogs were orally dosed with (^{14}C)-MCPA at 5 or 100 mg kg^{-1} and plasma toxicokinetics, rates and routes of excretion and biotransformation were investigated.

2. Elimination of radioactivity in rat plasma was biphasic and in dog was monophasic. Rat eliminated radioactivity from plasma significantly faster than dog (approximate values based on total radioactivity: 5 mg kg^{-1} rat: $t_{½dist}$ 3.5 h, $t_{½elim}$ 17.2–36.2 h, $AUC_{(0-\infty)}$ 230 µg equiv h g^{-1}; 5 mg kg^{-1} dog: $t_{½}$ 47 h, $AUC_{(0-\infty)}$ 2500 µg equiv h g^{-1}; 100 mg kg^{-1} rat: $t_{½dist}$ 10 h, $t_{½elim}$ 10.27–25.4 h, $AUC_{(0-\infty)}$ 5400 µg equiv h g^{-1}; 100 mg kg^{-1} dog: $t_{½}$ 41 h, $AUC_{(0-\infty)}$ 20 500 µg equiv h g^{-1}).

3. For both species, the principal route of excretion was in urine but renal elimination was notably more rapid and more extensive in rat.

4. In both rat and dog, excretion of radioactivity was mainly as MCPA and its hydroxylated metabolite hydroxymethylphenoxyacetic acid (HMCPA). In rat, both were mainly excreted as the free acids although a small proportion was conjugated. In dog, the proportion of HMCPA was increased and the majority of both species was excreted as glycine or taurine conjugates.

5. These data, along with previously published accounts, indicate that renal elimination of MCPA in dog is substantially slower than in rat resulting in disproportionate elevation of AUC (based on total radioactivity) in dog compared with rat.

Introduction

4-Chloro-2-methylphenoxyacetic acid (MCPA, CAS No. 94-74-6), a plant growth regulator-type herbicide developed in the 1940s, is used effectively to control a wide variety of broad-leaved weeds in cereals, grasses, orchards, grapes, flax, sugarcane, pulses and non-crop areas. MCPA is often formulated as a salt (alkali metal salt such as sodium or a dimethylamine (DMA) salt) in a concentrated solution or as an ester, e.g. 2-ethylhexyl (MCPA-2-EHE). MCPA-DMA and MCPA-2-EHE dissociate extremely rapidly to MCPA in soil and water (Chang 1992, Fernando and Kok 1993) and at pH > 5 (Lai 1993). It has therefore been established that the metabolism of both MCPA-DMA and MCPA-2-EHE can adequately be described by MCPA (i.e. the free acid), as this is the relevant form in

* Author for correspondence; CBAMS Ltd, Sand Hutton, York YO41 1LZ, UK; e-mail: graham.lappin@cbams.co.uk

Xenobiotica ISSN 0049–8254 print/ISSN 1366–5928 online © 2002 Taylor & Francis Ltd
http://www.tandf.co.uk/journals
DOI: 10.1080/00498250110098940

terms of exposure (MCPA Taskforce III, 2002). MCPA has a low acute toxicity in rat and rabbit (Kirsch and Hildebrand 1983a–d, Gelbke and Hellwig 1986). Subchronic oral studies in rat (90 days) indicated that the most common signs of toxicity were reduced weight gain, increased kidney weight and altered clinical chemistry (Bellet *et al.* 1999). The systemic no overall adverse effect level (NOAEL) for subchronic toxicity (90 days) in rat is $\sim 4\,mg\,kg^{-1}\,day^{-1}$ and for chronic toxicity it is 20 ppm (equivalent to $1.3\,mg\,kg^{-1}$ body weight) with little or no evidence for a cumulative effect. NOAEL in a subchronic dog study (Reuzel *et al.* 1980) was $1\,mg\,kg^{-1}$ body weight and the chronic NOAEL $= 0.2\,mg\,kg^{-1}$ body weight (Hellwig *et al.* 1986), although the acute toxicity (single dose) was not markedly different from other species. The effects seen in dog were more severe than those recorded in the rat study with clear hepatotoxicity and anaemia as well as severe renal toxicity. Although the reason for increased sensitivity of dogs to MCPA has not been investigated previously, two factors suggest that it may be related to differences in kidney function. First, the kidney is a typical target organ for MCPA toxicity (Bellet *et al.* 1999). Second, it is well known that the dog has only a limited capacity to excrete weak organic acids in urine (Timchalk and Nolan 1997). Since MCPA has a $pK_a = \sim 3.1$, it is possible that the difference in NOAEL reflected a slower rate of elimination by dog compared with rat. To test this hypothesis, rat and dog were orally dosed with (^{14}C)-MCPA and the toxicokinetics and metabolism studied at two dose levels. The low dose, $5\,mg\,kg^{-1}$, was close to the subchronic NOAEL. The high dose was $100\,mg\,kg^{-1}$, and as this resulted in mild toxicological effects, it represents a short-term maximum tolerated dose (MTD) in rat. At the time the study was designed, this high dose was considered to be above the threshold for saturation of renal clearance in rat. The dose is also sustainable as a single administration to dog, but is well beyond the maximum tolerated dose for repeated exposures. Thus, it was anticipated that any inter-species differences would be particularly evident at this high dose.

Materials and methods

Chemicals

MCPA (4-chloro-2-methylphenoxyacetic acid > 98% pure), (^{14}C)-MCPA (universally labelled in the aromatic ring, specific activity $8.17\,MBq\,mg^{-1}$, > 95% radiopurity) and hydroxymethylphenoxyacetic acid (HMCPA, > 95% pure) were supplied by BASF. General-purpose reagents and solvents of Analar grade were obtained principally from Merck Ltd (Poole, UK). Liquid scintillants (Emulsifier-Safe^{TM}, Hionic-Fluor^{TM}, Ultima flo^{TM}) were obtained from Canberra Packard (Pangbourne, UK). Permafluor^{R} E+, Carbo-Sorb^{R} and (^{14}C)-Spec Chec^{TM}, for use in the Sample Oxidizer, were obtained from Canberra Packard. (^{14}C)-*n*-hexadecane was obtained from Amersham Pharmacia Biotech (Aylesbury, UK).

Animals

Ten male and ten female Cr1:(WI)BR strain rats (~250g, 6–8 weeks old) were obtained from Charles River (UK) Ltd (Margate, UK). Rats were fed water and rat diet (SQC rat and mouse maintenance diet No. 1, Special Diet Services, Stepfiled, UK) *ad libitum*. Four male Beagle dogs (~6–12 months of age and between 10 and 15 kg) were obtained from Bantin and Kingman Universal Ltd (Hull, UK). Dogs were fed 400 g dog maintenance diet daily (SQC Laboratory Diet A Special Diets Services, Stepfield, UK) and water *ad libitum*.

Dosing

Rats were administered a single oral dose of (^{14}C)-MCPA, by gavage, at 5 or $100\,mg\,kg^{-1}$ body weight ($4\,ml\,kg^{-1}$, $2.2\,MBq\,kg^{-1}$), suspended in 1% carboxymethyl cellulose (CMC). Four dogs were administered a single oral dose of (^{14}C)-MCPA admixed with CMC in a capsule at 5 or $100\,mg\,kg^{-1}$

body weight (1 MBq kg^{-1}). Dogs were given the 5 mg kg^{-1} dose first. The same dogs were then dosed at 100 mg kg^{-1} after a 4-week 'wash out' period. (^{14}C)-MCPA was stable in the dosing formulations from the time of preparation to the time of dosing.

Sample collection

Five male and five female rats were group housed, by sex, in wire-floored cages. Blood (~150 µl) was sampled from the lateral caudal vein at the following times after dosing: 1.5, 3, 6, 9, 12, 24, 48, 72, 120 and 168 h.

Another five male and five female rats were housed in glass metabolism cages. Urine and faeces were collected at the following times after dosing: 6 (urine only), 12 (urine only), 24, 48, 96, 120, 144 and 168 h.

Four dogs were housed in metabolism cages. Blood (~10 ml) was sampled at the following times after dosing: 1, 2, 4, 6, 8, 12, 24, 48, 72, 96 and 120 h. Samples of urine and faeces were collected after 12 h from dosing and then every 24 h until 120 h post-dose.

For both species, collection vessels for excreta were cooled by solid carbon dioxide. Where animals were housed in metabolism cages, the cages were rinsed with water after each collection of excreta. At the end of the experiment, after the animals had been removed, the cages were rinsed with methanol.

Sample analysis (rat and dog)

Blood samples were centrifuged to produce plasma. Portions of urine, plasma and cage washings were added directly to Emulsifier-Safe^{TM} scintillant and assayed by liquid scintillation counting. Faeces were homogenized in an appropriate volume of de-ionized water and added to ashless floc in Combusto Cones^{TM} and combusted in oxygen using a Packard Sample Oxidizer. The combusted products were absorbed in Carbo-Sorb^{R}, mixed with Permafluor^{R} E^{+}, and the radioactivity determined by liquid scintillation counting. Radioassays were performed at least in duplicate. Radioactivity was measured for 5 min or 2 σ% using Packard Tri-Carb liquid scintillation counters (Canberra Packard) with the facilities for computing quench-corrected disintegrations per minute (dpm). Efficiency correlation curves were prepared for organic, aqueous and combusted sample types and was routinely checked by the use of (^{14}C)-*n*-hexadecane standards.

Calculation of toxicokinetic data

Non-compartmental toxicokinetic evaluations of blood and plasma data were performed with the aid of TopFit v.2 (Thomae, Shering and Gödecke, Germany). The input consisted of: sample time (h); sample concentration; units of concentration; dose administered; and units of dose administered. Non-detected values were not used in half-life calculations. Blood and plasma half-lives of total radioactivity following administration of the test article were calculated by regression analysis of the linear portion of the individual concentration–time curves when plotted semilogarithmically. The area under the blood and plasma concentration time curves (AUC) was calculated using the trapezoidal rule. $AUC_{(0-t)}$ was defined as the area under the curve between time zero and the last datum point. $AUC_{(0-\infty)}$ was extrapolated from the last datum point using the rate constant defined in the terminal elimination phase.

Identification of metabolites

Urine samples were centrifuged to remove particulate matter and subjected to HPLC, without further processing. MCPA and HMCPA were used as chromatographic markers. The HPLC column was a Spherisorb ODS2 (5 µm particle size, 250 × 4.6 mm i.d.) and the flow rate was 1 ml min^{-1}. The mobile phase consisted of 0.1% aqueous formic acid (solvent A) and 0.1% formic acid (Solvent B) in acetonitrile. The linear gradient was 70%A, 30%B to 0%A, 100%B over 21 min. Detection was by radiodetector using a 500 µl liquid cell (Ultima flo^{TM}scintillant) and UV detection at 230 nm. Samples of rat urine were pooled by sex over time, to account for at least 70% of the excreted dose. Samples of urine and faeces from dogs were analysed individually. Faeces samples from dogs were extracted using methanol containing 1% formic acid. Extraction efficiencies were > 90%. Urine samples from rat and dog were analysed by LC-MS using either a VG Quattro triple quadrupole mass spectrometer (Micromass, Manchester, UK) or a Finnigan LCQ ion trap (Thermo Finnigan, Hemel Hemstead, UK). Typically, negative-ion electrospray was used with a capillary temperature of 160 °C held at −9V. The scan range was typically m/z 100–500. Selected ions were chosen and daughter ion experiments performed to obtain further structural information.

Results

For rat, the mean total recovery of radioactivity was between 85 and 102%. Mean total recoveries for the dog ranged from 78 to 85%. For rat, between 75 and

80% of the administered dose was excreted in urine over 24 h irrespective of the dose administered. Rat faeces contained ~2–12% of the dose for the 5 and 100 mg kg^{-1} dose levels respectively. There was no significant difference between routes or rates of excretion for the male or female rat. The rate of elimination of radioactivity in urine for rat dosed at 100 mg kg^{-1} was slightly prolonged compared with the 5 mg kg^{-1} dose level.

Dogs dosed at 5 mg kg^{-1} eliminated 44–73% in urine over 120 h. Dog faeces, at this dose level, contained 15–20.2% of the dose, a significantly higher proportion than seen in rat. There was also a marked difference in the routes and rates of excretion in the dog when the and 100 mg kg^{-1} dose levels were compared. Urine from dogs dosed at 100 mg kg^{-1} contained 26–38% of the administered dose, with faeces containing 20–55%. For both dose levels, excretion from the dog was not complete at the end of the 120-h period (figures 1 and 2).

Remaining radioactivity, to account for the overall recoveries for both species reported above, was found in the cage washings.

For both dose levels, elimination of radioactivity from rat plasma was biphasic. The $t_{½dist}$ measured between 6 and 24 h for rats dosed at 5 mg kg^{-1} was 3.9 and 3.1 h for males and females respectively. The values, measured over the same period, for rats dosed at 100 mg kg^{-1} were 17.8 and 6.9 h for males and females respectively. The $t_{½elim}$ measured between 48 and the last measurable time point (120 h) for rats dosed at 5 mg kg^{-1} was 17.5 and 36.2 h for males and females respectively. The $t_{½elim}$, measured from 48 h to the last measurable time point (120 h) for rats dosed at 100 mg kg^{-1}, was 10.27 and 25.4 h for males and females respectively.

These results were in sharp contrast to those for the dog where elimination was monophasic and the single $t_{½}$ for both dose levels was 41–47 h (measured from 6 to 120 h).

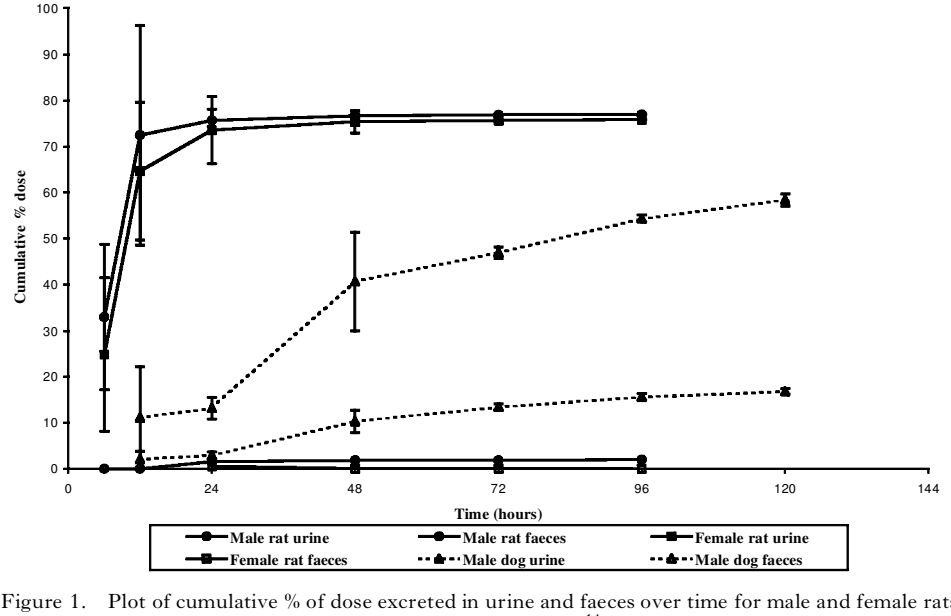


Figure 1. Plot of cumulative % of dose excreted in urine and faeces over time for male and female rats and male dogs administered 5 mg/kg body weight (^{14}C)-MCPA. Error bars are standard deviation ($n - 1$).

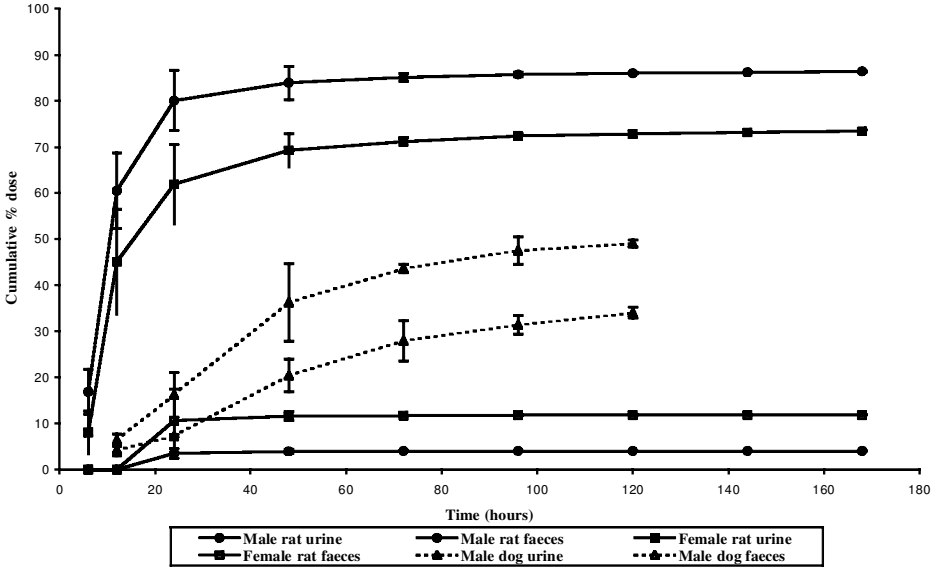


Figure 2. Plot of cumulative % of dose excreted in urine and faeces over time for male and female rats and male dogs administered 100 mg/kg body weight (^{14}C)-MCPA. Error bars are standard deviation ($n-1$).

For dogs dosed at 5 mg kg^{-1}, the $AUC_{(0-t)}$ was almost 10-fold that for the rat at the same dose level. For dogs dosed at 100 mg kg^{-1}, the $AUC_{(0-t)}$ was about three times higher than that in the rat. AUCs calculated for $0-t$ and $0-\infty$ in rat were virtually identical, showing that elimination was essentially complete at the end of the 120-h period (table 1). AUCs calculated from 0 to ∞ for dog were extrapolated from the $0-t$ by 20 and 16% for the 5 and 100 mg kg^{-1} dose levels respectively, thus showing elimination from dog plasma was not complete by 120 h (figures 3 and 4). AUCs for rats dosed at 100 mg kg^{-1} were ~25 times those for rats dosed at 5 mg kg^{-1} (i.e. for a 20-fold difference in dose level). For dog, however, a 20-fold increase in dose level lead to only a ~8.5-fold increase in AUC.

The C_{max} for the respective dose level between rat and dog were comparable (table 1). The T_{max} for dog was only slightly longer than for the rat (2.4–4.2 h in rat, 4.5–7 h in dog).

Rat urine and dog urine and faeces were analysed for the presence of metabolites of MCPA. Metabolites were identified from their mass spectra and, in the case of parent and HMCPA, by comparison with standards (figure 5).

In rat, parent compound was excreted mainly in urine (~65% of the dose). The only metabolic pathway of any significance in rat was hydroxylation of the 2-methyl moiety to form HMCPA. A trace of the glycine conjugate of MCPA was detected, but it was present in amounts too small to reliably quantify.

Dog urine contained a smaller proportion of MCPA (2–29%). There was significant interanimal variation in the amounts of metabolites present in dog samples. The glycine conjugate of MCPA was present in significantly higher amounts in dog urine (up to 37% of the dose) compared with rat. Dog urine also contained a taurine conjugate (up to 7% of the dose) which was not detected in rat. Because dog faeces contained a higher proportion of the dose than those from rat,

Table 1. Pharmacokinetic parameters calculated for the male and female rat and male dog administered either 5 or 100 mg kg^{-1} body weight (^{14}C)-MCPA.

	Rat				Dog	
	5 mg kg^{-1}		100 mg kg^{-1}		5 mg kg^{-1}	100 mg kg^{-1}
Pharmacokinetic parameter	Male	Female	Male	Female	Male	Male
C_{max} (μg eq. g^{-1})	26.78	33.19	373.1	357.8	35.95	341.2
T_{max} (h)	2.70	2.40	2.40	4.20	4.5	7.0
$t_{½dist}$ (h)	3.9	3.1	17.8	6.9	–	–
$t_{½elim}$ (h)	17.5	36.2	10.27	25.4	–	–
$t_{½}$ (h)	–	–	–	–	47.05	41.04
$AUC_{(0-t)}$ (μg eq. h g^{-1})	207.5	246.2	5150	5574	2030	17195
$AUC_{(0-\infty)}$ (μg eq. h g^{-1})	209.8	249.9	5180	5628	2539	20454
% extrapolation $AUC_{(0-t)}$ to $AUC_{(0-\infty)}$	0	0	0	1	20	16

$t_{½dist}$, distribution phase in rat calculated between 6 and 24 h; $t_{½elim}$, terminal elimination phase in rat calculated between 48 h to the last measurable time point; $t_{½}$, calculated in dog between 6 and 120 h.

Values below the limit of detection were excluded from calculations.

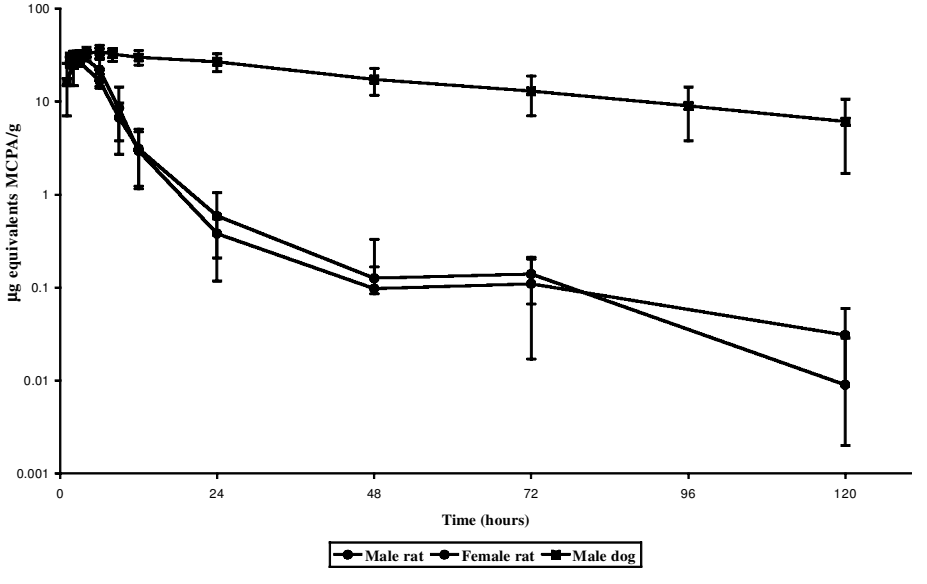


Figure 3. Semi log plot of concentration (μg equivalents MCPA/g) in plasma over time for male and female rats and male dogs administered 5 mg/kg body weight (^{14}C)-MCPA. Error bars are standard deviation ($n - 1$).

samples were extracted and analysed using HPLC and LC-MS/MS. Dog faeces contained parent compound and the glycine and taurine conjugates (table 2).

Discussion

It has been previously established (MCPA Taskforce III, 2002) that rat rapidly excretes MCPA. Biotransformation is limited to partial oxidation of the aromatic

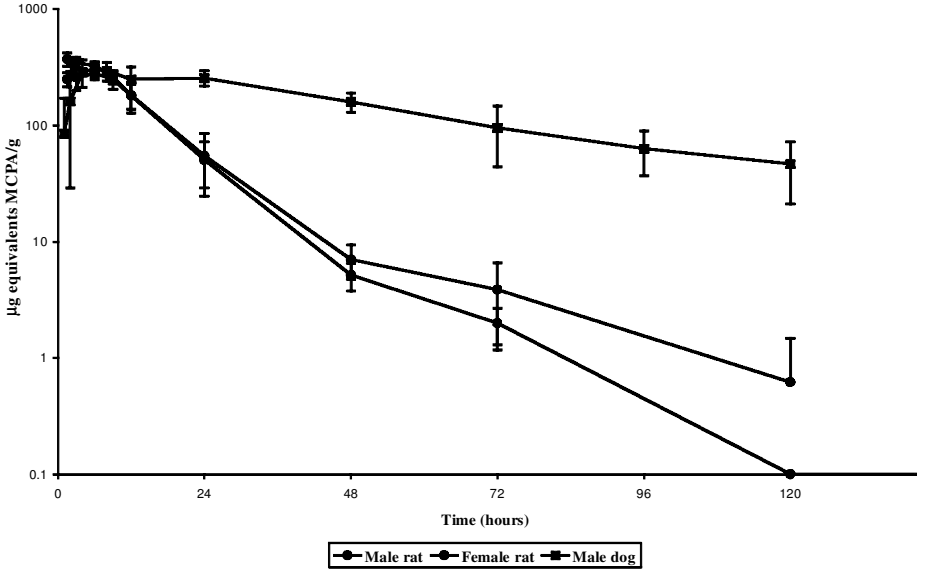
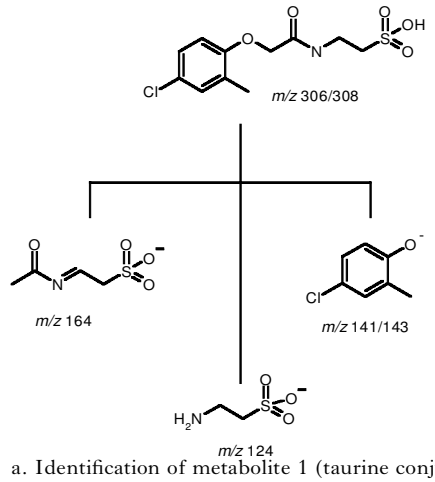


Figure 4. Semi log plot of concentration (µg equivalents MCPA/g) in plasma over time for male and female rats and male dogs administered 100 mg/kg body weight (^{14}C)-MCPA. Error bars are standard deviation ($n - 1$).

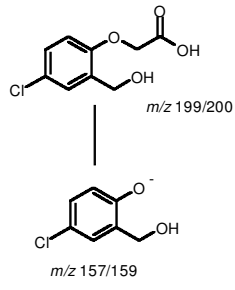
methyl group with ~10% of the dose transformed in this way. The excreted species are either the parent acid or metabolite in free form or as conjugates. The latter are usually regarded as devices to increase polarity and therefore aid excretion. They thus reduce toxicity rather than enhance it, but this has not been specifically examined for MCPA. MCPA does not accumulate in tissue, at least in the rat, and thus plasma concentration can be taken as a surrogate for body burden (MCPA Taskforce III, 2002). Measures of the increase and decrease of plasma concentrations are therefore useful indices of absorption and elimination. By contrast, dog is more sensitive to the effects of MCPA and repeated dosing indicates that there is a level of accumulation as the dose at which effects are observed decreases with increasing duration of exposure. Thus, indices relating to the level of radioactivity in plasma can be taken to represent the balance of assimilation and elimination in both rat and dog, although it is recognized that the nature of the circulating species may be different.

The interspecies differences in $t_{½}$ and AUC could be a reflection of slower absorption by dog or faster elimination in rat. Taken alone, it is not possible to differentiate these possibilities but as C_{max} and T_{max} were similar for rat and dog at each dose level, the latter explanation seems more probable. Thus, the data indicate a significantly reduced excretion in dog compared with rat at the lower dose. At the high dose, renal excretion is saturated for both species.

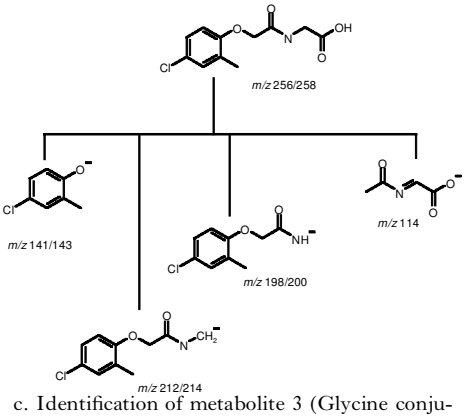
At the 100 mg kg^{-1} dose level, the dog excretes nearly 40% of the dose in faeces. This was present as a mixture of parent compound and amino acid conjugates, the latter accounting for up to 50% of the radioactivity present. This indicates that at least a proportion of the faecal radioactivity was first absorbed and then eliminated in the bile, as conjugation is unlikely to have occurred in the gut. However, definitive demonstration of this would require cannulation of the bile duct, which



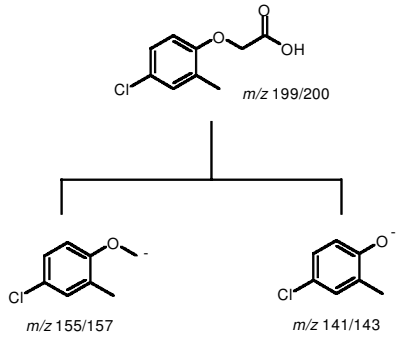
a. Identification of metabolite 1 (taurine conjugate)



b. Identification of metabolite 2 (HMCPA)



c. Identification of metabolite 3 (Glycine conjugate)



d. Identification of metabolite 4 (MCPA)

Figure 5. Fragment ions (negative ion electrospray MS/MS) and the identification of metabolites of MCPA in rat and dog

has not been undertaken to date. There is some evidence that phenoxy herbicides such as 2,4-dichlorophenoxy acetic acid may attain higher plasma concentrations in males (Erne 1966). However, generally these differences are limited and in the toxicity profiles of these compounds there is no evidence for a differential effect in females. In particular, there are no sex differences in the signs associated with MCPA administration or in the organs affected. Moreover, the recorded difference in $t_{½elim}$ between the male and female rat (table 1) should be viewed with caution as these values were calculated from only three data points. Thus, although the toxicokinetic differences observed may be real, they are of only minor importance. This is also true for the dog and to reduce animal usage, only male animals were used in the experiment. The rat experiments were performed ahead of the dog study and thus only one sex of dog was used. Although the rate and extent of absorption of MCPA in the rat and dog appeared equally rapid, the overall rate of elimination of radioactivity in dog was much slower. Elimination of radioactivity

Table 2. Percentage of dose for each metabolite of MCPA identified in the urine and faeces of rat and dog. The structures of metabolites are shown in figure 5.

		Rat				Dog			
		5 mg kg^{-1}		100 mg kg^{-1}		5 mg kg^{-1}		100 mg kg^{-1}	
	Retention time (min)	Urine		Urine		Urine	Faeces	Urine	Faeces
Metabolite		Male	Female	Male	Female	Male	Male	Male	Male
1	3	–	–	–	–	5	4	7	1–19
2	4	10	7.5	12.5	11	5–10	–	2–15	–
3	15	< 0.5	< 0.5	< 0.5	< 0.5	12–37	1	5	2
4	17.2	65	65	67	50	4–29	8	2	11–27

1, Taurine conjugate; 2, HMCPA; 3, glycine conjugate; 4, MCPA (parent).

from rat was biphasic, with the $t_{½dist}$ phase being significantly more rapid than the $t_{½elim}$ phase. The most rapid rate of elimination in rat ($t_{½dist}$ 3.1–3.9 h) compared with the single $t_{½}$ in dog of 41–47 h. Although the $t_{½elim}$ in rat was significantly slower than the $t_{½dist}$ phase, it was nevertheless still more rapid than the single $t_{½}$ obtained in dog. Although a comparison of the rates of excretion of MCPA in rat and dog has not been reported previously, data are available for other weak organic acids. 1-Aminocyclopanecarboxylic acid is rapidly cleared in mouse, rat, monkey and human but slower in dog (Cherkofsky 1995). Triclopyr is well absorbed in rat, monkey and dog, but excretion is slower in dog (Timchalk and Nolan 1997). The plasma $t_{½}$ for 2,4,5-trichlorophenoxy acetic acid in rat is 4–5 h but in dog is 77 h, with consequential slower excretion (Hook *et al.* 1976).

The precise reason why the dog is deficient in the elimination of weak organic acids is obscure. There is evidence to suggest that certain phenoxyacetic acids bind to plasma protein and perhaps their affinity for the protein is high enough to limit excretion (Bräunlich *et al.* 1989). MCPA is known to bind to plasma protein in the rat but it is nevertheless cleared via the kidneys very rapidly (Bräunlich *et al.* 1989). There is evidence that weak organic acids are actively reabsorbed in the dog kidney thus maintaining high plasma levels (Timchalk and Nolan 1997). Reabsorption of organic acids by the kidney of the possum has also been reported (Miller and Morris 1982). MCPA has been shown to be reabsorbed in rat kidney and the extent to which this occurs is affected by the urinary pH. An increase in pH leads to a reduction in reabsorption (Bräunlich *et al.* 1989). This is unlikely to explain the observed differences as MCPA has no influence on urinary pH in either the rat or dog over a range of dose levels used in the subchronic studies.

In the present study, MCPA was excreted in rat urine mainly as parent compound and the methyl-hydroxy metabolite, HMCPA. In dog urine, however, significant amounts of the glycine and taurine conjugates of MCPA were found (figure 6). The formation of taurine conjugates is commonly seen in dog but it is much rarer in other species. Dog and ferret form the taurine conjugate of clofibric acid but man, rat, guinea pig and rabbit produce mostly the ester glucuronide (Emudianughe *et al.* 1983). Muricholic acid forms the taurine conjugate in dog, which is excreted in bile. Hamster bile, however, contains mostly parent compound and some glycine along with only a small amount of taurine conjugates (Miki *et al.* 1993).

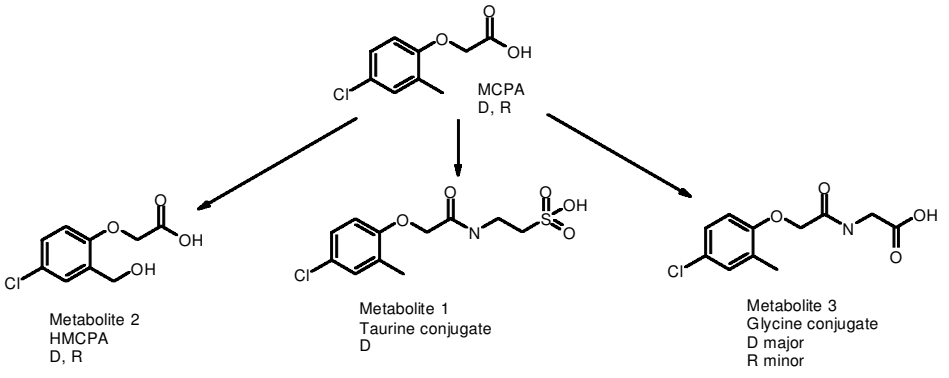


Figure 6. Proposed metabolic pathway of MCPA in rat and dog. (R — metabolite identified in rat excreta, D — metabolite identified in dog excreta.

Since the rat has the capability of readily eliminating the free acid, the urine contains mostly parent and elimination is much more rapid. It is interesting to note that the 6.5-fold difference in NOAEL for MCPA between rat and dog is broadly consistent with the difference in AUC between the species, thus suggesting that systemic exposure and toxicological effects are linked. It is concluded that the interspecies differences in both toxicokinetic profiles and extent of metabolism most probably reflect an increased rate of renal reabsorption in dog compared with rat.

The dog has also shown enhanced sensitivity to triclopyr (Timchalk and Nolan 1997) and 2,4,5-trichlorophenoxy acetic acid (Piper *et al*. 1973). In both cases, urinary elimination of the compounds in dog was deficient. The excretion of several other weak organic acids has been studied in a range of species (Miller and Morris 1982, Cherkofsky 1995, Timchalk and Nolan 1997) and in each case, dog showed significantly slower rates of elimination. The data presented here therefore add to a growing body of evidence showing that since the dog is deficient in the excretion of weak organic acids, the species is not appropriate for assessing the toxicological significance of this class of compound to man.

Acknowledgements

The work was sponsored by MCPA Task Force III.

References

Bellet, E. M., van Ravenzwaay, B., Pigott, G. and Leeming, N., 1999, Chronic dietary toxicity and oncogenicity evaluation of MCPA in rodents. *Regulatory Toxicology and Pharmacology*, **30**, 223–232.

Bräunlich, H., Bernhardt, H. and Bernhardt, I., 1989, Renal handling of 2-methyl-4-chlorophenoxyacetic acid (MCPA) in rats. *Journal of Applied Toxicology*, **9**, 255–258.

Chang, J., 1992, Dissociation of MCPA-DMA in water. Unpublished; DP Barcode D182938, Battelle, Columbus, OH.

Cherkofsky, S. C., 1995, 1-Aminocyclopanecarboxylic acid: mouse to man interspecies pharmacokinetic comparisons and allometric relationships. *Journal of Pharmaceutical Science*, **84**, 1231–1235.

Emudianughe, T. S., Caldwell, J., Sinclair, K. A. and Smith, R. L., 1983, Species differences in the metabolic conjugation of colfibric acid and colfibrate in laboratory animals and man. *Drug Metabolism and Disposition*, **11**, 97–102.

Erne, K., 1966, Distribution and elimination of chlorinated phenoxy-acetic acids in animals. *Acta Veterinica Scandinavica*, **7**, 240–256.

Fernando, T. R. and Kok, R., 1993, Hydrolysis of [^{14}C]-MCPA-2-EHE to MCPA-acid in a soil/water system. Unpublished Study No. SC920064; DP Barcode D189442, Battelle, Columbus, OH.

Gelbke, H. P. and Hellwig, J., 1986, Acute inhalation toxicity LC_{50} 4 hours (rat) dust aerosol study of MCPA. Unpublished, BASF Aktiengesellschaft, Ludwigshafen am Rhein, Germany.

Hellwig, J., Deckardt, K., Hasenoehrl, J. and Hildebrand, B. 1986. Report on the study of the toxicity of MCPA in Beagle dogs after 12-month administration in the diet. Unpublished, BASF Aktiengesellschaft, Ludwigshafen am Rhein, Germany.

Hook, J. B., Cardona, R., Osborn, J. L. and Baile, M. D., 1976, The renal handling of 2,4,5-trichlorophenoxy-acetic acid in the dog. *Food and Cosmetic Toxicology*, **14**, 19–23.

Kirsch, P. and Hildebrand, B., 1983a, Report on the study of the acute oral toxicity in rats of MCPA. Unpublished, BASF Aktiengesellschaft, Ludwigshafen am Rhein, Germany.

Kirsch, P. and Hildebrand, B., 1983b, Report on the study of the acute dermal toxicity in rats of MCPA. Unpublished, BASF Aktiengesellschaft, Ludwigshafen am Rhein, Germany.

Kirsch, P. and Hildebrand, B., 1983c, Report on the study of the irritation to the intact and abraided dorsal skin of the white rabbit based on draize of MCPA. Unpublished, BASF Aktiengesellschaft, Ludwigshafen am Rhein, Germany.

Kirsch, P. and Hildebrand, B., 1983d, Report on the study of the irritation to the eye of the white rabbit based on draize of MCPA. Unpublished, BASF Aktiengesellschaft, Ludwigshafen am Rhein, Germany.

Lai, I., 1993, Hydrolysis of [^{14}C]-MCPA-2-EHE in buffered aqueous solutions. Unpublished Study No. SC910087, DP Barcode D189760; Battelle, Columbus, OH.

MCPA Task Force III, 2002, Unpublished document. c/o the Technical Chairman, 7474 Creedmoor Rd., N.C., 27613, USA.

Miki, S., Mosbach, H., Cohen, B. I., Mikami, T., Infante, R., Ayyad, N. and McSherry, C. K., 1993, Metabolism of β-muricholic acid in the hamster and prairie dog. *Journal of Lipid Research*, **34**, 1709–1716.

Miller, J. H. and Morris, L. L., 1982, Mechanisms of organic acid and monosaccharide transport in the kidney of the brush-tailed possum. *Australian Journal of Biological Science*, **35**, 363–372.

Piper, W. N., Rose, J. Q., Leng, M. L. and Gehring, P. J., 1973, The fate of 2,4,5-trichlorophenoxy acetic acid following oral administration to rats and dogs. *Toxicology and Applied Pharmacology*, **26**, 339–401.

Reuzel, P. G. J., van der Heijden, C. A. and van Oostrum, E. C. M., 1980, Subchronic (13-week) oral toxicity study of MCPA in Beagle dogs. Unpublished; TNO Central Institute for Nutrition and Food Research, Zeist, The Netherlands.

Timchalk, C. and Nolan, R. L., 1997, Pharmacokinetics of tricopyr in the beagle dog and rhesus monkey: perspective on the reduced capacity of dogs to excrete this organic acid relative to the rat. *Toxicology and Applied Pharmacology*, **144**, 268–278.

XENOBIOTICA, 2002, VOL. 32, NO. 3, 165–206

Taylor & Francis
healthsciences

Topics in Xenobiochemistry

Receptor-dependent transcriptional activation of cytochrome P4503A genes: induction mechanisms, species differences and interindividual variation in man

G. G. GIBSON†*, N. J. PLANT†, K. E. SWALES†, A. AYRTON‡ and W. EL-SANKARY†

† Molecular Toxicology Group, School of Biomedical and Life Sciences, University of Surrey, Guildford, Surrey GU2 7XH, UK.
‡GlaxoSmithKline Pharmaceuticals, Department of Drug Metabolism and Pharmacokinetics, The Frythe, Welwyn, Hertfordshire AL6 9AR, UK.

Received August 23, 2001

1 The importance of CYP3A enzymes in drug metabolism and toxicology has yielded a wealth of information on the structure, function and regulation of this subfamily and recent research emphasis has been placed on the human forms, namely CYP3A4, CYP3A5, CYP3A7 and CYP3A43.

2 The current review will focus on the receptor-dependency of CYP3A regulation and includes consideration of the regulatory roles of the glucocorticoid (GR), pregnane X (PXR) and constitutive androstane (CAR) receptors.

3 Emphasis has been placed on the topics of expression and substrate specificity, assessment of induction, species differences in induction, CYP3A promoter sequences and regulation of gene expression, structural and functional aspects of receptor-mediated, CYP3A gene activation, receptor variants and interindividual variation in human CYP3A expression, the latter encompassing environmental, physiological and genetic aspects.

4 An outline of future research needs will be discussed in the context of receptor-mediated molecular mechanisms of CYP3A gene regulation and the impact on interindividual variations in CYP3A expression.

5 Taken collectively, this review highlights the importance of understanding the molecular mechanisms of CYP3A induction as a means of rationalizing human responses to many clinically used drugs, in addition to providing a mechanistically coherent platform to understand and predict interindividual variations in response and drug–drug interactions.

Introduction

Members of the cytochrome P4503A (CYP3A) (for abbreviations, see appendix A) subfamily play a pivotal role in the metabolism of clinically used drugs and certain toxic environmental chemicals and are highly expressed in human liver and intestine (Ioannides 1996). CYP3A4 is predominantly expressed in human liver and intestine where it comprises between 30 and 50% of the total cytochrome P450 population in these tissues (Watkins 1994). This isoform is highly inducible in man by synthetic glucocorticoids, macrolide antibiotics and phenobarbitone, amongst others, and, in addition to metabolizing a number of endogenous compounds such

* Author for correspondence; e-mail: g.gibson@surrey.ac.uk

Xenobiotica ISSN 0049–8254 print/ISSN 1366–5928 online © 2002 Taylor & Francis Ltd
http://www.tandf.co.uk/journals
DOI: 10.1080/00498250110102674

as testosterone and environmental xenobiotics such as aflatoxins, it has been estimated to be responsible for approximately 60% of the cytochrome P450-mediated metabolism of pharmaceuticals in therapeutic use today (Cholerton *et al*. 1992). In addition, CYP3A4 activity is inhibited by several clinically used drugs such as erythromycin, gestodene and ketoconazole (Newton *et al*. 1994).

This diverse range of substrates, inducers and inhibitors of CYP3A4 activity creates the potential for clinically significant drug interactions involving this enzyme, particularly in therapeutic areas where polypharmacy is common practice, e.g. in the elderly or in the long-term prophylaxis of psychiatric disorders (Thummel and Wilkinson 1998). Whereas it is recognized that not every drug–drug interaction involving induction or inhibition of CYP3A4-mediated metabolism results in altered clinical responses, there are sufficient reports in the literature where this is indeed the case. For example, induction of the metabolism of the CYP3A4 substrate cyclosporin by rifampicin in man has resulted in clinically defined organ graft rejection (Lucey *et al*. 1990). Thus, variation in the expression of the CYP3As can therefore affect substantial variation in the clinical usage (first-pass metabolism) and potential toxicity of drug–drug interactions in man. Because of the large number of substrates, inhibitors and inducers of human CYP3As, there is clearly a significant potential for drug–drug interactions and some illustrative examples of this phenomenon are described herein and as recently reviewed (Weaver 2001).

There is a substantial interindividual variation in CYP3A4 expression in man (10–100-fold; Shimada *et al*. 1994, Watkins 1994), but the molecular basis for this variation is not fully understood at present, and may possibly be attributed to factors of both environmental and/or genetic origin. For example, high-level expression may be rationalized by prior exposure to the inductive effects of drugs as mentioned above, whereas lower expression may result from either xenobiotic, disease or injury-related hepatocellular damage (Thummel *et al*. 1994). As CYP3A4 regulation is receptor-mediated (see below), clearly the absolute and relative expression levels of cellular receptors is an additional, potential source of interindividual variation in CYP3A4.

Genetic polymorphisms in cytochrome P450 gene expression have been identified and well-characterized for several isoforms, including CYP2A6, CYP2D6, CYP2C9 and CYP2C19 (Meyer and Zanger 1997), but it is only recently that functionally inactivating CYP3A4 polymorphisms have been described (see below). Nevertheless, it is intuitively apparent that any genetically derived variations in CYP3A4 expression may exacerbate clinical responses and contribute to the interindividual variation in expression, in addition to having substantial implications for the drug discovery and development process in the pharmaceutical industry (Ingelman-Sundberg 2001).

Given the importance of this subfamily in drug metabolism and toxicology, the molecular mechanisms of regulation of the CYP3A4 gene is an important topic for the clinical responses to many drugs and it is our purpose to review recent developments in this area. Although emphasis is placed on CYP3A4, other members of the CYP3A subfamily in man and other species will also be considered. For other related reviews on this topic, see Waxman (1999), Negishi and Konkakowski (2000), Wrighton *et al*. (2000), Quattrochi and Guzelian (2001), Savas *et al*. (1999), Smith (2000), Tzameli and Moore (2001), Moore and Kliewer (2000), Fuhr (2000), Weaver (2001) and Worboys and Carlile (2001).

Expression and substrate specificity of human CYP3As

Currently, four human CYP3A enzymes have been identified: CYP3A4, CYP3A5, CYP3A7 and CYP3A43. It is generally accepted that CYP3A4 is the major member of the CYP3A subfamily expressed in the majority of human livers, followed by CYP3A5. In those human livers expressing CYP3A5, the levels approximate those of CYP3A4, whereas CYP3A7 and CYP3A43 are expressed at much lower levels.

CYP3A4, 3A5 and 3A7 lie in a head-to-tail orientation in the order CYP3A4, 3A7 and 3A5 on chromosome 7q21-q22.1 (Brooks *et al.* 1988, Finta and Zaphiropoulos 2000. Finta and Zaphiropoulos discussed the evolution of the human CYP3A gene locus in terms of the capture of downstream exons).

The CYP3A subfamily is the major cytochrome P450 expressed in human liver at all stages of development with CYP3A7 predominating in foetal liver and CYP3A4 in adult liver (Schuetz *et al.* 1994, de Wildt *et al.* 1999). CYP3A7 is predominantly expressed in human foetal liver (Schuetz *et al.* 1984, Kitada *et al.* 1985) and in 54% of human adult livers examined (Schuetz *et al.* 1994, Gervot *et al.* 1996). CYP3A5 appears to be variably expressed in human adult liver as reported in three separate studies: in 11/46 (Wrighton *et al.* 1989), 19/66 (Wrighton *et al.* 1990) and 3/13 (Schuetz *et al.* 1994) livers examined.

The CYP3As are also expressed in other tissues, particularly the gastrointestinal tract (Kolars *et al.* 1994). CYP3A5 is the major CYP3A in the stomach and both CYP3A4 and CYP3A5 mRNA have been detected by polymerase chain reaction (PCR) in all regions of the digestive tract (Kolars *et al.* 1994). CYP3A4 has been reported to be the major CYP3A enzyme in the small intestine, whereas CYP3A5 is the main form in the human colon (Gervot *et al.* 1996). The expression of CYP3As in the gastrointestinal tract has substantial implications in toxicology and in the systemic bioavailability of xenobiotics. For example, CYP3A4 metabolizes aflatoxin B_1 in human small bowel enterocytes, resulting in the formation of intracellular aflatoxin B_1 molecular adducts that pass out in the stool as enterocytes are continuously sloughed off. Otherwise, the reactive metabolite may be absorbed into the systemic circulation and have the potential to form carcinogenic adducts in the liver (Aoyama *et al.* 1989, Kolars *et al.* 1992, Kolars *et al.* 1994). Whereas the expression of CYP3A4 in the small intestine is a protective mechanism in the case of aflatoxin B_1, the presence of CYP3A4 in enterocytes can be important in the first-pass metabolism of drugs, thereby limiting the systemic absorption of orally administered drugs. For example, 50% of an oral dose of cyclosporin A undergoes CYP3A4-dependent hydroxylation, thereby contributing to the poor oral bioavailability of the drug in man, a situation that can be exacerbated by the inducibility of the enzyme in the small intestine (Herbert *et al.* 1997).

Human CYP3A4 does not generally exhibit marked gender differences in expression because there are no distinct differences (pulsatile versus continuous secretion) in growth hormone regulation. However, we are aware of a report wherein erythromycin *N*-demethylation (catalysed by CYP3A4) is 24% greater ($p = 0.027$) in the female as compared with the male (Hunt *et al.* 1992), in agreement with pharmacokinetic studies *in vivo* where females show a 36% higher clearance of erythromycin than males (Austin *et al.* 1980) and a significantly higher rate of metabolism as determined by the erythromycin breath test (Watkins *et al.* 1989). In this context, it should be borne in mind that it is always difficult to

eliminate other confounding factors that may contribute to this apparent sex difference and further studies are required to substantiate whether there is indeed a clinically meaningful sex difference in the human population. CYP3A catalytic activity is not affected by age, smoking status, ethanol consumption or percentage ideal body weight (Hunt *et al*. 1992). Therefore, any age-related differences in the clearance of CYP3A substrates is probably due to changes in liver blood flow, liver size, or drug binding and distribution.

There appears to be no common structural factors that determine whether a compound is metabolized by the CYP3As (table 1), because the enzyme is capable of metabolizing both small molecules such as paracetamol and large molecules, including cyclosporin (molecular weights of 151 and 1203 respectively). In addition, CYP3A4 exhibits both homotropic and heterotropic cooperativity for some (but not all) substrates, wherein the initial binding of one drug facilitates either its own metabolism or the metabolism of a second substrate, in a dose-dependent manner. Although the specific molecular mechanisms underpinning this phenomenon have not been fully clarified, some progress in understanding the mechanisms involved has been made (Guengerich 1999).

CYP3A4

CYP3A4 mRNA is undetectable in the human foetal liver but is expressed in the new born and adult liver (Greuet *et al*. 1996). CYP3A4 is responsible for approximately 60% of the cytochrome P450-mediated metabolism of drugs in therapeutic use today (Cholerton *et al*. 1992) and is therefore an important enzyme with respect to the action and duration of drugs and their metabolites. Because CYP3A4 is induced by many of its substrates and other drugs (table 1), it also plays a significant role in drug–drug interactions. For example, rifampicin

Table 1. Representative substrates, inhibitors and inducers of human CYP3As.

Substrates	Inhibitors	Inducers
Endogenous		
Androstenedione, chenodeoxycholic acid, cortisol, deoxycholic acid, estradiol, lithocholic acid, progesterone, testosterone	Cimetidine, erythromycin fluconazole, fluoxetine, gestodene grapefruit juice, itraconazole, josamycin, ketoconazole, norfloxacin, ritonavir, troleandomycin	Corticosterone, chenodeoxycholic acid, growth hormone, hydrocortisone
Xenobiotic		
Aflatoxin B_1, alfentanil, carbemazepine, cyclophosphamide, cyclosporin, dextromethorphan, diazepam, erythromycin, 17-α-ethynylestradiol, heterocyclic amines, ifosfamide, imipramine, lansoprazole, lidocaine, midazolam, nifedipine, omeprazole, paracetamol, quinidine, ritonavir, saquinavir, simvastatin, tamoxifen, terfenadine, troleandomycin, verapamil		Carbemazepine, clotrimazole, cyclophosphamide, diazepam, fexofenadine, hyperforin, ifsofamide, lovastatin, metyrapone, moracizine, nevirapine, nonylphenol, omeprazole, PCN, phenobarbital, phenytoin, phenylbutazone, prednisolone, probenicid, rifampicin, RU-486, simvastatin, spironolactone, sulfinpyrazole, troglitazone, troleandomycin

(a CYP3A4 inducer in man) significantly increases the rate of cyclosporin A metabolism (a CYP3A4 substrate) and clearance resulting in ineffective blood levels and the resultant organ graft rejection in transplant patients (Lucey *et al.* 1990). Up regulation of CYP3A4 by inducers can also exaggerate toxic responses to drugs. For example, CYP3A4 produces the cytotoxic metabolite *N*-acetyl-*p*-aminobenzoquinoneimine from paracetamol and the CYP3A4 inducer rifampicin, may potentiate paracetamol hepatotoxicity when the drugs are co-administered (Thummel *et al.* 1993). Conversely, ketoconazole and erythromycin inhibit the metabolism of cyclosporin A, resulting in higher blood levels with concomitant nephrotoxicity (Lucey *et al.* 1990).

CYP3A4 catalyses a range of metabolic activities including C- and N-oxidation, N- and O-dealkylation, nitro reduction and dehydration. Although CYP3A4 can accommodate a wide variety of structurally diverse substrates, the enzyme exhibits regio- and stereoselectivity. For example human CYP3A4 catalyses the 2β-, 6β- and 15β-hydroxylation of testosterone and the 6β-hydroxylation of progesterone, and to a lesser extent the 16 α-hydroxylation (Komori *et al.* 1988, He *et al.* 1997). Based on molecular modelling and cassette/site-directed mutagenesis studies, several amino acid residues in CYP3A4 have been postulated to play an important role in determining substrate specificity, thereby indicating a relatively complex substrate-binding site(s) (He *et al.* 1997, Szklarz and Halpert 1997).

CYP3A5

CYP3A5 is a polymorphically expressed CYP3A subfamily member identified in 1989 in 11 of 46 human liver samples (Wrighton *et al.* 1989). A follow-up study by the same group identified CYP3A5 in only 19 of 66 livers and its expression did not correlate with gender, smoking or medical history (Wrighton *et al.* 1990). CYP3A5 has been detected in a statistically higher percentage of children and adolescents compared with the rest of the population and also in one of 10 human foetal livers examined (Wrighton *et al.* 1990). CYP3A5 mRNA was detected in all foetal livers examined and in three of 12 adult livers and therefore appears to be polymorphically expressed throughout development (Schuetz *et al.* 1994). The molecular basis for this polymorphic expression of CYP3A5 is not fully understood at present, but it is relevant to note that Paulussen *et al.* (2000) identified two linked mutations in the CYP3A5 promoter that are related to the metabolic ability to metabolize the CYP3A4/5 substrate midazolam. In addition, the presence of recently identified mutations in the CYP3A5 gene is an additional factor that may rationalize the polymorphic expression of this enzyme (Hseih *et al.* 2001, Kuehl *et al.* 2001). For a fuller discussion of this topic, see the section on genetic differences in the interindividual variation of human CYP3A expression below.

Although CYP3A5 actively metabolizes nifedipine, testosterone, oestradiol, dehydroepiandrosterone and cortisol, it appears to be more limited in its metabolic capacity than CYP3A4 and (unlike CYP3A4) poorly metabolizes erythromycin, quinidine, 17α-ethynyloestradiol, aflatoxins, cyclosporins and the 6β-hydroxylation of progesterone and androstenedione (Aoyama *et al.* 1989, Wrighton *et al.* 1990, Schuetz *et al.* 1994).

CYP3A7

CYP3A7 was initially purified and characterized in the late 1980s (Komori *et al.* 1988, Wrighton and van den Branden 1989) and is the major CYP3A expressed in the human foetal liver (Kitada *et al.* 1985, Schuetz *et al.* 1994). Unlike foetal liver in most experimental animals, the human foetal liver supports the oxidative metabolism of a wide range of drugs and other xenobiotics (Wrighton and van den Branden 1989). CYP3A7 is expressed in 54% of adult human livers (Schuetz *et al.* 1994, Gervot *et al.* 1996), in the placenta and endometrium, and is prominent in pregnant women and those in the secretory phase of the menstrual cycle (Scheutz *et al.* 1993). The amount of CYP3A7 increases in the second trimester of pregnancy in both placental and endometrial tissue (Scheutz *et al.* 1993), which is probably due to changes in endogenous hormones such as the increased systemic levels of dehydroepiandrosterone sulphate or increased CYP3A7 expression derived from induction by circulating glucocorticoids via up-regulated placental glucocorticoid receptors. It has been postulated that CYP3A7 may protect the foetus from the effects of endogenous steroids because the placenta and endometrium are important sites for the 6β- and 16α-hydroxylation of specific steroid precursors, such as cortisol. In addition, CYP3A7 catalyses the 16α-hydroxylation of dehydroepiandrosterone sulphate produced by the foetal adrenals (Scheutz *et al.* 1993), the latter being utilized by the placenta for oestrogen biosynthesis and which additionally inhibits progesterone biosynthesis (Powell *et al.* 1986), which the 16α-dehydroepiandrosterone sulphate does not. The comparative catalytic activities of CYP3A4, 3A5 and 3A7 have been compared in cDNA-expressing COS-7 cells, wherein the rate of 16α-hydroxylation of both dehydroepiandrosterone and dehydroepiandrosterone 3-sulphate were higher for CYP3A7 than CYP3A4, whereas the converse is true for the 6β-hydroxylation of testosterone and the 10,11-epoxidation of carbamazepine (Ohmori *et al.* 1998). Taken collectively, the above involvement of CYP3A7 emphasizes the overall importance of the regulation of this enzyme in steroid homeostasis related to the control of developmental processes and also in xenobiotic metabolism.

CYP3A43

Recently, a new member of the human CYP3A subfamily has been characterized and termed CYP3A43, whose amino acid sequence is 75% similar to CYP3A4 and CYP3A5 and 71% similar to CYP3A7 and is expressed at comparatively low levels in adult and foetal liver, kidney, pancreas, skeletal muscle, testis and prostate (Domanski *et al.* 2001, Westlind *et al.* 2001). Specifically, hepatic expression of CYP3A43 mRNA has been reported to be approximately 0.1 and 2% of CYP3A4 and CYP3A5 respectively (Westlind *et al.* 2001). The substrate specificity of this enzyme and its contribution to human drug metabolism still remains to be fully clarified, but preliminary studies have demonstrated that CYP3A43 has low testosterone 6β-hydroxylase activity, which may be rationalized by the fact that CYP3A43 differs from CYP3A4 at six amino acid residues in the putative substrate recognition site (Domanski *et al.* 2001).

Assessment of CYP3A4 induction

Historically much of the assessment of xenobiotic induction of the CYP3A subfamily has been carried out using *in vivo* and *in vitro* preclinical studies in animals. In man, induction *in vivo* has been the subject of much interest and debate and includes the use of biotransformation of CYP3A substrates including the erythromycin breath test, midazolam, nifedipine, dapsone and lignocaine, in addition to the urinary 6β-hydroxy cortisol:cortisol ratio (Watkins 1994, Smith *et al.* 1998). Extrapolation of animal *in vitro*/*in vivo* data to man can be problematical as marked species differences have been demonstrated in the response of the CYP3A subfamily to inducers. For example, rat does not readily respond to rifampicin and rabbit does not respond to pregnenolone 16α-carbonitrile (PCN) (Le Cluyse 2001a). To overcome this problem of species differences, human-derived *in vitro* systems have been used, particularly human hepatocytes (Le Cluyse 2001b), in addition to human liver slices or human-derived cell lines. Although informative, the use of human hepatocytes and liver slices has a number of drawbacks. For example, supply can be erratic, expensive and often from atypical/uncharacterized sources, with an unknown drug history. In addition, the levels of cytochrome P450 expression may be highly variable and may be lost during extended culture (Cashman 1996). Some human-derived cell lines such as Hep3B or Tong/HCC either fail to express the cytochromes P450 or demonstrate atypical expression (Ferro *et al.* 1993, Schuetz *et al.* 1993), although it should be noted that HepG2 cells are responsive to CYP3A4 inducers (Fukuda *et al.* 1992, Schuetz *et al.* 1993) as are HuH-7 cells for CYP3A5 and CYP3A7 expression (Pickwell *et al.* 1996, Schuetz *et al.* 1996a). *In vivo* studies in man, such as the erythromycin breath test, have been used to demonstrate the induction of CYP3A4 by xenobiotics (Watkins 1988). However, this latter approach poses ethical problems including the invasive administration of radioactive probe substances.

The ability of xenobiotics to regulate gene expression may be studied using *in vitro* reporter gene constructs in human liver cell lines. In this approach, the regulatory elements (promoter and/or enhancer regions) of the gene of interest are genetically engineered into a plasmid vector containing a readily assayed reporter gene enzyme. The expression of the reporter gene is thus directly regulated by the target gene regulatory elements, allowing the assessment of the ability of a compound to regulate the expression of the gene at the transcriptional level. This approach has been previously applied in our laboratory to the study of the induction of CYP3A4 by xenobiotics (Ogg *et al.* 1999, El-Sankary *et al.* 2000, 2001), using approximately 1 kb of the CYP3A4 regulatory region (-1067 to -57 bp) coupled to the reporter gene for secretory placental alkaline phosphatase (SEAP) in HepG2 cells and driven by the CMV promoter. The use of heterologous promoters in reporter gene constructs is a standard and widely accepted method of amplifying responses mediated by the homologous promoter and is fully controlled and accounted for in our data analysis (Plant *et al.* 2000). HepG2 cells (human liver-derived) are commonly used in such studies as they contain constitutive and inducible CYP3As (Fukuda *et al.* 1992, Schuetz *et al.* 1993) and have been successfully used to transactivate the CYP3A4 promoter, as originally reported (Hashimoto *et al.* 1993), in our recently published studies (Ogg *et al.* 1999) and additional studies described herein.

Our laboratory has taken the approach of using a CYP3A4 promoter–reporter gene in HepG2 cells to construct dose–response curves for known and putative

Table 2. Dose–response characteristics of known CYP3A4 *in vitro* inducers.

Compound	EC_{50}^{*} (μM)	I_{max}	Intrinsic activation (I_{max}/EC_{50})
Lovastatin	0.5	100	223
Simvastatin	0.8	82	101
Troglitazone	0.2	17	78
Rifampicin	1.2	48	40
Dexamethasone	1.9	47	25
Fexofenadine	2.4	47	20
PCN	2.5	44	18
Carbamazepine	0.9	14	16
Clotrimazole	1.1	15	14
Spironolactone	1.1	13	12
Cyproterone acetate	1.6	11	7
Phenobarbital	9.7	41	4
Metyrapone	6.6	21	3
Sulphinpyrazone	7.9	14	2
Phenytoin	25	28	1
Pravastatin	NI	NI	NI

*EC_{50} is defined as the concentration of the inducer producing half the maximum induction response (I_{max}). Intrinsic activation (I_{max}/EC_{50}) reflects the overall ability of the compound to induce CYP3A4 and incorporates both potency and extent of induction. The inducers are ranked in descending order of intrinsic activation. NI, not an inducer.

CYP3A4 inducers to determine their EC_{50} and I_{max} (interpolated maximum induction effect) and hence the overall induction ability, which we have termed intrinsic activation (I_{max}:EC_{50} ratio) as described by El-Sankary *et al*. (2001). As shown in table 2, inducers can be ranked with respect to their induction ability over two orders of magnitude and have the utility that putative human CYP3A4 inducers can be identified and ranked with the need for <100 mg of test compound, which is of particular advantage in the early stages of drug discovery in the pharmaceutical industry. The inducers in table 2 are a combination of known *in vivo* inducers and putative inducers that have been identified either in human hepatocytes or inferred from drug interaction observations in the clinic. Thus, we have categorized inducers as either being strong, medium or weak (dependent on their intrinsic activation) and hence new compounds can be categorized as such. The study represented by table 2 produced no false-positives and no false-negatives, with the only exception of pravastatin, which may be rationalized by the fact that it is taken up by the hepatocyte by a specific uptake mechanism (OATP-2; Tokui *et al*. 1999), and it would appear that this particular phenotype has been lost in the dedifferentiated HepG2 cell line. Whereas we recognize that this *in vitro* ranking procedure for inducers may well be different to that *in vivo* for several metabolic and pharmacokinetic reasons, we suggest that it serves as a useful adjunct to the drug-discovery process, particularly when ever-increasing numbers of candidate compounds derived from combinatorial libraries have to be screened.

Species differences in CYP3A induction

There are marked species differences in response to CYP3A inducers (Kocarek *et al*. 1995, Le Cluyse 2001a). This not only infers species-specific molecular

mechanisms of induction/regulation, but also additionally has clear consequences for the processes of drug discovery and development in the pharmaceutical industry. For example, inducibility of human CYP3As is an undesirable characteristic in that autoinduction of a drug's own metabolism or induction of the biotransformation of a second, co-administered drug (which are both mediated by CYP3A4), would produce variable pharmacokinetics and altered drug clearance on repeated exposure. This presents the clinician with an undesirable biological variable as individuals are most likely to vary in their response to CYP3A4 inducers as exemplified by the 4–8-fold variation in induction of enterocyte CYP3A4 mRNA and corresponding catalytic activity in patients receiving rifampicin, a known CYP3A4 inducer (Kolars *et al.* 1992). This latter variability in the human induction data is not inconsistent with the possible existence of genetic polymorphisms in the regulatory region of the CYP3A4 gene. However, it must be emphasized that evidence to support this view is only now beginning to emerge and that alternative mechanisms are possible, including prior exposure to drugs and other xenobiotics that induce or inhibit CYP3As. Accordingly, it is clear that human variability in susceptibility to CYP3A induction and the resultant differences in drug clearance would result in non-uniform patient blood levels, variable patient responses and, in extreme cases, to complete therapeutic failure (Venkatesan 1992).

With the above in mind, the early recognition and characterization of drug candidates as potential CYP3A inducers in man is an important milestone in the drug-discovery and -development processes (Worboys and Carlile 2001). Although testing in human subjects for CYP3A4 induction can be approached by the use of non-invasive CYP3A-specific substrates such as the erythromycin breath test or probe substrates such as nifedipine, dapsone or lignocaine (Watkins *et al.* 1988, Wilkinson 1996), the early *in vivo* testing of drugs in man is ethically impossible due to the lack of acute/chronic toxicological information at this stage. Traditionally, surrogate experimental animals have been used to assess CYP3A induction and an extrapolation made to man, but, as discussed below, species variations in response obscure a realistic assessment of induction in man.

Although the synthetic steroids, dexamethasone and PCN induce CYP3A1 in rat, both *in vitro* and *in vivo*, rifampicin is without effect (Li *et al.* 1995). However, rifampicin is a potent inducer of CYP3A4 both in human hepatocytes (Kocarek *et al.* 1995), in man (Damkier *et al.* 1999) and in rabbit (Lange *et al.* 1984, Sonderfan *et al.* 1987). Barwick *et al.* (1996) investigated the molecular basis for this species difference in induction by trans-species gene transfer of the 5′-regulatory sequences from rat (CYP3A2), human (CYP3A4, CYP3A5, CYP3A7) and rabbit (CYP3A6), coupled to a chloramphenicol acetyltransferase (CAT) reporter gene. All of the latter CYP3A reporter genes were activated by rifampicin when transfected into rabbit hepatocytes as the host cell, but not in rat hepatocytes. Thus, these experiments have indicated that the host cellular environment (namely transcription factors and receptors) in addition to gene promoter structure dictate the patterns of CYP3A inducibility. The opposite occurred when PCN was used as the inducer, as CAT activity in rabbit hepatocytes was refractory to CYP3A6 induction. Dexamethasone increased CAT activity in both rat and rabbit hepatocytes (Barwick *et al.* 1996). Other species differences in CYP3A inducibility include the α-naphthoflavone and diazepam induction of the cognate CYP3As in

man and dog, whereas these two compounds inhibited mouse and rat CYP3As, possibly by an allosteric mechanism (Zhao and Ishizaki 1997).

As will be discussed below, cellular receptors play an important role in regulating CYP3A gene expression and with respect to species differences in CYP3A inducibility, it is important to note that a 'humanized' transgenic mouse colony has been described where the constitutive mouse receptor has been deleted and the human orthologue inserted (Xie *et al.* 2000b). These receptor knock out/knock in mice respond to rifampicin-mediated induction of CYP3A, whereas the wild-type mouse does not.

Therefore, with these species differences in mind, the early identification of drug candidates as inducers of human CYP3As in the discovery phase is problematical. Fortunately, human CYP3A promoter/reporter gene constructs have been developed partially to address this problem, as discussed above.

Receptor-mediated transcriptional activation of the CYP3A4 gene

The molecular mechanisms of induction of the CYP3A subfamily remain a topic of current debate and substantial research effort. Phenobarbitone, dexamethasone, PCN and rifampicin have been reported to induce CYP3A expression at the level of transcription (Larsen *et al.* 1994, Barwick *et al.* 1996), whereas clotrimazole, triacetyloleandomycin (TAO) and erythromycin appear to induce at the post-transcriptional level either by mRNA or protein stabilization (Watkins *et al.* 1986, Hostetler *et al.* 1989). For those CYP3A genes whose transcriptional regulation is known to be receptor-dependent, many of the molecular mechanisms share common features between species, and for the sake of clarity, attention will be focussed on the CYP3A4 gene and substantial differences highlighted where appropriate.

Strictly speaking, the standardized nomenclature system for nuclear receptors based on sequence similarity and evolutionary relatedness should be used (Nuclear Receptor Nomenclature Committee 1999). Currently, approximately 50 such receptors are known, half of which are classified as orphan receptors as they have no known ligands (Tzameli and Moore 2001). This system currently categorizes the superfamily into seven groups and seven subfamilies, which are further divided into groups, wherein receptors in the same group share at least 80–90% identity in their DNA-binding domains and have at least a 40–60% identity within the ligand-binding domain (Nuclear Receptor Nomenclature Committee 1999). For example, the glucocorticoid receptor is alternatively termed NR3C1.

Role of the glucocorticoid receptor (NR3C1) in CYP3A4 gene regulation

Structural aspects

There has been much discussion about the role of the glucocorticoid receptor (GR) in the induction of the CYP3A subfamily by compounds such as dexamethasone because several aspects of putative GR-mediated regulation do not accord with the classical functions of this receptor. The GR contains a DNA-binding domain with two putative zinc-binding fingers, consisting of a zinc ion in tetrahedral coordination with two cysteine residues and it is highly conserved in

the steroid hormone receptor family (Evans 1988). The GR also contains a ligand-binding domain of approximately 30 amino acid residues near the carboxyl terminus of the molecule and is involved in hormone binding, nuclear translocation, transactivation and dimerization with other receptors (Evans 1988, Beato 1989). The precise sequence of molecular events resulting in GR-dependent gene regulation is still emerging, but it is thought that binding of the glucocorticoid to the GR promotes dissociation from the cytoplasmic hsp90/hsp70/hsp56 heteromeric complex (Pratt 1993), thereby exposing the nuclear localization signal (Picard and Yamamoto 1987), subsequent GR-homodimerization and translocation to and accumulation in the nucleus (Pariante *et al.* 2001) where the zinc fingers interact with the GR response elements in the promoter of GR-responsive genes (Ing and O'Malley 1995). The consensus sequence of GR response elements is GGTACAnnnTGTTCT and the GR also recognizes a consensus half site (TGTTCT) arranged in a pair as a palindrome (Beato 1989). Classical glucocorticoid-inducible genes such as tyrosine aminotransferase (TAT) and mouse mammary tumour virus (MMTV) contain consensus glucocorticoid response elements (GRE) (Evans 1988) and their induction by dexamethasone is antagonized by the antiglucocorticoids PCN and RU-486 (Wright and Paine 1994, Quattrochi *et al.* 1995).

Functional aspects

Defining a specific and 'classical' role for the GR in CYP3A gene regulation is problematical in that the concentrations of glucocorticoid required for induction exceed full GR occupancy (Schuetz and Guzelian 1984) and the observation that GR antagonists induce CYP3A4 (Wright *et al.* 1996) and also enhance dexamethasone-dependent induction (Wright and Paine 1994). The role of GR antagonists in CYP3A induction is particularly puzzling, but may be related to the observation that RU-486 activates the translocation of the GR from the cytoplasm to the nucleus in a mouse cell line (Pariante *et al.* 2001). Furthermore, a recent study in the GR-null mouse (−/−) showed no differences in either constitutive- or glucocorticoid/antiglucocorticoid-induction of hepatic CYP3As, as compared with the wild-type (+/+), suggesting a non-obligatory (but perhaps permissive?) role for the GR (Schuetz *et al.* 2000). Promoter sequences identified in rat CYP3A23, rabbit CYP3A6 and human CYP3A4, which have been reported to be responsible for the transcriptional activation by dexamethasone, PCN and rifampicin (Quattrochi *et al.* 1995, Barwick *et al.* 1996), display no sequence identity for the consensus GRE sequence (GGTACAnnnTGTTCT). Transfection of constructs containing components of the 5′-flanking regions of CYP3A7 into the human hepatoma line HuH-7, identified a dexamethasone-responsive sequence 835 bp upstream of the CYP3A7 promoter, but induction was only observed upon co-transfection with a plasmid encoding the human glucocorticoid receptor (Pickwell 1996). The glucocorticoid receptor has been implicated in the dexamethasone-mediated induction of a CYP3A5 reporter construct (−1109 bp to −891 bp) for the following reasons. First, dexamethasone induction was blocked by the antiglucocorticoid RU-486; second, two GRE half-sites (separated by 160 bp) were identified within the response element, both of which were required to achieve dexamethasone-mediated induction. Third, in

HepG2 cells, co-transfection with a plasmid encoding the glucocorticoid receptor was required to achieve induction (Schuetz 1996a).

Our laboratory has developed a validated reporter gene construct containing the first 1 kb of the CYP3A4 promoter and demonstrated it to be inducible in HepG2 cells both by dexamethasone and a glucocorticoid steroid (hydrocortisone) in a dose-dependent manner (Ogg *et al.* 1999, El-Sankary *et al.* 2000, 2001), a response which is increased 2–3-fold by the co-transfection of an expression plasmid encoding the full-length human GR (figure 1). Although rifampicin transactivated the CYP3A4 construct in basal HepG2 cells, this response was not significantly increased in hGR co-transfected cells (El-Sankary *et al.* 2000, 2001), consistent with the observation that this inducer is a better ligand for hPXR than it is for hGR (figure 1). Furthermore, we have reported that high passage HepG2 cells lose the ability to respond to dexamethasone (50 μM), the response being regained (3-fold induction) subsequent to co-transfection of the hGR (Ogg *et al.* 1999).

Further evidence implicating a role for the GR in CYP3A induction has been reported for the CYP3A1/CYP3A23 gene (Pereira *et al.* 1998). In this latter study, a 219 bp GRE in CYP3A1/CYP3A23 (−1882 to −2100 bp) was identified that mediated induction with physiological doses of glucocorticoids

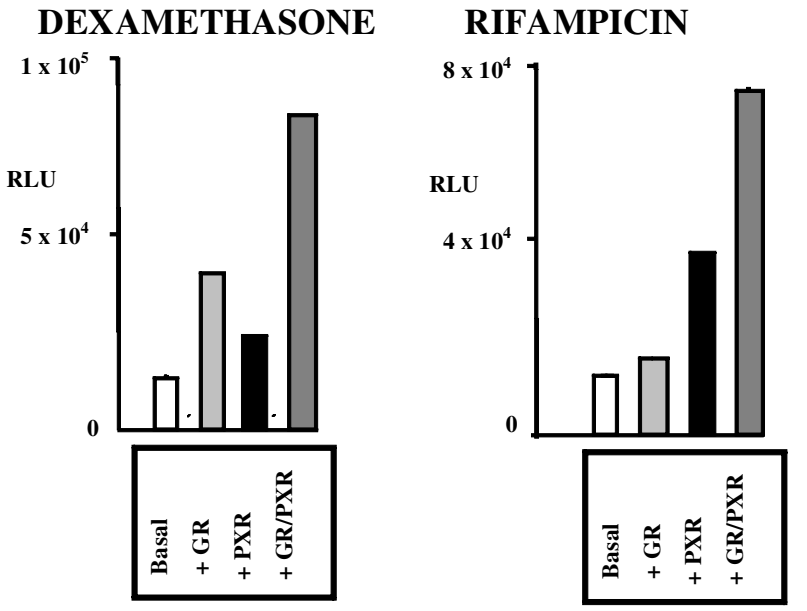


Figure 1. Role of cellular receptors in the activation of CYP3A4 by dexamethasone and rifampicin. HepG2 cells were transfected with a CYP3A4 proximal promoter–reporter gene system and transactivated with either dexamethasone or rifampicin, both at 50 μm concentration, which produced the maximum response in the absence of attendant cytotoxicity. Transactivation was carried out in either the basal system or HepG2 cells that had been transfected with expression plasmids encoding either GR, PXR or both, as described (El Sankary *et al.* 2000, 2001). Data are the mean ± SEM from eight replicate determinations and are all significantly different from the relevant control value (no inducer) at $p < 0.001$. RLU is relative light units for reporter gene activity as determined by enhanced chemiluminescence (ECL).

in HepG2 cells. DNase footprinting analysis identified two GR-protected sequences at −1960 to −1982 bp (footprint 1) and at −1968 to −2001 bp (footprint 2), but point mutations in footprint 1 completely abolished binding and transcriptional activation, whereas mutation of footprint 2 only decreased binding and had no influence on activation. Although this latter study is not inconsistent with a direct role for the GR, it was alternatively suggested that cooperation between the GRE and other regulatory elements, such as ER_6, could not be excluded.

The role of the GR in CYP3A4 gene activation is further complicated by the observation that recent evidence suggests that submicromolar concentrations of dexamethasone activate CYP3A4 via an GR-mediated increase in both hPXR and hRXRα, which parallels the time course and dexamethasone concentration-dependency of induction of the tyrosine aminotransferase gene, a classical, glucocorticoid-responsive gene (Pascussi *et al.* 2000a). Similarly, it has recently been reported that the glucocorticoid agonists dexamethasone, prednisolone and hydrocortisone also induces hCAR mRNA (see below) in cultured human hepatocytes, in parallel with accumulation of tyrosine aminotransferase, both of which are down-regulated by the concomitant treatment with RU-486 (Pascussi *et al.* 2000b). Thus, the role of the hGR in CYP3A4 regulation is complex and obscures a realistic assessment of whether hGR plays a direct or an indirect role, or indeed, both.

A further subtlety relating to the role of the GR involves the possible interaction of ligand activated GR and HNF-5 binding to the 5′-flanking region, a previously proposed mechanism for the transcriptional activation of glucocorticoid-dependent genes. Grange *et al.* (1991) proposed a 'hit and run' mechanism for GR-mediated activation of the rat tyrosine aminotransferase gene, wherein transient binding of the activated GR–ligand complex causes a stable binding of HNF-5 at neighbouring sites (in some cases in a mutually exclusive fashion), with subsequent transcriptional activation mediated by HNF-5. This is also consistent with recent evidence that the GR complexes with histone acetyltransferases, which are directly involved in removing histones from DNA, thus freeing binding sites for other transcription factors, possibly HNF-5 (Lemon 1999, Wallberg 1999). Whether the GR activates CYP3A4 transcription by this latter mechanism, in whole or in part, remains to be established, but it is instructive to note that in human hepatocytes transfected with the closely related HNF-4 antisense RNA, there is a dose-dependent down-regulation of CYP3A4 and CYP3A5 (Jover *et al.* 2001). Related to this are the observations that HNF-4 contributes to both the basal level and maximum induction by dexamethasone of CYP3A in rat (Huss and Kasper 1998, 2000).

A further issue to consider is that the GR function is becoming increasingly recognized as not simply an on/off switch for gene regulation, in that the recruitment of coactivators and other regulatory factors can confer receptor, promoter and cell specificity for target genes (Jenkins *et al.* 2001).

Thus, taken collectively, the GR does indeed contribute to CYP3A4 transcriptional gene activation for some but not all CYP3A inducers, and very likely does so by a 'non-classical', indirect molecular mechanisms, including functional cross talk between GR-, PXR- and CAR-signalling pathways.

Role of the pregnane X receptor (PXR, NR112) in CYP3A4 gene regulation

Structural aspects

Notwithstanding the role of the GR in CYP3A4 gene regulation, the apparent paradox that both glucocorticoid receptor agonists (e.g. dexamethasone and hydrocortisone) and antagonists (e.g. PCN and RU-486) up-regulate the gene (and other CYP3As) has been problematical to reconcile. However, this apparent paradox has been essentially resolved by the discovery that the PXR plays an important role in CYP3A4 gene regulation for several xenobiotic and endobiotic inducers in several species, first identified in mouse (Kliewer *et al.* 1998) and subsequently in man (Bertilsson *et al.* 1998, Lehmann *et al.* 1998), rat (Zhang *et al.* 1999), rabbit (Savas *et al.* 2000) and chicken (Handschin *et al.* 2000). The PXR is a member of the nuclear receptor family, the important structural features being a C-terminal, ligand (inducer)-binding domain and a DNA-binding domain (Nuclear Receptor Nomenclature Committee 1999). The PXRs have alternatively been termed SXR (steroid xenobiotic receptor) or PAR (pregnane-activated receptor).

Of the five PXRs isolated and characterized to date in rat, mouse, human, rabbit and chicken, rat shares an overall 95% sequence similarity to that of mouse, whereas the former is only 79% similar to the human form (Zhang *et al.* 1999), consistent with the observations that the CYP3A induction profile in rodents is different from that in man (Le Cluyse 2001a). The rabbit PXR shares an overall 73% sequence similarity to rat (Savas *et al.* 2000) and on this basis is more related to the human form. Of more importance to species differences in CYP3A induction is a comparison of the ligand-binding domains of PXR orthologues which are somewhat more divergent in the amino acid sequence of their ligand-binding domains (77–82% for the above five species), with the exception of a 97% similarity between rat and mouse (Savas *et al.* 2000). In contrast, the amino acid sequences of the DNA-binding domains in the above five species are more conserved (92–95% similar (Savas and Johnson 2000), inferring that the PXRs regulate CYP3A gene expression via binding to and activation of common (or very similar) response elements in their respective promoters.

The ligand-binding domain (amino acid residues 130–434) of human PXR has been crystallized in both the free and ligand (SR12813)-bound forms to a resolution of 2.5 and 2.75 Å respectively (Watkins *et al.* 2001). The ligand-binding cavity is substantially larger than for related nuclear receptors and has a pronounced lipophilic character, with 20 of the cavity-lining residues being hydrophobic in nature, with a minimum of charged residues. The SR12813 ligand binds in at least three energetically favourable conformations, and of the 20 residues involved in ligand contact, only Phe^{288} interacts with all three conformations. In this context, it is noteworthy that Phe^{288} is conserved in known PXR sequences reported to date. Thus, it would appear that the large ligand-binding pocket and its hydrophobic nature is consistent with the known spectrum of structurally diverse CYP3A inducers that act via the PXR.

Functional aspects

In man and other species, a PXR/RXR heterodimer is essential for the activation of CYP3A4 reporter gene constructs by xenobiotics and naturally

occurring pregnane steroids (Lehmann *et al*. 1998). The importance of the RXR as an obligate dimerization partner for PXR is underscored by *in vivo* studies in the mouse wherein *cre*/*lox*-mediated, recombinant disruption of the mRXRα gene ablated PXR-mediated responses, in addition to other nuclear receptors including PPARα, CARβ, LXR and FXR (Wan *et al*. 2000). In addition, submicromolar concentrations of dexamethasone in human hepatocytes have been reported to increase the expression of human RXRα mRNA (which is inhibited by RU-486, a GR antagonist), to induce the accumulation of RXRα-immunoreactive protein and to increase the nuclear level of RXRα: PXR heterodimers as determined by gel shift assays (Pascussi *et al*. 2000a). Thus, RXR plays a central role in the regulation of many diverse endobiotic and xenobiotic metabolic pathways, and as such, represents an additional locus of control for the PXR-mediated regulation of the CYP3A4 gene, particularly in cellular environments where the prevailing concentrations of RXR are limiting.

In the proximal promoter of CYP3A4, the PXR response element is localized to a sequence in the CYP3A4 promoter (at approximately -153 to -170 bp), containing two copies of the nuclear receptor half site sequence AG(G/T)TCA organized as an everted repeat (ER) and separated by 6 bp, collectively termed an ER_6 motif. The distal CYP3A4 enhancer, located approximately -7.8 kbp upstream of the transcription start site, contains three elements (termed dNR1, dNR2 and dNR3) capable of binding hPXR-RXR-α heterodimers, in addition to two additional *cis*-acting elements (termed FP1 and FP2) immediately upstream of the latter PXR-binding regions which are essential for full responsiveness to transactivation by rifampicin (Goodwin *et al*. 1999a). In addition, the latter group have reported on the preliminary characterization of transgenic mice carrying the essential elements of the human distal enhancer linked to the *lacZ* reporter gene, which when challenged with a broad range of CYP3A inducers, reflected the mouse *Cyp3a* induction profile, probably reflecting the ligand specificity of the mouse PXR (Robertson *et al*. 2000). This human regulatory CYP3A4 transgene in the mouse offers an excellent opportunity to delineate the relative contributions made by human regulatory elements and animal transcription factors to CYP3A induction in an *in vivo* setting. Furthermore, the latter authors have provided evidence that the proximal and distal CYP3A4 promoters interact with each other in a cooperative manner, highly reminiscent of a similar interaction of regulatory elements in the glucocorticoid-responsive tyrosine aminotransferase (Jantzen *et al*. 1987) and the phenobarbital-responsive CYP2B genes (Sueyoshi *et al*. 1999) amongst others. However, the precise molecular mechanisms underpinning the proximal/distal promoter interaction(s) in CYP3A4 remains an area for further exploration, as does the role of the liver-specific CAR receptor (see below).

PXR can bind to a number of response elements including ER_6, $DR_3$and DR_4 and these elements are not confined to the human CYP3A4 gene, but are also present in the promoters of rat CYP3A2, rabbit CYP3A6 and human CYP3A5 (Barwick *et al*. 1996), rat CYP3A23 (Huss and Kasper 1998) and human CYP3A7 (Pascussi *et al*. 1999).

To summarize, it appears that PXR/RXR heterodimers can bind to both DR_3 elements (RGKTCAknaAGTTCA) in CYP3A2, 3A4 and 3A23 and to ER_6 motifs (TKAACTcannggAGGTCA) in CYP3A4, 3A6, 3A7 and 3A23 (Negishi and Honkakoski 2000).

The rabbit CYP3A6 and human CYP3A4 promoters utilize ER_6 elements whereas the rat CYP3A2 and CYP3A23 promoters have similar DR3 elements (AGTTCAn3AGTTCA). Notwithstanding these species similarities in their PXR-binding regions, it is evident that the molecular mechanisms underpinning species differences in CYP3A induction profiles are either due to the participation of different sets of transcription factors and/or differences in the binding capacity/affinity of the PXR orthologues between species (see below), further emphasizing the importance of cellular factors as proposed by Barwick *et al*. (1996). A recent study emphasized the importance of PXRs in dictating species-specificity in inducer response by generating a null mouse PXR-transgenic/human PXR knock-in mouse colony that is 'humanized' in the sense that they respond to rifampicin induction of CYP3A, whereas the wild-type mouse does not (Xie *et al*. 2000b).

From the above discussion of the PXR, it is absolutely clear that xenobiotics and steroids are PXR ligands activating CYP3A genes, thereby indicating a possible physiological role for the latter group of compounds. The spectrum of PXR ligands has been expanded by the recent identification of lithocholic acid (a bile acid) as a PXR ligand in man, rat and mouse in addition to chenodeoxycholic acid and deoxycholic acid (Staudinger *et al*. 2001, Xie *et al*. 2001). Lithocholic acid is hepatotoxic (Taylor and Lesna 1997) and CYP3A enzymes protect against the liver from this bile acid by catalysing its hydroxylation. This has clearly been demonstrated by the use of the PXR knockout mouse whereby after 4 days of treatment with lithocholic acid, necrotic lesions in 100% of the knockout mice as compared with 58% in the wild-type were observed, consistent with the complete protection exhibited by transgenic mice harbouring the human PXR/SXR gene (Xie *et al*. 2001). These latter authors also directly demonstrated the involvement of CYP3A4 in producing several hydroxy metabolites of lithocholic acid, although CYP3A5 was much less active in this respect.

Regulation of PXR expression

Although classical P450 inducers (β-naphthoflavone, 3-methylcholanthrene, phenobarbital) marginally induce PXR mRNA in rat *in vivo*, significant increases have been reported for dexamethasone and PCN (1–3-fold), clofibrate (2-fold), perfluorodecanoic acid (10-fold) and isonizaid (8-fold), whereas troleandomycin slightly decreased expression (Zhang *et al*. 1999). Thus, taken collectively in the rat, xenobiotics induce CYP3As by acting as PXR inducers, ligands or both, thereby providing a rational molecular explanation for the structural diversity of CYP3A inducers. Whether this phenomenon of PXR induction by PXR ligands and CYP3A substrates is rat-specific remains to be determined, but if a similar regulatory paradigm exists in man, then this would represent an additional mechanistic basis for drug–drug interactions (e.g. HIV-positive patients on combination therapy with protease inhibitors [ritonavir, a CYP3A4 substrate] and antitubercular drugs [isoniazid and rifampicin, inducers]).

It remains to be determined whether the PXR is responsible for the regulation of other P450 subfamilies, although it should be noted that PXR-like response elements have been identified in several CYP2A, CYP2C and CYP2E genes (Blumberg *et al*. 1998), and PXR (in addition to GR and CAR) has been

implicated in the regulation of both CYP2C8 and CYP2C9 (Gerbal-Chaloin *et al.* 2001). In this context, it is interesting to note that PCN (a PXR ligand) acts to *down-regulate Cyp7a1* (cholesterol 7-α-hydroxylase) in C57BL/6J mice and that basal *Cyp7a1* mRNA expression is reduced in PXR $-/-$ mice as compared with the wild-type (Staudinger *et al.* 2001). Furthermore, the PXR $-/-$ phenotype was additionally refractory to the repressive effects of PCN on *Cyp7a1* expression, thereby strongly supporting a role for PXR in the regulation (albeit negative) of *Cyp7a1*.

The observation that several inducers of CYP3A4 are also inducers of P-glycoprotein (a transporter involved in the absorption and presystemic elimination of drugs, encoded by the MDR1 gene) would infer that both proteins share common elements in their regulation. The 5′-upstream regulatory region of the MDR1 gene has a complex regulatory cluster at approximately -8 kbp, containing a DR4 motif that serves as a locus for the binding of PXR (Geick *et al.* 2001), thereby conferring a broader role for PXR in drug disposition.

A further interesting aspect of PXR regulation involves the transcription factor HNF-4α, whereby deletion of this gene in the CD-1 mouse results in the complete ablation of both PXR and HNF-1α expression in the liver (Li *et al.* 2000). Whether HNF-4 acts alone in this context or additionally requires the participation of HNF-1 and other coactivators such as SRC-1 or GRIP1 (Wang *et al.* 1998) still remains to be determined.

In the perinatal mouse, expression of PXR mRNA has been reported to increase by 50-fold in the liver and ovary towards term and decrease postpartum, but is unaffected in the placenta (Masuyama *et al.* 2001). In the same report, these latter authors also reported interaction of the PXR with the nuclear receptor coactivators SRC1 (steroid hormone receptor coactivator-1), RIP140 (receptor interacting protein 140) and SUG1 (also known as p45 or thyroid hormone-receptor interacting protein [TRIP1'], an ATPase subunit of the 26 S proteasome and a putative transcriptional modulator). In separate experiments, the same authors reported that PXR interacts with SRC1 and RIP140 in the presence of phthalic acid or nonylphenol, two compounds capable of inducing CYP3A in primary human hepatocytes (Masuyama *et al.* 2000).

Role of the constitutive androstane receptor (CAR, NR1 13) in CYP3A4 regulation

CAR was originally identified as a receptor controlling the expression of the retinoic acid receptor β2 and alcohol dehydrogenase 3 genes (Baes *et al.* 1994). CAR belongs to a subgroup of the nuclear receptor superfamily, which includes vitamin D, farnesoid X (FXR) and the α- and β-oxysterol receptors, but its closest structural relative is the PXR (Tzameli and Moore 2001). CAR is an unusual receptor in that it is transcriptionally active in the absence of bound ligand and upon binding of its steroid ligands (the 3α-hydroxy, 5α-reduced androgens androstanol [5α-androstan-3α-ol] and androstenol [5α-androst-16-en-3α-ol]) is transcriptionally inactive, i.e. the steroid ligands function as suppressers of receptor activity thought to function by enhancing the release of necessary coactivators and often referred to as reverse agonists (Forman *et al.* 1998).

CAR is a liver-enriched nuclear receptor that participates in the regulation of CYP2B genes and interacts with a DR4 element (RGGTCAggaaAGTNCA) of

phenobarbital-responsive enhancer regions (PBREs) in CYP2B promoters (in conjunction with RXR), to confer phenobarbital-inducible transcriptional activation of CYP2B genes, such as CYP2B6 (Honkakoski *et al.* 1998, Sueyoshi *et al.* 1999, Sueyoshi and Negishi 2001) and CYP2B1, 2B2 and *2b10* (Negishi and Honkakoski 2000, Muangmoonchai *et al.* 2001). CAR–RXR heterodimers have been reported to bind to ER_6 elements in the CYP3A4 promoter (Sueyoshi *et al.* 1999, Tzameli *et al.* 2000, Xie *et al.* 2000) and when transfected into HepG2 cells, human CAR produces a 13-fold enhancement of constitutive CYP3A4 gene expression (Goodwin *et al.* 1999b). This latter CAR-dependent enhancement appears to reside in both the distal enhancer (Goodwin *et al.* 1999a and b) and the proximal promoter of CYP3A4 (Moore *et al.* 2000), and there appears to be a functional synergism between the distal and proximal promoters, the precise molecular details of which remain to be clarified.

Like the PXR, CAR is activated by a range of structurally diverse ligands (Blizard *et al.* 2001, Quattrochi and Guzelian 2001, Sueyoshi and Negishi 2001) and it should also be noted that direct binding of CAR activator ligands to the receptor has been demonstrated, substantiating the role of CAR as a receptor mediating CYP3A gene regulation (Moore *et al.* 2000).

In uninduced mice, CAR is localized in the cytoplasm and accumulates in the nucleus after exposure to phenobarbitone (Kawamoto *et al.* 1999), the nuclear translocation being mediated by a leucine-rich peptide in the C-terminus of the receptor, at least in the mouse (Zelco *et al.* 2001). Put another way, the exclusion of CAR from the nucleus provides a mechanism whereby CYP genes are (partially) transcriptionally suppressed in the absence of phenobarbitone and presumably, CYP3A inducers. As is the case for other nuclear receptors, once accumulated in the nucleus, CAR targets its cognate genes, but the precise molecular mechanism(s) whereby CAR activates CYP3A genes still remains to be clarified. It is plausible that inducer–CAR binding to responsive genes may involve the subsequent recruitment of cellular coactivators, crucial to the inductive response.

1,4-bis[2-(3,5-dichloropyridoxyloxy)] benzene (TCPOBOP), a highly potent phenobarbitone-like inducer of CYP2B genes (Sueyoshi *et al.* 1999), is also a highly potent, dose-dependent activator of CAR, wherein CAR–RXR heterodimers bind to both ER_6 elements in human CYP3A4 and DR-3 elements in the rat CYP3A1 promoter. The EC_{50} for TCPOBOP activation of CAR is 20 nM, substantially lower (250–400 nM) than that for the CAR suppresser androstanol (Tzameli *et al.* 2000). These latter authors have therefore suggested that TCPOBOP and androstanol compete with each other for binding to the CAR ligand-binding domain, a hypothesis substantiated by the observation that mutations in the ligand-binding domain of CAR block both the inhibitory effect of androstanes and TCPOBOP-dependent activation. It should be noted that direct binding of TCPOBOP to the mouse receptor has been reported and that this ligand binding significantly enhances coactivator recruitment both *in vitro* and *in vivo* (Tzameli *et al.* 2000).

It appears very likely that CAR plays a crucial role in the well-established glucocorticoid-mediated induction of CYP3As, as it has recently been reported that dexamethasone induces CAR mRNA levels in human hepatocytes (Pascussi *et al.* 2000b). Although this observation needs to be independently confirmed and further clarified, it does provide an attractive hypothesis to rationalize the 'non-classical' role of the hGR in CYP3A induction, as discussed above.

The importance of CAR in drug metabolism is emphasized by the lack of induction of the *Cyp2b10* gene in CAR knockout mice by both phenobarbitone and TCPOBOP (Wei *et al.* 2000). To our knowledge, CAR knockout mice have not been used to examine the effect of such a manipulation on *Cyp3a* inducibility, but would be an interesting set of experiments to attempt, as it may yield valuable information on the relative contribution made by CAR to the overall induction process by a variety of inducers.

Recently, the CAR gene has been stably incorporated into the genome of HEK293 cells, the receptor in the first generation cell line being suppressed by androstanes and reactivated by chlorpromazine, metyrapone, phenobabitone and clotrimazole (Honkakoski *et al.* 2001).

Receptor variants

PXR

Two variants of PXR (termed mPXR.1 and mPXR.2) have been characterized in the mouse (Kliewer *et al.* 1998). mPXR.2 is a splice variant of mPXR.1 (wild-type) and although both receptors bind to the CYP3A4 promoter, mPXR.2 is activated about 20-fold less than the mPXR.1 wild-type receptor and has a significantly restricted range of inducer activators. Recent evidence has supported the view that the hPXR gene is polymorphically expressed in normal and neoplastic human breast tissue, wherein both the wild-type (termed hPXR.1) and a splice variant (termed hPXR.2) are expressed (Dotzlaw *et al.* 1999). hPXR.2 contains an in-frame 123-nucleotide deletion in the ligand-binding domain and this variant is similar to the above mutation in the mPXR.2 gene. However, the functional impact of this deletion in hPXR.2 on gene expression, nor its presence/frequency in liver, has not been determined to date, and offers a fruitful area for further exploration.

CAR

In the mouse, the CAR gene expresses at least two variants, namely the wild-type (mCAR1, active) and the inactive mCAR2 species. mCAR2 is a truncated transcript missing the C-terminal portion of the ligand binding/dimerization domain, arising from a splicing defect that skips the eighth and last exon (Choi *et al.* 1997). mCAR2 does not bind to its target DNA, nor does it interfere with binding of mCAR1.

CYP3A promoter sequences and regulation of gene expression

As CYP3A inducers constitute a structurally diverse range of chemical structures, it is highly unlikely that they all act through a common mechanism of action and the cumulative experimental evidence available to date supports this view. Whereas the majority of inducers (e.g. dexamethasone and rifampicin) act through transcriptional activation of the 5′-flanking region, additional post-translational mechanisms have been reported, including mRNA stabilization produced by clotrimazole (Eliasson *et al.* 1994) and the triacetyloleandomycin-mediated stabilization of preformed CYP3A protein (Iribarne *et al.* 1997).

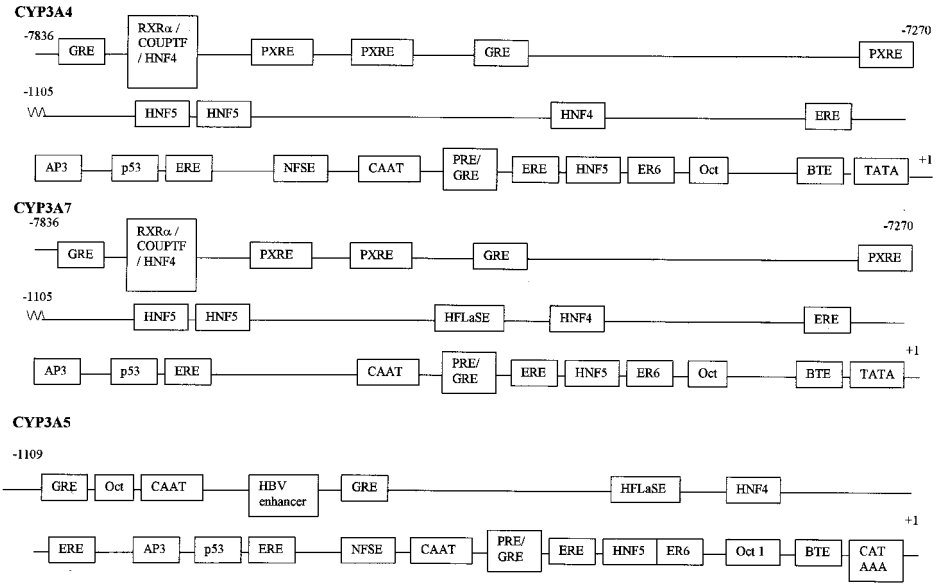


Figure 2. Comparison of proximal promoters and distal enhancers of CYP3A4, CYP3A5 and CYP3A7. The proximal promoters and distal enhancers are shown for CYP3A4 and CYP3A7 and the latter has not been characterized for CYP3A5. The response elements are boxed in at their approximate 5′-flanking location and are abbreviated/defined as in table 3. The promoter region for CYP3A43 has not been characterized to date. Compiled from Itoh *et al.* (1992), Hashimoto *et al.* (1993), Jounaidi *et al.* (1994), Barwick *et al.* (1996), Schuetz *et al.* (1996a), Goodwin *et al.* (1999a), Pascussi *et al.* (1999) and Bertilsson *et al.* (2001).

To rationalize the above species differences in CYP3A regulation and the molecular mechanisms involved, it is instructive to consider and compare the promoter regions in the CYP3A genes and to summarize the regulatory elements (transcription factors/receptors) involved in the induction processes (figure 2).

Rat CYP3A1/CYP3A23 promoter

The literature is somewhat confused about whether CYP3A1 and CYP3A23 are the same gene. In view of Quattrochi and Guzelian (2001), who stated that the 5′ non-coding region of CYP3A1 (Burger *et al.* 1992) is identical to that of CYP3A23 (Komori and Oda 1994), it would appear that they are the same gene. However, until this issue is completely resolved, the literature describing the promoters for CYP3A1 and CYP3A23 will be discussed separately, as follows.

For CYP3A1, a 164 bp fragment (−220 to −56 bp) confers dose-dependent responsiveness to both dexamethasone and PCN, independent of its orientation, although it does not contain a classical glucocorticoid response element. Sequence analysis further revealed a consensus sequence for a TATA box at −31 bp. Putative glucocorticoid response elements (GRE) similar to the TGTYCT motif (where Y is a pyrimidine) of the GRE consensus half palindrome have also been identified (Burger *et al.* 1992). However, there is no TGTYCT hexamer motif or the consensus 15-bp palindrome essential for optimal response to glucocorticoids. Two regions (−936 to −797 bp) and (−219 to −146 bp) contain GRE-like sequences in close proximity to sequences known to bind transcription factors

that interact with the glucocorticoid receptor (GR) such as nuclear factor 1 (NF1), octamer factor and a CACCC box binding factor (Burger *et al.* 1992). These latter experiments support the contention that CYP3A1 induction involves either a GR-like receptor with similar binding properties or a classical GR interacting directly or indirectly with altered GREs associated with PCN-responsive genes. In this context, it should be noted that the PCN receptor has been identified as a human nuclear orphan receptor termed the pregnane X receptor (PXR, see above) in the rat and mouse (Lehmann *et al.* 1998). The PXR binds to a response element in the CYP3A4 promoter and is activated by a range of drugs, natural steroids, synthetic glucocorticoids and antiglucocorticoids known to induce CYP3A4 expression (Kliewer *et al.* 1998, Lehmann *et al.* 1998).

Quattrochi *et al.* (1995) also examined the functionality of the CYP3A1 promoter from adult, male Sprague–Dawley rats and identified a 165-bp fragment (approximately 200 bp upstream of the transcription start site) that confers both dexamethasone and PCN inducibility. DNase 1 footprinting studies identified two extensively protected regions within this 165 bp fragment, which they termed FP1 (-135 to -117 bp) and FP2 (-108 to -85 bp). Only fragments containing the FP1 region (independent of orientation) were responsive to dexamethasone and PCN at a similar magnitude to that which occurs to endogenous CYP3A1 induction by dexamethasone. FP1 contained a palindromic sequence (ATGAACTTCAT) that overlaps one of the two ATGAACT direct repeats separated by two nucleotides (Quattrochi *et al.* 1995). A 6-bp fragment (AGTTCA) of these 7-bp repeated segments represents a high-affinity binding site for several types of nuclear receptors, including the peroxisome proliferator activated receptor (PPAR) and retinoic acid receptors, but the functional significance (if any) of these latter nuclear receptors in CYP3A1 regulation is currently unclear. The 33-bp FP1 motif suggests that multiple DNA-binding proteins may interact with sequences within this element, particularly in view of the fact that this direct repeat sequence also occurs in the rat CYP3A2 gene (Miyata *et al.* 1995).

An additional 219 bp, dexamethasone-responsive fragment has been reported for CYP3A1 at $-2100/-1882$ bp upstream of the transcription start site (Pereira *et al.* 1998). DNase footprinting analysis in this region revealed two glucocorticoid receptor-protected sites, one of which ($-1982/-1960$ bp) completely abolished both binding and transcriptional activation.

Recent work in rat liver hepatocytes has demonstrated the role of PXR and the constitutive androstane receptor (CAR) in activation of the rat CYP3A1 gene, wherein both receptors mediate activation via a DR3 site in the PXR response element of the CYP3A1 promoter (Smirlis *et al.* 2001).

Ogino *et al.* (1999) identified a role for the liver-enriched transcription factor HNF-4, wherein HNF-4 binds to a site in the CYP3A1 promoter (termed 6βB-A, -105 to -86 bp) and enhances transcriptional activation. It has been proposed that HNF-4 functions by recruiting transcriptional coactivators with histone acetylase activity, thereby facilitating gene activation by chromatin remodelling through relaxation of chromatin structure in enhancer and promoter regions (Li *et al.* 2000). However, the role of HNF-4 in regulating CYP genes is not universal as it does play a role in transcriptional activation of rabbit CYP2C2 and human CYP2D6 genes (Chen *et al.* 1994, 1999, Cairns *et al.* 1996) but not for CYP2C7, 2C11, 2C12 and 2C13 (Strom *et al.* 1995). In contrast, a negative regulatory role

for the transcription factors ARP-1 (apolipoprotein A1 regulatory protein 1) and EAR-3 (v-ErbA-related protein 3) in CYP3A1 regulation have been reported (Ogino *et al.* 1999), wherein ARP-1 and EAR-3 bind to a 6βB-B site (−139 to −118 bp) and suppress HNF-4 mediated activation of CYP3A1.

Regulation of the CYP3A23 proximal promoter by dexamethasone using a luciferase reporter gene has been reported and three sites of protection were identified by DNase 1 footprinting analysis in the region −167 to −60 bp (Huss *et al.* 1996). Site A (−91 to −110 bp) shared 80% sequence similarity with an HNF consensus element and was related to the 6-β A-A site in CYP3A2 (Miyata *et al.* 1995, Huss *et al.* 1996). Sites B (−118 to −136 bp) and C (−144 to −169 bp) are necessary for dexamethasone-dependent activation in a cooperative manner, but neither site contains a GRE. Site B contains a repeated ATGAACT sequence, which is also present in the CYP3A1 and CYP3A2 proximal promoters (Miyata *et al.* 1995, Quattrochi *et al.* 1995, Huss *et al.* 1996). Site C contains an imperfect AGGTCA repeat, but no DNA–protein interactions were detected at either the putative GRE half site or the CACCC consensus site (Huss *et al.* 1996). Site C is similar in sequence to the 6βA-C site in the CYP3A2 proximal promoter and the former was responsible for all of the dexamethasone responsiveness, and the sequence was homologous to the class of steroid response elements recognized by the oestrogen receptor (ER) family (Huss *et al.* 1996).

Schuetz *et al.* (1998) demonstrated the presence of a hormone- and xenobiotic-responsive element separated by three nucleotides in the rat CYP3A23 promoter (termed a DR-3), and that this motif required the presence of co-transfected PXR for inducer responsiveness. In addition to the classical CYP3A inducers, the organochlorine pesticides transnonachlor and chlordane and non-planar polychlorinated biphenyls have been demonstrated to activate CYP3A23, as mediated by the PXR at the DR3-3 element in the promoter. This PXR-dependency for CYP3A23 induction was recently confirmed and it has additionally been shown that the DexRE-1 and HNF-4 sites, although not ligand-responsive, are essential for optimal CYP3A23 promoter activity (Scheutz *et al.* 1998). Furthermore, the latter authors have postulated that, in addition to PXR-activation, the overall inductive response involves GR-mediated stimulation of PXR and RXR expression (Huss and Kasper 2000). In this latter model, induction of the CYP3A23 gene is thought to occur in a two-stage process with the initial involvement of a GR-dependent increase in PXR/retinoid X receptor (RXR) expression and subsequent, direct transcriptional activation of CYP2A23, which is dependent on inducer-activated PXR acting in concert with accessory factors bound to the DexRE-1 and HNF-4 sites as described above. This initial sequence of events (PXR/RXR up-regulation) has also been reported to occur in the dexamethasone-dependent activation of the CYP3A4 gene in human hepatocytes (Pascussi *et al.* 2000a).

Although CYP3A2 and CYP3A1/CYP3A23 share 90% sequence similarity in 110 bp in the 5′-regulatory sequences responsible for glucocorticoid induction, it is well established that these two rat genes display different patterns of gender-dependent basal expression and are differentially responsive to induction by glucocorticoids (Huss *et al.* 1999). Specifically, the CYP3A2 gene has been classified as male-specific (Gonzalez *et al.* 1986), represents the major CYP3A enzyme in uninduced rat liver and is approximately 20–25% less responsive to treatment with dexamethasone than is CYP3A1/CYP3A23, the latter being assessed by comparative hepatic mRNA levels (Telhada *et al.* 1992). The

molecular mechanisms mediating these differences in basal and inducible regulation have largely been clarified by promoter deletion studies wherein four nucleotide mismatches in two dexamethasone response elements (termed DexRe-1 and DexRE-2) confer reduced glucocorticoid responsiveness in CYP3A2 (Huss and Kasper 2000). In particular, the DexRe-1 site is preferentially occupied by the chicken ovalbumin upstream promoter-transcription factor (COUP-TF), thereby excluding the B-group proteins, which appear to function as auxiliary transcription factors acting in concert with PXR/RXR and HNF-5 (Huss and Kasper 2000). Therefore, COUP-TF appears to be a negative regulatory factor with respect to DexRE-1 CYP3A4 expression and a similar situation may exist for the DexRE-2 regulatory site (Huss and Kasper 2000).

The higher basal level of expression of CYP3A2 as compared with CYP3A1/CYP3A23 appears to be related to the A site in both promoters. Whereas both CYPs bind HNF-5, only CYP3A23 binds USF1 (a helix–loop–helix leucine zipper protein) via a CACGTG E-box consensus sequence, binding which is ablated in the CYP3A2 promoter because of a single base pair substitution.

Rat CYP3A2 promoter

Miyata *et al.* (1991) isolated a clone and characterized *cis*-acting elements in the proximal promoter of CYP3A2 (−165 to −73 bp), which bound components of a rat nuclear extract. These elements were termed 6βA-A (−106 to −87 bp), 6βA-B (−140 to −119 bp) and 6βA-C (−163 to −145 bp), and share a similar nucleotide sequence of T(A/C)(A/C)N(A/G)AAG(G/T)(C/T)CA. The promoter region was fused with a CAT reporter gene and CAT activity increased when nucleotides −164 to −111 bp were deleted, but decreased when the 6βA-A site was deleted. An oligonucleotide corresponding to 6βA-A interacted with liver nuclear factors, the interaction being inhibited by an oligonucleotide corresponding to HNF-4. Sites 6βA-B and 6βA-C contain direct repeats similar to the consensus sequences for nuclear receptors, including those for the retinoic acid and thyroid receptors (Miyata *et al.* 1995), suggesting that different transcription factors may bind to each site, thereby rationalizing the existence of a wide range of CYP3A2 inducers.

Rabbit CYP3A6 promoter

This promoter is relatively poorly characterized but sequence analysis of up to −257 bp from the transcription start, reveals regions of high homology to CYP3A4, 3A5, 3A7, 3A2 and 3A23, namely at −60 to −70, −150 to −170 and −230 to −250 bp (Barwick *et al.* 1996). Although these latter authors identified regions in the CYP3A6 promoter that appeared to confer inducer-responsiveness, their overall conclusion was that host cellular transcription factors play an important role in dictating the pattern of CYP3A responsiveness between species.

Mouse and dog CYP3As

Although CYP3A12 and 3A26 have been characterized in the dog (Ciaccio *et al.* 1991, Fraser *et al.* 1997) and *Cyp3a11, 3a13, 3a25 and 3a26* in the mouse (Yanagimoto *et al.* 1992, 1997, Itoh *et al.* 1994, Sakuma *et al.* 2000, Dai *et al.*

2001), essentially nothing is known about their promoters or molecular mechanisms of regulation, and therefore will not be considered further.

Human CYP3A4 promoter

The first 1 kb of the 5′-flanking regions of CYP3A4 and CYP3A7 share 91% sequence similarity, but each promoter has a characteristic fragment, namely a $P450_{NF}$-specific element (NFSE, −287 to −296 bp) and a $P450_{HFLa}$-specific element (HFLaSE, −729 to −737 bp) respectively (Hashimoto *et al.* 1993). The CYP3A4 5′-flanking region also contains a basic transcription element (BTE) and a TATA box, in addition to putative binding sites for transcriptional regulatory factors including an octamer-binding protein (Oct-1), CCAAT-binding protein (CP-1), activator protein 3 (AP-3), oestrogen receptor (ER), progesterone/glucocorticoid receptor (PR/GR), hepatic nuclear factors 4 and 5 (HNF-4 and HNF-5) and p53. Most importantly, the CP3A4 5′-flanking region contains an everted repeat sequence (termed ER_6) for the pregnane X receptor (PXR; Kliewer *et al.* 1998), which plays a major role in transactivation of the CYP3A4 gene by both steroid and xenobiotic ligands (see above for a fuller discussion of the role of the PXR).

The regulatory regions of the CYP3A4 promoter has been investigated using deletion mutations linked to a CAT reporter gene transfected into HepG2 cells and the −362 to −94 bp region has been identified as possessing promoter activity in response to inducers (Hashimoto *et al.* 1993). There are also two *cis*-acting elements in the region −290 to −445 bp which appear to repress transcription and another element (−445 to −254 bp), which appears necessary for efficient transcriptional activation by inducers in HepG2 cells. The latter region contains both CAAT and NFSE motifs, the former being defined as a *cis*-acting element involved in the enhancement of transcription. When the above reporter genes containing the above putative regulatory elements were transfected into FL cells (human amnion cells), no enhancement of CYP3A4 reporter gene activity by inducers was observed (Hashimoto *et al.* 1993), further underscoring the importance of cell-specific factors in regulation of the CYP3A4 gene.

The above role of the CYP3A4 proximal promoter has been recently augmented by the recognition of a distal enhancer module in the CYP3A4 promoter, located at −7607 to −7836 bp from the AUG start codon and responsive to rifampicin in HepG2 cells (Goodwin *et al.* 1999a). This responsive region contains ER_6 motifs and is functional irrespective of its position relative to the proximal promoter and cooperativity in induction was demonstrated between the distal element and *cis*-acting elements of the proximal promoter. DNase footprinting studies identified four protected sites in the CYP3A4 distal promoter sense strand, termed FP1 (−7811 to 7777 bp), FP2 (−7763 to −7740 bp), FP3 (−7738 to −7717 bp) and FP4 (−7698 to −7682 bp), two of which (FP3 and FP4) overlap with binding sites for the PXR.

It is interesting to note that other hormones also play a role in regulation of the CYP3A4 gene in that growth hormone (GH) up-regulates and triiodothyronine (T3) down-regulates CYP3A4 activity and mRNA expression in cultured human hepatocytes (Liddle *et al.* 1998) although the precise molecular mechanisms/receptorology underpinning these regulatory events have yet to be clarified.

Human CYP3A5 promoter

The 5′-flanking region of CYP3A5 (−1 to −1434 bp) shares 60 and 59% sequence similarity to that of CYP3A4 and CYP3A7 respectively (Jounaidi *et al.* 1994). However, the 5′-flanking genomic sequences of CYP3A4 and CYP3A7 appear to be more closely linked than that for CYP3A5, suggesting that a gene modification event (such as gene conversion with a non-CYP3A gene, a large deletion or a large insertion), has occurred upstream of −700 bp.

The CYP3A5 promoter region contains a CATAA box (−23 to −28 bp), rather than a TATA box (Jounaidi *et al.* 1994) and also contains a BTE (−35 to −50 bp) with two mutations, whereas CYP3A4 and CYP3A7 only contain one mutation. However, several other consensus sequences for transcription factors found in CYP3A4 and CYP3A7 are present in CYP3A5 with some modifications (Itoh *et al.* 1992, Hashimoto *et al.* 1993). These include Oct-1 (−64 to −71 bp), a CAAT box (−197 to −200 bp), an AP-3 site (−362 to −373 bp), three ER_6 motifs (−137 to −149, −293 to −305 and −428 to −440 bp), a PRE/GRE (−162 to −175 bp), HNF-4 and HNF-5 sites (−634 to −647 and −125 to −132 bp respectively) and a p53 site (−320 to −335 bp). The NFSE nucleotide sequence is present in both CYP3A5 and CYP3A4, but is absent from CYP3A7, whereas the HFLaSE is present in CYP3A5 and CYP3A7 but is absent in CYP3A4 (Hashimoto *et al.* 1993, Jounaidi *et al.* 1994). These sequences have several changes in CYP3A5. The CYP3A5 promoter sequence also contains a 12-nucleotide sequence at −308 to −320 bp (GAGGGAATTGCA), an eight-nucleotide sequence at −772 to −780 bp (TTTCCTTT) and a 50-bp deletion upstream of the BTE at −63 bp (Jounaidi *et al.* 1994).

There is only 47% sequence similarity between the CYP3A5 and CYP3A4 proximal promoters compared with 82% similarity between the proximal −644 bp of CYP3A5 and −690 bp of CYP3A4 (Scheutz *et al.* 1996a). Therefore, the 219-bp enhancer region is unique to CYP3A5. Prototypical CYP3A inducers do not induce CYP3A5, as reflected in the above lack of homology between CYP3A5 and CYP3A4. However, CYP3A5 appears to have retained many of the putative transcription factor binding sites found in the 5′-flanking region of other CYP3A subfamily members (Jounaidi *et al.* 1994).

Human CYP3A7 promoter

The original sequencing and functional analysis of the CYP3A7 promoter revealed that the PXR-binding fragment of the CYP3A7 gene (ER_6 motif) contained three mutations, two of which disrupted both half sites of the element (Itoh *et al.* 1992), with the resultant inability of the PXR to transcriptionally activate the gene, as independently confirmed by Blumberg *et al.* (1998). However, this view is in conflict with the observation that CYP3A7 is inducible by rifampicin (a PXR ligand) in human hepatocytes in primary culture and in the HuH7 and HepG2 human liver cell lines, thereby inferring a functional ER_6 motif (Yang *et al.* 1994). In an attempt to resolve this conflict, the CYP3A7 promoter was resequenced from two different human genomic libraries and no mutations were noted in the ER_6 motif (Pascussi *et al.* 1999). Furthermore, by the use of electrophoretic mobility shift assay and receptor transfection, these latter authors were able to demonstrate that PXR binds to the ER_6 motif and that the CYP3A7 gene is transcriptionally activated by rifampicin, clotrimazole and RU-486 (mifepristone),

known human PXR ligands. Thus, it appears that the original non-responsiveness may have arisen through isolation/sequencing artefacts in the CYP3A7 promoter.

More recently, it has been reported that a PXR- and CAR-responsive enhancer is approximately −8 kbp from the proximal promoter and it was termed a xenobiotic responsive enhancer module, XREM (Bertilsson *et al.* 2001).

Human CYP3A43 promoter

Only the full-length cDNA for this gene has been published (Domanski *et al.* 2001), and, to our knowledge, the promoter region has not been sequenced or characterized.

Taken collectively, the regulatory motifs found in the 5′-flanking region of CYP3A genes are summarized in table 3.

Interindividual variation in human CYP3A expression

It is now generally accepted that there is a substantial interindividual variation in human liver CYP3A4 expression, based on both *in vitro* (35–100-fold) and *in vivo* (20-fold) studies (Guengerich and Turvy 1991, Thummel *et al.* 1994, Wilkinson 1996, Westlind *et al.* 1999). In addition, it has been reported that CYP3A4 mRNA was only detected in 40% of human kidney samples (Haehner *et al.* 1996). Furthermore, treatment of patients with rifampicin results in a 4–8-fold variation in induction of CYP3A4 in the enterocyte as assessed by CYP3A4

Table 3. Regulatory motifs in CYP3A promoters.

Regulatory motif	Function
AP-3	consensus sequence recognized by the gene-activating factor, activating protein 3
BTE	basal transcription element involved in maintenance of the basal level of transcription in many genes, possible through the BTE-binding protein (BTEB) in the liver
CAAT box	consensus sequence present in many genes and binds the liver-specific protein C/EBP (CCAAT enhancer-binding protein) and the ubiquitous transcription factor CP1 (CCAAT-protein-1)... has a major role in determining the efficiency of the promoter
CACCC box	located upstream of the CAAT box and is thought to be involved in transcriptional activation; known to bind the transcription factor Sp-1
DRn	a direct repeat with *n* bp spacing (AGTTCA-N_3-AGTTCA) that binds PXR-RXR heterodimers and activates CYP3A-responsive genes
ERE/PRE/GRE	receptor-response elements with similar consensus sequences; binding of the ER, PR and GR receptors involved in both positive and negative regulation of gene transcription in response to oestrogens, progestogens and glucocorticoids
ER_6	two everted copies of the AG(G/T)TCA motif, separated by six nucleotides; binds the PXR–RXR receptor complex and activates xenobiotic-dependent gene transcription in CYP3As; also locus of CAR binding
HNF-4 and HNF-5	regulatory motifs (hepatocyte-specific, nuclear transcription factors) that bind liver-specific transcription factors HNF-4 and HNF-5; also involved in the regulation of CYP2B genes (HNF-4) and transferin gene (HNF-5)
OCT	conserved octamer motif present in many genes (including CYP1A1), binding members of the octamer factors family, resulting in the up/down regulation of responsive genes.
TATA box	found in all eucaryotic genes and essential for transcription; recognized by the TATA binding protein (TBP).
P53	consensus sequence that binds the tumour suppressor protein, p53

mRNA expression and catalytic activity determinations (Kolars *et al.* 1992), implying an additional interindividual variation in the CY3A4 inductive response. Similarly, other members of the human CYP3A subfamily are polymorphically expressed in man in that CYP3A5 has been reported to be expressed in only 10–25% of human adult livers (Aoyama *et al.* 1989, Gervot *et al.* 1996) and although CYP3A7 is the predominant form in human foetal liver, it is polymorphically expressed in 54% of human adult livers examined (Kitada *et al.* 1985, Schuetz *et al.* 1994, Gervot *et al.* 1996).

Identification of the precise biological reasons underpinning the above variations is a complex matter, arising from a multifactorial aetiology of both basal- and xenobiotic-modulated expression. Confounding factors such as tissue viability, patients versus healthy volunteer tissue sources, the relatively small number of patients/volunteers in any sample group studied to date, and specificities of the analytical techniques/substrates used to assess CYP3A expression and catalytic activities must also be taken into account when assessing interindividual variation. In addition, the specific statistical methods used to analyse both *in vitro* and *in vivo* human datasets of enzyme expression and activity in general is problematical. Specifically, although there appears to be substantial interindividual variation in human CYP3A expression, all studies reported to date appear to exhibit a unimodal distribution, the modality being determined by complex interactions between the nature of the statistical analysis of the data, the population size and the impact of genotype on phenotype, as elegantly discussed by Tucker *et al.* (1998) and Ozdemir *et al.* (2000).

Notwithstanding the above complications, a simplistic approach to classifying factors that influence human CYP3A expression (and therefore contribute to the apparent interindividual variability), would be on the basis of genetic, physiological and environmental influences, but the more challenging task is to assess the relative contributions made by these factors.

Environmental influences

As outlined above and summarized in table 1, it is abundantly clear that environmental factors have the ability to induce or inhibit the expression and/or activity of human CYP3As, and will not be discussed further here. Suffice it to say that prior exposure of man to drugs, environmental chemicals and dietary components is an important factor in rationalizing interindividual differences in CYP3A levels (Wrighton *et al.* 2000, Quattrochi *et al.* 2001).

Physiological influences

Although not a specific focus of this review, the interested reader should be mindful that physiological factors may additionally contribute to interindividual CYP3A expression in man. Contributing factors may include gender (Hunt *et al.* 1992, Low *et al.* 1994), although this remains to be firmly established and hormonal status including down-regulation by triiodothyronine and up-regulation mediated by growth hormone in human primary hepatocytes (Liddle *et al.* 1998). Furthermore, it has been recognized for a few years that inflammation impairs drug metabolism by switching off expression of several CYPs, including the CYP3A subfamily (Fukuda *et al.* 1992). The

molecular basis for this observation has recently been determined for the cytokine interleukin 6, which rapidly and extensively decreases expression of both human PXR and CAR mRNAs in human hepatocytes, without any change in the dioxin receptor (arylhydrocarbon receptor or AHR) nor the GR (Pascussi *et al*. 2000c). This receptor down-regulation phenomenon is accompanied by a reduced responsiveness of CYP3A4 to induction by both rifampicin and phenobarbital.

Of relevance in this context is the physiological drug transporters involved in the cellular efflux of steroids and antibiotics, as the activity of these transporters can alter the intracellular concentration of CYP3A inducers and hence the magnitude of the inductive response. The best characterized of these transporters are the products of the MDR (multiple drug resistance) *1a* gene, P-glycoprotein (Barnes *et al*. 1996). The importance of the P-glycoprotein pump is underscored in studies in *mdr1a* knockout mice, wherein rifampicin concentrations were 11 times higher in the *mdr 1a* (−/−) animals as compared with the *mdr 1a* (+/+) wild-type, concordant with a significantly higher induction of *Cyp3a*-mediated hydroxylation of midazolam in the *mdr 1a* (−/−) genotype (Schuetz *et al*. 1996b).

Genetic influences

It is well documented that genetic polymorphisms in drug-metabolizing enzymes result in the impaired ability to metabolize drugs in man, including the cytochromes P450 (Meyer and Zanger 1997). The recognition of this phenomenon led to original proposals for a unified nomenclature system for the human cytochromes P450 that uniquely identifies specific CYP alleles (Daly *et al*. 1996), which have now been generally accepted and a website for the recommended nomenclature for the human polymorphic CYP genes has been established, listing all known allelic variants (http://www.imm.ki.se/CYPalleles). To be assigned as a unique allele, the CYP should contain nucleotide changes that have been shown to affect transcription, splicing, translation, post-transcriptional or post-translational modifications or result in at least one amino acid change. For example, CYP2D6 has been the most extensively studied CYP to date, with 72 different CYP2D6 alleles have been identified at the time of writing (http://www.imm.ki.se/CYPalleles/cyp2d6). However, it must be emphasized that the functional impact of all of these latter allelic variants in the database have not been fully characterized in all cases, nor have their frequency incidence in the human population.

Because of their importance in human drug metabolism, the CYP3As have been the subject of recent intensive investigation and information on genetic variants of the human CYP3A subfamily is beginning to emerge. To date, 24, 8 and 5 allelic variants have been identified for CYP3A4, 3A5 and 3A7 respectively (http://www.imm.ki.se/CYPalleles), with none having been reported for CYP3A43 as yet. Again, it must be emphasized that our knowledge of the functional consequences and incidence of these 37 different alleles in the human CYP3A subfamily are far from complete, but the following examples clearly illustrate the substantial impact of genetic factors in interindividual variation in human CYP3A expression.

Promoter mutations

CYP3A4. Rebbeck *et al*. (1998) first reported a polymorphism in the CYP3A4 promoter wherein an A to G change occurred at −290 bp in the middle of the so-called nifedipine-specific element, NFSE, which demonstrated substantial interethnic variation with allele frequencies of 9% in Caucasians, 53% in African-Americans and 0% in a Taiwanese population (Walker *et al*. 1998). The NFSE was originally identified by Hashimoto *et al*. (1993) and it should be noted that the basis for naming this element as being nifedipine-specific is somewhat obscure in that no regulatory function has been ascribed to it. Rather, it was simply present in the CYP3A4 promoter but absent from CYP3A7.

To date, no known regulatory function has been identified for this NFSE and Rebbeck *et al*. (1998) offered no functional studies to relate this polymorphism to phenotypic changes. Subsequent investigations have cast doubt on the functional significance of this polymorphism, wherein the A/G promoter change was identified in three of 39 human livers but had no effect on the 6β-hydroxylation of testosterone *in vitro* (Westlind *et al*. 1999). In addition, three separate *in vivo* studies have confirmed the large interethnic variation in the allelic frequency of this mutation, but found no correlation between this mutation and the *in vivo* erythromycin breath test, the pharmacokinetics of nifedipine or its major metabolite, dehydronifedipine, nor cyclosporin clearance (Ball *et al*. 1999, Rivory *et al*. 2000). Thus, from the information available to date, it appears unlikely that this A/G promoter mutation in CYP3A4 confers a reduced capacity to metabolize CYP3A4 substrates in man, underscoring the importance of correlating mutations with a functional outcome.

CYP3A5. A more incisive study has been reported for functionally related polymorphisms in the CYP3A5 promoter, wherein an apparent, statistically distinct bimodality has been reported for the *in vitro* hydroxylation of midazolam in 39 human liver samples (Paulussen *et al*. 2000). These authors have taken advantage of the fact that CYP3A4 preferentially catalyses the 4-hydroxylation of midazolam, whereas CYP3A5-supported metabolism preferentially produces the 1-hydroxy metabolites (Gorski *et al*. 1994). Although the metabolite specificity is not absolute for either enzyme, the 1-hydroxy:4-hydroxy metabolite ratio (MR) is a not unreasonable surrogate marker for the CYP3A5:CYP3A4 ratio. In the same study, the group identified two linked mutations in the CYP3A5 promoter, namely an A to G change at −45 bp in the BTE (Sp1) regulatory element and a T to G change at −369 bp in the AP3 site, with allelic frequencies (600 samples examined) of 9.2% for the linked mutant and 91% for the wild-type gene. Noteworthy is the fact that 38 of 39 individuals harbouring the mutation had MR >5.0 (mean $=6.0\pm2.0$) compared with the wild-type with MR <3.5 (2.7 ± 0.42). Thus, in this particular instance, the mutation conferred an increase in CYP3A5-dependent metabolism, as rationalized by the fact that the mutation in the BTE increased the percentage identity from 80 to 90% of the consensus sequence for this element.

Coding mutations

*CYP3A4*2*. In a recent study, a Ser222Pro mutation, a known helix-breaker substitution, has been identified in a Finnish population (frequency of 2.7%), but

not in Chinese or African-Americans, and termed CYP3A4*2 (Sata *et al*. 2000). The wild-type and mutant cDNAs were constructed and their comparative activities towards nifedipine in a baculovirus-directed expression system yielded $K_m = 2$ and $11\,\mu M$ and $V_{max} = 36$ and $23\,min^{-1}$ for the wild-type and mutant respectively. Thus, the nifedipine intrinsic clearance ($V_{max} : K_m$) for the mutant is approximately 9-fold lower than the wild-type enzyme. Interestingly, both CYP3A4 forms showed no difference in their ability to catalyse the 6β-hydroxylation of testosterone, which may be related to the somewhat unusual features of the CYP3A4 active site(s), as described by Wrighton *et al*. (2000).

*CYP3A4*4, 3A4*5 and 3A4*6*. Hsieh *et al*. (2001) identified three mutant alleles in a Taiwan Chinese population, characterized by an ILE118Val change in exon 5 (CYP3A4*4), a Pro218Arg change in exon 7 (CYP3A4*5) and an $ARG^{17,776}$ insertion, introducing a premature stop codon in exon 9 (CYP3A4*6). In the same study, this population cohort of 102 samples was also assessed for the urinary ratio of 6β-hydroxycortisol: cortisol, an *in vivo* index of CYP3A4 activity and it turns out that the wild-type (CYP3A4*1) was phenotyped by a ratio of 5.92, whereas the mutant allele genotypes had ratios of 2.48, 3.10 and 0.88 for CYP3A4*4, 3A4*5 and 3A4*6, respectively. Thus, the existence of these three mutant alleles is not inconsistent with a compromised CYP3A4 phenotype and further studies on the *in vivo* clearance of CYP3A4 substrates would be valuable in directly assessing the impact on drug metabolism.

*CYP3A5*3 and CYP3A5*6*. Kuehl *et al*. (2001) characterized two functional coding mutations in the CYP3A5 gene. CYP3A5*3 is characterized by a single nucleotide polymorphism (SNP) at 22 893 bp in exon 3, creating a cryptic splice site which introduces a premature stop codon, yielding a truncated enzyme of 109 amino acids, which correlated with low expression of CYP3A5 protein and midazolam 1-hydroxylase activity. The second polymorphism is a G to A mutation at 30 597 bp in exon 7, resulting in the deletion of exon 7 and a corresponding low-activity enzyme (CYP3A5*6). These latter authors also demonstrated that the wild-type allele (CYP3A5*1 by convention) was expressed in 30% of Caucasians/Japanese/Mexican, 40% in Chinese and 50% in African-Americans.

These results bring into sharp relief the hitherto undefined importance of CYP3A5 in drug metabolism in those individuals expressing at least one CYP3A5*1 allele, wherein the expression of CYP3A4 and CYP3A5 are approximately equal in human liver. Thus, the above study has led to the conclusion that genetic variation in CYP3A5 expression is a major determinant of interindividual variation in CYP3A drug substrates in man. Related to this, the ratio of catalytically competent CYP3A4 to CYP3A5 expression in human liver may be a risk factor in the susceptibility to aflatoxin B_1 toxicity, in that CYP3A4 is approximately two orders of magnitude more efficient at 3α-hydroxylation (an inactivation pathway), whereas CYP3A5 is more efficient in catalysing the 8,9-epoxidation (an activation pathway) of aflatoxin B_1 (Gillam *et al*. 1995).

Perspectives and future research needs

The molecular aspects and receptor-dependency of the regulation of CYP3A genes are now beginning to clarify somewhat and have confirmed early suspicions that the process is indeed a complex one (figure 3). In addition, evidence is beginning to emerge that functional genetic polymorphisms in human CYP3As exist and may partially contribute to interindividual variations in drug biotransformation. This rapid accumulation of information has identified new avenues of basic and applied research in drug discovery/development and future areas of potential study include the following.

Relative receptor expression and CYP3A induction

Although binding and transactivation studies of CYP3A inducers in *in vitro* heterologous cell systems are of immense importance (and will continue to be so), a key question is how does this information relate to the *in vivo* situation in man? To date, the only study that has began to address this issue is the PXR (SXR) knockout/knock in humanized mouse experiments described by Xie *et al.* (2000a) and clearly more research along these lines is needed for other relevant receptors including CAR and GR, either alone or in combination. It would also be useful to know the relative expression ratios of CAR, GR and PXR in a bank of human liver samples that have been phenotyped for CYP3A4/CYP3A5 activities and inducibility in viable hepatocytes to examine the hypothesis that variation in receptor expression ratios may contribute to interindividual variation in CYP3A expression and inducibility.

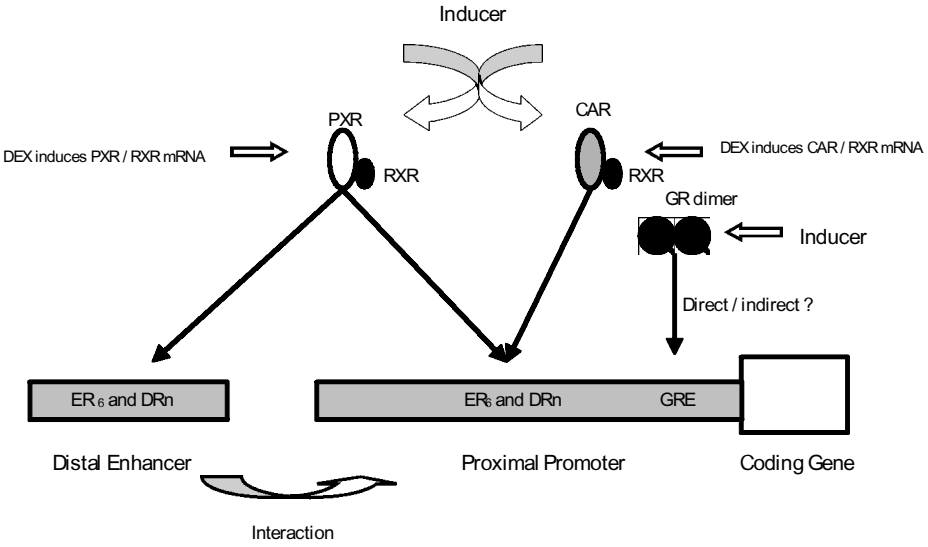


Figure 3. Receptor-dependent regulation of the CYP3A4 gene. Inducers are shown as either acting directly with individual receptors or interacting with both PXR and CAR. Dexamethasone is shown to act directly at a GRE via the GR or by inducing PXR, CAR or RXR mRNA. The complexity of receptor-dependent regulation of the CYP3A4 gene is further compounded by competition of both the receptors for other responsive genes and by inducers for other receptors (data not shown).

Receptor variants

Although the less active splice variant of the human PXR (PXR.2) has been identified in cancerous breast tissue as discussed above (Dotzlaw *et al.* 1999), it is not known if this variant is expressed in liver and if so, is there interindividual variation in wild-type/variant ratios in the human population. Similarly, more research is needed to determine if GR and CAR are polymorphically expressed in man and to examine the functional consequences of these.

Other CAR and PXR/SXR target genes

Whereas we know that a GenBank database search has identified SXR response elements in several gene promoters other than the CYP3As, including CYP2A1, CYP2A2, CYP2C1, CYP2C6, NADPH-cytochrome P450 reductase and a UDP-glucuronosyl transferase (Blumberg *et al.* 1998), more functional studies are required to examine the broader role of PXR in the regulation of drug metabolizing enzymes. Similarly, we have quite sparse knowledge of the complete battery of genes regulated by CAR and further knowledge of specific target genes for this receptor would allow a more comprehensive assessment of the competition for the limited cellular concentrations of CAR, and hence the attendant impact on CYP3A regulation.

Inducer-receptor specificity

From the foregoing discussion it appears that CAR and PXR share many ligands in common, and although there may be preferences of particular inducers for human and mouse CAR/PXR (Moore *et al.* 2000), no inducer has been identified to date that has absolute specificity for either of these receptors (or indeed GR). Identification of such specific ligands would be a valuable experimental tool in further dissecting out the relative roles of specific receptors in the induction process.

Receptor-dependent recruitment of cellular coactivators

An emerging view of nuclear receptors is that they are not simply on/off switches for gene expression, but function to recruit coactivators and other regulatory factors which can confer receptor, promoter and cell specificity for target genes (Jenkins *et al.* 2001). At present, we do not fully understand the entirety of these complex regulatory processes for GR, CAR and PXR and therefore is obviously a fertile area for further research.

Drug discovery and development

During drug discovery and development in the pharmaceutical industry, it is advantageous to identify human CYP3A inducers early on in the lead selection and development process. Inducers are often problematical in the clinic, producing altered pharmacokinetc profiles and drug–drug interactions (Smith 2000) at the end of a long and expensive developmental programme, and hence the scientific and financial need for early identification.

Towards this end, the transient transfection, CYP3A4 promoter–reporter gene approach described herein may be developed further to include CAR in the transfection protocol along with auxiliary transcription factors/coactivators that may emerge as contributing to the induction process. Furthermore, cell lines stably incorporating the promoter–reporter constructs into genomic DNA would be an approach that is generally more applicable and technically easier to use, but careful thought would have to be given to the choice of which particular cell line to use. In this context, the intestine-derived Caco-2 cell line would be an attractive candidate, as it currently is relatively extensively used to assess drug absorption and intestinal cells normally express CYP3As in man (Muenier *et al.* 1995, Paine *et al.* 1997), thus providing an engineered cell line that may be used to simultaneously assess both absorption and the intestinal first-pass effect of drugs

Dominant factors in dictating interindividual variation in metabolism of CYP3A substrates

Whereas a few brave attempts have been made to identify the relative contributions made by environmental, physiological or genetic factors to CYP3A expression (Tucker *et al.* 1998, Ozdemir *et al.* 2000), this has been an extremely complex and vexing area to investigate and delineate. However, there may be some light at the end of the tunnel in that the emerging area of functional human genomics may help to identify dominant genetic loci in individuals, but we are clearly still some way away from harnessing the enormous potential that this approach offers.

Acknowledgements

The authors thank GlaxoSmithKline, UK, for partial support of the studies described herein.

Appendix A: Abbreviations

AHR	arylhydrocarbon receptor
AP-3	activator protein 3
ARP-1	apolipoprotein A1 regulatory protein 1
BTE	basic transcription element
CAR	constitutive androstane receptor
CAT	chloramphenicol acetyltransferase
COUP-TF	chicken ovalbumin upstream promoter-transcription factors
CP-1	CCAAT-binding protein
CYP	cytochrome P450
DR3	hormone/xenobiotic response element separated by three nucleotides
EAR-3	v-ErbA-related protein 3
ER	oestrogen receptor
ER_6	everted repeat sequence separated by six nucleotides
FXR	farnesoid X receptor
GH	growth hormone
GR	glucocorticoid receptor
GRE	glucocorticoid response elements

GRIP1	glucocorticoid receptor interacting protein 1
HNF-4	hepatocyte nuclear factor 4
HNF-5	hepatocyte nuclear factor 5
LXR	liver X receptor
MDR	multiple drug resistance gene
MMTV	mouse mammary tumour virus
NF1	nuclear factor 1
NFSE	nifedipine specific element
Oct-1	octamer-binding protein
PBRE	phenobarbital-responsive enhancer regions
PCN	pregnenolone 16α-carbonitrile
PCR	polymerase chain reaction
PR	progesterone receptor
PXR	pregnane X receptor; alternatively named SXR (steroid xenobiotic receptor) or PAR (pregnane activated receptor)
RIP140	receptor interacting protein 140
RU-486	mifepristone
RXR	retinoid X receptor
SNP	single nucleotide polymorphism
SRC-1	steroid receptor coactivator 1
SUG1	also known as p45 or thyroid hormone-receptor interacting protein (TRIP1)
T_3	triiodothyronine
TAO	triacetyloleandomycin
TAT	tyrosine aminotransferase
XREM	xenobiotic responsive enhancer module

References

Aoyama, T., Yamano, S., Waxman, D. J., Lapenson, D. P., Meyer, U. A., Fischer, V., Tyndale, R., Inaba, T., Kalow, W., Gelboin, H. V. and Gonzalez, F. J., 1989, Cytochrome p450 hpcn3, a novel cytochrome p450 IIIA-gene product that is differentially expressed in adult human liver-cDNA and deduced amino-acid sequence and distinct specificities of cDNA-expressed hpcn1 and hpcn3 for the metabolism of steroid-hormones and cyclosporine. *Journal of Biological Chemistry*, **264**, 10388–10395.

Austin, K. L., Mather, L. E., Philpot, C. R. and McDonald, P. J., 1980, Inter-subject and dose-related variability after intravenous administration of erythromicin. *British Journal of Clinical Pharmacology*, **10**, 273–279.

Baes, M., Gulick, T., Choi, H. S., Martinoli, M. G., Simha, D. and Moore, D. D., 1994, A new orphan member of the nuclear hormone receptor family that interacts with a subset of retinoic acid response elements. *Molecular and Cellular Biology*, **14**, 1544–1551.

Ball, S., Scatina, J., Kao, J., Ferron, G., Fruncillo, R., Mayer, P., Hopkins, P., Warner, N. and Hall, J., 1999, Population distribution and effects on drug metabolism of a genetic variant in the 5′ promoter region of CYP3A4. *Clinical Pharmacology and Therapeutics*, **66**, 288–294.

Barnes, K. M., Dickstein, B., Cutler, G. B., Fojo, T. and Bates, S. E., 1996, Steroid transport, accumulation and antagonism of P-glycoprotein in multidrug-resistant cells. *Biochemistry*, **35**, 4820–4827.

Barwick, J. L., Quattrochi, L. C., Mills, A. S., Potenza, C., Tukey, R. H. and Guzelian, P. S., 1996, Trans-species gene transfer for analysis of glucocorticoid-inducible transcriptional activation of transiently expressed human CYP3A4 and rabbit CYP3A6 in primary cultures of adult rat and rabbit hepatocytes. *Molecular Pharmacology*, **50**, 10–16.

Beato, M., 1989, Gene regulation by steroid hormones. *Cell*, **56**, 335–344.

Bertilsson, F., Berkenstam, A. and Blomquist, P., 2001, Functionally conserved xenobiotic responsive enhancer in cytochrome P450 3A7. *Biochemical and Biophysical Research Communications*, **280**, 139–144.

Bertilsson, G., Heidrich, J., Svensson, K., Asman, M., Jendeberg, L., Sydow-Backman, M., Ohlsson, R., Postlind, H., Blomquist, P. and Berkenstam, A., 1998, Identification of a human nuclear receptor defines a new signalling pathway for CYP3A induction. *Proceedings of the National Academy of Sciences, USA*, **95**, 12208–12213.

Blizard, D., Sueyoshi, T., Negishi, M., Dehal, S. S. and Kupfer, D., 2001, Mechanism of induction of cytochrome P450 enzymes by the proestrogenic endocrine disrupter pesticide-methoxychlor: interactions of methoxychlor metabolites with the constitutive androstane receptor system. *Drug Metabolism and Disposition*, **29**, 781–785.

Blumberg, B., Sabbagh, W., Jr, Juguilon, H., Bolado, J., Jr, van Meter, C. M., Ong, E. S. and Evans, R. M., 1998, SXR, a novel steroid and xenobiotic-sensing nuclear receptor. *Genes and Development*, **12**, 3195–3205.

Brooks, B. A., McBride, O. W., Dolphin, C. T., Farrall, M., Scambler, P. J., Gonzalez, F. J. and Idle, J. R., 1988, The gene CYP3 encoding P450pcn1 (nifedipine oxidase) is tightly linked to the gene COL1A2 encoding collagen type 1 alpha on 7q21-q22. 1. *American Journal of Human Genetics*, **43**, 280–284.

Burger, H. J., Schuetz, J. D., Schuetz, E. G. and Guzelian, P. S., 1992, Paradoxical transcriptional activation of rat-liver cytochrome-P-450 3A1 by dexamethasone and the antiglucocorticoid pregnenolone 16-alpha-carbonitrile — analysis by transient transfection into primary monolayer-cultures of adult-rat hepatocytes. *Proceedings of the National Academy of Sciences, USA*, **89**, 2145–2149.

Cairns, W., Smith, C. A., McLaren, A. W. and Wolf, C. R., 1996, Characterization of the human cytochrome P4502D6 promoter. A potential role for antagonistic interactions between members of the nuclear receptor family. *Journal of Biological Chemistry*, **271**, 25269–25276.

Cashman, J. R., 1996, Drug discovery and drug metabolism. *Drug Discovery Today*, **1**, 209–216.

Chen, D., Lepar, G. and Kemper, B., 1994, A transcriptional regulatory element common to a large family of hepatic cytochrome P450 genes is afunctional binding site of the orphan receptor HNF-4. *Journal of Biological Chemistry*, **269**, 5420–5427.

Chen, H., Brzezinski, M. R., Fantel, A. G. and Juchau, M. R., 1999, Catalysis of drug oxidation during embryogenesis in human hepatic tissues using imipramine as a model substrate. *Drug Metabolism and Disposition*, **27**, 1306–1308.

Choi, H.-S., Chung, M., Tzameli, I., Simha, D., Lee, Y.-K., Seol, W. and Moore, D. D., 1997, Differential transactivation by two isoforms of the orphan nuclear hormone receptor CAR. *Journal of Biological Chemistry*, **272**, 23565–23571.

Cholerton, S., Daly, A. K. and Idle, J. R., 1992, The role of individual human cytochromes P450 in drug-metabolism and clinical-response. *Trends in Pharmacological Sciences*, **13**, 434–439.

Ciaccio, P. J., Graves, P. E., Bourque, D. P., Glinsmann-Gibson, B. and Halpert, J. R., 1991, cDNA and deduced amino acid sequences of a dog liver cytochrome P450 of the IIIa gene sub-family. *Biochimica et Biophysica Acta*, **1088**, 319–322.

Daly, A. K., Brockmoller, J., Broly, F., Eichelbaum, M., Evans, W. E., Gonzalez, F. J., Huang, J. D., Idle, J. R., Ingelman-Sundberg, M., Ishizaki, T., Jacqzaigrain, E., Meyer, U. A., Nebert, D. W., Steen, V. M., Wolf, C. R. and Zanger, U. M., 1996, Nomenclature for human CYP2D6 alleles. *Pharmacogenetics*, **6**, 193–201.

Damkier, P., Hansen, L. L. and Brosen, K., 1999, Rifampicin treatment greatly increases the apparent oral clearance of quinidine. *Pharmacology and Toxicology*, **85**, 257–262.

De Wildt, S. N., Kearns, G. L., Leeder, J. S. and van den Anker, J. N., 1999, Cytochrome P450 3A — ontogeny and drug disposition. *Clinical Pharmacokinetics*, **37**, 485–505.

Domanski, T., Finta, C., Halpert, J. and Zaphiropoulos, P., 2001, cDNA cloning and initial characterization of CYP3A43, a novel human cytochrome P450. *Molecular Pharmacology*, **59**, 386–392.

Dotzlaw, H., Leygue, E., Watson, P. and Murphy, L. C., 1999, The human orphan receptor PXR messenger RNA is expressed in both normal and neoplastic breast tissue. *Clinical Cancer Research*, **5**, 2103–2107.

El-Sankary, W., Plant, N. and Gibson, G., 2000, Regulation of the CYP3A4 gene by hydrocortisone and xenobiotics: role of the glucocorticoid and pregnane × receptors. *Drug Metabolism and Disposition*, **28**, 493–496.

El-Sankary, W., Plant, N. J. and Gibson, G. G., 2001, Use of a reporter gene assay to predict and rank the potency and efficacy of CYP3A4 inducers. *Drug Metabolism and Disposition*, **29**, 1499–1504.

Eliasson, E., Mkrtchian, S., Halpert, J. R. and Ingelman-Sundberg, M., 1994, Substrate-regulated, c-AMP-dependent phosphorylation, denaturation and degradation of glucocorticoid-inducible cytochrome P4503A1. *Journal of Biological Chemistry*, **269**, 18378–18383.

Evans, R. M., 1988, The steroid and thyroid hormone receptor superfamily. *Science*, **240**, 889–895.

Ferro, M., Bassi, A. M., Penco, S. and Nanni, G., 1993, Use of established hepatoma cell lines in biotoxicology. *Cytotechnology*, **11**, S126–129.

Finta, C. and Zaphiropoulos, P. G., 2000, The human cytochrome P450 3A locus. Gene evolution by capture of downstream exons. *Gene*, **260**, 13–23.

Forman, B. M., Tzameli, I., Choi, H. S., Chen, L., Simha, D., Seol, W., Evans, R. M. and Moore, D. D., 1998, Androstane metabolites bind to and deactivate the nuclear receptor CAR-beta. *Nature*, **395**, 612–615.

Fraser, D. J., Feyereisen, R., Harlow, G. R. and Halpert, J. R., 1997, Isolation, heterologous expression and functional characterisation of a novel cytochrome P450 3A enzyme from a canine liver cDNA library. *Journal of Pharmacology and Experimental Therapeutics*, **283**, 1425–1432.

Fuhr, U., 2000, Induction of drug metabolising enzymes — pharmacokinetic and toxicological consequences in humans. *Clinical Pharmacokinetics*, **38**, 493–504.

Fukuda, Y., Ishida, N., Noguchi, T., Kappas, A. and Sassa, S., 1992, Interleukin-6 down regulates the expression of transcripts encoding cytochrome P450 1A1, 1A2 and 3A3 in human hepatoma cells. *Biochemical and Biophysical Research Communications*, **184**, 960–965.

Geick, A., Eichelbaum, M. and Burk, O., 2001, Nuclear receptor response elements mediate induction of intestinal MDR1 by rifampin. *Journal of Biological Chemistry*, **276**, 14581–14587.

Gerbal-Chaloin, S., Pascussi, J. M., Pichard-Garcia, L., Daujat, M., Waechter, F., Fabre, J. M., Carrere, N. and Maurel, P., 2001, Induction of CYP2C genes in human hepatocytes in primary culture. *Drug Metabolism and Disposition*, **29**, 242–251.

Gervot, L., Carriere, V., Costet, P., Cugnenc, P. H., Berger, A., Beaune, P. H. and de Waziers, I., 1996, CYP3A5 is the major cytochrome P450 3A expressed in human colon and colonic cell lines. *Environmental Toxicology and Pharmacology*, **2**, 381–388.

Gillam, E. M., Guo, Z., Ueng, Y. F., Yamazaki, H., Cock, I., Reilly, P. E., Hooper, W. D. and Guengerich, F. P., 1995, Expression of cytochrome P450 3A5 in *Escherichia coli*: effects of 5′ modification, purification, spectral characterization, reconstitution conditions, and catalytic activities. *Archives of Biochemistry and Biophysics*, **317**, 374–378.

Gonzalez, F. J., Song, B. J. and Hardwick, J. P., 1986, Pregnenolone 16 alpha-carbonitrile-inducible P-450 gene family: gene conversion and differential regulation. *Molecular and Cellular Biology*, **6**, 2969–2976.

Goodwin, B., Hodgson, E. and Liddle, C., 1999a, The orphan human pregnane X receptor mediates the transcriptional activation of CYP3A4 by rifampicin through a distal enhancer module. *Molecular Pharmacology*, **56**, 1329–1339.

Goodwin, B. J., Hodgson, E. and Liddle, C., 1999b, The orphan nuclear receptor hCAR supports constitutive expression of the human cytochrome P450 3A4 gene in HepG2 cells. *Hepatology*, **30**, 929.

Gorski, J. C., Hall, S. D., Jones, D. R., Banden-Branden, M. and Wrigton, S. A., 1994, Regioselective biotransformation of midazolam by members of the human cytochrome P4503A (CYP3A) subfamily. *Biochemical Pharmacology*, **47**, 1643–1653.

Grange, T., Roux, J., Rigaud, G. and Pictet, R., 1991, Cell-type specific activity of two glucocorticoid responsive units of rat tyrosine aminotransferase gene is associated with multiple binding sites for c/e bp and a novel liver-specific nuclear factor. *Nucleic Acids Research*, **19**, 131–139.

Greuet, J., Pichard, L., Bonfils, C., Domergue, J. and Maurel, P., 1996, The fetal specific gene CYP3A7 is inducible by rifampicin in adult human hepatocytes in primary culture. *Biochemical and Biophysical Research Communications*, **225**, 689–694.

Guengerich, F., 1999, Cytochrome P450 3A4: regulation and role in drug metabolism. *Annual Review in Pharmacology and Toxicology*, **39**, 1–17.

Guengerich, F. P. and Turvy, C. G., 1991, Comparison of levels of several human microsomal cytochrome P-450 enzymes and epoxide hydrolase in normal and disease states using immunochemical analysis of surgical liver samples. *Journal of Pharmacology and Experimental Therapeutics*, **256**, 1189–1194.

Haehner, B. D., Gorski, J. C., Vandenbranden, M., Wrighton, S. A., Janardan, S. K., Watkins, P. B. and Hall, S. D., 1996, Bimodal distribution of renal cytochrome P450 3A activity in humans. *Molecular Pharmacology*, **50**, 52–59.

Handschin, C., Podvinec, M. and Meyer, U., 2000, CXR, a chicken xenobiotic-sensing orphan nuclear receptor is related to both mammalian pregnane X receptor (PXR) and constitutive androstane receptor (CAR). *Proceedings of the National Academy of Sciences, USA*, **97**, 10769–10774.

Hashimoto, H., Toide, K., Kitamura, R., Fujita, M., Tagawa, S., Itoh, S. and Kamataki, T., 1993, Gene structure of CYP3A4, and adult specific form of cytochrome P450 in human livers, and its transcriptional control. *European Journal of Biochemistry*, **218**, 585–595.

He, Y. A., He, Y. Q., Szklarz, G. D. and Halpert, J. R., 1997, Identification of three key residues in substrate recognition site 5 of human cytochrome P450 3A4 by cassette and site-directed mutagenesis. *Biochemistry*, **36**, 8831–8839.

Honkakoski, P., Jaaskelainen, I., Kortelahti, M. and Urtti, A., 2001, A novel drug-regulated gene expression system based on the nuclear receptor constitutive androstane receptor (CAR). *Pharmaceutical Research*, **18**, 146–150.

Honkakoski, P., Zelko, I., Sueyoshi, T. and Negishi, M., 1998, The nuclear orphan receptor CAR-retinoid × receptor heterodimer activates the phenobarbital-responsive enhancer module of the CYP2B6 gene. *Molecular and Cellular Biology*, **18**, 5652–5658.

Hostetler, K. A., Wrighton, S. A., Molowa, D. T., Thomas, P. E., Levin, W. and Guzelian, P. S., 1989, Co-induction of multiple hepatic cytochrome P-450 proteins and their messenger-RNAs in rats treated with imidazole antimycotic agents. *Molecular Pharmacology*, **35**, 279–285.

Hseih, K.-P., Lin, Y.-Y., Cheng, C.-L., Lai, M.-L., Lin, M.-S., Siest, J.-P. and Huang, J.-D., 2001, Novel mutations of CYP3A4 in Chinese. *Drug Metabolism and Disposition*, **29**, 268–273.

Hunt, C. M., Westerkam, W. R. and Stave, G. M., 1992, Effect of age and gender on the activity of human hepatic CYP3A. *Biochemical Pharmacology*, **44**, 275–283.

Huss, J. M. and Kasper, C. B., 1998, Nuclear receptor involvement in the regulation of rat cytochrome P450 3A23 expression. *Journal of Biological Chemistry*, **273**, 16155–16162.

Huss, J. M. and Kasper, C. B., 2000, Two-stage glucocorticoid induction of CYP3A23 through both the glucocorticoid and pregnane X receptors. *Molecular Pharmacology*, **58**, 48–57.

Huss, J. M., Wang, S. I., Astrom, A., McQuiddy, P. and Kasper, C. B., 1996, Dexamethasone responsiveness of a major glucocorticoid-inducible CYP3A gene is mediated by elements unrelated to a glucocorticoid receptor binding motif. *Proceedings of the National Academy of Sciences, USA*, **93**, 4666–4670.

Ing, N. H. and O'Malley, B., 1995, The steroid hormone receptor superfamily: molecular mechanisms of action. In B. D. Weintrub (ed.), *Endocrinology: Basic Concepts and Clinical Correlations* (New York: Raven), pp. 195–215.

Ingelman-Sundberg, M., 2001, Implications of polymorphic cytochrome P450-dependent drug metabolism for drug development. *Drug Metabolism and Disposition*, **29**, 570–573.

Ioannides, C., 1996, *Cytochromes P450: Metabolic and Toxicological Aspects* (Boca Raton: CRC Press).

Iribarne, C., Dreano, Y., Bardou, G., Menez, J. F. and Berthou, F., 1997, Interaction of methadone with substrates of human hepatic cytochrome P450. *Toxicology*, **117**, 13–23.

Itoh, Satoh, M., Abe, Y., Hashimoto, H., Yanagamito, T. and Kamataki, T., 1994, A novel form of mouse cytochrome P450 3A (*Cyp3a-16*): its cDNA cloning and expression in fetal liver. *European Journal of Biochemistry*, **226**, 877–882.

Itoh, S., Yanagimoto, T., Tagawa, S., Hashimoto, H., Kitamura, R., Nakajima, Y., Okochi, T., Fujimoto, S., Uchino, J. and Kamataki, T., 1992, Genomic organization of human fetal specific P-450IIIA7 (cytochrome P-450HFLa)-related gene(s) and interaction of transcriptional regulatory factor with its DNA element in the 5′ flanking region. *Biochimica et Biophysica Acta*, **1130**, 133–138.

Jantzen, H.M., Strahle, U., Gloss, B., Stewart, F., Schmid, W., Boshart, M., Miksicek, R. and Schutz, G., 1987, Cooperativity of glucocorticoid response elements located far upstream of the tyrosine aminotransferase gene. *Cell*, **49**, 29–38.

Jenkins, B. D., Pullen, C. B. and Darimont, D., 2001, Novel glucocorticoid receptor coactivator mechanisms. *Trends in Endocrinology and Metabolism*, **12**, 122–126.

Jounaidi, Y., Guzelian, P. S., Maurel, P. and Vilarem, M. J., 1994, Sequence of the 5′-flanking region of CYP3A5 — comparative-analysis with CYP3A4 and CYP3A7. *Biochemical and Biophysical Research Communications*, **205**, 1741–1747.

Jover, R., Bort, R., Gomez-Lechon, M. and Castell, J., 2001, Cytochrome P450 regulation by hepatocyte nuclear factor 4 in human hepatocytes: a study using adenovirus-mediated antisense targeting. *Hepatology*, **33**, 668–675.

Kawamoto, T., Sueyoshi, T., Zelco, I., Moore, R., Wasgburn, K. and Negishi, M., 1999, Phenobarbitone-responsive nuclear translocation of the receptor CAR in induction of the *Cyp2b* gene. *Molecular and Cell Biology*, **19**, 6318–6322.

Kitada, M., Kamataki, T., Itahashi, K., Rikihisi, M., Kato, R. and Kanakubo, Y., 1995, Purification and properties of cytochrome P450 from homogenates of human fetal livers. *Archives of Biochemistry and Biophysics*, **241**, 275–280.

Kliewer, S. A., Moore, J. T., Wade, L., Staudinger, J. L., Watson, M. A., Jones, S. A., McKee, D. D., Oliver, B. B., Willson, T. M., Zetterstrom, R. H., Perlmann, T. and Lehmann, J. M., 1998, An orphan nuclear receptor activated by pregnanes defines a novel steroid signalling pathway. *Cell*, **92**, 73–82.

Kocarek, T. A., Schuetz, E. G., Strom, S. C., Fisher, R. A. and Guzelian, P. S., 1995, Comparative-analysis of cytochrome P4503A induction in primary cultures of rat, rabbit, and human hepatocytes. *Drug Metabolism and Disposition*, **23**, 415–421.

Kolars, J. C., Lown, K. S., Schmiedlinren, P., Ghosh, M., Fang, C., Wrighton, S. A., Merion, R. M. and Watkins, P. B., 1994, CYP3A gene-expression in human gut epithelium. *Pharmacogenetics*, **4**, 247–259.

Kolars, J. C., Schmiedlinren, P., Schuetz, J. D., Fang, C. and Watkins, P. B., 1992, Identification of rifampin-inducible P450IIIA4 (CYP3A4) in human small-bowel enterocytes. *Journal of Clinical Investigation*, **90**, 1871–1878.

Komori, M., Hashizume, T., Ohi, H., Miura, T., Kitada, M., Nagashima, K. and Kamataki, T., 1998, Cytochrome P450 in human liver microsomes: high performance liquid chromatographic isolation of three forms and their characterisation. *Journal of Biochemistry*, **104**, 912–916.

Komori, M. and Oda, Y., 1994, A major glucocorticoid-inducible P450 in rat liver is not P450 3A1. *Journal of Biochemistry*, **116**, 114–120.

Kuehl, P., Zhang, J., Lin, Y., Lanba, J., Assem, M., Scheutz, J., Watkins, P., Daly, A., Wrighton, S., Hall, S., Maurel, P., Relling, M., Brimer, C., Yasuda, K., Venkataramanan, R., Strom, S., Thummel, K., Boguski, M. and Schuetz, E., 2001, Sequence diversity in CYP3A promoters and characterisation of the genetic basis of polymorphic CYP3A5 expression. *Nature Genetics*, **27**, 383–391.

Lange, B., Balny, C. and Maurel, P., 1984, Inductive and repressive effects of rifampicin on rabbit liver microsomal cytochrome P450. *Biochemical Pharmacology*, **33**, 2771–2776.

Larsen, M. C., Brake, P. B., Parmar, D. and Jefcoate, C. R., 1994, The induction of five rat hepatic P450 cytochromes by phenobarbital and similarly acting compounds is regulated by a sexually dimorphic, dietary-dependent endocrine factor that is highly strain specific. *Archives of Biochemistry and Biophysics*, **315**, 24–34.

Le Cluyse, E. L., 2001a, Pregnane X receptor: molecular basis for species differences in CYP3A induction by xenobiotics. *Chemico-Biological Interactions*, **134**, 283–289.

Le Cluyse, E. L., 2001b, Human hepatocyte culture systems for the *in vitro* evaluation of cytochrome P450 expression and regulation. *European Journal of Pharmaceutical Sciences*, **13**, 343–368.

Lehmann, J. M., McKee, D. D., Watson, M. A., Willson, T. M., Moore, J. T. and Kliewer, S. A., 1998, The human orphan nuclear receptor PXR is activated by compounds that regulate CYP3A4 gene expression and cause drug interactions. *Journal of Clinical Investigation*, **102**, 1016–1023.

Li, A. P., Kaminski, L. and Rasmussen, A., 1995, Substrates of human hepatic cytochrome P450 3A4. *Toxicology*, **104**, 1–8.

Li, J., Ning, G. and Duncan, S., 2000, Mammalian hepatocyte differentiation requires the transcription factor HNF-4 alpha. *Genes and Development*, **14**, 464–474.

Liddle, C., Goodwin, B. J., George, J., Tapner, M. and Farrell, G. C., 1998, Separate and interactive regulation of cytochrome P450 3A4 by triiodothyronine, dexamethasone, and growth hormone in cultured hepatocytes. *Journal of Clinical Endocrinology and Metabolism*, **83**, 2411–2416.

Lown, K. S., Kolars, J. C., Thummel, K. E., Barnett, J. L., Kunze, K. L., Wrighton, S. A. and Watkins, P. B., 1994, Interpatient heterogeneity in expression of CYP3A4 and CYP3A5 in small-bowel — lack of prediction by the erythromycin breath test. *Drug Metabolism and Disposition*, **22**, 947–955.

Lucey, M. R., Kolars, J. C., Merion, R. M., Campbell, D. A., Aldrich, M. and Watkins, P. B., 1990, Cyclosporin toxicity at therapeutic blood levels and cytochrome P4503A. *Lancet*, **335**, 11–15.

Masuyama, H., Hiramatsu, Y., Kunitomi, M., Kudo, T. and MacDonald, P. N., 2000, Endocrine disrupting chemicals, phthalic acid and nonylphenol activate pregnane X receptor-mediated transcription. *Molecular Endocrinology*, **14**, 421–428.

Masuyama, H., Hiramatsu, Y., Mizutani, Y., Inoshita, H. and Kudo, T., 2001, The expression of pregnane X receptor and its target gene, cytochrome P450 *3a1*, in perinatal mouse. *Molecular and Cellular Endocrinology*, **172**, 47–56.

Meyer, U. and Zanger, U., 1997, Molecular mechanisms of genetic polymorphisms of drug metabolism. *Annual Review of Pharmacology and Toxicology*, **37**, 269–296.

Miyata, M., Nagata, K., Yamazoe, Y. and Kato, R., 1991, A gene structure of testosterone 6 beta-hydroxylase (P450IIIA). *Biochemical and Biophysical Research Communications*, **31**, 68–73.

Miyata, M., Nagata, K., Yamazoe, Y. and Kato, R., 1995, Transcriptional elements directing a liver-specific expression of P450/6 beta A (CYP3A2) gene-encoding testosterone 6 beta-hydroxylase. *Archives of Biochemistry and Biophys*ics, **318**, 71–79.

Moore, L. B., Parks, D. J., Jones, S. A., Bledsoe, R. K., Consler, T. G., Stimmel, J. B., Goodwin, B., Liddle, C., Blanchard, G., Willson, T. M., Collins, J. L. and Kliewer, S. A., 2000, Orphan nuclear receptors CAR and PXR share xenobiotic and steroid ligands. *Journal of Biological Chemistry*, **275**, 15122–15127.

Muangmoonchai, R., Smirlis, D., Wong, S. C., Edwards, M., Phillips, I. R. and Shephard, E. A., 2001, Xenobiotic induction of cytochrome P4502b1 (CYP2B1) is mediated by the orphan nuclear receptor constitutive androstane receptor (CAR) and requires steroid co-activator 1 (src-1) and the transcription factor sp1. *Biochemical Journal*, **355**, 71–78.

Muenier, V., Bourrie, M., Berger, Y. and Fabre, G., 1995, The human intestinal epithelial cell line Caco-2: pharmacological and pharmacokinetic applications. *Cell Biology and Toxicology*, **11**, 187–194.

Negishi, M. and Honkakoski, P., 2000, Induction of drug metabolism by nuclear receptor CAR: molecular mechanisms and implications for drug research. *European Journal of Pharmaceutical Sciences*, **11**, 259–264.

Nelson, D. R., Koymans, L., Kamataki, T., Stegeman, J. J., Feyereisen, R., Waxman, D. J., Waterman, M. R., Gotoh, O., Coon, M. J., Estabrook, R. W., Gunsalus, I. C. and Nebert, D. W., 1996, P450 superfamily: update on new sequences, gene mapping, accession numbers and nomenclature. *Pharmacogenetics*, **6**, 1–42.

Newton, D. J., Wang, R. W. and Lu, A. Y. H., 1994, Cytochrome P450 inhibitors: evaluation of specificities in the *in vitro* metabolism of therapeutic agents by human liver microsomes. *Drug Metabolism and Disposition*, **23**, 154–158.

Nuclear Receptor Nomenclature Committee, 1999, A unified nomenclature system for the nuclear receptor superfamily. *Cell*, **97**, 161–163.

Ogg, M., Williams, J., Tarbit, M., Goldfarb, P., Gray, T. and Gibson, G., 1999, A reporter gene assay to assess the molecular mechanisms of xenobiotic-dependent induction of the human CYP3A4 gene *in vitro*. *Xenobiotica*, **29**, 269–279.

Ogino, M., Nagata, K., Miyata, M. and Yamazoe, Y., 1999, Hepatocyte nuclear factor 4-mediated activation of rat CYP3A1 gene and its modes of modulation by apolipoprotein A1 regulatory protein 1 and v-erba-related protein 3. *Archives of Biochemistry and Biophysics*, **362**, 32–37.

Ohmori, S., Nakasa, H., Asanome, K., Kurose, Y., Ishii, I., Hosokawa, M. and Kitada, M., 1998, Differential catalytic properties in metabolism of endogenous and exogenous substrates among CYP3A enzymes expressed in cos-7 cells. *Biochimica et Biophysica Acta*, **1380**, 297–304.

Ozdemir, V., Kalow, W., Tang, B.K., Paterson, A., Walker, S., Endrenyi, L. and Kashuba, A., 2000, Evaluation of the genetic component of variability in CYP3A4 activity: a repeated drug administration method. *Pharmacogenetics*, **10**, 373–388.

Paine, M. F., Khalighi, M., Fisher, J. M., Shen, D. D., Kunze, K. L., Marsh, C. L., Perkins, J. D. and Thummel, K. E., 1997, Characterisation of inter- and intra-intestinal differences in human CYP3A-mediated metabolism. *Journal of Pharmacology and Experimental Therapeutics*, **283**, 1552–1562.

Pariante, C. M., Pearce, B. D., Pisell, T. L., Su, C. and Miller, A. H., 2001, The steroid receptor antagonists RU40555 and RU486 activate glucocorticoid receptor translocation and are not excreted by the by the steroid hormones transporter in L929 cells. *Journal of Endocrinology*, **169**, 309–320.

Pascussi, J., Jounaidi, Y., Drocourt, L., Domergue, J., Balabaud, C., Maurel, P. and Vilarem, M., 1999, Evidence for the presence of a functional pregnane X receptor response element in the CYP3A7 promoter gene. *Biochemical and Biophysical Research Communications*, **260**, 377–381.

Pascussi, J.-M., Drocourt, L., Fabre, J.-M., Maurel, P. and Vilarem, M.J., 2000a, Dexamethasone induces pregnane X receptor and retinoid X receptor-α expression in human hepatocytes: synergistic increase of CYP3A4 induction by pregnane X receptor. *Molecular Pharmacology*, **58**, 361–372.

Pascussi, J. M., Gerbal-Chaloin, S., Fabre, J. M., Maurel, P. and Vilarem, M. J., 2000b, Dexamethasone enhances constitutive androstane receptor expression in human hepatocytes: consequences on cytochrome P450 gene regulation. *Molecular Pharmacology*, **58**, 1441–1450.

Pascussi, J. M., Gerbal-Chaloin, S., Pichard-Garcia, L., Daujat, M., Fabre, J. M., Maurel, P. and Vilarem, M. J., 2000c, Interleukin-6 negatively regulates the expression of pregnane X receptor and constitutively activated receptor in primary human hepatocytes. *Biochemical and Biophysical Research Communications*, **274**, 707–713.

Paulussen, A., Lavrijsen, K., Bohets, H., Hendrickx, J., Versasselt, P., Luyten, W. and Konings, F., 2000, Two linked mutations in transcriptional regulatory elements of the CYP3A5 gene constitute the major genetic determinant of polymorphic activity in humans. *Pharmacogentics*, **10**, 415–424.

Pereira, T. M., Carlstedt-Duke, J., Leckner, M. C. and Gustafsson, J. A., 1998, Identification of a functional glucocorticoid response element in the CYP3A1/igc2 gene. *DNA and Cell Biology*, **17**, 39–49.

Picard, D. and Yamamoto, K. R., 1987, Two signals mediate hormone-dependent nuclear localization of the glucocorticoid receptor. *EMBO Journal*, **6**, 3333–3340.

Pickwell, G. V., Quattrochi, L. C., Shih, H. and Guzelian, P. S., 1996, Transcriptional activation of human fetal cytochrome P450 CYP3A7. *FASEB Journal*, **10**, 1346.

Plant, N., Ogg, M., Crowder, M. and Gibson, G., 2000, Control and statistical analysis of *in vitro* reporter gene assays. *Analytical Biochemistry*, **278**, 170–174.

Powell, W. A., Mitchell, B. F. and Challis, J. R., 1986, Effect of steroids on progesterone output by explants of human chorion. *Gynecological and Obstetric Investigation*, **22**, 64–72.

Pratt, W. B., 1993, The role of heat shock proteins in regulating the function, folding and trafficking of the glucocorticoid receptor. *Journal of Biological Chemistry*, **268**, 21455–21458.

Quattrochi, L. and Guzelian, P., 2001, CYP3A regulation: from pharmacology to nuclear receptors. *Drug Metabolism and Disposition*, **29**, 615–622.

Quattrochi, L. C., Mills, A. S., Barwick, J. L., Yockey, C. B. and Guzelian, P. S., 1995, A novel *cis*-acting element in a liver cytochrome-P450 3A gene confers synergistic induction by glucocorticoids plus antiglucocorticoids. *Journal of Biological Chemistry*, **270**, 28917–28923.

Rebbeck, T., Jaffe, J., Walker, A., Vein, A. and Malkowicz, S., 1998, Modification of clinical presentation of prostate tumours by a novel genetic variant in CYP3A4. *Journal of the National Cancer Institute*, **90**, 1225–1230.

Rivory, L. P., Qin, H., Clarke, S. J., Eris, J., Duggin, G., Ray, E., Trent, R. J., Bishop, J. F., 2000, Frequency of cytochrome P450 3A4 variant genotype in transplant population and lack of association with cyclosporin clearance. *European Journal of Clinical Pharmacology*, **56**, 395–398.

Robertson, G., Goodwin, B., Field, J. and Liddle, C., 2000, Transgenic mouse models of CYP3A4 regulation. In *13th International Symposium on Microsomes and Drug Oxidations*, Stresa, Italy, abst 46.

Sakuma, T., Takai, M., Endo, Y., Kuroiwa, M., Ohara, A., Jarukamjorn, K., Honma, R. and Nemoto, N., 2000, A novel female-specific member of the CYP3A gene subfamily in the mouse liver. *Archives of Biochemistry and Biophysics*, **377**, 153–162.

Sata, F., Sapone, A., Elizondo, G., Stocker, P., Miller, V., Zheng, W., Raunio, H., Crespi, C. and Gonzalez, F., 2000, CYP3A4 allelic variants with amino acid substitutions in exons 7 and 12: evidence for an allelic variant with altered catalytic activity. *Clinical Pharmacology and Therapeutics*, **67**, 48–56.

Savas, U., Griffen, K. and Johnson, E., 1999, Molecular mechanisms of cytochrome P450 induction by xenobiotics: an expanded role for nuclear hormone receptors. *Molecular Pharmacology*, **56**, 851–857.

Savas, U., Wester, M. R., Griffin, K. J. and Johnson, E. F., 2000, Rabbit pregnane X receptor is activated by rifampicin. *Drug Metabolism and Disposition*, **28**, 529–537.

Schuetz, E. G., Brimer, C. and Scheutz, J. D., 1998, Environmental xenobiotics and the antihormones cyproterone acetate and spironolactone use the nuclear hormone pregnane X receptor to activate the CYP3A23 hormone response element. *Molecular Pharmacology*, **54**, 1113–1117.

Schuetz, E. G. and Guzelian, P. S, 1984, Induction of cytochrome P-450 by glucocorticoids in rat liver. II. Evidence that glucocorticoids regulate induction of cytochrome P-450 by a non-classical receptor mechanism. *Journal of Biological Chemistry*, **259**, 2007–2012.

Schuetz, E. G., Schinkel, A. H., Relling, M. V. and Schuetz, J. D., 1996b, P-glycoprotein: a major determinant of rifampicin-inducible expression of cytochrome P450 3A in mice and humans. *Proceedings of the National Academy of Sciences, USA*, **93**, 4001–4005.

Schuetz, E., Schmid, W., Schutz, G., Brimer, C., Yasuda, K., Kamataki, T., Bornheim, L., Myles, K. and Cole, T., 2000, The glucocorticoid receptor is essential for induction of cytochrome P-450 *2b* by steroids but not for drug or steroid induction of *cyp3a* or P-450 reductase in mouse liver. *Drug Metabolism and Disposition*, **28**, 268–277.

Schuetz, E. G., Schuetz, J. D., Strom, S. C., Thompson, M. T., Fisher, R. A., Molowa, D. T., Li, D. and Guzelian, P. S., 1993, Regulation of human liver cytochromes P-450 in family 3A in primary and continuous-culture of human hepatocytes. *Hepatology*, **18**, 1254–1262.

Schuetz, J., Beach, D. and Guzelian, P., 1994, Selective expression of cytochrome P450 CYP3A mRNA's in embryonic and adult human liver. *Pharmacogenetics*, **4**, 11–20.

Schuetz, J. D. and Guzelian, P. S., 1995, Isolation of CYP3A5p cDNA from human liver — a reflection of a novel cytochrome P-450 pseudogene. *Biochimica et Biophysica Acta*, 1261, 161–165.

Schuetz, J. D., Schuetz, E. G., Thottassery, J. V., Guzelian, P. S., Strom, S. and Sun, D., 1996a, Identification of a novel dexamethasone responsive enhancer in the human CYP3A5 gene and its activation in human and rat liver cells. *Molecular Pharmacology*, **49**, 63–72.

Shimada, T., Yamazaki, H., Mimura, M., Inui, Y. and Guengerich, F., 1994, Interindividual variations in human liver cytochrome P450 enzymes involved in the oxidation of drugs, carcinogens and toxic chemicals — studies with liver microsomes of 30 Japanese and 30 Caucasians. *Journal of Pharmacology and Experimental Therapeutics*, **270**, 414–423.

Smirlis, D., Muangmoonchai, R., Edwards, M., Phillips, I. R. and Shephard, E. A., 2001, Orphan receptor promiscuity in the induction of cytochromes P450 by xenobiotics. *Journal of Biological Chemistry*, **276**, 12822–12826.

Smith, D. A., Abel, S. M., Hyland, R. and Jones, B. C., 1998, Human cytochrome P450s: selectivity and measurement *in vivo*. *Xenobiotica*, **28**, 1095–1128.

Smith, D. A., 2000, Induction and drug development. *European Journal of Pharmaceutical Sciences*, **11**, 185–189.

Sonderfan, A. J., Arlotto, M. P., Dutton, D. R., McMillan, S. K. and Parkinson, A., 1987, Regulation of testosterone hydroxylation by rat liver microsomal cytochrome P450. *Archives of Biochemistry and Biophysics*, **255**, 27–41.

Staudinger, J., Goodwin, B., Jones, S., Hawkins-Brown, D., MacKenzie, K., LaTour, A., Liu, Y., Klaassen, C., Brown, K., Reinhard, J., Willson, T., Koller, B. and Kliewer, S., 2001, The nuclear receptor PXR is a lithocholic acid sensor that protects against liver toxicity. *Proceedings of the National Academy of Sciences, USA*, **98**, 3369–3374.

Strom, A., Westin, S., Eguchi, H., Gustafsson, J. A. and Mode, A., 1995, Characterization of orphan nuclear receptor binding elements in sex-differentiated members of the CYP2C gene family expressed in rat liver. *Journal of Biological Chemistry*, **12**, 11276–11281.

Sueyoshi, T., Kawamoto, T., Zelco, I., Honkakowski, P. and Negishi, M., 1999, The repressed nuclear receptor CAR responds to phenobarbital in activating the human CYP2B6 gene. *Journal of Biological Chemistry*, **274**, 6043–6046.

Sueyoshi, T. and Negishi, M., 2001, Phenobarbitone response elements of cytochrome P450 genes and nuclear receptors. *Annual Review of Pharmacology and Toxicology*, **41**, 123–143.

Szklarz, G. D. and Halpert, J. R., 1997, Molecular modelling of cytochrome P450 3A4. *Journal of Computer Aided Molecular Design*, **11**, 265–272.

Taylor, W. and Lesna, M., 1997, The hepatotoxicity of lithocholic acid in male mice. *British Journal of Pharmacology*, **61**, 133–134.

Telhada, M. B., Pereira, T. M. and Lechner, M. C., 1992, Effect of dexamethasone and phenobarbital on run-on transcription rate and CYP3A mRNA concentration in rat liver: changes during development. *Archives of Biochemistry and Biophysics*, **298**, 715–725.

Thummel, K. E., Lee, C. A., Kunze, K. L., Nelson, S. D. and Slattery, J. T., 1993, Oxidation of acetaminophen to *N*-acetyl-*p*-aminobenzoquinoneimine by human CYP3A4. *Biochemical Pharmacology*, **45**, 1563–1569.

Thummel, K. E., Shen, D. D., Podoll, T. D., Kunze, K. L., Trager, W. F., Bacchi, C. E., Marsh, C. L., McVicar, J. P., Barr, D. M., Perkins, J. D. and Carithers, R. L., 1994, Use of midazolam as a human cytochrome P4503A probe. 2. Characterization of interindividual and intraindividual hepatic CYP3A variability after liver-transplantation. *Journal of Pharmacology and Experimental Therapeutics*, **271**, 557–566.

Tokui, T., Nakai, D., Nakagomi, R., Yawo, H., Abe, T. and Sugiyama, Y., 1999, Pravastatin, an HMG-CoA reductase inhibitor, is transported by rat organic anion transporting polypeptide, OATP-2. *Pharmaceutical Research*, **16**, 904–9088.

Tucker, G. T., Rostami-Hodjegan, A. and Jackson, P. R., 1998, Determination of drug-metabolizing enzyme activity *in vivo*: pharmacokinetic and statistical issues. *Xenobiotica*, **28**, 1255–1273.

Tzameli, I. and Moore, D. D., 2001, Role reversal: new insights from new ligands for the xenobiotic receptor CAR. *Trends in Endocrinology and Metabolism*, **12**, 7–10.

Tzameli, I., Pissios, P., Scheutz, E. G. and Moore, D. D., 2000, The xenobiotic compound 1,4-bis[3,5-dichloropyridyloxy)] benzene is an agonist ligand for the nuclear receptor CAR. *Molecular and Cell Biology*, **20**, 2951–2958.

Venkatesan, K., 1992, Pharmacokinetic drug-interactions with rifampicin. *Clinical Pharmacokinetics*, **22**, 47–65.

Walker, A. H., Jaffe, J. M., Gunasegaram, S., Cummings, S. A., Huang, C. S., Chern, H. D., Olopade, O. I., Weber, B. L. and Rebbeck, T. R., 1998, Characterization of an allelic variant in the nifedipine-specific element of CYP3A4: ethnic distribution and implications for prostate cancer risk. *Human Mutation*, **12**, 289.

Wan, Y.U. Y., An, D., Cai, Y., Repa, J., Chen, T. H.-P., Flores, M., Postic, C., Magnuson, M., Chen, J., Chien, K., French, S., Mangelsdorf, D. and Sucov, H., 2000, Hepatocyte-specific mutation establishes retionid X receptor as a heterodimeric integrator of multiple physiological processes in the liver. *Molecular and Cellular Biology*, **20**, 4436–4444.

Wang, J. C., Stafford, J. M. and Granner, D. K., 1998, SRC-1 and GRIP1 coactivate transcription with hepatocyte nuclear factor 4. *Journal of Biological Chemistry*, **273**, 30847–30850.

Watkins, P., 1994, Noninvasive tests of CYP3A enzymes. *Pharmacogenetics*, **4**, 171–184.

Watkins, P., Murray, S., Winkelman, L., Heuman, D., Wrighton, S. and Guzelian, P., 1988, Erythromycin breath test as an assay of glucocorticoid-inducible liver cytochromes P450. *Journal of Clinical Investigation*, **83**, 688–697.

Watkins, P. B., Wrighton, S. A., Schuetz, E. G., Maurel, P. and Guzelian, P. S., 1986, Macrolide antibiotics inhibit the degradation of the glucocorticoid-responsive cytochrome P-450p in rat hepatocytes *in vivo* and in primary monolayer-culture. *Journal of Biological Chemistry*, **261**, 6264–6271.

Watkins, R. E., Wisely, G. B., Moore, L. B., Collins, J. L., Lambert, M. H., Williams, S. P., Willson, T. M., Kliewer, S. A. and Redinbo, M. R., 2001, The human nuclear xenobiotic receptor PXR: structural determinants of directed promiscuity. *Science*, **292**, 2329–2333.

Waxman, D. J., 1999, P450 gene induction by structurally diverse xenochemicals: central role of nuclear receptors CAR, PXR and PPAR. *Archives of Biochemistry and Biophysics*, **369**, 11–23.

Weaver, R. J., 2001, Assessment of drug–drug interactions: concepts and approaches. *Xenobiotica*, **31**, 499–538.

Wei, P., Zhang, J., Egan-Hafley, M., Liang, S. G. and Moore, D. D., 2000, The nuclear receptor CAR mediates specific xenobiotic induction of drug metabolism. *Nature*, **407**, 920–923.

Westlind, A., Lofberg, L., Tindberg, N., Andersson, T. B. and Ingelman-Sundberg, M., 1999, Interindividual differences in hepatic expression of CYP3A4: relationship to genetic polymorphism in the 5′-upstream regulatory region. *Biochemical and Biophysical Research Communications*, **259**, 201–205.

Westlind, A., Malmebo, S., Johansson, I., Otter, C., Andersson, T. B., Ingelman-Sundberg, M. and Oscarson, M., 2001, Cloning and tissue distribution of a novel human cytochrome P450 of the CYP3A subfamily, CYP3A43. *Biochemical and Biophysical Research Communications*, **281**, 1349–1355.

Wilkinson, G. R., 1996, Cytochrome P4503A (CYP3A) metabolism: prediction of *in vivo* activity in humans. *Journal of Pharmacokinetics and Biopharmaceutics*, **24**, 475–490.

Worboys, P. D. and Carlile, D. J., 2001, Implications and consequences of enzyme induction on preclinical and clinical drug development. *Xenobiotica*, **31**, 539–556.

Wright, M. C. and Paine, A. J., 1994, Induction of the cytochrome P450 3A subfamily in rat liver correlates with the binding of inducers to a microsomal protein. *Biochemical and Biophysical Research Communications*, **201**, 973–979.

Wright, M. C., Wang, X. J., Pimenta, M., Ribeiro, V., Paine, A. J. and Lechner, M. C., 1996, Glucocorticoid receptor-independent transcriptional induction of cytochrome P450 3A1 by metyrapone and its potentiation by glucocorticoid. *Molecular Pharmacology*, **50**, 856–863.

Wrighton, S. A., Brian, W. R., Sari, M. A., Iwasaki, M., Guengerich, F. P., Raucy, J. L., Molowa, D. T. and Vandenbranden, M., 1990, Studies on the expression and metabolic capabilities of human liver cytochrome P45IIIA5 (hlp3). *Molecular Pharmacology*, **38**, 207–213.

Wrighton, S. A., Ring, B. J., Watkins, P. B. and van den Branden, M., 1989, Identification of a polymorphically expressed member of the human cytochrome P-450III family. Molecular Pharmacology, **36**, 97–105.

Wrighton, S. A., Schuetz, E. G., Thummel, K. E., Shen, D. D., Korzekwa, P. B. and Watkins, P. B., 2000, The human CYP3A subfamily: practical considerations. *Drug Metabolism Reviews*, **32**, 339–362.

Wrighton, S. A. and van den Branden, M., 1989, Isolation and characterisation of human liver fetal liver cytochrome P450HLp2: a third member of the P450III gene family. *Archives of Biochemistry and Biophysics*, **268**, 144–151.

Xie, W., Barwick, J., Simmon, C., Pierce, A., Safe, S., Blumberg, B., Guzelian, P. and Evans, R., 2000a, Reciprocal activation of xenobiotic response genes by nuclear receptors SXR/PXR and CAR. *Genes and Development*, **14**, 3014–3023.

Xie, W., Barwick, J. L., Downes, M., Blumberg, B., Simon, C. M., Nelson, M. C., Neuschwander-Tetri, B. A., Bruntk, E. M., Guzelian, P. S. and Evans, R. M., 2000b, Humanized xenobiotic response in mice expressing nuclear receptor SXR. *Nature*, **406**, 435–439.

Xie, W., Radominska-Pandya, A., Shi, Y., Simon, C. M., Nelson, M. C., Ong, E. S., Waxman, D. J. and Evans, R. M., 2001, An essential role for nuclear receptors SXR/PXR in detoxification of cholestatic bile acids. *Proceedings of the National Academy of Sciences, USA*, **98**, 3375–3380.

Yanagimoto, T., Itoh, S., Muller-Enoch, D. and Kamataki, T., 1992, Mouse liver cytochrome P450(P-450IIIAM1): its cDNA cloning and inducibility by dexamethasone. *Biochimica et Biophysica Acta*, **1130**, 319–332.

Yanagimoto, T., Itoh, S., Sawada, M., Hashimoto, H. and Kamataki, T, 1994, Molecular cloning and functional expression of a mouse cytochrome P450 (*Cyp3a13)*: examination of *Cyp3a13* to activate aflatoxin B_1. *Biochimica et Biophysica Acta*, **1201**, 405–410.

Yanagimoto, T., Itoh, S., Sawada, M. and Kamataki, T., 1997, Mouse cytochrome P450 (*Cyp3A11*): predominant expression in liver and capacity to activate aflatoxin B_1. *Archives of Biochemistry and Biophysics*, **340**, 215–218.

Yang, H. Y., Lee, Q. P., Rettie, A. E. and Juchau, M. R., 1994, Functional cytochrome P4503A isoforms in human embryonic tissues: expression during organogenesis. *Molecular Pharmacology*, **46**, 922–928.

Zelco, I., Sueyoshi, T., Kawamoto, T., Moore, R. and Negishi, M., 2001, The peptide near the C-terminus regulates receptor CAR nuclear translocation induced by xenochemicals in mouse liver. *Molecular and Cellular Biology*, **21**, 2838–2846.

Zhang, H., Le Culyse, E., Liu, L., Hu, M., Matoney, L., Zhu, W. and Yan, B., 1999, Rat pregnane X receptor: molecular cloning, tissue distribution and xenobiotic regulation. *Archives of Biochemistry and Biophysics*, **368**, 14–22.

Zhao, X. J. and Ishizaki, T., 1997, The *in vitro* hepatic metabolism of quinine in mice, rats and dogs: comparison with human liver microsomes. *Journal of pharmacology and Experimental Therapeutics*, **283**, 1168–1176.

XENOBIOTICA, 2002, VOL. 32, NO. 3, 207–220

Taylor & Francis
healthsciences

Differences in the absorption, metabolism and biliary excretion of a diastereomeric pair of $\alpha_v\beta_3$-antagonists in rat: limited role of P-glycoprotein

T. PRUEKSARITANONT†*, Y. MENG†, B. MA†, P. LEPPERT†, J. HOCHMAN†, C. TANG†, J. PERKINS‡, M. ZRADA‡, R. MEISSNER‡, M. E. DUGGAN‡ and J. H. LIN†

† Departments of Drug Metabolism and ‡ Medicinal Chemistry, Merck Research Laboratories, West Point, PA 19486, USA

Received 19 July 2001

1. The study investigated mechanisms underlying the pharmacokinetic differences of two zwitterionic diastereomers ((3*S*)-3-{(3*R* or 3*S*)-2-oxo-3-[3-(5,6,7,8-tetrahydro-1,8-naphthyridin-2-yl)propyl]pyrrolidin-1-yl}-3-quinolin-3-ylpropanoic acid) with different lipophilicities using a combination of *in vivo* and *in vitro* approaches.

2. In rat, both isomers possessed comparable plasma clearances (CL). However, the more lipophilic diastereomer **I** exhibited a higher metabolic clearance (> 2-fold higher than **II**), whereas the hydrophilic zwitterion **II** exhibited a higher biliary clearance (~5-fold higher than **I**). Following oral administration, the bioavailability (*F*) of **I** (17%) was much higher than that of **II** (1%).

3. Consistent with these *in vivo* observations and the expectation based on their lipophilicity differences, the metabolism in rat liver microsomes was faster and the permeability in Caco-2 and LLC-PK1 cells and *in situ* rat intestinal loop was better for **I** than for **II**.

4. Only the absorption of the more lipophilic diastereomer **I** was subjected to an efflux system in the Caco-2 and *in situ* rat intestinal loop models. **I** was a good substrate for P-glycoprotein (P-gp) in both the human *MDR1* and mouse *mdr1a* transfected cell lines, and in the wild-type mdr1a (+/+) mouse when compared with the P-gp-deficient mdr1a (−/−) mouse. Concomitant administration of **I** with verapamil in rat caused significant increases in oral AUC, *F* and C_{max} of **I** without affecting its CL, further supporting the effect of P-gp in limiting the intestinal absorption of **I** *in vivo* in this animal model.

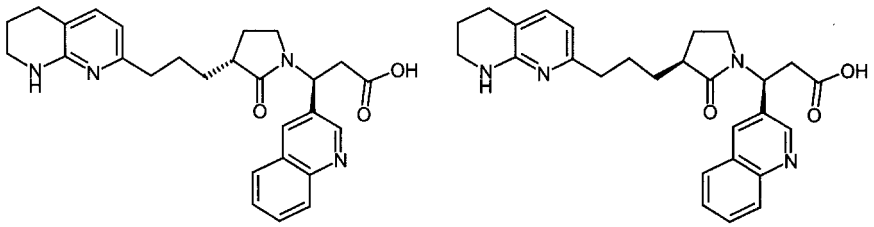
5. Since the findings that the lipophilic diastereomer **I**, but not **II**, was a good P-gp substrate were not in line with the observations that **I** was excreted to bile much slower than **II** and that **I** was absorbed better than **II**, the results suggested that P-gp played a minor role to the observed differences in the biliary excretion and intestinal absorption of the diastereomers **I** and **II** in rat.

Introduction

Compound **I** ((3*S*)-3-{(3*R*)-2-oxo-3-[3-(5,6,7,8-tetrahydro-1,8-naphthyridin-2-yl)propyl]pyrrolidin-1-yl}-3-quinolin-3-ylpropanoic acid) and its diastereomer **II** ((3*S*)-3-{(3*S*)-2-oxo-3-[3-(5,6,7,8-tetrahydro-1,8-naphthyridin-2-yl)propyl]-pyrrolidin-1-yl}-3-quinolin-3-ylpropanoic acid) (figure 1) are potent antagonists of the $\alpha_v\beta_3$-receptor, which is thought to play a key role in bone resorption processes (Hartman and Duggan 2000, Miller *et al.* 2000). The compounds contain both the basic tetrahydronaphthyridine moiety ($pK_a \sim 8$) and the acidic carboxylic ($pK_a \sim 3$) functional group, and are zwitterions at physiological pH. Early characterization of compounds revealed marked differences in their physicochem-

* Author for correspondence; e-mail: thomayant_prueksaritanont@merck.com

Xenobiotica ISSN 0049–8254 print/ISSN 1366–5928 online © 2002 Taylor & Francis Ltd
http://www.tandf.co.uk/journals
DOI: 10.1080/00498250110094403



I **II**

Figure 1. Chemical structures of **I** and **II**.

ical properties. **I** is more lipophilic than **II**; log *P* (octanol/buffer pH 7.4) = 1.04 for **I** versus log *P* = −0.05 for **II**. Preliminary studies also indicated considerable differences in their pharmacokinetic properties, especially after oral administration in rat and dog. Although stereoselectivity in pharmacokinetics and metabolism of chiral drugs has been well documented for decades (Watari *et al.* 1989, Davies 1998), there have been few reports describing in detail the pharmacokinetics of diastereomers with different lipophilicities. Lipophilicity is widely recognized as a major determinant in pharmacokinetic processes, including absorption and metabolism (Testa *et al.* 2000). Recently, it has been recognized increasingly that the absorption, distribution and excretion into bile and urine of a compound can also be influenced by secretory transport systems. One of the important and well-characterized transport systems is the multidrug resistance (MDR) transporter P-glycoprotein (P-gp) (Schinkel *et al.* 1995, Wacher *et al.* 1995), which is localized on epithelia of animal and human tissues, such as the intestine, kidney, liver and the blood–brain barrier (Thiebaut *et al.* 1987).

The present study was, therefore, set-up to gain some insight into mechanisms responsible for the observed pharmacokinetic differences of **I** and **II**. First, the absorption, metabolism and excretion of both diastereomers were characterized in rat. The intestinal transport and metabolism of **I** and **II** were then investigated using an *in situ* rat intestinal loop technique, the Caco-2 model, and *in vitro* rat liver microsomes. Involvement of P-gp in the absorption process of **I** and **II** was examined using the *in situ* rat intestinal loop model, and human *MDR1* (L-MDR1) and mouse *mdr1a* (L-mdr1a) transfected cell lines, coupled with *in vivo* studies in the rat and P-gp-deficient mdr1a (−/−) mouse. The results described here show that (1) there were quantitative differences in the intestinal absorption, hepatic metabolism and biliary excretion between the two diastereomers in rat, (2) the more lipophilic zwitterion **I**, but not the diastereomer **II**, was a good substrate for P-gp, and (3) P-gp transport was unlikely a major contributing factor to the observed differences in the absorption and biliary excretion between these zwitterionic diastereomers in rat.

Materials and methods

Materials

I and its diastereomer **II** (figure 1) (chemical purity > 98% and isomeric purity > 99%) and MK-571 were synthesized at Merck Research Laboratories (West Point, PA, USA). Verapamil, UDPGA and NADPH were purchased from Sigma Chemicals Co. (St Louis, MO, USA). Solvents used for analysis

were of analytical or HPLC grade (Fisher Scientific, Pittsburgh, PA, USA). Human intestinal cell line, Caco-2, was obtained from the American Type Culture Collection (Rockville, MD, USA). The cells were maintained in Opti-MEM supplemented with 10% foetal calf serum, non-essential amino acids and Glutamax, and were used at passage nos 20–50. Human *MDR1* transfectants L-MDR1, mouse *mdr1a* transfectants L-mdr1a, and their parenteral cell line LLC-PK1 pig kidney epithelial cells were kindly provided by Dr A. H. Schinkel (The Netherlands Cancer Institute, Amsterdam) and used under a license agreement. The cells were cultured in medium 199 (Life Technologies) supplemented with 2 mM L-glutamine, penicillin (50 units ml^{-1}), streptomycin (50 μg ml^{-1}) and 10% foetal calf serum. Male Sprague–Dawley rats were obtained from Taconic Laboratories (Germantown, NY, USA), and male mdr1a (–/–) and CF-1 mice were from Charles River Laboratories (Raleigh, NC, USA).

In vivo *studies*

All studies were reviewed and approved by the Merck Research Laboratories Institutional Animal Care and Use Committee.

Studies in rat. Male Sprague–Dawley rats (230–320 g) with an indwelling cannula implanted in a jugular vein for blood sampling and drug administration were used. Dosing solutions of **I** or **II** (0.5–2.0 mg ml^{-1}) were prepared in normal saline buffered to pH 7.4. **I** or **II** was given to rats at 1 mg kg^{-1} i.v. and 3 mg kg^{-1} p.o. In the experiments designed to investigate the effect of verapamil on the absorption and disposition of **I**, verapamil was given at 10 mg kg^{-1} p.o. ~30 min before administration of **I** (1 mg kg^{-1} i.v. or 3 mg kg^{-1} p.o.). Excretion studies of **I** or **II** were carried out at 1 mg kg^{-1} i.v. in the bile duct cannulated rat. Rats were housed individually in metabolism cages for urine collection. To minimize the hydrolysis of a glucuronide conjugate of **I** and **II** to **I** and **II**, respectively, bile and urine samples were acidified immediately after collection with 1% 1 N hydrochloric acid. Plasma, bile and urine samples were stored frozen until analysis by HPLC (see below).

Studies in mouse. Two separate groups of mice, the P-gp-deficient mdrla (–/–) (Schinkel *et al.* 1994) and the wild-type mdrla (+/+) CF-1, were given an oral dose of 5 mg kg^{-1} of **I**. After appropriate intervals, mice were exsanguinated under carbon dioxide via cardiac puncture. Three animals were used for each sampling time point. Blood samples were collected, centrifuged and plasma samples were separated and analysed by HPLC (see below). Brain was removed, weighed and homogenized. An aliquot of brain homogenate was mixed with acetonitrile (1:5 v/v) to precipitate proteins. Following centrifugation, the supernatant was evaporated, reconstituted with 20% acetonitrile in 25 mM potassium phosphate buffer, pH 6, and analysed for **I** by the HPLC method described below.

In vitro *plasma protein binding*

The binding of **I** and **II** to rat plasma proteins was determined, in triplicate, using an ultrafiltration method. Rat plasma (pH adjusted to 7.4) was spiked with **I** or **II** to yield final concentrations of 0.5 and 10 μm. Following incubation at 37°C for 15 min, an aliquot of plasma (3 × 1 ml) was transferred immediately to a centrifuge tube (Amicon Co., Danvers, MA, USA). The tube was centrifuged at 1500*g* for 15–30 min at 37°C to obtain ~0.2 ml filtrate. The filtrate and original plasma samples were analysed for **I** and **II** by HPLC. The unbound fraction was estimated directly from the ratio of the intact drug in the filtrate to that in the original plasma samples before centrifugation. Preliminary studies indicated that **I** or **II** was bound minimally to the ultrafiltrate device.

In vitro *metabolism studies*

The hepatic metabolism of **I** or **II** was examined initially using pooled liver microsomes from rats ($n = 6$). Liver microsomes (0.2 mg protein/0.2 ml) were incubated with **I** or **II** (2 μM) in the presence of NADPH (1 mM), or in the presence of UDPGA (5 mM) and D-saccharic acid 1,4-lactone (3 mM) following activation with 0.04 mg Brij 58, at 37°C, for up to 60 min. Studies on the kinetics of **I** and **II** metabolism also were conducted in the presence of NADPH or UDPGA using various concentrations of **I** and **II** (0.25–200 μM) and an incubation of 25 min (NADPH) or 30 min (UDPGA). The reaction was terminated by the addition of 2 ml acetonitrile. The supernatant was evaporated, reconstituted with 20% acetonitrile in 25 mM potassium phosphate buffer, pH 6, and analysed for **I** or **II** by HPLC.

In vitro *transport studies*

Caco-2 cells, grown on 12-mm millicel PCF filter inserts, at 100 000 cells cm^{-2} for 3 weeks, were used throughout. The integrity of the monolayer was monitored by determining transepithelial electrical resistance (320–490 Ω cm^2) and the lucifer yellow permeation. The transport study of **I** and **II** was carried out under identical conditions as described (Prueksaritanont *et al.* 1998), at 37°C, using 10 μM **I** or **II**, at the apical and basolateral compartment pH of 7.4 (10 mM HEPES buffer). The apparent

permeability coefficient constant (P_{app}) was determined by dividing the amount permeating cm^{-2} s^{-1}, during 90 min, by the membrane surface area and the drug concentration in solution in the donor. Solutions from the two compartments were injected directly on to HPLC for quantitative analysis of **I** and **II**. Over the concentration range studied, both compounds were soluble and had a recovery of $>95\%$, indicating negligible non-specific binding to the well or filter.

Transepithelial transport across L-MDR1, L-mdr1a and LLC-PK1 cells was carried out as described (Yamazaki *et al.* 2001). In brief, cells were plated at a density of 1.5×10^5 cells/6.4-mm well on collagen I-coated porous polycarbonate membrane filters, and were used for the transport experiments on the fifth day after plating. The directional transport studies of **I** and **II** was carried out in quadruplicate, at 37°C for 2 h, using 5 μM **I** or **II** in the apical and basolateral compartments. Aliquots from the two compartments were injected directly on to HPLC for quantitative analysis of **I** and **II**.

In situ *rat intestinal loop studies*

The studies were reviewed and approved by the Merck Research Laboratories Institutional Animal Care and Use Committee. Male Sprague–Dawley rats (230–320 g) were prepared for the intestinal absorption study according to the procedure of Barr and Riegelman (1970) as described (Prueksaritanont *et al.* 1998). In brief, dosing solution (0.5 mg **I** or **II**/2 ml normal saline), with or without verapamil or MK-571 (500 μM), was injected directly into the lumen of the intestinal loop. Blood samples were collected at appropriate intervals, and the blood lost from the mesenteric vein was replaced continuously with an equal volume of heparinized fresh rat blood through the cannulated jugular vein. At the end of the experiment (1 h), the remaining content in the intestinal loop was collected. The loop was rinsed with 2×3 ml saline, and the washes were combined. The intestinal wash was aliquoted and mixed with 3 ml acetone. The intestine was homogenized using 4 vols saline, and an aliquot was taken and extracted instantly with 3 ml acetone to terminate potential metabolic reactions. Blood samples (25–75 μl) were also extracted using 3 ml acetone. The acetone extracts were evaporated and reconstituted with the mobile phase and analysed for **I** and **II** by the HPLC methods described below.

Analytical procedure

An HPLC method with fluorescence detection was used for quantitative determination of **I** and **II** concentrations in samples obtained from the above studies. Plasma, bile and urine samples, with or without appropriate dilutions, were analysed after protein precipitation with acetonitrile (1:1 v/v). The system consisted of a Waters 600E multisolvent delivery system, a Waters 717 plus autosampler (Waters Co., Milford, MA, USA) and a Jasco 821-FP fluorescence detector (Jasco Co., Tokyo, Japan). The sample analysis of **I** or **II** was conducted on a Spherisorb SCX column (4.6×250 mm, 5 μm) (Phenomenex, Torrance, CA, USA), with the mobile phase (A, acetonitrile; B, 25 mM phosphate buffer, pH 6) delivered at a flow rate of 1 ml min^{-1} (27% A for 5 min, then to 60% A in 1 min and held at 60%A for 6 min). The effluent was monitored at λ_{ex} and λ_{em} of 330 and 395 nm, respectively. The linear calibration range was 2 nM (limit of quantitation, LOQ) to 1000 nM for the quantification of **I** and **II**. The intra- and interday assay precision (%CV) and accuracy throughout the calibration range was $<15\%$ for analytes **I** and **II** in all matrices examined. Owing to the unavailability of an analytical standard, quantitation of a glucuronide conjugate of **I** and **II** in the *in vitro* incubation mixtures supplemented with UDPGA was accomplished using standard curves for **I** and **II**, respectively, assuming identical extraction recoveries and extinction coefficients between the parent drug and its corresponding glucuronide conjugate.

Additionally, qualitative analysis was performed on bile and urine samples and microsomal incubates to determine metabolites of **I** and **II**. Samples were injected on to a BDS Hypersil C18 column (2×150 mm, 5 μm) (Keystone Scientific, Inc., Bellefonte, PA, USA) with a mobile phase consisting of 0.2% acetic acid (pH adjusted to 4.5 with ammonium hydroxide, solvent A) and acetonitrile (solvent B), delivered at a constant flow rate of 0.2 ml min^{-1}. The initial mobile phase consisted of 10% of solvent B, which increased linearly to 35% over 20 min. LC-MS and LC-MS/MS experiments were conducted on a Finnigan MAT LCQ ion-trap mass spectrometer (Finnigan MAT, San Jose, CA, USA) using electrospray ionization (ESI) in the positive mode.

Data analysis

CL of **I** and **II** was calculated as the dose divided by the AUC from time zero to infinity. The apparent elimination half-life was estimated from the slope of the terminal phase of the log plasma concentration–time data. V_{dss} and MRT were determined using a non-compartmental method (Benet and Galeazzi 1979). F was calculated by dividing dose-normalized AUC resulting from oral administration by that obtained from i.v. administration. The extent of metabolism (%) was estimated by subtracting the per cent of the i.v. dose recovered as unchanged in the 48-h excreta from 100, assuming complete recovery after the 48-h collection. The metabolic clearance, biliary clearance or renal clearance

was estimated as the CL multiplied by the fraction metabolized, eliminated unchanged in bile or in urine, respectively.

Apparent K_m and V_{max} were estimated using a non-linear regression program (Enfit from Biosoft, Ferguson, MO, USA). The CL_{int} was estimated by dividing V_{max} by K_m.

An unpaired Student's *t*-test was used to assess the significance of differences between the pharmacokinetic parameters determined for **I** and **II** in the control rat, and for **I** in the control and verapamil treated animals. One-way ANOVA assessed the significance of differences in per cent recovery of **I** or **II** in the absence and presence of inhibitors in the *in situ* rat experiments. In all cases, $p < 0.05$ was considered as statistically significant.

Results

Pharmacokinetic studies

Following i.v. administration, plasma concentrations of **I** and **II** declined in a multiphasic manner (figure 2A). Both **I** and **II** were moderate clearance compounds, with similar CL = 25–26 ml min^{-1} kg^{-1}. **I** possessed ~3-fold larger V_d, resulting in ~2–3-fold longer $t_{1/2}$ and MRT than **II**. Following oral administration, plasma concentrations of **I** were much higher than those of **II** over the entire sampling period (figure 2B); AUC, C_{max} and F for **I** were ~40-, 10- and 17-fold higher than **II**, respectively (table 1).

Table 1. Pharmacokinetic parameters of **I** and **II** following i.v. and p.o. administration of **I** and **II** and following i.v. and p.o. administration of **I** after 10 mg kg^{-1} p.o. verapamil (**I** + verapamil) to rat.

		I	**II**	**I** + verapamil
1 mg kg^{-1} i.v.				
CL	(ml min^{-1} kg^{-1})	24.9 ± 2.0	25.9 ± 1.4	26.6 ± 2.0
V_{dss}	(l kg^{-1})	1.3 ± 0.3	0.4 ± 0.1	2.5 ± 1.6
$t_{1/2}$	(h)	2.2 ± 0.8	1.0 ± 0.0	3.0 ± 1.8
MRT	(h)	1.0 ± 0.3	0.3 ± 0.05	1.6 ± 0.9
3 mg kg^{-1} p.o.				
AUC	(nM h)	763 ± 268	18.2 ± 8	1300 ± 276*
C_{max}	(nM)	174 ± 55	17 ± 1	644 ± 212*
T_{max}	(h)	0.3 ± 0	0.3 ± 0.15	0.3 ± 0.0
F	(%)	17	1	32

Values are means ± SD, $n = 4$.
* Significantly different ($p < 0.05$) from control.

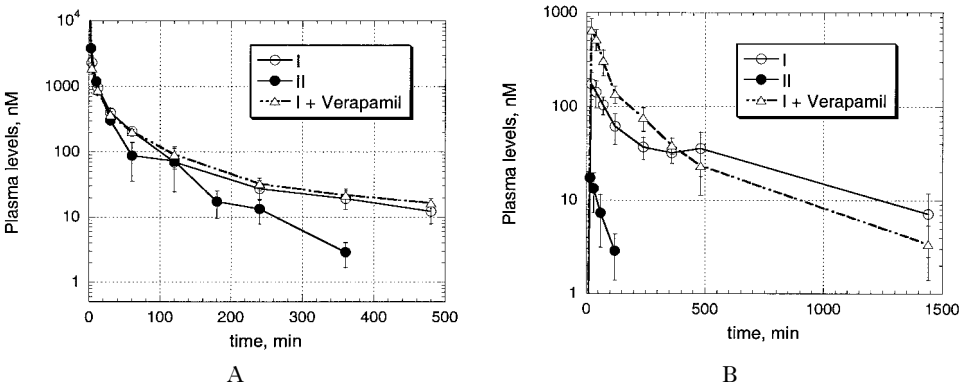


Figure 2. Plasma concentration–time profiles of **I** and **II** following 1 mg kg^{-1} i.v. administration (A) and 3 mg kg^{-1} p.o. administration (B) of **I** with or without co-administration of verapamil (10 mg kg^{-1} p.o.), and **II**, to rat. Results are the mean ± SD, $n = 4$.

Table 2. *In vivo* excretion/metabolism studies of **I** and **II** following 1 mg kg^{-1} i.v. administration to rat.

Compoud administered	Recovery (% of dose)			Clearance (ml min^{-1} kg^{-1})*		
	Bile	Urine	Total	Biliary	Renal	Metabolic
I	13 ± 4	14 ± 3	27 ± 1	3.2	3.5	18.2
II	58 ± 14	14 ± 12	72 ± 7	15.0	3.6	7.3

Values are means ± SD, $n = 3$.
* Estimated based on clearance methods described in Materials and methods.

Both **I** and **II** were bound substantially and comparably to rat plasma proteins over the concentration range studied. Unbound fractions were 6 ± 0.4% and 6 ± 0.2% for **I**, and 4 ± 0.5% and 4 ± 0.1% for **II**, at 0.5 and 10 μM, respectively.

Excretion and metabolism studies

Over 48 h, ~27% of the i.v. dose was excreted as unchanged drug in the bile (13%) and urine (14%) of rat following i.v. administration of **I** (table 2). In contrast, > 70% of the i.v. dose was recovered as unchanged drug in the excreta (58% in bile, 14% in urine) following i.v. administration of **II** (table 2). For both diastereomers, the majority of the unchanged drug recovered in the excreta during the first 8 h after dosing, with < 1% of the i.v. dose was recovered thereafter, in good agreement with their relatively short $t_{1/2}$ and suggesting that the 48-h collection period was sufficient for nearly complete recovery of the unchanged drug. The estimated extent of metabolism was higher for **I** (73%) than **II** (28%). Accordingly, **I** exhibited metabolic clearance ~2.5-fold higher than **II**, while **II** possessed ~5-fold higher biliary clearance than **I** (table 2). LC/MS/MS analysis of bile and urine samples suggested that both **I** and **II** formed a glucuronide conjugate (M + 176), and few oxidative products (M + 16). The glucuronide conjugate was likely an acyl glucuronide conjugate, based on enzymatic cleavage with β-glucuronidase and chemical stability (in buffers at different pHs) studies (data not shown). The glucuronide was detected mainly in bile and minimally in urine.

In vitro metabolism studies using liver microsomal preparations fortified with UDPGA showed that both **I** and **II** underwent glucuronidation. Formation of a glucuronide conjugate of **I** or **II** was time-, UDPGA- and microsome-dependent (data not shown). LC/MS/MS analysis suggested that the conjugate was likely the acyl glucuronide conjugate of **I** or **II**, similar to those observed in the bile samples. Formation of these glucuronides quantitatively mirrored the disappearance of its parent compound, supporting the assumption of identical extinction coefficients between the glucuronide and parent pair. In the presence of only NADPH, few oxidative metabolites (M + 16) were observed. Kinetic studies revealed that the glucuronidation as well as the oxidation of **I** was higher than that of **II** at all concentrations tested (data not shown). As a result, the intrinsic clearance of glucuronidation (based on glucuronide formation) and the intrinsic clearance of the oxidation (based on parent disappearance) pathway appeared to be higher for **I** than for **II**. The combined intrinsic clearance (V_{max}/K_m) of metabolism of **I** was ~3-fold of that of **II** (table 3).

Table 3. Kinetics of *in vitro* metabolism of **I** and **II** in rat liver microsomes.

	Glucuronidation		Oxidation		Total	
	I	**II**	**I**	**II**	**I**	**II**
V_{max} (pmol min^{-1} mg^{-1})	150 ± 6	373 ± 146	1225 ± 160	837 ± 213		
K_m (μM)	189 ± 13	975 ± 344	490 ± 75	1140 ± 312		
V_{max}/K_m (μl $min^{-1}mg^{-1}protein^{-1}$)	0.8	0.4	2.5	0.7	3.3	1.1

Table 4. Transcellular transport of **I** and **II** across monolayers of Caco-2, LLC-PK1 and LLC-PK1 transfected with human *MDR1* (LLC-PK1:MDR1) and mouse *mdrla* (LLC-PK1:mdrla).

Compound	Cell model	Direction[a]	Permeability $\times 10^6$ (cm s^{-1})	Transport ratio B-to-A/A-to-B
I	Caco-2	B-to-A	20.3 ± 2.0	7.0
		A-to-B	2.9 ± 0.7	
	LLC-PK1	B-to-A	8.9 ± 1.1	1.7
		A-to-B	5.3 ± 2.0	
	LLC-PK1:MDR1	B-to-A	5.9 ± 0.5	7.4
		A-to-B	0.8 ± 0.1	
	LLC-PK1:mdr1a	B-to-A	10 ± 2.3	20.0
		A-to-B	0.5 ± 0.2	
II	Caco-2	B-to-A	1.6 ± 0.4	1.3
		A-to-B	1.2 ± 0.2	
	LLC-PK1	B-to-A	1.1 ± 0.2	1.0
		A-to-B	1.1 ± 0.7	
	LLC-PK1:MDR1	B-to-A	1.1 ± 0.1	1.4
		A-to-B	0.8 ± 0.3	
	LLC-PK1:mdr1a	B-to-A	1.3 ± 0.1	4.3
		A-to-B	0.3 ± 0.1	

Transport of **I** and **II** was studied in triplicate or quadruplicate at 10 μM in Caco2 cells for 1.5 h and at 5 μM in LLC-PK1 with or without transfectants for 2 h.

[a] A, apical side; B, basolateral side.

In vitro *studies*

In Caco-2 cells, the transport of **I** was higher than that of **II** in both the apical-to-basolateral (~13-fold) and basolateral-to-apical (2.4-fold) directions (table 4). Transport of **I**, but not **II**, across Caco-2 monolayers was highly directional dependent; the ratio of secretory P_{app} (basolateral-to-apical) to absorptive P_{app} (apical-to-basolateral) was 7 for **I** and 1.3 for **II** at 10 μM substrate (table 4). Similar results also were observed at a substrate concentration of 50 μM (data not shown).

In the control LLC-PK1 cells (without the human MDR1 or mouse mdr1a gene), the transport of **I** was also much higher (5–8-fold) than that of **II** in both the apical-to-basolateral and basolateral-to-apical directions (table 4). There was slight polarized transport for **I**, but not **II** in the control cell line; the ratio of secretory P_{app} to absorptive P_{app} was 1.7 for **I** and 1 for **II** (table 4). Species differences in the P-gp-mediated transport for both **I** and **II** were apparent. In the human *MDR1* transfected cells, the transport of **I**, but not **II** was highly polarized (transport

ratio = 7.4 for **I** and 1.4 for **II**; table 4), suggesting that **I**, but not **II** was a good P-gp substrate for humans. In the mouse *mdr1a* transfected cells, transport of **I** and **II** exhibited directional dependent. However, **I** was a much better substrate for mouse P-gp than **II**; the transport ratio (secretory to absorptive) was 20 for **I** and 4 for **II** (table 4).

In situ *studies*

In the *in situ* rat intestinal loop studies, the majority of the dose administered ($\geq 75\%$) for both compounds was found in rat lumen, and the total recovery of **I** or **II** in all sections (blood, intestine, lumen) was $> 85\%$ (table 5). Although there were relatively large interindividual variations, the intestinal absorption, based on total recovery in blood and the intestinal tissue, of **I** (14%) was statistically higher than that of **II** (6%) in control animals (table 5). The absorption of **I** was increased significantly to 30% in the presence of verapamil, while it was not significantly affected (11%) in the presence of MK-571 (table 5). In blood, the recovery of **I** during the 60-min collection interval was significantly higher in the presence of verapamil, but not MK-571 (figure 3A). In contrast, the intestinal absorption of **II**

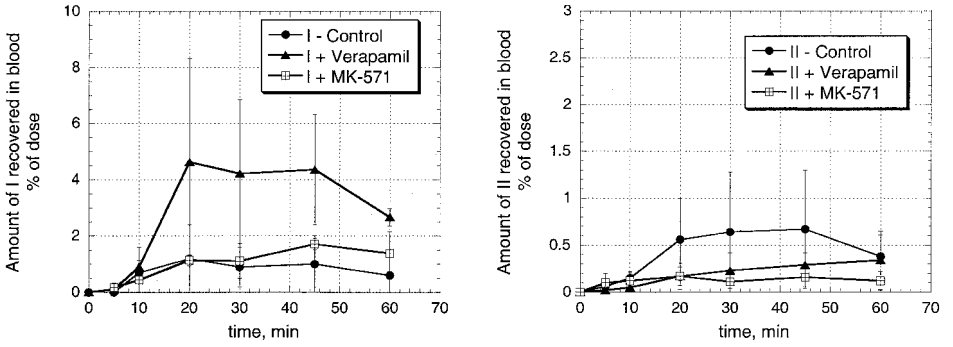


Figure 3. Recovery of **I** or **II** in rat blood as a function of sampling time following administration of **I** (A) or **II** (B). Results are the mean ± SD ($n = 4$) obtained following administration of **I** or **II** (0.5 mg/2 ml) in the rat intestinal loop, in the absence (control) or presence of verapamil or MK-571 (500 μM).

Table 5. *In situ* rat intenstinal absorption studies of **I** and **II**.

			% of Dose recovered				
Compound	Inhibitor	*n*	Lumen	Gut	Blood	Gut + blood	Total
I	none	4	84 ± 12	9.2 ± 2.3	4.4 ± 6	13.6 ± 7	97 ± 11
	verapamil	4	78 ± 10	10.9 ± 1.2	18.9 ± 8.1*	29.8 ± 8.9*	108 ± 9
	MK-571	4	75 ± 12	5.2 ± 0.6*	6.0 ± 4.8	11.2 ± 5.0	86 ± 12
II	none	4	92 ± 5	3.0 ± 1.3	2.9 ± 2.1	5.9 ± 2.5	98 ± 7
	verapamil	3	88 ± 9	5.8 ± 1.9	1.1 ± 0.8	6.9 ± 1.9	95 ± 7
	MK-571	4	84 ± 7	2.2 ± 0.5	0.8 ± 0.4	3.0 ± 0.8	87 ± 7

Values are mean ± SD ($n = 3$–4).
* Statistically different ($p < 0.05$) from control.

was not altered significantly by verapamil or MK-571. At the end of the experiment (60 min), the total dose absorbed, as reflected by the amount of **II** recovered in blood and intestine, was 7 and 3% in the presence of verapamil and MK-571, respectively, as compared with 6% in control animals (table 5). In blood, the amount of **II** recovered over the experimental time-course appeared to be decreased, although insignificantly due to large variations, by verapamil or MK-571 (figure 3B). For both compounds, the total recovery in the intestinal tissue or intestinal lumen was not affected by verapamil or MK-571 (table 5).

In vivo *studies in mouse*

To confirm that **I** was a P-gp substrate, disposition studies were carried out in the P-gp-deficient mdrla (−/−) and normal mdrla (+/+) mouse. After an oral dose of 5 mg kg^{-1} of **I**, plasma (figure 4A) and brain (figure 4B) concentrations of **I** rose rapidly, reaching C_{max} at 20 min. In both groups, the concentrations of **I** in brain were lower than those in plasma. In the mdr1a (−/−) mouse, the concentrations of **I** in brain were ~10% of that plasma, whereas in the mdr1a (+/+), the brain to plasma AUC ratio was only 0.02 (table 6). Both the plasma and brain concentra-

Table 6. Pharmacokinetic parameters of **I** following 5 mg kg^{-1} p.o. administration of **I** to mouse.

		mdr1a (−/−)	*mdr1a* (+/+)	(−/−)/(+/+) Ratio
Plasma	AUC (nM h)	2987.2	1350.0	2.2
	C_{max} (nM)	3028 ± 448	1180 ± 370	2.6
Brain	AUC (nM h)	311.5	24.1	12.9
	C_{max} (nM)	245 ± 38	18 ± 5	13.6
Brain/plasma AUC ratio		10.4	1.8	5.8

Values for AUC were calculated from a set of mean plasma concentrations. Three animals were used for each sampling time.

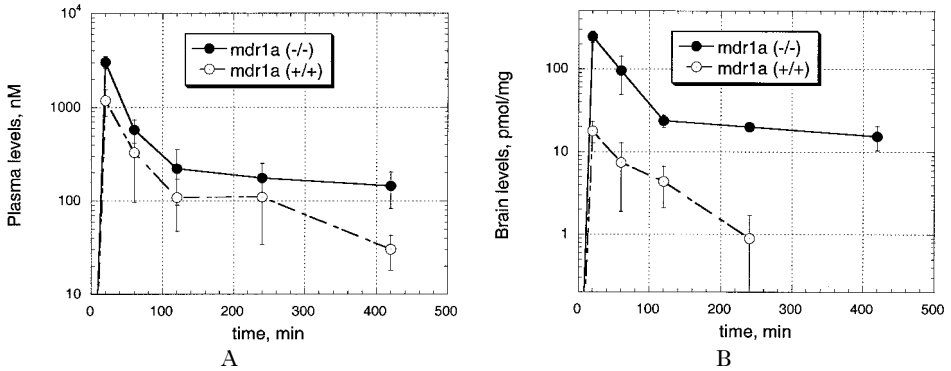


Figure 4. Plasma (A) and brain (B) concentration–time profiles of **I** after 5 mg kg^{-1} p.o. administration of **I** to the mdr1a (−/−) and mdr1a (+/+) mouse. Results are the mean ± SD ($n = 3$). Three different mice were used for each time point.

tions were higher in the P-gp-deficient mouse than those in the wild-type mouse. AUC ratios between the P-gp deficient mouse and the normal mouse were ~2 in plasma and 10 in brain (table 6). The ratio of brain AUC normalized to plasma AUC in the mdrla1 (−/−) mouse was ~6-fold higher than that in the normal mouse.

Effect of verapamil on pharmacokinetics of ***I***

The impact of P-gp on the absorption and disposition of **I** was subsequently examined in rat. Pretreatment with 10 mg kg^{-1} p.o. verapamil 30 min before i.v. administration of **I** did not alter the pharmacokinetic parameters of **I** (figure 2A and table 1). However, verapamil increased plasma levels of **I** significantly following p.o. administration of **I** (figure 2B). Oral plasma AUC (and F) and C_{max} of **I** were increased by ~2- and ~4-fold, respectively, while those for T_{max} were unchanged by co-administration with verapamil (table 1).

Discussion

In the current study, absorption and disposition of a diastereomeric pair with markedly different lipophilicity (>10-fold disparity in log P) were characterized using *in vivo* and *in vitro* approaches. Both the lipophilic zwitterion **I** and its hydrophilic isomer **II** exhibited comparable plasma protein binding and CL. However, there were quantitative differences in the major elimination pathway of these two isomers. The lipophilic isomer **I** was metabolized extensively (~70%), while the hydrophilic isomer **II** was excreted primarily unchanged in bile (58%). As a result, **I** exhibited higher metabolic clearance than **II**, while **II** possesses higher biliary clearance than **I**. In agreement with this observation, *in vitro* hepatic metabolism studies showed that **I** was intrinsically metabolized via glucuronidation and oxidation, at a rate faster than **II**. These results agree with the generally accepted belief that lipophilic compounds are more susceptible to biotransformation (Testa *et al*. 2000).

In vivo studies also showed that the lipophilic zwitterion **I** was more orally bioavailable than its diastereomer **II** (F = 17% for **I,** 1% for **II**). Marked differences in F could be attributed to differences in first-pass elimination and/or absorption. Considering that the sums of metabolic clearance and biliary clearance for **I** and **II** were comparable (table 2), the hepatic first-pass elimination is expected to be comparable between the two isomers and, therefore, should not be the primary cause for the observed difference in their oral bioavailability. To examine whether the difference in F could be attributed to the difference in intrinsic absorption, additional studies were subsequently carried out using *in vitro* Caco-2 cell monolayer and in *in situ* rat intestinal loop models. The results from both models showed that absorption of **I** was intrinsically higher than that of **II**, suggesting that the difference in absorption was likely the major contributing factor to the observed diastereomeric difference in F.

The above finding on compound absorption was expected based on physicochemical properties of the compounds. The relatively good permeability of **I** in both the intestinal models (Caco-2 cells and rat intestinal loop) and the renal cell line LLC-PK1 is in agreement with its lipophilicity (log P = 1.04 at pH 7.4). The rather poor permeability of **II** in all the models used in this study was also

consistent with its low lipophilicity (log $P = -0.05$ at pH 7.4) and ionic nature over the normal gastrointestinal pH range (pH ~2–8 versus pK_a ~3.3, 4.3 and 8.0). Similar findings have been reported previously for other zwitterionic compounds (Prueksaritanont *et al*. 1998). The low permeability of **II** also was not likely due mainly to polarized efflux systems since unlike **I**, directional transport could not be demonstrated in the Caco-2 cells, LLC-PK1 and human *MDR1* transfected cell line. Although **II** appeared to be a weak substrate for mouse mdr1a, P-gp is not expected to be involved in the low intestinal absorption observed in rat since there was no increase in intestinal absorption observed in the *in situ* experiment using verapamil, a known P-gp inhibitor (Wacher *et al*. 1995, Orlowski and Garrigos 1999). It is noteworthy that species differences in the P-gp-mediated efflux are common and have been described previously for several compounds (Yamazaki *et al*. 2001, *passim*). Involvement of MRP, another efflux transporter known to be present in both Caco-2 cells and rat intestines (Hunter *et al*. 1993, Flens *et al*. 1996, Hirohashi *et al*. 2000, Mottino *et al*. 2000), in the intestinal transport of **II** also was not evident here. In fact, in the *in situ* rat model, the presence of MK-571, a potent MRP inhibitor (Leier *et al*. 1994, Gekeler *et al*. 1995), appeared to decrease the absorption (per cent recovered in blood and gut) of **II** although statistically insignificant, as oppose to increasing its absorption. MK-571 also decreased the recovery of **I** in gut, although its overall absorption (per cent recovered in blood and gut) was not affected by MK-571. The underlying mechanism for these apparent decreases by MK-571 is presently unclear.

Surprisingly, in spite of possessing higher F, the lipophilic diastereomer **I** was a good substrate of P-gp in all systems used here. The highly polarized transport of **I** in the human intestinal cell line Caco-2 suggested that **I** was a substrate for an intestinal efflux system. *In situ* rat intestinal absorption studies suggested that **I** was a substrate for P-gp since the intestinal absorption of **I** in rat was increased by the P-gp inhibitor verapamil, but not the MRP inhibitor MK-571. Owing to unavailability of *in vitro* and *in vivo* P-gp models for rat, confirmation studies were carried out using the human *MDR1* and mouse *mdr1a* transfected cell lines, which indicated clearly that **I** was a good substrate for both human and mouse P-gp. This finding was further substantiated *in vivo*, which showed a significant, although modest, increase (~2-fold) in plasma AUC and a marked increase (~10-fold) in brain uptake in the mdr1a (−/−) mouse following p.o. administration of **I**. The apparently lesser effects of P-gp on oral absorption than in brain uptake is not unexpected and have also been observed earlier for several known P-gp substrates (Desrayaud *et al*. 1998, Kim *et al*. 1998, Yokogawa *et al*. 1999).

Further studies were subsequently conducted to demonstrate the impact of the efflux system P-gp on the intestinal absorption of **I** *in vivo* in the animal model used in this study, following concomitant administration of **I** with verapamil to rat. Since only the oral, but not the i.v., pharmacokinetic parameters of **I** were affected by verapamil (figure 2A and B, and table 1), the results suggested that the modest but significant increases (~2-fold) in oral plasma AUC and F of **I** were likely due to the inhibitory effect of verapamil on the intestinal P-gp activity, and not to inhibition of the hepatic first-pass elimination by verapamil. Consistent with this, preliminary *in vitro* metabolism studies suggested that **I** was not metabolized significantly in the rat intestinal tissue and that verapamil had a minimal effect on metabolism of **I** in rat liver microsomes (data not shown). Thus, the present results demonstrated that the oral absorption of the lipophilic zwitterion **I** was much

higher than the hydrophilic diastereomer **II**, in spite of the counter effect of P-gp on the intestinal absorption of **I** in rat. In other words, the impact of P-gp on overall intestinal transport process of **I** was relatively modest, as compared with its apparently high permeability. This view has also been noted earlier for other high-permeability compounds (Chiou *et al.* 2000).

To date, stereoselectivity in the P-gp-mediated transport has been reported for a number of chiral compounds (Szabo and Molnar 1998, Neuhoff *et al.* 2000). However, differences in P-gp susceptibility have not been well documented for enantiomers with different lipophilicity, as demonstrated for **I** and **II** in the present study. Noteworthy, the present finding that only the more lipophilic zwitterion **I**, but not the hydrophilic isomer **II**, was a good P-gp substrate, is consistent with the observation that lipophilicity is a common feature for known substrates for P-gp (Ford and Hait 1990). It is also interesting to note that both diastereomers contain a quinoline functional group and that several quinoline-based drugs have been shown to be P-gp substrates (Sato 1997, Vezmar *et al.* 1997, Vezmar and Georges 2000). Considering that P-gp is also expressed in rat canaliculi of hepatocytes (Flens *et al.* 1996) and that it has been shown to be involved in biliary excretion of several P-gp substrates (Kusuhara *et al.* 1998), the biliary excretion of **I** in rat could also be mediated in part by P-gp. However, the observation that biliary excretion of **II** was much faster than **I** (table 2) suggested that factor(s) other than the P-gp contributed to the observed difference in the biliary excretion of the diastereomers **I** and **II** in this species. Studies are ongoing in our laboratory to explore underlying mechanisms for the hepatic elimination of the two isomers.

In summary, the study provided an example of stereoselectivity in pharmacokinetics of zwitterionic disatereomers. By means of pharmacokinetics, *in vivo* and *in vitro* metabolism, *in vitro* transport, and *in situ* intestinal absorption, the present study demonstrated that (1) the absorption and disposition of the diastereomers **I** and **II** in rat were quantitatively different; the absorption and metabolism of the more lipophilic zwitterion **I** was higher than that of its hydrophilic diastereomer **II**, while the biliary excretion of **I** was much slower than **II**; and (2) the more lipophilic diastereomer **I**, and not **II** was a good substrate for P-gp. The aforementioned results were consistent with the difference in lipophilicity between the two isomers, but inconsistent with the finding of **I** being a much better P-gp substrate, suggesting that compound physicochemical property was an important determinant for, while P-gp played a limited role in the observed differences in the intestinal absorption and disposition of this diastereomeric pair. These findings exemplify the importance of compound physicochemical properties on xenobiotic disposition, complexity of P-gp substrate specificity, and the interplay between lipophilicity/permeability and P-gp activity in determining compound disposition.

Acknowledgements

The authors thank Ms Janice Brunner, Kimberly Michel, Polly Deluna, Judy Tran and Suzanne Ciccotto for their assistance in animal and transport studies.

References

Barr, W. H. and Riegelman, S., 1970, Intestinal drug absorption and metabolism. I. Comparison of methods and models to studying physiological factors of *in vitro* and *in vivo* intestinal absorption. *Journal of Pharmaceutical Sciences*, **59**, 154–163.

Benet, L. Z. and Galeazzi, R. L., 1979, Noncompartmental determination of the steady-state volume of distribution. *Journal of Pharmaceutical Sciences*, **68**, 1071–1074.

Chiou, W. L., Chung, S. M. and Wu, T. C., 2000, Apparent lack of effect of P-glycoprotein on the gastrointestinal absorption of a substrate, tacrolimus, in normal mice. *Pharmaceutical Research*, **17**, 205–208.

Davies, N. M., 1998, Clinical pharmacokinetics of ibuprofen. The first 30 years. *Clinical Pharmacokinetics*, **34**, 101–154.

Desrayaud, S., de Lange, E. C. M., Bruelisauer, A., de Boer, A. G. and Breimer, D. D., 1998, Effect of the *mdr1a* P-glycoprotein gene disruption on the tissue distribution of SDZ PSC 833, a multidrug resistance-reversing agent, in mice. *Journal of Pharmacology and Experimental Therapeutics*, **285**, 438–443.

Flens, M. J., Zaman, G. J. R., van der Valk, P., Izquierdo, M. A., Schroeijers, A. B., Scheffer, G. L., van der Groep, P., de Hass, M., Meijer, C. J. L. M. and Scheper, R. J., 1996, Tissue distribution of the multidrug resistance protein. *American Journal of Pathology*, **148**, 1237–1247.

Ford, J. M. and Hait, W. H., 1990, Pharmacology of drugs that alter multidrug resistance in cancer. *Pharmacological* Reviews, **42**, 155–199.

Gekeler, V., Sanders, K. H., Ulrich, W. R. and Beck, J., 1995, The leukotriene LTD4 receptor antagonist MK571 specifically modulates MRP associated multidrug resistance. *Biochemical and Biophysical Research Communications*, **208**, 345–353.

Hartman, G. D. and Duggan, M. E., 2000, Alpha (v) beta (3) integrin antagonists as inhibitors of bone resorption. *Expert Opinion on Investigational Drugs*, **9**, 1281–1291.

Hirohashi, T., Suzuki, H., Chu, X. Y., Tamai, I., Tsuji, A. and Sugiyama, Y., 2000, Function and expression of multidrug resistance-associated protein family in human colon adenocarcinoma cells (Caco-2). *Journal of Pharmacology and Experimental Therapeutics*, **292**, 265–270.

Hunter, J., Jepson, M. A., Tsuruo, T., Simmons, N. L. and Hirst, B. H., 1993, Functional expression of P-glycoprotein in apical membranes of human intestinal Caco-2 cells. *Journal of Biological Chemistry*, **268**, 14991–14997.

Kim, R. B., Fromm, M. F., Wandel, C., Leake, B., Wood, A. J. J., Roden, D. M. and Wilkinson, G. R., 1998, The drug transporter P-glycoprotein limits oral absorption and brain entry of HIV-1 protease inhibitors. *Journal of Clinical Investigation*, **101**, 289–294.

Kusuhara, H., Suzuki, H. and Sugiyama, Y., 1998, The role of P-glycoprotein and canalicular multispecific organic anion transporter in the hepatobiliary excretion of drugs. *Journal of Pharmaceutical Sciences*, **87**, 1025–1040.

Leier, I., Jedlitachky, G., Buchho, U., Cole, S. P. C., Deeley, R. G. and Keppler, D., 1994, The MRP gene encodes an ATP-dependent export pump for leukotriene C4 and structurally related conjugates. *Journal of Biological Chemistry*, **289**, 27807–27810.

Miller, W. H., Keenan, R. M., Willette, R. N. and Lark, M. W., 2000, Identification and *in vivo* efficacy of small-molecule antagonists of integrin $\alpha_v\beta_3$ (the vitronectin receptor). *Drug Discovery Today*, **5**, 397–408.

Mottino, A. D., Hoffman, T., Jennes, L. and Vore, M., 2000, Expression and localization of multidrug resistant protein mrp2 in rat small intestine. *Journal of Pharmacology and Experimental Therapeutics*, **293**, 717–723.

Neuhoff, S., Langguth, P, Dressler, C, Andersson, T. B., Regardh, C. G. and Spahn-Langguth, H., 2000, Affinities at the verapamil binding site of MDR1-encoded P-glycoprotein: drugs and analogs, stereoisomers and metabolites. *International Journal of Clinical Pharmacology and Therapeutics*, **38**, 168–179.

Orlowski, S. and Garrigos, M., 1999, Multiple recognition of various amphiphilic molecules by the multidrug resistance P-glycoprotein: molecular mechanisms and pharmacological consequences coming from functional interactions between various drugs. *Anticancer Research*, **19**, 3109–3123.

Prueksaritanont, T., Deluna, P., Gorham, L. M., Ma, B., Cohn, D., Pang, J., Xu, X., Leung, K. and Lin, J. H., 1998, *In vitro* and *in vivo* evaluations of intestinal barriers for the zwitterion L-767,679 and its carboxyl ester prodrug L-775,318: roles of efflux and metabolism. *Drug Metabolism and Disposition*, **26**, 520–527.

Sato, W. and Yano, O., 1997, Structure–activity relationship of newly synthesized quinoline derivatives for reversal of multidrug resistance in cancer. *Journal of Medicinal Chemistry*, **40**, 2047–2052.

Schinkel, A. H., Smit, J. J. M., van Tellingen, O., Beijnen, J. H., Wargenaar, E., van Deemter, L., Mol, C. A. A. M., van der Valk, M. A., Robanus-Maandag, E. C., te Riele, H. P. J, Berns, A. J. M. and Borst, P., 1994, Disruption of the mouse mdr1a P-glycoprotein gene leads to deficiency in the blood–brain barrier and to increased sensitivity to drugs. *Cell*, **77**, 491–502.

Schinkel, A. H., Wagenaar, E., van Deemter, L., Mol, C. A. A. M. and Borst, P., 1995, Absence of the mdr1a P-glycoprotein in mice affects tissue distribution and pharmacokinetics of dexamethasone, digoxin, and cyclosporin A. *Journal of Clinical Investigation*, **97**, 2517–2524.

Szabo, D. and Molnar, J., 1998, The role of stereoselectivity of chemosensitizers in the reversal of multidrug resistance of mouse lymphoma cells. *Anticancer Research*, **18**, 3039–3044.

Testa, B., Crivori, P., Reist, M. and Carrupt, P.-A., 2000, The influence of lipophilicity on the pharmacokinetic behavior of drugs: concepts and examples. *Perspectives in Drug Discovery and Design*, **19**, 179–211.

Thiebaut, F., Tsuruo, T., Hamada, H., Gottesman, M. M., Pastan, I. and Willingham, M. C., 1987, Cellular localization of the multidrug-resistance gene product P-glycoprotein in normal human tissues. *Proceedings of the National Academy of Sciences, USA*, **84**, 7735–7738.

Wacher, V. J., Wu, C. Y. and Benet, L. Z., 1995, Overlapping substrate specificities and tissue distribution of cytochrome P450 3A and P-glycoprotein: implications for drug delivery and activity in cancer chemotherapy. *Molecular Carcinogenesis*, **13**, 129–134.

Watari, N., Wakamatsu, A. and Kaneniwa, N., 1989, Comparison of disposition parameters of quinidine and quinine in the rats. *Journal of Pharmacobio-Dynamics*, **12**, 608–615.

Vezmar, M., Deady, L. W., Tilley, L. and Georges, E., 1997, The quinoline-based drug *N*-{4-[1-hydroxy-2(dibutylamino)ethyl]quinolin-8-yl}-4-azadosalicylamide, photoaffinity labels the multidrug resistance protein (MRP) at a biologically relevant site. *Biochemical and Biophysical Research Communications*, **241**, 104–111.

Vezmar, M. and Georges, E., 2000, Reversal of MRP mediated doxorubicin resistance with quinoline based drugs. *Biochemical Pharmacology*, 59, 1245–1252.

Yamazaki, M., Neway, W. E., Ohe, T., Chen, I. W., Rowe, J. F., Hochman, J. H., Chiba, M. and Lin, J. H., 2001, *In vitro* substrate identification studies for P-glycoprotein-mediated transport: species difference and predictability of *in vivo* results. *Journal of Pharmacology and Experimental Therapeutics*, **296**, 723–735.

Yokogawa, K., Takahashi, M., Tamai, I., Konishi, H., Nomura, M., Moritani, S., Miyamoto, K. and Tsuji, A., 1999, P-glycoprotein-dependent disposition kinetics of tacrolimus: studies in *mdr*1a knockout mice. *Pharmaceutical Research*, **16**, 1213–1218.

XENOBIOTICA, 2002, VOL. 32, NO. 3, 221–233

Taylor & Francis
healthsciences

SB-242235, a selective inhibitor of p38 mitogen-activated protein kinase. I: Preclinical pharmacokinetics

K. W. WARD†*, J. W. PROKSCH†‖, K. L. SALYERS‡, L. M. AZZARANO†, J. A. MORGAN†, T. J. ROETHKE†, J. E. MCSURDY-FREED†, M. A. LEVY§ and B. R. SMITH†

† Preclinical Drug Discovery, Cardiovascular, Urogenitary, and Oncology Centre for Excellence in Drug Discovery
‡ Preclinical Drug Discovery, Antimicrobial and Host Defense Centre for Excellence in Drug Discovery
§ Drug Metabolism and Pharmacokinetics, GlaxoSmithKline R&D, King of Prussia, PA 19406, USA

Received 12 July 2001

1. SB-242235 (1-(4-piperidinyl)-4-(4-fluorophenyl)-5-(2-methoxy-4-pyrimidinyl) imidazole) is a potent and selective p38 MAP kinase inhibitor that may be an effective therapy for cytokine-mediated diseases such as autoimmune or inflammatory diseases. The present studies were conducted to evaluate the pharmacokinetics of SB-242235 in several preclinical species, including rat, dog and monkey.

2. SB-242235 demonstrates generally favourable pharmacokinetic properties in all species examined. Systemic plasma clearance was high in rat, but in the non-rodent species SB-242235 demonstrated low to moderate clearance with plasma half-lives > 4 h. Oral bioavailability in each preclinical species was high. In rat and monkey, SB-242235 demonstrated non-linear elimination kinetics that manifested as a decrease in clearance with increasing dose and apparent oral bioavailability >100% at high oral doses. Furthermore, SB-242235 displayed concentration-dependent plasma protein binding over a concentration range of 1000–10,000 ng ml^{-1}.

3. In conclusion, SB-242235 demonstrates high oral bioavailability across the major preclinical species, and may thus be a useful tool compound for investigation of the role of p38 inhibition in various disease states. However, the observations of non-linear protein binding and disposition also suggest the need for caution in the design of and data interpretation from such studies.

Introduction

The mitogen-activated protein (MAP) kinases are a family of serine/threonine kinases that regulate a wide variety of cellular signal transduction processes (Cobb 1999). Members of the MAP kinase family have been implicated in multiple pathways that may play integral roles in disease states, including oncogenesis/metastasis, immune diseases, inflammatory processes, transplantation rejection, and others (Stein and Anderson 1996). Several different MAP kinases have been identified, including p38, also termed the cytokine-suppressive antiinflammatory drug (CSAID)-binding protein or reactivating kinase (Freshney *et al.* 1994, Han *et al.* 1994, Lee *et al.* 1994, Rouse *et al.* 1994). Inhibition of p38 results in an inhibition of cytokine biosynthesis, and may thus be an effective therapy for diseases such as autoimmune or inflammatory diseases.

* Author for correspondence; e-mail: keith_w_ward@gsk.com
‖ Present Address: Molecumetics, 2023 120th Avenue NE, Bellevue, WA, 98005, USA.

Xenobiotica ISSN 0049–8254 print/ISSN 1366–5928 online © 2002 Taylor & Francis Ltd
http://www.tandf.co.uk/journals
DOI: 10.1080/00498250110100720

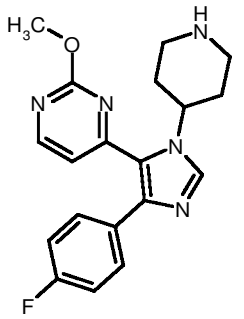


Figure 1. Chemical structure of SB-242235 (1-(4-piperidinyl)-4-(4-fluorophenyl)-5-(2-methoxy-4-pyrimidinyl) imidazole).

Potent and selective p38 inhibitors have been previously described and are typified by SB-203580 (4-(4-fluorophenyl)-2-(4-methylsulphinylphenyl)-5-(4-pyridyl)imidazole; Cuenda *et al.* 1995). SB-203580 has been extensively used by investigators as a tool compound both *in vivo* and *in vitro* to evaluate the effects of p38 inhibition in various systems. Furthermore, less-selective structural analogues of SB-203580, including SK&F-86002 and SK&F-105561, have also been used to investigate the potential effects of inhibition of cytokine biosynthesis in autoimmune and inflammatory diseases (Lee *et al.* 1993). Recently, a new member of this structural series, 1-(4-piperidinyl)-4-(4-fluorophenyl)-5-(2-methoxy-4-pyrimidinyl) imidazole (SB-242235; figure 1), has been characterized that demonstrates improved potency and selectivity over previous analogues. SB-242235 is a potent inhibitor of p38α ($IC_{50} = 0.019\,\mu M$) and p38β2 ($IC_{50} = 1\,\mu M$) MAP kinases, and provides significant reduction in symptoms of adjuvant-induced arthritis in the rat (Badger *et al.* 2000).

To date, no comprehensive study of the interspecies preclinical pharmacokinetics of this structural class of selective p38 inhibitors has been published. A determination of the dispositional properties of these compounds is needed not only to investigate further their potential use in therapeutic intervention in inflammatory disease, but also to aid in the design, conduct and data interpretation of *in vivo* and *in vitro* pharmacology studies employing CSAIDs as p38 inhibitors. Therefore, the present set of studies was conducted to evaluate the pharmacokinetic properties of SB-242235 in several preclinical species, including the rat, dog and monkey.

Materials and methods

Materials

SB-242235 (molecular weight = 353.399; clog P = 2.280) was synthesized by the Department of Medicinal Chemistry at SmithKline Beecham Pharmaceuticals and was determined to be >95% pure. All other reagents and materials were purchased from standard vendors, and were of the highest available purity.

Animals

Male outbred rats (Crl:CD(SD)IGS BR; Charles River, Raleigh, NC, USA) weighing 270–390 g, male pure-bred Beagle dogs (Marshall Research, North Rose, NY, USA) weighing 12.7–13.5 kg, and male Cynomolgus monkeys (*Macaca fascicularis*; Charles River Primate Labs, Houston, TX, USA) weighing 5.6–7.3 kg were used for the pharmacokinetic studies. All animals were housed according to the National Institutes of Health *Guide for the Care and Use of Laboratory Animals*. Filtered tap water

was available *ad libitum*. Animals were fed a standard animal diet (Purina Mills, St Louis, MO, USA); food was available *ad libitum* except for certain overnight periods before dosing, as described below. Whenever overnight fasting was employed, food was provided after the 240-min blood sample was obtained on the study day. All animal use was conducted according to protocols reviewed and approved by the Institutional Animal Care and Use Committee prior to the study, and all surgical procedures were conducted using aseptic techniques in special-purpose operating suites.

In vivo *pharmacokinetic studies*

All dose solutions were prepared in either isotonic saline (intravenous doses) or analytical-grade water (oral doses). For oral doses using suspension formulations, SB-242235 was triturated in a glass mortar and pestle and suspended in 1% aqueous methylcellulose (Aldrich Chemical, Milwaukee, WI, USA) before administration. For each dose solution, the concentration of SB-242235 was verified by HPLC/MS/MS to be ±10% of the target value. All studies were conducted in a crossover fashion, with the study legs at least two (rat) or seven (dog and monkey) days apart, except as noted below. A complete blood chemistry analysis was performed on each dog and monkey before each study day to obtain baseline values and ensure haematological recovery. Blood samples ($<10\%$ total blood volume withdrawn per 24 h) were collected from each study animal at various times during and after drug administration, as noted in the figures; plasma (50 µl) was isolated by centrifugation and stored at −70 °C until analysis. Predose blood samples also were analysed on each study day to confirm the absence of residual drug material from prior study legs.

Rat. Nine rats received surgically implanted femoral vein catheters for intravenous drug administration. Surgery was performed under ketamine/xylazine anaesthesia (87/13 mg kg^{-1}, i.m.) 4–5 days before the first day of the experiment; the catheters were filled with heparinized saline when not in use to prevent occlusion. Three rats received only a femoral vein catheter during the surgery, three received both femoral and hepatic portal vein catheters for intraportal vein administration, and three received both femoral vein and femoral artery catheters. On each study day, the rats were held in restrainers to facilitate drug administration and blood sampling (from a lateral tail vein) for up to 2 h before being returned to their cages. On study day 1, rats received SB-242235 (1.5 mg kg^{-1}, $n = 3$, femoral vein-only rats; or 3.0 mg kg^{-1}, $n = 3$; femoral and hepatic portal vein rats) as a 30-min intravenous infusion (4.0 ml kg^{-1} final volume). On study day 2, the femoral/hepatic portal-cannulated rats ($n = 3$) received SB-242235 (3.0 mg kg^{-1}) as a 60-min intraportal vein infusion. On study day 3, after an overnight fast, rats received SB-242235 (3.5 mg kg^{-1}, $n = 3$, femoral vein-only rats; or 12 mg kg^{-1}, $n = 3$, femoral and hepatic portal vein rats) as an oral solution by gavage (4 ml kg^{-1} final volume). Finally, on study day 4, to investigate the pharmacokinetic linearity of SB-242235, the three rats with both femoral vein and artery catheters were dosed with two consecutive steady-state infusions. The rats were not restrained during the course of the study but were tethered to infusion and sampling lines inside a standard cage. During the study, SB-242235 was administered to rats as a continuous intravenous infusion for 12 h (0.36 mg kg^{-1} h^{-1}; 1.1 ml kg^{-1} h^{-1}), followed immediately by an 8-h continuous intravenous infusion (3.6 mg kg^{-1} h^{-1}; 1.1 ml kg^{-1} h^{-1}). Blood samples were obtained from the femoral artery catheters at several time points near the end of each infusion regimen to confirm that steady-state plasma concentrations were attained.

Dog. On each study day, a cephalic vein catheter was placed in each dog for blood sampling; on study day 1, a catheter was also temporarily placed in the saphenous vein of each dog for drug administration. On each study day, the dogs were restrained in slings to facilitate drug administration and blood sampling for up to 2 h before being returned to their cages. On study day 1, the dogs ($n = 3$) received SB-242235 (2 mg kg^{-1}) as a 60-min intravenous infusion (4.0 ml kg^{-1} final volume). On study day 2, after an overnight fast, the same dogs received SB-242235 (4 mg kg^{-1}) as an oral gavage of a suspension formulation (4 ml kg^{-1} final volume).

Monkey. Seven monkeys were used. Each monkey had a previously chronically implanted vascular access port in a femoral vein that was used for blood sampling; on study day 1, a catheter was also temporarily placed in a saphenous vein for drug administration. On each study day, the monkeys were placed in restraining chairs for the first 4 h of the study to facilitate drug administration and blood sampling; monkeys were fasted overnight prior to each study day. On study day 1 all seven monkeys received SB-242235 (3 mg kg^{-1}) as a 60-min intravenous infusion (6 ml kg^{-1} final volume). On study day 2, four of these monkeys received SB-242235 (10 mg kg^{-1}) as a 60-min intravenous infusion (6 ml kg^{-1} final volume). On study day 3 the same four monkeys received SB-242235 (3 mg kg^{-1}) as a 60-min intraportal vein infusion (6 ml kg^{-1} final volume). The monkeys used in the intraportal infusion study possessed previously chronically implanted vascular access ports in the hepatic portal vein that were used for infusion of SB-242235. On study days 4 and 5, the monkeys received SB-242235 (3 mg kg^{-1}, $n = 3$ on day 4; 10 mg kg^{-1}, $n = 7$ on day 5) as an oral dosage in a capsule.

In vitro *plasma protein binding and blood-to-plasma ratio*

Plasma protein binding of SB-242235 was investigated in each species in which *in vivo* pharmacokinetic parameters were determined, as well as in man, by standard ultrafiltration techniques (Pacifici and Viani 1992). In addition, the blood-to-plasma ratio of SB-242235 was investigated in each species using standard techniques (Hinderling 1997). Briefly, ~25 ml whole blood was collected by cardiac puncture from rat, and by peripheral venipuncture from dog, monkey and one male human volunteer; plasma was obtained by centrifugation. Plasma from each source was determined to be within published reference ranges for pH, haematocrit, osmolality and protein content (data not shown). Blood-to-plasma partitioning was determined in whole blood to which was added SB-242235 to yield concentrations of 100, 1000 and 2000 ng ml^{-1}. Triplicate samples were obtained from the blood before and after a 1-h incubation at 37 °C, and centrifuged to obtain plasma; triplicate 50-µl aliquots were collected from each plasma sample for quantification of SB-242235. Plasma protein binding was determined by adding SB-242235 to plasma from each species to yield concentrations of 1000 and 10 000 ng ml^{-1}; similar solutions were prepared in Krebs' Ringer bicarbonate buffer (pH 7.4) to test for non-specific binding of SB-242235 to the filtration device. Each incubation mixture was vortexed gently to ensure uniform mixing, and triplicate 50-µl aliquots were collected and analysed to verify initial concentrations. Mixtures were incubated in a 37 °C water bath for at least 15 min. Following incubation, triplicate 1-ml aliquots were collected from each incubation mixture and placed into Centrifree micropartition devices (Amicon, Inc., Beverly, MA, USA). The tubes were centrifuged at ~200*g* for 60 min to generate an ultrafiltrate $\leq$ 10% of the volume of the original sample. One 50-µl aliquot was collected from the ultrafiltrate of each device, and one 50-µl aliquot was collected from the plasma in the top portion of the device after centrifugation and analysed to determine recovery of test compound. Each sample was quick-frozen on dry ice and stored at −70 °C until analysis.

Analytical procedure

Quantitative analysis of plasma, buffer and plasma ultrafiltrate samples for SB-242235 was performed using an LC/MS/MS method. For each matrix, 50 µl sample was subjected to protein precipitation/dilution with acetonitrile containing an internal standard (a proprietary compound). All tubes were capped, vortex-mixed and centrifuged for 10 min at 15 000*g*. Supernatant (125 µl) was transferred to autosampler vials containing 50 µl 10 mM ammonium acetate buffer (pH 6.5). The vials were capped and vortex-mixed and the samples injected (1–5 µl by Perkin-Elmer Series 200 autosampler) onto the LC/MS/MS.

The LC mobile phase was composed of an 85/15 (v/v) mixture of acetonitrile/10 mm ammonium acetate, pH 6.5. A quaternary pumping system with degasser was used to deliver the mobile phase to a 2 × 50 mm, 3 u, Hypersil Aminopropyl (APS2) analytical column preceded by a 0.5 µm precolumn filter. The flow rate was set at 300 µl min^{-1} and was introduced into the source of the mass spectrometer (Sciex API 365 triple quadrupole) with no post-column split. The mass spectrometer was coupled to the HPLC via a Turbo IonSpray interface (400 °C). Positive-ion multiple reaction monitoring was employed for the MS/MS detection of SB-242235 and the internal standard. The selected $[M + H]^+$ precursor ions were m/z 354 for SB-242235 and m/z 416 for the internal standard. The product ions monitored were at m/z 271 and 333 for SB-242235 and the internal standard, respectively. The lower limit of quantification for each experiment ranged from 2.00 to 10.0 ng ml^{-1}.

Pharmacokinetic analysis

Concentration-versus-time profiles after each route of administration of SB-242235 were obtained for each animal. Standard compartmental analysis techniques (Gabrielsson and Weiner 1997) were used for data analysis using WinNonlin Professional Version 2.1 (Pharsight, Mountain View, CA, USA). For each data set, with the exception of the oral dog and monkey data, the best-fit model was a two-compartment model with first-order elimination from the central compartment. For the oral dog and monkey data, a one-compartment model with first-order elimination provided the best model fit. WinNonlin was used to generate pharmacokinetic parameters including distribution and elimination half-lives ($t_{½\alpha}$ and $t_{½\beta}$, min), systemic plasma clearance (CL, ml min^{-1} kg^{-1}), mean residence time (MRT, min), and steady-state volume of distribution (V_{dSS}, ml kg^{-1}). Oral bioavailability (F,%) and first-pass hepatic extraction (E_h,%) also were estimated by standard non-compartmental techniques, based on the non-extrapolated dose-normalized areas under the concentration–time curve (DNAUC) for oral, intravenous and intraportal administration. Calculation of oral bioavailability was based on an assumption of linear and stationary pharmacokinetics, and was based on the lowest intravenous DNAUC in each instance to minimize any effects of non-linear elimination. To calculate blood-to-plasma ratios, the initial concentration of SB-242235 was divided by the post-incubation concentration. For analysis of plasma protein binding in each species, the concentration of SB-242235 in the plasma ultrafiltrate was divided by the concentration in the unfiltered plasma reservoir to yield the unbound fraction (f_u) in the sample.

Statistical analysis

An unpaired Student's *t*-test assessed the significance of differences in various parameters across groups determined for SB-242235, as described below. In instances where parameters possessed unequal variances, statistical comparison was made using the Mann–Whitney non-parametric U-test. One-way ANOVA with a Bonferroni *post-hoc* comparison was used to assess differences in parameters for SB-242235 across groups, where appropriate. In all cases, $p < 0.05$ was predetermined as the criterion of significance.

Results

The pharmacokinetic parameters describing the disposition of SB-242235 in rat are displayed in table 1. Representative concentration versus time profiles for rat are given in figure 2A and B. After a 1.5 mg kg^{-1} intravenous dose, SB-242235 exhibited high plasma clearance in rat (56 ± 9 ml min^{-1} kg^{-1}), with an elimination half-life of 93.5 ± 11.3 min, and a large steady-state volume of distribution ~10 times total body water. With a somewhat larger intravenous dose (3.0 mg kg^{-1}), approximate dose-proportionality was observed in maximal plasma concentration (C_{max}), and no statistically significant difference was observed between any of the pharmacokinetic parameters obtained at the two doses (paired two-tailed Student's *t*-tests, all $p > 0.05$). Clearance appeared to decrease slightly (25%) at the higher dose, suggesting the possibility of non-linear elimination of SB-242235, but the variability associated with this parameter precluded achieving statistical significance ($p = 0.11$). Further evidence of non-linear elimination kinetics was observed following oral administration of SB-242235. A 3.4-fold increase in the administered dose resulted in a 9-fold increase in the oral C_{max}; furthermore, apparent oral bioavailability was >100% in one of the animals receiving the 3.5 mg kg^{-1} dose, and in all three of the animals receiving the higher dose. Following intraportal vein infusion, SB-242235 demonstrated low and variable first-pass hepatic extraction (~5%), indicating that the primary mechanism for the high systemic clearance of the compound in the rat was non-hepatic in nature.

Given the suggestion of non-linearity in clearance from the intravenous studies in rat, as well as the apparent oral bioavailability >100% and the non-linear

Table 1. Pharmacokinetic parameters defining systemic disposition of SB-242235 in rat after various dosages and routes of administration.

	Dosing regimen				
Parameter	1.5 mg kg^{-1}, i.v.	3.0 mg kg^{-1}, i.v.	3 mg kg^{-1}, i.p.v.	3.5 mg kg^{-1}, p.o.	12 mg kg^{-1}, p.o.
C_{max} (ng ml^{-1}) [a]	280 ± 31	621 ± 155	507 ± 56	132 ± 47	1239 ± 263
T_{max} (min)[a]	60 ± 0	60 ± 0	55 ± 6	120 ± 52	110 ± 62
$t_{½\alpha}$ (min)	1.18 ± 0.18	1.75, 10.1, 26.1[b]	–[c]	–	–
$t_{½\beta}$ (min)	93.5 ± 11.3	123 ± 82	273 ± 215	154 ± 56	160 ± 57
MRT (min)	124 ± 15	127 ± 36	246 ± 190	274 ± 46	282 ± 37
CL (ml min^{-1} kg^{-1})	56.2 ± 8.9	42.9 ± 11.7	49.1 ± 3.9	–	–
$V_{d_{ss}}$ (l kg^{-1})	6.87 ± 0.56	5.26 ± 1.14	–	–	–
Oral F (%)[a]	–	–	–	107, 49.3, 42.9[b]	151, 192, 110[b]
IPV E_h (%)[a]	–	–	4.7 ± 3.1	–	–

Data are presented as the mean ± SD ($n = 3$) and were derived from compartmental analysis unless otherwise noted.

[a] Measured (not fitted) parameter.

[b] Individual values listed due to large variability, animals always listed in the same order.

[c] Not determined for this route of administration.

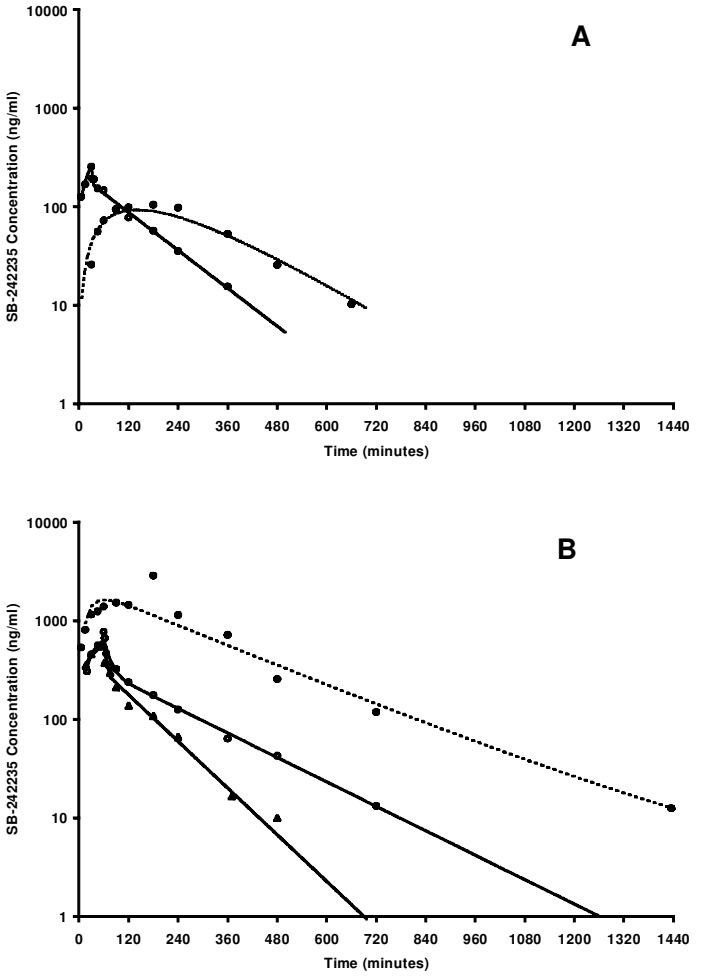


Figure 2. Representative plasma concentration–time profiles for SB-242235 in rat (selected from $n = 3$ animals). Symbols represent measured plasma concentrations after intravenous (open) or oral (solid) administration. Lines represent the best model fit to the observed intravenous (solid) or oral (dashed) data. Profiles were obtained after a 1.5 mg kg^{-1} intravenous dose and 3.5 mg kg^{-1} oral dose (A) or a 3.0 mg kg^{-1} intravenous or intraportal dose (triangles) and 12 mg kg^{-1} oral dose (B).

increase in exposure with increasing oral dose, an additional study was performed to investigate the pharmacokinetic linearity of SB-242235 in rat. In this experiment, SB-242235 was infused at two different rates to attain two different apparent steady-state plasma concentrations, and clearance was determined at each concentration. These data are displayed in table 2. For two of the three rats, clearance at the higher infusion rate was significantly lower than that determined based on the lower infusion rate, while for the third rat, the difference between the two values was not significant. The average clearances determined at the low and high infusion rates were 54.6 ± 16.1 and 39.9 ± 5.1 ml min^{-1} kg^{-1}, respectively, and were significantly different ($p = 0.03$) from one another.

In dog in contrast to rat, SB-242235 exhibited low plasma clearance (5.1 ± 0.9 ml min^{-1} kg^{-1}; ~15% hepatic blood flow), with an elimination half-life

Table 2. Apparent steady-state concentrations and the resulting clearance estimates at two different infusion rates of SB-242235 in rat.

Subject	Infusion regimen	Apparent steady-state concentration ($ng\,ml^{-1}$)	Plasma clearance ($ml\,min^{-1}\,kg^{-1}$)
Rat 1	12-h infusion; $0.36\,mg\,kg^{-1}\,h^{-1}$	81.8 ± 1.4	71.6 ± 1.2
	8-h infusion; $3.6\,mg\,kg^{-1}\,h^{-1}$	1615 ± 64	37.1 ± 1.5^a
Rat 2	12-h infusion; $0.36\,mg\,kg^{-1}\,h^{-1}$	103 ± 7	57.1 ± 3.8
	8-h infusion; $3.6\,mg\,kg^{-1}\,h^{-1}$	1538 ± 250	39.0 ± 5.9^a
Rat 3	12-h infusion; $0.36\,mg\,kg^{-1}\,h^{-1}$	167 ± 9	35.1 ± 2.1
	8-h infusion; $3.6\,mg\,kg^{-1}\,h^{-1}$	1392 ± 166	43.3 ± 5.5
Average	12-h infusion; $0.36\,mg\,kg^{-1}\,h^{-1}$	117 ± 39	54.6 ± 16.1
	8-h infusion; $3.6\,mg\,kg^{-1}\,h^{-1}$	1513 ± 187	39.9 ± 5.1^a

Data are the mean ± SD ($n = 3$–6 separate determinations).
[a] Significantly different from that derived from the low infusion rate.

Table 3. Pharmacokinetic parameters defining the systemic disposition of SB-242235 in dog after various dosages and routes of administration.

Parameter	Dosing regimen	
	$1.9\,mg\,kg^{-1}$, i.v.	$4.8\,mg\,kg^{-1}$, p.o.
C_{max} ($ng\,ml^{-1}$)[a]	698 ± 142	765 ± 160
T_{max} (min)[a]	60 ± 0	360 ± 1
$t_{½\alpha}$ (min)	1.11 ± 0.79	–[b]
$t_{½\beta}$ (min)	646 ± 93	357 ± 42
MRT (min)	892 ± 134	726 ± 62
CL ($ml\,min^{-1}\,kg^{-1}$)	5.08 ± 0.86	–
$V_{d_{ss}}$ ($L\,kg^{-1}$)	4.46 ± 0.34	–
Oral F (%) [a]	–	84.3 ± 7.6

Data are the mean ± SD ($n = 3$) and were derived from compartmental analysis, unless otherwise noted.
[a] Measured (not fitted) parameter.
[b] Not determined for this route of administration.

of 646 ± 93 min, and a large steady-state volume of distribution approximately six times total body water. Following oral administration as a suspension, SB-242235 demonstrated high bioavailability ($84 \pm 8\%$) in dog. The pharmacokinetic parameters describing the disposition of SB-242235 in dog are displayed in table 3. As with rat, the model provided a good fit to the observed data. Representative concentration versus time profiles for SB-242235 in dog are shown in figure 3.

The pharmacokinetic parameters obtained after administration of SB-242235 to the monkey are displayed in table 4, along with representative concentration versus time profiles in figure 4. At a $3.0\,mg\,kg^{-1}$ intravenous dose, SB-242235 demonstrated moderate plasma clearance in the monkey ($17 \pm 6\,ml\,min^{-1}\,kg^{-1}$), with an elimination half-life of 240 ± 82 min, and a large steady-state volume of distribution approximately seven times total body water. When the intravenous dose was increased 3-fold to $10\,mg\,kg^{-1}$, C_{max} was variable, and increased disproportionately to dose (an average of ~20-fold), suggestive of saturation of an elimination pathway. Furthermore, clearance at the $10\,mg\,kg^{-1}$ dose ($8.5 \pm 3.3\,ml\,min^{-1}\,kg^{-1}$) was significantly lower ($p = 0.037$) than at the $3\,mg\,kg^{-1}$ dose. Following oral administration as a capsule at either 3 or

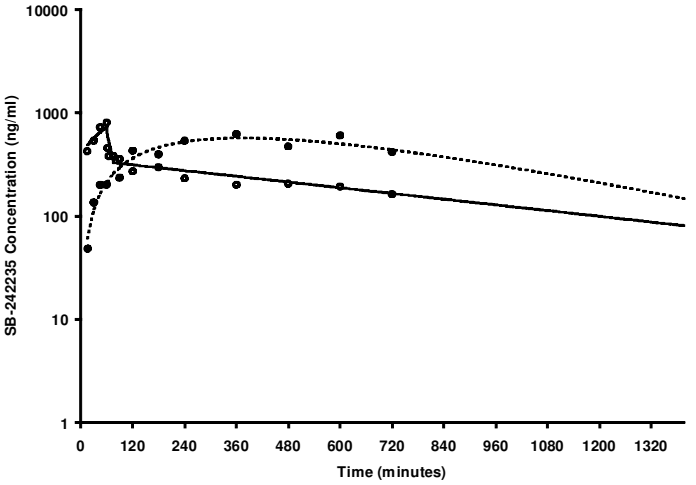


Figure 3. Representative plasma concentration–time profiles for SB-242235 in dog (selected from $n = 3$ animals). Symbols represent measured plasma concentrations after a 1.9 mg kg^{-1} intravenous (open) or 4.8 mg kg^{-1} oral (closed) dose. Lines represent the best model fit to the observed intravenous (solid) or oral (dashed) data.

Table 4. Pharmacokinetic parameters defining the systemic disposition of SB-242235 in monkey after various dosages and routes of administration.

	Dosing regimen				
Parameter	3.0 mg kg^{-1}, i.v. ($n = 7$)	10 mg kg^{-1}, i.v. ($n = 4$)	3.0 mg kg^{-1}, i.p.v. ($n = 4$)	3.0 mg kg^{-1}, p.o. ($n = 3$)	10 mg kg^{-1}, p.o. ($n = 7$)
C_{max} (ng ml^{-1})[a]	551 ± 170	2781, 28501, 2622, 9749[b]	580 ± 83	303 ± 13	1861 ± 320
T_{max} (min)[a]	60 ± 0	60 ± 0	60 ± 0	161 ± 69	228 ± 78
$t_{½\alpha}$ (min)	1.83 ± 1.42	0.47 ± 24	–[c]	–	–
$T_{½\beta}$ (min)	240 ± 82	429 ± 60	219 ± 87	238 ± 120	374 ± 103
MRT (min)	284 ± 118	407 ± 119	282 ± 92	484 ± 117	630 ± 112
CL (ml min^{-1} kg^{-1})	16.8 ± 6.2	8.50 ± 3.30	21.5 ± 10.2	–	–
$V_{d_{ss}}$ (l kg^{-1})	4.80 ± 2.56	3.48 ± 1.50	–	–	–
Oral F (%)[a]	–	–	–	90.7 ± 12.4	108 ± 26
IPV E_h (%)[a]	–	–	28 ± 8	–	–

Data are the mean ± SD ($n = 3$–7), and were derived from compartmental analysis, unless otherwise noted.

[a] Measured (not fitted) parameter.

[b] Individual values listed due to large variability, animals always listed in the same order.

[c] Not determined for this route of administration.

10 mg kg^{-1}, the bioavailability of SB-242235 in the monkey was high. As with the intravenous route, administration of a 3-fold higher oral dosage resulted in a disproportionate increase in C_{max} (6-fold increase), and produced an increase in apparent oral bioavailability (108 ± 26%; range = 65–126%).

In addition to the *in vivo* pharmacokinetic studies, *in vitro* plasma protein binding and blood-to-plasma partitioning of SB-242235 also were examined. As shown in table 5, the blood-to-plasma partitioning of SB-242235 in all species was ~1.0, suggesting that the distribution of SB-242235 in whole blood is homogenous, and that the plasma concentration of SB-242235 provides a reliable surrogate for whole blood concentrations. No evidence of concentration-depen-

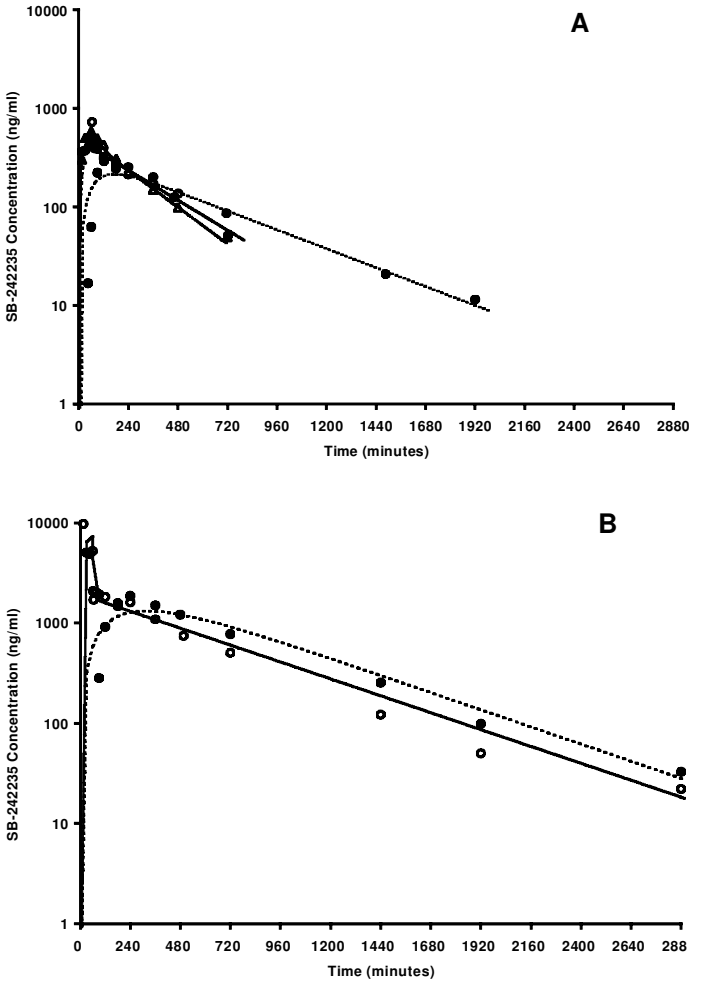


Figure 4. Representative plasma concentration–time profiles for SB-242235 in monkey (selected from $n = 3$–7 animals). Symbols represent measured plasma concentrations after intravenous (open) or oral (closed) administration. Lines represent the best model fit to the observed intravenous (solid) or oral (dashed) data. Profiles were obtained after a 3.0 mg kg^{-1} intravenous, intraportal (triangles), and oral dose (A) or a 10.0 mg kg^{-1} intravenous and oral dose (B).

dent blood cell association was noted over a concentration range of 100–2000 ng ml^{-1} in rat, monkey or human. In dog, however, a significant difference was observed at both 0 and 60 min between the blood-to-plasma ratio measured at each concentration. Cross-species comparison revealed a significant difference at both 0 and 60 min in the mean blood-to-plasma ratio ($p < 0.0001$; one-way ANOVA). *Post-hoc* comparisons with a Bonferroni correction using the results from the one-way ANOVA across species with the mean data revealed significantly lower blood-to-plasma ratios in rat and human versus both dog and monkey.

As detailed in table 6, plasma protein binding was relatively low in all species examined. Recovery of SB-242235 from the test device, as measured by SB-242235 concentrations in an ultrafiltrate generated from buffer incubations, was 86–96%. In the preclinical species, some evidence of saturable plasma protein

Table 5. Blood-to-plasma partitioning of SB-242235 in preclinical species and human.

Time (min)	Blood concentration ($ng\,ml^{-1}$)	Blood-to-plasma ratio			
		Rat	Dog[a]	Monkey	Human
0	100	0.954 ± 0.009	1.04 ± 0.02	1.17 ± 0.03	0.892 ± 0.003
	1000	0.962 ± 0.028	1.10 ± 0.04	1.08 ± 0.08	0.970 ± 0.049
	2000	0.965 ± 0.032	1.15 ± 0.04	1.15 ± 0.06	1.03 ± 0.09
	Average data [b]	0.960 ± 0.023	1.10 ± 0.05	1.13 ± 0.07	0.963 ± 0.078
60	100	1.13 ± 0.04	1.15 ± 0.02	1.29 ± 0.12	1.03 ± 0.06
	1000	1.10 ± 0.01	1.38 ± 0.04	1.32 ± 0.07	1.10 ± 0.08
	2000	1.17 ± 0.02	1.31 ± 0.12	1.34 ± 0.08	1.19 ± 0.10
	Average data [b]	1.13 ± 0.04	1.28 ± 0.12	1.31 ± 0.08	1.11 ± 0.10

Data are the mean $\pm$ SD ($n = 3$ determinations at each concentration for each species).

[a] Significantly different across concentrations at each time point ($p = 0.02$; one-way ANOVA).

[b] Significantly different across species ($p < 0.0001$; one-way ANOVA).

Table 6. Plasma protein binding of SB-242235 in preclinical species and human.

Concentration ($ng\,ml^{-1}$)	f_u (%)			
	Rat[a]	Dog[a]	Monkey[a]	Human
1000[b]	22.5 ± 6.0	45.7 ± 2.5	55.6 ± 3.3	50.4 ± 2.1
10 000[b]	64.4 ± 3.2	62.5 ± 3.0	72.9 ± 1.3	47.1 ± 10.5
Average data	43.5 ± 23.4	54.1 ± 9.5	50.4 ± 2.1	52.3 ± 4.2

Data are the mean $\pm$ SD ($n = 3$).

[a] Significantly different between concentrations ($p < 0.01$; two-tailed t-test).

[b] Significantly different across species ($p < 0.004$; one-way ANOVA).

binding was observed. In rat, dog and monkey, f_u determined at 1000 $ng\,ml^{-1}$ was significantly lower ($p < 0.001$) than that determined at 10 000 $ng\,ml^{-1}$. This phenomenon was not noted in human plasma. Cross-species comparison of f_u at both 1000 and 10 000 $ng\,ml^{-1}$ revealed significant differences across species ($p < 0.005$). *Post-hoc* comparisons with a Bonferroni correction using the results from the one-way ANOVA across species at the low concentration revealed significant differences between rat versus dog, monkey and human, while *post-hoc* comparisons at the high concentration demonstrated differences only between human versus rat and monkey ($p < 0.05$).

Discussion

Signal transduction pathways, including MAP kinase-mediated pathways, have been subject to extensive investigations in both basic and clinical research. As a therapeutic target, inhibition of p38 MAP kinase has been suggested for the potential treatment of a variety of inflammatory diseases, including rheumatoid arthritis (Lee *et al.* 1993), as well as other applications including pulmonary disease (Underwood *et al.* 2000). The importance of MAP kinases is also being increasingly recognized in other areas. For example, it was demonstrated that p38 MAP kinase negatively regulates Phase II metabolism of xenobiotics, suggesting

that this signalling pathway may play an important role in biotransformation pathways (Yu *et al.* 2000). It is clear that continued exploration of the role of MAP kinases in normal physiology and in various disease states will likely occur. The development and characterization of inhibitors of MAP kinase pathways will therefore be useful in furthering these lines of research.

The present work describes the preclinical pharmacokinetic characteristics of the novel p38 inhibitor, SB-242235. In general, this compound displayed favourable dispositional properties in each preclinical species examined. Systemic plasma clearance was high in the rat, but in the non-rodent species, SB-242235 demonstrated low to moderate clearance with plasma elimination half-lives >4 h. Oral bioavailability in each of the preclinical species was high. The high plasma clearance coupled with low first-pass hepatic extraction in the rat suggested that clearance of SB-242235 was non-hepatic in nature; subsequent investigations have revealed renal elimination of unchanged compound to be the primary route of clearance for SB-242235 (Ward *et al.* 2002). These pharmacokinetic data suggest that SB-242235 possesses dispositional properties conducive to further *in vitro* and *in vivo* investigation of the effects of p38 inhibition, and may be an effective oral agent for the treatment of human disease. A description of the pharmacokinetic behaviour of SB-242235 in man, as well as a detailed extrapolation exercise based in part on the present data, are presented separately (Fullerton *et al.* 2000, Ward *et al.* 2002).

Although no previous data have been published describing the pharmacokinetics of selective p38 inhibitors, prior results have been presented with structural analogues of SB-242235 that are less potent and selective. Newton *et al.* (1989) described the pharmacokinetics of SK&F-86002 (6-(4′-fluorophenyl)-5-(4′-pyridyl)-2,3-dihydroimidazo-[2,1-*b*]-thiazole) in rat. SK&F-86002 demonstrated moderate clearance in the rat, with a short half-life of $\sim$0.5 h, and an oral bioavailability of $\sim$45–100%. Notably, marked non-linear elimination properties were observed for SK&F-86002 as the oral dose was increased 8-fold over a range of 10–80 mg kg^{-1}, the AUC increased disproportionately, $\sim$22-fold, over this dose range. These pharmacokinetic data, including the observation of non-linear elimination kinetics, appear to be similar to those observed for SB-242235. In the present series of studies, evidence of non-linearity was noted for SB-242235 in both rat and monkey. The mechanism of this non-linearity was not evident, but is likely renal in nature, given the primarily renal elimination of SB-242235 (Ward *et al.* 2002). Non-linear renal elimination may arise through several mechanisms (reviewed by Bonate *et al.* 1998). However, the mechanism of non-linearity was beyond the scope of this investigation. Also, the large volume of distribution associated with SB-242235 precluded a determination of the range of linear pharmacokinetics for this compound using a rapid technique such as an accelerated infusion (Ward *et al.* 2000), consequently, an extensive investigation of the non-linear pharmacokinetics of SB-242235 was not conducted. However, this observation may be an important consideration when using SB-242235, and potentially other triaryl imidazole compounds, as *in vivo* tool compounds for investigating the role of p38 in various physiological functions. In *in vitro* settings, the target concentration may be precisely controlled, whereas greater-than-anticipated exposure may be generated with large doses of SB-242235 *in vivo*; appropriate caution should therefore be exercised in interpreting data from pharmacology studies with this class of compounds where systemic exposure data are not generated.

The *in vitro* data generated in the present investigation also may be valuable in the interpretation of future *in vivo* pharmacology studies with this series of compounds. First, the blood-to-plasma partitioning of SB-242235 approximated 1.0 in rats, dogs, monkeys and humans. Some interspecies differences were noted (ratios of 1.13 and 1.11 for rat and human versus 1.28 and 1.31 for dog and monkey, respectively), but in all cases, the blood-to-plasma ratio was < 2.0. These results indicate that measuring drug concentrations in whole blood rather than in plasma is not likely to increase the assay sensitivity for SB-242235 significantly (Hinderling 1997), and would not likely confer any advantage over the plasma assay developed in this investigation. Of greater consequence are the data describing the plasma protein binding of SB-242235. For SB-242235, each of the preclinical species demonstrated a significant concentration-dependent increase in unbound fraction as concentration increased from 1000 to 10 000 $ng\,ml^{-1}$. This concentration range ($\sim$3–30 μM) includes or exceeds the range likely to be investigated either *in vitro* or *in vivo* in pharmacology studies using SB-242235. It is generally recognized that only the free fraction of a drug is available to establish a transcellular equilibrium, and thus to achieve a pharmacological effect (Benet *et al.* 1990). Thus, data from any *in vivo* studies employing SB-242235, as well as from any *in vitro* cell-based assays that require protein, plasma, and/or serum in the culture medium, should be interpreted in the light of this concentration-dependent plasma protein-binding phenomenon.

In summary, the pharmacokinetics of SB-242235, a potent and selective p38 MAP kinase inhibitor, have been described across a variety of preclinical species. SB-242235 demonstrates favourable pharmacokinetic properties, including high oral bioavailability, in all species examined. This investigation further details several caveats, including the existence of non-linear elimination kinetics and concentration-dependent plasma protein binding for SB-242235, that may be important experimental considerations in interpreting data from studies employing this class of compounds in research to explore the role of p38 inhibition in various disease states.

Acknowledgements

The authors gratefully acknowledge the expert technical assistance of members of the Preclinical Pharmacokinetics group, including Michael Gould, Gary Stelman, Michael Walsh and Kelli Zeigler, and members of the Laboratory Animal Sciences Department, including Earl Jenkins, in the conduct of the in-life portions of the experiments described here. Furthermore, the work would not have been possible without the invaluable contribution of members of the Drug Analysis group, including Heather Yott, Maria Busz and Tina Molnar, for the analysis of plasma samples for SB-242235. Finally, the members of GSK Medicinal Chemistry who provided SB-242235 for evaluation, including Jerry Adams, are also gratefully acknowledged.

References

Badger, A. M., Griswold, D. E., Kapadia, R., Blake, S., Swift, B. A., Hoffman, S. J., Stroup, G. B., Webb, E., Rieman, D. J., Gowen, M., Boehm, J. C., Adams, J. L. and Lee, J. C., 2000, Disease-modifying activity of SB 242235, a selective inhibitor of p38 mitogen-activated protein kinase, in rat adjuvant-induced disease. *Arthritis Rheumatism*, **43**, 175–183.

Benet, L. Z., Mitchell, J. R. and Sheiner, L. B., 1990, Pharmacokinetics: the dynamics of drug absorption, distribution, and elimination. In A. G. Gilman, T. W. Rall, A. S. Nies and P. Taylor (eds), *Goodman and Gilman's The Pharmacological Basis of Therapeutics* (New York: Pergamon), pp. 3–32.

Bonate, P. L., Reith, K. and Weir, S., 1998, Drug interactions at the renal level: implications for drug development. *Clinical Pharmacokinetics*, **34**, 375–404.

Cobb, M. H., 1999, MAP kinase pathways. *Progress in Biophysics and Molecular Biology*, **71**, 479–500.

Cuenda, A., Rouse, J., Doza, Y. N., Meier, R., Cohen, P., Gallagher, T. F., Young, P. R. and Lee, J. C., 1995, SB 203580 is a specific inhibitor of a MAP kinase homologue which is stimulated by cellular stresses and interleukin-1. *FEBS Letters*, **364**, 229–233.

Freshney, N. W., Rawlinson, L., Guesdon, F., Jones, E., Cowley, S., Hsuan, J. and Saklatvala, J., 1994, Interleukin-1 activates a novel protein kinase cascade that results in the phosphorylation of Hsp27. *Cell*, **78**, 1039–1049.

Fullerton, T., Sharma, A., Prabhakar, U., Tucci, M., Boike, S. and Davis, H., 2000, Suppression of *ex vivo* cytokine production by SB 242235, a selective inhibitor of p38 MAP kinase. *Clinical Pharmacology and Therapeutics*, **114** (Meeting Abstract).

Gabrielsson, J. and Weiner, D., 1997, *Pharmacokinetic and Pharmacodynamic Data Analysis: Concepts and Applications* (Stockholm: Apotekarsocieteten).

Han, J., Lee, J.-D., Bibbs, L. and Ulevitch, R. J., 1994, A MAP kinase targeted by endotoxin and hyperosmolarity in mammalian cells. *Science*, **265**, 808–811.

Hinderling, P. H., 1997, Red blood cells: a neglected compartment in pharmacokinetics and pharmacodynamics. *Pharmacology Reviews*, **49**, 279–295.

Lee, J. C., Badger, A. M., Griswold, D. E., Dunnington, D., Truneh, A., Votta, B., White, J. R., Young, P. R. and Bender, P. E., 1993, Bicyclic imidazoles as a novel class of cytokine biosynthesis inhibitors. *Annals of the New York Academy of Sciences*, **696**, 149–170.

Lee, J. C., Laydon, J. T., McDonnell, P. C., Gallagher, T. F., Kumar, S., Green, D., McNulty, D., Blumenthal, M. J., Heys, J. R., Landvatter, S. W., Strickler, J. E., McLaughlin, M. M., Siemens, I. R., Fisher, S. M., Livi, G. P., White, J. R., Adams, J. L. and Young, P. R., 1994, A protein kinase involved in the regulation of inflammatory cytokine biosynthesis. *Nature*, **372**, 739–746.

Newton, J. F., Yodis, L. P., Keohane, D., Eckardt, R., Dewey, R., Dent, J. and Mico, B., 1989, Pharmacokinetics and metabolism of SK&F 86002 in male and female Sprague–Dawley rats. *Drug Metabolism and Disposition*, **17**, 174–179.

Pacifici, G. M. and Viani, A., 1992, Methods of determining plasma and tissue binding of drugs. *Clinical Pharmacokinetics*, **23**, 449–468.

Rouse, J., Cohen, P., Trigon, S., Morange, M., Alonso-Llamazares, A., Zamanillo, D., Hunt, T. and Nebreda, A. R., 1994, A novel kinase cascade triggered by stress and heat shock that stimulates MAPKAP kinase-2 and phosphorylation of the small heat shock proteins. *Cell*, **78**, 1027–1037.

Stein, B. and Anderson, D., 1996, The MAP kinase family: new 'MAPs' for signal transduction pathways and novel targets for drug discovery. *Annals in the Reporting of Medical Chemistry*, **31**, 289–298.

Underwood, D. C., Osborn, R. R., Kotzer, C. J., Adams, J. L., Lee, J. C., Webb, E. F., Carpenter, D. C., Bochnowicz, S., Thomas, H. C., Hay, D. W. P. and Griswold, D. E., 2000, SB 239063, a potent p38 MAP kinase inhibitor, reduces inflammatory cytokine production, airways eosinophil infiltration, and persistence. *Journal of Pharmacology and Experimental Therapeutics*, **293**, 281–288.

Ward, K. W., Griffiths, R., Levy, M. A. and Smith, B. R., 2000, Evaluation of the use of accelerated infusions for the determination of pharmacokinetic linearity. *Journal of Pharmacology and Experimental Therapeutics*, **293**, 468–479.

Ward, K. W., Proksch, J. W., Gorycki, P. D., Yu, C.-P., Ho, M. Y. K., Bush, B. D., Levy, M. A. and Smith, B. R., 2002, SB-242235, a selective inhibitor of p38 mitogen-activated protein kinase. II. *In vitro* and *in vivo* metabolism studies and pharmacokinetic extrapolation to man. *Xenobiotica*, **32**, 235–250.

Yu, R., Mandelkar, S., Lei, W., Fahl, W. E., Tan, T.-H. and Kong, A.-N. T., 2000, p38 mitogen-activated protein kinase negatively regulates the induction of Phase II drug-metabolizing enzymes that detoxify carcinogens. *Journal of Biological Chemistry*, **275**, 2322–2327.

XENOBIOTICA, 2002, VOL. 32, NO. 3, 235–250

Taylor & Francis
healthsciences

SB-242235, a selective inhibitor of p38 mitogen-activated protein kinase. II: *In vitro* and *in vivo* metabolism studies and pharmacokinetic extrapolation to man

K. W. WARD†*, J. W. PROKSCH†§, P. D. GORYCKI‡, C.-P. YU‡, M. Y. K. HO‡, B. D. BUSH‡, M. A. LEVY and B. R. SMITH†

† Preclinical Drug Discovery, Cardiovascular, Urogenitary, and Oncology Centre for Excellence in Drug Discovery
‡ Drug Metabolism and Pharmacokinetics, GlaxoSmithKline R&D, King of Prussia, PA 19406, USA

Received 12 July 2001

1. Inhibition of p38 MAP kinase has been investigated extensively as a potential therapy for cytokine-mediated diseases such as autoimmune and inflammatory diseases. SB-242235 (1-(4-piperidinyl)-4-(4-fluorophenyl)-5-(2-methoxy-4-pyrimidinyl) imidazole) is a potent and selective p38 MAP kinase inhibitor; the preclinical pharmacokinetics of SB-242235 have been described previously. The present studies were conducted to describe the *in vitro* metabolic rates and routes of SB-242235 metabolism, to characterize its *in vivo* preclinical metabolism, and to use these data to aid in the prediction of the pharmacokinetic behaviour of SB-242235 in man.

2. SB-242235 was metabolically stable in rat, dog, monkey and human hepatic microsomes, isolated hepatocytes and liver slices *in vitro*. The *in vivo* preclinical metabolism studies were consistent with the *in vitro* findings; SB-242235 was minimally metabolized, and was primarily excreted unchanged in the urine (45 and 67% of the administered dose in the rat and monkey, respectively).

3. Allometric scaling using various correction factors predicted that SB-242235 would have low clearance in man with a predicted half-life ranging from 11.5 to 18.7 h. This prediction was consistent with the observed mean half-life of 16.4 h in the first-in-man study for SB-242235. An allometric scaling method with a correction for interspecies differences in glomerular filtration rate provided the most accurate prediction of the pharmacokinetic behaviour of SB-242235 in humans, although the clinical data also highlight potential difficulties in conducting prospective allometry.

Introduction

In recent years, attention has been focused on the role of mitogen-activated protein (MAP) kinases in disease, including autoimmune and inflammatory diseases, and on the potential for using MAP kinase inhibitors as therapeutic agents (Lee *et al*. 1999). The *in vitro* and *in vivo* activity of many p38 inhibitors has been well-characterized (Stein and Anderson 1996, Lee *et al*. 2000). However, little information is available about the pharmacokinetics and metabolism of these compounds, particularly with regard to interspecies extrapolation of such parameters.

Recently, the *in vivo* activity of a novel p38 inhibitor, SB-242235 (1-(4-piperidinyl)-4-(4-fluorophenyl)-5-(2-methoxy-4-pyrimidinyl) imidazole) (figure 1),

* Author for correspondence; and reprint requests to: e-mail: keith_w_ward@gsk.com
§ Present address: Molecumetics, 2023 120th Avenue N.E., Bellevue, WA 98005, USA.

Xenobiotica ISSN 0049–8254 print/ISSN 1366–5928 online © 2002 Taylor & Francis Ltd
http://www.tandf.co.uk/journals
DOI: 10.1080/00498250110100711

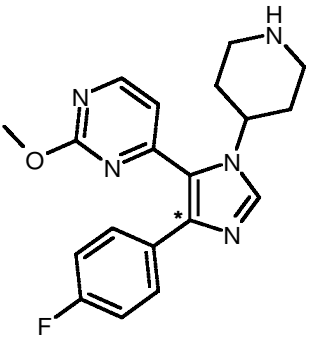


Figure 1. Chemical structure of SB-242235 (1-(4-piperidinyl)-4-(4-fluorophenyl)-5-(2-methoxy-4-pyrimidinyl) imidazole). *Site of radiolabel.

has been characterized (Badger *et al.* 2000). In a companion manuscript, the preclinical pharmacokinetics of SB-242235 are described (Ward *et al.* 2002). SB-242235 demonstrates high total clearance in rat (3.4 $l h^{-1} kg^{-1}$), and moderate clearance in dog and monkey (0.3 and 1.0 $l h^{-1} kg^{-1}$, respectively). Oral bioavailability in the preclinical species was excellent (50–100%). These data suggest that SB-242235 may provide sufficient exposure upon oral dosing to be useful both as a tool compound to probe the effects of p38 inhibition in biological systems, and in therapeutic intervention in p38-mediated disease. The objectives of the study were to describe the rates and routes of SB-242235 metabolism *in vitro*, to characterize its *in vivo* preclinical metabolism, and to use these data to help predict the pharmacokinetic behaviour of SB-242235 in man. This prediction was then compared with human pharmacokinetic data for SB-242235.

Materials and methods

Materials

[^{3}H]SB-242235 and [^{14}C]SB-242235 were provided by Radiochemistry, Department of Chemical Development, SmithKline Beecham (King of Prussia, PA, USA). Non-radiolabelled SB-242235 was provided by the SB Department of Medicinal Chemistry. The chemical and radiochemical purity (where appropriate) of all material used was $\geq$ 98%. The specific activities of [^{3}H]SB-242235 and [^{14}C]SB-242235 used in the *in vitro* experiments were 3028 and 150 $\mu Ci\, mg^{-1}$, respectively. The specific activities of [^{14}C]SB-242235 used in the *in vivo* rat and monkey studies were 5 and 7.2 $\mu Ci\, mg^{-1}$, respectively. All other materials were purchased from standard commercial vendors, and were of the highest available purity.

Animals

Male outbred rats (Crl:CD(SD)BR; Charles River, UK; 290–320 g) and male Cynomolgus monkeys (*Macaca fascicularis*; Covance Research Products, Denver, PA, USA; 4.3–5.6 kg) were used in the *in vivo* studies. Animals used for the collection of excreta or bile were housed according to the National Institutes of Health *Guide for the Care and Use of Laboratory Animals* in individual cages designed for the separation and collection of urine and faeces. Rats used for blood collection were housed individually in plastic cages. Filtered tap water was available *ad libitum*, and animals were fed a standard animal diet (Purina Mills, St Louis, MO, USA). For rodents, food was available *ad libitum* throughout the study. Monkeys were fasted overnight before dosing; food was returned after the 240-min blood samples were obtained. Studies were pre-approved by the Institutional Animal Care and Use Committee, and all surgical procedures were conducted using aseptic techniques.

In vitro *metabolism studies*

In vitro experiments were conducted in rat, dog, monkey, and human hepatic microsomal fractions and isolated hepatocytes and in precision-cut liver slices from rat, monkey and human. Microsomes and hepatocytes were prepared according to standard techniques (Ekins *et al.* 1999) or purchased from outside vendors; human hepatocytes were a generous gift from Dr Stephen C. Strom (University of Pittsburgh). Rat and monkey liver slices (~200 μm thick) were prepared as described (Parrish *et al.* 1995); human liver slices were obtained from the Anatomic Gift Foundation (Columbia, MD, USA). All slices were floated onto titanium mesh rollers (two slices per roller) and blotted to remove excess buffer. Each roller was loaded into a vial containing 1.7 ml Waymouth's supplemented culture medium (Waymouth's medium supplemented with 25 mM sodium bicarbonate, 25 mM Hepes, 25 mM D-glucose, 2 mM L-glutamine, 84 μg ml^{-1} gentamicin, and 5% serum, pH 7.4) containing 0.5, 5 or 50 μM [^{3}H]SB-242235. Slices were incubated for various times up to 6 h; incubations without either liver slices or test compound also were included as controls. Biochemical viability during the incubation period was confirmed by determining membrane integrity (LDH leakage) and protein synthesis by standard techniques. At the conclusion of each incubation period, slices and media were homogenized, and concentrations of SB-242235 and/or potential metabolites were determined. Microsomal incubations with hepatic microsomes also were conducted with both SB-242235 (1 μM, to assess metabolic rates), and [^{14}C]SB-242235 (10 μM, to assess metabolic routes). Incubations were conducted under standard conditions (Ekins *et al.* 1999) in the presence of NADPH and UDPGA to support both Phase I and II metabolic processes. Reactions were terminated at selected time points up to 30 min by adding an equal volume of acetonitrile; samples were stored frozen until analysis.

In vivo *rat studies*

The study design employed three intact rats for collection of urine and faeces, four bile duct-cannulated (BDC) rats for collection of bile, urine and faeces, and nine intact rats for collection of plasma at three separate time points. The common bile duct and duodenum of the BDC rats were cannulated with each cannula being exteriorized. The cannulae were maintained for 2 days post-surgery by infusion of saline through the duodenal cannula. Thereafter, the infusate was changed to a 0.05% solution of bile salts in 0.9% saline. The surgically prepared animals were maintained for 5 days before dosing. On the study day, each rat received a single oral gavage dose of a suspension of [^{14}C]SB-242235 in 1% aqueous methylcellulose (30 and 10 ml kg^{-1}). Bile, urine and faeces were collected into preweighed containers, cooled to −70 °C, at various periods up to 96 h after dosing. At 2, 12 and 24 h after dosing, the rats used for collection of plasma were euthanized with CO_2, and a terminal blood sample obtained from the vena cava. Blood was centrifuged to obtain plasma; all samples were stored frozen until analysis.

In vivo *monkey studies*

Three monkeys were used in this investigation. On the day of dosing, after an overnight fast, the monkeys received a single oral gavage dose of [^{14}C]SB-242235 (10 and 4 ml kg^{-1}) as a suspension in 1% aqueous methylcellulose. Urine and faeces were collected predose and at 24-h intervals through 240 h post-dose. Blood samples were obtained from a femoral vein of each monkey at 4, 12, 24, 48, 72 and 96 h post-dose; plasma was obtained by centrifugation. All samples were stored frozen until analysis.

Analytical procedures

For samples generated in the *in vitro* studies, qualitative analysis to identify potential metabolites of SB-242235 was conducted by HPLC/MS. Quantitative analysis of the amount of SB-242235 present (to determine the rate of metabolism) was performed using an HPLC/MS/MS method. Proteins were precipitated from a 50-μl aliquot of the incubation mixture with acetonitrile and concentrations of SB-242235 quantified with a Finnigan TSQ 700 mass spectrometer using positive-ion electrospray ionization. All samples generated during the in-life phase of the *in vivo* rat and monkey studies were analysed for total radioactivity to determine the routes of excretion of drug-related material. Urine, bile and plasma were analysed directly by liquid scintillation counting. Faeces were homogenized in water, aliquots of the homogenate combusted in a sample oxidizer, and the total radioactivity content determined by liquid scintillation counting (Tri-Carb 2700 TR, Packard Biosciences, Downers Grove, IL, USA). For metabolic analysis, samples of urine and bile were centrifuged briefly to pellet debris, with triplicate aliquots of the supernatant analysed for radioactivity. Similarly, proteins were precipitated from plasma by extraction with acetonitrile followed by centrifugation. The supernatants were evaporated to dryness and reconstituted in 1 ml 10 mM ammonium acetate for analysis. All samples were analysed by an appropriate radio-HPLC method, with selected samples being analysed also by HPLC/MS or HPLC/MS/MS to provide structural identification information; analysis for SB-242235 and metabolites was performed essentially as described (Ward *et al.* 2002).

Allometric scaling

For interspecies scaling, the total plasma clearance (CL, $l\,h^{-1}\,kg^{-1}$) and distributional volume (V_{SS}, $l\,kg^{-1}$) obtained previously for SB-242235 (Ward *et al.* 2002) were plotted against body weight (BW, kg) on a log–log scale (Ritschel *et al.* 1992). Linear least-squares regression analysis was performed on these plots using Excel to fit these relationships to the following equations:

$$CL = aBW^x \tag{1}$$

and

$$V_{SS} = bBW^y, \tag{2}$$

where a and b are the allometric coefficients, and x and y are the allometric exponents for clearance and distributional volume, respectively. A human half-life ($T_{½}$, h) was estimated from the predicted estimate of clearance and volume of distribution using the following relationship:

$$T_{1/2} = 0.693 \cdot \frac{V_{SS}}{CL}. \tag{3}$$

The relationship assumes a linear, mono-exponential elimination profile for SB-242235 in man. In addition, the effect of various correction factors on the allometric scaling was examined. These factors included a correction for plasma protein binding (van Hoogdalem *et al.* 1997), longevity (maximum lifespan potential, MLP; Boxenbaum 1982), and brain weight (BrW; Mahmood and Balian 1996). Finally, a correction factor designed to account for interspecies differences in renal excretion also was investigated (Mahmood 1998). In each case, the measured clearance or distributional volume was multiplied by the proposed scaling factor to generate an adjusted parameter estimate, and the adjusted parameter used in equation (1) or (2) to perform the allometry. Linear least-squares regression analysis was performed on each scaling set, with the correlation coefficient used to determine the goodness of fit of the regression analysis to the data.

Pharmacokinetic data analysis

Radioactivity plasma concentration versus time profiles after oral administration of [^{14}C]SB-242235 were obtained in the rat and monkey. Non-compartmental data analysis was performed on each data set using WinNonlin Professional Version 2.1 (Pharsight, Mountain View, CA, USA) to describe the critical pharmacokinetic parameters. For rat, because only a single plasma sample was obtained from each animal, average data were analysed. In monkey, data for each subject were analysed separately; data for each pharmacokinetic parameter were averaged and reported as mean ± SD.

Results

In vitro *metabolism*

Examination of all samples from microsomal incubations in all species revealed unchanged SB-242235 to be the major component (figure 2). SB-242235 concentrations were constant throughout the microsomal, hepatocyte and liver slice incubations. Therefore, a rate of metabolism could not be determined by analysis of the rate of disappearance of the parent. Minor metabolites were detected by qualitative analysis in most *in vitro* samples (apparently products of monooxygenation, dioxygenation, demethylation and glucuronidation; definitive metabolite analysis not conducted); as shown by figure 2, these metabolites accounted for $< 5\%$ of the total injected radioactivity. Similar data were obtained following analysis of liver slice and hepatocyte cultures (data not shown).

In vivo *metabolism in rat*

The *in vivo* biotransformation of SB-242235 in rat was investigated after a single $30\,mg\,kg^{-1}$ oral dose of [^{14}C]SB-242235. Mass balance data, including biliary secretion and urinary elimination, are displayed in table 1. Based on total recovery of radioactivity in bile and urine, absorption of total drug-related material was at least 60% of the administered dose. Urinary excretion was the predominant route of elimination of SB-242235, accounting for 51% of the administered dose

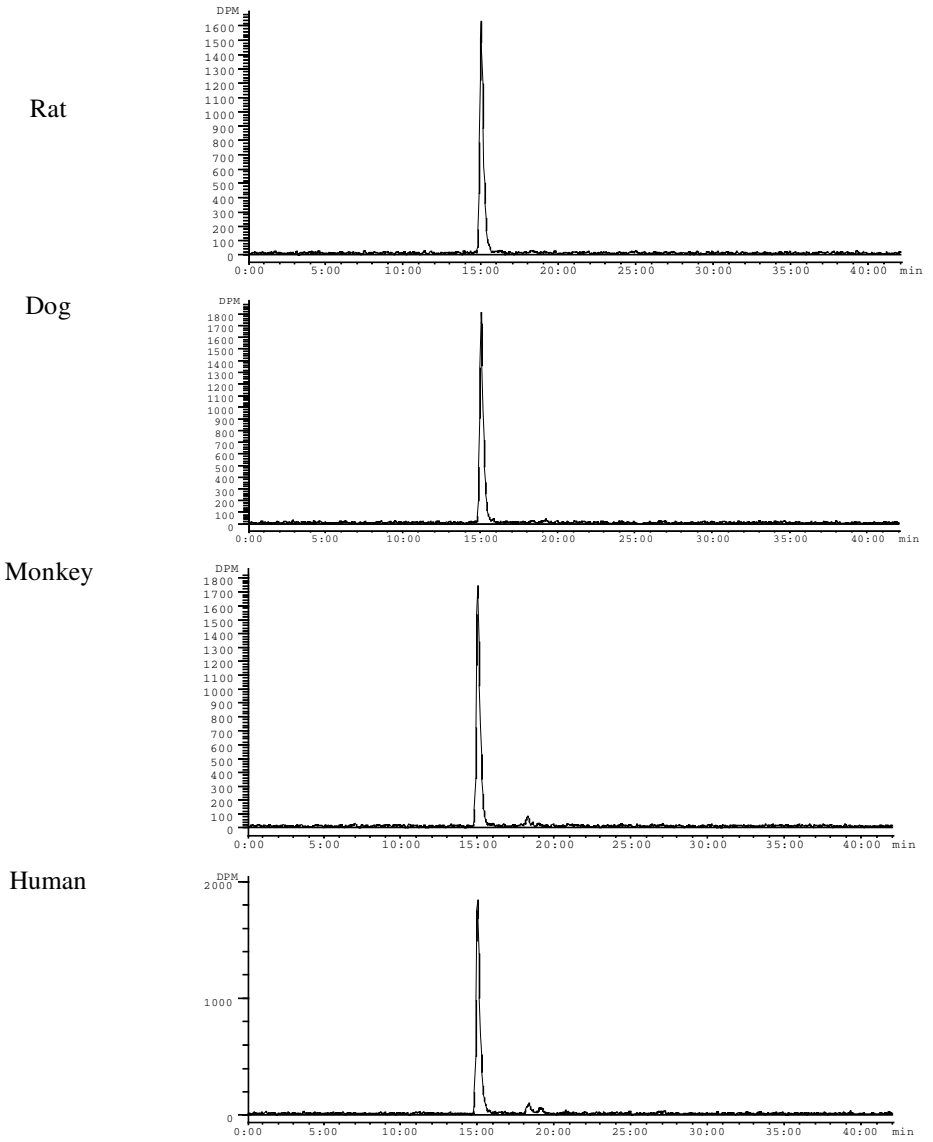


Figure 2. Representative radio-HPLC chromatograms of *in vitro* hepatic microsomal incubations of [C]SB-242235 (10 μM) from rat, dog, monkey and human microsomal preparations.

over the 96 h following dosing. Biliary excretion of radioactivity was low, accounting for only 9% of the administered dose. Elimination of radioactivity was rapid with the majority of radioactivity recovered within 24 h of dosing. Representative radio-HPLC chromatograms of rat urine are shown in figure 3. The predominant radiolabelled component in rat urine was unchanged SB-242235; no significant metabolites of SB-242235 were observed in rat urine. Rat bile contained very low levels of two uncharacterized metabolites in addition to low levels of unchanged parent compound (data not shown). However, rat bile was not further investigated due to the low percentage of dose excreted via this route. Plasma radioactivity

Table 1. Recovery of radioactivity (expressed as the percentage of the administered dose) following a single oral suspension dose of [^{14}C]SB-242235 (30 mg kg^{-1}) to the male rat.

		Recovery of radioactivity (% dose)	
Sample	Time (h)	Intact rat	BDC rat
Urine	0–6	15.2 ± 2.2	20.7 ± 5.8
	6–24	32.8 ± 4.6	29.4 ± 7.5
	24–48	0.8 ± 0.1	0.8 ± 0.2
	0–96	49.2 ± 2.4	51.4 ± 3.3
Bile	0–6	n/a	8.0 ± 0.7
	6–24	n/a	0.6 ± 0.2
	24–48	n/a	0.1 ± 0.1
	0–96	n/a	8.7 ± 0.8
Faeces	0–24	39.0 ± 1.6	27.0 ± 0.8
	24–48	4.6 ± 1.4	2.2 ± 0.8
	0–96	43.9 ± 0.9	29.6 ± 0.8
Total recovery*	0–96	98.0 ± 0.7	96.9 ± 0.1

Data are the mean ± SD from three to four animals per group.
* Includes radioactivity recovered in daily cage washes, GI tract and carcass at 96 h after dosing.

versus time data from the present study are shown in figure 4A. Because of the limited plasma data obtained, full pharmacokinetic characterization of SB-242235 was not performed. However, the data suggest that SB-242235 demonstrated an apparent plasma half-life of ~3 h in the rat. Rat plasma radio-HPLC profiles were similar to those obtained in urine, with the predominant component being SB-242235 (data not shown).

In vivo *metabolism in monkey*

The *in vivo* biotransformation of SB-242235 was investigated in monkey following a single 10 mg kg^{-1} oral dose of [^{14}C]SB-242235. Urinary elimination, faecal excretion and total radioactivity recovery from the study are shown in table 2. Based on total recovery of radioactivity from urine, absorption of drug-related material in monkey was at least 67% of the administered dose. The administered dose was primarily excreted in urine. Approximately 18% of the dose was recovered in faeces, resulting either from the non-absorbed fraction of the dose or from biliary secretion and/or direct intestinal excretion. Elimination of radioactivity was rapid, with the majority of radioactivity recovered within 48 h of dosing. Average plasma concentration–time profiles for [^{14}C]SB-242235 in monkey are shown in figure 4B. The approximate terminal plasma half-life of [^{14}C]SB-242235 in monkey was 29 ± 2 h. Monkey plasma radio-HPLC profiles were similar to those obtained in urine, with the predominant radiolabelled component being SB-242235 (data not shown).

Allometric scaling

Before initiating clinical studies with SB-242235, allometry was performed to predict SB-242235 disposition in man. Estimates for clearance, distributional volume and plasma protein binding previously determined for SB-242235 in rat,

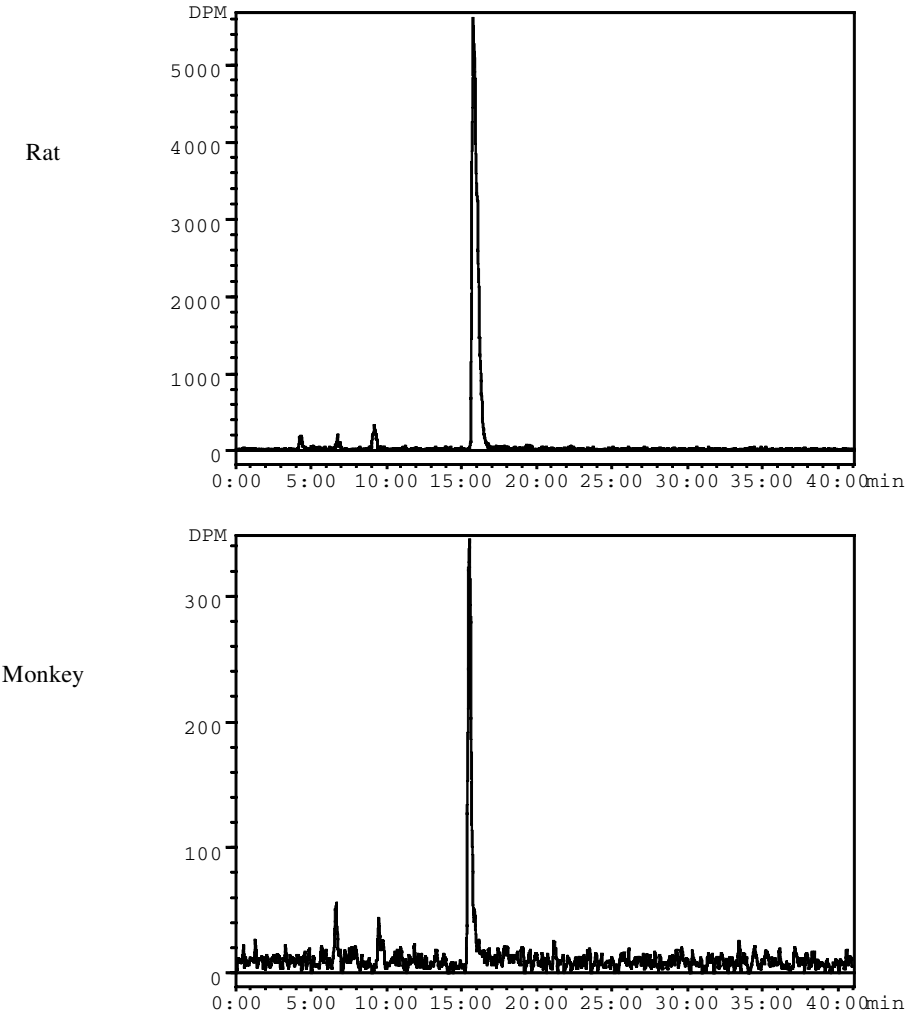


Figure 3. Representative radio-HPLC chromatograms of rat and monkey urine obtained following single oral doses of [^{14}C]SB-242235 to the male rat and monkey at nominal doses of 30 and 10 mg kg^{-1}, respectively.

dog and monkey were used for the interspecies scaling (Ward *et al*. 2002). Clinical data for SB-242235 (Fullerton *et al*. 2000) were used retrospectively to evaluate the accuracy of the allometric scaling and the various correction factors used. Because of the apparent non-linear elimination of SB-242235 in rat and monkey, only data from the lowest dosage group for each species were used for the extrapolation, in instances where more than one dosage was evaluated. Figure 5 demonstrates the standard log–log allometric plots for clearance and volume of distribution across species, without the inclusion of any correction factors. The allometric exponent and correlation coefficient of the allometric regression, as well as the predicted human pharmacokinetic parameters, for each allometric scaling iteration are displayed in table 3. Primarily owing to low clearance in dog, the exponent of the uncorrected allometric clearance relationship was only ~0.42, while the

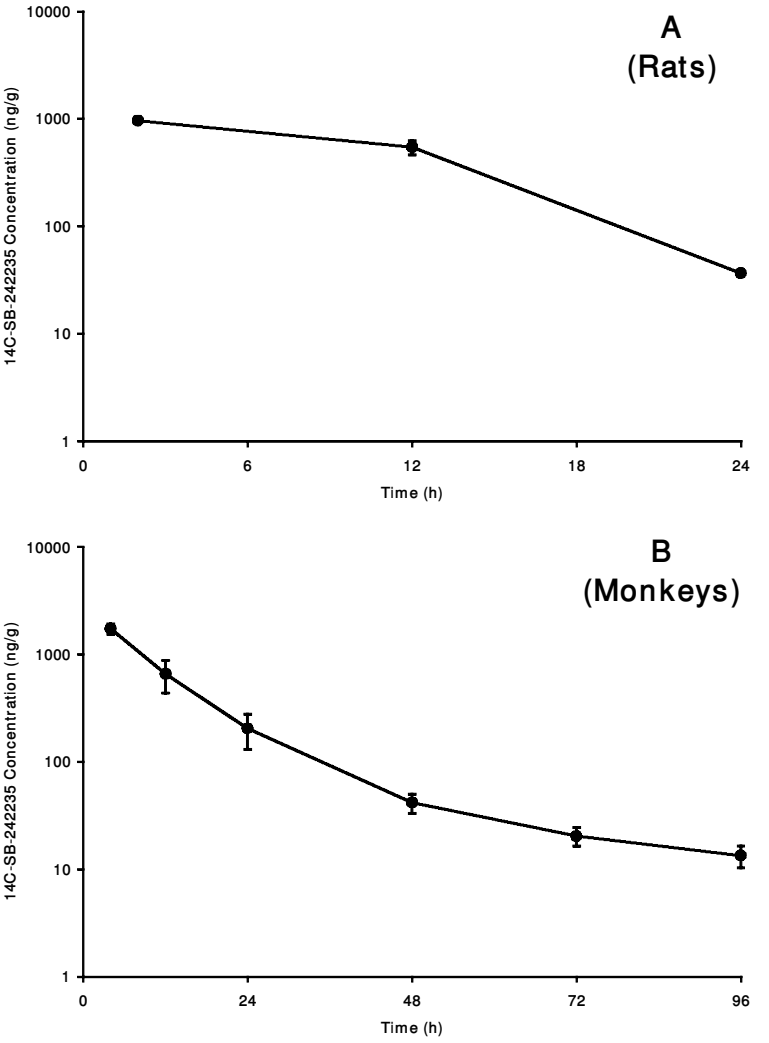


Figure 4. Plasma concentration versus time profiles for SB-242235 following a single oral administration of [^{14}C]SB-242235 in rat (30 mg kg^{-1}) (A) or in monkey following a single oral administration of 10 mg kg^{-1} [^{14}C]SB-242235 (B). Data are the mean ± SD for $n = 3$ animals.

uncorrected prediction of distributional volume yielded a more acceptable allometric exponent of ~0.84. Next, a correction for plasma protein binding was employed for both clearance and distributional volume. Because the *in vivo* pharmacokinetic profiles spanned the concentration range used to determine protein binding for each species (Ward *et al.* 2002), the average protein binding for each species was used for all corrections. Incorporation of protein binding did not improve the fit of the linear regression to the data or the allometric exponent of the relationship for either clearance or distributional volume. The predicted volume of distribution of SB-242235 was either 5.24 or 3.06 l kg^{-1}, estimated by including or not including plasma protein binding, respectively.

After completing the uncorrected and protein binding-corrected scaling, various additional clearance correction factors, including corrections for longevity,

Table 2. Recovery of radioactivity (expressed as the percentage of the administered dose) following a single oral suspension dose of [^{14}C]SB-242235 (10 mg/kg) to the male monkey.

Matrix	Collection interval (h)	Recovery of radioactivity (% administered dose)
Urine	0–24	54.3 ± 8.2
	24–48	7.1 ± 1.8
	48–72	2.2 ± 0.8
	0–240	66.6 ± 6.4
Faeces	0–24	4.75*
	24–48	7.1 ± 3.0
	48–72	2.8 ± 0.6
	0–240	17.7 ± 6.4
Daily pan rinses	0–216	11.6 ± 3.9
Total**	0–240	97.5 ± 3.9

Data are the mean ± SD from three animals per group.

* Standard deviation not calculated since no radioactivity was detected in one sample.

** Includes radioactivity recovered in cage washes and wipe at 240 h.

brain weight and glomerular filtration, were explored. Because these factors relate primarily to clearance processes, they were not applied to the allometry for distributional volume. The values for each factor are displayed in table 4; all data were derived from Davies and Morris (1993). In no instance did co-inclusion of a correction for plasma protein binding improve the interspecies scaling, as determined by the allometric exponent or the correlation coefficient for the linear regression. Use of maximum lifespan potential as a correction factor for scaling of clearance substantially improved both the regression fit and the allometric exponent (table 3). Similarly, inclusion of correction for interspecies differences in brain weight for scaling of clearance improved the fit of the linear regression to the data, although the brain weight correction also provided an unrealistically high allometric exponent of 1.6. Finally, because of the important role of renal processes in the elimination of SB-242235, correction factors were considered for interspecies differences in renal elimination. Initially, the calculated renal clearance normalization factor proposed by Mahmood (1998) was employed. This correction resulted in an improvement of the scaling of SB-242235 clearance compared with uncorrected allometry, but provided a less favourable correlation coefficient compared with the maximum lifespan correction. Subsequently, the renal correction factor of Mahmood (1998) was recalculated for each species based on physiological source data from Davies and Morris (1993), and used in the allometry. The recalculated interspecies scaling provided no apparent improvement over uncorrected allometry or any other correction factor, resulting in the lowest regression correlation coefficient of all corrections evaluated (figure 6).

Comparison of predicted and observed clinical pharmacokinetic parameters

SB-242235 demonstrates a terminal plasma half-life of 16.4 ± 1.6 h in healthy male human volunteers over a dose range of 25 to 300 mg (Fullerton *et al.* 2000). The deviation of the predicted human half-life from this measured value in the first-in-man study is displayed in table 3. In general, the various scaling methods

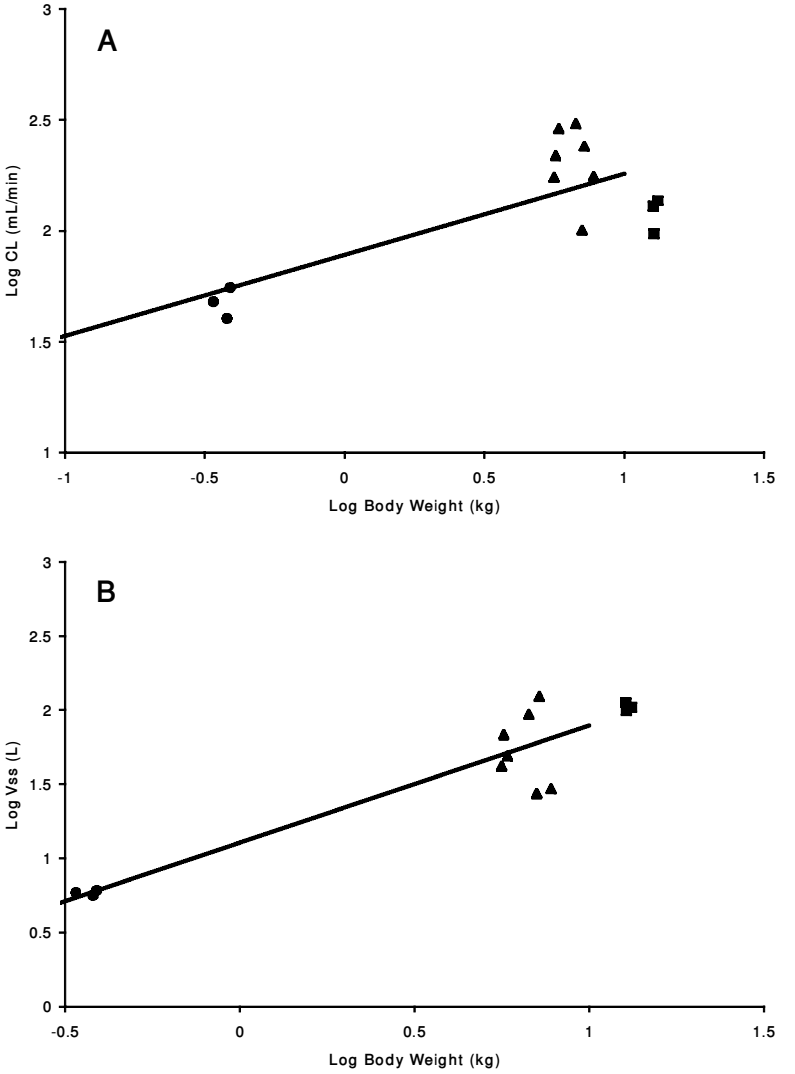


Figure 5. Uncorrected allometric scaling of clearance (A) and distributional volume (B) of SB-242235 from preclinical species to humans. Symbols represent the measured pharmacokinetic parameter in each animal; lines represent linear least-squares regression through all data points. Circles, triangles and squares represent data from rat ($n = 3$), monkey ($n = 7$) and dog ($n = 3$), respectively.

all provided a reasonable estimation of half-life, with the deviation from the actual value ranging from -30 to $+14\%$. There was no obvious correlation between the goodness of fit of the allometric linear regression analysis and the deviation from the measured human half-life. Retrospectively, of the allometric correction factors employed in this investigation, the correction for maximum lifespan potential and the recalculated renal correction factor provided the most accurate estimate of human half-life. Both correction methods resulted in a half-life estimation only 14% above the actual value, although the correlation coefficient for the renal correction was poor, and neither method provided the optimum regression coefficient. Recalculation of the renal correction factor of Mahmood (1998)

Table 3. Allometric interspecies scaling of the predicted clinical pharmacokinetics of SB-242235. Data result from the application of equations (1) and (2), with various correction factors, to previously obtained preclinical pharmacokinetic data, where a and x are the allometric coefficient and exponent, and r^2 is the correlation coefficient of the linear allometric regression.

Correction method	a	x	r^2	Predicted clearance ($l h^{-1} kg^{-1}$)	Predicted volume ($l kg^{-1}$)	Predicted half-life (h)	Deviation from measured half-life (%)
Uncorrected	1.552	0.4223	0.6407	0.18	3.06	11.5	−29.9
Plasma protein binding (PPB)	1.892	0.3650	0.5615	0.32	5.24	11.5	−29.9
Lifespan potential (MLP)	2.455	0.8865	0.8067	0.11	3.06	18.7	14.0
PPB + MLP	2.795	0.8292	0.7793	0.19	5.24	18.7	14.0
Brain weight	2.540	1.580	0.8881	0.17	3.06	12.1	−26.2
PPB + brain weight	2.880	1.523	0.8773	0.30	5.24	12.1	−26.2
Mahmood renal factor	1.141	0.6198	0.7119	0.17	3.06	12.9	−21.3
PPB + Mahmood renal factor	1.4802	0.5624	0.6624	0.28	5.24	12.9	−21.3
Present renal factor	1.130	0.5375	0.5045	0.11	3.06	18.7	14.0
PPB + present renal factor	1.470	0.4802	0.4407	0.19	5.24	18.7	14.0

a, x, r^2 are the allometric coefficient, allometric exponent and correlation coefficient for the allometric relationship, as shown in equations (1) and (2).

Table 4. Physiological and allometric scaling parameters employed in the interspecies scaling of SB-242235. Physiological data were derived from Davies and Morris (1993).

Parameter	Rat	Dog	Monkey	Human
MLP (years)	4.7	20	22	93
Brain weight (g)	1.8	80	90	1400
Kidney weight ($g\,kg^{-1}$)	8	5.5	5	4.4
Renal blood flow ($ml\,min^{-1}$)	13.6	279	181	1239
GFR ($ml\,min^{-1}$)	5.24	6.13	2.08	1.78
Renal clearance normalization factor (Mahmood 1998)[a]	3.3	1.9	1.6	1.0
Renal clearance normalization factor (present data)[a]	3.37	3.36	1.60	1.00

[a] Calculated as [(GFR · renal flow)/(body weight · kidney weight)].

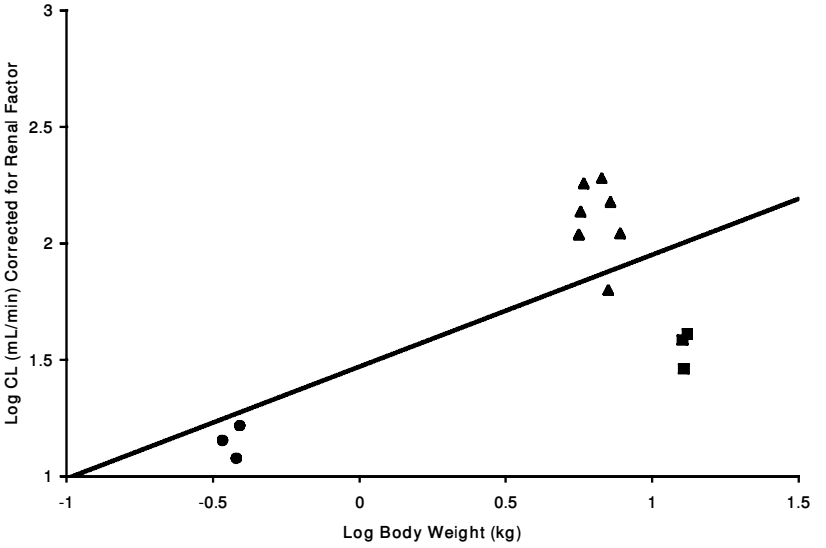


Figure 6. Allometric scaling of clearance of SB-242235 from preclinical species to humans corrected for interspecies differences in renal elimination. Symbols represent the measured pharmacokinetic parameter in each animal; lines represent linear least-squares regression through all data points. Circles, triangles and squares represent data from rat ($n = 3$), monkey ($n = 7$) and dog ($n = 3$), respectively.

based on literature physiological values, however, did improve the prediction provided by the renal correction method, from a 21% underestimate to a 14% overestimate of the true human value.

Discussion

In the current investigation, the *in vitro* and *in vivo* biotransformation of SB-242235, a novel p38 MAP kinase inhibitor, was explored. Inhibitors of p38 MAP kinase may have therapeutic utility in managing a variety of diseases, including inflammatory, autoimmune and pulmonary disease (Lee *et al.* 1993, Underwood *et al.* 2000). Although many potent and selective aryl imidazole p38 inhibitors have been synthesized, to date, a full description of their pharmacokinetics and

biotransformation has not been published. Previously, the metabolism of SK&F-86002 (6-(4′-fluorophenyl)-5-(4′-pyridyl)-2,3-dihydroimidazo-[2,1-b]-thiazole), a less potent and non-selective cytokine biosynthesis inhibitor, was investigated *in vitro* (Howard *et al.* 1990) and *in vivo* (Newton *et al.* 1989) in the rat. SK&F-86002 was extensively metabolized, but the metabolism was primarily cytochrome P450-mediated sulphoxidation on the thiazole moiety; other metabolites arising from the 4-fluorophenyl or the pyridine groups were not noted. SB-242235 lacks the metabolically labile thiazole found in SK&F-86002, and was metabolically stable, with no substantial metabolism around the 4-fluorophenyl or the methoxypyrimidine moieties.

The present data are similar to those obtained in a previous study of the preclinical pharmacokinetics of SB-242235 in rat and monkey (Ward *et al.* 2002). In the non-radiolabelled study, SB-242235 demonstrated maximal plasma concentrations following oral administration and areas under the plasma concentration versus time curve in both rat and monkey that were similar to those obtained from the limited profiles generated in the current study employing [^{14}C]SB-242235. In both rat and monkey, the large absorbed fraction observed in the present study with [^{14}C]SB-242235 was anticipated based on the excellent oral bioavailability previously seen for SB-242235 in these species. Finally, the predominantly renal elimination of [^{14}C]SB-242235 in the present study in rat is consistent with the low first-pass hepatic extraction ($< 5\%$) observed in the previous study using non-radiolabelled SB-242235.

In general, the preclinical pharmacokinetic data were predictive of the clinical pharmacokinetics of SB-242235. Exposure following oral administration was good across species, and good oral exposure was noted in the first-in-man study for SB-242235 (Fullerton *et al.* 2000). The complete preclinical pharmacokinetic and biotransformation data allowed rigorous prospective allometric interspecies scaling of SB-242235. Obviously, the preclinical pharmacokinetic data are used directly in performing extrapolation to man. In addition, the incorporation of the biotransformation data allowed for an appropriate, mechanism-based selection of an allometric correction factor for glomerular filtration, and directed effort away from alternate correction factors such as those employed for compounds eliminated primarily through oxidative metabolism. Retrospectively, allometry effectively predicted the clinical pharmacokinetics of SB-242235, regardless of correction factors employed. Despite the limitations of allometry (discussed below), this technique did provide a reasonable estimation of the half-life of SB-242235 in man, with $< 30\%$ deviation from the measured value regardless of the scaling method selected. In addition, the low plasma protein binding observed for SB-242235, and the minimal observed differences in average protein binding across species, correctly suggested that inclusion of a correction for plasma protein binding would not improve the allometry for SB-242235. SB-242235 demonstrates a free fraction in all species of $> 20\%$; it is generally recognized that plasma protein binding of < 80–90% will be of minimal pharmacokinetic significance (Welling 1993).

The predictive success of the allometric scaling for SB-242235 was not completely anticipated *a priori*, for several reasons. First, the overall interspecies correlation, as measured by the correlation coefficient of the allometric linear regression analysis, ranged from only 0.44 to 0.89, regardless of the correction method employed. This observation suggested that the scaling of SB-242235

might be unreliable, and gave low confidence in the final extrapolation. However, as shown in table 3, there was no correlation between r^2 for the regression and the accuracy of the correction technique in predicting human half-life; in fact, the method with the lowest correlation coefficient provided one of the most accurate predicted half-life estimates. This observation suggests that the goodness of fit of the linear regression may not be the most appropriate selection criterion when performing prospective allometry. Further investigation may be warranted to elucidate appropriate selection criteria for such allometric correction techniques.

Another factor that gave less certainty to the overall interspecies scaling for SB-242235 was the value obtained for the allometric exponent in the uncorrected allometric analysis. It has been observed that 'typical' values for the allometric exponent for clearance are generally around 0.75, while those for distributional volume typically pivot around 1.0 (Mahmood 1999). Mahmood and Balian (1996) suggested that if the uncorrected allometric exponent for clearance is <0.55, human clearance cannot be accurately predicted, even with correction factors; the uncorrected allometric exponent for SB-242235 clearance was 0.42. Also, although it is generally believed that compounds excreted unchanged in the urine are the most likely to allow successful allometric scaling, recent evidence suggests that total clearance of drugs that are primarily excreted renally often does not scale well (Mahmood 1999). Finally, the non-linearity in the preclinical species for SB-242235 added further uncertainty in the allometric analysis. To attempt to circumvent any scaling liabilities associated with this non-linearity, only preclinical pharmacokinetic data obtained at the lowest administered dose was used to develop the allometric scaling. This approach to minimizing the effect of saturable elimination is similar to that previously used for compounds exhibiting non-linear pharmacokinetics, including triclopyr (Timchalk and Nolan 1997) and the carbapenem antibiotic DA-1131 (Kim *et al.* 1998), and appeared to be successful in this instance.

In light of the failure of allometry for many compounds excreted in urine, Mahmood (1998) developed a correction factor to account for interspecies differences in renal excretion. In that study, the correction factor was calculated by dividing the product of glomerular filtration rate (GFR) and renal blood flow by the product of body weight and kidney weight. However, the source for these physiological data was not provided. As shown in table 4, the renal correction factor as estimated by Mahmood and that determined directly from the data of Davies and Morris (1993) were essentially identical except for the correction factor for dog. Mahmood used 0.05 kg, 216 ml min^{-1} and 45 ml min^{-1} for kidney weight, blood flow and GFR, respectively, to yield a correction factor of 1.9 for the dog, while the corresponding data from Davies and Morris (1993) produced estimates of 0.07 kg, 279 ml min^{-1} and 79 ml min^{-1} for these same parameters, yielding a final correction factor of 3.4. The two factors produced substantially different estimates of human half-life (12.9 versus 18.7 h for the Mahmood and recalculated values, respectively); the estimate based on the recalculated factor provided a better prediction of the human value. This observation suggests that although the correction approach proposed by Mahmood for renally excreted compounds appears to improve the scaling for SB-242235, caution is warranted in using the absolute correction factor for dog cited by Mahmood (1998).

In summary, the present study investigated the rates and routes of metabolism of SB-242235 *in vitro* and *in vivo*. The compound was only minimally metabolized,

and *in vivo* was primarily excreted in the urine in both rat and monkey. Various prospective allometric scaling approaches were also investigated for SB-242235, with optimal prediction achieved using a scaling factor to correct for interspecies differences in glomerular filtration, as expected based on the biotransformation characteristics of the compound. However, comparison with the observed clinical data for SB-242235 revealed that standard goodness of fit criteria were not well correlated with predictive accuracy for human half-life. Thus, although allometry was sufficient for SB-242235 to allow reasonable prediction of human pharmacokinetics regardless of the various scaling factors employed, these data highlight the importance of considering appropriate mechanism-based correction factors to achieve optimal accuracy in interspecies extrapolation.

Acknowledgements

The authors gratefully acknowledge the expert technical assistance of members of various groups within DMPK, including Biotransformation (Jim Politowski and Randy Sozio) and Preclinical Registration and Outsourcing (Vicki Horton and Dave Kenworthy). Furthermore, the work would not have been possible without the support of SB Radiochemistry, particularly Keith Garnes, for its synthesis of radiolabelled SB-242235. Appreciation is also extended to Jerry Adams, Amarnath Sharma, Terence Fullerton and William V. Williams for their critical review of the manuscript.

References

Badger, A. M., Griswold, D. E., Kapadia, R., Blake, S., Swift, B. A., Hoffman, S. J., Stroup, G. B., Webb, E., Rieman, D. J., Gowen, M., Boehm, J. C., Adams, J. L. and Lee, J. C., 2000, Disease-modifying activity of SB 242235, a selective inhibitor of p38 mitogen-activated protein kinase, in rat adjuvant-induced disease. *Arthritis Rheumatism*, **43**, 175–183.

Boxenbaum, H., 1982, Interspecies scaling, allometry, physiological time, and the ground plan of pharmacokinetics. *Journal of Pharmacokinetics and Biopharmacology*, **10**, 201–227.

Davies, B. and Morris, T., 1993, Physiological parameters in laboratory animals and humans. *Pharmaceutical Research*, **10**, 1093–1095.

Ekins, S., Mäenpää, J. and Wrighton, S. A., 1999, *In vitro* metabolism: subcellular fractions. In T. W. Woolf (ed.), *Handbook of Drug Metabolism* (New York: Marcel Dekker), pp 363–399.

Fullerton, T., Sharma, A., Prabhakar, U., Tucci, M., Boike, S. and Davis, H,. 2000, Suppression of *ex vivo* cytokine production by SB 242235, a selective inhibitor of p38 MAP kinase. *Clinical and Pharmacological Therapeutics*, **114** (Meeting Abstract).

Howard, M. O., Newton, J. F., Kohane, D. J., Yodis, L. P., Saverino, C. M., Qualls, C. W., Jr, and Schwartz, L. W., 1990, *In vitro* metabolism of the novel antiinflammatory agent 6-(4′-fluorophenyl)-5-(4′-pyridyl)-2,3-dihydroimidazo-{2,1-b}-thiazole. *Drug Metabolism and Disposition*, **18**, 607–612.

Kim, S. H., Kim, W. B. and Lee, M. G., 1998, Interspecies pharmacokinetic scaling of a new carbapenem, DA-1131, in mice, rats, rabbits and dogs, and prediction of human pharmacokinetics. *Biopharmacology and Drug Disposition*, **19**, 231–235.

Lee, J. C., Kassis, S., Kumar, S., Badger, A. and Adams, J. L., 1999, p38 Mitogen-activated protein kinase inhibitors—mechanisms and therapeutic potentials. *Pharmacological Therapeutics*, **82**, 389–397.

Lee, J. C., Kumar, S., Griswold, D. E., Underwood, D. C., Votta, B. J. and Adams, J. L., 2000, Inhibition of p38 MAP kinase as a therapeutic strategy. *Immunopharmacology*, **47**, 185–201.

Mahmood, I., 1998, Interspecies scaling of renally secreted drugs. *Life Sciences*, **63**, 2365–2371.

Mahmood, I., 1999, Allometric issues in drug development. *Journal of Pharmaceutical Sciences*, **11**, 1101–1106.

Mahmood, I. and Balian, J. D., 1996, Interspecies scaling: predicting clearance of drugs in humans. Three different approaches. *Xenobiotica*, **26**, 887–895.

Newton, J. F., Yodis, L. P., Keohane, D., Eckardt, R., Dewey, R., Dent, J. and Mico, B., 1989, Pharmacokinetics and metabolism of SK&F 86002 in male and female Sprague–Dawley rats. *Drug Metabolism and Disposition*, **17**, 174–179.

Parrish, A. R., Gandolfi, A. J. and Brendel, K., 1995, Precision-cut tissue slices: applications in pharmacology and toxicology. *Life Sciences*, **57**, 1887–1901.

Ritschel, W. A., Vachharajani, N. N., Johnson, R. D. and Hussain, A. S., 1992, The allometric approach for interspecies scaling of pharmacokinetic parameters. *Computers in Biological Physics*, **103C**, 249–253.

Stein, B. and Anderson, D., 1996, The MAP kinase family: New 'MAPs' for signal transduction pathways and novel targets for drug discovery. *Annals in the Reporting of Medical Chemistry*, **31**, 289–298.

Timchalk, C. and Nolan, R. J., 1997, Pharmacokinetics of triclopyr (3,5,6-trichloro-2-pyridinyloxyacetic acid) in the beagle dog and rhesus monkey: perspective on the reduced capacity of dogs to excrete this organic acid relative to the rat, monkey, and human. *Toxicology and Applied Pharmacology*, **144**, 268–278.

Underwood, D. C., Osborn, R. R., Kotzer, C. J., Adams, J. L., Lee, J. C., Webb, E. F., Carpenter, D. C., Bochnowicz, S., Thomas, H. C., Hay, D. W. P. and Griswold, D. E., 2000, SB 239063, a potent p38 MAP kinase inhibitor, reduces inflammatory cytokine production, airways eosinophil infiltration, and persistence. *Journal of Pharmacology and Experimental Therapeutics*, **293**, 281–288.

Van Hoogdalem, E. J., Soeishi, Y., Matsushima, H. and Higuchi, S., 1997, Disposition of the selective (1A-adrenoceptor antagonist tamsulosin in humans: Comparison of data from interspecies scaling. *Journal of Pharmaceutical Science*, **86**, 1156–1161.

Ward, K. W., Proksch, J. W., Salyers, K. L., Azzarano, L. M., Morgan, J. A., Roethke, T. J., McSurdy-Freed, J. E., Levy, M. A. and Smith, B. R., 2002, SB-242235, a selective inhibitor of p38 mitogen-activated protein kinase. I. Preclinical pharmacokinetics. *Xenobiotica*, **32**, 221–233.

Welling, P. G., 1993, Pharmacokinetic principles. Linear and nonlinear. In P. G. Welling (ed.), *Drug Toxicokinetics* (New York: Marcel Dekker), pp. 19–42.

XENOBIOTICA, 2002, VOL. 32, NO. 4, 251–265

Taylor & Francis
healthsciences

Metabolism and mode of action of *cis*- and *trans*-3-pinanones (the active ingredients of hyssop oil)

K. M. HÖLD, N. S. SIRISOMA, S. E. SPARKS and J. E. CASIDA*

Environmental Chemistry and Toxicology Laboratory, Department of Environmental Science, Policy and Management, 114 Wellman Hall, University of California, Berkeley, CA 94720-3112, USA.

Received 10 July 2001

1. Hyssop oil is an important food additive and herbal medicine and the principal active ingredients are (−)-*cis*- and (−)-*trans*-3-pinanones. No information is available on their metabolism or specific mode of action.

2. The metabolites of *cis*- and *trans*-3-pinanones were examined from mouse and human liver microsomes and human recombinant P4503A4 with NADPH and on administration to mouse by gas chromatography/chemical ionization mass spectrometry comparison with standards from synthesis.

3. The major metabolite of *cis*-3-pinanone in each P450 system and in brain of the i.p.-treated mouse in quantitative studies was 2-hydroxy-*cis*-3-pinanone, and two minor metabolites were hydroxypinanones other than 2-hydroxy-*trans*-3-pinanone and 4S-hydroxy-*cis*-3-pinanone. The urine from oral *cis*-3-pinanone treatment examined on a qualitative basis contained conjugates of metabolites observed in the microsomal systems plus 2,10-dehydro-3-pinanone.

4. *Trans*-3-pinanone was metabolized more slowly than the *cis*-isomer in each system to give hydroxy derivatives different than those derived from *cis*-3-pinanone.

5. *Cis*- and *trans*-3-pinanones and hyssop oil act as γ-aminobutyric acid type A ($GABA_A$) receptor antagonists based on inhibition of 4′-ethynyl-4-*n*-[2,3-$^3H_2$]propylbicycloorthobenzoate ([^{3}H]EBOB) binding in mouse brain membranes (IC_{50} of 35-64 μM) and supported by tonic/clonic convulsions in mouse (i.p. LD_{50} 175 to >250 mg kg^{-1}) alleviated by diazepam. The *cis*-3-pinanone metabolites 2-hydroxy-*cis*-3-pinanone and 2,10-dehydro-3-pinanone exhibit reduced toxicity and potency for inhibition of [^{3}H]EBOB binding.

Introduction

Hyssop oil is produced by steam distillation of the flowers and stalks of *Hyssopus officinalis* L. of the mint family (Lamiaceae). This essential oil is used as a flavouring for foods and liqueurs (Chartreuse and Benedictine) and a component in some perfumes with a spicy odour. It has also been employed for centuries (and possibly millennia) as an herbal medicine claimed to be effective for fever, colds, and liver and gallbladder complaints among a wide variety of problems (Crowfoot and Baldensperger 1932, Blumenthal 1998, Gruenwald *et al*. 1998, Alberta Agriculture 2001, Southall 2001).

Hyssop is 'generally regarded as safe' for food use by the US Food and Drug Administration (Duke 2001) and 'no health hazards are known in conjunction with the proper administration of designated therapeutic doses' (Gruenwald *et al*.

*Author for correspondence; e-mail: ectl@nature.berkeley.edu

Xenobiotica ISSN 0049–8254 print/ISSN 1366–5928 online © 2002 Taylor & Francis Ltd
http://www.tandf.co.uk/journals
DOI: 10.1080/00498250110095745

1998). However, hyssop oil does pose a risk to the central nervous system. An oral dose of 10–30 drops in the adult human or two to three drops in a child over several days resulted in clonic and/or clonic-tonic spasms and 130 mg kg^{-1} i.p. in rat caused similar poisoning signs (Millet *et al.* 1981, Blumenthal 1998, Gruenwald *et al.* 1998). These limited toxicological observations and studies are less than adequate for an important food flavouring and herbal medicine.

The principal constituents of hyssop oil are (−)-*cis*-3-pinanone (cP) and (−)-*trans*-3-pinanone (tP), also known as isopinocamphone and pinocamphone, respectively (figure 1) (Simonsen and Owen 1949, Phytochemical Database 2001). Hyssop oil generally contains more tP than cP (Garg *et al.* 1999, Aqua-Oleum 2000). It is considered a convulsant essential oil with epileptogenic components (Burkhard *et al.* 1999). Hyssop oil, tP and thujone induce the same type of electrocortical seizures associated with myoclonic activities (Millet *et al.* 1981), suggesting that hyssop oil and tP, as with thujone (Höld *et al.* 2000), are non-competitive blockers of the γ-aminobutyric acid (GABA)-gated chloride channel. On this basis, the GABA type A (GABAA) receptor is a candidate target for the action of hyssop oil and the 3-pinanones. The thujone diastereomers also serve as models for the 3-pinanones in another respect, i.e. α- and β-thujones are rapidly metabolized and detoxified by cytochrome P450 (Höld *et al.* 2000, 2001).

The present study takes the first steps in defining the metabolism and mode of action of cP and tP. The data demonstrate that they are metabolized *in vitro* and *in vivo* primarily by cytochrome P450 to a series of hydroxypinanones (quantitated in brain but not in urine, where they appear as conjugates), that they act as blockers of the GABA-gated chloride channel conveniently assayed as inhibition of 4′-ethynyl-4-*n*-[2,3-$^3H_2$]propylbicycloorthobenzoate ([^{3}H]EBOB) binding (Cole and

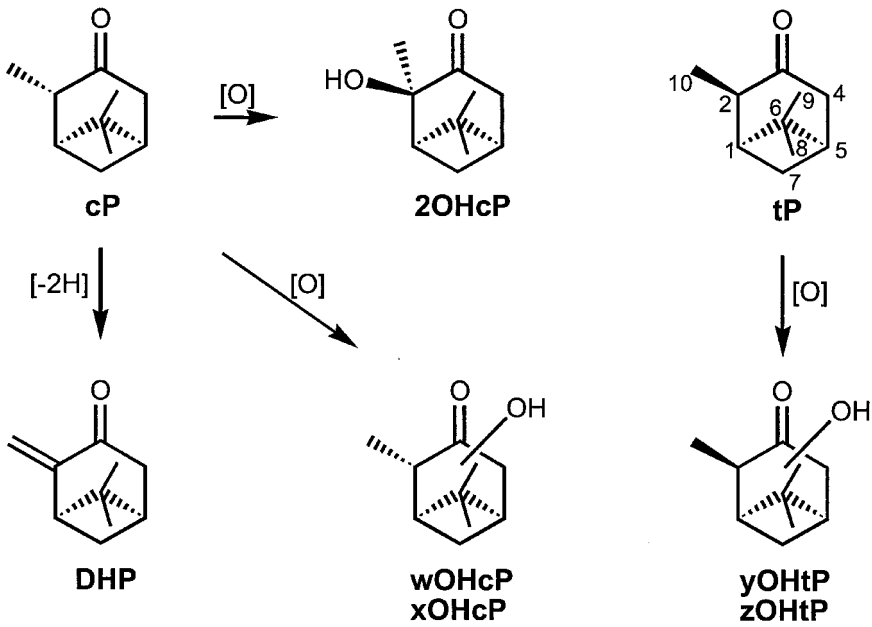


Figure 1. Partial metabolic pathways for *cis*-3-pinanone (cP) and *trans*-3-pinanone (tP). Metabolites are designated by the position of hydroxylation (2OHcP or unspecified for wOHcP, xOHcP, yOHtP and zOHtP) or dehydrogenation (DHP).

Casida 1992), and that metabolism is probably a detoxification process relative to their action at the GABAA receptor.

Materials and methods

Chemicals

Hyssop oil. The hyssop oil used was from steam-distilled flowering tops of *H. officinalis* var. *decumbens* grown in Switzerland and purchased from Lhasa Karnak Herb Co. (Berkeley, CA, USA).

General procedures. Preparation of cP, epi-cP, tP, and their hydroxy and dehydro derivatives involved procedures shown in figure 2 and described below. The products were purified by silica gel chromatography and characterized by ^{1}H-NMR (table 1), ^{13}C NMR (table 2) and GC/MS (table 3), which also established a purity in each case of 98–100%.

cP and epi-cP. cP was more easily obtained pure by oxidation of (+)-isopinocampheol (Aldrich, Milwaukee, WI, USA) than by chromatography of hyssop oil. Thus, pyridinium dichromate (1700 mg, 4.51 mmol) was added to (+)-isopinocampheol (500 mg, 3.24 mmol) dissolved in methylene chloride (5 ml) (Corey and Schmidt 1979). The reaction mixture was stirred overnight at room temperature, diluted with diethyl ether (50 ml), filtered through silica gel and the filtrate washed with 5% hydrochloric acid (50 ml), water (50 ml) and saturated sodium chloride (50 ml). The organic layer was dried (anhydrous magnesium sulphate) and chromatographed on a silica gel column using 5% ethyl acetate in hexane to obtain cP (482 mg, 3.2 mmol, 98%). (−)-Isopinocampheol (Aldrich) was converted to epi-cP in an analogous manner. As expected (Simonsen and Owen 1949), cP from both hyssop oil and the synthetic sample were observed to be levorotatory, whereas epi-cP was dextrorotatory.

tP. A cP/tP 1 : 2 diastereomeric mixture was used as the starting material rather than the more complex hyssop oil. This mixture was obtained by epimerizing cP to tP (using sodium methoxide in methanol) then conversion to the corresponding ketals (Satterwhite and Croteau 1987), leading to the observation that the ketal with (2*R*, 3*R*)-2,3-butanediol forms much more rapidly with cP than tP. The resulting reaction mixture greatly enriched in tP versus cP was chromatographed using 1–2% diethyl ether in hexane to elute (in sequence) cP-ketal, tP and cP.

Enol and epoxy acetates. The hydroxypinanones were prepared via the enol and epoxy acetates. To obtain the enol acetates, cP (1000 mg, 6.57 mmol) in isopropenyl acetate (6 ml) was treated with p-toluenesulphonic acid (54 mg, 0.32 mmol) and refluxed for 3 days. The reaction mixture was concentrated and chromatographed using 1–4% ethyl acetate in hexane to recover a non-resolved mixture (860 mg, 67%) of 56% 2,3-enol acetate and 14% 3,4-enol acetate by GC/MS analysis. To obtain the epoxy acetates, a solution of *m*-chloroperbenzoic acid (1.0 g, 75% pure, 4.4 mmol) in chloroform (8 ml) was added to a solution of the above enol acetates (800 mg, 4.11 mmol) in chloroform (8 ml) at 0°C. The mixture was stirred at 0°C for 0.5 h then another portion of *m*-chloroperbenzoic acid (500 mg) was added and warmed to room temperature with continued stirring for 3 h. The reaction mixture was diluted with ethyl acetate (100 ml) and washed in sequence with 5% sodium bisulphite (50 ml), 5% sodium bicarbonate (50 ml) and saturated sodium chloride (50 ml). The organic layer was dried, concentrated and chromatographed using 7% ethyl acetate in hexane to obtain the 2,3- and 3,4-epoxy acetates (852 mg, 4.1 mmol, 98%) as a mixture.

2-Hydroxy-cis-*3-pinanone (2OHcP) and (4S)-hydroxy*-cis-*3-pinanone (4SOHcP).* The epoxy acetates (210 mg, 1.0 mmol) were dissolved in absolute methanol (10 ml) and sodium methoxide (0.1 mmol in methanol) was added at room temperature. The rearrangement was complete after 2 h. A few drops of water were added then most of the solvent evaporated under vacuum and the residue dissolved in ethyl acetate (25 ml) and washed with water (25 ml) and saturated sodium chloride (25 ml). The organic layer was dried and concentrated to an oily residue that was chromatographed using 3–5% ethyl acetate in hexane to obtain 2OHcP (more polar product, 128 mg, 0.76 mmol) (Suga *et al.* 1968, Curci *et al.* 1993) and 4SOHcP (less polar product, 26 mg, 0.15 mmol).

2-Hydroxy-trans-*3-pinanone (2OHtP).* The mixture of epoxy acetates (120 mg, 0.57 mmol) in a 1 ml round-bottomed flask was heated at 170°C in an oil bath for 0.5 h. After cooling, the reaction mixture was chromatographed using 4–6% ethyl acetate in hexane to obtain 2-acetoxy-tP (68 mg, 0.32 mmol,

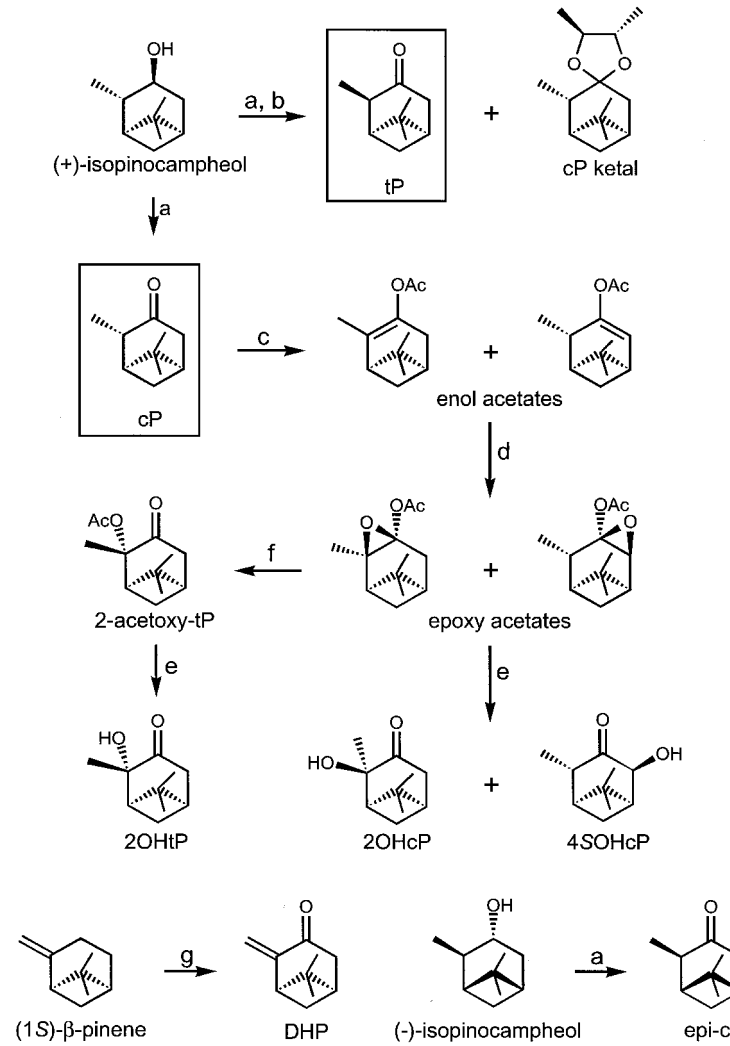


Figure 2. Procedures for preparation of 3-pinanone isomers and their hydroxy and dehydro derivatives. (a) Pyridinium dichromate, CH_2Cl_2, 25°C, (b, i) NaOMe, MeOH, 25°C, (b, ii) (2*R*, 3*R*)-(−)-2,3-butanediol, trimethylsilyl chloride, MeOH, 25°C (tP does not form the ketal so with a derivatized cP/tP mixture the unreacted tP is recovered by column chromatography), (c) isopropenyl acetate, anhydrous p-toluenesulphonic acid, 110°C, (d) *m*-chloroperbenzoic acid, $CHCl_3$, 0–25°C, (e) NaOMe, MeOH, 25°C, (f) neat, 140°C, (g) *tert*-butyl hydroperoxide, SeO_2, CH_2Cl_2, 25°C.

56%) as the major product. The acetate group was removed by treating with sodium methoxide in methanol as above and the crude product was chromatographed using 15% ethyl acetate in hexane to obtain 2OHtP (50 mg, 0.30 mmol, 94%).

2,10-Dehydro-3-pinanone (DHP). (1S)-β-pinene (Aldrich) (200 mg, 1.3 mmol) was dissolved in methylene chloride (3 ml) and selenium dioxide (6 mg, 0.054 mmol) was added followed by *tert*-butyl hydroperoxide (3 ml, 90% pure). The reaction was stirred for 1 day at room temperature. Hexane (50 ml) was then added and the mixture washed with 10% potassium carbonate (30 ml) and saturated sodium chloride (30 ml), dried over magnesium sulphate, filtered and concentrated. The oily residue was chromatographed using 3% ethyl acetate in hexane to obtain the enone DHP (180 mg, 1.21 mmol, 91%) (Mazzega *et al.* 1999).

Table 1. ^{1}H-NMR (300 MHz) data [δ, $\mathcal{J}$(Hz)] in $CDCl_3$

Hydrogen[a]	cP[b]		tP[b]		2OHcP[c]		2OHtP[d]		4*S*OHcP		DHP[e]	
1	2.05	dt (2.1, 6.2)	1.90	dt (2.6, 6.2)	2.62	m	2.63	m	1.94	dt (1.5, 6.2)	2.52	d (3.0)
2	2.62	m	2.60	m	–		–		2.79	m	–	
4a	2.52	m	2.40	m	2.11	m	2.13	m	2.25	m	2.18	m
4s	2.62	m	2.62	m	2.62	m	2.61	m	–		2.60	m
5	2.12	m	2.09	m	2.11	m	2.13	m	2.27	m	2.60	m
7a	1.18	d (10.3)	1.14	d (11.3)	1.69	d (11.3)	2.61	d (11.3)	1.12	d (10.3)	1.27	d (10.3)
7s	2.45	m	2.45	m	2.45	m	2.61	m	2.36	m	2.60	m
8	1.30	s	1.31	s	1.37	s	1.28	s	1.39	s	1.34	s
9	0.87	s	0.87	s	0.89	s	0.95	s	1.00	s	0.78	s
10	1.20	d (7.2)	1.10	d (7.2)	1.38	s	1.32	s	1.12	d (7.2)	4.98 5.93	d (1.5) d (1.5)
OH	–		–		2.37		2.80		3.04		–	

[a] For numbering, see figure 1.
[b] Assignment based on Badjah-Hadj-Ahmed *et al.* (1992).
[c] Assignment based on Solladié-Cavallo *et al.* (1994).
[d] Assignment based on Carlson and Pierce (1971).
[e] Assignment based on Mazzega *et al.* (1999).
s, Singlet; d, doublet; dt, double triplets; m, multiplet.

Table 2. ^{13}C-NMR (75 MHz) data (δ) in $CDCl_3$.

Carbon	cP[a]	tP[a]	2OHcP[b]	2OHtP[c]	4*S*OHcP	DHP[d]
CH_3	16.8	15.0	22.8	22.6	14.3	21.5
	21.9	19.7	25.3	27.0	19.3	26.0
	27.0	26.3	27.3	31.1	26.6	
CO	214.9	215.2	213.9	216.7	215.9	199.7
CHOH	–	–	77.1	79.0	76.9	-
Other	34.3	29.1	28.4	25.8	25.6	32.4
	39.0	38.4	38.4	39.0	40.2	38.6
	39.2	39.4	39.3	39.5	44.7	40.7
	44.7	44.3	42.9	43.2	44.9	42.4
	45.1	44.5	49.7	50.0	46.2	48.3
	51.3	46.4				117.2
						149.1

[a] Assignment based on Badjah-Hadj-Ahmed *et al.* (1992).
[b] Assignment based on Solladié-Cavallo *et a*l. (1994).
[c]Assignment based on Carlson and Pierce (1971).
[d] Assignment based on Mazzega *et al.* (1999).

GC/MS analysis

Using a previously described procedure (Höld *et al.* 2001) and briefly restated here, an HP5890 gas chromatograph equipped with a DB-5 fused silica gel capillary column (30 m, 0.25 mm i.d., 0.25 µm film thickness) coupled to the HP5971 mass selective detector was used in the positive chemical ionization mode. Helium was employed as the carrier gas and methane as the reagent gas at a flow rate of 0.8 ml min^{-1}. The temperature programme was first 80 to 200°C at 5°C min^{-1} and then 200 to 300°C at 20°C min^{-1}, holding this final temperature for 2 min. The injection port was at 250°C and the detector at 280°C. The GC/MS was operated both in the full-scan and selected ion-monitoring (SIM) modes, measuring m/z 135 for cP or 109 for tP (table 3) with α-thujone as the internal standard (m/z 135) and m/z 151 for DHP and hydroxy-3-pinanones (table 3) with 7-hydroxy-α-thujone (m/z 151) (Sirisoma *et al.* 2001) as the internal standard. Trimethylsilyl (TMS) ethers were formed by adding *N*-(trimethylsilyl)trifluoroacetamide (50 µl) to the extract residue and heating for 30 min at 80°C (Höld *et al.* 2000, 2001). In each type of analysis, a sample aliquot of 1.0µl was injected splitless onto the column.

cP and epi-cP were analysed as their ketals formed with (2*R*,3*R*)-2,3-butanediol as described by Satterwhite and Crotean (1987) for stereochemical assignment of the *cis*-pinanone fraction from hyssop oil. Epi-cP was prepared for this purpose from (−)-isopinocampheol (Aldrich) by the procedure above for conversion of (+)-isopinocampheol to cP.

Metabolism in cytochrome P450 (P450) systems

Mouse liver microsomes (10 000g supernatant, 100 000g pellet) prepared from a 20% (w/v) homogenate in phosphate buffer (100 mM, pH 7.4) were washed once with phosphate buffer and suspended in 0.25 M sucrose, 20 mM Tris, and 5.4 mM EDTA (pH 7.4). Other P450 sources were pooled human microsomes and human P4503A4 Supersomes (Gentest, Woburn, MA, USA). The preparations were stored frozen at −80°C.

Liver microsomes (1 mg protein, 1.1 and 0.49 nmol P450 for mouse and human, respectively) or P4503A4 (0.15 mg protein, 0.10 nmol P450) and NADPH (0 or 1 mM final concentration) were incubated with cP or tP (30 µg added in ethanol, final concentration 0.2 µM) in 100 mM phosphate, pH 7.4, buffer (1 ml) for 1 h at 37°C. Each reaction mixture was then cooled on ice, saturated with sodium chloride and extracted with ethyl acetate (3 ml). The ethyl acetate phase was evaporated to 200 µl for analysis of a 1.0-µl aliquot.

Table 3. GC t_R and postulated MS fragmentation patterns for 3-pinanones and their metabolites and derivatives.

Compound[a]	t_R (min)	m/z of protonated molecular ions and major fragments and their relative abundances				
		$[MH]^+$	$[MH\text{-}H_2O]^+$	$[MH\text{-}H_2O\text{-}CO]^+$	$[MH\text{-}H_2O\text{-}C_3H_6]^+$	Other
3-Pinanones and 2,10-dehydro-3-pinanone						
cP[b]	6.7	153(23)	135(100)		93(82)	109(23)
tP[b]	6.4	153(18)	135(26)		93(13)	109(100)
DHP						
Standard	6.6	151(100)				135(7);123(3);109(10)
Metabolite[c]	6.6	151(100)				135(7);123(5);109(12)
Hydroxy-3-pinanones						
2OHcP						
Standard	8.3	169(4)	151(100)	123(22)	109(89)	95(22)
Metabolite[c]	8.3	169(4)	151(100)	123(22)	109(86)	95(22)
4*S*OHcP	8.6	169(19)	151(65)	123(100)	109(47)	83(35)
wOHcP	9.6	169(4)	151(60)	123(100)	109(15)	
xOHcP	10.6	169(39)	151(70)	123(55)	109(58)	113(100)
2OHtP	7.6	169(3)	151(100)	123(9)	109(55)	
yOHtP	9.6	169(4)	151(100)	123(43)	109(16)	
zOHtP	10.1	169(33)	151(47)	123(53)	109(9)	113(100)
		$[MH]^+$	$[MH\text{-}CH_4]^+$	$[MH\text{-}TMSOH]^+$	$[MH\text{-}TMSOH\text{-}C_3H_6]^+$	Other
Trimethylsilyl derivatives						
2OHcP						
Standard	11.5	241(20)	225(97)	151(100)	109(53)	123(19)
Metabolite[c]	11.5	241(21)	225(93)	151(100)	109(56)	123(19)
4*S*OHcP	11.4	241(18)	225(100)	151(53)	109(32)	123(58)
wOHcP	12.9	241(100)	225(39)	151(29)		169(19);123(40)
xOHcP	11.4	241(18)	225(90)	151(100)	109(71)	123(22)
2OHtP	11.4	241(5)	225(100)	151(96)	109(81)	123(17)
yOHtP	12.3	241(100)	225(53)	151(100)	109(17)	169(36);123(38)
zOHtP	13.3	241(100)	225(43)	151(34)		169(31);123(43)

[a]Structures or compound types are given in figures 1 and 2.
[b]Fragmentation patterns of cP and tP were analysed according to Youssefi *et al.* (1994).
[c]DHP from urine of the cP-treated mouse and 2OHcP from incubation of cP with mouse microsomes and NADPH.

Animal treatment

Male albino Swiss-Webster mice (25–30 g) (Harlan, Indianapolis, IN, USA) were maintained under standard conditions of controlled light (12 h light-dark cycle), temperature (20–22°C) and relative humidity (50–55%) with access to food and water *ad libitum*. The studies were carried out in accordance with the *Guiding Principles in the Use of Animals in Toxicology* as adopted by the Society of Toxicology in 1989 and were approved before commencement by the Animal Care and Use Committee of the University of California at Berkeley.

Metabolites in the brain

Mice were treated i.p. with cP at 250 mg kg^{-1} in propylene glycol (2 µl g^{-1} mouse) and at appropriate times thereafter the animals were killed and whole brains removed for analysis. The brains were rinsed and homogenized in 100 mM phosphate, pH 7.4, buffer (10 ml). α-Thujone (0.5 µg) and 7-hydroxy-α-thujone (2.0 µg) were added as internal standards. After centrifugation (1500g, 10 min), the pellet was resuspended in 2 ml phosphate buffer, sonicated for 1 min and centrifuged, and the supernatant fractions were combined. The samples were extracted with ethyl acetate (6 ml) and analysed as with the extracts of microsomal incubations. Quantitation was based on standard curves for cP and 2OHcP corrected for recoveries by the use of internal standards (α-thujone for cP and 7-hydroxy-α-thujone for 2OHcP). Mice administered tP at 250 mg kg^{-1} were analysed the same way at 40 min after treatment.

Metabolites in the urine of mouse

Mice, as above, were treated orally with cP (100 mg kg^{-1}) in propylene glycol (2 µl g^{-1} mouse) and individually housed in all glass metabolism cages (Minor Metabowl, Jencons, Leighton Buzzard, UK). Urine was collected for 24 h, an aliquot (1 ml) mixed with 200 mM phosphate, pH 7.0, buffer (1 ml), saturated with sodium chloride and extracted with ethyl acetate (4 ml). The unconjugated metabolites in the ethyl acetate extract were analysed directly by GC/MS and the conjugate fraction in the aqueous phase was treated with β-glucuronidase/arylsulphatase as described (Höld *et al.* 2001) then analysed following deconjugation. Urine from the untreated mouse was used as a control but no interfering peaks were observed.

Inhibition of [^{3}H]EBOB binding

GABA-depleted mouse brain membranes (200 µg protein) (Cole *et al.* 1984) were incubated with the test compound (added in dimethyl sulphoxide, final concentration 1%) and [^{3}H]EBOB (0.7 nM) (38 Ci $mmol^{-1}$; NEN Life Science Products, Boston, MA, USA) in 1.0 ml phosphate buffer (10 mM, pH 7.5) containing 200 mM sodium chloride for 70 min at 37°C (Cole and Casida 1992). The mixtures were then filtered through GF/C glassfibre filters using a cell harvester, followed by two rinses with 5 ml ice-cold 0.9% sodium chloride. Specific binding was defined as the difference between total binding and non-specific binding determined in the presence of 5 µM α-endosulphan.

Toxicity to mouse

Mice, as above, were treated i.p. with the test compound dissolved in dimethyl sulphoxide (2–3 µl g^{-1} mouse) for observation of poisoning signs shortly after treatment and mortality at 24 h. Alternatively, mice were treated with diazepam (0 or 1 mg kg^{-1}) in dimethyl sulphoxide (2 µ g^{-1} mouse) and 15 min later with cP or hyssop oil at an approximate LD_{50} dose (200 mg kg^{-1}) for observation of poisoning signs and mortality.

Results

Analysis of hyssop oil and stereochemical assignment of 3-pinanones

The two principal constituents of the hyssop oil examined (66 and 22% of the total peak area at t_R 6.7 and 6.4 min, respectively) were identical in t_R and MS fragmentation patterns to cP prepared by oxidation of (+)-isopinocampheol and tP from epimerization of this synthetic cP sample, respectively (table 3). cP (both as a synthetic standard and as a constituent of hyssop oil), on conversion to the ketal with (2*R*, 3*S*)-2,3-butanediol (figure 2), gave $t_R = 11.3$ min with no peak at 11.0 min (as would be the case for epi-cP), which confirms the stereochemical assignment and enantiomeric purity of cP in hyssop oil.

GC/MS analysis of 3-pinanones and their metabolites and derivatives

Table 3 gives t_R and protonated molecular ions and major fragments with their relative abundances for each of the standards and metabolites. tP and cP are easily differentiated by t_R and relative abundances of their fragments at m/z 135, 109 and 93. DHP is baseline separated from tP and can be analysed in the presence of tP and cP by $[MH]^+$ at m/z 151 versus 153. Seven hydroxy-3-pinanones were analysed as standards or metabolites, four derived from cP and three from tP. Each hydroxy-3-pinanone gives a small protonated molecular ion and fragments as follows (m/z, relative abundance): $[MH]^+$ 169 (3–39), $[MH\text{-}H_2O]^+$ 151 (47–100), $[MH\text{-}H_2O\text{-}CO]^+$ 123 (9–100) and $[MH\text{-}H_2O\text{-}C_3H_6]^+$ 109 (9–89). The base peaks for xOHcP and zOHtP appear at m/z 113. Corresponding values for the trimethylsilyl derivatives are $[MH]^+$ 241 (5–100), $[MH\text{-}CH_4]^+$ 225 (39–100), [MH-TMSOH]$^+$ 151 (29–100), [MH-TMSOH-C_3H_6]$^+$ 109 (17–81 except for wOHcP and zOHtP) and other fragments at 169 (19–36 when present) and 123 (17–58).

Compounds identified as metabolites (DHP and 2OHcP) and the trimethylsilyl derivative of 2OHcP are identical to the standards in t_R and give essentially the same fragmentation patterns (table 3).

Metabolism of cis- *and* trans-*3-pinanones in cytochrome P450 systems*

cP and tP are stable on incubation with mouse or human liver microsomes or human P4503A4 but are metabolized (except for tP with P4503A4) when NADPH is added, with the extent of metabolism decreasing in the indicated order for P450 source (table 4). cP is much more extensively metabolized than tP in each system (figure 3, A and B). In every case there is a single major metabolite and one or two minor metabolites, each at longer t_R than the parent compound (figure 3, A and B, and table 4). The major metabolite of cP is identical in GC and MS features when analysed directly and as the trimethylsilyl derivative to synthetic 2OHcP (table 3) and the minor metabolites (wOHtP and xOHtP) differ in chromatographic properties and fragmentation patterns from synthetic standards of 4SOHcP and

Table 4. Metabolism of *cis*- and *trans*-3-pinanones in cytochrome P450 systems.

Substrate and products[a]	Relatively peak area (%)[b]		
	Mouse microsomes	Human microsomes	Human P4503A4
Cis-3-pinanone			
cP	43 ± 1	76 ± 13	94 ± 3
2OHcP	55 ± 5	18 ± 6	5 ± 1
wOHcP, xOHcP[c]	2 ± 4	6 ± 7	<1
Trans-3-Pinanone			
tP	86 ± 14	92 ± 7	100
yOHtP	3 ± 1	1 ± 1	<1
zOHtP	11 ± 14	7 ± 6	<1

[a] See figure 1 for structures and abbreviations.

[b] Area as total ion current of the indicated peak relative to that for the sum of all peaks (mean ± SD, n = 3). All metabolism was dependent on NADPH.

[c] wOHcP and xOHcP appear as approximately equal peak areas.

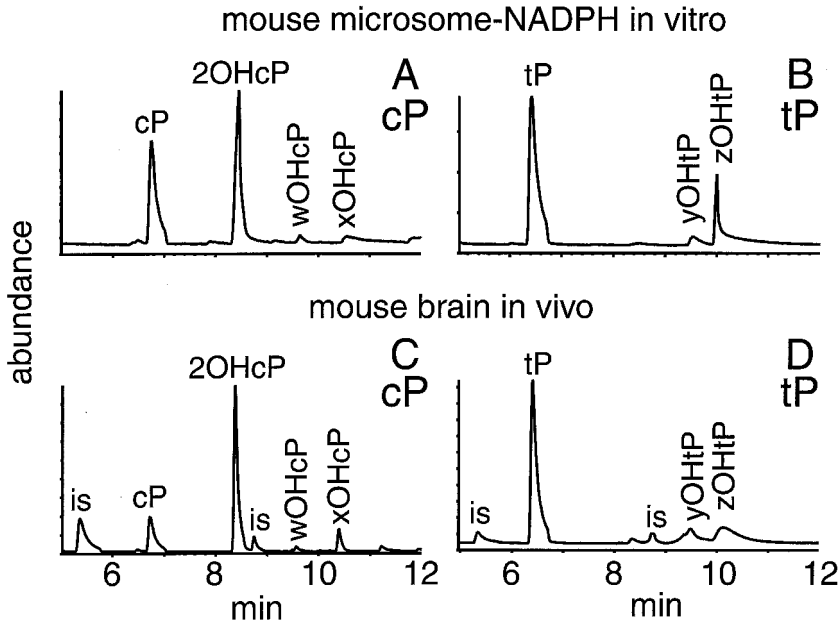


Figure 3. Representative GC/MS chromatograms for *cis*-3-pinanone (cP) and *trans*-3-pinanone (tP) and their metabolites (OHcP, OHtP) extracted from the mouse liver microsome-NADPH system and the brain of the treated mouse (250 mg kg^{-1}, i.p.; 40 min after treatment). (A) cP substrate, total ion current; (B) tP substrate, total ion current; (C) cP treatment, SIM at m/z 151 and 135, internal standard (is) α-thujone at 5.4 min and 7-hydroxy-α-thujone at 8.7 min; (D) tP treatment, SIM at m/z 151 and 109, internal standards as in (C). All metabolites fall within the chromatographic region shown. See figure 1 for structures and abbreviations.

2OHtP. The hydroxypinanone metabolites of tP (yOHtP and zOHtP) were not identified.

Metabolites of cis- *and* trans-*3-pinanones in the brain of mouse*

GC/MS analysis of the brain of mouse treated with cP reveals the parent compound, a single major metabolite and two minor metabolites (figure 3, C). The major metabolite is identified as 2OHcP by t_R and MS fragmentation pattern, both directly and as the trimethylsilyl derivative. The two minor hydroxypinanones in brain, although not identified, are the same ones (wOHcP and xOHcP) observed in the cytochrome P450 systems (figure 3, A and C). In a study relating brain levels to the time after treatment, the parent compound drops to about half its maximum amount in 10–20 min when 2OHcP reaches its maximum level (figure 4). The minor hydroxy metabolites (wOHcP and xOHcP) increase in amount up to 40–80 min. The mouse at this 250 mg kg^{-1} dose of cP with propylene glycol as the treatment vehicle exhibit neurological poisoning signs throughout the 80-min experimental period.

The level of cP in brain for the first 10 min after treatment greatly exceeds that of the hydroxypinanone metabolites whereas with α-thujone the 7-hydroxy metabolite during this period is at a much higher level than the parent compound (figure 4) (Höld *et al.* 2000).

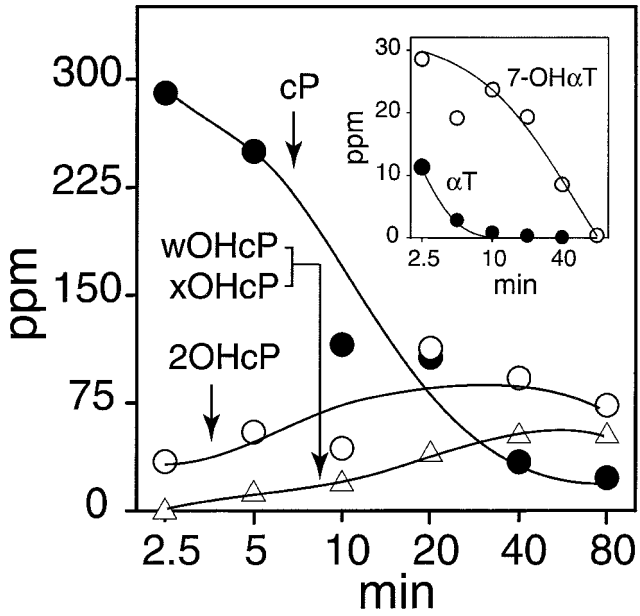


Figure 4. Brain levels of *cis*-3-pinanone (cP) and metabolites (2OHcP, wOHcP, xOHcP) as a function of time following i.p. treatment with cP at 250 mg kg^{-1}. The curve for minor metabolites wOHcP and xOHcP is based on the response factor for 2OHcP and because of their small amounts are increased by a factor of 5 for plotting. The insert figure shows corresponding data for α-thujone (αT) and its principal metabolite 7-hydroxy-α-thujone (7OHαT) after i.p. treatment with α-thujone at 50 mg kg^{-1} (Höld *et al.* 2000). Each datum point is the average of determinations on two mice.

tP was also administered i.p. at 250 mg kg^{-1} and the brain analysed 40 min after treatment. The principal GC peaks were identical to those for the P450 metabolites yOHtP and zOHtP (figure 3, B and D).

Metabolites of cis*-3-pinanone in the urine of mouse*

The urine, 18 h after oral treatment of mouse with cP at 100 mg kg^{-1}, contains DHP in the free but not the conjugate fraction with the same t_R and almost identical MS fragmentation pattern to the standard from synthesis (table 3). The three hydroxypinanones (2OHcP, wOHcP, xOHcP) noted above for cytochrome P450 systems *in vitro* and brain *in vivo* are also apparent in urine, but only in the conjugate fraction and not free. An additional metabolite appears as a major product in the free fraction of urine and the observed m/z 167 suggests that it may be an aldehyde. It is very minor or absent in the brain or cytochrome P450 systems examined.

Inhibition of [^{3}H]EBOB binding

The IC_{50} of hyssop oil and 3-pinanone isomers and derivatives for inhibiting [^{3}H]EBOB binding in mouse brain membranes increase in the order of cP and tP (35–36 μM), hyssop oil (64 μM), and DHP and 2OHcP (each 285 μM) (figure 5 and

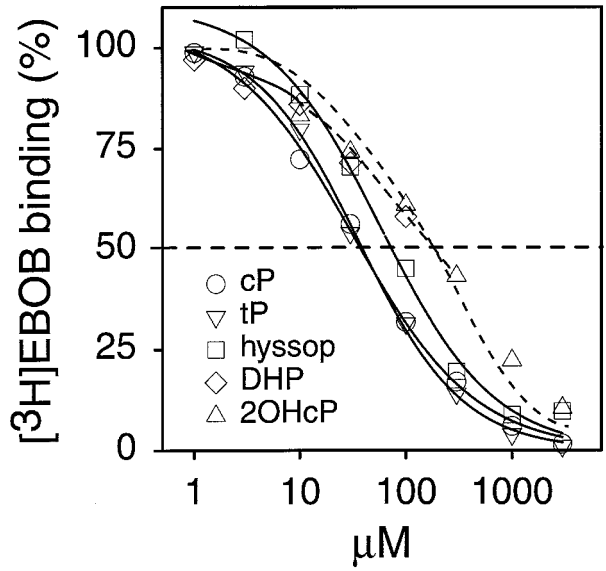


Figure 5. Inhibition of [^{3}H]EBOB binding in mouse brain membranes by hyssop oil and 3-pinanone isomers, metabolites and analogues. See figure 1 for structures and abbreviations. Data shown are derived from three determinations.

Table 5. Activities of hyssop oil and 3-pinanone isomers and derivatives as inhibitors of [^{3}H]EBOB binding and toxicants in mouse.

Compound	IC_{50} (μM)[a]	LD_{50} (mg kg^{-1})[b]
Hyssop oil and constituents		
Hyssop oil	64 ± 14	235
cP	36 ± 9	175
tP	35 ± 2	>250
Dehydro and hydroxy derivatives		
DHP	285[c]	>250
2OHcP	285 ± 48	250
2OHtP	1000[d]	–

[a] Mean ± SEM ($n = 4$). Hyssop oil is calculated as the molecular weight of 3-pinanone.
[b] I.p. treatment as 25% solution (w/v) in dimethyl sulphoxide.
[c] Extrapolation from 42% inhibition at the highest test concentration of 100 μM (solubility limitation) (figure 5).
[d] Highest test concentration of 1000 μM gave a 50% inhibition.

table 5). Although not a metabolite, 2OHtP gives an $IC_{50} = 1000\,\mu M$. For comparison, the IC_{50} of other monoterpenes is 13 μM for α-thujone and 29 μM for β-thujone (Höld *et al.* 2001) and 300–1000 μM for D- and L-camphor, fenchone and 1,8-cineole (also found in hyssop oil).

Toxicity in mouse

cP was more toxic than tP on i.p. administration to mouse with $LD_{50} = 175$ and $>250\,mg\,kg^{-1}$, respectively, consistent with cP being the principal acute

toxicant in the hyssop oil examined ($LD_{50} = 235\,mg\,kg^{-1}$) (table 5). Mouse treated i.p. with cP or hyssop oil at an LD_{50} dose exhibit neurological signs 1–2 min post-injection, manifested as tail-raising and forelimb paddling, followed by intermittent periods of dorsal and lateral trunk flexing and opisthotonos, progressing to generalized and unremitting convulsions with running, hopping, chattering and eventual death after 60–90 min or recovery from poisoning. DHP and 2OHcP were only slightly less toxic ($LD_{50} \geq 250\,mg\,kg^{-1}$).

Mouse treated with diazepam ($1\,mg\,kg^{-1}$) and 15 min later with cP or hyssop oil at the approximate LD_{50} dose (which caused neurological signs as above when administered alone) exhibited depression only and appeared to have recovered after 1 h.

Discussion

The current understanding of the metabolic fate of cP and tP is summarized in figure 1. 2OHcP is the principal metabolite of cP in P450 systems and mouse brain and it also appears as a conjugate (glucuronide or sulphate) in mouse urine. Two minor cP metabolites are hydroxypinanones (wOHcP and xOHcP with the positions of hydroxylation not identified) again appearing in P450 systems, brain and as conjugates in urine. DHP is present in urine but is not detected in P450 systems as was also the case for 7,8-dehydro-α-thujone as an α-thujone metabolite (Hold *et al.* 2001). The first steps have also been taken in comparing the metabolism of tP with that of cP. tP is converted to one principal hydroxypinanone (yOHtP) and a minor hydroxypinanone (zOHtP) in P450 systems and brain, with no common metabolite from cP and tP as currently understood. In each system examined, cP is much more extensively metabolized than tP, and correspondingly tP is more persistent. This may be due in part to the 2-position being more sterically protected in the *trans*- than the *cis*-isomer. Studies on the fate of other monoterpenes (Ishida *et al.* 1981, 1989, Scheline 1991, Höld *et al.* 2000, 2001) are relevant to the site specificity in oxidation and nature of the terminal metabolites of the 3-pinanones.

Three lines of evidence indicate that the toxicity of cP, tP and hyssop oil results from blocking the GABA-gated chloride channel. First, the similar potency of cP and tP in the [^{3}H]EBOB assay indicates their action at the non-competitive blocker site of the GABAA receptor. Next, the poisoning signs are the same as those of picrotoxinin, the classical chloride channel blocker, and of α-thujone and a variety of other 'small cage convulsants' (Casida *et al.* 1976, Höld *et al.* 2000). Finally, as with picrotoxinin and other GABAA receptor antagonists (Costa *et al.* 1975, Klaassen 2001), the GABAA receptor modulator diazepam greatly ameliorates the poisoning with life-sparing action.

The 2OHcP and DHP metabolites of cP are clearly detoxification products relative to cP based on reduced potency at the [^{3}H]EBOB binding site and they are also of lower i.p. toxicity to mouse. While not metabolites in systems examined here, 2OHtP and 4SOHcP are also of low activity in the [^{3}H]EBOB assay. This parallels the findings on α- and β-thujone metabolism where all of the hydroxy metabolites and 7,8-dehydrothujone are less potent inhibitors of [^{3}H]EBOB binding than the parent compounds (Höld *et al.* 2000, 2001).

The main constituent of hyssop oil may be either cP or tP depending on the source and purification. The present study indicates that these isomeric 3-pinanones are

of similar potency at the GABAA receptor with the *trans*- metabolized more slowly. cP is more toxic than tP on i.p. administration to mouse and appears to be the principal acute toxicant in the hyssop oil examined here

Acknowledgements

The work was supported by Grant R01 ES08419 from the National Institute of Environmental Health Sciences, NIH, and its contents are solely the responsibility of the authors and do not necessarily represent the official views of the NIEHS, NIH. They thank Gary Quistad of this laboratory for helpful suggestions. The first two authors contributed equally to the study.

References

Alberta Agriculture, 2001, Medicinal, culinary and aromatic crops. Food and rural development website [http://www.agric.gov.ab.ca/crops/special/hyssop.html].

Aqua-Oleum, 2000, Hyssop oil [http://www.aqua-oleum.co.uk/essentials/long/hyssop.htm].

Badjah-Hadj-Ahmed, A. Y., Meklati, B. Y., Waton, H. and Pham, Q. T., 1992, Structural studies in the bicyclo[3.1.1]heptane series by ^{1}H and ^{13}C NMR. *Magnetic Resonance Chemistry*, **30**, 807–816.

Blumenthal, M. (ed.), 1998, *The Complete German Commission E Monographs: Therapeutic Guide to Herbal Medicines* (Austin: American Botanical Council), pp. 338–339.

Burkhard, P. R., Burkhardt, K., Haenggeli, C. A. and Landis, T., 1999, Plant-induced seizures: reappearance of an old problem. *Journal of Neurology*, **246**, 667–670.

Carlson, R. G. and Pierce, J. K., 1971, The synthesis and stereochemistry of the four isomeric pinane-2,3-diols. *Journal of Organic Chemistry*, **36**, 2319–2324.

Casida, J. E., Eto, M., Moscioni, A. D., Engel, J. L., Milbrath, D. S. and Verkade, J. G., 1976, Structure-toxicity relationships of 2,6,7-trioxabicyclo[2.2.2]octanes and related compounds. *Toxicology and Applied Pharmacology*, **36**, 261–279.

Cole, L. M. and Casida, J. E., 1992, GABA-gated chloride channel: binding site for 4′-ethynyl-4-*n*-[2,3-$^{3}H_2$propylbicycloorthobenzoate ([^{3}H]EBOB) in vertebrate brain and insect head. *Pesticide Biochemistry and Physiology*, **44**, 1–8.

Cole, L. M., Lawrence, L. J. and Casida, J. E., 1984, Similar properties of [^{35}S]*t*-butylbicyclophosphorothionate receptor and coupled components of the GABA receptor–ionophore complex in brains of human, cow, rat, chicken and fish. *Life Sciences*, **35**, 1755–1762.

Corey, E. J. and Schmidt, G., 1979, Useful procedures for the oxidation of alcohols involving pyridinium dichromate in aprotic media. *Tetrahedron Letters*, 399–402.

Costa, E., Guidotti, A., Mao, C. C. and Suria, A., 1975, New concepts on the mechanism of action of benzodiazepines. *Life Sciences*, **17**, 167–186.

Crowfoot, G. M. and Baldensperger, L., 1932, *From Cedar to Hyssop: A Study in the Folklore of Plants in Palestine* (London: Sheldon and New York: Macmillan), pp. 71–78.

Curci, R., Daccolti, L., Detomaso, A., Fusco, C., Takeuchi, K., Ohga, Y., Eaton, P. E. and Yip, Y. C., 1993, Selective oxidation of tertiary-secondary *vic*-diols to α-hydroxy ketones by dioxiranes. *Tetrahedron Letters*, **34**, 4559–4562.

Duke, J. A., 2001, Syllabus of a mini-course in medical botany. Module 19 [http://www.ars-grin.gov/duke/syllabus/gras.htm].

Garg, S. N., Naqvi, A. A., Singh, A., Ram, G. and Kumar, S., 1999, Composition of essential oil from an annual crop of *Hyssopus officinalis* grown in Indian plains. *Flavour and Fragrance Journal*, **14**, 170–172.

Gruenwald, J., Brendler, T. and Jaenicke, C. (eds), 1998, *PDR for Herbal Medicines* (Montvale: Medical Economics), pp. 908–909.

Höld, K. M., Sirisoma, N. S. and Casida, J. E., 2001, Detoxification of α- and β-thujones (the active ingredients of absinthe): Site specificity and species differences in cytochrome P450 oxidation *in vitro* and *in vivo*. *Chemical Research in Toxicology*, **14**, 589–595.

Höld, K. M., Sirisoma, N. S., Ikeda, T., Narahashi, T. and Casida, J. E., 2000, α-Thujone (the active component of absinthe): γ-aminobutyric acid type A receptor modulation and metabolic detoxification. *Proceedings of the National Academy of Sciences, USA*, **97**, 3826–3831.

Ishida, T., Asakawa, Y., Tekemoto, T. and Aratani, T., 1981, Terpenoids biotransformation in mammals III: biotransformation of α-pinene, β-pinene, pinane, 3-carene, carane, myrcene, and *p*-cymene in rabbits. *Journal of Pharmaceutical Sciences*, **70**, 406–415.

Ishida, T., Toyota, M. and Asakawa, Y., 1989, Terpenoid biotransformation in mammals. V. Metabolism of (+)-citronellal, (±)-7-hydroxycitronellal, citral, (−)-perillaldehyde, (−)-myrtenal, cuminaldehyde, thujone, and (±)-carvone in rabbits. *Xenobiotica,* **19**, 843–855.

Klaassen, C. D. (ed.), 2001, *Casarett & Doull's Toxicology, The Basic Science of Poisons,* 6th edn (New York: McGraw-Hill).

Mazzega, M., Fabris, F., Cossu, S., De Lucchi, O., Lucchini, V. and Valle, G., 1999, Synthesis, atropoisomerism and chemistry of the dimers of *R*-(−)-carvone, *R*-(−)-hydrocarvone, 1*R*,5*R*-(+)-pinocarvone and other monoterpenic ketones. *Tetrahedron,* **55**, 4427–4440.

Millet, Y., Jouglard, J., Steinmetz, M. D., Tognetti, P., Joanny, P. and Arditti, J., 1981, Toxicity of some essential plant oils. Clinical and experimental study. *Clinical Toxicology,* **18**, 1485–1498.

Phytochemical Database, 2001, Chemicals in *Hyssop officinalis* L. (Lamiaceae)-Hyssop. In *Dr. Duke's Phytochemical and Ethnobotanical Databases.* USA-ARS-NGRL (Beltsville: Beltsville Agricultural Research Center) [http://ars-grin.gov/duke].

Satterwhite, D. M. and Croteau, R. B., 1987, Resolution of monoterpene enantiomers by gas chromatography. *Journal of Chromatography,* **407**, 243–252.

Scheline, R. R., 1991, *Handbook of Mammalian Metabolism of Plant Compounds* (Boca Raton: CRC Press), pp. 108–113.

Simonsen, J. and Owen, L. N., 1949, Pinocamphone. In *The Terpenes,* vol. 2: *The Dicyclic Terpenes and their Derivatives,* 2nd edn (Cambridge: Cambridge University Press), pp. 226–232.

Sirisoma, N. S., Höld, K. M. and Casida, J. E., 2001, α- and β-Thujones (herbal medicines and food additives): synthesis and analysis of hydroxy and dehydro metabolites. *Journal of Agricultural and Food Chemistry,* **49**, 1915–1921.

Solladié-Cavallo, A., Schwarz, J. and Burger, V., 1994, A four-step, highly enantioselective synthesis and enzymatic resolution of 3,4-dichloro-phenylalanine. *Tetrahedron: Asymmetry,* **5**, 1621–1626.

Southall, W., 2001, in D. Bible-Larson, P. Young and D. Lyle (eds), *Hyssop Superior Healing Power: A 21st Century Herb,* 2nd edn (Hollywood: Southall Research).

Suga, T., Shishibori, T., Hirata, T. and Matsuura, T., 1968, Stereochemical studies of monoterpene compounds. VI. The stereochemistry of 2-hydroxypinocamphone and its reduction products. *Bulletin of the Chemical Society of Japan,* **41**, 1180–1184.

Youssefi, M. J., Boschung, A. F. and Thomas, A. F., 1994, Conformation dependence in the chemical ionization mass spectra of 3-pinanones. *Rapid Communications in Mass Spectrometry,* **8**, 313–316.

XENOBIOTICA, 2002, VOL. 32, NO. 4, 267–277

Taylor & Francis
healthsciences

Structure–metabolism relationships of substituted anilines: prediction of *N*-acetylation and *N*-oxanilic acid formation using computational chemistry

G. B. SCARFE†§, I. D. WILSON‡, M. A. WARNE†, E. HOLMES, J. K. NICHOLSON† and J. C. LINDON†*

† Biological Chemistry, Biomedical Sciences Division, Faculty of Medicine, Imperial College of Science, Technology and Medicine, Sir Alexander Fleming Building, South Kensington, London SW7 2AZ, UK
‡ Department of Drug Metabolism and Pharmacokinetics, AstraZeneca Pharmaceuticals, Mereside, Alderley Park, Macclesfield SK10 4TG, UK

Received 10 July 2001

1. The relationship between the *in vivo* metabolism of substituted anilines, in particular *N*-acetylation and subsequent formation of oxanilic acids, and their molecular physico-chemical properties has been investigated using computational chemistry and pattern-recognition methods. The methods revealed that the physico-chemical properties most important for *N*-acetylation and subsequent oxanilic acid formation were electronic descriptors based on partial atomic charges and the susceptibility of the molecules to nucleophilic attack at certain ring positions.

2. The calculated partial atom charge on the amine nitrogen was the parameter most important for predicting that an aniline would be *N*-acetylated. The calculated nucleophilic susceptibility of the aromatic carbon *para* to the amino group (NS4) was the most significant parameter for determining oxanilic acid formation following *N*-acetylation. Thus, highly electron-withdrawing groups substituted at this position gave higher nucleophilic susceptibilities that were related to the presence of an oxanilic acid metabolite.

3. If the parameters relating to *N*-acetylation were modified by other electron-withdrawing groups in the ring (particularly at the position *ortho* to the amino group), then acetylation and subsequent oxanilic acid formation did not occur. The introduction of groups that allow the possibility of competing oxidative metabolic pathways elsewhere in the molecule (e.g. CH_3) also affected the production of oxanilic acids.

4. Using chemometric analysis of the computed physico-chemical properties, the result has been the generation of a model that classifies the metabolism of a number of anilines. This could be used to predict the acetylation and oxanilic formation propensity of a number of substituted anilines whose metabolism was unknown to the system, demonstrating that such techniques may be of use for predicting metabolism and hence could provide support for rational drug design.

Introduction

In vivo quantitative structure–metabolism relationships (QSMRs) using computational chemistry and pattern recognition techniques have previously been used for the prediction of urinary sulphate and glucuronide conjugate excretion for substituted phenols in rat (Holmes *et al.* 1995) and the prediction of urinary glycine and glucuronide conjugation for substituted benzoic acids in rat and rabbit

* Author for correspondence; e-mail: j.lindon@ic.ac.uk
§ Present address: Department of Drug Metabolism and Pharmacokinetics, Servier Research and Development Ltd, Fulmer Hall, Windmill Road, Fulmer, Slough SL3 6HH, UK.

Xenobiotica ISSN 0049–8254 print/ISSN 1366–5928 online © 2002 Taylor & Francis Ltd
http://www.tandf.co.uk/journals
DOI: 10.1080/00498250110100739

(Ghauri *et al.* 1992a, b, Cupid *et al.* 1996, 1999). If these techniques are to be used ultimately for metabolism support of rational drug design programmes, it is important that this methodology can be applied to compounds with more complex metabolism. The *in vivo* metabolism of substituted anilines is more varied and complex than either of the previous substrates analysed by these techniques and therefore represents a more realistic model system to evaluate the potential for QSAR techniques to predict metabolism. The metabolism of substituted anilines can be complex leading to a variety of products. For example, ring hydroxylation with or without Phase 2 conjugation to sulphates and glucuronides is possible. Conjugation at the amine nitrogen to form *N*- and *N*-*O*-glucuronides is also observed. In addition, substituents on the aniline ring system such as methyl groups can also undergo metabolism such as oxidation. One route of some interest is the *N*-acetylation of the amino group of an aniline followed by oxidation to an oxanilic acid via a glycol-anilide. To address the whole complex pattern of metabolism in anilines systematically, it was decided to investigate the individual routes separately and initially to study the acetylation/oxanilic acid pathway.

The conversion of substituted anilines to *N*-oxanilic acids is a relatively rare metabolic pathway involving oxidation of *N*-acetyl groups and only appears to occur with certain substituents at specific positions on the aromatic ring (Kiese and Lenk 1969, Fries *et al.* 1971, Wilson *et al.* 1985, Ehlardt and Howbert 1991, Scarfe *et al.* 2001). Therefore, one of the aims of the present work was to investigate the structure–metabolism relationships of these metabolic pathways using computational chemistry and pattern recognition techniques. The first stage of the metabolic process of *N*-oxanilic acid formation from an aniline is *N*-acetylation and clearly if this process does not occur, then an oxanilic acid will not be produced. The structure–metabolism relationships of a series of substituted anilines with known metabolic fates using data measured by ourselves as well as data taken from the literature with regard to *N*-acetylation (or not) and subsequent oxidation of the acetyl methyl, via a glycol-anilide intermediate, $R.NH.CO.CH_2OH$, to produce oxanilic acids has, therefore, been investigated. This has been accomplished using computational chemistry approaches to derive a series of molecular properties. Many such properties can have values that are highly dependent on molecular conformation, but in the simple substituted anilines studied here, this is unlikely to be a serious hindrance to the methods used. From these data, a prediction has been made of the metabolic fate (i.e. not acetylated, acetylated or oxanilic acid formation) of selected substituted anilines, the metabolism of which had not previously been studied.

Materials and methods

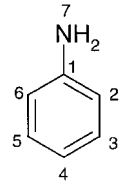
Metabolism studies

These have been reported previously in terms of dosing of compounds, sample collection, identification of metabolites and quantitation of metabolites (Kiese and Lenk 1969, Fries *et al.* 1971, Kao *et al.* 1978, Baldwin and Hutson 1980, Hutson *et al.* 1984, Wilson *et al.* 1985, Ehlhardt and Howbert 1991, Tugnait 1994, Scarfe *et al.* 1998, 1999a–c, 2000, 2001).

Computational chemistry

All molecular structure and property generation was performed using CAChe^{TM} v.3.9 (Oxford Molecular, Oxford, UK). Geometry optimization for all structures was carried out at the semi-empirical molecular orbital level using the AM1 parameterization (Dewar *et al.* 1985) performed on a Silicon

Table 1. Computed physiochemical properties, their abbreviations and the method of calculation.



Property (unit)	Abbreviation	Method of calculation
Heat of formation (kcal mol^{-1})	E	
Energy of the highest occupied molecular orbital (eV)	EHOMO	MO-AM1
Energy of the lowest unoccupied molecular orbital (eV)	ELUMO	MO-AM1
Dipole moment (debye)	DM	MO-AM1
Surface area of the electron density (Å^2)	SA	MO-AM1
Volume of the electron density (Å^3)	Vol	MO-AM1
Solvent accessible surface area (Å^2)	SASA	COSMO model (Klamt and Schuurman 1993)
Molecular weight (mass au)	MW	empirical
$\log_{10}$ octan-1-ol/water partition coefficient	log *P*	additivity scheme (Ghose *et al.* 1988)
Molar refractivity	MR	additivity scheme (Ghose *et al.* 1988)
0th to 2nd order molecular connectivity index	Chi0-Chi2	Kier and Hall (1986)
0th to 2nd order valence molecular connectivity index	Chi0V-Chi2V	Kier and Hall (1986)
Partial atomic charge	PAC1-PAC7	MO-AM1
Electrophilic superdelocalizability	ESD1-ESD7	Fukui *et al.* (1954)
Nucleophilic superdelocalizability	NSD1-NSD7	Fukui *et al.* (1954)
Nucleophilic susceptibility	NS1-NS7	Fukui *et al.* (1954)
Electrophilic susceptibility	ES1-ES7	Fukui *et al.* (1954)
Density highest occupied molecular orbital	ρHOMO1-ρHOMO7	Fukui *et al.* (1954)
Density lowest unoccupied molecular orbital	ρLUMO1-ρLUMO7	Fukui *et al.* (1954)

Graphics Origin 200 computer with twin R10000 processors. A list of calculated molecular and atomic physico-chemical properties at the minimum energy structure, and the molecular numbering system used is given in table 1.

The overall MO-generated molecular properties comprised the heat of formation (*E*), energies of the highest occupied and lowest unoccupied molecular orbitals (EHOMO and ELUMO), the total dipole moment (DM) and the surface area (SA) and volume (Vol) of the electron density to a threshold of 0.01 electron charge/Å^3, plus the solvent accessible surface area (SASA). Additional empirical molecular physico-chemical descriptors comprised the molecular weight (MW), molar refractivity (MR) and log to base 10 of the octan-1-ol/water partition coefficient (log *P*), along with a variety of connectivity indices (Chi0 – Chi2, Chi0V – Chi2V) as shown in table 1. These connectivity indices depend only on the arrangement of the atoms within the molecule and are thus independent of the effects of the geometry optimization.

The atom-centred electronic descriptors calculated at the MO level included those based upon HOMO and LUMO properties, as well as the partial atomic charge (PAC) at each ring carbon and at the nitrogen. The HOMO-based properties are the electron density in the HOMO orbital (ρHOMO) and the electrophilic susceptibility (ES) and the electrophilic superdelocalizability (ESD), all at each ring carbon atom and at the nitrogen. The LUMO-based properties are the electron density in the LUMO (ρLUMO), and the nucleophilic susceptibility (NS) and the nucleophilic superdelocalizability (NSD) again at each ring carbon atom and at the nitrogen.

Chemometrics methods

The calculated molecular properties were input into the JMP statistical package (v.3.2, SAS Institute, Inc., Cary, NC, USA) and investigated using the multivariate technique of principal components analysis (PCA). This constructs a new set of descriptors, known as principal components (PC), which are linear combinations of the input variables with appropriate weighting coefficients. These are calculated such that each PC is orthogonal to every other, the first PC (PC1) explains the

largest part of the variance in the data, and each subsequent PC (PC2, PC3, etc.) decreasing amounts. Results of PCA were evaluated using scores plots which indicate the relationships (clustering, similarity) between molecules based on their physico-chemical descriptors, and loadings plots which indicate the physico-chemical descriptors that are important for the clustering behaviour seen in the scores plots. Although not necessary, given that quantitative metabolic data are available in most cases, for simplicity, the metabolic fate of each compound was assigned to one of three classes (acetylated, not acetylated, oxanilic acid formation) and given a dummy class variable to allow regression of the physico-chemical descriptors against class and hence determine the important properties for class differentiation. The alternative reaction of oxidation of aromatic ring methyl groups was not considered as a separate class for the purpose here.

Results and discussion

Development of training and test sets of data

Table 2 shows details of the 24 substituted anilines used for these analyses. The compounds were classified according to their *in vivo* metabolic fate (almost all in

Table 2. Identity of the compounds studied with description of their metabolic fate.

Number	Substituents	Name	Classification of metabolism[1]	Reference
1	H	aniline	A	Kao *et al.* (1978)
2	2-F	2-fluoroaniline	A	Tugnait (1994)
3	3-F	3-fluoroaniline	A	Tugnait (1994)
4	4-F	4-fluoroaniline	A	Scarfe *et al.* (1999b)
5	4-Cl	4-chloroaniline	OA	Elhardt and Howbert (1991)
6	4-Br	4-bromoaniline	OA	Scarfe *et al.* (in press)
7	4-CN	4-cyanoaniline[2]	OA[3]	Hutson *et al.* (1984)
8	2-CF_3	2-trifluoromethylaniline	NA	Tugnait (1994)
9	3-CF_3	3-trifluoromethylaniline	A	Tugnait (1994)
10	4-CF_3	4-trifluoromethylaniline	OA	Wilson *et al.* (1985)
11	2-Cl, 4-CF_3	2-chloro-4-trifluoromethylaniline	NA	Scarfe *et al.* (1999a)
12	2-Br, 4-CF_3	2-bromo-4-trifluoromethylaniline	NA	Scarfe *et al.* (1998)
13	3-Me, 4-CF_3	3-methyl-4-trifluoromethylaniline	A	Scarfe *et al.* (1999c)
14	2,3,5,6-F, 4-CF_3	2,3,5,6-tetrafluoro-4-trifluoromethylaniline	NA	Scarfe *et al.* (2000)
15	2-Me, 4-CF_3	2-methyl-4-trifluoromethylaniline	unknown	
16	3-Br, 4-CF_3	3-bromo-4-trifluoromethylaniline	unknown	
17	2-CF_3, 4-Br	2-trifluoromethyl-4-bromoaniline	unknown	
18	3-CF_3, 4-Br	3-trifluoromethyl-4-bromoaniline	unknown	
19	2-Br	2-bromoaniline	unknown	
20	3-Br	3-bromoaniline	unknown	
21	3-Cl, 4-F	3-chloro-4-fluoroaniline	A	Baldwin and Hutson (1980)
22	2-F, 4-CF_3	2-fluoro-4-trifluoromethylaniline	unknown	
23	4-COC_2H_5	4-propionylaniline[4]	OA	Kiese and Lenk (1969)
24	4-SO_2NH_2	Sulphanilamide[5]	OA	Fries *et al.* (1971)

[1] NA, not acetylated; A, acetylated; OA, oxanilic acid.
[2] Metabolite of 4-cyano,*N*,*N*-dimethylaniline.
[3] Oxanilic acid not detected, other oxidized products at the *N*-acetyl methyl were detected.
[4] Acetanilide dosed to rabbit.
[5] Data in rabbit.

rat, but with a few examples in rabbit) as to whether they were acetylated (A), not acetylated (NA) or metabolized to produce an oxanilic acid (OA). This formed a training set of data used for generation of maps of compounds in the property space. Compound 7 was chosen at random from those compounds producing an oxanilic acid, compound 21 was chosen at random from compounds undergoing acetylation and both were omitted from the training set and used to test whether the observed groupings were useful for predicting metabolism. This model was then applied to the compounds whose *in vivo* metabolism was unknown (table 2).

Chemometrics analysis of the training set of data

A PC map of the 15 compound training set based on all 62 molecular and atomic parameters is shown in figure 1a. The first principal component (PC1) contained 51% of the variance with a further 16% in the second principal component (PC2). This map shows that in general the compounds with the same metabolic fate grouped together. Compounds that were not acetylated clustered together, however, those that were *N*-acetylated and those which formed oxanilic acids were largely separated except for compounds 10 and 13. The fact that most of the compounds tend to cluster according to their metabolic propensities using physicochemical descriptors indicated that there might be a subset of physicochemical characteristics that determine the selection of the metabolic route.

To explore the structure–metabolism relationships further and to ascertain whether it was possible to obtain a PC scores plot with more defined separation of the compounds in a particular class, the properties most correlated with *N*-acetylation and *N*-oxanilic production were determined. Each class was given a different indicator variable (e.g. not acetylated = 1, acetylated = 2 and oxanilic acid formation = 3). The Pearson correlation coefficients (r) of all 62 calculated parameters with *N*-acetylation and oxanilic acid formation were calculated and those with $r \geq 0.65$ used for further analysis. This resulted in eight significant parameters as shown in table 3 and these were all atom-based electronic descriptors. The four most significant parameters that were related to *N*-acetylation were PAC7, NSD2, PAC1 and ρHOMO1, whilst the four most important parameters related to oxanilic acid formation were NS4, ρLUMO7, NS3 and NS1. The properties pertaining to the whole molecule, unlike the atomic-centred properties, did not appear to be significant for *N*-oxanilic acid production. Since some of these parameters were likely to be highly correlated, these selected descriptors were then used for subsequent PCA where PC1 contained 55% of the variance with a further 29% in PC2. The contributions of each of these eight most significant parameters to PC1 and PC2 are given in table 3.

A PC map of the 15 compound training set based on the eight most significant parameters that correlated with both *N*-acetylation and oxanilic acid formation is shown in figure 1b. Apart from compound 13, the compounds now fell into three separate areas of the PC map depending on their ultimate urinary metabolic fate. The fate of the substituted anilines with regard to *N*-acetylation was separated on PC1 with the compounds that are acetylated falling to the left of the PC map and those that are not acetylated falling to the right. *N*-oxanilic acid production appears to be governed by the variance in PC2, with those compounds that do form oxanilic acids *in vivo* lying at the top of the PC map. It is noteworthy that compound 13 (3-methyl-4-trifluoromethylaniline) lies very close to the group that

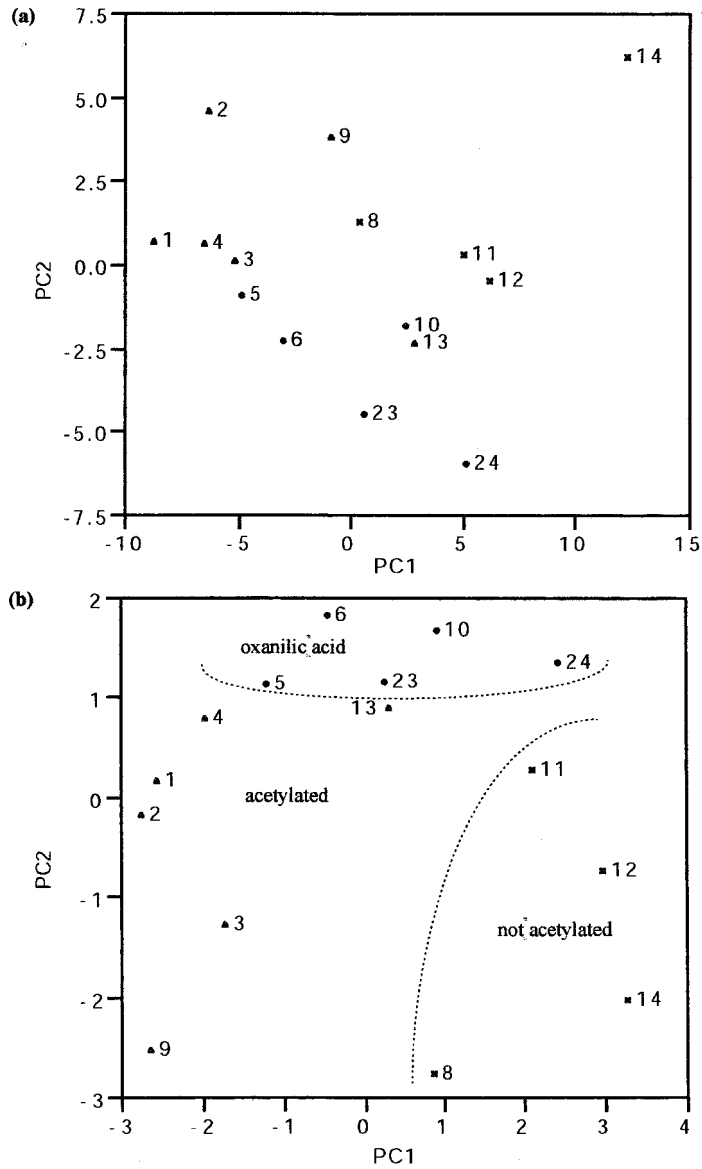


Figure 1. Plot of the scores for PC1 versus PC2 (a) based on all 62 calculated physicochemical properties and (b) based on the eight most significant parameters correlated with *N*-acetylation and *N*-oxanilic acid formation. ▲, Acetylated; ×, not acetylated; ●, oxanilic acid. Boundaries are a subjective assessment of the minimum area for the respective metabolic propensities and are indicative only.

form oxanilic acids, although no oxanilic acid was detected. 3-Methyl-4-trifluoromethylaniline was *N*-acetylated, a necessary precursor to oxanilic acid formation, but instead of the acetyl methyl group being oxidized to form an oxanilic acid, the ring methyl group was oxidized *in vivo* to produce 2-trifluoromethyl-5-acetamidobenzoic acid (Scarfe *et al.* 1999c). Such competing metabolic pathways are likely to complicate interpretation of the results.

Table 3. Most significant parameters from Pearson correlation coefficients (r) and their contribution to the principal components (PC1 and PC2).

Parameter	r(*N*-acetylation)	r(oxanilic acid formation)	Contribution to PC1	Contribution to PC2
PAC7	0.86		0.46	0.15
NSD2	0.84		0.38	0.25
PAC1	0.82		0.45	0.12
ρHOMO1	0.80		0.46	0.11
NS4		0.74	0.04	0.57
ρLUMO7		0.68	0.40	0.24
NS3		0.67	0.16	0.46
NS1		0.65	0.22	0.54

Model validation using test data

To test whether the observed groupings were useful for predicting metabolism, two test compounds whose metabolic fates were known, were mapped using the same model as applied to the training set. This is shown in figure 2a with the two test compounds (7 and 21) denoted by squares. Compound 21, (3-chloro-4-fluoroaniline), was *N*-acetylated when dosed to rat (Baldwin and Hutson 1980) and it can be clearly seen that the compound falls within the acetylated section of the PC map. Compound 7, (4-cyanoaniline), has itself not actually been studied *in vivo*. However, Hutson *et al.* (1984) studied the metabolic fate of 4-cyano-*N*,*N*-dimethylaniline in the rat and found *N*-demethylation to be a major metabolic pathway producing 4-cyanoaniline (compound 7). In that study, it was shown that 7 was subsequently *N*-acetylated and the acetyl methyl group was oxidized to the glycol-anilide and conjugated products of this were excreted in the urine. Although an oxanilic acid of 4-cyanoaniline was not detected in that study, it can be seen that the compound clearly falls within the oxanilic acid section of the map and this would suggest that the level of oxanilic acid was rather low or that the competing reaction of glycol-anilide conjugation was more efficient.

Prediction of unknown metabolic fate

Once the model had been tested, it was used to predict the metabolic fate of some compounds the metabolism of which were completely unknown. Figure 2b shows the PC map including the seven compounds (15–20 and 22) with unknown metabolic fates denoted by open squares. Two of these compounds mapped in the region of the map containing compounds which produced oxanilic acid metabolites. Compound 22 (2-fluoro-4-trifluoromethylaniline) was one of these compounds. This structure was chosen as a test to compare with compounds studied earlier, namely 2-chloro and 2-bromo-4-trifluoromethylaniline (Scarfe *et al.* 1998, 1999a), thus completing the 2-halogen-4-trifluoromethylaniline substituted series. 4-Trifluoromethylaniline (compound 10) is known to produce an oxanilic acid (Wilson *et al.* 1985), but, however, the chloro- and bromo-substituent at the 2-position in compounds 11 and 12 respectively caused the aniline not to be acetylated and therefore no oxanilic acid was produced. Fluorine substitution at the 2-position in 4-trifluoromethylaniline did not appear to effect *N*-acetylation and subsequently it is likely that an oxanilic acid metabolite of this substrate would be formed *in vivo*. It is interesting to note, however, that if the other aromatic ring

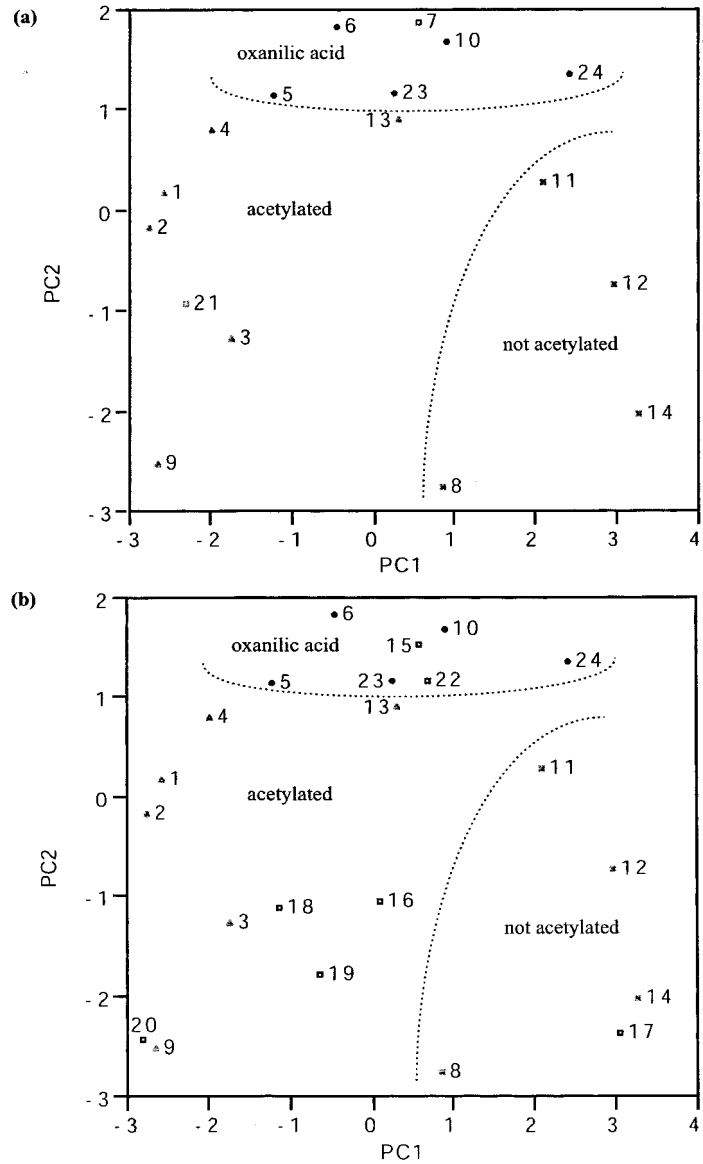


Figure 2. Plot of the scores for PC1 versus PC2 based on the eight most significant parameters correlated with *N*-acetylation and oxanilic acid formation, (a) known and (b) unknown test compounds. □, Known test (acetylated); □, known test (oxanilic acid); □, unknown tests; other symbols as defined in figure 1. Boundaries are a subjective assessment of the minimum area for the respective metabolic propensities and are indicative only.

positions in 4-trifluoromethylaniline are also substituted with fluorine (as in 2,3,5,6-tetrafluoro-4-trifluoromethylaniline, compound 14) the compound was not acetylated and an oxanilic acid was not detected (Scarfe *et al.* 2000). The other test compound with unknown metabolism that fell in the oxanilic acid section of the map was 2-methyl-4-trifluoromethylaniline (compound 15). This structure was also chosen to compare with the 2-substituted-4-trifluoromethylanilines and although this would suggest an oxanilic acid is formed, it is more likely

in vivo that the aromatic methyl would be oxidized instead of the acetyl methyl (as was the case with 3-methyl-4-trifluoromethylaniline, compound 13).

4-Bromoaniline and 4-chloroaniline produce oxanilic acids when dosed to rat (Ehlhardt and Howbert 1991, Scarfe *et al.* 2001) and these compounds (6 and 5) map in the region for oxanilic acid production. The *in vivo* metabolic fate of 2- and 3-bromoaniline (19 and 20) has not previously been studied, but it can be predicted in figure 2b that these compounds would be *N*-acetylated but not produce oxanilic acids. This prediction is supported by a recent publication on the metabolism of 2-chloroaniline in rat (Hong and Rankin 1998). 2-Chloroaniline was shown to be *N*-acetylated but there was no evidence of an oxanilic acid. This trend was also observed with the 4-trifluoromethylanilines, when the trifluoromethyl group was substituted at the 4-position (compound 10) an oxanilic acid was produced but compounds with substitution at the 2- or 3-positions (compounds 8 and 9) did not form oxanilic acid metabolites (Tugnait 1994). Compounds 16–18 all have a bromine and a trifluoromethyl group substituted at different positions in the aromatic ring. It appears that having two highly electron-withdrawing groups in the aromatic ring reduces the probability of oxanilic acid formation. The effect of the trifluoromethyl group at the 2-position in 2-trifluoromethyl-4-bromoaniline (compound 17) would probably cause the compound not to be acetylated, as was the case with its isomer, 2-bromo-4-trifluoromethylaniline (compound 11; Scarfe *et al.* 1998). In the isomers with an electron-withdrawing group substituted at the 3-position (compounds 16 and 18), the substrates would more than likely be acetylated but no oxanilic acid metabolites produced.

Derivation of the significant molecular properties

Eight of the physicochemical properties given in table 1 were most significant with regard to *N*-acetylation and subsequent production of oxanilic acids. Five of these parameters are all atom-based terms relating to attack on the ring carbon atoms by a nucleophile, namely NS1, NSD2, NS3, NS4 and ρLUMO7. This indicates the general importance of nucleophilic attack on substituted anilines in these pathways. From the clear separation in PC2 of figure 2b the significance of NS1, NS3 and NS4, or nucleophilic attack on the ring carbons, is evident. Of these the property most correlated with *N*-oxanilic acid formation was the nucleophilic susceptibility of carbon 4 (NS4) and a relatively high value for NS4 appears to be a prerequisite for *in vivo* oxanilic acid formation from a substituted aniline. This is consistent with the fact that all of the compounds found to produce oxanilic acids *in vivo* (compounds 5, 6, 10, 23 and 24) had a highly electron-withdrawing group (Cl, Br, CF_3, COR, SO_2NH_2) attached to the carbon at the 4-position and this would cause this position to have a partial positive charge and therefore be susceptible to attack by nucleophiles. However, oxanilic acid formation is the product of two separate metabolic processes; firstly *N*-acetylation, followed by oxidation of the acetyl methyl group to the glycol-anilide then further metabolism to the oxanilic acid ($Ar.NH_2 \rightarrow Ar.NH.CO.CH_3 \rightarrow Ar.NH.CO.CH_2OH \rightarrow$ Ar.NH.CO.COOH). Clearly, if *N*-acetylation does not occur then an oxanilic acid cannot be produced. This appears to have been the case with compounds 11, 12 and 14 where the extra electron-withdrawing groups in the aromatic ring, particularly at the position *ortho* to the amino group, must have affected the parameters governing *N*-acetylation (e.g. PAC7, NSD2, PAC1, ρHOMO1), thus

mitigating against *N*-acetylation and therefore preventing formation of oxanilic acid metabolites.

Conclusions

Computational chemistry and pattern recognition techniques have been shown to be applicable for investigating the underlying structure–metabolism relationships of a particular route of metabolism (i.e. *N*-oxanilic acid formation) of a series of compounds that can have very complex metabolism (i.e. anilines). Here, these structure–metabolism relationships have only been investigated qualitatively. However, there is no reason why similar methodology could not be applied to investigate the quantitative structure–metabolism relationships of this metabolic route as was the case with other substrates and metabolic pathways (Holmes *et al.* 1995, Cupid *et al.* 1996, 1999). Also, these other metabolic routes have not been ignored and indeed the techniques used here could be employed to investigate some of the many other metabolic routes of metabolism of anilines, such as aromatic ring hydroxylation and subsequent Phase II conjugation or *N*-conjugation, and this work will form the basis of future publications. This work has contributed to an ongoing goal of developing an expert system that can be used to predict metabolism of xenobiotic compounds, a technology useful in early-stage metabolism studies in rational drug design programmes.

References

Baldwin, M. K. and Hutson, D. H., 1980, The metabolism of 3-chloro-4-fluoro-aniline in dog and rat. *Xenobiotica*, **10**, 135–144.

Cupid, B. C., Beddell, C. R., Wilson, I. D., Lindon, J. C. and Nicholson, J. K., 1996, Quantitative structure–metabolism relationships for substituted benzoates in the rabbit: prediction of urinary excretion of glycine and glucuronide conjugates. *Xenobiotica*, **26**, 157–176.

Cupid, B. C., Holmes, E., Wilson, I. D., Lindon, J. C. and Nicholson, J. K., 1999, Quantitative structure–metabolism relationships (QSMR) using computational chemistry: pattern recognition analysis and statistical prediction of phase II conjugation reactions of substituted benzoic acids in the rat. *Xenobiotica*, **29**, 27–42.

Dewar, M. J. S., Zoebisch, E. G. and Stewart, J. J. P., 1985, The development and use of quantum-mechanical molecular-models. 76. AM1 – a new general purpose molecular-model. *Journal of the American Chemical Society*, **107**, 3902–3909.

Ehlhardt, W. J. and Howbert, J. J., 1991, Metabolism and disposition of *p*-chloroaniline in rat, mouse, and monkey. *Drug Metabolism and Disposition*, **19**, 366–369.

Fries, W., Kiese, M. and Lenk, W., 1971, Additional route in the metabolism of Sulphanilamide. *Xenobiotica*, **1**, 241–256.

Fukui, K., Yonezawa, T. and Shingu, H., 1954, Theory of substitution in conjugated molecules. *Bulletin of the Chemical Society of Japan*, **27**, 423–427.

Ghauri, F. Y., Blackledge, C. A., Glen, R. C., Sweatman, B. C., Lindon, J. C., Beddell, C. R., Wilson, I. D. and Nicholson, J. K., 1992a, An approach to a metabolic expert system: structure–metabolism relationships for benzoic acids in the rat. In E. Reid and I. D. Wilson (eds), *Methodological Surveys in Biochemistry and Analysis* (Cambridge: Royal Society of Chemistry), pp. 21–28.

Ghauri, F. Y., Blackledge, C. A., Glen, R. C., Sweatman, B. C., Lindon, J. C., Beddell, C. R., Wilson, I. D. and Nicholson, J. K., 1992b, Quantitative structure–metabolism relationships of substituted benzoic acids in the rat. Computational chemistry, NMR spectroscopy and computer pattern recognition studies. *Biochemical Pharmacology*, **44**, 1935–1946.

Ghose, A. K., Pritchett, A. and Crippen, G. M., 1988, Atomic physicochemical parameters for 3-dimensional structure directed quantitative structure–activity-relationships. 3. Modelling hydrophobic interactions. *Journal of Computational Chemistry*, **9**, 80–90.

Holmes, E., Sweatman, B. C., Bollard, M., Blackledge, C. A., Beddell, C. R., Wilson, I. D., Lindon, J. C. and Nicholson, J. K., 1995, Prediction of urinary sulphate and glucuronide excretion of substituted phenols in the rat using quantitative structure–metabolism relationships. *Xenobiotica*, **25**, 1269–1281.

Hong, S. K. and Rankin, G. O., 1998, Biotransformation of 2-chloroaniline in the Fischer 334 rat: identification of urinary metabolites. *Xenobiotica*, **28**, 985–994.

Hutson, D. H., Lakeman, S. K. and Logan, C. J., 1984, The fate of 4-cyano-*N*,*N*-dimethylaniline in rats; a novel involvement of glutathione in the metabolism of aniline. *Xenobiotica*, **14**, 925–934.

Kao, J., Faulkner, J. and Bridges, J. W., 1978, Metabolism of aniline in rats, pigs and sheep. *Drug Metabolism and Disposition*, **6**, 549–555.

Kier, L. B. and Hall, L. H., 1986, *Molecular Connectivity in Structure–Activity Analysis* (New York: Wiley).

Kiese, M. and Lenk, W., 1969, Oxidation of acetanilides to glycolanilides and oxanilic acids in rabbits. *Biochemical Pharmacology*, **18**, 1325–1333.

Klamt, A. and Schuurman, G., 1993, COSMO – a new approach to dielectric screening in solvents with explicit expressions for the screening energy and its gradient. *Journal of the Chemical Society, Perkin Transactions II*, pp. 799.

Scarfe, G. B., Clayton, E., Wilson, I. D. and Nicholson, J. K., 2000, Identification and quantification of metabolites of 2,3,5,6-tetrafluoro-4-trifluoromethylaniline in rat urine using ^{19}F nuclear magnetic resonance spectroscopy, high-performance liquid chromatography-nuclear magnetic resonance spectroscopy and high-performance liquid chromatography-mass spectrometry. *Journal of Chromatography B*, **748**, 311–319.

Scarfe, G. B., Lindon, J. C., Nicholson, J. K., Clayton, E., Wright, B., Taylor, S. and Wilson, I. D., 2001, The identification of the urinary metabolites of 4-bromoaniline and 4-bromo-[*carbonyl*-^{13}C]-acetanilide in the rat. *Xenobiotica*, **32**, 325–337.

Scarfe, G. B., Lindon, J. C., Nicholson, J. K., Wright, B., Clayton, E. and Wilson, I. D., 1999c, Investigation of the quantitative metabolic fate and urinary excretion of 3-methyl-4-trifluoromethylaniline and 3 methyl-4-trifluoromethylacetanilide in the rat. *Drug Metabolism and Disposition*, **27**, 1171–1178.

Scarfe, G. B., Tugnait, M., Wilson, I. D. and Nicholson, J. K., 1999b, Studies on the metabolism of 4-fluoroaniline and 4-fluoroacetanilide in the rat: formation of 4-acetamidophenol (paracetamol) and its metabolites *via* defluorination and *N*-acetylation. *Xenobiotica*, **29**, 205–216.

Scarfe, G. B., Wright, B., Clayton, E., Taylor, S., Wilson, I. D., Lindon, J. C. and Nicholson, J. K., 1998, ^{19}F NMR and directly coupled HPLC-NMR-MS investigations into the metabolism of 2-bromo-4-trifluoromethylaniline in the rat: a urinary excretion balance study without the use of radiolabelling. *Xenobiotica*, **28**, 373–388.

Scarfe, G. B., Wright, B., Clayton, E., Taylor, S., Wilson, I. D., Lindon, J. C. and Nicholson, J. K., 1999a, Quantitative studies on the urinary metabolic fate of 2-chloro-4-trifluoromethylaniline in the rat using ^{19}F NMR spectroscopy and directly coupled HPLC-NMR-MS. *Xenobiotica*, **29**, 77–92.

Tugnait, M., 1994, Multinuclear magnetic resonance studies on the metabolism of model fluoroaromatic xenobiotics. PhD thesis, University of London.

Wilson, I. D., Macdonald, C. M., Fromson, J. M., Troke, J. A. and Hillbeck, D., 1985, Species differences in the metabolism of ^{14}C-*p*-trifluoromethylaniline: production of an oxanilic acid as the major metabolite by the rat. *Biochemical Pharmacology*, **34**, 2025–2028.

XENOBIOTICA, 2002, VOL. 32, NO. 4, 279–287

Taylor & Francis
healthsciences

Metabolism of quercetin and kaempferol by rat hepatocytes and the identification of flavonoid glycosides in human plasma

E. J. OLIVEIRA†, D. G. WATSON†* and M. H. GRANT‡

†Department of Pharmaceutical Sciences, University of Strathclyde, 27 Taylor Street, Glasgow G4 0NR, UK
‡Bioengineering Unit, Wolfson Centre, University of Strathclyde, 106 Rottenrow, Glasgow G4 0NW, UK

Received 30 August 2001

1. The metabolism of the flavonoids quercetin and kaempferol by rat hepatocytes was investigated using liquid chromatography coupled with electrospray mass spectrometry (LC-ESI MS). Quercetin and kaempferol were extensively metabolized ($98.8 \pm 0.1\%$ and $81.0 \pm 5.1\%$ respectively, $n = 4$), with four glucuronides of quercetin and two of kaempferol being detected after incubation.

2. The glucuronides of quercetin and kaempferol formed upon incubation with rat hepatocytes were identified as the same ones formed after incubation with the UDP-glucuronosyltransferase isoform UGT1A9.

3. In addition, plasma samples from human volunteers taken after consumption of capsules of *Ginkgo biloba*, a plant rich in flavonoid glycosides, were analysed by LC-MS for the presence of flavonoid glucuronides and flavonoid glycosides. Reported is evidence for the presence of flavonoid glycosides in samples of plasma.

4. The results suggest that UGT1A9 is a key UDP-glucuronosyltransferase isoform for the metabolism of flavonoids, and that absorption of intact flavonoid glycosides is possible.

Introduction

Flavonoids are an important class of polyphenolic compounds that occur naturally in many vegetables and fruits, including apple, citrus, broccoli, grapefruit, and onion (Hollman and Katan 1999). Several pharmacological activities are attributed to flavonoids including antioxidant, anti-inflammatory, antitumour, antiviral and immunomodulatory properties (Middleton 1996). There has been considerable effort to characterize the pharmacological properties of plant flavonoids in biological models *in vitro*, but their metabolism still needs to be more thoroughly investigated, particularly when considering the potential health benefits of this class of compounds.

Quercetin and kaempferol (figure 1) are two widespread flavonoids and their main dietary sources are onion and tea. It is estimated that the average daily consumption of quercetin and kaempferol is about $30\,\mathrm{mg\,day^{-1}}$ (deVries *et al.* 1997).

Flavonoids occur mainly as glycosides and it was generally believed that absorption was dependent upon hydrolysis of the glycosidic bond by intestinal microflora with the consequent release of the corresponding aglycone (Hollman

* Author for correspondence; e-mail: d.g.watson@strath.ac.uk

Xenobiotica ISSN 0049–8254 print/ISSN 1366–5928 online © 2002 Taylor & Francis Ltd
http://www.tandf.co.uk/journals
DOI: 10.1080/00498250110107886

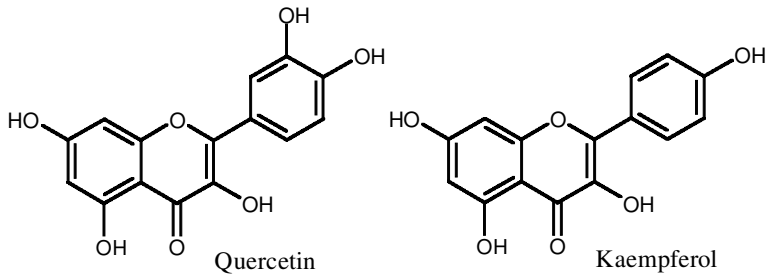


Figure 1. Chemical structures of quercetin and kaempferol.

1997). Recent studies, however, indicate that flavonoid glycosides can be absorbed without hydrolysis. Thus, absorption of pure quercetin was lower than that of quercetin glycosides present in onion (Hollman *et al.* 1997) and evidence for flavonoid glycosides being present in human plasma has been reported (Paganga and RiceEvans 1997). The present authors reported that quercetin and kaempferol are extensively metabolized by microsomes expressing a human form (UGT1A9) of the enzyme UDP-glucuronosyltransferase (Oliveira and Watson 2000).

It is reported here that rat hepatocytes metabolize quercetin and kaempferol to the same glucuronides found after incubation with microsomal preparations. We also investigated the presence of flavonoid glucuronides and glycosides in human plasma taken after consumption of *Ginkgo biloba*, a plant rich in kaempferol and quercetin glycosides. Taken together, the results suggest that glucuronidation is the main pathway for the metabolism of flavonoids and they support the view that flavonoid glycosides can be absorbed without hydrolysis.

Material and methods

Drugs

Quercetin (≥98%), kaempferol (> 90%), rutin (≥95%), [4-(2-hydroxyethyl)-1-piperazineethanesulphonic acid] (HEPES), and dimethylsulphoxide were purchased from Sigma-Aldrich Chemical Co. (Poole, UK). HPLC-grade solvents were obtained from Merck (Poole, UK). *G. biloba* tablets had a stated content of 28.8 mg total flavonoid glycosides and were purchased from Boots (Glasgow, UK). Nylon syringe filters were purchased from HPLC Technologies (Macclesfield, UK).

Hepatocyte incubations

Hepatocytes were prepared from livers of male Sprague–Dawley rats (190–210 g) by a two-step collagenase perfusion as described by Moldeus *et al.* (1978). Incubations were carried out at 37°C under an atmosphere of 95% O_2, 5% CO_2 with constant rotation in 50-ml round-bottomed flasks. Stock solutions of the flavonoids were prepared at a concentration of 100 mM in DMSO and diluted 1000 times in Krebs–Henseleit buffer, pH 7.4, containing 12.5 mM HEPES to give a final concentration of 100 μM. The final incubation volume was 5 ml. Incubations were started by adding a suspension of hepatocytes (2×10^6 viable cells ml^{-1} in Krebs–Henseleit buffer) to the incubation mixtures. Time-course experiments were carried out by removing 0.5-ml aliquots of incubation medium at each time point. Reactions were stopped by adding an equal volume of ice-cold methanol and the samples sonicated and centrifuged (5000*g* for 5 min) before analysis by LC-MS (see below).

Collection and preparation of plasma samples

Two tablets of *G. biloba* were administered daily to four volunteers without dietary restrictions (two men, two women, 29–45 years) for 4 consecutive days. On day 4 of the study, approximately 3 h after dosing, venous blood samples were collected in EDTA Vacutainer™ tubes. Blood samples were centrifuged (3000*g* for 10 min) and the collected plasma stored in a freezer at −20°C. To perform LC-MS analysis, 1 ml plasma was deproteinized by adding 2 ml acetonitrile, followed by centrifugation

(2000*g* for 10 min). The supernatant was collected, mixed with a further 1 ml acetronitrile and centrifuged as before. Samples were then evaporated at 77°C under a stream of nitrogen to about 0.5 ml. Then, 1 ml acetonitrile was added and the samples filtered through a nylon syringe filter (0.45 μm). Samples were then evaporated to dryness, and 200 μl 1:1 (v/v) solution of methanol and 0.1% acetic acid were added, the samples were transferred to a 0.5-ml Eppendorf tube and centrifuged (5000*g* for 5 min) in a microcentrifuge. The supernatant was transferred to a vial and 20 μl was injected into the LC/MS.

Analysis of flavonoid glycosides in G. biloba *capsules*

The contents of a capsule of *G. biloba* were transferred into a 5-ml glass vial and 3 ml HPLC-grade methanol was added. The vial was then heated at 80°C for 10 min in a heating block and the extract filtered (Whatmann, qualitative 1 paper) into a 20-ml volumetric flask. From this solution, a 1:5 dilution was made using water:methanol (8:2 v/v) as the solvent. The diluted solution was filtered using a nylon syringe filter (0.45 μm) and 20 μl was injected into the LC/MS.

LC/MS analysis

LC/MS experiments were carried out using an Automass multi-LC-GC/MS (Thermo Finnigan, UK). Separation was achieved on a Phenomenex Luna C18 column (75 × 4.6 mm, 3 μm). Samples (20 μl) were injected using a Spectra System AS 3000 autosampler and the flow rate (0.8 ml min^{-1}) was reduced by a zero-volume 'T' split, with 0.4 ml min^{-1} being introduced into the quadrupole mass spectrometer. The interface was operated in negative electrospray mode, with a cone voltage of −31 V and corona voltage of −2510 V. The drying gas temperature was 270°C. The mobile phase consisted of (A) 0.1% aqueous acetic acid and (B) methanol. Quercetin metabolites were separated using a linear gradient from 40 to 70% B in 20 min while kaempferol samples were analysed with a gradient from 40 to 88% B in 20 min. The percentage of the glucuronides formed at each time point was obtained by calculating the ratio between the areas of each glucuronide divided by the sum of the areas for all glucuronides taken at the time point at which their formation was maximal (22 min for quercetin and 70 min for kaempferol) (figure 3). The amount of flavonoid remaining after incubation was calculated based on the peak area for the particular flavonoid at each time point expressed as a percentage of its area at time zero.

Plasma samples and methanolic extracts of *G. biloba* capsules were analysed using the same mobile phase described above, but using a modified gradient of 40–59% B in 13 min, 59–40% B in 1 min and an isocratic step at 40% B for 3 min, giving a total run time of 17 min. For the analysis of plasma samples, the mass spectrometer was operated using selected ion monitoring and the ions corresponding to the molecular weight of the flavonoid glycosides detected in *G. biloba* capsules (table 1) were selected. To avoid the possibility of carry-over effects, plasma samples were analysed only after a blank injection (with water) produced no peaks with retention times similar with those of the flavonoid glycosides being screened. A semiquantitative estimate of the levels of glycosides in plasma samples was made based on a calibration curve for rutin from 1 to 100 ng ml^{-1}, since authentic standards for other flavonoid glycosides were not available. For this reason, the values quoted are a semiquantitative estimate based on the assumption that the flavonoid glycosides detected have similar response factors to that of rutin.

Results

Figure 2 shows extracted ion chromatograms of samples of quercetin and kaempferol after incubation with rat hepatocytes. Four glucuronides of quercetin and two of kaempferol were formed. Kaempferol and quercetin were both extensively metabolized with 81.0 ± 5.1% kaempferol and 98.8 ± 0.1% quercetin being conjugated after 40 min (mean ± SD of four determinations).

Figure 3 shows the time-course of the disappearance of kaempferol and quercetin, and the formation of glucuronides during incubation with rat hepatocytes. With kaempferol, only two monoglucuronides, KG1 and KG2, were detected and they were formed to an equal extent. Formation was approximately linear for up to 70 min and at this time point KG1 (retention of 7.23 min in figure 2) accounted for 51.4 ± 9.2% of the glucuronides formed and KG2 (retention of 8.49 min in figure 2) accounted for 48.6 ± 9.2% (mean ± SD, $n = 4$). In contrast, quercetin was conjugated to form four monoglucuronides: QG1 (retention of

Table 1. Flavonoid glycosides detected in the methanolic extract of *G. biloba* capsules by LC-MS and their mass spectral data. HPLC and mass spectrometry conditions are as described in the Materials and methods.

Compound no.	RT†	Tentative assignments‡	MW§	Relevant peaks in the mass spectrum
1	3.29	3-*O*-[2-*O*, 6-*O*-bis (α-L-rhamnosyl)-β-D-glucosyl] quercetin	756	755 [M−1]*, 300 [aglycone]
2	4.28	3-*O*-[2-*O*, 6-*O*-bis (α-L-rhamnosyl)-β-D-glucosyl] kaempferol	740	739 [M−1], 285 [aglycone]
3	5.31	3-*O*-[6-*O*-(α-L-rhamnosyl)-β-D-glucosyl] quercetin	610	609 [M−1], 301 [aglycone]
4	6.46	3-*O*-[2-*O*-(β-D-glucosyl)-α-L-rhamnosyl] quercetin	610	609 [M−1], 301 [aglycone]
5	7.23	3-*O*-[6-*O*-(α-L-rhamnosyl)-β-D-glucosyl] kaempferol	594	593 [M−1], 285 [aglycone]
6	7.98	3-*O*-{2-*O*-[6-*O*-(*p*-hydroxy-*trans*-cinnamoyl)-β-D-glucosyl]-α-L-rhamnosyl} quercetin	756	755 [M−1], 610 [M−145], 300 [aglycone]
7	8.56	3-*O*-[2-*O*-(β-D-glucosyl)-α-L-rhamnosyl] kaempferol	594	593 [M−1], 285 [aglycone]
8	10.11	3-*O*-{2-*O*-[6-*O*-(*p*-hydroxy-*trans*-cinnamoyl)-β-D-glucosyl]-α-L-rhamnosyl} kaempferol	740	739 [M−1], 285 [aglycone]

† RT, retention time.
‡ Positional isomers cannot be distinguished based only on the data presented.
§ MW, molecular weight.
* Base peak.

5.51 min in figure 2), QG2 (7.52 min), QG3 (9.40 min) and QG4 (12.07 min), which correspond to the four peaks in figure 2B. Formation of all four glucuronides was approximately linear up to 22 min of incubation. However, QG1 and QG4 were most abundant and accounted for 28.6 ± 1.7 and $55.0 \pm 8.5\%$ (mean $\pm$ SD, $n = 4$) of the glucuronides recovered at 22 min respectively. QG1 appeared to be formed more slowly than QG4. In contrast, QG2 accounted for $9.6 \pm 1.0\%$ of glucuronidation at 22 min and QG3 for $6.7 \pm 0.7\%$. After 22 min, there was a marked decrease in the amounts of both QG4 and QG1 detected, indicating that these glucuronides may undergo further metabolism. It is interesting to note that the conjugate that showed the greatest decrease in its formation rate after 22 min (QG4) is also the one that was formed at the highest rate before this time point and was thus the one most available for further metabolism. However, since mass spectrometry with selected ion monitoring was used for the detection of the conjugates, additional metabolites could not be identified. Thus, in rat hepatocytes, the levels of glucuronides of quercetin formed were in the order QG3 < QG2 < QG1 < QG4. The same four glucuronides were formed after incubation of quercetin with human microsomes expressing UGT1A9, but the pattern of glucuronidation was different, with the levels being QG3 = QG4 < QG1 = QG2 (Oliveira and Watson 2000). At present, it is not possible to define the position of glucuronidation in the metabolites.

The analysis of a methanolic extract of *G. biloba* capsules by LC-MS allowed the identification of several flavonoid glycosides (figure 4A). The assignment of the peaks (table 1) was based on mass spectral data and on a comparison with the

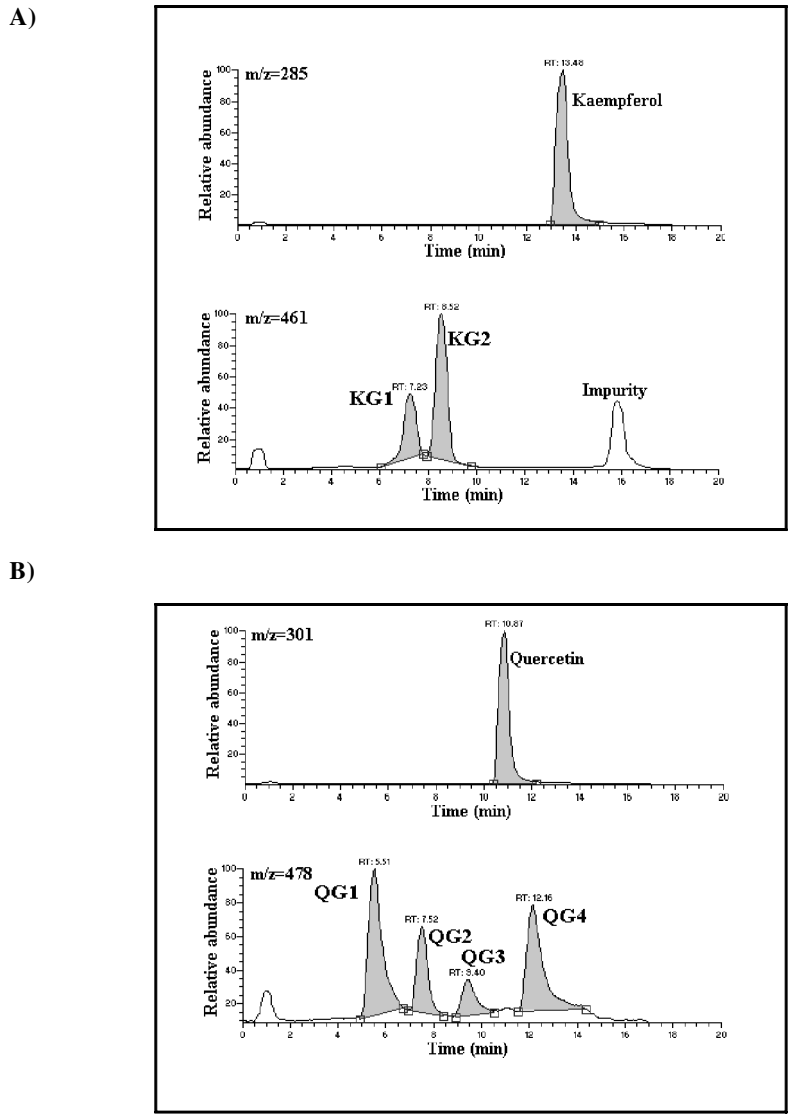


Figure 2. Ion chromatograms of kaempferol (A) and quercetin (B) samples before (top) and 40 min after incubation (bottom) with rat hepatocytes showing the formation of glucuronides.

elution order for flavonoid glycosides in *G. biloba* from the method of Hasler and Sticher (1992). Based on the data available, it is not possible to distinguish between positional isomers, but in all cases an ion for the aglycone was clearly distinguishable in the mass spectrum (table 1). Using the data obtained for the analysis of *G. biloba* capsules, we screened plasma samples taken from volunteers for the presence of flavonoid glycosides (figure 4).

In all the plasma samples, a peak having the same retention time and mass-to-charge ratio of compound 6 (table 1) was detected. In addition, compounds 5 and 7 were also detected in one of the plasma samples. The levels of flavonoid glycosides detected in plasma samples are shown in table 2. We could not detect any of the

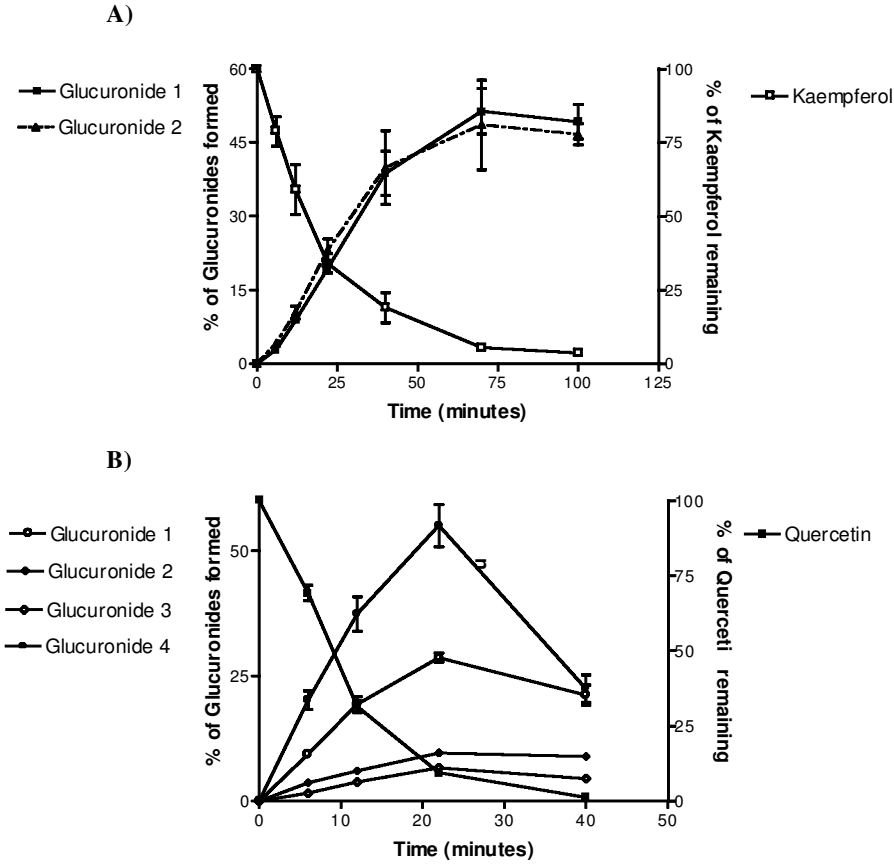


Figure 3. Time-course of glucuronidation of kaempferol (A) and quercetin (B) by rat hepatocytes. Each point is the mean ± SD of four separate determinations. For retention times of glucuronides, see figure 2, and for details of how the percentages were calculated, see above.

glucuronide metabolites in plasma; the LC-MS method has greater sensitivity with respect to the monitoring of glycosides.

Discussion

The metabolism of flavonoids in humans is an important aspect that must be taken into account when discussing their biological activities. Previous work has indicated that flavonoids and their glycosides have a low bioavailability in general, and, more importantly, has stressed the importance for absorption on the type of glycosidic bond and sugar moiety present. Thus, Hollman *et al.* (1997) reported that quercetin glucosides present in onion were better absorbed than pure quercetin or pure rutin (quercetin rhamnoside). This is in contrast with the generally accepted view that flavonoid glycosides have first to be hydrolysed to release the aglycone, which is then absorbed. Also, extensive metabolism of quercetin by HepG2 cell lines with the formation of isorhamnetin (quercetin 3′-methyl ether) and degradative products including protocatechuic acid has been reported (Boulton *et al.* 1999). The metabolism of chrisin (5,7-dihydroxyflavone)

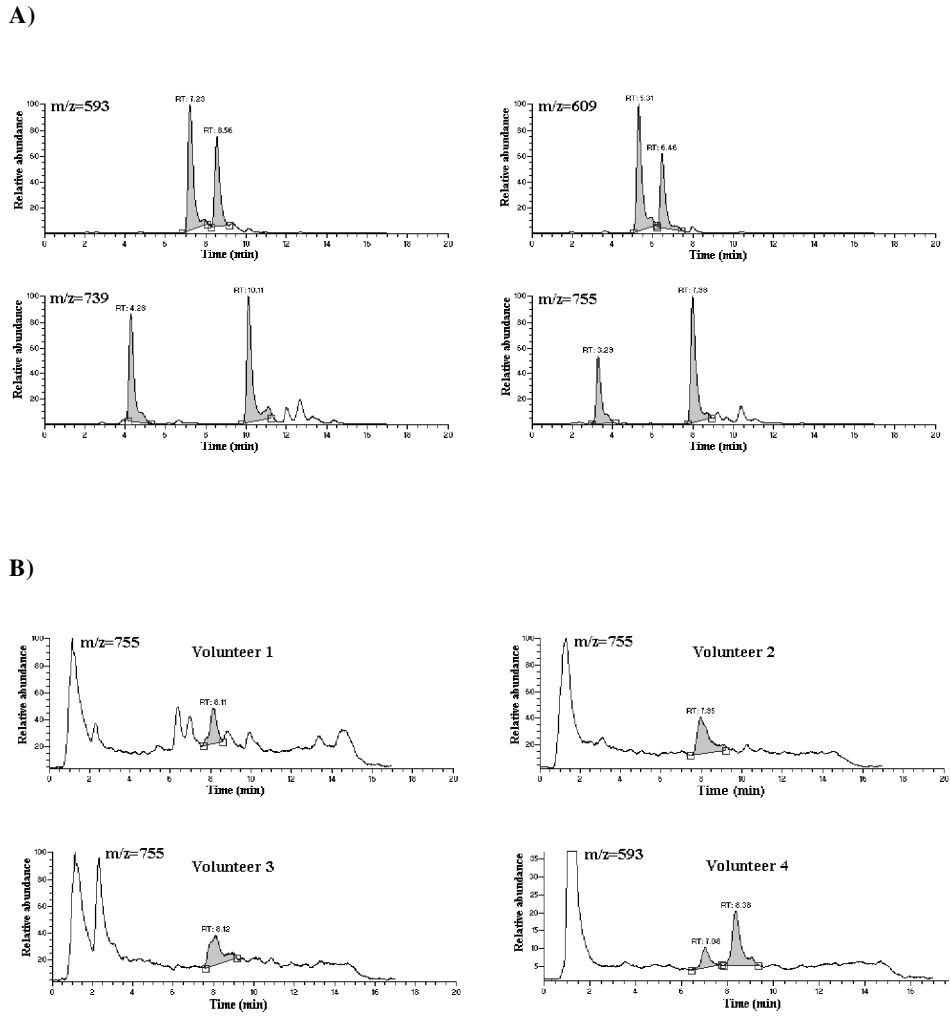


Figure 4. Ion chromatograms from a sample of *G. biloba* methanolic extract (A) and of samples of plasma from volunteers (B). See table 1 for peak identification, and table 2 for concentration of the flavonoids detected in plasma samples.

has also been investigated using human Hep G2 and CACO-2 cells, demonstrating that Hep G2 cells can conjugate this flavonoid into both glucuronic acid and sulphate conjugates (Galijatovic *et al.* 1999). Although some of the studies suggested that different metabolic routes compete for flavonoid metabolism, including methylation, sulphation, glucuronidation and oxidative degradation pathways, glucuronide conjugation seems to be a major reaction in the metabolism of polyphenols. Glucuronidation of diosmetin (3′,5,7-trihydroxy-4′methoxyflavone) in rat after oral administration leads to a rapid fall in the plasma levels of this flavonoid (Boutin *et al.* 1993). Similar results were obtained when the metabolism of diosmin (disometin 7-β-rutinoside) and diosmetin were investigated using rat perfused liver (Perego *et al.* 1993). In addition, it has been shown that the intestine can both absorb and glucuronidate flavonoids without the

Table 2. Levels of flavonoids detected in plasma samples taken from human volunteers after consumption of *G. biloba* capsules.

Volunteer	Flavonoid detected (see table 1 for identification)	Concentration* (ng ml^{-1})
1	6	11
2	6	21
3	6	10
4	6	12
	5	9
	7	23

* Based on a calibration curve with rutin.

need of intestinal microflora (Spencer *et al.* 1999), which suggests the intestine may play a more active role not only in the absorption, but also in the metabolism of flavonoids.

Oliveira and Watson (2000) reported that quercetin and kaempferol were extensively metabolized by microsomes expressing a human form (UGT1A9) of the enzyme UDP-glucuronosyltransferase (EC 2.4.1.17). While work with heterologously expressed enzyme systems has the advantage of allowing the identification of the particular enzymes responsible for metabolism, rat hepatocytes allow the simultaneous study of conjugative and oxidative metabolic pathways in a model that more closely resembles *in vivo* metabolism. The present results show that quercetin and kaempferol are extensively glucuronidated by rat hepatocytes (figure 2) with four glucuronides of quercetin and two of kaempferol being formed. The glucuronides formed by rat hepatocytes are the same ones formed by human UGT1A9-expressing microsomes, suggesting that this enzyme plays a key role in the glucuronidation of polyphenols. Other forms of UGT enzymes (such as UGT1A6) previously have been implicated in the metabolism of flavonoids (Galijatovic *et al.* 1999). The fact that quercetin and kaempferol are metabolized in a similar way by isolated rat hepatocytes and by an isolated UGT enzyme indicates that glucuronidation is an important pathway for the metabolism of flavonoids.

There has been considerable debate over whether not flavonoid glycosides can be absorbed intact or if hydrolysis of the glycosidic bond is required before absorption. Paganga and RiceEvans (1997) and Mauri *et al.* (1999) detected flavonoid glycosides (at nanogram levels) in plasma. Hollman *et al.* (1999) reported that the bioavailability of quercetin glucoside was 20 times higher than that of rutin (quercetin rutinoside), which suggests that the specific type of sugar moiety present on different flavonoid glycosides may influence their bioavailability. The present results are in agreement with these findings, confirming that some flavonoid glycosides can be absorbed, although the levels detected were low.

Considering the wide dietary occurrence of flavonoids and their alleged chemopreventive action, more work directed towards clarifying the extent to which they are absorbed and metabolized is still needed.

Acknowledgements

The authors thank the Wellcome Trust for supporting the purchase of an LC-MS system, and Dr Roy Rampling for taking blood samples.

References

Boulton, D. W., Walle, U. K. and Walle, T., 1999, Fate of the flavonoid quercetin in human cell lines: Chemical instability and metabolism. *Journal of Pharmacy and Pharmacology*, **51**, 353–359.

Boutin, J. A., Meunier, F., Lambert, P. H., Hennig, P., Bertin, D., Serkiz, B. and Volland, J. P., 1993, *In-vivo* and *in-vitro* glucuronidation of the flavonoid diosmetin in rats. *Drug Metabolism and Disposition*, **21**, 1157–1166.

DeVries, J. H. M., Janssen, P., Hollman, P. C. H., vanStaveren, W. A. and Katan, M. B., 1997, Consumption of quercetin and kaempferol in free-living subjects eating a variety of diets. *Cancer Letters*, **114**, 141–144.

Galijatovic, A., Otake, Y., Walle, U. K. and Walle, T., 1999, Extensive metabolism of the flavonoid chrysin by human Caco-2 and Hep G2 cells. *Xenobiotica*, **29**, 1241–1256.

Hasler, A. and Sticher, O., 1992, Identification and determination of the flavonoids from *Ginkgo biloba* by high-performance liquid chromatography. *Journal of Chromatography A*, **605**, 41–48.

Hollman, P. C. H., 1997, Bioavailability of flavonoids. *European Journal of Clinical Nutrition*, **51**, S66–S69.

Hollman, P. C. H., Bijsman, M., van Gameren, Y., Cnossen, E. P. J., de Vries, J. H. M. and Katan, M. B., 1999, The sugar moiety is a major determinant of the absorption of dietary flavonoid glycosides in man. *Free Radical Research*, **31**, 569–573.

Hollman, P. C. H. and Katan, M. B., 1999, Dietary flavonoids: intake, health effects and bioavailability. *Food and Chemical Toxicology*, **37**, 937–942.

Hollman, P. C. H., vanTrijp, J. M. P., Buysman, M., VanderGaag, M. S., Mengelers, M. J. B., deVries, J. H. M. and Katan, M. B., 1997, Relative bioavailability of the antioxidant flavonoid quercetin from various foods in man. *FEBS Letters*, **418**, 152–156.

Mauri, P. L., Iemoli, L., Gardana, C., Riso, P., Simonetti, P., Porrini, M. and Pietta, P. G., 1999, Liquid chromatography electrospray ionization mass spectrometric characterization of flavonol glycosides in tomato extracts and human plasma. *Rapid Communications in Mass Spectrometry*, **13**, 924–931.

Middleton, E., 1996, Biological properties of plant flavonoids: an overview. *International Journal of Pharmacology*, **34**, 344–348.

Moldeus, P., Hogberg, J. and Orrenius, S., 1978, Isolation and use of liver cells. *Methods in Enzymology*, **52**, 60–71.

Oliveira, E. J. and Watson, D. G., 2000, *In vitro* glucuronidation of kaempferol and quercetin by human UGT-1A9 microsomes. *FEBS Letters*, **471**, 1–6.

Paganga, G. and RiceEvans, C. A., 1997, The identification of flavonoids as glycosides in human plasma. *FEBS Letters*, **401**, 78–82.

Perego, R., Beccaglia, P., Angelini, M., Villa, P. and Cova, D., 1993, Pharmacokinetic studies of diosmin and diosmetin in perfused-rat liver. *Xenobiotica*, **23**, 1345–1352.

Spencer, J. P. E., Chowrimootoo, G., Choudhury, R., Debnam, E. S., Srai, S. K. and RiceEvans, C., 1999, The small intestine can both absorb and glucuronidate luminal flavonoids. *FEBS Letters*, **458**, 224–230.

XENOBIOTICA, 2002, VOL. 32, NO. 4, 289–303

Taylor & Francis
healthsciences

Metabolite of 2,2′,4′,5-tetrabromobiphenyl, 3-methylsulphonyl-2,2′,4′,5-tetrabromobiphenyl, a potent inducer of CYP2B1/2 in rat

Y. KATO†*, K. HARAGUCHI‡, S. YUMOTO†, T. YAMAZAKI†, Y. NAGANO†, N. KOGA§, Y. MASUDA‡ and R. KIMURA†

† School of Pharmaceutical Sciences, University of Shizuoka, 52-1, Yada, Shizuoka 422-8526, Japan
‡ Daiichi College of Pharmaceutical Sciences, 22-1, Tamagawa-cho, Minami-ku, Fukuoka 815-8511, Japan
§ Department of Food and Nutrition, Nakamura Gakuen University, 5-7-1 Befu, Johnan-ku, Fukuoka 814-0198, Japan

Received 10 July 2001

1. 3-Methylsulphonyl- and 4-methylsulphonyl-2,2′,4′,5-tetrabromobiphenyls (3-$MeSO_2$- and 4-$MeSO_2$-TetraBrBs) were detected in the liver, lung, kidney, adipose tissue and faeces of the 2,2′,4′,5-tetrabromobiphenyl (TetraBrB)-dosed rat.

2. The administration of 0.05–2.0 μmol kg^{-1} doses of 3-$MeSO_2$-TetraBrB produced corresponding increases in the hepatic concentration of the methyl sulphone metabolite, corresponding increases in the content of total cytochrome P450, and corresponding increases in the activities of 7-benzyloxy-, 7-ethoxy- and 7-pentoxyresorufin *O*-dealkylases. The inducing effects of the 3-$MeSO_2$-TetraBrB (0.2 μmol kg^{-1}), both on the content of total P450 and on the activities of the three alkoxyresorufin *O*-dealkylases, were higher than that of the parent TetraBrB (342 μmol kg^{-1}).

3. The major phenobarbital (PB)-inducible forms of P450, CYP2B1, CYP2B2, CYP3A2 and CYP2C6, were substantially induced by 3-$MeSO_2$-TetraBrB, but CYP1A1 and CYP1A2 were not. On the other hand, the activities of drug-metabolizing enzymes and the four PB-inducible forms of P450 were unchanged by 4-$MeSO_2$-TetraBrB treatment.

4. The induction profiles of these enzymes and P450 forms in rat treated with 3-$MeSO_2$-TetraBrB were similar to those treated with PB.

5. The inducing ability of 3-$MeSO_2$-TetraBrB (0.5 μmol kg^{-1}) both on the activities of the three alkoxyresorufin *O*-dealkylases and on the contents of four PB-inducible forms of P450 was roughly equal to that of PB (431 μmol kg^{-1} twice at a 24-h interval) or 3-$MeSO_2$-2,2′,4′,5-tetrachlorobiphenyl (1 μmol kg^{-1}). It is noteworthy that the effects of 3-$MeSO_2$-TetraBrB on the drug-metabolizing enzymes CYP2B1 and CYP2B2 were several thousand-fold higher than those of parent TetraBrB, while the effect of its isomeric 4-$MeSO_2$-TetraBrB were not.

6. The extent of hepatic accumulation of the 3-$MeSO_2$ metabolite after the administration of TetraBrB (342 μmol kg^{-1}) was almost the same as that after the administration of 3-$MeSO_2$-TetraBrB (0.1–0.2 μmol kg^{-1}). The relationship between the hepatic concentration of the 3-$MeSO_2$ metabolite and the extent of enzyme induction after the administration of TetraBrB or 3-$MeSO_2$-TetraBrB suggests that 3-$MeSO_2$-TetraBrB plays an important role in the induction of microsomal drug-metabolizing enzymes by TetraBrB.

* Author for correspondence; e-mail: kato@ys7.u-shizuoka-ken.ac.jp

Xenobiotica ISSN 0049–8254 print/ISSN 1366–5928 online © 2002 Taylor & Francis Ltd
http://www.tandf.co.uk/journals
DOI: 10.1080/00498250110107895

Introduction

Polybrominated biphenyls (PBrBs) have been used as fire retardants for moulded plastic parts such as the cases of televisions, typewriters and business machines (Carter 1976, WHO 1994). In 1973, for a few months, many Michigan residents unknowingly ate meat and dairy products contaminated with PBrBs (Dunckel 1975, Fries 1988). PBrBs are stable and lipophilic, and tend to accumulate in lipid-rich tissues in rat, cow and marine animals (Fries and Marrow 1975, Matthews *et al.* 1977, De Boer *et al.* 1998). Just like polychlorinated biphenyls (PCBs), PBrBs have been reported to elicit a number of toxic and other biological responses in diverse mammalian species (Garthoff *et al.* 1977, Hass *et al.* 1978, Fries 1988) and there are many studies of the toxicity of PBrBs (Garthoff *et al.* 1977, Dicarlo *et al.* 1978, Hass *et al.* 1978, Fries 1988). However, the biotransformation of PBrB to methylsulphonyl ($MeSO_2$) metabolite(s) in animals has not been reported to date. If PBrBs are biotransformed to $MeSO_2$ metabolite(s) in animals, $MeSO_2$-PBrBs may have biological activities and/or toxicological effects similar to the $MeSO_2$-PCBs.

We reported that the 3-$MeSO_2$ metabolites of PCBs are inducers of rat hepatic microsomal drug-metabolizing enzymes CYP2B1 and CYP2B2 (Kato *et al.* 1995a, b, 1997), and their inducing potency are several hundred times higher than the parent PCBs (Kato *et al.* 1995a, 1997). We also showed that the seven 3-$MeSO_2$ and two 4-$MeSO_2$ metabolites of tetra-, penta- and hexachlorobiphenyls reduced serum thyroxine (T_4) levels (Kato *et al.* 1998a, 1999), and the seven 3-$MeSO_2$-PCBs and 4-$MeSO_2$-2,2′,4′,5,5′-pentachlorobiphenyl increases in hepatic T_4 glucuronidation after the administration of the methyl sulphones possibly because of the induction of both UGT1A1 and UGT1A6 caused the reduction of serum T_4 levels (Kato *et al.* 2000).

The current study attempts to identify the $MeSO_2$ metabolites in the liver of rat after the administration of a PBrB congener, 2,2′,4′,5-tetrabromobiphenyl (TetraBrB), and, second, to compare the inductive effects of 3- and 4-$MeSO_2$-TetraBrBs on the drug-metabolizing enzyme system, with the parent TetraBrB.

Materials and methods

Chemicals

TetraBrB was synthesized by using the Cadogan (1962) coupling reactions. 3- and 4-$MeSO_2$-TetraBrBs and 3-$MeSO_2$-2,2′,4′,5-tetrachlorobiphenyl (3-$MeSO_2$-TetraCB) were prepared as described by Haraguchi *et al.* (1987). The purity of these compounds was >99% as determined by GC. 3-$MeSO_2$-4-methyl-2,3′,4′,5,5′-pentachlorobiphenyl (3-$MeSO_2$-4-Me-2,3′,4′,5,5′-pentaCB) was used as the internal standard. Panacete 810 (a mixture of medium-chain triglycerides) was purchased from Nippon Oils and Fats Co., Ltd (Tokyo, Japan); 7-benzyloxy-, 7-ethoxy- and 7-pentoxyresorufins were from Sigma Chemical Co., Ltd (St Louis, MO, USA); $NADP^+$, NADPH, glucose 6-phosphate disodium salt and glucose 6-phosphate dehydrogenase were from Oriental Yeast Co., Ltd (Osaka, Japan); and phenobarbital (PB) sodium was from Wako Pure Chemical Industries, Ltd (Osaka, Japan). The microsomal cytochrome P450 standards and antibodies against purified P450s were obtained from Daiichi Pure Chemicals Co., Ltd (Tokyo, Japan). A polyclonal antibody raised against rat CYP2B1, which detects both rat CYP2B1 and CYP2B2, a polyclonal antibody raised against rat CYP2C6 and CYP3A2, which detects rat CYP2C6 and CYP3A2, respectively, and a polyclonal antibody raised against rat CYP1A1, which detects both rat CYP1A1 and CYP1A2, were used. Other chemicals were obtained from commercial sources.

The spectroscopic properties of tetraBrB and its metabolites were as follows.

- TetraBrB: mass spectrum; *m/z* (relative abundance, %) 470 (100, M+4), 468 (74, M+2), 466 (18, M^+), 387 (33, M^+-Br), 308 (44, M^+-2Br).
- *3-MeSO$_2$-TetraBrB*: retention time on glc; 27.2 min. Mass spectrum; *m/z* (relative abundance, %):

548 (23, $M^+ + 4$), 546 (20, $M^+ + 2$), 544 (6, M^+), 465 (38, M^+-Br), 469 (100, M^+-Br + 4), 386 (8, M^+-2Br), 228 (36, M^+-MeSO$_2$-3Br); ^{1}H-NMR δ (ppm): 3.35 (3H, s, SO_2CH_3), 7.10 (1H, d, $J = 8.0$ Hz, 6′-H), 7.56 (1H, dd, $J = 1.8$, 8.0 Hz, 5′-H), 7.61 (1H, d, $J = 2.2$ Hz, 6-H), 7.87 (1H, d, $J = 1.8$ Hz, 3′-H), 8.40 (1H, d, $J = 2.2$ Hz, 4-H).

- *4-MeSO$_2$-TetraBrB*: retention time on glc; 28.1 min. Mass spectrum; *m/z* (relative abundance,%) 548 (100, $M^+ + 4$), 546 (75, $M^+ + 2$), 544 (20, M^+), 481 (5, M^+-MeSO), 465 (36, M^+-Br), 386 (22, M^+-2Br), 228 (62, M^+-MeSO$_2$-3Br); ^{1}H-NMR δ (ppm) 3.29 (3H, s, SO_2CH_3), 7.08 (1H, d, $J = 8.1$ Hz, 6′-H), 7.55 (1H, dd, $J = 1.8$, 8.1 Hz, 5′-H), 7.62 (1H, d, $J = 2.2$ Hz, 6-H), 7.88 (1H, d, $J = 1.8$ Hz, 3′-H), 8.43 (1H, d, $J = 2.2$ Hz, 3-H).

Animal treatment

Male Wistar rats, weighing 180–200 g, were housed three or four per cage with free access to food (MF, Oriental Yeast Co.) and tap water, and maintained on a 12-h dark/light cycle (08:00–20:00 hours light) in a room at a controlled temperature (24.5 ± 1°C) and humidity (55 ± 5%). Rats received an i.p. injection of TetraBrB (342 μmol kg^{-1}) and its MeSO$_2$ derivatives (0.05–2.0 μmol kg^{-1}) dissolved in Panacete 810 (5 ml kg^{-1}). Control animals received an equivalent volume of the vehicle. All rats were starved for 18 h before killing by decapitation at the designated time after the dosing.

Microsomal preparation and enzyme assays

Microsomes were prepared according to the procedure of Kato *et al.* (1995b). The protein content was determined by the method of Lowry *et al.* (1951) with bovine serum albumin as a standard. Total P450 content was estimated according to the method of Omura and Sato (1964). The activity of alkoxyresorufin *O*-dealkylase in microsomes was determined by the method of Burke *et al.* (1985). The immunoblotting and immunochemical quantitation were performed as described by Imaoka *et al.* (1987).

Isolation of metabolites

Sample cleanup and quantification were carried out according to our previous methods (Haraguchi *et al.* 1997). Briefly, liver samples were homogenized with acetone/*n*-hexane (2:1 v/v). An internal standard (3-MeSO$_2$-4-Me-2,3′,4′,5,5′-pentaCB, 70 ng) was added to each extract and the mixtures subjected to a gel permeation column packed with Bio-Beads S-X3 (50 g, Bio-Rad Laboratories, Hercules, CA, USA). Dichloromethane/*n*-hexane (1:1) was used as a mobile phase at a flow rate of 4 ml min^{-1}. The metabolite fraction (120–200 ml) was collected and subjected to GC analysis. Other tissue samples were purified as described for the liver.

Analytical methods

^{1}H-NMR spectra were obtained on a JEOL GSX-500 spectrometer (500 MHz). The samples were dissolved in chloroform-*d* with TMS as an internal standard. GC/MS was carried out on a JMS-AX505W (JEOL) apparatus connected to a JMA-DA5000 data system in the EI mode. The GC instrument was fitted with a DB-5MS fused silica capillary column (30 m × 0.25 mm i.d., J&W Scientific, Inc., Folsom, CA, USA) with helium as a carrier gas. Injection was carried out in the splitless mode. The oven temperature was programmed from 70 (2 min) to 220°C at 20°C min^{-1} and then to 280°C at 4°C min^{-1}. The GC for quantification was performed on a GC-14A (Shimadzu Co., Kyoto, Japan) instrument equipped with a ^{63}Ni electron-capture detector (ECD) with column conditions analogous to those described for GC/MS.

The metabolites in samples were identified on GC/MS by comparison with authentic synthesized metabolites. Recoveries of 3-MeSO$_2$-4-Me-2,3′,4′,5,5′-pentaCB added to liver samples before extraction were >85%. The quantification of metabolites was performed on a GC/ECD apparatus using 3-MeSO$_2$-4-Me-2,3′,4′,5,5′-pentaCB as an internal standard.

Statistics

The results were statistically analysed according to a Student's *t*-test.

Results

Identification of the MeSO$_2$ metabolites of TetraBrB

Figure 1 shows the GC/MS profiles of liver extracts from the TetraBrB-dosed rat. The mass spectra of metabolites MT-1 and MT-2 in the total ion chromatogram showed the molecular ion peaks (M^+) at *m/z* 544 and other characteristic

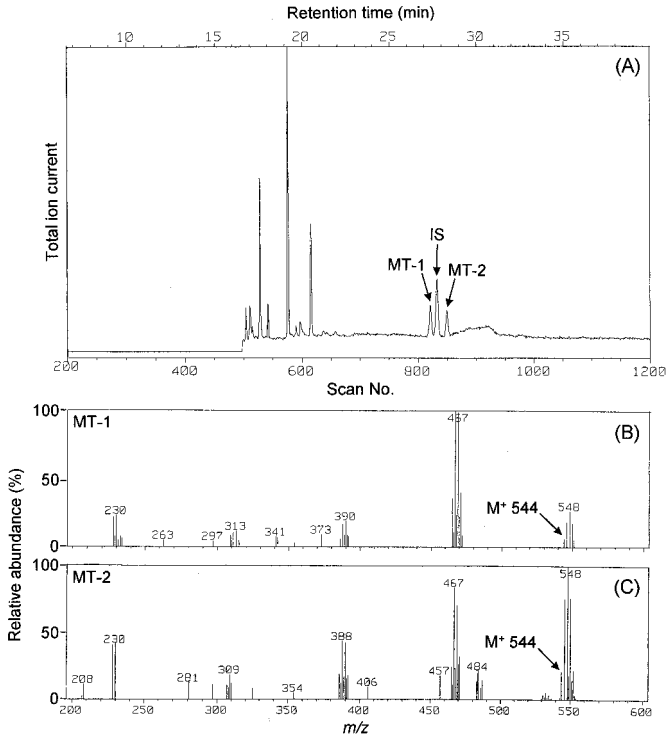


Figure 1. Total ion chromatogram (A) and mass spectra (B, C) of the liver extract from the TetraBrB-administered rat.

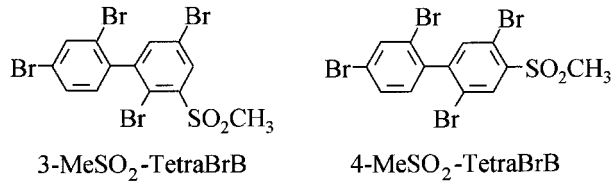


Figure 2. Chemical structures of the methyl sulphone metabolites of TetraBrB.

peaks at m/z 465, [M^+-Br]; at m/z 386, [M^+-2Br], and at m/z 228, [M^+-$MeSO_2$-3Br]. In addition, the mass spectra of MT-2 showed the characteristic peaks at m/z 481, [M^+-MeSO]. Thus, the spectral data suggested the presence of methylsulphone metabolites in the liver. The mass spectra and GCt_R of MT-1 and MT-2 (27.2 and 28.1 min, respectively) corresponded with those of authentic 3- and 4-$MeSO_2$-TetraBrBs, respectively. From these results, MT-1 and MT-2 were identified as 3- and 4-$MeSO_2$-TetraBrBs, respectively (figure 2). Both 3- and 4-$MeSO_2$-TetraBrBs were also detected in the lung, kidney, adipose tissue and faeces (data not shown).

Table 1 shows the concentration of TetraBrB, and 3-$MeSO_2$ and 4-$MeSO_2$ metabolites in the liver, lung, kidney and adipose tissue 96 h after the i.p. administration of 342 μmol kg^{-1} TetraBrB.

Table 1. Tissue concentrations of TetraBrB and its methyl sulphone metabolites after the administration of TetraBrB to rat.

	TetraBrB or methyl sulphone concentration (nmol g^{-1} tissue)		
Tissue	TetraBrB	3-MeSO$_2$-TetraBrB	4-MeSO$_2$-TetraBrB
Liver	4.54 ± 0.70	0.33 ± 0.05	0.28 ± 0.04
Lung	0.82 ± 0.03	0.08 ± 0.02	3.22 ± 0.58
Kidney	1.89 ± 0.30	0.06 ± 0.003	0.41 ± 0.05
Adipose tissue	151.83 ± 36.36	1.39 ± 0.34	1.80 ± 0.45

Rats were given 342 μmol kg^{-1} TetraBrB (i.p.) and killed 96 h after administration. Results are the mean ± SE for three to four animals.

The concentration of TetraBrB was highest (152 nmol g^{-1}) in adipose tissue, and was approximately 1–5 nmol g^{-1} in the liver, lung and kidney. The 3-MeSO$_2$ metabolite accumulated in the order adipose tissue > liver > lung > kidney. The concentration of the 4-MeSO$_2$ metabolite was the highest in the lung followed by adipose tissue, kidney and liver.

Induction of drug-metabolizing enzymes by 3-MeSO$_2$-TetraBrB

The time-course of accumulation of 3-MeSO$_2$-TetraBrB in the liver after the i.p. administration of 0.35 μmol kg^{-1} 3-MeSO$_2$-TetraBrB is shown in figure 3, reaching a maximum at around 168 h.

Figure 4 shows the time-courses of the content of total P450 and the activities of alkoxyresorufin *O*-dealkylases in liver microsomes after the i.p. administration of 0.35 μmol kg^{-1} 3-MeSO$_2$-TetraBrB. The content of total P450 and activities of 7-benzyloxy-, 7-ethoxy- and 7-pentoxyresorufin *O*-dealkylases significantly increased 48 h after dosing, and were 2.0-, 59-, 3.6- and 33-fold of control (0 h) levels, respectively, at 96 h, and remained elevated at 168 h post-dosing.

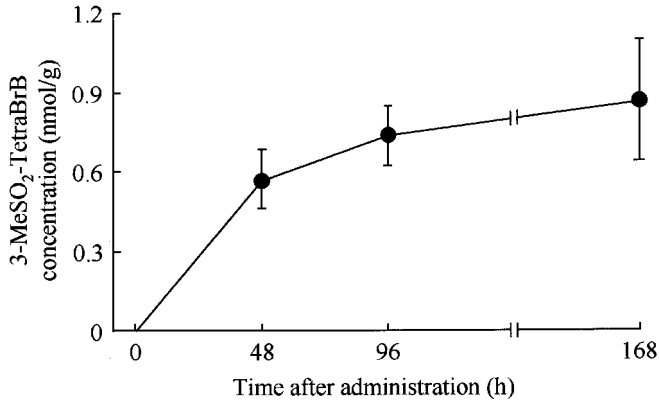


Figure 3. Time-course of the liver concentration of the methyl sulphone after the administration of 3-MeSO$_2$-TetraBrB to rat. Rats were given 0.35 μmol kg^{-1} 3-MeSO$_2$-TetraBrB (i.p.) and killed at the indicated times after administration. Each point represents the mean ± SEM (vertical bars) for four animals.

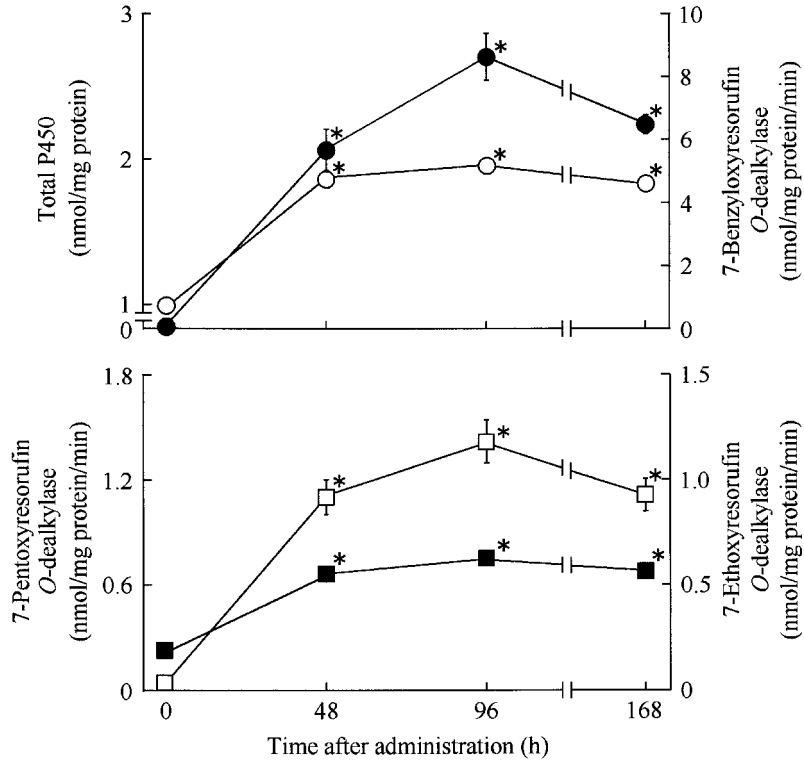


Figure 4. Effects of 3-$MeSO_2$-TetraBrB on the content of total P450 and the activities of drug-metabolizing enzymes of rat liver microsomes. The experimental conditions were the same as described in figure 3. ○, Total P450; ●, 7-benzyloxyresorufin *O*-dealkylase; □, 7-pentoxyresorufin *O*-dealkylase; ■, 7-ethoxyresorufin *O*-dealkylase. Each point represents the mean ± SEM (vertical bars) for five to eight animals. $^*P < 0.001$, significantly different from the control (0 h).

To clarify the relationship between hepatic concentration and the inducing effect on the drug-metabolizing enzymes, we examined the activities of drug-metabolizing enzymes, the contents of P450 forms and the hepatic concentration of methyl sulphone 96 h after the administration of 3-$MeSO_2$-TetraBrB at various doses.

As shown in figure 5, the hepatic concentration of 3-$MeSO_2$-TetraBrB increased in proportion to the dose of 3-$MeSO_2$-TetraBrB. As shown in figure 6, 0.05 μmol kg^{-1} 3-$MeSO_2$-TetraBrB significantly increased both the content of total P450 and activities of 7-benzyloxy-, 7-ethoxy- and 7-pentoxyresorufin *O*-dealkylases. The methyl sulphone caused dose-dependent increases in the content of total P450 and in the extent of dealkylation of 7-benzyloxyresorufin and 7-pentoxyresorufin in the range 0.05–2.0 μmol kg^{-1}, and of 7-ethoxyresorufin of liver microsomes in the range 0.05–0.35 μmol kg^{-1}.

The levels of PB-inducible forms of P450 in hepatic microsomes after the administration of 3-$MeSO_2$-TetraBrB to rat are shown in figure 7. A 0.1 μmol kg^{-1} dose of 3-$MeSO_2$-TetraBrB significantly induced CYP2B1, CYP2B2, CYP3A2 and CYP2C6. The methyl sulphone produced dose-related inductions of CYP2B1, CYP2B2 and CYP3A2 in liver microsomes in the range 0.1–0.5 μmol kg^{-1}. The

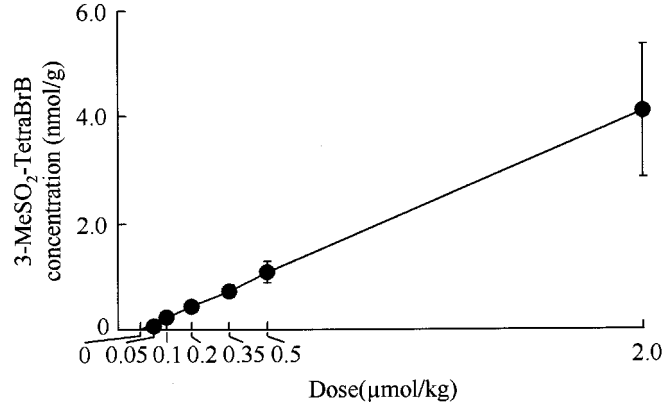


Figure 5. Liver concentrations of 3-MeSO$_2$-TetraBrB after the administration of 3-MeSO$_2$-TetraBrB in graded doses to rat. Rats were given 3-MeSO$_2$-TetraBrB (i.p.) at the various doses indicated and killed 96 h after administration. Each point represents the mean ± SEM (vertical bars) for four animals.

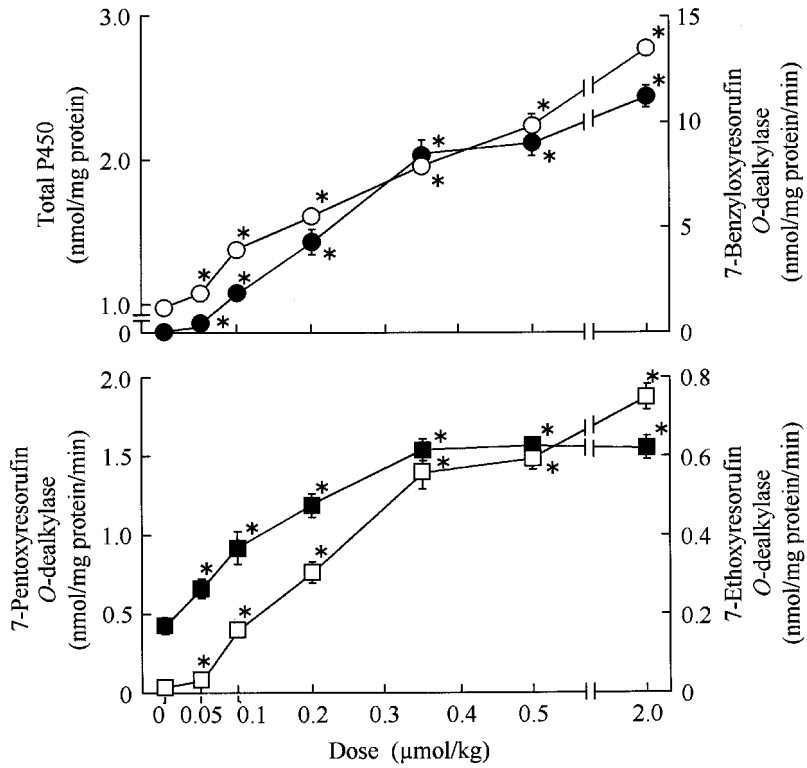


Figure 6. Effects of graded doses of 3-MeSO$_2$-TetraBrB on the content of total P450 and the activities of drug-metabolizing enzymes of liver microsomes in rat. The experimental conditions were the same as described in figure 5. ○, Total P450; ●, 7-benzyloxyresorufin *O*-dealkylase; □, 7-pentoxyresorufin *O*-dealkylase; ■, 7-ethoxyresorufin *O*-dealkylase. Each point represents the mean ± SEM (vertical bars) for five to eight animals. $^*P < 0.05$, significantly different from the control.

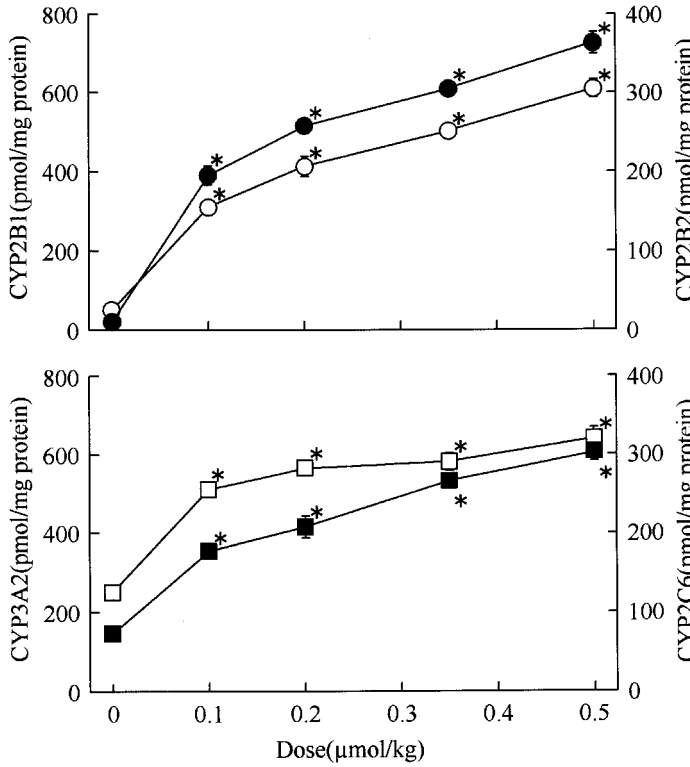


Figure 7. Effects of graded doses of 3-$MeSO_2$-TetraBrB on the contents of P450 forms in rat liver microsomes. The experimental conditions were the same as described in figure 5. The contents of P450 forms were assayed by densitometry of nitrocellulose immunoblotted from an SDS-polyacrylamide gel. Hepatic microsomes (1–5 μg protein) were analysed by Western blotting. Measurement was done with duplicates of three to seven different preparations of microsomes. ●, CYP2B1; ○, CYP2B2; ■, CYP3A2; □, CYP2C6. Each point represents the mean ± SEM (vertical bars) for three to seven animals. $^*P < 0.001$, significantly different from the control.

major PB-inducible forms, CYP2B1 and CYP2B2, were induced 35- and 11.4-fold of control by this methyl sulphone at 0.5 μmol kg^{-1}, respectively. In contrast, CYP1A1 was not detected, and no change was observed in CYP1A2 content after the administration of 3-$MeSO_2$-TetraBrB (0.5 μmol kg^{-1}) (data not shown).

Comparative studies of inducing effects

The effect of 3-$MeSO_2$-TetraBrB on the content of total P450, on the activities of drug-metabolizing enzymes and on the contents of P450 forms were compared with that of 3-$MeSO_2$-TetraCB and PB (figures 8 and 9).

The inducing abilities of 0.5 μmol kg^{-1} 3-$MeSO_2$-TetraBrB both on the content of total P450 and activities of the three alkoxyresorufin *O*-dealkylases were almost the same as that of 1 μmol kg^{-1} 3-$MeSO_2$-TetraCB or that of 431 μmol kg^{-1} PB twice at a 24-h interval (figure 8). A similar profile was observed for the induction of CYP2B1, CYP2B2, CYP3A2 and CYP2C6 (figure 9). CYP1A1 was not detected (data not shown) and CYP1A2 was not changed by 3-$MeSO_2$-TetraBrB (figure 9).

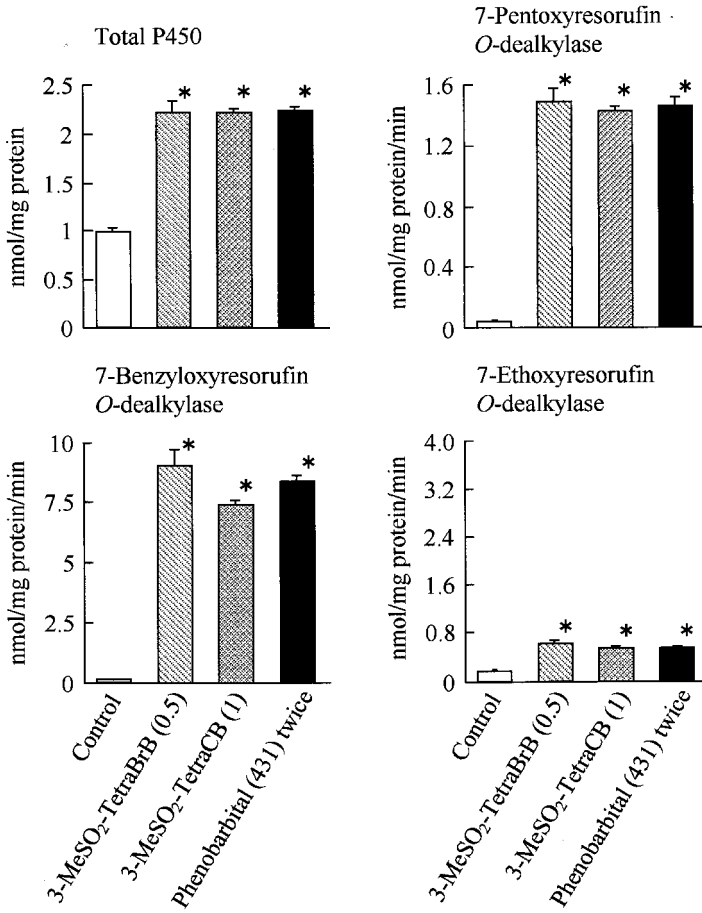


Figure 8. Effects of 3-$MeSO_2$-TetraBrB, 3-$MeSO_2$-TetraCB and phenobarbital on the content of total P450 and the activities of drug-metabolizing enzyme of rat liver microsomes. Rats were given 3-$MeSO_2$-TetraBrB or 3-$MeSO_2$-TetraCB (i.p.) and killed 96 h after administration. Phenobarbital was injected i.p. into rats twice with a 24-h interval and killed 24 h after the second injection. Results are the mean ± SEM for five to eight animals. The value in parentheses is a dose ($\mu mol\,kg^{-1}$) for each group. $^*P < 0.001$, significantly different from the control.

Role of 3-$MeSO_2$-TetraBrB

Figures 10 and 11 show the relationship between the concentrations of 3- and 4-$MeSO_2$-TetraBrBs with the activities of drug-metabolizing enzymes, and with the contents of P450 forms in the liver after the administration of TetraBrB and its $MeSO_2$ derivatives to rat.

The extents of both the hepatic accumulation of the 3-$MeSO_2$ metabolite and the induction of P450, 7-pentoxy- and 7-benzyloxyresorufin *O*-dealkylases, and CYP2B1, CYP2B2, CYP3A2 and CYP2C6 after the administration of TetraBrB ($342\,\mu mol\,kg^{-1}$) was almost the same as those after the administration of 3-$MeSO_2$-TetraBrB ($0.1–0.2\,\mu mol\,kg^{-1}$). The 4-$MeSO_2$-TetraBrB metabolite ($0.35\,\mu mol\,kg^{-1}$) had no effect on the content of P450, on the activities of the two alkoxyresorufin *O*-dealkylases and on the contents of PB-inducible forms of P450. Even $5\,\mu mol\,kg^{-1}$ 4-$MeSO_2$-TetraBrB had no effect (data not shown).

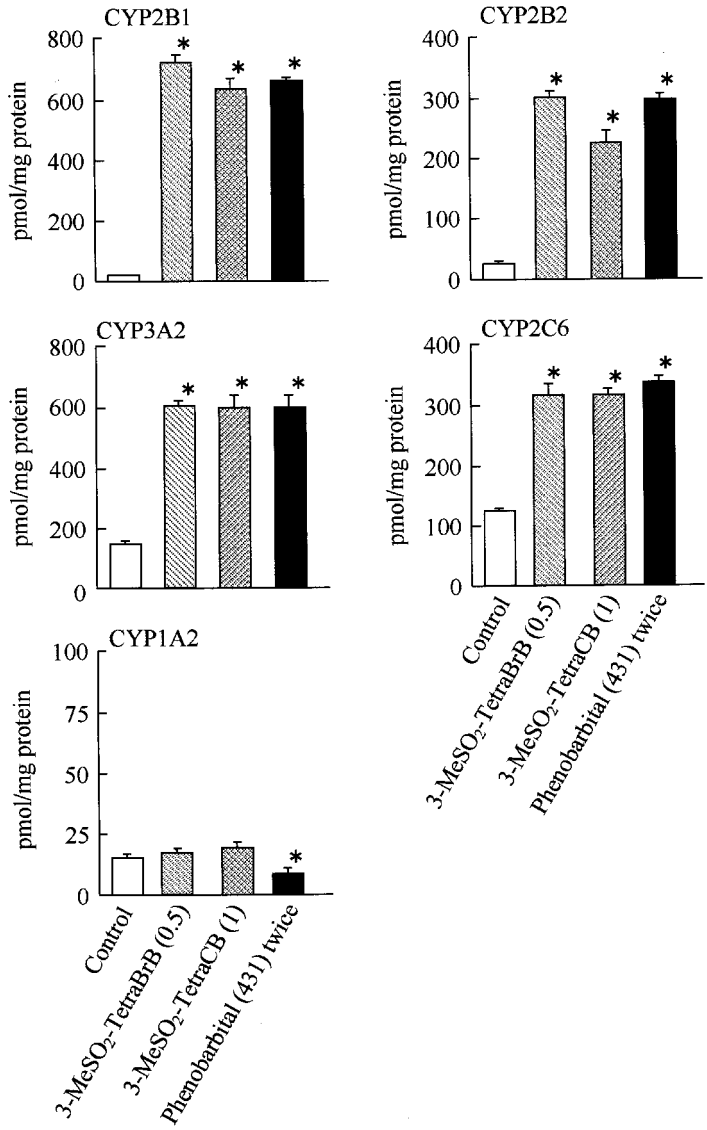


Figure 9. Effects of 3-$MeSO_2$-TetraBrB, 3-$MeSO_2$-TetraCB and phenobarbital on the contents of P450 forms of rat hepatic microsomes. The experimental conditions were the same as described in figure 8. Assays were done under same conditions as described in figure 7. Results are the mean ± SEM (vertical bars) for three to seven animals. The value in parentheses is a dose ($\mu mol\,kg^{-1}$) for each group. $^*P < 0.001$, significantly different from the control.

Discussion

The formation of sulphur-containing metabolites of PCBs in mouse and rat has been well established (Mio *et al.* 1976, Mizutani *et al.* 1978, Brandt *et al.* 1982). The current paper has shown that 3- and 4-$MeSO_2$-TetraBrBs (MT-1, MT-2) were present in the liver, lung, kidney, adipose tissue and faeces of rat administered TetraBrB. This suggests that 3- and 4-$MeSO_2$ metabolites may readily be formed from PBrB congeners and subsequently may accumulate in several tissues

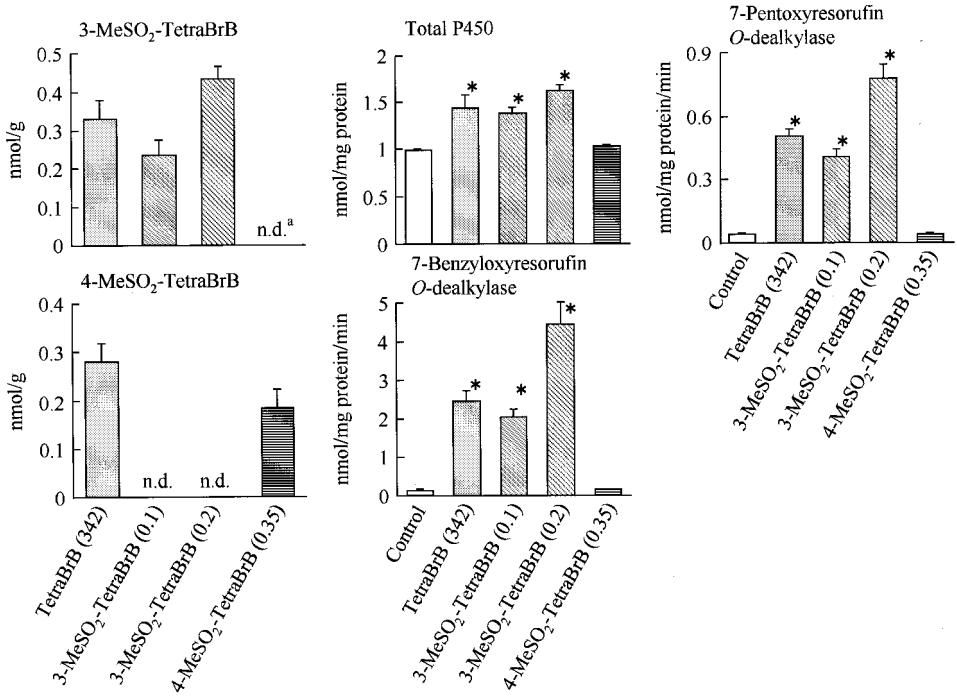


Figure 10. Relationship between the liver concentrations of 3- and 4-$MeSO_2$-TetraBrBs, the content of P450, and the activities of drug-metabolizing enzymes after the administration of TetraBrB and its $MeSO_2$ derivatives to rat. Rats were given TetraBrB or its $MeSO_2$ derivatives (i.p.) and killed 96 h after administration. Results are the mean ± SEM (vertical bars) for four to eight animals. The value in parentheses is the dose ($\mu mol\,kg^{-1}$) for each group. [a]Not detected. *$P < 0.01$, significantly different from the control.

of animals such as the 3- and 4-$MeSO_2$ metabolites of PCBs, which are formed in the tissues of mammals (Bergman *et al.* 1992, 1994, Haraguchi *et al.* 1992, Letcher *et al.* 1995) and man (Haraguchi *et al.* 1989, Norén *et al.* 1996, Weistrand and Norén 1997, Weistrand *et al.* 1997).

A specific affinity for 3-$MeSO_2$-PCBs for the liver has been observed in the gray seal (*Halichoerus grypus*) (Bergman *et al.* 1994), otter (*Lutra lutra*) (Bergman *et al.* 1994) and mink (*Mustela vison*) (Klasson-Wehler *et al.* 1996). In contrast, the specific retention of 4-$MeSO_2$-PCBs in the lung has been reported for rat (Haraguchi *et al.* 1999), mouse (Bergman *et al.* 1979, Klasson-Wehler *et al.* 1996) and mink (Klasson-Wehler *et al.* 1996). The binding proteins for 4-$MeSO_2$-PCBs have been identified as an uteroglobin-like protein residing in the pulmonary Clara cells (Härd *et al.* 1995, Gillner *et al.* 1988), or as a fatty acid-binding protein in the chicken liver (Larsen *et al.* 1992). The 4-$MeSO_2$ metabolites of 2,2′,4′,5-tetraBrB may also selectively accumulate in the lung through the same binding mechanism as that of the 4-$MeSO_2$ metabolites of PCBs, although this has yet to be confirmed.

The 3-$MeSO_2$-TetraBrB metabolite caused significant increases in both the content of total P450 and the activities of 7-pentoxy-, 7-benzyloxy- and 7-ethoxyresorufin *O*-dealkylases. The increased content and enzyme activities remained elevated up to 168 h after the administration of 3-$MeSO_2$-TetraBrB.

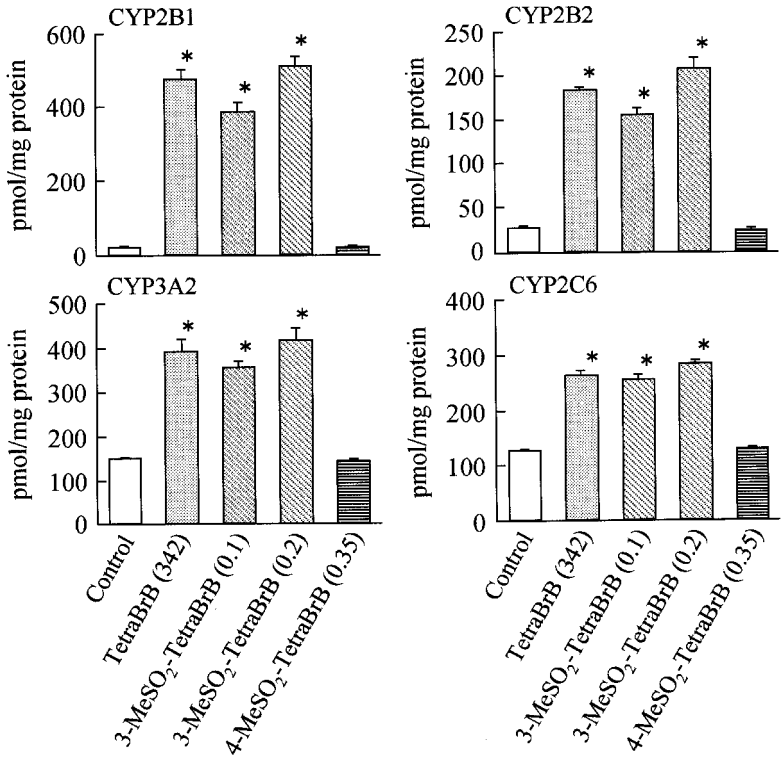


Figure 11. Relationship between the liver concentrations of 3- and 4-$MeSO_2$-TetraBrBs, and the contents of P450 forms after the administration of TetraBrB and its $MeSO_2$derivatives. The experimental conditions were the same as in figure 10. Assays were done under same conditions as described in figure 7. Results are the mean ± SEM (vertical bars) for four to six animals. The value in parentheses is a dose ($\mu mol\,kg^{-1}$) for each group. $^*P < 0.01$, significantly different from the control.

The prolonged induction of hepatic microsomal drug-metabolizing enzymes may be due to the prolonged presence of 3-$MeSO_2$-TetraBrB in the liver.

The dose-related increases in both the activities of drug-metabolizing enzymes and the contents of CYP2B1, CYP2B2, CYP3A2 and CYP2C6 after the administration of 3-$MeSO_2$-TetraBrB are considered to be due to the rise in the hepatic concentration of 3-$MeSO_2$-TetraBrB after dosing. The comparison of the inducing abilities of 3-$MeSO_2$-TetraBrB ($0.5\,\mu mol\,kg^{-1}$) with those of 3-$MeSO_2$-TetraCB ($1\,\mu mol\,kg^{-1}$), PB ($431\,\mu mol\,kg^{-1}$ twice), and the parent TetraBrB ($342\,\mu mol\,kg^{-1}$) indicated that 3-$MeSO_2$-TetraBrB has a comparatively pronounced inductive effect on the hepatic drug-metabolizing enzymes CYP2B1, CYP2B2, CYP3A2 and CYP2C6.

The induction profiles of the drug-metabolizing enzymes and four PB-inducible forms of P450 of rat treated with 3-$MeSO_2$-TetraBrB were similar to those of rat treated with PB. This finding indicates that 3-$MeSO_2$-TetraBrB is a PB-like inducer of microsomal drug-metabolizing enzymes, analogous to the 3-$MeSO_2$ metabolites of PCBs.

It has been reported that the potent PB-like inducer, 1,4-bis[2-(3,5-dichloropyridyloxy)]benzene, is 600 times more potent than PB as an inducer of *Cyp2b* in

mouse (Poland *et al.* 1980, 1981), and, by comparison, 3-MeSO$_2$-TetraBrB was 1700 times more potent than PB as an inducer of CYP2B1/2 in rat at an estimate in accordance with their doses and dose times. Therefore, 3-MeSO$_2$-TetraBrB is the most potent PB-like inducer of the CYP2B1 and CYP2B2 described to date, with an inducing potency several thousand times more than that of the parent TetraBrB.

When a 342 μmol kg^{-1} dose of TetraBrB was administered to rat, the hepatic concentration of 3-MeSO$_2$-TetraBrB 96 h after dosing was similar to that after the administration of 0.1–0.2 μmol kg^{-1} 3-MeSO$_2$-TetraBrB. The increases in the content of total P450 in the activities of 7-pentoxy- and 7-benzyloxyresorufin *O*-dealkylases and in the contents of CYP2B1, CYP2B2, CYP3A2 and CYP2C6 96 h after the administration of TetraBrB were almost equal to the increases 96 h after the administration of 3-MeSO$_2$-TetraBrB. Thus, 3-MeSO$_2$-TetraBrB is considered to play an important role in the induction mediated by the TetraBrB. On the other hand, 4-MeSO$_2$-TetraBrB did not appear to be involved in the induction process because it had no inducing effect, as was the case with the 4-MeSO$_2$ derivatives of PCB congeners (Kato *et al.* 1995a, b).

The above observations suggest that the inducing effect of TetraBrB on hepatic microsomal drug-metabolizing enzymes is attributable not to the action of TetraBrB *per se*, but to that of its MeSO$_2$ metabolite, 3-MeSO$_2$-TetraBrB.

Acknowledgements

Research was partially funded by a Grant-in-Aid for Scientific Research (C) (Nos 12680549, Y. K., and 12672180, K. H.) from the Japan Society for the Promotion of Science, and by a Health Sciences Research Grants for Research on Environmental Health from the Ministry of Health and Welfare.

References

Bergman, Å., Athanasiadou, M., Bergek, S., Haraguchi, K., Jensen, S. and Klasson-Wehler, E., 1992, PCB and PCB methyl sulfones in mink treated with PCB and various PCB fractions. *Ambio*, **21**, 570–576.

Bergman, Å., Brandt, I. and Jansson, B., 1979, Accumulation of methylsulphonyl derivatives of some bronchial-seeking polychlorinated biphenyls in the respiratory tract of mice. *Toxicology and Applied Pharmacology*, **48**, 213–220.

Bergman, Å., Norstrom, R. J., Haraguchi, K., Kuroki, H. and Béland, P., 1994, PCB and DDE methyl sulfones in mammals from Canada and Sweden. *Environmental and Toxicological Chemistry*, **13**, 121–128.

Brandt, I., Darnerud, P. O., Bergman, Å. and Larsson, Y., 1982, Metabolism of 2,4′,5-trichlorobiphenyl: Enrichment of hydroxylated and methyl sulphone metabolites in the uterine luminal fluid of pregnant mice. *Chemico-Biological Interactions*, **40**, 45–56.

Burke, M. D., Thompson, S., Elcombe, C. R., Halpert, J., Haaparanta, T. and Mayer, R. T., 1985, Ethoxy-, pentoxy- and benzyloxyphenoxazones and homologues: a series of substrates to distinguish between different induced cytochromes P-450. *Biochemical Pharmacology*, **34**, 3337–3345.

Cadogan, J. I. G., 1962, A convenient new method of aromatic arylation. *Journal of the Chemical Society*, 4257–4258.

Carter, L. J., 1976, Michigan's PBB incident: chemical mix-up leads to disaster. *Science*, **192**, 240–243.

De Boer, J., Wester, P. G., Klamer, H. J. C., Lewis, W. E. and Boon, J. P., 1998, Do flame retardants threaten ocean life? *Nature*, **394**, 28–29.

Dicarlo, F. J., Seifter, J. and Decarlo, V. J., 1978, Assessment of the hazards of polybrominated biphenyls. *Environmental Health Perspectives*, **23**, 351–365.

Dunckel, A. E., 1975, An updating of the polybrominated biphenyl disaster in Michigan. *Journal of the American Veterinary and Medical Association*, **167**, 838–841.

Fries, G. F., 1988, The PBB episode in Michigan: an overall appraisal. *CRC Critical Reviews in Toxicology*, **16**, 105–156.

Fries, G. F. and Marrow, G. S., 1975, Excretion of polybrominated biphenyls into the milk of cows. *Journal of Dairy Science*, **58**, 947–951.

Garthoff, L. H., Friedman, L., Farber, T. M., Locke, K. K., Sobotka, T. J., Green, S., Hurley, N. E., Peters, E. L., Story, G. E., Moreland, F. M., Graham, C. H., Keys, J. E., Taylor, M. J., Scalera, J. V., Rothlein, J. E., Marks, E. M., Cerra, F. E., Rodi, S. B. and Sporn, E. M., 1977, Biochemical and cytogenetic effects in rats caused by short-term ingestion of Aroclor 1254 or Firemaster BP-6. *Journal of Toxicology and Environmental Health*, **3**, 769–796.

Gillner, M., Lund, J., Cambillau, C., Alexandersson, M., Hurtig, U., Bergman, Å., Klasson-Wehler, E. and Gustafsson, J.-Å., 1988, The binding of methylsulfonyl-polychlorobiphenyls to uteroglobin. *Journal of Steroid Biochemistry*, **31**, 27–33.

Haraguchi, K., Athanasiadou, M., Bergman, Å., Hovander, L. and Jensen, S., 1992, PCB and PCB methyl sulfones in selected groups of seals from Swedish waters. *Ambio*, **21**, 546–549.

Haraguchi, K., Kato, Y., Kimura, R. and Masuda, Y., 1999, Tissue distribution of methylsulfonyl metabolites derived from 2,2′,4,5,5′-penta- and 2,2′,3,4′,5′,6-hexachlorobiphenyls in rats. *Archives of Environmental and Contamination Toxicology*, **37**, 135–142.

Haraguchi, K., Kato, Y., Masuda, Y. and Kimura, R., 1997, Metabolism of 3,3′,4,4′-tetrachlorobiphenyl via sulphur-containing pathway in rat: liver-specific retention of methylsulphonyl metabolite. *Xenobiotica*, **27**, 831–842.

Haraguchi, K., Kuroki, H. and Masuda, Y., 1987, Synthesis and characterization of tissue-retainable methylsulfonyl polychlorinated biphenyl isomers. *Journal of Agriculture and Food Chemistry*, **35**, 178–182.

Haraguchi, K., Kuroki, H. and Masuda, Y., 1989, Polychlorinated biphenyl methylsulfone congeners in human tissues: identification of methylsulfonyl dichlorobiphenyls. *Chemosphere*, **18**, 477–484.

Härd, T., Barnes, H. J., Larsson, C., Gustafsson, J.-Å. and Lund, J., 1995, Solution structure of a mammalian PCB-binding protein in complex with a PCB. *Nature Structural Biology*, **2**, 983–989.

Hass, J. R., McConnell, E. E. and Harvan, D. J., 1978, Chemical and toxicologic evaluation of firemaster BP-6. *Journal of Agriculture and Food Chemistry*, **26**, 94–99.

Imaoka, S., Terano, Y. and Funae, Y., 1987, Purification and characterization of two constitutive cytochromes P-450 (F-1 and F-2) from adult female rats: identification of P-450F-1 as the phenobarbital-inducible cytochrome P-450 in male rat liver. *Biochimica et Biophysica Acta*, **916**, 358–367.

Kato, Y., Haraguchi, K., Kawashima, M., Yamada, S., Isogai, M., Masuda, Y. and Kimura, R., 1995a, Characterization of hepatic microsomal cytochrome P-450 from rats treated with methylsulphonyl metabolites of polychlorinated biphenyl congeners. *Chemico-Biological Interactions*, **95**, 269–278.

Kato, Y., Haraguchi, K., Kawashima, M., Yamada, S., Masuda, Y. and Kimura, R., 1995b, Induction of hepatic microsomal drug-metabolizing enzymes by methylsulphonyl metabolites of polychlorinated biphenyl congeners in rats. *Chemico-Biological Interactions*, **95**, 257–268.

Kato, Y., Haraguchi, K., Shibahara, T., Masuda, Y. and Kimura, R., 1998, Reduction of thyroid hormone levels by methylsulfonyl metabolites of polychlorinated biphenyl congeners in rats. *Archives of Toxicology*, **72**, 541–544.

Kato, Y., Haraguchi, K., Shibahara, T., Shinmura, Y, Masuda, Y. and Kimura, R., 2000, The induction of hepatic microsomal UDP-glucuronosyltransferase by the methylsulfonyl metabolites of polychlorinated biphenyl congeners in rats. *Chemico-Biological Interactions*, **125**, 107–115.

Kato, Y., Haraguchi, K., Shibahara, T., Yumoto, S., Masuda, Y. and Kimura, R., 1999, Reduction of thyroid hormone levels by methylsulfonyl metabolites of tetra- and pentachlorinated biphenyls in male Sprague–Dawley rats. *Toxicology Science*, **48**, 51–54.

Kato, Y., Haraguchi, K., Tomiyasu, K., Saito, H., Isogai, M., Masuda, Y. and Kimura, R., 1997, Structure-dependent induction of CYP2B1/2 by 3-methylsulfonyl metabolites of polychlorinated biphenyl congeners in rats. *Environmental and Toxicological Pharmacology*, **3**, 137–144.

Klasson-Wehler, E., Hovander, L. and Lund, B.-O., 1996, 2,2′,4,5,5′-Pentachlorobiphenyl: Comparative metabolism in mink (*Mustela vison*) and mouse. *Chemical Research in Toxicology*, 9, 1340–1349.

Larsen, G. L., Huwe, J. K., Bergman, Å., Klasson-Wehler, E. and Hargis, P., 1992, Methylsulfonyl metabolites of xenobiotics can serve as ligands for fatty acid binding proteins in chicken liver and in intestinal mucosa. *Chemosphere*, **25**, 1189–1194.

Letcher, R. J., Norstrom, R. J. and Bergman, Å., 1995, Geographical distribution and identification of methyl sulphone PCB and DDE metabolites in pooled polar bear (*Ursus maritimus*) adipose tissue from western hemisphere Arctic and Subarctic regions. *Science of the Total Environment*, **160/161**, 409–420.

Lowry, O. H., Rosebrough, N. J., Farr, A. L. and Randall, R. J., 1951, Protein measurement with the Folin phenol reagent. *Journal of Biological Chemistry*, **193**, 265–275.

Matthews, H. B., Kato, S., Morales, N. M. and Tuey, D. B., 1977, Distribution and excretion of 2,4,5,2′,4′,5′-hexabromobiphenyl, the major component of Firemaster BP-6. *Journal of Toxicology and Environmental Health*, **3**, 599–605.

Mio, T., Sumino, K. and Mizutani, T., 1976, Sulfur-containing metabolites of 2,5,2′,5′-tetrachlorobiphenyl, a major component of commercial PCB's. *Chemical Pharmacology Bulletin*, **24**, 1958–1960.

Mizutani, T., Yamamoto, K. and Tajima, K., 1978, Sulfur-containing metabolites of chlorobiphenyl isomers, a comparative study. *Journal of Agriculture and Food Chemistry*, **26**, 862–866.

Norén, K., Lundén, Å., Pettersson, E. and Bergman, Å., 1996, Methylsulfonyl metabolites of PCBs and DDE in human milk in Sweden, 1972–1992. *Environmental Health Perspectives*, **104**, 766–772.

Omura, T. and Sato, R., 1964, The carbon monoxide-binding pigment of liver microsomes I. Evidence for its hemoprotein nature. *Journal of Biological Chemistry*, **239**, 2370–2378.

Poland, A., Mak, I. and Glover, E., 1981, Species differences in responsiveness to 1,4-bis[2-(3,5-dichloropyridyloxy)]-benzene, a potent phenobarbital-like inducer of microsomal monooxygenase activity. *Molecular Pharmacology*, **20**, 442–450.

Poland, A., Mak, I., Glover, E., Boatman, R. J., Ebetino, F. H. and Kende, A. S., 1980, 1,4-Bis[2-(3,5-dichloropyridyloxy)]benzene, a potent phenobarbital-like inducer of microsomal monooxygenase activity. *Molecular Pharmacology*, **18**, 571–580.

Weistrand, C. and Norén, K., 1997, Methylsulfonyl metabolites of PCBs and DDE in human tissues. *Environmental Health Perspectives*, **105**, 644–649.

Weistrand, C., Norén, K. and Nilsson, A., 1997, Occupational exposure, Organochlorine compounds in blood plasma from potentially exposed workers: PCB, PCN, PCDD/PCDF, HCB and methylsulphonyl metabolites of PCB. *Environment and the Science of Pollution Research*, **4**, 2–9.

World Health Organization, 1994, Polybrominated biphenyls. *International Programme on Chemical Safety, Environmental Health Criteria*, **152**.

XENOBIOTICA, 2002, VOL. 32, NO. 4, 305–323

Taylor & Francis
healthsciences

Homology modelling of human CYP2 family enzymes based on the CYP2C5 crystal structure

D. F. V. LEWIS*

Molecular Toxicology Group, School of Biomedical and Life Sciences, University of Surrey, Guildford GU2 7XH, UK

Received 10 July 2001

1. The construction of molecular models for human cytochromes P450 from the CYP2 family are reported, utilizing the recently available crystal structure of CYP2C5, which is also a mammalian (rabbit) form of the enzyme.

2. In particular, selective substrate interactions with CYP2A6, CYP2B6, CYP2C8, CYP2C9, CYP2C19, CYP2D6 and CYP2E1 are described in the context of favourable contacts with active site amino acid residues that appear to orientate each substrate for metabolism at the experimentally observed position.

3. The results are consistent with reported findings from site-directed mutagenesis experiments with the CYP2 family, and with published information on substrate metabolism.

Introduction

The cytochromes P450 (CYP) constitute a superfamily of haem-thiolate enzymes, for which over 1200 individual genes have been sequenced to date (Anzenbacher and Anzenbacherova 2001), and are involved primarily in the oxidative metabolism (although reductions are also known) of a large number and variety of chemicals, both exogenous and endogenous (Lewis 2001). In mammalia, most xenobiotic metabolism is mediated via P450s from families CYP1, CYP2 and CYP3; the human enzymes primarily associated with the metabolism of foreign compounds being CYP1A2, CYP2A6, CYP2B6, CYP2C8, CYP2C9, CYP2C19, CYP2D6, CYP2E1 and CYP3A4 (Rendic and DiCarlo 1997). The generation of homology models of these enzymes from the CYP102 haemoprotein domain has been reported previously (Lewis *et al.* 1996, 1997, 1998, 1999a–c, 2000) and it would appear that the results are largely consistent with available experimental evidence from site-directed mutagenesis (reviewed in Lewis 1998) and from substrate metabolic data relating to preferred sites of oxidation. Other groups have also reported similar findings using related techniques with bacterial P450 crystal structural templates (Chang *et al.* 1997, de Groot *et al.* 1999, Dai *et al.* 2000). The purpose of the current study is to produce refined structures of human enzymes from the CYP2 family based on homology with the recently available crystallographic coordinates of the mammalian P450, CYP2C5 (Williams *et al.* 2000), as it is anticipated that this new

* E-mail: d.lewis@surrey.ac.uk

Xenobiotica ISSN 0049–8254 print/ISSN 1366–5928 online © 2002 Taylor & Francis Ltd
http://www.tandf.co.uk/journals
DOI: 10.1080/00498250110112015

structural template should prove a better paradigm than CYP102, at least as far as the enzymes of the CYP2 family are concerned.

Materials and methods

Figure 1 shows a multiple sequence alignment between various CYP2 family enzymes and that of the CYP102 haemoprotein domain for comparison produced using the GCG package (Genetics Computer Group, Madison, WI, USA). The location of substrate recognition sites (Gotoh 1992) are provided in figure 1, together with the position of α-helices and β-sheets. There is a close commonality (table 1) between the CYP102 and CYP2C5 structures (Williams *et al.* 2000) in terms of secondary structural motifs, although the position of the peptide chain varies significantly within SRS1, which corresponds to the B–C loop. The orientation of the F-helix (containing SRS2) is also different between these two

```
                membrane   anchor   region
                1          10         20          30          40
cyp2a1   ...MLDTGLL LVVILASLSV MLLVSLWQQ. KIRGRLPPGP TPLPFIGNYL
cyp2a4   ...MLTSGLL LVAAVAFLSV LVLMSVWKQR KLSGKLPPGP TPLPFVGNFL
cyp2a5   ...MLTSGLL LVAAVAFLSV LVLMSVWKQR KLSGKLPPGP TPLPFIGNFL
cyp2a6   ...MLASGML LVALLVCLTV MVLMSVWQQR KSKGKLPPGP TPLPFIGNYL
cyp2b1   ......MEPT ILLLLALLVG FLLLLVRGHP KSRGNFPPGP RPLPLLGNLL
cyp2b4   ......MEFS LLLLIAFLAG LLLLLFRGHP KAHGRLPPGP SPLPVLGNLL
cyp2b6   ......MELS VLLFLALLTG LLLLLVQRHP NTHDRLPPGP RPLPLLGNLL
cyp2c2   .......MDL VVVLGLCLSC LLLPSLWKQS HGGGKLPPGP TPFPILGNVL
cyp2c3   .......MDL LIILGICLSC VVLLSLWKKT HGKGKLPPGP TPLPVVGNLL
cyp2c4   .......MDP VAGLVLGLCC LLLLSLWKQN SGRGKLPPGP TPFPIIGNIL
cyp2c5   .......MDP VVVLVLGLCC LLLLSIWKQN SGRGKLPPGP TPFPIIGNIL
cyp2c8   .......MEP FVVLVLCLSF MLLFSLWRQS CRRRKLPPGP TPLPIIGNML
cyp2c9   .......MDS LVVLVLCLSC LLLLSLWRQS SGRGKLPPGP TPLPVIGNIL
cyp2c19  .......MDP FVVLVLCLSC LLLLSIWRQS SGRGKLPPGP TPLPVIGNIL
cyp2d1   MELLNGTGLW SMAIFTVIFI LLVDLMHRRH RWTSRYPPGP VPWPVLGNLL
cyp2d6   ...MGLEALV PLAVIVAIFL LLVDLMHRRQ RWAARYPPGP LPLPGLGNLL
cyp2e1r  ....MAVLGI TVALLGWMVI LLFISVWKQI HSSWNLPPGP FPLPIIGNLL
cyp2e1h  ....MSALGV TVALLVWAAF LLLVSMWRQV HSSWNLPPGP FPLPIIGNLF
cyp2f1   ......MDSI STAILLLLLA LVCLLLTLSS RDKGKLPPGP RPLSILGNLL
cyp2f2   ......MDGV STAILLLLLA VISLSLTFSS RDKGQLPPGP KPLPILGNLL

                < Ahelix >                          <   B helix   >
                50          60          70          80          90
cyp2a1   QLNTKDVYSS ITQLSERYGP VFTIHLGPRR VVVLYGYDAV KEALVDQAEE
cyp2a4   QLNTEQMYNS LMKISQRYGP VFTIYLGSRR IVVLCGQEAV KEALVDQAEE
cyp2a5   QLNTEQMYNS LMKISQRYGP VFTIYLGPRR IVVLCGQEAV KEALVDQAEE
cyp2a6   QLNTEQMYNS LMKISERYGP VFTIHLGPRR VVVLCGHDAV REALVDQAEE
cyp2b1   QLDRGGLLNS FMQLREKYGD VFTVHLGPRP VVMLCGTDTI KEALVGQAED
cyp2b4   QMDRKGLLRS FLRLREKYGD VFTVYLGSRP VVVLCGTDAI REALVDQAEA
cyp2b6   QMDRRGLLKS FLRFREKYGD VFTVHLGPRP VVMLCGVEAI REALVDKAEA
cyp2c2   QLDFKDLSKS LTNLSKVYGP VFTVYLGMKP TVVVHGYEAV KEALVDLGHE
cyp2c3   QLETKDINKS LSMLAKEYGS IFTLYFGMKP AVVLYGYEGV IEALIYRGEE
cyp2c4   QIDVKDISKS LTKFSERYGP VFTVYLGMKP TVVLHGYKAV KEALVDLGEE
cyp2c5   QIDAKDISKS LTKFSECYGP VFTVYLGMKP TVVLHGYEAV KEALVDLGEE
cyp2c8   QIDVKDICKS FTNFSKVYGP VFTVYFGMNP IVVFHGYEAV KEALIDNGEE
cyp2c9   QIGIKDISKS LTNLSKVYGP VFTLYFGLKP IVVLHGYEAV KEALIDLGEE
cyp2c19  QIDIKDVSKS LTNLSKIYGP VFTLYFGLER MVVLHGYEVV KEALIDLGEE
cyp2d1   QVDLSNMPYS LYKLQHRYGD VFSLQKGWKP MVIVNRLKAV QEVLVTHGED
cyp2d6   HVDFQNTPYC FDQLRRRFGD VFSLQLAWTP VVVLNGLAAV REALVTHGED
cyp2e1r  QLDLKDIPKS FGRLAERFGP VFTVYLGSRR VVVLHGYKAV REMLLNHKNE
cyp2e1h  QLELKNIPKS FTRLAQRFGP VFTLYVGSQR MVVMHGYKAV KEALLDYKDE
cyp2f1   LLCSQDMLTS LTKLSKEYGS MYTVHLGPRR VVVLSGYQAV KEALVDQGEE
cyp2f2   QLRSQDLLTS LTKLSKEYGS VFTVYLGSRP VIVLSGYQTV KEALVDKGEE
```

```
                    SRS1                        <  C helix >
            100             110             120         130
cyp2a1  FSGRGEQATY NTLFKG...Y GVAFSS.GER AKQLRRLSIA TLRDFGVGKR
cyp2a4  FSGRGEQATF DWLFKG...Y GIAFSS.GER AKQLRSFSIA TLRDFGVGKR
cyp2a5  FSGRGEQATF DWLFKG...Y GVVFSS.GER AKQLRRFSIA TLRDFGVGKR
cyp2a6  FSGRGEQATF DWVFKG...Y GVVFSN.GER AKQLRRFSIA TLRDFGVGKR
cyp2b1  FSGRGTIAVI EPIFKE...Y GVIFAN.GER WKALRRFSLA TMRDFGMGKR
cyp2b4  FSGRGKIAVV DPIFQG...Y GVIFAN.GER WRALRRFSLA TMRDFGMGKR
cyp2b6  FSGRGKIAMV DPFFRG...Y GVIFAN.GNR WKVLRRFSVT TMRDFGMGKR
cyp2c2  LSGRSRFLVT AKLNKG...F GVIFSN.GKR WTETRRFSLM TLRNFGMGKR
cyp2c3  FSGRGIFPVF DRVTKG...L GIVFSS.GEK WKETRRFSLT VLRNLGMGKK
cyp2c4  FAGRGHFPIA EKVNKG...L GIVFTN.ANT WKEMRRFSLM TLRNFGMGKR
cyp2c5  FAGTGSVPIL EKVSKG...L GIAFSN.AKT WKEMRRFSLM TLRNFGMGKR
cyp2c8  FSGRGNSPIS QRITKG...L GIISSN.GKR WKEIRRFSLT TLRNFGMGKR
cyp2c9  FSGRGIFPLA ERANRG...F GIVFSN.GKK WKEIRRFSLM TLRNFGMGKR
cyp2c19 FSGRGHFPLA ERANRG...F GIVFSN.GKR WKEIRRFSLM TLRNFGMGKR
cyp2d1  TADRPPVPIF KCLGVKPRSQ GVILASYGPE WREQRRFSVS TLRTFGMGKK
cyp2d6  TADRPPVPIT QILGFGPRSQ GVFLARYGPA WREQRRFSVS TLRNLGLGKK
cyp2e1r FSGRGEIPAF .REFKD...K GIIFNN.GPT WKDTRRFSLT TLRDYGMGKQ
cyp2e1h FSGRGDLPAF .HAHRD...R GIIFNN.GPT WKDIRRFSLT TLRNYGMGKQ
cyp2f1  FSGRGDYPAF FNFTKG...N GIAFSS.GDR WKVLRQFSIQ ILRNFGMGKR
cyp2f2  FSGRGAYPVF FNFTRG...N GIAFSD.GER WKILRRFSVQ ILRNFGMGKR

         <     D helix    >          < D'> < Ehelix >
        140         150         160         170         180
cyp2a1  GVEERILEEA GYLIKMLQGT CGAPIDPTIY LSKTVSNVIS SIVFGERFDY
cyp2a4  GIEERIQEEA GFLIDSFRKT NGAFIDPTFY LSRTVSNVIS SIVFGDRFDY
cyp2a5  GIEERIQEEA GFLIDSFRKT NGAFIDPTFY LSRTVSNVIS SIVFGDRFDY
cyp2a6  GIEERIQEEA GFLIDAHRGT GGANIDPTFF LSRTVSNVIS SIVFGDRFDY
cyp2b1  SVEERIQEEA QCLVEELRKS QGAPLDPTFL FQCITANIIC SIVFGERFDY
cyp2b4  SVEERIQEEA RCLVEELRKS KGALLDNTLL FHSITSNIIC SIVFGKRFDY
cyp2b6  SVEERIQEEA QCLIEELRKS KGALMDPTFL FQSITANIIC SIVFGKRFHY
cyp2c2  SIEERVQEEA HCLVEELRKT NASPCDPTFI LGAAPCNVIC SVIFQNRFDY
cyp2c3  TIEERIQEEA LCLIQALRKT NASPCDPTFL LFCVPCNVIC SVIFQNRFDY
cyp2c4  SIEDRVQEEA RCLVEELRKT NALPCDPTFI LGCAPCNVIC SVILHNRFDY
cyp2c5  SIEDRIQEEA RCLVEELRKT NASPCDPTFI LGCAPCNVIC SVIFHNRFDY
cyp2c8  SIEDRVQEEA HCLVEELRKT KASPCDPTFI LGCAPCNVIC SVVFQKRFDY
cyp2c9  SIEDRVQEEA RCLVEELRKT KASPCDPTFI LGCAPCNVIC SIIFHKRFDY
cyp2c19 SIEDRVQEEA RCLVEELRKT KASPCDPTFI LGCAPCNVIC SIIFQKRFDY
cyp2d1  SLEEWVTKEA GHLCDAFTAQ AGQSINPKAM LNKALCNVIA SLIFARRFEY
cyp2d6  SLEQWVTEEA ACLCAAFANH SGRPFRPNGL LDKAVSNVIA SLTCGRRFEY
cyp2e1r GNEDRIQKEA HFLLEELRKT QGQPFDPTFV IGCTPFNVIA KILFNDRFDY
cyp2e1h GNESRIQREA HFLLEALRKT QGQPFDPTFL IGCAPCNVIA DILFRKHFDY
cyp2f1  SIEERILEEG SFLLADVRKT EGEPFDPTFV LSRSVSNIIC SVLFGSRFDY
cyp2f2  SIEERILEEG SFLLEVLRKM EGKPFDPVFI LSRSVSNIIC SVVFGSRFDY
```

enzymes (Williams *et al.* 2000) and this is of importance for the enzyme–substrate interactions because additional key amino acid residues (e.g. within the F-helix and B–C loop) become available for substrate binding, which would not have been considered in the case of CYP102-derived models. Moreover, the considerably higher sequence identities between CYP2C5 and other CYP2 family enzymes (42–78%) clearly facilitates protein sequence alignment (figure 1) and subsequent generation of structural models.

Homology models of CYP2A6, CYP2B6, CYP2C8, CYP2C9, CYP2C19, CYP2D6 and CYP2EI were constructed from the CYP2C5 crystallographic coordinates (pdb code 1dt6) on the basis of amino acid residue replacement according to the sequence alignment presented in figure 1. A small stretch of peptide 11 residues in length was added to the original CYP2C5 crystal structure (via protein databank loop search procedures implemented in Sybyl Biopolymer) due to a missing portion of the F–G loop, and the modified enzyme was energy minimized (100 iterative cycles of molecular mechanics using the Tripos force field) before its employment as the structural template for homology modelling of the human CYP2 family enzymes. Owing to the relatively high degree of sequence homology between CYP2C5 and the other CYP2 family enzymes constructed (identities varied from 42 to 78% for the matched sequences), the generation of each model was relatively straightforward, requiring very few insertions or deletions of amino acid residues (see alignment in figure 1). A very small stretch of peptide

```
          < F helix SRS2 >     <  F' >          <        SRS3
         190        200        210        220        230
cyp2a1   EDTEFLSLLQ MMGQMNRFAA SPTGQLYDMF HSVMKYLPGP QQQIIKVTQK
cyp2a4   EDKEFLSLLR MMLGSLQFTA TSMGQVYEMF SSVMKHLPGP QQQAFKELQG
cyp2a5   EDKEFLSLLR MMLGSFQFTA TSMGQLYEMF SSVMKHLPGP QQQAFKELQG
cyp2a6   KDKEFLSLLR MMLGIFQFTS TSTGQLYEMF SSVMKHLPGP QQQAFQLLQG
cyp2b1   TDRQFLRLLE LFYRTFSLLS SFSSQVFEFF SGFLKYFPGA HRQISKNLQE
cyp2b4   KDPVFLRLLD LFFQSFSLIS SFSSQVFELF PGFLKHFPGT HRQIYRNLQE
cyp2b6   QDQEFLKMLN LFYQTFSLIS SVFGQLFELF SGFLKYFPGA HRQVYKNLQE
cyp2c2   TDQDFLSLMG KFNENFKILN SPWVQFCNCF PILFDYFPGS HRKAVKNIFY
cyp2c3   DDEKFKTLIK YFHENFELLG TPWIQLYNIF PILGHYLPGS HRQLFKNIDG
cyp2c4   KDEEFLKLME RLNENIRILS SPWLQVYNNF PALLDYFPGI HKTLLKNADY
cyp2c5   KDEEFLKLME SLNENVRILS SPWLQVYNNF PALLDYFPGI HKTLLKNADY
cyp2c8   KDQNFLTLMK RFNENFRILN SPWIQVCNNF PLLIDCFPGT HNKVLKNVAL
cyp2c9   KDQQFLNLME KLNENIKILS SPWIQICNNF SPIIDYFPGT HNKLLKNVAF
cyp2c19  KDQQFLNLME KLNENIRIVS TPWIQICNNF PTIIDYFPGT HNKLLKNLAF
cyp2d1   EDPYLIRMVK LVEESLTEVS GFIPEVLNTF PALLR.IPGL ADKVFQGQKT
cyp2d6   DDPRFLRLLD LAQEGLKEES GFLREVLNAV PVLLH.IPAL AGKVLRFQKA
cyp2e1r  KDKQALRLMS LFNENFYLLS TPWLQVYNNF SNYLQYMPGS HRKVIKNVSE
cyp2e1h  NDEKFLRLMY LFNENFHLLS TPWLQLYNNF PSFLHYLPGS HRKVIKNVAE
cyp2f1   DDERLLTIIR LINDNFQIMS SPWGELYDIF PSLLDWVPGP HQRIFQNFKC
cyp2f2   DDERLLTIIH FINDNFKIMS SPWGEMYNIF PSVLDWIPGP HKRLFRNFGG

            G helix   >          < H  >                <
         240        250        260        270        280
cyp2a1   LEDFMIEKVR QNHSTLDPN. SPRNFIDSFL IRMQEE.KNG NSEFHMKNLV
cyp2a4   LEDFITKKVE HNQRTLDPN. SPRDFIDSFL IRMLEEKKNP NTEFYMKNLV
cyp2a5   LEDFITKKVE HNQRTLDPN. SPRDFIDSFL IRMLEEKKNP NTEFYMKNLV
cyp2a6   LEDFIAKKVE HNQRTLDPN. SPRDFIDSFL IRMQEEEKNP NTEFYLKNLV
cyp2b1   ILDYIGHIVE KHRATLDPS. APRDFIDTYL LRMEKEKSNH HTEFHHENLM
cyp2b4   INTFIGQSVE KHRATLDPS. NPRDFIDVYL LRMEKDKSDP SSEFHHQNLI
cyp2b6   INAYIGHSVE KHRETLDPS. APKDLIDTYL LHMEKEKSNA HSEFSHQNLN
cyp2c2   VKNYITEQIK EHQKSLDIN. NPRDFIDCFL IKMEQEKCNQ QSEFTIENLL
cyp2c3   QIKFILEKVQ EHQESLDSN. NPRDFVDHFL IKMEKEKHKK QSEFTMDNLI
cyp2c4   TKNFIMEKVK EHQKLLDVN. NPRDFIDCFL IKMEKE...N NLEFTLGSLV
cyp2c5   IKNFIMEKVK EHEKLLDVN. NPRDFIDCFL IKMEQE...N NLEFTLESLV
cyp2c8   TRSYIREKVK EHQASLDVN. NPRDFIDCFL IKMEQEKDNQ KSEFNIENLV
cyp2c9   MKSYILEKVK EHQESMDMN. NPQDFIDCFL MKMEKEKHNQ PSEFTIESLE
cyp2c19  MESDILEKVK EHQESMDIN. NPRDFIDCFL IKMEKEKQNQ QNEFTIENLV
cyp2d1   FMALLDNLLA ENRTTWDPAQ PPRNLTDAFL AEVEKAKGNP ESSFNDENLR
cyp2d6   FLTQLDELLT EHRMTWDPAQ PPRDLTEAFL AEMEKAKGNP ESSFNDENLR
cyp2e1r  IKEYTLARVK EHHKSLDPS. CPRDFIDSLL IEMEKDKHST EPLYTLENIA
cyp2e1h  VKEYVSERVK EHHQSLDPN. CPRDLTDCLL VEMEKEKHSA ERLYTMDGIT
cyp2f1   LRDLIAHSVH DHQASLDPR. SPRDFIQCFL TKMAEEKEDP LSHFHMDTLL
cyp2f2   MKDLIARSVR EHQDSLDPN. SPRDFIDCFL TKMAQEKQDF LSHFNMDTLL
```

two to three residues long was inserted within the H-I loop region in each case, following a search of the protein databank, and this corresponded to a slight extension of a surface turn at position 274 in the CYP2C5 template structure.

After the raw models had been produced, each P450 structure was inspected visually for the presence of unfavourable steric contacts between residues and these were relieved manually before energy minimization. Following 100 iterative cycles of molecular mechanics using the Tripos force field, the energy minimized geometries of each human CYP2 enzyme were screened for the presence of disallowed protein conformations (Sybyl Biopolymer module) before their being probed using selective substrates (as listed in table 2) and their preferred positions were obtained via interactive docking (using the DOCK algorithm as implemented in Sybyl) of the substrate molecules within the putative active site regions of the relevant enzymes. This procedure was facilitated by the presence of hydrogen bond donor/acceptor amino acid residues close to the haem and lying within the active site region, together with those containing aromatic sidechains, such that the most likely substrate orientations displaying optimal hydrogen-bonded and π–π stacking interactions could be definitively assigned on the basis of

```
           SRS4   I helix              > <   J helix    >
             290         300         310         320         330
cyp2a1  MTTLSLFFAG SETVSSTLRY GFLLLMKHPD VEAKVHEEIE QVIGRNRQPQ
cyp2a4  LTTLNLFFAG TETVSTTLRY GFLLLMKYPD IEAKVHEEID RVIGRNRQPK
cyp2a5  LTTLNLFFAG TETVSTTLRY GFLLLMKHPD IEAKVHEEID RVIGRNRQPK
cyp2a6  MTTLNLFIGG TETVSTTLRY GFLLLMKHPE VEAKVHEEID RVIGKNRQPK
cyp2b1  ISLLSLFFAG TETSSTTLRY GFLLMLKYPH VAEKVQKEID QVIGSHRLPT
cyp2b4  LTVLSLFFAG TETTSTTLRY GFLLMLKYPH VTERVQKEIE QVIGSHRPPA
cyp2b6  LNTLSLFFAG TETTSTTLRY GFLLMLKYPH VAERVYREIE QVIGPHRPPE
cyp2c2  TTVSDVFMAG TETTSTTLRY GLLLLMKHPE VIAKVQEEIE RVIGRHRSPC
cyp2c3  TTIWDVFSAG TDTTSNTLKF ALLLLLKHPE ITAKVQEEIE HVIGRHRSPC
cyp2c4  IAVFDLFGAG TETTSTTLRY SLLLLLKHPE VAARVQEEIE RVIGRHRSPC
cyp2c5  IAVSDLFGAG TETTSTTLRY SLLLLLKHPE VAARVQEEIE RVIGRHRSPC
cyp2c8  CTVADLFVAG TETTSTTLRY GLLLLLKHPE VTAKVQEEID HVIGRHRSPC
cyp2c9  NTAVDLFGAG TETTSTTLRY ALLLLLKHPE VTAKVQEEIE RVIGRNRSPC
cyp2c19 ITAADLLGAG TETTSTTLRY ALLLLLKHPE VTAKVQEEIE RVIGRNRSPC
cyp2d1  MVVVDLFTAG MVTTATTLTW ALLLMILYPD VQRRVQQEID EVIGQVRCPE
cyp2d6  IVVADLFSAG MVTTSTTLAW GLLLMILHPD VQRRVQQEID DVIGQVRRPE
cyp2e1r VTVADMFFAG TETTSTTLRY GLLILLKHPE IEEKLHEEID RVIGPSRMPS
cyp2e1h VTVADLFFAG TETTSTTLRY GLLILMKYPE IEEKLHEEID RVIGPSRIPA
cyp2f1  MTTHNLLFGG TKTVSTTLHH AFLALMKYPK VQARVQEEID LVVGRARLPA
cyp2f2  MTTHNLLFGG TETVGTTLRH AFLILMKYPK VQARVQEEID RVVGRSRMPT

        < J'>  <     K helix    > SRS5
             340         350         360         370         380
cyp2a1  YEDHMKMPYT QAVINEIQRF SNLAPLGIPR RIIKNTTFRG FFLPKATDVF
cyp2a4  YEDRMKMPYT EAVIHEIQRF ADLIPMGLAR RVTKDTKFRD FLLPKGTEVF
cyp2a5  YEDRMKMPYT EAVIHEIQRF ADMIPMGLAR RVTKDTKFRD FLLPKGTEVF
cyp2a6  FEDRAKMPYM EAVIHEIQRF GDVIPMSLAR RVKKDTKFRD FFLPKGTEVY
cyp2b1  LDDRSKMPYT DAVIHEIQRF SDLVPIGVPH RVTKDTMFRG YLLPKNTEVY
cyp2b4  LDDRAKMPYT DAVIHEIQRL GDLIPFGVPH TVTKDTQFRG YVIPKNTEVF
cyp2b6  LHDRAKMPYT EAVIYEIQRF SDLLPMGVPH IVTQHTSFRG YIIPKDTEVF
cyp2c2  MQDRSRMPYT DATVHEIQRY INLIPNNVPH TTICNLKFRN YLIPKGTDVL
cyp2c3  SQDRSRMPYT DAVMHEIQRY VDLVPTSLPH AVTQDIEFNG YLIPKGTDII
cyp2c4  MQDRSHMPYT DAVIHEIQRF IDLLPTNLPH AVTRDVKFRN YFIPKGTDII
cyp2c5  MQDRSRMPYT DAVIHEIQRF IDLLPTNLPH AVTRDVRFRN YFIPKGTDII
cyp2c8  MQDRSHMPYT DAVVHEIQRY SDLVPTGVPH AVTTDTKFRN YLIPKGTTIM
cyp2c9  MQDRSHMPYT DAVVHEVQRY IDLLPTSLPH AVTCDIKFRN YLIPKGTTIL
cyp2c19 MQDRGHMPYT DAVVHEVQRY IDLIPTSLPH AVTCDVKFRN YLIPKGTTIL
cyp2d1  MTDQAHMPYT NAVIHEVQRF GDIAPLNLPR FTSCDIEVQD FVIPKGTTLI
cyp2d6  MGDQAHMPYT TAVIHEVQRF GDIVPLGVTH MTSRDIEVQG FRIPKGTTLI
cyp2e1r VRDRVQMPYM DAVVHEIQRF IDLVPSNLPH EATRDTTFQG YVIPKGTVVI
cyp2e1h IKDRQEMPYM DAVVHEIQRF ITLVPSNLPH EATRDTIFRG YLIPKGTVVV
cyp2f1  LKDRAAMPYT DAVIHEVQRF ADIIPMNLPH RVTRDTAFRG FLIPKGTDVI
cyp2f2  LEDRTSMPYT DAVIHEVQRF ADVIPMNLPH RVTRDTPFRG FLIPKGTDVI
```

proximity to the haem iron for the site of metabolism in each case (and the relevant distances have been listed in table 3). All molecular modelling operations were carried out using the Sybyl software package (Tripos Associates, St Louis, MO, USA) implemented on a Silicon Graphics Indigo^2 IMPACT 10000 graphics workstation operating under UNIX.

Results and discussion

Table 3 provides information on the substrates modelled with each human CYP2 enzyme, together with their percentage sequence identity with CYP2C5 and the minimized energy of each enzyme model. A comparison between CYP2 family active site residues in contact with the substrates is provided as table 4. Each model will now be discussed in terms of specific substrate interactions.

```
           < K'>  <K">                                          <
             390        400        410        420        430
cyp2a1   PILGSLMTDP KFFPSPKDFD PQNFLDDKGQ LKKNAAFLPF STGKRFCLGD
cyp2a4   PMLGSVLKDP KFFSNPKDFN PKHFLDDKGQ FKKSDAFVPF SIGKRYCFGE
cyp2a5   PMLGSVLKDP KFFSNPKDFN PKHFLDDKGQ FKKNDAFVPF SIGKRYCFGE
cyp2a6   PMLGSVLRDP SFFSNPQDFN PQHFLNEKGQ FKKSDAFVPF SIGKRNCFGE
cyp2b1   PILSSALHDP QYFDHPDSFN PEHFLDANGA LKKSEAFMPF STGKRICLGE
cyp2b4   PVLSSALHDP RYFETPNTFN PGHFLDANGA LKRNEGFMPF SLGKRICLGE
cyp2b6   LILSTALHDP HYFEKPDAFN PDHFLDANGA LKKTEAFIPF SLGKRICLGE
cyp2c2   TSLSSVLHDD KEFPNPDRFD PGHFLDASGN FRKSDYFMPF STGKRVCVGE
cyp2c3   PSLTSVLYDD KEFPNPEKFD PGHFLDESGN FKKSDYFMPF STGKRACVGE
cyp2c4   TSLTSVLHDE KAFPNPKVFD PGHFLDESGN FKKSDYFMPF SAGKRMCVGE
cyp2c5   TSLTSVLHDE KAFPNPKVFD PGHFLDESGN FKKSDYFMPF SAGKRMCVGE
cyp2c8   ALLTSVLHDD KEFPNPNIFD PGHFLDKNGN FKKSDYFMPF SAGKRICAGE
cyp2c9   ISLTSVLHDN KEFPNPEMFD PHHFLDEGGN FKKSKYFMPF SAGKRICVGE
cyp2c19  TSLTSVLHDN KEFPNPEMFD PRHFLDEGGN FKKSNYFMPF SAGKRICVGE
cyp2d1   INLSSVLKDE TVWEKPHRFH PEHFLDAQGN FVKHEAFMPF SAGRRACLGE
cyp2d6   TNLSSVLKDE AVWEKPFRFH PEHFLDAQGH FVKPEAFLPF SAGRRACLGE
cyp2e1r  PTLDSLLYDK QEFPDPEKFK PEHFLNEEGK FKYSDYFKPF SAGKRVCVGE
cyp2e1h  PTLDSVLYDN QEFPDPEKFK PEHFLNENGK FKYSDYFKPF STGKRVCAGE
cyp2f1   TLLNTVHYDP SQFLTPQEFN PEHFLDANQS FKKSPAFMPF SAGRRLCLGE
cyp2f2   TLLNTVHYDS DQFKTPQEFN PEHFLDDNHS FKKSPAFMPF SAGRRLCLGE

           L helix     >                 SRS6
             440        450        460        470        480
cyp2a1   GLAKMELFLL LTTILQNFRF KFPMKLEDIN ESPKPLGFTR IIPKYTMSFMPI
cyp2a4   GLARMELFLF LTNIMQNFHF KSTQAPQDID VSPRLVGFVT IPPTYTMSFLSR
cyp2a5   GLARMELFLF LTNIMQNFHF KSTQAPQDID VSPRLVGFAT IPPTYTMSFLSR
cyp2a6   GLARMELFLF FTTVMQNFRL KSSQSPKDID VSPKHVGFAT IPRNYTMSFLPR
cyp2b1   GIARNELFLF FTTILQNFSV SSHLAPKDID LTPKESGIGK IPPTYQICFSAR
cyp2b4   GIARTELFLF FTTILQNFSI ASPVPPEDID LTPRESGVGN VPPSYQIRFLAR
cyp2b6   GIARAELFLF FTTILQNFSM ASPVAPEDID LTPQECGVGK IPPTYQIRFLPR
cyp2c2   ALARMELFLF LTAILQNFTP KPLVNPNNVD ENPFSSGIVR VPPLYRVSFIPV
cyp2c3   GLARMELFLL LTTILQHFTL KPLVDPKDID PTPVENGFVS VPPSYELCFVPV
cyp2c4   GLARMELFLF LTSILQNFKL QSLVEPKDLD ITAVVNGFVS VPPSYQLCFIPI
cyp2c5   GLARMELFLF LTSILQNFKL QSLVEPKDLD ITAVVNGFVS VPPSYQLCFIPI
cyp2c8   GLARMELFLF LTTILQNFNL KSVDDLKNLN TTAVTKGIVS LPPSYQICFPIV
cyp2c9   ALAGMELFLF LTSILQNFNL KSLVDPKNLD TTPVVNGFAS VPPFYQLCFIPV
cyp2c19  GLARMELFLF LTFILQNFNL KSLIDPKDLD TTPVVNGFAS VPPFYQLCFIPV
cyp2d1   PLARMELFLF FTCLLQRFSF .SVPVGQPRP STHGFFAFPV APLPYQLCAVVREQGL
cyp2d6   PLARMELFLF FTSLLQHFSF .SVPTGQPRP SHHGVTAFLV SPSPYELCAVPR
cyp2e1r  GLARMELFLL LSAILQHFNL KPLVDPEDID LPNITVGFGR VPPRYKLCVIPRS
cyp2e1h  GLARMELFLL LCAILQHFNL KPLVDPKDID LSPIHIGFGC IPPRYKLCVIPRS
cyp2f1   LLARMELFLY LTAILQSFSL QPLGAPEDID LTPLSSGLGN LPRPFQLCLRPR
cyp2f2   PLARMELFIY FTSILQNFTL QPLVDPEDID LTPLSSGLGN LPRPFQLCMHIR
```

Figure 1. Multiple sequence alignment of 20 CYP2 family P450s showing substrate recognition sites (SRS) and selected mutagenesis sites within the SRS regions (emboldened).

CYP2A6 model

Figures 2A and B show the putative active site of CYP2A6 containing the bound substrate, coumarin, orientated for 7-hydroxylation. Complementary contacts between substrate and active site amino acid residues cooperatively assist in positioning the coumarin molecule relative to the haem iron such that the 7-hydrogen is closest to the iron atom, lying at a distance of 3.025 Å (table 3). It would appear that the substrate can form a π–π stacking interaction with the aromatic sidechain of Phe205, and there is an asparagine residue (Asn290) in the I-helix that donates a hydrogen bond to the ketonic oxygen atom of the pyrone ring

Table 1. α-Helices in the CYP2C5 crystal structure.

Helix	Residues involved	Number of residues	Comments
A	I50–S58	9	analogous to A helix in CYP102
B	Y80–E93	14	analogous to B helix in CYP102
C	W120–T130	11	analogous to C helix in CYP102
D	I141–R157	17	analogous to D helix in CYP102
D′	T167–L170	4	probably forms part of the E helix
E	C172–S180	9	analogous to E helix in CYP102
F	E192–E206	15	analogous to F helix in CYP102
F′	P211–N217	7	part of loop added after PDB search
G	G228–Q252	25	analogous to G helix in CYP102
H	F263–L268	6	analogous to H helix in CYP102
I	L281–K312	32	analogous to I helix in CYP102
J	P314–V327	14	analogous to J helix in CYP102
J′	M336–S340	5	analogous to J′ helix in CYP102
K	P343–I356	14	analogous to K helix in CYP102
K′	L388–L392	5	analogous to K′ helix in CYP102
K″	E395–A397	3	analogous to K″ helix in substrate-bound CYP102
L	E435–Q451	17	analogous to L helix in CYP102

PDB, protein data bank (Ravichandran *et al.* 1993, Li and Poulos 1997, Williams *et al.* 2000).

Table 2. Selective high-affinity human CYP2 family substrates.

CYP	Substrate	Reaction	K_m (μM)
2A6	coumarin	7-hydroxylation	2.1
2B6	4-trifluoromethyl 7-ethoxycoumarin	7-deethylation	2.9
2C8	rosiglitazone	*N*-demethylation	10
2C9	diclofenac	4-hydroxylation	6
2C19	omeprazole	5-methyl hydroxylation	8.6
2D6	propranolol	4-hydroxylation	2.7*
2E1	4-nitrophenol	2-hydroxylation	20

*K_D was provided in this case (Lewis *et al.* 2001).

Table 3. Human CYP2 enzymes modelled from the CYP2C5 crystal structure.

CYP	Selective substrate	Sequence identity (%) †	Minimized energy (kcal min mol^{-1})*	Haem substrate distance (Å)
2A6	coumarin	52	−1306.836	3.025
2B6	4-trifluoromethyl-7-ethoxycoumarin	51	−1179.222	3.906
2C8	rosiglitazone	76	−1246.292	4.096
2C9	diclofenac	78	−1239.456	3.795
2C19	omeprazole	77	−1269.521	4.959
2D6	propranolol	42	−1080.602	3.145
2E1	4-nitrophenol	59	−1156.884	5.675

† Only matched sequences with the CYP2C5 crystal structure were considered, i.e. the comparisons commenced at residue 30.

* Minimized energy of the CYP2C5 crystallographic template was recorded as −1105.11 kcal min mol^{-1} (100 iterative cycles of molecular mechanics) after addition of the missing portion of the F-G loop region (11 residues in length).

Table 4. Amino acid residues in active sites of CYP2 family enzymes.

SRS*	CYP2C5	Region	CYP2A6	CYP2B6	CYP2C8	CYP2C9	CYP2C19	CYP2D6	CYP2E1
1	I102	B-C loop	T	M	I	L	L	I	A
1	A113	B-C loop	V	I	I	V	V	F	I
2	V205	F helix	F	F	F	I	I	L	F
2	L208	F helix	T	I	L	L	V	E	L
4	D290	I helix	N	S	D	D	D	D	D
4	A294	I helix	G	A	A	A	A	A	A
4	T298	I helix	T	T	T	T	T	T	T
5	L359	$\beta_1(4)$ sheet	I	L	V	L	I	V	V
5	L363	$\beta_1(4)$ sheet	L	V	V	L	L	V	L
6	F473	$\beta_4(2)$ sheet	F	V	I	F	F	F	F
6	V474	$\beta_4(2)$ sheet	A	G	V	A	A	L	G

SRS, substrate recognition site (Gotoh 1992).
*SRS3 does not appear to lie within the CYP2C5 active site region (Williams *et al*. 2000).

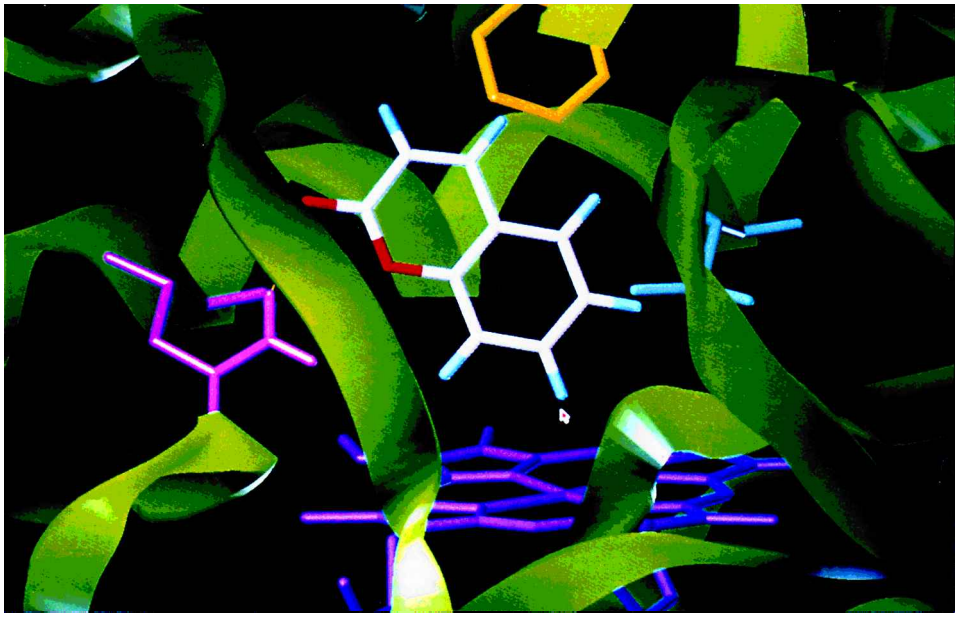


Figure 2A. Active site region of CYP2A6 showing the orientation of coumarin (colour-coded by atom type) within the haem environment. The haem moiety is displayed in purple, whereas the distal conserved threonine is in green. Amino acid residues interacting with the substrate are depicted in yellow (phenylalanine-205) and magenta (asparagine-290). The site of metabolism (7-hydrogen) is arrowed and the ribbon indicates the folding of the polypeptide chain in the vicinity of the active site.

(figure 2B). Of these active site contacts, the residue corresponding to Phe205 has been the subject of site-directed mutagenesis experiments in the mouse orthologue, CYP2A5 (Lindberg and Negishi 1989). As the analogous phenylalanine residue in CYP2A5 appears to be important for coumarin binding to the mouse orthologue, it is likely that Phe205 in the current model represents a key contact for CYP2A6 substrates containing aromatic rings such as coumarin, 4-nitroanisole, fadrozole and 2,6-dichlorobenzonitrile (Lewis *et al*. 1999b). Furthermore, the

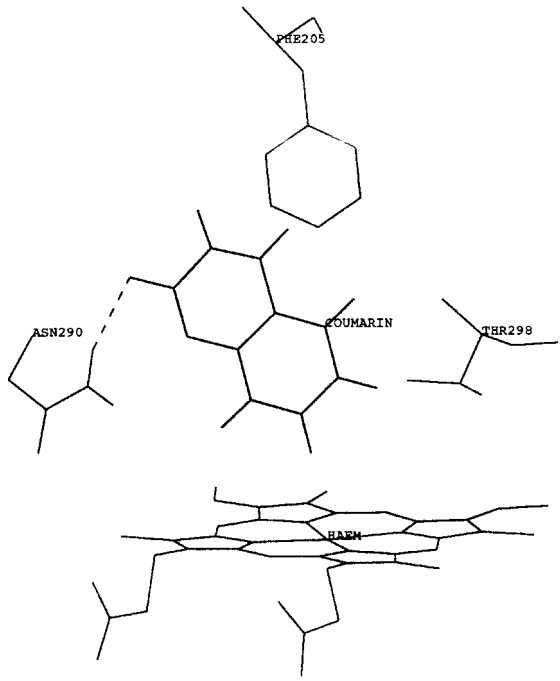


Figure 2B. Putative active site region of CYP2A6 showing the bound substrate, coumarin, orientated for 7-hydroxylation. Hydrogen bonds are displayed as dashed lines and residues are numbered according to those of the template crystal structure.

residue corresponding to Asn290 has been mutated in the rat orthologue, CYP2A1, and appears to affect the binding of testosterone (Hanioka *et al.* 1992). Consequently, the new model of CYP2A6 is in agreement with reported mutagenesis findings within the CYP2A subfamily (although data on CYP2A6 itself are not available) and with known metabolism of the selective high-affinity CYP2A6 substrate, coumarin, together with that of other substrates for this enzyme.

CYP2B6 model

The putative active site of CYP2B6 is presented as figure 3 and contains the selective substrate 4-trifluoromethyl-7-ethoxycoumarin orientated for *O*-deethylation. In particular, there are π–π stacking interactions between the substrate's coumarin ring system and the aromatic sidechains of Phe114 and Phe205, together with hydrogen bonding with Ser290, which donates a hydrogen bond to the pyrone carbonyl group. These complementary contacts between enzyme and substrate bring the methylene hydrogens of the ethoxy group close to the haem iron such that *O*-deethylation would be the preferred route of metabolism. Residues analogous to those mentioned above have been probed using site-directed mutagenesis in other CYP2B subfamily enzymes (reviewed in Lewis 1998, Szklarz *et al.* 1996) or are adjacent to them. Inspection of the molecular structures of other CYP2B6 substrates indicate that these are also likely to fit within the active site of the new CYP2B6 model such that metabolism at the

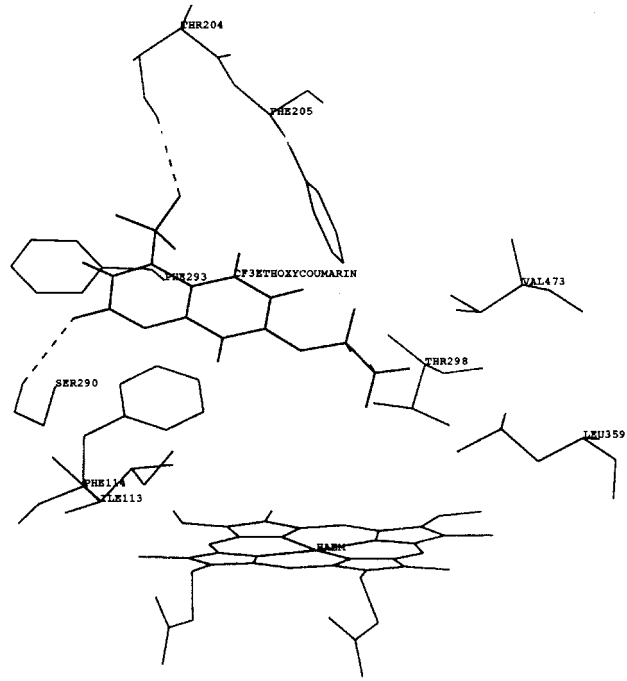


Figure 3. CYP2B6 active site region showing how the selective substrate, 4-trifluoromethyl-7-ethoxycoumarin, can become orientated for O-deethylation via contacts with complementary amino acid residues. Hydrogen bonds are shown as dashed lines and residues are numbered according to those of the CYP2C5 template structure.

observed positions can occur, and this is in keeping with previous findings using superimposed structural templates (Lewis *et al.* 1999a).

CYP2C8 model

Figure 4 shows the putative site of CYP2C8 containing the bound substrate, rosiglitazone orientated for *N*-demethylation. The molecule is held in position by a combination of hydrogen bonding to Asn99 and Ser114 with a π-π stacking interaction to the phenyl ring of Phe205. There are also hydrophobic contacts between the substrate and the sidechains of Ile113, Val363, Val474 and Ala294. Each residue has been the subject of site-specific mutagenesis in CYP2 family enzymes, including those of the CYP2C subfamily in the cases of positions 99, 113 and 114 (table 5). Other selective CYP2C8 substrates such as taxol and retinoic acid also fit the putative active site in orientations consistent with their known positions of metabolism. However, in the case of rosiglitazone, the *N*-methyl group lies directly above the haem iron at a distance of 4.1 Å, which is in agreement with its reported metabolism.

CYP2C9 model

The putative active site region of CYP2C9 is presented as figure 5, showing the selective substrate diclofenac orientated for 4-hydroxylation. The molecule forms

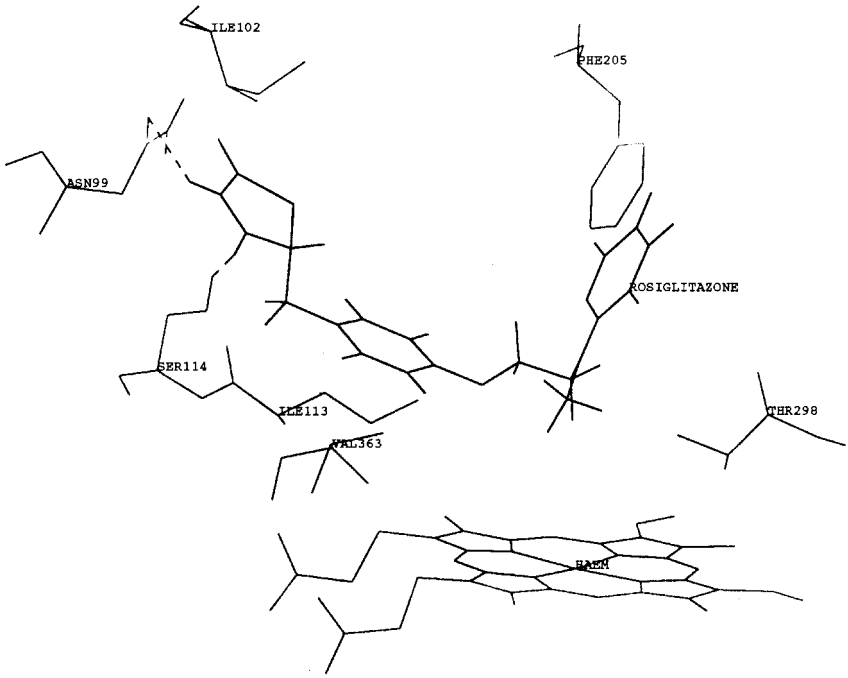


Figure 4. Putative active site of CYP2C8 containing the bound substrate, rosiglitazone, orientated for *N*-demethylation. Hydrogen bonds are displayed as dashed lines and residues are numbered according to that of the template structure.

π–π stacking interactions with the sidechains of Phe114 and Phe473. The first of these has been the subject of site-directed mutagenesis experiments in CYP2C9 (Haining *et al.* 1999) and is known to affect *S*-warfarin metabolism. Table 5 presents a summary of site-directed mutagenesis experiments within the CYP2C subfamily, such that various likely contacts with substrates can be appreciated – especially for those residues lying within the SRS regions. The sidechain of Gln214 forms a hydrogen bond with the carboxylate moiety of diclofenac, and these complementary contacts position the substrate for metabolism at the experimentally observed site. The 4-hydrogen atom lies at a distance of 3.8 Å from the haem iron and is the closest point in the substrate for oxygenation to occur. Consequently, there is a good agreement between experimental findings and the modelled interaction in the case of CYP2C9. Ridderstrom *et al.* (2000) reported that an arginine residue, Arg97, may play a role in CYP2C9-mediated metabolism. This residue lies just within SRS1 (figure 1) and is close to the putative active site in the current model. However, as this surface residue points away from the haem pocket both in the CYP2C9 model and in the CYP2C5 crystal structure, it is possible that Arg97 may be involved in redox partner interactions or for guiding the entry of substrates to the active site.

CYP2C19 model

Figure 6 presents the docked interaction of omeprazole in the CYP2C19 active site. In this example, there are π–π stacking interactions between the substrate's

Table 5. Site-directed mutagenesis and allelic variants in the CYP2C subfamily.

CYP	Change	2C5	SRS	Region/comments	Reference
2C11	P3DA	P30	–	polyproline motif	Yamazaki *et al.* (1993), Chen and Kemper (1996)
2C11	P33A	P33	–	polyproline motif	Yamazaki *et al.* (1993), Chen and Kemper (1996)
2C11	P35A	P35	–	polyproline motif	Yamazaki *et al.* (1993), Chen and Kemper (1996)
2C11	P37A	P37	–	polyproline motif	Yamazaki *et al.* (1993), Chen and Kemper (1996)
2C9	R97A	T97	1	B-C loop	Ridderstrom *et al.* (2000)
2C9	I99H	S99	1	B-C loop: substrate interaction	Ibeanu *et al.* (1996)
2C9	L102A	I102	1	B-C loop: substrate interaction	Ridderstrom *et al.* (2000)
2C9	R105A	K105	1	B-C loop	Ridderstrom *et al.* (2000)
2C2	G111V	G111	1	B-C loop	Straub *et al.* (1993)
2C2	I113C	A113	1	B-C loop: substrate interaction	Straub *et al.* (1993), Richardson and Johnson (1994)
2C2	F114L	F114	1	B-C loop: substrate interaction	Straub *et al.* (1993), Haining *et al.* (1999)
2C2	S115R	S115	1	B-C loop	Straub *et al.* (1993)
2C2	G117V	A117	–	B-C loop	Straub *et al.* (1993), Kronbach *et al.* (1989)
2C2	W120L	W120	–	C helix: conserved tryptophan	Straub *et al.* (1993)
2C9	R144C	R144	–	D helix: reductase interaction	Tracy *et al.* (1995), Kaminsky *et al.* (1993)
2C3	I178M	I178	–	E helix: contact with I helix	Hsu *et al.* (1993)
2C13	S180C	S180	–	E helix: close to R144 position	Faletto *et al.* (1992)
2C9	S220P	P220	–	F-G loop	Ibeanu *et al.* (1996)
2C9	P221T	A221	–	F-G loop	Ibeanu *et al.* (1996)
2C9	E241K	K241	–	G helix	Jung *et al.* (1998)
2C9	E274-	E274	–	H-I loop	Ohgiya *et al.* (1992)
2C9	K275-	N275	–	H-I loop	Ohgiya *et al.* (1992)
2C9	N286S	S283	–	I helix	Jung *et al.* (1998), Klose *et al.* (1998)
2C9	I289N	I286	–	I helix	Jung *et al.* (1998), Klose *et al.* (1998)
2C14	T301S	T298	4	I helix: conserved distal threonine	Imai and Nakamura (1989)
2C9	Y358C	F355	–	K helix	Kaminsky *et al.* (1993)
2C9	I359L	I356	–	K helix	Takanashi *et al.* (2000), Haining *et al.* (1996)
2C3	S364T	N362	5	$\beta_1(4)$ sheet	Hsu *et al.* (1993), Richardson and Johnson (1994)
2C1	H368R	H365	5	$\beta_1(4)$ sheet: heme propionate interaction	Ramarao *et al.* (1995)
2C1	T369A	T366	5	$\beta_1(4)$ sheet	Ramarao *et al.* (1995)
2C1	L374V	V371	–	$\beta_2(1)$ sheet	Ramarao *et al.* (1995)
2C1	D386A	D383	–	$\beta_1(3)$ sheet: close to reductase site	Ramarao *et al.* (1995)
2C1	L388I	I385	–	$\beta_1(3)$ sheet	Ramarao *et al.* (1995)
2C9	G417D	G414	–	F_1 helix	Kaminsky *et al.* (1993), Veronese *et al.* (1993)
2C2	S473V	V470	6	$\beta_4(2)$ sheet: substrate interaction	Uno *et al.* (1993)
2C2	P480A	P477	–	$\beta_3(2)$ sheet: close to active site	Uno *et al.* (1993)
2C2	P481T	P478	–	$\beta_3(2)$ sheet: close to active site	Uno *et al.* (1993)

SRS, substrate recognition site (Gotoh 1992). Also Lewis (1998, 2001), Lewis *et al.* (1998), von Wachenfeldt and Johnson (1995).

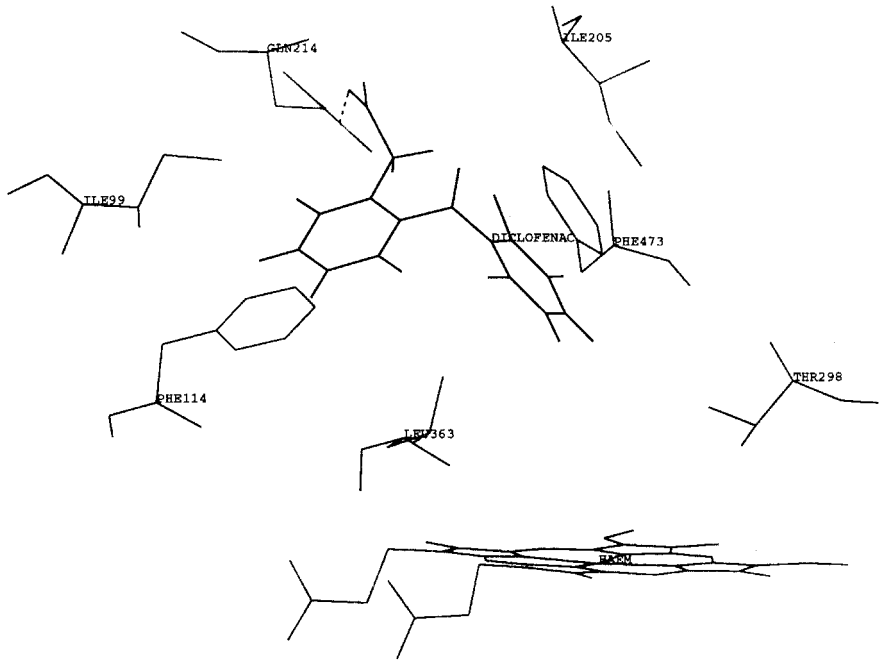


Figure 5. Active site region of CYP2C9 where the selective substrate diclofenac is positioned for 4-hydroxylation via a combination of π–π stacking and hydrogen-bonded interactions. Hydrogen bonds are shown as dashed lines and residues are numbered according to that of the template structure.

benzimidazole and pyridine rings and the aromatic sidechains of Phe114 and Phe473, together with hydrogen bonding from His99 and Gln214 residues which serve to anchor the omeprazole molecule for 5-methyl hydroxylation. One of the 5-methyl hydrogens lies directly above the haem iron at a distance of 4.96 Å and a nearby methoxy group forms a hydrophobic contact with Leu363. Both His99 (Ibeanu *et al.* 1996) and the position adjacent to Leu363 (Richardson and Johnson 1996) have been mutated in CYP2C enzymes (Lewis 1998, for a review) and, consequently, the CYP2C19 model is in close agreement with reported experimental findings. Table 5 provides a summary of published site-specific mutagenesis data for the CYP2C subfamily from which it can be appreciated that several key residue positions have been probed using this technique which map closely with the interactions described in the models.

CYP2D6 model

The putative active site of CYP2D6 is presented as figure 7. In this case, the selective substrate propranolol is shown docked within the haem pocket for 4-hydroxylation. There are two π–π stacking interactions that serve to position the substrate such that the 4-hydrogen lies at a distance of 3.1 Å from the haem iron. These cooperatively assist the ion-paired contact between the protonated basic nitrogen of propranolol and the sidechain of Asp301 (Asp290 in figure 7). One of the phenylalanine residues that π-stacks with propranolol has been mutated (Smith

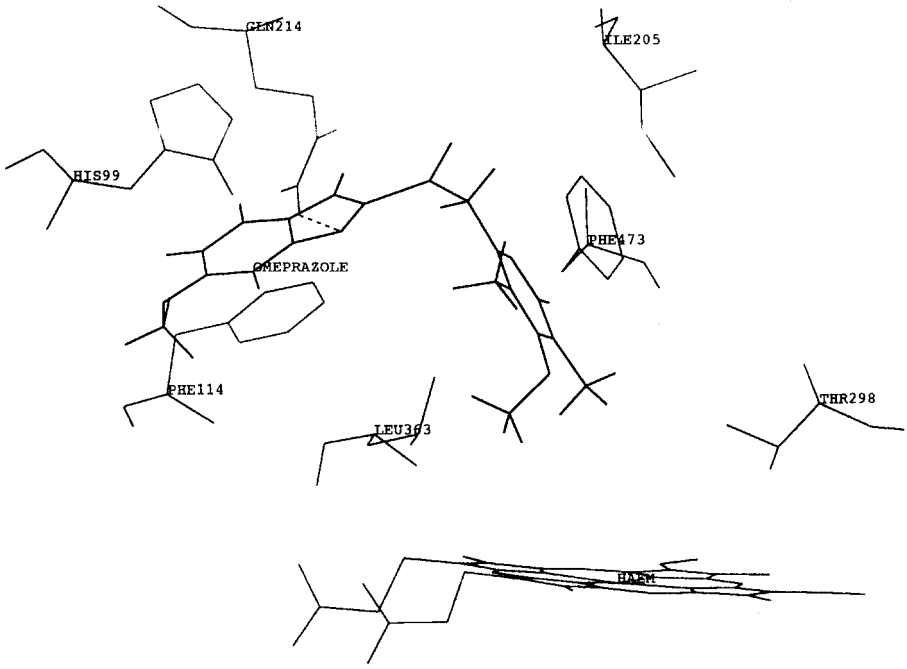


Figure 6. CYP2C19 active site showing omeprazole docked for 5-methyl hydroxylation by cooperative binding interactions to aromatic and polar amino acid residues. Hydrogen bonds are displayed as dashed lines and residues are numbered according to that of the template structure.

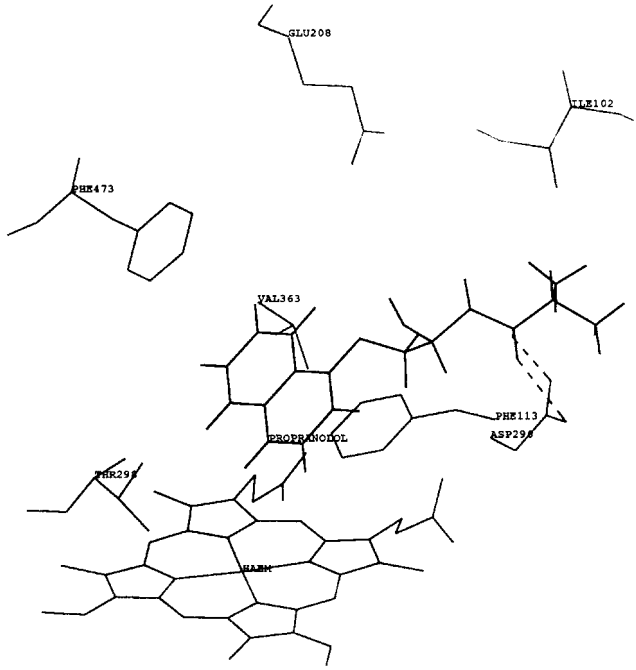


Figure 7. Active site region of CYP2D6 showing the substrate propranolol docked for 4-hydroxylation via contacts with complementary amino acid residues. Residues are labelled according to that of the template structure, and hydrogen bonds are displayed as dashed lines.

et al. 1998) in this enzyme with resulting loss in activity, and the aspartate residue has also been the subject of site-specific mutation in CYP2D6 (Ellis *et al*. 1995). Furthermore, other typical CYP2D6 substrates such as debrisoquine and bufuralol can also fit the putative binding site of this enzyme in a similar manner, thus strengthening its overall validity.

CYP2E1 model

Figure 8 shows how the substrate 4-nitrophenol can be orientated for 2-hydroxylation in the putative active site of human CYP2E1. The substrate forms a π–π stacking interaction with Phe205 and there are hydrogen-bonded contacts with the sidechains of Asn202 and Thr298. These cooperative interactions with active site amino acid residues position the 2-hydrogen of 4-nitrophenol closest to the haem iron at a distance of 5.6 Å. Chlorzoxazone, a selective CYP2E1 substrate, also fits within the putative active site region, where a combination π–π-stacking and hydrogen bonded interactions (via Phe205 and Asn202, respectively) orientates the substrate for hydroxylation at the 6-position. Of the aforementioned residues, only Thr298 has been the subject of mutagenesis experiments in the CYP2E subfamily, however (reviewed in Lewis 1998). Nevertheless, the interactions are consistent with site-specific mutations of corresponding residues in other CYP2 family enzymes, especially that of Phe205, which

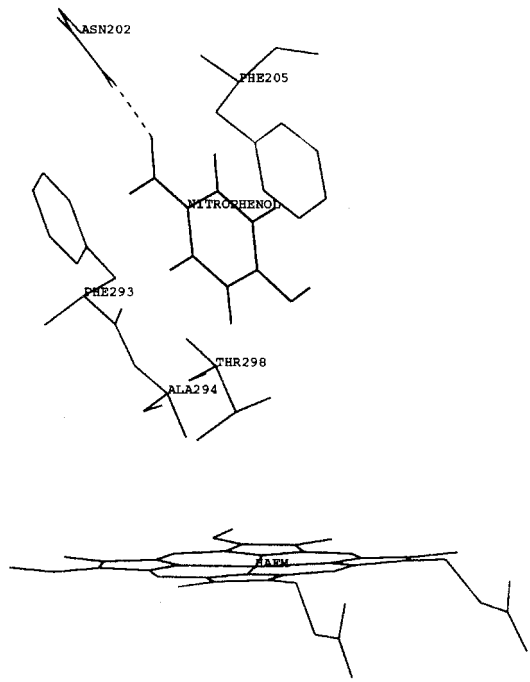


Figure 8. Selective substrate 4-nitrophenol shown within the putative active site of CYP2E1 where a combination of hydrogen bonded (dashed lines) and π–π interactions position the molecule for 2-hydroxylation. Residues are labelled according to that of the template crystal structure.

Table 6. Comparison between experimental and calculated binding affinities (kcal mol^{-1}) for substrates of human CYP2 family enzymes.

CYP	Substrate	K_m(μM)	ΔG_{bind}	Active site interactions	log P	ΔG_{part}	ΔG_{rotors}	ΔG_{bind}^{calc}
2A6	coumarin	2.1	−8.0537	2 hydrogen bonds: 2π-stacks	1.39	−1.9717	0	−7.7717
	losigamone	10.0	−7.0923	2 hydrogen bonds: 1π-stack	1.46	−2.0710	0	−6.9710
	cotinine	264.7	−5.0742	2 hydrogen bonds: 1π-stack	0.07	−0.0993	0	−4.9993
2B6	4-trifluoromethyl-7-ethoxycoumarin	2.9	−7.8549	2 hydrogen bonds: 2π-stacks	3.31	−4.6951	2.4	−8.0951
	7-benzyloxyresorufin	1.28	−8.3587	1 hydrogen bond: 2π-stacks	4.75	−6.7377	1.8	−8.7377
	benzphetamine	93.4	−5.7159	1 hydrogen bond: 2π-stacks	2.27	−3.2199	1.8	−5.2199
2C8	rosiglitazone	10	−7.0923	2 hydrogen bonds: 1π-stack	2.43	−3.4469	1.2	−7.1469
	retinoic acid	9	−7.1572	1 hydrogen bond	6.58	−9.3335	4.2	−7.1335
	taxol	5	−7.5193	4 hydrogen bonds: 1π-stack	2.28	−3.2341	4.8	−7.3341
2C9	tobutamide	132	−5.5028	1 hydrogen bond: 1π-stack	2.34	−3.3192	2.4	−5.6192
	diclofenac	6	−7.4070	1 hydrogen bond: 1π-stack	4.40	−6.2413	1.8	−7.3413
	ibuprofen	52	−6.0767	1 hydrogen bond: 1π-stack	3.51	−4.9788	1.8	−6.0788
2C19	omeprazole	8.6	−7.1852	2 hydrogen bonds: 1π-stack	2.23	−3.1632	0.6	−7.4632
	S-mephenytoin	49.8	−6.1037	2 hydrogen bonds: 1π-stack	1.74	−2.4681	1.2	−6.1681
	proguanil	96	−5.6990	1 hydrogen bond: 1π-stack	2.53	−3.5887	0.6	−5.8887
2D6	propranolol	2.73	−7.6375	1 ion-pair: 1π-stack: 1 hydrogen bond	3.37	−4.7802	4.2	−7.4802
	bufuralol	8.6	−6.9535	1 ion-pair: 1π-stack: 1 hydrogen bond	3.50	−4.9646	4.8	−7.0646
	debrisoquine	13	−6.7071	1 ion-pair: 1π-stack: 1 hydrogen bond	0.75	−1.0638	1.2	−6.7638
2E1	chlorzoxazone	40	−6.2539	1 hydrogen bond: 1π-stack	2.36	−3.3476	0	−6.2476
	4-nitrophenol	21	−6.6353	2 hydrogen bonds: 1π-stack	1.91	−2.7093	1.2	−6.4093
	halothane	500	−4.6824	1 hydrogen bond	2.30	−3.2625	0.6	−4.6625

K_m, Michaelis constant (μM) for substrate metabolism; ΔG_{bind}, experimental binding affinity given by $RT \ln K_m$ where R is the gas constant and T is the absolute temperature (310 K); log P, experimental log P, where P is the octanol/water partition coefficient; ΔG_{part}, partitioning free energy given by $RT \ln P$; ΔG_{rotors}, energy loss due to rigidity of rotatable bonds produced by substrate binding (0.6 kcal mol^{-1} per rotatable bond); ΔG_{bind}^{calc}, calculated binding affinity obtained by a summation of the ΔG_{part}, ΔG_{rotors}, ΔG_{hbond} and $\Delta G\pi$-π terms, where the latter two refer to hydrogen bond and π–π stacking interactions with average energies of −2.0 and −0.9 kcal mol^{-1}, respectively (Lewis 2000). The agreement between experimental and calculated ΔG_{bind} is 98% for the substrates tabulated.

appears to be a common contact for substrates containing aromatic rings irrespective of the P450 enzyme involved.

Table 6 shows that it is possible to make estimates of substrate binding energies that agree well with the experimental values, provided that one takes into account the various components of the overall binding energy (Lewis 2000). These include the partitioning free energy, ΔG_{part}, the energy loss caused by rotatable bonds in the substrate which become fixed on binding (ΔG_{rotors}) and the active site interactions made up from hydrogen bond and π–π stacking contributions (Lewis 2000) with averages of -2.0 and $-0.9\,\text{kcal mol}^{-1}$, respectively. The method used is based on the original work of Andrews *et al.* (1984) with later developments by Williams *et al.* (1991) and Bohn (1994). In general, it can be appreciated that there is a good agreement between experimental and calculated binding affinities for the substrates investigated, as shown in table 6, thus demonstrating that this approach can be applicable to P450–substrate interactions. Although the use of K_s would be preferable to K_m data, only the latter were available and the satisfactory agreement shown in table 6 tends to justify the utility of this procedure, despite such limitations.

Conclusions

All seven CYP2 family enzyme models are consistent with known experimental information in the form of substrate metabolism and site-specific mutagenesis data. In each case, a preferred substrate (usually of high affinity) can be shown to interact favourably within the putative active site region where hydrogen-bonded and π–π stacking interactions cooperatively assist in orientating each molecule relative to the haem iron such that metabolism at the known position can be explained, including the enzyme–substrate K_m. Consequently, it would appear that each human CYP2 family enzyme model investigated displays binding site characteristics consistent with the requirements of selective substrates of the individual enzymes themselves.

Acknowledgements

The financial support of GlaxoSmithKline Research & Development Ltd, Merck, Sharp & Dohme Ltd and the University of Surrey Foundation Fund is gratefully acknowledged. The author also thanks Sandeep Modi and Maurice Dickins (GlaxoSmithKline) for their assistance in obtaining the CYP2C5 crystallographic coordinates.

References

Andrews, P. R., Craik, D. J. and Martin, J. L., 1984, Functional group contributions to drug–receptor interactions. *Journal of Medicinal Chemistry*, **28**, 1648–1657.

Anzenbacher, P. and Anzenbacherova, E., 2001, Cytochromes P450 and metabolism of xenobiotics. *Cellular and Molecular Life Sciences*, **58**, 737–747.

Bohm, H.-J., 1994, The development of a simple empirical scoring function to estimate the binding constant for a protein ligand of known 3-dimensional structure. *Journal of Computer-Aided Molecular Design*, **8**, 243–256.

Chang, Y. T., Stiffelman, O. B., Vasker, I. A., Loew, G. H., Bridges, A. and Waskell, L., 1997, Construction of a 3D model of cytochrome P4502B4. *Protein Engineering*, **10**, 119–129.

Chen, C.-D. and Kemper, B., 1996, Different structural requirements at specific proline residue positions in the conserved proline-rich region of cytochrome P450 2C2, *Journal of Biological Chemistry*, **271**, 28607–28611.

Dai, R., Pincus, M. R. and Friedman, F. K., 2000, Molecular modelling of mammalian cytochrome P450s. *Cellular and Molecular Life Sciences*, **57**, 487–499.

De Groot, M. J., Ackland, M. J., Horne, V. A., Alex, A. A. and Jones, B. C., 1999, Novel approach to predicting P450-mediated drug metabolism: development of a combined protein and pharmacophore model for CYP2D6. *Journal of Medicinal Chemistry*, **42**, 1515–1524.

Ellis, S. W., Hayhurst, G. P., Smith, G., Lightfoot, R., Wong, M. M. S., Simula, A. P., Ackland, M. J., Sternberg, M. J. E., Lennard, M. S., Tucker, G. T. and Wolf, C. R., 1995, Evidence that aspartic acid 301 is a critical substate-contact residue in the active site of cytochrome P450 2D6. *Journal of Biological Chemistry*, **270**, 29055–29058.

Faletto, M. B., Linko, P. and Goldstein, J. A., 1992, A single amino acid mutation, Ser^{180}, Cys, determines the polymorphism in cytochrome P450g, P4502C13, by altering protein stability, *Journal of Biological Chemistry*, **267**, 2032–2037.

Gotoh, O., 1992, Substrate recognition sites in cytochrome P450 family 2 (CYP2) proteins inferred from comparative analyses of amino acid and coding nucleotide sequences, *Journal of Biological Chemistry*, **267**, 83–90.

Haining, R. L., Jones, J. P., Henne, K. R., Fisher, M. B. and Koop, D. R., 1999, Enzymatic determinants of the substrate specificity of CYP2C9: role of B-C loop residues in providing the pi-stacking anchor site for warfarin binding. *Biochemistry*, **38**, 3225–3292.

Hanioka, N., Gonzalez, F. J., Lindberg, N. A., Liu, G., Gelboin, H. V. and Korzekwa, K. R., 1992, Site-directed mutagenesis of cytochrome P450s CYP2A1 and CYP2A2: influence of the distal helix on the kinetics of testosterone metabolism. *Biochemistry*, **31**, 3364–3370.

Hsu, M.-H., Griffin, K. J., Wang, Y., Kemper, B. and Johnson, E. F., 1993, A single amino acid substitution confers progesterone 6, -hydroxylase activity to rabbit cytochrome P450 2C3, *Journal of Biological Chemistry*, **268**, 6939–6944.

Ibeanu, G. C., Ghanayen, B. I., Linko, P., Li, L., Pedersen, L. G. and Goldstein, J. A., 1996, Identification of residues 99, 220, and 221 of human cytochrome P450 2C19 as key determinants of omeprazole hydroxylase activity, *Journal of Biological Chemistry*, **271**, 12496–12501.

Imai, Y. and Nakamura, M., 1989, Point mutations at threonine-301 modify substrate specificity of rabbit liver microsomal cytochromes P-450 (laurate, ω-1) -hydroxylase and testosterone 16α-hydroxylase), *Biochemical and Biophysical Research Communications*, **158**, 717–722.

Kaminsky, L. S. de Morais, S. M. F. Faletto, M. B., Dunbar, D. A. and Goldstein, J. A., 1993, Correlation of human cytochrome P4502C substrate specificities with primary structure: warfarin as a probe, *Molecular Pharmacology*, **43**, 234–239.

Kronbach, T., Larabee, T. M. and Johnson, E. F., 1989, Hybrid cytochromes P-450 identify a substrate binding domain in P-450IIC5 and P450IIC4, *Proceedings of the National Academy of Sciences, USA*, **86**, 8262–8265.

Lewis, D. F. V., 1996, *Cytochromes P450: Structure, Function and Mechanism* (London: Taylor & Francis).

Lewis, D. F. V., 1998, The CYP2 family: models, mutants and interactions. *Xenobiotica*, **28**, 617–661.

Lewis, D. F. V., 2000, On the recognition of mammalian microsomal cytochrome P450 substrates and their characteristics. *Biochemical Pharmacology*, **60**, 293–306.

Lewis, D. F. V., 2001, *Guide to Cytochromes P450 Structure and Function* (London: Taylor & Francis).

Lewis, D. F. V., Dickins, M., Eddershaw, P. J., Goldfarb, P. S. and Tarbit, M. H., 1998, Molecular modelling of human CYP2C subfamily enzymes CYP2C9 and CYP2C19: rationalization of substrate specificity and site-directed mutagenesis experiments in the CYP2C subfamily. *Xenobiotica*, **28**, 235–268.

Lewis, D. F. V., Dickins, M., Lake, B. G., Eddershaw, P. J., Tabit, M. H. and Goldfarb, P. S., 1999c, Molecular modelling of the human cytochrome P450 isoform CYP2A6 and investigations of CYP2A substrate selectivity. *Toxicology*, **133**, 1–33.

Lewis, D. F. V., Eddershaw, P. J., Goldfarb, P. S. and Tarbit, M. H., 1996, Molecular modelling of CYP3A4 from an alignment with CYP102: identification of key interactions between putative active site residues and CYP3A-specific chemicals. *Xenobiotica*, **26**, 1067–1086.

Lewis, D. V. F., Eddershaw, P. J., Goldfarb, P. S. and Tarbit, M. H., 1997, Molecular modelling of cytochrome P4502D6 (CYP2D6) based on an alignment with CYP102: Structural studies on specific CYP2D6 substrate metabolism. *Xenobiotica*, **27**, 319–340.

Lewis, D. F. V., Lake, B. G., Bird, M. G., Dickins, M., Eddershaw, P. J., Tarbit, M. H. and Goldfarb, P. S., 2000, Molecular modelling of human CYP2E1 by homology with the CYP102 haemoprotein domain: investigation of the interactions of substrates and inhibitors within the putative active site of the CYP2E1 isoform. *Xenobiotica*, **30**, 1–25.

Lewis, D. F. V., Lake, B. G., Dickens, M., Eddershaw, P. J., Tarbit, M. H. and Goldfarb, P. S., 1999a, Molecular modelling of the phenobarbital-inducible P450 isoforms: CYP2B1, CYP2B4 and CYP2B6 by homology with the substrate-bound CYP102 crystal structure, and evaluation of CYP2B substrate binding affinity. *Xenobiotica*, **29**, 361–393.

Lewis, D. F. V., Lake, B. G., George, S. G., Dickins, M., Beresford, A. P., Eddershaw, P. J., Tarbit, M. H., Goldfarb, P. S. and Guengerich, F. P., 1999b, Molecular modelling of CYP1 family isoforms: CYP1A1, CYP1A2, CYP1A6 and CYP1B1 based on sequence homology with CYP102. *Toxicology*, **139**, 53–79.

Lewis, D. F. V., Modi, S. and Dickins, M., 2002, Structure-activity relationships for human cytochrome P450 substrates and inhibitors. *Drug Metabolism Reviews* (in press).

Li, H. and Poulos, T. L., 1997, The structure of the cytochrome P450BM-3 haem domain complexed with the fatty acid substrate, palmitoleic acid. *Nature and Structural Biology*, **4**, 140–146.

Lindberg, R. L. P. and Negishi, M., 1989, Alteration of mouse cytochrome $P450_{coh}$ substrate specificity by mutation of a single amino acid residue. *Nature*, **339**, 632–674.

Ohgiya, S., Komori, M., Ohi, H., Shiramatsu, K., Shinriki, N. and Kamataki, T., 1992, Six-base deletion occurring in messages of human cytochrome P-450 in the CYP2C subfamily results in reduction of tolbutamide hydroxylase activity, *Biochemistry International*, **27**, 1073–1081.

Ramarao, M. K., Straub, P. and Kemper, B., 1995, Identification by *in vitro* mutagenesis of the interaction of two segments of C2MstC1, a chimera of cytochromes P450 2C2 and P450 2C1, *Journal of Biological Chemistry*, **270**, 1873–1880.

Ravichandran, K. G., Boddupalli, S. S., Hasemann, C. A., Peterson, J. A. and Deisenhofer, J., 1993, Crystal structure of hemoprotein domain of P450BM-3, a prototype for microsomal P450s. *Science*, **261**, 731–736.

Rendic, S. and DiCarlo, F. J., 1997, Human cytochrome P450 enzymes: a status report summarizing their reactions, substrates, inducers and inhibitors. *Drug Metabolism Reviews*, **29**, 413–580.

Richardson, T. H. and Johnson, E. F., 1994, Alterations of the regiospecificity of progesterone metabolism by the mutagenesis of two key amino acid residues in rabbit cytochrome P450 2C3v. *Journal of Biological Chemistry*, **269**, 23927–23943.

Richardson, T. H. and Johnson, E. F., 1996, The CYP2C subfamily. In C. Ioannides (ed.), *Cytochromes P450: Metabolic and Toxicological Aspects* (Boca Raton: CRC Press) pp. 161–181.

Ridderstrom, M., Masimirembara, C., Trump-Kallmeyer, S., Ahlefelt, M., Otter, C. and Andersson, T. B., 2000, Arginines 97 and 108 in CYP2C9 are important determinants of the catalytic function. *Biochemical and Biophysical Research Communications*, **270**, 983–987.

Smith, G., Modi, S., Pillai, I., Lian, L.-Y., Sutcliffe, M. J., Pritchard, M. P., Friedberg, T., Roberts, G. C. K. and Wolf, C. R., 1998, Determinants of the substrate specificity of human cytochrome P450 CYP2D6: design and construction of mutant with testosterone hydroxylase activity. *Biochemical Journal*, **331**, 783–792.

Straub, P., Johnson, E. F. and Kemper, B., 1993b, Hydrophobic side chain requirements for lauric acid and progesterone hydroxylation at amino acid 113 in cytochrome P450 2C2, a potential determinant of substrate specificity, *Archives of Biochemistry and Biophysics*, **306**, 521–527.

Straub, P., Lloyd, M., Johnson, E. F. and Kemper, B., 1993a, Cassette mutagenesis of a potential substrate recognition region of cytochrome P450 2C2, *Journal of Biological Chemistry*, **268**, 21997–22003.

Szklarz, G. D., He, Y. Q., Kedzie, K. M., Halpert, J. R. and Burnett, V. L., 1996, Elucidation of amino acid residues critical for unique activities of rabbit cytochrome P4502B5 using hybrid enzymes and reciprocal site-directed mutagenesis with rabbit cytochrome P4502B4. *Archives of Biochemistry and Biophysics*, **327**, 308–318.

Veronese, M. E., Doecke, C. J., Mackenzie, P. I., McManus, M. E., Miners, J. O., Rees, D. L. P., Gasser, R., Meyer, U. A. and Birkett, D. J., 1993, Site-directed mutation studies of human liver cytochrome P-450 isoenzymes in the CYP2C subfamily, *Biochemical Journal*, **289**, 533–538.

Von Wachenfeldt, C. and Johnson, E. F., 1995, Structures of eukaryotic cytochrome P450 enzymes. In P. R. Ortiz de Montellano (ed.), *Cytochrome P450* (New York: Plenum), pp. 183–244.

Williams, D. H., Cox, J. P. L., Doig, A. J., Gardner, M., Gerhard, U., Kaye, P. T., Lal, A. R., Nicholls, I. A., Salter, C. J. and Mitchell, R. C., 1991, Toward the semiquantitative estimation of binding constants. *Journal of the American Chemical Society*, **113**, 7020–7030.

Williams, P. A., Cosme, J., Sridhar, V., Johnson, E. F. and McRee, D. E., 2000, Mammalian microsomal cytochrome P450 monooxygenase: structure adaptions for membrane binding and functional diversity. *Molecular Cell*, **5**, 121–131.

Yamazaki, S., Sato, K., Suhaka, K., Sakaguchi, M., Mihara, K. and Omura, T., 1993, Importance of the proline-rich region following signal-anchor sequence in the formation of correct conformation of microsomal cytochrome P-450s, *Journal of Biochemistry*, **114**, 652–657.

XENOBIOTICA, 2002, VOL. 32, NO. 4, 325–337

Taylor & Francis
healthsciences

Identification of the urinary metabolites of 4-bromoaniline and 4-bromo-[*carbonyl*-^{13}C]-acetanilide in rat

G. B. SCARFE†§, J. K NICHOLSON†, J. C. LINDON†, I. D. WILSON‡*, S. TAYLOR‡, E. CLAYTON‡ and B. WRIGHT‡

† Biological Chemistry, Division of Biomedical Sciences, Imperial College of Science, Technology and Medicine, University of London, Sir Alexander Fleming Building, South Kensington, London SW7 2AZ, UK
‡ Department of Drug Metabolism and Pharmacokinetics, AstraZeneca Pharmaceuticals, Mereside, Alderely Park, Macclesfield SK10 4TG, UK

Received 14 May 2001

1. The urinary excretion of 4-bromoaniline and its [*carbonyl*-^{13}C]-labelled *N*-acetanilide, together with their corresponding metabolites, have been investigated in the rat following i.p. administration at 50 mg kg^{-1}.

2. Metabolite profiling was performed by reversed-phase HPLC with UV detection, whilst identification was performed using a combination of enzymic hydrolysis and directly coupled HPLC-NMR-MS analysis. The urinary metabolite profile was quantitatively and qualitatively similar for both compounds with little of either excreted unchanged.

3. The major metabolite present in urine was 2-amino-5-bromophenylsulphate, but, in addition, a number of metabolites with modification of the *N*-acetyl moiety were identified (from both the [^{13}C]-acetanilide or produced following acetylation of the free bromoaniline).

4. For 4-bromoacetanilide, *N*-deacetylation was a major route of metabolism, but despite the detection of the acetanilide following the administration of the free aniline, there was no evidence of reacetylation (futile deacetylation).

5. Metabolites resulting from the oxidation of the acetyl group included a novel glucuronide of an *N*-glycolanilide, an unusual *N*-oxanilic acid and a novel *N*-acetyl cysteine conjugate.

Introduction

Anilines and their derivatives are used as intermediates in many industrial applications including the production of plastics, dyes, pesticides and pharmaceuticals. They can also arise as the result of the metabolism of many xenobiotics (e.g. paracetamol and phenacetin, Nicholls *et al.* 1997a, b, 1999; salicylazosulphapyridine Schroder *et al.* 1973; flutamide, Shulz *et al.* 1988; sulofenur, Ehlardt *et al.* 1992; and casodex, Boyle *et al.* 1993, Mckillop *et al.* 1993). Exposure to such compounds is, therefore, widespread and such exposure may result in a range of undesirable and toxic effects, including haemolysis, methaemoglobinaemia, nephro- and hepatoxicity and carcinogenesis (e.g. Radomski 1979). Many of the adverse effects seen with this class of compounds result from the production of

* Author for correspondence; ian.wilson@astrazeneca.com
§ Present address: Department of Drug Metabolism and Pharmacokinetics, Servier Research and Development Ltd, Fulmer Hall, Windmill Road, Fulmer, Slough SL3 6HH, UK.

Xenobiotica ISSN 0049–8254 print/ISSN 1366–5928 online © 2002 Taylor & Francis Ltd
http://www.tandf.co.uk/journals
DOI: 10.1080/00498250110079806

toxic and/or reactive metabolites. Hence, a better understanding of the metabolic fate of these compounds is likely to be of benefit in understanding their toxicity. Despite their structural simplicity, substituted anilines can undergo complex metabolic reactions making accurate prediction of metabolic fate problematic. We have therefore undertaken a series of studies aimed at determining the effects of different substituents and substitution patterns on the metabolism of anilines (Wilson *et al.* 1985, Wade *et al.* 1988, Nicholls *et al.* 1987a, b, Scarfe *et al.* 1997, 1998, 1999a, b, 2000) to develop *in vivo* quantitative structure–metabolism relationships (QSMRs) of the type that we have obtained for aromatic carboxylic acids (Ghauri *et al.* 1992 a, b, Cupid *et al.* 1996, 1999) and phenols (Holmes *et al.* 1995) that will enable accurate prediction of their fate, thereby minimizing the use of animals in future metabolic studies. In addition to models for predicting the overall metabolism of anilines, we wished to determine molecular physicochemical factors that result in the propensity of certain *para*-substituted anilines, or their acetanilides, to undergo oxidation of the acetyl group to form *N*-oxanilic acids. Compounds that have been found to give rise to significant amounts of *N*-oxanilic acids include 4-chloroaniline and 4-chloroacetanilide (Kiese and Lenk 1969, 1970, 1971, Ehlhardt and Howbert 1991), 4-propionylacetanilide (Kiese and Lenk 1969) and 4-trifluoromethylaniline (Wilson *et al.* 1985, Wade *et al.* 1988). Presented here are the results of an investigation of the metabolic fate of 4-bromoaniline (4-BrA) and its [*carbonyl*-^{13}C]-labelled acetanilide (4-BrAc) in the rat.

Materials and methods

Solvents and chemicals used were the purest available (analytical or HPLC grade).

*4-Bromoaniline and 4-bromo[*carbonyl-^{13}*C]-acetanilide*

4-BrA (97% chemical purity) was obtained from Aldrich (Gillingham, UK) and was used as received. 4-BrAc was prepared by dissolving 3 mmol 4-bromoaniline in the minimum volume of dichloromethane followed by the addition of 3.5 mmol acetyl-1-[^{13}C]chloride (Aldrich). After the reaction had occurred, the dichloromethane was removed by rotary evaporation. The solid residue was then washed with water to remove excess acetyl chloride. The resulting material was then recrystallized from ethanol to give a product that was >95% pure as determined by ^{1}H-NMR spectroscopy.

Animal dosing

Before dosing, groups of three male Sprague–Dawley rats (200–330 g) were allowed to acclimatize individually for 24 h in metabolism cages designed for the separate collection of urine and faeces. The rats were permitted free access to food (rat maintenance diet TRM 9607) and water throughout the study. 4-BrA was dissolved in ethanol–water (50:50 v/v) at a concentration of 50 mg ml^{-1}, 4-BrAc was dissolved in corn oil at a concentration of 25 mg ml^{-1}. The test compounds were administered i.p. at a nominal dose level of 50 mg kg^{-1}. Urine was collected over solid carbon dioxide for –24–0, 0–8, 8–24 and 24–48 h post-dose (p.d.). Urinary weights were recorded and samples stored at −20 °C until analysed. Before analysis by ^{1}H-NMR samples were centrifuged at low speed (500 g) for 10 min to remove solid debris.

Metabolite profiling by HPLC-UV

HPLC with UV detection (254 nm) was performed on samples (50 or 100 µl, predose, 0–8, 8–24 and 24–48 h p.d.) following the removal of particulate matter by filtration through a 0.45 µm filter. The HPLC system consisted of a Bruker LC22 pump and a Bischoff Lambda 1100 variable wavelength detector (Bruker UK, Coventry, UK). The separation was performed on a Hypersil H5BDS 5 µm C18 column (250 × 4.6 mm i.d.; Hichrom, Reading, UK) at a flow rate of 1 ml min^{-1}. A solvent gradient was used, controlled via Bruker Chromstar software, with the mobile phase formed from 0.01 M ammonium formate (adjusted to pH 7.0 with aqueous ammonia) and acetonitrile. Initially an isocratic period of 10 min with 100% ammonium formate was followed by a linear increase in acetonitrile concentration to 30% over 35 min and then to 50% at 45 min.

Concentrations of compound-related material were estimated by comparison of the peak areas against a standard curve prepared from 4-BrA, making the assumption for the purposes of quantification that all components had the same UV extinction coefficient and absorption maximum as the parent. These data are therefore at best semiquantitative and indicative only.

Enzymic hydrolysis

Selected samples were subjected to hydrolysis with either β-glucuronidase or aryl sulphatase to determine the presence of glucuronide and sulphate conjugates. For these experiments aliquots (600 µl) of urine were taken and the pH adjusted to 5.0 (sulphatase) or 7.0 (glucuronidase) with 1 M hydrochloric acid or sodium hydroxide solution. Either 2500 IU β-glucuronidase (*E. coli* type VII-A, sulphatase free; Sigma, Poole, UK) or 75–200 IU aryl sulphatase (*H. pomatia*, type H-1, Sigma) were added to the samples. In addition, 50 µl 0.1 M solution of D-saccharic acid-1,4-lactone (Sigma) was added to the sulphatase incubations to inhibit glucuronidase activity. Test and control samples (at the appropriate pH) were then incubated overnight at 37 °C in a shaking water bath.

Metabolite identification by HPLC-NMR-MS

For the identification of metabolites, the system used was as follows. Chromatography was performed on a Hypersil H5BDS 5 µm C18 bonded column (250 × 4.6 mm i.d.; Hichrom) using the conditions described above but with D_2O instead of water and employing Pestanal-grade acetonitrile (Reidel de Haen, Germany). Following UV detection (254 nm), the flow was split ~95:5 with the major portion directed to the flow probe of a Bruker DRX 500 NMR spectrometer operating at 500.13 MHz for ^1H, and the minor portion to a Micromass Quattro LC triple-quadrupole mass spectrometer fitted with a Z-spray interface (Micromass UK, Wythenshawe, UK). Stopped flow NMR spectra were obtained by acquiring 600–5000 free induction decays (FIDs), depending upon the concentration of the analytes. FIDs were collected over a spectral width of 8278 Hz into 16 384 data points using an acquisition time of 0.99 s. Residual water and solvent resonances were suppressed using a presaturation pulse sequence (NOESYPRESAT, Bruker) with pre-irradiation during the interpulse relaxation delay of 2.0 s and a mixing time of 0.10 s. ^1H chemical shifts were referenced internally to the organic solvent signal (acetonitrile at δ2.0 relative to external tetramethylsilane δ0.0).

Mass spectra were obtained using electrospray in negative ionization mode up to mass m/z 600 using alternating low (20–30 V) and high (50 V) cone voltages to provide molecular ion and fragmentation data.

Results

Chromatographic profiling of samples

Following the administration of both 4-BrA and 4-BrAc, chromatographic profiles generated by reversed-phase gradient HPLC revealed a number of new peaks, compared with the predose controls. These peaks had retention times of between ~29 and 35 min, with 4-BrA and 4-BrAc, small amounts of which were present in the samples, eluting at 44.4 and 43.0 min respectively. The UV profiles for urine samples obtained after dosing both compounds were qualitatively very similar, implying a similar metabolic fate. A typical HPLC profile for 4-BrA is shown in figure 1.

In total 1.0 ± 1% (mean ± SD) of the 4-BrA dose was excreted in the urine as unchanged parent compound with a further 1% as the acetanilide. When 4-BrAc was administered, no 4-BrA was detected and 1.0 ± 2% of the dose was excreted unchanged.

Metabolite identification

Enzymic hydrolysis. Incubation of urine samples, from both 4-BrA- and 4-BrAc-dosed animals, with β-glucuronidase gave equivocal results as, although peaks were seen to decline in intensity following treatment with the enzyme, the same peaks were also observed to decrease in the control incubations. This meant that it

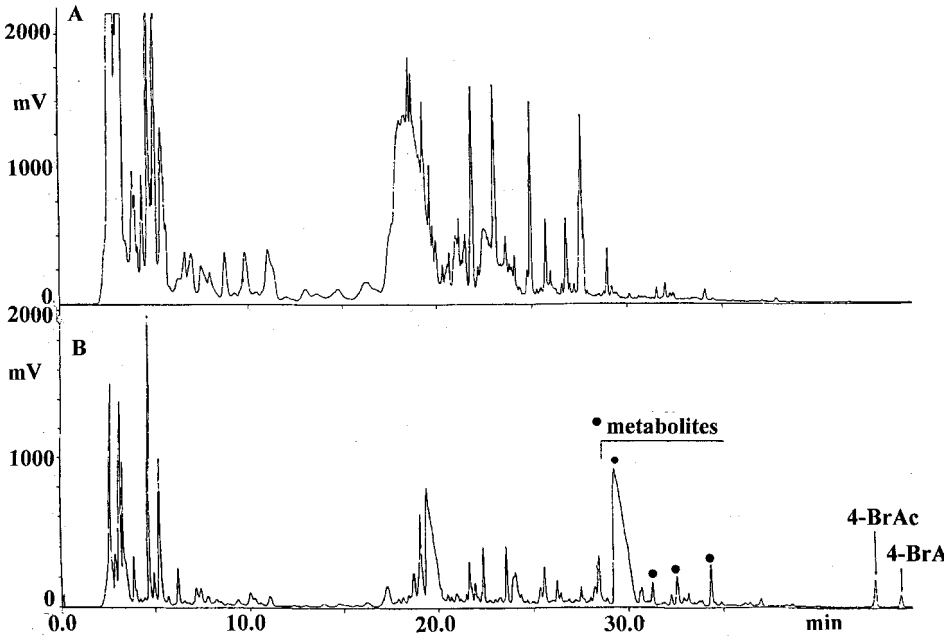


Figure 1. Typical gradient HPLC-UV profile for (A) a predose control sample and (B) a 0–8-h sample of urine obtained following the administration of 4-BrA. Putative metabolites (indicated with a solid circle) were detected as new peaks eluting between 29 and 35 min. 4-BrA and 4-BrAc eluted at 44.4 and 43.0 min respectively.

was not possible to make any tentative identifications of peaks as potential glucuronides. It was possible to be more definite after treatment with aryl sulphatase as the decrease of the peak of the major metabolite eluting at ~29.2 min and concomitant appearance of a previously unobserved peak at 36.5 min (not seen in control incubations) indicated that the major metabolite of 4-BrA and 4-BrAc was most probably a sulphate of a phase 1 hydroxylated metabolite.

HPLC-NMR-MS of urine extracts. As described above, examination of the UV chromatogram clearly showed the presence of compound-related material and, therefore, studies were undertaken to identify these metabolites. Solid-phase extraction was used partially to purify and concentrate representative 0–8-h p.d. samples to optimize them for HPLC-NMR-MS. Gradient HPLC was then performed as described above. The HPLC-UV and corresponding MS-TIC (total ion current) traces are shown in figure 2a, b for the 0–8-h p.d. 4-BrA sample.

Identification of the metabolite 2-amino-5-bromophenyl sulphate. The major metabolite peak for both 4-BrA and 4-BrAc eluted with a retention time of 30.0 min and, based on the experiments with hydrolytic enzymes, was tentatively identified as a sulphate. The negative-ion mass spectrum of this peak gave a molecular ion $[M\text{-}D]^-$ at m/z 268/270, with a loss of 80 Da consistent with the presence of (SO_3). Both 4-BrA and 4-BrAc gave the same molecular ions, indicating the loss of the [^{13}C]-labelled acetyl from the acetanilide. Thus, the

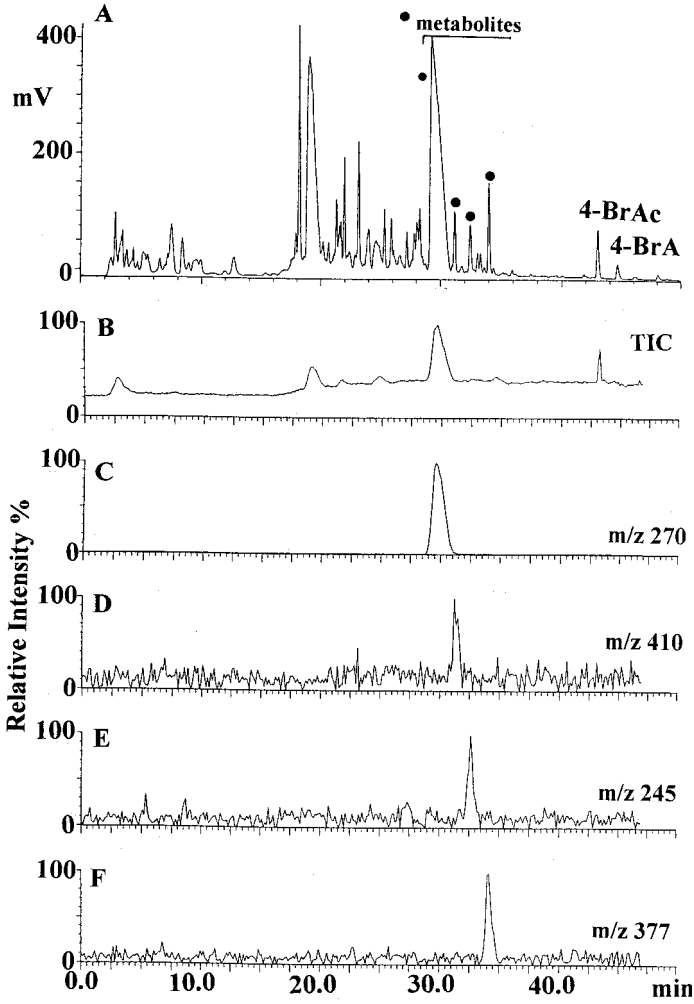


Figure 2. HPLC-UV (A) and HPLC-MS total ion current (B) traces obtained for an extract of 0–8-h post-dose rat urine following administration of 4-BrA. Traces C–F correspond to the $[M\text{-}D]^-$ ions for the metabolites (C) 2-amino-5-bromophenyl sulphate, (D) 4-bromoglycolanilide-*O*-glucuronide, (E) 4-bromooxanilic acid and (F) *N*-acetyl-*S*-[2-keto-2(4-bromoanilino)ethyl-cysteine.

molecular mass was consistent with the presence of a hydroxy-sulphate of the parent aniline. Stopped-flow ^{1}H-NMR spectroscopy showed the *p*-di-substituted pattern of the parent compounds was no longer present, indicating that metabolite had been modified on the aromatic ring rather than the amino group. Three signals were present for the remaining protons. The two *ortho*-coupled protons ($^3\mathcal{J}_{H\text{-}H} = 9$ Hz) at δ6.80 and δ7.18 were, based on their chemical shifts, located next to the NH_2- and Br-substituents respectively, whilst the remaining *meta*-coupled proton ($^4\mathcal{J}_{H\text{-}H} = 2.2$) at δ7.37 was adjacent to the Br. The site of hydroxylation was thus the position *ortho* to the amino group. Representative ^{1}H-NMR and mass spectra are shown in figure 3. Assuming that this material had a similar UV extinction coefficient to the parent, ~25% of the dose was recovered in the first 24 h p.d. (with the bulk excreted in the first 0–8-h sample). For 4-BrAc,

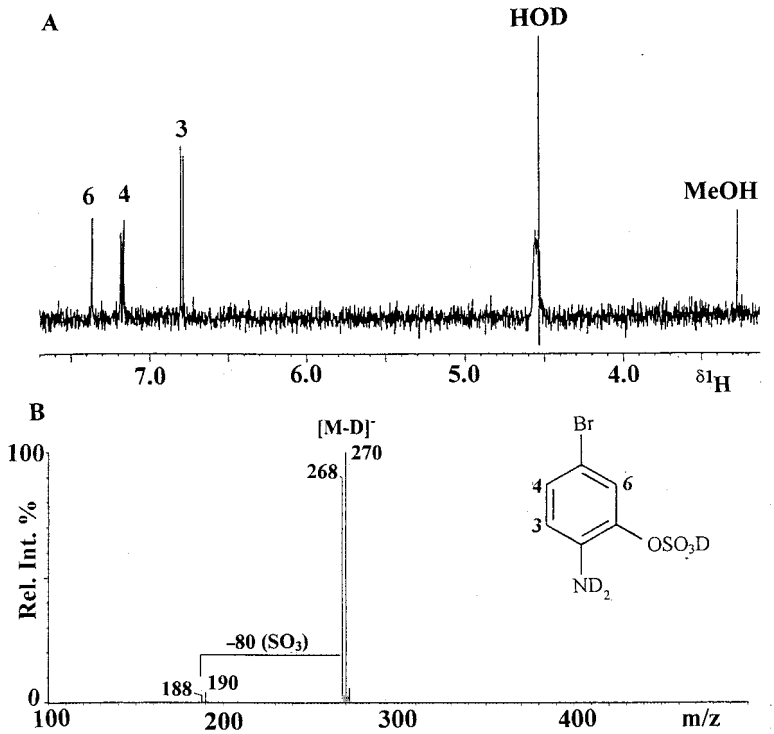


Figure 3. Representative ^{1}H-NMR (A) and mass spectra (B) of 2-amino-5-bromophenyl sulphate obtained following HPLC-NMR-MS of a sample obtained after dosing 4-BrA, as shown in figure 2.

the equivalent figure was ~16% (equally divided between the 0–8- and 8–24-h samples). Little variation was observed between animals (±1%) in the proportions of this material excreted in the urine.

Identification of the metabolite 4-bromoglycolanilide-O-glucuronide. Following the administration of 4-BrA, the minor UV peak eluting at 31.1 min, shortly after the phenolic sulphate metabolite, gave molecular ions $[M-D]^-$ at m/z 408/410 with the characteristic isotope pattern for a bromine-containing compound. When 4-BrAc was dosed, the same metabolite had molecular ions at m/z 409/411, indicating that the [^{13}C]-labelled acetyl had been retained. Stopped-flow ^{1}H-NMR spectroscopy on this peak revealed that the *para*-di-substituted pattern for the aromatic protons had been retained, indicating that metabolism had occurred elsewhere. The aliphatic portion of the NMR spectrum of the 4-BrA-derived metabolite showed clear signals for a glucuronide conjugate. In addition, an *AB*-quartet was observed (δ4.38) showing two non-equivalent protons as the result of the presence of a chiral glucuronide. The equivalent spectrum for the 4-BrAc-derived glucuronide showed this resonance as an ABX system, with the further splitting resulting from the adjacent [^{13}C]-labelled carbonyl group (the spectra are shown in figure 4). All of these data are consistent with the metabolism of both 4-BrA and 4-BrAc to an *O*-glucuronide of a glycolanilide (structure inset

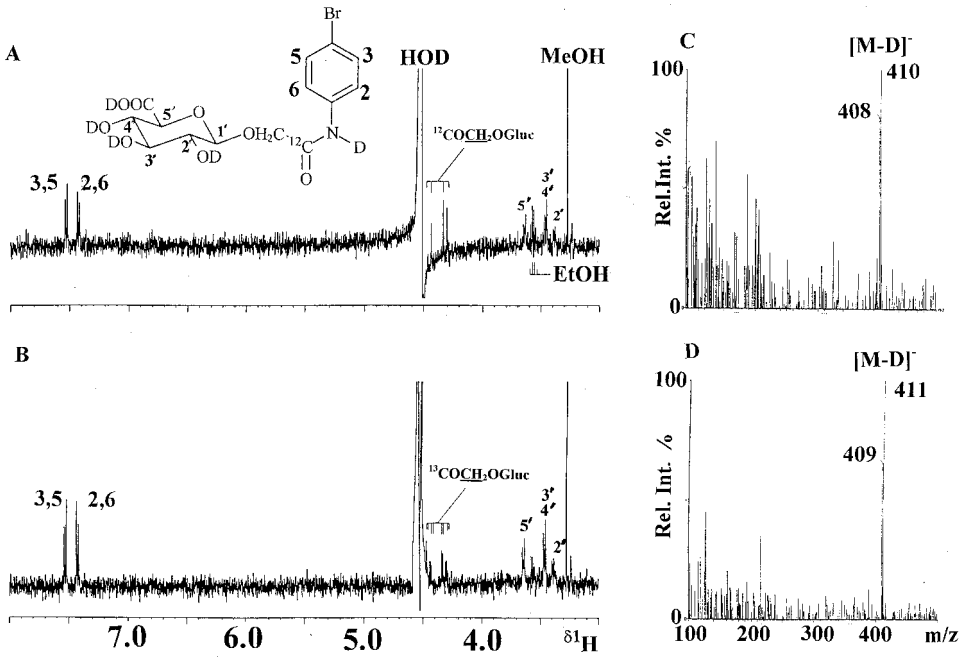


Figure 4. Representative ^{1}H-NMR (A, B) and mass spectra (C, D) of 4-bromoglycoanilide-*O*-glucuronide obtained via the HPLC-NMR-MS of samples obtained following administration of 4-BrA (spectra A, C) and [^{13}C]-4-BrAc (spectra B, D).

to figure 4). Previously Kiese and Lenk (1969) identified the free, unconjugated, glycolanilide of 4-BrAc in rabbit.

For both 4-BrA and 4-BrAc, the 4-bromoglycoanilide-*O*-glucuronide was a minor component of the urinary metabolite profile comprising ~1.0–2.0% of the dose.

Identification of the metabolite 4-bromooxanilic acid. The peak eluting with a retention time of 32.5 min gave a molecular ion at an *m/z* 243/245 or 244/246 amu after the administration of 4-BrA and 4-BrAc respectively, indicating the retention of the [^{13}C]-label in this metabolite. These mass spectra showed a major loss of either 72 or 73 resulting from the loss of either $COCO_2$ or $^{13}COCO_2$ consistent with the metabolite being an *N*-oxanilic acid. Stopped-flow ^{1}H-NMR spectroscopy on this metabolite revealed a *para*-di-substituted aromatic ring pattern confirming that the ring protons were all intact, and that there were no other signals associated with this metabolite (figure 5). Similar proportions of the dose were eliminated as this metabolite in the urine after either 4-BrA or 4-BrAc administration. Assuming similar UV properties this metabolite accounted for ~7 and ~9% of the dose respectively following 4-BrA or 4-BrAc administration. This metabolite was not reported when 4-BrAc was administered to rabbit (Kiese and Lenk 1969).

Identification of the metabolite N-*acetyl*-S-*[2-keto-2(4-bromoanilino)ethyl]-cysteine.* The minor metabolite eluting at 34.0 min gave [M-D]$^-$ ions at *m/z*

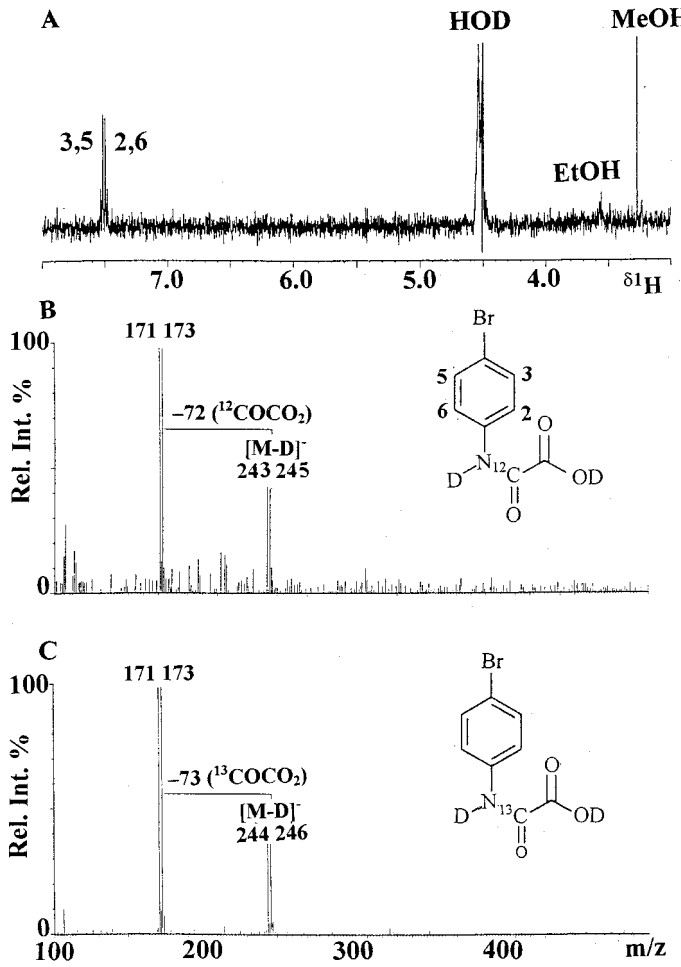


Figure 5. Representative ^{1}H-NMR (A) and mass spectra (B, C) of 4-bromooxanilic acid obtained via the HPLC-NMR-MS of samples obtained following the administration of 4-BrA (spectra A, B) and [^{13}C]-BrAc (spectrum C).

375/377 and 376/378 following the administration of 4-BrA and 4-BrAc respectively, again indicating the retention of the [^{13}C]-label in this latter metabolite. Stopped-flow ^{1}H-NMR spectroscopy of this peak showed firstly that the *para*-di-substituted pattern had been retained, demonstrating that metabolism had not occurred on the aromatic ring and, in addition, signals in the aliphatic portion of the spectrum were also observed. Thus, the AB component of an ABX spin system (two protons) was observed centred at δ2.97 together with a one-proton multiplet (the X part of the ABX system) at δ4.32 characteristic of the -SCH_2CH- moiety of a cysteinyl residue. In addition, the methyl signal of an *N*-acetyl group could be observed at δ1.92 (between the acetonitrile resonance and its ^{13}C satellite). These data suggest that an *N*-acetyl-l-cysteinyl (mercapturic acid) conjugate was present. Further examination of the NMR spectrum showed the presence of a methylene group (derived from the acetyl methyl of the acetanilide) present as either a singlet at or doublet at δ3.37 for the 4-BrA and 4-BrAc dosed

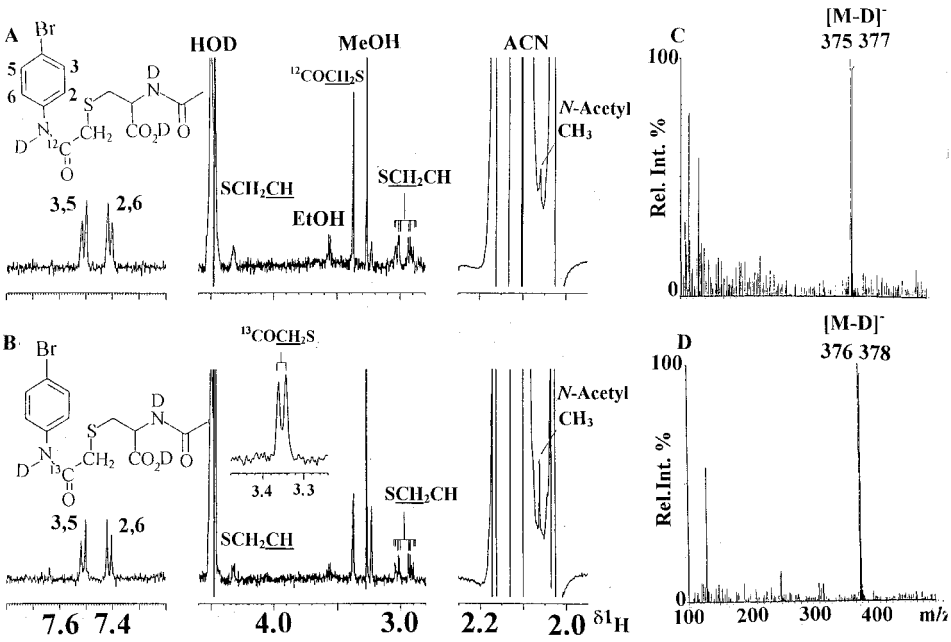


Figure 6. Representative ^{1}H-NMR (A, B) and mass spectra (C, D) for *N*-acetyl-*S*-[2-keto-2(4-bromoanilino)ethyl-cysteine obtained via HPLC-NMR-MS of samples obtained following the administration of 4-BrA (spectra A, C) and [^{13}C]-4-BrAc (spectra B, D).

animals respectively. The combination of NMR and MS data (figure 6) therefore show this metabolite to be the *N*-acetyl-S-[2-keto-2 (4-bromoanilino) ethyl] cysteine metabolite.

As with the other metabolites detected in this study, the amounts excreted in the urine were similar for both 4-BrA and 4-BrAc-dosed animals (~5 and 6% respectively, assuming similar UV properties to 4-BrA). The bulk of the urinary excretion of this metabolite was observed in the 8–24 h p.d. samples (~4% for both 4-BrA and 4-BrAc).

Discussion

As indicated above, in the absence of labelled material or authentic standards, it is not possible to provide a fully quantitative description of the metabolic fate and excretion balance for 4-BrA and 4-BrAc. However, if the assumption is made that the extinction coefficients of the metabolites are not too dissimilar to the parent compounds, then ~40% of the doses of both compounds were excreted in the urine (with the remainder presumably eliminated via the bile). The qualitative fate of both compounds was determined by comparison of both MS and UV data, thereby obtaining the relative proportions of the various metabolites, and these were identical for 4-BrA and 4-BrAc. Based on the metabolites of 4-BrA and 4-BrAc identified in urine in this study, a complex metabolic fate emerges with the bromoaniline metabolized by a combination of ring hydroxylation and sulphation with *N*-acetylation (and subsequent further metabolism) as an alternative route.

Ring hydroxylation might either be direct, e.g. Cnubben *et al*. (1992) and Anderson *et al*. (1984), or result from the rearrangement of an *N*-hydroxylamine metabolite (Booth and Boyland 1964, Gutmann and Erikson 1969, Sternson and Gammans 1974). For 4-BrAc, *N*-deacetylation was a major route of metabolism, followed by ring hydroxylation and sulphation as seen with 4-BrA. However, a portion of the dosed acetanilide was metabolized directly at the *N*-acetyl group to give a range of oxidized metabolites. Interestingly, little or no 'futile acetylation' of the bromoacetanilide was observed, unlike several other acetanilides (Nicholls *et al*. 1997a, b 1999), as the [^{13}C]-label was completely retained in all of the acetanilide metabolites of 4-BrAc identified in these samples.

The metabolism of the acetyl group of both the dosed acetanilide and that derived from 4-BrA was partly via the glycolanilide (evidenced by the *O*-glucuronide) to the *N*-oxanilic acid. Such glycolanilide and oxanilic acid metabolites have been detected as metabolites of 4-chloroaniline (Kiese and Lenk 1969, 1970, 1971, Ehlhardt and Howbert 1991), 4-propionacetanilide (Kiese and Lenk 1969) and sulphanilamide (Fries *et al*. 1971). The formation of *N*-oxanilic acids has also been reported for 4-trifluoromethylaniline and its acetanilide (Wilson *et al*. 1985, Wade *et al*. 1988). Metabolism to form oxanilic acids seems to require the presence of a *para*-substituent with appropriate electron withdrawing properties.

A particularly interesting finding was the identification of the *N*-acetyl-*S*-[2-keto-2-(4-bromoanilino)ethylcysteine conjugate. Such conjugates are generally observed when metabolism generates highly active electrophilic sites that react with glutathione. The best known example perhaps being the well-documented reactive *N*-acetyl-*p*-benzoquinone imine metabolite of paracetamol (acetaminophen) (e.g. Hinson 1983). Glutathione conjugation is then followed by metabolism via the mercapturic acid pathway to give the *N*-acetyl-l-cysteinyl conjugate (Silverman 1992). A similar metabolite to the one detected in this study was also seen following the administration of 4-cyano-*N*,*N*-dimethylaniline (Hutson *et al*. 1984a, b). A probable route for the formation of this type of metabolite is via a reactive sulphate conjugate, analogous to the glucuronide metabolite detected in this study (e.g. Rietvald *et al*. 1980, Seutter-Berlage *et al*. 1982). Irrespective of its route of formation, the presence of the *N*-acetylcyteinyl conjugate is clear evidence for the generation of a reactive electrophilic centre at this methylene carbon, with all of the potential toxicological sequelae that this observation implies.

Recently, we examined the metabolic fate of *p*-fluoroaniline using the same methodology and noted the presence of metabolites due to metabolic de-fluorination (Scarfe *et al*. 1999a). Whilst the loss of bromine from aromatic systems during metabolism is not uncommon, we did not detect any evidence of the products of such reactions for either 4-BrA or 4-BrAc in this study. The postulated metabolic fate of 4-BrA and 4-BrAc in the rat, as revealed by the metabolites excreted in urine identified in this study, is summarized in figure 7.

In summary, the use of HPLC-NMR-MS has provided a rapid and efficient method for the determination of the major metabolites of 4-BrA and 4-BrAc excreted in the urine of rats dosed i.p. with these compounds. The complementary nature of mass spectrometry and ^{1}H-NMR spectroscopy, with the former providing mass and fragmentation data whilst the latter allows the site of metabolism to be elucidated, was evident here. The metabolic fate of both 4-BrA and 4-BrAc was

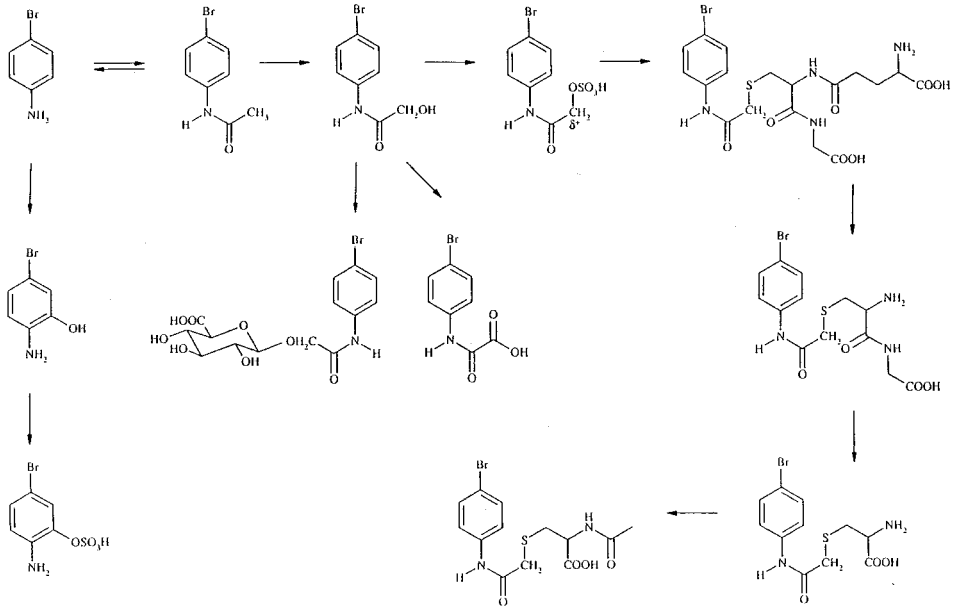


Figure 7. Metabolic fate of 4-BrA and 4-BrAc.

very similar with the ring-hydroxylated sulphate forming the major metabolite of both compounds. Extensive metabolism of the *N*-acetyl group was also observed to a range of unusual metabolites.

Acknowledgements

The authors acknowledge the Analytical Division of the Royal Society of Chemistry and AstraZeneca Pharmaceuticals for provision of a studentship (G. B. S.). They are also grateful to the ULIRS for use of the NMR facilities at Birkbeck and QMW Colleges, London University.

References

Anderson, M. M., Mays, J. B., Mitchum, R. K and Hinson, J. A., 1984, Metabolism of 4-nitroaniline by rat liver microsomes. *Drug Metabolism and Disposition*, **12**, 179–185.

Booth, J. and Boyland, E., 1964, The biochemistry of aromatic amines: enzymic *N*-hydroxylation of arylamines and conversion of arylhydroxylamines into *o*-aminophenols. *Biochemical Journal*, **91**, 362–669.

Boyle, G. W., Mckillop, D., Phillips, P. J., Harding, J. R., Pickford, R. and McCormick A. D., 1993a, Metabolism of casodex in laboratory animals. *Xenobiotica*, **23**, 781–798.

Cnubben, H. H. P., Vervoort, J., Veeger, C. and Rietjens, I. M. C. M., 1992, Study on the regioselectivity and mechanism of the aromatic hydroxylation of monofluoroanilines. *Chemico-Biological Interactions*, **85**, 151–172.

Cupid, B. C., Beddell, C. R., Wilson, I. D., Lindon, J. C. and Nicholson, J. K., 1996, Quantitative structure–metabolism relationships for substituted benzoates in the rabbit: prediction of urinary excretion of glycine and glucuronide conjugates. *Xenobiotica*, **26**, 157–176.

Cupid, B. C., Holmes, E., Wilson, I. D., Lindon, J. C. and Nicholson, J. K., 1999, Quantitative structure–metabolism relationships (QSMR) using computational chemistry: pattern recognition analysis and statistical prediction of phase II conjugation reactions of substituted benzoic acids in the rat. *Xenobiotica*, **29**, 22–42.

Ehlhardt, W. J. and Howbert, J. J., 1991, Metabolism and disposition of *p*-chloroaniline in rat mouse and monkey. *Drug Metabolism and Disposition*, **19**, 366–369

Ehlhardt, W. J., Woodland, J. M., Worazalla, J. F., Bewley, J. R., Grindey, G. B., Todd, G. C., Toth, J. E. and Howbert, J. J., 1992, Comparison of metabolism and toxicity to the structures of the anticancer agent sulofenur and related sulfonylureas. *Chemical Research in Toxicology*, **5**, 667–673.

Fries, W., Keise, M. and Lenk, W., 1971, Additional route in the metabolism of sulphanilamide. *Xenobiotica*, **1**, 241–256.

Ghauri, F. Y. K., Blackledge, C. A., Glen, R. C., Lindon, J. C., Bedell, C. R., Wilson, I. D. and Nicholson, J. K., 1992b, Quantitative structure–metabolism relationships for substituted benzoic acids in the rat: computational chemistry, NMR spectroscopy and pattern recognition studies. *Biochemical Pharmacology*, **44**, 1935–1946.

Ghauri, F. Y. K., Blackledge, C. A., Glen, R. C., Sweatman, B. C., Lindon. J. C., Beddell, C. R., Wilson, I. D. and Nicholson, J. K., 1992a, An approach to a metabolic expert system: structure–metabolism relationships for benzoic acids in the rat. In E. Reid and I. D. Wilson (eds), *Methodological Surveys in Biochemistry and Analysis, 20* (Cambridge: Royal Society of Chemistry), pp. 21–28.

Gutmann, H. R. and Erickson, R. R., 1969, The conversion of the carcinogen *N*-hydroxy-2-fluorenylacetamide to *o*-amidophenols by rat liver *in vitro*. *Journal of Biological Chemistry*, 244, 1729–1740.

Holmes, E., Sweatman, B. C., Bollard, M. E., Blackledge, C. A., Beddell, C. R., Wilson, I. D., Lindon, J. C. and Nicholson, J. K., 1995, Prediction of urinary sulphate and glucuronide conjugate excretion for substituted phenols in the rat using quantitative structure–metabolism relationships. *Xenobiotica*, **25**, 1269–1281.

Hinson, J. A., 1983, Reactive metabolites of phenacetin and acetaminophen. A review. *Environmental Health Perspectives*, **49**, 71–79.

Hutson, D. H., Lakeman, S. K. and Logan, C. J., 1984b, The fate of 4-cyano-*N*,*N*-dimethylaniline in rats: a novel involvement of glutathione in the metabolism of aniline. *Xenobiotica*, **14**, 925–934.

Hutson, D. H., Logan, C. J. and Regan, P. D., 1984a, Evidence for the formation of a novel glutathione conjugate in the metabolism of an aromatic amine derivative. *Drug Metabolism and Disposition*, **12**, 523–524.

Kiese, M. and Lenk, W., 1969, Oxidation of acetanilides to glycolanilides and oxanilic acids in rabbits. *Biochemical Pharmacology*, **18**, 1325–1333.

Kiese, M. and Lenk, W., 1970, Hydroxylation of *N*-(4-chlorophenyl)[$^{14}C_1$]acetamide to *N*-(4-chlorophenyl)-[$^{14}C_1$]glycolamide in rabbits. *Biochimica et Biophysica Acta*, **222**, 549–551.

Kiese, M. and Lenk, W., 1971, Metabolites of 4-chloroaniline and chloroacetanilides produced by rabbits and pigs. *Biochemical Pharmacology*, **20**, 379–391.

Nicholls, A. W., Farrant, R. D., Shockcor, J. P., Unger, S. E., Wilson, I. D., Lindon, J. C. and Nicholson, J. K., 1997a, NMR and HPLC-NMR spectroscopic studies on the metabolism and futile deacetylation of paracetamol metabolites in rat and man. *Biochemical Pharmacology*, **49**, 1155–1164.

Nicholls, A. W., Lindon, J. C., Caddick, S., Farrant, R. D., Wilson, I. D. and Nicholson, J. K., 1997b, NMR spectroscopic studies on the metabolism and futile deacetylation of phenacetin in the rat. *Xenobiotica*, **27**, 1175–1186.

Nicholls, A. W., Lindon, J. C., Farrant, R. D., Shockor, J. P., Wilson, I. D. and Nicholson, J. K., 1999, Directly-coupled HPLC-NMR spectroscopic studies of metabolism and futile deacetylation of phenacetin in the rat. *Journal of Pharmaceutical and Biomedical Analysis*, **20**, 865–873.

Radomski, J. L., 1979, The primary aromatic amines: their biological properties and structure–activity relationships. *Annual Reviews in Pharmacological Toxicology*, **19**, 129–157.

Rietvald, E. C., Plate, R. and Seutter-Berlage, F., 1980, Mechanism of formation of mercapturic acids from aromatic aldehydes *in vivo*. *Archives of Toxicology*, **52**, 199–207.

Scarfe, G. B., Clayton, E., Wilson I. D. and Nicholson, J. K., 2000, Identification and quantification of metabolites of 2,3,5,6-tetrafluoro-4-trifluoromethylaniline in rat urine using ^{19}F nuclear magnetic resonance spectroscopy, high performance liquid chromatography-nuclear magnetic resonance spectroscopy and high performance liquid chromatography-mass spectroscopy. *Journal of Chromatography B*, **748**, 311–319.

Scarfe, G. B., Lindon, J. C., Nicholson, J. K., Wright, B., Clayton, E. and Wilson, I. D., 1999b, Investigation of the quantitative metabolic fate and urinary excretion of 3-methyl-4-trifluoromethylaniline and 3-methyl-4-trifluoromethylacetanilde in the rat. *Drug Metabolism and Disposition*, **27**, 1171–1178.

Scarfe, G. B., Tugnait, M., Wilson, I. D. and Nicholson, J. K., 1999a, Studies on the metabolism of 4-fluoroaniline and 4-fluoroacetanilide in rat: formation of 4-actamidophenol (paracetamol) and its metabolites via defluorination and *N*-acetylation. *Xenobiotica*, **29**, 205–216.

Scarfe, G. B., Wilson, I. D., Spraul, M., Hofmann, M, Brauman, U., Lindon. J. C. and Nicholson, J. K., 1997, Application of directly coupled high performance liquid chromatography-nuclear magnetic resonance-mass spectrometry to the detection and characterisation of the metabolites of 2-bromo-4-trifluoromethylaniline in rat urine. *Analytical Communications*, **34**, 37–39.

Scarfe, G. B., Wright G. B., Clayton, E., Taylor S., Wilson, I. D., Lindon, J. C. and Nicholson, J. K., 1998, ^{19}F-NMR and directly coupled HPLC-NMR-MS investigations into the metabolism of 2-bromo-4-trifluromethylaniline in the rat: urinary excretion balance study without the use of radiolabelling. *Xenobiotica*, **28**, 373–388.

Schroder, H., Lewkonia, R. M. and Price-Evans, D. A., 1973, Metabolism of salicylazosulfapyridine in healthy subjects and patients with ulcerative colitis. *Clinical Pharmacology and Therapeutics*, **14**, 802–809.

Schulz, M., Schmoldt, A., Donn, F. and Becker, H., 1988, The pharmacokinetics of flutamide and its major metabolites after a single oral dose and during chronic treatment. *European Journal of Clinical Pharmacology*, **34**, 633–636.

Seutter-Berlage, F., Rietveld, E. C., Plate, R. and Kippert, P. J. M, 1982, Mercapturic acids as metabolites of aromatic aldehydes and alcohols. In R. Snyder, D. V. Parke, J. Koesis, D. J. Jollow and G. G. Gibson (eds), *Biological Reactive Intermediates IIA: Chemical Mechanisms and Biological Effects* (New York: Plenum), pp. 359–368.

Silverman, R. B., 1992, *The Organic Chemistry of Drug Design and Drug Action* (San Diego: Academic Press), pp. 277–351.

Sternson, L. A. and Gammans, R. E., 1974, A mechanisitic study of aromatic hydroxylamine rearrangement in the rat. *Bioinorganic Chemistry*, **4**, 58–63.

Wade, K. E., Troke, J., MacDonald, C. M., Wilson. I. D. and Nicholson, J. K., 1988, NMR studies of the metabolism of trifluoromethylaniline. In E. Reid, J. D. Robinson and I. D. Wilson (eds), *Methodological Surveys in Biochemistry and Analysis, 18* (New York: Plenum), pp. 383–388.

Wilson, I. D., MacDonald, C. M., Fromson, J. M., Troke, J. A. and Hillbeck, D., 1985, Species differences in the metabolism of ^{14}C-*p*-trifluoromethylaniline: production of an oxanilic acid as the major metabolite by the rat. *Biochemical Pharmacology*, **34**, 2025–2028.

XENOBIOTICA, 2002, VOL. 32, NO. 4, 339–347

Taylor & Francis
healthsciences

Plasma pharmacokinetics of a liver-selective nitric oxide-donating diazeniumdiolate in the male C57BL/6 mouse

S. F. STINSON†*, T. HOUSE†, C. BRAMHALL†,
J. E. SAAVEDRA‡, L. K. KEEFER§ and R. W. NIMS§

† Developmental Therapeutics Program, ‡ Intramural Research Support Program and § Chemistry Section, Laboratory of Comparative Carcinogenesis, National Cancer Institute at Frederick, Frederick, MD 20702-1201, USA.

Received 26 July 2001

1. The single-dose plasma pharmacokinetics of O^2-vinyl 1-(pyrrolidin-1-yl)diazen-1-ium-1,2-diolate (V-PYRRO/NO) following intravenous (i.v.) and intraperitoneal (i.p.) bolus administration to the male C57BL/6 mouse was studied in an effort to characterize the disposition of the agent and to serve as a basis for the design of *in vivo* efficacy studies.

2. Plasma V-PYRRO/NO concentrations declined rapidly in a bi-exponential manner after i.v. administration of 5 mg kg^{-1} body weight to mouse. The terminal half-life was 9.4 min and the mean residence time was 3.4 min.

3. V-PYRRO/NO was absorbed rapidly following i.p. administration, with peak plasma concentrations being observed 3 min after injection. Levels then declined with a terminal half-life of 11.7 min. The bioavailable fraction from the i.p. compartment was 19%, indicating a high first-pass effect.

4. The results provide additional evidence for a liver-selective metabolism of this nitric oxide-donating prodrug.

Introduction

Nitric oxide (NO)-donating agents have received considerable attention in the past decade as a result of the contribution of such compounds in elucidating the biological roles of NO and due to the potential utility of these agents as pharmaceutical leads for the development of therapeutic interventions involving NO delivery (Feelisch and Stamler 1996, Keefer 2000, Lehmann 2000). Most available NO-donating agents are not tissue selective, i.e. they either decompose to NO spontaneously or are metabolized to NO by a multiplicity of tissues, thereby producing NO-mediated effects in a variety of organ systems when administered systemically (Keefer 2000). On the other hand, the diazeniumdiolate O^2-vinyl 1-(pyrrolidin-1-yl)diazen-1-ium-1,2-diolate (V-PYRRO/NO) (figure 1) was designed to be a liver-selective NO-donating agent (Saavedra *et al.* 1997). The NO-donating prodrug was created by adding a vinyl functional group to the terminal (O^2) oxygen of pyrrolidine diazeniumdiolate (PYRRO/NO) (figure 1). The prodrug does not spontaneously decompose in physiological solutions, but the vinyl-protecting group is thought to be susceptible to oxidation by hepatic monoxygenases such as the cytochromes P450 and the resulting epoxide is

* Author for correspondence at: Building 1052, Room 121, National Cancer Institute at Frederick, Frederick, MD 21702-1201, USA; e-mail: stinson@dtpax2.ncifcrf.gov

Xenobiotica ISSN 0049–8254 print/ISSN 1366–5928 online © 2002 Taylor & Francis Ltd
http://www.tandf.co.uk/journals
DOI: 10.1080/00498250110102665

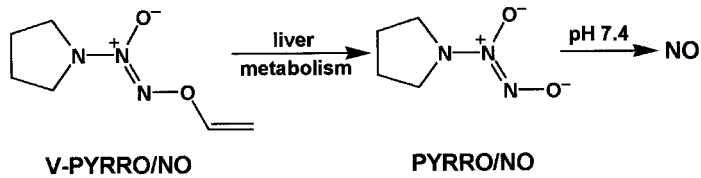


Figure 1. Structural formulae of V-PYRRO/NO and the proximal NO-donating compound, PYRRO/NO, which is generated *in vivo*.

expected to undergo hydrolysis, either spontaneously or catalysed by hepatic epoxide hydrolase. These metabolic steps generate the parent compound, which spontaneously releases NO under physiological conditions (37°C, pH 7.4) with a half-life of 3 s (Saavedra *et al.* 1997).

In vitro and *in vivo* experiments have demonstrated that the administration of this agent results in effects in liver tissue without the systemic effects usually associated with NO release (e.g. systemic blood pressure lowering) (Saavedra *et al.* 1997, Ricciardi *et al.* 2001). The present study was conducted to evaluate the single-dose pharmacokinetics of this agent. The terminal plasma half-life and bioavailability results obtained provide additional evidence of the liver-selectivity of this NO-donating prodrug.

Materials and methods

Chemicals

V-PYRRO/NO was synthesized and purified by flash chromatography as described (Saavedra *et al.* 1997). Its purity was confirmed by elemental analysis; C, H, and N were all within 0.2% of theoretical. All other chemicals were of HPLC grade or of the highest obtainable purity, and were purchased from various sources.

Animal treatment and preparation of samples

Studies were carried out using 61 young adult male (body weights 25.2–28.7 g) C57BL/6 mice (Harlan Sprague–Dawley; Frederick, MD, USA). The mice were housed on hardwood bedding in rooms maintained at 20°C with a 12-h light–dark cycle. Water and standard 18% protein mouse and rat diet (PMI Nutrition International, Inc., Brentwood, MO, USA) were provided *ad libitum*. Animal care and all experimental manipulations and procedures were conducted in an American Association for Laboratory Animal Care-certified laboratory under strict compliance with the National Institutes of Health guidelines for the care and use of laboratory animals.

Thirty-three mice (mean body weight 26.8 ± 1.0 g) were given 5 mg kg^{-1} V-PYRRO/NO as a uniform 0.5-min i.v. infusion in the tail vein. The dose was selected based on the results of a pilot toxicity study indicating doses in this range were well tolerated in the animal. V-PYRRO/NO was dissolved in sterile water and administered using a dose volume of 1 ml kg^{-1} body weight. Groups of three mice were lightly anaesthetized with methoxyfluorane, and exsanguinated from the retro-orbital sinus at 2, 4, 6, 8, 10, 15, 20, 25, 30, 45 and 60 min following injection. Twenty-eight mice (mean body weight 26.7 ± 1.9 g) were given 5 mg kg^{-1} V-PYRRO/NO as a bolus i.p. injection. The vehicle and dose volume were the same as for the i.v. study. Groups of three mice were terminally bled from the retro-orbital sinus at 3, 6, 9, 12, 15, 20, 30, 40 and 60 min following injection. In addition, the results of a preliminary study, consisting of three mice samples at 6, 15 and 60 min, were combined with those of the more comprehensive study, yielding a total of six mice at each time point. Blood was collected into heparinized microfuge tubes; plasma was separated by centrifugation at 13 000*g* for 3 min, immediately frozen, and stored at –70°C until assayed. For both the i.v. and i.p. studies, the times for the beginning and end of the injection and blood collection intervals were recorded to the nearest second.

V-PYRRO/NO analysis in blood plasma samples

Plasma samples (50 µl) were prepared for analysis by precipitation of plasma proteins with acetonitrile (100 µl). Following centrifugation at 13 000*g* for 5 min, 100 µl supernatant was mixed with 150 µl water, and 200 µl of the mixture was injected onto a 4.6×150 mm YMC Pack J-Sphere

ODS-H80 column (YMC, Inc., Wilmington, NC, USA) coupled to a HP 1050 Series quaternary pump and autosampler (Hewlett Packard, Inc., Palo Alto, CA, USA). The column was maintained at ambient temperature and eluted isocratically at a flow rate of $1\,ml\,min^{-1}$ with a mobile phase composed of acetonitrile:water (40:60 v/v). The column effluent was monitored at a wavelength of 266 nm using a HP 1050 Series UV detector. The analytical system was interfaced with a computer with HP software installed, which was responsible for module control and data acquisition and analysis. Using this method, the absolute recovery of V-PYRRO/NO from plasma was >95%.

Calibration curves were constructed by plotting the chromatographic peak area for V-PYRRO/NO against the known analyte concentration in plasma standards. The calibration curve was composed of 16 standards covering the concentration range 0.01–10 μM. The curve was linear over this range, and the coefficient of variation for 10 replicate determinations of each of the standards was less than 15%. Linear least-squares regression analysis was performed to determine the slope and y-intercept of the best-fit line. Analyte concentrations in unknown samples were calculated by interpolation from the regression line. Each unknown sample was initially assayed in duplicate, with additional analyses performed if the replicate determinations deviated from their average by >10%. Samples with concentrations above the range of the calibration curve were diluted with mouse plasma, and re-assayed.

Pharmacokinetic analysis

Plasma concentration versus time profiles were constructed using the geometric mean of the plasma concentrations for the three individual animals, and the mean of the times of collection for each time point. The time of collection was calculated from the beginning of the injection to the midpoint of the sample collection interval. Computer-assisted, iterative, non-linear least-squares regression analysis of plasma concentration versus time data was conducted using the software package TableCurve* (Jandel Scientific, San Rafael, CA, USA). For the i.v. study, the data were fitted to the polyexponential equation:

$$C = \sum_{i=1}^{z} \frac{C_i}{\lambda_i T}(e^{(-\lambda_i f)} - e^{(-\lambda_i t)})$$

where C is the plasma concentration at a time, t, C_i and l_i are the y-intercept and rate constant (slope) for each respective phase, T is the duration of the infusion, and when $t \leq T$, $f = 0$ or when $> T$, $f = (t - T)$. The slopes and y-intercepts of the regression lines were the primary iterated parameters. The line of best fit was determined from analysis of residuals, and the standard errors for the primary parameters and the fit. Secondary pharmacokinetic parameters were calculated from the primary parameters using non-compartmental methods (Notari 1987). For the i.p. study, the area under the plasma concentration–time curve was determined by trapezoidal rule and extrapolated to infinity ($AUC_{0-\infty}$) using the slope (rate constant) of the regression line determined by non-linear least-squares regression analysis of the data points.

Results

Intravenous administration

Following i.v. administration to mouse at $5\,mg\,kg^{-1}$ body weight, plasma concentrations of V-PYRRO/NO declined in a biphasic manner from approximately 21 μM at 2 min to 0.02 μM after 1 h (figure 2). Primary and selected secondary pharmacokinetic parameters determined by non-linear regression analysis and subsequent calculations are shown in table 1. Half-lives for the initial, distribution phase and the terminal elimination phase were 1.6 and 9.4 min, respectively, and the mean residence time was 3.4 min. The total plasma clearance rate was rapid ($0.19\,l\,min^{-1}\,kg^{-1}$). The ratio of the apparent volumes of distribution for the central compartment to the whole body suggests moderate distribution of the compound into non-sampled compartments. The high proportion of the total area under the plasma concentration–time profile represented by the initial phase (91%) indicates that rapid distribution into tissues may be a controlling factor in the pharmacokinetics of this compound after i.v. injection.

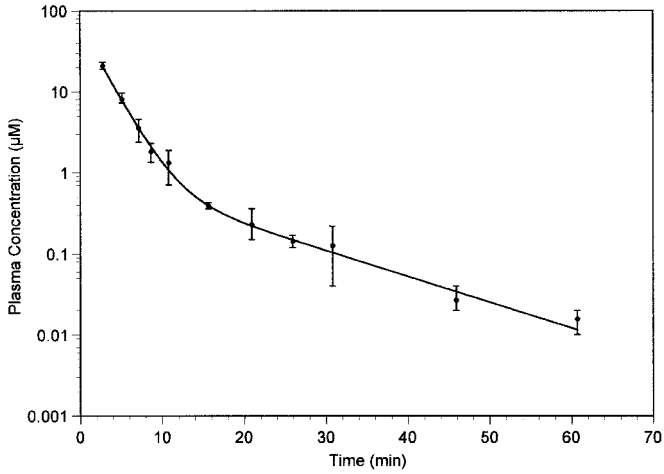


Figure 2. Blood plasma concentrations of V-PYRRO/NO following bolus i.v. injection of 5 mg kg^{-1} body weight in the male C57BL/6 mouse. Each time point represents the geometric mean (± range) of data obtained from three mice. The line of best fit was determined by non-linear regression analysis.

Table 1. Primary and secondary pharmacokinetic parameters derived from non-linear least-squares regression analysis of V-PYRRO/NO plasma concentration versus time data obtained following i.v. injection of 5 mg kg^{-1} body weight in the male C57BL/6 mouse.

Parameter	Unit	Value
C_1	μM	57
C_z	μM	1.0
λ_1	min^{-1}	0.43
λ_z	min^{-1}	0.07
$t_{\frac{1}{2},1}$	min	1.6
$t_{\frac{1}{2},z}$	min	9.4
MRT	min	3.4
CL	l min^{-1} kg^{-1}	0.19
V_1	l kg^{-1}	0.5
V_z	l kg^{-1}	2.6
$AUC_{0\text{-}\infty}$	μM × min	146
AUC_1	%	91
AUC_z	%	9

C_1 and C_z are the y-intercepts, and λ_1 and λ_z the slopes (rate constants) for the regression lines representing the initial and terminal phases, respectively. These primary iterated parameters were used to derive the following secondary pharmacokinetic parameters: $t_{\frac{1}{2},1}$, initial phase half-life; $t_{\frac{1}{2},z}$, terminal phase half-life; MRT, mean residence time; CL, total plasma clearance rate; V_1, apparent volume of distribution for the central compartment; V_z apparent volume of distribution; $AUC_{0\text{-}\infty}$ area under the plasma concentration versus time curve extrapolated to time infinity; and AUC_1 and AUC_z, percentage of the total area under the curve represented by the initial and terminal phases, respectively. Parameters are derived from 11 data points, each representing the geometric mean from determinations in three animals.

Intraperitoneal administration

The plasma concentration–time profile following i.p. administration and the results of pharmacokinetic analysis are shown in figure 3 and table 2, respectively. Intraperitoneal administration of V-PYRRO/NO to mouse at 5 mg kg^{-1} body

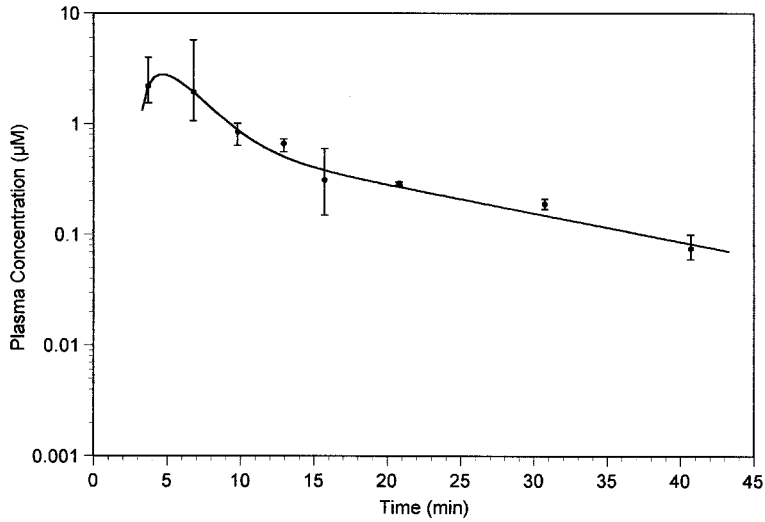


Figure 3. Blood plasma concentrations of V-PYRRO/NO following bolus i.p. injection of 5 mg kg^{-1} body weight in the male C57BL/6 mouse. Each time point represents the geometric mean (± range) of data obtained from three or six (6- and 15-min time points) mice. The line of best fit was determined by non-linear regression analysis.

Table 2. Pharmacokinetic parameters derived from non-linear least-squares regression analysis of V-PYRRO/NO plasma concentration versus time data obtained following i.p. injection of 5 mg kg^{-1} body weight in the male C57BL/6 mouse.

Parameter	Unit	Value
$t_{\frac{1}{2}\lambda 1}$	min	11.7
AUC	μM × min	29.0
f		0.19

$t_{\frac{1}{2}\lambda 1}$, terminal phase half-life; $AUC_{0-\infty}$, area under the plasma concentration versus time curve extrapolated to time infinity; *f*, bioavailable fraction. Parameters are derived from eight data points each representing the geometric mean from determinations in three or six (six and 15 min time points) animals.

weight produced a geometric mean peak plasma concentration of 2.2 μM after 3 min. This declined in an apparent bi-exponential manner to 0.08 μM by 40 min. The terminal half-life was 11.7 min. V-PYRRO/NO levels were below the limit of detection by 1 h following administration. The $AUC_{0-\infty}$ was 29.0 μM × min. A comparison of this with the $AUC_{0-\infty}$ obtained following i.v administration revealed a bioavailable fraction (*f*) of 0.19, indicating that < 20% of the i.p. dose reached the systemic circulation after first pass through the liver.

Discussion

The diazeniumdiolate class of nitric oxide-donating agents has been exploited in a variety of research contexts since the first report characterizing certain of these agents appeared (Maragos *et al.* 1991). The ability to alter, in a predictable manner, the solution half-life and thereby the rate of NO generation through

structural modification has contributed greatly to the utility of these agents as research tools. The initial modifications to the basic structure included variation of the nucleophile residue attached to the $N_2O_2^-$ functional group to achieve a wide range of solution decomposition (NO release) rates (Keefer *et al.* 1996). More recently, attempts have been made to synthesize compounds containing the $N_2O_2^-$ group that could be targeted to specific tissues within the body. These have included the infusion of ultrafast NO releasers directly at the desired location (Saavedra *et al.* 1996, Chen *et al.* 1997, Pluta *et al.* 1997) and incorporation of the $N_2O_2^-$group into solid polymeric matrices that can be placed in contact with the desired tissue (Hanson *et al.* 1995, Smith *et al.* 1996, Espadas-Torre *et al.* 1997, Annich *et al.* 2000, Mowery *et al.* 2000). In the case of V-PYRRO/NO, the intended target tissue was the liver. It was expected that derivatization of the $N_2O_2^-$group with a protecting group subject to metabolism by one or more hepatic phase I drug-metabolizing enzymes would target the NO release from V-PYRRO/NO to that organ. Possible therapeutic applications for a liver-selective NO donor include improvement of hepatic blood flow following ischaemia/reperfusion injury such as that experienced during organ transplant (Ricciardi *et al.* 2001).

Demonstration of such a liver-selective NO donation has been provided by a variety of experimental observations. When administered by i.v. injection to animals, the expected vasodilatory effects of NO have been confined to the liver and more general effects (such as systemic blood pressure decrease) have been minimal (Saavedra *et al.* 1997, Ricciardi *et al.* 2001). In addition, the expected effects of the locally released NO on hepatic tissue have been observed following i.v. administration of V-PYRRO/NO. These effects have included: (1) increases in hepatic cGMP levels (Saavedra *et al.* 1997); (2) the protection of hepatocytes from the expected cytotoxic and apoptosis-inducing effects of tumour necrosis factor-α (TNFα) plus galactosamine (Saavedra *et al.* 1997), endotoxin (Ou *et al.* 1997), and endotoxin plus galactosamine (Liu *et al.* 2001); and (3) suppression in liver tissue of the expression of a variety of genes associated with apoptosis pathways (Liu *et al.* 2001). *In vitro* studies have demonstrated that hepatocytes can metabolize V-PYRRO/NO, resulting in the generation of nitrite and nitrate (the oxidative metabolites of NO), while other cell types, including liver non-parenchymal cells, pulmonary artery smooth muscle cells, endothelial cells and macrophages, displayed a minimal ability to metabolize this compound (Saavedra *et al.* 1997). The enzymes within hepatocytes that are responsible for the metabolism of V-PYRRO/NO have not been fully characterized, although initial studies have suggested a role for one or more subfamilies (CYP1A, 2B, 2E1, 3A) of the cytochromes P450 (A. Cederbaum *et al.*, Mt Sinai School of Medicine, unpublished data). A further expectation for a liver-selective NO-donating agent would be that it exhibits a relatively low bioavailability (high first-pass metabolic effect or presystemic elimination) following i.p. administration. The present study was, therefore, conducted to investigate the pharmacokinetics of V-PYRRO/NO following i.v. and i.p. administration to the male mouse.

The pharmacokinetic analysis presented here reveals that V-PYRRO/NO is rapidly cleared from the plasma following i.v. administration in the male mouse. This rapid clearance was characterized by a distribution phase of only 1.6 min, and a terminal elimination phase of 9.4 min. Likewise, plasma levels declined with a half-life of 11.7 min after i.p. administration. The bioavailable fraction (f) by the

i.p. route was only 0.19. The limited (19%) bioavailability of the compound when administered by this route is consistent with metabolism of the agent in liver, since the entire i.p. dose would be collected by the hepatic portal circulation and delivered to the liver. Only the amount of V-PYRRO/NO escaping metabolism in the liver can enter the systemic circulation (the compartment ultimately sampled). Assuming that intestinal metabolism would be minimal following i.p. administration, the liver extraction ratio (ER) for V-PYRRO/NO can be estimated (Shargel and Yu 1985) as $1 - f$, or 0.81. The results, therefore, provide additional evidence that V-PYRRO/NO is a liver-selective NO-donating prodrug.

While comparing the area under the plasma concentration–time profile following i.p. administration with that obtained after i.v. dosing can be a convenient and efficient method for estimating a hepatic first-pass metabolic effect, there are number of factors that might complicate interpretation of such studies. These include incomplete absorption of the dose, partial absorption of the dose into the general circulation through the parietal peritoneum, partial absorption of the dose through the intestinal wall and subsequent metabolism by the intestinal mucosa, and saturation of first-pass hepatic metabolism owing to rapid absorption (Lukas *et al.* 1971, Gillette and Pang 1977, Pang and Gillette 1978, Nickerson and Toler 1997), among others. Efficiency of absorption into the peritoneal circulation is largely controlled by the physicochemical properties of an agent, which determine both its availability to the peritoneal membranes and the rate at which it diffuses through them. Considering its aqueous solubility, and the rapid kinetics of its absorption it is likely that V-PYRRO/NO is efficiently absorbed from the peritoneal cavity. The extent to which V-PYRRO/NO is absorbed via the parietal peritoneum, or through the intestinal wall is not known. Direct absorption into the general circulation of a chemically diverse set of i.p. administered compounds was unsubstantial (Lukas *et al.* 1971). While absorption of compounds from the peritoneal cavity through the intestinal wall has not, to our knowledge, been systematically studied, it was suggested on theoretical grounds (Pang and Gillette 1978). It would seem, however, that the barrier provided by the visceral peritoneum combined with two layers of musculature before the submucosa and mucosa of the intestine are reached would diminish the potential for this effect. Administration into the hepatic portal vein avoids these complicating factors (Lukas *et al.* 1971, Gillette and Pang 1977, Pang and Gillette 1978, Nickerson and Toler 1997), but such studies are more efficiently accomplished in larger species than the mouse. In instances where hepatic metabolism is a major route of elimination, as is suggested by our results, saturation of metabolizing capacity would be accompanied by a prolonged elimination half-life. The rapid elimination of V-PYRRO/NO following i.p. administration argues against the presence of substantial metabolic saturation, although studies of the linearity of pharmacokinetics in this dose range are required to address the question definitively.

Optimization of a dosing regimen for V-PYRRO/NO may be most efficiently accomplished through a knowledge of the levels required for efficacy against a specific target, and characterization of the pharmacokinetic properties of the compound. The pharmacokinetic results obtained here may be used to determine the feasibility of maintaining continuous V-PYRRO/NO plasma concentrations in the range of 0.1 μM, the theoretical level that was effective in blocking TNFα-mediated liver damage in rat (Saavedra *et al.* 1997). In light of the plasma clearance rate and low bioavailability after oral or i.p. administration, a continuous infusion

at 1.15 μmol h^{-1} kg^{-1}, or 5 μg h^{-1} per mouse for a 25-g mouse, would appear to be required. A model 2001 Alzet osmotic pump will discharge at 1 μl h^{-1}. Filled with a 5 mg ml^{-1} solution, the delivery rate would be 5 μg h^{-1}, making this a feasible approach to test.

In summary, the plasma pharmacokinetics of the diazeniumdiolate V-PYRRO/NO were determined in the male C57BL/6 mouse following i.v. and i.p. administration. The results indicate that the compound is rapidly cleared, with elimination half-lives of 9.4 and 11.7 min following i.v. and i.p. administration, respectively. The relatively low bioavailability (19%) of V-PYRRO/NO following i.p. administration is consistent with metabolism within the liver, providing additional evidence for a liver-selective mode of action for this NO-donating agent.

Acknowledgements

The authors acknowledge the skilled technical assistance of Dan Logsdon and Craig Driver. The project was funded in part by the National Cancer Institute, Contract No. NO1-CO-56000.

References

Annich, G. M., Meinhardt, J. P., Mowery, K. A., Ashton, B. A., Merz, S. I., Hirschl, R. B., Meyerhoff, M. E. and Bartlett, R. H., 2000, Reduced platelet activation and thrombosis in extracorporeal circuits coated with nitric oxide release polymers. *Critical Care Medicine*, **28**, 915–920.

Chen, C., Hanson, S. R., Keefer, L. K., Saavedra, J. E., Davies, K. M., Hutsell, T. C., Hughes, J. D., Ku, D. N. and Lumsden, A. B., 1997, Boundary layer infusion of nitric oxide reduces early smooth muscle cell proliferation in the endarterectomized canine artery. *Journal of Surgical Research*, **67**, 26–32.

Espadas-Torre, C., Oklejas, V., Mowery, K. and Meyerhoff, M. E., 1997, Thromboresistant chemical sensors using combined nitric oxide release/ion sensing polymeric films. *Journal of the American Chemical Society*, **119**, 2321–2322.

Feelisch, M. and Stamler, J. S., 1996, Donors of nitrogen oxides. In M. Feelisch and J. S. Stamler (eds), *Methods in Nitric Oxide Research* (New York: Wiley), pp. 71–115.

Hanson, S. R., Hutsell, T. C., Keefer, L. K., Mooradian, D. L. and Smith, D. J., 1995, Nitric oxide donors: a continuing opportunity in drug design. *Advances in Pharmacology*, **34**, 383–398.

Keefer, L. K., 2000, Design of nitric oxide-releasing drugs. *Pharmaceutical News*, **7**, 27–32.

Keefer, L. K., Nims, R. W., Davies, K. M. and Wink, D. A., 1996, 'NONOates' (1-substituted diazen-1-ium-1,2-diolates) as nitric oxide donors: convenient nitric oxide dosage forms. *Methods in Enzymology*, **268**, 281–293.

Gillette, J. R. and Pang, K. S., 1977, Theoretic aspects of pharmacokinetic drug interactions. *Clinical Pharmacology and Therapeutics*, **22**, 623–639.

Lehmann, J., 2000, Nitric oxide donors — current trends in therapeutic applications. *Expert Opinion on Therapeutic Patents*, **10**, 579–594.

Liu, J., Saavedra, J. E., Lu, T., Song, J.-G., Waalkes, M. P. and Keefer, L. K., 2002, The liver-selective nitric oxide donor, V-PYRRO/NO, protects against d-galactosamine/endotoxin-induced hepatotoxicity in mice. *Journal of Pharmacology and Experimental Therapeutics*, **300**, 1–8.

Lukas, G., Brindle, S. D. and Greengard, P., 1971, The route of absorption of intraperitoneally administered compounds. *Journal of Pharmacology and Experimental Therapeutics*, **178**, 562–566.

Maragos, C. M., Morley, D., Wink, D. A., Dunams, T. M., Saavedra, J. E., Hoffman, A., Bove, A. A., Isaac, L., Hrabie, J. A. and Keefer, L. K., 1991, Complexes of NO with nucleophiles as agents for the controlled biological release of nitric oxide. Vasorelaxant effects. *Journal of Medicinal Chemistry*, **34**, 3242–3247.

Mowery, K. A., Schoensch, M. H., Saavedra, J. E., Keefer, L. K. and Meyerhoff, M. E., 2000, Preparation and characterization of hydrophobic polymeric films that are thromboresistant via nitric oxide release. *Biomaterials*, **21**, 9–21.

Nickerson, D. F. and Toler, S. M., 1997, Intraperitoneal and intraportal administration of droloxifene to the Sprague–Dawley rat: assessing the first-pass effect. *Xenobiotica*, **27**, 627–632.

Notari, R. E., 1987, *Biopharmaceutics and Clinical Pharmacokinetics* (New York: Marcel Dekker).

Ou, J., Carlos, T. M., Watkins, S. C., Saavedra, J. E., Keefer, L. K., Kim, Y.-M., Harbrecht, B. G. and Billiar, T. R., 1997, Differential effects of nonselective nitric oxide synthase (NOS) and selective inducible NOS inhibition on hepatic necrosis, apoptosis, ICAM-1 expression, and neutrophil accumulation during endotoxemia. *Nitric Oxide: Biology and Chemistry*, **1**, 404–416.

Pang, K. S. and Gillette, J. R., 1978, Complications in the estimation of hepatic blood flow in vivo by pharmacokinetic parameters. The area under the curve after the concomitant intravenous and intraperitoneal (or intraportal) administration of acetaminophen in the rat. *Drug Metabolism and Disposition*, **6**, 566–576.

Pluta, R. M., Oldfield, E. H. and Boock, R. J., 1997, Reversal and prevention of cerebral vasospasm by intracarotid infusions of nitric oxide donors in a primate model of subarachnoid hemorrhage. *Journal of Neurosurgery*, **87**, 746–751.

Ricciardi, R., Foley, D. P., Quarfordt, S. H., Saavedra, J. E., Keefer, L. K., Wheeler, S. M., Donohue, S. E., Callery, M. P. and Meyers, W. C., 2001, V-PYRRO/NO: an hepato-selective nitric oxide donor improves porcine liver hemodynamics and function after ischemia reperfusion. *Transplantation*, **71**, 193–198.

Saavedra, J. E., Billiar, T. R., Williams, D. L., Kim, Y.-M., Watkins, S. C. and Keefer, L. K., 1997, Targeting nitric oxide (NO) delivery *in vivo*. Design of a liver-selective NO donor prodrug that blocks tumor necrosis factor-a-induced apoptosis and toxicity in the liver. *Journal of Medicinal Chemistry*, **40**, 1947–1954.

Saavedra, J. E., Southan, G. J., Davies, K. M., Lundell, A., Markou, C., Hanson, S. R., Adrie, C., Hurford, W. E., Zapol, W. M. and Keefer, L. K., 1996, Localizing antithrombotic and vasodilatory activity with a novel, ultrafast nitric oxide donor. *Journal of Medicinal Chemistry*, **39**, 4361–4365.

Shargel, L. and Yu, A. B. C. 1985, *Applied Biopharmaceutics and Pharmacokinetics* (Norwalk: Appleton-Century-Crofts).

Smith, D. J., Chakravarthy, D., Pulfer, S., Simmons, M. L., Hrabie, J. A., Citro, M. L., Saavedra, J. E., Davies, K. M., Hutsell, T. C., Mooradian, D. L., Hanson, S. R. and Keefer, L. K., 1996, Nitric oxide-releasing polymers containing the $[N(O)NO]^-$ group. *Journal of Medicinal Chemistry*, **39**, 1148–1156.

XENOBIOTICA, 2002, VOL. 32, NO. 5, 349–362

Taylor & Francis
healthsciences

Drug-metabolizing activity of human and rat liver, lung, kidney and intestine slices

R. DE KANTER†*, M. H. DE JAGER†, A. L. DRAAISMA†, J. U. JURVA‡, P. OLINGA†, D. K. F. MEIJER† and G. M. M. GROOTHUIS†

† Groningen University Institute for Drug Exploration (GUIDE), Department Pharmacokinetics & Drug Delivery, and ‡ Department of Medical Chemistry, Ant. Deusinglaan 1, 9713 AV Groningen, The Netherlands

Received 22 August 2001

1. Organ-specific biotransformation was studied in human and rat liver, lung, kidney and small intestine slices and compared on a protein basis, using four model substances.

2. Deethylation of lidocaine was highest in liver slices from both man and rat, followed by the small intestine.

3. Metabolism of testosterone was highest in liver slices, but a different overall metabolic pattern was found between the different organs.

4. Lung, kidney and intestine slices prepared from human and rat organs showed mainly an unknown metabolite of 7-ethoxycoumarin identified as 4-ethoxy-2-hydroxyphenyl propionic acid (EPPA).

5. The maximal metabolism of 7-ethoxycoumarin in slices was equal with *in vivo* V_{max} in the rat.

6. Phase II metabolism of 7-hydroxycoumarin in kidney and intestinal slices was about 60% of the activity in liver slices.

7. In conclusion, organs other than the liver show a surprisingly high drug-metabolizing activity. Thus, the use of precision-cut slices of a combination of drug metabolizing organs in an *in vitro* test system from both animal and human origin is required for a proper systematic prediction of drug metabolism in man.

Introduction

The use of precision-cut liver slices from both animal and human origin is now a widely used model to study drug metabolism and toxicity (Bach *et al*. 1996, Olinga *et al*. 1998a, Lerche-Langrand and Toutain 2000). Lung and kidney slices have also been used for these purposes but not as extensively as liver slices (de Kanter *et al*. 2002). The use of slices prepared from the small intestine has been only very limited (Vickers *et al*. 1992, 1995).

Although the liver is generally considered to be the most important organ for the biotransformation of drugs, it is also recognized that the lung, kidney and intestine can make an important contribution to the fate of drugs in the body (Krishna and Klotz 1994). In addition, many examples of metabolism-induced toxicity in these organs have been described (Boyd *et al*. 1983). The role of the small intestine in metabolism of drugs is considered particularly substantial due to

* Author for correspondence; e-mail: rdekanter@mac.com

Xenobiotica ISSN 0049–8254 print/ISSN 1366–5928 online © 2002 Taylor & Francis Ltd
http://www.tandf.co.uk/journals
DOI: 10.1080/00498250110112006

its high drug-metabolizing enzyme content (Krishna and Klotz 1994) and the first-pass phenomenon after oral drug administration.

When studying extrahepatic metabolism, whole cell systems are preferably used instead of microsomal preparations, because the latter does not contain all of the various drug-metabolizing enzymes (Pacifici *et al.* 1988). One example of such a whole cell model is that of precision-cut slices. It has the important advantage over the use of isolated cells that invasive cell isolation techniques, which are different for each organ and species, are not required. Moreover, in the use of precision-cut slices, preparation and incubation can be performed in essentially the same manner, which is important when comparing organ-specific metabolic capacity and species differences therein. Another advantage of the use of precision-cut slices is that the *in vivo* situation (including the presence of all cell types, cell–cell contacts and extracellular matrix) is more closely approached than in most other *in vitro* systems, such as isolated hepatocytes (liver), Clara or alveolar cells (lung), renal tubule fragments (kidney), or enterocytes (intestines).

Therefore, we have developed an *in vitro* test system using liver, lung, kidney and intestine slices to compare organ-specific metabolism and study differences between rat and man. Some preliminary data from this work on human lung slices and rat liver, lung and kidney slices have been described by de Kanter *et al.* (1999). The present paper expands our preliminary results on liver, kidney and intestine slices from both human and rat origin. To monitor the viability of these slices, ATP levels were measured during the 24 h of incubation and compared with *in vivo* values. Four representative test substrates were used to study xenobiotic phase I and II metabolism, i.e. testosterone (TST), lidocaine, 7-ethoxycoumarin (7-EC) and 7-hydroxycoumarin (7-HC), which are metabolized via different pathways. Slices were incubated with these test substrates at relatively high concentrations to be able to detect sufficient amounts of metabolites to study organ and species differences in metabolic pattern, and in metabolism capacity between rat and man.

Materials and methods

Materials

The following compounds were obtained from the sources indicated: lidocaine from Centrachemie (Etten-Leur, The Netherlands); 2α-, 7α-, 11α-, 19-, 16α- and 16β-hydroxytestosterone (TOH) from Steraloids (Newport, RI, USA); 7-EC from Fluka (Buchs, Germany); 2β-, 6α-, 6β-, 11β-, 14α- and 15α-TOH, TST, androstenedione, 7-methoxycoumarin, 7-HC, 7-hydroxycoumarin glucuronide (7-HC GLUC) and low melting agarose (type VII-A) from Sigma-Aldrich Chemie (Zwijndrecht, The Netherlands); University of Wisconsin organ preservation (UW) solution from DuPont Pharmaceuticals (Waukegan, IL, USA); Amphotericin B (Fungizone), penicillin-streptomycin solution and Williams' medium E (with Glutamax) from Gibco (Paisley, UK). Monoethylglycinexylidide (MEGX) was a kind gift of AstraZeneca (Södertälje, Sweden), and 7-hydroxycoumarin sulphate (7-HC SULF) was a kind gift from Mr P. Mutch, GlaxoWellcome (Herts, UK). All other chemicals were of analytical grade and were obtained from commercial sources.

Human organ tissue

Human liver tissue was obtained from redundant donor tissue after liver transplantation as part of a transplantation related research project. Human kidney, lung and intestine tissue was obtained from patients subjected to surgery for cancer in the organs concerned. Tumour free tissue considered as surgical waste was used. Human liver tissue was perfused with and stored in ice-cold UW (maximum 36 h) (Olinga *et al.* 1998b) while human lung, kidney and intestine (jejunum) material was stored in ice-cold Krebs–Henseleit buffer during transport from the hospital until arrival in the lab (maximum 2 h).

The research protocols were approved by the medical ethical committee of the Academic Hospital in Groningen, The Netherlands, and informed consent from the patients concerned was obtained.

Rat organ tissue

Male Wistar (HsdCpb:WU) rats (Harlan, Horst, The Netherlands) were housed in standard cages and had free access to food (standard chow, Hope Farms, Woerden, The Netherlands) and tap water. Rats (mean body weight 390 g) were anaesthetized by isofurane and N_2O/O_2, and the liver, lungs, kidneys and the small intestine were excized and placed in ice-cold Krebs–Henseleit, containing 10 mM Hepes and 25 mM glucose (pH 7.4). The intestines were flushed with ice-cold Krebs–Henseleit buffer to remove the contents, directly after excision, and all organs were weighed after removal of tissue (table 4). The trachea (rat) or the biggest bronchiole available (human) were cannulated and lungs instilled with 1.5% (w/v) low melting agarose solution containing 0.9% (w/v) NaCl at 37°C and allowed to gel in UW on ice. Small pieces of each organ were cut off before the organs were excized and snap-frozen to determine *in vivo* ATP levels as described below.

Preparation of slices

Tissue cylinders from liver, agarose-filled lung and kidney were prepared with a coring tool (i.d. 8 mm) (Alabama R&D, Munford, AL, USA) attached to a drilling machine with a variable rotation speed. The organ cylinders were stored in ice-cold UW until slicing (maximum 1 h).

Intestinal slices were punched out of the intestine with an 8 mm (human) or 3 mm (rat) biopsy core. After (human) or before (rat) coring the mucosa was carefully separated from the muscle layer and only the mucosa (upper 15 cm of the jejunum) was used for incubation. Precision-cut liver, lung and kidney slices were prepared using a Krumdieck tissue slicer (Alabama R&D) precooled and filled with oxygenated, ice-cold Krebs–Henseleit buffer. Kidney slices were derived mainly from cortex tissue. All slices were stored in ice-cold UW until incubation (time gap between coring and incubation: maximum 2 h).

Incubation of slices

Slices were incubated in 3.2 ml Williams' medium E, which was prewarmed and gassed with 95% O_2/5% CO_2 and supplemented with glucose (final concentration 25 mM) and for liver and lung slices gentamicin (50 $\mu g\,ml^{-1}$) was added. For kidney slices, penicillin (100 $U\,ml^{-1}$) plus streptomycin (100 $\mu g\,ml^{-1}$) was used, while for intestine slices gentamicin (50 $\mu g\,ml^{-1}$) and amphotericin B (2.5 $\mu g\,ml^{-1}$) was added, agents that are poorly metabolized and therefore considered not to interfere with biotransformation enzymes. Slices were individually incubated in six-well culture plates, which were placed in a plastic container, continuously gassed with humidified 95% O_2/5% CO_2, and shaken back and forth (90 times min^{-1}) in a cabinet at 37°C.

Viability of slices

The viability of the slices before and during incubation was determined by measurement of ATP content of individual slices. For this purpose, slices were placed in 1 ml 70% ethanol (v/v) containing 2 mM EDTA (pH 10.9) and snap-frozen in liquid nitrogen. After storage at −80°C and homogenization by sonication, ATP extracts were diluted 10 times with 0.1 M Tris HCl/2 mM EDTA solution (pH 7.8) buffer to lower the ethanol concentration. The ATP content was measured using ATP Bioluminescence Assay Kit CLS II from Roche (Mannheim, Germany) and a 96-well Lucy1 luminometer (Anthos, Durham, NC, USA) against an ATP-calibration curve.

Metabolic activity of slices

Metabolism of lidocaine (5 mM), TST (0.25 mM), 7-EC (0.5 mM) and 7-HC (0.5 mM) was studied by the addition of 32 µl stock-solution (to 3.2 ml Williams' medium E) in water (lidocaine), or methanol (TST, 7-EC, 7-HC). Metabolism was studied for 3 h of incubation, except in the case of rat liver slices incubated with TST, which was performed for 15 min to circumvent considerable substrate depletion. Medium samples (1 ml) of 7-EC incubations were acidified by directly adding 10 µl 2 M HCl after sampling, in order to prevent spontaneous formation of metabolites (if the pH of the incubation > 8.0). Medium incubated for 3 h with substrates, but without slices, served as controls and showed the absence of the particular metabolites (data not shown). Lidocaine, 7-EC and 7-HC medium samples were stored at −20°C until analysis. Preliminary experiments showed that no significant amounts of metabolites were retained in the slices (data not shown). After thawing, sodium azide was added to inhibit bacterial contamination (final concentration 0.1 $mg\,ml^{-1}$) and 50 µl of the centrifuged sample was analysed using HPLC as described above for the MEGX metabolite of lidocaine (Bargetzi *et al.* 1989) and for the metabolites of 7-EC (Walsh *et al.* 1995). For the metabolic biotransformation of TST, slices and incubation medium were harvested together and homogenized using sonication to extract the metabolites from the slice. Control experiments showed that metabolites of TST were significantly retained in

the slices (about 1.5 times the amount in medium, although metabolite profiles were similar) at the concentration used (data not shown). The homogenates were stored at −20°C. After thawing, 5 µl 11β-TOH, dissolved in methanol, was added as internal standard to 1 ml homogenate and 6 ml dichloromethane was then added. After removal of the water phase and protein interphase, the organic phase was evaporated and TST and its metabolites were dissolved in 130 µl 50% (v/v) methanol which was analysed using HPLC (van 't Klooster *et al.* 1993).

Protein content of slices

After incubation, five slices from each organ were taken and homogenized in their own incubation medium by sonication and diluted with 0.1 M NaOH. The protein content of the diluted homogenate was determined using the Bio-Rad protein assay dye reagent (Bio-Rad, Munich, Germany) against a BSA standard curve. Together with the wet weight of the slices, the percentage protein in the slices was determined (table 4). All metabolic activities and ATP levels are expressed as µg protein^{-1}.

Mass spectrometry

Samples were injected on to an Alltech Alltima C_{18} column (150 × 2.1 mm, 5 µm, Alltech Associates, Deerfield, IL, USA). Two series 200 micro-LC pumps (Perkin Elmer, Norwalk, CT, USA) delivered a gradient starting at 15% acetonitrile and 85% ammonium acetate (10 mM). One minute after the injection, the acetonitrile concentration was then linearly increased to 95% during 15 min. The system was operated at room temperature at 0.2 ml min^{-1}. The HPLC system was connected on-line with an API 3000 triple quadrupole mass spectrometer (PE-Sciex, Concord, Ontario, Canada) equipped with a TurboIonSpray interface. The conditions were set for negative ions, and full-scan spectra or product ion scan spectra were taken continuously. The MS was operated at such a low orifice voltage that 'up front' collision induced dissociation did not take place.

Results

Viability

To determine the relative viability of tissue slices in culture, ATP levels were assessed directly after slicing and after 1, 3 and 24 h of incubation (figure 1). ATP levels in both human and rat liver, lung and kidney slices showed an increase during 3 h of incubation and after 3 h a plateau level was reached, which was maintained during the incubation period (up to 24 h). However, the ATP level of intestine slices was lower than that in liver, lung and kidney slices, and did not increase during incubation.

To compare ATP results with *in vivo* levels, we determined the ATP content of small sections of organs taken from anaesthetized rats just before excizing the organs (table 1). Remarkably, ATP levels in rat liver, kidney and lung slices were higher (figure 1) than the *in vivo* levels (table 1). In contrast, ATP levels in intestine slices were the same as *in vivo* levels.

Metabolism studies

To determine the metabolic capacity of slices, incubations were performed with lidocaine, TST, 7-EC and 7-HC and the formation of metabolites was analysed. In this study, the *N*-deethylated metabolite, MEGX, of lidocaine was quantified. From table 2, it can be concluded that both rat and human liver slices have the highest capacity to form MEGX when compared with other organs. Rat liver shows a threefold higher formation rate of MEGX when compared with human slices.

As shown in table 3, a substantial organ-specific metabolic pattern of TST was observed for both rat and human slices. Human liver slices mainly formed 6β-TOH and androstenedione, whereas in human lung, kidney and intestine slices,

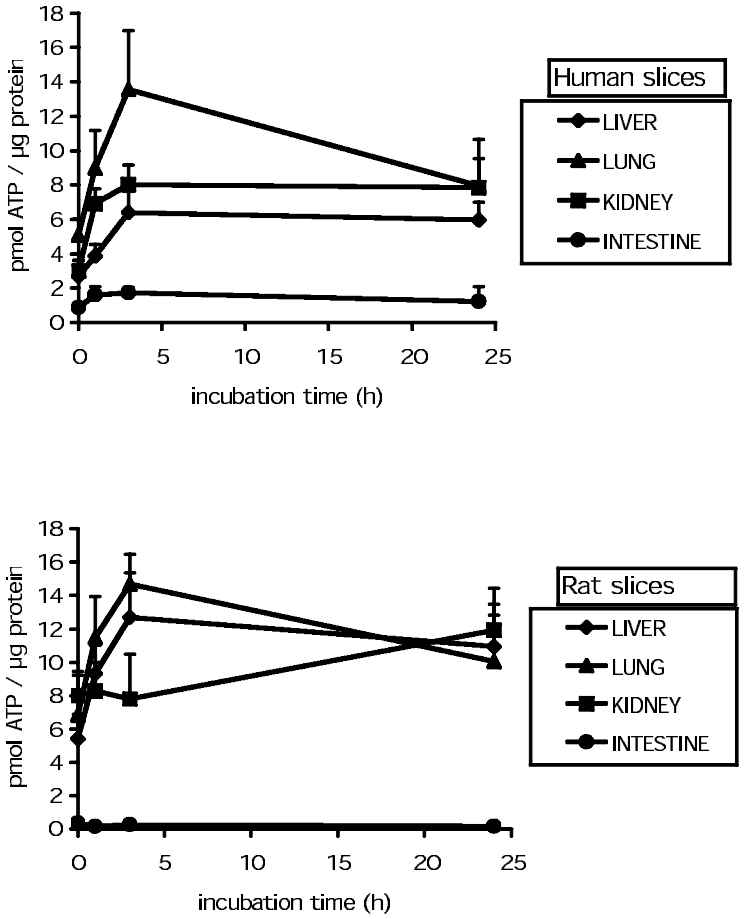


Figure 1. ATP levels in liver, lung, kidney and intestinal slices during 24 h of incubation (each time point representing the mean ± SEM of at least three organs, and three slices per organ).

Table 1. *In vivo* ATP levels in rat tissues.

Rat organ	ATP level[a]
Liver	1.81 ± 0.96
Lung	3.21 ± 0.15
Kidney	1.01 ± 0.41
Intestine	1.85 ± 0.88

[a] pmol ATP/µg protein
Data shown are the mean ± SEM from four organs.

mainly androstenedione was formed. Rat liver slices formed several metabolites, including 2α-TOH, which was not formed by human slices, and showed the highest activity of TST metabolism when compared with lung, kidney or intestine slices (15, 14 and 25% of rat liver slices, respectively). In addition, when regarding human organ slices, liver slices were most active but this was less pronounced than for rat organ slices (45, 63 and 61% of human liver slices, respectively).

Table 2. Metabolism of lidocaine in tissue slices.

MEGX formation[a]	*Human slices*	Rat slices
Liver	109 ± 16	363 ± 62
Lung	48 ± 24	25 ± 3
Kidney	6 ± 2	4 ± 3
Intestine	59 ± 30	71 ± 19

[a] pmol MEGX/3 h/μg protein.

Data are the means of at least four organs ± SEM, and three slices per organ.

Table 3a. Metabolism of testosterone in human tissue slices[a].

Metabolite	Human liver	Human lung	Human kidney	Human intestine
6α-TOH	0.8 ± 0.3	1.8 ± 1.6	n.d.	n.d.
6β-TOH	11.7 ± 1.7	3.9 ± 1.7	0.9 ± 0.2	0.8 ± 0.7
7α-TOH	1.3 ± 0.6	n.d.	n.d.	n.d.
15α-TOH	1.3 ± 0.8	n.d.	n.d.	0.4 ± 0.3
19-TOH	0.5 ± 0.2	n.d.	0.4 ± 0.2	n.d.
16α-TOH	0.9 ± 0.4	n.d.	0.5 ± 0.3	0.3 ± 0.3
16β-TOH	1.0 ± 0.5	0.2 ± 0.2	0.0 ± 0.0	n.d.
2α-TOH	0.1 ± 0.0	n.d.	0.2 ± 0.2	n.d.
2β-TOH	4.4 ± 1.5	n.d.	2.2 ± 2.2	0.2 ± 0.2
Androstenedione	40.1 ± 6.9	22.0 ± 13.4	34.6 ± 5.6	35.6 ± 15.6
Total	62.1 ± 12.8	27.9 ± 10.3	38.9 ± 13.0	37.4 ± 17.0

[a] pmol metabolite/3h/μg protein.

n.d. not detected.

Data are the means of at least four organs ± SEM, and three slices per organ.

Table 3b. Metabolism of testosterone in rat tissue slices[a].

Metabolite	Rat liver	Rat lung	Rat kidney	Rat intestine
6α-TOH	n.d.	2.2 ± 1.8	0.5 ± 0.5	n.d.
6β-TOH	15.7 ± 5.9	2.2 ± 1.7	0.7 ± 0.4	5.8 ± 1.7
7α-TOH	n.d.	1.0 ± 1.0	n.d.	n.d.
15α-TOH	0.4 ± 0.4	1.0 ± 1.0	n.d.	n.d.
19-TOH	9.2 ± 3.0	3.6 ± 1.3	0.6 ± 0.6	n.d.
16α-TOH	28.8 ± 8.4	1.5 ± 1.4	0.6 ± 0.4	1.5 ± 1.2
16β-TOH	1.5 ± 1.5	1.5 ± 1.5	0.9 ± 0.9	3.1 ± 2.4
2α-TOH	22.6 ± 7.3	1.1 ± 0.9	1.5 ± 0.2	n.d.
2β-TOH	n.d.	1.0 ± 1.0	n.d.	1.8 ± 1.1
Androstenedione	97.2 ± 24.6	11.3 ± 1.0	19.5 ± 2.2	31.4 ± 7.2
Total	175.3 ± 51.1	26.3 ± 12.5	24.4 ± 5.1	43.7 ± 13.6

[a] pmol metabolite/3 h/μg protein.

n.d. not detected.

Data are the means of at least four organs ± SEM, and three slices per organ.

Unlike liver slices that formed predominantly 7-HC and the conjugate 7-HC GLUC from 7-EC, lung, kidney and intestine slices from both man and rat formed mainly an, as yet, unidentified metabolite (figure 2). Minor amounts of this metabolite were also present in incubations without slice when the medium was not acidified (see above). Usually, the pH of WE increases towards 8.5 when the CO_2 atmosphere was not present. Incubations without slices or, with slices but

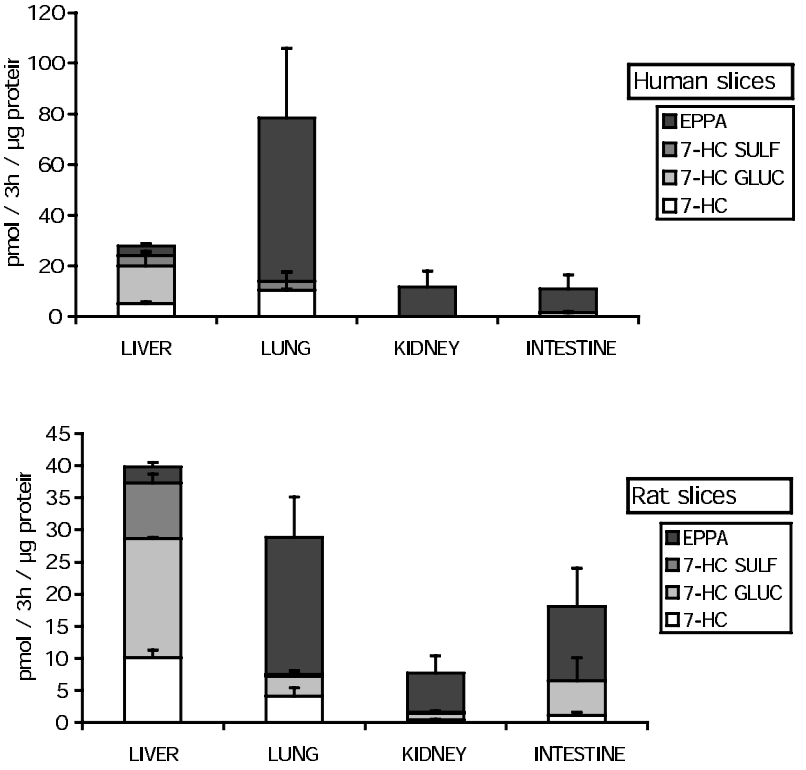


Figure 2. 7-EC (0.5 mM) metabolism during 3 h of incubation (data are means ± SEM of at least three organs, and three slices per organ).

performed at 4°C, showed no detectable formation of this metabolite when the medium was acidified after incubation.

To identify this metabolite, larger amounts of it were prepared by adding 5 µl 1M NaOH solution to 1 ml 0.5 mM solution of 7-EC in water (pH > 9). HPLC-MS analysis of this mixture showed mainly two molecular ions at m/z 207 $[M\text{-}H]^-$, with an empirical formula of $C_{11}H_{11}O_4$. A product ion scan of the $[M\text{-}H]^-$ ion at m/z 207 gave daughter ions at m/z 163, 133, 105 and 77, which are consistent with the loss of $[CO_2]$, $[C_2H_6]$, and twice [CO] from the parent ions. The structure of the metabolite was therefore presumed to be 4-ethoxy-2-hydroxyphenyl propionic acid (EPPA) (figure 3). This metabolite is in agreement with the finding that EPPA was not formed from 7-HC incubations (figure 4) and that similar additional HPLC peaks were formed when this experiment (increasing pH) was performed with 7-methoxycoumarin, analogous to 7-EC. The two peaks in the HPLC are thought to be the *cis* and *trans* forms of EPPA and its analogue formed from 7-methoxycoumarin, although this remains to be established.

To quantify the formation of EPPA we used a 7-EC standard curve, because the absorption coefficient at 320 nm appeared to be the same for EPPA and 7-EC, as is also the case for 7-HC and its conjugates (data not shown), which is in agreement with the preservation of the conjugated structure as depicted in figure 3.

Human and rat organ slices incubated with 7-HC at a concentration of 0.5 mm mainly formed 7-HC GLUC from 7-HC incubations, except human lung slices that produced only minor amounts of 7-HC SULF (figure 4). In contrast, rat lung

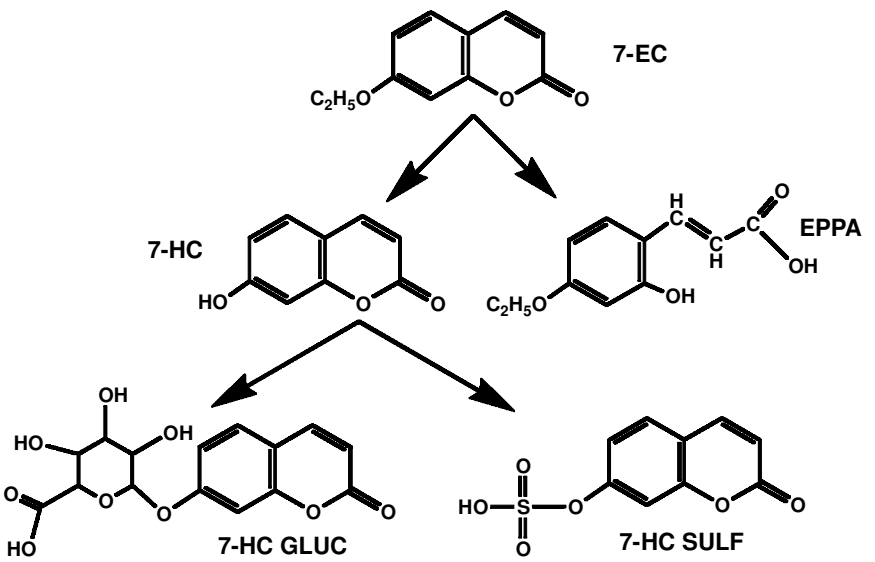


Figure 3. Metabolic pathway of 7-EC.

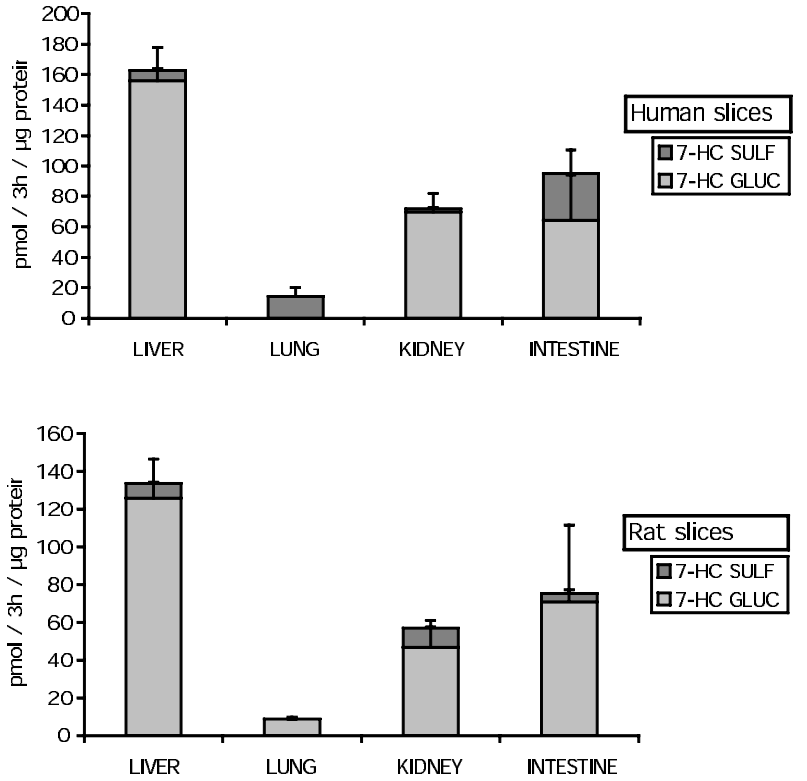


Figure 4. Phase II metabolism of 7-HC (0.5 mM), during 3 h of incubation (data are means ± SEM of at least four organs, and three slices per organ).

slices only produced some 7-HC GLUC. Both in man and rat, slices from kidney and intestine formed about equal quantities, of conjugate from 7-HC, that were about 60% of liver slices, when compared on a protein basis.

Discussion

The present study has shown for man and rat that the most important organs for drug metabolism (liver, lung, kidney, intestine) can be studied under similar conditions (preparation, handling, incubation) using tissue slices. Moreover, it has been shown that both phase I and II reactions can be studied simultaneously in tissue slices, being a major advantage above the use of microsomes. Metabolism in rat organs can also be studied simultaneously, using slices from the same animal. Tissue slices of human origin were made whenever tissue was available (normally one organ at a time). The period between explantation and slicing was much longer for liver (up to 36 h) than for the other human organs (maximum 2 h). It has been shown that this cold preservation time has no effects on ATP levels or metabolic capacity of liver slices (Olinga *et al*. 1998b).

We monitored tissue viability by measuring ATP levels in the slices. ATP concentrations in liver, lung and kidney slices increased during the first 3 h of incubation and were ultimately higher than the *in vivo* levels, as was shown for rat liver slices (Chapman *et al*. 1994), and then remained constant (figure 1 and table 1). However, it should be noted that it is very difficult to determine actual *in vivo* levels of ATP due to its rapid breakdown, even in small tissue samples (Faupel *et al*. 1972). As far as we know, the ATP content of human liver, lung, kidney or intestine slices has not been previously reported. However, another measure of viability, potassium content has been determined in human liver slices but it decreased during incubation (VandenBranden *et al*. 1998). Literature data on rat liver ATP levels (Wang *et al*. 1999), lung (Monteil *et al*. 1999) and kidney slices (Obatomi and Bach 2000) are in the same range as described herein. No data on ATP levels from rat intestine slices could be retrieved from literature. ATP levels from both rat and human intestine slices decreased slightly with time, unlike the slices from other organs. Therefore, it is concluded that for slices from liver, lung and kidney, viability is sufficient for our purposes. However, for intestine slices this might not be the case because ATP levels are quite low and did not increase with time of incubation (figure 1). Current research in our laboratory is ongoing to improve intestinal ATP levels and to study viability more extensively by examination of the morphology of the slices. Nevertheless, the results show that despite this relatively low viability, metabolic activity is remarkably high.

In the current study, the *N*-deethylated metabolite of lidocaine, MEGX, has been quantified. At the concentration used (5 mM), MEGX is by far the major metabolite both in rat liver (Hoke and Ravis 1991), rat lung and kidney (Tanaka *et al*. 1994) and man liver slices (Parker *et al*. 1996), although other metabolites have been reported at lower concentrations. It can be concluded from table 2 that liver slices have the highest capacity in both rat and man to metabolize lidocaine, although extrahepatic metabolism of lidocaine does takes place, which is in agreement with *in vivo* results in man (Sallie *et al*. 1992).

The current study analysed the phase I products of TST by HPLC. It was found that in human liver slices, 6β-TOH accounted for 19% of total metabolism. It was stated that 6β-TOH accounted for 75–80% of all metabolites in human liver

microsomes (Draper *et al.* 1998). This difference may be explained because only cytochrome P450-catalysed reactions were considered in the latter study using microsomes, in contrast to the circumstances in the present study, using human liver slices.

Apart from metabolism of TST towards TOHs by CYPs as discussed by de Kanter *et al.* (1999), TST can be metabolized by 17β-hydroxysteroid dehydrogenase, forming androstenedione (Farthing *et al.* 1981, 1982). Because we observed mainly androstenedione formation in lung, kidney and intestine slices (and only minor amounts of TOHs) (table 3), together with the finding that this enzyme is found in the small intestine (Farthing *et al.* 1981, 1982), it is possible that 17β-hydroxysteroid dehydrogenase is involved in the formation of androstenedione in the intestine, and possibly in lung and kidney too.

Many reports in the literature describe only three metabolites of 7-EC, namely 7-HC, 7-HC GLUC and 7-HC SULF. The main reason for this is that 7-HC and 7-HC conjugates (after enzymatic deconjugation) are often analysed by fluorescence (Rogiers *et al.* 1986). As shown in figure 3, these three metabolites are indeed the most abundant metabolites of 7-EC formed by liver slices from both rat and man. However, the main metabolite in lung, kidney and intestine slices appear to be EPPA, a metabolite that has not been described until now. Unidentified metabolites of 7-EC have been previously reported *in vivo* (Ritschel and Hardt 1983), in rat liver slices (Price *et al.* 1995, Walsh *et al.* 1995, Ball *et al.* 1996) and in rat microsomes (Jung *et al.* 1985). The latter study reported that 3-hydroxylation of 7-EC took place. By comparing the effect of deconjugation of rat liver slice metabolites, Ball *et al.* (1996) reported that out of 11 unidentified metabolites, three are glucuronic acid conjugates and four sulphate conjugates. A study on guinea pig and dog liver slices reported that ring opening of 7-EC can also take place, forming 4-ethoxy-2-hydroxyphenylacetic acid (EHPA) (Terada *et al.* 1996). However, EHPA differs from EPPA with respect to the length of the carboxyl moiety. In addition, EPPA appears to have the same absorption coefficient at 320 nm as 7-EC (and as 7-HC and its conjugates), unlike EHPA (Terada *et al.* 1996), most likely because of the difference between the structures.

We studied metabolism using relatively high substrate concentrations (0.25 mM for TST, 0.5 mM for 7-EC and 7-HC, 5 mM for lidocaine). In fact, these concentrations are probably sufficient to saturate the enzyme systems involved, implying that we actually measured V_{max} (capacity) rates. This opened the possibility to compare these V_{max} found *in vitro* with *in vivo* values. It has been reported in several studies that V_{max} and clearances were lower in slices when compared with isolated hepatocytes, especially when high clearance drugs such as 7-EC are considered (Ekins *et al.* 1995, Worboys *et al.* 1996a, b, 1997, Houston and Carlile 1997, Carlile *et al.* 1999). However, the rate of metabolism of lidocaine, which also results in a relatively high clearance, was similar for human liver slices and isolated hepatocytes (Olinga *et al.* 1993, 1998b). Moreover, even higher values have been reported for the metabolism of biphenyl using human and dog (but not rat) liver slices compared with isolated hepatocytes (Powis *et al.* 1989). Apart from species and substrate differences herein, we believe that it is difficult to compare slices and cells quantitatively. When normalizing to wet weight, adhering water may cause an underestimation of slices and this may also be the case for dry weight or protein content, because damaged cells on the cutting edges will contribute to

Table 4. *In vivo* scaling factors of rat slices.

Rat organ	Organ weight (g)	Percentage protein in slices[a]	Scaling factor (×1000)[b]
Liver	15.3	10.6	1631
Lung (agarose filled)	6.9	1.1	78
Kidney	2.9	9.3	268
Small intestine	7.2	12.0	865

[a] Determined through the wet weight and protein content of the slices.
[b] Calculated by multiplying the organ weight with the percentage slice protein.
Data are the means of 6 organs ± SEM (of each, organ five slices were determined).

the weight or protein content but are not metabolically active. In the case of isolated cells, damaged cells are simply removed by (Percoll) centrifugation.

An alternative approach to establish if metabolism rates in slices reflect *in vivo* values correctly is to compare the metabolic capacity of slices with *in vivo* values. The measured metabolic rates, which are expressed μg protein, can be scaled to the metabolic rates per μg organ using the protein percentage in slices and subsequently scaled to the total organ value by extrapolation to total organ weight. This scaling results in the scaling factors as indicated in table 4. In the present case, when the sum of the four measured metabolites of 7-EC from rat liver slices are taken from figure 2, and multiplied with the scaling factor from table 4, and corrected for rat weight, a $V_{max} = 0.42\,\mu mol\,min^{-1}\,SRW^{-1}$ (Standard Rat Weight of 250 g) for 7-EC metabolism in rat liver is derived. This value may largely underestimate the total rate of 7-EC metabolism because other organs than the liver contribute significantly (figure 2). When a similar calculation is made for lung, kidney and intestine, by summing all the metabolites from figure 2 of each organ, and multiplying by the scaling factors from table 4 for each organ, the following V_{max} are derived: lung, 0.01, kidney 0.01 and intestine 0.10 μmol $SRW^{-1}\,min^{-1}$.

The sum of V_{max} of liver, lung, kidney and intestine then gives a $V_{max} = 0.51\,\mu mol\,SRW^{-1}\,min^{-1}$, which correlates well for the reported V_{max} *in vivo*, namely 0.49 $mol\,SRW^{-1}\,min^{-1}$ (Carlile *et al*. 1998). Therefore, it is concluded that in the case of 7-EC metabolism, the use of slices reflects the *in vivo* metabolizing capacity correctly. Clearly, other organs than the liver contribute significantly to the total metabolism of the test compound.

Conclusions

It was reported (de Kanter *et al*. 1999) that using slices, it was possible to study xenobiotic metabolism, not only in liver, but also in lung and kidney from both rat and man, under similar experimental conditions. The present study has additionally examined intestinal slices and shown that, apart from the liver, lung and kidney, the intestine can also contribute considerably to the overall capacity of xenobiotic metabolism in the body of both rat and man. As shown, it is also possible to compare the results of slices (after up-scaling) to the *in vivo* situation.

This technology may lead to a more adequate choice of animal species used during drug development and can result in a considerable reduction in the use of experimental animals.

The use of a combination of liver, lung, kidney and intestine slices might be appropriate for most substrates because the most important organs involved in metabolism are included. Nevertheless, in a minority of cases significant drug metabolism takes also place in skin, nasal mucosa or other tissue and this aspect should not be neglected.

Acknowledgements

The authors thank Dr J. R. de Haas, Dr J. Nieken, Professor Dr H. J. A. Mensink, Professor Dr M. J. H Slooff for supplying human tissue. M. T. Merema, R. N. Patty and C. Driessen are thanked for their technical contribution, and A. van Dam, C. M. Jeronimus-Stratingh and Dr A. P. Bruins for their work on the mass spectrometry. The work was supported by a grant from The Netherlands Alternatives to Animal Experiments Platform (P. A. D.).

References

Bach, P. H., Vickers, A. E. M., Fisher, R., Baumann, A., Brittebo, E., Carlile, D. J., Koster, H. J., Lake, B. G., Salmon, F., Sawyer, T. W. and Skibinski, G., 1996, The use of tissue slices for pharmacotoxicology studies. The report and recommendations of ECVAM workshop 20. *Alternatives to Laboratory Animals*, **24**, 893–923.

Ball, S. E., Thiel, V. E., Tio, C. O., Lim, H.-K., Kao, J., Sisenwine, S. F. and Scatina, J., 1996, [^{14}C]-7-ethoxycoumarin metabolism by precision-cut rat hepatic slices. *Drug Metabolism and Disposition*, **24**, 383–389.

Bargetzi, M., Aoyama, T., Gonzalez, F. and Meyer, U., 1989, Lidocaine metabolism in human liver microsomes by cytochrome P450IIIA4. *Clinical Pharmacology and Therapeutics*, **46**, 521–527.

Boyd, M. R., Grygiel, J. J. and Minchin, R. F., 1983, Metabolic activation as a basis for organ-selective toxicity. *Clinical and Experimental Pharmacology and Physiology*, **10**, 87–99.

Carlile, D. J., Hakooz, N. and Houston, J. B., 1999, Kinetics of drug metabolism in rat liver slices: IV. Comparison of ethoxycoumarin clearance by liver slices, isolated hepatocytes, and hepatic microsomes from rats pretreated with known modifiers of cytochrome P-450 activity. *Drug Metabolism and Disposition*, **27**, 526–532.

Carlile, D. J., Stevens, A. J., Ashforth, E. I., Waghela, D. and Houston, J. B., 1998, *In vivo* clearance of ethoxycoumarin and its prediction from *in vitro* systems. Use of drug depletion and metabolite formation methods in hepatic microsomes and isolated hepatocytes. *Drug Metabolism and Disposition*, **26**, 216–221.

Chapman, D. E., Michener, S. R. and Powis, G., 1994, Adenine and pyridine nucleotide concentrations and relationships to 2,6-dinitrotoluene metabolism in cultured rat liver slices. *Toxicology In Vitro*, **8**, 343–349.

De Kanter, R., Monshouwer, M., Meijer, D. K. F. and Groothuis, G. M. M., 2002, Precision-cut organ slices as a tool to study toxicity and metabolism of xenobiotics with special reference to non-hepatic tissues. *Current Drug Metabolism* (in press).

De Kanter, R., Olinga, P., de Jager, M. H., Merema, M. T., Meijer, D. K. F. and Groothuis, G. M. M., 1999, Organ slices as an *in vitro* test system for drug metabolism in human liver, lung and kidney. *Toxicology In Vitro*, **13**, 737–744.

Draper, A. J., Madan, A., Smith, K. and Parkinson, A., 1998, Development of a non-high pressure liquid chromatography assay to determine testosterone hydroxylase (CYP3A) activity in human liver microsomes. *Drug Metabolism and Disposition*, **26**, 299–304.

Ekins, S., Murray, G. I., Burke, M. D., Williams, J. A., Marchant, N. C. and Hawksworth, G. M., 1995, Quantitative differences in phase I and II metabolism between rat precision-cut liver slices and isolated hepatocytes. *Drug Metabolism and Disposition*, **23**, 1274–1279.

Farthing, M. J., Vinson, G. P., Edwards, C. R. and Dawson, A. M., 1981, 17 Beta-hydroxysteroid dehydrogenase activity in the mucosa of rat and human small intestine. *Journal of Steroid Biochemistry*, **14**, 1107–1113.

Farthing, M. J., Vinson, G. P., Edwards, C. R. and Dawson, A. M., 1982, Testosterone metabolism by the rat gastrointestinal tract, *in vitro* and *in vivo*. *Gut*, **23**, 226–234.

Faupel, R. P., Seitz, H. J., Tarnowski, W., Thiemann, V. and Weiss, C., 1972, The problem of tissue sampling from experimental animals with respect to freezing technique, anoxia, stress and narcosis. A new method for sampling rat liver tissue and the physiological values of glycolytic intermediates and related compounds. *Archives of Biochemistry and Biophysics*, **148**, 509–522.

Hoke, J. F. and Ravis, W. R., 1991, Effect of a perfluorochemical erythrocyte substitute on the *in vitro* metabolism of lidocaine using rat liver slices. *Research Communications in Chemical Pathology and Pharmacology*, **73**, 333–353.

Houston, J. B. and Carlile, D. J., 1997, Prediction of hepatic clearance from microsomes, hepatocytes, and liver slices. *Drug Metabolism Reviews*, **29**, 891–922.

Jung, B., Graf, H. and Ullrich, V., 1985, A new monooxygenase product from 7-ethoxycoumarin and its relation to the *O*-dealkylation reaction. *Biological Chemistry Hoppe-Seyler*, **366**, 23–31.

Krishna, D. R. and Klotz, U., 1994, Extrahepatic metabolism of drugs in humans. *Clinical Pharmacokinetics*, **26**, 144–160.

Lerche-Langrand, C. and Toutain, H. J., 2000, Precision-cut liver slices: characteristics and use for *in vitro* pharmaco-toxicology. *Toxicology*, **153**, 221–253.

Monteil, C., Le Prieur, E., Buisson, S., Morin, J. P., Guerbet, M. and Jouany, J. M., 1999, Acrolein toxicity: comparative *in vitro* study with lung slices and pneumocytes type II cell line from rats. *Toxicology*, **133**, 129–138.

Obatomi, D. K. and Bach, P. H., 2000, Atractyloside nephrotoxicity: *in vitro* studies with suspensions of rat renal fragments and precision-cut cortical slices. *In Vitro Molecular Toxicology*, **13**, 25–36.

Olinga, P., Meijer, D. K. F., Slooff, M. J. H. and Groothuis, G. M. M., 1998a, Liver slices in *in vitro* pharmacotoxicology with special reference to the use of human liver tissue. *Toxicology In Vitro*, **12**, 77–100.

Olinga, P., Merema, M., Hof, I. H., de Jong, K. P., Slooff, M. J. H., Meijer, D. K. F. and Groothuis, G. M. M., 1998b, Effect of human liver source on the functionality of isolated hepatocytes and liver slices. *Drug Metabolism and Disposition*, **26**, 5–11.

Olinga, P., Merema, M. T., Meijer, D. K. F., Slooff, M. J. H. and Groothuis, G. M. M., 1993, Human liver slices express the same lidocaine biotransformation rate as isolated human hepatocytes. *Alternatives to Laboratory Animals*, **21**, 466–468.

Pacifici, G. M., Franchi, M., Bencini, C., Repetti, F., Di Lascio, N. and Muraro, G. B., 1988, Tissue distribution of drug-metabolizing enzymes in humans. *Xenobiotica*, **18**, 849–856.

Parker, R. J., Collins, J. M. and Strong, J. M., 1996, Identification of 2,6-xylidine as a major lidocaine metabolite in human liver slices. *Drug Metabolism and Disposition*, **24**, 1167–1173.

Powis, G., Melder, D. C. and Wilke, T. J., 1989, Human and dog, but not rat, isolated hepatocytes have decreased foreign compound-metabolizing activity compared to liver slices. *Drug Metabolism and Disposition*, **17**, 526–531.

Price, R. J., Renwick, A. B., Beamand, J. A., Esclangon, F., Wield, P. T., Walters, D. G. and Lake, B. G., 1995, Comparison of the metabolism of 7-ethoxycoumarin and coumarin in precision-cut rat liver and lung slices. *Food and Chemical Toxicology*, **33**, 233–237.

Ritschel, W. A. and Hardt, T., 1983, Tissue distribution of coumarin, 7-hydroxycoumarin and their 7-hydroxy metabolites following parenteral administration of 14C-labeled compound in the DBA/lac mouse. *Arzneimittel-Forschung/Drug Research*, **33**, 836–840.

Rogiers, V., Adriaenssens, L., Vandenberghe, Y., Gepts, E., Callaerts, A. and Vercruysse, A., 1986, Critical evaluation of 7-ethoxycoumarin *O*-deethylase activity measurement in intact isolated rat hepatocytes. *Xenobiotica*, **16**, 817–826.

Sallie, R. W., Tredger, J. M. and Williams, R., 1992, Extrahepatic production of the lignocaine metabolite monoethylglycinexylidide (MEGX). *Biopharmacology and Drug Disposition*, **13**, 555–558.

Tanaka, K., Oda, Y., Asada, A., Fujimori, M. and Funae, Y., 1994, Metabolism of lidocaine by rat pulmonary cytochrome P450. *Biochemical Pharmacology*, **47**, 1061–1066.

Terada, T., Kaneko, H., Terashita, S., Tozuka, Z., Tokuma, Y. and Hata, T., 1996, A species comparison of ^{14}C-labeled 7-ethoxycoumarin metabolism in precision-cut liver slices from guinea pig and dog using a phosphor imaging system. *Research Communications in Molecular Pathology and Pharmacology*, **91**, 41–56.

Van 't Klooster, G. A. E., Blaauboer, B. J., Noordhoek, J. and van Miert, A. S. J. P. A. M., 1993, Cytochrome P450 induction and metabolism of alkoxyresofurins, ethylmorphine and testosterone in cultured hepatocytes from goats, sheep and cattle. *Biochemical Pharmacology*, **46**, 1781–1790.

VandenBranden, M., Wrighton, S. A., Ekins, S., Gillespie, J. S., Binkley, S. N., Ring, B. J., Gadberry, M. G., Mullins, D. C., Strom, S. C. and Jensen, C. B., 1998, Alterations of the catalytic activities of drug-metabolizing enzymes in cultures of human liver slices. *Drug Metabolism and Disposition*, **26**, 1063–1068.

Vickers, A. E. M., Fisher, R. L., Brendel, K., Guertler, J., Dannecker, R., Keller, B. and Fischer, V., 1995, Sites of biotransformation for the cyclosporin derivative SDZ IMM 125 using human liver and kidney slices and intestine. Comparison with rat liver slices and cyclosporin A metabolism. *Drug Metabolism and Disposition*, **23**, 327–333.

Vickers, A. E., Fischer, V., Connors, S., Fisher, R. L., Baldeck, J. P., Maurer, G. and Brendel, K., 1992, Cyclosporin A metabolism in human liver, kidney, and intestine slices. Comparison to rat and dog slices and human cell lines. *Drug Metabolism and Disposition*, **20**, 802–809.

Walsh, J. S., Patanella, J. E., Halm, K. A. and Facchine, K. L., 1995, An improved HPLC assay for the assessment of liver slice metabolic viability using 7-ethoxycoumarin. *Drug Metabolism and Disposition*, **23**, 869–874.

Wang, B. H., Zuzel, K. A., Rahman, K. and Billington, D., 1999, Treatment with aged garlic extract protects against bromobenzene toxicity to precision cut rat liver slices. *Toxicology*, **132**, 215–225.

Worboys, P. D., Bradbury, A. and Houston, J. B., 1996a, Kinetics of drug metabolism in rat liver slices. II. Comparison of clearance by liver slices and freshly isolated hepatocytes. *Drug Metabolism and Disposition*, **24**, 676–681.

Worboys, P. D., Bradbury, A. and Houston, J. B., 1997, Kinetics of drug metabolism in rat liver slices. III. Relations between metabolic clearance and slice uptake rate. *Drug Metabolism and Disposition*, **25**, 460–467.

Worboys, P. D., Brennan, B., Bradbury, A. and Houston, J. B., 1996b, Metabolic kinetics of ondansetron in rat. Comparison of hepatic microsomes, isolated hepatocytes and liver slices with *in vivo* disposition. *Xenobiotica*, **26**, 897–907.

XENOBIOTICA, 2002, VOL. 32, NO. 5, 363–368

Taylor & Francis
healthsciences

Inhibition of phenol sulfotransferase (SULT1A1) by quercetin in human adult and foetal livers

C. DE SANTI†, A. PIETRABISSA‡, F. MOSCA‡, A. RANE§ and G. M. PACIFICI†*

† Department of Neurosciences, Section of Pharmacology, Medical School, University of Pisa, Via Roma 55, I-56126 Pisa, Italy
‡ Department of Oncology, Section of Surgery, Cisanello Hospital at the University of Pisa, I-56124 Cisanello, Pisa, Italy
§ Department of Medical Laboratory Sciences, Division of Clinical Pharmacology, Karolinska Institutet at Huddinge University Hospital, SE-141 86 Stockholm, Sweden

Received 27 September 2001

1. Quercetin is one of the most abundant flavonoids in edible vegetables, fruit and wine. The aim was to study the type of inhibition of SULT1A1 by quercetin in the human adult and foetal livers.

2. The activity of SULT1A1 was measured with 4 μM 4-nitrophenol and 0.4 μM 3′-phosphoadenosine-5′-phosphosulphate-[^{35}S], and its mean (±SD) and median were 769 ± 311 and 740 pmol min^{-1} mg^{-1}, respectively (adult liver, $n = 10$), and 185 ± 98 and 201 pmol min^{-1} mg^{-1}, respectively (foetal liver, $n = 8$, $p < 0.0001$).

3. In non-inhibited samples, K_m for SULT1A1 (mean ± SD) was 0.31 ± 0.14 μM (adult liver) and 0.49 ± 0.17 μM (foetal liver, n.s.). V_{max} for SULT1A1 (mean ± SD) was 885 ± 135 pmol min^{-1} mg^{-1} (adult liver) and 267 ± 93 pmol min^{-1} mg^{-1} (foetal liver, $p = 0.007$).

4. The IC_{50} of quercetin for SULT1A1 was measured in three samples of adult and foetal livers and was 13 ± 2.1 and 12 ± 1.4 nM, respectively.

5. The type of inhibition was mixed non-competitive in adult and foetal livers and K_i was 4.7 ± 2.5 nM (adult liver) and 4.8 ± 1.6 nM (foetal liver).

6. In the adult liver, the intrinsic clearance (mean ± SD) was 3.3 ± 1.5 ml min^{-1} mg^{-1} (non-inhibited samples), 0.9 ± 0.4 ml min^{-1} mg^{-1} (12.5 nM quercetin) and 0.5 ± 0.06 ml min^{-1} mg^{-1} (25 nM quercetin). In the foetal liver, the intrinsic clearance (mean ± SD) was 0.5 ± 0.2 ml min^{-1} mg^{-1} (non-inhibited samples), 0.12 ± 0.01 ml min^{-1} mg^{-1} (12.5 nM quercetin) and 0.2 ± 0.09 ml min^{-1} mg^{-1} (25 nM quercetin).

7. In conclusion, quercetin is a potent inhibitor of human adult and foetal liver SULT1A1. It reduces the sulphation rate and intrinsic clearance of 4-nitrophenol in both human adult and foetal livers. This suggests that quercetin may inhibit the sulfation rate of those drugs sulphated by SULT1A1. The inhibition of SULT1A1 is complex and not due solely to competition at the catalytic site of SULT1A1.

Introduction

Quercetin is one of the most abundant flavonoids in edible vegetables, fruit and wine. In wine, the concentration of quercetin varies from 1 to 33 μM and drinking two glasses (300 ml) of wine leads to the ingestion of up to 10 μmole quercetin (Goldberg *et al.* 1996). After the administration of fried onions (equivalent to 225 μmole quercetin) and apples (325 μmole), the peak plasma levels of

* Author for correspondence; e-mail: pacifici@biomed.unipi.it

Xenobiotica ISSN 0049–8254 print/ISSN 1366–5928 online © 2002 Taylor & Francis Ltd
http://www.tandf.co.uk/journals
DOI: 10.1080/00498250110119108

quercetin have been reported to be 0.74 and 0.30 μM, respectively (Hollman *et al.* 1997).

It was shown that quercetin inhibits the sulfation of resveratrol (De Santi *et al.* 2000a, b) and 4-nitrophenol, dopamine, (–)-salbutamol, minoxidil and paracetamol (Marchetti *et al.* 2001). The latter authors observed that quercetin was a better inhibitor of 4-nitrophenol than dopamine sulfation in the human adult liver and the IC_{50} of quercetin for the former was two orders of magnitude lower than that for the latter.

4-Nitrophenol and dopamine are diagnostic substrates of two forms of phenol sulfotransferase, namely SULT1A1 and SULT1A3, respectively (Cappiello *et al.* 1990, Couhtrie and Johnston 2001). The former is preferentially expressed in the liver, whereas the latter is preferentially expressed in the intestinal mucosa (Cappiello *et al.* 1990). Up to now, the inhibition type of SULT1A1 by quercetin has not been studied. Therefore, the first aim of the present investigation was to study the inhibition type of SULT1A1 by quercetin in the human adult liver.

Drugs cross the human placenta and act on the foetus (Pacifici and Nottoli 1995) and quercetin may thus cross the human placenta and accumulate in foetal tissues. SULT1A1 is developed in the mid-gestational human foetal liver (Cappiello 1991). A recent study showed that mefenamic acid and salicylic acid inhibit human foetal liver SULT1A1 (Vietri *et al.* 2001). Therefore, the second aim of this study was to see whether quercetin inhibited the human foetal liver SULT1A1, and if so, to study the inhibition type of SULT1A1.

Materials and methods

Chemicals

3′-Phosphoadenosine-5′-phosphosulfate-[^{35}S] (PAPS, specific activity 1.71 Ci mmol^{-1}, radiochemical purity 99%) was obtained from NEN Life Science Products Inc. (Brussels, Belgium). 4-Nitrophenol, dithiothreitol (DTT), quercetin and bovine serum albumin (BSA) were obtained from Sigma Chemical Company (Milan, Italy). Mono- and dibasic potassium phosphate, acetone, sodium hydroxide, barium hydroxide, barium acetate, and zinc sulphate were obtained from Carlo Erba (Milan, Italy).

Biological material

Specimens of human adult livers were obtained after clinically indicated partial hepatotectomy to remove a tumour. The Ethics Committee of the Medical School of Pisa University approved the study. Liver samples were obtained from 10 patients (seven men, three women) aged between 19 and 85 years (mean ± SD, 60 ± 18 years), and relevant clinical data for liver function are summarized in table 1. Specimens of human foetal liver were obtained from eight foetuses at legal abortion performed for socio-medical reasons. The foetus's ages ranged from 9 to 21 weeks (mean ± SD, 15 ± 4 weeks). Foetal liver samples were obtained within 15 min after the abortion. The Ethics Committee of the Karolinska Institute at Huddinge University Hospital approved the project.

Isolation of tissue cytosolic fractions

About 1 g adult and foetal livers was homogenized in 5 vols 0.25 M sucrose dissolved in 5 mM potassium orthophosphate buffer (pH 7.4) using a glass–Teflon homogenizer. The homogenates were centrifuged at 12 000 *g* for 15 min and the resulting supernatants were centrifuged again at 105 000 *g* for 1 h. The high-speed cytosolic fraction was divided in aliquots, stored at –80 °C and designated as the cytosolic fraction. The protein concentration was measured as described by Lowry *et al.* (1951) using bovine serum albumin as a standard.

Assays for SULT1A1

The activity of SULT1A1 was measured with 4 μM 4-nitrophenol and 0.4 μM PAPS as substrates. This assay was as described by Foldes and Meek (1973), modified by Anderson *et al.* (1980) and adapted

Table 1. Liver function tests of patients undergoing clinically indicated partial hepatectomy from whom liver samples were derived.

	Minimum	Maximum	Mean ± SD	Median	Normal*
Albumin ($g\,l^{-1}$)[1]	3.4	4.5	3.9 ± 0.4	4.0	3.5–5.5 $g\,dl^{-1}$
Bilirubin ($mg\,dl^{-1}$)[2]	0.2	0.9	0.6 ± 0.2	0.6	$<$1.1 $mg\,dl^{-1}$
GOT ($U\,l^{-1}$)	11	83	36 ± 24	28	$<$45 $U\,l^{-1}$
GPT ($U\,l^{-1}$)	5	96	30 ± 29	17	$<$45 $U\,l^{-1}$
PT (s)	11.5	12	11.7 ± 0.2	11.6	10.9–12.8 s

[1] Plasma albumin concentration; [2] total bilirubin plasma concentration; GOT, glutamic-oxalacetic transaminase activity; GPT, glutamic-pyruvic transaminase activity; PT, prothrombin time.

*Derived from the Hospital of Pisa.

to the human adult and foetal livers by Cappiello *et al.* (1990, 1991). The incubation buffer was 8.3 mM orthophosphate potassium (pH 6.0) with a 20-min incubation time. The adult and foetal liver cytosolic fractions were diluted 10 000- and 400-fold, respectively. Dilutions were carried out with 5 mM orthophosphate potassium buffer (pH 7.4) containing 1.54 $mg\,ml^{-1}$ DTT and BSA (0.625 $mg\,ml^{-1}$). The final protein concentration per ml incubation mixture ranged from 0.9 to 1.7 $\mu g\,ml^{-1}$ (adult liver) and from 8.3 to 16 $\mu g\,ml^{-1}$ (foetal liver). Quercetin was dissolved in acetone and 2 µl were added to the incubation mixture (final volume of 150 µl). This volume of acetone did not affect the activities of adult and foetal liver SULT1A1.

Kinetics of SULT1A1

The kinetics of SULT1A1 were studied in three samples of human adult and foetal livers. The adult liver was obtained from two men and one woman aged from 58 to 85 years, and the foetal liver was obtained from three foetuses aged from 12 to 21 weeks. The following concentrations of 4-nitrophenol were used: 0.12, 0.25, 0.5, 1.0, 2 and 4 µM both in adult and foetal livers.

Inhibition of SULT1A1

The inhibition of SULT1A1 by quercetin was studied in three samples of adult and foetal livers. The inhibition curves were constructed using the following concentration of quercetin: 3.12, 6.25, 12.5, 25 and 50 nM. The concentrations of 4-nitrophenol and PAPS were kept constant at 4 and 0.4 µM, respectively.

Inhibition type of SULT1A1

The study was carried out with adult human liver obtained from two men and one woman aged from 58 to 85 years, and foetal liver obtained from three foetuses aged from 12 and 21 weeks. Each assay consisted of three saturation curves obtained with the following concentrations of 4-nitrophenol: 0.12, 0.25, 0.5, 1.0, 2 and 4 µM. One saturation curve did not contain quercetin (control) and the other two contained 12.5 and 25 nM quercetin.

Calculations

The kinetic parameters V_{max} and K_m were determined using the non-linear correlation option of the software package Prism 3 (GraphPad Software, San Diego, CA, USA). IC_{50} was calculated using the software package Dose–Effect Analysis (Biosoft, Cambridge, UK). ANOVA analysis, followed by the Tukey–Kramer multiple comparisons test, assessed the difference of K_m, V_{max} and the intrinsic clearances measured in the absence and presence of two concentrations of quercetin. The intrinsic clearance was measured by dividing V_{max} by K_m. The software package used for statistical analysis was Instat for Windows (GraphPad Software). The difference between groups was examined by the *t*-test with Welch correction for groups having different SD. The correlations were tested by the Spearman-rank test. K_i and K_{ies} were calculated by using the computer program 'Enzpack 3' (Biosoft). The effectiveness of inhibitor binding to free enzyme was measured by the dissociation constant K_i of the reaction, which was defined as:

$$K_i = ([E] \times [I])/[EI],$$

and the effectiveness of its binding to the enzyme substrate complex was measured by K_{ies}, which was defined as:

$$K_{ies} = ([ES] \times [I])/[EIS],$$

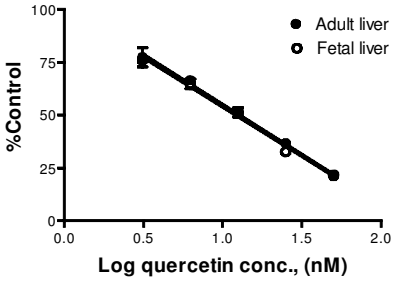


Figure 1. Inhibition of SULT1A1 by quercetin. Data points are the mean ± SD of three adult and three foetal livers. IC_{50} (mean ± SD) is 13 ± 2.1 nM (adult liver) and 12 ± 1.4 nM (foetal liver).

where [E] is the concentration of the enzyme, [I] is the concentration of the inhibitor, [ES] is the concentration of the enzyme–substrate complex and [EIS] is the concentration of the enzyme–inhibitor–substrate complex. In a mixed, non-competitive inhibition type, when $K_i < K_{ies}$, the binding of the substrate to the enzyme decreases the affinity of the enzyme for the inhibitor.

Results and discussion

The activity of SULT1A1 was measured in 10 samples of adult liver and in eight samples of foetal liver. The mean (±SD) and the median were 769 ± 311 and 740 pmol min^{-1} mg^{-1}, respectively (adult liver), and 185 ± 98 and 201 pmol min^{-1} mg^{-1}, respectively (foetal liver). The activity in adult liver was higher than that in the foetal liver ($p < 0.0001$).

The IC_{50} of quercetin for 4-nitrophenol sulfation was measured in three samples of adult and foetal livers and was (mean ± SD) 13 ± 2.1 and 12 ± 1.4 nM (n.s.), respectively. The inhibition curves are shown in figure 1.

The type of inhibition of 4-nitrophenol sulfation by quercetin was studied in the three adult and foetal livers and the representative results of an adult and foetal livers are shown in figure 2. The type of inhibition was mixed non-competitive. K_i and K_{ies} were 4.7 ± 2.5 and 15 ± 2.9 nM, respectively (adult liver, $p = 0.008$), and 4.8 ± 1.6 and 13 ± 2.1 nM, respectively (foetal liver, $p = 0.005$). The kinetic parameters (K_m, V_{max}) obtained in the adult and foetal livers are summarized in table 2. In non-inhibited samples, K_m (mean ± SD) was 0.31 ± 0.14 μM (adult liver) and 0.49 ± 0.17 μM (foetal liver, n.s.), while V_{max} (mean ± SD) was 885 ± 135 pmol min^{-1} mg^{-1} (adult liver) and 267 ± 93 pmol min^{-1} mg^{-1} (foetal liver, $p = 0.007$).

The intrinsic clearance of 4-nitrophenol was measured in adult and foetal livers and the results are summarized in table 3. In non-inhibited samples, the intrinsic clearance was 3.3 ± 1.5 ml min^{-1} mg^{-1} (adult liver) and 0.5 ± 0.2 ml min^{-1} mg^{-1} (foetal liver, $p = 0.04$). The presence of quercetin lowered the V_{max} of SULT1A1 and consequently reduced the intrinsic clearance of 4-nitrophenol.

The results show that the activity of SULT1A1 is better developed in the adult livers than in foetal livers, consistent with Cappiello *et al.* (1991) and Vietri *et al.* (2001). Therefore, quercetin inhibits SULT1A1 and the IC_{50} is similar in adult and foetal livers. Quercetin may inhibit the sulfation of drugs or chemicals sulfated by SULT1A1 both in the human adult and foetal livers. As figure 2 shows, the inhibition type of SULT1A1 by quercetin is mixed non-competitive both in adult and foetal livers. This suggests that the inhibition of quercetin is complex and not due solely to competition at the catalytic site of SULT1A1. K_i is similar in the

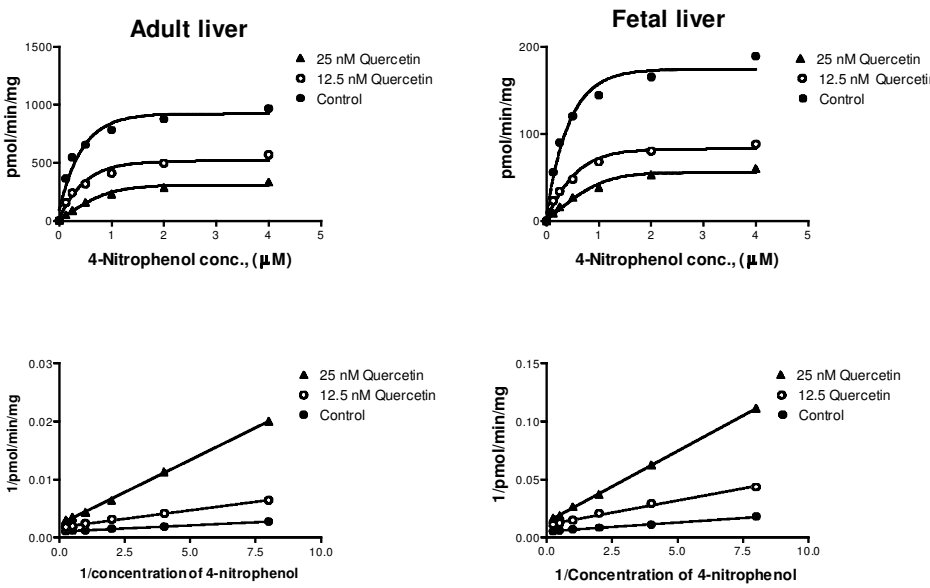


Figure 2. Effect of 4-nitrophenol concentration on the activity of SULT1A1. Each panel shows three curves, one obtained in the absence of quercetin (control) and the other 2 obtained in presence of 12.5 nM and 25 nM quercetin. Saturation curves (top) and transformation of the enzyme activity into Lineweaver-Burk plots (bottom) are shown. The Km and Vmax values are summarised in table 2. The adult liver was derived from a woman 85 years old and the fetal liver derived from a fetus 17 weeks old.

Table 2. V_{max} and K_m of SULT1A1 in the absence and presence of two concentrations of quercetin.

	Control	12.4 nM Quercetin	25 nM Quercetin
Adult liver			
V_{max} (pmol min^{-1} mg^{-1})	885 ± 135	514 ± 111	336 ± 91
K_m (μM)	0.31 ± 0.14	0.62 ± 0.19	0.62 ± 0.18
	A	B	C
Foetal liver			
V_{max} (pmol min^{-1} mg^{-1})	267 ± 93	130 ± 41	92 ± 31
K_m (μM)	0.49 ± 0.17	1.0 ± 0.2	0.5 ± 0.4
	D	E	F

Data are the mean ± SD of three liver samples.

Adult liver: V_{max}: A versus B, $p < 0.05$; A versus C, $p < 0.01$; B versus C, $p > 0.05$; K_m: figures are not different; ANOVA test, $p = 0.104$.

Foetal liver: V_{max}: D versus E, $p > 0.05$, D versus F, $p < 0.05$; E versus F, $p > 0.05$; K_m: D versus E, $p < 0.05$; D versus F, $p > 0.05$; E versus F, $p < 0.05$.

adult and foetal livers and in the order of nM, whereas the K_m for 4-nitrophenol is in the order of μM indicating that the affinity of the inhibitor for SULT1A1 is greater than that of its diagnostic substrate 4-nitrophenol.

The K_m for SULT1A1 is similar in adult and foetal livers, whereas V_{max} is one-third in the foetal than the adult liver. Accordingly, the intrinsic clearance of 4-nitrophenol is smaller in the foetal than in the adult liver. Quercetin lowers the activity of SULT1A1 both in the adult and foetal livers with a consequent reduction of 4-nitrophenol intrinsic clearance. Taken collectively, the present data suggest that quercetin may impair the sulphation of drugs in the human adult and foetal livers.

Table 3. Intrinsic clearance (ml min^{-1} mg^{-1}) of 4-nitrophenol in the absence and presence of two concentrations of quercetin.

Control	12.5 nM Quercetin	25 nM Quercetin
Adult liver		
3.3 ± 1.5	0.9 ± 0.4	0.5 ± 0.06
A	B	C
Foetal liver		
0.5 ± 0.2	0.12 ± 0.01	0.2 ± 0.09
D	E	F

Data are the mean ± SD of three liver samples.
Adult liver: A versus B, $p < 0.05$; A versus C, $p < 0.05$; B versus C, $p > 0.05$.
Foetal liver: D versus E, $p < 0.05$; D versus F, $p < 0.05$; E versus F, $p > 0.05$.

Acknowledgements

The work was supported by Contract BMH1-CT94-1622 of the European Commission (Brussels, Belgium), by the Italian Ministry of the University (Rome, Italy), the Italian Association for Cancer Research (Milan, Italy), and by the Swedish Medical Research Council (04496) and the Swedish Cancer Society.

References

Anderson, R. J., Wei, N. S. and Hilboum, R. M., 1980, Phenolsulphotransferase in human tissues: radiochemical enzymatic assay and biochemical properties. *Clinica et Chimica Acta*, **103**, 79–90.

Cappiello, M., Giuliani, L. and Pacifici, G. M., 1990, Differential distribution of phenol and catechol sulphotransferase in human liver and intestinal mucosa. *Pharmacology*, **40**, 69–76.

Cappiello, M., Giuliani, L., Rane, A. and Pacifici, G. M., 1991, Dopamine sulphotransferase is better developed than *p*-nitrophenol sulphotransferase in the human fetus. *Developmental Pharmacology and Therapeutics*, **16**, 83–88.

Couhtrie, M. W. H., John, S. and Ton, L. E., 2001, Interactions between dietary chemicals and human sulfotransferases – molecular mechanisms and clinical significance. *Drug Metabolism and Disposition*, **29**, 522–528.

De Santi, C., Pietrabissa, A., Spisni, R., Mosca, F. and Pacifici, G. M., 2000a, The sulfation of resveratrol, a natural compound present in wine, is inhibited by natural flavonoids. *Xenobiotica*, **30**, 857–866.

De Santi, C., Pietrabissa, A., Spisni, R., Mosca, F. and Pacifici, G. M., 2000b, Sulphation of resveratrol, a natural product present in grapes and wine, in the human liver and duodenum. *Xenobiotica*, **30**, 609–617.

Foldes, A. and Meek, J., 1973, Rat brain phenolsulphotransferase-partial purification and some properties. *Biochimica et Biophysica Acta*, **327**, 365–374.

Goldberg, D. M., Tsang, E., Karumanchiri, A., Diamandis, E. P., Soleas, G. and Ng, E., 1996, Method to assay the concentrations of phenolic constituents of biological interest in wines. *Analytical Chemistry*, **68**, 1688–1694.

Hollman, P. C. H., van Trijp, J. M. P., Buysman, M. N. C. P., Gaag, M. S. V. D., Mengelers, M. J. B., de Vries, J. H. M. and Katan, M. B., 1997, Relative bioavailability of the antioxidant flavonoid quercetin from various foods in man. *FEBS Letters*, **418**, 152–156.

Lowry, O. H., Rosebrough, N. J., Farr, A. and Randall R. J., 1951, Protein measurement with Folin phenol reagent. *Journal of Biological Chemistry*, **193**, 265–275.

Marchetti, F., De Santi, C., Vietri, M., Pietrabissa, A., Spisni, F., Mosca, F. and Pacifici, G. M., 2001, Differential inhibition of human liver and duodenum sulfotransferase activities by quercetin, a flavonoid present in vegetables, fruit and wine. *Xenobiotica*, **31**, 841–847.

Pacifici, G. M. and Nottoli, R., 1995, Placental transfer of drugs administered to the mother. *Clinical Pharmacokinetics*, **28**, 235–269.

Vietri, M., Pietrabissa, A., Mosca, F., Rane, A. and Pacifici, G. M., 2001, Human adult and foetal liver sulphotransferases inhibition by mefenamic acid and salicylic acid. *Xenobiotica*, **31**, 153–161.

XENOBIOTICA, 2002, VOL. 32, NO. 5, 369–382

Taylor & Francis
healthsciences

Tissue disposition, excretion and metabolism of 2,2′,4,4′,5-pentabromodiphenyl ether (BDE-99) in the male Sprague–Dawley rat

H. HAKK†*, G. LARSEN† and E. KLASSON-WEHLER‡§

† USDA, ARS, Biosciences Research Laboratory, PO Box 5674, Fargo, ND 58105-5647 USA

‡ Department of Environmental Chemistry, Stockholm University, SE-106 91 Stockholm, Sweden

Received 7 August 2001

1. A disposition, metabolism and excretion study of orally administered 2,2′,4,4′,5-pentabromodiphenyl ether (BDE-99) was conducted in the conventional and bile duct-cannulated male rat.

2. In the conventional rat, > 50% of the radiolabelled dose was retained at 72 h, and lipophilic tissues were the preferred sites for disposition, i.e. adipose tissue, adrenals, gastrointestinal tract and skin.

3. Urinary excretion of BDE-99 was very low (< 1% of dose), and glucuronidation of phenolic metabolites was suggested.

4. Biliary excretion of BDE-99 was slightly greater than observed in urine, i.e. 3.6% at 72 h.

5. Over 43% of the dose in the conventional male rat and 86% in the bile duct-cannulated rat was excreted in the faeces, mainly as the unmetabolized parent compound.

6. Metabolites in bile and faeces were not conjugated. Mono- and di-hydroxylated pentabromodiphenyl ether metabolites were characterized by mass spectrometry. Two thiol metabolites were characterized in the bile. Oxidative debromination was also observed in the faecal metabolites.

7. Tissue BDE-99 was readily extractable, except for in the liver. The tissue ^{14}C was not associated with lipids and was mainly the unmetabolized parent compound.

8. Total thyroxine (T4) plasma levels were elevated at 3 and 6 days, and returned to control levels by day 12.

Introduction

Polybrominated-diphenyl ethers (PBDEs), -biphenyls (PBBs) and -bisphenol-A (i.e. TBBP-A) are synthesized in large quantities and serve as flame retardants in textiles and in electronic equipment, such as computer circuit boards. Owing to their structural similarity to polychlorinated dibenzo-*p*-dioxins and biphenyls, and the increase in their commercial synthesis over the past 20 years, currently at 150 000 tons per year globally (Sellstrom and Jansson 1995), there is a growing concern that environmental levels may be increasing, leading to a future toxicological problem. Bioaccumulation of PBDEs in the environment is expected because of their high lipophilicity, which ranges between log K_{ow} 4.3–9.9. The occurrence of PBDEs in the environment was first reported 20 years ago in

* Author for correspondence; e-mail: hakkh@fargo.ars.usda.gov

§ Present address: AstraZeneca R&D Södertälje, DMPK&BAC, SE-151 85 Södertälje, Sweden.

Xenobiotica ISSN 0049-8254 print/ISSN 1366–5928 online © 2002 Taylor & Francis Ltd
http://www.tandf.co.uk/journals
DOI: 10.1080/00498250110119117

sediments from the USA (Zweidinger *et al.* 1979), and shortly thereafter in fish from Sweden (Anderson and Blomkvist 1981). They have now been identified in human plasma (Klasson-Wehler *et al.* 1997) and Baltic biota (Haglund *et al.* 1997). A continuous increase has been reported for all measured congeners in human milk banked from 1972 to 1997 in Sweden (Norén and Meironyté 2000). Both PBDEs and PBBs have recently been found in relatively high levels in the sperm whale, an organism that spends most of its time in deep ocean waters (De Boer *et al.* 1998).

The PBDE congener of greatest concentration in biological tissues is 2,2′,4,4′-tetrabromodiphenyl ether (BDE-47), followed by 2,2′,4,4′,5-pentabromodiphenyl ether (BDE-99). BDE-47 and BDE-99 are the principal components of commercial pentabromodiphenyl ether (PeBDE). World-wide production figures for PeBDE indicate that it makes up $<10\%$ of the total PBDE market. Therefore, one can hypothesize that either biological tissues selectively accumulate these lesser brominated diphenyl ethers over the more highly brominated congeners, or that debromination of more highly brominated PBDEs leads to the formation and bioaccumulation of BDE-47 and BDE-99.

Relatively little is known about the metabolism and tissue disposition of individual PBDEs in mammalian systems. Therefore, the aim of the present paper is to administer a single, radiolabelled oral dose of BDE-99 to the male Sprague–Dawley rat and study the tissue disposition, excretion and metabolite formation after 72 h in conventional and bile duct-cannulated animals.

Materials and methods

Chemicals

2,2′,4,4′,5-Pentabromo-[^{14}C and ^{12}C]diphenyl ether (BDE-99) was synthesized in-house by the method of Örn *et al.* (1996). The radiolabelled purity of [^{14}C] BDE-99 ($>98\%$) was determined by silica TLC (50:50 hexane:methylene chloride) and HPLC (C18, H_2O:CH_3CN gradient). Chemical purity of [^{12}C]BDE-99 (97%) was determined by ^{1}H-NMR analysis. Radiolabelled BDE-99 was diluted with unlabelled material until the desired specific activity was achieved (995 dpm μg^{-1}). Diazomethane was generated in-house using Diazald® (Aldrich Chemical Co., Milwaukee, WI, USA) according to the manufacturer's procedure. Regisil® [*N*,*O*-bis(trimethylsilyl)trifluoroacetamide] was purchased from Regis Technologies, Inc. (Morton Grove, IL, USA).

Instrumentation

A Polytron Tissue-mizer (Brinkman Instruments, Westbury, NY, USA) homogenized tissues for extraction analysis.

Gas chromatography-electron impact mass spectrometry (GC/MS) was performed on a VG Auto Spec mass spectrometer operating at 70 eV, using a Model 5890 GC (Hewlett-Packard, Palo Alto, CA, USA) with a 15 m DB-5ms column (J&W Scientific, Folsom, CA, USA) run from 70 to 310 °C at 10 °C min^{-1}.

HPLC analyses were performed on a Gilson System 45NC Gradient Analytical instrument (Gilson Medical Electronics, Middleton, WI, USA) equipped with a variable wavelength UV detector set to 254 nm, and a liquid scintillation flow-through radioactivity detector in series. Injections were made with a Model 7125 Rheodyne injector. HPLC fractionations were accomplished in reversed-phase mode with a C18 Delta-Pak column (8 × 100 mm; Waters Associates, Milford, MA, USA).

Quantitation of radioactivity

Urine, bile and plasma were assayed for radioactivity by counting aliquots in a Packard Model 1900 CA liquid scintillation counter (LSC). Air-dried faeces and lyophilized tissues were homogenized, and the aliquots were removed in triplicate, weighed and combusted with a Packard Model 307 tissue oxidizer (0.5 g most tissues, 0.1 g adipose). Radiolabelled CO_2 was trapped in CARBO-SORB® E (Packard, Meridan, CT, USA), and measured for ^{14}C in a Permafluor scintillator (Packard) with a LSC. Radiolabelled bands on silica TLC plates were quantitated using a System 2000 Imaging Scanner (Bioscan, Inc., Washington, DC, USA).

Animals

The radiolabelled dose was administered orally (2.2 mg/rat in corn oil; 1.0 μCi/rat) to three conventional male rats (Sprague–Dawley, 271 ± 21 g; 14.5 μmol kg^{-1}) and five bile duct-cannulated rats (238 ± 11 g; 16.5 μmol kg^{-1}). The rats were housed in steel metabolism cages. Urine, faeces and bile were collected at 24 h intervals for 72 h. The rats were anesthetized with halothane and exsanguinated. Adrenals, adipose, gastrointestinal tract, heart, kidneys, liver, lungs, testes and thymus were removed and stored at –20 °C until analyses could be performed.

The same methodology was employed for parallel metabolism studies with two other groups of rat ($n = 3$), in which the first group was killed after 6 days and the second at 12 days. The only difference in these studies was the 6- and 12-day rats were completely skinned immediately upon killing, which allowed disposition data from the skin and the remaining carcass to be determined.

Urine

Two aliquots of 0–24 h conventional urine were stored at 4 °C for 1 and 21 months, and at the appropriate time the aliquots were extracted with hexane. Pooled 0–72 h urine was also analysed by TLC using the following development conditions: (1) hexane/methylene chloride (50:50) for parent BDE-99, (2) tetrahydrofuran/ethyl acetate/hexane (12.5:12.5:25) for Phase I metabolites and (3) tetrahydrofuran/methanol/acetic acid (27:27:4) for Phase II conjugates.

Bile

Pooled bile from each day was concentrated with a centrifugal vacuum concentrator (Savant Instruments, Holbrook, NY, USA), and injected onto a C18 DeltaPak HPLC column (8 × 30 cm; Waters Associates). The mobile phase consisted of a binary gradient system: A, methanol/water (20:80); B, methanol. The column was equilibrated with A and ramped to B over 20 min. The trapped radioactivity was further fractionated by HPLC under the same conditions, except that acetonitrile replaced methanol. Samples were treated with diazomethane or Regisil® and analysed by GC/MS.

Plasma

Plasma from each rat was analysed for thyroxine (T4) concentrations by reversed fluorescence polarization kits (Axxsum, Abbott Laboratories, Northfield, IL, USA). The values are the total plasma T4, including bound and free forms of T4.

Faeces

The pooled, air-dried faeces were extracted three times each with hexane, ethyl acetate and methanol. Silica gel TLC plates were developed with 50:50 hexane:methylene chloride using BDE-99 as a standard. HPLC analysis was performed as described above. HPLC fractions were evaporated to dryness on a rotary evaporator, derivatized with diazomethane or Regisil® and analysed by GC/MS.

Tissues

Selected tissues, i.e. adipose tissue, kidney, liver and lung, were solvent extracted. Two columns (3.5 × 16 cm) with stopcocks were assembled one above the other. The tissue samples were cut into small pieces with a razor blade and homogenized with a Polytron Tissue-mizer™ in acetone (35 ml) and hexane (10 ml). The homogenate was transferred to the upper column, which was equipped with a sintered glass frit. The acetone:hexane mixture was filtered into the lower column, which contained 0.9% sodium chloride in 0.1 M orthophosphoric acid. The tissue samples were rehomogenized twice with hexane (20 ml) and passed into the lower column. The lower column was shaken and the organic layer set aside. The aqueous layer was re-extracted with hexane (10 ml) twice. A gravimetric lipid determination was performed on the combined organic layers.

Gel permeation chromatography (GPC) was performed on the tissue extracts using Biobeads SX-3 (Bio-Rad Laboratories, Richmond, CA, USA) according to Klasson-Wehler *et al.* (1987), except that the column flow rate was 2.0 ml min^{-1} and a pump was not used. Each tube was assayed for radioactivity by LSC. Unbound parent or metabolites eluted at 50–76 ml. Radioactive fractions were silylated and analysed by GC/MS.

Results

The metabolism of BDE-99 to water-soluble metabolites or conjugates was low, as evidenced by the low daily excretion observed in the urine and bile. Cumulative recovery of radiolabel in urine was $< 1\%$ in the conventional rat at

Table 1. Recoveries of ^{14}C from 3-day-old male rats receiving a single oral dose of 2,2′,4,4′,5-pentabromo-[^{14}C]diphenyl ether (BDE-99; 2.2 mg/rat) in a conventional (14.5 μmol kg^{-1} body weight) and bile duct-cannulated (16.5 μmol kg^{-1} body weight) study.

	% of Dose	
Tissue/excreta	Conventional ($n = 3$)	Cannulated ($n = 5$)
Urine		
0–24 h	0.4 ± 0.06	0.1 ± 0.08
24–48 h	0.3 ± 0.1	0.2 ± 0.2
48–72 h	0.2 ± 0.01	0.05 ± 0.03
Bile		
0–24 h	–	0.7 ± 0.8
24–48 h	–	1.8 ± 1.1
48–72 h	–	1.4 ± 1.0
Faeces		
0–24 h	22.3 ± 15.8	52.5 ± 26.9
24–48 h	14.8 ± 5.4	30.4 ± 19.9
48–72 h	6.0 ± 1.6	3.6 ± 5.9
Adrenals	0.1 ± 0.02	0.01 ± 0.006
Adipose (epididymal)	3.8 ± 1.1	0.8 ± 0.6
Blood	0.03 ± 0.02	0.007 ± 0.007
Carcass	38.8 ± 5.2	2.0 ± 1.2
Gastrointestinal tract	6.1 ± 0.7	1.5 ± 1.4
Heart	0.03 ± 0.005	0.01 ± 0.009
Kidney	0.1 ± 0.005	0.03 ± 0.02
Liver	0.9 ± 0.20	0.3 ± 0.1
Lungs	0.1 ± 0.02	0.04 ± 0.04
Testes	0.06 ± 0.02	0.08 ± 0.06
Thymus	0.06 ± 0.03	0.01 ± 0.006
Total recovery	94.0	98.4

Data are the mean ± SD from three animals.

72 h, and approximately 0.3% in the bile duct-cannulated rat (table 1). Radiolabel amounts in bile were only 3.9% over the same period. No ^{14}C from the urine could be extracted into hexane at either the time of collection or following 1 or 21 months of storage at 4 °C. This indicated that parent BDE-99 was not present in the urine either at the outset or via decomposition from labile metabolites over time. Therefore, metabolism of BDE-99 controls the rate of excretion via the urine. Quantitative TLC analysis demonstrated that the majority of the urinary ^{14}C was that of conjugated metabolites (data not shown).

Faeces were the major route of elimination of BDE-99. In conventional rat faeces, 43% of the dose was excreted and > 86% was excreted in the faeces of the bile duct-cannulated rat in 72 h (table 1). Evidence for labile metabolites was obtained in the faecal extracts where reversion of chromatographed metabolites back to parent was observed on several occasions. In addition, the presence of reactive intermediates in the gut was suggested by the extraction recoveries. Approximately 82% of the ^{14}C could be extracted from 0–24 h conventional faeces, but < 48% could be extracted from 48–72 h faeces (table 2).

TLC and HPLC quantitative analysis of the faecal extracts from the conventional rat indicated that only minor amounts (< 10% of extracted ^{14}C) of metabolites were present. Methyl derivatives of hydroxy and thiol metabolites were not methoxy or methylthiol metabolites by derivatization with Regisil® and deutero

Table 2. Average percentage lipid content of selected tissues and the relative distribution of [^{14}C]BDE-99 in selected tissues and in 0–24, 24–48 and 48–72 h faeces from 3-day-old conventional rats extracted according to the materials and methods.

Tissue	% Lipid content	% Extractable ^{14}C	% Non-extractable ^{14}C
Adipose	70.9	98.7	0.04
Kidney	14.2	94.7	5.3
Liver	4.9	41.8	57.0
Lungs	8.8	95.0	5.0
Faeces			
0–24 h	n.d.*	81.5	18.5
24–48 h	n.d.	55.2	44.7
48–72 h	n.d.	47.6	52.4

* n.d., Not determined.
Data are the mean of three animals.

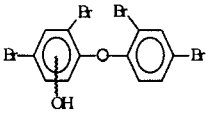
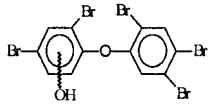
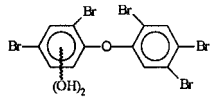
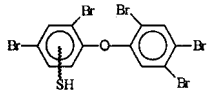
Regisil® (table 3). GC/MS analysis (table 3), following methylation of faecal extracts, indicated the presence of two methyl derivatives of monohydroxy pentabromodiphenyl ether metabolites [M^{+} 590 (5 Br); M-15 (575); M-80 (512, 4 Br); M-158 (432)], and two methyl derivatives of debrominated monohydroxy tetrabromodiphenyl ether metabolites [M^{+} 512 (4 Br); M-15 (497); M-80 (434, 3 Br); M-94 (418)]. Sufficient amounts of purified material were not available to perform ^{1}H-NMR spectroscopy on these metabolites. Therefore, absolute stereochemical assignments could not be made. The majority of the ^{14}C in the faecal extracts (> 90%, from TLC data) was present as parent BDE-99. This was confirmed by GC/MS [M^{+} 560 (5 Br); M-78 (482, 4 Br); M-158 (402); M-265 (295)] and ^{1}H-NMR [8.10 (s), 7.95 (s), 7.62 (d), 7.33 (s), 7.11 (d); in acetone-d_6].

Bile was fractionated by HPLC and analysed for metabolites. The metabolites were characterized after methylation by GC/MS (table 3). Two methyl derivatives of monohydroxy pentabromodiphenyl ether metabolites were identified [M^{+} 590 (5 Br); M-15 (575); M-31 (559); M-80 (512)]. Three dimethyl derivatives of dihydroxy pentabromodiphenyl ethers were characterized by mass spectrometry [M^{+} 620 (5 Br); M-15 (605)]. Mass spectral evidence was also obtained to suggest the presence of two methyl derivatives of thio-substituted pentabromodiphenyl ethers [M^{+} 606 (5 Br); M-15 (591); M-80 (526)].

Disposition data on a per cent of dose basis at 72 h revealed that BDE-99 was preferentially found in lipophilic tissues, i.e. adipose tissue, carcass and gastrointestinal tract (table 1). No other tissues in the conventional or bile duct-cannulated rat contained > 1% of the ^{14}C at 72 h. Bile salts were apparently necessary for the intestinal absorption of BDE-99, because tissue retention data for the bile duct-cannulated rat was much lower when compared with the conventional rat. The remaining carcass from the conventional rat contained nearly 39% of the dosed ^{14}C, therefore it was further fractionated into skin, bone, brain, eyes and muscle. The majority of the carcass ^{14}C partitioned into the skin. If an average weight of 55 g for skin is assumed, then > 21% of the BDE-99 deposited in the skin at 72 h in the conventional rat.

When the tissue disposition data were expressed on a concentration basis, the most lipophilic tissues, i.e. adipose tissue, adrenals, gastrointestinal tract and skin, contained the highest concentrations of ^{14}C (table 4). The lipid content of selected tissues was determined (table 2), but the observed disposition pattern for BDE-99

Table 3. Mass spectra of compounds characterized in 3-day-old conventional male rats as either methyl, silyl or deutero silyl derivatives in bile and faeces derived from [^{14}C]BDE-99 administered as a single oral dose.

Compound	Methyl derivative	Silyl derivative	Deutero silyl
 OH-TBDE (faeces)	$M_{\cdot}^{+}$512 (4 Br) M-15 (497) M-80 (434, 3 Br) M-94 (418)	n/a	n/a
 OH-PeBDE (faeces and bile)	$M_{\cdot}^{+}$590 (5 Br) M-15 (575) M-31 (559) M-80 (512) M-158 (432) M-173 (417) M-201 (389)	$M_{\cdot}^{+}$648 (5 Br) M-15 (633, 5 Br) M-79 (569; 4 Br) M-136 (512, 4 Br)	$M_{\cdot}^{+}$657 (5 Br) M-18 (639)
 Di-OH-PeBDE (bile)	$M_{\cdot}^{+}$620 (5 Br) M-15 (605) M-94 (526) M-107 (513)	$M_{\cdot}^{+}$736 (5 Br) M-15 (721) M-73 (663; 5 Br) M-88 (648; 5 Br)	$M_{\cdot}^{+}$745 (5 Br) M-18 (727)
 SH-PeBDE (bile)	$M_{\cdot}^{+}$606 (5 Br) M-15 (591) M-80 (526) M-94 (512) M-158 (448)	$M_{\cdot}^{+}$664 (5 Br) M-15 (649, 5 Br) M-72 (592) M-93 (571; 4 Br)	$M_{\cdot}^{+}$673 (5 Br) M-18 (655) M-96 (577)

did not consistently correlate with tissue lipid content. Although adipose tissue had the highest lipid content and the highest BDE-99 concentration, kidney and lung had a higher lipid content than liver, and yet lower BDE-99 concentrations (0.7 and 1.7 μg BDE-99 g^{-1} kidney and lung, respectively versus 4.9 μg BDE-99 g^{-1} liver) (table 4). Other halogenated aromatics, i.e. toxic dioxins and furans, are known to distribute in extrahepatic tissue based on the lipid content of the tissue. The liver:fat (L:F) ratio of BDE-99 in the male rat was only 0.12, an indication that no selectivity in hepatic retention was occurring.

The radioactivity from adipose tissue, liver, kidney and lung was extracted. None of the extracted ^{14}C was associated with lipid by means of GPC analyses (data not shown). Essentially all the ^{14}C isolated from the tissues was that of parent [$M_{\cdot}^{+}$ 560 (5 Br), M-Br (482; 4 Br), M-2Br (402; 3 Br)]. Only trace amounts of hydroxylated metabolites in the liver extracts were detected by mass spectrometry [$M_{\cdot}^{+}$ 648, M-15 (633) as TMS ether] (table 3).

The total thyroid hormone, thyroxine (T4), in the plasma of the control rat was determined as 1.7 ± 0.2 μg dl^{-1}, whereas in the conventional rat (14.5 μmol BDE-99 kg^{-1} body weight), T4 levels rose to 3.2 ± 0.5 μg dl^{-1} at day 3 (figure 1). At day 6, the levels of T4 remained elevated at 3.0 ± 0.3 μg dl^{-1}, but by day 12 the levels fell to 1.9 ± 0.4 μg dl^{-1} in these conventional rats. T4 levels in plasma of the bile duct-cannulated rat were not significantly different from control levels at 1.7 ± 0.4 μg dl^{-1}.

Table 4. Average concentration of [^{14}C]BDE-99 in fresh tissues from 3-day-old conventional rats following a single oral dose in peanut oil (2.0 mg kg^{-1}; 1.0 μCi μmole^{-1}; $n = 3$ for most tissues, $n = 2$ for bone, eyes, hair and skin). It was assumed that all the tissue ^{14}C was parent BDE-99.

Tissue	μg BDE-99 g^{-1} tissue
Adipose (epididymal)	40.3
Adrenals	24.3
Brain	0.4
Bone	
Femur	1.4
Femur marrow	2.1
Humerus	0.5
Humerus marrow	1.1
Shoulder blade	0.8
Eyes	0.03
Gastrointestinal tract	16.4
Hair	1.3
Heart	0.6
Kidney	0.7
Liver	4.9
Lungs	1.7
Muscle (longisimus dorsi)	1.6
Red blood cells	0.02
Skin	8.5
Testes	0.0006
Thymus	1.6

Discussion

The urine excretion data for BDE-99 were similar to those observed in the male rat following an oral dose of BDE-47 in which the cumulative excretion in the urine was $< 0.5\%$ of the dose at 5 days (Örn and Klasson-Wehler 1998). Essentially, all the ^{14}C present in the urine of both the conventional and bile duct-cannulated rat was present as metabolites of BDE-99, as determined by TLC analysis with standard [^{14}C]BDE-99. Furthermore, TLC analysis with a protonated mobile phase (see the Materials and methods) suggested that the urine metabolites were conjugated and not simply Phase I metabolites (data not shown). Hydrolysis with β-glucuronidase (*E. coli*; Sigma Chemical Co., St Louis, MO, USA) resulted in deconjugation, as determined by TLC. Therefore, conjugation of phenolic metabolites with glucuronic acid was implied for BDE-99.

The largest amount of radioactivity was recovered in the faeces in both the conventional and bile duct-cannulated rat at 72 h (43 and 86%, respectively) (table 1). In both groups of animals, the faecal radioactivity peaked at 0–24 h (22 and 52%, respectively) and declined steadily with time. This suggested that enterohepatic circulation of BDE-99, if it occurred, played a minor role in the male rat. These faecal excretion data are higher than those obtained following a single oral dose of BDE-47 to the conventional male rat, where only 14% was recovered in faeces over 5 days (Örn and Klasson-Wehler 1998). The low faecal excretion of BDE-47 was due to facile intestinal absorption and tissue retention. A higher brominated PBDE congener, decabromodiphenyl ether (BDE-209), was sparingly absorbed from the gut when administered in feed at 0.025–5.0% of the diet (El Dareer *et al.* 1987). This resulted in about 85% of the dose being excreted in the

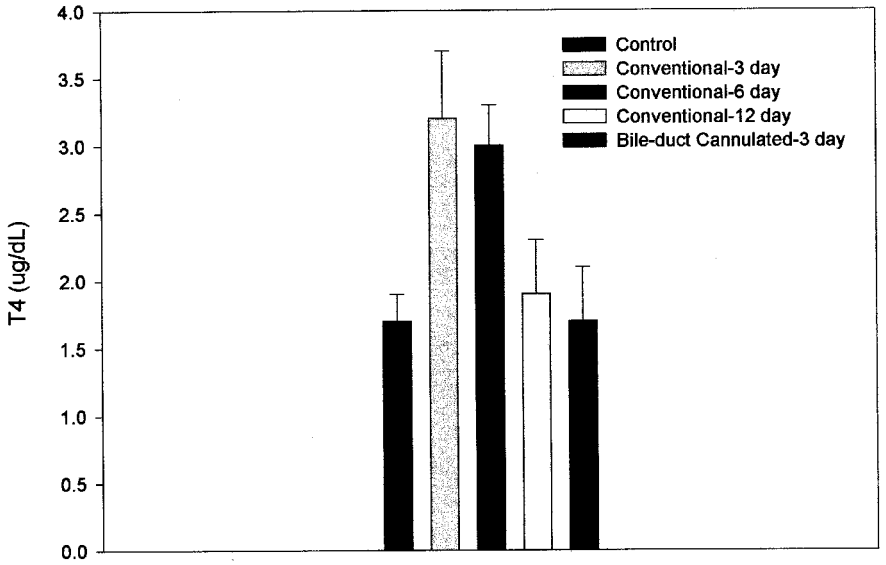


Figure 1. Average concentration of total thyroxine (T4) in the plasma of the male Sprague–Dawley rat at various times following a single oral dose of BDE-99 in corn oil ($n = 3$). Error bars are the SD.

faeces in 72 h, with the amount of parent BDE-209 ranging from 72 to 98%. The lack of intestinal absorption of BDE-209 and subsequent metabolism may be the result of a vehicle dependence because other work has shown that 2.2 and 0.5% of a BDE-209 dose (2.9 mg kg^{-1} body weight) was retained in the liver and lungs, respectively, of the conventional rat at 72 h, while $>9\%$ was excreted in the bile of the bile duct-cannulated rat at 72 h when Lutrol F127, soya phospholipid and water was used as the vehicle (Hakk *et al.* 2000, Mörck and Klasson-Wehler 2001).

The present *in vivo* excretion results are in agreement with standard *in vitro* biotransformation results conducted on a series of PBDEs, where no significant metabolism was observed for any PBDE tested (De Boer *et al.* 1998). It was concluded from the latter data that a substantial environmental persistence was likely for the PBDE family because of the low observed biotransformation.

A sizable portion of the ^{14}C in faeces could not be extracted (table 2). At 0–24 h in the conventional rat, 18.5% of the ^{14}C in faeces was non-extractable, and this increased to 52.4% by 72 h. The non-extractable [^{14}C]BDE-99 was presumably metabolically activated to a reactive intermediate, e.g. arene oxide, which efficiently formed covalent bonds with reactive groups in the intestinal proteins or lipids. Relatively high levels of non-extractable ^{14}C were also observed in the liver (57%) (table 2), the site of highest metabolic activity. In contrast, the bulk of the ^{14}C in adipose tissue, kidney and lung could be readily extracted ($\geq$95%). The extractable BDE-99 derived radioactivity in the tissues was not associated with lipid by GPC analysis (data not shown). It was concluded that adipose tissue, kidney and lung had no significant activity towards BDE-99. Örn and Klasson-Wehler (1998) observed covalent binding of parent BDE-47 and metabolites to faecal macromolecules, and non-covalent binding to lipids in faeces and tissues. Therefore, the GPC data suggest a different metabolic pathway in tissues for BDE-99 compared with BDE-47. Lipid-associated metabolites in faeces and

tissues have also been observed with PCB and polychlorinated naphthalene congeners (Klasson-Wehler *et al*. 1989, 1993, Jakobsson 1994).

The presence of thiol metabolites in the bile was confirmed by precise mass determinations from mass spectra after silyl derivatization. At a resolution of 5000 mass units, the elemental composition with the best fit for the molecular ion cluster peak of 667 was $C_{15}H_{13}OSiS\ ^{79}Br_3{}^{81}Br_2$. Reasonable elemental compositions with < 2 ppm deviation were also observed with the other molecular ion cluster peaks. In addition, the normal silyl mass spectrum of the pentabromo thiol metabolite displayed the molecular ion at M^{+} 664, while the molecular ion of the deuterated compound was nine mass units higher at M^{+} 673 (table 3). A molecular ion at M^{+} 736 would have been expected for the deuterated di-OTMS pentabromodiphenyl ether metabolite, which has the same underivatized molecular weight (table 3). Metabolism studies with BDE-47 have also suggested the presence of a thiol metabolite in addition to five monohydroxy tetrabromodiphenyl ether metabolites in the faeces of the male rat (Örn and Klasson-Wehler 1998). Normally, sulphur metabolites result from glutathione conjugation of an arene oxide, followed by enzymatic hydrolysis by γ-glutamyltransferase and carboxypeptidase to a cysteine conjugate via the mercapturic acid pathway (MAP). Cysteine conjugate β-lyase, which is known to exist in rat liver, can cleave a cysteine conjugate to a free thiol. However, apart from thiols that can result from cysteine conjugates, none of the intermediates of the MAP were observed in the present study. Therefore, if glutathione and cysteine conjugated metabolites of BDE-99 were formed in rat metabolism, then these putative intermediates were labile or rapidly converted to other compounds. Occasionally, thiols can be methylated and oxidized to methyl sulphones, which have been observed with PCBs and chlorinated benzenes (Bakke and Gustafsson 1986), but they were also not detected in the present study.

It was clear that BDE-99 preferentially deposited in the most lipophilic tissues, i.e. adipose, adrenals, gastrointestinal tract and skin (table 4). However, measurable levels of BDE-99 derived radioactivity were observed in every tissue examined in the 3-day conventional rat. Even hair and bone contained 0.5–2.1 μg BDE-99 g^{-1} tissue (table 4). BDE-99 was only slowly mobilized from skin and fat deposits. In the 3-day conventional rat, 21% of the dose deposited in the skin. At 6 days, over 18% of the dose to the conventional rat was still in the skin, while at 12 days the levels in the skin had only declined to 12% (table 5). A substantial portion of the dose, i.e. 14 and 10% for the 6- and 12-day conventional rat, respectively, was in the carcass remains (less skin and removed tissues), the majority of which was probably in the remaining adipose tissue. Based on the disposition and excretion results in tables 1 and 5, the estimated whole-body half-life of BDE-99 in the male rat was slightly less than 6 days. Therefore, the data would indicate that the bioaccumulation potential of BDE-99 is relatively high.

The L:F ratio in the conventional rat was less than unity, i.e. 0.12, an indication that no specificity for hepatic sequestration was occurring. High xenobiotic L:F ratios have been described in numerous studies, particularly with toxic dioxin and furan congeners. Dioxins and furans, i.e. TCDD and PeCDF, can tightly, but non-covalently, associate with cytochrome P4501A2 in mouse hepatocytes (Diliberto *et al*. 1997, 1999).

Following a single oral dose, both BDE-99 and BDE-47 deposited in adipose tissue with the highest concentration of the tissues analysed (table 4 and Örn and Klasson-Wehler 1998, respectively). However, the resulting L:F ratio in the

Table 5. Recoveries of ^{14}C from 6- and 12-day-old conventional male rats dosed orally with 2,2′,4,4′,5-pentabromo-[^{14}C]diphenyl ether (BDE-99) in corn oil.

	% of Dose	
	6 Day	12 Day
Urine		
0–24 h	0.34 ± 0.06	0.29 ± 0.09
24–48 h	0.21 ± 0.04	0.19 ± 0.04
48–72 h	0.14 ± 0.11	0.12 ± 0.043
72–96 h	0.07 ± 0.06	0.08 ± 0.03
96–120 h	0.048 ± 0.043	0.051 ± 0.042
120–144 h	0.071 ± 0.033	0.042 ± 0.024
144–168 h	–	0
168–192 h	–	0.056 ± 0.034
192–216 h	–	0.037 ± 0.017
216–240 h	–	0.056 ± 0.042
240–264 h	–	0.023 ± 0.026
264–288 h	–	0.024 ± 0.019
Faeces		
0–24 h	21.97 ± 4.39	27.97 ± 6.98
24–48 h	15.12 ± 0.61	12.60 ± 0.70
48–72 h	5.87 ± 0.51	5.69 ± 0.045
72–96 h	3.85 ± 0.14	3.89 ± 0.27
86–120 h	3.16 ± 0.30	3.22 ± 0.26
120–144 h	2.79 ± 0.12	2.64 ± 0.36
144–168 h	–	2.23 ± 0.066
168–192 h	–	1.98 ± 0.17
192–216 h	–	1.75 ± 0.15
216–240 h	–	1.72 ± 0.17
240–264 h	–	1.49 ± 0.14
264–288 h	–	1.46 ± 0.16
Adipose (epididymal)	4.22 ± 0.48	3.04 ± 0.59
Adrenals	0.042 ± 0.019	0.033 ± 0.012
Blood	0.023 ± 0.001	0.011 ± 0.0075
Carcass (less skin)	13.86 ± 1.88	10.26 ± 3.08
Gastrointestinal tract	4.49 ± 0.37	3.00 ± 0.96
Heart	0.027 ± 0.014	0.010 ± 0.0019
Kidneys	0.058 ± 0.0054	0.033 ± 0.0036
Liver	0.068 ± 0.023	0.40 ± 0.019
Lung	0.061 ± 0.007	0.047 ± 0.0030
Skin	18.16 ± 1.63	12.09 ± 2.10
Testes	0.088 ± 0.033	0.37 ± 0.11
Thymus	0.039 ± 0.015	0.028 ± 0.0073
Total recovery	94.8	96.9

Data are the mean ± SD from three animals.

BDE-99 rat was 17-fold greater, indicating that BDE-47 had a stronger preference for adipose tissue than BDE-99. Assuming equal exposures, the currently available pharmacokinetic data would predict that BDE-47 would probably be the most abundant PBDE congener detected in the adipose tissue. However, these present pharmacokinetic data also suggest that a significant portion of the total body burden of BDE-99 would be excluded if only adipose tissue was examined. This demonstrates the value of conducting whole-body metabolism studies of new classes of environmental contaminants before widespread environmental analyses as a means of guiding the tissue-sampling process. Current environmental analyses of PBDEs have utilized blubber (Ikonomou *et al.* 2000), muscle (Hale *et al.* 2000),

adipose tissue (She *et al*. 2000) or the entire organism (Dodder *et al*. 2000, Luross *et al*. 2000). Reliance on a single tissue for environmental analyses may inadvertently favour one congener at the expense of others due to differential pharmacokinetics.

Based on previous data with other halogenated, aromatic compounds, the metabolism of BDE-99 in the male rat probably proceeded via the formation of an arene oxide intermediate catalysed by a cytochrome P450 (figure 2). The 2,4-dibromo ring may have been the preferred site of oxidation because fewer bromines would produce less steric hindrance. Aromatic hydroxylation generally proceeds through an arene oxide (Timbrell 1991). A strong preference for hydroxylation *ortho* or *meta* to the ether linkage has been shown for chlorinated diphenyl ethers (Tulp *et al*. 1979). Since two hydroxylated BDE-99 metabolites were characterized in both the bile and faeces, it is possible that one represented an *ortho* product on the 2,4-dibromo ring, while the other represented the *meta* product on the same ring. No synthetic standards were available. Therefore, observed differences in mass spectral ion intensities of the methoxy BDE-99 derivatives could not be used to correlate each with a particular isomer. The arene oxide was probably subject to microsomal epoxide hydrolase and cytosolic dihydrodiol dehydrogenase that resulted in three different pentabromo diphenyl ether diols of BDE-99. Since only one pentabromominated diol could have formed with BDE-99 without bromine atom migration, these data suggested that an NIH-shift had occurred in the rat.

Nucleophilic attack of the arene oxide by glutathione would have yielded a glutathione conjugate, which was not detected. Through a series of cleavage reactions along a portion of the mercapturic acid pathway, some of which are bacterial (Bakke and Gustafsson 1986), and cleavage of the intermediary cysteine conjugate, a glutathione conjugate could have yielded a free thiol of BDE-99. A pentabromodiphenyl ether thiol was identified in the bile as two isomers (figure 2). No labile metabolites were observed in the urine, as had been reported for BDE-47 (Örn and Klasson-Wehler 1998). However, labile metabolites were observed in the faeces and may provide circumstantial evidence for a glutathione intermediate. Spontaneous degradation of 1,2-dihydro-1-hydroxy-2-(*N*-acetyl)cysteinyl-naphthalene has been observed during storage at −4 to −15 °C (Bakke *et al*. 1983). Varying amounts (5–30%) of degradation products were isolated by reversed-phase HPLC and characterized by GC/MS, including naphthalene. Arene oxides of chlorinated diphenyl ethers were subject to ether ring scission as a minor metabolic route (Tulp *et al*. 1979), but brominated phenols were not identified as metabolites of BDE-99. Non-oxidized tetrabromodiphenyl ethers were not isolated in the metabolite fraction from either bile or faeces. Therefore, the observed hydroxylated tetrabromodiphenyl ether metabolites of BDE-99 characterized in the faeces (table 3) were probably formed by oxidative debromination (figure 2).

The analysis of total thyroxine (T4) demonstrated that plasma T4 levels increased approximately twofold during the 6 days after receiving BDE-99, but that these levels decreased to control levels at 12 days (figure 1). Decreased total serum T4 levels were previously observed in rat and mouse following exposure to commercial PBDE mixtures (Fowles *et al*. 1994) and to BDE-47 (Darnerud and Sinjari 1996). Plasma T4 levels were also sharply reduced when rat was exposed to toxic dioxins, and this was believed to occur through an aryl hydrocarbon receptor-mediated process that resulted in increased T4 glucuronidation and

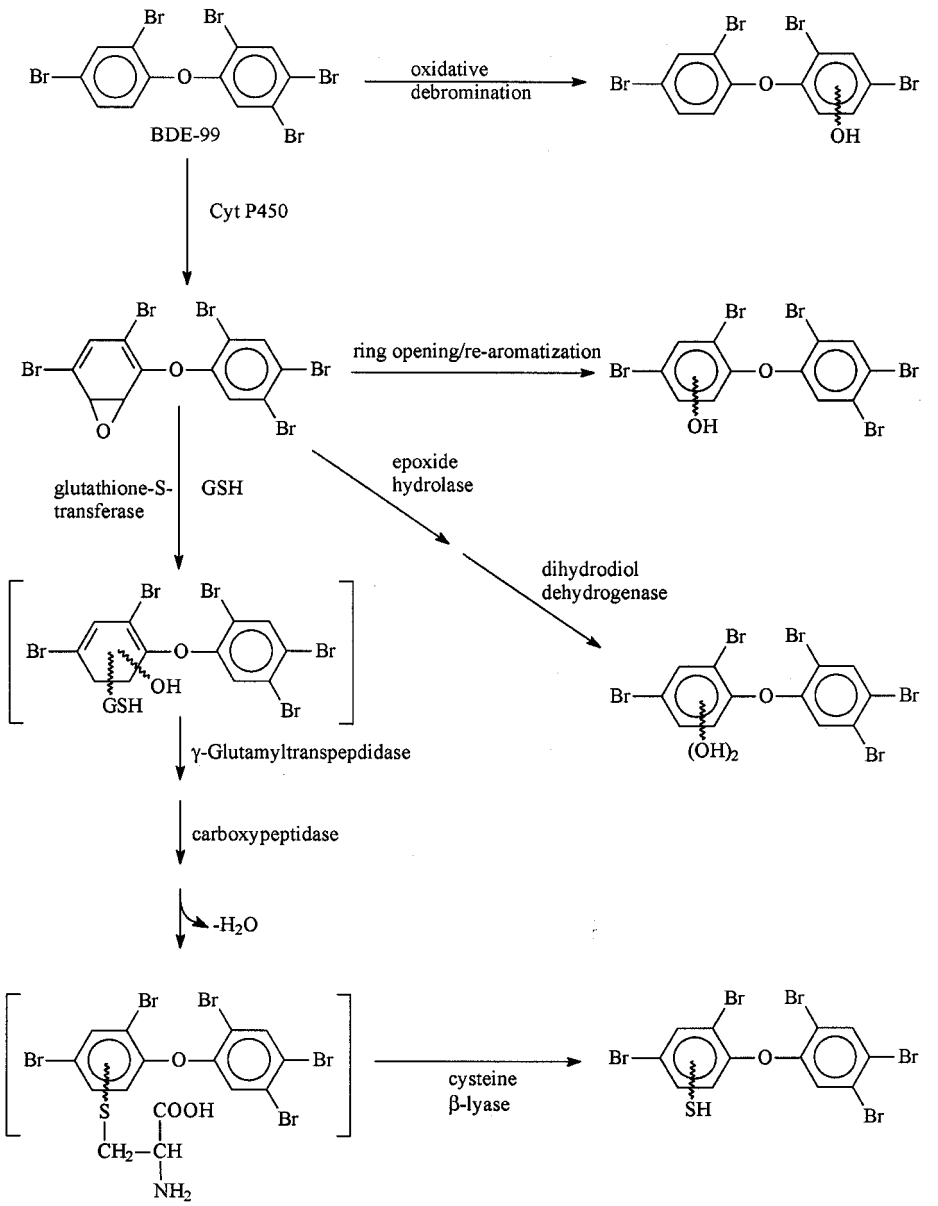


Figure 2. Proposed pathway for the metabolism of BDE-99 in the male rat. Cyt P450, cytochrome P450; GSH, glutathione.

excretion (Beestra *et al.* 1991). A strong structural similarity exists between some halogenated aromatic hydrocarbons (HAH) and T4, and this is particularly true when the HAHs are hydroxylated. Many hydroxylated dioxins (Lans *et al.* 1993) have greater affinities for transthyretin, the native plasma carrier protein for thyroid hormones, than does T4. Increased T4 levels, 3–6 days after receiving BDE-99, may reflect a competition between T4 and hydroxylated BDE-99 metabolites for transthyretin binding sites. Lower protein-bound T4 levels may have been interpreted by the hypothalamus as a signal to increase T4 synthesis via

the cascade of thyroid releasing and stimulating hormones. Further study may resolve these opposing effects on T4 by various HAHs and may lead to an understanding of the possible mechanism of BDE-99 interference with thyroid hormone homeostasis.

Acknowledgements

The authors acknowledge the synthesis of radiolabelled and unlabelled BDE-99 by Ulrika Örn and Åke Bergman (Department of Environmental Chemistry, University of Stockholm, Sweden), and the technical assistance of Barbara Magelky, Colleen Pfaff and Margaret Lorentzsen (USDA-ARS Biosciences Research Laboratory, Fargo, ND, USA). The use of trade, firm or corporation names in this paper is for the information and convenience of the reader. Such use does not constitute an official endorsement or approval by the US Department of Agriculture or the Agricultural Research Service of any product or service to the exclusion of others that may be suitable.

References

Anderson, O. and Blomkvist, G., 1981, Polybrominated aromatic pollutants found in fish in Sweden. *Chemosphere*, **10**, 1051–1060.

Bakke, J. E. and Gustafsson, J.-Å., 1986, Role of the intestinal microflora in metabolism of agrochemicals conjugated with glutathoine. *Xenobiotica*, **16**, 1047–1056.

Bakke, J. E., Struble, C., Gustafsson, J.A. and Gustafsson, B., 1983, Enterohepatic circulation and catabolism of mercapturic acid pathway metabolites of naphthalene. In J. Rydstrom, J. Montelius and M. Bengtsson (eds), *Extrahepatic Drug Metabolism and Chemical Carcinogenesis* (Amsterdam: Elsevier), pp. 257–274.

Beestra, J. B., Van Engelen, J. G. M., Karels, P., Van Der Hoek, H. G., De Jong, M., Docter, R., Krenning, E. P., Heeneman, G., Brouwer, A. and Visser, T. J., 1991, Thyroxine and 3,3′,5-triiodothyronine are glucuronidated in rat liver by different uridine diphosphate glucuronyltransferases. *Endocrinology*, **128**, 741–746.

Darnerud, P. O. and Sinjari, T., 1996, Effects of polybrominated diphenyl ethers (PBDEs) and polychlorinated biphenyls (PCBs) on thyroxin and TSH blood levels in rats and mice. *Organohalogen Compounds*, **29**, 316–319.

De Boer, J., Wester, P. C., Klamer, H. J. C., Lewis, W. E. and Boon, J. P., 1998, Do flame retardants threaten ocean life? *Nature*, **394**, 28–29.

Diliberto, J. J., Burgin, D. and Birnbaum, L. S., 1997, Role of CYP1A2 in the hepatic sequestration of dioxin: studies using CYP1A2 knockout mice. *Biochemical and Biophysical Research Communications*, **236**, 431–433.

Diliberto, J. J., Burgin, D. and Birnbaum, L. S., 1999, Effects of CYP1A2 on disposition of 2,3,7,8-tetrachlorodibenzo-*p*-dioxin, 2,4,7,8-pentachlorodibenzofuran, and 2,2′,4,4′,5,5′-hexachlorobiphenyl in CYP1A2 knockout and parental (C57BL/6N and 129/Sv) strains of mice. *Toxicology and Applied Pharmacology*, **159**, 52–64.

Dodder, N. G., Strandberg, B. and Hites, R. A., 2000, Concentrations and spatial variations of polybrominated diphenyl ethers in fish and air from the northeastern United States. *Organohalogen Compounds*, **47**, 69–72.

El Dareer, S. M., Kalin, J. R., Tillery, K. F. and Hill, D. L., 1987, Disposition of decabromodiphenyl ether in rats dosed intravenously or by feeding. *Journal of Toxicology and Environmental Health*, **22**, 405–415.

Fowles, J. R., Fairbrother, A., Baecher-Steppan, L. and Kerkvliet, N. I., 1994, Immunologic and endocrine effects of the flame retardant pentabromodiphenyl ether (DE-71) in C57BL/6J mice. *Toxicology*, **86**, 49–61.

Haglund, P., Zook, D. R., Buser, H.R. and Hu, J., 1997, Identification and quantification of polybrominated diphenyl ethers and methoxy polybrominated diphenyl ethers in Baltic biota. *Journal of Environmental and Science Technology*, **31**, 3281–3287.

Hakk, H., Larsen, G. L., Örn, U. and Bergman, A., 2000, Association of decabromodiphenyl ether with urinary and biliary carrier proteins. *Organohalogen Compounds*, **49**, 108–111.

Hale, R. C., La Guiddia, M. J., Harvey, E. P., Mainor, T. M., Duff, W. H., Gaylor, M. O., Jacobs, E. M. and Mears, G. L., 2000, Comparison of brominated diphenyl ether flame retardant and organochlorine burdens in fish from Virginia rivers (USA). *Organohalogen Compounds*, **47**, 65–68.

Ikonomou, M. G., Fischer, M., He, T., Addison, R. F. and Smith, T., 2000, Congener patterns, spatial and temporal trends of polybrominated diphenyl ethers in biota samples from the Canadian west coast and the Northwest Territories. *Organohalogen Compounds*, **47**, 77–80.

Jakobsson, E., 1994, Synthesis and analysis of chlorinated naphthalenes. Doctoral thesis, Environmental Chemistry, Stockholm University.

Klasson-Wehler, E., Bergman, A., Darnerud, P. O. and Wachmeister, C. A., 1989, Excretion and tissue retention of hydroxylated metabolites in the mouse. *Drug Metabolism and Disposition*, **17**, 441–448.

Klasson-Wehler, E., Bergman, Å., Kowalski, B. and Brandt, I., 1987, Metabolism of 2,3,4′,6-tetrachlorobiphenyl: formation and tissue localization of mercapturic acid metabolites in mice. *Xenobiotica*, **16**, 477–486.

Klasson-Wehler, E., Hovander, L. and Bergman, Å., 1997, New organohalogens in human plasma – identification and quantification. *Organohalogen Compounds*, **33**, 420–425.

Klasson-Wehler, E., Lindberg, T., Jönsson, C. J. and Bergman, Å., 1993, Tissue retention and metabolism of 2,3,3′,4,4′-pentachlorobiphenyl in mink and mouse. *Chemosphere*, **27**, 2397–2412.

Lans, M. C., Klasson-Wehler, E., Willemsen, M., Meussen, E., Safe, S., Brouwer, A., 1993, Structure-dependent, competitive interaction of hydroxy-polychlorobiphenyls, -dibenzo-*p*-dioxins and dibenzofurans with human transthyretin. *Chemico-Biological Interactions*, **88**, 7–21.

Luross, J. M., Alaee, M., Sergeant, D. B., Whittle, D. M. and Solomon, K. R., 2000, Spatial and temporal distribution of polybrominated diphenyl ethers in lake trout from the Great Lakes. *Organohalogen Compounds*, **47**, 73–76.

Mörck, A. and Klasson-Wehler, E., 2001, Metabolism of decabromodiphenyl ether (BDE-209) in the rat. *Organohalogen Compounds*, **52**, 9–12.

Norén, K. and Meironyté, D., 2000, Certain organochlorine and organobromine contaminants in Swedish human milk in perspective of past 20–30 years. *Chemosphere*, **40**, 1111–1123.

Örn, U., Eriksson, L., Jakobsson, E. and Bergman, A., 1996, Synthesis and characterization of polybrominated diphenyl ethers – unlabelled and radiolabelled tetra-, penta-, and hexa-bromodiphenyl ethers. *Acta Chimica Scandinavica*, **50**, 802–807.

Örn, U. and Klasson-Wehler, E., 1998, Metabolism of 2,2′,4,4′-tetrabromodiphenyl ether in rat and mouse. *Xenobiotica*, **28**, 199–211.

Sellstrom, U. and Jansson, B., 1995, Analysis of tetrabromobisphenol A in a product and environmental samples. *Chemosphere*, **31**, 3085–3092.

She, J., Winkler, J., Visita, P., McKinney, M. and Petreas, M., 2000, Analysis of PBDEs in seal blubber and human breast adipose tissue samples. *Organohalogen Compounds*, **47**, 53–56.

Timbrell, J. A., 1991, *Principles of Biochemical Toxicology*, 2nd edn (London: Taylor & Francis).

Tulp, M. Th. M., Sundström, G., Martron, L. B. J. M. and Hutzinger, O., 1979, Metabolism of chlorodiphenyl ethers and Irgasan® DP 300. *Xenobiotica*, **9**, 65–77.

Zweidinger, R. A., Cooper, S. D. and Pellizzari, E. D., 1979, Sampling and analysis for semi volatile brominated organics in ambient air. In D. Schuetzle (ed.), *Monitoring Toxic Substances, 686*. ACS Symposium Series No. 94 (ACS), pp. 217–231.

XENOBIOTICA, 2002, VOL. 32, NO. 5, 383–397

Taylor & Francis
healthsciences

Microsomal metabolism and enyzme kinetics of the terpene *p*-cymene in the common brushtail possum (*Trichosurus vulpecula*), koala (*Phascolarctos cinereus*) and rat

G. J. PASS†¶, S. MCLEAN†*, I. STUPANS‡ and N. W. DAVIES§

† School of Pharmacy, University of Tasmania, Hobart 7001, Australia
‡ School of Pharmaceutical, Molecular and Biomedical Sciences, University of South Australia, Adelaide 5000, Australia
§ Central Science Laboratory, University of Tasmania, Hobart, 7001, Australia
¶ Present address: Institut für Pharmakologie und Toxikologie, Medizinische Fakultät der RWTH Aachen, Wendlingweg 2, D-52057, Aachen, Germany.

Received 24 September 2001

1. *p*-Cymene is an aromatic monoterpene found in the leaves of *Eucalyptus* spp. and is ingested in the diet of two marsupial folivores, the brushtail possum (*Trichosurus vulpecula*) and koala (*Phascolarctos cinereus*). The metabolism of *p*-cymene by liver microsomes from the possum, koala and rat (an animal whose diet is not terpene-rich) was examined.

2. The major *p*-cymene metabolite in each species was cuminyl alcohol, with smaller amounts of other side-chain alcohols being formed. No phenolic metabolites were detected. Possum and koala microsomes further oxidized cuminyl alcohol to cumic acid.

3. Pretreatment with a terpene diet more than doubled the V_{max} for cuminyl alcohol formation by possum microsomes. This is similar to a previous finding by our group with 1,8-cineole and indicates that a terpene-containing diet results in induction of the enzymes responsible for terpene metabolism.

4. The rank order of the ability to metabolize *p*-cymene, measured by intrinsic clearance ($Cl_{int} = V_{max}/K_m$ [$\mu l\,mg\,protein^{-1}\,min^{-1}$]) was: terpene-treated possum (128) > control possum (107) > koala (69) > rat (38).

5. The findings support the hypothesis that animals that have adapted to a diet of *Eucalypus* leaf have a greater capacity than generalist feeders to metabolize dietary terpenes.

Introduction

For over 25 years it has been proposed that cytochrome P450 microsomal enzymes (CYPs) are important in protecting herbivorous mammals against the effects of potentially toxic plant secondary metabolites (PSMs) (Freeland and Janzen 1974, McManus and Ilett 1976, 1977, McManus *et al.* 1978, Foley *et al.* 1999), yet research on the xenobiotic-metabolizing system of mammalian herbivores has, to date, been largely overlooked.

Australian forests offer excellent opportunities to study the involvement of CYPs in plant–mammal interactions because of the dominance of a single tree

* Author for correspondence; email: Stuart.McLean@utas.edu.au

Xenobiotica ISSN 0049–8254 print/ISSN 1366–5928 online © 2002 Taylor & Francis Ltd
http://www.tandf.co.uk/journals
DOI: 10.1080/00498250210124138

genus, *Eucalyptus*, which makes up more than 90% of trees in temperate forests and woodlands around Australia (Kelly 1969). In spite of this dominance, only four Australian marsupials, the koala (*Phascolarctos cinereus*), the greater glider (*Petauroides volans*), the common ringtail possum (*Pseudocheirus peregrinus*) and the common brushtail possum (*Trichosurus vulpecula*), utilize *Eucalyptus* foliage as a food source and each species has varying degrees of specialization.

In addition to the low levels of protein and high levels of lignified fibre (Hume 1982), *Eucalyptus* leaves contain a significant amount of potentially toxic PSMs, mostly phenolics and terpenes. Up to 10% of the dry leaf mass of the leaves of *Eucalyptus* can consist of essential oils, comprising mixtures of terpenes whose composition varies with species and the locality of the tree (Boland and Brophy 1991, Li 1993). It is therefore thought that the marsupials that utilize *Eucalyptus* foliage have developed highly specialized detoxification systems, enabling them to metabolize these terpenes.

Recently, our group reported that the CYP activity and content of the liver of common brushtail possums was increased after the animals had been fed for 10 days on a mixture of four common *Eucalyptus* terpenes (Pass *et al*. 1999). We also reported on the *in vitro* metabolism of 1,8-cineole, the major dietary terpene for *Eucalyptus*-eating marsupials, by liver microsomes from brushtail possums, koalas, rats and humans (Pass *et al*. 2001). The rank order of *in vitro* 1,8-cineole metabolism, based on the overall intrinsic clearance between species, was: terpene-treated possum $>$ koala $\geq$ control possum $\gg$ rat $>$ human. To clarify these findings, we set out to study the *in vitro* metabolism and enzyme kinetics of another *Eucalyptus* terpene, *p*-cymene, which is chemically dissimilar to 1,8-cineole.

p-Cymene is a simple aromatic monoterpene that occurs in the essential oils of many plant species. It is commonly found in the leaves of *Eucalyptus* spp. and is therefore encountered in the diets of koalas and common brushtail possums. The *in vivo* metabolism of *p*-cymene has been studied in a number of species, including the rat, guinea pig and rabbit (Ishida *et al*. 1981, Walde *et al*. 1983). The *in vivo* metabolism of this terpene has also been compared in the four *Eucalyptus*-eating marsupials and the rat (Boyle *et al*. 1999, 2000a). A species-specific pattern of metabolism was found, with a higher level of oxidation in animals that had a greater degree of feeding specialization on *Eucalyptus* leaves. The rat, which has not adapted to a *Eucalyptus* diet, relied mostly on conjugation for the excretion of *p*-cymene metabolites. The common brushtail possum, which is a generalist *Eucalyptus* browser, also relied on conjugation, but to a lesser extent. On the other hand, very little conjugation was observed in the specialized *Eucayptus* herbivores, the ringtail possum, glider and koala, in which most of the *p*-cymene dose was excreted as highly oxidized, unconjugated metabolites. It was concluded that the enzymatic system of the specialized feeders was better adapted for the oxidation of *p*-cymene. Similar *in vivo* findings have recently been reported for 1,8-cineole (Boyle *et al*. 2000b, 2001).

The present study extends these observations to the *in vitro* metabolism of *p*-cymene in liver microsomes from two marsupials and the rat to gain further insight into the mechanisms used by herbivores to detoxify plant secondary metabolites.

Materials and methods

General

The research was approved by the Animal Experimentation Ethics Committee of the University of Tasmania and conforms to the Australian Code of Practice for the Care and Use of Animals for Scientific Purposes.

Chemicals

p-Cymene, cuminyl alcohol, cumic acid, $NADP^+$, isocitric dehydrogenase and isocitric acid were purchased from Sigma Chemical Co. (Castle Hill, Australia). *N*,*O*-bis(trimethylsilyl)-trifluoroacetamide (BSTFA) was purchased from Alltech Associates Pty Ltd (Sydney, Australia). Solvents and other chemicals were of analytical grade. The isolation from urine and identification of metabolites of *p*-cymene was described by Boyle *et al.* (1999, 2000a).

Animals

The acquisition and treatment of the brushtail possums, koalas and rats has been described, together with the preparation of liver microsomes (Pass *et al.* 1999, 2001). In brief, male brushtail possums were captured around Hobart and acclimated to an artificial diet of fruits and vegetables. For 10 days before sacrifice, the diet of terpene-treated animals included a mixture of terpenes similar to that present in *E. melliodora*, a preferred dietary foliage. Hooded Wistar rats were maintained on a standard laboratory chow, and for 6 days before sacrifice were gavaged daily with either the same mix of terpenes ($400\,mg\,kg^{-1}$) in peanut oil (terpene-treated group) or the vehicle (control group). Koala livers were obtained from two adult males collected near Adelaide, South Australia, which were euthanized because of road injury. Veterinary inspection concluded that the liver was not affected by the injuries.

Instrumentation

Gas chromatography-mass spectrometry (GC-MS) for the identification and quantitation of *p*-cymene metabolites was carried out as described (Pass *et al.* 2001). Briefly, GC-MS chromatography was carried out on a 25 m HP-1 (cross-linked phenyl methyl silicone) capillary column. The GC-MS operating conditions were: splitless injector 250 °C, detector 290 °C, oven 50 °C for 1 min and then $10\,°C\,min^{-1}$ to 250 °C and then 250 to 290 °C at $30\,°C\,min^{-1}$ and held at 290 °C for 3 min. MS detector conditions required a solvent delay of 5 min, an EM voltage of 2200 V and a selected mass range of m/z 40–400. Selected ion monitoring (SIM) was required to quantitate the low concentrations of metabolites formed.

Identification of metabolites

Microsomal incubations. To identify the metabolites formed, bulk incubations were performed using a 3-ml reaction mixture containing microsomal protein (0.75 mg), isocitric acid (4 mM), isocitric dehydrogenase (1.2 IU), $MgCl_2$ (8 mM), $NADP^+$ (1 mM) and *p*-cymene (100 μM) in ethanol (15 μl), made up to volume (3 ml) with phosphate buffer (0.1 M, pH 7.4). The microsomes used for this part of the study were from one individual animal in the terpene-treated and control possum groups, the terpene-treated, control and phenobarbitone rat groups and the koala. The reaction was initiated by the addition of the NADPH-generating system and the mixture was incubated at 37 °C for 60 min. The incubations were carried out in capped 25-ml glass centrifuge tubes to reduce the loss of terpene due to the heating process. This technique has been shown to maximize the metabolism of another volatile terpene, 1,8-cineole (Pass *et al.* 2001).

Extraction and derivatization. After incubation, each sample was placed on ice and internal standard added (2,5-dimethylbenzoic acid, 75 μg in 75 μl water). The incubate containing the internal standard was acidified to about pH 1 using 5 M HCl (~60 μl) and the sample was then extracted three times with ethyl acetate (1×6 ml, 2×3 ml). The ethyl acetate extract was reduced under low pressure to approximately 100 μl. Trimethylsilyl (TMS) derivatives were then prepared. An aliquot of extract (20 μl) was placed into an autosample vial, BSTFA (20 μl) was added, and the vial capped and heated at 60 °C for 20 min. The samples were then analysed by gas chromatography.

GC-MS analysis. The methods to identify *p*-cymene metabolites in the microsomal extract had been previously developed by our group for the identification of these metabolites in the urine of possums (Boyle *et al.* 1999). The metabolites found in microsomal extracts were compared with those detected in urine and all were identical from mass spectral data. Metabolites in the microsomal extract that had not been detected in urine from possums were found by searching total-ion current (TIC) chromatograms

of the microsomal extracts for diagnostic ions of all the metabolites that Southwell *et al.* (1980), Ishida *et al.* (1981) and Walde *et al.* (1983) identified in the urinary extracts of brushtail possum, guinea pig, rabbit and rat.

Enzyme kinetics

Microsomes (0.25 mg protein) were incubated with *p*-cymene in ethanol (5 µl) and the NADPH-generating system (200 µl consisting of 1 mM $NADP^+$, 4 mm isocitric acid, 0.4 IU isocitric dehydrogenase and 8 mM $MgCl_2$) and made up to a final volume of 1.0 ml with phosphate buffer (0.1 M, pH 7.4). For microsomes from both possum groups and rat ($n = 4$), one incubation was carried out for each substrate concentration. For koala microsomes ($n = 2$), incubations were done in duplicate. Substrate concentrations ranged from 5 to 400 µM. The reaction was started by the addition of the NADPH-generating system. Incubations were performed at 37 °C for 10 min. The reaction was then stopped by the placing sample tubes on ice, internal standard was added (4 µg 2,5-dimethylbenzoic acid in 25 µl water) and then the samples were acidified, extracted, derivatized and analysed by GC-MS as outlined above. All reactions were linear with respect to substrate, protein and time. For microsomes from possum and rat, one incubation was done at each substrate concentration, while koala incubations were done in duplicate.

Owing to the low concentrations of metabolites, once the characteristic masses and retention times of each metabolite were determined from full scans, the quantitation of the major metabolites was carried out using GC-SIM-MS. The ions monitored were those that were most abundant and characteristic in the spectrum of the metabolite of interest.

Further kinetic studies were carried out on the conversion of the *p*-cymene metabolite, cuminyl alcohol, to cumic acid. Incubation conditions were the same as for *p*-cymene. However, the incubation time was reduced to 5 min. Cuminyl alcohol was added in 5 µl ethanol to give concentrations ranging from 0.5 to 100 µM.

Quantitation of metabolites

Standard solutions were made up in methanol for two *p*-cymene metabolites (cuminyl alcohol, cumic acid). Then, varying amounts of metabolite solutions, covering appropriate concentration ranges, were placed into the 7-ml glass vial. Microsomes (0.25 mg, 100 µl) and the NADPH-generating system (200 µl, described below) were then added to these tubes and the mixture was made up to a final volume of 1 ml with phosphate buffer (0.1 M, pH 7.4). Internal standard (4 µg 2,5-dimethylbenzoic acid) was added and the mixture acidified, extracted and derivatized as described above for metabolite identification and it was analysed by GC-SIM-MS.

Calibration curves for cuminyl alcohol and cumic acid were linear ($r^2 = 0.97$–1.00) with high reproducibility. Calibration curves were prepared with each day's analysis and the coefficient of variation between days was 4.7 and 5.1% for cuminyl alcohol and cumic acid respectively ($n = 6$). The cuminyl alcohol curve was used for 2-*p*-tolypropan-1-ol.

Data analysis

For the determination of apparent enzyme kinetics of *p*-cymene and cuminyl alcohol metabolism, data were analysed by non-linear least-squares regression using GraphPad Prism 3.02 (GraphPad Software, Inc., CA, USA). For *p*-cymene and cuminyl alcohol metabolism, in many cases the relationship between rate and substrate concentration was described using the one-enzyme Michaelis–Menten model:

$$V = \frac{V_{\max} \cdot S}{K_m + S}, \tag{1}$$

where V is the velocity of the reaction, S is the substrate concentration, K_m is the apparent Michaelis–Menten constant and $V_{\max}$ is the maximum velocity. For some sets of data, a significant departure from linearity was detected, as determined initially by visual inspection of Eadie–Hofstee plots (non-linearity suggested that more than one enzyme was involved). Consequently, the data were additionally analysed using the reduced two-enzyme Michaelis–Menten model:

$$V = \frac{V_{\max} \cdot S}{K_m + S} + CL_{\text{int2}} \cdot S, \tag{2}$$

where V is the velocity of the reaction, S is the substrate concentration, K_m and $V_{\max}$ are the apparent Michaelis–Menten constant and the maximum velocity for the high-affinity enzyme respectively, and CL_{int2} is the intrinsic clearance ($V_{\max}/K_m$) by the low-affinity enzyme. Comparison of the two equations was carried out by an *F*-test using the same statistical package (GraphPad Prism, 3.02) to determine the equation that best fitted the data.

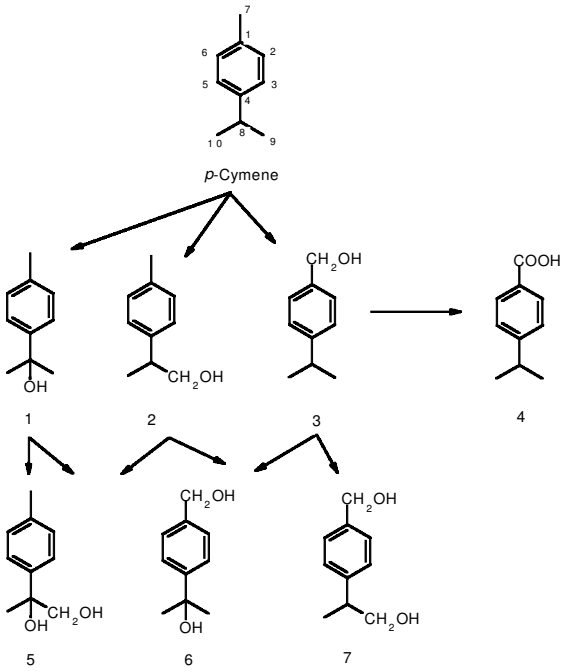


Figure 1. Chemical structure of *p*-cymene metabolites detected in possum liver microsomes *in vitro* and probable metabolic pathways. All metabolites are shown in their underivatized forms.

Statistics

All data were expressed as means with standard errors (SE). The mean differences between the terpene-treated and control groups were compared using an independent sample *t*-test (SPSS 7.5, SPSS, Inc., Chicago, IL, USA). The differences in total CL_{int} for each species was compared by one-way ANOVA using the same statistical package.

Results

Metabolites of p-*cymene*

Identification. The structure of each metabolite, identified from 60-min microsomal incubations with *p*-cymene, and the proposed metabolic pathways are shown in figure 1. The chemical names of *p*-cymene metabolites and their mass spectral data are reported in table 1. The need for SIM analysis of metabolites is shown in figure 2, which compares the GC-MS analysis of a possum microsomal extract by total-ion current (TIC) and by monitoring diagnostic metabolite ions (SIM). The ion selected for quantitative analysis of each metabolite and its per cent contribution to the TIC are outlined in table 2. The proportions of metabolites detected in bulk incubates in each species are summarized in table 3. The method of calculating the relative proportions of metabolites has been described by Pass *et al.* (2001).

Possum. Total-ion monitoring of the mass chromatograms of extracts from the bulk microsomal incubations with *p*-cymene showed the presence of six metabolites derived from *p*-cymene in control possum microsomes, and seven

Table 1. Chemical names of structures, published mass spectral data, retention times and mass spectral data for all *p*-cymene metabolites identified *in vitro* in the brushtail possum, koala or rat. All mass spectra of *p*-cymene metabolites, with the exception of (1), are reported as the TMS derivatives.

	Metabolite (reference)	Retention time (min)[a]	$M^{+\cdot}$, Prominent fragments (m/z) and relative abundances (%)[b]
(1)	2-*p*-tolylpropan-2-ol (Ishida *et al.* 1981)	7.92*	150 (4), 135 (25), 91 (6), 75 (17), 73 (36), 65 (5), 43 (100)
(2)	2-*p*-tolypropan-1-ol (Ishida *et al.* 1981)	10.72	222 (10), 207 (25), 119 (100), 103 (77), 91 (32), 75 (56)
(3)	*p*-isopropylbenzyl alcohol (cuminyl alcohol) (Walde *et al.* 1983)	11.18	222 (13), 207 (49), 179 (50), 177 (23), 133 (100), 117 (23), 91 (22), 75 (34), 73 (57)
(4)	*p*-isopropylbenzoic acid (cumic acid) (Ishida *et al.* 1981)	12.78	236 (9), 221 (100), 177 (54), 156 (6), 147 (57), 131 (12), 103 (27), 91 (14), 73 (65)
(5)	2-*p*-(hydroxymethyl)phenyl-propan-2-ol (Walde *et al.* 1983)	13.14	238 (4), 223 (100), 133 (20), 119 (10), 103 (19), 91 (49), 73 (61), 59 (33), 43 (90)
(6)	2-*p*-tolypropan-1,2-diol (Walde *et al.* 1983)	13.51	310 (0), 295 (2), 207 (100), 147 (12), 73 (38), 43 (11)
(7)	2-*p*-(hydroxymethyl)phenyl-propan-1-ol (Walde *et al.* 1983)	15.13	310 (0), 295 (10), 207 (6), 177 (9), 119 (6), 118 (100), 103 (17), 79 (10), 43 (29)

* Underivatized.
[a] Retention times were measured by GC-MS.
[b] Relative abundances are given in parentheses.

metabolites in microsomes from terpene-treated possums (table 3). In control possum microsomes, the major metabolite detected was *p*-isopropylbenzyl alcohol (cuminyl alcohol; **3**) followed by *p*-isopropylbenzoic acid (cumic acid; **4**), 2-*p*-tolylpropan-1-ol (**2**) and 2-*p*-tolypropan-2-ol (**1**). Trace amounts of 2-*p*-(hydroxymethyl)phenylpropan-2-ol (**5**) and 2-*p*-(hydroxymethyl)phenylpropan-1-ol (**7**) were also detected.

The major differences between terpene-treated and control possums were the formation of less cuminyl alcohol and a 10-fold greater proportion of 2-*p*-(hydroxymethyl)phenylpropan-2-ol (**5**) of all metabolites found (24.6 compared with 2.6%). A small amount of a dihydroxylated metabolite, 2-*p*-tolypropan-1,2-diol (**6**), not detected in control microsomes, was formed in terpene-treated microsomes.

Koala. All seven *p*-cymene metabolites were detected in koala microsomal incubations (table 3). As for the possum, cuminyl alcohol (**4**) was the major metabolite, comprising 90% of all metabolites found, followed by 6% 2-*p*-tolypropan-2-ol (**1**) and only trace amounts of the other five metabolites.

Rat. The pattern of *p*-cymene metabolism in rat microsomes was very similar to that observed in the koala (table 3). There were some differences between the control and treated rat microsomes, e.g. the absence of some metabolites after terpene-treatment (**4**, **7**) and phenobarbitone-treatment (**2**).

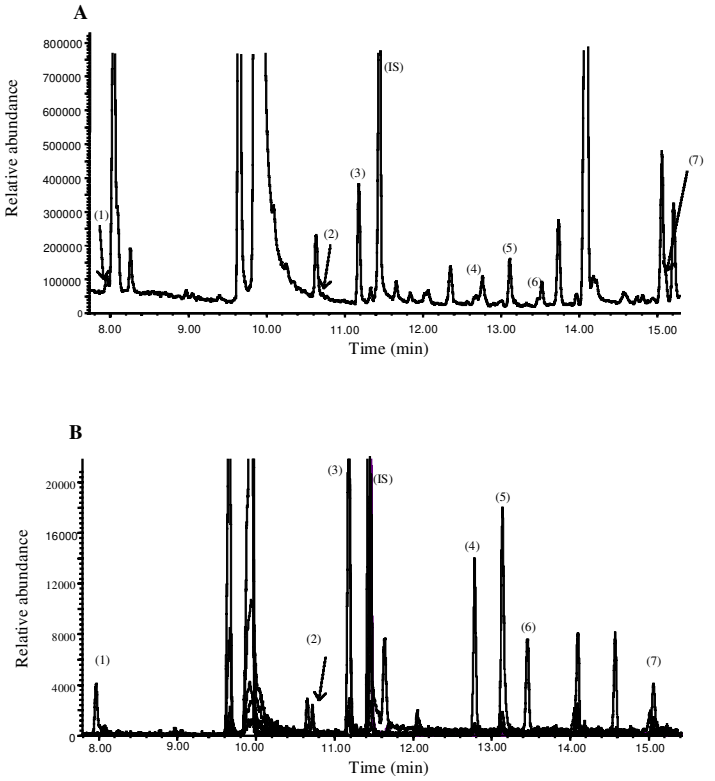


Figure 2. GC-MS analysis of bulk possum microsomal extract (TMS derivatized) after 60-min incubation with *p*-cymene (100 μM). Total ion current chromatogram (A) and corresponding mass chromatogram of diagnostic *p*-cymene metabolite ions (*m*/*z* 135, 119, 179, 164, 221, 223, 207, 295, 118) to highlight metabolites (B).

Enzyme kinetics

Reactions and quantitation. After the brief (10-min) incubation time, only cuminyl alcohol and cumic acid formation could be quantitated in all microsomes. In addition, 2-*p*-tolypropan-1-ol (**2**) could be quantitatively measured in both groups of possum microsomes.

p-*Cymene metabolism.* Michaelis–Menten and Eadie–Hofstee plots for the metabolism of *p*-cymene to the major metabolite detected in all species, cuminyl alcohol, are shown in figure 3. In both possum groups, the further oxidation of cuminyl alcohol to cumic acid (figure 1) occurred very quickly and at low substrate concentrations. This was also the case for the koala microsomes, but to a lesser extent. Therefore, total cuminyl alcohol formation in these species was taken as the sum of both cuminyl alcohol and cumic acid. Eadie–Hofstee plots for the formation of total cuminyl alcohol showed a linear relationship for all livers studied in the possum and rat groups. However, curved lines were found for the koala. Therefore, for the possum and rat, the data for this reaction were analysed with the one-enzyme Michaelis–Menten model (equation 1), and for the koala, data were analysed with the reduced two-enzyme model (equation 2). The kinetic parameters obtained (K_m, V_{max}, CL_{int}) are summarized in table 4.

Table 2. *p*-Cymene metabolites detected in possum microsomal incubations, diagnostic ion monitored and per cent contribution to total ion current of the mass spectrum of that metabolite.

	Metabolite	Ion monitored (*m*/*z*)	% Contribution to TIC
(IS)	2,5-dimethylbenzoic acid	164	–
(1)	2- *p*-tolylpropan-2-ol	135	14.5
(2)	2-*p*-tolypropan-1-ol	119	21.9
(3)	cuminyl alcohol	179	12.5
(4)	cumic acid	177	17.3
(5)	2-*p*-(hydroxymethyl)phenylpropan-2-ol	223	24.4
(6)	2-*p*-tolypropan-1,2-diol	207	48.9
(7)	2-*p*-(hydroxymethyl)phenylpropan-1-ol	118	54.2

Table 3. *p*-Cymene metabolites detected *in vitro* and per cent contribution based on the total ion current of mass spectra of all metabolites detected in each species.

	Species					
	Possum			Rat		
Metabolite	Control	Terpene-treated	Koala	Control	Terpene-treated	Phenobarbitol-treated
(1) 2-*p*-tolypropan-2-ol	5.5	6.8	5.6	7.3	10.6	9.2
(2) 2-*p*-tolypropan-1-ol	7.5	2.3	1.5	1.1	0.6	n.d.
(3) *p*-isopropylbenzyl alcohol (cuminyl alcohol)	73.1	51.2	89.8	84.4	86.8	80.2
(4) *p*-isopropylbenzoic acid (cumic acid)	9.0	9.2	1.4	1.7	0.6	6.6
(5) 2-*p*-(hydroxymethyl)phenyl-propan-2-ol	2.6	24.6	0.7	3.1	n.d.	1.5
(6) 2-*p*-tolypropan-1,2-diol	n.d.	3.9	0.7	2.1	1.3	2.0
(7) 2-*p*-(hydroxymethyl)phenyl-propan-1-ol	2.2	1.9	<0.5	<0.5	n.d.	0.5

n.d., Not detected.

All data were determined from 60-min microsomal incubations from one individual for each species.

Possum. V_{max} for total cuminyl alcohol formation was significantly higher in terpene-treated possum microsomes. However, although the CL_{int} to cuminyl alcohol was also higher, this difference was not significant (table 4). The rate of formation of total cuminyl alcohol was considerably higher than that found for 2-*p*-tolypropan-1-ol (table 4). CL_{int} to the combined cuminyl alcohol and cumic acid was around 5–6 times greater than that for 2-*p*-tolypropan-1-ol for control- and terpene-treated microsomes respectively. No significant differences were found in kinetic parameters between the terpene-treated and control possum microsomes, as a considerable amount of variability was found in both groups.

A comparison of the total CL_{int} for all metabolites quantified for each species, as determined by taking the sum of the CL_{int} of all metabolites, is shown in table 4.

The kinetics of the further oxidation of cuminyl alcohol to cumic acid was studied in possum microsomes. Figure 4 shows the velocity of cumic acid formation at different concentrations of both *p*-cymene and cuminyl alcohol formed *in situ*. The concentration of cuminyl alcohol formed *in situ* was calculated for each *p*-cymene concentration and plotted against cumic acid formation. Substrate inhibition was observed in both plots.

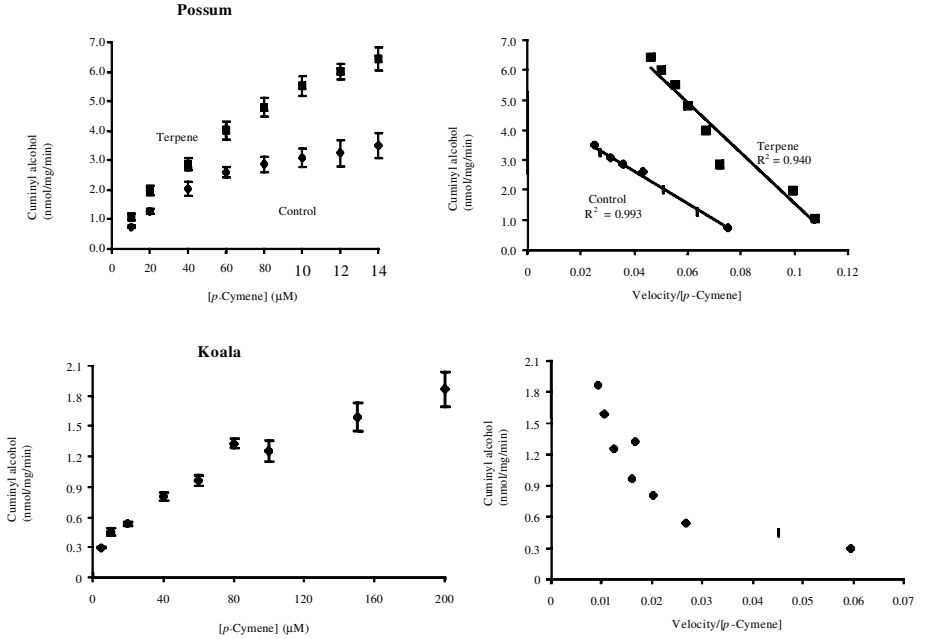


Figure 3. Formation of cuminyl alcohol in microsomes from the control ($n = 4$) and terpene-treated ($n = 4$) possum and koala ($n = 2$). Michaelis–Menten plots (left) and crresponding Eadie–Hofstee plots (right). Total cuminyl alcohol formation included cumic acid.

Koala. For the conversion of *p*-cymene to cuminyl alcohol by microsomes from both koalas, Eadie–Hofstee plots were not linear (figure 3) and therefore were consistent with at least a two-enzyme system. This was confirmed with significant differences between the two models in the comparison of fit *F*-test (koala 1, $F = 38.85$, d.f. 1,15, $p < 0.001$; koala 2, $F = 12.58$, d.f. 1,14, $p = 0.003$). The apparent K_m and V_{max} for total cuminyl alcohol formation were lower in koala microsomes than for all other groups (table 4). However, because there appeared to be two enzymes involved in the formation of cuminyl alcohol in the koala, it is difficult to make comparisons of these kinetic parameters, and instead clearances were compared.

The total CL_{int} to cuminyl alcohol in koala microsomes, determined from the sum of CL_{int} by the high- and low-affinity enzymes, was approximately 69 $\mu l\,mg^{-1}$ protein min^{-1} (table 4). This was significantly lower ($p = 0.023$) than the CL_{int} for the formation of this metabolite in terpene-treated possum microsomes (110 $\mu l\,mg^{-1}$ protein min^{-1}), but not significantly different from that in control possum microsomes (89 $\mu l\,mg^{-1}$ protein min^{-1}). Although this clearance tended to be higher in koala than rat microsomes, the difference was not significant ($p = 0.073$).

Rat. The apparent K_m for the oxidation of *p*-cymene to cuminyl alcohol in rat microsomes was greater than those determined for terpene-treated and control possum microsomes (table 4), suggesting that a low-affinity enzyme is responsible for this reaction in rat. V_{max} for the formation of cuminyl alcohol was be relatively high (around 8.5 $nmol\,mg^{-1}\,min^{-1}$), falling between the values for control- and

Table 4. Michaelis–Menten parameters (mean ± SE) for three metabolic reactions catalysed by liver microsomes from the brushtail possum, koala and rat.

	Species			
	Possum			
Reaction	Control ($n = 4$)	Terpene-treated ($n = 4$)	Koala ($n = 2$)	Rat ($n = 4$)
p-Cymene to cuminyl alcohol*				
Apparent K_m (μM)	55.2 ± 9.4	116.8 ± 32.4	14.8 ± 6.5	222.9 ± 25.7
p		0.091	0.339	< 0.001
V_{max} (nmol mg^{-1} min^{-1})	4.92 ± 0.82	11.81 ± 2.17	0.81 ± 0.14	8.53 ± 0.12
p		0.007	0.128	0.125
CL_{int1} (μl mg^{-1} min^{-1})	89.4 ± 2.0	109.5 ± 13.2	63.1 ± 18.5	38.4 ± 2.7
p		0.135	0.106	0.002
CL_{int2} (μl mg^{-1} min^{-1})			5.7 ± 2.1	
p-Cymene to 2-*p*-tolylpropan-1-ol				
Apparent K_m (μM)	12.8 ± 3.8	33.0 ± 10.9		
p		0.130		
V_{max} (nmol mg^{-1} min^{-1})	0.20 ± 0.05	0.36 ± 0.06		
p		0.071		
CL_{int} (μl mg^{-1} min^{-1})	17.9 ± 4.3	18.0 ± 9.6		
p		0.977		
Total clearance of *p*-cymene**				
CL_{int} (μl mg^{-1} min^{-1})	107.4 ± 18.4	127.4 ± 34.3	68.8 + 29.1	38.4 ± 5.3
p		0.253	0.086	0.002
Cuminyl alcohol to cumic acid				
Apparent K_m (μM)	23.0 ± 6.1	14.6 ± 2.3	18.9 + 5.0	
p		0.217	0.713	
V_{max} (nmol mg^{-1} min^{-1})	0.86 ± 0.19	1.14 ± 0.18	0.87 ± 0.15	
p		0.290	0.949	
CL_{int1} (μl mg^{-1} min^{-1})	38.7 ± 5.0	82.6 ± 13.4	45.8 ± 13.1	
p		0.017	0.676	
CL_{int2} (μl mg^{-1} min^{-1})			2.4 ± 1.1	

p versus control possum.

* In the possum and koala, the total cuminyl alcohol formation was equal to the sum of cuminyl alcohol and cumic acid.

** Sum of partial clearances of *p*-cymene.

terpene-treated possum microsomes, but not significantly different from either. CL_{int} for cuminyl alcohol formation was, however, significantly lower in rat than in both possum groups ($p < 0.005$ for both groups).

Cuminyl alcohol metabolism. The kinetics of cumic acid formation were studied after adding cuminyl alcohol as a substrate to microsomes from terpene-treated and control possums and the koala (figure 5). The Eadie–Hofstee plot for the formation of cumic acid from cuminyl alcohol showed a linear relationship for all livers studied in the two possum groups. However, Eadie–Hofstee plots for the data obtained from the koala appeared to be curved, suggesting the involvement of more than one enzyme. Therefore, for the possum, data for this reaction were analysed with the one enzyme Michaelis–Menten model (equation 1) and for the koala, the reduced two-enzyme model (equation 2). The kinetic parameters obtained are summarized in table 4.

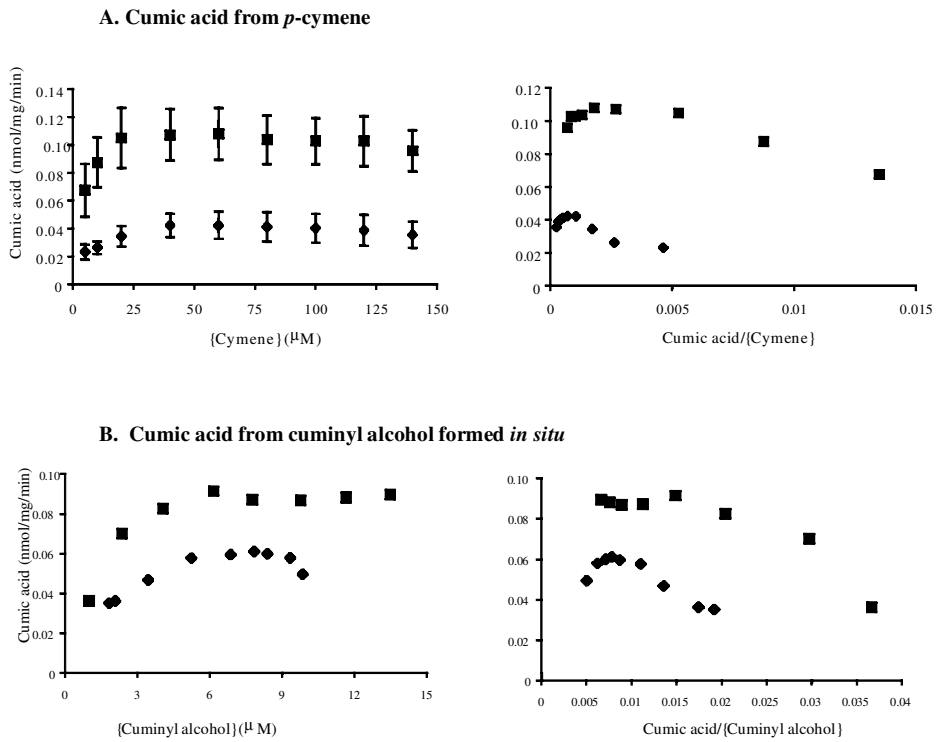


Figure 4. Formation of cumic acid in microsomes from the control (◆) and terpene-treated (■) possum microsomes. (upper) (A) From *p*-cymene ($n = 4$); (lower) (B) from cuminyl alcohol formed *in situ* in microsomes (for each group, $n = 1$). Michaelis–Menten plots (left) and corresponding Eadie–Hofstee plots (right).

In the possum, terpene treatment significantly increased CL_{int} to cumic acid although the differences from controls in the apparent K_m and V_{max} were not significant. In the koala, the total CL_{int} (sum of CL_{int} of the low- and high-affinity components, 49 μl mg^{-1} min^{-1}) fell between the values for the control and treated possum microsomes (table 4).

Discussion

Microsomal metabolites of p-*cymene*

This study has shown that the pathways of *in vitro* metabolism of *p*-cymene are similar across the three species studied. In microsomes from possum, koala and rat, the most rapid oxidation was at C7, with much slower oxidation at C8 or C9 or both sites. Three diols were detected, one of which (**5**) was greatly increased following terpene-treatment of possum microsomes, suggesting induction of specific CYPs which oxidize at C8/C9. Associated with this was a commensurate fall in cuminyl alcohol formation, a competing pathway. There was little other change in the pattern of microsomal metabolites after terpene treatment in possum or rat, or phenobarbitone treatment in rat. However, oxidation of cuminyl alcohol to cumic acid was significant in the possum, koala and phenobarbitone-induced rat microsomes.

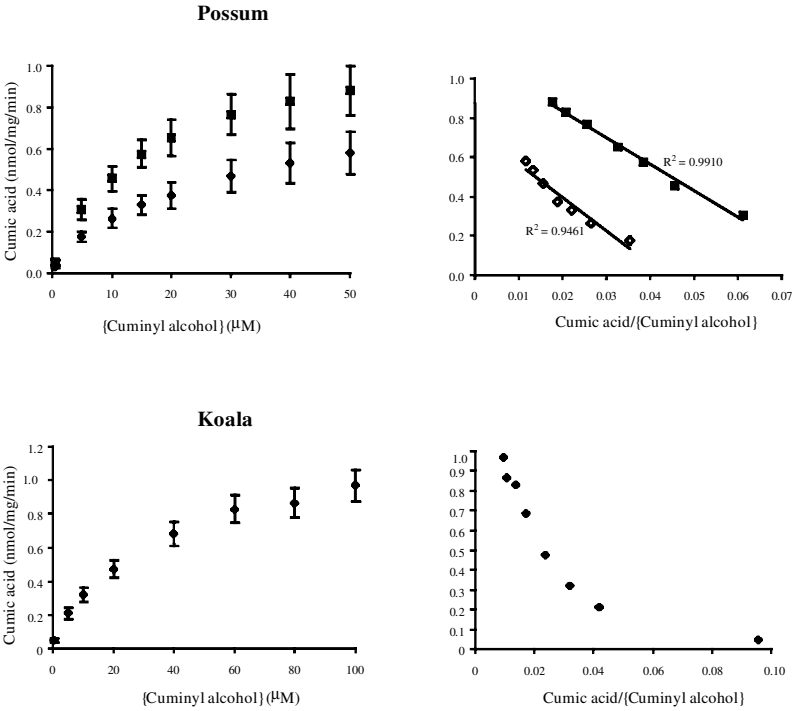


Figure 5. Formation of cumic acid from cuminyl alcohol in microsomes from the control (◇) and terpene-treated (■) possums (above; each group, $n = 4$) and koalas (below; $n = 2$). Michaelis–Menten plots (left) and corresponding Eadie–Hofstee plots (right).

It is interesting to compare these findings with the *in vivo* metabolism of *p*-cymene in the same animal species. In both the possum and koala, the urinary metabolites were hydroxy carboxylic acids and mono- and di-carboxylic acids (Boyle *et al*. 1999, 2000a). No alcohols were excreted, although these were the major *in vitro* metabolites. This *in vivo–in vitro* difference is presumably due to a combination of slow renal clearance of alcohols and the rapid *in vivo* oxidation of alcohols to carboxylic acids. In humans, ethanol is mainly oxidized in the liver cytosol by alcohol dehydrogenase, forming acetaldehyde which is itself oxidized to acetic acid by mitochondrial aldehyde dehydrogenase (Riveros-Rosas *et al*. 1997). Thus, the microsomal alcohol dehydrogenase (which is mainly CYP2E1) makes a minor contribution to alcohol metabolism, although as it is inducible and has a high K_m it becomes more important with continued and high alcohol consumption. In marsupials eating a terpene-rich diet, induction of alcohol oxidation appears likely through exposure to the alcohol metabolites of terpenes.

The major *in vivo* metabolites of *p*-cymene in the possum resulted from oxidation at both C7 and C9, accounting for 75% of all urinary metabolites (Boyle *et al*. 1999). The *in vitro* diol metabolite **7** (figure 1) is a possible precursor of these major urinary metabolites. The koala also mostly oxidized *p*-cymene at C7 and C9, with over half of all urinary metabolites comprising 4-(1,2-dihydroxy-1-methylethyl)-benzoic acid. This urinary metabolite is oxidized at C7–9 (Boyle *et al*. 2000a) and, therefore, represents all three *in vitro* sites of attack (figure 1). The koala, as a specialized *Eucalyptus* herbivore, has a greater capacity than the generalist brushtail possum to oxidize dietary terpenes (Boyle *et al*. 2000a,

2001). Although this was not reflected in a higher CL_{int}, the koala liver samples were taken from injured wild animals whose nutritional status and general health were unknown. Consequently, direct comparison with data from captive animals is difficult.

In vivo, rat did excrete an alcohol metabolite, 2-p-tolylpropan-2-ol (**1**), accounting for about one-third of the dose (Boyle *et al*. 1999). However, this metabolite was mostly conjugated with glucuronic acid, which would increase its renal clearance and thus prevent further oxidative metabolism. Most urinary metabolites in rat were hydroxy carboxylic acids and carboxylic acids, although oxidation was less extensive than in the possum or koala (Boyle *et al*. 1999, 2000a). Two-thirds of the urinary metabolites had been oxidized at C7, in keeping with the *in vitro* data.

The *in vitro* microsomal metabolism of *p*-cymene may be compared with that of another monoterpene, 1,8-cineole (Pass *et al*. 2001). The major sites of oxidation of 1,8-cineole were at C9 in possum and koala and the ring positions C3 and C2 in rat, with very minor C7 oxidation in possum and koala. Human liver microsomes and induced rat liver microsomes primarily formed 2-hydroxy cineole (Miyazawa *et al*. 2001, Pass *et al*. 2001). In 1,8-cineole, C8 is linked to C1 via the oxygen bridge and is unavailable for oxidation. Despite this, the oxidative attack on 1,8-cineole tended to be spread over more positions than for *p*-cymene, resulting in a larger number of significant *in vitro* metabolites (Pass *et al*. 2001). Similarly, the *in vivo* metabolism of *p*-cymene in possums showed only eight metabolites (Boyle *et al*. 1999) in contrast to the nineteen 1,8-cineole metabolites (Boyle *et al*. 2000b).

It appears that the CYP isoforms involved in terpene metabolism preferentially oxidize at the saturated sites as opposed to the aromatic carbons. The same regioselectivity is seen for toluene and the three isomeric xylenes in rat and human liver microsomes, in which they are predominantly oxidized to the corresponding benzyl alcohols with only minor amounts of phenolic metabolites (Tassaneeyakul *et al*. 1996, Kim *et al*. 1997, Nakajima 1997). These authors concluded that CYP2E1 was the form principally responsible for the oxidation of methyl groups and CYP1A2 for the minor ring oxidation reactions.

It is tempting to propose that a form analogous to human CYP2E1 is also responsible for the methyl hydroxylation of *p*-cymene in marsupials. Since CYP2E1 is also responsible for alcohol oxidation in microsomes, this could explain the inhibition of cumic acid formation seen at higher *p*-cymene concentrations (see below).

Kinetics of p-*cymene metabolism*

Kinetic analysis of *p*-cymene metabolite formation confirmed that the CYPs primarily attack the C7 position, as in most cases cuminyl alcohol was the only metabolite formed in high enough quantities to measure quantitatively. In possum microsomes, although 2-*p*-tolypropan-1-ol (the C9 hydroxylated metabolite) was also present in measurable amounts, the CL_{int} to cuminyl alcohol was far greater than that found for 2-*p*-tolypropan-1-ol ($\sim$100 compared with $\sim 18\,\mu l\,mg^{-1}\,min^{-1}$) (table 4).

The apparent K_m for the conversion to cuminyl alcohol were relatively high in microsomes from terpene-treated possums compared with those found in control possum microsomes, suggesting that a low-affinity enzyme contributed to this

conversion in terpene-treated microsomes. However, V_{max} for total cuminyl alcohol formation in terpene-treated possum microsomes was also high. The fact that cuminyl alcohol was further oxidized to cumic acid complicated the kinetics of cuminyl alcohol formation. Formation of cumic acid also appeared to be inhibited as concentrations of *p*-cymene increased, suggesting that either *p*-cymene, or one of its metabolites (cuminyl alcohol or 2-*p*-tolypropan-1-ol), inhibited the conversion of cuminyl alcohol to cumic acid (figure 4).

As for the possum, kinetic analysis of cuminyl alcohol formation in koala microsomes was not straightforward. Two enzymes appeared to be involved, but the intrinsic clearance of the high-affinity enzyme (CL_{int1}) was around 10 times higher than the intrinsic clearance of the low-affinity enzyme (CL_{int2}), suggesting that the low-affinity enzyme has a very minor role in the overall metabolism of *p*-cymene.

Cuminyl alcohol formation in the rat liver followed typical Michaelis–Menten kinetics and negligible cumic acid was detected after the 10-min incubation. Therefore, kinetic analysis was not as complicated as for the two marsupial species. The higher K_m for this reaction in rat liver microsomes explains the relatively low CL_{int} to cuminyl alcohol. These results, coupled with the absence of cumic acid, support the *in vivo* finding (Boyle *et al.* 1999, 2000a) that rat has a lower capacity than the two marsupials to oxidize *p*-cymene.

Kinetics of cuminyl alcohol metabolism

As cumic acid was formed by marsupial microsomes even at low concentrations of cuminyl alcohol, a kinetic study of this reaction was undertaken. Pretreatment of possums with terpenes significantly increased the CL_{int} to cumic acid, thereby verifying that dietary terpenes increase the capacity to oxidize alcohols in this animal.

In koala microsomes, kinetic analysis of the conversion of cuminyl alcohol to cumic acid indicated the involvement of more than one enzyme. As with cuminyl alcohol formation, the CL_{int1} by the high-affinity enzyme was significantly greater than the CL_{int2} by the low-affinity component. This suggests that the low-affinity enzymes have a very minor role in the oxidation of *p*-cymene and cuminyl alcohol.

Overall, although the *in vitro* metabolism of *p*-cymene appears to be considerably more complicated than that of 1,8-cineole, the pattern between the adapted *Eucalyptus* feeders, the koala and possum, compared with the non-adapted feeder, the rat, was similar. The rank order of oxidative capacity of *p*-cymene, in terms of the overall CL_{int}, was: terpene-treated possum $\geq$ control possum $>$ koala $\geq$ rat. Although the difference between the CL_{int} of *p*-cymene in koala and rat microsomes was not significant, microsomes from koalas had a higher capacity for the further oxidation of cuminyl alcohol to cumic acid.

References

Boland, K. J. and Brophy, J. J., 1991, *Eucalyptus Leaf Oils: Use, Chemistry, Distillation and Marketing* (Melbourne: Inkata).

Boyle, R. R., McLean, S. and Davies, N., 2000b, Biotransformation of 1,8-cineole in the brushtail possum (*Trichosurus vulpecula*). *Xenobiotica*, **30**, 915–932.

Boyle, R. R., McLean, S., Foley, W. J. and Davies, N., 1999, Comparative metabolism of dietary terpene, *p*-cymene, in generalist and specialist folivorous marsupials. *Journal of Chemical Ecology*, **25**, 2109–2126.

Boyle, R., McLean, S., Foley, W. J., Davies, N. W., Peacock, E. J. and Moore, B. D., 2001, Metabolites of dietary 1,8-cineole in the male koala (*Phascolarctos cinereus*). *Comparative Biochemistry and Physiology Part C*, **129**, 385–395.

Boyle, R., McLean, S., Foley, W. J., Moore, B. D., Davies, N. W. and Brandon, S., 2000a, Fate of the dietary terpene, *p*-cymene, in the male koala. *Journal of Chemical Ecology*, **25**, 1095–1111.

Foley, W. J., Iason, G. R. and McArthur, C., 1999, Nutritional ecology of herbivores. In H.-J. G. Jung and G. C. Fahey (eds), *Proceedings of the 5th International Symposium of the Nutrition of Herbivores* (San Antonio: American Society of Animal Science), pp. 130–209.

Freeland, W. J. and Janzen, D. H., 1974, Strategies in herbivory by mammals: the role of plant secondary compounds. *American Naturalist*, **108**, 269–287.

Hume, I. D., 1982, *Digestive Physiology and Nutrition of Marsupials* (Melbourne: Cambridge University Press).

Ishida, T., Asakawa, Y., Takemoto, T. and Aratani, T., 1981, Terpenoid biotransformation in mammals. III: Biotransformation of α-pinene, β-pinene, pinane, 3-carene, carane, myrcene, and *p*-cymene in rabbits. *Journal of Pharmaceutical Sciences*, **70**, 406–415.

Kelly, S., 1969, *Eucalypts* (Melbourne: Nelson).

Kim, H., Wang, R. S., Elovaara, E., Raunio, H., Pelkonen, O., Aoyama, T., Vainio, H. and Nakajima, T., 1997, Cytochrome P450 isozymes responsible for the metabolism of toluene and styrene in human liver microsomes. *Xenobiotica*, **27**, 657–665.

Li, H., 1993, Phytochemistry of *Eucalyptus* spp. and its role in insect–host–tree selection. PhD thesis, University of Tasmania, Hobart.

McManus, M. E. and Ilett, K. F., 1976, Mixed function oxidase activity in a marsupial, the quokka (*Setonix brachyurus*). *Drug Metabolism and Disposition*, **4**, 199–202.

McManus, M. E. and Ilett, K. F., 1977, Microsomal xenobiotic metabolism in marsupials. *Drug Metabolism and Disposition*, **5**, 503–510.

McManus, M. E., McGeachis, J. K. and Ilett, K. F., 1978, Development of the hepatic mixed function oxidase system in a marsupial, the quokka (*Setonix brachyurus*). *Toxicology and Applied Pharmacology*, **46**, 117–124.

Miyazawa, M., Shindo, M. and Shimada, T., 2001, Oxidation of 1,8-cineole, the monoterpene cyclic ether originated from *Eucalyptus polybractea*, by cytochrome P450 3A enzymes in rat and human liver microsomes. *Drug Metabolism and Disposition*, **29**, 200–205.

Nakajima, M., 1997, Cytochrome P450 isoforms and the metabolism of volatile hydrocarbons of low relative molecular mass. *Journal of Occupational Health*, **39**, 83–91.

Pass, G. J., McLean, S. and Stupans, I., 1999, Induction of xenobiotic metabolising enzymes in the common brushtail possum, *Trichosurus vulpecula*, by *Eucalyptus* terpenes. *Comparative Biochemistry and Physiology Part C*, **124**, 239–246.

Pass, G. J., McLean, S., Stupans, I. and Davies, N., 2001, Microsomal metabolism of the terpene, 1,8-cineole, in the common brushtail possum (*Trichosurus vulpecula*), koala (*Phascolarctos cinereus*), rat and human. *Xenobiotica*, **31**, 205–221.

Riveros-Rosas, H., Julian-Sanchez, A. and Pina, E., 1997, Enzymology of ethanol and acetaldehyde metabolism in mammals. *Archives of Medical Research*, **28**, 453–471.

Southwell, I. A., Flynn, T. M. and Degabriele, R., 1980, Metabolism of α- and β-pinene, *p*-cymene and 1,8-cineole in the brushtail possum, *Trichosurus vulpecula*. *Xenobiotica*, **10**, 17–23.

Tassaneeyakul, W., Birkett, D. J., Edwards, J. W., Veronese, M. E., Tassaneeyakul, W., Tukey, R. H. and Miners, J. O., 1996, Human cytochrome P450 isoform specificity in the regioselective metabolism of toluene and *o*-, *m*- and *p*-xylene. *Journal of Pharmacology and Experimental Therapeutics*, **276**, 101–108.

Walde, A., Ve, B., Scheline, R. R. and Monge, P., 1983, *p*-Cymene metabolism in rats and guinea-pigs. *Xenobiotica*, **13**, 503–512.

XENOBIOTICA, 2002, VOL. 32, NO. 5, 399–409

Taylor & Francis
healthsciences

Long-term disposition of a novel lipophilic platinum complex SM-11355 in dog after intrahepatic arterial administration: highly sensitive detection of platinum and radioactivity

J. SHIMAKURA*, K. FUJIMOTO, S. KOMURO, M. NAKANO and H. KANAMARU

Environmental Health Science Laboratory, Sumitomo Chemical Co., Ltd, 1-98 Kasugade-naka 3-chome, Konohana-ku, Osaka, 554-8558, Japan

Received 22 August 2001

1. The disposition of SM-11355, an anticancer platinum complex for hepatocellular carcinoma, was investigated in dog by measuring platinum (Pt) and radioactivity levels following intrahepatic arterial administration of ^{14}C-SM-11355 suspended in Lipiodol, an oily lymphographic agent. Plasma and excretion profiles were monitored in six animals, with tissue distribution studied after 1 day, 4 and 13 weeks ($n = 2$/time point).

2. SM-11355 was released very slowly into the systemic circulation from Lipiodol, resulting in very low levels of Pt compounds in plasma, urine, faeces and organs. Plasma levels of Pt and radioactivity declined with apparent half-lives of 5–7 weeks. Excretion continued even at 3 months after the administration with proportions excreted for Pt and radioactivity up to 30–60% in urine and 8–10% in faeces.

3. The Pt and radioactivity in the liver accounted for 80–100% of the dose at 1 day and for 20–50% at 13 weeks after the administration, predominately as intact SM-11355. The concentrations were highest in the left lobe of the liver, the administration site, but levels in the remainder of the liver were also markedly higher than those in plasma and other tissues.

4. The results strongly support the concept that SM-11355 targets the liver with highly selectivity and sustained release of Pt compounds.

Introduction

SM-11355, *cis*[((1*R*,2*R*)-1,2-cyclohexanediamine-*N*,*N*')bis(myristato)]platinum(II) (figure 1) is a lipophilic platinum (Pt) complex under clinical development as a antineoplastic agent for the treatment of primary hepatocellular carcinoma in combination with Lipiodol as a carrier. The oily lymphographic agent Lipiodol (the ester of iodinated fatty acids of poppy seed oil) remains in tumour sites for a long period after intrahepatic arterial injection (Iwai *et al*. 1984). Therefore, various anticancer agents such as cisplatin (Shibata *et al*. 1989, Ikeda *et al*. 1992, Isomoto *et al*. 1992) and doxorubicin (Horiguchi *et al*. 1992, Ikeda *et al*. 1992) have been examined for the therapy of hepatocellular carcinoma with intrahepatic arterial injection with Lipiodol as a carrier. However, most of these drugs are released rapidly from Lipiodol, resulting in adverse effects and reduced anticancer efficacy. SM-11355 is designed to be highly lipophilic to be stabley suspended in Lipiodol, so that selective and sustained antitumour effects are expected in clinical use. Indeed, efficacy and safety of SM-11355/Lipiodol have been already demon-

* Author for correspondence; e-mail: shimakura@sc.sumitomo-chem.co.jp

Xenobiotica ISSN 0049–8254 print/ISSN 1366–5928 online © 2002 Taylor & Francis Ltd
http://www.tandf.co.uk/journals
DOI: 10.1080/00498250110111999

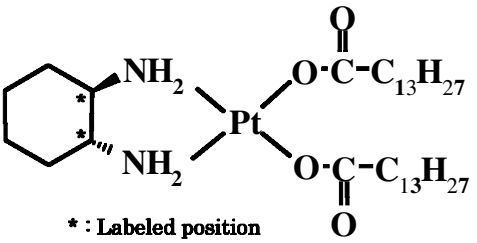


Figure 1. Chemical structure of [cyclohexyl-1,2-^{14}C]SM-11355.

strated in animal models (Kishimoto *et al.* 1992, Kishimoto *et al.* 2000) and are now under clinical trial.

The disposition of SM-11355 released from Lipiodol after intrahepatic arterial administration is fundamental for the safety assessment of the compound. However, initial attempts to measure Pt using conventional atomic absorption spectrometry techniques proved unsatisfactory with respect to the sensitivity because very low levels of the Pt compounds are released from Lipiodol into the systemic circulation. The inductively coupled plasma-mass spectrometry (ICP-MS) approach, which is widely used for the analysis of trace elements in industrial fields, has been reported for Pt determination in biological samples (Tothill *et al.* 1990, 1992) in the last decade. We have succeeded in establishing a highly sensitive method for determination of Pt in dog plasma, urine, faeces and tissues by using ICP-MS (the limits of quantification 0.05 ng g^{-1} or ng ml^{-1} for plasma and tissues, 0.1 ng ml^{-1} for urine and 1 ng g^{-1} for faeces), facilitating examination of the disposition of SM-11355/Lipiodol in dog after intrahepatic arterial administration.

The beagle dog was selected as a test species since it is possible to apply the same administration method as in humans, i.e. intrahepatic arterial administration via a femoral artery using an angiocatheter.

In the current study, the disposition of SM-11355/Lipiodol in dog after intrahepatic arterial administration was investigated for up to 3 months. In addition to Pt, by employing radioactive SM-11355 labelled with ^{14}C at the diamino cyclohexane (DACH) moiety, radioactivity was also measured, allowing an analysis of the metabolic fate and disposition of the complex.

Materials and methods

Chemicals

[Cyclohexyl-1,2-^{14}C]SM-11355 (^{14}C-SM-11355) (figure 1) was synthesized in our laboratory. The specific activity was 2.4 MBq mg^{-1}, and the radiochemical purity was > 95%, as determined by HPLC analysis with a SUMIPAX ODS A212 column, 150 × 6 mm i.d. (Sumika chemical analysis service, Osaka, Japan) eluted with methanol-acetonitrile-water (77/22/1 v/v/v) at a flow rate of 1 ml min^{-1}. Lipiodol (Lipiodol Ultra-Fluid, Laboratorie Guerbert, France) was purchased from Kodama Co. (Tokyo, Japan). All other chemicals were of reagent grade.

Animals

Male beagle dogs, purchased from Kasho Co. (Tokyo, Japan), weighing 10–12 kg, were used at 7 months of age. They were housed individually in aluminium cages and fed a pellet diet (Lab Rations 4360, Purina, St Louis, MO, USA) once a day and filtered water *ad libitum* in a temperature- and humidity-controlled room.

Administration of SM-11355/Lipiodol

^{14}C-SM-11355 (20 mg) was mixed with Lipiodol (1 ml) to form a stable colloidal suspension (SM-11355/Lipiodol). Dogs were anaesthetized by an intravenous injection of pentobarbital sodium solution (Nembutal^{TM}, 25 mg kg^{-1}; Abott Laboratories, North Chicago, IL, USA), and a catheter was inserted from the femur artery into the hepatic artery under X-ray imaging. Contrast media (Conray^{TM}, Daiichi Pharmaceuticals Co., Tokyo, Japan) was administered to check the selective targeting of the catheter to the liver. After confirmation, 2.4 mg kg^{-1} SM-11355/Lipiodol was infused through the catheter at 0.12 ml kg^{-1} over 20 min.

Sample collection

Two animals at each time point were killed by exsanguination under pentobarbital anaesthesia at 1 day, 4 and 13 weeks after administration. Blood, urine and faeces samples were regularly collected from each animal until sacrifice. Blood samples were collected into heparinized tubes from the cephalic vessels to obtain plasma at various times. Urine and faeces excreted were collected every 24 h. Tissue samples were excized at the time of sacrifice. Liver samples were further divided into six lobes: left lateral, left medial, right lateral, right medial, caudate and quadrate. All the excized tissues and faeces were homogenized by a polytron with an appropriate amount of water.

Measurement of radioactivity

Appropriate amounts of plasma or tissue homogenate (about 0.1 g) were digested in 1 ml tissue solubilizer (NCS-2^{R}, Amersham, Uppsala, Sweden), and 15 ml liquid scintillator (Hionic-Fluor^{TM}, Packard, Meriden, CT, USA) was added. Urine and bile samples (about 0.1 g) were mixed with 15 ml liquid scintillator (Emusifier Scintillator Plus^{TM}, Packard). Faeces homogenates, blood and bone marrow samples (about 0.2 g) were combusted by a sample oxidizer (Model 306, Packard). The radioactivity of these pretreated samples was counted using a liquid scintillation counter (TRI-CARB 2500TR, Packard).

Measurement of Pt

Each sample (about 1 ml) was heated with 68% HNO_3 (0.6 ml) in a glass beaker covered with a watch glass on a hot plate and evaporated to dryness. The residue was mixed with 68% HNO_3 (0.6 ml) again and evaporated to dryness by heating. This step was repeated twice more. The residue was mixed with H_2O_2 (0.6 ml) and evaporated to dryness by heating. After cooling, the inside of the beaker and watch glass were washed with 10 ml 4% aqua regia, 25-fold diluted mixture of 36% HCl and 68% HNO_3 (3/1 v/v). The wash solution was heated and concentrated to about 1 ml. After cooling, the solution was transferred to a polystyrene tube and made up to 4 ml (plasma and tissues) or 10 ml (urine and faeces) with 4% aqua regia. $Na_3IrCl_6 10H_2O$ was added to this solution to make a concentration of iridium (Ir) of 1 ng ml^{-1} as an internal standard. Calibration lines were prepared with standard solutions of 0, 1.25 and 2.5 ng ml^{-1} Pt for plasma, urine and tissue samples, or 0, 1 and 10 ng ml^{-1} Pt for faeces samples. When measured values were outwith the calibration range, the sample solution was appropriately diluted with 4% aqua regia and re-analysed.

The instruments used were a VG Plasma Trace (Micromass, Manchester, UK) for plasma, urine and tissues, and a SPQ6500 (Seiko Instruments, Chiba, Japan) for faeces. The instrument conditions for the VG Plasma Trace were as follows: plasma power 1.35 kW; plasma flow 15 l min^{-1}; auxiliary gas 0.5 l min^{-1}; nebulizer gas flow 0.8 l min^{-1}; element/mass Pt/195, Ir/193; dwell time 160 ms for Pt, 80 ms for Ir. The instrument conditions for the SPQ6500 were as follows: plasma power 1.5 kW; plasma flow 16 l min^{-1}; auxiliary gas 1 l min^{-1}; nebulizer gas flow 1 l min^{-1}; element/mass Pt/195, Ir/193; dwell time 25 ms.

The limits of quantification were 0.05 ng ml^{-1} for plasma, 0.1 ng ml^{-1} for urine, 1 ng g^{-1} for faeces and 0.05 ng g^{-1} for tissues.

HPLC analysis

Left liver lobe homogenates were extracted with a fourfold volume of chloroform-methanol (2/1 v/v). The extracts were analysed by reverse-phase HPLC with radioactivity detection on the column of SUMIPAX ODS A212 (150 × 6 mm i.d., Sumika chemical analysis service, Osaka, Japan) eluting with methanol-acetonitrile-water (77/22/1 v/v/v) at 1 ml min^{-1}.

Pharmacokinetic analysis

C_{max} and T_{max} were individually observed values. AUCs were calculated by the linear trapezoidal rule for 0–4 weeks and 0–13 weeks. The apparent half-liveswere calculated from the slope of the log–linear regression line from 6 to 13 weeks.

Results

Plasma concentrations of Pt and radioactivity

The plasma concentrations of Pt and radioactivity generally reached C_{max} after 8 hr, although T_{max} for one animal was at 2 weeks, and showed a slight peak at 1 or 2 weeks after administration (figure 2 and tables 1 and 2). Thereafter, plasma levels of Pt and radioactivity decreased gradually with apparent half-livesof 5.0–7.1 weeks for Pt and 3.2–5.4 weeks for radioactivity. The concentrations in the plasma were essentially similar for Pt and radioactivity throughout the study.

Excretion of Pt and radioactivity

Proportions of Pt excreted into urine and faeces were $23 \pm 12\%$ and $8 \pm 0.5\%$ (mean $\pm$ SD, $n = 4$) by week 4, and 29–51% and 9–10% ($n = 2$) by week 13, respectively (figure 3). Radioactivity excreted into urine and faeces was $27 \pm 12\%$ and $7 \pm 0.7\%$ (mean $\pm$ SD, $n = 4$) of the total by week 4, and 35–57% and 8–10% ($n = 2$) by week 13, respectively. The excretion of Pt and radioactivity continued even at 13 weeks after administration. The urinary excretion rate showed three phases, being highest between weeks 1 and 2. Urinary excretion of Pt was slightly lower than that for radioactivity.

Distribution of Pt and radioactivity

The tissue distributions of Pt and radioactivity at day 1, weeks 4 and 13 after dosing are presented in tables 3 and 4. At all time points, Pt and radioactivity were detected in all tissues except the brain, with the majority in the liver. In contrast to

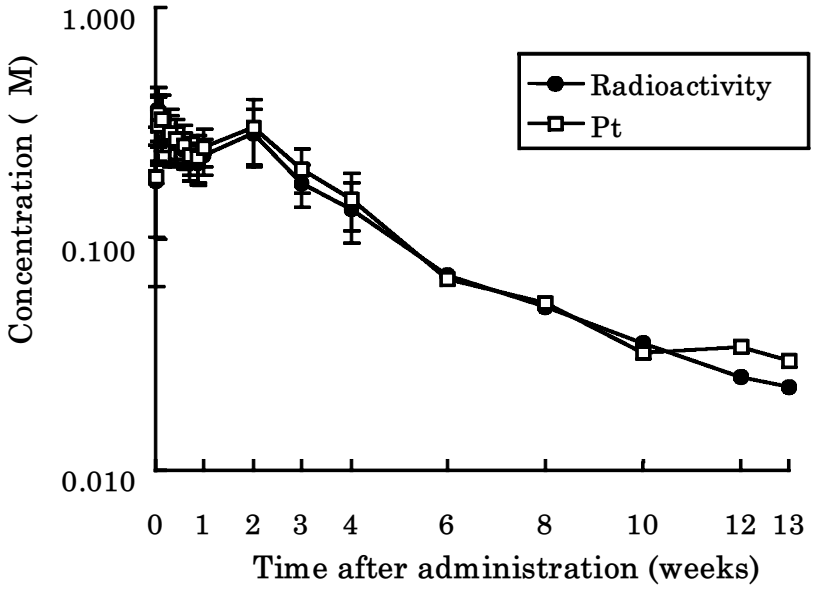


Figure 2. Plasma concentrations of Pt and radioactivity after a single intrahepatic arterial administration of ^{14}C-SM-11355/Lipiodol to dog at 2.4 mg kg^{-1}. Each point with a vertical line represents the mean $\pm$ SD for 6 (1–24 h) and 4 dogs (48 h to week 4), and represents the mean of 2 dogs (weeks 4–13).

Table 1. Pharmacokinetic parameters of Pt after a single intrahepatic arterial administration of ^{14}C-SM-11355/Lipiodol to dog at 2.4 mg kg^{-1}.

Animal no.	C_{max} (ng ml^{-1})	T_{max}	$AUC_{0\text{-}4W}$ (ng week ml^{-1})	$AUC_{0\text{-}13W}$ (ng week ml^{-1})	$t_{1/2}$ (week)
4001	94.0	8 h	228	327	5.0
4005	47.7	8 h	130	227	7.1
4010	63.7	week 2	191	–	–
4014	84.9	24 h	210	–	–
4015	76.2	8 h	–	–	–
4021	62.2	24 hr	–	–	–
Mean	71.4	–	189	277	6.1
SD	16.9	–	42.8	–	–

–, Not calculated.

Table 2. Pharmacokinetic parameters of radioactivity after a single intra-hepatic arterial administration of ^{14}C-SM-11355/Lipiodol to dog at 2.4 mg kg^{-1}.

	Pharmacokinetic parameters				
Animal no.	C_{max} (μg eq. ml^{-1})	T_{max}	$AUC_{0\text{-}4W}$ (μg eq. week ml^{-1})	$AUC_{0\text{-}13W}$ (μg eq. week ml^{-1})	$t_{1/2}$ (week)
4001	0.372	8 h	0.811	1.16	3.2
4005	0.197	8 h	0.502	0.894	5.4
4010	0.219	week 2	0.664	–	–
4014	0.339	8 h	0.775	–	–
4015	0.301	8 h	–	–	–
4021	0.255	24 h	–	–	–
Mean	0.281	–	0.688	1.03	4.3
SD	0.069	–	0.139	–	–

–, Not calculated.

the high levels of Pt and radioactivity in the left lateral lobe, the administration site, relatively low levels were found in the right lateral lobe on the opposite side. The amounts of Pt remaining in the body of each pair of dogs were 79 and 97% at day 1, 47 and 70% at week 4, and 31 and 54% at week 13, respectively. The corresponding amounts of radioactivity were 87 and 101% at day 1, 44 and 65% at week 4, and 20 and 49% at week 13. The Pt and radioactivity in the liver accounted for $>96\%$ of that in the whole body at all time points. No other tissue accounted for $>1\%$ of the dose.

The highest concentrations of Pt and radioactivity were present at day 1 or week 4 in most tissues. At day 1, the concentrations were relatively high in spleen, lungs and kidney cortex, similar to the plasma level. Otherwise, tissue concentrations were lower. At week 4, tissues containing significantly greater Pt or radioactivity concentrations than plasma were kidney cortex, spleen and lungs. At week 13, concentrations of Pt and radioactivity in most tissues had declined from the week 4 values, but were greater than in plasma.

The Pt/radioactivity ratios (calculated as nmol units) in representative tissues are given in figure 4. In the liver, the Pt/radioactivity ratios were near 1 at 1 day after dosing, but showed a tendency to increase, especially in the right medial lobe

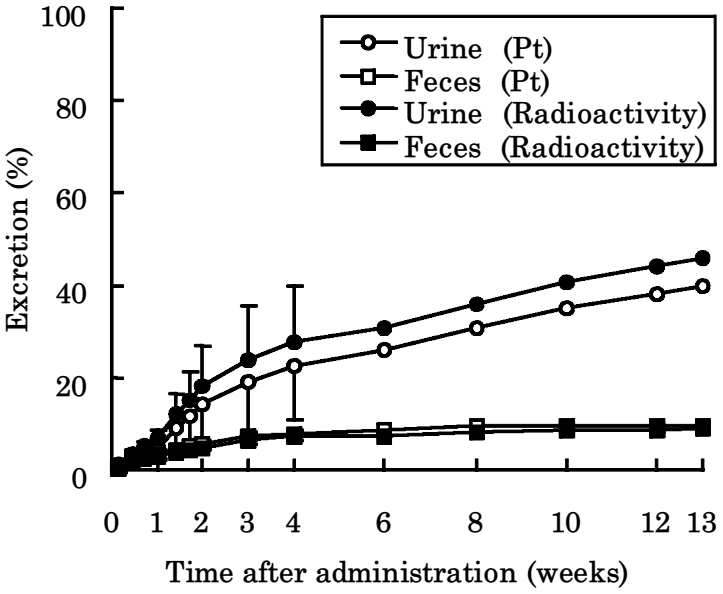


Figure 3. Cumulative excretion (% dose) of Pt and radioactivity after a single intrahepatic arterial administration of ^{14}C-SM-11355/Lipiodol to dog at 2.4 mg kg^{-1}. Each point with a vertical line represents the mean ± SD of 4 dogs (0 to week 4), and the mean of 2 dogs (weeks 4–13).

at weeks 4 or 13. In addition, the Pt/radioactivity ratios were significantly elevated in the kidney cortex.

The chloroform-methanol extracts of liver left lobes (day 1, weeks 4 and 13) were analysed by reverse-phase HPLC. At every time point, the main peak corresponded to the unchanged parent drug, SM-11355 (data not shown).

Discussion

After the intrahepatic arterial administration of ^{14}C-SM-11355/Lipiodol, most of administered Pt and radioactivity was distributed to the liver as expected. SM-11355/Lipiodol was assumed to be trapped in sinusoids or arteries in the liver, similarly to the case of Lipiodol alone (Kan *et al.* 1993, Kishi *et al.* 1994). Unchanged SM-11355 was the major component in the extracted radioactivity of the liver at every time point (day 1, weeks 4 and 13) based on radio-HPLC analysis. Thus, most of administered SM-11355 appears to be retained in the liver as the intact form for a long period. Plasma concentrations of Pt and radioactivity were very low as compared with those in the liver with long persistence, reflecting sustained release from Lipiodol. The plasma Pt levels observed in this study were 50 ng ml^{-1} just after administration and 100 ng ml^{-1} even at T_{max}. For comparison, plasma Pt levels of dogs intravenously dosed with cisplatin at 1 mg kg^{-1} were reported to be 1–4 μg ml^{-1} immediately after dosing, and > 0.5 μg ml^{-1} at 24 h after dosing (Irie *et al.* 1983). Plasma Pt concentrations in man after intravenous administration of cisplatin or carboplatin at clinical doses are generally 0.5 to several μg ml^{-1} (Gullo *et al.* 1980, van der Vijgh 1991). The fact that side-effects of

Table 3. Tissue distribution of Pt after a single intrahepatic arterial administration of ^{14}C-SM-11355/Lipiodol to dog at 2.4 mg kg^{-1}.

	ng g^{-1} or ml^{-1} (% of dose[a])											
	Day 1				Week 4				Week 13			
	No. 4015		No. 4021		No. 4010		No. 4014		No. 4001		No. 4005	
Plasma	71.1	–	59.1	–	19.5	–	38.8	–	3.9	–	5.9	–
Blood	49.2	–	42.2	–	22.0	–	35.7	–	6.3	–	7.5	–
Brain	0.7	*< 0.01*	< 0.5	*< 0.01*	< 0.5	*< 0.01*	0.8	*< 0.01*	0.7	*< 0.01*	0.5	*< 0.01*
Heart	11.0	*0.01*	6.4	*< 0.01*	14.8	*0.02*	14.7	*0.02*	6.4	*< 0.01*	4.4	*< 0.01*
Lung	5.6	*0.05*	64.4	*0.09*	31.5	*0.05*	35.5	*0.04*	39.4	*0.06*	28.7	*0.04*
Liver (left lateral)	35 800	*46.44*	35 000	*62.32*	11 900	*20.83*	29 400	*41.79*	9080	*12.93*	25 500	*30.88*
Liver (left medial)	24 000	*15.61*	13 000	*9.03*	21 900	*16.11*	21 300	*13.71*	4900	*3.59*	23 100	*12.92*
Liver (right medial)	281	*0.24*	5420	*4.01*	418	*0.49*	420	*0.40*	410	*0.43*	342	*0.24*
Liver (right lateral)	164	*0.07*	1990	*1.32*	1680	*1.50*	5860	*5.79*	562	*0.22*	*8190*	*5.35*
Liver (caudate)	25 000	*6.62*	380	*0.13*	10 400	*3.71*	11 300	*4.13*	13 000	*4.87*	7790	*1.84*
Liver (quadrate)	8910	*8.98*	15 200	*19.54*	2290	*2.65*	2440	*3.00*	10 600	*7.46*	2530	*2.31*
Liver (subtotal)		*77.96*		*96.35*		*45.29*		*68.80*		*29.50*		*53.53*
Gallbladder	8590	*0.29*	390	*0.02*	148	*< 0.01*	59.7	*< 0.01*	12 000	*0.66*	2330	*0.04*
Spleen	115	*0.05*	98.8	*0.06*	175	*0.08*	209	*0.09*	132	*0.06*	84.8	*0.06*
Pancreas	12.2	*< 0.01*	9.4	*< 0.01*	20.2	*< 0.01*	21.4	*< 0.01*	11.9	*< 0.01*	9.8	*< 0.01*
Kidney (cortex)	76.0	*0.04*	41.2	*0.03*	1190	*0.80*	1300	*0.91*	492	*0.25*	761	*0.33*
Kidney (medulla)	11.5	*< 0.01*	15.3	*< 0.01*	22.4	*< 0.01*	19.9	*< 0.01*	38.9	*< 0.01*	39.2	*0.01*
Bone marrow	30.7	–	27.0	–	36.9	–	40.5	–	12.9	–	34.7	–
Stomach (fundus)	8.1	*0.01*	6.9	*< 0.01*	16.0	*0.02*	12.4	*0.02*	36.0	*0.05*	7.2	*0.01*
Jejunum	15.1	*0.03*	13.1	*0.03*	14.1	*0.04*	21.2	*0.04*	23.9	*0.04*	6.6	*0.01*
Bile	1160	–	1140	–	28.2	–	107	–	11.1	–	7.9	–
Recovery												
Tissues		*78.50*		*96.67*		*47.33*		*70.06*		*30.74*		*54.11*
Urine		*0.39*		*0.15*		*34.65*		*17.62*		*50.71*		*28.89*
Faeces		*0.00*		*0.00*		*8.96*		*8.35*		*9.18*		*9.72*
Total		*78.90*		*96.81*		*90.93*		*96.03*		*90.64*		*92.71*

[a] *Italic* figures are the percentages of the dose.

Table 4. Tissue distribution of radioactivity after a single intrahepatic arterial administration of ^{14}C-SM-11355/Lipiodol to dog at 2.4 mg kg^{-1}.

	μg eq. g^{-1} or ml^{-1} (% of dose[a])											
	Day 1				Week 4				Week 13			
	No. 4015		No. 4021		No. 4010		No. 4014		No. 4001		No. 4005	
Plasma	0.298	–	0.227	–	0.062	–	0.143	–	0.011	–	0.023	–
Blood	0.192	–	0.167	–	0.081	–	0.132	–	0.021	–	0.026	–
Brain	0.005	*< 0.01*	0.004	*< 0.01*	0.012	*< 0.01*	0.016	*< 0.01*	0.005	*< 0.01*	0.005	*< 0.01*
Heart	0.046	*0.01*	0.039	*0.01*	0.036	*0.01*	0.051	*0.02*	0.016	*< 0.01*	0.013	*< 0.01*
Lung	0.371	*0.09*	0.482	*0.18*	0.187	*0.07*	0.316	*0.11*	0.098	*0.03*	0.181	*0.07*
Liver (left lateral)	161	*54.81*	141	*63.65*	47.6	*21.47*	98.6	*37.37*	23.5	*8.32*	94.3	*29.55*
Liver (left medial)	104	*17.75*	60.8	*10.71*	75.1	*14.17*	92.0	*15.78*	12.7	*2.32*	81.6	*11.79*
Liver (right medial)	1.06	*0.24*	22.7	*4.25*	0.568	*0.17*	0.749	*0.19*	0.509	*0.13*	0.359	*0.06*
Liver (right lateral)	0.760	*0.08*	6.78	*1.14*	4.26	*0.97*	20.7	*5.45*	0.457	*0.05*	20.4	*3.44*
Liver caudate)	82.3	*5.72*	1.49	*0.13*	41.0	*3.74*	33.7	*3.28*	36.3	*3.37*	32.8	*2.00*
Liver (quadrate)	31.4	*8.32*	63.1	*20.60*	8.62	*2.56*	7.31	*2.39*	30.2	*5.25*	9.21	*2.17*
Liver (subtotal)		*86.91*		*100.49*		*43.09*		*64.47*		*19.43*		*49.02*
Gall bladder	26.9	*0.24*	1.78	*0.02*	0.226	*< 0.01*	0.155	*< 0.01*	37.5	*0.52*	6.23	*0.03*
Spleen	0.495	*0.05*	0.547	*0.09*	0.522	*0.06*	0.662	*0.08*	0.361	*0.04*	0.285	*0.05*
Pancreas	0.068	*< 0.01*	0.055	*< 0.01*	0.112	*0.01*	0.115	*0.01*	0.035	*< 0.01*	0.049	*< 0.01*
Kidney (cortex)	0.283	*0.04*	0.297	*0.05*	1.19	*0.21*	1.38	*0.26*	0.234	*0.03*	0.447	*0.05*
Kidney (medulla)	0.105	*< 0.01*	0.137	*< 0.01*	0.079	*< 0.01*	0.116	*< 0.01*	0.098	*< 0.01*	0.201	*0.02*
Bone	0.012	–	0.005	–	0.009	–	0.014	–	0.009	–	0.007	–
Bone marrow	0.107	–	0.080	–	0.114	–	0.121	–	0.061	–	0.069	–
Stomach (fundus)	0.035	*0.01*	0.037	*0.01*	0.054	*0.02*	0.073	*0.03*	0.032	*0.01*	0.023	*< 0.01*
Jejunum	0.068	*0.03*	0.049	*0.03*	0.041	*0.03*	0.070	*0.04*	0.024	*0.01*	0.018	*< 0.01*
Bile	4.99	–	3.96	–	0.116	–	0.254	–	0.041	–	0.030	–
Recovery												
Tissues		*87.48*		*100.97*		*44.31*		*65.14*		*20.12*		*49.31*
Urine		*0.47*		*0.17*		*39.05*		*24.23*		*57.40*		*34.57*
Faeces		*0.00*		*0.01*		*8.01*		*8.26*		*7.85*		*10.11*
Total		*87.95*		*101.15*		*91.37*		*97.63*		*85.37*		*93.99*

[a] *Italic* figures are the percentages of the dose.

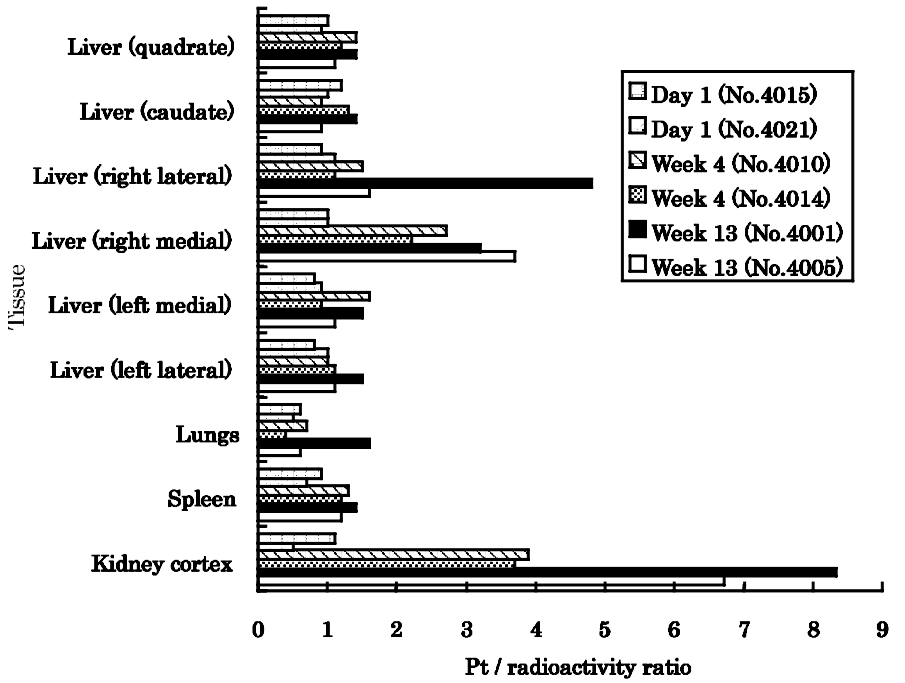


Figure 4. Pt/radioactivity ratios (calculated as molar units) in tissues after a single intrahepatic arterial administration of ^{14}C-SM-11355/Lipiodol to dog at 2.4 mg kg^{-1}.

SM-11355 were very slight (Kitamoto *et al.* 2000) may be attributable to this low level of systemic exposure.

The amount of Pt and radioactivity in the liver accounted for most of the dose at 1 day after administration with gradual elimination to 20–50% of the maximum at week 13. The excretion route was mainly into the urine, as for other Pt complexes (Irie *et al.* 1983, van der Vijgh 1991, Graham *et al.* 2000), suggesting excretion via the kidneys after release into the systemic circulation. The total percentages excreted into urine and faeces were 40–60% after 13 weeks, which indicated on-going excretion. In animal nos 4001 and 4010, the fact that the excretion rate showed three phases, highest at between week 1 and 2, presumably reflects the second peak of plasma concentration at week 2.

Although Pt and radioactivity were detected in all the investigated tissues, the levels were very low. The relatively high levels in the gall bladder and spleen might indicate direct delivery, taking into account the blood supply near the common hepatic artery. It is also possible that a small amount of dosing suspension passed through the sinusoids into the hepatic vein and into the lungs, resulting in extensive retention. The high levels in kidneys are in agreement with reports for other Pt complexes, such as cisplatin (Siddik *et al.* 1988) and ormaplatin (Kido *et al.* 1992), presumably related to the excretory function. The levels of Pt and radioactivity tended to decrease in many tissues, although the elimination half-lives were uncertain due to the individual differences.

Excretion of Pt was less than that of radioactivity, and Pt/radioactivity ratios tended to increase with time, being relatively high in the liver (right lobe), and

high in the kidneys. In the liver left lobe, however, Pt/radioactivity ratios remained unchanged, as expected from the HPLC analysis. These results indicate that the diaminocyclohexane (DACH) moiety was released from Pt after entry of SM-11355 into the systemic circulation, and eliminated more rapidly, consistent with previous *in vivo* findings for ormaplatin which possesses a similar DACH moiety (Kido *et al*. 1992).

As for the metabolism of SM-11355, it was difficult to identify metabolites in plasma or urine here because of the very low concentrations. Oxaliplatin and ormaplatin have been reported to undergo ligand exchange reactions with nucleophiles of amino acids such as methionine and cysteine to form biotransformation products (Luo *et al*. 1999). SM-11355 also forms a methionine complex by exchange of the myristato ligand with methionine when SM-11355/Lipiodol was incubated with serum *in vitro* (data not shown). Therefore, SM-11355 is likely to form complexes with certain amino acids *in vivo*.

In conclusion, SM-11355 was distributed mainly in the liver by selective targeting of intrahepatic arterial administration, and retained there for a long time with sustained release of Pt compounds. The high efficacy and low side-effects of SM-11355 may be attributable to these pharmacokinetic features.

References

Graham, M. A., Lockwood, G. F., Greenslade, D., Brienza, S., Bayssas, M. and Gamelin, E., 2000, Clinical pharmacokinetics of oxaliplatin: a critical review. *Clinical Cancer Research*, **6**, 1205–1218.

Gullo, J. J., Litterst, C. L., Maguire, P. J., Sikic, B. I., Hoth, D. F. and Woolley, P. V., 1980, Pharmacokinetics and protein binding of *cis*-dichlorodiammine platinum(II) administered as a one hour or as a twenty hour infusion. *Cancer Chemotherapy and Pharmacology*, **5**, 21–26.

Horiguchi, Y., Itoh, M., Takagawa, H., Imai, H., Kamei, A., Sekoguchi, B. and Nagamura, Y., 1992, Assessment of chemoembolization therapy for primary liver cancer using a stabilized adriamycin-lipiodol suspension. *Cancer Chemotherapy and Pharmacology*, **31**, S60–S64.

Ikeda, K., Inoue, H., Yano, T., Kobayashi, H. and Nakajo, M., 1992, Comparison of the anticancer effect of ADMOS alone and ADMOS with CDDP in the treatment of hepatocellular carcinoma by intra-arterial injection. *Cancer Chemotherapy and Pharmacology*, **31**, S65–S68.

Irie, T., Hashimoto, Y., Irie, A., Ishibashi. M., Miyazaki, H., Machida, H., Karasawa, Y. and Nakamori, K., 1983, Absorption, excretion and distribution of cisplatin in dogs and rats. *Iyakuhin Kenkyu*, **14**, 384–410.

Isomoto, I., Akikawa, H., Mori, H., Matsunaga, N., Ajima, A., Fukuda, T. and Ogasawara, M., 1992, Intraarterial injection therapy of newly developed cisplatin-phosphatidyl choline-lipiodol suspension for hepatocellular carcinoma. *Radiation Medicine*, **10**, 19–25.

Iwai, K., Maeda, H. and Konno, T., 1984, Use of oily contrast medium for selective drug targeting to tumor: enhanced therapeutic effect and X-ray image. *Cancer Research*, **44**, 2115–2121.

Kan, Z., Satoh, M., Ivancev, K., Uchida, B., Hedgpeth, P., Lunderquist, A., Rosch, J. and Yamada, R., 1993, Distribution and effect of iodized poppy seed oil in the liver after hepatic artery embolization: experimental study in several animal species. *Radiology*, **186**, 861–866.

Kido, Y., Khokhar, A. R. and Siddik, Z. H., 1992, Pharmacokinetics of intravenously injected [^{3}H]tetrachloro(D,L-*trans*)1,2-diaminicyclohexane platinum (IV) (tetraplatin) in mice. *Drug Metabolism and Disposition*, **20**, 673–678.

Kishi, K., Sonomura, T., Satoh, M., Nishida, N., Terada, M., Shioyama, Y. and Yamada, R., 1994, Acute toxicity of Lipiodol infusion in to the hepatic arteries of dogs. *Investigative Radiology*, **29**, 882–889.

Kishimoto, S., Fukui, M., Fukushima, S. and Nakano, M., 1992, Application of a lipophilic platinum derivative contained in an oily lymphographic agent to intra-hepatic arterial chemotherapy. *Regular Cancer Treatment*, **1–2**, 25–29.

Kishimoto, S., Noguchi, T., Yamaoka, T., Fukushima, S. and Takeuchi, Y., 2000, Antitumor effects of a novel lipophilic platinum complex (SM-11355) against a slowly-growing rat hepatic tumor after intra-hepatic arterial administration. *Biological and Pharmacological Bulletin*, **23**, 344–348.

Kitamoto, M, Nakanishi, T., Okada, S., Fujiyama, S. and Kubo, Y., 2000, Phase II trial of intra-arterial chemotherapy using a novel lipophilic platinum derivative (SM-11355) in patients with hepatocellular carcinoma. *Gut*, 47(suppl. III), A191.

Luo, F. R., Wyrick, S. D. and Chaney, S. G., 1999, Pharmacokinetics and biotransformations of oxaliplatin in comparison with ormaplatin following a single bolus intravenous injection in rats. *Cancer Chemotherapy and Pharmacology*, **44**, 19–28.

Shibata, J., Fujiyama, S., Sato, T., Kishimoto, S., Fukushima, S. and Nakano, M., 1989, Hepatic arterial injection chemotherapy with cisplatin suspended in an oily lymphographic agent for hepatocellular carcinoma. *Cancer*, **64**, 1586–1594.

Siddik, Z. H., Jones, M., Boxall, F. E. and Harrap, K. R., 1988, Comparative distribution and excretion of carboplatin and cisplatin in mice. *Cancer Chemotherapy and Pharmacology*, **21**, 19–24.

Tothill, P., Klys, H. S., Matheson, L. M., McKay, K. and Smyth, J. F., 1992, The long-term retention of platinum in human tissues following the administration of cisplatin or carboplatin for cancer chemotherapy. *European Journal of Cancer*, **28**, 1358–1361.

Tothill, P., Matheson, L. M., Smyth, J. F. and McKay, K., 1990, Inductively coupled plasma mass spectrometry for the determination of platinum in animal tissues and a comparison with atomic absorption spectrometry. *Journal of Analysis and Atomic Spectrometry*, **5**, 619–622.

Van der Vijgh, W. J. F., 1991, Clinical pharmacokinetics of carboplatin. *Clinical Pharmacokinetics*, **21**, 242–261.

XENOBIOTICA, 2002, VOL. 32, NO. 5, 411–425

Taylor & Francis
healthsciences

Metabolism of the analgesic drug ULTRAM® (tramadol hydrochloride) in humans: API-MS and MS/MS characterization of metabolites

W. N. WU*, L. A. MCKOWN and S. LIAO

Division of Preclinical Development, The R. W. Johnson Pharmaceutical Research Institute, Spring House, PA 19477, USA

Received 22 August 2001

1. Metabolism of the analgesic agent tramadol hydrochloride has been investigated after a single oral administration of tramadol to three male volunteers (100 mg/subject), and a urine pool (4–12 h) was obtained.

2. Unchanged tramadol and a total of 23 metabolites, consisting of 11 Phase I metabolites (M1–11) and 12 conjugates (seven glucuronides, five sulphates), were profiled, characterized and tentatively identified in urine on the basis of API ionspray-MS and MS/MS data.

3. Of the metabolites, five (M1–5) had been previously identified.

4. The metabolites were formed via the following six metabolic pathways: (1) *O*-demethylation, (2) *N*-demethylation, (3) cyclohexyl oxidation, (4) oxidative *N*-dealkylation, (5) dehydration and (6) conjugation.

5. Pathways 1–3 appear to be major routes, forming seven *O*-desmethyl/*N*-desmethyl and hydroxycyclohexyl metabolites.

6. Pathways 1–3 in conjunction with pathway 6 produced seven glucuronides along with five sulphates.

7. In addition, the *in vitro* metabolism of tramadol was conducted using a human liver microsomal fraction in the presence of an NADPH-generating system. Unchanged tramadol (82% of the sample) plus eight metabolites (M1, M2, M4–6, tramadol-*N*-oxide (M31), OH-cyclohexyl-M1 (M32) and dehydrated tramadol-*N*-oxide), were profiled and tentatively identified on the basis of MS and MS/MS data.

Introduction

Tramadol hydrochloride (ULTRAM®), (1 *RS*, 2 *RS*)-2-[(dimethylaminomethyl]-1-(3-methoxyphenyl)-cyclohexanol HCl (figure 1), is an orally active, centrally acting opioid analgesic currently being marketed in the USA and more than 90 other nations. Following oral administration, tramadol is well absorbed and extensively metabolized, and its metabolites are excreted primarily in the urine (Lintz *et al*. 1981, Wu *et al*. 1997a–c, 2001). The mechanism of action, pharmacokinetics and clinical attributes of tramadol have been published (Flohe' *et al*. 1978, Fridericks *et al*. 1978, Lintz *et al*. 1981, Lintz and Besker 1986, Hills *et al*. 1992, Liao *et al*. 1992, Raffa *et al*. 1992, 1993, 1955, Lee *et al*. 1993, Sunshine 1994, Abel 1995, Dayer *et al*. 1997). The excretion and metabolism of tramadol in animals and humans have also been investigated, and five metabolites (M1–5), *O*-desmethyl tramadol (M1), *N*-desmethyl tramadol (M2), *N*,*N*-didesmethyl tramadol (M3), *N*,*N*,*O*-tridesmethyl tramadol (M4), *N*,*O*-didesmethyl tramadol

* Author for correspondence.

Xenobiotica ISSN 0049–8254 print/ISSN 1366–5928 online © 2002 Taylor & Francis Ltd
http://www.tandf.co.uk/journals
DOI: 10.1080/00498250110113230

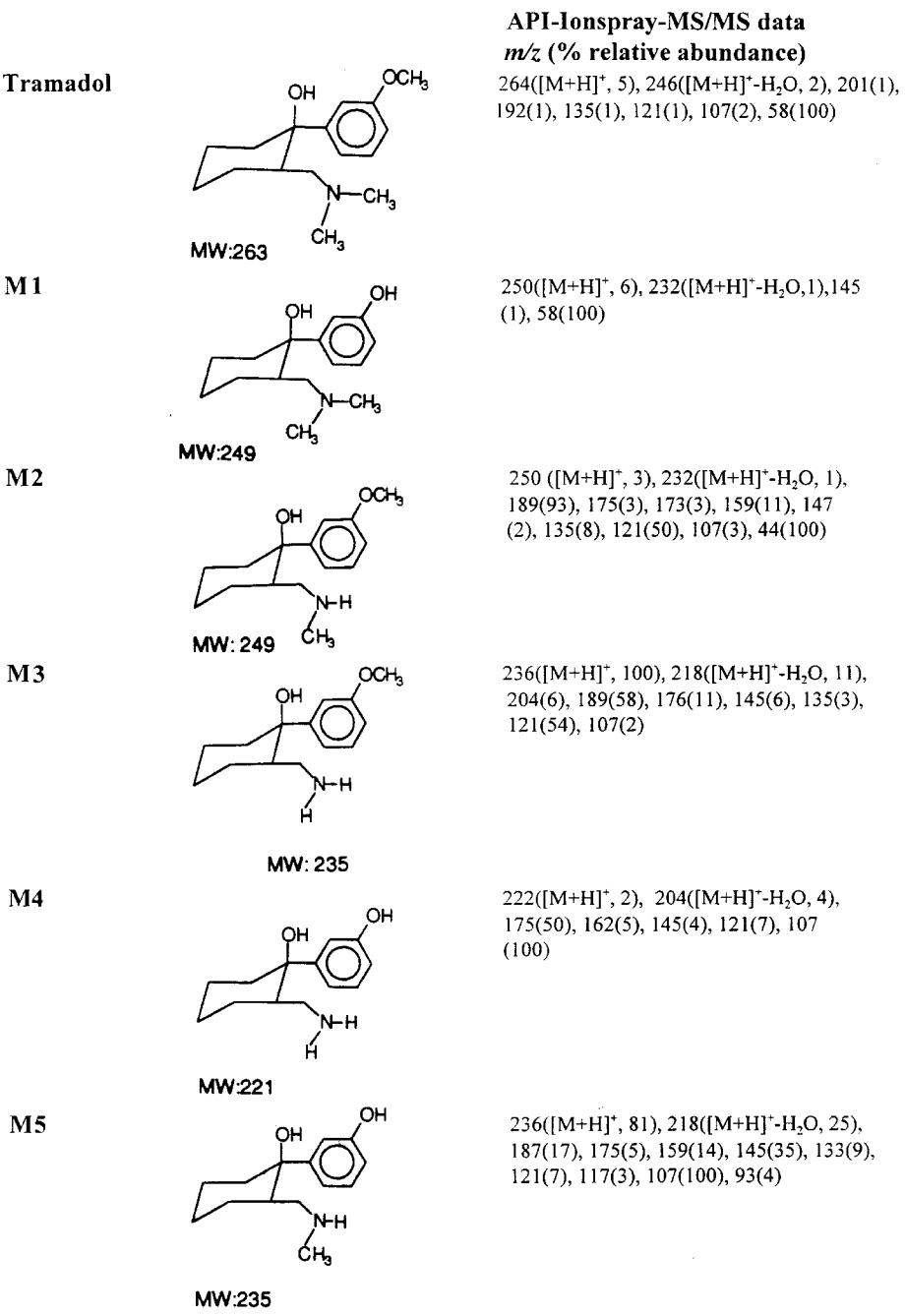
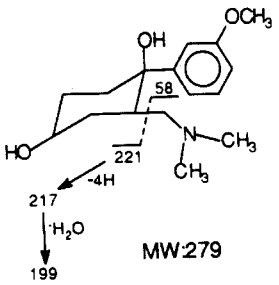


Figure 1. Structures and mass spectral data for tramadol and its metabolites.

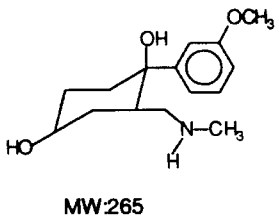
(M5), and three uncharacterized conjugates of M1, M4 and M5 have been reported (Lintz *et al.* 1981). The *in vitro* metabolism of tramadol has also been investigated and CYP2D6 and CYP3A4 identified as the principal cytochrome P450 enzymes catalysing *O*-demethylation and *N*-demethylation of tramadol in human liver microsomes (Paar *et al.* 1992, 1993, Dayer *et al.* 1997, Subrahmanyam

M6



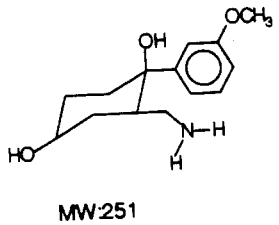
280([M+H]$^+$, 20), 262([M+H]$^+$-H_2O, 11), 217 (5), 201(2), 199(17), 184(5), 149(3), 135(10), 121(3), 107(2), 91(4), 58(100)

M7



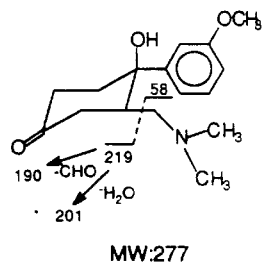
266([M+H]$^+$, 25), 248([M+H]$^+$-H_2O, 12), 187 (10), 121(26), 58(7), 44(100)

M8



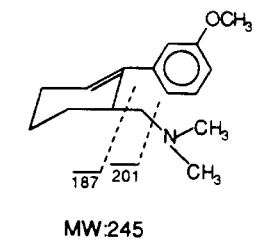
252([M+H]$^+$, 100), 234([M+H]$^+$-H_2O, 45), 217 (5), 205(86), 187(60), 121(5), 101(38)

M9



278([M+H]$^+$, 66), 260([M+H]$^+$-H_2O, 3), 219(3), 201(100), 189(2), 135(24), 121(14), 72(27), 58(28)

M10

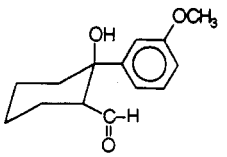


246([M+H]$^+$, 16), 201(25), 187(30), 159(10), 145(8), 135(2), 121(10), 107(2), 72(11), 58 (100)

Figure 1—(*continued*)

et al. 2001). In animal models, M1 is up to six times more potent than tramadol in producing analgesia and 200 times more potent in μ-opioid binding (Raffa *et al.* 1992). Preliminary results from our laboratories on the metabolism of tramadol in man have been reported (Wu *et al.* 1997c). The metabolism of tramadol in rat and dog describing the identification of 26 metabolites has also been reported (Wu *et al.* 2001).

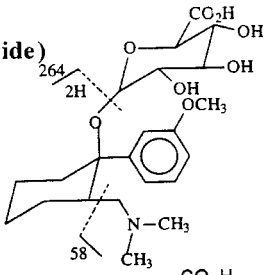
M11



235([M+H]$^+$, 60), 217([M+H]$^+$-H_2O, 78), 189 ([M+H]$^+$-H_2O-CO, 58), 171(100), 135(20), 121(22), 107(22)

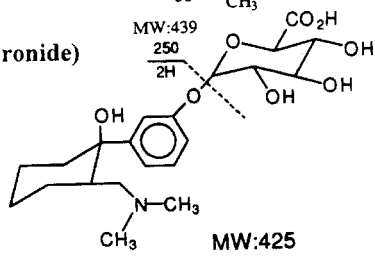
MW:234

M12
(tramadol-glucuronide)



440([M+H]$^+$, 88), 422([M+H]$^+$-H_2O, 3), 264 ([tramadol+H]$^+$, 99), 246([tramadol+H]$^+$-H_2O, 53) 187(100), 87(35), 58(7)

M13
(M1 glucuronide)

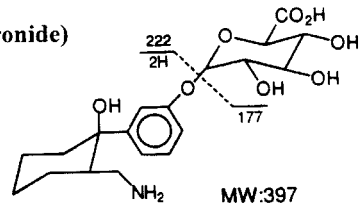


MW:439

426([M+H]$^+$, 70), 408([M+H]$^+$-H_2O, 2), 250 ([M1+H]$^+$, 17), 232([M1+H]$^+$-H_2O, 3), 58(100)

MW:425

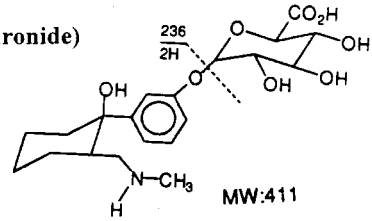
M14
(M4 glucuronide)



398([M+H]$^+$, 100), 380([M+H]$^+$-H_2O, 10), 222 (M4+H]$^+$, 42), 204([M4+H]$^+$-H_2O, 50), 117(2), 103(12)

MW:397

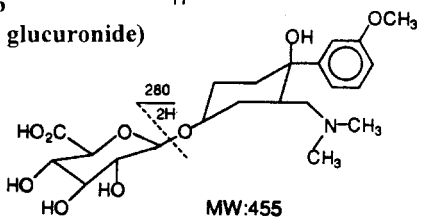
M15
(M5 glucuronide)



412([M+H]$^+$, 100), 394([M+H]$^+$-H_2O, 3), 236([M5+H]$^+$, 30), 218([M5+H]$^+$-H_2O, 4), 117(3)

MW:411

M16
(M6 glucuronide)



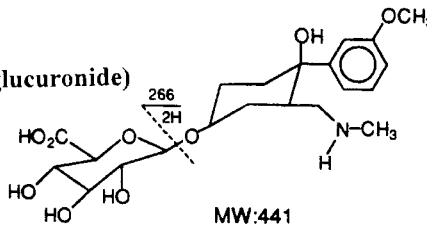
456([M+H]$^+$, 72), 438([M+H]$^+$-H_2O, 2), 280 ([M6+H]$^+$, 14), 262([M6+H]$^+$-H_2O, 4), 131(26), 58(100)

MW:455

Figure 1—(*continued*)

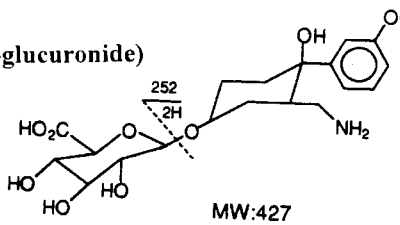
The purpose of the present study was: (1) to reconfirm the previously identified metabolites, (2) to characterize the nature of M1, M4 and M5 conjugates, and (3) to identify any other metabolites in man. The paper describes the profiling, characterization and identification of unchanged tramadol, its 23 metabolites in

M17
(M7-glucuronide)



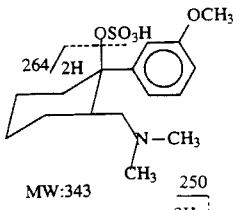
442([M+H]$^+$, 25), 424([M+H]$^+$-H_2O, 2), 266 ([M7+H]$^+$, 5), 248([M7+H]$^+$-H_2O, 12), 187 (5), 135(8), 121(3), 117(20), 58(10), 44(100)

M18
(M8-glucuronide)



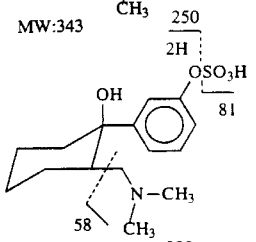
428([M+H]$^+$, 100), 410([M+H]$^+$-H_2O, 18), 252([M8+H]$^+$, 22), 235([M8+H]$^+$-NH_3, 11), 234([M8+H]$^+$-H_2O, 4), 217(21), 206(20), 130(5)

M19
(Tramadol sulphate)



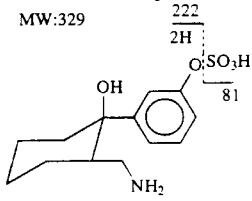
344([M+H]$^+$, 100), 327([M+H]$^+$-NH_3, 6), 262 ([tramadol+H]$^+$, 6), 165(24), 151(73), 133(94), 81(8)

M20
(M1 sulphate)



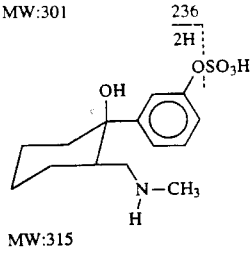
330([M+H]$^+$, 38), 313([M+H]$^+$-NH_3, 2), 250 ([M1+H]$^+$, 2), 127(23), 109(29), 85(33), 81(3), 58(100)

M21
(M4 sulphate)



302([M+H]$^+$, 100), 285([M+H]$^+$-NH_3, 15), 222 ([M4+H]$^+$, 8), 159(15), 141(38), 81(31)

M22
(M5 sulphate)

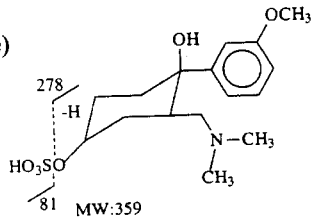


316([M+H]$^+$, 100), 299([M+H]$^+$-NH_3, 6), 281(2) 236([M5+H]$^+$, 3), 155(14), 135(5), 121(2), 113 (16)

Figure 1—(*continued*)

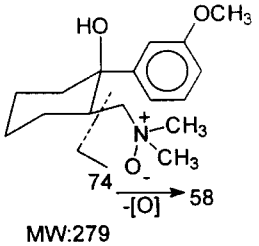
urine consisting of 11 Phase I metabolites (five known metabolites; six new metabolites) and 12 conjugates (seven glucuronides, five sulphates), and eight metabolites in liver microsomal incubates. Metabolic pathways have been proposed in a human liver microsomal fraction and in urine after oral administration of tramadol.

M23
(M6 sulphate)



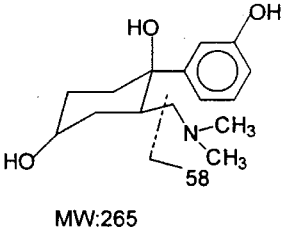
360([M+H]$^+$, 100), 343([M+H]$^+$-NH_3, 2), 278 ([M6+H]$^+$-H, 3), 201(16), 184(31), 121(33), 85(24), 81(3)

M31



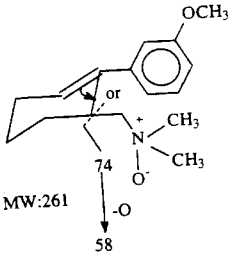
280([M+H]$^+$, 48), 262([M+H]$^+$-H_2O, 68), 201(45) 191(5), 159(8), 149(23), 135(100), 121(6), 110 (26), 107(4), 74(5), 58(58)

M32



266([M+H]$^+$, 27), 248([M+H]$^+$-H_2O, 4), 225(2), 187(1), 121(2), 58(100), 44(1)

M33



262([M+H]$^+$, 100), 202(4), 191(3), 135(80, +CH_2CH_2PhOMe), 110(32), 107(4), 74(14), 58(45), 44(76)

Figure 1—(*continued*)

Materials and methods

Chemicals and materials

Tramadol hydrochloride, (±) *cis*-2[(dimethylamino)-methyl]-1-(3-methoxyphenyl)-cyclohexanol hydrochloride (figure 1) was supplied by The R. W. Johnson Pharmaceutical Research Institute (Spring House, PA, USA). Tramadol (RWJ-26898), RWJ-41907 (M1), RWJ-41908 (M2), RWJ-41909 (M3), RWJ-41910 (M4), RWJ-41911 (M5) and RWJ-50803 (M6) (figure 1) were synthesized at the same institute. Each of the previous compounds was >97% pure by HPLC and MS. Diazald and *N*-ethyl-*N'*-nitroso guanidine were purchased from Aldrich Chemical Co. (Milwaukee, WI, USA). Glusulase was obtained from Endo Laboratory (Wilmington, DE, USA). HPLC grade solvents were obtained from Fisher Scientific (Fair Lawn, NJ, USA), and glass-distilled solvents were purchased from Burdick and Jackson Laboratories (Muskegon, MI, USA). The incubation components for hepatic S9, Tris, potassium chloride, magnesium chloride, NADPH and glucose-6-phosphate, were purchased from Sigma Co. (St Louis, MO, USA).

Hepatic S9 fraction

The human liver microsomal fraction was purchased from XenoTech LLC (Kansas City, KS, USA).

Incubation

Chilled, freshly made components were added to each flask (on ice) in the following order: 1.15% KCl in 0.05 M Tris buffer (pH 7.4), 5 mM $MgCl_2$, 5 mM glucose-6-phosphate, 0.5 mM NADPH, test substrate (microsomes) and tramadol spike to obtain a final volume of 5 ml and a tramadol concentration of 10 μg ml^{-1}. After the addition of the last component, each flask was incubated in a 37 °C Dubnoff Metabolic Shaker Incubator (Precision Scientific, Chicago, IL, USA). Samples were removed at 0, 30 and 60 min. A control flask was incubated without a rat subcellular fraction to determine drug stability under incubation conditions.

Human urine

Tramadol (100 mg/subject) was administered orally to each of three healthy male volunteers (18–45 years old, 60–75 kg) (Liao *et al.* 1992). Urine samples were obtained from 4 to 12 h post-dose and stored frozen at −20 °C.

Analytical equipment

API-ionspray MS and MS/MS spectra were obtained in a PE Sciex API-III Plus (Perkin-Elmer Sciex, Thornhill, Ontario, Canada), a triple quadrupole mass spectrometer interfaced to a Hitachi HPLC solvent delivery system (L-6200A, Intelligent Pump, Hitachi Co., Tokyo, Japan) via an ionsprayer using nitrogen as a curtain and nebulizing gas and argon as a collision gas for MS/MS and multiple reaction monitoring (MRM) analysis.

Sample preparation

A urine sample pool (4–12 h) was generated from equal aliquots of urine from each of three volunteers. The Glusulase-hydrolysed urine sample was prepared from the urine pool (5 ml) in the following manner: the urine sample was adjusted to pH 5.1 with acetic acid and buffered with 1 M sodium acetate solution (10% urine volume). Glusulase (2% by vol.) was added to this mixture and hydrolysed for 16 h at 37 °C. Each hydrolysed urine sample was twice extracted with a one-third urine volume of Amberlite XAD-2. The combined XAD-2 resin was washed with water and hexane followed by methanol extraction. Each methanol extract residue was reconstituted in a small volume of methanol and further separated and purified using LC/ionspray-MS, MS/MS and MRM. Phenolic metabolites were further derivatized as methyl and ethyl ethers by diazomethane and diazoethane, respectively. For sample preparation of untreated urine, 5 ml untreated urine pool (4–12 h) was extracted with Amberlite XAD-2/methanol, as described previously. Each methanol extract residue was reconstituted in a small volume of methanol and further analysed using LC/Ionspray-MS and MS/MS techniques.

Metabolite profiling, isolation and identification

Each HPLC analysis was conducted using a gradient programme, from 1% methanol (99% water) to 100% methanol in 10 min and 100% methanol in 2 min with both methanol and water containing 0.2% ammonium acetate at a flow rate of 1 ml min^{-1}. Unchanged tramadol and its metabolites were fractionated from the above LC system and analysed using PE Sciex API-Ionspray MS, MS/MS and MRM. The mobile phase for this system was acetonitrile/water with 2.5 mM ammonium acetate buffer (pH 4.0, 50/50, v/v) at a flow rate of 0.1 ml min^{-1}.

Data analysis

An estimate of the relative percentages of unchanged tramadol and each metabolite in a given sample was made using the integrated chromatogram, and the Sciex API III-Q1 scan MS (TIC, total ion chromatogram).

Results

Unchanged tramadol plus 26 metabolites were characterized and tentatively identified from the human urine, and human liver microsomal incubations (table 1). The *in vitro* metabolism of tramadol was conducted in the human liver microsomal fraction, and unchanged tramadol plus eight metabolites were profiled and identified in the 60-min incubation. The structures of tramadol and each metabolite and their MS data (figure 1) are presented. API-Q1 scan MS (TIC) profiles were obtained for untreated and Glusulase-treated urine (figure 2). Representative mass spectra for tramadol and its glucuronide, and M1 glucuronide

Table 1. Estimated per cent of sample of unchanged tramadol and its metabolites in the urine of subjects receiving an oral dose of tramadol (100 mg) and in human hepatic microsomes.

Analyte	Chemical	Per cent in urine (4–12 h)[a]	Per cent in microsomes (1 h)[a]
Tramadol	(±)-*cis*-2-[(dimethylamino)methyl]-1-(3-methoxyphenyl) cyclohexanol	>10	82
M1 (RWJ-41907)	*O*-desmethyl tramadol	>10	5
M2 (RWJ-41908)	*N*-desmethyl tramadol	>10	6
M3 (RWJ-41909)	*N*, *N*-didesmethyl tramadol	5–10	–
M4 (RWJ-41910)	*O*, *N*, *N*-tridesmethyl tramadol	<2	<0.5
M5 (RWJ-41911)	*O*, *N*-didesmethyl tramadol	5–10	<0.5
M6 (RWJ-50803)	4-OH-cyclohexyl tramadol	2–5	3
M7	4-OH-cyclohexyl-*N*-desmethyl tramadol	<2	–
M8	4-OH-cyclohexyl-*N*,*N*-didesmethyl tramadol	<2	–
M9	4-oxo-cyclohexyl tramadol	<2	–
M10	dehydrated tramadol	<2	–
M11	2-formyl-1-(3-methoxyphenyl) cyclohexanol	<2	–
M12	tramadol glucuronide	<2	–
M13	M1 glucuronide	2–5	–
M14	M4 glucuronide	<2	–
M15	M5 glucuronide	2–5	–
M16	M6 glucuronide	2–5	–
M17	M7 glucuronide	<2	–
M18	M8 glucuronide	<2	–
M19	tramadol sulphate	<2	–
M20	M1 sulphate	2–5	–
M21	M4 sulphate	2–5	–
M22	M5 sulphate	5–10	–
M23	M6 sulphate	<2	–
M31	tramadol *N*-oxide	–	2
M32	hydroxy-M1	–	<1
M33	dehydrated M31	–	<2

[a] Values are relative percentages of a total ion chromatogram for each analyte of the sample matrix only and, due to potential differences in the degree of ionization of each analyte, are not absolutely quantitative.

–, Not detected.

and sulphate are presented in figure 3. The proposed metabolic pathways for tramadol in humans are depicted in figure 4.

Unchanged tramadol and M1–5

Unchanged tramadol (major compound in urine: 82% in microsomes) and known metabolites 1–5 (Lintz *et al.* 1981) were reconfirmed as major metabolic products (table 1) in both untreated and Glusulase-treated urine using API-ionspray-MS, MS/MS and MRM techniques, and by comparison with synthetic samples. Following an oral dose of ^{14}C-tramadol, 30% of unchanged tramadol was excreted in the urine over 0–72 h (Lintz *et al.* 1981). The MS data are shown in figure 1. In human microsomal incubations (60 min), unchanged tramadol (82% of the sample) plus M1 and M2 as major, and M4 as trace metabolites were profiled, quantified and tentatively identified (table 1). M1 was derivatized to M1 ethyl ether ($[M + H]^+$: m/z 278).

M6–11

M6–11 were not previously identified in the human, but have been previously reported in the rat and dog (Wu *et al.* 2001). Q1 scan MS analysis of M6 revealed

an apparent protonated molecular ion at *m/z* 280 (figure 1). MS/MS analysis of protonated molecular ion displayed important daughter ions at *m/z* 262, 199, 135, 121 and 58 (base peak), together with *m/z* 280 (figure 1). On the basis of MS data and by comparison with a synthetic sample (RWJ-50803), M6 was identified as 4-hydroxycyclohexyl tramadol. API-ionspray Q1 scan MS analysis of M7–9 showed protonated molecular ions at *m/z* 266, 252 and 278, respectively (figure 1). MS/MS analysis of *m/z* 266 (protonated M7) exhibited diagnostic daughter ions at *m/z* 248, 187 and 44, along with protonated parent ion (figure 1). MS/MS analysis of protonated M8 indicated informative daughter ions at *m/z* 234, 205, 187 and 121 (figure 1). MS/MS analysis of protonated M9 revealed prominent daughter ions at *m/z* 260, 219, 201, 135, 121 and 58 (figure 1). On the basis of MS data, M7–9 were tentatively identified as 4-hydroxycyclohexyl *N*-desmethyl tramadol, 4-hydroxycyclohexyl *N*,*N*-didesmethyl tramadol, and 4-oxo-cyclohexyl tramadol, respectively. M6–9 are present in minor quantities in human urine and microsomal incubations (table 1). The stereoconfiguration of the 4-hydroxycyclohexyl metabolites of tramadol (M6–8) is still uncertain. M10 and M11 were present in trace quantities (table 1), and were not previously identified in man. MS/MS analysis of protonated M10, *m/z* 246, displayed important daughter ions at *m/z* 201, 187, 145, 135, 121, 107, 72 and 58 for the structural assignment of M10, dehydrotramadol (figure 1). MS/MS analysis of *m/z* 235 (protonated M11) revealed product ions at *m/z* 217, 189, 171, 135, 121 and 107 (figure 1). M11 was tentatively identified to be an aldehyde, an oxidative *N*-dealkylated product of tramadol.

M12–18

M12–18 were identified as glucuronides present in minor amounts in urine, and M13–15 were previously reported as M1, M4 and M5 conjugates (Lintz *et al.* 1981) (table 1). M13–18 were reported in the rat and dog (Wu *et al.* 2001). Q1 scan MS analysis of M12–18 provided apparent protonated molecular ions of glucuronides at *m/z* 440, 426, 398, 412, 456, 442 and 428 for glucuronides of tramadol, M1 and M4–8, respectively (figure 1). MS/MS analysis of each glucuronide exhibited a protonated molecular ion and a diagnostic aglycon ion as well as informative daughter ions (figure 1). These seven glucuronides of tramadol, M1 and M4–8 were tentatively elucidated on the basis of MS and MS/MS data.

M19–23

M19–23 were identified as new sulphate conjugates in human urine. M22 was present in moderate amounts, and the others were minor. Q1 scan MS analysis of M19–23 revealed apparent protonated molecular ions at *m/z* 344, 330, 302, 316 and 360 for sulphate conjugates of tramadol, M1 and M4–6, respectively (figure 1). MS/MS analysis of each sulphate displayed a protonated molecular ion and informative product ions (figure 1). The structures of the five sulphates were tentatively elucidated on the basis of MS and MS/MS data.

M31–33

M31–33 were present in minor quantities in the human liver microsomal incubations (table 1). Ionspray Q1 scan MS analysis of M31 provided an apparent

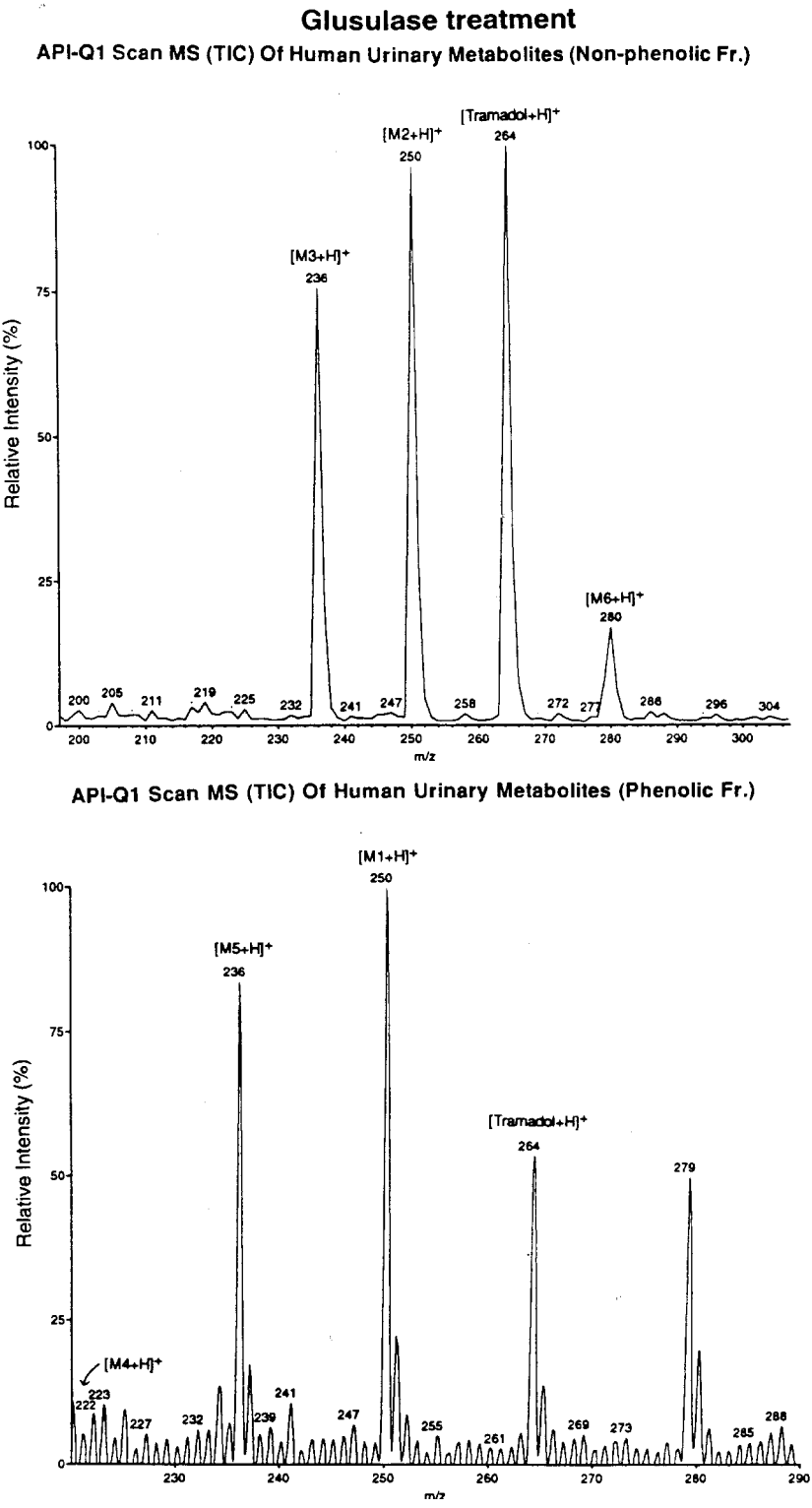


Figure 2. API-Q1 MS of tramadol metabolites in human urine.

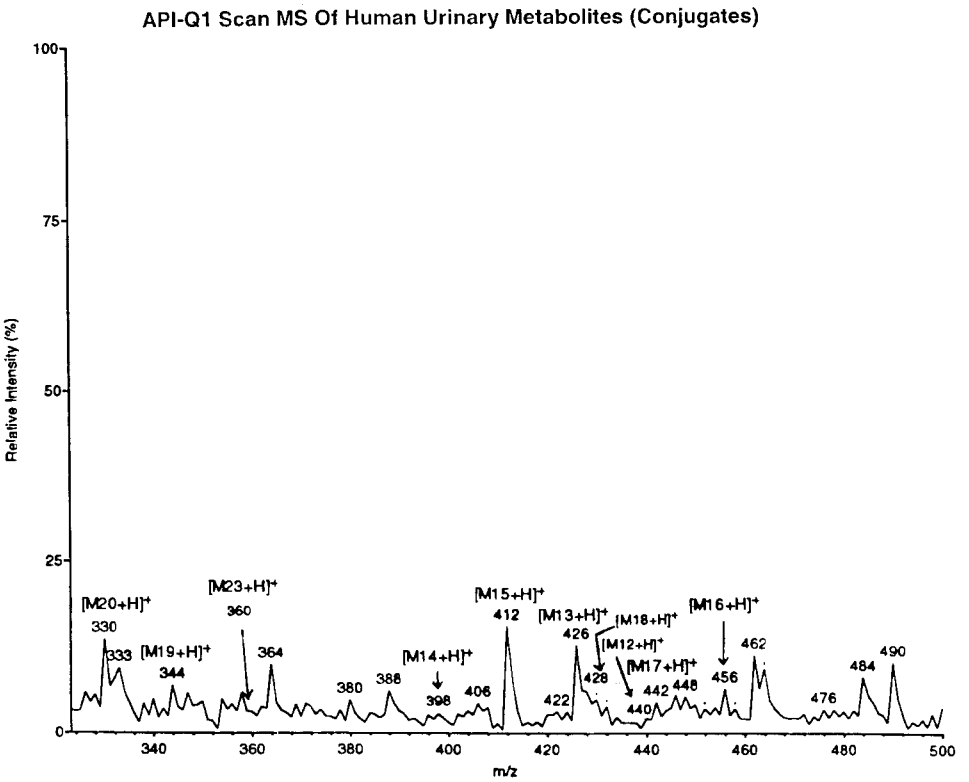


Figure 2—(*continued*)

protonated molecular ion at m/z 280, which revealed diagnostic product ions at m/z 262, 201, 159, 135, 121, 110, 107, 74 and 58 in MS/MS, and these data were identical to those MS data of synthetic tramadol-*N*-oxide (figure 1). M32 produced a protonated molecular ion at m/z 266 and product ions at m/z 248, 121 and 58 in MS/MS spectrum, and was tentatively assigned to be hydroxycyclohexyl-M1 (figure 1). Diazomethane and diazoethane converted M32 to its methyl ether (M6: $[M + H]^+$: m/z 280) and ethyl ether ($[M + H]^+$: m/z 294), respectively, which were confirmed by MS data. M33 showed a protonated molecular ion at m/z 262 with product ions at m/z 191, 135, 110, 74, 58 and 44 in MS/MS spectrum (figure 1) and was identical to those MS data of dehydrated tramadol-*N*-oxide generated by the dehydration of tramadol-*N*-oxide with methanolic potassium hydroxide solution.

Discussion

In a previous metabolism study of ^{14}C-tramadol in humans, it was determined that 90% of the radioactive dose was recovered in the 0–72-h urine (Lintz *et al.* 1981). In this investigation, unchanged tramadol and a total of 26 metabolites consisting of 14 Phase I metabolites (M1–11, 31–33) and 12 conjugates (seven glucuronides, M12–18, five sulphates, M19–23) have been characterized and tentatively identified by means of API ionspray-MS and MS/MS data in human urine and liver microsomal fractions. API ionspray-MS and MS/MS revealed

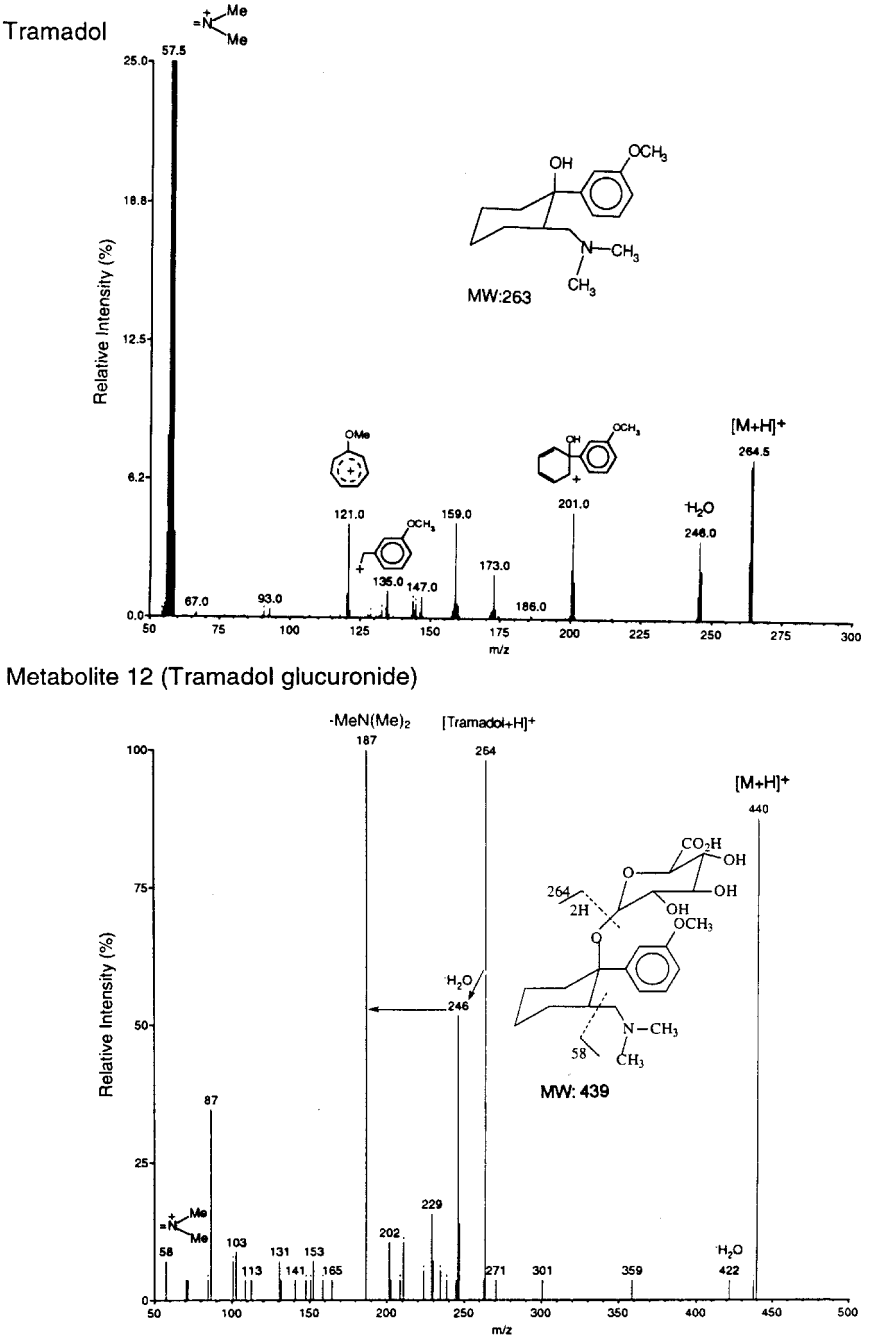


Figure 3. MS/MS spectra of tramadol, tramadol glucuronide, and M1 glucuronide and sulphate.

apparent protonated molecular ions, and prominent as well as diagnostic product ions for the structural elucidation of tramadol and its metabolites. Formation of these metabolites can be explained by six proposed pathways: *O*-demethylation, *N*-demethylation, cyclohexyl oxidation, oxidative *N*-dealkylation, dehydration

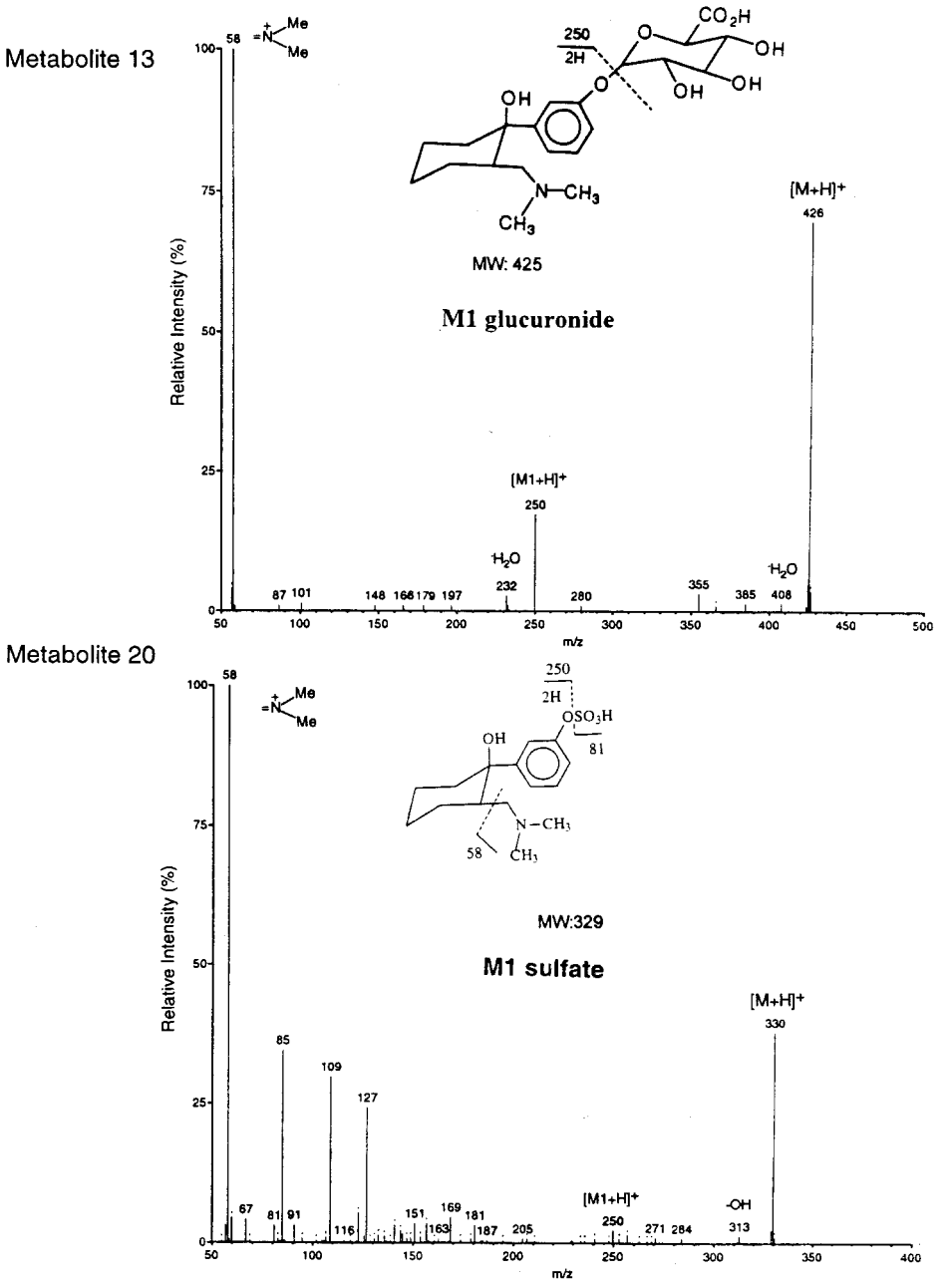


Figure 3—(*continued*)

and conjugation (figure 4). The first three and last steps appear to be the major pathways forming ten *O*-desmethyl/*N*-desmethyl metabolites and hydroxycyclohexyl metabolites of tramadol, M1–7 in both human urine and microsomal fractions as major/moderate quantities, and M31–33 in hepatic microsomes as minor Phase I metabolites (table 1). M1 is the only metabolite that has shown to have more analgesic activity than tramadol (Flick *et al.* 1978, Frankus *et al.* 1978,

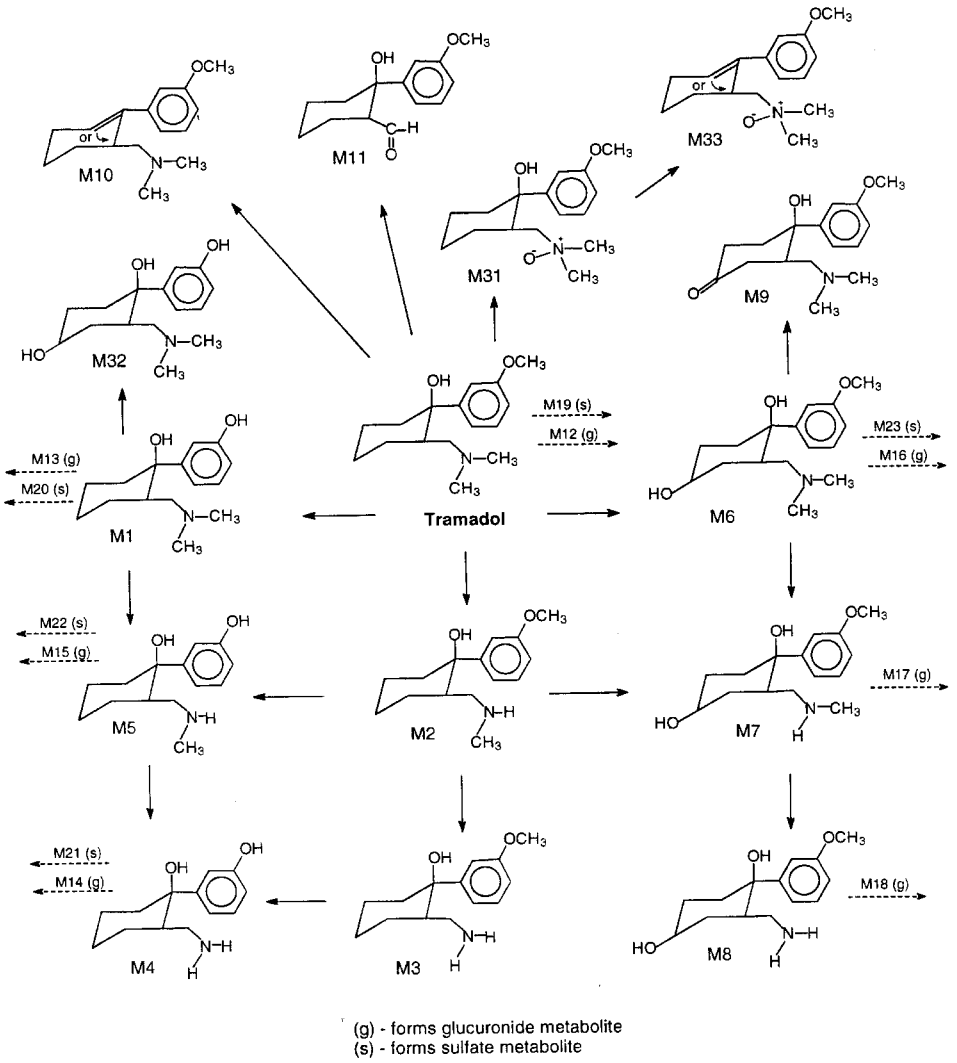


Figure 4. Proposed metabolic pathways for tramadol in humans.

Raffa *et al.* 1992, 1993). The cyclohexyl oxidation of tramadol, forming M6–9 and their subsequent glucuronides, is a newly identified pathway that is only significant in the rat and dog. The first three steps in conjunction with the last step produced seven minor glucuronides (M12–18) and five sulphates (M19–23) in urine (table 1). Of the 26 identified metabolites in man, seven metabolites (M12, 19–23, 33) have not been found in the rat and dog (Wu *et al.* 2001). In summary, tramadol was rapidly and extensively metabolized after oral administration, and renal excretion was the major route of elimination of tramadol and its metabolites.

Acknowledgement

The authors thank Dr K. L. Sorgi and Miss L. Scott for synthesizing the tramadol metabolites.

References

Abel, S. R., 1995, Tramadol: an alternative analgesic to traditional opioids and NSAIDs. *Journal Pharmaceutical Care in Pain and Symptom Control*, **3**, 5–29.

Dayer, P., Desmeules, J. and Collart, L., 1997, Pharmacologie du tramadol. *Drugs*, **53 (suppl. 2)**, 18–24.

Flick, K., Frankus, E. and Fridericks, E., 1978, Studies on chemical structure and analgesic activity of phenyl substituted aminomethylcyclohexanols. *Arzneim-Forsch/Drug Research*, **28**, 107–113.

Flohe', L., Arend, I., Cogal, A., Richter, W. and Simon, W., 1978, Klinische prufung der abhangigkeitsentwicklung nach langzeitapplikation von tramadol. *Arzneim-Forsch/Drug Research*, **28**, 213–217.

Frankus, E., Fridericks, E., Kim, S. M. and Osterloh, G., 1978, On separation of isomers, structural elucidation and pharmacological characterization of 1-(*m*-methoxyphenyl)-2-(dimethylamino-methyl)-cyclohexan-1-ol. *Arzneim-Forsch/Drug Research*, **28**, 114–121.

Fridericks, E., Felgenhauer, F., Jonschaap, P. and Osterloh, G., 1978, Pharmakologische untersuchungen zur analgesie, abhangigkeits und toleranzen-twicklung von tramadol, einem stark wirkenden analgetikum. *Arzneim-Forsch/Drug Research*, **28**, 122–134.

Hills, J. F., Liao, S. and Nayak, R. K., 1992, The effect of food on the bioavailability of tramadol. 1992 AAPS Eastern Regional Meeting, abst 32.

Lee, R. C., McTavish, D. and Sorkin, E. M., 1993, Tramadol, a preliminary review of its pharmacodynamic and pharmacokinetic properties, and therapeutic potential in acute and chronic pain states. *Drugs*, **46**, 313–340.

Liao, S., Hill, J. F. and Nayak, R. K., Pharmacokinetics of tramadol following single and multiple oral doses in man. 1992 AAPS Annual Meeting, abst PPDM 8206; *Pharmaceutical. Research*, **9 (suppl. 1)**, 308.

Lintz, W. and Besker, R., 1986, Determination of tramadol in human serum by capillary gas chromatography with nitrogen-selective detection. *Journal of Chromatography*, **377**, 213–220.

Lintz, W., Erlacin, S., Frankus, E. and Uragg, H., 1981, Metabolismus von tramadol bei mensch und tier. *Arzneim-Forsch/Drug Research*, **31**, 1932–1943.

Paar, W. D., Frankus, P. and Dengler, H. J., 1992, The metabolism of tramadol by human liver microsomes. *Clinical Investigation*, **70**, 708–710.

Paar, W. D., Poche, S., Gerlo, J. and Dengler, H. J., 1993, *In vivo* investigation of the metabolism of tramadol – further evidence for *O*-demethylation polymorphism. *Naunyn-Schmiedeberg's Archives of Pharmacology*, **347 (suppl. R39)**, 154.

Raffa, R. B., Friderichs, E., Reimann, W., Shank, R. P., Codd, E. E. and Vaught, J. L., 1992, Opioid and nonopioid components independently contribute to the mechanism of action of tramadol, an 'atypical' opioid analgesic. *Journal of Pharmacology and Experimental Therapeutics*, **260**, 275–285.

Raffa, R. B., Friderichs, E., Reimann, W., Shank, R. P., Codd, E. E., Vaught, J. L., Jacoby, H. I. and Selve, N., 1993, Complementary and synergistic antinociceptive interaction between the enantiomers of tramadol. *Journal of Pharmacology and Experimental Therapeutics*, **267**, 331–340.

Raffa, R. B., Nayak, R. K. and Liao, S., 1995, The mechanism(s) of action and pharmacokinetics of tramadol. *Reviews in Contemporary Pharmacotherapeutics*, **6**, 485–497.

Subrahmanyam, V., Renwick A. B., Walters D. G., Young P. J., Price R. J., Tonelli A. P. and Lake, B. G., 2001, Identification of cytochrome p-450 isoforms responsible for *cis*-tramadol metabolism in human liver microsomes. *Drug Metabolism and Disposition*, **29**, 1146–1155.

Sunshine, A., 1994, New clinical experience with tramadol. *Drugs*, **47 (suppl. 1)**, 8–18.

Wu, W. N., Desai, D., McKown, L. A., Gauthier, A. D., Jones, W. J., Takacs, A. R., Scott, L., Sorgi, K. L. and Raffa, R. B., 1997a, Metabolism of Ultram® (tramadol) in the dog. In *ISSX Proceedings of the 6th European ISSX Meeting*, **11**, 160 (abst).

Wu, W. N., McKown, L. A., Jones, W. J., Gauthier, A. D. and Takacs, A. R., 1997b, Metabolism of Ultram® (tramadol) in the rat. In *ISSX Proceedings of the 8th North American ISSX Meeting*, **12**, 107 (abst).

Wu, W. N., Liao, S., McKown, L. A. and Takacs, A. R., 1997c, Metabolism of Ultram® (tramadol) in the human. *ISSX Proceedings of the 6th European ISSX Meeting*, **11**, 159 (abst).

Wu, W. N., McKown, L. A., Gauthier, A. D., Jones. W. J. and Raffa, R. B., 2001, Metabolism of the analgesic drug, tramadol hydrochloride, in rats and dogs. *Xenobiotica*, **31**, 423–441.

XENOBIOTICA, 2002, VOL. 32, NO. 5, 427–439

Taylor & Francis
healthsciences

Hydromorphone metabolites: isolation and identification from pooled urine samples of a cancer patient

M. ZHENG†§, K. M. MCERLANE†* and M. C. ONG‡

† Faculty of Pharmaceutical Sciences, University of British Columbia, 2146 East Mall, Vancouver, BC V6T 1Z3, Canada
‡ Chronic Pain Day Program, St Paul's Hospital, Vancouver, BC V6Z 1Y6, Canada

Received 28 August 2001

1. Hydromorphone-3-glucuronide, dihydromorphine, dihydroisomorphine, dihydromorphine-3-glucuronide and dihydroisomorphine-3-glucuronide were isolated from a cancer patient's urine and identified as metabolites of hydromorphone by comparison with synthetic standards using LC/MS/MS with gradient elution.

2. The relative urinary recovery of dihydroisomorphine-3-glucuronide was estimated to be 17-fold higher than previously reported.

3. Three new metabolites, including hydromorphone-3-sulphate, norhydromorphone and nordihydroisomorphine, were tentatively identified.

Introduction

Hydromorphone, or dihydromorphinone, is a semisynthetic potent opioid that is about eight times more potent than morphine (Mahler and Forrest 1975). Since its first clinical use in 1926 (Eddy 1993), hydromorphone has been commonly used to relieve both cancer pain (Bruera *et al.* 1988, Ferris *et al.* 1990, Moulin *et al.* 1991, Vanier *et al.* 1993, Hays *et al.* 1994) and postoperative pain (Dougherty *et al.* 1989, Brodsky *et al.* 1990, Wallenstein *et al.* 1990, Searle *et al.* 1994, Liu *et al.* 1995). Hydromorphone provides a useful alternative to morphine in situations where adverse effects, such as nausea, sedation and myoclonus, remain significant problems (Librach 1991). In addition, the high water solubility of hydromorphone hydrochloride (five times more soluble than morphine sulphate (Budavari 1989) is an important advantage over morphine when concentrated preparations or small volume delivery, such as subcutaneous infusion, are required. Subcutaneous infusion of hydromorphone has been widely accepted for the management of chronic cancer pain (Ferris *et al.* 1990, Moulin *et al.* 1991, Bruera *et al.* 1993, Vanier *et al.* 1993).

Structurally, hydromorphone differs from morphine in two respects, namely the saturation of the 7,8-double bond and the replacement of the 6-hydroxy group by a 6-keto group. Although hydromorphone is commonly prescribed for pain management, information on its metabolic fate is scant. Roerig *et al.* (1973) reported the isolation of hydromorphone-3-glucuronide and dihydromorphine-3-glucuronide from rabbit urine after hydromorphone administration. A more

* Author for correspondence; e-mail: tuit@interchange.ubc.ca.
§ Present address: Metabolism and Pharmacokinetics, Pharmaceutical Research Institute, Bristol-Myers Squibb Co., Wallingford, CT06067, USA

Xenobiotica ISSN 0049–8254 print/ISSN 1366–5928 online © 2002 Taylor & Francis Ltd
http://www.tandf.co.uk/journals
DOI: 10.1080/00498250110119090

extensive study by Cone *et al.* (1977) in several species, including humans, indicated that hydromorphone was metabolized to conjugated hydromorphone, dihydromorphine (6α-hydroxy hydromorphone) and dihydroisomorphine (6β-hydroxy hydromorphone). The precise identities of these conjugates, however, were not characterized. The overall urinary recoveries of these metabolites plus hydromorphone in humans only accounted for 43.5% of the administered dose. Dihydromorphine and dihydroisomorphine have been reported to exhibit 65 and 21% of the analgesic activity of hydromorphone, respectively, as determined by mechanical clip test (Small *et al.* 1938).

Morphine undergoes extensive metabolism and forms morphine-3-glucuronide, morphine-6-glucuronide, morphine-3-sulphate, normorphine and some other minor metabolites (Boerner *et al.* 1975). Both morphine-6-glucuronide and normorphine possess analgesic activity (Hanna *et al.* 1990, Gong *et al.* 1991, Osborne *et al.* 1992, Zaw-Tun and Bruera 1992, Thompson *et al.* 1995). In view of the structural similarities between hydromorphone and morphine and the unaccounted mass balance, the existence of additional unidentified metabolites of hydromorphone was considered a possibility. Thus, the objectives of the present study were to isolate and identify the above known metabolites as well as to search for the presence of new metabolites in cancer patients' urine using HPLC/mass spectrometry/mass spectrometry (LC/MS/MS).

Materials and methods

Materials

Hydromorphone hydrochloride was a generous gift from Knoll Pharma, Inc. (Mississauga, ON, Canada). Morphine sulphate·$5H_2O$ was obtained from BDH, Inc. (Toronto, ON, Canada). Amberlite XAD-2 resin was obtained from Supelco (Oakvill, ON, Canada). Palladium on activated carbon (Pd 10%) was obtained from Aldrich (Milwaukee, WI, USA). Formamidinesulphinic acid and 2,3,4-tri-*O*-acetyl-1α-bromo-1-deoxy-D-glucopyranuronyl methyl ester were obtained from Sigma Chemical Co. (St Louis, MO, USA). Lithium hydroxide·H_2O was obtained from Anachemia Science (Montreal, PQ, Canada). Trifluoroacetic acid (TFA) was obtained from Fisher (Fair Lawn, NJ, USA). D_6-DMSO was obtained from Matheson (Miamisburg, OH, USA). Other reagents were of analytical grade and the solvents were of HPLC grade. Purified water was produced using a Milli-Q water purification system (Mississauga, ON, Canada).

Isolation of hydromorphone and its metabolites from patient urine

The urine sample was obtained from a female patient with multiple myeloma and who had been under chronic hydromorphone monotherapy for analgesia for 2 weeks (subcutaneous infusion, 4 mg every 3 h) in St Paul's hospital, Vancouver, British Columbia. The urine was collected over 48 h. An aliquot of 1300 ml urine was applied to an Amberlite XAD-2 resin column (4 × 18 cm). The column was washed with 180 ml water and the analytes were subsequently eluted with 240 ml methanol. The methanol eluent was concentrated under vacuum. The residue was reconstituted in 13 ml water and the pH was adjusted to 9.5–10 with 5% ammonium hydroxide. The aqueous solution was extracted with 25 ml ethyl acetate (twice). The organic and aqueous phases were separated and both were concentrated under vacuum. Before the LC/MS/MS analysis, the residues from the aqueous phase were dissolved in 1 ml water, whereas the residues from the organic phase were dissolved in 700 µl methanol. An aliquot of 100 µl was taken from each sample and both were further diluted 20 times. An aliquot of 20 µl of the final solution was analysed by LC/MS/MS.

LC/MS/MS system

The LC/MS/MS system consisted of a HP Series II 1090 liquid chromatograph (Hewlett Packard, Avondale, PA, USA), a Zorbax SB-phenyl column (4.6 mm × 25 cm) (Rockland Technologies, Inc., Newport, DE, USA) and a VG Quattro triple quadrupole mass spectrometer equipped with an electrospray interface (Fisons, Altrincham, UK).

The separation of hydromorphone and its metabolites was achieved by HPLC using gradient elution. Mobile phase A consisted of 0.05% TFA in 10% methanol; mobile phase B consisted of 0.05% TFA in 90% methanol. The initial elution condition was 10% of B maintained for 6 min and increased to 30% of B over the next 8 min and 80% of B over a further 16 min. The flow rate was 0.7 ml min^{-1}. The LC effluent was split and 10% of the effluent was introduced into MS.

The electrospray source was operated with a capillary voltage of 3.4 kV, a cone voltage of 29 V and a source temperature of 100 °C. The MS/MS analysis was performed in the multiple reaction monitoring (MRM) mode. The first MS (MS1) was static at a preselected parent ion masses. The selected parent ions were introduced into the collision cell and the fragmentation occurred at a collision energy of 70 eV. Argon was used as a collision gas at a pressure of 3×10^{-3} mbar. The second MS (MS2) was static at pre-determined daughter ion masses produced from the fragmentation in the collision cell. A dwell time of 0.5 s was used for monitoring.

Synthesis of dihydromorphine

Dihydromorphine was synthesized by catalytic hydrogenation of morphine following the method reported by Small and Lutz (1932). Accordingly, 40 mg 10% palladium on activated carbon was added to 3.3 g (8 mmol morphine base) of morphine sulphate in 85 ml water. This solution was shaken with hydrogen at 44 psi for 45 min. After filtration, the pH of the reaction mixture was adjusted to 9.8 by the addition of 1.5 M Na_2CO_3 solution and dihydromorphine base separated as needles. The product was recrystallized from methanol with a yield of 2.3 g (92%), m.p. 150–155 °C with decomposition at 155–157 °C (lit. m.p. 155–157 °C with decomposition (Small and Lutz 1932). The ^{1}H-NMR spectrum in d_6-DMSO exhibited signals at: δ2.22 (s, 3H, NCH_3; 3.80 (m, 1H, 6β-H); 4.44 (d, $J = 5$ Hz, 1H, 5β-H); 6.40, 6.53 (d, $J = 8$ Hz, 2H, 1-H, 2-H), 8.73 (s, 1H, 3-OH).

The hydrochloride salt was obtained by dissolving the base in methanol and treating with ethanolic HCl solution. LC/MS: $[M + 1]^+$ 288 (100%); IR (Nujol mull): 3390 cm^{-1} (free OH), 3140 cm^{-1} (bonded OH), 2687 cm^{-1} (tertiary amine salt); UV λ_{max} (water): 284 nm; UV λ_{max} (0.1 N NaOH): 296 nm. Anal. calcd. for $C_{17}H_{21}NO_3 \cdot HCl$: C, 63.05; H, 6.86; N, 4.33. Found: C, 62.95; H, 7.05; N, 4.31.

Synthesis of dihydroisomorphine

The synthesis of dihydroisomorphine was accomplished by adaptation of a method for stereospecific synthesis of 6-β-hydroxy metabolites of naltrexone and naloxone (Chatterjie *et al.* 1975). Water (20 ml) was added to dissolve 1.3 g (4 mmol) hydromorphone hydrochloride. To the above solution was added, drop wise with magnetic stirring, 1.7 g (16 mmol) acid dissolved in 170 ml 0.2 N NaOH. The reaction mixture was heated on a water bath at 80–85 °C with magnetic stirring for 3.5 h. The mixture was allowed to cool and the pH was adjusted to 9.8 with sodium hydroxide solution. The solution was extracted with 150 ml ethyl acetate four times. The base was obtained by evaporation of the organic extract to dryness with a rotary evaporator. The product was recrystallized from methanol with a yield of 0.3 g (26%), m.p. 225–227 °C with decomposition at 227 °C. The ^{1}H-NMR spectrum in d_6-DMSO exhibited signals at: δ2.29 (s, 3H, NCH_3); 3.10 (m, 1H, 6α-H); 4.12 (d, $J = 6$ Hz, 1H, 5β-H); 6.45, 6.54 (d, $J = 8$ Hz, 2H, 1-H, 2-H), 8.95 (s, 1H, 3-OH).

The hydrochloride salt was obtained by dissolving the base in methanol and treating with ethanolic HCl solution. LC/MS: $[M + 1]^+$ 288 (100%). IR (Nujol mull): 3363 cm^{-1} (free OH), 3127 cm^{-1} (bonded OH), 2644 cm^{-1} (tertiary amine salt); UV λ_{max} (water): 282 nm; UV λ_{max} (0.1 N NaOH): 296 nm. Anal. calcd. for $C_{17}H_{21}NO_3 \cdot HCl$: C, 63.05; H, 6.86; N, 4.33. Found: C, 63.19; H, 6.83; N, 4.31.

Synthesis of hydromorphone-3-glucuronide

Hydromorphone-3-glucuronide was prepared by adaptation of a method described by Berrang *et al.* (1975) for the preparation of morphine-3-glucuronide. To a solution of hydromorphone base (2.3 g, 8 mmol) and lithium hydroxide (0.3 g) in methanol (13 ml) was added 2.3 g (6 mmol) of 2,3,4-tri-*O*-acetyl-1α-bromo-1-deoxy-D-glucopyranuronic methyl ester as a solid. The mixture was stirred and allowed to stand at room temperature for 4 h. A solution of lithium hydroxide (0.68 g) in water (13 ml) was then added and the mixture stirred for an additional 1 h. The pH of the mixture was reduced to about 9.5 with acetic acid. Unreacted hydromorphone (1.2 g) was recovered by extraction with 4 vol ethyl acetate. The remaining reaction mixture was concentrated to a viscous liquid under vacuum and taken up in 29 ml methanol. The solution was treated with ethanolic hydrochloric acid solution to pH 7–8 and crystallization occurred at −10 °C overnight. The crystals were filtered and recrystallized from methanol/water (50/50 v/v). The yield was 0.54 g (15%); m.p. 225–227 °C with decomposition. The ^{1}H-NMR spectrum in d_6-DMSO exhibited signals at: δ2.40 (s, 3H, $=N^+HCH_3$), 4.92 (s, 1H, 5β-H), 5.23 (d, $J = 7$ Hz, 1H, 1′-H), 6.65, 6.82 (d, $J = 9$ Hz, 2H, 1-H, 2-H). LC/MS: $[M + 1]^+$ 462 (100%); IR (Nujol mull): 3650–3110 cm^{-1} (broad, bonded and free OH), 2670 cm^{-1} (tertiary ammonium ion), 1724 cm^{-1} ($\nu_{C=O}$), 1590 cm^{-1} ($-COO^-$); UV λ_{max} (water): 278 nm; UV λ_{max} (0.1 N NaOH), 278 nm. Anal. calcd. for $C_{23}H_{27}NO_9 \cdot 3H_2O$: C, 53.59; H, 6.26; N, 2.72. Found: C, 53.61; H, 6.31; N, 2.73.

Synthesis of dihydromorphine-3-glucuronide

Dihyromorphine-3-glucuronide was prepared following the same procedures as for the synthesis of hydromorphone-3-glucuronide. To a solution of dihydromorphine hydrochloride (1.0 g, 3.1 mmol) and lithium hydroxide (0.25 g) in methanol (5 ml) was added 1.0 g (2.5 mmol) of 2,3,4-tri-*O*-acetyl-1α-bromo-l-deoxy-D-glucopyranuronic methyl ester as a solid. After recrystallization, a yield of 0.36 g (25%) was obtained; m.p. 230–233 °C with decomposition. The ^{1}H-NMR spectrum in d_6-DMSO exhibited signals at: δ2.56 (s, 3H, $=N^+NCH_3$), 3.86 (m, 1H, 6β-H), 4.53 (d, $J = 5$ Hz, 1H, 5β-H), 5.19 (d, $J = 7$ Hz, 1H, 1′-H), 6.59, 6.70 (d, $J = 9$ Hz, 2H, 1-H, 2-H). LC/MS: $[M + 1]^+$ 464 (100%); IR (Nujol mill): 3650–3110 cm^{-1} (broad, bonded and free OH), 2660 cm^{-1} (tertiary ammonium ion), 1597 cm^{-1} ($-COO^-$); UV λ_{max} (water): 280 nm; UV λ_{max} (0.1 N NaOH): 280 nm. Anal. calcd. for $C_{23}H_{29}NO_9 \cdot 2.5H_2O$: C, 54.32; H, 6.74; N, 2.75. Found: C, 54.33; H, 6.58; N, 2.76.

Synthesis of dihydroisomorphine-3-glucuronide

Dihyroisomorphine-3-glucuronide was prepared following the same procedures as for the synthesis of hydromorphone-3-glucuronide. To a solution of dihydroisomorphine base (0.4 g, 1.4 mmol) and lithium hydroxide (0.056 g) in methanol (3 ml) was added 0.4 g (1 mmol) of 2,3,4-tri-*O*-acetyl-1α-bromo-l-deoxy-D-glucopyranuronic methyl ester as a solid. After recrystallization, a yield of 0.27 g (42%) was obtained; m.p. 245–248 °C with decomposition. The ^{1}H-NMR spectrum in d_6-DMSO exhibited signals at: δ2.55 (s, 3H, $=N^+HCH_3$), 4.23 (d, $J = 7$ Hz, 1H, 5β-H), 5.30 (d, $J = 7$ Hz, 1H, 1′-H), 6.64, 6.80 (d, $J = 9$ Hz, 2H, 1-H, 2-H). LC/MS: $[M + 1]^+$ 464 (100%); IR (Nujol mull): 3650–3110 cm^{-1} (broad, bonded and free OH), 2650 cm^{-1} (tertiary ammonium ion), 1585 cm^{-1} ($-COO^-$); UV λ_{max} (water): 278 nm; UV λ_{max} (0.1 N NaOH): 278 nm. Anal. calcd. for $C_{23}H_{29}NO_9 \cdot 2H_2O$: C, 55.30; H, 6.66; N, 2.80. Found: C, 55.28; H, 6.53; N, 2.79.

Results

Synthesis

Dihydromorphine, dihydroisomorphine and the 3-*O*-glucuronides of hydromorphone, dihydromorphine and dihydroisomorphine were synthesized by adaptation of methods for the preparation of structurally similar compounds. Dihydroisomorphine was synthesized according to the method of stereospecific synthesis of the 6β-hydroxy derivatives of naltrexone and naloxone (Chatterjie *et al.* 1975). The 6β-hydroxy derivatives of naltrexone and naloxone were synthesized with no indication of the presence of 6α isomers. In our case, however, we observed the presence of about 10% of the 6α isomer (dihydromorphine). Dihydroisomorphine was further purified by recrystallization. The orientation of the 6β-hydroxy group was confirmed by the observed upfield shifts in NMR due to 5β-H and 6α-H, as compared with the values due to 5β-H and 6β-H on dihydromorphine (Okuda *et al.* 1964).

The 3-*O*-glucuronide conjugates were prepared, with modifications, following the method of Berrang *et al.* (1975) for the synthesis of morphine-3-glucuronide. This method simplified the procedure of Yoshimura *et al.* (1968). The crystallization of these glucuronides from methanol was facilitated by adjusting the pH to 7–8 with ethanolic hydrochloric acid solution. No precipitation was observed after 1.2 mg of each of the glucuronides was added to 1.5 ml 0.1 N $AgNO_3$ solution, which indicated that hydrochloride salt was not formed for these glucuronides. In contrast, 0.5 mg hydromorphone hydrochloride showed a strong positive result.

The β-configuration of the glycosidic linkage in the glucuronides was supported by the NMR results that showed a resonance signal at δ5.19–5.30 due to the axial 1′-H on the glucuronic acid moiety, whereas a signal would have appeared at around δ6.31 due to an equatorial 1′-H if it were the α-isomer (Yoshimura *et al.* 1968). An absence of a bathochromic shift in UV λ_{max} in the alkaline medium, which would occur in compounds possessing a free phenolic group as seen with

dihydromorphine and dihydroisomorphine, further supported the formation of the 3-*O*-glucuronide conjugate. Furthermore, NMR results also confirmed the formation of the 3-*O*-glucuronide conjugate because a singlet due to the 3-hydroxy proton, which appeared at δ8.73 and 8.95 for dihydromorphine and dihydroisomorphine, respectively, was not seen with hydromorphone-3-glucuronide. The IR results showed a strong peak at 1585–1597 cm^{-1} and a broad absorption around 2650–2670 cm^{-1}, suggesting the existence of a carboxylate anion and a positive charge on the piperidine nitrogen.

Identification of hydromorphone and its metabolites in cancer patient urine by LC/MS/MS

The separation of hydromorphone and the five synthetic standards was achieved by a gradient elution followed by MS/MS detection performed in the MRM mode, which is a highly specific technique for rapid screening of biological sample for known or new metabolites. Figure 1 shows the mass chromatograms of the six standards and table 1 presents the mass/charge ratios (m/z) and the retention times of the parent and daughter ions. The daughter ions of the three glucuronide conjugates were produced by the common loss of the glucuronic acid moiety (m/z 176), whereas the three free compounds produced a common daughter ion of m/z 185. The relative elution orders of dihydromorphine-3-glucuronide to dihydroisomorphine-3-glucuronide, and dihydromorphine to dihydroisomorphine had been previously determined on a HPLC-UV system with the same gradient elution program.

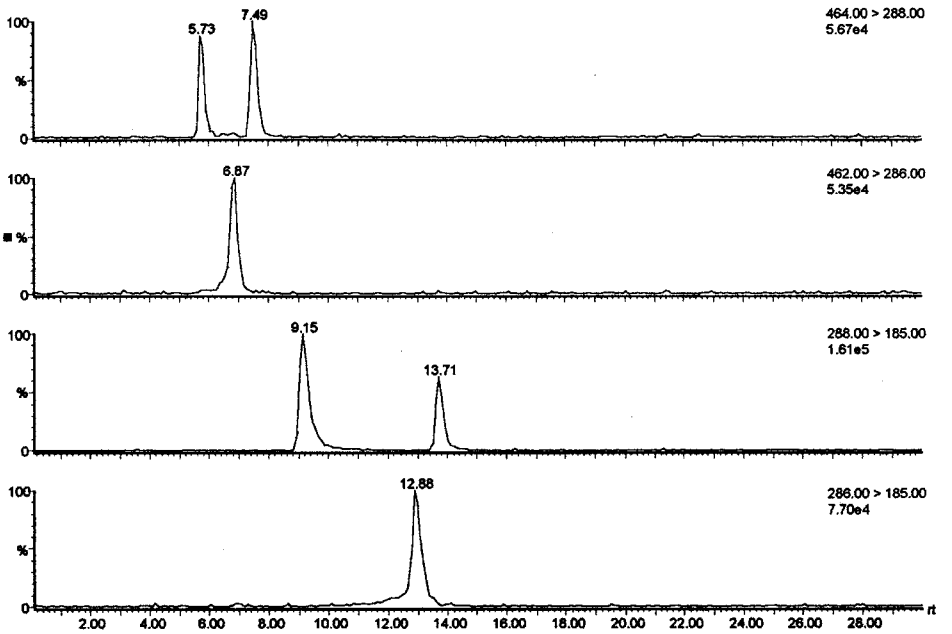


Figure 1. MRM traces of standards: dihydromorphine-3-glucuronide, 5.73 min; hydromorphone-3-glucuronide, 6.87 min; dihydroisomorphine-3-glucuronide, 7.49 min; dihydromorphine, 9.15 min; hydromorphone, 12.88 min; dihydroisomorphine, 13.71 min.

Table 1. LC/MS/MS characteristics of hydromorphone and its metabolites.

Compound	Parent $(M+1)^+$ (m/z)	Daughter (m/z)	Retention times (min)	
			Standard	Urine
Dihydromorphine-3-glucuronide	464	288 $(M+1)^+$	5.73	5.62
Hydromorphone-3-glucuronide	462	296 $(M+1)^+$	6.87	6.66
Dihydroisomorphine-3-glucuronide	464	288 $(M+1)^+$	7.49	7.39
Dihydromorphine	288	185	9.15	9.15
Hydromorphone	286	185	12.88	12.78
Dihydroisomorphine	288	185	13.71	13.71

Figures 2 and 3 show the mass chromatograms of metabolites isolated from patient urine samples dissolved in methanol and water, respectively. The presence of all of the five metabolites plus hydromorphone were confirmed by comparing the retention times with those of the standards (table 1). Owing to the differences in hydrophilicity of the compounds, the three glucuronide conjugates are present at much higher levels in the aqueous sample than in the methanolic sample, whereas the unconjugated compounds are present in much higher concentrations in the methanolic sample than in the aqueous sample.

To obtain an estimation of the relative levels of the six compounds in the above urine samples, a standard solution was prepared with known amounts of the six standards added (table 2). This standard solution was analysed under the same chromatographic conditions as used for the urine sample, but without prior extraction. The peak areas for each compound were recorded. Only compounds with similar physicochemical properties were compared because the glucuronide

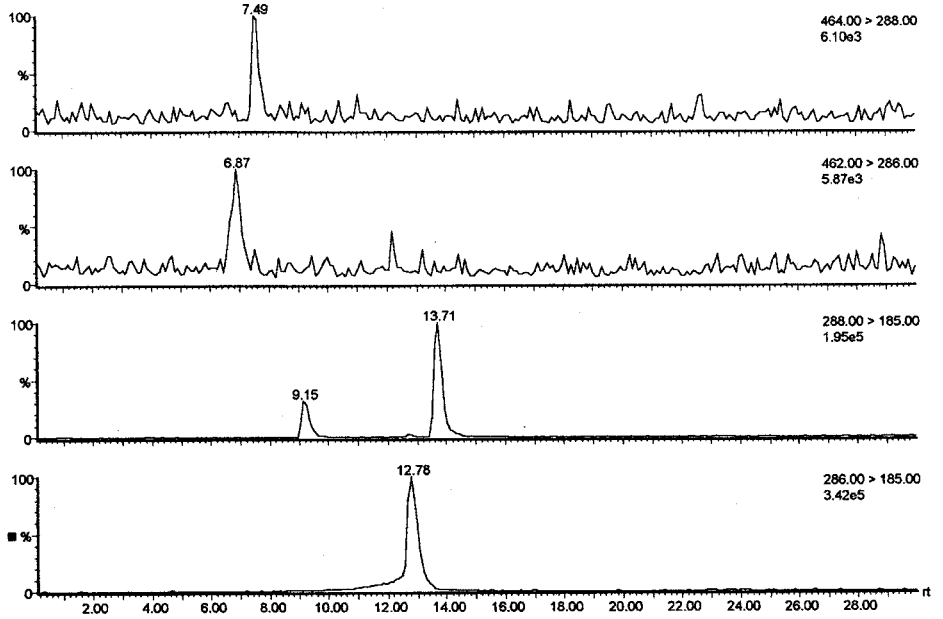


Figure 2. MRM traces of the urinary extract dissolved in methanol: hydromorphone-3-glucuronide, 6.87 min; dihydroisomorphine-3-glucuronide, 7.49 min; dihydromorphine, 9.15 min, hydromorphone, 12.78 min; dihydroisomorphine, 13.71 min.

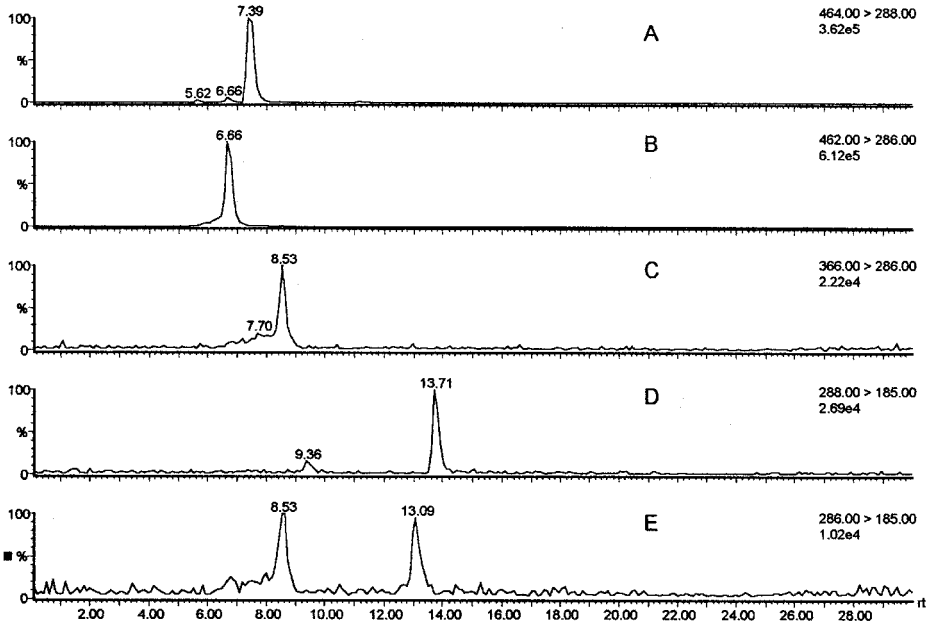


Figure 3. MRM traces of the urinary extract dissolved in water: dihydromorphine-3-glucuronide, 5.62 min; hydromorphone-3-glucuronide, 6.66 min (B); dihydroisomorphine-3-glucuronide, 7.39 min; hydromorphone-3-sulphate, 8.53 min (C); dihydromorphine, 9.36 min; hydromorphone, 13.09 min; dihydroisomorphine, 13.71 min. Note that the peak at 8.53 min that appeared in E was apparently due to the fragmentation of hydromorphone-3-sulphate in the MS1.

conjugates and the unconjugated compounds might have considerably different recoveries during the isolation with Amberlite XAD-2 column, which could lead to an invalid comparison. As shown in table 2, when corrected for the same concentration, the peak area ratios between dihydromorphine/hydromorphone/dihydroisomorphine standards are about 2.3/1.0/2.4. Thus, the relative levels of these three compounds in urine, when corrected for this response factor, are about 1/18/3, respectively. Likewise, the relative levels of the conjugated dihydromorphine/hydromorphone/dihydroisomorphine in urine are about 1/82/37, respectively. As the reported urinary recovery of hydromorphone-3-glucuronide

Table 2. Peak areas of hydromorphone and its metabolites as determined by MRM.

Compound	Concentration of standard ($\mu g\,ml^{-1}$)	Peak areas	
		Standard	Urine
Dihydromorphine	5.0	57 794	18 305
Hydromorphone	5.0	24 751	142 499
Dihydroisomorphine	2.5	30 136 (60 272)†	58 050
Dihydromorphine-3-glucuronide	2.9	10 908 (18 807)	2 688
Hydromorphone-3-glucuronide	5.0	14 525	169 569
Dihydroisomorphine-3-glucuronide	3.3	13 947 (21 132)	111 656

† Values in parentheses are peak areas corrected for $5\,\mu g\,ml^{-1}$.

accounted for 37% of the administered dose (Cone *et al.* 1977), the urinary recovery of dihydroisomorphine-3-glucuronide in the current study would account for 17% of the given dose. This is much higher than the result of Cone *et al.* who reported that the urinary recovery of total dihydroisomorphine, present almost exclusively as conjugate, only accounted for 1.0% of the given dose. Using the same calculation, the urinary recovery of dihydromorphine-3-glucuronide was about 0.45%, which is in general agreement with the urinary recovery of 0.1% reported by Cone *et al.* when considering the possible analytical errors involved.

Tentative identification of hydromorphone-3-sulphate, norhydromorphone and nordihydroisomorphine

Because of the structural similarities between hydromorphone and morphine, the same LC/MS/MS conditions were used for screening additional previously unidentified metabolites of hydromorphone. The aqueous and the methanolic samples were screened for conjugated and unconjugated metabolites, respectively. The parent ion and daughter ion masses were determined for the proposed structures of the new metabolites. The potential metabolites screened are summarized in table 3.

The presence of previously unidentified hydromorphone-3-sulphate is shown in figure 3C. A significant amount of hydromorphone-3-sulphate underwent fragmentation to hydromorphone in MS1 before entering the collision cell as shown by the presence of a peak at a retention time of 8.53 min (figure 3E), which coincided with the retention time of hydromorphone-3-sulphate. The presence of other potential conjugates could not be confirmed (figure 4).

The presence of unconjugated nordihydroisomorphine and norhydromorphone is shown in figure 5C, D, respectively. The peak at 11.77 min in figure 5C is proposed to be nordihydroisomorphine with reference to the relative elution order between dihydroisomorphine and hydromorphone (figure 5A, B). Both nordihy-

Table 3. LC/MS/MS characteristics of the potential metabolites of hydromorphone.

Compound screened	Parent $(M+1)^+$ (m/z)	Daughter (m/z)	Retention times (min) for urine
Hydromorphone-3-sulphate	366	286 $(M+)^+$	8.53
Norhydromorphone-3-glucuronide	448	272 $(M+1)^+$ (norhydromorphone)	n.d.
Nordihydromorphine- or nordihydroisomorphine-3-glucuronide	450	274 $(M+1)^+$ (nordihydromorphine or nordihydroisomorphine)	n.d.
Dihydromorphine- or dihydroisomorphine-di-glucuronide	640	464 $(M+1)^+$ and 288 $(M+1)^+$	n.d.
Nordihydromorphine	274	185	n.d.
Nordihydroisomorphine	274	185	11.77
Norhydromorphone	272	185	11.49

n.d., not detected.

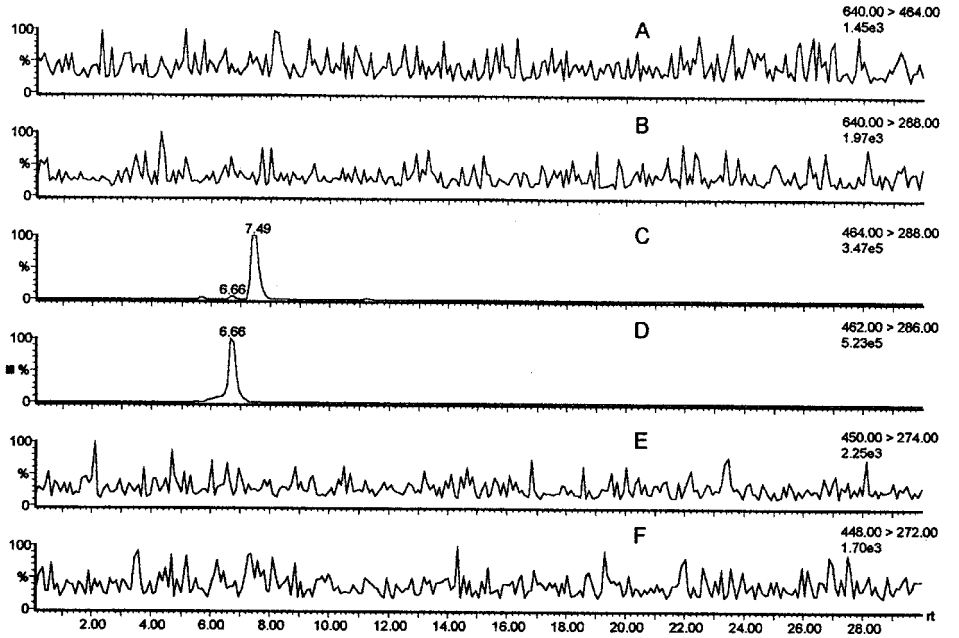


Figure 4. Screening for additional urinary conjugates in the urinary extract dissolved in water. Channel A was for monitoring the possible fragmentation of dihydromorphine- or dihydroisomorphine-di-glucuronide to dihydromorphine or dihydroisomorphine glucuronide; channel B for dihydromorphine- or dihydroisomorphine-di-glucuronide to dihydromorphine or dihydroisomorphine; dihydroisomorphine-3-glucuronide, 7.49 min (C); hydromorphone-3-glucuronide, 6.66 min (D); channel E for nordihydromorphine glucuronide or nordihydroisomorphine glucuronide to nordihydromorphine or nordihydroisomorphine; channel F for norhydromorphone glucuronide to norhydromorphone.

droisomorphine and norhydromorphone appear to be present at much lower levels than the other three metabolities (figure 5A, B).

Discussion

Although hydromorphone is being increasingly used for pain management, the metabolic profile of this opioid analgesic is poorly understood. Hydromorphone-3-glucuronide and dihydromorphine-3-glucuronide have been identified as metabolites in the rabbit (Roerig *et al.* 1973). A more extensive study by Cone *et al.* (1977) examined the differences in the metabolism of hydromorphone between different species. In particular, the urinary recoveries of dihydromorphine and dihydroisomorphine in guinea pig, mostly present in unconjugated forms, accounted for 8.3 and 19.3% of the administered dose, respectively, which were much higher than the level in rat, dog, rabbit and human. In human, the urinary recoveries of dihydromorphine and dihydroisomorphine were only 0.1 and 1.0%, respectively, with only the conjugated forms detected. The exact identities of these conjugates, however, were not determined. In chicken, opioids with a hydromorphone structure, such as naltrexone and naloxone, were preferentially metabolized to 6α-hydroxy metabolites (Roerig *et al.* 1976).

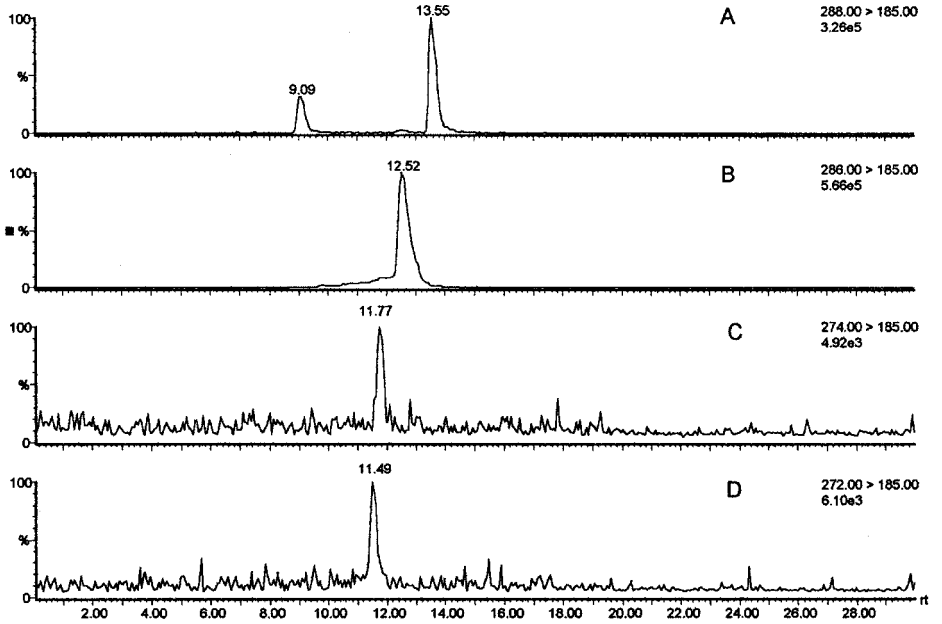


Figure 5. Screening for additional unconjugated metabolites in the urinary extract dissolved in methanol: Dihydromorphine, 9.09 min; hydromorphone, 12.52 min; dihydroisomorphine, 13.55 min; nordihydroisomorphine, 11.77 min; norhydromorphone, 11.49 min.

In the present study, both free and conjugated dihydromorphine and dihydroisomorphine were identified in the patients' urine. More specifically, the conjugated metabolites were identified as dihydromorphine-3-glucuronide and dihydroisomorphine-3-glucuronide. A surprising finding of the study was that the urinary recovery of dihydroisomorphine-3-glucuronide was about 17-fold higher than the result reported by Cone *et al.* (1977). A possible explanation is the interindividual variations in the metabolism of hydromorphone. The subjects studied by Cone *et al.* were healthy, adult male prisoners. In the present study, the subject was a female patient suffering from multiple myeloma. Large variations in hepatic metabolism of hydromorphone have been reported in normal healthy volunteers (Parab *et al.* 1988). The particular physiological conditions of our patient could cause even larger deviation from the already highly variable metabolism of hydromorphone among the healthy population. Since the objective of the present study was the identification of the metabolites rather than quantitation, a more accurate quantitation assay and a larger patient number are required to confirm the above differences between the two studies.

Hydromorphone-3-glucuronide and unchanged hydromorphone were also identified in the patient's urine. The overall urinary recovery of hydromorphone, dihydromorphine and dihydroisomorphine (free plus conjugated) in humans was about 43.5% as determined by Cone *et al.* (1977). According to the results of the present study, although dihydroisomorphine was present at a much higher level, there is still a lack of mass balance between the administered dose and the urinary recovery. Alternate excretion routes such as biliary excretion and/or the presence of additional metabolites are possible explanations (Cone and Darwin 1978).

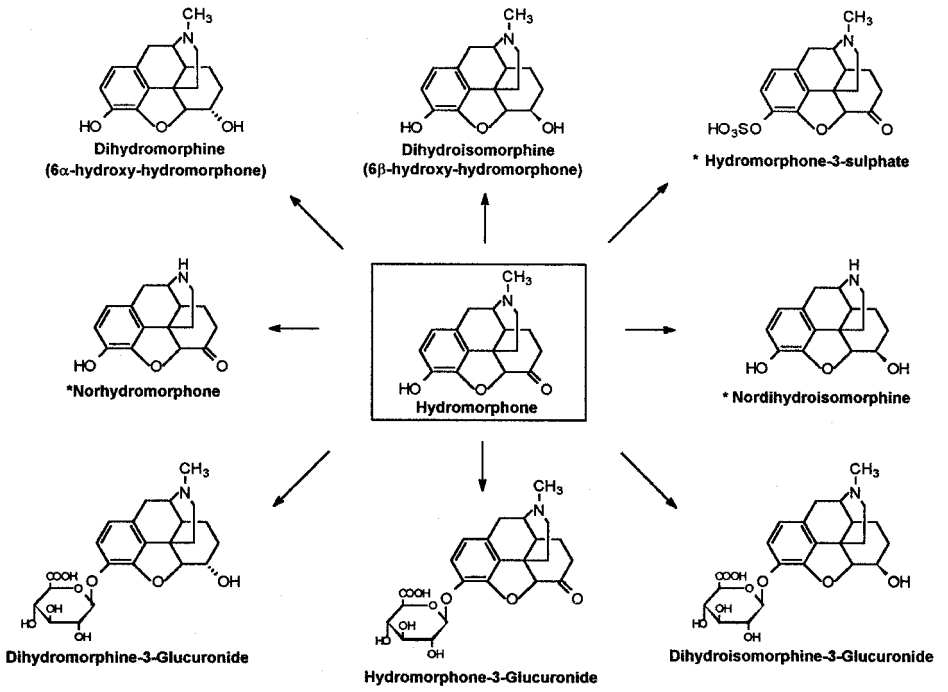


Figure 6. Chemical structures of hydromorphone and its metabolites detected in this study.
* Metabolites tentatively identified but not confirmed due to lack of standards.

Because of the structural similarities between hydromorphone and morphine, we explored the presence of previous unidentified metabolites. As expected, hydromorphone-3-sulphate, norhydromorphone and nordihydroisomorphine were tentatively identified as new metabolites of hydromorphone by LC/MS/MS. The retention times of these new metabolites were in general agreement relative to the other identified metabolites.

In analogy to morphine-6-glucuronide, the existence of hydromorphone-6-glucuronide has always been speculated (Lee *et al.* 1991, Hagen *et al.* 1995). The 6-glucuronides of dihydromorphine and dihydroisomorphine have been referred as hydromorphone-6-glucuronide based on the work of Cone *et al.* (1977). As we understand, however, Cone *et al.* did not discuss the presence of hydromorphone-6-glucuronide and, furthermore, they had never made the above comparison. As a matter of fact, as already mentioned, the exact identities of the dihydromorphine and dihydroisomorphine conjugates were not characterized by Cone *et al.*

It is believed that, structurally, hydromorphone-6-glucuronide is different from the 6-glucuronides of dihydromorphine and dihydroisomorphine. Hydromorphone-6-glucuronide is formed via the conversion of the 6-keto group on hydromorphone to its enol form followed by further glucuronidation, whereas the 6-glucuronides of dihydromorphine and dihydroisomorphine are simply formed through the glucuronidation of the 6-hydroxy group on dihydromorphine and dihydroisomorphine. There has been no report on glucuronidation via a keto group. In addition, neither hydromorphone-6-glucuronide nor the 6-glucuronides of dihydromorphine and dihydroisomorphine were detected in the present study.

Thus, unlike morphine, the formation of hydromorphone-6-glucuronide is probably not favoured for hydromorphone.

In conclusion, we have identified an unchanged hydromorphone, hydromorphone-3-glucuronide, and both free and conjugated dihydromorphine and dihydroisomorphine in the cancer patient's urine using LC/MS/MS. More specifically, the conjugated dihydromorphine and dihydroisomorphine were identified as dihydromorphine-3-glucuronide and dihydroisomorphine-3-glucuronide. The above metabolites were confirmed by comparison of the retention times with those of the synthetic standards using LC/MS/MS. In addition, we have for the first time tentatively identified three new metabolites of hydromorphone including hydromorphone-3-sulphate, norhydromorphone and nordihydroisomorphine (figure 6). Some of the disagreements between the present study and previous work need to be investigated further.

Acknowledgements

The work was partially supported by Knoll Pharma, Inc. (Canada). The authors thank Dr Frank Abbott, Mr Wei Tang and Mr Roland Burton for technical assistance in the LC/MS/MS experiments.

References

Berrang, B., Twine, C. E., Hennessee, G. L. and Carroll, F. I., 1975, Synthesis of morphine-3-glucuronide. *Synthetic Communications*, **5**, 231–236.

Boerner, U., Abbott, S. and Roe, R. L., 1975, The metabolism of morphine and heroin in man. *Drug Metabolism Reviews*, **4**, 39–73.

Brodsky, J. B., Chaplan, S. R., Brose, W. G. and Mark, J. B. D., 1990, Continuous epidural hydromorphone for postthoracotomy pain relief. *Annals of Thoracic Surgery*, **50**, 888–893.

Bruera, E., Brenneis, C., Michaud, M., Macmillan, K., Hanson, J. and Macdonald, R. N., 1988, Patient-controlled subcutaneous hydromorphone versus continuous subcutaneous infusion for the treatment of cancer pain. *Journal of the National Cancer Institute*, **80**, 1152–1154.

Bruera, E., Maceachern, T., Macmillan, K., Miller, M. J. and Hanson, J., 1993, Local tolerance to subcutaneous infusions of high concentrations of hydromorphone: a prospective study. *Journal of Pain Symptoms and Management*, **8**, 201–204.

Budavari, S. (ed.), *Merck Index*, 1989, 11th edn (Rahway: Merck).

Chatterjie, N., Inturrisi, C. E., Dayton, H. B. and Blumberg, H., 1975, Stereospecific synthesis of the 6β-hydroxy metabolites of naltrexone and naloxone. *Journal of Medicinal Chemistry*, **18**, 490–492.

Cone, E. J. and Darwin, W. D., 1978, Simultaneous determination of hydromorphone, hydrocodone and their 6α- and 6β-hydroxy metabolites in urine using selected ion recording with methane chemical ionization. *Biomedical Mass Spectrometry*, **5**, 291–295.

Cone, E. J., Phelps, B. A. and Gorodetzky, C. W., 1977, Urinary extraction of hydromorphone and metabolites in humans, rats, dogs, guinea pigs, and rabbits. *Journal of Pharmaceutical Sciences*, **66**, 1709–1713.

Dougherty, T. B., Baysinger, C. L., Henenberger, J. C. and Gooding, D. J., 1989, Epidural hydromorphone with and without epinephrine for post-operative analgesia after cesarean delivery. *Anesthesia and Analgesia*, **68**, 318–322.

Eddy, N. B., 1933, Dilaudid (dihydromorphinone hydrochloride). *Journal of the American Medical Association*, **100**, 1032–1035.

Ferris, F. D., Kerr, I. G., De Angelis, C., Sone, M and Hume, S., 1990, Inpatient narcotic infusions for patients with cancer pain. *Journal of Palliative Care*, **6**, 51–59.

Gong, Q.-L., Hedner, T., Hedner, J., Björkman, R. and Nordberg, G., 1991, Antinociceptive and ventilatory effects of the morphine metabolites: morphine-6-glucuronide and morphine-3-glucuronide. *European Journal of Pharmacology*, **193**, 47–56.

Hagen, N., Thirlwell, M. P., Dhaliwal, H. S., Babul, N., Harsanyi, Z. and Darke, A. C., 1995, Steady-state pharmacokinetics of hydromorphone and hydromorphone-3-glucuronide in cancer patients after immediate and controlled-release hydromorphone. *Journal of Clinical Pharmacology*, **35**, 37–44.

Hanna, M. H., Peat, S. J., Woodham, M., Knibb, A. and Fung, C., 1990, Analgesic efficacy and CSF pharmacokinetics of intrathecal morphine-6-glucuronide: comparison with morphone. *British Journal of Anaesthesia*, **64**, 547–550.

Hays, H., Hagen, N., Thirwell, M., Dhaliwal, H., Babul, N., Harsanyi, Z. and Darke, A. C., 1994, Comparative clinical efficacy and safety of immediate release and controlled release hydromorphone for chronic severe cancer pain. *Cancer*, **74**, 1808–1816.

Lee, J. W., Pedersen, J. E., Moravetz, T. L., Dzerk, A. M., Mundt, A. D. and Shepard, K. V., 1991, Sensitive and specific radioimmunoassays for opiates using commercially available materials. I: Methods for the determinations of morphine and hydromorphone. *Journal of Pharmaceutical Sciences*, **80**, 284–288.

Librach, S. L., 1991, Adverse effects of opioids. In *The Pain Manual: Principles and Issues in Cancer Pain Management* (Montreal: Pegasus Healthcare), pp. 58–66.

Liu, S., Carpenter, R. L., Mulroy, M. F., Weissman, R. M., McGill, T. J., Rupp, S. M. and Allen, H. M., 1995, Intravenous versus epidural administration of hydromorphone. *Anesthesiology*, **82**, 682–688.

Mahler, D. L. and Forrest, W. H., Jr., 1975, Relative analgesic potencies of morphine and hydromorphone in postoperative pain. *Anesthesiology*, **42**, 602–607.

Moulin, D. E., Kreeft, J. H., Murray-Parsons, N. and Bouquillon, A. I., 1991, Comparison of continuous subcutaneous and intravenous hydromorphone infusions for management of cancer pain. *Lancet*, **337**, 465–468.

Okuda, S., Yamaguchi, S., Kawazoe, Y. and Tsuda, K., 1964, Studies on morphine alkaloids. I. Nuclear magnetic resonance spectral studies on morphine alkaloids. *Chemical and Pharmaceutical Bulletin*, **12**, 104–112.

Osborne, R., Thompson, P., Joel, S., Trew, D., Patel, N. and Slevin, M., 1992, The analgesic activity of morphine-6-glucuronide. *British Journal of Clinical Pharmacology*, **34**, 130–138.

Parab, P. V., Ritschel, W. A., Coyle, D. E., Gregg, R. V. and Denson, D. D., 1988, Pharmacokinetics of hydromorphone after intravenous, peroral and rectal administration to human subjects. *Biopharmaceutics and Drug Disposition*, **9**, 187–199.

Roerig, S., Fujimoto, J. M. and Wang, R. I. H., 1973, Isolation of hydromorphone and dihydromorphine glucuronides from urine of the rabbit after hydromorphone administration (37291). *Proceedings of the Society for Experimental Biology and Medicine*, **143**, 230–233.

Roerig, S., Fujimoto, J. M., Wang, R. I. H., Pollock, S. H. and Lange, D., 1976, Preliminary characterization of enzymes for reduction of naloxone and naltrexone in rabbit and chicken liver. *Drug Metabolism and Disposition*, **4**, 53–58.

Searle, N. R., Roy, M., Bergeron, G., Perrault, J., Roof, J., Heermans, C., Courtemanche, M., Demers, C. and Carter, R., 1994, Hydromorphone patient-controlled analgesia (PCA) after coronary artery bypass surgery. *Canadian Journal of Anaesthesia*, **41**, 198–205.

Small, L. F., Eddy, N. B., Mosettig, E. and Himmelsbach, C. K., 1938, Studies on drug addiction. *United States Public Health Reports*, **Suppl. 138**, 1–35.

Small, L. F. and Lutz, R. E., 1932, Chemistry of the opium alkaloids. *United States Public Health Reports*, **Suppl. 103**, 159.

Thompson, P. I., Joel, S. P., John, L., Wedzicha, J. A., Maclean, M. and Slevin, M. L., 1995, Respiratory depression following morphine and morphine-6-glucuronide in normal subjects. *British Journal of Clinical Pharmacology*, **40**, 145–152.

Vanier, M.-C., Labrecque, G., Lepage-Savary, D., Poulin, E., Provencher, L. and Lamontagne, C., 1993, Comparison of hydromorphone continuous subcutaneous infusion and basal rate subcutaneous infusion plus PCA in cancer pain. *Pain*, **53**, 27–32.

Wallenstein, S. L., Houde, R. W., Portenoy, R., Lapin, J., Rogers, A. and Foley. K. M., 1990, Clinical analgesic assay of repeated and single doses of heroin and hydromorphone. *Pain*, **41**, 5–13.

Yoshimura, H., Oguri, K. and Tsukamoto, H., 1968, Metabolism of drugs. LX. The synthesis of codeine and morphine glucuronides. *Chemical and Pharmaceutical Bulletin*, **16**, 2114–2119.

Zaw-Tun, N. and Bruera, E., 1992, Active metabolites of morphine. *Journal of Palliative Care*, **8**, 48–50.

XENOBIOTICA, 2002, VOL. 32, NO. 5, 441–450

Taylor & Francis
healthsciences

Pharmacokinetic analysis of factors determining elimination pathways for sulfate and glucuronide metabolites of drugs. I: Studies by *in vivo* constant infusion

M. ISHII, M. KANAYAMA, H. ESUMI, K.-I. OGAWARA, T. KIMURA and K. HIGAKI*

Department of Pharmaceutics, Faculty of Pharmaceutical Sciences, Okayama University, Okayama 700-8530, Japan

Received 3 September 2001

1. The hepatic and renal handling of glucuronides and sulphates of three phenolic compounds, 4-methylumbelliferone (4-MU), *p*-nitrophenol (pNP) and acetaminophen (APAP), were evaluated pharmacokinetically by *in vivo* constant infusion experiments in rat. It was shown that the urinary excretion rate at steady-state was larger than the biliary excretion rate for both glucuronides and sulfates, and sulfates, in particular, were extensively excreted into the urine.

2. For each glucuronide, however, biliary excretion clearances (CL_b) calculated based on the total concentration and unbound concentration in the liver were much larger than the corresponding renal excretion clearances (CL_r). Even in the case of sulfates, there was not any large difference between CL_r and CL_b based on the total and unbound concentration in tissues, which could not explain their extensive urinary excretion. From these results, these excretion clearances were recognized not to reflect necessarily the actual excretion rate obtained.

3. On the other hand, the tissue-to-plasma concentration ratio (K_p) of both glucuronides and sulfates for every phenolic compound was much higher in the kidney than that in the liver. The results suggested that one of the most important determinants for the preferential excretion of these conjugates into the bile or urine is the extent of disposition of each compound to the liver or kidney.

4. In addition, K_p of both glucuronides and sulfates in the liver, where these conjugates are mainly formed, was small. The K_p of sulfates was quite low, suggesting that sulfates generated in the liver were subject to extensive sinusoidal efflux.

Introduction

Biliary and renal excretion are the major ways of clearing the internal milieu from potentially dangerous exogenous and endogenous substances including drugs and their metabolites. Conjugation reactions such as glucuronidation and sulfation, mainly in the liver, are also an important process for the detoxification of xenobiotics. Only in the case of a few compounds such as *p*-aminohippuric acid (Fleck and Braunlich 1986) and indocyanine green (Guarino and Anderson 1976, Fleck and Braunlich 1986) are xenobiotics excreted via almost entirely by one of these two pathways, urinary or biliary excretion, whereas most xenobiotics are eliminated via both pathways (Fleck and Braunlich 1990). It has been reported that damage to one system could be compensated by the other (Siegers and Klaassen 1984, Besseghir and Roch-Ramel 1987). Glucuronides and sulfates are categorized

* Author for correspondence; e-mail: higaki@pheasant.pharm.okayama-u.ac.jp

Xenobiotica ISSN 0049–8254 print/ISSN 1366–5928 online © 2002 Taylor & Francis Ltd
http://www.tandf.co.uk/journals
DOI: 10.1080/00498250210123094

into the group that Fleck and Braunlich (1990) defined as an intermediate one, where the compounds can be handled by both the liver and kidney. However, glucuronides are usually excreted into both the urine (Moller and Sheikh 1983) and bile (Klassen and Watkins 1984), whereas sulfates are extensively excreted into the urine (De Vries *et al*. 1985, Mulder *et al*. 1985).

To predict the pharmacokinetics and drug–drug interactions in terms of excretion kinetics and to design safer and more effective drugs, the elucidation of the mechanisms behind the renal and hepatic handling of drugs and their relationship is very important. Lipophilic compounds of molecular weight >300–500 appear to be preferentially eliminated by the liver, while the kidney would dispose preferentially of hydrophilic substances of molecular weight <500 (Besseghir and Roch-Ramel 1987). However, it is an empirical rule and the specific determinants of the preferential excretion pathway of drugs including glucuronides and sulfates have not been fully clarified to date. Although molecular biological studies have been being reported on the transporters that are involved in the biliary (Kusuhara *et al*. 1998) and renal (Burckhardt and Wolff, 2000) excretion of xenobiotics, macroscopic studies are still needed to elucidate the processes determining their preferential excretion.

The present study has evaluated the hepatic and renal handling of three phenolic compounds, 4-methylumbelliferone (4-MU), *p*-nitrophenol (pNP) and acetaminophen (APAP), and of their glucuronides and sulfates in an *in vivo* constant infusion study and it has attempted to elucidate the important pharmacokinetic factors for the preferential excretion of those conjugates into the bile or urine.

Materials and methods

Materials

4-MU, APAP, glucuronides or sulfates of 4-MU and of pNP, of which the chemical purities are $>98\%$, were obtained from Sigma Chemical Co. (St Louis, MO, USA). pNP, its chemical purity is $>98.5\%$, was purchased from Ishizu Pharmaceutical Co. (Osaka, Japan). As the internal standard for the determination of 4-MU, APAP, pNP and their conjugates, umbelliferone, benzamide (Tokyo Chemical Co., Tokyo, Japan) and phenol (Sigma), respectively, were used. All other reagents were of the highest grade available.

Animals

Male Wistar rats (Japan SLC, Hamamatsu, Japan), maintained at 25 °C and 55% humidity, were allowed free access to standard laboratory chow (Clea Japan, Tokyo, Japan) and water before the experiments. Rats weighing 240–290 g were assigned randomly to each experimental group. The investigations were performed after approval by the local ethical committee at Okayama University and in accordance with *Interdisciplinary Principles and Guidelines of the Use of Animals in Research.*

In vivo *constant infusion experiments*

All animals were anaesthetized before surgery by the intraperitoneal injection of urethane ($1\,g\,kg^{-1}$). Heat lamps helped the animals maintain their body temperature during the experiment. The femoral vein, bile duct and urinary bladder were cannulated with vinyl tubing (i.d. 0.5×0.8 mm for the femoral vein and bile duct; i.d. 0.28×0.61 mm for the urine bladder; Dural Plastic & Engineering, Dural, Australia). After a loading dose equivalent to the amount infused in 30 min, 4-MU (50, 300, $600\,\mu g\,min^{-1}\,kg^{-1}$), pNP (300, 600, $1200\,\mu g\,min^{-1}\,kg^{-1}$) and APAP (300, 600, $1200\,\mu g\,min^{-1}\,kg^{-1}$) dissolved in isotonic saline solution containing D-mannitol, delivered at $3000\,\mu g\,min^{-1}\,kg^{-1}$ to ascertain constant urine flow, were infused through the femoral vein throughout the experiments. After reaching steady-state, the liver and kidneys were excized and the drug concentrations in these tissues determined. Bile and urine were collected from the cannulae in fractions and blood samples were withdrawn via the jugular vein into heparinized plastic tubes.

Determination of drug concentrations

Drug concentrations in plasma, bile, urine, liver and kidney were determined by HPLC. 4-MU, pNP and APAP and their conjugates were assayed according to the methods of Zimmerman (1991), Morris and Hansel (1990) and Klaassen (1984), respectively, with minor modifications. Briefly, the collected plasma was deproteinized with methanol after the addition of an internal standard. Urine or bile were diluted with the mobile phase used in the HPLC analysis after the addition of an internal standard. The excized liver and kidneys were homogenized in NaOH–glycine buffer (pH 10.5), and the resultant homogenate was deproteinized with methanol after the addition of an internal standard. An aliquot of each supernatant was introduced onto the HPLC system described below. The HPLC system consisted of a model LC-6A HPLC pump (Shimadzu, Kyoto, Japan), a model SIL-9A system controller (Shimadzu), and a model SPD-2A UV detector (Shimadzu) set at 313, 280 and 254 nm for the cases of 4-MU, pNP and APAP, respectively. A ChemcoPak Nucleosil column (150 × 4.6 mm i.d.; pore size 120Å; particle size 5 μm; Macherey-Nagel, Inc., Easton, PA, USA) was used at room temperature. The mobile phase for determination of 4-MU and its conjugated metabolites consisted of 25% methanol in 0.05 M KH_2PO_4, and that for pNP, APAP and their conjugates consisted of acetic acid–methanol–0.05 M KH_2PO_4, 1:10:10 or 7.5:15:1000 (v/v), respectively, both of which were delivered at 1.0 ml min^{-1}. The coefficient of variation (CV) for each standard curve ranged from 0.3 to 5% and the squared correlation coefficient was > 0.998. The quantity of each APAP conjugate was determined by using the standard curve for APAP because its molar extinction coefficient has been reported to be the same as APAP (Howie *et al*. 1977).

Determination of free fraction in plasma

An aliquot of collected plasma was transferred to an ultrafiltration tube (MPS-1; Amicon Co., Tokyo, Japan), and centrifuged at 1000*g* for 5 min. The drug concentration in the filtrate was determined as the unbound plasma concentration of drugs.

Statistical analysis

Statistical significance was evaluated by using the Student's *t*-test. Results are expressed as the mean ± SD of at least three experiments.

Results and discussion

The plasma concentration, biliary excretion rate and urinary excretion rate of 4-MU, pNP, APAP and their conjugates (glucuronide or sulfate) during the constant infusion of each parent drug were determined (figure 1). Since preliminary experiments revealed that the distribution equilibrium was completely achieved within 90 min after starting the infusion for all chemicals concerned, we determined their plasma concentrations, biliary excretion and urinary excretion between 100 and 150 min. The pharmacokinetic parameters at steady-state are summarized in table 1. No common pattern was observed in the plasma concentrations for the phenolic compounds examined, but the unbound fraction in plasma (f_p) for the glucuronide or sulfate was determined to be larger or smaller than that for each parent compound, respectively. The conjugate of each compound predominantly excreted into the bile was the glucuronide, whereas a preferential urinary excretion of sulfate was observed for pNP and APAP. Even for 4-MU, the ratio of sulfate to glucuronide in the excretion rates was much larger for the urinary excretion (0.23) than that for the biliary excretion (0.06). Figure 1 and table 1 also show that the urinary excretion rate at steady-state is larger than the biliary excretion rate for each compound, suggesting that these phenolic compounds and their conjugates are likely to be excreted into the urine. However, the contribution of urinary excretion to the total excretion was much greater for sulfates (about 88, 98 and 93% for 4-MUS, pNPS and APAPS, respectively) than that for glucuronides (about 65, 58 and 53% for 4-MUG, pNPG and APAPG, respectively) (figure 1 and table 1). The results suggest that glucuronides are preferential substrates for biliary excretion and sulfates for urinary excretion. The

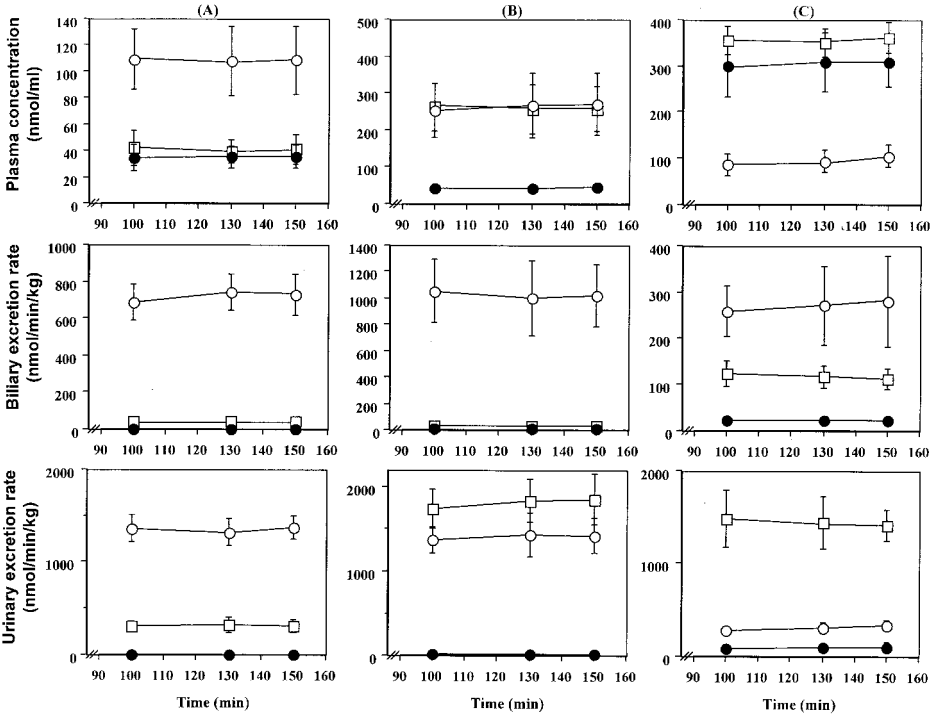


Figure 1. Plasma concentrations, biliary excretion rates and urinary excretion rates of 4-MU, pNP, APAP and their conjugated metabolites during the *in vivo* constant infusion of (A) 4-MU, (B) pNP and (C) APAP at an infusion rate of 600 μg min^{-1} kg^{-1} in rat. Parent drug (●); glucuronide (○); sulfate (□) Results are the mean ± SD of at least three experiments.

renal excretion clearances of sulfates based on the plasma concentration at steady-state (7.7, 7.0 and 4.1 ml min^{-1} kg^{-1} for 4-MUS, pNPS and APAPS, respectively) were much larger than the glomerular filtration rate (GFR) of the free molecule – 0.37, 0.79 and 2.0 ml min^{-1} kg^{-1} for 4-MUS, pNPS and APAPS, respectively – which are the products of each f_p with the reported value for rat GFR being 5.24 ml min^{-1} kg^{-1} (Davies and Morris 1993). The extensive difference of the renal excretion clearance from GFR suggests that the secretion from renal epithelial cells is involved in the urinary excretion of the sulfates examined. As for the tissue concentrations, the higher concentration of the glucuronide than the corresponding sulfate was observed in both the liver and kidney. Concentrations of APAP and its conjugates in the liver and kidney could not be quantitatively measured because the separation from biological substances was not successful.

To estimate excretion from the tissue to the bile or urine, the biliary excretion clearance (CL_b) or renal excretion clearance (CL_r) was calculated based on the concentration of compound in the liver or kidney, respectively (figure 2). The tissue-to-plasma concentration ratios (K_p) for 4-MUG, 4-MUS, pNPG and pNPS are also summarized in figure 2. CL_b for 4-MUG or pNPG was about 5.0 or 2.0 times larger than that for 4-MUS or pNPS, respectively. On the other hand, CL_r for 4-MUG or pNPG was smaller than that for 4-MUS or pNPS, respectively. Even considering their unbound fraction obtained preliminarily in the 16% homogenate of the liver and kidney (4-MUG; $f_{T,liver} = 0.72 \pm 0.02$, $f_{T,kidney} = 0.94 \pm 0.01$: 4-MUS; $f_{T,liver} = 0.23 \pm 0.04$, $f_{T,kidney} = 0.77 \pm 0.07$:

Table 1. Excretion kinetics of 4-MU, pNP, APAP and their conjugates under steady-state during constant infusion of each parent compound.

Drug/metabolite		$C_{p,ss}$ (nmol ml^{-1})	f_p	$C_{liver,ss}$ (nmol g^{-1})	Biliary excretion rate (nmol min^{-1} kg^{-1})	$C_{kidney,ss}$ (nmol g^{-1})	Urinary excretion rate (nmol min^{-1} kg^{-1})
	4-MU	34.7 ± 8.6	0.23 ± 0.05	39.2 ± 13.3	0.1 ± 0.3	70.3 ± 41.6	2.4 ± 1.3
4-MU	4-MUG	108.3 ± 23.7	0.61 ± 0.03	226.1 ± 72.2	718.0 ± 99.3	2038.4 ± 552.5	1350.1 ± 130.0
	4-MUS	40.7 ± 10.7***	0.07 ± 0.02***	58.9 ± 21.1***	40.9 ± 7.3***	250.4 ± 103.5***	312.4 ± 64.2***
	pNP	43.0 ± 7.7	0.42 ± 0.05	12.2 ± 3.0	7.8 ± 1.9	67.9 ± 24.1	15.1 ± 4.7
pNP	pNPG	262.1 ± 73.8	0.92 ± 0.08	101.0 ± 15.6	1021.8 ± 230.0	345.4 ± 74.0	1405.4 ± 193.6
	pNPS	257.5 ± 57.9$^{n.s.}$	0.15 ± 0.04***	6.7 ± 2.2***	31.4 ± 4.0***	291.8 ± 24.9$^{n.s.}$	1806.8 ± 244.6$^{n.s.}$
	APAP	304.7 ± 56.9	0.75 ± 0.04	–[a]	22.1 ± 6.2	–	94.7 ± 37.3
APAP	APAPG	94.1 ± 23.5	1.01 ± 0.02	–	269.2 ± 75.8	–	309.0 ± 52.0
	APAPS	355.5 ± 29.9***	0.38 ± 0.05***	–	116.9 ± 22.8**	–	1444.6 ± 240.4***

Results are the mean ± SD of at least three experiments. The infusion rate of each parent drug was 600 μg min^{-1} kg^{-1}. $C_{p,ss}$, $C_{liver,ss}$ and $C_{kidney,ss}$ are the plasma, hepatic and renal concentrations at steady-state, respectively. f_p is the free fraction in plasma.

[a] Not determined; n.s., not significant; $^{**}p < 0.01$, $^{***}p < 0.001$, compared with the corresponding glucuronide.

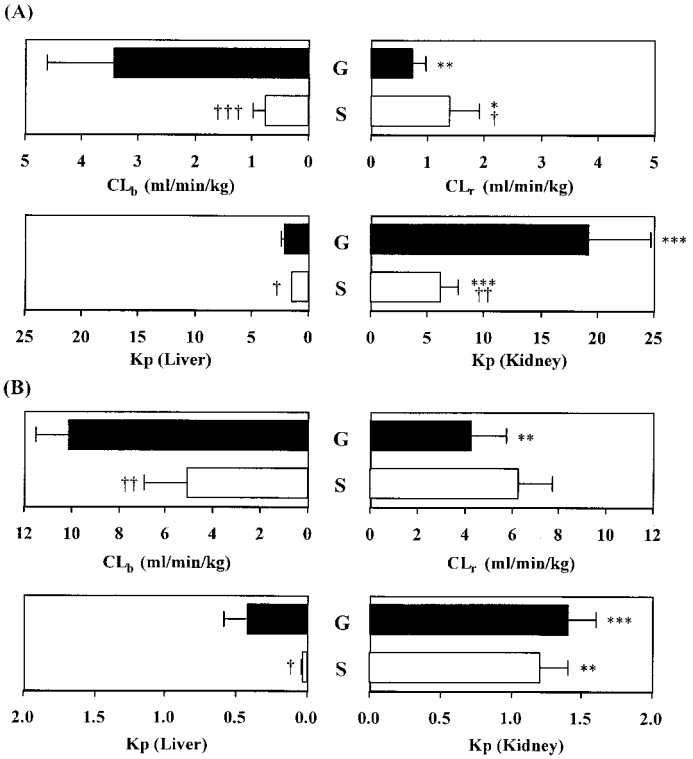


Figure 2. CL_b, CL_r and K_p of (A) 4-MUG or 4-MUS and (B) pNPG or pNPS during the *in vivo* constant infusion of 4-MU and pNP, respectively, at an infusion rate of 600 μg min^{-1} kg^{-1} in rat. CL_b and CL_r are the biliary excretion clearance based on the drug concentration in the liver and urinary excretion clearance based on those in the kidney, respectively. K_p is the tissue-to-plasma concentration ratio. G and S are the glucuronide and sulfate, respectively. Results are the mean ± SD of at least three experiments. Statistical significance: $*p < 0.05$, $**p < 0.01$, $***p < 0.001$ compared with K_p of liver. $\dagger p < 0.05$, $\dagger\dagger p < 0.01$, $\dagger\dagger\dagger p < 0.001$ compared with glucuronide.

pNPG; $f_{T,liver} = 0.66 \pm 0.21$, $f_{T,kidney} = 0.88 \pm 0.01$: pNPS; $f_{T,liver} = 0.51 \pm 0.12$, $f_{T,kidney} = 0.48$ 0.06), the CL_b/f_T values of glucuronides are larger than those of sulfates and CL_r/f_T of sulfates were smaller than those of glucuronides. From these results, it is suggested that glucuronides in the liver or sulfates in the kidney were more preferentially excreted into the bile or urine, respectively. Comparing CL_b with CL_r in terms of glucuronides, CL_b was much larger than CL_r for both 4-MUG and pNPG. This is also the case with the clearances for the unbound concentration. On the contrary, in the case of sulfates, there is not any large difference between CL_b and CL_r based on total or unbound concentration for both 4-MUS and pNPS. However, the actual excretion rates indicated that glucuronides were excreted into the bile and urine more equally compared with sulfates and that sulfates were excreted into the urine extensively (figure 1 and table 1). These results indicate that CL or CL/f_T, corresponding to the intrinsic excretion ability from the tissue to the bile or urine, do not necessarily reflect the actual excretion of drugs, i.e. their preference of excretion.

As for K_p, it was determined that the concentrations of both glucuronides and sulfates were substantially higher in the kidney than those in the plasma, and that

K_p for 4-MUG, 4-MUS, pNPG and pNPS for the kidney was about 9.0, 4.3, 3.4 and 44 times larger than those for the liver, respectively. These results strongly suggest that the high concentration of conjugates in the kidney influence crucially their actual excretion rates, indicating that the disposition of each compound to the liver or kidney is one of the most important determinants for their preferential excretion into the bile or urine. Thus, the bile-oriented excretion is cancelled out by the extremely larger K_p for the kidney compared with the liver, although glucuronides have larger CL_b than CL_r (figure 2). On the other hand, in the case of sulfates, the substantially larger K_p for the kidney than that for the liver does enhance its preference for urinary excretion, leading to the extensive urinary excretion of sulfates (figure 2).

The disposition of a compound in a tissue can be determined by its influx from plasma, its efflux to plasma and its tissue binding. The uptake and biliary excretion of glucuronides and sulfates of various drugs across the sinusoidal membrane and the apical membrane of hepatocytes, respectively, have been proposed to be mediated by carrier-mediated transport systems in rat hepatocytes (Sundheimer and Brendel 1983, Iida *et al.* 1989, Studenberg and Brouwer 1993, Takenaka *et al.* 1995, Hassen *et al.* 1996). On the other hand, there are also many carrier-mediated transport systems involved in the renal handling of organic anions on both sides of the plasma membrane of renal epithelial cells. However, both the substrate specificity and role for the direction of drug transport of transporters has yet to be established, except for a limited number of compounds (Bergwerk *et al.* 1996, Kullak-Ublick 1999, Tojo *et al.* 1999, van Aubel *et al.* 2000). Therefore, the localization of these transporters and their substrate specificity can determine the tissue level of each compound in the liver or kidney, resulting in the preferential excretion of drugs into the bile or urine. GFR is also an important factor for the urinary excretion of the glucuronide because its f_p is much larger than that of the corresponding sulfate (table 1).

Considering that conjugated metabolites were mainly formed in the liver, K_p for both glucuronides and sulfates in the liver were determined to be quite small, especially for sulfates (1.4 or 0.028 for 4-MUS or pNPS, respectively) (figure 2). As it has been reported that an extrahepatic conjugation reaction occurs for several phenolic compounds including 4-MU and pNP (Mulder *et al.* 1984), sulfates-generated extrahepatically may decrease their K_p in the liver to some extent. However, sulfates extensively excreted in the urine must be mainly supplied by the liver, which means sulfates generated in the liver are needed to be subject to efflux to the blood. In fact, it has been reported that harmol sulfate is subject to sinusoidal efflux via a carrier-mediated mechanism (De Vries *et al.* 1985), and that the Oatp transporters, mediating not only the uptake, but also the efflux of the organic anions across the sinusoidal membrane in the liver (Satlin *et al.* 1997), may function as anion exchangers. In addition, our preliminary experiment showed that the net efflux of sulfate into the perfusate from the liver is more predominant than its biliary excretion during the constant infusion of 4-MU or pNP in the isolated liver perfusion study. Therefore, the sinusoidal efflux of sulfates is mainly responsible for the low K_p of sulfates, although further studies are required to substantiate this fact. On the other hand, the conjugates excreted into urine are mainly derived from plasma. Therefore, the comparison between $CL_r/f_{T,kidney}$ and CL_r/f_p will give some information about the process that will be more important for the urinary excretion. CL_r/f_p (about 6–110 $ml\,min^{-1}\,kg^{-1}$) was larger than

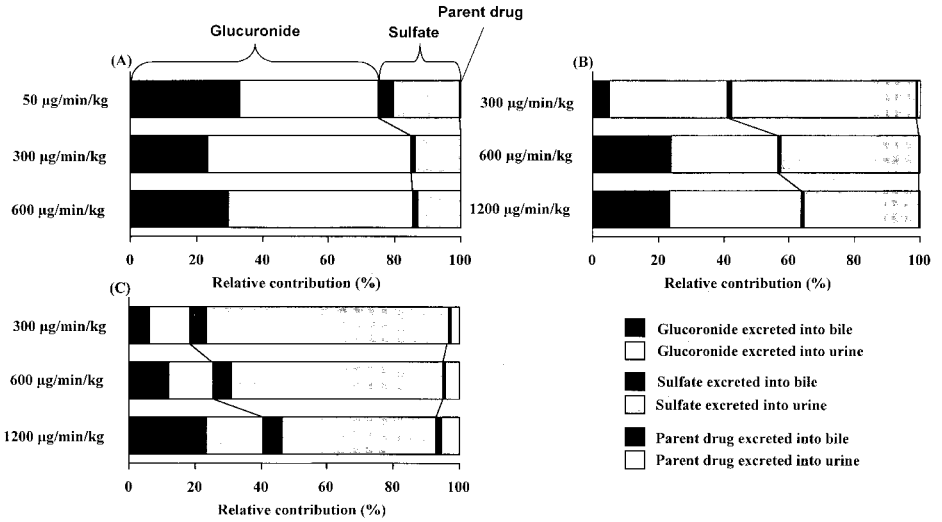


Figure 3. Relative contribution of excretion of glucuronide, sulphate and the parent drug of (A) 4-MU, (B) pNP and (C) APAP into the bile and urine at steady-state during *in vivo* constant infusion into rat at various infusion rates. Results are the mean of at least three experiments.

$CL_r/f_{T,kidney}$ (about 0.7–13 ml min^{-1} kg^{-1}) for both conjugates of 4-MU and pNP, suggesting that the uptake from plasma may be more responsible for the preferential urinary excretion. Furthermore, CL_r/f_p of sulfates (4-MUS, 110 ml min^{-1} kg^{-1}; pNPS, 47 ml min^{-1} kg^{-1}) were much larger than those of glucuronides (4-MUG, 21 ml min^{-1} kg^{-1}; pNPG, 6 ml min^{-1} kg^{-1}), indicating strongly that the urine-oriented excretion of sulfates should be attributed to their high distribution into the kidney based on the high uptake clearance from plasma.

The relative contributions of the biliary and urinary excretion of glucuronides, sulfates and parent drugs for 4-MU, pNP and APAP were determined under various infusion rates and are summarized in figure 3. As the infusion rate increased, the relative contribution of sulfate excretion to the total excretion decreased for all model compounds, although that of glucuronide excretion conversely increased. The decrease in the relative contribution of sulfate excretion was markedly observed in its urinary excretion. On the other hand, the increase in the relative contribution of glucuronide excretion was ascribed to its biliary excretion. The proportion of the sulfate formed in the liver has been reported to decrease with the increasing intracellular concentration of the parent drug, accompanied by a compensatory increase in the glucuronide (Pang *et al.* 1981, 1983). Generally, it is well known that the relatively higher affinity and lower capacity of the sulfotransferases than the glucuronosyltransferases lead to the formation of phenolic sulfate at low doses, but they favour the glucuronide at high doses (Benet *et al.* 1995), which is responsible for the relative decrease in sulfate excretion and the relative increase in glucuronide excretion with an increase in infusion rate. This speculation can be supported by our two findings. The first is that no significant decrease in CL_r with increased infusion rate was observed for 4-MUS or pNPS (data not shown), suggesting that the relative decrease in the urinary excretion might be ascribed to the relatively lower concentration of sulfates in the kidney at the higher infusion rate. Second, the increase in CL_b with

increased infusion rate was observed for 4-MUG or pNPG, although K_p for the liver was almost the same. Since the binding of drugs to certain cytosolic proteins and/or organelles must influence their subsequent sequestration and disposition, the increase in the amount of 4-MUG or pNPG excreted into the bile may be partially ascribed to the increase in free fraction in the cytosol due to the saturation of their binding with intracellular components. However, the actual mechanism involved in this saturable nature of excretion kinetics remains to be elucidated.

In conclusion, one of the most important determinants for the preferential excretion of glucuronides and sulfates into the bile or urine is the extent of disposition of each compound to the liver or kidney, and that the sinusoidal efflux is also an important factor for their hepatic handling and subsequent disposition to the kidney, especially for sulfates.

References

Benet, L. Z., Kroety, D. L. and Sheiner, L. B. 1995, Pharmacokinetics: the dynamics of drug absorption, distribution, and elimination. In J. G. Hardman, L. E. Limbird, P. B. Molinoff, R. W. Ruddon and A. G. Gilman (eds), *Goodman & Gilman's The Pharmacological Basis of Therapeutics* (New York: McGraw-Hill), pp. 2–27.

Bergwerk, A. J., Shi, X., Ford, A. C., Kanai, N., Jacquemin, E., Burk, R. D., Bai, S., Novikoff, P. M., Stieger, B., Meier, P. J., Schuster, V. L. and Wolkoff, A. W., 1996, Immunologic distribution of an organic anion transport protein in rat liver and kidney. *American Journal of Physiology*, **271**, G231–G238.

Besseghir, K. and Roch-Ramel, F., 1987, Renal excretion of drugs and other xenobiotics. *Renal Physiology*, **10**, 221–241.

Burckhardt, G. and Wolff, N. A., 2000, Structure of renal anion and cation transporters. *American Journal of Physiology*, **278**, F853–F866.

Davies, B. and Morris, T., 1993, Physiological parameters in laboratory animals and humans. *Pharmacology Research*, **10**, 1093–1095.

De Vries, M. H., Groothuis, G. M. M., Mulder, G. J., Nguyen, H. and Meijer, D. K. F., 1985, Secretion of the organic anion harmol sulfate from liver into blood. *Biochemical Pharmacology*, **34**, 2129–2135.

Fleck, C. and Braunlich, H., 1986, Relation between renal and hepatic excretion of drugs: I. Phenol red in comparison with *p*-aminohippurate and indocyanine green. *Experimental Pathology*, **29**, 179–192.

Fleck, C. and Braunlich, H., 1990, Factors determining the relationship between renal and hepatic excretion of xenobiotics. *Arzneim. Forsch./Drug Research*, **40**, 942–946.

Guarino, A. M. and Anderson, J. B., 1976, Excretion of phenol red and its glucuronide in the dogfish shark. *Xenobiotica*, **6**, 1–13.

Hassen, A. M., Lam, D., Chiba, M., Tan, E., Geng, W. and Pang, K. S., 1996, Uptake of sulfate conjugates by isolated rat hepatocytes. *Drug Metabolism and Disposition*, **24**, 792–798.

Howie, D., Adriaenssens, P. I. and Prescott, L. F., 1977, Paracetamol metabolism following overdosage: application of high performance liquid chromatography. *Journal of Pharmaceutics and Pharmacology*, **29**, 235–237.

Iida, S., Mizuma, T., Sakuma, N., Hayashi, M. and Awazu, S., 1989, Transport of acetaminophen conjugates in isolated rat hepatocytes. *Drug Metabolism and Disposition*, **17**, 341–344.

Klaassen, C. D. and Watkins, J. B. III, 1984, Mechanisms of bile formation, hepatic uptake, and biliary excretion. *Pharmacology Reviews*, **36**, 1–67.

Kullak-Ublick, G. A., 1999, Regulation of organic anion and drug transporters of the sinusoidal membrane. *Journal of Hepatology*, **31**, 563–573.

Kusuhara, H., Suzuki, H. and Sugiyama, Y., 1998, The role of P-glycoprotein and canalicular multispecific organic anion transporter in the hepatobiliary excretion of drugs. *Journal of Pharmaceutical Science*, **87**, 1025–1040.

Moller, J. V. and Sheikh, M. I., 1983, Renal organic anion transport system: Pharmacological, physiological, and biochemical aspects. *Pharmacology Reviews*, **34**, 315–368.

Mulder, G. J., Brouwer, S. and Scholtens, E., 1984, High-rate intestinal conjugation of 4-mehtylumbelliferone during intravenous constant infusion in the rat *in vivo*. *Biochemical Pharmacology*, **34**, 2129–2135.

Mulder, G. J., Brouwer, S., Weitering, J. G., Scholtens, E. and Pang, K. S., 1985, Glucronidation and sulfation in the rat *in vivo*: the role of the liver and the intestine in the *in vivo* clearance of 4-methylumbelliferone. *Biochemical Pharmacology*, **34**, 1325–1329.

Pang, K. S., Koster, H., Halsema, I. C. M., Scholtens, E. and Mulder, G. J., 1981, Aberrant pharmacokinetics of harmol in the perfused rat liver preparation: sulfate and glucuronide conjugations. *Journal of Pharmacology and Experimental Therapeutics*, **219**, 134–140.

Pang, K. S., Koster, H., Halsema, I. C. M., Scholtens, E., Mulder, G. J. and Stillwell, R. N., 1983, Normal and retrograde perfusion to probe the zonal distribution of sulfation and glucronidation activities of harmol in the perfused rat liver preparation. *Journal of Pharmacology and Experimental Therapeutics*, **224**, 647–653.

Satlin, L. M., Amnin, V. and Wolkoff, A. W., 1997, Organic anion transporting polypeptide mediates organic anion/HCO_3 exchange. *Journal of Biological Chemistry*, **272**, 26340–26345.

Siegers, C. P. and Klaassen, C. D., 1984, Biliary excretion of acetaminophen in ureter-ligated rats. *Pharmacology*, **28**, 177–180.

Studenberg, S. D. and Brouwer, K. L. M., 1993, Effect of phenobarbital and *p*-hydroxyphenobarbital glucuronide on acetaminophen metabolites in isolated rat hepatocytes: Use of a kinetic model to examine the rates of formation and egress. *Journal of Pharmacokinetics and Biopharmacology*, **21**, 175–194.

Sundheimer, D. W. and Brendel, A. K., 1983, Metabolism of harmol and transport of harmol conjugates in isolated rat hepatocytes. *Drug Metabolism and Disposition*, **11**, 433–440.

Takenaka, O., Horie, T., Kobayashi, K., Suzuki, H. and Sugiyama, Y., 1995, Kinetic analysis of hepatobiliary transport for conjugated metabolites in the perfused liver of mutant rats (EHBR) with hereditary conjugated hyperbilirunemia. *Pharmacology Research*, **12**, 1746–1755.

Tojo, A., Sekine, T., Takeda, M., Cha, S. H., Kanai, Y., Kimura, K. and Endou, H., 1999, Immunohistochemical localization of multispecific organic anion transporter 1 in rat kidney. *Journal of the American Society of Nephrology*, **10**, 464–471.

Van Aubel, R. A. M. H., Masereeuw, R. and Russel, F. G. M., 2000, Molecular pharmacology of renal organic anion transporters. *American Journal of Physiology*, **279**, F216–F232.

XENOBIOTICA, 2002, VOL. 32, NO. 6, 451–478

Taylor & Francis
healthsciences

Topics in Xenobiochemistry

Pharmacokinetic interactions between herbal remedies and medicinal drugs

C. IOANNIDES*

Molecular Toxicology Group, School of Biomedical and Life Sciences, University of Surrey, Guildford GU2 7XH, UK

Received 21 September 2001

1. The use of herbal products to treat a wide range of conditions is rising rapidly, leading to increased intake of phytochemicals. Recent studies revealed potentially fatal interactions between herbal remedies and traditional drugs.

2. In transplant patients, self-medication with St John's wort (*Hypericum perforatum*) has led to a drop in plasma levels of the immunosuppressant drug cyclosporine, causing tissue rejection.

3. Intake of St John's wort increases the expression of intestinal P-glycoprotein and the expression of CYP3A4 in the liver and intestine. The combined up-regulation in intestinal P-glycoprotein and hepatic and intestinal CYP3A4 impairs the absorption and stimulates the metabolism of cyclosporine, leading to subtherapeutic plasma levels. The St John's wort component, hyperforin, contributes to the induction of CYP3A4.

4. St John's wort also enhances the metabolism of other CYP3A4 substrates including the protease inhibitors indinavir and nevirapine, oral contraceptives, and tricyclic antidepressants such as amitriptyline.

5. Other herbal remedies with the potential to modulate cytochrome P450 activity and thus participate in interactions with conventional drugs include Milk thistle, *Angelica dahurica*, ginseng, garlic preparations, Danshen and liquorice.

6. Herbal products are currently not subject to the rigorous testing indispensable for conventional drugs. However, if potential drug interactions are to be predicted, it is essential that the ability of herbal products to interfere with drug-metabolizing enzyme systems is fully established.

Introduction

Exposure of the human body to exogenous chemicals is a continuous process that is both inevitable and unavoidable. Although anthropogenic chemicals attract most attention, the vast majority of chemicals to which man is exposed to are naturally occurring, of plant origin. It has been estimated that >99% of the chemicals ingested by humans are naturally occurring (Ames and Gold 1998). Phytochemicals, similar to their anthropogenic counterparts, may be biologically active and thus capable of modulating physiological processes, to the benefit or detriment of humans. Undoubtedly, the major sources of human exposure to chemicals are the diet and, increasingly, herbal remedies. Most of the dietary chemicals are inherent to the diet, such as the carcinogenic hydrazines in the edible mushroom *Agaricus bisporus*, and safrole and estragole in spices (Mori *et al*. 1998).

* Author for correspondence; e-mail: c.ioannides@surrey.ac.uk

Xenobiotica ISSN 0049–8254 print/ISSN 1366–5928 online © 2002 Taylor & Francis Ltd
http://www.tandf.co.uk/journals
DOI: 10.1080/00498250210124147

Furthermore, food may be contaminated by chemicals derived from the packaging or generated during storage, such as the mycotoxins, an important class of hepatocarcinogens (Wang *et al.* 1998). Finally, the cooking process can generate novel chemicals such as heterocyclic amines and polycyclic aromatic hydrocarbons, both being major classes of chemical carcinogens (Skog and Jägerstadt 1998). The biological activity of naturally occurring chemicals, however, is not always detrimental to the living organism, and it is increasingly being recognized that plant constituents in food, such as polyphenols and organosulfates, may possess anticancer activity (Ahmad *et al.* 1998, Mori and Nishikawa 1998). This realization has led to an enormous current research effort aimed at defining these dietary anticancer chemicals better and elucidating their mechanism of action.

The use of herbs to treat disease emanates from the ancient Greek, Egyptian and Chinese civilizations, long before the chemist was able to synthesize bioactive compounds. Mandrake (*Mandragora officinarum*), a perennial herb containing alkaloids (e.g. atropine and scopolamine), native to South East Mediterranean, was used as a narcotic by the ancients, and in the Middle Ages found use as a painkiller. However, at the same time, the ancient civilizations also recognized that plant chemicals could be detrimental to the human body and did not hesitate to exploit them. Poison hemlock (*Conium maculatum*), another alkaloid-containing herb, was used by the ancient Greeks in executions, the most renowned victim being the philosopher Socrates. There can be no doubt that the plant kingdom presented humanity with some of its most efficacious medicines. The digitalis drugs, derived from foxglove (*Digitalis purpurea*), are still used widely today to treat major heart conditions. Even modern drugs such as the anticancer agents tamoxifen and taxol, used in the treatment of breast cancer, owe their existence to the Pacific yew (*Taxus brevifolia*). The recent upsurge in popularity of herbal remedies and other plant preparations to treat and prevent disease lie in the belief that these are at least as efficacious as their 'chemical' counterparts without the side-effects associated usually with the latter.

Metabolism of xenobiotics

The body cannot discern between a natural chemical emanating from the garden and a synthetic chemical generated in a laboratory, and consequently it deals with both in the same way. As these chemicals cannot be exploited beneficially by the body, they are recognized as being foreign (xenobiotics), and potentially deleterious, so the immediate response of the body is to eliminate them. A large number of xenobiotics that gain access to the systemic circulation tend to be lipophilic, and consequently difficult to excrete; the body renders these hydrophilic through metabolism to facilitate their excretion (Ioannides 2000). A number of enzyme systems adept at converting xenobiotics to excretable polar metabolites are ubiquitous in the body but principally found in the liver, and are intracellularly localized on the endoplasmic reticulum and in the cytosol (Ioannides 2001). Metabolism, in most instances, terminates the biological activity of the xenobiotic as the metabolites are unable to gain access and/or interact with the appropriate receptors to elicit a biological response. Undoubtedly, the most versatile enzyme system involved in xenobiotic metabolism is the cytochromes P450. By virtue of existing as a number of distinct proteins, cytochromes P450 display unprecedented substrate specificity, being able to metabolize a myriad of

structurally dissimilar chemicals including medicinal drugs (Ioannides 1996, Guengerich 1999). Since the same enzyme system is responsible for the metabolism of naturally occurring chemicals, the increasing awareness of interactions between dietary components or herbal remedies on one hand and conventional drugs on the other, similar to drug–drug interactions, should not come as a surprise.

It is now established that naturally occurring chemicals, at dietary levels of intake, can modulate the hepatic and extrahepatic expression of cytochrome P450 levels resulting in marked changes in the metabolism of drugs that lead to adverse drug interactions (Guengerich 1984, Parke and Ioannides 1994, Ioannides 1998, 1999). Changes in cytochrome P450 activity will be particularly relevant in the clinic when they concern drugs with a low therapeutic index, where plasma levels have to be maintained within a narrow concentration range to ensure maximum benefit with the minimum of adverse effects. Elevated cytochrome P450 activity, translated into a more rapid metabolic rate, may result in a decrease in drug plasma concentrations to subtherapeutic levels and total loss of the pharmacological effect. Conversely, suppression of cytochrome P450 activity may trigger a rise in plasma drug levels leading to an undesirable exaggerated pharmacological effect and the appearance of toxic symptoms commensurate with overdose.

Effects of phytochemicals on cytochrome P450 expression

The first reports indicating that dietary chemicals interacted with medicinal drugs were published in the 1970s, showing that consumption of cruciferous vegetables resulted in lower plasma levels of the analgesic drug phenacetin, and it suggested that indoles, which are present in such vegetables in substantial amounts, could be responsible (Pantuck *et al.* 1976, 1979). In further studies, broccoli, when added to the diet, up-regulated a number of cytochrome P450 enzymes in the liver and colon of rats (Vang *et al.* 1991). Subsequent studies in humans indicated, using the caffeine metabolic ratio as an *in vivo* probe for CYP1A2 activity, that broccoli intake up-regulated selectively this isoform (Vistisen *et al.* 1992, Kall *et al.* 1996, Lampe *et al.* 2000). It was eventually established that indole-3-carbinol, present in these vegetables as the glucosinolate, glucobrassicin, and released by the action of the enzyme myrosinase, was indeed responsible for the effects of cruciferous vegetables; in the stomach it undergoes non-enzymic condensation to generate dimers and other oligomers that appear to mediate its effects on the cytochrome P450 system (Vang *et al.* 1990, de Kruif *et al.* 1991, Stresser *et al.* 1994). Both indole-3-carbinol and its dimer, 3,3′-diindolylmethane are currently marketed in the USA as dietary supplements, largely to treat and prevent breast cancer.

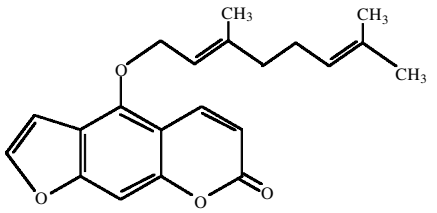
Cruciferous vegetables also contain other compounds, the isothiocyanates, such as phenethyl isothiocyanate and sulforaphane, present in the form of glucosinolates, which are also capable of selectively modulating cytochrome P450 activity (Ishizaki *et al.* 1990, Barcelo *et al.* 1992, Mahéo *et al.* 1997). However, the picture is more complex as cruciferous vegetables also influence other enzyme systems, so that the effects of these vegetables on the metabolism of a certain drug will be very much dependent on the nature of the principal enzymes responsible for its metabolic breakdown. For example, cruciferous vegetables and indoles also modify the activity of other enzyme systems, up-regulating conjugation reactions such as

glutathione *S*-transferases and glucuronyl transferases (Pantuck *et al*. 1984), but down-regulating the flavin monooxygenase system (Cashman *et al*. 1999, Katchamart *et al*. 2000).

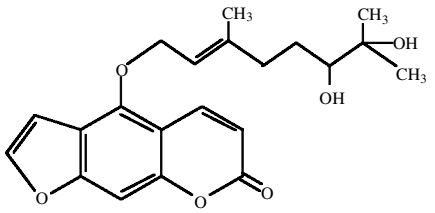
Other common foods that appear to up-regulate cytochrome P450 expression include tea. In studies conducted in rat, exposure to normal-strength green and black tea brews resulted in up-regulation of CYP1A2; as decaffeinated tea failed to induce the same enzyme, it was concluded that caffeine, also present in many other foods, is responsible for the effect (Bu-Abbas *et al*. 1994, 1999, Sohn *et al*. 1994). Indeed, exposure of rats to caffeine in drinking water elevated CYP1A2, and to a lesser extent CYP2B, activity (Ayalogu *et al*. 1995). Treatment by all three types of tea also stimulated the activity also of some Phase II conjugation enzymes (Bu-Abbas *et al*. 1998). Thus, phytochemicals in tea, at dietary levels of intake, are capable of altering the hepatic cytochrome P450 profile, and modulating the activity of conjugation. It is worth noting that heavy coffee drinkers may consume as much as 3 g caffeine daily (Barone and Roberts 1996).

Diet can also suppress cytochrome P450 activity. Indeed, recent work employing the caffeine metabolic ratio to monitor CYP1A2 activity in humans has shown that consumption of diets containing apiaceous vegetables, such as carrots, parsnips and celery, leads to lower activity (Lampe *et al*. 2000). Thus, vegetables have the potential both to enhance and impair cytochrome P450 activity. Perhaps the best-researched, clinically relevant interaction between diet and drugs involves grapefruit juice (Ameer and Weintraub 1997, Bailey *et al*. 1998a, Fuhr 1998). Simultaneous consumption of grapefruit juice with a number of drugs that are subject to extensive first-pass effect leads to a rise in their plasma levels and an increase in the bioavailability of the drug, with a consequent intensification of the pharmacological effect and the appearance of adverse effects associated with overdose (Bailey *et al*. 1991, Kupferschmidt *et al*. 1995, 1998, Yee *et al*. 1995, Kantola *et al*. 1998, Lilja *et al*. 1998). The effect becomes even more pronounced after the repeated intake of the juice (Lilja *et al*. 2000a). What is of particular concern, is that the effect may be sustained for at least up to 3 days following the last consumption of grapefruit juice (Lundahl *et al*. 1995, Lilja *et al*. 2000b, Takanaga *et al*. 2000). Grapefruit juice acts by inhibiting intestinal CYP3A4 activity, which is responsible for the presystemic metabolism of these drugs, so that more of the drug enters the systemic circulation reaching undesirable high concentrations (Lown *et al*. 1997). In contrast, grapefruit juice has no effect on the hepatic activity as exemplified by the erythromycin breath test, although repeated intake of concentrated grapefruit juice has been reported to prolong the biological half-life of triazolam (Lilja *et al*. 2000a). Enterocyte CYP3A4 levels, determined immunologically, were reduced almost by half, 4 h following intake of grapefruit juice (Schmiedlin-Ren *et al*. 1997). Since the mRNA levels were not altered (Lown *et al*. 1997), mechanism-based degradation of enterocyte CYP3A4 content by component(s) of grapefruit remains the likely mechanism. Following repeated intake of grapefruit juice, intestinal levels of CYP3A5, a less abundant enzyme with catalytic properties similar to those of CYP3A4, also diminished (Lown *et al*. 1997). Such mechanism-based inhibitors cause marked loss in activity and their effects are long lasting, requiring the synthesis of new enzyme protein for the effect to disappear.

Grapefruit constituents that appear to promote this effect are furanocoumarins (psoralens), such as bergamottin and its derivative 6′,7′-dihydroxy-



Bergamottin



6',7'-Dihyroxybergamottin

Figure 1. Components of grapefruit juice that contribute to its interactions with drugs.

bergamottin (figure 1), and dimers derived from these (Edwards *et al.* 1996, Fukuda *et al.* 1997, Schmiedlin-Ren *et al.* 1997, Bailey *et al.* 1998b, 2000, He *et al.* 1998). Furanocoumarins, in general, are known to inactivate cytochrome P450, in many cases through mechanism-based inhibition processes (Cai *et al.* 1993, Koenigs and Trager 1998a, b, Guo *et al.* 2000). Among these, bergamottin has been shown to reduce CYP3A4 activity more effectively than its dihydroxylated metabolite (He *et al.* 1998). Bergamottin is converted to a reactive intermediate by CYP3A4, which then interacts covalently with the apoprotein moiety of the cytochrome, leading to loss of activity (He *et al.* 1998). Such a metabolite could be an epoxide formed because of oxidation of the double bond on the furano ring. In a recent *in vitro* study, dimers and trimers of furanocoumarins were particularly potent inhibitors of human microsomal CYP3A activity as assessed by the 6β-hydroxylation of testosterone, implicating these compounds in the grapefruit-mediated suppression of CYP3A4 levels (Guo *et al.* 2000). In extensive kinetic studies evaluating the cytochrome P450 inhibitory potency of grapefruit juice furanocoumarins, it was observed that dimeric furanocoumarins were markedly more potent inhibitors of CYP3A4 activities in human liver microsomes than the monomers bergamottin and its 6′,7′-dihydroxyderivative, and mechanism-based inhibition appears to have been involved (Tassaeenyakul *et al.* 2000). In the colon cell line Caco-2, 6′,7′-dihydroxybergamottin and a dimer have been shown selectively to inhibit CYP3A4 activity and decrease the apoprotein levels through a mechanism-based process (Schmiedlin-Ren *et al.* 1997). Furthermore, bergamottin is a more potent mechanism-based inhibitor of the intestinal oxidation of nifedipine in rat than 6′,7′-dihydroxybergamottin (Mohri and Uesawa 2001). However, other authors have presented experimental evidence leading to the conclusion that 6′,7′-dihydroxybergamottin is not responsible for the interaction of grapefruit juice with drugs such as felodipine and cyclosporin (Bailey *et al.* 1998b, Edwards *et al.* 1999). When grapefruit juice was fractionated and the influence of the fractions on the pharmacokinetics of felodipine was studied in humans, no correlation was obtained between the levels of 6′,7′-dihydroxybergamottin and the area under the curve (AUC) and C_{max} of the drug (Bailey *et al.* 1998b). In a recent *in vivo* study performed in rat, grapefruit juice and bergamottin, but not 6′,7′-dihydroxybergamottin, increased the AUC of nifedipine, supporting a role for bergamottin, but not for its more hydrophilic dihydroxy metabolite, in this interaction (Mohri and Uesawa 2001). Overall, it appears that bergamottin and furanocoumarin dimers present in grapefruit juice, albeit at lower concentrations, may be the major contributors to the pronounced inhibitory effect

of grapefruit juice on CYP3A4 activity. Precise clarification of the role of individual compounds must await the completion of *in vivo* studies in humans.

It is also worth emphasizing that the activity of other cytochromes P450 is also suppressed by grapefruit juice and its component furanocoumarins (Tassaeenyakul *et al*. 2000), such that interactions may conceivably occur if these forms play a dominant role in the presystemic metabolism of drugs. In murine microsomes, bergamottin is a potent inhibitor of the CYP1A-mediated *O*-deethylation of ethoxyresorufin and of the CYP2B-mediated *O*-dependentylation of pentoxyresorufin (Cai *et al*. 1993). Finally, it is worth pointing out that other furanocoumarins, such as methoxsalen (8-methoxy-3′,2′:6,7-furanocoumarin), also influence cytochrome P450 activity, but in this case it leads to the transcriptional up-regulation of cytochrome P450 proteins belonging to the CYP1A and 2B subfamilies in rat (Gwang 1996). In *in vitro* studies, methoxsalen inhibited markedly the activity of a number of human cytochrome P450 enzymes, especially CY3A4/5, 2A6 and 1A2 (Ono *et al*. 1996). Further studies on CYP2A6 indicated that its inhibition by methoxsalen involves a mechanism-based process (Draper *et al*. 1997).

Herbal remedies

During the last decade, an explosion in the consumption of herbal remedies, especially among older people, has been witnessed in North America and Europe, particularly in Germany, which leads the world in the sales of such remedies, and France. In England, nearly one in four adults purchases a homeopathic or herbal remedy annually, the latter being the more frequently used (Thomas *et al*. 2001), and their use is considerably higher in women. Herbal preparations such as ginkgo, biloba, echinacea, feverfew, garlic, ginseng, kava, liquorice (licorice), saw palmetto and St John's wort are increasingly taken to treat a number of conditions ranging from depression to high blood pressure, or to improve general well-being (Wills *et al*. 2000). Other plant preparations, such as polyphenol supplements, believed to afford protection against cancer and cardiovascular disease and to boost the immune system, are also gaining favour, and may be further complemented by healthcare products such as vitamins and minerals. Such herbal remedies and dietary supplements are now widely available over-the-counter in pharmacies as well as specialist 'health' and 'herbalist' shops, without the need for a prescription, so that self-medication is prevalent. Thus, the intake of herbal remedies, especially on a chronic basis, may increase dramatically the intake of phytochemicals that would otherwise be consumed at low levels through the diet.

A major cause of current concern is that herbal remedies may interact with medicinal drugs, altering the pharmacokinetic characteristics of the latter and leading to clinically significant interactions. Herbal medications are taken not only by healthy persons who want to protect themselves from the onset of disease or to improve their well being, but also by patients suffering from life-threatening conditions who simultaneously receive one or more medicinal drugs (Liu *et al*. 2000). Herbal preparations may interact with a drug at the site of absorption, reducing the amount of drug absorbed or its rate of absorption, thus modifying the pharmacological effect of the drug. Phytochemicals may interact with the ATP-depended transporter proteins such as the intestinal P-glycoprotein and other multidrug resistance proteins that facilitate the efflux of drugs (Hunter and Hirst 1997, Evans 2000, Leslie *et al*. 2001, van Tellingen 2001). Phytochemicals thus

have the potential to compete with traditional drugs for the transporter proteins. Furthermore, the P-glycoprotein transporter may be also induced by xenobiotics such as dexamethasone (Ayrton and Morgan 2001). Finally, phytochemicals can impair or facilitate drug absorption by a number of additional mechanisms (Thomas *et al*. 1998).

A number of cases have been described where herbal products appear to have interacted with anticoagulants such as warfarin, although it is not clear whether the underlying mechanisms are pharmacokinetic in nature (Heck *et al*. 2000). Warfarin is a highly protein-bound drug so that displacement from its binding sites may form the basis for such interaction. Warfarin has a narrow therapeutic range, so that displacement by constituents of diet or herbal products will increase plasma levels and facilitate its distribution, enhancing its pharmacological activity with the risk of haemorrhage.

Herbal remedies may participate in interactions with medicinal drugs in the same way as any dietary phytochemical by modulating the activity of the cytochromes P450 and other drug-metabolizing enzyme systems. For example, coumarins, which are responsible for the grapefruit effect, are very abundant in nature and have been detected in many herbal remedies. Indeed, a wide variety of naturally occurring coumarins have been shown effectively and selectively to inhibit and inactivate a number of cytochrome P450 enzymes (Cai *et al*. 1993). Consequently, they may exaggerate the effect of a drug and lead to the appearance of adverse effects that are not normally manifested when the drug is taken alone. Indeed, in *in vitro* investigations, commercial ethanolic extracts of many herbs extensively inhibit the CYP3A4-mediated debenzylation of benzyloxyresorufin (Budzinski *et al*. 2000). Similarly, hot water decoctions or 40% ethanol infusions of many herbal remedies impair CYP3A activity, monitored by the 6β-hydroxylation of testosterone, in human hepatic microsomes (Guo *et al*. 2001). However, such *in vitro* observations can not be extrapolated confidently to the *in vivo* situation, since inhibition may reflect nothing more than competitive inhibition by constituent(s) present in the extract; induction of the cytochrome P450 system may result *in vivo*. For example, the phytochemical anthraflavic acid, a planar anthraquinone, is a potent inhibitor of hepatic CYP1A activity *in vitro* (Ayrton *et al*. 1987), but when administered to rat it up-regulated the hepatic expression of this subfamily (Ayrton *et al*. 1988). Similarly, safrole, another phytochemical, is metabolized *in vitro* to a carbene intermediate that interacts with cytochrome P450 impairing its activity. However, *in vivo* the initial inhibitory phase is followed by one of potent induction of cytochrome P450 enzymes belonging to the CYP1A and CYP2B subfamilies (Ioannides *et al*. 1981).

Phytochemicals in herbal products are not subject to the same level of rigorous testing in animals and humans which is routinely undertaken with synthetic chemicals, so that their ability to perturb xenobiotic-metabolizing enzyme systems is not known and, as a result, possible interactions with medicinal drugs cannot be predicted. This problem is further compounded by the fact that the purity and composition of herbal products is not always assured and may vary considerably among various preparations and between batches, in marked contrast to synthetic drugs. Furthermore, herbal products are particularly popular among older people who are more likely to be receiving conventional medication and are also more sensitive to chemicals.

St John's wort

St John's wort, an extract of the plant *Hypericum perforatum*, is an extensively used herb product prepared from the flowers and leaves of the plant, indigenous to Europe, North Africa and North America, and it is used largely as an antidepressant to treat mild to moderate depression (Josey and Tackett 1999, Barnes *et al.* 2001). It is available in many forms, pulverized in to powder, brewed in to tea, extracts in oil, as tablets, capsules, etc. In some preparations, it is the sole ingredient, whereas in others it is found in combination with others. In many countries, including the UK, it is marketed as a food supplement whereas in others, such as Sweden, it is marketed as herbal remedy and in Germany as a drug. Moreover, this is one of the most extensively studied herbal products (Greeson *et al.* 2001). Preparations of the herb are standardized with respect to hypericin, believed to be one of its active components. The hypericin content of St John's wort is subject to marked seasonal variations (Southwell and Bourke 2001).

St John's wort has been implicated in a number of clinically important life-threatening interactions with a number of conventional drugs. Indeed, in *in vitro* studies, crude extracts of St John's wort inhibit cytochrome P450 enzymes belonging to all the xenobiotic-metabolizing families (Obach 2000), raising the possibility of drug interactions. The same study identified hyperforin, hypericin, quercetin and I3,II8-biapigenin as the components that may contribute to this inhibitory effect. In most cases, the inhibition is of a competitive nature suggesting that these compounds may serve as cytochrome P450 substrates, and *in vivo* they may also have the potential to induce cytochrome P450 expression, assuming that the necessary intracellular levels can be attained.

St John's wort: cyclosporin. This is one of the most serious, and potentially fatal, interactions between a herbal remedy and a conventional drug, and is also one of the most extensively researched, with the mechanism of action being relatively well understood. Cyclosporin is one of the most widely used immunosuppressant drugs following transplantation, but it is essential that blood levels are maintained within a narrow concentration range; a fall below the effective concentration may lead to tissue rejection whereas an increase is associated with hepato- and kidney toxicity. A number of cases have been reported, particularly from Germany, of a potentially fatal interaction between cylosporin and the herbal remedy. The common features of these cases are that patients stabilized effectively on cyclosporin experienced tissue rejection after taking St John's wort even at dose levels of the herb below those recommended (table 1). The clinical picture improved in all cases following abstinence from the herb. Each case will be dealt with separately. In a case reported from Switzerland (Ruschitzka *et al.* 2000), a heart transplant patient was stabilized on cyclosporin since having the transplant 11 months earlier. The patient, 3 weeks before admission to hospital for elective endomyocardial biopsy, self-medicated with the St John's wort extract LI160 at a total daily dose level of 900 mg, taken in three doses. Endomyocardial biopsy revealed acute cellular transplant rejection. Cyclosporin levels were determined and found to have dropped below $100\,\mu g\,l^{-1}$ (the desirable effective therapeutic range is in the region of $200–350\,\mu g\,l^{-1}$). St John's wort was discontinued and the cyclosporin dose was increased to improve the subtherapeutic levels. The levels remained within the therapeutic range without further tissue rejection. Ruschitzka *et al.*

Table 1. Documented cases of interaction between cyclosporin and St John's wort.

Period and organ(s) of transplantation	Cyclosporin dose (mg)	St John's wort dose (mg)	Cyclosporin plasma levels before St John's wort ($ng\,ml^{-1}$)	Cyclosporin plasma levels after St John's wort ($ng\,ml^{-1}$)	Reference
Heart – 11 months	2 × 125 daily	3 × 300 daily for 3 weeks	200	95	Ruschitzka *et al.* (2000)
Heart – 20 months	2 × 125 daily	3 × 300 daily for 3 weeks	230	87	Ruschitzka *et al.* (2000)
Kidney – 25 years	2 × 75 daily	300 daily for 4 weeks	126*	72*	Mai *et al.* (2000)
Liver – 14 months	2 × 175 daily	2 × 900 daily for 2 weeks	200	48	Karliova *et al.* (2000)
Kidney and pancreas – 54 months	2 × 100 daily	1 or 2 × 300 daily for 7 weeks	250–300*	97*	Barone *et al.* (2000)
Kidney – 3 years and 10 months	2 × 175 daily	2 or 3 × 300 daily for 6 months	275*†	90–150*	Barone *et al.* (2001)

* Whole blood trough concentrations; † concentration 2 weeks after ceasing St John's wort intake.

(2000) also reported a second case where the patient was referred to the clinic 20 months after heart transplant for elective endomyocardial biopsy which indicated acute rejection. The patient had also been stabilized on cyclosporin. Three weeks earlier, treatment was commenced with the same dose of St John's wort as the previous patient; plasma levels of cyclosporin were subtherapeutic ($87\,\mu g\,l^{-1}$). The plasma levels of the immunosuppressant returned to therapeutic values when the St John's wort treatment was discontinued, and no other rejection episodes were reported. A few weeks later, a publication originating from Germany (Breidebach *et al.* 2000) referred to 30 kidney transplant patients whose plasma cyclosporin levels were nearly halved after taking St John's wort; the dose(s) used by the patients was not specified. The cyclosporin dose was increased to attain once again the therapeutic levels; when the herbal remedy was withdrawn, the immunosuppressant levels rose sharply and the drug dose was lowered to that taken before the intake of St John's wort. In a further case reported from Germany (Mai *et al.* 2000), a female kidney transplant patient was maintained successfully on cyclosporin for 25 years, but suddenly blood levels dropped following medication for 4 weeks with St John's wort, at the low dose of $300\,mg\,day^{-1}$; on discontinuation of the St John's wort intake, blood levels rose. When the intake of the herbal remedy was reintroduced 3 months later, the decline in the plasma levels of cyclosporin was reproduced. In another case from Germany (Karliova *et al.* 2000), a liver transplant patient maintained on cyclosporin began taking a high dose of St John's wort ($2 \times 900\,mg\,day^{-1}$), 14 months after the transplantation. Two weeks after the commencement of the herbal intake, the patient attended the clinic for routine examination and it was noted that the plasma levels of the immunosuppressant were very low ($48\,\mu g\,l^{-1}$). Liver function tests were abnormal and liver biopsy revealed acute cellular rejection. The cyclosporin dose was increased to bring the plasma levels within the therapeutic range. Following the discontinuation of the herbal remedy, the cyclosporin dose was reduced and the plasma levels returned to normal, with liver function tests recovering. Similar cases have also been reported from the USA involving two transplant patients on cyclosporin. One of these was transplanted with a kidney and the other a combined kidney and pancreas (Barone *et al.* 2000, 2001). Following self-medication with St John's wort (600–900 mg daily, taken in two to three doses), the blood levels of the immunosuppressant became subtherapeutic with one of the patients developing rejection of the graft, so that the dose of the immunosuppressant had to be increased to bring plasma levels within the therapeutic range. Cyclosporin levels overshot in both cases following discontinuation of St John's wort. All the above reports demonstrate unequivocally that treatment with the recommended dose of St John's wort lead to a fall in the levels of cyclosporin with life-threatening consequences. The possible underlying mechanisms may include St John's wort-mediated impaired absorption, possibly concerned with the intestinal P-glycoprotein transporter, and/or increased metabolism of cyclosporin.

In *in vitro* studies, methanolic and ethanolic extracts of St John's wort act as inhibitors of CYP3A4 activity (Budzinski *et al.* 2000, Carson *et al.* 2000), showing that components of this herbal product can interact with this enzyme. In a study conducted in rat, however, administration of a St John's wort extract led to increased expression of hepatic, but not intestinal, CYP3A2. The same treatment also elevated the expression of intestinal P-glycoprotein (Dürr *et al.* 2000). The

same group demonstrated that exposure of healthy volunteers to St John's wort for 2 weeks ($3 \times 300\,\text{mg}\,\text{day}^{-1}$) resulted in increased expression of duodenal P-glycoprotein and CYP3A4, determined immunologically, and hepatic CYP3A4 as exemplified by the erythromycin breath test. Cyclosporin is a good substrate of the intestinal P-glycoprotein (Ayrton and Morgan 2001). The combined up-regulation in duodenal P-glycoprotein and duodenal and hepatic CYP3A4 will be expected to limit severely the bioavailability of drugs that rely on these proteins for their absorption and metabolism, respectively. Using a different approach, Roby *et al.* (2000) monitored CYP3A4 activity through the 6β-hydroxycortisol: cortisol urinary ratio and confirmed that treatment with St John's wort ($3 \times 300\,\text{mg}$ daily) for 2 weeks elevated the ratio. Cyclosporin is metabolized through hydroxylation and *N*-demethylation by CYP3A4 to a large number of pharmacologically inactive products. Clearly, the St John's wort doses that have been reported to lower plasma cyclosporin concentrations to subtherapeutic levels are sufficient to stimulate CYP3A4 activity in the liver and intestine, and increase the expression of the P-glycoprotein.

Two components of St John's wort, hypericin, a polycyclic aromatic dianthroquinine (4,5,7,4′,5′,7′-hexahydroxy-2,2′-dimethylnaphthodianthrone), and hyperforin, a lipophilic acylphloroglucinol, are believed to be responsible for its antidepressant effects (figure 2). Exposure of primary human hepatocytes to hyperforin (1 μM) led to a very marked increase in *CYP3A4* mRNA levels (Moore *et al.* 2000). St John's wort as well as hyperforin, but not hypericin, interact avidly with the pregnane X receptor, a member of the steroid/thyroid receptor family that regulates CYP3A4 expression (Moore *et al.* 2000, Wentworth *et al.* 2000). Thus, it is likely that the induction of CYP3A4 may be mediated, at least partly, by hyperforin. It is worth pointing out that hyperforin is a potent inhibitor of CYP3A4 activity *in vitro* (Budzinski *et al.* 2000). The selective interaction of hyperforin with CYP3A4 is perhaps not surprising since this is a large molecular weight compound. Among the cytochrome P450 enzymes, the haem pocket of CYP3A4 has a large and open substrate-binding site that can accommodate large molecular weight compounds (Lewis *et al.* 1996).

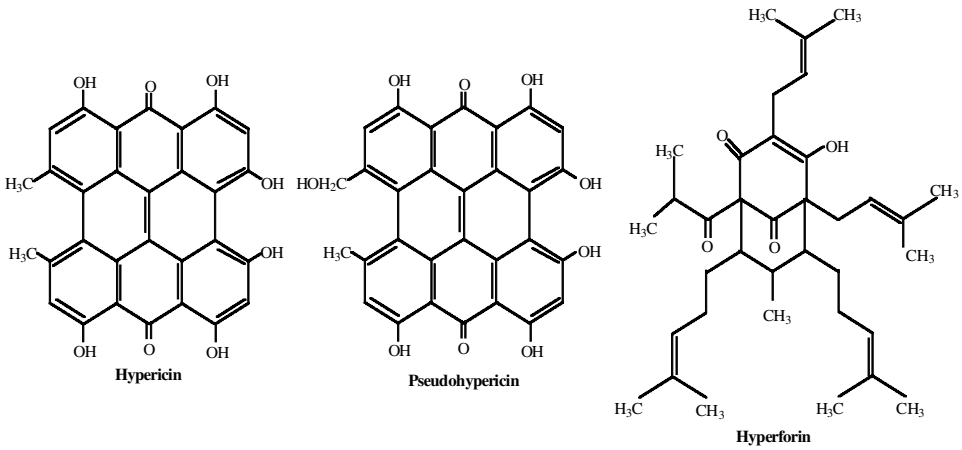


Figure 2. Bioactive constituents of St John's wort.

In human volunteers, after intake of hypericum extracts equivalent to 14.8 mg hyperforin, hyperforin was well absorbed with maximum plasma levels achieved 3.5 h after administration, with a plasma half-life of 9 h (Biber *et al.* 1998). Hypericin, the bioactive component of St John's wort on which the samples are quality controlled, has a terminal half-life of about 40 h in man, and that of pseudohypericin (2′-hydroxymethylhypericin) (figure 2) is about 25 h (Kerb *et al.* 1996, Brockmöller *et al.* 1997). Ingestion of St John's wort (LI 160) resulted in maximum plasma total hypericin (hypericin plus pseudohypericin) levels being achieved in 4 h (Brockmöller *et al.* 1997). Following the intake of the recommended doses of St John's wort ($3 \times 300\,\text{mg day}^{-1}$), steady-state was attained after 4 days (Staffeldt *et al.* 1994). The three bioactive compounds hypericin, pseudohypericin and hyperforin have good bioavailability when taken orally in tablets of St John's extracts (Kerb *et al.* 1996, Biber *et al.* 1998). The bioavailability of hypericin and pseudohypericin in humans appears to be about 15 and 20% respectively (Kerb *et al.* 1996). The effects of St John's wort on P-glycoprotein are likely to be mediated by flavonoids present in St John's wort, as these compounds are known to interact with this transporter (Conseil *et al.* 1998). In more recent studies (Leslie *et al.* 2001), flavonoids including naringenin, a grapefruit polyphenol, have been shown to also interact with the multidrug resistance protein 1 (MRP1).

Interactions involving St John's wort have also been reported for a number of other important drugs (table 2).

St John's wort: protease inhibitors. The European Medicine Evaluation Agency (EMEA) has recommended (1999) that patients receiving the protease inhibitor indinavir, a CYP3A4 substrate (Chiba *et al.* 1996), for the treatment of human immunodeficiency virus-1 (HIV-1) infection should not take St John's wort and other products containing this herb. Protease inhibitors retard the progress of the disease and thus prolong survival. Intake of St John's wort ($3 \times 300\,\text{mg day}^{-1}$) for 2 weeks led to a marked drop in the plasma concentrations of indinavir, halving the AUC (Piscitelli *et al.* 2000), which could compromise the effectiveness of the antiretroviral drug in persons infected with HIV.

It has also been reported that the oral clearance of another antiretroviral drug, nevirapine, is also elevated following consumption of St John's wort (de Maat *et al.* 2001). Thus, the drug may be rendered ineffective if taken concurrently with St John's wort. The principal catalysts of nevirapine metabolism are CYP3A4 and CYP2B6 (Erickson *et al.* 1999). It is important to point out that other protease inhibitors, such as amprenavir and saquinavir (Fitzsimmons and Collins 1997, Decker *et al.* 1998), are also metabolized by the CYP3A4 isoform and thus may be adversely influenced by concomitant intake of St John's wort.

St John's wort: oral contraceptives. Bleeding has been reported in women on the contraceptive pill when also taking St John's wort, and this has also been attributed to increased deactivation of the steroids through CYP3A-mediated metabolism (Ernst 1999). Ethinyloestradiol is a major component of the contraceptive pill and is also used in hormone-replacement therapy in postmenopausal women. It is metabolized and deactivated through hydroxylation at the 2-position, the reaction being catalysed by CYP3A4 (Guengerich 1988, Ball

Table 2. Investigated interactions between St John's wort and drugs other than cyclosporin.

St John's wort dose (mg)	Interacting drug	Pharmacokinetic consequences	Clinical implications	Reference
900 daily for 3 days	Alprazolam	none	–	Markowicz *et al.* (2000)
900 daily for 2 weeks	Amitriptyline	↓AUC	loss of antidepressant activity?	Roots *et al.* (2000)
900 daily for 2 weeks	Carbamazepine	none	–	Burstein *et al.* (2000)
900 daily for 3 days	Dextromethorphan	none	–	Markowicz *et al.* (2000)
900 daily for 10 days	Digoxin	↓AUC, ↓ C_{max}, ↓ C_{trough}	no change in blood pressure and PQ interval from electrocardiogram	Johne *et al.* (1999b)
900 daily for 2 weeks	Digoxin	↓AUC	?	Dürr *et al.* (2000)
900 daily for 2 weeks	Indinavir	↓AUC, ↓ C_{max},	loss of antiretroviral activity?	Piscitelli *et al.* (2000)
Not specified	Nevirapine	↑Cl	loss of antiretroviral activity?	De Maat *et al.* (2001)
Not specified	oral contraceptives	–	intermenstrual bleeding. Recovery when St John's wort withdrawn	Yue *et al.* (2000)
900 daily for 11 days	Phenprocoumon	↓AUC	loss of anticoagulant activity?	Maurer *et al.* (1999)
300 for 2 months	Theophylline	↓plasma levels	loss of bronchodilator activity?	Nebel *et al.* (1999)
Not specified	Warfarin	–	reduced anticoagulant activity	Yue *et al.* (2000)

↑, Increase; ↓, decrease.

et al. 1990). It has already been observed that in female tuberculosis patients the contraceptive pill may fail to afford the expected protection. Rifampicin, an antitubercular drug, was found responsible by virtue of its ability to elevate CYP3A4 activity (Bolt 1994). Since St John's wort is clearly an inducer of CYP3A4, an interaction with the contraceptive pill is a distinct possibility, and is particularly likely when the ethinyloestradiol content is lowered to avoid the undesirable oestrogenic effects (Shader and Greenblatt 2000). In seven cases reported to the Swedish Medical Products Agency, intermenstrual bleeding was experienced by mainly young women on oral contraceptives after they had taken St John's wort for as little as 1 week; the dose of the herbal remedy was not given (Yue *et al*. 2000). Termination of the intake of St John's wort led to recovery in those cases where the outcome was known.

St John's wort: alprazolam. Short-term ingestion (900 mg daily for 3 days) of St John's wort before and during oral intake of the benzodiazepine alprazolam failed to alter the pharmacokinetic characteristics of the drug in seven healthy volunteers (Markowicz *et al*. 2000). Alprazolam metabolism, like that of many other benzodiazepines, is catalysed in humans primarily by CYP3A4 (von Moltke *et al*. 1996). The lack of effect seen following exposure to St John's wort may simply reflect the short duration of treatment. In studies where the plasma/blood levels of CYP3A4-metabolized drugs such as cyclosporin were reduced (see above) involved exposure to St John's wort for at least 2 weeks.

St John's wort: anticoagulants. Seven cases have been reported to the Swedish Medical Products Agency where the use of St John's wort compromised the anticoagulant action of warfarin (Yue *et al*. 2000). Concomitant intake of St John's wort was associated with loss of anticoagulant activity in patients stabilized on warfarin. Although no thromboembolic episodes occurred, the decrease in anticoagulant activity was considered clinically significant. Anticoagulant activity was restored when St John's wort was discontinued or the warfarin dose was increased. These observations imply increased clearance of the drug. The human metabolism of warfarin involves a number of cytochrome P450 proteins, including CYP1A2, CYP2C9 and CYP3A4 (Kaminsky and Zhang 1997). It is feasible that induction of CYP3A4 by the intake of St John's wort may have contributed to the loss of the anticoagulant activity.

In a cross-over study, volunteers that took a 900-mg daily dose of St John's wort (LI 160) for 11 days before a single dose of phenprocoumon, another anticoagulant, had a lower AUC of the free fraction than when they received the placebo (Maurer *et al*. 1999).

St John's wort: carbamazepine. In a study aimed at investigating the possible interaction between St John's wort and orally administered carbamazepine, ingestion of the herbal remedy (3×300 mg daily) for 2 weeks failed to influence the pharmacokinetic characteristics of the drug taken by volunteers for 3 weeks before commencement of the St John's wort intake (Burstein *et al*. 2000). The predominant enzyme catalysing the metabolism of this drug is CYP3A4, but other enzymes, such as CYP2C8, also make a substantial contribution (Kerr *et al*. 1994).

It has been suggested (Burstein *et al.* 2000) that the reason for the inability of St John's wort to influence the clearance of carbamazepine, as a result of CYP3A4 induction, is that the enzyme may have already been maximally induced by the repeated intake of carbamazepine (Rapeport *et al.* 1982, Bertilsson *et al.* 1986, Kudriakova *et al.* 1992), or alternatively carbamazepine may not function as a substrate of P-glycoprotein, which is also activated by St John's wort.

St John's wort: digoxin. The possible interaction of digoxin with the St John's wort extract LI160, following a single dose or treatment for 10 days with the latter (900 mg daily), was studied in volunteers where digoxin levels had attained steady-state (Johne *et al.* 1999a, b). No significant effect was observed following single exposure to the herbal remedy, but following the repeated intake the AUC decreased by 25% and, moreover, the plasma C_{max} and C_{trough} were similarly reduced; the decline in C_{trough} became more pronounced as the duration of St John's wort intake increased. $t_{1/2}$ was unaffected showing that the metabolism of the digoxin was not influenced by the St John's wort intake. In fact, digoxin is not significantly metabolized by the cytochrome P450 system in human hepatocytes and human liver microsomes (Lacarelle *et al.* 1991). However, in contrast to human microsomes, microsomal CYP3A proteins have been shown to catalyse the sequential oxidative cleavage of digoxin in rat (Salphati and Benet 1999). In a subsequent study, intake of St John's wort for 2 weeks, at a daily dose of 900 mg, decreased the oral bioavailability of digoxin (Dürr *et al.* 2000). It was suggested that the underlying mechanism involved induction of the P-glycoprotein drug transporter facilitating the efflux of the drug from the enterocytes to the intestinal lumen (Johne *et al.* 1999b) and that flavonoids present in the herbal extract may contribute to the activation of the P-glycoprotein transporter (Conseil *et al.* 1998); digoxin is a good substrate of the P-glycoprotein transporter (Schinkel *et al.* 1995).

St John's wort: amitriptyline. In a study published in abstract form (Roots *et al.* 2000), the effect of St John's wort intake on the steady-state pharmacokinetics of the tricyclic antidepressant amitriptyline and its demethylated metabolite nortriptyline was evaluated in depressed patients. Concomitant consumption of the hypericum extract LI160, 900 mg daily for at least 2 weeks, led to a decrease in the AUC of amitriptyline and nortriptyline by >20 and 40% respectively. The underlying mechanisms have not been investigated. The demethylation of amitripyline to nortriptyline is primarily catalysed by CYP2C19 and CYP3A4 (Olesen and Linnet 1997, Venkatakrishnan *et al.* 1998). The further metabolism of nortriptyline through hydroxylation at the 10-position is mediated by CYP3A4 and CYP2D6 (Venkatakrishnan *et al.* 1999). Thus, again, up-regulation of CYP3A4 may have caused the decrease in the AUC of amitriptyline and nortriptyline.

St John's wort: theophylline. A case has been reported where a female patient required high doses of theophylline to attain therapeutic plasma levels (Nebel *et al.* 1999). The use of a high dose of this drug became necessary when the patient started taking St John's wort (300 mg daily). These observations would suggest that the intake of St John's wort stimulates the metabolism of theophylline. In fact,

when the ingestion of the herb was discontinued, theophylline plasma levels doubled requiring dose reduction, supporting a mechanism entailing induction of theophylline metabolism by the herbal product.

Theophylline is metabolized primarily through 8-hydroxylation, the principal catalyst being CYP1A2 (Fuhr *et al.* 1992), implying that a component(s) of the St John's wort up-regulates the expression of this cytochrome P450 in the liver.

St John's wort: dextromethorphan. The antitussive drug dextromethorphan is routinely used selectively to monitor in humans the activity of CYP2D6, a polymorphically expressed form of cytochrome P450 (Gonzalez 1996). In a study designed to evaluate the influence of St John's wort intake on the orally administered drug, no interaction was evident when the drug was taken after exposure for 3 days to the herb, at a dose of 900 mg daily (3×300 mg), and being continued during the sampling period (Markowitz *et al.* 2000). The herbal preparation did not alter the metabolic ratio in the urine (ratio of dextromethorphan to the metabolite dextrorphan).

Other herbal remedies also contain components with the potential to interfere with the cytochrome P450 metabolism of drugs.

Milk thistle

Silymarin, a mixture of flavonolignans, is a component of milk thistle (*Silybum marianum*), the seed extracts of which are used as a hepatoprotectant in a number of conditions including alcoholic cirrhosis and hepatitis. In hepatocyte cultures, silymarin suppresses CYP3A4 activity and, in addition, inhibits glucuronosyl transferase activity (Venkataramanan *et al.* 2000). If these effects are operative *in vivo*, then silymarin-containing products such as milk thistle have the potential to impair the metabolism of drugs by interfering with both the Phase I and II pathways of biotransformation.

Angelica dahurica

The root of the Chinese herb *Angelica dahurica* (Bai Zhi) is used to relieve cold symptoms. A single, albeit large, oral dose ($1\,g\,kg^{-1}$) of an aqueous root extract of the herb suppressed the rat hepatic hydroxylation of testosterone at positions 2α- catalysed by CYP2C11, 16β- catalysed by CYP2C11 and CYP2B and 6β- catalysed by CYP3A, and the CYP3A-mediated nifedipine oxidation and CYP2D1-catalysed bufurarol 1′-hydroxylase (Ishihara *et al.* 2000). Inhibition was maximum at about 6 h after administration but was still evident, in some of the activities, after 24 h. At the same dose level, *A. dahurica* prolonged the half-life and reduced the clearance of intravenously administered tolbutamide in rat, accompanied by a decrease in hepatic tolbutamide hydroxylase activity, an activity catalysed by CYP2C, but had no influence on the pharmacokinetic characteristics of diazepam (Ishihara *et al.* 2000). However, when diazepam was given orally, plasma levels of the drug rose sharply with concomitant administration of the herbal remedy, suggesting an effect on its presystemic metabolism. In the human liver, diazepam is extensively metabolized by oxidation catalysed by CYP3A4 and CYP2C19 (Andersson *et al.* 1994).

In *in vitro* studies, infusions and decoctions from *A. dahurica* inhibit the CYP3A-mediated 6β-hydroxylation of testosterone in human hepatic microsomes (Guo *et al.* 2001). Furthermore, the extent of inhibition was more pronounced following pre-incubation, alluding to mechanism-based inhibition that may involve furanocoumarins, as described for grapefruit juice (He *et al.* 1998). Furanocoumarins are found in abundance in preparations of *A. dahurica* (Bergendorff *et al.* 1997, Baek *et al.* 2000), and CYP3A inhibition was clearly related to the furanocoumarin concentration (Guo *et al.* 2001).

Ginseng

A number of varieties of ginseng, a tropical herb prepared from the root of *Panax ginseng*, are available from various countries in South East Asia. They are believed to boost well-being by combating physical and mental fatigue, and are often utilized by athletes to enhance physical endurance and stamina.

The ability of six ginsenosides and two eleutherosides, all constituents of ginseng, were evaluated *in vitro* for their ability to inhibit the activity of a number of cDNA-expressed cytochrome P450 enzymes (Henderson *et al.* 1999). None of the compounds caused marked inhibition of activity that was likely to lead to interactions with conventional drugs. However, *in vitro* red ginseng total saponins inhibited, in a concentration-dependent manner, cytochrome P450 activity in rat liver microsomes (Kim *et al.* 1997). The inhibitory effect was most marked against CYP2E1-mediated *p*-nitrophenol oxidation and CYP3A-mediated *N*-demethylation of erythromycin (Kim *et al.* 1997). The effect of the whole ginseng, as it reaches the consumer, on drug-metabolizing systems has not, to my knowledge, been addressed.

Garlic

Garlic (*Allium sativum*) is taken, in a variety of formulations, to reduce hypertension and hyperlipidaemia, thus decreasing the risk of blood clot formation. In addition, epidemiological studies have established an inverse relationship between garlic consumption and colon cancer (Steinmetz *et al.* 1994). In animal studies, organosulfur compounds present in garlic in substantial amounts, such as the lipophilic thioethers allyl sulfides, products of allicin (*S*-allylcysteine sulfoxide) oxidation, have displayed anticarcinogenic activity (Mori and Nishikawa 1998), and this prompted research into their mechanism of action, including their effects on the cytochrome P450 system, because of its role in the bioactivation of chemical carcinogens. Treatment of rat with diallyl sulfide, diallyl disulfide, allyl methyl sulfide and allyl mercaptan selectively led to suppression of hepatic CYP2E1 (Brady *et al.* 1991a, Haber *et al.* 1994, Kwak *et al.* 1994, Reicks and Crankshaw 1996, Guyonnet *et al.* 2000, Yang *et al.* 2001). In contrast, the hepatic expression of CYP2B, CYP3A and, to a lesser extent, CYP1A was elevated following treatment with diallyl disulfide, diallyl sulfide, dipropyl sulfide and dipropyl disulfide (Dragnev *et al.* 1995, Guyonnet *et al.* 2000). The decline in CYP2E1 activity was accompanied by a drop in apoprotein levels without change in mRNA levels, suggesting that these compounds were functioning as mechanism-based inhibitors (Kwak *et al.* 1994, Reicks and Crankshaw 1996). Indeed, it appears that these organosulfates are metabolized by CYP2E1 to generate metabolites that

interact irreversibly with, and impair the activity of, this cytochrome P450 enzyme (Brady *et al.* 1991b, Jin and Baillie 1997, Yang *et al.* 2001). Diallyl sulfide is converted to diallyl sulfoxide, which is further metabolized to the sulfone (Jin and Baillie 1997). The metabolite responsible for the inactivation of CYP2E1 appears to be an epoxide of diallyl sulfone (Premdas *et al.* 2000). This cytochrome P450 isoform catalyses the metabolism of volatile halogenated anaesthetics such as enflurane and halothane, and it is feasible that intake of garlic supplements may prolong their anaesthetic effect. It is relevant to point out that, at least in rat, exposure to organosulfates such as diallyl disulfide also stimulates the activities of conjugating enzymes such as glutathione *S*-transferases, UDP-glucuronosyl transferases and quinone reductase (Wargovich *et al.* 1992, Haber *et al.* 1995, Guyonnet *et al.* 1999, Munday and Mundsay 1999). However, it must be borne in mind that the effects of the garlic oraganosulfates have been observed at doses that cannot be attained at normal dietary intakes, and whether intake of garlic supplements can alter the activity of the xenobiotic-metabolizing enzymes remains to be established. Taken for medical reasons, however, garlic may be consumed daily in gram quantities either raw or in capsule and tablet forms to minimize the odour.

Danshen

Danshen, derived from the dried root and rhizome of *Salvia miltiorrhiza*, is a popular Chinese herb taken as a decoction to treat cardiovascular diseases, and when taken with warfarin it may exaggerate its anticoagulant effect leading to bleeding (Yu *et al.* 1997). Intraperitoneal administration of danshen root extracts, twice daily ($5\,g\,kg^{-1}$), for 3 days followed by a single oral dose of racemic warfarin resulted in a rise in the plasma concentrations of both enantiomers of the anticoagulant in rat, and prolonged the prothrombin time; a similar effect was observed at steady levels of warfarin (Chan *et al.* 1995). Danshen itself had no effect on prothrombin time at this dose level (Lo *et al.* 1992). The same treatment with Danshen increased the rate of absorption, AUC and maximum concentration of warfarin, prolonged the half-life and decreased clearance (Chan *et al.* 1995), suggesting impairment of its metabolism as a possible mechanism of the interaction. A number of cases have been reported where patients on long-term warfarin therapy have displayed exaggerated anticoagulant activity when taking danshen concomitantly (Chan 2001). These patients were also taking other medications at the time, and the contribution of danshen to the interaction is difficult to evaluate. Moreover, as danshen exhibits itself anticoagulant activity (Chan 2001), the possibility that the basis of this interaction is pharmacodynamic can not be ruled out.

Liquorice

Aqueous extracts of liquorice (*Glycyrrhiza glabra* L.) are used world-wide to treat a number of conditions including gastric ulcers, arthritis and viral infections, and it may be consumed at very high doses, up to 100 g daily (Bernardi *et al.* 1994). Ethanolic extracts of the herb inhibit the CYP3A4-mediated metabolism of benzyloxyresorufin (Budzinski *et al.* 2000), alluding to possible interactions with medicinal drugs. In studies conducted in mouse, liquorice extracts ($6.3\,g\,kg^{-1}$) as

well as the glycoside glycyrrhizin (480 mg kg^{-1}), an important component of the herb, altered the hepatic expression of cytochrome P450 activities (Paolini *et al.* 1998). Repeated exposure to either glycyrrhizin or liquorice extracts elevated the metabolism of diagnostic substrates associated with CYP3A, and this was paralleled by an increase in the apoprotein and mRNA levels, indicating transcriptional activation and/or mRNA stabilization. To a lesser extent, an increase in the activity of CYP2B, CYP1A2 and CYP2A1 was also noted. Paolini *et al.* (1999) also conducted similar studies in rat using the same dose regimens. Neither the liquorice extract nor glycyrrhizin modulated hepatic cytochrome P450 activity following a single oral dose. However, when the animals were treated for 4 days, the liquorice intake doubled the CYP1A-mediated *O*-deethylation of ethoxyresorufin and, in the female animals only, also stimulated the *O*-demethylation of methoxyresorufin. The most marked increase, however, was in the CYP3A-mediated 6β-hydroxylation of testosterone. In the male rat only, a marked rise in the male-specific CYP2C11-mediated 2α-hydroxylation of testosterone was also observed. Glycyrrhizin induced modestly the *O*-deethylation of ethoxyresorufin in the male rat and the *O*-demethylation of methoxyresorufin and the CYP2B-mediated *O*-dependentylation of pentoxyresorufin in the female; an increase in the CYP3A-mediated 6β-hydroxylation of testosterone was also evident in both sexes and a rise in 2α-hydroxylation only in the male. It has also been reported, in abstract form, that a liquorice extract could modulate glucuronosyl transferase activity in a hepatoma line (Leung and Ho 2000). These observations emphasize the potential involvement of liquorice in interactions with medicinal drugs. However, in a recent abstract, it was reported that daily intake by volunteers of 1 g aqueous extracts of liquorice (*Radix glycyrrhizae*) for 7 days did not influence the pharmacokinetics of midazolam (Shon *et al.* 2001), the principal catalyst of its metabolism being CYP3A4 (Kronbach *et al.* 1989). Moreover, the pharmacological effect of midazolam was not modified by the liquorice intake. Whether this discrepancy reflects the lower doses employed in this study remains to be clarified.

Conclusions

Interactions between herbal remedies and conventional drugs are not any more just a theoretical possibility. The interaction between cyclosporin and St John's wort is now well documented and the underlying mechanisms are reasonably well understood, but future interactions can only be avoided if this under-researched crucial area of pharmacology (Ernst 2000a) receives the attention it so urgently merits. A number of other potential pharmacokinetic interactions have now been recognized, although cause-and-effect relationships have not always been established. Herbal remedies, similar to other plant products, contain phytochemicals which, on repeated exposure or even following a single intake, may modify the activity of cytochromes P450 and of other drug-metabolizing enzyme systems. Such chemicals include flavonoids (Trela and Carlson 1987, Obermeier *et al.* 1995, Canivenc-Lavier *et al.* 1996), coumarins and particularly furanocoumarins (Cai *et al.* 1993, Hoult and Payá 1996, Guo *et al.* 2000, 2001), anthraquinones (Ayrton *et al.* 1988, Longo *et al.* 2000), caffeine (Ayalogu *et al.* 1995) and terpenes (Maltzman *et al.* 1991). An additional complication results from poor standardization of herbal preparations, the chemical profile of which varies substantially among batches. As herbal remedies are usually taken for prolonged periods, co-

administration with medicinal drugs is frequent and the likelihood of a clinically relevant interaction high. It is likely that such interactions are more common than generally thought, but are under-reported and appearance of adverse effects may be attributed to the disease for which the treatment is taken. Unfortunately, many professionals in the medical world unwisely still consider herbal preparations as innocuous.

Modulation of CYP3A4 activity, as observed in the case of St John's wort, is particularly worrying bearing in mind the abundance of this enzyme in the liver and intestine, and its crucial role in the metabolism of drugs (Maurel 1996, Guengerich 1999). It is responsible for the metabolism of immunosuppressants (cyclosporin), antibiotics (erythromycin), antiepileptics (diphenylhydantoin), steroids (ethinyloestradiol), antidepressants (imipramine), and of drugs employed in the treatment of heart disease (nifedipine) and cancer (tamoxifen).

Many of today's consumers are not satisfied with the traditional medicinal drugs because of the side-effects associated with these, so they resort to herbal products on the false premise that these are totally devoid of any risk. In developed, industrialized nations, there is a clear tendency of substituting anthropogenic chemicals with phytochemicals as a result of this misconception that they are safer, being natural. The general population is completely unaware of the fact that herbal products have the potential to induce adverse effects.

It has been proposed that to tackle this problem, herbal products are appropriately labelled to alert consumers to possible interactions with other concomitantly ingested drugs and to recommend a consultation with their general practitioners and other medical carers. Patients are generally reluctant to inform their physicians that they are exposed to alternative treatments, including intake of herbal products (Liu *et al*. 2000), for fear of offending them or because they believe it is irrelevant. However, it is very difficult to envisage how even a sympathetic physician can respond to such information about the intake of herbal preparations, bearing in mind the paucity of quality research data on which to base rational, science-based advice. Furthermore, it is unlikely that the physician has received formal training in this area, which is not taught in the curricula of British medical schools (Rampes *et al*. 1997).

Herbal products are not subject to the scientific rigorous testing indispensable for conventional drugs and this attitude in itself fuels the belief that plant chemicals are far safer compared with their synthetic counterparts. Regrettably, at present there is no comparable regulatory system in the countries of use to ensure the safety of these compounds when taken alone, or in combination with traditional medicinal preparations. Germany, the most important market for herbal remedies, has taken the lead in this, and through the German Federal Health Agency has set up the commission E Group that obtains information on the safety and effectiveness of herbal products available in Germany and produces informative monographs. In the USA, herbal products are not reviewed by the FDA since they make no medical claims; they are considered as 'food supplements'.

Herbal products are a booming, multibillion-pound global business that must ensure the safety of its products and protect the consumer. Studies to evaluate the effects of their products on the cytochrome P450 and other enzyme systems that metabolize drugs are neither difficult nor expensive to perform. Such a knowledge would allow us to either alter the doses to account for the interaction between

phytochemicals and medicinal drugs or to choose alternative combinations that are not subject to such interactions. Failure to investigate such interactions may lead to a general advice to abstain from herbal products when receiving treatment with medicinal drugs, particularly when these are characterized by a narrow therapeutic index. It should be emphasized that the present review has addressed pharmacokinetic interactions and pharmacodynamic interactions between herbal products and conventional drugs have also been documented (Ernst 2000a, b, Fugh-Berman 2000, Heck *et al*. 2000).

Clearly, the notion that herbal products are problem-free is incorrect, and some degree of regulation is desirable and, perhaps, inevitable if we are to avoid adverse interactions between phytochemicals and medicinal drugs.

Acknowledgements

The author thanks Miss Sheila Evans for the preparation of the figures.

References

Ahmad, N., Katiyar, S. K. and Mukhtar, H., 1998, Cancer chemoprevention by tea polyphenols. In C. Ioannides (ed.), *Nutrition and Chemical Toxicity* (Chichester: Wiley), pp. 301–343.

Ameer, B. and Weintraub, R. A., 1997, Drug interactions with grapefruit juice. *Clinical Pharmacokinetics*, **33**, 103–121.

Ames, B. N. and Gold, L. S., 1998, The prevention of cancer. *Drug Metabolism Reviews*, **30**, 201–223.

Andersson, T., Miners, J. O., Veronese, M. E. and Birkett, D. J., 1994, Diazepam metabolism by human liver microsomes is mediated by both *S*-mephenytoin hydroxylase and CYP3A isoforms. *British Journal of Clinical Pharmacology*, **38**, 131–137.

Ayalogu, E. O., Snelling, J., Lewis, D. F. V., Talwar, S., Clifford, M. N. and Ioannides, C., 1995, Induction of hepatic CYP1A2 by the oral administration of caffeine to rats: Lack of association with the Ah locus. *Biochimica et Biophysica Acta*, **1272**, 89–94.

Ayrton, A. D, Ioannides, C. and Walker, R., 1988, Induction of rat hepatic cytochrome P-450I proteins by the antimutagen anthraflavic acid. *Food and Chemical Toxicology*, **26**, 909–915.

Ayrton, A. D. and Morgan, P., 2001, Role of transport proteins in drug absorption, distribution and excretion. *Xenobiotica*, **31**, 469–497.

Ayrton, A. D., Lewis, D. F. V., Ioannides, C. and Walker, R., 1987, Anthraflavic acid is a potent and specific inhibitor of cytochrome P-448 activity. *Biochimica et Biophysica Acta*, **916**, 328–333.

Baek, N. I., Ahn, E. M., Kim, H. Y. and Pauk, Y. D., 2000, Furanocoumarins from the root of Angelica dahurica. *Archives of Pharmaceutical Research*, **23**, 467–470.

Bailey, D. G., Arnold, M. O. and Spence, J. D., 1998a, Grapefruit juice–drug interactions. *British Journal of Clinical Pharmacology*, **46**, 101–110.

Bailey, D. G., Dresser, G. K., Kreeft, J. H., Munoz, C., Freeman, D. J. and Bend, J. R., 2000, Grapefruit–felodipine interaction: effect of unprocessed fruit and probable active ingredients. *Clinical Pharmacology and Therapeutics*, **68**, 468–477.

Bailey, D. G., Kreeft, J. H., Munoz, C., Freeman, D. J. and Bend, J. R., 1998b, Grapefruit juice–felodipine interaction: effect of naringin and 6′,7′-dihydrobergamottin in humans. *Clinical Pharmacology and Therapeutics*, **64**, 248–256.

Bailey, D. G., Spence, J. D., Munoz, C. and Arnold, J. M. O., 1991, Interaction of citrus juices with felodipine and nifedipine. *Lancet*, **337**, 268–269.

Ball, S. E., Forrester, L. M., Wolf, C. R. and Backs, D. J., 1990, Differences in the cytochrome P-450 isoenzymes involved in the 2-hydroxylation of oestradiol and 17α-ethinyloestradiol. *Biochemistry Journal*, **267**, 221–226.

Barcelo, S., Gardiner, J. M., Gescher, A. and Chipman, J. K., 1996, CYP2E1-mediated mechanism of anti-genotoxicity of the broccoli constituent sulforaphane. *Carcinogenesis*, **17**, 277–282.

Barnes, J., Anderson, L. A. and Phillipson, J. D., 2001, St. John's wort (*Hypericum perforatum* L): a review of its chemistry, pharmacology and clinical properties. *Journal of Pharmacy and Pharmacology*, **53**, 583–600.

Barone, G. W., Curley, B. J., Ketel, B. L. and Abul-Ezz, S. R., 2001, Herbal supplements: a potential for drug interactions in transplant recipients. *Transplantation*, **71**, 239–241.

Barone, G. W., Curley, B. J., Ketel, B. L., Lightfoot, M. L. and Abul-Ezz, S. R., 2000, Drug interaction between St. John's wort and cyclosporine. *Annals of Pharmacotherapy*, **34**, 1013–1016.

Barone, J. J. and Roberts, H. R., 1996, Caffeine consumption. *Food and Chemical Toxicology*, **34**, 119–129.

Bergendorff, O., Dekermedjian, K., Nielsen, M., Shan, Rd., Witt, R., Ai, J. L. and Sterner, O., 1997, Furanocoumarins with affinity to brain benzodiazepine receptors *in vitro*. *Phytochemistry*, **44**, 1121–1124.

Bernardi, M., D'Intino, P. E., Trevisani, F., Cantelli-Forti, G., Raggi, M. A., Turchetto, E. and Gasbarrini, G., 1999, Effects of prolonged ingestion of graded doses of licorice by healthy volunteers. *Life Sciences*, **55**, 863–872.

Bertilsson, L., Tomson, T. and Tybring, G., 1986, Pharmacokinetics: time-dependent changes – autoinduction of carbamazepine epoxidation. *Journal of Clinical Pharmacology*, **26**, 459–462.

Biber, A., Fischer, H., Römer, A. and Chatterjee, S. S., 1998, Oral bioavailability of hyperforin from hypericum extracts in rats and human volunteers. *Pharmacopsychiatry*, **31**, 36–43.

Bolt, H. M., 1994, Interactions between clinically used drugs and oral contraceptives. *Environmental Health Perspectives*, **102**, 35–38.

Brady, J. F., Ishizaki, H., Fukuto, J. M., Lin, M. C., Fadel, A., Gapac, J. M. and Yang, C. S., 1991b, Inhibition of cytochrome P-450 2E1 by diallyl sulfide and its metabolites. *Chemical Research in Toxicology*, **4**, 642–647.

Brady, J. F., Wang, M.-H., Hong, J.-Y., Xiao, F., Li, Y., Yoo, J.-S., Ning, S. M., Fukuto, J. M., Gapac, J. M. and Yang, C. S., 1991a, Modulation of rat hepatic microsomal monooxygenase activities and cytotoxicity by diallyl sulfide. *Toxicology and Applied Pharmacology*, **108**, 342–354.

Breidebach, Th., Kliem, V., Burg, M., Radermacher, J. and Hoffmann, M. W., 2000, Profound drop of cyclosporin A whole blood levels caused by St John's wort (*Hypericum perforatum*). *Transplantation*, **69**, 2229–2232.

Brockmöller, J., Reum, T., Bauer, S., Kerb, R., Hubner, W. D. and Roots, I., 1997, Hypericin and pseudohypericin: pharmacokinetics and effects on photosensitivity in humans. *Pharmacopsychiatry*, **30**, 94–101.

Bu-Abbas, A., Clifford, M. N., Walker, R. and Ioannides, C., 1994, Selective induction of rat hepatic CYP1 and CYP4 proteins and of peroxisomal proliferation by green tea. *Carcinogenesis*, **15**, 2575–2579.

Bu-Abbas, A., Clifford, M. N., Walker, R. and Ioannides, C., 1998, Contribution of caffeine and flavanols in the induction of phase II activities by green tea. *Food and Chemical Toxicology*, **36**, 617–621.

Bu-Abbas, A., Copeland, E., Clifford, M. N., Walker, R. and Ioannides, C., 1999, Cytochrome P450 induction by tea, and its consequences on the bioactivation of chemical carcinogens: contribution of caffeine and flavanols. *Environmental Toxicology and Pharmacology*, **7**, 41–47.

Budzinski, J. W., Foster, B. C., Vandenhoek, S. and Arnason, J. T., 2000, An *in vitro* evaluation of human cytochrome P450 3A4 inhibition by selected commercial herbal extracts and tinctures. *Phytomedicine*, **7**, 273–282.

Burstein, A. H., Horton, R. L., Dunn, T., Alfaro, R. M., Piscitelli, S. C. and Theodore, W., 2000, Lack of effect of St. John's wort on carbamazepine pharmacokinetics in healthy volunteers. *Clinical Pharmacology and Therapeutics*, **68**, 605–612.

Cai, Y., Bennett, D., Nair, R. V., Ceska, O., Ashwood-Smith, M. J. and Diiovanni, J., 1993, Inhibition and inactivation of murine hepatic ethoxy- and pentoxyresorufin *O*-dealkylase by naturally occurring coumarins. *Chemical Research in Toxicology*, **6**, 872–879.

Canivenc-Lavier, M.-C., Vernevaut, M.-F., Totis, M., Siess, M.-H., Magdalou, J. and Suschetet, M., 1996, Comparative effects of flavonoids and model inducers on drug-metabolizing enzymes in rat liver. *Toxicology*, **114**, 19–27.

Carson, S. W., Hill-Zabala, C. E., Roberts, S. H. and Hawke, R. L., 2000, Inhibitory effect of methanolic solution of St. John's wort (*Hypericum perforatum*) on cytochrome P450 3A4 activity in human liver microsomes. *Clinical Pharmacology and Therapeutics*, **67**, 99.

Cashman, J. R., Xiong, Y., Lin, J., Verhagen, H., Van Poppel, G., Van Bladeren, P. J., Larsen-Su, S. and Williams, D. E., 1999, *In vitro* and *in vivo* inhibition of human flavin-containing monooxygenase form 3 (FMO3) in the presence of dietary indoles. *Biochemical Pharmacology*, **58**, 1047–1055.

Chan, K., Lo, A. C. T., Yeung, J. H. K. and Woo, K. S., 1995, The effects of danshen (*Salvia miltiorrhiza*) on warfarin pharmacodynamics and pharmacokinetics of warfarin enantiomers in the rats. *Journal of Pharmacy and Pharmacology*, **47**, 402–406.

Chan, T. Y. K., 2001, Interaction between warfarin and danshen (*Salvia miltiorrhiza*). *Annals of Pharmacotherapy*, **35**, 501–504.

Chiba, M., Hensleigh, M., Nishime, J. A., Balani, S. and Lin, J. J., 1996, Role of cytochrome P450 3A4 in human metabolism of MK-639, a potent human immunodeficiency virus protease inhibitor. *Drug Metabolism and Disposition*, **24**, 307–314.

Conseil, G., Baubichon-Cortay, H., Dayan, G., Jault, J. M., Barron, D. and Di Pietro, A., 1998, Flavonoids: a class of modulators with bifunctional interactions at vicinal ATP- and steroid-binding sites on mouse P-glycoprotein. *Proceedings of the National Academy of Sciences, USA*, **95**, 9831–9836.

De Kruif, C. A., Marsman, J. W., Venekamp, J. C., Noordhoek, J., Blaauboer, B. J. and Wortelboer, H. M., 1991, Structure elucidation of acid reaction products of indole-3-carbinol: detection *in vivo* and enzyme induction *in vitro*. *Chemico-Biological Interactions*, **80**, 303–315.

De Maat, M. M. R., Hoetelmans, R. M. W., Mathôt, R. A. A., Van Gorp, E. C. M., Meenhorst, P. L., Mulder, J. W. and Beijnen, J. H., 2001, Drug interaction between St. John's wort and nevirapine. *AIDS*, **15**, 420–421.

Decker, C. J., Laitinen, L. M., Bridson, G. W., Raybuck, S. A., Tung, R. D. and Chatuverdi, P. R., 1998, Metabolism of amprenavir in liver microsomes: role of CYP3A4 inhibition for drug interactions. *Journal of Pharmaceutical Sciences*, **87**, 803–807.

Dragnev, K. H., Nims, R. W. and Lubet, R. A., 1995, The chemopreventive agent diallyl sulfide. A structurally atypical phenobarbital-type inducer. *Biochemical Pharmacology*, **50**, 2099–2104.

Draper, A. J., Madan, A. and Parkinson, A., 1997, Inhibition of coumarin 7-hydroxylase activity in human liver microsomes. *Archives of Biochemistry and Biophysics*, **341**, 47–61.

Dürr, D., Stieger, B., Kullak-Ublick, G. A., Rentsch, K. M., Steinert, H. C., Meier, P. J. and Fattinger, K., 2000, St. John's wort induces intestinal P-glycoprotein/MDR1 and intestinal and hepatic CYP3A4. *Clinical Pharmacology and Therapeutics*, **68**, 598–604.

Edwards, D. J., Bellevue Iii, F. H. and Woster, P. M., 1996, Identification of 6′,7′-dihydroxybergamottin, a cytochrome P450 inhibitor, in grapefruit juice. *Drug Metabolism and Disposition*, **24**, 1287–1290.

Edwards, D. J., Fitzsimmons, M. E., Schuetz, E. G., Yasuda, K., Ducharme, M. P., Warbasse, L. H., Woster, P. M., Schuetz, J. D. and Watkins, P., 1999, 6′,7′-Dihydroxybergamottin in grapefruit juice and Seville orange juice: effects on cyclosporine disposition, enterocyte CYP3A4, and P-glycoprotein. *Clinical Pharmacology and Therapeutics*, **65**, 237–244.

EMEA, 1999, *Report from the Ad Hoc Working Group on Herbal Medicinal Products* (European Medicine Evaluation Agency).

Erickson, D. A., Mather, G., Trager, W. F., Levy, R. H. and Keirns, J. J., 1999, Chacterization of the *in vitro* biotransformation of the HIV-1 reverse transcriptase inhibitor nevirapine by human hepatic cytochromes P-450. *Drug Metabolism and Disposition*, **27**, 1488–1495.

Ernst, E., 1999, Second thoughts about safety of St. John's wort. *Lancet*, **354**, 2014–2016.

Ernst, E., 2000a, Herb–drug interactions: potentially important but woefully under-researched. *European Journal of Clinical Pharmacology*, **56**, 523–534.

Ernst, E., 2000b, Possible interactions between synthetic and herbal medicinal products. Part I: Systematic review of indirect evidence. *Perfusion*, **13**, 4–15.

Evans, A. M., 2000, Influence of dietary components on the gastrointestinal metabolism and transport of drugs. *Therapeutic Drug Monitoring*, **22**, 131–136.

Fitzsimmons, M. E. and Collins, J. M., 1997, Selective biotransformation of the human immunodeficiency virus protease inhibitor sequinavir by human small-intestinal cytochrome P4503A4 — potential contribution to high first-pass metabolism. *Drug Metabolism and Disposition*, **25**, 256–266.

Fugh-Berman, A., 2000, Herb–drug interactions. *Lancet*, **355**, 134–138.

Fuhr, U., 1998, Drug interactions with grapefruit juice. Extent, probable mechanism and clinical relevance. *Drug Safety*, **18**, 251–272.

Fuhr, U., Doehmer, J., Battula, N., Wolfel, C., Kudla, C., Keita, Y. and Staib, A. H., 1992, Biotransformation of caffeine and theophylline in mammalian cell lines genetically engineered for expression of single cytochrome-P450 isoforms. *Biochemical Pharmacology*, **43**, 225–235.

Fukuda, K., Ohta, T., Oshima, Y., Ohashi, N., Yoshikawa, M. and Yamazoe, Y., 1997, Specific CYP3A4 inhibitors in grapefruit juice: furocoumarin dimers as components of drug interaction. *Pharmacogenetics*, **7**, 391–396.

Gonzalez, F. J., 1996, The CYP2D subfamily. In C. Ioannides (ed.), *Cytochromes P450: Metabolic and Toxicological Aspects* (Boca Raton: CRC Press), pp. 183–210.

Greeson, J. M., Sanford, B. and Monti, D. A., 2001, St. John's wort (*Hypericum perforatum*): a review of the current pharmacological, toxicological, and clinical literature. *Psychopharmacology*, **153**, 402–414.

Guengerich, F. P, 1984, Effects of nutritive factors on metabolic processes involving bioactivation and detoxication of chemicals. *Annual Reviews in Nutrition*, **4**, 207–231.

Guengerich, F. P, 1988, Oxidation of 17α-ethynyloestradiol by human liver cytochrome P-450. *Molecular Pharmacology*, **33**, 500–508.

Guengerich, F. P., 1999, Cytochrome P-450 3A4: regulation and role in drug metabolism. *Annual Review of Pharmacology and Toxicology*, **39**, 1–17.

Guo, L.-Q., Taniguchi, M., Chen, Q. Y., Baba, K. and Yamazoe, Y., 2001, Inhibitory potential of herbal medicines on human cytochrome P450-mediated oxidation: properties of umbelliferous or citrus crude drugs and their relative prescriptions. *Japanese Journal of Pharmacology*, **85**, 399–408.

Guo, L.-Q., Taniguchi, M., Chen, Q. Y., Xio, Y.-Q., Baba, K., Ohta, T. and Yamazoe, Y., 2000, Inhibitory effect of natural furanocoumarins on human microsomal cytochrome P450 3A activity. *Japanese Journal of Pharmacology*, **82**, 122–129.

Guyonnet, D., Belloir, C., Suscetet, M., Siess, M.-H. and Le Bon, A.-M., 2000, Liver subcellular fractions from rats treated by organosulfur compounds from *Allium* modulate mutagen activation. *Mutation Research*, **466**, 17–26.

Guyonnet, D., Siess, M.-H., Le Bon, A.-M. and Suscetet, M., 1999, Modulation of phase II enzymes by organosulfur compounds form *Allium* vegetables in rat tissues. *Toxicology and Applied Toxicology*, **154**, 50–58.

Gwang, J. H., 1996, Induction of rat hepatic cytochrome P4501A and P4502B by the methoxsalen. *Cancer Letters*, **108**, 115–120.

Haber, D., Siess, M.-H., De Waziers, I,. Beaune, P. and Suschetet, M., 1994, Modification of hepatic drug-metabolizing enzymes in rats fed naturally occurring allyl sulphides. *Xenobiotica*, **24**, 169–182.

He, K., Iyer, K. R., Hayes, R. N., Sinz, M. W., Woolf, T. F. and Hollenberg, P. F., 1998, Inactivation of cytochrome P450 3A4 by bergamottin, a component of grapefruit juice. *Chemical Research in Toxicology*, **11**, 252–259.

Heck, A. M., Dewitt, B. A. and Lukes, A. L., 2000, Potential interactions between alternative therapies with warfarin. *American Journal of Health-System Pharmacy*, **57**, 1221–1230.

Henderson, C. L., Harkey, M. R., Gershwin, M. E., Hackman, R. M., Stern, J. S. and Stresser, D. M., 1999, Effects of ginseng components on c-DNA expressed cytochrome P450 enzyme catalytic activity. *Life Sciences*, **65**, 209–214.

Hoult, J. R. S. and Paya, M., 1996, Pharmacological and biochemical actions of simple coumarins: natural products with therapeutic potential. *General Pharmacology*, **27**, 713–722.

Hunter, J. and Hirst, B. H., 1997, Intestinal secretion of drugs. The role of P-glycoprotein and related drug efflux systems in limiting oral drug absorption. *Advanced Drug Delivery Reviews*, **25**, 129–157.

Ioannides, C. (ed.), 1996, *Cytochromes P450: Metabolic and Toxicological Aspects* (Boca Raton: CRC Press).

Ioannides, C., 1998, Nutritional modulation of cytochromes P450. In C. Ioannides (ed.), *Nutrition and Chemical Toxicity* (Chichester: Wiley), pp. 115–159.

Ioannides, C., 1999, Effect of diet and nutrition on the expression of cytochromes P450. *Xenobiotica*, **29**, 109–154.

Ioannides, C., 2000, Xenobiotic metabolism and bioactivation by cytochrome P-450. In H. Wiseman, P. Goldfarb, T. Ridgway and A. Wiseman (eds), *Biomolecular Free Radical Toxicity: Causes and Prevention* (Chichester: Wiley), pp. 103–144.

Ioannides, C. ed., 2002, *Enzyme Systems that Metabolise Drugs and Other Xenobiotics* (Chichester: Wiley).

Ioannides, C., Delaforge, M. and Parke, D. V., 1981, Safrole: its metabolism, carcinogenicity and interactions with cytochrome P-450. *Food and Cosmetics Toxicology*, **19**, 657–666.

Ishihara, K., Kushida, H., Yuzurihara, M., Wakui, Y., Yanagisawa, T., Kamei, H., Ohmori, S. and Kitada, M., 2000, Interaction of drugs and Chinese herbs: pharmacokinetic changes of tolbutamide and diazepam caused by extract of *Angelica dahurica*. *Journal of Pharmacy and Pharmacology*, **52**, 1023–1029.

Ishizaki, H., Brady, J. F., Ning, S. M. and Yang, C. S., 1990, Effect of phenethyl isothiocyanate on microsomal *N*-nitrosodimethylamine (NDMA) metabolism and other monooxygenase activities. *Xenobiotica*, **20**, 255–264.

Jin, L. and Baillie, T. A., 1997, Metabolism of the chemopreventive agent diallyl sulphide to glutathione conjugates in rats. *Chemical Research in Toxicology*, **10**, 318–327.

Johne, A., Brockmöller, J., Bauer, S., Maurer, A., Langheinrich, M. and Roots, I., 1999a, Interaction of St. John's wort extract with digoxin. *European Journal of Clinical Pharmacology*, **55**, A22.

Johne, A., Brockmöller, J., Bauer, S., Maurer, A., Langheinrich, M. and Roots, I., 1999b, Pharmacokinetic interaction of digoxin with an herbal extract from St. John's wort (*Hypericum perforatum*). *Clinical Pharmacology and Therapeutics*, **66**, 338–345.

Josey, E. S. and Tackett, R. L., 1999, St John's wort: a new alternative for depression? *International Journal of Clinical Pharmacology and Therapeutics*, **37**, 111–119.

Kall, M. A., Vang, O. and Clausen, J., 1996, Effects of dietary broccoli in human *in vivo* drug metabolizing enzymes: evaluation of caffeine, oestrone and chlorzoxazone metabolism. *Carcinogenesis*, **17**, 793–799.

Kaminsky, L. C. and Zhang, Z. Y., 1997, Human P450 metabolism of warfarin. *Pharmacology and Therapeutics*, **73**, 67–74.

Kantola, T., Kivistö, K. T. and Neuvonen, P. J., 1998, Grapefruit juice greatly increases serum concentrations of lovastatin and lovastatin acid. *Clinical Pharmacology and Therapeutics*, **63**, 394–402.

Karliova, M., Treichel, U., Malagò, M, Frilling, A., Gerken, G. and Broelsch, C. E., 2000, Interaction of *Hypericum perforatum* (St. John's wort) with cyclosporin A metabolism in a patient after liver transplantation. *Journal of Hepatology*, **33**, 853–855.

Katchamart, S., Stresser, D. M., Dehal, S. S., Kupfer, D. and Williams, D. E., 2000, Concurrent flavin-containing monooxygenase down-regulation and cytochrome P-450 induction by dietary indoles in the rat: implications for drug–drug interaction. *Drug Metabolism and Disposition*, **28**, 930–936.

Kerb, R., Brockmöller, J., Staffeldt, B., Ploch, M. and Roots, I., 1996, Single-dose and steady-state pharmacokinetics of hypericin and pseudohypericin. *Antimicrobial Agents and Chemotherapy*, **40**, 2087–2093.

Kerr, B. M., Thummel, K. E., Wurden, C. J., Klein, S. M., Kroetz, D. L., Gonzalez, F. J. and Levy, R. J., 1994, Human liver carbamazepine metabolism: role of CYP3A4 and CYP2C8 in 10,11-epoxide formation. *Biochemical Pharmacology*, **47**, 1969–1979.

Kim, H. J., Chum, Y. J., Park, J. D., Kim, S. I., Roh, J. K. and Jeong, T. C., 1997, Protection of rat liver microsomes against carbon tetrachloride-induced lipid peroxidation by red ginseng saponin through cytochrome P450 inhibition. *Planta Medica*, **63**, 415–418.

Koenigs, L. L. and Trager, W. F., 1998a, Mechanism-based inactivation of cytochrome P450 2B1 by 8-methoxypsoralen and several other furanocoumarins. *Biochemistry*, **37**, 13184–13193.

Koenigs, L. L. and Trager, W. F., 1998b, Mechanism-based inactivation of P450 2A6 by furanocoumarins. *Biochemistry*, **37**, 10047–10061.

Kronbach, T., Mathys, D., Umeno, M., Gonzalez, F. J. and Meyer, U. A., 1989, Oxidation of midazolam and triazolam by human liver cytochrome P450IIIA4. *Molecular Pharmacology*, **36**, 89–96

Kudriakova, T. B., Sirota, L. A., Rozova, G. I. and Gorkov, V. A., 1992, Autoinduction and steady-state pharmacokinetics of carbamazepine and its major metabolites. *British Journal of Clinical Pharmacology*, **33**, 611–615.

Kupferschmidt, H., Ha, H., Ziegler, W., Meier, P. and Krähenbühl, S., 1995, Interaction between grapefruit juice and midazolam in humans. *Clinical Pharmacology and Therapeutics*, **58**, 20–28.

Kupferschmidt, H. H., Fattinger, K. E., Ha, H. R., Follath, F. and Krähenbühl, S., 1998, Grapefruit juice enhances the bioavailability of the HIV protease inhibitor saquinavir in man. *British Journal of Clinical Pharmacology*, **45**, 355–359.

Kwak, M. K., Kim, S. G., Kwak, J. Y., Novak, R. F. and Kim, N. D., 1994, Inhibition of cytochrome P4502E1 expression by organosulfur compounds allylsulfide, allylmercaptan and allyl methylsulfide in rats. *Biochemical Pharmacology*, **47**, 531–539.

Lacarelle, B., Rahmani, R., Desousa, G., Durand, A., Placidi, M. and Cano, J. P.,1991, Metabolism of digoxin, digoxigenin digitoxosides and digoxigenin in human hepatocytes and liver-microsomes. *Fundamental and Clinical Pharmacology*, **5**, 567–582.

Lampe, J. W., King, I. B., Li, S., Grate, M. T., Barale, K. V., Chen, C., Feng, Z. and Potter, J. D., 2000, *Brassica* vegetables increase and apiaceous vegetables decrease cytochrome P450 1A2 in humans: changes in caffeine metabolite ratios in response to controlled vegetable diets. *Carcinogenesis*, **21**, 1157–1162.

Leslie, E. M., Mao, Q., Oleschuk, C. J., Deeley, R. G. and Cole, S. P. C., 2001, Modulation of multidrug resistance protein 1 (MRP1/ABCC1) transport and ATPase activities by interaction with dietary flavonoids. *Molecular Pharmacology*, **59**, 1171–1180.

Leung, Y. K. and Ho, J., 2000, Effects of liquorice on the expression of UGT1A isozymes in rat hepatoma cells. *FASEB Journal*, **14**, abst 1221.

Lewis, D. F. V., Eddershaw, P. J., Goldfarb, P. J. and Tarbit, M. H., 1996, Molecular modelling of CYP3A4 from an alignment with CYP102: identification of key interactions between putative active site residues and CYP3A-specific chemicals. *Xenobiotica*, **26**, 1067–1086.

Lilja, J. J., Kivistö, K. T. and Neuvonen, P. J., 1998, Grapefruit juice–simvastatin interaction; effect on serum concentrations of simvastatin, simvastatin acid, and HMG-CoA reductase inhibitors. *Clinical Pharmacology and Therapeutics*, **64**, 477–483.

Lilja, J. J., Kivistö, K. T. and Neuvonen, P. J., 2000b, Duration of effect of grapefruit juice on the pharmacokinetics of the CYP3A4 substrate simvastatin. *Clinical Pharmacology and Therapeutics*, **68**, 384–390.

Lilja, J. J., Kivistö, K. T., Backman, J. T. and Neuvonen, P. J., 2000a, Effect of grapefruit dose on grapefruit juice–triazolam interaction. *European Journal of Clinical Pharmacology*, **56**, 411–415.

Liu, E. H., Turner, L. M., Lin, S. X., Klaus, L., Choi, L. Y., Whitworth, H., Ting, W. and Oz, M. C., 2000, Use of alternative medicine by patients undergoing cardiac surgery. *Journal of Thoracic and Cardiovascular Surgery*, **120**, 335–341.

Lo, A. C. T., Chan, K., Yeung, J. H. K. and Woo, K. S., 1992, The effects of Danshen (*Salvia miltiorrhiza*) on pharmacokinetics and pharmacodynamics of warfarin in rats. *European Journal of Drug Metabolism and Pharmacokinetics*, **17**, 257–262.

Longo, V., Amato, G., Salvetti, A. and Gervasi, P. G., 2000, Heterogeneous effects of anthraquinones on drug-metabolizing enzymes in the liver and small intestine of rat. *Chemico-Biological Interactions*, **126**, 63–77.

Lown, K. S., Bailey, D. G., Fontana, R. J., Janardan, S. K., Adair, C. H., Fortlage, L. A., Brown, M. B., Guo, W. and Watkins, P. B., 1997, Grapefruit juice increases felodipine oral bioavailability in humans by decreasing intestinal CYP3A protein expression. *Journal of Clinical Investigation*, **99**, 2545–2553.

Lundahl, J., Regårdh, C. G., Edgar, B. and Johnson, G., 1995, Relationship between the time of intake of grapefruit juice and its effect on pharmacokinetics and pharmacodynamics of felodipine in healthy subjects. *European Journal of Clinical Pharmacology*, **49**, 61–67.

Mahéo, K., Morewl, F., Langouët, S., Kramer, H., Le Ferrec, E., Ketterer, B. and Guillouzo, A., 1997, Inhibition of cytochromes P-450 and induction of glutathione *S*-transferases by sulphoraphane in primary human and rat hepatocytes. *Cancer Research*, **57**, 3649–3652.

Mai, I., Krüger, H., Budde, K., Johne, A., Brockmöller, H., Neumayer, H.-H. and Roots, I., 2000, Hazardous pharmacokinetic interaction of St John's wort (*Hypericum perforatum*) with the immunosuppressant cyclosporin. *International Journal of Clinical Pharmacology and Therapeutics*, **38**, 500–502.

Maltzman, T. H, Christou, M., Gould, M. N. and Jefcoate, C. R., 1991, Effects of monoterpenoids on *in vivo* DMBA–DNA adduct formation and on phase I hepatic metabolizing enzymes. *Carcinogenesis*, **12**, 2081–2087.

Markowitz, J. S., De Vane, C. L., Boulton, D. W., Carson, S. W., Nahas, Z. and Risch, S. C., 2000, Effect of St. John's wort (*Hypericum perforatum*) on cytochrome P-450 2D6 and 3A4 activity in healthy volunteers. *Life Sciences*, **66**, PL133–PL139.

Maurel, P., 1996, The CYP3 family. In C. Ioannides (ed.), *Cytochromes P450: Metabolic and Toxicological Aspects* (Boca Raton: CRC Press), pp. 241–270.

Maurer, A., Johne, A., Bauer, S., Brockmöller, F., Donath, F., Roots, I., Langheinrich, M. and Hübner, W. D., 1999, Interaction of St. John's wort extract with phenprocoumon. *European Journal of Clinical Pharmacology*, **55**, A22.

Mohri, K. and Uesawa, Y., 2001, Effects of furanocoumarin derivatives in grapefruit juice on nifedipine pharmacokinetics in rats. *Pharmaceutical Research*, **18**, 177–182.

Moore, L. B., Goodwin, B., Jones, S. A., Wisely, G. B., Serabjit-Singh, C. J., Willson, T. M., Collins, J. L. and Kliewer, S. A., 2000, St John's wort induces drug metabolism through activation of the pregnane X receptor. *Proceedings of the National Academy of Sciences, USA*, **97**, 7500–7502.

Mori, H. and Nishikawa, H., 1998, Naturally occurring organosulphur compounds as potential anticarcinogens. In C. Ioannides (ed.), *Nutrition and Chemical Toxicity* (Chichester: Wiley), pp. 285–299.

Mori, H., Tanaka, T. and Hirono, I., 1998, Toxicants in food: naturally occurring. In C. Ioannides (ed.), *Nutrition and Chemical Toxicity* (Chichester: Wiley), pp. 1–27.

Munday, R. and Mundsay, C. M., 1999, Low doses of diallyl sulfide, a compound derived from garlic, increase tissue activities of quinone reductase and glutathione transferase in the gastrointestinal tract of the rat. *Nutrition and Cancer*, **34**, 42–48.

Nebel, A., Schneider, B. J., Baker, R. K. and Kroll, D. J., 1999, Potential metabolic interaction between St. John's wort and theophylline. *Annals of Pharmacotherapy*, **33**, 502.

Obach, R. S., 2000, Inhibition of cytochrome P450 enzymes by constituents of St John's wort, and herbal preparation used in the treatment of depression. *Journal of Pharmacology and Experimental Therapeutics*, **294**, 88–95.

Obermeier, M. T., White, R. E. and Yang, C. S., 1995, Effects of bioflavonoids on hepatic P450 activities. *Xenobiotica*, **25**, 575–584.

Olesen, O. V. and Linnet, K., 1997, Metabolism of the tricyclic antidepressant amitriptyline by cDNA-expressed human cytochrome P450 enzymes. *Pharmacology*, **55**, 235–243.

Ono, S., Hatanaka, T., Hotta, H. Satoh, T., Gonzalez, F. J. and Tsutsui, M., 1996, Specificity of substrates and inhibitor probes for cytochrome cytochromes P450: evaluation of *in vitro* metabolism using cDNA-expressed human P450s and human liver microsomes. *Xenobiotica*, **26**, 681–693.

Pantuck, E. J., Hsiao, K.-C., Loub, W. D., Wattenberg, L. W., Kuntzman, R. and Conney, A. H., 1976, Stimulatory effects of vegetables on intestinal drug metabolism in the rat. *Journal of Pharmacology and Experimental Therapeutics*, **198**, 278–283.

Pantuck, E. J., Pantuck, C. B., Anderson, K. E., Wattenberg, L. W., Conney, A. H. and Kappas, A., 1984, Effects of brussel sprouts and cabbage on drug conjugation. *Clinical Pharmacology and Therapeutics*, **35**, 161–169.

Pantuck, E. J., Pantuck, E. B., Garland, W. A., Min, B. H., Wattenberg, L. W., Anderson, K. E., Kappas, A. and Conney, A. H., 1979, Stimulatory effect of Brussel sprouts and cabbage on human drug metabolism. *Clinical Pharmacology and Therapeutics*, **25**, 88–95.

Paolini, M., Barillari, J., Broccoli, M., Pozzetti, L., Perocco, P. and Cantelli-Forti, G., 1999, Effect of liquorice and glycyrrhizin on rat liver carcinogen metabolising enzymes. *Cancer Letters*, **145**, 35042.

Paolini, M., Pozzetti, L., Sapone, A. and Cantelli-Forti, G., 1998, Effect of licorice and glycyrrhizin on murine liver CYP-dependent monooxygenases. *Life Sciences*, **62**, 571–582.

Parke, D. V. and Ioannides, C., 1994, The effects of nutrition on chemical toxicity. *Drug Metabolism Reviews*, **26**, 739–765.

Piscitelli, S. C., Burstein, A. H., Chaitt, D., Alfaro, R. M. and Falloon, J., 2000, Indinavir concentrations and St John's wort. *Lancet*, **355**, 547–548.

Premdas, P. D., Bowers, R. J. and Forkert, P.K., 2000, Inactivation of hepatic CYP2E1 by an epoxide of diallyl sulfone. *Journal of Pharmacology and Experimental Therapeutics*, **293**, 1112–1120.

Rampes, H., Sharples, F., Maragh, S. and Fisher, P., 1997, Introducing complementary medicine into the medical curriculum. *Journal of the Royal Society of Medicine*, **90**, 19–22.

Rapeport, W. G., McInnes, G. T., Forrest, G., Thompson, C. G., Moore, M. R., Smith, D. A. S., Goldberg, A., Park, B. K. and Brodie, M. J., 1982, Auto- and hetero-induction with carbamazepine in man. *British Journal of Clinical Pharmacology*, **14**, P619–P620.

Reicks, M. M. and Crankshaw, D. L., 1996, Modulation of rat hepatic cytochrome P-450 activity by garlic organosulfur compounds. *Nutrition and Cancer*, **25**, 242–248.

Roby, C. A., Anderson, G. D., Kantor, E., Dryer, D. A. and Burstein, A. H., 2000, St. John's wort: effect on CYP3A4 activity. *Clinical Pharmacology and Therapeutics*, **67**, 451–457.

Roots, I., Johne, A., Schmider, J., Brockmöller, A., Maurer, A., Störmer, E. and Donath, F., 2000, Interaction from herbal extract from St. John's wort with amitriptyline and its metabolites. *Clinical Pharmacology and Therapeutics*, **67**, PIII69.

Ruschitzka, F., Meier, P. J., Turina, M., Lüscher, T. F. and Noll, G., 2000, Acute heart transplant rejection due to St John's wort. *Lancet*, **355**, 548–549.

Salphati, L. and Benet, Z., 1999, Metabolism of digoxin and digoxigenin digitoxosides in rat liver microsomes: involvement of cytochrome P4503A. *Xenobiotica*, **29**, 171–185.

Schmiedlin-Ren, P., Edwards, D. J., Fitzsimmons, M. E., He, K., Lown, K. S., Woster, P. M., Rahman, A., Thummel, K. E., Fisher, J. M., Hollenberg, P. F. and Watkins, P. B., 1997, Mechanisms of enhanced oral availability of CYP3A4 substrates by grapefruit constituents. *Drug Metabolism and Disposition*, **25**, 1228–1233.

Schinkel, A. H., Waenaar, E., Van Deemter, L., Mol, C. A. A. M. and Borst, P., 1995, Absence of the mdr1a P-glycoprotein in mice affects tissue distribution and pharmacokinetics of dexamethasone, digoxin, and cyclosporine A. *Journal of Clinical Investigation*, **96**, 1698–1705.

Shader, R. I. and Greenblatt, D. J., 2000, More on oral contraceptives, drug interactions, herbal medicines, and hormone replacement therapy. *Journal of Clinical Psychopharmacology*, **20**, 397–398.

Shon, J. H., Park, J. Y., Kim, M. S., Cha, I. J., Chun, B. H. and Shin, J. G., 2001, Effect of licorice (*Radix glycyrrhizae*) on the pharmacokinetic (PK) and pharmacodynamics (PD) of midazolam in healthy subjects. *Clinical Pharmacology and Therapeutics*, **69**, P78

Skog, K. I. and Jägerstad, M., 1998, Toxicants in food: generated during cooking. In C. Ioannides (ed.), *Nutrition and Chemical Toxicity* (Chichester: Wiley), pp. 59–79.

Sohn, O. S., Surace, A, Fiala E. S., Richie, J. P., Jr, Colosimo, S., Zang, E. and Weisburger, J. H., 1994, Effects of green and black tea on hepatic xenobiotic metabolizing systems in male F344 rats. *Xenobiotica*, **24**, 119–127.

Southwell, I. A. and Bourke, C. A., 2001, Seasonal variation in hypericin content of *Hypericum perforatum* L. (St John's wort). *Phytochemistry*, **56**, 437–441.

Staffeldt, B., Kerb, R., Brockmöller, J., Ploch, M. and Roots, I., 1994, Pharmacokinetics of hypericin and pseudohypericin after oral intake of the hypericum perforatum extract LI 160 in healthy volunteers. *Journal of Geriatric Psychiatry and Neurology*, **7**, S47–S53.

Steinmetz, K. A., Kushi, L. H., Bostick, R. M., Folsom, A. R. and Potter, J. D., 1994, Vegetables, fruit and colon cancer in the Iowa Women's Health Study. *American Journal of Epidemiology*, **139**, 1–15.

Stresser, D. M., Bailey, G. S. and Williams, D. E., 1994, Indole-3-carbinol and β-naphthoflavone induction of aflatoxin B_1 metabolism and cytochromes P-450 associated with bioactivation and detoxication of aflatoxin B_1 in the rat. *Drug Metabolism and Disposition*, **22**, 383–391.

Takanaga, H., Ohnishi, A., Murakami, H., Matsuo, H., Higuchi, S., Urae, A., Irie, S., Furuie, H, Matsukuma, K, Kimura, M., Kawano, K., Orii, Y., Tanaka, T. and Sawada, Y., 2000, Relationship between time after intake of grapefruit juice and the effect on pharmacokinetics and pharmacodynamics of nisoldipine in healthy subjects. *Clinical Pharmacology and Therapeutics*, **67**, 201–214.

Tassaeenyakul, W., Guo, L.-Q., Fukuda, K., Ohta, T. and Yamazoe, Y., 2000, Inhibition selectivity of grapefruit components on human cytochromes P450. *Archives of Biochemistry and Biophysics*, **378**, 356–363.

Thomas, J. A., Stargel, W. W. and Tschanz, C., 1998, Interactions between drugs and diet. In C. Ioannides (ed.), *Nutrition and Chemical Toxicity* (Chichester: Wiley), pp. 161–182.

Thomas, K. J., Nicholl, J. P. and Coleman, P., 2001, Use and expenditure on complementary medicine in England; a population based survey. *Complementary Therapies in Medicine*, **9**, 2–11.

Trela, B. A. and Carlson, G. P., 1987, Effect of flavanone on mixed-function oxidase and conjugation reactions in rats. *Xenobiotica*, **17**, 11–16.

Van Tellingen, O., 2001, The importance of drug-transporting P-glycoproteins in toxicology. *Toxicology Letters*, **120**, 31–41.

Vang, O., Jensen, M. B. and Autrup, H., 1990, Induction of cytochrome P4501A1 in rat colon and liver by indole-3-carbinol and 5,6-benzoflavone. *Carcinogenesis*, **11**, 1259–1263.

Vang, O., Jensen, M. B. and Autrup, H., 1991, Induction of cytochrome P-450IA1, IA2, IIB1 and IIE1 by broccoli in rat liver and colon. *Chemico-Biological Interactions*, **78**, 85–96.

Venkatakrishnan, K., Greenblatt, D. J., Von Moltke, L. L., Schmider, J., Harmatz, J. S. and Shader, R. I., 1998, Five distinct human cytochromes mediate amitriptyline *N*-demethylation *in vitro*: dominance of CYP2C19 and 3A4. *Journal of Clinical Pharmacology*, **38**, 112–121.

Venkatakrishnan, K., von Moltke, L. L. and Greenblatt, D. J., 1999, Nortriptyline E-10-hydroxylation *in vitro* is mediated by human CYP2D6 (high affinity) and CYP3A4 (low affinity): implications for interactions with enzyme-inducing drugs. *Journal of Clinical Pharmacology*, **39**, 567–577.

Venkataramanan, R., Ramachandran, V., Komoroski, B. J., Zhang, S., Schiff, P. L. and Strom, S. C., 2000, Milk thistle, a herbal supplement, decreases the activity of CYP3A4 and uridine diphosphoglucuronosyl transferase in human hepatocyte cultures. *Drug Metabolism and Disposition*, **28**, 1270–1273.

Vistisen, K., Poulsen, H. E. and Loft, S., 1992, Foreign compound metabolism capacity in man measured from metabolites of dietary caffeine. *Carcinogenesis*, **13**, 1561–1568.

Von Moltke, L. L., Greenblatt, D. J., Harmatz, J. S., Duan, X. S., Harrel, L. M., Contreau-Bibbo, M. M., Prichard, G. A., Wright, C. E. and Shader, R. I., 1996, Triazolam biotransformation by human liver microsomes *in vitro*: effects of metabolic inhibitors and clinical confirmation of a predicted interaction with ketoconazole. *Journal of Pharmacology and Experimental Therapeutics*, **276**, 370–379.

Wang, J.-S., Kensler, T. W. and Groopman, J. D., 1998, Toxicants in food: Fungal contaminants. In *Nutrition and Chemical Toxicity*, edited by C. Ioannides (Chichester: John Wiley & Sons), pp. 29–57.

Wargovich, M. J., Imada, O. and Stephen, L. C., 1992, Initiation and post-initiation chemopreventive effects of diallyl sulfide in esophageal carcinogenesis. *Cancer Letters*, **64**, 39–42.

Wentworth, J. M., Agostini, M., Schwabe, J. W. and Chatterjee, V. K. K., 2000, St John's wort, a herbal antidepressant, activates the steroid X receptor. *Journal of Endocrinology*, **166**, R11–R16.

Wills, R. B. H., Bone, K. and Morgan, M., 2000, Herbal products: active constituents, modes of action and quality control. *Nutrition Research Reviews*, **13**, 47–77.

Yang, C. S., Chhabra, S. K., Hong, J.-Y. and Smith, T. J., 2001, Mechanisms of inhibition of chemical toxicity and carcinogenesis by diallyl sulfide (DAS) and related compounds. *Journal of Nutrition*, **131**, 1041S–1045S.

Yee, G. D., Stanley, D. L., Pessa, L., Dalla Costa, T., Beltz, S. E., Ruiz, J. and Lowenthal, D. T., 1995, Effect of grapefruit juice on blood cyclosporin concentration. *Lancet*, **345**, 955–956.

Yu, C. M., Chan, J. C. N. and Sanderson, J. E., 2000, Chinese herbs and warfarin potentiation by 'Danshen'. *Journal of Internal Medicine*, **241**, 337–339.

Yue, Q.-Y., Bergquist, C. and Gerdén, B., 2000, Safety of St. John's wort (*Hypericum perforatum*). *Lancet*, **355**, 576–577.

XENOBIOTICA, 2002, VOL. 32, NO. 6, 479–490

Taylor & Francis
healthsciences

Metabolism of 4-fluoroaniline and 4-fluorobiphenyl in the earthworm *Eisenia veneta* characterized by high-resolution NMR spectroscopy with directly coupled HPLC-NMR and HPLC-MS

J. G. BUNDY†*, E. M. LENZ†§, D. OSBORN‡, J. M. WEEKS‡¶, J. C. LINDON† and J. K. NICHOLSON†

† Biological Chemistry, Biomedical Sciences Division, Faculty of Medicine, Imperial College of Science, Technology and Medicine, Sir Alexander Fleming Building, South Kensington, London SW7 2AZ, UK
‡ Centre for Ecology and Hydrology, Monks Wood, Abbots Ripton, Huntingdon PE28 2LS, UK

Received 1 October 2001

1. Little is known about metabolism of xenobiotics by earthworms, despite their importance in soil ecotoxicity testing. Normal earthworms and earthworms treated with antibiotics to ensure inhibition of gut microflora were exposed to two model xenobiotic compounds, 4-fluoroaniline and 4-fluorobiphenyl, to determine which metabolites were produced, and whether the pattern of metabolism was affected by the presence of microbial transformation ability.

2. ^{19}F-NMR spectroscopy detected the number and relative proportions of metabolites and directly coupled HPLC-^{1}H-NMR spectroscopy and HPLC-MS then identified the metabolites.

3. Despite uptake, no metabolism of 4-fluorobiphenyl was observed at any stage, which appears to be a consequence of the lack of oxidative Phase I metabolic activity of the earthworms towards this substrate. In contrast, 4-fluoroaniline exhibited dose-dependent metabolism. At high doses (leading to mortality within 24 h) one predominant metabolite was observed, which was identified as the *N*-β-glucoside conjugate. At lower dose levels, the predominant metabolite was the γ-glutamyl conjugate, although the glucoside and another as yet unidentified metabolite were also detected.

4. The inhibition of gut microflora did not have any influence on metabolism. The study represents the first evidence for glucoside and glutamyl conjugation as a pathway for xenobiotic metabolism in earthworms.

Introduction

Although earthworms are standard organisms for ecotoxicity testing, there are still many areas where knowledge is lacking about their biological and biochemical responses to xenobiotics (Lagadic and Caquet 1998). In particular, the metabolism of xenobiotics by earthworms is not fully understood (Stenersen 1992), although they are known to possess cytochrome P450 enzyme systems, and hence have the capacity for Phase I oxidative metabolism of xenobiotics (Lee 1998). However,

* Author for correspondence; e-mail j.bundy@ic.ac.uk
§ Present address: Department of Drug Metabolism and Pharmacokinetics, AstraZeneca Pharmaceuticals, Mereside, Alderley Park, Macclesfield SK10 4TG, UK.
¶ Present address: National Centre for Environmental Toxicology, WRc-NSF, Henley Road, Medmenham, Marlow SL2 2HD, UK.

Xenobiotica ISSN 0049–8254 print/ISSN 1366–5928 online © 2002 Taylor & Francis Ltd
http://www.tandf.co.uk/journals
DOI: 10.1080/00498250210124156

there is evidence that earthworm cytochrome P450 systems may not metabolize xenobiotic substrates that are readily metabolized by vertebrates. For example, it has been reported that P450 expression in earthworms is not inducible by exposure to polycyclic aromatic hydrocarbons (PAHs) (Milligan *et al.* 1986, Achazi *et al.* 1998). This may be because annelids and other invertebrates lack the aryl hydrocarbon receptor, and thus earthworm cytochrome P450 would not be induced by PAHs and other planar aromatic compounds (Hahn and Stegemann 1992). Phase II metabolism is also possible since earthworms have been shown to possess glutathione *S*-transferase (GST) activity, the activity of which is enhanced by the pesticide quintozene (Stenersen and Øien 1981), although there is evidence that GSTs may not be inducible by other xenobiotics (Stokke and Stenersen 1993). Other Phase II metabolic transformations that have been reported include methyl and spermine conjugation of pesticides (Khalil *et al.* 1990, as cited in Stenersen 1992, Curl *et al.* 1987). Compared with the state of knowledge of xenobiotic metabolism in vertebrates, there is a clear need for more understanding of metabolism in earthworms. In particular, there is a requirement for studies that include full characterization of the metabolites produced and that do not solely rely on reporting levels of enzyme activity. For studies of metabolism by soil invertebrates, it is also important to distinguish the possible contribution made by the gut and soil microorganisms.

^{19}F-nuclear magnetic resonance (NMR) spectroscopy can provide an approach for determining the metabolic fate of fluorinated compounds. The ^{19}F isotope is present at 100% natural abundance, removing the need for isotopic labelling, and gives about 83% of the sensitivity of ^{1}H-NMR spectroscopy (the most NMR sensitive naturally occurring isotope) at an equivalent field strength. ^{19}F-containing molecules are not generally present in endogenous biological systems of terrestrial annelids, hence all the resonances observed in a spectrum can be attributed to fluorine-containing xenobiotics and their metabolites. This lack of interference from background resonances allows detection at concentrations as low as 0.1 μM given the use of reasonable data acquisition periods (Bollard *et al.* 1996). The ^{19}F nucleus possesses a wide natural chemical shift range (of around 250 ppm for fluorine in organic chemicals), and is thus sensitive to chemical changes even if occurring at a site distant from that of the fluorine substituent in the molecule: changes up to nine bonds away can be detected (Everett 1995, Boersma *et al.* 2001). Each fluorine-containing compound (if there is only a single fluorine substituent in the parent xenobiotic) gives rise to a single resonance in the NMR spectrum, thus allowing simultaneous, non-destructive detection and quantitation of all of the metabolites that have been produced with no need for a physical separation step. As a consequence, ^{19}F-NMR spectroscopy has been used to identify the pathways of metabolism in a wide variety of cases, including in vertebrates, microbes, cultured cell lines and in soil (Vervoort *et al.* 1990, Wade *et al.* 1990, Vervoort *et al.* 1991, Boersma *et al.* 1998, Green *et al.* 1999a, b).

Although ^{19}F-NMR spectroscopy is an ideal technique for detecting and quantifying all major fluorine-containing metabolites in a sample, it is not possible to identify the metabolites on the basis of their ^{19}F-NMR spectra alone. This is particularly the case when the routes of metabolism and possible conjugates are not well known. It is, therefore, desirable to combine ^{19}F-NMR spectroscopy with complementary analytical techniques for the full elucidation of the target analytes. HPLC-^{1}H-NMR spectroscopy provides a powerful tool for identification of

unknown metabolites by combining the chromatographic separating power of high-pressure liquid chromatography (HPLC) with the highly structurally informative technique of ^{1}H-NMR spectroscopy (Lindon *et al.* 1996, Wolfender *et al.* 1998, Lindon *et al.* 2000). The technique provides complementary information to that from HPLC-MS, and the two detectors can be combined in parallel to give HPLC-MS-NMR. HPLC-NMR spectroscopy has been used to identify products of drug metabolism and for natural product analysis (e.g. Shockcor *et al.* 1996, Scarfe *et al.* 1998, Bobzin *et al.* 2000).

The aims of the present study were to investigate the metabolism of two model compounds in the earthworm *Eisenia veneta* by ^{19}F-NMR and HPLC-NMR spectroscopy, and to determine the contribution of the gut microflora to the metabolic fate of these two compounds. ^{19}F-NMR spectroscopy has been used to characterize the number and relative quantity of metabolites, and HPLC-MS and HPLC-NMR have been used for metabolite identification.

Materials and methods

Chemicals

4-fluoroaniline (4FA) and 4-fluorobiphenyl (4FBP), purity 99%, were obtained from Sigma-Aldrich (Poole, UK) and Lancaster Synthesis (Morecambe, UK) respectively. Tetracycline hydrochloride, gentamycin sulphate, carbenicillin and nalidixic acid sodium salt were obtained from Sigma-Aldrich.

Earthworms

Individual adult (clitellate) *Eisenia veneta* were taken from a culture maintained at CEH Monks Wood. Earthworms were allowed to empty their gut contents before antibiotic treatment by keeping them on moist filter paper for 48 h in the dark at 15°C.

Antibiotic treatment

Earthworms were exposed to antibiotics in 10 mM $CaCl_2$ agar plates (0.5% bacteriological agar) and incubated at 15°C in the dark. The antibiotics were filter-sterilized and added to the agar solution after autoclaving immediately before the plates were poured. Antibiotic-containing plates were stored at 4°C for no longer than 1 week. The Petri dishes were filled as completely as possible with agar solution to encourage the worms to burrow through the agar by minimizing the space between the top of the agar and the lid of the dish. A two-step antibiotic regime was followed, based on that described by Whiston and Seal (1988):

- Step A: the earthworms (two per plate) were added to agar containing nalidixic acid and tetracyclin hydrochloride (both 50 mg l^{-1}) for 48 h.
- Step B: the earthworms were transferred to fresh agar plates containing carbenicillin (200 mg l^{-1}) and gentamycin sulphate (50 mg l^{-1}) for 72 h.

The earthworms were then removed from the agar and exposed to xenobiotics via contact with filter paper for 24 h as detailed below.

The number of bacteria found in the earthworms was checked by plate counts on nutrient agar (Oxoid, Basingstoke, UK). Each worm was rinsed in sterile water, then cut into 10–12 pieces in 10 ml sterile quarter-strength microbiological Ringer's solution. The solution plus worm segments was transferred to a tightly stoppered vial, shaken vigorously by hand and then vortex-mixed for 1 min. Tenfold serial dilutions were then made of the resultant suspension, spread on nutrient agar plates and colonies counted after incubation for 72 h at 15°C.

Xenobiotic exposure

A filter paper contact test was used based on the OECD standard earthworm acute toxicity test (OECD 1984). Filter paper (Whatman no. 2) was cut to fit exactly inside glass vials with aluminium foil-lined lids. Each piece of filter paper measured 55 cm^2. The vials were loosely capped and sterilized by autoclaving. Xenobiotic solutions were then made up in acetone, such that 0.6 ml acetone applied to the filter paper would result in the desired concentration. The xenobiotic solutions were added to the filter paper, and the acetone allowed to evaporate with the vial lying on its side (approximately 20 min). The

filter paper was then wetted with 1 ml sterile de-ionized water. Earthworms were taken from agar plates (antibiotic containing for microbially inhibited earthworms, or plain agar for normal worms), rinsed in sterile water and transferred aseptically to the filter paper-lined vials. The vials were capped and incubated in the dark at 15°C for 24 h. At the end of the exposure period, survival was recorded and all earthworms (dead and surviving) frozen in liquid N_2, and stored at –20°C until analysis.

Extraction and sample preparation

Tissue extracts were made in 1:1 acetonitrile–water solution, using HPLC-NMR grade acetonitrile and de-ionized water. Each worm was added to 2 ml acetonitrile–water and ground in a mortar and pestle. The resulting homogenate was centrifuged to remove particulate matter and precipitated proteins (10 min, 17 000*g*), and the supernatant used for both ^{19}F-NMR spectroscopy and for identification of metabolite peaks using HPLC-MS and HPLC-NMR.

^{19}F-NMR spectroscopy

Samples were analysed on a Bruker Avance 500 MHz NMR spectrometer (Bruker UK, Coventry, UK) equipped with a 5 mm QNP probe and operating at a ^{19}F frequency of 470.59 MHz. Samples were held at 300 K during acquisition. 550 µl sample was added to 50 µl D_2O containing 11 mM trifluoroethanol (TFE) in a 5-mm NMR tube, i.e. such that the final TFE concentration was 1.1 mM. The D_2O provided a field-frequency lock for the spectrometer and the TFE provided an internal chemical shift reference ($\delta_F = -77.023$, expressed relative to $CFCl_3$ at $\delta_F = 0$). Proton-decoupled ^{19}F spectra (^{19}F-{^{1}H}) were acquired with a 55° tip angle and a 2 s relaxation delay between scans. Each free induction decay (FID) was collected into 64 K data points with a spectral width of 37 600 Hz. A total of 512 FIDs were collected for each sample and multiplied by an exponential function equivalent to 2 Hz line broadening before Fourier transformation (FT).

HPLC-MS and HPLC-NMR spectroscopy

Chromatography was performed with a HiChrom 150 × 4.6 mm column with 5 µm C18 BDS packing (HiChrom, Theale, UK) with an Hewlett-Packard pump, and detection by a UV detector set at 254 nm. Samples were eluted using an aqueous buffer comprising 10 mM ammonium formate adjusted to pH 7 with a few drops of ammonia solution (A) and acetonitrile (B). For HPLC-NMR spectroscopy, buffer A was made up using D_2O and deuterated ammonium formate. Chromatography was carried out at a constant flow rate of 1 ml min^{-1}. Samples were eluted isocratically for 10 min at a ratio of 98% A/2% B, followed by a linear gradient to 70% A/30% B by 35 min, followed by a linear gradient to 50% A/50% B by 45 min. The post-UV detector flow was directed to a splitter such that 5% was sent to the MS and 95% was either sent to waste (during HPLC-MS experiments) or to the NMR spectrometer (for HPLC-NMR). HPLC-MS utilized a Bruker Esquire ion-trap mass spectrometer with electrospray ionization interface operated in the positive-ion mode.

HPLC-NMR spectroscopy was performed in stop-flow mode using a Bruker Avance 600 MHz spectrometer with a dedicated HPLC probe with a sample cell volume of 120 µl. Samples were held at 300 K during acquisition. A field-frequency lock was obtained from the D_2O in the eluent. The pulse program used a standard presaturation pulse sequence for solvent suppression at the residual water (HDO) and at the acetonitrile frequencies. Spectra were acquired into 32 K data points over a spectral width of 7200 Hz. Between 2 and 10 K scans were collected depending on metabolite concentration, and an exponential apodization function equivalent to 1 Hz line broadening applied before FT. Chemical shifts were referenced to that of acetonitrile at δ2.00.

Results

Effectiveness of antibiotic treatment

Plate counts showed that the microflora of antibiotic-treated earthworms was inhibited by at least three orders of magnitude compared with untreated worms, and that this inhibition remained 24 h after the earthworms had been transferred from agar to sterile moist filter paper (table 1). The protocol for antibiotic treatment differed from that used previously (Whiston and Seal 1988) in two respects: (1) the fungicide cycloheximide was omitted and (2) agar was used as a carrier for the antibiotics. Agar jelly has been shown to be a suitable medium for depuration of earthworms for ecotoxicity testing (Pokarzhevskii *et al.* 2000). In the

Table 1. Inhibition of the microflora of earthworms after antibiotic treatment. Data are the number of colony-forming units per worm (nutrient agar, 3 days incubation) ± SEM.

	Step A[a]	Step B[b]	Filter paper [c]
Antibiotic-treated worms	$1.4 \pm 1.4 \times 10^3$	$2.5 \pm 1.4 \times 10^2$	$3.8 \pm 2.4 \times 10^2$
Control worms	$1.6 \pm 0.6 \times 10^6$	$4.7 \pm 1.7 \times 10^6$	$5.5 \pm 1.1 \times 10^5$

[a] 2 days, exposed to tetracyclin and nalidixic acid.
[b] 5 days, exposed to tetracyclin and nalidixic acid followed by carbenicillin and gentamycin.
[c] 6 days, exposed to tetracyclin and nalidixic acid followed by carbenicillin and gentamycin, followed by 24 h on filter paper.

Table 2. Numbers of antibiotic-treated and untreated (control) earthworms surviving after 24-H exposure to 4FA or 4FBP at different doses.

	0 (no xenobiotics)	4FA, 5 μg cm^{-2}	4FA, 25 μg cm^{-2}	4FA, 125 μg cm^{-2}	4FBP, 2 μg cm^{-2}	4FBP, 10 μg cm^{-2}	4FBP 50 μg cm^{-2}
Treated	100	100	75	0	75	50	0
Control	100	100	50	0	50	0	0

Data are per cent survival ($n = 4$ except for concentration 0, no xenobiotics, when $n = 8$).

present study, they were observed to burrow readily into the agar, with no signs of reluctance to burrow in antibiotic-containing agar.

The concentration ranges tested of the selected xenobiotics caused mortality at the highest concentrations for both 4FA and 4FBP and details of the numbers surviving is given in table 2. Both live and dead earthworms were analysed at the end of the 24-h exposure.

^{19}F-*NMR spectroscopy*

No metabolites of 4FBP were observed in any of the earthworms. A single resonance corresponding to the parent compound was observed in all worms that had been dosed with 4FBP, demonstrating that uptake had taken place.

For 4FA, up to three separate metabolite resonances were observed, although not all resonances were observed in every individual animal. The quantitative pattern of metabolism was markedly different at the highest dose level (125 μg cm^{-2}) compared with the two lower dose levels in that the major metabolite resonance (metabolite 1) was observed at $\delta_F - 127.07$ (figure 1A), whilst at 25 and 5 μg cm^{-2}, the major metabolite resonance (metabolite 2) was observed at $\delta_F - 118.53$ (figure 1B). In addition, at the lower two dose levels, a third metabolite was observed in some worms at $\delta_F - 114.45$ (metabolite 3).

Antibiotic treatment of the worms was not found to exert any statistically significant effect on the pattern of metabolites observed ($p = 0.22$, ANOVA). The relative percentages of the parent compound and the three detected metabolites after dosing with 4FA at different concentrations for the combined set of normal and antibiotic treated worms as determined by ^{19}F-NMR spectroscopy is given in table 3. It should be noted that any metabolites arising from defluorination would not have been directly observable by ^{19}F-NMR spectroscopy. However, in this case, one would expect to see a resonance from fluoride ion, which was not

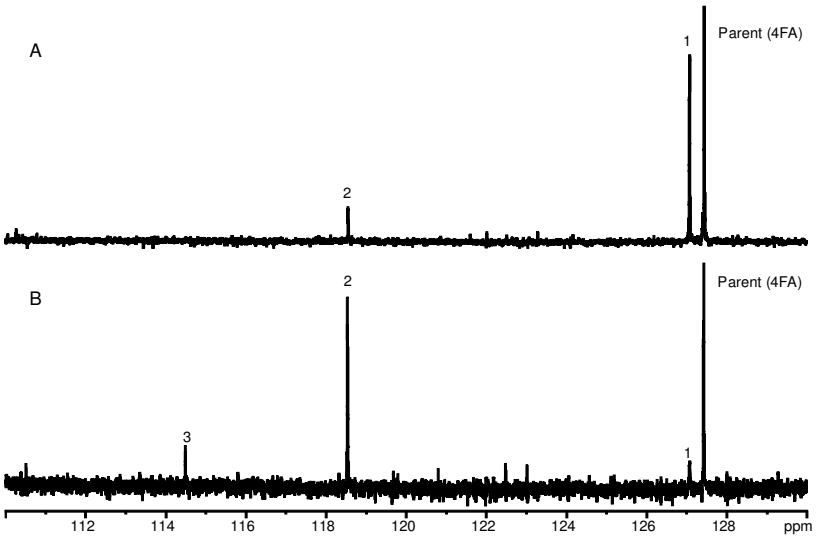


Figure 1. ^{19}F-NMR spectra of acetonitrile/water tissue extracts of *Eisenia veneta* dosed with 4-fluoroaniline at two different dose levels: (A) 125 μg cm^{-2}; (B) 25 μg cm^{-2} dose level. Spectra are scaled vertically to the height of the largest metabolite resonance.

Table 3. Distribution of the metabolites of 4FA measured by ^{19}F-NMR spectroscopy.

	4FA	1	2	3
Chemical shift (δF)	−127.44	−127.07	−118.57	−114.45
% label at 125 μg cm^{-2} dose	70 ± 16	25 ± 16	4.6 ± 1.4	0
% label at 25 μg cm^{-2} dose	75 ± 11	2.9 ± 3.9	21 ± 7	0.7 ± 2
% label at 5 μg cm^{-2} dose	54 ± 19	0	34 ± 18	12 ± 9

Data are per cent (of the total concentration of all recovered metabolites plus unmetabolized parent compound as shown by ^{19}F label) ± SD.

observed in any of the samples. Thus, by inference, defluorination is not an important pathway for these compounds.

HPLC-NMR and HPLC-MS

There were no apparent effects of the gut microflora on metabolism (data not shown) and so it was decided to use only the normal, i.e. non-antibiotic-treated, earthworms for metabolite identification. Initially, samples taken from the worms dosed at 125 μg cm^{-2} were used. A single additional metabolite peak was observed by HPLC with UV detection for dosed compared to control worms, at a retention time of 18.5 min (metabolite 1). A peak was also observed at 22.0 min, which corresponded to unmetabolized 4FA, as shown by co-elution with an added standard and by exhibiting the same observed ions as standard 4FA in the HPLC-MS. The ^{19}F-NMR spectrum of the high dose extract (figure 1A) showed that at least one other 4FA metabolite was present in lower concentration (metabolite 2), but this was not detected in the HPLC-UV chromatogram. The peak at 18.5 min gave rise to ions in the HPLC-MS at m/z 112, 274 and 296. ^{1}H-NMR spectroscopy, using HPLC-NMR, of the peak at 18.5 min showed two

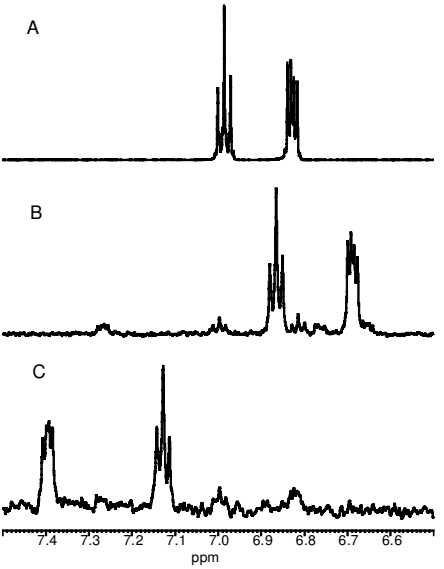


Figure 2. HPLC-^{1}H-NMR spectra of earthworm tissue extracts after dosing with 4FA, aromatic region only. (A) Spectrum of authentic 4FA; (B) metabolite 1 from a high dose level ($125\,\mu g\,cm^{-2}$); (C) metabolite 2 from a medium dose level ($25\,\mu g\,cm^{-2}$).

aromatic resonances of equal intensity (figure 2B), very similar in pattern to 4FA (figure 2A). This indicated that there was neither loss of fluorine nor any substitution in the aromatic ring. The ion observed at $m/z = 112$ using HPLC-MS corresponded to 4FA, also showing that there had been no substitution on the aromatic ring. These two observations taken together imply that the major metabolite involved *N*-conjugation of 4FA. HPLC-^{1}H-NMR spectroscopy of the peak from metabolite 1 showed additional resonances in the region $\delta 3.2$–3.8 (figure 3A), in a chemical shift range that is typical of sugars and integrating to six protons. Close examination shows an ABX spin system at $\delta 3.70/3.53/3.37$, with the remaining resonances possessing 9 Hz couplings indicative of all-axial couplings around the sugar ring. The presence of all-axial couplings indicates that the sugar is in the β form. On the basis of the combined HPLC-MS and HPLC-NMR results, this metabolite was assigned as the β-glucoside conjugate of 4FA (figure 4A). The resonance for the proton in the β-H1 position is not observed, as this is expected to be close to that of water and thus attenuated by water suppression. However, the assignment is confirmed by the HPLC-MS data which showed ions at m/z 112 corresponding to the 4FA fragment ion, m/z 274 corresponding to the expected molecular ion MH^+, and m/z 296 arising from a sodium adduct MNa^+. The MS results confirm that the metabolite is an *N*-glucoside and not an *N-O*-glucoside.

For samples from worms dosed at $25\,\mu g\,cm^{-2}$, the major metabolite resonance in the ^{19}F-NMR spectrum (figure 1B, metabolite 2) is at $\delta_F - 118.57$ ppm. Again, apart from parent 4FA, a single metabolite peak was observed by HPLC-UV with a retention time of 17.5 min. HPLC-MS showed that the ions associated with the peak were (in order of intensity) 224, 130, 112, 241, 263, 285, 310 and 414. The corresponding ^{1}H-NMR spectrum obtained using HPLC-NMR is given in figures 2C and 3B. The multiplicity of the aromatic resonances (figure 2C) again

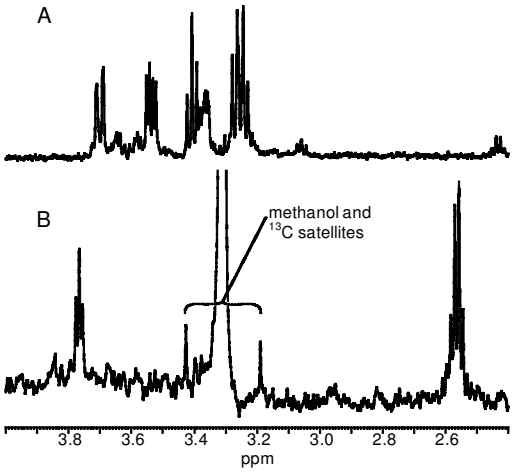


Figure 3. HPLC-^{1}H-NMR spectra of 4FA earthworm tissue extracts after dosing with 4FA, aliphatic region only. (A) Metabolite 1 from a high dose level (125 μg cm^{-2}); (B) metabolite 2 from a medium dose level (25 μg cm^{-2}). Contamination by methanol is visible in B – the resonances from methanol are labelled on the spectrum.

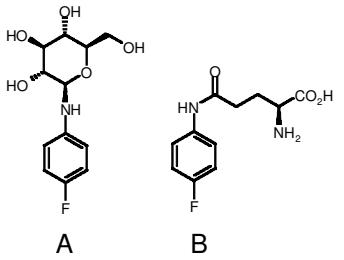


Figure 4. Structure of 4FA metabolites. (A) β-Glucoside conjugate; (B) γ-glutamyl conjugate.

demonstrated that the metabolite was a conjugate of 4FA, although the pattern of resonances was reversed, i.e. the apparent doublet of doublets (corresponding to the protons *ortho* to the aniline nitrogen) now appears to high frequency of the pseudo-triplet (corresponding to the protons *meta* to the nitrogen). This indicates that the conjugating group caused considerable deshielding of the protons *ortho* to the nitrogen and suggests conjugation at the amine group to form an amide linkage. The other resonances (figure 3B) include a triplet at δ3.75 and a multiplet at δ2.60. These integrate to one and two protons respectively, relative to the two-proton aromatic resonance at δ7.13. Large signals were also seen from a contaminant, presumed to be methanol. The resonance at δ3.75 is typical of an amino acid α proton. The ^{1}H-NMR spectrum is consistent with a γ-glutamyl conjugate of 4Fα (figure 4B): the multiplet at δ2.57 is assigned to the γ-protons. There must be another resonance in order to produce the multiplicity of the observed resonances: this is most probably obscured by the large residual signal of the suppressed acetonitrile resonance and its unsuppressed ^{13}C satellites. The resonance of the unobserved β-protons of the glutamyl conjugate would be expected to come at around that chemical shift. The suggested γ-glutamyl conjugate is

confirmed by the HPLC-MS evidence with the ion at 241 being the molecular ion MH^+, and the ions at 112 and 130 being the two daughter ions produced by loss of the conjugate in the mass spectrometer. The peak at m/z 224 may possibly be caused by dimerization of the parent compound in the vapour phase, thus accounting for the four largest peaks observed in the mass spectrum. Conjugation of the aniline with the α-carbonyl function of glutamate can be ruled out on the basis of the observed ^{1}H chemical shifts, in particular that of the α-CH proton which is at a typical value for free glutamate.

^{19}F-NMR spectroscopy of the worms dosed at 5 and 25 $\mu g\,cm^{-2}$ showed that another metabolite was present with a chemical shift of $\delta_F - 114.53$ ppm. Neither HPLC-UV nor HPLC-MS detected any peaks that could be attributed to this low-concentration metabolite, thus its structure could not be determined. However, some information is provided by the ^{19}F-NMR spectrum, with the fluorine substituent of the unidentified metabolite being deshielded by $\Delta\delta$ 13 relative to 4FA. The glucoside conjugate ^{19}F-NMR chemical shift showed a high frequency shift of $\Delta\delta$ 0.4 relative to 4FA, but the glutamyl conjugate – in which the aromatic amine is biotransformed to an aromatic amide – has a larger shift of $\Delta\delta$ 8.50. Hence, it is probable that the unidentified metabolite may also possess an amide linkage.

Discussion

Production of microbially inhibited animals and effects on metabolism

The use of a combined antibiotic regime in agar was shown to be effective in producing microbially inhibited individuals of the earthworm *Eisenia veneta*, and that the effect of antibiotics continued for 24 h after completion of antibiotic dosing. This appears to be a highly suitable approach for future metabolic studies. In this study, the inhibition of the worms' commensal microbiological activity had no effect on the metabolism of the xenobiotic compounds (data not shown).

Previous studies of xenobiotic metabolism in earthworms have tended to focus on compounds of perceived ecological concern, i.e. known biocides and in particular pesticides (Stenersen *et al.* 1973). Interest in metabolism and metabolic enzymes has also centred on known mechanisms of activation or detoxification of bioactive compounds, such as the transformation of the P=S to P=O moiety in organophosphorus pesticides (Park *et al.* 1990, 1992). Thus, many previous studies on metabolism by earthworms have been limited to measuring the appearance of initial oxidized metabolites. Studies on other xenobiotics, i.e. compounds which are not specifically applied as biocides, are scarce. Albro *et al.* (1993) studied the metabolism of di-(2-ethylhexyl) phthalate (DEHP) by *Lumbricus terrestris*, including the effects of inhibiting the gut microflora by gentamycin treatment. They reported that *L. terrestris* could oxidize DEHP to mono-(2-ethylhexyl) phthalate and to phthalic acid, and concluded that all further metabolism of these intermediates to CO_2 was carried out by an intestinal bacterial strain. However, antibiotic treatment slightly increased rather than decreased the amount of bacterial metabolism observed. The system used by Albro *et al.* followed metabolism over 7 days. This longer duration presumably afforded time for degradative microbial populations to develop, and it is possible that if the study reported here

had been carried out over an extended period, effects of bacterial biodegradation may have been observed.

This study did not employ soil exposure of xenobiotics, as the primary aim was the investigation of xenobiotic metabolism in the worm. Simplified systems, such as the filter paper contact test used in this case, provide a controllable environment in which it can be determined whether intestinal bacteria affect metabolic fate. Experiments carried out in soil have the complicating factor that the major contributors to metabolism at the ecosystem level may be the soil microbes themselves. 4-Fluorobiphenyl was not metabolized at all by *E. veneta* in the current study, for instance, but has been shown to be rapidly incorporated into soil organic matter in the absence of earthworms, presumably through metabolism by soil microbiota (Green *et al.* 1999b). However, the presence of earthworms in a contaminated soil may still have a major effect on environmental fate: it has been reported that biodegradation is enhanced by the presence of earthworms, possibly by direct metabolism of the contaminants present, but also by turning over soil and increasing the numbers and/or activity of soil microbes (e.g. Renoux *et al.* 1999).

Metabolism of 4-fluoroaniline

The two major metabolites of 4FA observed in this study were both products of Phase II metabolism, i.e. conjugated derivatives rather than resulting from oxidative biotransformation. Conjugation by glutamate in the earthworm *Lumbricus terrestris* has been observed in the context of its normal biochemistry: the γ-glutamyl conjugate of the neurochemical 5-hydroxytryptamine (serotonin) has been reported by Sloley (1994), who speculated that this enzyme system might also used by earthworms as a pathway for conjugation and detoxification of xenobiotics.

Glucoside conjugates have not been previously reported in earthworms, but typically glucosidation appears to be a more important route than β-glucuronidation in invertebrates compared to vertebrates (Livingstone 1998). Thus, the conversion of 4FA to the glucoside appears entirely reasonable. However, the shift in metabolism between the high and low dose levels of 4FA was unexpected. Possibly high concentrations of xenobiotic are required to induce the β-glucose conjugation mechanism, and glutamyl conjugation is seen at less extreme biochemical levels. An alternative explanation might be that the earthworm glutamyl transferases are easily saturated, and are only capable of dealing with xenobiotics at low doses.

Clearly Phase II (conjugative) metabolism is a major pathway in earthworms for dealing with xenobiotics. Curl *et al.* (1987) investigated the metabolism of cypermethrin by *L. terrestris* and reported that, in addition to a major product (spermine conjugated to two xenobiotic molecules), there were several minor products which were also probably Phase II metabolites. It has been suggested that P450-type oxygenase activity is low in earthworms because, as detritus feeders, they have less need to detoxify plant defence compounds (Stenersen 1992). Indeed, low cytochrome P450 activity relative to vertebrates appears to be a characteristic of invertebrates in general (Livingstone 1998). This may explain the lack of any observed metabolism of 4FBP: the compound was not oxidized, and there are no heteroatom sites in the molecule available for conjugation.

This study provides the first report of xenobiotic metabolism in earthworms by conversion to β-glucoside and γ-glutamyl conjugates. The combination of ^{19}F-

NMR spectroscopy with HPLC-^{1}H-NMR was shown to be a powerful combined approach for the probing of xenobiotic metabolism in a typical ecotoxicological invertebrate test species such as *E. veneta*.

Acknowledgements

Funding for research was provided under a NERC Environmental Diagnostics grant. Dr Rob Eaton, University of London Intercollegiate Research Service, Birkbeck College, is thanked for access to the ^{19}F-NMR spectroscopy facility.

References

Achazi, R. K., Flenner, C., Livingstone, D. R., Peters, L. D., Schaub, K. and Scheiwe, E., 1998, Cytochrome P450 and dependent activities in unexposed and PAH-exposed terrestrial annelids. *Comparative Biochemistry and Physiology*, **C121**, 339–350.

Albro, P. W., Corbett, J. T. and Schroeder, J. L., 1993, The metabolism of di-(2-ethylhexyl) phthalate in the earthworm *Lumbricus terrestris*. *Comparative Biochemistry and Physiology*, **C104**, 335–344.

Bobzin, S. C., Yang, S. and Kasten, T. P., 2000, Application of liquid-chromatography-nuclear magnetic resonance spectroscopy to the identification of natural products. *Journal of Chromatography B*, **748**, 259–267.

Boersma, M. G., Dinarieva, T. Y., Middelhoven, W. J., van Berkel, W. J. H., Doran, J., Vervoort, J. and Rietjens, I. M. C. M., 1998, ^{19}F-NMR magnetic resonance as a tool to investigate microbial degradation of fluorophenols to fluorocatechols and fluoromuconates. *Applied and Environmental Microbiology*, **64**, 1256–1263.

Boersma, M. G., Solyanikova, I. P., van Berkel, W. J. H., Vervoort, J., Golovleva, L. A. and Rietjens, I. M. C. M., 2001, ^{19}F-NMR metabolomics for the elucidation of microbial degradation pathways of fluorophenols. *Journal of Industrial Microbiology and Biotechnology*, **26**, 22–34.

Bollard, M. E., Holmes, E., Blackledge, C. A., Lindon, J. C., Wilson, I. D. and Nicholson, J. K., 1996, ^{1}H and ^{19}F-NMR spectroscopic studies on the metabolism and urinary excretion of mono- and disubstituted phenols in the rat. *Xenobiotica*, **26**, 255–273.

Everett, T. S., 1995, Nuclear magnetic resonance spectroscopy of organofluorine compounds. In *Chemistry of Organic Fluorine Compounds II*, pp. 1037–1087.

Green, N. A., Meharg, A. A., Till, C., Troke, J. A. and Nicholson, J. K., 1999a, Degradation of 4-fluorobiphenyl by mycorrhizal fungi as determined by ^{19}F nuclear magnetic resonance spectroscopy and ^{14}C radiolabelling analysis. *Applied and Environmental Microbiology*, **65**, 4021–4027.

Green, N. A., Meharg, A. A., Till, C., Troke, J. A. and Nicholson, J. K., 1999b, Degradation of 4-fluorobiphenyl in soil investigated by ^{19}F-NMR spectroscopy and ^{14}C radiolabelling analysis. *Chemosphere*, **38**, 1085–1101.

Hahn, M. A. and Stegemann, J. J., 1992, Phylogenetic distribution of the Ah receptor in non-mammalian species: implications for dioxin toxicity and Ah receptor evolution. *Chemosphere*, **25**, 931–937.

Lagadic, L. and Caquet, T., 1998, Invertebrates in testing of environmental chemicals: are they alternatives? *Environmental Health Perspectives*, **106**, 593–611.

Lee, R. F., 1998, Annelid cytochrome P-450. *Comparative Biochemistry and Physiology*, **C121**, 173–179.

Lindon, J. C., Nicholson, J. K. and Wilson, I. D., 1996, Direct coupling of chromatographic separations to NMR spectroscopy. *Progress in NMR Spectroscopy*, **29**, 1–49.

Lindon, J. C., Nicholson, J. K. and Wilson, I. D., 2000, Directly coupled HPLC–NMR and HPLC–NMR–MS in pharmaceutical research and development. *Journal of Chromatography B*, **748**, 233–258.

Livingstone, D. R., 1998, The fate of organic xenobiotics in aquatic ecosystems: quantitative and qualitative differences in biotransformation by invertebrates and fish. *Comparative Biochemistry and Physiology*, **A120**, 43–49.

Milligan, D. L., Babish, J. G. and Neuhauser, E. F., 1986, Noninducibility of cytochrome P-450 in the earthworm *Dendrobaena veneta*. *Comparative Biochemistry and Physiology*, **C85**, 85–87.

OECD, 1984, *Earthworm, Acute Toxicity Tests*. OECD Guideline for Testing of Chemicals, No. 7 (Organization for Economic Co-operation and Development).

Park, S. C., Smith, T. J. and Bisesi, M. S., 1990, Hydrolysis of bis(4-nitrophenyl) phosphate by the earthworm *Lumbricus terrestris*. *Soil Biology and Biochemistry*, **22**, 729–730.

Park, S. C., Smith, T. J. and Bisesi, M. S., 1992, Activities of phosphomonoesterase and phosphodiesterase from *Lumbricus terrestris*. *Soil Biology and Biochemistry*, **24**, 873–976.

Scarfe, G. B., Wright, B., Clayton, E., Taylor, S., Wilson, I. D., Lindon, J. C. and Nicholson, J. K., 1998, F-19-NMR and directly coupled HPLC-NMR-MS investigations into the metabolism of 2-bromo-4-trifluoromethylaniline in rat: a urinary excretion balance study without the use of radiolabelling. *Xenobiotica*, **28**, 373–388.

Shockcor, J. P., Unger, S. E., Wilson, I. D., Foxall P. J. D., Nicholson, J. K. and Lindon, J. C., 1996, Combined HPLC, NMR spectroscopy, and ion-trap mass spectrometry with application to the detection and characterization of xenobiotic and endogenous metabolites in human urine. *Analytical Chemistry*, **68**, 4431–4435.

Sloley, B. D., 1994, γ-Glutamyl conjugation of 5-hydroxytryptamine (serotonin) in the earthworm (*Lumbricus terrestris*). *Neurochemical Research*, **19**, 217–222.

Stenersen, J., 1992, Uptake and metabolism of xenobiotics by earthworms. In P. W. Greig-Smith, H. Becker, P. J. Edwards and F. Heimbach (eds), *Ecotoxicology of Earthworms* (Andover: Intercept), pp. 129–138.

Stenersen, J., Gilman, A. and Vardanis, A., 1973, Carbofuran: its toxicity to and metabolism by earthworm (*Lumbricus terrestris*). *Journal of Agricultural and Food Chemistry*, **21**, 166–171.

Stenersen, J. and Øien, N, 1981, Glutathione *S*-transferases in earthworms (*Lumbricidae*). Substrate specificity, tissue and species distribution and molecular weight. *Comparative Biochemistry and Physiology*, **C69**, 243–252.

Stokke, K. and Stenersen, J., 1993, Non-inducibility of the glutathione transferases of the earthworm *Eisenia andrei*. *Comparative Biochemistry and Physiology*, **C106**, 753–756.

Vervoort, J., de Jager, P. A., Steenbergen, J. and Rietjens, I. M. C. M., 1990, Development of a ^{19}F-NMR method for studies on the *in vivo* and *in vitro* metabolism of 2-fluoroaniline. *Xenobiotica*, **20**, 657–670.

Vervoort, J., Rietjens, I. M. C. M., Moonen, C. T. W., von Kienlin, M. and Despres, D., 1991, Biotransformation of 2-fluoroaniline in rats studied by *in vivo* ^{19}F-NMR. *NMR in Biomedicine*, **4**, 255–261.

Wade, K. E., Wilson, I. D., Troke, J. A. and Nicholson, J. K., 1990, ^{19}F and ^{1}H magnetic resonance strategies for metabolic studies on fluorinated xenobiotics: application to flurbiprofen [2-(2-fluoro-4-biphenylyl)propionic acid]. *Journal of Pharmaceutical and Biomedical Analysis*, **8**, 401–410.

Whiston, R. A. and Seal, K. J., 1988, Rapid production of axenic specimens of the earthworm *Eisenia foetida* using microcrystalline cellulose as a carrier medium for antibiotics. *Soil Biology and Biochemistry*, **20**, 407–408.

XENOBIOTICA, 2002, VOL. 32, NO. 6, 491–503

Taylor & Francis
healthsciences

In vitro and *in vivo* studies on the stereoselective pharmacokinetics and biotransformation of an (*S*)-(−)- and (*R*)-(+)-pyrazolotriazine sulfoxide in the male rat

S. NAITO* and M. NISHIMURA

Laboratory of Drug Metabolism Research, Naruto Research Institute, Otsuka Pharmaceutical Factory, Inc., Naruto, Tokushima 772-8601, Japan

Received 14 April 2000

1. BOF-4272 (a pyrazolotriazine sulfoxide) is a new drug for the treatment of hyperuricemia. The pharmacokinetics and biotransformation of both BOF-4272 enantiomers were investigated in rat.

2. Plasma concentrations after intravenous or oral administration of racemic BOF-4272 to rat were significantly higher for (*S*)- than for (*R*)-BOF-4272.

3. The concentration of (*S*)-BOF-4272 in hepatocyte culture medium 24 h after the addition of racemic BOF-4272 was higher than that of (*R*)-BOF-4272.

4. Liver concentrations after oral adminstration of racemic BOF-4272 to rat were significantly higher for (*R*)- than for (*S*)-BOF-4272. Kidney concentrations were significantly higher for (*S*)- than for (*R*)-BOF-4272.

5. Hepatic biotransformation from BOF-4272 to unknown metabolites, possibly conjugates, is stereoselective. Biotransformation of both enantiomers to the sulfone metabolite by cytochrome P450 in rat liver may also be stereoselective.

6. Biotransformation of the sulfide metabolite of BOF-4272 to BOF-4272 may be stereoselective, possibly due to the stereospecificity of flavin-containing mono-oxidase and/or cyrochrome P450.

7. The stereoselectivity of plasma concentrations of racemic BOF-4272 after intravenous or oral administration appears to be due to differences in the hepatic uptake of the two enantiomers as well as the stereoselective biotransformation of the sulfide metabolite to BOF-4272 in rat liver. Biotransformation of BOF-4272 in rat liver may also be stereoselective.

Introduction

BOF-4272, a sulfoxide derivative of pyrazolotriazine, is a new drug that has been developed for the treatment of hyperuricemia and ischemic reperfusion injury (Sato *et al.* 1991, Yamamoto *et al.* 1993, Iwahara *et al.* 1994, Uematsu and Nakashima 1994). BOF-4272 inhibits the *de novo* biosynthesis of uric acid by blocking the xanthine oxidase/xanthine dehydrogenase system, which catalyses the last step of purine catabolism (Sato *et al.* 1991, Uematsu and Nakashima 1994). The mechanism of the inhibitory action of BOF-4272 was elucidated by an *in vitro* study using milk xanthine oxidase/xanthine dehydrogenase (Okamoto and Nishino 1995). BOF-4272 significantly decreases the concentration of free radicals generated by xanthine oxidase and consequently reduced cellular necrosis (Suzuki *et al.*

* Author for correspondence; e-mail: naitousn@otsukakj.co.jp

Xenobiotica ISSN 0049–8254 print/ISSN 1366–5928 online © 2002 Taylor & Francis Ltd
http://www.tandf.co.uk/journals
DOI: 10.1080/00498250210125 34

1994). Earlier reports have suggested that BOF-4272 is not absorbed from any specific point in the digestive tract (Terao *et al.* 1995).

Since BOF-4272 contains an asymmetric sulfoxide group, it exists as (*S*)-(−)- and (*R*)-(+)-BOF-4272 enantiomers. Recently, an asymmetric synthesis of (*S*)-BOF-4272 was reported by Matsugi *et al.* (1995). We reported the metabolic pathways and pharmacokinetic properties of racemic BOF-4272 in rat (Naito and Nishimura 1999, Naito *et al.* 1999a). It was demonstrated in previous *in situ* studies that the hepatic elimination of BOF-4272 was relatively high in rat (Nishimura *et al.* 1994, 1995, 1996). It was also demonstrated in a previous *in situ* study that the hepatic extraction ratio of (*R*)-BOF-4272 was significantly greater than that of (*S*)-BOF-4272 in rat (Nishimura *et al.* 1997).

The present paper describes the detailed stereoselective pharmacokinetics and biotransformation of (*S*)- and (*R*)-BOF-4272 in rat. In addition, it discusses the stereoselective biotransformation of BOF-4269 (the sulfide metabolite of BOF-4272), which is metabolized by the intestinal flora, absorbed from the intestinal tract and biotransformed to BOF-4272 in the rat liver.

Materials and methods

Materials

^{14}C-labelled racemic BOF-4272 (3.89 MBq mg^{-1}) was obtained from Amersham International (Amersham, UK), and the radiochemical purity was >97%. Racemic BOF-4272 and the metabolites of (*S*)- and (*R*)-BOF-4272 used were synthesized at Otsuka Pharmaceutical Factory, Inc. (Tokushima, Japan), and their chemical purity was >99%. The isomeric purity of both enantiomers of BOF-4272 and the metabolite M-4 (hydroxy-BOF-4272) were >99% enantiomeric excess. Carboxymethyl cellulose sodium salt (CMC), diethyl ether, acetonitrile, ethyl acetate, dexamethasone, collagenase and perchloric acid (PCA) were purchased from Wako Pure Chemical Industries, Ltd (Osaka, Japan). Polyethylene glycol 400 (Peg 400) was purchased from Nacalai Tesque, Inc. (Kyoto, Japan). Trypsin inhibitor, insulin, $NADP^+$, glucose 6-phosphate and glucose 6-phosphate dehydrogenase were purchased from Sigma Chemical Co. (St Louis, MO, USA). Trypan blue was purchased from Flow Laboratories, Ltd (Irvine, UK). Williams' medium E and calf bovine serum were purchased from Dainippon Pharmaceutical Co., Ltd (Osaka, Japan).

All other chemicals and reagents were of analytical reagent grade.

Animals

The rats used were male Wistar rats of 7 weeks of age and weighing between 172 and 240 g. They were purchased from Charles River Japan (Kanagawa, Japan). During the experiments, the rats were housed individually in metabolic cages at a temperature of 23 ± 2 °C and relative humidity of 55% ± 10% with a 12-h night/day cycle. Animals were allowed free access to food (CRF-1-RE, Oriental Yeast Co., Ltd, Tokyo, Japan), except during periods of fasting, and to drinking water

Chromatography

BOF-4272 and M-4 concentrations were measured using high-performance liquid chromatography (HPLC) systems (CCP & 8010 Series, Tosoh Co., Tokyo, Japan) with a stationary phase of LiChrospher 100 NH_2 (250 × 4.0 mm i.d.; Merck, Darmstadt, Germany) on an extraction column and two CHIRALCELL ODs (50 × 4.6 mm i.d.; Daicel Chemical Industries, Ltd, Tokyo, Japan) on a chiral separation column. The concentrations of (*S*)- and (*R*)-BOF-4272 were determined using a fluorescence photometer (Tosoh Co.) with excitation and emission wavelengths of 319 and 400 nm, respectively. The concentrations of (*S*)- and (*R*)-M-4 were determined using a UV detector (UV-8010, Tosoh Co.) with a detector wavelength of 313 nm. The integrated data analyser was a C-R4AX Chromatopac (Shimadzu Co., Kyoto, Japan). The flow rate and the column temperature were 0.6 ml min^{-1} and 43 °C, respectively. The mobile phase was a mixture of *n*-hexane, ethnaol and formic acid (650:250:4 v/v).

The concentrations of BOF-4276 (the sulfone metabolite of BOF-4272) were measured using HPLC systems (CCP & 8010 Series) with a stationary phase of TSKgel ODS-120T (250 × 4.6 mm i.d.; all Tosoh Co.). The HPLC systems consisted of a system controller (PX-8010), pump (CCPM), autosampler (AS-48), UV detector (UV-8010) and integrated data analyser (C-R4AX Chromatopac, Shimadzu Co.). The detector wavelength and the flow rate were 323 nm and 1.0 ml min^{-1}, respectively.

The column temperature was ambient. The mobile phase was a mixture of solution A (10 mM $NH_4H_2PO_4$, pH 3.0) and solution B (acetonitrole and solution A, 80:20 v/v), with a linear gradient from 70/30 to 0/100% over 31 min.

Animal studies

The rats were fasted from 20 h before to 4 h after the intravenous administration of the test drugs, but were allowed free access to food when oral administration was employed. Racemic BOF-4272 was dissolved in 50% PEG 400 for intravenous administration, and in 0.5% CMC solution for oral administration. BOF-4269 was dissolved in 50% PEG 400 for intravenous administration. Racemic BOF-4272 was administered to rats intravenously at a dose of 5 mg kg^{-1}, and orally at a dose of 25 mg kg^{-1}. BOF-4269 was administered intravenously at a dose of 5 mg kg^{-1}.

The rats were decapitated and blood samples obtained. Blood samples were drawn into heparinized test tubes at 0 (predose), 0.083, 0.25, 0.5, 1, 2, 3, 4, 6 and 8 h after intravenous administration and at 0 (predose), 0.25, 0.5, 1, 2, 4, 6, 8, 12, 16 and 24 h after oral administration. All blood samples were immediately centrifuged to obtain the plasma. The livers and kidneys at 0 (predose), 0.25, 0.5, 1, 2, 4, 6, 8, 12, 16 and 24 h after oral administration were perfused with saline solution at 4 °C, resected and frozen on dry ice.

Tissue distribution

The tissue distribution of ^{14}C-labelled racemic BOF-4272 after intravenous administrations to rat was studied using whole-body autoradiography. At the designated time points (5, 15, 60 min) after the administration of ^{14}C-labelled racemic BOF-4272 (5 mg kg^{-1}, 0.74 MBq kg^{-1}), the animals were sacrificed by anaesthesia with diethyl ether and immersed in dry ice-acetone at −70 °C. The frozen animals, embedded in 5% CMC solution, were mounted on the stage of a cryomicrotome (LKB2250, PMV Co., Stockholm, Sweden) at −18 °C and sliced to obtain whole-body sections 40 μm in thickness. The thin sections were dried and placed at the bottom of a cassette. They were then placed in contact with an imaging plate (IP, Fuji Photo Co., Ltd, Tokyo, Japan). After exposure for 48 h in a light-proof lead-shielded box (Fujix Bas Shs 2040), the IPs were processed automatically using a BAS 2000 (all Fuji Photo Co., Ltd) at room temperature to obtain whole-body autoradiograms.

Isolation and monolayer culture of hepatocytes

Liver perfusion was performed as described by Moldeus *et al.* (1978). Briefly, the rat liver was perfused at 37 °C for 4 min with Ca^{2+}- and Mg^{2+}-free Hanks' solution (pH 7.4) containing 0.5 mM EGTA and for 6 min with Hanks' solution (pH 7.4) containing 0.1% collagenase and 0.05% trypsin inhibitor. Hepatocytes were liberated from the perfumed liver by blunt dissection and dispersed by gentle shaking in Ca^{2+}- and Mg^{2+}-free Hanks' solution (pH 7.4). After filtration through gauze, the hepatocytes were separated from non-parenchymal cells by centrifugation three times, with the cells washed and resuspended in Ca^{2+}- and Mg^{2+}-free Hanks' solution (pH 7.4) each time. Finally, the cells were resuspended in Williams' medium E (pH 7.4) containing 10% calf bovine serum, 1 nM insulin, and 10 nM dexamethasone. Cell suspensions with viability >90 as assessed by trypan blue exclusion were used for the experiments. The number of cells was counted using a Coulter counter. The cell suspensions were diluted to a final concentration of 10^6 viable cells ml^{-1}, and inocula of 4×10^6 viable cells ml^{-1} were introduced into 60-mm-diameter dishes that had been coated with collagen. The cells were cultured for 6 h after inoculation under 5% CO_2 and 95% air at 37 °C. The medium was then replaced with fresh medium, and the cells were used for experiments at 24 h after inoculation.

Experiments using monolayer cultures of hepatocytes

The medium was replaced with the same medium containing racemic BOF-4272, BOF-4269, or racemic M-4 at 2 μg ml^{-1}. The concentrations of each enantiomer of BOF-4272 or M-4 were determined at 24 h after the addition of substrate.

*Liver specimens and preparation of liver 9000*g *homogenate*

The liver of each rat was perfused with saline solution at 4 °C. Each liver sample was homogenized in ice-cold 0.01 M phosphate-buffered (pH 7.4) 1.15% potassium chloride solution (1:3 w/v), and the homogenate was centrifuged (9000*g*, 4 °C) for 20 min. The 9000*g* supernatant (S9) was used in the experiments. Proteins in the S9 fraction were quantified according to the technique of Lowry *et al.* (1951) using bovine serum albumin as a standard.

Incubation with S9

A typical incubation mixture, in a final volume of 1.2 ml, contained 0.2 ml S9, 2.4 μg (*S*)- or (*R*)-BOF-4272, 1.25 mM $NADP^+$, 2.5 mM glucose 6-phosphate, 0.75-U ml^{-1} glucose 6-phosphate dehy-

drogenase, and 6.25 mM $MgCl_2$ in 0.1 M potassium phosphate buffer (pH 7.4). The incubation mixtures in air at 37 °C were incubated for 0, 2, 5, 10, 15, 30, 60 and 120 min after the addition of (*S*)- or (*R*)-BOF-4272. The incubation mixtures were mixed with 2.4 ml acetonitrile to terminate the enzymatic reaction and then vortexed for 1 min. After centrifugation, 1.5 ml was used for analysis of both enantiomers of BOF-4272 and M-4, and 1 ml was used for analysis of BOF-4276.

After centrifugation, 1.5 ml of the acetonitrile mixture was mixed with ethyl acetate (3 ml) and shaken. After a second centrifugation, 2 ml of the ethyl acetate layer was transferred to another tube and dried under reduced pressure. The dried sample was dissolved in 200 µl of the mobile phase for analysis, shaken, and filtered through a membrane filter (pore size, 0.2 µm). A 50-µl aliquot of the filtrate was injected into the HPLC system for analysis of both enantiomers of BOF-4272 and M-4.

After centrifugation, 1 ml of the acetonitrile mixture was transferred to another tube, 2 ml 10 mM $NH_4H_2PO_4$ (pH 3.0) was added, and the mixture was shaken. The mixture was then filtered through a membrane filter (pore size, 0.2 µm) and a 500-µl aliquot of the filtrate was injected into the HPLC system for analysis of BOF-4276.

Preparation of HPLC samples from culture medium and plasma

Each sample (0.5 ml) was mixed with ethyl acetate (3 ml) and shaken. After centrifugation, 2 ml of the ethyl acetate layer was transferred to another tube and dried under reduced pressure. The dried sample was dissolved in 200 µl of the HPLC mobile phase for analysis, shaken and filtered through a membrane filter (pore size, 0.2 µm). A 50-µl aliquot of the filtrate was injected into the HPLC system for analysis of BOF-4272 and M-4.

Preparation of HPLC samples from liver and kidney

Each frozen liver sample (about 500 mg) was prepared by the successive addition of 5 vols of perchloric acid at 4 °C with shaking. After centrifugation, the supernatant was transferred to another tube, mixed with ethyl acetate (4 ml), and shaken again. After a second centrifugation, 1 ml of the ethyl acetate layer was transferred to another tube and dried under reduced pressure. The dried sample was dissolved in 200 µl of the HPLC mobile phase for analysis of BOF-4272, shaken and filtered through a membrane filter (pore size, 0.2 µm). A 50-µl aliquot of the filtrate was injected onto the HPLC system for analysis of BOF-4272.

Data analysis

The concentration at time 0 (C_0) for intravenous administration was estimated by the residual method. The maximum concentration (C_{max}) and the time to reach the maximum concentration (t_{max}) after oral administration were read directly from the mean concentration data. The elimination half-life ($t_{1/2}$) after intravenous or oral administration was calculated using the equation $t_{1/2} = \ln 2/K$, where K is the slope of the terminal portion of the natural logarithm of the concentration–time curve obtained by linear regression. The area under the concentration–time curve from time 0 to the measurement time point ($AUC_{0\text{-}t}$), and the mean residence time (MRT) after intravenous or oral administration were calculated according to the trapezoidal rule (Yamaoka *et al.* 1978). Total systemic clearance (CL) and volume of distribution at steady state (V_{dss}) were calculated according to the following equations:

$$CL = D/AUC$$

$$V_{dss} = D \cdot MRT/AUC,$$

where D is the administered dose. The bioavailability (F) was assessed by comparing AUC after oral and intravenous administration.

Result

The tissue distribution of radioactivity after the intravenous administration of ^{14}C-labelled racemic BOF-4272 to the male rat was examined using autoradiography. Whole-body autoradiograms at 5, 15 and 60 min after the single intravenous administration of ^{14}C-labelled racemic BOF-4272 to the fasted rat at a dose of 5 mg kg^{-1} (0.74 MBq kg^{-1}) are shown in figure 1. At all time points after administration, the highest level of radioactivity (except for the intestinal contents) was detected in the liver, followed by the kidney. At all time points after administration, no radioactivity was detected in the brain, and only low levels of radioactivity

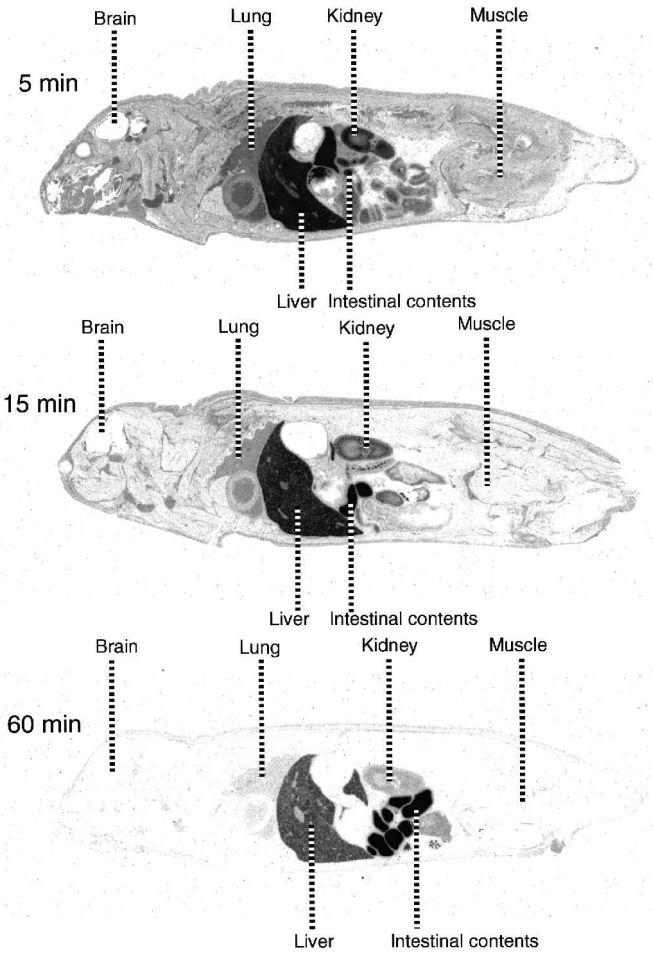


Figure 1. Whole-body autoradiograms on imaging plates after the single intravenous administration of ^{14}C-labelled racemic BOF-4272 to the fasted rat at a dose of 5 mg kg^{-1}.

were detected in other tissues. In the intestinal contents, the highest level of radioactivity was observed at 60 min.

Figure 2A shows the metabolic data after the addition of the (*S*)- or (*R*)-BOF-4272 substrate to liver S9 fractions from rat. The amounts of the parent compound depleted within 0.5 and 2 h after the addition of (*S*)-BOF-4272 were 264 and 499 ng mg^{-1} (48 and 91% of the total added dose), respectively. On the other hand, the amount of the parent compound depleted up to 0.5 h after the addition of (*R*)-BOF-4272 was 520 ng mg^{-1} (95% of the total added dose). The amount of (*S*)-M-4 increased, with (*S*)-M-4 reaching about 25% of the total added dose at 2 h after the addition of (*S*)-BOF-4272 (figure 2B). As shown in figure 2C, the BOF-4276 concentration increased up to 0.17 h, with BOF-4276 reaching about 6% of the total added dose at 0.17 h after the addition of (*S*)-BOF-4272, and decreased after 0.17 h, falling to about 3% at 2 h. On the other hand, (*R*)-M-4 and BOF-4276 concentrations increased up to 0.17 h, with (*R*)-M-4 (figure 2B) and BOF-4276 (figure 2C) reaching about 4 and 2% of the total added dose, respectively, at 0.17 h after the addition of (*R*)-BOF-4272, followed by a decrease after 0.17 h. (*R*)-M-4

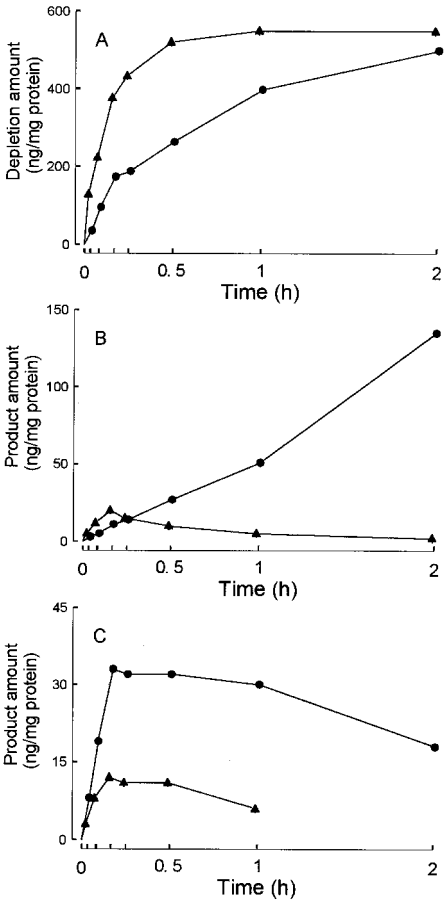


Figure 2. Metabolic data after the addition of the substrate (*S*)- or (*R*)-BOF-4272 to the liver S9 fraction obtained from rat. Experiments were performed in duplicate. Means are shown. The data are for one study in one rat, which are representative results for three separate studies in three rats. The amount of protein in the liver S9 fraction was 3.7 mg ml^{-1}. The concentration of (*S*)- or (*R*)-BOF-4272 at time 0 of incubation was 2 μg ml^{-1} (0.55 μg mg^{-1} protein). The closed circles (●) and triangles (▲) in (A) indicate the amounts of (*S*)- and (*R*)-BOF-4272 depleted, respectively. The closed circles (●) and triangles (▲) in (B) indicate the amount of (*S*)-M-4 produced after the addition of (*S*)-BOF-4272 and the amount of (*R*)-M-4 produced after the addition of (*R*)-BOF-4272, respectively. The closed circles (●) and triangles (▲) in (C) indicate the amounts of BOF-4276 produced after the addition of (*S*)- and (*R*)-BOF-4272, respectively.

was detected in small amounts and BOF-4276 was not detected at 2 h after the addition of (*R*)-BOF-4272. (*R*)-BOF-4272 and (*R*)-M-4 were not detected at any time point after the addition of (*S*)-BOF-4272, and (*S*)-BOF-4272 and (*S*)-M-4 were not detected at any time point after the addition of (*R*)-BOF-4272.

Table 1 shows the concentrations of both enantiomers of BOF-4272 and M-4 in the hepatocyte culture medium at 24 h after the addition of substrate (racemic BOF-4272, BOF-4269 or racemic M-4). The concentrations of (*S*)-BOF-4272 and (*S*)-M-4 in the culture medium were 1.7- and 4.3-fold higher than those of (*R*)-BOF-4272 and (*R*)-M-4, respectively, after the addition of racemic BOF-4272. The concentrations of (*S*)-BOF-4272 in the culture medium after the addition of BOF-4269 were 3.3-fold higher than those of (*R*)-BOF-4272, and (*S*)-M-4 was the only metabolite detected in the culture medium. The concentratoin of (*S*)-M-4

Table 1. Concentrations of both enantiomers of BOF-4272 and M-4 in hepatocyte culture medium at 24 h after the addition of substrate (2 μg ml^{-1}).

Substrate	(*S*)-BOF-4272 (ng ml^{-1})	(*R*)-BOF-4272 (ng ml^{-1})	(*S*)-M-4 (ng ml^{-1})	(*R*)-M-4 (ng ml^{-1})
Racemic BOF-4272 ($n = 2$)	129	75	275	65
BOF-4269 ($n = 2$)	40	12	53	n.d.
Racemic M-4 ($n = 2$)	n.d.	n.d.	715	687

Experiments were performed in duplicate. Means are shown.
n.d., Not detected.

was almost the same as that of (*R*)-M-4 and neither of the BOF-4272 enantiomers were detected in the culture medium after the addition of racemic M-4.

Figure 3 shows the plasma concentration profiles of (*S*)- and (*R*)-BOF-4272 after the intravenous administration of racemic BOF-4272 (5 mg kg^{-1}) to the fasted rat. Plasma concentrations at all time points after administration were significantly higher for (*S*)- than for (*R*)-BOF-4272. Figure 4 shows the plasma, liver and kidney concentration profiles of (*S*)- and (*R*)-BOF-4272 after the oral administrations of racemic BOF-4272 (25 mg kg^{-1}) to the fed rat. Plasma and kidney concentrations at all time points were significantly higher for (*S*)- than for (*R*)-BOF-4272 (figure 4A and C). On the other hand, liver concentrations at all time points were significantly higher for (*R*)- than for (*S*)-BOF-4272 (figure 4B). (*S*)- and (*R*)-BOF-4272 were not detected in plasma at 16 and 24 h after oral administration to rat. (*S*)- and (*R*)-BOF-4272 were not detected in the kidney at 24 h and from 16 to 24 h after oral administration to rat, respectively.

Table 2 shows the pharmacokinetic parameters for (*S*)- and (*R*)-BOF-4272 in plasma after the single intravenous administration of racemic BOF-4272 to rats at a dose of 5 mg kg^{-1}. The $t_{1/2}(\beta)$ for (*S*)- and (*R*)-BOF-4272 were 4.9 and 2.3 h, respectively. The $AUC_{0\text{-}t}$ for (*S*)- and (*R*)-BOF-4272 were 3866 and 1612 ng h ml^{-1}, respectively. Table 3 shows the pharmacokinetic parameters for (*S*)- and (*R*)-BOF-4272 in plasma, liver and kidney after the single oral administration of racemic BOF-4272 to rat at a dose of 25 mg kg^{-1}. The $AUC_{0\text{-}t}$ for (*S*)- and (*R*)-BOF-4272 in plasma were 626 and 180 ng h ml^{-1}, respectively The $AUC_{0\text{-}t}$ for (*S*)- and (*R*)-BOF-4272 in the liver were 4065 and 9633 ng h ml^{-1}, respectively. The $AUC_{0\text{-}t}$ for (*S*)- and (*R*)-BOF-4272 in the kidney were 1892 and 830 ng h ml^{-1}, respectively. The bioavailability (*F*) for (*S*)- and (*R*)-BOF-4272 were 3.2 and 2.2%, respectively.

Figure 5 shows the plasma concentration profiles of (*S*)- and (*R*)-BOF-4272 after the intravenous administration of BOF-4269 (5 mg kg^{-1}) to the fasted rat. Plasma concentrations at all time points were significantly higher for (*S*)- than for (*R*)-BOF-4272. (*S*)- and (*R*)-BOF-4272 were not detected in plasma from 6 h and from 4 to 8 h after the administration of BOF-4269 to rat, respectively. Table 4 shows the pharmacokinetic parameters for (*S*)- and (*R*)-BOF-4272 in plasma after the single intravenous administration of BOF-4269 to rat at a dose of 5 mg kg^{-1}. The $AUC_{0\text{-}t}$ for (*S*)- and (*R*)-BOF-4272 were 487 and 38 ng h ml^{-1}, respectively.

Discussion

The study has clarified the reasons for the stereoselectivity of the plasma concentrations of BOF-4272 after intravenous and oral administration to rat. The

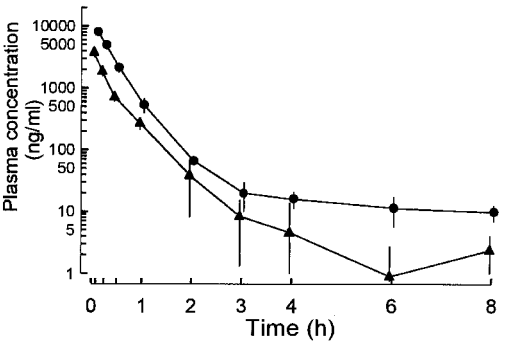


Figure 3. Time-courses of plasma concentrations of (*S*)- (●) and (*R*)-BOF-4272 (▲) after the single intravenous administration of racemic BOF-4272 to the fasted rat at a dose of 5 mg kg^{-1}. Each point represents the mean ± SD of four rats.

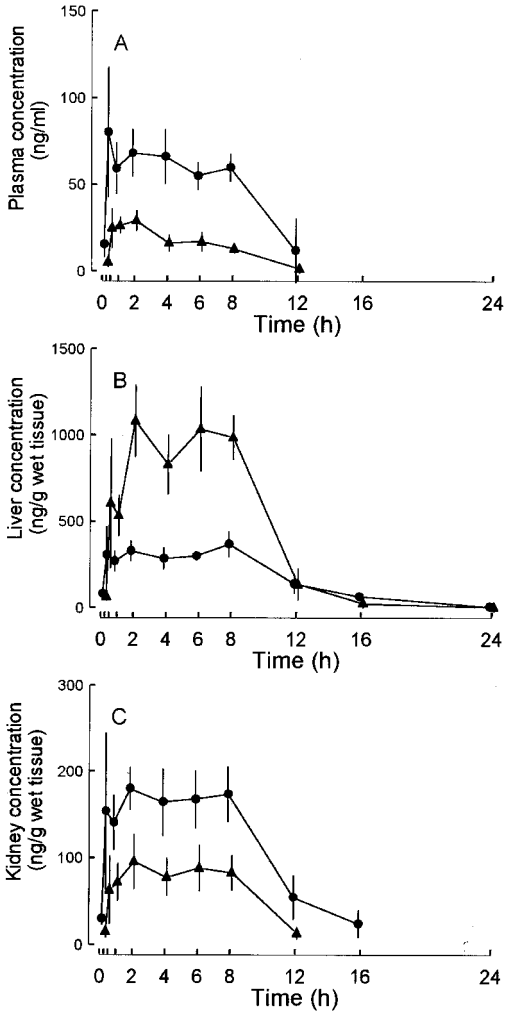


Figure 4. Time-courses of plasma, liver and kidney concentrations of (*S*)- (●) and (*R*)-BOF-4272 (▲) after the single oral administration of racemic BOF-4272 to the fed rat at a dose of 25 mg kg^{-1}. Each point in A, B and C represents the mean ± SD of six rats.

Table 2. Pharmacokinetic parameters for (*S*)- and (*R*)-BOF-4272 in plasma after the single intravenous administration of racemic BOF-4272 to rat (5 mg kg^{-1}).

		(*S*)-BOF-4272	(*R*)-BOF-4272	(*S*)/(*R*) ratio
C_0	(ng ml^{-1})	10 810	5166	2.1
$t_{1/2}$ (β)	(h)	4.9	2.3	2.1
$AUC_{0\text{-}t}$	(ng h ml^{-1})	3866	1612	2.4
MRT	(h)	0.68	0.43	1.6
V_{dss}	(ng kg^{-1})	440	667	0.66
CL	(ml h kg^{-1})	647	1551	0.42

C_0, plasma concentration at time 0; $t_{1/2}$ (β), elimination half-life of the terminal elimination phase; $AUC_{0\text{-}t}$; area under the plasma concentration–time curve from time 0 to the last measurement point; MRT, mean residence time; V_{dss}, volume of distribution; CL, clearance = dose/$AUC_{0\text{-}t}$. Data are calculated from the means obtained from four rats.

Table 3. Pharmacokinetic parameters for (*S*)- and (*R*)-BOF-4272 in plasma, liver and kidney after the single oral adminstration of racemic BOF-4272 to rat (25 mg kg^{-1}).

		(*S*)-BOF-4272	(*R*)-BOF-4272	(*S*)/(*R*) ratio
Plasma				
C_{max}	(ng ml^{-1})	80	29	2.8
t_{max}	(h)	0.5	2	–
$t_{1/2}$	(h)	2.5	1.5	1.7
$AUC_{0\text{-}t}$	(ng h ml^{-1})	626	180	3.5
MRT	(h)	5.82	4.50	1.3
F	(%)	3.2	2.2	1.5
Liver				
C_{max}	(ng ml^{-1})	369	1081	0.34
t_{max}	(h)	8	2	–
$t_{1/2}$	(h)	2.6	1.9	1.4
$AUC_{0\text{-}t}$	(ng h ml^{-1})	4065	9633	0.42
Kidney				
C_{max}	(ng ml^{-1})	180	96	1.9
t_{max}	(h)	2	2	–
$t_{1/2}$	(h)	2.8	2.0	1.4
$AUC_{0\text{-}t}$	(ng h ml^{-1})	1892	830	2.3

C_{max}, maximum concentration; t_{max}, time to maximum concentration; $t_{1/2}$, elimination half-life; $AUC_{0\text{-}t}$, area under the concentration–time curve from time 0 to the last measurement point; MRT, mean residence time; *F*, bioavailability based on $AUC_{0\text{-}t}$. Data are calculated from the means obtained from six rats.

results showed that the plasma concentration of (*S*)-BOF-4272 was significantly higher than that of (*R*)-BOF-4272 after the intravenous or oral administration of racemic BOF-4272 to rat. Generally, stereoselectivity in pharmacokinetics is known to result from stereospecificity in one or more of the processes of drug absorption, distribution, metabolism and excretion. After the intravenous administration of racemic ^{14}C-labelled BOF-4272 to rat, its tissue distribution was examined by autoradiography. At all time points after administration, the highest level of radioactivity was observed in the liver, followed by the kidney, and little radioactivity was detected in other tissues. High levels of radioactivity were detected in the intestinal contents. These results suggest that the stereoselectivity observed in the pharmacokinetics of BOF-4272 may be due to differences in the distribution, metabolism and/or excretion of the two enantiomers of BOF-4272 in the liver and kidney. We therefore investigated the disposition of the enantiomers in the liver and kidney in rat.

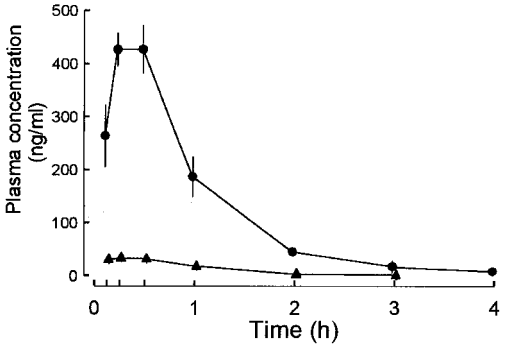


Figure 5. Time-courses of plasma concentrations of (*S*)- (●) and (*R*)-BOF-4272 (▲) metabolized from BOF-4269 in the liver after the single intravenous administration of BOF-4269 to the fasted rat at a dose of 5 mg kg^{-1}. Each point represents mean ± SD of four rats.

Table 4. Pharmacokinetic parameters for the metabolites (*S*)- and (*R*)-BOF-4272 in plasma after the single intravenous administration of BOF-4269 to rat (5 mg kg^{-1}).

		(*S*)-BOF-4272	(*R*)-BOF-4272	(*S*)/(*R*) ratio
C_{max}	(ng ml^{-1})	427	33	12.9
t_{max}	(h)	0.5	0.25	–
$t_{1/2}$	(h)	0.81	0.48	1.7
AUC_{0-t}	(ng h ml^{-1})	487	38	12.8

C_{max}, maxima plasma concentration; t_{max}, time to maximum plasma concentration; $t_{1/2}$, elimination half-life; AUC_{0-t}, area under the plasma concentration–time curve from time 0 to the last measurement point. Data are calculated from the means obtained from four rats.

In the *in vitro* experiments, deletion of the parent compound after the addition of (*S*)-BOF-4272 to the liver S9 fraction was greater than that after the addition of (*R*)-BOF-4272. However, the liver concentrations at all time points after the oral administration of racemic BOF-4272 *in vivo* were significantly higher for (*R*)- than for (*S*)-BOF-4272. In the *in vitro* experiments using hepatocytes, the concentration of (*S*)-BOF-4272 in the culture medium at 24 h after the addition of racemic BOF-4272 was higher than that of (*R*)-BOF-4272. Furthermore, the hepatic extraction ratio of (*R*)-BOF-4272 has been reported to be significantly higher than that of (*S*)-BOF-4272 in rat (Nishimura *et al.* 1997).

On the other hand, the kidney concentrations of (*S*)-BOF-4272 were significantly higher than those of (*R*)-BOF-4272. The stereoselectivity of the renal uptake of BOF-4272 enantiomers has little effect on the stereoselectivity of BOF-4272 in the systemic circulation in rat. This may be related to the cumulative urinary excretion of racemic BOF-4272 after intravenous and oral administration to rat that has been reported to be lower than about 5 and 2%, respectively (Naito and Nishimura 1999).

BOF-4272 is metabolized by the intestinal flora to BOF-4269 and absorbed from the intestinal tract. BOF-4269 was the main metabolite in plasma and faeces after the oral administration of BOF-4272 (Naito and Nishimiura 1999). In our previous studies using the loop method in the rat gastrointestinal tract, it was concluded that BOF-4269 is absorbed from the intestine, and particularly the colon, much more readily than BOF-4272 (Terao *et al.* 1995, Naito *et al.* 1999b).

Plasma concentrations at all time points after the intravenous administration in BOF-4269 were significantly higher for (*S*)- than for (*R*)-BOF-4272 and the $AUC_{0\text{-}t}$ of (*S*)-BOF-4272 after the intravenous administration of BOF-4269 was 12.8-fold higher than that of (*R*)-BOF-4272. The (*S*)-BOF-4272 concentration in the culture medium at 24 h after the addition of BOF-4269 was higher than that of (*R*)-BOF-4272. The bioavailability (*F*) of (*S*)-BOF-4272 was 1.5-fold higher than that of (*R*)-BOF-4272. However, *F* for both BOF-4272 enantiomers was $< 4\%$. We therefore conclude that the difference in *F* for the two enantiomers of BOF-4272 may be, to a small degree, due to the stereoselective absorption of BOF-4272 from the rat gastrointestinal tract and, to a large degree, to the stereoselective biotransformation of BOF-4269 to BOF-4272 in the rat liver.

These findings suggest that the reason that the plasma concentrations observed at all time points after the intravenous and oral administration of racemic BOF-4272 were significantly higher for (*S*)- than for (*R*)-BOF-4272 is related to differences in the hepatic uptake of the two enantiomers. In addition, these findings suggest that the stereoselective biotransformation of BOF-4269 to BOF-4272 in the rat liver is also a factor.

The results of the present study leads us to propose the metabolic pathways for both BOF-4272 enantiomers in the rat (figure 6). The chiral conversion of either BOF-4272 enantiomer was not observed in the rat liver. (*S*)-M-4 increased, with (*S*)-M-4 reaching about 25% of the total added dose at 2 h after the addition of (*S*)-BOF-4272 to the liver S9 fraction. On the other hand, (*R*)-M-4 increased up to 0.17 h, with (*R*)-M-4 reaching about 4% of the total added dose at 0.17 h after the addition of (*R*)-BOF-4272 to the liver S9 fraction. Subsequently, (*R*)-M-4 decreased after 0.17 h, with only small amounts of (*R*)-M-4 detected at 2 h after the addition of (*R*)-BOF-4272 to the liver S9 fraction. These findings suggest that the biotransformation from BOF-4272 to unknown metabolites, possibly conjugates via M-4, is stereoselective. They also suggest that the biotranformation from (*S*)-M-4 to unknown metabolites is slower than the biotransformation from (*R*)-M-4 to unknown metabolites. Sulfoxides are metabolized to their sulfones by rat liver cytochrome P450 (Benoit *et al*. 1994). BOF-4272 may be metabolized to BOF-4276 by cytochrome P450 in the rat liver (Naito and Nishimura 1999). BOF-4276 increased up to 0.17 h after the addition of both (*S*)- and (*R*)-BOF-4272 to the liver S9 fraction, and decreased after 0.17 h. However, in the S9 fraction at all time points, the concentration of BOF-4276 after the addition of (*S*)-BOF-4272 was higher than that after the addition of (*R*)-BOF-4272. Therefore, the biotransformation of both BOF-4272 enantiomers to BOF-4276 by cytochrome P450 in the rat liver may be stereoselective.

Sulfides are oxidized to their sulfoxides by flavin-containing mono-oxidase (Buronfasse *et al*. 1995, Rettie *et al*. 1995) and cytochrome P450 (Benoit *et al*. 1994, Buronfosse *et al*. 1995). BOF-4269, which is metabolized by the intestinal flora and absorbed from the intestinal tract, may be metabolized to BOF-4272 by these enzymes in the rat liver (Naito and Nishimura 1999). Plasma concentrations at all time points after the intravenous administration of BOF-4269 to rat were significantly higher for (*S*)- than for (*R*)-BOF-4272. In the *in vitro* experiments using hepatocytes, the concentration of (*S*)-BOF-4272 in the culture medium at 24 h after the addition of BOF-4269 was higher than that of (*R*)-BOF-4272. This finding indicates that the hepatic biotransformation of BOF-4269 to BOF-4272 may be stereoselective, and that the differences in its biotransformation may be

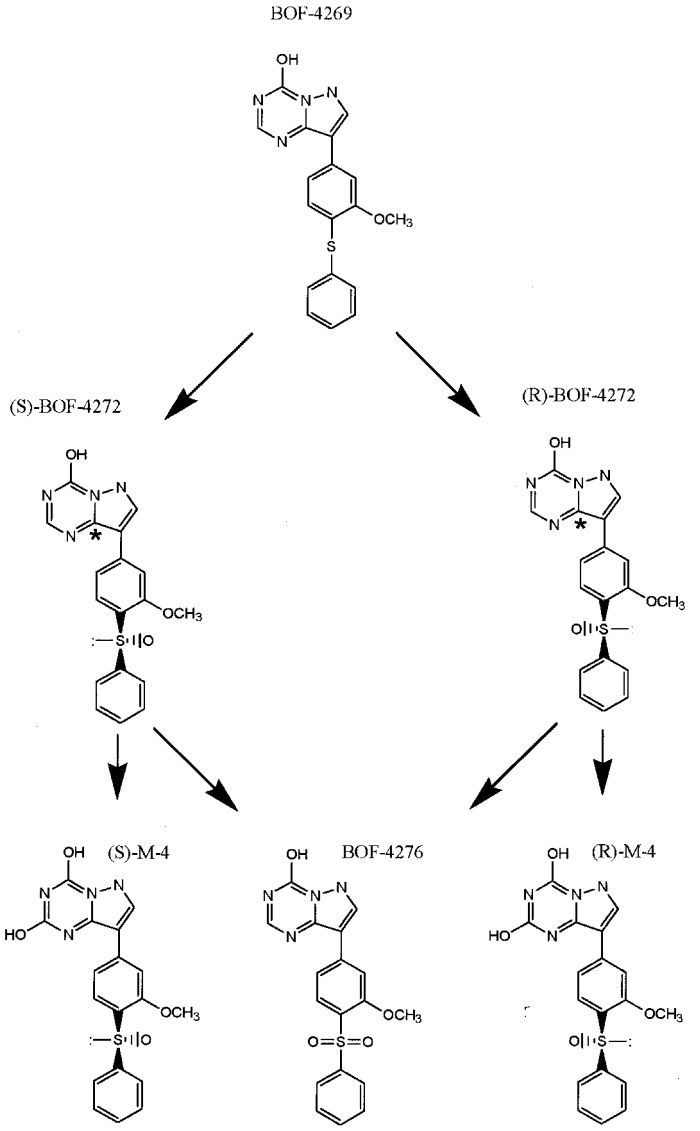


Figure 6. Chemical structures of BOF-4272 and its metabolites. *Position of ^{14}C.

due to differences in the stereospecificity of flavin-containing mono-oxidase and/or cytochrome P450.

In conclusion, the results of the present study indicate that the stereoselectivity of plasma concentrations after the intravenous and oral administration of racemic BOF-4272 is due to differences in the hepatic uptake of the two enantiomers of BOF-4272, and may also be due to the stereoselective biotransformation of BOF-4269 to BOF-4272 in the rat liver. The results also indicate that, in the rat liver, the biotransformation of BOF-4272 to unknown metabolites via M-4, the biotransformation of BOF-4272 to BOF-4276, and the biotransformation of BOF-4269 to BOF-4272 are stereoselective.

References

Benoit, E., Buronfosse, T. and Delatour, P., 1994, Effect of cytochrome P-450 1A induction on enantioselective metabolism and pharmacokinetics of an aryltrifluoromethyl sulfide in the rat. *Chirality*, **6**, 372–377.

Buronfosse, T., Moroni, P., Benoit, E. and Riviere, J. L., 1995, Stereoselective sulfoxidation of the pesticide methiocarb by flavin-containing monooxygenase and cytochrome P450-dependent monooxygenases of rat liver microsomes: anticholinesterase activity of the two sulfoxide enantiomers. *Journal of Biochemical Toxicology*, **10**, 179–189.

Iwahara, R., Emoto, S., Kaga, J., Imura, Y., Aoki, M. and Asakawa, K., 1994, Chemical structure, physico-chemical properties and stability of sodium (±)-8-(3-methoxy-4-phenylsulfinylphenyl)pyrazolo[1,5-*a*]-1,3,5-triazine-4-olate monohydrate (BOF-4272). *Iyakuhin Kenkyu*, **25**, 426–438. [In Japanese]

Lowry, O. H., Rosebrough, N. J., Farr, A. L. and Randall, R. J., 1951, Protein measurement with the Folin phenol reagent. *Journal of Biological Chemistry*, **193**, 265–275.

Matsugi, M., Hashimoto, K., Inai, M., Fukuda, N., Furuta, T., Minamikawa, J. and Otsuka, S., 1995, Asymmetric synthesis of a xanthine dehydrogenase inhibitor (*S*)-(−)-BOF-4272: utility of chiral alkoxysulfonium salts. *Tetrahedron: Asymmetry*, **6**, 2991–3000.

Moldeus, P., Hogberg, J. and Orrenius, S., 1978, Isolation and use of liver cells. *Methods in Enzymology*, **52**, 60–71.

Naito, S. and Nishimura, M., 1999, Pharmacokinetics and proposed metabolic pathways of BOF-4272, a sulphoxide-containing drug, based on *in-vivo* and *in-vitro* studies in rats. *Pharmacy and Pharmacology Communications*, **5**, 123–131.

Naito, S., Nishimura, M. and Nogawa, H., 1999a, Pharmacokinetics of BOF-4272, a xanthine oxidase inhibitor, after single intravenous or oral administration to male mice and rats. *Journal of Pharmacy and Pharmacology*, **51**, 347–351.

Naito, S., Nishimura, M., Yoshitsugu, H. and Nogawa, H., 1999b, Metabolic pathways and pharmacokinetics of BOF-4272, a sulfoxide-containing drug, in the dog: *in vivo* and *in vitro* studies. *Biological and Pharmaceutical Bulletin*, **22**, 1391–1395.

Nishimura, M., Yamaoka, K., Naito, S. and Nakagawa, T., 1996, Hepatic local disposition of a drug with high protein binding and high hepatic clearance using BOF-4272 as a model drug. *Biological and Pharmaceutical Bulletin*, **19**, 1197–1202.

Nishimura, M., Yamaoka, K., Naito, S. and Nakagawa, T., 1997, Influence of albumin on enantioselective local disposition of BOF-4272, a xanthine oxidase inhibitor with chiral sulfoxide, in rat liver. *Biological and Pharmaceutical Bulletin*, **20**, 1285–1289.

Nishimura, M., Yamaoka, K., Yasui, H., Naito, S. and Nakagawa, T., 1994, Local disposition of new xanthine oxidase/xanthine dehydrogenase inhibitor, BOF-4272, in rat liver. *Biological and Pharmaceutical Bulletin*, **17**, 1301–1304.

Nishimura, M., Yamaoka, K., Yasui, H., Naito, S. and Nakagawa, T., 1995, Effect of temperature in perfusate on local hepatic disposition of BOF-4272, a new xanthine oxidase inhibitor. *Biological and Pharmaceutical Bulletin*, **18**, 980–983.

Okamoto, K. and Nishino, T., 1995, Mechanism of inhibition of xanthine oxidase with a new tight binding inhibitor. *Journal of Biological Chemistry*, **270**, 7816–7821.

Rettie, A. E., Meier, G. P. and Sadeque, A. J., 1995, Prochiral sulfides as in vitro probes for multiple forms of the flavin-containing monooxygenase. *Chemico-Biological Interactions*, **96**, 3–15.

Sato, D., Tatsumi, K. and Nishino, T., 1991, A novel xanthine dehydrogenase inhibitor, BOF-4272. *Advances in Experimental Medicine and Biology*, **309A**, 135–138.

Suzuki, H., Suematsu, M., Ishii, H., Kato, S., Miki, H., Mori, M., Ishimiura, Y., Nishino, T. and Tsuchiya, M., 1994, Prostaglandin E_1 abrogates early reductive stress and zone-specific paradoxical oxidative injury in hypoperfused rat liver. *Journal of Clinical Investigation*, **93**, 155–164.

Terao, T., Matsubara, T., Kaga, J., Kobatake, H. and Naito, S., 1995, Improvement of gastrointestinal absorption of a new oral xanthine oxidase/dehydrogenase inhibitor, sodium (±)-8-(3-methoxy-4-phenylsulfinylphenyl)-pyrazolo[1,5-*a*]-1,3,5-triazine-4-olate monohydrate, in rats and dogs. *Yakuzaigaku*, **55**, 36–43. [In Japanese]

Uematsu, T. and Nakashima, M., 1994, Pharmacokinetic and pharmacodynamic properties of a novel xanthine oxidase inhibitor, BOF-4272, in health volunteers. *Journal of Pharmacology and Experimental Therapeutics*, **270**, 453–459.

Yamamoto, T., Moriwaki, Y., Suda, M., Nasako, Y., Takahashi, S., Hiroishi, K., Nakano, T., Hada, T. and Higashino, K., 1993, Effect of BOF-4272 on the oxidation of allopurinol and pyrazinamide *in vivo*. Is xanthine dehydrogenase or aldehyde oxidase more important in oxidizing both allopurinol and pyrazinamide? *Biochemical Pharmacology*, **46**, 2277–2284.

Yamaoka, K., Nakagawa, T. and Uno, T., 1978, Statistical moments in pharmacokinetics. *Journal of Pharmacokinetics and Biopharmaceutics*, **6**, 547–558.

XENOBIOTICA, 2002, VOL. 32, NO. 6, 505–520

Taylor & Francis
healthsciences

Cytochrome P450 expression in human hepatocytes and hepatoma cell lines: molecular mechanisms that determine lower expression in cultured cells

C. RODRÍGUEZ-ANTONA†, M. T. DONATO‡, A. BOOBIS§, R. J. EDWARDS§, P. S. WATTS§, J. VICENTE CASTELL†‡ and M.-J. GÓMEZ-LECHÓN‡*

† Departamento de Bioquímica y Biología Molecular, Facultad de Medicina, Avenida Blasco Ibáñez, 20, E-46010, Spain
‡ Unidad de Hepatología Experimental, Centro de Investigación, Hospital Universitario La Fe, Avenida Campanar 21, E-46009 Valencia, Spain
§ Section on Clinical Pharmacology, Division of Medicine, Imperial College School of Medicine, Ducane Road, London W12 0NN, UK

Received 17 September 2001

1. Cultured hepatic cells have reduced cytochrome P450 (CYP) activities in comparison with human liver, but the mechanism(s) that underlies this circumstance is not clear. We investigated the causes of this low CYP activity by analysing the activity, protein, mRNA and heterologous nuclear RNA contents of the most important CYPs involved in drug metabolism (1A1, 1A2, 2A6, 2B6, 2C9, 2C19, 2D6, 2E1, 3A4, 3A5) in cultured human hepatocytes, and in HepG2 and Mz-Hep-1 hepatoma cell lines.

2. After 24 h of culture, hepatocytes retained most of their CYP activities and protein contents, but the mRNA decreased 20-fold. However, the mRNA content of most CYPs in 24-h hepatocytes was still 400-fold higher than in hepatoma cells. When we examined the transcriptional activity of the CYP genes, this decreased during culture time in hepatocytes and it was poor in hepatoma cell lines.

3. We investigated the abundance of key hepatic transcription factors that govern CYP transcription (C/EBP-β: LAP and LIP, HNF-3α, HNF-4α, RXR-α) and observed that the expression of some factors was altered in the hepatoma cells.

4. In conclusion, the loss of biotransformation activity in cultured hepatic cells is caused by a decrease in CYP transcription, which correlates with an alteration in the expression of key transcription factors.

Introduction

Liver biotransformation mediates many of the biological effects, both toxic and therapeutic, of toxic compounds and clinical drugs (Meyer 1996). Among the drug-metabolizing enzymes in human liver, CYPs are the most important (Murray and Burke 1995, Paine 1995, Wrighton *et al.* 1996) and they catalyse the oxidation of many endogenous and exogenous compounds and provide the main route for xenobiotic biotransformation. Therefore, understanding the regulation of these genes and their encoded enzymes has a major clinical significance.

Presently, human hepatocytes in culture and hepatoma cell lines are the most frequently used *in vitro* systems to investigate drug metabolism and toxicity.

* Author for correspondence; e-mail: gomez_mjo@gva.es

Xenobiotica ISSN 0049–8254 print/ISSN 1366–5928 online © 2002 Taylor & Francis Ltd
http://www.tandf.co.uk/journals
DOI: 10.1080/00498250210128675

Human cultured hepatocytes contain the entire hepatic drug-metabolizing enzyme system in an integrated form and they provide an *in vitro* model that has been successfully used to investigate drug effects on specific liver functions and hepatic drug metabolism (Maurel 1996, Gómez-Lechón *et al.* 1997, Guillouzo 1998). However, cultured hepatocyte drug detoxification capacity decreases during culture. Hepatoma cell lines have an unlimited life-span, a more stable phenotype than primary cultures and are always available, but they have a low CYP expression (Castell *et al.* 1998, Guillouzo 1998). HepG2 cells (Aden *et al.* 1979) are commonly used and Mz-Hep-1 cells (Dippold *et al.* 1985) are also human hepatoma cells. However, expression of the different CYPs has not been studied in Mz-Hep-1 cells and in HepG2 cells it has not been thoroughly characterized to date (Roe *et al.* 1993, Nakama *et al.* 1995, Sumida *et al.* 2000).

The mechanism that leads to decreased CYP activities in human cultured hepatic cells (both in primary cultures and in continuous cell lines) is still largely unknown. An inactivation of CYP enzymes, a decreased stability of the apoprotein, a decreased mRNA production or mRNA stability, etc., could all lead to the observed loss. The phenotypic instability of CYPs in primary cultures has been studied in rat, where an early decrease in CYP mRNA contents precedes the decline in activities (Padgham *et al.* 1992, Woodcroft and Novak 1998). In human hepatocytes in culture, protein and activity contents decrease gradually, although slower, than in rat hepatocytes (Guillouzo and Guguen-Guillouzo 1992). Up to now, CYP expression in cultured human hepatocytes has not been analysed at activity, protein and mRNA level in the same cell preparation. Hepatocyte isolation procedures and culture conditions greatly affect CYP expression, making it impossible to use data from different studies to investigate at which level CYP expression is altered. Furthermore, time-dependent expression of CYP mRNAs in human hepatocytes in culture has been poorly characterized and the results obtained are contradictory (Morel *et al.* 1990, George *et al.* 1997). To shed light on the regulatory mechanism that accounts for the decreased expression of the most important drug-metabolizing CYPs (1A1, 1A2, 2A6, 2B6, 2C9, 2C19, 2D6, 2E1, 3A4, 3A5) we analysed the activity, protein, mRNA and heterologous nuclear RNA (*hn*RNA) contents in human cultured hepatocytes and in HepG2 and Mz-Hep-1 cell lines.

Liver-specific gene expression in adult hepatocytes relies on four families of transcription factors that are liver-enriched [enhancer-binding protein (C/EBP), hepatocyte nuclear factor (HNF)-1, HNF-3 and HNF-4] (Cereghini 1996) and, although the mechanisms of liver-specific expression of the CYP genes are diverse, these liver enriched transcription factors (LETFs) govern the transcription of CYPs (Gonzalez and Lee 1996). The content of these LETFs has been related to CYP expression during primary culture (Padgham *et al.* 1993, Gómez-Lechón *et al.* 1998). Therefore, we analysed the cellular contents of some key transcription factors, namely C/EBP-β, HNF-3α and -4α, and retinoid X receptor (RXR)-α in hepatocytes and cell lines.

The results of the present study show that the low expression of CYPs in human cultured cells is caused by a decrease in CYP gene transcription and that an alteration in the expression of LETFs could be involved in this process.

Materials and methods

Chemicals and reagents

7-Ethoxyresorufin, 7-benzoxyresorufin and collagenase were from Roche (Mannheim, Germany). 7-Methoxyresorufin was from Molecular Probes Europe BV (Leiden, The Netherlands). Diclofenac sodium, coumarin, 7-ethoxycoumarin, 7-hydroxycoumarin, *p*-nitrophenol, 4-nitrocatechol, resorufin, testosterone, 16α- and 11β-hydroxy-testosterone (OHT) androstenedione, phenobarbital (PB), rifampicin (Rif) and 3-methylcholanthrene (MC) were from Sigma (St Louis, MO, USA). The 6β- and 16β-hydroxy derivatives of testosterone were supplied by Steraloids, Inc. (Wilton, NH, USA). 2β-Hydroxy-testosterone was from the Steroid Reference Collection (London, UK). 15β-Hydroxy-testosterone (G. D. Searle and Co., Skokie, IL, USA) was kindly supplied by Dr B. Blaauboer (Utrecht, The Netherlands). Plastic culture plates were obtained from Nunc (Roskilde, Denmark). All other reagents used were of analytical grade. Ham F-12, Leibovitz L-15 media, foetal calf serum and all RNA/DNA-modifying enzymes were from Lifetechnologies (Barcelona, Spain), who also custom-synthesized the oligo d(T)14 primer and all the oligonucleotide primers used. Ribogreen and picogreen were from Molecular Probes, and the Rneasy Total RNA Kit was from Quiagen (Basel, Switzerland). The High Pure PCR Product Purification Kit was from Roche.

Cell culture

Surgical liver biopsies were obtained in conformity with the rules of the Hospital's Ethics Committee and after informed consent from patients undergoing programmed cholecystectomy. Patients had no known liver pathology, were not habitual consumers of alcohol and other drugs, and did not receive any medication during the weeks before surgery. Human hepatocytes were isolated using a two-step perfusion technique (Gómez-Lechón *et al.* 1990) and seeded on fibronectin-coated plates (3.6 $\mu g\,cm^{-2}$) at a density of 8×10^4 cells cm^{-2} in an appropriate volume of the medium. The culture medium was Ham F-12/Leibovitz L-15 (1:1 v/v), supplemented with 2% newborn calf serum, 5 mM glucose, 50 U ml^{-1} penicillin, 50 $\mu g\,ml^{-1}$ streptomycin, 0.2% bovine serum albumin and 10^{-8} M insulin. The medium was changed 1 h later to remove unattached hepatocytes. By 24 h, the cultures were shifted to serum-free medium and 10^{-8} M dexamethasone was added. Thereafter, the medium was renewed daily. HepG2 and Mz-Hep-1 cells were plated in Ham's F-12/Leibovitz L-15 (1:1 v/v) supplemented with 7% newborn calf serum, 50 U ml^{-1} penicillin and 50 $\mu g\,ml^{-1}$ streptomycin. HeLa cells were grown in DMEM supplemented with 10% newborn calf serum, 50 U ml^{-1} penicillin and 50 $\mu g\,ml^{-1}$ streptomycin. For subculturing, cells were harvested after trypsin/EDTA (0.05%/0.02%) treatment at 37 °C. Cells were used at the 75% monolayer confluency.

Treatment of cultures

Human hepatocytes and cell lines were exposed to inducers 24 h after plating. PB was prepared as an aqueous solution and added directly to cultures at a final concentration of 1 mM. MC and Rif were dissolved in DMSO and added to the culture medium to give a final concentration of 2 and 50 μM, respectively. The DMSO concentration in culture medium never exceeded 0.1% (v/v). Control cultures were treated with the same concentration of the respective solvent.

Isolation, quantification and purification of total RNA from cell cultures

Total RNA was extracted from 6-cm diameter culture plates of human hepatocytes and HepG2 and Mz-Hep-1 cell lines using 'Rneasy Total RNA Kit'. The amount of purified RNA was estimated by ribogreen fluorescence and its purity by the absorbance ratio at 260/280 nm. RNA was incubated for 15 min at 23 °C with DNase I (1 unit μg^{-1}) according to the recommendations of the supplier, followed by thermal inactivation of the enzyme (65 °C for 10 min) in the presence of 2.5 mM EDTA and rapid cooling to 4 °C.

Measurement of mRNAs by RT-PCR

The reverse transcription (RT) reaction mixture consisted of 1 μg total RNA, which was reverse-transcribed in 20 μl 1× reverse transcriptase buffer, 10 mM DTT, 500 μM dNTPs, 3 μM oligo d(T)14 primer, 60 U RNase OUT and 250 U RTase H. The reaction was allowed to proceed for 60 min at 42 °C, followed by 5 min of heating at 95 °C and then rapid cooling on ice. The cDNA was stored at −20°C until use. The conditions used for the quantitative polymerase chain reaction (PCR), the specific primers and the strategy of quantification were previously described (Rodríguez-Antona *et al.* 2000).

Intron-specific RT-PCR assay

A total of 1 μg total RNA was reverse-transcribed as described before but using an intron-specific RT primer corresponding to the intron 2 of the human *CYP3A4* gene, 5′-CCT TCT TTC TGG CGC GCT CAC A-3′, together with the oligo d(T) 14 primer. PCR analysis of the CYP3A4 *hn*RNA used an

upstream primer located on the intron 1 of *CYP3A4*, 5′-ATC TCA TCA TCA CTG CGG AAG A-3′ and a downstream primer located on the intron 2 of *CYP3A4*, 5′-AGA GCC CTT GGG TAA ACA TTG C-3′. The CYP3A4 *hn*RNA fragment, which is 686 bp long, was amplified using the same PCR conditions described before (Rodríguez-Antona *et al.* 2000).

Measurement of drug-metabolizing protein

Human hepatocytes that had been cultured on 6-cm diameter fibronectin-coated plates were solubilized in approximately 1 ml 20 mm potassium phosphate buffer, pH 7.4, containing 0.15 M sodium chloride, 0.1 mM EDTA, 0.02% (v/v) Nonidet P-40, 1% (w/v) sodium cholate and 20% (v/v) glycerol. Insoluble material was removed by centrifugation (100 000*g* for 30 min at 4 °C) and the protein content of the supernatant was determined as described (Lowry *et al.* 1951). Samples were subjected to immunoblotting as described using antipeptide antibodies which specifically recognized CYP2C forms (CYP2C8, CYP2C9, CYP2C19), CYP2E1, CYP3A4 (Edwards *et al.* 1998).

The relative intensity of immunoreactive bands was determined by laser densitometry using an LKB UltroScan XL Enhanced Laser Densitometer (Amersham Pharmacia Biotech, Little Chalfont, UK) and analysed using FigP 6.0a software (Biosoft, Cambridge, UK).

Measurement of transcription factor protein

The immunoblotting analysis of transcription factors was performed as described (Jover *et al.* 1998). In brief, protein extracts were obtained from cells in suspension, electrophoresed in a SDS-polyacrylamide gel (20 g protein/lane). Proteins were transferred to Immobilon-P membranes (Millipore) and sheets were incubated with the first polyclonal antibody (Santa Cruz Biotechnology, Santa Cruz, CA, USA). After washing, blots were developed with horseradish peroxidase-labelled IgG, using an Enhanced Chemiluminence Kit (Amersham Pharmacia Biotech).

Measurement of drug-metabolizing activities

CYP activities were measured by incubating intact cell monolayers with specific substrates, namely 8 μM 7-ethoxyresorufin, 10 μM 7-methoxyresorufin, 15 μM 7-benzoxyresorufin, 50 μM coumarin, 800 μM 7-ethoxycoumarin, 200 μM dextormethorphan, 500 μM *p*-nitrophenol, 300 μM diclofenac or 250 μM testosterone (Gomez-Lechon *et al.* 2001). Reactions were stopped by aspirating the incubation medium from plates and medium samples were then incubated with β-glucuronidase/arylsulfatase for 2 h at 37 °C (Donato *et al.* 1993). Resorufin formed during 7-ethoxyresorufin *O*-deethylation, 7-methoxyresorufin *O*-demethylation (EROD and MROD, CYP1A1/2 and CYP1A2, respectively) and 7-benzoxyresorufin *O*-debenzylation (BROD, CYP2B6) assays and 7-hydroxycoumarin formed in the coumarin 7-hydroxylase (CH, CYP2A6) and 7-ethoxycoumarin *O*-deethylase (ECOD, various CYPs) assays were quantified fluorimetrically as described (Edwards *et al.* 1984, Donato *et al.* 1993). The 4-nitrocatechol formed during the *p*-nitrophenol hydroxylase (PNH, CYP2E1) assay was determined spectrophotometrically as described (Dicker *et al.* 1990). The products of diclofenac 4′-hydroxylation (4′OH-DIC, CYP2C9) and dextromethorphan *O*-demethylation (DXOD, CYP2D6) were measured by HPLC analysis (Kronbach *et al.* 1987, Bort *et al.* 1996). Hydroxylated metabolites formed from testosterone were extracted and analysed by HPLC as described (Donato *et al.* 1995).

Statistical analysis

Statistical analysis was by Student's *t*-test.

Results

CYP expression during primary culture of human hepatocytes

Hepatocytes were isolated from four different human liver biopsies and cultured as described in the Materials and methods. After different culture times, we determined CYP expression by measuring the mRNA contents and the specific catalytic activities of CYP1A1, 1A2, 2A6, 2B6, 2C9, 2D6, 2E1 and 3A4 and the apoprotein levels of CYP2C9, 2E1 and 3A4. The reason for quantifying the protein only in three CYPs was that the amount of material required for this analysis is large and with the material available only the most abundant CYPs could be assayed.

Protein and activity levels generally declined in parallel (figure 1). Whereas all of the CYPs declined with time, the rate of decline was not the same. For some

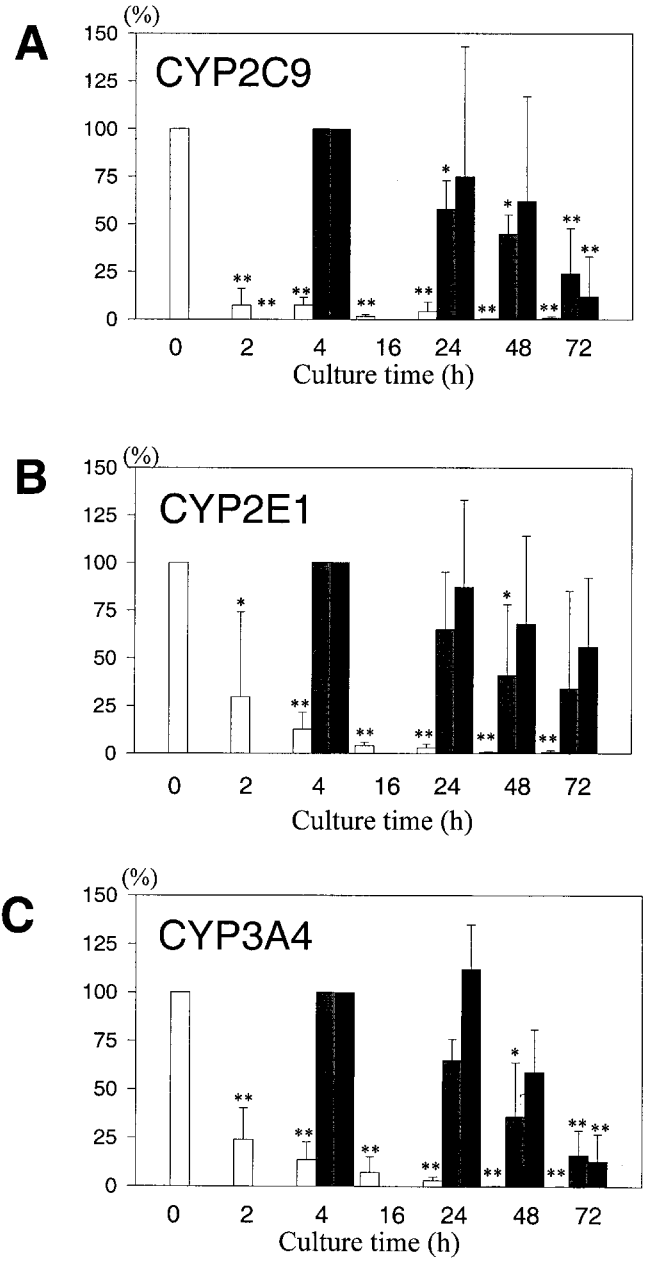


Figure 1. Stability of cytochrome P450s in culture: CYP2C9, 2E1 and 3A4 specific activities, mRNA and protein content in human cultured hepatocytes. mRNA content (assayed by RT-PCR) was measured in a small piece of liver and at 2, 4, 16, 24, 48 and 72 h of culture. Protein content (measured by immunoblot using specific antibodies) and metabolic activities (assayed using specific substrates) were measured at 4, 16, 24, 48 and 72 h of culture. mRNA is expressed as the per cent of that in the liver and protein contents and activities are expressed as the per cent of that at 4 h of culture. Open bars correspond to mRNA contents; grey bars correspond to activity; black bars correspond to protein content. (A) CYP2C9 mRNA, CYP2C9 protein and 4′-OH-Dic activity. (B) CYP2E1 mRNA, CYP2E1 protein and PNP activity. (C) CYP3A4 mRNA, CYP3A4 protein and 6β-OHT. Data are the mean ± SD of four different human primary cultures. *$p < 0.05$ and **$p < 0.01$ with respect to liver for mRNA or from 4-h hepatocytes for protein and activity.

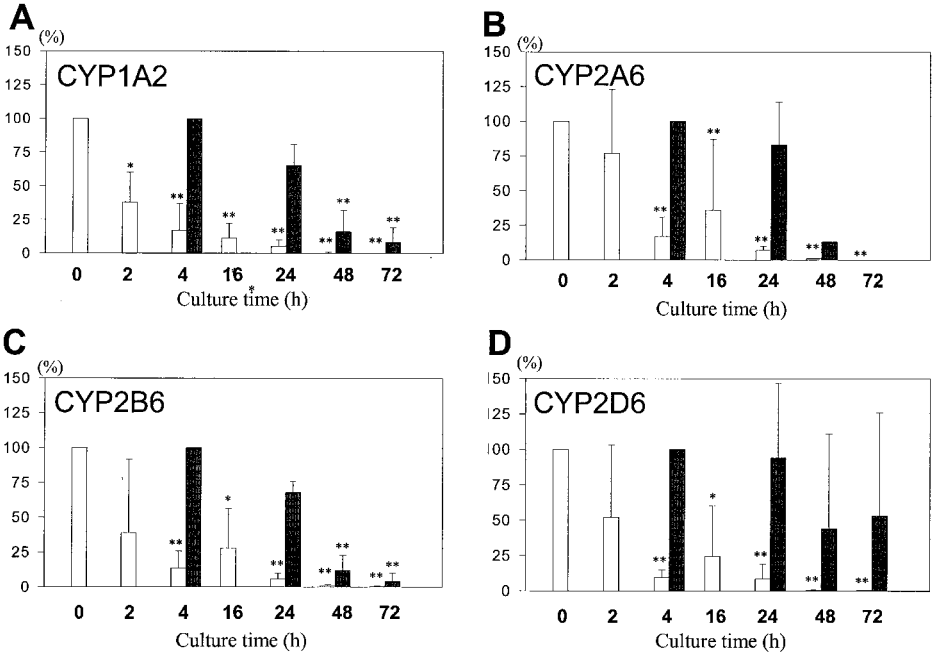


Figure 2. Stability of cytochrome P450s in culture: CYP1A2, 2A6, 2B6 and 2D6 specific activities and mRNA were quantified in human cultured hepatocytes. mRNA content (assayed by RT-PCR) was measured in a small piece of liver and at 2, 4, 16, 24, 48 and 72 h of culture. Metabolic activities (assayed using specific substrates) were measured at 4, 16, 24, 48 and 72 h of culture. mRNA is expressed as the per cent of that in liver and activities expressed as the per cent of that at 4 h of culture. Open bars correspond to mRNA contents; grey bars correspond to activity. (A) CYP1A2 mRNA and MROD activity; (B) CYP2A6 mRNA and CH activity; (C) CYP2B6 mRNA and BROD; and (D) CYP2D6 mRNA and DXOD. Data are the mean ± SD of four different human primary cultures. $*p < 0.05$ and $**p < 0.01$ with respect to liver for mRNA or from 4-h hepatocytes for activity.

enzymes, after 48 h of culture, residual protein and/or activity levels were 40% of those at 4 h (i.e. CYP2C9, CYP2D6, CYP2E1, CYP3A4), whereas for other isoforms residual levels at this time were 20% of those at 4 h (i.e. CYP1A2, CYP2A6, CYP2B6).

Protein and activity levels were expressed relative to those at 4 h of culture and hence it is not appropriate to compare the absolute percentage changes in protein level or CYP activity with those in mRNA expression. However, it is possible to compare the rates of decline and it becomes apparent that, for all of the CYPs, the decline in mRNA levels after 4 h was much more rapid than in either protein or activity levels. The CYP mRNA contents declined rapidly during the first few hours after hepatocyte isolation and after 4 h of culture the mRNA contents of all of the CYPs studied were < 15% of those in fresh liver. After 24 h of culture mean mRNA content was 5.2% of that in liver and all enzymes had mRNA levels lower than 10%. The mRNA content continued to decrease during culture and at 72 h of culture, mean CYP mRNA content was < 0.5% of that in liver (figures 1 and 2).

CYP expression in cell lines compared with hepatocytes

The activities and mRNA contents of the major drug-metabolizing CYPs were determined in human cultured hepatocytes and HepG2 and Mz-Hep-1 cell lines 24 h after seeding. CYP activities were examined using specific substrates and CYP mRNA contents were quantitatively determined by RT-PCR. In general, HepG2 cells showed higher CYP expression than Mz-Hep-1 cells, but these values were significantly lower than those of human hepatocytes (tables 1 and 2). EROD activity (CYP1A1) was the highest with 20 and 9% of that in 24 h cultured hepatocytes (HepG2 and Mz-Hep-1, respectively). CYP1A1 mRNA was 7 and 1% of that in 24 h cultured hepatocytes (HepG2 and Mz-Hep-1, respectively). BROD (CYP2B6) and MROD (CYP1A2) activities presented also quite high levels and CYP3A5 and CYP2B6 mRNA contents in HepG2 were among the highest (1 and 0.2% of that in 24 h cultured hepatocytes, respectively). CH (CYP2A6), PNP (CYP2E1) and 6β-OHT (CYP3A4) activities were $< 1.0\%$ of that in 24 h cultured hepatocytes and mRNA contents of CYP1A2, 2A6, 2B6, 2C9, 2C19, 2D6, 2E1 and 3A4 were $< 0.25\%$.

Testosterone metabolism profiles by primary hepatocytes and cell lines

CYP functionality was assessed by measuring the profile of testosterone metabolism. Testosterone is metabolized in a regioselective manner by different CYPs and can be used as a multi-enzymatic substrate to investigate the activities of multiple enzymes simultaneously (Komori *et al.* 1988, Waxman *et al.* 1991). The major metabolites produced by hepatocytes cultured for 4 h were 6β-OHT (CYP3A4) and androstenedione, followed by 2β- and 15β-OHT (CYP3A4-5), whereas 16α- and 16β-OHT were less abundant. The profile of metabolites released by hepatocytes cultured for longer periods was similar to that observed after 4 h of culture. The HepG2 and Mz-Hep-1 testosterone metabolic profiles were also determined and only formation of 6β- and 16α-OHT metabolites was observed (figure 3).

CYP inducibility in primary hepatocyte culture and cell lines

A relevant pharmaco-toxicological issue is CYP induction by drugs, which can have important clinical consequences by influencing their therapeutic efficacy (Li *et al.* 1996, Li 1997). CYP inducibility in HepG2 and Mz-Hep-1 cells was compared with that of cultured hepatocytes by measuring mRNA content and activity. The inducers were added to 24-h cultured cells and were incubated for 48 h as described in the Materials and methods. Non-treated cells were used as controls. MC induction was assessed by measuring MROD activity and CYP1A2 mRNA content, PB induction was determined by BROD activity and by CYP2B6 mRNA content and Rif induction was assessed by measuring 6β-OHT activity and CYP3A4 mRNA content.

The results are summarized in table 3 and show that in all three cell systems MC induced MROD activity (mean 10.7-fold induction) and CYP1A2 mRNA (mean 10.3-fold). Whereas PB induction of BROD activity and CYP2B6 mRNA was not significant. Rif induced 6β-OHT activity in hepatocytes and HepG2 cells and CYP3A4 mRNA levels were increased in hepatocytes (15.3-fold) and Mz-Hep-1 cells (2.6-fold).

Table 1. Cytochrome P450 activity in 24-h cultured human hepatocytes, HepG2 and Mz-Hep-1.

CYP activity	ECOD (CYPs)	EROD (CYP1A1/2)	MROD (CYP1A2)	CH (CYP2A6)	BROD (CYP2B6)	PNP (CYP2E1)	TEST (CYP3A4)
Hepatocytes ($n = 6$)	24.2 ± 11.3	4.5 ± 2.0	5.04 ± 1.87	121 ± 70	2.46 ± 1.95	104 ± 57	253 ± 110
HepG2 ($n = 5$)	0.5 ± 0.2**	0.9 ± 0.5**	0.35 ± 0.34**	0.05 ± 0.04**	0.28 ± 0.26*	< 1	0.18 ± 0.16**
Mz-Hep-1 ($n = 3$)	< 0.1	0.4 ± 0.3**	< 0.1	< 0.01	< 0.1	< 1	0.15 ± 0.33**

Activities are given as pmol production mg^{-1} protein min^{-1}. Data are the mean $\pm$ SD.
*$p < 0.05$ and **$p < 0.01$ with respect to hepatocytes.

Table 2. Cytochrome P450 mRNA content in 24-h cultured human hepatocytes, HepG2 and Mz-Hep-1 cells.

CYP	1A1	1A2	2A6	2B6	2C9	2C19	2D6	2E1	3A4	3A5
Hepatocytes ($n = 6$)	10.2 ± 18.1	162 ± 210	4.07 ± 7.18	22.4 ± 15.7	288 ± 428	21.7 ± 22.8	263 ± 409	479 ± 303	327 ± 255	30.1 ± 30.3
HepG2 ($n = 3$)	0.68 ± 0.08	0.04 ± 0.02	< 0.01	0.04 ± 0.05*	< 0.01	< 0.01	0.03 ± 0.01	0.06 ± 0.05*	0.10 ± 0.04	0.35 ± 0.18
Mz-Hep-1 ($n = 3$)	0.14 ± 0.03	0.05 ± 0.03	< 0.01	0.02 ± 0.01*	< 0.01	< 0.01	0.03 ± 0.01	0.03 ± 0.2*	0.01 ± 0.01	< 0.01

Data are mRNA CYP molecules/10^3 molecule β-actin. Data are mean $\pm$ SD.
*$p < 0.05$ with respect to hepatocytes

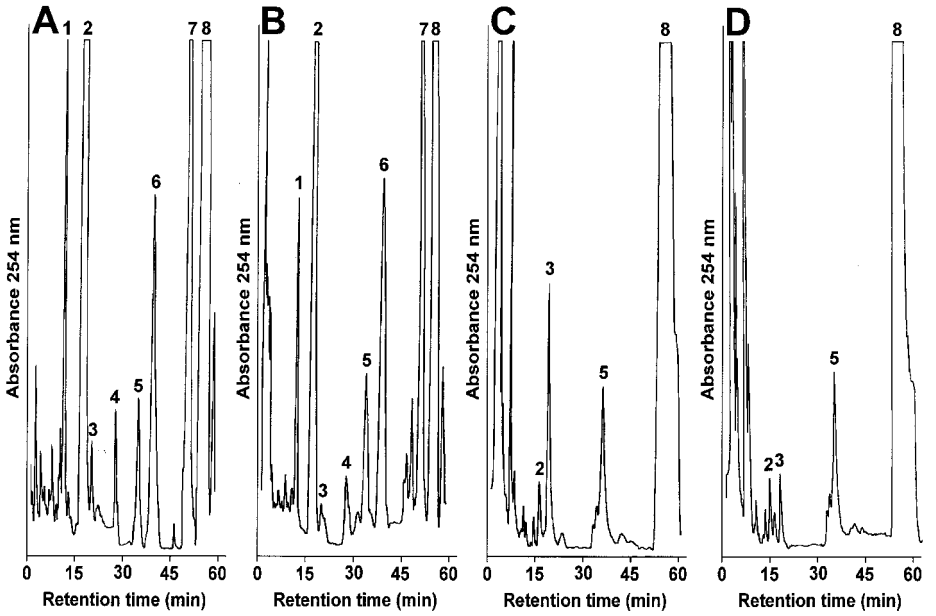


Figure 3. Metabolite profile of testosterone by human hepatocytes and HepG2 and Mz-Hep-1 cells. (A) Human hepatocytes after 4 h of culture; (B) human hepatocytes after 72 h of culture; (C) HepG2 cells after 24 h of culture; (D) Mz-Hep-1 cells after 24 h of culture. Cells were incubated for 1 h with 250 μM testosterone and the hydroxylated metabolites formed were extracted and analysed by HPLC. Peaks 1, 15β-OHT; 2, 6β-OHT; 3, 16α-OHT; 4, 16β-OHT; 5, 11β-OHT (internal standard); 6, 2β-OHT; 7, androstenedione; 8, testosterone.

Table 3. Cytochrome P450 activity and mRNA induction by MC, PB and Rif in cultured human hepatocytes, HepG2 and Mz-Hep-1 cells.[a]

Inducer	MC		PB		Rif	
Induction[b]	MROD	CYP1A2 mRNA	BROD	CYP2B6 mRNA	6β-OHT	CYP3A4 mRNA
Hepatocytes ($n = 3$)	12.7 ± 6.0*	11.1 ± 9.9	1.5 ± 0.6	6.1 ± 3.8	2.5 ± 0.8*	15.3 ± 8.3*
HepG2 ($n = 3$)	14.2 ± 8.2*	11.6 ± 5.6*	3.5 ± 2.2	1.6 ± 0.3	4.2 ± 1.9*	1.3 ± 0.5
Mz-Hep-1 (n = 3)	5.2 ± 2.7*	8.1 ± 1.9**	nd	1.3 ± 0.5	1.4 ± 0.8	2.6 ± 0.9*

[a] After 24 h of culture, cells were exposed to 2 μM MC, 1 mM PB or 50 μM Rif for 48 h, and specific activities and mRNA contents were evaluated as described in the Materials and methods.
[b] Results are expressed as fold induction over control cells.
* $p < 0.05$ with respect to control.
** $p < 0.01$ with respect to control.

CYP3A4 hnRNA expression in human hepatocytes and cell lines

The decreased CYP mRNA contents that we observed in the cultured hepatic cells could be caused by decreased CYP transcription, an altered RNA processing, or a mRNA instability. The determination of CYP *hn*RNA expression constitutes a reliable method for the measurement of the gene transcriptional activity (Elferink and Reiners 1996, Backlund *et al.* 1997). The expression of the CYP3A4 gene at the transcriptional level was determined by RT-PCR-based determination of CYP3A4 *hn*RNA using a 686-bp fragment corresponding to exon 2 and parts of the flanking intron sequences of the CYP3A4 gene as a target. CYP3A4 mRNA

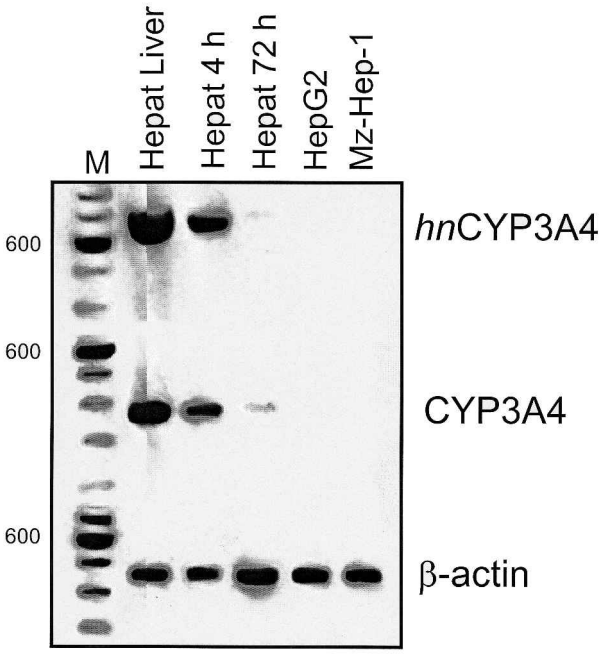


Figure 4. CYP3A4 *hn*RNA levels in cultured hepatic cells. Total RNA was extracted from a piece of human liver (Hepat Liver), 4 and 72 h human cultured hepatocytes (Hepat 4 and 72 h), HepG2, and Mz-Hep-1 cells. A total of 1 μg total RNA was reverse-transcribed using both oligo(dT) and an intron-specific CYP3A4 RT primer and amplified by PCR using different specific primers for CYP3A4 *hn*RNA, CYP3A4 mRNA and β-actin mRNA. The PCR products were analysed on a 1.5% agarose/TBE gel and visualized with UV light using ethidium bromide staining. M, 100-bp DNA ladder.

was quantified by RT-PCR using primers specific for cDNA. In the same RT preparations CYP3A4 *hn*RNA and CYP3A4 mRNA were quantified and β-actin mRNA was used as an internal standard. The assay of *hn*RNA expression revealed that CYP3A4 *hn*RNA decreased in hepatocytes with culture time in a similar way as CYP3A4 mRNA and that the levels in hepatoma cell lines were far lower than those in liver (figure 4).

Expression of transcription factors in human hepatocytes, HepG2, Mz-Hep-1 and HeLa cells

The expression of several LETFs and nuclear receptors involved in CYP transcription was analysed by Western blot analysis in a fresh suspension of human hepatocytes, HepG2 and Mz-Hep-1 (hepatic cell lines) and HeLa (non-hepatic cell line). As a quality test of the samples used we studied the expression of the nuclear receptor STAT-3α which should be similar in all the cells tested (Runge *et al.* 1999). As shown in figure 5, STAT-3α levels were similar in the different cells. HNF-4α exhibited the highest levels in HepG2, followed by hepatocytes and HeLa cells, but was not detected in Mz-Hep-1 cells and the expression of nuclear receptor RXR-α was the same in the different cells. The *C/EBP-β* gene produces different isoforms by alternative initiation of translation, the full-length isoform

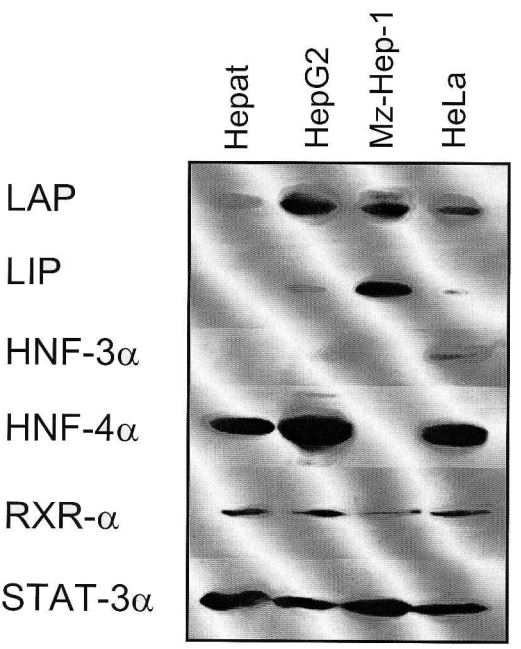


Figure 5. Western-blot of transcription factors and nuclear receptors in human hepatocytes and cell lines. Total extracts of protein were obtained from a fresh suspension of human hepatocytes, HepG2, MzHep-1 or HeLa cells and 20 g were elecrophoresed and transferred to a membrane. LAP, LIP, HNF-3α, HNF-4α, RXR-α and STAT-3α protein contents in the different samples were detected using specific antibodies.

liver-enriched transcriptional activator protein (LAP) and the truncated isoform liver-enriched transcriptional inhibitory protein (LIP), which lacks most of the transactivation domain. As shown in figure 5, LAP was detected in all the cells tested and was highest in HepG2 cells. LIP (the inhibitory isoform of C/EBP-β) expression was not detected in hepatocytes and the highest levels were detected in Mz-Hep-1 cells. HNF-3α was only detected in the non-hepatic cell line HeLa, and in similar experiments HNF-1α was not detected in any of the cell lines used.

Discussion

The expression of many hepatic specific proteins (including CYPs), decline during the primary culture of hepatocytes and the cells dedifferentiate becoming more similar to hepatic cell lines. The decrease in CYP activities could be caused by enzymatic inhibition (CYP protein and mRNA contents would remain unchanged), by a decrease in protein stability (mRNA contents should be unaltered) or by a decrease in mRNA synthesis or stability (mRNA and protein levels should be diminished). The study of mRNA, protein and activity will provide information about the regulatory mechanism(s) that is altered resulting in decreased CYP expression.

In the study, CYP protein contents and activities of all CYPs examined declined in parallel, thus indicating that intact apoprotein in hepatocytes remains in the form of holoenzyme during culture. Similar results have been described with cultured cells (Wu *et al.* 1990) and with cultured human liver slices (Renwick

et al. 2000). In contrast to CYP protein content and activity, the mRNA declined substantially, reaching very low levels after 24 h of culture. These results differ from those of George *et al*. (1997) in which the protein content of CYP1A2, 2C9 and 3A4 decreased, whereas mRNA contents increased. Our results resemble those reported for cultured rat hepatocytes (Padgham *et al*. 1993, Wang *et al*. 1997, Woodcroft and Novak 1998) and support the conclusion that a decreased CYP mRNA content is responsible for the decline of human CYP activities during culture.

When we compared CYP mRNA contents and activities of cultured hepatocytes with those of HepG2 and Mz-Hep-1 cells, we found substantially reduced levels in the hepatoma cells (tables 1 and 2). The data showed again that a decrease in the CYP mRNA content is responsible for the low enzymatic activities in hepatoma cells, clearly indicating that human hepatocytes are a much better *in vitro* system for drug-metabolism studies than cell lines.

To investigate if the low mRNA contents were consequence of a decreased transcription of the *CYP* genes rather than a post-transcriptional mechanism (processing of the RNA in the nucleus and mRNA stability) we measured the levels of CYP3A4 *hn*RNA. The results obtained were similar to those of CYP3A4 mRNA (figure 4), indicating that transcription of the *CYP* genes is the cause of the decreased mRNA levels.

Two different mechanisms could account for the decreased transcription rate: (1) a decreased expression of activatory transcription factors needed for *CYPs* transcription or (2) an increase in the expression of inhibitory factors. The LETFs are responsible for the hepatic specific transcription of CYPs in liver (i.e. HepG2 cells stably transfected with C/EBPα have increased CYPs levels (Jover *et al*. 1998), a decrease in the expression of key LETFs appears to cause the down-regulation of CYP expression during hepatocyte culture (Padgham *et al*. 1993, Gómez-Lechón *et al*. 1998, Jover *et al*. 1998). Interestingly, in our study the highest CYP mRNA levels in hepatoma cells corresponded to CYP1A1 and 3A5 (table 2), which are not liver specific (Guengerich 1995, Haehner *et al*. 1996). Our hypothesis was that the decreased transcription of *CYPs* in cultured hepatic cells could be caused by changes in the expression of LETFs implicated in CYP regulation. Therefore, we carried out a detailed examination of activatory (HNF-4α, RXR-αLAP) and inhibitory (LIP and HNF-3α) transcription factors.

According to the stimulatory effect of HNF-4α on expression of HNF-1 (Kuo *et al*. 1992) and some CYPs (Jover *et al*. 2001) as well as many other hepatic genes (Späth and Weiss *et al*. 1997), the absence of HNF-4α in Mz-Hep-1 cells correlates with its lower CYP expression. However, the presence of the largest amounts of HNF-4α in HepG2 cells would suggest that HNF-4α alone does not determine CYP expression. CYP induction by PB and Rif requires heterodimerization of the nuclear receptors constitutive androstane receptor (CAR) and pregnane X receptor (PXR) with RXR (Savas *et al*. 1999, Waxman *et al*. 1999). The similar RXR-α contents found in hepatocytes and hepatoma cells, suggest that the lack of response of hepatoma cell lines to PB and Rif treatments (table 3) is not due to differences in this protein. C/EBP-β has been related to the expression of CYPs (Lee *et al*. 1997, Gómez-Lechón *et al*. 2001) and can be transcribed from the same gene as a full-length isoform (LAP) and a truncated isoform (LIP). The LIP isoform lacks the transactivatory domain and antagonizes the transactivation of C/EBP-α and LAP (Descombes and Schibler 1991, Ossipow *et al*. 1993). In our

study LAP expression, though similar in the different cells, was largest in HepG2 cells, which does not correlate with CYP expression. However, the inhibitory factor LIP was highest in Mz-Hep-1 cells, followed by HepG2 and HeLa cells and no expression in freshly isolated hepatocytes. As a moderate increase in the LAP/LIP ratio can result in a significantly higher transcriptional activation of an appropriate target gene (Descombes and Schibler 1991), the LAP/LIP ratio found in hepatocytes and hepatoma cells correlates with their differentiation state and CYP expression. HNF-3 plays an important role in the expression of liver-specific genes and different *CYP2Cs* genes (Legraverend *et al*. 1994, Shaw *et al*. 1994, Vallet *et al*. 1995, Delesque-Touchard *et al*. 2000). In our study, the only cells with a detectable expression of HNF-3α were HeLa cells. It has been reported that HNF-3α acts as a negative regulator with antagonistic transcriptional regulatory functions with HNF-3β (Duncan *et al*. 1998), which is in accordance with the HeLa non-hepatic phenotype.

In summary, as a step towards further understanding the mechanisms leading to low CYP activity in the cultured hepatic cells, our results provide evidence that: (1) human hepatocytes constitute a useful liver model for drug biotransformation and CYP regulation studies whereas HepG2 and Mz-Hep-1 are not; (2) the low drug-metabolizing capacity of human cultured hepatic cells is the consequence of a decrease in CYP gene transcription; and (3) the expression of key inhibitory and activatory LETFs is altered in the hepatoma cell lines and could be linked to decreased CYP expression and functionality of these cells.

Acknowledgements

The work was supported by the EU, BIOTECH Contract BIO4-CT96-0052 and BIOMED Contract BMH4-CT86-0254 (Eurocyp). C. R.-A. was the recipient of a fellowship from the Generalitat Valenciana. The authors acknowledge the expert technical assistance of E. Belenchón, C. Corchero and M. C. Lorenzo.

References

Aden, D. P., Fogel, A., Plotkin, S., Damjanov, I. and Knowles, B. B., 1979, Controlled synthesis of HBsAg in a differentiated human liver carcinoma-derived cell line. *Nature*, **282**, 615–616.

Backlund, M., Johansson, I., Mkrtchian, S. and Ingelman-Sundberg, M., 1997, Signal transduction-mediated activation of the aryl hydrocarbon receptor in rat hepatoma H4IIE cells. *Journal of Biological Chemistry*, **272**, 31755–31763.

Bort, R., Ponsoda, X., Carrasco, E., Gómez-Lechón, M. J. and Castell, J. V., 1996, Metabolism of aceclofenac in humans. *Drug Metabolism and Disposition*, **24**, 834–841.

Castell, J. V., Jover, R., Bort, R. and Gómez-Lechón, M. J., 1998, The challenge of using hepatic cell using cell lines for drug metabolism studies. In *Proceedings of COST B1 European Symposium on the Prediction of Drug Metabolism in Man: Progress and Problems* (Luxembourg: European Commission) pp. 77–92.

Cereghini, S., 1996, Liver-enriched transcription factors and hepatocyte differentiation. *FASEB Journal*, **10**, 267–282.

Delesque-Touchard, N., Park, S. H. and Waxman, D. J., 2000, Synergistic action of hepatocyte nuclear factors 3 and 6 on CYP2C12 gene expression and suppression by growth hormone-activated STAT5b. Proposed model for female specific expression of CYP2C12 in adult rat liver. *Journal of Biological Chemistry*, **275**, 34173–34182.

Descombes, P. and Schibler, U., 1991, A liver-enriched transcriptional activator protein, LAP, and a transcriptional inhibitory protein, LIP, are translated from the same mRNA. *Cell*, **67**, 569–579.

Dicker, E., McHugh, T. and Cederbaum, A. I., 1990, Increased oxidation of *p*-nitrophenol and aniline by intact hepatocytes isolated from pyrazole-treated rats. *Biochimica et Biophysica Acta*, **1035**, 249–256.

Dippold, W. G., Dienes, H. P., Knuth, A., Sachsse, W., Prellwitz, W., Bitter Suermann, D. and Meyer Zum Buschenfelde, K. H., 1985, Hepatocellular carcinoma after thorotrast exposure: establishment of a new cell line (Mz-Hep-1). *Hepatology*, **5**, 1112–1119.

Donato, M. T., Castell, J. V. and Gómez-Lechón, M. J., 1995, Effect of model inducers on cytochrome P450 activities of human hepatocytes in primary cultures. *Drug Metabolism and Disposition*, **25**, 553–558.

Donato, M. T., Gómez-Lechón, M. J. and Castell, J. V., 1993, A microassay for measuring cytochrome P450IA1 and P450IIB1 activities in intact human and rat hepatocytes cultured on 96-well plates. *Analytical Biochemistry*, **213**, 29–33.

Duncan, S. A., Navas, M. A., Dufort, D., Rossant, J. and Stoel, M., 1998, Regulation of a transcription factor network required for differentiation and metabolism. *Science*, **281**, 692–695.

Edwards, A. M., Glistak, M. L., Lucas, C. M. and Wilson, P. A., 1984, Ethoxycoumarin deethylase activity as a convenient measure of liver drug metabolizing enzymes: regulation in cultured rat hepatocytes. *Biochemical Pharmacology*, **33**, 1537–1546.

Edwards, R. J., Adams, D. A., Watts, P. S., Davies, D. S. and Boobis, A. R., 1998, Development of a comprehensive panel of antibodies against the major xenobiotic metabolising forms of cytochrome P450 in human. *Biochemical Pharmacology*, **56**, 377–387.

Elferink, C. J. and Reiners, J. J. J, 1996, Quantitative RT-PCR on CYP1A1 heterogeneous nuclear RNA: a surrogate for the *in vitro* transcription run-on assay. *Biotechniques*, **20**, 470–477.

George, J., Goodwin, B., Liddle, C., Tapner, M. and Farrell, G. C., 1997, Time-dependent expression of cytochrome P450 genes in primary cultures of well-differentiated human hepatocytes. *Journal of Laboratory and Clinical Medicine*, **129**, 638–648.

Gómez-Lechón, M., Jover, R., Donato, M. T., Ponsoda, X., Rodriguez, C., Stenzel, K. G., Klocke, R., Paul, D., Guillén, I., Bort, R. and Castell, J. V., 1998, Long-term expression of differentiated functions in hepatocytes cultured in three-dimensional collagen matrix. *Journal of Cellular Physiology*, **177**, 553–562.

Gómez-Lechón, M. J., Donato, M. T., Ponsoda, X., Fabra, R., Trullenque, R. and Castell, J. V., 1997, Isolation, culture and use of human hepatocytes in drug research. In *In Vitro Methods in Pharmaceutical Research* (San Diego: Academic Press), pp. 129–154.

Gómez-Lechón, M. J., Donato, T., Jover, R., Rodriguez, C., Ponsoda, X., Glaise, D., Castell, J. V. and Guguen-Guillouzo, C., 2001, Expression and induction of a large set of drug metabolism enzymes by the highly differentiated human hepatoma cell line BC2. *European Journal of Biochemistry*, **268**, 1448–1459.

Gómez-Lechón, M. J., López, P., Donato, T., Montoya, A., Larrauri, A., Giménez, P., Trullenque, R., Fabra, R. and Castell, J. V., 1990, Culture of human hepatocytes from small surgical liver biopsies. Biochemical characterization and comparison with *in vivo*. *In Vitro Cellular and Developmental Biology*, **26**, 67–74.

Gonzalez, F. and Lee, Y., 1996, Constitutive expression of hepatic cytochrome P450 genes. *FASEB Journal*, **10**, 1112–1117.

Guengerich, F. P., 1995, Human cytochrome P450 enzymes. In *Cytochromes P-450: Structure, Mechanism and Biochemistry* (New York: Plenum), pp. 473–535.

Guillouzo, A. and Guguen-Guillouzo, C., 1992, *In vitro* approaches to hepatotoxicity studies. In *In Vitro Methods in Toxicology* (London: Academic Press), pp 133–160.

Guillouzo, A., 1998, Liver cell models in *in vitro* toxicology. *Environmental Health Perspectives*, **106**, 511–531.

Haehner, B. D., Gorski, J. C., Vandenbranden, M., Wrighton, S. A., Janardan, S. K., Watkins, P. B. and Hall, S. D., 1996, Bimodal distribution of renal cytochrome P450 3A activity in humans. *Molecular Pharmacology*, **50**, 52–59.

Jover, R., Bort, R., Gomez, L., M. J. and Castell, J., 1998, Re-expression of C/EBP alpha induces CYP2B6, CYP2C9 and CYP2D6 genes in HepG2 cells. *FEBS Letters*, **431**, 227–230.

Jover, R., Bort, R., Gomez-Lechon, M. J. and Castell, J. V., 2001, Cytochrome P450 regulation by hepatocyte nuclear factor 4 in human hepatocytes: a study using adenovirus-mediated antisense targeting. *Hepatology*, **33**, 668–675.

Komori, M., Hahizume, T., Ohi, H., Miura, T., Kitada, M., Nagashima, K. and Kamataki, T., 1988, Cytochrome P-450 in human liver microsomes: high-performance liquid chromatographic isolation of three forms and their characterization. *Journal of Biochemistry*, **104**, 912–916.

Kronbach, T., Mathys, D., Gut, J., Catin, T. and Meyer, U. A., 1987, High-performance liquid chromatographic assays for bufuralol 1′-hydroxylase, debrisoquine 4-hydroxylase, and dextromethorphan *O*-demethylase in microsomes and purified cytochrome P-450 isozymes of human liver. *Analytical Biochemistry*, **162**, 24–32.

Kuo, C. J., Conley, P. B., Chen, L., Sladek, F. M., Darnell, J. E. and Crabtree, G. R., 1992, A transcriptional hierarchy involved in mammalian cell-type specification. *Nature*, **355**, 457–461.

Lee, Y. H., Williams, S. C., Baer, M., Sterneck, E., Gonzalez, F. J. and Johnson, P. F., 1997, The ability of C/EBP β but not C/EBP α to synergize with an Sp1 protein is specified by the leucine zipper and activation domain. *Molecular and Cellular Biology*, **17**, 2038–2047.

Legraverend, C., Eguchi, H., Strom, A., Lahuna, O., Mode, A., Tollet, P., Westin, S. and Gustafsson, J., 1994, Transactivation of the rat CYP2C13 gene promoter involves HNF-1, HNF-3, and members of the orphan receptor subfamily. *Biochemistry*, **33**, 9889–9897.

Li, A. P., 1997, Primary hepatocyte cultures as an *in vitro* experimental model for the evaluation of pharmacokinetic drug–drug interactions. In *Advances in Pharmacology: Drug–Drug Interactions, Scientific and Regulatory Perspectives* (London: Academic Press), pp. 103–129.

Li, A. P., Maurel, P., Gómez-Lechón, M. J., Cheng, L. C. and Jurima Romert, M., 1996, Preclinical evaluation of drug–drug interaction potential: present status of the application of primary human hepatocytes in the evaluation of cytochrome P450 induction. *Chemico-Biological Interactions*, **107**, 5–16.

Lowry, O. H., Rosenbrough, N. J., Farr, A. L. and Randal, R. J., 1951, Protein measurement with the Folin phenol reagent. *Journal of Biological Chemistry*, **193**, 265–275.

Maurel, P., 1996, The use of adult human hepatocytes in primary culture and other *in vitro* systems to investigate drug metabolism in man. *Advanced Drug Delivery Reviews*, **22**, 105–132.

Meyer, U. A., 1996, Overview of enzymes of drug metabolism. *Journal of Pharmacokinetics and Biopharmacy*, **24**, 449–459.

Morel, F., Beaune, P. H., Ratanasavanh, D., Flinois, J. P., Yang, C. S., Guengerich, F. P. and Guillouzo, A., 1990, Expression of cytochrome P-450 enzymes in cultured human hepatocytes. *European Journal of Biochemistry*, **191**, 437–444.

Murray, G. I. and Burke, D. M., 1995, Immunochemistry of drug metabolizing enzymes. *Biochemical Pharmacology*, **50**, 895–903.

Nakama, A., Kuroda, K. and Yamada, A., 1995, Induction of cytochrome P450-dependent monooxygenase in serum-free cultured HepG2. *Biochemical Pharmacology*, **50**, 1407–1412.

Ossipow, V., Descombes, P. and Schibler, U., 1993, CCAAT/enhancer-binding protein mRNA is translated into multiple proteins with different transcription activation potentials. *Proceedings of the National Academy of Sciences, USA*, **90**, 8219–8223.

Padgham, C. R., Boyle, C. C., Wang, X. J., Raleigh, S. M., Wright, M. C. and Paine, A. J., 1993, Alteration of transcription factor mRNAs during the isolation and culture of rat hepatocytes suggests the activation of a proliferative mode underlies their de-differentiation. *Biochemical Biophysical Research Communications*, **197**, 599–605.

Padgham, C. R., Paine, A. J., Phillips, I. R. and Shephard, E. A., 1992, Maintenance of total cytochrome P-450 content in rat hepatocyte culture and the abundance of CYP1A2 and CYP2B1/2 mRNAs. *Biochemical Journal*, **285**, 929–932.

Paine, A. J., 1995, Heterogeneity of cytochrome P450 and its toxicological significance. *Human Experimental Toxicology*, **14**, 1–7.

Renwick, A. B., Watts, P. S., Edwards, R. J., Barton, P. T., Guyonnet, I., Price, R. J., Tredger, J. M., Pelkonen, O., Boobis, A. R. and Lake, B. G., 2000, Differential maintenance of cytochrome P450 enzymes in cultured precision-cut human liver slices. *Drug Metabolism and Disposition*, **28**, 1202–1209.

Rodríguez-Antona, C., Jover, R., Gómez-Lechón, M. J. and Castell, J. V, 2000, Quantitative RT-PCR measurement of human cytochrome P-450s: application to drug induction studies. *Archives of Biochemistry and Biophysics*, **376**, 109–116.

Roe, A. L., Snawder, J. E., Benson, R. W., Roberts, D. W. and Casciano, D. A., 1993, HepG2 cells: an *in vitro* model for P450-dependent metabolism of acetaminophen. *Biochemical Biophysical Research Communications*, **190**, 15–19.

Runge, D. M., Runge, D., Foth, H., Strom, S. C. and Michalopoulos, G. K., 1999, STAT 1alpha/1beta, STAT 3 and STAT 5: expression and association with c-MET and EGF-receptor in long-term cultures of human hepatocytes. *Biochemical Biophysical Research Communications*, **265**, 376–381.

Savas, U., Grin, K. J. and Johnson, E. F., 1999, Molecular mechanisms of cytochrome P-450 induction by xenobiotics: an expanded role for nuclear receptors. *Molecular Pharmacology*, **56**, 851–857.

Shaw, P. M., Weiss, M. C. and Adesnik, M., 1994, Hepatocyte nuclear factor 3 is a major determinant of CYP2C6 promoter activity in hepatoma. *Molecular Pharmacology*, **46**, 79–87.

Späth, G. F. and Weiss, M. C., 1997, Hepatocyte nuclear factor 4 expression overcomes repression of the hepatic phenotye in dedifferentiated hepatoma cells. *Molecular and Cellular Biology*, **17**, 1931–1942.

Sumida, A., Fukuen, S., Yamamoto, I., Matsuda, H., Naohara, M. and Azuma, J., 2000, Quantitative analysis of constitutive and inducible CYPs mRNA expression in the HepG2 cell line using reverse transcription-competitive PCR. *Biochemical Biophysical Research Communications*, **267**, 756–760.

Vallet, V., Antoine, B., Chafey, P., Vandewalle, A. and Kahn, A., 1995, Overproduction of a truncated hepatocyte nuclear factor 3 protein inhibits expression of liver-specific genes in hepatoma cells. *Molecular and Cellular Biology*, **15**, 5453–5460.

WANG, X. J., HODGKINSON, C. P., WRIGHT, M. C. and PAINE, A. J., 1997, Temperature-sensitive mRNA degradation is an early event in hepatocyte de-differentiation. *Biochemical Journal*, **328**, 937–944.

WAXMAN, D. J., 1999, P450 gene induction by structurally diverse xenochemicals: central role of nuclear receptors CAR, PXR, and PPAR. *Archives of Biochemistry and Biophysics*, **369**, 11–23.

WAXMAN, D. J., LAPENSON, D. P., AOYAMA, T., GELBOIN, H. V., GONZALEZ, F. J. and KORZEKWA, K., 1991, Steroid hormone hydroxylase specificities of eleven cDNA-expressed human cytochrome P450s. *Archives of Biochemistry and Biophysics*, **290**, 160–166.

WOODCROFT, K. J. and NOVAK, R. F., 1998, Xenobiotic-enhanced expression of cytochromes P450 2E1 and 2B in primary cultured rat hepatocytes. *Drug Metabolism and Disposition*, **26**, 372–378.

WRIGHTON, S. A., VANDENBRANDEN, M. and RING, B. J., 1996, The human drug metabolizing cytochromes P450. *Journal of Pharmacokinetics and Biopharmacy*, **24**, 461–473.

WU, D. F., CLEJAN, L., POTTER, B. and CEDERBAUM, A. I., 1990, Rapid decrease of cytochrome P-450IIE1 in primary hepatocyte culture and its maintenance by added 4-methylpyrazole. *Hepatology*, **12**, 1379–1389.

XENOBIOTICA, 2002, VOL. 32, NO. 6, 521–534

Taylor & Francis
healthsciences

Metabolism of a novel phosphodiesterase-IV inhibitor (V11294) by human hepatic cytochrome P450 forms

V. SUBRAHMANYAM†§, A. B. RENWICK‡, D. G. WALTERS‡, R. J. PRICE‡, A. P. TONELLI†§ and B. G. LAKE‡*

† Purdue Pharma L.P., 444 Sawmill River Road, Ardsley, NY 10502, USA
‡ TNO BIBRA International Ltd, Woodmansterne Road, Carshalton SM5 4DS, UK

Received 17 September 2001

1. The metabolism of a novel phosphodiesterase-IV inhibitor (V11294) was studied in human liver microsomal and cytosol preparations and in cDNA-expressed human hepatic CYP forms.

2. Human liver microsomes, but not cytosol, catalysed the NADPH-dependent metabolism of V11294 to V10331 (formed by hydroxylation of the cyclopentyl ring), V10332 (*N*-desethyl V11294) and V11689 (formed by hydroxylation of the isopropyl side chain). In addition, smaller amounts of a secondary metabolite V11690 (which can be formed from either V10332 or V11689) were also produced.

3. Kinetic analysis of V11294 metabolism to V10331, V10332 and V11689 in two preparations of pooled human liver microsomes revealed average $K_m = 2.5$, 8.1 and 3.9 μM, respectively.

4. The metabolism of V11294 was determined with a characterized bank of 16 individual human liver microsomal preparations employing a V11294 substrate concentration of 8 μM (i.e. approximately the K_m for V10332 formation and around twice the K_m for V10331 and V11689 formation). Good correlations ($r^2 = 0.570$–0.903) were observed between V10331, V10332 and V11689 formation and markers of CYP3A forms. In contrast, poorer correlations ($r^2 = 0.0002$–0.428) were observed with markers of CYP1A2, CYP2A6, CYP2B6, CYP2C8, CYP2C9, CYP2C19, CYP2D6, CYP2E1 and CYP4A9/11.

5. Using human B-lymphoblastoid cell microsomes containing cDNA-expressed CYP forms, V11294 (8 μM) was metabolized by cDNA-expressed CYP3A4 to V10331, V10332 and V11689, with lower amounts of V11690 also being formed. Lower rates of V11294 metabolism to some V11294 metabolites were also observed with cDNA-expressed CYP2C9, CYP2C19 and CYP2D6, whereas only very low or undetectable rates of V11294 metabolism were observed with cDNA-expressed CYP1A2, CYP2A6, CYP2B6, CYP2C8 and CYP2E1.

6. The metabolism of V11294 (8 μM) to V10331, V10332 and V11689 was markedly inhibited by the CYP3A mechanism-based inhibitor troleandomycin. In contrast, V11294 metabolism was not significantly affected by inhibitors of CYP1A2, CYP2C9, CYP2D6 and CYP2E1 or by the CYP2C19 substrate *S*-mephenytoin.

7. In summary, by correlation analysis, chemical inhibition studies and the use of cDNA-expressed CYPs, V11294 metabolism in human liver to V10331, V10332 and V11689 appears to be primarily catalysed by CYP3A forms.

* Author for correspondence; e-mail: blake@tnobibra.co.uk
§ Present address: R. W. Johnson Pharmaceutical Research Institute, PO Box 300, Raritan, NJ 08869, USA.

Xenobiotica ISSN 0049-8254 print/ISSN 1366–5928 online © 2002 Taylor & Francis Ltd
http://www.tandf.co.uk/journals
DOI: 10.1080/00498250210128684

Introduction

Members of the cytochrome P450 (CYP) superfamily are known to play a major role in the oxidative metabolism of both xenobiotics and certain endogenous compounds (Parkinson 1996). Human hepatic CYP1A, CYP2A, CYP2B, CYP2C, CYP2D, CYP2E and CYP3A forms can metabolize a wide variety of therapeutic agents (Wrighton *et al.* 1993, Nelson *et al.* 1996, Parkinson 1996, Pelkonen *et al.* 1998).

V11294 (3-(3-cyclopentyloxy-4-methoxybenzyl)-6-ethylamino-8-isopropyl-3*H*-purine) is a novel phosphodiesterase-IV inhibitor which was under development as an anti-asthma agent. The inhibition of phosphodiesterase-IV by such agents leads to increased levels of cAMP in the affected cells (smooth muscle, macrophages and other immune cells), which initiates a cascade of physiological responses including bronchorelaxation and reduction in the immune response to different stimuli (Giembycz 2000).

V11294 has been administered to human subjects at oral dose levels of 25–300 mg and has been shown to be metabolized to various products (Subrahmanyam and Tonelli, unpublished observations), including *N*-desethyl V11294 (metabolite V10332). The structure of V11294 and some pathways of V11294 metabolism are shown in figure 1.

The objective of the current study was to elucidate the CYP forms responsible for V11294 metabolism in human liver. 'Reaction phenotyping' studies (Parkinson 1996) were performed by correlation analysis, chemical inhibition and the use of cDNA-expressed human CYP forms.

Materials and methods

Materials

NADPH, Tris, diethyldithiocarbamate, quinidine, sulfaphenazole and troleandomycin were obtained from Sigma-Aldrich Co. (Poole, UK) and furafylline and *S*(+)-mephenytoin from Salford Ultrafine Chemicals and Research (Manchester, UK). Samples of V11294, V10331, V10332, V11689, V11690 and V10388 (internal standard for high-performance liquid chromatography [HPLC]) were supplied by Department of Drug Metabolism and Pharmacokinetics, Purdue Pharma L.P. (Ardsley, NY, USA). A reaction phenotyping kit (Product No. H0500), containing 16 separate human liver microsomal preparations characterized for total CYP content and a range of CYP form enzyme activities (table 2), was purchased from XenoTech LLC (Kansas City, KS, USA) and stored at −80°C. Samples of microsomes from human B-lymphoblastoid cell lines engineered to express stably cDNAs for human cytochrome P450 forms (GENTEST Corporation, Woburn, MA, USA) were obtained from Cambridge Bioscience (Cambridge, UK). The samples of GENTEST cell microsomes comprised control cell microsomes (i.e. no transfected human cytochrome P450 form cDNA but contains native CYP1A1 activity) and cell microsomes containing CYP1A2, CYP2A6 + OR (i.e. CYP2A6 cDNA plus human NADPH-cytochrome P450 reductase (OR) cDNA), CYP2B6, CYP2C8 + OR, CYP2C9 + OR, CYP2C19, CYP2D6 + OR, CYP2E1 + OR and CYP3A4 + OR.

Human liver microsomes

Samples of human liver were transported on ice to TNO BIBRA and stored at −80°C. The Research Ethics Committee of King's College Hospital (London, UK) granted approval for the use of this tissue, which was surplus to clinical requirements. Washed liver microsomal fractions were prepared in 0.154 M KCl containing 50 mM Tris-HCl as described (Lake 1987). Washed microsomal fractions were assayed for total CYP content (Lake 1987) and for protein (Lowry *et al.* 1951) employing bovine serum albumin as standard. The washed microsomal fractions were diluted to 10 mg ml^{-1} and aliquots stored at −80°C. Two separate batches, designated pools A and B, of pooled human liver microsomes were prepared, with each batch consisting of pooled liver samples from five subjects. Pool A comprised liver samples from males aged 15, 17 and 29 years and females aged 31 and 42 years, whereas pool B comprised liver samples, from males aged 2.5 and 58 years and females, aged 14, 59 and 74 years.

Metabolism of V11294 by human liver microsomes

The NADPH-dependent metabolism of V11294 was studied in incubation mixtures containing 0–100 μM V11294 (added in 5 μl methanol), 10 mM $MgCl_2$, 2 mM EDTA, 80 mM phosphate buffer pH 7.4 and 0.5–2.0 mg microsomal protein in a final volume of 1 ml. After 5-min pre-incubation at 37 °C in a shaking water bath, the reaction was initiated by the addition of 1 mM NADPH. Incubations were performed for 5–30 min at 37 °C and were terminated by the addition of 3 ml ice-cold acetonitrile, followed by the addition of 0.05 ml 0.8 mM V10388 (internal standard) in methanol. Blank incubations contained all components except NADPH, which was added after the reaction was terminated with acetonitrile. For each V11294 substrate concentration, incubation time and microsomal protein concentration, incubations were conducted in duplicate with a single blank (no NADPH) tube. Tubes were left on ice for 30 min and then centrifuged at 1730*g* average for 10 min at 4 °C. A 3-ml sample of the supernatant was removed into a clean glass tube and the solvent removed in a gyrovap at 50 °C for 60–90 min. The residue in each tube was reconstituted with either 1 or 2 ml HPLC mobile phase (see below), centrifuged at 10 000*g* for 5 min in a benchtop centrifuge and subsequently filtered through a 10 mm 0.2 μm Anotop 10 Plus syringe filter (Whatman International, Maidstone, UK). The samples were then stored at 4 °C before HPLC analysis. The HPLC method employed was based on a fully validated procedure for analysis of V11294 and V11294 metabolites in human plasma developed by Purdue Pharma L.P. (Ardsley, NY, USA). Chromatography of 50 μl aliquots of the filtered incubate extracts was performed with a 150 × 2.1 mm Waters Symmetry C8 3.5 μm column (Catalogue No. WAT 106011) protected by a 10 × 2.1 Waters Symmetry C8 3.5 μm guard column (WAT 106128) and isocratic elution with a mobile phase of 27% (v/v) acetonitrile in water containing 0.2% (v/v) glacial acetic acid and 0.1% triethylamine. Elution was achieved at a flow rate of 0.4 ml min^{-1} with a column temperature of 40 °C. The eluent was monitored at 290 nm. Retention times of V10331, V11690, V10332, V11689, V10388 (internal standard) and V11294 were approximately 3.5, 6.2, 11.7, 13.3, 22.8 and 25.9 min, respectively.

Metabolism of V11294 by human liver cytosol

Incubation mixtures contained 1 mM NADPH, 10 mM $MgCl_2$, 2 mM EDTA, 1 mg protein and 80 mM phosphate buffer pH 7.4 in a final volume of 1 ml. After a 5-min pre-incubation at 37 °C in a shaking water bath, the reaction was initiated by adding 100 μM V11294 (added in 5 μl methanol). Incubations were also performed in the absence of NADPH. Duplicate incubations were terminated after 15, 30 and 60 min with 3 ml ice-cold acetonitrile, followed by the addition of 0.05 ml 0.4 mM V10388 (internal standard) in methanol. For these studies, blank incubations comprised tubes stopped at zero time. Incubations were processed for HPLC analysis as described above.

V11294 metabolism correlation analysis

Incubation mixtures contained 8 μM V11294 (added in 5 μl methanol), 10 mM $MgCl_2$, 2 mM EDTA, 0.5 mg microsomal protein and 87 mM phosphate buffer pH 7.4 in a final volume of 1 ml. After 5-min pre-incubation at 37 °C in a shaking water bath, the reaction was initiated by addition of 1 mm (final concentration) NADPH. Incubations were conducted in triplicate with a single blank (no NADPH) for each of the 16 preparations of characterized human liver microsomes and were terminated after 5 min by addition of 3 ml ice-cold acetonitrile, followed by the addition of 0.05 ml 0.8 mM V10388 (internal standard) in methanol. Incubations were processed for HPLC analysis as described above.

V11294 metabolism by cDNA-expressed CYP forms

Incubation mixtures contained 8 μM V11294 (added in 0.25 ml 100 mM Tris-HCl buffer pH 7.4) 10 mM $MgCl_2$, 2 mM EDTA, 1 mM NADPH and 80 mM Tris-HCl buffer pH 7.4 in a final volume of 0.5 ml. After 5-min pre-incubation in a 37 °C water bath, the reaction was initiated by adding 0.5 mg GENTEST cell microsomal protein with gentle mixing. The incubations were conducted in duplicate with a single blank (no NADPH) for each CYP form preparation. Reactions were terminated after 20, 45 and 120 min with 1.5 ml ice-cold acetonitrile, followed by 0.05 ml 0.8 mM V10388 (internal standard) in methanol. Incubations were processed for HPLC analysis as described above.

V11294 metabolism inhibition studies

For the compounds requiring pre-incubation with NADPH, incubation mixtures contained 10 mM $MgCl_2$, 2 mM EDTA, 1 mM NADPH, 85 mM phosphate buffer pH 7.4, 0.5 mg microsomal protein and either furafylline (5–50 μM), diethyldithiocarbamate (5–100 μM) or troleandomycin (5–100 μM) in a volume of 0.85 ml. All the inhibitors were added in DMSO (5 μl/tube) and the concentrations refer to the final concentrations in a 1 ml incubation. Following a 30 min pre-incubation at 37 °C in a shaking water bath, 8 μM V11294 (added in 0.1 ml 100 mM phosphate buffer pH 7.4) and another aliquot of NADPH (final concentration 2 mM) were added. Incubations were performed for 5 min at 37 °C and were terminated by the addition of 3 ml ice-cold acetonitrile, followed by 0.05 ml 0.8 mM V10388

(internal standard) in methanol. All test incubations were performed in either triplicate (no inhibitor added but containing 5 µl DMSO/tube) or duplicate (for each concentration of each inhibitor), with single blank tubes where V11294 was added after the ice-cold acetonitrile. Incubations were processed for HPLC analysis as described above. For the compounds not requiring pre-incubation with NADPH, incubation mixtures contained 8 µM V11294 (added in 0.1 ml 100 mM phosphate buffer pH 7.4), 10 mM $MgCl_2$, 2 mM EDTA, 0.5 mg microsomal protein, 85 mM phosphate buffer pH 7.4 and either sulfaphenazole (2–50 µM), quinidine (2–20 µM) or *S*-mephenytoin (50–500 µM) in a volume of 0.95 ml. All the inhibitors were added in DMSO (5 µl/tube) and the concentrations refer to the final concentrations in a 1 ml incubation. Following a 10 min pre-incubation at 37 °C in a shaking water bath, 1 mM NADPH was added. Incubations were performed for 5 min at 37 °C and were terminated by the addition of 3 ml ice-cold acetonitrile, followed by 0.05 ml 0.8 mM V10388 (internal standard) in methanol. All test incubations were performed in either triplicate (no inhibitor added but containing 5 µl DMSO/tube) or duplicate (for each concentration of each inhibitor), with single blank tubes where NADPH was added after the ice-cold acetonitrile. Incubations were processed for HPLC analysis as described above.

Results

Kinetics of V11294 metabolism

Initial V11294 metabolism studies were conducted with 100 µM substrate and the pool A and B human liver microsomal preparations. V11294 was metabolized by human liver microsomes in the presence of NADPH to a number of metabolites. The major metabolites detected were V10331 (formed by hydroxylation of the cyclopentyl ring), V10332 (*N*-desethyl V11294) and V11689 (formed by hydroxylation of the isopropyl side chain), together with smaller amounts of the secondary metabolite V11690, which can be formed from either V10332 or V11689 (figure 1). With both human liver microsomal preparations, V11294 metabolism to V10331, V10332 and V11689 was linear with respect to incubation time for up to 10 min and microsomal protein concentration up to 1.5 mg protein ml^{-1} (data not shown).

V11294 was incubated at a substrate concentration of 100 µM in both the presence and absence of 1 mm NADPH with 1 mg of cytosolic protein from both the A and B human liver pools for up to 60 min. Under these conditions only trace amounts ($\leqslant$1 pmol per incubation) of V10331, V10332, V11689 and V11690 were formed (data not shown). These data suggest that cytosolic enzymes do not contribute to V11294 metabolism.

Using the pool A and B human liver microsomal preparations, the metabolism of V11294 was investigated over a substrate concentration range of 0.5–50 µM. Kinetic analysis of Eadie–Hofstee plots revealed K_m for V10331, V10332 and V11689 formation between 1.8 and 11.9 µM (table 1). The pool B human liver microsomal preparation was more active than the pool A preparation as indicated by the higher V_{max} (expressed per unit of microsomal protein) for formation of V10331, V10332 and V11689. The total CYP contents of the pool A and B human liver microsomal preparations were 0.39 and 0.72 nmol mg^{-1} protein, respectively. When V_{max} was expressed per unit of total CYP, the differences between the two pools were much less marked (table 1).

Average K_m was for V11294 metabolism to V10331, V10332 and V11689 by the pool A and B human liver microsomal preparations were 2.5, 8.1 and 3.9 µM, respectively (table 1). For subsequent studies, a V11294 substrate concentration of 8 µM was selected as being approximately the K_m for V10332 formation and around twice K_m for V10331 and V11689 formation. This substrate concentration

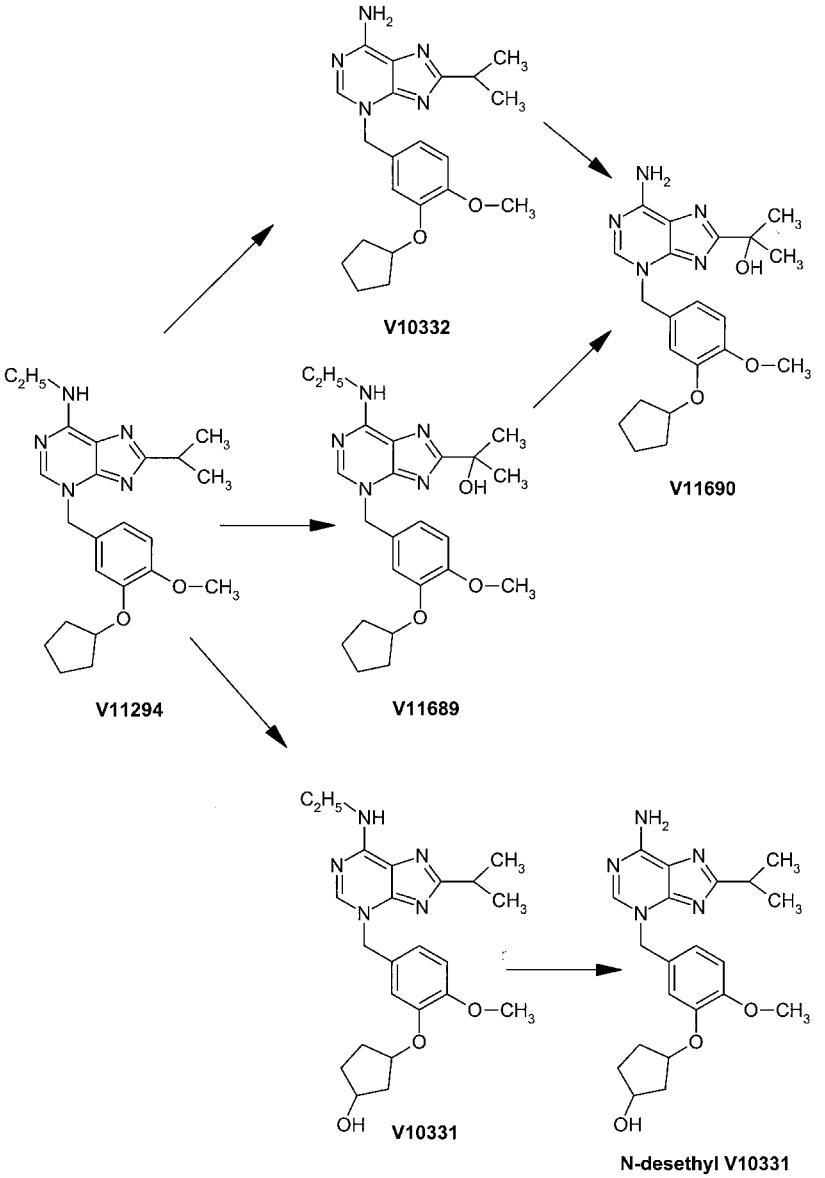


Figure 1. Some pathways of V11294 metabolism.

was also similar to plasma levels of V11294 observed after oral administration to human subjects (unpublished observations).

V11294 metabolism correlation analysis

The metabolism of V11294 was examined with a characterized panel of 16 human liver microsomal preparations employing a V11294 substrate concentration of 8 μM. V11294 was metabolized to V10331, V10332 and V11689 by all 16 human liver microsomal preparations examined (figure 2). Some of these microsomal preparations were more active than the pool A and B human liver microsomal

Table 1. Kinetic analysis of V11294 metabolism to V10331, V10332 and V11689 in two preparations of human liver microsomes.

Microsomal preparation	V11294 metabolism kinetics[a]								
	K_m (μM)			V_{max} (pmol min^{-1} mg^{-1} protein)			V_{max} (pmol min^{-1} $nmol^{-1}$ CYP)		
	V10331	V10332	V11689	V10331	V10332	V11689	V10331	V10332	V11689
Pool A	3.1	4.3	3.0	68.0	68.3	47.0	174	175	121
Pool B	1.8	11.9	4.7	98.5	163.1	108.4	137	227	151
Average	2.5	8.1	3.9	83.3	115.7	77.7	156	201	136

[a] Duplicate incubations were performed with each V11294 substrate concentration and 1 mg microsomal protein for 10 min.

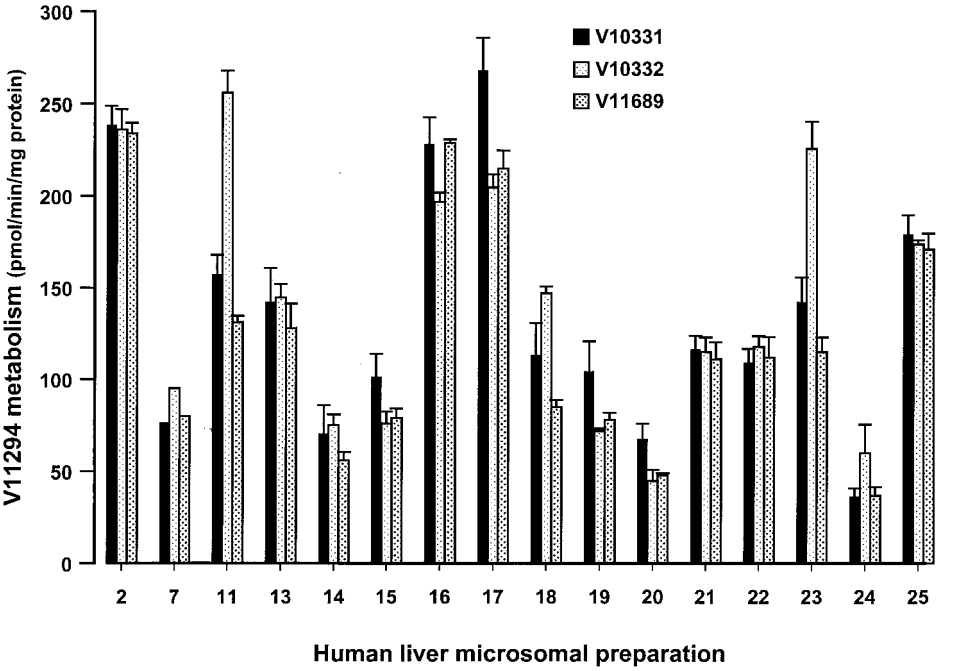


Figure 2. Variability in the metabolism of 8 μM V11294 to V10331, V10332 and V11689 in a panel of 16 individual human liver microsomal preparations. Incubations were performed with 0.5 mg protein for 5 min. Results are either the average of duplicate incubations (preparation number 7) or as mean ± SEM of triplicate incubations (all other preparations).

preparations. With the majority of the 16 characterized human liver microsomal preparations examined, similar amounts of V10331, V10332 and V11689 were formed. Although preparations 11 and 23 produced somewhat greater quantities of V10322 (figure 2), this could not be attributed to any obvious differences in the CYP enzyme profiles of these two preparations compared to those of the other liver microsomal preparations examined (data not shown). In 12 of the 16 microsomal preparations examined, smaller amounts of the secondary metabolite V11690 ranging from 1 to 57 pmol min^{-1} mg^{-1} protein were also formed (data not shown).

The rates of V11294 metabolism to V10331, V10332 and V11689 were correlated with data for total CYP content and a range of CYP form-dependent enzyme activities in the 16 human liver microsomal preparations. The best correlations (table 2) for V11294 metabolism to V10331, V10332 and V11689 were observed with total CYP content ($r^2 = 0.559$–0.654) and two markers of CYP3A forms, namely testosterone 6β-hydroxylase ($r^2 = 0.776$–0.903) and dextromethorphan *N*-demethylase ($r^2 = 0.570$–0.710). For V11294 metabolism to V10331, V10332 and V11689 and CYP form markers for CYP1A2, CYP2A6, CYP2B6, CYP2C8, CYP2C9, CYP2C19, CYP2D6, CYP2E1 and CYP4A9/11, r^2 of 0.0002–0.428 were observed (table 2). These latter enzyme activities comprised 7-ethoxyresorufin *O*-deethylase, coumarin 7-hydroxylase, *S*-mephenytoin *N*-demethylase, taxol 6α-hydroxylase, tolbutamide methylhydroxylase, *S*-mephenytoin 4′-hydroxylase, dextromethorphan *O*-demethylase, chlorzoxazone 6-hydroxylase and 4-nitrophenol hydroxylase and lauric acid 12-hydroxylase, respectively.

Table 2. Correlation analysis for V11294 metabolism to V10331, V10332 and V11689 with various CYP-dependent enzyme activities in human liver microsomes.

		V11294 metabolism correlation (r^2)		
CYP form	Enzyme activity[a]	V10331	V10332	V11689
–	total CYP content	0.652	0.654	0.559
1A2	7-ethoxyresorufin *O*-deethylase	0.001	0.072	0.0002
2A6	coumarin 7-hydroxylase	0.345	0.183	0.277
2B6	*S*-mephenytoin *N*-demethylase	0.380	0.286	0.428
2C8	taxol 6α-hydroxylase	0.329	0.424	0.309
2C9	tolbutamide methylhydroxylase	0.290	0.055	0.271
2C19	*S*-mephenytoin 4′-hydroxylase	0.137	0.049	0.121
2D6	dextromethorphan *O*-demethylase	0.042	0.061	0.035
2E1	chlorzoxazone 6-hydroxylase	0.102	0.036	0.115
	4-nitrophenol hydroxlyase	0.304	0.103	0.295
3A4/5	testosterone 6β-hydroxylase	0.873	0.776	0.903
	dextromethorphan *N*-demethylase	0.694	0.570	0.710
4A9/11	lauric acid 12-hydroxylase	0.020	0.019	0.016

[a] Total CYP content and the enzyme activities shown were correlated with data obtained from the metabolism of 8 μM V11294 to V10331, V10332 and V11689 (figure 2) in a panel of 16 individual human liver microsomal preparations.

Metabolism of V11294 by cDNA-expressed CYP forms

The metabolism of 8 μM V11294 was examined in GENTEST B-lymphoblastoid cell microsomes containing cDNA-expressed CYP1A2, CYP2A6, CYP2B6, CYP2C8, CYP2C9, CYP2C19, CYP2D6, CYP2E1 and CYP3A4, together with microsomes from control (wild type) cells which contain native CYP1A1. V11294 was metabolized in a time-dependent manner by B-lymphoblastoid cell microsomes containing cDNA-expressed CYP2C9, CYP2C19, CYP2D6 and CYP3A4 (data not shown). With the cDNA-expressed CYP3A4 preparation V11294 was metabolized to V10331, V10332, V11689 and V11690, the former three V11294 metabolites being produced in much greater amounts than V11690. V11294 was also metabolized to V10331, V10332 and V11689 by the cDNA-expressed CYP2C9 preparation, with a small quantity of V11690 also being formed after 120 min of incubation. The cDNA-expressed CYP2D6 preparation metabolized V11294 to V10331 and V10332, with a small amount of V11689 being formed after 120 min of incubation. With the cDNA-expressed CYP2C19 preparation, V10332 was the primary metabolite of V11294, with a trace amount of V10331 being formed after 120 min of incubation. Data for 20-min incubations with the cDNA-expressed CYP2C9, CYP2C19, CYP2D6 and CYP3A4 preparation is shown in figure 3. Overall, the CYP3A4 preparation was the most active CYP form examined.

In contrast to the above cDNA-expressed CYP forms, V11294 was not metabolized by control B-lymphoblastoid cell microsomes or by microsomes containing cDNA-expressed CYP1A2, CYP2B6, CYP2C8 and CYP2E1 (data not shown). With cDNA-expressed CYP2A6, trace amounts of V10332 (< 0.5 pmol min^{-1} mg^{-1} protein) were formed after 120 min of incubation.

Inhibition of V11294 metabolism

The effect of some known human CYP inhibitors and one substrate (*S*-mephenytoin) on the metabolism of 8 μM V11294 in human liver microsomes was

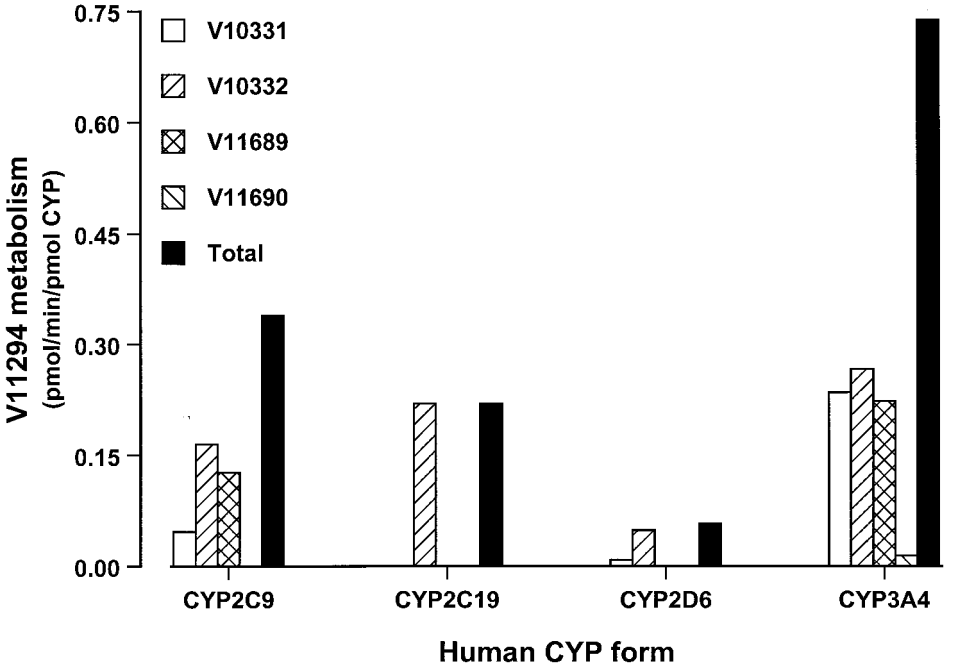


Figure 3. Metabolism of 8 μM V11294 by cDNA-expressed CYP2C9, CYP2C19, CYP2D6 and CYP3A4. Results are the averages of duplicate 20-min incubations with 0.5 mg B-lymphoblastoid cell microsomal protein expressed as pmol V11294 metabolite min^{-1} $pmol^{-1}$ CYP. Total metabolism refers to the sum of V11294 metabolism to V10331, V10332, V11689 and V11690.

studied. For the mechanism-based inhibitors (Newton *et al.* 1995) furafylline (CYP1A2), diethyldithiocarbamate (CYP2E1) and troleandomycin (CYP3A4), the compounds were pre-incubated with NADPH and the liver microsomes for 30 min at 37 °C prior to the addition of 8 μM V11294 and another aliquot of NADPH. In the studies with the inhibitors sulfaphenazole (CYP2C9) and quinidine (CYP2D6) and the substrate *S*-mephenytoin (CYP2C19), the compounds were pre-incubated with liver microsomes for 10 min at 37 °C prior to the addition of 8 μM V11294 and NADPH. The pool B human liver microsomal preparation was used for these studies, except for the investigations with troleandomycin where both the pool A and B microsomal preparations were employed. None of the CYP inhibitors and the one CYP substrate appeared to interfere with the HPLC analysis of V11294 metabolism to V10332 and V11689. However, an interfering component present in incubations containing sulfaphenazole precluded the determination of the effect of this inhibitor on V11294 metabolism to V10331.

Treatment with all five CYP inhibitors and the one CYP substrate studied had similar effects on the three pathways of V11294 metabolism examined. V11294 metabolism to V10332 was not markedly affected by furafylline and diethyldithiocarbamate (figure 4A) and by sulfaphenazole, *S*-mephenytoin and quinidine (figure 4B). Similarly, furafylline, diethyldithiocarbamate, *S*-mephenytoin and quinidine did not markedly inhibit V11294 metabolism to V10331 and V11689 and sulfaphenazole did not markedly inhibit V11294 metabolism to

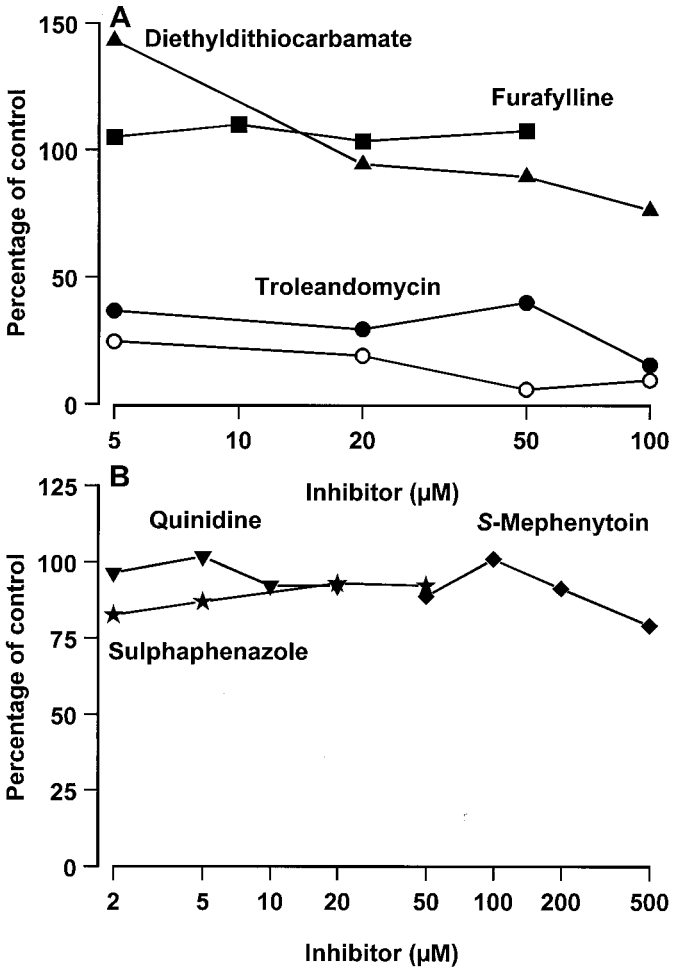


Figure 4. Inhibition of 8 μM V11294 metabolism to V10332 in human liver microsomes. To study the effects of 5–50 μM furafylline (■), 5–100 μM diethyldithiocarbamate (▲) and 5–100 μM troleandomycin (○●) (A), but not 2–50 μM sulfaphenazole (⋆), 50–500 μM *S*-mephenytoin (◆) and 2–20 μM quinidine (▼) (B), the compounds were pre-incubated with liver microsomes and NADPH for 30 min at 37°C prior to the addition of 8 μM V11294. Duplicate incubations were performed with 0.5 mg of either the pool A (open symbols) or B (closed symbols) microsomal preparations for 5 min, and the results expressed as the percentage of triplicate control (no inhibitor added) incubations. Control (no inhibitor added) rates of V11294 metabolism to V10332 were 53 and 123 pmol min^{-1} mg^{-1} protein for the pool A and B microsomal preparations, respectively.

V11689 (data not shown). In contrast, 5 μM troleandomycin markedly inhibited V11294 metabolism to V10332 to 25 and 37% of control in the pool A and B microsomal preparations, respectively (figure 4A). Treatment with 20–100 μM troleandomycin inhibited V11294 metabolism to V10332 to 5–19 and 15–40% of control in the pool A and B microsomal preparations, respectively (figure 4A). V11294 metabolism to both V10331 and V11689 was inhibited by 20–100 μM troleandomycin to 0–17 and 2–24% of control in the pool A and B microsomal preparations, respectively (data not shown).

Discussion

In this study the metabolism of V11294 by human hepatic microsomal and cytosolic fractions and cDNA-expressed human hepatic CYP isoforms has been investigated. The NADPH-dependent metabolism of V11294 to the major metabolites V10331, V10332 and V11689 was observed in two preparations of pooled human liver microsomes and in 16 individual preparations. In addition, V11690 was also identified as a minor secondary metabolite of V11294 in human liver microsomes. V11294 can thus be metabolized by human liver microsomes by *N*-deethylation, hydroxylation of the isopropyl side chain and hydroxylation of the cyclopentyl ring to yield V10332, V11689 and V10331, respectively (figure 1). Both V10332 and V11689 can be further oxidized to yield the minor secondary metabolite V11690 (figure 1). Kinetic analysis of microsomal V11294 metabolism revealed similar K_m for V10331, V10332 and V11689 formation, with a mean of 4.8 μM (table 1). Whereas V11294 was metabolized by human liver microsomal fractions to various products, the compound was not metabolized to any significant extent by cytosolic fractions in either the presence or absence of NADPH.

To identify the CYP forms responsible for V11294 metabolism in human liver, 'reaction phenotyping' studies were performed (Parkinson 1996, Clarke 1998). Such investigations can include the use of correlation analysis, chemical inhibitors, inhibitory antibodies and cDNA-expressed CYP forms. For the current study, 'reaction phenotyping' was performed by correlation analysis with a panel of characterized microsomal preparations, chemical inhibition and the use of cDNA-expressed human CYP forms. A V11294 substrate concentration of 8 μM was selected as being approximately the K_m for V10332 formation and around twice K_m for V10331 and V11689 formation. In addition, this V11294 substrate concentration is similar to the plasma C_{max} of 2.4 μM observed after oral administration of a 200 mg dose of V11294 to human subjects (Subrahmanyam and Tonelli, unpublished observations).

The metabolism of 8 μM V11294 was determined in a panel of 16 characterized human liver microsomal preparations. Good correlations were obtained between V11294 metabolism to V10331, V10332 and V11689 and testosterone 6β-hydroxylase ($r^2 = 0.776$–0.903) and dextromethorphan *N*-demethylase ($r^2 = 0.570$–0.710) activities. Both these enzyme activities are considered to be relatively specific markers for CYP3A forms in human liver (Wrighton *et al.* 1993, Gorski *et al.* 1994, Parkinson 1996, Clarke 1998, Pelkonen *et al.* 1998). V11294 biotransformation to all three primary metabolites also correlated with total CYP content ($r^2 = 0.559$–0.654). This may be attributable to the fact that CYP3A forms account for around 20–50% of the total CYP content of human liver (Wrighton *et al.* 1993, Shimada *et al.* 1994, Rodrigues 1999). In addition, while V_{max} (expressed per unit protein) for V11294 metabolite formation was higher in the pool B human liver microsomal preparation, when expressed per unit of total CYP V_{max} was similar in the pool A and B microsomal preparations. In contrast, to the markers of CYP3A forms and total CYP content, poorer correlations ($r^2 = 0.0002$–0.428) were observed between V11294 metabolism and 7-ethoxyresorufin *O*-deethylase, coumarin 7-hydroxylase *S*-mephenytoin *N*-demethylase, taxol 6α-hydroxylase, tolbutamide methylhydroxylase, *S*-mephenytoin 4′-hydroxylase, dextromethorphan *O*-demethylase, chlorzoxazone 6-hydroxylase and 4-nitrophenol hydroxylase and lauric acid 12-hydroxylase. These latter enzyme activities are considered markers of CYP1A2, CYP2A6, CYP2B6, CYP2C8, CYP2C9, CYP2C19,

CYP2D6, CYP2E1 and CYP4A9/11, respectively (Wrighton *et al.* 1993, Heyn *et al.* 1996, Parkinson 1996, Clarke 1998, Pelkonen *et al.* 1998).

The conclusions of the correlation analysis study are supported by the results of the chemical inhibition studies. Previous work has demonstrated that furafylline, sulfaphenazole, *S*-mephenytoin, quinidine, diethyldithiocarbamate and troleandomycin may be considered either inhibitors or substrates of human hepatic CYP1A2, CYP2C9, CYP2C19, CYP2D6, CYP2E1 and CYP3A4, respectively (Wrighton *et al.* 1993, Chang *et al.* 1994, Clarke *et al.* 1994, Baldwin *et al.* 1995, Newton *et al.* 1995, Ono *et al.* 1996, Parkinson 1996, Clarke 1998, Pelkonen *et al.* 1998, Tucker *et al.* 2001). The substrate *S*-mephenytoin was employed as a CYP2C19 inhibitor owing to the lack of specific chemical inhibitor for this CYP form (Clarke 1998, Tucker *et al.* 2001). Using two separate human liver microsomal preparations (pools A and B), 20–100 μM troleandomycin inhibited V11294 metabolism to V10331, V10332 and V11689 to 0–40% of control. Previous studies have demonstrated that troleandomycin is a relatively specific mechanism-based inhibitor of CYP3A forms in human liver (Chang *et al.* 1994, Newton *et al.* 1995, Ono *et al.* 1996). Unlike the effect of troleandomycin, 5–50 μM furafylline, 5–100 μM diethyldithiocarbamate, 50–500 μM *S*-mephenytoin and 2–20 μM quinidine did not markedly inhibit V11294 metabolism to either V10331, V10332 or V11689. In addition, V11294 metabolism to V10332 and V11689 was not markedly inhibited by 2–20 μM sulfaphenazole.

V11294 was metabolized by some of the cDNA-expressed human CYP forms examined. Using human B-lymphoblastoid cell microsomal preparations containing cDNA-expressed CYP3A4, V11294 was metabolized in a time-dependent manner to V10331, V10332, V11689 and V11690. V11294 was also metabolized to V10331 by cDNA-expressed CYP2C9 and CYP2D6, to V10332 by cDNA-expressed CYP2C9, CYP2C19 and CYP2D6 and to V11689 by cDNA-expressed CYP2C9. At extended incubation times, V11294 was also metabolized to V10331 by cDNA-expressed CYP2C19, to V10332 by cDNA-expressed CYP2A6, to V11689 by cDNA-expressed CYP2D6 and to V11690 by cDNA-expressed CYP2C9. In contrast, V11294 was not metabolized by control human B-lymphoblastoid cell microsomal preparations and microsomal preparations containing cDNA-expressed CYP1A2, CYP2B6, CYP2C8 and CYP2E1.

Although V11294 could be metabolized to some products by cDNA-expressed CYP2C9, CYP2C19 and CYP2D6, V11294 metabolism to any product was greatest with the cDNA-expressed CYP3A4 preparation (figure 3). Previous studies have demonstrated that levels of CYP2C19 and CYP2D6 are much lower than levels of CYP3A4 in human liver (Lecoeur *et al.* 1994, Shimada *et al.* 1994, Rodrigues 1999). Thus assuming these CYP forms have similar affinities (i.e. K_m values) for V11294 biotransformation, neither CYP2C19 nor CYP2D6 would have any major role in V11294 metabolism *in vivo*. In contrast, levels of CYP2C9 are relatively abundant in human liver (Lecoeur *et al.* 1994, Shimada *et al.* 1994, Rodrigues 1999), suggesting that this CYP form may have a minor role in hepatic V11294 metabolism.

In summary, the results of this study demonstrate that V11294 can be metabolized to V10331, V10332, V11689 and V11690 by human liver microsomal preparations. The three primary metabolites, namely V10331, V10332 and V11689, constitute major metabolites, whereas the secondary metabolite V11690, which can be formed from either V10332 or V11689, is only a minor

metabolite. By correlation analysis, chemical inhibition and the use of cDNA-expressed CYP isoforms, V11294 metabolism in human liver microsomes appears to be primarily catalysed by CYP3A forms.

Acknowledgements

The work was supported by a research grant from Purdue Pharma L.P. (Ardsley, NY, USA). The authors thank Dr J. M. Tredger (Institute of Liver Studies, Guy's, King's and St Thomas' School of Medicine, London, UK) for the supply of liver samples.

References

Baldwin, S. J., Bloomer, J. C., Smith, G. J., Ayrton, A. D., Clarke, S. E. and Chenery, R. J., 1995, Ketoconazole and sulphaphenazole as the respective selective inhibitors of P4503A and 2C9. *Xenobiotica*, **25**, 261–270.

Chang, T. K. H., Gonzalez, F. J. and Waxman, D. J., 1994, Evaluation of triacetyloleandomycin, α-naphthoflavone and diethyldithiocarbamate as selective chemical probes for inhibition of human cytochromes P450. *Archives of Biochemistry and Biophysics*, **311**, 437–442.

Clarke, S. E., 1998, *In vitro* assessment of human cytochrome P450. *Xenobiotica*, **28**, 1167–1202.

Clarke, S. E., Ayrton, A. D. and Chenery, R. J., 1994, Characterization of the inhibition of P4501A2 by furafylline. *Xenobiotica*, **24**, 517–526.

Giembycz, M. A., 2000, Phosphodiesterase 4 inhibitors and the treatment of asthma, where we are now and where do we go from here? *Drugs*, **59**, 193–212.

Gorski, J. C., Jones, D. R., Wrighton, S. A. and Hall, S. D., 1994, Characterization of dextromethorphan *N*-demethylation by human liver microsomes. Contribution of the cytochrome P450 3A (CYP3A) subfamily. *Biochemical Pharmacology*, **48**, 173–182.

Heyn, H., White, R. B. and Stevens, J. C., 1996, Catalytic role of P4502B6 in the *N*-demethylation of *S*-mephenytoin. *Drug Metabolism and Disposition*, **24**, 948–954.

Lake, B. G., 1987, Preparation and characterisation of microsomal fractions for studies of xenobiotic metabolism. In K. Snell and B. Mullock (eds), *Biochemical Toxicology: A Practical Approach* (Oxford: IRL Press), pp. 183–215.

Lecoeur, S., Bonierbale, E., Challine, D., Gauter, J.-C., Valadon, P., Dansette, P. M., Catinot, R., Ballet, F., Mansuy, D. and Beaune, P. H., 1994, Specificity of *in vitro* covalent binding of tienilic acid metabolites to human liver microsomes in relationship to the type of hepatotoxicity: comparison with two directly hepatotoxic drugs. *Chemical Research in Toxicology*, **7**, 434–442.

Lowry, O. H., Rosebrough, N. J., Farr, A. L. and Randall, R. J. 1951, Protein measurement with the Folin phenol reagent. *Journal of Biological Chemistry*, **193**, 265–275.

Nelson, D. R., Koymans, L., Kamataki, T., Stegeman, J. J., Feyereisen, R., Waxman, D. J., Waterman, M. R., Gotoh, O., Coon, M. J., Estabrook, R. W., Gunsalus, I. C. and Nebert, D. W., 1996, P450 superfamily: update on new sequences, gene mapping, accession numbers and nomenclature. *Pharmacogenetics*, **6**, 1–42.

Newton, D. J., Wang, R. W. and Lu, A. Y. H., 1995, Cytochrome P450 inhibitors. Evaluation of specificities in the *in vitro* metabolism of therapeutic agents by human liver microsomes. *Drug Metabolism and Disposition*, **23**, 154–158.

Ono, S., Hatanaka, T., Hotta, H., Satoh, T., Gonzalez, F. J. and Tsutsui, M., 1996, Specificity of substrate and inhibitor probes for cytochrome P450s: evaluation of *in vitro* metabolism using cDNA-expressed human P450s and human liver microsomes. *Xenobiotica*, **26**, 681–693.

Parkinson, A., 1996, Biotransformation of xenobiotics. In C. D. Klaassen (ed.), *Casarett and Doull's Toxicology: The Basic Science of Poisons*, 5th edn (New York: McGraw-Hill), pp. 113–186.

Pelkonen, O., Mäenpää, J., Taavitsainen, P., Rautio, A. and Raunio, H., 1998, Inhibition and induction of human cytochrome P450 (CYP) enzymes. *Xenobiotica*, **28**, 1203–1253.

Rodrigues, A. D., 1999, Integrated cytochrome P450 reaction phenotyping. Attempting to bridge the gap between cDNA-expressed cytochromes P450 and native human liver microsomes. *Biochemical Pharmacology*, **57**, 465–480.

Shimada, T., Yamazaki, H., Mimura, M., Inui, Y. and Guengerich, F. P., 1994, Interindividual variations in human liver cytochrome P-450 enzymes involved in the oxidation of drugs, carcinogens and toxic chemicals: studies with liver microsomes of 30 Japanese and 30 Caucasians. *Journal of Pharmacology and Experimental Therapeutics*, **270**, 414–423.

Tucker, G. T., Houston, J. B. and Huang, S.-M., 2001, Optimizing drug development: strategies to assess drug metabolism/transporter interaction potential-towards a consensus. *British Journal of Clinical Pharmacology*, **52**, 107–117.

Wrighton, S. A., Vandenbranden, M., Stevens, J. C., Shipley, L. A., Ring, B. J., Rettie, A. E. and Cashman, J. R., 1993, *In vitro* methods for assessing human hepatic drug metabolism: their use in drug development. *Drug Metabolism Reviews*, **25**, 453–484.

XENOBIOTICA, 2002, VOL. 32, NO. 6, 535–546

Taylor & Francis
healthsciences

^{19}F-NMR and directly coupled ^{19}F/^{1}H-HPLC-NMR spectroscopic investigations of the metabolism of the model ecotoxin 3-trifluoromethylaniline in the earthworm species *Eisenia veneta*

E. M. LENZ†*, J. C. LINDON†, J. K. NICHOLSON†, J. M. WEEKS‡§ and D. OSBORN

† Biological Chemistry, Division of Biomedical Sciences, Imperial College of Science Technology and Medicine, Sir Alexander Fleming Building, South Kensington, London SW7 2AZ, UK
‡ Institute of Terrestrial Ecology, Monks Wood, Abbots Ripton, Huntingdon PE17 2LS, UK

Received 22 October 2001

1. The metabolic fate of the model ecotoxin 3-trifluoromethylaniline (3-TFMA) in earthworm was studied by ^{19}F- and directly coupled ^{19}F/^{1}H-HPLC-NMR spectroscopy. Earthworms of *Eisenia veneta* spp. were subjected to the ecotoxin during a filter paper-contact toxicity test at exposure levels of 1000, 100, 10, 1 and 0.1 μg cm^{-2}. A metabolic profile was obtained previously by ^{19}F-NMR spectroscopy and metabolites were observed at all the exposure levels.

2. Identification of metabolites in individual worm extracts at the (lethal) exposure levels of 1000 and 100 μg cm^{-2} could be achieved on-line without sample preparation by ^{19}F/^{1}H-HPLC-NMR spectroscopy. ^{19}F-HPLC-NMR spectroscopy was used in the continuous-flow mode, which enabled the HPLC chromatographic retention times (t_R) of the metabolites to be established in a single analytical step.

3. In total, three ^{19}F-NMR signals could be detected, of which one was identified as the parent compound. Two earlier eluting metabolites were identified to be α- and β-glucoside conjugates of 3-TFMA.

4. Metabolites at the lower (sublethal) exposure levels of 10, 1 and 0.1 μg cm^{-2} escaped identification by ^{19}F/^{1}H-HPLC-NMR spectroscopy as outlined here and will require concentration prior to analysis.

Introduction

Much research is carried out with earthworms in ecotoxicology studies, based on their ecological function in soil and their role as susceptible pollutant biomonitors (Stenersen *et al.* 1992, Christensen and Mather 1994). However, relatively little is known about the reaction of earthworms to organic chemicals or how soil organisms metabolize or react to toxic organic chemicals (van Gestel and van Dis 1988, van Gestel *et al.* 1992, Haimi *et al.* 1992, Belfroid *et al.* 1993, 1995). The current study, therefore, concentrated on the metabolism of earthworms exposed to 3-trifluormethylaniline (3-TFMA) as a representative model ecotoxin. Aniline

* Author for correspondence; 24F5, DMPK, AstraZeneca Pharmaceuticals, Mereside, Alderley Park, Macclesfield SK10 4TG, UK; e-mail: Eva.Lenz@astrazeneca.com
§ Present address: WRc-NSF, Henley Road, Medmenham, Marlow SL2 2HD, UK.

Xenobiotica ISSN 0049-8254 print/ISSN 1366-5928 online © 2002 Taylor & Francis Ltd
http://www.tandf.co.uk/journals
DOI: 10.1080/00498250210128666

is one of the oldest and most widely used industrial compounds (Radomski 1979), hence its contamination potential is considerable. The widespread occurrence of primary aromatic amines/anilines in the chemical industry and their association with toxicological properties and carcinogenicity have led to their extensive use as model compounds in the areas of pharmaceutical and environmental research (Kiese and Lenk 1971, Wilson *et al.* 1985; Eadsforth *et al.* 1986, Rietjens *et al.* 1989, Vervoort *et al.* 1990, Ehlhardt and Howbert 1991).

Much data in the literature deals with anilines in experimental animals (rat, dog, rabbit), and Phase I and II metabolism appears to be extensive (Radomski 1979, Scarfe *et al.* 2000, Tugnait *et al.* 2001). The relative amounts of the various metabolites formed appear to vary considerably from species to species (Radomski 1979, Eadsforth *et al.* 1986, Ehlhardt and Howbert 1991). However, there is still little information on metabolites produced by invertebrate species.

In a previous study, we examined the uptake of the model toxin itself, and a metabolic profile was obtained by ^{19}F-NMR spectroscopy (Lenz *et al.* 2001). There is a substantial amount of literature data supporting the use of ^{19}F-NMR spectroscopy as a metabolic probe (e.g. Lindon 1995, Bundy *et al.* 2001, Lenz *et al.* 2001), based on the high natural abundance (100%) of the ^{19}F isotope, its selectivity and sensitivity (83% of ^{1}H). The large total chemical shift range inherent to ^{19}F (about 250 ppm for organic compounds containing ^{19}F) (Wade *et al.* 1990, Akitt 1992) minimizes signal overlap and makes the ^{19}F resonance frequency very sensitive to even small changes in the chemical environment of the molecule. Most importantly, however, ^{19}F is not naturally contained in biological samples, hence, ^{19}F-NMR spectroscopy is an ideal tool for detecting the relative quantities (and absolute quantities once an internal standard has been added) of metabolites that are present in a sample. However, it gives no information about the structure of the metabolites themselves. Techniques such as spiking of parent and suspected synthetic metabolites enable identification, but this requires prior knowledge of the metabolic pathway. Enzyme hydrolysis monitored by ^{19}F-NMR spectroscopy enables the identification of glucuronide and sulphate conjugates. However, this approach is relatively labour intensive and information on detailed structural modifications (e.g. hydroxylation and site of substitution) as a consequence of metabolism cannot be provided.

HPLC-NMR is a powerful tool for the identification of metabolites as it combines the isolation of analytes/metabolites from the complex biological matrix and their identification in a single analytical step (Lindon *et al.* 2000). The NMR spectrometer operates as a secondary detector, which provides the structural information on-line. Provided the analytes/metabolites have a characteristic handle (e.g. NMR active X-nucleus) and are present in high enough concentrations, a preliminary continuous-flow experiment can be carried out. This enables the calculation of the exact chromatographic retention times of the metabolites/analytes taking into account the transfer time between the UV-cell and the centre of the NMR flow-cell. However, this experiment generally suffers from poor signal-to-noise as only a limited number of scans can be acquired while the analytes are flowing through the flow-cell of the NMR magnet. Alternatively or subsequently, ^{1}H-NMR spectra are acquired in stop-flow mode, which allows the capture of the metabolite in question inside the NMR flow-probe. This enables

good quality ^{1}H-NMR spectra to be obtained (with sufficient signal-to-noise) and the structure to be determined.

Studies concerning trifluoromethylated (-CF_3) aromatic compounds benefit from maximum sensitivity, as all three ^{19}F atoms are magnetically equivalent giving rise to a singlet. ^{1}H decoupling is not necessary as couplings (over four bonds) between ^{19}F and aromatic ring protons are generally too small to be observed. This has the added advantage that dedicated proton NMR probes can be manually tuned to the ^{19}F frequency (470.59 MHz cf. 500 MHz for ^{1}H), hence allowing the observation of ^{19}F and ^{1}H spectra sequentially on the same sample in the NMR spectrometer.

In the current study, the 'CF_3-handle' was used selectively to detect ^{19}F-containing peaks during the chromatographic separation in the continuous-flow mode. The chromatographic separation could then be repeated in stop-flow mode, which enabled successful structural identification of the 3-TFMA metabolites to be carried out by ^{1}H-NMR spectroscopy. The results and limitations of this approach are discussed.

Materials and methods

Experimental design and sample preparation

A filter-paper contact toxicity test was conducted following the OECD guidelines (OECD 1984). After a depuration period of 24 h (at 17 °C and 54% humidity), five replicas were used per exposure level. Earthworms of the species *Eisenia veneta* were subjected to the model ecotoxin 3-TFMA at exposure levels of 1000, 100, 10, 1 and 0.1 μg cm^{-2}. After the carrier solvent (hexane) had evaporated (10 min), the filter paper was remoistened before the introduction of the earthworms. The earthworms were exposed to the volatile 3-TFMA model toxin for a duration of 3 days (while being incubated in the dark at 17 °C and 54% humidity). At the end of the exposure period or following death, the earthworms were frozen in liquid N_2 and homogenized directly into ice-cold methanol-d_4 (MeOH-d_4, 1 ml) using an Ultra Turrax homogenizer (Model T25). This ensured maximum extraction efficiency and prevented loss of the volatile parent and/or its metabolites due to evaporation during extensive sample preparation procedures. The homogenates were subsequently ultracentrifuged (MSE, Micro Centaur, 18 950*g* for 5 min). The supernatants were stored frozen at −20 °C until NMR and on-line HPLC-NMR spectroscopic measurements were carried out.

^{19}F-NMR spectroscopic measurements/spectroscopy: ^{19}F-NMR measurements were carried out on a Bruker AMX600 spectrometer fitted with a TXI-probe (triple resonance: ^{1}H, ^{13}C, ^{15}N) of which the ^{1}H channel was tuned to the ^{19}F frequency of 564.68 MHz. The 90 pulse width was measured to be 11.03 μs, and spectra were acquired with a spectral width of 42 ppm (23 629.49 Hz). Spectra were acquired with 128 scans into 64 K data points. Full T_1 relaxation was ensured by applying/allowing a relaxation delay of 8 s. This resulted in a spectrum acquisition time per sample of about 20 min. Spectra were referenced to external TFE (trifluoroethanol) $\delta 19_F$ −77.023 spiked into a control earthworm homogenate.

Directly coupled HPLC-NMR analysis of 3-TFMA metabolites in worm homogenates

The on-line HPLC system consisted of a Bruker LC22 pump (Bruker, Coventry, UK) connected to a Bishoff Lambda 1000 variable wavelength UV detector and a Bruker BPSU-12 collector. The chromatography was controlled by the Bruker Chromstar^{TM} software. The separation of the analytes was carried out on a Hypersil BDS C_{18} column (250 × 4.6 mm i.d., packing/particle size: 5 μm; Hichrom, Reading, UK) at 25 °C. The mobile phase consisted of a H_2O/D_2O mixture (50:50 v/v) (Fluorochem, Old Glossop, UK) containing 0.01 mol l^{-1} ammonium formate (Fisons Ltd, Loughborough, UK) adjusted to pH 7 with ammonia solution and 'Pestanal'-grade acetonitrile (ACN; Riedel-de Haën, Seelze, Germany). With a flow-rate of 1 ml min^{-1}, a linear gradient was employed starting at 5% ACN increasing to 65% in 40 min. The column eluates were monitored by UV-detection at 254 nm and on-line ^{19}F-NMR spectroscopy in the continuous-flow mode. Continuous-flow HPLC-NMR comprises the acquisition of sequential NMR spectra while the column eluates flow through the flow-cell (TXI probe ^{1}H, ^{13}C, ^{15}N; cell volume of 120 μl) of the Bruker DRX 500 NMR spectrometer. NMR spectra were measured at 500.13 MHz (for stop-flow ^{1}H) and manually tuned to the ^{19}F resonance frequency of 470.59 MHz for the continuous-flow experiments.

Instrument parameters for ^{19}F- and ^{1}H-HPLC-NMR spectroscopy

Continuous-flow ^{19}F-HPLC-NMR spectroscopy. Sequential ^{19}F-HPLC-NMR spectra in the continuous-flow mode were acquired at 470.59 MHz with a pulse width of 5 µs over a spectral width of 60 ppm (28 235.4 Hz). Spectra were collected into 32 K data points resulting in an acquisition time of 0.58 s. For speed of acquisition, a relaxation delay of 1 s and 16 scans per increment were applied. Hence, the time of acquisition for each increment/sequential spectrum was 25.76 s.

For continuous sequential acquisition of 1D ^{19}F-NMR spectra, a pulse sequence was applied suitable for x-nucleus detection without decoupling and solvent suppression requirements (Bruker Spectrospin Ltd). The resulting 'pseudo-2D matrix' comprises sequential 1D spectra versus time of elution (figure 1).

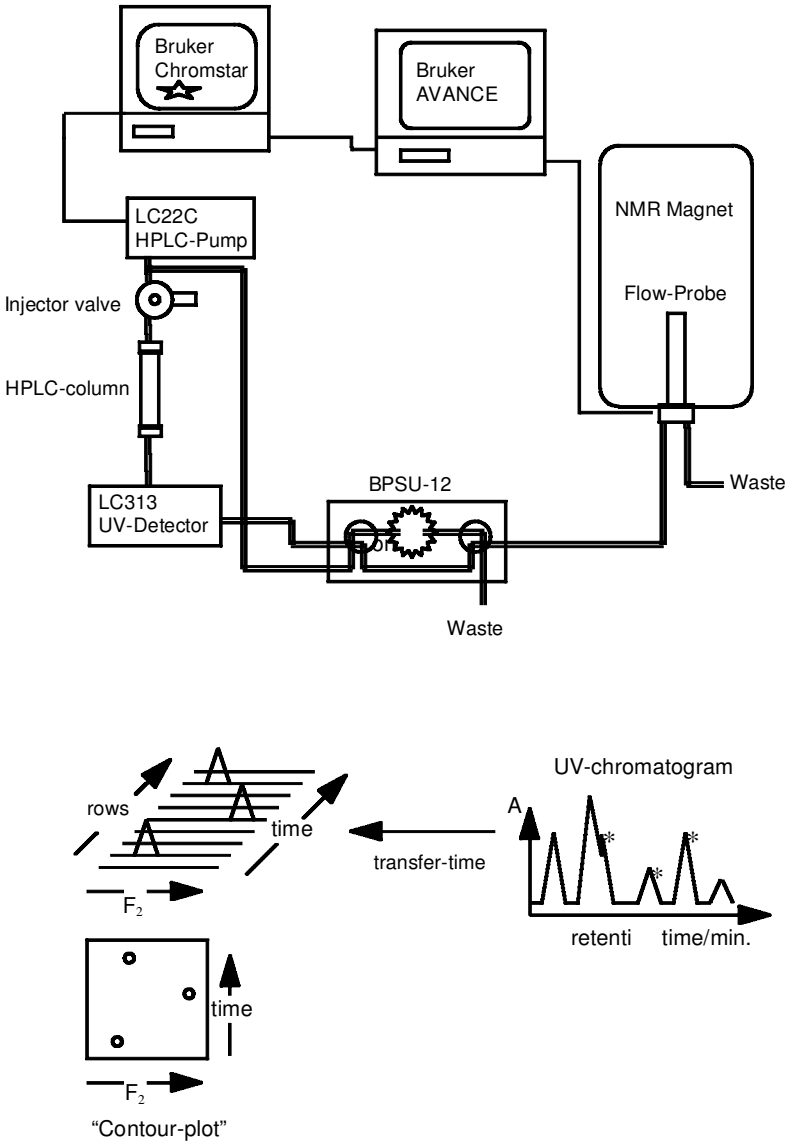


Figure 1. Set-up of the HPLC-NMR system. Depicted schematically is a 'pseudo-2D contour-plot' obtained from sequential acquisition of 1D NMR data (f2-axis) in continuous-flow mode, and its reference to the UV-chromatogram. BPSU-12, Bruker Peak Sampling Unit.

Aliquots of 100–110 µl of a sample after exposure to 1000 and 100 µg cm^{-2} were injected onto the column and the chromatographic separation was monitored by UV and ^{19}F-NMR detection. In total, 128 increments were collected, covering 54.95 min and, hence, the chromatographic run time of 40 min. Spectra were referenced to external TFE (trifluoroethanol) $\delta 19_F$ −77.023.

Stop-flow ^{1}H-HPLC-NMR spectroscopy. Stop-flow ^{1}H-HPLC-NMR spectra were acquired at 500.13 MHz utilizing a version of the NOESYPRESAT pulse sequence with double solvent suppression (Bruker Spectrospin) to attenuate the residual water and ACN in the mobile phase. This was achieved by irradiation of their frequencies during the relaxation delay of 1.8 s and during the mixing time of 80 ms. Spectra were acquired with 90 pulse angles (7.5 µs) into 32 K data points over a spectral width of 24 ppm, with 64–1024 scans depending on the concentration of the analytes. The temperature was kept constant at 30 °C. Stop-flow ^{1}H-HPLC-NMR spectra were referenced to internal ACN $\delta 1_H$ 2.0.

Typically, the injection volume (V_i) was 100l or 110 µl of individual methanolic earthworm extracts.

Results

The ^{19}F-NMR spectra of earthworm extracts following exposure to 1000 and 100 µg cm^{-2} 3-TFMA are displayed in figure 2. The ^{19}F-NMR spectra reveal a similar profile of metabolites at both exposure levels. The strong resonance at $\delta 19_F$ −61.38 is from 3-TFMA, as confirmed by spiking of the authentic standard (data not shown).

The results from the continuous-flow ^{19}F-HPLC-NMR experiment following exposure at 1000 µg cm^{-2} are shown in figure 3, with the corresponding HPLC UV chromatogram ($\lambda = 254$ nm) in figure 4. The 'pseudo-2D contour plot' represents a series of 1D ^{19}F-NMR spectra of the column eluates acquired sequentially in time (figure 1). As the spectrometer was specifically tuned to the ^{19}F frequency and since ^{19}F is not naturally abundant in earthworm samples, only 3-TFMA-related metabolites are visible. The difference in ^{19}F chemical shifts compared with the worm extracts as shown in figure 2 is due to the difference in solvent composition. An electronic spike was observed at $\delta 19_F$ −74 throughout the run, but did not interfere with the analysis. Three ^{19}F-NMR signals/metabolites could be observed, labelled as rows/increments 40, 43 and 62, which correspond to chromatographic retention times (t_R) of 16.4, 18.1 and 26.3 min, respectively.

Repeating the HPLC-NMR experiment in the ^{1}H-NMR stop-flow mode enabled structure identification and, hence, metabolite characterization. The

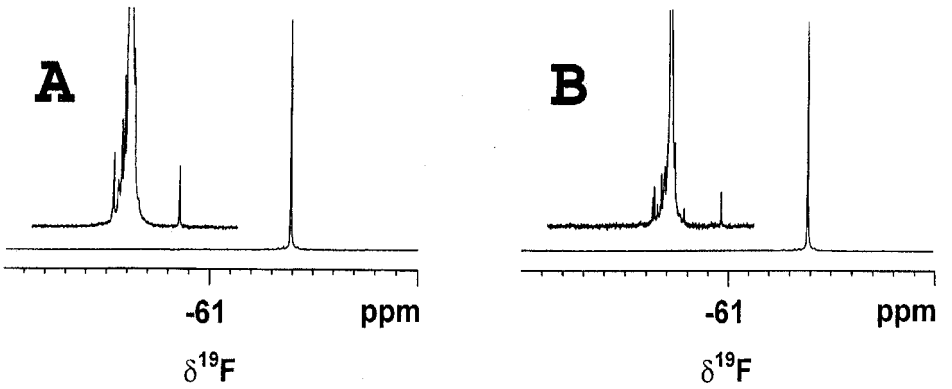


Figure 2. ^{19}F-NMR spectra of methanolic earthworm extracts following exposure to (A) 1000 and (B) 100 µg cm^{-2}. Expansions are shown in the inset.

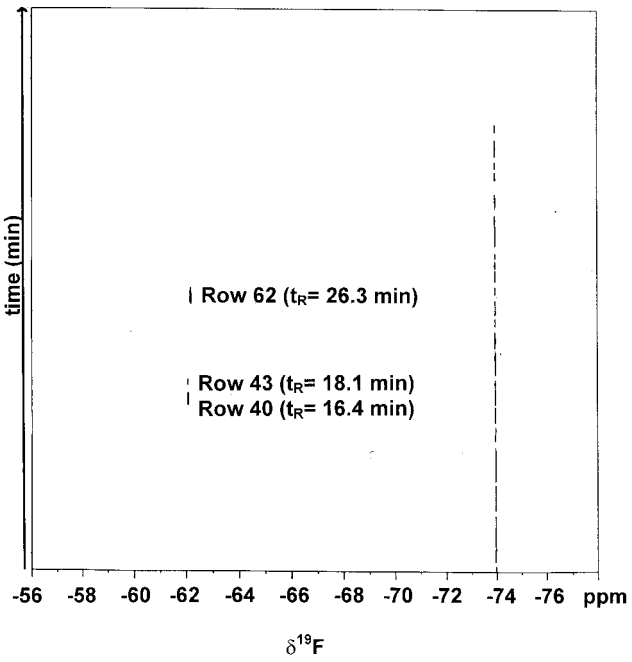


Figure 3. Pseudo-2D contour-plot of the ^{19}F-NMR monitored reversed-phase gradient HPLC-separation of the methanolic earthworm extract following 1000 µg cm^{-2} 3-TFMA exposure.

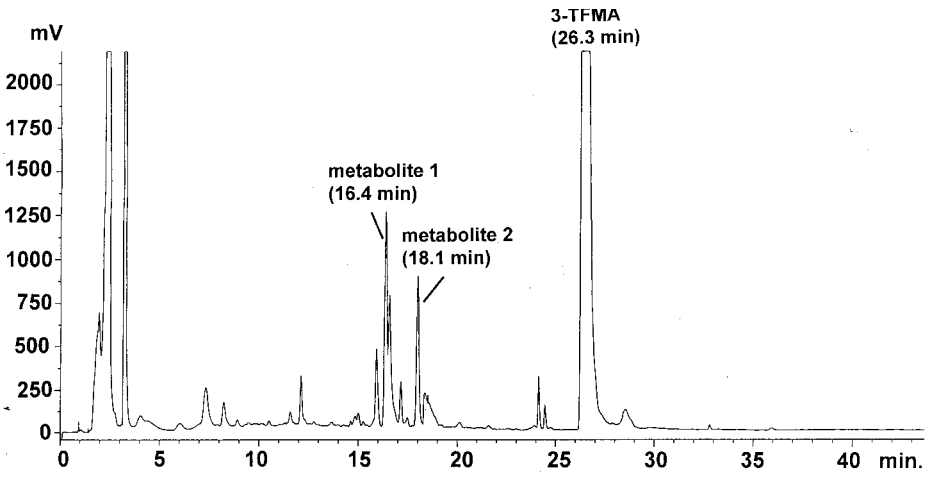


Figure 4. Reversed-phase gradient HPLC-separation of the methanolic earthworm extract following 1000 µg cm^{-2} 3-TFMA exposure.

^{1}H-NMR stop-flow spectrum of the first eluting metabolite with t_R = 16.4 min is shown in figure 5. The aromatic signals at $\delta 1_H$ 7.35, 7.05, 7.02 and 7.00 with a splitting pattern of triplet, doublet, singlet, doublet, respectively, is characteristic of unsubstituted 3-TFMA. However, the presence of a doublet at $\delta 1_H$ 4.65 with a coupling constant ($^3\mathcal{J}_{H-H}$) of 8.8 Hz is characteristic of the anomeric proton of a β-glucose conjugate. The signal intensity of the anomeric proton doublet was slightly

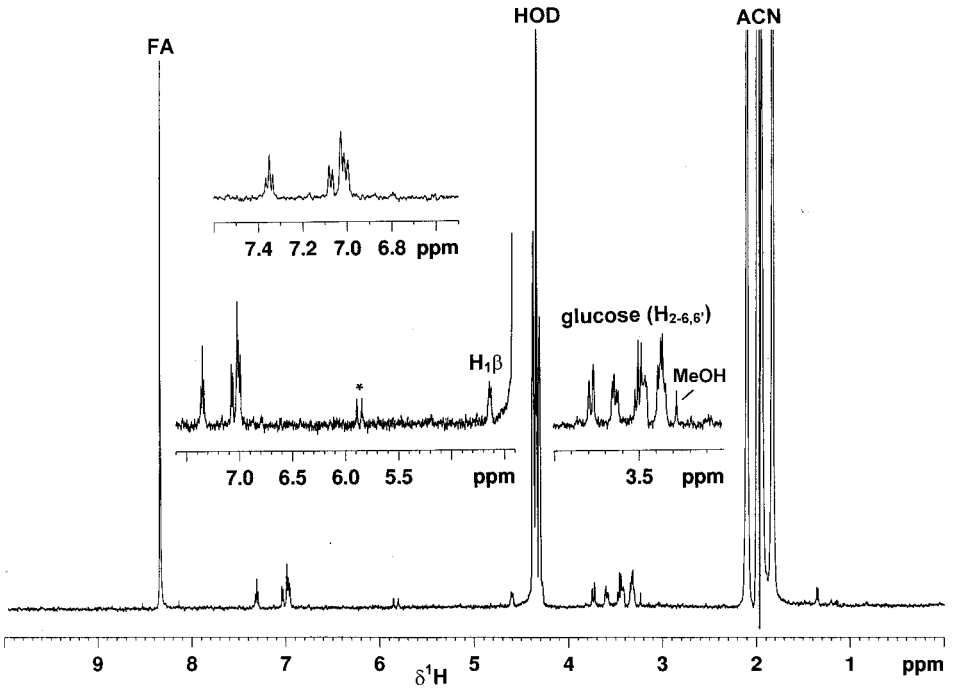


Figure 5. Stop-flow ^{1}H-NMR spectrum of metabolite 1 with a retention time of 16.4 min (acquired with 256 scans). FA, formic acid; HOD, residual water; ACN, acetonitrile. *ACN-impurity.

reduced as it appeared to be affected by the presaturation of the nearby residual water peak. The residual glucose resonances resonated at $\delta 1_H$ 3.78 (doublet; H_6), 3.65 (doublet-of-doublet; $H_{6'}$), 3.49 (multiplet) and 3.36 (multiplet). The singlet at $\delta 1_H$ 3.37 is a known impurtity (MeOH) contained in the solvent and/or the HPLC system, and is commonly observed in HPLC-NMR analyses (e.g. Scarfe *et al.* 2000, Bundy *et al.* 2001). The MeOH-d_4 used in the earthworm extraction did not give rise to a signal, as the expected quintet pattern was not observed. Also shown are suppressed but still dominant signals from the mobile phase constituents, residual water at $\delta 1_H$ 4.32 and ACN at $\delta 1_H$ 2.0. The large singlet at $\delta 1_H$ 8.33 is from formate, the buffer contained in the mobile phase. Another impurity signal appeared consistently, giving rise to signals at $\delta 1_H$ 5.9 and 5.85, which has been identified as an impurity in the ACN.

As the 3-TFMA splitting was preserved in this metabolite, i.e. ruling out substitution on the aromatic ring, it appeared that this metabolite is an *N*- or possibly a *NO*-glucoside conjugate of 3-TFMA. However, the chemical shift of the anomeric proton is indicative of *N*- rather than *NO*-conjugation (Scarfe *et al.* 2000).

The metabolite eluting after $t_R = 18.1$ min still preserved the pattern of unsubstituted 3-TFMA (figure 6), however, a slight change in the chemical shifts of the signals have been observed compared with the previous eluting metabolite. The aromatic protons of this minor metabolite appeared at $\delta 1_H$ 7.37 (triplet), 7.15 (singlet), 7.1 (doublet) and 7.07 (doublet). Again, a doublet from an anomeric proton could also be observed at $\delta 1_H$ 5.17 with $^3\mathcal{J}_{H-H} = 4.8$ Hz, indicating conjugation with α-glucose. The residual glucose resonances were not as clearly

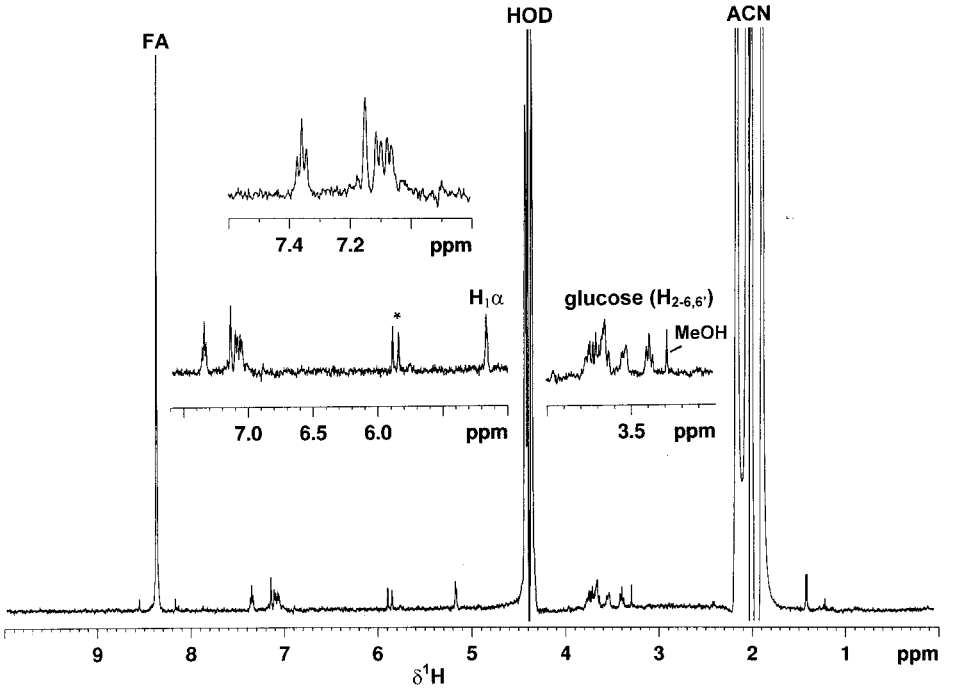


Figure 6. Stop-flow ^{1}H-NMR spectrum of metabolite 2 with a retention time of 18.1 min (acquired with 512 scans). FA, formic acid; HOD, residual water; ACN, acetonitrile. *ACN-impurity.

defined and appeared as heavily overlapped multiplets in the region of $\delta 1_H$ 3.8–3.38. However, the total integral of the signals indicated the presence of six protons.

The methanol impurity at $\delta 1_H$ 3.27 was also contained in this chromatographic fraction, as well as the signals at $\delta 1_H$ 6.0 and 5.95 from the ACN impurity. Fortunately, they did not perturb signal assignment. The more challenging (dynamic range) problem was provided by the presence of the solvent peaks ($\delta 1_H$ 4.38 and 2.0) and the formate singlet at $\delta 1_H$ 8.36. The doublet at $\delta 1_H$ 1.39 and the corresponding quartet at $\delta 1_H$ 2.4 derive from an isopropanol impurity in the solvent (ACN).

The chemical shift differences observed for the aromatic signals *ortho* to the amino-group can be accounted for by the differences in conformation because of conjugation with α- and β-glucose.

The identity of the parent compound could be confirmed by stopping the chromatographic separation at its characteristic $t_R = 26.3$ min and by recording a ^{1}H stop-flow NMR spectrum (figure 7). Although, 3-TFMA could be chromatographically identified, based on its high concentration and characteristic retention time, stop-flow ^{1}H-HPLC-NMR provided an unequivocal means for its unambiguous structural characterization. Owing to the high concentration of the parent compound, only 64 scans were required. The aromatic resonances appeared at $\delta 1_H$ 7.28 (triplet, ^{1}H *meta* to amino group), 6.98 (doublet), 6.97 (singlet, ^{1}H *ortho* to amino and CF_3-groups) and 6.92 (doublet). The solvent resonances at $\delta 1_H$ 4.25 (residual water) and $\delta 1_H$ 2.0 (ACN), and the mobile phase buffer constituent

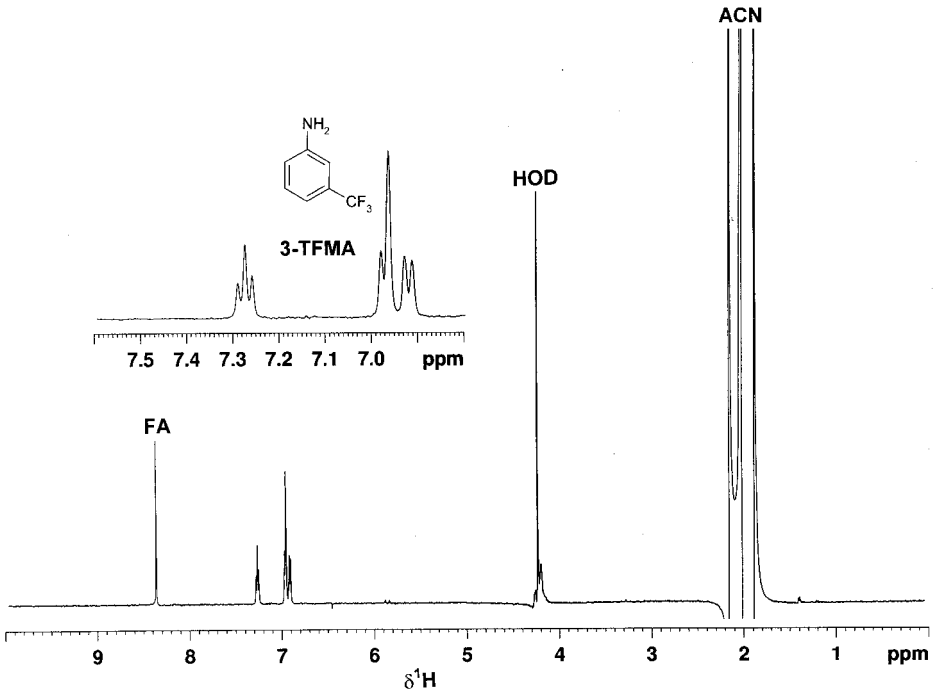


Figure 7. Stop-flow ^{1}H-NMR spectrum of 3-TFMA parent compound with a retention time of 26.3 min (acquired with 64 scans). FA, formic acid; HOD, residual water; ACN, acetonitrile. *ACN-impurity.

formate ($\delta 1_{H}$ 8.39) were also present, however, they did not present a severe dynamic range problem for this late eluting analyte, as the residual water and, therefore, the buffer salt proportions were reduced as a consequence of the linear gradient with increasing organic solvent composition.

The same metabolites could be identified following exposure to 100 $\mu g\,cm^{-2}$ (data not shown). In this case, the ^{19}F-NMR monitored continuous-flow experiment was able to detect signals from the β-glucoside conjugate and parent compound, however, failed to detect the weaker contour from the α-glucose conjugate. The identity of the metabolites and parent could be verified by stop-flow ^{1}H-NMR spectroscopy, although longer acquisition times were required to counteract the lower concentrations at this exposure level. The chromatographic peak with the expected retention time for the α-glucose conjugate was additionally verified by stop-flow ^{19}F-NMR spectroscopy prior to its structural identification by ^{1}H-NMR spectroscopy, an approach that will be very useful for the identification of the metabolites at the lower (sublethal) exposure levels.

Following the same method/protocol, the minor metabolites at the lethal exposure levels and the metabolites contained in the extracts from the sublethal doses (10, 1, 0.1 $\mu g\,cm^{-2}$) could not be detected by continuous-flow ^{19}F-NMR spectroscopy. Owing to the chromatographic limit in sample loading, the metabolites will have to be concentrated in future work and the analysis will have to be carried out entirely by stop-flow ^{19}F and ^{1}H-NMR.

Discussion

The component complexity of ^{1}H-NMR spectra of earthworm extracts was highlighted in Lenz *et al.* (2001). The most striking differences between the earthworm extracts following exposure to 1000 and 100 μg cm^{-2} 3-TFMA and the controls comprised increased concentrations of lactate and alanine (doublets at $\delta 1_H$ 1.34 and 1.48, respectively), a toxicological effect discussed further in Warne *et al.* 2000, and the presence of signals from 3-TFMA itself (Lenz *et al.* 2001). Although detection of parent compound was possible at the highest exposure levels, excessive peak overlap with endogenous metabolites impaired detection and identification of the 3-TFMA metabolites.

The corresponding ^{19}F-NMR spectra demonstrated the selectivity of ^{19}F-NMR and revealed the simplicity of the worm extract spectra as ^{19}F species are not naturally present in biological samples. The use of ^{19}F as a specific handle for the HPLC-NMR analysis is obvious, especially since problems presented by chemical noise and signal overlap (from endogenous material), and dynamic range (from the mobile phase's water/solvent signals) inherent to ^{1}H-NMR spectroscopic detection could be eliminated. However, above all, it provided an analytical challenge. This work represents the first application of a ^{19}F-NMR-monitored separation of an invertebrate sample.

The continuous-flow NMR experiment demonstrated the real value of ^{19}F-NMR detection as it allowed the ecotoxin related metabolites to be selectively identified in the UV chromatogram in a single analytical step. The signals comprised single lines of triple intensity (due to the presence of the CF_3-group), which facilitated their detection on-flow.

At this point, metabolite identification was severely limited as structural information was not given by ^{19}F-NMR spectroscopy alone, however, the elution characteristics indicated that the metabolites must have been more polar than the parent compound.

The subsequent stop-flow ^{1}H-NMR spectra were sufficiently clean for full structural identification, hence, successful chromatographic separation of the metabolites from the endogenous worm metabolites has been achieved. The only interferences encountered were from the mobile phase constituents and solvent impurities.

The detection of metabolites at the dose levels of 1000 and 100 μg cm^{-2} is noteworthy, considering that mortality was observed virtually instantly (between 0 and 30 min and 0 and 120 min in the 1000 and 100 μg cm^{-2} dose groups, respectively). It therefore appears that absorption was rapid allowing metabolism to occur during the short exposure time before their deaths. Alternatively, some contribution by the worm's microflora possibly during sample preparation (e.g. homogenization) had to be assumed.

N-β-glucoside conjugates have been previously identified in plants and earthworms (Bailey *et al.* 2000, Bundy *et al.* 2001, respectively). In the earthworm study, ridding the earthworm of bacteria did not affect the metabolite profile. Hence, it appears more likely that the metabolites observed in this study are metabolic products produced by the earthworm itself. The results in this study confirm Phase II conjugation to be an important metabolic pathway in earthworms dealing with xenobiotics (Bundy *et al.* 2001) and to the best of our knowledge, present the first evidence of α-glucose conjugation of xenobiotics in earthworms.

The earthworms were extracted directly into MeOH-d_4 to ensure solubility of the hydrophobic 3-TFMA, hence, maximizing extraction efficiency, and to reduce the risk of evaporation during extensive sample preparation steps (i.e. freeze-drying). A total of 100–110 µl methanolic earthworm extract were injected directly onto the HPLC column. Unfortunately, injection of larger volumes resulted in overloading and loss of retention of the analytes.

Conclusions

The advantages of continuous-flow ^{19}F-HPLC-NMR spectroscopy have been demonstrated. The 3-TFMA metabolites could be selectively detected and their retention times determined in a single step entirely without sample preparation. The subsequent stop-flow ^{1}H-NMR spectra enabled full structural identification of the metabolites as isolation from the endogenous worm metabolites could be achieved on-line. This enabled the identification of α- and β-glucoside conjugates of 3-TFMA following exposure to 1000 and 100 µg cm^{-2} in individual earthworm extracts.

Although the HPLC-NMR experiment as demonstrated in this study appeared to be a suitable approach for concentrated samples, the metabolites from earthworms exposed to the sublethal dose levels (10, 1, 0.1 µg) could not be detected on-flow by ^{19}F-monitored HPLC-NMR spectroscopy. In fact, these levels severely challenge the detection limits of continuous-flow HPLC-NMR spectroscopy, as the residence time of each analyte inside the flow-cell is very limited at the given flow-rate.

Obviously, improved detection may be achieved by reducing the flow-rate, therefore, enabling the acquisition of an increased number of scans per NMR increment. However, further work will require pooling and concentrating of the metabolites and analysis solely under ^{19}F- and ^{1}H-NMR stop-flow conditions, preferably at higher field strengths. In addition, identification by mass spectrometry will be invaluable.

Acknowledgements

The authors thank the NERC for funding E. M. L. and for provision of facilities for the earthworm experiments. They are also very grateful to the ULIRS for the use of the 600 MHz spectrometer at Q. M. W. College, London, and the 500 MHz spectrometer at Birkbeck College, London.

References

Akitt, J. W., 1992, *NMR and Chemistry: An Introduction to Modern NMR Spectroscopy*, 3rd edn (London: Chapman & Hall).

Bailey, N. J. C., Cooper, P., Hadeld, S. T., Lenz, E. M., Lindon, J. C., Nicholson, J. K., Stanley, P. D., Wilson, I. D., Wright, B. and Taylor, S., 2000, Application of directly coupled HPLC-NMR-MS/MS to the identification of metabolites of 5-trifluoro-methylpyridone (2-hydroxy-5-trifluoromethylpyridine) in hydroponically grown plants. *Journal of Agriculture and Food Chemistry*, **48**, 42–46.

Belfroid, A., Seinen, W., van Gestel, K. and Hermens, J., 1993, The acute toxicity of chlorobenzenes for earthworms (*Eisenia andrei*) in different exposure systems. *Chemosphere*, **26**, 2265–2277.

Belfroid, A., van den Berg, M., Seine, N. W., Hermens, J. and van Gestel, K., 1995, Uptake, bioavailability and elimination of hydrophobic compounds in earthworms (*Eisenia andrei*) in field-contaminated soil. *Environmental Toxicology and Chemistry*, **14**, 605–612.

Bundy, J. G., Lenz, E. M., Osborn, D., Weeks, J. M., Lindon, J. C. and Nicholson, J. K., 2001, Metabolism of 4-fluoroaniline and 4-fluorobiphenyl in the earthworm *Eisenia veneta* characterized by NMR spectroscopy, HPLC-NMR, and HPLC-MS. *Xenobiotica*, **32**, 479–490.

Christensen, O. M. and Mather, J. G., 1994, *Earthworms as Ecotoxicological Test-Organisms.* No. 5 (Copenhagen: Danish Environmental Protection Agency, Ministry of the Environment).

Eadsforth, C. V., Coveney, P. C., Hutson, D. H., Logan, C. J. and Samuel, A. J., 1986, The metabolism of *o*-fluoroaniline by rats, rabbits and marmosets. *Xenobiotica*, **16**, 555–566.

Ehlhardt, W. J. and Howbert, J. J., 1991, Metabolism and disposition of *p*-chloro-aniline in rat, mouse and monkey. *Drug Metabolism and Disposition*, **19**, 366–369.

Haimi, J., Salminen, J., Huhta, V., Knuutinen, J. and Palm, H., 1992, Bioaccumulation of organochlorine compounds in earthworms. *Soil Biology and Biochemistry*, **24**, 1699–1703.

Kiese, M. and Lenk, W., 1971, Metabolites of 4-chloroaniline and chloroacetanilides produced by rabbits and pigs. *Biochemistry and. Pharmacology*, **20**, 379–391.

Lenz, E. M., Lindon, J. C., Nicholson, J. K., Weeks, J. M. and Osborn, D., 2001, ^{19}F-NMR spectroscopic investigation into the absorption and metabolism of the model ecotoxin, 3-trifluoromethylaniline, in *Eisenia veneta. Ecotoxicology and Environmental Safety* (submitted).

Lindon, J. C., 1995, Fluorine nuclear magnetic resonance. In *Encyclopedia of Analytical Science* (London: Academic Press), p. 3408.

Lindon, J. C., Nicholson, J. K. and Wilson, I. D., 2000. Directly coupled HPLC-NMR and HPLC-NMR-MS in pharmaceutical research and development. *Journal of Chromatography* B, **748**, 233–258.

OECD, 1984, *Earthworm, Acute Toxicity Tests.* Guideline for Testing of Chemicals, No. 7 (Paris: Organization for Economic Co-operation and Development).

Radomski, J. L., 1979, The primary aromatic amines: their biological properties and structure–activity relationships. *Annual Review in Pharmacology and Toxicology*, **19**, 129–157.

Rietjens, I. M. C. M. and Vervoort, J., 1989, Microsomal metabolism of fluoro-anilines. *Xenobiotica*, **19**, 1297–1305.

Scarfe, G. B., Clayton, E., Wilson, I. D. and Nicholson, J. K., 2000, Identification and quantification of metabolites of 2,3,5,6-tetrafluoro-4-trifluoromethylaniline in rat urine using ^{19}F-NMR spectroscopy, HPLC-NMR spectroscopy and HPLC-MS spectrometry. *Journal of Chromatography* B, **748**, 311–319.

Stenersen, J., Brekke, E. and Engelstadt, F., 1992, Earthworms for toxicity testing; species differences in response towards cholinesterase inhibiting insecticides. *Soil Biology and Biochemistry*, **24**, 1761–1764.

Tugnait, M., Lenz, E. M., Phillips, P., Hofmann, M., Spraul, M., Lindon, J. C., Nicholson, J. K. and Wilson, I. D., 2001, The metabolism of 4-trifluoromethoxyaniline and [^{13}C]-4-trifluoromethoxyacetanilide in the rat: detection and identification of metabolites excreted in the urine by NMR and HPLC-NMR. *Journal of Pharmaceutical and Biomedical Analysis* (in press).

Van Gestel, C. A. M. and van Dis, W. A., 1988, The influence of soil characteristics on the toxicity of four chemicals to the earthworm *Eisenia andrei. Biology and Fertility of Soils*, **6**, 262–265.

Van Gestel, C. A. M., Dirven-Van Bremen, E. M., Baerselman, R., Emans, H. J. B., Jannsen, J. A. M., Postuma, R. and van Vliet, P. J. M., 1992, Comparison of sublethal and lethal criteria for nine different chemicals in standardized toxicity tests using the earthworm *Eisenia andrei. Ecotoxicology and Environmental Safety*, **23**, 206–220.

Vervoort, J., De Jager, P. A., Steenbergen, J. and Rietjens, I. M. C. M., 1990, Development of a ^{19}F-NMR method for studies on the *in vivo* and *in vitro* metabolism of 2-fluoroaniline. *Xenobiotica*, **20**, 657–670.

Vervoort, J., Rietjens, I. M. C. M., Moonen, C. T. W., von Kienlin, M. and Despres, D., 1991, Biotransformation of 2-fluoroaniline in rats by *in vivo* ^{19}F-NMR. *NMR in Biomedicine*, **4**, 255–261.

Wade, K. E., Wilson, I. D., Troke, J. A. and Nicholson, J. K., 1990, ^{19}F and ^{1}H magnetic resonance strategies for metabolic studies on fluorinated xenobiotics: application to flurbiprofen [2-(2-fluoro-4-biphenylyl)propionic acid]. *Journal of Pharmacological and Biomedical Analysis*, **8**, 401–410.

Warne, M. A., Lenz, E., Osborn, D., Weeks, J. M. and Nicholson, J. K., 2000, An NMR-based metabonomic investigation of the toxic effects of 3-trifluoromethylaniline on the earthworm *Eisenia veneta. Biomarkers*, **5**, 56–72.

Wilson, I. D., MacDonald, C. M., Fromson, J. M., Troke, J. A. and Hillbeck, D., 1985, Species differences in the metabolism of ^{14}C-*p*-trifluoromethyl aniline: production of an oxanilic acid as the major metabolite by the rat. *Biochemical Pharmacology*, **34**, 2025–2028.

XENOBIOTICA, 2002, VOL. 32, NO. 7, 547–561

Taylor & Francis
healthsciences

Species differences in coumarin metabolism: a molecular modelling evaluation of CYP2A interactions

D. F. V. LEWIS†* and B. G. LAKE‡

† School of Biomedical and Life Sciences, University of Surrey, Guildford GU2 7XH, UK
‡ TNO BIBRA International Ltd, Woodmansterne Road, Carshalton, SM5 4DS, UK

Received 17 September 2001

1. An account of the differences in coumarin metabolism between several mammalian species, including man, is reported.

2. The metabolism of coumarin via 7-hydroxylation in the human (CYP2A6) and mouse (CYP2A5) enzymes is explained in terms of molecular modelling of the active site interactions, whereas the rat orthologue (CYP2A1) exhibits 3,4-epoxidation of coumarin, which is also consistent with the modelled interaction between enzyme and substrate.

3. In addition, quantitative structure–activity relationships (QSARs) for coumarin 7-hydroxylation in wild-type and mutant CYP2A5 show the importance of amino acid residue properties for substrate binding, whereas QSARs for CYP2A6 substrates indicate the importance of hydrogen bonding and lipophilicity for favourable interactions with the enzyme.

Introduction

The cytochromes P450 (CYP) constitute a superfamily of haem-thiolate enzymes present in most species and are associated with Phase I metabolism of a large number and variety of drugs and other xenobiotics (Rendic and DiCarlo 1997). In mammalia, a relatively small number of hepatic microsomal P450s catalyse the oxidation of most foreign compounds, and these enzymes constitute P450s from families CYP1, CYP2 and CYP3; the situation in *Homo sapiens* is similar to that encountered in other mammalian species studied, with > 90% of all drug oxidations being mediated by P450s from the same three families (Rendic and DiCarlo 1997). Coumarin is generally regarded as a selective marker substrate for CYP2A6, where 7-hydroxylation is the specifically catalysed pathway for coumarin metabolism in man (Pelkonen *et al.* 2000, Cok *et al.* 2001). In rat, however, the route of metabolism is thought to involve 3,4-epoxidation (reviewed in Lake 1999, Born *et al.* 2000) whereas the mouse isoform, CYPA5, resembles the human orthologue in catalysing 7-hydroxylation of coumarin. Although not exclusively involved, the rat orthologue CYP2A1 is thought to mediate in the 3,4-epoxidation pathway leading to coumarin clearance (reviewed in Lewis and Lake 1995) but CYP2A1 does not appear to catalyse the 7-hydroxylation of coumarin.

Consequently, it is anticipated that the species differences in coumarin metabolism can be explained in terms of active site modelling of the relevant CYP2A subfamily enzymes. With the advent of a new mammalian microsomal P450 crystal

* Author for correspondence; e-mail: d.lewis@surrey.ac.uk

Xenobiotica ISSN 0049–8254 print/ISSN 1366–5928 online © 2002 Taylor & Francis Ltd
http://www.tandf.co.uk/journals
DOI: 10.1080/00498250210128693

structure, namely that of the rabbit enzyme CYP2C5 (Williams *et al.* 2000), there is an opportunity of generating homology models of CYP2 family enzymes, including those of the CYP2A subfamily which show about 50% sequence identity with the crystallographic template (Lewis 2002). Consequently, the use of CYP2C5 enables more accurate models of CYP2 family enzymes to be developed than those based on the CYP102 template (Lewis and Lake 1995, Lewis *et al.* 1999). However, it is unfortunate that the CYP2C5 structure does not contain a bound substrate, although a molecule of progesterone was docked interactively within the active site following generation of the crystallographic coordinates (Williams *et al.* 2000). It is apparent from a comparison between the substrate-bound and -free forms of CYP101 and CYP102 that there is some degree of structural change accompanying substrate binding, although the differences are minimal for CYP101 (Poulos *et al.* 1986, 1987). For CYP102, there are significant conformational changes in the structure when the substrate palmitoleic acid is bound to the enzyme, as can be appreciated by comparison of the substrate-free (Ravichandran *et al.* 1993) and -bound forms (Li and Poulos 1997). However, while one awaits elucidation of a substrate-bound CYP2C5 crystal structure, it is reasonable to make use of the current substrate-free form provided that it is appreciated that models based on these coordinates are likely to represent only approximations of the true situation *in vivo*. Nevertheless, the use of CYP2C5 is justifiable as it represents an advance on previously available crystal structures, which are all from prokaryotic sources and, consequently, of much lower sequence homology with mammalian P450s than is CYP2C5 (Lewis 2002).

Materials and methods

From the recently available atomic coordinates of CYP2C5 (Williams *et al.* 2000), the structures of CYP2A1, CYP2A5 and CYP2A6 were modelled by homology using the Sybyl Bipolymer module (Tripos Associates, St Louis, MO, USA) according to multiple sequence alignment of the CYP2 family as shown in figure 1 (Lewis 2002). This alignment was produced via the GCG software (Genetics Computer Group, Madison, WI, USA) and figure 1 indicates the location of substrate recognition sites (SRS) regions (Gotoh 1992) and membrane anchor peptide via shaded boxes, whereas residues that have been the subject of site-directed mutagenesis experiments have been emboldened. Following generation of a raw model via amino acid residue replacement, the structure in each case was energy minimized using molecular mechanics (Tripos force field) to obtain a low-energy geometry by relaxing the original protein molecule such that any unfavourable steric interactions between both bonded and non-bonded atoms are either reduced or removed (Lewis 2002).

Once a satisfactory low-energy conformation had been obtained, the coumarin molecule was docked interactively within each enzyme active site such that favourable binding associations between amino acid residues and the substrate could orientate coumarin relative to the haem moiety for oxidation at the experimentally observed positions. The total energy of interaction between the substrate and enzyme was then estimated on the basis of these interactions. All molecular modelling procedures were carried out using Sybyl as implemented on a Silicon Graphics Indigo^2 IMPACT 10000 graphics workstation operating under the UNIX system.

Quantitative structure–activity relationships (QSARs) were generated for CYP2A6 substrates based on K_m data (Rendic and DiCarlo 1997) and physicochemical properties such as log P (Suzuki and Kudo 1990).

Results and discussion

Table 1 shows the similarities and differences between the three CYP2A subfamily enzymes as mapped against the CYP2C5 active site within their putative active site regions, and the results of previously reported site-directed mutagenesis experiments in the CYP2A subfamily are summarized in table 2. These give

ALIGNMENT BETWEEN VARIOUS CYP2 FAMILY SEQUENCES

```
                membrane   anchor   region
                1          10       20          30          40
cyp2a1   ...MLDTGLL LVVILASLSV MLLVSLWQQ. KIRGRLPPGP TPLPFIGNYL
cyp2a4   ...MLTSGLL LVAAVAFLSV LVLMSVWKQR KLSGKLPPGP TPLPFVGNFL
cyp2a5   ...MLTSGLL LVAAVAFLSV LVLMSVWKQR KLSGKLPPGP TPLPFIGNFL
cyp2a6   ...MLASGML LVALLVCLTV MVLMSVWQQR KSKGKLPPGP TPLPFIGNYL
cyp2b1   ......MEPT ILLLLALLVG FLLLLVRGHP KSRGNFPPGP RPLPLLGNLL
cyp2b4   ......MEFS LLLLLAFLAG LLLLLFRGHP KAHGRLPPGP SPLPVLGNLL
cyp2b6   ......MELS VLLFLALLTG LLLLLVQRHP NTHDRLPPGP RPLPLLGNLL
cyp2c2   ........MDL VVVLGLCLSC LLLPSLWKQS HGGGKLPPGP TPFPILGNVL
cyp2c3   ........MDL LIILGICLSC VVLLSLWKKT HGKGKLPPGP TPLPVVGNLL
cyp2c4   ........MDP VAGLVLGLCC LLLLSLWKQN SGRGKLPPGP TPFPIIGNIL
cyp2c5   ........MDP VVVLVLGLCC LLLLSIWKQN SGRGKLPPGP TPFPIIGNIL
cyp2c8   ........MEP FVVLVLCLSF MLLFSLWRQS CRRRKLPPGP TPLPIIGNML
cyp2c9   ........MDS LVVLVLCLSC LLLLSLWRQS SGRGKLPPGP TPLPVIGNIL
cyp2c19  ........MDP FVVLVLCLSC LLLLSIWRQS SGRGKLPPGP TPLPVIGNIL
cyp2d1   MELLNGTGLW SMAIFTVIFI LLVDLMHRRH RWTSRYPPGP VPWPVLGNLL
cyp2d6   ...MGLEALV PLAVIVAIFL LLVDLMHRRQ RWAARYPPGP LPLPGLGNLL
cyp2e1r  ....MAVLGI TVALLGWMVI LLFISVWKQI HSSWNLPPGP FPLPIIGNLL
cyp2e1h  ....MSALGV TVALLVWAAF LLLVSMWRQV HSSWNLPPGP FPLPIIGNLF
cyp2f1   ......MDSI STAILLLLLA LVCLLLTLSS RDKGKLPPGP RPLSILGNLL
cyp2f2   ......MDGV STAILLLLLA VISLSLTFSS RDKGQLPPGP KPLPILGNLL

                < Ahelix >      |1-1|  | 1-2 |   <   B helix   >
                50         60         70          80          90
cyp2a1   QLNTKDVYSS ITQLSERYGP VFTIHLGPRR VVVLYGYDAV KEALVDQAEE
cyp2a4   QLNTEQMYNS LMKISQRYGP VFTIYLGSRR IVVLCGQEAV KEALVDQAEE
cyp2a5   QLNTEQMYNS LMKISQRYGP VFTIYLGPRR IVVLCGQEAV KEALVDQAEE
cyp2a6   QLNTEQMYNS LMKISERYGP VFTIHLGPRR VVVLCGHDAV REALVDQAEE
cyp2b1   QLDRGGLLNS FMQLREKYGD VFTVHLGPRP VVMLCGTDTI KEALVGQAED
cyp2b4   QMDRKGLLRS FLRLREKYGD VFTVYLGSRP VVVLCGTDAI REALVDQAEA
cyp2b6   QMDRRGLLKS FLRFREKYGD VFTVHLGPRP VVMLCGVEAI REALVDKAEA
cyp2c2   QLDFKDLSKS LTNLSKVYGP VFTVYLGMKP TVVVHGYEAV KEALVDLGHE
cyp2c3   QLETKDINKS LSMLAKEYGS IFTLYFGMKP AVVLYGYEGV IEALIYRGEE
cyp2c4   QIDVKDISKS LTKFSERYGP VFTVYLGMKP TVVLHGYKAV KEALVDLGEE
cyp2c5   QIDAKDISKS LTKFSECYGP VFTVYLGMKP TVVLHGYEAV KEALVDLGEE
cyp2c8   QIDVKDICKS FTNFSKVYGP VFTVYFGMNP IVVFHGYEAV KEALIDNGEE
cyp2c9   QIGIKDISKS LTNLSKVYGP VFTLYFGLKP IVVLHGYEAV KEALIDLGEE
cyp2c19  QIDIKDVSKS LTNLSKIYGP VFTLYFGLER MVVLHGYEVV KEALIDLGEE
cyp2d1   QVDLSNMPYS LYKLQHRYGD VFSLQKGWKP MVIVNRLKAV QEVLVTHGED
cyp2d6   HVDFQNTPYC FDQLRRRFGD VFSLQLAWTP VVVLNGLAAV REALVTHGED
cyp2e1r  QLDLKDIPKS FGRLAERFGP VFTVYLGSRR VVVLHGYKAV REMLLNHKNE
cyp2e1h  QLELKNIPKS FTRLAQRFGP VFTLYVGSQR MVVMHGYKAV KEALLDYKDE
cyp2f1   LLCSQDMLTS LTKLSKEYGS MYTVHLGPRR VVVLSGYQAV KEALVDQGEE
cyp2f2   QLRSQDLLTS LTKLSKEYGS VFTVYLGSRP VIVLSGYQTV KEALVDKGEE
```

```
                    SRS1                          <  C helix >
            100             110             120             130
cyp2a1  FSGRGEQATY NTLFKG...Y GVAFSS.GER AKQLRRLSIA TLRDFGVGKR
cyp2a4  FSGRGEQATF DWLFKG...Y GIAFSS.GER AKQLRSFSIA TLRDFGVGKR
cyp2a5  FSGRGEQATF DWLFKG...Y GVVFSS.GER AKQLRRFSIA TLRDFGVGKR
cyp2a6  FSGRGEQATF DWVFKG...Y GVVFSN.GER AKQLRRFSIA TLRDFGVGKR
cyp2b1  FSGRGTIAVI EPIFKE...Y GVIFAN.GER WKALRRFSLA TMRDFGMGKR
cyp2b4  FSGRGKIAVV DPIFQG...Y GVIFAN.GER WRALRRFSLA TMRDFGMGKR
cyp2b6  FSGRGKIAMV DPFFRG...Y GVIFAN.GNR WKVLRRFSVT TMRDFGMGKR
cyp2c2  LSGRSRFLVT AKLNKG...F GVIFSN.GKR WTETRRFSLM TLRNFGMGKR
cyp2c3  FSGRGIFPVF DRVTKG...L GIVFSS.GEK WKETRRFSLT VLRNLGMGKK
cyp2c4  FAGRGHFPIA EKVNKG...L GIVFTN.ANT WKEMRRFSLM TLRNFGMGKR
cyp2c5  FAGTGSVPIL EKVSKG...L GIAFSN.AKT WKEMRRFSLM TLRNFGMGKR
cyp2c8  FSGRGNSPIS QRITKG...L GIISSN.GKR WKEIRRFSLT TLRNFGMGKR
cyp2c9  FSGRGIFPLA ERANRG...F GIVFSN.GKK WKEIRRFSLM TLRNFGMGKR
cyp2c19 FSGRGHFPLA ERANRG...F GIVFSN.GKR WKEIRRFSLM TLRNFGMGKR
cyp2d1  TADRPPVPIF KCLGVKPRSQ GVILASYGPE WREQRRFSVS TLRTFGMGKK
cyp2d6  TADRPPVPIT QILGFGPRSQ GVFLARYGPA WREQRRFSVS TLRNLGLGKK
cyp2e1r FSGRGEIPAF .REFKD...K GIIFNN.GPT WKDTRRFSLT TLRDYGMGKQ
cyp2e1h FSGRGDLPAF .HAHRD...R GIIFNN.GPT WKDIRRFSLT TLRNYGMGKQ
cyp2f1  FSGRGDYPAF FNFTKG...N GIAFSS.GDR WKVLRQFSIQ ILRNFGMGKR
cyp2f2  FSGRGAYPVF FNFTRG...N GIAFSD.GER WKILRRFSVQ ILRNFGMGKR
```

```
        <     D helix    >          < D'> < Ehelix >
        140         150         160         170         180
cyp2a1  GVEERILEEA GYLIKMLQGT CGAPIDPTIY LSKTVSNVIS SIVFGERFDY
cyp2a4  GIEERIQEEA GFLIDSFRKT NGAFIDPTFY LSRTVSNVIS SIVFGDRFDY
cyp2a5  GIEERIQEEA GFLIDSFRKT NGAFIDPTFY LSRTVSNVIS SIVFGDRFDY
cyp2a6  GIEERIQEEA GFLIDAHRGT GGANIDPTFF LSRTVSNVIS SIVFGDRFDY
cyp2b1  SVEERIQEEA QCLVEELRKS QGAPLDPTFL FQCITANIIC SIVFGERFDY
cyp2b4  SVEERIQEEA RCLVEELRKS KGALLDNTLL FHSITSNIIC SIVFGKRFDY
cyp2b6  SVEERIQEEA QCLIEELRKS KGALMDPTFL FQSITANIIC SIVFGKRFHY
cyp2c2  SIEERVQEEA HCLVEELRKT NASPCDPTFI LGAAPCNVIC SVIFQNRFDY
cyp2c3  TIEERIQEEA LCLIQALRKT NASPCDPTFL LFCVPCNVIC SVIFQNRFDY
cyp2c4  SIEDRVQEEA RCLVEELRKT NALPCDPTFI LGCAPCNVIC SVILHNRFDY
cyp2c5  SIEDRIQEEA RCLVEELRKT NASPCDPTFI LGCAPCNVIC SVIFHNRFDY
cyp2c8  SIEDRVQEEA HCLVEELRKT KASPCDPTFI LGCAPCNVIC SVVFQKRFDY
cyp2c9  SIEDRVQEEA RCLVEELRKT KASPCDPTFI LGCAPCNVIC SIIFHKRFDY
cyp2c19 SIEDRVQEEA RCLVEELRKT KASPCDPTFI LGCAPCNVIC SIIFQKRFDY
cyp2d1  SLEEWVTKEA GHLCDAFTAQ AGQSINPKAM LNKALCNVIA SLIFARRFEY
cyp2d6  SLEQWVTEEA ACLCAAFANH SGRPFRPNGL LDKAVSNVIA SLTCGRRFEY
cyp2e1r GNEDRIQKEA HFLLEELRKT QGQPFDPTFV IGCTPFNVIA KILFNDRFDY
cyp2e1h GNESRIQREA HFLLEALRKT QGQPFDPTFL IGCAPCNVIA DILFRKHFDY
cyp2f1  SIEERILEEG SFLLADVRKT EGEPFDPTFV LSRSVSNIIC SVLFGSRFDY
cyp2f2  SIEERILEEG SFLLEVLRKM EGKPFDPVFI LSRSVSNIIC SVVFGSRFDY
```

indications of likely substrate contact points, and it is apparent from the models discussed below that certain amino acid residues that have been probed via site-specific mutation do, in fact, interact with the coumarin substrate via hydrogen bonding or π-π stacking contacts. Table 3 provides a summary of the minimized internal energies of CYP2A1, CYP2A5 and CYP2A6, together with a listing of the

```
          < F helix SRS2 >      <  F' >          <        SRS3
         190         200         210         220         230
cyp2a1   EDTEFLSLLQ MMGQMNRFAA SPTGQLYDMF HSVMKYLPGP QQQIIKVTQK
cyp2a4   EDKEFLSLLR MMLGSLQFTA TSMGQVYEMF SSVMKHLPGP QQQAFKELQG
cyp2a5   EDKEFLSLLR MMLGSFQFTA TSMGQLYEMF SSVMKHLPGP QQQAFKELQG
cyp2a6   KDKEFLSLLR MMLGIFQFTS TSTGQLYEMF SSVMKHLPGP QQQAFQLLQG
cyp2b1   TDRQFLRLLE LFYRTFSLLS SFSSQVFEFF SGFLKYFPGA HRQISKNLQE
cyp2b4   KDPVFLRLLD LFFQSFSLIS SFSSQVFELF PGFLKHFPGT HRQIYRNLQE
cyp2b6   QDQEFLKMLN LFYQTFSLIS SVFGQLFELF SGFLKYFPGA HRQVYKNLQE
cyp2c2   TDQDFLSLMG KFNENFKILN SPWVQFCNCF PILFDYFPGS HRKAVKNIFY
cyp2c3   DDEKFKTLIK YFHENFELLG TPWIQLYNIF PILGHYLPGS HRQLFKNIDG
cyp2c4   KDEEFLKLME RLNENIRILS SPWLQVYNNF PALLDYFPGI HKTLLKNADY
cyp2c5   KDEEFLKLME SLNENVRILS SPWLQVYNNF PALLDYFPGI HKTLLKNADY
cyp2c8   KDQNFLTLMK RFNENFRILN SPWIQVCNNF PLLIDCFPGT HNKVLKNVAL
cyp2c9   KDQQFLNLME KLNENIKILS SPWIQICNNF SPIIDYFPGT HNKLLKNVAF
cyp2c19  KDQQFLNLME KLNENIRIVS TPWIQICNNF PTIIDYFPGT HNKLLKNLAF
cyp2d1   EDPYLIRMVK LVEESLTEVS GFIPEVLNTF PALLR.IPGL ADKVFQGQKT
cyp2d6   DDPRFLRLLD LAQEGLKEES GFLREVLNAV PVLLH.IPAL AGKVLRFQKA
cyp2e1r  KDKQALRLMS LFNENFYLLS TPWLQVYNNF SNYLQYMPGS HRKVIKNVSE
cyp2e1h  NDEKFLRLMY LFNENFHLLS TPWLQLYNNF PSFLHYLPGS HRKVIKNVAE
cyp2f1   DDERLLTIIR LINDNFQIMS SPWGELYDIF PSLLDWVPGP HQRIFQNFKC
cyp2f2   DDERLLTIIH FINDNFKIMS SPWGEMYNIF PSVLDWIPGP HKRLFRNFGG

            G helix   >           < H  >                  <
         240         250         260         270         280
cyp2a1   LEDFMIEKVR QNHSTLDPN. SPRNFIDSFL IRMQEE.KNG NSEFHMKNLV
cyp2a4   LEDFITKKVE HNQRTLDPN. SPRDFIDSFL IRMLEEKKNP NTEFYMKNLV
cyp2a5   LEDFITKKVE HNQRTLDPN. SPRDFIDSFL IRMLEEKKNP NTEFYMKNLV
cyp2a6   LEDFIAKKVE HNQRTLDPN. SPRDFIDSFL IRMQEEEKNP NTEFYLKNLV
cyp2b1   ILDYIGHIVE KHRATLDPS. APRDFIDTYL LRMEKEKSNH HTEFHHENLM
cyp2b4   INTFIGQSVE KHRATLDPS. NPRDFIDVYL LRMEKDKSDP SSEFHHQNLI
cyp2b6   INAYIGHSVE KHRETLDPS. APKDLIDTYL LHMEKEKSNA HSEFSHQNLN
cyp2c2   VKNYITEQIK EHQKSLDIN. NPRDFIDCFL IKMEQEKCNQ QSEFTIENLL
cyp2c3   QIKFILEKVQ EHQESLDSN. NPRDFVDHFL IKMEKEKHKK QSEFTMDNLI
cyp2c4   TKNFIMEKVK EHQKLLDVN. NPRDFIDCFL IKMEKE...N NLEFTLGSLV
cyp2c5   IKNFIMEKVK EHEKLLDVN. NPRDFIDCFL IKMEQE...N NLEFTLESLV
cyp2c8   TRSYIREKVK EHQASLDVN. NPRDFIDCFL IKMEQEKDNQ KSEFNIENLV
cyp2c9   MKSYILEKVK EHQESMDMN. NPQDFIDCFL MKMEKEKHNQ PSEFTIESLE
cyp2c19  MESDILEKVK EHQESMDIN. NPRDFIDCFL IKMEKEKQNQ QNEFTIENLV
cyp2d1   FMALLDNLLA ENRTTWDPAQ PPRNLTDAFL AEVEKAKGNP ESSFNDENLR
cyp2d6   FLTQLDELLT EHRMTWDPAQ PPRDLTEAFL AEMEKAKGNP ESSFNDENLR
cyp2e1r  IKEYTLARVK EHHKSLDPS. CPRDFIDSLL IEMEKDKHST EPLYTLENIA
cyp2e1h  VKEYVSERVK EHHQSLDPN. CPRDLTDCLL VEMEKEKHSA ERLYTMDGIT
cyp2f1   LRDLIAHSVH DHQASLDPR. SPRDFIQCFL TKMAEEKEDP LSHFHMDTLL
cyp2f2   MKDLIARSVR EHQDSLDPN. SPRDFIDCFL TKMAQEKQDF LSHFNMDTLL
```

relevant interatomic distances between the known site of coumarin metabolism (namely, the 7-hydrogen for CYP2A5 and CYP2A6, and the 4-hydrogen for CYP2A1) and the haem iron in each P450 model. These will now be discussed in each case for the three species, human, rat and mouse, respectively.

```
                SRS4    I helix              > <   J helix    >
                290         300         310         320         330
cyp2a1   MTTLSLFFAG SETVSSTLRY GFLLLMKHPD VEAKVHEEIE QVIGRNRQPQ
cyp2a4   LTTLNLFFAG TETVSTTLRY GFLLLMKYPD IEAKVHEEID RVIGRNRQPK
cyp2a5   LTTLNLFFAG TETVSTTLRY GFLLLMKHPD IEAKVHEEID RVIGRNRQPK
cyp2a6   MTTLNLFIGG TETVSTTLRY GFLLLMKHPE VEAKVHEEID RVIGKNRQPK
cyp2b1   ISLLSLFFAG TETSSTTLRY GFLLMLKYPH VAEKVQKEID QVIGSHRLPT
cyp2b4   LTVLSLFFAG TETTSTTLRY GFLLMLKYPH VTERVQKEIE QVIGSHRPPA
cyp2b6   LNTLSLFFAG TETTSTTLRY GFLLMLKYPH VAERVYREIE QVIGPHRPPE
cyp2c2   TTVSDVFMAG TETTSTTLRY GLLLLMKHPE VIAKVQEEIE RVIGRHRSPC
cyp2c3   TTIWDVFSAG TDTTSNTLKF ALLLLLKHPE ITAKVQEEIE HVIGRHRSPC
cyp2c4   IAVFDLFGAG TETTSTTLRY SLLLLLKHPE VAARVQEEIE RVIGRHRSPC
cyp2c5   IAVSDLFGAG TETTSTTLRY SLLLLLKHPE VAARVQEEIE RVIGRHRSPC
cyp2c8   CTVADLFVAG TETTSTTLRY GLLLLLKHPE VTAKVQEEID HVIGRHRSPC
cyp2c9   NTAVDLFGAG TETTSTTLRY ALLLLLKHPE VTAKVQEEIE RVIGRNRSPC
cyp2c19  ITAADLLGAG TETTSTTLRY ALLLLLKHPE VTAKVQEEIE RVIGRNRSPC
cyp2d1   MVVVDLFTAG MVTTATTLTW ALLLMILYPD VQRRVQQEID EVIGQVRCPE
cyp2d6   IVVADLFSAG MVTTSTTLAW GLLLMILHPD VQRRVQQEID DVIGQVRRPE
cyp2e1r  VTVADMFFAG TETTSTTLRY GLLILLKHPE IEEKLHEEID RVIGPSRMPS
cyp2e1h  VTVADLFFAG TETTSTTLRY GLLILMKYPE IEEKLHEEID RVIGPSRIPA
cyp2f1   MTTHNLLFGG TKTVSTTLHH AFLALMKYPK VQARVQEEID LVVGRARLPA
cyp2f2   MTTHNLLFGG TETVGTTLRH AFLILMKYPK VQARVQEEID RVVGRSRMPT

         < J'>  <     K helix    > SRS5    |1-4|              |1-3|
              340         350         360         370         380
cyp2a1   YEDHMKMPYT QAVINEIQRF SNLAPLGIPR RIIKNTTFRG FFLPKATDVF
cyp2a4   YEDRMKMPYT EAVIHEIQRF ADLIPMGLAR RVTKDTKFRD FLLPKGTEVF
cyp2a5   YEDRMKMPYT EAVIHEIQRF ADMIPMGLAR RVTKDTKFRD FLLPKGTEVF
cyp2a6   FEDRAKMPYM EAVIHEIQRF GDVIPMSLAR RVKKDTKFRD FFLPKGTEVY
cyp2b1   LDDRSKMPYT DAVIHEIQRF SDLVPIGVPH RVTKDTMFRG YLLPKNTEVY
cyp2b4   LDDRAKMPYT DAVIHEIQRL GDLIPFGVPH TVTKDTQFRG YVIPKNTEVF
cyp2b6   LHDRAKMPYT EAVIYEIQRF SDLLPMGVPH IVTQHTSFRG YIIPKDTEVF
cyp2c2   MQDRSRMPYT DATVHEIQRY INLIPNNVPH TTICNLKFRN YLIPKGTDVL
cyp2c3   SQDRSRMPYT DAVMHEIQRY VDLVPTSLPH AVTQDIEFNG YLIPKGTDII
cyp2c4   MQDRSHMPYT DAVIHEIQRF IDLLPTNLPH AVTRDVKFRN YFIPKGTDII
cyp2c5   MQDRSRMPYT DAVIHEIQRF IDLLPTNLPH AVTRDVRFRN YFIPKGTDII
cyp2c8   MQDRSHMPYT DAVVHEIQRY SDLVPTGVPH AVTTDTKFRN YLIPKGTTIM
cyp2c9   MQDRSHMPYT DAVVHEVQRY IDLLPTSLPH AVTCDIKFRN YLIPKGTTIL
cyp2c19  MQDRGHMPYT DAVVHEVQRY IDLIPTSLPH AVTCDVKFRN YLIPKGTTIL
cyp2d1   MTDQAHMPYT NAVIHEVQRF GDIAPLNLPR FTSCDIEVQD FVIPKGTTLI
cyp2d6   MGDQAHMPYT TAVIHEVQRF GDIVPLGVTH MTSRDIEVQG FRIPKGTTLI
cyp2e1r  VRDRVQMPYM DAVVHEIQRF IDLVPSNLPH EATRDTTFQG YVIPKGTVVI
cyp2e1h  IKDRQEMPYM DAVVHEIQRF ITLVPSNLPH EATRDTIFRG YLIPKGTVVV
cyp2f1   LKDRAAMPYT DAVIHEVQRF ADIIPMNLPH RVTRDTAFRG FLIPKGTDVI
cyp2f2   LEDRTSMPYT DAVIHEVQRF ADVIPMNLPH RVTRDTPFRG FLIPKGTDVI
```

Human CYP2A6 interaction with coumarin

Figure 2 shows a possible interaction between the coumarin molecule and the putative active site of CYP2A6. A π-π stacking interaction between the coumarin ring system and a complementary phenyl group on phenylalanine-205, cooperatively assisted by a hydrogen-bonded contact between the sidechain of

```
           < K'>  <K">                                              <
             390        400        410        420        430
cyp2a1   PILGSLMTDP KFFPSPKDFD PQNFLDDKGQ LKKNAAFLPF STGKRFCLGD
cyp2a4   PMLGSVLKDP KFFSNPKDFN PKHFLDDKGQ FKKSDAFVPF SIGKRYCFGE
cyp2a5   PMLGSVLKDP KFFSNPKDFN PKHFLDDKGQ FKKNDAFVPF SIGKRYCFGE
cyp2a6   PMLGSVLRDP SFFSNPQDFN PQHFLNEKGQ FKKSDAFVPF SIGKRNCFGE
cyp2b1   PILSSALHDP QYFDHPDSFN PEHFLDANGA LKKSEAFMPF STGKRICLGE
cyp2b4   PVLSSALHDP RYFETPNTFN PGHFLDANGA LKRNEGFMPF SLGKRICLGE
cyp2b6   LILSTALHDP HYFEKPDAFN PDHFLDANGA LKKTEAFIPF SLGKRICLGE
cyp2c2   TSLSSVLHDD KEFPNPDRFD PGHFLDASGN FRKSDYFMPF STGKRVCVGE
cyp2c3   PSLTSVLYDD KEFPNPEKFD PGHFLDESGN FKKSDYFMPF STGKRACVGE
cyp2c4   TSLTSVLHDE KAFPNPKVFD PGHFLDESGN FKKSDYFMPF SAGKRMCVGE
cyp2c5   TSLTSVLHDE KAFPNPKVFD PGHFLDESGN FKKSDYFMPF SAGKRMCVGE
cyp2c8   ALLTSVLHDD KEFPNPNIFD PGHFLDKNGN FKKSDYFMPF SAGKRICAGE
cyp2c9   ISLTSVLHDN KEFPNPEMFD PHHFLDEGGN FKKSKYFMPF SAGKRICVGE
cyp2c19  TSLTSVLHDN KEFPNPEMFD PRHFLDEGGN FKKSNYFMPF SAGKRICVGE
cyp2d1   INLSSVLKDE TVWEKPHRFH PEHFLDAQGN FVKHEAFMPF SAGRRACLGE
cyp2d6   TNLSSVLKDE AVWEKPFRFH PEHFLDAQGH FVKPEAFLPF SAGRRACLGE
cyp2e1r  PTLDSLLYDK QEFPDPEKFK PEHFLNEEGK FKYSDYFKPF SAGKRVCVGE
cyp2e1h  PTLDSVLYDN QEFPDPEKFK PEHFLNENGK FKYSDYFKPF STGKRVCAGE
cyp2f1   TLLNTVHYDP SQFLTPQEFN PEHFLDANQS FKKSPAFMPF SAGRRLCLGE
cyp2f2   TLLNTVHYDS DQFKTPQEFN PEHFLDDNHS FKKSPAFMPF SAGRRLCLGE

           L helix     > |3-1|            SRS6          |3-2|
             440        450        460        470        480
cyp2a1   GLAKMELFLL LTTILQNFRF KFPMKLEDIN ESPKPLGFTR IIPKYTMSFMPI
cyp2a4   GLARMELFLF LTNIMQNFHF KSTQAPQDID VSPRLVGFVT IPPTYTMSFLSR
cyp2a5   GLARMELFLF LTNIMQNFHF KSTQAPQDID VSPRLVGFAT IPPTYTMSFLSR
cyp2a6   GLARMELFLF FTTVMQNFRL KSSQSPKDID VSPKHVGFAT IPRNYTMSFLPR
cyp2b1   GIARNELFLF FTTILQNFSV SSHLAPKDID LTPKESGIGK IPPTYQICFSAR
cyp2b4   GIARTELFLF FTTILQNFSI ASPVPPEDID LTPRESGVGN VPPSYQIRFLAR
cyp2b6   GIARAELFLF FTTILQNFSM ASPVAPEDID LTPQECGVGK IPPTYQIRFLPR
cyp2c2   ALARMELFLF LTAILQNFTP KPLVNPNNVD ENPFSSGIVR VPPLYRVSFIPV
cyp2c3   GLARMELFLL LTTILQHFTL KPLVDPKDID PTPVENGFVS VPPSYELCFVPV
cyp2c4   GLARMELFLF LTSILQNFKL QSLVEPKDLD ITAVVNGFVS VPPSYQLCFIPI
cyp2c5   GLARMELFLF LTSILQNFKL QSLVEPKDLD ITAVVNGFVS VPPSYQLCFIPI
cyp2c8   GLARMELFLF LTTILQNFNL KSVDDLKNLN TTAVTKGIVS LPPSYQICFPIV
cyp2c9   ALAGMELFLF LTSILQNFNL KSLVDPKNLD TTPVVNGFAS VPPFYQLCFIPV
cyp2c19  GLARMELFLF LTFILQNFNL KSLIDPKDLD TTPVVNGFAS VPPFYQLCFIPV
cyp2d1   PLARMELFLF FTCLLQRFSF .SVPVGQPRP STHGFFAFPV APLPYQLCAVVREQGL
cyp2d6   PLARMELFLF FTSLLQHFSF .SVPTGQPRP SHHGVFAFLV SPSPYELCAVPR
cyp2e1r  GLARMELFLL LSAILQHFNL KPLVDPEDID LRNITVGFGR VPPRYKLCVIPRS
cyp2e1h  GLARMELFLL LCAILQHFNL KPLVDPKDID LSPIHIGFGC IPPRYKLCVIPRS
cyp2f1   LLARMELFLY LTAILQSFSL QPLGAPEDID LTPLSSGLGN LPRPFQLCLRPR
cyp2f2   PLARMELFIY FTSILQNFTL QPLVDPEDID LTPLSSGLGN LPRPFQLCMHIR
```

Figure 1. Multiple sequence alignment of enzymes from the CYP2 family, including some from the CYP2A subfamily of relevance to this study. The substrate recognition sites (SRSs) identified by Gotoh (1992) and the membrane anchor peptides are shown as shaded boxes, whereas residues which have been mutated in the wild-type enzymes are emboldened.

Table 1. Similarities and differences between putative active site residues in the CYP2A enzymes based on the alignment with CYP2C5.

SRS	CYP2C5	CYP2A6	CYP2A5	CYP2A1	Comments
1	A113	V	V	A	in active site region
–	L156	L	F	L	L160H is present in an allelic variant of CYP2A6
2	V205	F	F	N	substrate contact in CYP2A1, CYP2A5 and CYP2A6
4	D290	N	N	S	substrate contact in CYP2A5 and CYP2A6
4	T298	T	T	T	conserved distal theonine
5	L358	V	M	L	in active site region
5	L359	I	I	A	in active site region
6	V474	A	A	T	in active site region

A, alanine; V, valine; L, leucine; F, phenylalanine; N, asparagine; S, serine; T, threonine; D, aspartate; I, isoleucine.

SRS, substrate recognition site (Gotoh 1992).

Table 2. A summary of site-directed mutagenesis data for CYP2A enzymes*.

CYP	Change	CYP2C5 position	SRS	Comments	Reference
2A11	Q104L	V100	1	at access to active site	Ding *et al.* (1994)
2A5	V117A	A113	1	in active site region	Lindberg and Negishi (1989)
2A5	G207P	E205	2	in active site region	Lindberg and Negishi (1989)
2A5	F209L	V205	2	in active site region	Lindberg and Negishi (1989)
2A1	S295G	D290	4	in active site region	Hanioka *et al.* (1992)
2A1	T303S	T298	4	distal threonine residue	Hanioka *et al.* (1992)
2A5	M365L	L358	5	in active site region	Lindberg and Negishi (1989)
2A11	R372H	H365	5	forms ion-pair with a haem proprionate group	Ding *et al.* (1994)
2A5	R481V	V474	6	in active site region	Lindberg and Negishi (1989)

Q, glutamine; V, valine; G, glycine; P, proline; E, glutamate; F, phenylalanine; L, leucine; S, serine; D, aspartate; T, threonine; M, methionine; R, arginine; H, histidine.

SRS, substrate recognition site (Gotoh 1992).

*CYP2A1 is a rat orthologue; CYP2A5 is a mouse orthologue; CYP2A11 is a rabbit orthologue. Reference to summarized mutagenesis data: Lewis (1998).

Table 3. Energies of minimized structures[a] and haem substrate distances[b].

CYP	Minimized energy (kcal mol^{-1})	Coumarin to haem iron distance (Å)
2A1	−1446.0	4.5 (4-hydrogen)
2A5	−1432.6	4.1 (7-hydrogen)
2A6	−1306.8	3.0 (7-hydrogen)

[a] The minimized energy in kcal mol^{-1} of the geometry-optimized structures of CYP2A1, CYP2A5 and CYP2A6 are provided following 100 iterative cycles of energy minimization via molecular mechanics using the Tripos force field. These values represent the total internal energy of the molecule in each case, being a summation of the bond energies over all atoms in the structure, and are calculated relative to atoms of the elements in their standard states. The fact that these values are all relatively large and negative indicates that the enzyme structures are all energetically stable and do not contain any regions of high energy indicative of unacceptable protein conformations.

[b] The distance (Å) between the coumarin substrate (site of metabolism) and haem iron are shown following interactive docking with the energy-minimized structures of CYP2A1, CYP2A5 and CYP2A6. These values are given to one decimal place as this reflects the degree of precision afforded by the crystal structure template.

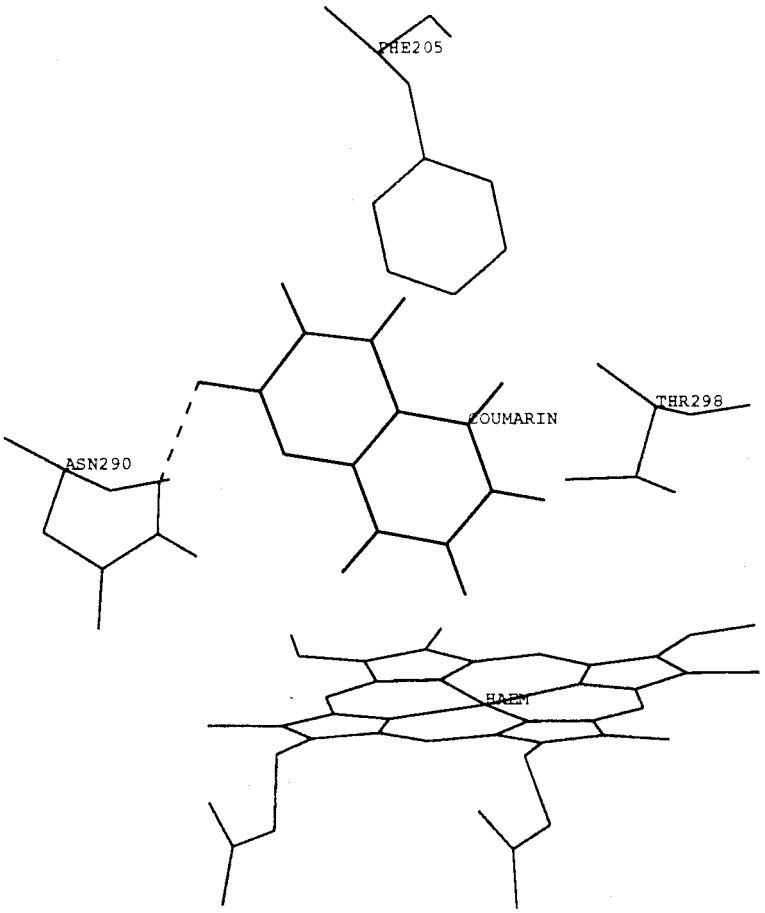


Figure 2. Putative active site region of CYP2A6 showing a possible binding interaction between coumarin and the enzyme. Hydrogen bonds are shown as dashed lines. Interacting residues are labelled according to that of the template structure, CYP2C5.

asparagine-290 and the ketone oxygen of coumarin, serves to orientate the substrate for oxygenation at the 7-position. The 7-hydrogen is situated directly above the haem iron in this orientation and is 3.025 Å from the iron atom, thus enabling the binding of a dioxygen molecule to the haem before hydroxylation of coumarin. The phenylalanine residue mentioned above has been the subject of site-directed mutagenesis experiments in the mouse orthologues CYP2A4 and CYP2A5 (Lindberg and Negishi 1989) and the asparagine residue position has also been investigated in CYP2A1 (Hanioka *et al.* 1992) via this procedure (see table 2 for a summary of mutagenesis data for CYP2A enzymes).

Rat CYP2A1 interaction with coumarin

Figure 3 shows how coumarin may interact with amino acid residues within the putative active site of CYP2A1. In this case, the key phenylalanine residue mentioned above (namely Phe205) is replaced by asparagine. This appears to bring about a reorientation to the substrate molecule due to hydrogen bonding

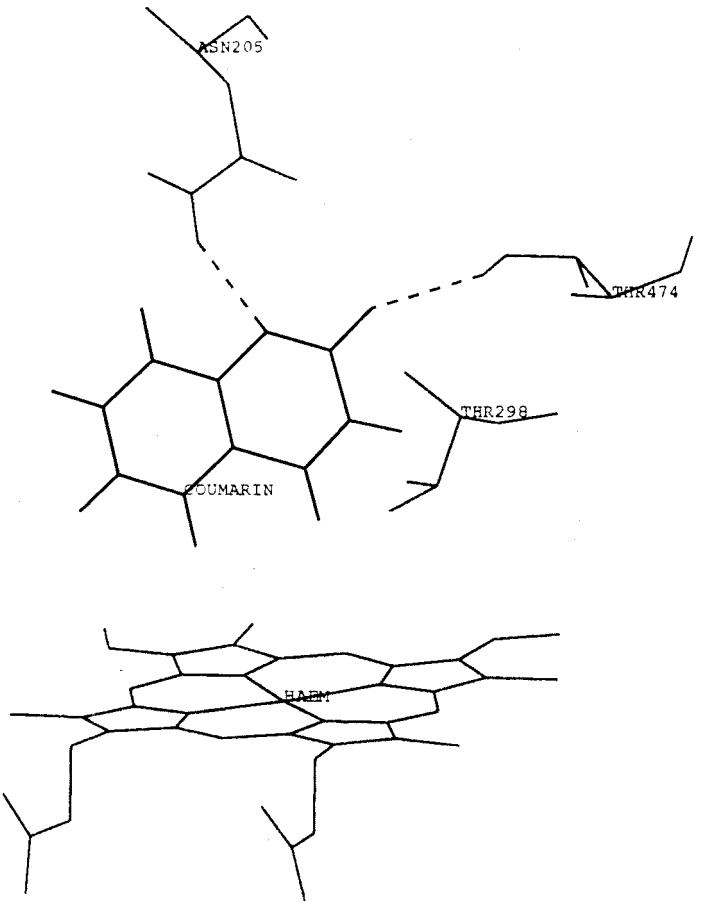


Figure 3. Putative active site region of CYP2A1 showing a possible binding interaction between coumarin and the enzyme. Hydrogen bonds are shown as dashed lines. Interacting residues are labelled according to that of the template structure, CYP2C5.

between the amide side-chain and the ketonic oxygen on coumarin. In addition, a threonine residue in SRS6 donates a second hydrogen bond to coumarin, thus anchoring the substrate for oxygenation at the 4-position. Consequently, as coumarin enters the CYP2A1 active site region, it will experience a positive electrostatic field due to the end-of-chain hydrogens on Asn205 (via its $CONH_2$ group) and Thr474 (via its OH group) residues within the haem environment. Furthermore, a number of phenylalanines present within the hydrophobic pocket (namely in SRS1, SRS4 and SRS6) will probably incline the coumarin molecule via π-π stacking interactions with the substrate's bicyclic ring system, although these are unlikely to play a role in its final orientation relative to the haem for 3,4-epoxidation.

Mouse CYP2A5 interaction with coumarin

The active site of CYP2A5 is presented as figure 4, from which it can be appreciated that, like the situation encountered in CYP2A6, coumarin is orientated for 7-hydroxylation via π-π stacking interactions with Phe205 and hydrogen

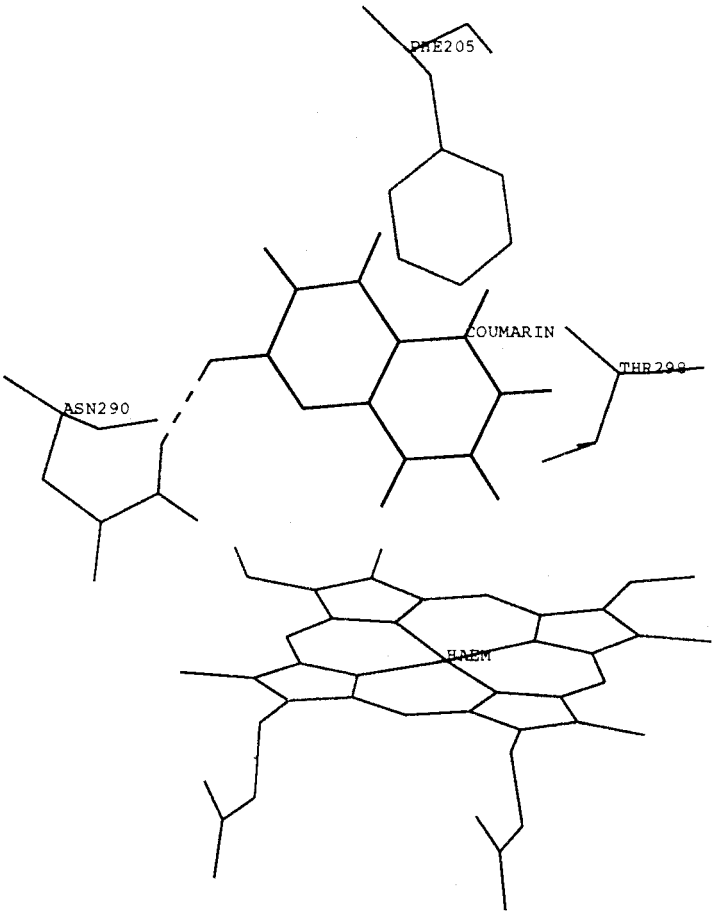


Figure 4. Putative active site region CYP2A5 showing a possible binding interaction between coumarin and the enzyme. Hydrogen bonds are shown as dashed lines. Interacting residues are labelled according to that of the template structure, CYP2C5.

bonding to Asn290. These contacts cooperatively assist in positioning the substrate relative to the haem iron such that the 7-hydrogen lies at a distance of 4.077 Å from the iron atom. The phenylalanine residue has been mutated and shown to have importance for substrate binding in CYP2A5 (Lindberg and Negishi 1989), whereas the residue corresponding to Asn290 as been the subject of mutagenesis experiments in the rat orthologue CYP2A1 (Hanioka *et al.* 1992). Consequently, the CYP2A5 model is consistent with the known pathway of coumarin metabolism, namely 7-hydroxylation. Although the mouse can metabolize coumarin via 3,4-epoxidation, this metabolic pathway will be catalysed by enzymes from another P450 family or subfamily.

Quantitative Structure–Activity Relationship (QSAR) for coumarin binding to wild-type and mutant CYP2A5

Table 4 provides the relevant data on CYP2A5 mutants and their coumarin 7-hydroxylase activities (K_m) relative to that of the wild-type enzyme (Juvonen *et al.*

Table 4. Physicochemical and coumarin 7-hydroxylase data (K_m) for wild-type (Phe209) and mutant CYP2A5 enzymes.

Residue	M_r (Da)	Hydrophobicity	$\log K_m$
1. Phenylalanine (WT)	147.18	−2.27	0.28
2. Leucine	113.16	−1.82	0.95
3. Valine	99.14	−1.30	1.66
4. Alanine	71.09	−0.39	2.63
5. Glycine	57.05	0.0	2.70
6. Asparagine	114.11	1.91	1.72
7. Serine	87.08	1.24	2.20
8. Lysine	128.17	2.77	1.35

K_m, Michaelis constant (μM) for Coumarin 7-hydroxylation (Juvonenen *et al.* 1991, Negishi *et al.* 1996); M_r, relative molecular mass (Da) of the amino acid (Creighton 1993); hydrophobicity, relative hydrophobicity of the amino acid sidechain (Creighton 1993); WT, wild-type enzyme (CYP2A5).

QSAR expression	*n*	SE	*R*	*F*
$\log K_m = 0.25$ hydrophobicity $- 0.024 M_r + 4.246$ (± 0.05) (± 0.002)	8	0.145	0.99	113.2

n, number of points; SE, standard error; *R*, correlation coefficient ($R^2 = 0.98$); *F*, variance ratio (*F*-test).

References to biological and physicochemical data: Juvonen *et al.* (1991), Negishi *et al.* (1996), Creighton (1993).

1991, Negishi *et al.* 1996). QSAR analysis of the data shows that the variation in $\log K_m$ can be attributable ($R = 0.99$) to a combination of residue hydrophobicity and relative molecular mass (M_r) of the relevant amino acid (data taken from Creighton 1993). This emphasizes the importance of a phenylalanine residue at position 209 for the binding of coumarin to the wild-type enzyme (lowest K_m) and also demonstrates that both the size and hydrophobic character of the amino acid side-chain have a bearing on the binding affinity of coumarin for 7-hydroxylation by CYP2A5. Consequently, it appears that the presence of a phenylalanine residue at position 209 in the structure is essential for high-affinity binding of the coumarin substrate, in accordance with the evidence from homology modelling and site-specific mutagenesis (Lindberg and Negishi 1989).

QSAR studies on CYP2A6 substrates

Table 5 presents information on six substrates of CYP2A6, which has been used to generate a QSAR for substrate-binding affinity (ΔG_{bind}) based on K_m (Rendic and DiCarlo 1997). It is found that a combination between $\log P$ and the number of active site hydrogen bonds gives a good correlation ($R = 0.97$) with substrate affinity for CYP2A6-catalysed metabolism. These findings emphasize the importance of lipophilicity and hydrogen-bonded interactions to CYP2A6 binding avidity, and also show that consideration of enzyme active site interactions can provide useful information for correlations with substrate binding affinity. In fact, a single regression involving the number of hydrogen bonds in the enzyme–substrate interaction gives a satisfactory correlation ($R = 0.87$) with binding affinity. This indicates that the number of hydrogen bonds and their associated energy makes a major contribution to the overall binding energy, although compound lipophilicity

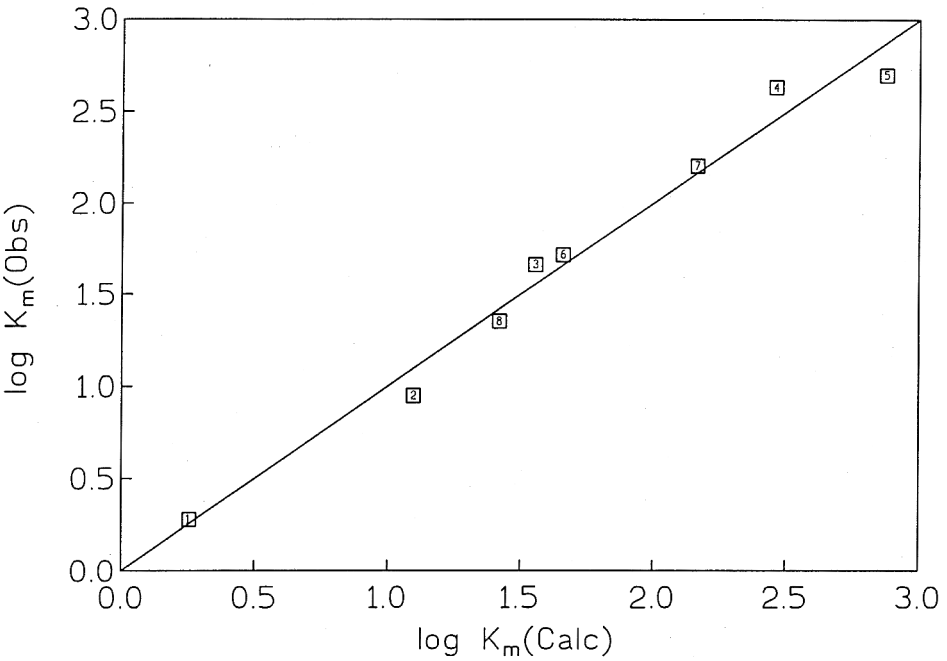


Figure 5. Agreement between experimental and calculated log K_m for coumarin binding to wild-type and mutant CYP2A5 enzymes, based on the data presented in table 4.

Table 5. Substrate binding to CYP2A6: data employed in QSAR analysis.

Substrate	N_{HB}	log P	K_m (μM)	ΔG_{bind}^{expt} (kcal mol^{-1})	ΔG_{bind}^{calc}
1. Coumarin	3	1.39	2.1	−8.05	−7.84
2. Losigamone	2	1.46	10.0	−7.09	−7.12
3. SM-12502	3	1.06	4.7	−7.56	−7.58
4. Cotinine	1	0.07	264.7	−5.07	−5.28
5. Nicotine	1	1.17	25.5	−6.52	−6.13
6. 4-Nitroanisole	2	2.94	9.0	−7.16	−7.50

QSAR expression	n	SE	R	F
$\Delta G_{bind} = -0.77 N_{HB} - 0.78 \log P - 4.45$ (±0.19) (±0.27)	6	0.343	0.97	21.2

n, number of points; SE, standard error; R, correlation coefficient ($R^2 = 0.94$); F, variance ratio.

N_{HB}, number of active site hydrogen bonds between substrate and enzyme; log P, logarithm of the octanol/water partition coefficient (Suzuki and Kudo 1990); K_m, Michaelis constant for CYP2A6-mediated metabolism (Rendic and DiCarlo 1997); ΔG_{bind}^{expt}, binding energy given by RT ln K_m, where R is the gas constant and T is the absolute temperature (310 K).

SM12502 = (+)*cis*-3,5,dimethyl-2-(3-pyridyl)thiazolidin-4-one.

represents an additional factor. This could be related to the π-π stacking interaction between the substrate and Phe209, although it is possible that there are other hydrophobic contacts within the active site which are important, and liphophilic character may also play a role in progress of the substrate along an access channel to the haem where desolvation of the local environment is a feature likely to make some contribution to the binding energy between enzyme and substrate.

Conclusions

The 7-hydroxylation of coumarin in *H. sapiens*, mediated via CYP2A6, can be explained by the homology modelling of this isoform, and the same is true of the mouse orthogue, CYPA5. However, in the case of CYP2A1, coumarin becomes orientated for metabolism at a different position, namely that of 3,4-epoxidation, due to the presence of differently interacting amino acid residues within the CYP2A1 active site. The results of QSAR are consistent with the findings obtained from homology modelling, and future studies will explore further substrate and inhibitor interactions within the CYP2A subfamily. However, the limitations of the current approach include the fact that we are using a substrate-free crystal structure to investigate the ways in which another substrate (namely, coumarin) may interact with an enzyme from a different subfamily, despite a high sequence homology. Moreover, there is a relative lack of available site-directed mutagenesis information for CYP2A6, and although more allelic variants are being reported in the literature, the majority of these do not map to the putative active site region. Furthermore, these studies involve consideration of the enzyme–substrate complex in the absence of either the microsomal membrane in which it is embedded or bound redox partner, and it is generally accepted that conformational changes are likely to occur following reduction of the enzyme–substrate complex. Consequently, although an ultimate goal of this approach to understanding the P450 system is to predict the rate of substrate metabolism, it is possible to rationalize regioselectivity of coumarin oxidation within the CYP2A subfamily in terms of specific interactions with amino acid residues which orientate the substrate for metabolism at the experimentally observed positions. QSAR studies can assist in the prediction of rates and clearance (Lewis and Dickins 2002), but progress of the substrate along its access channel before interaction within the haem locus would be an important process to investigate in future structural studies, as this probably has an influence on the overall rate of substrate metabolism.

Acknowledgements

The financial support of GlaxoSmithKline Research and Development Ltd, Merck, Sharp & Dohme Ltd, and the University of Surrey Foundation Fund is gratefully acknowledged by D.F.V.L.

References

Born, S. L., Caudill, D., Smith, B. J. and Lehman-McKeeman, L. D., 2000, *In vitro* kinetics of coumarin 3,4-epoxidation: application to species differences in toxicity and carcinogenicity, *Toxocological Sciences*, **58**, 23–31.

Born, S. L., Rodriguez, P. A., Eddy, C. L. and Lehman-McKeeman, L. D., 1997, Synthesis and reactivity of coumarin 3,4-epoxide. *Drug Metabolism and Disposition*, **35**, 1318–1323.

Cok, I., Kocabas, N. A., Cholerton, S., Karakaya, A. E. and Sardas, S., 2001, Determination of coumarin metabolism in Turkish population. *Human and Experimental Toxicology*, **20**, 179–184.

Creighton, T. E., 1993, *Proteins: Structure and Molecular Properties* (New York: Freeman).

Ding, X., Peng, H.-M. and Coon, M. J., 1994, Heterologous expression and structure–function analysis of CYP2A10 and CYP2A11 which differ in only eight amino acids but have strikingly different activities toward testosterone and coumarin. In M. C. Lechner (ed.), *Cytochrome P450 8th International Conference* (Paris: Libbey), pp. 885–888.

Gotoh, O., 1992, Substrate recognition sites in cytochrome P450 family 2 (CYP2) inferred from comparative analyses of amino acid and coding nucelotide sequences. *Journal of Biological Chemistry*, **267**, 83–90.

Hanioka, N., Gonzalez, F. J., Lindberg, N. A., Liu, G., Gelboin, H. V. and Korzekwa, K. R., 1992, Site-directged mutagenesis of cytochromes P405 CYP2A1 and CYP2A2: influence of the distal helix on the kinetics of testosterone hydroxylation. *Biochemistry*, **31**, 3364–3370.

Juvonen, R. O., Iwasaki, M. and Negishi, M., 1991, Structural function of residue 209 in coumarin 7-hydroxylase ($P450_{coh}$). *Journal of Biological Chemistry*, **266**, 16431–16435.

Lake, B. G., 1999, Coumarin metabolism, toxicity and carcinogenicity: relevance for human risk assessment. *Food and Chemical Toxicology*, **37**, 423–453.

Lewis, D. F. V., 1998, The CYP2 family: models, mutants and interactions. *Xenobiotica*, **28**, 617–661.

Lewis, D. F. V., 2002, Homology modelling of CYP2 family enzymes based on the CYP2C5 crystal structure. *Xenobiotica*, **32**, 305–323.

Lewis, D. F. V. and Dickins, M., 2002, Factors influencing rates and clearance in P450-mediated reactions. *Toxicology*, **170**, 45–53.

Lewis, D. F. V. and Lake, B. G., 1995, Molecular modelling of members of the P4502A subfamily: application to studies of enzyme specificity. *Xenobiotica*, **25**, 585–598.

Lewis, D. F. V., Dickins, M., Lake, B. G., Eddershaw, P. J., Tarbit, M. H. and Goldfarb, P. S., 1999, Molecular modelling of the human cytochrome P450 isoform CYP2A6 and investigations of CYP2A substrate selectivity. *Toxicology*, **133**, 1–33.

Lewis, D. F. V., Modi, S. and Dickins, M., 2002, Quantitative structure-activity relationships for substrates and inhibitors of human cytochromes P450. *Drug Metabolism Reviews*, **34** (in press).

Li, H. and Pouulos, T. L., 1997, The structure of the cytochrome $P450_{BM-3}$ haem domain complexed with the fatty acid substrate, palmitoleic acid. *Nature Structural Biology*, **4**, 140–146.

Lindberg, R. L. P. and Negishi, M., 1989, Alteration of mouse cytochrome $P450_{coh}$ substrate specificity by mutation of a single acid residue. *Nature*, **339**, 617–661.

Negishi, M., Iwasaki, M., Juvonen, R. O., Sueyoshi, T., Darden, T. A. and Pedersen, L. G., 1996, Structural flexibility and functional versatility of cytochrome P450 and rapid evolution. *Mutation Research*, **350**, 43–50.

Pelkonen, O., Rautio, A., Raunio, H. and Pasanen, M., 2000, CYP2A6: a human coumarin 7-hydroxylase. *Toxicology*, **144**, 139–147.

Poulos, T. L., Finzel, B. C. and Howard, A. J., 1986, Crystal structure of substrate-free *Pseudomonas putida* cytochrome P450. *Biochemistry*, **25**, 5314–5322.

Poulos, T. L., Finzel, B. C. and Howard, A. J., 1987, High-resolution crystal structure of cytochrome $P450_{cam}$. *Journal of Molecular Biology*, **195**, 687–700.

Ravichandran, K. G., Boddupalli, S. S., Hasemann, C. A., Peterson, J. A. and Deisenhofer, J., 1993, Crystal structure of hemoprotein domain of $P450_{BM-3}$, a prototype for microsomal P450s. *Science*, **261**, 731–736.

Rendic, S. and DiCarlo, F. J., 1997, Human cytochrome P450 enzymes: a status report summarizing their reactions, substrates, inducers and inhibitors. *Drug Metabolism Reviews*, **29**, 413–580.

Suzuki, T. and Kudo, Y., 1990, Automatic log P estimation based on combined additive modeling methods. *Journal of Computer-Aided Molecular Design*, **4**, 155–198.

Williams, P. A., Cosme, J., Sridhar, V., Johnson, E. F. and McRee, D. E., 2000, Mammalian microsomal cytochrome P450 monooxygenase: structural adaptations for membrane binding and functional diversity. *Molecular Cell*, **5**, 121–131.

XENOBIOTICA, 2002, VOL. 32, NO. 7, 563–571

Taylor & Francis
healthsciences

7-OH-flavone is sulfated in the human liver and duodenum, whereas 5-OH-flavone and 3-OH-flavone are potent inhibitors of SULT1A1 activity and 7-OH-flavone sulfation rate

M. VIETRI†, A. PIETRABISSA‡, R. SPISNI§, F. MOSCA‡ and G. M. PACIFICI†*

† Department of Neurosciences, Section of Pharmacology, Medical School, and §Department of Surgery, Via Roma 55, I-56126 Pisa, Italy
‡ Department of Oncology, Section of Surgery, Cisanello Hospital at the University of Pisa, I-56124 Cisanello, Italy

Received 14 August 2001

1. The aim of this investigation was to see whether 7-OH-flavone, 5-OH-flavone and 3-OH-flavone, which are present in edible vegetables, fruit and wine, are substrates or inhibitors of human liver and duodenum sulfotransferase.

2. An assay was set up to study the sulfation of 7-OH-flavone, and using this assay, it was observed that 7-OH-flavone was sulfated and the rate of sulfation (mean ± SD) was 324 ± 87 pmol min^{-1} mg^{-1} (liver) and 584 ± 164 pmol min^{-1} mg^{-1} (duodenum; $p < 0.0001$).

3. 7-OH-flavone sulfotransferase followed Michaelis–Menten kinetics and the K_m (mean ± SD) was 0.2 ± 0.04 μM (liver) and 1.1 ± 0.3 μM (duodenum; $p = 0.008$). V_{max} (mean ± SD) was 392 ± 134 pmol min^{-1} mg^{-1} (liver) and 815 ± 233 pmol min^{-1} mg^{-1} (duodenum; $p = 0.016$).

4. 5-OH-flavone and 3-OH-flavone were not sulfated and were inhibitors of human liver and duodenum SULT1A1 activity and 7-OH-flavone sulfation rate.

5. The IC_{50} of 5-OH-flavone for SULT1A1 was 0.3 ± 0.06 μM (liver) and 0.3 ± 0.1 μM (duodenum; n.s.) and those of 3-OH-flavone were 1.0 ± 0.1 μM (liver) and 1.6 ± 0.03 μM (duodenum; $p = 0.0006$).

6. There was inhibition of 7-OH-flavone sulfation rate by 5-OH-flavone and 3-OH-flavone. The IC_{50} of 5-OH-flavone for the sulfation rate of 7-OH-flavone was 3.5 ± 0.5 μM (liver) and 69 ± 18 μM (duodenum; $p < 0.0001$) and for 3-OH-flavone it was 18 ± 3.4 μM (liver) and 213 ± 47 μM (duodenum; $p < 0.0001$).

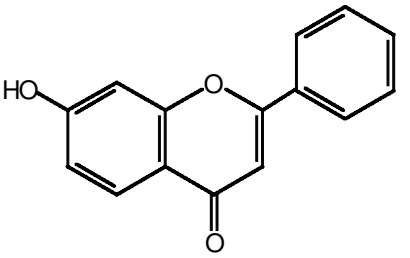
7. The position of the hydroxy group confers to the molecules of OH-flavones the quality of substrate or inhibitor of sulfotransferase.

Introduction

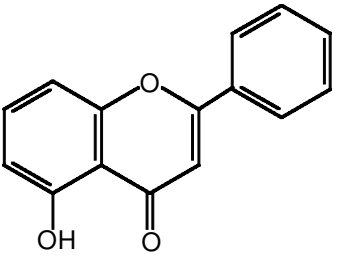
Flavones are present in edible vegetables, fruits and wine (McDonald *et al.* 1998, Hollman and Katan 1999, Aray *et al.* 2000, de Pascual-Teresa *et al.* 2000, Scalbert and Williamson 2000). The chemical structures of 3-OH-flavone, 5-OH-flavone and 7-OH-flavone vary for the position of the hydroxy group and are shown in figure 1. It was observed that resveratrol (De Santi *et al.* 2000a, b) and chrysin (De Santi 2000b) are sulfated, whereas quercetin, fisetin, apigenin, myricetein and kaempferol are inhibitors of sulfotransferase (De Santi 2000b).

* Author for correspondence; pacifici@biomed.unipi.it

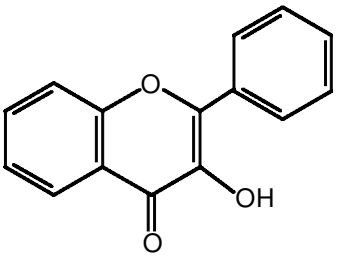
Xenobiotica ISSN 0049–8254 print/ISSN 1366–5928 online © 2002 Taylor & Francis Ltd
http://www.tandf.co.uk/journals
DOI: 10.1080/00498250210130582



7-OH-FLAVONE
Substrate of sulfotransferase



5-OH-FLAVONE
Inhibitor of SULT1A1



3-OH-FLAVONE
Inhibitor of SULT1A1

Figure 1. Chemical structures of 7-OH-flavone, 5-OH-flavone and 3-OH-flavone.

The question arose whether the position of the hydroxy group in hydroxy flavones molecules modifies their reaction profile with sulfotransferase.

Flavones protect from heart infarction (Hirvonen *et al.* 2001). The sulfation of flavones in the gut and liver should reduce their bioavailability and consequently their plasma concentrations, and their protective effect against heart infarction should be reduced. The aim was to see whether there was a relationship between the position of hydroxy group in the molecules of OH-flavones and their rate of sulfation.

There are several forms of phenol sulfotransferase (EC 2.8.2.1) (Coughtrie and Jonston 2001) and two of them have been characterized with regards to their

substrate specificity, inhibitor sensitivity, thermal stability and regulation. One form, named SULT1A1, whose diagnostic substrate is 4-nitrophenol, is sensitive to the inhibition of 2,6-dichloro-4-phenol (Campbell *et al.* 1987), is better expressed in the liver than gut (Cappiello *et al.* 1990) and is relatively thermostabile. The other form of phenol sulfotransferase, SULT1A3 is less susceptible to inhibition by 2,6-dichloro-4-phenol (Sundaram *et al.* 1989), is thermolabile and is better expressed in the gut than liver (Cappiello *et al.* 1990), and dopamine is its diagnostic substrate.Therefore, the liver and duodenum differ as regards the expression of SULT1A1 and SULT1A3, and these tissues were included in the present study.

During the study, it was observed that 5-OH-flavone and 3-OH-flavone were inhibitors of SULT1A1, and another aim was to study the inhibition of SULT1A1 by these two flavones in the human liver and duodenum. Finally, the inhibition rate of 7-OH-flavone sulfation by 5-OH-flavone and 3-OH-flavone was followed.

Materials and methods

Chemicals

3′-Phosphoadenosine-5′-phosphosulfate-[^{35}S] (PAPS, specific activity 1.93 Ci mmol^{-1}, chemical purity 99%) was from NEN Life Science Products, Inc. (Brussels, Belgium). 4-Nitrophenol, dithiothreitol (DTT), bovine serum albumin (BSA), 7-OH-flavone, 5-OH-flavone and 3-OH-flavone were from Sigma Chemical Co. (Milan, Italy). Mono- and dibasic potassium phosphate, sodium hydroxide, barium hydroxide, barium acetate, and zinc sulphate were from Carlo Erba (Milan, Italy).

Biological material

Liver samples. The Ethical Committee of our Medical School approved the project. Liver specimens were obtained after clinically indicated partial hepatectomy to remove a cancer from five men and five women aged between 47 and 81 years with a mean ± SD of 65 ± 9 years. A sample of normal liver, as far as possible from the tumour, was made available for the study. A specimen of liver was sampled immediately after part of the organ was removed, placed on ice and transferred to the laboratory within a few minutes where it was frozen and stored at −80 °C. The liver function tests of the patients from whom liver samples derived are summarized in table 1.

Duodenum samples. The duodenum samples derived from 6 men and 4 women aged between 19 and 73 years with a mean ± SD of 60 ± 15 years. Biopsies of duodenum were sampled after the informed consent was obtained from the patients. Biopsies of duodenal mucosa, of about 5 mg in weight, were sampled from the second portion of the duodenum in patients that underwent clinically indicated gastro-intestinal enteroscopy. Several biopsies of duodenum were obtained from the same patient, were combined and analysed as a single sample. As the samples of duodenum were available, they were immediately placed on ice and transferred to the laboratory within a few minutes where they were frozen and stored at −80 °C.

Table 1. Function liver tests of the patients undergoing clinically indicated partial hepatectomy from whom liver samples were derived.

	Minimum	Maximum	Mean ± SD	Median	Normal
Age (years)	47	81	65 ± 9	66	–
Albumin (g dl^{-1})†	3.4	4.6	4.0 ± 0.4	4.0	3.5–5.5
Bilirubin (mg dl^{-1})‡	0.3	1.2	0.6 ± 0.3	0.7	≤1.1
GOT (U l^{-1})	15	69	27 ± 18	20	< 45
GPT (U l^{-1})	14	96	30 ± 27	24	< 45
PT (s)	10.5	12.3	11.6 ± 0.6	11.8	10.9–12.8

† Plasma albumin concentration; ‡ total bilirubin plasma concentration.

GOT, glutamic-oxalacetic transaminase activity; GPT, glutamic-pyruvic transaminase activity; PT, prothrombin time.

Isolation of the cytosolic function

After the tissue specimens were sampled, they were immediately chilled in ice and transported to our laboratory within a few minutes, where they were frozen and stored at −80 °C. Liver samples (about 1 g) were homogenized in 5 vols 0.25 M sucrose dissolved in 5 mM potassium orthophosphate buffer (pH 7.4). The biopsies of duodenum were homogenized in 0.3 ml 0.25 M sucrose (buffered at pH 7.4 with 5 mM potassium orthophosphate buffer) using a glass–Teflon homogenizer ('size 0', Thomas, Philadelphia, PA, USA). The homogenates were aspirated using a Pasteur pipette and transferred into centrifuge tubes. The grinding chamber and pestle were rinsed with 0.2 ml 0.25 M sucrose (buffered at pH 7.4 with 5 mM potassium orthophosphate buffer) and the washings were combined with the homogenates. The homogenates were centrifuged at 12 000*g* for 15 min and the supernatants were centrifuged again at 105 000*g* for 1 h. The high-speed supernatants were divided into aliquots, stored at −80 °C and designated as the cytosolic fraction.

Assays

Protein concentration assay. The protein concentration was measured as described by Lowry *et al.* (1951) using BSA as a standard.

7-OH-flavone sulfotransferase assay. The assay of 7-OH-flavone was based on that described by Foldes and Meek (1973) and modified by Anderson and Weinshilboum (1980). The unreacted PAPS-(^{35}S) was precipitated with barium hydroxide, barium acetate and zinc sulphate. The final saturating concentrations of 7-OH-flavone were 1 μM (liver) and 4 μM (duodenum), and that of PAPS was 0.4 μM (about 500 000 dpm). The enzyme activity was measured on the specific radioactivity of PAPS-[^{35}S] after correction of the test samples for the blank samples. 7-OH-flavone was dissolved in acetone and added in 2 μl to the incubation mixture (final volume 150 μl) and this volume of acetone did not affect the activity of sulphotransferase. The cytosolic fraction was diluted 2000-fold (liver) and 500-fold (duodenum) in 5 mM potassium orthophosphate buffer (pH 7.4) containing 0.625 mg ml^{-1} BSA and 1.54 mg ml^{-1} DTT. The final protein concentration ranged from 3.5 to 6.7 (liver) and from 1.0 to 3.2 (duodenum) μg cytosolic protein per ml incubation mixture. The incubation time was 20 min for both the liver and duodenum. Each sample was assayed in duplicate and had two blank samples that had the same composition of the test samples with the exception that 7-OH-flavone was replaced by 2 μl acetone.

Kinetics of 7-OH-flavone sulfotransferase. The kinetics of 7-OH-flavone sulfotransferase were studied in five liver samples obtained from three men and two women aged from 58 to 81 years, mean ± SD = 69 ± 7 years and from five samples of duodenum obtained from two men and three women aged from 19 to 69 years mean ± SD = 56 ± 20 years. The following concentrations of 7-OH-flavone were used: 0.062, 0.125, 0.25, 0.50 and 1 μM (liver), and 0.125, 0.25, 0.5, 1 and 2 μM (duodenum). The final concentration of PAPS was kept constant at 0.4 μM.

SULT1A1 sulfotransferase assay. The activity of SULT1A1 was measured with 4 μM 4-nitrophenol, as the sulphate acceptor substrate, and with 0.4 μM PAPS-(^{35}S), as the sulphate donor substrate. The assay was as described by Foldes and Meek (1973) and modified by Anders and Weinshilboum (1980). The unreacted PAPS was precipitated with barium hydroxide, barium acetate and zinc sulphate.

Inhibition of SULT1A1 activity by 5-OH-flavone and 3-OH-flavone

The inhibition of SULT1A1 was studied in three samples of liver and duodenum. The liver samples were obtained from two men and one woman, aged from 58 to 71 years, mean ± SD = 65 ± 5 years, and the duodenum samples derived from two men and one woman aged between 55 and 69 years, mean ± SD = 60 ± 7 years. The inhibition curves were constructed using the following concentrations of 5-OH-flavone: 0.312, 0.625, 1.25, 2.5, 5 and 10 μM (liver and duodenum). The concentrations of 3-OH-flavone were: 0.062, 0.125, 0.25, 0.5 and 1 μM (liver and duodenum). The final concentrations of the reaction substrates, 4-nitrophenol and PAPS, were 4 and 0.4 μM, respectively.

Inhibition of 7-OH-flavone sulfation rate by 5-OH-flavone and 3-OH-flavone

The inhibition of 7-OH-flavone sulfation rate was studied in five samples of liver and duodenum. The liver was obtained from three men and two women aged from 58 to 81 years, mean ± SD = 69 ± 7 years. The duodenum derived from two men and three women aged from 19 and 69 years, mean ± SD = 56 ± 20 years. The concentrations of 5-OH-flavone were: 0.78, 1.56, 3.25, 6.25 and 12.5 μM (liver) and 12.5, 25, 50 and 200 μM (duodenum). The concentrations of 3-OH-flavone were: 1.56, 3.12, 6.25, 12.5 and 25 μM (liver) and 31.25, 62.5, 125, 250 and 500 μM (duodenum).

Calculations

The kinetic parameters, V_{max} and K_m, were determined using the non-linear correlation option of the software package Prism 3 (GraphPad Software, San Diego, CA, USA). IC_{50} was calculated using the software package Dose–Effect Analysis (Biosoft, Cambridge, UK). Differences between groups were tested by the *t* test with Welch correction for groups with different SD. The correlations between groups were tested by the Spearman-rank correlation test.

Results and discussion

Optimal assay conditions for 7-OH-flavone sulfation in human liver and duodenum were determined first. The amounts of 7-OH-flavone sulfate increased linearly with incubation time up to at least 40 min (liver) and 30 min (duodenum) (figure 2, a) and up to at least a protein concentration of 26 μg (liver) and 13 μg (duodenum) of cytosolic protein per ml of incubation mixture (figure 2, b).

The kinetics of 7-OH-flavone sulfotransferase were studied in five samples of human liver and duodenum and the results of a representative experiment are shown in figure 2 (c, d). Sulfotransferase towards 7-OH-flavone followed Michaelis–Menten kinetics both in liver and duodenum and the K_m (mean ± SD) was $0.2 \pm 0.04\,\mu M$ (liver) and $1.1 \pm 0.3\,\mu M$ (duodenum; $p = 0.008$). V_{max} (mean ± SD) was $392 \pm 134\,pmol\,min^{-1}\,mg^{-1}$ (liver) and $815 \pm 233\,pmol\,min^{-1}\,mg^{-1}$ (duodenum; $p = 0.016$).

The sulfation of 7-OH-flavone was measured in ten samples of liver and duodenum and ranged from 215 to 503 $pmol\,min^{-1}\,mg^{-1}$ (liver) and from 399 to 931 $pmol\,min^{-1}\,mg^{-1}$ (duodenum) (figure 2, e). The rates (mean ± SD) of 7-OH-flavone sulfation were $324 \pm 87\,pmol\,min^{-1}\,mg^{-1}$ (liver) and $584 \pm 164\,pmol\,min^{-1}\,mg^{-1}$ (duodenum; $p < 0.0001$). 7-OH-flavone sulphation rate did not correlate with the liver donor's age ($r = 0.013$; $p = 0.971$) and with the donor's duodenum age ($r = 0.470$; $p = 0.171$). The rate (mean ± SD) of 7-OH-flavone sulfation was $321 \pm 51\,pmol\,min^{-1}\,mg^{-1}$ (men) and $326 \pm 120\,pmol\,min^{-1}\,mg^{-1}$ (women; n.s.) in liver and $619 \pm 197\,pmol\,min^{-1}\,mg^{-1}$ (men) and $530 \pm 95\,pmol\,min^{-1}\,mg^{-1}$ (women; n.s.) in duodenum.

5-OH-flavone and 3-OH-flavone were not sulfated but inhibited SULT1A1 activity (figure 3). The IC_{50} (mean ± SD) of 5-OH-flavone was $0.3 \pm 0.06\,\mu M$ (liver) and $0.3 \pm 0.07\,\mu M$ (duodenum; n.s.) and that of 3-OH-flavone was $1.0 \pm 0.1\,\mu M$ (liver) and $1.6 \pm 0.03\,\mu M$ (duodenum; $p = 0.0006$). In the liver, the IC_{50} of 5-OH-flavone was smaller than that of 3-OH-flavone ($p = 0.0007$), and the same occurred in the duodenum ($p < 0.0001$).

The inhibition of the 7-OH-flavone sulfation rate was studied by 5-OH-flavone and 3-OH-flavone (figure 4). The IC_{50} of 5-OH-flavone was $3.5 \pm 0.5\,\mu M$ (liver) and $69 \pm 18\,\mu M$ (duodenum; $p < 0.0001$), and that of 3-OH-flavone was $18 \pm 3.4\,\mu M$ (liver) and $213 \pm 47\,\mu M$ (duodenum; $p < 0.0001$). 5-OH-flavone is a better inhibitor than 3-OH-flavone of 7-OH-flavone sulfation rate and both inhibitors have a lower IC_{50} in the liver than in the duodenum.

The present results show that the position of the hydroxy group in the molecule of OH-flavones determines the properties of substrate or inhibitor of these compounds for sulfotransferase. The K_m of 7-OH-flavone is in the order of μM both in the liver and duodenum as the K_m of 4-nitrophenol and dopamine, the diagnostic substrates of SULT1A1 and SULT1A3, respectively (Cappiello *et al.* 1990). The form(s) of sulfotransferase that catalyses the sulfation of 7-OH-flavone

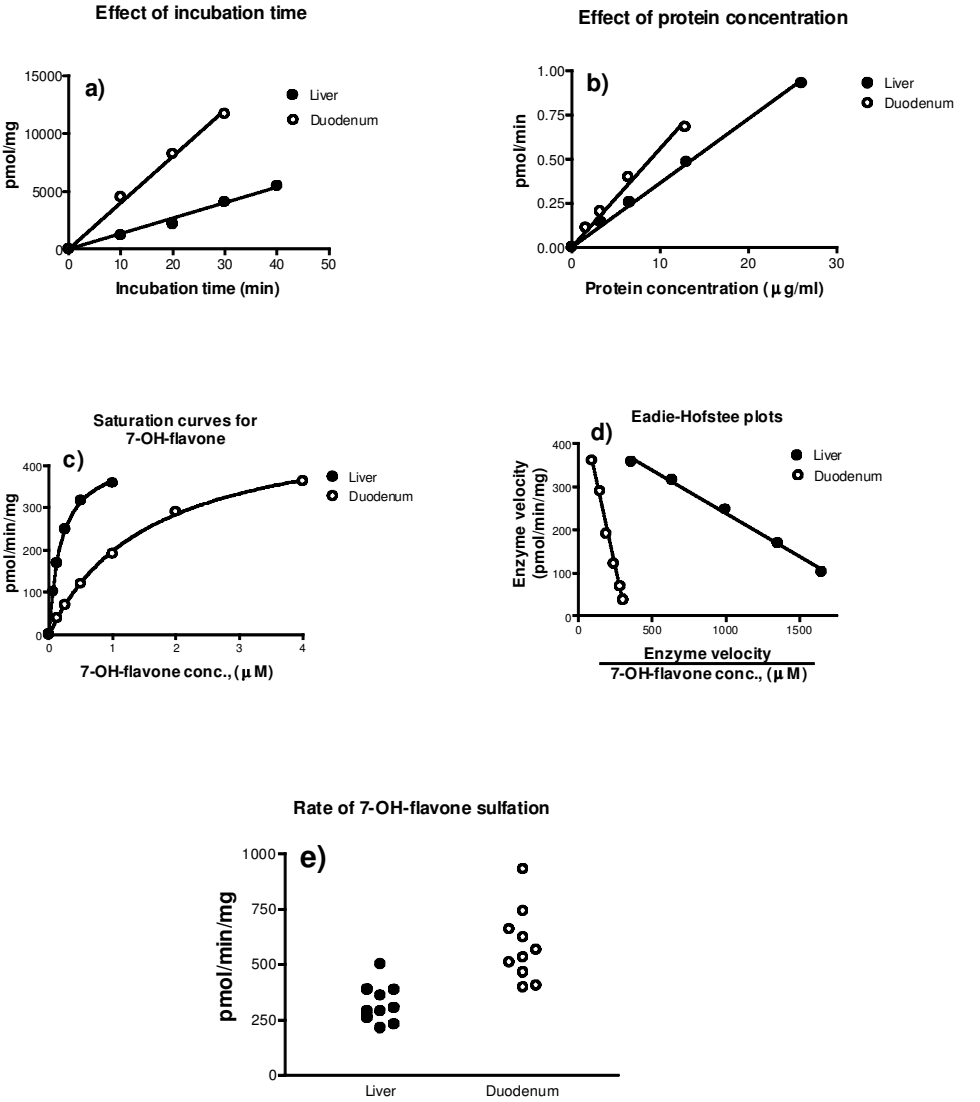


Figure 2. Sulfation of 7-OH-flavone in the human liver and duodenum. Effects of incubation time (a), protein concentration (b) and 7-OH-flavone concentration (c) on the rate of 7-OH-flavone sulfation. Transformation of the enzyme activity into a Lineweaver–Burk plot (d). Activities of 7-OH-flavone sulfation in 10 samples of the human liver and duodenum (e).

is unknown. SULT1A1 activity is higher in the liver than duodenum, whereas SULT1A3 activity is higher in duodenum than liver (Cappiello *et al.* 1990). The rate of 7-OH-flavone sulfation was higher in the duodenum than liver.

5-OH-flavone is a better inhibitor than 3-OH-flavone of SULT1A1 activity both in the liver and duodenum, and the same applies to the sulfation of 7-OH-flavone. The IC_{50} of 5-OH-flavone was similar in the liver and in the duodenum, whereas that of 3-OH-flavone was higher in the latter than in the former. The findings accord with previous results. Quercetin inhibited the sulfation rates of 4-

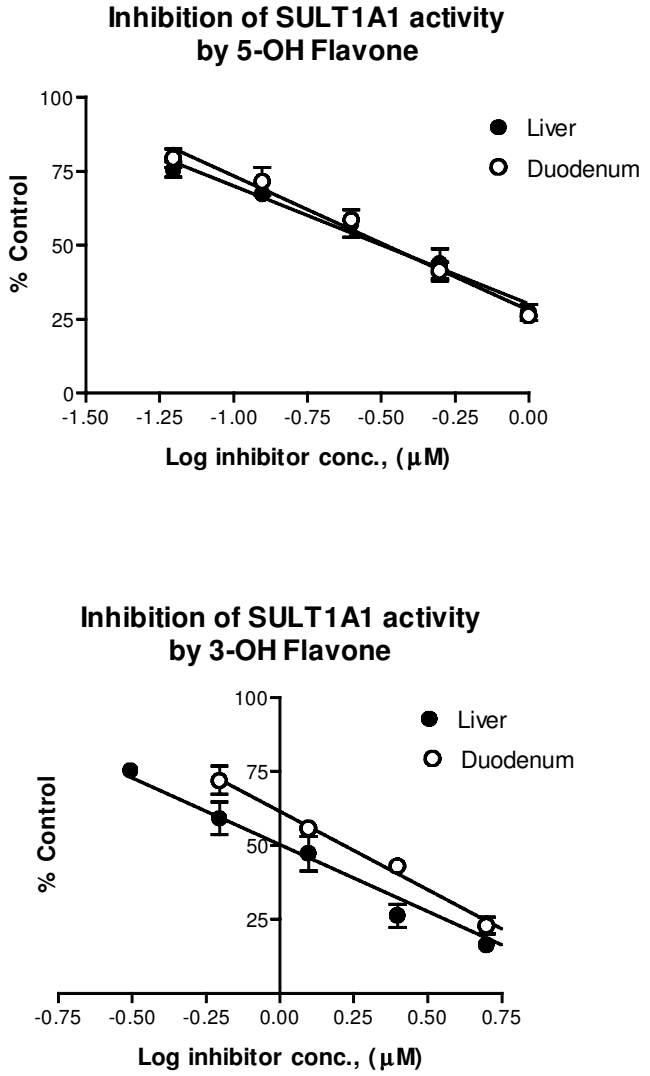


Figure 3. Inhibition of 4-nitrophenol sulfation rate by 5-OH-flavone (top) and 3-OH-flavone (bottom) in the human liver (filled circles) and duodenum (unfilled circles). Data are the mean of three tissue samples; vertical bars are 2 × SD.

nitrophenol, dopamine, (−)-salbutamol, minoxidil and paracetamol in the liver and duodenum. The IC_{50} of 4-nitrophenol was similar in the liver and duodenum, whereas the IC_{50} of dopamine, (−)-salbutamol, monoxidil and paracetamol were lower in liver than duodenum (Marchetti *et al.* 2001). Consistent results were obtained with the non-steroidal anti-inflammatory drugs mefenamic acid and salicylic acid. These compounds were better inhibitors of the sulfation of (−)-salbutamol and minoxidil in the liver than in the duodenum (Vietri *et al.* 2000). Under particular circumstances, the duodenum sulfotransferase is less susceptible than liver sulfotransferase to the inhibition by 5-OH-flavone, 3-OH-flavone, quercetin, mefenamic acid and salicylic acid.

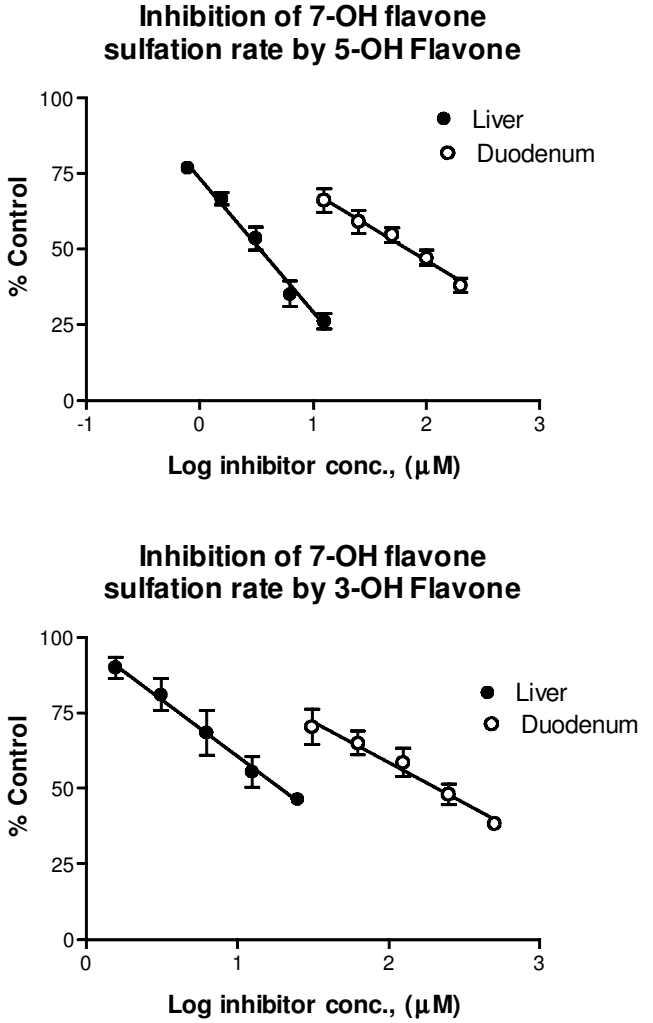


Figure 4. Inhibiton of 7-OH-flavone sulfation rate by 5-OH-flavone (top) and 3-OH-flavone (bottom) in the human liver (filled circles) and duodenum (unfilled circles). Data are the mean of five tissue samples; vertical bars are 2 × SD.

In conclusion, it is difficult to predict whether a flavone is a substrate or an inhibitor of sulfotransferase. This consideration is applicable to other natural compounds such as flavonoids (De Santi *et al*. 2000b); chrysin is a substrate of sulfotransferase, whereas quercetin is an inhibitor of this enzyme.

Acknowledgements

The work was supported by Contract BMH1-CT94-1622 of the European Commission (Brussels, Belgium), by the Italian Ministry of the University (Rome, Italy) and by the Italian Association for Cancer Research (Milan, Italy).

References

Anderson, R. J. and Weinshilboum, R. M., 1980, Phenolsulphotransferase in human tissues: radiochemical enzymatic assay and biochemical properties. *Clinica et Chimica Acta*, **103**, 79–90.

Arai, Y., Watanabe, S., Kimira, M., Shimoi, K., Mochizuki, R. and Kinae, N., 2000, Dietary intakes of flavonols, flavones and isoflavones by Japanese women and the inverse correlation between quercetin intake and plasma LDL cholesterol concentration. *Journal of Nutrition*, **130**, 2243–2250.

Campbell, N. R. C., Van Loon, J. A. and Winshilboum, R. M., 1987, Human liver phenol sulfotransferase: assay conditions, biochemical properties and partial purification of isoenzymes of the thermostable form. *Biochemical Pharmacology*, **36**, 1435–1446.

Cappiello, M., Giuliani, L. and Pacifici, G. M., 1990, Differential distribution of phenol and catechol sulphotransferase in human liver and intestinal mucosa. *Pharmacology*, **40**, 69–76.

Coughtrie, M. W. H. and Johnston, L. E., 2001, Interactions between dietary chemicals and human sulfotransferases – molecular mechanism and clinical significance. *Drug Metabolism and Disposition*, **29**, 522–528.

De Pascual-Teresa, S., Santos-Buelga, C. and Rivas-Gonzalo, J. C., 2000, Quantitative analysis of flavan-3-ols in Spanish foodstuffs and beverages. *Journal of Agriculture and Food Chemistry*, **48**, 5331–5337.

De Santi, C., Pietrabissa, A., Spisni, R., Mosca, F. and Pacifici, G. M., 2000a, The sulfation of resveratrol, a natural compound present in wine, is inhibited by natural flavonoids. *Xenobiotica*, **30**, 857–866.

De Santi, C., Pietrabissa, A., Spisni, R., Mosca, F. and Pacifici, G. M., 2000b, Sulphation of resveratrol, a natural product present in grapes and wine, in the human liver and duodenum. *Xenobiotica*, **30**, 609–617.

Foldes, A. and Meek, J., 1973, Rat brain phenolsulphotransferase-partial purification and some properties. *Biochimica et Biophysica Acta*, **327**, 365–374.

Hirvonen, T., Pietinen, P., Ovaskainen, M. L., Hakkinen, S., Albanes, D. and Virtamo, J., 2001, Intake of flavonols and flavones and risk of coronary heart disease in male smokers. *Epidemiology*, **12**, 62–67.

Hollman, P. C. and Katan, M. B., 1999, Dietary flavonoids: intake, health effects and bioavailability. *Food and Chemical Toxicology*, **37**, 937–942.

Lowry, O. H., Rosebrough, N. J., Farr, A. and Randall, R. J., 1951, Protein measurement with Folin phenol reagent. *Journal of Biological Chemistry*, **193**, 265–275.

Marchetti, F., De Santi, C., Vietri, M., Pietrabissa, A., Spisni, R., Mosca, F. and Pacifici, G. M., 2001, Differential inhibition of human liver and duodenum sulphotransferase activities by quercetin, a flavonoid present in vegetables, fruit and wine. *Xenobiotica*, **31**, 841–847.

McDonald, M. S., Hughes, M., Lean, M. E. and Matthews, D., 1998, The free and corrugated myricetin and quercetin content of red wines of different geographical origins. *Journal of Agriculture and Food Chemistry*, **46**, 368–375.

Scalbert, A. and Williamson, G., 2000, Dietary intake and bioavailability of polyphenols. *Journal of Nutrition*, **130**, 2073S–2085S.

Sundaram, R. S., Val Loon, J., Tucker, R. and Weinshilboum, R. M., 1989, Sulfation pharmacogenetics: correlation of human platelet and small intestinal phenol sulfotransferase. *Clinical Pharmacology and Therapeutics*, **46**, 501–509.

Vietri, M., Pietrabissa, A., Spisni, R., Mosca, F. and Pacifici, G. M., 2000, Differential inhibition of hepatic and duodenal sulfation of (−)-salbutamol and minoxidil by mefenamic acid. *European Journal of Clinical Pharmacology*, **56**, 477–479.

XENOBIOTICA, 2002, VOL. 32, NO. 7, 573–586

Taylor & Francis
healthsciences

Involvement of cytochrome P450 in the metabolism of rebamipide by the human liver

N. KOYAMA*, H. SASABE and G. MIYAMOTO

Tokushima Research Institute, Otsuka Pharmaceutical Co., Ltd, 463-10 Kagasuno, Kawauchi-cho, Tokushima 771-0192, Japan

Received 15 October 2001

1. The metabolism of rebamipide, a gastroprotective agent, was investigated using human liver microsomes and cDNA-expressed human cytochrome P450 systems.

2. 6-Hydroxy and 8-hydroxyrebamipide were produced by human cytochrome P450 enzyme(s), and 8-hydroxylation was the major metabolic pathway. K_m and V_{max} for 8-hydroxylation were 1.35 ± 0.20 mM and 0.32 ± 0.34 nmol min^{-1} mg protein^{-1}, respectively (mean $\pm$ SD, $n = 6$). Kinetic analysis showed that the 8-hydroxylation reaction consisted of a single component.

3. 8-Hydroxylation was inhibited by the addition of CYP3A4 antibodies as well as troleandomycin, a specific inhibitor of CYP3A4. Furthermore, the metabolism of rebamipide in human liver microsomes was compatible with that in a human cDNA-expressed CYP3A4 system, but not for other human P450 expression systems. It is therefore suggested that the hydroxylation of rebamipide only involves CYP3A4.

4. Rebampide showed no inhibitory effect on CYP1A2-, 2C9-, 2C19-, 2D6-, 2E1- and 3A4-catalysed metabolism. In addition, the metabolic contribution by CYP3A4 was considered to be slight for the overall elimination of rebamipide in man. It is therefore considered that drug interactions with cytochrome P450 enzymes are not involved in either the metabolism of rebamipide or the metabolism of other drugs concomitantly administered with rebamipide.

Introduction

Rebamipide (Mucosta; 2-(4-chlorobenzoylamino)-3-[2(1*H*)-quinolinon-4-yl]-propionic acid) is a quinolinone-derived gastroprotective agent that is widely used for the treatment of chronic gastritis, acute gastritis and gastric ulcer (Yamasaki *et al*. 1989). The drug enhances the production of endogenous prostaglandins (Yamasaki *et al*. 1987, Kleine *et al*. 1993), it has the potential to increase gastric mucus secretion (Ishihara *et al*. 1992) and it has an antioxidant effect on lipid peroxidation mediated by oxygen radicals (Yoshikawa *et al*. 1993a, b). These effects of rebamipide are considered to protect the gastric mucosa. It has been reported that the anti-ulcer activity of the metabolites is lower than that of the parent compound (Uchida *et al*. 1986).

To reduce gastric damage, rebamipide may be administered concomitantly with non-steroidal anti-inflammatory drugs (NSAIDs), which are widely used in many therapeutic areas. However, it is known that NSAIDs cause ulceration and erosion in the stomach and small intestine as adverse effects (Wallance 1994).

The aim of the present study was to identify which cytochrome P450 enzymes were involved in the hydroxylation reactions by examining the *in vitro* metabolism of rebamipide using human liver microsomes and cDNA-expressed human

* Author for correspondence; n_koyama@research.otsuka.co.jp

Xenobiotica ISSN 0049–8254 print/ISSN 1366–5928 online © 2002 Taylor & Francis Ltd
http://www.tandf.co.uk/journals
DOI: 10.1080/00498250210130591

cytochrome P450 systems. The inhibitory effect of rebamipide on cytochrome P450-catalysed metabolism was also investigated. In addition, a prediction of the drug interaction between rebamipide and NSAIDs was also performed.

Materials and methods

Chemicals and regents

Rebamipide, 6-hydroxyrebamipide and 8-hydroxyrebamipide were synthesized in Otsuka Pharmaceutical Co., Ltd (Tokyo, Japan), and were >97% chemically pure. The chemical structures are shown in figure 1. β-Nicotinamide adenine dinucleotide phosphate, reduced form (β-NADPH), β-nicotinamide adenine dinucleotide, reduced form (β-NADH), chlorzoxazone, propranolol, quinidine hydrochloride monohydrate, sulphaphenazole, testosterone, 6β-hydroxytestosterone, tolbutamide, tranylcypromine and troleandomycin were from Sigma Chemical Co. (St Louis, MO, USA). Diethyldithiocarbamate (DDC) was from Wako Pure Chemical Industries, Ltd (Osaka, Japan). (±)-Bufuralol HCl salt, 1′-hydroxybufuralol maleate salt, furafylline, *S*(+)-mephenytoin, quinidine, sulphaphenazole, *R*(+)-warfarin and 6-hydroxywarfarin were from Salford Ultrafine Chemicals and Research, Ltd (Manchester, UK). Furafylline, 6-hydroxychlorzoxazone, 4′-hydroxymephenytoin and 4-hydroxytolbutamide were purchased from Research Biochemicals, Inc. (Natick, MA, USA). Ketoconazole was purchased from Biomol Research Laboratories, Inc. (Plymouth Meeting, PA, USA). All other reagents and solvents were of special or HPLC grade and used without further purification.

Human liver microsomes, cDNA-expressed cytochrome P450 systems and antibodies

Microsomes derived from 10 human livers (Lot Nos 0101-960003, -960008, -960010, -960012, -960014, -960016, -970017, -970024, -970027, -970030) were prepared and supplied by the Biomedical Research Institute of Human and Animal Bridge (Chiba, Japan). The samples were from non-transplantable livers of donors and legally procured according to the legitimate protocol from the National Disease Research Interchange (NDRI, PA, USA) based on the international partnership between the NDRI and the Human and Animal Bridge Discussion Group (HAB) in Japan. Microsomes were stored at approximately −80 °C until use.

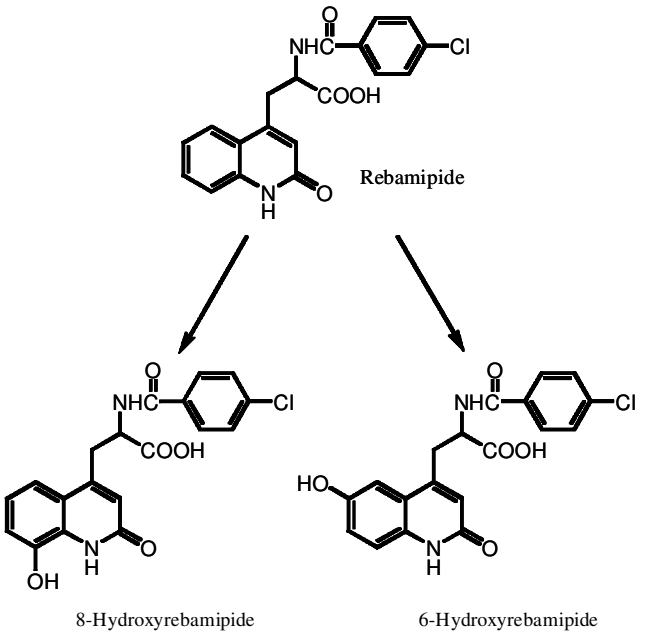


Figure 1. Metabolic pathways of rebamipide in man.

Microsomes from human AHH-1 TK+/− cells expressing cDNA-derived human cytochrome P450 enzymes (CYP1A1, 1A2, 2A6, 2B6, 2C8, 2C9, 2C19, 2D6, 2E1, 3A4) and control microsomes from a cell line containing an empty cDNA expression plasmid were purchased from Gentest Corporation (Woburn, MA, USA). Monoclonal antibodies (CYP2A6 [MAB-2A6], 2E1 [MAB-2E1] and 3A4 [MAB-3A4]) were also from Gentest. Polyclonal antibodies (goat antiserum for human NADPH P-450 reductase, rabbit antiserum for human CYP1A1/1A2, goat antiserum for human CYP2C, rabbit anti-human CYP2D6, rabbit antiserum for human CYP3A4) were purchased from Daiichi Pure Chemicals Co., Ltd (Tokyo, Japan). MAB-2A6 specifically inhibits human CYP2A6 catalytic activity with some cross-reactivity with CYP2E1, and MAB-2E1 and 3A4 specifically inhibit human CYP2E1 and 3A (3A4 and 3A5) catalytic activities, respectively. Antiserum for human NADPH P-450 reductase inhibits human CYP1A1, 1A2, 2A6, 2B6, 2C9, 2D6, 2E1 and 3A4 catalytic activities. Antiserum for human CYP1A1/1A2, 2C, 2D6 and 3A4 specifically inhibit human CYP1A (1A1 and 1A2), 2C (2C9 and 2C19), 2D6 and 3A4 catalytic activities, respectively.

Rebamipide metabolism in human liver microsomes

Rebamipide, dissolved in dimethylsulphoxide (DMSO), was added to reaction mixtures containing microsomes (pooled or individuals) in 0.1 M potassium phosphate buffer (pH 7.4). The reaction was started by the addition of a β-NADPH and β-NADH mixture following a 3-min pre-incubation, and the mixtures (final incubation volume 0.5 ml) were incubated at 37 °C for the designed time. The reaction was terminated by the addition of 2 mol l^{-1} hydrochloric acid (0.2 ml), and the mixtures were extracted with 5 ml ethyl acetate. Of the organic layer, 4 ml was transferred to another grass tube and dried under a stream of air. The residue was dissolved in 100 µl DMSO and analysed by a HPLC system from Waters Associates (Milford, MA, USA).

The formation of metabolites was linear for 15 min of incubation. The final concentration of rebamipide varied from 0.1 to 2 mM, and for β-NADPH, β-NADH and DMSO final concentrations were 5, 2.5mM and 1%, respectively. The final concentration of microsomal protein was 1 mg ml^{-1}, except for the microsomes of Lot No. 960010, which was 0.796 mg ml^{-1}.

Aliquots of the samples (60 µl) were injected on a TSK-gel ODS-80Ts column (5 µm, 4.6 × 150 mm, Tosoh Co., Tokyo, Japan), and the metabolites of rebmipide were separated with a linear gradient eluent, consisting of water:acetonitrile:acetic acid from 82:18:0.8 to 50:50:0.8, for 25 min. Analysis was performed at room temperature at 1 ml min^{-1} using Model 510 pumps. The eluates were monitored at UV 280 nm with a Model 486 detector (all Waters).

Inhibition experiments using human liver microsomes

Rebamipide (1 mM) was incubated together with CYP-specific chemical inhibitors (0, 0.1, 1, 10, 100 µM) in the reaction mixtures at 37 °C for 15 min. Cytochrome P450 inhibitors included sulphaphenazole (CYP2C9), tranylcypromine (CYP2C19), quinidine and propranolol (CYP2D6) dissolved in DMSO and were added simultaneously with rebampide to the reaction mixture. Mechanism-based inhibitors (furafylline [CYP1A2], DDC [CYP2A6 and 2E1] and troleandomycin [CYP3A4]) were pre-incubated at 37 °C for 15 min in the reaction mixtures before the addition of rebamipide, and were subsequently incubated at 37 °C for 30 min.

Monoclonal (MAB-2A6, 2E1 and 3A4) and polyclonal antibodies (antiserum for human NADPH-cytochrome P450 reductase, CYP1A1/1A2, 2C, 2D6 and 3A4) were mixed with microsomes and incubated before the addition to the reaction mixtures. Rebamipide (1 mM) was incubated with microsomes (0.4 mg ml^{-1}) and antibodies (0, 0.5, 1, 2 and 4 mg mg microsomal $protein^{-1}$) at 37 °C for 30 min in the presence of β-NADPH (5 mM).

The samples containing sulphaphenazole were exceptionally analysed (injection volume 10 µl) with a linear gradient eluent, consisting of water:acetonitrile:phosphoric acid from 82:18:0.1 to 50:50:0.1, for 30 min to separate the metabolite of rebamipide from the metabolite or the decomposition products of sulphaphenazole.

Rebamipide metabolism in cDNA-expressed human cytochrome P450 systems

Rebamipide, dissolved in *N*,*N*-dimethylformamide (DMF), was added to reaction mixtures containing microsomes expressing cDNA-derived CYP1A1, 1A2, 2A6, 2B6, 2C8, 2C9, 2C19, 2D6, 2E1 and 3A4, and the mixtures were incubated at 37 °C for 2 h after the addition of β-NADPH. The reaction mixtures (0.5 ml) consisted of microsomes (1 mg ml^{-1}), rebamipide (1 mM), β-NADPH (10 mM) and DMF (1%) in 0.1 M potassium phosphate buffer (pH 7.4), except for CYP2A6 and 2C9, which was in 0.1 M Tris-HCl buffer (pH 7.4). The reaction was terminated by the addition of methanol (0.5 ml), and the mixtures were centrifuged at 9000*g* for 10 min. Of the supernatant, 50 µl was injected into the HPLC.

For the determination of K_m and V_{max}, rebamipide (dissolved in DMF) was added to reaction mixtures containing microsomes expressing cDNA-derived CYP3A4 in 0.1 M potassium phosphate buffer (pH 7.4), and incubated at 37 °C for 10 min after the addition of β-NADPH. The final

concentration of rebamipide varied from 0.05 to 2 mM, and for microsomes, β-NADPH and DMF final concentrations were 1 mg ml^{-1}, 5 mM and 1%, respectively. The reaction was terminated by the addition of 2 mol l^{-1} hydrochloric acid and extracted with ethyl acetate according to the method described above. Of the sample, 60 µl was injected into the HPLC. The analytes were separated with a linear gradient eluent, consisting of water: acetonitrile: acetic acid from 95:5:1 to 30:70:1, for 40 min.

Effect of rebamipide on CYP1A2, 2C9, 2C19, 2D6, 2E1 and 3A4-catalysed reactions and NSAID metabolism

The possible inhibitory effects of rebamipide on *R*(+)-warfarin 6-hydroxylation (CYP1A2), tolbutamide methylhydroxylation (CYP2C9), *S*(+)-mephenytoin 4′-hydroxylation (CYP2C19), (±)-bufuralol 1′-hydroxylation (CYP2D6), chlorzoxazone 6-hydroxylation (CYP2E1) and testosterone 6β-hydroxylation (CYP3A4) were examined. The inhibitory effect of rebamipide on NSAID metabolism (diclofenac 4′-hydroxylation and naproxen 6-desmethylation, CYP2C9) was also examined. The reaction mixtures (0.5 ml) consisted of cDNA-derived, human CYP-expressing microsomes (1 mg ml^{-1}), β-NADPH (5 mM), the substrate, rebamipide or CYP-specific inhibitors (0, 0.5, 5, 50 and 500 µM) and DMSO (1%) in 0.1 M potassium phosphate buffer (pH 7.4), except for the CYP2C9 reaction, which was in 0.1 M tris-HCl buffer (pH 7.4). The reaction mixtures were incubated at 37 °C for 10 min, except for the CYP1A2 and 2C19 reactions, which were incubated for 20 min. The concentrations of the substrates were designed around the K_m determined in the present study. The final concentrations of the substrates were 500 µM *R*(+)-warfarin, 100 µM tolbutamide, 50 µM *S*(+)-mephenytoin, 10 µM (±)-bufuralol, 500 µM chlorzoxazone, 100 µM testosterone, 25 µM diclofenac and 150 µM naproxen.

The metabolites were extracted by deproteinization with methanol or extracted with ethyl acetate under acidic conditions, and analysed by the HPLC system described above.

Calculations and kinetic analysis

The concentrations of the analytes in the reaction mixtures were calculated from the calibration curves constructed based on the peak areas in the HPLC chromatograms. The velocity and per cent inhibition were calculated using the concentration data. Kinetic parameters for these reactions were estimated using the following equation:

$$V_0 = \frac{V_{max} \times S}{K_m + S},$$

where V_0 is the initial velocity (nmol min^{-1} mg $protein^{-1}$), S is the drug concentration (mM) in the reaction mixtures, K_m is the Michaelis–Menten constant (mM) and V_{max} is the maximum velocity (nmol min^{-1} mg $protein^{-1}$). The data sets were fitted to the equation by an iterative non-linear least-squares method using WinNonlin v.2.1 (Pharsight Corporation, Mountain View, CA, USA). The input data were weighted as the reciprocal of the observed and the Damping Gauss Newton method algorithm was used for the fitting algorithm.

Results

Rebamipide metabolism in human liver microsomes

When rebamipide was incubated at 37 °C for 1 h with human liver microsomes in the presence of β-NADPH, the production of 6-hydroxy and 8-hydroxyrebamipide was observed in all individual microsomes (figure 2). The quantitation of metabolites was achieved in nine of 10 microsomes because the activity in one sample (Lot No. 960010) was below the limit of quantitation (0.05 µM in reaction mixtures). The activities of 8- and 6-hydroxylation ranged from 0.38 to 17.13 nmol h^{-1} mg $protein^{-1}$ and from 0.18 to 1.13 nmol h^{-1} mg $protein^{-1}$, respectively (figure 3). The activity of 8-hydroxylation was approximately 10 times that of 6-hydroxylation. Six microsomal samples (Lot Nos 960008, 960012, 960014, 960016, 970017, 970027) in which the metabolic activity was relatively high were selected and used to determine the kinetic parameters.

Initial velocities of 8-hydroxyrebamipide were determined by incubation of rebamipide (0.1–2 mM) for 15 min in six human liver microsomal samples. The

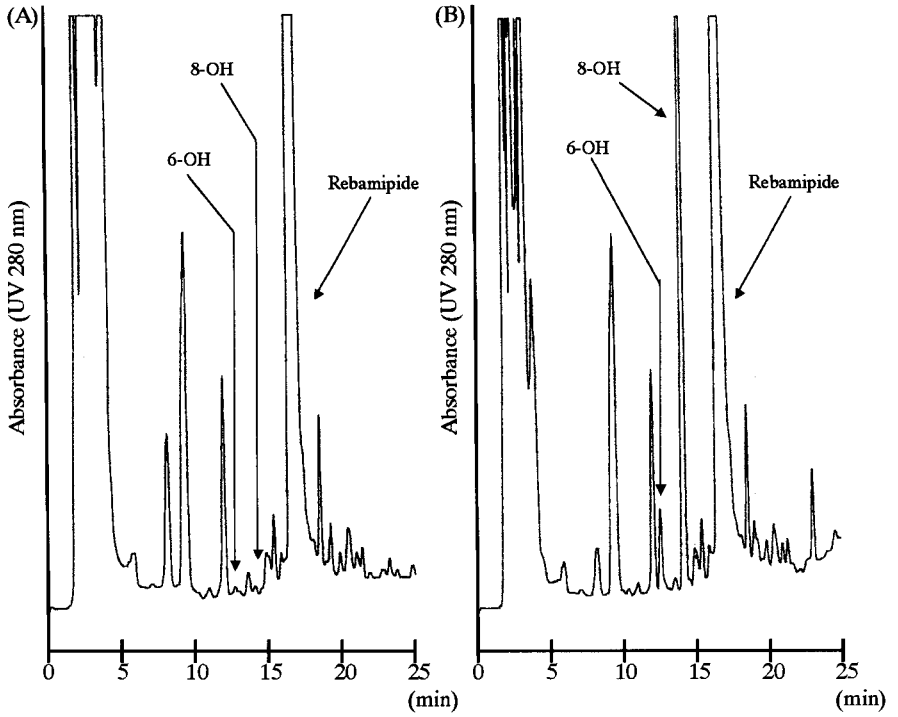


Figure 2. Identification of the 6- and 8-hydroxy metabolites of rebamipide. The reaction mixture (0.5 ml) consisted of 1 mg ml^{-1} human liver microsomal protein, 1 mM rebamipide, 5 mM β-NADPH, 2.5 mM β-NADH and 1% DMSO in potassium phosphate buffer (0.1 M, pH 7.4). The reaction mixture (A) was not incubated, and (B) was incubated at 37 °C for 1 h. Metabolites were identified by HPLC analysis as described in the Materials and methods.

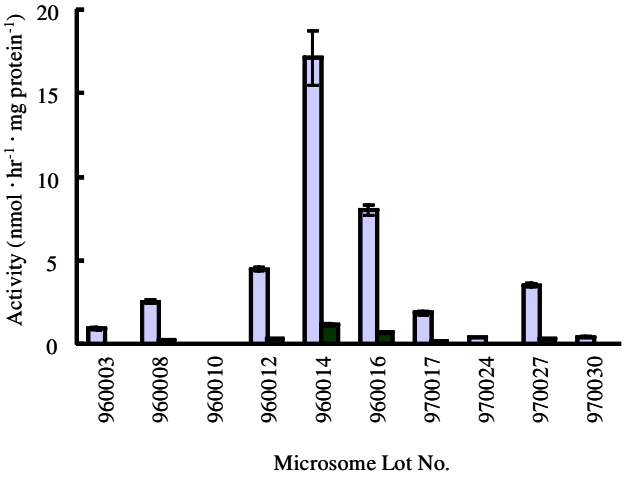


Figure 3. Metabolic activity for the production of 6-hydroxyrebamipide (■) and 8-hydroxyrebamipide (■) in 10 individual microsomes derived from human livers. Rebamipide (1 mM) was incubated at 37 °C for 1 h with 1 mg ml^{-1} individual microsomal protein (Lot No. 960010: 0.796 mg ml^{-1}), 5 mM β-NADPH, 2.5 mM β-NADH and 1% DMSO in potassium phosphate buffer (0.1 M, pH 7.4). Incubations were performed in triplicate and are shown as mean ± SD.

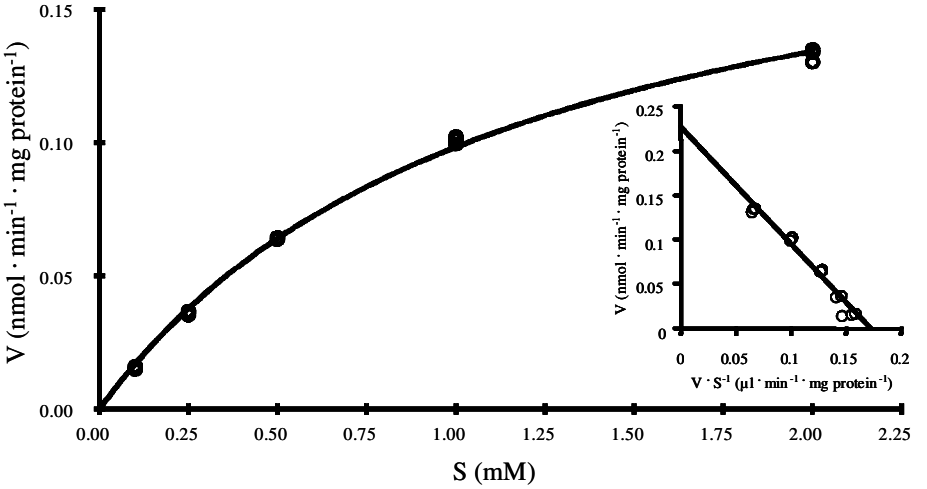


Figure 4. Typical plots for the kinetic analysis of rebamipide 8-hydroxylation in human liver microsomes. The solid line represents the estimated initial velocity. The inset shows an Eadie–Hofstee plot for the 8-hydroxylation of rebamipide. Rebamipide (0.1, 0.25, 0.5, 1 and 2 mM) was incubated at 37 °C for 15 min with 1 mg ml^{-1} microsomal protein, 5 mM β-NADPH, 2.5 mM β-NADH and 1% DMSO in potassium phosphate buffer (0.1 M, pH 7.4). Incubations were performed in triplicate, and these are shown separately in the figures.

profiles of the Eadie–Hofstee plots demonstrated that the 8-hydroxylation reaction consisted of one component (figure 4). K_m, V_{max} and CL_{int} ranged from 1.04 to 1.65 mM (1.35 ± 0.20 mM), from 0.08 to 0.99 nmol min^{-1} mg protein^{-1} (0.32 ± 0.34 nmol min^{-1} mg protein^{-1}) and from 0.06 to 0.60 µl min^{-1} mg protein^{-1} (0.22 ± 0.20 µl min^{-1} mg protein^{-1}), respectively (table 1).

Table 1. Kinetic parameters for the 8-hydroxylation of rebamipide in human liver microsomes (A) and cDNA-derived, CYP3A4-expressing microsomes (B)

A

Microsome Lot No.	K_m (mM)	V_{max} (nmol min^{-1} mg protein^{-1})	Intrinsic clearance (µl min^{-1} mg protein^{-1})
960008	1.30	0.12	0.09
960012	1.04	0.20	0.19
960014	1.65	0.99	0.60
960016	1.28	0.35	0.27
970017	1.39	0.08	0.06
970027	1.45	0.16	0.11
Mean	1.35	0.32	0.22
SD	0.20	0.34	0.20
Pooled (n = 10)	1.15	0.21	0.18

B

cDNA-expressed cytochrome P450			
CYP3A4	1.01	3.36	3.33

Effects of chemical inhibitors and antibodies on the 8-hydroxylation of rebamipide

The effects of chemical inhibitors on the 8-hydroxylation of rebamipide are shown in figure 5. The production of the metabolite was inhibited >80% in the presence of 10 μM troleandomycin, a mechanism-based inhibitor of CYP3A4 (Chang *et al.* 1994). The other inhibitors, furafylline (Sesardic *et al.* 1990, Kunze and Trager 1993), sulfaphenazole (Brian *et al.* 1989) tranylcypromine (Inaba *et al.* 1985, Wienkers *et al.* 1996) and DDC (Guengerich *et al.* 1991, Chang *et al.* 1994), did not inhibit 8-hydroxylation activity at a concentration of 100 μM. Production of 8-hydroxyrebamipide was markedly increased by the addition of quinidine and propranolol, both inhibitors of CYP2D6 (Inaba *et al.* 1985, Otton *et al.* 1990). When rebamipide and 1, 10 and 100 μM quinidine were co-incubated in reaction mixtures, the production of 8-hydroxyrebamipide was increased by about 1.2-, 3- and 8-fold compared with that of the control. Propranolol (100 μM) increased metabolite production by about 5-fold. Therefore, the inhibition of rebamipide 8-hydroxylation using chemical inhibitors of CYP2D6 could not be achieved.

The inhibitory effects of polyclonal antibodies for human NADPH-cytochrome P450 reductase, CYP1A1/1A2, 2C, 2D6 and 3A4 on the 8-hydroxylation are shown in figure 6(A), and those of monoclonal antibodies for CYP2A6, 2E1 and 3A4 are shown in figure 6(B). The presence of NADPH-cytochrome P450 reductase and CYP3A4 antibodies reduced the production of the metabolite by more than 80%. The other antibodies examined were without effect.

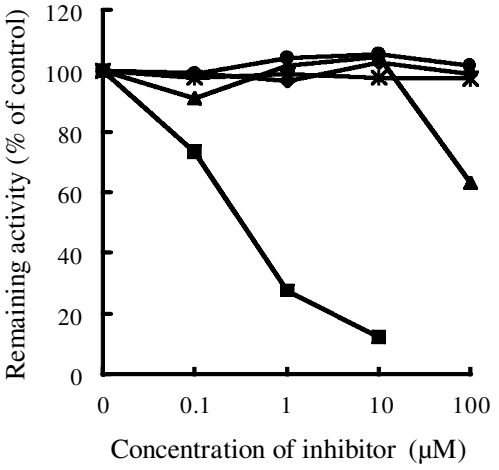


Figure 5. Effects of chemical inhibitors on rebamipide 8-hydroxylation activity in human liver microsomes. Rebamipide (1 mM) and inhibitors [0 (control), 0.1, 1,10 and 100 μM] were incubated at 37 °C for 15 min with 1 mg ml^{-1} microsomal protein, 5 mM β-NADPH, 2.5 mM β-NADH and 1% DMSO in potassium phosphate buffer (0.1 μM, pH 7.4). Each datum point represents the average of duplicate incubations. The control rebamipide 8-hydroxylation activities for furafylline, sulfaphenazole, tranylcypromine, DDC and troleandomycin inhibitory assay were 0.12, 0.15, 0.14, 0.14 and 0.12 nmol min^{-1} mg $protein^{-1}$, respectively. ●, Furafylline; ▲, sulfaphenazole; ∗, tranylcypromine; ◆, DDC (diethyldithiocarbamate); ■, troleandomycin.

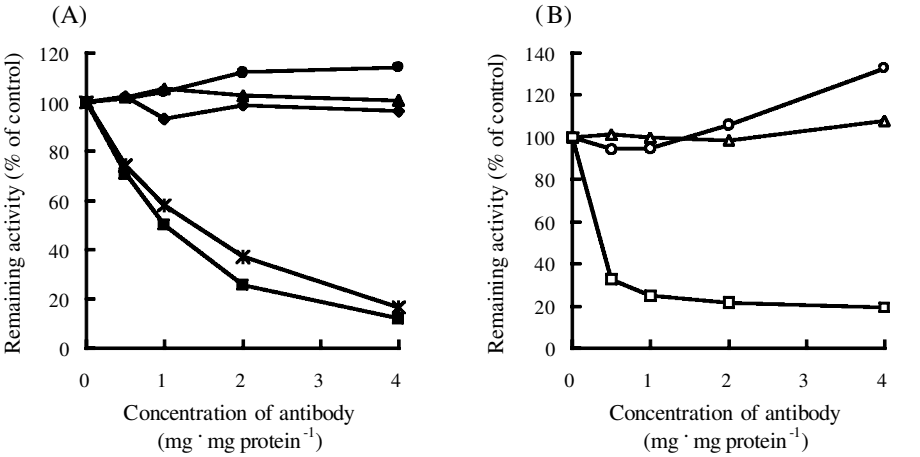


Figure 6. Effects of polyclonal (A) and monoclonal (B) antibodies on rebamipide 8-hydroxylation activity in human liver microsomes. Rebamipide (1 mM) was incubated at 37 °C for 30 min with 0.4 mg ml^{-1} microsomal protein, antibody [0 (control), 0.5, 1,2 and 4 mg mg $protein^{-1}$], 5 mM β-NADPH and 1% DMSO in potassium phosphate buffer (0.1 M, pH 7.4). Each datum point represents the average of duplicate incubations. The control rebamipide 8-hydroxylation activities for polyclonal anti-human cytochrome P450, CYP1A1/1A2, CYP2C, CYP2D6 and CYP3A4 inhibitory assay were 0.16, 0.16, 0.14, 0.16 and 0.16 nmol min^{-1} mg $protein^{-1}$, respectively, and those for monoclonal anti-human CYP2A6, CYP2E1 and CYP3A4 inhibitory assay were 0.19, 0.20 and 0.14 nmol min^{-1} mg $protein^{-1}$, respectively. *, Antiserum for human NADPH P-450 reductase; ●, antiserum for human CYP1A1/1A2, ▲, antiserum for human CYP2C; ◆ anti-human CYP2D6; ■, antiserum for human CYP3A4; △, MAB-2A6; ○, MAB-2E1; □, MAB-3A4.

Rebamipide metabolism in cDNA-expressed human cytochrome P450 systems

Rebamipide was incubated for 2 h in reaction mixtures containing cDNA-derived, human cytochrome P450-expressing microsomes. 8-Hydroxy and 6-hydroxyrebamipide were observed only in CYP3A4-expressing microsomes, and not in control microsomes, CYP1A1, 1A2, 2A6, 2B6, 2C8, 2C9, 2C19, 2D6 or 2E1-expressing microsomes. The activities of 8- and 6-hydroxylation were 79.73 ± 0.40 and 6.56 ± 0.28 pmol 2 h^{-1} pmol $CYP3A4^{-1}$, respectively (mean ± SD, $n = 3$) (figure 7). The K_m for 8-hydroxylation in CYP3A4-expressing microsomes was 1.01 mM, which was comparable with that in human liver microsomes (table 1).

Effect of rebamipide on CYP1A2, 2C9, 2C19, 2D6, 2E1 and 3A4-catalysed reactions and NSAID metabolism

The effects of rebamipide on the following reactions are shown in table 2: CYP1A2-catalysed $R(+)$-warfarin 6-hydroxylation (Rettie *et al.* 1992), CYP2C9-catalysed tolbutamide methylhydroxylation (Relling *et al.* 1990), CYP2C19-catalysed $S(+)$-mephenytoin 4′-hydroxylation (Wrighton *et al.* 1993), CYP2D6-catalysed (±)-bufuralol 1′-hydroxylation (Kronbach *et al.* 1987), CYP2E1-catalysed chlorzoxazone 6-hydroxylation (Peter *et al.* 1990) and CYP3A4-catalysed testosterone 6β-hydroxylation (Waxman *et al.* 1988, Brian *et al.* 1990). All the above probe substrate reactions examined were not inhibited by rebamipide until a 500 μM concentration.

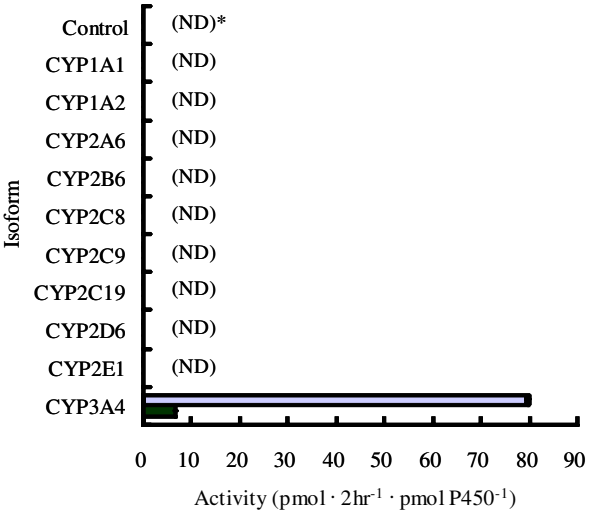


Figure 7. Metabolic activity for the production of 6-hydroxyrebamipide (■) and 8-hydroxyrebamipide (■) in cDNA-derived, human cytochrome P450-expressing microsomes. Rebamipide (1 mM) was incubated at 37 °C for 2 h with 1 mg ml^{-1} microsomal protein, 10 mM β-NADPH and 1% DMF in potassium phosphate buffer (0.1 M, pH 7.4) except for CYP2A6 and 2C9 in which tris-HCl buffer (0.1 M, pH 7.4) was used. Incubations were performed in triplicate and are shown as the mean ± SD. *ND indicates that the peaks of the metabolites were not detected in the chromatograms of the incubated reaction mixtures.

Table 2. Effects of rebamipide on CYP1A2, 2C9, 2C19, 2D6, 2E1 and 3A4-catalysed metabolism in cDNA-derived human cytochrome P450-expressing microsomes

Cytochrome P450	Parameter K_m (μM) V_{max} (pmol min^{-1} pmol P450^{-1})	Percentage of inhibition				
			Concentration of inhibitor (μM)			
		Inhibitors	0.5	5	50	500
CYP1A2	*R*(+)-warfarin 6-hydroxylation	rebamipide	2.3	4.3	3.0	−3.4
	K_m = 707.0, V_{max} = 0.50	furafylline	9.9	51.4	87.7	>96.2
CYP2C9	tolbutamide hydroxylation	rebamipide	−3.2	6.1	2.9	16.1
	K_m = 77.8, V_{max} = 14.46	sulphaphenazole	62.2	>86.8	>86.8	>86.8
CYP2C19	*S*(+)-mephenytoin 4′-hydroxylation	rebamipide	−8.6	−3.7	−1.7	−14.0
		tranylcypromine	−4.0	26.4	82.7	not done
	K_m = 48.6, V_{max} = 1.49					
CYP2D6	(±)-bufuralol 1′-hydroxylation	rebamipide	1.4	3.4	1.7	11.5
	K_m = 7.2, V_{max} = 4.03	quinidine	>83.1	>83.1	>83.1	>83.1
CYP2E1	chloroxazone 6-hydroxylation	rebamipide	5.0	2.9	6.3	3.5
	K_m = 465.8, V_{max} = 14.27	DDC	8.1	6.7	27.0	73.2
CYPeA4	testosterone 6β-hydroxylation	rebamipide	0.0	−0.4	4.5	1.4
	K_m = 71.6, V_{max} = 24.22	ketoconazole	80.4	>93.4	>93.4	not done

The concentrations of substrates used for each assay were 500 μM *R*(+)-warfarin, 100 μM tolbutamide, 50 μM *S*(+)-mephenytoin, 10 μM (±)-bufuralol, 500 μM chlorzoxazone or 100 μM testosterone. Substrate and inhibitor were incubated at 37 °C for 10 min (CYP2C9, 2D6, 2E1 and 3A4) or 20 min (CYP1A2 and 2C19) with 1 mg ml^{-1} microsomal protein, 5 mM β-NADPH and 1% DMSO in potassium phosphate buffer (0.1 M, pH 7.4) except for CYP2A6 and 2C9 in which Tris-HCl buffer (0.1 M, pH 7.4) was used. Data are the average of duplicate incubations. The control activities of probe substrate reactions for CYP1A2, 2C9, 2C19, 2D6, 2E1 and 3A4 were 0.20, 12.19, 0.58, 2.27, 4.14 and 14.92 pmol min^{-1} pmol P450^{-1}, respectively.

DDC, diethyldithiocarbamate.

Table 3. Effects of rebamipide on the metabolism of diclofenac and naproxen in cDNA-derived human CYP2C9-expressing microsomes.

Parameter K_m (μM) V_{max} (pmol eq. of substrate min^{-1} pmol $P450^{-1}$)	Inhibitors	Percentage of inhibition Concentration of inhibitor (μM) 0.5	5	50	500
Diclofenac 4′-hydroxylation $K_m = 19.6$, $V_{max} = 93.67$	rebamipide	−2.5	−1.9	−0.6	6.9
	sulfaphenazole	22.0	71.6	95.4	> 96.9
Naproxen 6-desmethylation $K_m = 206.0$, $V_{max} = 57.89$	rebamipide	0.7	1.5	5.9	27.8
	sulfaphenazole	42.6	89.6	not determined	not determined

The concentrations of substrates used for each assay were 25 μM diclofenac or 150 μM naproxen. Substrate and inhibitor were incubated at 37 °C for 10 min (diclofenac) or 20 min (naproxen) with 1 mg ml^{-1} microsomal protein, 5 mM β-NADPH and 1% DMSO in Tris-HCl buffer (0.1 M, pH 7.4). Data are average of duplicate incubations. The control activities of probe substrate reactions for diclofenac and naproxen were 51.29 and 21.94 pmol eq. of substrate min^{-1} pmol $P450^{-1}$, respectively.

The effects of rebamipide on diclofenac 4′-hydroxylation (Leemann *et al.* 1993) and naproxen 6-desmethylation (Miners *et al.* 1996, Rodrigues *et al.* 1996) are shown in table 3. Diclofenac 4′-hydroxylation was not inhibited by rebamipide until 500 μM. Rebamipide inhibited naproxen 6-desmethylation by 27.8% at 500 μM, while sulfaphenazole, a CYP2C9 inhibitor (Brian *et al.* 1989), inhibited it completely.

Discussion

The *In vitro* metabolism of rebamipide using human liver microsomes yielded two metabolites: 6-hydroxy and 8-hydroxyrebamipide. The hydroxylation of rebamipide showed a huge individual difference between microsomes (6-hydroxylation: 0.18–1.13 nmol h^{-1} mg $protein^{-1}$, 8-hydroxylation: 0.38–17.13 nmol h^{-1} mg $protein^{-1}$) (figure 3). When the activity of diazepam 3-hydroxylation (mediated by CYP3A4; Andersson *et al.* 1994) was assayed by the HAB using the microsomes derived from the same human livers, all the samples showed CYP3A4 activity, and the activity was from 120 to 2100 nmol min^{-1} mg $protein^{-1}$ (http://www2.odn.ne.jp/hab). The activities of diazepam 3-hydroxylation are also relatively low in the microsomes that show low activities in the hydroxylation of rebamipide. The individual difference of these metabolic activities is considered to be due to the variation of CYP3A4 activities in the microsomes, and CYP3A4 contents in the livers, and so on.

In six individual microsomes, the K_m for the production of 8-hydroxyrebamipide was 1.35 mM, which was comparatively high, suggesting that rebamipide had a low affinity for the microsomal enzyme. The 8-hydroxylation reaction was inhibited by human NADPH-cytochrome P450 reductase antibody in human liver microsomes (figure 6 (A)), suggesting that a cytochrome P450 enzyme was involved in the metabolism of rebamipide. This reaction was inhibited > 80% in the presence of 10 μM troleandomycin, a mechanism-based inhibitor of CYP3A4 (Chang *et al.* 1994) (figure 5). On the other hand, furafylline, an inhibitor of CYP1A2 (Sesardic *et al.* 1990, Kunze and Trager 1993), sulphaphenazole, an

inhibitor of CYP2C9 (Brian *et al*. 1989), tranylcypromine, an inhibitor of CYP2C19 (Inaba *et al*. 1985, Wienkers *et al*. 1996), and DDC, an inhibitor of CYP2A6 and 2E1 (Guengerich *et al*. 1991, Chang *et al*. 1994), did not inhibit the reaction at a high concentration (100 μM) (figure 5), which was higher than the corresponding K_i (approximately between 0.1 and 10 μM) (Inaba *et al*. 1985, Bourrié *et al*. 1996, Eagling *et al*. 1998). In addition, only the CYP3A4 antibody inhibited the 8-hydroxylation activity (figure 6). The 8-hydroxylation of rebamipide was observed only in a human cDNA-expressed CYP3A4 system, whereas CYP1A1, 1A2, 2A6, 2B6, 2C8, 2C9, 2C19, 2D6 and 2E1 were not involved in this reaction (figure 7). These results demonstrate that CYP3A4 is responsible for the 8-hydroxylation reaction. The Eadie–Hofstee plots of the initial velocity of 8-hydroxylation showed a linear profile, indicating that the metabolic reaction consisted of one component and was mediated by a single enzyme (figure 4). In addition, the K_m in human liver microsomes (1.35 mM) was close to that in a human cDNA-expressed CYP3A4 system (1.01 mM). It is therefore concluded that the K_m in human liver microsomes is predominantly governed by the K_m for CYP3A4. This conclusion is in agreement with the results of inhibition studies using specific chemical inhibitors and antibodies.

Production of 8-hydroxyrebamipide was markedly increased by the addition of quinidine and propranolol, both inhibitors of CYP2D6 (Inaba *et al*. 1985, Otton *et al*. 1990). This phenomenon was dependent on the concentration of the inhibitors. Although the mechanism is not clear, the affinity for the microsomal enzyme may be increased by the presence of a CYP2D6 inhibitor, accompanied by a conformational change of the enzyme. However, taking into account that the antibody for CYP2D6 does not inhibit 8-hydroxylation of rebamipide and that the hydroxylation does not occur in a human cDNA-expressed CYP2D6 system, it can be concluded that CYP2D6 is not involved in the 8-hydroxylation reaction.

The involvement of CYP3A4 in the 6-hydroxylation of rebamipide was supported by the results of the experiments using cDNA-derived, human cytochrome P450-expressing microsomes (figure 7). The kinetic and inhibition studies for the 6-hydroxylation were not performed in the present study because the production of the 6-hydroxy metabolite was much smaller than 8-hydroxy metabolite, and was not enough to quantitate under this analytical condition. It is, however, considered that the 6-hydroxylation of the substrate is not a major pathway in the metabolism of rebamipide in man.

A high concentration of rebamipide (500 μM) did not inhibit CYP1A2-catalysed *R*(+)-warfarin 6-hydroxylation (Rettie *et al*. 1992), CYP2C9-catalysed tolbutamide methylhydroxylation (Relling *et al*. 1990), CYP2C19-catalysed *S*(+)-mephenytoin 4′-hydroxylation (Wrighton *et al*. 1993), CYP2D6-catalysed (±)-bufuralol 1′-hydroxylation (Kronbach *et al*. 1987), CYP2E1-catalysed chlorzoxazone 6-hydroxylation (Peter *et al*. 1990) and CYP3A4-catalysed testosterone 6β-hydroxylation (Waxman *et al*. 1988, Brian *et al*. 1990), although specific inhibitors for cytochrome P450 inhibited them completely at low concentrations. These results suggest that rebamipide have no inhibitory effect on any CYP-catalysed reaction examined herein. Diclofenac 4′-hydroxylation and naproxen 6-desmethylation are known to be mediated by CYP2C9 (Leemann *et al*. 1993, Miners *et al*. 1996, Rodrigues *et al*. 1996). Rebamipide had little inhibition on the metabolism of these NSAIDs. Taking into account that the C_{max} level of rebamipide in human plasma after a single oral administration is approximately

1 μM (390 ng ml^{-1} at a dose of 600 mg/body) (Kishi and Ogawa 1989), it can be concluded that rebamipide has little inhibitory effect on drug metabolism mediated by CYP1A2, 2C9, 2C19, 2D6, 2E1 and 3A4 or on the metabolism of NSAIDs by CYP2C9.

The 8-hydroxy metabolite of rebamipide was predominantly formed by CYP3A4. Therefore, 8-hydroxylation might be inhibited by other drugs metabolized by CYP3A4. The degree of drug interaction *in vivo* is dependent on the contribution of metabolism to the overall elimination of the drug. To compare with urinary clearance, the *in vivo* hepatic clearance by 8-hydroxylation was predicted using the results of the *in vitro* data described in the present study. The intrinsic clearance of 8-hydroxylation ranged from 0.06 to 0.60 μl min^{-1} mg $protein^{-1}$, and it was consequently calculated to be from 3 to 32 μl min^{-1} g $liver^{-1}$ using the microsomal protein content in human liver (52.5 mg protein g $liver^{-1}$) (Iwatsubo *et al.* 1997). These are much lower than the hepatic blood flow rate in man (approximately 1 ml min^{-1} g $liver^{-1}$) (Boxenbaum 1980), suggesting that the activity of 8-hydroxylation is very low in human liver. Furthermore, the organ clearance of drug metabolism is dependent on the degree of intrinsic clearance. The organ clearance by 8-hydroxylation obtained from intrinsic clearance, protein binding (0.985) (Shioya *et al.* 1989) and liver weight (24.2 g kg^{-1}) (Boxenbaum 1980) was up to 11 μl min^{-1} kg^{-1}, which was $<1\%$ of the urinary excretion clearance in a Phase I clinical study in man (approximately between 2 and 4 ml min^{-1} kg^{-1}) (Kishi and Ogawa 1989). This prediction suggests that rebamipide absorbed from the gastrointestinal tract is predominantly excreted in urine without being metabolized in human liver. It is therefore concluded that the plasma concentration of rebamipide is marginally influenced if CYP3A4 activity in human liver is reduced by drug interactions.

It is known that rebamipide undergoes glucuronidation as well as hydroxylation *in vivo*, although the activity of glucuronidation is very low. Actually, when rebamipide was orally administered to man in a Phase I clinical study (Kishi and Ogawa 1989), the parent compound was predominantly present in plasma and urine, and the quantities of hydroxyl metabolites and the glucuronide conjugates were very low. The low activity in the *in vitro* metabolism of rebamipide is comparable with the result of the *in vivo* study.

In conclusion, the 6- and 8-hydroxylation of rebamipide is only catalysed by CYP3A4. It is, however, considered that drug interactions with cytochrome P450 enzymes is not involved in either the metabolism of rebamipide or the metabolism of the other drugs concomitantly administered with rebamipide examined herein. This takes into account the fact that the plasma concentration of rebamipide in clinical therapy is much smaller than the concentration that causes inhibition, and that the metabolic contribution by CYP3A4 is marginal in the overall elimination of rebamipide in man.

References

Andersson, T., Miners, J. O., Veronese, M. E. and Birkett, D. J., 1994, Diazepam metabolism by human liver microsomes is mediated by both *S*-mephenytoin hydroxylase and CYP3A isoforms. *British Journal of Clinical Pharmacology*, **38**, 131–137.

Bourrié, M., Meunier, V., Berger, Y. and Fabre, G., 1996, Cytochrome P450 isoform inhibitors as a tool for the investigation of metabolic reactions catalysed by human liver microsomes. *Journal of Pharmacology and Experimental Therapeutics*, **277**, 321–332.

Boxenbaum, H., 1980, Interspecies variation in liver weight, hepatic blood flow, and antipyrine intrinsic clearance: extrapolation of data to benzodiazepines and phenytoin. *Journal of Pharmacokinetics and Biopharmaceutics*, **8**, 165–176.

Brian, W. R., Sari, M. A., Iwasaki, M., Shimada, T., Kaminsky, L. S. and Guengerich, F. P., 1990, Catalytic activities of human liver cytochrome P-450 IIIA4 expressed in *Saccharomyces cerevisiae*. *Biochemistry*, **29**, 11280–11292.

Brian, W. R., Srivastava, P. K., Umbenhauer, D. R., Lloyd, R. S. and Guengerich, F. P., 1989, Expression of a human liver cytochrome P-450 protein with tolbutamide hydroxylase activity in *Saccharomyces cerevisiae*. *Biochemistry*, **28**, 4993–4999.

Chang, T. K. H., Gonzalez, F. J. and Waxman, D. J., 1994, Evaluation of triacetyloleandomycin, α-naphthoflavone and diethyldithiocarbamate as selective chemical probes for inhibition of human cytochromes P450. *Archives of Biochemistry and Biophysics*, **311**, 437–442.

Eagling, V. A., Tjia, J. F. and Back, D. J., 1998, Differential selectivity of cytochrome P450 inhibitors against probe substrates in human and rat liver microsomes. *British Journal of Clinical Pharmacology*, **45**, 107–114.

Guengerich, F. P., Kim, D. H. and Iwasaki, M., 1991, Role of human cytochrome P-450 IIE1 in the oxidation of many low molecular weight cancer suspects. *Chemical Research in Toxicology*, **4**, 168–179.

Inaba, T., Jurima, M., Mahon, W. A. and Kalow, W., 1985, *In vitro* inhibition studies of two isozymes of human liver cytochrome P-450: mephenytoin *p*-hydroxylase and sparteine monooxygenase. *Drug Metabolism and Disposition*, **13**, 443–448.

Ishihara, K., Komuro, Y., Nishiyama, N., Yamasaki, K. and Hotta, K., 1992, Effect of rebamipide on mucus secretion by endogenous prostaglandin-independent mechanism in rat gastric mucosa. *Arzneimittel-Forschung/Drug Research*, **42**, 1462–1466.

Iwatsubo, T., Hirota, N., Ooie, T., Suzuki, H., Shimada, N., Chiba, K., Ishizaki, T., Green, C. E., Tyson, C. A. and Sugiyama, Y., 1997, Prediction of *in vivo* drug metabolism in the human liver from *in vitro* metabolism data. *Pharmacology and Therapeutics*, **73**, 147–171.

Kishi, S. and Ogawa, N., 1989, Phase I clinical study of the anti-ulcer drug proamipide (OPC-12759). *Journal of Adult Diseases*, **19**, 355–363.

Kleine, A., Kluge, S. and Peskar, B. M., 1993, Stimulation of prostaglandin biosynthesis mediates gastroprotective effect of rebamipide in rats. *Digestive Diseases and Sciences*, **38**, 1441–1449.

Kronbach, T., Mathys, D., Gut, J., Catin, T. and Meyer, U. A., 1987, High-performance liquid chromatographic assays for bufuralol 1′-hydroxylase, debrisoquine 4-hydroxylase, and dextromethorphan *O*-demethylase in microsomes and purified cytochrome P-450 isozymes of human liver. *Analytical Biochemistry*, **162**, 24–32.

Kunze, K. L. and Trager, W. F., 1993, Isoform-selective mechanism-based inhibition of human cytochrome P450 1A2 by furafylline. *Chemical Research in Toxicology*, **6**, 649–656.

Leemann, T., Transon, C. and Dayer, P., 1993, Cytochrome $P450_{TB}$ (CYP2C): a major monooxygenase catalyzing diclofenac 4′-hydroxylation in human liver. *Life Sciences*, **52**, 29–34.

Miners, J. O., Coulter, S., Tukey, R. H., Veronese, M. E. and Birkett, D. J., 1996, Cytochromes P450, 1A2, and 2C9 are responsible for the human hepatic *O*-demethylation of *R*- and *S*-naproxen. *Biochemical Pharmacology*, **51**, 1003–1008.

Otton, S. V., Gillam, E. M. J., Lennard, M. S., Tucker, G. T. and Woods, H. F., 1990, Propranolol oxidation by human liver microsomes – the use of cumene hydroperoxide to probe isoenzymes specificity and regio- and stereoselectivity. *British Journal of Clinical Pharmacology*, **30**, 751–760.

Peter, R., Böcker, R., Beaune, P. H., Iwasaki, M., Guengerich, F. P. and Yang, C. S., 1990, Hydroxylation of chlorzoxazone as a specific probe for human liver cytochrome P450IIE1. *Chemical Research in Toxicology*, **3**, 566–573.

Relling, M. V., Aoyama, T., Gonzalez, F. J. and Meyer, U. A., 1990, Tolbutamide and mephenytoin hydroxylation by human cytochrome P450s in the *CYP2C* subfamily. *Journal of Pharmacology and Experimental Therapeutics*, **252**, 442–447.

Rettie, A. E., Korzekwa, K. R., Kunze, K. L., Lawrence, R. F., Eddy, A. C., Aoyama, T., Gelboin, H. V., Gonzalez, F. J. and Trager, W. F., 1992, Hydroxylation of warfarin by human cDNA-expressed cytochrome P-450: a role for P-4502C9 in the etiology of (*S*)-warfarin-drug interactions. *Chemical Research in Toxicology*, **5**, 54–59.

Rodrigues, A. D., Kukulka, M. J., Roberts, E. M., Ouellet, D. and Rodgers, T. R., 1996, [*O*-Methyl ^{14}C] naproxen *O*-demethylase activity in human liver microsomes: Evidence for the involvement of cytochrome P4501A2 and P4502C9/10. *Drug Metabolism and Disposition*, **24**, 126–136.

Sesardic, D., Boobis, A. R., Murray, B. P., Murray, S., Segura, J., De La Torre, R. and Davies, D. S., 1990, Furafylline in a potent and selective inhibitor of cytochrome P450IA2 in man. *British Journal of Clinical Pharmacology*, **29**, 651–663.

Shioya, Y., Kashiyama, E., Okada, K., Kusumoto, N., Abe, Y., Uchida, M. and Shimizu, T., 1989, Metabolic fate of the anti-ulcer agent, (±)-2-(4-chlorobenzoylamino)-3-[2(1*H*)-quinolinon-4-yl]propionic acid (OPC-12759) – absorption, distribution and excretion in rats and dogs. *Iyakuhin Kenkyu*, **20**, 522–533.

Uchida, M., Tabusa, F., Komatsu, M., Morita, S., Kanbe, T. and Nakagawa, K., 1986, Studies on 2(1*H*)-quinolinone derivatives as gastric antiulcer active agents. Synthesis and antiulcer activity of the metabolites of 2-(4-chlorobenzoylamino)-3-[2(1*H*)-quinolinon-4-yl]propionic acid. *Chemical and Pharmaceutical Bulletin*, **34**, 4821–4824.

Wallance, J. L., 1994, The 1994 Merck Frosst Award. Mechanisms of nonsteroidal anti-inflammatory drug (NSAID) induced gastrointestinal damage – potential for development of gastrointestinal tract safe NSAIDs. *Canadian Journal of Physiology and Pharmacology*, **72**, 1493–1498.

Waxman, D. J., Attisano, C., Guengerich, F. P. and Lapenson, D. P., 1988, Human liver microsomal steroid metabolism: Identification of the major microsomal steroid hormone 6β-hydroxylase cytochrome P-450 enzyme. *Archives of Biochemistry and Biophysics*, **263**, 424–436.

Wienkers, L. C., Wurden, C. J., Storch, E., Kunze, K. L., Rettie, A. E. and Trager, W. F., 1996, Formation of (*R*)-8-hydroxywarfarin in human liver microsomes: a new metabolic marker for the (*S*)-mephenytoin hydroxylase, P4502C19. *Drug Metabolism and Disposition*, **24**, 610–614.

Wrighton, S. A., Stevens, J. C., Becker, G. W. and VandenBranden, M., 1993, Isolation and characterization of human liver cytochrome P450 2C19: correlation between 2C19 and *S*-mephenytoin 4′-hydroxylation. *Archives of Biochemistry and Biophysics*, **306**, 240–245.

Yamasaki, K., Ishiyama, H., Imaizumi, T., Kanbe, T. and Yabuuchi, Y., 1989, Effect of OPC-12759, a novel antiulcer agent, on chronic and acute experimental gastric ulcer, and gastric secretion in rats. *Japanese Journal of Pharmacology*, **49**, 441–448.

Yamasaki, K., Kanbe, T., Chijiwa, T., Ishiyama, H. and Morita, S., 1987, Gastric mucosal protection by OPC-12759, a novel antiulcer compound, in the rat. *European Journal of Pharmacology*, **142**, 23–29.

Yoshikawa, T., Naito, Y., Nakamura, S., Nishimura, S., Kaneko, T., Iinuma, S., Takahashi, S., Kondo, M. and Yamasaki, K., 1993a, Effect of rebamipide on lipid peroxidation and gastric mucosal injury induced by indomethacin in rats. *Arzneimittel-Forschung/Drug Research*, **43**, 1327–1330.

Yoshikawa, T., Naito, Y., Tanigawa, T. and Kondo, M., 1993b, Free radical scavenging activity of the novel anti-ulcer agent rebamipide studied by electron spin resonance. *Arzneimittel-Forschung/Drug Research*, **43**, 363–366.

XENOBIOTICA, 2002, VOL. 32, NO. 7, 587–594

Taylor & Francis
healthsciences

Sulfation of *R*(−)-apomorphine in the human liver and duodenum, and its inhibition by mefenamic acid, salicylic acid and quercetin

M. VIETRI†, F. VAGLINI†, A. PIETRABISSA§, R. SPISNI‡, F. MOSCA§ and G. M. PACIFICI†*

† Department of Neurosciences, Section of Pharmacology, and ‡ Department of Surgery, Medical School, Via Roma 55, I-56126 Pisa, Italy
§ Department of Oncology, Section of Surgery, Cisanello Hospital at the University of Pisa, I-56124 Cisanello, Pisa, Italy

Received 13 December 2001

1. The aims were to study the sulfation of *R*-(−)-apomorphine (hereafter apomorphine) in the human liver and duodenum, and to study the rate of inhibition of apomorphine sulphation by mefenamic acid, salicylic acid and quercetin also in the human liver and duodenum.

2. A rapid and sensitive method was developed to measure the sulfation rate of apomorphine in the human liver and duodenum. The method was based on the use of 0.4 μM 3′-phosphoadenosine-5′-phosphosulfate-[^{35}S] (PAPS) and 50 μM apomorphine. The unreacted PAPS was precipitated with barium hydroxide, barium acetate and zinc sulfate.

3. The rate of apomorphine sulfation (mean ± SD and median) was 261 ± 82 and 242 pmol min^{-1} mg^{-1}, respectively (liver), and 433 ± 157 and 443 pmol min^{-1} mg^{-1}, respectively (duodenum). The apomorphine sulfation rate was higher in the duodenum than in the liver ($p = 0.0005$).

4. Apomorphine sulfation was correlated with SULT1A1 activity in the liver ($r^2 = 0.363$, $p = 0.005$) and duodenum ($r^2 = 0.494$, $p = 0.0005$), but it did not correlate with SULT1A3 activity both in the liver and duodenum.

5. The K_m estimate of apomorphine sulfation rate was 20 ± 3.6 (liver) and 6.5 ± 0.2 μM (duodenum, $p = 0.024$), and the V_{max} estimate was 248 ± 99 (liver) and 636 ± 104 pmol min^{-1} mg^{-1} (duodenum, $p = 0.018$).

6. Mefenamic acid, salicylic acid and quercetin were potent inhibitors of apomorphine sulfation rate in the liver, and the IC_{50} estimates were 16 ± 0.2 nM, 54 ± 8.6 μM and 18 ± 2.8 nM, respectively. These compounds were poor inhibitors of apomorphine sulfation in the duodenum.

7. Apomorphine is sulfated by the human liver and duodenum, the highest activity being associated with the duodenum. The K_m of apomorphine sulfotransferase is in the order of μM both in the liver and duodenum. The non-steroidal anti-inflammatory drug mefenamic acid and the natural flavonoid quercetin inhibit the hepatic sulfation of apomorphine with an IC_{50} in the order of nM.

Introduction

Apomorphine is a dopamine agonist used in association with levodopa in the treatment of Parkinson's disease. It undergoes an extensive metabolism, and although oxidation is the major metabolic pathway of apomorphine, sulfation

* Author for correspondence; e-mail: pacifici@biomed.unipi.it

Xenobiotica ISSN 0049-8254 print/ISSN 1366-5928 online © 2002 Taylor & Francis Ltd
http://www.tandf.co.uk/journals
DOI: 10.1080/00498250210131581

contributes to the overall metabolism of this drug for 5–10% (Neef and Laar 1999). Up to now, the *in vitro* sulfation of apomorphine has not been studied.

Ernst (1965) demonstrated that the chemical structure of apomorphine resembles that of dopamine and both possess a catechol group. Dopamine is sulfated by the human liver and gut (Cappiello *et al.* 1990), and the first aim of the present paper was to study apomorphine sulfation in the human liver and duodenum, the organs being the major sites of absorption and potential first-pass effect.

Apomorphine contains a chiral centre generating two enantiomers defined as *R*(−)- and *S*(+)-apomorphine. In clinical practice, *R*(−)-apomorphine is predominantly used. Consequently, it was used as a substrate for sulfotransferases in the present study and hereafter is referred to as apomorphine.

Previous studies have reported that the non-steroidal anti-inflammatory drugs (NSAIDs) mefenamic acid and salicylic acid and quercetin, a natural flavonoid present in edible vegetables, fruits and wine (Marchetti *et al.* 2001), are potent inhibitors of human liver SULT1A1 (Vietri *et al.* 2000a, b) whose diagnostic substrate is 4-nitrophenol. The aim of the current study was to determine if the sulfation of apomorphine is inhibited by mefenamic acid, salicylic acid and quercetin in the human liver and duodenum.

Materials and methods

Chemicals

3′-Phosphoadenosine-5′-phosphosulfate-[^{35}S] (PAPS, specific activity 1.93 Ci mmol^{-1}, radiochemical purity 99%) was obtained from NEN Life Science Products, Inc., (Brussels, Belgium). 4-Nitrophenol, dithiothreitol and bovine serum albumin were obtained from Sigma Chemical Co. (Milan, Italy). *R*(−)-apomorphine was obtained from ICN (Milan, Italy). Mono- and dibasic potassium phosphate, sodium hydroxide, barium hydroxide, barium acetate and zinc sulfate were obtained from Carlo Erba (Milan, Italy).

Human tissues

The Ethical Committee of Pisa Medical School approved the project. The liver samples were obtained after clinically indicated partial hepatectomy from 9 men and 11 women aged between 36 and 81 years, with a mean ± SD of 63 ± 13 years. The patients' liver function tests are summarized in table 1. Liver specimens were sampled from a normal part of the organ as far as possible from the tumour, were placed on ice and were transferred to the laboratory within a few minutes. Liver samples were stored frozen at −80 °C.

The duodenum samples derived from 10 men and 10 women aged between 19 and 73 years, with a mean ± SD of 59 ± 16 years. Biopsies of duodenum were sampled after informed consent was obtained from the patients. Biopsies of duodenal mucosa, of about 5 mg, were sampled from the second portion of the duodenum in patients that underwent clinically indicated gastrointestinal enteroscopy. Four or five biopsies of duodenum were obtained from the same patient and were combined and analysed as a single sample. Duodenum biopsies were chilled on ice, transported to the laboratory, frozen and stored at −80 °C.

Isolation of the cytosolic fraction

Liver samples (about 1 g) were homogenized in 5 vols 0.25 M sucrose dissolved in 5 mM potassium orthophosphate buffer (pH 7.4). The duodenum biopsies were homogenized in 0.3 ml 0.25 M sucrose (buffered at pH 7.4 with 5 mM potassium orthophosphate buffer) using a glass–Teflon homogenizer ('Size 0', Thomas, Philadelphia, PA, USA). The homogenates were aspirated using a Pasteur pipette and transferred into centrifuge tubes. The grinding chamber and pestle were rinsed with 0.2 ml 0.25 M sucrose (buffered at 7.4 with 5 mM potassium orthophosphate buffer) and the washings were combined with the homogenates. The homogenates were centrifuged at 12 000*g* for 15 min and the supernatants were centrifuged again at 105 000*g* for 1 h. The high-speed supernatants were divided into aliquots and stored at −80 °C, and were designated as the cytosolic fraction.

Table 1. Liver function tests of patients undergoing clinically indicated partial hepatectomy from whom liver samples were derived.

	Minimum	Maximum	Mean ± SD	Median	Normal
Age (year)	36	81	63 ± 13	66	–
Albumin ($g\,dl^{-1}$)*	3.3	4.6	4.0 ± 0.4	4.1	3.5–5.5
Bilirubin ($mg\,dl^{-1}$)**	0.3	12.1	1.3 ± 2.7	0.73	≤1.1
GOT ($U\,l^{-1}$)	11	56	22 ± 10	18.5	< 45
GPT ($U\,l^{-1}$)	5	61	23 ± 15	19.5	< 45
PT (s)	10.9	12.3	11.7 ± 0.3	11.8	10.9–12.8

*Plasma albumin concentration; **total bilirubin plasma concentration; GOT, glutamic-oxalacetic transaminase activity; GPT, glutamic-pyruvic transaminase activity; PT, prothrombin time.

Assays

Protein concentration assay. The protein concentration was measured as described by Lowry *et al.* (1951) using bovine serum albumin as a standard.

Apomorphine sulfation assay. The apomorphine sulfation assay was based on that described by Foldes and Meek (1973) and modified by Anderson and Weinshilboum (1980). The unreacted PAPS-(^{35}S) was precipitated with barium hydroxide, barium acetate and zinc sulphate. The final saturating concentration of apomorphine was 50 µM and the saturating concentration of PAPS was 0.4 µM (about 500 000 dpm) both in the liver and duodenum. Enzyme activity was measured by the specific radioactivity of PAPS-[^{35}S] after correction of the test samples for the blank samples. Apomorphine was dissolved in water and added in 5-µl aliquots to the incubation mixture (final volume 155 µl). The cytosolic fraction was diluted 2000- (liver) and 500-fold (duodenum) in 5 mM potassium orthophosphate buffer (pH 7.4) containing 0.63 $mg\,ml^{-1}$ bovine serum albumin and 1.54 $mg\,ml^{-1}$ dithiothreitol. The final protein concentration ranged between 1.3 and 6.4 (liver) and between 0.9 and 3.2 (duodenum) µg cytosolic protein per ml incubation mixture. The incubation time was 20 min for both the liver and duodenum. Each sample was assayed in duplicate and had two blank samples that had the same composition of the test samples with the exception that apomorphine was replaced by 5 µl water.

The interassay variability was measured by assaying the rate of apomorphine sulfation in a liver sample for 10 different days. The intra-assay variability was measured by assaying the rate of apomorphine sulphation 10 times in the same assay. The intra- and interassay variabilities were determined by dividing the SD by the mean.

Assay of SULT1A1 and SULT1A3. The activities of SULT1A1 and SULT1A3 were measured with 4 µM 4-nitrophenol and 60 µM dopamine, respectively, as the sulfate acceptor substrates, and 0.4 µM PAPS-[^{35}S] (about 500 000 dpm) as the sulfate donor substrate. These assays were as described by Foldes and Meek (1973) and modified by Anderson and Weinshilboum (1980). The incubation buffer was 8.3 mm orthophosphate potassium (pH 6.0) and the incubation time was 20 (SULT1A1) and 5 min (SULT1A3). The unreacted PAPS was precipitated with barium hydroxide, barium acetate and zinc sulfate. In the SULT1A1 assay, the cytosolic fractions were diluted 1000- (liver) and 500-fold (duodenum) and the final cytosolic protein concentration ranged from 0.72 to 1.5 $\mu g\,ml^{-1}$ (liver) and from 0.9 to 3.2 $\mu g\,ml^{-1}$ (duodenum). In the SULT1A3 assay, the cytosolic fractions were diluted 100- (liver) and 500-fold (duodenum), and the final cytosolic protein concentration ranged from 72 to 147 $\mu g\,ml^{-1}$ (liver) and from 0.9 to 3.2 $\mu g\,ml^{-1}$ (duodenum). Dilutions were carried out with 5 mM orthophosphate potassium buffer (pH 7.4) containing 1.54 $mg\,ml^{-1}$ dithiothreitol and 0.63 $mg\,ml^{-1}$ bovine serum albumin.

Kinetics of apomorphine sulfotransferase

The kinetics of apomorphine sulfotransferase were studied in three liver samples obtained from one man aged 66 years old and two women aged 36 and 55 years old, and from three samples of duodenum obtained from one man aged 69 years old and two women aged 45 and 55 years old. The following concentrations of apomorphine were used: 1.56, 3.12, 6.25, 12.5, 25 and 50 µM both in the liver and duodenum, and the concentration of PAPS was kept constant at 0.4 µm.

Inhibition of apomorphine sulfation by mefenamic acid, salicylic acid and quercetin.

The inhibition of apomorphine sulfation rate was studied with mefenamic acid, salicylic acid and quercetin. The inhibition was studied in three samples of liver and duodenum. The liver samples were obtained from one man aged 66 years old and two women aged 36 and 55 years old, and the duodenum

samples were derived from one man aged 69 years old and two women aged 45 and 55 years old. The inhibition curves were constructed using the following concentrations of mefenamic acid: 3.9, 7.8, 15.6, 31, 62 and 125 nM (liver) and 31, 62, 125, 250 and 500 μM (duodenum). The concentrations of salicylic acid were: 12.5, 25, 50, 100 and 200 μM (liver) and 125, 250, 500, 1000 and 2000 μM (duodenum). The concentrations of quercetin were: 3.9, 7.8, 15.6, 31.2 and 62.5 nM (liver) and 2, 4, 8, 16 and 32 μM (duodenum).

Calculations

The kinetic parameters V_{max} and K_m were determined using the non-linear correlation option of the software package Prism 3 (GraphPad Software, San Diego, CA, USA). The intrinsic clearance was determined by dividing V_{max} by K_m. IC_{50} was calculated using the software package Dose–Effect Analysis (Biosoft, Cambridge, UK). Differences between groups were tested by the Mann–Whitney *U*-test, and the correlations between groups were tested by the Spearman-rank correlation test.

Results

Initially, the optimal conditions for the apomorphine sulfation assay were determined first. The amount of apomorphine sulfated increased linearly up to 30 min of incubation both in the liver and duodenum, and up to at least a cytosolic protein concentration of 9 μg (liver) and 4 μg (duodenum) per ml incubation mixture (data not shown). The inter-assay variability was 10%, the intra-assay variability 1%.

The apomorphine sulfation rate was measured in 20 samples of human liver and duodenum. The mean ± SD and the median of apomorphine sulfation were 261 ± 82 and 242 pmol min^{-1} mg^{-1} (liver), respectively, and 433 ± 157 and 443 pmol min^{-1} mg^{-1} (duodenum), respectively. The apomorphine sulfation rate was higher in the duodenum than in the liver ($p = 0.0005$).

The activities of SULT1A1 and SULT1A3 were measured in the same liver and duodenum samples used to measure apomorphine sulfation rate. In the liver, the mean ± SD and median were 725 ± 200 and 624 pmol min^{-1} mg^{-1}, respectively (SULT1A1) and 33 ± 19 and 28 pmol min^{-1} mg^{-1}, respectively (SULT1A3). In the duodenum, the mean ± SD and median were 275 ± 112 and 288 pmol min^{-1} mg^{-1}, respectively (SULT1A1) and 871 ± 294 and 847 pmol min^{-1} mg^{-1}, respectively (SULT1A3).

The apomorphine sulfation rate was correlated with the activity of SULT1A1 in the liver ($r^2 = 0.363$, $p = 0.005$) and duodenum ($r^2 = 0.494$, $p = 0.0005$), but was not correlated with the activity of SULT1A3 in the liver ($r^2 = 0.068$, $p = 0.268$) and duodenum ($r^2 = 0.012$, $p = 0.645$). Figure 1 shows the correlations of apomorphine sulfation rate with SULT1A1 and SULT1A3 activities in the liver and duodenum.

The kinetics of sulfotransferase towards apomorphine were studied in three samples of human liver and duodenum and followed Michaelis–Menten kinetics. The K_m estimates were 20 ± 3.6 (liver) and 6.5 ± 0.2 μM (duodenum, $p = 0.024$), and the V_{max} estimates were 248 ± 99 (liver) and 636 ± 104 pmol min^{-1} mg^{-1} (duodenum, $p = 0.018$). Figure 2 shows representative results obtained in one liver and one duodenum. The intrinsic clearance estimate was $12 \pm 3.2 \times 10^{-3}$ (liver) and $98 \pm 16 \times 10^{-3}$ ml min^{-1} mg^{-1} (duodenum, $p = 0.011$).

The inhibition of apomorphine sulfation was studied with mefenamic acid, salicylic acid and quercetin in three samples of human liver and duodenum. The inhibition curves are shown in figure 3 and the IC_{50} estimates are summarized in table 2. Mefenamic acid, salicylic acid and quercetin were potent inhibitors of

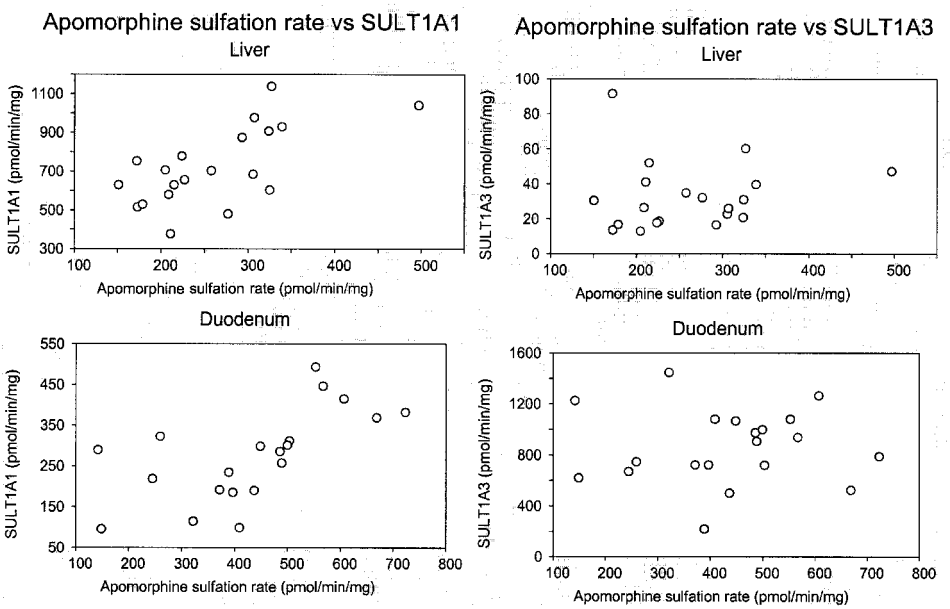


Figure 1. Correlation of the apomorphine sulfation rate with the activities of SULT1A1 and SULT1A3 in the human liver and duodenum. The correlation was based on 20 samples of liver and duodenum. The correlation coefficient and level of significance of each correlation are given in the text.

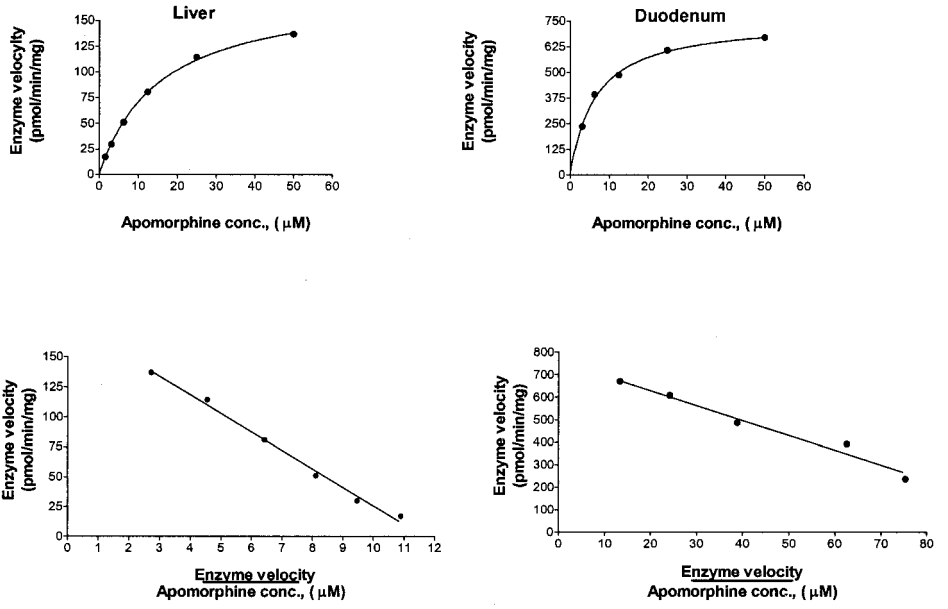


Figure 2. Effect of apomorphine concentration on the apomorphine sulfation rate in the liver and duodenum. Saturation curves (top) and transformation of the enzyme activity into a Eadie–Hofstee plot (bottom) are shown. The liver was derived from a 60-year-old man, the duodenum from a 55-year-old woman.

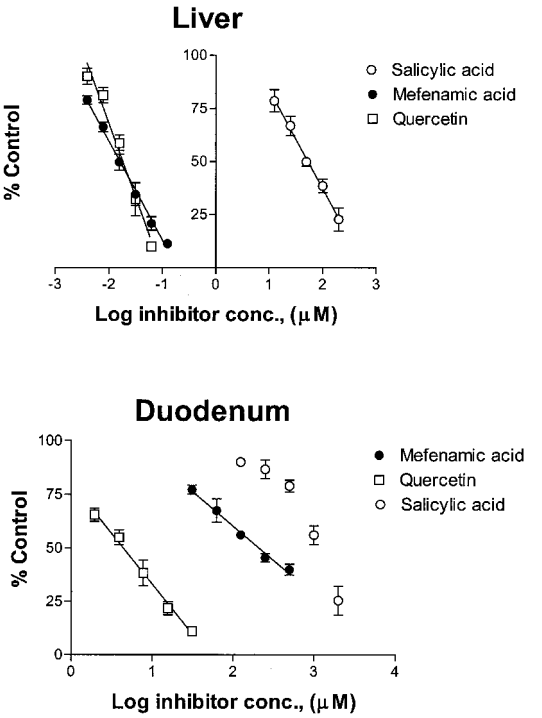


Figure 3. Inhibition curves of mefenamic acid, salicylic acid and quercetin in the human liver and duodenum. The IC_{50} estimates are summarized in table 2. The absolute mean ± SD were 190 ± 43 pmol min^{-1} mg^{-1} (liver) and 441 ± 204 pmol min^{-1} mg^{-1} (duodenum). Data points are the average of three determinations.

Table 2. IC_{50} of mefenamic acid, salicylic acid and quercetin for the sulfation of apomorphine.

Drug	$IC_{50} \pm SD$		p	Therapeutic plasma concentrations
	Liver	Duodenum		
Mefenamic acid	16 ± 0.2 nM	221 ± 24 μM	0.004	28 μM*
Salicylic acid	54 ± 8.6 μM	–	–	1.1.– 2.2 mM**
Quercetin	18 ± 2.8 nM	4.3 ± 0.7 μM	0.01	–

Data are the mean ± SD of three liver and duodenum samples.
* Neuvonen and Kivisto (1988); ** Benet *et al.* (1996).

apomorphine sulfation rate in the liver whereas they were poor inhibitors in the duodenum. In particular, salicylic acid was a poor inhibitor of apomorphine sulphation rate in the duodenum.

Discussion

Human liver and duodenum sulfate apomorphine and the rate of sulfation are higher in the duodenum than in the liver. The apomorphine sulfation rate correlates with SULT1A1 activity both in the liver and duodenum, whereas it does not correlate with SULT1A3 activity. This result is unexpected as dopamine, the diagnostic substrate of SULT1A3, and apomorphine posses a catechol group that is the functional moiety for sulfation by SULT1A3.

The liver-to-duodenum ratios for apomorphine sulfation rates and for the activities of SULT1A1 and SULT1A3 were 0.6, 2.6 and 0.04, respectively. These different ratios suggest that the sulfation of apomorphine is complex and not due solely to SULT1A1 or SULT1A3. Interestingly, the apomorphine sulfation rate correlates with the activity of SULT1A1 and is higher in the duodenum than in the liver as it is the activity of SULT1A3.

Apomorphine sulfotransferase follows Michaelis–Menten kinetics with K_m estimates in the order of μM indicating that the affinity of apomorphine for sulfotransferase is in the same order as those for 4-nitrophenol and dopamine (Cappiello *et al*. 1990), the diagnostic substrates of SULT1A1 and SULT1A3, respectively.

Apomorphine sulfation is inhibited by mefenamic acid, salicylic acid and quercetin, and the IC_{50} estimates are lower in the liver than in the duodenum. Comparable results were obtained for the inhibition of SULT1A1 by mefenamic acid and salicylic acid (Vietri *et al*. 2000b). The IC_{50} estimates of mefenamic acid and salicylic acid for apomorphine sulfation were 16 nm and 54 μM, respectively, which are similar to those for SULT1A1 (Vietri *et al*. 2000a, b). Thus, mefenamic and salicylic acid produce similar inhibition of the sulfation of apomorphine and 4-nitrophenol, the latter being a diagnostic substrate for SULT1A1.

The IC_{50} estimate of mefenamic acid for human liver apomorphine sulfation is three orders of magnitude lower than the peak plasma concentration (28 μM) after single oral administration of 500 mg of the drug (Neuvonen and Kivisto 1988). Assuming, hypothetically, that the intracellular concentration of mefenamic acid equilibrates with the unbound plasma concentration and the unbound fraction of mefenamic acid is 1%, as it is for the congener drug tolfenamic acid (Anon. 1998), the unbound plasma concentration of mefenamic acid is 0.28 μm, i.e. one order of magnitude greater than its IC_{50} estimate in the liver. Thus, mefenamic acid is likely to inhibit apomorphine sulfation *in vivo* in the liver.

The IC_{50} estimate of salicylic acid is about 20 times lower than the lower limit of the therapeutic concentrations. The unbound plasma fraction of salicylic acid is 19.6% in young healthy subjects (Viani *et al*. 1992). Therefore the plasma concentration of unbound salicylic acid is 4-fold greater than its IC_{50} estimate and apomorphine sulfation is likely to be inhibited by salicylic acid when it is administered at therapeutic doses.

Information about the bioavailability of quercetin in food is limited. The intake of flavonoids and flavones ranges between 16.7 and 47.2 mg day^{-1} in a Japanese population (Arai *et al*. 2000). In wine, the concentration of quercetin varies from 1 to 33 μM (Goldberg *et al*. 1996). Drinking two glasses of wine (300 ml) leads to the ingestion of up to 10 μmole quercetin (Goldberg *et al*. 1996). After the consumption of fried onions (equivalent to 225 μmole quercetin) and apples (equivalent to 325 (μ mole quercetin), the peak plasma levels of quercetin are 0.74 and 0.30 μM, respectively (Hollman *et al*. 1997). These concentrations are higher than the IC_{50} estimate of quercetin for apomorphine sulfation in the liver.

In conclusion, apomorphine is sulfated in the human liver and duodenum. Mefenamic acid and quercetin are potent inhibitors of apomorphine sulphation in the human liver with an IC_{50} estimate in the order of nM. Further work needs to be done to determine whether mefenamic acid and quercetin inhibit apomorphine sulfation in other organs.

Acknowledgements

The work was supported by Contract BMH1-CT94-1622 of the European Commission (Brussels, Belgium), by the Italian Ministry of the University (Rome, Italy) and by the Italian Association for Cancer Research (Milan, Italy).

References

Anderson, R. J. and Weinshilboum, R. M., 1980, Phenolsulphotransferase in human tissue: radiochemical enzymatic assay and biochemical properties. *Clinica et Chimica Acta*, **103**, 79–90.

Anon., 1998, *Drug Data Handbook*, 3rd edn (Auckland: Adis), pp. 1–52.

Arai, Y., Watanabe, S., Kimira, M., Shimoi, K., Mochizuki, R. and Kinae, N., 2000, Dietary intakes of flavonols, flavones and isoflavones by Japanese women and the inverse correlation between quercetin intake and plasma LDL cholesterol concentration. *Journal of Nutrition*, **130**, 2243–2250.

Benet, L. Z., Oie, S. and Schwartz, J. B., 1996, Design and optimization of dosage regimens; pharmacokinetic data. In J. G. Hardman, L. E. Limbird, P. B. Molinoff, R. W. Ruddon and A. G. Gilman (eds), *The Pharmacological Basis of Therapeutics*, 9th edn (New York: McGraw-Hill), pp. 1707–1793.

Cappiello, M., Giuliani, L. and Pacifici, G. M., 1990, Differential distribution of phenol and catechol sulphotransferase in human liver and intestinal mucosa. *Pharmacology*, **40**, 69–76.

Ernst, A. M., 1965, Relation between action of dopamine and apomorphine and the *O*-methylated derivatives upon CNS. *Psychopharmacologia*, **7**, 391–399.

Foldes, A. and Meek, J., 1973, Rat brain phenolsulphotransferase-partial purification and some properties. *Biochimica et Biopsyca Acta*, **327**, 365–374.

Goldberg, D. M., Tsang, E., Karumanchiri, A., Diamandis, E. P., Soleas, G. and Ng, E., 1996, Method to assay the concentrations of phenolic constituents of biological interest in wines. *Analytical Chemistry*, **68**, 1688–1694.

Hollman, P. C. H., van Trijp, J. M. P., Buysman, M. N. C. P., Gaag, M. S. V. D., Mengelers M. J. B., De Vries J. H. M. and Katan, M. B., 1997, Relative bioavailability of the antioxidant flavonoid quercetin from various foods in man. *FEBS Letters*, **418**, 152–156.

Lowry, O. H., Rosebrough, N. J., Farr, A. and Randall, R. J., 1951, Protein measurement with the Folin phenol reagent. *Journal of Biological Chemistry*, **193**, 265–275.

Marchetti, F., De Santi, C., Vietri, M., Pietrabissa, A., Spisni, R. and Pacifici, G. M., 2001, Differential inhibition of human liver and duodenum sulphotransferase activities by quercetin, a flavonoid present in vegetables, fruit and wine. *Xenobiotica*, **31**, 841–847.

Neef, C. and van Laar, T., 1999, Pharmacokinetic–pharmacodynamic relationships of apomorphine in patients with Parkinson's disease. *Clinical Pharmacokinetics*, **37**, 257–271.

Neuvonen, P. J. and Kivisto, K. T., 1988, Effect of magnesium hydroxide on the absorption of tolfenamic and mefenamic acids. *European Journal of Clinical Pharmacology*, **35**, 495–501.

Viani, A., Rizzo, G., Carrai, M. and Pacifici, G. M., 1992, The effect of ageing on plasma albumin and plasma protein binding of diazepam, salicylic acid and digitoxin in healthy subjects and patients with renal impairment. *British Journal of Clinical Pharmacology*, **33**, 299–304.

Vietri, M., De Santi, C., Pietrabissa, A., Mosca, F. and Pacifici, G. M., 2000a, Inhibition of human liver phenol sulphotransferase by nonsteroidal anti-inflammatory drugs. *European Journal of Clinical Pharmacology*, **56**, 81–87.

Vietri, M., Pietrabissa, A., Spisni, R., Mosca, F. and Pacifici, G. M., 2000b, Differential inhibition of hepatic and duodenal sulphation of (−)-salbutamol and minoxidil by mefenamic acid. *European Journal of Clinical Pharmacology*, **56**, 477–479.

XENOBIOTICA, 2002, VOL. 32, NO. 7, 595–604

Taylor & Francis
healthsciences

Developmental changes in the expression of enterocytic and hepatic cytochromes P4501A in rat

T. N. JOHNSON†*, M. S. TANNER‡ and G. T. TUCKER

† University of Sheffield, Academic Unit of Molecular Pharmacology and Pharmacogenetics, Division of Clinical Sciences, Royal Hallamshire Hospital, Sheffield S10 2JF, UK
‡ University of Sheffield, Academic Unit of Child Health, Children's Hospital Sheffield S10 2TH, UK

Received 15 October 2001

1. The development of CYP1A enzymes was studied in enterocytic and hepatic microsomes from 1-day-old to adult male and female rats. Microsomes were prepared by calcium precipitation. Enzyme expression was determined by Western blotting using a polyclonal CYP1A1 antibody.

2. The developmental expression of CYP1A in enterocytic and hepatic microsomes was similar for males and females.

3. Enterocytic CYP1A (CYP1A1) showed a sharp increase at weaning, plateauing at adult levels by 60 days.

4. Hepatic CYP1A (mostly CYP1A2) increased sharply just before weaning. However, in contrast to the enterocytic enzyme, there was a 4-fold decrease in enzyme expression down to adult levels by day 60.

Introduction

CYP1A1 and CYP1A2 are expressed predominantly in extrahepatic and hepatic tissues, respectively (Guengerich 1995), and are inducible by environmental carcinogens and by mycotoxins (Conney *et al.* 1982, Sinha *et al.* 1994, Buchthal *et al.* 1995).

The strategic expression of CYP1A1 alongside CYP3A at the villous tips in enterocytes of the duodenum and jejunum represents an important frontline defence against ingested toxic compounds. CYP1A1 can activate polycyclic aromatic hydrocarbons (PAH) to products that covalently bind within mature enterocytes, which then slough off and are replaced, thereby eliminating these potentially carcinogenic compounds before they can enter the systemic circulation (Zhang *et al.* 1997). An inverse relationship was observed between hepatic CYP1A2 expression and systemic exposure to carcinogenic heterocyclic amines (HA) (Sinha and Caporosa 1997, Stillwell *et al.* 1997). In a study of the effects of chargrilled meat on CYP1A expression, those subjects with high levels of hepatic CYP1A2 or intestinal CYP1A1 had lower white blood cell concentrations of PAH DNA adducts (Fontana *et al.* 1999).

In man, the levels of CYP1A1 and CYP1A2 in enterocytes and hepatocytes, respectively, are relatively low, although the enzymes are inducible by HA and

* Author for correspondence; e-mail: t.n.johnson@sheffield.ac.uk

Xenobiotica ISSN 0049–8254 print/ISSN 1366–5928 online © 2002 Taylor & Francis Ltd
http://www.tandf.co.uk/journals
DOI: 10.1080/00498250210131888

PAH (Gonzalez 1993). In contrast to man, where CYP3A is the major expressed enterocytic CYP enzyme, CYP1A1 predominates in the small bowel of the rat (Zhang *et al.* 1996). However, adult levels of CYP1A2 in liver are low (1% of total CYP) (Thomas *et al.* 1981). There is no correlation between the magnitude of enterocytic CYP1A1 and hepatic CYP1A2 induction, although transcriptional activation of both enzymes is considered to be mediated by the aryl hydrocarbon (Ah) receptor (Landers and Vunce 1991). This may be due to site-dependent differences in concentrations of the inducer at the receptor or in the level of receptor expression.

To our knowledge, little is known about the ontogeny of enterocytic or hepatic CYP1A enzymes in rat or man. Waxman *et al.* (1985) reported expressed levels of hepatic CYP1A1 and CYP1A2 to be low and mostly unaffected by age, sex and hormonal status in the 0–14-week-old rat. The present paper documents their expression in hepatic and enterocytic microsomes from 1-day-old to the adult male and female rat.

Materials and methods

Materials

Acrylamide solution (40% v/v) was purchased from Bio-Rad Micromeasurements (York, UK), Immobilon-P from Millipore (Watford, UK), buffered formaldehyde from Genta Medical (York, UK), enhanced chemiluminescent reagents (Tropix) from PE Applied Biosystems (Warrington, UK), bovine serum albumin from Pierce and Warriner (Chester, UK), goat anti-rat polyclonal cytochrome P4501A1 antibody (reacts with both CYP1A1 and CYP1A2 with minor cross-reactivity with CYP2E1) and control rat hepatic 3-methylcholanthrene-induced microsomes (containing 380 ρmol CYP1A per mg microsomal protein) from Cambridge Biosciences (Cambridge, UK), and normal rabbit serum, rabbit anti-goat antibody and streptavidin from Dako (Ely, UK). All other chemicals were purchased from Sigma (Poole, UK) and were of analytical or electrophoresis grade.

Animals

Male and female Wistar rats, divided into age groups (days 1, 10, 15, 20, 25, 30, 40, 60, 80 and adults), were obtained from the University of Sheffield Field Laboratories. They were housed in plastic cages and fed a standard cereal-based diet (CRM diet feed); free access was allowed to food and water. The animals were stunned and killed by cervical dislocation according to UK Home Office procedures.

Isolation of enterocytes

Tissue comprising the first third of the small bowel from the duodenum onwards was dissected from six male and six female animals in each age group. The bowel sections were placed immediately in ice-cold buffer (phosphate-buffered saline containing 5 mM EDTA, 0.5 mM dithiothreitol and 40 $\mu g\,ml^{-1}$ phenylmethylsulphonyl fluoride). The bowel contents were flushed out and the tissue transferred to fresh buffer. A small cross-section of duodenum (1–2 mm) was taken from each bowel length and placed in buffered formaldehyde for histochemical staining. The remaining bowel samples were dissected longitudinally, chopped into 2–3-cm lengths and placed in 100 ml ice-cold modified Weiser solution (Weiser 1973). After stirring gently for 15 min the enterocyte-containing suspension was decanted into a glass beaker on ice. This process was repeated with 100 ml fresh ice-cold Weiser solution. The two Weiser fractions were then combined and centrifuged in 50-ml aliquots at 800*g* for 10 min. The cell pellets were combined, resuspended and washed twice with 10 ml buffer (histidine 5 mM, sucrose 0.25 M, EDTA 0.5 mM and phenylmethylsulphonyl fluoride 40 $\mu g\,ml^{-1}$, pH 7.4), and centrifuged at 800*g* for 10 min.

Preparation of microsomes

Enterocytic microsomes were prepared by a calcium precipitation method (Bonkovsky 1985). All steps were carried out at 0–4° C. Washed enterocytes (2–5 g wet weight) were resuspended in 5 ml buffer using 10 up and 10 down strokes of a Potter–Elvehjem homogenizer. The homogenate was then centrifuged at 15 000*g* for 10 min. The supernatant was carefully removed using a Pasteur pipette and placed in two glass tubes to which were added 1.25 ml 52 mM calcium chloride solution (the final calcium

concentration was approximately 10 mM). After six inversions, the tubes were kept on ice for 15 min then centrifuged at 2000*g* for 10 min. The supernatant was discarded and the microsomes resuspended in 1–2 ml microsome buffer (20% w/v glycerol, 100 mM Tris-HCl, 10 mM EDTA, pH 7.4).

Liver (5 g minced wet weight) from at least four animals was finely chopped and 15 ml buffer (0.25 M sucrose, 10 mM Tris-HCl, pH 7.4) was added. The tissue was homogenized using 10 up and 10 down strokes of a Potter–Elvehjem homogenizer, centrifuged at 10 000*g* for 10 min and the supernatant carefully removed into glass tubes. Microsomes were sedimented by calcium aggregation as described for intestinal microsomes. The supernatant was discarded and the microsomes resuspended in 7 ml 0.15 M potassium chloride solution. After centrifugation at 100 000*g* for 60 min, the supernatant was again discarded and the microsomes resuspended in 5 ml microsome buffer.

Microsomal recovery was calculated using:

Microsomal recovery (%) = (total amount of microsomal protein)/(wet weight of enterocytes/liver) × 100.

Microsomal protein content was determined by the method of Lowry *et al.* (1951) using bovine serum albumin as standard.

Immunoblotting

Western blots from microsomal protein were obtained after denaturation and reduction by boiling for 2 min in treatment buffer (62.5 mM Tris-HCl, 2% w/v SDS, 20% w/v glycerol, 10% v/v mercaptoethanol). A Flowgen G31010 electrophoresis unit (Lichfield, UK) was used with 10% resolving and 2.7% stacking SDS-PAGE gels. Alternate lanes were loaded with 5–10 μg microsomal protein and control buffer along with Novex Mark 12™ and Seeblue™ (San Diego CA, USA) molecular weight markers. One lane on each gel was loaded with 10 μg control microsomes. The unit was attached to a Biorad 500/200 power supply (Hercules, CA, USA), adjusted to 150 mV and left to run for 2 h. Transfer onto Immobilon-P membranes was performed using a CBS semi-dry blotter (EU-4000) (CBS Scientific Co., St Francisco, CA, USA) at 80 mA for 50 min. Membranes were probed with goat anti-rat CYP1A1 polyclonal antibody (1:50 000). Antibody binding was detected using an alkaline phosphatase-conjugated rabbit anti-goat immunoglobulin type G (1:20 000). The Tropix Western Light™ (Tropix, Bedford, MA, USA) chemiluminescent detection system was used for visualization, and the blots were recorded using Kodak X-OMAT film (Kodak Eastman Co., Rochester, NY, USA). Western blots were compared both visually and by densitometric analysis. Densitometric analysis was performed on triplicate blots from two sets of microsomes ($n = 6$) using a Kodak DC120 digital camera and the KDS 1d image analysis software. CYP1A expression was calculated from the known concentration (380 ρmol mg protein^{-1}; Gentest Corporation, Woburn, MA, USA) in the control microsomes.

Immunohistochemistry

Samples of rat duodenum across the age range were fixed in buffered formaldehyde overnight, dehydrated in a graded series of ethanol solutions and embedded in paraffin wax. Sections were cut onto glass slides using a Leica Scientific microtome (Unterentfelden, Switzerland) and dried at 37° C. The paraffin wax was removed with xylene and decreasing concentrations of ethanol solution. The sections were then incubated for 30 min in methanol containing 1.7% v/v (100 vol.) hydrogen peroxide to block any endogenous peroxidase activity. All subsequent operations were carried out in a humidified chamber, washing the sections with Tris buffer (pH 7.6) between each incubation. Incubation with 20% normal rabbit serum for 15 min was followed by 30 min with an optimal dilution of primary antibody (1:500 goat anti-rat CYP1A1 polyclonal), 30 min with an optimal dilution of secondary antibody (1:400 biotinylated rabbit anti-goat) and 30 min with a 1:600 dilution of streptavidin–biotin–peroxidase complex. Peroxidase activity was visualized using a 0.035% w/v solution of 3,3-diaminobenzidine tetra-hydrochloride containing 0.3% v/v 100 vol. hydrogen peroxide.

Statistical analysis

Statistical analysis was performed using SPSS v.6.0 (SPSS, Inc., Chicago, IL, USA). Two-way analysis of variance compared the expression of CYP1A1 between sexes at the various ages.

Results

Microsomal recovery

Microsomal recovery was relatively constant over the age range of animals used. It was 1.4% ± 0.8 SD of the wet weight of liver and 1.2% ±0.9SD of the wet weight of enterocytes.

Immunoblotting

The chemiluminescence detection system gave a linear response to microsomal standards with respect to CYP1A content over the range 0–300 ρmol ($r^2 = 0.92 - 0.98$) (data not shown).

Western blots prepared from male and female enterocytic microsomes using the polyclonal CYP1A1 antibody revealed a single band at approximately 50 KDa (figure 1a, b). Visual and densitometric analysis revealed a similar developmental pattern for males and females, with a marked increase in band intensity between days 20 and 40 followed by a plateau up to 1 year (figure 2a). A statistical difference in enzyme expression between male and female animals at the various ages was not detected ($p = 0.42$).

Male and female rat liver microsomes showed two bands at approximately 50 KDa, a strong one together with a faint second band in some of the samples at a slightly higher molecular weight (figure 3). Visual and densitometric analysis revealed a marked increase in hepatic CYP1A expression between days 15 and 25 followed by a sharp decline through to 1 year (figure 2b). No statistical

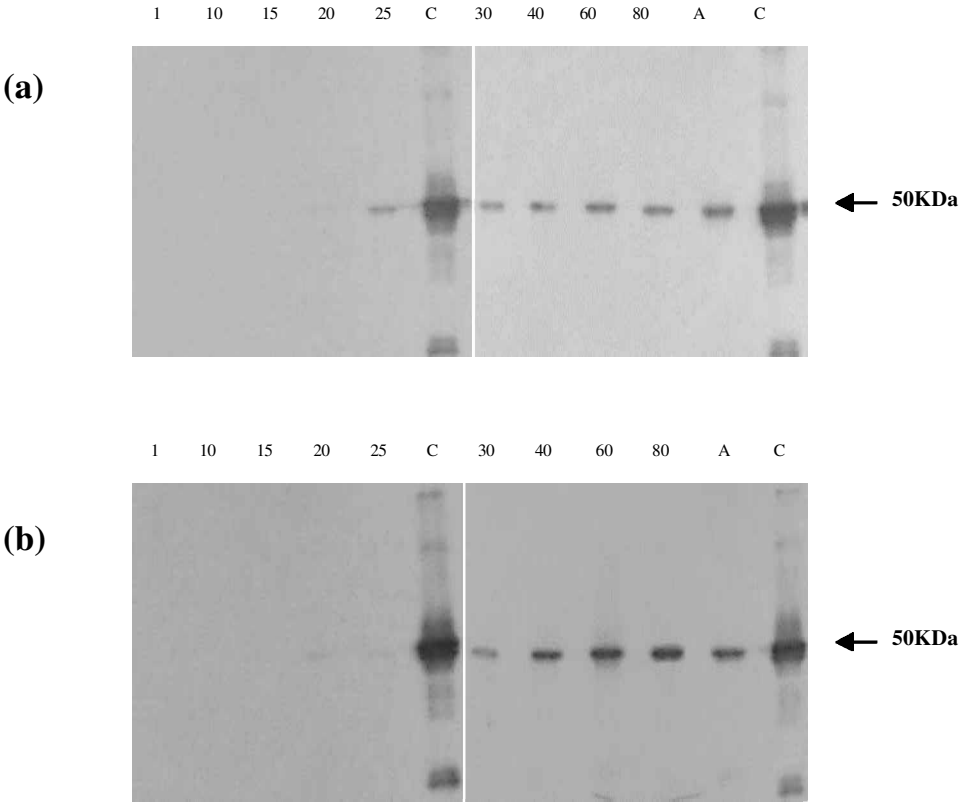


Figure 1. Western blots of enterocytic microsomes from the (a) male and (b) female rat aged from 1 day to 1 year (A, adult) produced using a polyclonal goat anti-rat CYP1A1 antibody. Numbers refer to the age (days) of the animals. C is a rat liver CYP1A1 standard. Of microsomal protein, 10 µg was loaded onto each lane.

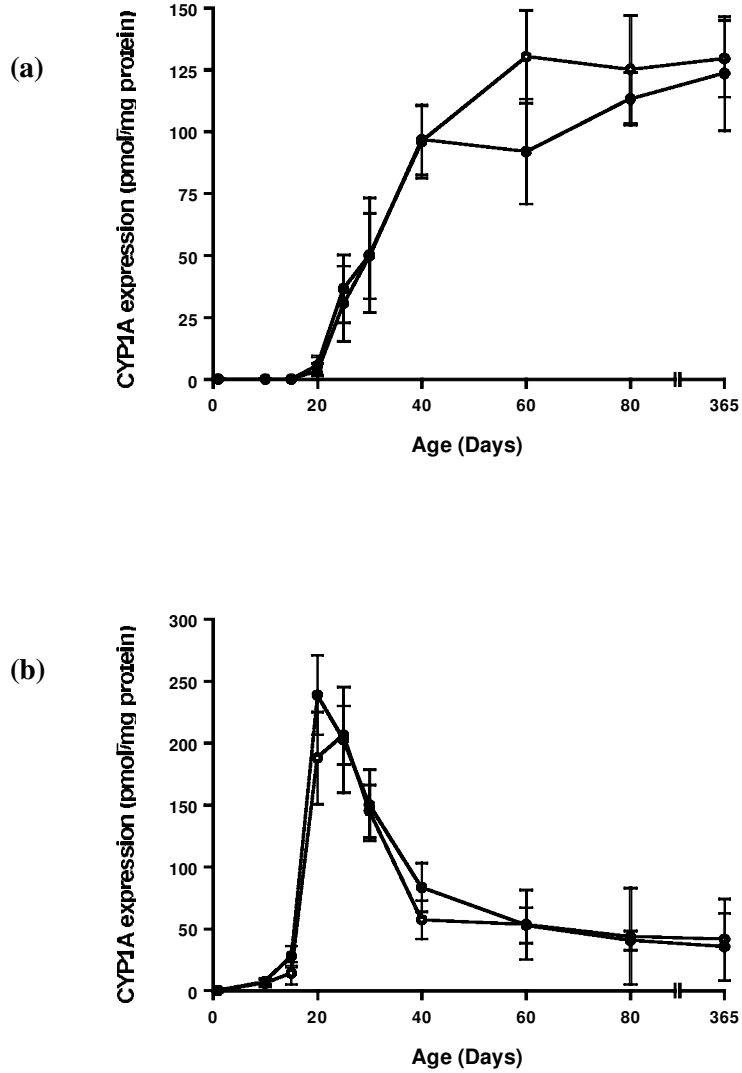


Figure 2. Development of CYP1A expression in the male (●) and female (○) rat (a) enterocytic and (b) hepatic microsomes with age, quantified by densitometry of immunoblots. Date points are the mean ± SD for six replicate experiments.

difference between male and female animals at the various ages was detected ($p = 0.58$).

Immunohistochemistry

Figure 4 shows cross-sections of duodenum from the 1- and 60-day-old male rat immunostained with the polyclonal CYP1A1 antibody. The presence of enzyme was evident in the brush border cells of the villi of the older animals. Subjective estimation of stain intensity suggested an age-related increase in enterocytic CYP1A1 expression (data not shown).

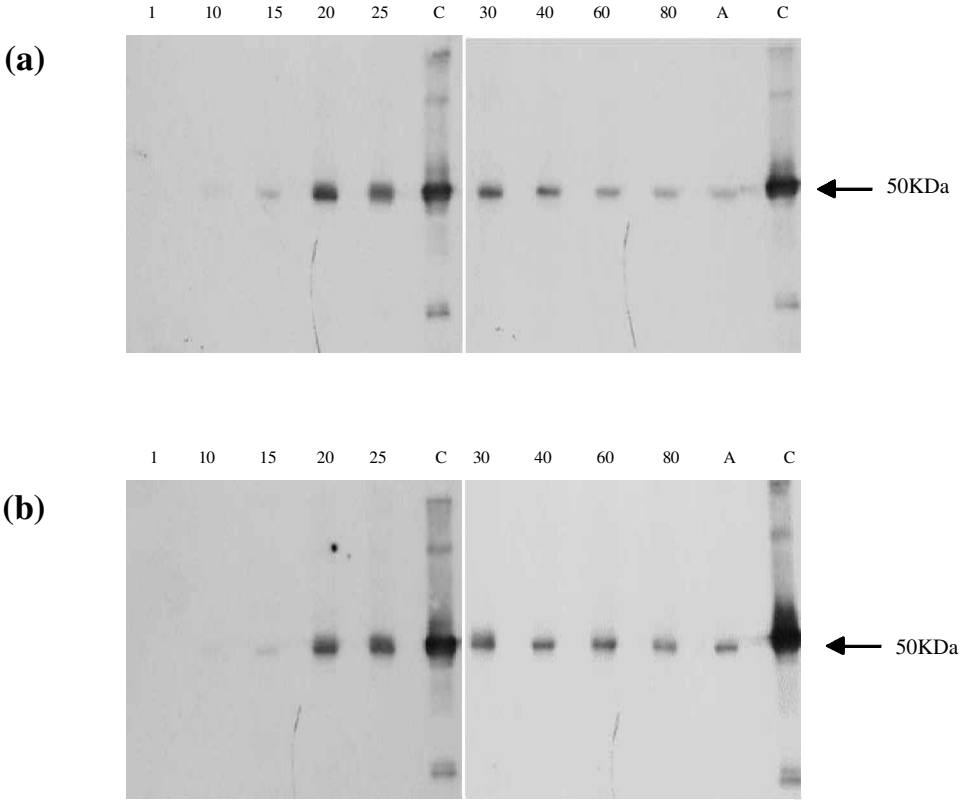


Figure 3. Western blots of hepatic microsomes from the (a) male and (b) female rat aged from 1 day to 1 year (A, adult) produced using a polyclonal goat anti-rat CYP1A1 antibody. Numbers refer to the age (days) of the animals. C is a standard 3-MC-induced rat liver microsome preparation. Of microsomal protein, 5 μg was loaded onto each lane.

Discussion

The antibody used in the study reacted with both CYP1A1 and CYP1A2, and it has a very weak cross-reactivity with CYP2E1 (Technical Support, Gentest). The single band seen in immunoblots from rat enterocytic microsomes was assumed to correspond to CYP1A1. Others have not detected CYP1A2 and CYP2E1 in the rat small intestine (de Waziers *et al.* 1990, Zhang *et al.* 1996). In rat hepatic microsomes, CYP1A2 is the predominant enzyme (de Waziers *et al.* 1990) and it showed as a strong band on the immunoblot. The weaker band of slightly higher molecular weight evident in some blots was assumed to correspond to CYP1A1. No third band of lower molecular weight corresponding to CYP2E1 was observed.

Enterocytic CYP1A expression was low before weaning and then surged after 20 days. Thereafter, it remained constant and comparable in both sexes up to 1 year. The pattern of CYP1A development with age is similar to that observed for enterocytic CYP3A (CYP3A1, CYP3A9) expression and activity in rat (Johnson *et al.* 2000). The surge in both CYP1A and CYP3A expression around the time of weaning may be an adaptation to the ingestion of solid food and xenobiotics. The adult expression of CYP1A is higher than that observed for rat enterocytic CYP3A



A



B

Figure 4. Cross-sections of rat duodenum immunostained using a polyclonal goat anti-rat CYP1A1 antibody: (A) 1-; and (B) 60-day-old animal. The enzyme is indicated by the brown stain.

in previous studies (Zhang *et al*. 1996, Johnson *et al*. 2000). Thus, the strategic expression of CYP1A in the small bowel enterocytes, coupled with its higher level of expression and its inducibility by potential dietary carcinogens such as HA and PAH, indicate that it has an important role as a first-line defence against ingestion

of such compounds. A strictly formulated enteral nutrition feed was found to decrease the expression of enterocytic CYP1A1 in the rat (Hakkak *et al.* 1993), probably due to the removal from the diet of potent enzyme inducers such as PAHs and dioxin.

The pattern of CYP1A development in rat hepatic microsomes is unusual, showing a marked surge just before weaning followed by a sharp decline to adult levels by day 80. Thomas *et al.* (1981) reported a decrease in CYP1A from 4% of total hepatic CYP content in the immature (50–60 g) rat to 1% in the mature (150–190 g) animal. Our values for hepatic CYP1A in the adult rat of around 30–50 ρmol mg protein^{-1} are in agreement with those reported by others (Thomas *et al.* 1981, Guengerich *et al.* 1982, Imaoka *et al.* 1990).

The mechanism regulating the surge in hepatic and enterocytic CYP1A enzymes is unknown but may involve endogenous compounds known to be involved in the weaning process such as corticosteroids and thyroxine (Henning 1985). Regulation of the enzymes at the two sites appears to be independent (Fontana *et al.* 1999), consistent with our observation that the surge and decline of hepatic CYP1A occurred before the maximal expression of intestinal CYP1A. The decline of hepatic CYP1A levels after day 25 may reflect a corresponding decrease in levels of an endogenous CYP1A inducer after weaning. In contrast to a marked sex difference in the ontogeny of rat hepatic CYP3A expression, where the weaning process precedes a rapid period of sexual differentiation (Wright *et al.* 1997, Johnson *et al.* 2000), there was no such sex difference in the development of CYP1A. Kamataki *et al.* (1983) showed no sex difference in the expression of hepatic CYP1A2 in the adult rat.

Both enterocytic and microsomal yields were invariate across the age bands, suggesting a consistent methodology in the preparation of microsomes from different ages of animals. The ontogeny of enterocytic CYP1A measured by immunoblotting was confirmed by the immunohistochemical results.

Despite similarities in rat and man with respect to CYP1A enzymes (Nelson *et al.* 1996), developmental differences are likely to be marked. Whereas hepatic CYP1A2 expression reaches a peak during development in the rat, in man it is absent in foetal and neonatal liver, increases in infants aged 1–3 months, and attains 50% of the adult value at 1 year (Sonnier and Cresteil 1998).

Although a systematic study of the ontogeny of human enterocytic CYP1A1 is lacking, this may also differ from that in rat. Whereas the small bowel of the latter continues to develop after birth (Cummins *et al.* 1988), that of man is fully developed *in utero*, with function generally being ahead of need at birth (Menard 1994).

Acknowledgements

The work was supported by Grant S/F/0763 from Action Research and by the Children's Appeal, Sheffield Children's Hospital, UK.

References

Bonkovsky, H. L., Hauri, H. P., Marti, U., Gasser, R. and Meyer, U. A., 1985, Cytochrome P450 of small intestinal epithelial cells. *Gastroenterology*, **88**, 458–467.

Buchthal, J., Grund, K. E., Buchmann, A., Schrenk, D., Beaune, P. and Bock, K. W., 1995, Induction of P4501A by smoking or omeprazole in comparison with UDP-glucuronosyltransferase in biopsies of human duodenal mucosa. *European Journal of Clinical Pharmacology*, **47**, 431–435.

Conney, A. H., 1982, Induction of microsomal enzymes by foreign chemicals and carcinogenesis by polycyclic aromatic hydrocarbons. *Cancer Research*, **42**, 4875–4917.

Cummings, A. G., Steele, T. W., Labrooy, J. T. and Shearman, D. J. C., 1988, Maturation of the rat small intestine at weaning: changes in epithelial cell kinetics, bacterial flora, and mucosal immune activity. *Gut*, **29**, 1672–1679.

De Waziers, I., Cugenee, P. H., Yang, C. S., Lefous, J. P. and Beaune P. H., 1990, Cytochrome P450 isoenzymes, epoxide hydrolase and glutathione transferase in rat and human hepatic and extrahepatic tissue. *Journal of Pharmacology and Experimental Therapeutics*, **253**, 387–394.

Fontana, R. J., Lown, K. S., Paine, M. F., Fortlage, L., Santella, R. M., Felton, J. S., Knize, M. G., Greenberg, A. and Watkins, P. B., 1999, Effects of chargrilled meat diet on expression of CYP3A, CYP1A, and P-glycoprotein levels in healthy volunteers. *Gastroenterology*, **117**, 89–98.

Gonzalez, F. J., 1993, Cytochrome P450 in humans. In J. B. Schenkman and H Greim (eds), *Cytochrome P450* (Berlin: Springer), pp. 239–257.

Guengerich, F. P., 1995, Human cytochrome P450 enzymes. In P Ortiz de Montellano (ed.), *Cytochrome P450: Structure, Mechanism and Biochemistry* (New York: Plenum), pp. 473–535.

Guengerich, F. P., Dannan, G. A., Wright, S. T., Martin, M. V. and Kaminsky, L. S., 1982, Purification and characterization of liver microsomal cytochrome P-450: electrophoretic, spectral, catalytic and immunochemical properties and inducibility of eight isozymes isolated from rats treated with phenobarbital or β naphthoflavone. *Biochemistry*, **21**, 6019–6030.

Hakkak, R., Ronis, M. J. and Badger, T. M., 1993, Effects of enteral nutrition and ethanol on cytochrome P450 distribution in small intestine of male rats. *Gastroenterology*, **104**, 1611–1618.

Henning, S. J., 1985, Ontogeny of enzymes in the small bowel. *Annual Review of Physiology*, **47**, 231–245.

Imaoka, S., Terano, Y. and Funae, Y., 1990, Changes in the amount of cytochrome P450s in rat hepatic microsomes with starvation. *Archives of Biochemistry and Biophysics*, **278**, 168–178.

Johnson, T. N., Tanner, M. S. and Tucker, G. T., 2000, Ontogeny of enterocytic and hepatic cytochrome P450 3A in the rat. *Biochemical Pharmacology*, **60**, 1601–1610.

Kamataki, T., Maeda, K., Yamazoe, Y., Nagai, T. and Kato, R., 1983, Sex differences of cytochrome P-450 in the rat: purification, characterisation, and quantification of constitutive forms of cytochrome P-450 from liver microsomes of male and female rats. *Archives of Biochemistry and Biophysics*, **225**, 758–770.

Landers, J. P. and Vunce, N. J., 1991, The Ah receptor and the mechanism of dioxin toxicity. *Biochemical Journal*, **276**, 273–278.

Lowry, O. H., Rosebrough, N. J., Farr, A. L. and Randall, R. J., 1951, Protein measurement with the Folin phenol reagent. *Journal of Biological Chemistry*, **193**, 265–275.

Menard, D., 1994, Development of human intestinal and gastric enzymes. *Acta Paediatrica*, **405 (suppl.)**, 1–6.

Nelson, D. R., Koymans, L., Kamataki, T., Stegeman, J. J., Feyereisen, R., Waxman, D. J., Waterman, M. R., Gotoh, O., Coon, M. J., Estabrook, R. W., Gunsalus, I. C. and Nebert, D. W., 1996, P450 superfamily: update on new sequences, gene mapping, accession numbers and nomenclature. *Pharmacogenetics*, **6**, 1–42.

Sinha, R. and Caporosa, N., 1997, Heterocyclic amines, cytochrome P450 1A2, and *N*-acetyltransferase: issues involved in incorporating putative genetic susceptibility markers into epidemiological studies. *Annals of Epidemiology*, **7**, 350–356.

Sinha, R., Rothman, N., Brown, E. D., Mark, S. D., Hoover, R. N., Caporaso, N. E., Levander, O. A., Knize, M. G., Lang, N. P. and Kadlubar, F. F., 1994, Pan-fried meat contains high levels of heterocyclic aromatic amines but low levels of polycyclic aromatic hydrocarbons induces cytochrome P450 1A2 activity in humans. *Cancer Research*, **54**, 6154–6159.

Sonnier, M. and Cresteil, T., 1998, Delayed ontogenesis of CYP1A2 in the human liver. *European Journal of Biochemistry*, **251**, 893–898.

Stillwell, W. G., Kidd, L. C., Wishnok, J. S., Tannerbaun, S. R. and Sinha, R., 1997, Urinary excretion of unmetabolized and phase 1 conjugates of 1-amino-1-methyl-6-phyenylimidazo [4,5-*f*] quinoxaline in humans: relationship to cytochrome P4501A2 and *N*-acetyltransferase activity. *Cancer Research*, **57**, 3457–3464.

Thomas, P. E., Reik, L. M., Ryan, D. E. and Levin, W., 1981, Regulation of three forms of cytochrome P-450 and epoxide hydrolase in rat liver microsomes. *Journal of Biological Chemistry*, **256**, 1044–1052.

Waxman, D. J., Dannan, G. A. and Guengerich, F. P., 1985, Regulation of rat hepatic cytochrome P-450: age-dependent expression, hormonal imprinting, and xenobiotic inducibility of sex-specific isozymes. *Biochemistry*, **24**, 4409–4417.

Weiser, M. M., 1973, Intestinal epithelial cell surface membrane glycoprotein synthesis I. An indicator of cellular differentiation. *Journal of Biological Chemistry*, **248**, 2536–2541.

Wright, M. C., Edwards, R. J., Pimenta, M., Ribeiro, V. and Ratra, G. S., 1997, Developmental changes in the constitutive and inducible expression of cytochrome P450 3A2. *Biochemical Pharmacology*, **54**, 841–846.

Zhang, Q. Y., Wikoff, J., Dunbar, D., Fasco, M. and Kaminsky, L., 1997, Regulation of cytochrome P4501A1 expression in rat small intestine. *Drug Metabolism and Disposition*, **25**, 21–26.

Zhang, Q. Y., Wikoff, J., Dunbar, D. and Kaminsky, L., 1996, Characterization of rat small intestinal cytochrome P450 composition and inducibility. *Drug Metabolism and Disposition*, **24**, 322–328.

XENOBIOTICA, 2002, VOL. 32, NO. 7, 605–613

Taylor & Francis
healthsciences

Application of ^{1}H- and ^{19}F-NMR spectroscopy in the investigation of the urinary and biliary excretion of 3,5-, 2,4-ditrifluoromethylbenzoic and pentafluorobenzoic acids in rat

C. A. BLACKLEDGE†, J. K. NICHOLSON†,
J. A. EVANS‡, C. RODGERS‡ and I. D. WILSON‡*

† Department of Biological Chemistry, Biomedical Sciences Division, Sir Alexander Fleming Building, Imperial College of Science Technology and Medicine, South Kensington, London SW7 2AZ, UK
‡ Department of Drug Metabolism and Pharmacokinetics, AstraZeneca Pharmaceuticals, Mereside, Alderley Park, Macclesfield SK10 4TG, UK

Received 13 December 2001

1. The metabolism and excretion of 2,4-, 3,5-ditrifluoromethyl- and pentafluorobenzoic acids were studied in the bile-cannulated rat using ^{1}H- and ^{19}F-NMR spectroscopy following intraperitoneal administration at 50 mg kg^{-1}.

2. Pentafluorobenzoic acid was excreted in the urine entirely unchanged. No detectable compound or metabolites were eliminated in the bile. A total of 63.5 ± 6.7% of the dose was recovered in the 24-h collection period.

3. In the case of 2,4-ditrifluromethyl benzoic acid, 83.9 ± 5.2% of the dose was recovered in the 24 h after administration, with about 52% being excreted in the urine and 32% in the bile. The majority of the material present in the urine was unchanged parent compound. In bile, some 60% of the compound-related material excreted was present as transacylated ester glucuronide conjugates.

4. For 3,5-ditrifluoromethylbenzoic acid, 49.6 ± 5.3% of the dose was recovered in the 24-h collection period, with about 22% being excreted in the urine and 28% in the bile. The material excreted in both the urine and bile was a mixture of the parent acid and transacylated ester glucuronides.

5. Urinary excretion in bile-cannulated animals was similar to that found in studies using non-cannulated animals dosed at 100 mg kg^{-1}.

Introduction

Substituted benzoic acids are of interest because of the widespread human exposure to them, not least because they are often important substituents in drugs. The metabolic fate of substituted benzoic acids is also of interest because they provide a useful model system for the determination of structure–metabolism relationships (SMRs) (e.g. Caldwell 1978) including the development of quantitative models (QSMRs) (Ghauri *et al*. 1992a, b, Cupid *et al*. 1996, 1999).

Fluorinated benzoic acids, bearing a range of substituents and substitution patterns, are of particular usefulness because ^{19}F-NMR spectroscopy can be used for metabolite profiling and quantification, thereby eliminating the need for radiolabelled studies. However, while ^{19}F-NMR-based studies are well suited to compounds when elimination is largely via the urine, where faecal excretion is

* Author for correspondence; e-mail: ian.wilson@astrazeneca.com

Xenobiotica ISSN 0049–8254 print/ISSN 1366–5928 online © 2002 Taylor & Francis Ltd
http://www.tandf.co.uk/journals
DOI: 10.1080/00498250210131590

significant, the data that can readily be obtained are more limited as more extensive sample work up is needed (e.g. solvent extraction with unknown extraction efficiency). Where the bile forms a major route of excretion, the only method by which reliable data can currently be obtained on the metabolic fate of a compound using NMR-based methods is via the use of bile-cannulated animals (e.g. Spurway *et al.* 1990, Lenz *et al.* 2002). Here, the metabolic fate of pentafluorobenzoic acid (PFBA), 2,4-ditrifluoromethylbenzoic acid (2,4-DTFMBA) and 3,5-ditrifluoromethylbenzoic acid (3,5-DTFMBA) in the biliary-cannulated rat is described and compared with studies in non-cannulated animals. This study provides a further demonstration of the utility of ^{19}F-NMR spectroscopy as a means of performing metabolism and excretion balance studies in the rat.

Materials and methods

Chemicals

PFBA, 2,4- and 3,5-DTFMBAs were obtained from Fluorochem (Old Glossop, UK). The compounds were pure by ^{1}H- and ^{19}F-NMR (> 99%) and were used as received.

Dosing

Male Alpk:APfSD (Wistar derived) bile duct-cannulated rats (200–250g) were divided into groups of three animals. Each group was dosed (i.p.) with one of the substituted benzoic acids (50 mg kg^{-1}, in 2 ml kg^{-1} 0.9% saline). The surgery to perform the biliary cannulation was carried out 24 h before dosing (Lenz *et al.* 2002). The animals were housed individually in plastic metabolism cages, designed for the separate collection of urine and faeces, in a well-ventilated room with regular cycles of light and dark (12 h). Food (Modified R and M No. 1 irradiated diet) and drinking water, supplemented with glucose (5% w/v), sodium chloride (0.9% w/v) and potassium chloride (0.05% w/v), were available *ad libitum*.

Sample collection

Urine was collected over solid carbon dioxide for 24 h before dosing and for 0–24 h postdose (p.d.). Bile was collected over solid carbon dioxide for 0–6, 6–12 and 12–24 h p.d. The samples were stored frozen at −20 °C until analysed. The urinary and biliary volumes were recorded and the samples centrifuged at about 600*g* for 10 min (4 °C) before analysis to remove particulate matter.

^{1}H- and ^{19}F-NMR spectroscopy

^{1}H-NMR spectra of urine, bile and urine extracts were obtained on a Jeol GSX 500 spectrometer operating a field strength of 11.75T (500 MHz ^{1}H frequency) at ambient probe temperature. Typically, 128 free induction decays (FIDs) were collected for each sample into 32 768 data points using a spectral width of 6000 Hz and acquisition time of 2.73 s. A further delay of 2.27 s was used between pulses to ensure that spectra were fully T_1-relaxed. The residual signal for HOD protons was suppressed by applying a gated secondary irradiation field (off during acquisition) at the water resonance frequency. An exponential line-broadening factor of 0.2 Hz was applied before Fourier transformation (FT). Chemical shifts were referenced internally to sodium 3-trimethylsilyl-[2,2,3,3,^{2}H$_4$]-1-propionic acid (TSP, 1.0 mg ml^{-1}) (δ0.0).

^{19}F-NMR spectra of urine, bile and urine extracts were measured on a Bruker AM 400 NMR spectrometer operating at a field strength of 9.8T (376 MHz ^{19}F frequency) using 45° pulses with a 10 000 Hz spectral width. Typically, 128 scans were collected into 8192 data points with an acquisition time of 0.819 s. A further delay of 2.5 s was used between pulses to allow T_1-relaxation. An exponential line-broadening factor of 0.5 Hz was applied before FT. Chemical shifts were referenced externally to $CFCl_3$ (δ0.0) and to the secondary reference compound trifluoroethanol (δ −77.0). ^{19}F-^{1}H couplings were eliminated using broadband decoupling. For quantification, a known amount of 2-trifluoromethylbenzoic acid (for 3,5-DTFMBA), 4(-trifluoromethoxy)-phenol (for 2,4-DTFMBA) or 2-fluorophenol (for PFBA) was added to each sample to act as an internal standard and a delay of 5T_1 between pulses was used to ensure complete T_1-relaxation.

Metabolite isolation and identification

Chemical hydrolysis. To identify ester glucuronides, samples were incubated at pH 12.9 (with 0.1 M NaOD) at room temperature overnight (16 h). Hydrolysis was monitored by ^{19}F-NMR, as described above.

Enzymic hydrolysis. Samples (0.5 ml) were incubated with type B10, β-glucuronidase (0.5 ml, 1 mg ml^{-1}, sulphatase free) obtained from bovine liver (Sigma, Poole, UK). Samples were adjusted to pH 5.0 with 0.2 m sodium acetate buffer (0.5 ml) and incubated at 37 °C overnight. Phenolphthalein glucuronide was used as a positive control whilst saccharolactone (100 mM, 19.2 mg ml^{-1}, 0.05 ml) was used as a specific inhibitor of the enzyme. NMR monitored hydrolysis, as described above.

Solid-phase extraction/chromatography (SPEC). To concentrate and (partially) purify metabolites, selected urine samples were subjected to solid-phase extraction followed by stepwise gradient elution (Wilson and Ismail 1986, Wilson and Nicholson 1987, 1988). Samples (pH 2.2 with 0.1 M HCl) were applied to C18 Bond Elut columns (Jones Chromatography, Hengoed, UK) containing 500 mg sorbent. The cartridges had been conditioned with methanol (5 ml) and 0.1 M HCl (1 ml). Following sample application, the cartridges were washed with 0.1 M HCl (1 ml) and then sequentially with 1-ml aliquots of methanol–water mixtures of increasing eluotropic strength (20:80, 40:60, 60:40, 20:80, 0:100). The column eluates were collected, following which methanol was removed using a stream of nitrogen (room temperature) and any remaining water was removed by freeze-drying. Samples obtained in this way were reconstituted in 600 µl D_2O before spectroscopy.

Results

Pentafluorobenzoic acid (PFBA)

^{1}H-NMR spectroscopic examination of the urine obtained following the administration of 50 mg kg^{-1} PFBA to the male rat provided no evidence for the presence of any putative metabolites (e.g. glycine or glucuronide conjugates). The absence of protons in PFBA itself meant that this compound, if present, would not be detected by ^{1}H-NMR. ^{19}F-NMR spectroscopy, in contrast, revealed large quantities of unchanged PFBA in the urine (data not shown). Similar spectroscopic analysis of the bile samples obtained showed that there was no detectable excretion of either parent compound or metabolites by this route.

Quantification of the amount of PFBA excreted in the urine showed that 63.5 ± 6.7% (SE) of the dose was eliminated by this route over the 24-h collection period of the experiment.

2,4-Ditrifluoromethylbenzoic acid (2,4-DTFMBA)

^{1}H-NMR spectra of the 0–24-h p.d. urine samples from the biliary-cannulated rat dosed with 2,4-DTFMBA revealed resonances at δ8.08 (singlet), δ7.98 (double) and δ7.66 (doublet) (figure 1a) consistent with the presence of the unchanged compound (confirmed by addition of a standard). Examination of these samples by ^{19}F-NMR confirmed these observations (figure 2a). Similarly, ^{1}H-NMR spectroscopy of the 0–6-h p.d. bile sample revealed signals consistent with the presence of 2,4-DTFMBA together with additional resonances for metabolites (Figure 1b). Analysis for the 0–6-h p.d. bile sample by ^{19}F-NMR spectroscopy showed unchanged 2,4-DTFBMA to be present, together with a complex set of overlapping signals between δ −59.261 and δ −59.316, and another group between δ −63.117 and δ −63.140 (figure 2b). No signals for fluorine-containing compounds were detectable in subsequent bile samples. In an attempt to identify the metabolite resonances in the 0–6-h p.d. bile sample the pH was adjusted to 12.9 and incubated to hydrolyse ester glucuronides. This resulted in

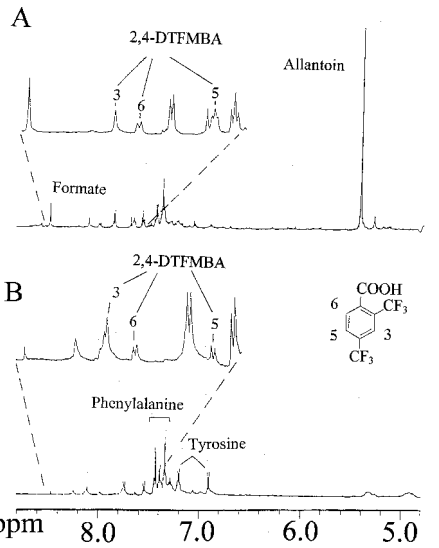


Figure 1. Typical ^{1}H-NMR spectra of (a) a 0–24-h p.d. urine sample and (b) a 0–6-h p.d. bile sample obtained following the administration of 2,4-DTFMBA 50 mg kg^{-1} to the bile cannulated rat.

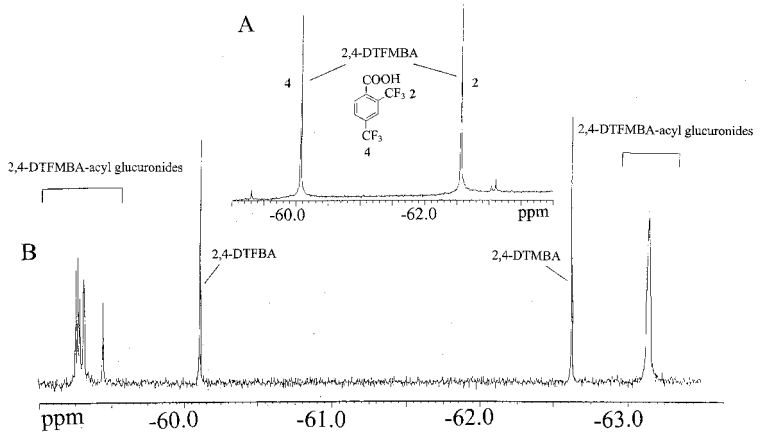


Figure 2. Typical ^{19}F-NMR spectra of (a) a 0–24-h p.d. urine sample and (b) a 0–6-h p.d. bile sample obtained following the administration of 2,4-DTFMBA 50 mg kg^{-1} to the bile cannulated rat.

the disappearance of the complex resonances at about δ −59.3 and δ −63.1 ppm, whilst the signals due to 2,4-DTFMBA increased. Such behaviour was consistent with the presence of labile ester glucuronides. When 0–6-h p.d. bile samples were treated with β-glucuronidase, the bulk of the signals were unaffected, suggesting that a significant amount of transacylation to enzyme-resistant glucuronides had occurred. To confirm the identity of these putative transacylated glucuronide conjugates, their isolation and partial purification was undertaken using SPEC (see Materials and methods). ^{19}F-NMR showed that these metabolites were eluted in the 60 and 80% methanolic eluates, while 2,4-DTFMBA was eluted predominantly in the 100% methanol fraction. The ^{1}H-NMR spectrum of the 100 and 80% methanolic eluates are shown in figure 3a, b. In the 80% fraction, a range of α- and β-anomeric protons can be seen corresponding to the various transacylated ester glucuronides of 2,4-DTFMBA.

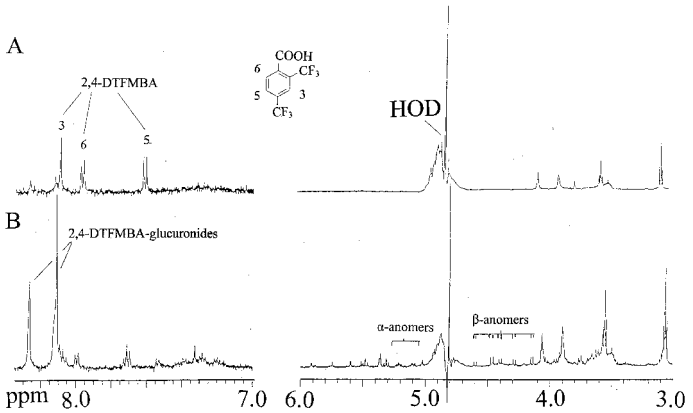


Figure 3. ^{1}H-NMR spectra of the (a) 100% and (b) 80% methanolic eluates obtained for the SPEC fractionation of 2,4-DTFMBA-related material present in the 0–6-h p.d. bile samples following administration at 50 mg kg^{-1} to the bile cannulated rat. HOD, residual water.

Table 1. Recovery of 2,4-DTFMBA and its ester glucuronides in urine and bile following i.p. administration at 50 mg kg^{-1} to rat.

Time point (h)	2,4-DTFMBA (% of dose)	Ester glucuronides (% of dose)	Total (% of dose)
Urine (0–24)	52.2 ± 1.2	n.d.	52.2 ± 1.2
(0–48)	(56.1 ± 7.8)[#]	(n.d.)[#]	(56.1 ± 7.8)[#]
Bile (0–6)	12.5 ± 1.5	19.2 ± 5.2	31.7 ± 6.4
Bile (6–12)	n.d.	n.d.	–
Bile (12–24)	n.d.	n.d.	–
Total (0–24)	64.7 ± 1.1	19.2 ± 5.2	83.9 ± 5.2

$n = 3$, ± SE.
n.d., not detected.
[#] Data in parentheses for urinary excretion are for non-cannulated animals dosed at 100 mg kg^{-1} (0–48-h collection period) (Blackledge 1996).

The quantification of 2,4-DTFMBA and the associated ester glucuronides revealed that some 65% of the administered dose was recovered as the parent benzoic acid itself, while about a further 20% was eliminated as the ester glucuronide. The overall recovery rate was 83.9% ± 5.2% (table 1). The bulk of the dose was excreted via the urine (about 52%), with the remainder eliminated rapidly in the bile.

3,5-Ditrifluoromethylbenzoic acid (3,5-DTFMBA)

Analysis of the 0–24-h p.d. urine sample using ^{1}H-NMR spectroscopy revealed signals at δ8.38 and 8.21 consistent with the presence of unchanged 3,5-DTFMBA (figure 4a). Analysis by ^{19}F-NMR confirmed that these urine samples contained unchanged parent compound and, in addition, showed two additional overlapped signals (δ −62.84 and δ −62.85) consistent with the presence of metabolites (figure 5a). Similarly, ^{1}H-NMR of the bile showed the presence of 3,5-DTFMBA in all of the post-administration samples. The ^{1}H-NMR spectrum of a typical 0–6-h p.d. bile sample is shown in figure 4b. ^{19}F-NMR spectra of the bile confirmed that

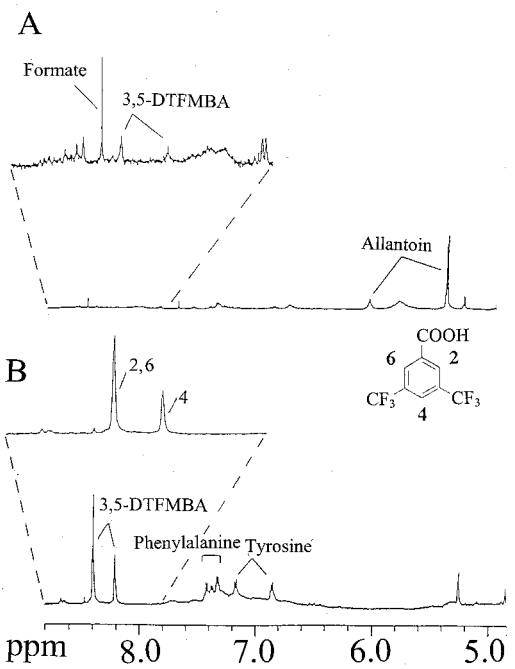


Figure 4. Typical ^{1}H-NMR spectra of (a) a 0–24-h p.d. urine sample and (b) a 0–6-h p.d. bile sample obtained following the administration of 3,5-DTFMBA 50 mg kg^{-1} to the bile cannulated rat.

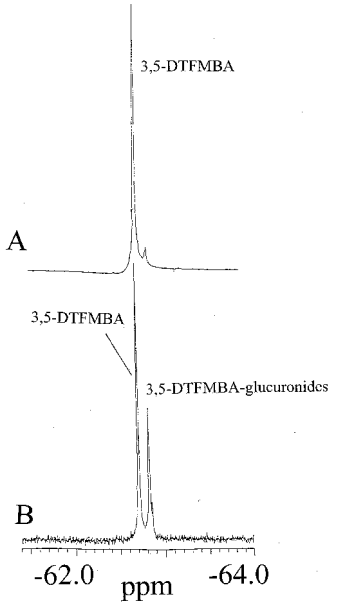


Figure 5. Typical ^{19}F-NMR spectra of (a) a 0–24-h p.d. urine sample and (b) a 0–6-h p.d. bile sample obtained following the administration of 3,5-DTFMBA 50 mg kg^{-1} to the bile cannulated rat.

these samples contained 3,5-DTFMBA and also showed a signal for small quantities of a metabolite at δ −62.95 (figure 5b). When the 0–24-h p.d. urine samples were incubated with alkali, the minor metabolite signals at δ −62.84 and δ −62.85 disappeared, suggesting that they were ester glucuronides. These peaks proved largely refractory to β-glucuronidase, suggesting that, like the 2,4-

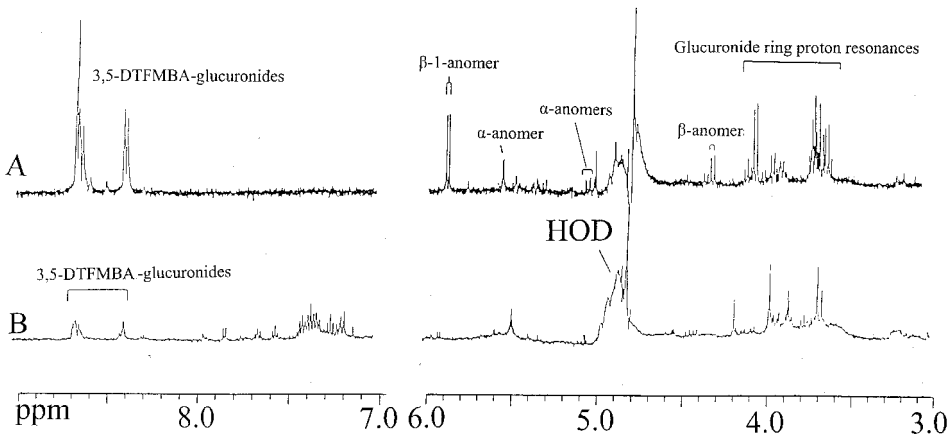


Figure 6. ^{1}H-NMR spectra of the (a) 80% and (b) 60% methanolic eluates obtained for the SPEC fractionation of 3,5-DTFMBA-related material present in the 0–6-h p.d. bile samples obtained following administration at 50 mg kg^{-1} to the bile cannulated rat. HOD, residual water.

Table 2. Recovery of 3,5-DTFMBA and its ester glucuronides in urine and bile following i.p. administration at 50 mg kg^{-1} to rat.

Time point (h)	3,5-DTFMBA (% of dose)	Ester glucuronides (% of dose)	Total (% of dose)
Urine (0–24)	10.9 ± 2.1	11.0 ± 6.7	21.9 ± 8.7
(0–48)	(4.1 ± 1.5)[#]	(9.0 ± 1.3)[#]	(13.1 ± 2.4)[#]
Bile (0–6)	13.7 ± 7.0	2.3 ± 0.8	15.9 ± 7.7
Bile (6–12)	8.1 ± 0.3	1.2 ± 0.3	9.4 ± 4.7
Bile (12–24)	1.7 ± 1.0	0.9 ± 0.4	2.6 ± 1.2
Total (0–24)	34.4 ± 10.1	15.3 ± 5.3	49.6 ± 5.3

$n = 3$, ± SE.
[#] Data in parentheses for urinary excretion are for non-cannulated animals dosed at 100 mg kg^{-1} (48-h collection period) (Blackledge 1996).

DTFMBA glucuronides described above, they were composed mainly of transacylated glucuronides rather than of the biosynthetic β-1-D-*O*-acyl glucuronide itself. When the 0–24-h p.d. urine samples were fractionated using SPEC analysis, ^{1}H-NMR revealed that the 60 and 80% methanolic eluates contained the transacylated glucuronides (figure 6a, b) with parent compound eluting in the 100% methanol fraction (spectrum not shown).

Quantification of 3,5-DTFMBA and its ester glucuronides in urine and bile indicated that about 50% of the administered material had been eliminated over the 24 h of the experiment (table 2), with the bulk excreted in the bile (27.9%). The majority of the excreted dose was unchanged parent with the remainder as the glucuronide.

Discussion

When using biliary cannulation as a means of obtaining metabolic and excretion balance data, there is always the concern that the metabolism and disposition of the test compounds will be affected by the surgical procedure. Whilst exactly comparable data are not available for these compounds in intact animals, studies

have been performed in non-cannulated animals dosed i.p. at 100 mg kg^{-1} (Blackledge 1996). Comparison of these data with those from the present study shows that similar urinary excretion and metabolite profiles were obtained for PFBA in both the biliary cannulated and non-cannulated animal. Thus, at 100 mg kg^{-1} the urinary recovery of unchanged PFBA was 52.8% ± 8.5% for the 0–48-h p.d. collection period compared with the 63.5% ± 6.7% over 24 h observed in the present study. Similarly, for 2,4-DTFMBA, some 56.1% ± 7.85% of the dose was recovered as unchanged parent compound over the 48 h p.d. in the urine of the non-cannulated rat dosed at 100 mg kg^{-1} dose compared with 52.2% ± 1.2% over the 24 h in the bile cannulated animal. For 3,5-DTFMBA, the corresponding rates over 48 h p.d. were 13.1% ± 2.4% at 100 mg kg^{-1} versus 21.9% ± 8.7% over 24 h at 50 mg kg^{-1}, and again the similarity in the urinary recoveries implies that the disposition of the compound was essentially unaltered. However, in the bile cannulated animals, roughly equal amounts of free and conjugated material were excreted via the urine, while in non-cannulated animals dosed at 100 mg kg^{-1}, the ratio was 2:1 in favour of the conjugates. This difference may in part be due to the chemical instability of the metabolites. Thus, for both of the di-trifluoromethylbenzoic acids, the major metabolites detected in the samples were transacylated ester glucuronides. Given the well-known ease with which these metabolites can hydrolyse, it is possible that despite efforts to ensure stability by freezing the samples on collection, some hydrolysis to the free acids may have occurred. The incomplete overall recoveries of the dosed acids may also be due in part to the formation of these reactive ester glucuronides that may have been retained in the body following the formation of covalent adducts to macromolecules such as proteins, etc. Alternatively, these compounds may have become incorporated into hybrid fatty acids and triglycerides via acyl-CoA thioesters (Caldwell 1984, 1985).

This study provides a further example of the usefulness of ^{19}F-NMR spectroscopy and of bile cannulated animals as a means of obtaining metabolic and disposition data without the use of radiolabelled material. Using this methodology, the formation and biliary excretion of the ester glucuronide of 2,4-DTFMBA was observed, which would have gone undetected if only urine had been monitored.

References

Blackledge, C. A., 1996, High resolution ^{19}F and ^{1}H nuclear magnetic resonance spectroscopic studies of substituted aromatic compounds in the rat. Thesis, University of London.

Caldwell, J., 1978, Structure–metabolism relationships in amino acid conjugation. In A. Aitio (ed.), *Conjugation Reactions in Drug Biotransformation* (Amsterdam: Elsevier/North Holland), pp 111–121.

Caldwell. J., 1984, Xenobiotic acyl-coenzymes A: critical intermediates in the biochemical pharmacology and toxicology of carboxylic acids. *Biochemical Society Transactions*, **12**, 9–11.

Caldwell, J., 1985, Novel xenobiotic-lipid conjugates. *Biochemical Society Transactions*, **13**, 852–854.

Cupid, B. C., Beddell, C. R., Wilson, I. D., Lindon, J. C. and Nicholson, J. K., 1996, Quantitative structure–metabolism relationships for substituted benzoates in the rabbit: prediction of urinary excretion of glycine and glucuronide conjugates. *Xenobiotica*, **26**, 157–176.

Cupid, B. C., Holmes, E., Wilson, I. D., Lindon, J. C. and Nicholson, J. K., 1999, Quantitative structure–metabolism relationships (QSMR) using computational chemistry: pattern recognition analysis and statistical prediction of phase II conjugation reactions of substituted benzoic acids in the rat. *Xenobiotica*, **29**, 27–42.

Ghauri, F. Y., Blackledge, C. A., Glen, R. C., Sweatman, B. C., Lindon, J. C., Beddell, C. R., Wilson, I. D and Nicholson, J. K., 1992a, An approach to a metabolic expert system: structure–metabolism relationships for benzoic acids in the rat. In E. Reid and I. D. Wilson (eds), *Methodological Surveys in Biochemistry and Analysis* (Cambridge: Royal Society of Chemistry), pp. 21–28.

Ghauri, F. Y., Blackledge, C. A., Glen, R. C., Sweatman, B. C., Lindon, J. C., Beddell, C. R., Wilson, I. D. and Nicholson, J. K., 1992b, Quantitative structure–metabolism relationships of substituted benzoic acids in the rat. Computational chemistry, NMR spectroscopy and computer pattern recognition studies. *Biochemical Pharmacology*, **44**, 1935–1946.

Lenz, E. M., Wilson, I. D., Wright, B., Partridge, E. A., Rodgers, C. T., Lindon, J. C. and Nicholson, J. K., 2002, A comparison of quantitative NMR and radiolabelling studies of the metabolism and excretion of Statil (3-(4-bromo-2-fluorobenzyl)-4-oxo-3H-phthalazin-1-ylacetic acid in the rat. *Journal of Pharmaceutical and Biomedical Analysis*, **28**, 31–43.

Spurway, T. D., Gartland, K. P. R., Warrander, A., Pickford, R., Nicholson, J. K. and Wilson, I. D., 1990, Proton nuclear magnetic resonance of urine and bile from paracetamol dosed rats. *Journal of Pharmaceutical and Biomedical Anal*ysis, **8**, 969–973.

Wilson, I. D. and Ismail, I. M., 1986, A rapid method for the isolation and identification of drug metabolites from human urine using solid phase extraction and proton NMR spectroscopy. *Journal of Pharmaceutical and Biomedical Anal*ysis, **4**, 663–665.

Wilson, I. D. and Nicholson, J. K., 1988, Solid phase extraction and NMR spectroscopy (SPE-NMR) for the rapid identification of drug metabolites in urine. *Journal of Pharmaceutical and Biomedical Anal*ysis, **6**, 151–165.

Wilson, I. D. and Nicholson, J. K., 1987, Solid phase extraction chromatography and nuclear magnetic resonance spectroscopy for the isolation of drug metabolites in urine. *Analytical Chemistry*, **59**, 2830–2832.

XENOBIOTICA, 2002, VOL. 32, NO. 7, 615–623

Taylor & Francis
healthsciences

Absolute bioavailability and stereoselective pharmacokinetics of doxepin

J.-H. YAN†, J. W. HUBBARD†‡* G. MCKAY†‡,
E. D. KORCHINSKI§ and K. K. MIDHA†‡§

† College of Pharmacy & Nutrition, ‡ PharmaLytics, Inc. and § College of Medicine, University of Saskatchewan, Saskatoon, Saskatchewan, Canada S7N 5C9

Received 17 September 2001

1. Commercial doxepin contains geometric isomers in the proportions $Z{:}E = 15{:}85$. *Z*-doxepin and its metabolite *Z*-*N*-desmethyldoxepin are both active antidepressants, whereas the corresponding *E*-isomers are less active therapeutically.

2. The present pharmacokinetic study was a balanced, randomized, two-treatment, two-period, two-sequence crossover design in which 12 healthy male volunteers were given single doses of commercial doxepin intravenously and orally on two occasions separated by a washout period.

3. A two-compartment model with no lag time and first-order elimination fitted the plasma concentration–time curves after intravenous dosing. Pharmacokinetic parameters estimated from the model were comparable with those estimated by non-compartmental methods.

4. All pharmacokinetic parameters displayed a wide between-subject variability. Both isomers of doxepin showed large volumes of distribution and relatively short half-lives in plasma, suggestive of extensive distribution and/or tissue binding. The mean fraction absorbed after oral administration was 0.29 for each isomer. Renal clearances of each isomer were very low after either oral or intravenous dosing, although all four analytes were quantifiable in the urine for prolonged periods.

5. After oral dosing, plasma concentrations of the doxepin isomers remained roughly in the ratio $Z{:}E = 15{:}85$, whereas those of *N*-desmethyldoxepin were closer to 1:1 in all but two outliers, who had high levels *E*-*N*-desmethyldoxepin.

Introduction

Doxepin is a tricyclic antidepressant (figure 1) marketed as a mixture of geometric isomers in a ratio of $Z{:}E = 15{:}85$, although animal studies suggest that the *Z*-doxepin is the more active isomer (Pinder *et al.* 1977). The *N*-desmethyl metabolite is also known to be active, and it has been suggested that the total plasma concentration of *Z*- + *E*-doxepin and *Z*- + *E*-*N*-desmethyldoxepin may show better correlation with antidepressant effects than the parent drug alone (Faulkner *et al.* 1983). Several other studies have also included correlations between clinical effect and plasma or serum concentrations of *N*-desmethyldoxepin (Friedel and Raskin 1975, Green 1978, Ward *et al.* 1982). Rosseel *et al.* (1978) reported that plasma concentrations of *E*-doxepin in two patients were higher than *Z*-doxepin, such that the *Z*:*E* ratio was approximately the same as that in the administered dosage form (= 15:85), whereas plasma concentrations of *Z*-*N*-desmethyldoxepin were similar to those of the *E*-isomer, a finding subsequently confirmed by Bogaert *et al.* (1981) and Hrdina *et al.* (1990).

* Author for correspondence; e-mail: Hubbard@duke.usask.ca

Xenobiotica ISSN 0049-8254 print/ISSN 1366–5928 online © 2002 Taylor & Francis Ltd
http://www.tandf.co.uk/journals
DOI: 10.1080/00498250210131879

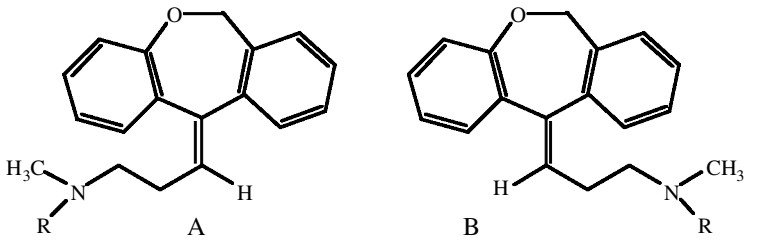


Figure 1. *Z*- (A) and *E*- (B) geometric isomers of doxepin (R = CH_3) and *N*-desmethyldoxepin (R = H).

These observations fuelled speculation that the change in the *Z*:*E* ratio of *N*-desmethyldoxepin isomers in plasma or serum of patents may have come about as a result of enrichment of *Z*-*N*-desmethyldoxepin at the expense of the less active *E*-isomer. Ghabrial *et al.* (1991) administered 25 mg *Z*-doxepin and 25 mg tetra-deuterated *E*-doxepin to eight healthy volunteers. Urinary recoveries of all four analytes were very low, being consistent with extensive metabolism of both doxepin and *N*-desmethyldoxepin (Hobbs 1969, Kimura *et al.* 1972, Shu *et al.* 1990a, b, Luo *et al.* 1991). There was no evidence of interconversion between the doxepin isomers, but deuterium-labelled *Z*-*N*-desmethyldoxepin was detected, suggesting that isomerization occurred during the formation of *N*-desmethyldoxepin. More recently, a phenolic metabolite of *N*-desmethyldoxepin hydrated at the exocyclic double-bond was identified by mass spectromety in the urine of patients medicated with doxepin (Shu *et al.* 1990a). This finding gives tentative support for the existence of a possible mechanism for interconversion mediated by a process involving hydration of the exocyclic double-bond followed by rotation from the *E*- to the *Z*-configuration and subsequent dehydration to reform the exocyclic double-bond.

Earlier non-stereoselective single-dose pharmacokinetic studies of doxepin and *N*-desmethyldoxepin (Ziegler *et al.* 1978, Virtanen *et al.* 1980, Wecker *et al.* 1986) reported that doxepin was rapidly absorbed from the gastrointestinal tract with maximum plasma concentrations (C_{max}) occurring approximately 2 h after oral administration. However, there was considerable between-subject variability in other pharmacokinetic parameters, as had previously been reported in patients under medication with doxepin (Hrdina *et al.* 1990). Stereoselective single-dose pharmacokinetic studies in humans have proven difficult to carry out because of the extremely low concentrations of *Z*-doxepin, such that earlier analytical methods have proven inadequate (Rosseel *et al.* 1978, Whall and Dokladalova 1979, Bogaert *et al.* 1981, Dilger *et al.* 1988, Midha *et al.* 1992, Adamczyk *et al.* 1995). For example, the single-dose oral pharmacokinetics of doxepin and *N*-desmethyldoxepin were examined in 30 healthy volunteers who each received 75 mg commercial doxepin hydrochloride (Midha *et al.* 1992). Unfortunately, plasma concentrations of the parent drug were so low that it was possible to monitor *Z*-doxepin concentrations in only three subjects. The *Z*:*E* ratio in these three subjects remained close to that in the administered dose (15:85). Stereoselective analysis of *N*-desmethyldoxepin, however, was possible in all subjects. The area under the plasma concentration–time curve (AUC) of *Z*-*N*-desmethyldoxepin exceeded that of *E*-*N*-desmethyldoxepin in all but two subjects who appeared to be outliers. The present stereoselective study was undertaken after the

development of more sensitive high-performance liquid chromatography (HPLC) assay procedures for which the lower limit of quantitation was 1.0 ng ml^{-1} *Z*- and *E*-doxepin and of *Z*- and *E*-*N*-desmethyldoxepin (Yan *et al.* 1997).

The objectives of the current two period cross over study were: (1) to define for the first time the stereoselective pharmacokinetics of doxepin after single intravenous (i.v.) doses in healthy volunteers, and (2) to examine the stereoselective single-dose oral pharmacokinetics of doxepin and *N*-desmethyldoxepin after administration of doxepin to healthy volunteers.

Materials and methods

Clinical study design

The study was carried out in 12 healthy male volunteers who were non-smokers, 21–36 years of age inclusive and deviating by no more than 10% from the ideal weight for height according to the Metropolitan Life Insurance Company Bulletin (1983). Each subject was required to be free of cardiovascular, hepatic, renal, gastrointestinal diseases, or drug abuse or alcohol dependence, as assessed by physical examination and a review of their medical history. In addition, the blood pressure, electrocardiogram and results of clinical laboratory tests (blood chemistry, haematology, urinalysis) were required to be within normal ranges. Written informed consent was obtained from all volunteers prior to their participation in the study. The local institutional review board approved the study protocol. All subjects were required to abstain from the use of all other drugs (including non-prescription drugs) for at least 1 week prior to and until after completion of the study. The subjects were also required to refrain from consuming alcoholic- or caffeine-containing beverages from 48 h prior to dosing to after the collection of the last blood sample.

The study was a balanced, randomised, two-treatment, two-period, two-sequence crossover design. The washout period between the two dosing periods was 2 weeks. USP-grade doxepin (Wiler, Lot 36938, Exp. 07-30-2000) was used for the preparation of i.v. dosage form (5 mg ml^{-1} solution in normal saline) by the Royal University Hospital dispensary, Saskatoon. This formulation was shown to be sterile and pyrogen-free (Nucro Technics, Inc., Scarborough, Ontario, Canada). The i.v. and oral formulations were validated by HPLC (Yan *et al.* 1997) and shown to contain an isomeric ratio of *Z*:*E* = 16:84. No impurities were detectable in the HPLC chromatograms. All doses were administered under medical supervision. After an overnight fast, the i.v. group received 25 mg doxepin hydrochloride (equivalent to 22.12 mg free base containing 3.54 mg *Z*-doxepin + 18.58 mg *E*-doxepin) by an injection administered slowly over 2 min (timed with a stopwatch). Blood samples (14 ml) were drawn in evacuated tubes containing heparin, immediately before dosing, and at 0.1, 0.2, 0.3, 0.5, 0.8, 1, 2, 3, 5, 7, 10, 12, 24, 36, 48, 72, 96 and 120 h. The oral group received 85.5 mg doxepin hydrochloride (equivalent to 75 mg free base containing 12.0 mg *Z*-doxepin + 63.0 mg *E*-doxepin, Apo-doxepin^{TM}, Apotex, Inc., Weston, Ontario, Canada) taken with 100 ml water. Blood samples (14 ml) were drawn in heparinized evacuated tubes immediately before dosing and at 0.3, 0.5, 1, 1.5, 2, 2.5, 3, 4, 6, 8, 10, 12, 24, 36, 48, 72, 96 and 120 h. Each blood sample was immediately centrifuged at 1000*g* to separate plasma, which was then divided into two aliquots and frozen (−20 °C) until analysis. Control samples of urine were collected immediately before dosing. Total urine was then collected in 12-h segments up to 120 h after i.v. or oral administration. The volume and pH of urine of each segment were recorded, and a portion of each sample was stored at –20 °C until analysis.

Analytical methods

Plasma and urine samples were analysed by means of validated, stereoselective HPLC procedures for *Z*- and *E*- doxepin and for *Z*- and *E*-*N*-desmethyldoxepin, as described by Yan *et al.* (1997). The lower limit of quantification was 1.0 ng ml^{-1} for each isomer of the parent drug and for the *N*-desmethyl metabolite. Standard curves were run daily. Acceptance criteria were based on quality-control samples (analyst 'blind') representing the low, medium and high regions of the standard curve. Plasma or urine samples from both i.v. and oral treatments of any given volunteer were analysed on the same day. To assess the stability of plasma and urine samples during storage, eight control samples (5 ng ml^{-1}) for *E*-doxepin and *E*-N-desmethyldoxepin in plasma or urine were analysed at various times during and at the end of the 3- (plasma) or 5-month (urine) periods of storage at −20 °C.

Non-compartmental pharmacokinetic analysis

Non-compartmental pharmacokinetic parameters were calculated by means of WinNonLin (v.1.1, Scientific Consulting, Inc.). Briefly, the elimination rate constant (λz) was estimated by log–linear

regression of the terminal phase (last four plasma concentrations) of the plasma concentration–time curve. After oral dosing, the area under the plasma concentration–time curve up to the last measurable plasma concentration (AUC_{last}) was computed by means of the linear trapezoidal rule for ascending portions of the curve and the log trapezoidal rule for descending portions, whereas for i.v. administration the log trapezoidal rule was used throughout. Extrapolated areas (AUC_{∞}) were determined by adding to the appropriate AUC_{last} the quotient $C_{last\,t}$ and the appropriate λz. Terminal phase half-lives ($t_{1/2}$) were calculated from the quotient of ln 2 and λz. Clearance (CL) was determined as the quotient of dose (i.v.) and the appropriate AUC_{∞}. Apparent oral clearance (CL_o) was determined in a similar manner from oral data. The fraction reaching the systemic circulation after oral administration (F) was calculated as the quotient of CL and CL_o. Mean residence time (MRT) was estimated as the quotient of area under the first moment curve (AUMC) and AUC. The amount of drug eliminated in the urine, $A_{e(\infty)}$, was estimated from the total urine collection period (up to 120 h after the drug administration). The per cent dose excreted unchanged was calculated based on $A_{e(\infty)}$ and the total administrated dose. Renal clearance (CL_R) was calculated as the quotient of $A_{e(\infty)}$ and AUC_{∞}.

Compartmental pharmacokinetic analysis

Compartmental pharmacokinetic analysis (WinNonLin using a two-compartment model, no lag time, and first-order elimination) was fitted to the mean plasma concentration–time data obtained after i.v. administration of doxepin:

$$C = A\,e^{\alpha t} + B\,e^{\beta t}, \tag{1}$$

where C is the plasma concentration at time t, A is the zero-time intercept associated with the α-phase, α is the macro rate constant associated with the distribution phase, B is the zero-time intercept associated with the β-phase, and β is the macro-rate constant associated with the elimination phase. A weighting factor of $1/C^2$ (predicted values) was selected to minimize optimally the weighted sums of squared residuals. The method of Gauss–Newton (Levenberg and Hartley) was used for minimization. Model selection was based on evaluation of Akaike's Information Criterion (AIC) (Akaike 1974, Yamaoka 1978) and Schwarz's Criterion (SC) (Schwarz 1978).

Statistical analysis

Statistics of the pharmacokinetic parameters in non-compartmental and compartmental analysis were performed in WinNonlin (v.1.1, Scientific Consulting, Inc., Cary, NC, USA). Analysis of variance (ANOVA) was carried out on urinary recoveries of doxepin or *N*-desmethyldoxepin isomers expressed as percentages of dose as the dependent variable (SuperANOVA v.1.11, Abacus Concepts, Inc., Berkley, CA, USA). Effects in the ANOVA model were Subject, Route, Isomer, Subject*Route, Subject*Isomer, Route*Isomer and Residual Error. Subject*Route was used as the error term for Route, and Subject*Isomer was used as the error term for Isomer. The level of significance was set at $\alpha = 0.05$.

Results

All 12 subjects who met the entry requirements completed the study. No blood or urine samples were missed during either phase of the study. Generally, the doses were well tolerated in all subjects after either i.v. or oral doxepin administration. The most common side-effects included dry mouth, drowsiness and sleepiness, the onset of which started earlier after i.v. than oral administration (onset approximately 1 h post-dose). All symptoms of these side-effects generally disappeared after 24 h. There was no evidence of deterioration of either plasma or urine samples during frozen storage (3–5 months). Concentrations of analytes in stability samples deviated from nominal concentrations in the range 1.0–2.5%.

After i.v. administration, plasma concentrations of *Z*-doxepin were measurable up to 24 h in 10/12 subjects, and plasma concentrations of *E*-doxepin were measurable up to 48 h in 9/12 subjects (figure 2A). Similarly, after oral administration, plasma concentrations of *Z*-doxepin were measurable up to 24 h in 10/12 subjects (figure 2C), whereas concentrations of *E*-doxepin were measurable in 9/12 subjects at 48 h post-oral dosing.

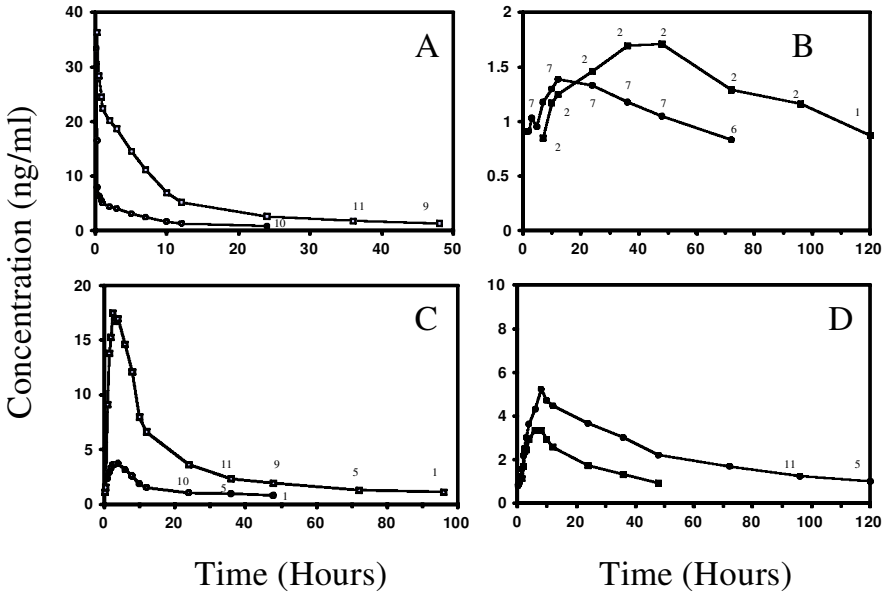


Figure 2. Mean ($n = 12$, unless indicated otherwise) plasma concentration–time curves after intravenous administration of commercial doxepin: A, *Z*-doxepin (grey circles) and *E*-doxepin (grey squares); B, *Z*-*N*-desmethyldoxepin (black circles) and *E*-*N*-desmethyldoxepin (black squares). Mean plasma concentration–time curves after oral administration of commercial doxepin: C, *Z*-doxepin (grey circles) and *E*-doxepin (grey squares); D, *Z*-*N*-desmethyldoxepin (black circles) and *E*-*N*-desmethyldoxepin (black squares). The latter plot includes values for one randomly selected subject (no. 11) because of very wide between-subject variation in plasma concentrations.

Pharmacokinetic parameters derived from non-compartmental analysis are listed in tables 1 and 2 for i.v. and oral administration, respectively. There was wide between-subject variability in all pharmacokinetic parameters. For example, the mean absolute oral bioavailability was 29% for both doxepin isomers, but in each case the coefficient of variation >50% (table 2). A two-compartment model (i.v. bolus, no lag time, first-order elimination) fitted the data after i.v. administration of doxepin (*Z*-doxepin: AIC = −7.62; SC = −10.49; *E*-doxepin: AIC = 5.98; SC = 3.40). Pharmacokinetic parameters estimated from the model were comparable with those estimated by non-compartmental methods (table 1).

The ratio of *Z*- to *E*-doxepin in plasma appeared very close to that in the administered dosage form (16:84) in that the mean percentage of the *Z*-isomer ranged from 18 to 20 in all volunteers after either i.v. or oral administration. Plasma concentrations of the *N*-desmethyldoxepin isomers, however, were so low after i.v. administration of doxepin that their pharmacokinetics could be determined only in seven subjects for the *Z*-isomer and in two subjects (nos 4 and 6) for *E*-isomer (figure 2B). By contrast, the pharmacokinetics of *Z*-*N*-desmethyldoxepin after oral administration of doxepin could be determined in all 12 subjects for up to 72 h post-dose (figure 2D). However, plasma concentrations of *E*-*N*-desmethyldoxepin ranged from very low in subject 3 to very high in subjects 4 and 6, resulting in very wide between-subject variability. Therefore, we selected randomly the plasma concentration–time curve subject 11 as an illustration in figure 2D. In general, plasma AUCs of *Z*-*N*-desmethyldoxepin after either i.v. or oral

Table 1. Pharmacokinetics of the *Z*- and *E*-isomers of doxepin and *N*-desmethyldoxepin in 12 healthy men after 22.12 mg (base) intravenous administration of doxepin ($Z/E = 16/84$).

	C_{max} (ng ml^{-1})	t_{max} (h)	λz (h^{-1})	$t_{1/2}$ (h)	CL (l h^{-1})	V_{SS} (l)	V_Z (l)	MRT (h)	CL_R (l h^{-1})
Z-doxepin	–	–	0.0719	11.7	53.7	677	822	13.8	0.5
	–	–	(55.03)	(40.3)	(32.3)	(33)	(25)	(47.3)	(46.36)
E-doxepin	–	–	0.0475	17.7	62.1	957	1436	16.7	0.5
	–	–	(44.89)	(47.3)	(29.5)	(35)	(29)	(52.0)	(41.9)
Z-*N*-desmethyldoxepin[a]	1.5	15.9	0.0110	65.7	–	–	–	99.5	–
	(19.9)	(48.9)	(20.77)	(21.60)	–	–	–	(20.5)	–
E-*S*-desmethyldoxepin[b]	1.8	42.0	0.0089	78.0	–	–	–	127.0	–

Figures in parentheses are the percentage coefficients of variation.
[a] $n = 7$.
[b] $n = 2$ (*E*-*N*-desmethyldoxepin detectable in subjects 4 and 6 who appeared to be outliers).

Table 2. Pharmacokinetics of *Z*- and *E*-isomers of doxepin and *N*-desmethyldoxepin in 12 healthy men after 75 mg (base) oral administration of doxepin ($Z/E = 16/84$).

	C_{max} (ng ml^{-1})	t_{max} (h)	λz (h^{-1})	$t_{1/2}$ (h)	CL_0 (l h^{-1})	V_Z (l)	F_{abs}	MRT (h)	CL_R (l h^{-1})
Z-doxepin	4.3	2.9	0.0594	14.8	238	1102	0.29	20.7	0.69
	(44.1)	(43.1)	(59.77)	(42.0)	(59)	(44)	(51.95)	(40.2)	(63.56)
E-doxepin	20.4	3.0	0.0366	20.4	262	17 547	0.29	24.7	0.65
	(52.6)	(41.7)	(27.70)	(29.8)	(50)	(26)	(50.09)	(26.5)	(55.85)
Z-*N*-desmethyldoxepin[a]	5.4	7.8	0.0159	45.8	–	–	–	67.3	–
	(22.3)	(17.1)	(25.50)	(20.7)	–	–	–	(20.0)	–
E-*N*-desmethyldoxepin[b]	3.3	5.8	0.0468	23.4[c]	–	–	–	34.8	–
	(30.7)	(39.5)	(84.00)	(62.0)	–	–	–	(59)	–

Figures in parentheses are the percentage coefficients of variation.
[a] $n = 12$ (no outliers detected).
[b] $n = 9$ (volunteers 4 and 6 are not included in calculations for the outlier status; volunteer 3 could not be calculated due to low plasma concentrations).
[c] The half-life of subject 4 was 83.0 h; that of subject 6 was 56.6 h.

doxepin tended to be much greater than those of its geometric antipode in all subjects except for subjects 4 and 6, in whom the AUC of the *E*-isomer was greater than that of *Z*-isomer.

Examination of urinary data revealed that the four analytes under investigation in the present study represented only a small percentage of the administered dose of doxepin (< 3%), which is extensively metabolized by routes other than *N*-desmethylation. Nevertheless, it was possible to monitor both *E*- and *Z*-isomers of doxepin and of *N*-desmethyldoxepin for at least 60 h in all subjects after either i.v. or oral administration. As in the case of plasma, the urinary ratio of the doxepin isomers remained similar to that in the original dosage form, whereas there was marked distortion in the ratio of the *N*-desmethyldoxepin isomers. Again, with the exception of subjects 4 and 6, percentage recoveries of *Z*-*N*-desmethyldoxepin were higher than those of the *E*-isomer.

Factorial ANOVA was carried out to examine between-subject effects within the time segments of the harvested urine. With doxepin as the dependent variable, route of administration was significant in the earliest time segments (0–12 and 12–24 h), which reflect extensive first-pass metabolism after oral administration. The effect of the doxepin isomer was also significant in the two earlier time segments

because there was a tendency for the percentage of the dose of the *Z*-isomer excreted in the urine to be higher than that of the *E*-isomer in all subjects. Neither route nor isomer was significant in later time segments. With urinary *N*-desmethyldoxepin as the dependent variable, the effect of isomer was significant in all time segments, whereas route of administration was significant only in the earliest time segment (0–12 h).

Discussion

To the best of our knowledge, this is the first report of the i.v. pharmacokinetics of doxepin in man. Intravenous administration of doxepin in healthy volunteers revealed both isomers to have large volumes of distribution and relatively short half-lives (table 1), which suggests that both isomers were subject to extensive tissue distribution and/or binding. Prolonged low-level excretion of both isomers in the urine suggested that there was a late phase of elimination that was not measurable in the plasma because all four analytes were below the lower limit of quantification of the assay method (1.0 ng ml^{-1} for each analyte). A two-compartment model fitted the i.v. plasma concentration–time data and gave reasonable estimates of clearances and volumes of distribution of the doxepin isomers, comparable with estimates from non-compartmental methods.

Despite large between-subject variability, the mean fraction of the dose reaching the systemic circulation intact after oral administration was 0.29 for both isomers (table 2). This is consistent with earlier estimates (Ziegler *et al.* 1978, Virtanen *et al.* 1980, Faulkner *et al.* 1983) based on Gibaldi *et al.*'s (1971) method for the calculation of hepatic availability in which it was assumed that the drug is completely absorbed from the gastrointestinal tract into the hepatoportal system and that liver blood flow is 90 l h^{-1}. This suggests that metabolism of both doxepin isomers was largely hepatic in nature. After oral administration, both doxepin isomers exhibited large apparent volumes of distribution and relatively short half-lives. The fact that the ratio of the doxepin isomers in plasma remained close to that in the dosage form administered (16:84) suggested stereoselective metabolism was not a factor after either route of administration. Furthermore, renal clearances were very similar for the two isomers after i.v. (table 1) or oral (table 2) administration, which suggests that stereoselective renal excretion of the parent drug was not a factor either. The fact that the effect of isomer was significant in factorial ANOVA of the early urinary time segments arose because the recovery of *Z*-doxepin was slightly but consistently higher than that of the *E*-isomer in all subjects.

Z-*N*-desmethyldoxepin was quantifiable in 7 of 12 individuals after i.v. administration of commercial doxepin (figure 2B), whereas *E*-*N*-desmethyldoxepin was quantifiable in only two subjects (nos 4 and 6) who had high concentrations of the *E*-isomer and appeared to be outliers (table 1). Similarly, after oral administration, much higher concentrations of *E*-*N*-desmethyldoxepin were found in the plasma of subjects 4 and 6 compared with the other subjects. These data are consistent with the study of Midha *et al.* (1992) on the oral single dose pharmacokinetics of doxepin in which two subjects appeared to be outliers in that they had high levels of *E*-*N*-desmethyldoxepin in comparison with other subjects. Recent *in vitro* studies (unpublished data) suggest that *N*-glucuronidation may be an important stereoselective route of metabolism of *N*-desmethyldoxepin, and it is

tempting to speculate that subjects 4 and 6 may have been poor metabolizers in terms of glucuronosyl transferase(s). The clinical consequences of this apparent polymorphism are unknown beyond the increase in between-subject pharmacokinetic variability. In the present treatment, it was decided not to include data from subjects 4 and 6 in pharmacokinetic calculations involving the *E*-*N*-desmethyl isomer after oral dosing. Removal of data from the outliers led to substantial reductions in C_{max}, t_{max} and $t_{1/2}$ in the case of the *E*-isomer, but had little effect on the same parameters in the case of the *Z*-isomer. The mean half-life of *Z*-*N*-desmethyldoxepin was very long after i.v. (table 1) or oral (table 2) administration. The half-life of the *E*-*N*-desmethyl isomer was much shorter after oral administration (table 2) in all but the two outliers (subjects 4 and 6) in whom the half-lives were 83.01 and 56.55 h respectively.

In conclusion, the study showed that both geometric isomers of doxepin gave plasma concentration–time curves that fitted a two-compartment model after i.v. injection in man. Both isomers of the parent drug were extensively eliminated by metabolism, such that renal clearances were very low after either i.v. or oral administration. There was wide between-subject variability in all pharmacokinetic measures, and particularly so in the oral data. For example, the mean fraction absorbed from the gastrointestinal tract was approximately 30% for each isomer, but the coefficient of variation was 50% in each case. These data show that pharmacokinetic variability is a factor contributing to between-patient variability in clinical response to doxepin.

References

Adamczyk, M., Fishpaugh, J. R. and Harrington, C., 1995, Quantitative determination of *E*- and *Z*-doxepin and *E*- and *Z*-desmethyldoxepin by high-performance liquid chromatography. *Therapeutics and Drug Monitoring*, **17**, 371–376.

Akaike, H., 1974, A new look at the statistical model identification. *IEEE Transactions on Automatic Control*, **19**, 716–723.

Bogaert, M. G., Rosseel, M. T., Deberdt, R. and Vranckx, C., 1981, Plasma levels of the *cis*- and *trans*-isomers of doxepin and desmethyldoxepin after administration of doxepin to patients. *Arzneimittelforschung/Drug Research*, **31**, 113–115.

Dilger, C., Salama, Z. and Jaeger, H., 1988, High-performance liquid chromatographic determination of *trans*-doxepin and desmethyldoxepin. *Arzneimittelforschung/Drug Research*, **38**, 1525–1528.

Faulkner, R. D., Pitts, W. M., Lee, C. S., Lewis, W. A. and Fann, W. E., 1983, Multiple-dose doxepin kinetics in depressed patients. *Clinical and Pharmacological Therapeutics*, **34**, 509–515.

Friedel, R. and Raskin, M., 1975, Relationship of blood levels of Sinequan to clinical effects in the treatment of depression in aged patients. In J. Mendels (ed.), *Sinequan: A Monograph of Recent Studies* (New York: Elsevier).

Ghabrial, H., Prakash, C., Tacke, U. G., Blair, I. A. and Wilkinson, G. R., 1991, Geometric isomerization of doxepin during its *N*-demethylation in humans. *Drug Metabolism and Disposition*, **19**, 596–599.

Gibaldi, M., Boys, R. and Feldman, S., 1971, Influence of first pass effect on availability of drugs on oral administration. *Journal of Pharmaceutical Science*, **60**, 1338–1340.

Green, D., 1978, Clinical importance of doxepin plasma levels. *Journal of Clinical Psychiatry*, **39**, 481–482.

Hobbs, D. C., 1969, Distribution and metabolism of doxepin. *Biochemical Pharmacology*, **18**, 1941–1954.

Hrdina, P. D., Bakish, D., Swenson, S. and Lapierre, Y. D., 1990, *Cis*- and *trans*-isomers of doxepin and desmethyldoxepin in the plasma of depressed patients treated with doxepin. *Therapeutics and Drug Monitoring*, **12**, 129–133.

Kimura, Y., Kume, M. and Kageyama, K., 1972, Doxepin hydrochloride: absorption, distribution, excretion and metabolism of doxepin. *Pharmacometrics*, **6**, 955–971.

Luo, H., Hawes, E. M., McKay, G., Korchinski, E. D. and Midha, K. K., 1991, The quaternary ammonium-linked glucuronide of doxepin: a major metabolite in depressed patients treated with doxepin. *Drug Metabolism and Disposition*, **19**, 722–724.

Midha, K. K., Hubbard, J. W., McKay, G., Hawes, E. M., Korchinski, E. D., Gurnsey, T., Cooper, J. K. and Schwede, R., 1992, Stereoselective pharmacokinetics of doxepin isomers. *European Journal of Clinical Pharmacology*, **42**, 539–544.

Pinder, R. M., Brogden, R. N., Speight, T. M. and Avery, G. S., 1977, Doxepin up-to-date: a review of its pharmacological properties and therapeutic efficacy with particular reference to depression. *Drugs*, **13**, 161–218.

Rosseel, M. T., Bogaert, M. G. and Claeys, M., 1978. Quantitative GLC determination of *cis*- and *trans*-isomers of doxepin and desmethyldoxepin. *Journal of Pharmaceutical Science*, **67**, 802–805.

Schwarz, G., 1978, Estimating the dimension of a model. *Annals of Statistics*, **6**, 461–464.

Shu, Y. Z., Hubbard, J. W., Cooper, J. K., McKay, G., Korchinski, E. D., Kumar, R. and Midha, K. K., 1990a, The identification of urinary metabolites of doxepin in patients. *Drug Metabolism and Disposition*, **18**, 735–741.

Shu, Y. Z., Hubbard, J. W., McKay, G. and Midha, K. K., 1990b, Identification of phenolic doxepin glucuronides from patient urine and rat bile. *Drug Metabolism and Disposition*, **18**, 1096–1099.

Virtanen, R., Scheinin, M. and Iisalo, E., 1980, Single dose pharmacokinetics of doxepin in healthy volunteers. *Acta Pharmacologica et Toxicologica Copenhagen*, **47**, 371–376.

Ward, N. G., Bloom, V. L., Wilson, L., Raskind, M. and Raisys, V. A., 1982, Doxepin plasma levels and therapeutic response in depression: preliminary findings. *Journal of Clinical Psychopharmacology*, **2**, 126–128.

Wecker, M. T., Woodworth, J. R., Amsel, L. P., Hinsvark, O. N. and Rotenberg, K. S., 1986, Pharmacokinetic evaluation of two doxepin products. *Clinical Therapeutics*, **8**, 342–347.

Whall, T. J. and Dokladalova, J., 1979, High-performance liquid chromatographic determination of (*Z*)- and (*E*)-doxepin hydrochloride isomers. *Journal of Pharmaceutical Science*, **68**, 1454–1456.

Yamaoka, K. T., 1978, Application of Akaike's information criterion (AIC) in the evaluation of linear pharmacokinetic equations. *Journal of Pharmacokinetics and Biopharmacology*, **6**, 165–175.

Yan, J. H., Hubbard, J. W., McKay, G. and Midha, K. K., 1997, Stereoselective and simultaneous measurement of *cis*- and *trans*-isomers of doxepin and *N*-desmethyldoxepin in plasma or urine by high-performance liquid chromatography. *Journal of Chromatography B*, **691**, 131–138.

Ziegler, V. E., Biggs, J. T., Wylie, L. T., Rosen, S. H., Hawf, D. J. and Coryell, W. H., 1978, Doxepin kinetics. *Clinical and Pharmacological Therapeutics*, **23**, 573–579.

XENOBIOTICA, 2002, VOL. 32, NO. 7, 625–640

Taylor & Francis
healthsciences

Covalent binding of PCB metabolites to lipids: route of formation and characterization

A. MÖRCK†*, G. LARSEN‡ and E. KLASSON WEHLER§

† Department of Environmental Chemistry, Stockholm University, S-106 91 Stockholm, Sweden
‡ USDA, ARS, Bioscience Research Laboratory, Fargo, ND 58105, USA

Received 4 July 2001

1. After an oral dose of ^{14}C-labelled 3,3′,4,4′-tetrachlorobiphenyl (CB-77), the conventional germ-free and bile-duct cannulated male Sprague–Dawley rat excreted approximately 80% of the dose in faeces and/or bile within 3 days.

2. For the germ-free and conventional rat, 15% of the dose was excreted via the faeces as metabolites covalently bound to lipids. Bile-duct-cannulated rats excreted similar amounts of lipid-bound metabolites in the bile. The lipid-bound metabolites appear to be formed in the liver and excreted via the bile, and the microflora did not seem essential for the formation of lipid-bound metabolites.

3. The novel CB-77 metabolites had chemical and physical properties similar to those of lipids with regard to solubility and polarity, as determined by partition characteristics on various chromatographic systems.

4. In addition to identification of hydroxylated CB-77 metabolites, several fatty acid esters of hydroxy-chlorobiphenyls were indicated and one hydroxy-tetrachlorobiphenylol palmitoate was identified, but fatty acid esters were minor metabolites.

5. Approximately 70% of the lipid-bound metabolites were present in the fraction that contained phospholipids. The formation of lipid-bound CB-77 metabolites seems a spontaneous reaction rather than an enzymatically catalysed reaction, as indicated by the large number of different lipid-bound metabolites.

Introduction

Lipophilic organic compounds are generally metabolized to products with higher polarity and water solubility to facilitate excretion. The introduction or uncovering of a functional group or conjugation to an endogenous reactant (usually glucuronic acid or sulphate) can also occur.

Although less frequently reported, conjugation or other binding to lipids also occurs. Xenobiotics having a hydroxy-group or those hydroxylated during metabolism may be conjugated to endogenous carboxylic acids, e.g. fatty acids (Hutson 1982, Fears 1985, Dodds 1995). Examples of this are pentachlorophenol (Ansari *et al.* 1995), tetrahydrocannabinol (Leighty *et al.* 1976, Yisak *et al.* 1987), the 1,1-di(4-chlorophenyl)-2,2,2-trichloroethane (DDT) metabolite 2,2′-di(4-chlorophenyl)-ethanol (DDOH) (Leighty *et al.* 1980) and the asthma drug Budesonid (Tunek *et al.* 1997), which have been observed to form esters with palmitic acid, stearic acid, oleic acid and/or linoleic acid. Fatty acid ester formation has also been shown for ethanol and haloethanols (Kaphalia and Ansari 1989, Bhat and Ansari

* Author for correspondence;
§ Present address: AstraZeneca R&D, S-151 85 Södertälje, Sweden.

Xenobiotica ISSN 0049–8254 print/ISSN 1366–5928 online © 2002 Taylor & Francis Ltd
http://www.tandf.co.uk/journals
DOI: 10.1080/00498250210130573

1990, Treloar *et al.* 1996). The esters are formed by liver microsomal systems (Leighty *et al.* 1980) and have been observed in *in vivo* experiments both retained in tissues and excreted in faeces (Leighty *et al.* 1976). The palmitic acid ester of pentachlorophenol has been reported to be present in human adipose tissue at a concentration of 240 ng g^{-1} lipid weight (Ansari *et al.* 1985). The incorporation of xenobiotics into pathways of lipid biosynthesis has been reviewed by Dodds (1995).

Reports of conjugation of xenobiotics with phospholipids are less frequent. One example is the reaction between phosphatidyl ethanolamine and the reactive electrophilic site of halogenated alkene cysteine conjugates (Hayden *et al.* 1992). Primary aminophospholipids, e.g. phosphatidyl ethanolamine (PE) and phosphatidyl serine (PS), have been shown to form Michael products, Schiffs bases and/or pyrrole derivates with 4-hydroxynonenal, *p*-hydroxyphenylacetaldehyde and glucose (Bucala *et al.* 1993, Guichardant *et al.* 1998, Hazen *et al.* 1999).

Polychlorinated biphenyls (PCBs), ubiquitous environmental pollutants, are mainly metabolized via the same routes as many other aromatic xenobiotics, e.g. via arene oxides to phenolic metabolites, although they may also react with glutathione, eventually resulting in the formation of PCB-methylsulphonyl metabolites (Bakke *et al.* 1983, Safe 1984). In a metabolism study of ^{14}C-labelled 3,3′,4,4′-tetrachlorobiphenyl (CB-77) in mouse, 20% of the dose was reported to be excreted in the faeces as metabolites with characteristics similar to lipids (Klasson Wehler *et al.* 1989). Similar types of metabolites have been observed in the metabolism study of two other PCB congeners, 2,3,3′,4,4′-pentachlorobiphenyl (CB-105) and 2,2′,4,5,5′-pentachlorobiphenyl (CB-101), in mouse and mink (Klasson Wehler *et al.* 1993, 1996). In these latter studies, radiolabelled metabolites in the gel permeation chromatography (GPC) lipid fraction were also identified in tissues. Preliminary characterization of the lipid-bound metabolites obtained from exposure to CB-77 has shown that they cover a wide range of polarity and were only partly hydrolysable under alkaline conditions (unpublished data). The large number of lipid-bound metabolites indicated several and/or random routes of formation that might include random formation via reactive intermediates and/or metabolism by the intestinal microflora.

The intestinal microflora perform important steps in metabolism, such as reduction of nitro-groups to amines (Goldman 1989), deconjugation of glucuronides and sulphates, and also to cleave the C-S bond of cysteine conjugates (Larsen 1988). The intestinal microflora also have an important role for the bioactivation of many carcinogens (Chadwick *et al.* 1992).

The present study aimed to investigate the role of the microflora in the formation of lipophilic CB-77 conjugates/adducts, and the characterization of the lipophilic metabolites. Conventional germ-free and bile-duct cannulated rats were dosed orally with ^{14}C-labelled CB-77. The faeces and bile were collected and analysed for the potential presence of lipid-bound CB-77 metabolites.

Materials and methods

Animals

Three groups of male Sprague–Dawley rats (from Harlan Sprague Dawley, WI, USA), conventional ($n = 4$), germ free ($n = 4$), and bile-duct cannulated ($n = 4$), were dosed orally with ^{14}C-labelled CB-77 (34 μmol kg^{-1}, 1 Ci mol^{-1}). The ^{14}C-labelled CB-77 was dissolved in peanut oil and the dose volume

was 1 ml kg^{-1} bw. The conventional Sprague–Dawley rats and those subjected to bile-duct cannulation weighed approximately 250 g. Bile-duct cannulation was performed as described by Larsen and Bakke (1981). The germ-free rats (190–220 g, males) were obtained from Taconic Farms, Inc. (Germantown, NY, USA) and maintained in a flexible-film isolator (Trexler and Reynolds 1957). The animals were kept in metabolism cages, and urine and faeces were collected daily for 3 days. Bile from the bile-duct cannulated rats was collected at 0–4, 4–12, 12–24, 24–48 and 48–72 h. The radioactivity content was determined in the faeces, urine and bile.

Chemicals

3,3′,4,4′-Tetrachloro-[^{14}C]biphenyl (CB-77), with a specific activity of 15 Ci mol^{-1} and a purity > 95%, was purchased from Sigma Chemical Co. (St Louis, MO, USA). The specific activity was diluted to 1 Ci mol^{-1} with unlabelled CB-77 (> 99%) (Bergman *et al.* 1990). 4-Methoxy-3,3′,4′,5-tetrachlorobiphenyl (4-MeO-tetraCB), 3-methoxy-3′,4,4′,5-tetrachlorobiphenyl (3-MeO-tetraCB) and 4-methoxy-3,3′,4′-trichlorobiphenyl (3-MeO-triCB) were synthesized as described (Bergman *et al.* 1995) and used as standards for the GC/MS analysis of non-conjugated metabolites. 2,3,3′,4,4′,5,5′-Heptachlorobiphenyl (CB-189, synthesized according to Sundström 1973) and 4-OH-2,3,3′,4′,5,5′,6-heptachlorobiphenyl (Bergman *et al.* 1995) were used as internal standards in the GC/MS analysis of non-conjugated metabolites.

The lipid standards phosphatidyl choline (PC), phosphatidyl ethanolamine (PE), phosphatidyl inositol (PI), phosphatidyl serine (PS), phosphatidic acid (PA), lysophosphatidyl choline, sphingomyelin, neutral lipids mixture, fatty acid methyl ester mixture and cholesterol were all purchased from Sigma, and trilaurin was from Eastman Kodak Co. (Rochester, NY, USA).

Solvents and chemicals were of pro-analysis (p.a.) quality, HPLC grade or of pesticide grade, unless otherwise stated. Hexane (Fison, Loughborough, UK), dichloromethane (Riedel de Haen, Seelze, Germany), methanol and chloroform (Merck, Darmstadt, Germany), and ammonia AnalR (BDH Chemicals, Rathburn, UK) were of p.a. quality or pesticide grade. Hydrochloric acid (37%) was obtained from Riedel de Haen; the citrate-hydrochloric acid buffer (pH 4) was from Merck. Diazomethane was synthesized according to Fieser and Fieser (1967). For HPLC analysis, hexane and 2-propanol were used (p.a. grade, Merck). Silica gel 60 (particle size 0.063–0.200 mm, 70–230 mesh) was from Merck.

Thin-layer chromatography (TLC) was performed on straight-phase silica gel TLC plates (silica gel 60 F-254, 0.25 mm thickness) obtained from Merck, using chloroform/methanol/ammonia (65/25/5 v/v/v) as the mobile phase. The plates were developed in iodine vapour to detect lipids, and the radioactivity was detected using a Raytest RITA 3200 TLC scanner (gas: 10% methane in argon, counting time 1800 s) (Raytek Scientific, Sheffield, UK).

Synthesis of fatty acid biphenylol esters (FABEs) 4-hydroxy-3,3′,4′,5-tetrachlorobiphenyl palmitic acid and stearic acid esters, 4-hydroxy-2,3,3′,4′-tetrachlorobiphenyl palmitic acid, stearic acid and lauric acid esters were prepared. The biphenylol obtained by demethylation of the corresponding MeO-tetraCB (Bergman *et al.* 1995) and an excess of the fatty acid (10–26-fold) were dissolved in pyridine. Thionyl chloride was added and the reaction mixture stirred for 18 h at room temperature. The product was extracted with hexane, washed with water and isolated by liquid chromatography on a silica gel column (silica gel, particle size < 0.063 mm; Merck) with dichloromethane/hexane (2/1 v/v) as the mobile phase. All esters were synthesized under the same conditions except the two palmitic acid esters where an excess of palmitoyl chloride (fivefold) was used instead of palmitic acid and thionyl chloride, and the reagents were refluxed for 1 h. The identities of the products were verified by mass spectrometry on a Finnigan TSQ Instrument (ThermoQuest, Bremen, Germany) by a direct inlet probe, operated at electronic ionization (EI) mode. The ion source temperature was 150 °C and the probe was programmed from 50 to 350 °C within 2 min and kept at 350 °C for 5 min. The molecular ion for tetrachlorobiphenylol palmitic acid ester was observed at m/z 544 with fragments for the palmitic acid, m/z 239, and for the tetrachlorobiphenylol, m/z 306. For tetrachlorobiphenylol stearic acid ester, the molecular ion was m/z 572, with a fragment at m/z 267 for stearic acid and at m/z 306 the tetrachlorobiphenylol. For tetrachlorobiphenylol lauric acid ester, the molecular ion was m/z 488 with ions at m/z 183 for the lauric acid and m/z 306 for the tetrachlorobiphenylol fragments, respectively. The products were purified on TLC using dichloromethane/hexane (3/1 v/v) as the mobile phase, with resulting purities of 92–99%.

Instruments

Gel permeation chromatography (GPC) was performed using Bio Beads SX-3 (200–400 mesh, 50 g) from Bio-Rad (Richmond, CA, USA) and hexane/dichloromethane (1/1) as the mobile phase (Klasson Wehler *et al.* 1987). The samples were filtered (0.45 µm MILLEX filter unit, Millipore Corporation, MA, USA) before injection. The GPC column was connected on-line with a Gilson 112 UV/VIS detector (254 nm) and a radioactivity detector (Packards Flow One 500). The radiodetector was equipped with a splitter and a flow cell (500 µl), using Ultima Flo M (Packard Instrument, Meriden, CT, USA) as the scintillator liquid. Of the effluent, 10% was split to the radiodetector.

Analysis of isolated lipid-related metabolites was performed on straight-phase silica (SP)-HPLC with a Shimadzu LC-4A pump from Schimadzu Corporation (Kyoto, Japan) equipped with a spectrophotometric detector SPD-2AS (Schimadzu), an Evaporate Light Scattering Detector (ELSD) (DDL 21, Cunow, Lergy, France) and a radioactivity detector (GPC). An AS3W-1516 column, protected by a precolumn S3W-103C from Hichrom (Berkshire, UK) was used. The mobile phases consisted of hexane (A) and hexane/2-propanol/water (B; 3/4/0.7 v/v/v). The mobile phases were eluted in a gradient starting with 0% B for 5 min, linearly increased to 50% B after 15 min, further linearly increased to 100% after 45 min and held at 100% for 10 min.

The gas chromatography/mass spectrometry (GC/MS) analyses of fatty acid esters were performed on a Finnigan GCQ instrument with a Varian 3400 GC equipped with a DB-5HT capillary column (30 m × 0.25 mm i.d., 0.1 μm film, J&W Scientific, Folsom, CA, USA). Helium was used as the carrier gas. The oven temperature was programmed; 80 °C (1 min), 20 °C min^{-1} to 360 °C (6 min). The ion source was 180 °C. Samples were injected in the splitless mode on a split-splitless injector, at an injector temperature of 260 °C. The instrument was operated in the positive chemical ionization (PCI) mode. Scanning range was m/z 450–650.

The GC/MS analyses of non-conjugated metabolites were performed on a Finnigan ITS 40 instrument with a Varian 3400 GC equipped with a CP-Sil 8 CB (low bleed/MS DF 0.25) capillary column (30 m × 0.25 mm i.d., Chrompack International, Middelburg, The Netherlands). Helium was used as the carrier gas. The oven temperature was programmed; 80 °C (2 min), 10 °C min^{-1} to 270 °C (20 min). Samples were injected in the splitless mode on a split-splitless injector, at an injector temperature of 260 °C. The mass spectrometer was operated at EI energy of 70 eV and an ion source temperature of 210 °C. Mass spectra were collected at a speed of 1 scan s^{-1}, scanning for ions in the range of m/z 50–400.

Radioactivity measurements were performed on a Wallac 1409 using emulsifier scintillator 299 (Packard Instrument, Meriden, CT, USA) and Opti Scint Hisafe (Wallac Oy, Turku, Finland) as scintillation cocktails for lipophilic samples. Aqueous samples were mixed with Optiphase II (Wallac Oy). Solid samples (approximately 20 mg dry weight) were moistened with 100 μl water for 30 min before digestion in Soluene-350 (Packard Instrument, 1 ml) for 4 h, or until fully dissolved. Hydrogen peroxide/2-propanol (2/3 v/v 1 ml) was added and the samples stored in darkness for 2 h before measurement. The scintillation counter's function for automatic compensation for chemiluminescence was applied.

Extraction

A scheme of the sample clean up applied in this study is shown in figure 1. Faecal and bile samples from individual rats within each treatment group were analysed separately, but at a later stage, samples were pooled as indicated.

Faeces. Individual faecal samples were freeze-dried and ground before extraction in a Soxhlet-apparatus with chloroform/methanol (2/1 v/v 200 ml) for at least 15 cycles (Klasson Wehler *et al.* 1989). The solvent was evaporated and the lipid weight determined. The radioactivity content in extracts and extract residues were determined.

The extracted compounds were fractionated by GPC. The UV and radioactivity signals were recorded and the fractions collected accordingly – generally one fraction contained lipids (GPC-lipid fraction, 0–132 ml) and one was essentially a lipid-free fraction containing CB-77 and non-conjugated metabolites (GPC-metabolite fraction, 132–200 ml). The GPC-metabolite fractions were pooled by day for each group and internal standards were added. The GPC-metabolite fractions were partitioned into neutral and phenolic compounds as described by Klasson Wehler *et al.* (1996). The phenolic fraction was derivatized with diazomethane and both the neutral and phenolic fractions were analysed by GC/MS. The neutral and phenolic metabolites were quantified by comparing their GC/MS peak area with that of the internal standards peak area. The GPC-lipid fractions were analysed individually by TLC and then pooled by group and day.

Bile. After determination of ^{14}C content, bile samples were pooled groupwise for each sample collection time point. The pooled bile samples were diluted with one volume of citrate-hydrochloric acid buffer (pH 4) and the pH adjusted to 3 with hydrochloric acid (4 M). Lipophilic material was extracted with dichloromethane (three times). The lipid weight and radioactivity content was determined. The extracts were fractionated by GPC and analysed as described above.

Lipid class separation

The pooled GPC-lipid fractions from bile and faeces, respectively, were separated into lipid classes on a silica gel column using a succession of solvents of different polarity. The method used was a slight modification of that of Radwan (1984). The lipids were eluted with hexane (silica-1), chloroform (silica-2), chloroform/methanol (1/1 v/v, silica-3) and finally methanol (silica-4). Ten void volumes of solvent

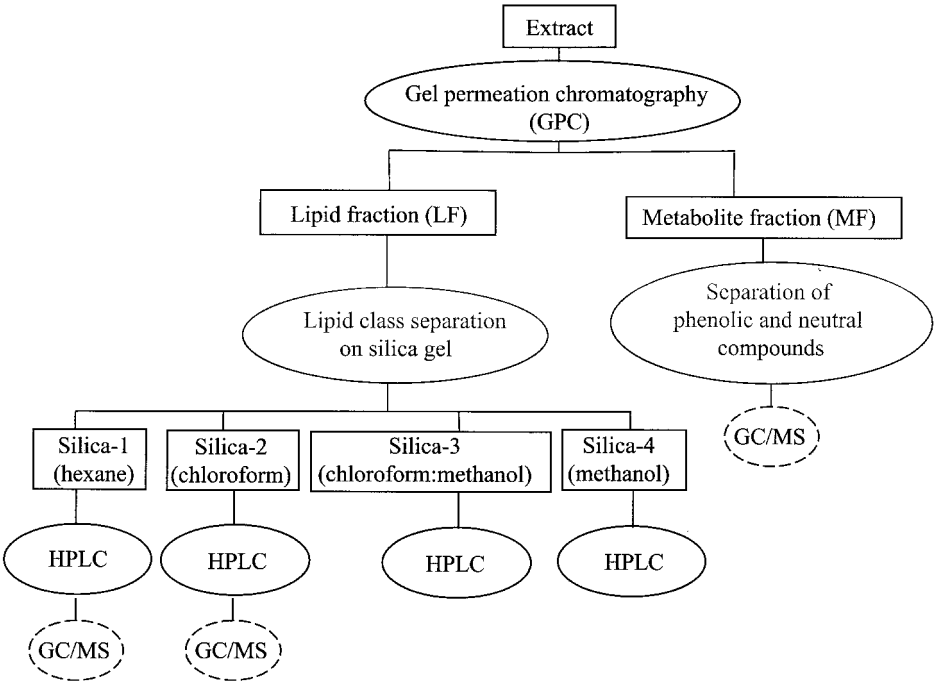


Figure 1. General outline of the clean up of faecal and bile samples.

were generally used, except for the bile samples where only five void volumes were needed for silica-1 and silica-2. Separation of a mixture of lipid standards (PC, PE, PI, PS PA, lysophospatidyl choline, cholesterol, fatty acid methyl ester and trilaurin) and analysis (by TLC developed with I_2 and by monitoring of ^{14}C with a radioscanner [RITA], by HPLC analysis of the samples and by comparison with lipid standards) of the collected fraction from the samples verified the separation. Silica-1 contained mainly fatty acid esters and/or cholesterol esters (TLC R_f = 0.9–1.0), silica-2 contained neutral lipids such as triacylglycerol (TLC R_f = 0.35–0.85), and silica-3 (TLC R_f = 0.2–0.45) and silica-4 (TLC R_f = 0–0.35), contained phospholipids.

Hydrolysis

Aliquots of faecal GPC-lipid fractions from conventional rats were subjected to alkaline hydrolysis according to the method of Christie (1989). Potassium hydroxide (1 m) in ethanol (95%) was added to the lipid sample and stirred overnight at room temperature. The reaction mixture was extracted with hexane/diethyl ether (1/1, three times) and then acidified with hydrochloric acid (6 M) and re-extracted with hexane/diethyl ether (1/1, three times). The ^{14}C content in the organic extracts and the remaining aqueous phase were determined and the second extract fractionated by GPC into a lipid and a metabolite fraction. The latter fractions were analysed by GC/MS.

Results

Excretion

Faeces was the dominant route of excretion for both conventional and germ-free rats, with 80% of the CB-77 dose excreted within 3 days (table 1). The bile-duct cannulated rats excreted 46% of the dose in the faeces and 32% of the dose in the bile, but there were large individual variations for the bile excretion (19–45%). Urinary excretion was low for all groups, $1.2 \pm 0.2\%$ of the dose from the conventional rats, $1.6 \pm 0.3\%$ from the germ-free rats and $0.5 \pm 0.03\%$ from the bile-duct cannulated rats. Urine was not further analysed in this study.

Table 1. Daily excretion of ^{14}C (% of the dose) in the faeces and bile, and the relative distribution of ^{14}C for different types of metabolites from conventional (C), germ free (GF) and bile-duct cannulated (BD) rats after oral dosing of 3,3′,4,4′-tetrachloro-[^{14}C]biphenyl.

			Relative distribution of ^{14}C			
Sample ($n = 4$)	Time point after dose	% of dose	Non-extracted ^{14}C	Lipid bound ^{14}C	Non-conjugated ^{14}C	Ratio of non-conjugated ^{14}C/lipid bound ^{14}C
C rats, faeces	Day 1	41.6 ± 6.4	40.5 ± 0.7	13.0 ± 0	46.5 ± 0.7	3.6
	Day 2	28.4 ± 6.6	7.7 ± 9.3	25.7 ± 4.2	66.7 ± 5.1	3.0
	Day 3	9.9 ± 2.0	17.5 ± 3.7	23.8 ± 2.5	58.8 ± 4.9	2.6
GF rats, faeces	Day 1	48.7 ± 5.7	46.8 ± 6.4	13.3 ± 6.7	40.0 ± 7.5	3.8
	Day 2	22.9 ± 2.3	43.0 ± 8.2	31.7 ± 6.5	25.7 ± 3.1	0.7
	Day 3	8.6 ± 1.2	47.7 ± 4.7	19.7 ± 3.8	32.7 ± 3.1	1.7
BD rats, faeces	Day 1	35.6 ± 2.6	14.5 ± 7.8	3.0 ± 1.4	82.5 ± 6.4	28
	Day 2	9.0 ± 6.0	1.5 ± 1.9	9.3 ± 6.0	89.3 ± 7.9	13
	Day 3	1.6 ± 1.5	40.0 ± 49.5	10.5 ± 2.2	49.5 ± 51.6	8.5
BD rats, bile†	0–4 h	0.6 ± 0.3	n.a.	n.a.	n.a.	n.a.
	4–12 h	16.1 ± 9.2	45	35	20	0.6
	12–24 h	8.2 ± 2.6	26	48	26	0.5
	24–48 h	5.6 ± 0.7	18	56	17	0.3
	48–72 h	1.8 ± 0.1	n.a.	n.a.	n.a.	n.a.

n.a., not analysed.
† Bile samples were pooled before extraction

Extraction and GPC fractionation

In faeces from conventional and bile-duct cannulated rats, the major part of the radioactivity was extracted with chloroform/methanol, whereas about 50% was extracted from the germ-free rat faeces and almost 50% of the ^{14}C remained in the faecal residue at all time points (table 1). No attempts were made to extract other than lipophilic material from the faeces and it can therefore not be excluded that the non-extracted ^{14}C to some extent correspond to water-soluble metabolites. In a previous study, 60–75% of the radioactivity in faeces from mice dosed with CB-77 was extracted by the Soxhlet method used here and an additional 15–30% could be extracted with boiling 0.2 M $(NH_4)_2CO_3$ in ethanol. No attempts were made to identify the additionally extracted material (Klasson Wehler *et al.* 1989).

The faeces extracts were fractionated by GPC and the two fractions collected, lipids (GPC-lipid fraction) and the fraction containing parent CB-77 and non-conjugated metabolites (GPC-metabolite fraction), both contained radiolabelled material though the relative amounts varied as indicated by the GPC-metabolite fraction to GPC-lipid fraction ratio in table 1. The major part of the faecal ^{14}C was found in the GPC-metabolite fractions and all samples contained ^{14}C also in the GPC-lipid fractions. The cumulated ^{14}C in the GPC-lipid fractions from days 1 to 3 were similar for conventional and germ-free rats, 15% of the dose. For the faecal samples from bile-duct cannulated rats only about 2% of the dose was obtained in the GPC-lipid fraction (table 2).

More than 95% of the ^{14}C excreted in the bile was collected between 4 and 48 h after dosing. The major portion (55–74%) of the ^{14}C in the bile was lipophilic enough at pH 3 to be extracted with dichloromethane, and the relative amount of ^{14}C in this lipophilic fraction increased with time (GPC-metabolite fraction +

Table 2. Total amount (% of dose) of different metabolite types excreted in the faeces and bile (data from days 1–3 and 4–48 h, combined), after an oral dose 3,3′,4,4′-tetrachloro [^{14}C]biphenyl (CB-77) to conventional (C), germ free (GF) and bile-duct cannulated (BD) rats.

Sample	CB-77 and/or non-conjugated metabolites (% of the dose)	Non-extracted metabolites (% of the dose)	Lipid-bound metabolites (% of the dose)
C rats (faeces) days 1–3	44	22	15
GF rats (faeces) days 1–3	28	39	15
BD rats (faeces) days 1–3	39	6.2	1.8
BD rats (bile) 4–48 h	6.3	10	13

GPC-lipid fraction in table 1). The water-soluble metabolites present in the aqueous phase were not further analysed in this study.

A large part (35–56%) of the ^{14}C in the bile extract eluted in the GPC-lipid fraction, and thus represented metabolites with similar properties as the lipids with regard to lipophilicity and size (table 1, 2). About 20% of the total ^{14}C in the bile represented non-conjugated metabolites and/or parent CB-77 (GPC-metabolite fraction) (table 2).

Characterization of ^{14}C in the lipid fractions

According to TLC analysis, the GPC-lipid fractions from conventional and germ-free rat faeces both contained several ^{14}C-labelled compounds with large variations in polarity (R_f = 0.01–0.9, data not shown). The radiolabelled material was most abundant in the region of phospholipids (R_f = 0.03–0.3). There were no apparent differences in the relative distribution by TLC between the germ-free and conventional rats.

The faecal GPC-lipid fractions, pooled daywise for germ-free and conventional rats, respectively, were separated into lipid classes. The relative distribution of ^{14}C in the different lipid classes was similar within each group of rats and unrelated to the day of excretion (data not shown). The data on distribution of ^{14}C in the lipid classes for the GPC-lipid fractions from faeces days 1–3 were therefore combined and the result is shown in table 3. Approximately 70% of the radiolabelled material from both conventional and germ-free rats were associated with polar lipids, e.g. phospholipids eluting in silica column fractions 3 and 4 (silica-3 and silica-4) (table 3). Only 1% of the ^{14}C from GPC-lipid fraction from conventional rats, and 9% from germ-free rats, eluted with hexane (silica-1) – the fatty acid ester fraction.

The GPC-lipid fraction from bile also contained mainly polar radiolabelled compounds (table 3) and HPLC/ELSD analysis revealed that PC dominated in both silica-3 and silica-4 (figure 2). The radiolabelled metabolite(s) in these two fractions eluted as a narrow peak with a retention time between PE and PC, whereas the radiolabelled material in silica-1 and approximately 50% of the radioactivity in silica-2 eluted with the solvent front. Reference compounds of fatty acid biphenylol esters, triglycerides and cholesterols also eluted with the front.

GC/MS analysis of silica-1 and silica-2 showed the presence of approximately six compounds with characteristics indicating FABEs. Most were present in trace amounts but one metabolite was present in concentrations allowing a full scan

Table 3. Relative distribution of lipid-bound ^{14}C in different silica column fractions in samples from conventional (C), germ free (GF) and bile-duct cannulated (BD) rats. Silica-1 and 2 represent non-polar lipids (fatty acid esters and triacylglycerols), and silica-3 and 4 polar lipids (phospholipids).

	Lipid-bound metabolites (% of the dose)†	Relative distribution of lipid-bound metabolites			
		Silica 1	Silica 2	Silica 3	Silica 4
C rats (faeces) days 1–3	15	1	29	38	32
GF rats (faeces) days 1–3	15	9	24	36	31
BD rats (bile) 4–48 h	13	< 1	4	13	82

† Mean from table 1.

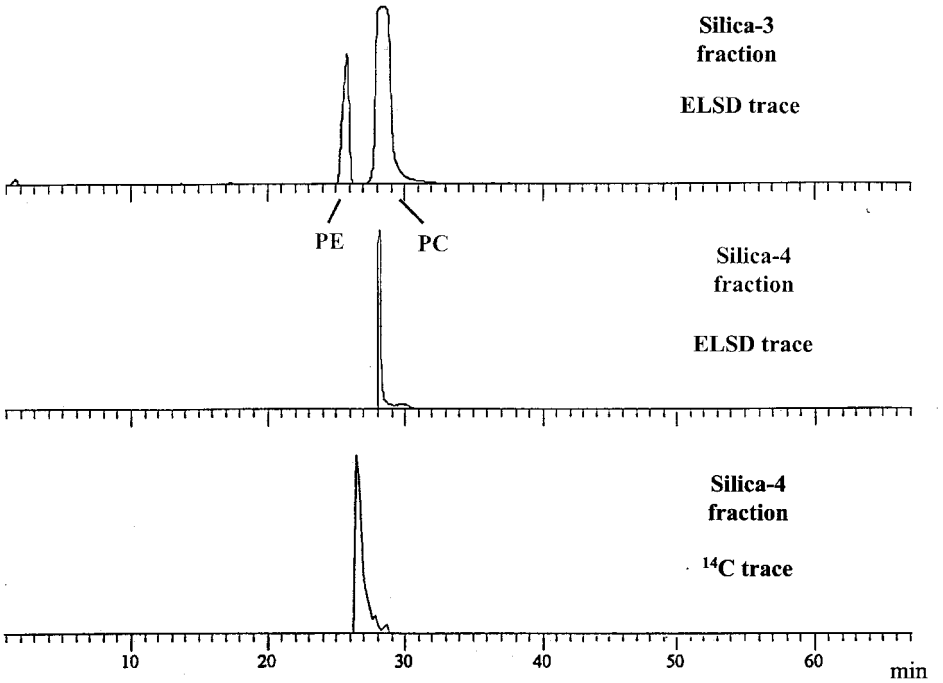


Figure 2. HPLC chromatograms of the polar lipid fractions silica 3 (upper) and silica 4 fractions (middle and lower) from bile extracts. The upper and middle traces were detected with a light-scattering detector, the lower trace by a radioactivity detector. The retention times for the phospholipids phosphatidylethanolamine (PE) and phosphatidylcholine (PC) standards are indicated in the chromatogram.

spectrum. A molecular ion at m/z 545, with an isotope pattern consistent with four chlorine atoms, suggested a hydroxylated tetrachlorobiphenyl palmitic acid ester (figure 3). The MS data were consistent with those of the synthesized hydroxylated tetrachlorobiphenyl palmitic acid esters but the retention times differed. Two OH-tetraCB metabolites are formed from CB-77, 4-OH-tetraCB and 5-OH-tetraCB (see below) (figure 4). Only 4-OH-tetraCB was available for synthesis of fatty acid esters. The observed tetrachlorobiphenylol palmitic acid ester may thus represent a conjugate of 5-OH-tetraCB. None of the indicated metabolites in the GC/MS chromatograms had retention times identical to any of the synthesized standards and may thus be isomeric metabolites.

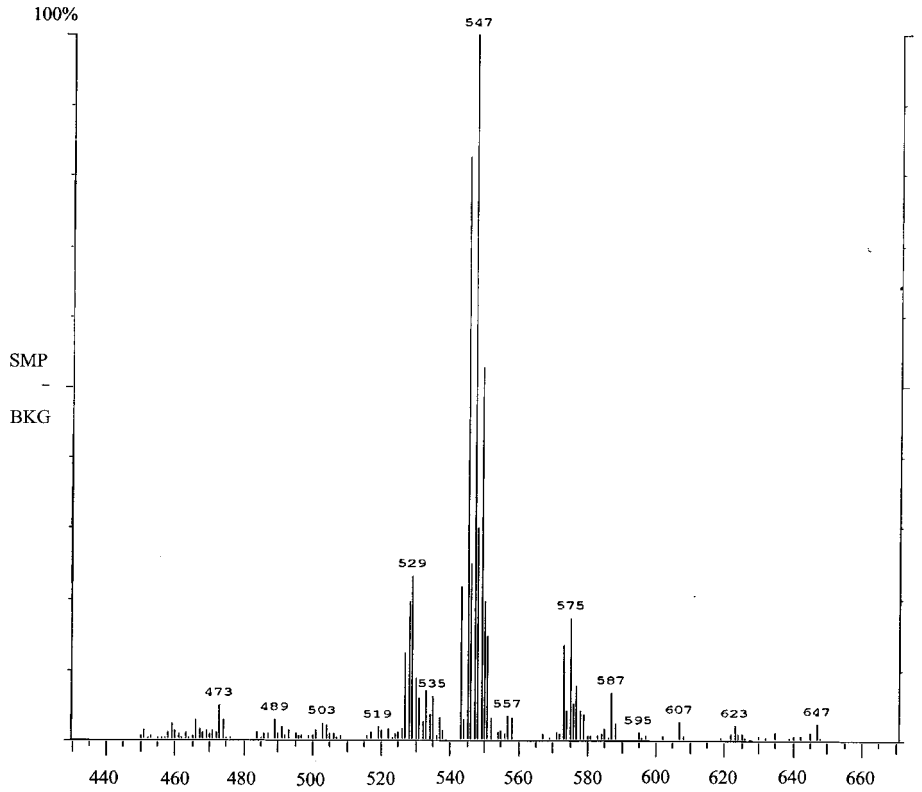


Figure 3. GC/MS-spectra (positive chemical ionization) of a metabolite in the non-polar fraction (silica-1) found in bile extracts. A hydroxy tetrachlorobiphenyl palmitic acid ester is the proposed structure.

GC/MS analysis of non-conjugated metabolites

According to GC/MS analysis of faecal GPC-metabolite fraction day 1 samples from the conventional rats, parent CB-77 constituted approximately 55% of the identified compounds in this fraction (on a molar basis) (table 4), and this corresponded to approximately 11% of the dose. The major metabolites in the GPC-metabolite fraction were hydroxylated, 5-OH-3,4,3′,4′-tetraCB (5-OH-tetraCB), 4-OH-3,5,3′,4′-tetraCB (4-OH-tetraCB) and 4-OH-3,3′,4′-triCB (4-OH-triCB), identified as their methyl derivatives (table 4). Trace amounts of a dihydroxylated tetraCB metabolite were also observed. The metabolites found in this study are shown in figure 4.

For the germ-free rats, parent CB-77 constituted approximately 88% of the GPC-metabolite fraction day 1, which corresponded to approximately 17% of the dose. As for conventional rats, the concentrations of CB-77 were much lower on days 2 and 3. The same hydroxylated metabolites were observed as in the conventional rats (table 4).

The faecal GPC-metabolite fraction from the bile-duct cannulated rats contained mainly parent CB-77 (table 4). On the first day, only parent CB-77 could be detected, but in days 2 and 3, small amounts of 5-OH-tetraCB and 4-OH-tetraCB were also found. In the bile, only traces of parent CB-77 were detected and the

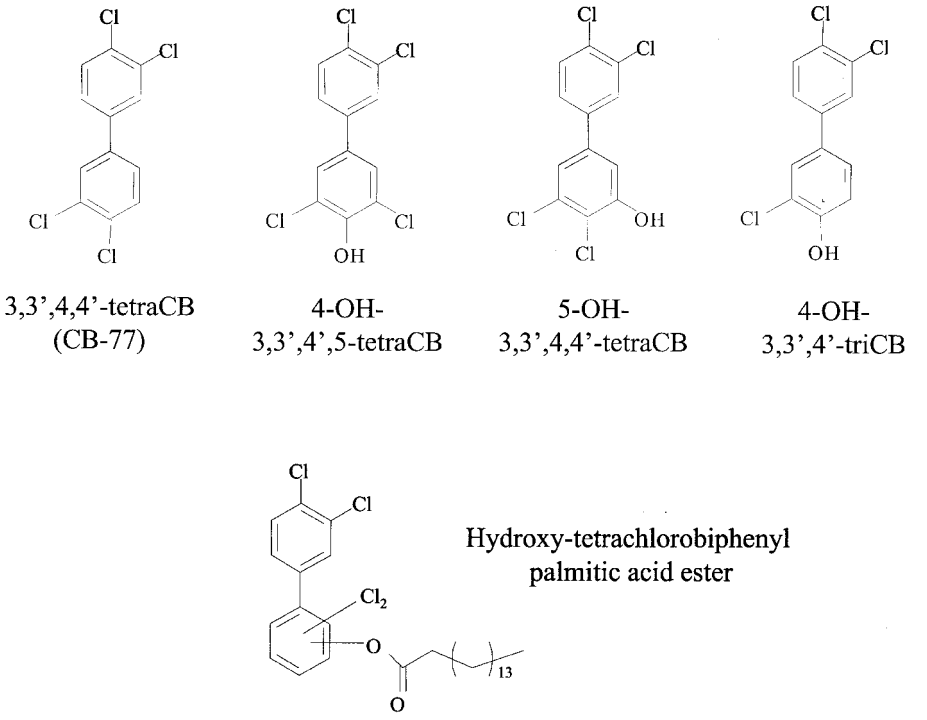


Figure 4. Structures of 3,3′,4,4′-tetrachlorobiphenyl (CB-77) metabolites found by GC/MS.

Table 4. Relative distribution of 3,3′,4,4′-tetrachlorobiphenyl (CB-77) and phenolic metabolites, 4-hydroxy-3,3′,4′-trichlorobiphenyl (4-OH-triCB), 5-hydroxy-3,3′,4,4′-tetrachlorobiphenyl (5-OH-tetraCB) and 4-hydroxy-3,3′,4′,5-tetrachlorobiphenyl (4-OH-tetraCB), in GPC metabolite fractions from faeces and bile. The fraction of dose in the analysed sample is also given.

Sample	Time point after dose	Non-conjugated metabolites (% of the dose) ($n = 4$)†	Relative distribution of identified metabolites in the non-conjugated metabolites fraction				
			CB-77 (%)	4-OH-triCB (%)	5-OH-tetraCB (%)	4-OH-tetraCB (%)	Ratio of 5-OH-tetraCB/4-OH-tetraCB
C rats (faeces)	day 1	19	55	1	38	6	6.3
	day 2	19	4	2	68	25	2.7
	day 3	6	2	2	60	36	1.7
GF rats (faeces)	day 1	19	88	0.3	8	3	2.5
	day 2	6	28	n.d.	62	10	6.2
	day 3	3	3	n.d.	17	79	0.2
BD rats (faeces)	day 1	29	100	n.d.	n.d.	n.d.	—
	day 2	8	94	0.2	4	2	2.0
	day 3	1	96	n.d.	4	n.d.	—
BD rats (bile)	4–12 h	20	0.6	4	73	22	3.3
pooled	12–24 h	26	0.7	4	44	51	0.9

n.d., Not detected

† Mean value from table 1.

same phenolic metabolites as determined in faecal samples dominated in the sample.

Hydrolysis of ^{14}C-labelled material in the GPC-lipid fraction

After alkaline treatment of aliquots of faecal GPC-lipid fraction from conventional rats from day 2, 98% of the radioactivity remained in the aqueous solution. After acidification of the aqueous phase, 61% was extracted. Thus, 37% of the radioactivity remained in the aqueous phase at both alkaline and acidic pH. Only 24% of the total radioactivity was obtained in the metabolite-fraction after GPC of the second extract and almost 40% remained lipophilic and large enough to elute in the lipid-fraction. However, the GPC elution profile (radioactivity trace) had changed slightly compared with non-hydrolysed material (data not shown).

Phenolic metabolites were found by GC analysis of the GPC-metabolite fraction from hydrolysed GPC-lipid fraction. The dominating metabolite was 4-OH-tetraCB (94% of the totally identified compounds in the chromatogram) followed by 5-OH-tetraCB (6%). The 5-OH-tetraCB to 4-OH-tetraCB ratio was 0.07 after hydrolysis, compared with 2.3 in non-hydrolysed GPC-metabolite fraction (table 4), indicating a preference of the 4-OH-tetraCB for lipid binding. Traces of CB-77 and OH-triCB were also found.

Discussion

In the present study, novel types of lipophilic CB-77 metabolites have been characterized and the role of the intestinal microflora for their formation investigated. The characterization included partitioning between organic solvent and aqueous solutions, size exclusion chromatography (GPC) and separation based on polarity (lipid class separation, straight phase HPLC).

The GPC method to separate lipids from CB-77 and its non-conjugated metabolites is mainly based on size exclusion and is frequently used as a lipid removal step for analysis of lipophilic xenobiotics, including their metabolites (Steinwandter 1982, Norstrom *et al.* 1986, Klasson Wehler *et al.* 1987). In the present study, radioactivity corresponding to approximately 15% of the dose, or 25% of the extracts (from conventional rat faeces) (table 2), eluted together with the lipids, whereas parent compound and phenolic metabolites eluted in a separate fraction (GPC-metabolite fraction) with a longer elution time. The method is robust and neither a roughly treated mixture of a radiolabelled pentachlorobiphenyl standard and a lipid extract (adipose tissue from an unexposed animal), nor urine extract from the present study, assumingly containing aqueous conjugates (Bakke *et al.* 1983, Klasson Wehler *et al.* 1989), resulted in radioactivity co-eluting in the lipid fraction (data not shown). The presence of radioactivity in the lipid fraction was therefore taken as an indication that CB-77 metabolites were present in this fraction and that their properties were similar to those of lipids, e.g. lipid-bound metabolites.

Faeces have previously been shown to be the major excretion route for PCB congeners (Bergman *et al.* 1982, Bakke *et al.* 1983, Klasson Wehler *et al.* 1989, 1993, 1996). PCB metabolites have also been shown to be substrates for intestinal microflora metabolism, eventually resulting in lipophilic and persistent methyl-

sulphonyl metabolites (Bakke and Gustavsson 1986). We therefore compared the formation of lipid-bound metabolites in germ-free, conventional and bile-duct cannulated rats. For conventional and germ-free rats, 80% of the dose was excreted in faeces within 3 days (table 1) and for both groups, approximately 19% of the faecal excreted radioactivity, or 15% of the dose, was bound to lipids (table 2). The intestinal microflora was thus not essential for the formation of the lipid-bound metabolites.

In rats lacking microflora, the proportion of non-extractable radioactivity was higher than for conventional rats. This is likely to be, at least in part, due to covalent binding to macromolecules. However, the non-extracted ^{14}C could also consist of water-soluble metabolites since the extraction method not was designed to extract water-soluble material (Klasson Wehler *et al.* 1989). The intestinal microflora are capable of deconjugating a number of biliary metabolites such as glucuronic, sulphate and cysteine conjugates (Larsen 1988), and it is also possible that other conjugates, e.g. fatty acid esters, are hydrolysed by the microflora. Lack of microflora could therefore result in an increased excretion of water-soluble and lipophilic conjugates in faeces. The larger relative amount of ^{14}C in silica-1 from the germ-free rats compared with that from conventional rats (table 3) could thus to some extent be due to fatty acid esters of biphenylols.

Lipid-bound metabolites were found in the bile, but only in trace amounts in the faeces, from the bile-duct cannulated rats. The amounts excreted in bile were similar to those excreted from conventional and germ-free rats, close to 13% of dose (table 1). It thus seems clear that the lipid-bound metabolites of CB-77 were formed in the liver and subsequently excreted via the bile to faeces. Binding of xenobiotics to lipids, e.g. formation of fatty acid esters of 2,2′-di(4-chlorophenyl)-ethanol (DDOH), tetrahydrocannabinol, ethanol, haloethanols and Budesonide are formed *in vitro* by the microsomal systems, but also *in vivo* followed by excretion via faeces (Leighty *et al.* 1976, 1980, Leighty and Fentiman 1981, Treloar *et al.* 1996, Tunek *et al.* 1997). Xenobiotics may also be incorporated in the biosynthesis of several lipid classes, as has been reviewed by Dodds (1995).

Further characterization of the lipid-bound metabolites in the present study demonstrated that the polarity of the metabolites varied from non-polar, a minor part, to a polarity similar to phospholipids (table 3). This suggests that the formation route is non-specific, takes place via reactive intermediates and/or that several pathways exist. Potential fatty acid esters of hydroxylated CB-77 metabolites would be obtained in the non-polar silica-1 fraction (table 3). CB-77 forms several hydroxylated metabolites (figure 4) (Yoshimura *et al.* 1987, Klasson Wehler *et al.* 1989, Koga *et al.* 1990) and conjugation to fatty acids is thus possible. One fatty acid ester was interpreted as a hydroxylated tetrachlorobiphenyl palmitic acid ester by GC/MS (figure 3). Three isomeric phenolic metabolites are formed (figure 4) and all three can theoretically form FABEs. Two FABEs, 4-hydroxy-3,3′,4′,5-tetrachlorobiphenyl palmitic and stearic acid ester, were available as reference compounds but none had the same relative retention time as the identified FABE metabolite. It is therefore proposed that the fatty acid conjugate observed is 5-OH-3,3′,4,4′-tetrachlorobiphenyl palmitic acid ester, as the 5-OH-3,3′,4,4′-tetraCB is the remaining possible OH-tetraCB isomer. Further studies are in progress to identify the metabolites in the non-polar fraction.

The major parts of the lipid-bound metabolites in faecal and bile samples were highly polar and co-eluted with phospholipids from the silica gel column (in the

silica-3 and silica-4 fractions) (table 3). HPLC analysis of the bile samples and comparison with reference compounds confirmed the presence of mainly PC and PE in these fractions and showed that a radiolabelled compound, present in both the silica-3 and silica-4 fractions, eluted between PE and PC (figure 2).

Reactions between phospholipids and xenobiotics may occur either by a nucleophilic reaction by the amine on the head group of PE or at an electrophilic site of the xenobiotic, such as has been reported by Hayden *et al*. (1992) for cysteinyl conjugates of halogenated alkenes. Another type of reaction is exchange of the fatty acid ester on the glycerol by a carboxylic acid group on the xenobiotic, as reported for several benzoic acids and 2- and 3-substituted propanoic acids. A third reaction is displacement of the headgroup and formation of a xenobiotic phosphate ester. This latter reaction has been reported for ethanolamine (Dodds 1995).

Two of these reactions seem possible in this case; (1) the reaction of a lipid nucleophile, e.g. the PE amine, with an electrophilic position on a CB-77 metabolite, (2) the reaction between a hydroxylated metabolite and the phosphate group. CB-77 is metabolized via an arene oxide, as evidenced by the 1,2-shifted metabolite 4-OH-tetraCB (Jerina and Daly 1974, Klasson Wehler *et al*. 1989, Koga *et al*. 1990). The large number of different lipid-bound metabolites indicates a spontaneous reaction rather than an enzymatically catalysed reaction. In addition, the results of the hydrolysis of the compounds in the lipid fractions indicate that several types of reactions occur. A comparably large fraction of the hydrolysed material was obtained in the GPC-lipid fraction also after hydrolysis, indicating that the CB-77 metabolite remained firmly bound to the lipid, by a non-ester bond.

An alternative reactive intermediate could be a quinone-like structure as previously reported for several other PCB congeners (Amaro *et al*. 1996). Such reactions have been suggested for the formation of protein adducts of 2,2′,5,5′-tetrachlorobiphenyl (CB-52), where a quinonoid metabolite reacts in a Michael addition and covalently binds to lipoproteins (Lin *et al*. 2000). PCB-derived quinones of mono- and di-chlorinated biphenyls have been reported to react with both nitrogen and sulphur nucleophiles in the cell (Amaro *et al*. 1996). Dihydroxylated metabolites of CB-77 have been indicated in the present study and were previously identified (Klasson Wehler *et al*. 1989).

A large fraction (37%) of the hydrolysed aliquot also remained in the aqueous phase at both acidic and alkaline pH. If a biphenylol phosphate ester had been formed, it likely would survive alkaline treatment (Dawson 1984, Evstigneeva 1993) and would be expected in the aqueous phase. A substitution reaction of the phospholipid polar head group has been reported to occur for several xenobiotics, although so far generally involving smaller molecules, such as halogenated alkenes (Hayden *et al*. 1992). Further structural analyses of these metabolites are in progress, which require the development of a new analytical mass spectrometric method. In the present case, although the reaction may have occurred by substitution of the polar head group by a hydroxylated metabolite, an attack of phosphate-oxygen on a reactive intermediate, e.g. the arene oxide is also possible. The 4-hydroxylated isomer predominates after hydrolysis of the lipid fraction. The difference in ratio of the 5- and 4-hydroxylated isomer in the hydrolysed material compared with the metabolites in the GCP-metabolite fraction is notable. The 4-OH-substituted metabolite dominates also in the GPC-lipid fraction, with

the 5-OH-substituted metabolite virtually absent in the hydrolysed material. This seems to indicate that the arene oxide plays an important role in the binding to lipids.

Lipid conjugation has also been detected in the metabolism of other PCB congeners although these have not been further characterized (Klasson Wehler *et al*. 1993, 1996, unpublished results). In metabolism studies of 2,2′,4,4′-tetrabromodiphenyl ether (BDE-47) and polychlorinated naphthalenes (PCNs) lipid-bound metabolites have also been observed (Örn and Klasson Wehler 1998, unpublished data). The relative amounts of lipid-bound material in these studies varies from 2% (BDE-47) to 42% (PCN) of excreted ^{14}C. The formation of lipid-bound metabolites may thus be a general metabolic route for xenobiotics, such as environmental organic contaminants.

The reaction between lipophilic environmental contaminants and endogenous lipids may constitute can otherwise overlooked elimination route for these compounds via bile and faeces. The occurrence of lipid adducts/conjugates is likely indicative of reactive intermediates and potential toxicity caused by reactions with DNA. Reactions of reactive intermediates and lipids need to be further studied and correlated with reactions with other biomacromolecules such as DNA and proteins. It will be of fundamental interest to further clarify the formation and identity of the lipophilic excretion products.

Acknowledgement

The assistance of, and valuable discussion with, Dr Kerstin Bernström (ITM, Stockholm University) is gratefully acknowledged, as are the valuable discussions with Professor Åke Bergman (Department of Environmental Chemistry; Stockholm University) and Dr PeO Edlund (Biovitrum AB, Stockholm).

References

Amaro, A. R., Oakley, G. G., Bauer, U., Spielmann, H.-P. and Robertsson, L. W., 1996, Metabolic activation of PCBs to quinones: reactivity toward nitrogen and sulfur nucleophiles and influence of superoxide dismutase. *Chemical Research in Toxicology*, **9**, 623–629.

Ansari, G. A. S., Britt, S. G. and Reynolds, E. S., 1985, Isolation and characterisation of palmitoyl-pentachlorophenol from human fat. *Bulletin of Environmental Contamination and Toxicology*, **34**, 661–667.

Ansari, G. A. S., Kaphalia, B. S. and Khan, M. F., 1995, Mini Review. Fatty acid conjugates of xenobiotics. *Toxicology Letters*, **75**, 1–17.

Bakke, J., Feil, V. and Bergman, Å., 1983, Metabolites of 2,4′,5-trichlorobiphenyl in rats. *Xenobiotica*, **13**, 555–564.

Bakke, J. and Gustavsson, J.-Å., 1986, Role of the intestinal microflora in metabolism of polychlorinated biphenyls. In B. Hallgren *et al.* (eds), *Diet and Prevention of Coronary Heart Disease and Cancer* (New York: Raven), pp. 47–54.

Bergman, Å., Klasson Wehler, E., Nilsson, A. and Kuroki, H., 1995, Synthesis and mass spectrometry of methoxylated PCBs. *Chemosphere*, **30**, 1921–1938.

Bergman, Å., Larsen, G. L. and Bakke, J. E., 1982, Biliary secretion, retention and excretion of five ^{14}C-labelled polychlorinated biphenyls in the rat. *Chemosphere*, **11**, 249–253.

Bergman, Å., Nilsson, A., Riego, J. and Örn, U., 1990, Synthesis of ^{14}C-labelled and unlabelled coplanar polychlorinated biphenyls (PCBs). *Acta Chemica Scandinavica*, **44**, 1071–1076.

Bhat, H. K. and Ansari, G. A., 1990, Cholesterol ester hydrolase mediated conjugation of haloethanols with fatty acids. *Chemical Research in Toxicology*, **3**, 311–317.

Bucala, R., Makita, Z., Koschinsky, T., Cerami, A. and Vlassara, H., 1993, Lipid advanced glycosylation: pathway for lipid oxidation *in vivo*. *Proceedings of the National Academy of Sciences*, **90**, 6434–6438.

Chadwick, R. W., George, S. E. and Claxton, L. D., 1992, Role of the gastrointestinal mucosa and microflora in the bioactivation of the dietary and environmental mutagens or carcinogens. *Drug Metabolism Reviews*, **24**, 425–492.

Christie, W. W., 1989, The preparation of derivates of fatty acids. In W. W. Christie (ed.), *Gas Chromatography and Lipids* (Ayr: Oily Press), pp. 65–66.

Dawson, R. M. C., 1984, Products of degradation of phospholipids. In G. Zweig, J. Sherma and H. K. Mangold (eds), *Handbook of Chromatography, Lipids* (Boca Raton: CRC Press), pp. 545–554.

Dodds, P. F., 1995, Xenobiotic lipids: the inclusion of xenobiotic compounds in pathways of lipid biosynthesis. *Progress in Lipid Research*, **34**, 219–247.

Evstigneeva, R., 1993, Chemical stability. In G. Ceve (ed.), *Phospholipids Handbook* (New York: Marcel Dekker), pp. 323–333.

Fears, R., 1985, Lipophilic xenobiotic conjugates: the pharmacological and toxicological consequences of the participation of drugs and other foreign compounds as substrates in lipid biosynthesis. *Progress in Lipid Research*, **24**, 177–195.

Fieser, L. F. and Fieser, M., 1967, *Reagents for Organic Synthesis*, vol. 1 (New York: Wiley), pp. 191–192.

Goldman, P., 1989, Germ free rats in the study of the metabolites of xenobiotics compounds. In D. H. Hutson, J. Caldwell and G. D. Paulsen (eds), *Intermediary Xenobiotic Metabolism in Animals: Methodology, Mechanism and Significance* (London: Taylor & Francis), pp. 263–276.

Guichardant, M., Taibe-Tronche, P., Fay, L. B. and Lagarde, M., 1998, Covalent modification of aminophospholipids by 4-hydroxynonenal. *Free Radicals in Biology and Medicine*, **25**, 1049–1056.

Hayden, P., Welsh, J., Yang, Y., Schaefer, W., Ward, A. and Stevens, J., 1992, Formation of mitochondrial phospholipid adducts by nephrotoxic cystein conjugate metabolites. *Chemical Research in Toxicology*, **5**, 231–237.

Hazen, S. L., Heller, J., Hsu, F.-F., D'Avignon, A. and Heinecke, J. W., 1999, Synthesis, isolation and characterization of the adduct formed in the reaction of *p*-hydroxyphenylacetaldehyde with the amino headgroup of phosphatidylethanolamine and phosphatidylserine. *Chemical Research in Toxicology*, **12**, 19–27.

Hutson, D. H., 1982, Formation of lipophilic conjugates of pesticides and other xenobiotic compounds. In D. H. Hutson and T. R. Roberts (eds), *Progress in Pesticide Biochemistry*, vol. 2 (Chichester: Wiley), pp. 171–184.

Jerina, D. M. and Daly, J. W., 1974, Arene oxides: a new aspect of drug metabolism. *Science*, **185**, 573–581.

Kaphalia, B. S. and Ansari, G. A., 1989, Hepatic fatty acid conjugation of 2-chloroethanol and 2-bromoethanol in rats. *Journal of Biochemical Toxicology*, **4**, 183–188.

Klasson Wehler, E., Bergman, Å., Brandt, I., Darnerud, P. O. and Wachtmeister, C. A., 1989, 3,3′,4,4′-Tetrachlorobiphenyl: excretion and tissue retention of hydroxylated metabolites in the mouse. *Drug Metabolism and Disposition*, **17**, 441–448.

Klasson Wehler, E., Hovander, L. and Lund, B.-O., 1996, 2,2′,4,5,5′-Pentachlorobiphenyl: comparative metabolism in the mink (*Mustela vison*) and the mouse. *Chemical Research in Toxicology*, **9**, 1340–1349.

Klasson Wehler, E., Kowalski, B., Bergman, Å. and Brandt, I., 1987, Metabolism of 2,3,4′,6-tetrachlorobiphenyl: formation and tissue localization of mercapturic acid pathway metabolites in mice. *Xenobiotica*, **17**, 477–486.

Klasson Wehler, E., Lindberg, L., Brandt, I., Jönsson, C. J. and Bergman Å., 1993, Tissue retention and metabolism of 2,3,3′,4,4′-pentachlorobiphenyl in mink and mouse. *Chemosphere*, **27**, 2397–2412.

Koga, N., Beppu, M. and Yoshimura, H., 1990, Metabolism *in vivo* of 3,4,5,3′,4′-pentachlorobiphenyl and toxicological assessment of the metabolite in rats. *Journal of Pharmaco-Biological Dynamics*, **13**, 499–506.

Larsen, G., 1988, Deconjugation of biliary metabolites by microfloral-glucuroniases, sulphatases and cysteine conjugate β-lyases and their subsequent enterohepatic circulation. In I. Rowland (ed.), *Role of the Gut Flora in Toxicity and Cancer* (London: Academic Press), pp. 79–107.

Larsen, G. and Bakke, J. E., 1981, Enterohepatic circulation in formation of propachlor (2-chloro-l-isopropylacetanilide) metabolites in the rat. *Xenobiotica*, **11**, 423–480.

Leighty, E. and Fentiman, A., Jr, 1981, *In vitro* conjugation of the trichloroethylene metabolite trichloroethanol to a fatty acid. *Research Communications in Chemical Pathology and Pharmacology*, **32**, 569–572.

Leighty, E., Fentiman, A. and Foltz, R., 1976, Long-retained metabolites of Δ^9- and Δ^8-tetrahydrocannabinols identified as novel fatty acid conjugates. *Research Communications in Chemical Pathology and Pharmacology*, **14**, 13–28.

Leighty, E., Fentiman, A., Jr and Thompson, R., 1980, Conjugation of fatty acids to DDT in the rat: possible mechanism for retention. *Toxicology*, **15**, 77–82.

Lin, P.-H., Sangaiah, R., Ranasinghe, A., Upton, P. B., La, D. K., Gold, A. and Swenberg, J. A., 2000, Formation of quinonoid-derived protein adducts in the liver and brain of Sprague–Dawley rats treated with 2,2′,5,5′-tetrachlorobiphenyl. *Chemical Research in Toxicology*, **13**, 710–718.

Norstrom, R. J., Simon, M. and Mulvihill, M. J., 1986, A gel permeation/column chromatography cleanup method for the determination of CDDs in animal tissue. *International Journal of Environmental and Analytical Chemistry*, **23**, 267–287.

Örn, U. and Klasson Wehler, E., 1998, Metabolism of 2,2′,4,4′-tetrabrominated diphenyl ether in rat and mouse. *Xenobiotica*, **28**, 199–211.

Radwan, S. S., 1984, Glycerophospholipids. In H. K. Mangold, G. Zweig and J. Sherma (ed.), *Handbook of Chromatography*, vol. 1: *Lipids* (Boca Raton: CRC Press), pp. 486–487.

Safe, S., 1984, Polychlorinated biphenyls (PCBs) and polybrominated biphenyls (PBBs): biochemistry, toxicology, and mechanism of action. *CRC Critical Reviews in Toxicology*, **13**, 319–395.

Steinwandter, H., 1982, Contributions to the application of gel permeation chromatography in residue analysis. 1. Gel-chromatographic separation of chlorinated pesticides and polychlorinated biphenyls (PCBs) in the binary solvent system dichloromethane-cyclohexane. *Fresenius Z. Analytical Chemistry*, **313**, 536–538.

Sundström, G., 1973, Polychlorinated biphenyls II. Synthesis of some tetra- and pentachlorobiphenyls. *Acta Chemica Scandinavica*, **27**, 600–604.

Treloar, T., Madden, L. J., Winter, J. S., Smith, J. L. and De Jersey, J., 1996, Fatty acid ethyl ester synthesis by human liver microsomes. *Biochimica et Biophysica Acta*, **19**, 160–166.

Trexler, P. and Reynolds, L., 1957, Flexible film apparatus for rearing and use of germ free animals. *Applied Microbiology*, **5**, 406–442.

Tunek, A., Sjodin, K. and Hallström, G., 1997, Reversible formation of fatty acid esters of Budesonide, an antiasthma glucocorticoid, in human lung and liver microsomes. *Drug Metabolism and Disposition*, **25**, 1311–1317.

Yisak, W., Agurell, S., Lindgren, J.E. and Widman, M., 1987, *In vivo* metabolites of cannabinol identified as fatty acid conjugates. *Journal of Pharmaceutics and Pharmacology*, **30**, 462–463.

Yoshimura, H., Yonemoto, Y., Yamada, H., Koga N., Oguri, K. and Saeki, S., 1987, Metabolism *in vivo* of 3,3′,4,4′-tetrachlorobiphenyl and toxicological assessment of the metabolites in rats. *Xenobiotica*, **17**, 897–910.

XENOBIOTICA, 2002, VOL. 32, NO. 8, 641–651

Taylor & Francis
healthsciences

Quantitative assessment of foetal exposure to trenbolone acetate, zeranol and melengestrol acetate, following maternal dosing in rabbits

I. G. LANGE†*, A. DAXENBERGER†, H. H. D. MEYER†, E. RAJPERT-DE MEYTS‡, N. E. SKAKKEBÆK‡ and D. N. R. VEERAMACHANENI§

† Institute of Physiology, Technical University Munich-Weihenstephan, D-85354 Freising, Germany
‡ Department of Growth and Reproduction, Section GR 5064, Rigshospitalet, DK-2100 Copenhagen, Denmark
§ Animal Reproduction and Biotechnology Laboratory, Department of Physiology, Colorado State University, Fort Collins, CO 80523-1683, USA

Received 17 September 2001

1. Residues of commonly used growth-promoting agents found in animal meat can be hormonally active and they have been implicated as possible endocrine disruptors in man. Although these compounds could be potentially detrimental to the developing foetus, it is not clear whether and to what extent they pass through placental barrier.

2. This issue was addressed using the rabbit as an animal model. Pregnant rabbits were treated with trenbolone acetate, zeranol or melengestrol acetate beginning at gestation day 14. Levels of active substances in plasma were screened by means of specific ELISA systems. The residues of parent compounds and their metabolites were quantified in maternal and foetal tissues on gestation day 27 using validated, sensitive HPLC/ELISA methods.

3. All three compounds crossed the placental barrier and were detectable in foetal tissues. The extent of tissue concentration varied depending on the compound and tissue analysed. Gender differences were observed in some instances.

Introduction

Environmental endocrine disruptors may have a profound influence on the differentiation and development of vertebrates (Danzo 1998, Gray and Ostby 1998). In this context, the widespread use of growth-promoting agents with potent hormonal activity in animal husbandry has recently become a matter of concern (Andersson and Skakkebæk 1999, EC 1999, Skakkebæk *et al.* 2000).

A substantial majority of endocrine disruptors identified so far possess either oestrogenic or anti-androgenic activity. In addition to xenobiotics, such effects are also attributed to phytoestrogens or mycoestrogens (Fritsche and Steinhart 1999). Sex hormones play a pivotal role in the regulation of behaviour and morphogenesis and functional differentiation of the reproductive system during all stages of life, but primarily during early foetal development (Knobil and Neill 1988). The reproductive system, the development of which depends upon a perfect balance between androgenic and oestrogenic effects, is probably one of the most vulnerable to endocrine disrupters (Toppari *et al.* 1996). The recently observed apparent

* Author for correspondence; e-mail: lange@weihenstephan.de

Xenobiotica ISSN 0049–8254 print/ISSN 1366–5928 online © 2002 Taylor & Francis Ltd
http://www.tandf.co.uk/journals
DOI: 10.1080/00498250210143010

decline in male reproductive health and a rise in some endocrine cancers such as breast and testicular cancers may be a phenomenon causally linked to the widespread presence of endocrine-disrupting environmental pollutants, although this relationship remains presumptive at best (Skakkebæk *et al.* 1998, 2001, Sonnenschein and Soto 1998, Veeramachaneni 2000). Detrimental factors acting *in utero* and perinatally, including hormonal imbalances, have been implicated in the pathogenesis of all these diseases (Weir *et al.* 2000, Skakkebæk *et al.* 2001). It is, therefore, obligatory to investigate the consequences of prenatal exposures at least to commonly used hormonally active substances.

The study focuses on the three most commonly used hormonal growth-promoting agents, melengestrol acetate (MGA), trenbolone acetate (TBA) and zeranol, licensed for use in meat-producing animals in several countries outside the EU, e.g. in the USA (Code of Federal Regulations 1999). MGA is an orally active progestin whose affinity for the bovine progestin receptor is about five times higher than that of progesterone (Bauer *et al.* 2000). According to Lauderdale *et al.* (1977), cattle is the species most sensitive to MGA. The relative daily oral dose per body weight of MGA necessary to inhibit the reproductive cycle in cows is about 230 times lower than in women. TBA is rapidly hydrolysed to its active form, trenbolone (TbOH)-17β (Pottier 1981). TbOH-17β is a potent anabolic agent since it has androgenic, gestagenic and anti-glucocorticoid effects (Meyer and Rapp 1985, Danhaive and Rousseau 1986, Bauer *et al.* 2000). Zeranol (α-zearalanol) is a non-steroidal oestrogen derived from the mycotoxin zearalenone, which is synthesized by *Fusarium* spp.

As an initial first step, it was necessary to determine whether these compounds actually reach the developing foetus or not. Thus, the objective of the study was to determine the extent of transplacental passage and residue formation in foetal tissues of MGA, TBA and zeranol and their metabolites following maternal exposure. The results will be used in follow-up studies to establish a causal link between maternal exposures and possible detrimental effects on the foetus or to form a basis for *in vitro* studies. The rabbit was used as an animal model because unlike rodents, it has a relatively long phase of reproductive development and differentiation (Gondos *et al.* 1973, 1976), thus simulating the natural situation in children better. Furthermore, testicular pre-invasive neoplasia, similar to human carcinoma *in situ* has been described in rabbit (Veeramachaneni and Vandewoude 1999, Veeramachaneni 2000), but not in rodents. In addition, the use of rabbit facilitates multiple evaluations of sexual capacity and seminal quality (Veeramachaneni *et al.* 2001).

Materials and methods

Animal exposures and sampling

All animals in the experiments were treated according to the Code of Ethics of the World Medical Association (Declaration of Helsinki) and the Guiding Principles in the Care and Use of Animals (DHEW Publication NIH, 80–23).

Dutch-Belted rabbits were treated with MGA, TBA or zeranol between gestation days (GD) 14 and 27 (the second half of pregnancy). Two animals (rabbits 832 and 840) were fed daily with 0.5 mg MGA kg^{-1} body weight in corn syrup from GD 14 to 27. Two animals (rabbits 781 and 841) were injected subcutaneously with 0.5 mg TBA kg^{-1} body weight in safflower oil on GD 14, 21 and 27. One animal (rabbit 838) was implanted subcutaneously with a zeranol implant (0.25 mg kg^{-1} body weight) on GD 14. Two untreated animals (rabbits 795 and 831) served as controls.

Table 1. Sampling scheme.

Tissue	Tissue:buffer ratio	Aliquot [g]
Maternal muscle	1:2	4
Maternal liver/kidney	1:2	1
Maternal fat	–	1
Placenta	1:3	6
Foetal muscle	1:10	1–2
Foetal liver	1:5	2
Foetal kidney	1:10	1
Foetal fat	–	0.1–0.2

Blood plasma samples were taken from the dams (untreated and treated animals) before ('pre') and 2 h after treatment ('post'; treated ones only) on GD 14, 21 and 27. Plasma samples from foetuses were taken upon euthanasia on GD 27. In addition, samples of skeletal muscle, liver, kidney and fat also were taken from dams and foetuses on GD 27. Corresponding placentas were also collected. The samples were shipped on dry ice and stored at −20°C until analyses were performed. Tissues from two male and two female foetuses of each treatment group (rabbit 795-M, 795-F, 831-M, etc.) were taken for analyses.

The tissues, except fat, were cut into small pieces and homogenized in buffer. Muscle and all tissues that were analysed for MGA were homogenized in 67 mM phosphate buffer, pH 7.2; the remaining liver, kidney and placenta samples were homogenized in 0.5 M sodium acetate buffer, pH 4.8. Because of technical demands smaller amounts of tissue (< 1 g) had to be homogenized in larger volumes of buffer (table 1).

Screening of plasma samples

The concentrations of TbOH, MGA and zeranol in plasma were screened after liquid extraction by specific and sensitive enzyme-linked immunosorbent assay (ELISA) systems as previously described (Meyer and Hoffmann 1987, Hageleit *et al.* 2001, Lange *et al.* 2001). A total of 200 µl (MGA 100 µl) of plasma were extracted with 3 ml *tert*-butyl methyl ether (TBME)/petroleum ether (PE) 70/30 (v/v) (MGA: PE only) for 1 h at room temperature. Before extraction TbOH and zeranol conjugates were hydrolysed for 2 h at 37°C after adding 500 µl 0.4% *β*-glucuronidase (EC 3.2.1.31)/arylsulfatase (EC 3.1.6.1) from *Helix pomatia* (Merck, Darmstadt, Germany) in 0.05 M sodium acetate, pH 4.8. After extraction the organic phases were evaporated, redissolved in 200 µl methanol/purified water 40/60 (v/v) and the hormone contents were quantified by means of ELISA.

Extraction of tissue

The extraction of the analytes was performed as previously described (Lange *et al.* 2001). After adding internal standard, the samples were extracted twice with 5 ml TBME at room temperature with the exception of fat which was extracted at 40°C. The MGA samples were extracted twice with PE at 40°C (Hageleit *et al.* 2001). Before extraction, liver, kidney and placenta samples from TbOH- and zeranol-treated animals were hydrolysed with β-glucuronidase (EC 3.2.1.31)/arylsulfatase (EC 3.1.6.1) from *H. pomatia* (Merck) for 2 h at 37°C. The organic phases were decanted and evaporated to dryness. To remove fat, the dry residues were redissolved in 1.25 ml methanol and frozen. After centrifugation the methanolic phase was diluted with 5 ml purified water and applied to octadecylsilica gel (RP18) solid-phase extraction (Baker, Inc., Phillipsburg, NJ, USA). The eluate was evaporated to dryness and redissolved in 300 µl 20 mM Tris-acetate pH 7.2/acetonitrile 80/20 (v/v) (TbOH and zeranol) or 20 mM Tris-acetate pH 7.2/methanol 60/40 (v/v) (MGA).

HPLC-ELISA of tissue samples

According to previously established procedures (Lange *et al.* 2001), 250 µl extract were applied to a RP18-HPLC column (PRONTOSIL®, 250 × 4.0 mm; Bischoff, Leonberg, Germany), which was protected by a RP18-cartridge (Phenomenex, Torrance, USA). Acetonitrile/20 mM Tris-acetate pH 7.2 36/64 (v/v) (flow rate 1 ml min^{-1}, $T = 25°C$) served as mobile phase for the separation of TbOH-17β, TbOH-17α and trendione (TbO) and for zeranol analysis in liver and kidney (mobile phase A) (table 2); and at a ratio of 42/58 (v/v) for zeranol analysis in muscle, fat and placenta (mobile phase B). Fractions of 500 µl were collected, except those of TbOH-17β and TbOH-17α, which were 200 µl fractions. The solvent was evaporated completely and the residue was redissolved in 150 µl (200 µl for maternal kidney and placenta) methanol/purified water 40/60 (v/v).

Table 2. HPLC/ELISA retention times.

Mobile phase	Analyte	Retention time (min)
A	TbOH-17β	13.5
	TbOH-17α	15.0
	zeranol	20.5
	TbO	22.0
	equilenine	27.0
B	zeranol	12.3
	equilenine	15.5
C	melengestrol acetate	12.6
	16α-methylprogesterone	18.0

For the detection of MGA, a shorter RP18-column, also protected by an octadecylsilica gel cartridge (as above), was used (NUCLEOSIL®, 150 × 4.6 mm, Macherey-Nagel, Düren, Germany) with methanol/20 mM Tris-acetate pH 7.2 70/30 (v/v) as eluent (mobile phase C). Fractions of 500 µl were collected. After evaporation the samples were redissolved in 200 µl methanol/purified water 40/60 (v/v) (foetal fat, maternal liver: 300 µl, maternal fat 500 µl; method validation: muscle, kidney and placenta: 200 µl, liver and fat: 300 µl). The fractions of maternal liver samples had to be diluted 1:25, to minimize endogenous noise signals.

The ELISAs were performed as described previously (Meyer and Hoffmann 1987, Hageleit *et al.* 2001, Lange *et al.* 2001). TbOH-17β, TbOH-17α and TbO were quantified by means of specific calibration curves.

Method validation of HPLC-ELISA

The efficacy of the trenbolone and zeranol extraction and the specificity of the HPLC separation were confirmed in previous studies using GC-MS (Daxenberger *et al.* 2000). Analysis of samples from MGA-treated animals using GC/LC-MS (Daxenberger *et al.* 1999, Hageleit *et al.* 2001) corroborated results obtained from MGA-ELISA. To check the applicability of the HPLC/ELISA method to rabbit samples, commercially available rabbit samples of Hungarian provenience (muscle, liver, kidney, fat) were prepared as described above for maternal tissues, fortified and analysed. Placental tissue was taken from a pool of the four untreated foetuses; at this point the amount of samples had to be reduced because of a shortage of material (table 3).

Wherever applicable, internal standardization was applied to fulfil the requirements of the EC concerning methods used for detecting residues of substances having a hormonal or thyrostatic action (Commission of the European Communities 1993). In this context, internal standardization means correction of the measured analyte concentration by the recovery factor of the internal standard. A known amount of this substance was added to the sample before the extraction procedure to determine procedural losses. If internal standardization led to an overestimation of the results, external standardization was applied, although concordance with the guidelines could not be achieved in every case (table 3). External standardization means the correction of the measured analyte concentration by the average recovery factor of the analyte in fortified validation samples.

The detection limits could be determined separately in each test, because in each ELISA negative and positive samples were measured. They were calculated as difference of the mean relative binding of all blank samples and its threefold standard deviation (table 3, column 2). Sensitivities within the pg g^{-1} range could be reached.

Results

In treated rabbits, MGA, TbOH or zeranol could be detected in all corresponding maternal and foetal plasma and tissue samples except in case of foetal fat in which no zeranol could be determined and in case of foetal muscle in which zeranol was detected only in one of the four samples (tables 4–6).

After TBA injection levels of total TbOH in plasma rose up to > 4.4 ng TbOH-17β-equivalents ml^{-1} and declined to < 0.048 ng ml^{-1} by the 7th day (before the next injection). In rabbit 781, the rise of plasma TbOH was higher than in rabbit 841 (rabbits 781 and 841: GD 14 pre-: both < 0.048 ng ml^{-1}, post-: 16 and

Table 3. HPLC/ELISA validation parameters.

Analyte	Matrix	Detection limit ($pg\,g^{-1}$)	Fortification ($pg\,g^{-1}$)	Accuracy/precision after standardization[a,b] (%)
TbOH-17β	muscle	1.7	30/60/120	82/16[b]
TbOH-17α		1.8	9/15/30	112/15[b]
TbO		0.76	9/15/30	111/2.0[b]
TbOH-17β	liver	3.8	150/300/600	54/11[b]
TbOH-17α		2.8	1500/3000/6000	81/3.8[b]
TbO		2.6	12/24/48	49/21[b]
TbOH-17β	kidney	1.3	30/60/120	65/26[b]
TbOH-17α		4.2	150/300/600	64/12[b]
TbO		5.3	24/48/96	76/14[b]
TbOH-17β	fat	1.8	100/200/400	108/4.3[b]
TbOH-17α		1.9	10/20/40	117/7.1[b]
TbO		3.1	50/100/200	102/10[b]
TbOH-17β	placenta	0.56	1500/6000	122/14[b]
TbOH-17α		1.1	1500/6000	139/8.8[b]
TbO		1.4	75/300	138/21[b]
Zeranol	muscle	1.1	3.4/6.8/14	67/24[b]
	liver	11	720/1400/2900	61/18[a]
	kidney	6.1	360/720/1400	58/20[a]
	fat	1.3	25/50/100	84/23[a]
	placenta	1.5	120	58/–[a]
MGA	muscle	4.6	750/1500/3000	111/16[b]
	liver	40	600/1200/2400	83/13[b]
	kidney	32	3000/6000/12 000	92/4.2[a]
	fat	7.2	200/400/800	98/4.9[b]
	placenta	9.0	1250/5000	121/11[b]

[a]External standardization; [b]internal standardization

8.3 $ng\,ml^{-1}$; GD 21 pre-: both $< 0.048\,ng\,ml^{-1}$, post-: 14 and 4.5 $ng\,ml^{-1}$; GD 27 pre-: both $< 0.048\,ng\,ml^{-1}$, post-: 12 and 9.8 $ng\,ml^{-1}$). Mean plasma levels of TBA in foetuses were 5 $ng\,ml^{-1}$. The concentration of total trenbolone was lower in foetuses of rabbit 841 than in those of 781 reflecting the difference already observed in dams themselves. In both sibling pairs female foetuses had lower plasma concentrations than males (781-M: 6.0 $ng\,ml^{-1}$, 781-F: 5.2 $ng\,ml^{-1}$; 841-M: 4.8 $ng\,ml^{-1}$; 841-F: 4.4 $ng\,ml^{-1}$). In samples of all untreated rabbits plasma concentrations were below the detection limit of 0.048 $ng\,ml^{-1}$.

In foetal muscle samples the total concentration of TbOH reached 50% of the concentration found in maternal muscle samples (100%), 100% in liver, 10% in kidney and 30% in fat (table 4). The main metabolite of TBA found in maternal as well as foetal liver and kidney was TbOH-17α (95–99% of total metabolites) (table 7). Whereas the proportions of this metabolite in maternal muscle and fat were 24 and 33%, respectively, those for corresponding foetal tissues were 82 and 63%. The predominant metabolite in maternal muscle and fat was TbOH-17β (74 and 63%, respectively). In the placenta, the proportions of TbOH-17α and TbOH-17β were 57 and 42%.

Because of the different mode of administration (lower dose, depot preparation) and the more hydrophilic properties, zeranol residues in maternal and foetal samples were well less than those of the TbOH-treated animals. The concentration of zeranol in the foetal liver was 71% relative to that in maternal liver (100%) and in the kidney 16%. In foetal fat, < 25% of the amount found in that of the mother was measured (table 5).

Table 4. Residues after TBA treatment.

Tissue	Animal no.	TbOH-17β ($pg\,g^{-1}$)	TbOH-17α ($pg\,g^{-1}$)	TbO ($pg\,g^{-1}$)
Muscle	maternal controls	< 0.85	< 1.3	< 0.94
	781	8200	2800	220
	841	8100	2500	170
	foetal controls	< 9.1	< 20	< 11
	781-M	990	5300	54
	841-M	1100	5600	13
	781-F	1100	4500	< 6.4
	841-F	580	2100	< 5.9
Liver	maternal controls	< 11	< 4.2	< 7.9
	781	390	12 000	57
	841	370	8700	79
	foetal controls	< 4.3	< 7.1	< 2.7
	781-M	51	9100	27
	841-M	43	11 000	53
	781-F	110	18 000	66
	841-F	33	9700	25
Kidney	maternal controls	< 7.9	< 15	< 7.2
	781	5900	160 000	1000
	841	4800	48 000	500
	foetal controls	< 11	< 17	< 8.0
	781-M	43	1800	43
	841-M	370	15 000	< 19
	781-F	260	16 000	< 15
	841-F	–	–	–
Fat	maternal controls	< 2.9	< 3.8	< 0.86
	781	40 000	22 000	2500
	841	26 000	12 000	1700
	foetal controls	< 29	< 10	< 4.0
	781-M	7400	13 000	170
	841-M	8100	9900	230
	781-F	4600	10 000	183
	841-F	2600	7100	240
Placenta	foetal controls	< 1.4	< 2.5	< 2.4
	781-M	6300	7500	150
	841-M	5400	7900	110
	781-F	7600	10 000	240
	841-F	7600	9400	190

[a]M, male foetus, [b]F, female foetus

In maternal plasma, the zeranol concentration reached $190\,pg\,ml^{-1}$ 2 h after administration of the implant on GD 14 and was $99\,pg\,ml^{-1}$ on GD 21 and $120\,pg\,ml^{-1}$ on GD 27, indicating a steady release of active ingredient from the preparation. Foetal plasma samples taken on GD 27 had higher zeranol contents than the maternal one, female foetuses had higher contents than male ones (838-1M: $130\,pg\,ml^{-1}$, 838-2M: $140\,pg\,ml^{-1}$, 838-1F: $210\,pg\,ml^{-1}$, 838-2F: $160\,pg\,ml^{-1}$). In samples of untreated dams and foetuses no zeranol was detectable (detection limit: $13\,pg\,ml^{-1}$).

After feeding of MGA, residues in plasma rose to the $ng\,ml^{-1}$ range and did not fall below the detection limit until the next sampling. Rabbit 832 showed a higher amplitude among the MGA concentrations before and after feeding than rabbit 840 (rabbits 832 and 840: GD 14 pre-: both $< 0.043\,ng\,ml^{-1}$, post-: 1.08 and $0.45\,ng\,ml^{-1}$; GD 21 pre-: 0.11 and $0.35\,ng\,ml^{-1}$, post-: 1.19 and $0.82\,ng\,ml^{-1}$; GD

Table 5. Residues after zeranol treatment.

Animal no.	Muscle zeranol ($pg\,g^{-1}$)	Liver zeranol ($pg\,g^{-1}$)	Kidney zeranol ($pg\,g^{-1}$)	Fat zeranol ($pg\,g^{-1}$)	Placenta zeranol ($pg\,g^{-1}$)
Maternal controls	< 3.4	< 10	< 11	< 4.7	–
838	24	180	860	55	–
Foetal controls	< 16	< 5.6	< 15	< 14	< 3.2
838-1M	< 6.2	97	36	< 10	140
838-2M	< 6.2	76	60	< 10	140
838-1F	65	140	240	< 13	97
838-2F	< 11	200	210	< 13	90

Table 6. Residues after melengestrol acetate treatment.

Animal no.	Muscle MGA ($pg\,g^{-1}$)	Liver MGA ($pg\,g^{-1}$)	Kidney MGA ($pg\,g^{-1}$)	Fat MGA ($pg\,g^{-1}$)	Placenta MGA ($pg\,g^{-1}$)
Maternal controls	< 6.8	< 650	< 22	< 46	–
832	290	190 000	2800	28 000	–
840	700	160 000	2500	72 000	–
Foetal controls	< 83	< 28	< 86	< 250	< 4.4
832-M	990	5300	1100	3100	750
840-M	950	7700	1000	4700	690
832-F	1000	5100	600	5600	950
840-F	880	6200	1000	7000	810

Table 7. Metabolite pattern of TbOH.

	Ratio of metabolites [%]								
	Muscle		Liver		Kidney		Fat		
Analyte	Maternal	Foetal	Maternal	Foetal	Maternal	Foetal	Maternal	Foetal	Foetal placenta
TbOH-17β	74	18	3.5	0.5	4.8	2.0	63	36	42
TbOH-17α	24	82	96	99	95	98	33	63	57
TbO	1.8	0.3	0.6	0.4	0.7	0.1	4.1	1.3	1.1

27 pre-: 0.072 and 0.13 $ng\,ml^{-1}$, post-: 0.85 and 0.42 $ng\,ml^{-1}$). Foetuses of rabbit 832 had higher plasma MGA levels than those of rabbit 840, female foetuses had higher levels than their male littermates (832-M: 0.39 $ng\,ml^{-1}$, 832-F: 0.48 $ng\,ml^{-1}$, 840-M: 0.27 $ng\,ml^{-1}$, 840-F: 0.31 $ng\,ml^{-1}$). MGA concentrations in samples of all untreated rabbits were below the detection limit of 0.043 $ng\,ml^{-1}$. In maternal tissues, MGA accumulated especially in the liver (mean: 175 ng MGA g^{-1}) and in fat (50 $ng\,g^{-1}$) in which the difference between maternal and corresponding foetal tissues also was the highest (table 6). The residues found in the foetus were 4% (of that of the mother) in liver, 12% in fat and 39% in kidney. In foetal muscle of rabbit 840, however, nearly one and half times as much MGA was detected compared with maternal muscle, and in foetal muscle of rabbit 832, three times as much.

Discussion

Placental transfer of TbOH, zeranol and MGA was quantified in rabbit by means of a specific and sensitive method combining HPLC and ELISA. Plasma concentrations of TBA and MGA showed a pulsatile profile while those of zeranol a steady release, reflecting modes of their administration. Plasma levels indicate that zeranol passes the placenta unrestrictedly while only 40–50% of TbOH and 50–70% of MGA reach the foetal circulation. Female foetuses tend to show higher residues of zeranol and MGA. Male foetuses show slightly higher plasma levels of TbOH than their female littermates. These gender differences also are partly reflected in tissue residues. Even though statistically not significant, it is striking that in the fat the residues of TbOH-17β and MGA show a considerable gender difference. While TbOH-17β is found to a higher degree in male foetuses, MGA prevailed in females. Interestingly, MGA and the three TbOH metabolites were higher in placentas associated with female foetuses than males. This observation contrasts the fact that higher plasma levels of TbOH-17β were detected in male foetuses than in females. After zeranol treatment, the female foetuses showed higher residues in their tissues than males, which is in accordance with the gender differences in plasma residues. In placenta, however, the zeranol contents were lower in the female foetuses. The proportion of the contents in liver and kidney also showed gender differences. In the male foetal kidneys the zeranol concentrations constituted about one half of those in liver, while in female kidneys the amount was 1.3-fold compared with that of liver. Although these tendencies are based only on the observations of two animals, this probably indicates possible sexual differences, which need to be confirmed.

With regard to the tissue distribution kinetics, the three substances studied show different patterns. Although plasma levels of zeranol in foetuses were elevated compared with those in dams, zeranol did not appear to have accumulated in the foetal tissues. On the other hand, plasma levels of TbOH and MGA indicated that these substances did not enter the foetal circulation completely, but both of them were elevated in foetal tissues, TbOH-17α in liver and MGA in muscle. In TBA- and zeranol-treated dams, the highest residues were detected in the kidney, whereas in MGA-treated animals most residue accumulated in the liver. In these tissues, the differences between maternal and foetal samples were the highest. In foetal kidney 10% of the total trenbolone content and 16% of the zeranol content found in maternal kidney could be detected. The residues in foetal liver of MGA-treated animals reached only 4% of those in maternal liver samples. In foetal kidney, the MGA concentrations were even sixfold lower than in the liver, while in TBA- and zeranol-treated animals the concentrations in the foetal kidneys and livers were comparable.

Although the differences between dams and foetuses indicate that the detoxification mechanisms and/or excretory capacity of foetal liver and kidney are not fully established in the foetus and not comparable with that of the mother, the elevation of residues in foetal liver and kidney compared with muscle indicate that these organs are developed to a considerable degree in the second half of gestation. As we know, the foetal kidneys start production of urine early in development although their function is not vital at this point of time, as the metabolic products of the foetus are excreted via the placenta. Besides this, the placenta also contributes to the metabolic activity of the foetus, while the contribution of the foetal liver remains unclear. In human foetal liver, there are signs for active

metabolism and conjugation already in the second trimester (Tsukamoto 1984). Experiments with late gestational age placenta of rhesus monkeys perfused by either 17α-ethinylestradiol (EE2) or oestradiol-17β (E2) revealed that 96% of the E2 was metabolized to oestrone, while EE2 escaped the placental metabolic conversion. This could be explained by the inability of the synthetic EE2 to undergo 17β-steroid dehydrogenase oxidation (Slikker *et al.* 1982). Thus, the relatively high proportion of TbOH-17α in foetal tissues could indicate that TbOH-17β, which reaches the placental barrier, is further metabolized in the foetus, presumably by 17β-steroid dehydrogenase mediated oxidation/epimerization.

For delineation of the toxicological consequences of individual metabolites of the compounds used in this study it is also important to compare the similarity of metabolic patterns of the substances in rabbit and man. The metabolism of TbOH has been studied in the male Sprague–Dawley rat, Friesian heifer (Pottier 1981) as well as in a male human subject (Spranger and Metzler 1991). Unlike in rat and cow, the major route of excretion in man is via the urine. The major fraction of metabolites is eliminated as glucuronides, which consist mostly of TbOH-17α (Spranger and Metzler 1991). This metabolic conversion decreases the androgenic potency significantly. The relative affinity of the different metabolites for the recombinant human androgen receptor is 109% for TbOH-17β, 4.5% for TbOH-17α and 0.36% for TbO (5α-dihydrotestosterone 100%) (Bauer *et al.* 2000). The gestagenic potency given as relative affinity for the bovine progestin receptor is 137% for TbOH-17β, 2.0% for TbOH-17α and 1.0% for TbO (progesterone 100%) (Bauer *et al.* 2000). The metabolic pattern of zeranol has been studied in the female Wistar rat, New Zealand rabbit, beagle dog, Rhesus monkey and man (Migdalof *et al.* 1983). Only in rabbit and man urinary excretion predominated. The metabolites included conjugates of zeranol and the major metabolite zearalanone. Taleranol (β-zearalanol) was identified as urinary metabolite in a female rabbit (Migdalof *et al.* 1983). Assessment of the oestrogenic potency of zeranol as uterotrophic agent in the sexually immature rat led to 0.67% (oestradiol-17β 100%), 0.29% for taleranol and 0.25% for zearalanone (Everett *et al.* 1987). The relative affinity for the recombinant human oestrogen receptor α is 57% for zeranol, 19% for taleranol and 13% for zeralanone (Seifert *et al.* 1999). Our results suggest the possibility that in rabbit TbOH, like zeranol, is predominantly excreted via the urine. Thus, in both man and rabbit zeranol and possibly also TbOH are mainly excreted via the urine (WHO 1988), whereas in rat biliary excretion is predominant (Pottier 1981). Another parallelism is that in rabbit, the main metabolite of TBA is TbOH-17α. With a maximum of 4% in maternal fat, TbO is presumably only an intermediate product in the biotransformation of TbOH in rabbit. However, in rat, which is commonly used in developmental and reproductive toxicology studies, 16α-hydroxytrendione and 16α- hydroxy-17β-trenbolone prevail (WHO 1988). These unique aspects have to be considered, if risk assessment for man is extrapolated from animal studies.

In the context of current health concerns and debates on possible endocrine disruption in man, these new data on placental transfer and residue formation in the foetus are valuable for designing strategies for assessment of risk associated with hormonally active compounds such as residues resulting from extensive use of anabolic agents in cattle.

Acknowledgements

The authors thank Inge Celler, Ty Higuchi, Jennifer Palmer and Ginger Sammonds for diligent assistance. The study was supported financially by the European Commission.

References

Andersson, A. M. and Skakkebæk, N. E., 1999, Exposure to exogenous estrogens in food: Possible impact on human development and health. *European Journal of Endocrinology*, **140**, 477–485.

Bauer, E. R. S., Daxenberger, A., Petri, T., Sauerwein, H. and Meyer, H. H. D., 2000, Characterization of the affinity of different anabolics and synthetic hormones to the human androgen receptor, human sex hormone binding globulin and to the bovine progestin receptor. *Acta Pathologica, Microbiologica et Immunologica Scandinavica*, **108**, 838–846.

Code of Federal Regulations, 1999, *Title 21, Volume 6, Chapter I, Part 522, Section 522.842, 522.2478 and 522.2680* (Washington, DC: US Government Printing Office) [http://www.access.gpo.gov/nara/cfr/waisidx_99/21cfrv6_99.html] (cited 26 June 2001).

Commission of the European Communities, 1993, Commission Decision 93/256/EC of 14 April 1993 laying down the methods to be used for detecting residues of substances having a hormonal or thyrostatic action. *Official Journal of the European Community*, **L118**, 64–74.

Danhaive, P. A. and Rousseau, G. G., 1986, Binding of glucocorticoid antagonists to androgen and glucocorticoid hormone receptors in rat skeletal muscle. *Journal of Steroid Biochemistry*, **24**, 481–487.

Danzo, B. J., 1998, The effects of environmental hormones on reproduction. *Cellular and Molecular Life Sciences*, **54**, 1249–1264.

Daxenberger, A., Lange, I. G., Meyer, K. and Meyer, H. H. D., 2000, Detection of anabolic residues in misplaced implantation sites in cattle. *Journal of the Association of Official Analytical Chemists International*, **83**, 809–819.

Daxenberger, A., Meyer, K., Hageleit, M. and Meyer, H. H. D., 1999, Detection of melengestrol acetate residues in plasma and edible tissues of heifers. *Veterinary Quarterly*, **21**, 154–158.

European Commission, 1999, Opinion of the scientific committee on veterinary measures relating to public health: assessment of potential risks to human health from hormone residues in bovine meat and meat products (30 April 1999) [http://europa.eu.int/comm/food/fs/sc/scv/out21_en.html] (cited 26 June 2001).

Everett, D. J., Perry, C. J., Scott, K. A., Martin, B. W. and Terry, M. K., 1987, Estrogenic potencies of resorcylic acid lactones and 17-β-estradiol in female rats. *Journal of Toxicology and Environmental Health*, **20**, 435–443.

Fritsche, S. and Steinhart, H., 1999, Occurrence of hormonally active compounds in food: a review. *European Food Research and Technology*, **209**, 153–179.

Gondos, B., Renston, R. H. and Conner, L. A., 1973, Ultrastructure of germ cells and Sertoli cells in the postnatal rabbit testis. *American Journal of Anatomy*, **136**, 427–439.

Gondos, B., Renston, R. H. and Goldstein, D. A., 1976, Postnatal differentiation of Leydig cells in the rabbit testis. *American Journal of Anatomy*, **145**, 167–181.

Gray, L. E., Jr and Ostby, J., 1998, Effects of pesticides and toxic substances on behavioural and morphological reproductive development: endocrine versus nonendocrine mechanisms. *Toxicology and Industrial Health*, **14**, 159–184.

Hageleit, M., Daxenberger, A. and Meyer, H. H. D., 2001, A sensitive enzyme immunoassay (EIA) for the determination of melengestrol acetate (MGA) in adipose and muscle tissues. *Food Additives and Contaminants*, **18**, 285–291.

Knobil, E. and Neill, J. D., 1988, *The Physiology of Reproduction*, vol. 2. (New York: Raven).

Lange, I. G., Daxenberger, A. and Meyer, H. H. D., 2001, Hormone contents in peripheral tissues after correct and off-label use of growth promoting hormones in cattle: Effect of the implant preparations Finaplix-H®, Ralgro®, Synovex-H® and Synovex Plus®. *Acta Pathologica, Microbiologica et Immunologica Scandinavica*, **109**, 53–65.

Lauderdale, J. W., Goyings, L. S., Krzeminski, L. F. and Zimbelman, R. G., 1977, Studies of a progestogen (MGA) as related to residues and human consumption. *Journal of Toxicology and Environmental Health*, **3**, 5–33.

Meyer, H. H. D. and Hoffmann, S., 1987, Development of a sensitive microtitration plate enzyme-immunoassay for the anabolic steroid trenbolone. *Food Additives and Contaminants*, **4**, 149–160.

Meyer, H. H. D. and Rapp, M., 1985, Reversible binding of the anabolic steroid trenbolone to steroid receptors. *Acta Endocrinologica*, **108 (suppl. 267)**, 129.

Migdalof, B. H., Dugger, H. A., Heider, J. G., Coombs, R. A. and Terry, M. K., 1983, Biotransformation of zeranol. I. Disposition and metabolism in the female rat, rabbit, dog, monkey and man. *Xenobiotica*, **13**, 209–221.

Pottier, J., Cousty, C., Heitzman, R. J. and Reynolds, I. P., 1981, Differences in the biotransformation of a 17β-hydroxylated steroid, trenbolone acetate, in rat and cow. *Xenobiotica*, **11**, 489–500.

Seifert, M., Haindl, S. and Hock, B., 1999, Development of an enzyme linked receptor assay (ELRA) for estrogens and xenoestrogens. *Analytica Chimica Acta*, **386**, 191–199.

Skakkebæk, N. E., Leffers, H., Rajpert-De Meyts, E., Carlsen, E. and Grigor, K. M., 2000, Should we watch what we eat and drink? Report on the international workshop on hormones and endocrine disrupters in food and water: possible impact on human health, Copenhagen, Denmark, 27–30 May 2000. *Trends in Endocrinology and Metabolism*, **11**, 291–293.

Skakkebæk, N. E., Rajpert-De Meyts, E., Jørgensen, N., Carlsen, E., Petersen, P. M., Giwercman, A., Andersen, A. G., Jensen, T. K., Andersson, A. M. and Müller, J., 1998, Germ cell cancer and disorders of spermatogenesis: an environmental connection?, *Acta Pathologica, Microbiologica et Immunologica Scandinavica*, **106**, 3–12.

Skakkebæk, N. E., Rajpert-De Meyts, E. and Main, K. M., 2001, Testicular dysgenesis syndrome: an increasingly common developmental disorder with environmental aspects. *Human Reproduction*, **16**, 972–978.

Slikker, W., Jr, Bailey, J. R., Newport, G. D., Lipe, G. W. and Hill, D. E., 1982, Placental transfer and metabolism of 17α-ethinylestradiol and estradiol-17β in the rhesus monkey. *Journal of Pharmacology and Experimental Therapeutics*, **223**, 483–489.

Sonnenschein, C. and Soto, A. M., 1998, An updated review of environmental estrogen and androgen mimics and antagonists. *Journal of Steroid Biochemistry and Molecular Biology*, **65**, 143–150.

Spranger, B. and Metzler, M., 1991, Disposition of 17β-trenbolone in humans. *Journal of Chromatography Biomedical Applications*, **564**, 485–492.

Toppari, J., Larsen, J. C., Christiansen, P., Giwercman, A., Grandjean, P., Guillette, L. J., Jr, Jégou, B., Jensen, T. K., Jouannet, P., Keiding, N., Leffers, H., Mclachlan, J. A., Meyer, O., Muller, J., Rajpert-De Meyts, E., Scheike, T., Sharpe, R., Sumpter, J. and Skakkebæk, N. E., 1996, Male reproductive health and environmental xenoestrogens. *Environmental Health Perspectives*, **104 (suppl. 4)**, 741–803.

Tsukamoto, K., 1984, The metabolism and conjugation of estrogens in the human foetus. *Nippon Naibunpi Gakkai Zasshi*, **60**, 1091–1111.

Veeramachaneni, D. N. R., 2000, Deteriorating trends in male reproduction: idiopathic or environmental? *Animal Reproduction Science*, **60–61**, 121–130.

Veeramachaneni, D. N. R., Palmer, J. S. and Amann, R. P., 2001, Long-term effects on male reproduction of early exposure to common chemical contaminants in drinking water. *Human Reproduction*, 16, 979–987.

Veeramachaneni, D. N. R. and Vandewoude, S., 1999, Interstitial cell tumour and germ cell tumour with carcinoma *in situ* in rabbit testes. *International Journal of Andrology*, **22**, 97–101.

Weir, H. K., Marrett, L. D., Kreiger, N., Darlington, G. A. and Sugar, L., 2000, Pre-natal and peri-natal exposures and risk of testicular germ-cell cancer. *International Journal of Cancer*, 87, 438–443.

WHO, 1988, Toxicological evaluation of certain veterinary drug residues in food. *WHO Food Additives Series*, **23**, 73–151.

XENOBIOTICA, 2002, VOL. 32, NO. 8, 653–666

Taylor & Francis
healthsciences

Permissive and suppressive effects of dexamethasone on enzyme induction in hepatocyte co-cultures

M. RINGEL†, F. OESCH†, M. GERL‡, M. KLEBACH‡, M. QUINT‡, A. BADER§, T. BÖTTGER§ and J. G. HENGSTLER¶*

† Institute of Toxicology, Obere Zahlbacher Str. 67, D-55131 Mainz, Germany
‡ Aventis Pharma Deutschland GmbH, D-65926 Frankfurt, Germany
§ Leibnitz Laboratory, Hospital Hannover Oststadt, D-30659 Hannover, Germany
¶ Department of Surgery, University of Mainz, D-55131 Mainz, Germany

Received 14 August 2001

1. Steroids are known to act as permissive factors in hepatocytes. This study shows that dexamethasone (DEX) is a permissive factor for induction of CYP2B1/2, CYP3A1, CYP2A1 and probably also CYP2C11 in cultures with primary rat hepatocytes.

2. The induction factor of phenobarbital (PB)-induced formation of 16β-hydroxytestosterone (OHT), a testosterone biotransformation product predominantly formed by CYP2B1, is increased 18-fold by the addition of 32 nM DEX to the culture medium. Interestingly, higher concentrations of DEX up to 1000 nM led to a concentration-dependent maximally 5-fold decrease ($p = 0.002$) of phenobarbital-induced 16β-OHT formation compared with the effect observed with 32 nM DEX. Thus, DEX shows permissive and suppressive effects on enzyme induction depending on the concentration of the glucocorticoid.

3. Qualitatively similar but smaller permissive and suppressive effects of DEX were observed for PB-induced CYP3A1 activity as evidenced by formation of 2β-, 6β- and 15β-OHT.

4. DEX is a permissive factor for induction of CYP2A1 activity by 3-methylcholanthrene (3MC), as evidenced by the formation of 7α-OHT. Without addition of DEX, 3MC did not induce formation of 7α-OHT, whereas an almost 3-fold induction occurred in the presence of DEX. In contrast to CYP2B and CYP3A, concentrations up to 1000 nM DEX were not suppressive for the induction of CYP2A1.

5. We described recently a technique that allows preparation of cultures from cryopreserved hepatocytes. An almost identical influence of dexamethasone on enzyme induction was observed here in cultures from cryopreserved compared with freshly isolated hepatocytes.

6. Cultures with primary hepatocyte cultures represent a well-established technique for the study of drug–drug interactions. However, a large interlaboratory variation is known. Our study provides evidence that differences in glucocorticoid concentration in the culture medium contribute to this variation.

Introduction

The use of hepatocyte cultures is now well established for the study of drug–drug interactions. The observation that data reflecting the *in vivo* situation can be obtained with hepatocytes *in vitro* has led to the increased use of *in vitro* systems

* Author for correspondence; e-mail: hengstle@mail.Uni-Mainz.de

Xenobiotica ISSN 0049–8254 print/ISSN 1366–5928 online © 2002 Taylor & Francis Ltd
http://www.tandf.co.uk/journals
DOI: 10.1080/00498250210144811

with hepatocytes (Dou *et al.* 1992, Utesch *et al.* 1992, Li *et al.* 1999, Steinberg *et al.* 1999, Hengstler *et al.* 2000a, b, Runge *et al.* 2000). An important application of hepatocyte cultures is identification of drugs acting as inducers or inhibitors of biotransformation enzymes that alter metabolic clearance of other therapeutic agents. Well-known examples represent induction of cytochrome P4503A4 (CYP3A4) by rifampicin, carbamazepine or phenytoin leading to loss of protection in women taking oral contraceptives or to lowered serum concentrations of the immunosuppressant cyclosporin, causing serious clinical complications such as organ rejection after transplantation (Freeman *et al.* 1984, DeSouza *et al.* 1988, Cooney *et al.* 1995, Li *et al.* 1997).

Although hepatocyte cultures are well established for studies of enzyme induction, very large quantitative interlaboratory differences are known. For instance, induction factors of 2.1-fold (Wortelboer *et al.* 1991) and >10-fold (Hengstler *et al.* 2000b) have been reported for induction of PROD activity by phenobarbital in rat hepatocyte cultures. Probably these differences are due to different hepatocyte culture techniques related to differences in the hormonal additives to the culture medium. Researchers in independent laboratories have made the observation that addition of insulin (Yoshida *et al.* 1996, Sidhu and Omiecinski 1999) and a glucocorticoid is essential (Edwards and Lucas 1985a, b, Donato *et al.* 1990, Silver *et al.* 1990, Waxman *et al.* 1990, Sidhu *et al.* 1993, Nemoto *et al.* 1995, Sidhu and Omiecinski 1995, Kocarek and Reddy 1998, Jemnitz *et al.* 2000). The latter may be explained by the existence of glucocorticoid response elements that confer maximal inducibility of some biotransformation enzymes. For instance, a glucocorticoid response element has been identified in the 5′-region of rat CYP2B2 (Stoltz *et al.* 1998). Site directed mutagenesis indicated that this glucocorticoid response element as well as a nuclear factor 1 site and a nuclear receptor hexamer half-site are essential for conferring maximal phenobarbital induction of CYP2B2.

Although there is a general consensus that a glucocorticoid should be added to the hepatocyte culture medium for examination of enzyme induction, large differences exist in the type and concentration of glucocorticoids. Mostly dexamethasone (Utesch and Oesch 1992), hydrocortisone (Koebe *et al.* 1990, Wortelboer *et al.* 1991, Bader *et al.* 1992) and prednisolone (Bader *et al.* 1996) have been used as hormonal medium additives for culturing rat hepatocytes. For culturing rat hepatocytes, dexamethasone concentrations ranged from 100 nM (Madan *et al.* 1999) to 1 μM (Utesch and Oesch 1992) and hydrocortisone from 0.6 μM (Bader *et al.* 1992) to 20 μM (Koebe *et al.* 1990).

In the present study, we have examined the influence of glucocorticoid concentrations in the culture medium on the extent of enzyme induction. We report that dexamethasone is a permissive factor for induction of CYP2B, CYP2A and CYP3A activities, but it also suppresses enzyme induction if dexamethasone concentrations are higher than optimal. In our hepatocyte culture system, a concentration of 1 μM dexamethasone caused a clear reduction in inducibility of CYP2B compared with dexamethasone concentrations ranging between 32 and 100 nM. Since some investigators routinely use 1 μM dexamethasone as a hormonal additive to hepatocyte culture medium, whereas others use lower concentrations. The differences in glucocorticoid additives probably contribute to the large quantitative interlaboratory differences concerning studies of enzyme induction.

Materials and methods

Chemicals

3-Methylcholanthrene, phenobarbital, William's medium E (WME, without glutamine and phenolred), dexamethasone, 7-ethoxyresorufin, 7-pentoxyresorufin, trypan blue, insulin and Percoll were obtained from Sigma Chemical Co. (Deisenhofen, Germany). Bovine serum albumin (BSA) was obtained from Roth (Karlsruhe, Germany). Collagenase (type CLSII; 255 U mg^{-1}) and foetal calf serum (FCS) were supplied by Biochrom (Berlin, Germany). Penicillin/streptomycin (10 000 U ml^{-1} to 10 mg ml^{-1}) was obtained from Gibco (Paisley, UK) and pentobarbital sodium by Boehringer Ingelheim (Ingelheim, Germany). HBSS (10×) was obtained from PAN (Aidenbach, Germany). Petri dishes (9 cm diameter) were coated with collagen type 6 (C-7521) from human placenta (Sigma). All other chemicals of analytical grade were obtained from Merck (Darmstadt, Germany).

Animals

Male Sprague–Dawley rats (200–300 g body weight, 6–9 weeks old) (Charles River, Sulzfeld, Germany) were fed *ad libitum* with Sniff diet R/M-H (Sniff GmbH, Soest, Germany) and had free access to drinking water.

Hepatocyte isolation and cell culture

Rat hepatocytes were isolated using the two-step collagenase perfusion technique described by Seglen (1976) with slight modifications. The rats were anesthetized with an i.p. injection of pentobarbital (150 mg kg^{-1}). The liver was perfused via the vena portae for 20 min with an EGTA-buffer at 37 °C consisting of 124 ml glucose-solution (50 mM D-glucose), 20 ml KH-buffer (1 M NaCl, 24 mM KCl, and 12 mM KH_2PO_4; adjusted to pH 7.6 with NaOH), 20 ml HEPES-buffer (250 mM HEPES; adjusted to pH 8.5 with NaOH), 30 ml amino acid solution (3.0 mM L-alanine, 1.0 mM L-aspartic acid, 3.0 mM L-asparagine, 1.5 mM L-citrulline, 0.8 mM L-cysteine, 6.4 mM L-histidine, 6.8 mM L-glutamic acid, 13.3 mM L-glycin, 3.0 mM L-isoleucine, 6.1 mM L-leucine, 7.1 mM L-lysine, 3.7 mM L-methionine, 3.8 mM L-ornithine, 3.3 mM L-phenylalanine, 4.8 mM L-proline, 6.2 mM L-serine, 11.3 mM L-threonine, 3.2 mM L-tryptophan, 3.0 mM L-tyrosine, 6.8 mM L-valine; amino acids that could not be dissolved at neutral pH were dissolved by addition of 10 N NaOH at pH 11.0 and thereafter adjusted to pH 7.6 by 37% HCl), 2 ml glutamine solution (48 mM L-glutamine; freshly prepared), 1.0 ml insulin solution (I-5500; 0.35 mM insulin dissolved with 1 N NaOH, adjusted to pH 7.6 by 1 N HCl; freshly prepared) and 0.8 ml EGTA-solution (125 mM EGTA; dissolved by addition of NaOH, adjusted to pH 7.6 by HCl). Subsequently, perfusion was continued for 25 min by the collagenase buffer (37 °C) consisting of 155 ml glucose solution, 25 ml KH-buffer, 25 ml HEPES-buffer, 38 ml amino acid solution, 1.2 ml insulin solution, 10 ml $CaCl_2$ solution (129 mM $CaCl_2 \times 2\ H_2O$), 2.5 ml glutamine solution and 125 mg collagenase that were dissolved in the prewarmed mixture of the above mentioned solutions immediately before use. The flow for the EGTA and collagenase buffers was 10 ml min^{-1} and the pressure of perfusion did not exceed a 20-cm water column. After perfusion the liver was removed from the animal and dissociated in suspension buffer (620 ml glucose-solution, 100 ml KH buffer, 100 ml HEPES buffer, 150 ml amino acid solution, 10 ml glutamine solution, 5 ml insulin solution, 8 ml $CaCl_2$ solution, 4 ml $MgSO_4$ solution (100 mM $MgSO_4 \times 7\ H_2O$) and 2 g bovine serum albumin l^{-1} dissolved in the mixture of the above mentioned solutions). The liver cell suspension was filtered through gauze, centrifuged for 10 min at 15*g*, washed twice with suspension buffer, centrifuged again and resuspended in 30 ml suspension buffer. Hepatocytes were isolated by the 'warm technique' (Hengstler *et al.* 2000a) including the use of carbogen (95% O_2/5% CO_2) equilibrated buffers at 37 °C. Trypan blue exclusion rate was determined after 1:1 dilution of the hepatocyte suspension with an aqueous trypan blue solution (4 g l^{-1} trypan blue). The trypan blue exclusion rate (viability) of the hepatocytes varied from 74.6 to 84.8%.

Cryopreservation and thawing of hepatocytes

Cryopreservation was performed as described by Hengstler *et al.* (2000a). Hepatocytes were adjusted to 3×10^6 cells ml^{-1} in suspension buffer. The HEPES-buffer was adjusted to pH 7.6 and the suspension buffer is not gassed with carbogen. The volume was determined and the suspension was centrifuged for 10 min at 15*g*. A volume equal to two-thirds of the original volume was discarded from the supernatant and the cell pellet was resuspended in the remaining suspension buffer (one-third of the original volume) by shaking gently. Suspension buffer containing 12% (v/v) of DMSO was added to the cell suspension up to 50% of the original volume, resulting in a DMSO concentration of 4% and 6×10^6 ml^{-1} hepatocytes. After 5 min, suspension buffer containing 16% (v/v) of DMSO was added up to the original volume of the cell suspension, resulting in a DMSO concentration of 10% and 3×10^6 hepatocytes ml^{-1}. After 5 min, the hepatocyte suspension was transferred to cryovials with 1.5 ml per vial and the freezing programme was started within 5 min. The period between the second addition of DMSO and initiation of cryopreservation did not exceed 10 min. The freezing procedure was performed by a computer controlled freezing machine, BV-8 (Consarctic, Heidelberg, Germany) and

included: cooling in 10 min to 0 °C, 8 min at 0 °C, in 4 min to –8 °C, in 0.1 min to –28 °C, in 2 min to –33 °C, in 2 min up to –28 °C, in 16 min to –60 °C, in 4 min to –100 °C. The temperature in the chamber and in one sample was monitored during freezing by a chart recorder. Immediately after the freezing programme had been completed, cryovials were transferred into a liquid nitrogen atmosphere.

The frozen hepatocytes were thawed quickly by gentle shaking in a 37 °C water bath. Immediately after thawing the hepatocyte suspension was transferred into ice cold Erlenmeyer flasks and DMSO was gradually diluted by addition of cold suspension buffer, 0.5-, 1-, 2-, 3- and 6-fold the volume of the thawed hepatocyte suspension. Suspension buffer was added dropwise and hepatocytes placed for 5 min on ice before the next dilution step took place. After centrifugation (4 °C, 15*g*, 10 min) and resuspension in 10 ml suspension buffer, hepatocytes were purified by Percoll centrifugation.

Percoll purification

A modification of the method of Kreamer *et al.* (1986) was applied. A total of 10 ml hepatocytes in suspension buffer (containing maximally 20×10^6 hepatocytes), 22 ml suspension buffer and 18 ml Percoll solution were mixed gently and centrifuged at 50*g*, 4 °C, for 20 min. The Percoll solution consists of 16.2 ml Percoll and 1.8 ml HBSS-10× solution. After centrifugation the cell pellet containing the intact hepatocytes were resuspended and washed twice in suspension buffer (centrifugation at 15*g*, 10 min, 4 °C).

Cell culture and incubation with enzyme inducers

Hepatocytes were plated on 9-cm tissue culture dishes at a density of 5×10^6 cells/dish in 10 ml culture medium consisting of William's medium E supplemented with 10% FCS, 7 μM insulin (I-6634; 28.5 IU mg^{-1} insulin), dexamethasone (1–1000 nM as indicated in results), 4 mM L-glutamine and 1% penicillin/streptomycin solution. This insulin concentration was used since it was found adequate in Hengstler *et al.* (2000a). Media were replaced by 10 ml fresh media containing 10^6 NEC2 cells/dish, a rat liver non-parenchymal epithelial cell line (Hengstler *et al.* 2000a), after 3 and 15 h in the case of freshly isolated and cryopreserved hepatocytes, respectively. After 24 h of culture, hepatocytes were exposed to phenobarbital (PB, 0.75 mM) or 3-methylcholanthrene (3-MC, 5 μM) for 72 h. PB and 3-MC were dissolved in DMSO (0.5% in the incubation medium). Cell culture media contained 10% FCS throughout the experiment. The cells were cultured in a humidified incubator (5% CO_2) at 37.5 °C.

Enzyme assays

After incubation with inducers, the medium was removed and the attached cells were scraped off the plates using a rubber policeman. Than the cells were washed with phosphate-buffered saline (PBS). After centrifugation (50*g*, 10 min, 4 °C) the pellet was suspended in 2 ml PBS, homogenized by sonification, shock frozen and stored in liquid nitrogen. All enzyme assays were performed with these cell homogenates. The protein content of the cell homogenates was determined as described by Bradford (1969). 7-Ethoxyresorufin-*O*-deethylase (EROD) and 7-pentoxyresorufin-*O*-dependentylase (PROD) activities were measured as described by Burke and Mayer (1974) in the presence of dicumarol as suggested by Lubet *et al.* (1985) using 1.5 μM ethoxyresorufin or 9.8 μM pentoxyresorufin as CYP substrates and 6 mM NAD^+ in the buffer instead of nicotinamide (Lubet *et al.* 1985). The testosterone hydroxylation assay was performed according to Oesch *et al.* (1992) using 1.3 mM testosterone as substrate.

Statistical analysis

For enzyme activities and induction factors, statistical significance was analysed using Student's *t*-test (two-sided).

Results

To examine the influence of the dexamethasone concentration on enzyme induction, we incubated rat hepatocyte co-cultures with 0.75 mM phenobarbital for 3 days using culture media that contained dexamethasone concentrations ranging from 1 to 1000 nM. The concentration of 0.75 mM phenobarbital was chosen because it caused a maximal PROD induction (data not shown). Regio- and stereoselective hydroxylation of testosterone was examined (table 1). To facilitate interpretation we include an overview on biotransformation of testosterone by specific cytochrome P450 isoforms (table 2).

Table 1. Influence of dexamethasone concentrations (1.0–1000 nM) in the culture medium on induction of testosterone hydroxylation by 5 μM 3-methylcholanthrene (3-MC) and 0.75 mM phenobarbital (PB). DMSO (0.5% dimethylsulfoxide) served as a solvent control.

		Hydroxylation of testosterone (pmol min^{-1} × mg^{-1} protein) in position:								
Dexamathasone (nM)	Inducer	2α	2β	6α	6β	7α	15β	16α	16β	Androstendione
0	DMSO	55.0 ± 32.8	1.21 ± 0.04	19.6 ± 9.21	31.0 ± 10.6	18.4 ± 5.89	1.72 ± 0.70	56.5 ± 32.6	1.72 ± 0.25	105.4 ± 40.8
	3-MC	44.3 ± 30.7	2.03 ± 0.58	15.5 ± 2.32	29.9 ± 7.19	19.3 ± 6.17	1.64 ± 0.75	45.0 ± 30.3	1.92 ± 0.72	101.9 ± 45.3
	PB	24.5 ± 7.02	2.76 ± 1.00	12.6 ± 1.21	31.8 ± 4.79	45.1 ± 11.8	3.82 ± 0.43	29.0 ± 8.52	4.69 ± 1.91	87.6 ± 33.2
1.0	DMSO	51.5 ± 28.8	1.50 ± 0.43	16.1 ± 0.79	26.8 ± 2.70	22.1 ± 2.19	1.53 ± 0.52	52.3 ± 27.8	1.75 ± 0.49	105.3 ± 25.3
	3-MC	47.6 ± 31.5	2.44 ± 0.80	15.9 ± 1.90	31.5 ± 6.81	28.8 ± 5.47	1.94 ± 0.99	48.9 ± 30.1	1.85 ± 0.49	105.9 ± 53.0
	PB	30.5 ± 8.10	4.56 ± 2.44	13.4 ± 0.79	38.1 ± 8.67	60.7 ± 19.7	5.37 ± 1.77	43.4 ± 1.82*	15.0 ± 11.3	107.8 ± 26.6
3.2	DMSO	39.2 ± 18.6	1.42 ± 0.25	16.1 ± 1.20	24.5 ± 1.95	21.5 ± 2.04	1.16 ± 0.25	39.5 ± 18.2	1.39 ± 0.33	91.3 ± 16.6
	3-MC	42.3 ± 31.5	2.55 ± 1.02	16.8 ± 2.40	33.0 ± 9.05	41.6 ± 16.2	1.81 ± 1.03	42.1 ± 29.8	1.53 ± 0.56	101.5 ± 51.0
	PB	30.5 ± 9.90	5.72 ± 2.95	13.6 ± 1.48	42.6 ± 6.76	67.5 ± 15.8	6.81 ± 2.19	51.3 ± 9.45*	22.8 ± 8.06*	115.4 ± 27.2
10.0	DMSO	38.0 ± 29.4	1.57 ± 0.57	15.4 ± 1.25	25.4 ± 5.80	27.5 ± 9.33	1.75 ± 1.30	37.3 ± 26.8	1.42 ± 0.47	81.0 ± 29.6
	3-MC	30.5 ± 22.2	2.48 ± 1.13	16.1 ± 2.26	32.2 ± 8.98	52.9 ± 22.2	2.11 ± 1.37	30.8 ± 21.7	1.59 ± 0.50	85.1 ± 29.8
	PB	25.0 ± 5.60	11.1 ± 8.80	13.3 ± 1.27	56.5 ± 21.8	74.7 ± 26.4	11.1 ± 6.46	58.5 ± 21.3	40.8 ± 22.8	111.9 ± 4.59
32.0	DMSO	34.8 ± 26.7	1.72 ± 0.72	15.7 ± 1.37	28.1 ± 6.80	31.1 ± 15.3	2.03 ± 1.37	35.2 ± 25.0	1.72 ± 0.42	85.1 ± 26.0
	3-MC	26.0 ± 19.1	2.81 ± 1.42	17.1 ± 4.19	32.7 ± 10.8	68.4 ± 32.7	2.05 ± 1.08	26.2 ± 18.3	1.59 ± 0.55	70.5 ± 24.3
	PB	26.1 ± 14.4	14.9 ± 10.0	13.5 ± 0.81	71.2 ± 23.3*	75.5 ± 22.9	14.8 ± 6.69*	73.9 ± 39.1	82.5 ± 35.5*	130.9 ± 22.7
100.0	DMSO	33.4 ± 33.0	3.05 ± 1.01*	15.0 ± 2.65	32.8 ± 11.3	34.4 ± 27.0	4.08 ± 2.80	32.7 ± 30.4	1.98 ± 0.77	65.1 ± 27.9
	3-MC	32.7 ± 34.5	4.39 ± 1.18*	17.6 ± 5.31	42.6 ± 14.0	101.0 ± 79.5	4.78 ± 2.11	33.2 ± 30.7	2.38 ± 0.63	78.5 ± 37.4
	PB	32.5 ± 28.7	35.7 ± 11.0*	15.3 ± 3.51	148.1 ± 47.9*	127.9 ± 75.0	35.7 ± 13.4*	108.5 ± 52.6	90.3 ± 34.4*	177.6 ± 72.8
320.0	DMSO	33.2 ± 32.1	13.1 ± 2.44*	14.5 ± 1.39	65.0 ± 7.99*	31.3 ± 19.7	13.2 ± 1.55*	34.2 ± 29.1	3.84 ± 0.77*	70.1 ± 20.5
	3-MC	29.2 ± 29.5	16.6 ± 1.84*	16.5 ± 5.24	76.3 ± 8.16*	93.0 ± 78.5	14.0 ± 0.92*	31.1 ± 27.1	3.88 ± 0.59*	73.4 ± 27.5
	PB	36.6 ± 42.4	70.7 ± 27.6*	20.8 ± 14.8	250.7 ± 127.2*	146.5 ± 127.5	62.7 ± 31.7*	131.1 ± 77.3	109.7 ± 46.9*	230.2 ± 158.0
1000.0	DMSO	21.5 ± 12.8	41.1 ± 19.6*	13.5 ± 0.19	122.7 ± 45.8*	16.7 ± 6.09	31.7 ± 13.4*	23.1 ± 12.9	6.28 ± 2.66*	71.5 ± 18.4
	3-MC	28.1 ± 26.1	51.5 ± 16.2*	15.8 ± 3.20	156.4 ± 37.2*	77.4 ± 66.4	37.5 ± 10.8*	29.9 ± 26.2	7.12 ± 1.97	75.9 ± 25.3
	PB	36.5 ± 38.9	138 ± 31.9*	20.1 ± 13.5	400.9 ± 132.1*	118.1 ± 99.0	108.2 ± 32.7*	76.9 ± 63.0	57.5 ± 25.2*	173.4 ± 138.6

Data are means ± SD of three separate hepatocyte isolations.
* Significantly different ($p \leq 0.05$, Student's t-test) from the corresponding sample (0 nM dexamethasone).

Table 2. Regio- and stereoselective biotransformation of testosterone by cytochrome P450 enzymes of rat liver. Enzymes with the highest activities are shown in **bold**

Testosterone hydroxylation product (OHT)	Cytochrome P450 isoenzymes
2α-OHT	2C11[c]
2β-OHT	**3A1**[e], 3A2[e], 1A1[e]
6α-OHT	2A1[e]
6β-OHT	**3A1**[c], **2C13**[e], 2A2[e], 3A2[d], 1A1[d]
7α-OHT	**2A1**[a], 2A2[e]
15β-OHT	3A1[c], 2A2[e]
16α-OHT	**2B1**[d], **2C11**[d], 2B2[d], 2C7[d], 2C13[d]
16β-OHT	**2B1**[b], **2B2**[e], 3A1[e]
4-Androsten-3,17-dione	**2B1**[d], **2C11**[d], 2A2[e], 2B2[d], 3A1[e]

[a] Levin *et al.* (1987); [b] Waxmann *et al.* (1983); [c] Sonderfan *et al.* (1987); Waxmann (1988); [d] Utesch *et al.* (1992), [e] Hengstler *et al.* (2000a).

A substantial influence of the dexamethasone concentration on phenobarbital induced testosterone hydroxylation was observed in positions 16α and 16β that both are catalysed predominantly by CYP2B1 and CYP2B2 (table 3a). The phenobarbital-mediated induction of 16β-hydroxylation of testosterone was enhanced by addition of dexamethasone, reaching a maximum between 32 and 100 nM. Interestingly, a decrease in 16β-hydroxylation was obtained for higher dexamethasone concentrations (32 nM dexamethasone versus 1000 nM; $p = 0.002$). Although hydroxylation in the 16α-position was also dependent on dexamethasone, also reaching a maximum between 32 and 100 nM, the decrease at higher dexamethasone concentrations was less pronounced compared with 16β-OHT.

Similar results were also observed for phenobarbital-induced testosterone hydroxylation products predominantly formed by CYP3A1, namely 2β-, 6β- and 15β-OHT (table 3a). A substantial influence of dexamethasone was observed for 2β-OHT formation, reaching a maximum between 32 and 100 nM and decreasing at higher concentrations (100 nM dexamethasone versus 1000 nM; $p = 0.005$).

Phenobarbital induction of 6α- and 7α-OHT was also influenced by dexamethasone (table 3a). The latter testosterone hydroxylation products are predominantly formed by CYP2A1. However, the influence of dexamethasone on formation of 6α- and 7α-OHT was much smaller compared with hydroxylation products formed predominantly by CYP2B and CYP3A and did not reach statistical significance.

Hydroxylation of testosterone in position 2α is catalysed predominantly by the male-specific isoform CYP2C11. Similar to CYP2B1, CYP3A and CYP2A, dexamethasone also increased inducibility of CYP2C11 by phenobarbital (0 nM dexamethasone versus 100 nM; $p = 0.022$). However, in contrast to CYP2B and CYP3A inducibility of CYP2C11 was enhanced up to the highest tested dexamethasone concentration of 1000 nM.

Similar experiments as for phenobarbital were also performed for 3-methylcholanthrene. A concentration of 5 μM 3-methylcholanthrene, since this concentration caused a maximal induction of EROD (data not shown). As expected, 7α-OHT was the only testosterone hydroxylation product that could be induced by 3-methylcholanthrene (tables 1 and 3b). 7α-OHT is predominantly formed by CYP2A1. However, no induction of 7α-OHT was observed without addition of dexamethasone to the culture medium (table 3b). Addition of only 10 nM dex-

Table 3a. Influence of dexamethasone concentrations (1.0–1000 nM) in the culture medium on induction of testosterone hydroxylation by 0.75 mM phenobarbital (PB). Values are the corresponding induction factors of the data shown in table 1. DMSO (0.5% dimethylsulfoxide) served as a solvent control. Means ± SD of three separate hepatocyte isolations are given.

	Induction factors of testosterone hydroxylation after 72 h incubation with 0.75 mM phenobarbital								
Dexamethasone (nM)	2α	2β	6α	6β	7α	15β	16α	16β	Androstendione
0	0.51 ± 0.17	2.66 ± 0.85	0.71 ± 0.23	1.11 ± 0.40	2.59 ± 0.83	2.54 ± 1.21	0.57 ± 0.16	2.88 ± 1.65	0.84 ± 0.12
1.0	0.66 ± 0.18	3.28 ± 1.88	0.83 ± 0.04	1.45 ± 0.44	2.72 ± 0.63	3.91 ± 1.87	0.99 ± 0.49	10.6 ± 11.2	1.06 ± 0.35
3.2	0.82 ± 0.14	4.30 ± 2.69	0.84 ± 0.10	1.75 ± 0.43	3.16 ± 0.78	6.28 ± 2.99	1.44 ± 0.47*	17.8 ± 9.66	1.29 ± 0.33
10.0	0.86 ± 0.41	8.17 ± 7.20	0.86 ± 0.11	2.39 ± 1.27	2.94 ± 1.30	9.42 ± 6.61	2.19 ± 1.35	45.3 ± 12.1*	1.50 ± 0.49
32.0	0.84 ± 0.18	11.0 ± 8.91	0.86 ± 0.08	2.76 ± 1.42	2.95 ± 1.58	10.5 ± 7.26	3.07 ± 2.08	51.5 ± 7.33*	1.62 ± 0.47*
100.0	1.07 ± 0.20*	11.8 ± 0.83*	1.02 ± 0.13	4.54 ± 0.81*	4.07 ± 0.83	10.4 ± 3.65*	4.33 ± 1.94*	47.5 ± 20.7*	2.74 ± 0.40*
320.0	0.98 ± 0.23*	5.78 ± 3.32	1.38 ± 0.85	3.76 ± 1.47*	4.24 ± 1.06	4.64 ± 1.82	4.39 ± 1.27*	27.5 ± 7.57*	3.05 ± 1.22*
1000.0	1.48 ± 0.78	4.00 ± 2.27	1.48 ± 1.00	3.71 ± 2.12	6.33 ± 3.12	3.99 ± 2.33	3.09 ± 0.87*	10.4 ± 6.80	2.53 ± 2.01

* Significantly different ($p \leq 0.05$, Student's t-test) from the corresponding sample (0 nM dexamethasone).

Table 3b. Influence of dexamethasone concentrations (1.0–1000 nM) in the culture medium on induction of testosterone hydroxylation by 5 μM 3-methylcholanthrene (3-MC). Values are the corresponding induction factors of the data shown in table 1. DMSO (0.5% dimethylsulfoxide) served as a solvent control. Means ± SD of three separate hepatocyte isolations are given.

	Induction factors of testosterone hydroxylation after 72 h incubation with 5 μM 3-methylcholanthrene								
Dexamethasone (nM)	2α	2β	6α	6β	7α	15β	16α	16β	Androstendione
0	0.78 ± 0.08	1.41 ± 0.20	0.86 ± 0.22	0.99 ± 0.09	1.05 ± 0.09	0.94 ± 0.06	0.77 ± 0.08	1.11 ± 0.36	0.95 ± 0.05
1.0	0.89 ± 0.09	1.65 ± 0.39	1.07 ± 0.01	1.17 ± 0.13	1.18 ± 0.38	1.23 ± 0.21	0.91 ± 0.08	1.07 ± 0.15	1.03 ± 0.30
3.2	1.00 ± 0.29	1.75 ± 0.38	1.04 ± 0.11	1.34 ± 0.28	1.99 ± 0.94	1.50 ± 0.59	1.00 ± 0.27	1.10 ± 0.28	1.11 ± 0.49
10.0	0.81 ± 0.17	1.55 ± 0.14	1.04 ± 0.07	1.25 ± 0.06*	1.91 ± 0.24*	1.28 ± 0.16*	0.82 ± 0.16	1.13 ± 0.03	1.04 ± 0.06
32.0	0.77 ± 0.08	1.60 ± 0.12	1.05 ± 0.26	1.15 ± 0.18	2.21 ± 0.22*	1.08 ± 0.35	0.78 ± 0.13	0.94 ± 0.25	0.85 ± 0.22
100.0	0.93 ± 0.07	1.48 ± 0.23	1.16 ± 0.17	1.31 ± 0.09*	2.96 ± 0.36*	1.42 ± 0.68	1.01 ± 0.02*	1.24 ± 0.30	1.19 ± 0.08*
320.0	0.86 ± 0.06	1.28 ± 0.18	1.17 ± 0.25	1.18 ± 0.11	2.72 ± 0.61*	1.08 ± 0.20	0.90 ± 0.03	1.02 ± 0.09	1.03 ± 0.08
1000.0	1.13 ± 0.46	1.23 ± 0.37	1.16 ± 0.30	1.33 ± 0.35	2.97 ± 0.27*	1.23 ± 0.29	1.14 ± 0.42	1.18 ± 0.25	1.09 ± 0.39

* Significantly different ($p \leq 0.05$, Student's t-test) from the corresponding sample (0 nM dexamethasone).

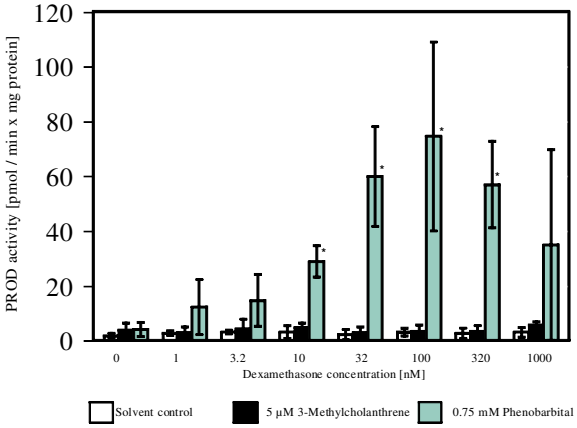


Figure 1. Effect of dexamethasone on PROD (7-pentoxyresorufin-*O*-deethylase) activities in cultured rat hepatocytes. Data are the mean and SD of three separate hepatocyte isolations. *Significantly different ($p \leq 0.05$, Student's *t*-test) from the corresponding sample (0 nM dexamethasone).

amethasone caused an approximately 2-fold increase in 3-methylcholanthrene induced hydroxylation of testosterone in position 7α (versus 0 nM dexamethsone; $p = 0.004$). A further increase was obtained for higher dexamethasone concentrations reaching a plateau between 100 nM (versus 0 nM dexamethasone; $p = 0.0009$) and 1000 nM (versus 0 nM dexamethasone; $p = 0.001$).

In addition to testosterone hydroxylation, we also examined 7-pentoxyresorufin-*O*-dealkylation (PROD; figure 1) and 7-ethoxyresorufin-*O*-deethylation (EROD; figure 2) activities. Activity of PROD after treatment with 0.75 mM phenobarbital was 4.0 pmol min^{-1} mg^{-1} without addition of dexamethasone to the culture medium (figure 1). A maximal PROD activity (74.4 pmol min^{-1} mg^{-1}) was observed for 100 nM dexamethasone (versus 0 nM dexamethasone; $p = 0.024$). The influence of dexamethasone on EROD activity after induction by 5 µM 3-methylcholanthrene was less prominent compared with PROD activity after incubation by phenobarbital (figure 2). Nevertheless, addition of 32 nM dexamethasone increased 3-methylcholanthrene mediated EROD induction 2.6-fold compared with incubations without addition of dexamethasone ($p = 0.013$).

All experiments described so far were performed with freshly isolated hepatocytes. We described recently a technique that allows establishment of cultures with cryopreserved hepatocytes (Hengstler *et al.* 2000a). Thus, we examined whether dexamethasone influences enzyme induction also in cultures prepared with cryopreserved hepatocytes. A similar scenario was observed as for fresh cultures (table 4). Dexamethasone concentrations up to 1000 nM did not influence viability and morphology of hepatocyte co-cultures during the incubation time of 72 h (data not shown).

Discussion

Glucocorticoids are usually included into media for hepatocyte cultures, since several hepatic functions depend on steroid hormones. For instance phenobarbital induced DNA synthesis in cultured rat hepatocytes was enhanced by 30 nM dexamethasone, while dexamethasone alone had almost no effect (Edwards and

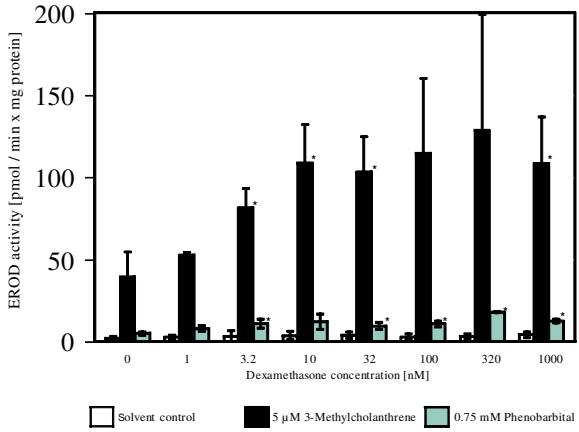


Figure 2. Effect of dexamethasone on EROD (7-ethoxyresorufin-*O*-deethylase) activities in cultured rat hepatocytes. Data are the mean and SD of three separate hepatocyte isolations. *Significantly different ($p \leq 0.05$, Student's *t*-test) from the corresponding sample (0 nM dexamethasone).

Lucas 1985a). Similarly, steroids enhance induction of γ-glutamyltranspeptidase by phenobarbital (Edwards and Lucas 1985b), induction of UDP-glucuronosyltransferase 1A6 by polycyclic aromatic hydrocarbons (Jemnitz *et al.* 2000) and the glucagon-dependent activation of the phosphoenol-pyruvate carboxykinase gene (Runge *et al.* 1991) in rat hepatocytes. In addition, steroids enhance induction of ECOD by phenobarbital in human hepatocytes (Donato *et al.* 1990). A permissive effect of dexamethasone has already been reported for CYP2B1/2 and CYP3A1 mRNA expression: concentrations up to 100 nM potentiated phenobarbital induced mRNA expression in primary cultures of rat hepatocytes (Sidhu *et al.* 1993, Sidhu and Omiecinski 1995, Kocarek and Reddy 1998, Burczynski *et al.* 2001). However, data concerning permissive effects of dexamethasone in rat hepatocytes are not completely consistent. Consistent with previous reports Burczynski *et al.* (2001) observed also a permissive effect of dexamethasone concerning CYP2B1 induction in rat hepatocytes. However, rat hepatocytes cultured in the absence of dexamethasone gave much higher fold inductions for CYP1A1 and CYP3A1 in the presence of inducers (Burczynski *et al.* 2001).

In the current study, we have shown that dexamethasone is a permissive factor for induction of rat CYP2B1/2, 3A1 and 2C11 by phenobarbital and also for CYP2A1 by 3-methylcholanthrene. Phenobarbital induction of CYP2B1, as evidenced by formation of 16β-OHT, is 18-fold higher in the presence of 32 nM dexamethasone, whereas phenobarbital induction of CYP3A1 activity (2β-, 6β-, 15β-OHT) was enhanced only 4-fold in the presence of 100 nM dexamethasone. Interestingly, induction of both CYP2B1/2 and CYP3A1 activities was maximal at 32–100 nM dexamethasone, whereas higher dexamethasone concentrations suppressed the effect of phenobarbital. Compared with the maximal induction, a 5- and 3-fold decrease in CYP2B1 and CYP3A1 induction, respectively, was obtained at a dexamethasone concentration of 1 µM. This observation is of practical relevance, since a large number of studies on enzyme induction have been performed using 1 µM dexamethasone as a hormonal culture medium additive (e.g. Utesch *et al.* 1992), whereas others have used 0.1 µM dexamethasone (Madan *et al.* 1999). Thus, the difference in steroid concentrations is likely to contribute to

Table 4. Influence of dexamethasone concentrations (100 versus 1000 nM) on enzyme induction in cultures of cryopreserved hepatopcytes. (A) Induction of 7-ethoxyresorufin-*O*-deethylase (EROD) by 5 μM 3-methylcholanthrene (3-MC) as well as induction of 7-pentoxyresorufin-*O*-deethylase (PROD) by 0.75 mM phenobarbital (PB). (B) Induction of regio- and stereospecific testosterone hydroxylation by 3-MC and PB. DMSO (dimethylsulfoxide, 0.5%) served as a solvent control.

		Activity (pmol min^{-1} mg^{-1})		Induction factor	
		Dexamethasone concentration		Dexamethasone concentration	
	Inducer	100 nM	1000 nM	100 nM	1000 nM
(A) Assay					
EROD	DMSO	2.08 ± 0.41	3.77 ± 1.92		
	3-MC	109.0 ± 53.9	58.3 ± 0.69	52.4	15.5
	PB	10.5 ± 7.15	23.3 ± 14.3	5.05	6.18
PROD	DMSO	2.05 ± 0.09*	5.43 ± 1.53		
	3-MC	3.47 ± 1.58	5.25 ± 1.02	1.69	0.97
	PB	40.0 ± 27.5	14.2 ± 2.22	19.5	2.61
(B) Testosterone-hydroxylation at position:					
2α	DMSO	8.93 ± 5.32	4.32 ± 0.77		
	3-MC	7.95 ± 2.96	5.52 ± 5.59	0.89	1.28
	PB	14.0 ± 4.53	6.97 ± 4.42	1.57	1.61
2β	DMSO	≤ 0.20*	31.2 ± 12.0		
	3-MC	0.79 ± 0.45*	27.7 ± 14.7	≥ 3.95	0.89
	PB	5.78 ± 1.84*	68.6 ± 19.5	≥ 28.9	2.20
6α	DMSO	14.2 ± 5.45	14.6 ± 3.44		
	3-MC	15.0 ± 5.85	11.7 ± 0.65	1.06	0.80
	PB	14.6 ± 5.98	14.1 ± 2.56	1.03	0.96
6β	DMSO	15.9 ± 4.86*	88.8 ± 32.3		
	3-MC	23.5 ± 7.49	80.3 ± 39.3	1.48	0.90
	PB	36.8 ± 20.4*	188.7 ± 47.8	2.31	2.12
7α	DMSO	6.96 ± 4.80	4.21 ± 2.70		
	3-MC	35.7 ± 16.6	27.8 ± 23.8	5.13	6.60
	PB	33.2 ± 19.4	23.7 ± 15.9	4.80	5.63
15β	DMSO	0.92 ± ≤0.01*	20.2 ± 8.68		
	3-MC	1.18 ± 0.44*	20.2 ± 9.68	1.28	1.00
	PB	5.32 ± 3.28*	47.9 ± 11.4	5.78	2.37
16	DMSO	13.2 ± 6.64	6.13 ± 1.41		
	3-MC	12.1 ± 4.34	7.88 ± 5.21	0.92	1.28
	PB	106.7 ± 59.7*	22.0 ± 9.61	8.08	3.59
16β	DMSO	1.25 ± 0.98*	4.98 ± 1.75		
	3-MC	0.98 ± 0.79	3.91 ± 2.28	0.78	0.78
	PB	58.5 ± 37.8	22.4 ± 14.5	46.8	4.50
Androstendione	DMSO	48.0 ± 23.6	80.4 ± 52.2		
	3-MC	51.9 ± 32.4	45.7 ± 15.3	1.08	0.57
	PB	119.9 ± 61.3	72.6 ± 28.5	2.50	0.90

Data are means ± SD of at least three separate hepatocyte isolations.

* Enzyme activity significantly different ($p \leq 0.05$, Student's *t*-test) from the corresponding sample (1000 nM dexamathasone).

the large quantitative interlaboratory differences in enzyme induction studies. Furthermore, it can be expected that the optimal dexamethasone concentrations differ between various *in vitro* systems, such as hepatocyte monocultures, co-cultures, sandwich cultures, microencapsulated hepatocytes and liver slices. Thus, dexamethasone concentrations should be optimized for each individual system to achieve an optimal sensitivity for studies of enzyme induction.

Interestingly, dexamethasone also showed a permissive effect for induction of CYP2A1 by 3-methylcholanthrene as evidenced by 7α-OHT formation ($p \leq 0.05$ for dexamethasone concentrations 0 nM versus ≥10 nM; table 3b).

Dexamethasone also appeared to be a permissive factor for phenobarbital induction of the male-specific CYP2C11. However, this effect must be interpreted with caution: without addition of dexamethasone the induction factor due to phenobarbital was 0.51 showing that phenobarbital alone suppressed formation of 2α-OHT (table 3A). A small increase in phenobarbital induced 2α-OHT formation was observed when dexamethasone concentrations were increased up to 1000 nM. However, this observation is complicated because dexamethasone alone suppressed formation of 2α-OHT. In previously published studies, suppression of CYP2C11 by high concentrations of glucocorticoid was also observed (Iber *et al.* 1997, Murray 2000). Thus, the influence of dexamethasone on basal and induced CYP2C11 seems to be complex. Taken together, the data show that in our hepatocyte co-culture system, addition of 100 nM dexamethasone is optimal for enzyme induction studies. The latter concentration yields maximal induction of CYP2B and CYP3A1, but still does not cause enzyme induction per se.

Taken together with previous studies (Silver *et al.* 1990, Waxman *et al.* 1990, Sidhu *et al.* 1993, Sidhu and Omiecinsky 1995) steroids strongly influence inducibility of cytochrome P450 mRNA (Silver *et al.* 1990, Sidhu *et al.* 1993, Sidhu and Omiecinsky 1995), protein (Waxman *et al.* 1990) and activity (present study). However, the molecular mechanisms whereby glucocorticoids confer maximal phenobarbital inducibility remain unsolved. Recently, a putative glucocorticoid response element has been identified in the phenobarbital response unit 5′ of the rat CYP2B2 gene (Stoltz *et al.* 1998). Site-directed mutagenesis indicated that this glucocorticoid response element is essential for conferring maximal phenobarbital inducibility. However, recent research suggested that mechanisms independent from glucocorticoid-response elements may be involved (Kende *et al.* 1985, Forman *et al.* 1998, Edwards 1999, Sueyoshi *et al.* 1999, Waxman 1999): the orphan receptor CAR (constitutive androstane receptor) binds to DNA as a heterodimer with the retinoid-X receptor (RXR). The (CAR-RXR)–DNA complex associates with the nuclear receptor coactivator SRC-1. SRC-1 serves as a general transducer between DNA-bound nuclear receptors and the transcriptional machinery and confers transcription of, for instance, CYP2B2. In this context it seems to be relevant that dexamethasone has been demonstrated to increase CAR mRNA expression as well as phenobarbital-mediated nuclear translocation of CAR, explaining the synergistic effect of this glucocorticoid on phenobarbital-mediated induction of CYP2B genes (Pascussi *et al.* 2000). The steroids androstanol (5α-androstan-3α-ol) and androstenol (5α-androst-16-en-3α-ol) interact with CAR and inhibit its transcriptional activity. This inhibition is mediated by a mechanism that involves dissociation of SRC-1 from the (CAR-RXR)–DNA complex as a consequence of binding of androstanes (androstanol and androstenol) to CAR. It has been suggested that in the presence of phenobarbital or phenobarbital-like inducers, the binding of androstanes to CAR is abolished and that CYP2B transcription is thereby derepressed (Sueyoshi *et al.* 1999, Waxman 1999). It is tempting to speculate that steroids other than androstanes, for instance dexamethasone, might interfere with transcriptional repression/derepression of CYP2B transcription. Possibly high concentrations of dexamethasone inhibit

transcription of CYP2B by a similar mechanism as suggested for androstanol and androstenol. However, this assumption still remains speculative.

In conclusion, we have shown that glucocorticoids represent permissive factors for induction of rat CYP3A1, CYP2B1/2, CYP2A1 and possibly also of CYP2C11 activity. However, high steroid concentrations suppress CYP2B1/2 and 3A1/2 (but not CYP2A1 and 2C11) inducibility. Taken together, our results emphasize the importance of optimizing steroid concentrations in culture media of hepatic *in vitro* systems for the study of enzyme induction.

Acknowledgements

This paper is dedicated to Prof. Dr. A. Kröger (Frankfurt, Germany). The study was supported by the BMBF, Project No. 0312500.

References

Bader, A., Borel Rinkes, I. H., Closs, E. I., Ryan, C. M., Toner, M., Cunningham, J. M., Tompkins, R. G. and Yarmush, M. L., 1992, A stable long-term hepatocyte culture system for studies of physiologic processes: cytokine stimulation of the acute phase response in rat and human hepatocytes. *Biotechnology Progress*, **8**, 219–225.

Bader, A., Knop, E., Boker, K. H., Crome, O., Fruhauf, N., Gonschior, A. K., Christians, U., Esselmann, H., Pichlmayr, R. and Sewing, K. F., 1996, Tacrolimus (FK 506) biotransformation in primary rat hepatocytes depends on extracellular matrix geometry. *Naunyn Schmiedebergs Archives of Pharmacology*, **353**, 461–473.

Bradford, M. M., 1969, A rapid and sensitive method for the quantification of microgram quantities of protein utilizing the principle of protein–dye binding. *Analytical Biochemistry*, **27**, 502–522.

Burczynski, M. E., McMillan, M., Parker, J. B., Bryant, S., Leone, A., Grant, E. R., Thorne, J. M., Zhong, Z., Zivin, R. A. and Johnson, M. D.., 2001, Cytochrome P450 induction in rat hepatocytes assessed by quantitative real-time reverse-transcription polymerase chain reaction and the RNA invasive cleavage assay. *Drug Metabolism and Disposition*, 29, 1243–1250.

Burke, M. D. and Mayer, R. T., 1974, Ethoxyresorufin: direct fluorimetric assay of a microsomal *O*-dealkylation which is preferentially by 3-methylcholanthrene. *Drug Metabolism and Disposition*, **2**, 583–588.

Cooney, G. F., Mochon, M., Kaiser, B., Dunn, S. P. and Goldsmith, B., 1995, Effects of carbamazepine on cyclosporine metabolism in pediatric renal transplant recipients. *Pharmacotherap*, **15**, 353–356.

Donato, M. T., Gomez Lechon, M. J. and Castell, J. V., 1990, Effect of xenobiotics on monooxygenase activities in cultured human hepatocytes. *Biochemical Pharmacology*, **39**, 1321–1326.

Dou, M., De Sousa, G., Lacarelle, B., Placidi, M., Lechene De La Porte, P., Domingo, M., Lafont, H. and Rahmani, R., 1992, Thawed human hepatocytes in primary culture. *Cryobiology*, **29**, 454–469.

DeSouza, M. J., Pollock, S. H. and Solomon, H. M., 1988, Cyclosporine-phenytoin interaction. *Drug Metabolism and Disposition*, **16**, 256–258.

Edwards, D. P., 1999, Coregulatory proteins in nuclear hormone receptor action. *Vitamins and hormones*, **55**, 165–218.

Edwards, A. M. and Lucas, C. M., 1985a, Phenobarbital and some other liver tumor promoters stimulate DNA synthesis in cultured rat hepatocytes. *Biochemical and Biophysical Research Communications*, **131**, 103–108.

Edwards, A. M. and Lucas, C. M., 1985b, Induction of gamma-glutamyl transpeptidase in primary cultures of normal rat hepatocytes by liver tumor promoters and structurally related compounds. *Carcinogenesis*, **6**, 733–739.

Forman, B. M., Tzameli, I., Choi, H. S., Chen, J., Simha, D., Seol, W., Evans, R. M. and Moore, D. D., 1998, Androstane metabolites bind to and deactivate the nuclear receptor CAR-beta. *Nature*, **395**, 612–615.

Freeman, D. J., Laupacis, A., Keown, P. A., Stiller, C. R. and Carruthers, S. G., 1984, Evaluation of cyclosporin-phenytoin interaction with observations on cyclosporin metabolites. *British Journal of Clinical Pharmacology*, **18**, 887–893.

Hengstler, J. G., Ringel, M., Biefang, K., Hammel, S., Milbert, U., Gerl, M., Klebach, M., Diener, B., Platt, K. L., Bottger, T., Steinberg, P. and Oesch, F., 2000a, Cultures with cryopreserved hepatocytes: applicability for studies of enzyme induction. *Chemico-Biological Interactions*, **125**, 51–73.

Hengstler, J. G., Utesch, D., Steinberg, P., Platt, K. L., Diener, B., Ringel, M., Swales, N., Fischer, T., Biefang, K., Gerl, M., Bottger, T. and Oesch, F., 2000b, Cryopreserved primary hepatocytes as a constantly available *in vitro* model for the evaluation of human and animal drug metabolism and enzyme induction. *Drug Metabolism Reviews*, **32**, 81–118.

Iber, H., Chen, Q., Sewer, M. and Morgan, E. T., 1997, Regulation of hepatic cytochrome P450 2C11 by glucocorticoids. *Archives of Biochemistry and Biophysics*, **345**, 305–310.

Jemnitz, K., Veres, Z., Monostory, K. and Vereczkey, L., 2000, Glucuronidation of thyroxine in primary monolayer cultures of rat hepatocytes: *in vitro* induction of UDP-glucuronosyltranferases by methylcholanthrene, clofibrate, and dexamethasone alone and in combination. *Drug Metabolism and Disposition*, **28**, 34–37.

Kende, A. S., Ebetino, F. H., Drendel, W. B., Sundaralingam, M., Glover, E. and Poland, A., 1985, Structure–activity relationship of bispyridyloxybenzene for induction of mouse hepatic aminopyrine *N*-demethylase activity. Chemical biological, and X-ray crystallographic studies. *Molecular Pharmacology*, **28**, 445–453.

Kocarek, T. A. and Reddy, A. B., 1998, Negative regulation by dexamethasone of fluvastatin-inducible CYP2B expression in primary cultures of rat hepatocytes: role of CYP3A. *Biochemical Pharmacology*, **55**, 1435–1443.

Koebe, H. G., Dunn, J. C., Toner, M., Sterling, L. M., Hubel, A., Cravalho, E. G., Yarmush, M. L. and Tompkins, R. G., 1990, A new approach to the cryopreservation of hepatocytes in a sandwich culture configuration. *Cryobiology*, **27**, 576–584.

Kreamer, B. L., Staecker, J. L., Sawada, N., Sattler, G. L., Hsia, M. T. and Pitot, H. C., 1986, Use of a low-speed, iso-density Percoll centrifugation method to increase the viability of isolated rat hepatocyte preparations. *In Vitro Cellular and Developmental Biology*, **22**, 201–211.

Levin, W., Thomas, P. E., Ryan, D. E. and Wood, A. W., 1987, Isoenzyme specificity of testosterone 7 alpha-hydroxylation in rat hepatic microsomes: is cytochrome P-450a the sole catalyst? *Archives of Biochemistry and Biophysics*, **258**, 630–635.

Li, A. P., Gorycki, P. D., Hengstler, J. G., Kedderis, G. L., Koebe, H. G., Rahmani, R., De Sousas, G., Silva, J. M. and Skett, P., 1999, Present status of the application of cryopreserved hepatocytes in the evaluation of xenobiotics: consensus of an international expert panel. *Chemico-Biological Interactions*, **121**, 117–123.

Li, A. P., Maurel, P., Gomez Lechon, M. J., Cheng, L. C. and Jurima Romet, M., 1997, Preclinical evaluation of drug–drug interaction potential; present status of the application of primary human hepatocytes in the evaluation of cytochrome P450 induction. *Chemico-Biological Interactions*, **107**, 5–16.

Lubet, R. A., Nims, R. W., Mayer, R. T., Cameron, J. W. and Schechtman, L. M., 1985, Measurement of cytochrome P-450 dependent dealkylation of alkoxyphenoxazones in hepatic S9s and hepatocyte homogenates: effects of dicumarol. *Mutation Research*, **142**, 127–131.

Madan, A., Dehaan, R., Mudra, D., Carroll, K., Lecluyse, E. and Parkinson, A., 1999, Effect of cryopreservation on cytochrome P-450 enzyme induction in cultured rat hepatocytes. *Drug Metabolism and Disposition*, **27**, 327–335.

Murray, M., 2000, Glucocorticoid-dependent maintenance of CYP2C11-dependent oxidation in male rat liver *in vivo*. *Human and Experimental Toxicology*, **19**, 126–131.

Nemoto, N., Sakurai, J. and Funae, Y., 1995, Maintenance of phenobarbital-inducible Cyp2b gene expression in C57BL/6 mouse hepatocytes in primary culture as spheroids. *Archives of Biochemistry and Biophysics*, **316**, 362–369.

Oesch, F., Wagner, H., Platt, K. L. and Arand, M., 1992, Improved sample preparation for the testosterone hydroxylation assay using disposable extraction columns. *Journal of Chromatography*, **582**, 232–235.

Pascussi, J. M., Gerbal-Chaloin, S., Fabre, J. M., Maurel, P. and Vilarem, M. J., 2000, Dexamethasone enhances constitutive androstane receptor expression in human hepatocytes: consequences on cytochrome P450 gene regulation. *Molecular Pharmacology*, **58**, 1441–1450.

Runge, D., Kohler, C., Kostrubsky, V. E., Jager, D., Lehmann, T., Runge, D. M., May, U., Stolz, D. B., Strom, S. C., Fleig, W. E. and Michalopoulos, G. K., 2000, Induction of cytochrome P450 (CYP)1A1, CYP1A2, and CYP3A4 but not of CYP2C9, CYP2C19, multidrug resistance (MDR-1) and multidrug resistance associated protein (MRP-1) by prototypical inducers in human hepatocytes. *Biochemical and Biophysical Research Communications*, **273**, 333–341.

Runge, D., Schmidt, H., Christ, B. and Jungermann, K., 1991, Mechanism of the permissive action of dexamethasone on the glucagon-dependent activation of the phosphoenolpyruvate carboxykinase gene in cultured rat hepatocytes. *European Journal of Biochemistry*, **198**, 641–649.

Seglen, P. O., 1976, Preparation of isolated rat liver cells. In D. M. Prescott (ed.), *Methods in Cell Biology* (New York: Academic Press), pp. 29–83.

Sidhu, J. S., Farin, F. M. and Omiecinski, C. J., 1993, Influence of extracellular matrix overlay on phenobarbital-mediated induction of CYP2B1, 2B2, and 3A1 genes in primary adult rat hepatocyte culture. *Archives of Biochemistry and Biophysics*, **301**, 103–113.

Sidhu, J. S. and Omiecinski, C. J., 1995, Modulation of xenobiotic-inducible cytochrome P450 gene expression by dexamethasone in primary rat hepatocytes. *Pharmacogenetics*, **5**, 24–36.

Sidhu, J. S. and Omiecinski, C. J., 1999, Insulin-mediated modulation of cytochrome P450 gene induction profiles in primary rat hepatocyte cultures. *Journal of Biochemical and Molecular Toxicology*, **13**, 1–9.

Silver, G., Reid, L. M. and Krauter, K. S., 1990, Dexamethasone-mediated regulation of 3-methylcholanthrene-induced cytochrome P-450d mRNA accumulation in primary rat hepatocyte cultures. *Journal of Biological Chemistry*, **265**, 3134–3138.

Sonderfan, A. J., Arlotto, M. P., Dutton, D. R., McMillen, S. K. and Parkinson, A., 1987, Regulation of testosterone hydroxylation by rat liver microsomal cytochrome P-450. *Archives of Biochemistry and Biophysics*, **255**, 27–41.

Steinberg, P., Fischer, T., Kiulies, S., Biefang, K., Platt, K. L., Oesch, F., Bottger, T., Bulitta, C., Kempf, P. and Hengstler, J., 1999, Drug metabolizing capacity of cryopreserved human, rat, and mouse liver parenchymal cells in suspension. *Drug Metabolism and Disposition*, **27**, 1415–1422.

Stoltz, C., Vachon, M. H., Trottier, E., Dubois, S., Paquet, Y. and Anderson, A., 1998, The CYP2B2 phenobarbital response unit contains an accessory factor element and a putative glucocorticoid response element essential for conferring maximal phenobarbital responsiveness. *Journal of Biological Chemistry*, **273**, 8528–8536.

Sueyoshi, T., Kawamoto, T., Zelko, I., Honkakoski, P. and Negishi, M., 1999, The repressed nuclear receptor CAR responds to phenobarbital in activating the human CYP2B6 gene. *Journal of Biological Chemistry*, **274**, 6043–6046.

Utesch, D., Diener, B., Molitor, E., Oesch, F. and Platt, K. L., 1992, Characterization of cryopreserved rat liver parenchymal cells by metabolism of diagnostic substrates and activities of related enzymes. *Biochemical Pharmacology*, **44**, 309–315.

Utesch, D. and Oesch, F., 1992, Dependency of the *in vitro* stabilization of differentiated functions in liver parenchymal cells on the type of cell line used for co-culture. *In vitro Cellular and Developmental Biology*, **28A**, 193–198.

Waxman, D. J., 1988 Interactions of hepatic cytochromes P-450 with steroid hormones. Regioselectivity and stereospecificity of steroid metabolism and hormonal regulation of rat P-450 enzyme expression. *Biochemical Pharmacology*, **37**, 71–84.

Waxman, D. J., 1999, P450 gene induction by structurally diverse xenochemicals: central role of nuclear receptors CAR, PXR, and PPAR. *Archives of Biochemistry and Biophysics*, **369**, 11–23.

Waxman, D. J., Ko, A. and Walsh, C., 1983, Regioselectivity and stereoselectivity of androgen hydroxylations catalyzed by cytochrome P-450 isoenzymes purified from phenobarbital-induced rat liver. *Journal of Biological Chemistry*, **258**, 11937–11947.

Waxman, D. J., Morrissey, J. J., Naik, S. and Jauregui, H. O., 1990, Phenobarbital induction of cytochromes P-450. High-level long-term responsiveness of primary rat hepatocyte cultures to drug induction, and glucocorticoid dependence of the phenobarbital response. *Biochemical Journal*, **271**, 113–119.

Wortelboer, H. M., De Kruif, C. A., Van Iersel, A. A., Falke, H. E., Noordhoek, J. and Blaauboer, B. J., 1991, Comparison of cytochrome P450 isoenzyme profiles in rat liver and hepatocyte cultures. The effects of model inducers on apoproteins and biotransformation activities. *Biochemical Pharmacology*, **42**, 381–390.

XENOBIOTICA, 2002, VOL. 32, NO. 8, 667–682

Taylor & Francis
healthsciences

Metabolism of 2-nitrofluorene, an environmental pollutant, by liver preparations of sea bream, *Pagrus major*

O. UEDA, S. KITAMURA* and S. OHTA

Institute of Pharmaceutical Science, Hiroshima University, School of Medicine, Kasumi 1-2-3, Minami-ku, Hiroshima 734-8551, Japan

Received 5 October 2001

1. The *in vitro* metabolism of 2-nitrofluorene (NF), an environmental pollutant, was examined in fish, focusing on nitro-reduction followed by *N*-acylation and hydroxylation.

2. When NF was incubated with liver microsomes or cytosol of sea bream, *Pagrus major*, in the presence of NADPH or 2-hydroxypyrimidine, 2-aminofluorene (AF) was formed.

3. When AF was incubated with liver cytosol in the presence of acetyl-CoA or *N*-formyl-L-kynurenine, 2-acetylaminofluorene (AAF) or 2-formylaminofluorene (FAF) was formed, respectively. AAF and FAF thus formed were deacylated to the parent AF by the liver preparations.

4. AF, AAF and FAF were oxidized to 7-hydroxy or 5-hydroxy derivatives by the liver microsomes.

5. Nitro-reduction, *N*-acylation and ring-hydroxylation of NF and the metabolites were also observed in rat liver preparations. These activities in sea bream livers were lower than those of rat liver. However, the order of magnitude of these activities in fish was the same as in rat.

6. It is suggested that NF is effectively reduced to AF by the cytochrome P450 system or aldehyde oxidase, and the acylated metabolites, AAF and FAF, generated by arylamine acetyltransferase and formamidase were hydroxylated by the cytochrome P450 system in fish in the same way as in rat. Further, the acetylamino and formylamino derivatives were interconverted via amino derivatives in the fish.

Introduction

Nitropolycyclic aromatic hydrocarbons (nitro-PAHs), which are widespread environmental pollutants found in automobile exhaust, the urban atmosphere, the wastewater from gasoline stations, cigarette smoke, airplane engine emissions, coal fly ash, etc., enter waterways via the release of urban wastewater into the environment and by atmospheric fallout of airborne particles associated with smog (Wang *et al*. 1980, El-Bayoumy *et al*. 1982, Rosenkranz and Mermelstein 1983, Manabe *et al*. 1984, Hayakawa *et al*. 1995). Nitro-PAHs exhibit a range of biological activities including mutagenicity and carcinogenicity. They are strong mutagens and multi-site carcinogens. For instance, 2-nitrofluorene (NF) causes liver, mammary gland and intestine/forestomach tumours and is a typical mutagen. It is particularly important as nitro-PAHs that these compounds usually require metabolic activation to become mutagenic, and nitro-reduction leads to direct acting mutagens (Möller *et al*. 1989, Fu 1990, Purohit and Basu 2000). NF

* Author for correspondence; e-mail: skitamu@hiroshima-u.ac.jp

Xenobiotica ISSN 0049–8254 print/ISSN 1366–5928 online © 2002 Taylor & Francis Ltd
http://www.tandf.co.uk/journals
DOI: 10.1080/00498250210144839

has been detected as a major component in diesel particles, together with nitropyrenes (Campbell and Milton 1984, Beije and Möller 1988). It has also been reported that NF forms DNA adducts (Möller *et al.* 1994, Cui *et al.* 1999).

Recently, we examined the *in vivo* metabolism of NF in rat, reporting that NF was metabolized to 2-aminofluorene (AF), 2-acetylaminofluorene (AAF) and 2-formylaminofluorene (FAF). These metabolites were subsequently hydroxylated at the 7-, 5- or 3-position of the fluorene moiety. Finally, the hydroxylated metabolites were conjugated with glucuronic acid or sulfuric acid and excreted in the urine or faeces. We suggested that intestinal bacteria played an important role in the reduction and acylation (Ueda *et al.* 2001a). Möller *et al.* (1987) also examined the *in vivo* metabolism in rat, and identified 7-hydroxy-2-acetylaminofluorene (7-OH-AAF) and 5-hydroxy-2-acetylaminofluorene (5-OH-AAF) as urinary metabolites. Furthermore, we examined the *in vitro* mammalian metabolism of NF, focusing on nitro-reduction (Kitamura *et al.* 1983, Tatsumi *et al.* 1986, 1989). When the nitro compound was incubated with liver cytosol or microsomes of rabbit, its reduction product AF was isolated from the mixture. The nitro-reduction of NF was followed by *N*-acylation and hydroxylation. We obtained evidence that liver aldehyde oxidase catalysed this nitro reduction in the cytosolic fraction and that cytochrome P450 functioned in the reduction in the liver microsomal fraction of rat.

Several investigators have demonstrated that fish have the ability to metabolize a variety of compounds such as pesticides, environmental contaminants and antimicrobials used for cultured fish, as well as for mammalian species (Bend and James 1978, Stegeman 1981, Binder *et al.* 1984, Livingstone 1998). Many drug-metabolizing enzymes, i.e. the microsomal cytochrome P450 system and flavin-containing monooxygenase, cytosolic quinone oxidoreductase and double-bond reductase, and Phase II enzymes exist in fish as do mammalian species (Tatsumi *et al.* 1992, Stegeman and Hahn 1994, Kitamura and Tatsumi 1997a, Buhler and Wang-Buhler 1998, Livingstone and Goldfarb 1998, Schlenk 1998). We have also examined reductive metabolism in fish. Nitro compounds such as 1-nitropyrene, an environmental pollutant, and sodium nifurstyrenate, a veterinary antimicrobial nitrofuran, are reduced to amino derivatives and are further metabolized to acetylamino derivatives in goldfish (*Carassius auratus*) and sea bream (*Pagrus major*) (Tatsumi *et al.* 1992, Kitamura and Tatsumi 1996). Recently, we examined the *in vivo* metabolism of NF in fish (Ueda *et al.* 2001b). When goldfish were bathed in a solution of NF, its reduction product AF, its acylated products AAF and FAF, and its hydroxylated metabolites were isolated from the solution and identified. Of these metabolites, 7-OH-AAF and its conjugates with glucuronic acid and sulfate were mainly detected. To our knowledge, such metabolic reactions of nitro-PAHs have not been studied with fish liver preparations except for our brief communication concerning the metabolism of 1-nitropyrene by goldfish hepatopancreas (Kitamura and Tatsumi 1997b).

In the present study, nitro-reductase activity toward NF, acylating activity toward AF, and hydroxylating activity toward its reduction and acylated products have been examined using liver preparations from sea bream, which is frequently used for drug metabolism studies (Mizukami *et al.* 1994, Sen and Arinc 1997, Bagnasco *et al.* 1991), and these activities in fish were compared with those of rat. Furthermore, we demonstrated that the acetylamino and the formylamino derivatives were interconverted via the amino derivative in fish.

Materials and methods

Materials

NF (98% pure), AF (> 98%) and AAF (> 98%) were purchased from Tokyo Chemical Industry Co., Ltd (Tokyo, Japan). NADPH and acetyl-CoA were from Sigma Chemical Co. (St Louis, MO, USA). *N*-formyl-L-kynurenine was from Calbiochem (La Jolla, CA, USA). FAF was prepared as described by Tatsumi and Amano 1987). 7-Hydroxy-2-aminofluorene (96%; 7-OH-AF) and 7-OH-AAF (98%) were prepared by the method of Bielschowsky (1945). 5-Hydroxy-2-aminofluorene (94%; 5-OH-AF) and 5-OH-AAF (95%) were synthesized by the method of Weisburger and Weisburger (1955). 7-Hydroxy-2-formylaminoflurene (97%; 7-OH-FAF) and 5-hydroxy-2-formylaminofluorene (96%; 5-OH-FAF) were prepared from 7-OH-AF and 5-OH-AF, respectively, by formylation according to the method of Ueda *et al.* (1996).

Liver preparations

Living marine fish, red sea bream (*Pagrus major*) (mixed sex, body weight 0.8—1.2 kg) were obtained from a local fresh fish shop. Male Wistar (Slc:Wistar/ST) rat, 120–150 g, were obtained from Japan SLC, Inc. (Shizuoka, Japan). The livers were excized and immediately homogenized in 3 vols 1.15% KCl containing 0.1 mM ethylenediaminetetraacetic acid disodium salt (EDTA), 0.1 mM ethylene glycol bis (β-aminoethyl ether)-*N,N,N′,N′*-tetraacetic acid (EGTA), 0.1 mM dithiothreitol and 0.1 mM phenylmethanesulfonyl fluoride. The homogenate was centrifuged for 20 min at 9000*g*, and the supernatant fraction was separated into microsomes and cytosol by centrifugation for 60 min at 105 000*g*. The microsomes were washed by resuspension in 2 vols KCl solution and by resedimentation for 60 min at 105 000*g*. The pellets were resuspended in the solution to make 1 ml equivalent to 1 g liver. Protein contents in the liver microsomes and cytosol of sea bream were 5.5–7.5 and 7.2–9.8 mg ml^{-1}, and those of rat were 16.8–19.7 and 12.9–15.4 mg protein ml^{-1}, respectively, as determined by the method of Lowry *et al.* (1951). Heat treatment was performed as below. Of liver cytosol, 3 ml was treated at 45 °C for various times. After centrifugation, the supernatant was used as heat-treated liver cytosol.

Assay of aldehyde oxidase activity

Benzaldehyde oxidase activity was assayed by the method of Johns (1967). The decrease in absorbance at 249 nm upon the oxidation of benzaldehyde to benzoate at 25 °C was monitored.

Identification of the metabolites of NF generated by liver preparations

Large-scale incubations with liver preparations were performed to identify the *in vitro* metabolites. The incubation mixture consisted of 1 μmol NF, AF, AAF or FAF, 5 μmol a cofactor, and a liver preparation equivalent to 2.5 g sea bream liver in a final volume of 10 ml 0.1 M K,Na phosphate buffer (pH 7.4). The incubation was performed at 30 °C for 30 min in nitrogen or in air. The incubation mixture was extracted with equal volumes of ethyl acetate, and the extracts were evaporated to dryness *in vacuo*. Thin-layer chromatography (TLC) and high-performance liquid chromatography (HPLC) showed that the extract contained the metabolites with R_f's and retention times corresponding to those of authentic samples. These metabolites were purified by preparative TLC. AF formed by liver preparations was identified as a metabolite of NF by comparing the mass and UV spectra with those of an authentic sample. AAF and FAF formed by liver cytosol were also identified as for metabolites of AF. Furthermore, hydroxylated metabolites of AF, AAF and FAF were unequivocally identified by comparing the mass and UV spectra with those of authentic samples.

Assay of NF-reductase activity

The incubation mixture consisted of 0.1 μmol NF, 0.5 μmol an electron donor, and a liver preparation equivalent to 0.25 g liver in a final volume of 2 ml 0.1 M K,Na phosphate buffer (pH 7.4). The incubation was performed at 30 °C for 30 min in nitrogen or in air in the case of sea bream. In control experiments, boiled liver preparations were used. After incubation, 30 μg phenacetin was added to the mixture as an internal standard, and the mixture was extracted with 5 ml ethyl acetate. The extract was evaporated to dryness *in vacuo* and the residue was subjected to HPLC. AF formed was determined from its peak area. The time-course of the cytosolic reductase activity toward NF was linear at least for the initial 30 min. When NF was incubated with the liver microsomes at 10, 15, 20, 25, 30, 37, 40 and 45 °C, the amounts of AF formed increased according to the incubation temperature up to 30 °C and decreased above that temperature. In contrast, when NF was incubated with cytosol, the amounts of AF formed increased according to the incubation temperature up to 37 °C and decreased above that temperature.

Assay of N-acylase activity toward AF

For the assay of *N*-acetylase and *N*-formylase activities, the incubation mixture consisted of 0.1 μmol AF, 0.5 μmol acetyl-CoA or *N*-formyl-L-kynurenine, and a liver preparation equivalent to 0.25 g liver in a final volume of 2 ml 0.1 M K,Na phosphate buffer (pH 7.4). The incubation was performed at 30 °C for 30 min in air. In control experiments, boiled liver preparations were used. After incubation, 30 μg phenacetin was added to the mixture as an internal standard, and then the mixture was extracted with 5-ml portions of ethyl acetate. The extract was evaporated to dryness *in vacuo* and the residue was subjected to HPLC for the determination of AAF and FAF.

Assay of N-deacylase activity with AAF and FAF as substrates

For the assay of *N*-deacetylase and *N*-deformylase activities, the incubation mixture consisted of 0.1 μmol AAF or FAF, and a liver preparation equivalent to 0.25 g liver in a final volume of 2 ml 0.1 M K,Na phosphate buffer (pH 7.4). The incubation was performed at 30 °C for 30 min in air. In control experiments, boiled liver preparations were used. After incubation, 30 mg phenacetin (internal standard) was added to the mixture, and the mixture extracted with 5 ml ethyl acetate. The extract was evaporated to dryness *in vacuo* and the residue was subjected to HPLC. AF formed was determined from its peak area.

Assay of hydroxylase activity

In the assay for hydroxylase activity, the incubation mixture consisted of 0.1 μmol AF, AAF or FAF, 0.5 μmol NADPH and liver microsomes of sea bream equivalent to 0.25 g liver wet weight or those of rat equivalent to 0.1 g in a final volume of 2 ml 0.1 M phosphate buffer (pH 7.4). The incubation was performed at 30 °C in air. In control experiments, boiled microsomes were used. After incubation, phenacetin was added to the mixture, and was extracted with ethyl acetate in the same manner as described above. The ethyl acetate extract, after removal of the solvent, was subjected to HPLC for the determination of 7-hydroxy or 5-hydroxy derivatives of AF, AAF or FAF.

TLC

Silica gel plates (Kieselgel 60 GF_{254}, 0.25 mm thick; E. Merck, Darmstadt, Germany) were developed in benzene–acetone (7:3 v/v). Spots were visualized under UV light (254 nm). The R_f's of authentic samples were: 7-OH-AAF, 0.17; 5-OH-AAF, 0.23; 7-OH-FAF, 0.17; 5-OH-FAF, 0.23; 7-OH-AF, 0.17; 5-OH-AF, 0.23; AAF, 0.45; FAF, 0.48; AF, 0.64; and NF, 0.78.

HPLC

HPLC was performed in a Hitachi L-6000 chromatograph (Tokyo, Japan) fitted with a 125 × 4 mm LiChrosorb RP-18 column (Merck). For the determination of AF, AAF and FAF, the mobile phase was acetonitrile–H_2O (7:3 v/v). The chromatograph was operated at a flow rate of 0.6 ml min^{-1} at a wavelength of 280 nm. The elution times of phenacetin (an internal standard), FAF, AAF, AF and NF were 4.8, 6.5, 8.3 and 16.8 min, respectively. For the determination of hydroxylated metabolites of AF, AAF and FAF, the mobile phase was acetonitrile–H_2O (3:7 v/v) for 25 min, acetonitrile–H_2O (linear gradient from 3:7 to 7:3 v/v) for 25 min and acetonitrile–H_2O (7:3 v/v) for 20 min. The chromatograph was operated at a flow rate of 0.6 ml min^{-1} at a wavelength of 280 nm. The elution times of NF and its metabolites were: 7-OH-AAF, 14.2; 7-OH-AF, 15.3; 5-OH-AAF, 23.0; 7-OH-FAF, 12.7; 5-OH-AF, 23.7; 5-OH-FAF, 21.4; FAF, 48.8; AAF, 51.6; AF, 53.5; diethylstilbestrol (an internal standard), 56.9; and NF, 63.2 min. The amounts of the metabolites were determined from the peak areas.

Analytical procedures

Electron-impact mass spectra were taken with a Japan Electron Optics (JEOL, Tokyo, Japan) JMS-SX102GCG mass spectrometer. UV spectra were recorded with a Hitachi (Tokyo, Japan) 320 spectrophotometer.

Results

Metabolites of NF generated by sea bream liver preparations

After incubation of NF with liver microsomes and cytosol of sea bream, NF metabolites were extracted with ethyl acetate, and the extract was subjected to HPLC as described in the Materials and methods. One metabolite detected at 8.3 min corresponded to authentic AF (figure 1). The metabolite was isolated from

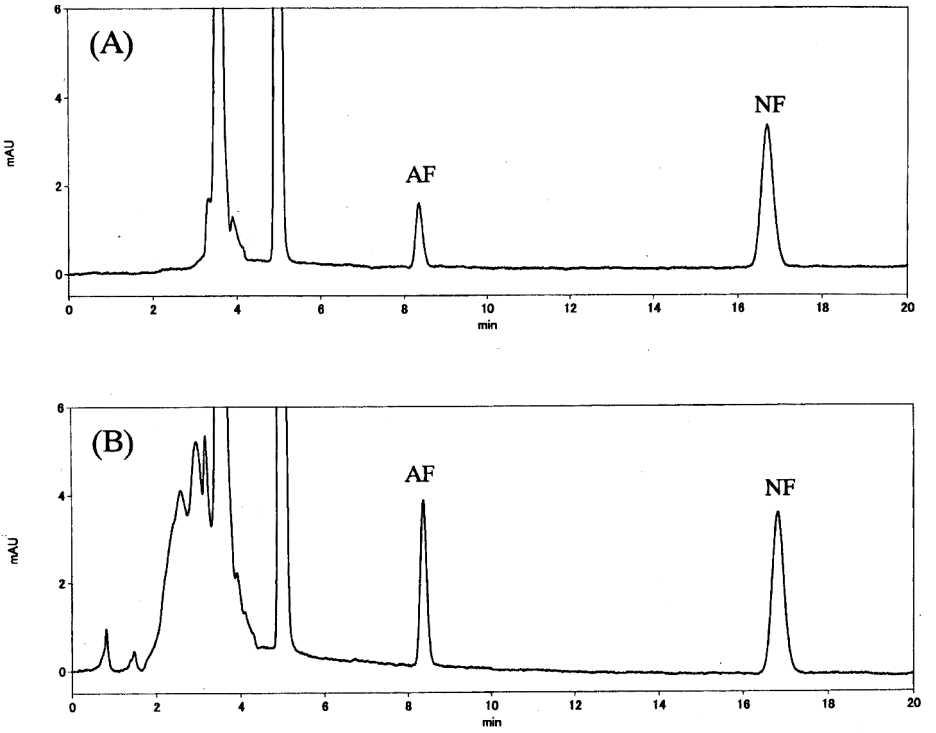


Figure 1. HPLC of the metabolites of 2-nitrofluorene (NF) generated by liver microsomes (A) and cytosol (B) of sea bream. The absorbance was measured at 280 nm. AF, 2-aminofluorene.

the extract by TLC as described in the Materials and methods. The mass spectrum of the metabolite showed a molecular ion at m/z 181, and fragment ions at m/z 165 (M^+–NH_2) and 152. The mass and UV spectra, the R_f's in TLC and the elution times in HPLC of the metabolite were identical with those of an authentic sample of AF. Based on these facts, we concluded that NF was metabolized to the reduced metabolite, AF.

NF-reductase activity of sea bream liver preparations

The ability of liver microsomes and cytosol of sea bream to reduce NF to AF was examined (figure 2). Sea bream liver microsomes exhibited an NADPH-dependent reductase activity under anaerobic conditions. The NADPH-dependent activity was completely inhibited by α-naphthoflavone and carbon monoxide. In this case, NADH was less effective than NADPH. On the other hand, when 2-hydroxypyrimidine, which is an electron donor for aldehyde oxidase, was added, the liver cytosol exhibited a significant reductase activity toward the nitro compound under anaerobic conditions. Other electron donors to aldehyde oxidase, N^1-methylnicotinamide and benzaldehyde, were also effective for reduction. The 2-hydroxypyrimidine-dependent activity was markedly inhibited by menadione, an inhibitor of aldehyde oxidase. The cytosolic activity was much higher than the NADPH-dependent microsomal activity. In the cytosolic reduction, xanthine (an electron donor for xanthine oxidase), NADPH and NADH (electron donors for

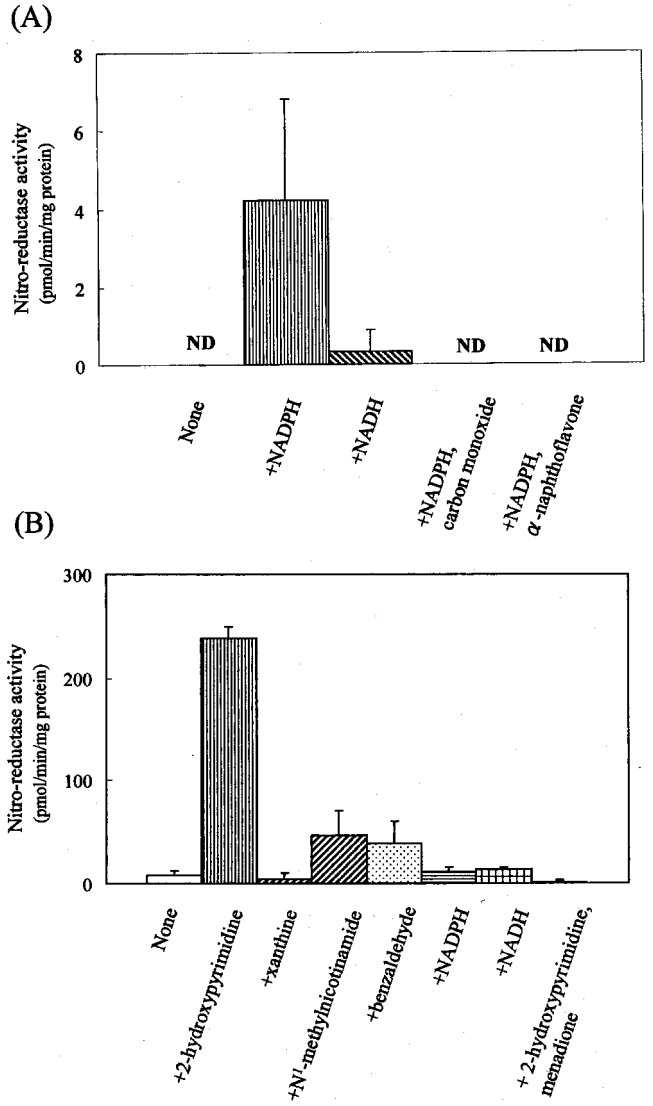


Figure 2. 2-Nitrofluorene reductase activity in liver microsomes (A) and cytosol (B) of sea bream. Each bar is the mean ± SD of four fish. The incubation was performed as described in the Materials and methods. The amount of 2-aminofluorene formed was determined by HPLC. α-Naphthoflavone and menadione were added at 10^{-4} M. ND, not detected.

DT-diaphorase) were much less effective than 2-hydroxypyrimidine. Furthermore, these activities were not influenced by oxypurinol or dicumarol, which is an inhibitor for xanthine oxidase or DT-diaphorase. When the liver microsomes and cytosols were boiled, their reductase activities were completely abolished (data not shown). When these activities were calculated per original liver wet weight, the NADPH-linked microsomal activity and the 2-hydroxypyrimidine-linked cytosolic activity were 0.1 and 11.2 nmol min^{-1} g^{-1} liver, respectively. Thus, the nitroreductase activity toward NF in sea bream liver is predominantly cytosolic.

NF reductase activity and aldehyde oxidase activity in liver cytosol of sea bream were subsequently compared. After heat-treatment of sea bream liver

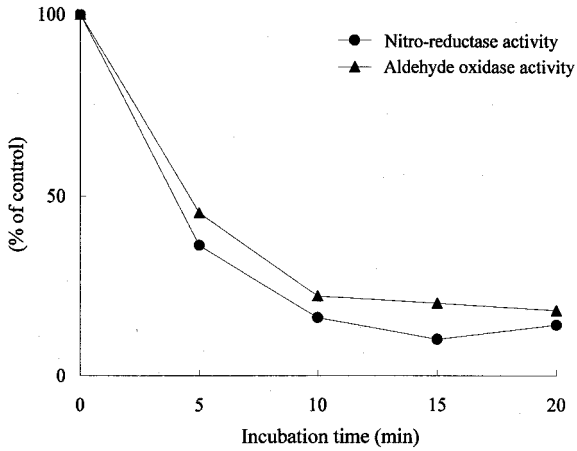


Figure 3. Heat inactivation of nitro-reductase and aldehyde-oxidase activities in sea bream. Each value is the mean of three fish. 2-Nitrofluorene reductase and benzaldehyde oxidase activities in liver cytosol were assayed after heat-treatment at 45 °C for 0, 5, 10, 15 and 20 min. 2-Nitrofluorene reductase and benzaldehyde oxidase activities before heat-treatment were 0.23 and 4.35 nmol min^{-1} mg^{-1} protein, respectively. Other details are described in the Materials and methods.

cytosol at 45 °C, nitro-reductase and benzaldehyde oxidase activities were assayed (figure 3). About half the nitro-reductase activity was destroyed in the initial 5 min, and by 10 min, most of the activity was abolished. Benzaldehyde oxidase activity due to aldehyde oxidase of liver cytosol decreased similarly. These results suggest that the cytosolic nitro-reductase activity was due to aldehyde oxidase. Furthermore, the liver cytosol was fractionated with ammonium sulfate, and the NF reductase and benzaldehyde oxidase activities were assayed. The nitro-reductase activity was found in the 30–45% ammonium sulfate saturation fraction, which also contained the aldehyde oxidase activity (data not shown). We further examined the components in liver cytosol that mediate the nitro-reduction in the presence of 2-hydroxypyrimidine, by means of DEAE-cellulose column chromatography. The 30–45% ammonium sulfate fraction of the liver cytosol was subjected to DEAE-cellulose column chromatography, and the fractions were assayed for NF reductase activity. The fractions that exhibited reducing activity in the presence of 2-hydroxypyrimidine also showed aldehyde oxidase activity (figure 4). These results suggest that aldehyde oxidase in sea bream liver cytosol is involved in the reduction of NF.

N-acylase activity of sea bream liver preparations

The reduction product, AF, was further metabolized to AAF, when incubated with sea bream liver cytosol in the presence of acetyl-CoA, an acetyl donor for mammalian arylamine acetyltransferase. The amount of AAF formed increased depending on incubation time up to 20 min (figure 5). Furthermore, when AF was incubated with liver cytosol in the presence of *N*-formyl-L-kynurenine, a formyl donor for mammalian formamidase (formyl transferase), FAF was formed. In this case, the amount of FAF formed also increased during the initial 10 min and then markedly decreased (figure 5).

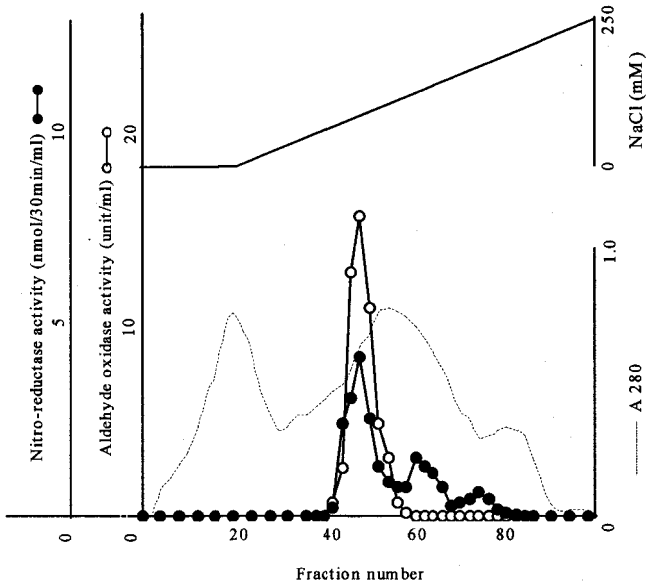


Figure 4. Elution pattern of 2-nitrofluorene reductase activity in DEAE-cellulose column chromatography of the 30–45% ammonium sulfate fraction of sea bream liver cytosol. 2-Nitrofluorene reductase activity was assayed with 0.2 ml each fraction in the presence of 2-hydroxypyrimidine at 30 °C for 30 min under anaerobic conditions. 2-Aminofluorene formed was determined by HPLC. Aldehyde oxidase activity was measured in terms of the oxidation of benzaldehyde. Other details are described in the Materials and methods.

N-deacylase activity of sea bream liver preparations

N-deacylation of AAF or FAF to AF by sea bream liver cytosol was also examined. When AAF was incubated with liver cytosol, AAF gradually decreased concomitantly with the increase of AF (figure 6). Furthermore, when FAF was incubated with liver cytosol, FAF was also deacylated to AF. The deacylase activity toward FAF was much higher than that toward AAF (figure 6). This is presumably the reason why FAF formed from AF markedly decreased after the initial formation of FAF noted above.

Hydroxylase activity of sea bream liver preparations

Hydroxylation of AF, AAF and FAF were further examined using sea bream liver microsomes. When AF was incubated with liver microsomes in the presence of NADPH, 7-OH-AF was formed. Liver microsomes also exhibited hydroxylase activity toward AAF and FAF. In these cases, 7-hydroxyl derivatives were formed to a greater extent than 5-hydroxyl derivatives. However, the amount of the hydroxylated metabolites of AAF and FAF were much higher than those of AF (table 1). NADPH-linked 7-hydroxylase activity of liver microsomes toward AAF was inhibited by about 50% by α-naphthoflavone (10^{-4} M), and to about 90% by SKF 525-A (10^{-4} M) and carbon monoxide. The hydroxylation was less effective with NADH in place of NADPH (data not shown).

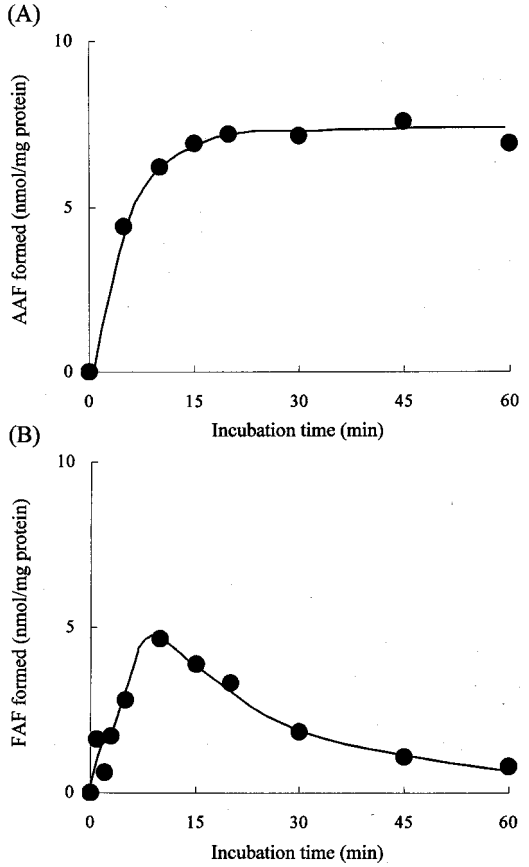


Figure 5. Time-courses of *N*-acylation of 2-aminofluorene to 2-acetylaminofluorene (A) and 2-formylaminofluorene (B) by sea bream liver cytosol. Each value is the mean of three fish. The incubation was performed in the presence of acetyl-CoA or *N*-formyl-L-kynurenine as described in the Materials and methods. The amount of 2-acetylaminofluorene or 2-formylaminofluorene formed was determined by HPLC.

Metabolism of NF by rat liver preparations

The metabolism of NF by rat liver preparations was examined in the same way as that by sea bream liver. When NF was incubated with liver microsomes or cytosol in the presence of NADPH or 2-hydroxypyrimidine, respectively, AF was detected in the HPLC chromatogram of the extract of the incubation mixture. The nitro-reductase activities based on cytochrome P450 in the microsomes and aldehyde oxidase in the liver cytosol were almost the same as those of sea bream liver microsomes and cytosol (figure 7). The cytosolic reductase activity was also inhibited by menadione at a concentration of 10^{-4} M (data not shown). In contrast, *N*-acetylase and *N*-formylase activities of rat liver cytosol toward AF in the presence of acetyl-CoA or *N*-formyl-L-kynurenine were also observed. These activities in rat liver were also higher than those of sea bream liver. However, the same order of the activities were observed in the fish (figure 7).

The oxidative metabolism of AF, AAF and FAF in rat liver microsomes was also examined (table 2). In this case, the activity was similar to that of sea bream liver microsomes. 7-Hydroxylated metabolites were detected as major metabolites,

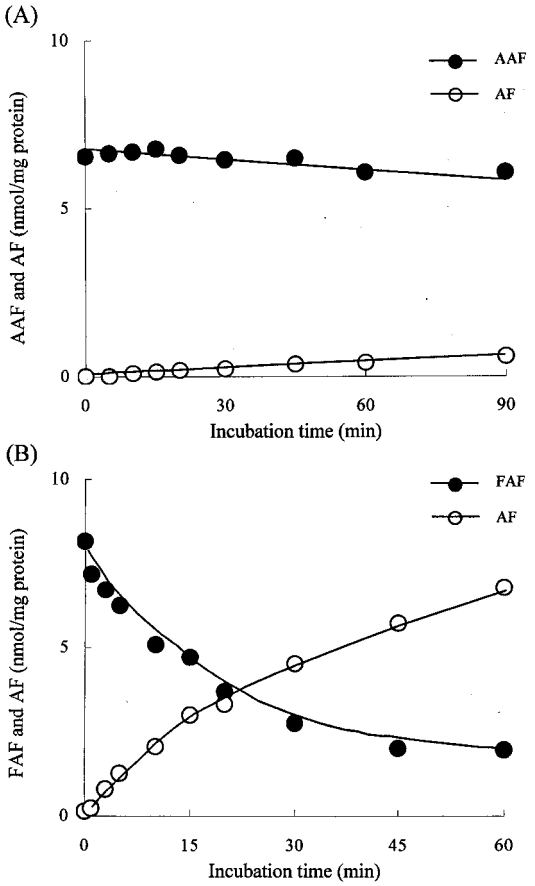


Figure 6. Time-courses of *N*-deacylation of 2-acetylaminofluorene and 2-formylaminofluorene to 2-aminofluorene by sea bream liver cytosol. (A) 2-Aminofluorene formed from 2-acetylaminofluorene. (B) 2-Aminofluorene formed from 2-formylaminofluorene. Each value is the mean of three fish. The incubation was performed as described in the Materials and methods. The amount of 2-aminofluorene formed was determined by HPLC.

together with the 5-hydroxylated product. The activity toward AF in the rat was higher than that in liver microsomes from sea bream. The activity toward AAF was highest among the tested compounds (table 2).

From these results, we concluded that NF was readily reduced to AF, AF was acylated to AAF and FAF, and these metabolites were subsequently oxidized to 7- or 5-hydroxylated products in fish, in a similar manner to mammalian species.

Discussion

Comparison of nitro-reductase between fish and mammals

Several reports have indicated that nitro-PAHs are mainly metabolized by nitro-reduction, ring hydroxylation, acylation and conjugation in mammalian species (Fu 1990). In rabbit, our previous studies concluded that the liver microsomal cytochrome P450 system and liver cytosolic aldehyde oxidase catalyse

Table 1. Oxidation of 2-aminofluorene, 2-acetylaminofluorene and 2-formylaminofluorene to 7-hydroxy and 5-hydroxy derivatives by liver microsomes of sea bream.

Substrate	7-Hydroxylase activity (pmol min^{-1} mg^{-1} protein)	5-Hydroxylase activity (pmol min^{-1} mg^{-1} protein)
2-Aminofluorene	6 ± 2	n.d.
2-Acetylaminofluorene	67 ± 12	5 ± 2
2-Formylaminofluorene	66 ± 8	6 ± 3

Data are the mean ± SD of three fish.
n.d., Not detected.
Incubation was carried out in the presence of NADPH. Hydroxylated products formed were measured by HPLC as described in the Materials and methods.

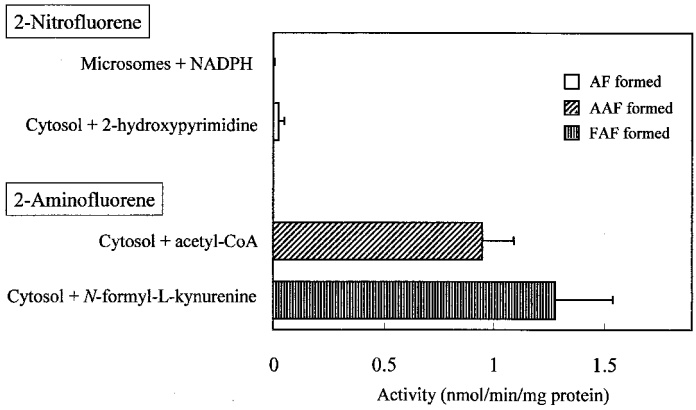


Figure 7. Nitro-reduction of 2-nitrofluorene and *N*-acylation of 2-aminofluorene by rat liver preparations. Each bar is the mean ± SD of four fish. 2-Nitrofluorene was incubated with liver microsomes or cytosol in the presence of NADPH or 2-hydroxypyrimidine under anaerobic conditions. 2-Aminofluorene was incubated with liver cytosol in the presence of acetyl-CoA or *N*-formyl-L-kynurenine at 37 °C for 30 min under aerobic conditions. The amount of 2-aminofluorene, 2-acetylaminofluorene or 2-formylaminofluorene formed was determined by HPLC as described in the Materials and methods.

Table 2. Oxidation of 2-aminofluorene, 2-acetylaminofluorene and 2-formal-aminofluorene to 7-hydroxy and 5-hydroxy derivatives by liver microsomes of rat.

Substrate	7-Hydroxylase activity (pmol min^{-1} mg^{-1} protein)	5-Hydroxylase activity (pmol min^{-1} mg^{-1} protein)
2-Aminofluorene	48 ± 8	1 ± 1
2-Acetylaminofluorene	181 ± 21	6 ± 2
2-Formylaminofluorene	99 ± 14	6 ± 2

Data are the mean ± SD of three rats.
Incubation carried out in the presence of NADPH. Hydroxylated products formed were measured by HPLC as described in the Materials and methods.

the reduction of NF and 1-nitropyrene to the corresponding amines (Tatsumi *et al.* 1986). In fish, an early study by Hitchcock and Murphy (1966) reported that under appropriate anaerobic conditions, liver preparations could reduce the nitro group of parathion to give the less toxic amino compound. In addition, nitro-reductase activity toward *p*-nitrobenzoic acid was reported by Buhler and Rasmusson (1968) in liver preparations from several fish species. We have also reported that sodium

nifurstyrenate, a nitrofuran derivative, and 1-nitropyrene are reduced to the amino derivatives by liver of sea bream or carp (Tatsumi *et al.* 1992, Kitamura and Tatsumi 1997b). The present study suggested that in fish as well as mammals, liver cytosolic aldehyde oxidase and microsomal cytochrome P450 system are involved in the nitroreduction of NF, and that aldehyde oxidase is mainly involved. In our preliminary study, aldehyde oxidase activity in sea bream liver was examined using benzaldehyde as a model substrate. Benzaldehyde oxidase activity was about 41% of the one of liver cytosol of rat (Sea:SD strain). In the current study, the electron donors for xanthine oxidase and DT-diaphorase were not effective on the nitro-reduction of NF. Furthermore, the inhibitors for these enzymes did not effect on the nitro-reduction. It is thought that xanthine oxidase and DT-diaphorase, which are known to act as nitro-reductase in mammalian livers, are not involved in nitro-reduction of NF in sea bream liver.

Comparison of N*-acylation between fish and mammals*

In mammals, there is an ample evidence of metabolic *N*-acetylation of arylamines, including AF. Liver cytosol from several mammalian species exhibit a significant *N*-acetylating activity toward aromatic amino compounds in the presence of acetyl-CoA (Weber and Hein 1985). We reported that various type of arylamines were acylated to the acetylamino and formylamino derivatives in rabbit (Tatsumi *et al.* 1989). Arylamine acetyltransferase or formamidase are responsible for the acetylation or formylation, respectively. In fish, Huang and Collins (1962) reported that 2-, 3- and 4-aminobenzoic acids were partly acetylated and excreted in urine as the *N*-acetyl derivatives. Grondel *et al.* (1986) reported that sulfadimidine was acetylated in carp (*Cyprinus carpio*). To our knowledge, *N*-acylating pathways have not been extensively studied in aquatic species *in vitro*. The present study strongly suggests that arylamine acetyltransferase and formamidase exist in fish livers, as in mammalian livers, and catalyse *N*-acetylation and *N*-formylation of aromatic amino compounds. It is noteworthy that *N*-acylation of arylamines also proceeds in fish.

In contrast, acetylamino derivatives are known to be deacetylated by liver preparations of mammalians, and the reaction is catalysed by carboxylesterases (Heymann and Mentlein 1988). Furthermore, formylamino derivatives are also hydrolysed to the parent aromatic amines (Ueda *et al.* 1996). In the current study, we demonstrate that AAF and FAF are deacylated by liver cytosol of sea bream. In particular, FAF was markedly deformylated to AF by liver cytosol. The balance between formylation and deformylation seems to favour strongly deformylation in the fish.

Comparison of oxidase activities toward AF, AAF and FAF between fish and mammals

In mammalian liver microsomes, AAF was reported to be oxidized by the cytochrome P4501A subfamily (Lewis 1996). Cytochrome P450 in fish includes the P4501A subfamily (Goksøyr 1995, Livingstone and Goldfarb 1998). The oxidative metabolism of AAF may be catalysed by P4501A forms, because the oxidase activity was inhibited by α-naphthoflavone in the current study. Lotlikar *et al.* (1967) also demonstrated that AAF is metabolized to 7-hydroxyl and 5-

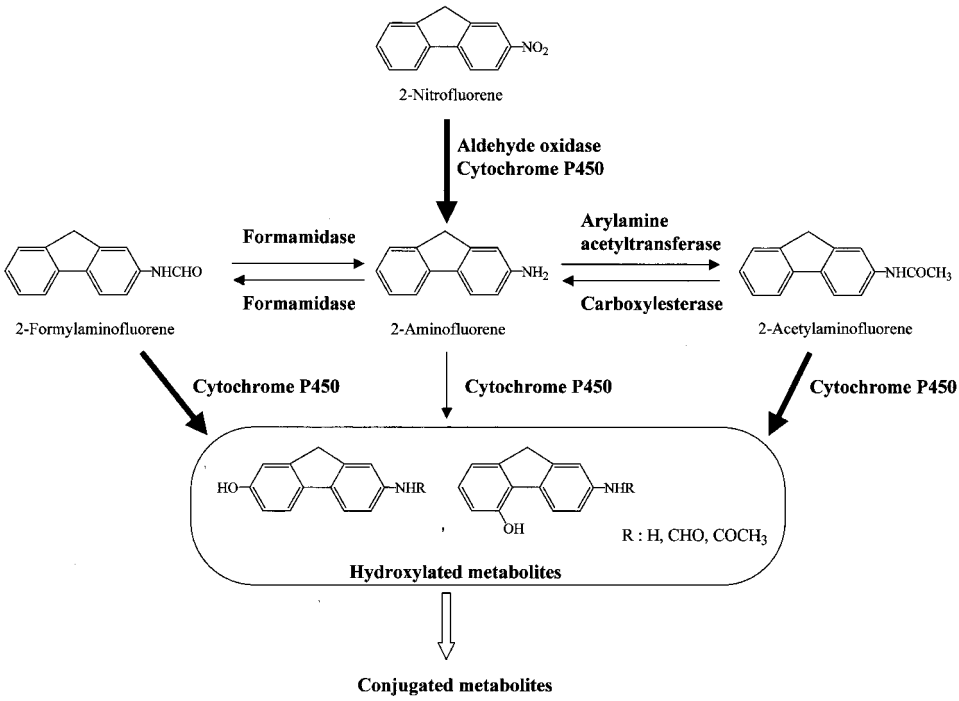


Figure 8. Postulated metabolic pathways of 2-nitrofluorene by liver preparations of sea bream.

hydroxyl derivatives in rainbow trout *in vivo*. The specific activities of the hydroxylases per protein in the current study based on cytochrome P450 in rat liver were almost the same as those of sea bream liver. In our preliminary study, the microsomal drug-oxidase activity of sea bream liver towards model substrates was examined. Ethoxyresorufin-*O*-dealkylase and methoxyresorufin-*O*-dealkylase activities were about 27 and 20% of those of liver microsomes of the untreated rat, respectively. However, pentoxyresorufin-*O*-dealkylase activity was not observed in sea bream liver.

Metabolic pathway of NF in fish

Recently, we demonstrated that NF is converted to reduced, *N*-acylated and hydroxylated metabolites, AF, AAF, FAF, 7-OH-AF, 5-OH-AF, 7-OH-AAF, 5-OH-AAF, 3-OH-AAF, 7-OH-FAF and 5-OH-FAF, and suggested that these reactions are catalysed by enzymes in rat tissues and intestinal bacteria (Ueda *et al.* 2001a). Furthermore, we demonstrated that NF was metabolized *in vivo* in goldfish (*Carassius auratus*) (Ueda *et al.* 2001b); five metabolites of NF, i.e. AF, AAF, 7-OH-AAF, FAF and 5-OH-AAF, were identified. In the latter study, we demonstrated that NF is metabolized similarly *in vitro* by sea bream liver preparations. We propose that the metabolism of NF by liver preparation of sea bream is as shown in figure 8. In other words, the reductive metabolism of NF is mainly catalysed by aldehyde oxidase and the P450 system in sea bream liver preparations. Acetylation and formylation of AF involve arylamine acetyltransferase and formamidase, respectively. In contrast, we demonstrated that AAF and

FAF were deacylated to AF, suggesting that AAF and FAF are interconverted via AF in fish. Furthermore, AF, AAF and FAF are oxidized mainly to 7-hydroxy derivatives and also to 5-hydroxy derivatives. Acylated 2-aminofluorene was highly oxidized to hydroxylated metabolites compared with 2-aminofluorene by the liver microsomes. These hydroxylated metabolites are conjugated with glucuronic acid or sulfuric acid, because conjugated metabolites have been detected as major metabolites *in vivo* in fish (Ueda *et al.* 2001b). In conclusion, we have demonstrated that NF is metabolized by fish liver enzyme systems similar to those operating in mammals.

Acknowledgements

This work was supported by Grant-in-Aid for Scientific Research on Priority Area (13027256) from the Japanese Ministry of Education, Science, Sports and Culture, and a Grant-in-Aid for Scientific Research (C13672343) from the Japan Society for the Promotion of Science.

References

Bagnasco, M., Camoirano, A., De Flora, S., Melodia, F. and Arillo, A., 1991, Enhanced liver metabolism of mutagens and carcinogens in fish living in polluted seawater. *Mutation Research*, **262**, 129–137.

Bend, J. R. and James, M. O., 1978, Xenobiotic metabolism in marine and freshwater species. In D. C. Malins and J. A. Sargent (eds), *Biochemical and Biophysical Perspectives in Marine Biology*, vol. 4 (New York: Academic Press), pp. 125–188.

Bielschowsky, F., 1945, A metabolite of 2-acetamidofluorene. *Biochemical Journal*, **39**, 287–289.

Beije, B. and Möller, L., 1988, 2-Nitrofluorene and related compounds: prevalence and biological effects. *Mutation Research*, **196**, 177–209.

Binder, R. L., Melancon, M. J. and Lech, J. J., 1984, Factors influencing the persistence and metabolism of chemicals in fish. *Drug Metabolism Reviews*, **15**, 697–724.

Buhler, D. R. and Rasmusson, M. E., 1968, Reduction of *p*-nitrobenzoic acid by fishes. *Archives of Biochemistry Biophysics*, **103**, 582–595.

Buhler, D. R. and Wang-Buhler, J. L., 1998, Rainbow trout cytochrome P450: purification, molecular aspects, metabolic activity, induction and role in environmental monitoring. *Comparative Biochemistry and Physiology*, **121C**, 107–138.

Campbell, R. M. and Milton, L. L., 1984, Capillary column gas chromatographic determination of nitro polycyclic aromatic compounds in particulate extracts. *Analytical Chemistry*, **56**, 1026–1030.

Cui, X.-S., Eriksson, L. C. and Möller, L., 1999, Formation and persistence of DNA adducts during and after a long-term administration of 2-nitrofluorene. *Mutation Research*, **442**, 9–18.

El-Bayoumy, K., Hecht, S. S. and Hoffmann, D., 1982, Comparative tumor initiating activity on mouse skin of 6-nitrobenzo[*a*]pyrene, 6-nitrochrysene, 3-nitroperylene, 1-nitropyrene and their parent hydrocarbons. *Cancer Letters*, **16**, 333–337.

Fu, P. P., 1990, Metabolism of nitro-polycyclic aromatic hydrocarbons. *Drug Metabolism Reviews*, **22**, 209–268.

Goksøyr, A., 1995, Use of cytochrome P450 1A (CYP1A) in fish as a biomarker of aquatic pollution. *Archives of Toxicology Supplement*, **17**, 80–95.

Grondel, J. L., Nouws, J. F. M. and Haenen, O. L. M., 1986, Fish and antibiotics: Pharmacokinetics of sulphadimidine in carp (*Cyprinus carpio*). *Veterinary Immunology and Immunopathology*, **2**, 281–286.

Hayakawa, K., Murahashi, T., Butoh, M. and Miyazaki, M., 1995, Determination of 1,3-, 1,6-, and 1,8-dinitropyrenes and 1-nitropyrene in urban air by high-performance liquid chromatography using chemiluminescence detection. *Environmental Science and Technology*, **29**, 928–932.

Heymann, E. and Mentlein, R., 1988, Identification, localization and specificity of detoxifying hydrolases in rat tissues. In J. W. Gorrod, H. Oelschläger and J. Caldwel (eds), *Metabolism of Xenobiotics* (London: Taylor & Francis), pp. 189–197.

Hitchcock, M. and Murphy, S. D., 1966, Reduction of parathion, paraoxon and EPN by tissues of mammals, birds and fishes. *Federation Proceedings*, **25**, 687.

Huang, K. C. and Collins, S. F., 1962, Conjugation and excretion of aminobenzoic acid isomers in marine fishes. *Journal of Cellular and Comparative Physiology*, **60**, 49–52.

John, D. G., 1967, Human liver aldehyde oxidase: Differential inhibition of oxidation charged and uncharged substrates. *Journal of Clinical Investigation*, **46**, 1492–1505.

Kitamura, S., Narai, N., Hayashi, M. and Tatsumi, K., 1983, Rabbit liver enzymes responsible for reduction of nitropolycyclic aromatic hydrocarbons. *Chemical and Pharmaceutical Bulletin*, **31**, 776–779.

Kitamura, S. and Tatsumi, K., 1996, Metabolism *in vivo* of 1-nitropyrene, an enironmental pollutant, in fish. *Biological and Pharmaceutical Bulletin*, **19**, 1524–1526.

Kitamura, S. and Tatsumi, K., 1997b, 1-Nitropyrene-metabolizing activities of fish liver preparations. *Bulletin of Environmental Contamination and Toxicology*, **58**, 448–455.

Kitamura, S. and Tatsumi, K., 1997a, Purification of NADPH-linked and NADH-linked quinone reductases from liver cytosol of sea bream, *Pagrus major*. *Comparative Biochemistry and Physiology*, **118B**, 675–680.

Lewis, D. F., 1996, *Cytochromes P450: Structure, Function and Mechanism* (London: Taylor & Francis).

Livingstone, D. R., 1998, The fate of organic xenobiotics in aquatic ecosystems: quantitative and qualitative differences in biotransformation by invertebrates and fish. *Comparative Biochemistry and Physiology*, **120A**, 43–49.

Livingstone, D. R. and Goldfab, P. S., 1998, Aquatic environmental biomonitoring: Use of cytochrome P450 1A and other molecular biomarkers in fish and mussels. In J. Lynch and A. Wiseman (eds), *Environmental Biomonitoring*, vol. 6: *The Biotechnology Ecotoxicology Interface* (Cambridge: Cambridge University Press), pp. 101–129.

Lotlikar, P. D., Miller, E. C., Miller, J. A. and Halver, J. E., 1967, Metabolism of the carcinogen 2-acetylaminofluorene by rainbow trout. *Proceedings of the Society for Experimental Biology Medicine*, **124**, 160–163.

Lowry, O. H., Rosebrough, N. J., Farr, A. L. and Randall, R. J., 1951, Protein measurement with the Folin phenol reagent. *Journal of Biological Chemistry*, **193**, 265–275.

Manabe, Y., Kinouchi, Y., Wakisaka, K., Tahara, I. and Ohnishi, Y., 1984, Mutagenic 1-nitropyrene in wastewater from oil-water separating tanks of gasoline stations and in used crankcase oil. *Environmental Mutagenesis*, **6**, 669–681.

Mizukami, M., Okauchi, M., Ariyoshi, T. and Kito, H., 1994, The isolation and sequence of cDNA encoding a 3-methylcholanthrene-inducible cytochrome *P*450 from wild red sea bream. *Pagrus major*. *Marine Biology*, **120**, 343–349.

Möller, L., Rafter, J. and Gustafsson, J.-Å., 1987, Metabolism of the carcinogenic air pollutant 2-nitrofluorene in the rat. *Carcinogenesis*, **8**, 637–645.

Möller, L., Torndal., U.-B., Eriksson, L. C. and Gustafsson, J.-Å., 1989, The air pollutant 2-nitrofluorene as initiator and promoter in a liver model for chemical carcinogenesis. *Carcinogenesis*, **10**, 435–440.

Möller, L., Zeisig, M., Midtvedt, T. and Gustafsson, J.-Å., 1994, Intestinal microflora enhances formation of DNA adducts following administration of 2-NF and 2-AAF. *Carcinogenesis*, **15**, 857–861.

Purohit, V. and Basu, A. K., 2000, Mutagenicity of nitroaromatic compounds. *Chemical Research in Toxicology*, **13**, 673–692.

Rosenkranz, H. S. and Mermelstein, R., 1983, Mutagenicity and genotoxicity of nitroarenes. All nitro-containing chemicals were not created equal. *Mutation Research*, **114**, 217–267.

Schlenk, D., 1998, Occurrence of flavin-containing monooxygenases in non-mammalian eukaryotic organisms. *Comparative Biochemistry and Physiology*, **121C**, 185–195.

Sen, A. and Arinc, E., 1997, Separation of three P450 isozymes from liver microsomes of gilthead seabream treated with β-NF and partial purification of cytochrome P4501A1. *Biochemistry and Molecular Biology International*, **41**, 131–141.

Stegeman, J. J. and Hahn, M. E., 1994, Biochemistry and molecular biology of monooxygenases: current perspectives on forms, functions, and regulation of cytochrome P450 in aquatic species. In D. C. Malins and G. K. Ostrander (eds), *Aquatic Toxicology: Molecular, Biochemical, and Cellular Perspectves* (Florida: Lewis), pp. 87–206.

Stegeman, J. J., 1981, Polynuclear aromatic hydrocarbons and their metabolism in the marine environment. *Polycyclic Hydrocarbons and Cancer*, **3**, 1–60.

Tatsumi, K. and Amano, H., 1987, Biotransformation of 1-nitropyrene and 2-nitrofluorene to novel metabolites, the corresponding formylamino compounds, in animal bodies. *Biochemical and Biophysical Research Communications*, **142**, 376–382.

Tatsumi, K., Kitamura, S., Amano, H. and Ueda, K., 1989, Comparative study on metabolic formation of *N*-arylformamides and *N*-arylacetamides from carcinogenic arylamines in mammalian species. *Cancer Research*, **49**, 2059–2064.

Tatsumi, K., Kitamura, S., Kato, M. and Hiraoka, K., 1992, Metabolism of sodium nifurstyrenate, a veterinary antimicrobial nitrofuran, in animals and fish. *Drug Metabolism and Disposition*, **20**, 226–233.

Tatsumi, K., Kiramura, S. and Narai, N., 1986, Reductive metabolism of aromatic nitro compounds including carcinogens by rabbit liver preparations. *Cancer Research*, **46**, 1089–1093.

Ueda, O., Kitamura, S., Huruse, Y., Saito, T., Kanzaki, Y., Yano, Y., Kanzaki, Y., Tatsumi, K. and Ohta, S., 2001b, Metabolism of 2-nitrofluorene, an environmental pollutant, and 2-acetylaminofluorene in fish. *Bulletin of Environmental Contamination and Toxicology*, **66**, 371–378.

Ueda, O., Kitamura, S., Kubo, R., Yano, Y., Kanzaki, Y., Fujimoto, T. Tatsumi, K. and Ohta, S. 2001a, Metabolism of 2-nitrofluorene, 2-aminofluorene and 2-acylaminofluorenes in rat and dog and the role of intestinal bacteria. *Xenobiotica*, **31**, 33–49.

Ueda, O., Kitamura, S. and Tatsumi, K., 1996, Further metabolism of 2-formylaminofluorene, a metabolite of 2-aminofluorene, in rats. *Biological and Pharmaceutical Bulletin*, **19**, 330—333.

Wang, C. Y., Lee, M. S., King, C. M. and Warner, P. O., 1980, Evidence for nitroaromatics as direct-acting mutagens of airborne particulates. *Chemosphere*, **9**, 83–87.

Weber, W. W. and Hein, D. C., 1985, *N*-acetylation pharmacogenetics. *Pharmacological Reviews*, **37**, 25–79.

Weisburger, E. K. and Weisburger, J. H., 1955, 2-Acetylamino-5-hydroxyfluorene, a metabolite of the carcinogen 2-acetylaminofluorene. *Journal of Organic Chemistry*, **20**, 1396–1401.

XENOBIOTICA, 2002, VOL. 32, NO. 8, 683–697

Taylor & Francis
healthsciences

Stereoselectivity of ibuprofen metabolism and pharmacokinetics following the administration of the racemate to healthy volunteers

S. C. TAN†§, B. K. PATEL†*, S. H. D. JACKSON‡,
C. G. SWIFT‡ and A. J. HUTT†

† Department of Pharmacy, King's College London, Franklin-Wilkins Building, Stamford Street, London SE1 9NN, UK.
‡ Clinical Age Research Unit, Department of Health Care of the Elderly, GKT School of Medicine and Dentistry, Denmark Hill, London, SE5 9RS, UK.

Received 14 December 2001

1. The stereoselective metabolism and pharmacokinetics of the enantiomers of ibuprofen have been investigated following the oral administration of the racemic drug (400 mg) to 12 healthy volunteers.

2. The stereochemical composition of the drug in serum, both total and unbound, and drug and metabolites, both free and conjugated, in urine were determined by a combination of the direct and indirect chromatographic procedures to enantiomeric analysis.

3. The oral clearance of (*S*)-ibuprofen was significantly greater than that of the *R*-enantiomer (74.5 ± 18.1 versus 57.1 ± 11.7 ml min^{-1}; $p < 0.05$) and the clearance of (*R*)-ibuprofen via inversion was *ca* two fold that via alternative pathways.

4. Some $74.0 \pm 9.6\%$ of the dose was recovered in urine over 24 h as ibuprofen, 2-hydroxyibuprofen and carboxyibuprofen, both free and conjugated with glucuronic acid. Analysis of the stereochemical composition of the urinary excretion products indicated that 68% of the dose of (*R*)-ibuprofen had undergone chiral inversion.

5. Metabolism via glucuronidation and both routes of oxidation, showed enantioselectivity for (*S*)-ibuprofen, the enantiomeric ratios (*S*/*R*) in partial metabolic clearance being 7.1, 4.8 and 3.4 for formation of ibuprofen glucuronide, 2-hydroxyibuprofen and carboxyibuprofen respectively.

6. Modest stereoselectivity was observed in the formation of (2′*R*, 2*R*)- and (2′*S*, 2*S*)-carboxyibuprofen in comparison to the alternative diastereoisomers, the ratios in formation clearance being 1.6 and 1.2 respectively.

Introduction

The metabolism and pharmacokinetics of (*R*,*S*)-ibuprofen [(±)-(*R*,*S*)-2-(4-isobutylphenyl)propionic acid] have been extensively investigated both *in vitro* and *in vivo*, since its introduction into therapeutics. In recent years these investigations have been primarily directed towards studies concerned with the stereoselectivity of drug disposition following the administration of the racemate and/or individual enantiomers to both healthy volunteers and patients (Lee *et al*. 1985, Avgerinos and Hutt, 1990, Evans *et al*. 1990, Geisslinger *et al*. 1990, Rudy *et al*. 1992, Li *et al*. 1993, Chen and Chen 1994, Smith *et al*. 1994) or with the elucidation of the

* Author for correspondence; e-mail : bhavesh.patel@kcl.ac.uk
§ Present address: Doping Control Centre, Universiti Sains Malaysia, 11800 Minden, Penang, Malaysia.

Xenobiotica ISSN 0049–8254 print/ISSN 1366–5928 online © 2002 Taylor & Francis Ltd
http://www.tandf.co.uk/journals
DOI: 10.1080/00498250210142994

chemical and biochemical mechanism of the chiral inversion reaction (see below) (Baillie *et al.* 1989, Knihinicki *et al.* 1989, 1991, Sanins *et al.* 1991, Knights *et al.*, 1992, Shieh and Chen 1993, Shieh *et al.* 1993, Tracy *et al.* 1993, Menzel *et al.* 1994, Roy-De Vos *et al.* 1996, Scheuerer *et al.* 1998) and its biological consequences (Williams *et al.* 1986, Freneaux *et al.* 1990, Zhao *et al.* 1992). However, relatively little attention has been directed towards the stereochemical composition of the two major urinary metabolites of the drug.

The metabolism of ibuprofen (**I**, figure 1) in man involves conjugation with glucuronic acid, which is stereoselective for the *S*-enantiomer (Lee *et al.* 1985, El-Mouelhi *et al.* 1987) and oxidation to yield two major metabolites, 2-hydroxyibu-

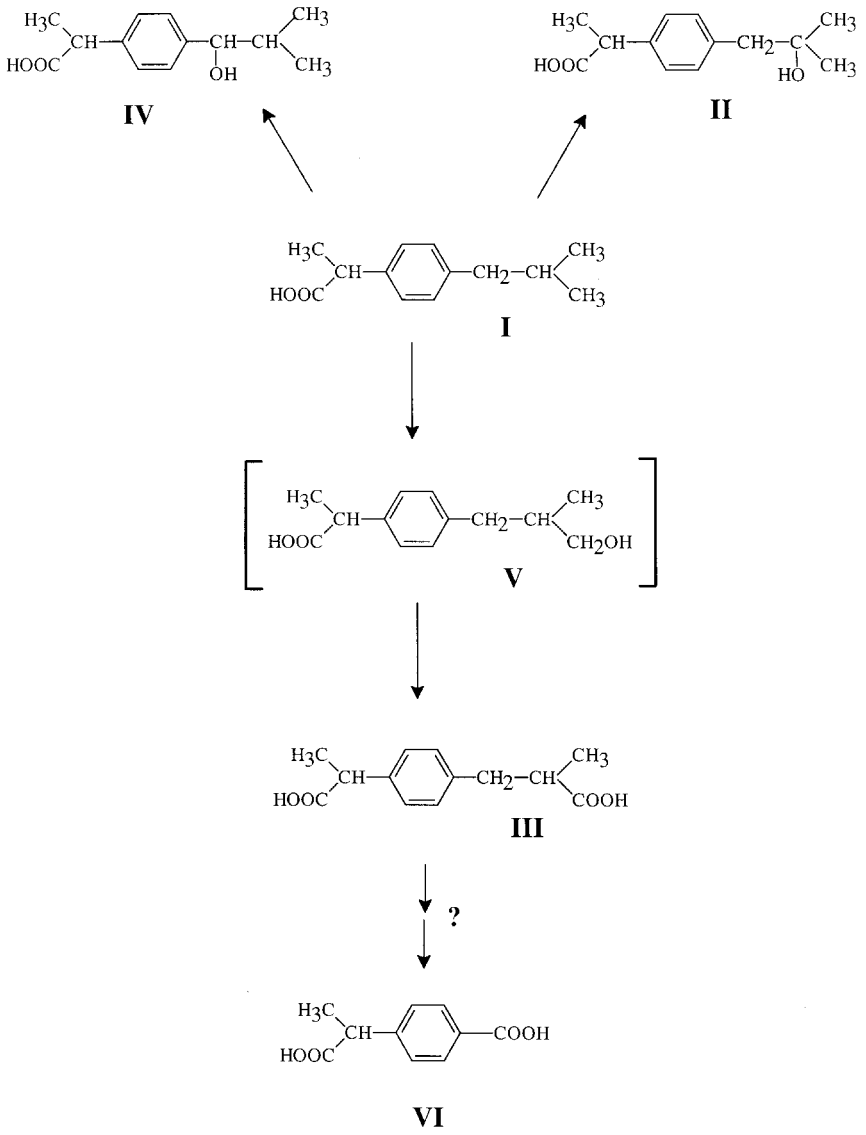


Figure 1. Oxidative metabolism of ibuprofen (**I**) in man

profen (2-[4-(2-hydroxy-2-methylpropyl)phenyl]propionic acid, **II**) and carboxyibuprofen (2-[4-(2-carboxypropyl)phenyl]propionic acid, **III**) (Adams *et al*. 1967, Mills *et al*. 1973, Brooks and Gilbert 1974, Kaiser *et al*. 1976, Petterson *et al*. 1978). The urinary excretion of these two latter metabolites together with ibuprofen, both free and conjugated with glucuronic acid, accounts for between 74 and 86% of an oral dose following the administration of the racemate to man (Lockwood *et al*. 1983, Evans *et al*. 1989a, 1990, Smith *et al*. 1994). Conjugation of the regioisomeric hydroxy metabolites and carboxyibuprofen with glucuronic acid has been shown to take place preferentially at the propionic acid moiety (Kepp *et al*. 1997). In addition to the above, two minor oxidation products, 1-hydroxy- (**IV**) and 3-hydroxyibuprofen (**V**) have been identified in human urine (Brooks and Gilbert 1974, Petterson *et al*. 1978, Kepp *et al*. 1997) and 2-(4-carboxyphenyl)-propionic acid (**VI**) has been identified in dialysis fluid following administration of the drug to a nephrectomized patient (Petterson *et al*. 1978) (figure 1). More recently, Shirley *et al*. (1994) have reported the identification of a taurine conjugate of ibuprofen in urine accounting for about 1.5% of the dose following oral administration of the racemate.

In addition to what maybe regarded as conventional routes of metabolism, the essentially inactive (*R*)-ibuprofen also undergoes chiral inversion to the pharmacologically active *S*-enantiomer. The observation that both major urinary metabolites, 2-hydroxy- and carboxyibuprofen, were excreted predominantly in the dextrorotatory form, irrespective of the stereochemical composition of the administered drug, ultimately resulted in the discovery of the chiral inversion reaction for ibuprofen (Adams *et al*. 1967, Mills *et al*. 1973, Wechter *et al*. 1974, Kaiser *et al*. 1976) and the related 2-arylpropionic acid non-steroidal antiinflammatory drugs (Hutt and Caldwell 1983, Caldwell *et al*. 1988, Mayer 1990, Hayball 1996).

Several investigations concerned with the stereoselective plasma pharmacokinetics of ibuprofen have also examined the urinary recovery of the drug and the two major metabolites (e.g. Evans *et al*. 1989a, 1990, Smith *et al*. 1994, Rudy *et al*. 1991, 1995). However, few of these studies have addressed the stereochemical composition of the metabolic products due to methodological problems associated with the chromatographic resolution of the four possible stereoisomeric forms of carboxyibuprofen, quantitatively the most important urinary metabolite accounting for about 40% of the dose (Lockwood *et al*. 1983, Baillie *et al*. 1989, Evans *et al*. 1989a, 1990, Rudy *et al*. 1991, Smith *et al*. 1994). We have recently reported the chromatographic resolution and characterization of the four stereoisomers of carboxyibuprofen (Tan *et al*. 1997a), and the chromatographic methodology employed has been developed into a validated sequential achiral-chiral technique for the determination of the stereochemical composition of both major oxidation products in urine (Tan *et al*. 1997b). We now report on the application of this methodology to an examination of the stereoselective metabolism and pharmacokinetics of ibuprofen following the administration of the racemic drug to healthy volunteers.

Material and Methods

Nomenclature

In the case of carboxyibuprofen, 2-[4-(2-carboxypropyl)phenyl]propionic acid, the position of both chiral centres are indicated as the second carbon atom in each of the two side chains. In the present

report the chiral centre introduced by metabolic oxidation of the terminal methyl groups of the isobutyl moiety in ibuprofen will be designated as the 2′-position, whereas the original chiral centre in the propionic acid moiety will be indicated as the 2-position.

Chemicals

The individual enantiomers (enantiomeric purity $\geq 99.6\%$), (*R,S*)-ibuprofen and (*R,S*)-2-hydroxyibuprofen, together with (*R,S*)-flurbiprofen were the generous gifts of Boots Co. Ltd (Nottingham, UK). Carboxyibuprofen was synthesized, with a chemical purity $>98\%$, as described by Tan *et al.* (1997a). Radiolabelled [^{14}C]-ibuprofen with a specific activity of 21.6 mCi g^{-1} and a radiochemical purity of $>99\%$ post-HPLC purification (Tan *et al.* 1997c) was generously donated by Knoll Pharmaceuticals (Nottingham, UK). (*R*)-1-(Naphthen-1-yl)ethylamine and 1-(3-dimethylaminopropyl)-3-ethylcarbodiimide hydrochloride were purchased from Aldrich (Gillingham, UK); 1-hydroxybenzotriazole and 4-chlorophenoxyacetic acid were obtained from Fluka Chemicals (Poole, UK) and Sigma Chemicals (Poole, UK) respectively. HPLC solvents were purchased from Rathburn (Walkerburn, UK) and all other reagents and solvents from BDH (Poole, UK). Protein assay reagents based on the Coomassie blue method were obtained from Bio-Rad (Hemel Hempstead, UK) and dialysis membranes (Spectrapor 2) were obtained from Pierce and Warriner (Chester, UK).

Chromatography columns

The C_{18} column (Waters Resolve C_{18}), (5 µm, 150 × 3.9 mm i.d.) was obtained from Anachem Ltd (Luton, UK) and the Partisil silica column (5 µm, 250 × 4.6 mm i.d.) was obtained from Whatman (Maidstone, UK). Refillable guard columns (10 × 2.1 mm), pellicular silica (40–63 µm) and pellicular C_{18} (40–60 µm) were obtained from Alltech Associates (Carnforth, UK). The chiral-phase columns, amylose tris(3,5-dimethylphenylcarbamate) (Chiralpak AD) (10 µm, 250 × 4.6 mm i.d.) and cellulose tris(3,5-dimethylphenylcarbamate) (Chiralcel OD) (10 µm, 250 × 4.6 mm i.d.), together with matching guard columns (10 µm, 50 × 4.6 mm i.d.), were supplied by HPLC Technology Ltd (Macclesfield, UK).

Instrumentation

High-performance liquid chromatography (HPLC) was carried out using an LDC Constametric 3000 pump, and either an LDC Spectromonitor 3100 UV detector or Merck-Hitachi spectrofluorometer, depending on the analytes under examination, linked to an LDC CI 4000 computing integrator. Samples were introduced on-column using either an Perkin-Elmer ISIS 100 or an LKB 2157 autosampler fitted with 100-µl sample loops. Liquid scintillation spectrometry was carried out using an LKB 1209 Wallac Rackbeta liquid scintillation spectrometer. The liquid scintillation cocktail used was Quickscint flow 302 (Zinsser Analytical, Maidenhead, UK).

Analytical methods

Full details of the analytical methodologies employed in the present investigation, including their development, validation and preliminary application to samples of biological origin, have been reported elsewhere (Tan *et al.* 1997b and c). Brief details of each method are presented below.

Ibuprofen enantiomers. The enantiomeric composition of ibuprofen in serum and urine was determined by the indirect approach to enantiomeric analysis (Tan *et al.* 1997c). Following the addition of the internal standard, (*R,S*)-flurbiprofen (1 µg, 10 µl of a 100 µg ml^{-1} solution in acetonitrile) to either serum (0.5 ml) or urine (0.5 ml for free and 0.1 ml for total, free plus conjugated drug, following alkaline hydrolysis) the analytes were isolated by liquid–liquid extraction (serum samples, diethylether, 3ml; urine samples, hexane:isopropanol [9:1 v/v], 5 ml) at pH 3.8. Following phase separation and evaporation of the organic solvent, the residue was derivatized by the addition of (*R*)-1-(naphthen-1-yl)ethylamine in dichloromethane, to yield the corresponding diastereoisomeric amides using 1-(3-dimethylaminopropyl)-3-ethylcarbodiimide and 1-hydroxybenzotriazole as coupling agents. Under these conditions the derivatization is essentially quantitative (Tan *et al.* 1997c). Chromatographic resolution of the derivatives was achieved under reversed-phase conditions using the C_{18}-stationary phase and a mobile phase of phosphate buffer (pH 3.5, 0.01 M):acetonitrile (1:1 v/v) at a flow rate of 1.5 ml min^{-1}. Quantification was carried out using a spectrofluorometer with excitation and emission wavelengths of 290 and 330 nm respectively. Under these conditions the (*R*)-1-(naphthen-1-yl)ethylamides of (*R*)- and (*S*)-flurbiprofen and (*R*)- and (*S*)-ibuprofen eluted at 14.5, 17.8, 22.2 and 25.6 min respectively.

Metabolite Analysis. The concentrations and stereochemical composition of 2-hydroxy- and carboxyibuprofen in urine were determined by sequential achiral-chiral chromatography (Tan *et al.* 1997b). Following the addition of the internal standard (4-chlorophenoxyacetic acid, 25 µg per sample) urine (0.5 ml aliquots for the determination of free and 0.1 ml aliquots for the determination of total

concentrations following alkaline hydrolysis) was extracted under acidic conditions with dichloromethane:ethyl acetate (14:1 v/v). Following phase separation, the organic layer was removed, evaporated to dryness and the residue reconstituted in 150 µl of the mobile phase employed for achiral chromatography and 50 µl injected on column. Achiral analysis was carried out using the Partisil column with a mobile phase of hexane:ethanol (98.2:1.8 v/v) containing trifluoroacetic acid (TFA; 0.05% v/v) at a flow rate of 2.0 ml min^{-1} with UV detection at 220 nm. Under these conditions the internal standard, carboxyibuprofen and 2-hydroxyibuprofen eluted with retention times of 4.9, 12.6 and 15.8 min respectively. The HPLC eluate containing the two metabolites was separately collected between 12.2–13.0 min and 15.3–16.3 min, evaporated under nitrogen and the residue dissolved in the mobile phase used for chiral chromatography. Chiral-phase analysis was carried out using a Chiralpak AD CSP with a mobile phase of hexane:ethanol (92:8 v/v) containing TFA (0.05% v/v) at a flow rate of 1.0 ml min^{-1}, and UV detection at 220 nm. Under these conditions (*R*)- and (*S*)-2-hydroxyibuprofen eluted with retention times of 13.9 and 16.1 min respectively and the retention times of the four stereoisomers of carboxyibuprofen were 2′*S*,2*R*-, 11.0; 2′*R*,2*R*-, 12.1; 2′*R*,2*S*-, 16.9 and 2′*S*,2*S*-, 20.1 min. The stereochemical composition of both metabolites was determined by comparison of peak areas following chiral-phase chromatography and the individual concentrations were calculated from a knowledge of stereochemical composition and urinary concentration.

Protein binding of ibuprofen. Protein binding of the enantiomers of ibuprofen was carried out by equilibrium dialysis using 2.5 ml volume dialysis cells and Spectrapor 2 membranes preconditioned by soaking overnight in phosphate buffered saline (PBS) (Tan *et al.* 1997c). Five determinations, using serum samples obtained at 0.5, 1.0, 2.0, 3.0 and 4.0 hours post drug administration, were carried out for each volunteer. Serum samples (1 ml) were transferred into three adjacent dialysis cells and equal volumes of PBS were added to the opposite sides of the membranes. The cells were then placed in a water bath (37°C) and allowed to equilibrate for 8 h. Analysis of the stereochemical composition of ibuprofen in the dialysate buffer was initially carried out by HPLC using the methodology for the determination of the drug enantiomers in serum but employing a semi-microbore column (150 × 2.1 mm i.d.) packed 'in-house' with Resolve C_{18} media obtained by emptying the packing material from a Radialpak Resolve C_{18} cartridge (5 µm) (Anachem Ltd, Luton, UK), as neither a smaller bore column or the packing material were commercially available. The mobile phase employed was the same as that used previously (see above) but at a flow rate of 0.6 ml min^{-1} with fluorescence detection as described above. During the course of this investigation a sample of racemic [^{14}C]-ibuprofen became available and the above analytical methodology was validated against a previously reported procedure using radiolabelled material (Evans *et al.* 1989b). Both methods yielded similar data, the determined unbound enantiomer fractions showing no statistically significant differences (Tan *et al.* 1997c). Subsequently, the approach utilising the radiolabelled material was adopted and enantiomeric resolution performed using a Chiralcel OD CSP with a mobile phase of hexane:isopropanol (100:1.1 v/v) containing TFA (0.1% v/v) at a flow rate of 1.0 ml min^{-1}, with UV detection at 220 nm. Under these conditions (*R*)- and (*S*)-ibuprofen eluted with retention times of 12.5 and 15.9 minutes respectively. The eluate fractions of the drug enantiomers were collected between 12.0 to 13.2 min and 15.4 to 17.2 min into individual scintillation vials and supplemented with 4 ml scintillation cocktail for radiochemical analysis. In this manner, higher throughput was achieved and also loss of analyte by additional manipulation was minimized.

The unbound enantiomer fractions determined were corrected for volume shift changes occurring during dialysis (Huang 1983), following determination of the protein concentrations both before and after dialysis using the Coomassie blue procedure (Tan *et al.* 1997c).

Volunteer study

Approval for the investigation was obtained from the Local Research Ethics Committee of King's College Hospital. Twelve healthy volunteers (6M, 6F) between the ages of 20 and 29 years (mean ± SD; M: 23 ± 3 years, weight 78 ± 13 kg; F: 25 ± 3 years, weight 70 ± 5 kg) gave written informed consent and participated in the study. Each volunteer underwent a thorough physical examination and routine biochemical tests prior to recruitment and none of the subjects were receiving drug treatment and had not been involved in research studies within the last three months. The volunteers were required to abstain from any medication, alcohol and caffeine containing beverages for 24 hours prior to the investigation and to fast overnight. On the morning of the study each subject swallowed a single 400 mg tablet of racemic ibuprofen (Brufen®) with approximately 150 ml of water. Blood samples (10 ml) were collected from a cannulated forearm vein immediately prior to and at 0.25, 0.5, 0.75, 1.0, 1.5, 2.0, 2.5, 3.0, 3.5, 4.0, 6.0, 8.0 and 10.0 hours post drug administration. A 24 h blood sample was obtained by venepuncture. The samples were collected into plain vacutainers and allowed to clot prior to centrifugation and separation of serum. Urine samples were collected immediately prior to drug administration and then continuously for 24 hours at the following time intervals: 0–2, 2–4, 4–6, 6–8, 8–10 and 10–24 h, from which a pooled 24 h sample was prepared. All serum and urine samples were frozen and stored at −20°C until required for analysis. All analyses were carried out in duplicate.

Data Analysis

Pharmacokinetic analysis of the serum concentration-time curves for the individual enantiomers was carried out by the non-compartmental approach using the TOPFIT program (Heinzel *et al.*, 1993). The terminal disposition constant (λ_z) and the apparent elimination half-life ($t_{1/2}$) for each profile were calculated by linear regression of the log-linear portions of the serum concentration-time curves. The area under the concentration-time curves (AUC) from time zero to 24 hours were calculated using the trapezoidal method and extrapolated to infinity by dividing the last measurable serum concentration by λ_z. The extrapolated areas were typically less than 2% of the total AUC. The maximum serum concentration (C_{max}) and the time to attain it (t_{max}) were determined by visual inspection of the data. The apparent total clearance (CL/F) and volume of distribution (V_D/F) were calculated as follows:

$$CL/F = D/AUC$$

$$V_D/F = D/(AUC.\lambda_z)$$

where F is the fraction of the dose (D) reaching the systemic circulation.

The fraction of (*R*)-ibuprofen undergoing inversion (F_{inv}) was calculated from an examination of the stereochemical composition of ibuprofen and both major oxidation products (both free and conjugated) excreted in urine over 24 hours, from:

$$F_{inv} = \frac{S\text{-metabolites (\%)} - S\text{-dose (\%)}}{R\text{-dose (\%)}}$$

where *S*-metabolites (%) is the sum of ibuprofen, and both oxidation products, excreted with the *S*-configuration of the propionic acid moiety expressed as a percentage of the total drug recovery, and *S*- and *R*-dose (%) are the percentages of the administered dose in that form, i.e. 50% as a racemate was administered. The systemic exposure (i.e. the 'dose') of (*S*)-ibuprofen was calculated from:

$$\text{'dose'} = (1 + F_{inv}).D,$$

where D is equal to the dose administered, i.e. 200 mg. The metabolite formation clearances were calculated from:

$$CL_{metab.} = A_m/AUC$$

where A_m is the amount of metabolite recovered in urine over 24 h and AUC corresponds to the area under the concentration-time curve of the drug enantiomer from which the metabolite was derived (Rowland and Tozer 1995).

Statistical comparisons of pharmacokinetic data derived from an examination of individual enantiomers may prove problematic unless their systemic availability is known to be equivalent. In the case of ibuprofen previous investigations, following intravenous and oral administration of the racemic drug, have indicated that the bioavailability of the individual enantiomers is essentially equivalent and approximates to unity (Hall *et al.* 1993). Statistical analysis of the data was carried out using Student's *t*-test for paired and independent samples.

Results

A representative ibuprofen enantiomer serum concentration time profile following oral administration of the racemic drug (400 mg) to a healthy volunteer is presented in figure 2 and the pharmacokinetic parameters derived from an examination of the individual data are presented in table 1. Peak serum concentrations (C_{max}) of both enantiomers were achieved within 3.0 h post dosing, with only one subject showing delayed absorption for both enantiomers with a t_{max} at 6.0 h. The mean values of C_{max} for (*S*)- and (*R*)-ibuprofen were 17.5 and 16.3 $\mu g\,ml^{-1}$ respectively. The mean serum concentrations of (*S*)-ibuprofen were greater than those of the *R*-enantiomer at all time points following four hours post drug administration, resulting in a significantly greater AUC for the *S*-enantiomer (table 1). The mean apparent elimination half-life of (*R*)-ibuprofen (1.4 ± 0.3 h) was significantly shorter than that of the *S*-enantiomer (2.3 ± 0.5 h; $p < 0.001$) resulting in a progressive predominance of (*S*)-ibuprofen with respect to the total drug serum concentration.

Examination of protein binding indicated stereoselectivity with the unbound fraction of (*S*)-ibuprofen being significantly greater than that of the *R*-enantiomer

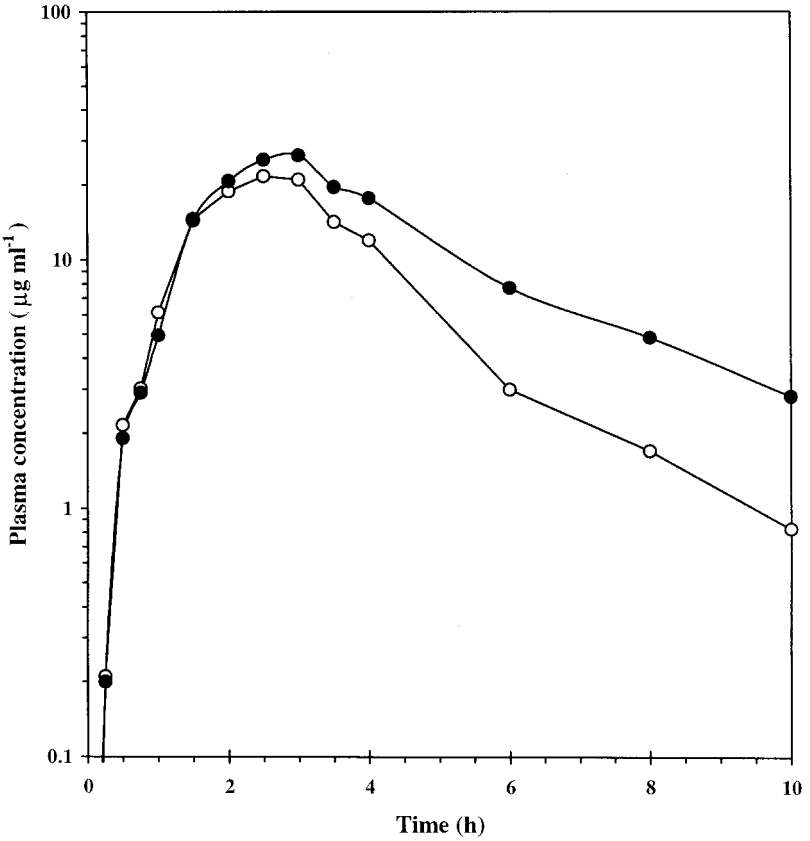


Figure 2. Representative serum concentration profiles of (*R*)-ibuprofen (open circles) and (*S*)-ibuprofen (closed circles) following the oral administration of the racemic drug (400 mg) to a healthy female volunteer. Individual data points are the average of duplicate determinations

(table 1) ($p < 0.001$) yielding an enantiomeric ratio (S/R) of the unbound fraction of 2.04.

The stereochemical composition of the drug and metabolites in urine (see below) was used to estimate the fraction of the dose of (*R*)-ibuprofen undergoing chiral inversion for each subject (table 1). Some 68% of the administered dose of the *R*-enantiomer was found to undergo inversion and the clearance via inversion was significantly greater than that via alternative routes (38.9 ± 9.0 ml min^{-1} compared to 18.3 ± 3.4 ml min^{-1}; $p < 0.00001$). The fraction of the dose inverted was also used to establish the exposure of the volunteers to (*S*)-ibuprofen and the parameters derived for the *S*-enantiomer (table 1) were calculated taking this increased 'dose' into account.

The urinary recovery of ibuprofen, 2-hydroxy- and carboxyibuprofen, both free and conjugated, accounted for approximately 11%, 23% and 40% of the dose respectively during the 24 h collection period (table 2). Examination of the stereochemical composition of the drug and both metabolites in urine indicated that 84% of the recovered material (74% of the dose) had the *S*-configuration in the propionic acid moiety. The stereochemical composition (S/R) of ibuprofen, 2-hydroxyibuprofen and carboxyibuprofen (considering the 2-position only) being 9,

Table 1. Pharmacokinetic parameters of the enantiomers of ibuprofen following the oral administration of the racemic drug (400 mg) to healthy volunteers.

	R		*S*	
Parameter (units)	Mean ± SD	Range	Mean ± SD	Range
C_{max} ($\mu g\,ml^{-1}$)	16.3 ± 3.8	11.3–21.6	17.5 ± 4.3	12.6–26.2
t_{max} (h)	2.4 ± 1.3	1.0–6.0	2.6 ± 1.4	1.0–6.0
$t_{1/2}$ (h)	1.4 ± 0.3	1.1–2.1	2.3 ± 0.5*	1.9–3.6
AUC ($\mu g.h\,ml^{-1}$)	60.6 ± 12.0	42.9–80.7	79.3 ± 19.7*	53.6–120.0
CL/*F* ($ml\,min^{-1}$)	57.1 ± 11.7	41.3–77.7	74.5 ± 18.1*	45.0–120.6
V_D /*F* (L)	7.0 ± 1.6	5.0–9.8	15.0 ± 4.2*	8.2–22.9
fu (%)	0.23 ± 0.04	0.19–0.32	0.47 ± 0.11*	0.33–0.69
F_{inv}	0.68 ± 0.03	0.62–0.74	–	–
CL_{inv}/F ($ml\,min^{-1}$)	38.9 ± 9.0	25.6–54.1	–	–
CL_{other}/F ($ml\,min^{-1}$)	18.3 ± 3.4	13.7–24.9	–	–

C_{max}, maximum observed concentration; t_{max}, time to C_{max}; $t_{1/2}$, terminal elimination half-life; AUC, area under the curve; CL/*F*, oral clearance; V_D/F, volume of distribution; *fu*, fraction unbound; F_{inv}, fraction inverted; CL_{inv}/F, clearance via inversion; CL_{other}/F, clearance via other metabolic routes.

* Significant differences between enantiomers, ($p < 0.05$; $n = 12$).

6.3 and 4.3 respectively. Examination of the stereochemistry of the metabolically introduced chiral centre in carboxyibuprofen, i.e. the 2′-position, indicated preferential oxidation of the drug to yield the diastereoisomeric metabolite having the same configuration at the new chiral centre as that in the substrate. Thus, oxidation of (*R*)-ibuprofen preferentially yields the $2'R,2R$-diastereoisomer (ratio $2'R,2R/2'S,2R = 1.6$) whereas oxidation of (*S*)-ibuprofen preferentially yields the $2'S,2S$-diastereoisomer (ratio $2'S,2S/2'R,2S = 1.2$).

The partial metabolic clearances for each ibuprofen enantiomer are presented in table 3. In each case the clearance of the *S*-enantiomer is significantly greater than that of (*R*)-ibuprofen and the formation clearance of the two preferentially formed diastereoisomers of carboxyibuprofen are significantly greater ($p < 0.001$) than those of the alternative stereoisomers (table 3).

The majority of the urinary ibuprofen was excreted as alkali labile conjugates, presumably the acyl glucuronides, with relatively minor quantities (< 1%) of either enantiomer being detected in the free form. Such minor quantities of the free drug may be due to hydrolysis of the conjugate during sample manipulation, i.e. collection, storage and analysis. In contrast, the 2-hydroxy- and carboxyibuprofen metabolites were excreted as alkali labile conjugates in variable amounts (table 2). 2-Hydroxyibuprofen showed stereoselectivity with respect to conjugation with the *S*-enantiomer being excreted predominantly as the conjugate (ratio conjugate/free ~2.1) whereas the *R*-enantiomer was excreted predominantly in the free form (ratio conjugate/free ~0.45). In the case of the diacid all four stereoisomers were preferentially excreted in the free form with ratios of conjugate/free varying from 0.45 for the $2'S,2R$-isomer to 0.58 for the $2'S,2S$-diastereoisomer.

Discussion

The pharmacokinetics of ibuprofen following administration of either racemate or the *R*-enantiomer are complicated as a result of the metabolic chiral inversion of (*R*)-ibuprofen. A number of approaches have been adopted in order to determine

Table 2. Urinary recovery of ibuprofen, 2-hydroxyibuprofen and carboxyibuprofen stereoisomers, both free and conjugated, following oral administration of the racemic drug (400 mg) to healthy volunteers.

		Free		Conjugated		Total	
Analyte	Stereochemistry	Mean ± SD	Range	Mean ± SD	Range	Mean ± SD	Range
Ibuprofen	*R*	0.06 ± 0.06	0.01–0.21	1.0 ± 0.3	0.8–1.7	1.1 ± 0.3	0.9–1.8
	S	0.70 ± 0.50	0.18–1.90	9.2 ± 2.8	4.7–13.5	9.9 ± 3.0	5.0–14.0
2-Hydroxyibuprofen	*R*	2.2 ± 0.6	1.4–3.5	1.0 ± 0.5	0.2–1.7	3.1 ± 0.5	2.4–3.8
	S	6.4 ± 2.4	3.4–11.5	13.3 ± 3.6	6.9–18.4	19.5 ± 2.9	15.7–24.4
Carboxyibuprofen	$2'S, 2R$	2.0 ± 0.4	1.4–2.8	0.9 ± 0.6	0.2–1.8	2.9 ± 0.5	2.1–3.7
	$2'R, 2R$	3.0 ± 0.6	1.5–3.9	1.7 ± 1.0	0.02–3.0	4.7 ± 0.8	3.8–6.3
	$2'R, 2S$	9.7 ± 2.8	5.6–15.6	5.1 ± 2.9	0.5–9.8	14.8 ± 3.2	11.3–21.7
	$2'S, 2S$	11.3 ± 3.3	6.2–18.1	6.5 ± 3.0	1.0–10.7	17.8 ± 3.1	14.3–23.3
Total recovery		35.4 ± 9.6	21.5–46.3	38.6 ± 11.1	21.0–55.6	74.0 ± 9.6	66.4–91.3

Data are the percentage of the dose administered; ($n = 12$).

Table 3. Metabolite formation clearances of ibuprofen glucuronide, 2-hydroxyibuprofen and carboxyibuprofen stereoisomers following oral administration of the racemic drug (400 mg) to healthy volunteers

Analyte	Stereochemistry	Formation clearance (ml min^{-1}) Mean ± SD	Range
Ibuprofen-glucuronide	R	1.2 ± 0.4	0.7–2.0
	S	8.5 ± 2.3[a]	3.9–13.1
2-Hydroxyibuprofen	R	3.6 ± 1.0	2.4–5.3
	S	17.3 ± 5.3[a]	11.0–29.1
Carboxyibuprofen	$2'S, 2R$	3.3 ± 0.9	2.1–4.8
	$2'R, 2R$	5.4 ± 1.4[b]	3.8–7.9
	$2'R, 2S$	13.4 ± 5.2	7.1–26.3
	$2'S, 2S$	16.0 ± 5.3[b]	7.9–28.3
	$2'S, 2R + 2'R, 2R$	8.7 ± 2.1	5.9–12.4
	$2'R, 2S + 2'S, 2S$	29.3 ± 10.3[a]	15.0–54.6

Data presented as $(2'S, 2R + 2R, 2R)$ and $(2'R, 2S + 2'S, 2S)$ for carboxyibuprofen represent the clearances of (R)- and (S)-ibuprofen via the formation of the diacid metabolite respectively.

[a] Significant differences between the drug enantiomers ($p < 0.001; n = 12$).

[b] Significant differences between the formation clearances of the individual diastereoisomers of the diacid arising from either enantiomer of ibuprofen ($p < 0.001; n = 12$).

the extent of chiral inversion including: administration of the individual enantiomers and comparison of the areas under the plasma concentration time curve of (S)-ibuprofen following administration as such and that resulting from inversion following dosing of the R-enantiomer (Lee *et al.* 1985); simultaneous administration of deuterated (S)-ibuprofen with unlabelled drug followed by quantification using gas-chromatography mass spectrometry (Rudy *et al.* 1991); and determination of the fraction of drug related material excreted in urine with the S-configuration in the propionic acid moiety (Baillie *et al.* 1989, Rudy *et al.* 1991). Comparison of the values obtained using all three approaches have indicated similar mean estimates for the fraction of the dose undergoing inversion. However, the interindividual variability using the administration of the individual enantiomer approach was found to be greater, and in some cases results in considerable errors in the estimate, in comparison to the alternative approaches (Rudy *et al.* 1991). This is presumably associated with intraindividual variability in drug handling on different occasions and possible enantiomer-enantiomer interactions during drug disposition following administration of the racemate.

The approach based on determination of the stereochemical composition of material excreted in urine, i.e. that adopted in the present investigation, has been reported to yield estimates of fraction inverted consistently greater, but with reduced interindividual variability in comparison to the approaches based on plasma determinations (Rudy *et al.* 1991). In one report these differences were found to be significantly greater, whereas in another this was not the case (Rudy *et al.* 1991, Hall *et al.* 1993). For the urinary analysis approach to be successful a high recovery of drug related material is essential and the observed greater estimates of fraction inverted may be associated with incomplete drug recovery. For example in the present investigation 74 ± 9.6% of the dose was accounted for with about 84% of the material having the S-configuration in the propionic acid moiety (table 2). If the proportion of the $2S$-configured material is reduced in the

unrecovered fraction then the estimated extent of inversion will be reduced. However, this approach does have the advantage of not requiring single enantiomer deuterated standards and quantification by mass spectrometry or repeated administration of single enantiomer doses. In addition, the urinary metabolite analysis approach would not be susceptible to the nonlinear kinetics of the drug with increased doses associated with concentration dependent protein binding (Evans *et al.* 1989b, 1990, Paliwal *et al.* 1993). However, an essential prerequisite for the urinary approach to be adopted is the availability of methodology capable of determining the stereochemical composition of the metabolites.

In comparison to the parent drug, relatively few studies have examined the stereochemical composition of the two major metabolic products. This is in part due to the limited availability of the material, particularly with respect to stereochemically defined standards, and also due to methodological problems associated with the chromatographic resolution of the four stereoisomers of carboxyibuprofen. Several investigations have determined the enantiomeric composition of the drug in plasma and reported the total urinary recovery of the metabolic products (Evans *et al.* 1990, Geisslinger *et al.* 1993) and a number of investigations have combined the data for the two carboxyibuprofen stereoisomers which are difficult to resolve chromatographically (Baillie *et al.* 1989, Smith *et al.* 1994). Two recent publications have successfully addressed this analytical problem using capillary electrophoresis (Bjørnsdottir *et al.* 1998, Fanali *et al.* 1998), however these have not as yet been applied to pharmacokinetic investigations. The only reports to date which refer to the stereochemical composition of both the drug and both major metabolites are those of Hall and coworkers (Rudy *et al.* 1990, 1991, 1995, Hall *et al.* 1993) who determined the stereochemical composition of the metabolites using the indirect approach to enantiomeric analysis. However, due to the lack of stereochemically defined standards of the carboxy metabolite, the chromatographic elution order could not be unequivocally assigned and was established by reference to a previously published method by Kaiser *et al.* (1976), which was empirical.

In the present investigation, using our sequential achiral-chiral approach to enantiomeric analysis (Tan *et al.* 1997b) we were able to determine the stereochemical composition of both major oxidative metabolites of ibuprofen, both free and conjugated with glucuronic acid, and estimate the fraction of (*R*)-ibuprofen undergoing inversion following administration of the racemate. Using this approach the fraction undergoing inversion was determined to be 0.68 ± 0.03 (range 0.62–0.74), data in good agreement with that of Rudy *et al.* (1991) using the urinary analysis approach, and within the range of values 0.52–0.71 reported by others (see Davies 1998 for review). It is noteworthy that, in comparison to other pharmacokinetic parameters, the variability observed in fractional inversion was relatively low (table 1) within this group of healthy young volunteers. It would be of interest to examine, using a similar approach, the extent of inversion within other defined subgroups to establish if the minimal variability observed in the present investigation is consistent within the population.

The significance of inversion versus noninversion mechanisms in the clearance of (*R*)-ibuprofen is difficult to ascertain from the literature. Rudy *et al.* (1991) reported similar values for both pathways whereas in subsequent studies these workers, and others, have reported that clearance via inversion is the predominant pathway (Hall *et al.* 1993, Smith *et al.* 1994, Rudy *et al.* 1995). Our observations support the latter view, the about two fold greater clearance of (*R*)-ibuprofen via

inversion (38.9 ± 9.0 ml min^{-1}) being significantly greater than that via noninversion pathways (18.3 ± 3.4 ml min^{-1}; $p < 0.00001$). The values obtained being similar to those reported by Smith *et al.* (1994) and lower than those obtained by Rudy *et al.* (1991).

The total clearance of (*S*)-ibuprofen was significantly greater than that of the *R*-enantiomer (table 1), the values obtained being similar to those of Smith *et al.* (1994) following administration of the individual enantiomers. The partial metabolic clearance of the drug via the three alternative pathways, i.e. conjugation with glucuronic acid and oxidation at the 2- and 3- positions of the isobutyl side chain, all showed a stereo preference for (*S*)-ibuprofen. The most marked stereoselectivity being found for conjugation with glucuronic acid (ratio S/R 7.1; table 3), with oxidation at the 2′-position yielding a ratio S/R of 4.8 and a substrate selectivity S/R of 3.4 for the carboxy metabolite. Examination of the diastereomeric composition of carboxyibuprofen indicated a more modest selectivity with respect to product formation, the diastereoisomer formed in excess in each case having the same configuration at the metabolically introduced centre as that in the substrate. Thus, the predominantly formed diastereoisomers are of the 2′*R*, 2*R*- and 2′*S*, 2*S*- absolute configurations, the product diastereoselectivity being 1.6 and 1.2 fold respectively (table 3). An observation in agreement with that of Rudy *et al.* (1991). The significance of this product selectivity is by no means clear as obviously multiple oxidative transformations are involved in the formation of carboxyibuprofen each of which may exhibit its own stereoselectivity.

Examination of the influence of gender on the enantiomeric disposition of ibuprofen revealed no significant differences in either drug recovery or pharmacokinetic parameters between males and females (data not shown), in agreement with the observations of Knights *et al.* (1995) who examined the pharmacokinetics of (*R*)-ibuprofen following administration of the single enantiomer to male, female and oral contraceptive-using females.

In conclusion, the data presented above represents the first investigation involving the unequivocal assignment of the stereochemical composition of both major urinary metabolites of ibuprofen and has confirmed the utility of the urinary metabolite approach as a facile means for the estimation of the fraction of (*R*)-ibuprofen undergoing inversion.

Acknowledgements

We gratefully acknowledge the award of a University of London Triangle Trust Postgraduate Studentship to BKP and a King's College Research Strategy Fund award to SHDJ, CGS and AJH.

References

Adams, S. S., Cliffe, E. E., Lessel, B. and Nicholson, J. S., 1967, Some biological properties of 2-(4-isobutylphenyl)propionic acid. *Journal of Pharmaceutical Sciences*, **56**, 1686.

Avgerinos, A. and Hutt, A. J., 1990, Interindividual variability in the enantiomeric disposition of ibuprofen following the oral administration of the racemic drug to healthy volunteers. *Chirality*, **2**, 249–256.

Baillie, T. A., Adams, W. J., Kaiser, D. G., Olanoff, L. S., Halstead, G. W., Harpootlian, H. and Van Giessen, G. J., 1989, Mechanistic studies of the metabolic chiral inversion of (*R*)-ibuprofen in humans. *Journal of Pharmacology and Experimental Therapeutics*, **249**, 517–523.

Bjørnsdottir, I., Kepp, D. R. Tjørnelund, J. and Hansen, S. H., 1998, Separation of the enantiomers of ibuprofen and its major phase I metabolites in urine using capillary-electrophoresis. *Electrophoresis*, **19**, 455–460.

Brooks, C. J. W. and Gilbert, M. T., 1974, Studies of urinary metabolites of 2-(4-isobutylphenyl)propionic acid by gas-liquid chromatography-mass spectrometry. *Journal of Chromatography*, **99**, 541–551.

Caldwell, J., Hutt, A. J. and Fournel-Gigleux, S., 1988, The metabolic chiral inversion and dispositional enantioselectivity of the 2-arylpropionic acids and their biological consequences. *Biochemical Pharmacology*, **37**, 105–114.

Chen, C.-Y. and Chen, C.-S., 1994, Stereoselective disposition of ibuprofen in patients with renal dysfunction. *Journal of Pharmacology and Experimental Therapeutics*, **268**, 590–594.

Davies, N. M., 1998, Clinical pharmacokinetics of ibuprofen. The first 30 years. *Clinical Pharmacokinetics*, **34**, 101–154.

El-Mouelhi, M., Ruelius, H. W., Fenselau, C. and Dulik, D. M., 1987, Species-dependent enantioselective glucuronidation of three 2-arylpropionic acids. Naproxen, ibuprofen and benoxaprofen. *Drug Metabolism and Disposition*, **15**, 767–772.

Evans, A. M., Nation, R. L. and Sansom, L. N., 1989a, Lack of effect of cimetidine on the pharmacokinetics of *R*(-)- and *S*(+)-ibuprofen. *British Journal of Clinical Pharmacology*, **28**, 143–149.

Evans, A. M., Nation, R. L., Sansom, L. N. Bochner, F. and Somogyi, A. A., 1989b, Stereoselective plasma protein binding of ibuprofen enantiomers. *European Journal of Clinical Pharmacology*, **36**, 283–290.

Evans, A. M., Nation, R. L., Sansom, L. N. Bochner, F. and Somogyi, A. A., 1990, The relationship between the pharmacokinetics of ibuprofen enantiomers and the dose of racemic ibuprofen in humans. *Biopharmaceutics and Drug Disposition*, **11**, 507–518.

Fanali, S., Desiderio, C., Schulte, G., Heitmeier, S., Strickmann, D., Chankvetadze, B. and Blaschke, G., 1998, Chiral capillary electrophoresis-electrospray mass spectrometry coupling using vancomycin as chiral selector. *Journal of Chromatography A*, **800**, 69–76.

Freneaux, E., Fromenty, B., Berson, A., Labbe, G., Degott, C., Letteron, P., Larrey, D. and Pessayne, D., 1990, Stereoselective and nonstereoselective effects of ibuprofen enantiomers on mitochondrial β-oxidation of fatty acids. *Journal of Pharmacology and Experimental Therapeutics*, **255**, 529–535.

Geisslinger, G., Schuster, O., Stock, K. P., Loew, D., Bach, G. L. and Brune, K., 1990, Pharmacokinetics of S(+)- and R(-)-ibuprofen in volunteers and first clinical experience of S(+)-ibuprofen in rheumatoid arthritis. *European Journal of Clinical Pharmacology*, **38**, 493–497.

Geisslinger, G., Stock, K. P., Loew, D., Bach, G. L. and Brune, K., 1993, Variability in the stereoselective disposition of ibuprofen in patients with rheumatoid arthritis. *British Journal of Clinical Pharmacology*, **35**, 603–607.

Hall, S. D., Rudy, A. C. Knight, P. M. and Brater, D. C., 1993, Lack of presystemic inversion of (*R*)- to (*S*)-ibuprofen in humans. *Clinical Pharmacology and Therapeutics*, **53**, 393–400.

Hayball, P. J., 1996, Chirality and nonsteroidal anti-inflammatory drugs. *Drugs*, **52 (Suppl 5)**, 47–58.

Heinzel, G., Woloszczak, P. and Thomann, P. (eds), 1993, Non-compartment analysis-methods manual. In *TOPFIT 2.0-Pharmacodynamic Data Analysis System* (Stuttgart: Fischer), pp 5–64.

Huang, J. D., 1983, Errors in estimating the unbound fraction of drugs due to the volume shift in equilibrium dialysis. *Journal of Pharmaceutical Sciences*, **72**, 1368–1369.

Hutt, A. J. and Caldwell, J., 1983, The metabolic chiral inversion of 2-arylpropionic acids – a novel route with pharmacological consequences. *Journal of Pharmacy and Pharmacology*, **35**, 693–704.

Kaiser, D. G., Van Giessen, G. J., Reischer, R. J. and Wechter, W. J., 1976, Isomeric inversion of ibuprofen (*R*)-enantiomer in humans. *Journal of Pharmaceutical Sciences*, **65**, 269-273.

Kepp, D. R., Sidelmann, U. G. and Hansen, S. H., 1997, Isolation and characterization of major phase I and II metabolites of ibuprofen. *Pharmaceutical Research*, **14**, 676–680.

Knights, K. M., McLean, C. F., Tonkin, A. L. and Miners, J. O., 1995, Lack of effect of gender and oral contraceptive steroids on the pharmacokinetics of (*R*)-ibuprofen in humans. *British Journal of Clinical Pharmacology*, **40**, 153–156.

Knights, K. M., Talbot, U. M. and Baillie, T. A., 1992, Evidence of multiple forms of rat liver microsomal coenzyme A ligase catalysing the formation of 2-arylpropionyl-coenzyme A thioesters. *Biochemical Pharmacology*, **44**, 2415-2417.

Knihinicki, R. D., Day, R. O. and Williams, K. M., 1989, Chiral inversion of 2-arylpropionic acid non-steroidal anti-inflammatory drugs I. *In vitro* studies of ibuprofen and flurbiprofen. *Biochemical Pharmacology*, **38**, 4389–4395.

Knihinicki, R. D., Day, R. O. and Williams, K. M., 1991, Chiral inversion of 2-arylpropionic acid non-steroidal anti-inflammatory drugs II. Racemization and hydrolysis of (*R*)- and (*S*)-ibuprofen-CoA thioesters. *Biochemical Pharmacology*, **42**, 1905–1911.

Lee, E. J. D., Williams, K., Day, R., Graham, G. and Champion, D., 1985, Stereoselective disposition of ibuprofen enantiomers in man. *British Journal of Clinical Pharmacology*, **19**, 669–674.

Li, G., Treiber, G., Maier, K., Walker, S. and Klotz, U., 1993, Disposition of ibuprofen in patients with liver cirrhosis. Stereochemical considerations. *Clinical Pharmacokinetics*, **25**, 154–163.

Lockwood, G. F., Albert, K. S., Gillespie, W. R., Bole, G. G., Harkcom, T. M., Szpunar, G. J. and Wagner, J. G., 1983, Pharmacokinetics of ibuprofen in man I. Free and total area/dose relationships. *Clinical Pharmacology and Therapeutics*, **34**, 97–103.

Mayer, J. M., 1990, Stereoselective metabolism of anti-inflammatory 2-arylpropionates. *Acta Pharmaceutica Nordica*, **2**, 197–215.

Menzel, S., Waibel, R., Brune, K. and Geisslinger, G., 1994, Is the formation of *R*-ibuprofenyl-adenylate the first stereoselective step of chiral inversion? *Biochemical Pharmacology*, **48**, 1056–1058.

Mills, R. F. N., Adams, S. S., Cliffe, E. E., Dickinson, W. and Nicholson, J. S., 1973, The metabolism of ibuprofen. *Xenobiotica*, **3**, 589–598.

Paliwal, J. K., Smith, D. E., Cox, S. R., Berardi, R. R., Dunn-Kucharski, V. A. and Elta, G. H., 1993, Stereoselective, competitive and nonlinear plasma protein binding of ibuprofen enantiomers as determined *in vivo* in healthy subjects. *Journal of Pharmacokinetics and Biopharmaceutics*, **21**, 145–161.

Petterson, J. E., Ulsaker, G. A. and Jellum, E., 1978, Studies on the metabolism of 2,4′-isobutylphenylpropionic acid (ibuprofen) by gas-chromatography and mass spectrometry. Dialysis fluid, a convenient medium for studies on drug metabolism. *Journal of Chromatography. Biomedical Applications*, **145**, 413–420.

Rowland, M. and Tozer, T. N., 1995, Metabolite kinetics. In M. Rowland and T. N. Tozer (eds), *Clinical Pharmacokinetics*, (Philadelphia: Lea & Febiger) pp. 367–394.

Roy-De Vos, M., Mayer, J. M., Etter, J.C. and Testa, B., 1996, Clofibric acid increases the unidirectional chiral inversion of ibuprofen in rat liver preparations. *Xenobiotica*, **26**, 571–582.

Rudy, A. C., Anliker, K. S. and Hall, S. D., 1990, High-performance liquid chromatographic determination of the stereoisomeric metabolites of ibuprofen. *Journal of Chromatography. Biomedical Applications*, **528**, 395–405.

Rudy, A. C., Bradley, J. D., Ryan, S. I., Kalasinski, L. A., Xiaotao, Q. and Hall, S. D., 1992, Variability in the disposition of ibuprofen enantiomers in osteoarthritis patients. *Therapeutic Drug Monitoring*, **14**, 464–470.

Rudy, A. C., Knight, P. M., Brater, D. C. and Hall, S. D., 1991, Stereoselective metabolism of ibuprofen in humans: administration of *R*- and *S*- and racemic ibuprofen. *Journal of Pharmacology and Experimental Therapeutics*, **259**, 1133–1139.

Rudy, A. C., Knight, P. M., Brater, D. C. and Hall, S. D., 1995, Enantioselective disposition of ibuprofen in elderly persons with and without renal impairment. *Journal of Pharmacology and Experimental Therapeutics*, **273**, 88–93.

Sanins, S. M., Adams, W. J., Kaiser, D. G., Halstead, G. W., Hosley, J., Barnes, H. and Baillie, T. A., 1991, Mechanistic studies on the metabolic chiral inversion of *R*-ibuprofen in the rat. *Drug Metabolism and Disposition*, **19**, 405–410.

Scheuerer, S., Hall, S. D., Williams, K. M. and Geisslinger, G., 1998, Effect of clofibrate on the chiral inversion of ibuprofen in healthy volunteers. *Clinical Pharmacology and Therapeutics*, **64**, 168–176.

Shieh, W.-R. and Chen, C.-S., 1993, Purification and characterization of novel '2-arylpropionyl-CoA epimerases' from rat liver cytosol and mitochondria. *Journal of Biological Chemistry*, **268**, 3487-3493.

Shieh, W.-R., Gou, D.-M., Liu, Y.-C., Chen, C.-S. and Chen, C.-Y., 1993, A ^{13}C-NMR study on ibuprofen metabolism in isolated rat liver mitochondria. *Analytical Biochemistry*, **212**, 143–149.

Shirley, M. A., Guan, X., Kaiser, D. G., Halstead, G. W. and Baillie, T. A., 1994, Taurine conjugation of ibuprofen in humans and in rat liver *in vitro*. Relationship to metabolic chiral inversion. *Journal of Pharmacology and Experimental Therapeutics*, **269**, 1166–1175.

Smith, D. E., Paliwal, J. K., Cox, S. R., Berardi, R. R., Dunn-Kucharski, V. A. and Elta, G. H., 1994, The effect of competitive and non-linear plasma protein binding on the stereoselective disposition and metabolic inversion of ibuprofen in healthy subjects. *Biopharmaceutics and Drug Disposition*, **15**, 545–561.

Tan, S. C., Baker, J. A., Stevens, N., de Biasi, V., Salter, C., Chalaux, M., Afarinkia, K. and Hutt, A. J., 1997a, Synthesis, chromatographic resolution and chiroptical properties of carboxyibuprofen stereoisomers: major metabolites of ibuprofen in man. *Chirality*, **9**, 75–87.

Tan, S. C., Jackson, S. H. D., Swift, C. G. and Hutt A. J., 1997b, Stereospecific analysis of the major metabolites of ibuprofen in urine by sequential achiral-chiral high-performance liquid chromatography. *Journal of Chromatography B*, **701**, 53–63.

Tan, S. C., Jackson, S. H. D., Swift, C. G. and Hutt A. J., 1997c, Enantiospecific analysis of ibuprofen by high-performance liquid chromatography: determination of free and total drug enantiomer concentrations in serum and urine. *Chromatographia*, **46**, 23–32.

Tracy, T. S., Wirthwein, D. P. and Hall, S. D., 1993, Metabolic inversion of (*R*)-ibuprofen. Formation of ibuprofenyl-coenzyme A. *Drug Metabolism and Disposition*, **21**, 114–120.

Wechter, W. J., Loughhead, D. G., Reischer, R. J., Van Giessen, G. J. and Kaiser, D. G., 1974, Enzymatic inversion at saturated carbon: nature and mechanism of the inversion of *R*(-)-*p*-isobutylhydratropic acid. *Biochemical and Biophysical Research Communications*, **61**, 833–837.

Williams, K. M., Day, R. O., Knihinicki, R. D. and Duffield, A., 1986, The stereoselective uptake of ibuprofen enantiomers into adipose tissue. *Biochemical Pharmacology*, **35**, 3403–3405.

Zhao, B., Geisslinger, G., Hall, I., Day, R. O. and Williams, K. M., 1992, The effect of the enantiomers of ibuprofen and flurbiprofen on the β-oxidation of palmitate in the rat. *Chirality*, **4**, 137–141.

XENOBIOTICA, 2002, VOL. 32, NO. 8, 699–713

Taylor & Francis
healthsciences

Pharmacokinetics and metabolism of the anti-oestrogen droloxifene in female human subjects

B. A. JOHN†*, R. R. BRODIE†, G. A. BALDOCK†, A. MCBURNEY†, L. F. CHASSEAUD†, P. JANK‡ and A. VON NIECIECKI‡

† Department of Metabolism and Pharmacokinetics, Huntingdon Life Sciences, Huntingdon PE28 4HS, UK.
‡ Klinge Pharma GmbH, 81673, Munich, Germany.

Received 13 December 2001

1. Single oral doses of a solution formulation of ^{14}C-droloxifene citrate (141 mg) appeared to be rapidly and well absorbed in four post-menopausal female subjects. Peak plasma concentrations (C_{max}) of total ^{14}C (1260 ng eq. ml^{-1}), droloxifene (196 ng ml^{-1}) and the major metabolite droloxifene glucuronide (851 ng eq. ml^{-1}) occurred at 0.9–1.1 h (T_{max}) and declined bi-exponentially with terminal half-lives of 45.0, 31.6 and 32.0 h respectively. The mean AUCs of droloxifene and the major metabolite were 21 and 37% respectively that of total ^{14}C.

2. Total ^{14}C was excreted slowly, mainly in the faeces. Mean totals of 6.6 and 90.3% of the dose were excreted in the urine and faeces respectively during 11 days. The data were consistent with biliary excretion and enterohepatic circulation of the major metabolite, droloxifene glucuronide.

3. GC-MS showed that the major ^{14}C-components in 0–24-h urine were droloxifene (mean 0.4% dose) and its glucuronide (2.3% dose), and in faeces were droloxifene (60.2% dose) and *N*-desmethyldroloxifene (4.2% dose). Other components in faeces corresponded chromatographically to reference standards, droloxifene *N*-oxide (1.9% dose), side-chain hydroxylated droloxifene (dimethylamine moiety of droloxifene side-chain replaced by hydroxyl, 1.3% dose) and droloxifene glucuronide (10.7% dose). The latter was resistant to enzymic hydrolysis by the β-glucuronidase used.

4. Intersubject variability in the pharmacokinetics of droloxifene in this study was relatively low (CV $< 20\%$ for AUC and half-life).

Introduction

Droloxifene citrate, (E)-1-[4′-(2-dimethylaminoethoxy)phenyl]-1-(3-hydroxyphenyl)-2-phenylbut-1-ene citrate, is a non-steroidal anti-oestrogen structurally related to tamoxifen but differing from it by a hydroxyl group. Droloxifene is 3-hydroxytamoxifen. It has been developed for the treatment of hormone-receptor-dependent tumours such as breast cancer, as well as for osteoporosis. Pharmacological studies have shown that compared with tamoxifen, droloxifene citrate is a more potent anti-oestrogen (Ahlemann *et al.* 1988). It has less intrinsic oestrogenicity, potent antiproliferative activity and is cytotoxic to tumour cells (Löser *et al.* 1985, 1986, Hasmann *et al.* 1994). Droloxifene has undergone clinical trials (Rauschning and Pritchard 1994) and its pharmacokinetics in breast cancer patients has been reported (Grill and Pollow 1991).

* Author for correspondence;

Xenobiotica ISSN 0049-8254 print/ISSN 1366–5928 online © 2002 Taylor & Francis Ltd
http://www.tandf.co.uk/journals
DOI: 10.1080/00498250210143029

The present study was designed to evaluate the pharmacokinetics and metabolism of droloxifene citrate in man using the ^{14}C-labelled compound. It was carried out in female subjects as they would mainly comprise the patient population for droloxifene citrate.

Materials and methods

Materials

Droloxifene citrate and the reference compounds listed in table 3 were provided by Klinge Pharma GmbH (Munich, Germany). ^{14}C-droloxifene citrate of specific activity 16.6 μCi mg^{-1} was obtained from Amersham International Plc (Amersham, UK).

β-Glucuronidase (Type VIIA from *E. coli*) was obtained from Sigma Chemical Co. Ltd (Poole, UK). The scintillator systems MI-31 and Permafluor-E, and Carbo-Sorb, were from Packard Instrument Ltd (Pangbourne, UK). Other analytical grade reagents were commercially available.

Dose formulation

This was prepared by dissolving a spray-dried powder containing droloxifene citrate and β-cyclodextrin in a 1:2 molar ratio, in distilled water: ^{14}C-droloxifene citrate was then added. The resultant aqueous formulation contained 141 mg ^{14}C-droloxifene citrate (47.2 μCi) in each 200 ml water. Its radiochemical purity was at least 98% (HPLC-radioactivity/UV detectors). The dose formulation was prepared under low-lighting conditions and protected from light.

Clinical phase

The clinical phase of this study was conducted at Leicester Clinical Research Centre (Leicester, UK) under the supervision of the Medical Director (Dr M. D. Eve). The study was approved by the local ethics committee and the UK Administration of Radioactive Substances Advisory Committee.

Four post-menopausal non-smoking female subjects (three Caucasian, one African-Caribbean, mean (range) age 57 (48–62) years; bodyweight 65 (54–78) kg, volunteered for this study after its purpose, procedures and possible adverse events were explained to them. They were enrolled on the study following acceptable medical histories and results in physical and laboratory screening, and they provided informed consent.

The subjects were resident in the clinical unit from the night preceding dose administration through to sample collection during 11 days. They were rescreened on completion of the study to ensure that the administered drug had no detectable effect on their health.

Following an overnight fast of at least 8 h, individual doses (141 mg ^{14}C-droloxifene citrate in 200 ml water) were ingested by the subjects from glass beakers, which were then rinsed with distilled water (2 × 50 ml). These rinsings were also ingested and measurement showed that $< 0.01\%$ of the radioactivity remained in any beaker after this process. The volunteers were permitted food at 4 h after dosing.

Sample collection

Blood samples were withdrawn from an indwelling cannula in an arm vein at predose and at 0.25, 0.5, 0.75, 1.0, 1.5, 2, 2.5, 3, 4, 6, 8, 10, 12, 14, 20, 24, 28, 36, 48, 60, 72, 84, 96, 108, 120, 132, 156, 180, 204, 228 and 252 h postdose. Urines were collected predose and during 0–2, 2–4, 4–8, 8–12, 12–16, 16–24 and then at 24-h intervals up to 262 h postdose. Faeces were similarly collected but at 24 h intervals.

All samples were stored at about −20°C until taken for analysis except whole blood which was stored at about 4°C.

Preparation of samples for measurement of radioactivity

Plasma (1 ml) and urine (1–2 ml) were mixed with MI-31 scintillator. Whole blood (0.5 ml) and aq. (1:1 w/v) faecal homogenates (about 0.2 g) were combusted in an automatic sample oxidizer (Model 307, Canberra Packard Ltd, Pangbourne, UK). The combustion products were absorbed in Carbo-Sorb to which Permafluor-E was added before liquid scintillation analysis in an LKB-Wallac 1219 RackBeta scintillation counter (Wallac Oy, Turku, Finland). Combustion recoveries using either ^{14}C-standards (Amersham) or ^{14}C-droloxifene citrate $> 95\%$ for which the results were corrected. The concentrations of radioactivity in blood cells were calculated from those in whole blood and plasma using measured haematocrit values at each time point. These ranged between 31 and 46% and tended to diminish during the course of blood withdrawals, as would be expected.

Plasma protein binding

The binding of droloxifene to human plasma proteins was measured *in vitro* in control human plasma to which ^{14}C-droloxifene citrate was added over a concentration range similar to that measured *in vivo*, by ultrafiltration (micropartition system, Amicon Ltd, Stonehouse, UK).

Determination of droloxifene and its metabolites in plasma

Plasma concentrations of droloxifene and its metabolites *N*-desmethyldroloxifene and 4-methoxydroloxifene were measured by an HPLC procedure involving a post-column photoreactor and fluorescence detection. The photoreactor converts these analytes to their corresponding fluorescent phenanthrene derivatives (Jank *et al*. 1987, Lien *et al*. 1995). The limit of quantification was set at 0.2 ng ml^{-1}. Throughout the concentration range of droloxifene measured, between-day or within-day accuracy and precision were < 10 and 13.5% respectively. Plasma concentrations of the metabolites *N*-desmethyldroloxifene and 4-methoxydroloxifene were measured with reference to the calibration line for droloxifene, and the data corrected for the relative fluorescence intensity of the phenanthrene derivatives of these two metabolites. As might be expected, the fluorescence intensity of the phenanthrene derivative of *N*-desmethyldroloxifene was similar to that of the corresponding derivative of droloxifene whereas that of 4-methoxydroloxifene was one half. Plasma concentrations of droloxifene were again measured after hydrolysis of plasma samples (100 µl) with β-glucuronidase (4 units), pH 6.8 at 37°C for 1 h.

The above procedure was also used to determine the amounts of droloxifene and three of its potential metabolites in methanol extracts (20 ml) of aq. (1:1 w/w) faecal homogenates (0.5–1 g). Partial validation of the procedure showed that at the set limit of quantification of 1 µg g^{-1} for droloxifene and 0.2 µg g^{-1} for each of the metabolites, within-day and between-day precision and accuracy were no worse than 11 and 7.2% respectively for any analyte. The respective retention times of droloxifene, *N*-desmethyldroloxifene, 4-methoxydroloxifene and droloxifene *N*-oxide were 26.3, 22.1, 29.2 and 18.5 min respectively. A reference compound 3-methoxy-4-hydroxy-tamoxifen (table 3), structurally similar to 4-methoxydroloxifene, had a retention time between that of the latter and of droloxifene.

Thin-layer chromatography (TLC)

TLC was carried out on prelayered Merck silica gel 60F254 plates (E. Merck AG, Darmstadt, Germany) of layer thickness 0.25 min in the following solvent systems: (1) chloroform:methanol:ammonia (50:50:1 v/v/v); chloroform:isopropanol:ammonia (60:50:1 v/v/v). Radioactive components present on TLC plates were detected by apposition autoradiography using Hyperfilm β-max X-ray film (Amersham) and quantified by radiochromatogram scanning using a Berthold Automatic TLC Analyser (Model LB 3832 with online data collection).

Enzymic hydrolysis

Samples of plasma and urine were incubated with β-glucuronidase (500 units ml^{-1} biological sample) in 0.1 M phosphate buffer, pH 6.8, for about 18 h at 37°C.

Preparation of samples before TLC

Plasma. Samples were freeze-dried and the resultant residue extracted with methanol (2×5 ml). The combined extracts were evaporated to a small volume, under N_2 at 37°C and subjected to TLC.

Urine. Samples (2 ml) were applied to preconditioned C_{18} Bond Elut columns (Analytichem, Harbor City, CA, USA). After removing unwanted material with methanol:water (20:80 v/v), ^{14}C-components were eluted with methanol (10 ml). The eluates were evaporated to dryness under N_2 at 37°C, and the residues reconstituted in methanol. The methanol solution was subjected to TLC

Faeces. Faecal homogenates (about 0.25 g) were freeze-dried and the resultant residue extracted with methanol (1×3 ml, 2×2 ml). The combined extracts were evaporated to dryness under N_2 at 37°C and the residues reconstituted in methanol. The methanol extract was subjected to TLC.

Isolation of metabolites

Urine. Urine was processed as described for TLC, and the methanol extract subjected to GC-MS.

Faeces. For isolation of the major component (M3), faecal homogenates were processed as described for TLC, and the residue reconstituted in water before solid phase extraction as previously described for urine. This component was separated from other faecal ^{14}C-components by TLC and isolated from the TLC silica gel by methanol extraction. The extract, after evaporation to a small volume, was subjected to GC-MS.

M6 was isolated following separation from other faecal ^{14}C-components by TLC and methanol extraction of the TLC silica gel. The extract, after evaporation to a small volume, was subjected to GC-MS.

Mass spectrometry

Urine. Extracts were evaporated to dryness, and the residues silylated (BSTFA/TMCS). The silylated material was introduced into a medium resolution VG TS-250 mass spectrometer (VG Analytical Ltd, Manchester, UK) via an HP 5890 gas chromatograph (Hewlett Packard, Bracknell, UK) fitted with a DB-5 (15 m × 0.25 mm i.d.), fused silica column (FSA Laboratory Supplies, Loughborough, UK). The column outlet was passed directly into the ion source of the mass spectrometer. Samples were injected into the GC column using the splitless mode with the injector at 250°C, the oven at 100°C and the split valve closed for 0.4 min; the split valve was then opened, and the oven heated at 20°C min^{-1} up to 300°C. Electron impact mass spectra were recorded at 70 eV and a source temperature of 200°C.

Faeces. Using the direct insertion probe, M3 was introduced into the ion source of a high resolution VG 7070E double focussing mass spectrometer (VG Analytical Ltd) operating in the electron impact mode at 70 eV and a source temperature of 200°C.

M6 was derivatized before mass spectrometry. The derivatives were introduced into the VG 7070E via a gas chromatograph (HP 5790) operated under similar conditions to those described for urine samples. M6 derivatives were formed by silylation (BSTFA/TMCS) or by trifluoroacetylation (TFAA) using standard conditions.

Pharmacokinetic data processing

Concentrations of radioactivity in plasma and whole-blood are expressed throughout this report in terms of ng equivalents droloxifene base ml^{-1} as are plasma concentrations of droloxifene glucuronide, *N*-desmethyldroloxifene and its glucuronide, and 4-methoxydroloxifene so that the data can be compared.

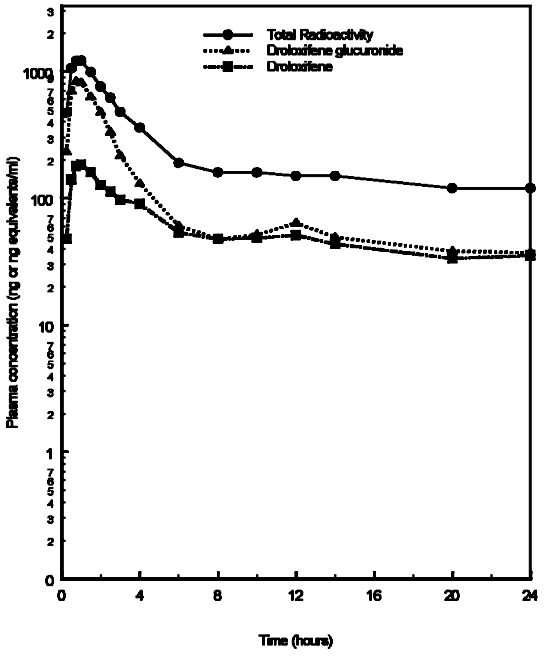
Maximum plasma concentrations of radioactivity and of other analytes (C_{max}) and their times of occurrence (T_{max}) were the observed values. The respective areas under the plasma concentration versus time curves were estimated by the linear trapezoidal rule to the last sampling time at which concentrations were above the limit of accurate detection (AUC_t) and, where acceptable, extrapolated to infinite time (AUC) by the addition of C/λ_z where λ_z is the terminal rate constant calculated by linear regression of ln concentration on time using at least three data points which appeared to be randomly distributed about a single straight line, and C is the plasma concentration at the last measurable sampling time given by the regression. Terminal half-lives were calculated from $\ln 2/\lambda_z$. Mean residence time after oral doses was calculated as AUMC/AUC, where AUMC is the area under the first moment of the plasma droloxifene concentration–time curve estimated by the log–linear trapezoidal rule.

Results

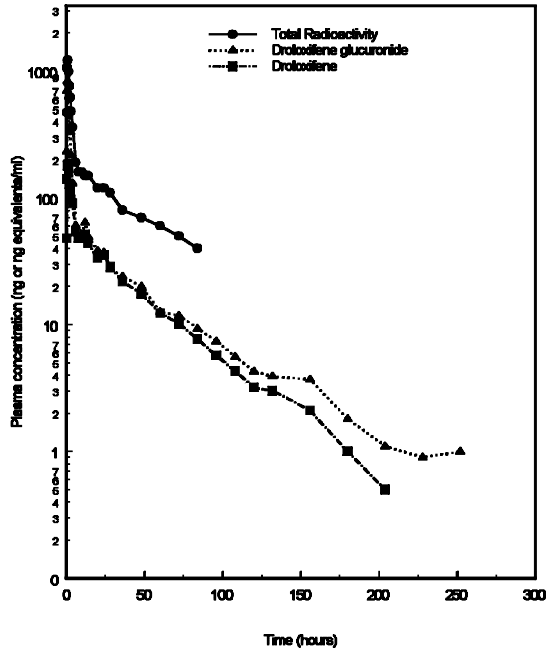
Mean concentrations of total ^{14}C, droloxifene and its glucuronic acid conjugate are shown in figure 1a, b and pharmacokinetic parameters in table 1. The peak mean concentration of total ^{14}C was 1220 ng eq. ml^{-1} at 1 h compared with that of droloxifene of 184 ng ml^{-1} and that of the glucuronide of 816 ng eq. ml^{-1}. Mean concentrations of all three analytes declined biexponentially. Plasma concentrations of droloxifene were 10–34% (mean 23%) of those of total ^{14}C during 0.25–84 h, implying that droloxifene is subjected to first-pass metabolism during its absorption from the gut into the systemic circulation.

Mean concentrations of droloxifene and its glucuronic acid conjugate were detected for longer than were those for total ^{14}C (figure 1) owing to the greater sensitivity of the HPLC-fluorescence method (0.2 ng ml^{-1}) than that for total ^{14}C (about 30 ng eq. ml^{-1}).

Comparison of the mean areas under the respective plasma concentration–time curves (AUC) indicated that the mean AUC of droloxifene was 21% of that for total ^{14}C and its glucuronic acid conjugate was 37%, indicating that these two components accounted for much of the circulating total ^{14}C (table 1). The data obtained from metabolite profiling suggested that the values obtained for drolox-



a



b

Figure 1. (a, b) Mean plasma concentration–time profiles of total ^{14}C (●), droloxifene (■) and droloxifene glucuronide (▲) after oral administration of 141 mg ^{14}C-droloxifene citrate to four healthy female subjects. (a) 0–24 h; (b) 0–254 h.

Table 1. Pharmacokinetic parameters of total ^{14}C, droloxifene and its metabolites in plasma after oral administration of ^{14}C-droloxifene citrate (141 mg) to healthy female subjects

Subject no.	C_{max} (ng ml^{-1})*	T_{max} (h)	$t_{1/2}$, (h)†	AUC (ng.h ml^{-1})*
Total ^{14}C				
1	1300	0.75	66.1	17 373
2	610	1.0	82.0	10 398
3	1450	1.0	28.4	11 753
4	1680	0.75	37.7	13 572
Mean	1260	0.9	45.0	13 274
SD	461	0.1	23.0	3026
Droloxifene				
1	212	0.75	36.3	3239
2	124	1.5	34.7	2072
3	304	1.0	25.2	3030
4	142	1.0	32.8	2579
Mean	196	1.1	31.6	2730
SD	82	0.3	5.8	518
Droloxifene glucuronide				
1	848	0.75	46.0	5264
2	342	1.0	NC	2535‡
3	934	1.0	25.7	3784
4	1280	0.75	24.4	5793
Mean	851	0.9	32.0	4947
SD	387	0.1	12.1	1041
N-Desmethyldroloxifene				
1	7.4	1.5	54.8	419‡
2	5.2	2.5	NC	193‡
3	10.9	1.5	36.8	299‡
4	5.6	1.5	NC	327‡
Mean	7.3	1.8	–	310
SD	2.6	0.5		93
N-Desmethyldroloxifene glucuronide				
1	21.0	2.0	NC	454‡
2	10.8	1.5	NC	958‡
3	28.6	2.0	NC	1035‡
4	25.6	1.5	77.4	823‡
Mean	21.5	1.8	–	820
SD	7.8	0.3		258
4-Methoxydroloxifene				
1	7.4	4.0	NC	468‡
2	3.8	8.0	NC	432‡
3	6.4	2.5	NC	384‡
4	4.2	4.0	NC	239‡
Mean	5.5	4.6	–	381
SD	1.7	2.4		101

* ng eq. to droloxifene so that data can be compared.
† Harmonic mean.
‡ AUC_{254}, value excluded from the mean for droloxifene glucuronide.
NC, not calculable.

ifene glucuronide were underestimates owing to its incomplete hydrolysis by β-glucuronidase used during analysis. However, other minor droloxifene-related components were also present in plasma. The mean AUCs of *N*-desmethyldroloxifene and 4-methoxydroloxifene each accounted for 2 and 3% respectively of the

mean AUC of total ^{14}C, and the glucuronic acid conjugate of the former also accounted for 6%. There was little evidence for the presence of a glucuronic acid conjugate of 4-methoxydroloxifene in plasma.

Plasma concentrations of droloxifene declined with a mean terminal half-life of 31.6 h and those of its glucuronic acid conjugate with a similar mean half-life of 32.0 h.

The mean residence time of droloxifene in plasma ranged between 28.5 and 49.3 h (mean 39.4 ± 8.9 h) consistent with its slow elimination from the body.

The whole-blood concentration–time profile of total ^{14}C paralleled that for plasma, and whole blood to plasma ratios of total ^{14}C were in the range 0.55–0.75 suggesting that uptake of ^{14}C into blood cells was minimal.

Plasma protein binding

Over the concentration range 100–2000 ng ml^{-1}, ^{14}C-droloxifene was extensively bound (99%) to plasma proteins *in vitro*.

Excretion

Following oral doses of ^{14}C-droloxifene citrate, ^{14}C was excreted slowly, mainly in the faeces (Table 2). During the first 24 h, means of 3.3% dose were excreted in the urine and 0.5% dose in faeces increasing to 5.4 and 41.8% dose respectively during 72 h, 6.6 and 80.6% dose respectively during 7 days and a total of 6.6 and 90.4% dose respectively during the 11-day collection period. The total proportions of the dose excreted by the individual subjects were remarkably consistent; urinary excretion ranged between 6.2 and 7.3% dose and faecal excretion between 89.5 and 91.3% dose. The corresponding coefficients of variation were < 8 and 1% respectively for the total percentage dose excreted in the urine and faeces.

Assuming complete absorption of the ^{14}C-dose, the relationship between the mean proportion of the ^{14}C-dose remaining to be excreted in faeces with time was linear when plotted on a log–linear scale. It declined with a mean half-life of 45.8 h, virtually identical to the half-life (45.0 h) for the decline of ^{14}C concentrations in plasma.

Metabolite profiles

The R_f of available reference standards in the two TLC solvent systems used are shown in table 3. Presumably because they have similar physicochemical properties, some of the reference standards are not resolved by either of the solvent systems and accordingly are given the same metabolite designation. However, the identities of major components M3, M6 and M8 were established by other methods.

Plasma. Recovery of ^{14}C in plasma extracts $> 91\%$. In accordance with the HPLC-fluorescence data, the major components in 26 individual samples of plasma obtained during 0.25–3.0 h after dosing, corresponded chromatographically to droloxifene and its glucuronic acid conjugate. These components accounted for 4–21 and 59–94% of the ^{14}C in 'unhydrolysed' plasma and for 44–87 and 4–56% in enzyme hydrolysed plasma. The component in plasma

Table 2. Excretion of ^{14}C in the urine and faeces after oral administration of ^{14}C-droloxifene citrate (141 mg) to four healthy female subjects

	Subject number				
Time interval (h)	1	2	3	4	Mean ± SD
Urine					
0–2	0.6	0.8	0.9	0.8	0.8 ± 0.1
2–4	0.5	0.6	0.4	0.5	0.5 ± 0.1
4–8	0.4	0.5	0.7	0.6	0.6 ± 0.1
8–12	0.4	0.3	0.5	0.5	0.4 ± 0.1
12–16	0.2	0.4	0.5	0.5	0.4 ± 0.1
16–24	0.6	0.4	0.6	0.6	0.6 ± 0.1
24–48	1.7	0.8	1.3	1.3	1.3 ± 0.4
48–72	0.9	1.1	0.6	0.6	0.8 ± 0.2
72–96	0.8	0.6	0.3	0.4	0.5 ± 0.2
96–120	0.5	0.4	0.2	0.2	0.3 ± 0.1
120–144	0.3	0.3	0.1	0.1	0.2 ± 0.1
144–168	0.2	0.2	0.1	0.1	0.2 ± 0.1
168–192	0.1	0.1	< 0.1	< 0.1	–
192–216	0.1	ND	ND	ND	–
216–240	ND	ND	ND	ND	ND
240–264	ND	ND	ND	ND	ND
Total urine (0–264)	7.3	6.5	6.2	6.2	6.6 ± 0.5
Faeces					
0–24	NS	0.1	0.2	1.6	0.5 ± 0.8
24–48	NS	NS	35.2	6.6	10.5 ± 16.8
48–72	4.7	34.9	31.7	51.7	30.8 ± 19.5
72–96	25.1	NS	5.5	10.5	10.3 ± 10.8
96–120	NS	20.0	6.0	7.7	8.4 ± 8.4
120–144	28.0	12.8	6.6	5.0	13.1 ± 10.5
144–168	11.6	12.0	1.9	2.6	7.0 ± 5.5
168–192	NS	2.1	1.6	2.0	1.4 ± 1.0
192–216	13.4	5.2	1.2	0.9	5.2 ± 5.8
216–240	6.2	1.6	0.1	0.4	2.1 ± 2.8
240–264	2.3	1.1	0.6	0.5	1.1 ± 0.8
Total faeces (0–264)	91.3	89.8	90.6	89.5	90.3 ± 0.8
Total excretion (0–264)	98.6	96.3	96.8	95.7	96.9 ± 1.2

Results are shown as the percentage administered dose.
NS, no sample excreted.

Table 3. R_f values of reference compounds in solvent systems 1 (SSI) and (SS2) and correlation with ^{14}C components

	R_f		^{14}C component with similar R_f
Reference compound	SS1	SS2	
Side-chain-hydroxylated	0.81	0.74	M1
Droloxifene	0.69	0.43	M3
4-Methoxydroloxifene	0.69	0.43	M3
3-Methoxy-4-hydroxytamoxifen	0.69	0.43	M3
Di-*N*-desmethyldroloxifene	0.50	0.24	M6
N-desmethyldroloxifene	0.50	0.24	M6
N-desmethyl-4-methoxydroloxifene	0.50	0.24	M6
N-desmethyl-3-methoxy-4-hydroxytamoxifen	0.50	0.24	M6
Droloxifene-*N*-oxide	0.38	0.05	M7
Droloxifene glucuronide	0.29	0	M8

corresponding to droloxifene glucuronide was not completely hydrolysed by the β-glucuronidase used in all samples as shown by the 'spread' in the data obtained. However, conversion of the data to weight ml^{-1} units provided reasonable agreement between the data obtained from metabolite profiling and those obtained from HPLC-fluorescence (range 64–112%, mean difference $<15\%$). TLC/radioactivity measurement generally yielded lower values (weight ml^{-1}) than did HPLC-fluorescence.

In some samples, a third component (designated M5) and more polar than droloxifene was detected after enzyme hydrolysis (2–8% ^{14}C) that did not correspond chromatographically to the available reference standards.

Urine. Recovery of ^{14}C in urine extracts ranged between 76 and 88%. Urine extracts (0–24 h) contained one major component corresponding chromatographically either to droloxifene or to its glucuronic acid conjugate. In either case, these components accounted for up to 88 or 95% respectively of the ^{14}C in individual samples and to a mean total of 0.4 and 2.3% dose respectively in 0–24-h urine. The identity of droloxifene was confirmed by GC-MS. Several other minor components were detected, especially after enzyme hydrolysis of urine, but none accounted for $>7\%$ of the ^{14}C (i.e. 0.03% dose), and consequently these were not further characterized. Enzyme hydrolysis of urine generally increased the proportion of the component corresponding to droloxifene (up to 92% ^{14}C) and decreased that of the component corresponding to the glucuronic acid conjugate to 5% ^{14}C or less in individual samples. Unlike plasma, β-glucuronidase treatment of urine essentially hydrolysed all of the glucuronide.

Faeces (TLC). At least six faeces samples from each subject were extracted for metabolite profiling. Recovery of ^{14}C from most extracts was essentially complete: the lowest recovery was 74%. There was one major component in faeces corresponding to droloxifene, which accounted for 44–84% of the sample ^{14}C (table 4). There were at least five other ^{14}C-components present of which the most abundant (5–28% sample ^{14}C) had an R_f similar to droloxifene glucuronide (figure 2). Another minor component, designated M6, accounted for 3–10% sample ^{14}C. The data for the percentage dose excreted in faeces as the different components by individual subjects are shown in table 4. A representative radiochromatogram is shown in figure 2.

Faeces (HPLC). A mean of 79% (range 50–100%) of the radioactivity in faecal homogenates was extracted with methanol. Droloxifene was measurable in most samples as was its metabolite *N*-desmethyldroloxifene. 4-Methoxydroloxifene and droloxifene *N*-oxide were measurable in about one-third to one-half of the samples respectively. The amounts of droloxifene present accounted for most (mean 90%) of what was measured. The metabolites, *N*-desmethyldroloxifene (mean 5%), and 4-methoxydroloxifene and droloxifene *N*-oxide (mean $<1\%$ each) were measured in much lower proportions. Furthermore, a component corresponding to an available reference compound 3-methoxy-4-hydroxytamoxifen was also measurable (with reference to the calibration line for 4-methoxydroloxifene); it accounted for a mean of 4% of what was measured.

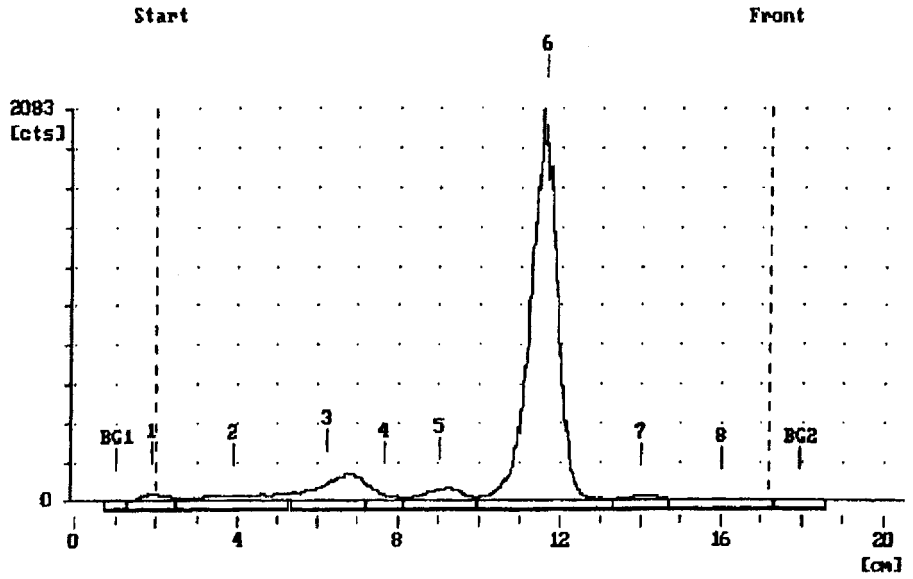


Figure 2. Thin layer radiochromatogram of a 24–48-h extract of faeces obtained after oral administration of 141 mg ^{14}C-droloxifene citrate to a healthy female subject (no. 3).

Table 4. Proportions of ^{14}C-components excreted in faeces after oral administration of ^{14}C-droloxifene citrate (141 mg) to healthy female subjects

	Subject number				
Component	1	2	3	4	Mean ± SD
M1	0.9	1.3	1.4	1.5	1.3 ± 0.3
M2*	ND	ND	ND	ND	ND
M3	59.1	57.3	61.2	63.2	60.2 ± 2.6
M4	2.2	1.9	0.7	1.1	1.5 ± 0.7
M5*	ND	ND	ND	ND	ND
M6	4.5	3.7	4.8	3.9	4.2 ± 0.5
M7	2.1	1.9	2.0	1.5	1.9 ± 0.3
M8	10.9	13.7	10.6	7.4	10.7 ± 2.6
M9		ND	ND		
Origin	6.3	1.1	(1.0)	1.2	2.4 ± 2.6

Results are the percentage of administered dose.

*Traces of M2 were detected in urine and M5 in plasma and urine, particularly after enzymic hydrolysis.

Identification of droloxifene and its metabolites in urine and faeces

Urine. An extract of enzyme-hydrolysed pooled urine was silylated, and the product subject to GC-MS. The ion chromatogram of summed masses m/z 58, 72, 444 and 459 contained one prominent peak. The mass spectrum obtained from the component corresponding to this peak was consistent with that of the trimethylsilyl derivative of droloxifene (table 5).

Table 5. Mass spectral data of droloxifene and its metabolites.

Component	*m/z* (assignment)	Relative intensity %
Droloxifene	459 (mol. ion M^+)	18
(mono-TMS in urine)	444 ($M^+ - CH_3$)	5
	72 ($CH_3CH{=}N^+(CH_3)_2$)	54
	58 ($CH_2{=}N^+(CH_3)_2$)	100
Droloxifene (underivatized in faeces)	387 (mol. ion M^+)	33
	72 ($CH_3CH{=}N^+(CH_3)_2$)	100
	58 ($CH_2{=}N^+(CH_3)_2$)	100
N-desmethyldroloxifene (mono-TMS in faeces)	445 (mol. ion M^+)	56
	388 (M^+-($CH_3CH{=}NCH_3$)	100
N-desmethyldroloxifene (di-TFA in faeces)	565 (mol. ion M^+)	12
	154 ($CH_2CH_2N(CH_3)COF_3$)	100

The ion chromatogram of summed masses 58, 72, 474 and 489 also contained a prominent peak but there was insufficient material present to yield a mass spectrum. However, such masses would be expected to be present in the mass spectrum of a trimethylsilyl derivative of a methoxydroloxifene, such as 4-methoxydroloxifene which was measurable in plasma by HPLC-fluorescence.

Faeces. The electron impact mass spectrum of isolated faeces component M3 was essentially identical to that of the reference standard of droloxifene containing a prominent molecular ion at *m/z* 387 and base peaks at *m/z* 58 (corresponding to $CH_2{=}N(CH_3)_2$ and at *m/z* 72 (corresponding to $CH_3CH{=}N(CH_3)_2$) both derived by fragmentation of the dimethylaminoethoxy side-chain of droloxifene. Similar fragmentation of the side-chain of tamoxifen has been reported (Poon *et al.* 1993). Other low abundance ions common to both mass spectra were at *m/z* 316, 239, 178, 165 and 91 (table 5).

The faecal extract containing component M6 was silylated and subjected to GC-MS. It yielded a complex total ion chromatogram. However, by monitoring characteristic ions (*m/z* 388 and 445), a peak was observed in the ion chromatogram at the same retention time (10.29 min) as that obtained when a reference standard of *N*-desmethyldroloxifene was silylated and subjected to GC-MS. The mass spectrum of the component corresponding to this peak was identical in both cases, confirming the identity of M6 as *N*-desmethyldroloxifene (table 5). Furthermore, the thermal degradation product of the reference standard *N*-desmethyldroloxifene results in a di-phenol by loss of the methylaminoethyl side-chain which forms a bis-trimethylsilyl derivative when silylated. This derivative was also present in the ion chromatogram at 9.12 min when *m/z* 445 and 460 were monitored. The mass spectrum obtained from the component corresponding to this peak was identical for M6 and for the reference standard *N*-desmethyldroloxifene after thermal degradation.

Additional confirmation of the identity of M6 as *N*-desmethyldroloxifene was obtained by trifluorocetylation of the faeces extract containing M6. When the trifluoracetylated M6 was subjected to GC-MS, a peak was present in the ion chromatogram at 10.15 min (as also for trifluoracetylated *N*-desmethyldroloxifene standard). The mass spectra of both trifluoroacetylated derivatives were essentially identical (table 5).

Discussion

In the absence of data from intravenous route administration or extensive urinary excretion, it is usually not feasible to assess the extent of absorption of an oral dose. However, in the case of ^{14}C-droloxifene citrate, it would appear that the dose was well absorbed because of the low faecal excretion of ^{14}C (< 1% dose) during the first 24 h following dose administration (table 2). Extensive faecal excretion of an unabsorbed drug would be expected during this period.

Absorbed droloxifene is subjected to first-pass metabolism since at C_{max} at 1 h, the plasma concentration of unchanged drug was a mean of 16% of that of total ^{14}C whereas its major metabolite, a glucuronide, accounted for at least a mean of 68%. Furthermore the AUC of unchanged drug was 21% of that of total ^{14}C (table 1).

The above interpretation is supported by data from a study in rats that showed that the systemic availability of droloxifene following oral administration and intraportal infusion was similar, and was about 25% of that of an intravenous dose (Nickerson *et al*. 1997). The systemic availability of droloxifene in the mouse and monkey was lower than that in the rat (Tanaka *et al*. 1994).

Intersubject variability in droloxifene's pharmacokinetics was relatively low in this study (table 1). The coefficients of variation for C_{max}, AUC and half-life were 42, 19 and 18% respectively. Droloxifene has a relatively long half-life of 31.6 h, which should render this drug suitable for once-a-day administration as is the case for tamoxifen. After once daily doses, 90% of steady-state concentrations would be reached after about 5 days and the accumulation of droloxifene would be less than twofold. The half-life of droloxifene obtained in a pharmacokinetic study of seven Japanese post-menopausal breast cancer patients was similar to that shown in table 1, ranging between 17 and 41 h (mean ± SD 26 ± 9 h) (Tanaka *et al*. 1994). In another pharmacokinetic study of droloxifene (100 mg) in 12 healthy postmenopausal women (mean age 53 years), a similar half-life (about 25 h) was observed (Grill and Pollow 1991) as in the present study (table 1); however, C_{max} and AUC were about 40% lower than obtained in the present study (table 1). In the present study and that of Grill and Pollow (1991), the C_{max} of droloxifene glucuronide was about four times that of droloxifene. Plasma concentrations of droloxifene and its glucuronide declined exponentially with similar terminal half-lives (table 1) suggesting that the elimination of the latter was rate-limited by its formation from the former. Other minor metabolites present in plasma in similar concentrations included *N*-desmethyldroloxifene and 4-methoxydroloxifene: the former is also an anti-oestrogen (Hasmann *et al*. 1994). Droloxifene was bound by plasma proteins to about the same extent as are the anti-oestrogens tamoxifen and toremifene (IARC 1996).

The prolonged excretion of ^{14}C in faeces after administration of ^{14}C-droloxifene citrate is, at least, partly explained by biliary excretion of the major metabolite of ^{14}C-droloxifene, an ether glucuronide, and enterohepatic circulation. In rats, biliary excretion was an important part of the disposition of droloxifene (Tanaka *et al*. 1994), and enterohepatic circulation has been demonstrated (Nickerson *et al*. 1997). Droloxifene glucuronide has the requisite physicochemical properties for facile biliary excretion: its molecular weight is 563.7 and exceeds the molecular weight threshold for biliary excretion in humans (Hirom *et al*. 1977). Furthermore, the intersubject variability for the urinary and faecal excretion of ^{14}C in this study was remarkably low with coefficients of variation for total percentage dose in urine and faeces of < 8 and 1% respectively (table 2).

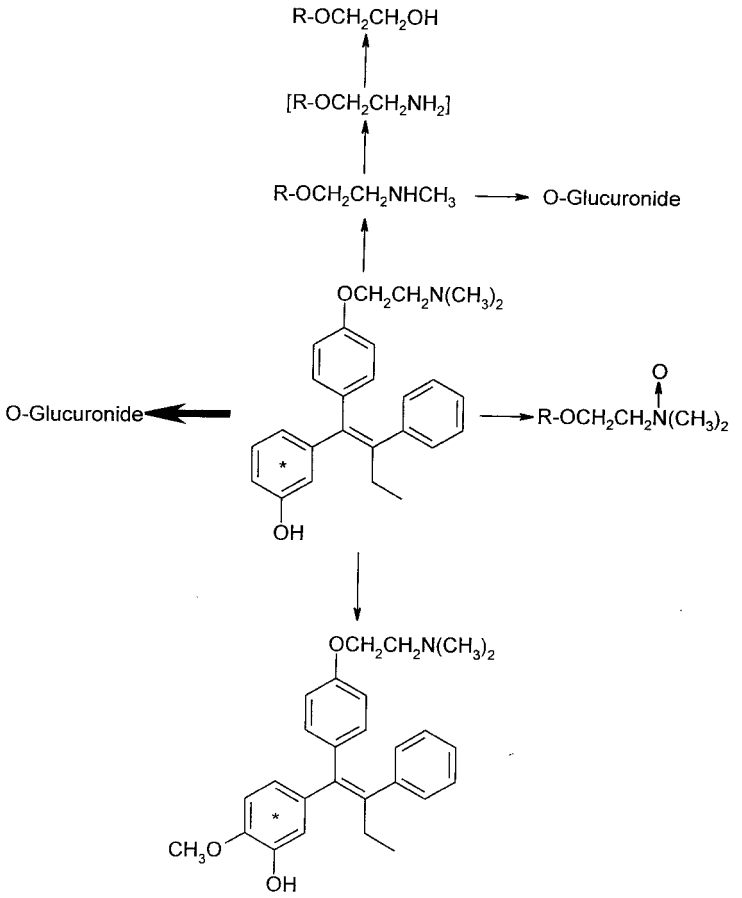


Figure 3. Proposed metabolism pathway of droloxifene in humans. * indicates position of radiolabel.

This study showed that droloxifene is mainly metabolized by conjugation with glucuronic acid (figure 3). The conjugate is present in plasma in relatively large concentrations and in urine, as the major urinary metabolite. Evidence for its presence in faeces was not obtained other than the presence in faeces of a ^{14}C-component with similar chromatographic properties to the glucuronide. It is noteworthy that the 'glucuronide' in faeces, if present, is resistant to enzymic hydrolysis, that in plasma also seems partly resistant whereas that in urine is readily hydrolysed. Indeed large quantities of the glucuronide would not be expected in the faeces even if it is excreted in the bile because it would be hydrolysed by the gut flora during its passage through the intestinal tract. Indeed this is an essential process if enterohepatic cycling is to occur (Gibson and Skett 1986). Minor metabolites of droloxifene include those formed by mono-*N*-desmethylation of the side-chain, *N*-oxidation, ring hydroxylation followed by *O*-methylation (presumably in the ring containing the existing hydroxyl group), and hydroxylation of the side-chain. This latter metabolite requires the prior formation of di-*N*-desmethyldroloxifene. These minor metabolites were also detected in faecal extracts by HPLC-fluorescence. However, the excretion of an *N*-oxide in faeces is surprising as it would have been expected to have been

reduced to the parent compound by the gut flora (Scheline, 1973). The metabolism of droloxifene in mice, rats and monkeys has been reported (O'Donnell *et al.* 1998), and a variety of Phase I and II metabolites have been characterized in plasma, bile and faeces. The metabolism of droloxifene in the monkey (Tanaka *et al.* 1994, O'Donnell *et al.* 1998) most resembled that in humans (table 4) when the data are compared.

Droloxifene differs structurally from tamoxifen only in that it has a hydroxyl group in one of its three phenyl rings. This is an important difference from a metabolism viewpoint as droloxifene possesses a functional group for conjugation, and consequently this drug is mostly metabolized by glucuronidation, a Phase II reaction (Gibson and Skett 1986). Consequently, it has a shorter half-life than tamoxifen (e.g. about 7 days) (Lonnig *et al* 1992). By contrast, tamoxifen is first metabolized by Phase I reactions (Wisemann 1994). Some of the Phase I metabolism reported for tamoxifen (Poon *et al.* 1993) also occurred for droloxifene, namely *N*-desmethylation and perhaps *N*-oxidation as well as di-*N*-desmethylation and amine oxidation (in the side-chain) to yield the primary alcohol (referred to in table 3 as side-chain hydroxylated droloxifene). Plasma concentrations of *N*-desmethyltamoxifen exceed those of the parent drug in females with breast cancer (Lonning *et al* 1992): by contrast, *N*-desmethyldroloxifene is a minor metabolite of droloxifene.

There was no evidence in this study for oxidation of the ethyl side-chain of droloxifene, a process thought to lead to the hepatotoxicity of tamoxifen in the rat as well as DNA-adduct formation (Phillips 2001). However, droloxifene does not cause liver tumours in rats (IARC 1996) and nor does it form detectable DNA-adducts in rat liver when investigated by ^{32}P-postlabelling (White *et al.* 1992).

Another anti-oestrogen structurally related to droloxifene is toremifene, which also has a longer half-life approaching that of tamoxifen. Unlike droloxifene, toremifene is mainly metabolized by Phase I pathways: major circulating metabolites include the *N*-desmethyl and side-chain hydroxylated analogues (Taras *et al.* 2000). Of these two structural types, the former is only a minor circulating metabolite of droloxifene and the latter was only detected in the faeces. Thus the pharmacological action of droloxifene is probably almost entirely due to the parent compound whereas in the case of tamoxifen and toremifene, it is likely that phase I metabolites contribute to drug action.

Acknowledgement

The authors thank Leicester Clinical Research Centre for its care of the female subjects which participated in the study and also K. N. Cheng, C. A. Graham, G. R. Morris and S. G. Wood for their respective contributions.

References

Ahlemann, L. M., Staab, H.-J., Loser, R., Seibel, K. and Huber, H.-J., 1988, Inhibition of growth of human cancer by intermittent exposure to the antiestrogen droloxifene. *Tumordiagnostik und Therapie*, **9**, 41–46.

Gibson, G. G. and Skett, P., 1986, *Introduction to Drug Metabolism* (London: Chapman & Hall).

Grill, H. J. and Pollow, K., 1991, Pharmacokinetics of droloxifene and its metabolites in breast cancer patients. *American Journal of Clinical Oncology*, **14 (suppl. 2)**, S21–S29.

Hasmann, M., Rattel, B. and Löser, R., 1994, Preclinical data for droloxifene. *Cancer Letters*, **84**, 101–116.

Hirom, P. C., Idle, J. R. and Millburn, P., 1977, Comparative aspects of the biosynthesis and excretion of xenobiotic conjugates by non-primate mammals. In D. V. Parke and R. L. Smith (eds), *Drug Metabolism: From Microbe to Man* (London: Taylor & Francis), pp. 299–329.

IARC, 1996, *Droloxifene.* IARC Monographs on the Evaluation of Carcinogenic Risks to Humans, Vol. 66 (Lyon: IARC) pp. 241–251.

Jank, P., Kern, D., Huber, H. J. and Stanislaus, F. D., 1987, Direct determination of droloxifene in serum using HPLC with precolumn switching, post-column photochemical derivatisation and fluorescence detection. In J. M. Aiache and J. Hirtz (eds), *Proceedings of the 3rd European Congress of Biopharmaceutics and Pharmacokinetics*, Clermont-Ferrand, vol. 1, pp. 511–520.

Lien, E. A., Anker, G., Lonning, P. E. and Ueland, D. M., 1995, Determination of droloxifene and two metabolites in serum by high-pressure liquid chromatography. *Therapeutic Drug Monitoring*, **17**, 259–265.

Lonning, P. E., Lien, E. A., Lundgren, S. and Kvinnsland, S., 1992, Clinical pharmacokinetics of endocrine agents used in advanced breast cancer. *Clinical Pharmacokinetics*, **22**, 327–358.

Löser, R., Seibel, K., Liehn, H. D. and Staab, H. J., 1986, Pharmacology and toxicology of the antiestrogen, droloxifene. *Control of Oncology*, **24**, 64–72.

Löser, R., Seibel, K., Roos, W. and Eppenberger, U., 1985, *In vivo* and *in vitro* antiestrogenic action of 3-hydroxytamoxifen, tamoxifen and 4-hydroxytamoxifen. *European Journal Cancer and Clinical Oncology*, **21**, 985–990.

Nickerson, D. F., Tess, D. A. and Toler, S. M., 1997, First-pass metabolism and biliary recirculation of droloxifene in the female Sprague–Dawley rat. *Xenobiotica*, **27**, 257–264.

O'Donnell, J. P., Khosla, N. B. and Dalvie, D. K., 1998, Metabolism of droloxifene in the CD-1 mouse, Fischer-344 rat and cynomolgus monkey. *Xenobiotica*, **28**, 153–166.

Poon, G. K., Chui, Y. C., McCague, R., Lonning, P. E., Feng, R., Rowlands, M. G. and Jarman, M., 1993, Analysis of Phase 1 and Phase II metabolites of tamoxifen in breast cancer patients. *Drug Metabolism and Disposition*, **21**, 1119–1124.

Rauschning, W. and Pritchard, K. I., 1994, Droloxifene: a new antiestrogen: its role in metastatic breast cancer. *Breast Cancer Research and Treatment*, **31**, 83–94.

Scheline, R. R., 1973, Metabolism of foreign compounds by gastrointestinal microorganisms. *Pharmacological Reviews*, **25**, 451–523.

Tanaka, Y., Sekiguchi, M., Sawamoto, T., Hata, T., Esumi, Y., Sugai, S. and Ninomiya, S., 1994, Pharmacokinetics of droloxifene in mice, rats, monkeys, premenopausal and postmenopausal patients. *European Journal of Drug Metabolism and Pharmacokinetics*, **19**, 47–58.

Taras, T. L., Wurz, G. T., Linares, G. R. and Degregorio, M. W., 2000, Clinical pharmacokinetics of toremifene. *Clinical Pharmacokinetics*, **39**, 327–334.

White, I. N. H., Dematteis, F., Davies, A., Smith, L. L., Crofton-Sleigh, C., Venitt, S., Hewer, A. and Phillips, D. H., 1992, Genotoxic potential of tamoxifen and analogues in female Fischer F344/n rats, DBA/2 and C57BL/6 mice and in human MCL-5 cells. *Carcinogenesis*, **13**, 2197–2203.

Wiseman, H., 1994, *Tamoxifen: Molecular Basis of Use in Cancer Treatment and Prevention* (Chichester: Wiley).

XENOBIOTICA, 2002, VOL. 32, NO. 8, 715–727

Taylor & Francis
healthsciences

Pharmacokinetics and disposition of rosuvastatin, a new 3-hydroxy-3-methylglutaryl coenzyme A reductase inhibitor, in rat

K. NEZASA†*, A. TAKAO‡, K. KIMURA‡, M. TAKAICHI‡, K. INAZAWA† and M. KOIKE†

† Developmental Research Laboratories, Shionogi and Co., Ltd, 3-1-1, Futaba-cho, Toyonaka, Osaka 561-0825, Japan
‡ Tokai Research Laboratories, Daiichi Pure Chemicals Co., Ltd, Ibaraki, Japan

Received 13 December 2001

1. The pharmacokinetics and disposition of rosuvastatin, a new 3-hydroxy-3-methylglutaryl coenzyme A (HMG-CoA) reductase inhibitor, were investigated following single administration of ^{14}C-rosuvastatin in the Sprague–Dawley rat.

2. Following oral administration of ^{14}C-rosuvastatin at 1, 5 and 25 mg kg^{-1}, the C_{max} and AUC of the radioactivity in the plasma increased more than the increase in dose ratio.

3. Excretion of radioactivity was 98.0% of the dose in the faeces and 0.4% in the urine up to 168 h after oral administration in the intact rat, and was 55.1% in the bile and 0.5% in the urine up to 48 h post-dosing in the bile duct-cannulated rat. The unchanged compound mainly accounted for the radioactivity in the bile and faeces.

4. In the tissue distribution study, the concentration of the radioactivity in the liver was markedly higher than those in the other tissues, and the radioactivity concentration ratios of the liver to the plasma were between 8 and 25 up to 48 h after oral administration. The liver-specific distribution of rosuvastatin was similarly recognized in whole-body autoradiography.

5. Metabolic profiling studies indicated that rosuvastatin would not be metabolized by CYP enzymes.

6. These results clarified that rosuvastatin selectively distributed in the liver – the target organ – and was excreted in the bile mainly as the unchanged compound.

Introduction

Rosuvastatin (Crestor™), calcium bis[(+)-(3*R*,5*S*,6*E*)-7-[4-(*p*-fluorophenyl)-6-isopropyl-2-(*N*-methylmethanesulfonamido)-5-pyrimidinyl]-3,5-dihydroxy-6-heptenoate], discovered at Shionogi and Co., Ltd (Watanabe *et al.* 1997), is expected to be used for the treatment of hyperlipidemia. It is a new and potent inhibitor of 3-hydroxy-3-methylglutaryl-CoA (HMG-CoA) reductase, which is the rate-limiting enzyme in cholesterol biosynthesis in the liver. *In vitro* studies have indicated that rosuvastatin has a higher inhibitory potency to cholesterol synthesis in rat hepatocytes (IC_{50} 0.16 nM), compared with other statins, in the range 1.16–6.93 nM (McTaggart *et al.* 2001). Furthermore, in a clinical study, rosuvastatin was shown to produce a more effective reduction in blood cholesterol levels than atorvastatin (Olsson 2001).

The present paper describes the absorption, distribution, metabolism and excretion of rosuvastatin after single administration in rat.

* Author for correspondence; e-mail: kenichi.nezasa@shionogi.co.jp

Xenobiotica ISSN 0049–8254 print/ISSN 1366–5928 online © 2002 Taylor & Francis Ltd
http://www.tandf.co.uk/journals
DOI: 10.1080/00498250210144820

Materials and methods

Materials

^{14}C-rosuvastatin (0.31–1.16 MBq mg^{-1}) was synthesized at the Developmental Research Laboratories, Shionogi and Co., Ltd, and the radiochemical purity was 98% or more as determined by TLC. The chemical structure of ^{14}C-rosuvastatin and the ^{14}C-labelled position are shown in figure 1. Unlabeled rosuvastatin, the pentenoic acid derivative, 5*S*-lactone and the taurine conjugate of pentenoic acid derivative synthesized at the Discovery Research Laboratories, Shionogi and Co., Ltd, were used as authentic standards. The chemical structures of the pentenoic acid derivative, 5*S*-lactone and taurine conjugate of pentenoic acid derivative are shown in figure 2. All other chemicals were of analytical grade and were obtained from commercial sources.

Animals

Male and female rats of the Jcl:SD (Sprague–Dawley) strain purchased from CLEA Japan, Inc., were used in the experiments at age 7–8 weeks. Male and female rats weighed 248–313 and 174–178 g, respectively. After purchase, the rats were allowed water and pellet food (MF, Oriental Yeast, Tokyo, Japan) *ad libitum*, and were acclimatized for at least 2 weeks to conditions of 23 ± 2 °C, 55 ± 10% relative humidity and lighting with a 12-h light/dark cycle from 06:00 to 18:00 hours. Each group consisted of three animals.

Animal studies

Administration of the drug. Oral administration study: ^{14}C-rosuvastatin was sonicated in distilled water to dissolve at 1, 5 and 25 mg ml^{-1} as the calcium salt (1.13, 1.49–5.78 and 7.41 MBq ml^{-1}, respectively). ^{14}C-rosuvastatin dosing solution was administered to rats by oral intubation at 1 ml kg^{-1}. Before administration, the animals were not fasted unless otherwise described. In the fasting group, the animals were fasted from about 17:00 hours the day before administration (water was given freely), and fed 8 h after administration.

Intravenous dosing study: ^{14}C-rosuvastatin was sonicated in saline for injection, being dissolved at 5 mg ml^{-1} as the calcium salt (5.63 MBq ml^{-1}). ^{14}C-rosuvastatin in the dosing solution was administered into the metatarsal vein of rats at 1 ml kg^{-1}.

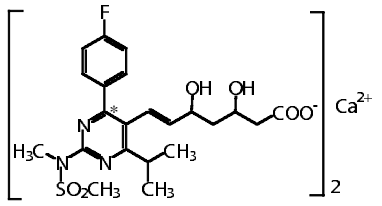


Figure 1. Chemical structure of ^{14}C-labelled rosuvastatin. *Labelled position.

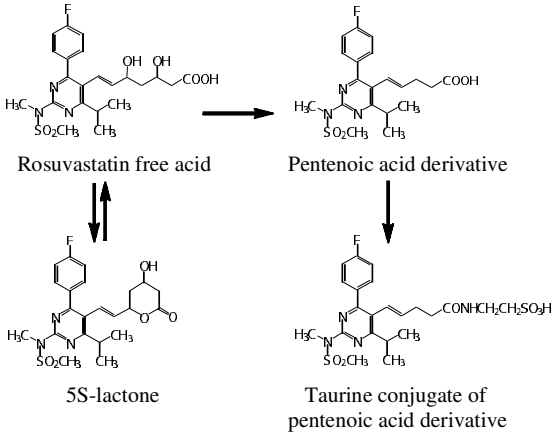


Figure 2. Postulated metabolic pathways of rosuvastatin in rat.

Pharmacokinetics of radioactivity in blood. Blood samples (about 250 µl) were collected from the caudal vein at 5, 15, 30 min, 1, 1.5, 2, 4, 6, 8 and 24 h after oral administration and 2, 5, 10, 30 min, 1, 1.5, 2, 4, 6, 8 and 24 h after intravenous dosing. Each blood sample was taken into a microtube containing heparin sodium and centrifuged (2000*g*, room temperature, 2 min) to separate the plasma.

Tissue distribution of radioactivity. Following oral administration of ^{14}C-rosuvastatin at 5 mg kg^{-1} in the male rat, the animals were killed by exsanguination from the vena cava under diethyl ether anaesthesia at 15 min, 1.5, 4, 8, 24, 48 and 120 h. The following tissues and organs were collected for determination of radioactivity: plasma, blood, cerebrum, cerebellum, spinal cord, pituitary gland, eyeball, Harderian gland, thyroid gland, mandibular gland, thymus, heart, lung, liver, kidney, adrenal gland, spleen, pancreas, fat (around the kidney), brown fat, skeletal muscle (femoral region), skin (latero-abdominal region), bone marrow, mesenteric lymph node, aorta, testis, epididymis and prostate gland.

Whole-body autoradiography. Following the oral administration of ^{14}C-rosuvastatin at 5 mg kg^{-1} in the male rat, the animals were killed by deep anaesthesia with diethyl ether/chloroform (3/1, v/v) at 15 min, 1.5, 4 and 24 h, and frozen with liquid nitrogen. The frozen animal bodies were embedded in 4% carboxymethylcellulose, and whole-body sections of 40 µm in thickness were prepared using a microtome (450MP, PMV). After lyophilization of the sections for 3 days, they were covered with Lumilar membrane and placed in contact with X-ray films (RX-type, Fuji Film) to prepare autoradiograms by exposure for 9 weeks at room temperature.

Urinary and faecal excretion of radioactivity. Male rats were housed in stainless steel metabolic cages after oral administration of ^{14}C-rosuvastatin at 5 mg kg^{-1}, and naturally excreted urine and faeces were collected every 24 h up to 168 h post-dosing. 24-h urines were collected in sampling bottles set in an ice bath.

Biliary excretion of radioactivity. Male rats were anesthetized with diethyl ether and their common bile ducts were cannulated with polyethylene tubes for bile collection. Further polyethylene tubes were inserted into the duodenum via the common bile duct for continuous bile provision. The rats were kept in Bollman cages. After they had recovered from anaesthesia, ^{14}C-rosuvastatin (5 mg kg^{-1}) was administered orally while bile, collected in an ice bath from other undosed rats, was fed into the duodenum at the rate of 1 ml h^{-1}. Bile was then collected 0–2, –4, –6, –8, –24 and –48 h after ^{14}C-rosuvastatin administration. Urine and faeces were collected 0–24 and –48 h post-dosing. The rats were killed by deep anaesthesia with diethyl ether at 48 h and the gastrointestinal contents were collected.

Enterohepatic circulation. Male rats were anesthetized with diethyl ether and the common bile ducts of the donor and recipient rats were cannulated with polyethylene tubes. The bile from the donor rat was introduced into the duodenum of the recipient rat via the common bile duct; donor and recipient rats were kept individually in Bollman cages. Another polyethylene tube was inserted into the duodenum of the donor rat via the common bile duct to provide the route for the bile provision (1 ml h^{-1}) collected from other rats. After recovering from anaesthesia, the donor rat was dosed orally with ^{14}C-rosuvastatin (5 mg kg^{-1}). Urine and faeces from the donor rat were collected 0–48 h after ^{14}C-rosuvastatin administration. Bile was collected from the recipient rat at 0–2, –4, –6, –8, –24 and –48 h post-dosing, and urine and faeces were collected 0–24 and –48 h after administration. The rats were killed at 48 h with diethyl ether overdose and the gastrointestinal contents of the recipient rat were collected.

Collection of bile for quantitative metabolic profiling. Bile duct-cannulated rats were prepared as described above. ^{14}C-rosuvastatin (5 mg kg^{-1}) was administered orally to the rats while bile collected from other undosed rats was fed into the duodenum at 1 ml h^{-1}. Bile was collected 0–24 h after ^{14}C-rosuvastatin administration.

Measurement of radioactivity

The radioactivity in each sample described below was counted in a liquid scintillation counter (LSC-903, Aloka). The counting efficiency was corrected by the channel ratio method using an external standard source.

Plasma and blood. Aliquots of the plasma and blood were weighed and dissolved in 2 ml tissue solubilizer Soluene-350 (Packard). The blood sample was decolourized with 0.4 ml benzene saturated with benzoyl peroxide. Radioactivity in the plasma and blood was measured after addition of 13 ml scintillator Econofluor (Du Pont NEN Research Products, Boston, MA, USA).

Tissues and organs. The cerebrum and kidney were each weighed and solubilized in 10 ml Soluene-350; the resultant solution was diluted with toluene to 20 ml. Radioactivity in 2 ml of the diluent was measured after addition of 13 ml scintillator Econofluor. For all other tissues, whole or tissue-sections were each weighed and solubilized in 2 ml Soluene-350. The radioactivity of each sample was measured after addition of 13 ml the scintillator Econofluor, and the concentrations of the radioactivity in the tissues were determined.

Urine, bile and faeces. The urine and bile were diluted with water to 100 and 50 ml, respectively. The faeces were mixed with water to make 300 ml, and the mixture was homogenized. Radioactivity in aliquots of the diluents and homogenates (0.5–1 ml) were measured after the addition of 10 ml scintillator Atomlight (Du Pont NEN Research Products) to determine the excretion rates of radioactivity in the excreta.

Gastrointestinal contents and carcass. The gastrointestinal contents were brought to 300 ml with water and then homogenized. The carcasses of the rats in the biliary excretion and enterohepatic circulation studies were solubilized in 500 ml 0.5 M sodium hydroxide and 80 ml toluene by refluxing for 72 h. Each resultant mixture was made up to 1000 ml with water and then homogenized. Radioactivity in 0.5-ml aliquots of the each homogenate was measured after the addition of 10 ml of the scintillator Atomlight. Each residual percentage of the radioactivity in the gastrointestinal contents and carcass was determined.

Quantitative metabolic profiling

Plasma and liver samples obtained in the tissue distribution study and the faeces obtained in the urinary and faecal excretion study were analysed, as well as the bile.

Individual liver samples obtained at 15 min, 1.5, 4, 8, 24 and 48 h after administration were homogenized with a 5-fold volume of distilled water. An aliquot of liver homogenate, plasma at 15 min, 1.5, 4 and 8 h post-dosing and faecal homogenate collected 0–24 h after administration was mixed with a 3-fold volume of methanol and centrifuged (1800*g*, 4 °C, 10 min), and the supernatant was separated. To the residue, a 3-fold volume of methanol was added and the extraction procedure was repeated twice. Methanol extracts from the plasma, liver and faeces were each evaporated to dryness under reduced pressure in a rotary evaporator. The residue was reconstituted in a small volume of methanol and subjected to TLC. The bile was applied directly to a TLC plate. In addition, authentic standards were applied to the plate to overlap each sample. The TLC plates, after development with chloroform/methanol/acetic acid (20/10/1, by vol.) or ethyl acetate/methanol/*n*-hexane/acetic acid (20/2/8/1, by vol.), were placed in contact with phosphorous imagings (TYPE-BA, Fuji Film) and exposed in a lead shield box for 24 h. After exposure, radioactive images on the plates were analysed with a Bio-image analyser system (FUJIX BA100, Fuji Film) to obtain the radioluminograms. Silica gel on the plates was scraped off based on the location of radioactive bands on the radioluminograms and the radioactivity was measured after addition of 1 ml 70% methanol and 10 ml scintillator Atomlight to determine the relative amounts (%) of the unchanged compound and metabolites.

Survey of urinary metabolites

The urine collected 0–24 h after ^{14}C-rosuvastatin administration in the urinary and faecal excretion study was acidified to pH 4.0 by addition of 0.5 M acetate buffer and applied to a Bond Elut C_{18} cartridge (Varian), preconditioned with methanol and acetate buffer. The cartridge was washed with 8 ml distilled water and eluted with 8 ml methanol. After the methanol eluate was evaporated to dryness under reduced pressure in a rotary evaporator, the residue was reconstituted in a small volume of methanol and subjected to TLC. The radioactivity on the TLC plates was measured as described above.

Pharmacokinetic analysis

Radioactivity concentration was expressed as equivalents of rosuvastatin free acid. The area under the radioactivity concentration in the plasma versus time curve (AUC) was calculated by the trapezoidal method.

Results

Plasma concentration of radioactivity

The plasma concentrations of the radioactivity after single oral and intravenous administration of ^{14}C-rosuvastatin in the male rat are shown in figure 3 and the

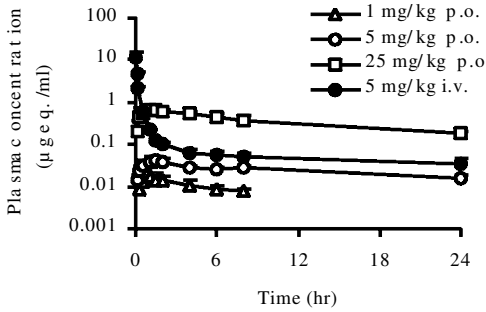


Figure 3. Plasma concentrations of radioactivity after single oral and intravenous administration of ^{14}C-rosuvastatin in the male rat. Each datum point is the mean ± SD of three animals.

Table 1. Pharmacokinetic parameters of radioactivity after single oral and intravenous administration of ^{14}C-rosuvastatin in rat.

				Pharmacokinetic parameter		
Sex	Dose (mg kg^{-1})	Dosing route	Dosing condition	C_{max} (nq eq. ml^{-1})	AUC* (nq eq. h ml^{-1})	T_{max} (h)
Male	1	p.o.	non-fasted	16.7 ± 11.6	88.4	1.0
	5	p.o.	non-fasted	42.1 ± 11.2	599	1.5
	25	p.o.	non-fasted	656 ± 84	8440	1.5
	5	i.v.	non-fasted	–	3100	–
	5	p.o.	fasted	99.5 ± 41.8	849	0.25
Female	5	p.o.	non-fasted	47.2 ± 15.4	658	1.0

Each C_{max} is the mean ± SD of three animals.
AUC and T_{max} were calculated from the means of plasma concentration.
*AUC was calculated with values from 0 to 24 h after administration except for 1 mg kg^{-1} dosing (from 0 to 8 h post-dosing).
–, not determined.

pharmacokinetic parameters are listed in table 1. Following oral administration of ^{14}C-rosuvastatin at 1, 5 and 25 mg kg^{-1}, the radioactivity in the plasma reached maximum levels within 1.5 h; the C_{max} were markedly low and determined as 16.7, 42.1 and 656 ng eq. ml^{-1}, respectively. The AUC of the radioactivity in the plasma after oral administration at 1, 5 and 25 mg kg^{-1} were 88.4, 599 and 8440 ng eq. h ml^{-1}, respectively. Following intravenous administration of ^{14}C-rosuvastatin at 5 mg kg^{-1}, the AUC of the radioactivity in the plasma was calculated as 3100 ng eq. h ml^{-1}.

The plasma concentrations of the radioactivity after single oral administration of ^{14}C-rosuvastatin at 5 mg kg^{-1} in the fasted and non-fasted male rat are shown in figure 4, and the calculated pharmacokinetic parameters are summarized in table 1. In the fasted rat, the radioactivity in the plasma reached maximum concentration, 99.5 ng eq. ml^{-1}, at 0.25 h after administration, and the AUC was determined as 849 ng eq. h ml^{-1}. This indicates, therefore, that the plasma level of radioactivity was affected by the food intake.

The plasma concentrations of the radioactivity after single oral administration of ^{14}C-rosuvastatin 5 mg kg^{-1} in the male and female rat are shown in figure 5, and the calculated pharmacokinetic parameters are summarized in table 1. In the female rat, the C_{max} of the radioactivity in the plasma was 47.2 ng eq. ml^{-1} and

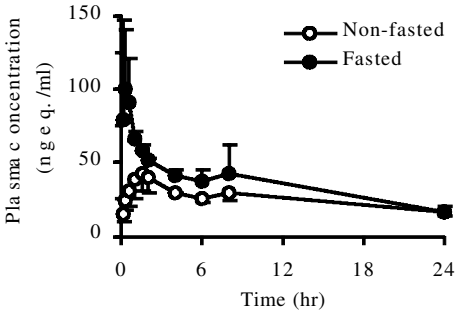


Figure 4. Plasma concentrations of radioactivity after single oral administration of ^{14}C-rosuvastatin at 5 mg kg^{-1} in the fasted and non-fasted male rat. Each datum point is the mean ± SD of three animals.

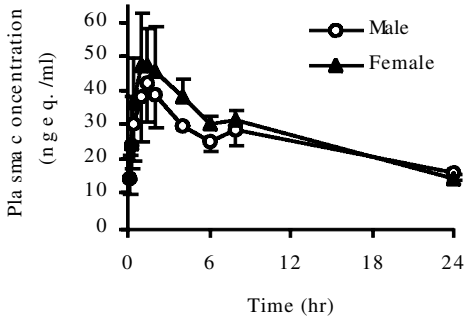


Figure 5. Plasma concentrations of radioactivity after single oral administration of ^{14}C-rosuvastatin at 5 mg kg^{-1} in the male and female rat. Each datum point is the mean ± SD of three animals.

AUC was 658 ng eq. h ml^{-1}; the C_{max} and AUC in the male and female rat were comparable. These results indicated that there were no sex differences in the profile of the radioactivity in the plasma.

Tissue distribution of radioactivity

The concentrations of the radioactivity in the tissues and organs after oral administration of ^{14}C-rosuvastatin at 5 mg kg^{-1} in the male rat are shown in table 2. The maximum concentrations of radioactivity were observed at 15 min, the first sampling time, in the liver, at 4 h in the Harderian gland, fat, skin, testis and epididymis and at 1.5 h in the other tissues.

The highest concentration of radioactivity was observed in the liver, the target organ of rosuvastatin, for almost all sampling times. Up to 48 h post-dosing, the radioactivity concentration ratios in the liver relative to the plasma were calculated to be between 8 and 25, and the radioactivity concentrations in most other tissues were comparable with or less than the concentrations in the plasma. At 120 h after administration, radioactivity was detected only in the liver. The radioactivity concentrations in the cerebrum, cerebellum, spinal cord, pituitary gland, eyeball, thyroid gland, bone marrow and aorta were below the detection limit at all the sampling times.

Table 2. Tissue concentration of radioactivity after single oral administration of ^{14}C-rosuvastatin at 5 mg kg^{-1} in the male rat.

Tissue	Radioactivity concentration (ng eq. g^{-1} or ml^{-1})						
	15 min	1.5 h	4 h	8 h	24 h	48 h	120 h
Plasma	38.6 ± 12.0	79.4 ± 14.7	68.1 ± 8.1	44.8 ± 15.3	28.9 ± 12.7	10.9 ± 3.3	n.d.
Blood	24.8 ± 5.7	48.5 ± 12.2	47.7 ± 9.6	29.6 ± 8.7	n.d.	n.d.	n.d.
Cerebrum	n.d.	n.d.	n.d.	n.d.	n.d.	n.d.	n.d.
Cerebellum	n.d.	n.d.	n.d.	n.d.	n.d.	n.d.	n.d.
Spinal cord	n.d.	n.d.	n.d.	n.d.	n.d.	n.d.	n.d.
Pituitary gland	n.d.	n.d.	n.d.	n.d.	n.d.	n.d.	n.d.
Eye ball	n.d.	n.d.	n.d.	n.d.	n.d.	n.d.	n.d.
Harderian gland	21.0 ± 3.8	45.8 ± 6.6	49.2 ± 17.0	21.1 ± 5.5	n.d.	n.d.	n.d.
Thyroid gland	n.d.	n.d.	n.d.	n.d.	n.d.	n.d.	n.d.
Mandibular gland	14.1 ± 0.6	27.0 ± 1.5	23.2 ± 3.9	12.0 ± 3.5	n.d.	n.d.	n.d.
Thymus	n.d.	14.5 ± 1.7	n.d.	n.d.	n.d.	n.d.	n.d.
Heart	17.5 ± 2.5	31.5 ± 1.6	27.7 ± 7.3	16.6 ± 4.3	9.0 ± 1.9	n.d.	n.d.
Lung	16.5 ± 1.9	31.7 ± 2.7	31.6 ± 8.8	16.7 ± 2.8	n.d.	n.d.	n.d.
Liver	965.0 ± 302.0	843.6 ± 139.1	722.1 ± 100.0	477.4 ± 71.8	239.3 ± 67.4	89.3 ± 13.1	19.8 ± 6.0
Kidney	42.6 ± 9.1	89.5 ± 10.5	84.4 ± 13.9	49.3 ± 8.5	19.3 ± 4.3	9.8 ± 2.7	n.d.
Adrenal gland	n.d.	65.7 ± 11.2	49.4 ± 11.2	n.d.	n.d.	n.d.	n.d.
Spleen	11.3 ± 1.8	18.0 ± 1.4	14.4 ± 5.3	8.8 ± 3.0	7.0 ± 2.5	n.d.	n.d.
Pancreas	26.1 ± 7.8	34.3 ± 6.3	26.4 ± 5.3	18.5 ± 11.1	n.d.	n.d.	n.d.
Fat	n.d.	41.5 ± 6.3	69.5 ± 14.4	27.7 ± 4.5	15.7 ± 1.7	n.d.	n.d.
Brown fat	33.7 ± 6.6	65.5 ± 8.3	57.2 ± 19.5	30.0 ± 4.3	25.3 ± 9.0	n.d.	n.d.
Skeletal muscle	n.d.	15.8 ± 5.1	14.1 ± 3.8	n.d.	n.d.	n.d.	n.d.
Skin	11.8 ± 0.8	30.1 ± 5.0	34.8 ± 7.6	23.0 ± 8.4	10.0 ± 1.3	n.d.	n.d.
Bone marrow	n.d.	n.d.	n.d.	n.d.	n.d.	n.d.	n.d.
Mesenteric lymph node	64.5 ± 27.0	1041.8 ± 386.8	355.2 ± 188.9	74.4 ± 8.6	14.8 ± 7.6	n.d.	n.d.
Aorta	n.d.	n.d.	n.d.	n.d.	n.d.	n.d.	n.d.
Testis	n.d.	10.4 ± 1.1	11.3 ± 4.8	n.d.	n.d.	n.d.	n.d.
Epididymis	n.d.	19.0 ± 1.7	22.4 ± 5.6	12.4 ± 3.2	n.d.	n.d.	n.d.
Prostate gland	n.d.	20.3 ± 0.8	18.2 ± 2.4	n.d.	n.d.	n.d.	n.d.

Each value is the mean ± SD of three animals.
n.d., not detected.

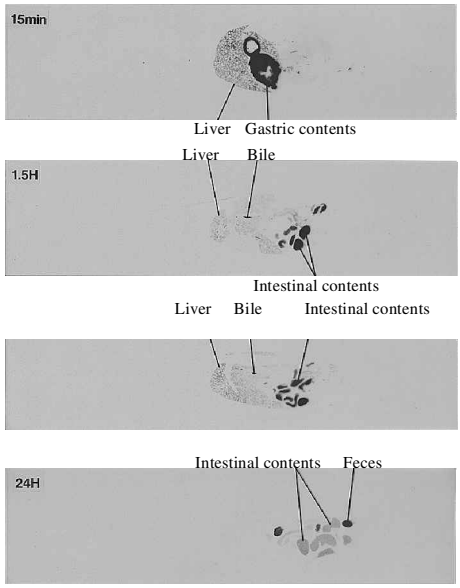


Figure 6. Whole-body autoradiograms showing the distribution of radioactivity at various times after oral administration of ^{14}C-rosuvastatin at 5 mg kg^{-1} in the male rat.

Whole-body autoradiography

The whole-body autoradiograms after oral administration of ^{14}C-rosuvastatin at 5 mg kg^{-1} in the male rat are shown in figure 6. At 15 min after dosing, high levels of radioactivity were observed in the liver and gastrointestinal contents. At 1.5 h post-dosing, the radioactivity in the liver was reduced compared with that observed at 15 min. From 1.5 to 4 h after dosing, high levels of radioactivity were observed in the bile and gastrointestinal contents, and the distribution profile of the radioactivity was unchanged. At 24 h post-dosing, the radioactivity was detectable only in the intestinal contents. Only in the liver was the radioactivity observed throughout all the periods.

Excretion of radioactivity

The excretion of the radioactivity in the urine and faeces after oral administration of ^{14}C-rosuvastatin at 5 mg kg^{-1} in the intact male rat is shown in figure 7A. The excretion of the radioactivity was $0.4 \pm 0.1\%$ of the dose in the urine and $98.0 \pm 0.3\%$ in the faeces up to 168 h after administration. The total recovery was $98.3 \pm 0.3\%$ up to 168 h post-dosing.

The excretion of the radioactivity in the bile, urine and faeces after oral administration of ^{14}C-rosuvastatin at 5 mg kg^{-1} in the bile duct-cannulated male rat is shown in figure 7B. The excretion of radioactivity was $55.1 \pm 9.4\%$ of the dose in the bile, $0.5 \pm 0.1\%$ in the urine and $41.0 \pm 11.4\%$ in the faeces up to 48 h after administration. The residual radioactivity was $1.8 \pm 1.4\%$ in the gastrointestinal contents and $0.5 \pm 0.4\%$ in the carcass at 48 h post-dosing, thus the total recovery was $98.3 \pm 0.3\%$ up to 48 h after administration.

The enterohepatic circulation of the radioactivity after oral administration of ^{14}C-rosuvastatin at 5 mg kg^{-1} in the bile duct-cannulated male rat is shown in

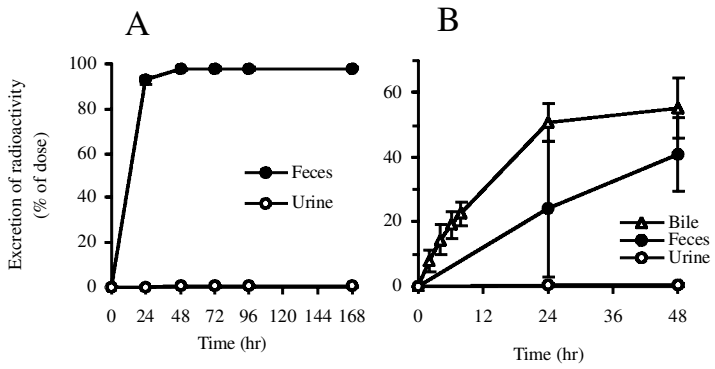


Figure 7. Excretion of radioactivity after single oral administration of ^{14}C-rosuvastatin at 5 mg kg^{-1} in the male rat. (A) Urinary and faecal excretion of radioactivity in the intact rat; (B) biliary, urinary and faecal excretion of radioactivity in the bile duct-cannulated rat. Each datum point is the mean ± SD of three animals.

Table 3. Enterohepatic circulation of radioactivity after single oral administration of ^{14}C-rosuvastatin at 5 mg kg^{-1} in the bile duct-cannulated male rat.

	Cumulative excretion (% of dose)				
	Donor rat		Recipient rat		
Time (h)	Urine	Faeces	Bile	Urine	Faeces
0–2	–	–	0.2 ± 0.1	–	–
0–4	–	–	1.2 ± 0.2	–	–
0–6	–	–	2.0 ± 0.4	–	–
0–8	–	–	2.8 ± 0.8	–	-
0–24	–	–	9.9 ± 2.1	0.0 ± 0.0	4.3 ± 2.5
0–48	0.4 ± 0.2	42.3 ± 11.1	19.1 ± 1.1	0.0 ± 0.1	21.0 ± 6.9
Gastrointestinal contents (at 48 h)					8.9 ± 9.0
Carcass (at 48 h)		6.9 ± 6.1			0.6 ± 0.5
Total recovery					99.3 ± 0.8

Each value is the mean ± SD of three animals.
–, not determined

table 3. In the recipient rats, the excretion of radioactivity was 19.1% of the dose in the bile, 0.0% in the urine and 21.0% in the faeces up to 48 h post-dosing. In addition, the residual radioactivity in the recipient rats was 8.9% in the gastrointestinal contents and 0.6% in the carcass at 48 h after administration. These results indicated that about 20% of the dose (about 40% of the radioactivity in the bile) was reabsorbed and most of the reabsorbed radioactivity was excreted in bile again.

Quantitative metabolic profiling

The metabolic pathways of rosuvastatin were postulated as shown in figure 2. The radioactivity concentrations and the compositions of the unchanged compound and metabolites in the plasma and liver after oral administration of ^{14}C-rosuvastatin at 5 mg kg^{-1} in the male rat are summarized in table 4. In the plasma,

Table 4. Metabolites in plasma, liver, bile and faeces after single oral administration of ^{14}C-rosuvastatin at 5 mg kg^{-1} in the male rat.

Sample	Time	Radioactivity concentration (ng eq. ml^{-1} or g^{-1})	Percentage of radioactivity in each sample			
			Rosuvastatin	Pentenoic acid derivative	5*S*-lactone	Taurine conjugate of pentenoic acid derivative
Plasma	15 min	38.6 ± 12.0	36.9 ± 14.4	10.3 ± 9.6	3.2 ± 3.8	3.0 ± 3.1
	1.5 h	79.4 ± 14.7	34.5 ± 14.6	10.1 ± 4.2	7.1 ± 3.0	4.5 ± 3.1
	4 h	68.1 ± 8.1	13.0 ± 2.2	17.4 ± 4.2	1.5 ± 2.6	3.4 ± 4.0
	8 h	44.8 ± 15.3	7.9 ± 7.0	26.7 ± 9.3	7.9 ± 4.2	3.0 ± 2.7
Liver	15 min	965.0 ± 302.0	66.1 ± 8.4	3.8 ± 1.3	1.7 ± 1.5	2.3 ± 1.1
	1.5 h	843.6 ± 139.1	57.4 ± 8.3	10.9 ± 4.3	1.6 ± 0.9	5.5 ± 1.2
	4 h	722.1 ± 100.0	25.1 ± 0.0	21.7 ± 1.7	2.1 ± 1.9	12.8 ± 1.4
	8 h	477.4 ± 71.8	29.3 ± 4.7	26.1 ± 7.3	1.7 ± 2.0	4.3 ± 2.8
	24 h	239.3 ± 67.4	5.5 ± 3.4	43.8 ± 11.3	2.1 ± 1.8	–
	48 h	89.3 ± 13.1	–	47.5 ± 18.0	–	0.1 ± 0.2

Each value is the mean ± SD of three animals.
–, below the detection limit.

the unchanged compound accounted for about 35% of plasma radioactivity up to 1.5 h after oral administration, and its percentage decreased with time. The major metabolite in the plasma was pentenoic acid derivative and its percentage increased with time. In the liver, the target organ of rosuvastatin, the unchanged compound represented about 60–70% of the hepatic radioactivity up to 1.5 h post-dosing, and its percentage decreased to < 30% after 4 h post-dosing. The major metabolite in the liver was also pentenoic acid derivative and the percentage increased with time.

The compositions of the unchanged compound and metabolites in the bile and faeces after oral administration of ^{14}C-rosuvastatin at 5 mg kg^{-1} in the male rat are summarized in table 5. The unchanged compound accounted for 88.3% of biliary radioactivity and 87.5% of faecal radioactivity. The percentages of other metabolites (pentenoic acid derivative, 5*S*-lactone and taurine conjugate of pentenoic acid derivative) were < 3% in the bile and faeces.

Although the concentration of the radioactivity in the urine was extremely low, a survey of the urinary metabolites was performed. The excretion of the unchanged compound and the pentenoic acid derivative in the urine was 28.6 and 23.5% of urinary radioactivity, respectively. 5*S*-lactone and taurine conjugate of pentenoic acid derivative were detected as minor metabolites.

Discussion

Following single oral administration of ^{14}C-rosuvastatin at 1, 5 and 25 mg kg^{-1} in non-fasted male rats, the C_{max} and AUC of the radioactivity in the plasma increased more than the increase in dose ratio. On the other hand, T_{max} did not change at 1 or 1.5 h at all doses. These results indicate that ^{14}C-rosuvastatin was absorbed rapidly from the small intestine, and the pharmacokinetics of the radioactivity is clearly non-linear over the dose range. In the fasted rat, smaller T_{max} and larger C_{max} and AUC compared with those in the non-fasted rat were observed, suggesting that the gastric emptying time of rosuvastatin decreased under fasting conditions and that faster absorption of ^{14}C-rosuvastatin occurred in

Table 5. Metabolites in bile and faeces after single oral administration of ^{14}C-rosuvastatin at 5 mg kg^{-1} in the male rat.

		Percentage of radioactivity in each sample			
Sample	Time (h)	Rosuvastatin	Pentenoic acid derivative	5*S*-lactone	Taurine conjugate of pentenoic acid derivative
Bile	0–24	88.3 ± 1.9	≤0.5	≤0.5	2.6 ± 0.7
Faeces	0–24	87.5 ± 1.6	≤0.9	≤0.9	≤0.9

Each value is the mean ± SD of three animals.

the fasted rat than in the non-fasted rat. The tissue distribution study showed the hepatic extraction of rosuvastatin to be high. In addition, following single oral administration of ^{14}C-rosuvastatin at 5 mg kg^{-1} in the bile duct-cannulated rat, 88.3% of the radioactivity in the bile was attributed to the unchanged compound (table 5), indicating that rosuvastatin was mainly excreted into the bile as the unchanged compound. Considering these findings, it is possible that the hepatic extraction and/or the biliary excretion of rosuvastatin may be saturated in the case of a high dose or fasting.

Following oral administration of ^{14}C-rosuvastatin at 5 mg kg^{-1}, the excretion of the radioactivity in the intact rat was 0.4% of the dose in the urine and 98.0% in the faeces, and that in the bile duct-cannulated rat was 55.1% in the bile and 0.5% in the urine. These results demonstrated that most of the absorbed radioactivity was excreted into the faeces via the bile. From the results of the biliary excretion study, the extent of absorption of rosuvastatin was estimated to be 56%, being similar to that of pravastatin in rats (Komai *et al.* 1992a). On the other hand, the transfer ratio of the radioactivity into the circulating plasma after oral administration at 5 mg kg^{-1}, as estimated by the plasma AUC obtained after oral and intravenous administration (table 1), was calculated as 19%. Therefore, it was suggested that rosuvastatin absorbed from the intestine would be mainly extracted by the liver and excreted into bile.

The proportion of the unchanged compound in the liver was higher than that in the plasma (table 4), and the hepatic concentration ratios of the unchanged compound to the plasma were calculated to be between 18 to 45 up to 8 h post-dosing. The concentrations of the radioactivity in the liver were the highest among all tissues at almost all times examined. The concentrations of the radioactivity in the other tissues were similar to or lower than that in the plasma. Moreover, in the whole-body autoradiograms (figure 6), only the distribution of the radioactivity into the liver was detectable. These results indicated that absorbed rosuvastatin distributed selectively to the liver, the target organ of rosuvastatin. Selective distribution of other HMG-CoA reductase inhibitors to the liver have been reported (Tse *et al.* 1990 for fluvastatin; Koga *et al.* 1992 for pravastatin; Sirtori 1993 for BMY-22089, pravastatin and CI-981). Furthermore, it has also been reported that carrier-mediated transport systems participate in the liver uptake of other HMG-CoA reducutase inhibitors, such as pravastatin (Komai *et al.* 1992b), fluvastatin (Ohtawa *et al.* 1999) and cerivastatin (Hirayama *et al.* 2000). Our present results also suggested that rosuvastatin would be taken up selectively into the liver similarly to other HMG-CoA reducutase inhibitors.

Quantitative metabolic profiling indicated that the major metabolite of rosuvastatin in the plasma and liver is the pentenoic acid derivative, formed by β-oxidation of the side chain of rosuvastatin. Furthermore, the pentenoic acid derivative undergoes taurine conjugation at the carboxylic acid, as shown in figure 2. There was little evidence that rosuvastatin was metabolized *via* CYP enzyme-mediated oxidation, as evidenced by the result that unchanged compound accounted for most of the radioactivity in the bile and faeces.

Recently, many reports have indicated drug–drug interaction among other HMG-CoA reductase inhibitors and CYP substrates and/or inhibitors (Azie *et al.* 1998 for lovastatin; Kantola *et al.* 1998 for atorvastatin; Mück *et al.* 1999 for cerivastatin; review by Beaird 2000). On the other hand, no marked inhibitory effect of rosuvastatin was noted for any CYP enzymes in human liver microsomes (McCormick *et al.* 2000), suggesting that rosuvastatin appears to have a low potential for interactions with CYP enzymes.

In summary, in rat, rosuvastatin was well absorbed and selectively distributed to the liver. Rosuvastatin was eliminated, principally as the parent compound, via bile secretion. There was little evidence of P450-mediated metabolism.

Acknowledgements

The authors thank T. Nagasaki, Y. Katsuyama and M. Segawa for synthesizing and purifying the ^{14}C-rosuvastatin used in this study.

References

Azie, N. E., Brater, D. C., Becker, P. A., Jones, D. R. and Hall, S. D., 1998, The interaction of diltiazem with lovastatin and pravastatin. *Clinical Pharmacology and Therapeutics*, **64**, 369–377.

Beaird, S. L., 2000, HMG-CoA reductase inhibitors: assessing differences in drug interactions and safety profiles. *Journal of the American Pharmaceutical Association*, **40**, 637–644.

Hirayama, M., Yoshimura, Y. and Moriyasu, M., 2000, Carrier-mediated uptake of cerivastatin in primary cultured rat hepatocytes. *Xenobiotic Metabolism and Disposition*, **15**, 219–225.

Kantola, T., Kivisto, K. T. and Neuvonen, P. J., 1998, Effect of itraconazole on the pharmacokinetics of atorvastatin. *Clinical Pharmacology and Therapeutics*, **64**, 58–65.

Koga, T., Fukuda, K., Shimada, Y., Fukami, M., Koike, H. and Tsujita, Y., 1992, Tissue selectivity of pravastatin sodium, lovastain and simvastatin. *European Journal of Biochemistry*, **209**, 315–319.

Komai, T., Kawai, K., Tokui, T., Tokui, Y., Kuroiwa, C., Shigehara, E. and Tanaka, M., 1992a, Disposition and metabolism of pravastatin sodium in rats, dogs and monkeys. *European Journal of Drug Metabolism and Pharmacokinetics*, **17**, 103–113.

Komai, T., Shigehara, E., Tokui, T., Koga, T., Ishigami, M., Kuroiwa, C. and Horiuchi, S., 1992b, Carrier-mediated uptake of pravastatin by rat hepatocytes in primary culture. *Biochemical Pharmacology*, **43**, 667–670.

McCormick, A. D., McKillop, D., Butters, C. J., Miles, G. S., Baba, T., Touchi, A. and Yamaguchi, Y., 2000, ZD4522 – an HMG-CoA reductase inhibitor free of metabolically mediated drug interactions: Metabolic studies in human *in vitro* systems. *Journal of Clinical Pharmacology*, **40**, 1055.

McTaggart, F., Buckett, L., Davidson, R., Holdgate, G., McCormick, A., Schneck, D., Smith, G. and Warwick, M., 2001, Preclinical and clinical pharmacology of rosuvastatin, a new 3-hydroxy-3-methylglutaryl coenzyme A reductase inhibitor. *American Journal of Cardiology*, **87**, 28B–32B.

Muck, W., Mai, I., Fritsche, L., Ochmann, K., Rohde, G., Unger, S., Johne, A., Bauer, S., Budde, K., Roots, I., Neumayer, H. H. and Kuhlmann, J., 1999, Increase in cerivastatin systemic exposure after single and multiple dosing in cyclosporine-treated kidney transplant recipients. *Clinical Pharmacology and Therapeutics*, **65**, 251–261.

Ohtawa, M., Masuda, N., Akasaka, I., Nakashima, A., Ochiai, K. and Moriyasu, M., 1999, Cellular uptake of fluvastatin, an inhibitor of HMG-CoA reductase, by rat cultured hepatocytes and human aortic endothelial cells. *British Journal of Clinical Pharmacology*, **47**, 383–389.

Olsson, A. G., 2001, Statin therapy and reductions in low-density lipoprotein cholesterol: initial clinical data on the potent new statin rosuvastatin. *American Journal of Cardiology*, **87**, 33B–36B.

Sirtori, C. R., 1993, Tissue selectivity of hydroxymethylglutaryl coenzyme A (HMG-CoA) reductase inhibitors. *Pharmacology and Therapeutics*, **60**, 431–459.

Tse, F. L. S., Smith, H. T., Ballard, F. H. and Nicoletti, J., 1990, Disposition of fluvastatin, an inhibitor of HMG-CoA reductase, in mouse, rat, dog, and monkey. *Biopharmaceutics and Drug Disposition*, **11**, 519–531.

Watanabe, M., Koike, H., Ishiba, T., Okada, T., Seo, S. and Hirai, K., 1997, Synthesis and biological activity of methanesulfonamide pyrimidine- and *N*-methanesulfonyl pyrrole-substituted 3,5-dihydroxy-6-heptenoates, a novel series of HMG-CoA reductase inhibitors. *Bioorganic and Medical Chemistry*, **5**, 437–444.

XENOBIOTICA, 2002, VOL. 32, NO. 9, 729–737

Taylor & Francis
healthsciences

Differential hormonal regulation of carbonyl reductase activities in liver and kidney microsomes of rat

Y. IMAMURA*, H. TAKADA, R. KAMIZONO and M. OTAGIRI

Faculty of Pharmaceutical Sciences, Kumamoto University, 5-1, Oe-honmachi, Kumamoto 862-0973, Japan

Received 13 December 2001

1. In the male rat, hepatic microsomal carbonyl reductase (CR) activity decreased by testectomy (Tx) was restored to the control level by the treatment with testosterone propionate (TP), even though the enzyme activity decreased by hypophysectomy (Hx) was not increased by the treatment with TP. On the other hand, renal microsomal CR activities decreased by Tx and Hx were markedly increased by the treatment with TP.

2. The treatment with TP had no effect on the CR activity in liver microsomes of the ovariectomized or hypophysectomized female rat. On the other hand, the CR activities in kidney microsomes of the ovariectomized and hypophysectomized female rat were significantly increased by the treatment with TP.

3. The results indicate that in rat programmed by neonatal androgens, the hepatic microsomal CR activity is regulated indirectly by androgens through the hypothalamus–pituitary system, whereas the hormonal regulation of the renal microsomal CR activity is not via the pituitary. We conclude that the regulatory mechanism of the CR activity in liver microsomes is distinguishable from that in kidney microsomes.

Introduction

Carbonyl reductase (CR) (EC 1.1.1.184) belonging to the short-chain dehydrogenase/reductase superfamily (Jörnvall *et al*. 1995, Tanaka *et al*. 2001) is a key enzyme catalysing the ketone-reduction of drugs such as acetohexamide, haloperidol and daunorubicin to their corresponding alcohol metabolites (Jakoby and Ziegler 1990, Oppermann and Maser 2000). This enzyme is widely distributed in various subcellular fractions in the liver and kidney of mammalian species (Forrest and Gonzalez 2000). We have also previously demonstrated that when acetohexamide, an oral antidiabetic drug, is used as a substrate, the CR activity is detected not only in liver and kidney cytosols, but also in liver and kidney microsomes of rat (Imamura *et al*. 1993). Note that in rat, the microsomal enzyme activity, unlike the cytosolic enzyme activity, is much higher in the male than in the female, and is regulated by testosterone propionate (TP) (Imamura *et al*. 1987, 1993).

Rat hepatic cytochrome P450 (CYP) 2C11, one of the CYP enzymes that play an important role in the oxidative metabolism of a variety of drugs, is known to be a male-specific and androgen-dependent enzyme (Ryan and Levin 1993). Many investigators (Morgan *et al*. 1985, Kato and Yamazoe 1993, Oinonen and Lindros 1998) have reported that the primary factor responsible for male-specific expression of hepatic CYP2C11 is the pulsatile pattern of growth hormone (GH) secretion, indicating that androgens do not act on the liver, but rather through

* Author for correspondence; e-mail: yorishig@gpo.kumamoto-u.ac.jp

Xenobiotica ISSN 0049–8254 print/ISSN 1366–5928 online © 2002 Taylor & Francis Ltd
http://www.tandf.co.uk/journals
DOI: 10.1080/00498250210144848

the hypothalamic–pituitary system. On the other hand, male-specific expression of rat renal CYP2C11 is regulated directly by androgens (Chen *et al.* 1997). These clearly indicate that rat hepatic and renal CYP2C11 genes are expressed by different mechanisms. However, no information on tissue-specific hormonal regulation of drug-reducing enzymes including carbonyl reductase is available so far. Most recently, our preliminary studies observed that the hormonal regulation of CR activity in liver microsomes of the male rat differs from that in kidney microsomes of the male rat (unpublished data). The purpose of this paper is to elucidate the mechanism for differential hormonal regulation of hepatic and renal microsomal CR activities.

Materials and methods

Materials

Acetohexamide was supplied from Shionogi Co. (Osaka, Japan). Hydroxyhexamide was synthesized from acetohexamide according to the method of Girgis-Takla and Chroneos (1979). The melting point was 143–146 °C. The infrared (IR) spectrum (in KBr) showed a hydroxyl band at 3520 cm^{-1}. Testosterone propionate (TP) was purchased from Nacalai Tesque (Kyoto, Japan). Recombinant human growth hormone (GH) was a gift from Novo Nordisk Pharma Ltd (Baggsvaerd, Denmark). $NADP^+$, glucose 6-phosphate and glucose 6-phosphate dehydrogenase were obtained from Oriental Yeast Co. (Tokyo, Japan).

Animals and treatments

Male and female Fischer (F344/NSlc) rat at 6 weeks of age (male, 110–120 g; female, 85–95 g) were purchased from Japan SLC (Shizuoka, Japan). All animal experiments were undertaken in accordance with the guideline principles for the care and use of laboratory animals. Gonadectomy [testectomy (Tx) and ovariectomy (Ox)] and hypophysectomy (Hx) of the animals were performed at 6 and 7 weeks of age, respectively. The testectomized, ovariectomized and hypophysectomized rat were raised up to 8 weeks of age under controlling lighting (12 h light/dark cycle), temperature (20 ± 2 °C) and humidity (50 ± 10%). TP (10 mg kg^{-1} body weight) dissolved in corn oil was injected subcutaneously to the testectomized, ovariectomized and hypophysectomized rat once every day for 7 days. Corn oil used as vehicle was given to control, Tx only, Ox only or Hx only animals. Recombinant human GH (0.34 IU/body) dissolved in saline solution was injected subcutaneously to the hypophysectomized rat twice daily for 7 days. Saline solution was given to control or Hx only animals. Animals were killed by decapitation after 7 days of hormonal replacement.

Preparation of liver and kidney microsomes

After perfusion with ice-cold 1.15% KCl solution, the livers and kidneys of the male and female rat were immediately removed and homogenized in a Potter-Elvehjem homogenizer with 3 vols 10 mM sodium-potassium phosphate buffer containing 1.15% KCl (pH 7.4). All subsequent procedures were performed at 3–5 °C. The homogenates were centrifuged at 10 000*g* for 20 min and the resulting supernatants were centrifuged at 105 000*g* for 60 min to obtain the microsomal pellets. The microsomal pellets were suspended in 10 mM sodium-potassium phosphate buffer containing 1.15% KCl (pH 7.4) and recentrifuged at 105 000*g* for 60 min. The microsomal pellets obtained were used for the assay of enzyme activity.

Assay of CR activity

The assay of CR activity was conducted in an NADPH-generating system, using acetohexamide as the substrate. The reaction mixture consisted of substrate (1.0 mM acetohexamide), NADPH-generating system (0.25 mM $NADP^+$, 6.25 mM glucose 6-phosphate, 0.25 U glucose 6-phospate dehydrogenase and 6.25 mM $MgCl_2$), enzyme (microsomal preparation) and 100 mM sodium-potassium phosphate buffer (pH 7.4) in a final volume of 2.0 ml. The mixture was incubated at 37 °C for 10 min, and the reaction was stopped by the addition of 1.0 M HCl (0.5 ml) to the mixture. The reduction product (hydroxyhexamide) of acetohexamide was determined by high-performance liquid chromatography (HPLC) (Takagishi *et al.* 1979). Briefly, the reaction mixture was extracted with 5.0 ml benzene–ethylacetate (1:1 v/v) mixture containing fenbufen (a gift from Lederle Japan, Tokyo, Japan) as the internal standard. The organic phase (4.0 ml) was removed and evaporated under reduced pressure. The residue was

dissolved in acetonitrile (0.3 ml) and injected into the HPLC system. HPLC was carried out using a Hitachi 655A-11 HPLC apparatus equipped with a LiChrosorb RP-18 column and a Hitachi 638-41 UV monitor (230 nm). The enzyme activity was expressed as nmol min^{-1} mg^{-1} protein. Protein concentration was estimated by the method of Bradford (1976) with bovine serum albumin as the standard.

Western blot analysis

Microsomal protein (5 μg) from the liver of each male rat was subjected to sodium dodecyl sulfate-polyacrylamide gel electrophoresis (SDS-PAGE). SDS-PAGE was performed using 10% gels according to the method of Laemmli. Separated proteins were transferred to PVDF membranes and probed with a goat polyclonal antibody (Daiichi Chemical Co., Tokyo, Japan) directed against rat CYP2C11. Rabbit anti-goat IgG conjugated horseradish peroxidase (Sigma Chemical Co., St Louis, MO, USA) was used as the secondary antibody. Peroxidase activity was determined with Immunostain HRP-1000 kit (Konica Co., Tokyo, Japan). Immunoquantification was accomplished by densitomeric scanning.

Statistical analysis

Data were analysed by a one-way analysis of variance. When the analysis indicated a significant difference, the significance of difference between two groups was evaluated using Duncan's multiple range test. $p < 0.05$ was considered as statistically significant.

Results

Effect of TP treatment on CR activity in liver microsomes of the testectomized and hypophysectomized male rat

To elucidate the mechanism underlying the male-specific expression of hepatic microsomal CR, we attempted to compare the effects of the treatment with TP on CR activity in liver microsomes of the testectomized and hypophysectomized male rat. As shown in figure 1, the hepatic microsomal CR activity was decreased by Tx, but the decreased enzyme activity was restored to control level by the treatment with TP. On the other hand, treatment with TP had no significant effect on the hepatic microsomal CR activity decreased by Hx. These findings provide evidence

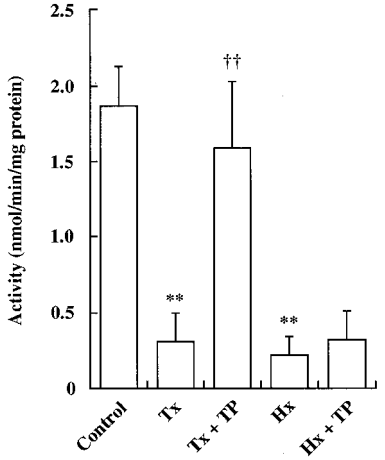


Figure 1. Effects of Tx, Hx and the tretment with TP on CR activity in liver microsomes of the male rat. Each bar is the mean ± SD of at least four rats. One-way analysis of variance indicated a significant different among all groups ($p < 0.001$). **$p < 0.01$, significantly different from control; ††$p < 0.01$, significantly different from Tx (Duncan's multiple range test).

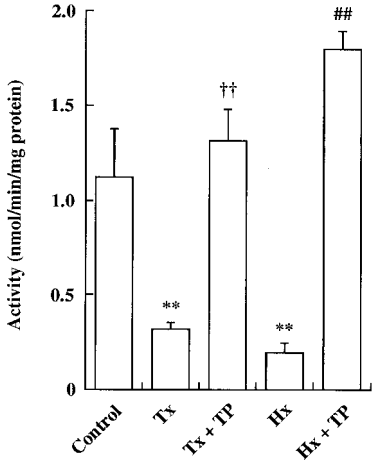


Figure 2. Effects of Tx, Hx and the treatment with TP on CR activity in kidney microsomes of the male rat. Each bar is the mean ± SD of at least four rats. One-way analysis of variance indicated a significant difference among all groups ($p < 0.001$). **$p < 0.01$, significantly different from control; ††$p < 0.01$, significantly different from Tx; ##$p < 0.01$, significantly different from Hx (Duncan's multiple range test).

that the hepatic microsomal CR activity is regulated indirectly by androgens through the hypothalamus–pituitary system.

Effect of TP treatment on CR activity in kidney microsomes of the testectomized and hypophysectomized male rat

Figure 2 shows the effects of TP treatment on CR activity in kidney microsomes of the testectomized and hypophysectomized male rat. Treatment with TP caused marked increases in the renal microsomal CR activities decreased by Tx and Hx. These findings, unlike in the case of the hepatic microsomal CR activity described above, indicate that TP treatment regulates the renal microsomal CR activity without mediating the hypothalamus–pituitary system.

Effect of the intermittent treatment with GH on CR activity in liver microsomes of the hypophysectomized male rat

It has been reported that in the adult male rat, the secretion of GH exhibits a pulsatile profile that is androgen-dependent (Edén 1979, Mode *et al.* 1982, Skett and Young 1982). Thus, we attempted to examine the effect of a male-type intermittent treatment with GH on CR activity in liver microsomes of the hypophysectomized male rat. At first, to establish whether the intermittent treatment with GH stimulates the expression of CYP2C11 protein, the protein level in liver microsomes of the male rat was determined by Western blot analysis. As expected, although Hx decreased the CYP2C11 protein level, the decreased protein level was increased by the intermittent treatment with GH (figure 3). Nevertheless, the hepatic microsomal CR activity decreased by Hx was not increased by the intermittent treatment with GH; its treatment showed a tendency to decrease rather than to increase the enzyme activity decreased by Hx (figure 4).

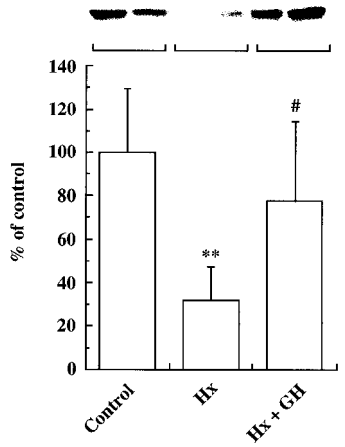


Figure 3. Effects of Hx and the intermittent treatment with GH on CYP2C11 protein level in liver microsomes of the male rat. The top section is Western blot data for liver microsomes of two rats untreated (control) treated with Hx and with Hx plus GH. Quantification of CYP2C11 bands from Western blots was obtained by using densitomeric scanning and the value (densitomeric unit) of control was defined as 100%. Each bar is the mean ± SD of at least four rats. One-way analysis of variance indicated a significant difference among all groups ($p < 0.01$). **$p < 0.01$, significantly different from control; #$p < 0.05$, significantly different from Hx (Duncan's multiple range test).

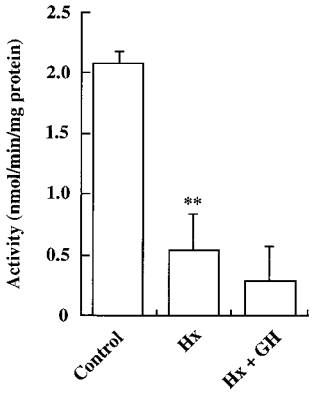


Figure 4. Effects of Hx and the intermittent treatment with GH on CR activity in liver microsomes of the male rat. Each bar is the mean ± SD of at least four rats. One-way analysis of variance indicated a significant difference among all groups ($p < 0.01$). **$p < 0.01$, significantly different from control (Duncan's multiple range test).

Effect of TP treatment on CR activities in liver and kidney microsomes of the ovariectomized and hypophysectomized female rat

We also compared the effects of TP treatment on CR activities in liver and kidney microsomes of the ovariectomized and hypophysectomized female rat. The CR activity in liver microsomes of the ovariectomized or hypophysectomized female rat was unaffected by the treatment with TP (figure 5). However, as shown in figure 6, TP treatment significantly increased the CR activities in kidney microsomes of the ovariectomized and hypophysectomized female rat.

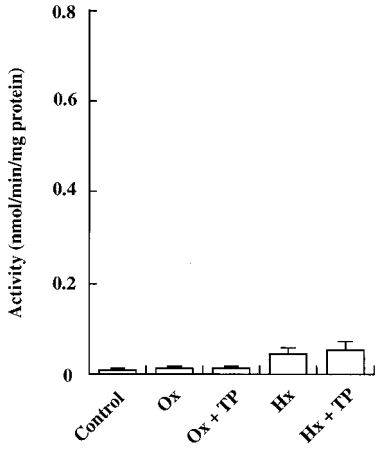


Figure 5. Effects of Ox, Hx and the treatment with TP on CR activity in liver microsomes of female rats. Each bar is the mean ± SD of at least four rats.

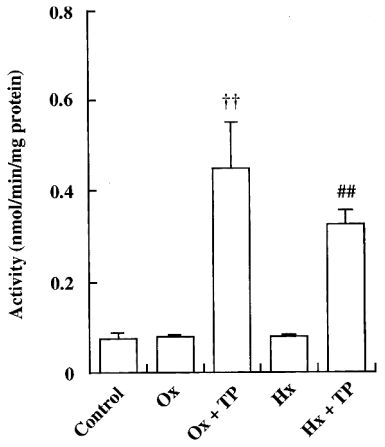


Figure 6. Effects of Ox, Hx and the treatment with TP on CR activity in kidney microsomes of the female rat. Each bar is the mean ± SD of at least four rats. One-way analysis of variance indicated a significant difference among all groups ($p < 0.001$). ††$p < 0.01$, significantly different from Ox; ##$p < 0.01$, significantly different from Hx (Duncan's multiple range test).

Discussion

A typical tissue-specific hormonal regulation has been observed in the expression of rat hepatic and renal CYP2C11, as described in the Introduction (Chen *et al.* 1997). The present study demonstrated that in the male rat, although hepatic microsomal CR activity decreased by Tx is restored to control level by the treatment with TP, the enzyme activity decreased by Hx is not increased by the treatment with TP. On the other hand, TP treatment caused a marked increase not only in the renal microsomal CR activity decreased by Tx, but also in the enzyme activity decreased by Hx. These results indicate that the hepatic microsomal CR activity is regulated indirectly by androgens through the hypothalamus–pituitary system, whereas the hormonal regulation of the renal microsomal CR activity is not via the pituitary. We conclude that the regulatory mechanism of the CR activity in liver microsomes is distinguishable from that in kidney microsomes.

The adult male rat is known to exhibit a pulsatile pattern in the secretion of GH from the pituitary gland. Interestingly, the pulsatile pattern of GH secretion is regulated by androgens and plays an important role in the male-specific expression of rat hepatic CYP2C11 (Kato and Yamazoe 1993). In the current study, we confirmed that CYP2C11 protein level in liver microsomes of the male rat decreased by Hx is restored to the control level by a male-type intermittent treatment with GH. However, the hepatic microsomal CR activity decreased by Hx was not increased by the intermittent treatment with GH. Additional studies including different dose and treatment schedule with GH will be necessary to elucidate this discrepancy. Furthermore, it is possible that since Hx accompanies the loss of pituitary hormones such as prolactin, adrenocorticotropic hormone (ACTH), follicle-stimulating hormone (FSH) and luteinizing hormone (LH), the pituitary hormone(s) other than GH is involved in the regulation of CR activity in the liver microsomes of the male rat. The dwarf rat, which was spontaneously derived from a colony of Sprague–Dawley strain (Okuma 1984), has low or undetectable level of circulating GH due to a selective defect in its pituitary system, although other pituitary hormones are secreted (Charlton *et al*. 1988, Nogami *et al*. 1989). The GH deficiency is caused by a point mutation in the GH gene, resulting in an abnormal splicing of GH mRNA (Takeuchi *et al*. 1990). This mutant rat may be useful to elucidate the detailed mechanism for the hormonal regulation of the hepatic microsomal CR activity (Shimada *et al*. 1997).

Treatment with TP had no effect on the CR activity in the liver microsomes of the ovariectomized or hypophysectomized female rat, even though it significantly increased the CR activities in kidney microsomes of the ovariectomized and hypophysectomized female rat. These results also indicate that the regulatory mechanisms of CR activity in liver and kidney microsomes of rat differ from each other. It has been reported that some drug-metabolizing enzymes can be programmed for its induction at puberty by androgens secreted during neonatal period in the male rat (Kamataki *et al*. 1984, Jansson *et al*. 1985, Waxman *et al*. 1985). This androgenic programming is referred to as neonatal imprinting and results in the different secretory patterns of GH in the male and female rat (Edén 1979, Mode *et al*. 1982, Skett 1988). We have shown that the expression of CR in liver microsomes of the male rat depends on neonatal imprinting mediated by the hypothalamus–pituitary system (Imamura *et al*. 1993). Alternatively, neonatal androgens are essential for programming the expression of hepatic microsomal CR. However, the female rat cannot be programmed due to the lack of neonatal androgen secretion. Thus, it is likely that the CR activity in liver microsomes of the ovariectomized female rat, unlike that in liver microsomes of the testectomized male rat, is unaffected by the treatment with TP.

The hypophysectomized male and female rat did not show the same CR activity in liver microsomes. Furthermore, the castrated male and female rat did not show the same CR activity in kidney microsomes. The reason for these may be that the CR activity was determined using an oral antidiabetic drug acetohexamide as the substrate. Since acetohexamide is a xenobiotic compound, it is reasonable to assume that minor but male-specific enzymes, in addition to the CR, somewhat contribute to the reductive metabolism of acetohexamide, namely CR activity, in liver and kidney microsomes of the male rat.

In conclusion, the present study provides evidence that in rat programmed by neonatal androgens, the hepatic microsomal CR activity is regulated indirectly by

androgens through the hypothalamus–pituitary system, whereas the hormonal regulation of the renal microsomal CR activity is not via the pituitary.

References

Bradford, M. M., 1976, A rapid and sensitive method for the quantitation of microgram quantities of protein utilizing the principle of protein–dye binding. *Analytical Biochemistry*, **72**, 247–254.

Charlton, H. M., Clark, R. G., Robinson, I. C. A. F., Porter-Go, A E., Cox, B. S., Bugnon, C. and Bloch, B. S., 1988, Growth hormone-deficient dwarfism in the rat: A new mutation. *Journal of Endocrinology*, **119**, 51–58.

Chen, G.-F., Ronis, M. J. J., Thomas, P. E., Flint, D. J. and Badger, T. M., 1997, Hormonal regulation of microsomal cytochrome P450 2C11 in rat liver and kidney. *Journal of Pharmacology and Experimental Therapeutics*, **283**, 1486–1494.

Edén, S., 1979, Age- and sex-related differences in episodic growth hormone secretion in the rat. *Endocrinology*, **105**, 555–560.

Forrest, G. L. and Gonzalez, B., 2000, Carbonyl reductase. *Chemico-Biological Interactions*, **129**, 21–40.

Girgis-Takla, P. and Chroneos, I., 1979, Fluorometric determination of acetohexamide in plasma and tablet formulation using 1-methylnicotinamide. *Analyst*, **104**, 117–123.

Imamura, Y., Iwamoto, K., Yanachi, Y., Higuchi, T. and Otagiri, M., 1993, Postnatal development, sex-related difference and hormonal regulation of acetohexamide reductase activities in rat liver and kidney. *Journal of Pharmacology and Experimental Therapeutics*, **264**, 166–171.

Imamura, Y., Kojima, Y. and Otagiri, M., 1987, Sex difference of acetohexamide reduction in rat liver. *Journal of Pharmacobio-Dynamics*, **10**, 285–286.

Jakoby, W. B. and Ziegler, D. M., 1990, The enzymes of detoxication. *Journal of Biological Chemistry*, **265**, 20715–20718.

Jansson, J.-O., Ekberg, S., Isaksson, O., Mode, A. and Gustafsson, J.-Å., 1985, Imprinting of growth hormone secretion, body growth and hepatic steroid metabolism by neonatal testosterone. *Endocrinology*, **117**, 1881–1889.

Jörnvall, H., Persson, B., Krook, M., Atrian, S., Gnozàlez-Duarte, R., Jeffery, J. and Ghosh, D., 1995, Short-chain dehydrogenase/reductase (SDR). *Biochemistry*, **34**, 6003–6013.

Kamataki, T., Maeda, K., Shimada, M., Nagai, T. and Kato, R., 1984, Neonatal testosterone imprinting of hepatic microsomal drug metabolism and a male-specific form of cytochrome P-450 in the rat. *Journal of Biochemistry* (Tokyo), **96**, 1939–1942.

Kato, R. and Yamazoe, Y., 1993, Hormonal regulation of cytochrome P450 in rat liver. In J. B. Schenkman and H. Greim (eds), *Handbook of Experimental Pharmacology*, vol. 105: *Cytochrome P450* (Berlin: Springer), pp. 447–459.

Mode, A., Gustafsson, J.-Å., Jansson, J.-O., Edén, S. and Isaksson, O., 1982, Association between plasma levels of growth hormone and sex differentiation of hepatic steroid metabolism in the rat. *Endocrinology*, **111**, 1692–1697.

Morgan, E. T., MacGeogh, C. and Gustafsson, J.-Å., 1985, Hormonal and developmental regulation of the expression of the hepatic microsomal steroid 16a-hydroxylase cytochrome P-450 apoprotein in the rat. *Journal of Biological Chemistry*, **260**, 11895–11898.

Nogami, H., Takeuchi, T., Suzuki, K., Okuma, S. and Ishikawa, H., 1989, Studies on prolactin and growth hormone gene expression in the pituitary gland of spontaneous dwarf rat. *Endocrinology*, **125**, 964–970.

Oinonen, T. and Lindros, K. O., 1998, Zonation of hepatic cytochrome P-450 expression and regulation. *Biochemical Journal*, **329**, 17–35.

Okuma, S., 1984, Study of growth hormone in spontaneous dwarf rat. *Nippon Naibunpi Gakkai Zasshi*, **60**, 1005–1014.

Oppermann, U. C. T. and Maser, E., 2000, Molecular and structural aspects of xenobiotic metabolizing enzymes. Role of reductases and dehydrogenases in xenobiotic phase I reactions. *Toxicology*, **144**, 71–81.

Ryan, D. E. and Levin, W., 1993, Age- and gender-related expression of rat liver cytochrome P450. In J. B. Schenkman and H. Greim (eds), *Handbook of Experimental Pharmacology*, vol. 105: *Cytochrome P450* (Berlin: Springer), pp. 461–476.

Shimada, M., Murayama, N., Nagata, K., Hashimoto, H., Ishikawa H. and Yamazoe, Y., 1997, A specific loss of growth hormone abolished sex-dependent expression of hepatic cytochrome P450 in Dwarf rat: reversal of the profile by growth hormone-treatment. *Archives of Biochemistry and Biophysics*, **337**, 34–42.

Skett, P., 1988, Biochemical basis of sex differences in drug metabolism. *Pharmacology and Therapeutics*, **38**, 269–304.

Skett, P. and Young, C., 1982, The effect of pituitary hormones on hepatic drug metabolism in the rat. *Acta Endocrinologica*, **100**, 421–426.

Takagishi, Y., Sato, K., Tomita, K. and Sakamoto, T., 1979, High-performance liquid chromatographic determination of acetohexamide and its metabolite hydroxyhexamide. *Yakugaku Zasshi*, **99**, 961–963.

Takeuchi, T., Suzuki, S., Nogami, H., Okuma, S. and Ishikawa, H., 1990, Molecular mechanism of growth hormone (GH) deficiency in the spontaneous dwarf rat: detection of abnormal splicing of GH messenger ribonucleic acid by the polymerase chain reaction. *Endocrinology*, **126**, 31–38.

Tanaka, N., Nonaka, T., Nakamura, K. T. and Hara, A., 2001, SDR: structural mechanism of action, and substrate recognition. *Current Organic Chemistry*, **5**, 89–111.

Waxman, D .J., Dannan, G. A. and Guengerich, F. P., 1985, Regulation of hepatic cytochrome P-450: age-dependent expression, hormonal imprinting and xenobiotic inducibility of sex-specific isoenzymes. *Biochemistry*, **24**, 4409–4417.

XENOBIOTICA, 2002, VOL. 32, NO. 9, 739–747

Taylor & Francis
healthsciences

Use of a quantitative real-time reverse transcription-polymerase chain reaction method to study the induction of CYP1A, CYP2B and CYP4A forms in precision-cut rat liver slices

J. PAN†§, Q. XIANG†, A. B. RENWICK‡, R. J. PRICE‡, S. E. BALL†, J. KAO†, J. A. SCATINA§ and B. G. LAKE‡*

† Wyeth-Ayerst Research, Drug Metabolism Division, CN8000, Princeton, NJ 08543-8000, USA
‡ TNO BIBRA International Ltd, Woodmansterne Road, Carshalton SM5 4DS, UK

Received 14 March 2002

1. The aim was to employ real-time quantitative reverse transcription-polymerase chain reaction (RT-PCR) technology (TaqMan®) to examine the induction of some selected cytochrome P450 (CYP) forms in precision-cut rat liver slices.

2. Taqman® primers and probe sets were developed for rat CYP1A1, CYP1A2, CYP2B1 and CYP4A1 forms.

3. Rat liver slices were cultured in control medium or medium containing either 10 μg ml^{-1} Aroclor 1254 (ARO), 500 μM sodium phenobarbitone (NaPB) or 50 μM Wy-14,643 (WY) for 3, 6 and 24 h.

4. Compared with control liver slices, treatment with ARO for 3 and 6 h produced 24- and 184-fold increases, respectively, in CYP1A1 mRNA levels, and after 24 h produced an 85-fold increase in CYP1A2 mRNA levels. Levels of CYP1A1 and CYP1A2 mRNA were not markedly affected by NaPB and WY.

5. Treatment with ARO and PB for 24 h produced 10.6- and 23.8-fold increases, respectively, in CYP2B1 mRNA. Levels of CYP2B1 mRNA were not markedly affected by WY.

6. Treatment with WY, but not ARO and NaPB, for 24 h produced a 20.4-fold increase in levels of CYP4A1 mRNA.

7. These results demonstrate that cultured liver slices may be used to evaluate the effect of xenobiotics on CYP form mRNA levels.

Introduction

Cytochrome P450 (CYP) forms have a major role in the oxidative metabolism of drugs and other xenobiotics (Conney 1986, Nelson *et al*. 1996, Parkinson 1996). In the development of new therapeutic agents, it is important to ascertain whether the compounds will be either inducers or inhibitors of CYP forms in order to minimize potential drug interactions. CYP induction can also be important in preclinical studies as several non-genotoxic CYP2B, CYP3A and CYP4A inducers have been shown to induce liver tumours in rodents (Nims *et al*. 1987, Grasso and Hinton 1991, Lake 1995, Whysner *et al*. 1996).

* Author for correspondence; e-mail: blake@tnobibra.co.uk
§ Present address: Aventis Pharmaceuticals, Department of Drug Metabolism and Pharmacokinetics – Pre-Clinical PK, PO Box 6800, Bridgewater, NJ 08807, USA.

Xenobiotica ISSN 0049-8254 print/ISSN 1366-5928 online © 2002 Taylor & Francis Ltd
http://www.tandf.co.uk/journals
DOI: 10.1080/00498250210147115

The effects of xenobiotics on hepatic CYP forms can be evaluated by both *in vivo* and *in vitro* techniques. Many studies have utilized cultured rat hepatocytes to evaluate the induction of CYP1A, CYP2B, CYP3A and CYP4A subfamily forms (LeCluyse *et al*. 1996, Davila and Morris 1999, Burczynski *et al*. 2001). The induction of CYP forms can also be evaluated in precision-cut rat liver slices (Lake *et al*. 1998, Lerche-Langrand and Toutain 2000). As with cultured hepatocytes, CYP induction has been assessed by measurement of enzyme activities, Western immunoblotting for CYP apoprotein levels and in a few studies only by measurement of CYP mRNA levels. The induction of CYP1A2 and/or CYP1A1 mRNA in rat liver slices has been reported by a number of laboratories (Gokhale *et al*. 1995, Drahushuk *et al*. 1996, Müller *et al*. 1998) and one report has also described the induction of CYP2B1 mRNA (Müller *et al*. 2000).

While the measurement of mRNA levels can provide a sensitive measure of the effects of chemicals in CYP forms, conventional reverse transcription-polymerase chain reaction (RT-PCR) methods require relatively large amounts of RNA and provide only semiquantitative data due to problems of saturation that can occur in the PCR amplification process. This can complicate 'endpoint' assays leading to an incorrect estimation of the starting mRNA abundance (Murphy *et al*. 1990, Wiesner *et al*. 1992). Recently, a real-time quantitative RT-PCR method (TaqMan®) has been developed to overcome the limitations of conventional RT-PCR methods (Gibson *et al*. 1996, Heid *et al*. 1996). Unlike endpoint methods (e.g. band densitometry), real-time quantitative RT-PCR is capable of monitoring signal amplification during the course of each PCR cycle. To date, there have been only a few published applications of TaqMan® methodology to determine mammalian hepatic CYP mRNA levels. Recently, the TaqMan® methodology has been employed to study the effects of cytokines on some CYPs in mouse liver (Pan *et al*. 2000), the effects of some chemicals on CYP1A1 and CYP3A4 levels in cultured human hepatocytes (Bowen *et al*. 2000), and levels of CYP3A in human duodenal enterocytes and colorectal tissues (Nakamura *et al*. 2002).

The objective of the current study was to examine the induction of some selected CYP forms in cultured rat liver slices employing TaqMan® methodology to quantify CYP mRNA levels. To undertake the liver slice studies, TaqMan® primers and probe sets were developed for rat CYP1A1, CYP1A2, CYP2B1 and CYP4A1 forms. Rat liver slices were treated with Aroclor 1254 (ARO), sodium phenobarbitone (NaPB) and Wy-14,643 (WY) and the effects on CYP1A1, CYP1A2, CYP2B1 and CYP4A1 mRNA levels were determined. Previous studies have demonstrated that the polychlorinated biphenyl mixture ARO induces several rat CYP subfamilies including CYP1A, CYP2B and CYP3A, whereas NaPB induces CYP2B, CYP3A and other forms and the peroxisome proliferator WY induces CYP4A forms (Conney 1986, Okey 1990, Lake and Lewis 1996, Nims and Lubet 1996).

Materials and methods

Materials

Tissue culture materials and recombinant RNase inhibitor (cat. no. 10777-019) were obtained from Life Technologies Ltd (Paisley, UK) and FastPrep® tubes (cat. no. 6040-601) for RNA isolation from Qbiogene (Harefeld, UK). Sodium phenobarbitone was obtained from BDH Chemicals (Poole, UK) and Wy-14,643 from Chemsyn Science Laboratories (Lenexa, KS, USA). Aroclor 1254 was the generous gift of Monsanto Chemical Co. (St Louis, MO, USA). Trizol reagents were purchased

from Life Technologies (Rockwille, MD, USA). TaqMan® RT-PCR universal master mix reagents (cat. no. 4309169) and TaqMan® primers and probe for 18S rRNA were obtained from Applied Biosystems (Foster City, CA, USA). The oligonucleotide primers and probes for CYP1A1, 1A2, 2B1 and 4A1 were synthesized by Keystone Labs at Biosources (Camarillo, CA, USA).

Animals

Male Sprague–Dawley rats were obtained from Harlan Olac (Bicester, UK) and were allowed free access to R&M No. 1 laboratory animal diet (Special Diets Services, Witham, UK) and water. The animals were housed in polypropylene cages with stainless-steel grid tops and floors in rooms maintained at $22 \pm 3\,^{\circ}C$ with a relative humidity of 40–70% and were allowed to acclimatize to these conditions for at least 14 days before use.

Preparation of liver slices

Rats (10–12 weeks old, 330–360 g body weight) were killed by carbon dioxide asphyxiation followed by cervical dislocation. The livers were immediately excized and placed in ice-cold Earle's balanced salt solution (EBSS) containing 25 mM D-glucose, $50\,\mu g\,ml^{-1}$ gentamicin and $2.5\,\mu g\,ml^{-1}$ fungizone previously gassed with 95% O_2/5% CO_2. Tissue cylinders from liver samples were prepared with a 10-mm diameter motor-driven tissue-coring tool. From the cylinders, liver slices of around 250 µm thickness were prepared in cold oxygenated EBSS containing the above additions using a Krumdieck tissue slicer (Alabama Research and Development, Munford, AL, USA). Liver slice thickness was determined as described (Price *et al.* 1998), whereas protein content was determined by the method of Lowry *et al.* (1951) employing bovine serum albumin as standard.

Culture of liver slices

Liver slices were floated onto Vitron, Inc. (Tucson, AZ, USA) type C titanium roller inserts (two slices per insert) and cultured in glass vials containing 1.7 ml culture medium employing a Vitron dynamic organ culture incubator. The culture medium consisted of Williams' medium E containing 2 mM L-glutamine, 0.1 µM insulin, 0.1 µM dexamethasone, $50\,\mu g\,ml^{-1}$ gentamicin and $2.5\,\mu g\,ml^{-1}$ fungizone. Liver slice cultures were maintained at $37\,^{\circ}C$ in an atmosphere of 95% O_2/5% CO_2. After 1 h, treatment was commenced by replacing the culture medium with medium containing the required concentrations of the test compounds. Test compounds were dissolved in dimethyl sulphoxide (DMSO) and added to the culture medium so that the final DMSO concentration was 0.4% (v/v) in all vials including the control cultures. At the end of the 3, 6 or 24 h of treatment periods, the liver slices were washed in 0.154 M KCl containing 50 mM Tris-HCl, pH 7.4 and 100 units ml^{-1} of the RNase inhibitor, blotted dry with tissue and placed in FastPrep® RNA isolation tubes. The liver slices were rapidly frozen in dry ice and then stored at $-80\,^{\circ}C$ before transportation in dry ice to Wyeth-Ayerst Research (Princeton, NJ, USA).

RNA extraction from liver slices

Total RNA was isolated from the liver slices using Trizol reagents (Life Technologies, Rockville, MD, USA). Batches of 12 samples were homogenized for 0.5 min employing a FastPrep FP120 instrument (Bio 101, Inc., San Diego, CA, USA). The homogenized samples were phase separated by the addition of chloroform (1:0.2 v/v, Trizol:chloroform) and centrifuged as described in the manufacturer instructions. The aqueous phase was transferred to a fresh tube and mixed with isopropyl alcohol for RNA precipitation. The quality of the isolated RNA was assessed as the 260/280 nm absorbance ratio (range 1.8–2.0 indicates a highly pure sample). Selected samples were subjected to electrophoresis on 1% agarose gels and stained with ethidium bromide to confirm the integrity of the 28S and 18S bands. RNA concentration was determined as described (Pan *et al.* 2000).

Design of TaqMan® primers and probes

CYP primers and probes (table 1) were designed using PrimerExpress software (Applied Biosystems). The RNA sequences of CYP1A1, CYP1A2, CYP2B1 and CYP4A1 were obtained from GenBank with accession nos X00469, K02422, L00318 and M14972, respectively. Where possible, to avoid genomic DNA amplification, one of the primers or the probe was on an exon–exon border. The CYP1A1 forward primer crosses exons 3 and 4, the CYP1A2 probe crosses exons 4 and 5, and the CYP4A1 forward primer crosses exons 2 and 3. Owing to the high homology (97% of amino acid sequences) between CYP2B1 and CYP2B2, the exon 7 sequence (most variable region) was used to design CYP2B1 primers and probe to obtain its specificity from CYP2B2. Appropriate controls demonstrated that there was no significant contamination of the isolated RNA samples by genomic DNA (data not shown).

Real-time quantitative RT-PCR

Real-time quantitative RT-PCR for rat CYP mRNA levels was performed employing a TaqMan® 7700 sequence detector system (Applied Biosystems). The sample preparation for mRNA level quantification was conducted automatically in 96-well plate format using a 6700 automated nucleic acid purification workstation (Applied Biosystems). The reaction mixture (20 µl per well) for RT-PCR was prepared in a single tube with final concentrations as follows: 1x master mix reagents (containing AmpliTaq Gold DNA polymerase, dATP, dGTP, dCTP, dUTP, passive reference and optimized buffer components), 200 nM of each primer and 100 nM probe for each CYP mRNA assay. Total RNA (10 µg) in 5 µl diethyl pyrocarbonate-treated distilled water was added to each well and the final volume was 25 µl with master mix for RT-PCR reaction. The thermal cycle condition for RT reaction was 30 min at 48 °C and then 10 min at 95 °C to activate AmpliTaq Gold DNA polymerase. The PCR reaction was performed for 40 cycles: denaturation at 95 °C for 15 s and anneal/extension at 60 °C for 1 min. Quantitative RT-PCR for 18S rRNA was also performed to normalize for RNA loading. The concentration of primers and probe of 18S rRNA were 50 nM each for the reaction employing 10 ng total RNA from each sample.

Results

Development of rat CYP TaqMan® primers and probes

TaqMan® primers and probe sets were developed for rat CYP1A1, CYP1A2, CYP2B1 and CYP4A1 and used to quantify CYP mRNA levels in cultured rat liver slices. Table 1 shows the primers and probe sequences and their locations for all four CYPs studied. Where possible, one of the TaqMan® primers or the probe for each CYP was selected to cross an exon–exon border in order to avoid amplification of any contaminating genomic DNA present in the liver slice RNA samples. For all four CYP mRNAs studied, a good linearity of response was observed in standard curves of TaqMan® threshold cycle values obtained in the amplication plots and the amount of total RNA added (data not shown).

Rat liver slice CYP mRNA induction studies

Freshly cut rat liver slices were prepared with a Krumdieck tissue slicer. Liver slice thickness and protein content (mean ± SEM of eight slices) was determined to be 253 ± 3 µm and 3.1 ± 0.1 mg protein/slice, respectively. Rat liver slices were cultured for 3, 6 and 24 h in control medium (containing 0.4% v/v DMSO) or medium containing either 10 µg ml^{-1} ARO, 500 µm NaPB or 50 µm WY. These

Table 1. TaqMan® rat at CYP mRNA primers and probe sequences.

CYP form	Primers/ probes	Location	5′ → 3′ sequence	Amplicon size (bp)
1A1	forward	1107–1131	AAAGATCCAGGAGGAGTTAGACACA	68
	reverse	1174–1155	GAGGTCTGTCAGAAAGCCGG	
	probe	1133–1153	TGATTGGCAGGGATCGGCAGC	
1A2	forward	1140–1161	CGATACACATCCTTTGTCCCCT	66
	reverse	1205–1186	GCCATTCAGTGAGGTGACCC	
	probe	1163–1184	CACCATCCCCCAGAGCACAACG	
2B1	forward	46–64[a]	GGTTCACACCGGCTACCAA	74
	reverse	119–96	TGAATCTCATGGATAACTGCATCA	
	probe	66–94	CCTTGATGACCGCAGTAAAATGCCATACA	
4A1	forward	329–348	TGATTCTCGGGCGATCAGAT	70
	reverse	398–379	CCATATCCGATCCAAGGAGC	
	probe	350–376	CAAAGGCCAATGGCGTCTACAGATTGC	

[a] Location of CYP2B1 primers and probe were derviced from exon 7 DNA sequences.

concentrations of ARO, NaPB and WY were selected from the results of previous studies on the induction of CYP forms and peroxisomal enzyme activities in cultured rat liver slices (Beamand *et al.* 1993, Lake *et al.* 1993, 1996). At the end of the treatment periods, the slices were harvested, total RNA extracted and cDNA prepared as described in the Methods section. Levels of each rat CYP mRNA were determined by real-time quantitative RT-PCR and expressed as a ratio to levels of 18S rRNA which was employed to normalize RNA loading.

Compared with control (DMSO only treated liver slices), treatment with 10 μg ml^{-1} ARO for 3 and 6 h produced 24- and 184-fold increases in levels of CYP1A1 mRNA (figure 1A). In contrast, treatment with 500 μM NaPB and 50 μM WY for 3 and 6 h had no marked effect on CYP1A1 mRNA levels. Levels of CYP1A1 mRNA increased in 24-h cultured control rat liver slices that precluded the evaluation of the effect of treatment with the CYP inducers. The treatment of liver slices with ARO for 24 h resulted in an 85-fold increase in CYP1A2 mRNA

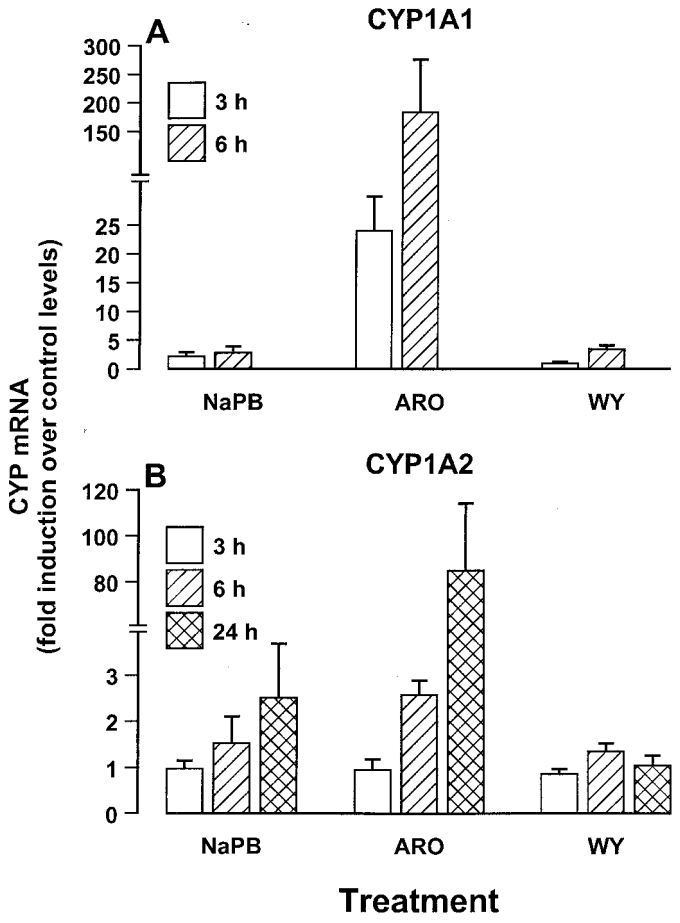


Figure 1. Effect of treatment of rat liver slices for up to 24 h with 500 μM NaPB, 10 μg/ml^{-1} ARO and 50 μM WY on levels of CYP1A1 (A) and CYP1A2 (B) mRNA. Levels of CYP1A1 and CYP1A2 mRNA were expressed as ratios of levels of 18S rRNA, which was used to normalize RNA loading. Values are the fold induction over mRNA levels in control (DMSO only treated) liver slices at each time point. Results are the mean ± SEM ($n = 4$) for two separate experiments, with replicate incubations being performed for each treatment and time point in both experiments.

levels (figure 1B). While WY had no effect on CYP1A2 mRNA levels, treatment with NaPB for 24 h produced a small 2.5-fold increase.

Levels of CYP2B1 mRNA were increased by treatment of rat liver slices with NaPB and ARO, but not by treatment with WY (figure 2A). NaPB produced 10.8- and 10.6-fold increases after 3 and 24 h, respectively, whereas the greatest induction of CYP2B1 mRNA by ARO was a 23.8-fold increase after 24 h of treatment. WY produced a time-dependent increase in CYP4A1 mRNA levels, with a 20.4-fold increase being observed after 24 h of treatment (figure 2B). In contrast, treatment with NaPB and ARO had no marked effect on CYP4A1 mRNA levels.

Discussion

The aim was to utilize TaqMan® methodology to quantify the induction of some selected CYP mRNA levels in cultured rat liver slices. By employing

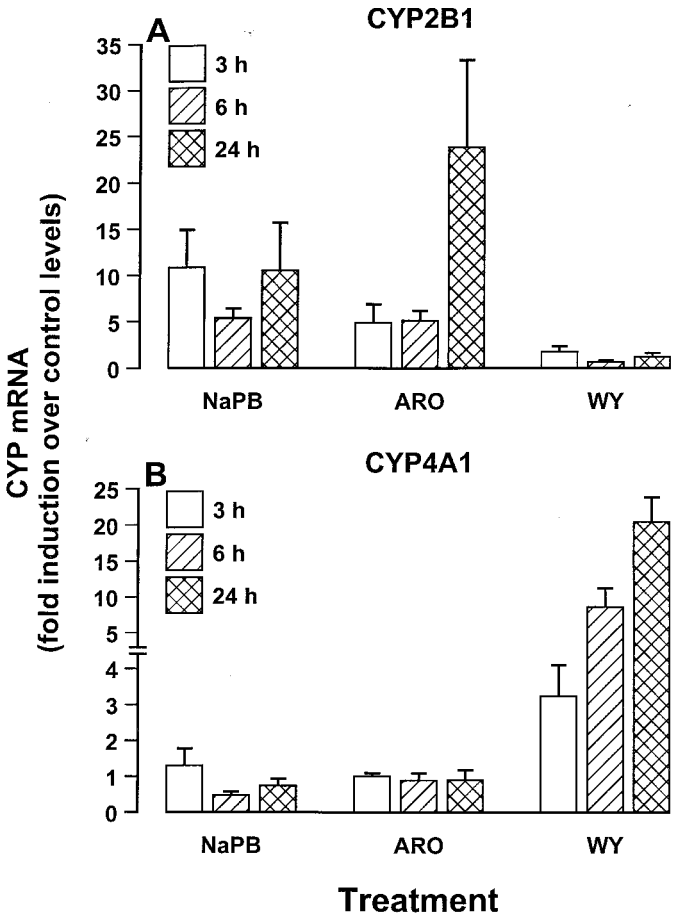


Figure 2. Effect of treatment of rat liver slices for up to 24 h with 500 μM NaPB, 10 μg/ml^{-1} ARO and 50 μM WY on levels of CYP2B1 (A) and CYP4A1 (B) mRNA. Levels of CYP2B1 and CYP4A1 mRNA were expressed as ratios of levels of 18S rRNA, which was used to normalize RNA loading. Values are the fold induction over mRNA levels in control (DMSO only treated) liver slices at each time point. Results are the mean ± SEM ($n = 4$) for two separate experiments, with replicate incubations being performed for each treatment and time point in both experiments.

commercially available software, TaqMan® primers and probe sets were developed for rat CYP1A1, CYP1A2, CYP2B1 and CYP4A1 forms.

Rat liver slices were cultured for up to 24 h with three known CYP inducers: NaPB, ARO and WY. Treatment with ARO, but not NaPB and WY, markedly induced levels of CYP1A1 mRNA. ARO also produced a marked increase in levels of CYP1A2 mRNA after 24 h of treatment, whereas WY had no effect. Although NaPB produced a small 2.5-fold increase in CYP1A2 mRNA levels, this was minor in comparison with the 85-fold increase observed after treatment with ARO. While treatment with ARO and NaPB increased levels of CYP2B1 mRNA, only treatment with WY increased levels of CYP4A1 mRNA. The effects of these CYP inducers on the four CYP mRNA levels studied are largely in agreement with previous *in vivo* and *in vitro* studies. The polychlorinated biphenyl mixture ARO is known to induce rat CYP1A and CYP2B forms, NaPB to induce CYP2B forms and WY to induce CYP4A forms (Conney 1986, Okey 1990, Lake *et al*. 1993, 1996, Lake and Lewis 1996, Nims and Lubet 1996).

Whereas the induction of CYP1A and CYP2B mRNAs has been observed in rat liver slices (Gokhale *et al*. 1995, Drahushuk *et al*. 1996, Müller *et al*. 1998, 2000), the induction of CYP4A1 mRNA has not been reported. However, as with cultured hepatocytes, the induction of peroxisomal and microsomal fatty acid oxidizing enzymes, organelle proliferation and CYP4A1 apoprotein has been observed in cultured rat liver slices (Lake *et al*. 1993, 1996, Lake and Lewis 1996). In the current study, WY only induced CYP4A1 mRNA, whereas in other studies peroxisome proliferators have also been shown to induce other CYP forms (Lake and Lewis 1996). For example, in cultured rat hepatocytes clofibric acid (a peroxisome proliferator) has been shown to induce CYP2B1 mRNA and apoprotein (Bars *et al*. 1989, 1993) and WY to induce CYP2B1 mRNA (Pan and Xiang, Wyeth-Ayerst Research, unpublished data). Additional studies would be required to ascertain if there are any differences between cultured rat hepatocytes and liver slices in the induction of CYP2B forms by peroxisome proliferators.

The use of TaqMan® methodology has a number of potential advantages over other procedures for assessing CYP form induction in cultured liver slices. For example, the real-time quantitative RT-PCR procedure employed in this study is highly sensitive with a single liver slice containing sufficient RNA to permit the subsequent determination of mRNA levels of a number of CYP forms. Moreover, as demonstrated by the present study, large increases in mRNA levels can be obtained within 24 h, whereas for CYP induction studies utilizing enzymatic or Western immunoblotting endpoints, longer treatment times may be required (Lake *et al*. 1993, 1996, 1998, Gokhale *et al*. 1995, Lerche-Langrand and Toutain 2000). The monitoring of mRNA levels is also more specific for individual CYP forms than the determination of marker enzyme activities. Overall, the measurement of mRNA levels by TaqMan® methodology requires shorter liver slice culture periods and, with appropriate automation, can result in more rapid sample throughout. TaqMan® methodology may also be useful to study mechanisms of induction of CYP forms in liver slices, including the effects of supplementation of the culture medium with hormones and other components.

At the concentrations of the CYP inducers employed in this study, the induction of CYP1A1 mRNA could be observed after 3 h of treatment, whereas 6 and 24 h of treatment times were required to observe a clear induction of CYP4A1 and CYP1A2 mRNA, respectively. For CYP2B1 mRNA, ARO pro-

duced a similar increase after 3 and 6 h, with a much greater increase being obtained after 24 h. For NaPB no clear time-course was discernible, as similar-fold increases in CYP2B1 mRNA levels were observed after 3 and 24 h culture. Although a single treatment time may be suitable to assess the effects of chemicals on one particular CYP mRNA, multiple treatment times appear to be preferable for studies where effects on a number of CYP mRNA levels are to be examined.

In summary, a real-time quantitative RT-PCR methodology has been developed to study CYP mRNA induction in cultured rat liver slices. TaqMan® primer and probe sets were developed for four rat CYP forms and induction profiles obtained after treatment with NaPB, ARO and WY. Cultured precision-cut liver slices appear to be a useful *in vitro* model system for screening xenobiotics for effects on CYP mRNA levels. Additional studies are required to examine the effects of more CYP inducers on a wider range of CYP forms.

Acknowledgements

The work was supported by a research grant from Wyeth-Ayerst Research Drug Metabolism Division (Princeton, NJ, USA).

References

Bars, R. G., Bell, D. R. and Elcombe, C. R., 1993, Induction of cytochrome P450 and peroxisomal enzymes by clofibric acid *in vivo* and *in vitro*. *Biochemical Pharmacology*, **45**, 2045–2053.

Bars, R. G., Mitchell, A. M., Wolf, C. R. and Elcombe, C. R., 1989, Induction of cytochrome *P*-450 in cultured rat hepatocytes. The heterogeneous localization of specific isoenzymes using immunocytochemistry. *Biochemical Journal*, **262**, 151–158.

Beamand, J. A., Price, R. J., Cunninghame, M. E. and Lake, B. G., 1993, Culture of precision-cut liver slices: effect of some peroxisome proliferators. *Food and Chemical Toxicology*, **31**, 137–147.

Bowen, W. P., Carey, J. E., Miah, A., McMurray, H. F., Munday, P. W., James, R. S., Coleman, R. A. and Brown, A. M., 2000, Measurement of cytochrome P450 gene induction in human hepatocytes using quantitative real-time reverse transcriptase-polymerase chain reaction. *Drug Metabolism and Disposition*, **28**, 781–788.

Burczynski, M. E., McMillian, M., Parker, J. B., Bryant, S., Leone, A., Grant, E. R., Thorne, J. M., Zhong, Z., Zivin, R. A. and Johnson, M. D., 2001, Cytochrome P450 induction in rat hepatocytes assessed by quantitative real-time reverse-transcription polymerase chain reaction and the RNA invasive cleavage assay. *Drug Metabolism and Disposition*, **29**, 1243–1250.

Conney, A. J., 1986, Induction of microsomal cytochrome P-450 enzymes: the first Bernard B. Brodie lecture at Pennsylvania State University. *Life Sciences*, **39**, 2493–2518.

Davila, J. C. and Morris, D. L., 1999, Analysis of cytochrome P450 and phase II conjugating enzyme expression in adult male rat hepatocytes. *In Vitro Cellular and Developmental Biology*, **35**, 120–130.

Drahushuk, A. T., McGarrigle, B. P., Tai, H.-L. Kitareewan, S., Goldstein, J. A. and Olson, J. R, 1996, Validation of precision-cut liver slices in dynamic organ culture as an *in vitro* model for studying CYP1A1 and CYP1A2 induction. *Toxicology and Applied Pharmacology*, **140**, 393–403.

Gibson, U. E. M., Heid, C. A. and Williams, P. M., 1996, A novel method for real-time quantitative PCR. *Genome Research*, **6**, 995–1001.

Gokhale, M. S., Bunton, T. E., Zurlo, J. and Yager, J. D., 1995, Cytochrome P-450 1A1/1A2 induction, albumin secretion, and histological changes in cultured liver slices. *In vitro Toxicology*, **8**, 357–368.

Grasso, P. and Hinton, R. H., 1991, Evidence for and possible mechanisms of non-genotoxic carcinogenesis in rodent liver. *Mutation Research*, **248**, 271–290.

Heid, C. A., Stevens, J., Livak, K. J. and Williams, P. M., 1996, Real-time quantitative PCR. *Genome Research*, **6**, 986–994.

Lake, B. G., 1995, Mechanisms of hepatocarcinogenicity of peroxisome-proliferating drugs and chemicals. *Annual Review of Pharmacology and Toxicology*, **35**, 483–507.

Lake, B. G., Beamand, J. A., Japenga, A. C., Renwick, A., Davies, S. and Price, R. J., 1993, Induction of cytochrome P-450-dependent enzyme activities in cultured rat liver slices. *Food and Chemical Toxicology*, **31**, 377–386.

Lake, B. G., Charzat, C., Tredger, J. M., Renwick, A. B., Beamand, J. A. and Price, R. J., 1996, Induction of cytochrome P450 isoenzymes in cultured precision-cut rat and human liver slices. *Xenobiotica*, **26**, 297–306.

Lake, B. G. and Lewis, D. F. V., 1996, The CYP4 family. In C. Ioannides (ed.), *Cytochromes P450: Metabolic and Toxicological Aspects* (Boca Raton: CRC Press), pp. 271–297.

Lake, B. G., Price, R. J., Renwick, A. B. and Beamand, J. A., 1998, Maintenance of intracellular organization in liver slices: importance in studies of drug metabolism. In A. R. Boobis, P. Kremers, O. Pelkonen and K. Pithan (eds), *COST B1 European Symposium on the Prediction of Drug Metabolism in Man: Progress and Problems* (Luxembourg: European Community), pp. 61–76.

LeCluyse, E. L., Bullock, P. L. and Parkinson, A., 1996, Strategies for restoration and maintenance of normal hepatic structure and function in long-term cultures of rat hepatocytes. *Advanced Drug Delivery Reviews*, **22**, 133–186.

Lerche-Langrand, C. and Toutain, H. J., 2000, Precision-cut liver slices: characteristics and use for in vitro pharmaco-toxicology. *Toxicology*, **153**, 221–253.

Lowry, O. H., Rosebrough, N. J., Farr, A. L. and Randall, R. J., 1951, Protein measurement with the Folin phenol reagent. *Journal of Biological Chemistry*, **193**, 265–275.

Müller, D, Glöckner, R., Rost, M. and Steinmetzer, P., 1998, Monooxygenation, cytochrome P450-mRNA expression and other functions in precision-cut rat liver slices. *Experimental Toxicology and Pathology*, **50**, 507–513.

Müller, D., Steinmetzer, P., Pissowotzki, K. and Glöckner, R., 2000, Induction of cytochrome P450 2B1-mRNA and pentoxyresorufin *O*-dependentylation after exposure of precision-cut rat liver slices to phenobarbital. *Toxicology*, **44**, 93–97.

Murphy, L. D., Herzog, C. E., Rudick, J. B., Fojo, A. T. and Bates, S. E., 1990, Use of the polymerase chain reaction in the quantitation of *mdr*-1 gene expression. *Biochemistry*, **29**, 10351–10356.

Nakamura, T., Sakaeda, T., Ohmoto, N., Tamura, T., Aoyama, N., Shirakawa, T., Kamigaki, T., Nakamura, T., Kim, K. I., Kim, S. R., Kuroda, Y., Matsuo, M., Kasuga, M. and Okumura, K., 2002, Real-time quantitative polymerase chain reaction for MDR1, MRP1, MRP2, and CYP3A-mRNA levels in Caco-2 cell lines, human duodenal enterocytes, normal colorectal tissues, and colorectal adenocarcinomas. *Drug Metabolism and Disposition*, **30**, 4–6.

Nelson, D. R., Koymans, L., Kamataki, T., Stegeman, J. J., Feyereisen, R., Waxman, D. J., Waterman, M. R., Gotoh, O., Coon, M. J., Estabrook, R. W., Gunsalus, I. C. and Nebert, D. W., 1996, P450 superfamily: update on new sequences, gene mapping, accession numbers and nomenclature. *Pharmacogenetics*, **6**, 1–42.

Nims, R. W., Devor, D. E., Henneman, J. R. and Lubet, R. A., 1987, Induction of alkoxyresorufin *O*-dealkylases, epoxide hydrolase, and liver weight gain: correlation with tumor-promoting potential in a series of barbiturates. *Carcinogenesis*, **8**, 67–71.

Nims, R. W. and Lubet, R. A., 1996, The CYP2B subfamily. In C. Ioannides (ed.), *Cytochromes P450: Metabolic and Toxicological Aspects* (Boca Raton: CRC press), pp. 135–160.

Okey, A. B., 1990, Enzyme induction in the cytochrome P-450 system. *Pharmacology and Therapeutics*, **45**, 241–298.

Pan, J., Xiang, Q. and Ball, S., 2000, Use of a novel real-time quantitative reverse transcription-polymerase chain reaction method to study the effects of cytokines on cytochrome P450 mRNA expression in mouse liver. *Drug Metabolism and Disposition*, **28**, 709–713.

Parkinson, A., 1996, Biotransformation of xenobiotics. In C. D. Klaassen (ed.), *Casarett and Doull's Toxicology: The Basic Science of Poisons*, 5th edn (New York: McGraw-Hill), pp. 113–186.

Price, R. J., Renwick, A. B., Barton, P. T., Houston, J. B. and Lake, B. G., 1998, Influence of slice thickness and culture conditions on the metabolism of 7-ethoxycoumarin in precision-cut rat liver slices. *Alternatives to Laboratory Animals*, **26**, 541–548.

Whysner, J., Ross, P. M. and Williams, G. M., 1996, Phenobarbital mechanistic data and risk assessment: enzyme induction, enhanced cell proliferation, and tumor promotion. *Pharmacology and Therapeutics*, **71**, 153–191.

Wiesner, R., Ruegg, J. C. and Morano, I., 1992, Counting target molecules by exponential polymerase chain reaction: copy number of mitochondrial DNA in rat tissues. *Biochemical and Biophysical Research Communications*, **183**, 553–559.

XENOBIOTICA, 2002, VOL. 32, NO. 9, 749–759

Taylor & Francis
healthsciences

Characterization of mixtures of recombinant human cytochrome P450s as a screening model for metabolic stability in drug discovery

N. HAGEN*, A. K. OLSEN‡, J. V. ANDERSEN‡, J. TJØRNELUND†§ and S. H. HANSEN†

† Department of Analytical and Pharmaceutical Chemistry, The Royal Danish School of Pharmacy, DK-2100 Copenhagen, Denmark
‡ Department of Drug Metabolism, Novo Nordisk A/S, DK-2760 Måløv, Denmark

Received 22 January 2002

1. Recombinant human cytochrome P450 (*rh*CYP) has become an important screening model in drug metabolism studies due to the high cost of human and animal hepatic tissue. Until now, *rh*CYPs have been evaluated and used as separate forms, but a mixture of CYP forms comparable with the human liver could be of value in early drug discovery.

2. In the present study, *rh*CYP2C9, *rh*CYP2D6 and *rh*CYP3A4 co-expressed with reductase in *Escerichia coli* were mixed and evaluated with regards to kinetic properties (K_m and V_{max}). Furthermore, antioxidant was added to investigate whether a free radical scavenger would affect the kinetic parameters. Results were compared with data obtained in human liver microsomes (HLM).

3. Results showed a good correlation between mixed *rh*CYP data and HLM data for K_m and V_{max}. K_m varied < 3-fold between matrices for CYP2C9 and CYP3A4, whereas the K_m for CYP2D6 varied up to 4.5-fold. V_{max} differed up to 3-fold between matrices for the CYP forms investigated. However, the discrepancy in V_{max} may depend on the anticipated level of each form in HLM. The addition of antioxidant increased V_{max} for CYP2C9 and CYP2D6 by 75 and 50%, respectively, whereas V_{max} for CYP3A4 was unchanged.

4. In conclusion, the *rh*CYP mixture shows promising results as a predictor of CYP kinetic parameters. Furthermore, addition of antioxidant can in certain cases increase catalytic activity.

Introduction

In vitro drug metabolism studies, investigating the extent and route of candidate drug metabolism, have been recognized as important methods in the early discovery screening of new drug candidates (White 1998, Eddershaw and Dickins 1999). The number of new drug candidates and thereby screening expenses has increased significantly due to combinatorial chemistry and other developments in medicinal research (Roberts *et al.* 2001). Therefore, efficient low-cost metabolism study protocols are needed.

Cytochrome P450 (CYP) is the major family of Phase I drug-metabolizing enzymes in the human liver. CYP-catalysed reactions are often the main reason for drugs failing to make it to the market and therefore of great interest for the drug metabolism scientist (Bajpai and Adkison 2000). Hepatic microsomes have proven

* Author for correspondence; e-mail: nhag@novonordisk.com
§ Present address: Analytical Support, H. Lundbeck A/S, DK-2500 Valby, Denmark.

Xenobiotica ISSN 0049–8254 print/ISSN 1366–5928 online © 2002 Taylor & Francis Ltd
http://www.tandf.co.uk/journals
DOI: 10.1080/00498250210147124

to be the simplest and best suited model for high-throughput screening among the traditional metabolic stability *in vitro* models (Roberts *et al.* 2001). As the supply of human tissue is expensive and of varying quality, animal liver tissue is often used for early metabolic stability screening purposes presently. However, due to interspecies differences, a more human-like alternative would be preferable. Therefore, it is an advantage to have other *in vitro* possibilities for human metabolism screening than hepatic microsomes.

cDNA-expressed human cytochrome P450 enzymes provide a reproducible, consistent source of single CYP forms for many types of studies. Owing to its rapid and inexpensive production in, for example, bacterial systems, recombinant human CYPs (*rh*CYP) have become a common tool in drug metabolism studies (Crespi and Miller 1999). *rh*CYPs expressed in *Escherichia coli* have been reported generally to exhibit the same kinetic profiles and inhibition properties as shown in HLM experiments when incubated separately (Jung *et al.* 1997, McGinnity *et al.* 1999, Moody *et al.* 1999). However, others have reported that enzyme activity varies among the *in vitro* systems (Crespi and Penman 1997). The level of NADPH-cytochrome P450 oxidoreductase (reductase) and/or other cofactors may be suboptimal, as the catalytic activity is not solely determined by the CYP itself but, also, by the electron transport partners present. For example, the reductase:CYP ratio is higher in expression systems compared with *in vivo* thereby increasing the risk for accumulation of reactive oxygen species (Crespi and Miller 1999). Single *rh*CYPs are typically used to determine potential inhibition of the specific enzymes or they are used in the identification of specific enzymes involved in metabolism (McGinnity *et al.* 2000).

The use of single enzyme systems, relative to multi-enzyme systems, has distinct advantages and disadvantages depending on the specific application. Mixing the *rh*CYPs in levels comparable with HLM would be another approach to study metabolic stability in the early discovery phase with reduced cost and would be a way to produce 'artificial livers' representing subpopulations (e.g. alcoholics, polymorphisms). Crespi and Miller (1999) and Eddershaw and Dickins (1999) have reported a reasonable correlation to HLM metabolism profiles by this approach, but a formal evaluation has not been published. Hence, it is essential to know whether the *rh*CYPs affect the catalytic activity of each other *in vitro* and to study the conditions that are likely to affect this.

The aim of the present study was, therefore, to compare the enzyme kinetics of a mixture of *rh*CYPs to HLM, and furthermore to evaluate the effect of antioxidant addition. A simplified mixture containing *rh*CYP2C9, *rh*CYP2D6, and *rh*CYP3A4 (expressed in *E. coli*) in ratios equivalent to those reported to be present in HLM has been studied. The three forms were chosen based on their high contribution to the total CYP-catalysed metabolism of marketed drug substances. Furthermore, they represent CYPs with both high and low natural abundance in human liver.

Kinetic profiles for reactions containing both separate and mixed *rh*CYPs were compared with data obtained in HLM incubations. Also, the addition of a free radical scavenger, the antioxidant ascorbate, was investigated. Ascorbate was added to decrease possible accumulation of reactive oxygen species caused by an excess of reductase or uncoupling of the CYP catalytic cycle in order to test its effect on the enzyme kinetics.

Materials and methods

Chemicals

S-warfarin, 7-hydroxywarfarin and dextrorphan were purchased from Ultrafine Chemicals (Manchester, UK). Dextromethorphan hydrobromide, testosterone, 6 β-hydroxytestosterone and corticosterone were purchased from Sigma (St Louis, MO, USA). All other chemicals were of analytical grade.

Test systems

HLM (mixed pool, 15 donors) were obtained from In Vitro Technologies (Baltimore, MD, USA). Transformed *E. coli* co-expressing either CYP2C9, CYP2D6 or CYP3A4 with reductase were provided by the LINK consortium (a collaboration between University of Dundee, UK, and a number of pharmaceutical companies). Expression of the recombinant proteins and the subsequent preparation of *E. coli* membranes were carried out according to earlier published protocols (Pritchard *et al.* 1998, Voice *et al.* 1999).

Cytochrome P450 content was determined by CO-difference UV spectrum as described by Omura and Sato (1964). Protein content was determined by the method described by Lowry *et al.* (1951) using BSA as standard protein for quantification. Reductase activity was estimated by its ability to reduce cytochrome *c* in the presence of NADPH in a 300 mM potassium phosphate buffer at pH 7.7 (Vermilion and Coon 1978).

Testosterone 6 β-hydroxylase assay. Incubations (500 µl) contained (1) 24 pmol *rh*CYP3A4, or (2) 24 pmol *rh*CYP3A4, 3.5 pmol *rh*CYP2D6 and 15.5 pmol *rh*CYP2C9, or (3) HLM (0.2 mg protein) in 0.1 M sodium phosphate buffer (pH 7.4). Microsomal incubations furthermore contained magnesium chloride (5 mM). Testosterone dissolved in methanol was added to the incubation mixture in eight concentrations covering a range around the expected K_m (9–230 µM). The final methanol concentration was 1% v/v. For samples testing the effect of antioxidant, ascorbate was added to a final concentration of 5 mM. The incubation mixture was pre-incubated at 37 °C for 5 min before 1 mM NADPH was added to start the reaction. Incubation was carried out for 5 min at 37 °C and stopped by the addition of 3 ml dichloromethane. Corticosterone (1 µM) was subsequently added as an internal standard and the samples were vigorously shaken and centrifuged. The aqueous phase was then removed followed by evaporation of 2 ml dichloromethane phase at 35 °C in the presence of N_2. The residue was redissolved in 100 µl methanol before analysis (injection volume 35 µl). The metabolites were separated by HPLC on a LiChrospher 100 RP-18 endcapped (5 µm) 250 × 4 mm column (Merck, Darmstadt, Germany) operating at 40 °C using a gradient based on (A) methanol/water (30/70 v/v), (B) methanol/water (70/30 v/v) and (C) tetrahydrofuran/water (50/50 v/v) at a flow rate of 1 ml min^{-1}. Gradient: Isocratic from 0 to 8 min at 87% A/13% C, linear gradient from 8 to 28 min going from 87% A/13% C to 17% A/70% B/13% C and from 28 to 29 min going to 100% B. Isocratic from 29 to 34 min at 100% B, and linear gradient from 34 to 35 min going to 87% A/13% C. UV detection was performed at 240 nm. The assay was based on protocols published by Van der Hoeven (1984) and Reinerink *et al.* (1991).

S-warfarin 7-hydroxylase assay. Incubations (200 µl) contained (1) 6.2 pmol *rh*CYP2C9, or (2) 6.2 pmol *rh*CYP2C9, 1.4 pmol *rh*CYP2D6 and 9.6 pmol *rh*CYP3A4 or (3) HLM (0.08 mg protein) in 0.1 M sodium phosphate buffer (pH 7.4). Microsomal incubations furthermore contained magnesium chloride (5 mM). *S*-warfarin dissolved in acetonitrile was added to the incubation mixture in eight concentrations covering a range around the expected K_m (0.4–53 µM). The *S*-warfarin concentration was 9 µM in the experiment investigating time dependency. The final acetonitrile concentration was 0.1%. For samples testing the effect of antioxidant, ascorbate was added to a final concentration of 5 mM. The incubation mixture was pre-incubated for 5 min at 37 °C before 1 mM NADPH was added to start the reaction. Incubations were carried out at 37 °C for 15 min (or 10, 20, 30, 45, 60, 90 and 120 min for the time dependency experiment) then stopped by the addition of 100 µl 12% perchloric acid. Following centrifugation, the metabolites in the supernatant were separated by HPLC on a LiChrospher 100 RP-18 endcapped (5 µm) 250 × 4 mm column (Merck) operating at 40 °C using an eluent containing 0.5% phosphoric acid/acetonitrile (67/33 v/v) at a flow rate of 1 ml min^{-1}. The injection volume was 100 µl. Fluorescence detection at λ_{ex} 315 nm and λ_{em} 395 nm was performed. The HPLC assay was based on the method described by Lang and Böcker (1995).

Dextromethorphan O-*demethylase assay.* Incubations (200 µl) contained (1) 1.4 pmol *rh*CYP2D6, or (2) 1.4 pmol *rh*CYP2D6, 9.6 pmol *rh*CYP3A4 and 6.2 pmol *rh*CYP2C9, or (3) HLM (0.08 mg protein) in 0.1 M sodium phosphate buffer (pH 7.4). Microsomal incubations furthermore contained magnesium chloride (5 mM). Dextromethorphan dissolved in sodium phosphate buffer was added to the incubation mixture in eight concentrations covering a range around the expected K_m (0.25–22 µM). For samples testing the effect of antioxidant, ascorbate was added to a final concentration of 5 mM. The incubation mixture was then pre-incubated for 2 min at 37 °C followed by the addition of 1 mM NADPH to start the

reaction. Incubation was carried out for 10 min at 37 °C and stopped by the addition of 200 µl acetonitrile. Following centrifugation, the metabolites in the supernatant were separated by HPLC on a LiChrospher 100 CN (5 µM) 125 × 4 mm column (Merck) operating at 40 °C using an eluent containing 100 mM ammonium acetate (pH 5.0)/triethylamine/acetonitrile (80/0.06/20 v/v/v). The samples were diluted 1:1 with eluent. The injection volume was 50 µl. The flow rate was 1 ml min^{-1}. Fluorescence detection was performed at λ_{ex} 220 nm and λ_{em} 305 nm. The HPLC method was based on a protocol by Jones *et al.* (1996).

Kinetic analysis

K_m and V_{max} were determined by non-linear regression fit to Michaelis–Menten enzyme kinetics (GraphPad Prism version 3.0 for Windows, GraphPad Software, San Diego, CA, USA).

Results

CYP content and reductase activity of the *rh*CYPs used are shown in table 1. The CYP content in the recombinant systems was essentially the same for the three forms. The reductase activity in the *rh*CYP3A4 preparation was approximately 3-fold higher than in *rh*CYP2C9 and *rh*CYP2D6 preparations.

Mixture of rh*CYPs versus separate* rh*CYPs*

Comparisons of kinetic parameters between *rh*CYPs incubated separately and as a mixture with other *rh*CYPs as well as those determined in HLM incubations are shown in table 2. The data for maximal catalytic activity (V_{max}) in HLM are in this study corrected for the average content in a Caucasian human liver of the CYP in question, i.e. 18% CYP2C9, 4% CYP2D6 and 28% CYP3A4 (Guengerich 1995, Lewis 1998). In this way the results obtained in HLM incubations can be directly compared with the results obtained in the recombinant system. V_{max} for the *rh*CYP mixture was comparable with *rh*CYPs incubated separately for CYP2C9 and CYP2D6 (table 2 and figure 1). In contrast, CYP3A4 V_{max} was slightly decreased when the other *rh*CYPs were included in the incubation (table 2 and figure 1). However, V_{max} determined in separate *rh*CYP or the *rh*CYP mixture were 2–3-fold lower than obtained in HLM for both CYP2D6 and CYP3A4, whereas for CYP2C9 the results were opposite with approximately 2-fold higher V_{max} for the *rh*CYPs compared with HLM.

Apparent affinity constants (K_m) determined in single *rh*CYP forms, the *rh*CYP mixture, and HLM varied < 3-fold for CYP2C9 and CYP3A4, whereas K_m for CYP2D6 varied up to 4.5-fold between matrices (table 2).

Table 1. CYP content and reductase activity of the recombinant systems used determined by spectral analysis (CO-difference spectrum), as described by Omura and Sato (1964), and the activity towards cytochrome c (Vermillion and Coon 1978). All values are means of duplicate determinations.

CYP form	CYP-specific content (pmol mg^{-1} protein)	Reductase activity (nmol *cyt c* min^{-1} mg^{-1} protein)	Reductase activity/CYP (nmol *cyt c* min^{-1} $pmol^{-1}$ CYP)
*rh*CYP2C9	349	72	0.206
*rh*CYP2D6	306	61	0.199
*rh*CYP3A4	387	205	0.530

Table 2. K_m and V_{max} for the studied CYPs as determined in incubations including a single *rh*CYP, mixed *rh*CYPs and HLM for CYP2C9 catalysed *S*-warfarin 7-hydroxylation, CYP2D6-catalysed dextromethorphan *O*-demethylation, and CYP3A4-catalysed testosterone 6β-hydroxylation ($n = 3, \pm$SD). HLM data are corrected for the expected contant of CYP2C9 (18%), CYP2D6 (4%) and CYP3A4 (28%) (Guengerich 1995, Lewis 1998).

CYP form	Matrix	K_m (μM)	V_{max} (pmol min^{-1} nmol^{-1} relevant CYP)
CYP2C9	single *rh*CYP	7.5 ± 0.7	74 ± 2
	*rh*CYP mixture	6.4 ± 0.5	80 ± 2
	HLM	3.4 ± 1.0	37 ± 3
CYP2D6	single *rh*CYP	1.1 ± 0.1	2700 ± 100
	*rh*CYP mixture	0.6 ± 0.2	2700 ± 300
	HLM	2.7 ± 0.7	8000 ± 600
CYP3A4	single *rh*CYP	37 ± 8	21000 ± 2000
	*rh*CYP mixture	50 ± 18	14000 ± 2000
	HLM	53 ± 12	31000 ± 2000

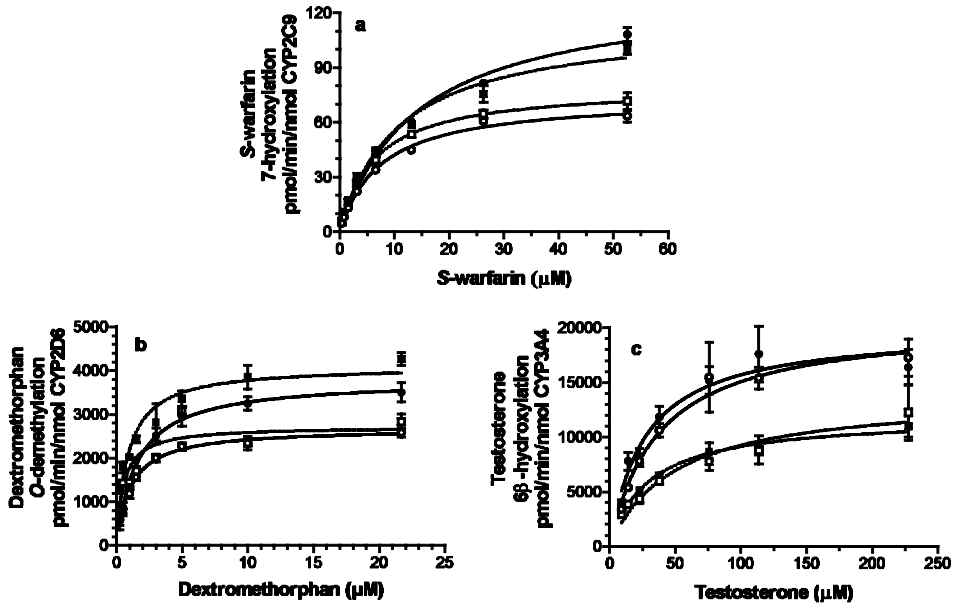


Figure 1. Effect of addition of ascorbate on (a) CYP2C9 catalysed *S*-warfarin 7-hydroxylation, (b) CYP2D6 catalysed dextromethorphan *O*-demethylation and (c) CYP3A4-catalysed testosterone 6β-hydroxylation using *rh*CYPs separately (○, solid line) and in a *rh*CYP mixture (□, dashed line). Data from experiments where ascorbate was added are presented with closed legends. Control data (no ascorbate) is presented with open legends ($n = 3 \pm$ S.D.).

Antioxidant addition

Results from *rh*CYP2C9, *rh*CYP2D6 and *rh*CYP3A4 experiments where ascorbate was added are shown fitted to the Michaelis–Menten equation in figure 1a–c. V_{max} and K_m are listed in table 3. Addition of ascorbate gave rise to an increased V_{max} for *rh*CYP2C9 (about 75%) and *rh*CYP2D6 (about 50%) incubated separately. Likewise, an increase was observed for K_m when ascorbate was added to *rh*CYP2C9 (2-fold) and *rh*CYP2D6 (50%). Results obtained in experiments using the *rh*CYP mixture were comparable with those obtained using the separate *rh*CYPs. For *rh*CYP3A4, on the other hand, ascorbate addition appeared to result

Table 3. Effect of ascorbate addition on K_m and V_{max} as determined in *rh*CYPs both separately and mixed for CYP2C9-catalysed *S*-warfarin 7-hydroxylation, CYP2D6-catalysed dextromethorphan *O*-demethylation and CYP3A4 catalysed testosterone 6 β-hydroxylation ($n = 3 \pm$ SD).

CYP form	Matrix	K_m (μM)	V_{max} (pmol min^{-1} nmol^{-1} relevant CYP)
CYP2C9	single *rh*CYP	14 ± 2	130 ± 6
	*rh*CYP mixture	11 ± 2	115 ± 6
CYP2D6	single *rh*CYP	1.6 ± 0.2	3800 ± 100
	*rh*CYP mixture	0.9 ± 0.2	4100 ± 200
CYP3A4	single *rh*CYP	27 ± 8	20000 ± 2000
	*rh*CYP mixture	30 ± 7	12000 ± 1000

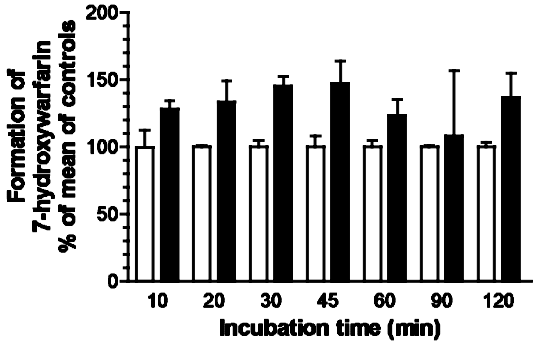


Figure 2. Time dependence of the effect of ascorbate on the 7-hydroxylation of *S*-warfarin in *rh*CYP mixture ($n = 3 \pm$ SD). Controls (no ascorbate added) are presented as open bars.

in a greater affinity towards testosterone (K_m decreased) whereas no change in V_{max} was observed. Experiments to determine the potential time-dependent effect of ascorbate addition in prolonged incubations versus short incubations showed no time dependency (figure 2).

Discussion

The yields of *rh*CYP in the *E. coli* expression system are similar to those reported by Pritchard *et al.* (1997, 1998) and McGinnity *et al.* (1999) for similar cDNA-constructs from the LINK consortium. The reductase activities were typically between 100 and 600 nmol cytochrome *c* reduced min^{-1} mg^{-1} protein in the above-mentioned papers, thus the reductase activities reported here are slightly lower for the *rh*CYP2C9 and *rh*CYP2D6 membrane preparations (72 and 61 nmol cytochrome *c* reduced min^{-1} mg^{-1} protein, respectively) as shown in table 1.

Mixture of rh*CYPs versus separate* rh*CYPs*

The mixture of *rh*CYPs investigated was based on the relative abundance of the CYP2C9, CYP2D6 and CYP3A4 in a Caucasian human liver. Generally, CYP2C9 is reported to account for 15–20% of the total cytochrome P450 content, whereas CYP2D6 and CYP3A4 have been reported to account for 1–5% and approximately 30%, respectively (Shimada *et al.* 1994, Guengerich 1995, Inoue *et al.* 1997, Lewis 1998, Pelkonen *et al.* 1998). However, human hepatic tissue is subject to large

interindividual differences in CYP expression due to both genetic polymorphisms and induction/inhibition caused by environmental exposures or drug treatments. Polymorphisms have been reported for CYP2C9 (Crespi and Miller 1997, Kimura *et al*. 1998, Yamazaki *et al*. 1998), CYP2D6 (Gut *et al*. 1986, Köhler *et al*. 1997), and recently for CYP3A4 (Eiselt *et al*. 2001, Dai *et al*. 2001). CYP2D6 polymorphisms are due to both inactive alleles (Köhler *et al*. 1997) as well of gene multiplication (Ingelman-Sundberg 1997) leading to an expression variability of 1000-fold or more (Guengerich 1995). CYP2C9 allelic variants have been shown to change the catalytic activity as well as the substrate affinity rather than affect the expression level (Crespi and Miller 1997, Inoue *et al*. 1997). Among the CYP3A4 allelic variants, one is reported to be expressed at significantly lower levels than wild type CYP3A4, and for another variant an altered testosterone metabolite profile is observed (Eiselt *et al*. 2001). With regard to induction, several inducers of CYP2C9 and CYP3A4 are known (e.g. barbiturates and rifampicin), but no induction of CYP2D6 has been detected so far. In an attempt to minimize the large interindividual differences in our study, a pool of 15 different donors was used. However, a comparison of the catalytic activities reported by the supplier of 14 mixed pools of HLM revealed a 10-fold variation with regards to CYP2C9 catalytic activity, CYP2D6 catalytic activity varied 4-fold, and CYP3A4 catalytic activity varied 5-fold (data not shown). Furthermore, it has to be kept in mind that even larger variability is observed between individuals. The overall levels of total CYP vary only a few fold among most humans (Guengerich 1995), which was also reflected by the fact that the total CYP content varied < 3-fold and reductase activity varied < 4-fold in the above-mentioned mixed pools of HLM. In short, the CYP ratios chosen, i.e. 18% CYP2C9, 4% CYP2D6 and 28% CYP3A4 (Guengerich 1995, Lewis 1998), reflect an 'average' Caucasian liver, without being an absolute standard.

The kinetic properties (K_m and V_{max}) of *rh*CYP2C9 were not significantly affected by the addition of CYP2D6 and CYP3A4 (table 2 and figure 1a). Furthermore, these kinetic parameters are within 2-fold range of the HLM data. This suggests that *rh*CYP2C9 co-expressed with reductase can be mixed with other *rh*CYPs for kinetic investigations without affecting the kinetic parameters. CYP2D6 substrate affinity and maximal catalytic activity show a good correlation between *rh*CYP2D6 and the *rh*CYP mixture. K_m determined in *rh*CYP2D6 and the *rh*CYP mixture were, however, low compared with data obtained in incubations with HLM. V_{max} determinations in *rh*CYP2D6 and the *rh*CYP mixture were 3-fold lower than in HLM (table 2). Both K_m and V_{max} determined in *rh*CYP3A4 were within 2-fold of the values obtained in HLM (table 2). For *rh*CYP3A4, V_{max} was somewhat decreased by the addition of *rh*CYP2C9 and *rh*CYP2D6 (table 2 and figure 1c). On the contrary, the K_m for CYP3A4 was not affected. It could be speculated that competition for reductase takes place as shown by Li *et al*. (1999). This latter group co-expressed *rh*CYP2D6 and *rh*CYP3A4 in the same system. By adding substrate for both CYP forms it was demonstrated that competition did take place. The experiments described in the current paper were, however, different as CYP2D6 and CYP3A4 were expressed in separate systems. Furthermore, one substrate only was added in each experiment. The decrease in CYP3A4 activity upon mixing forms is rather surprising considering that more *rh*CYP3A4 is present in the *rh*CYP mixture than *rh*CYP2C9 and *rh*CYP2D6 in total. On the other hand, it may not be surprising that CYP3A4 seems to be the one enzyme

showing peculiar kinetics when considering various reports on CYP3A4 complexity such as non Michaelis–Menten kinetics and variability in kinetic behaviour due to cofactors such as cytochrome b_5 or the use of different buffers (Korzekwa *et al.* 1998, Houston and Kenworthy 2000).

The above-mentioned comparisons of *rh*CYP catalytic activity and substrate affinity to values obtained in HLM agree with earlier published reports where separate *rh*CYPs were compared with HLM. Generally, the variation between the two *in vitro* models are reported to be up to 3-fold with regard to K_m and up to 6-fold with regard to V_{max} (Rettie *et al.* 1992, Yamazaki and Shimada 1997, Von Moltke *et al.* 1998, McGinnity *et al.* 1999). The higher variability between V_{max} is most likely due to the above-mentioned possible discrepancy between anticipated and real expression level of the specific forms in the HLM used. These variations do not seem to be increased when the *rh*CYPs are mixed.

Crespi and Miller (1999) mixed *rh*CYPs according to another approach where catalytic activity was used as a marker and the *rh*CYP mixture was 'formulated to achieve ratios of individual enzyme activities similar to those observed in pooled HLMs'. The latter authors have reported a reasonable correlation of the catalytic activity of pooled HLM preparations with catalytic activities of the *rh*CYP mixtures generally being 2-fold higher than for HLM. Furthermore, Crespi and Miller (1999) stated that individually expressed *rh*CYPs can be 'predictably combined to prepare mixtures whose profile of metabolic activities is similar to pooled HLMs'.

Antioxidant addition

The level of NADPH-cytochrome P450 oxidoreductase (reductase) and/or other cofactors could be suboptimal, as the catalytic activity is not solely determined by the CYP itself but, also, by the electron transport partners present. For example, the reductase/CYP ratio is higher in expression systems compared with liver microsomes (Crespi and Miller 1999) thereby increasing the possibility of accumulation of reactive oxygen species. Calculated from data of Venkatakrishnan *et al.* (2000), the reductase to CYP ratio is about 1:5 or more in HLM depending on the CYP level/induction state compared with the typical 1:2 or more ratio in the *E. coli* expression system. This renders the reductase to be the limiting component in HLM, as the different CYP forms may have to compete for the reductase. However, reductase is known to transfer electrons much faster than CYP can use them (Parkinson 1996) and could thereby make up for the difference between CYP and reductase expression. Furthermore, the low reductase level may be a protective measure by the cells to avoid one-electron reduction reactions catalysed by reductase (Parkinson 1996). The possible accumulation of reactive oxygen species could also be caused by uncoupling of the catalytic cycle, e.g. oxygen would be released as a superoxide anion if the catalytic cycle was interrupted following introduction of the first electron (Parkinson 1996). Such uncoupling could be speculated to be more likely to occur in the 'foreign' environment of an *E. coli* membrane than in HLM, the native environment of human CYP.

Addition of an antioxidant to the *rh*CYPs and the *rh*CYP mixture was therefore expected to result in an increase in enzyme stability, as the negative influence of accumulating free radicals would be suppressed. Thereby, the V_{max} for the reactions would be anticipated to increase due to more active enzyme available.

*rh*CYP2C9 and *rh*CYP2D6 both exhibited an increased V_{max} when the antioxidant ascorbate was added to the incubation mixture (figure 1). The increase was about 75% for *S*-warfarin 7-hydroxylation and about 50% for dextromethorphan *O*-demethylation. Thereby, *rh*CYP2C9 V_{max} was further increased to a higher level than observed in HLM; *rh*CYP2D6 V_{max} was still 2-fold below the HLM V_{max} level. These changes all fit with the hypothesis of the free radical suppression described above. K_m was also affected demonstrating a 2-fold increase for both *rh*CYP2C9 and *rh*CYP2D6. In contrast, *rh*CYP3A4 V_{max} in testosterone incubations was not affected by the addition of ascorbate, although the reductase activity of the *rh*CYP3A4 preparation was slightly higher than for the other two *rh*CYP preparations. The affinity of *rh*CYP3A4 was, on the other hand, slightly increased (table 3).

The effect of addition of antioxidant could possibly be related to incubation time, i.e. there was no effect towards *rh*CYP3A4 catalytic activity (5-min incubation) whereas *rh*CYP2C9 catalytic activity (15-min incubation) was substantially affected. However, there was no increase of the effect of ascorbate when the incubation time was prolonged (figure 2). Therefore, the effect of ascorbate appears to be related to the specific CYP form or specific substrate metabolism rather than the experimental procedure.

In conclusion, K_m and V_{max} determinations in *rh*CYP mixtures produce results comparable with those obtained in HLM. The *rh*CYP mixture would, therefore, even with more CYP forms incorporated, be an *in vitro* model to use in early drug discovery screenings of metabolic stability with the advantages of consisting of human enzymes, being lower-cost, well-defined, reproducible and biohazard-free. Finally, addition of antioxidant can, in certain cases, be used as a means to obtain an increase in V_{max}.

Acknowledgements

Portions of the paper were presented at the 9th and 10th North American ISSX Meetings in October 1999 and October 2000.

References

Bajpai, M. and Adkison, K. K., 2000, High-throughput screening for lead optimization: a rational approach. *Current Opinions in Drug Discovery and Development*, **3**, 63–71.

Crespi, C. L. and Miller, V. P., 1997, The R144C change in the CYP2C9*2 allele alters interaction of the cytochrome P450 with NADPH:cytochrome P450 oxidoreductase. *Pharmacogenetics*, **7**, 203–210.

Crespi, C. L. and Miller, V. P., 1999, The use of heterologously expressed drug metabolizing enzymes – state of the art and prospects for the future. *Pharmacology and Therapeutics*, **84**, 121–131.

Crespi, C. L. and Penman, B. W., 1997, Use of cDNA-expressed human cytochrome P450 enzymes to study potential drug–drug interactions. *Advances in Pharmacology*, **43**, 171–188.

Dai, D., Tang, J., Rose, R., Hodgson, E., Bienstock, R. J., Mohrenweiser, H. W. and Goldstein, J. A., 2001, Identification of variants of CYP3A4 and characterization of their abilities to metabolise testosterone and chlorpyrifos. *Journal of Pharmacology and Experimental Therapeutics*, **299**, 825–831.

Eddershaw, P. J. and Dickins, M., 1999, Advances in *in-vitro* drug metabolism screening. *Pharmaceutical Science and Technology Today*, **2**, 13–19.

Eiselt, R., Domanski, T. L., Zibat, A., Mueller, R., Presecan-Siedel, E., Hustert, E., Zanger, U. M., Brockmoller, J., Klenk, H.P., Meyer, U. A., Khan, K. K., He, Y.A., Halpert, J. R. and Wojnowski, L., 2001, Identification and functional characterization of eight CYP3A4 protein variants. *Pharmacogenetics*, **11**, 447–458.

Guengerich, F. P., 1995, Human cytochrome P450 enzymes. In P. R. Ortiz de Montellano (ed.), *Cytochrome P450: Structure, Mechanism, and Biochemistry*, 2nd edn (New York: Plenum), pp. 473–535.

Gut, J., Catin, T., Dayer, P., Kronbach, T., Zanger, U. and Meyer, U. A., 1986, Debrisoquine/sparteine-type polymorphism of drug oxidation. *Journal of Biological Chemistry*, **261**, 11734–11743.

Houston, J. B. and Kenworthy, K. E., 2000, *In vitro–in vivo* scaling of CYP kinetic data not consistent with the classical Michaelis–Menten model. *Drug Metabolism and Disposition*, **28**, 246–254.

Inoue, K., Yamazaki, H., Imiya, K., Akasaka, S., Guengerich, F. P. and Shimada, T., 1997, Relationship between CYP2C9 and CYP2C19 genotypes and tolbutamide methyl hydroxylation and *S*-mephenytoin 4′-hydroxylation activities in livers of Japanese and Caucasian populations. *Pharmacogenetics*, **7**, 103–113.

Jones, D. R., Gorski, J. C., Hamman, M. A. and Hall, S. D., 1996, Quantification of dextromethorphan and metabolites: a dual phenotypic marker for cytochrome P450 3A4/5 and 2D6 activity. *Journal of Chromatography* B, **678**, 105–111.

Jung, F., Richardson, T. H., Raucy, J. L. and Johnson, E. F., 1997, Diazepam metabolism by cDNA-expressed human 2C P450s. *Drug Metabolism and Disposition*, **25**, 133–139.

Kimura, M., Ieiri, I., Mamiya, K., Urae, A. and Higuchi, S., 1998, Genetic polymorphism of cytochrome P450s, CYP2C19, and CYP2C9 in a Japanese population. *Therapeutic Drug Monitoring*, **20**, 243–247.

Kohler, D., Härtter, S., Fuchs, K., Sieghart, W. and Hiemke, C., 1997, CYP2D6 genotype and phenotyping by determination of dextromethorphan and metabolites in serum of healthy controls and of patients under psychotropic medication. *Pharmacogenetics*, **7**, 453–461.

Korzekwa, K. R., Krishnamachary, N., Shou, M., Ogai, A., Parise, R. A., Rettie, A. E., Gonzalez, F. J. and Tracy, T. S., 1998, Evaluation of atypical cytochrome P450 kinetics with two-substrate models: evidence that multiple substrates can simultaneously bind to cytochrome P450 active sites. *Biochemistry*, **37**, 4137–4147.

Lang, D. and Böcker, R., 1995, Highly sensitive and specific high-performance liquid chromatographic analysis of 7-hydroxywarfarin, a marker for human cytochrome P4502C9 activity. *Journal of Chromatography* B, **672**, 305–309.

Lewis, D. F. V., 1998, The CYP2 family: models, mutants and interactions. *Xenobiotica*, **28**, 617–661.

Li, D. N., Pritchard, M. P., Hanlon, S. P., Burchell, B., Wolf, C. R. and Friedberg, T., 1999, Competition between cytochrome P450 isozymes for NADPH-cytochrome P-450 oxidoreductase affects drug metabolism. *Journal of Pharmacology and Experimental Therapeutics*, **289**, 661–667.

Lowry, O. H., Rosebrough, N. J., Farr, A. L. and Randall, R. J., 1951, Protein measurement with the Folin phenol reagent. *Journal of Biological Chemistry*, **193**, 265–275.

McGinnity, D. F., Griffin, S. J., Moody, G. C., Voice, M., Hanlon, S., Friedberg, T. and Riley, R. J., 1999, Rapid characterization of the major drug-metabolizing human hepatic cytochrome P-450 enzymes expressed in *Escherichia coli*. *Drug Metabolism and Disposition*, 27, 1017–1023.

McGinnity, D. F., Parker, A. J., Soars, M. and Riley, R. J., 2000, Automated definition of the enzymology of drug oxidation by the major human drug metabolizing cytochrome P450s. *Drug Metabolism and Disposition*, **28**, 1327–1334.

Moody, G. C., Griffin, S. J., Mather, A. N., McGinnity, D. F. and Riley, R. J., 1999, Fully automated analysis of activities catalysed by the major human liver cytochrome P450 (CYP) enzymes: assessment of human CYP inhibition potential. *Xenobiotica*, **29**, 53–75.

Omura, T. and Sato, R., 1964, The carbon monoxide-binding pigment of liver microsomes. *Journal of Biological Chemistry*, **239**, 2370–2378.

Parkinson, A., 1996, Biotransformation of xenobiotics. In C. D. Klaassen (ed.), *Casarett & Doull's Toxicology: The Basic Science of Poisons*, 5th edn (New York: McGraw-Hill), pp. 113–186.

Pelkonen, O., Mäenp, J., Taavitsainen, P., Rautio, A. and Raunio, H., 1998, Inhibition and induction of human cytochrome P450 (CYP) enzymes. *Xenobiotica*, **28**, 1203–1253.

Pritchard, M. P., Glancey, M. J., Blake, J. A. R., Gilham, D. E., Burchell, B., Wolf, C. R. and Friedberg, T., 1998, Functional co-expression of CYP2D6 and human NADPH-cytochrome P450 reductase in *Escherichia coli*. *Pharmacogenetics*, **8**, 33–42.

Pritchard, M. P., Ossetian, R., Li, D. N., Henderson, C. J., Burchell, B., Wolf, C. R. and Friedberg, T., 1997, A general strategy for the expression of recombinant human cytochrome P450s in *Escherichia coli* using bacterial signal peptides: expression of CYP3A4, CYP2A6, and CYP2E1. *Archives of Biochemistry and Biophysics*, **345**, 342–354.

Reinerink, E. J., Doorn, L., Jansen, E. H. and Van Iersel, A. A., 1991, Measurement of enzyme activities of cytochrome P-450 isoenzymes by high-performance liquid chromatographic analysis of products. *Journal of Chromatography*, **553**, 233–241.

Rettie, A. E., Korzekwa, K. R., Kunze, K. L., Lawrence, R. F., Eddy, A. C., Aoyama, T., Gelboin, H. V., Gonzalez, F. J. and Trager, W. F., 1992, Hydroxylation of warfarin by human cDNA-expressed cytochrome P450: a role for P-4502C9 in the etiology of (*S*)-warfarin–drug interactions. *Chemical Research in Toxicology*, **5**, 54–59.

Roberts, S. A., 2001, High-throughput screening approaches for investigating drug metabolism and pharmacokinetics. *Xenobiotica*, **31**, 557–589.

Shimada, T., Yamazaki, H., Mimura, M., Inui, Y. and Guengerich, F. P., 1994, Interindividual variation in human liver cytochrome P-450 enzymes involved in the oxidation of drugs, carcinogens and toxic chemicals: studies with liver microsomes of 30 Japanese and 30 Caucasians. *Journal of Pharmacology and Experimental Therapeutics*, **270**, 414–423.

Van der Hoeven, T., 1984, Assay of hepatic microsomal testosterone hydroxylases by high performance liquid chromatography. *Analytical Biochemistry*, **138**, 57–65.

Venkatakrishnan, K., Von Moltke, L. L., Court, M. H., Harmatz, J. S., Crespi, C. L. and Greenblatt, D. J., 2000, Comparison between cytochrome P450 (CYP) content and relative activity approaches to scaling from cDNA-expressed CYPs to human liver microsomes: ratios of accessory proteins as sources of discrepancies between the approaches. *Drug Metabolism and Disposition*, **28**, 1493–1504.

Vermilion, J. L. and Coon, M. J., 1978, Purified liver microsomal NADPH-cytochrome P450 reductase. *Journal of Biological Chemistry*, **253**, 2694–2704.

Voice, M. W., Zhang, Y., Wolf, C. R., Burchell, B. and Friedberg, T., 1999, Effects of human cytochrome b_5 on CYP3A4 activity and stability *in vivo*. *Archives of Biochemistry and Biophysics*, **366**, 116–124.

Von Moltke, L. L., Greenblatt, D. J., Grassi, J. M., Granda, B. W., Venkatakrishnan, K., Schmider, J., Harmatz, J. S. and Shader, R. I., 1998, Multiple human cytochromes contribute to biotransformation of dextromethorphan *in-vitro*: role of CYP2C9, CYP2C19, CYP2D6, and CYP3A. *Journal of Pharmacy and Pharmacology*, **50**, 997–1004.

White, R. E., 1998, Short- and long-term projections about the use of drug metabolism in drug discovery and development. *Drug Metabolism and Disposition*, **26**, 1213–1216.

Yamazaki, H. and Shimada, T., 1997, Progesterone and testosterone hydroxylation by cytochromes P450 2C19, 2C9, and 3A4 in human liver microsomes. *Archives of Biochemistry and Biophysics*, **346**, 161–169.

Yamazaki, H., Inoue, K. and Shimada, T., 1998, Roles of two allelic variants (Arg144Cys and Ile359Leu) of cytochrome P4502C9 in the oxidation of tolbutamide and warfarin by human liver microsomes. *Xenobiotica*, **28**, 103–115.

XENOBIOTICA, 2002, VOL. 32, NO. 9, 761–770

Taylor & Francis
healthsciences

Pharmacokinetic and mass balance study of unlabelled and ^{14}C-labelled emedastine difumarate in healthy volunteers

M. BRUNNER†, K. KLETTER‡, A. ASSANDRI§, M. ERMANNO CORRADO§, H. G. EICHLER† and M. MÜLLER†*

Departments of ‡Clinical Pharmacology, Division of Clinical Pharmacokinetics and ‡Nuclear Medicine, University of Vienna Medical School, Allgemeines Krankenhaus, Währinger Gürtel 18–20, A-1090 Vienna, Austria
§CROSS S.A., Arzo, Switzerland

Received 17 October 2001

1. In a mass balance study, six healthy male volunteers received a single oral dose of 4 mg ^{14}C-labelled emedastine difumarate. The pharmacokinetics of the total radioactivity and unchanged drug were assessed over 48 h. Urinary and faecal excretion were measured over 120 h. Additionally, urinary metabolites were investigated.

2. In a single- and multiple-dose pharmacokinetic study, nine male and nine female healthy volunteers received 2 mg oral emedastine difumarate b.i.d. or 4 mg o.d. for 7 consecutive days. The plasma pharmacokinetics were assessed on day 1 and at steady-state.

3. The mass balance study demonstrated almost complete gastrointestinal absorption of the administered dose. A total of 94.2% of the radioactivity was eliminated via the kidneys. Unchanged emedastine in the urine accounted for $< 5\%$ of dose. 5-Hydroxy, 6-hydroxy and *N*-oxide metabolites previously identified in the Japanese were present in Caucasian subjects.

4. AUC after single and multiple dosing were dose-proportional. On day 7, no statistical difference in AUC_{0-24} could be detected between the two regimens, with $AUC = 70.6 \pm 36.1$ and 71.7 ± 52.3 ng h ml^{-1}, respectively. There were no gender differences in the pharmacokinetics of emedastine.

5. The results corroborate the use of emedastine in a Caucasian population and support the extrapolation of safety and efficacy data from Asians to Caucasians.

Introduction

Emedastine difumarate [1-(2-ethoxyethyl)-2-(hexahydro-4-methyl-1-H-1,4-diazepin-1-yl) benzimidazole difumarate], a second-generation H_1-receptor antagonist, belongs to the same chemical class as other new antihistmines, e.g. mizolastine (Slater *et al.* 1999). Emedastine has been shown to suppress anaphylactic shock, passive cutaneous anaphylaxis and allergic rhinitis in various experimental models in rat and guinea pig (Fukuda *et al.* 1984a, b, Saito *et al.* 1987). In man, emedastine qualified as a suitable alternative to reference H_1-receptor antagonists due to its high therapeutic index and less potent effects on the circulation and central nervous system compared with established antihistamines (Tasaka *et al.* 1986, Saito *et al.* 1988a, b). Since 1993, emedastine has been licensed in Japan for the use in allergic rhinitis and urticaria. Currently, two dosages are

* Author for correspondence; e-mail: markus.mueller@univie.ac.at

Xenobiotica ISSN 0049–8254 print/ISSN 1366–5928 online © 2002 Taylor & Francis Ltd
http://www.tandf.co.uk/journals
DOI: 10.1080/00498250210143001

administered, i.e. 2 mg b.i.d. or 4 mg o.d., both providing 24-h effectiveness (Jansen *et al.* 2000).

To date, most information on the pharmacokinetics and tolerability of emedastine in man has been obtained from young Asian volunteers (Nakajima *et al.* 1989, Amada *et al.* 1990). Although several studies were recently conducted in Caucasians (Jansen *et al.* 2000, Herranz *et al.* 2001, Joukhadar *et al.* 2001), some steps in the cascade of absorption, metabolism and excretion of emedastine still need to be investigated for a comprehensive understanding of its pharmacokinetics in Caucasians. Therefore, a mass-balance study was conducted and both total radioactivity and unchanged drug were measured in blood, plasma, urine and faeces after a single oral dose of 4 mg ^{14}C-labelled emedastine as the immediate-release formulation. Thereafter, the plasma pharmacokinetics of the two approved dosage regimens, i.e. slow-release formulations, were compared after single-dose administration and at steady-state in male and female Caucasian volunteers.

Materials and methods

The studies were approved by the local ethics committee. All volunteers were given a detailed description of their study and provided informed consent. Studies were performed in accordance with the Declaration of Helsinki and the Good Clinical Practice Guideline of the European Commission (EC-GCP guideline).

Healthy volunteers

Two studies were conducted in different study populations. The first involved six healthy male volunteers (mean age 28 ± 5 (SD), mean weight 72 ± 8 kg, mean height 177 ± 8 cm). The second involved nine male and nine female, healthy, drug-free, normal weight volunteers (mean age 27 ± 5 years, mean weight 71 ± 7 kg and 59 ± 10 kg, mean height 176 ± 5 cm and 166 ± 6 cm for men and women, respectively). Each volunteer was subjected to a screening examination including a medical history, physical examination, 12-lead ECG, blood pressure, complete blood count with differential blood analysis, urinalysis, urine drug screen, clinical blood chemistry, blood coagulation tests, HBs antigen and HIV antibody test. Subjects were excluded if they were taking any prescribed medication or OTC drugs within a period of two weeks before the study. For each study day, volunteers were fasted for 12 h before the start of the experiments.

Overall study design and plan of trial

The first study was carried out as a single-centre, uncontrolled trial involving six healthy young male volunteers who received a single oral dose of 4 mg ^{14}C-labelled emedastine difumarate. Volunteers attended the Clinical Trial Center the evening before drug administration and remained under observation for 48 h post-dose. ^{14}C-labelled emedastine difumarate was administered as powder in one capsule between 08:00 and 10:00 hours. Blood samples were taken up to 48 h post-dose. Urine and faeces were collected during predefined intervals up to 120 h post-dose. Upon discharge, volunteers were advised to continue urine and faeces collection and to return to the Clinical Trial Center for each of the next 3 days to deliver urine and faeces and to receive the next collection containers.

The second study was conducted as a single-centre, randomized, open, two-way crossover trial involving nine healthy female and nine healthy male volunteers. Each volunteer participated in both treatment phases and was randomly assigned to receive either emedastine difumarate slow-release capsules in a dose of 2 mg twice daily or 4 mg once daily for 7 consecutive days. Treatment phases were separated by a 14-day washout period. Capsules were administered at 08:00 hours (±1 h) after an overnight fast and at 20:00 hours (±1 h) (2 mg b.i.d. treatment phase only). Standardized light meals were given 2 and 5 h after the morning dose and 1 h after the evening dose of the 2 mg b.i.d. regimen. Plasma pharmacokinetics of emedastine were assessed after morning administration on days 1 and 7 of each study period. Volunteers were hospitalized from the evening before the first administration up to 25 h after the last morning dose.

Drugs and metabolites

Emedastine difumarate and ^{14}C-labelled emedastine difumarate were provided by Kanebo Pharmaceuticals Ltd (Osaka, Japan), represented for this product in the EU by Saluc Pharma SA (Geneva,

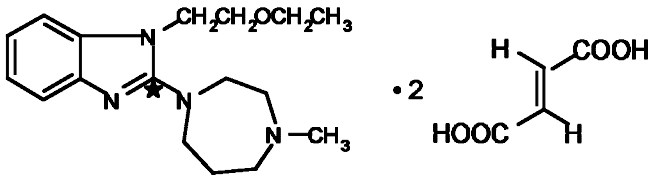


Figure 1. Structural formula.

Switzerland). The study medication included slow-release capsules containing 2 or 4 mg of the drug, while ^{14}C-emedastine difumarate was provided as 4 mg immediate-release capsules. Chemical purity of emedastine was > 99%. Radiochemical purity of ^{14}C-emedastine (> 97.7%) was assessed by thin-layer chromatography (TLC). The administered radioactive dose averaged 68.74 ± 5.76 μCi (0.947 ± 0.138 μCi kg^{-1}). This value was established based on the EURATOM directives 80/836, 84/467, 84/466, 89/618, 90/641 and 92/3 and in compliance with the general guidelines of the WHO.

The structural formula is as shown in figure 1 (★^{14}C). For the synthesis route see Awata *et al.* (1986).

In addition, 5-hydroxy and 6-hydroxy emedastine were provided as reference metabolites by Kanebo.

Sampling of venous plasma

- Venous plasma samples were drawn from a forearm vein using an indwelling catheter with a switch valve. Blood samples were collected into lithium heparinized tubes at the following times after the morning administration of each study period:
- Mass balance study: 0 (predose), 0.25, 0.5, 1, 1.5, 2, 3, 4, 5, 6, 8, 10, 12, 24, 32 and 48 h.
- 4 mg o.d. kinetics: 0 (predose), 0.5, 1, 2, 3, 4, 6, 8, 10, 12, 16 and 24 h post-dose.
- 2 mg b.i.d kinetics: 0 (predose), 0.5, 1, 2, 3, 4, 6, 8, 10, 12, 12.5, 13, 14, 15, 16, 18, 20 and 24 h (the evening dose was given 12 h after the morning dose).

The specimens were immediately centrifuged at 4°C at 2500g for 5 min. The plasma obtained was immediately frozen and stored at −20°C until analysis.

Urine and faeces collection (mass balance study)

Urine. The total volume of urine excreted during the following intervals after administration was collected: predose blank, 0–4, 4–8, 8–12, 12–24, 24–48, 48–72, 72–96 and 96–120 h. The volume of each urine sample, up to 120 h, was measured and stored at −20°C.

Faeces. The total amount of faeces obtained during the following intervals after administration was collected: predose blank, 0–24, 24–48, 48–72, 72–96 and 96–120 h. Faeces samples, stored frozen at −20°C, were weighed, diluted with water (1:4 w/v) homogenized and the final volume was measured.

Sample analyses

Emedastine. The concentration of emedastine was measured by radioreceptor assay (RRA) with [pyridinyl-5-^{3}H] pyrilamine tracer to histamine receptors of guinea pig cerebellum membrane as described by Hamada *et al.* (1987). Between assay precision was < 30% (concentration range of the calibration line: 0.025–2.5 ng ml^{-1}). Limit of quantification was 0.1 ng ml^{-1} emedastine base. Regarding RRA specificity, two emedastine metabolites (i.e. 1-(2-ethoxyethyl)-2-(1-homopiperazinyl)benzimidazole and 1-(2-ethoxyethyl)-5-hydroxy-2-(4-methyl-1-homopiperazinyl)benzimidazole showed a cross-reactivity of 28.6 and 21.1% respectively. The precision of the duplicate measurements was high: all CVs averaged 4.3 ± 0.74%. The lower and higher limits of quantification were established between 0.1 and 1.6 ng ml^{-1}. Emedastine in plasma was stable after 1 year of storage at −20°C. Samples in the present study were stored for a maximum of 5 months.

Total radioactivity. Determination of radioactivity in blood, plasma, urine and faeces was performed by liquid scintillation counting using a WALLAC 1410 liquid scintillation counter with an external standard source to correct for sample quenching. All biological samples were counted for 20 min or up to a statistical confidence level of 2σ error, < 5%. Radioactivity amount/concentration was given as emedastine equivalents (i.e. mg eq./ng eq. ml^{-1}).

Sample preparation

Blood. A total of 1 ml BTS-450/isopropanol (1:2 v/v) was added to 0.15 ml blood and incubated for 1 h at 40°C. BTS-450, a quaternary ammonium hydroxide (0.5 N) in toluene, is a tissue solubilizer, rapidly digesting tissues and tissue homogenates. Afterwards, 0.5 ml 30% hydrogen peroxide was added dropwise while swirling. Samples were then incubated for 60 min at 40°C. Finally, 10 ml Ready Safe scintillation cocktail containing glacial acetic acid (7 ml l^{-1}) were added and the samples counted.

Plasma. A total of 0.5 ml 0.1 N HCl and 10 ml Ready Safe were added to a 0.5-ml aliquot of each plasma sample. After shaking samples were counted.

Urine. A total of 10 ml Ready Safe was added to an aliquot (0.5–1 ml) of each urine sample. Thereafter samples were shaken and counted.

Faeces. Samples were homogenized by Stomacher® 3500 (SEWARD Medical Ltd, London, UK) after adding distilled water 4:1 (v/w). 0.5 ml water was added to 0.2 ml faeces homogenate and rehydrated for 1 h. Thereafter, the following steps were performed: (1) addition of 1 ml BTS-450 with swirling; (2) incubation for 1–2 h at 40°C; (3) addition of 0.5 ml isopropanol with stirring; (4) addition of 0.2 ml 30% hydrogen peroxide; and (5) 10 min at room temperature and then a second 2-h incubation period at 40°C. The dissolved samples were then diluted with 5 ml water and added 10 ml Ready Safe containing 7 ml l^{-1} glacial acetic acid. After gentle shaking, the stable gel was counted.

Metabolites profile. In the mass balance study, 0–4-, 4–8-, 8–12- and 12–24-h urine samples from each subject were taken to investigate the pattern of main emedastine urinary metabolites (5-hydroxy, 6-hydroxy emedastine and their conjugated metabolites and emedastine *N*-oxide). Urine analysis was carried out by two-dimensional TLC according to Wada *et al.* (1990).

Data analysis

The pharmacokinetic analysis was carried out according to a compartment model-independent analysis. The individual plasma (blood) concentration of radioactivity (ng eq. ml^{-1}) and emedastine (ng ml^{-1}) versus time (h) curves underwent a non-linear fitting procedure using Kinetica™ software (v.2.02.200, InnaPhase Corporation, Philadelphia, PA, USA).

The following pharmacokinetic parameters were assessed either after a single dose or at steady-state: time to reach peak concentration after morning administration ($t_{maxa.m.}$); time to reach peak concentration after evening administration ($t_{maxp.m.}$); peak concentration after morning administration ($C_{maxa.m.}$); peak concentration after evening administration ($C_{maxp.m.}$); minimum plasma concentration (C_{min}), steady-state average concentration ($C_{average}$,), peak trough fluctuation (PTF%), area under the plasma concentration–time curve (AUC); terminal elimination half-life ($t_{1/2}$); mean residence time (MRT); total clearance (Cl/F); renal clearance (Cl_r); and volume of distribution (V_d/F). For the mass balance study, parameters were calculated up to 48 h, for the 2 mg b.i.d. regimen up to 12 and 24 h post-dose and for the 4 mg o.d. regimen up to 24 h.

Statistical analysis

A descriptive statistical analysis was performed on the demographic data of the enrolled volunteers by means of PharmStat software (SIMED, Paris, France) and Excel® 7.0 for Windows 95. For the main pharmacokinetic parameters statistics were made using Kinetica™ Software. All emedastine AUC and C_{max} comparisons were made by the complete analysis of variance (ANOVA) after logarithmic transformation of data. T_{max} was compared by the non-parametric Friedman test (non-transformed data).

Results

Mass balance study

Concentration–time profiles of plasma ^{14}C and emedastine after the administration of 4 mg ^{14}C-labelled drug to six male volunteers is shown in figure 2. Table 1 summarizes the pharmacokinetic parameters of ^{14}C in blood, plasma and urine and the plasma pharmacokinetics of emedastine following single-dose administration of 4 mg ^{14}C-emedastine. Cl/F and V_d/F for plasma emedastine were 0.658 ± 0.284 and 4.6 ± 3.3 l kg^{-1}, respectively. The mean cumulative urinary and faecal ^{14}C excretion given as the percentage of dose are shown in figure 3. ^{14}C

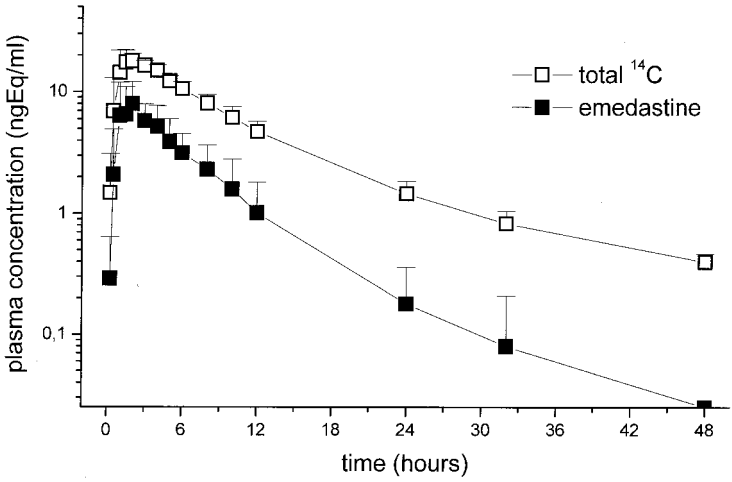


Figure 2. Time versus plasma profile for total ^{14}C and emedastine concentrations obtained in six healthy male Caucasian volunteers following administration of a single dose of 4 mg ^{14}C-emedastine difumarate immediate-release capsules.

Table 1. Pharmacokinetic parameters for emedastine.

	^{14}C blood	^{14}C plasma	Plasma emedastine
t_{max} (h)	2.0 ± 0.8	2.0 ± 0.8	1.4 ± 0.5
C_{max} (ng eq. ml^{-1})	13.9 ± 2.2	18.8 ± 3.0	9.4 ± 5.0
$AUC_{0\text{-}48}$ (ng eq. h ml^{-1})	130.0 ± 20.0	176.8 ± 26.0	48.1 ± 25.7
$t_{1/2}$ (h)	10.7 ± 4.6	13.3 ± 1.4	4.8 ± 2.1
MRT (h)	11.7 ± 2.5	12.5 ± 1.0	6.7 ± 2.1

Data are means $\pm$ SD of ($n = 6$).

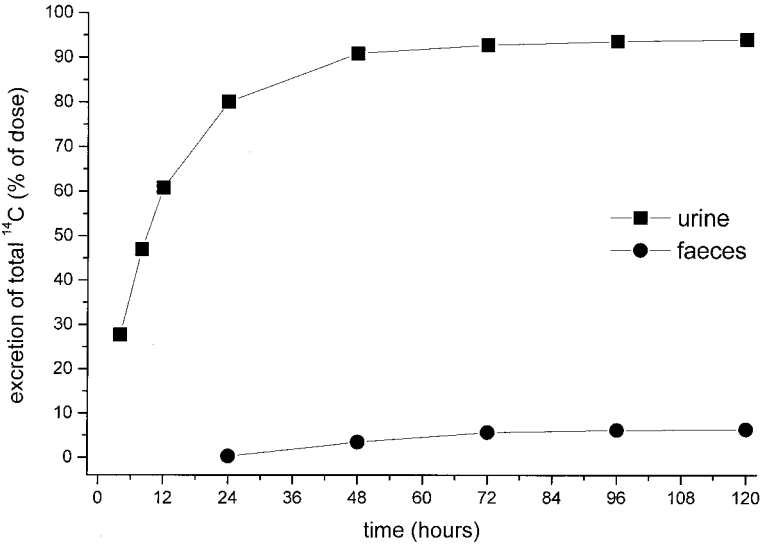


Figure 3. Mean cumulative urinary and faecal excretion of total ^{14}C following oral single-dose administration of 4 mg ^{14}C-emedastine difumarate to six male healthy volunteers. Excretion of radioactivity is given as the percentage of the ^{14}C-administered dose.

in urine was mainly excreted in the 0–12 h collection interval (60.8 ± 15.1%), whereas ^{14}C in faeces was detectable not earlier than 12–24-h post-administration with excretion occurring mostly 48–120 h post-dose. The mean total recovery of radioactivity in urine and faeces was 94.16 ± 13.71% and 6.37 ± 13.67% of dose, respectively, in the 120 h collection interval. Consistent with the almost complete absorption and urinary excretion, renal clearance (143.34 ± 41.03 ml h^{-1} kg) accounted for most of total clearance (147.54 ± 26.37 ml h^{-1} kg).

In urine samples, analysed for urinary metabolites, unchanged emedastine accounted for 4.3 ± 2.2% of the administered dose in the 0–4 h fraction and for 2.4 ± 1.1% in the 4–8 h fraction, then decreased to undetectable values. Free 5-hydroxy and 6-hydroxy emedastine ranged from 7.1 ± 3.5 and 3.8 ± 2.9% from the first to the last collection interval. Free emedastine *N*-oxide was present in only minor amounts (2.1 ± 1.3% in the 0–4 h fraction), and afterwards declined to lower percentages. Conjugated metabolites were detected in small amounts in all the collected urine fractions (4–5% of total urinary ^{14}C).

Single-multiple dose pharmacokinetic study

Mean time versus plasma concentration profiles of emedastine obtained, after a single dose and at the steady-state, in nine male and nine female healthy volunteers administered emedastine difumarate for 7 consecutive days according to 2 mg b.i.d. and 4 mg o.d. dose regimens are shown in figure 4. The main pharmacokinetic parameters for both treatment regimens calculated on days 1 and 7 are shown in table 2. Between days 1 and 7, average C_{max} after 2 mg b.i.d increased by a factor of 1.8 ($p = 0.001$). Accordingly, the cumulation factor for AUC_{0-12} was 1.9 ($p = 0.001$). In contrast, there was no relevant increase in C_{max} or AUC_{0-24} between days 1 and 7 for the 4 mg o.d. regimen (n.s. between days). AUC_{0-24} measured on day 1 were 1.4 times higher for the 4 mg o.d. formulation as

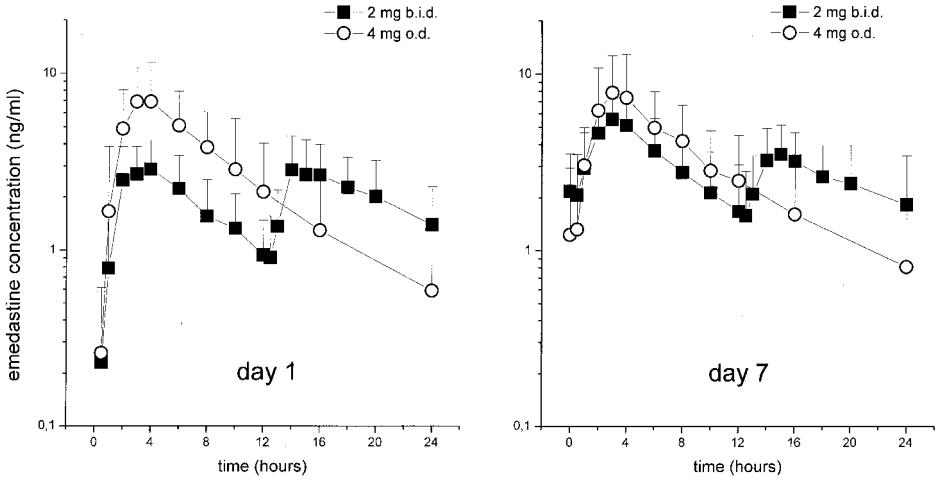


Figure 4. Mean time versus plasma emedastine concentration profiles obtained in nine healthy male and nine female Caucasian volunteers administered either emedastine slow-release capsules 2 mg b.i.d. or 4 mg o.d. for 7 consecutive days. The left panel shows concentration profiles after single-dose administration on day 1. Steady-state pharmacokinetics on day 7 are shown in the right panel. Results are means ± SD.

Table 2. Pharmacokinetic parameters on days 1 and 7 for 2 mg b.i.d. or 4 mg o.d. emedastine difumarate regimens in nine male and nine female healthy volunteers.

	Day 1		Day 2	
	2 mg b.i.d.	4 mg o.d.	2 mg b.i.d.	4 mg o.d.
C_{min}, a.m. (ng ml^{-1})	–	–	1.4 ± 1.2	0.7 ± 1.2
C_{min}, p.m. (ng ml^{-1})	–	–	1.1 ± 0.75	–
t_{max}, a.m. (h)	3.5 ± 1.5	3.6 ± 1.2	3.0 ± 0.7	3.3 ± 1.5
t_{max}, p.m. (h)	3.5 ± 1.7	–	3.6 ± 1.6	–
C_{max}, a.m. (ng ml^{-1})	3.3 ± 1.3*	7.7 ± 4.7	5.8 ± 2.7*	8.7 ± 5.1
C_{max}, p.m. (ng ml^{-1})	3.5 ± 1.6*	–	4.1 ± 1.8*	–
$C_{average}$, a.m. (ng ml^{-1})	–	–	3.4 ± 1.7	3.0 ± 2.2
$C_{average}$, p.m. (ng ml^{-1})	–	–	2.5 ± 1.3	–
PTF, a.m. (%)	–	–	142.2 ± 50.7	295.4 ± 76.4
PTF, p.m. (%)	–	–	130.0 ± 52.1	–
AUC_{0-12} (ng h ml^{-1})	21.2 ± 10.1	–	40.3 ± 20.4	–
AUC_{0-24} (ng h ml^{-1})	45.8 ± 21.2**	62.6 ± 42.1**	70.6 ± 36.1	71.7 ± 52.3
$t_{1/2}$ (h)	–	6.9 ± 4.0	–	7.0 ± 2.9
MRT (h)	9.6 ± 3.1	10.8 ± 4.4	–	10.7 ± 3.8
Cl/F (L kg h^{-1})	–	1.2 ± 0.5	–	1.0 ± 0.4
V_d/F (L kg^{-1})	–	11.3 ± 7.5	–	9.3 ± 3.5

Results are presented as means ± SD.
*$p < 0.05$ between days, **$p < 0.05$ between groups.
a.m., given in the morning; p.m., given in the evening.

compared with 2 mg b.i.d. ($p = 0.001$), whereas on day 7 no significant difference in AUC_{0-24} could be detected between the two regimens. The pharmacokinetic parameters obtained on days 1 and 7 were not significantly different between men and women (data not shown). At steady-state the ratio between C_{max} and C_{min} was higher for the 4 mg o.d. regime than for 2 mg b.i.d., with a mean PTF of 295.41 ± 76.44% as compared with 147.17 ± 50.69% after the morning dose and 129.97 ± 52.12% after the evening dose, with mean $C_{average} = 2.99 \pm 2.18$ and 3.36 ± 1.70 and 2.52 ± 1.32 ng ml^{-1}, respectively.

After the administration of 4 mg emedastine o.d., 67% of volunteers reported, at least once, mild somnolence and 11% mild headache, whereas after 2 mg b.i.d. 11% somnolence episodes and 11% headache were reported, respectively. No other adverse events occurred and no laboratory abnormalities or ECG changes were detected.

Discussion

After administration of ^{14}C-labelled emedastine difumarate, absorption of both radioactivity and unchanged emedastine was rapid with maximum concentrations reached after 2 and 1.4 h for plasma ^{14}C and emedastine, respectively (figure 2 and table 1). The observed delay in t_{max} for ^{14}C accompanied by a higher C_{max} for ^{14}C might be the result of a hepatic first-pass effect of emedastine, which has been described in previous experimental studies (Sakai 1987, Wada 1989). Concentrations of total radioactivity were different between blood and plasma. When corrected for individual hematocrits, the distribution into blood cells could be estimated by determining the ratio of ^{14}C concentrations in plasma and blood cells. A mean plasma/blood cell concentration ratio of 2.7 ± 0.4 thus indicated a poor penetration of emedastine and/or its metabolites into blood cells.

Our data indicate that emedastine undergoes extensive metabolism before being excreted via the kidney. This was shown by the ratio between plasma radioactivity and unchanged emedastine as given by AUC_{0-48} of 176.8 ng h ml^{-1} for ^{14}C and 48.1 ng h ml^{-1} for emedastine, respectively, which demonstrate that in plasma, emedastine accounts for about 27% of total ^{14}C, the difference being represented by metabolites.

Emedastine was primarily excreted by the kidneys. During the 120-h observation, 94.2% of total administered radioactivity was excretion with urine, while during the same interval recovery of radioactivity in faeces accounted for 6.4% of the dose (figure 3). Urinary excretion occurred mainly during the first 12 h post-dose, declined thereafter and accounted for $< 1\%$ of the administered dose in the last collection interval from 96 to 120 h. Unchanged emedastine in urine accounted for $< 5\%$ of total urinary radioactivity. Urinary metabolites (5-hydroxy, 6-hydroxy emedastine and their conjugated metabolites and emedastine *N*-oxide), previously identified in Japanese volunteers (Amada *et al.* 1990), were also measurable. Faecal elimination of total ^{14}C was less pronounced with a maximum elimination on days 2 and 3 post-dose and might be interpreted as a result of the excretion of an unabsorbed dose fraction or minor excretion via the bile.

After the administration of emedastine difumarate according to 2 mg b.i.d. or 4 mg o.d. dosing regimens, mean t_{max} ranged from 3.0 to 3.6 h both after the first dose and at steady-state, which was assumed to be achieved within 7 days of multiple dose administration (Joukhadar *et al.* 2001). Between days 1 and 7, average C_{max} after 2 mg b.i.d increased by a factor of 1.8 ($p = 0.001$). Mean C_{min} on day 1 were 0.94 ± 0.55 ng ml^{-1}. Accordingly, the cumulation factor for AUC_{0-12} was 1.9 ($p = 0.001$). In contrast, there was no relevant increase in C_{max} or AUC_{0-24} between days 1 and 7 for the 4 mg o.d. regimen (n.s. between days). C_{max} proportionality increased with dose with C_{max} after 4 mg o.d being 2.3 and 1.5 times higher on days 1 and 7, respectively, compared with b.i.d. administration. AUC_{0-24} measured on day 1 were 1.4 times higher for the 4 mg o.d. formulation as compared with 2 mg b.i.d. ($p = 0.001$), whereas on day 7 no statistic difference in AUC_{0-24} could be detected between the two regimens. MRT, clearance and volume of distribution were not significantly different between treatments, indicating pharmacokinetic linearity of both dosages within the studied dose range. However, note that clearance and volume of distribution are only valid provided that the bioavailability does not change from days 1 to 7. Plasma concentrations declined with a mono-exponential profile for both dosages (figure 4). Experiments performed in a small number of Asian subjects indicated comparable absorption and elimination rates between Asian and Caucasian subjects ($t_{max} = 3.05 \pm 0.03$ h; $t_{1/2} = 6.98 \pm 0.43$ h; MRT $= 10.8 \pm 0.7$ h; Nakajima *et al.*, Kanebo Ltd, personal communication). Minor pharmacokinetic differences, i.e. higher C_{max} and AUC, might be due to differences in body weight between Asians and Caucasians.

No significant pharmacokinetic difference between genders could be detected for AUC, MRT, $t_{1/2}$, clearance and volume of distribution after single- and multiple-dose administration of 4 mg emedastine, which indicates that emedastine is equally absorbed, distributed, metabolized and excreted in men and women.

After 4 mg o.d. the mean volume of distribution at steady-state was 9.3 l kg^{-1}, i.e. about 600 litres, if an average body weight of 65 kg is taken for the present study. Based on this observation, one might conclude that emedastine either

distributes specifically to 'deep' tissue or is stored and pooled somewhere in a peripheral compartment, such as in adipose tissue, or that emedastine is specifically bound. An extensive distribution to body fluids and tissues with the involvement of peripheral compartments could also be confirmed by the results obtained after the administration of ^{14}C-labelled emedastine with a volume of distribution of 2.9 and 4.6 $l kg^{-1}$ for plasma ^{14}C and plasma emedastine concentrations, respectively (table 1).

Emedastine was well tolerated with no systemic or gastrointestinal side effects. The most commonly observed adverse reaction was the occurrence of somnolence and mild headache. The frequency of somnolence episodes was highest for the 4 mg o.d. dosage on the first treatment day and decreased during the course of the treatment. The degree of somnolence after 2 mg b.i.d. was lower with a reduced incidence after seven days. Similar findings have been reported previously (Jansen *et al*. 2000) and the observed differences have been ascribed to lower peak concentrations after b.i.d. dosage and lower fluctuations of drug concentrations.

In conclusion, there were no gender differences in the pharmacokinetics of orally administered emedastine. Apart from characterizing the same urinary metabolites already identified in Asians, the results of the present study corroborate the use of emedastine in a Caucasian population and support the extrapolation of safety and efficacy data from Asians to Caucasians.

References

Amada, T. and Awata, N., 1990, Metabolism of a new antiallergic agent, emedastine difumarate, in human. *Xenobiotics Metabolism and Disposition*, **5**, 871–881.

Awata, N. and Satomi, O., 1986, Synthesis of 1-(2-ethoxyethyl)-2-(4-methyl-1-homopiperazinyl)-[2-14c] benzimidazole difumarate ([^{14}C] KB-2413). *Journal of Labelled Compounds and Radiopharmaceuticals*, **24**, 331–338.

Fukuda, T., Morimoto, Y., Iemura, R., Kawashima, T., Tsukamoto, G. and Ito, K., 1984b, Effect of 1-(2-ethoxyethyl)-2-(4-methyl-1-homopiperazinyl)-benzimidazole (KB-2413), a new antiallergic, on chemical mediators. *Arzneimittelforschung*, **34**, 801–805.

Fukuda, T., Saito, T., Tajima, S., Shimohara, K. and Ito, K., 1984a, Antiallergic effect of 1-(2-ethoxyethyl)-2-(4-methyl-1-homopiperazinyl)benzimidazole difumarate (KB-2413). *Arzneimittelforschung*, **34**, 805–810.

Hamada, T., Kadowaki, M. and Awata, N., 1987, Radioreceptor assay for a new antiallergic agent, 1-(2-ethoxyethyl)-2-(4-methyl-1-homopiperazinyl)benzimidazole difumarate (KB-2413), in plasma. *Chemical and Pharmaceutical Bulletin (Tokyo)*, **35**, 3329–3335.

Herranz, U., Rusca, A. and Assandri, A., 2001, Emedastine–ketoconazole: pharmacokinetic and pharmacodynamic interactions in healthy volunteers. *International Journal of Clinical Pharmacology and Therapeutics*, **39**, 102–109.

Jansen, B., Graselli, U., Dallinger, S., Kiss, B., Wacheck, V., Schlagbauer-Wadl, H., Assandri, A. and Müller, M., 2000, Pharmacokinetics and pharmacodynamics of the novel H_1-receptor antagonist emedastine in healthy volunteers. *European Journal of Clinical Pharmacology*, **55**, 837–841.

Joukhadar, C., Herranz, U., Pernerstorfer, T., Assandri, A., Klein, N., Schrolnberger, C., Lackner, E., Eichler, H. G. and Müller, M., 2001, Pharmacokinetics of emedastine difumarate, a new anti-histaminic agent in patients with renal impairment. *European Journal of Clinical Pharmacology*, **56**, 905–910.

Nakajima, S., Tsutani, Y., Ohishi, M., Doi, Y., Yamazaki, K. and Ohba, Y., 1989, Phase I study on emedastine difumarate (KG-2413). Single and consecutive administration with KG-2413 tablets. *Kiso to Rinsho*, **23**, 5419–5430.

Saito, T., Fukuda, T., Sukamoto, T., Yoshidomi, M., Morimoto, Y., Shimohara, K. and Ito, K., 1988a, General pharmacology of 1-(2-ethoxyethyl)-2-(4-methyl-1-homopiperazinyl)benzimidazole difumarate. 1st Communication: Effects on the central nervous system. *Arzneimittelforschung*, **38**, 66–69.

Saito, T., Fukuda, T., Tajima, S., Sukamoto, T., Yamashita, A., Kanazawa, T., Morimoto, Y., Shimohara, K., Nishimura, N., Yokota, K. *et al.* 1988b, General pharmacology of 1-(2-ethoxyethyl)-2-(4-methyl-1-homopiperazinyl) benzimidazole difumarate. 2nd Communication: Effects on the circulation and the other systems. *Arzneimittelforschung*, **38**, 267–272.

Saito, T., Nishimura, N., Tajima, S., Fukuda, T. and Ito, K., 1987, Anti-allergic effects of 1-(2-ethoxyethyl)-2-(4-methyl-1-homopiperazinyl)benzimidazole fumarate (KB-2413). *Nippon Yakurigaku Zasshi*, **89**, 55–62.

Sakai, T., 1987, The biological fate of emedastine difumarate. Absorption and excretion after oral administration to rats and guinea pigs. *Xenobiotics Metabolism and Disposition*, **2**, 123–131.

Slater, J. W., Zechnich, A. D. and Haxby, D. G., 1999, Second-generation antihistamines: a comparative review. *Drugs*, **57**, 31–47.

Tasaka, K., Kamei, C., Katayama, S., Kitazumi, K., Akahori, H. and Hokonohara, T., 1986, Comparative study of various H_1-blockers on neuropharmacological and behavioral effects including 1-(2-ethoxethyl)-2-(4-methyl-1-homopiperazinyl) benzimidazole difumarate (KB-2413), a new antiallergic agent. *Archives of International Pharmacodynamics*, **280**, 275–291.

Wada, Y., 1989, Absorption, metabolism and excretion of an antiallergic agent, emedastine difumarate, in dogs. *Xenobiotics Metabolism and Disposition*, **4**, 471–480.

Wada, Y., Hamada, T., Kawashima, T. and Awata, N., 1990, In vitro metabolism of an antiallergic agent, emedastine difumarate, in rats and guinea pigs. *Yakugaku Zasshi*, **10**, 40–48.

XENOBIOTICA, 2002, VOL. 32, NO. 9, 771–782

Taylor & Francis
healthsciences

Fate of the anthelmintic, phenothiazine, in man

S. C. MITCHELL†*, P. KESTELL‡, G. B. STEVENTON§ and R. H. WARING¶

† Biological Chemistry, Division of Biomedical Sciences, Faculty of Medicine, Imperial College, South Kensington, London SW7 2AZ, UK.
‡ Cancer Research Laboratory, Auckland Medical School, University of Auckland, Private Bag 92019, Auckland, New Zealand.
§Department of Pharmacy, King's College London, Franklin-Wilkins Building, 150 Stamford Street, London SE1 8WA, UK.
¶ School of Biosciences, University of Birmingham, PO Box 363, Edgbaston, Birmingham B15 2TT, UK

Received 13 December 2001

1. Radiolabelled [^{35}S]-phenothiazine has been administered orally to two healthy adult male volunteers (6 mg kg^{-1} body weight). Faeces were the major route of excretion of radioactivity (68%), the remainder being eliminated via the urine (32%) with an estimated urinary half-life (biphasic) of 6–16 h. Over the 5 days of the study a complete recovery of radioactivity was achieved.

2. From urinary data, it was shown that metabolism occurred via ring carbon oxidation to form phenothiazone and thionol and via ring sulphur oxidation to form phenothiazine sulphoxide. The majority of urinary material (92%) was present in the form of conjugates of phenothiazine and phenothiazone. Only unchanged phenothiazine was detected in the faeces. Phenothiazine sulphoxide was reduced to phenothiazine during incubation with faecal homogenates.

Introduction

The synthesis of phenothiazine (thiodiphenylamine, dibenzothiazine) was first published in 1883 during researches into the chemical structure of methylene blue and its derivatives (Bernthsen 1883, 1885). It remained a chemical curiosity for 50 years until it was shown to possess several biological properties (antifungal, bacteriocidal, insecticidal, vermifugal) and then quickly became regarded as the panacea for parasitic infestation. It was the first of the 'modern' anthelmintics and was extensively used during the Second World War enabling the provision of many tons of desperately needed infection-free food and sheep intestines (catgut sutures/ligatures). However, its potential adverse reactions including haemolytic anaemia, dermatitis, photosensitization and neuromuscular incoordination (Mitchell 1994), coupled with the development of more potent agents, have now limited its use. Nevertheless, low-dose phenothiazine has been shown to be active against strains of nematodes that have become resistant to more recently developed products and this property, together with its relative cheapness, still secures it a place on the world scene (Kelly *et al.* 1981, Lyons *et al.* 1993). Indeed, it is quoted as the 'drug of choice' for treatment of caecal nematode (*Heterakis gallinae*) infestations in poultry (Jacobs *et al.* 1997).

* Author for correspondence; e-mail: s.c.mitchell@ic.ac.uk

Xenobiotica ISSN 0049–8254 print/ISSN 1366–5928 online © 2002 Taylor & Francis Ltd
http://www.tandf.co.uk/journals
DOI: 10.1080/00498250210143038

Despite its wide-scale application amongst many animal species, investigations of the fate of phenothiazine have been limited (Mitchell 1982) and data for man are scant. This is surprising, since vast amounts of the compound have been used and exposure in man, through accidental ingestion, inhalation and potential dermal absorption, has been inevitable. The few studies undertaken (DeEds *et al.* 1938, DeEds and Thomas 1941, 1942) have shown the presence of red/purple quinoidal compounds in human urine after its relatively harsh chemical treatment and suggest extensive metabolism, but no advantage has been taken of the use of radiolabelled material. Any estimate of the persistence of phenothiazine within man necessarily requires the inclusion of all metabolic products, whether known or not, and would be aided greatly by the incorporation of a readily quantifiable marker within the parent molecule. The present paper describes the fate of [^{35}S]-phenothiazine in two adult men.

Materials and methods

Chemicals

Phenothiazine was obtained from Sigma-Aldrich Ltd (Dorset, UK) and purified by recrystallization from diethyl ether (Smith 1938) then aqueous ethanol to give light tan crystals, m.p. 181–183 °C, UV absorption peaks at 254 and 317 nm, mass spectrum M^+ m/z 199 (mol. wt 199) (Shine and Mach 1965, McLafferty and Stauffer 1989). Radiolabelled phenothiazine was synthesized by refluxing elementary [^{35}S]-sulphur (Nycomed-Amersham, Amersham, UK) with diphenylamine in the molar ratio of 2:1.3 respectively, for 1 h at 180 °C in 1,2-dichlorobenzene under an atmosphere of nitrogen, 1% (w/w) iodine being added as a catalyst (Lannung 1941, Massie 1954, Coffey 1978). The evolved radioactive hydrogen sulphide was trapped in an aqueous solution of $FeCl_3$ (1 M). The solvent was removed by distillation, the excess diphenylamine precipitated in anhydrous ethereal solution by dry HCl gas and the phenothiazine recrystallized twice from aqueous ethanol to give light yellow crystals of specific activity 189.4 mCi mol^{-1}, radiochemical purity > 98% (TLC), mixed m.p. 181–183 °C, with spectral properties as above.

Phenothiazine sulphoxide (phenothiazine-5-oxide) was prepared by oxidizing phenothiazine with 3-chloroperbenzoic acid in cold dry acetone (Beckett *et al.* 1975) to give light green crystals, m.p. 247–248 °C, UV absorption peaks 229, 271, 303 and 336 nm, IR sharp band at 1070 cm^{-1}, mass spectrum M^+ m/z 215 (mol. wt 215) (McLafferty and Stauffer 1989). Phenothiazone (phenothiaz-3-one) was synthesized by the oxidation of phenothiazine with ferric chloride in hot water (Pummerer and Gabner 1913, Houston *et al.* 1949a). The crude residue was extracted with hot ethanol and the crystalline product obtained by chilling (Granick *et al.* 1940). Further purification by elution from aluminium oxide columns with chloroform, followed by preparative thin-layer chromatography (TLC) (2.0 mm silica gel G) in carbon tetrachloride/acetone, 4/1 (v/v), gave red crystals, m.p. 161–163 °C, UV/vis. absorption peaks at 236, 258, 272, 368 and 508 nm, mass spectrum M^+ m/z 213 (mol. wt 213) (McLafferty and Stauffer 1989). Thionol (7-hydroxyphenothiaz-3-one) was prepared by refluxing phenothiazine with 80% (v/v) sulphuric acid at 160–165 °C for 6 h, the residue being poured into excess iced-water and filtered (Houston *et al.* 1949b, Granick and Michaelis 1947). The crude product was purified by elution with 10% (v/v) aqueous NH_4OH from aluminium oxide columns, followed by preparative TLC (2.0 mm silica gel G) in carbon tetrachloride/acetone, 4/1 (v/v), to give red/purple crystals, m.p. > 300 °C, UV/vis. absorption peaks at 232, 276 and 592 nm, mass spectrum M^+ m/z 229 (mol. wt 229).

Human excretion study

Two healthy male volunteers (aged 27 and 28 years, weight 70.5 and 74 kg, height 1.85 and 1.80 m) were given a single oral dose of [^{35}S]-phenothiazine (423 mg (40.3 μCi) and 444 mg (42.3 μCi); dose-rate 6 mg kg^{-1} body weight) in a gelatin capsule with water (100 ml) during the early morning at least 2 h after a light breakfast. The subjects were non-smokers and no alcohol or medication was permitted for 1 week before or during the study. Urine was collected for known intervals for the first 0–24 h and then daily for the following 4 days, all samples being stored in darkened bottles at −70 °C until analysis. Faeces were collected daily for 0–5 days directly into lyophilization containers (plastic drums) and then stored at −70 °C until processing. Ethical approval for the study was obtained from the local ethics committee, following consultation with the local radiation protection panel.

Faecal metabolism

The possible contribution to metabolism by the lower gut contents was investigated by the separate incubation of phenothiazine, phenothiazine sulphoxide, phenothiaz-3-one and thionol (50 mg) with aqueous human faecal homogenate (2 ml) in sealed tubes under nitrogen at 37 °C for 48 h (Scheline 1966). The solutions were then lyophilized, extracted with methanol and analysed by TLC and HPLC as described below. Incubates with phosphate buffer (0.1 M, pH 7.4) instead of homogenates were included as controls.

Quantification of radioactivity

Aliquots of urine and HPLC eluant (100 µl–1.0 ml) and areas of silica from thin-layer plates were added directly to vials containing scintillation fluid ('Ecoscint', National Diagnostics, NJ, USA) and analysed by liquid scintillation spectrometry using a Packard model 385 scintillation counter (Ambac Industries, Inc., Downers Green, IL, USA), efficiency being determined by automatic external standardization and previously prepared quench-correction curves. Faeces were lyophilized, ground to a mixed powder, weighed and triplicate samples (about 100 mg) combusted in oxygen (Harvey Biological Material Oxidizer, ICN Tracer Labs, High Wycombe, Surrey, UK), the [$^{35}SO_2$] so produced being trapped in an alkaline scintillation mixture containing 2-phenylethylamine and then analysed as above.

Chromatography

Thin-layer chromatography (TLC) was carried out in nitrogen flushed tanks at 4 °C in the absence of light on plates coated with silica gel G (20 × 20 cm, 0.4 mm thick; Merck, Darmstadt, Germany) using solvents A (chloroform/acetone, 9/2 v/v), B (carbon tetrachloride/acetone, 4/1 v/v) and C (hexane/acetone, 3/2 v/v). Phenothiazine and its derivatives were detected under UV light and by spraying the dried plates with either (1) 50% v/v aqueous H_2SO_4, (2) 1% (w/v) I_2 in methanol, (3) 0.8% w/v HgI_2 in ethanol (with gentle warming), (4) 5% (w/v) $AgNO_3$ in 10% (v/v) aqueous NH_4OH or (5) 1% w/v $PdCl_2$ in 60 ml 0.1 M HCl plus 40 ml ethanol (Elliot 1959).

High-performance liquid chromatography (HPLC) was undertaken using a Perkin-Elmer LC sample processor ISS200 (PerkinElmer Analytical Instruments, Buckinghamshire, UK) connected to a Dionex quaternary gradient pump (Dionex Ltd, Camberley, Surrey, UK) in line with an LDC SpectroMonitor 5000 photodiode array detector (LDC/Milton Roy, Riviera Beach, FL, USA) and a fraction collector (LKB Bromma; Pharmacia LKB, Piscataway, NJ, USA). Data acquisition was by Chromquest chromatography software (ThermoFinnigan, Hemel Hempstead, Hertfordshire, UK). A reverse phase Zorbax Rx-C8 (5 µ, 250 × 4.6 mm) analytical column (Phenomenex UK Ltd, Macclesfield, Cheshire, UK) was used together with a gradient elution programme at an overall solvent flow rate of 1 ml min^{-1}. The mobile phase consisted of aqueous acetic acid (0.1% v/v) with its acetonitrile component increasing linearly from an initial 5% to 90% over 15 min, thereafter rapidly returning to 5% during the next 3 min and remaining at these proportions for another 7 min (a total run time of 25 min).

Investigation of metabolites

Urine (0–24 h) was examined both neat (concentrated by lyophilization where necessary) and following incubation with a β-glucuronidase/sulphatase mixture (type H-1 from *Helix pomatia*, Sigma-Aldrich) in acetate buffer (equal vol.; 0.05 M, pH 5) at 37 °C for 18 h (to hydrolyse any conjugates present). Incubations with standard phenolphthalein glucuronide or *p*-nitrophenol sulphate confirmed activity of this enzyme preparation. Lyophilized powdered faeces (0–48 h) were extracted with cold methanol (3 × 1 ml g^{-1}). The combined extracts were then filtered and decreased in volume by rotary evaporation at room temperature under reduced pressure. The extracted faecal residues were lyophilized and combusted as described above to detect any residual radioactivity. Known amounts of [^{35}S]-phenothiazine added to control faeces and then extracted gave recoveries of 88.6 ± 4.2% ($n = 6$) and the results obtained were corrected for this.

These fluids (urine, incubates, extracts) were examined, as spots (10–50 µl) or streaks (100–500 µl), by TLC in the solvent systems A, B and C. On some plates where urine spots had been used (as opposed to streaks), once the non-conjugated material had been removed, cold HCl (9.7 M; about 100 µl) was applied to the origin, and the plates dried and rerun at an angle of 90° in the same solvent to give a two-dimensional separation. When developed and dried, the thin-layer plates were scanned directly for radioactivity using a Berthold Series 272 computerized radiochromatogram scanner (Berthold Instruments, Inc., Aliquippa, PA, USA) or otherwise cut into 0.3-cm strips and analysed for radioactivity as described above. Quantification was also undertaken by adding the relevant eluant fractions obtained from HPLC examination to scintillation fluid and counting as above. Authentic metabolites, dissolved in urine or methanolic extracts of faeces, were co-chromatographed by both TLC and HPLC to provide provisional identification. Radioactive areas removed from preparative plates (2 mm thick) were extracted with methanol, concentrated, redissolved in minimum quantities of methanol and, after filtration, examined by UV and mass spectral techniques. Similarly, the collection of relevant HPLC

eluant fractions, with their lyophilization and reconstitution in methanol, provided further samples for spectral analysis.

Spectrometry

UV and visible spectra were recorded in methanolic solution on a Pye-Unicam SP 1800 UV spectrophotometer (Pye-Unicam, Cambridge, UK). IR spectra were measured using a potassium bromide disc and a Pye-Unicam SP200 IR spectrophotometer (Pye-Unicam). Electron impact mass spectrometry was carried out on a Kratos MS80 instrument (Kratos Ltd, Manchester, UK) with Kratos D555 (data generator) computerized display and printout facilities. The sample was inserted directly into the ionization chamber at 70 eV with a source temperature of 200 °C.

Results

Excretion study

The studies showed similar results for both subjects. About one-third of the administered radioactivity was recovered from the urine, with the majority (about 26% dose, about 84% of that in the 0–5-day urine) being voided during the first day. The portion of the dose that was absorbed appeared to be so quite rapidly; with 9% of the radioactive dose (about 29% of that in the 0–5-day urine) being detected in the urine within 0–3 h. The remaining two-thirds of the radioactive dose was recovered from the faeces over 3–4 days with excretion tapering off towards the end of the study. Overall, excellent total recoveries (98.4 and 100.4%) were achieved (table 1).

Metabolism

Separate examination by TLC of the complete 0–24-h urine collected from each volunteer showed the presence of five areas of radioactivity at various distances along the plate from the origin to the solvent front. This pattern was identical for both subjects. For identification purposes the R_F obtained in all three TLC solvents systems are given in the order A, B and C.

Table 1. Excretion of radioactivity by two adult male subjects following the oral administration of [^{35}S]-phenothiazine (6 mg/kg body weight).

	Subject 1		Subject 2	
Period	Urine	Faeces	Urine	Faeces
Day 1				
0–3 h	8.4		10.2	
3–6 h	8.0		7.2	
6–9 h	3.3		4.8	
9–12 h	2.0		2.0	
12–18 h	2.7		1.8	
18–24 h	1.3		1.2	
Day 1	25.7	19.6	27.2	28.8
Day 2	3.6	32.0	4.2	29.8
Day 3	0.9	14.0	1.1	6.7
Day 4	0.2	4.2	0.1	0.3
Day 5	0.1	0.1	0.1	0.1
Subtotal	30.5	69.9	32.7	65.7
Total	100.4		98.4	

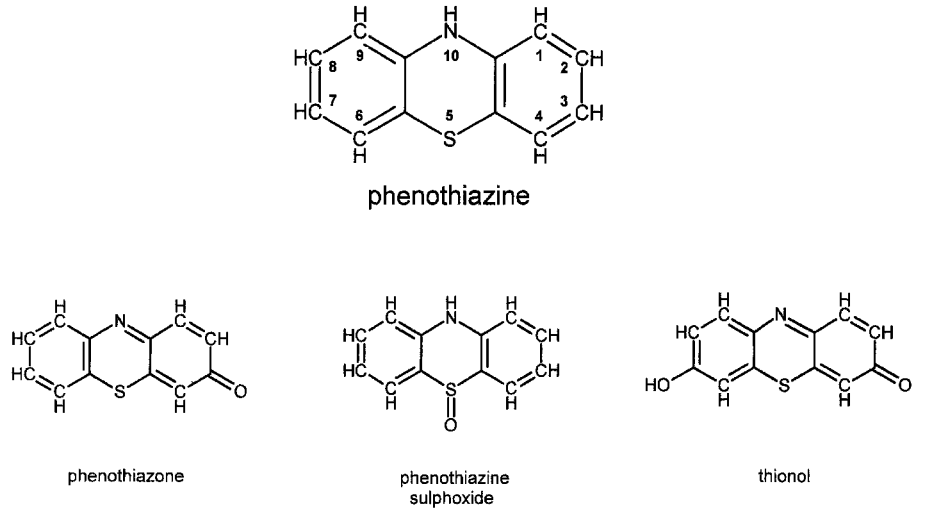


Figure 1. Structure of the anthelmintic, phenothiazine, and its oxidized metabolites, phenothiazone (phenothiaz-3-one), phenothiazine sulphoxide (phenothiazine-5-oxide) and thionol (7-hydroxyphenothiaz-3-one).

Area 1 (R_F 0.0, 0.0, 0.0) (conjugated material)

The majority of radioactivity within the urine (91.0, 92.3%) remained on the TLC plate origin, where the urine sample had been applied, in all of the solvent systems examined. Two-dimensional chromatography following *in situ* acid hydrolysis of the material on the origin, and examination of urine following enzyme hydrolysis, both demonstrated no radioactivity at the TLC plate origin but displayed concomitant increases in phenothiazone (area 4) and phenothiazine (area 5). This general pattern was confirmed by HPLC examination.

Cold butanol extraction of powdered lyophilized urine provided a radioactive product that remained on the TLC origin and was unstable in concentrations of cold HCl > 0.5 M, decomposing to yield phenothiazine and glucuronic acid only, as detected by TLC (Elliot 1959). This conjugate was tentatively assigned the structure of phenothiazine *N*-glucuronide (Mitchell and Waring 1979). Rapid cooling of concentrated urine (by lyophilization) provided a crude white precipitate that turned purple on heating in air. This precipitate provided a radioactive product that remained on the TLC origin and decomposed in warm HCl (9.7 M) to yield phenothiazone and inorganic sulphate (Mitchell and Waring 1978). Infrared analysis (bands at 1100–1200 cm^{-1}, sulphur-oxygen bond vibrations, covalent sulphate) (Bellamy 1954, Avram and Mateescu 1972) and a mass spectrum (*inter alia*, mass peak at m/z 278, M^+-16) were consistent with the tentative assignment of this conjugate as leucophenothiazone sulphate (Collier *et al.* 1943, Clare 1962, Mitchell and Waring 1979).

Area 2 (R_F 0.26, 0.19, 0.42) (thionol)

This radioactive metabolite co-chromatographed with authentic thionol (7-hydroxyphenothiaz-3-one) in all TLC solvent systems and by HPLC (R_T 5.8 min) following methanolic elution. The pink/purple tint was decolourized by covering

the TLC spot with a saturated solution of sodium dithionite. This reduces thionol to leucothionol (3,7-dihydroxyphenothiazine) thereby removing the quinoidal chromophore. Authentic thionol behaved in an identical manner. Absorption maxima were recorded at 232, 276 and 592 nm and mass spectral analysis gave a molecular ion at m/z 229 and a fragmentation pattern identical to the authentic compound (table 2).

Area 3 (R_F 0.35, 0.13, 0.37) (phenothiazine sulphoxide)

Co-chromatography of this radioactive excretion product was obtained with phenothiazine sulphoxide (phenothiazine-5-oxide) in all TLC solvent systems and by HPLC (R_T 4.0 min) following methanolic elution. Characteristic ultraviolet absorption maxima were observed at 229, 271, 303 and 336 nm. The molecular ion obtained for this metabolite was at m/z 215 with a fragmentation pattern identical to the authentic compound (McLafferty and Stauffer 1989, Sutherland *et al.* 2001) (table 2).

Area 4 (R_F 0.87, 0.77, 0.75) (phenothiazone)

This radioactive compound was shown clearly to co-chromatograph with authentic phenothiazone (phenothiaz-3-one) in all three TLC solvent systems employed and also by HPLC (R_T 7.4 min) when eluted and examined. Absorption maxima were recorded at 236, 258, 272, 368 and 508 nm and mass spectral analysis of this material gave a molecular ion at m/z 213 and fragment ions identical to those obtained from the authentic compound (McLafferty and Stauffer 1989, Sutherland *et al.* 2001) (table 2).

Area 5 (R_F 0.96, 0.87, 0.91) (phenothiazine)

Co-chromatography with authentic phenothiazine was achieved for this radioactive metabolite in all three solvent systems used for TLC and also by HPLC (R_T 13.7 min) following elution and rechromatography. Distinctive colorations, produced by authentic phenothiazine, were also noticed with various TLC reagents; green with ammoniacal $AgNO_3$, blue with $PdCl_2$ and brown with I_2 and HgI_2. UV absorption maxima were recorded at 254 and 317 nm. Mass spectral examination gave a molecular ion at m/z 199 and an expected splitting pattern characteristic of this molecule (Shine and Mach 1965, McLafferty and Stauffer 1989) (table 2).

For both subjects, the majority of radioactivity present within the urine was in the form of conjugated material (91.0 and 92.3% of the total radioactivity in the 0–24 h urine corresponding to 23.4 and 25.1% of the administered radioactive dose). Non-conjugated metabolites together accounted for $< 10\%$ (9.0 and 7.7% in urine; 2.3 and 2.1% dose), with phenothiazine sulphoxide being the most prominent (table 3).

The only radioactive component found in methanolic extracts of faeces showed chromatographic and spectral properties identical to those of the parent compound, phenothiazine (table 2). Methanolic extraction, although efficient in removing [^{35}S]-phenothiazine added to control faeces, only removed $82.4 \pm 5.2\%$

Table 2. Chromatographic and spectral properties of phenothiazine and its derivatives.

Compound/metabolite	Chromatographic properties				Spectral properties		
	TLC R_f Solvent system					Mass spectral fragmentation (m/z)*	
	A	B	C	HPLC R_t (min)	Ultraviolet/visible absorption maxima (nm)	Molecular ion (base peak)	Other diagnostic ions
Phenothiazine	0.96	0.87	0.91	13.7	254, 317	199	198, 167, 154
Phenothiazine sulphoxide	0.35	0.13	0.37	4.0	229, 271, 303, 336	215	199, 198, 186, 167, 154
Phenothiazone	0.87	0.77	0.75	7.4	236, 258, 272, 368, 508	213	199, 197, 185/6, 135
Thionol	0.26	0.19	0.42	5.8	232, 276, 592	229	215, 213, 199, 186, 167

* Although interpretation of mass spectra may be complex, the majority of daughter ions observed might be explained by the loss of fragments to yield phenyl sulphide ($C_{12}H_{10}S$, mol. wt 186), carbazole ($C_{12}H_9N$, mol. wt 167) and diphenyl ($C_{12}H_{10}$, mol. wt 154); all degradation products readily observed during chemical reaction of phenothiazine in the presence of metal ions (e.g. Goske 1887, Orlow 1931, Shah *et al.* 1948). The ion at m/z 135 observed with phenothiazone may represent the loss of a benzene moiety (M^+, 213 – C_6H_6, 78).

Table 3. Excretion of metabolites in urine (0–24 h) following the ingestion of [^{35}S]-phenothiazine (6 mg/kg) by two male subjects

Metabolite	Percentage radioactivity in urine (0-24 h)		Percentage of the administered radioactive dose	
	Subject 1	Subject 2	Subject 1	Subject 2
Phenothiazine	2.4	1.9	0.6	0.5
Phenothiazine sulphoxide	4.0	3.3	1.0	0.9
Phenothiazone	2.1	1.5	0.6	0.4
Thionol	0.5	1.0	0.1	0.3
Phenothiazine conjugate*	53.2	62.2	13.7	16.9
Phenothiazone conjugate**	37.8	30.1	9.7	8.2
	100.0	100.0	25.7	27.2

The conjugates have been tentatively assigned the structures of *phenothiazine *N*-glucuronide and **leucophenothiazone sulphate.

of the radioactivity associated with the faeces. This meant that the chemical identity of around 10% (9.1%, 10.3%) of the radioactive material within the faeces (0–48 h) obtained from both subjects was unaccounted for; probably remaining bound to the cellulose and other polyphenolic components of the faeces. Incubation of metabolites with faecal homogenates produced no chemical alterations to phenothiazine or its derivatives except for the almost quantitative (90%+) reduction of phenothiazine sulphoxide to phenothiazine (data not shown).

Discussion

In agreement with the present results for man, other workers have reported low urinary recoveries following oral administration; 5 and 10% for sheep (Lipson 1940, Swales and Collier 1940), 14% for the horse (Swales *et al.* 1942), 23% for the rabbit (Benham 1945) and 25% for the cow (Guyton *et al.* 1976). In addition, traces of large doses of phenothiazine have been shown to remain within calves for between 5 and 15 days (Sundukov 1963) and in sheep for 14–16 days (Dobryina 1963). However, the proportion of the dose that does enter the body appears to be absorbed quickly from the upper gastrointestinal tract and then rapidly voided in the urine. The greatest rate of urinary excretion of a single dose of phenothiazine has previously been shown to occur within 0–9 h in the cow, sheep and horse (Swales and Collier 1940, Swales *et al.* 1942, Ellison and Todd 1957) and this is consistent with the findings presented here for man. Simple graphical plotting of the present 0–24-h urinary data was suggestive of a biphasic excretion pattern with an initial half-life of around 6 h (0–12 h period) and a latter half-life of 16 h (12–24-h period). However, it must be appreciated that there are only a few data points during this first day, and there are only two subjects. Recalculated urinary data from the literature gives half-life values ranging from 11 to 18 h for both the sheep and the horse (Swales and Collier 1940, Swales *et al.* 1942).

The delay in excretion via the gastrointestinal tract is indicative of a decreased transit time through the gut, perhaps assisted by enterohepatic cycling (DeEds and Thomas 1941, Davey and Innes 1942, Mitchell 1982). This cycling may be a mechanism that prolongs its residence and assists its mode of action as an anthelmintic. Local effects of phenothiazine on the gut may also produce a

decrease in gastrointestinal motility. Phenothiazine has been shown to inhibit horse serum cholinesterase (Collier 1942, Collier and Allen 1942) and interfere with neuromuscular transmission in the crab (Collier 1940b). This has led to the suggestion that phenothiazine acts, in part, by paralysing the infesting helminths, thereby causing their detachment from anchorage and promoting their passage through and expulsion from the gut (Collier 1942, Mackie and Raeburn 1952, Mackie 1953). Colonic impaction has been reported in horses that have received large doses of phenothiazine but, conversely, so has diarrhoea (Habermann *et al.* 1941, Wolfe and Dennis 1941). The two volunteers in the present study reported no gastrointestinal disturbances although gut irritation in man has been cited elsewhere (Nour El-Din 1946). Persistence of phenothiazine, observed in some animals as measured by trace amount in their urine, may be related to the relatively large doses that these animals have received (up to 1 kg in the horse; Habermann *et al.* 1941). The effective formation of a slow moving bolus within the gut and the slight but constant absorption from this reservoir mimics a multiple or continuous dosing situation which would persist for many days following the original oral administration.

The pattern of metabolism found in man is in general agreement with that found for other species examined and there is nothing unusual or unexpected in the human profile. All of the phenothiazine metabolites identified in the present study have been previously reported (Mitchell 1982). The carbon oxidation products, phenothiazone and thionol have been demonstrated in the urine of the cow, dog, gerbil, horse, mouse, pig, rabbit, rat and sheep and the sulphur oxidation product, phenothiazine sulphoxide in the cow, guinea pig and sheep (Lipson 1940, Swales and Collier 1940, Taylor and Sanderson 1940, DeEds and Thomas 1941, Swales *et al.* 1942, Collier *et al.* 1943, Clare 1947, 1962, Richardson and Todd 1958, Mitchell and Waring 1979, Mitchell 1980). Conjugated forms of phenothiazine (phenothiazine-*N*-glucuronide) and phenothiazone (leucophenothiazone sulphate) have been also previously reported in the urine from the cow, gerbil, guinea pig, hamster, pig, rat and sheep (Lipson 1940, Swales and Collier 1940, Taylor and Sanderson 1940, DeEds and Thomas 1941, Swales *et al.* 1942, Collier *et al.* 1943, Clare 1947, 1962, Richardson and Todd 1958, Mitchell and Waring 1979, Mitchell 1980). The glucuronic acid conjugate of thionol appears to be absent from human urine, unlike that of the gerbil, mouse, rabbit and rat (Benham 1945, Mitchell 1980).

Phenothiazine is the only compound that has been positively identified as being present in the faeces of cows, guinea pigs, horses, rabbits, rats and sheep, presumably unabsorbed, although trace amounts of phenothiazone and thionol have been found in rat faeces and phenothiazone and the sulphoxide in guinea pig faeces (Collier 1940a, Lipson and Gordon 1940, Swales *et al.* 1942, Richardson and Todd 1958, Waddell 1959, Mitchell and Waring 1979, Mitchell 1982). Phenothiazone and phenothiazine sulphoxide have been detected in the gut of sheep distal to the bile duct and *in vitro* incubation experiments with rumen contents have shown that phenothiazine was not converted into any detectable derivatives, except for minute traces of phenothiazone ascribed to air oxidation (Waddell 1959), suggesting that the metabolites probably entered the enteric tract via the bile (Clare 1947, Harpur *et al.* 1950a, b). Phenothiazine and thionol have been observed in bile from one human subject but the harsh chemical detection methods employed did not permit differentiation between phenothiazine and its

N-glucuronide or even between the C-oxidation products (DeEds and Thomas 1941). No such metabolites made their way into the faeces to be detected in the present study.

By analogy with its water-soluble *N*-substituted derivatives, the carbon and sulphur oxidations of phenothiazine are presumably undertaken by cytochromes P450 as these positions present favourable electromolecular environments for these enzyme systems. Delocalization of electrons from the sulphur (and nitrogen) moiety into the adjacent unsaturated tricyclic ring system decreases the nucleophilicity of this heteroatom and renders it less susceptible to oxidation by the flavin monoxygenase family of enzymes. The lipophilic nature of phenothiazine (log $P_{(\text{heptane})}$ 3.88, log $P_{(\text{octanol})}$ 4.15; Cymerman-Craig and Warburton 1956, Leo *et al.* 1971) and its negligible solubility in water (both 51 and 125 μg $100\,\text{ml}^{-1}$ quoted; Davey and Innes 1942, Cymerman-Craig and Warburton 1956), although presumably aiding its uptake and retention within the cuticle of the parasite (Lazarus and Rogers 1951), prevents *in vitro* investigations and precludes any attempts at intravenous studies. Investigations are therefore limited and any useful data obtained concerning the interaction of phenothiazine with living systems are thus welcomed.

References

Avram, M. and Mateescu, G. H. D., 1972, *Infrared Spectroscopy: Applications in Organic Chemistry* (New York: Wiley Interscience), pp. 290–302.

Beckett, A. H., Al-Sarraj, S. and Essien, E. E., 1975, Metabolism of chlorpromazine and promethazine to give new pink spots. *Xenobiotica*, **5**, 325–355.

Bellamy, L. J., 1954, *The Infra-red Spectra of Complex Molecules* (London: Metheun), pp. 288–302.

Benham, G. H., 1945, The fate of phenothiazine in rabbits. I. The detection of a new conjugate in rabbits' urine after feeding of phenothiazine. *Canadian Journal of Research*, **23E**, 71–79.

Bernthsen, A., 1883, Zur Kenntniss des Methylenblau und verrwander Farbstoffe. *Berichte der Deutschen chemischen Gesellschaft*, **16**, 2896–2904.

Bernthsen, A., 1885, Studien in der Methylenblau-gruppe. *Justus Liebigs Annalen der Chemie*, **230**, 73–211.

Clare, N. T., 1962, Metabolic products of phenothiazine in farm animals. *Psychopharmacology Service Center Bulletin*, **2**, 44.

Clare, N. T., 1947, A photosensitised keratitis in young cattle following the use of phenothiazine as an anthelmintic. II. The metabolism of phenothiazine in ruminants. *Australian Veterinary Journal*, **23**, 340–344.

Coey, S. (ed.), 1978, Phenothiazines. In *Rodd's Chemistry of Carbon Compounds*, 2nd edn (Amsterdam: Elsevier), vol. 4, Part H, pp. 516–535.

Collier, H. B., 1940a, The fate of phenothiazine in the sheep. *Canadian Journal of Research*, **18D**, 272–278.

Collier, H. B. (presented by Cameron, T. W. M.), 1942, The mode of action of phenothiazine as an anthelmintic. *Proceedings of Transactions of the Royal Society of Canada*, 3rd Ser., **36**, 163 (abst 51).

Collier, H. B. and Allen, D. E., 1942, Enzyme inhibition by derivatives of phenothiazine. II. Inhibition of cholinesterase. *Canadian Journal of Research*, **20B**, 189–193.

Collier, H. B., Allen, D. E. and Swales, W. E. 1943, Observations on the fate of phenothiazine in domestic animals. *Canadian Journal of Research*, **21D**, 151–159.

Collier, H. O. J., 1940b, Depression of neuromuscular transmission in a crab by phenothiazine. *Nature*, **146**, 232–233.

Cymerman-Craig, J. and Warburton, W. K., 1956, Lipoid–water partition coefficients of some phenothiazines. *Australian Journal of Chemistry*, **9**, 294–295.

Davey, D. G. and Innes, J. R. M., 1942, The present position of phenothiazine as an anthelmintic. *Veterinary Bulletin (Weybridge)*, **12**, 7–14.

DeEds, F., Eddy, C. W. and Thomas, J. O., 1938, Studies on phenothiazine. V. Fate of phenothiazine in the body. *Journal of Pharmacology and Experimental Therapeutics*, **64**, 250–262.

DeEds, F. and Thomas, J. O., 1941, Studies on phenothiazine. IX. The biliary excretion and anthelmintic action of thionol. *Journal of Parasitology*, **27**, 143–151.

DeEds, F. and Thomas, J. O., 1942, Studies on phenothiazine. XI. The excretion of phenothiazine. *Journal of Parasitology*, **28**, 363–367.

Dobryina, V. I., 1963, Absorption, distribution, conversion, and excretion of phenothiazine in sheep. *Materialy 8-oi [Vos'moi] Nauchnii Konferentsia po Farmakologii (Moscow) Sbornik*, 78–80; *Zhurnal Biologii i Khimii*, 1963, 21F851; *Chemical Abstracts*, 1964, **60**, 13744b.

Elliot, D. C., 1959, Methods for the detection of biochemical compounds on paper. In R. M. C. Dawson, D. C. Elliot, W. H. Elliot and K. M. Jones (eds), *Data for Biochemical Research* (London: Clarendon), pp. 210–272.

Ellison, T. and Todd, A. C., 1957, The metabolism of phenothiazine, N. F., in diary calves. I. Chronological distribution of drug in digestive tract contents. *American Journal of Veterinary Research*, **18**, 519–529.

Goske, A., 1887, Carbazol aus Thiodiphenylamin. *Berichte der Deutschen chemischen Gesellschaft*, **20**, 232–234.

Granick, S. and Michaelis, L., 1947, Thionol and its semiquinone radical. *Journal of the American Chemical Society*, **69**, 2983–2986.

Granick, S., Michaelis, L. and Schubert, M. P., 1940, Semiquinones of oxazines, thiazines and selenazines. *Journal of the American Chemical Society*, **62**, 1802–1810.

Guyton, C. L., Missaghi, E. and Marshall, P. M., 1976, Metabolic disposition of radioactive phenothiazine in calves. *American Journal of Veterinary Research*, **37**, 1287–1289.

Habermann, R. T., Harwood, P. D. and Hunt, W. H., 1941, Critical tests with phenothiazine as an anthelmintic in horses. *North American Veterinarian*, **22**, 85–92.

Harpur, R. P., Swales, W. E. and Denstedt, O. F., 1950a, Fate of phenothiazine in the gut of sheep. *Canadian Journal of Research*, **28D**, 143–161.

Harpur, R. P., Swales, W. E. and Denstedt, O. F., 1950b, Absorption of phenothiazine from sheep rumen. *Canadian Journal of Research*, **28D**, 162–172.

Houston, D. F., Kester, E. B. and DeEds, F., 1949a, Phenothiazine derivatives: monooxygenated compounds. *Journal of the American Chemical Society*, **71**, 3816–3818.

Houston, D. F., Kester, E. B. and DeEds, F., 1949b, Phenothiazine derivatives: dioxygenated compounds. *Journal of the American Chemical Society*, **71,** 3819–3822.

Jacobs, R. D., Hogsette, J. A. and Butcher, G. D., 1997, *Nematode Parasites of Poultry (And Where to Find Them)*. Fact sheet PS-18 (Gainesville, Florida: Dairy and Poultry Sciences Department, Florida Cooperative Extension Service, Institute of Food and Agricultural Sciences, University of Florida) [http://edis.ifas.ufl.edu/BODY_PS012].

Kelly, J. D., Whitlock, H. V., Gunawan, M., Griffin, D. and Porter, C. J., 1981, Anthelmintic efficacy of low dose phenothiazine against strains of sheep's nematodes susceptible or resistant to thiabendazole, levamisole and morantel tartrate; effect on patent infections. *Research in Veterinary Science*, **30**, 161–169.

Lannung, A., 1941, The synthesis, analysis, toxicology and therapeutic use of phenothiazine. *Archives of Pharmaceutical Chemistry*, **48**, 141–152.

Lazarus, M. and Rogers, W. P., 1951, Mode of action of phenothiazine as an anthelmintic. The uptake of S^{35}-labelled phenothiazine by the tissues of nematode parasites and their hosts. *Australian Journal of Scientific Research*, **B4**, 163–179.

Leo, A., Hansch, C. and Elkins, D., 1971, Partition coefficients and their uses. *Chemical Reviews*, **71**, 525–616.

Lipson, M., 1940, An examination of the urine of sheep dosed with phenothiazine. *Australian Journal of Experimental Biology and Medical Science*, **18**, 269–272.

Lipson, M. and Gordon, H. McL., 1940, The passage of phenothiazine through the alimentary canal of the sheep. *Journal of the Council for Scientific and Industrial Research, Australia*, **13**, 240–244.

Lyons, E. T., Drudge, J. H., Tolliver, S. C. and Stamper, S., 1993, Controlled tests of activity of several antiparasitic compounds against natural infections of *Haemonchus contortus* and other helminths in lambs from a flock established in 1962. *American Journal of Veterinary Research*, **54**, 406–410.

Mackie, A., 1953, The effects of some oxidation products of phenothiazine on *Ascaris lumbricoides in vitro*. *Archives Internationales de Pharmacodynamie et Thérapie*, **52**, 301–304.

Mackie, A. and Raeburn, J., 1952, Effects of some oxidation products of phenothiazine on liver fluke (*Fasciola hepatica*) *in vitro*. *British Journal of Pharmacology*, **7**, 215–218.

Massie, S. P., 1954, The chemistry of phenothiazine. *Chemical Reviews*, **54**, 797–833.

McLafferty, F. W. and Stauffer, D. B., 1989, *The Wiley/NBS Registry of Mass Spectral Data* (New York: Wiley), vol. 2, 1049, 1310, 1341.

Mitchell, S. C., 1980, Comparative metabolism of phenothiazine in the rat (*Rattus norvegicus*), mouse (*Mus musculus*), hamster (*Mesocricetus auratus*) and gerbil (*Gerbillus gerbillus*). *Comparative Biochemistry and Physiology*, **67C**, 199–202.

Mitchell, S. C., 1982, Mammalian metabolism of orally administered phenothiazine. *Drug Metabolism Reviews*, **13**, 319–343.

Mitchell, S. C., 1994, The toxicity of phenothiazine. *Drug Metabolism and Drug Interactions*, **11**, 201–235.

Mitchell, S. C. and Waring, R. H., 1978, Detection of inorganic sulphate and other anions on paper and thin-layer chromatograms. *Journal of Chromatography*, **166**, 341–343.

Mitchell, S. C. and Waring, R. H., 1979, Metabolism of phenothiazine in the guinea pig. *Drug Metabolism and Disposition*, **7**, 399–403.

Nour El-Din, Ge.-D., 1946, Recent advances in chemotherapy of tropical diseases. VIII. Anthelmintics. *Royal Egyptian Medical Association*, **29**, 167–172.

Orlow, N. A., 1931, Berginisierung einiger heterocyclischer Verbindungen. *Berichte der Deutschen chemischen Gesellschaft,* **64**, 2631–2636.

Pummerer, R. and Gabner, S., 1913, Uber die Desmotropie σ- und ρ-chinoider Salze in der Thiazinreihe. *Berichte der Deutschen chemischen Gesellschaft*, **46**, 2310–2327.

Richardson, T. and Todd, A. C., 1958, Elimination of phenothiazine by lactating diary cows. *American Journal of Veterinary Research*, **19**, 610–619.

Scheline, R. R., 1966, Decarboxylation and demethylation of some phenolic benzoic acid derivatives by rat caecal contents. *Journal of Pharmacy and Pharmacology*, **18**, 664–669.

Shah, K. H., Tilak, B. D. and Venkataraman, K., 1948, Raney nickel reductions. *Proceedings of the Indian Academy of Sciences*, **28A**, 142–150.

Shine, H. J. and Mach, E. E., 1965, Ion Radicals. V. Phenothiazine, phenothiazine-5-oxide, and phenothiazine-3 in acid solutions. *Journal of Organic Chemistry*, **30**, 2130–2139.

Smith, L. E., 1938, Analysis of commercial phenothiazine used as an insecticide. *Industrial and Engineering Chemistry, Analytical Edition*, **10**, 60.

Sundukov, A. I., 1963, Absorption, secretion, and distribution of phenothiazine in calves. *Materialy 8-oi [Vos'moi] Nauchnii Konferentsia po Farmakologii (Moscow) Sbornik*, 80–81; *Zhurnal Biologii i Khimii*, 1963, 21F850; *Chemical Abstracts*, 1964, **60**: 13744c.

Sutherland, J. B., Freeman, J. P., Heinze, T. M., Moody, J. D., Parshikov, I. A., Williams, A. J. and Zhang, D., 2001, Oxidation of phenothiazine and phenoxazine by *Cunninghamella elegans*. *Xenobiotica*, **31**, 799–809.

Swales, W. E. and Collier, H. B., 1940, Effects and excretion of phenothiazine when used as an anthelmintic for sheep. *Canadian Journal of Research*, **18D**, 279–287.

Swales, W. E., Collier, H. B. and Allen, D. E., 1942, Effects of phenothiazine on horses. I. Studies in haematology and pharmacology. *Canadian Journal of Research*, **20D**, 349–361.

Taylor, E. L. and Sanderson, K. M., 1940, A remarkably efficient anthelmintic. *Veterinary Record*, **52**, 635–647.

Waddell, A. W., 1959, Observations on the excretion of phenothiazine and oxidation products in sheep and rabbits. *Archives Internationales de Pharmacodynamie et de Thérapie*, **121**, 368–379.

Wolfe, W. R. and Dennis, W. R., 1941, Toxemia resulting from the use of phenothiazine. *Veterinary Bulletin of the US Army*, **35**, 171–174; *Veterinary Bulletin*, 1942, **12**, 306.

XENOBIOTICA, 2002, VOL. 32, NO. 9, 783–794

Taylor & Francis
healthsciences

Effect of intestinal microflora on the urinary metabolic profile of rats: a ^{1}H-nuclear magnetic resonance spectroscopy study

R. E. WILLIAMS*, H. W. EYTON-JONES, M. J. FARNWORTH, R. GALLAGHER and W. M. PROVAN

Syngenta Central Toxicology Laboratory, Alderley Park, Macclesfield, SK10 4TJ, UK

Received 13 December 2001

1. Analysis of urine by ^{1}H-nuclear magnetic resonance (NMR) spectroscopy is used to detect biochemical disturbances predictive of toxicological changes. Recent studies, using ^{1}H-NMR spectroscopy have suggested that Alderley Park rats can be classified as hippuric acid (HA) or *m*-(hydroxyphenyl)propionic acid (*m*-HPPA) excretors. Evidence exists for the role of intestinal microflora in the excretion of aromatic phenolic compounds including HA and *m*-HPPA.

2. We sought to investigate whether intestinal microflora contribute to the difference in excretion. Urinary HA and *m*-HPPA levels were monitored to characterize excretion over time. The effect of intestinal microflora on the ^{1}H-NMR spectrum was also investigated using antibiotics to sterilize the intestine. Finally, the levels of *m*-HPPA and phenylpropionic acid (a precursor for HA) were analysed in the caecum and colon (entire tissue, including contents).

3. Characterization confirmed the presence of HA and *m*-HPPA excretors; enquiries revealed that the rats were obtained from two floors within a barriered breeding unit. Housing the rats from the two floors together for 21 days resulted in comparable levels of HA and *m*-HPPA excretion demonstrating that the profiles are not stable.

4. Following antibiotic treatment, HA and *m*-HPPA excretion decreased, indicating that intestinal microflora contribute to the excretion of these compounds. Finally, *m*-HPPA levels were higher in the colon of rats that excreted *m*-HPPA whilst PPA was increased in the caecum and colon of rats that excreted HA.

5. These results demonstrate that the observed difference in HA/*m*-HPPA excretion is due to differences in the intestinal microflora.

Introduction

Analysis of urine by ^{1}H-nuclear magnetic resonance (NMR) spectroscopy combined with multivariate data analysis has become widely used as a method to non-invasively detect biochemical disturbances predictive of toxicological changes in laboratory animals (Beckwith Hall *et al.* 1998, Holmes *et al.* 1998, Nicholson *et al.* 1999). Using this method, an elevation in the endogenous levels of urinary taurine, creatine and bile acids has been reported to be associated with exposure of rats to the hepatotoxic agents α-naphthyl isothiocyanate and D-(+)-galactosamine (Beckwith-Hall *et al.* 1998). Furthermore, the ability of this technique to differentiate between the urinary profile of endogenous metabolites collected from rats following exposure to nephrotoxins that act at either the renal papilla (i.e. 2-bromoethanamine) or the proximal tubule (i.e. mercury (II)

* Author for correspondence; e-mail: becky.williams@syngenta.com

Xenobiotica ISSN 0049–8254 print/ISSN 1366–5928 online © 2002 Taylor & Francis Ltd
http://www.tandf.co.uk/journals
DOI: 10.1080/00498250210143047

chloride) has been demonstrated (Holmes *et al.* 1992). In addition to contributing to the biochemical and toxicological understanding of xenobiotics, the technique has also been successfully applied to the determination of factors governing physiological and biochemical variation within control populations (Gavaghan *et al.* 2000, Bollard *et al.* 2001, Tate *et al.* 2001). Recent work has demonstrated that urine from mice, analysed by ^{1}H-NMR spectroscopy, can be distinguished based on the genetic background of the animal (Gavaghan *et al.* 2000). Furthermore, metabolic variation has been characterized in urine collected from rat at different intervals during the day (Bollard *et al.* 2001, Tate *et al.* 2001) and at different stages of the oestrus cycle in the female rat (Bollard *et al.* 2001).

Currently, we are using this approach in our laboratories to aid in the safety evaluation of potential agrochemical products. Recent studies have suggested that urine obtained from the control Alderley Park (AP; Wistar-derived) rat can be separated into two distinct metabolic profiles when analysed using ^{1}H-NMR spectroscopy. Typically, 50% of the animals obtained from the breeding unit were found to excrete significant amounts of hippuric acid (HA) and low levels of *m*-(hydroxyphenyl)propionic acid (*m*-HPPA). The remaining rats, which excreted low levels of HA, excreted large amounts of *m*-HPPA. It was assumed that this was a local phenomenon, until we learned of the same distinction in urinary metabolic profile reported in the male Sprague–Dawley rat in a separate laboratory (Gavaghan *et al.* 2001).

The presence of two distinct subgroups within a control population of rats is the cause of fundamental difficulties when aiming to apply multivariate data analysis to the ^{1}H-NMR spectra acquired in our studies. Furthermore, it is possible that the biochemical or physiological parameters that lead to the observed distinction may contribute to variation between individual animals in experimental studies.

Previous work with the AP rat has reported that an alteration in the diet can cause the urinary metabolic profile to alter in the aromatic region of the ^{1}H-NMR spectrum. Rats fed an SDS diet excreted *m*-HPPA as the major urinary aromatic metabolite. However, when the diet was changed to a Teklad diet *m*-HPPA excretion was replaced by HA (Phipps *et al.* 1998). Although it was suggested that the change in urinary profile was related to a difference in the dietary precursors available in the two diets used, on return to the SDS diet HA excretion was maintained. Consequently, it was proposed that a modification in the activity or components of the intestinal microflora might also be involved in altering the urinary output of *m*-HPPA and HA in these animals (Phipps *et al.* 1998, Gavaghan *et al.* 2001).

Substantial evidence exists to associate the activity of intestinal microflora with the production of *m*-HPPA and other phenolic acid-related metabolites in the rat (Scheline 1968, Peppercorn and Goldman 1972, Smith and MacFarlane 1996). The contents of the rat caecum are capable of metabolizing several phenolic compounds, the main reactions being reduction, dehydroxylation, demethylation and decarboxylation (Scheline 1968). For example, it was demonstrated that 3,4-dihydroxycinnamic acid (caffeic acid) could be reduced and dehydroxylated to *m*-HPPA by caecal bacteria.

The aim was to determine the reason for the presence of two different urinary profiles (as determined by ^{1}H-NMR spectroscopy) within a control rat population. The first part of the study monitored urinary *m*-HPPA and HA levels in control

rats to characterize the two groups and determine the stability of the two profiles over time. Second, we investigated the effect of intestinal microflora on the ^{1}H-NMR spectroscopy urinary profile using antibiotics to sterilize the intestine and suppress the microflora. Finally, the levels of *m*-HPPA and phenylpropionic acid (PPA; a major precursor for HA synthesis in the liver) were analysed in the caecum and colon to determine whether the intestinal production of these phenolic acid-related metabolites differs in the two groups of animals.

Materials and methods

Materials

Deuterium oxide was purchased from Fluorochem Ltd (Glossop, UK). *m*-HPPA was from Lancaster Synthesis (Morecambe, UK). All other chemicals were from Sigma Aldrich (Poole, UK).

Animal treatment

Male Alderley Park (AP; Wistar-derived) rats (190–220 g) were obtained from the animal breeding unit at Alderley Park. Rats were either housed individually in metabolism cages for the collection of urine or were housed five per cage according to the experimental protocol. Controlled humidity (30–70%), temperature ($22 \pm 3\,^{\circ}$C) and a 12-h light/dark cycle were maintained. The animals' bodyweight and clinical observations were recorded immediately before housing in metabolism cages. Measurements were repeated every 24 h in situations where animals were housed in metabolism cages for > 24 h. All animals had free access to food (RM-1 diet; Special Diet Services; Witham, UK) and water throughout the study. Animal procedures were performed in accordance with licenses issued under the Animals (Scientific Procedures) Act 1986.

Experimental protocols

All urine samples were collected frozen over dry ice and analysed within 4 h of defrosting in order to exclude artefacts arising from sample collection.

Characterization of urinary metabolic profile

To characterize and monitor the urinary metabolic profile of the rat, two separate experimental protocols were used.

Initial study. Twenty animals were allowed to acclimatize at the Central Toxicology Laboratory (CTL) for 6 days before going into metabolism cages. Urine was then collected from all of the animals at 12-h intervals for 96 h.

Profile stability. Ten animals were obtained from the breeding unit (five from floor A, five from floor B) and immediately housed in metabolism cages for the collection of urine over 24 h (day 1 of the study). The animals were then rehoused in stock cages with those animals from floor A in one cage and those from floor B in a second cage. Further 24-h urine samples were collected on days 7, 14, 21, 28 and 35; on the intervening days, the animals were returned to their stock cages.

Effect of antibiotic treatment on the urinary metabolic profile

Twenty animals were obtained from the breeding unit (10 from floor A, 10 from floor B) and housed in stock cages according to the floor that they originated from. The animals were allowed to acclimatize at CTL for 6 days and then 24-h urine samples were collected from all of the animals for 48 h. After 48 h, five HA excretors and five *m*-HPPA excretors were selected and dosed with a mixture of antibiotics (neomycin sulphate, 400 mg kg^{-1}; tetracycline hydrochloride, 200 mg kg^{-1}; bacitracin 200 mg kg^{-1} at 10 ml kg^{-1} p.o. in saline; Gingell *et al*. 1971) or saline (as control). The dose was administered every 12 h, for 48 h, to maintain suppression of the intestinal flora during the collection of a further two 24-h urine samples. At the end of the dosing regimen, the animals were killed by inhalation overdose (halothane) followed by exsanguination by cardiac puncture. The caecum was removed for examination of the bacterial species present in order to confirm suppression of the intestinal microflora.

Determination of the bacteriology of the caecum

Ten animals were obtained from the breeding unit (five from floor A, five from floor B) and immediately housed in metabolism cages for the collection of urine over 24 h. The rats were then killed by inhalation overdose (halothane) followed by exsanguination by cardiac puncture. The caecum was removed for examination of the bacterial species present.

Determination of m-HPPA and PPA content in the caecum and colon

Ten animals were obtained from the breeding unit (five from floor A, five from floor B) and immediately housed in metabolism cages for the collection of urine over 24 h. The rats were then killed by exposure to rising carbon dioxide followed by exsanguination by cardiac puncture. The colon and caecum were removed and the entire tissue, including the contents, was homogenized (Polytron) immediately in perchloric acid (6% v/v; 10 ml; 0 °C). The homogenate was centrifuged (1430*g*; 20 min; 4 °C) and then the pellet was resuspended in perchloric acid (6% v/v; 2 ml; 0 °C) before a second centrifugation step. The supernatants from each centrifugation were combined and neutralized using potassium hydroxide (3M). The neutralized extract was centrifuged (1430*g*; 20 min; 4 °C) and the resulting supernatant was submitted for analysis by LC-MS to quantitate *m*-HPPA and PPA levels.

Analytical procedures

Analysis of urine by ^{1}*H-NMR spectroscopy*. The samples were prepared according to the method of Holmes *et al.* (1998). Phosphate buffer (0.2 M Na_2HPO_4/0.2 m NaH_2PO_4, pH 7.4; prepared in D_2O) containing sodium 3(trimethylsilyl)propionate-2,2,3,3-d_4 (TSP; 0.5 mg TSP ml^{-1} buffer; quantitation and internal chemical shift reference standard) was added to each urine sample (250 µl buffer; 500 µl sample). The samples were then centrifuged (14 000*g*; 10 min; 4 °C) and 600 µl of each supernatant was placed into a 5-mm NMR tube (Wilmad).

^{1}H-NMR spectra were acquired using a Bruker DPX400 spectrometer operating at 400.13 MHz for proton spectroscopy. The standard 'noesypr1d' pulse sequence (Bruker Analytik GmbH, Germany) was used for data acquisition; this pulse sequence efficiently suppresses the large signal that arises from water. Sixty-four free induction decays were accumulated into 64 k data points with a spectral width of 8012.821 Hz, an acquisition time of 4.09 s and an interpulse delay of 2 s. A line broadening of 0.3 Hz was applied and the spectra were phase and baseline corrected.

The chemical shifts of *m*-HPPA and HA resonances were confirmed by the addition of standards. The resonances were integrated and the total number of mmoles of *m*-HPPA and HA in the entire urine sample were calculated by comparison of the integrals with the integral obtained from the TSP resonance. *m*-HPPA and HA levels were corrected for the bodyweight of the animal and expressed as a function of the collection time (µmoles kg^{-1} bodyweight.12 h or µmoles kg^{-1} bodyweight.24 h).

Caecal bacteriology. The caecal contents were plated onto the following growth media to characterize the bacterial species present: MacConkey (allows growth of Gram ± ve cocci and bacilli); Kanamycin (selective for *Clostridia perfringens*); Campylobacter (selective for *Campylobacter*); Listeria broth (selective for *Listeria*); Selente/XLD (selective for *Salmonella*). Where growth occurred, the bacterial species were identified using the API Lab identification kit and their presence recorded.

Analysis of m-*HPPA and PPA content in the caecum and colon*. The samples (10 µl) were injected onto a reversed-phase HPLC column (250 × 4.6 mm; Jupiter C18; 5 µm; Phenomenex, UK). The mobile phase, water (35%) and 0.1% formic acid in acetonitrile (65%), was delivered at 1 ml min^{-1}. The eluent was coupled directly to a mass spectrometer fitted with an atmospheric pressure chemical ionization source operating in the negative-ion mode. The instrument was set to monitor two multiple reactions: for *m*-HPPA, m/z 164.9 to 121.0 at a collision energy of 14 eV; for PPA m/z 148.9 to 105.0 at a collision energy of 12 eV. The collision gas used was nitrogen. For quantitation, calibration curves were prepared of the two standards, *m*-HPPA and PPA.

The HPLC system employed a Perkin Elmer series 200 (Perkin Elmer Ltd, Beaconsfield, UK); MS analysis was carried out using a Sciex API 365 triple quadruplole mass spectrometer (Applied Biosystems, Foster City, CA, USA).

Statistics

Data are the mean ± SD. The Student's *t*-test determined significant differences between measurements at the 5% level.

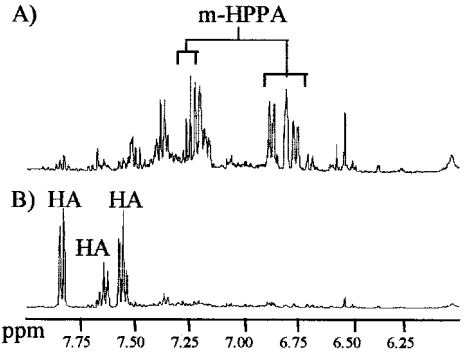


Figure 1. ^{1}H-NMR spectra (6.0–8.0 ppm) of urine obtained from two different rats demonstrating the different excretion profiles identified. (A) Spectrum of urine collected from a rat that excreted predominantly *m*-(hydroxyphenyl)propionic acid (*m*-HPPA). (B) Spectrum of urine collected from a rat that excreted predominantly hippuric acid (HA). Urine samples were collected from rats that had been acclimatized at CTL for 6 days and then had been in metabolism cages for 0–12 h.

Results

Characterization of urinary metabolic profile (initial study)

Analysis of the 0–12-h urine samples collected from untreated rats confirmed the presence of two distinct urinary profiles. Figure 1 shows the region of the ^{1}H-NMR spectrum of urine that is predominantly contributed to by resonances from aromatic compounds (6.00–8.00 ppm). Figure 1A is representative of the 10 urine samples characterized by the presence of phenolic acid-related metabolites, *m*-HPPA being the prominent metabolite. In these spectra, HA was either absent or barely detectable. These 10 animals were classified as *m*-HPPA excretors. Figure 1B is representative of the animals that had prominent HA resonances in the ^{1}H-NMR spectra of their urine; *m*-HPPA was present at low levels in these spectra. These 10 animals were classified as HA excretors. There were no other obvious perturbations in any other region of the spectrum.

Urinary HA levels were significantly higher in the urine collected from rats classed as HA excretors compared with rats classed as *m*-HPPA excretors for all eight urine samples collected over 96 h (figure 2A). The amount of *m*-HPPA excreted by the *m*-HPPA excretors was greater than for the HA excretors for the first four urine samples collected (0–48 h); however, after 48 h the urinary *m*-HPPA levels became indistinguishable (figure 2B). One rat, which was not included in the analysis shown in figure 2, exhibited an alteration in its urinary profile after 48 h. It was originally classified as an excretor of *m*-HPPA. HA excretion was low in this animal over the first 48 h in metabolism cages (14.33 ± 2.96 μmoles hippurate $kg^{-1}.12$ h). During the 48–60-h collection, a sharp rise in HA excretion was observed. The level of HA excreted in the urine by this animal continued to increase reaching 217.46 μmoles hippurate $kg^{-1}.12$ h by 84–96 h.

No difference was observed in the body weight of these animals when they were initially housed in the metabolism cages (after 6 days' acclimatization at CTL) (*m*-HPPA excretors $= 257.2 \pm 6.8$ g; HA excretors $= 258.0 \pm 10.3$ g). Additionally, no difference in body weight gain (%) was observed over the 96-h urine collection (*m*-HPPA excretors $= 8.64 \pm 1.61$; HA excretors $= 8.33 \pm 2.39$%).

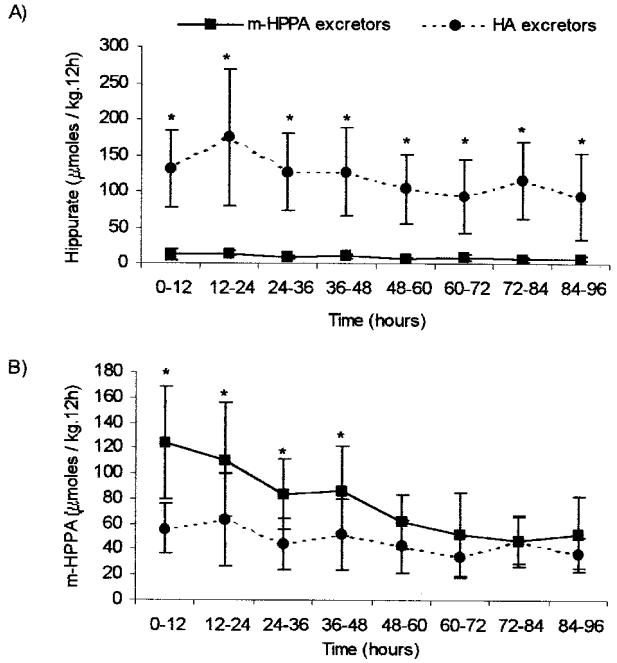


Figure 2. Quantitation of (A) hippuric acid (HA) and (B) *m*-(hydroxyphenyl)propionic acid (*m*-HPPA) (μmoles kg^{-1}.12 h) in urine obtained from rats. Urine samples were collected at 12 h intervals from rats that had been acclimatized at CTL for 6 days and then had been in metabolism cages for 96 h. *$p < 0.05$ *m*-HPPA excretors ($n = 9$) versus HA excretors ($n = 10$) at specified time points (Student's *t*-test). One rat is not included in this analysis as discussed in the text.

Enquiries into the origin of the animals used in this initial characterization study revealed that the animals that were classed as *m*-HPPA excretors originated from a different floor within the breeding unit than those classed as HA excretors. As a result of this observation, the remainder of the studies used groups of animals from different floors: A and B.

Characterization of urinary metabolic profile (profile stability)

Analysis of urine collected on day 1 at CTL and after 7 and 14 days allowed the separation of two distinct subgroups within the 10 animals (figure 3A, B; *m*-HPPA excretors, floor A and HA excretors, floor B). After 21 days at CTL and for the remainder of the study, the urinary *m*-HPPA and HA levels within the two groups were not statistically different. Figure 3C shows a typical spectrum obtained from a rat after 21 days at CTL, both HA and *m*-HPPA are present in the spectrum. The rat was initially an excretor of *m*-HPPA.

At the end of this study, the rats were 13 weeks old. To exclude the effect of age on the alteration of urinary profile over time, ten 13-week-old rats were obtained from the breeding unit (five from floor A, five from floor B) for the collection of a 24 h urine sample. Two subgroups were identified within these animals (*m*-HPPA: floor A, 141.4 ± 61.6; floor B, 27.7 ± 7.5; $p = 0.013$ (Student's *t*-test) HA: floor A, 15.0 ± 2.7; floor B, 316.7 ± 187.7; $p = 0.001$ (*t*-test) (μmoles kg^{-1}.24 h)).

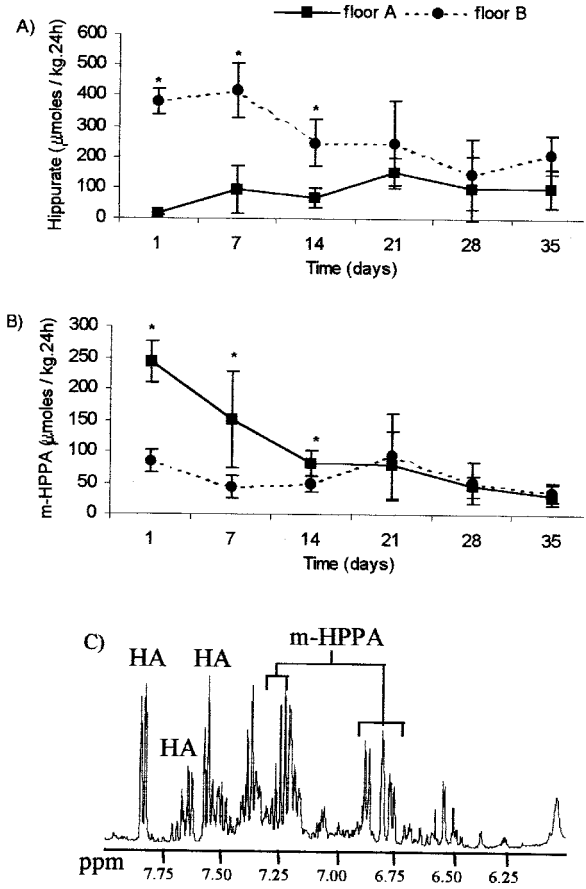


Figure 3. Quantitation of (A) hippuric acid (HA) and (B) *m*-(hydroxyphenyl)propionic acid (*m*-HPPA) (μmoles kg^{-1}.24 h) in urine obtained from rats. Urine samples were collected for 24 h from rats that had been at CTL for 1, 7, 14, 21, 28 and 35 days (with no prior acclimatization). The animals were housed in stock cages according to their initial excretion profile on the intervening days. *$p < 0.05$ floor A (*m*-HPPA excretors; $n = 5$) versus floor B (HA excretors; $n = 5$) at specified time points (Student's *t*-test). (C) Typical ^{1}H-NMR spectra (6.0–8.0 ppm) of urine obtained from a rat after housing at CTL for 21 days. The rat excretes significant amounts of both HA and *m*-HPPA. The rat was from floor A.

Effect of antibiotic treatment on the urinary metabolic profile

Before treatment with antibiotics, it was possible to identify two distinct subgroups within the 20 animals based on the excretion of *m*-HPPA and HA. There was a significant decrease ($p < 0.05$ compared with the predose value) in HA excretion in the urine of animals from floor B that were treated with antibiotics compared with saline (predose, 281.9 ± 166.6; saline, 216.6 ± 172.9; antibiotics 8.14 ± 1.69 moles HA kg^{-1}.24 h). Furthermore, *m*-HPPA excretion was significantly decreased ($p < 0.05$ compared with the predose value) in the urine of animals from floor A that were treated with antibiotics compared with saline (predose, 126.8 ± 41.1; saline, 80.8 ± 16.9; antibiotics, 8.8 ± 2.8 μmoles *m*-HPPA kg^{-1}.24 h). Figure 4 demonstrates the effect of antibiotic treatment on the aromatic region of the ^{1}H-NMR spectrum of urine for animals from floors A and B. Analysis of the bacterial species present in the caecum of these animals

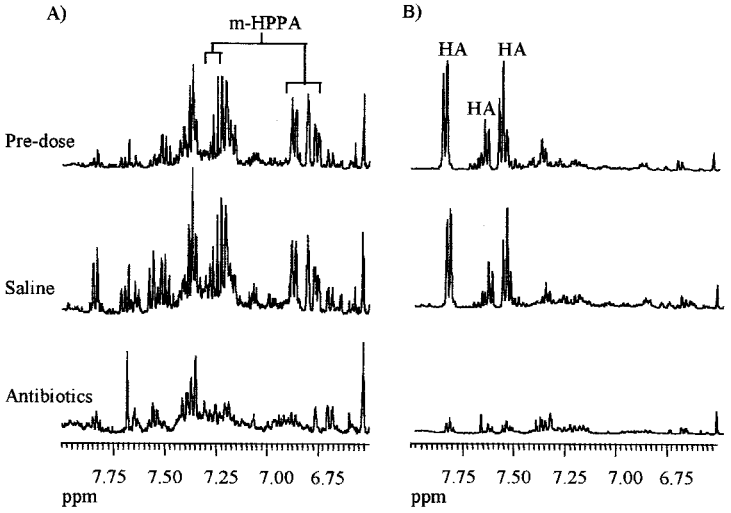


Figure 4. (A) ^{1}H-NMR spectra (6.5–8.0 ppm) of urine collected from rats obtained from floor A (excretors of *m*-(hydroxyphenyl)propionic acid (*m*-HPPA)). (B) ^{1}H-NMR spectra (6.5–8.0 ppm) of urine collected from rats obtained from floor B (excretors of hippuric acid (HA)). The predose urine was collected from each rat over 24 h immediately before the start of the dosing regimen. The post-dose urine was collected from each rat over 24 h starting 24 h after the initial dose of either saline or antibiotics.

confirmed that the antibiotic regimen had suppressed the bacterial growth (data not shown)

There was no difference in the body weight gain throughout the study between the animals from each floor and between those that were treated with antibiotics compared with saline (data not shown).

Determination of the bacteriology of the caecum

Urinary ^{1}H-NMR spectroscopic analysis confirmed the classification of these animals as *m*-HPPA or HA excretors according to their floor of origin within the breeding unit.

Streptococci and *E. coli* were present in the caecum of five out of five *m*-HPPA excretors (floor A) and five out of five HA excretors (floor B); *Proteus* spp. was present in four out of five animals from each floor and coagulase-negative *Staphylococcus* was found in four out of five *m*-HPPA excretors (floor A) and five out of five HA excretors (floor B).

Determination of m-HPPA and PPA content in the caecum and colon

Urinary ^{1}H-NMR spectroscopic analysis confirmed the classification of these animals as *m*-HPPA or HA excretors according to their floor of origin within the breeding unit.

The amount of *m*-HPPA present in the caecum did not differ between the two groups of animals; however, significantly more *m*-HPPA was present in the colon of animals from floor A compared with floor B. PPA was not detectable in either

Table 1. Quantitation of *m*-(hydroxyphenyl)propionic acid (*m*-HPPA) and phenylpropionic acid (PPA) in the caecum and colon obtained from rats from floor A (*m*-HPPA excretors) or floor B (hippurate excretors).

	m-HPPA (mmoles g^{-1} tissue)		PPA (mmoles g^{-1} tissue)	
	Floor A	Floor B	Floor A	Floor B
Caecum	0.67 ± 0.55	0.78 ± 0.17	n.d.	0.31 ± 0.13
Colon	0.31 ± 0.51	0.19 ± 0.05*	n.d.	0.45 ± 0.16

Data are mean ± SD with five animals in each group.
* $p < 0.05$ floor A versus floor B (Student's *t*-test). n.d., not detectable.

the caecum or colon obtained from animals from floor A whilst it was readily detected in these two regions in animals from floor B (table 1).

Discussion

Characterization of urinary metabolic profile

^{1}H-NMR spectroscopy of urine from rats confirmed the presence of two separate subgroups, *m*-HPPA and HA excretors, within the control population.

Considerable variability in the amount of HA present in rat urine has been reported in the literature. The level of urinary HA observed in this study for the HA excretors was comparable with that reported elsewhere (100–300 μmoles kg^{-1}.24 h) (Linhart and Smejkal 1987). A decrease in the level of urinary HA has previously been described as a result of housing Wistar rats in glass metabolism cages for 2 days following 14 days' acclimatization (Linhart and Smejkal 1987) suggesting that the animals' environment can affect HA excretion.

Enquiries into the origin of the animals revealed that the animals that excreted *m*-HPPA originated from a different floor within the breeding unit than those animals that excreted HA. All the animals were of the same genetic lineage and housed under the same environmental conditions, thus ruling out genetic and environmental differences as a factor in the distinction of the metabolic profiles. The diet received by the rats is derived from the same source and at any one time the same batch of diet is being fed to both groups of animals. Furthermore, whilst the animals were housed at CTL, body weight gain was comparable for both groups demonstrating that there was no significant difference in food intake. Therefore, in contrast to the observations of Phipps *et al.* (1998), differences in dietary precursors do not contribute to the observed distinction in urinary excretion profile reported in this study.

One of the animals used in the initial characterization study switched profile after it had been at CTL for 9 days, demonstrating that it is possible for the profile to alter. Monitoring of the urinary profiles over time demonstrated that within 3 weeks of arriving at CTL, HA and *m*-HPPA excretion levels were similar for both groups. Furthermore, when animals from each floor were housed together within the same cages, the excretion profiles became harmonized after only 7 days (unpublished data). Profile harmonization due to contact between the two groups of animals supports suggestions that differences in intestinal microflora might be responsible for the distinct profiles. Repopulation of the intestines of germ free rats with intestinal flora can be achieved by housing the rats in the cages of

conventional rats demonstrating the infectious nature of the intestinal bacteria (Kitamura *et al.* 1997). The breeding unit that these animals were obtained from is a barriered unit and therefore any cross-contamination with bacteria cannot occur between the separate floors. Transfer to CTL removes the animals from the barriered environment and will allow bacterial species present in the intestines to populate all animals.

Intestinal microflora metabolism

The intestines are inhabited by several hundred different species of bacteria that reside predominantly in the caecum and colon. Intestinal bacteria derive their growth nutrients from the fermentative degradation of various dietary residues including plant phenolic compounds and aromatic amino acids. Metabolites formed as a result of bacterial metabolism are absorbed in the caecum and colon.

Conjugated hydroxycinnamic acids, such as chlorogenic acid, are plant phenolic compounds metabolized by the intestinal microflora (the metabolic pathway is shown in Phipps *et al.* 1998). Caffeic acid, a product of the hydrolysis of chlorogenic acid by caecal and colonic bacteria (Couteau *et al.* 2001), is extensively metabolized by intestinal bacteria. The major pathway is the reduction of caffeic acid to 3,4-dihydroxyphenylpropionic acid followed by dehydroxylation to *m*-HPPA (Booth and Williams 1963, Scheline 1968). Finally, bacteria exist in the large intestine that can produce PPA by dehydroxylation of *m*-HPPA (Smith and MacFarlane 1996, Phipps *et al.* 1998). Aromatic amino acids, including tyrosine, tryptophan and phenylalanine, are also dietary precursors of phenolic acid-related metabolites (Smith and MacFarlane 1996). The metabolic endpoints of the intestinal metabolism of tyrosine include PPA and *m*-HPPA (Curtius *et al.* 1976). PPA is readily absorbed from the intestine (Cremin *et al.* 1995) and undergoes b-oxidation followed by glycine conjugation in the liver to produce HA (Scheline 1978). It has therefore been thoroughly documented that intestinal microflora are capable of producing *m*-HPPA as well as PPA as a precursor for HA synthesis in the liver.

HA and m*-HPPA excretion in the rat: involvement of intestinal microflora*

Sterilization of the intestine by treatment with antibiotics clearly demonstrated that the aromatic region of urinary ^{1}H-NMR spectra is dependent on the presence and activity of the intestinal microflora. These results indicate that the two distinct urinary profiles observed in this study could occur as a result of differences in the metabolism of compounds within the large intestines.

Different bacterial species have been reported to be capable of catalysing specific reactions involved in the production of phenolic acid-related metabolites (Peppercorn and Goldman 1971). For example, *Clostridium perfringens* can reduce caffeic acid to dihydrocaffeic acid, but cannot dehydroxylate dihydrocaffeic acid further to *m*-HPPA (Peppercorn and Goldman 1971). Whilst we have been unable to demonstrate specific differences in the bacterial species present in the caecum of the two groups of animal, it is likely to be a result of the limitations of the technique used. In particular, the procedure used does not fully evaluate anaerobes or specific strains of bacterial species; a full evaluation is outside the scope of this study.

Quantitation of the amount of *m*-HPPA and PPA present in the large intestine was, however, able to demonstrate a difference in the amount of these metabolites between the two groups of animals. In the colon, *m*-HPPA levels were greater in those animals from floor A, suggesting that these animals have a different metabolic capability with regard to their intestinal flora than those from floor B. This is strongly supported by analysis of PPA. PPA was not detectable in the caecum or colon of animals from floor A corresponding to the absence of HA in their urine. In contrast, the animals from floor B produced readily detectable amounts of PPA.

Conclusions

This study has demonstrated that the level of urinary HA and *m*-HPPA can be affected by differences in the metabolic capability of the intestinal microflora. Furthermore, using ^{1}H-NMR spectroscopic analysis of urine it is possible to detect alterations to the intestinal microflora, thus providing information that may help in understanding physiological variations that occur within control populations. The toxicological implications of an altered metabolic capability of the intestinal microflora is clearly of importance. Extensive work has been carried out demonstrating the involvement of intestinal microflora in the metabolism of orally dosed xenobiotics (Wheeler *et al*. 1975, Rowland *et al*. 1977, Kitamura *et al*. 1997). The work reported here has demonstrated the importance of the acclimatization period when using animals for experimental studies. An acclimatization period of 7 days before the use of these animals for toxicological studies provides control data that is suitable for analysis by multivariate data analysis as well as allowing the intestinal microflora to become consistent within all of the animals.

Acknowledgements

The authors thank June MacKay and Bruce Wilson for their work in determining the bacteriology of the caecum. They also thank Ted Lock and Doug Brown for helpful discussions during the course of this work.

References

Beckwith-Hall, B. M., Nicholson, J. K., Nicholls, A. W., Foxall, P. J., Lindon, J. C., Connor, S. C., Abdi, M., Connelly, J. and Holmes, E., 1998, Nuclear magnetic resonance spectroscopic and principal components analysis investigations into biochemical effects of three model hepatotoxins. *Chemical Research in Toxicology*, **11**, 260–272.

Bollard, M. E., Holmes, E., Lindon, J. C., Mitchell, S. C., Branstetter, D., Zhang, W. and Nicholson, J. K., 2001, Investigations into biochemical changes due to diurnal variation and estrus cycle in female rats using high-resolution (1)H-NMR spectroscopy of urine and pattern recognition. *Annals in Biochemistry*, **295**, 194–202.

Booth, A. N. and Williams, R. T., 1963, Dehydroxylation of caffeic acid by rat and rabbit caecal contents and sheep rumen liquor. *Nature (London)*, **198**, 684–685.

Couteau, D., McCartney, A. L., Gibson, G. R., Williamson, G. and Faulds, C. B., 2001, Isolation and characterisation of human colonic bacteria able to hydrolyse chlorogenic acid. *Journal of Applied Microbiology*, **90**, 873–881.

Cremin, J. D., Jr, Drackley, J. K., Hansen, L. R., Grum, D. E., Odle, J. and Fahey, G., C. Jr, 1995, Effects of glycine and bovine serum albumin on inhibition of propionate metabolism in ovine hepatcoytes caused by reduced phenolic monomers. *Journal of Animal Science*, **73**, 3009–3021.

Curtius, H., Mettler, M. and Ettlinger, L., 1976, Studies of the intestinal tyrosine metabolism using stable isotopes and gas chromatography–mass spectrometry. *Journal of Chromatography*, **126**, 569–580.

Gavaghan, C. L., Holmes, E., Lenz, E., Wilson, I. D. and Nicholson, J. K., 2000, An NMR-based metabonomic approach to investigate the biochemical consequences of genetic strain differences: application to the C57BL10J and Alpk:ApfCD mouse. *FEBS Letters*, **484**, 169–174.

Gavaghan, C. L., Nicholson, J. K., Connor, S. C., Wilson, I. D., Wright, B. and Holmes, E., 2001, Directly coupled high-performance liquid chromatography and nuclear magnetic resonance spectroscopic with chemometric studies on metabolic variation in Sprague–Dawley rats. *Annals in Biochemistry*, **291**, 245–252.

Gingell, R., Bridges, J. W. and Williams, R. T., 1971, The role of intestinal flora in the metabolism of prontosil and neoprontosil in the rat. *Xenobiotica*, **1**, 143–156.

Holmes, E., Bonner, F. W., Sweatman, B. C., Lindon, J. C., Beddell, C. R., Rahr, E. and Nicholson, J. K., 1992, Nuclear magnetic resonance spectroscopy and pattern recognition analysis of the biochemical processes associated with the progression of and recovery from nephrotoxic lesions in the rat induced by mercury(II) chloride and 2-bromoethanamine. *Molecular Pharmacology*, **42**, 922–930.

Holmes, E., Nicholls, A. W., Lindon, J. C., Ramos, S., Spraul, M., Neidig, P., Connor, S. C., Connelly, J., Damment, S. J. P., Haselden, J. and Nicholson, J. K., 1998, Development of a model for classification of toxin-induced lesions using ^{1}H-NMR spectroscopy of urine combined with pattern recognition. *NMR in Biomedicine*, 11, 235–244.

Kitamura, S., Sugihara, K., Kuwasako, M. and Tatsumi, K., 1997, The role of mammalian intestinal bacteria in the reductive metabolism of zonisamide. *Journal of Pharmaceutics and Pharmacology*, **49**, 253–256.

Linhart, I. and Smejkal, J., 1987, Changes in the excretion of endogenous glycine conjugate as a possible artifact in toxicological experiments. *Archives in Toxicology*, **61**, 83–85.

Nicholson, J. K., Lindon, J. C. and Holmes, E., 1999, 'Metabonomics': understanding the metabolic responses of living systems to pathophysiological stimuli via multivariate statistical analysis of biological NMR spectroscopic data. *Xenobiotica*, **29**, 1181–1189.

Peppercorn, M. A. and Goldman, P., 1971, Caffeic acid metabolism by bacteria of the human gastrointestinal tract. *Journal of Bacteriology*, **108**, 996–1000.

Peppercorn, M. A. and Goldman, P., 1972, Caffeic acid metabolism by gnotobiotic rats and their intestinal bacteria. *Proceedings of the National Academy of Sciences, USA*, **69**, 1413–1415.

Phipps, A. N., Stewart, J., Wright, B. and Wilson, I. D., 1998, Effect of diet on the urinary excretion of hippuric acid and other dietary-derived aromatics in rat. A complex interaction between diet, intestinal microflora and substrate specificity. *Xenobiotica*, **28**, 527–537.

Rowland, I., Davies, M. and Grasso, P., 1977, Biosynthesis of methylmercury compounds by the intestinal flora of the rat. *Archives of Environmental Health*, **32**, 24–28.

Scheline, R. R., 1968, Metabolism of phenolic acids by the rat intestinal microflora. *Acta Pharmacologica et Toxicologica*, **26**, 189–205.

Scheline, R. R., 1978, Metabolism of acids, lactones and esters. In R. R. Scheline (ed.), *Mammalian Metabolism of Plant Xenobiotics* (New York: Academic Press), 70.

Smith, E. A. and MacFarlane, G. T., 1996, Formation of phenolic and indolic compounds by anaerobic bacteria in the human large intestine. *Microbial Ecology*, **33**, 180–188.

Tate, A. R., Damment, S. J. P. and Lindon, J. C., 2001, Investigation of the metabolite variation in control rats urine using ^{1}H-NMR spectroscopy. *Annals in Biochemistry*, **291**, 17–26.

Wheeler, L. A., Soderberg, F. B. and Goldman, P., 1975, The relationship between nitrogroup reduction and the intestinal microflora. *Journal of Pharmacology and Experimental Therapeutics*, **194**, 135–144.

XENOBIOTICA, 2002, VOL. 32, NO. 9, 795–807

Taylor & Francis
healthsciences

Biotransformation of cyclizine in greyhounds. 1: identification and analysis of cyclizine and some basic metabolites in canine urine by gas chromatography-mass spectrometry

M. C. DUMASIA*, L. GRAINGER and E. HOUGHTON

Department of Drug Metabolism, Research Division, Horseracing Forensic Laboratory Ltd, PO Box 150, Newmarket Road, Fordham, Ely CB7 5WP, UK

Received 17 January 2002

1. The partial *in vivo* biotransformation of Marezine® [(cyclizine.HCl); 1-diphenylmethyl-4-methylpiperazine hydrochloride] in the racing greyhound and the excretion of the unconjugated and conjugated (Phase II) basic metabolites of cyclizine in canine urine are reported.

2. Using copolymeric bonded mixed-mode solid-phase extraction cartridges, the basic isolates from both unhydrolysed and enzyme hydrolysed urine samples were isolated, derivatized as trimethylsilyl ethers and analysed by positive-ion electron ionization gas chromatography-mass spectrometry (EI^+-GC-MS). Selected samples were analysed by positive-ion methane chemical ionization (CI^+)-GC-MS to aid structure elucidation of the putative metabolites.

3. Cyclizine was the major component excreted in post-administration urine. Five substrate-related basic compounds (M1 → M5) were tentatively identified by EI^+- and CI^+-GC-MS. The major Phase I metabolite was identified as norcyclizine [1-diphenylmethylpiperazine] (M1), the other metabolites (M2 → M5) were tentatively identified as monohydroxylated products based on MS data.

4. Cyclizine and the N_4-desmethyl metabolite (M1) are excreted unconjugated; the other four hydroxylated metabolites are excreted as Phase II conjugates (glucuronides and/or sulphates). Structures of the putative basic metabolites are presented. At least four other basic metabolites were also detected in post-administration urine, but could not be characterized from GC-MS data.

5. All unhydrolysed post-administration urine samples were analysed by selected ion monitoring EI^+-GC-MS to quantify cyclizine and norcyclizine (M1) using authentic cyclizine as the analyte and chlorcyclizine as the internal standard. The level of M1 is expressed as 'cyclizine equivalents'. The duration of urinary elimination of cyclizine and M1 was obtained from their excretion profiles.

6. From these studies, cyclizine and norcyclizine (M1) would be the target compounds of choice in the development of screening and confirmatory methods for the detection of cyclizine administration to racing greyhounds. Information on any of the other metabolites may also be of some value for confirmatory analysis.

Introduction

Cyclizine is an antihistaminic (H1 antagonist), anticholinergic and anti-emetic drug of the diphenylmethane class used for the prevention and treatment of nausea, vomiting and dizziness of motion sickness (Walder and Aitkenhead 1994, Weinstein and Stern 1997, Cholwill *et al.* 1999). Possible side-effects such as blurred vision and dry mouth, nose and throat are due to its anticholinergic

* Author for correspondence; e-mail: mdumasia@hfl.co.uk

Xenobiotica ISSN 0049–8254 print/ISSN 1366–5928 online © 2002 Taylor & Francis Ltd
http://www.tandf.co.uk/journals
DOI: 10.1080/00498250210144802

properties. There are also effects due to its antihistaminic properties such as drowsiness, although cyclizine has a less sedative effect than promethazine and dimenhydrinate (Pendse and Madan 1969). Cyclizine may aggravate heart disease, as well as causing intestinal and urinary problems. It may also have hypotensive action (Madan and Pendse 1969) and teratogenic effects (Sadusk and Palmisano 1965). Fatalities resulting from its use and overdose have been reported (Backer *et al*. 1989). Therefore, cyclizine should only be administered to dogs in good overall health. The dose of the drug depends on the size of the dog. Tablets are administered 20–30 min before travelling and the dose may be repeated every 4–6 h.

The determination of some diphenylmethane antihistaminics by solid-phase extraction (SPE) and GC with surface ionization detection (Hattori *et al*. 1992), GC-MS (Seno *et al*. 1993) and by headspace solid-phase micro-extraction capillary GC-MS (Nishikawa *et al*. 1997) has been reported. Solid-phase cation-exchange extraction of basic drugs from greyhound urine has been described (Moore 1990). The determination of cyclizine and norcyclizine in biological fluids by gas–liquid chromatography with nitrogen-selective detection (Land *et al*. 1981, Griffin and Baselt 1984) and high-performance liquid chromatography with coulometric detection (Walker and Kanfer 1995) has also been reported. The importance of tissue and plasma protein binding in the retention of norcyclizine in man, dog and rat has also been reported (Kuntzman *et al*. 1967).

In the current study, after a single dose oral administration to racing greyhounds, cyclizine and its *in vivo* Phase I basic metabolites were isolated from hydrolysed urine using copolymeric mixed-mode cartridges as described (Dumasia and Houghton 1991, Dumasia *et al*. 2002), and analysed, both qualitatively and quantitatively, by EI^+-GC-MS. The compounds were characterized by CI^+-GC-MS.

The objective was to identify suitable urinary metabolites indicative of cyclizine (Marezine®) administration that could be used as analytes to develop methods to detect and confirm its possible abuse/misuse in racing greyhounds. In addition, semiquantitative analysis of metabolites was performed to determine urinary excretion profiles, indicate a detection period for this drug and give an estimated concentration of the analyte in a particular sample.

Materials and methods

Chemicals and reagents

Glass distilled-grade organic solvents were purchased from Rathburn Chemicals Ltd (Walkerburn, UK). Marezine® tablets (50 mg, scored tablets as HCl) were obtained from Himmel Pharmaceuticals, Inc. (North Lake Worth, FL, USA). β-Glucuronidase from *Helix pomatia* [G 7017, type HP2; a mixture of β-glucuronidase (EC 3.2.1.31); 100 000 units ml^{-1} and aryl sulfatase enzymes, ≥7500 units] and *N*-methyl-*N*-(trimethylsilyl)trifluoroacetamide (MSTFA) were obtained from Sigma Chemical Co. Ltd (Poole, UK). Bond-Elut Certify® mixed-mode SPE cartridges were obtained from Anachem (Luton, UK). Worldwide Monitoring XTRACT® mixed-mode solid-phase extraction cartridges (XRDAH, 150 mg, 3 ml) were obtained from Anachem (Luton, UK). A 20-port SPE vacuum extraction manifold was obtained from Whatman International Ltd (Maidstone, Kent, UK). Cyclizine.HCl ($C_{18}H_{22}N_2$.HCl, pure drug) and chlorcyclizine.HCl ($C_{18}H_{21}N_2Cl$.HCl, pure drug) used as the analyte and internal standard respectively were a gift from Burroughs Wellcome (Durham, NC, USA).

Animal administration

Animal administrations were performed at Racing Chemistry, Veterinary Diagnostic Laboratory, Iowa State University, Ames, IA, USA (Director: Professor W. Hyde). Two male greyhounds [dog 640

(6 years, 30 kg) and dog 4691 (6 years, 43 kg)] were used. Marezine® (1 tablet = 50.0 mg cyclizine. HCl ≡ 44.0 mg free base per animal) was administered orally, mixed with cat food. Urine samples were collected at 0 h (blank) and 2.5, 4.5, 8.5, 24, 33.5, 48, 51.5 and 72 h post-dose. For urine collection at each time point, the dogs were taken out into the yard, exercized, allowed to urinate naturally and the voided samples collected. The samples were stored at −20 °C and on completion of the collection period were transported frozen to the Horseracing Forensic Laboratory (UK) for analysis.

Sample preparation

For analysis of unconjugated (free) metabolites, each urine sample (1 ml) was made up to 5 ml with phosphate buffer (0.1 M, pH 6). For the determination of total metabolites, each urine aliquot was adjusted to pH 5.0 by addition of phosphate buffer (0.1 M, 4 ml) and hydrolysed with *H. pomatia* (20 µl; 50 °C, 2 h). After hydrolysis, the urine was adjusted to pH 6 for extraction.

Solid-phase extraction method

Samples (hydrolysed or non-hydrolysed) were centrifuged (15 min, 2000*g*). Supernatant (5 ml ≡ 1 ml neat urine) was applied on mixed mode SPE (Certify® or XTRACT®) columns primed with methanol (4 ml) and phosphate buffer (0.1 M, pH 6.0; 4 ml) and drawn through the columns at about 1 ml min^{-1}. The columns were washed with 1 M acetic acid (2 ml), dried under full vacuum suction for 5 min, then washed with methanol (5 ml) and dried again for 2 min. The retained basic metabolites were eluted with ethyl acetate: concentrated ammonia mixture (98:2 v/v; 5 ml). The solvents were removed under oxygen free nitrogen (OFN) at 60 °C and the residue derivatized as TMS ethers.

Derivatization

The urine isolates were dissolved in toluene (25 µl) and treated with MSTFA (25 µl). After vigorous mixing, the solution was heated at 80 °C for 30 min. After removal of the solvents under OFN at 60 °C, the derivatized extracts were dissolved in toluene (50 µl) for analysis by GC-MS in the EI^+ and methane CI^+ modes.

Full-scan GC-MS analysis for identification of metabolites

Samples were analysed using either a Fisons MD800 bench top GC-MS (for EI^+) or a Finnigan MAT TSQ 700 Triple Quadrupole mass spectrometer (for CI^+) interfaced to a Varian 3400 gas chromatograph. A BPX5 column (about 25 m × 0.25 mm id, 0.25 µm film thickness, SGE) was used with helium as carrier gas. The initial column temperature, 90 °C, was maintained for 1 min. The oven was then programmed at 15 °C min^{-1} to 320 °C and then maintained at 320 °C for 5 min. The injector and transfer line temperatures were 260 and 250 °C respectively. Aliquots (1 µl) of the derivatized urine isolates were injected in the splitless mode (1 min) using an autosamlper (CTC model A200S, Zwingen, Switzerland). Positive-ion EI and methane CI mass spectra were recorded at 70 eV. The ion source temperature was 150 °C. The mass spectrometer was operated in the repetitive scan mode with a scan time of 1.5 s for the mass range between 40 and 550 amu acquiring full-scan data from 8 to 18 min.

Semiquantitative analysis of cyclizine and norcyclizine

Semiquantitative analysis of the parent drug and its major metabolite norcyclizine was performed on unhydrolysed urine as the isolates were cleaner and the ion profiles less complex. The pre- and all post-administration samples from both administrations were analysed together. The 4.5-h urine voids from both dogs were initially diluted 1:5 and the 8.5-h voids were diluted 1:5 and 1:2 with phosphate buffer (pH 6). From all samples, 2 × 1-ml aliquots were taken for analysis. A calibration line (in duplicate) covering the range 0–500 ng ml^{-1} was constructed from calibration standards ($n = 6$) in phosphate buffer (0.1 M, pH 6, 1 ml) using cyclizine as the analyte. QC samples were prepared at 150 and 350 ng ml^{-1} in phosphate buffer (1 ml). Chlorcyclizine was used as the internal standard added at a constant level of 200 ng ml^{-1} to all samples. All samples were then made up to 5 ml with the addition of phosphate buffer (0.1 M, pH 6.0, 4 ml), vortex-mixed and centrifuged (15 min, 2000*g*). The unhydrolysed samples were extracted and derivatized as described above for qualitative analysis.

The derivatized isolates were analysed by SIM-EI^+-GC-MS using the Fisons MD800 bench top instrument acquiring data from 6 to 18 min. The ions (m/z) of interest acquired are shown in table 1.

Peak area integration, ion ratios, the calibration line and the concentration of the analytes in pre- and post-administration urine samples were obtained using the Mass Lynx™ automated quantification software program (version 6.11). For semiquantification, the peak area of the ion at m/z 165.2 was integrated for cyclizine, norcyclizine and chlorcyclizine. The calibration line was constructed for the peak area ratio (cyclizine/chlorcyclizine) against the amount (ng ml^{-1}) of fortified cyclizine. The non-weighted linear regression line of the peak area ratios was fitted over the entire concentration range to include the origin (0 ng point) and the urinary concentration of cyclizine (ng ml^{-1}) was determined for all samples. Since no authentic standard of norcyclizine was available as the analyte, the apparent

Table 1.

Channel	Ion (m/z)	Compounds detected
1	165.2	all basic metabolites
2	167.2	cyclizine and norcyclizine
3	194.2	cyclizine
4	207.2	cyclizine
5	252.3	norcyclizine
6	266.3	cyclizine

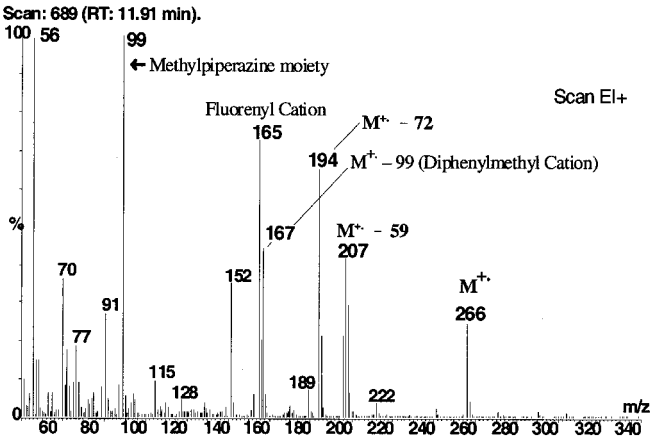


Figure 1. Full-scan EI^+ mass spectrum of authentic standard cyclizine.

norcyclizine concentration (ng ml^{-1}, as 'cyclizine equivalents') was determined from the peak area ratio of norcyclizine/chlorcyclizine using the cyclizine calibration line. The urinary excretion profiles of the apparent concentrations of cyclizine and norcyclizine against time after administration were plotted for each dog administration using the Fig-PWIN scientific processor (Biosoft, Cambridge, UK).

Results and discussion

GC-MS analysis of pre- and post-administration canine urine

Cyclizine and its Phase I metabolites are readily isolated by the copolymeric mixed-mode SPE cartridges using the targeted basic extraction procedure described previously (Dumasia and Houghton 1991, Dumasia *et al.* 2002). Substrate-related compounds that could be used as indicators of cyclizine administration to a greyhound were detected in the TMS-derivatized basic isolates of hydrolysed urine samples from both administrations by GC-MS. The parent drug and five substrate-related basic compounds (M1 → M5) were tentatively identified from their mass-spectral fragmentation patterns using EI^+ and methane CI^+ data.

The full-scan EI^+ mass spectrum of authentic cyclizine (figure 1) shows the molecular ion ($M^{+\cdot}$) at m/z 266, with fragment ions at m/z 207 ($M^{+\cdot}$ -59; $C_3H_9N^{\cdot}$), m/z 194 ($M^{+\cdot}$ -72; $C_4H_{10}N^{\cdot}$) and m/z 56 ($C_3H_8N^{\cdot}$) formed by proton transfers and scissions of the C-C and N-C bonds of the heterocyclic piperazine ring. The ion at m/z 167 ($C_{13}H_{11}^+$) can be attributed to the diphenylmethyl cation formed by cleavage of the diphenylmethylamino bond and loss of the methylpiperazine moiety as a radical. The abstraction of two protons from this ion results in the formation of the stable fluorenyl cation carbocycle ($C_{13}H_9^+$) at m/z 165. The ion at

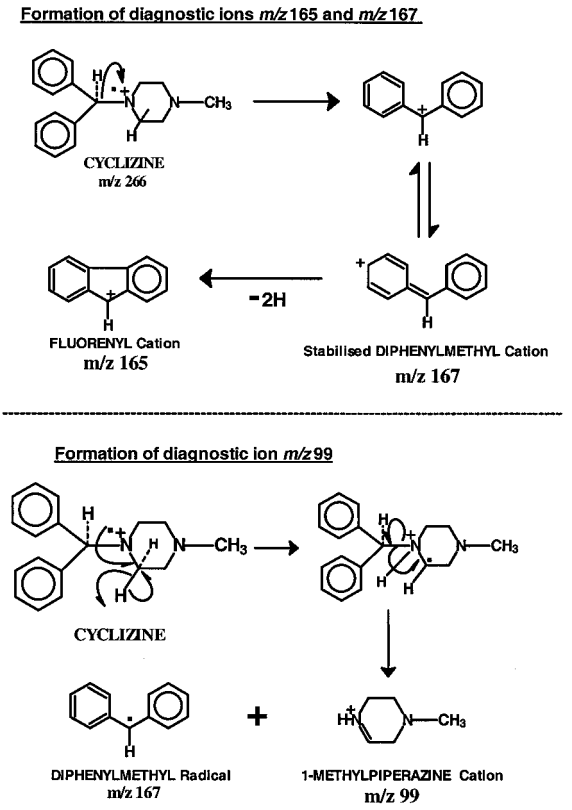


Figure 2. Proposed EI^+ fragmentation mechanisms for formation of the diagnostic ions m/z 165,167 and 99.

m/z 99 results from the charge retention on the *N*-methylpiperazine heterocycle and loss of the diphenylmethyl moiety as a radical. The proposed mechanisms for the formation of these diagnostic ions are shown in figure 2.

Figure 3a, b shows the total ion chromatograms (TIC) and mass chromatograms (ions m/z 167, 252, 266, 340 and 354) for the TMS-derivatized basic isolates of hydrolysed urine samples from one dog: (A) the predose urine showing negative responses and (B) the 4.5-h post-dose urine sample showing the presence of substrate-related peaks $1 \rightarrow 6$. Figure 4 shows the full-scan EI^+ mass spectra of peaks $1 \rightarrow 6$ (cyclizine and $M1 \rightarrow M5$ respectively) tentatively identified in the post-administration urine isolate. Similar data were obtained for the second animal. Only the parent drug and one metabolite were detected in unhydrolysed urine (data not shown).

The unchanged parent drug cyclizine was identified from a comparison of its retention time and mass spectrum (**1**, figure 4) with that of authentic standard (figure 1). The twin ions m/z 165/167, present in the spectra of cyclizine and of the compounds M1, M2 and M5 (figure 4), show that the unchanged diphenylmethylene substructure has been retained. Hydroxylation on either of the aromatic carbocycles (benzene rings) and formation of the *O*-TMS derivative results in an increase in the mass of this ion to m/z 255 (spectra M3 and M4; figure 4) and a molecular ion ($M^{+\cdot}$) at m/z 354. Aromatic oxidation (hydroxylation) is also reflected in the shift of the ions m/z 194 and m/z 207 present in cyclizine

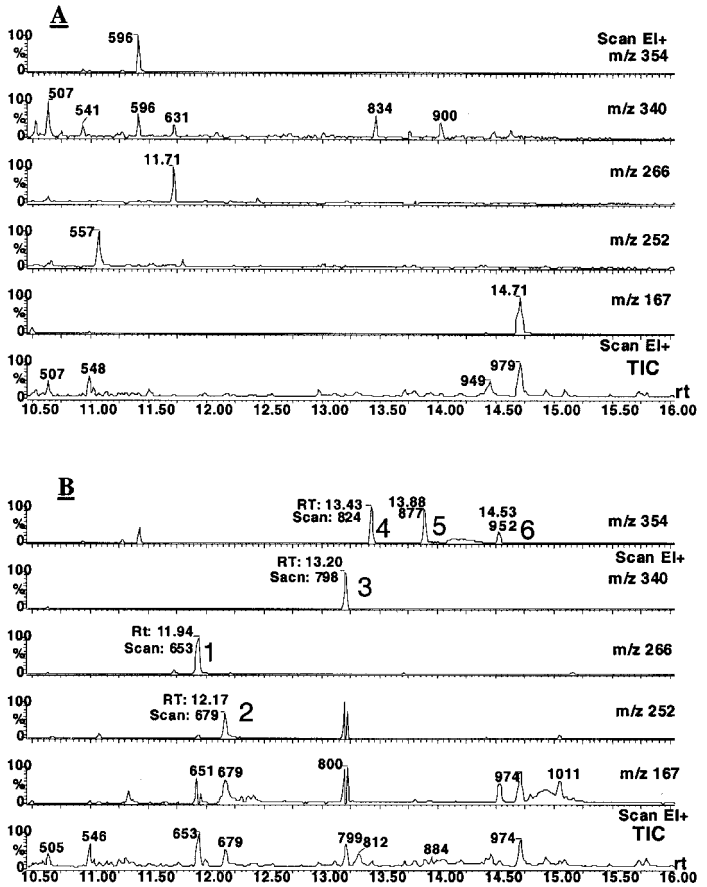


Figure 3. TIC and mass chromatograms of ions (m/z) 167, 252, 266, 340 and 354 associated with the major metabolites of cyclizine, obtained from the TMS-derivatized isolates of the hydrolysed (A) pre-administration blank dog urine sample showing negative responses and (B) 4.5 h post-administration urine sample from the same dog, showing positive responses. The diagnostic ions for the metabolites are: m/z 167 [common to all compounds ($1 \rightarrow 6$)], m/z 252 ($M^{+\cdot}$, norcyclizine; M1), m/z 266 ($M^{+\cdot}$, cyclizine), m/z 340 ($M^{+\cdot}$, hydroxynorcyclizine; M2), and m/z 354 ($M^{+\cdot}$, regio-isomers of hydroxycyclizine; M3 $\rightarrow$ M5).

(figure 1) by 88 u (O + TMS) to m/z 282 and 295 respectively. The ions at m/z 99 and 56 (seen in the mass spectra of cyclizine, M3, and M4, figure 4) indicate the unchanged N_4-methylpiperazine heterocycle. The ion at m/z 85, seen in the spectrum of M2 (norcyclizine, **2**; figure 4), represents demethylation at the N_4 heteroatom. Heterocyclic oxidation, however, is reflected by the absence of the ions m/z 85, 99 and 56, the presence of the twin ions m/z 165/167 and the concomitant increase in the derivatized molecular weight ($M^{+\cdot}$) to m/z 340 (M2) and 354 (M5). The derivatized molecular weights and fragmentation patterns of these metabolites were confirmed by methane CI^+-MS (figures 5 and 6). From these data, the structures (figure 10) attributed to the compounds detected by GC-MS (figure 4) were norcyclizine (M1), hydroxynorcyclizine (M2) and three regio-isomers of monohydroxycyclizine (M3 $\rightarrow$ M5).

Norcyclizine (M1) was the major unconjugated basic metabolite in canine urine. M2 was identified as hydroxynorcyclizine with oxidation occurring on the

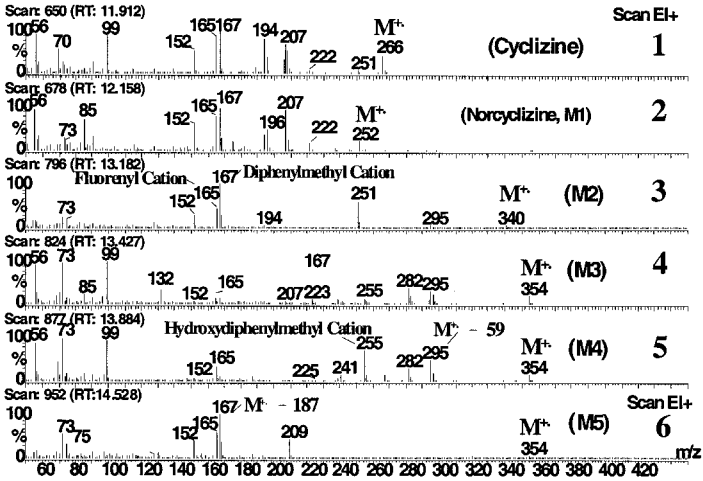


Figure 4. Positive-ion EI mass spectra of (1) underivatized cyclizine (1-diphenylmethyl-4-methylpiperazine), (2) underivatized norcyclizine (1-diphenylmethylpiperazine, M1), (3) hydroxynorcyclizine (1-diphenylmethyl-hydroxypiperazine (M2, as a *mono*-TMS derivative), (4, 5) two regio-isomers of monohydroxycyclizine (M3 and M4, hydroxylation on the phenyl ring, as *mono*-TMS derivatives) and (6) monohydroxycyclizine regio-isomer [M5, hydroxylated on the 4-methylpiperazine moiety (a carbinolamine), as a *mono*-TMS derivative] obtained from the TMS-derivatized isolate of a hydrolysed canine urine (4.5 h post-cyclizine administration).

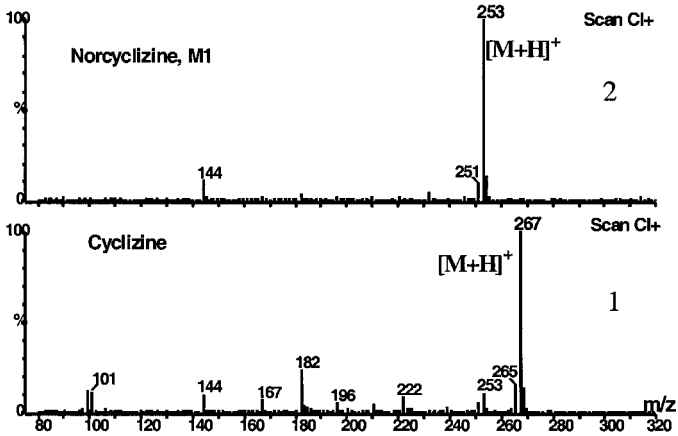


Figure 5. Full-scan positive-ion methane CI mass spectrum of (1) cyclizine and (2) norcyclizine (M1) obtained from the TMS-derivatized isolate of a hydrolysed canine urine sample (4.5 h post-administration).

piperazine substructure (either at N_4- or on carbons 2, 3, 5 or 6) resulting in the formation of either an *N*-hydroxy or a hemi-aminal (cyclic α-carbinolamine) type metabolite. The other three compounds (M3 → 5) were identified as monohydroxycyclizine regio-isomers. From the mass spectral data, the site of oxidation for the regio-isomers M3 and M4 can be attributed to the *para*, *ortho* or possibly *meta* positions on the phenyl ring. For the hydroxycyclizine regio-isomer M5, oxidation was again attributed to the piperazine ring and the resultant formation of a hemi-aminal type structure. The site of oxidation on carbons 2, 3, 5 or 6 of the piperazine ring could not be determined. At least four other compounds

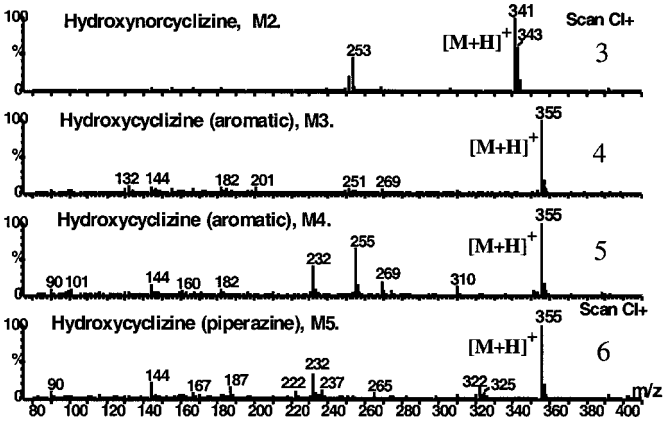


Figure 6. Full-scan positive-ion methane CI mass spectra of (3) hydroxynorcyclizine (M2) and (4 → 6) the three regio-isomers of hydroxycyclizine (M3 → M5) obtained from the TMS-derivatized isolate of a hydrolysed canine urine sample (4.5 h post-administration).

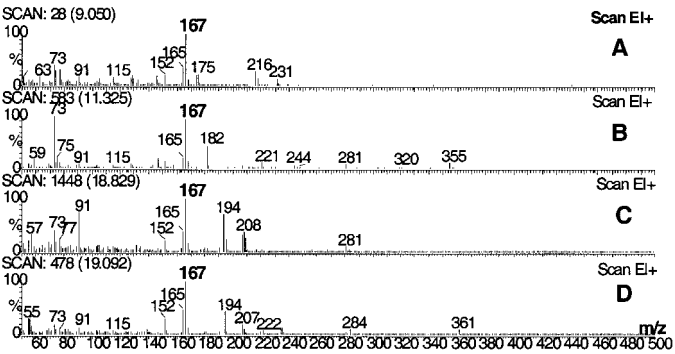


Figure 7. Positive-ion EI mass spectra of some *unidentified* cyclizine-related compounds (A → D), detected in and obtained from the TMS-derivatized isolate of the hydrolysed 4.5-h post-cyclizine administration canine urine sample. All spectra show the twin ions m/z 165 and 167 characteristic of compounds containing the diphenylmethylene moiety (m/z 167) and the subsequent formation of the fluorenyl cation (m/z 165). These compounds were detected in the post-administration urine isolates from both animals and were not present in the pre-administration blank urine.

containing the diphenylmethyl moiety and showing the doublet of ions m/z 165 and 167 (figure 7) were detected but are not characterized at present.

Semiquantification of cyclizine and metabolite in urine

Cyclizine and norcyclizine (M1) were the two major unconjugated compounds excreted in greyhound urine after oral administration. Cyclizine was quantified using chlorcyclizine as the internal standard. Since authentic reference standard for norcyclizine is unavailable, the concentration of this analyte was calculated as 'cyclizine equivalents' using the cyclizine calibration line. Following preparation of the calibration and pre- and post-administration samples, the isolates were derivatized (TMS) and analysed by GC-MS in the SIM mode as described. The peak area of the ion m/z 165 was integrated for both analytes as well as the internal marker. With respect to the internal standard, the calibration plot

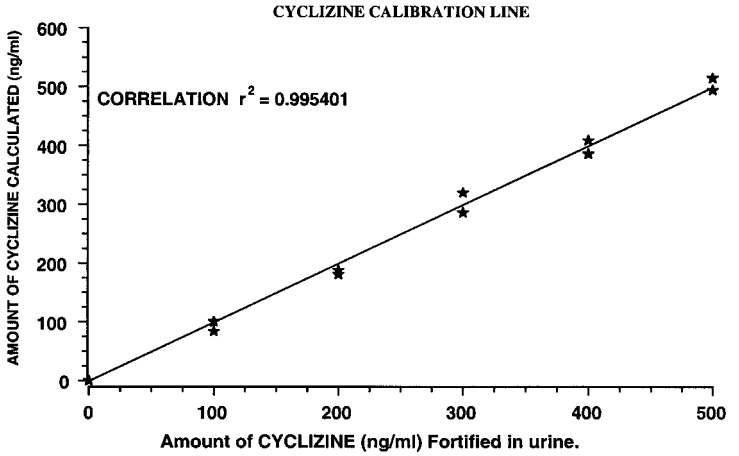


Figure 8. Typical calibration line obtained by SIM-GC-MS analysis for the semiquantification of total cyclizine in post-administration canine urine.

(figure 8) was linear in the range between 0 and 500 ng ml^{-1} (correlation coefficient 0.9954) and the responses of the internal marker and quality control samples were acceptable. The levels (ng ml^{-1}) of the two analytes in sequential urine samples were determined and the urinary excretion profiles of apparent concentration against time after drug administration were plotted.

The excretion profiles of cyclizine and norcyclizine for the two animal administrations are shown in figure 9a, b providing an indication of the clearance of the parent drug and its major metabolite in post-cyclizine administration greyhound urine. Both compounds were rapidly excreted and could be detected by SIR for up to 33 h in unhydrolysed post-administration canine urine.

Cyclizine metabolism

After oral administration of Marezine® to the racing greyhound, *in vivo* Phase I metabolism of cyclizine leads to the formation of several basic metabolites excreted/detected both as unconjugated and Phase II conjugates in post-administration urine samples. The parent drug and five substrate-related compounds (M1 → M5) were tentatively identified by GC-MS (figure 10). Cyclizine and the N_4-demethylated metabolite (norcyclizine; M1) were detected as unconjugated, the remainder (M2 → M5) after enzyme hydrolysis. The major EI-fragmentation pathways of cyclizine leading to the formation of the diagnostic ions m/z 99, 165 and 167 are shown in figure 2.

In the present study, the partial *in vivo* biotransformation of cyclizine in racing greyhounds leading to the formation of the basic Phase I metabolites has been shown to proceed via N_4-demethylation of the piperazine heterocycle and by aromatic and heterocyclic oxidations (hydroxylation). The major pathway involved the loss of the N_4-methyl moiety leading to the formation of norcyclizine. Either *N*- or *C*-oxidation of the piperazine heterocycle led to the formation of hydroxynorcyclizine (M2). Aromatic oxidations on the diphenylmethyl substructure led to the formation of two monohydroxycyclizine regio-isomers (M3 and M4). Heterocyclic (piperazine) ring oxidation gave rise to the third hydroxycyclizine

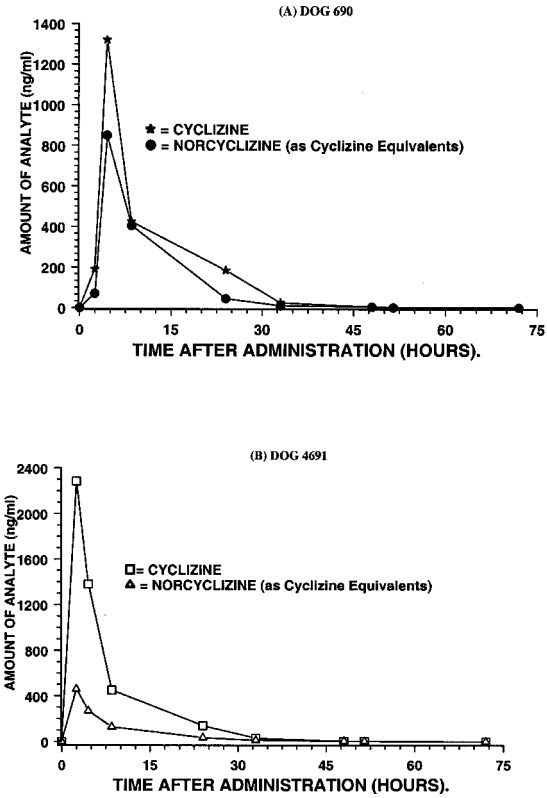


Figure 9. Urinary excretion profile of cyclizine and norcyclizine for (a) dog 690 and (b) dog 4691 after oral administration of Marezine® (50.0 mg) to each animal.

regio-isomer (M5). The hydroxylated metabolites are subjected to Phase II metabolism (conjugation with glucuronic and/or sulphuric acids). Oxidation of the piperazine ring and the identification of mono- and di-hydroxypiperazine metabolites have been previously reported for sildenafil (Walker *et al.* 1999), UK-343,664 (Walker *et al.* 2001) and CP93,393 (Prakash and Soliman 1997). The stability of carbinolamines in aqueous media has been reported by Urbansky (2000) and stable carbinolamine metabolites of a number of drugs have also been isolated (Jackson *et al.* 1991, Lang *et al.* 1997, Upthagrove and Nelson 2001).

A number of other basic metabolites were present (figure 7) but could not be identified. These could arise by formation of iminium species (Gorrod and Aislaitner 1994) or by oxidation of the α-carbinolamines to alicyclic amides (lactams) and further cleavages of the piperazine ring from both cyclizine and norcyclizine (Vickers and Polsky 2000). Following chronic administration of chlorcyclizine and meclizine to rats, metabolites containing an ethylenediamine group resulting from piperazine ring cleavages have been reported (Gaertner *et al.* 1973). No attempt was made in the present study to identify the Phase II conjugates of cyclizine or for any of its Phase I metabolites identified in canine urine, including the formation of quaternary ammonium-linked glucuronides reported previously (Luo *et al.* 1991, Hawes 1998, Kowalczyk 2000). The formation and identification of neutral and phenolic metabolites (benzhydrol, diphenyl-

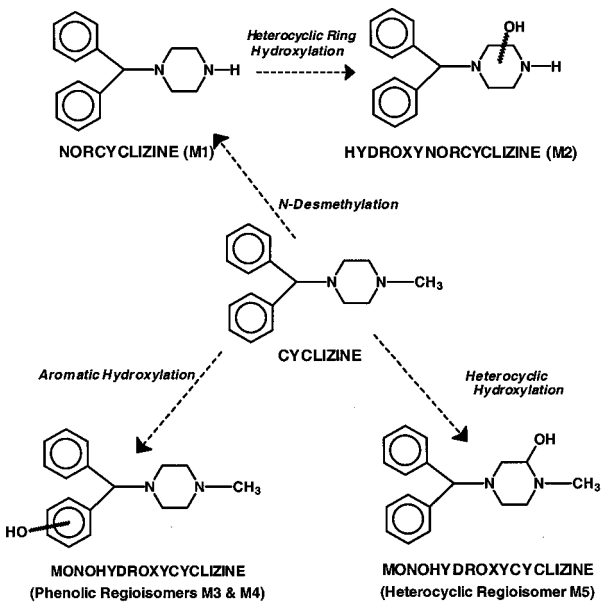


Figure 10. Partial *in vivo* biotransformation of cyclizine in the greyhound. The chemical structures of cyclizine and its putative basic metabolites are identified in canine urine by GC-MS.

methane, benzophenone and their secondary phenolic products) following N_1-dealkylation of cyclizine will be reported in (Dumasia 2002).

Conclusions

In the greyhound, a number of *in vivo* Phase I functionalization pathways were observed for the detoxification and elimination of cyclizine, leading to the formation of a large number of metabolites. In the present study, some of the basic metabolites were identified by EI^+-and CI^+-GC-MS from their derivatized (TMS) molecular weights ($M^{+\cdot}$), and an interpretation of their mass spectral fragmentation patterns. Neither authentic reference compounds nor literature data are available on all the metabolites. Phase II biotransformation (conjugation with either glucuronic acid or sulphate) was observed for some functionalized metabolites. Qualitative and semiquantitative analysis of the isolates of post-administration urine samples showed significant concentrations of unchanged cyclizine and norcyclizine in both animals. This compound (M1) along with the parent drug could be used as possible target indicator compound for the detection and confirmation of cyclizine administration to greyhounds by GC-MS.

From the urinary excretion profiles (figure 9), the peak urinary concentrations of cyclizine and norcyclizine were observed between 2.5 and 4.5 h for the two studies. From semiquantitative analysis, it was evident that significant concentrations of cyclizine were present in samples up to 24 h post-administration in both animals. Some variation in the metabolism and urinary excretion of cyclizine and its metabolite between the two animals was observed.

Using the analytical methods described here and depending on the level of the major metabolite in the urine, it should be possible to confirm the administration

of cyclizine by screening urine samples for the presence the parent drug and one of the major metabolites-norcyclizine.

Acknowledgements

This project was entirely funded by the National Greyhound Racing Club (NGRC) of Great Britain. Animal administrations were performed and the urine samples collected and provided by Professor Walter Hyde and staff at Racing Chemistry, Iowa State University, Ames, IA, USA.

References

Backer, R. C., McFeeley, P. and Wohlenberg, N., 1989, Fatality resulting from cyclizine overdose. *Journal of Analytical Toxicology*, **13**, 308–309.

Cholwill, J. M., Wright, W., Hobbs, G. J. and Curran, J., 1999, Comparison of ondansetron and cyclizine for prevention of nausea and vomiting after day-case gynaecological laparoscopy. *British Journal of Anaesthesia*, **83**, 611–614.

Dumasia, M. C., 2002, Biotransformation of cyclizine in greyhounds. 2: N_1-dealkylation and identification of some neutral and phenolic metabolites in canine urine by gas chromatography-mass spectrometry. *Xenobiotica*, **32**, 809–821.

Dumasia, M. C. and Houghton. E., 1991, Screening and confirmatory analysis of beta-agonists, beta-antagonists and their metabolites in horse urine by capillary gas chromatography-mass spectrometry. *Journal of Chromatography B: Biomedical Applications*, **564**, 503–513.

Dumasia, M. C., Houghton. E., Hyde, W., Greulich, D., Nelson, T. and Peterson, J., 2002, Detection of Fenspiride and identification of *in vivo* metabolites in horse body fluids by capillary gas chromatography-mass spectrometry: administration, biotransformation and urinary excretion after a single oral dose. *Journal of Chromatography B: Biomedical Sciences and Applications*, **767**, 131–144.

Gaertner, H. J., Breyer, U. and Liomin, G., 1973, Chronic administration of chlorcyclizine and meclizine to rats: accumulation of a metabolite formed by piperazine ring cleavage. *Journal of Pharmacology and Experimental Therapeutics*, **185**, 195–201.

Gorrod, J. W. and Aislaitner, G., 1994, The metabolism of alicyclic amines to reactive iminium ion intermediates. *European Journal of Drug Metabolism and Pharmacokinetics*, **19**, 209–217.

Griffin, D. S. and Baselt, R. C., 1984, Blood and urine concentrations of cyclizine by nitrogen-phosphorus gas–liquid chromatography. *Journal of Analytical Toxicology*, **8**, 97–99.

Hattori, H., Yamamoto, S., Iwata, M., Takashima, E., Yamada, T. and Suzuki, O., 1992, Determination of diphenylmethane antihistaminic drugs and their analogues in body fluids by gas chromatography with surface ionisation detection. *Journal of Chromatography*, **581**, 213–218.

Hawes, E. M., 1998, N^+-glucuronidation, a common pathway in human metabolism of drugs with a tertiary amine group. *Drug Metabolism and Disposition*, **26**, 830–837.

Jackson, C., Crabb, T. A., Gibson, M., Godfrey, R., Saunders, R. and Thurston, D. E., 1991, Studies on the stability of trimelamol, a carbinol containing antitumor drug. *Journal of Pharmaceutical Science*, **80**, 245–251.

Kowalczyk, I., Hawes, E. M. and McKay G., 2000, Stability and enzymatic hydrolysis of quaternary ammonium-linked glucuronide metabolites of drugs with an aliphatic tertiary amine-implications for analysis. *Journal of Pharmaceutical and Biomedical Analysis*, **22**, 803–811.

Kuntzman, R., Tsai, I. and Burns, J. J., 1967, Importance of tissue and plasma binding in determining the retention of norchlorcyclizine and norcyclizine in man, dog and rat. *Journal of Pharmacology and Experimental Therapeutics*, **158**, 332–339.

Land, G., Dean, K. and Bye, A., 1981, Determination of cyclizine and norcyclizine in plasma and urine using gas–liquid chromatography with nitrogen selective detection. *Journal of Chromatography*, **222**, 135–140.

Lang, D. H., Rettie, A. E. and Bocker, R. H., 1997, Identification of enzymes involved in the metabolism of atrazine, terbuthylazine, ametryne and terbutryne in human liver microsomes. *Chemical Research in Toxicology*, **10**, 1037–1044.

Luo, H., Hawes, E. M., McKay, G., Korchinski, E. D. and Midha, K. K., 1991, $N(^+)$-glucuronidation of aliphatic tertiary amines, a general phenomenon in the metabolism of H1-antihistamines in humans. *Xenobiotica*, **21**, 1281–1288.

Madan, B. R. and Pendse, V. K., 1969, Some cardiovascular actions of cyclizine, chlorcyclizine and homchlorcyclizine. *Indian Journal of Physiology and Pharmacology*, **13**, 113–121.

Moore, C. M., 1990, Solid-phase cation-exchange extraction of basic drugs from urine of racing greyhounds. *Journal of the Forensic Science Society*, **30**, 123–129.

Nishikawa, M., Seno, H., Ishii, A., Suzuki, O., Kumazawa, T., Watanabe, K. and Hattori, H. 1997, Simple analysis of diphenylmethane antihistaminics and their analogues in body fluids by headspace solid-phase microextraction-capillary gas chromatography. *Journal of Chromatographic Science*, **35**, 275–279.

Pendse, V. K. and Madan, B. R., 1969, Some pharmacological actions of cyclizine, chlorcyclizine and homochlorcyclizine. *Indian Journal of Physiology and Pharmacology*, **13**, 31–36.

Prakash, C. and Soliman, V., 1997, Metabolism and excretion of a novel anti-anxiety drug candidate CP-93,393 in Long–Evans rats. Differentiation of regioisomeric glucuronides by LC/MS/MS. *Drug Metabolism and Disposition*, **25**, 1288–1297.

Sadusk, J. F. and Palmisano, P. A., 1965, Teratogenic effect of meclizine, cyclizine, and chlorcyclizine *Journal of the American Medical Association*, **194**, 987–989.

Seno, H., Hattori, H., Kumazawa, T. and Suzuki, O. 1993, Positive- and negative-ion mass spectrometry of diphenylmethane antihistaminics and their analogues and rapid clean-up of them from biological samples. *Forensic Science International*, **62**, 187–208.

Upthagrove, A. L. and Nelson, W. L., 2001, Carbinolamines, imines and oxazolidines from fluorinated propranolol analogs. ^{19}F NMR and mass spectral characterization and evidence for formation as intermediates in cytochrome P450-catalysed *N*-dealkylation. *Drug Metabolism and Disposition*, **29**, 1114–1122.

Urbansky, E. T., 2000, Carbinolamines and geminal diols in aqueous environmental organic chemistry. *Journal of Chemical Education*, **77**, 1644–1647.

Vickers, S. and Polsky, S. L., 2000, Biotransformation of nitrogen containing xenobiotics to lactams. *Current Drug Metabolism*, **1**, 357–389.

Walder, A. D. and Aitkenhead, A. R., 1994, Anti-emetic efficacy of metoclopramide when induced in a patient-controlled analgesia infusion. *Anaesthesia*, **49**, 804–806.

Walker, D. K., Ackland, M. J., James, G. C., Muirhead, G. J., Rance, D. J., Wastall, P. and Wright, P. A., 1999, Pharmacokinetics and metabolism of sildenafil in mouse, rat, rabbit, dog and man. *Xenobiotica*, **29**, 297–210.

Walker, D. K., Beaumont, K. C., Comby, P., Evans, K. M., Gedge, J. I., Halliday, R. C., Roey, S. J. and Wright, P. A., 2001, Pharmacokinetics and metabolism of a selective PDE5 inhibitor (UK-343,664) in rat and dog. *Xenobiotica*, **31**, 651–654.

Walker, R. B. and Kanfer, I., 1995, Sensitive high-performance liquid chromatographic determination of cyclizine and its demethylated metabolite, norcyclizine, in biological fluids using coulometric detection. *Journal of Chromatography B: Biomedical Applications*, **672**, 172–177.

Weinstein, S. E. and Stern, R. M., 1997, Comparison of marezine and dramamine in preventing symptoms of motion sickness. *Aviation Space Environmental Medicine*, **68**, 890–894.

XENOBIOTICA, 2002, VOL. 32, NO. 9, 809–821

Taylor & Francis
healthsciences

Biotransformation of cyclizine in greyhounds. 2: N_1-dealkylation and identification of some neutral and phenolic metabolites in canine urine by gas chromatography-mass spectrometry

M. C. DUMASIA*

Department of Drug Metabolism, Research Division, Horseracing Forensic Laboratory Ltd, PO Box 150, Newmarket Road, Fordham, Ely CB7 5WP, UK

Received 17 January 2002

1. The *in vivo* enzymatic Phase I biotransformation of cyclizine (Marezine®) in the racing greyhound has been shown to proceed via several different pathways. Aromatic and heterocyclic oxidation and the N_4-demethylation of cyclizine lead to the formation of unconjugated and conjugated (Phase II) basic metabolites excreted in canine urine.

2. Enzymatic N_1-dealkylation of cyclizine and its basic metabolites leads to the formation of the neutral and phenolic Phase I metabolites containing the diphenylmethane/methylene substructures. Further, Phase I metabolism of the neutral metabolites could also lead to the formation of several secondary phenolic products. These neutral and phenolic compounds are then excreted as unconjugated and Phase II conjugates in greyhound urine.

3. Following enzymatic deconjugation of selected post-Marezine administration urine samples from two greyhounds, the total aglycones were extracted and separated into neutral/acidic and basic fractions using copolymeric mixed-mode solid-phase extraction cartridges.

4. The neutral/acid isolates were further separated into neutral and phenolic fractions by column chromatography on a lipophilic strong anion-exchanger gel, triethylaminohydroxypropyl Sephadex LH-20 in OH^- form.

5. The individual neutral and phenolic fractions obtained from the acid/neutral isolate were derivatized as trimethylsilyl ethers and analysed by positive-ion electron ionization gas chromatography-mass spectrometry (EI^+-GC-MS).

6. Three compounds, diphenylmethane (M1), benzophenone (or diphenyl ketone, M2) and benzhydrol (M3), were identified in the neutral isolates by comparison of their EI^+ mass spectra with authentic standards. At least seven secondary compounds containing the functionalized diphenylmethylene substructure were detected in the phenolic isolates. As no authentic compounds are available, the structures of these putative metabolites (M4 → M10) were elucidated from an interpretation of the EI^+-GC-mass spectra of their TMS derivatives.

Introduction

Cyclizine is an antihistaminic (H1 antagonist), anticholinergic and anti-emetic drug used for the prevention and treatment of nausea, vomiting and dizziness of motion sickness (Walder and Aitkenhead 1994, Weinstein and Stern 1997, Cholwill *et al*. 1999). Extraction of basic drugs from greyhound urine by solid-

* Author for correspondence; e-mail: mdumasia@hfl.co.uk

Xenobiotica ISSN 0049–8254 print/ISSN 1366–5928 online © 2002 Taylor & Francis Ltd
http://www.tandf.co.uk/journals
DOI: 10.1080/00498250210144794

phase cation-exchange columns has been reported by Moore (1990). Determination of the basic compounds cyclizine and norcyclizine in biological fluids by gas–liquid chromatography with nitrogen-selective detection (Land *et al*. 1981, Griffin and Baselt 1984) and high-performance liquid chromatography with coulometric detection (Walker and Kanfer 1995) has been reported previously.

Cycline is used to prevent motion sickness during the transport of the animals to various racetracks. In a previous study, after administration of a single oral dose of Marezine® (50.0 mg) to two racing greyhounds, cyclizine and five basic metabolites were isolated from hydrolysed post-administration urine by a targeted cation-exchange mixed-mode SPE method and characterized by EI^+ and positive-ion methane chemical ionization (CI^+)-GC-MS (Dumasia *et al*. 2002a). The objective was to identify suitable metabolites that could be used to develop routine screening and confirmatory procedures to detect the administration of cyclizine to the racing greyhound. In addition, excretion profiles were determined by semi-quantitative analysis to indicate a period for the detection of this drug in canine urine.

Cyclizine is one of a number of drugs that contain either a diphenylmethylene ether or a diphenylmethyleneamino group as part of the molecule. In 1949, Glazko and Dill suggested that benzhydrol and benzophenone might be metabolites of diphenhydramine, which is also an antihistaminic drug containing the benzhydrylether group. Since then several other drugs containing the diphenylmethyl group have been reported to yield diphenylmethane, benzhydrol, benzophenone and their substituted derivatives (Hespe *et al*. 1965, Narrod *et al*. 1965, Soudijn and van Wijnaarden 1968, Ellison 1972, Remberg *et al*. 1977). Kariya *et al*. (1992, 1996) identified benzophenone as a metabolite of cinnarizine in rat liver microsomes and described the enzymes involved in aromatic oxidation and *N*-dealkylation pathways. Kageura *et al*. (1986) identified 4-chlorodiphenylmethane and 4-chlorobenzophenone as metabolites of hydroxyzine in human urine. DeLoach *et al*. (1978), Stocklinski *et al*. (1979) and Stocklinski (1981) identified benzhydrol, 2- and 4-hydroxydiphenylmethane and 2,2′- and 4,4′-dihydroxydiphenylmethane as metabolites of diphenyl[^{14}C]ethane in rat urine, bile and faeces. Stocklinski *et al*. (1980) also identified *p*-hydroxybenzophenone as a metabolite of benzophenone in rat urine.

The present study was conducted specifically to determine conclusively the *in vivo* N_1-dealkylation pathway of Marezine® in the racing greyhound and to detect and characterize the formation of the neutral and phenolic metabolites containing only the diphenylmethane or diphenylmethylene substructures. To this end, some early (2.5–4.5 h) post-Marezine® administration canine urine samples were used to isolate the proposed metabolites. The isolation technique uses a combination of hydrolysis, solid-phase (liquid–solid) extraction (SPE), lipophilic anion exchange chromatography, derivatization and capillary column GC-MS, which permits the detailed determination of the neutral, phenolic and basic metabolites of Marezine® in canine urine. This paper describes the isolation, detection and EI^+-GC-MS characterization of diphenylmethane (M1), the primary neutral metabolite of cyclizine and some of the secondary Phase I functionalized metabolites (M2 → M10) formed *in vivo*. Some of these compounds also undergo Phase II biotransformations and are then excreted in greyhound urine as glucuronide and/or sulfoconjugates.

Materials and methods

Chemicals and reagents

Glass distilled-grade organic solvents were purchased from Rathburn Chemicals Ltd. (Walkerburn, UK). Marezine® tablets (50 mg, scored tablets as HCl) were obtained from Himmel Pharmaceuticals, Inc. (North Lake Worth, FL, USA). β-Glucuronidase from *Helix pomatia* [G 7017, type HP2; a mixture of β-glucuronidase (EC 3.2.1.31); 100 000 units ml^{-1} and aryl sulfatase enzymes, ≥7500 units], diphenylmethane (Fluka Chemie GmbH, Buchs, Switzerland), benzophenone and benzhydrol (Aldrich Chemie GmbH, Steinheim, Germany), *N*-methyl-*N*-(trimethylsilyl)trifluoroacetamide (MSTFA) and lipophilic Sephadex LH-20 were obtained from Sigma Chemical Co. Ltd (Poole, UK). Bond-Elut Certify® mixed-mode SPE cartridges (Part No. 12102082; Varian), Worldwide Monitoring XTRACT® mixed-mode SPE cartridges (XRDAH, 150 mg, 3 ml) and Sep-Pac® Vac C_{18} SPR cartridges (Part No. WAT043395; Waters Corp., Milford, USA) were obtained from Anachem (Luton, UK). A 20-port SPE vacuum extraction manifold was obtained from Whatman International Ltd (Maidstone, Kent, UK).

Synthesis of triethylaminohydroxypropyl Sephadex LH-20 (TEAP-LH-20)

The lipophilic strong anion exchange TEAP-LH-20 gel was synthesized according to the methods of Axelson and Sjövall (1977) and Axelson *et al.* (1981). It was stored at −20 °C in its acetate form. Before use, a required amount of the acetate was converted to its active OH^- form by washing with NaOH. It is stable in the active form for 1 month at 4 °C, and then can be regenerated by washing with NaOH.

Animal administration

Animal administrations were performed at Racing Chemistry, Veterinary Diagnostic Laboratory, Iowa State University, Ames, IA, USA (Director: Professor W. Hyde). Two male greyhounds [dog 640 (6 years, 30 kg) and dog 4691 (6 years, 43 kg)] were used. Marezine® (1 tablet = 50.0 mg cyclizine. HCl ≡ 44.0 mg free base per animal) was administered orally, mixed with cat food. Urine samples were collected predose and at 2.5, 4.5, 8.5, 24, 33.5, 48, 51.5 and 72 h post-dose. The samples were stored frozen at −20 °C and on completion of the collection period were transported frozen to the Horseracing Forensic Laboratory (UK) for analysis.

Extraction, hydrolysis and fractionation of urinary aglycones

Pre-administration blank (0 h) and post-Marezine® administration canine urine samples collected at 2.5 and 4.5 h from both animals were used. Sep-Pac® Vac C_{18} SPE columns were primed by successive washes with methanol (5 ml) and de-ionized water (5 ml). Blank and post-administration urine samples (10 ml) were centrifuged (2000*g*, 15 min) to remove solids. The clear supernatant was applied on and drawn through the columns at about 1 ml min^{-1}. The columns were washed with de-ionized water (5 ml) and *n*-hexane (2 ml). After each step, the SPE column was dried under full vacuum suction for 5 min. The retained organic material was eluted with methanol (5 ml). The methanol eluates were reduced to dryness under nitrogen at 40 °C and the residues were dissolved in acetate buffer (0.2 M, pH 4.8; 5 ml). Following addition of *H. pomatia* mixed enzymes (50 µl), the Phase II conjugates were hydrolysed at 37 °C overnight. After hydrolysis, the aqueous hydrolysate was adjusted to pH 5.8, centrifuged (2000*g*, 15 min) and the aglycones were separated into acid/neutral and basic fractions by SPE using mixed-mode extraction columns as described below.

The aqueous supernatant (5 ml) was applied on copolymeric mixed mode SPE columns (Certify® or XTRACT®) primed with methanol (4 ml) and phosphate buffer (0.1 M, pH 6.0; 4 ml) and drawn through the columns at about 1 ml min^{-1}. The columns were washed with 1 M acetic acid (2 ml), *n*-hexane (2 ml) and dried under full vacuum suction for at least 5 min. The acid/neutral metabolites were recovered by elution with dichloromethane:ethyl acetate mixture (3:1 v/v; 5 ml). The column was then washed with methanol (5 ml) to remove the polar materials and dried again for 2 min. Following the methanol wash, the retained basic metabolites were eluted with ethyl acetate:concentrated ammonia mixture (98:2 v/v; 5 ml) as described by Dumasia *et al.* (2002a). The solvents were removed under oxygen free nitrogen (OFN) at 40 °C.

Triethylaminohydroxypropyl Sephadex LH-20 (TEAP-LH-20) chromatographic fractionation of the aglycone isolates

The acid/neutral and basic isolates obtained from the mixed mode SPE columns were separated by TEAP-LH-20 (OH^- form) ion-exchange column chromatography into neutral and phenolic (acidic) residues as described previously for steroids (Dumasia *et al.* 1989). Briefly, a stoppered glass column (diameter 10 mm) was plugged with cotton wool. The activated gel was slurry-packed (solvent, $CHCl_3$–methanol, 85:15 v/v) under gentle pressure to a height of 5 cm. The acid/neutral isolates dissolved in the above solvent (0.25 ml) were loaded on the column followed by two washes (0.25 ml). The neutral

fraction was then eluted with $CHCl_3$–methanol (85:15 v/v; 10 ml). The eluant was then changed and the phenolic fraction was eluted with $CHCl_3$–methanol–acetic acid (85:15:1 v/v/v; 10 ml). The organic solvents were reduced to dryness under nitrogen at 40 °C and the residues were derivatized for analysis by EI^+-GC-MS.

Derivatization

The dry isolates were dissolved in toluene (25 µl) and treated with MSTFA (25 µl). After vigorous mixing, the solution was heated at 80 °C for 30 min. After removal of the solvents under OFN at 60 °C, the derivatized extracts were dissolved in toluene (50 µl) for analysis by GC-MS in the EI^+ mode.

Full-scan GC-MS analysis for identification of metabolites

Samples were analysed using a Fisons MD800 bench top GC-MS instrument. A BPX5 column (about 25 m × 0.25 mm i.d., 0.25 µm film thickness, SGE) was used with helium as carrier gas. The initial column temperature, 90 °C, was maintained for 1 min. The oven was then programmed at 15 °C min^{-1} to 320 °C and then maintained at 320 °C for 5 min. The injector and transfer line temperatures were 260 and 250 °C respectively. Aliquots (1 µl) of the derivatized fractions were injected in the splitless mode (1 min) using an autosamlper (CTC model A200S, Zwingen, Switzerland). Positive-ion EI mass spectra were recorded at 70 eV. The ion source temperature was 150 °C. The mass spectrometer was operated in the repetitive scan mode with a scan time of 1.5 s for the mass range between 40 and 550 amu acquiring full-scan data from 5 to 18 min.

Results and discussion

Extraction and fractionation of pre- and post-administration canine urine

Unconjugated and conjugated (Phase II) metabolites of cyclizine excreted in selected early post-Marezine® urine samples were initially preconcentrated by extraction using C_{18} (ODS) SPE columns. The conjugated metabolites were enzyme-hydrolysed in buffer. The total aglycones were separated into acid/neutral and basic fractions by the cation-exchange copolymeric mixed-mode SPE cartridges, using a modification of the targeted basic extraction procedure described previously (Dumasia and Houghton 1991, Dumasia *et al.* 2002b). Substrate-related compounds containing the diphenylmethane substructure formed *in vivo* from initial N_1-dealkylation were eluted in the acid/neutral fraction. Cyclizine and Phase I metabolites containing the piperazine heterocycle were eluted in the basic isolate.

Separation of the total acid/neutral isolates into individual neutral and phenolic fractions was achieved by column chromatography on TEAP-Sephadex LH-20 ion-exchange gel as described previously for the separation of steroids (Axelson and Sahlberg 1983, Dumasia *et al.* 1989). Individual fractions were then derivatized (TMS-ethers) and analysed by EI^+-GC-MS to characterize the substrate-related metabolites. In the neutral fraction, three substrate-related compounds diphenylmethane (M1), benzophenone (M2) and benzhydrol (M3) were unequivocally identified by comparison with authentic standards. In the phenolic fraction, seven compounds (M4 → M10) also containing the diphenylmethane or diphenylmethylene nucleus were detected and tentatively identified from an interpretation of the EI^+ mass-spectral fragmentation patterns of the *O*-TMS ether derivatives.

EI^+-GC-MS identification of cyclizine-related metabolites in the neutral isolate

The full-scan EI^+ mass spectrum (A; figure 1) of a compound detected by GC-MS analysis in the TEAP-LH-20 neutral fraction of the acid/neutral isolate shows a molecular ion ($M^{+\cdot}$) at m/z 168 with fragment ions at m/z 167 [($M^{+\cdot}$-H), base

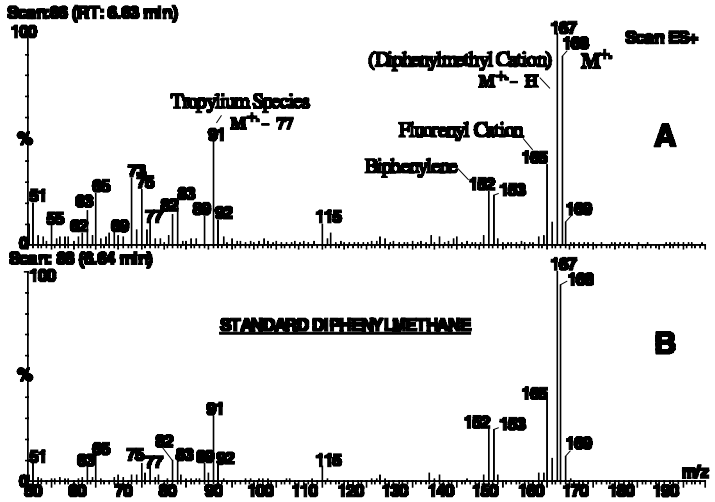


Figure 1. Full-scan EI^+ mass spectra of diphenylmethane (A) isolated from the TEAP-LH-20 neutral isolate of a post-Marezine® administration canine urine sample (M1) and (B) authentic standard.

peak; $(C_{13}H_{11})^+$, diphenylmethylene cation], m/z 152 [biphenylene; $(C_{12}H_8)^{+\cdot}$] and m/z 91 [$(M^{+\cdot}$ -77), $(C_7H_7)^+$ or tropylium species]. From a comparison of the retention time and EI^+ mass spectrum (A) with those of the authentic standard diphenylmethane (spectrum B, figure 1), this compound was identified as diphenylmethane [$(C_6H_5)_2CH_2$; (M1)]. This neutral metabolite is formed *in vivo* by oxidative N_1-dealkylation and loss of the piperazine heterocycle from either cyclizine (parent drug) or its major basic N_4-desmethyl metabolite norcyclizine and is excreted as unconjugated in canine urine. The halogenated analogue of this compound has been identified as a metabolite of hydroxyzine in human urine (Kageura *et al.* 1986). Oxidative N_1- and N_4-dealkylations of the piperazine heterocycle have been reported in the biotransformation of cinnarizine and flunarizine (Meuldermans *et al.* 1983, Lavrijsen *et al.* 1992) and the involvement of cytochromes P450 in these transformations has been studied by Karia *et al.* (1996).

The full-scan EI^+ mass spectrum (A; figure 2) of a second compound detected by GC-MS analysis in the TEAP-LH-20 neutral fraction, shows a molecular ion ($M^{+\cdot}$) at m/z 182, with fragment ions at m/z 152 [biphenylene; $(C_{12}H_8)^{+\cdot}$], m/z 105 [$M^{+\cdot}$ -77, $(C_6H_5)^{\cdot}$; base peak] and m/z 77 [phenyl cation $(C_6H_5)^+$]. From a comparison of the retention time and EI^+ mass spectrum (A) of the urinary metabolite with those of the authentic standard (spectrum B, figure 2), this compound was identified as benzophenone [$(C_6H_5)_2CO$;(M2)]. This neutral compound could be formed *in vivo* either by oxidation of the benzhydrol metabolite (M3) or during the N_1-dealkylation of either cyclizine or norcyclizine. Benzophenone has previously been identified as a metabolite of cinnarizine in rat liver microsomes (Kariya *et al.* 1992) and as a metabolite of diphenylmethane in rat urine (Stocklinski *et al.* 1980).

The full-scan EI^+ mass spectrum (A; figure 3) of the third compound detected by GC-MS analysis in the TEAP-LH-20 neutral fraction shows a molecular ion ($M^{+\cdot}$) at m/z 256, with fragment ions at m/z 241 ($M^{+\cdot}$ -15), m/z 179 ($M^{+\cdot}$ -77),

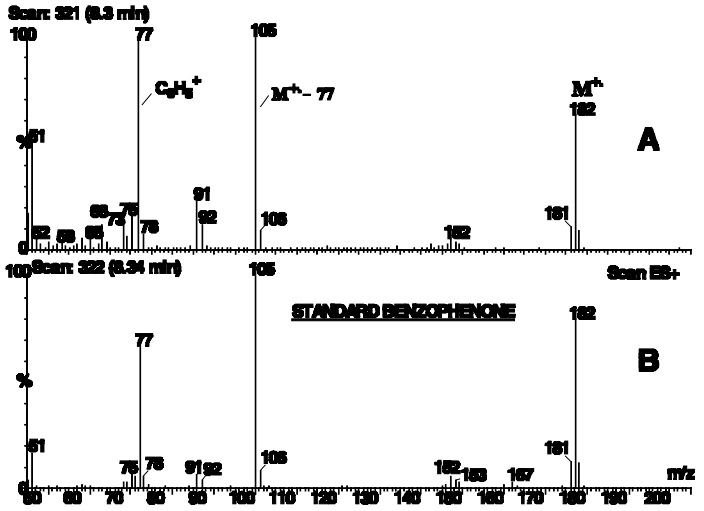


Figure 2. Full-scan EI^+ mass spectra of benzophenone (A) isolated from the TEAP-LH-20 neutral isolate of a post-Marezine® administration canine urine sample (M2) and (B) authentic standard.

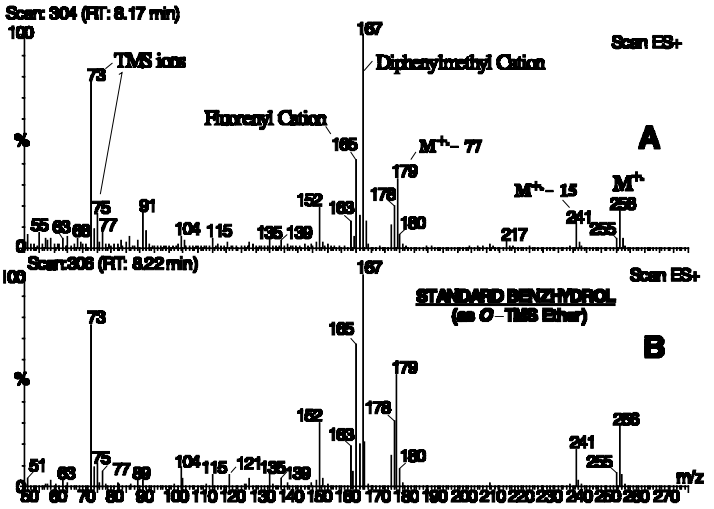


Figure 3. Full-scan EI^+ mass spectra of benzhydrol (as *O*-TMS derivative) (A) isolated from the TEAP-LH-20 neutral isolate of a post-Marezine® administration canine urine sample (M3) and (B) authentic standard.

m/z 167 [diphenylmethylene cation $(C_{13}H_{11})^+$, base peak], *m/z* 165, [fluorenyl cation $(C_{13}H_9)^+$], *m/z* 152 [biphenylene; $(C_{12}H_8)^{+\cdot}$] and *m/z* 73 (a TMS species). The doublet of ions at *m/z* 165 and 167 is characteristic of compounds containing the diphenylmethane nucleus and shows that the substructure is retained. From a comparison of the retention time and EI^+ mass spectrum (A) of the urinary metabolite with those of the TMS derivative of authentic standard benzhydrol (spectrum B, figure 3), this compound was identified as benzhydrol [$(C_6H_5)_2CHOH$; (M3)] detected as its *O*-TMS ether derivative. This compound could be formed *in vivo* by three possible mechanisms: (1) from a reduction of the benzophenone metabolite (M2), (2) from P450 monooxygenase mediated oxidation

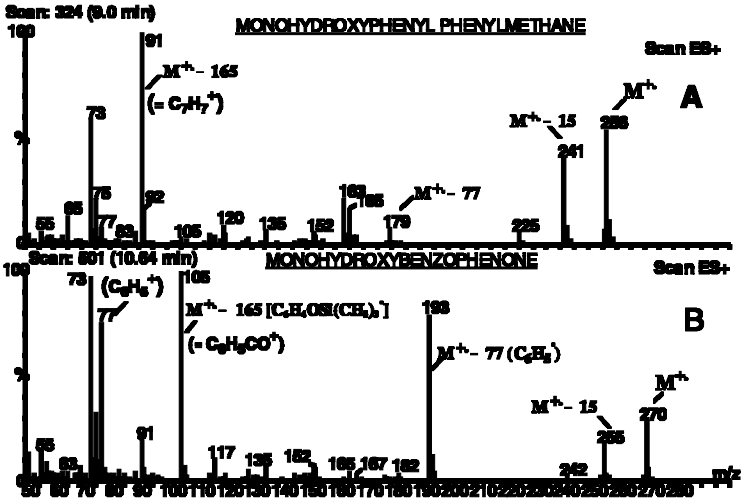


Figure 4. Full-scan EI^+ mass spectra of the *O*-TMS derivatives of (A) an isomer of (monohydroxyphenyl)phenylmethane (M4) and (B) an isomer of monohydroxybenzophenone (M5) isolated from the TEAP-LH-20 phenolic isolate of a post-Marezine® administration canine urine sample.

of the methylene moiety of M1 and (3) from enzymatic hydrolysis of the C-N_1 bond during N_1-dealkylation of the piperazine heterocycle of either cyclizine or norcyclizine. Benzhydrol has previously been identified as a metabolite of diphenylmethane in rat urine faeces and bile (Stocklinski 1981) and of benzophenone from rat hepatocyte incubation studies (Nakagawa *et al.* 2000).

EI^+-GC-MS identification of cyclizine-related metabolites in the phenolic isolate

The full-scan EI^+ mass spectrum of a minor phenolic compound (figure 4a) detected by GC-MS analysis in the TEAP-LH-20 phenolic fraction of the acid/neutral isolate shows the molecular ion ($M^{+\cdot}$) at m/z 256, with fragment ions at m/z 241 ($M^{+\cdot}$-15), m/z 179 ($M^{+\cdot}$-77; $C_6H_5^{\cdot}$), m/z 165 $[C_6H_4OSi(CH_3)_3]^+$ and m/z 91 [($M^{+\cdot}$-165) or $(C_7H_7)^+$-tropylium species; the base peak). On basis of this data, this phenolic compound was assigned the structure (hydroxyphenyl)phenylmethane (M4) detected as its *O*-TMS ether derivative and is isobaric with the neutral M3. This compound (M4) is possibly formed from diphenylmethane (M1) by aromatic oxidation possibly at the 4-(*para*) position on a phenyl ring and excreted as a Phase II conjugate. 4-Hydroxydiphenylmethane [(4-hydroxyphenyl)phenylmethane] has previously been identified as a metabolite of diphenylmethane in rat urine faeces and bile (Stocklinski 1981).

The full-scan EI^+ mass spectrum of another phenolic compound (figure 4b) detected by GC-MS analysis in the TEAP-LH-20 phenolic fraction of the acid/neutral isolate shows the molecular ion ($M^{+\cdot}$) at m/z 270, with fragment ions at m/z 255 ($M^{+\cdot}$-15), m/z 193 [$M^{+\cdot}$-77; $(C_6H_5)^{\cdot}$], m/z 105 [$(M^{+\cdot}$-165)$^{\cdot}$ or $(C_6H_5CO)^+$-base peak] and m/z 77 [$(C_6H_5)^+$]. On basis of this data, this compound was assigned the structure hydroxybenzophenone (M5) detected as its *O*-TMS ether derivative. This compound again is possibly formed from

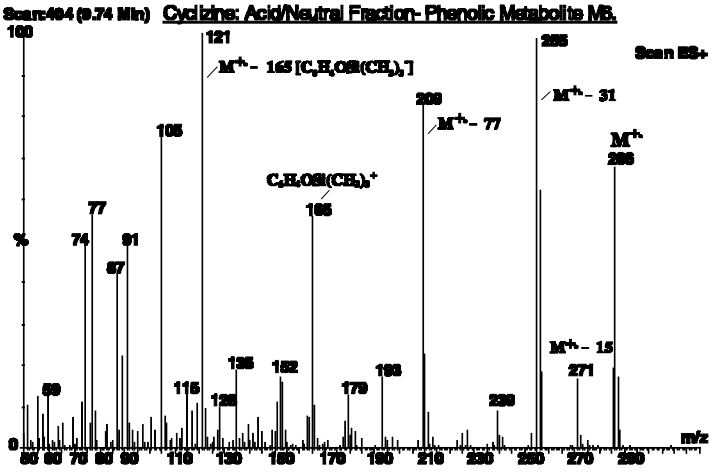


Figure 5. Full-scan EI$^+$ mass spectrum of the *O*-TMS derivative of an isomer of monohydroxybenzhydrylmethyl ether (M6), isolated from the TEAP-LH-20 phenolic isolate of a post-Marezine® administration canine urine sample.

benzophenone (M2) by aromatic oxidation possibly at the 4-(*para*) position on a phenyl ring. It is excreted as a Phase II conjugate and is a minor metabolite detected in the phenolic isolate. 4-Hydroxybenzophenone and its sulfate conjugate were identified as metabolites of benzophenone obtained from rat hepatocyte incubations (Nakagawa *et al.* 2000).

The full-scan EI$^+$ mass spectrum of a phenolic compound (figure 5) detected by GC-MS analysis in the TEAP-LH-20 phenolic fraction of the acid/neutral isolate shows the molecular ion ($M^{+\cdot}$) at m/z 286, with fragment ions at m/z 255 ($M^{+\cdot}$-31, loss of OCH_3; base peak), m/z 209 [$M^{+\cdot}$-77; $(C_6H_5)^{\cdot}$], m/z 165 $[C_6H_4OSi(CH_3)_3]^+$, m/z 121 [$(M^{+\cdot}$-165)$^{\cdot}$], m/z 105 and m/z 91 (the tropylium species). On basis of this data, this compound was assigned the structure hydroxybenzhydrylmethylether (M6) detected as its *O*-TMS ether derivative. This compound could possibly be formed from benzhydrol (M3) by two enzymatic Phase I biotransformation processes: (1) *O*-methylation of the benzhydrol and (2) aromatic oxidation. It is excreted as a Phase II conjugate and is the major phenolic metabolite detected in the phenolic isolate.

The full-scan EI$^+$ mass spectra (figure 6a, b) of two isobaric regioisomeric compounds, detected in the TEAP-LH-20 phenolic fraction of the acid neutral fraction by GC-MS analysis, show a molecular ion ($M^{+\cdot}$) at m/z 344 with fragment ions at m/z 267 [$M^{+\cdot}$-77; $(C_6H_5)^{\cdot}$], m/z 255 {$M^{+\cdot}$-89; loss of an $[OSi(CH_3)_3]^{\cdot}$ group as a radical}, m/z 179 {$M^{+\cdot}$-165; $[C_6H_4OSi(CH_3)_3]^{\cdot}$}, m/z 165 $[C_6H_4OSi(CH_3)_3]$, m/z 91 (tropylium species) and m/z 73 and 75 (both TMS species). On basis of this data, these compounds are assigned the structure hydroxybenzhydrol (regio-isomers M7 and M8) detected as their *bis*-*O*-TMS ether derivatives. These compounds could possibly be formed from benzhydrol (M3) by cytochrome P450 monooxygenase mediated aromatic oxidations at the 4-(*para*) and 2-(*ortho*) or possibly 3-(*meta*) positions on the phenyl ring.

Figure 7 shows the full-scan EI$^+$ mass spectra of two isobaric compounds having the derivatized molecular weight of 432 amu detected by GC-MS analysis

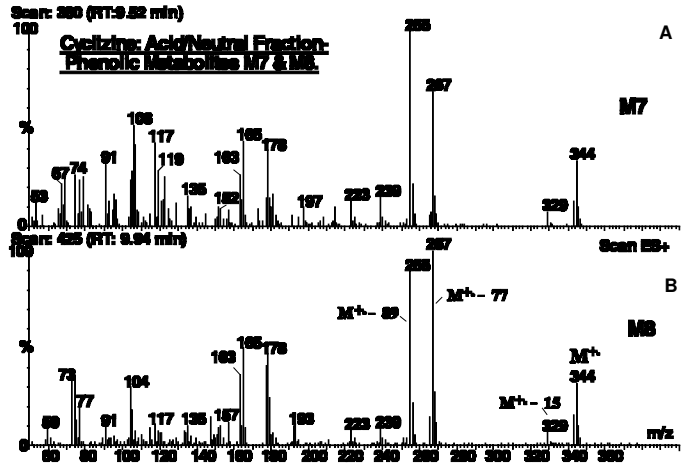


Figure 6. Full-scan EI$^+$ mass spectra (A) and (B) of the bis *O*-TMS derivatives of two isobaric compounds (M7 and M8) identified as monohydroxybenzhydrol regio-isomers isolated from the TEAP-LH-20 phenolic isolate of a post-Marezine® administration canine urine sample.

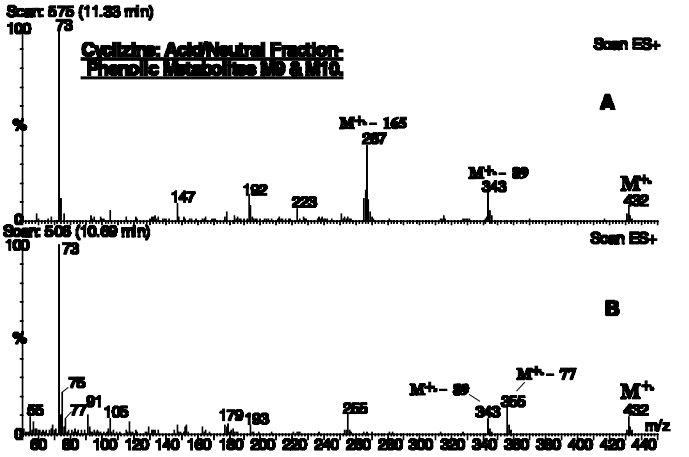


Figure 7. Full-scan EI$^+$ mass spectra of the tris *O*-TMS derivatives of two isobaric compounds isolated from the TEAP-LH-20 phenolic isolate of a post-Marezine® administration canine urine sample. (A) A compound identified as 4,4′-dihydroxybenzhydrol (M9) and (B) a regio-isomer of dihydroxybenzhydrol (M10) with both oxidations present only on one phenyl ring.

of the TEAP-LH-20 phenolic fraction. The full-scan EI$^+$ mass spectrum (figure 7a) of a minor compound shows a weak molecular ion ($M^{+\cdot}$) at m/z 432 with minor fragment ions at m/z 343 {$M^{+\cdot}$-89; loss of an $[OSi(CH_3)_3]^\cdot$ group as a radical}, m/z 267 {$M^{+\cdot}$-165; $C_6H_4[OSi(CH_3)_3]^\cdot$}, m/z 147 TMS rearrangement ion $[(CH_3)_2Si{=}O^+\text{-}Si(CH_3)_3]$. The TMS species m/z 73 forms the base peak in the spectrum. The most probable sites of aromatic oxidation (hydroxylation) in this compound are the 4 and 4′ positions on the two phenyl carbocycles. On basis of this data, this isobaric compound (M9) was assigned the structure 4,4′-dihydroxybenzhydrol detected as its *tris*-*O*-TMS ether derivative and possibly

could also be formed as described above for the phenolic metabolites M7 and M8. It has been reported previously as a metabolite of diphenylmethane in rat urine (Stocklinski 1981).

The full-scan EI^+ mass spectrum (figure 7b) of the other minor isobaric phenolic compound shows a weak molecular ion ($M^{+\cdot}$) at m/z 432 with minor fragment ions at m/z 355 ($M^{+\cdot}$-77), m/z 343 {$M^{+\cdot}$-89; loss of an $[OSi(CH_3)_3]^{\cdot}$ group as a radical}, m/z 255, m/z 179 {$M^{+\cdot}$-253; $(C_6H_3[OSi(CH_3)_3]_2)^{\cdot}$} and m/z 91 (tropylium species). The TMS species m/z 73 forms the base peak in the spectrum. The most probable sites of aromatic oxidation (hydroxylation) in this compound are the C-2 and C-4 positions on one of the phenyl rings as reported previously (Stocklinski 1981). However, the possibility of vicinal oxidations resulting in the formation of a catechol cannot be excluded. On basis of this data, this regioisomeric compound was assigned the structure dihydroxybenzhydrol (M10) detected as its *tris*-*O*-TMS ether derivative. This compound also could possibly be formed by the P450 monooxygenase oxidations on one of the phenyl rings of benzhydrol (M3).

Cyclizine metabolism

After oral administration to the greyhound, *in vivo* Phase I metabolism of cyclizine leads to the formation of several neutral, phenolic and basic metabolites excreted/detected both as unconjugated and Phase II conjugates in post-administration urine samples. The parent drug and five substrate-related basic compounds have previously been tentatively identified (Dumasia *et al*. 2002a).

In the present study, the *in vivo* biotransformation pathway leading to the formation of neutral metabolites of cyclizine detected in greyhound urine has been unequivocally shown to proceed via N_1-dealkylation with the concomitant loss of the methylpiperazine heterocycle. The neutral metabolites formed from primary or secondary metabolism of cyclizine are diphenylmethane (M1), benzophenone (M2) and benzhydrol (M3). These compounds were identified from a comparison of their EI^+ mass spectra with those of authentic reference compounds. Oxidation of the methylene moiety of M1 or reduction of M2 could lead to the formation of benzhydrol (M3). The formation of M2 and M3 during the *in vivo* biotransformation of diphenhydramine was first reported by Glazko and Dill (1949).

Aromatic oxidations on the diphenylmethyl substructure by cytochrome P450 monooxygenases led to the formation of several phenolic metabolites. These are secondary metabolites formed either from diphenylmethane or its hydroxylated (phenolic) basic primary metabolites. As no authentic reference compounds are available, some of these putative metabolites (M4–M10) have been tentatively identified from an interpretation of their EI^+ mass spectral data. The formation and identification of some phenolic compounds from diphenylmethane, benzophenone and cinnarizine have been reported previously (Stocklinski *et al*. 1980, Stocklinski 1981, Kariya *et al*. 1992, Nakagawa *et al*. 2000). The hydroxylated metabolites are subjected to Phase II metabolism (conjugation with glucuronic and/or sulfuric acids) and then excreted in canine urine. The structures of these neutral and the putative phenolic metabolites formed *in vivo* following administration of cyclizine to greyhounds are shown in figure 8. None of these compounds were detected by GC-MS analysis in the pre-administration (blank) urine isolates from both dogs.

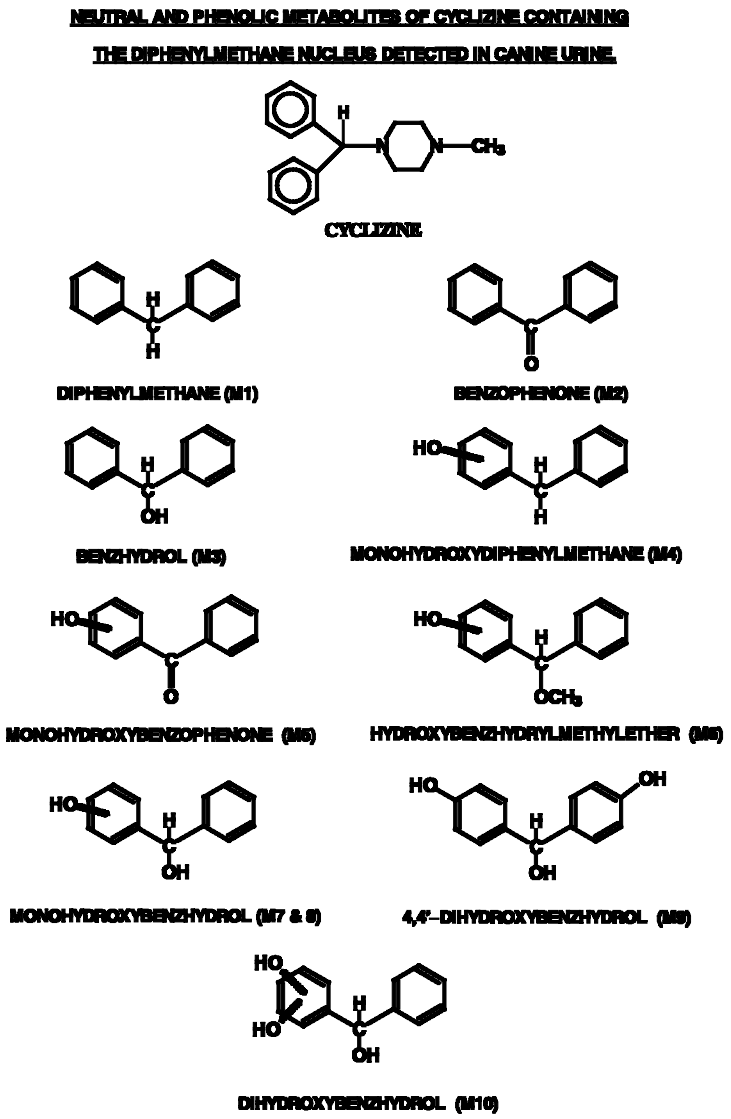


Figure 8. Chemical structure of cyclizine and of the neutral (M1 → M3) and phenolic metabolites (M4 → M10) formed as partial *in vivo* biotransformation products after N_1-dealkylation of cyclizine and identified by GC-MS in the acid/neutral fraction of post-Marezine® administration canine urine sample.

Conclusions

In the greyhound, a number of *in vivo* Phase I functionalization pathways were observed for the detoxification and elimination of cyclizine. In the present study, some of the neutral and phenolic metabolites formed via N_1-dealkylation with concomitant loss of the methylpiperazine heterocycle were identified by EI^+-GC-MS from their derivatized (TMS) molecular weights ($M^{+\cdot}$) and an interpretation of their mass spectral fragmentation patterns. Neither authentic reference compounds nor literature data are available for all the metabolites. Phase II biotrans-

formation (conjugation with either glucuronic acid or sulfate) was observed for some functionalized metabolites.

Acknowledgements

This project was entirely funded by the National Greyhound Racing Club (NGRC) of Great Britain. Animal administrations were performed and the urine samples collected and provided by Professor Walter Hyde and staff at Racing Chemistry, Iowa State University, Ames, IA, USA.

References

Axelson, M. and Sahlberg, B.-L., 1983, Group separation and gas chromatography-mass spectrometry of conjugated steroids in plasma. *Journal of Steroid Biochemistry*, **18**, 313–321.

Axelson, M., Sahlberg, B.-L. and Sjövall, J., 1981, Analysis of profiles of conjugated steroids in urine by ion-exchange separation and gas chromatography-mass spectrometry. *Journal of Chromatography*, **224**, 355–370.

Axelson, M. and Sjövall, J., 1977, Analysis of unconjugated steroids in plasma by liquid–gel chromatography and glass capillary gas chromatography-mass spectrometry. *Journal of Steroid Biochemistry*, **8**, 683–692.

Cholwill, J. M., Wright, W., Hobbs, G. J. and Curran, J., 1999, Comparison of ondansetron and cyclizine for prevention of nausea and vomiting after day-case gynaecological laparoscopy. *British Journal of Anaesthesia*, **83**, 611–614.

DeLoach, G. D., Leary, H. W. and Stocklinski, A. W., 1978, Identification of *p*-hydroxydiphenylmethane as a urinary and fecal metabolite of diphenylmethane in the rat. *Research Communications in Chemical Pathology and Pharmacology*, **22**, 419–422.

Dumasia, M. C. and Houghton, E., 1991, Screening and confirmatory analysis of beta-agonists, beta-antagonists and their metabolites in horse urine by capillary gas chromatography-mass spectrometry. *Journal of Chromatography B: Biomedical Applications*, **564**, 503–513.

Dumasia, M. C., Grainger, L. and Houghton. E., 2002a, Detection and partial *in vivo* biotransformation of cyclizine in greyhounds. 1: identification and semi-quantitative analysis of some basic metabolites in canine urine by gas chromatography-mass spectrometry. *Xenobiotica*, **32**, 795–807.

Dumasia, M. C., Houghton. E., Hyde, W., Greulich, D., Nelson T. and Peterson, J., 2002b, Detection of Fenspiride and identification of *in vivo* metabolites in horse body fluids by capillary gas chromatography-mass spectrometry: Administration, biotransformation and urinary excretion after a single oral dose. *Journal of Chromatography B: Biomedical Sciences and Applications*, **767**, 131–144.

Dumasia, M. C., Houghton, E., Moss, M., Gower, D. B. and Marshall, D. E., 1989, Gas chromatographic-mass spectrometric identification of some 3,16-dioxygenated steroids in the non-pregnant and in pregnant mare urine and placental tissues. *Biochemical Society Transactions*, **17**, 148–150.

Ellison, T., 1972, Metabolic studies of ^{3}H-orphenadrine citrate in the rat, dog and rhesus monkey. *Archives Internationales de Pharmacodynamie et de Therapie*, **147**, 213–230.

Glazko, A. J. and Dill, W. A., 1949, Biochemical studies on diphenhydramine (Benadryl). IV. Degradation of benadryl by tissue enzymes. *Journal of Biological Chemistry*, **179**, 417–421.

Griffin, D. S. and Baselt, R. C., 1984, Blood and urine concentrations of cyclizine by nitrogen-phosphorus gas–liquid chromatography. *Journal of Analytical Toxicology*, **8**, 97–99.

Hespe, W., De Roos, A. M. and Nauta, W. Th., 1965, Investigation into the metabolic fate of orphenadrine hydrochloride after oral administration to male rats. *Archives Internationales de Pharmacodynamie et de Therapie*, **156**, 180–200.

Kageura, M., Kataoka, M., Hara, K. and Nagata, T., 1986, Changed compounds of hydroxyzine in a human urine. *Forensic Science International*, **32**, 229–235.

Kariya, S., Isozaki, S., Natimatsu, S. and Suzuki, T., 1992, Oxidative metabolism of cinnarizine in rat liver microsomes. *Biochemical Pharmacology*, **44**, 1471–1474.

Kariya, S., Isozaki, S., Uchino, K., Suzuki, T. and Natimatsu, S., 1996, Oxidative metabolism of flunarizine and cinnarizine by microsomes from B-lymphoblastoid cell lines expressing human cytochrome P-450 enzymes. *Biological and Pharmaceutical Bulletin*, **19**, 1511–1514.

Land, G., Dean, K. and Bye, A., 1981, Determination of cyclizine and norcyclizine in plasma and urine using gas–liquid chromatography with nitrogen selective detection. *Journal of Chromatography*, **222**, 135–140.

Lavrijsen, K., van Houdt, J., van Dyck, D., Hendrickx, J., Bockx, M., Hurkmans, R., Meuldermans, W., LeJeune, L., Lauwers, W. and Heykants, J., 1992, Comparative metabolism of flunarizine in rats, dogs and man: an in vitro study with subcellular liver fractions and isolated Lepatocytes. *Xenobiotica*, **22**, 815–836.

Meuldermans, W., Hendrickx, J., Hurkmans, R., Swysen, E., Woestenburghs, R., Lauwers, W. and Heykants, J., 1983, Excretion and metabolism of flunarizine in rats and dogs. *Arzneimettelforschung*, **33**, 1142–1151.

Moore, C. M., 1990, Solid-phase cation exchange extraction of basic drugs from urine of racing greyhounds. *Journal of the Forensic Science Society*, **30**, 123–129.

Nakagawa, Y., Susuki, T. and Tayama, S., 2000, Metabolism and toxicity of benzophenone in isolated rat hepatocytes and estrogenic activity of its metabolites in MC cells. *Toxicology*, **156**, 27–36.

Narrod, S. A., Wilk, A. L. and King, C. T. G., 1965, Metabolism of meclizine in the rat. *Journal of Pharmacology and Experimental Therapeutics*, **147**, 380.

Remberg, G., Eichelbaum, M., Spiteller G. and Dengler, H. J., 1977, Metaboliosm of dl-[^{14}C]-prenylamine in man. *Biomedical Mass Spectrometry*, **4**, 213–230.

Soudijn, W. and van Wijnaarden, I., 1968, The metabolism and excretion of cinnarizine by rats. *Life Sciences*, **7**, 231–238.

Stocklinski, A. W., 1981, Semi-quantitative profile of regioisomeric monohydroxydiphenylmethane metabolites in rat urine, faeces and bile. *Xenobiotica*, **11**, 425–432.

Stocklinski, A. W., DeLoach, G. D. and Williams, H., 1979, Identification of benzhydrol as a urinary metabolite of diphenylmethane in the rat. *Research Communications in Chemical Pathology and Pharmacology*, **24**, 397–422.

Stocklinski, A. W., Ware, O. B. and Oberst, T. J., 1980, Benzophenone metabolism. I. Isolation of *p*-hydroxybenzophenone from rat urine. *Life Sciences*, **26**, 365–369.

Walder, A. D. and Aitkenhead, A. R., 1994, Anti-emetic efficacy of metoclopramide when induced in a patient-controlled analgesia infusion. *Anaesthesia*, **49**, 804–806.

Walker, R. B. and Kanfer, I., 1995, Sensitive high-performance liquid chromatographic determination of cyclizine and its demethylated metabolite, norcyclizine in biological fluids using coulometric detection. *Journal of Chromatography B: Biomedical Applications*, **672**, 172–177.

Weinstein, S. E. and Stern, R. M., 1997, Comparison of marezine and dramamine in preventing symptoms of motion sickness. *Aviation Space Environmental Medicine*, **68**, 890–894.

XENOBIOTICA, 2002, VOL. 32, NO. 9, 823–831

Taylor & Francis
healthsciences

Urinary excretion of selegiline *N*-oxide, a new indicator for selegiline administration in man

M. KATAGI*, M. TATSUNO, H. TSUTSUMI, A. MIKI, T. KAMATA, H. NISHIOKA, K. NAKAJIMA, M. NISHIKAWA and H. TSUCHIHASHI

Forensic Science Laboratory, Osaka Prefectural Police HQ, 1-3-18, Hommachi, Chuo-ku, Osaka 541-0053, Japan

Received 22 January 2002

1. The metabolism of selegiline (SG) has been studied by investigating the time-course of urinary excretion of SG and its metabolites using high-performance liquid chromatography-electrospray ionization mass spectrometry (LC-ESI MS) in combination with solid-phase extraction.

2. The excretion profiles of SG and its four major metabolites, selegiline-*N*-oxide (SGO), *N*-desmethylselegiline (DM-SG), methamphetamine (MA) and amphetamine (AP), were investigated in six healthy volunteers after oral administrations of SG hydrochloride in a single dose of 2.5 or 7.5 mg, and a repeat twice-daily dose of 5.0 mg day^{-1} (for 3 days).

3. The cumulative amount of SGO excreted within approximately the first 8–12 h was comparable with MA, and the amount in the first 72 h was 2.0–7.8 times larger (2.8–13.2% of the dose) than that of DM-SG.

4. These results demonstrate that SGO can be used in place of DM-SG, which is known to be a main specific metabolite of SG, as a new indicator for the discrimination of SG use compared with MA abuse.

Introduction

Selegiline [(*R*)-(–)-*N*,α-dimethyl-*N*-2-propynylphenethylamine] (SG) is a potent, irreversible and selective inhibitor of monoamine oxidase type-B (Knoll 1978). It has been widely prescribed alone or in combination with levodopa, a dopamine precursor, in the treatment of Parkinson's disease (Heinonen and Lammintausta 1991), and has also been sold as a prescription medicine in Japan since 1998 under the trade name FP. In 1996, the Japanese authorities classified SG as a precursor of the illicit stimulant methamphetamine (MA), and began to regulate its possession and use.

It is well established that SG is predominantly metabolized to MA and amphetamine (AP) along with its specific metabolite, *N*-desmethylselegiline (DM-SG) (Szatmari and Toth 1992, Heinonen *et al.* 1994, Lengyel *et al.* 1997, Shin 1997), which has been reported as an indicator for distinguishing SG use from MA abuse in clinical and forensic toxicology.

It is also known that tertiary amine compounds are readily *N*-oxidized in man by flavin-containing monooxygenase (FMO) (Poulsen and Ziegler 1979, Ziegler 1988). We expected that SG would be appreciably metabolized to selegiline *N*-oxide (SGO), and that this could serve as a novel indicator for SG administration.

* Author for correspondence; e-mail: kataginohito@mth.biglobe.ne.jp

Xenobiotica ISSN 0049–8254 print/ISSN 1366–5928 online © 2002 Taylor & Francis Ltd
http://www.tandf.co.uk/journals
DOI: 10.1080/00498250210144857

In fact, as previously reported, we found that SGO was excreted in two long-term SG users' urine, as identified by a solid-phase extraction and high-performance liquid chromatography-electrospray ionization mass spectrometry (LC-ESI MS) procedure (Katagi *et al.* 2001).

Although the excretion of several metabolites of SG in human urine has been reported (Szatmari and Toth 1992, Heinonen *et al.* 1994, Lengyel *et al.* 1997, Shin 1997), no research except for our previous study has been described on the metabolism of SG to SGO.

In the current study, SG was orally administered to healthy volunteers in single and repeat doses, and the time-course urinary excretion of SG, SGO and the well-known metabolites MA, AP and DM-SG was investigated by an LC-MS procedure. In addition, urinary metabolites of long-term SG users were further investigated.

Materials and methods

Chemicals

SG hydrochloride and DM-SG hydrochloride were kind gifts of Fujimoto Pharmaceuticals (Osaka, Japan). MA hydrochloride and AP sulphate were purchased from Dainippon Pharmaceuticals (Osaka, Japan) and Takeda Pharmaceutical Industries (Osaka, Japan), respectively. SGO was synthesized according to the procedure described in Katagi *et al.* (2001) and was >98% pure based on LC-MS analysis. Standard stock solutions of SGO were prepared in methanol, and those of SG, DM-SG, MA and AP in distilled water (each concentration of 1 mg ml^{-1}). These standards were diluted to appropriate concentrations with distilled water or control human urine immediately before use. The internal standard (IS) ethylamphetamine (EAP) was synthesized according to the procedure of Crossley and Moore (1944), and a solution was prepared in distilled water (concentration 1 μg ml^{-1}). Acetonitrile and methanol were of HPLC grade, and other chemicals used were of analytical grade. Sep-pak C_{18} cartridges were purchased from Waters Associates (Milford, MA, USA).

Drug administration and sample collection.

After informed consent, six healthy male volunteers (V1: 27 years, 64 kg body wt, V2: 36, 66 kg; V3: 54, 61 kg, V4: 39, 60 kg; V5: 43, 56 kg; V6: 46, 51 kg) received a single oral dose of 2.5 mg (V1–3) or 7.5 mg (V4–6) of SG hydrochloride (FP Tablet 2.5®, Fujimoto Pharmaceuticals, Osaka, Japan). A separate repeat, oral twice-daily dose of 5.0 mg day^{-1} (2.5 mg each after breakfast and lunch) for 3 days was administered for V4–6. The urine samples were collected for 4 and 6 days after administration in the single and repeat dosing experiments, respectively. Urine samples were stored at −20 °C until analysis. Blank urine samples were collected immediately before drug administration. Urine samples were also voluntarily obtained from six long-term SG patients (2.5 or 5 mg day^{-1}).

Sample preparation

Sep-pak C_{18} cartridges were prewashed successively with 10 ml distilled water, 10 ml methanol and 10 ml distilled water. Urine samples (1 ml) were loaded on the prewashed cartridges. The cartridges were subsequently rinsed with 1 ml distilled water and 5 ml 20% aqueous methanol solution. The retained analytes were eluted with 3 ml methanol. After acidification with acetic acid, the eluates were evaporated to dryness under a gentle stream of nitrogen. The residue was reconstituted in 100 μl the IS aqueous solution and filtered through a 0.2-μm membrane filter. An aliquot of 10 μl was injected into the LC-MS system with an auto-injector.

LC-ESI MS determination of SG metabolites

LC-MS was performed on an alliance-Platform LCZ system equipped with an ESI interface (Waters). The capillary voltage was 3 kV and the cone voltage was set at 20 V. The other ESI-operating parameters were: source temperature, 120 °C; desolvation temperature, 350 °C; nitrogen gas, 450 l h^{-1}; and multiplier voltage, 650 V. Under these conditions, full-scan data acquisition was performed in the centroid mode (from m/z 100 to 500; a cycle time, 1.0 s; an interscan time, 0.1 s) for identification of metabolites. The quantitative measurements were accomplished in the selected ion-monitoring (SIM) mode by monitoring each protonated molecule (m/z 204 for SGO, 188 for SG, 174 for DM-SG, 164 for EAP, 150 for MA, and 136 for AP) by an internal standard method.

The chromatographic separation was carried out on a semimicro SCX column (2.0 mm i.d. × 150 mm; Shizeido, Tokyo, Japan) with a mobile phase consisting of acetonitrile-10 mM ammonium formate (pH 3.0) (70:30, v/v). The flow rate was set at 0.1 ml min^{-1}, and the entire effluent was introduced into the ESI source.

Results and discussion

Identification of SG metabolites in human urine

It is well known that SG is primarily metabolized in man to MA, AP and DM-SG and excreted in the urine (Szatmari and Toth 1992, Heinonen *et al.* 1994, Lengyel *et al.* 1997, Shin 1997). In Katagi *et al.* (2001), it was also reported that SGO was detected in two long-term SG users' urine. SG metabolites in urine of subjects exposed to it have been re-identified.

Figure 1 shows a typical total-ion chromatogram and extracted mass chromatograms obtained from a urine sample taken from a subject after a single oral administration of SG (V4, 2 h post-dosing). By comparison of the mass spectrum and retention time of each peak with those of the standards, the peaks 1–3, 5 and 6 in figure 1 were identified as SGO, SG, DM-SG, MA and AP, respectively. This demonstrates that SG is metabolized and excreted into urine as SGO along with other metabolites in man. The main metabolic pathways for SG in man are summarized in figure 2.

Urinary excretion of SG metabolites

The time-course of urinary levels of SG metabolites observed for the six subjects following a single oral dose is shown in table 1. The urinary levels of the five metabolites were almost dependent on dose of SG, though the level of SGO for the subject 3 was extremely high compared with those for the other subjects. Peak urinary levels of SGO were attained between 2 and 4 h post-dosing for all six subjects. These levels were also comparable with those of MA and reached

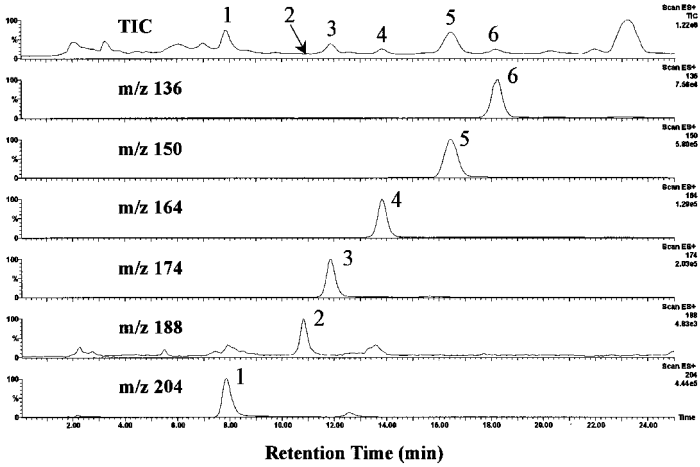


Figure 1. Total ion chromatogram and extracted ion chromatograms obtained from a urine sample (2 h after dosing) taken from subject 4 after a single oral administration of 7.5 mg SG hydrochloride. Peaks 1, selegiline *N*-oxide (SGO); 2, selegiline (SG); 3, *N*-desmethylselegiline (DM-SG); 4, ethylamphetamine (EAP, IS); 5, methamphetamine (MA); 6, amphetamine (AP).

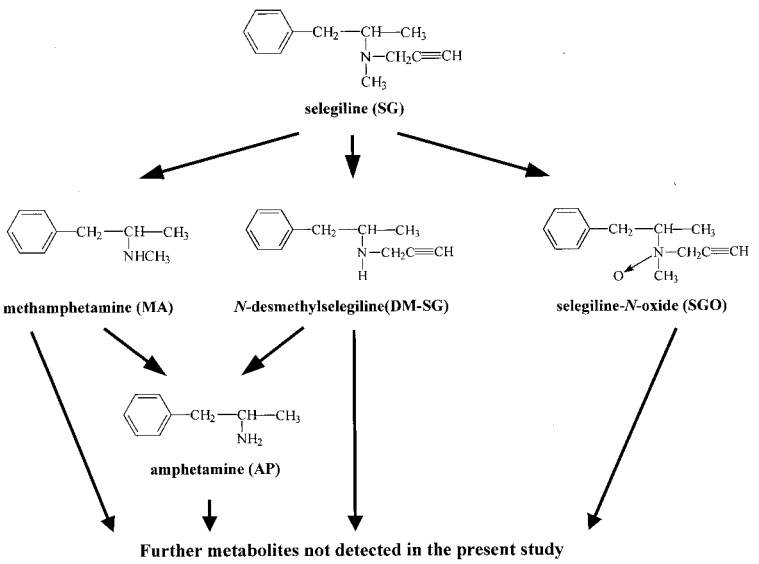


Figure 2. Proposed main metabolic pathways for selegiline (SG) in man.

Table 1. Urinary excretion of selegiline and its metabolites following the oral administration of selegiline to six human subjects.

Subject (dose)	Vol[a] (ml)	pH	Hours post-dosing	SD (ng ml^{-1})	SGO (ng ml^{-1})	DM-SG (ng ml^{-1})	MA (ng ml^{-1})	AP (ng ml^{-1})
1	141	7.04	2.0	0.3	226	77	51	20
(2.5 mg)	132	6.79	4.0	0.3	230	41	209	65
	101	5.98	6.0	0[b]	109	15	462	141
	110	6.47	8.0	0	34	4	116	30
	579	5.85	12.0	0	5	2	106	42
	580	5.52	24.0	0	1	2	234	73
	385	6.36	30.0	0	0	0	59	21
	254	5.60	36.0	0	0	0	103	39
	450	5.80	48.0	0	0	0	47	17
	501	5.68	60.0	0	0	0	35	11
	369	5.78	72.0	0	0	0	26	7
	575	6.49	84.0	0	0	0	4	2
	365	5.74	96.0	0	0	0	8	4
2	200	5.16	2.0	2	163	93	81	26
(2.5 mg)	111	5.14	4.0	0.7	279	88	280	111
	112	6.00	6.0	0	105	15	178	66
	101	6.06	8.0	0	57	8	184	68
	239	6.25	12.0	0	18	4	114	47
	1100	6.40	24.0	0	2	0.4	56	22
	348	5.70	30.0	0	0.8	0.7	125	57
	333	5.97	36.0	0	0.6	0	78	36
	1252	6.80	48.0	0	0	0	11	5
	1303	6.71	60.0	0	0	0	9	4
	980	6.64	72.0	0	0	0	8	3
	532	5.95	84.0	0	0	0	27	13
	1049	6.84	96.0	0	0	0	2	0.8
3	223	6.70	2.0	0.5	872	64	111	34
(2.5 mg)	105	6.32	4.0	0.8	614	17	238	69
	141	6.20	6.0	0.4	107	4	109	52
	114	5.86	8.0	0	128	4	232	119
	225	5.69	12.0	0	36	2	224	123

	901	5.98	24.0	0	2	0	51	36
	270	5.80	30.0	0	1	0	78	57
	244	5.94	36.0	0	0.5	0	41	43
	490	5.82	48.0	0	0	0	49	44
	1150	5.86	60.0	0	0	0	15	14
	562	5.55	72.0	0	0	0	11	12
	1031	5.90	84.0	0	0	0	5	3
	390	6.10	96.0	0	0	0	2	2
4	150	6.08	2.0	12	609	240	715	141
(7.5 mg)	88	5.16	4.0	11	525	227	1342	357
	62	5.92	6.0	2	538	102	1307	418
	78	6.57	8.0	0[b]	175	37	554	163
	112	5.52	12.0	0	69	99	1380	490
	333	5.30	24.0	0	5	30	970	249
	247	5.55	30.0	0	2	11	635	199
	264	5.70	36.0	0	0.8	3	313	102
	334	5.68	48.0	0	0.9	4	324	125
	492	5.66	60.0	0	0	0.8	106	50
	377	5.84	72.0	0	0	0	118	43
	403	5.54	84.0	0	0	0	50	36
	292	5.27	96.0	0	0	0	42	23
5	163	6.16	2.0	2	493	115	678	176
(7.5 mg)	76	5.17	4.0	6	566	149	1363	437
	120	6.39	6.0	1	232	22	615	223
	148	6.18	8.0	0	109	11	573	204
	219	5.83	12.0	0	49	8	874	324
	935	6.30	24.0	0	2	2	458	114
	350	5.99	30.0	0	0.4	0.4	408	119
	420	5.63	36.0	0	0	0	310	89
	711	5.82	48.0	0	0	0	130	62
	680	5.95	60.0	0	0	0	75	26
	527	5.89	72.0	0	0	0	49	25
	950	6.40	84.0	0	0	0	9	6
	149	6.37	96.0	0	0	0	15	6
6	215	6.49	2.0	0.9	450	67	278	54
(7.5 mg)	98	6.11	4.0	2	437	99	676	202
	133	6.95	6.0	0.7	218	22	290	76
	125	7.22	8.0	0	98	10	60	23
	245	6.48	12.0	0	41	14	278	92
	485	6.03	24.0	0	7	7	632	200
	135	5.45	30.0	0	4	4	727	290
	242	6.09	36.0	0	1	1	377	122
	305	5.92	48.0	0	2	2	476	236
	590	6.48	60.0	0	0.5	0	87	40
	341	5.81	72.0	0	0	0	200	96
	272	5.48	84.0	0	0	0	124	59
	447	5.35	96.0	0	0	0	50	30

Data were calculated as the free base.

[a] Urine volume.

[b] Zero means not detected.

SG, selegiline; SGO, selegiline *N*-oxide; DM-SG, *N*-desmethylselegiline; MA, methamphetamine; AP, amphetamine.

approximately 3–17 times those of DM-SG. The SGO levels rapidly decreased to the detection limit level (0.1 ng ml^{-1}) in 24–36 and 30–60 h post-dosing of 2.5 mg and 7.5 mg administration, respectively. The urinary levels of DM-SG dropped to the detection limit levels (0.2 ng ml^{-1}) in 12–30 and 30–60 h post-dosing of 2.5 and 7.5 mg administration, respectively. MA and AP were detectable even up to 96 h post-dosing, whereas unchanged SG was detected in 4–6 and 6–12 h post-dosing of 2.5 and 7.5 mg administration, respectively.

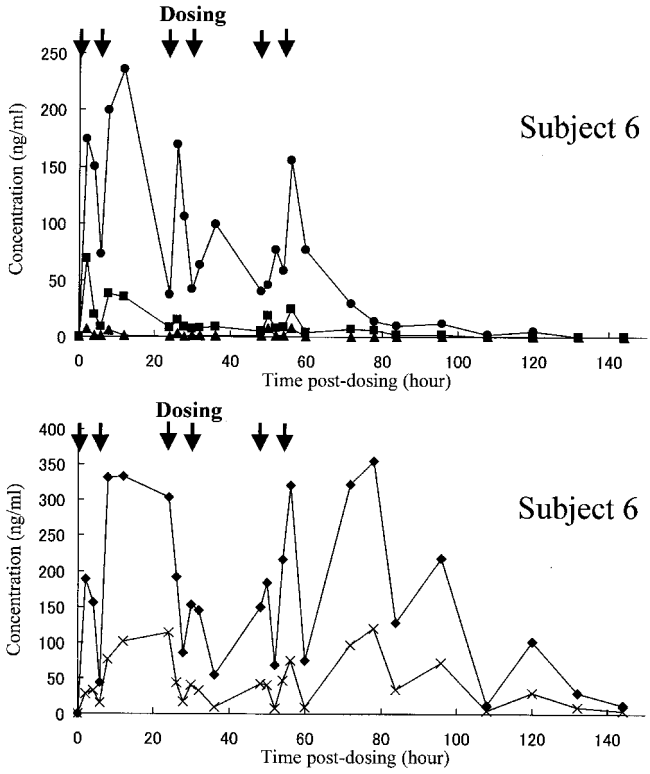


Figure 3. Time-course of urinary levels of selegiline (SG) and its metabolites after a repeat, twice-daily dosing of 5.0 mg day^{-1} for 3 days. ●, Selegiline *N*-oxide (SGO); ▲, selegiline (SG); ■, *N*-desmethylselegiline (DM-SG), □, methamphetamine (MA); ×, amphetamine (AP).

The time-course of urinary levels of SG metabolites were investigated for the three subjects following a repeat, twice-daily dosing of 5.0 mg day^{-1} for 3 days. Figure 3 shows an example (V6) of the excretion profile of the metabolites. The excretion patterns were essentially almost the same as those for single dosing: for SGO, the characteristic pattern, which is substantially increased in 2–4 h post-dosing, followed by rapid decrease, was repeated.

The total amounts of SG, SGO, DM-SG, MA and AP excreted in urine as a percentage of the parent drug after single oral dosing are shown in table 2. The total amount of each metabolite excreted within 72 h post-dosing was, on the whole, in the order MA, AP, SGO, DM-SG and SG. The amount of SGO was 2.0–7.8 times greater than that of DM-SG. However, within 4 h post-dosing, the amount of SGO was almost equal to that of MA. Unusually, subject 3 had substantially greater amounts of SGO compared with other subjects. SGO was mostly excreted within 8–12 h post-dosing for all six subjects.

It is well known that the cytochrome P450 (CYP) enzymes, including CYP2D6, CYP3A4 and CYP2B6, amongst others, are responsible for the metabolism of SG to MA, AP and DM-SG (Grace *et al.* 1994, Bach *et al.* 2000, Taavitsainen *et al.* 2000, Hidestrand *et al.* 2001). On the other hand, it has also been reported that tertiary amine compounds are readily *N*-oxidized in man by FMO (Poulsen and Ziegler 1979, Ziegler 1988). On the presumption that SGO is

Table 2. Per cent of selegiline dose excreted as selegiline and its metabolites in human urine.

Subject (dose)	Hours post-dosing	SG	SGO	DM-SG	MA	AP	Total[a]
1	0–4	< 0.1	2.7	0.8	2.1	0.7	6.3
(2.5 mg)	4–8	< 0.1	0.6	< 0.1	3.6	1.2	5.5
	8–12	0[b]	0.1	< 0.1	3.7	1.6	5.5
	12–24	0	< 0.1	< 0.1	8.2	2.8	11.1
	24–48	0	0	0	4.2	1.8	6.0
	48–72	0	0	0	1.6	0.5	2.1
	Total[c]	< 0.1	3.5	1.0	23.4	8.6	36.5
2	0–4	< 0.1	2.8	1.5	2.8	1.1	8.2
(2.5 mg)	4–8	0	0.8	0.1	2.3	0.9	4.1
	8–12	0	0.2	< 0.1	1.7	0.7	2.7
	12–24	0	0.1	< 0.1	3.7	1.6	5.4
	24–48	0	< 0.1	< 0.1	5.1	2.5	7.7
	48–72	0	0	0	1.2	0.5	1.7
	Total	< 0.1	4.0	1.8	16.8	7.3	29.9
3	0–4	< 0.1	11.4	1.6	3.0	1.0	17.0
(2.5 mg)	4–8	< 0.1	1.3	< 0.1	2.5	1.4	5.3
	8–12	0	0.4	< 0.1	3.0	1.8	5.3
	12–24	0	< 0.1	0	2.8	2.2	5.0
	24–48	0	< 0.1	0	3.4	3.2	6.6
	48–72	0	0	0	1.4	1.5	2.9
	Total	< 0.1	13.2	1.7	16.1	11.1	42.1
4	0–4	< 0.1	2.0	0.9	4.5	1.2	8.6
(7.5 mg)	4–8	< 0.1	0.7	0.2	2.5	0.9	4.3
	8–12	< 0.1	0.1	0.2	3.1	1.2	4.6
	12–24	0	< 0.1	< 0.1	6.5	1.9	8.5
	24–48	0	< 0.1	< 0.1	7.0	2.6	9.7
	48–72	0	< 0.1	< 0.1	1.9	0.9	2.8
	Total	< 0.1	3.0	1.5	25.5	8.7	38.7
5	0–4	< 0.1	1.8	0.5	4.5	1.4	8.2
(7.5 mg)	4–8	< 0.1	0.6	< 0.1	3.4	1.3	5.4
	8–12	0	0.2	< 0.1	4.0	1.6	5.8
	12–24	0	< 0.1	< 0.1	8.9	2.4	11.4
	24–48	0	< 0.1	< 0.1	7.4	2.7	10.1
	48–72	0	< 0.1	0	1.5	0.7	2.2
	Total	< 0.1	2.8	0.6	29.7	10.1	43.2
6	0–4	< 0.1	2.1	0.4	2.5	0.7	5.7
(7.5 mg)	4–8	< 0.1	0.6	< 0.1	0.9	0.3	1.9
	8–12	0	0.1	< 0.1	1.4	0.5	2.0
	12–24	0	< 0.1	< 0.1	6.2	2.1	8.4
	24–48	0	< 0.1	< 0.1	6.7	3.1	9.9
	48–72	0	< 0.1	< 0.1	2.4	1.2	3.7
	Total	< 0.1	3.0	0.6	20.1	7.9	31.6

Data are the percentage of the dose of SG.

[a]Combined total of SG, SGO, DM-SG, MA and AP.

[b]Zero means not detected.

[c]Combined total of each compound excreted within 72 h post-dosing.

SG, selegiline; SGO, selegiline *N*-oxide; DM-SG, *N*-desmethylselegiline; MA, methamphetamine; AP, amphetamine.

also formed by the FMO systems, the urinary excretion rate of SGO compared with those of other metabolites would, therefore, largely depend on CYP- and FMO-catalysed activities. Additionally, the substantial difference in urinary excretion of SGO among the subjects in this study may be caused by high extent of interindividual variation of FMO activities. However, only a few studies on FMO in man exist (Poulsen and Ziegler 1979, Ziegler 1988, Lemoine *et al*. 1990,

Table 3. Urinary excretion of selegiline and its metabolites for six long term selegiline patients.

Patient	dosing ($mg\,day^{-1}$)	pH	Hours post-last dosing	SG ($ng\,ml^{-1}$)	SGO ($ng\,ml^{-1}$)	DM-SG ($ng\,ml^{-1}$)	MA ($ng\,ml^{-1}$)	AP ($ng\,ml^{-1}$)
1	2.5×2	5.72	3.7	4	180	22	784	240
2	2.5×1	6.64	13.5	0.7	20	8	550	157
	2.5×2	5.58	2.3	5	150	32	1550	667
3	2.5×1	6.13	1.8	10	275	15	629	200
4	2.5×2	9.42	2.3	0[a]	111	8	46	26
5	2.5×2	5.67	3.8	7	402	70	1257	416
6	2.5×2	6.53	1.5	2	159	15	563	132

Data were calculated as the free base.
[a]Zero means not detected.
SG, selegiline; SGO, selegiline *N*-oxide; DM-SG, *N*-desmethylselegiline; MA, methamphetamine; AP, amphetamine.

Yamazaki *et al.* 1999), and future studies on this subject will be required to clarify the detailed metabolism of SG to SGO.

Urinary excretion of SG metabolites for long term SG patients

In previous research on long-term SG patients ($10\,mg\,day^{-1}$), Maurer and Kraemer (1992) reported that DM-SG was not detected in any urine samples. Thus, the urinary excretion of SG metabolites was studied by us for six long-term SG patients (2.5 or $5.0\,mg\,day^{-1}$). In this study, SGO was detected at high concentration in all urine samples collected from long-term SG patients, and DM-SG was also detected at lower levels than SGO in all the samples (table 3). This difference for DM-SG detection between the present study and the previous report may be caused by a difference in the dose.

One subject (patient 4) had a substantially higher level of SGO compared with levels of other metabolites, whereas the other five subjects had higher MA levels compared with SGO levels. The urinary pH of sample from patient 4 was 9.42 and those from the others were all < 7.0. Additionally, the fluctuations of concentrations of the metabolites (other than SGO) can be seen in the data summarized in table 1. It is well known that MA and AP are excreted depending largely on urinary pH (Beckett and Rowland 1965); alkaline conditions lower the extraction rate of both drugs. It is also reported that urinary pH scarcely influenced the excretion of *N*-oxides (Jenner 1971). These latter reports may help to explain such large fluctuations in concentration of the metabolites and low fluctuations in SGO excretion, though only preliminary data relating to the influence of urinary pH on the urinary excretion rate of SGO was obtained in this study.

In conclusion, the data from the present study have demonstrated that the main metabolic pathways for SG to SGO (by *N*-oxidation) as well as to MA, DM-SG and AP (by dealkylation) exist in all subjects. The cumulative amount of SGO excreted into urine within 72 h post-dosing ranged from 2.8 to 13.2% and was several times larger than that of DM-SG, which has previously considered to be a main specific metabolite and a marker of SG use. In the current study, SGO has proved to be an important abundant and specific metabolite of SG, and can serve

as a new indicator of SG administration, even in discrimination of SG use from MA abuse.

Acknowledgements

The authors thank Dr Azuma at Osaka Police Hospital for providing urine specimens from long-term SG patients.

References

Bach, M. V., Coutts, R. T. and Baker, G. B., 2000, Metabolism of *N*,*N*-dialkylated amphetamines, including deprenyl, by CYP2D6 expressed in a human cell line. *Xenobiotica*, **30**, 297–306.

Beckett, A. H. and Rowland, M., 1965, Urinary excretion kinetics of methyl-amphetamine in man. *Journal of Pharmacy and Pharmacology*, **17**, 109S–114S.

Crossley, F. S. and Moore, M. L., 1944, Studies on the Leuckart reaction. *Journal of Organic Chemistry*, **9**, 529–536.

Grace, J. M., Kinter, M. T. and Macdonald, T. L., 1994, Typical metabolism of deprenyl and its enantiomer, (*S*)-(+)-*N*, α-dimethyl-*N*-propynylphenethylamine, by cytochrome P450 2D6. *Chemical Research in Toxicology*, **7**, 286–290.

Heinonen, E. H. and Lammintausta, R., 1991, A review of the pharmacology of selegiline. *Acta Neurologica Scandinavica*, **84(suppl.)**, 44–59.

Heinonen, E. H., Anttila, M. I. and Lammintausta, R. A., 1994, Pharmacokinetic aspects of *l*-deprenyl (selegiline) and its metabolites. *Clinical Pharmacology and Therapeutics*, **56**, 742–749.

Hidestrand, M., Oscarson, M., Salonen, J. S., Nyman, L., Pelkonen, O., Turpeinen, M. and IngelmanSundberg, M., 2001, CYP2B6 and CYP2C19 as the major enzymes responsible for the metabolism of selegiline, a drug used in the treatment of Parkinson's disease, as revealed from experiments with recombinant enzymes. *Drug Metabolism and Disposition*, **29**, 1480–1484.

Jenner, P., 1971, The role of nitrogen oxidation in the excretion of drugs and foreign compounds. *Xenobiotica*, **1**, 399–418.

Katagi, M., Tatsuno, M., Miki, A., Nishikawa, M., Nakajima, K. and Tsuchihashi, H., 2001, Simultaneous determination of selegiline-*N*-oxide, a new indicator for selegiline administration, and other metabolites in urine by high-performance liquid chromatography-electrospray ionization mass spectrometry. *Journal of Chromatography B*, **759**, 125–133.

Knoll, J., 1978, The possible mechanisms of action of (–)deprenyl in Parkinson's disease. *Journal of Neural Transmission*, **43**, 177–198.

Lemoine, A., Johann, M. and Cresteil, T., 1990, Evidence for the presence of distinct flavin-containing monooxygenases in human tissues. *Archives of Biochemistry and Biophysics*, **276**, 336–342.

Lengyel, J., Magyar, K., Hollói, I., Bartók, T., Báthori, M., Kalász, H. and Fürst, S., 1997, Urinary excretion of deprenyl metabolites. *Journal of Chromatography A*, **762**, 321–326.

Maurer, H. H. and Kraemer, T., 1992, Toxicological detection of selegiline and its metabolites in urine using fluorescence polarization immunoassay (FPIA) and gas chromatography-mass spectrometry (GC-MS) and differentiation by enantioselective GC-MS of the intake of selegiline from abuse of methamphetamine or amphetamine. *Archives of Toxicology*, **66**, 675–678.

Poulsen, L. L. and Ziegler, D. M., 1979, The liver microsomal FAD-containing monooxygenase. Spectral characterization and kinetic studies. *Journal of Biological Chemistry*, **254**, 6449–6455.

Shin, H. S., 1997, Metabolism of selegiline in humans. Identification, excretion, and stereochemistry of urine metabolites. *Drug Metabolism and Disposition*, **25**, 657–662.

Szatmari, I. and Toth, K., 1992, Pharmacokinetics and metabolism of selegiline. *Acta Pharmaceutica Hungarica*, **62**, 243–248.

Taavitsainen, P., Anttila, M., Nyman, L., Karnani, H., Salonen, J. S. and Pelkonen, O., 2000, Selegiline metabolism and cytochrome P450 enzymes: in vitro study in human liver microsomes. *Pharmacology and Toxicology*, **86**, 215–221.

Yamazaki, M., Islam, M. N., Takikita, S., Ogura, Y., Terada, M., Nakatome, M., Kuroki, H. and Honda, K., 1999, Immunohistochemical and enzymological studies of flavin (FAD)-containing monooxygenase in human liver. *Japanese Journal of Forensic Toxicology*, **17**, 30–41.

Ziegler, D. M., 1988, Flavin-containing monooxygenase: catalytic mechanism and substrate specificities. *Drug Metabolism Reviews*, **19**, 1–32.

XENOBIOTICA, 2002, VOL. 32, NO. 10, 835–847

Taylor & Francis
healthsciences

Metabolism of zaleplon by human liver: evidence for involvement of aldehyde oxidase

B. G. LAKE†*, S. E. BALL‡, J. KAO‡, A. B. RENWICK†, R. J. PRICE† and J. A. SCATINA‡

† TNO BIBRA International Ltd, Woodmansterne Road, Carshalton, Surrey SM5 4DS, UK

‡ Wyeth-Ayerst Research, Drug Metabolism Division, CN8000, Princeton, NJ 08543-8000, USA

Received 12 March 2002

1. The metabolism of Zaleplon (CL-284,846; ZAL) has been studied in precision-cut human liver slices and liver cytosol preparations.

2. Human liver slices metabolized ZAL to a number of products including 5-oxo-ZAL (M2), N-desethyl-5-oxo-ZAL (M1) and N-desethyl-ZAL (DZAL), the latter metabolite being known to be formed by CYP3A forms.

3. Human liver cytosol preparations catalysed the metabolism of ZAL to M2. Kinetic analysis of three cytosol preparations revealed mean (± SEM) K_m and V_{max} of 93 ± 18 mm and 317 ± 241 pmol/min/mg protein, respectively.

4. Using 16 individual human liver cytosol preparations a 33-fold variability in the metabolism of 80 μM ZAL to M2 was observed. Correlations were observed between M2 formation and the metabolism of the aldehyde oxidase substrates phenanthridine ($r^2 = 0.774$) and phthalazine ($r^2 = 0.460$).

5. The metabolism of 80 μM ZAL to M2 in liver cytosol preparations was markedly inhibited by the aldehyde oxidase inhibitors chlorpromazine, promethazine, hydralazine and menadione. Additional kinetic analysis suggested that chlorpromazine and promethazine were non-competitive inhibitors of M2 formation with K_i of 2.3 and 1.9 μM, respectively. ZAL metabolism to M2 was also inhibited by cimetidine.

6. Incubations conducted with human liver cytosol and $H_2{}^{18}O$ demonstrated that the oxygen atom incorporated into ZAL and DZAL to form M2 and M1, respectively, was derived from water and not from molecular oxygen.

7. In summary, by correlation analysis, chemical inhibition and $H_2{}^{18}O$ incorporation studies, ZAL metabolism to M2 in human liver appears to be catalysed by aldehyde oxidase. With human liver slices, ZAL was metabolized to products dependent on both aldehyde oxidase and CYP3A forms.

Introduction

Zaleplon (*N*-[3-(3-cyanopyrazolo[1,5-*a*]pyrimidin-7-yl)phenyl]-*N*-ethylacetamide; CL-284,846; ZAL) is a novel non-benzodiazepine sedative-hypnotic agent for the treatment of insomnia. Studies in man have demonstrated that ZAL is extensively metabolized with 88% of the dose appearing in the urine (71%) and faeces (17%) as metabolites (Wu *et al*. 1996, Rosen *et al*. 1999). Investigations in both experimental animals and man (Beer *et al*. 1994, Chaudhary *et al*. 1994, Wu *et al*. 1996, Kawashima *et al*. 1999) have demonstrated that ZAL may be metabolized (figure 1) by oxidation to metabolite M2 (5-oxo-ZAL; (*N*-[3-(3-cyano-4,5-dihydro-5-oxopyrazolo[1,5-*a*]pyrimidin-7-yl)phenyl]-N-ethylacetamide)

* Author for correspondence; e-mail: blake@tnobibra.co.uk

Xenobiotica ISSN 0049–8254 print/ISSN 1366–5928 online © 2002 Taylor & Francis Ltd
http://www.tandf.co.uk/journals
DOI: 10.1080/00498250210158915

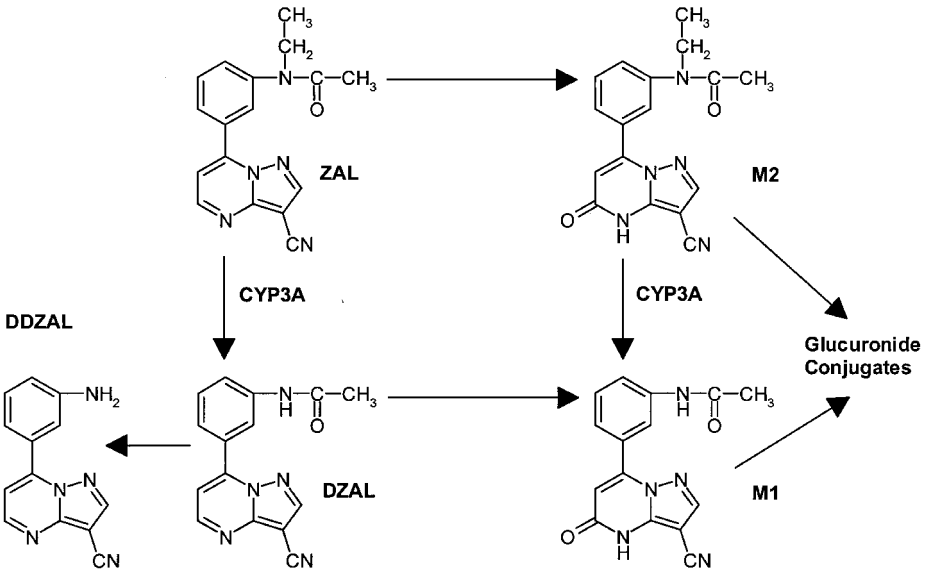


Figure 1. Some pathways of zaleplon (ZAL) metabolism.

and by *N*-deethylation to DZAL (*N*-desethyl-ZAL; *N*-[3-(3-cyanopyrazolo[1,5-*a*]pyrimidin-7-yl)phenyl]-acetamide). Other metabolites include M1 (*N*-desethyl-5-oxo-ZAL; *N*-[3-(3-cyano-4,5-dihydro-5-oxopyrazolo[1,5-a]pyrimidin-7-yl)-phenyl]-acetamide), which may be derived from M2 and DZAL (figure 1) and DDZAL (7-(3-aminophenyl)pyrazolo[1,5-*a*]pyrimidine-3-carbonitrile), which is derived from the deacetylation of DZAL (figure 1). Both M2 and M1 can form glucuronide conjugates. In man, M1 and M2 with their glucuronide conjugates account for some 9 and 57%, respectively, of the administered dose recovered in urine (Wu *et al*. 1996). Species differences in ZAL metabolism have been reported as M2 is the major plasma metabolite in man, whereas DZAL and/or DDZAL are the major plasma metabolites in the rat, mouse and dog (Chaudhary *et al*. 1994).

In a previous *in vitro* study, the NADPH-dependent *N*-deethylation of ZAL to DZAL by human liver microsomes was investigated (Renwick *et al*. 1998). Reaction phenotyping studies demonstrated that DZAL formation was predominantly catalysed by cytochrome P450 (CYP) 3A forms. Unlike ZAL metabolism to DZAL, the CYP3A-catalysed *N*-deethylation of M2 to M1 proceeded at only a very low rate.

In another *in vitro* investigation, Kawashima *et al*. (1999) examined the metabolism of ZAL by hepatic subcellular fractions from male Sprague–Dawley rats and from one male Cynomolgus monkey. ZAL metabolism to DZAL was NADPH-dependent and catalysed by liver microsomes, but not cytosol. From studies with a number of known inhibitors of CYP forms, the authors concluded that DZAL formation in both species was catalysed by several CYP forms including members of the CYP2B, CYP2C and CYP2D subfamilies. Unlike DZAL formation, ZAL metabolism to M2 was NADPH-independent and catalysed by liver cytosol, but not by microsomes. Additional studies provided

evidence that ZAL was metabolized to M2 in both species by cytosolic aldehyde oxidase.

While ZAL metabolism in human liver to DZAL is known to be catalysed by CYP3A forms (Renwick *et al.* 1998), the enzymes involved in M2 formation have not been elucidated. The aim of the present study was to ascertain the role of aldehyde oxidase in the metabolism of ZAL to M2 in human liver. In addition, the metabolism of ZAL was also studied in freshly cut and cultured human liver slices.

Materials and methods

Materials

Samples of CL-284,846 (ZAL), CL-284,859 (DZAL), CL-314,475 (DDZAL), CL-345,644 (M1) and CL-345,905 (M2) (purities > 99% for ZAL and > 97% for the other compounds) and [^{14}C]ZAL (specific activity 9.66 μCi/μmol; radiochemical purity 98%) were supplied by Wyeth-Ayerst Research Drug Metabolism Division (Princeton, NJ, USA). The sources of the tissue culture materials were as described by Beamand *et al.* (1993). Chlorpromazine, cimetidine, hydralazine, menadione and promethazine were obtained from Sigma Chemical Co. (St Louis, MO, USA) and phenanthridine and phthalazine from Aldrich Chemical Co. (Milwaukee, MI, USA). Samples of human liver were obtained from IIAM (Exton, PA, USA) and used to prepare cytosol fractions.

Preparation of liver slices

Samples of human liver (surplus to transplant requirements) were transported on ice to TNO BIBRA. Tissue cylinders from liver samples were prepared using a 10-mm diameter motor-driven tissue-coring tool. From the cylinders, tissue slices (200–300 μm) thick were prepared in oxygenated (95% O_2/5% CO_2) Earle s balanced salt solution containing 25 mM D-glucose, 50 μg/ml gentamicin and 2.5 μg/ml fungizone using a Krumdieck tissue slicer (Alabama Research and Development Corp., Munford, AL, USA).

Culture of liver slices

Liver slices were floated onto Vitron, Inc. (Tucson, AZ, USA) type C titanium roller inserts (two slices per insert) and cultured in glass vials containing 1.7 ml culture medium employing a Vitron dynamic organ incubator. The culture medium consisted of RPMI 1640 containing 5% (v/v) foetal calf serum, 0.5 mM (final concentration) L-methionine, 1 μm insulin, 0.1 mM hydrocortisone-21-hemisuccinate, 50 μg/ml gentamicin and 2.5 μg/ml fungizone. Liver slice cultures were maintained at 37°C in an atmosphere of 95% O_2/5% CO_2. After 1 h, liver slices were either incubated with fresh medium containing [^{14}C]ZAL (see below) or the medium was changed and the slices cultured for 72 h, with the medium being replaced every 24 h.

ZAL metabolism in liver slices

Freshly cut (i.e. after a 1-h preculture) and 72-h cultured human liver slices were cultured for 2 h in RPMI 1640 medium containing 120 μm [^{14}C]ZAL (approximately 1 μCi/ml, added in 4 μl dimethyl sulphoxide ml/medium), 1 μM insulin and 0.1 mM hydrocortisone-21-hemisuccinate. At the end of the incubation period, the liver slices were homogenized in the culture medium by sonication (Beamand *et al.* 1993) and the liver slice/medium homogenates stored at −80°C before analysis. Liver slice/medium homogenates were hydrolysed with β-glucuronidase and sulphatase as described by Steensma *et al.* (1994) and then treated with 3 vols ice-cold acetonitrile. Analysis of the deproteinized extracts was performed by high-performance liquid chromatography (HPLC) as described by Renwick *et al.* (1998), except that the ZAL metabolites were quantified by radiometric detection. Liver slice protein content was determined by the method of Lowry *et al.* (1951) employing bovine serum albumin as standard.

ZAL metabolism in liver cytosol

All ZAL metabolism studies with human liver cytosol preparations were performed at Wyeth-Ayerst (Princeton, NJ, USA). ZAL metabolism was studied with incubation mixtures containing 80 μM [^{14}C]ZAL (10–500 μM for kinetic studies, 0.1 μCi/tube), 2 mg cytosol protein and 0.1 M phosphate buffer in a final volume of 1 ml. Incubations were performed for 10 min at 37°C and terminated with 3 ml ice-cold acetonitrile. Blank incubations contained all components except cytosol, which was added after the reaction was terminated with acetonitrile. Precipitated protein was removed by centrifugation and the supernatants were blown to dryness under nitrogen gas. The residues were dissolved in 300 μl 20 mM

ammonium formate/acetonitrile (81:19 v/v) before analysis by HPLC. Chromatography was performed with a 150 × 4.6 mm column of Zorbax rx-C8 and mobile phases consisting of 20 mM ammonium formate pH 6.5 (A) and acetonitrile (B). Elution was achieved at 1 ml/min starting with 99% A and 1% B, changing to 81% A and 19% B over 6 min, to 75% A and 25% B over 15 min, to 69% A and 31% B over 11 min, to 42% A and 58% B over 1 min and then holding at 58% A and 42% B for 10 min. M2 formation was quantified by online radiometric detection. Inhibition studies were conducted by adding the selected compounds (namely chlorpromazine, promethazine, hydralazine, menadione and cimetidine) dissolved in either ethanol or water (10 µl/incubation) at final concentrations of 10, 125 and 250 µM. Control incubations (no inhibitor added) contained the appropriate solvent. The kinetics of inhibition by chlorpromazine and promethazine was studied using [^{14}C]ZAL concentrations of 20–200 µM and inhibitor concentrations of 0–5 and 0–10 µM, respectively.

Assay of aldehyde oxidase enzyme activities

Assays of phenanthridine and phthalazine metabolism were performed directly in spectrophotometer cuvettes at 37°C employing previously published procedures (Rajagopalan and Handler 1966, Johnson *et al.* 1984, Rodrigues 1994). For phenanthridine metabolism, cuvettes contained 1 mM substrate, 0.1 mM EDTA, 1 mg cytosol protein and 67 mM phosphate buffer, pH 7.8, in a final volume of 1 ml. The formation of oxidized phenanthridine (6-phenanthridone) was monitored at 322 nm and quantified using an extinction coefficient of 9 mM^{-1} cm^{-1}. For phthalazine metabolism, cuvettes contained 0.05 mM substrate, 1 mM potassium ferricyanide (as an artificial electron acceptor), 0.1 mM EDTA, 1 mg cytosol protein and 67 mM phosphate buffer, pH 7.8, in a final volume of 1 ml. The reduction of potassium ferricyanide (corrected for non-substrate dependent reduction) was monitored at 420 nm and quantified using an extinction coefficient of 1.02 mM^{-1} cm^{-1}.

$H_2{}^{18}O$ incorporation studies

To confirm whether the oxygen atom incorporated into either M2 or M1 was derived from water, either 50 µm ZAL or 100 µm DZAL were incubated at 37°C for either 15 or 60 min, respectively, with 1 mg human liver cytosol protein and 0.1 M phosphate buffer, pH 7.4, containing $H_2{}^{18}O$ in a final volume of 1 ml. $H_2{}^{18}O$ comprised around 70–80% of the total water in the incubations. The incubations were terminated with 3 ml ice-cold acetonitrile, precipitated proteins removed by centrifugation and the supernatants blown to dryness under nitrogen gas. Positive-ion electrospray liquid chromatography-mass spectrometry (LC/MS) analysis of the incubate extracts was performed with a Finnigan SSQ 710 mass spectrometer. Chromatography was performed with a 150 × 2.1 mm column of Zorbax rx-C8 employing gradient elution with mobile phases of 0.5% formic acid in water/acetonitrile (1000:20 v/v) and 0.5% formic acid in acetonitrile/water (1000:20 v/v). Positive-ion electrospray spectra were acquired at a unit mass resolution by flow injection of 20 µl of the incubation extracts. The sample solution was desolvated at a capillary temperature of 200°C. The electrospray needle voltage and the conversion dynode were set at 4.5 and −15 kV respectively, with the electron multiplier being set at 1.0 and 1.4 kV for M2 and M1, respectively.

Results

Metabolism of ZAL by human liver slices

The metabolism of 120 µm [^{14}C]ZAL by three preparations of human liver slices was investigated. Metabolism studies were performed employing a 2 h incubation time with either freshly cut slices (i.e. used immediately after preparation) or with slices that had been cultured in control medium for 72 h. ZAL was metabolized by all three freshly cut human liver slice preparations to a number of metabolites including M1, M2, DZAL and DDZAL (figure 2A). Liver slice/medium homogenates were treated with β-glucuronidase and sulphatase before HPLC analysis and hence no attempt was made to quantify free as well as conjugated M1 and M2. With all three human liver slice preparations M2 was the major metabolite formed, together with smaller amounts of M1, DZAL/DDZAL (quantified together owing to an incomplete separation by the HPLC method used) and an unknown metabolite (termed 'X'). In freshly cut slices, the formation of M1, M2, 'X' and DZAL/DDZAL accounted for 18, 59, 3 and 20% of total ZAL metabolism, respectively. When human liver slices were cultured for

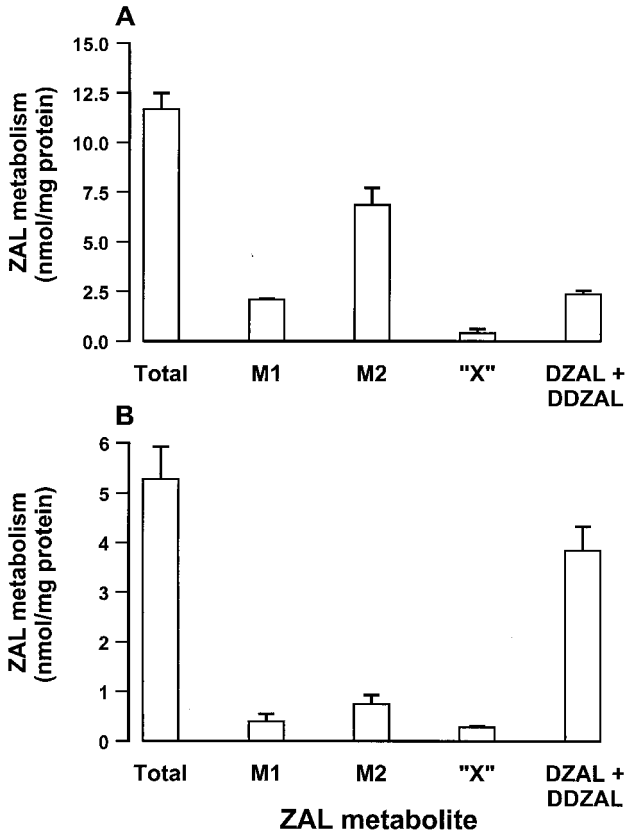


Figure 2. Metabolism of [^{14}C]ZAL by precision-cut human liver slices. Results are the mean ± SEM for three human liver slice preparations. Liver slices were prepared and either freshly cut slices were incubated with 120 μM [^{14}C]ZAL for 2 h (A) or the liver slices were cultured for 72 h before being incubated with 120 μM [^{14}C]ZAL for 2 h (B). Liver slice/medium homogenates were analysed by HPLC for ZAL metabolites.

72 h before incubation with [^{14}C]ZAL, total ZAL metabolism was only 45% of freshly cut slice levels (figure 2B). The formation of DZAL/DDZAL accounted for 73% of total ZAL metabolism, with M2 formation being only 14% of total ZAL metabolism.

Kinetics of M2 formation in liver cytosol

[^{14}C]ZAL was metabolized to M2 by human hepatic cytosolic fractions. M2 formation did not require the presence of NADPH (data not shown). Using three human liver cytosol preparations the kinetics of M2 formation was investigated over a substrate concentration range of 10–500 μM. Kinetic analysis of Michaelis–Menten plots revealed K_m of 57, 117 and 106 μM, respectively. Corresponding V_{max} were 132, 796 and 24 pmol/min/mg cytosolic protein, respectively. For these three human liver cytosol preparations, the mean (± SEM) K_m and V_{max} were 93 ± 18 μM and 317 ± 241 pmol/min/mg protein, respectively.

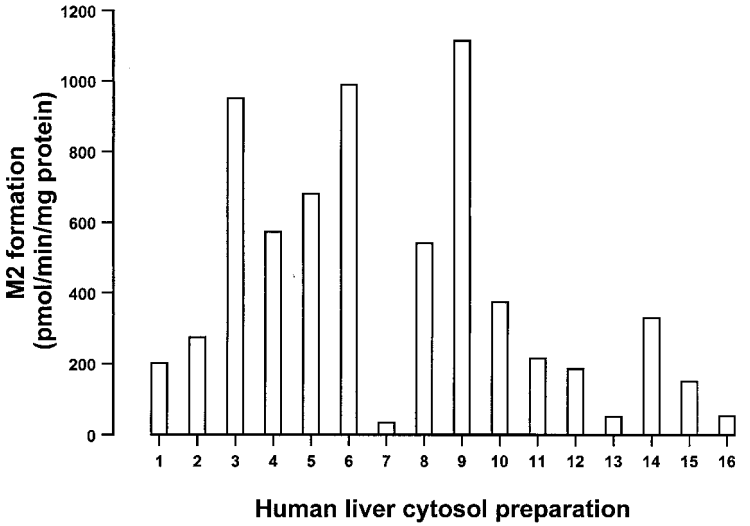


Figure 3. Variability in the metabolism of 80 μM [^{14}C]ZAL to M2 in a panel of 16 individual human liver cytosol preparations. Duplicate incubations were performed for 10 min with 2 mg human liver liver cytosol protein.

Correlation analysis studies

The metabolism of ZAL to M2 was examined with 16 individual human liver cytosol preparations employing a substrate concentration of 80 μM (i.e. around the observed mean K_m for M2 formation). A marked variability was observed between the 16 human liver cytosol samples examined. Rates of M2 formation ranged from 33.7 to 1114 pmol/min/mg protein (figure 3), resulting in an overall 33-fold variation between the 16 human liver cytosol preparations examined.

The rates of ZAL metabolism to M2 were correlated with rates of metabolism of two aldehyde oxidase substrates, namely phenanthridine and phthalazine, employing 16 human liver cytosol preparations. For M2 formation and phenanthridine metabolism a correlation of $r^2 = 0.774$ was observed (figure 4A), whereas for M2 formation and phthalazine metabolism a correlation of $r^2 = 0.460$ (figure 4B) was observed.

Inhibition studies

The effect of 10, 125 and 250 μM of the aldehyde oxidase inhibitors chlorpromazine, promethazine, hydralazine and menadione (Johns 1967, Johnson *et al.* 1985, Yoshihara and Tatsumi 1986, Beedham 1987, Rashidi *et al.* 1995) on ZAL metabolism in human liver cytosol preparations was examined. Studies were also performed with 10, 125 and 250 μM cimetidine, which is known to inhibit both aldehyde oxidase and CYP enzymes (Somogyi and Muirhead 1987, Rashidi *et al.* 1995, Tanaka 1998). Treatment with all five compounds resulted in a concentration-dependent inhibition of M2 formation (figure 5). Chlorpromazine and promethazine were the most potent inhibitors, reducing M2 formation at an inhibitor concentration of 10 μM to 26 and 32% of control, respectively. Hydralazine and menadione also markedly inhibited M2 formation, whereas cimetidine was the least potent inhibitor over the concentration range examined.

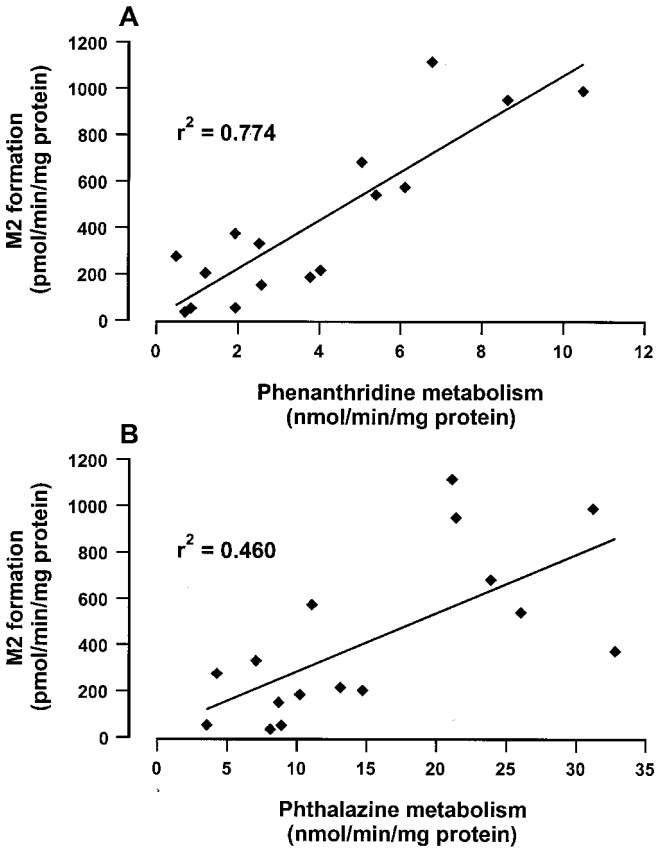


Figure 4. Correlation between the metabolism of 80 μM [^{14}C]ZAL to M2 and phenanthridine (A) and phthalazine (B) metabolism in a panel of 16 individual human liver cytosol preparations. Duplicate incubations were performed as described in the Materials and methods with 1 mg human liver cytosol protein.

The kinetics of inhibition of M2 formation by the two most potent inhibitors, namely chlorpromazine and promethazine, was studied employing ZAL substrate concentrations of 20–200 μM and inhibitor concentrations of 0–5 and 0–10 μM, respectively. Kinetic analysis of Dixon plots (Dixon 1953) suggested that both compounds were non-competitive inhibitors of M2 formation. Calculated K_i for chlorpromazine (figure 6A) and promethazine (figure 6B) inhibition were 2.3 and 1.9 μM, respectively.

$H_2{}^{18}O$ incorporation studies

One human liver cytosol preparation was incubated with 50 μM ZAL in buffer prepared with $H_2{}^{18}O$ (95–98%) and the incubate extract analysed by LC/MS (figure 7). Compared with the mass spectrum of normal M2 (figure 7A), 73% of the M2 formed in the incubation with $H_2{}^{18}O$ had a molecular ion two mass units higher (figure 7B), indicating that the ^{18}O-isotope in the metabolite was derived from water and not from molecular oxygen. The remaining 27% of the M2 contained ^{16}O-isotope (figure 7B), which is consistent with isotope dilution by

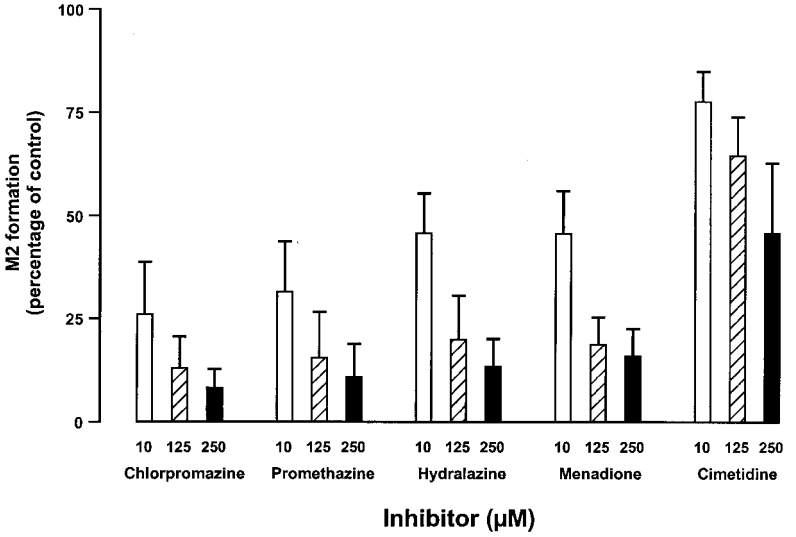


Figure 5. Inhibition of metabolism of 80 μM [^{14}C]ZAL to M2 in human liver cytosol preparations. Results are the mean ± SEM for three human liver cytosol preparations. Triplicate incubations were performed in the presence of either 10, 125 or 250 μM of either chlorpromazine, promethazine, hydralazine, menadione or cimetidine, and enzyme activity is expressed as a percentage of control (no inhibitor added) incubations.

^{16}O-isotope as the human liver cytosol preparation was prepared in 0.15 M KCl with 50 mM Tris-HCl, pH 7.4, containing $H_2{}^{16}O$ not $H_2{}^{18}O$.

A human liver cytosol preparation was also incubated with 100 μM DZAL in buffer prepared with $H_2{}^{18}O$ (95–98%) and the incubate extract analysed by LC/MS/MS. Compared with the mass spectrum of normal M1, about 83% of the M1 formed had a molecular ion two mass units higher (data not shown).

Discussion

In keeping with previous *in vitro* and *in vivo* studies (Beer *et al.* 1994, Chaudhary *et al.* 1994, Wu *et al.* 1996), ZAL was metabolized by precision-cut human liver slices to a number of metabolites including M1, M2, DZAL and DDZAL (figure 1). Using freshly cut liver slices M2, the major plasma metabolite of ZAL in man (Chaudhary *et al.* 1994), was the major metabolite observed in three separate human liver slice preparations. However, in 72-h cultured human liver slices, while total ZAL metabolism was reduced, there was a marked loss of M2 and M1 formation. These results suggest that freshly cut, rather than cultured, human liver slices are preferable for ZAL metabolism studies as there appears to be a differential loss of the enzymes involved in ZAL metabolism in cultured human liver slices. While CYP forms are known to be inducible in cultured human liver slices (Lake *et al.* 1997, 1998), the differential loss of the enzymes involved in ZAL metabolism precludes the use of cultured liver slices for *in vitro* studies aimed at evaluating the effect of enzyme inducers on ZAL metabolism. In contrast, freshly cut human liver slices appear to be a useful *in vitro* intact cell system for studying both CYP3A- and aldehyde oxidase-dependent pathways of ZAL metabolism. Moreover, liver slices have previously been used to study the biotransfor-

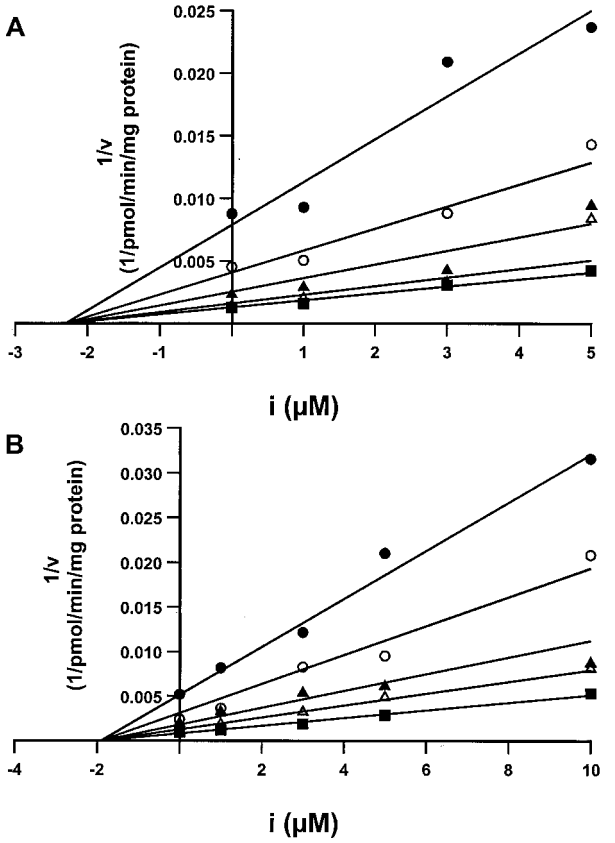


Figure 6. Dixon plots of the kinetics of inhibition of [^{14}C]ZAL metabolism to M2 by chlorpromazine (A) and promethazine (B) in a human liver cytosol preparation. Triplicate incubations were performed with 20 (●), 40 (○), 60 (▲), 80 (△) and 200 (■) μM [^{14}C]ZAL substrate and either 0–5 μM chlorpromazine (A) or 0–10 μM promethazine (B).

mation of other drugs which are substrates for aldehyde oxidase (Rodrigues *et al.* 1994, Acheampong *et al.* 1996).

In a previous study with human liver microsomal preparations, the metabolism of ZAL to DZAL and M2 to M1, respectively, was shown to be catalysed by CYP3A enzymes (Renwick *et al.* 1998). The major objective of the present investigation was to examine the enzymology of ZAL metabolism to M2 by human liver cytosol preparations. Whereas ZAL was metabolized to M2 by all human liver cytosol preparations examined, there was a marked variability between liver cytosol preparations from individual donors (figure 3). Although some other studies have suggested that hepatic aldehyde oxidase activity may have a high freeze–thaw lability (Johns 1967, Beedham 1987, Rodrigues 1994), this was not observed in the present study when liver cytosols were prepared from both fresh and frozen liver samples (S. E. Ball, unpublished data).

The present results demonstrate that ZAL is metabolized to M2 by human liver cytosol preparations with a mean K_m ($n = 3$ subjects) of 93 μM, this being lower than the S_{50} (i.e. the substrate concentration resulting in 50% of V_{max}) of 559 μM ($n = 2$ subjects) reported for microsomal CYP3A-dependent ZAL

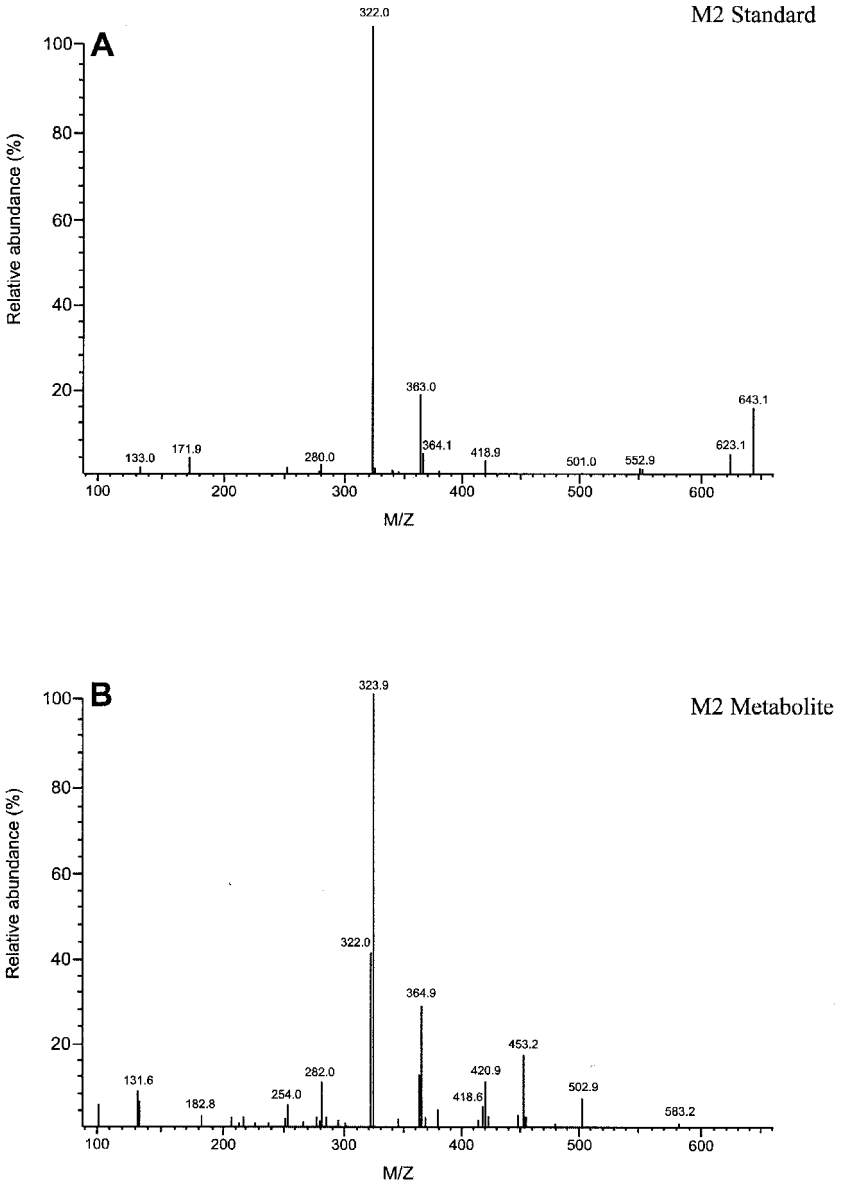


Figure 7. Metabolism of 50 μM ZAL to M2 in the absence (A) and presence (B) of $H_2{}^{18}O$. Incubations were performed for 15 min with 1 mg human liver cytosol protein in either normal 0.1 M phosphate buffer, pH 7.4, or buffer containing $H_2{}^{18}O$, and the incubate extracts were analysed by positive-ion electrospray LC/MS. M2 formed in the presence of $H_2{}^{18}O$ (B) had a molecular ion 2 mass units higher than normal M2 (A), indicating that the oxygen atom in the metabolites was derived from water and not from molecular oxygen.

metabolism to DZAL (Renwick *et al.* 1998). Based on the results of correlation analysis, chemical inhibition and $H_2{}^{18}O$ incorporation studies, ZAL metabolism to M2 appears to be catalysed by human hepatic aldehyde oxidase.

A good correlation ($r^2 = 0.774$) was observed between M2 formation in human liver cytosol preparations and phenanthridine metabolism, with a lower correlation

($r^2 = 0.460$) being observed between M2 formation and phthalazine metabolism. Both phenanthridine and phthalazine are known substrates of aldehyde oxidase in human liver (Beedham 1987, Beedham *et al.* 1987, Rashidi *et al.* 1997). In the 16 individual human liver cytosol preparations examined, ZAL metabolism to M2 varied by 33-fold, whereas phenanthridine and phthalazine metabolism varied by 22- and 9.2-fold, respectively. In a study on the metabolism of three other aldehyde oxidase substrates by human liver post-mitochondrial supernatant fractions, Rodrigues (1994) reported a variability between samples of 2.3-, 3.6- and >40-fold. It remains to be elucidated if the range of variability in activity of different aldehyde oxidase substrates is attributable to the presence of multiple aldehyde oxidase forms in human liver.

ZAL metabolism to M2 was markedly inhibited to 26–46% of control by the addition of 10 μM chlorpromazine, promethazine, hydralazine and menadione (figure 5). These four compounds are all known inhibitors of aldehyde oxidase (Johns 1967, Johnson *et al.* 1985, Beedham 1987, Rashidi *et al.* 1995, 1997). Additional studies indicated that both chlorpromazine and promethazine appeared to be non-competitive inhibitors of aldehyde oxidase-catalysed M2 formation in human liver (figure 6). ZAL metabolism to M2 was also inhibited to some extent by cimetidine, a known inhibitor of both aldehyde oxidase and CYP enzymes (Somogyi and Muirhead 1987, Rashidi *et al.* 1995, Tanaka 1998). In a recent *in vivo* study, cimetidine was reported to inhibit ZAL clearance in human volunteers (Darwish, Cevallos, Martin, Tse and Troy, unpublished data). The effect of cimetidine on ZAL metabolism by human liver slices and subcellular fractions is currently being investigated in our laboratories.

Aldehyde oxidase and xanthine oxidase are molybdenum-containing enzymes which can catalyse the oxidation of many aldehydes and nitrogen heterocycles (Beedham 1987). Both enzymes are known to be present in the liver of many species including humans. From the present data, ZAL appears to be metabolized to M2 by human hepatic aldehyde oxidase, rather than by xanthine oxidase. M2 formation was markedly inhibited by menadione and hydralazine, which are specific inhibitors of aldehyde oxidase activity (Johnson *et al.* 1985, Yoshihara and Tatsumi 1986, Beedham 1987). Moreover, whereas ZAL metabolism to M2 by both rat and Cynomolgus monkey liver cytosol preparations was markedly inhibited by menadione, the addition of allopurinol and other xanthine oxidase inhibitors had little effect on M2 formation (Kawashima *et al.* 1999). In addition, the observed species differences in ZAL metabolism, with M2 being the major plasma metabolite in humans and primates and DZAL being the major plasma metabolite in the rat and dog (Chaudhary *et al.* 1994), is in agreement with known species differences in levels of hepatic aldehyde oxidase (Beedham 1987, Beedham *et al.* 1987).

Unlike CYP-catalysed reactions, the oxygen atom incorporated in aldehyde oxidase-catalysed reactions is derived from water and not from molecular oxygen (Beedham 1987, Kawashima *et al.* 1999). In the present study, the incubation of ZAL with a human liver cytosol preparation in the presence of $H_2{}^{18}O$ resulted in a molecular ion two mass units higher (figure 7B) than that of M2 formed in normal incubations (i.e. with $H_2{}^{16}O$). This finding is in agreement with that of Kawashima *et al.* (1999) for the metabolism of ZAL to M2 by a single partially purified rat liver aldehyde oxidase preparation. Moreover, in the present study the oxygen atom incorporated in the metabolism of DZAL to M1 was also shown to be derived from

water and not from molecular oxygen, suggesting that this reaction is also catalysed by aldehyde oxidase. Additional studies are required to confirm the role of aldehyde oxidase in the metabolism of DZAL to M1 by human liver. Overall, whereas ZAL metabolism to DZAL and M2 metabolism to M1 are CYP3A-catalysed reactions (figure 1), ZAL metabolism to M2 and DZAL metabolism to M1 appear to be aldehyde oxidase-catalysed reactions. As the rate of M2 metabolism to M1 is very low (Renwick *et al.* 1998), the formation of M1 *in vivo* is more likely to proceed via the metabolism of DZAL, presumably catalysed by aldehyde oxidase, rather than by CYP3A-catalysed M2 metabolism.

In summary, by correlation analysis, chemical inhibition and $H_2{}^{18}O$ incorporation studies, ZAL metabolism to M2 is catalysed by human hepatic cytosolic aldehyde oxidase. The metabolism of DZAL to M1 also appears to be aldehyde oxidase dependent. As ZAL was metabolized to a number of known metabolites by precision-cut human liver slices, this *in vitro* model system may be useful for studying the interaction of other drugs with both the aldehyde oxidase- and CYP3A-dependent pathways of ZAL metabolism.

Acknowledgements

This work was supported by a research grant from Wyeth-Ayerst Research Drug Metabolism Division (Princeton, NJ, USA).

References

Acheampong, A. A., Chien, D.-S., Lam, S., Vekich, S., Breau, A., Usansky, J., Harcourt, D., Munk, S. A., Nguyen, H., Garst, M. and Tang-Liu, D., 1996, Characterization of brimonidine metabolism with rat, rabbit, dog, monkey and human liver fractions and rabbit liver aldehyde oxidase. *Xenobiotica*, **26**, 1035–1055.

Beamand, J. A., Price, R. J., Cunninghame, M. E. and Lake, B. G., 1993, Culture of precision-cut liver slices: effect of some peroxisome proliferators. *Food and Chemical Toxicology*, **31**, 137–147.

Beedham, C., 1987, Molybdenum hydroxylases: biological distribution and substrate-inhibitor specificity. In G. P. Ellis and G. B. West (eds), *Progress in Medicinal Chemistry*, vol. 24 (Amsterdam: Elsevier), pp. 85–127.

Beedham, C., Bruce, S. E., Critchley, D. J., Al-Tayib, Y. and Rance, D. J., 1987, Species variation in hepatic aldehyde oxidase activity. *European Journal of Drug Metabolism and Pharmacokinetics*, **12**, 307–310.

Beer, B., Ieni, J. R., Wu, W.-H., Clody, D., Amorusi, P., Rose, J., Mant, T., Gaudreault, J., Cato, A. and Stern, W., 1994, A placebo-controlled evaluation of single, escalating doses of CL-284,846, a non-benzodiazepine hypnotic. *Journal of Clinical Pharmacology*, **34**, 335–344.

Chaudhary, I., Demalo, W. and Kantrowitz, J., 1994, Species comparison of *in vitro* and *in vivo* metabolism of CL-284,846, a non-benzodiazepine sedative/hypnotic agent. *Pharmaceutical Research*, **11**, S391.

Dixon, M., 1953, The determination of enzyme inhibitor constants. *Biochemical Journal*, **55**, 170–171.

Johns, D. G., 1967, Human liver aldehyde oxidase: differential inhibition of oxidation of charged and uncharged substrates. *Journal of Clinical Investigation*, **46**, 1492–1505.

Johnson, C., Stubley-Beedham, C. and Stell, J. G. P., 1984, Elevation of molybdenum hydroxylase levels in rabbit liver after ingestion of phthalazine or its hydroxylated metabolite. *Biochemical Pharmacology*, **33**, 3699–3705.

Johnson, C., Stubbley-Beedham, C. and Stell, J. G. P., 1985, Hydralazine: a potent inhibitor of aldehyde oxidase activity *in vitro* and *in vivo*. *Biochemical Pharmacology*, **34**, 4251–4256.

Kawashima, K., Hosoi, K., Naruke, T., Shiba, T., Kitamura, M. and Watabe, T., 1999, Aldehyde oxidase-dependent marked species difference in hepatic metabolism of the sedative-hypnotic, zaleplon, between monkeys and rats. *Drug Metabolism and Disposition*, **27**, 422–428.

Lake, B. G., Ball, S. E., Renwick, A. B., Tredger, J. M., Kao, J., Beamand, J. A. and Price, R. J., 1997, Induction of CYP3A isoforms in cultured precision-cut human liver slices. *Xenobiotica*, **27**, 1165–1173.

Lake, B. G., Tredger, J. M., Renwick, A. B., Barton, P. B. and Price, R. J., 1998, 3,3′-Diindolylmethane induces CYP1A2 in cultured precision-cut human liver slices. *Xenobiotica*, **28**, 803–811.

Lowry, O. H., Rosebrough, N. J., Farr, A. L. and Randall, R. J., 1951, Protein measurement with the Folin phenol reagent. *Journal of Biological Chemistry*, **193**, 265–275.

Rajagopalan, K. V. and Handler, P., 1966, Aldehyde oxidase. *Methods in Enzymology*, **9**, 364–368.

Rashidi, M. R., Smith, J. A., Clarke, S. E. and Beedham, C., 1995, Inhibition of human and guinea-pig liver aldehyde oxidases *in-vitro*. *Journal of Pharmacy and Pharmacology*, **47**, 1090.

Rashidi, M. R., Smith, J. A., Clarke, S. E. and Beedham, C., 1997, *In vitro* oxidation of famciclovir and 6-deoxypenciclovir by aldehyde oxidase from human, guinea pig, rabbit, and rat liver. *Drug Metabolism and Disposition*, **25**, 805–813.

Renwick, A. B., Mistry, H., Ball, S. E., Walters, D. G., Kao, J. and Lake, B. G., 1998, Metabolism of zaleplon by human hepatic microsomal cytochrome P450 isoforms. *Xenobiotica*, **28**, 337–348.

Rodrigues, A. D., 1994, Comparison of levels of aldehyde oxidase with cytochrome P450 activities in human liver *in vitro*. *Biochemical Pharmacology*, **48**, 197–200.

Rodrigues, A. D., Ferrero, J. L., Amann, M. T., Rotert, G. A., Cepa, S. P., Surber, B. W., Machinist, J. M., Tich, N. R., Sullivan, J. P., Garvey, D. S., Fitzgerald, M. and Arneric, S. P., 1994, The *in vitro* hepatic metabolism of ABT-418, a cholinergic channel activator, in rats, dogs, Cynomolgus monkeys, and humans. *Drug Metabolism and Disposition*, **22**, 788–798.

Rosen, A. S., Fournie, P., Darwish, M., Danjou, P. and Troy, S. M., 1999, Zaleplon pharmacokinetics and absolute bioavailability. *Biopharmaceutics and Drug Disposition*, **20**, 171–175.

Somogyi, A. and Muirhead, M., 1987, Pharmacokinetic interactions of cimetidine 1987. *Clinical Pharmacokinetics*, **12**, 321–366.

Steensma, A., Beamand, J. A., Walters, D. G., Price, R. J. and Lake, B. G., 1994, Metabolism of coumarin and 7-ethoxycoumarin by rat, guinea pig, Cynomolgus monkey and human precision-cut liver slices. *Xenobiotica*, **24**, 893–907.

Tanaka, E., 1998, Clinically important pharmacokinetic drug–drug interactions: role of cytochrome P450 enzymes. *Journal of Clinical Pharmacy and Therapeutics*, **23**, 403–416.

Wu, W. H., Dicioccio, A. T., Demaio, W., Amorusi, P., Tonelli, A. P. and Mayer, P. R., 1996, Mass balance and pharmacokinetics of zaleplon, a non-benzodiazepine sedative/hypnotic, in man. *Pharmaceutical Research*, **13**, S487.

Yoshihara, S. and Tatsumi, K., 1986, Kinetic and inhibition studies on reduction of diphenyl sulphoxide by guinea pig liver aldehyde oxidase. *Archives of Biochemistry and Biophysics*, **249**, 8–14.

XENOBIOTICA, 2002, VOL. 32, NO. 10, 849–862

Taylor & Francis
healthsciences

Inhibition of zaleplon metabolism by cimetidine in the human liver: *in vitro* studies with subcellular fractions and precision-cut liver slices

A. B. RENWICK†, S. E. BALL‡, J. M. TREDGER§, R. J. PRICE†, D. G. WALTERS†, J. KAO‡, J. A. SCATINA‡ and B. G. LAKE†*

† TNO BIBRA International Ltd, Woodmansterne Road, Carshalton, Surrey SM5 4DS, UK

‡ Wyeth-Ayerst Research, Drug Metabolism Division, CN8000, Princeton, NJ 08543-8000, USA

§ Institute of Liver Studies, Guy's, King's and St Thomas' School of Medicine, London SE5 9PJ, UK

Received 25 March 2002

1. The effect of cimetidine on the metabolism of zaleplon (ZAL) in human liver subcellular fractions and precision-cut liver slices was investigated.

2. ZAL was metabolized to a number of products including 5-oxo-ZAL (M2), which is known to be formed by aldehyde oxidase, *N*-desethyl-ZAL (DZAL), which is known to be formed by CYP3A forms, and *N*-desethyl-5-oxo-ZAL (M1).

3. Human liver microsomes catalysed the NADPH-dependent metabolism of ZAL to DZAL. Kinetic analysis of three microsomal preparations revealed mean (±SEM) S_{50} and V_{max} of 310 ± 24 μM and 920 ± 274 pmol/min/mg protein, respectively.

4. Human liver cytosol preparations catalysed the metabolism of ZAL to M2. Kinetic analysis of three cytosol preparations revealed mean (±SEM), K_m and V_{max} of 124 ± 14 μM and 564 ± 143 pmol/min/mg protein, respectively.

5. Cimetidine inhibited ZAL metabolism to DZAL in liver microsomes and to M2 in the liver cytosol. With a ZAL substrate concentration of 62 μM, the calculated mean (±SEM, $n = 3$) IC_{50} were 596 ± 103 and 231 ± 23 μM for DZAL and M2 formation, respectively. Kinetic analysis revealed that cimetidine was a competitive inhibitor of M2 formation in liver cytosol with a mean (±SEM, $n = 3$) K_i of 155 ± 16 μM.

6. Freshly cut human liver slices metabolized ZAL to a number of products including M1, M2 and DZAL.

7. Cimetidine inhibited ZAL metabolism in liver slices to M1 and M2, but not to DZAL. Kinetic analysis revealed that cimetidine was a competitive inhibitor of M2 formation in liver slices with an average ($n = 2$ preparations) K_i of 506 μM.

8. The results demonstrate that cimetidine can inhibit both the CYP3A and aldehyde oxidase pathways of ZAL metabolism in the human liver. Cimetidine appears to be a more potent inhibitor of aldehyde oxidase than of CYP3A forms and hence *in vivo* is likely to have a more marked effect on ZAL metabolism to M2 than on DZAL formation.

9. The results also demonstrate that precision-cut liver slices may be a useful model system for *in vitro* drug-interaction studies.

Introduction

Zaleplon (*N*-[3-(3-cyanopyrazolo[1,5-*a*]pyrimidin-7-yl)phenyl]-*N*-ethylacetamide; CL-284,846; ZAL) (figure 1) is a novel non-benzodiazepine sedative-

* Author for correspondence; e-mail: blake@tnobibra.co.uk

Xenobiotica ISSN 0049–8254 print/ISSN 1366–5928 online © 2002 Taylor & Francis Ltd
http://www.tandf.co.uk/journals
DOI: 10.1080/00498250210158221

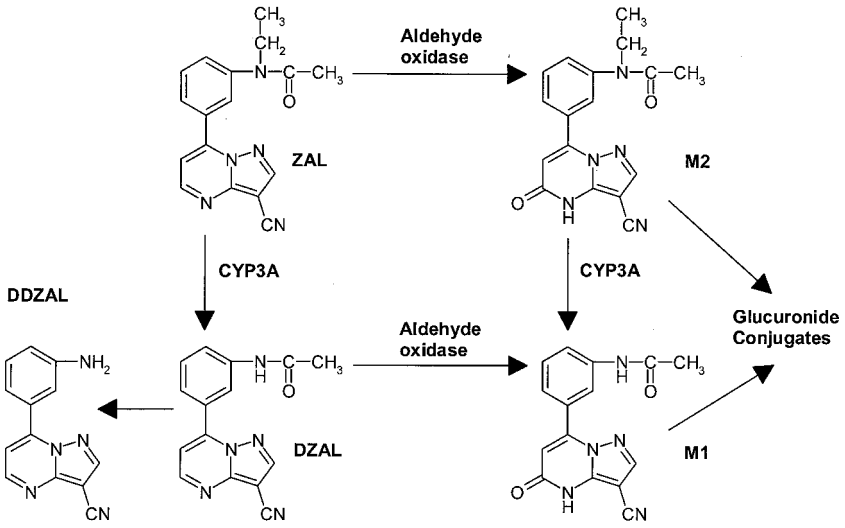


Figure 1. Some pathways of zaleplon (ZAL) metabolism.

hypnotic agent for the treatment of insomnia. Studies in man have demonstrated that ZAL is rapidly absorbed and extensively metabolized with 88% of the dose appearing in the urine (71%) and faeces (17%) as metabolites (Wu *et al.* 1996, Rosen *et al.* 1999). *In vivo* and *in vitro* studies in both experimental animals and man (Beer *et al.* 1994, Chaudhary *et al.* 1994, Wu *et al.* 1996, Renwick *et al.* 1998, Kawashima *et al.* 1999, Lake *et al.* 2002) have demonstrated that ZAL may be metabolized (figure 1) by oxidation to metabolite M2 (5-oxo-ZAL; *N*-[3-(3-cyano-4,5-dihydro-5-oxopyrazolo[1,5-*a*]pyrimidin-7-yl)phenyl]-*N*-ethylacetamide) and by *N*-deethylation to DZAL (*N*-desethyl-ZAL; *N*-[3-(3-cyanopyrazolo[1,5-*a*]-pyrimidin-7-yl)phenyl]-acetamide). Other metabolites include metabolite M1 (*N*-desethyl-5-oxo-ZAL; *N*-[3-(3-cyano-4,5-dihydro-5-oxopyrazolo[1,5-*a*]pyrimidin-7-yl)phenyl]-acetamide), which may be derived from M2 and DZAL, and DDZAL (7-(3-aminophenyl)pyrazolo[1,5-*a*]pyrimidine-3-carbonitrile), which is derived from the deacetylation of DZAL (figure 1). Both M1 and M2 can form glucuronide conjugates and in man M1 and M2 with their glucuronide conjugates account for some 9 and 57%, respectively, of the administered dose recovered in urine (Wu *et al.* 1996). Species differences in ZAL metabolism have been reported as M2 is the major plasma metabolite in man, whereas DZAL and/or DDZAL is the major plasma metabolite in the rat, mouse and dog (Chaudhary *et al.* 1994).

Previous studies with human, rat and Cynomolgus monkey liver microsomes have demonstrated that the NADPH-dependent *N*-deethylation of ZAL to DZAL is catalysed by cytochrome P450 (CYP) forms (Renwick *et al.* 1998, Kawashima *et al.* 1999). In human liver microsomes, reaction phenotyping studies have demonstrated that DZAL formation was predominantly catalysed by CYP3A forms (Renwick *et al.* 1998). Unlike ZAL metabolism to DZAL, the CYP3A-catalysed *N*-deethylation of M2 to M1 proceeded at only a very low rate. Studies with human, rat and Cynomolgus monkey subcellular fractions have demonstrated that ZAL metabolism to M2 was NADPH-independent and catalysed by liver cytosol, but not by microsomes (Kawashima *et al.* 1999, Lake *et al.* 2002).

Additional investigations, including correlation analysis, chemical inhibition and $H_2{}^{18}O$ incorporation studies, have demonstrated that ZAL metabolism to M2 in human liver is catalysed by cytosolic aldehyde oxidase (Lake *et al*. 2002).

In a study with healthy human volunteers, the pharmacokinetics of a 10 mg oral dose of ZAL was compared either alone or 1 h after an 800 mg oral dose of cimetidine (Darwish, Cevallos, Martin, Tse and Troy, Wyeth-Ayerst Research, unpublished data). Plasma samples were analysed for ZAL and M2, but not for other ZAL metabolites. Cimetidine treatment significantly inhibited the oral clearance of zaleplon and increased the observed maximum plasma concentration (C_{max}) and the area under the plasma concentration–time curve (AUC). In addition, analysis of plasma samples revealed that M2 formation occurred more slowly after cimetidine administration.

Many studies have demonstrated that cimetidine can produce drug interactions in man by binding to CYP forms and inhibiting the metabolism of other drugs (Somogyi and Muirhead 1987, Lin and Lu 1998, Smith and Kendall 1988, Tanaka 1998). In other studies, cimetidine has been shown to inhibit human, guinea pig and rat aldehyde oxidase-catalysed reactions (Robertson and Bland 1993, Rashidi *et al*. 1995) including ZAL metabolism to M2 by human liver cytosol preparations (Lake *et al*. 2002).

The aim of the current study was to investigate the inhibition of ZAL metabolism by cimetidine *in vitro* using human liver subcellular fractions. As an additional objective, investigations were also performed with precision-cut human liver slices in order to ascertain if this liver model would be useful for *in vitro* drug-interaction studies. Previous studies with ZAL and other compounds have demonstrated that precision-cut human liver slices can be used to study both CYP- and aldehyde oxidase-dependent pathways of xenobiotic metabolism (Rodrigues *et al*. 1994, Acheampong *et al*. 1996, Lake *et al*. 2002).

Materials and methods

Materials

Samples of CL-284,846 (ZAL), CL-284,859 (DZAL), CL-285,489 (internal standard for high-performance liquid chromatography [HPLC]), CL-314,475 (DDZAL), CL-345,644 (M1) and CL-345,905 (M2) (purities > 99% for ZAL and > 97% for the other compounds) and [^{14}C]ZAL (specific activity 9.66 μCi/μmol; radiochemical purity 98%) were supplied by Wyeth-Ayerst Research Drug Metabolism Division (Princeton, NJ, USA). The sources of the tissue culture materials were as described by Beamand *et al*. (1993). NADPH and cimetidine were obtained from Sigma-Aldrich Co. (Poole, UK).

Human liver

Samples of human liver were collected and transported to TNO BIBRA on ice. The Research Ethics Committee of King's College Hospital granted approval for this tissue, which was surplus to clinical requirements. Tissue for the preparation of liver slices was used immediately, whereas tissue for the preparation of hepatic subcellular fractions was stored at −80 °C.

Preparation of subcellular fractions

Thawed liver samples were homogenized (0.25 g tissue/ml) in 0.154 M KCl containing 50 mM Tris-HCl, pH 7.4, as described by Lake (1987). Liver whole homogenates were centrifuged at 10 000*g* av for 20 min to obtain the post-mitochondrial supernatant fraction and subsequently at 105 000*g* h to separate the microsomal fraction from the cytosol. Aliquots of the liver cytosol fraction were stored at −80 °C. Liver microsomes were resuspended in fresh homogenizing medium and again centrifuged at 105 000*g* h to obtain washed microsomal fractions. Liver washed microsomal fractions were assayed for total CYP content (Lake 1987) and for protein (Lowry *et al*. 1951) employing bovine serum albumin as standard.

The washed microsomal fractions were diluted to 10 mg protein/ml and aliquots were stored at −80 °C. Three separate preparations (designated A, B and C) of liver microsomes and cytosol were used. The donors of the liver samples were a female aged 11 years and males aged 50 and 10 years, respectively.

Metabolism of ZAL by human liver microsomes

The NADPH-dependent metabolism of ZAL to DZAL was studied in incubation mixtures containing 50–2000 μM ZAL (added in 5 μl dimethyl sulphoxide [DMSO]), 10 mM $MgCl_2$, 2 mM EDTA, 70 mM phosphate buffer, pH 7.4, and 1.5 mg microsomal protein in a final volume of 1 ml. After a 5-min pre-incubation at 37 °C in a shaking water bath, the reaction was initiated by the addition of 1 mM NADPH. Incubations were performed for 10 min at 37 °C in a shaking water bath and terminated by the addition of 3 ml ice-cold acetonitrite containing 30 μg/ml of the CL-285,489 internal standard. Blank incubations contained all components except NADPH, which was added after the addition of acetonitrile. Tubes were left on ice for 30 min and then centrifuged at 1730*g* av for 10 min at 4 °C. Analysis of the deproteinized extracts was performed by HPLC as described by Renwick *et al.* (1998).

Metabolism of ZAL by human liver cytosol

The metabolism of ZAL to M2 was studied in incubation mixtures containing 10–500 μM ZAL (added in 5 μl DMSO), 100 mM phosphate buffer, pH 7.4, and 2.0 mg cytosol protein in a final volume of 1 ml. After a 5-min pre-incubation at 37 °C in a shaking water bath, the reaction was initiated by adding the ZAL substrate. Incubations were performed for 10 min at 37 °C in a shaking water bath and terminated by the addition of 3 ml ice-cold acetonitrile containing 30 μg/ml of the CL-285,489 internal standard. Blank incubations contained all components except ZAL, which was added after the addition of acetonitrile. Tubes were processed for HPLC analysis as described above.

Inhibition of ZAL metabolism in human liver microsomes and cytosol

Incubations were performed with liver microsomes and cytosol as described above, except that the reaction mixtures also contained 0–1.0 mM cimetidine (added in 5 μl DMSO).

ZAL metabolism kinetic analysis

Because microsomal NADPH-dependent ZAL metabolism to DZAL exhibits sigmoidal kinetics due to substrate activation (Ueng *et al.* 1997, Renwick *et al.* 1998, Houston and Kenworthy 2000), kinetic analysis of data was performed with the Hill equation. To obtain an estimate of the maximal clearance due to autoactivation (CL_{max}), the following equation (Houston and Kenworthy 2000) was used:

$$CL_{max} = (V_{max}/S_{50}) \times (n-1)/n(n-1)^{1/n},$$

where S_{50} is the substrate concentration resulting in 50% of V_{max} and n is the Hill coefficient. The metabolism of ZAL to M2 by liver cytosol fractions was analysed by Michaelis–Menten and Eadie–Hofstee plots (Clarke 1998) and intrinsic clearance (CL_{int}) was calculated as V_{max}/K_m. Dixon (1953) plots were employed to analyse the effects of cimetidine on ZAL metabolism to M2 in liver cytosol and liver slices.

Preparation of precision-cut human liver slices

Tissue cylinders from liver samples were prepared using a 10-mm diameter motor-driven tissue-coring tool. From the cylinders, tissue slices (200–300 μM thick) were prepared in oxygenated (95% O_2/5% CO_2) Earle's balanced salt solution containing 25 mM D-glucose, 50 μg/ml gentamicin and 2.5 μg/ml fungizone using a Krumdieck tissue slicer (Alabama Research and Development Corp., Munford, AL, USA). Three separate preparations (designated B, D and E) of liver slices were used. The donors of the liver samples were males aged 50, 11 and 14 years, respectively.

Metabolism of ZAL by human liver slices

Liver slices were floated onto Vitron (Vitron, Inc., Tucson, AZ, USA) type C titanium roller inserts (two slices per insert) and cultured in glass vials containing 1.7 ml culture medium employing a Vitron dynamic organ incubator. The culture medium consisted of phenol red free RPMI 1640 containing 0.1 μM insulin and 0.1 μM dexamethasone. Liver slices were maintained at 37 °C in an atmosphere of 95% O_2/5% CO_2. After 1 h, liver slices were incubated in fresh medium containing 52–400 μM [^{14}C]ZAL (approximately 1 μCi/ml, added in 4 μl DMSO ml^{-1} medium) for 30 min. At the end of the incubation period, the liver slices were homogenized in the culture medium by sonication (Beamand *et al.* 1993) and the liver slice/medium homogenates stored at −80 °C before analysis. Liver slice/medium homogenates were hydrolysed with β-glucuronidase and sulphatase as described by Steensma *et al.*

(1994) and then treated with 3 vols ice-cold acetonitrile. Analysis of the deproteinized extracts was performed by HPLC as described by Renwick *et al.* (1998), except that the ZAL metabolites were quantified by radiometric detection. Liver slice protein content was determined by the method of Lowry *et al.* (1951).

Inhibition of ZAL metabolism in human livers slices

Studies on the effect of cimetidine on ZAL metabolism were performed as described above, except that the culture medium also contained 0–2.0 mM cimetidine (added in 4 µl DMSO ml^{-1} medium).

Results

Kinetics of ZAL metabolism in human liver microsomes and cytosol

The metabolism of ZAL was investigated with three preparations (subjects A–C) of human liver microsomes and three preparations of liver cytosol. The total CYP content of the A, B and C liver microsomal preparations were determined as 0.30, 0.43 and 0.32 nmol/mg protein, respectively. All three preparations of liver microsomes catalysed the NADPH-dependent metabolism of ZAL to DZAL and all three cytosol preparations catalysed the aldehyde oxidase-dependent metabolism of ZAL to M2. Initial experiments established that ZAL metabolism in the two liver subcellular fractions was linear with respect to incubation time and protein concentration (data not shown). DZAL and M2 were the major metabolites of ZAL formed in human liver microsomes and cytosol, respectively. For example, at a substrate concentration of 500 µM, the formation of DDZAL in liver microsomes was only around 2% of that of DZAL, with only trace amounts ($< 0.5\%$ of DZAL formation) of M1 and M2 being observed. At a substrate concentration of 100 µM, the formation of M1, DZAL and DDZAL in liver cytosol were all $< 2\%$ of that of M2 formation.

The kinetics of NADPH-dependent ZAL metabolism to DZAL in human liver microsomes was examined over a substrate concentration range of 50–2000 µM (figure 2). Sigmoidal kinetic plots for DZAL formation were observed for all three

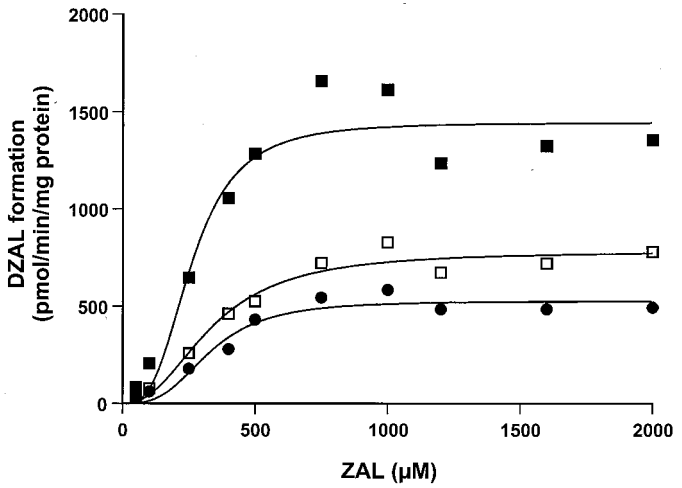


Figure 2. Kinetics of ZAL metabolism to DZAL in human liver microsomes. Duplicate incubations (1.5 mg protein for 10 min) were performed at each ZAL substrate concentration with the A (□), B (■) and C (●) liver microsomal preparations.

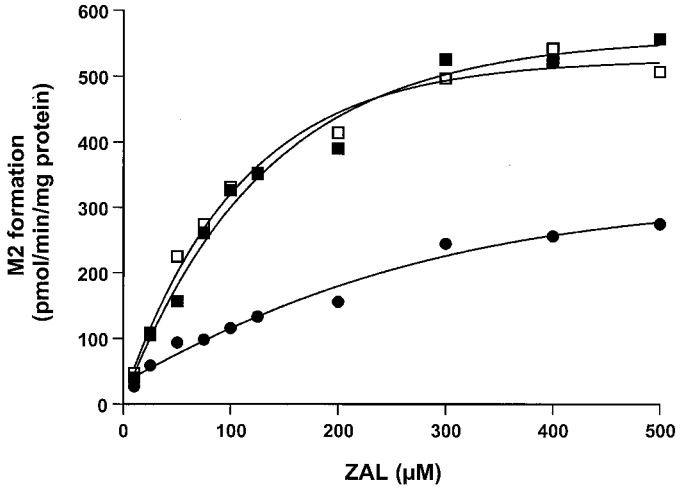


Figure 3. Kinetics of ZAL metabolism to M2 in human liver cytosol. Duplicate incubations (2.0 mg protein for 10 min) were performed at each ZAL substrate concentration with the A (□), B (■) and C (●) liver cytosol preparations.

Table 1. Kinetic analysis of ZAL metabolism in human liver microsomes and cytosol.

Subcellular fraction	ZAL metabolite	S_{50} [a]	K_m [a]	V_{max} [b]	CL_{max} [c]	CL_{int} [c]
Microsomes	DZAL	310 ± 24 [d]	–	920 ± 274	1.65 ± 0.65	–
Cytosol	M2	–	124 ± 14	564 ± 143	–	4.44 ± 0.88

[a] Units: μM.
[b] Units: pmol/min/mg protein.
[c] Units: μl/min/mg protein. Data calculated are as described in the Materials and methods.
[d] Results are the mean ± SEM for three microsomal and three cytosol preparations (subjects A–C).

microsomal preparations indicating positive cooperativity (Ueng *et al.* 1997, Houston and Kenworthy 2000). Kinetic analysis of the data by the Hill equation revealed S_{50} (i.e. substrate concentration resulting in 50% of V_{max}) of 338, 262 and 331 μM, V_{max} of 785, 1448 and 528 pmol/min/mg protein and Hill constants (n) of 2.32, 3.02 and 3.06 for the A, B and C liver microsomal preparations, respectively. Mean S_{50}, V_{max} and CL_{max} (calculated as described in Materials and Methods) for all three liver microsomal preparations are shown in table 1.

The kinetics of ZAL metabolism to M2 in human liver cytosol was examined over a substrate concentration range of 10–500 μM (figure 3). Similar K_m and V_{max} for M2 formation were obtained from Michaelis–Menten and Eadie–Hofstee plots (data not shown). For the A, B and C liver cytosol preparations, K_m were 119, 151 and 102 μM, and V_{max} were 677, 735 and 280 pmol/min/mg protein, respectively. Mean K_m, V_{max} and CL_{int} for all three liver cytosol preparations are shown in table 1.

Effect of cimetidine on ZAL metabolism in human liver microsomes and cytosol

The effect of 0.1–1.0 mM cimetidine on ZAL metabolism to DZAL and M2 was evaluated in all three preparations (subjects A–C) of liver microsomes and cytosol.

Table 2. Inhibition of ZAL metabolism in human liver microsomes and cytosol by cimetidine.

ZAL substrate concentration (μM)	Cimetidine inhibition IC_{50} (μM)[a,b]	
	Microsomal DZAL formation	Cytosol M2 formation
25	n.d.[c]	235 ± 28
62	596 ± 103	231 ± 23
103	545 ± 41	n.d.
124	n.d.	368 ± 36
310	534 ± 17	581 ± 48
620	469 ± 30	n.d.

[a] Results are the mean ± SEM for three microsomal and three cytosol preparations (subjects A–C).
[b] IC_{50} were determined over a cimetidine concentration of 0.1–1.0 mM.
[c] n.d., Not determined.

For both subcellular fractions, IC_{50} for cimetidine inhibition were determined at four ZAL substrate concentrations. With liver microsomes the ZAL substrate concentrations were 62, 103, 310 and 620 μM (corresponding to 1/5, 1/3, 1/1 and 2/1 the mean S_{50}), whereas for liver cytosol the ZAL substrate concentrations were 25, 62, 124 and 310 μM (corresponding to 1/5, 1/2, 1/1 and 2.5/1 of the mean K_m).

Cimetidine inhibited ZAL metabolism to DZAL in liver microsomes and to M2 in liver cytosol at all ZAL substrate concentrations examined. For DZAL formation, IC_{50} were relatively constant ranging from 469 to 596 μM over the 62–620 μM ZAL substrate concentration range examined (table 2). In contrast, for M2 formation, the IC_{50} were more variable ranging from 231 to 581 μM, with the lowest IC_{50} being observed at ZAL substrate concentrations of 25 and 62 μM and the highest IC_{50} at a ZAL substrate concentration of 310 μM. Whereas similar IC_{50} were observed for DZAL and M2 formation at a ZAL substrate concentration of 310 μM, the IC_{50} for M2 formation at a ZAL substrate concentration of 62 μM was only around 40% of the IC_{50} for DZAL formation.

The kinetics of cimetidine inhibition of M2 formation in liver cytosol was studied employing inhibitor concentrations of 0–1.0 mm and ZAL substrate concentrations of 25–310 μM. Kinetic analysis of Dixon (1953) plots indicated that cimetidine was a competitive inhibitor of aldehyde oxidase-dependent ZAL metabolism to M2 in human liver cytosol (figure 4). The calculated K_i (inhibitor constant) for cimetidine inhibition of M2 formation in the human liver A–C cytosol preparations was 141, 136 and 187 μM, respectively, with a mean (±SEM) of 155 ± 16 μM. Analysis of the data by Cornish-Bowden (1974) plots also indicated that cimetidine was a competitive inhibitor of M2 formation (data not shown). Because of the observed sigmoidal kinetics for ZAL metabolism to DZAL by liver microsomes, it was not possible to investigate the kinetics of cimetidine inhibition by Dixon (1953) plots.

Metabolism of ZAL in precision-cut human liver slices

Initial ZAL metabolism studies were performed with 52 μM [^{14}C]ZAL in three preparations (subjects B, D and E) of freshly cut human liver slices. ZAL was metabolized by all three liver slice preparations (figure 5) to M1, M2, DZAL, DDZAL and an unknown metabolite (termed 'X'). No attempt was made in

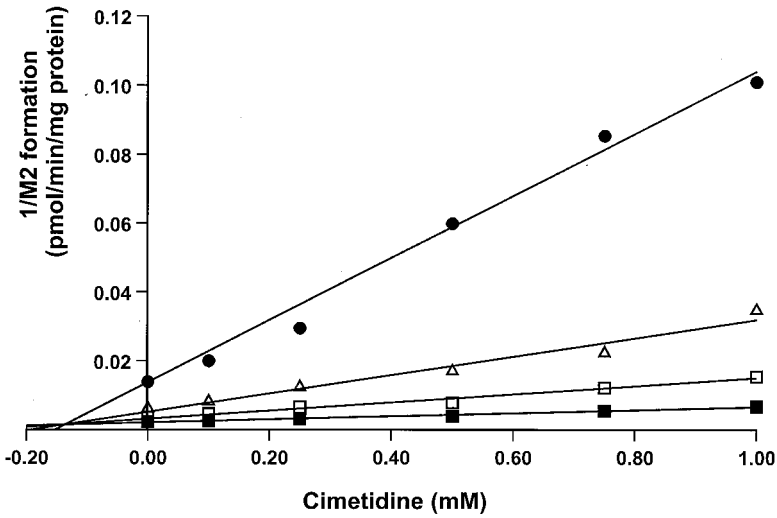


Figure 4. Dixon plot of the kinetics of inhibition of ZAL metabolism to M2 in human liver cytosol. Duplicate incubations were performed with 2.0 mg cytosol protein (subject B) for 10 min with 0–1.0 mM cimetidine and 25 (●), 62 (△), 124 (□) and 310 (■) μM ZAL substrate.

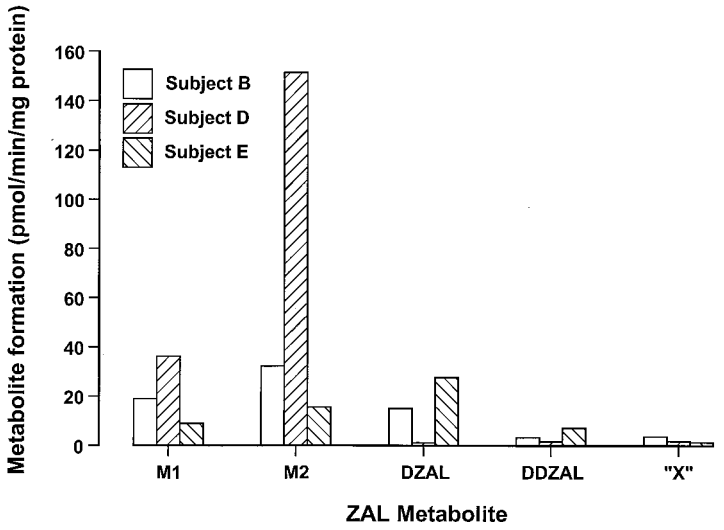


Figure 5. Metabolism of [^{14}C]ZAL by precision-cut human liver slices. Duplicate vials of freshly cut slices from subjects B, D and E were incubated with 52 μM [^{14}C]ZAL for 30 min. Liver slice/medium homogenates were analysed by HPLC for ZAL metabolites.

these studies to identify the unknown ZAL metabolite. Preliminary studies demonstrated that M1 and M2 were extensively conjugated with D-glucuronic acid and/or sulphate and hence liver slice/medium homogenates were treated with β-glucuronidase and sulphatase before HPLC analysis. No attempt was made to quantify free as well as conjugated M1 and M2 in these studies. Overall mean (±SEM) rates of ZAL metabolism to M1, M2, DZAL, DDZAL and 'X' in the three liver slice preparations were 21.4 ± 8.0, 66.4 ± 42.8, 14.6 ± 7.6, 4.1 ± 1.6 and 2.3 ± 0.7 pmol/min/mg liver slice protein, respectively.

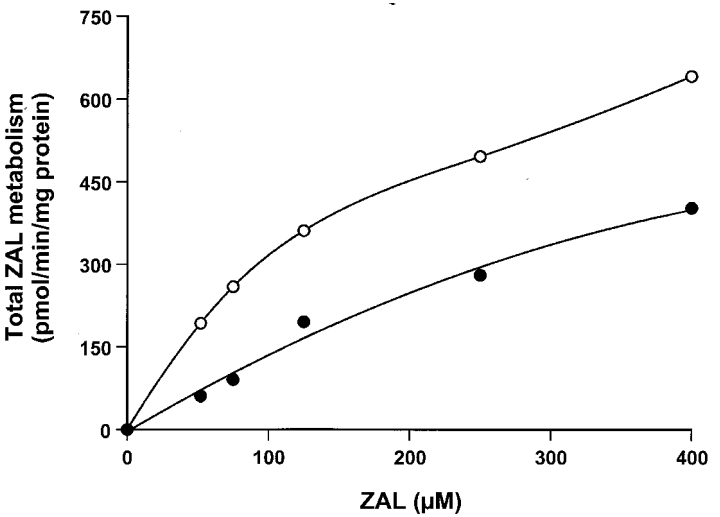


Figure 6. Metabolism of [^{14}C]ZAL by precision-cut human liver slices. Duplicate vials of freshly cut slices from subjects D (○) and E (●) were incubated with 52–400 μM [^{14}C]ZAL for 30 min. Liver slice/medium homogenates were analysed by HPLC for total ZAL metabolites (i.e. sum of M1, M2, DZAL, DDZAL and 'X').

With two liver slice preparations (subjects D and E), the metabolism of ZAL to total ZAL metabolites was examined over a substrate concentration range of 52–400 μM, the highest concentration being around the limit of ZAL solubility in tissue culture medium. Over this concentration range, ZAL metabolism in human liver slices to total metabolites (i.e. sum of M1, M2, DZAL, DDZAL and 'X') did not appear to be saturated (figure 6). The lowest substrate concentration examined, namely 52 μm ZAL, was selected for the studies on the inhibition of ZAL metabolism in human liver slices.

Effect of cimetidine on ZAL metabolism in human liver slices

The effect of 1.0 mM cimetidine on the metabolism of 52 μM ZAL was studied in three human liver slice preparations (subjects B, D and E). Cimetidine markedly inhibited ZAL metabolism to M1 and M2 in all three human liver slice preparations (figure 7). Whereas cimetidine had little effect on ZAL metabolism to DDZAL and a variable effect on 'X', ZAL metabolism to DZAL was stimulated by cimetidine treatment. The greatest stimulation of DZAL metabolism was observed with the liver slice preparation from subject D (figure 7), this subject having the highest rate of M2 formation (figure 5).

As cimetidine did not inhibit DZAL formation in human liver slices, only the effect of cimetidine on M1 and/or M2 formation was investigated in further studies. The effect of 0.05–2.0 mM cimetidine on the metabolism of 52 μM ZAL was examined. Cimetidine inhibited M1 and M2 formation in all three human liver slice preparations examined. For the liver slice preparations from subjects B, D and E, calculated IC_{50} for M1 formation were 645, 2056 and 500 μM, respectively, and for M2 formation were 606, 348 and 478 μM, respectively. The overall

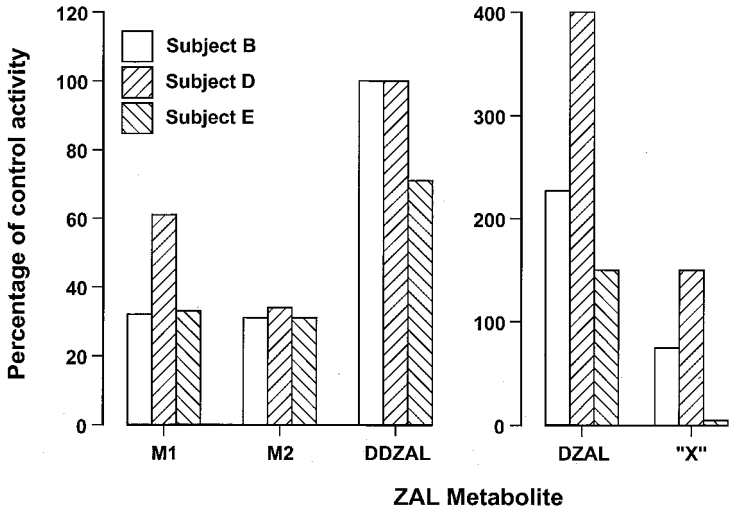


Figure 7. Effect of cimetidine on the metabolism of [^{14}C]ZAL by freshly cut human liver slices. Duplicate vials of liver slices from subjects B, D and E were incubated with 1.0 mM cimetidine and 52 μM [^{14}C]ZAL for 30 min. Liver slice/medium homogenates were analysed by HPLC for ZAL metabolites.

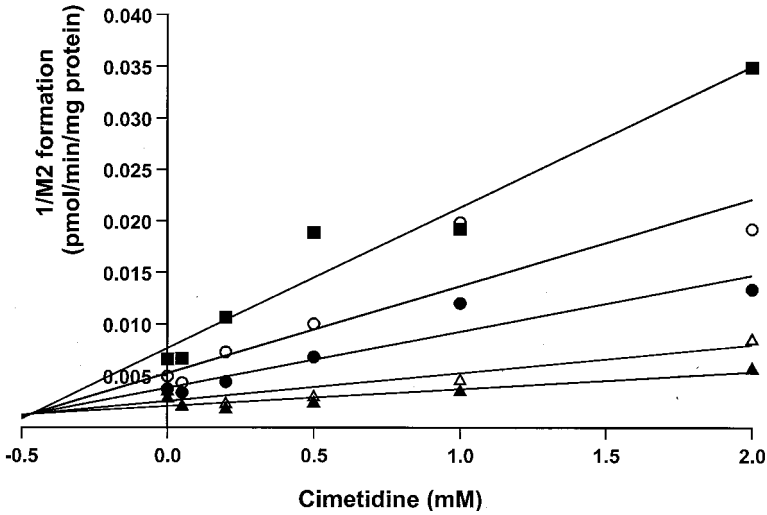


Figure 8. Dixon plot of the kinetics of inhibition of ZAL metabolism to M2 in freshly cut human liver slices (subject D). Duplicate vials were incubated for 30 min with 0–2.0 mM cimetidine and 52 (■), 75 (○), 125 (●), 250 (△) and 400 (▲) μM [^{14}C]ZAL substrate.

mean (±SEM) IC_{50} for cimetidine inhibition of M1 and M2 formation were 1067 ± 496 and 477 ± 75 μM, respectively.

The kinetics of cimetidine inhibition of M2 formation in two human liver slice preparations (subjects D and E) was studied employing inhibitor concentrations of 0–2.0 mm and ZAL substrate concentrations of 52–400 μM. Kinetic analysis of Dixon (1953) plots indicated that cimetidine was a competitive inhibitor of ZAL metabolism to M2 in human liver slices (figure 8). The calculated K_i for

cimetidine inhibition of M2 formation in the liver slice preparations from subjects D and E were 466 and 546 μM, respectively, with an average of 506 μM.

Discussion

In this study, the metabolism of ZAL (figure 1) by human hepatic microsomal and cytosol fractions and precision-cut liver slices has been investigated. As with previous investigations, liver microsomes catalysed the CYP-dependent metabolism of ZAL to DZAL, whereas liver cytosol catalysed the aldehyde oxidase-dependent metabolism of ZAL to M2 and liver slices catalysed the metabolism of ZAL to DZAL, M2 and other metabolites (Renwick *et al*. 1998, Kawashima *et al*. 1999, Lake *et al*. 2002).

Kinetic analysis was performed of ZAL metabolism to DZAL in liver microsomes and ZAL metabolism to M2 in liver cytosol (table 1). DZAL and M2 were the major metabolites formed from ZAL metabolism in liver microsomes and cytosol, respectively. The NADPH-dependent metabolism to ZAL to DZAL in liver microsomes was shown to exhibit sigmoidal kinetics, with a mean ($n = 3$) S_{50} of 310 μM, this value being similar to S_{50} observed previously with other human hepatic microsomal preparations (Renwick *et al*. 1998). The metabolism of ZAL to M2 by aldehyde oxidase in three human liver cytosol preparations exhibited a mean K_m of 124 μM, this value being similar to that observed in previous studies with other human liver cytosol preparations (Lake *et al*. 2002).

Previous studies have demonstrated that M2 is the major metabolite of ZAL in man, whereas DZAL and/or DDZAL formation is the major pathway of ZAL metabolism in the rat, mouse and dog (Beer *et al*. 1994, Chaudhary *et al*. 1994, Wu *et al*. 1996). These observations are supported by the present findings with human liver microsomal and cytosol fractions. For example, the mean K_m for M2 formation by aldehyde oxidase is lower than the mean S_{50} for CYP3A-catalysed DZAL formation (table 1). Moreover, the mean calculated CL_{int} for M2 formation in liver cytosol was around 2.5 times greater than the CL_{max} for DZAL formation in liver microsomes. This difference would be even greater if the CL_{int} and CL_{max} were expressed per g liver and not per unit protein. In this study, the mean liver cytosol protein content was determined as 96.5 mg protein/g liver, whereas allowing for losses during subcellular fractionation, microsomal protein content is considered to be around 45–50 mg protein/g liver (Andersson *et al*. 2001, Pelkonen *et al*. 2001). Overall, the *in vitro* kinetic data with human liver subcellular fractions supports *in vivo* findings that M2 is the major metabolite of ZAL in man.

Whereas the kinetic data demonstrates that M2 formation *in vivo* would be greater than that of DZAL formation, there was some variability between the subjects studied in these two pathways of ZAL metabolism. In keeping with the higher total CYP content, DZAL formation was greater in liver microsomes from subject B than from subjects A and C (figure 2), whereas rates of M2 formation were higher in liver cytosol preparations from subjects A and B than from subject C (figure 3). Marked interindividual variability in M2 and DZAL formation was also observed in the three preparations of freshly cut human liver slices examined (figure 5). At a ZAL substrate concentration of 52 μM, M2 formation was greater than DZAL formation in two of three preparations examined. In a previous study with 120 μM ZAL substrate, M2 formation was greater than DZAL formation in three other preparations of human liver slices (Lake *et al*. 2002).

In a study with healthy human volunteers, subjects were given either a 10 mg oral dose of ZAL alone or an 800 mg dose of cimetidine followed by a 10 mg dose of ZAL 1 h later (Darwish, Cevallos, Martin, Tse and Troy, Wyeth-Ayerst Research, unpublished data). Cimetidine treatment significantly reduced the oral clearance of ZAL to 56% of control (no cimetidine treatment) and significantly increased ZAL C_{max} and AUC to 183 and 185% of control, respectively. In addition, M2 formation occurred more slowly after cimetidine treatment.

The present results demonstrate that cimetidine can inhibit ZAL metabolism in human liver subcellular fractions and in freshly cut liver slices. Many studies have demonstrated that cimetidine can inhibit human CYP-dependent enzyme activities both *in vitro* and *in vivo* (Somogyi and Muirhead 1987, Smith and Kendall 1988, Wrighton and Ring 1994, Lin and Lu 1998, Tanaka 1998). In addition, cimetidine has also been reported to inhibit aldehyde oxidase-catalysed activities in the liver of humans and other species (Robertson and Bland 1993, Rashidi *et al*. 1995).

The effect of cimetidine on ZAL metabolism was compared by determining IC_{50} values for DZAL formation in liver microsomes at substrate concentrations of one-fifth to twice the mean S_{50} and for M2 formation in liver cytosol at substrate concentrations of one-fifth to 2.5 times the mean K_m (table 2). For cimetidine inhibition of microsomal DZAL formation, the observed IC_{50} are fairly similar over the 10-fold substrate concentration range examined. However, the IC_{50} for M2 formation in liver cytosol decreased with ZAL substrate concentration, suggesting that cimetidine was a competitive inhibitor of aldehyde oxidase. Kinetic analysis of the effect of cimetidine on M2 formation by Dixon (1953) plots confirmed that cimetidine was a competitive inhibitor of human hepatic aldehyde oxidase (figure 4).

The effect of cimetidine on ZAL metabolism in precision-cut human liver slices was also evaluated to ascertain if this liver intact cell model could be used for *in vitro* drug-interaction studies. As with the studies with liver subcellular fractions, cimetidine also inhibited ZAL metabolism in freshly cut human liver slices. Using a ZAL substrate concentration of 52 μM, cimetidine markedly inhibited M1 and M2 formation, whereas DZAL formation was enhanced (figure 7). The apparent increase in DZAL formation is attributable to a more marked effect of cimetidine on aldehyde oxidase-catalysed M1 and M2 formation than on CYP3A-catalysed DZAL formation. Previous studies have demonstrated that M2 is metabolized to M1 by CYP3A forms at only a low rate (Renwick *et al*. 1998). As such, M1 is largely formed from the metabolism of DZAL by aldehyde oxidase and not from M2 by CYP3A forms (figure 1). Hence, the greater inhibition of aldehyde oxidase than CYP3A form activity by cimetidine will increase the apparent formation of DZAL as the subsequent conversion of DZAL to M1 will occur at a lower rate than DZAL formation from ZAL. The present studies with human liver slices are also in agreement with *in vivo* findings where cimetidine was shown to inhibit both ZAL clearance and M2 formation (Darwish, Cevallos, Martin, Tse and Troy, Wyeth-Ayerst Research, unpublished data). Finally, as with the studies with human liver cytosol fractions, kinetic analysis by Dixon plots (1953) of cimetidine inhibition of M2 formation in liver slices also suggested that cimetidine was a competitive inhibitor of aldehyde oxidase.

While liver slices are a valuable liver intact cell model system for studying pathways of drug metabolism, they have been reported to be less useful for

obtaining estimates of CL_{int} due to problems of drug uptake into all cells of a liver slice (Houston and Carlile 1997, Worboys *et al*. 1997). This diffusion problem can result in lower estimates of CL_{int} than those obtained with other liver *in vitro* models (Houston and Carlile 1997, Worboys *et al*. 1997, Andersson *et al*. 2001, Pelkonen *et al*. 2001). However, the present investigations suggest that liver slices may be a good liver intact cell model for *in vitro* drug-interaction studies. As with the studies with liver subcellular fractions, cimetidine produced a marked inhibition of aldehyde oxidase-catalysed pathways of ZAL metabolism in human liver slices.

In summary, the metabolism of ZAL has been investigated in human hepatic subcellular fractions and in freshly cut human liver slices. Cimetidine inhibited ZAL metabolism to DZAL and M2, which are catalysed by CYP3A forms and aldehyde oxidase, respectively. Overall, cimetidine appeared to be a more potent inhibitor of aldehyde oxidase than of CYP3A forms and, hence, *in vivo* it is likely to have a more marked effect on M2 than on DZAL formation.

Acknowledgements

This work was supported by a research grant from Wyeth-Ayerst Research Drug Metabolism Division (Princeton, NJ, USA).

References

Acheampong, A. A., Chien, D.-S., Lam, S., Vekich, S., Breau, A., Usansky, J., Harcourt, D., Munk, S. A., Nguyen, H., Garst, M. and Tang-Liu, D., 1996, Characterization of brimonidine metabolism with rat, rabbit, dog, monkey and human liver fractions and rabbit liver aldehyde oxidase. *Xenobiotica*, **26**, 1035–1055.

Andersson, T. B., Sjöberg, H., Hoffmann, K.-J., Boobis, A. R., Watts, P., Edwards, R. J., Lake, B. G., Price, R. J., Renwick, A. B., Gómez-Lechón, M. J., Castell, J. V., Ingelman-Sundberg, M., Hidestrand, M., Goldfarb, P. S., Lewis, D. F. V., Corcos, L., Guillouzo, A., Taavitsainen, P. and Pelkonen, O., 2001, An assessment of human liver-derived *in vitro* systems to predict the *in vivo* metabolism and clearance of almokalant. *Drug Metabolism and Disposition*, **29**, 712–720.

Beamand, J. A., Price, R. J., Cunninghame, M. E. and Lake, B. G., 1993, Culture of precision-cut liver slices: effect of some peroxisome proliferators. *Food and Chemical Toxicology*, **31**, 137–147.

Beer, B., Ieni, J. R., Wu, W.-H., Clody, D., Amorusi, P., Rose, J., Mant, T., Gaudreault, J., Cato, A. and Stern, W., 1994, A placebo-controlled evaluation of single, escalating doses of CL-284,846, a non-benzodiazepine hypnotic. *Journal of Clinical Pharmacology*, **34**, 335–344.

Chaudhary, I., Demalo, W. and Kantrowitz, J., 1994, Species comparison of *in vitro* and *in vivo* metabolism of CL-284,846, a non-benzodiazepine sedative/hypnotic agent. *Pharmaceutical Research*, **11**, S391.

Clarke, S. E., 1998, *In vitro* assessment of human cytochrome P450. *Xenobiotica*, **28**, 1167–1202.

Cornish-Bowden, A., 1974, A simple graphical method for determining the inhibition constants of mixed, uncompetitive and non-competitive inhibitors. *Biochemical Journal*, **137**, 143–144.

Dixon, M., 1953, The determination of enzyme inhibitor constants. *Biochemical Journal*, **55**, 170–171.

Houston, J. B. and Carlile, D. J., 1997, Prediction of hepatic clearance from microsomes, hepatocytes, and liver slices. *Drug Metabolism Reviews*, **29**, 891–922.

Houston, J. B. and Kenworthy, K. E., 2000, In vitro–in vivo scaling of CYP kinetic data not consistent with the classical Michaelis–Menten model. *Drug Metabolism and Disposition*, **28**, 246–254.

Kawashima, K., Hosoi, K., Naruke, T., Shiba, T., Kitamura, M. and Watabe, T., 1999, Aldehyde oxidase-dependent marked species difference in hepatic metabolism of the sedative-hypnotic, zaleplon, between monkeys and rats. *Drug Metabolism and Disposition*, **27**, 422–428.

Lake, B. G., 1987, Preparation and characterisation of microsomal fractions for studies of xenobiotic metabolism. In K. Snell and B. Mullock (eds), *Biochemical Toxicology: A Practical Approach* (Oxford: IRL Press), pp. 183–215.

Lake, B. G., Ball, S. E., Kao, J., Renwick, A. B., Price, R. J. and Scatina, J. A., 2002, Metabolism of zaleplon by human liver: evidence for involvement of aldehyde oxidase. *Xenobiotica*, **32**, 835–847.

Lin, J. H. and Lu, A. Y. H., 1998, Inhibition and induction of cytochrome P450 and the clinical implications. *Clinical Pharmacokinetics*, **35**, 361–390.

Lowry, O. H., Rosebrough, N. J., Farr, A. L. and Randall, R. J., 1951, Protein measurement with the Folin phenol reagent. *Journal of Biological Chemistry*, **193**, 265–275.

Pelkonen, O., Myllynen, P., Taavitsainen, P., Boobis, A. R., Watts, P., Lake, B. G., Price, R. J., Renwick, A. B., Gómez-Lechón, M.-J., Castell, J. V., Ingelman-Sundberg, M., Hidestrand, M., Guillouzo, A., Corcos, L., Goldfarb, P. S. and Lewis, D. F. V., 2001, Carbamazepine: a 'blind' assessment of CYP-associated metabolism and interactions in human liver-derived *in vitro* systems. *Xenobiotica*, **31**, 321–343.

Rashidi, M. R., Smith, J. A., Clarke, S. E. and Beedham, C., 1995, Inhibition of human and guinea-pig liver aldehyde oxidases *in-vitro*. *Journal of Pharmacy and Pharmacology*, **47**, 1090.

Renwick, A. B., Mistry, H., Ball, S. E., Walters, D. G., Kao, J. and Lake, B. G., 1998, Metabolism of zaleplon by human hepatic microsomal cytochrome P450 isoforms. *Xenobiotica*, **28**, 337–348.

Robertson, I. G. C. and Bland, T. J., 1993, Inhibition by SKF-525A of the aldehyde oxidase-mediated metabolism of the experimental antitumour agent acridine carboxamide. *Biochemical Pharmacology*, **45**, 2159–2162.

Rodrigues, A. D., Ferrero, J. L., Amann, M. T., Rotert, G. A., Cepa, S. P., Surber, B. W., Machinist, J. M., Tich, N. R. Sullivan, J. P., Garvey, D. S. Fitzgerald, M. and Arneric, S. P., 1994, The *in vitro* hepatic metabolism of ABT-418, a cholinergic channel activator, in rats, dogs, Cynomolgus monkeys, and humans. *Drug Metabolism and Disposition*, **22**, 788–798.

Rosen, A. S., Fournie, P., Darwish, M., Danjou, P. and Troy, S. M., 1999, Zaleplon pharmacokinetics and absolute bioavailability. *Biopharmaceutics and Drug Disposition*, **20**, 171–175.

Smith, S. R. and Kendall, M. J., 1988, Ranitidine *versus* cimetidine: a comparison of their potential to cause clinically important drug interactions. *Clinical Pharmacokinetics*, **15**, 44–56.

Somogyi, A. and Muirhead, M., 1987, Pharmacokinetic interactions of cimetidine 1987. *Clinical Pharmacokinetics*, **12**, 321–366.

Steensma, A., Beamand, J. A., Walters, D. G., Price, R. J. and Lake, B. G., 1994, Metabolism of coumarin and 7-ethoxycoumarin by rat, guinea pig, Cynomolgus monkey and human precision-cut liver slices. *Xenobiotica*, **24**, 893–907.

Tanaka, E., 1998, Clinically important pharmacokinetic drug–drug interactions: role of cytochrome P450 enzymes. *Journal of Clinical Pharmacy and Therapeutics*, **23**, 403–416.

Ueng, Y.-F., Kuwabara, T., Chun, Y.-J. and Guengerich, F. P., 1997, Cooperativity in oxidations catalyzed by cytochrome P450 3A4. *Biochemistry*, **36**, 370–381.

Worboys, P. D., Bradbury, A. and Houston, J. B., 1997, Kinetics of drug metabolism in rat liver slices. III. Relationship between metabolic clearance and slice uptake rate. *Drug Metabolism and Disposition*, **25**, 460–467.

Wrighton, S. A. and Ring, B. J., 1994, Inhibition of human CYP3A catalyzed 1′-hydroxy midazolam formation by ketoconazole, nifedipine, erythromycin, cimetidine and nizatidine. *Pharmaceutical Research*, **11**, 921–924.

Wu, W. H., Dicioccio, A. T., Demaio, W., Amorusi, P., Tonelli, A. P. and Mayer, P. R., 1996, Mass balance and pharmacokinetics of zaleplon, a non-benzodiazepine sedative/hypnotic, in man. *Pharmaceutical Research*, **13**, S487.

XENOBIOTICA, 2002, VOL. 32, NO. 10, 863–878

Taylor & Francis
healthsciences

Reversible and irreversible inhibition of CYP3A enzymes by tamoxifen and metabolites

XUE-JUN ZHAO†, D. R. JONES†, YING-HONG WANG†, S. W. GRIMM‡ and S. D. HALL†

† Division of Clinical Pharmacology, Department of Medicine, Indiana University School of Medicine, Indianapolis, IN 46202, USA
‡ Drug Metabolism and Pharmacokinetics Department, AstraZeneca Pharmaceuticals LP, Wilmington DE 19803, USA

Received 7 February 2002

1. Preliminary studies have identified cytochrome P450 (CYP) 3A4 and CYP1B1 as the human CYPs inhibited by tamoxifen. To quantify the inhibitory potency of tamoxifen and its major metabolites, the metabolism of three substrates of CYP3A, midazolam, diltiazem and testosterone, and 7-ethoxyresorufin as a substrate of CYP1B1 were examined in catalytic assays carried out using human liver microsomes and cDNA-expression systems.

2. Tamoxifen, *N*-desmethyltamoxifen, 4-hydroxytamoxifen and 3-hydroxytamoxifen reversibly inhibited midazolam 1′-hydroxylation, diltiazem *N*-demethylation and testosterone 6β-hydroxylation with K_i ranging from 3 to 37 μM in human liver microsomes. Tamoxifen, *N*-desmethyltamoxifen, 4-hydroxytamoxifen and 3-hydroxytamoxifen also reversibly inhibited the activity of cDNA-expressed CYP3A4, CYP3A5 and CYP1B1.

3. Tamoxifen and *N*-desmethyltamoxifen exhibited time-dependent inactivation of testosterone 6β-hydroxylation by cDNA-expressed CYP3A4 (+ cytochrome b5) yielding k_{inact} and K_i of 0.04 min^{-1} and 0.2 μM for tamoxifen and 0.08 min^{-1} and 2.6 μM for *N*-desmethyltamoxifen. A metabolic intermediate complex (MIC) was also formed by tamoxifen and *N*-desmethyltamoxifen with CYP3A4 (+ cytochrome b5) and CYP3A4 but not with CYP3A5 or CYP3A7. Pre-incubation with 4-hydroxytamoxifen and 3-hydroxytamoxifen did not result in any CYP3A inactivation or detectable MIC formation. There was no detectable time-dependent inactivation or MIC formation with tamoxifen or metabolites with CYP1B1.

4. These data indicate that tamoxifen and its three major metabolites are effective inhibitors of CYP3A *in vitro* and that tamoxifen and *N*-desmethyltamoxifen are effective mechanism-based inhibitors. Thus, caution should be exercised when tamoxifen is coadministered with other CYP3A substrates.

Introduction

The oestrogen receptor antagonist tamoxifen is widely used for the treatment of hormone-dependent breast cancer and has been approved by the Food and Drug Administration (FDA) to reduce the risk of breast cancer in 'at risk' healthy women. This is due to results of large-scale clinical trials in which tamoxifen affords protection in 45% of the women considered at risk of breast cancer (Fisher *et al.* 1998).

The pharmacokinetics of tamoxifen are characterized by extensive metabolism and a long elimination half-life of approximately 7 days (Buckley and Goa 1989). Wide interpatient variability in exposure to tamoxifen and its metabolites is

* Author for correspondence; e-mail: drjones1@iupui.edu

Xenobiotica ISSN 0049–8254 print/ISSN 1366–5928 online © 2002 Taylor & Francis Ltd
http://www.tandf.co.uk/journals
DOI: 10.1080/00498250210158230

observed while median concentrations of tamoxifen and its desmethyl metabolites significantly increase with age (Peyrade *et al.* 1996). The metabolism of tamoxifen shows a considerable interindividual variation that may be a determinant of the efficacy and toxicity of the drug (Buckley and Goa 1989). Tamoxifen undergoes extensive metabolism by human and animal liver microsomal preparations to *N*-desmethyltamoxifen, 4-hydroxytamoxifen, tamoxifen-*N*-oxide and other minor metabolites (Reunitz *et al.* 1984, Mani *et al.* 1993a, b, Poon *et al.* 1993, Lim *et al.* 1994). Among these metabolites, 4-hydroxytamoxifen is approximately a 100-fold more potent anti-oestrogen than tamoxifen (Borgna and Rochefort 1981, Furr and Jordan 1984). The transformation of tamoxifen to *N*-desmethyltamoxifen and 4-hydroxytamoxifen derivatives is catalysed by human hepatic cytochrome P450 enzymes (CYPs) (Jacolot *et al.* 1991, Mani *et al.* 1993a, Crewe *et al.* 1997), whereas tamoxifen-*N*-oxidation is catalysed primarily by the flavin-containing monooxygenase (Mani *et al.* 1993b). The *N*-demethylation of tamoxifen in human liver is catalysed mainly by CYP3A enzymes (Jacolot *et al.* 1991, Mani *et al.* 1993a), but CYP2D6, CYP2C9 and CYP3A catalyse tamoxifen-4-hydroxylation although the relative contribution of these enzymes is unclear (Crewe *et al.* 1997, Dehal and Kupfer 1997).

The widespread use of tamoxifen and the paucity of information about its involvement in drug–drug interactions prompted us to characterize the potency and spectrum of CYP inhibition *in vitro* by tamoxifen and its metabolites. This is particularly important because tamoxifen, like other tertiary amines that are *N*-demethylated by CYP3A enzymes, forms a metabolic intermediate complex in the rat liver *in vivo* (Bensoussan *et al.* 1995). The formation of such a complex causes irreversible inhibition of catalysis. In turn, this inactivation might be expected to cause drug–drug interactions and possibly to modulate the pharmacological actions of tamoxifen by diverting metabolism towards non-CYP3A pathways, such as 4-hydroxytamoxifen formation.

Materials and methods

Materials

Tamoxifen, 4-hydroxytamoxifen, diltiazem, testosterone, 6β-hydroxytestosterone, *N*-desmethyldiazepam, 7-ethoxyresorufin and resorufin were purchased from Sigma Chemical Co. (St Louis, MO, USA). Midazolam and 1′-hydroxymidazolam were gifts from Hoffmann-LaRoche (Nutley, NJ, USA). *N*-desmethyldiltiazem and *N*-desmethyltamoxifen were a gift from Tanabe Seiyaku Co. (Osaka, Japan) and Zeneca Pharmaceuticals (Wilmington, DE, USA), respectively. 3-Hydroxytamoxifen was purchased from RBI (Natick, MA, USA). Sodium phosphate and magnesium chloride were obtained from Fisher Scientific (Pittsburgh, PA, USA), and NADPH (98%) from Boehringer Mannheim (Indianapolis, IN, USA). Microsomal preparations from baculovirus-transfected insect cells (CYP1A1, CYP1A2, CYP1B1, CYP2B6, CYP2C8, CYP2C9(-Arg 144), CYP2C19, CYP2D6(Val), CYP3A4, CYP3A4 (+b5), CYP3A5, CYP4A11, and Supermix (a mixture of CYP1A2, 2C8, 2C9, 2C19, 2D6 and 3A4)) and human lymphoblastoid cell lines (CYP2A6 and CYP3A4) were purchased from Gentest Corp. (Woburn, MA, USA). All other reagents and solvents were products at the highest quality available.

Human liver microsomes

Human adult liver specimens (IUL-10 and IUL-11; unknown gender) were obtained at surgery in accordance with protocols approved by the Institutional Review Board of Indiana University (Indianapolis, IN, USA). Microsomes from these specimens were prepared by differential centrifugation and stored at $-70\,^{\circ}$C in a 100 mM potassium phosphate buffer (pH 7.25) as described by Gorski *et al.* (1994). Protein and CYP concentrations were determined by the methods of Lowry *et al.* (1951) and Omura and Sato (1964), respectively.

Midazolam 1′-hydroxylation

The rates of midazolam hydroxylation by two different liver microsome preparations were determined using the method of Gorski *et al.* (1994). The incubations contained 50 μg microsomal protein, 100 mM sodium phosphate buffer (pH 7.4) containing 5 mM magnesium chloride, 1 mM NADPH and a range of midazolam concentrations up to 50 μM, in a final volume of 1000 μl. For cDNA-expressed CYP3A, 40 pmol were employed. Incubations were conducted at 37 °C for 1 or 2 min, which corresponded to initial rate conditions. After the reaction was stopped by addition of 1000 μl ice-cold acetonitrile, 200 ng desmethyldiazepam were added to the samples as an internal standard.

1′-Hydroxymidazolam formed in the incubation mixtures was determined according to a modified method of Gorski *et al.* (1994). Incubation samples were extracted into 5 ml cyclohexane:methylene chloride (7:3) after the addition of 0.5 ml 1 M NaOH/glycine buffer (pH 11.3). After evaporation of solvent, the residue was reconstituted with 150 μl mobile phase (methanol:acetonitrile:Na_2HPO_4 buffer, pH 7.0; 22:30:48) and 10–120 μl were injected onto a 5 μm C18 column (150 × 4.6 mm, Ultrasphere, Beckman Instrument, San Ramon, CA, USA). The mobile phase flow was set at 1 ml min^{-1} and ultraviolet detection wavelength was set at 230 nm. Standard curves ranged from 10 ng ml^{-1} (limit of quantification) to 2000 ng ml^{-1}. Quality control samples ($n = 3$; concentrations from 30 to 1500 ng ml^{-1}) were run with each set of unknowns. Standard curves were deemed acceptable if the quality controls concentrations estimated from the standard curve were within 10% of their prepared concentrations. If the estimates were >10%, then the standard curve and unknown samples were discarded and repeated.

Diltiazem N*-demethylation*

Microsomes from two human livers were used to characterize diltiazem *N*-demethylation. Microsomal incubations contained the same protein, buffer and NADPH as above. Diltiazem concentrations varied from 6.25 to 1600 μM in a final volume of 1 ml. The same concentration of cDNA-expressed CYP3A was used as above. The reaction was started by adding NADPH (1 mM) with incubation at 37°C for 5 min. These incubation conditions corresponded to initial rate conditions. After the reaction was stopped by addition of 1000 μl ice-cold methanol, 200 ng desmethyldiazepam were added to the samples as an internal standard.

N-desmethyldiltiazem was quantified by HPLC with UV detection (237 nm) (Jones *et al.* 1999). Samples were made basic by the addition of 0.2 m NaOH/glycine buffer (pH 8.5) and then extracted with 6 ml ethyl acetate. Following evaporation of the solvent, the residue was reconstituted with 150 μl mobile phase (methanol:acetonitrile:Na_2HPO_4 buffer, pH 6.3; 43:20:37) and 10–120 μl were injected onto a 5 μm C18 column (150 × 4.6 mm, Ultrasphere, Beckman Instrument) eluted at 1 ml min^{-1}. Standard curves ranged from 13 ng ml^{-1} (limit of quantification) to 2000 ng ml^{-1}. Quality control samples ($n = 3$; concentrations from 30 to 1500 ng ml^{-1}) were run with each set of unknowns. Standard curves were deemed acceptable if the quality controls concentrations estimated from the standard curve were within 10% of their prepared concentrations. If the estimates were >10%, then the standard curve and unknown samples were discarded and repeated.

Testosterone 6β-hydroxylation

Microsomal samples containing 50 μg protein and up to 400 μM testosterone were incubated at 37°C, in a final volume of 1000 μl, with 1 mM NADPH. Microsomal incubations of cDNA-expressed CYP3A used 20 pmol CYP. After 10-min incubation, the reaction was stopped by addition of 1000 μl ice-cold acetonitrile. Then, 400 ng desmethyldiazepam were added as an internal standard. These incubation conditions corresponded to initial rate conditions.

6β-Hydroxytestosterone formed during the incubations was quantified by a reverse-phase HPLC method with UV detection (254 nm). Samples were extracted with 6 ml ethyl acetate and following evaporation of the solvent, the residue was reconstituted using 150 μl mobile phase (methanol: Na_2HPO_4, pH 6.3; 58:42). An aliquot of 10–120 μl was injected onto an HPLC column. Standard curves ranged from 25 ng ml^{-1} (limit of quantification) to 2000 ng ml^{-1}. Quality control samples ($n = 2$; concentrations of 150 and 1500 ng ml^{-1}) were run with each set of unknowns. Standard curves were deemed acceptable if the quality controls concentrations estimated from the standard curve were within 10% of their prepared concentrations. If the estimates were >10%, then the standard curve and unknown samples were discarded and repeated.

7-Ethoxyresorufin O*-deethylation*

The rates of 7-ethoxyresorufin *O*-deethylation by cDNA-expressed CYP1B1 (Supersomes, Gentest Corp., Woburn, MA, USA) were determined using the method of Crespi *et al.* (1997). The incubation medium contained 20 or 40 pmol CYP1B1, 100 mM sodium phosphate buffer (pH 7.4) containing 5 mM magnesium chloride, 1 mM NADPH and 5 μM 7-ethoxyresorufin in a final volume of 1 ml. The mixture was incubated at 37°C for 10 min. These incubation conditions corresponded to initial rate conditions. After the reaction was stopped by addition of 50 μl trichloroacetic acid (10%), 200 μl of the mixture was transferred to a 24-well culture plate (Falcon), followed by addition of 1.8 ml 100 mM Tris buffer (pH 9)

to each well. The formation of resorufin from 7-ethoxyresorufin was quantified by a spectrofluorometer (CytoFluor^{TM} 2350, Millipore, Milford, MA, USA) with excitation and emission wavelengths of 550 and 586 nm, respectively. Standard curves ranged from 10 ng ml^{-1} (limit of quantification) to 1000 ng ml^{-1}. Quality control samples ($n = 2$; concentrations of 25 and 750 ng ml^{-1}) were run with each set of unknowns. Standard curves were deemed acceptable if the quality controls concentrations estimated from the standard curve were within 10% of their prepared concentrations. If the estimates were >10%, then the standard curve and unknown samples were discarded and repeated.

Binding to human liver microsomes

A 100 μM concentration of tamoxifen, *N*-desmethyltamoxifen or 4-hydroxytamoxifen was incubated with buffer and 100 μg human liver microsomal protein at 37°C for 10 min then transferred to an ultrafiltration apparatus (MPS-1; Amicon, Danvers, MA, USA) containing YMT membranes (30 000 MW cut-off). The samples were centrifuged at 2000*g* for 20 min at room temperature in sealed ultrafiltration cartridges. Aliquots of incubate and ultrafiltrate were supplemented with nelfinavir, the internal standard, and then extracted with 6 ml ethyl acetate. After evaporation of the solvent, the residue was reconstituted with mobile phase (acetonitrile: 50 mM ammonium acetate buffer (pH 8), 62:38 v/v) that was injected into a 5 μm C-18 column (150 × 4.6 mm, Luna, Phenomenex) attached to a ultraviolet detector (254 nm). The fraction unbound in microsomes (f_{um}) was estimated by comparing the ratio of ultrafiltrate concentration to the concentration of drug added to the ultrafiltration device. Preliminary experiments showed that tamoxifen and 4-hydroxytamoxifen did not bind to the ultrafiltration device, but the tube containing the ultrafiltrate bound *N*-desmethyltamoxifen so the unbound concentration was corrected for this. Each sample was assayed in triplicate and the values are the mean (± SD).

Screen for CYP inhibition

As a screen to assess inhibition of CYP activities, tamoxifen (10 μM) was pre-incubated with individual cDNA-expressed CYPs (CYP1A1, CYP1A2, CYP1B1, CYP2A6, CYP2B6, CYP2C8, CYP2C9-Arg144, CYP2C19, CYP2D6-Val, CYP2E1, CYP3A4 (+b5), CYP3A4, CYP3A5, and CYP4A11; Supersomes or B-lymphoblastoid cells, Gentest) and NADPH for 30 min. Following pre-incubation, an aliquot was removed and added to a tube containing the selective substrate for each CYP and NADPH. The selective substrates, enzyme concentrations, procedures and descriptions of control samples are described in Jones *et al.* (1999). The dilution of the aliquot from the pre-incubation tube with the contents of the tube containing the selective substrate was 1:10 (v/v) to eliminate reversible inhibition as a possible cause of the inhibitory effect. After a 5–15-min incubation, the reaction was terminated and then assayed for activity. Activity was expressed as per cent inhibition compared with the control activity.

Inhibition studies

Four different concentrations (5–80 μM) of tamoxifen or its three metabolites were respectively co-incubated with midazolam (0.5–50 μM), diltiazem (6.25–50 μM) or testosterone (10–100 μM) in human liver microsomes or cDNA-expressed CYP3A (Supersomes) to characterize and quantify the reversible inhibition. Inhibition of 7-ethoxyresorufin *O*-deethylation was performed by the co-incubation of 7-ethoxyresorufin (5 μM) with tamoxifen or its metabolites (100 μM) in cDNA-expressed CYP1B1.

To identify irreversible inhibition of CYP3A, tamoxifen or each metabolite (0.5–50 μM) was pre-incubated in human liver microsomes (IUL-10, 250 μg protein/250 μl), CYP3A4 (+b5) (Supersomes, 48 pmol/120 μl), CYP3A4 (Supersomes, 120 pmol/120 μl), and CYP3A5 (Supersomes, 120 pmol/120 μl) with NADPH from 0 to 30 min. Then, an aliquot (50 or 100 μl) was removed and added to a tube containing NADPH and midazolam (50 μM), diltiazem (1000 μM) or testosterone (200 μM) in a final volume of 1 ml. After appropriate incubation times, the reaction was stopped then assayed for metabolite formation. The dilution of pre-incubate with the contents of the incubation tube was 1:10 or 1:20 to prevent any reversible inhibition by the inhibitor. Activity was expressed as a percentage of control activity, which was the average activity at zero pre-incubation time for a given inhibitor concentration.

To test for irreversible inhibition of CYP1B1, tamoxifen or each metabolite (100 μM) was pre-incubated with CYP1B1 and NADPH for 30 min. Then an aliquot was removed and added to a tube containing NADPH and 7-ethoxyresorufin (5 μM). Activity was expressed in the same way as above.

Metabolic intermediate complex formation

Microsomes from human livers and cDNA-expressed CYP3A were used to characterize metabolic intermediate complex (MIC) formation by tamoxifen (1–50 μM), *N*-desmethyltamoxifen (1–50 μm), 4-hydroxytamoxifen (10 μM) and 3-hydroxytamoxifen (10 μM). MIC formation was characterized by dual wavelength spectroscopy (Uvikon 933 double beam UV/VIS Spectrophotometer; Research Instru-

ments International, San Diego, CA, USA) by scanning from 380 to 500 nm and was quantified by wavelength programming of two wavelengths selected from the original scans at 30-s intervals. The procedure was the same as that reported in Jones *et al.* (1999).

Data analysis

The microsomal activity data represent the mean of duplicate assays for every experiment. Untransformed kinetic data were analysed by non-linear regression without weighting (WinNonlin v.1.1 SCI Software, Apex, NC, USA). The appropriateness of the fit was determined by the visual inspection of fit and residual patterns, residual sums of squares, and precision of the parameter estimates (Boxenbaum *et al.* 1974).

Enzyme kinetic parameters, V_{max} and K_m, were estimated by fitting data to the Michaelis–Menten equation. The inhibition rate constant, K_i, was estimated with fits of data to competitive, non-competitive and uncompetitive inhibition models (Segel 1975).

Irreversible inhibition constants, K_I, the inactivator concentration that produces half the maximal rate of inactivation, analogous to a K_m, and k_{inact}, the maximal rate constant for inactivation (Silverman 1988) were estimated from the inhibition of activity and MIC formation data. The inactivation clearance, CL_{inact}, is defined as k_{inact}/K_I. The residual activity (percentage of remaining activity) versus pre-incubation time was fit for one inhibitor concentration to estimate k_{obs}, the slope of the line of equation (1):

$$\text{Percentage of remaining activity} = 100 \times e^{-(k_{obs} \times t)}. \quad (1)$$

Then, k_{obs} for each inhibitor concentration was fit to equation (3) to estimate k_{inact} and K_I:

$$k_{obs} = \frac{k_{inact} \times I}{K_I + I}, \quad (2)$$

where I is the concentration of irreversible inhibitor. It was assumed that there is negligible change of I in the incubation period and that loss of enzyme is due to inactivation. The MIC formation data (0–10 min) for a given inhibitor concentration were fit to equation (3) to estimate k_{obs}:

$$\text{AbsDiff}_{(t)} = \text{AbsDiff}_{max} \times (1 - e^{-(k_{obs} \times t)}), \quad (3)$$

where $\text{AbsDiff}_{(t)}$ is the absorbance difference measured at time t and $\text{AbsDiff}_{(max)}$ is the maximum absorbance difference. Again, k_{obs} for each inhibitor concentration was fit to equation (2) to estimate k_{inact} and K_I.

Results

The ability of tamoxifen (10 μM) to inhibit the human hepatic drug-metabolizing CYPs upon pre-incubation was evaluated by screening cDNA-expressed human drug-metabolizing CYPs: CYP1A1, CYP1A2, CYP1B1, CYP2A6, CYP2B6, CYP2C8, CYP2C9-Arg144, CYP2C19, CYP2D6-Val, CYP2E1, CYP3A4 (+b5), CYP3A4, CYP3A5 and CYP4A11. CYP3A4 (+b5) and CYP1B1 were identified as the targets of tamoxifen inhibition because they were inhibited by >30% compared with control activity (table 1). All the other CYPs exhibited less than a 5% inhibition. Although useful as a screen, this experimental design fails to distinguish between reversible and irreversible mechanisms of inhibition.

The potential for inhibition of 7-ethoxyresorufin *O*-deethylation by CYP1B1 was investigated using tamoxifen and its three metabolites, both by co-incubation and by pre-incubation (30 min), with cDNA-expressed enzyme. Tamoxifen and its three metabolites (100 μM) inhibited 7-ethoxyresorufin (5 μM) *O*-deethylation by up to 40% during the co-incubation experiment (tamoxifen, 22% inhibition; desmethyltamoxifen, 37%; 4-hydroxytamoxifen, 39%, 3-hydroxytamoxifen, 27%). However, there was no inhibition after a 30 min pre-incubation of tamoxifen and its three metabolites (40 μM) with cDNA-expressed CYP1B1 (data not shown), indicating that tamoxifen and its metabolites are not irreversible inhibitors of CYP1B1. The concentrations of tamoxifen and metabolites were 100 μM, which is

Table 1. Effect of tamoxifen (10 μM) pre-incubation on expressed CYP activity.

CYP	Substrate	Percentage inhibition
1A1	caffeine	0
1A2	caffeine	0
1B1	7-ethoxyresorufin	35
2A6	coumarin	0
2B6	7-ethoxytrifluoromethylcoumarin	0
2C8	tolbutamide	0
2C9-Arg 144	tolbutamide	4
2C19	*S*-mephenytoin	0
2D6-Val	dextromethorphan	0
2E1	chlorzoxazone	0
3A4(+b5)	midazolam	53
3A4	midazolam	0
3A5	midazolam	2
4A11	lauric acid	0

Tamoxifen was pre-incubated with cDNA-expressed CYPs and NADPH for 30 min. Control samples consisted of tamoxifen pre-incubated with cDNA-expressed CYPs for 30 min in the absence of NADPH.

All substrate concentrations were at least five times greater than K_m.

approximately 100 times greater than the reported plasma concentrations (Millward *et al.* 1992), therefore little to no inhibition of CYP1B1 would be expected *in vivo*.

The assessment of inhibitory potency towards CYP3A4 can be dependent on the substrate chosen to assess catalytic activity (Kenworthy *et al.* 1999). Therefore, to quantify the inhibitory potency of tamoxifen and its three metabolites, midazolam, diltiazem and testosterone were employed as CYP3A substrates. All three CYP3A substrates exhibit catalytic activities that are highly correlated at saturating substrate concentrations in an adult human liver microsomal bank ($n = 21$ for diltiazem and midazolam, $n = 4$ for testosterone) in our laboratory (Jones *et al.* 1999). Single concentrations of tamoxifen or its metabolites (20–100 μM) were tested on selective substrate activities (midazolam, 50 μM; diltiazem, 20 μM; testosterone, 25 μM) in human liver microsomes (IUL-11) and cDNA-expressed CYP3A enzymes to determine whether these compounds were reversible inhibitors of CYP3A activity. Tamoxifen and its metabolites (20–100 μM) caused varying degrees of inhibition of CYP3A activity in all tissues (table 2). The inhibition was independent of the source of CYP3A enzyme and comparable for CYP3A4 and 3A5.

Four different concentrations (5–80 μM) of tamoxifen and its three metabolites were respectively co-incubated with midazolam (0.5–50 μM), diltiazem (6.25–50 μM) and testosterone (10–100 μM) in human liver microsomes (IUL-10) to identify the type of reversible inhibition and K_i. All of the tested compounds exhibited a low K_i for each of the CYP3A substrates (table 3). The mode of inhibition was competitive for testosterone and diltiazem (figure 1), but in the case of midazolam, a complex interaction was noted and this precluded the fit of any hyperbolic model. When the control and 20 μM concentration of inhibitor were considered, a non-competitive (for *N*-desmethyltamoxifen) or an uncompetitive (for tamoxifen, 4-hydroxytamoxifen and 3-hydroxytamoxifen) model best described the midazolam data and the corresponding K_i are listed in table 2. The two human liver microsomes (IUL-10 and IUL-11) that were examined in the co-

Table 2. Effect of co-incubation of tamoxifen or metabolites on CYP3A activity.

Compound	Activity (% of control)*					
	HLM	CYP3A4(+b5)	CYP3A4	CYP3A4-B	CYP3A5	Supermix
Tamoxifen	53	55	75	92	70	78
Desmethyltamoxifen	59	17	87	92	83	81
4-hydroxytamoxifen	33	27	51	83	48	63
3-hydroxytamoxifen	51	58	75	83	58	43

*Activity is the mean of duplicate measurements.

Control activity: HLM, midazolam 1′-hydroxylation, 11,717 pmol/(mg × min); CYP3A4(+b5), testosterone 6β-hydroxylation, 56 pmol/(pmol CYP × min); CYP3A4, diltiazem *N*-demethylation, 2.9 pmol/(pmol CYP × min); CYP3A4-B, diltiazem *N*-demethylation, 7.2 pmol/(pmol CYP × min), CYP3A5, midazolam 1′-hydroxylation, 24 pmol/(pmol CYP × min); Supermix, diltiazem *N*-demethylation, 3.3 pmol/(pmol CYP × min)

Inhibitor concentration: 20–80 μM.

HLM, human liver microsomes (IUL-11); CYP3A4-B, microsomes from B-lymphoblastoid cells; all others are Supersomes.

Midazolam (50 μM) was the substrate for HLM and CYP3A5.

Testosterone (200 μM) was the substrate for CYP3A4(+b5).

Diltiazem (100 μM) was the substrate for CYP3A4, CYP3A4-B and Supermix (a mixture of CYP1A2, 2C8, 2C9, 2C19, 2D6, and 3A4).

Table 3. Estimates of K_i (μM) for tamoxifen and metabolites with CYP3A substrates in human liver microsomes (IUL-10).

Compound	Testosterone 6β-hydroxylation	Diltiazem *N*-demethylation	Midazolam 1′-hydroxylation
Tamoxifen	22	11	6
Desmethyltamoxifen	23	9	8
4-hydroxytamoxifen	< 5	10	< 5
3-hydroxytamoxifen	37	18	24

incubation experiments varied in CYP3A activity (the range of testosterone 6β-hydroxylation was 13 914–23 889 pmol mg^{-1} min^{-1}), but were not different in percent inhibition by tamoxifen or metabolites based on rank order of inhibition.

A range of pre-incubation times (1–30 min) was examined to characterize the time-course of irreversible CYP3A inhibition by tamoxifen and metabolites (10 μM). Tamoxifen inhibited CYP3A activity by 9% after 1 min in human liver (IUL-10), but there was no further inhibition between 1 and 30 min. *N*-desmethyltamoxifen and 3-hydroxytamoxifen inhibited CYP3A activity by approximately 30% after a 30-min pre-incubation in human liver microsomes relative to control. For pre-incubations with cDNA-expressed CYP3A4 (+b5), a significant loss of CYP3A activity (6β-hydroxytestosterone formation) at 30 min was observed for tamoxifen (71% loss of activity) and *N*-desmethyltamoxifen (63% loss of activity), whereas, 3-hydroxytamoxifen showed less than a 10% inhibition. 4-Hydroxytamoxifen did not exhibit any time-dependent inhibition in human liver microsomes or CYP3A4 (+b5). In view of the significant inhibition of CYP3A4 (+b5) by tamoxifen and *N*-desmethyltamoxifen, they were also pre-incubated with CYP3A4 or CYP3A5 and NADPH. Tamoxifen (30 μM) caused a 14 and 11% loss of activity compared with control in CYP3A4 and CYP3A5, respectively, after a 20-min pre-incubation. *N*-desmethyltamoxifen (50 μM)

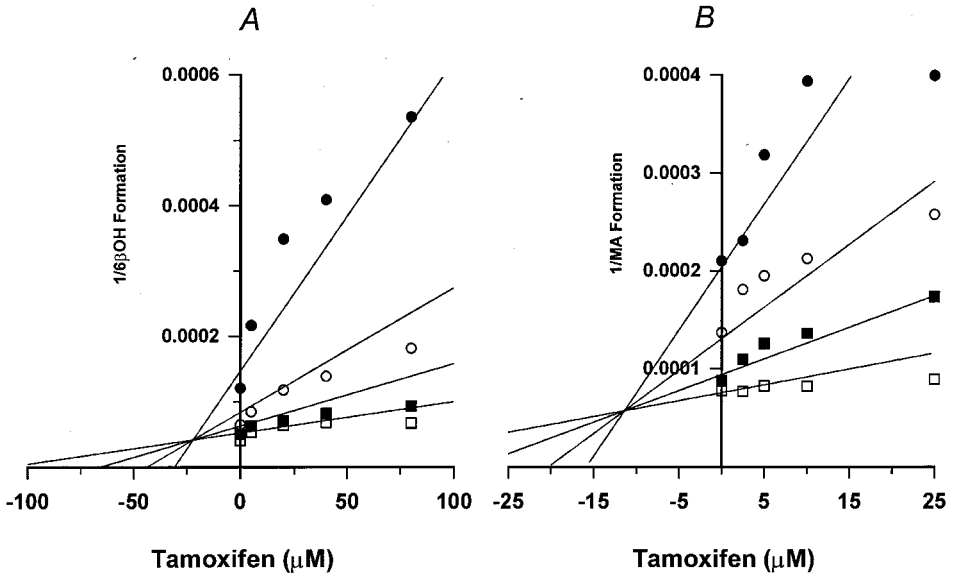


Figure 1. Dixon plots of tamoxifen inhibition of CYP3A-mediated metabolism in human liver microsomes. (A) Tamoxifen (5–80 μM) was co-incubated with testosterone (10–100 μM), human liver microsomes and NADPH. B. Tamoxifen (2.5–25 μM) was co-incubated with diltiazem (6.25–50 μM), human liver microsomes and NADPH. The data points represent averages of duplicate determinations. [Testosterone] = 10 (●), 25 (○), 50 (■), 100 μM (□); [diltiazem] = 6.25 (●), 12.5 (○), 25 (■), 50 μM (□). The lines represent WinNonlin estimates of the line of best fit at a given concentration when all the data were simultaneously fit to a competitive inhibition model.

exhibited a similar loss of activity, 11% for CYP3A4 and 8% for CYP3A5, after a 10-min pre-incubation.

In addition to the inhibition of catalytic activity, significant MIC formation was observed after a 60-min incubation in human liver microsomes, CYP3A4 (+b5) (figure 2), and CYP3A4 in the presence of tamoxifen (10 μM) and *N*-desmethyltamoxifen (10 μM). MIC formation by tamoxifen accounted for 92% of total CYP3A4 (+b5) (200 pmol) and 38% of total CYP3A4 (200 pmol). No MIC was detectable for tamoxifen incubated for 1 h with CYP3A5 (500 pmol) or CYP3A7(+b5) (100 pmol). The MIC formation by *N*-desmethyltamoxifen also accounted for 92% of total CYP3A4 (+b5) (100 pmol) and 31% of total CYP3A4 (200 pmol) but was undetectable for CYP3A5 (500 pmol) and CYP3A7(+b5) (100 pmol). 4-Hydroxytamoxifen and 3-hydroxytamoxifen did not form any detectable MIC with CYP3A4 (+b5) and were not studied in the other CYP3A systems.

To quantify the irreversible inhibition of CYP3A4 by tamoxifen and *N*-desmethyltamoxifen, k_{inact} and K_I were estimated from the inhibition of activity by varying time and inhibitor concentration. The pre-incubation of tamoxifen (0.5–30 μM) or *N*-desmethyltamoxifen (1–50 μM) in cDNA-expressed CYP3A4 (+b5) and NADPH resulted in the inhibition of CYP3A-mediated metabolism in the form of testosterone 6β-hydroxylation (figure 3). The slope, k_{obs}, of the residual CYP3A activity versus pre-incubation time was estimated for each inhibitor concentration. Then, k_{obs} was fit to equation (2) to estimate k_{inact} and K_I. The parameter estimates (±SE) of k_{inact} and K_I for tamoxifen were 0.04 (± 0.002 min^{-1}) and 0.2 (± 0.09 μM), respectively. For *N*-desmethyltamoxifen,

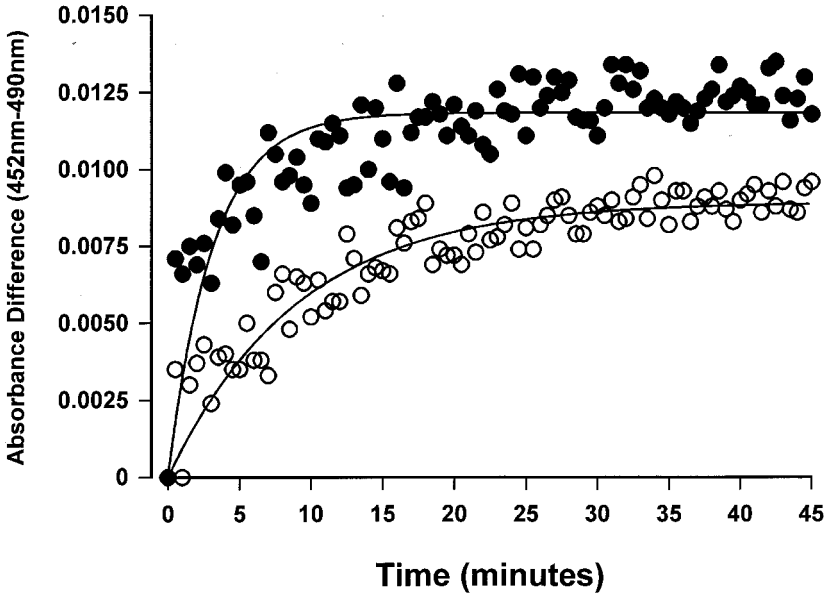


Figure 2. Metabolic intermediate complex formation of tamoxifen (●) and *N*-desmethyltamoxifen (○) with in CYP3A4 (+b5). The sample cuvette contained CYP3A4 (+b5), substrate (10 μM) and NADPH, whereas the reference cuvette contained CYP3A4 (+ b5), vehicle and NADPH. Absorbance was monitored at 452 and 490 nm every 30 s for 45 min. Each datum point represents the absorbance difference of 452–490 nm. The lines represent those of best fit of the data.

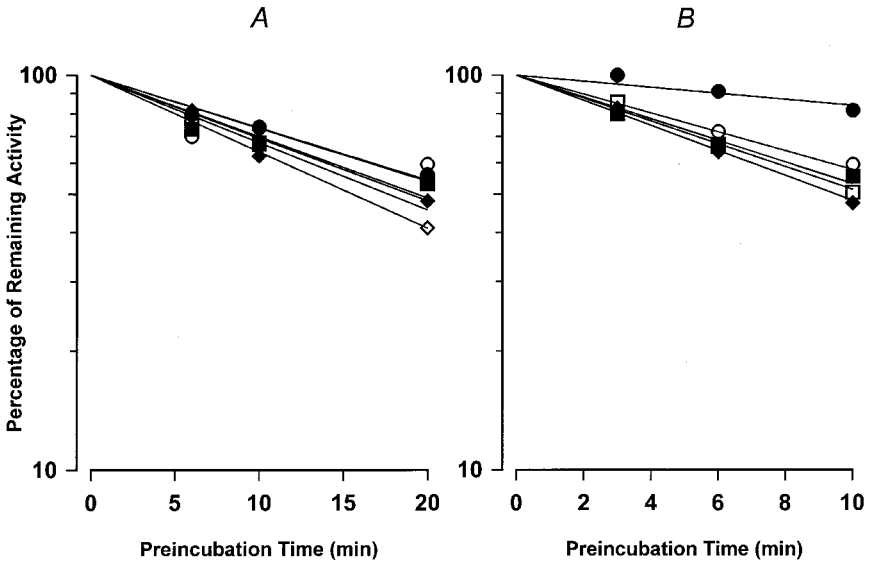


Figure 3. Effect of tamoxifen (A) and *N*-desmethyltamoxifen (B) pre-incubation on CYP3A4 (+b5) activity. CYP3A4 (+b5) was pre-incubated with NADPH and tamoxifen or *N*-desmethyltamoxifen then added to a tube containing testosterone and NADPH. (A) Tamoxifen: (●) 0.5 μM; (○) 1 μM; (■) 2.5 μM; (□) 5 μM; (◆) 10 μM; and (◇) 30 μM; (B) *N*-desmethyltamoxifen: (●) 1 μM; (○) 5 μM; (■) 10 μM; (□) 20 μM; and (◆) 50 μM. The results are expressed as the percentage of the remaining activity compared with the 0 min pre-incubation time sample average. The points are averages of duplicate determinations and the lines represent WinNonlin estimates of the line of best fit of the data at a given concentration applying equation (1).

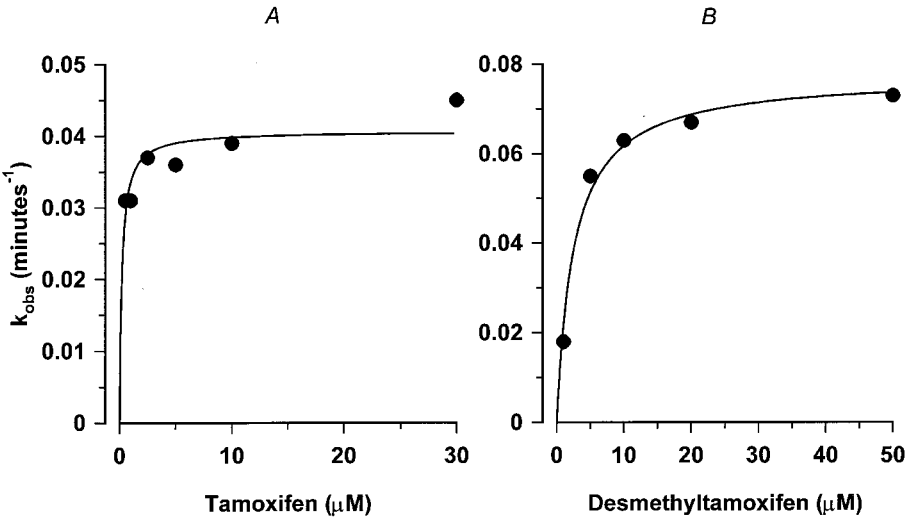


Figure 4. Plots of k_{obs} versus tamoxifen (A) or *N*-desmethyltamoxifen (B) pre-incubation with CYP3A4 (+ b5) to estimate mechanism-based inactivation constants. The lines are the lines of best fit from equation (2) using WinNonlin. Estimates of k_{obs} were obtained from the slope of the line of best fit of residual activity data (figure 3).

the estimates (±SE) of k_{inact} and K_I from k_{obs} applying equation (2) were 0.08 ($\pm 0.003\,min^{-1}$) and 2.6($\pm 0.52\,\mu M$), respectively (figure 4). The binding of tamoxifen, *N*-desmethyltamoxifen and 4-hydroxytamoxifen to human liver microsomes resulted in an average (SD) fraction unbound (f_{um}) of 0.007 (± 0.0010), 0.21 (± 0.077) and 0.35 (± 0.042), respectively. The f_{um} were then applied to the K_I to estimate the unbound K_I, which were 0.0014 and 0.55 μM for tamoxifen and *N*-desmethyltamoxifen, respectively.

When the inhibitor forms a MIC, then the k_{inact} may be estimated from the initial slope of the absorbance difference plots (equation 3). From the MIC formation data, the estimate of k_{inact} for tamoxifen (1–50 μM) was 0.10 min^{-1}, but the data did not allow an estimate of K_I because all the k_{obs} estimates were equal to k_{inact}. Estimates of k_{inact} and K_I for *N*-desmethyltamoxifen (1–50 μM) were 0.13 min^{-1} and 1.7 μM, respectively. These values are similar to those estimated from the inhibition of activity data, which provides additional evidence that tamoxifen and *N*-desmethyltamoxifen are relatively potent mechanism-based inactivators of CYP3A4 that is due mainly to MIC formation.

Discussion

Many anticancer drugs, including tamoxifen, exhibit a high degree of interindividual variability in pharmacokinetics (Buckley and Goa 1989, Evans and Relling 1989). This interindividual variability can be enhanced by metabolism-based drug interactions between anticancer drugs because many of these agents are metabolized primarily by CYP3A (Kivistö *et al.* 1995), the most abundant CYP in the liver (Guengerich *et al.* 1986, Shimada *et al.* 1994) and small intestinal epithelium (Watkins *et al.* 1987, Kolars *et al.* 1992). Several studies with human liver microsomes have indicated that the main metabolic pathway of tamoxifen (i.e.

N-demethylation) is catalysed principally by CYP3A (Jacolot *et al*. 1991, Mani *et al*. 1993a). CYP3A is also involved in the formation of 4-hydroxytamoxifen (Crewe *et al*. 1997) and 3,4-dihydroxytamoxifen (Dehal and Kupfer 1999), although CYP2D6 and CYP2C19 contribute to the formation of 4-hydroxytamoxifen. The experiments reported here examined the ability of tamoxifen and its three metabolites to inhibit the metabolism of substrates of CYP3A.

The interactions of tamoxifen, *N*-desmethyltamoxifen, 4-hydroxytamoxifen and 3-hydroxytamoxifen with diltiazem, midazolam and testosterone were studied in human liver microsomes and cDNA-expressed CYP3A. The results provide evidence that tamoxifen and its three metabolites are effective inhibitors of CYP3A activity, but the potency and the type of inhibition differed between CYP3A substrates (i.e. midazolam, diltiazem and testosterone) (tables 1 and 2). The differences in inhibition between substrates may be explained in part by Kenworthy *et al*. (1999) who showed that compounds used to quantify CYP3A activity may be classified into different 'groups' based on their catalytic properties. Testosterone and midazolam were two of the many CYP3A substrates tested in that study and were shown to represent different 'groups'. Therefore, the different K_i estimates of tamoxifen and metabolites with testosterone and midazolam as substrates may be explained on this basis.

Another reason for the differences between CYP3A substrates may be explained by the substrate specific involvement of CYP3A5 in midazolam 1′-hydroxylation, diltiazem *N*-demethylation and testosterone 6β-hydroxylation (Gorski *et al*. 1994, Sutton *et al*. 1997, Jones *et al*. 1999). The substrate specificity by CYP3A5 has been demonstrated by Gibbs *et al*. (1999), who noted that the expression of this protein in microsomes played a key role in the estimate of different inhibition constants (K_i) of ketoconazole and fluconazole when midazolam 1′-hydroxylation was employed as the marker of activity. A more recent study reported that CYP3A5 represents approximately 50% of the total hepatic CYP3A content in people that express this protein. This suggests that the contribution of CYP3A5 to the overall metabolism by a CYP3A substrate in such livers may be greater than expected when compared with livers without CYP3A5 (Kuehl *et al*. 2001). Note that CYP3A5 was not quantified in the human liver microsomes in our study.

In recent years, mechanism-based inactivators of CYP have been identified and some have been shown to inactivate the enzyme by formation of a MIC (Koudriakova *et al*. 1998, Jones *et al*. 1999). A MIC is a complex of a metabolite and CYP thought to be due to an amine or methylenedioxy constituent that quasi-irreversibly binds to the haem of the CYP. The MIC is catalytically inactive, thus reducing the pool of active CYP, and is measurable by dual-wavelength spectroscopy (Bensoussan *et al*. 1995, Franklin 1977). To assess any mechanistic inhibition of tamoxifen and its three metabolites on CYP3A substrate activity, pre-incubation and MIC formation experiments were performed with human liver microsomes and cDNA-expressed CYPs. Tamoxifen did not inhibit CYP3A activity upon pre-incubation experiments in human liver microsomes, but did exhibit MIC formation. The reason that tamoxifen produced MIC but did not inhibit CYP3A upon pre-incubation is unclear. The type of control used for the pre-incubation experiments in CYP3A may explain the differences in observations between the pre-incubation and MIC formation experiments. The pre-incubation of tamoxifen was compared with the pre-incubation of NADPH

alone. If CYP3A were inactivated in the presence of NADPH without substrate, then comparing one with the other would result in the apparently contradictory data presented here. Up to 40% inhibition of CYP3A activity was observed in the control of NADPH alone compared with the data from inhibitors (tamoxifen, *N*-desmethyltamoxifen, 4-hydroxytamoxifen and 3-hydroxytamoxifen) alone. This observation is consistent with the data of Chiba *et al.* (1995) who found a time-dependent loss (up to 40%) of the CYP3A activity (testosterone 6β-hydroxylation) in the presence of NADPH. The destructive effects of reactive oxygen products formed during NADPH-dependent electron transfer have been reported by Guengerich (1986) and Schaefer *et al.* (1985), and, therefore, the formation of reactive oxygen species may explain the inhibition of CYP3A activity in the presence of NADPH without inhibitors.

An earlier study reported that tamoxifen and *N*-desmethyltamoxifen formed MIC in liver microsomes from rat treated with dexamethasone (Bensoussan *et al.* 1995), but our paper is the first to show MIC formation by these compounds in human liver microsomes, CYP3A4 (+ b5) (figure 2) and CYP3A4. MIC formation by tamoxifen and *N*-desmethyltamoxifen in CYP3A4 (+ b5) accounted for nearly the total enzyme amount but accounted for $< 50\%$ in CYP3A4. The reason for the higher percentage in CYP3A4 (+ b5) is unknown but may be due to the increased turnover of the enzyme. Neither tamoxifen nor *N*-desmethyltamoxifen formed detectable MIC with CYP3A5 or CYP3A7, which suggests that in contrast to CYP3A4, the active sites of these enzymes are not conducive to complexation of the haem by these amines.

Tamoxifen and *N*-desmethyltamoxifen inhibited CYP3A-mediated metabolism in a time- and concentration-dependent manner (figure 3). This mechanism-based inhibition of CYP3A4 (+ b5) exhibited k_{inact} of 0.04 and 0.08 min^{-1} and K_I of 0.2 and 2.6 μM for tamoxifen and *N*-desmethyltamoxifen, respectively. The estimate of k_{inact} from MIC formation data with the same enzyme was similar to that of the inhibition of activity data. This suggests that mechanism-based inhibition of CYP3A by tamoxifen and *N*-desmethyltamoxifen occurs by MIC formation. There was a slight loss of activity when tamoxifen or *N*-desmethyltamoxifen was pre-incubated with CYP3A4 and CYP3A5. However, MIC formation was only observed for CYP3A4 and this formation was greater than predicted from the loss of CYP3A activity. Thus, these data further substantiate that inhibition of CYP3A4 is due to MIC formation. The inhibition rate constants, k_{inact} and K_I, for tamoxifen and *N*-desmethyltamoxifen that were estimated in the present study are similar to those that have been previously reported for tamoxifen inhibition of CYP2B6, k_{inact} of 0.02 min^{-1} and K_I of 0.9 μM (Sridor *et al.* 1999). The inhibition rate constants for tamoxifen and *N*-desmethyltamoxifen with CYP3A are also similar in magnitude to other potent CYP3A mechanistic inhibitors (e.g. diltiazem, clarithromycin) that our laboratory has studied (Jones *et al.* 1999, Mayhew *et al.* 2000) illustrating that tamoxifen and *N*-desmethyltamoxifen are potent mechanism-based inhibitors of CYP3A. In contrast to *N*-desmethyltamoxifen, the other metabolites of tamoxifen metabolism, 4-hydroxytamoxifen and 3-hydroxytamoxifen, did not produce significant inhibition of CYP3A activity.

The steady-state plasma tamoxifen concentration after a conventional clinical dose (20–40 mg day^{-1}) in man is 0.25–1.1 μM, but may attain levels as high as 3.6 μM (Millward *et al.* 1992). The K_i of tamoxifen obtained from three different CYP3A

substrates in our study (table 2) are similar to the steady-state plasma concentrations. This suggests that tamoxifen concentrations *in vivo* may cause some reversible CYP3A inhibition. *N*-desmethyltamoxifen and 4-hydroxytamoxifen exhibited low K_i for CYP3A activity (table 2) and may contribute to the *in vivo* inhibition of CYP3A activity in man when tamoxifen is administered because *N*-desmethyltamoxifen and 4-hydroxytamoxifen can reach plasma concentrations of 1.9 and 0.1 μM, respectively (Millward *et al.* 1992). In addition to the reversible inhibition, tamoxifen and *N*-desmethyltamoxifen are mechanism-based inactivators of CYP3A. The K_I for tamoxifen and *N*-desmethyltamoxifen are 0.2 and 2.6 μM, respectively, which approximate to the estimated steady-state plasma concentrations. However, the K_I for tamoxifen may be an overestimate because the k_{obs} obtained from the pre-incubation experiments do not illustrate a hyperbolic pattern (figure 4A), i.e. k_{obs} at very low tamoxifen were not detected. Thus, the K_I for tamoxifen may in fact be considerably less than that estimated from our pre-incubation experiments, which would suggest that considerable mechanism-based inhibition by tamoxifen is ongoing in the clinical setting. The mechanism-based inactivation is irreversible and may result in a prolonged inhibition of CYP3A, particularly after chronic administration of tamoxifen to patients. Full activity of this important drug-metabolizing enzyme would return only after cessation of treatment and resynthesis of new holoenzyme. An *in vivo* study that supports the prolonged inhibition of CYP by tamoxifen was performed in monkeys (Comoglio *et al.* 1996). In this latter study, the metabolism of marker compounds by liver microsomes of the tamoxifen chronic treatment group was inhibited when compared with the control group. Further study showed that a tamoxifen metabolite didesmethyltamoxifen bound to the haem of the CYP thus causing the irreversible inhibition.

All these data suggest that medication co-prescribed with tamoxifen that is significantly metabolized by CYP3A may exhibit decreased elimination that could result in increased side-effects, particularly during a longer tamoxifen administration period. However, there are no reported clinical drug–drug interaction data with tamoxifen to substantiate this conclusion. Letrozole, a non-steroidal aromatase inhibitor, is metabolized by both CYP2A6 and CYP3A4 (Wirz *et al.* 1996). The combination of tamoxifen with letrozole therapy was shown to cause a 38% decrease in letrozole AUC, suggesting induction of one or both of these two enzymes (Dowsett *et al.* 1999). A clinical study with specific CYP3A probe drugs such as midazolam would be necessary to establish the potential extent of interactions between tamoxifen and drugs that are CYP3A4 substrates. A possible positive contribution of CYP3A inhibition by *N*-desmethyltamoxifen *in vivo* may be an increase in the production of 4-hydroxytamoxifen. This metabolite has been shown to produce the more beneficial effects on breast cancer (Borgna and Rochefort 1981, Furr and Jordan 1984).

In conclusion, tamoxifen and *N*-desmethyltamoxifen are effective mechanism-based inactivators of CYP3A and tamoxifen, *N*-desmethyltamoxifen, 4-hydroxytamoxifen and 3-hydroxytamoxifen are relatively effective reversible inhibitors of CYP3A. Thus, caution may need to be exercised when tamoxifen is co-administered with other drugs where CYP3A enzymes contribute significantly to their metabolic elimination. There is a need to develop drugs for the treatment of breast cancer that do not interact with CYP3A-mediated metabolism.

Acknowledgements

This work was supported in part by a grant from Astra Zeneca and FD-T-001756 from the FDA. X.-J. Z. was the recipient of a Merck International Fellowship in Clinical Pharmacology.

References

Bensoussan, C., Delaforge, M. and Mansuy, D., 1995, Particular ability of cytochromes P450 3A to form inhibitory P450–iron-metabolite complexes upon metabolic oxidation of aminodrugs. *Biochemical Pharmacology*, **49**, 591–602.

Borgna, J. L. and Rochefort, H., 1981, Hydroxylated metabolites of tamoxifen are formed *in vivo* and bound to estrogen receptor in target tissues. *Journal of Biological Chemistry*, **256**, 859–868.

Boxenbaum, H. G., Riegelman, S. and Elasho, R. M., 1974, Statistical estimations in pharmacokinetics. *Journal of Pharmacokinetics and Biopharmaceutics*, **2**, 123–148.

Buckley, M. M. and Goa, K. L., 1989, Tamoxifen: a reappraisal of its pharmacodynamic and pharmacokinetic properties and therapeutic use. *Drugs*, **37**, 451–490.

Chiba, M., Nishime, J. A. and Lin, J. H., 1995, Potent and selective inactivation of human liver microsomal cytochrome P-450 isoforms by L-754,394, an investigational human immune deficiency virus protease inhibitor. *Journal of Pharmacology and Experimental Therapeutics*, **275**, 1527–1534.

Comoglio, A., Gibbs, A. H., White, I. N. H., Gant, T., Martin, E. A., Smith, L. L., Gamalero, S. R. and DeMatteis, F., 1996, Effect of tamoxifen feeding on metabolic activation of tamoxifen by the liver of the Rhesus monkey: does liver accumulation of inhibitory metabolites protect from tamoxifen-dependent genotoxicity and cancer? *Carcinogenesis*, **17**, 1687–1693.

Crespi, C. L., Penman, B. W., Steimel, D. T., Smith, T., Yang, C. S. and Sutter, T. R., 1997, Development of a human lymphoblastoid cell line constitutively expressing human CYP1B1 cDNA: substrate specificity with model substrates and promutagens. *Mutagenesis*, **12**, 83–89.

Crewe, H. K., Ellis, S. W., Lennard, M. S. and Tucker, G. T., 1997, Variable contribution of cytochromes P450 2D6, 2C9 and 3A4 to the 4-hydroxylation of tamoxifen by human liver microsomes. *Biochemical Pharmacology*, **53**, 171–178.

Dehal, S. and Kupfer, D., 1997, CYP2D6 catalyzes tamoxifen 4-hydroxylation in human liver. *Cancer Research*, **57**, 3402–3406.

Dehal, S. and Kupfer, D., 1999, Cytochrome P-450 3A and 2D6 catalyze *ortho* hydroxylation of 4-hydroxytamoxifen and 3-hydroxytamoxifen (droloxifene) yielding tamoxifen catechol: Involvement of catechols in covalent binding to hepatic proteins. *Drug Metabolism and Disposition*, **27**, 681–688.

Diver, J. M. J., Jackson, I. M. and Fitzgerald, J. D., 1986, Tamoxifen and nonmalignant indications. *Lancet*, **i**, 733.

Dowsett, M., Pster, C., Johnston, S. R. D., Miles, D. W., Houston, S. J., Verbeek, J. A., Gundacker, H., Siou, A. and Smith, I. E., 1999, Impact of tamoxifen on the pharmacokinetics and endocrine effects of the aromatase inhibitor letrozole in postmenopausal women with breast cancer. *Clinical Cancer Research*, **5**, 2338–2343.

Evans, W. E. and Relling, M. V., 1989, Clinical pharmacokinetics–pharmacodynamics of anticancer drugs. *Clinical Pharmacokinetics*, **16**, 327–336.

Fisher, B., Costantino, J. P., Wickerham, D. L., Redmond, C. K., Kavanah, M., Cronin, W. M., Vogel, V., Robidoux, A., Dimitrov, N., Atkins, J., Daly, M., Wieand, S., Tan-Chiu, E., Ford, L. and Wolmark, N., 1998, Tamoxifen for prevention of breast cancer: report of the National Surgical Adjuvant Breast and Bowl Project-1 Study. *Journal of the National Cancer Institute*, **90**, 1371–1388.

Franklin, M. R., 1977, Inhibition of mixed-function oxidations by substrates forming reduced cytochrome P-450 metabolic-intermediate complexes. *Pharmacological Therapeutics*, **2**, 227–245.

Furr, B. J. A and Jordan, V. C., 1984, The pharmacology and clinical uses of tamoxifen. *Pharmacological Therapeutics*, **25**, 127–205.

Gibbs, M. A., Thummel, K. E., Shen, D. and Kunze, K. L., 1999, Inhibition of cytochrome P-450 3A (CYP3A) in human intestinal and liver microsomes: Comparison of K_i values and impact of CYP3A5 expression. *Drug Metabolism and Disposition*, **27**, 180–187.

Gorski, J. C., Hall, S. D., Jones, D. R., VandenBranden, M. and Wrighton, S. A., 1994, Regioselective biotransformation of midazolam by members of the human cytochrome P450 3A (CYP3A) subfamily. *Biochemical Pharmacology*, **47**, 1643–1653.

Guengerich, F. P., 1986, Covalent binding to apoprotein is a major fate of heme in a variety of reactions in which cytochrome P-450 is destroyed. *Biochemistry and Biophysical Research Communications*, **138**, 193–198.

Guengerich, F. P., Martin, M. V., Beaune, P. H., Kremers, P., Wol, T. and Waxman, D. J., 1986, Characterization of rat and human liver microsomal cytochrome P-450 forms involved in nifedipine oxidation, a prototype for genetic polymorphism in oxidative drug metabolism. *Journal of Biological Chemistry*, **261**, 5051–5060.

Jacolot, F., Simon, I., Dreano, Y., Beaune, P., Riche, C. and Berthou, F., 1991, Identification of the cytochrome P450 IIIA family as the enzymes involved in the *N*-demethylation of tamoxifen in human liver microsomes. *Biochemical Pharmacology*, **41**, 1911–1919.

Jones, D. R., Gorski, J. C., Hamman, M. A., Mayhew, B. S., Rider, S. and Hall, S. D., 1999, Diltiazem inhibition of CYP3A activity is due to metabolite intermediate complex formation. *Journal of Pharmacology and Experimental Therapeutics*, **290**, 1116–1125.

Kenworthy, K. E., Bloomer, J. C., Clarke, S. E. and Houston, J. B., 1999, CYP3A4 drug interactions: correlation of 10 *in vitro* probe substrates. *British Journal of Clinical Pharmacology*, **48**, 716–727.

King, C. M., 1995, Tamoxifen and the induction of cancer. *Carcinogenesis*, **16**, 1449–1454.

Kivistö, K. T., Kroemer, H. K. and Eichelbaum, M., 1995, The role of human cytochrome P450 enzymes in the metabolism of anticancer agents: implications for drug interactions. *British Journal of Clinical Pharmacology*, **40**, 523–530.

Kolars, J. C., Schmiedlin-Ren, P., Schuetz, J. D., Fang, C. and Watkins, P. B., 1992, Identification of rifampin-inducible P450IIIA4 (CYP3A4) in human small bowel enterocytes. *Journal of Clinical Investigation*, **90**, 1871–1878.

Koudriakova, T., Iatsimirskaia, E., Utkin, I., Gangl, E., Vouros, P., Elena, S., Orza, D., Marinna, J. and Gerber, N., 1998, Metabolism of the human immunodeficiency virus protease inhibitors indinavir and ritonavir by human intestinal microsomes and expressed cytochrome P4503A4/3A5: mechanism-based inactivation of cytochrome P4503A by ritonavir. *Drug Metabolism and Disposition*, **26**, 552–561.

Kuehl, P., Zhang, J., Lin, Y., Lamba, J., Assem, M., Schuetz, J., Watkins, P. B. Daly, A., Wrighton, S. A., Hall S. D., Maurel, P., Relling, M., Brimer, C., Yasuda, K., Venkataramanan, R., Strom, S., Thummel, K., Boguski, M. S. and Schuetz, E., 2001, Sequence diversity in CYP3A promoters and characterization of the genetic basis of polymorphic CYP3A5 expression. *Nature Genetics*, **27**, 383–391.

Lim, C. K., Yuan, Z.H., Lamb, J. H., White, I. N. H., de Matteis, F. and Smith, L. L., 1994, A comparative study of tamoxifen metabolism in female rat, mouse and human liver microsomes. *Carcinogenesis (Oxf)*, **15**, 589–593.

Lowry, O. H., Rosebrough, N. J., Farr, A. L. and Randall, R. J., 1951, Protein measurement with the Folin phenol reagent. *Journal of Biological Chemistry*, **193**, 265–275.

Mani, C., Gelboin, H. V., Park, S. S., Pearce, R., Parkinson, A. and Kupfer, D. 1993a, Metabolism of the antimammary cancer antiestrogenic agent tamoxifen: I. Cytochrome P-450-catalyzed *N*-demethylation and 4-hydroxylation. *Drug Metabolism and Disposition*, **21**, 645–656.

Mani, C., Hodgson, E. and Kupfer, D., 1993b, Metabolism of the antimammary cancer antiestrogenic agent tamoxifen: II. Flavin-containing monooxygenase-mediated *N*-oxidation. *Drug Metabolism and Disposition*, **21**, 657–661.

Mayhew, B. S., Jones, D. R. and Hall, S. D., 2000, An *in vitro* model for predicting *in vivo* inhibition of cytochrome P450 3A4 by metabolic intermediate complex formation. *Drug Metabolism and Disposition*, **28,** 1031–1037.

Millward, M. J., Cantwell, B. M. J., Lien, E. A., Carmichael, J. and Harris, A. L., 1992, Intermittent high-dose tamoxifen as a potential modifier of multidrug resistance. *European Journal of Cancer*, **28A**, 805–810.

Omura, T. and Sato, R., 1964, The carbon monoxide-binding pigment of liver microsomes. I. Evidence for its hemoprotein nature. *Journal of Biological Chemistry*, **239**, 2379–2385.

Peyrade, F., Frenay, M., Etienne, M.-C, Ruch, F., Guillemare, C., Francois, E., Namer, M., Ferrero, J.-M. and Milano, G., 1996, Age-related difference in tamoxifen disposition. *Clinical Pharmacology and Therapeutics*, **59**, 401–410.

Poon, G. K., Chui, Y. C., McCague, R., Lonning, P. E., Feng, R., Rowlands, M. G. and Jarman, M., 1993, Analysis of phase I and phase II metabolites of tamoxifen in breast cancer patients. *Drug Metabolism and Disposition*, **21**, 1119–1124.

Reunitz, P. C., Bagley, J. R. and Pape, C. W., 1984, Some chemical and biochemical aspects of liver microsomal metabolism of tamoxifen. *Drug Metabolism and Disposition*, **12**, 478–483.

Schaefer, W. H., Harris, T. M. and Guengerich, F. P., 1985, Characterization of the enzymatic and nonenzymatic peroxidative degradation of iron porphyrins and cytochrome P450 heme. *Biochemistry*, **24**, 3254–3263.

Segel, I. H., 1975, *Enzyme Kinetics: Behavior and Analysis of Rapid Equilibrium and Steady-State Enzyme Systems* (New York: Wiley).

Shimada, T., Yamazaki, H., Mimura, M., Inui, Y. and Guengrich, F. P., 1994, Interindividual variations in human liver cytochrome P-450 enzymes involved in the oxidation of drugs, carcinogens and toxic chemicals: studies with liver microsomes of 30 Japanese and 30 Caucasians. *Journal of Pharmacology and Experimental Therapeutics*, **270**, 414–423.

Silverman, R. B., 1988, *Mechanism-based Enzyme Inactivation: Chemistry and Enzymology* (Boca Raton: CRC Press), vol. 1, pp. 3–30.

Sridor, C., Kent, U. M. and Hollenberg, P. F., 1999, Effect of tamoxifen on the enzymatic activity of human cytochrome P450 2B6. *ISSX Proceedings*, **15**, 99.

Sutton, D., Butler, A. M., Nadlin, L. and Murray, M., 1997, Role of CYP3A4 in human hepatic diltiazem *N*-demethylation: inhibition of CYP3A4 activity by oxidized diltiazem metabolites. *Journal of Pharmacology and Experimental Therapeutics*, **282**, 294–300.

Watkins, P. B., Wrighton, S. A., Schuetz, E. G., Molowa, D. T. and Guzelian, P. S., 1987, Identification of glucocorticoid-inducible cytochromes P-450 in the intestinal mucosa of rats and man. *Journal of Clinical Investigation*, **80**, 1029–1036.

Wirz, B., Valles, B., Parkinson, A., Madan, A., Probst, A., Zimmerlin, A. and Gut, J., 1996, CYP3A4 and CYP2A6 are involved in the biotransformation of letrozole (FEMARA®). *ISSX Proceedings*, **10**, 359.

XENOBIOTICA, 2002, VOL. 32, NO. 10, 879–893

Taylor & Francis
healthsciences

Pharmacokinetic evaluation of high pulmonary disposition of clarithromycin after systemic administration

J.-I. KUBO†, Y. OHIGASHI†, M. HAMABE†, K.-I. OGAWARA†, K. HIGAKI†, H. SAITO‡ and T. KIMURA†*

†Department of Pharmaceutics, Faculty of Pharmaceutical Sciences, Okayama University, Okayama 700-8530, Japan.
‡ Research Center, Taisho Pharmaceutical Co., Ltd, 1-403 Yoshino-cho, Saitama 330-8530, Japan.

Received 7 February 2002

1. The distribution characteristics of clarithromycin to the lung were investigated *in vivo* and in isolated lung perfusion experiments. The in-vivo integration plot analysis showed that the pulmonary uptake and extracellular distribution in the lung were significantly higher for clarithromycin than for erythromycin.

2. In the rat lung single-pass perfusion study, the pulmonary extraction ratio (E_{ss}) of clarithromycin at steady-state was significantly higher than that of erythromycin, and the E_{ss} of clarithromycin tended to decrease as the inflow concentration increased, suggesting the involvement of carrier-mediated transport in the pulmonary disposition of clarithromycin.

3. The outflow patterns of clarithromycin or erythromycin at various inflow concentrations were simultaneously analysed based on a pharmacokinetic model, which consists of the non-specific binding site, the specific binding site and the subsequent uptake process. The parameters obtained suggested that clarithromycin would have the higher affinity and higher capacity for the specific binding site, and the higher equilibrium constant for the non-specific binding site than erythromycin.

4. The simulation study using those parameters demonstrated that clarithromycin could be bound to the specific binding site and subsequently taken up more extensively than erythromycin.

5. A multiple-indicator dilution study also indicated that clarithromycin was more readily associated and extracted with the lung than with erythromycin. In the inhibition study, it was suggested that the pulmonary uptake of clarithromycin could be ascribed not only to the non-specific binding depending on its lipophilic nature, but also in part to some specialized mechanisms such as organic cation transporters.

Introduction

Clarithromycin is widely used in the treatment of Gram-positive infection because of its wide spectrum of antimicrobial activity. Clarithromycin is a 14-membered macrolide antibiotic (figure 1) and was synthesized by the methylation of the hydroxy group of erythromycin at the C6 position of the lactone ring to improve the stability of erythromycin. Erythromycin is well known to be rapidly inactivated by gastric acid and its absorption is reduced when the drug is given with meals (Posti and Salonen 1983).

Both clarithromycin and erythromycin are cationic antibiotics and Kohno *et al.* (1989) reported that the accumulation of clarithromycin in several tissues was

* Author for correspondence; e-mail: kimura@pheasant.pharm.okayama-u.ac.jp

Xenobiotica ISSN 0049–8254 print/ISSN 1366–5928 online © 2002 Taylor & Francis Ltd
http://www.tandf.co.uk/journals
DOI: 10.1080/00498250210160741

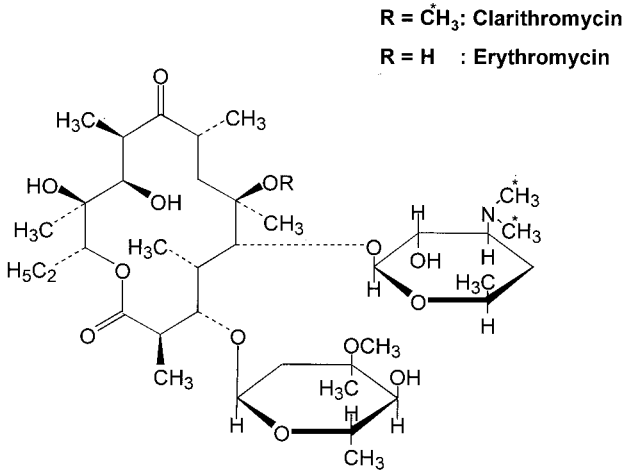


Figure 1. Chemical structures of clarithromycin and erythromycin. *Position of ^{14}C.

more than that of erythromycin after oral administration. The distribution to the lung was particularly high. Generally, the tissue distribution of drugs is considered to be determined by physicochemical properties of the drugs and physiological conditions of the experimental animals (Terasaki *et al.* 1984). Many studies have been performed on the pulmonary distribution of cationic drugs such as imipramine (Eling *et al.* 1975), lidocaine (Post *et al.* 1978), propranolol (Dollery and Junod 1976) and chlorpromazine (Hackman *et al.* 1970). Okumura *et al.* (1978, 1989) and Yoshida *et al.* (1987, 1989) reported that specific common binding sites for cationic drugs exist in lung tissue, and that the affinity for these sites was dependent on the lipid solubility of the cationic drugs. However, the mechanisms behind the high pulmonary distribution of clarithromycin still remain to be clarified.

Because clarithromycin is expected to be used to treat pulmonary infections, it is important to clarify its distribution mechanisms to the lung. We tried, therefore, to estimate quantitatively the pulmonary distribution characteristics of clarithromycin after intravenous administration and also examined the mechanism involved in its pulmonary uptake by using the isolated lung perfusion technique in rat.

Materials and methods

Materials

Clarithromycin, [^{14}C]clarithromycin (1.83 GBq mmol^{-1}) and erythromycin were supplied from Taisho Pharmaceuticals Co., Ltd (Saitama, Japan). Chemical purities of clarithromycin and erythromycin were 98%. [^{14}C]erythromycin (2.04 GBq mmol^{-1}) and [^{3}H]inulin (5.5 MBq mg^{-1}) were purchased from American Radiolabeled Chemicals, Inc. (St Louis, MO, USA). Radiochemical purities of [^{14}C]clarithromycin and [^{14}C]erythromycin were >97 and 99%, respectively. All other reagents were of the highest grade available. [^{14}C]clarithromycin and [^{14}C]erythromycin were used throughout the study by changing their final specific activities with each unlabeled compound to 26.5 and 29.6 MBq mmol^{-1}, respectively.

Animals

Male Wistar rats (Japan SLC, Hamamatsu, Japan), maintained at 25°C and 55% humidity, were allowed free access to standard laboratory chow (Clea Japan, Tokyo, Japan) and water before the experiments. Rats weighing 240–270 g were randomly assigned to each experimental group. Investiga-

tions were performed after approval by our local Ethical Committee at Okayama University and in accordance with *Interdisciplinary Principles and Guidelines of the Use of Animals in Research*.

Determination of unidirectional uptake clearance to organs

The unidirectional uptake clearance from the plasma to the tissue was estimated according to the method reported by Yamazaki *et al*. (1993) with minor modification. After bolus intravenous injection of clarithromycin or erythromycin at 1 mg kg^{-1}, blood and several tissues including lung were taken at 0.25, 0.5, 0.75, 1 and 2 min after dosing. The dose, 1 mg kg^{-1}, was chosen because our preliminary study indicated that the pharmacokinetics of both antibiotics should be linear at <5 mg kg^{-1}. After determination of total radioactivity in the plasma and tissues, an 'integration plot' was made as follows. As it can be assumed that the efflux of clarithromycin or erythromycin from the tissue to the plasma is negligible within short periods after intravenous administration when the integration plot gives a straight line, the uptake rate of clarithromycin or erythromycin in the tissue is given by:

$$\frac{dX_{t,i}}{dt} = CL_{uptake,i} \cdot C_p(t), \tag{1}$$

where $X_{t,i}$, $CL_{uptake,i}$ and $C_p(t)$ are the amount of drug in the tissue i at time t, the uptake clearance of drug from the plasma to the tissue i and the plasma concentration of the drug at time t, respectively. Integration of equation (1) from 0 to time t gives $X_{t,i}$ by equation (2):

$$X_{t,i} = CL_{uptake,i} \cdot AUC_{0-t} + V_{ex,i} \cdot C_p(0), \tag{2}$$

where AUC_{0-t} and $V_{ex,i}$ are the area under the plasma concentration–time curve from 0 to time t and the apparent extracellular volume of distribution in the tissue i, respectively. Equation (3) is obtained by dividing equation (2) by $C_p(t)$:

$$\frac{X_{t,i}}{C_p(t)} = CL_{uptake,i} \cdot \frac{AUC_{0-t}}{C_p(t)} + V_{ex,i} \cdot \frac{C_p(0)}{C_p(t)}. \tag{3}$$

$CL_{uptake,i}$ was estimated from the initial slope. The y intercept of the integration plot corresponds to $V_{ex,i}$, because equation (3) can be simplified as $X_{t,i}/C_p(t) = V_{ex,i}$ when time is zero.

Lung perfusion experiment

Rats were anaesthetized with an intraperitoneal injection of sodium pentobarbital (50 mg kg^{-1}) and the abdomen and chest opened after an intravenous injection of heparin (500 unit kg^{-1}). The main pulmonary artery and the left ventricle were cannulated, and Krebs–Ringer bicarbonate buffer (pH 7.4) freshly prepared was immediately perfused just after the exsanguination by cutting the aorta. Krebs–Ringer bicarbonate buffer was supplemented with 10 mM glucose and was oxygenated with 95% O_2:5% CO_2 before use. The lung was perfused at a constant flow rate of 8 ml min^{-1} using a peristaltic pump. An initial stabilization period of 5 min was allowed before introducing compounds into the pulmonary artery. Total radioactivity was determined for both clarithromycin and erythromycin because it has been previously reported that $>90\%$ of both drugs were found as unchanged in both the lung cell and the medium in an *in-vitro* study after a 5-min incubation (Kohno *et al*. 1988, 1990).

Single-pass perfusion study. Clarithromycin or erythromycin dissolved in the perfusate were continuously infused for 5 min at 0.294, 2.94 and 29.4 or 0.0294 and 0.294 μg ml^{-1}, respectively. From the venous outflow patterns obtained, the extraction ratio (E_{ss}) and the pulmonary clearance (CL_{lung}) at steady-state for clarithromycin or erythromycin were calculated using:

$$E_{ss} = \frac{C_{in} - C_{out}}{C_{in}} \tag{4}$$

$$CL_{lung} = Q \cdot E_{ss}, \tag{5}$$

where C_{in} and C_{out} are the drug concentrations in the inflow and outflow perfusates under the steady-state condition, respectively, and Q is the perfusion rate (8 ml min^{-1}).

Multiple-indicator dilution study. The perfused rat lung was prepared by the same procedure described above. Clarithromycin or erythromycin was injected at a dose of 294 ng with inulin (50 μg) as a vascular reference. The venous outflow was collected every second for 30 s. According to our preliminary study, the dose gives the maximum concentration of non-extractable compounds around 0.3 ng ml^{-1} in the outflow perfusate. The obtained dilution curve was analysed based on the statistical moment theory (Nishida *et al*. 1989, Higaki *et al*. 1998) and the extraction ratio (E), mean transit time (MTT) and distribution volume (V_d) were calculated according to the following equations:

$$E = 1 - \int_0^\infty F(t)_{\text{test}}\,\mathrm{d}t \Big/ \int_0^\infty F(t)_{\text{ref}}\,\mathrm{d}t \tag{6}$$

$$\text{MTT} = \int_0^\infty t \cdot F(t)_{\text{test}}\,\mathrm{d}t \Big/ \int_0^\infty F(t)_{\text{test}}\,\mathrm{d}t \tag{7}$$

$$V_{\text{d}} = Q \cdot \text{MTT}/(1 - E), \tag{8}$$

where $F(t)$ is the fraction of dose for each venous outflow sample. The subscript 'test' or 'ref' means test compounds (clarithromycin, erythromycin) or inulin, respectively.

Pharmacokinetic analysis using a one-organ pharmacokinetic model

The outflow patterns obtained in the single-pass perfusion study were analysed by a one-organ pharmacokinetic model reported by Ogawara *et al.* (1998) with some modification (figure 2). The model consists of a vascular compartment and a binding one. The vascular compartment is assumed to be under the well-stirred condition such that the drug concentration in the vascular compartment is equal to the concentration in the outflow (C_{out}). The volume of the vascular compartment (V) is assumed to be the distribution volume for inulin, a vascular reference, which was calculated as 0.654 ml/lung from the multiple-indicator dilution study. The binding compartment was divided into two independent subcompartments, i.e. a specific binding compartment and a non-specific binding one. The specific binding compartment is characterized by a maximum binding amount (X_∞) and a binding constant (K_{sp}), and subsequent uptake into the intracellular space is assumed to occur. Drugs bound to the non-specific binding compartment are assumed not to contribute to their uptake into the intracellular space because the analysis with the model including the uptake process following the non-specific binding did not converge. The rapid equilibration is assumed to be between the vascular and the binding compartments.

Assuming that the uptake process follows first-order kinetics, the uptake rate ($\mathrm{d}X_{\text{sp}}/\mathrm{d}t$) is expressed as a product of a specific binding amount (X_{sp}) and its rate constant (k_{uptake}). Then, in the vascular and the binding compartments, a mass-balance equation is defined as follows:

$$V \cdot \frac{\mathrm{d}C_{\text{out}}}{\mathrm{d}t} + \frac{\mathrm{d}X_{\text{non}}}{\mathrm{d}t} + \frac{\mathrm{d}X_{\text{sp}}}{\mathrm{d}t} = Q \cdot C_{\text{in}} - Q \cdot C_{\text{out}} - k_{\text{uptake}} \cdot X_{\text{sp}}, \tag{9}$$

where X_{non} is the drug amount bound to the non-specific site. The specific binding of clarithromycin or erythromycin is defined as Langmuir-type binding. The non-specific binding amount (X_{non}) is assumed to be proportional to the drug concentration in the vascular compartment as described by equation (10):

$$X = X_{\text{sp}} + X_{\text{non}} = \frac{X_\infty \cdot K_{\text{sp}} \cdot C_{\text{out}}}{1 + K_{\text{sp}} \cdot C_{\text{out}}} + K_{\text{non}} \cdot C_{\text{out}}, \tag{10}$$

where X and K_{non} are the total binding amount and equilibrium constant for the non-specific binding, respectively.

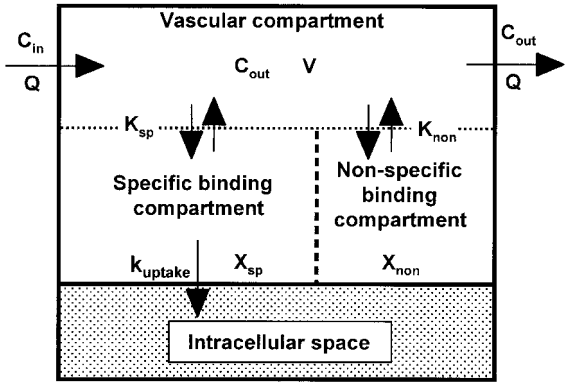


Figure 2. Physiological pharmacokinetic model for analysing the pulmonary uptake of clarithromycin and erythromycin. Q, perfusion rate ($\text{ml}\,\text{min}^{-1}$); C_{in}, inflow concentration ($\mu\text{g}\,\text{ml}^{1}$); C_{out}, concentration in venous outflow ($\mu\text{g}\,\text{ml}^{1}$); V, vascular compartment volume (ml); X_{sp}, specific binding amount (μg/lung); X_{non}, non-specific binding amount (μg/lung); X_∞, maximum binding amount (μg/lung); K_{sp}, binding constant for specific binding site ($\text{ml}\,\mu\text{g}^{1}$); K_{non}, equilibrium constant for non-specific binding site (ml); k_{uptake}, uptake rate constant (min^{-1}).

Differentiation of equation (10) with respect to t gives equation (11).

$$\frac{dX}{dt} = \left\{ \frac{X_\infty \cdot K_{sp}}{(1 + K_{sp} \cdot C_{out})^2} + K_{non} \right\} \cdot \frac{dC_{out}}{dt}. \quad (11)$$

Substituting in equation (9) for $dX_{non}/dt + dX_{sp}/dt$ by dX/dt from equation (11), and for X_{sp} by expression in equation (10) gives:

$$\left\{ V + K_{non} + \frac{X_\infty \cdot K_{sp}}{(1 + K_{sp} \cdot C_{out})^2} \right\} \cdot \frac{dC_{out}}{dt} = Q \cdot C_{in} - Q \cdot C_{out} - \frac{k_{uptake} \cdot X_\infty \cdot K_{sp} \cdot C_{out}}{1 + K_{sp} \cdot C_{out}}. \quad (12)$$

The differential equations derived from equation (12) for various inflow concentrations were numerically solved using the Runge–Kutta–Gill method. The initial condition is $C_{out} = 0$ when $t = 0$. Fitting of the equations to the outflow curves obtained in the single-pass perfusion studies with various inflow concentrations was simultaneously conducted using the MULTI (RUNGE) program (Yamaoka and Nakagawa 1983).

Inhibition studies

Inhibition studies were performed using the multiple-indicator dilution method in the isolated lung preparation. Each inhibitor (1 mM) dissolved in the perfusate was constantly infused into the lung throughout the experiments. Ice-cold buffer was also used to decrease the temperature of the isolated lung preparation. Clarithromycin or erythromycin was injected at 294 ng and inulin at 50 μg.

Analytical methods

The total radioactivity in the plasma in the *in-vivo* study and the collected outflow perfusate samples in the lung perfusion studies was measured using a liquid scintillation counter (TRI-CARB 2260XL, Packard, CT, USA) after the addition of scintillation medium (Clear-sol I, Nacalai Tesque, Tokyo, Japan). As for the radioactivity in the tissue samples, tissues (about 50 mg aliquot) were solubilized with 700 μl Soluene-350 (Packard Instruments Co., Downers Grove, IL, USA) overnight. The mixture was neutralized with 180 μl HCl and was, if necessary, decolourized with 150 μl 30% H_2O_2. Total radioactivity was then measured after adding Clear-sol I in the same manner as for plasma samples.

Statistical analysis

Results are the mean ± SD of three or four experiments. Statistical significance was evaluated with a Student's t-test or Dunnet test for single or multiple comparison of the results, respectively.

Results

The tissue distribution kinetics of clarithromycin and erythromycin was examined after intravenous administration to rat. CL_{uptake} and V_{ex} for each tissue were estimated by the integration plot (figure 3) and the results are summarized in table 1. The CL_{uptake} of clarithromycin was significantly larger than that of erythromycin for every tissue. Particularly, the uptake of clarithromycin by the lung ($CL_{uptake,lung}$; 2.35 ± 0.36 ml min^{-1} g^{-1} tissue) was about 10 times larger than that of erythromycin (0.233 ± 0.037 ml min^{-1} g^{-1} tissue). Furthermore, clarithromycin also distributed rapidly to the kidney. The V_{ex} of clarithromycin for the lung (2.96 ± 0.54 ml g^{-1} tissue) was much higher than those for other tissues or for erythromycin in all tissues examined (table 1). These results suggest that clarithromycin is rapidly distributed and reaches high levels in the lung.

To investigate the pulmonary distribution of clarithromycin and erythromycin in detail, the single-pass perfusion was performed with the rat isolated lung preparation (figure 4). The recovery ratio (C_{out}/C_{in}) of both compounds reached steady-state after 2 or 3 min after starting the perfusion, and the extraction ratio (E_{ss}) and pulmonary clearance (CL_{lung}) at steady-state are summarized in table 2. At the inflow concentration of 0.294 μg ml^{-1}, clarithromycin was extracted ($E_{ss} = 0.55$) much more than erythromycin ($E_{ss} = 0.13$) by the lung at steady-state. For clarithromycin, the CL_{lung} tended to decrease as the inflow concentration

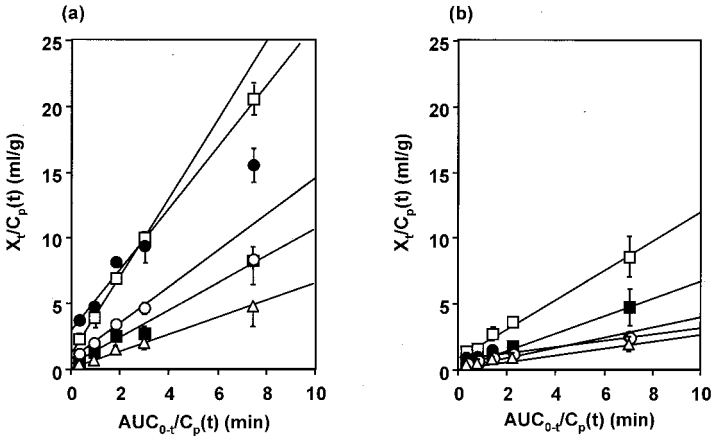


Figure 3. Integration plots for the tissue distribution of clarithromycin (a) and erythromycin (b). Lung (●), liver (■), kidney (□), spleen (△), heart (○). Each symbol and vertical bar represents the mean and SD of at least three experiments, respectively.

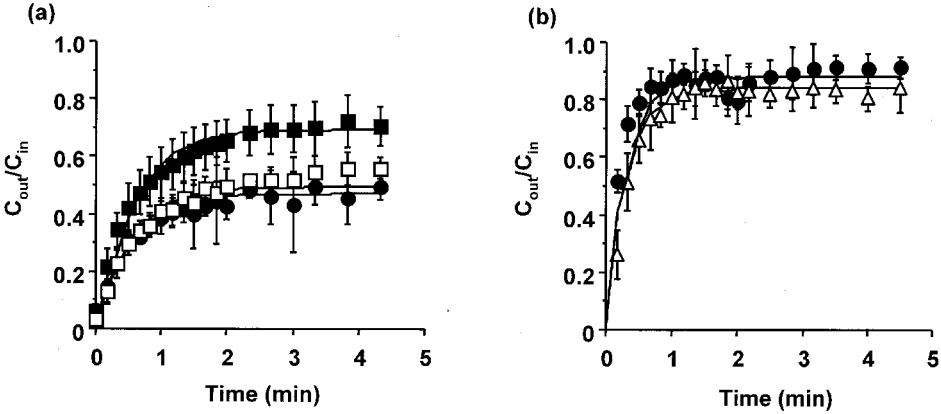


Figure 4. Recovery ratio (C_{out}/C_{in}) versus time profiles of clarithromycin (a) and erythromycin (b) at various inflow concentrations in the single-pass lung perfusion experiments. Solid lines were obtained by the fitting study as described in the Materials and methods. Each line was significantly correlated with its corresponding observed data ($p < 0.001$). Inflow concentrations: 0.0294 μg ml^{-1} (△), 0.294 μg ml^{-1} (●), 2.94 μg ml^{-1} (□) and 29.4 μg ml^{-1} (■). Results are the mean ± SD of at least three experiments.

increased to $> 2.94\,\mu g\,ml^{-1}$. On the other hand, there was no statistically significant difference in CL_{lung} between 0.0294 and $0.294\,\mu g\,ml^{-1}$ for erythromycin.

The integration plots show that the pulmonary distribution of both compounds could be via two different processes, the very rapid distribution reflected by $V_{ex,lung}$ and the uptake process by $CL_{uptake,lung}$. Therefore, the recovery ratio–time profiles were analysed based on the one-organ physiological model (figure 2), which is composed of the binding processes and the subsequent uptake process. The solid lines in figure 4 were drawn by simultaneous fitting to three or two different time-courses for clarithromycin or erythromycin, respectively. The pharmacokinetic parameters obtained are summarized in table 3. The specific binding constant (K_{sp}) for clarithromycin was about twice that for erythromycin and the difference was statistically significant ($p < 0.05$). The maximum binding

Table 1. Uptake clearance and extracellular distribution volume (± SD) of clarithromycin and erythromycin for five organs after intravenous administration.

		Lung	Liver	Kidney	Spleen	Heart
Clarithromycin	CL_{uptake} (ml min^{-1} g^{-1} tissue)	$2.35 \pm 0.36^{**}$	$1.03 \pm 0.01^{**,\dagger\dagger}$	$2.96 \pm 0.09^{***,\dagger}$	$0.635 \pm 0.040^{***,\dagger\dagger}$	$1.38 \pm 0.095^{***,\dagger}$
	V_{ex} (ml g^{-1} tissue)	$2.96 \pm 0.54^{**}$	$0.277 \pm 0.190^{n.s.,\dagger\dagger}$	$1.36 \pm 0.12^{*,\dagger\dagger}$	$0.180 \pm 0.076^{*,\dagger\dagger\dagger}$	$0.758 \pm 0.128^{*,\dagger\dagger}$
Erythromycin	CL_{uptake} (ml min^{-1} g^{-1} tissue)	0.233 ± 0.037	$0.649 \pm 0.025^{\dagger\dagger\dagger}$	$1.10 \pm 0.06^{\dagger\dagger\dagger}$	$0.245 \pm 0.030^{n.s.}$	$0.363 \pm 0.015^{\dagger}$
	V_{ex} (ml g^{-1} tissue)	0.963 ± 0.095	$0.299 \pm 0.044^{\dagger\dagger\dagger}$	$1.03 \pm 0.12^{n.s.}$	$0.355 \pm 0.063^{\dagger\dagger\dagger}$	$0.436 \pm 0.018^{\dagger\dagger}$

Uptake clearances (CL_{uptake}) and extracellular distribution volume (V_{ex}) were obtained by the integration plot analysis as described in the Materials and methods. $^{*}p < 0.05$, $^{**}p < 0.01$, $^{***}p < 0.001$ compared with erythromycin. $^{\dagger}p < 0.05$, $^{\dagger\dagger}p < 0.01$, $^{\dagger\dagger\dagger}p < 0.001$ compared with each value obtained for the lung.

Table 2. Pulmonary extraction of clarithromycin and erythromycin in the lung single-pass perfusion experiment.

Inflow concentration ($\mu g\,ml^{-1}$)	Clarithromycin		Erythromycin	
	E_{ss}	CL_{lung} ($ml\,min^{-1}$)	E_{ss}	CL_{lung} ($ml\,min^{-1}$)
0.0294	n.e.	n.e.	0.17 ± 0.01	1.3 ± 0.1
0.294	$0.55 \pm 0.05^{\dagger\dagger}$	$4.4 \pm 0.4^{\dagger\dagger}$	$0.13 \pm 0.07^{n.s.}$	$1.0 \pm 0.6^{n.s.}$
2.94	$0.49 \pm 0.05^{n.s.}$	$3.9 \pm 0.4^{n.s.}$	n.e.	n.e.
29.4	$0.32 \pm 0.08^{**}$	$2.6 \pm 0.6^{*}$	n.e.	n.e.

Results are the mean $\pm$SD of at least three experiments. E_{ss} and CL_{lung} are the pulmonary extraction ratio and the pulmonary clearance at steady-state, respectively. n.e., Not examined.

†† $p < 0.01$ compared with the parameters obtained for erythromycin. n.s., Not significant; * $p < 0.05$, ** $p < 0.001$ compared with the results obtained at the lowest inflow concentration.

Table 3. Pharmacokinetic parameters ($\pm$SD) for pulmonary uptake of clarithromycin and erythromycin based on a one-organ pharmacokinetic model.

	Clarithromycin	Erythromycin
K_{sp} ($ml\,\mu g^{-1}$)	$0.077 \pm 0.014^{*}$	0.039 ± 0.016
X_{∞} (μg)	$62.4 \pm 30.0^{n.s.}$	20.4 ± 8.1
K_{uptake} (min^{-1})	$1.90 \pm 0.70^{n.s.}$	1.64 ± 0.96
K_{non} (ml)	$3.51 \pm 1.28^{*}$	1.44 ± 0.92

Binding constant (K_{sp}) and maximum binding amount (X_{∞}) for the specific binding site, the uptake rate constant (K_{uptake}) and the equilibrium constant (K_{non}) for the non-specific binding site were obtained by fitting the differential equations based on a one-organ pharmacokinetic model.

n.s., Not significant; * $p < 0.05$ compared with parameters obtained for erythromycin.

amount (X_{∞}) for clarithromycin also tended to be larger than that for erythromycin on average, although it was not statistically significant. The uptake rate constant (k_{uptake}) was almost the same for clarithromycin and erythromycin, and the equilibrium constant for the non-specific binding (K_{non}) for clarithromycin was significantly larger than that for erythromycin ($p < 0.05$).

By using the pharmacokinetic parameters obtained above, the total binding amount (X), the specific binding amount (X_{sp}), and the uptake amount of clarithromycin and erythromycin by the lung were simulated (figure 5). The simulation curves clearly reveal that clarithromycin could be bound to the specific site and be subsequently taken up by the lung more extensively than erythromycin.

To examine the distribution kinetics in more detail, the multiple-indicator dilution study was performed by using the isolated lung preparation. Figure 6 shows typical outflow patterns of clarithromycin and erythromycin after a bolus injection with inulin. The injected inulin was almost completely recovered into the venous outflow. The obtained dilution curves of clarithromycin and erythromycin were assessed by moment analysis, and the moment parameters calculated are summarized in table 4. The V_d of both compounds were significantly larger than that of inulin, meaning that the two compounds distribute to the extravascular space including the endothelium of blood vessels in the lung. Furthermore, V_d of clarithromycin was significantly larger than that of erythromycin, suggesting the higher affinity of clarithromycin to the extracellular space than erythromycin. A similar tendency was also obtained for the mean transit time. The larger mean

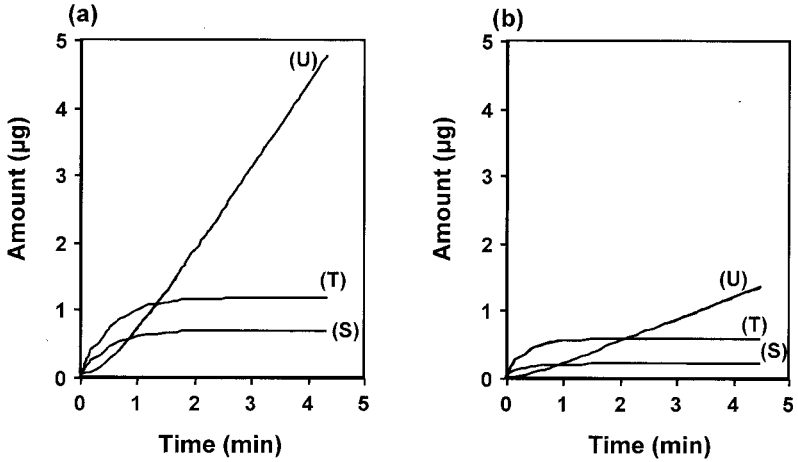


Figure 5. Simulation of the pulmonary disposition characteristics of clarithromycin (a) and erythromycin (b) based on a one-organ pharmacokinetic model. *U*, uptake amount; *T*, total binding amount; *S*, specific binding amount.

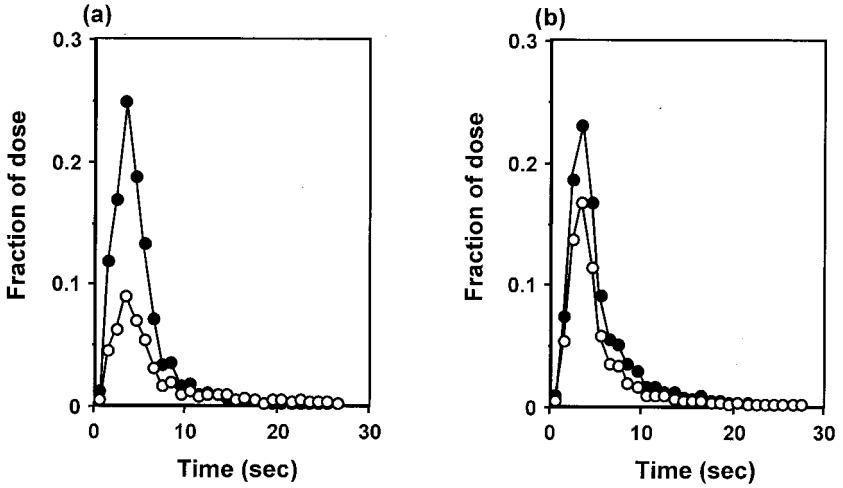


Figure 6. Typical outflow patterns of clarithromycin (a) and erythromycin (b) (○) after bolus injection with inulin (●) in the multiple-indicator dilution study with the isolated rat lung preparation. The dose of clarithromycin or erythromycin was 294 ng. Perfusate was delivered constantly at 8 ml min^{-1} and the outflow was collected every 1 s. Three experiments were performed at least for each compound and the dilution curve was analysed based on the statistical moment theory. The parameters obtained were summarized in table 4.

transit time for clarithromycin suggests that clarithromycin is more readily associated with the lung than erythromycin. The larger extraction ratio of clarithromycin than that of erythromycin coincides with the result from the single-pass perfusion study (figure 3 and table 2).

Because the *in-vivo* and the isolated lung perfusion studies suggested that specific binding and/or specialized mechanisms were possibly involved in the pulmonary disposition of both compounds, the effects of various experimental conditions on the pulmonary extraction (*E*) of clarithromycin or erythromycin were investigated using the isolated lung preparations by the multiple-indicator

Table 4. Moment parameters of clarithromycin and erythromycin in multiple-indicator dilution experiments.

	Clarithromycin	Erythromycin	Inulin
E	$0.592 \pm 0.022^{**}$	0.319 ± 0.009	–
MTT (s)	$6.87 \pm 0.28^{*,\dagger\dagger}$	$5.71 \pm 0.50^{n.s.}$	4.90 ± 0.31
V_d (ml)	$2.25 \pm 0.20^{**,\ \dagger\dagger}$	$1.12 \pm 0.10^{\dagger\dagger}$	0.654 ± 0.041

Results are the mean ± SD of at least three experiments. E, MTT and V_d stand for the pulmonary extraction ratio, the mean transit time and the volume of distribution, respectively.

$^{*}p < 0.05$, $^{**}p < 0.01$ compared with the parameters obtained for erythromycin. n.s., Not significant; $^{\dagger\dagger}p < 0.01$ compared with the parameters obtained for inulin.

dilution method (figure 7). Ice-cold buffer significantly reduced the E of both clarithromycin and erythromycin, while NaN_3 did not. In addition, the extraction of both compounds was significantly reduced by the presence of verapamil, quinine, quinidine or imipramine in the perfusate. Furthermore, procainamide and guanidine slightly, but significantly, reduced the E of clarithromycin. On the contrary, the pulmonary extraction of clarithromycin tended to be enhanced in the presence of N^1-methylnicotinamide or scopolamine methylbromide. These results suggest that specialized mechanisms are possibly involved in the uptake and/or efflux of clarithromycin in the lung.

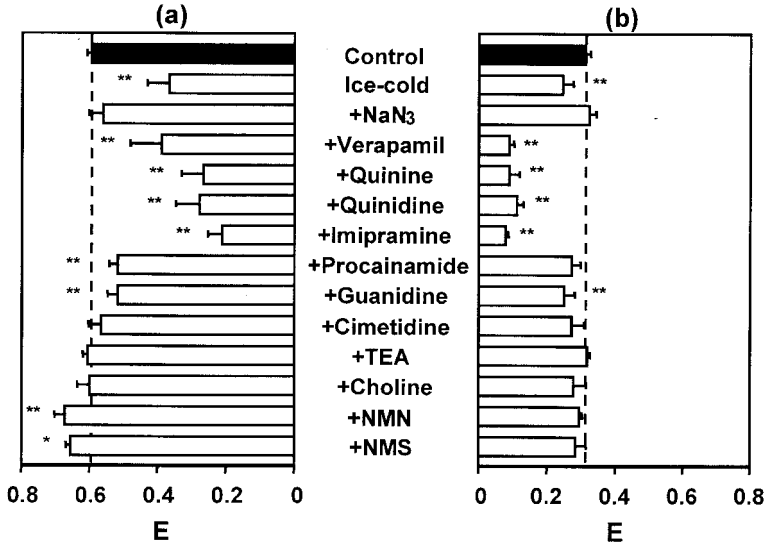


Figure 7. Effect of various experimental conditions on the pulmonary extraction (E) of clarithromycin (a) and erythromycin (b) in the multiple-indicator dilution study with the isolated rat lung preparation. TEA, NMN and NMS stand for tetraethylammonium, N^1-methylnicothinamide and scopolamine methylbromide, respectively. The dose of clarithromycin or erythromycin was 294 ng. The concentrations of inhibitors in the perfusate were 1 mM $^{*}p < 0.05$, $^{**}p < 0.01$ compared with control value. Results are the mean ± SD of at least three experiments.

Discussion

The main function of the lung is well known to be the exchange of O_2 and CO_2 between the alveolar gas and pulmonary capillary blood. The lung also plays other important roles such as metabolism (Said 1982, Bend *et al.* 1985) and accumulation of drugs in drug disposition (Hackman *et al.* 1970, Brown 1974). Some endogenous substances such as 5-hydroxytryptamine, norepinephrine, bradykinine and prostaglandins are rapidly removed from the circulation and subsequently inactivated by the lung (Said 1982, Bend *et al.* 1985). Several reports have also shown drug accumulation in the lung (Hackman *et al.* 1970, Brown 1974). Some exogenous amines such as imipramine (Eling *et al.* 1975) and chlorpromazine (Hackman *et al.* 1970) are known to be concentrated preferentially in the lung. However, the mechanisms of the selective pulmonary distribution of cationic compounds still remain unclear, although their interaction with acidic phospholipids has been suggested to be important (Nishiura *et al.* 1986, 1987).

In the present study, the CL_{uptake} of clarithromycin was significantly higher than that of erythromycin for every tissue examined, but particularly for the lung. The CL_{uptake} of clarithromycin to the lung was about 10 times larger than that of erythromycin by the integration plot analysis (figure 3 and table 1). In addition, the V_{ex} of clarithromycin for the lung ($2.96 \pm 0.54\,ml\,g^{-1}$ tissue) was much higher than those for other tissues or those obtained for erythromycin (table 1). Considering that the interstitial fluid volume of the lung is about 0.6 ml/lung in a rat weighing 240 g (Tsuji *et al.* 1983), the V_{ex} in the lung obtained for clarithromycin is quite large. These results suggest that efficient uptake and high-affinity binding onto the luminal surface of the vascular endothelium of the lung probably are involved in the high and rapid pulmonary disposition of clarithromycin.

The single-pass perfusion studies using the isolated lung preparation showed that the CL_{lung} of clarithromycin significantly decreased as the inflow concentration increased to $>2.94\,\mu g\,ml^{-1}$. This phenomenon is a typical one suggesting the possible involvement of some saturable processes or carrier-mediated transport systems in the pulmonary disposition of clarithromycin (table 2). The pulmonary extraction of clarithromycin was also significantly larger than that of erythromycin at the inflow concentration of $0.294\,\mu g\,ml^{-1}$ (figure 4 and table 2) as was observed in the multiple-indicator dilution study (table 4). In addition, the mean transit time and V_d for clarithromycin obtained by the moment analysis showed that clarithromycin was more readily associated with the lung than erythromycin (figure 6 and table 4). From these results, it is strongly suggested that clarithromycin should be distributed to the lung more efficiently via some carrier-mediated transport systems. Therefore, we tried pharmacokinetically to analyse the pulmonary uptake of clarithromycin by using the physiological pharmacokinetic model (figure 2). The model consists of the vascular and the binding compartments with the non-specific binding site and the specific one. The binding to the latter site is assumed to lead to the pulmonary uptake, but the binding to the former site does not, because our preliminary analysis with the model including the uptake process following the non-specific binding did not converge, suggesting its incorporation to the model should be inadequate in this case. The pharmacokinetic parameters obtained by analysing the venous outflow patterns indicate the higher binding property in both non-specific and specific binding sites for clarithromycin than erythromycin (table 3). Since there is no significant difference in k_{uptake} between the two compounds, the more efficient pulmonary uptake of

clarithromycin is possibly ascribed to the higher K_{sp} and X_{∞}. The specific binding of clarithromycin and erythromycin might reflect the binding to some membrane protein acting as a transporter. Our simulation study clearly demonstrated that clarithromycin could be taken up more efficiently following specific binding than erythromycin (figure 5).

As for the uptake mechanism by the lung, an ice-cold buffer significantly reduced the E for both clarithromycin and erythromycin, while NaN_3 did not (figure 7), suggesting that a facilitative transport system should be involved in the pulmonary uptake of clarithromycin and erythromycin. Furthermore, the pulmonary extraction for clarithromycin was profoundly reduced in the presence of verapamil, quinine, quinidine or imipramine, all of which are considerably lipophilic cations (figure 7). However, guanidine and procainamide, relatively hydrophilic cations, also inhibited their pulmonary extraction.

Many specific transport systems have been identified in mammalian cells and are responsible for the influx of organic cations into the cells as well as their efflux out of the cells (Ullrich 1994). Considering the substrate specificity and/or inhibitor specificity in this case, OCTN2, which is a member of a new subfamily of organic cation transporters, might be involved in the pulmonary uptake of these antibiotics. It has been reported that this organic cation transporter is expressed in the rat lung (Schomig *et al.* 1998) and that it can recognize both hydrophilic cations such as procainamide (Wu *et al.* 1998) and lipophilic ones such as verapamil (Dresser *et al.* 2001). OCTN1 might also be possible, but OCTN1 accepts only prototypical organic cations, small and hydrophilic ones (Dresser *et al.* 2001), and it functions as an antiporter with an H^+ gradient. Therefore, OCTN2 might be more likely because the transporter is reported to be Na^+- and H^+-independent (Dresser *et al.* 2001). The contribution of OCT3 can not be excluded because it has also been reported to be expressed in the lung as well as other tissues including the placenta, intestine, heart, brain and kidney in rat (Kekuda *et al.* 1998) and because it was also reported that OCT3 interacts with a variety of cationic xenobiotics such as 1-methyl-4-phenyl-pyridinium, clonidine, imipramine, desipramine, procainamide and guanidine (Wu *et al.* 2000). In the present study, the disposition of clarithromycin to the lung was also significantly inhibited with the presence of imipramine, procainamide and guanidine in the perfusate. Although tetraethylammonium did not inhibit the pulmonary extraction of the two antibiotics in the present study, the concentration of tetraethylammonium, 1 mM, might be not high enough to interact with the organic cation transporter. In any case, more detailed studies should be needed to clarify the actual mechanisms.

As for the pulmonary distribution of cationic drugs, it has been reported that quinidine and several drugs readily bind to tissues such as the lung, in which phosphatidylserine is abundant as a lipid component in the plasma membranes (Nishiura *et al.* 1986, 1987, Yata *et al.* 1990). The association with phosphatidylserine, therefore, has been considered as a factor for the pulmonary accumulation of cationic drugs. The non-specific pulmonary binding of the two antibiotics is possibly ascribed to their interaction with phosphatidylserine, and clarithromycin, a more lipophilic cation compared with erythromycin (Nakagawa *et al.* 1992), may have a higher affinity for phosphatidylserine as shown by the K_{non} (table 3). On the other hand, clarithromycin has been reported to inhibit the efflux of digoxin via P-glycoprotein in LLC-PK_1 cells (Wakasugi *et al.* 1998), and it was also reported

that P-glycoprotein could be involved, at least in part, in the transport of erythromycin in Caco-2 cells (Takano *et al*. 1998). As P-glycoprotein has been recently reported to be expressed in the luminal membranes of the vascular endothelium in the lung (Beaulieu *et al*. 1997), an influence of P-glycoprotein on the pulmonary disposition of clarithromycin and erythromycin might be predicted. In fact, our preliminary studies have shown that the pulmonary extraction of both clarithromycin (0.181 ± 0.014) and erythromycin (0.165 ± 0.030) at a lower dose of 29.4 ng were significantly smaller than those at a dose of 294 ng (table 4) in the multiple-indicator dilution study, suggesting that the efflux system, probably P-glycoprotein, also participates in the pulmonary disposition of clarithromycin and erythromycin at a lower dose. However, considering the fact that verapamil, a well-known substrate for P-glycoprotein, did not enhance but inhibited the pulmonary disposition of clarithromycin and erythromycin at a dose of 294 ng (figure 7), the capacity of this efflux system should be very small and that the efflux of clarithromycin and erythromycin from the lung should not, if any, affect the pulmonary disposition of these compounds at the clinical plasma concentration.

In conclusion, we have analysed the comparative pulmonary disposition characteristics of clarithromycin and erythromycin, through which the binding and uptake processes of clarithromycin were quantitatively evaluated and the extensive pulmonary uptake of clarithromycin could be ascribed to non-specific binding owing to its lipophilic nature and, in part, to some specialized mechanisms such as organic cation transporters. However, the specific transport systems involved in the uptake of these antibiotics still remain to be identified. Further studies including the uptake and/or transport studies using alveolar epithelial cells would be needed to elucidate the molecular mechanism behind the high disposition of clarithromycin to the lung.

References

Beaulieu, E., Demuele, M., Ghitescu, L. and Beliveau, R., 1997, P-glycoprotein is strongly expressed in the luminal membranes ofthe endothekium of blood vessels in the brain. *Biochemical Journal*, **326**, 539–544.

Bend, J. R., Serabjit-Singh, C. E. and Philot, R. M., 1985, The pulmonary uptake, accumulation, and metabolism of xenobiotics. *Annual Review of Pharmacology and Toxicology*, **25**, 97–125.

Brown, E. A. B., 1974, The localization, metabolism and effects of drugs and toxicants in lung. *Drug Metabolism Reviews*, **3**, 33–87.

Dollery, C. T. and Junod, A. F., 1976, Concentration of (±)-propranolol in isolated, perfused lungs of rat. *British Journal of Pharmacology*, **57**, 67–71.

Dresser, M. J., Leabman, M. K. and Giacomini, K. M., 2001, Transporter involved in the elimination of drugs in the kidney: organic anion transporters and organic cation transporters. *Journal of Pharmaceutical Sciences*, **90**, 397–421.

Eling, T. E., Pickett, R. D., Orton, T. C. and Anderson, M. W., 1975, A study of the dynamic of imipramine accumulation in the isolated perfused rabbit lung. *Drug Metabolism and Disposition*, **3**, 389–399.

Hackman, C. R., Rosengard, S. and Vappatolo, H., 1970, Tissue distribution of chlorpromadine studied by microautoradiography. *European Journal of Pharmacology*, **9**, 59–66.

Higaki, K., Yukawa, T., Takeuchi, M., Nezasa, K. and Nakano, M., 1998, Stereoselective uptake of an organic anion across the renal basolateral membrane in isolated perfused rat kidney. *Drug Metabolism and Disposition*, **26**, 138–145.

Kekuda, R., Prasad, P. D., Wu, X., Wang, H., Fei, Y. J., Leibach, F. H. and Ganapathy, V., 1998, Cloning and functional characterization of a potential-sensitive, polyspecific organic cation transporter (OCT3) most abundantly expressed in placenta. *Journal of Biological Chemistry*, **273**, 15971–15979.

Kohno, Y., Yoshida, H., Suwa, T. and Suga, T., 1989, Comparative pharmacokinetics of clarithromycin (TE-031), a new macrolide antibiotic, and erythromycin in rats. *Antimicrobial Agents and Chemotherapy*, **33**, 751–756.

Kohno, Y., Yoshida, H., Suwa, T. and Suga, T., 1990, Uptake of clarithromycin by rat lung cells. *Journal of Antimicrobial Chemotherapy*, **26**, 503–513.

Kohno, Y., Yoshida, H., Yoshitomi, S. and Suwa, T., 1988, Pharmacokinetics of TE-031 VII: its pulmonary disposition. *Chemotherapy*, **36**, 257–263.

Nakagawa, Y., Itai, S., Yoshida, T. and Nagai, T., 1992, Physicochemical properties and stability in the acidic solution of a new macrolide antibiotic, clarithromycin, in comparison with erythromycin. *Chemical and Pharmaceutical Bulletin*, **40**, 725–728.

Nishida, K., Tonegawa, C., Kakutani, T., Hashida, M. and Sezaki, H., 1989, Statistical moment analysis of hepatobiliary transport of phenol red in the perfused rat liver, *Pharmaceutical Research*, **6**, 140–146.

Nishiura, A., Higashi, J., Murakami, T., Higashi, Y. and Yata, N., 1986, A possible contribution of phospholipids in tissue distribution of quinidine in rats. *Journal of Pharmacobio-Dynamics*, **9**, 819–828.

Nishiura, A., Murakami, T., Higashi, Y. and Yata, N., 1987, Role of acidic phospholipids in tissue distribution of quinidine in rats. *Journal of Pharmacobio-Dynamics*, **10**, 135–141.

Ogawara, K., Nishikawa, M., Takakura, Y. and Hashida, M., 1998, Pharmacokinetic analysis of hepatic uptake of galactosylated bovine serum albumin in a perfused rat liver. *Journal of Controlled Release*, **50**, 309–317.

Okumura, K., Yoshida, H. and Hori, R., 1978, Tissue distribution and metabolism of drugs III accumulation of drugs by the isolated perfused rat lung. *Journal of Pharmacobio-Dynamics*, **1**, 230–237.

Okumura, K., Yoshida, H., Kamiya, A. and Hori, R., 1989, Mitochondrial distribution of basic drugs in the isolated perfused lung. *Chemical and Pharmaceutical Bulletin*, **37**, 1109–1111.

Post, C., Anderson, R. G. G., Ryrfeldt, A. and Nilsson, E., 1978, Transport and binding of lidocaine by lung slices and perfused lung of rats. *Acta Pharmcologica et Toxicologica*, **43**, 156–163.

Posti, J. and Salonen, M., 1983, Effect of formulation factors and food intake on the bioavailability of erythromycin stearate tablets. *International Journal of Pharmaceutics*, **17**, 225–235.

Said, S. I., 1982, Pulmonary metabolism of prostaglandins and vasoactive peptides. *Annual Review of Physiology*, **44**, 257–268.

Schomig, E., Spitzenberger, F., Engelhardt, M., Martel, F., Ording, N. and Grundemann, D., 1998, Molecular cloning and characterization of two novel transport proteins from rat kidney. *FEBS Letters*, **425**, 79–86.

Takano, M., Hasegawa, R., Fukuda, T. Yumoto, R., Nagai, J. and Murakami, T., 1998, Interaction with P-glycoprotein and transport of erythromycin, midazolam and ketoconazole in Caco-2 cells. *European Journal of Pharmacology*, **358**, 289–294.

Terasaki, T., Iga, T., Sugiyama, Y. and Hanano, M., 1984, Pharmacokinetic study on the mechanism of tissue distribution of doxorubicin: interorgan and interspecies of variation of tissue-to-plasma partition coefficients in rats. *Journal of Pharmaceutical Sciences*, **73**, 1359–1363.

Tsuji, A., Yoshikawa, T., Nishide, K., Minami, H., Kimura, M., Nakashima, E., Terasaki, T., Miyamoto, E., Nightingale, C. H. and Yamana, T., 1983, Physiologically based pharmacokinetic model for β-lactam antibiotics. I: Tissue distribution and elimination in rats. *Journal of Pharmaceutical Sciences*, **72**, 1239–1251.

Ullrich, K. J., 1994, Specificity of transporters for 'organic anions' and 'organic cations' in the kidney. Biochimica et Biophysica Acta, **1197**, 45–62.

Wakasugi, H., Yano, I., Ito, T., Hashida, T., Futumi, T., Nohara, R., Sasayama, S. and Inui, K., 1998, Effect of clarithromycin on renal excretion of digoxin: interaction with P-glycoprotein. *Clinical Pharmacology and Therapeutics*, **64**, 123–128.

Wu, X., Huang, W., Ganapathy, M. E., Wang, H., Kekuda, R., Conway, S. J., Leibach, F. H. and Ganapathy, V., 2000, Structure, function, and regional distribution of the organic cation transporter OCT3 in the kidney. *American Journal of Physiology*, **279**, F449–F458.

Wu, X., Prasad, P. D., Leibach, F. H. and Ganapathy, V., 1998, cDNA sequence, transport function, and genomic organization of human OCTN2, a new member of the organic cation transporter family. *Biochemical and Biophysical Research Communications*, **246**, 589–595.

Yamaoka, K. and Nakagawa, T., 1983, A nonlinear least squares program based on differential equations, MULTI (RUNGE), for microcomputers. *Journal of Pharmacobio-Dynamics*, **6**, 595–606.

Yamazaki, M., Suzuki, H., Hanano, M., Tokui, T., Komai, T. and Sugiyama, Y., 1993, N^+-independent multispecific anion transporter mediates active transport of pravastatin into rat liver. *American Journal of Physiology*, **264**, G36–G44.

Yata, N., Toyoda, T., Murakami, T., Nishiura, A. and Higashi, Y., 1990, Phosphatidylserine as a determinant for the tissue distribution of weakly basic drugs accumulated in the isolated perfused lung. *Pharmaceutical Research*, **7**, 1019–1025.

Yoshida, H., Okumura, K. and Hori, R., 1987, Subcellular distribution of basic drugs accumulated in the isolated perfused lung. *Pharmaceutical Research*, **4**, 50–53.
Yoshida, H., Okumura, K., Kamiya, A. and Hori, R., 1989, Accumulation mechanism of basic drugs in the isolated perfused rat lung. *Chemical and Pharmaceutical Bulletin*, **37**, 450–453.

XENOBIOTICA, 2002, VOL. 32, NO. 10, 895–906

Taylor & Francis
healthsciences

Modelling the loss of metabolic capacities of cultured hepatocytes: application to measurement of Michaelis–Menten kinetic parameters in *in vitro* systems

A. BOUSQUET-MELOU*, C. M. LAFFONT, V. LAROUTE and P.-L. TOUTAIN

Unité Associée INRA de Physiopathologie et Toxicologie Expérimentales, Ecole Nationale Vétérinaire de Toulouse, 23 chemin des Capelles, F-31076 Toulouse, France

Received 7 January 2002

1. The loss of metabolic capacities during culture time constitutes a major limitation for the use of hepatocyte primary cultures in *in vitro* metabolism measurements. A new strategy is presented that permits one to calculate the Michaelis–Menten parameters V_{max} and K_m from extended experiments, by modelling V_{max} as a variable dependent on time using exponential or sigmoidal equations.

2. This method was tested with cortisol depletion in cultured rat hepatocytes. V_{max} and K_m were used to calculate intrinsic clearance, and comparisons were made with methods already described in the literature. Intrinsic clearances given by our method were scaled to *in vivo* hepatic clearances that were close to those reported in the literature.

3. Our method could quantify the V_{max} decrease with culture time from estimates of time parameters, $t_{1/2}$ or t_{50}. In our system, this V_{max} decrease was in agreement with P450 cytochrome inactivation rates published for the rat liver.

4. In conclusion, we propose a convenient, simple and useful general method for both Michaelis–Menten parameter estimation and modelling of variations in the metabolic capacities observed in *in vitro* systems. Such an approach should improve the usefulness of hepatocytes in primary cultures for long-term metabolism experiments.

Introduction

Isolated or cultured hepatocytes represent extensively used models for studying the hepatic metabolism of xenobiotics. Their main limitations are the instability of their functions and especially their metabolic capacities. For hepatocytes in suspension, extended experiments are limited because survival of liver cells does not exceed a few hours, and primary cultures of hepatocytes exhibit a well-described decrease in enzyme expression and the progressive drift of their metabolic capacities with culture time (Maurel 1996, Boobis 1998, LeCluyse 2001). In particular, the activity of P450 enzymes in rat hepatocytes can decline to 10–30% of its original activity after 4 days *in vitro* (Bégué *et al.* 1984).

As standard culture techniques cannot preserve P450-dependent reactions in the long-term, attempts have been made to overcome this CYP decrease by modifying cell-culture technology. Various techniques have been developed, such as the use of co-cultures, biomatrix, particular constituents of the medium or immobilization, to maintain the stability of drug-metabolizing enzymes in hepatocytes (Maurel 1996, Boobis 1998). One drawback of these approaches is that they require specific adaptations for hepatocytes of different species and

* Author for correspondence; e-mail: a.bousquet-melou@envt.fr

Xenobiotica ISSN 0049–8254 print/ISSN 1366–5928 online © 2002 Taylor & Francis Ltd
http://www.tandf.co.uk/journals
DOI: 10.1080/00498250210163261

consequently are not adapted for routine drug screening. The consequences of model instability are particularly important for experiments requiring precise quantification of metabolism, such as intrinsic clearance predictions for which the estimations of the kinetic parameters V_{max} and K_m are needed.

From a kinetic point of view, it can be considered that the loss of enzymatic capacities in cultured hepatocytes corresponds to a progressive decrease of V_{max} during drug incubation, i.e. the parameter V_{max} becomes variable with time and the *in vitro* system can be described as non-stationary. In the present study, we propose a new strategy that consists of modelling V_{max} as a function of time, thus enabling the influence of the CYP decrease on *in vitro* drug metabolism to be quantified.

Our strategy was tested in the context of using drug disappearance versus time profiles to measure *in vitro* metabolism, which is an alternative to the more classical measurement of metabolite appearance in the incubation medium. The main advantage is that this approach does not require precise knowledge of the metabolic pathways of the analyte under investigation and it can be adapted for drugs with complicated metabolic pathways (Carlile *et al.* 1998). The present study used cortisol as a probe analyte for drugs exhibiting complex metabolic pathways for hepatic elimination (Abel *et al.* 1993).

Materials and methods

Chemicals

Cortisol, pentobarbital sodium, heparin, HEPES, KCl, NaCl, glucose, EGTA, $CaCl_2$, foetal bovin serum (FBS), glutamine, RPMI 1640 medium and collagenase were purchased from Sigma Chemical Co. (St Quentin Fallavier, France). The collagen-coated dishes Iwaki® were obtained from Fisher Scientific (Elancourt, France). The SPE C_8 cartridges were from Varian (Les Ulis, France). The organic solvents were obtained from Scharlau (Barcelona, Spain).

Animals

Male Wistar rats (300–350 g) were from Iffa Credo (L'Arbresle, France). The animals were housed at 20–22°C with a 12-h light–dark cycle and fed with UAR rat diet (UAR, Epinay-S/orge, France) and water *ad libitum*.

Preparation of hepatocytes

A liver perfusion technique based on the multistep collagenase protocol of Berry and Friend (1969) was used to isolate hepatocytes. The rats were anaesthetized with pentobarbital sodium (50 mg kg^{-1}, i.p.) and heparin (500 U, penial vein) was administered. The portal vein was cannulated with a polyethylene catheter and the liver was perfused *in situ* with sterile prewarmed (37°C) perfusates at a constant rate of 20 ml min^{-1}. Medium 1 (HEPES 10 mM, KCl 5 mM, NaCl 8 g l^{-1}, glucose 5 g l^{-1}) was perfused for 5 min to wash out the blood from the liver lobes. Medium 2 (medium 1 + EGTA 0.5 mM) was then perfused for 5 min. Medium 1 was again used for 5 min to remove EGTA. Finally, medium 3 (medium 1 + collagenase 0.04% and $CaCl_2$ 2 mM) was perfused for 15 min. The liver was then removed and placed in 40 ml medium 4 (medium 1 + collagenase 0.008% and $CaCl_2$ 0.4 mM) to achieve collagenase digestion. The capsule was cut and the hepatocytes dispersed by gentle shaking. The cell suspension was filtered then through two nylon filters (250 and 150 µm, successively) and centrifuged (70*g*, 3 min, 4°C). The resulting pellet was resuspended in medium 5 (medium 1 + $CaCl_2$ 1 mM and BSA 0.25%) and recentrifuged. The washing procedure was repeated again with culture medium in place of medium 5. The final pellet was resuspended in a suitable volume of culture medium.

Cell viability was assessed by the Trypan blue exclusion test and > 90% for all hepatocyte preparations.

Primary culture of hepatocytes

Hepatocytes were plated at a density of approximately 4×10^6 cells/dish in 60-mm collagen-coated dishes containing 3 ml culture medium. The medium consisted of RPMI supplemented with 10% FBS,

3 mM glutamine and 55 μg ml^{-1} kanamycin. The hepatocytes were allowed to attach at 37°C in a humidified 95%/5% air/CO_2 atmosphere. After 3–4 h of incubation, the medium containing unattached cells was aspirated and substituted with fresh supplemented RPMI without kanamycin.

Metabolic activities in cultured hepatocytes

The primary hepatocyte cultures were then incubated in a final volume of 4 ml with two or three initial concentrations of cortisol, classified as low, intermediate and high. The low and high concentrations were used in all the experiments. Fifteen concentration–time curves (performed in duplicate) were obtained. The culture medium was collected at various sampling times and immediately stored at −20°C until analysis.

Cortisol stability in hepatocyte-free medium was checked under similar experimental conditions.

Analytical methods

After solid-phase extraction of samples, 10 μl eluate were analysed by HPLC using an HP 1050 system (Hewlett-Packard, les Ulis, France). Cortisol was separated on a Prontosil C_{18} 3 μm column (125 × 3.1 mm) and detected at 254 nm. The mobile phase consisted of a mixture of methanol–water (50:50 v/v) with a flow rate of 0.3 ml min^{-1}. The limit of quantification was 2 ng ml^{-1} and the coefficients of repeatibility and reproducibility were < 10%.

Kinetic analysis

Kinetic analysis was performed to calculate the intrinsic clearance (Cl_{int}) corresponding to linear kinetic conditions.

The five methods considered in this study can be classified in two categories: (1) methods providing a direct estimation of Cl_{int} without determination of the kinetic parameters V_{max} and K_m (hereafter the AUC method and k_{10} method), and (2) methods based on determination of V_{max} and K_m, parameters of the Michaelis–Menten equation (MM methods).

AUC method. *In vitro* Cl_{int} was calculated using equation (1):

$$Cl_{int} = A_0/\mathrm{AUC}, \tag{1}$$

where A_0 is the amount of substrate in the incubation medium at time zero and AUC is the area under the cortisol concentration–time curve extrapolated to infinity. The AUC from 0 to the last time point (t_{last}) was calculated using the linear trapezoidal rule. For equation (1) to be valid, the kinetics of cortisol consumption must be linear, i.e. cortisol consumption must occur with a first-order rate constant.

K_{10} method. For cortisol concentration–time profiles obtained under conditions of kinetic linearity, the data can be fitted to equation (2):

$$C(t) = C_0 \times \exp(-k_{10} \times t), \tag{2}$$

where $C(t)$ is the cortisol concentration at time t, C_0 is the cortisol concentration for time zero and k_{10} is the first-order elimination rate constant of cortisol obtained by non-linear regression analysis. With this model, Cl_{int} is given by equation (3):

$$Cl_{int} = k_{10} \times V, \tag{3}$$

where V is the actual volume incubated.

Michaelis–Menten methods. Cortisol concentration–time profiles were described by the Michaelis–Menten differential equation:

$$-\frac{dC(t)}{dt} = \frac{V_{max}^{conc} \times C(t)}{K_m + C(t)}, \tag{4}$$

where V_{max}^{conc} is the maximal rate of metabolism expressed in concentration per time unit and K_m is the apparent Michaelis–Menten constant. V_{max}, the maximal rate of metabolism expressed in amount per time unit, was obtained using:

$$V_{max} = V_{max}^{conc} \times V \tag{5}$$

and Cl_{int} was given by equation (6):

$$Cl_{int} = V_{max}/K_m \tag{6}$$

We tested three different modelling options that enabled the non-stationarity of the *in vitro* system to be taken into account in the context of Michaelis–Menten kinetics. In these MM methods, the concentration–time profiles corresponding to the low and high initial cortisol concentrations were fitted simultaneously.

MM method 1. It was assumed here that the metabolic capacities of the system did not change during the first 6 h of cortisol incubation. Equations (4) and (5) were used to fit simultaneously the data corresponding to the low and high initial cortisol concentrations, the latter being truncated after 6 h of incubation.

MM method 2. Here, V_{max} was assumed to follow a sigmoidal decrease as a function of incubation time. The data were fitted with equations (4) and (5) in which V_{max}^{conc} becomes a variable described by equation (7):

$$V_{max}^{conc}(t) = V_{max0}^{conc} \times \left(1 - \frac{(t - t_{lag})}{t_{50} + (t - t_{lag})}\right), \quad (7)$$

where t is the cortisol incubation time, V_{max0}^{conc} the V_{max}^{conc} for time zero, t_{50} the time for which half of the maximal effect (maximal V_{max} decrease) is obtained, and t_{lag} the lag time between time zero and the beginning of the V_{max} decrease.

MM method 3. Here, V_{max} was assumed to follow an exponential decrease as a function of incubation time. The data were fitted with equations (4) and (5) in which V_{max}^{conc} becomes a variable described by equation (8):

$$V_{max}^{conc}(t) = V_{max0}^{conc} \times \exp(-k \times (t - t_{lag})), \quad (8)$$

where t, V_{max0}^{conc} and t_{lag} are as already defined, and k is the first-order rate constant of the V_{max} decrease. This process can be characterized by its half-life (equation 9):

$$t_{1/2} = \ln 2/k. \quad (9)$$

Hepatic clearance prediction. The prediction of Cl_H was performed in two steps: (1) scaling-up of Cl_{int} to the whole organ using an hepatocyte yield of 1.35×10^8 cells g^{-1} liver and a liver weight of 45 g kg^{-1} body weight (Houston 1994), and (2) incorporation of Cl_{int} into a classical model of Cl_H (well-stirred model) with a liver blood flow of 1.8 ml min^{-1} g^{-1} liver (Houston 1994) and the unbound fraction (f_u) = 1.

Fitting and statistical analysis

Data fitting by non-linear regression was conducted with the program SCIENTIST v. 2.01 (MicroMath Software, Salt Lake City, UT, USA). The weighting scheme of 1/observation^2 was used. Goodness of fit was assessed by visual inspection of the lines of best-fit and residual patterns, and consideration of a modified Akaike information criterion.

Statistical analysis was performed with SYSTAT 8.0 (SPSS, Inc., Chicago, IL, USA). All data are the means ± SD. The paired Student's t-test or ANOVA followed by pairwise comparisons using the Bonferroni procedure were used for comparison of the means. The level of significance was set at $p = 0.05$.

Results

Cell culture

Hepatocyte viability was assessed after the isolation procedure and the results are shown in table 1. Viability >90% for all samples, with a mean around 95%. A

Table 1. Parameters of primary hepatocyte cultures.

	Cases						
	1	2	3	4	5	6	Mean (SD)
Viability	94	100	98	90.7	90.7	95.6	94.8 (3.60)
Plated cells	4.4	4	4.7	4.5	4.4	4.5	4.4 (0.23)
Attached cells	1	1	1.6	1.35	2	2.4	1.56 (0.56)

Viability is the per cent of viable cells. Numbers of plated and attached cells are expressed in million ($\times 10^6$) cells.

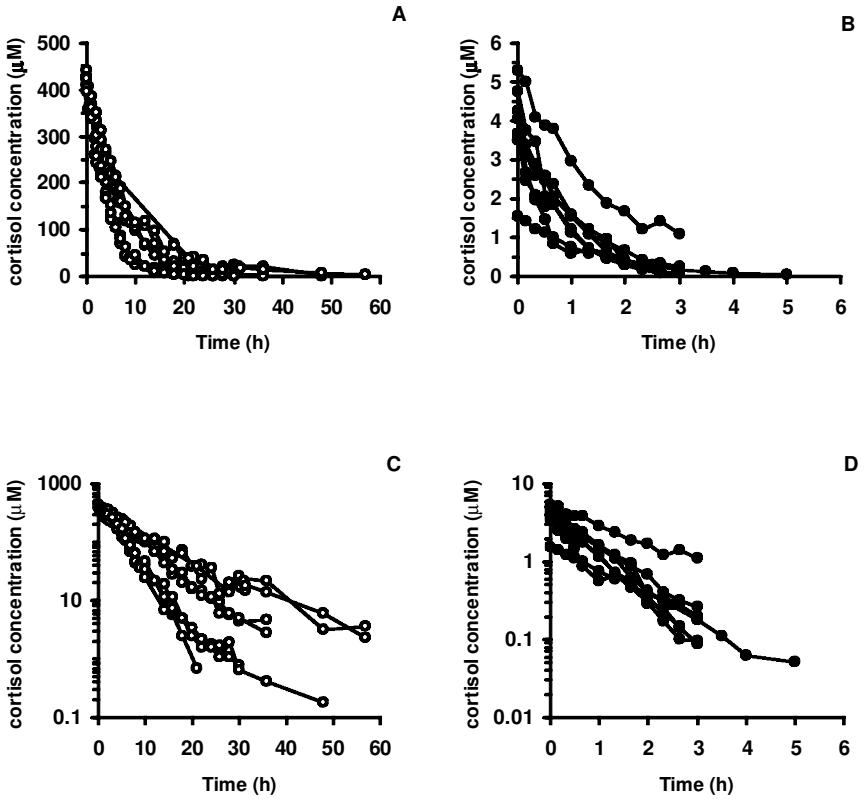


Figure 1. Plots of observed cortisol concentrations versus time after high (A, C) and low (B, D) initial cortisol concentrations. Data from six different hepatocyte cultures are presented in arithmetic (A, B) and semilogarithmic (C, D) scales.

mean of 4.4 ± 0.3 million cells were inoculated on plates and 1.56 ± 0.56 million cells were attached at the beginning of the cortisol incubations.

Intrinsic clearance calculation without V_{max} *and* K_m *measurement*

Cortisol disappearance in the presence of cultured rat hepatocytes was studied with three different cortisol initial concentrations. The cortisol depletion curves after the low and high doses are shown in figure 1. The range of initial cortisol concentrations was (1.3–5.31) and (416–555) micromolar for the low and high doses, respectively.

AUC method. Total AUC (from time zero to infinity) and the A_0/AUC ratios are shown in table 2. The extrapolated AUC (from t_{last} to infinity) did not exceed 7 and 5% of the total AUC for the low and high doses, respectively.

The ratio of high to low initial concentrations was >100 and the corresponding ratio of A_0/AUC (low to high initial concentrations) was around 7, indicating the non-linearity of cortisol kinetics within this concentration range. A first-order consumption of cortisol was expected after the low initial cortisol concentrations.

Table 2. Kinetics of cortisol depletion in cultured rat hepatocytes.

		AUC method		k_{10} method	
Initial concentration	(μM)	AUC ($\mu mol\,h\,l^{-1}$)	A_0/AUC ($\mu l\,min^{-1}$)	k_{10} (h^{-1})	$k_{10}V$ ($\mu l\,min^{-1}$)
High	439 ± 57	3512 ± 2662	6.45 ± 2.68	n.d.[a]	n.d.
Intermediate	46.1 ± 7.74	125 ± 64	29.0 ± 8.58	0.455 ± 0.162	27.3 ± 6.1
Low	3.68 ± 1.17	4.03 ± 2.11	47.5 ± 19.4	0.944 ± 0.273	47.2 ± 14.2

Data are the mean ± SD of six (high, low) or three (intermediate) determinations. A_0/AUC and k_{10}V are expressed per 10^6 cells.
[a] n.d., not determined.

Under this assumption, Cl_{int} is given by the ratio A_0/AUC and was $47.5 \pm 19.4\,\mu l\,min^{-1}$ per 10^6 cells.

K10 method. The calculation of Cl_{int} from the cortisol depletion data after the low initial cortisol concentrations, using the k_{10} method, gave a mean of $47.2 \pm 14.2\,\mu l\,min^{-1}$ per 10^6 cells (table 2). The k_{10} method applied to intermediate dose data provided a mean clearance of $27.3 \pm 6.1\,\mu l\,min^{-1}$ per 10^6 cells.

Intrinsic clearance calculation using V_{max} *and* K_m *measurement*

When parent compound depletion data are used, accurate estimations of both V_{max} and K_m require drug concentrations corresponding to the saturating phase (zero-order rate constant) and to the linear phase (first-order rate constant) of drug metabolism. We assumed *a priori* that these conditions were obtained after the high and low initial cortisol concentrations, respectively. For this reason, we analysed the concentration–time profiles obtained after the high and low initial cortisol concentrations simultaneously. Figure 2 shows a representative experiment (after the low and high initial cortisol concentrations) and the curves were fitted by the MM method 1, which ignores the data obtained after a 6-h incubation (figure 2, A). The theoretical curve corresponding to an invariant V_{max} throughout the incubation period is also shown (figure 2, B). This curve dramatically misfitted data corresponding to the longer incubation period (> 10 h) and overestimated the actual rate of cortisol disappearance at these times.

The entire concentration–time profiles at high cortisol concentration were fitted simultaneously with the low concentration profiles using both models that assume a time-dependent decrease of V_{max}, corresponding to equations (7) and (8). The fitted curves obtained with the two models are shown together with the observed data for a typical experiment in figure 3. These two models adequately fitted the experimental data, and especially the terminal part of the depletion curve after the high initial cortisol concentrations.

The means of the kinetic parameters V_{max}, K_m and Cl_{int} estimated by the three methods are shown in table 3. The V_{max} and K_m were significantly ($p < 0.05$) underestimated with method 1 compared with methods 2 and 3. Cl_{int} did not differ significantly between the three methods.

Methods 2 and 3 enabled the parameters of the V_{max} time-dependency to be estimated (table 4). The ranges of individual t_{lag} for the V_{max} decrease process were (0–5.55) and (0–1.44) h for methods 2 and 3, respectively. Moreover, t_{lag} close to

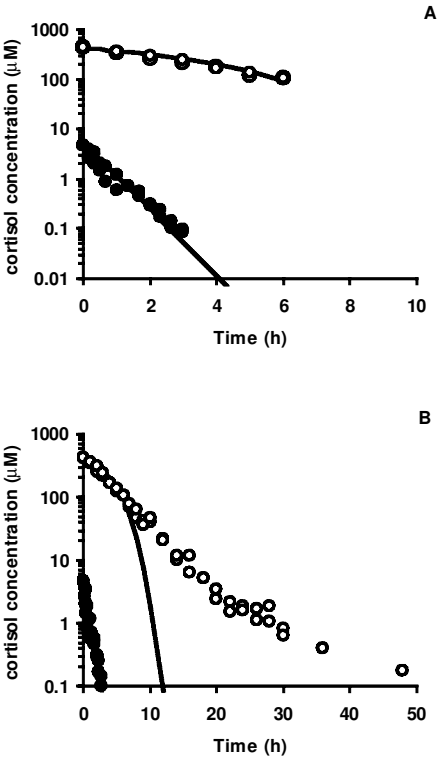


Figure 2. Semilogarithmic plots for observed (●, ○) and fitted (–) cortisol concentrations after low (●) and high (○) initial cortisol concentrations in a representative experiment. Fitting was obtained with a classical Michaelis–Menten equation (4), corresponding to an invariant V_{max} parameter. Data are duplicate determinations. (A) Data used in the curve fitting (0–6 h of incubation); (B) data corresponding to the total incubation time for high initial cortisol concentration (0–48 h).

zero were obtained in one experiment for method 2 and in three experiments for method 3. The means of the parameters describing the rate of V_{max} decrease, i.e. t_{50} for method 2 and $t_{1/2}$ for method 3, were similar for the two V_{max} models: 7.37 ± 1.55 h (range 4.65–8.87) and 6.78 ± 0.32 h (4.66–9.42), respectively.

Hepatic clearance prediction

The predicted Cl_H was obtained using Cl_{int} derived from methods 1–3. The Cl_H were very similar, ranging from 62.4 ml kg^{-1} min^{-1} for method 1 to 64.7 ml kg^{-1} min^{-1} for method 3.

Discussion

The main objective here was to demonstrate that the problem of non-stationarity of primary cultures of hepatocytes, for metabolism measurement may be tackled by a modelling strategy that takes into account the time-dependent variation of enzyme kinetic parameters. We propose kinetic data analysis based on two modelling hypotheses: (1) the overall metabolic clearance of a drug can be adequately described by a classical Michaelis–Menten model, and (2) the non-

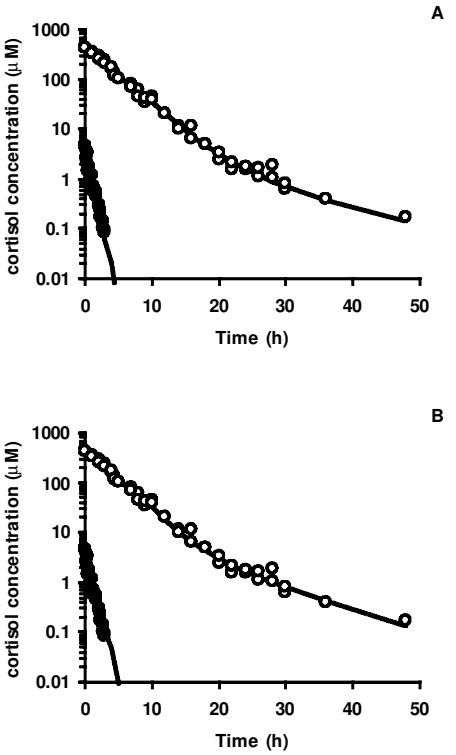


Figure 3. Semilogarithmic plots for observed (●, ○) and fitted (–) cortisol concentrations after low (●) and high (○) initial cortisol concentrations in a representative experiment. Data are duplicate determinations. (A) Fitting was obtained with a classical Michaelis–Menten equation (4), in which V_{max} is described as a time-dependent variable by a sigmoidal equation (7); (B) fitting was obtained with a classical Michaelis–Menten equation (4), in which V_{max} is described as a time-dependent variable by an exponential equation (8).

stationarity of the *in vitro* model can be taken into account by modelling the parameter V_{max} as a function of time.

The first assumption has already been presented in the literature and led to the notion of pooled Michaelis–Menten parameters, permitting description of the overall metabolism of a drug undergoing several parallel metabolic pathways. Sedman and Wagner (1974) demonstrated that the sum of Michaelis–Menten equations is equivalent to a single Michaelis–Menten equation when the drug concentrations are much higher or much lower than the individual K_m. The pooled V_{max} corresponds to the sum of the individual V_{max} and the pooled Cl_{int} corresponds to the sum of the individual Cl_{int}. These pooled parameters can be simply interpreted and have relevant meaning for the overall quantification of a drug's metabolism. The pooled K_m corresponds to the sum of the individual K_m weighted by the ratio of the corresponding individual Cl_{int} on the pooled Cl_{int}, and therefore cannot be simply interpreted.

Regarding the second assumption of our modelling strategy, we hypothesized that the modifications of the metabolic characteristics of rat hepatocytes in primary cultures had repercussions on the Michaelis–Menten parameter V_{max}, which is supported by the following considerations: (1) the *in vitro* modifications of metabolic capacities of cultured hepatocytes occurring with time are mainly

Table 3. Michaelis–Menten parameters for cortisol depletion in cultured rat hepatocytes.

	V_{max} (pmol min^{-1})	K_m (μM)	Cl_{int} (μl min^{-1})
1[a]	2416 ± 806[d]	48 ± 8[d]	47.7 ± 15.4[d]
2[b]	4046 ± 1475[e]	62 ± 13[e]	55.8 ± 21.5[d]
3[c]	4025 ± 1389[e]	65 ± 14[e]	57.9 ± 21.9[d]

Data are the mean ± SD ($n = 6$). For methods 2 and 3; the V_{max} for $t = 0$ (V_{max0}) is shown. V_{max} and Cl_{int} are expressed per 10^6 cells.

[a] MM method 1: V_{max} was invariant and data from $t = 0$–6 h were analysed.

[b] MM method 2: V_{max} was time-dependent with a sigmoidal relationship (equation 7).

[c] MM method 3: V_{max} was time-dependent with an exponential relationship (equation 8).

[d,e] Different indices in the same column are significantly different ($p < 0.05$).

Table 4. Parameters of V_{max} time-dependency in cultured rat hepatocytes.

Parameters (units)	MM 2[a]	MM 3[b]
t_{lag} (h)[c]	1.99 ± 1.90	0.43 ± 0.63
t_{50} (h)[d]	7.37 ± 1.55	–
k (h^{-1})[e]	–	0.102 ± 0.026
$t_{1/2}$ (h)[f]	–	6.78 ± 0.32

Data are the mean ± SD ($n = 6$).

[a] MM method 2: V_{max} is time-dependent with a sigmoidal relationship (equation 7).

[b] MM method 3: V_{max} is time-dependent with an exponential relationship (equation 8).

[c] t_{lag}, Lag time to V_{max} decrease.

[d] t_{50}, Time for which half of the maximal V_{max} decrease was obtained.

[e] k, First-order rate constant of V_{max} decrease.

[f] $t_{1/2}$, Half-life of V_{max} decrease.

associated with a decrease in CYP expression (Maurel 1996), and (2) the amount of functional enzymes present in the system is the main biological determinant of V_{max}. Therefore, it appears justified to consider that the time-dependent modification of cultured hepatocyte enzymes has a direct effect on V_{max}.

In our modelling strategy, we also chose to consider K_m as invariant, even though modifications of the pooled K_m during the culture time might be expected. These modifications might be due to changes in the environment influencing drug–enzyme interactions or to changes in the relative contribution of each individual metabolic pathway to overall drug metabolism. This latter phenomenon might occur if the time-dependent decrease of CYP expression is different between enzyme forms, which is likely to occur (LeCluyse 2001). Modifications of plasma membrane permeability to drugs might also be involved in the non-stationarity of hepatocyte models.

Finally, even if they did not take into account all the mechanisms potentially involved in the non-stationarity of *in vitro* systems, models assuming V_{max} to be a

variable and K_m a parameter succeeded in describing adequately the cortisol depletion curves and in providing accurate estimations of relevant parameters.

Two models describing the decrease of V_{max} with time are presented here. Although CYP depletion can be considered as a continuous phenomenon, we incorporated a t_{lag} in the V_{max} decrease equations because this parameter still provides relevant information on *in vitro* system stationarity. Indeed, the presence of a significant t_{lag} indicates that system stability might be assumed during this time interval. Our results revealed a high interexperiment dispersion probably due to the intrinsic variability of primary hepatocyte cultures, for which even well-standardized isolation steps can have uncontrolled repercussions on liver cell phenotype during the culture period. The ranges of estimated t_{lag} suggest that the time-dependent decrease of V_{max} occurred early during the incubation period, justifying the modelling of this parameter as a variable. Conversely, models considering V_{max} as a constant, even for a short incubation period, are likely to provide underestimations of V_{max}, as we observed for comparison of the MM-1 with MM-2 and 3 methods (table 3). Furthermore, an early V_{max} decrease during the incubation period can be the cause of underestimates of Cl_{int} measured with the AUC or k_{10} methods, particularly for drugs that are slowly metabolized and thus require longer incubation periods. This phenomenon should be taken into account in *in vitro* models classically used for *in vitro*/*in vivo* extrapolations of intrinsic clearance (microsomes, suspensions of freshly isolated hepatocytes).

Considering the shape of the V_{max} decrease with time curve, the two models presented here correspond to different classes of curves. The exponential model assumed a first-order process, characterized by its half-life; the second model assumed a sigmoidal decrease of V_{max}, characterized by t_{50}. Half-life and t_{50} provided the same information and their means were similar: around 7 h. Several models combining different relations between time and V_{max} decrease were tested, with results close to those of the exponential and sigmoidal models (data not shown). Particularly, the incorporation of the Hill coefficient in the sigmoidal model did not significantly improve the model performance.

The degradation rates of cellular proteins have previously been investigated, particularly those of liver CYPs (Correia 1991, Maurel 1996). Shiraki and Guengerich (1984) reported that the degradation of CYPs in rat liver was described by a first-order process with an half-life of microsomal CYP3A2 around 12 h for the protein and 7 h for the haem, and Watkins *et al.* (1986) published a CYP half-life in cultured rat hepatocytes of approximately 9 h. Our results on cortisol V_{max} decline (half-life and t_{50}) are in close agreement with these data, suggesting that enzyme degradation/inactivation is the major determinant of the non-stationarity of this *in vitro* system. Moreover, the rates of inactivation of the CYP enzymes can be investigated with our modelling approach, which presents the following advantages: (1) to study the time-dependent activity of the overall pool of enzymes involved in the metabolism of a drug, and (2) the possibility of exploring the influence of the substrate on the enzymes of its own metabolism.

The AUC and k_{10} methods, the latter being mathematically identical to the *in vitro* $t_{1/2}$ method proposed by Obach *et al.* (1997) for microsomal data, provide a direct estimate of Cl_{int} but cannot estimate the Michaelis–Menten parameters V_{max} and K_m. Moreover, as stated by Obach (1999), the validity of these methods requires substrate concentrations much lower than the apparent K_m (first-order kinetics) and this value is not known *a priori* for new compounds. An estimation of

the pooled K_m is therefore of paramount importance in our modelling approach, because it can be used to check *a posteriori* the assumption of first-order kinetics after low initial cortisol concentrations. In our experiments, the range of mean K_m obtained with the MM methods was 48.3–65.3 μM, indicating that low initial cortisol concentrations were in all cases > 10-fold lower than the K_m and thus that our *a priori* assumption was correct. This was confirmed by the Cl_{int} estimations with the AUC or k_{10} methods (table 2, low initial concentrations), which were not significantly different to the values obtained with the MM methods (table 3). Moreover, the AUC and k_{10} methods applied to data obtained after the intermediate initial cortisol concentrations, which were close to the K_m, gave Cl_{int} estimations that were 2-fold lower than the Cl_{int} obtained within the range of first-order kinetics (table 2). Finally, the simultaneous determinations of K_m and Cl_{int} confer an advantage to the MM methods, compared with AUC and k_{10} methods, especially for drugs under investigation for which the K_m are not known.

We used the Cl_{int} estimated by the three MM methods to predict cortisol Cl_H in rat. Chanoine and Junien (1984) published a cortisol total clearance in rat of 78.3 ml kg^{-1} min^{-1} and established that clearance by metabolism represented 80% of the total clearance, i.e. 62.7 ml kg^{-1} min^{-1}, which is close to our predictions (62.4–64.7 ml kg^{-1} min^{-1}).

In conclusion, we have demonstrated that the time-dependent decrease of enzymatic capacities in cultured rat hepatocytes can be simply investigated using a modelling approach. Because it allows the use of standard culture techniques easily available for different species, our strategy constitutes a clear-cut advantageous alternative to the time-consuming strategies aimed to reduce this phenomenon. Our approach can be easily applied and/or adapted to a variety of compounds and *in vitro* models (liver microsomes, suspensions of freshly isolated hepatocytes) and it could be used to perform retrospective analyses on *in vitro* metabolism data.

Acknowledgments

The authors thank N. Arpaillange and N. Gautier for technical assistance.

References

Abel, S. M., Back, J. D., Maggs, J. L. and Park, B. K., 1993, Cortisol metabolism *in vitro* — II. Species differences. *Journal of Steroid Biochemistry and Molecular Biology*, **45**, 445–453.

Bégué, J. M., Guguen-Guillouzo, C., Pasdeloup, N. and Guillouzo, A., 1984, Prolonged maintenance of active cytochrome P450 in adult rat hepatocytes co-cultured with another liver cell type. *Hepatology*, **4**, 839–842.

Berry, M. N. and Friend, D. S., 1969, High yield preparation of isolated rat liver parenchymal cells. *Journal of Cell Biology*, **43**, 506–520.

Boobis, A. R., 1998, Changing the *in vivo* extrapolation of *in vitro* drug metabolism data from fantasy to reality. In A. R. Boobis, P. Kremers, O. Pelkonen and K. Pithan (eds), *European Symposium on the Prediction of Drug Metabolism in Man: Progress and Problems*, pp. 1–35.

Carlile, D. J., Stevens, A. J., Ashforth, E. I., Waghela, D. and Houston, J. B., 1998, *In vivo* clearance of ethoxycoumarin and its prediction from *in vitro* systems. Use of drug depletion and metabolite formation methods in hepatic microsomes and isolated hepatocytes. *Drug Metabolism and Disposition*, **26**, 216–221.

Chanoine, F. and Junien, J. L., 1984, Comparative pharmacokinetic studies of tixocortol pivalate and cortisol in the rat. *Journal of Steroid Biochemistry and Molecular Biology*, **21**, 453–459.

Correia, M. A., 1991, Cytochrome P450 turnover. *Methods in Enzymology*, **206**, 315–325.

Houston, J. B., 1994, Utility of *in vitro* drug metabolism data in predicting *in vivo* metabolic clearance. *Biochemical Pharmacology*, **47**, 1469–1479.

LeCluyse, E. L., 2001, Human hepatocyte culture systems for the *in vitro* evaluation of cytochrome P450 expression and regulation. *European Journal of Pharmaceutical Sciences*, **13**, 343–368.

Maurel, P., 1996, The use of adult human hepatocytes in primary culture and other *in vitro* systems to investigate drug metabolism in man. *Advanced Drug Delivery Reviews*, **22**, 105–132.

Obach, R. S., 1999, Prediction of human clearance of twenty-nine drugs from hepatic microsomal intrinsic clearance data: an examination of *in vitro* half-life approach and nonspecific binding to microsomes. *Drug Metabolism and Disposition*, **27**, 1350–1359.

Obach, R. S., Baxter, J. G., Liston, T. E., Silber, B. M., Jones, B. C., MacIntyre, F., Rance, D. J. and Wastall, P., 1997, The prediction of human pharmacokinetic parameters from preclinical and *in vitro* metabolism data. *Journal of Pharmacology and Experimental Therapeutics*, **283**, 46–58.

Sedman, A. J. and Wagner, J. G., 1974, Quantitative pooling of Michaelis–Menten equations in models with parallel metabolite formation paths. *Journal of Pharmacokinetics and Biopharmaceutics*, **2**, 149–160.

Shiraki, H. and Guengerich, F. P., 1984, Turnover of membrane proteins: kinetics of induction and degradation of seven forms of rat liver microsomal cytochrome P-450, NADPH-cytochrome P-450 reductase, and epoxide hydrolase. *Archives of Biochemistry and Biophysics*, **235**, 86–96.

Watkins, P. B., Wrighton, S. A., Schuetz, E. G., Maurel, P. and Guzelian, P. S., 1986, Macrolide antibiotics inhibit the degradation of the glucocorticoid-responsive cytochrome P-450p in rat hepatocytes *in vivo* and in primary monolayer culture. *Journal of Biological Chemistry*, **261**, 6264–6271.

XENOBIOTICA, 2002, VOL. 32, NO. 10, 907–924

Taylor & Francis
healthsciences

Pharmacokinetics, toxicokinetics, distribution, metabolism and excretion of linezolid in mouse, rat and dog

J. G. SLATTER†, L. A. ADAMS‡, E. C. BUSH‡, K. CHIBA¶, P. T. DALEY-YATES||, K. L. FEENSTRA‡, S. KOIKE§, N. OZAWA¶, G. W. PENG‡, J. P. SAMS‡, M. R. SCHUETTE‡ and S. YAMAZAKI‡

†Product Life Cycle Management, Pharmacia Corp., 100 Route 206 N, PPK 121, Peapack, NJ 07977, USA.
‡Global Drug Metabolism and §Global Toxicology, Pharmacia Corp., Kalamazoo, MI, USA
¶Pharmacia K.K., Tokyo, Japan

Received 7 February 2002

1. Linezolid (ZYVOX^{TM}), the first of a new class of antibiotics, the oxazolidinones, is approved for treatment of Gram-positive bacterial infections.

2. The aim was to determine the absorption, distribution, metabolism and excretion (ADME) of linezolid in mouse, rat and dog in support of preclinical safety studies and clinical development.

3. Conventional replicate study designs were employed in animal experiments, and biofluids were assayed by HPLC or HPLC-MS.

4. Linezolid was rapidly absorbed after p.o. dosing with an p.o. bioavailability of $>95\%$ in rat and dog, and $>70\%$ in mouse. Twenty-eight-day i.v./p.o. toxicokinetic studies in rat (20–200 mg kg^{-1} day^{-1}) and dog (10–80 mg kg^{-1} day^{-1}) revealed neither a meaningful increase in clearance nor accumulation upon multiple dosing.

5. Linezolid had limited protein binding ($<35\%$) and was very well distributed to most extravascular sites, with a volume of distribution at steady-state (V_{ss}) approximately equal to total body water.

6. Linezolid circulated mainly as parent drug and was excreted mainly as parent drug and two inactive carboxylic acids, PNU-142586 and PNU-142300. Minor secondary metabolites were also characterized. In all species, the clearance rate was determined by metabolism.

7. Radioactivity recovery was essentially complete within 24–48 h. Renal excretion of parent drug and metabolites was a major elimination route. Parent drug underwent renal tubular reabsorption, significantly slowing parent drug excretion and allowing a slow metabolic process to become rate-limiting in overall clearance.

8. It is concluded that ADME data were relatively consistent across species and supported the rat and dog as the principal non-clinical safety species.

Introduction

Linezolid ((S)-*N*-[[3-[3-fluoro-4-(4-morpholinyl)phenyl]-2-oxo-5-oxazolidinyl]methyl]-acetamide, ZYVOX^{TM} (figure 1) is the first in a new class of synthetic antibiotics, the oxazolidinones. The oxazolidinones selectively inhibit the initiation phase of bacterial protein synthesis (Demyan *et al.* 1997, Lin *et al.* 1997,

* Author for correspondence; e-mail: j.greg.slatter@pharmacia.com
|| Present address: Pharmacokinetics Department, GlaxoSmithKline R&D, Middlesex, UK

Xenobiotica ISSN 0049–8254 print/ISSN 1366–5928 online © 2002 Taylor & Francis Ltd
http://www.tandf.co.uk/journals
DOI: 10.1080/00498250210158249

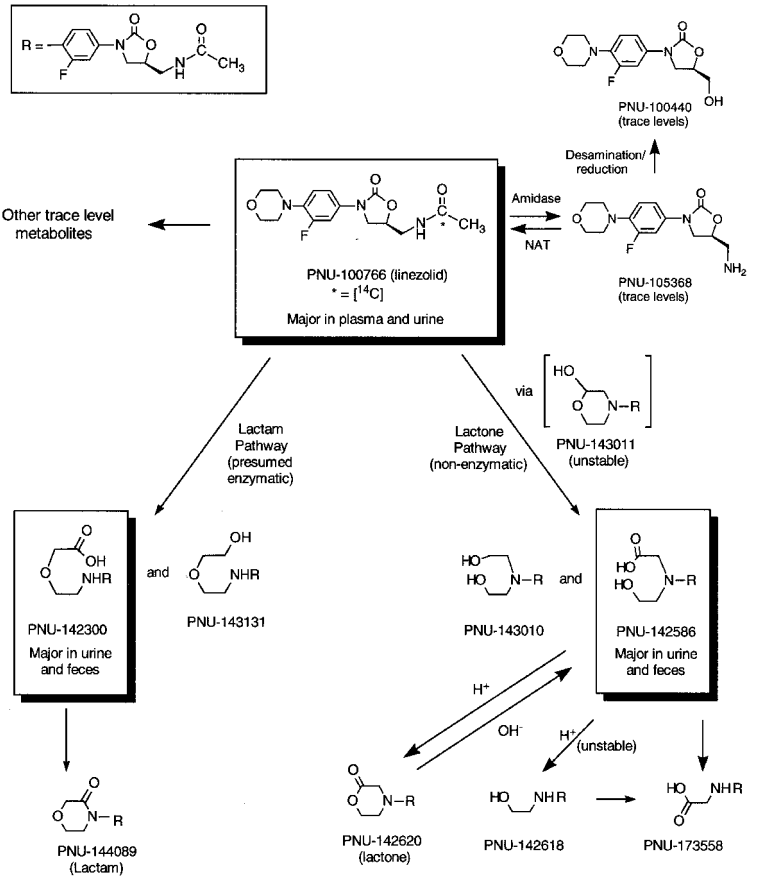


Figure 1. Linezolid metabolic pathways (used with permission from Slatter *et al.* 2001). The pathways are qualitatively similar across the species mouse, rat, dog and man. *Position of the ^{14}C radiolabel. NAT, *N*-acetyltransferase.

Shinabarger *et al.* 1997, Swaney and Shinabarger 1997). Linezolid is now approved in the USA and other countries world-wide for the treatment of Gram-positive bacterial infections.

Preliminary work on toxicokinetics and ADME in rat (Koike *et al.* 1995, Chiba *et al.* 1998) and *in vitro* metabolism studies (Wienkers *et al.* 1999) showed that linezolid had several ADME characteristics that were well suited to an effective new antibiotic agent. In man, linezolid is dosed intravenously (i.v.) or orally (p.o.) at a dose of 600 mg twice daily. Since bioavailability is approximately 100%, no change in dose is necessary when switching from i.v. to p.o. therapy. After a 600 mg twice daily p.o. dose regimen, a steady-state C_{max} of 21.2 ± 5.78 μg ml^{-1} is obtained at t_{max} 1.03 ± 0.62 h. Clearance is 80 ± 29 ml min^{-1} and occurs by both renal and non-renal (65%) mechanisms. The elimination half-life in plasma is 5.40 ± 2.06 h. Plasma protein binding is 31%, and the volume of distribution is close to that of total body water (40–50 litres) (Pawsey *et al.* 1996, Stalker *et al.* 1997a, b, Pharmacia 2000). Linezolid is neutral at physiological pH and undergoes renal tubular reabsorption (Chiba *et al.* 1998).

The objective of the current study was to determine the pharmacokinetics, toxicokinetics, distribution, metabolism and excretion of linezolid in the three main preclinical toxicology species, and to integrate these results with *in vitro* metabolism data (Wienkers *et al.* 1999, Wynalda *et al.* 2000) and human ADME data (Slatter *et al.* 2001).

Materials and methods

Pharmacokinetics and bioavailability

Formulations and dose administration. Non-fasted female CD-1 mice (22–26 g, $n = 3$/time point/route, serial sacrifice design) were given a single dextrose/sodium citrate solution dose of 10 mg kg^{-1} i.v. (tail vein bolus) or 10 mg kg^{-1} p.o. Blood was collected by exsanguinations from CO_2 euthanized mice, three per time point, by cardiac puncture over K_3EDTA over the 0–24 h post-dose period. Plasma was quenched with acetonitrile containing an internal standard, centrifuged and analysed for linezolid by HPLC/MS/MS. Non-compartmental pharmacokinetic parameters were calculated using a Microsoft Excel spreadsheet (Microsoft Corp., Redmond, WA, USA).

Fasted male Sprague–Dawley rats (190–230 g, $n = 3$/group, parallel design) were given a single saline solution dose of 10 mg kg^{-1} i.v. (cannula bolus) or 25 mg kg^{-1} p.o., then fed 4 h after dosing. Blood (0.25 ml) was collected from an indwelling superior vena cava cannula over K_3EDTA over the 0–24 h post-dose period. Plasma was quenched with an aqueous internal standard and acetonitrile, centrifuged and analysed for linezolid by HPLC. Non-compartmental pharmacokinetic parameters were calculated using TOPFIT (Heinzel *et al.* 1993).

Fasted male Beagle dogs (9–11 kg, $n = 3$/group, three-way crossover design with 2 weeks between doses) were given a single saline solution dose of 25 mg kg^{-1} i.v. (cephalic vein rapid infusion) or 25 mg kg^{-1} p.o. as an aqueous solution, or as solid drug in capsules, then fed 4 h after dosing. Blood (1.5 ml) was collected from the cephalic vein in heparinized syringes over the 0–48 h post-dose period. Plasma was mixed with an aqueous internal standard and concentrated by solid-phase extraction (SPE) before reconstitution and analysis by HPLC. Non-compartmental pharmacokinetic parameters were calculated using an internal Microsoft Excel spreadsheet.

Renal clearance in mouse and rat. Female CD-1 mice (22–26 g, $n = 3$) were housed together in metabolism cages and urine (0–24 h) was collected and weighed. Internal standard was added, then the urine was analysed directly by HPLC/MS/MS. Linezolid renal clearance (CL_r) was determined from the amount of linezolid excreted in urine, the area under the plasma concentration–time curve (AUC) and the mean body weight. An estimate of mean renal clearance (ml min^{-1} kg^{-1}) for three animals was calculated as CL_r = (μg linezolid in 24 h urine/3)/AUC_{0-24} kg^{-1}. AUC_{0-24} was determined in a separate set of serially sacrificed animals. Total clearance (ml min^{-1} kg^{-1}) was calculated as CL = dose/AUC. Fractional renal clearance was calculated as $CL_{fr} = CL_r/GFR$ using a value estimated from the literature of 9.1 ml min^{-1} kg^{-1} for glomerular filtration rate (Orloff and Berliner 1973).

Male Sprague–Dawley rats (> 200g, $n = 4$) with cannulae in the right jugular, left carotid and bladder were maintained under pentobarbital anaesthesia for the duration of the renal clearance experiments. A loading dose and fixed rate jugular co-infusion of inulin and linezolid was given to quickly attain linezolid steady-state and simultaneously determine both GFR and linezolid renal clearance. Carotid blood was taken at 0, 15, 30, 55, 75 and 95 min post-dose. Urine was collected and weighed over 0–20, 20–45, 45–65, 65–85 and 85–105 min and diluted for direct analysis by HPLC. Plasma was concentrated by solid-phase extraction (SPE) and analysed for linezolid by HPLC. Inulin was determined in plasma and diluted urine samples spectrophotometrically at 620 nm using an anthrone reagent (Heyrovsky 1956). Renal plasma flow was determined using an inulin and *p*-aminohippuric acid (PAH) co-administration ($n = 3$). PAH in diluted urine and plasma was determined colorimetrically (540 nm) using a modified method of Bratton and Marshall (1939). Linezolid CL_r and inulin CL_r (equals GFR) were determined from the linezolid and inulin concentrations in urine, urine flow rates and unbound plasma concentrations over three steady-state collection intervals. Plasma protein binding was determined separately to be 32%. Renal clearance was calculated as $CL_r = ([U]/[P]) \times$ urine flow rate, where $[U]$ and $[P]$ are steady-state urine concentration ($\mu g\,ml^{-1}$) and unbound plasma concentration ($\mu g\,ml^{-1}$), respectively. Total clearance ($ml\,min^{-1}\,kg^{-1}$) was calculated as CL = infusion rate/C_{ss} using the total plasma concentration ($\mu g\,ml^{-1}$) and an infusion rate of $23.27 \pm 0.81\,\mu g\,min^{-1}\,kg^{-1}$ for linezolid and $2753 \pm 96\,\mu g\,min^{-1}\,kg^{-1}$ for inulin. Urine flow rate was determined experimentally as $6.25 \pm 2.26\,\mu l\,min^{-1}$. Fractional renal clearance was calculated as $CL_{fr} = CL_r/GFR$.

Excretion and plasma/blood ^{14}C pharmacokinetics

Formulations and dose administration. Fasted female mice (22–25 g, $n = 4$ total) received a single $50\,mg\,kg^{-1}$ [^{14}C] linezolid p.o. suspension dose. Four mice were transferred to individual metabolism cages for the separate collection of urine and faeces over the 0–48 h post-dose period. In addition to excreta, $^{14}CO_2$ was collected from two of these mice by passage of cage air through an alkaline solution collection tower over the 0–48 h post-dose period.

Fasted male and female rats (212–220 g male, 157–173g female, $n = 3$/route) received $10\,mg\,kg^{-1}$ linezolid i.v. (tail vein) or $25\,mg\,kg^{-1}$ p.o. solution doses of [^{14}C] linezolid in a parallel design. Rats were housed individually in metabolism cages for the separate collection of urine and faeces over the 0–72 h post-dose period. In one preliminary experiment, four male rats (228–235 g) were dosed p.o. ($25\,mg\,kg^{-1}$), and in addition to excreta, $^{14}CO_2$ was collected by passage of cage air through an alkaline solution collection tower. In another experiment, three chronically bile duct-exteriorized, taurocholate-supplemented male rats (305–320 g) were administered a single $25\,mg\,kg^{-1}$ p.o. dose of [$^{2}H_3$][^{14}C] linezolid, and urine, bile and faeces were collected over the 0–48 h post-dose period. The animals were fully recovered from surgery and tubing containing bile was routed through a swivel-tether to chilled collection vessels.

Fasted male and female Beagle dogs (10–12 kg male, 7–9 kg female, $n = 3$/group, parallel design) were given a single saline solution dose of $10\,mg\,kg^{-1}$ by rapid infusion into the cephalic vein. The p.o. dose was given as a $25\,mg\,kg^{-1}$

aqueous solution (males) or 1% avicel/5% Tween 80 suspension in sodium acetate pH 4.5 (females). Animals were placed in stainless steel metabolism cages, blood was sampled and excreta were collected over 168 h post-dose.

Tissue distribution

Whole-body autoradiography study. Male rats (169–174g, $n = 1$/time point) received a 10 mg kg^{-1} i.v. bolus dose via the tail vein. Animals were euthanized at 20 min, 4, 10, and 24 h, frozen, embedded and sectioned in a PMV 450 (LKB Instruments, Stockholm, Sweden) or Leica CM3600 (Leica Instruments GmbH, Nussloch, Germany) cryomicrotome. Sections (20 μm) were apposed to Kodak Biomax MR film. Developed autoradiograms were digitally imaged and quantified using an MCID image analysis system (MCID Imaging Research, St Catherine's, Canada).

Tissue excision study. Fasted male and female rats (231–288 g male, 167–185 g female, $n = 3$/time point) received 10 mg kg^{-1} linezolid i.v. (tail vein) or 25 mg kg^{-1} p.o. solution doses of [^{14}C] linezolid in a serial sacrifice design. Male Sprague–Dawley rats were killed at 0.33, 4, 24 and 72 h post-dose. Female Sprague–Dawley rats were killed at 0.33 and 24 h post-dose. Twenty-nine tissues were collected for combustion and radio-analysis. The 72-h dose groups were housed in metabolism cages for radiochemical mass balance determination.

Protein binding. Protein binding was determined by ultrafiltration of [^{14}C] linezolid in plasma at 37 °C over a concentration range of 0.1–100 μg ml^{-1}.

One-month i.v. and p.o. toxicokinetics in rat and dog

In toxicology studies, linezolid was formulated as a suspension in Avicel-Tween-80-sodium acetate vehicle for p.o. dose administration to rat, and as a capsule to dog. For i.v. administration, linezolid was prepared as a solution in sodium citrate-dextrose. The doses given to rat were: i.v. (tail vein) 0, 20, 60 and 200 mg kg^{-1} day^{-1} or p.o. (gavage) 0, 20, 50 and 125 mg kg^{-1} day^{-1}. Doses were divided in two parts, given 8 h apart (p.o.) or 6 h apart (i.v.). The doses given to dog were: i.v. (cephalic vein) 0, 10, 20 and 40 mg kg^{-1} day^{-1} or p.o. (gavage) 0, 20, 40 and 80 mg kg^{-1} day^{-1}. Study doses were divided in two parts, given 8 h apart (p.o.) or 6 h apart (i.v.). Plasma was collected from dog and from satellite groups of rat and was assayed for linezolid by HPLC with UV detection. Non-compartmental pharmacokinetic analysis was applied to samples taken at selected time points on the first and last days of dosing.

Analytical methods

Sample isolation and bioanalytical methods. Procedures for excreta and plasma radio-analysis, quantitative metabolite extraction, radiometric HPLC profiling and non-compartmental pharmacokinetic analyses are described by Slatter *et al.* (2001). A variety of preliminary HPLC and HPLC/MS/MS methods were

employed during the conduct of these studies. Details on a robust and facile HPLC method (Peng *et al.* 2000) and HPLC/MS/MS method for linezolid and major metabolite quantification in plasma are available elsewhere (Slatter *et al.* 2001) and are generally applicable to urine or plasma from any species.

Pharmacokinetic analysis

Non-compartmental pharmacokinetic parameters were calculated as described by Slatter *et al.* (2001). Briefly, C_{max} and t_{max} for intact linezolid, metabolites in plasma, and radioactivity in plasma and whole blood were determined from individual subject concentration–time curves. The apparent terminal elimination half-life ($t_{1/2}$) was calculated as ($\ln 2/\lambda z$). The areas under the curve for intact linezolid, and metabolites in plasma and radioactivity in plasma and whole blood ($AUC_{0-t(last)}$) were determined using trapezoidals from time zero to the last quantifiable drug concentration ($C_{t(last)}$). For single-dose data, the area under the plasma linezolid, metabolite and radioactivity concentration–time curves through infinite time ($AUC_{0-\infty}$) was calculated by adding ($C_{t(last)}/\lambda z$) to $AUC_{0-t(last)}$. Total systemic clearance (CL) of linezolid was calculated as actual dose/AUC. The apparent volume of distribution (Vz/F) was calculated as $CL/\lambda z$.

Results

Pharmacokinetic and bioavailability study in mouse

Single-dose pharmacokinetic parameters for linezolid in the female mouse are summarized in table 1. Plasma linezolid decreased bi-exponentially after the i.v. dose and had a similar apparent terminal elimination $t_{½}$ (about 0.60 h) following the 10 mg kg^{-1} i.v. and p.o. doses. The volume of distribution (V_{ss} 0.629 l kg^{-1}) approximated the volume of total body water. Linezolid was rapidly absorbed after the p.o. dose, with a t_{max} at about 20 min after dosing, a C_{max} of 6.5 μg ml^{-1} and an absolute bioavailability of 72.5%. The total plasma clearance was 16.3 ml min^{-1} kg^{-1}, threefold lower than an estimated 47 ml min^{-1} kg^{-1} for hepatic plasma flow rate (derived from hepatic blood flow rate) (Boxenbaum 1980).

Pharmacokinetic and bioavailability study in rat

Single-dose pharmacokinetic parameters for linezolid in the male rat are summarized in table 2. Plasma linezolid decreased bi-exponentially after the 10 mg kg^{-1} i.v. dose and had a similar apparent terminal elimination half-life

Table 1. Summary of linezolid single-dose pharmacokinetic data for the female mouse.

Route (dose)	t_{max} (h)	C_{max} (μg ml^{-1})	AUC (μg h ml^{-1})	$t_{1/2}$ (h)	V_{ss} (l kg^{-1})	CL (mL min^{-1} kg^{-1})	F (%)
i.v. (10 mg/kg)	–	–	10.1	0.550	0.63	16.3	–
p.o. (10 mg/kg)	0.333	6.5	7.34	0.649	–	–	72.5

Data are from a serial sacrifice design, $n = 3$/time point.

Table 2. Summary of linezolid single-dose pharmacokinetic data for the male rat.

Route (dose)	t_{max} (h)	C_{max} ($\mu g\,ml^{-1}$) ($\mu g\,eq\,g^{-1}$)[a]	AUC ($\mu g\,h\,ml^{-1}$) ($\mu g\,eq\,h\,g^{-1}$)[a]	$t_{1/2}$ (h)	V_{ss} ($l\,kg^{-1}$)	CL ($ml\,min^{-1}\,kg^{-1}$)	F (%)
i.v. ($10\,mg\,kg^{-1}$)	–	15.0 ± 0.8[b]	15.5 ± 1.6	1.0 ± 0.1	0.72 ± 0.02	10.5 ± 1.1	100
p.o. ($25\,mg\,kg^{-1}$)	0.3 ± 0.2	15.8 ± 3.3	42.6 ± 6.6	1.1 ± 0.3	–	–	109
i.v.[a] ($10\,mg\,kg^{-1}$)	–	21.0 ± 13.8[ab]	29.8 ± 5.9[a]	33.1 ± 5.6[ac]	–	–	–
p.o.[a] ($25\,mg\,kg^{-1}$)	1.7 ± 0.6[a]	17.2 ± 0.8[ad]	78.1 ± 7.3[a]	25.3 ± 3.1[ac]	–	–	–

[a] Radioactivity.
[b] Concentration in sample at 0.083 h post-dose.
[c] Terminal half-life of radioactivity calculated from 72 h is related to radiolabel instability (see the text).
[d] Radioactivity was comprised of 77.6–67.5% linezolid over the period 20 min to 6 h.
Data are from three animals per dose and are the mean ± SD.

(about 1 h) following both i.v. and $25\,mg\,kg^{-1}$ p.o. dose administration. The volume of distribution ($V_{ss} = 0.72\ l\,kg^{-1}$) was similar to the volume of total body water. Linezolid was rapidly and completely absorbed after a $25\,mg\,kg^{-1}$ p.o. dose, with a t_{max} between 10 and 30 min of dosing, a mean C_{max} of $15.8\,\mu g\,ml^{-1}$, and a mean bioavailability of 109%. The C_{max} obtained from a $25\,mg\,kg^{-1}$ p.o. dose in rat is just below the steady-state human p.o. C_{max} ($21.2\,\mu g\,ml^{-1}$) obtained after a 600 mg therapeutic p.o. dose (Pharmacia 2000). The total plasma clearance was low ($10.5\,ml\,min^{-1}\,kg^{-1}$), relative to an estimated hepatic plasma flow reference of $36\,ml\,min^{-1}\,kg^{-1}$ (calculated from hepatic blood flow) (Boxenbaum 1980).

Pharmacokinetic and bioavailability study in dogs

Single-dose pharmacokinetic parameters for linezolid in the male dog are shown in table 3. In a three-way crossover study, $25\,mg\,kg^{-1}$ linezolid was given i.v. in normal saline solution, p.o. in distilled water solution and p.o. as solid drug in capsules. After the i.v. dose, linezolid plasma concentration declined bi-exponentially. The elimination phase mean $t_{1/2}$ was 3.91 h. The mean total plasma clearance was $1.99\,ml\,min^{-1}\,kg^{-1}$, and the mean steady-state volume of distribution (V_{ss}) was $0.63\,l\,kg^{-1}$. The CL was low relative to an estimate of hepatic plasma flow ($22\,ml\,min^{-1}\,kg^{-1}$, derived from hepatic blood flow) (Boxenbaum 1980). The V_{ss} was approximately equal to the volume of total body water (about $0.6\,l\,kg^{-1}$). Solution and solid capsule p.o. doses afforded similar pharmacokinetic parameters, whereby plasma concentration reached C_{max} rapidly (means 28.2 and 26.8 $\mu g\,ml^{-1}$, respectively) with mean t_{max} of 0.78 and 0.95 h for solution and capsule, respectively. This is just above the steady-state human p.o. C_{max} ($21.2\,\mu g\,ml^{-1}$) obtained after a 600 mg therapeutic p.o. dose (Pharmacia 2000). Plasma concentrations declined mono-exponentially with a mean $t_{1/2}$ of 3.6 h. The absolute bioavailability (F) was 97.3 and 96.6% for the solution and capsule, respectively.

Table 3. Summary of linezolid single-dose pharmacokinetic data for the male dog.

Route (dose)	t_{max} (h)	C_{max} ($\mu g\,ml^{-1}$) ($\mu g\,eq\,g^{-1}$)[d]	AUC ($\mu g\,h\,ml^{-1}$) ($\mu g\,eq\,h\,g^{-1}$)[d]	$t_{1/2}$ (h)	V_{ss} ($1\,kg^{-1}$)	CL ($ml\,min^{-1}\,kg^{-1}$)	F (%)
i.v. ($25\,mg\,kg^{-1}$)	–	67.2 ± 21.2[b]	214 ± 37	3.91 ± 0.38	0.63 ± 0.05	1.99 ± 0.33	100
p.o. solution ($25\,mg\,kg^{-1}$)	0.78 ± 0.19	28.2 ± 4.1	206 ± 51	3.61 ± 0.36	–	–	97.3 ± 24.3
p.o. capsule ($25\,mg\,kg^{-1}$)	0.95 ± 0.48	26.8 ± 1.5	206 ± 19	3.57 ± 0.06	–	–	96.6 ± 20.7
i.v. ($10\,mg\,kg^{-1}$)	–	23.2 ± 3.5[bd] radioactivity	71.7 ± 4.6[d] radioactivity	83.4 ± 16.3[cd] radioactivity	–	–	–
	–	20.8 ± 3.6[b] linezolid	58.8 ± 2.5[b] linezolid	2.8 ± 0.2 linezolid	0.68 ± 0.03	2.8 ± 0.1	–
p.o. ($25\,mg\,kg^{-1}$)	0.7 ± 0.7[d]	29.7 ± 3.4[bd] radioactivity	205 ± 13[d] radioactivity	87.5 ± 12.4[cd] radioactivity	–	–	–
	0.6 ± 0.8[a]	27.3 ± 3.2[b] linezolid	164 ± 11[b] linezolid	3.03 ± 0.5 linezolid	–	–	–

[a] Concentration in sample at 0.08 h.
[b] Concentration in sample at 0.02 h.
[c] Terminal half-life of radioactivity calculated from 168 h is related to radiolabel instability (see the text).
[d] Radioactivity.
Data are from three animals per dose and are the mean ± SD.

Renal clearance in mouse and rat

The renal clearance (CL_r) of linezolid in mouse resulting from an i.v. dose administration was $3.68\,ml\,min^{-1}\,kg^{-1}$. CL_r was less than a reference value for the GFR of mouse of $9.1\,ml\,min^{-1}\,kg^{-1}$ (Orloff and Berliner 1973), and the ratio of CL_r/GFR is approximately 0.4, indicating a net tubular reabsorption of the drug.

In the unconscious, cannulated rat, linezolid C_{ss} (unbound) was $1.18\,\mu g\,ml^{-1}$, allowing for 32% protein binding. Total clearance of linezolid was $13.5 \pm 1.4\,ml\,min^{-1}\,kg^{-1}$. This was similar to total inulin clearance ($15.2 \pm 8.5\,ml\,min^{-1}\,kg^{-1}$). Linezolid had very low renal clearance (CL_r) ($0.9 \pm 0.6\,ml\,min^{-1}\,kg^{-1}$), however, relative to the measured GFR of 12.4 ± 6.9, CL_r/GFR was therefore 0.08 (8%) indicating extensive net renal tubular reabsorption of linezolid. Renal tubular reabsorption is therefore a significant contributor to linezolid's low to moderate total clearance. The low CL_r indicates that there was a significant non-renal component of the total clearance of linezolid in rat. No effect of urine pH on clearance was observed, in accord with the fact that linezolid is neutral throughout the physiological pH range (data not shown). Tubular reabsorption is assumed to be passive.

Radiolabel excretion studies

Mouse. Linezolid was radiolabelled in the carbonyl carbon of the acetamide moiety (figure 1). In the female mouse, recovery of radioactivity in urine and faeces was largely complete by 48 h (table 4), with a total recovery of >95%. Urinary excretion accounted for 50–60% of the dose. An average of 4.1% of the dose was recovered as $^{14}CO_2$.

Table 4. Summary of linezolid single-dose radioactivity recoveries for the female mouse and male rat and dog.

Route	Matrix	Radioactivity recovery (mean % of dose ± SD) Mouse (0–48 h)	Rat (0–72 h)	Dog (0–168 h)
i.v.	Urine	–	66.0 ± 1.8	47.8 ± 3.8
	Faeces	–	30.4 ± 1.4	50.2 ± 1.8
	Total recovery	–	96.5 ± 0.6[b]	98.4 ± 2.0[b]
p.o.	Urine	56.4 ± 5.4	68.6 ± 0.9	50.9 ± 4.9
solution	Faeces	31.2 ± 5.1	26.3 ± 1.0	46.4 ± 4.8
	Total recovery	95.7 ± 1.0[ac]	95.0 ± 0.1[ab]	98.9 ± 0.7[b]

[a] Preliminary label stability in rat recovered 0.6 ± 0.1% of dose in carcass at 120 h and 2.7% of dose as $^{14}CO_2$ over 72 h, mice expired approximately 4% of dose as $^{14}CO_2$.
[b] Total radioactivity – includes cagewash.
[c] Total radioactivity – includes expired air, carcass, cagewash.
Data are from four mice or three rats or dogs per dose and are the mean ± SD.

Rat. Single-dose pharmacokinetic parameters for radioactivity in the male rat are shown in table 2 (female data are not tabulated). There were no obvious gender-related differences in the radioactivity pharmacokinetic parameters. After a 10 mg kg^{-1} i.v. dose, bi-exponential decay of radioactivity afforded a mean terminal half life of 33.1 and 29.6 h in the male and female, respectively. The longer terminal phase half-life of radioactivity relative to parent drug reflected cycling of endogenous by-products of a small amount of metabolically released [^{14}C] acetate (data not shown). After an p.o. 25 mg kg^{-1} dose, C_{max} was 17.2 μg eq. ml^{-1} with t_{max} at 2 h in the male rat and 17.4 μg eq. ml^{-1} with t_{max} at 1 h in the female. Linezolid accounted for 60–70% of the plasma radioactivity during the first 4 h after i.v. dosing; and 70–80% during the first 6 h after p.o. dosing.

Recovery of radioactivity in urine and faeces was essentially complete by 48 h (table 4). Total 0–72 h recovery was > 95% and urinary excretion accounted for about 60–70% of dose. A mean of 2.7% of the dose was recovered as $^{14}CO_2$. The carcass radioactivity burden at 72 h post-dose was 0.6% of dose.

Three bile duct-exteriorized, taurocholate-supplemented male rats were administered a single 25 mg kg^{-1} p.o. dose of [$^{2}H_3$][^{14}C] linezolid, then urine, bile and faeces were collected. The mean recoveries of radioactivity in 48 h excreta were 72.9 ± 3.7%, 6.7 ± 0.1% and 15.6 ± 4.9% for urine, faeces and bile, respectively, for a total recovery of 95.2 ± 2.0% of dose. The initial harmonic mean excretion half-life (amount remaining to be excreted (ARE) half-life) of radioactivity in bile was 3.2 ± 0.2 h.

Dog. After an i.v. dose, radioactivity concentrations decreased bi-exponentially over 0–168 h with a terminal phase half-life in the male dog of 83.4 h (table 3) (female data are not tabulated). The terminal phase did not commence until 48 h, after a 2-log decrease in plasma radioactivity concentration. The longer terminal phase of radioactivity relative to parent drug is presumed to be primarily due to cycling of endogenous by-products of a small amount of metabolically released [^{14}C] acetate. Linezolid had a half-life of 2.8 h in the male dog, and was not detectable past 24 h. Intact linezolid accounted for > 85% of plasma radioactivity up to 10 h post-dose.

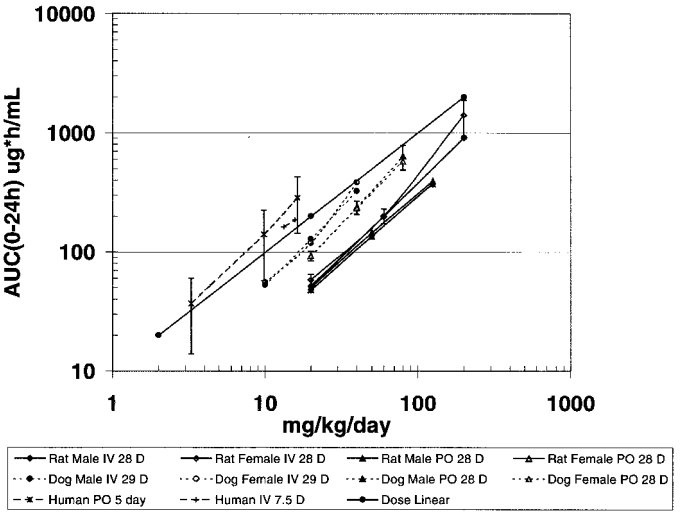


Figure 2. Comparison of linezolid steady-state 0–24 h AUC in 4-week i.v. and p.o. toxicology studies in rat and dog, to steady-state 0–24 h AUC data from i.v. and p.o. human clinical studies. For clarity, error bars (±SD) are shown for only one group per species. A line showing a hypothetical linear response is shown for comparison.

Table 5. Summary of steady-state linezolid exposure data for the male rat and dog on the last day of 4-week toxicology studies.

Species	Dose and route[a]	Mean C_{max} ($\mu g\,ml^{-1}$)	Mean C_{min}[b] ($\mu g\,ml^{-1}$)	Mean AUC[bf] ($\mu g\,h\,ml^{-1}$)
Rat	i.v., b.i.d.	–		–
	20 mg kg^{-1} day^{-1}	7.88 ± 0.46[c]	g	52.1 ± 4.0
	60 mg kg^{-1} day^{-1}	28.2 ± 1.7[c]	0.02 ± 0.01	199 ± 34
	200 mg kg^{-1} day^{-1}	110 ± 12[c]	0.70 ± 0.77	909 ± 73
	p.o., b.i.d	–		–
	20 mg kg^{-1} day^{-1}	7.55 ± 1.11[e]	0.12 ± 0.09	47.9 ± 11.7
	50 mg kg^{-1} day^{-1}	15.6 ± 3.6[e]	0.46 ± 0.18	135 ± 32
	125 mg kg^{-1} day^{-1}	36.4 ± 4.8[e]	4.52 ± 3.08	373 ± 37
Dog	i.v., b.i.d.	–		–
	10 mg kg^{-1} day^{-1}	10.4 ± 1.2[d]	0.13 ± 0.08	52.7 ± 7.1
	20 mg kg^{-1} day^{-1}	19.7 ± 1.8[d]	0.37 ± 0.10	128 ± 14
	40 mg kg^{-1} day^{-1}	42.3 ± 10.6[d]	1.96 ± 0.87	325 ± 39
	p.o., b.i.d.	–		–
	20 mg kg^{-1} day^{-1}	8.27 ± 6.89[e]	0.53 ± 0.17	93.1 ± 8.9
	40 mg kg^{-1} day^{-1}	19.7 ± 2.7[e]	2.14 ± 0.65	238 ± 31
	80 mg kg^{-1} day^{-1}	40.0 ± 15.0[e]	12.9 ± 2.6[e]	637 ± 147

[a] Dose divided into two portions given 6 or 8 h apart.
[b] C_{min} just before the morning dose.
[c] 1-h sample.
[d] 2-min sample after the afternoon dose.
[e] C_{max} afternoon dose.
[f] AUC0h–24h.
[g] Below the limit of quantitation.
Data are from three animals per dose (rats) or four animals per dose (dogs) and are the mean ± SD.

After an p.o. dose, the C_{max} for radioactivity (29.7 μg eq. ml^{-1}) was reached at 0.7 h (table 3). The plasma linezolid C_{max} was 27.3 $\mu g\,ml^{-1}$. The blood:plasma partitioning coefficient (k_p) for radioactivity (Sun *et al.* 1987) was initially about 0.8, declining to about 0.6 at 8 h post-dose. Since a value of 1 represents equal

partitioning between plasma and blood cell fractions, a slight exclusion of linezolid from blood cells in inferred. The small temporal decline in k_p over 8 h may indicate that the major anionic metabolites are excluded from the blood cell fraction to a slightly greater extent.

Approximately 50% (i.v., 48%; p.o., 51%) of the radioactive dose was recovered in urine over 48 h (table 4). The remaining radioactivity was recovered in faeces (i.v., 50%; p.o., 46%), with near quantitative recovery of radioactivity (i.v., 98%; p.o., 99%). Data from the female beagle dog were similar to data from the male dog (data not tabulated).

Four-week i.v. and p.o. toxicokinetic studies in rat and dog

Steady-state i.v. C_{max} and AUC_{0-24} data from 1-month rat and dog toxicology studies are shown in table 5 (female data are not tabulated). Oral and i.v. AUC_{0-24} data from rat and dog (both genders) are compared with steady-state human AUC_{0-24} data in figure 2.

After i.v. dosing for 4 weeks in rat, the mean AUC and mean nadir concentration did not change significantly with dosing day (day 1 data not shown). Mean AUC increased and C_{max} increased slightly greater than in proportion to the 10-fold increase in dose. As shown in figure 2, AUC increased in a predictable fashion, with each dose increment (dose multiple) adding about 10% above a proportional increase to the AUC. Differences in AUC and C_{max} between the male and female rat were minor.

Linezolid was administered to dog i.v. at doses of 10, 20 and 40 mg kg^{-1} day^{-1} in two equally divided doses with 6 h between the two daily doses. The $t_{1/2}$ and V_{ss} estimated on day 1 were in the range 2.55–3.56 h and 0.755–0.859 l kg^{-1}, respectively. Both AUC and the nadir concentrations increased with dosing day, indicating some accumulation on multiple dose administration. On day 28, the AUC and C_{max} increased in a linear fashion but were slightly greater than in proportion to the 4-fold increase in dose (figure 2). There were no significant gender differences in the pharmacokinetic parameters.

Linezolid was administered in capsules to male and female dogs at dose levels of 10, 20 and 40 mg kg^{-1} twice daily with an 8-h interval between the two daily doses (total dose 20, 40 and 80 mg kg^{-1} day^{-1}) for 30 days. The AUC increased from days 1 to 15, especially following a 80 mg kg^{-1} day^{-1} dose, but did not increase further between days 15 and 29 (day 1 and 15 data not shown). At the 80 mg kg^{-1} day^{-1} dose, the nadir concentrations of linezolid also increased with dosing day. There were no significant gender differences in the pharmacokinetic parameters.

Tissue distribution in rat

Excision study. Tissue distribution data for i.v. 10 mg kg^{-1} [^{14}C] linezolid is summarized in table 6. Consistent with the volume of distribution and bioavailability of linezolid, radioactivity was widely distributed, with most tissue concentrations similar to blood concentrations. Lower levels were observed in brain, eye, white fat, cortical bone and testis. The tissues containing radioactivity higher than the blood were liver, kidney, adrenal gland and gastrointestinal tract.

Table 6. Concentration of radioactivity ($\mu g\,eq\,g^{-1}$) in tissues of rat after a $10\,mg\,kg^{-1}$ intravenous dose of [^{14}C]linezolid.

Tissue	0.3 h	4 h	24 h
Blood	10.5 ± 0.20	0.87 ± 0.18	0.04 ± 0.00
Plasma	11.3 ± 0.10	1.04 ± 0.19	0.03 ± 0.00
Brain	1.98 ± 0.10	0.24 ± 0.04	0.02 ± 0.00
Pituitary gland	9.58 ± 0.25	0.71 ± 0.18	b
Eyeball	4.44 ± 0.25	0.68 ± 0.12	0.04 ± 0.00
Harderian gland	13.9 ± 0.90	16.1 ± 3.80	15.1 ± 1.30
Thyroid	9.13 ± 0.73	1.99 ± 0.11	1.30 ± 0.19
Thymus	9.22 ± 0.23	0.62 ± 0.15	0.06 ± 0.01
Lung	10.4 ± 0.20	0.81 ± 0.14	0.06 ± 0.00
Heart	11.0 ± 0.30	0.98 ± 0.38	0.03 ± 0.00
Liver	19.8 ± 0.90	3.01 ± 0.28	0.16 ± 0.01
Kidney	18.6 ± 1.60	3.04 ± 0.95	0.25 ± 0.03
Adrenal	18.9 ± 1.00	2.25 ± 0.49	0.30 ± 0.01
Spleen	9.62 ± 0.12	0.68 ± 0.17	0.08 ± 0.01
Pancreas	8.78 ± 0.47	0.80 ± 0.24	0.04 ± 0.00
White fat	1.74 ± 0.08	0.27 ± 0.14	0.06 ± 0.01
Brown fat	7.84 ± 0.64	0.64 ± 0.11	0.16 ± 0.02
Skin	7.82 ± 1.13	0.72 ± 0.11	0.08 ± 0.03
Muscle	9.12 ± 0.44	0.61 ± 0.17	0.02 ± 0.00
Bone marrow	9.42 ± 0.19	0.67 ± 0.15	0.09 ± 0.01
Bone mineral	1.70 ± 0.28	0.19 ± 0.06	0.02 ± 0.01
Mes. lymph node	9.18 ± 0.46	0.76 ± 0.15	0.06 ± 0.01
Stomach	10.1 ± 2.10	1.10 ± 0.28	0.57 ± 0.49
Small intestine	26.7 ± 0.40	51.8 ± 9.50	1.21 ± 0.51
Large intestine	9.38 ± 0.69	46.8 ± 3.70	9.02 ± 2.80
Bladder	11.6 ± 0.10	3.59 ± 0.17	0.06 ± 0.01
Testis	4.19 ± 0.19	0.84 ± 0.16	0.08 ± 0.01
Ovary[a]	8.79 ± 0.40	c	0.12 ± 0.04
Uterus[a]	9.55 ± 0.05	c	0.07 ± 0.03
Carcass	3.15 ± 0.10	0.24 ± 0.08	0.03 ± 0.00

[a] Data from female rats, all other tissues from male rats, tissue concentrations were similar across gender.
[b] Less than the limit of quantitation.
[c] No sample.
Data are from a serial sacrifice design using three animals per time point and are the mean ± SD.

The distribution after i.v. dosing was similar to that after p.o. dosing, except for the concentration in the gastrointestinal tract, which was higher after p.o. dosing, as expected. In the female rat, a similar distribution of radioactivity was observed. Radioactivity levels in some tissues were still measurable at 72 h. However, no long-lived residues were apparent except for the Harderian gland and thyroid. A small amount of radiolabel retention was anticipated owing to incorporation of metabolically released [^{14}C] acetate into endogenous molecules.

Whole-body autoradiography (WBA) study. Digitally coloured rat autoradiograms are shown in figure 3, where red regions represent radioactivity concentrations $> 4\,\mu g\,eq.\,g^{-1}$, the minimum inhibitory concentration (MIC) of some linezolid sensitive *Staphylococcus aureus* species. Quantitative WBA data were very similar to tissue excision results, and autoradiograms illustrate visually the homogeneous distribution of radioactivity to total body water at 20 min after the i.v. dose. Somewhat lower radioactivity concentrations were observed in brain,

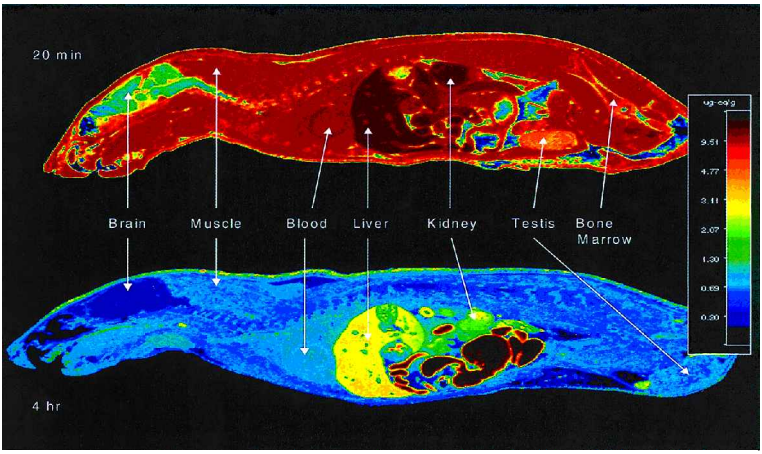


Figure 3. Colour images of representative autoradiograms from the male rat taken at 20 min and 4 h following a single 10 mg kg^{-1} i.v. administration of [^{14}C] linezolid. Red represents tissue concentrations greater than the highest MIC of susceptible organisms (> 4 μg ml^{-1}).

eye and testis, consistent with a moderate exclusion by the protective vasculature in these tissues. A pattern of exocrine secretion of radioactivity in sebaceous, ceruminous, mammary (data not shown) and Harderian glands was observed, implying that these glands excrete small amounts of the drug in sebum, earwax, milk and tears, respectively. Cortical bone was not well exposed, consistent with a low water content. However, all well-vascularized regions of bones and joints were well exposed to radioactivity. Most tissues attained similar radioactivity concentrations to blood, therefore extensive distribution to lungs, skin and other soft tissues supports the current clinical indications.

Protein binding. Protein binding of [^{14}C] linezolid at concentrations of 0.1–100 μg ml^{-1} as determined by ultrafiltration in rat, dog and human plasma was 32, 24 and 31%, respectively, and was not concentration-dependent.

Biotransformation

The metabolic pathways of linezolid are shown in figure 1. Metabolite structures were confirmed by radiometric HPLC retention time, HPLC-mass spectrometry, ^{19}F-NMR spectroscopy and by comparison with synthetic standards. Recoveries of radioactivity following extraction and concentration steps were determined experimentally to be near quantitative (data not shown). The overall metabolite abundance in excreta is summarized for mouse, rat and dog in table 7. Representative radiometric HPLC profiles of urine, bile and faeces from rat are shown in figure 4. Quantitative profiling of radioactivity related to [^{14}C] linezolid showed the three major drug-related compounds in mouse, rat and dog excreta were parent drug and the carboxylic acid metabolites, PNU-142300 and PNU-142586. Faeces generally contained the metabolites but little parent drug. In plasma, parent drug was the major radioactive component and the major metabolites, PNU-142300 and PNU-143586, were present in low relative abundance (data not shown). This observation is consistent with slow systemic formation and

Table 7. Species' comparison of [^{14}C]linezolid and metabolite abundance in excreta (faeces plus urine) after a 50 mg kg^{-1} oral dose in mouse and a 25 mg kg^{-1} oral dose in rat and dog.

Species (gender)	Parent linezolid	PNU-142300	PNU-142586	PNU-173558	PNU-142618	Sum of other (highest individual)[a]
Mouse (female)	34.0 ± 2.9	16.1 ± 0.4	3.2 ± 0.1	7.6 ± 0.4	3.4 ± 0.2	11.5 (2.0%)
Rat (male)	32.4 ± 2.1	29.6 ± 2.3	6.9 ± 1.4	4.6 ± 0.9	2.2 ± 0.3	13.8 (5.0%)
Rat (female)	32.5 ± 0.9	20.6 ± 1.1	5.4 ± 0.5	4.2 ± 0.5	1.5 ± 0.3	24.6 (5.2%)
Rat (male)[b]	31.8 ± 0.7	33.5 ± 0.7	7.5 ± 2.6	6.0 ± 1.1	4.2 ± 1.8	7.5 (1.1%)
Dog (male)	28.5	23.3	16.8	10.7	1.8	15.3 (3.3%)
Dog (female)	21.0 ± 2.5	28.1 ± 1.7	19.2 ± 0.6	11.9 ± 0.3	2.3 ± 0.2	7.7 (1.6%)

[a] Only metabolites >1% of dose in humans are shown individually. Many minor metabolites were quantified.

[b] Bile duct-exteriorized rat, recoveries include metabolites in urine, faeces and bile. Taurocholate supplemented during bile collection.

Data are derived from three animals per dose level (rat and dog) or four animals per dose level (mouse) and are the mean ± SD.

Data are the metabolite abundance (% of radioactive dose).

relatively rapid renal clearance of the carboxylic acid metabolites. The plasma metabolite profile was reasonably consistent across species, although mouse, rat and dog had relatively more circulating PNU-142300 than did man. Higher formation of PNU-142300 may account for the lower exposure to linezolid in mouse, rat and dog relative to man. Therefore, mouse, rat and dog were exposed to the major human metabolites PNU-142586 and PNU-142300. However, unlike man, where PNU-142586 formation is rate-limiting in linezolid clearance (Slatter *et al.* 2001), PNU-142300 formation appears to be clearance rate limiting in rat.

Discussion

Preclinical species similarity to human ADME

The ADME data collected to date on linezolid in mouse, rat, dog and man were reasonably consistent across i.v. and p.o. dosing routes and across species, supporting the use of the rat and dog as the principal non-clinical safety species. Linezolid was rapidly absorbed after p.o. dosing in all species examined, with essentially complete p.o. bioavailability in rat, dog and man. This attribute allows i.v. to p.o. switches to be made in the clinic without a dose adjustment.

There were no gender-related differences in linezolid pharmacokinetics in dog, or after a single dose in rat. After repeated doses, the female rat tended to have somewhat higher AUC than the male. The differences were minor (10–20%) and not consistent across studies. Similarly, in a single-dose study, female human subjects had about 20% lower body weight-normalized clearance than males (Sisson *et al.* 1999), although the mechanisms underlying these subtle gender differences may not be the same in rat and man.

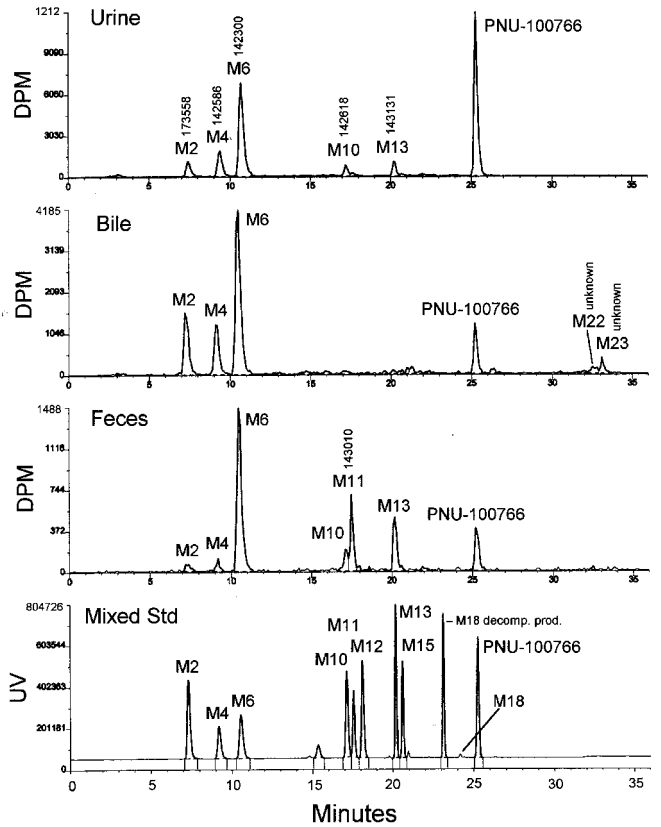


Figure 4. Representative radiometric HPLC profiles of urine, bile and faeces from a bile-duct exteriorized, taurocholate-supplemented rat after a 25 mg kg^{-1} p.o. dose of [^{14}C] linezolid, compared with a mixed standard. In the mixed standard, peaks not labelled in the excreta chromatograms are: M12 is PHA-105368 (not radioactive), M15 is the lactam PHA-144089, and M18 is the lactone PHA 142620 (structures shown in figure 1).

Linezolid circulates mainly as parent drug in mouse, rat, dog and man and circulating metabolites have no significant antibacterial efficacy (data not shown). Protein binding of linezolid is uniformly low ($\leqslant$35%) in both preclinical species and in man, therefore free linezolid is well distributed to most extravascular sites. Accordingly, volumes of distribution were on the order of total body water in all species. The homogeneous distribution of drug related radioactivity shown in figure 3 is an ideal requisite for an antibiotic agent that is indicated for pneumonia or other soft tissue infections. Exceptions to this homogeneous distribution occurred in brain, vitreous humour and bone, where drug concentrations were measurable, but lower than in tissues without tight junction barriers (brain and eye) or a higher water content (bone).

No significant induction, inhibition or metabolism by cytochrome P450 enzymes has been detected, and clinical drug interactions related to cytochrome P450 are not anticipated (Wienkers *et al.* 1999, Wynalda *et al.* 2000). The rate-limiting step in linezolid clearance in man was shown to be the formation of PNU-143011, a precursor of the major human metabolite PNU-142586 (Wienkers *et al.* 1999, Wynalda *et al.* 2000, Slatter *et al.* 2001). *In vitro*, this oxidation is not

catalysed by any known cytochrome P450s and is proposed to occur by a non-enzymatic mechanism. This implied that the morpholine ring of linezolid has weak antioxidant character, and this was proven by electrochemical measurements and a variety of *in vitro* experiments (Wienkers *et al.* 1999) and is supported by some examples of antioxidant morpholine compounds in the literature (Tanni *et al.* 1994).

Renal excretion of drug-related material was a major elimination route in rat and man, and was approximately equivalent to faecal elimination in the mouse and dog. Little parent drug was observed in the faeces, making enterohepatic recirculation of parent drug likely, since bioavailability was near 100%. In all species, both parent drug and metabolites were excreted extensively in urine. Renal clearance was less than GFR, implying renal tubular reabsorption of the neutral parent drug is a factor in the overall moderate clearance of linezolid. Accordingly, renal tubular absorption was extensive (CL_r was 8% of GFR) in the anaesthetized-cannulated rat model.

Species differences in the lactone and lactam metabolism pathways

The two major metabolism pathways are initiated by oxidation either adjacent to the morpholine nitrogen (denoted the lactam pathway) or adjacent to the morpholine oxygen (denoted the lactone pathway) (Slatter *et al.* 2001, figure 1). The major oxidation products of the lactam and lactone pathways in all species were the inactive carboxylic acids PNU-142300 and PNU-142586, respectively. Minor by-products of these metabolites were also observed and have been discussed elsewhere (Slatter *et al.* 2001). These morpholine oxidations are in accord with the metabolism pathways of other morpholine containing drugs, such as timolol and moclobemide (Tocco *et al.* 1980, Jauch *et al.* 1990). A list of morpholino compounds metabolized by the lactam pathway was compiled in a recent review, and included moclobemide, timolol, nitrimidazine, doxapram, viloxazine, minaprine, indelloxazine, reboxetine and AWD 122-14 (Vickers and Polsky 2000).

The lactone pathway of linezolid metabolism was favoured by 2–4-fold in man (Slatter *et al.* 2001), whereas the lactam pathway was favoured in rat by 2-fold. Therefore, the rate-limiting clearance step in rat, unlike man, may be PNU-142300 formation. The mouse favoured neither pathway whereas dog favoured lactone formation only slightly with a lactone/lactam ratio of 1.2, so both metabolism pathways contributed about equally to overall clearance.

At an equivalent mg kg^{-1} dose level, the exposure (AUC) of linezolid to man is greater than in animals in the order: human > dog > rat (figure 2). Since the ratio of lactone to lactam pathways increases in the same order, we speculate that species differences in the relative amount of the lactone or lactam metabolic pathways may account for the shift in the linear dose–AUC relationship across species. Regardless of which metabolic pathway was favoured, systemic clearance in all species was low to moderate. This was a result of relatively inefficient oxidative biotransformations that proceed as a consequence of renal tubular reabsorption of the neutral parent drug.

Metabolic pathways involving loss of the ^{14}C label (desacetylation of the oxazolidinone ring side-chain) or oxidation on the non-morpholine portion were minor in all species. Rat and mouse dosed with PNU-105368, produced linezolid

as a major metabolite (Slatter *et al.*, unpublished data), therefore any deacetylation of linezolid is likely to be reversible *in vivo* and is quantitatively less than the total recovery of radioactive carbon dioxide (< 5% of dose). The reacetylation of PNU-105368 is presumed to involve *N*-acetyltransferase (NAT), which affords non radioactive linezolid. Nicholls (1999) has described a similar futile deacetylation/reacetylation for phenacetin.

In summary, the overall metabolism of linezolid was qualitatively similar across species and no metabolites were unique to man. Collectively, the preclinical *in vivo* ADME data support the use of rat and dog as suitable preclinical safety species since man, rat and dog share these general ADME characteristics: 100% p.o. bioavailability, low protein binding, mainly parent drug in circulation, distribution to total body water, slow but extensive oxidative metabolism to the same inactive, anionic major metabolites, renal tubular reabsorption and significant urinary excretion. These ADME features contribute to the safety and efficacy of this novel oxazolidinone antibiotic.

Acknowledgements

This paper encompasses a portion of the preclinical ADME work done during the development of Linezolid (Zyvox^{TM}). As such, the authors gratefully acknowledge the following study contributors: B. E. Bothwell, D. Branstetter, K. S. Cathcart, M. Courtney, J. N. Duncan, J. A. Easter, P. E. Fagerness, M. J. Hauer, M. G. Johnson, B. W. Jones, G. Jungbluth, M. D. Koets, M. T. Kuo, J. Moe, J. L. Nederhoed, L. R. Norris, R. J. Ouding, J. Palandra, P. E. Sanders, F. J. Schwende, E. M. Shobe, R. P. Stryd, T. L. VandeGiessen, M. T. Verburg, J. J. Vrbanac, K. F. Wilkinson and R. J. Zielinski of Pharmacia Corp., Kalamazoo, MI. M. R. Howard, I. J. Martin, H. G. Parks, B. J. Passingham, R. J. Simmonds, W. Speed and D. Yallop of the former Pharmacia and Upjohn Corp. Laboratories, Crawley, UK. H. Aoyama, M. Aoyama, T. Fukuda, J. Hatanaka, E. Hisamatsu, S. Iida, Y. Kaneko, K. Kobayashi, S. Komatsu, T. Mitsui, H. Miura, S. Murata, R. Nakamura, K. Tsukamoto, F. Uda, K. Yamamoto and T. Zenki of the former Upjohn Pharmaceuticals Ltd, Tsukuba Laboratories. D. Pilon and A. Pombo-Gentile of Phoenix Laboratories, Montreal, Canada.

References

Boxenbaum, H., 1980, Interspecies variation in liver weight, hepatic blood flow, and antipyrine intrinsic clearance: extrapolation of data to benzodiazepines and phenytoin. *Journal of Pharmacokinetics and Biopharmaceutics*, **8**, 165–176.

Bratton, C. and Marshall, E. K., 1939, A new coupling agent for sulfanilamide determination. *Journal of Biological Chemistry*, **128**, 537–539.

Chiba, K., Feenstra, K. L., Slatter, J. G., Daley-Yates, P., Duncan, J. N., Fagerness, P. E., Howard, M. R., Martin, I. J., Ozawa, N., Passingham, B. J., Parks, H. G., Peng, G. W., Simmonds, R. J., Speed, W., Yallop, D. and Yamazaki, S., 1998, Absorption, distribution, metabolism and excretion of the oxazolidinone antibiotic linezolid (PNU-100766) in the Sprague–Dawley rat. Poster at the 38th Interscience Conference on Antimicrobial Agents and Chemotherapy, San Diego, CA, USA, Poster A-123.

Demyan, W. F., Swaney, S. M. and Shinabarger, D. L., 1997, The oxazolidinone linezolid inhibits translation initiation in bacteria. In *Proceedings of the 37th Interscience Conference on Antimicrobial Agents and Chemotherapy*, Toronto, Canada, Abstract 5375.

Heinzel, G., Wolosczak, R. and Thomman, P., 1993, *TOPFIT 2.0. Pharmacokinetic and Pharmacodynamic Data Analysis System for the PC* (Stuttgart: Gustav Fischer).

Heyrovsky, A., 1956, A new method for the determination of inulin in plasma and urine. *Clinica Chimica Acta*, **1**, 470.

Jauch, R., Griesser, E., Oesterhelt, G., Arnold, W., Meister, W., Ziegler, W. H. and Guentert, T. W., 1990, Biotransformation of moclobemide in humans. *Acta Psychiatrica Scandinavica Supplement*, **360**, 87–90.

Koike, S., Miura, H., Nakamura, R., Chiba, K. and Moe, J. B., 1995, Drug safety studies with a novel oxazolidinone U-100766. In *Proceedings of the 35th Interscience Conference on Antimicrobial Agents and Chemotherapy*, San Francisco, CA, USA, Abstract 5375.

Lin, A. H., Murray, R. W., Vidmar, T. J. and Marotti, K. R., 1997, The oxazolidinone eperezolid binds to the 50S ribosomal subunit and competes with the binding of chloramphenicol and lincomycin. *Antimicrobial Agents and Chemotherapy*, **41**, 2127–2131.

Nicholls, A. W., Lindon, J. C., Farrant, R. D., Shockcor, J. P., Wilson, I. D. and Nicholson, J. K. 1999, Directly-coupled HPLC-NMR spectroscopic studies of metabolism and futile deacetylation of phenacetin in the rat. *Journal of Pharmaceutical and Biomedical Analysis*, **20**, 865–873.

Orloff, J. and Berliner, R. W., 1973, *Handbook of Physiology, Section 8, Renal Physiology* (Washington, DC: American Physiological Society), p. 229.

Pawsey, S. D., Daley-Yates, P. T., Wajszczuk, C. P. and Stalker, D. J., 1996, U-100766 Safety, toleration and pharmacokinetics after oral and intravenous administration. In *Proceedings of the European Congress of Antimicrobial Chemotherapy*, Abstract F151.

Peng, G. W., Stryd, R. P., Murata, S., Igarashi, M., Chiba, K., Aoyama, H., Aoyama, M., Zenki, T. and Ozawa, N., 1999, Determination of linezolid in plasma by reversed-phase high-performance liquid chromatography. *Journal of Pharmaceutical and Biomedical Analysis*, **20,** 65–73.

Pharmacia Corp., 2000, Zyvox package insert. In *Physicians' Desk Reference* (Montvale: Medical Economics) [http://www.pdrel.com].

Shinabarger, D. L., Marotti, K. R., Murray, R. W., Lin, A. H. and Melchior, E. P., 1997, Mechanism of action of oxazolidinones: effects of linezolid and eperezolid on translation reactions. *Antimicrobial Agents and Chemotherapy*, **41**, 2132–2136.

Sisson, T. A., Jungbluth, G. L. and Hopkins, N. K., 1999, Effect of age and gender on linezolid pharmacokinetics. In *Proceedings of the 39th Interscience Conference on Antimicrobial Agents and Chemotherapy*, San Francisco, CA, USA, Abstract 32.

Slatter, J. G., Stalker, D. J., Feenstra, K. L., Welshman, I. R., Bruss, J. B., Sams, J. P., Johnson, M. G., Sanders, P. E., Hauer, M. J., Fagerness, P. E., Stryd, R. P., Peng, G. W. and Shobe, E. M., 2001, Pharmacokinetics, metabolism, and excretion of linezolid following an oral dose of [^{14}C] linezolid to healthy human subjects. *Drug Metabolism and Disposition*, **29**, 1136–1145.

Stalker, D. J., Wajszczuk, C. P. and Batts, D. H., 1997a, Linezolid safety, tolerance, and pharmacokinetics following oral dosing twice daily for 14.5 days. In *Proceedings of the 37th Interscience Conference on Antimicrobial Agents and Chemotherapy*, Toronto, Canada.

Stalker, D. J., Wajszczuk, C. P. and Batts, D. H., 1997b, Linezolid safety, tolerance, and pharmacokinetics after intravenous dosing twice daily for 7.5 days. In *Proceedings of the 37th Interscience Conference on Antimicrobe Agents and Chemotherapy*, Toronto, Canada.

Sun, J. X. S., Embil, K., Chow, D. S. L. and Lee, C. C. S., 1987, High-performance liquid chromatographic analysis, plasma protein binding and red blood cell partitioning of phenprobamate. *Biopharmaceutics and Drug Disposition*, **8**, 341–351.

Swaney, S. M. and Shinabarger, D. L, 1997, Oxazolidinone mechanism of action: eperezolid inhibits the initiation event of protein synthesis in bacteria. In *Proceedings of the 97th General Meeting of the American Society for Microbiology*, Miami Beach, FL, USA, Abstract A-57.

Tanni, E, Rekka, E. and Kourounakis, P. N., 1994, Synthesis and effect on free radical processes of some substituted morpholine derivatives with potential biological activity. *Arzeimittel Forschung/ Drug Research*, **44**, 992–994.

Tocco, D. J., Duncan, A. E., deLuna, F. A., Smith, J. L., Walker, R. W. and Vandenheuvel, W. J., 1980, Timolol metabolism in man and laboratory animals. *Drug Metabolism and Disposition*, **8**, 236–240.

Vickers, S. and Polsky, S. L., 2000, The biotransformation of nitrogen containing xenobiotics to lactams. *Current Drug Metabolism*, **1**, 357–389.

Wienkers, L. C., Wynalda, M. A., Feenstra, K. L., Gao, P. and Slatter, J. G., 1999, *In vitro* metabolism of linezolid (PNU-100766): lack of induction or inhibition of cytochrome P450 enzymes and studies on the mechanism of formation of the major human metabolite, PNU-142586. In *Proceedings of the 39th Interscience Conference on Antimicrobial Agents and Chemotherapy*, San Francisco, CA, USA.

Wynalda, M. A., Hauer, M. J. and Wienkers, L. C., 2000, Oxidation of the novel oxazolidinone antibiotic linezolid in human liver microsomes. *Drug Metabolism and Disposition*, **28**, 1014–1017.

XENOBIOTICA, 2002, VOL. 32, NO. 10, 925–934

Taylor & Francis
healthsciences

Pharmacokinetic scaling of bisphenol A by species-invariant time methods

CHANG YOUN CHO†, BEOM SOO SHIN†, JI HOON JUNG†, DONG HWAN KIM†, KANG CHOON LEE†, SOON-YOUNG HAN‡, HYUNG SIK KIM‡, BYUNG MU LEE† and SUN DONG YOO†*

† College of Pharmacy, Sungkyunkwan University, 300 Chonchon-dong, Changan-gu, Suwon, Kyonggi-do, 440-746, Korea
‡ Division of Reproductive and Developmental Toxicology, National Institute of Toxicological Research, 5 Nokbon-dong, Eunpyung-ku, Seoul, 122-704, Korea

Received 14 March 2002

1. The study was performed to predict the pharmacokinetic disposition of bisphenol A in humans using simple allometry and several species-invariant time methods based on animal data. Bisphenol A was injected intravenously to mouse, rat, rabbit and dog (1–2 mg kg^{-1} doses).

2. The obtained serum concentration–time profiles were best described by bi-exponential equations in all these animal species, with the mean Cl, V_{ss} and $t_{1/2}$ of 0.3 l h^{-1}, 0.1 litres and 39.9 min in mouse, 1.9 l h^{-1}, 1.3 litres and 37.6 min in rat, 12.6 l h^{-1}, 7.1 litres and 40.8 min in rabbit, and 27.1 l h^{-1}, 20.0 litres and 43.7 min in dog, respectively.

3. The human pharmacokinetic parameters of Cl, V_{ss} and $t_{1/2}$ were predicted by simple allometry as well as by normalization according to species-invariant times of kallynochrons, apolysichrons and dienetichrons.

4. The simple allometric scaling and different time transformation methods predicted the human Cl, V_{ss} and $t_{1/2}$ ranging from 46.0 to 127.1 l h^{-1}, 125.3 to 229.7 litres and 43.6 to 196.2 min, respectively. Species-invariant time transformations showed that all animal data from the four species were superimposable. These preliminary parameter values may be useful in interpreting toxicity data in humans on environmental exposure to bisphenol A.

Introduction

Bisphenol A [2,2-bis(*p*-hydroxyphenyl)propane] is a chemical used primarily in the production of epoxy resins and polycarbonate plastics (Keith 1997). Because these resins and plastics are widely used in the food, drink and medical packaging industries (Krishinan *et al.* 1993, Olea *et al.* 1996), there is a potential for exposure in humans to bisphenol A. Bisphenol A is listed by the US Environmental Protection Agency (EPA) as an endocrine-modifying chemical (Keith 1997) and it has been shown to increase cell proliferation significantly in various human breast cancer cell lines (Krishnan *et al.* 1993, Schafer *et al.* 1999) and in the rat mammary gland (Colerangle and Roy 1997). In addition, the reproductive, foetal, perinatal and postnatal toxicities of bisphenol A have been extensively examined at relatively high or physiologically relevant doses (Morrissey *et al.* 1987, vom Saal *et al.* 1998, Fisher *et al.* 1999, Nagao *et al.* 1999).

* Author for correspondence; e-mail: sdyoo@skku.ac.kr

Xenobiotica ISSN 0049–8254 print/ISSN 1366–5928 online © 2002 Taylor & Francis Ltd
http://www.tandf.co.uk/journals
DOI: 10.1080/00498250210163315

Recently, a number of studies have reported on the absorption and pharmacokinetic disposition of bisphenol A in animals (Pottenger *et al.* 1997, Snyder *et al.* 2000, Upmeier *et al.* 2000, Yoo *et al.* 2000, 2001). The pharmacokinetics of bisphenol A are linear in rat over an intravenous (i.v.) dose ranging from 0.2 to 2 mg kg^{-1} (Yoo *et al.* 2000). In this latter animal species, bisphenol A was rapidly metabolized and excreted unchanged in urine in small quantities (Pottenger *et al.* 1997, Yoo *et al.* 2000). The absolute oral bioavailability is low (5.3 ± 2.1%) (Yoo *et al.* 2001), and a majority (52.28–83.17%) of the administered radioactivity is found in the faeces after administration of ^{14}C-bisphenol A by oral, subcutaneous (s.c.) and intraperitoneal (i.p.) routes (Pottenger *et al.* 2000). To our knowledge, only limited information is available on the pharmacokinetic disposition of bisphenol A in humans, i.e. this chemical has been detected in the human placenta at concentrations of 3–100 ng g^{-1} (Schönfelder *et al.* 2000).

This study examined the pharmacokinetics of bisphenol A in mouse, rat, rabbit and dog after i.v. injection. In addition, the pharmacokinetic disposition and parameter values of bisphenol A were predicted in humans from the animal data using simple allometric scaling as well as various other species-invariant pharmacokinetic space times.

Materials and methods

Chemicals

Bisphenol A, butyl paraben, hydrochloric acid, xylazine and triethylamine were purchased from Sigma Chemical Co. (St Louis, MO, USA). Phosphoric acid and polyethylene glycol 400 were obtained from Wako Pure Chemicals Co. (Kyoto, Japan) and Yakuri Pure Chemicals Co. (Osaka, Japan), respectively. Ketamine hydrochloride was obtained from Yuhan Co. (Seoul, Korea). Acetonitrile, methanol and methylene chloride (all HPLC grades) were purchased from J. T. Baker (Phillipsburg, NJ, USA).

Animal study

Male ICR mice (20–29 g) and male New Zealand white rabbits (2.07–2.65 kg) were purchased from Hanlim Co. (Hwasung, Korea); male Sprague–Dawley rats (265–305 g) from Jeil Co. (Ansung, Korea). The animals were maintained at 23 ± 2 °C with a 12-h light/dark cycle and relative humidity of 50 ± 10%, and they had free access to standard animal diet (Samyang, Seoul, Korea) and water. Bisphenol A was injected i.v. to mouse (2 mg kg^{-1}, $n = 5$ at each sampling time), rat (1 mg kg^{-1}, $n = 7$) and rabbit (1 mg kg^{-1}, $n = 6$), and serial blood samples were obtained for plasma concentration determination before and 2, 5, 10, 15, 30 min, 1, 1.5, 2, 3, 4 and 6 h after drug administration. Bisphenol A was administered to mouse through the tail vein, and blood samples were taken by heart puncture. The rats were cannulated with PE tubing (0.58 mm i.d., 0.96 mm o.d., Natsume Co., Tokyo, Japan) in the right jugular and left femoral veins. After 2 days of recovery, the rats were injected with bisphenol A into the femoral vein, and blood samples were taken from the jugular vein. The rabbits were injected with bisphenol A into the left marginal ear vein and blood samples were collected from the right marginal ear vein. The male beagle dogs (10.2–11.0 kg; Jeil Co. Ansung, Korea) were injected i.v. with a single bolus dose of bisphenol A (1 mg kg^{-1}, $n = 5$) in the left tarsal vein and blood samples were taken from the right lateral tarsal vein at the times described above. All serum samples were harvested by centrifugation at 1500g for 10 min and were kept at −20 °C until drug analysis.

Analysis of bisphenol A

Bisphenol A concentrations in serum were determined by a validated HPLC method with fluorescence detection (Shin *et al.* 2001). Briefly, to aliquots (100 µl) of serum samples in borosilicate tubes (Scientific Glass, Inc., Rockwood, TN, USA) were added 100 µl internal standard (butyl paraben, 3 µg ml^{-1} in methanol) and 0.1 N HCl. The mixture was extracted with 2 ml methylene chloride on a vortex mixer for 3 min and centrifuged at 7000g for 10 min. The supernatant was transferred into a fresh tube and dried under nitrogen gas at 40 °C (Dry Thermo Bath MG-2000, Tokyo Rikakikai Co., Tokyo, Japan). The residue was reconstituted with 80 µl of the HPLC mobile phase on a vortex mixer for 3 min. The resulting solution was centrifuged at 1500g for 30 s and the supernatant (50 µl) was injected into the

chromatograph. A Shimadzu (Tokyo, Japan) HPLC system consisting of a model RF-10AXL fluorescence detector, SCL-10A system controller, LC-10AT pump, SIL-10A auto-sampler and CTO-10A column oven was used in the assay. Chromatographic separations were achieved using a Spherisorb S5 ODS2 analytical column (4.6×250 mm, 5 μm) and a guard column (4.6×10 mm, 5 μm) supplied by Waters (Milford, MA, USA). The mobile phase was a mixture of acetonitrile and 0.1% triethylamine in deionized water (54:46 v/v %) (Puris Ultrapure Water System, Mirae Scientific, Seoul, Korea). The mobile phase was filtered and degassed by ultrasonication under vacuum before use. The flow rate of the mobile phase was maintained at 0.5 ml min^{-1} at 40 °C. The excitation and emission wavelengths were set at 278 and 315 nm, respectively. The retention times of bisphenol A and the internal standard were 9.4 and 13.6 min, respectively. The standard curves from the biological samples was linear over the concentration range 1–1000 ng ml^{-1}, with a typical correlation coefficient (r) > 0.999. The extraction recovery of bisphenol A was > 91.3%. The intra- and interday assay accuracies were > 91.5 and > 90.8%, respectively, with the assay coefficients of variation being < 5.7 and < 10.5%, respectively.

Data analysis

The serum concentration of bisphenol A versus time data were analysed by a non-compartmental method using the non-linear least-squares regression program WinNonlin (Scientific Consulting, Inc., Cary, NC, USA). The area under the serum concentration–time curve (AUC) and the area under the first moment curve (AUMC) were calculated using the trapezoidal rule extrapolated to infinite time. The extrapolation of AUC and AUMC to infinite time was obtained by adding C_n/λ_z to AUC and $t_nC_n/\lambda_z + C_n/\lambda_z^2$ to AUMC, where C_n is the concentration of the last sampling time (t_n). The slope of the terminal logarithmic concentration–time curve (λ_z) was determined by linear regression of the last six to seven data points. The terminal elimination half-life ($t_{1/2}$) was calculated as $0.693/\lambda_z$. The systemic clearance (Cl) and the volume of distribution (V_{ss}) were calculated as dose/AUC and dose AUMC/AUC^2. The pharmacokinetic parameter values were expressed as the mean ± SD. For allometric scaling, the means of Cl, V_{ss} and $t_{1/2}$ obtained in animals were correlated with the mean animal body weight using the following equations:

$$\mathrm{Cl} = aB^x \tag{1}$$

$$V_{ss} = bB^y \tag{2}$$

$$t_{1/2} = cB^z, \tag{3}$$

where a, b and c are the coefficients, x, y and z are the exponents of the allometric equations, and B is body weight (kg). The systemic clearance was also investigated using the concept of maximum lifespan potential (Sacher 1959) using equations (4) and (5), i.e. the clearances in different animal species were multiplied by their respective MLP and plotted as a function of the body weight on a log–log scale:

$$\mathrm{MLP\ (years)} = 185.4\ \mathrm{BW}^{0.636}B^{-0.225} \tag{4}$$

$$\mathrm{Cl\ MLP} = pB^q, \tag{5}$$

where both the brain weight (BW) and the body weight (B) were in kilograms. The pharmacokinetic parameters of bisphenol A in a 70-kg human was then predicted by the allometric equations (1–3) and (5), as described above. In addition, the pharmacokinetic time concepts, kallynochrons, apolysichrons and dienetichrons, were calculated as outlined below (Dedrick 1973, Boxenbaum and Ronfeld 1983, Boxenbaum 1984), and the concentration–chronological time curves obtained in these animal species were converted into a human concentration–human time curve using the power functions x, y and q:

kallynochrons (elementary Dedrick plot):

$$\mathrm{Time_H} = \mathrm{Time_A} \cdot \left(\frac{B_\mathrm{H}}{B_\mathrm{A}}\right)^{1-x} \tag{6}$$

$$\mathrm{Conc._H} = \mathrm{Conc._A} \cdot \left(\frac{\mathrm{Dose_H}}{\mathrm{Dose_A}}\right) \cdot \left(\frac{B_\mathrm{A}}{B_\mathrm{H}}\right) \tag{7}$$

apolysichrons (complex Dedrick plot)

$$\mathrm{Time_H} = \mathrm{Time_A} \cdot \left(\frac{B_\mathrm{H}}{B_\mathrm{A}}\right)^{y-x} \tag{8}$$

$$\mathrm{Conc._H} = \mathrm{Conc._A} \cdot \left(\frac{\mathrm{Dose_H}}{\mathrm{Dose_A}}\right) \cdot \left(\frac{B_\mathrm{A}}{B_\mathrm{H}}\right)^{y} \tag{9}$$

dienetichrons:

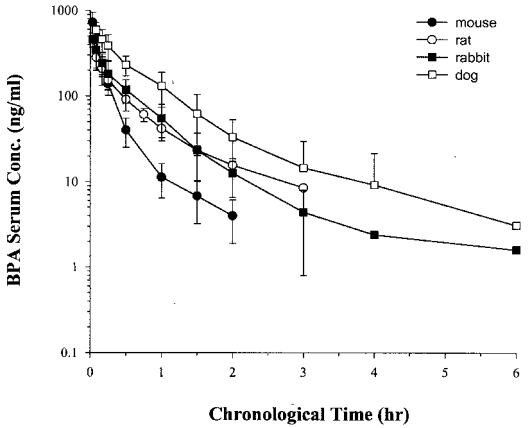


Figure 1. Mean serum bisphenol A concentration–time profiles obtained after i.v. injection to mouse ($2\,mg\,kg^{-1}$), rat ($1\,mg\,kg^{-1}$), rabbit ($1\,mg\,kg^{-1}$) and dog ($1\,mg\,kg^{-1}$). Data are the mean ± SD of five, seven, six and five determinations for mouse, rat, rabbit and dog, respectively.

Table 1. Mean pharmacokinetic parameters of bisphenol A obtained after i.v. injection to mouse ($2\,mg\,kg^{-1}$), rat ($1\,mg\,kg^{-1}$), rabbit ($1\,mg\,kg^{-1}$) and dog ($1\,mg\,kg^{-1}$).

Parameter	Mouse	Rat	Rabbit	Dog
Brain weight[1] (BW, g)	0.36	1.8	14	80
Body weight (B, kg)	0.024 ± 0.002	0.29 ± 0.001	2.34 ± 0.20	10.58 ± 0.29
Cl ($L\,h^{-1}$)	0.3	1.9 ± 0.4	12.6 ± 4.9	27.1 ± 8.0
V_{ss} (litres)	0.1	1.3 ± 0.4	7.1 ± 2.3	20.0 ± 5.4
$t_{1/2}$ (min)	39.9	37.6 ± 12.8	40.8 ± 17.1	43.7 ± 21.9

[1]Davies and Morris (1993).

Data are the mean ±SD of five, seven, six and five determinations for mouse, rat, rabbit and dog, respectively.

$$\mathrm{Time_H} = \mathrm{Time_A} \cdot \left(\frac{\mathrm{MLP_H}}{\mathrm{MLP_A}}\right) \cdot \left(\frac{B_\mathrm{H}}{B_\mathrm{A}}\right)^{y-q} \tag{10}$$

$$\mathrm{Conc._H} = \mathrm{Conc._A} \cdot \left(\frac{\mathrm{Dose_H}}{\mathrm{Dose_A}}\right) \cdot \left(\frac{B_\mathrm{A}}{B_\mathrm{H}}\right)^{y}, \tag{11}$$

where B_A and B_H are the animal and human body weights (kg), respectively, and the dose was in milligrams. The human concentration–time curves were used to calculate the pharmacokinetic parameters in humans, including Cl, V_{ss}, $t_{1/2}$, by a two-compartmental method (WinNonlin). The superimpositions of the concentration–time curves obtained from different animal species for respective pharmacokinetic time units were evaluated by coefficient of variation (r^2) and Akaike Information Criteria (AIC).

Results

The mean serum concentration–time curves of bisphenol A obtained after i.v. injection to mouse, rat, rabbit and dog are shown in figure 1. The serum concentration–time profiles were best described by bi-exponential equations in these four animal species (mouse, rat, rabbit, dog). Table 1 shows the mean body weights and pharmacokinetic parameters of bisphenol A obtained in these animals. The mean Cl and V_{ss} were $0.3\,l\,h^{-1}$ and 0.1 litres in mouse, $1.9\,l\,h^{-1}$ and 1.3 litres

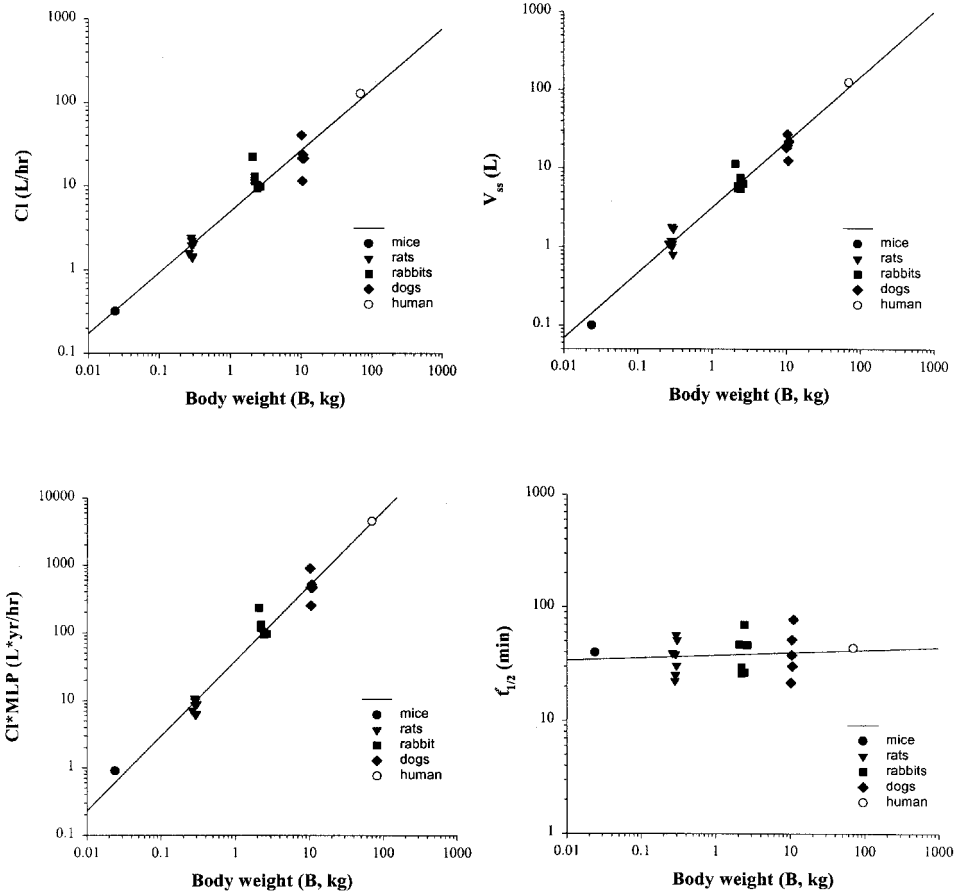


Figure 2. Interspecies' correlation between pharmacokinetic parameters and body weights. The regression line was obtained by least-squares analysis of the four animal species data. The extrapolated human parameter values based on a 70-kg body weight are also shown.

Table 2. Allometric equations and pharmacokinetic parameters of bisphenol A predicted in man based on allometric scaling of data obtained from mouse, rat, rabbit and dog.

Parameter	Allometric equation	Predicted value in man
Cl ($1h^{-1}$)	$5.264B^{0.749}$ ($r^2 = 0.993$)	127.1
V_{ss} (litres)	$2.994B^{0.879}$ ($r^2 = 0.993$)	125.3
$t_{1/2}$ (min)	$40.723B^{0.0158}$ ($r^2 = 0.451$)	43.6
Cl MLP ($1 year\,h^{-1}$)	$44.041B^{1.088}$ ($r^2 = 0.994$)	47.9[1]

[1] Calculated as the human Cl MLP divided by the human maximum lifespan potential of 8.18×10^5 h ($1h^{-1}$).

in rat, $12.61h^{-1}$ and 7.1 litres in rabbit, and $27.11h^{-1}$ and 20.0 litres in dog, respectively. There were increases in Cl, V_{ss}, Cl*MLP with increasing species body weights. The apparent terminal elimination half-life, however, remained relatively constant across the animal species tested (figure 2). Equations (1–3) and (5) were fitted to the animal data, and the resulting allometric equations were used to predict the pharmacokinetic parameter values for a 70-kg human. The predicted

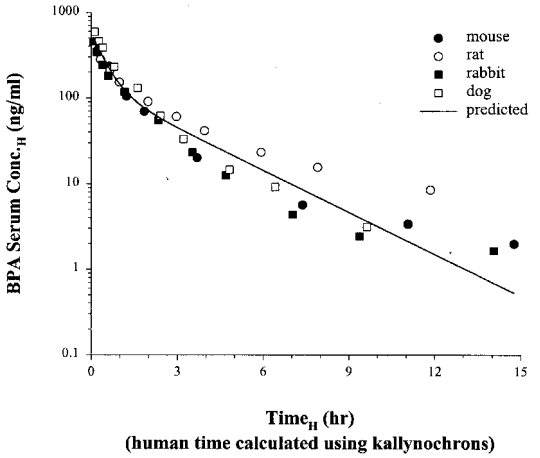


Figure 3. Estimated serum concentration–time profile in humans following a single i.v. injection (1 mg kg^{-1}) of bisphenol A obtained by a concentration–time transformation using the pharmacokinetic time, kallynochrons.

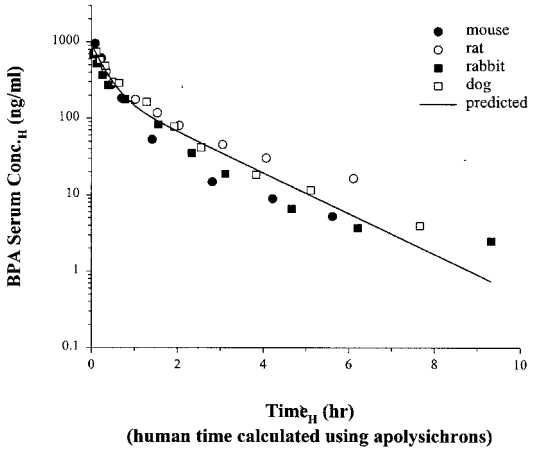


Figure 4. Estimated serum concentration–time profile in humans following a single i.v. injection (1 mg kg^{-1}) of bisphenol A obtained by a concentration–time transformation using the pharmacokinetic time, apolysichrons.

human pharmacokinetic parameters of Cl, V_{ss} and $t_{1/2}$ based on simple allometric scaling were 127.1 l h^{-1}, 125.3 litres and 43.6 min (table 2). The Cl calculated by incorporating the concept of human maximum lifespan potential was lower than predicted by the simple allometric scaling (47.9 versus 125.3 l h^{-1}).

Separately, obtained concentration–time data from animals were normalized according to the pharmacokinetic times, kallynochrons, apolysichrons and dienetichrons. The predicted human concentration–time curves of bisphenol A after i.v. injection (1 mg kg^{-1}) are shown in figures 3–5, respectively. The predicted pharmacokinetic parameters for a 70-kg human according to these species-invariant time methods are shown in table 3. Cl, V_{ss} and $t_{1/2}$ based on the apolysichron time transformation (120.7 l h^{-1}, 138.0 litres and 67.8 min, respectively) were comparable with those obtained from simple allometric scaling. The kallynochron time transformation, however, resulted in greater V_{ss} (229.7 litres) and $t_{1/2}$ (110.4 min). The dienetichron time transformation resulted in reduced Cl

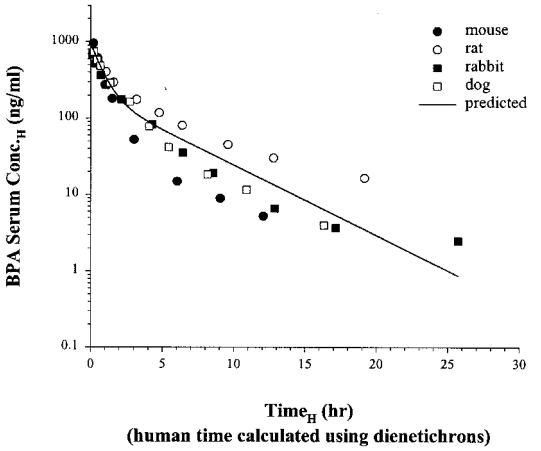


Figure 5. Estimated serum concentration–time profile in humans following a single i.v. injection (1 mg kg^{-1}) of bisphenol A obtained by a concentration–time transformation using the pharmacokinetic time, dienetichrons.

Table 3. Predicted pharmacokinetic parameters of bisphenol A in man using various concentration–time transformations.

Parameter	Kallynochrons	Apolysichrons	Dienetichrons
Cl (l h^{-1})	123.0	120.7	46.0
V_{ss} (litres)	229.7	138.0	149.3
$t_{1/2}$ (min)	110.4	67.8	196.2
r^2	0.940	0.940	0.949
AIC	221.0	233.5	244.1

(46.01 h^{-1}) and prolonged $t_{1/2}$ (196.2 min), but V_{ss} was comparable with those obtained by simple allometric scaling and apolysichron time transformation. The Cl calculated according to dienetichron times (46.01 h^{-1}) was comparable with that predicted from the simple allometric scaling of Cl MLP (47.91 h^{-1}). The superimposition and goodness of curve fitting evaluated by r^2 and AIC were comparable among different time transformations (table 3).

Discussion

Interspecies scaling is based on the assumption that similarities exist for the anatomy, biochemical and physiological functions among different animal species (Dedrick 1973, McNamara 1991). The current study discussed the interspecies' variations in the pharmacokinetics of bisphenol A as a function of body size scaling using simple allometric scaling and several other pharmacokinetic space–time transformations of kallynochrons, apolysichrons and dienetichrons (Boxenbaum and Ronfeld 1983, Ings 1990). The i.v. dose of bisphenol A used in this study (1–2 mg kg^{-1}) was less than the lowest observed adverse effect level (LOAEL 50 mg kg^{-1} day^{-1}) multiplied by an oral bioavailability of 5.3% in rat (Keith 1997, Yoo *et al.* 2001). The simple allometric scaling resulted in a relatively high Cl (127.11 h^{-1}) and V_{ss} (125.3 litres) and a short terminal elimination half-life

(43.6 min) for a 70-kg human. When serum concentrations of bisphenol A versus time data were normalized according to kallynochrons (elementary Dedrick plot), apolysichrons (complex Dedrick plot) and dienetichrons, all data obtained from mouse, rat, rabbit and dog were superimposable (figures 3–5, respectively). With the kallynochron time transformation, the volume of distribution was assumed to be directly proportional to the species body weight. Since this was not the case, i.e. y (0.879) in equation (2) was not equal to unity (table 2), the apolysichron time transformation was applied (figure 4). The superimposability of the animal data was, however, not improved as reflected by unaltered r^2 and increased AIC values (table 3). The predicted V_{ss} based on apolysichron times (138.0 litres) was comparable with that obtained by simple allometry and dienetichron time transformation, but was less than calculated by kallynochron time transformation (229.7 litres) (tables 2 and 3). The Cl predicted by kallynochron and apolysichron times were comparable with that predicted by allometric scaling (120.7–127.1 $l\,h^{-1}$). In the case of dienetichron time transformation, Cl was much lower (46.01 $l\,h^{-1}$) than predicted by other pharmacokinetic time transformations (tables 2 and 3) but was comparable with that determined by simple allometry incorporating the concept of maximum lifespan potential (47.91 $l\,h^{-1}$). The human $t_{1/2}$ predicted by different time transformations (67.8–196.2 min) were higher than that from simple allometric scaling (43.6 min). Generally, prediction of $t_{1/2}$ by interspecies scaling is considered not as successful as for Cl and V_{ss}. This poor correlation may arise in part by the fact that $t_{1/2}$ is a hybrid parameter indirectly relating to physiological functions (McNamara 1991).

A limitation of this study is that no literature information is available on the pharmacokinetics of bisphenol A in humans and, therefore, the validity of the prediction methods cannot be demonstrated. Bisphenol A is an environmental endocrine-modifying chemical and its administration to humans is unacceptable. Therefore, the pharmacokinetic parameter values predicted here may be used in interpreting bisphenol A exposure data until observed human parameter values become available. The daily human exposure to bisphenol A may be estimated as the product of the systemic clearance and AUC_{0-24h} (amount exposed daily = Cl $AUC_{0\text{-}24h}$), where AUC is obtained by determining the concentrations of bisphenol A in serial blood samples. Alternatively, under steady-state conditions, the exposure rate may be calculated as the product of the systemic clearance and the steady-state concentration (F dose/τ = Cl $C_{steady\text{-}state}$), where F is the extravascular bioavailability and τ is the exposure time. The predicted systemic clearance of bisphenol A in humans together with blood level data that may be achieved in future studies can help in the estimation of human exposure (human exposure = Cl AUC). Once the human exposure or AUC is determined, these parameters may be used to examine the toxicity-exposure relationship.

In summary, the pharmacokinetic disposition of bisphenol A was studied in the four animal species of mouse, rat, rabbit and dog after i.v. injection. In addition, the pharmacokinetics behaviour was predicted in humans using simple allometric scaling and several species-invariant time methods. These methods provide an approximate range of the systemic clearance of 46.0–123.01 $l\,h^{-1}$ and the volume of distribution of 125.3–229.7 litres for a 70-kg human. These preliminary parameter values may be useful in interpreting toxicity data in humans upon environmental exposure to bisphenol A.

Acknowledgements

The work was supported by an NITR/Korea FDA Grant No. ED2001-17 for Endocrine Disrupters Research. Partial financial support from the Brain Korea 21 by the Ministry of Education is appreciated.

References

Boxenbaum, H., 1984, Interspecies pharmacokinetic scaling and the evolutionary-comparative paradigm. *Drug Metabolism Reviews*, **15**, 1071–1121.

Boxenbaum, H. and Ronfeld, R., 1983, Interspecies pharmacokinetic scaling and the Dedrick plots. *American Journal of Physiology*, **245**, R768–R775.

Colerangle, J. B. and Roy, D., 1997, Profound effects of the weak environmental estrogen-like chemical bisphenol A on the growth of the mammary gland of Noble rats. *Journal of Steroid Biochemistry and Molecular Biology*, **60**, 153–160.

Davies, B. and Morris, T., 1993, Physiological parameters in laboratory animals and humans. *Pharmacology Research*, **10**, 1093–1095.

Dedrick, R. L., 1973, Animal scale-up. *Journal of Pharmacokinetics and Biopharmacology*, **1**, 435–461.

Fisher, J. S., Turner, K. J., Brown, D. and Sharpe, R. M., 1999, Effect of neonatal exposure to estrogenic compounds on development of the excurrent ducts of the rat testis through puberty to adulthood. *Environmental Health Perspectives*, **107**, 397–405.

Ings, R. M. J., 1990, Interspecies scaling and comparisons in drug development and toxicokinetics. *Xenobiotica*, **20**, 1201–1231.

Keith, L. H., 1997, *Environmental Endocrine Disruptors: A Handbook of Property Data* (New York: Wiley), pp. 261–270.

Krishnan, A. V., Starhis, P., Permuth, S. F., Tokes, L. and Feldman, D., 1993, Bisphenol A: an estrogenic substance is released from polycarbonate flasks during autoclaving. *Endocrinology*, **132**, 2279–2286.

McNamara, P. J., 1991, Interspecies scaling in pharmacokinetics. In P. G. Welling, F. L. S. Tse and S. V. Dighe (eds), *Pharmaceutical Bioequivalence* (New York: Marcel Dekker), pp. 267–300.

Morrissey, R. E., George, J. D., Price, C. J., Tyl, R. W., Marr, M. C. and Kimmel, C. A., 1987, The developmental toxicity of bisphenol A in rats and mice. *Fundamentals of Applied Toxicology*, **8**, 571–582.

Nagao, T., Saito, Y., Usumi, K., Kuwagata, M. and Imai, K., 1999, Reproductive function in rats exposed neonatally to bisphenol A and estradiol benzoate. *Reproductive Toxicology*, **13**, 303–311.

Olea, N., Pulgar, R., Perez, P., Olea-serrano, F., Rivas, A., Novillo-Fertrell, A., Pedraza, V., Soto, A. M. and Sonnenschein, C., 1996, Estrogenicity of resin-based composites and sealants used in dentistry. *Environmental Health Perspectives*, **104**, 298–305.

Pottenger, L. H., Domoradzki, J. Y., Markham, D. A. and Hansen, S. C., 1997, *Bioavailability of ^{14}C-bisphenol A in Fischer Rats following Oral, s.c. or Intraperitoneal Administration*. Report to the Bisphenol A Task Force Group (Society of the Plastics Industry).

Pottenger, L. H., Domoradzki, J. Y., Markham, D. A., Hansen, S. C., Cagen, S. Z. and Waechter, J. M., 2000, The relative bioavailability and metabolism of bisphenol A in rats is dependent upon the route of administration. *Toxicology Science*, **54**, 3–18.

Sacher, G., 1959, in G. E. W. Wolstenholme and M. O'Connor (eds), *CIBA Foundation Colloquia on Aging* (London: Churchill), pp. 115–133.

Schafer, T. E., Lapp, C. A., Hanes, C. M., Lewis, J. B., Wataha, J. C. and Schuster, G. S., 1999, Estrogenicity of bisphenol A and bisphenol A dimethacrylate in vitro. *Journal of Biomedical and Materials Research*, **45**, 192–197.

Schönfelder, G., Wittfoht, W., Hopp, H., Mutz, A., Halis, G., Talsness, C., Paul, M. and Chahoud, I., 2000, Bisphenol A concentration in human umbilical cord blood and placenta. Paper presented at the Symposium on Bisphenol A: Low Dose Effects–High Dose Effects, 18–20 November, Berlin, Germany.

Shin, B. S., Park, K. L., Han, S. Y., Lee, B. M., Kim, H. S., Lee, K. C., Eom, H. J. and Yoo, S. D., 2001, Sensitive micro-sample analysis of bisphenol A in serum by high-performance liquid chromatography with fluorescence detection. *Chromatographia*, **53**, 669–672.

Snyder, R. W., Maness, S. C., Gaido, K. W., Welsch, F., Sumner, S. C. J. and Fennel, T. R., 2000, Metabolism and disposition of bisphenol A in female rats. *Toxicology Science*, **168**, 225–234.

Upmeier, A., Degen, G. H., Diel, P., Michna, H. and Bolt, H. M., 2000, Toxicokinetics of bisphenol A in female DA/Han rats after a single i.v. and oral administration. *Archives of Toxicology*, **74**, 431–436.

VOM SAAL, F. S., COOKE, P. S., BUCHANAN, D. L., PALANZA, P., THAYER, K. A., NAGEL, S. C., PARMIGIANI, S. and WELSHONS, W. V., 1998, A physiologically based approach to the study of bisphenol A and other estrogenic chemicals on the size of reproductive organs, daily sperm production, and behavior. *Toxicology and Industrial Health*, **14**, 239–260.

YOO, S. D., SHIN, B. S., KWACK, S. J., LEE, B. M., PARK, K. L., HAN, S. Y. and KIM, H. S., 2000, Pharmacokinetic disposition and tissue distribution of bisphenol A in rats after intravenous administration. *Journal of Toxicology and Environmental Health, Part A*, **61**, 131–139.

YOO, S. D., SHIN, B. S., LEE, B. M., LEE, K. C., HAN, S. Y., KIM, H. S, KWACK, S. J. and PARK, K. L., 2001, Bioavailability and mammary excretion of bisphenol A in rats. *Journal of Toxicology and Environmental Health, Part A*, **64**, 417–426.

XENOBIOTICA, 2002, VOL. 32, NO. 11, 937–947

Taylor & Francis
healthsciences

Comparative study of the metabolism of drug substrates by human cytochrome P450 3A4 expressed in bacterial, yeast and human lymphoblastoid cells

J. ANDREWS†*, M. F. ABD-ELLAH†, N. L. RANDOLPH†, K. E. KENWORTHY†, D. J. CARLILE†, T. FRIEDBERG‡ and J. B. HOUSTON†

† School of Pharmacy and Pharmaceutical Sciences, University of Manchester, Manchester M13 9PL, UK
‡ Biomedical Research Centre, Ninewells Hospital and Medical School, University of Dundee, Dundee DD1 9SY, UK

Received 20 February 2002

1. The aim was to compare the metabolic activity of human CYP3A4 expressed in bacteria (*E. coli*), yeast (*S. cerevisiae*) and human lymphoblastoid cells (hBl), with the native CYP3A4 activity observed in a panel of human livers.

2. Three CYP3A4 substrates were selected for study: dextromethorphan (DEM), midazolam (MDZ) and diazepam (DZ). The substrate metabolism in each of the four systems was characterized by deriving the kinetic parameters K_m or S_{50}, V_{max} and intrinsic clearance (CL_{int}) or maximum clearance (CL_{max}) from the kinetic profiles; the latter differing by 100-fold across the three substrates.

3. The K_m or S_{50} for the formation of metabolites 3-methoxymorphinan (MEM), 1′-hydroxymidazolam (1′-OH MDZ) and 3-hydroxydiazepam (3HDZ) compared well in all systems. For CYP3A4-mediated metabolism of DEM, MDZ and DZ, the V_{max} for hBl microsomes were generally 2–9-fold higher than the respective yeast and human liver microsomes and *E. coli* membrane preparations, resulting in greater CL_{int} or CL_{max}. In the case of 3HDZ formation, non-linear kinetics were observed for *E. coli*, hBl microsomes and human liver microsomes, whereas the kinetics observed for *S. cerevisiae* were linear.

4. The use of native human liver microsomes for drug metabolic studies will always be preferable. However, owing to the limited availability of human tissues, we find it is reasonable to use any of the recombinant systems described herein, since all three recombinant systems gave good predictions of the native human liver enzyme activities.

Introduction

Cytochrome P450 (CYP) 3A4 is one of the major P450 enzymes in the human liver and it plays a key role in the oxidative biotransformation of structurally diverse endogenous and exogenous compounds, such as pharmaceutical drugs, pesticides and food additives (Friedberg and Wolf 1996, Voice *et al.* 1999). However, the interpretation of drug metabolic studies carried out with human liver microsomes (HLM) is complex due to the varying amounts and activities of the numerous CYP forms present (Shimada *et al.* 1994). To date, CYP3A4 has been expressed in a variety of heterologous systems, including bacteria (Gillam *et al.* 1993, Blake *et al.* 1996), yeast (Peyronneau *et al.* 1992), insect cells (Lee *et al.*

* Author for correspondence; e-mail julie.andrews@man.ac.uk

Xenobiotica ISSN 0049–8254 print/ISSN 1366–5928 online © 2002 Taylor & Francis Ltd
http://www.tandf.co.uk/journals
DOI: 10.1080/00498250210163289

1995) and mammalian cells (Gonzalez and Korzekwa 1995). Of these, bacterial and yeast models are the most desirable in terms of the ease of manipulation, the availability of cloning and expression vectors, and the low cost of culture. Although several authors have presented data on expression levels and enzyme activity in a single recombinant system, only two reports have presented comparative metabolic data for a range of substrates, in a variety of recombinant systems (McGinnity *et al.* 1999, Yamazaki *et al.* 1999). We therefore wanted to extend these studies by selecting a further group of CYP3A4 substrates for which we would derive comparative pharmacokinetic data, again in a variety of recombinant systems. Three CYP3A4 substrates were selected for study: dextromethorphan (DEM), midazolam (MDZ) and diazepam (DZ). DEM, an antitussive drug, is *O*-demethylated to dextrophan (DEX) via CYP2D6 and *N*-demethylated to 3-methoxymorphinan (MEM) via CYP3A4 (Ducharme *et al.* 1996). MDZ is a short-acting benzodiazepine used as a hypnotic and anaesthetic induction agent and its major metabolic pathway in humans is 1′-hydroxylation, accounting for 60–80% of an orally administered dose. The other important pathway is 4-hydroxylation (Amrein and Hetzel 1990). DZ is used world-wide as a muscle relaxant, anxiolytic and hypnotic drug. DZ undergoes *N*-demethylation and C_3-hydroxylation to form nordiazepam (NDZ) and 3-hydroxydiazepam (3HDZ), respectively. Whilst CYP3A4 is the major form involved in the formation of 3HDZ, both CYP2C19 and CYP3A4 contribute to the *N*-demethylation pathway (Jung *et al.* 1997).

In the current study, substrate metabolism in each of the three recombinant systems (*E. coli*, *S. cerevisiae* and human lymphoblastoid (hBl) cells) plus native human liver samples, has been characterized by deriving the kinetic parameters K_m or S_{50}, V_{max} and intrinsic clearance (CL_{int}) or maximum clearance (CL_{max}) from the kinetic profiles. The main aim of this study was to determine whether recombinant expression systems can yield pharmacokinetic data, for the metabolism of drugs by individual CYP enzymes, which are comparable with those obtained from native human liver microsomes.

Materials and methods

Materials

DEM, MEM and DZ were gifts from Roche Products Ltd (Welwyn Garden City, UK). MDZ and 1′-OH MDZ were purchased from Sigma Chemical Co. (Poole, UK). 3HDZ was a gift from Wyeth (Maidenhead, UK). Prazepam (internal standard) was obtained from Warner Co. (Pontypool, UK). All other chemicals were of the highest quality commercially available.

Methods

Enzyme preparations

Expression in E. coli. Membranes were prepared from *E. coli* JM109 transformed with pB216, a plasmid containing the human cDNAs for CYP3A4 and NADPH P450 reductase (NPR). Growth of the cells, co-expression levels, and the methods for harvesting and fractionating the cell membranes have been described by Blake *et al.* (1996).

Expression in S. cerevisiae. Yeast microsomes were prepared from *S. cerevisiae* INVSc1 cotransformed with the plasmids pMA91/3A4 (containing the human cDNA for CYP3A4 under the control of the PGK promoter) and pFBY8 containing a hybrid NADPH-P450 reductase (constructed from rat NPR cDNA fused to a yeast *N*-terminal sequence) under the control of an ADH1 promoter. Growth of the cells, co-expression levels and the methods for preparing the yeast microsomes have all been described by Guengerich *et al.* (1991).

Expression in human lymphoblastoid cells. Microsomes from human B-lymphoblastoid cells, expressing human CYP3A4 and NADPH-P450 reductase, were obtained from Gentest Corporation (Woburn, MA, USA) and used according to the manufacturer's instructions.

Native human liver microsomes. Human liver samples obtained from nine donors (five males, four females, 22–62 years old) were purchased from the Keystone Skin Bank, USA. Native liver microsomes were prepared using the ultracentrifugation method described by Ashforth *et al.* (1995), suspended in 0.1 M phosphate buffer (pH 7.4) and stored at −80 °C until used.

Determination of protein, P450 and NPR levels. Concentrations of protein and P450 in microsomes and membranes were estimated spectrally by the methods of Lowry *et al.* (1951) and Omura and Sato (1964), respectively. NPR activity was determined following the method of Vermilion and Coon (1978) using cytochrome c as a substrate. The kinetic parameters for the HLM were normalized for CYP3A4, using the value of Shimada *et al.* (1994), who reported CYP3A to represent 28.8% of the total CYP content in the liver.

Incubation conditions

Dextromethorphan. Incubations were carried out under linear conditions with respect to time (15 min for *E. coli* membranes, 20 min for yeast and hBl microsomes, 30 min for HLM) and protein concentration (0.5 mg ml^{-1} for yeast and hBl microsomes, 1 mg ml^{-1} for HLM and *E. coli* membranes). The substrate (final concentration 25–1500 μM) was added to each incubation in phosphate buffer. All incubations were carried out in duplicate. The reaction was started with the addition of an NADPH-regenerating system (100 μl) consisting of 1 mM $NADP^+$, 7.5 mM isocitric acid, 1 U isocitrate dehydrogenase ml^{-1}, 15 mM magnesium chloride and 0.1 M phosphate buffer, pH 7.4. The final incubation volume was 200 μl. The reaction was terminated by the addition of 30 μl 60% perchloric acid. Samples were then centrifuged (11 600*xg*) in a microcentrifuge for 5 min to precipitate protein.

Midazolam. Incubations were performed in duplicate over a substrate concentration range of 0.5–50 μM (*E. coli* membranes, yeast and hBl microsomes) or 5–60 μM (HLM) under linear conditions. A 0.2-ml incubation volume containing microsomal or membrane protein (0.5 mg ml^{-1} for yeast microsomes, 1 mg ml^{-1} for *E. coli* membranes, hBl and human liver microsomes), MDZ (added in methanol) and 0.1 M potassium phosphate buffer, pH 7.4, was used. The final concentration of methanol in the incubation mixture was 1% (v/v). The reaction was initiated by the addition of 100 μl of an NADPH-regenerating system. The incubation was terminated after 4 min (yeast microsomes) and 5 min (*E. coli* membranes, hBl and human liver microsomes) by the addition of 100 μl methanol. Samples were then centrifuged (11 600*xg*) for 5 min and the supernatants directly injected for HPLC analysis.

Diazepam. Incubation mixtures contained microsomal or membrane protein (0.4 mg ml^{-1} for HLM, 0.5 mg ml^{-1} for yeast and hBl microsomes, 1 mg ml^{-1} for *E. coli* membranes), 0.1 M potassium phosphate buffer (pH 7.4) and DZ (in dimethylformamide, final concentration 1%) at various concentrations (2.5–250 μM for *E. coli* membranes and hBl microsomes, 1–500 μM for yeast microsomes, 1–1500 μM for HLM). The final volume was 200 μl for the three expression systems and 500 μl for HLM. The mixture was pre-incubated for 5 min at 37 °C in a shaking water bath, and the reaction was initiated by the addition of 100 μl of an NADPH-regenerating system and incubated for 5 min (HLM), 15 min (hBl microsomes and *E. coli* membranes) and 20 min (yeast microsomes). Linearity with respect to time and protein concentration was confirmed. The incubation mixture was extracted with ethylacetate (3 ml) after adding the internal standard (prazepam, 100 μl, 70 μM in methanol) and carbonate buffer (1 ml, 100 mM, pH 10) by rotary mixing for 25 min. The organic phase was allowed to evaporate to dryness under a stream of nitrogen and the residue was reconstituted in the mobile phase (200 μl) for HPLC analysis.

HPLC analysis

Dextromethorphan. The method used was based on that of Chen *et al.* (1990). The supernatant (100 μl) was injected onto a 25 cm × 4.6 mm Spherisorb C8 column with a mobile phase of 57.9% water, 42% acetonitrile, 0.1% triethylamine, pH 3, at 0.6 ml min^{-1} (Gilson International, The Hague, Netherlands 302 pump). Fluorescence detection (Hewlett Packard, Bristol, UK 1046A) was used with excitation and emission wavelengths of 280 and 310 nm, respectively. The retention times were 10.5 and 12 min for MEM and DEM, respectively. Quantification was achieved by comparison of peak areas with those of the standard curve.

Midazolam. The method followed was a modification of that of Kronbach *et al.* (1989). Supernatant (100 μl) was injected onto a Supelcosil LC-ABZ, 5 μM, 15 cm × 4.6 mm column. The mobile phase (65%

0.025 M ammonium acetate (pH 5):40% acetonitrile) was delivered at 1 ml min^{-1} and the column effluent was monitored at 240 nm. Peak height was used for quantification. 1-hydroxymidazolam eluted at 7.7 min.

Diazepam. The method used is based on that of Reilly *et al.* (1990). The reconstituted samples (100 µl) were injected onto a Spherisorb S5 ODS2 250 × 5 mm column eluted with a mobile phase (delivered at a flow rate of 1 ml min^{-1}) consisting of 65% methanol/35% water containing 0.02% triethylamine adjusted to pH 7.0 with phosphoric acid. The eluate was monitored by UV absorbance at 236 nm. DZ and metabolite concentrations were determined by a peak height ratio method with respect to the internal standard (prazepam). The approximate retention times of 3HDZ, DZ and internal standard were 9, 12 and 26 min, respectively.

Data analysis

In vitro kinetic data were analysed using least-squares non-linear regression (GraFit, Erithacus Software Ltd) with a weighting factor of $1/y$.

Formation of MEM and 1′-OH MDZ was best described by the classical Michaelis–Menten equation (1):

$$v = \frac{V_{max} \times S}{K_m + S}, \tag{1}$$

where v and V_{max} are the observed and maximal rate of metabolism, K_m is the substrate concentration at which the reaction is half of its maximal value, and S is the substrate concentration.

The formation of 3HDZ in all enzyme systems except yeast microsomes was best described by the Hill equation (2):

$$f = \frac{V_{max} \times S^n}{S_{50}^n + S^n}, \tag{2}$$

where S_{50} is the concentration at half V_{max} and n is the Hill coefficient. In this case, CL_{int} cannot be determined by the ratio V_{max}/K_m; instead the parameter CL_{max} was used (Witherow and Houston 1999, Houston and Kenworthy 2000). CL_{max} is the clearance obtained when the enzyme is fully activated and is calculated using equation (3):

$$\frac{v}{S} = \frac{V_{max}}{S_{50}} \times \frac{(n-1)}{n(n-1)^{1/n}}. \tag{3}$$

Results

CYP content and reductase activities of human liver microsomes and recombinant systems

Typical levels of spectrally active CYP were 0.23 ± 0.09, 0.33 ± 0.08, 0.086 ± 0.008 and 0.27 ± 0.10 nmol mg^{-1} protein for *E. coli* membranes, yeast, hBl and human liver microsomes, respectively. NADPH-P450 reductase activities for *E. coli* membranes, yeast, hBl and human liver microsomes were determined as 719 ± 197, 289 ± 026, 207 ± 016 and 206 ± 056 nmol min^{-1} mg^{-1} protein, respectively. Levels of CYP3A4 and NPR for hBl microsomes were given on the manufacturer's data sheet and varied slightly according to the batch used.

DEM N*-demethylation in human liver microsomes and recombinant CYP3A4*

The monophasic kinetic profiles obtained for the formation of MEM in recombinant CYP3A4 is given in figure 1A. Table 1 summarizes the kinetic parameters obtained for DEM *N*-demethylation. The K_m for DEM *N*-demethylation compared well in all the expression systems and were also in agreement with those for human liver microsomes. The V_{max} for the hBl microsomes was higher than the respective HLM, yeast microsomes and *E. coli* membranes, and this was

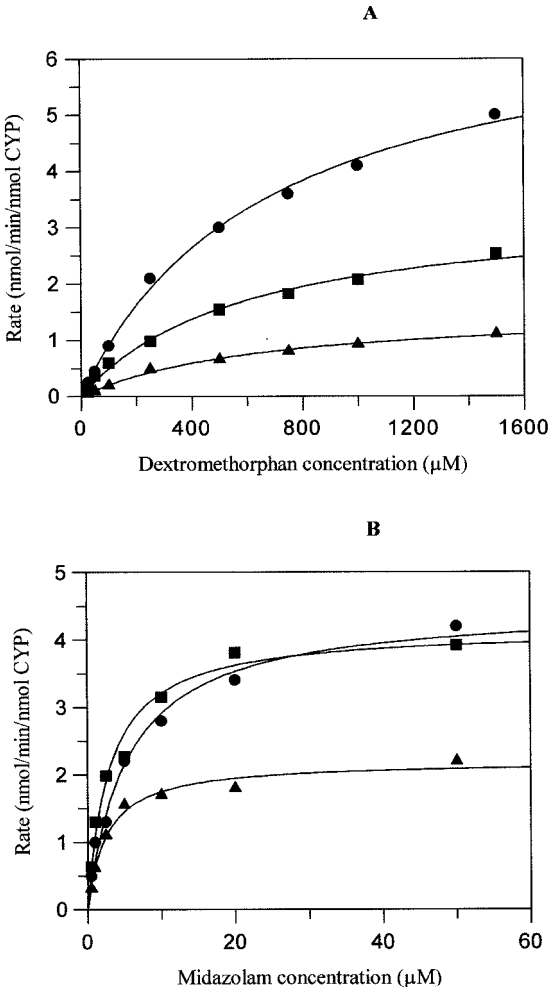


Figure 1. Kinetics of formation of metabolites for two different CYP3A4 substrates: (A) dextromethorphan (MEM formation) and (B) midazolam (1′-OH MDZ formation) in (●) hBl microsomes, (■) *E. coli* membranes and (χ) *S. cerevisiae* microsomes. Data are the mean of duplicate determinations.

reflected in the CL_{int} with 4- and 2-fold differences, respectively. There was no difference in CL_{int} between human liver microsomes and yeast microsomes. The CL_{int} for the three investigated expression systems were all within the range for the human liver microsomes.

MDZ 1′-hydroxylation in human liver microsomes and recombinant CYP3A4

The activity in the hBl microsomes was higher than in the respective yeast microsomes and *E. coli* membranes, resulting in greater CL_{int}. A 2-fold difference was observed between hBl microsomes and *E. coli* membranes. The K_m for the formation of 1′-OH MDZ compared well in all four systems. The CL_{int} for all the yeast microsomes, hBl microsomes and *E. coli* membranes were within the range of those determined for the human liver microsomes (table 2). As shown in figure 1B,

Table 1. Kinetic parameters for dextromethorphan *N*-demethylation.

Enzyme system	V_{max} (nmol min^{-1} nmol^{-1} CYP3A4)	K_m (μM)	CL_{int} (μl min^{-1} nmol^{-1} CYP3A4)
HLM ($n = 9$)	1.8 (0.45–4.8)	850 (162–1500)	2.8 (0.7–9.7)
hBl microsomes ($n = 1$)	6.7	660	10
Yeast microsomes ($n = 4$)	1.7 (1.1–2.6)	670 (550–790)	2.5 (2.0–3.2)
E. coli membranes ($n = 3$)	3.6 (3.0–4.3)	703 (590–840)	5.2 (3.6–6.3)

Results are the mean (range where appropriate).

Table 2. Kinetic parameters for 1′-OH MDZ formation in *in vitro* systems.

Enzyme system	V_{max} (nmol min^{-1} nmol^{-1} CYP3A4)	K_m (μM)	CL_{int} (μl min^{-1} nmol^{-1} CYP3A4)
HLM ($n = 9$)	4.0 (0.7–16)	11.7 (3.6–19.9)	368 (57–1100)
hBl microsomes ($n = 1$)	4.5	5.4	833
Yeast microsomes ($n = 4$)	1.9 (1.2–2.5)	3.1 (2.6–3.8)	600 (450–800)
E. coli membranes ($n = 3$)	2.3 (1.4–3.4)	4.4 (2.7–5.8)	521 (457–586)

Results are the mean (range where appropriate).

the formation of 1′-OH MDZ in cDNA-expressed CYP3A4 followed Michaelis–Menten kinetics.

Diazepam 3-hydroxylation in human liver microsomes and recombinant CYP3A4

Substrate versus velocity plots for formation of 3HDZ by recombinant CYP3A4 are shown in figure 2A, and the corresponding Eadie–Hofstee plots in figure 2B. Kinetic parameters for the formation of 3HDZ are presented in table 3. The mean S_{50}'s for the human livers compare favourably with those obtained in the three expression systems. V_{max} and CL_{max} in the hBl microsomes are much greater than in the HLM and *E. coli* membranes.

Discussion

The current study describes the utility of three expression systems (*E. coli, S. cerevisiae* and human lymphoblastoid cells), for obtaining *in vitro* kinetic data for drug metabolism. Data were collected for three CYP3A4 substrates (DEM, MDZ and DZ) and the recombinant data were compared with results obtained for native HLM.

During the past 30 years, HLM have been used as a tool to predict human drug metabolism. However, with HLM, the CYPs are present as a mixture and immunochemical inhibitors or correlation analysis with marker activities must be used to identify which CYP form metabolizes the compound of interest (Crespi and Penman 1997). Another disadvantage of the use of HLM is the low levels of CYP in biological materials, which are, in some cases, insufficient to generate adequate amounts of metabolite for novel drug studies. Moreover, the levels of a particular CYP in individual HLM samples can vary considerably according to the medical background of the donor patient (Iwata *et al*. 1998).

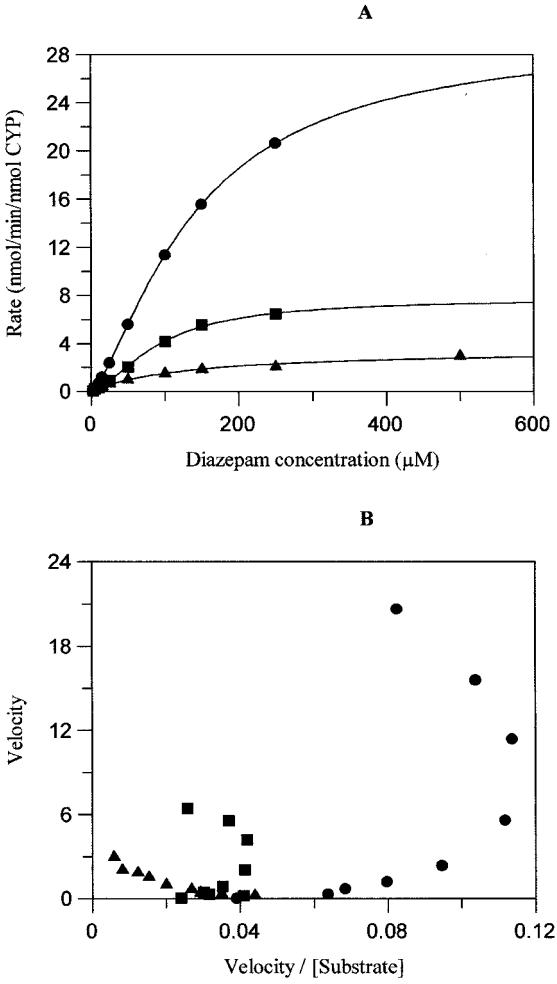


Figure 2. (A) Substrate versus velocity plots and (B) Eadie–Hofstee plots for 3HDZ formation in (●) hBl microsomes, (■) *E. coli* membranes and (χ) *S. cerevisiae* microsomes showing sigmoidal kinetics for hBl and *E. coli*. Data are the mean of duplicate determinations.

Following recent developments in molecular biology and recombinant DNA technology, it has now become possible to express mammalian CYPs in heterologous systems, including bacterial, yeast, insect and mammalian cells (Gonzalez and Korzekwa 1995, Friedberg and Wolf 1996). The principal advantages of recombinant systems are the relatively low cost, the ease of use and the high level of expression. In addition, with recombinant systems, only a single active CYP is present. Therefore, immunochemical inhibition and correlation analyses are not required to assign specific biotransformations to specific enzymes (Crespi and Penman 1997).

It has been reported that the *N*-demethylation of DEM is catalysed by CYP3A4 and, to a lesser extent, by CYP3A5 *in vitro* in humans (Jacqz-Aigrain *et al.* 1993, Gorski *et al.* 1994a). Results obtained from *E. coli* membranes, yeast and hBl microsomes containing recombinant CYP3A4 confirm that this CYP is involved in the production of MEM. Previous investigators have described single

Table 3. Kinetic parameters for 3-HDZ formation in *in vitro* systems.

Enzyme system	V_{max} (nmol min^{-1} nmol^{-1} CYP3A4)	S_{50} or K_m (μM)	Hill coefficient (n)	CL_{int} or CL_{max} (μl min^{-1} nmol^{-1} CYP3A4)
HLM[a] ($n = 9$)	16.2 (1.5–36.1)	230 (145–311)	1.47 (1.27–1.73)	37.6 (4.47–81.8)
hBl microsomes[a] ($n = 1$)	30	140	1.42	117
Yeast microsomes[b] ($n = 2$)	3.4 (3.2–3.6)	140 (130–150)	–	24.5 (21.3–27.7)
E. coli membranes[a] ($n = 3$)	9.3 (7.1–13)	129 (90–160)	1.41 (1.21–1.62)	41.5 (28.5–51.5)

[a] Data generated from HLM, hBl microsomes and *E. coli* membranes were fitted to the Hill equation (parameters V_{max}, S_{50} and CL_{max}.

[b] Data generated from yeast microsomes were fitted to the Michaelis–Menten equation (parameters V_{max}, K_m and CL_{int}).

enzyme Michaelis–Menten kinetics for DEM *N*-demethylation in HLM (Gorski *et al.* 1994a, Kerry *et al.* 1994, Hickman *et al.* 1998). Our findings are in agreement with those workers. The K_m and V_{max} for MEM formation in the present study were consistent with several previous studies in HLM ($K_m = 633\,\mu M$, $V_{max} = 6.15\,nmol\,min^{-1}\,nmol^{-1}$ CYP; Gorski *et al.* 1994a; $K_m = 217\,\mu M$, $V_{max} = 16.1\,nmol\,min^{-1}\,nmol^{-1}$ CYP; Hickman *et al.* 1998). Using a baculovirus expression system, Yu and Haining (2001) reported a $V_{max} = 21.3\,nmol\,min^{-1}\,nmol^{-1}$ CYP3A4, which is higher than the values reported in the present study. This may be due to enhanced expression of CYP3A4 in the baculovirus system or differences in the assay conditions used.

This paper also confirms that MDZ 1′-hydroxylation is catalysed almost exclusively by the CYP3A subfamily (Gorski *et al.* 1994b). It was found that 1′-OH MDZ formation was best described by a simple Michaelis–Menten kinetic model (equation 1). This observation is in good agreement with Gorski *et al.* (1994b). On the other hand, substrate inhibition of 1′-OH MDZ has been reported in HLM and cDNA-expressed enzymes (Ghosal *et al.* 1996). For MDZ 1′-hydroxylation, the K_m were consistent for the three expression systems and comparable with the values of HLM from this study and the available literature data (Gorski *et al.* 1994b, Ghosal *et al.* 1996). CL_{int} was also shown to be comparable in HLM and recombinant systems. Similar results were obtained by Ghosal *et al.* (1996) using just hBl microsomes and HLM. Yamazaki *et al.* (1999) previously investigated MDZ 1′-hydroxylation in microsomes of insect cells with baculovirus system containing CYP3A4/NPR (1:4.6). The activity for 1′-OH MDZ production in baculovirus ($13\,nmol\,min^{-1}\,nmol^{-1}$ CYP3A4) was greater than that observed in the present study.

The metabolism of DZ in HLM has been reported as exhibiting sigmoidal kinetics (Andersson *et al.* 1994, Shou *et al.* 1999). However, Zomorodi and Houston (1996) did not detect atypical kinetics of DZ metabolism in HLM. In the current study, with the exception of *S. cerevisiae* microsomes, sigmoidal kinetic profiles, with non-linear Eadie–Hofstee plots, were observed for *E. coli* membranes, hBl microsomes and HLM. Similar atypical formation kinetics for 3HDZ have been reported (Shou *et al.* 1999) using baculovirus-expressed CYP3A4. The atypical formation kinetics for 3HDZ suggest that the CYP3A4 enzyme may possess multiple affinity sites for this substrate. The substrate in this case is also a modifier or an activator of the enzyme (Shou *et al.* 1999). Interestingly, 3HDZ formation in yeast microsomes was best described by simple Michaelis–Menten

kinetics and showed no evidence of a sigmoidal nature. It is important to note that the CYP:NPR ratio, the lipid membrane composition and the orientation of the CYP protein complex in the membrane may differ in the yeast system and may be critical for the manifestation of the sigmoidal effects. The mean S_{50} (230 μM) for the formation of 3HDZ in HLM compares well with the 188 μM reported by Andersson *et al.* (1994) in HLM. However, the mean V_{max} (16.2 nmol min^{-1} nmol^{-1} CYP) presented here is lower than Andersson's 68 nmol min^{-1} nmol^{-1} CYP. Our observed mean V_{max} in *E. coli* membranes (9.3 nmol min^{-1} nmol^{-1} CYP) is in good agreement with the 7.2 nmol min^{-1} nmol^{-1} CYP reported by Yang *et al.* (1998) for HepG2 cells expressing CYP3A4. However, the mean V_{max} in hBl microsomes was 4-fold higher than that in Yang *et al.*

Because different cDNA-expressed enzyme preparations were used to assay three substrates, the V_{max} obtained are dependent on the factors that influence the absolute enzyme activity in any given preparation. These factors include the specific CYP content, the level of endogenous or expressed NPR, and the level of cytochrome b_5 (Crespi and Penman 1997, McGinnity *et al.* 1999, Yamazaki *et al.* 1999). In addition, factors such as ionic strength, organic solvents and membrane composition can all affect V_{max} estimates (Hickman *et al.* 1998, Mäenpää *et al.* 1998).

Expressing data obtained in HLM as nmol of metabolite per nmol CYP may not always be appropriate since human liver does not contain equimolar concentrations of the different P450 forms (Shimada *et al.* 1994). Moreover, the level of NPR also differs for each individual liver sample and the mean HLM may also differ from the values determined for different cDNA-expressed preparations. Consequently, V_{max} can vary substantially between HLM and recombinant enzymes. To address this problem, the Relative Activity Factor (RAF) approach, for relating rates of metabolism for cDNA-expressed enzymes with the rates observed for HLM, has been proposed by Crespi (1995). RAFs are determined as the ratio of the activity of the enzyme (per unit protein) in HLM to the activity in the cDNA expression system. The RAF approach reflects both the relative abundance of an individual enzyme in the human liver and accounts for the turnover number of the cDNA-expressed form. For HLM (the incubation matrix with the highest protein concentrations), microsomal binding was determined as $< 10\%$ and, therefore, was not considered important for our comparative studies.

In conclusion, it will always be preferable to use a panel of human livers to generate microsomes for drug metabolic studies in order to evaluate fully the range of metabolic capabilities within the population. However, owing to the limited availability of human liver tissues and the variability of CYP3A4 expression levels in the human population, we find it both useful and scientifically valid to substitute any of the three recombinant systems described, since no significant differences were observed. In all cases, the data derived from the recombinant systems were much more tightly clustered and always within the range observed for HLM.

Acknowledgements

The authors thank the Egyptian Government (MA), BBSRC (NLR) and SKB (KEK) for their support.

References

Amrein, R. and Hetzel, W., 1990, Pharmacology of Dormicum® (midazolam) and Anexate® (flumazenil). *Acta Anaesthesiologica Scandinavica*, **34**, 6–15.

Andersson, T., Miners, J. O., Veronese, M. E. and Birkett, D. J., 1994, Diazepam metabolism by human liver microsomes is mediated by both *S*-mephenytoin hydroxylase and CYP3A isoforms. *British Journal of Clinical Pharmacology*, **38**, 131–137.

Ashforth, E. I. L., Carlile, D. J., Chenery, R. and Houston, J. B., 1995, Prediction of *in vivo* disposition from *in vitro* systems: clearance of phenytoin and tolbutamide using rat hepatic microsomal and hepatocyte data. *Journal of Pharmacology and Experimental Therapeutics*, **274**, 761–766.

Blake, J. A. R., Pritchard, M., Ding, S., Smith, G. C. M., Burchell, B., Wolf, C. R. and Friedberg, T., 1996, Coexpression of a human P450 (CYP3A4) and P450 reductase generates a highly functional monooxygenase system in *Escherichia coli*. *Federation of European Biochemical Societies Letters*, **397**, 210–214.

Chen, Z. R., Somogyi, A. A. and Bochner, F., 1990, Simultaneous determination of dextromethorphan and three metabolites in plasma and urine using high performance liquid chromatography with application to their disposition in man. *Therapeutic Drug Monitoring*, **12**, 97–104.

Crespi, C. L., 1995, Xenobiotic-metabolising human cells as tools for pharmacological and toxicological research. *Advances in Drug Research*, **26**, 179–235.

Crespi, C. L. and Penman, B. W., 1997, Use of cDNA-expressed human cytochrome P450 enzymes to study potential drug–drug interactions. *Advances in Pharmacology*, **43**, 171–188.

Ducharme, J., Abdullah, S. and Wainer, I. W., 1996, Dextromethorphan as an *in vitro* probe for the simultaneous determination of CYP2D6 and CYP3A4 activity. *Journal of Chromatography B*, **678**, 113–128.

Friedberg, T. and Wolf, C. R., 1996, Recombinant DNA technology as an investigative tool in drug metabolism research. *Advanced Drug Delivery Reviews*, **22**, 187–213.

Ghosal, A., Satoh, H., Thomas, P. E., Bush, E. and Moore, D., 1996, Inhibition and kinetic of cytochrome P4503A activity in microsomes from rat, human and cDNA-expressed human cytochrome P450. *Drug Metabolism and Disposition*, **24**, 940–947.

Gillam, E. M. J., Baba, T., Kim, B.-R., Ohmori, S. and Guengerich, F. P., 1993, Expression of modified human cytochrome P450 3A4 in *Escherichia coli* and purification and reconstitution of the enzyme. *Archives of Biochemistry and Biophysics*, **305**, 123–131.

Gonzalez, F. J. and Korzekwa, K. R., 1995, Cytochrome P450 expression systems. *Annual Review of Pharmacology and Toxicology*, **35**, 369–390.

Gorski, J. C., Hall, S. D., Jones, D. R., Vandenbranden, M. and Wrighton, S. A., 1994b, Regioselective biotransformation of midazolam by members of the human cytochrome P450 3A (CYP3A) subfamily. *Biochemical Pharmacology*, **47**, 1643–1653.

Gorski, J. C., Jones, D. R., Wrighton, S. A. and Hall, S. D., 1994a, Characterisation of dextromethorphan *N*-demethylation by human liver microsomes: Contribution of the cytochrome P450 3A subfamily. *Biochemical Pharmacology*, **48**, 173–182.

Guengerich, F. P., Brian, W. R., Sari, M. A. and Ross, J. T., 1991, Expression of mammalian cytochrome P450 enzymes using yeast-based vectors. In M. R. Waterman and E. F. Johnson (eds), *Methods in Enzymology* (New York: Academic Press), pp. 130–148.

Hickman, D., Wang, J., Wang, Y. and Unadkat, J. D., 1998, Evaluation of the selectivity of *in vitro* probes and suitability of organic solvents for the measurement of human cytochrome P450 monooxygenase activities. *Drug Metabolism and Disposition*, **26**, 207–215.

Houston, J. B. and Kenworthy, K. E., 2000, *In vitro–in vivo* scaling of CYP kinetic data not consistent with the classical Michaelis–Menten model. *Drug Metabolism and Disposition*, **28**, 246–254.

Iwata, H., Fujita, K.-I., Kushida, H., Suzuki, A., Konno, Y., Nakamura, K., Fujino, A. and Kamataki, T., 1998, High catalytic activity of human cytochrome P450 co-expressed with human NADPH-cytochrome P450 reductase in *Escherichia coli*. *Biochemical Pharmacology*, **55**, 1315–1325.

Jacqz-Aigrain, E., Funck-Brentano, C. and Cresteil, T., 1993, CYP2D6- and CYP3A-dependent metabolism of dextromethorphan in humans. *Pharmacogenetics*, **3**, 197–204.

Jung, F., Richardson, T. H., Raucy, J. L. and Johnson, E. F., 1997, Diazepam metabolism by cDNA-expressed human 2C P450s identification of P4502C18 and P4502C19 as low K_m diazepam *N*-demethylases. *Drug Metabolism and Disposition*, **25**, 133–139.

Kerry, N. L., Somogyi, A. A., Bochner, F. and Mikus, G., 1994, The role of CYP2D6 in primary and secondary oxidative metabolism of dextromethorphan: *in vitro* studies using human liver microsomes. *British Journal of Clinical Pharmacology*, **38**, 243–248.

Kronbach, T., Mathys, D., Umeno, M., Gonzalez, F. J. and Meyer, U. A., 1989, Oxidation of midazolam and triazolam by human liver cytochrome P450 IIIA4. *Molecular Pharmacology*, **36**, 89–96.

LEE, C. A., KADWELL, S. H., KOST, T. A. and SERBJIT-SINGH, C. J., 1995, CYP3A4 expressed by insect cells infected with a recombinant baculovirus containing both CYP3A4 and human NADPH-cytochrome P450 reductase is catalytically similar to human liver microsomal CYP3A4. *Archives of Biochemistry and Biophysics*, **319**, 157–167.

LOWRY, O. H., ROSEBROUGH, N. J., FARR, A. L. and RANDALL, R. J., 1951, Protein measurement with the Folin phenol reagent. *Journal of Biological Chemistry*, **193**, 265–275.

MÄENPÄÄ, J., HALL, S. D., RING, B. J., STROM, S. C. and WRIGHTON, S. A., 1998, Human cytochrome P450 3A (CYP3A) mediated midazolam metabolism: the effect of assay conditions and regioselective stimulation by a-naphthoflavone, terfenadine and testosterone. *Pharmacogenetics*, **8**, 137–155.

MCGINNITY, D. F., GRIFFIN, S. J., MOODY, G. C., VOICE, M., HANLON, S., FRIEDBERG, T. and RILEY, R. J., 1999, Rapid characterisation of the major drug-metabolising human hepatic cytochrome P-450 enzyme expressed in *Escherichia coli*. *Drug Metabolism and Disposition*, **27**, 1017–1023.

OMURA, T. and SATO, R., 1964, The carbon monoxide-binding pigment of liver microsomes. I. Evidence for its hemoprotein nature. *Journal of Biological Chemistry*, **239**, 2370–2378.

PEYRONNEAU, M.-A., RENAUD, J.-P., TRUAN, G., URBAN, P., POMPON, D. and MANSUY, D., 1992, Optimisation of yeast-expressed human liver cytochrome P450 3A4 catalytic activities by coexpressing NADPH-cytochrome P450 reductase and cytochrome b_5. *European Journal of Biochemistry*, **207**, 109–116.

REILLY, P. E. B., THOMPSON, D. A., MASON, S. R. and HOOPER, W. D., 1990, Cytochrome P450IIIA enzymes in rat microsomes: involvement in C_3-hydroxylation of diazepam and nordazepam but not *N*-dealkylation of diazepam and temazepam. *Molecular Pharmacology*, **37**, 767–774.

SHIMADA, T., YAMAZAKI, H., MIMURA, M., INUI, Y. and GUENGERICH, F. P., 1994, Interindividual variations in human liver cytochrome P-450 enzymes involved in the oxidation of drugs, carcinogens and toxic chemicals of 30 Japanese and 30 Caucasians. *Journal of Pharmacology and Experimental Therapeutics*, **270**, 414–423.

SHOU, M., MEI, Q., ETTORE, M. W., DAI, R., BAILLIE, T. A. and RUSHMORE, T. H., 1999, Sigmoidal kinetic model for two co-operative substrate-binding sites in a cytochrome P450 3A4 active site: an example of the metabolism of diazepam and its derivatives. *Biochemical Journal*, **340**, 845–853.

VERMILION, J. L. and COON, M. J., 1978, Purified liver microsomal NADPH-cytochrome P-450 reductase. Spectral characterisation of oxidation–reduction states. *Journal of Biological Chemistry*, **253**, 2694–2704.

VOICE, M. W., ZHANG, Y., WOLF, C. R., BURCHELL, B. and FRIEDBERG, T., 1999, Effects of human cytochrome b_5 on CYP3A4 activity and stability *in vivo*. *Archives of Biochemistry and Biophysics*, **366**, 116–124.

WITHEROW, L. E. and HOUSTON, J. B., 1999, Sigmoidal kinetics of CYP3A substrates: An approach for scaling dextromethorphan metabolism in hepatic microsomes and isolated hepatocytes to predict *in vivo* clearance in rat. *Journal of Pharmacology and Experimental Therapeutics*, **290**, 58–65.

YAMAZAKI, H., NAKAJIMA, M., NAKAMURA, M., ASAHI, S., SHIMADA, N., GILLAM, E. M. J., GUENGERICH, F. P., SHIMADA, T. and YOKOI, T., 1999, Enhancement of cytochrome P-450 3A4 catalytic activities by cytochrome b_5 in bacterial membranes. *Drug Metabolism and Disposition*, **27**, 999–1004.

YANG, T. J., SHOU, M., KORZEKWA, K. R., GONZALEZ, F. J., GELBOIN, H. V. and YANG, S. K., 1998, Role of cDNA-expressed human cytochromes P450 in the metabolism of diazepam. *Biochemical Pharmacology*, **55**, 889–896.

YU, A. and HAINING, L. R., 2001, Comparative contribution to dextromethorphan metabolism by cytochrome P450 isoforms *in vitro*: can dextromethorphan be used as a dual probe for both CYP2D6 and CYP3A activities? *Drug Metabolism and Disposition*, **29**, 1514–1520.

ZOMORODI, K. and HOUSTON, J. B., 1996, Diazepam–omeprazole inhibition interactions: an *in vitro* investigation using human liver microsomes. *British Journal of Clinical Pharmacology*, **42**, 157–162.

XENOBIOTICA, 2002, VOL. 32, NO. 11, 949–962

Taylor & Francis
healthsciences

In vitro identification of metabolic pathways and cytochrome P450 enzymes involved in the metabolism of etoperidone

Z. YAN†*, G. W. CALDWELL†, W. N. WU‡, L. A. MCKOWN‡, B. RAFFERTY†, W. JONES† and J. A. MASUCCI†

† Division of Drug Discovery and ‡ Division of Preclinical Development, Johnson & Johnson Pharmaceutical Research & Development, Spring House, PA 19477, USA

Received 7 March 2002

1. *In vitro* studies have been carried out to investigate the metabolic pathways and identify the hepatic cytochrome P450 (CYP) enzymes involved in etoperidone (Et) metabolism.

2. Ten *in vitro* metabolites were profiled, quantified and tentatively identified after incubation with human hepatic S9 fractions. Et was metabolized via three metabolic pathways: (A) alkyl hydroxylation to form OH-ethyl-Et (M1); (B) phenyl hydroxylation to form OH-phenyl-Et (M2); and (C) *N*-dealkylation to form 1-*m*-chlorophenylpiperazine (*m*CPP, M8) and triazole propyl aldehyde (M6). Six additional metabolites were formed by further metabolism of M1, M2, M6 and M8.

3. Kinetic studies revealed that all metabolic pathways were monophasic, and the pathway leading to the formation of OH-ethyl-Et was the most efficient at eliminating the drug. On incubation with microsomes expressing individual recombinant CYPs, formation rates of M1–3 and M8 were 10–100-fold greater for CYP3A4 than that for other CYP forms. The formation of these metabolites was markedly inhibited by the CYP3A4-specific inhibitor ketoconazole, whereas other CYP-specific inhibitors did not show significant effects. In addition, the production of M1–3 and M8 was strongly correlated with CYP3A4-mediated testosterone 6β-hydroxylase activities in 13 different human liver microsome samples.

4. Dealkylation of the major metabolite M1 to form *m*CPP (M8) was also investigated using microsomes containing recombinant CYP enzymes. The rate of conversion of M1 to *m*CPP by CYP3A4 was 503.0 ± 3.1 pmole nmole^{-1} min^{-1}. Metabolism of M1 to M8 by other CYP enzymes was insignificant. In addition, this metabolism in human liver microsomes was extensively inhibited by the CYP3A4 inhibitor ketoconazole, but not by other CYP-specific inhibitors. In addition, conversion of M1 to M8 was highly correlated with CYP3A4-mediated testosterone 6β-hydroxylase activity.

5. The results strongly suggest that CYP3A4 is the predominant enzyme-metabolizing Et in humans.

Introduction

Etoperidone (Et), trazodone and nefazodone are all 1,2,4-triazole-3-one heterocyclic drugs currently prescribed for the treatment for depression. The compounds are potent serotonin 5-hydroxytryptamine (5-HT) receptor antagonists that inhibit serotonin and noradrenaline re-uptake (Raffa *et al*. 1992). Metabolism of these compounds all results in the formation of 1-*m*-chlorophenylpiperazine (*m*CPP), which is thought to contribute to the antidepressant effects of the parent drugs (Przegalinski and Lewandowska 1979, Fong *et al*. 1982, Raffa *et al*. 1992,

* Author for correspondence; e-mail: zyan@prius.jnj.com

Xenobiotica ISSN 0049–8254 print/ISSN 1366–5928 online © 2002 Taylor & Francis Ltd
http://www.tandf.co.uk/journals
DOI: 10.1080/00498250210163298

Maes *et al*. 1997). Detailed studies have been conducted to identify cytochrome P4503A4 (CYP3A4) as the major enzyme mediating the formation of *m*CPP from trazodone (Rotzinger *et al*. 1998, Zalma *et al*. 2000) and nefazodone (von Moltke *et al*. 1999). Similar studies are still required for Et.

After oral administration, Et is well absorbed and extensively metabolized in the liver (Baldwin *et al*. 1982). Twenty-two Et metabolites have been identified in animals (Wu *et al*. 1995, Wu and McKown 2000) and humans (Caldwell *et al*. 2001). Preliminary results of the *in vitro* metabolism of Et in human hepatic S9 fractions has been reported (Wu and McKown 2001). In man, the major circulating metabolites of Et include 5-(1-hydroxyethyl) etoperidone, 4-hydroxy-phenyl-etoperidone and *m*CPP. To date, the metabolic pathways generating those Et metabolites have not been fully characterized.

This study describes *in vitro* studies to identify the *in vitro* metabolites in human hepatic S9 fractions as well as CYP enzymes mediating the formation of major metabolites and to evaluate the potential inhibitory effects of Et on CYP enzymes.

Materials and Methods

Drugs and chemicals

Etoperidone (RWJ-26872), 2-[3-[4-(3-chlorphenyl)-1-piperazinyl]propyl]-4,5-diethyl-2,4-dihydro-3H-1,2,4-triazol, 5-(1-hydroxyethyl) etoperidone (RWJ–36766, M1), 5-(1-oxyethy) etoperidone (RWJ–36771, M3), 1-*m*-chlorophenylpiperazine (*m*CPP, RWJ–24315, M8) and 4-hydroxy-phenyl-etoperidone (M2) were synthesized at Johnson & Johnson Pharmaceutical Research & Development, LLC (Spring House, PA, USA). Each compound was >95% pure, verified by high-performance liquid chromatography (HPLC). Phenacetin, acetaminophan, testosterone, 6β-hydroxy-testosterone, tolbutamide, dextromethorphan, dextrorphan, midazolam, α-naphthoflavone, sulfaphenazole, tranylcypromine, quinidine, ketoconazole, β-nicotinamide adenine dinucleotide phosphate ($NADP^+$), glucose 6-phosphate and glucose 6-phosphate dehydrogenase were purchased from Sigma Chemical Co. (St Louis, MO, USA). (*S*)-mephenytoin, 4′-hydroxy-mephenytoin, 1-hydroxy-midazolam and 4-hydroxy-tolbutamide were all supplied by Ultrafine Chemicals (Manchester, UK). Human hepatic S9 fractions (mixed genders) were purchased from Xenotech, LLC (Kansas City, KS, USA). All microsomes were obtained from Gentest Corp. (Woburn, MA, USA). Pooled human liver microsomes were prepared from livers of 16 donors with mixed gender, and the supplier determined the protein content. Recombinant human microsomes containing individual CYPs (1A2, 2A6, 2B6, 2C9, 2C19, 2E1, 2D6, 3A4) were derived from human B-lymphoblastoid cells transfected with specific CYP cDNAs. The supplier (Gentest) also determined specific CYP contents in derived microsomes.

Incubations using human liver microsomes

All microsomal incubations were performed in triplicate in 96-well plates at 37 °C in a water bath. Et, at desired concentrations, was pre-incubated with human microsomal protein in 50 mM potassium phosphate buffer (pH 7.4) for 5 min. Incubations were initiated by the addition of an NADPH-generating system (final concentration 1.3 mM $NADP^+$, 3.3 mM glucose 6-phosphate, 0.4 U ml^{-1} glucose 6-phosphate dehydrogenase, 3.3 mM magnesium chloride), to give a final volume of 250 µl. The microsomal protein concentration in the reaction mixture varied from 0.125 to 1 mg ml^{-1}, depending upon the experiment. Reactions were terminated by the addition of 75 µl ice-cold acetonitrile. Samples were centrifuged at 1875 rpm for 30 min at 4 °C to pellet the precipitated protein, and supernatants were transferred to HPLC vials for liquid chromatography tandem mass spectrometry (LC-MS/MS) analysis.

Human hepatic S9 incubation

Et (10 µg ml^{-1}) was incubated with human hepatic S9 (1 mg ml^{-1}) in the presence of an NADPH generation system. The incubations were performed at 37 °C in a Dubnoff metabolic shaker incubator for 90 min in a total volume of 5 ml. After incubation, the unchanged Et and its metabolites were extracted with ethyl acetate and identified by LC-MS/MS combined with diazomethane derivatization.

Determination of the kinetic constants for metabolites from Et

The kinetic constants K_m and V_{max} were determined for four Et metabolites by incubating varying concentrations of Et (0, 1, 2, 5, 10, 20, 40, 60, 100, 200, 300 μM) with pooled human liver microsomes (0.25 mg ml^{-1}) under the conditions described above. The data were analysed by iterative non-linear least-squares regression analysis (GraphPad Prism), fitting the data to the Michaelis–Menten equation.

Incubations using microsomes containing cDNA-expressed CYPs

An initial screen with microsomes containing individual cDNA-expressed cytochrome CYPs (1A2, 2A6, 2B6, 2C8, 2C9, 2C19, 2D6, 2E1 or 3A4) was performed at an Et concentration of 10 μM. Incubations were carried out as described above for human liver microsomes, except that microsomes derived from specific cDNA-transfected human B-lymphoblastoid cells were used in place of human liver microsomes. The final concentration of cDNA-expressed enzymes in the mixture was adjusted to 100 pmoles ml^{-1}. An identical study was also conducted to determine the involvement of individual CYPs in the conversion M1 to M8, by using 10 μM M1 as a substrate in the incubation.

Correlation with marker substrate activities

A panel of 13 human livers was used to assess Et metabolism. Microsomes prepared from these livers had been previously characterized for individual CYP marker activities by the supplier (Gentest). Marker substrates used to determine specific CYP activities were: phenacetin (CYP1A2), coumarin (CYP2A6), (*S*)-mephenytoin (CYP2C19, CYP2B6), paclitaxel (CYP2C8), diclofenac (CYP2C9), bufuralol (CYP2D6), chlorzoxazone (CYP2E1), testosterone (CYP3A4) and lauric acid (CYP4A). A correlation study was conducted between the formation of Et metabolites and catalytic activities of specific CYP enzymes across the entire human liver microsome panel.

Inhibition studies

The effect of specific inhibitors of individual CYP enzymes on the metabolism of Et was investigated. The specific inhibitors α-naphthoflavone (1 μM), sulfaphenazole (5 μM), tranylcypromine (12.5 μM), quinidine (2 μM) and ketoconzole (1 μM) were added to incubation mixtures containing Et (10 μM) to investigate the involvement of CYP1A2 (Tassaneeyakul *et al.* 1993, Chang *et al.* 1994), CYP2C9 (Baldwin *et al.* 1995, Mancy *et al.* 1996), CYP2C19 (Ono *et al.* 1996), CYP2D6 (Otton *et al.* 1988) and CYP3A4 (Baldwin *et al.* 1995, Chenery *et al.* 1995), respectively. The effect of inhibitors on Et metabolism was studied using pooled human liver microsomes. The microsomal protein concentration was 0.25 mg ml^{-1}, the incubation time 10 min. The effect of specific inhibitors of individual CYP enzymes on the conversion of M1 to M8 was also investigated under the same experimental conditions except that M1 (10 μM) was used in place of Et.

Inhibition of CYP enzymes by Et

The effect of Et (0.01, 0.1, 1.0, 10.0, 100 μM) on the metabolism of marker substrates by corresponding CYP enzymes was investigated using pooled human liver microsomes. Drugs used as CYP marker substrates were 10 μM phenacetin (CYP1A2), 100 μM (*S*)-mephenytoin (CYP2C19), 500 μM tolbutamide (CYP2C9), 80 μM dextromethorphan (CYP2D6), 150 μM testosterone (CYP3A4) and 10 μM midazolam (CYP3A4). Individual marker substrates were pre-incubated with human liver microsomes in the presence and absence of Et for 5 min at 37 °C before the addition of an NADPH-generating solution. The incubation time was 15 min for CYP1A2, CYP2C9, CYP2D6 and CYP3A4, and 30 min for CYP2C19. After incubation, the reactions were terminated, and metabolites generated from individual CYP marker substrates were analysed by the LC-MS/MS method described below. A comparison was made with the controls (no Et) and activity was expressed as the percentage of control activity remaining. IC_{50} were determined by linear interpolation.

LC-MS/MS analysis

LC-MS/MS was performed on a Micromass (Manchester, UK) Quattro Ultima triple quadrupole mass spectrometer interfaced with an Agilent 1100 HPLC system. LC-MS/MS analyses were conducted using an electrospray ionization source with positive or negative ion detection, depending upon the analytes. The capillary voltage was 3.1 kV. The source temperature was set at 120 °C, the desolvation temperature at 350 °C. The collision energy was tuned for individual ions to achieve optimal sensitivity. The collision gas was nitrogen. The mass spectrometer was operated in the multiple reaction monitoring (MRM) mode to detect multiple metabolites simultaneously.

For analysis of Et metabolites, the electrospray ionization source was operated in the positive-ion detection mode, and transitions monitored at m/z 394 → 198 for 5-(1-hydroxyethyl) etoperidone (M1), 392 → 196 for 5-(1-oxyethy) etoperidone (M3), 197 → 154 for 1-*m*-chlorophenylpiperazine (M8) and 394 → 182 for 4-hydroxy-phenyl-etoperidone (M2).

For analysis of metabolites generated from CYP marker substrates, the electrospray ionization source was operated in the positive-ion mode detecting 6β-hydroxy-testosterone, dextrorphan and 1-hydroxy-midazolam, and in the negative-ion mode detecting acetaminophan, 4-hydroxy-tolbutamide and 4′-hydroxy-mephenytoin. The transitions monitored were m/z 233 → 190 for 4′-hydroxy-mephenytoin, 342 → 324 for 1-hydroxy-midazolam, 285 → 186 for 4-hydroxy-tolbutamide, 150 → 107 for acetaminophan, 305 → 269 for 6β-hydroxy-testosterone and 258 → 157 for dextrorphan.

An Agilent Zorbax SB C18 column (2.1 × 50 mm) was used for chromatographic separation. The starting mobile phase consisted of 95% water (0.5% acetic acid), and metabolites were eluted using a single gradient from 95% water to 95% acetonitrile over 12 min at 0.3 ml min^{-1}. At 12 min, the column was flushed with 95% acetonitrile for 3 min before re-equilibration at the initial conditions. During the run, the divert valve was activated to divert the HPLC eluant to waste in the first 1 min of elution, and then switched eluant to the mass spectrometer for analysis. LC-MS/MS analyses were carried out on 10-μl aliquots from incubations. Data were processed using Masslynx v3.5 software from Micromass (Manchester, UK).

Data analysis

All results are the mean ± SE (standard deviation) of three replicates. Correlation analysis and determination of apparent K_m and V_{max} were obtained using Graphpad Prism software.

Results

Identification of Et metabolites in human hepatic S9

Following hepatic S9 incubation and sample extraction, unchanged Et and 10 metabolites were profiled, quantified and tentatively identified using LC-MS/MS and methyl derivatization techniques and by comparison with synthetic samples as described by Caldwell *et al.* (2001). All MS data are summarized in table 1. In the incubation mixture, unchanged Et (about 46% of the sample), and three major metabolites, OH-ethyl-Et (M1) (18%), OH-phenyl-Et (M2) (11%) and *m*CPP (M8, 8%), were the major products resulting from the incubation. Seven minor identified metabolites were: oxo-ethyl-Et (M3, 2%), OH-phenyl-OH-ethyl-Et (M4, 3%), OH-phenyl-oxo-ethyl-Et (M5, 1%), triazole propyl aldehyde (M6, 1%), triazole propyl acid (M7, 1%), OH-phenyl-*m*CPP (M9, 1%) and triazole propyl alcohol (M10, < 1%). The proposed metabolic pathways are shown in figure 1. In summary, Et metabolites were mainly formed via three pathways: A, alkyl hydroxylation to form OH-ethyl-Et (M1); B, phenyl hydroxylation to form OH-phenyl-Et (M2); and C, *N*-dealkylation to form *m*CPP (M8) and TP aldehyde

Table 1. MS fragments of etoperidone and its metabolites from human hepatic S9.

Metabolite	Per cent of sample	MS/MS (m/z, relative abundance%)
Et	46	378 (MH^+, 96), 237(1), 225(1), 209(1), 197(1), 182(100), 154(55), 126(1) and 111(2)
M1	18	394 (MH^+, 9), 237(1), 209(2), 198(100), 197(5), 170(82), 140(1) and 126(2)
M2	11	394 (MH^+, 9), 253(1), 225(1), 213(1), 182(100), 154(88) and 142(1) Methyl ether: 408 (MH^+, 4), 267(1), 227(1), 182(100), 170(2) and 154(75)
M3	2	392 (MH^+, 9), 237(1), 196(49), 182(100), 168(16), 154(24) and 140(2)
M4	3	410 (MH^+, 4), 198(100), 170(56), 154(2) and 126(1) Methyl ether: 424 (MH^+)
M5	1	408 (MH^+, 4), 196(100), 182(7), 168(84), 154(6) and 126(1) Methyl ether: 422 (MH^+)
M6	1	198 (MH^+, 8), 167(14), 155(100), 154(26), 141(14)
M7	1	214 (MH^+, 10), 196(69), 168(100), 154(13) and 140(71)
M8	8	197 (MH^+, 42), 180(1), 154(100), 140(3) and 119(33)
M9	1	213 (MH^+, 19), 196(19), 170(100) and 135(89)
M10	< 1	200 (MH^+, 100), 182(45), 154(50), 142(86), 141(45)

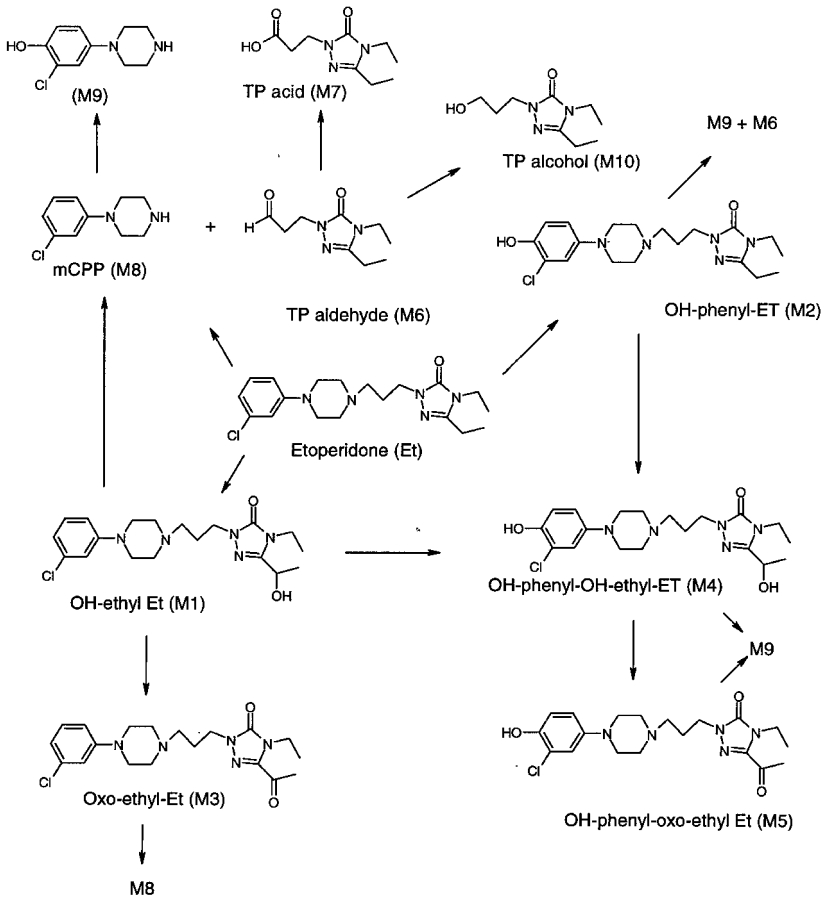


Figure 1. Proposed metabolic pathways of etoperidone in human.

(M6). M1 was further metabolized to form OH-phenyl-OH-ethyl-Et (M4) and oxo-ethyl-Et (M3) by oxidation, and *m*CPP (M8) by *N*-dealkylation. Oxidation of M2 formed OH-phenyl-OH-ethyl-Et (M4) that was presumably oxidized to form OH-phenyl-oxo-ethyl-Et (M5). M8 and M6 were further oxidized to form OH-phenyl-*m*CPP (M9) and triazole propyl acid (M7), respectively. Reduction of M6 formed triazole propyl alcohol (M10) in trace amounts.

Kinetic analyses

Kinetics studies were focused on the formation of major metabolites M1–3 and M8 via different pathways. Initial velocity conditions were established, which were linear with respect to both protein concentration and incubation time. It was found that the formation of four metabolites, M1–3 and M8, was all NADPH-dependent. Primary data also indicated the formation rates of these four metabolites were linear with incubation time up to 15 min and microsomal protein concentration up to 0.25 mg ml^{-1}. Therefore, kinetics studies of Et metabolism were carried out at a protein concentration of 0.25 mg ml^{-1} over 10 min. Incubations of Et over the concentration range 1–300 μM with pooled human liver microsomes resulted in a concentration-dependent formation of four metabolites, M1–3 and *m*CPP (M8)

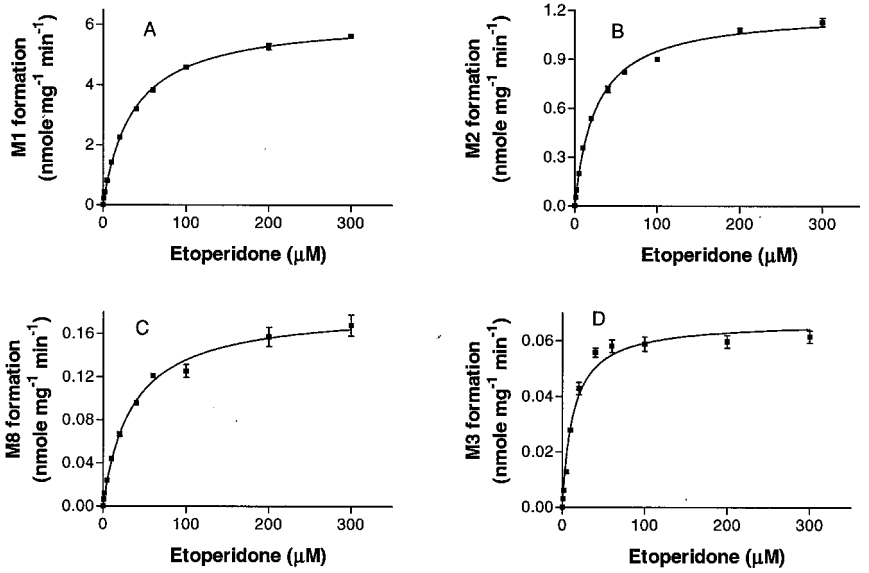


Figure 2. Michaelis–Menten plots for the conversion of etoperidone to M1 (A), M2 (B), M8 (C) and M3 (D). Data shown are from pooled human liver microsomes. Each point represents the mean of three replicates.

Table 2. Kinetic parameters of the metabolism of etoperidone in human liver microsomes.

Metabolite	K_m (μM)	V_{max} (nmole mg^{-1} min^{-1})	V_{max}/K_m (nmole mg^{-1} min^{-1} μM)
M1	36.02 ± 0.99	6.231 ± 0.053	0.173
M2	25.56 ± 1.14	1.192 ± 0.015	0.047
M3	13.20 ± 1.35	0.067 ± 0.002	0.005
M8	34.71 ± 2.88	0.183 ± 0.005	0.005

Data are the mean ± SD of three determinations.

(figure 2). The conversion of Et into these metabolites followed Michaelis–Menten kinetics, and the apparent kinetic constants were estimated and are summarized in table 2. The calculated intrinsic clearances (V_{max}/K_m) for the formation of M1 and M2 were 0.173 and 0.047 nmole mg^{-1} min^{-1} μM^{-1}, respectively, greater than those of M3 (0.005 nmole mg^{-1} min^{-1} μM^{-1}) and M8 (0.005 nmole mg^{-1} min^{-1} μM^{-1}), respectively. Examination of the Eadie–Hofstee transformation (figure 3) revealed a monophasic plot for M1, M2 and M8. In contrast, the Eadie–Hofstee plot of M3 was non-linear (figure 3).

Metabolite formation in expressed recombinant CYP enzymes

The formation of four metabolites of Et was investigated in microsomes derived from human B-lymphoblastoid cells expressing recombinant human CYP1A2, CYP2A6, CYP2B6, CYP2C8, CYP2C9, CYP2C19, CYP2D6, CYP2E1 and CYP3A4. As shown in table 3, at 10 μM Et, the rate of CYP3A4-mediated formation of hydroxylated M1 was 765.0 pmole nmole^{-1} min^{-1}, approximately > 10-fold of CYP2C19 (72.0 pmole nmole^{-1} min^{-1}) and > 100-fold of other

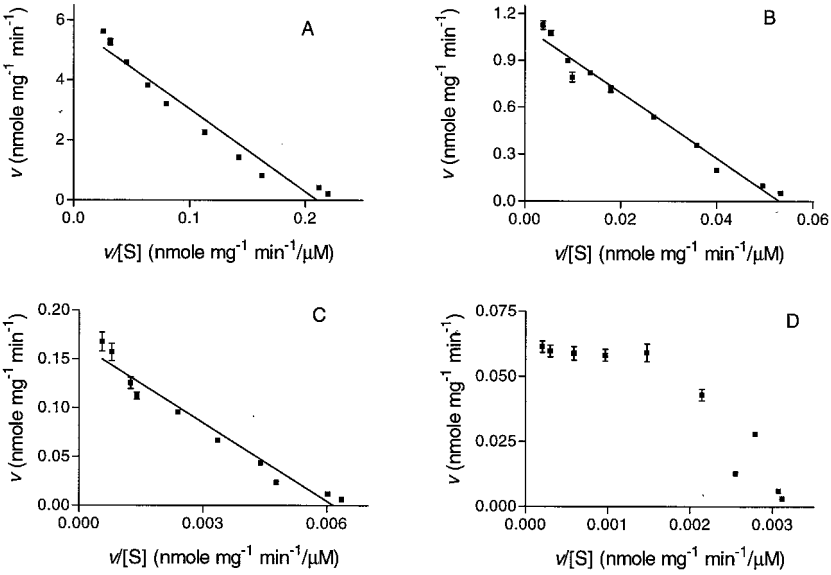


Figure 3. Eadie–Hofstee plots for the conversion of etoperidone to M1 (A), M2 (B), M8 (C) and M3 (D). Correlation coefficients (r^2) are 0.95 for M1, 0.97 for M2 and 0.95 for M8. Data shown are from pooled human liver microsomes. Each point represents the mean of three replicates.

Table 3. Rate of metabolite formation by recombinant CYP enzymes.

	Rate of metabolite formation (pmole nmole^{-1} CYP min^{-1})			
CYP	M1	M2	M3	M8
1A2	n.d.*	n.d.	n.d.	n.d.
2A6	n.d.	4.0 ± 0.3	n.d.	n.d.
2B6	n.d.	n.d.	n.d.	n.d.
2C8	n.d.	n.d.	n.d.	n.d.
2C9	3.0 ± 0.2	9.0 ± 0.7	n.d.	n.d.
2C19	72.0 ± 1.0	4.0 ± 0.3	n.d.	n.d.
2D6	8.0 ± 0.1	5.0 ± 0.2	n.d.	n.d.
2E1	8.0 ± 4.9	5.0 ± 1.0	n.d.	n.d.
3A4	765.0 ± 3.8	165.0 ± 3.8	20.0 ± 0.5	447.0 ± 18.0

Data are the mean ± SD of three determinations.
* n.d., Not detected.

forms; the formation of *N*-dealkylated metabolite *m*CPP (M8) was detected only in microsomes expressing CYP3A4, at a rate of 447.0 pmole nmole^{-1} min^{-1}. Similarly, the rate of CYP3A4-mediated formation of oxidized M3 was 20.0 pmole nmole^{-1} min^{-1}, whereas other enzymes did not show significant activity. The formation rate of phenyl hydroxylated metabolite (M2) was about 20–40 times greater for CYP3A4 compared with other enzymes including CYP2C9, CYP2C19, CYP2E1 and CYP2D6.

The formation of M8 (*m*CPP) via the metabolism of M1 was also investigated in microsomes derived from human B-lymphoblastoid cells expressing recombinant CYP enzymes. It was found that the rate of M8 (*m*CPP) formation from M1 was 503.0 ± 3.1 pmole nmole^{-1} min^{-1} for CYP3A4. Conversion of M1 to M8 was

not detected using derived microsomes containing other CYP enzymes including CYP1A2, CYP2A6, CYP2B6, CYP2C9, CYP2C19, CYP2D6 and CYP2E1.

Inhibition of Et metabolism in human liver microsomes

The inhibitory effect of specific inhibitors of individual CYP enzymes on the metabolism of Et was examined. These studies were conducted in pooled human liver microsomes prepared from 16 human liver samples. Since the concentrations of inhibitors used in the inhibition study varied widely among different laboratories (Newton *et al*. 1995, Zhou *et al*. 2000, Hyland *et al*. 2001), and inappropriate concentrations directly affect specificity of inhibitors (Ono *et al*. 1996, Eagling *et al*. 1998, Sai *et al*. 2000), the effective concentrations were previously determined in-house using pooled human liver microsomes and CYP marker substrates. The concentrations were chosen to inhibit the corresponding CYP enzyme significantly (> 60% inhibition) without causing non-specific effects on other enzymes. As shown in table 4, ketoconazole (1 μM), a CYP3A4 selective inhibitor, inhibited testosterone 6β-hydroxylase activity by 70%, and it also markedly blocked the formation of all four metabolites, M1–3 and M8, by 86, 75, 93 and 98%, respectively. However, the inhibitory effect on metabolite formation was only marginal (< 12%) for other CYP-selective inhibitors including α-naphthoflavone (CYP1A2), sulfaphenazole (CYP2C9), tranylcypromine (CYP2C19) and quinidine (CYP2D6), although extensive inhibition (> 60%) by these selective inhibitors was observed in the metabolism of corresponding CYP marker substrates (table 4).

The inhibitory effect of CYP-specific inhibitors on the formation of *m*CPP converted from M1 was also examined under the same conditions. As shown in table 4, ketoconazole, a CYP3A4 inhibitor, showed approximately 98% inhibition of conversion of M1 into *m*CPP, while other enzyme inhibitors (α-naphthoflavone, sulfaphenazole, tranylcypromine and quinidine) exhibited insignificant effects (< 15%) on the formation of *m*CPP (M8).

Etoperidone metabolism in a panel of human liver microsomes

Studies were carried out to investigate the correlation between the formation of four metabolites and the enzymatic activities of individual CYP enzymes (1A2, 2A6, 2B6, 2C8, 2C9, 2C19, 2D6, 2E1, 3A4). As shown in table 5, a significant correlation was observed between testosterone 6β-hydroxylase activity, a CYP3A4 marker activity and the rate of formation of all four metabolites, M1 ($r = 0.84$, $p < 0.005$), M2 ($r = 0.64$, $p < 0.05$), M3 ($r = 0.64$, $p < 0.05$) and M8 ($r = 0.98$, $p < 0.0001$). A good correlation ($r = 0.79$, $p < 0.005$) was also found between the rate of formation of M3 and (*S*)-mephenytoin *N*-demethylase activity, a CYP2B6 marker activity. In contrast, correlations of metabolite formation with all other CYP isoforms were statistically insignificant (table 5).

A correlation study was also conducted for the conversion of M1 to M8. Similarly, production of M8 from M1 was highly correlated with testosterone 6β-hydroxylase activity ($r = 0.71$, $p < 0.005$) (table 5), but not with any other CYP marker activities.

Table 4. Effects of CYP450 inhibitors on the metabolism of etoperidone in human liver microsomes.

Inhibitor (CYP) activity	(μM)	Inhibition of metabolite formation (% control)					CYP marker (% control)
		M1	M2	M3	M8	M1 → M8	
α-Naphthoflavone (1A2)	1.0	11.1 ± 0.6	2.2 ± 0.9	8.4 ± 1.9	9.2 ± 3.4	8.4 ± 1.4	22.1 ± 0.6[a]
sulfaphenazole (2C9)	5.0	10.3 ± 2.5	9.5 ± 2.5	11.9 ± 1.9	9.2 ± 0.8	8.2 ± 0.7	30.4 ± 1.2[b]
Tranylcypromine (2C19)	12.5	6.0 ± 2.8	11.8 ± 1.4	11.5 ± 3.0	−3.0 ± 2.8	−1.2 ± 2.8	37.3 ± 1.4[c]
Quinidine (2D6)	2.0	−4.7 ± 0.5	1.4 ± 0.3	−18.7 ± 0.5	−20.8 ± 1.6	−18.8 ± 1.2	21.6 ± 0.8[d]
Ketoconazole (3A4)	1.0	86.3 ± 1.1	74.8 ± 0.6	92.9 ± 0.5	98.6 ± 0.6	98.4 ± 0.2	29.5 ± 0.7[e]

[a] Phenacetin *O*-deethylation.
[b] Tolbutamide methylhydroxylation activity.
[c] (*S*)-Mephenytoin 4′-hydroxylation activity.
[d] Dextromethorphan *O*-demethylation activity.
[e] Testosterone 6β-hydroxylation.
Data are from pooled human liver microsomes and are the mean ± SD of three determinations.

Table 5. Correlation of etoperidone metabolism with marker activities of cytochrome P450s.

CYP	Isoform marker activity	Correlation coefficient (r)				
		M1	M8	M3	M2	M1 → *M8**
1A2	phenacetin *O*-deethylation	0.19	0.00	0.29	0.29	0.11
2A6	coumarin 7-hydroxylation	0.41	0.20	0.49	0.53	0.13
2B6	(*S*)-mephenytoin *N*-demethylation	0.52	0.79[a]	0.31	0.35	0.37
2C8	paclitaxel 6α-hydroxylation	0.10	0.29	0.05	0.07	0.05
2C9	diclofenac 4′-hydroxylation	0.08	0.24	0.00	0.00	0.03
2C19	(*S*)-mephenytoin 4′-hydroxylation	0.26	0.17	0.13	0.14	0.11
2D6	bufuralol 1′-hydroxylation	0.00	0.00	0.00	0.00	0.01
2E1	chlorzoxazone 6-hydroxylation	0.30	0.16	0.27	0.25	0.12
3A4	testosterone 6β-hydroxylation	0.84[b]	0.98[c]	0.64[d]	0.64[e]	0.71[f]
4A	lauric acid 12-hydroxylation	0.36	0.22	0.36	0.41	0.21

* Conversion of M1 to M8.

[a, f] Significantly correlated ($p < 0.005$); [b] significantly correlated ($p < 0.001$); [c] significantly correlated ($p < 0.0001$); [d, e] significantly correlated ($p < 0.05$). All other correlations were not statistically significant. The correlation study was carried out using human microsomes prepared from 13 different donors, and it represents the average of three determinations.

Table 6. *In vitro* inhibition of CYP activities by etoperidone.

CYP enzyme	Marker activity	IC_{50} (μM)
CYP1A2	phenacetin *O*-deethylation	> 100
CYP2C9	tolbutamide methylhydroxylation	> 100
CYP2C19	(*S*)-mephenytoin 4′-hydroxylation	> 100
CYP2D6	dextromethorphan *O*-demethylation	70.0 ± 4.1
CYP3A4	testosterone 6β-hydroxylation	> 100
	midazolam 1-hydroxylation	> 100

Data are from pooled human liver microsomes and are the average of three determinations.

Effects of Et on CYP enzymes

Inhibition of CYP activity by Et was investigated at concentrations up to 100 μM. Over this concentration range, Et was a weak inhibitor, with $IC_{50} > 100\,\mu M$ against all tested CYP marker substrates, with the exception of CYP2D6 ($IC_{50} = 70\,\mu M$) (table 6).

Discussion

Etoperidone was rapidly and extensively metabolized in human hepatic S9 fractions to form 10 metabolites via three metabolic pathways (figure 1). Alkyl and phenyl hydroxylations formed two major metabolites, M1 (18%) and M2 (11%), respectively, and *N*-dealkylation produced another major metabolite, M8 (*m*CPP, 8%). These three metabolites were further metabolized to form several minor metabolites, including M3–7, M9 and M10. These metabolites were all found in human, except for M6, M9 and M10 (Caldwell *et al.* 2001). M9 was previously identified in dog (Wu *et al.* 1995). In man, metabolism of Et produced a major circulating metabolite, M1, in plasma; both M2 and M4 are the major metabolites found in faecal extracts; M7 is the most predominant metabolite found in urine and the second most abundant metabolite detected in plasma (Caldwell *et al.* 2001). It therefore appears that both *in vivo* and *in vitro* studies revealed similar metabolite profiles.

Previous studies have demonstrated that *m*CPP formation from tradzodone and nefazodone was mainly mediated by CYP3A4 (Rotzinger *et al*. 1998, von Moltke *et al*. 1999, Zalma *et al*. 2000). In the present paper, efforts were made to identify CYP forms responsible for Et metabolism. Three metabolites, M1, M2 and M8, were chosen to represent three different metabolic pathways (figure 1). M3 formed from the primary metabolite M1 was also included in the study because it was found in all human samples including plasma, urine and faecal extract (Caldwell *et al*. 2001). The production of these metabolites in human liver microsomes was NADPH-dependent, suggesting that transformation of Et into these four metabolites was mediated by CYPs. Kinetics studies indicated these three pathways were all mediated by single CYP enzyme(s), as seen by monophasic Eadie–Hofstee plots of three primary metabolites, M1, M2 and M8. The V_{max}/K_m for M1 formation ($0.173\,nmole\,mg^{-1}\,min^{-1}\,\mu M^{-1}$) was approximately four times of that of M2 ($0.047\,nmole\,mg^{-1}\,min^{-1}\,\mu M^{-1}$), suggesting that alkyl hydroxylation is the most predominant metabolic pathway to eliminate Et in man. This conclusion is supported by the fact that M1 was a major metabolite found in man (Caldwell *et al*. 2001). Although M8, generated by *N*-dealkylation of Et, is thought to mediate pharmacological effects of the drug, the V_{max}/K_m for its formation was the lowest ($0.005\,nmole\,mg^{-1}\,min^{-1}\,\mu M^{-1}$) as compared with alkyl and phenyl oxidation reactions. These results were consistent with *in vivo* data (Caldwell *et al*. 2001). An Eadie–Hofstee plot of M3 was non-monophasic, which could be explained by the fact that M3 was not a primary metabolite and its formation rate was not directly related to Et.

The CYP enzymes mediating these three metabolic pathways were characterized by using recombinant CYP enzymes, chemical inhibition and correlation studies. Primary evidence for the involvement of CYP3A4 was provided by kinetics studies using recombinant CYP enzymes. The rate of M1 formation by CYP3A4 was the highest ($765.0\,pmole\,nmole^{-1}\,min^{-1}$), about 10-fold higher than that by CYP2C19 ($72.0\,pmole\,nmole^{-1}\,min^{-1}$) and hundreds of times higher than that by other CYP forms (2C9, 2D6, 2E1). Similarly, M2 formation rate was 20–40-fold greater for recombinant CYP3A4 compared with that for other CYP forms. M8 (*m*CPP) and M3 were only formed by CYP3A4 and not generated by any other CYP forms. Since CYP3A4 is the most abundant form in the human liver (Lin and Lu 1998), these results suggested CYP3A4 was the major enzyme mediating these three metabolic pathways. Although CYP2C19 showed activity, to some degree, in M1 formation, this form is unlikely to play a significant role in Et metabolism in man because its activity is relatively much lower and it only accounts for approximately 1% of total human hepatic CYPs compared with CYP3A4 (about 30%) (Lin and Lu 1998).

Further evidence for the involvement of CYP3A4 was provided by chemical inhibition studies. Of the various specific CYP inhibitors examined, the CYP3A4-selective inhibitor ketoconazole was the only one that extensively inhibited formation of M1–3 and M8. These data also suggested a major role of CYP3A4 in Et metabolism, which is in agreement with the results obtained using recombinant CYP enzymes. Tranylcypromine, a CYP2C19 selective inhibitor, inhibited $>60\%$ of (*S*)-mephenytoin 4′-hydroxylation, a CYP2C19 marker activity, but did not show significant effect ($<15\%$) on formation of M1–3 and M8. These results also indicate that CYP2C19 is not a major enzyme involved in Et metabolism. Quinidine, a CYP2D6-specific inhibitor, did not inhibit metabolite production but

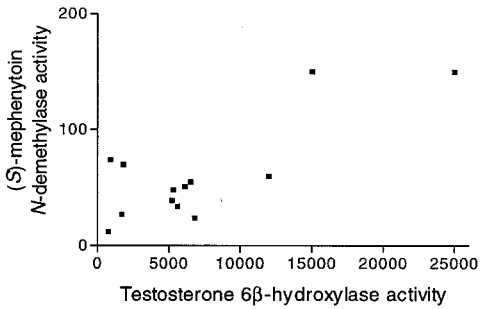


Figure 4. Correlation between (*S*)-mephenytoin *N*-demethylase activity and 6β-testosterone hydroxylase activity in human liver microsomes from 13 different donors. Activities were determined by the supplier (Gentest Corp.).

increased M8 and M3 formation by about 20%. Similar effects of quinidine on CYP3A4 activity have also been reported recently by Ngui *et al.* (2000, 2001). One possible explanation is that two substrates bind simultaneously to CYP3A4 active sites (Shou *et al.* 1994, Wang *et al.* 2000) and cooperative interactions may exist between two molecules bound to the enzyme (Maenpaa *et al.* 1998, Domanski *et al.* 2001, Atkins *et al.* 2001, Tang and Stearns 2001).

In the correlation study, formation of M1–3 and M8 from Et was highly correlated with testosterone 6β-hydroxylase activity in 13 different human liver microsomes. In addition, the conversion of M1 to M8 was significantly correlated with testosterone 6β-hydroxylase activity, which is a marker of CYP3A4 activity. Therefore, results from the correlation study also indicated that CYP3A4 played a predominant role in all three metabolic pathways. In the correlation study, it was also found that M3 formation correlated highly with (*S*)-mephenytoin *N*-demethylase activity, a marker activity of CYP2B6. However, recombinant CYP2B6 did not significantly produce M3 from Et (table 3). Further examination of specific CYP activities revealed that, surprisingly, a good correlation (figure 4) existed between (*S*)-mephenytoin *N*-demethylase activity and testosterone 6β-hydroxylase activity in those 13 human liver microsomes used in correlation studies. A similar correlation between (*S*)-mephenytoin *N*-demethylase activity and testosterone 6β-hydroxylase activity was observed by Prakash *et al.* (2000) in a different human liver microsome pool. Although a clear explanation is currently lacking, such a correlation should not be interpreted as the evidence indicating the involvement of CYP2B6 in Et metabolism.

Data from the correlation study indicated that metabolite formation was not significantly correlated with (*S*)-mephenytoin 4′-hydroxylase activity, further suggesting that CYP2C19 does not play a significant role in Et metabolism. This is consistent with the results obtained from inhibition studies and recombinant CYP incubation experiments.

M1 is the most predominant metabolite that was likely to be further converted into *m*CPP *in vivo*. Since *m*CPP is thought to mediate the pharmacological effects of the drug (Fong *et al.* 1982, Raffa *et al.* 1992), similar efforts were made to identify CYP forms involved in the conversion of M1 to M8. Data from chemical inhibition, correlation and kinetics studies suggested that CYP3A4 played the major role in this transformation.

The effect of Et on the activity of the five major drug-metabolizing CYPs was studied. It was found that Et was a weak inhibitor of all these enzymes; the most potent inhibition was against CYP2D6 activity, with an $IC_{50} = 70\,\mu M$. Owing to the predominant role of CYP3A4 in the metabolism of Et, interactions with two CYP3A4 substrates were investigated. It was found that Et was a very weak inhibitor for both testosterone and midazlam, with an $IC_{50} > 100\,\mu M$.

In conclusion, the results of this study show that three metabolic pathways, *N*-dealkylation, alkly and phenyl hydroxylation, are involved in Et metabolism, and that CYP3A4 is the principal CYP enzyme responsible for these metabolic transformations of Et in man.

References

Atkins, W. M., Wang, R. W. and Lu, A. Y. H., 2001, Allosteric behavior in cytochrome P450-dependent *in vitro* drug–drug interactions: a prospective based on conformational dynamics. *Chemical Research in Toxicology*, **14**, 338–347.

Baldwin, S. J., Bloomer, J. C., Smith, G. J, Ayrton, A. D., Clarke, S. E., Catanese, B., Barillari, G. and Galli Angeli, D., 1982, Studies on the oral absorption in man of etoperidone tablets and capsules. *Bollettino Chimica Farmaceutico*, **121**, 530–534.

Caldwell, G. W., Wu, W. N. and Masucci, J. A., 2001, Evaluation of the absorption, excretion and metabolism of [^{14}C] etoperidone in man. *Xenobiotica*, **31**, 823–839.

Chang, T. K. H., Gonzalez, F. J. and Waxman, D. J., 1994, Evaluation of triacetyloleandomycin, α-naphthoflavone and diethyldithiocarbamate as selective chemical probes for inhibition of human cytochromes P450. *Archives of Biochemistry and Biophysics*, **311**, 437–442.

Chenery, R. J., 1995, Ketoconazole and sulphaphenazole as the respective selective inhibitors of P4503A and 2C9. *Xenobiotica*, **25**, 261–270.

Domanski, T. L., He, Y. A., Khan, K. K., Roussel, F., Wang, Q. and Halpert, J. R., 2001, Phenylalanine and tryptophan scanning mutagenesis of CYP3A4 substrate recognition site residues and effect on substrate oxidation and cooperativity. *Biochemistry*, **40**, 10150–10160.

Eagling, V. A., Tjia, J. F. and Back, D. J., 1998, Differential selectivity of cytochrome P450 inhibitors against probe substrates in human and rat liver microsomes. *British Journal of Clinical Pharmacology*, **45**,107–114.

Fong, M. H., Garattini, S. and Caccia, S., 1982, 1-*m*-Chlorophenylpiperazine is an active metabolite common to the psychotropic drugs trazodone, etoperidone, and mepiprazole. *Journal of Pharmaceutics and Pharmacology*, **34**, 674–675.

Hyland, R., Roe, E. G. H., Jones, B. C. and Smith, D. A., 2001, Identification of the cytochrome P450 enzymes involved in the *N*-demethylation of sildenafil. *British Journal of Clinical Pharmacology*, **51**, 239–248.

Lin, J. H. and Lu, A. H. Y., 1998, Inhibition and induction of cytochrome P450 and the clinical implications. *Clinical Pharmacokinetics*, **35**, 361–390.

Maenpaa, J., Hall, S. D., Ring, B. J., Strom, S. C. and Wrighton, S. A., 1998, Human cytochrome P450 3A (CYP3A) mediated midazolam metabolism: the effect of assay conditions and regioselective stimulation by α-naphthoflavone, terfenadine and testosterone. *Pharmacogenetics*, **8**, 137–155.

Maes, M., Westenberg, H., Vandoolaeghe, E., Demedts, P., Wauters, A., Neels, H. and Meltzer, H. Y., 1997, Effects of trazodone and fluoxetine in the treatment of major depression: therapeutic pharmacokinetic and pharmacodynamic interactions through formation of meta-chlorophenylpiperazine. *Journal of Clinical Psychopharmacology*, **17**, 358–364.

Mancy, A., Dijols, S., Poli, S., Guengerich, P. and Mansuy, D., 1996, Interaction of sulfaphenazole derivatives with human liver cytochromes P450 2C: molecular origin of the specific inhibitory effects of sulfaphenazole on CYP 2C9 and consequences for the substrate binding site topology of CYP 2C9. *Biochemistry*, **35**, 16205–16212.

Newton, D. J., Wang, R. W. and Lu, A. Y. H., 1995, Cytochrome P450 inhibitors: evaluation of specificities in the *in vitro* metabolism of therapeutic agents by human liver microsomes. *Drug Metabolism and Disposition*, **23**, 154–158.

Ngui, J. S., Chen, Q., Shou, M., Wang, R. W., Stearns, R. A., Baillie, T. A. and Tang, W., 2001, *In vitro* stimulation of warfarin metabolism by quinidine: increases in the formation of 4- and 10-hydroxywarfarin. *Drug Metabolism and Disposition*, **29**, 877–886.

Ngui, J. S., Tang, W., Stearns, R. A., Shou, M., Miller, R. R., Zhang, Y., Lin, J. H. and Baillie, T. A., 2000, Cytochrome P450 3A4-mediated interaction of diclofenac and quinidine. *Drug Metabolism and Disposition*, **28**, 1043–1050.

Ono, S., Hatanaka, T., Hotta, H., Satoh, T., Gonzalez, F. J. and Tsutsui, M., 1996, Specificity of substrate and inhibitor probes for cytochrome P450s: evaluation of *in vitro* metabolism using cDNA-expressed human P450s and human liver microsomes. *Xenobiotica*, **26**, 681–693.

Otton, S. V., Crewe, H. K., Lennard, M. S., Tucker, G. T. and Woods, H. F., 1988, Use of quinidine inhibition to define the role of the sparteine/debrisoquine cytochrome P450 in metoprolol oxidation by human liver microsomes. *Journal of Pharmacology and Experimental Therapeutics*, **247**, 242–247.

Prakash, C., Kamel, A., Cui, D., Whalen, R. D., Miceli, J. J. and Tweedie, D., 2000, Identification of the major human liver cytochrome P450 isoform(s) responsible for the formation of the primary metabolites of ziprasidone and prediction of possible drug interactions. *British Journal of Clinical Pharmacology*, **49 (suppl. 1)**, 35S–42S.

Przegalinski, E. and Lewandowska, A., 1979, The effect of etoperidone a new potential antidepressant drug, on the central serotonin system. *Journal of Neural Transmission*, **46**, 303–312.

Raffa, R. B., Shank, R. P. and Vaught, J. L. 1992, Etoperidone, trazodone and MCPP: *in vitro* and *in vivo* identification of serotonin 5-HT1A (antagonistic) activity. *Psychopharmacology*, **108**, 320–326.

Rotzinger, S., Fang, J. and Baker, G. B., 1998, Trazodone is metabolized to *m*-chlorophenylpiperazine by CYP3A4 from human sources. *Drug Metabolism and Disposition*, **26**, 572–575.

Sai, Y., Dai, R., Yang, T. J., Krausz, K. W., Gonzalez, F. J., Gelboin, H. V. and Shou, M., 2000, Assessment of specificity of eight chemical inhibitors using cDNA-expressed cytochromes P450. *Xenobiotica*, **30**, 327–343.

Shou, M., Grogan, J., Mancewicz, J. A., Krausz, K. W., Gonzalez, F. J., Gelboin, H. V. and Korzekwa, K. R., 1994, Activation of CYP3A4: evidence for the simultaneous binding of two substrates in a cytochrome p450 active site. *Biochemistry*, **33**, 6450–6455.

Tang, W. and Stearns, R. A., 2001, Heterotropic cooperativity of cytochrome P450 3A4 and potential drug–drug interactions. *Current Drug Metabolism*, **2**, 185–198.

Tassaneeyakul, W., Birkett, D. J., Veronese, M. E., McManus, M. E., Tukey, R. H., Quattrochi, L. C., Gelboin, H. V. and Miners, J. O., 1993, Specificity of substrate and inhibitor probes for human cytochromes P450 1A1 and 1A2. *Journal of Pharmacology and Experimental Therapeutics*, **265**, 401–407.

Von Moltke, L. L., Greenblatt, D. J., Granda, B. W., Grassi, J. M., Schmider, J., Harmatz, J. S. and Shader, R. I., 1999, Nefazodone, meta-chlorophenylpiperazine, and their metabolites *in vitro*: cytochromes mediating transformation, and P450-3A4 inhibitory actions. *Psychopharmacology*, **145**, 113–122.

Wang, R. W., Newton, D. J., Liu, N., Atkins, W. M. and Lu, A. Y. H., 2000, Human cytochrome P-450 3A4: *in vitro* drug–drug interaction patterns are substrate-dependent. *Drug Metabolism and Disposition*, **28**, 360–366.

Wu, W. N., Caldwell, G. W. and Uetz, J. A., 1991, Biotransformation of etoperidone in man. *Pharmacologist*, **33**, 208–212.

Wu, W. N., Masucci, J. A., McKown, L. A. and Rodgers, J. D., 1995, Identification of four plasma metabolites of etoperidone in dogs. *Journal of Pharmaceutics and Biomedical Analysis*, **13**, 177–184.

Wu, W. N. and McKown, L. A., 2000, Recent advances in biotransformation of CNS and cardiovascular agents. *Current Drug Metabolism*, **1**, 255–270.

Wu, W. N. and McKown, L. A., 2001, *In vitro* metabolism of etoperidone in human hepatic S9 fraction. *Drug Metabolism Reviews*, **33**, 123.

Zalma, A., von Moltke, L. L., Granda, B. W., Harmatz, J. S., Shader, R. I. and Greenblatt, D. J., 2000, *In vitro* metabolism of trazodone by CYP3A: inhibition by ketoconazole and human immunodeficiency viral protease inhibitors. *Biology and Psychiatry*, **47**, 655–661.

Zhou, S., Paxton, J. W., Tingle, M. D. and Kestell, P., 2000, Identification of the human liver cytochrome P450 isoenzyme responsible for the 6-methylhydroxylation of the novel anticancer drug 5,6-dimethylxanthenone-4-acetic acid. *Drug Metabolism and Disposition*, **28**, 1449–1456.

XENOBIOTICA, 2002, VOL. 32, NO. 11, 963–973

Taylor & Francis
healthsciences

Decreased activity of hepatic P-glycoprotein in the isolated perfused liver of the adjuvant arthritis rat

M. ACHIRA, R. TOTSUKA and T. KUME

Discovery Research Laboratory, Tanabe Seiyaku Co., Ltd, 2-2-50 Kawagishi Toda Saitama 335-8505, Japan

Received 24 April 2002

1. We investigated the hepatobiliary transport of doxorubicin in the isolated perfused liver prepared from the adjuvant arthritis rat, an animal model for rheumatoid arthritis, to examine the hepatic P-glycoprotein activity in the adjuvant arthritis rat.

2 Liver was isolated from the normal and the adjuvant arthritis rat and perfused for 60 min with recirculating buffer and the perfusate and bile samples were collected at timed interval.

3. The elimination of doxorubicin in the adjuvant arthritis rat tended to be reduced, but it was not significantly different from the normal rat. Biliary clearance (CL_{bile}) in the normal rat was $1.93 \pm 0.48\,ml\,min^{-1}$, whereas, CL_{bile} in the adjuvant arthritis rat was significantly decreased to $0.40 \pm 0.13\,ml\,min^{-1}$.

4. CL_{bile} was markedly decreased to about $0.15\,ml\,min^{-1}$ in the presence of 100 μM verapamil in both types of rat. Methotrexate treatment had no effect on CL_{bile} in both the normal and adjuvant arthritis rat (2.18 ± 0.22 and $0.47 \pm 0.22\,ml\,min^{-1}$, respectively).

5. The results suggest that the hepatic P-glycoprotein activity was markedly decreased in the adjuvant arthritis rat and the effect of methotrexate on the hepatic P-glycoprotein activity did not corresponded to its anti-inflammatory effect.

Introduction

Rheumatic diseases are estimated to affect up to 1.1% of the world_fs population (Harris 1981) and patients are often treated with either steroids, non-steroidal anti-inflammatory drugs (NSAIDs), disease-modifying anti-rheumatic drugs (DMARDs) and/or immunosuppressive drugs. The adjuvant arthritis (AA) rat has been used as an animal model for rheumatoid arthritis (RA) because it represents a systemic inflammatory disease with bone and cartilage changes similar to those observed in RA (Williams *et al*. 1992). Altered pharmacokinetics or pharmacological effects in the AA rat have been reported, e.g. elevated plasma concentrations of cyclosporine A, acebutolol and propranolol (Piquette-Miller and Jamali 1992, 1993, Shibata *et al*. 1993) and the prolongation of pentobarbital sleeping time (Dipasquale *et al*. 1974). The change in the level in the α_1-acid glycoprotein content in plasma and the activities of cytochrome P450 and other hepatic enzymes such as UDP-glucuronosyltransferase are involved in these changes (Bishop *et al*. 1981, Belpaire *et al*. 1989, Meunier and Verbeeck 1999). Buchar and Janku (1985) suggested that AA alters the phospholipid composition of endoplasmic reticulum in the liver as a result of decreased synthesis of phosphatidylcholine and phosphatidylethanolamine, and that this alteration might lead to

* Author for correspondence; e-mail: m-achira@tanabe.co.jp

Xenobiotica ISSN 0049–8254 print/ISSN 1366–5928 online © 2002 Taylor & Francis Ltd
http://www.tandf.co.uk/journals
DOI: 10.1080/00498250210012664

an impairment of the function of microsomal enzymes. Altered plasma protein binding and metabolism in the liver have been the main focus in studies on changes in pharmacokinetics in the AA rat.

In addition to hepatic metabolism, urinary and biliary excretion are also important in the removal of xenobiotics, and many active transporters such as P-glycoprotein (P-gp), multidrug resistance-associated protein 2 (MRP2) and organic anion transporter 1 (OAT1) are involved in the urinary and biliary excretion (He *et al.* 1991, Masuda *et al.* 1997, Booth *et al.* 1998). However, little has been reported about the effect of AA on the activities and expressions of these active transporters. Recently, it was reported that lipopolysaccharide (LPS)-induced cholestasis causes the reduction of the expression and activity of P-gp in rat liver (Piquette-Miller *et al.* 1998). Some cytokines such as tumour necrosis factor-α (TNFα) and interleukin 1 (IL-1) modulate P-gp activity and expression level of *MDR1*, which encodes P-gp, in human carcinoma cells (Borsellino *et al.* 1994, Varga *et al.* 1996). Moreover, we have confirmed that the expression level of hepatic P-gp was significantly decreased in the AA rat by using an immunohistochemical detection method. Although the expression level of hepatic P-gp was decreased, alternation in the plasma concentration of doxorubicin (DOX) was not observed following intravenous administration to the AA rat (Achira *et al.* 2002a).

In the current study, we have investigated the effect of AA on hepatic P-gp activity in the isolated perfused rat liver. The isolated liver perfusion method can avoid the influence of altered hepatic blood flow rate, plasma protein binding and extrahepatic elimination in the AA rat. Moreover, we investigated the effects of methotrexate (MTX), a disease-modifying anti-rheumatic drug, on hepatic P-gp activity in the AA rat. MTX is a potent inhibitor of dihydrofolate reductase (Andersson *et al.* 2000) and patients with RA have been commonly treated with MTX.

Materials and methods

Chemicals and reagents

Doxorubicin (DOX) was purchased from Wako Pure Chemical Industries Ltd (Osaka, Japan). *Mycobacterium butyricum* was purchased from Difco Lab. (Detroit, MI, USA). Methotrexate (MTX)was purchased from Sigma Chemical Co. (St Louis, MO, USA). Other reagents used this study were analytical grade.

Animals

Female Lewis rats (8 weeks, about 120–150 g body weight) were purchased from Charles River Japan (Tokyo, Japan). The animals were allowed free access to standard laboratory chow (CE2, Japan Crea, Tokyo, Japan) and water. Studies were approved by the animal ethics committee of Tanabe Seiyaku Co., Ltd.

AA was induced by an injection of *M. butyricum* suspended in liquid paraffin (0.5 mg/0.1 ml/animal) into the subplantar region of the right hindpaw. Rats were studied approximately 17–21 days after adjuvant injection when they had developed swelling of the left hindpaw (secondary inflammation). MTX was given subcutaneously to the AA rat at a dose of 0.1 mg kg^{-1} day^{-1} from 0 to 20 days after adjuvant injection and rats were studied at 21 days after adjuvant injection. MTX was also given to the normal rat at the corresponding date. The swellings of the right injected hindpaw and left contralateral hindpaw were measured at 0, 3, 7, 10, 14, 17 and 21 days after adjuvant injection.

Isolated liver perfusion

The liver was isolated and perfused as described by Watanabe *et al.* (1993). Each rat was anesthetized with urethane (1 g kg^{-1} intraperitoneally), and cannulated into the bile duct, portal vein and superior vena cava. The liver was perfused *in situ* with oxygenated Krebs–Ringer buffer supplement

with 5 mM glucose (pH 7.4) and constantly gassed with 95% O_2/5% CO_2 by a recirculating method at a flow rate of 20 ml min^{-1}. The temperature of the liver perfusion system was kept at 37 °C. The liver was allowed to equilibrate for about 10 min before the addition of DOX. Following equilibration of the liver, 10 μM DOX with or without 100 μM verapamil, a P-gp inhibitor, was added to the reservoir. The isolated liver was perfused for 60 min after addition of DOX. Perfusate samples (0.5 ml) were collected at timed intervals, and bile samples were collected at 15-min intervals. At the end of perfusion, the whole liver was homogenized with 20 ml saline with a Polytron homogenizer (PT20 'OD'S Kinematica GmbH, Switzerland). Liver viability was determined based on bile flow rate and glutamic-oxaloacetic transaminase (GOT) activity of perfusate samples. Perfusate, bile and liver homogenate samples were stored at −20 °C until analysis.

High-performance liquid chromatography (HPLC) assay

Concentrations of DOX in the perfusate, bile and liver homogenate samples were determined by high-performance liquid chromatography as described by Álvarez-Cedrón *et al.* (1999) with slight modifications. A high-performance liquid chromatograph (D-7000 Liquid Chromatograph) was equipped with a fluorescence detector (L-7480; Hitachi, Tokyo, Japan) set at an excitation wavelength of 480 nm and an emission wavelength of 560 nm. An ODS column (Mightysil RP-18, 150 4.6 mm i.d., particle size 5 μm; Kanto Chemical Co., Inc., Tokyo, Japan) was used, and the mobile phase was a mixture of methanol and 0.5% phosphoric acid, 43:57 (v/v). The flow rate was 1.0 ml min^{-1}.

The liver homogenate and bile samples were deproteinized by adding a 1:1 mixture of 40% $ZnSO_4$/methanol containing daunorubicin as an internal standard (0.09 nmol). After centrifugation (10 000*g* for 5 min), the supernatant was injected into the chromatograph. Perfusate samples were directly injected into chromatograph.

Data analysis

The remaining DOX in the perfusate (FR) versus time profiles were fitted to the mono-exponential equation:

$$\mathrm{FR}\,(\%) = \mathrm{FR}_0 \times \mathrm{e}^{-k\mathrm{el}\cdot t},$$

where FR_0 is the extrapolated remaining fraction at 0 time, k_{el} is the elimination rate constant, by using a non-linear regression program, WinNonlin, and t is perfusion time. The apparent hepatic clearance defined in terms of DOX elimination from the perfusate (CL_{eli}) was obtained by multiplying k_{el} by the distribution volume:

$$V_d = V/\mathrm{FR}_0,$$

where V is the volume of perfusate (= 100 ml). Biliary clearance (CL_{bile}) was obtained from the following equation:

$$\mathrm{CL}_{\mathrm{bile}} = \text{total amount of DOX in the bile/AUC}, \quad (1)$$

where AUC is the area under the perfusate concentration profile.

Statistical analysis

The results are means ± SD. A Student's t-test was used to determine the significance of differences between the normal and the AA rat.

Results

The profiles of DOX concentration in the perfusate versus time are shown in figure 1. The GOT activities in the perfusate samples were in the normal range in every perfusion (< 60 Karmen U). The elimination of DOX in the normal and the AA rat followed first-order kinetics and the elimination rate constants (k_{el}) were estimated by non-linear regression analysis and multiplied by the volume of distribution to estimate the hepatic clearance defined in terms of DOX elimination from the perfusate (CL_{eli}). These pharmacokinetic parameters of DOX in the normal and the AA rat are shown in table 1. The elimination of DOX in the AA rat tended to be delayed compared with the normal rat, but a significant difference was not observed. DOX elimination from the perfusate in the normal and the AA rat was rapid, with a $t_{1/2}$ = 11.0 and 14.7 min, respectively. The extrapolated remain-

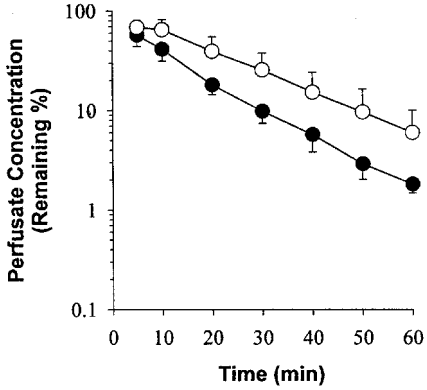


Figure 1. Time-course of residual DOX in the perfusate of a liver perfusion prepared from the normal and AA rat. Data are the mean ± SD ($n = 3$). ●, Normal rat; ○, AA rat. The initial concentration of DOX was 10 μM.

Table 1. Comparison of pharmacokinetic parameters for doxorubicin (DOX) in liver perfusion between the normal and the AA rat.

	Normal rat		AA rat	
	Verapamil (−)	Verapamil (+)	Verapamil (−)	Verapamil (+)
FR_0 (%)	82.6 ± 19.1	79.8 ± 13.8	97.0 ± 15.7	92.5 ± 10.0
k_{el} (min^{-1})	0.07 ± 0.01	0.05 ± 0.01	0.049 ± 0.010	0.05 ± 0.00
$T_{1/2}$ (min)	11.0 ± 1.3	14.3 ± 5.3	14.7 ± 3.1	13.5 ± 0.9
AUC_{0-60} (nmol min ml^{-1})	141 ± 23	162 ± 51	212 ± 80	182 ± 28
V_d (ml)	121 ± 47	127 ± 21	104 ± 16	107.5 ± 12.2
CL_{eli} (ml min^{-1})	7.6 ± 2.0	6.7 ± 2.6	5.1 ± 1.7	5.6 ± 0.9
Hepatic amount (nmol)	585 ± 165	725 ± 150	686 ± 68	792 ± 249
CL_{bile} (ml min^{-1})	1.93 ± 0.48	0.18 ± 0.11**	0.40 ± 0.13**	0.14 ± 0.09†

Data are the mean ± SD ($n = 3$); ** $p < 0.01$ for the value compared with verapamil (−) in the normal rat; † $p < 0.05$ for the value compared with verapamil (−) in the AA rat.

ing fraction of DOX at 0 min (i.e. FR_0) in the normal and the AA rat was 82.6 and 97.0%, respectively, giving a $V_d = 121$ and 104 ml, respectively (table 1). These parameters were statistically not significant between the normal and the AA rat. Although the hepatic clearance defined in term of DOX elimination from the perfusate (CL_{eli}) in the AA rat tended to be low compared with that found in the normal rat, there was no significant difference. The profiles of DOX concentration in the perfusate in the presence of 100 μM verapamil are shown in figure 2, and their pharmacokinetic parameters are also shown in table 1. The elimination of DOX versus time in the presence of verapamil also followed the first-order kinetics with $t_{1/2}$ of about 14 min in both groups of rat. Verapamil had no effect on each parameter for the elimination of DOX from the perfusate in both the normal and the AA rat.

The cumulative biliary excretion of DOX in the normal and the AA rat are shown in figure 3. A total of 21.4 ± 5.9% of the dose was recovered from the bile within 60 min in the normal rat. The cumulative biliary excretion of DOX in the AA rat was significantly decreased to 7.5 ± 0.8% of the dose. Moreover, in both groups of rat, the cumulative biliary excretion of DOX was markedly decreased to

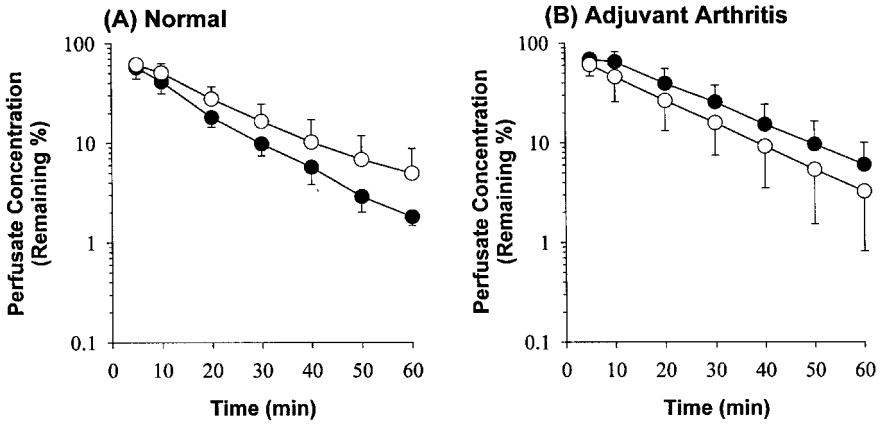


Figure 2. Effect of verapamil on the disappearance of DOX in the perfusate of a liver perfusion prepared from the normal (A) and AA (B) rat. Data are the mean ± SD (n = 3). ●, In the absence of verapamil; ○, in the presence of verapamil. The initial concentrations of DOX and verapamil were 10 and 100 μM, respectively.

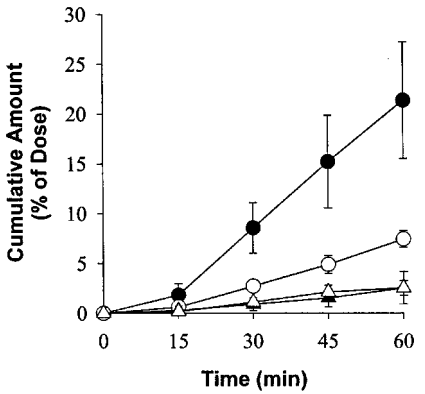


Figure 3. Cumulative biliary excretion of DOX in a liver perfusion prepared from the normal and AA rat. Data are the mean ± SD (n = 3). ●, ▲, Normal rat; ○, □, AA rat; ●, ○, in the absence of verapamil; ▲, □, in the presence of verapamil. The initial concentrations of DOX and verapamil were 10 and 100 μM, respectively.

about 2.5% of the dose in the presence of 100 μM verapamil. The biliary clearances (CL_{bile}) in the normal and the AA rat estimated from equation (1) are shown in table 1. CL_{bile} in the normal rat was 1.93 ml min^{-1}, whereas in the AA rat it was significantly decreased to 0.40 ml min^{-1}. CL_{bile} was markedly decreased to about 0.15 ml min^{-1} in the presence of 100 μM verapamil in both types of rat. These latter values were lower than the perfusion flow rate (= 20 ml min^{-1}).

The amounts of DOX in the liver at the end of perfusion are shown in table 1. The amounts of DOX in the normal and the AA rat were 585 and 686 nmol, respectively, and a significant difference was not observed. The liver concentration of DOX calculated by dividing by liver weight (about 7 g) was about 90 nmol g^{-1} liver, this amount being markedly higher than the perfusate concentration. Verapamil had no effect on the amount of DOX in the liver in both groups of rat (table 1). The recovery of DOX from the perfusate, bile and liver are summarized in table 2. The majority (58.4–68.4%) of DOX administered to the

Table 2. Recovery of doxorubicin (DOX) 60 min after liver perfusion in the normal and the AA rat.

	Normal (% of dose)		Adjuvant arthritis (% of dose)	
	Verapamil (−)	Verapamil (+)	Verapamil (−)	Verapamil (+)
Perfusate	1.8 ± 0.3	5.0 ± 3.9	6.0 ± 4.0	3.3 ± 2.4
Liver	58.4 ± 16.7	72.6 ± 15.0	68.4 ± 6.6	79.1 ± 24.9
Bile	21.4 ± 5.9	2.5 ± 0.8**	7.5 ± 0.8**	2.6 ± 1.6‡

Data are the mean ± SD ($n = 3$); ** $p < 0.01$ for the value compared with verapamil (−) in the normal rat; ‡ $p < 0.01$ for the value compared with verapamil (−) in the AA rat.

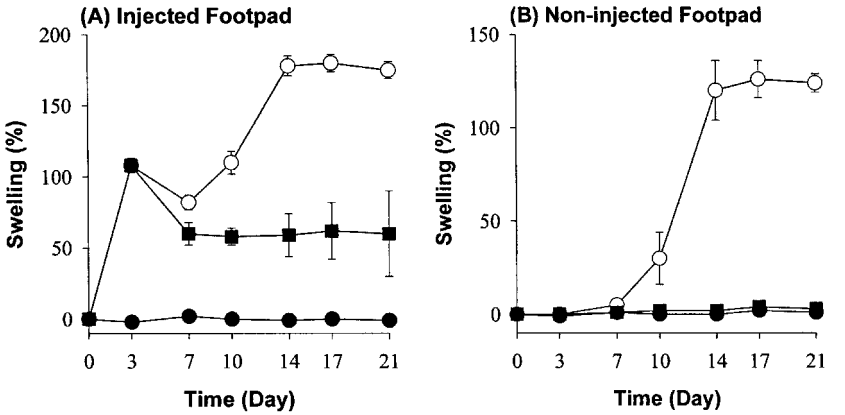


Figure 4. Effect of methotrexate (MTX) on the swelling of the adjuvant injected and non-injected footpad in the AA rat. Data are the mean ± SD ($n = 3$). ■, MTX-treated AA rat; ●, normal rat (without MTX treatment); ○, AA rat (without MTX treatment).

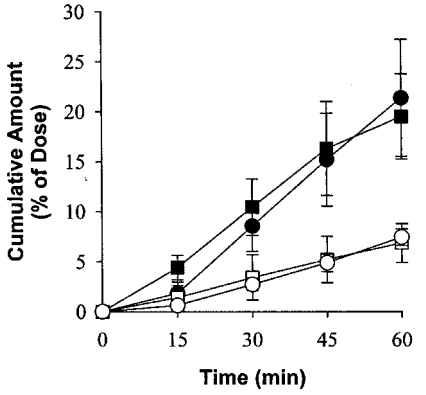


Figure 5. Cumulative biliary excretion of DOX in a liver perfusion prepared from the methotrexate (MTX)-treated normal and AA rat. Data are the mean ± SD ($n = 3$). ■, MTX-treated normal rat; □, MTX-treated AA rat; ●, normal rat (without MTX treatment); ○, AA rat (without MTX treatment).

isolated perfused rat liver was recovered in the liver homogenate at the end of the DOX perfusion.

The daily administration of MTX prevented the swelling of the hindpaw in the AA rat (figure 4). The profiles of DOX concentration in the perfusate were similar

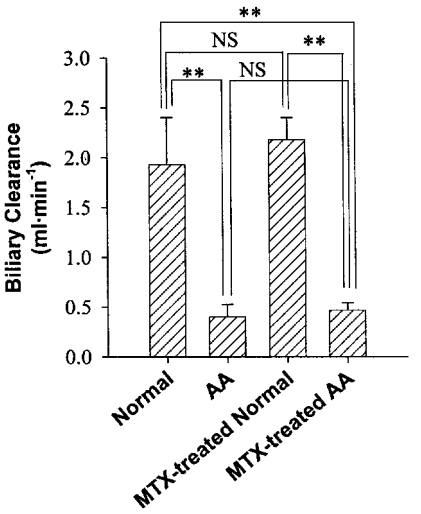


Figure 6. Biliary clearance of DOX in the methotrexate (MTX)-treated normal and AA rat. Data are the mean ± SD ($n = 3$). $^{**}p < 0.01$; $^{*}p < 0.05$; NS, no significant difference.

to those found in the MTX-untreated normal and AA rat (data not shown). Cumulative biliary excretion and biliary clearance of DOX in the MTX-treated normal and AA rat are shown in figures 5 and 6, respectively. A total of 19.5 ± 4.3% and 6.9 ± 2.0% of the dose was recovered from bile within 60 min in the MTX-treated normal and AA rat, respectively. CL_{bile} in the MTX-treated normal and AA rat was 2.18 ± 0.22 and 0.47 ± 0.07 ml min^{-1}, respectively. The reduction of the biliary excretion of DOX in the AA rat was not prevented by the daily administration of MTX.

Discussion

The AA rat is commonly used as an animal model for inflammatory disease such as RA. Cyclosporine A, tacrolimus and steroids are effective against AA and RA, and are known as substrates of P-gp (Marsaud *et al.* 1998, Wacher *et al.* 2001). It has been demonstrated that the expression of the hepatic P-gp in the AA rat is decreased, and that the plasma concentration of DOX after intravenous administration to the AA rat was not different from that in the normal rat (Achira *et al.* 2002a). The purpose of the current study was to examine the effect of AA on the activity of hepatic P-gp using the isolated rat liver perfusion method, because the method avoids the effects of changes in hepatic blood flow rate and plasma protein binding and extrahepatic elimination in the AA rat. DOX was used as a P-gp substrate and DOX is eliminated primarily by the liver and approximately 24% of dose is excreted into the bile via P-gp over 10 hours (Tavoloni and Guarino 1980).

The elimination of DOX from the perfusate was rapid in the normal and the AA rat and the hepatic clearance estimated from DOX elimination from the perfusate (CL_{eli}) was not altered in the AA rat (figure 4 and table 1). Although the elimination of DOX in the AA rat tended to be delayed compared with the normal rat, these results are in agreement with our previous *in vivo* study (Achira *et al.* 2002a). It has been reported that the distribution of DOX into the liver is very

rapid compared with the efflux to the perfusate, and the metabolism and excretion into the bile in the isolated perfused liver (Booth *et al.* 1998), and that this characteristic of DOX suggests that CL_{eli} represents only the uptake process of DOX into the liver (Booth *et al.* 1998). Although it has been reported that a carrier-mediated active transport system may also be involved in the hepatic uptake of DOX (Lane *et al.* 1987), its contribution to the hepatic uptake process was minor, and involvement of the active transport system is not observed *in vivo* (Colombo *et al.* 1994). Thus, DOX is mainly taken up into the liver by simple diffusion and these results suggest that AA has no effect on the uptake of drugs into the liver by simple diffusion.

The amount in the liver at the end of perfusion was not altered in the AA rat, although biliary clearance (CL_{bile}) in the AA rat was significantly decreased. If decreased biliary excretion in the AA rat resulted in sequestration of DOX in the liver, a significant alteration in the amount of DOX in the liver may not be detectable because the overwhelming majority of the recovered dose was in the liver homogenate (table 2). Moreover, DOX is localized in the nucleus in normal hepatocytes (Nicolo *et al.* 1982). The rapid passive uptake into the liver and the 'pool effect' in the nucleus may contribute to the high amount of DOX in the liver of the normal and the AA rat and the non-significant difference between the normal and the AA rat. Booth *et al.* (1998) reported that quinidine and GF120918, both potent P-gp inhibitors, had an effect on the biliary clearance of DOX, but not on the amount in the isolated perfused rat liver. These latter results are agreement with the present results. The CL_{bile} in the presence of verapamil was markedly decreased and comparable between the normal and the AA rat. Moderate concentrations of verapamil inhibit only P-gp in the liver (Watanabe *et al.* 1992), suggesting that DOX is mainly excreted into the bile via P-gp and that the reduction of CL_{bile} of DOX in the AA rat is mainly due to the reduction of hepatic P-gp activity. Moreover, the expression level of hepatic P-gp in the AA rat is two- or threefold lower than that in the normal rat (Achira *et al.* 2002a), again in agreement with the current results. Protein binding to liver proteins may affect the CL_{bile}. For example, the increased unbound fraction of YM796, a selective M1-receptor agonist, in the hepatocytes changes the clearance (Iwatsubo *et al.* 1999). We studied the unbound fraction of DOX in the liver using the method described by Lin *et al.* (1982). No significant difference was observed between the normal and the AA rat (0.004 ± 0.001 versus 0.005 ± 0.001, respectively). It has recently been reported that DOX is also a substrate for MRP2 (Cui *et al.* 1999). We have previously demonstrated that the activity and expression level of MRP2 in liver is decreased in the AA rat, hence a decreased MRP2 activity may also be involved in a decreased biliary excretion of DOX in the AA rat (Achira *et al.* 2002b). There are reports demonstrating that AA decreases the activity of cytochrome P450 and other metabolic enzymes (Piquette-Miller and Jamali 1993). DOX is known to be partially metabolized by aldo-ketoreductase, cytochrome P450 and glucuronide-conjugating enzymes (Arcamone *et al.* 1984). Although we focused on the hepatobiliary transport of DOX in the AA rat in the current investigation and did not clarify the effect of AA on DOX metabolism, the changes in these metabolic enzyme activities must have an effect on the DOX elimination in the AA rat.

MTX, commonly used as an anti-rheumatic drug, is effective in AA (figure 4). Hence, we investigated the effect of MTX on the decreased activity of the hepatic

P-gp in the AA rat. The biliary excretion of the MTX-treated AA rat remained low and no significant difference was observed compared with the MTX-untreated AA rat. The biliary excretion of the MTX-treated normal rat was similar to the untreated normal rat. MTX is a potent inhibitor of dihydrofolate reductase, but has no effect on the production of cytokines (Taki *et al.* 1998), and these pharmacological effects may cause different effects on the anti-inflammatory and on the hepatic P-gp activities. In rats treated with LPS, an animal model for cholestasis, the expression of the hepatic MRP2 is decreased (Nakamura *et al.* 1999). It has been reported that the level of MRP2 in parenchymal hetatocytes is decreased when normal parenchymal hepatocytes are co-cultured with Kupffer cells prepared from rats treated with LPS. The Kupffer cells activated by the LPS treatment produce and release cytokines such as TNFα and/or IL-1. From these results, the cytokine released from activated Kupffer cells results in the down-regulation of MRP2 in parenchymal hepatocytes (Nakamura *et al.* 1999). A similar mechanism may be involved in the case of hepatic P-gp in LPS-treated rats, because it has been reported that TNFα modulates MDR1 expression and P-gp function in human carcinoma cells (Borsellino *et al.* 1994, Varga *et al.* 1996) and the secretion of rhodamine-123, a P-gp substrate, from rat hepatocytes is significantly decreased after LPS treatment (Piquette-Miller *et al.* 1998). Moreover, Sukhai *et al.* (2001) reported that IL-6 has an effect on the expressions of *mdr1a* and *mdr1b* in rat hepatocytes. In the AA rat, the precise molecular mechanism of alternation of hepatic P-gp activity is unclear at present. The systemic levels of some cytokines such as TNFα and IL-6, but not IL-1β, are elevated in the AA rat, particularly plasma IL-6, which is sixfold higher than that found in the normal rat (Philippe *et al.* 1997). These cytokines may decrease hepatic P-gp activity in the AA rat as for the LPS-treated rat. Although we only studied activities at steady-state (17–21 days after adjuvant injection) in the current study, we could gain more information by investigating the time-course of change in hepatic P-gp activity in the AA rat and its relation to the systemic cytokines levels, because the systemic levels of TNFα and IL-6 depend on the time after adjuvant injection (Philippe *et al.* 1997).

The present results have confirmed the effect of AA on hepatic P-gp activity. The AA rat is a useful animal model for RA, but changes in pharmacokinetics must be considered when P-gp substrates such as cyclosporine A, tacrolimus and some steroids are used in the AA rat. Although there is no information about the expression and activity of hepatic P-gp in patients with RA, we suggest that the hepatobiliary transport of cyclosporine A, tacrolimus and steroids may be altered because of the altered expression and activity of hepatic P-gp.

References

Achira, M., Totsuka, R., Fujimura, H. and Kume, T., 2002a, Tissue-specific regulation of expression and activity of P-glycoprotein in adjuvant arthritis rats. *European Journal of Pharmaceutical Sciences*, **16**, 29–36.

Achira, M., Totsuka, R., Fujimura, H. and Kume, T., 2002b, Decreased hepatobiliary transport of methotrexate in adjuvant arthritis rats, *Xenobiotica* (accepted).

Alvarez-Cedrón, L., Sayalero, M. L. and Lanao, J. M., 1999, High-performance liquid chromatographic validated assay of doxorubicin in rat plasma and tissues. *Journal of Chromatography*, **721**, 271–278.

Andersson, S. E., Johansson, L. H., Lexmüller, K. and Ekström, G. M., 2000, Anti-arthritic effect of methotrexate: is it really mediated by adenosine? *European Journal of Pharmaceutical Sciences*, **9**, 333–343.

Arcamone, F., Lazzati, M., Vicario, G. P. and Zini, G., 1984, Disposition of ^{14}C-labelled 4′-epidoxorubicin and doxorubicin in the rat. A comparative study. *Cancer Chemotherapy and Pharmacology*, **12**, 157–166.

Belpaire, F. M., Smet, F. De., Chindavijak, B., Fraeyman, N. and Bogaert, M. G., 1989, Effect of turpentine-induced inflammation on the disposition kinetics of propranolol, metoprolol and antipyrine in the rat. *Fundamentals in Clinical Pharmacology*, **3**, 79–88.

Bishop, H., Schneider, R. E. and Welling, P., 1981, Plasma propranolol concentrations in rats with adjuvant-induced arthritis. *Biopharmacology and Drug Disposition*, **2**, 291–297.

Booth, C. L., Brouwer, K. R. and Brouwer, K. L. R., 1998, Effect of multidrug resistance modulators on the hepatobiliary disposition of doxorubicin in the isolated perfused rat liver. *Cancer Research*, **58**, 3641–3648.

Borsellino, D., Crescimanno, M., Flandina, C., Flugy, A. and D'Alessandro, N., 1994, Combined activity of interleukin-1alpha or TNF-alpha and doxorubicin on multidrug resistant cell lines: evidence that TNF and DXR have synergistic antitumor and differentiation-inducing effects. *Anticancer Research*, **14**, 2643–2548.

Buchar, E. and Janku, I., 1985, The effect of adjuvant-induced arthritis on rat liver microsomal phospholipid metabolism. *Methods and Findings in Experimental Clinical Pharmacology*, **7**, 469–472.

Colombo, T., Zucchetti, M. and D'Incalci, M., 1994, Cyclosporin A markedly changes the distribution of doxorubicin in mice and rats. *Journal of Pharmacology and Experimental Therapeutics*, **269**, 22–27.

Cui, Y., Konig, J., Buchholz, J. K., Spring, H., Leier, I. and Keppler, D., 1999, Drug resistance and ATP-dependent conjugate transport mediated by the apical multidrug resistance protein, MRP2, permanently expressed in human and canine cells. *Molecular Pharmacology*, **55**, 929–937.

Dipasquale, G., Welaj, P. and Rassaert, C. L., 1974, Prolonged pentobarbital sleeping time in adjuvant-induced polyarthritic rats. *Research Communications in Chemical Pathology and Pharmacology*, **9**, 253–264.

Harris, E. D., 1981, Rheumatoid arthritis: the clinical spectrum. In *Textbook of Rheumatology* (Philadelphia: WB Saunders), pp. 928–963.

He, Y. L., Tanigawara, Y., Yasuhara, M. and Hori, R., 1991, Effect of folinic acid on tissue residence and excretion of methotrexate in rats. *Drug Metabolism and Disposition*, **19**, 729–734.

Iwatsubo, T., Suzuki, H. and Sugiyama, Y., 1999, Determination of the rate-limiting step in the hepatic elimination of YM796 by isolated rat hepatocytes. *Pharmaceutical Research*, **16**, 110–116.

Lane, P., Vichi, P., Bain, D. L. and Tritton, T. R., 1987, Temperature dependence studies of adriamycin uptake and cytotoxicity. *Cancer Research*, **47**, 4038–4042.

Lin, J. H., Sugiyama, Y., Awazu, S. and Hanano, M., 1982, *In vitro* and *in vivo* evaluation of the tissue-to-blood partition coefficient for physiological pharmacokinetic models. *Journal of Pharmacokinetics and Biopharmacology*, **10**, 637–647.

Marsaud, V., Mercier-Bodard, C., Fortin, D., Le Bihan, S. and Renoir, J. M., 1998, Dexametasone and triamcinolone acetonide accumulation in rat fibroblast is differently modulated by the immunosuppressants cyclosporin A, FK506, rapamycin and their analogues, as well as other P-glycoprotein ligants. *Journal of Steroid Biochemistry and Molecular Biology*, **66**, 11–25.

Masuda, M., I'izuka, Y., Yamazaki, M., Nishigaki, R., Kato, Y., Ni'inuma, K., Suzuki, H. and Sugiyama, Y., 1997, Methotrexate is excreted into the bile by canalicular multispecific organic anion transporter in rats. *Cancer Research*, **57**, 3506–3510.

Meunier, C. J. and Verbeeck, R. K., 1999, Glucuronidation of *R*- and *S*-ketoprofen, acetoaminophen, and diflunisal by liver microsomes of adjuvant-induced arthritic rats. *Drug Metabolism and Disposition*, **27**, 26–31.

Nakamura, J., Nishida, T., Hayashi, K., Kawada, N., Ueshima, S., Sugiyama, Y., Ito, T., Sobue, K. and Matsuda, H., 1999, Kupffer cell-mediated down regulation of rat hepatic CMOAT/MRP2 gene expression. *Biochemical and Biophysical Research Communications*, **255**, 143–149.

Nicolo, G., Esposito, M., Belcastro, A., Rovida, S., Margallo, E. and Santi, L., 1982, Cytophotometric analysis of nuclear uptake of adriamycin in *in vivo* normal mouse liver and kidney cells. *Analytical and Quantitative Cytology*, **4**, 295–301.

Philippe, L., Gegout-Pottie, P., Guingamp, C., Bordji, K., Terlain, B., Netter, P. and Gillet, P., 1997, Relations between functional, inflammatory, and degenerative parameters during adjuvant arthritis in rats. *American Journal of Physiology*, **273**, R1550–R1556.

Piquette-Miller, M. and Jamali, F., 1992, Effect of adjuvant arthritis on the disposition of acebutolol enantiomer in rats. *Agent Actions*, **37**, 290–296.

Piquette-Miller, M. and Jamali, F., 1993, Selective effect of adjuvant arthritis on the disposition of propranolol enantiomer in rats detected using a stereospecific HPLC assay. *Pharmaceutical Research*, **10**, 294–299.

Piquette-Miller, M., Pak, A., Kim, H., Anari, R. and Shahzamani, A., 1998, Decreased expression and activity of P-glycoprotein in rat liver during acute inflammation. *Pharmaceutical Research*, **15**, 706–711.

Shibata, N., Shimakawa, H., Minouchi, T. and Yamaji, A., 1993, Pharmacokinetics of cyclosporin A after intravenous administration to rats in various disease states. *Biological and Pharmacological Bulletin*, **16**, 1130–1135.

Sukhai, M., Yong, A., Pak, A. and Piquette-Miller, M., 2001, Decreased expression of P-glycoprotein in interleukin-1beta and interleukin-6 treated rat hepatocytes. *Inflammation Research*, **50**, 362–370.

Taki, H., Sugiyama, E., Mino, T., Kuroda, A. and Kobayashi, M., 1998, Differential inhibitory effects of indomethacin, dexamethasone, and interferon-gamma (IFN-gamma) on IL-11 production by rheumatoid synovial cells. *Clinical and Experimental Immunology*, **1**, 133–138.

Tavoloni, N. and Guarino, A. M., 1980, Disposition and metabolism of adriamycin in the rat. *Pharmacology*, **21**, 244–255.

Varga, A., Nugel, H., Baehr, R., Marx, U., Hevér, A., Nacsa, J., Ocsovszky, I. and Molnar, J., 1996, Reversal of multidrug resistance by amitriptyline *in vitro*. *Anticancer Research*, **16**, 209–212.

Wacher, V. J., Salphati, L. and Benet, L. Z., 2001, Active secretion and enterocytic drug metabolism barriers to drug absorption. *Advances in Drug Delivery Reviews*, **46**, 89–102.

Watanabe, J., Kondo, H., Muranishi, H., Urano, K., Haba, M. and Yuasa, H., 1993, Macromolecule–macromolecule interaction in drug distribution. III. Kinetic characterization of the uptake of fractionated [^{3}H]heparin and the effect of plasma proteins in the perfused rat liver. *Biological and Pharmacological Bulletin*, **16**, 1035–1039.

Watanabe, T., Miyauchi, S., Sawada, Y., Iga, T., Hanano, M., Inaba, M. and Sugiyama, Y., 1992, Kinetic analysis of hepatobiliary transport of vincristine in perfused rat liver. Possible roles of P-glycoprotein in biliary excretion of vincristine. *Journal of Hepatology*, **16**, 77–88.

Williams, R. O., Feldmann, M. and Maini, R. N., 1992, Anti-tumor necrosis factor ameliorates joint disease in murine collagen-induced arthritis. *Proceedings of the National Academy of Sciences, USA*, **89**, 9784–9788.

XENOBIOTICA, 2002, VOL. 32, NO. 11, 975–984

Taylor & Francis
healthsciences

Differential induction of midazolam metabolism in the small intestine and liver by oral and intravenous dexamethasone pretreatment in rat

S. L. EECKHOUDT, Y. HORSMANS†* and R. K. VERBEECK‡

Departments of † Pharmaceutical Sciences and ‡ Gastroenterology, Catholic University of Louvain (UCL), B-1200 Brussels, Belgium

Received 25 March 2002

1. Midazolam is metabolized in the rat by CYP3A enzymes to 4-OH-midazolam (4-OH-MDZ) and 1′-OH-midazolam (1′-OH-MDZ). The induction of midazolam metabolism was studied in male Wistar rats treated with dexamethasone ($50\,mg\,kg^{-1}\,day^{-1}$) during 4 days via the oral or intravenous routes. Microsomes were prepared from the liver and the proximal small intestine and *in vitro* metabolism of midazolam was determined. In addition, CYP3A1- and CYP3A2-like protein levels were measured by gel electrophoresis and immunoblotting.

2. The V_{max}'s (mean SEM) for 4-OH-MDZ and 1′-OH-MDZ formation were much lower in intestinal (0.078 ± 0.002 and $0.074 \pm 0.002\,\mu M\,min^{-1}\,mg^{-1}$ protein, respectively) compared with hepatic microsomes prepared from the uninduced rat (0.870 ± 0.007 and $0.310 \pm 0.020\,\mu M\,min^{-1}\,mg^{-1}$ protein, respectively). Induction by oral or intravenous dexamethasone pretreatment led to significant increases in V_{max} for 4-OH-MDZ and 1′-OH-MDZ by both intestinal and hepatic microsomes. Oral dexamethasone pretreatment via the oral route resulted in a more pronounced increase in V_{max} compared with intravenous administration of the inducer.

3. CYP3A1 and CYP3A2 protein levels in liver microsomes were significantly increased following oral (3.7- and 3.2-fold, respectively) or intravenous (2.6- and 2.1-fold, respectively) pretreatment with dexamethasone. On the contrary, only oral dexamethasone pretreatment resulted in a significant change in intestinal CYP3A2-like protein (7.3-fold). A slight difference in the migration distance of the immunoreactive band for CYP3A2 was also observed for intestinal microsomes.

4. These results suggest that intestinal CYP3A enzymes in the rat differ from hepatic CYP3A1 and CYP3A2. They also demonstrate that systemic dexamethasone administration can induce intestinal microsome activity.

Introduction

Cytochrome P450 (CYP) enzymes play an important role in the metabolism of a large number of both endogenous and exogenous substances (Lu and West 1979, Porter and Coon 1991). Multiple forms of CYP exist and several enzymes can be expressed simultaneously in different tissues such as the liver, gut, lung, kidney and brain (Kaminsky and Fasco 1992, Krishna and Klotz 1994). It is now recognized that members of the CYP3A subfamily are among the most important of all drug-metabolizing enzymes and catalyse the metabolism of many drugs including cyclosporin, terfenadine, nifedipine, erythromycin and midazolam (Rendic and Di Carlo 1997). Certain members of this CYP subfamily, e.g. CYP3A4 in man and CYP3A1/3A2 in rat, are present in intestinal epithelial cells and have been shown to contribute significantly to the so-called first-pass

* Author for correspondence; e-mail: horsmans@gaen.ucl.ac.be

Xenobiotica ISSN 0049–8254 print/ISSN 1366–5928 online © 2002 Taylor & Francis Ltd
http://www.tandf.co.uk/journals
DOI: 10.1080/00498250210012655

effect following oral administration of a number of drugs (Wu *et al.* 1995, Thummel *et al.* 1996). More recently, Gushchin *et al.* (1999) demonstrated the existence of new CYP enzymes in the rat intestine. In addition, the activity of these CYP3A enzymes is modulated by inducers (e.g. dexamethasone, phenobarbital, rifampicin) and inhibitors (ketoconazole, grapefruit juice) and this may lead to clinically significant drug interactions (Thummel and Wilkinson 1998).

The induction of intestinal CYP3A enzymes could be expected to be influenced by the route of administration of the inducing agent (Zhang *et al.* 1996). Indeed, the exposure of the enterocytes to an orally administered inducing agent may be very different from the enterocyte exposure to the same agent administered systemically. The primary objective of the current study was to evaluate the effect of the route of administration, i.e. oral (p.o.) versus intravenous (i.v.), of the inducing agent dexamethasone on the expression and activity of CYP3A enzymes in the rat intestinal epithelium and liver. The rate of midazolam metabolism by intestinal and hepatic microsomes was used as a marker of CYP3A activity (Ghosal *et al.* 1996). In addition, CYP3A1 and CYP3A2 protein levels in control and dexamethasone-induced intestinal and hepatic microsomes were measured by immunoblot analysis.

Material and methods

Chemicals

Flunitrazepam, midazolam (MDZ), 1′-hydroxymidazolam (1′-OH-MDZ) and 4-hydroxymidazolam (4-OH-MDZ) were kindly donated by Dr T. W. Guentert, Hoffman-La Roche Ltd (Basel, Switzerland). $NADP^+$, NADPH, isocitric acid, isocitrate dehydrogenase and dexamethasone 21-phosphate disodium salt were purchased from ICN (Costa Mesa, CA, USA). Rat CYP3A1 and CYP3A2 supersomes were purchased from Gentest Corp. (Woburn, MA, USA). Polyclonal antibodies against CYP3A1 and CYP3A2 were obtained from Chemicon International, Inc. (Temecula, CA, USA). Reagents used for sodium dodecyl sulphate-polyacrylamide gel electrophoresis (SDS-PAGE) and Western blotting were obtained from Bio-Rad Laboratories (Watford, UK). The ECL kit used for the detection of immunoreactive bands was obtained from Amersham. HPLC-grade acetonitrile and methanol were purchased from Baker (Deventer, The Netherlands). All other chemicals used were of the highest purity available from standard commercial sources.

Animals

Male Wistar rats (Iffa Credo, Belgium), 8 weeks old (approximately 250 g) at the time of sacrifice, were housed in an environmentally controlled room at 20–22 °C with a 12-h light/dark cycle and had free access to food (type AO4, U.A.R., Espinay-sur-Orge, France) and tap water. Rats were always fasted overnight before sacrifice.

Study protocol

The experimental protocol was approved by the Animals Ethics Committee of the Catholic University of Louvain. The animals were divided into four groups of 12 rats each: (1) control-receiving vehicle p.o., (2) dexamethasone p.o., (3) control i.v. and (4) dexamethasone i.v. Rats were treated with dexamethasone ($50\,mg\,kg^{-1}\,day^{-1}$) for 4 days via the oral (gavage) or i.v. route (jugular vein). Control rats were treated with vehicle only. Rats receiving dexamethasone by the i.v. route, as well as their controls, were fitted with jugular vein cannulae. They were operated under Thalamonal® (Janssen Pharmaceutica, Beerse, Belgium) anaesthesia on the day before the start of dexamethasone treatment and a piece of silastic tubing (0.94 mm o.d., 0.51 mm i.d., Intramedic, The Netherlands) was implanted in the right and left jugular veins. The control p.o. and dexamethasone p.o. treatment rats were killed by decapitation. The control i.v. and dexamethasone i.v. treatment rats were killed by an i.v. injection of air. The liver was removed as well as the small intestine, which was cut in two equal parts: the proximal and distal small intestine. In each treatment group, the liver and proximal part of the small intestine of three rats were pooled for the preparation of microsomes.

Preparation of microsomes

Liver microsomes were prepared by the method of Leclercq *et al.* (1997). Briefly, livers were homogenized in microsomal buffer (0.1 M phosphate buffer, pH 7.4, 0.1 M KCl, 1 mM EDTA) using a Potter Elvehjem homogenizer. The homogenate was centrifuged at 9000*g* for 10 min at 4 °C. The supernatant was transferred to a clean tube and centrifuged at 11 000*g* for 60 min at 4 °C. The microsomal pellet corresponding to 3.5 g liver was resuspended in 10 ml microsomal buffer. Enterocytes were isolated by the method of Keelan *et al.* (1994). Subsequently, intestinal microsomes were prepared by the same method as the one used for the preparation of liver microsomes. Microsomal fractions were stored at −80 °C until used. The protein concentration of the microsomal preparations was determined by the method of Lowry *et al.* (1951).

Immunoquantification of CYP3A1 and CYP3A2

A total of 0.4–6.2 μg intestinal microsomal protein and 0.5–3.1 μg hepatic protein was used for the immunoquantification of CYP3A1 and CYP3A2. Electrophoresis was performed using a 10% acrylamide gel under 125 V for 90 min. Proteins were then electrophoretically transferred to polyvinylidene difluoride membranes under 30 V overnight. The membranes were blocked for 60 min in TBS (20 mM Tris-HCl, pH 7.6, 137 mM NaCl) containing 5% (w/v) defatted milk and incubated for 2 h with anti-CYP3A1 (1:16 000) or anti-CYP3A2 (1:8000). The membranes were washed five times in TBS containing 0.1% Tween 20 before incubation for 1 h with horseradish peroxidase-conjugated anti-rabbit IgG (1:10 000) diluted in blocking buffer. After washing as described above, the membranes were rinsed in TBS and the immunoreactive bands detected using the ECL kit. The optical density (OD) of the immunoreactive bands was determined using the Image Master 1.10 program (Pharmacia Biotech, Roosendaal, The Netherlands). The results are expressed as $OD\,mm^2\,mg^{-1}$ protein.

Microsomal incubations

The incubation mixture contained (in a total volume of 1 ml): intestinal or hepatic microsomes ($0.6\,mg\,protein\,ml^{-1}$), 0.1 m sodium phosphate buffer, pH 7.4, 0.1 M KCl, 1 mM EDTA, 6 mM $MgCl_2.6H_2O$, 10 mM isocitric acid, 0.3 units isocitric dehydrogenase and MDZ at concentrations ranging from 5 to 370 μM. The mixture was incubated in a shaking water bath at 37°C. After a preincubation period of 5 min, the reaction was started by the addition of 0.2 μM $NADP^+$ and 0.2 μM NADPH. After 16 min, the reaction was terminated by adding 40 μl NaOH (2%) and placing the samples on ice. The internal standard (IS) flunitrazepam was added to the incubation mixture (30 μl of $106\,\mu g\,ml^{-1}$ for hepatic microsomal incubations, 50 μl of $5\,\mu g\,ml^{-1}$ for intestinal microsomal incubations). MDZ metabolites were quantified by capillary HPLC by using a slight modification of a previously described method (Eeckhoudt *et al.* 1998). Briefly, the incubation mixtures were extracted with 4.5 ml diethyl ether:cyclohexane (69:31 v/v). After centrifugation, the organic layer was transferred to a clean tube and evaporated to dryness at 40C under a stream of nitrogen. The residue was dissolved in 100–1000 μl of a mixture of water:acetonitrile (95:5 v/v) and 20 μl were injected into the capillary HPLC system. The three MDZ metabolites and flunitrazepam (IS) eluted from the column with retention times of approximately 7 min (di-OH-MDZ), 9 min (4-OH-MDZ), 10 min (1′-OH-MDZ) and 12 min (flunitrazepam), respectively.

Supersomes ($0.21\,mg\,protein\,ml^{-1}$) were incubated following the same method as described above for hepatic and intestinal microsomes, but in the presence of a high concentration of MDZ (400 μM). The incubation mixture was extracted and analysed by HPLC as described above.

Data analysis

Untransformed enzyme kinetic data were analysed by non-linear regression analysis using PCNonlin (SCI Software, Lexington, KY, USA). A simple Michaelis–Menten model or Hill equation was fitted to the metabolite formation rates versus the substrate concentration. The choice between the two models was based on the Akaike Information Criterion, the Schwartz Criterion and the *F*-test (Gorski *et al.* 1994). Values in the text, tables and graphs are given as mean ± SEM. Means of V_{max}, K_m and OD obtained in the four treatment groups were compared by ANOVA followed by the Newman–Keuls test. The results of the *post-hoc* test were taken into account for the following comparisons: control p.o. versus dexamethasone p.o., control i.v. versus dexamethasone i.v. control p.o. versus control i.v. The last comparison allowed us to evaluate the effect of surgery on the enzyme kinetic parameters. Independent sample *t*-tests were carried out to compare mean V_{max} for the formation of 4-OH-MDZ and 1′-OH-MDZ between control p.o. control i.v. microsomes. $p \leq 0.05$ was considered as significant.

Results

Induction of hepatic MDZ metabolism by p.o. and i.v. dexamethasone treatment

Incubation of midazolam with liver microsomes from control p.o. and control i.v. rats resulted in the formation of two metabolites (figure 1). K_m and V_{max} were estimated for 1′-OH-MDZ and 4-OH-MDZ using the Hill equation (table 1).

In the p.o. and i.v. control rats, V_{max} for the formation of 4-OH-MDZ by hepatic microsomes were substantially higher (2–3-fold) than for the formation of 1′-OH-MDZ.

Induction by p.o. or i.v. pretreatment of rats with dexamethasone resulted in a substantial increase in the formation of all three metabolites. V_{max} for the formation of 1′-OH-MDZ was on average 4.6 and 3.3 times higher after p.o. and i.v. dexamethasone pretreatment, respectively. Similarly, statistically significant increases in V_{max} for the formation of 4-OH-MDZ, i.e. 4.5 times for the p.o. dexamethasone group and 3.7 times for the i.v. dexamethasone treatment group, were observed. Whereas V_{max} for the formation of 1′-OH-MDZ and 4-OH-MDZ were not significantly different between the i.v. and p.o. control rats, V_{max} for the formation of both metabolites were significantly higher following pretreatment with dexamethasone p.o. compared with the i.v. route (table 1). Pretreatment of the rats by p.o. or i.v. dexamethasone was also associated with statistically significant increases in the K_m for the formation of both MDZ metabolites (table 1). For both 1′-OH-MDZ and 4-OH-MDZ, the mean K_m following p.o. administration of dexamethasone (34.1 ± 2.6 and $44.0 \pm 3.0\,\mu M$, respectively) were statistically significantly higher than the mean K_m observed following i.v. administration of dexamethasone (25.9 ± 1.6 and $37.3 \pm 1.1\,\mu M$, respectively).

Induction of intestinal MDZ metabolism by p.o. and i.v. dexamethasone

Following incubation of MDZ in the presence of proximal intestinal microsomes of control p.o. and control i.v. rats, the formation rates of 1′-OH-MDZ and

Table 1. V_{max}, K_m and the Hill coefficient (Hill equation) for the formation of 4-OH-midazolam and 1′-OH-midazolam in liver microsomes of the control and dexamethasone treated rat. The statistical significance for the comparisons oral (p.o.) control versus intravenous (i.v.) dexa and p.o. dexa versus i.v. control are not shown.

Parameter	Treatment	1′-OH-midazolam	4-OH-midazolam
V_{max} ($\mu M\,min^{-1}\,mg^{-1}$ protein)	p.o. control	0.310 ± 0.020^{a}	0.870 ± 0.007^{d}
	p.o. dexa	$1.438 \pm 0.127^{a,c}$	$3.928 \pm 0.316^{d,f}$
	i.v. control	0.253 ± 0.026^{b}	0.773 ± 0.085^{e}
	i.v. dexa	$0.840 \pm 0.047^{b,c}$	$2.840 \pm 0.114^{e,f}$
K_m (μM)	p.o. control	13.1 ± 1.4^{g}	14.4 ± 0.5^{j}
	p.o. dexa	$34.1 \pm 2.6^{g,l}$	$44.0 \pm 3.0^{j,l}$
	i.v. control	13.3 ± 1.1^{h}	15.0 ± 1.8^{k}
	i.v. dexa	$25.9 \pm 1.7^{h,i}$	$37.3 \pm 1.1^{k,l}$
Hill coefficient	p.o. control	1.58 ± 0.27	1.34 ± 0.18
	p.o. dexa	2.12 ± 0.48	2.03 ± 0.35
	i.v. control	1.67 ± 0.25	1.52 ± 0.27
	i.v. dexa	2.42 ± 0.84	2.35 ± 0.52

Common superscripts are statistically different ($p < 0.05$, ANOVA)[a–l]
Data are the mean ± SEM of $n = 4$ determinations.

Table 2. V_{max} and K_m (Michaelis–Menten equation) for the formation of 4-OH-midazolam and 1′-OH-midazolam in intestinal microsomes of the control and dexamethasone treated rat. The statistical significance for the comparisons oral (p.o.) control versus intravenous (dexa) and p.o. dexa versus i.v. control are not shown.

Parameter	Treatment	1′-OH-midazolam	4-OH-midazolam
V_{max} ($\mu M\,min^{-1}\,mg^{-1}$ protein)	p.o. control	0.074 ± 0.002^{a}	0.078 ± 0.002^{d}
	p.o. dexa	$0.439 \pm 0.039^{a,c}$	$0.435 \pm 0.041^{d,f}$
	i.v. control	0.076 ± 0.001^{b}	0.078 ± 0.001^{e}
	i.v. dexa	$0.159 \pm 0.010^{b,c}$	$0.180 \pm 0.007^{e,f}$
K_m (μM)	p.o. control	7.3 ± 0.9	23.0 ± 1.3^{h}
	p.o. dexa	6.3 ± 0.6^{g}	28.9 ± 0.9^{h}
	i.v. control	4.7 ± 0.1	21.6 ± 1.7^{I}
	i.v. dexa	3.7 ± 0.8^{g}	30.0 ± 0.9^{i}

Common superscripts are statistically different ($p < 0.05$, ANOVA).
Data are the mean ± SEM of $n = 4$ determinations.

4-OH-MDZ were determined (figure 1). V_{max} and K_m were estimated using a simple Michaelis–Menten equation. No statistically significant difference was observed in V_{max} for the formation of 1′-OH-MDZ and 4-OH-MDZ between the control p.o. and control i.v. rats (table 2). Compared with the results obtained with control liver microsomes, mean V_{max} for 1′-OH-MDZ and 4-OH-MDZ formation by intestinal microsomes were approximately three and 10 times lower, respectively.

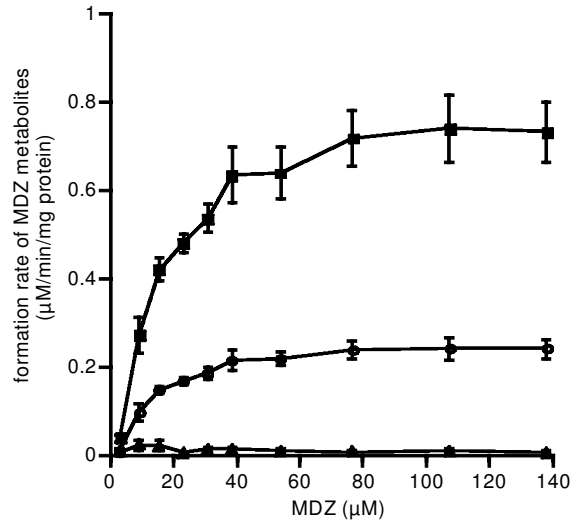
Induction by p.o. or i.v. dexamethasone pretreatment led to a significant increase in the formation rates of both 1′-OH-MDZ and 4-OH-MDZ. V_{max} for the formation of 1′-OH-MDZ were on average 5.9 and 2.1 times higher following p.o. and i.v. dexamethasone pretreatment, respectively (table 2). Similarly, statistically significant increases in V_{max} were observed for the formation of 4-OH-MDZ, i.e. 5.6 times for the p.o. dexamethasone group and 2.3 times for the i.v. dexamethasone treatment group. Whereas dexamethasone pretreatment did not lead to significant changes in the K_m for the formation of 1′-OH-MDZ, it slightly but significantly increased the K_m for the formation of 4-OH-MDZ (table 2).

MDZ metabolism by supersomes expressing CYP3A1 and CYP3A2

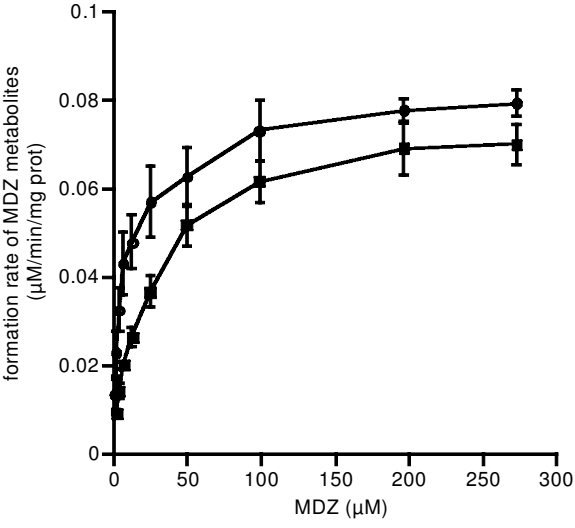
Incubation of MDZ (at a concentration of 400 μM) in the presence of supersomes expressing CYP3A1 resulted in comparable formation rates for 1′-OH-MDZ and 4-OH-MDZ. In the case of CYP3A2 supersomes, incubation with 400 μM MDZ also resulted in the formation of both MDZ metabolites, but the formation rate of 4-OH-MDZ was approximately twice as high compared with the 1′-OH-MDZ formation rate (data not shown).

Immunoquantification of CYP3A1 and CYP3A2 in control and induced hepatic and intestinal microsomes

CYP3A1 and CYP3A2 were expressed in hepatic and intestinal microsomes of control rats, and p.o. and i.v. pretreatment with dexamethasone led to an increase in their expression. No statistical differences in CYP3A1 and CYP3A2



(A)



(B)

Figure 1. (A) Kinetics of formation of midazolam (MDZ) metabolites in rat liver microsomes (control i.v. treatment): —, 4-OH-midazolam; ○, 1′-OH-midazolam; △, 1′,4-diOH-midazolam. (B) Kinetics of formation of MDZ metabolites in rat intestinal microsomes (control i.v. treatment): —, 4-OH-midazolam; ○, 1′-OH-midazolam.

levels were observed between the p.o. and i.v. control rats (figure 2a, b). Our results suggest that CYP3A2 levels in liver microsomes seems to be higher (approximately 3–5-fold in p.o. and i.v. control rats, respectively) than CYP3A1 levels (figure 2a). Expression of both CYP3A1 and CYP3A2 in liver microsomes was significantly increased following p.o. (3.7- and 3.2-fold, respectively) or i.v. (2.6- and 2.1-fold, respectively) pretreatment with dexamethasone (figure 2a). In intestinal microsomes of both groups of control rats, CYP3A1- and CYP3A2-like

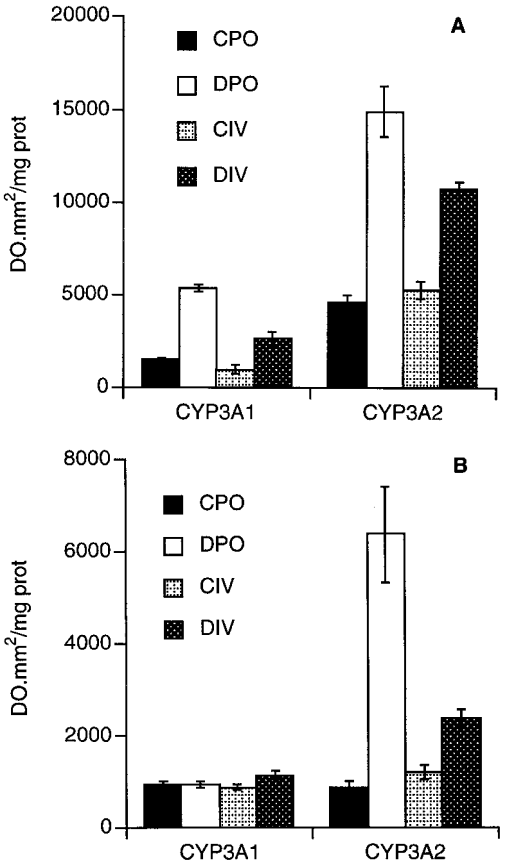


Figure 2. (A). CYP3A1 and CYP3A2 protein levels in rat liver microsomes: CPO, control oral (p.o.) rat; DPO, dexamethasone p.o.-treated rat; CIV, control intravenous (i.v.) rat; DIV, dexamethasone i.v.-treated rat. (B) CYP3A1 and CYP3A2 protein levels in rat intestinal microsomes: CPO, control p.o. rat; DPO, dexamethasone p.o.-treated rat; CIV, control i.v. rat; DIV, dexamethasone i.v.-treated rat.

protein expression seems to be similar (figure 2b). Intravenous or p.o. dexamethasone treatment did not result in a significant change in CYP3A1 levels in intestinal microsomes. On the contrary, treatment with dexamethasone led to an increase in CYP3A2-like protein levels in intestinal microsomes, but this increase was only statistically significant (7.3-fold) in the case of p.o. dexamethasone pretreatment (figure 2b). In microsomes of the control rat, expression of CYP3A1 was slightly lower (n.s.) in hepatic compared with intestinal microsomes, but CYP3A2 levels were significantly higher ($p \leq 0.001$) in hepatic microsomes.

As expected, no immunoreactive band was observed when the CYP3A1 supersomes were incubated with anti-CYP3A2 antibodies nor when the CYP3A2 supersomes were incubated with anti-CYP3A1 antibodies (figure 3). A slight difference in the migration distance of the immunoreactive band was observed for CYP3A2-like protein in intestinal microsomes compared with liver microsomes and supersomes (figure 3).



Figure 3. Western blot analysis showing the formation of protein–antibody complexes when CYP3A1 supersomes, CYP3A2 supersomes, control liver microsomes and control intestinal microsomes were incubated with CYP3A1 antibodies (lanes 1–4) or CYP3A2 antibodies (5–8). Samples of supersomes or microsomes were applied as follows: lanes 1, CYP3A2 supersomes; 2, CYP3A1 supersomes; 3, control liver microsomes; 4, control intestinal microsomes; 5, CYP3A1 supersomes; 6, CYP3A2 supersomes; 7, control liver microsomes; 8, control intestinal microsomes.

Discussion

Biotransformation of midazolam to 1′-OH-MDZ and 4-OH-MDZ is catalysed in man as well as in rat by enzymes of the CYP3A subfamily (Gorski *et al.* 1994, Ghosal *et al.* 1996). The results of the present study show that pretreatment with dexamethasone, a known inducer of CYP3A enzymes in rat (Telkada *et al.* 1992, Higashikawa *et al.* 1995), resulted in significant increases in V_{max} for the formation of both primary midazolam metabolites by hepatic and intestinal microsomes. In terms of the quantity of dexamethasone reaching the liver or intestine, oral administration was more effective than i.v. administration to induce both intestinal and hepatic CYP3A activity, but the difference was particularly pronounced in the small intestine.

The induction of intestinal CYP450 enzymes could be expected to be influenced by the route of administration of the inducing agent. Following p.o. administration of an enzyme inducer, the enterocytes are exposed to high concentrations of the inducer during its absorption across the intestinal epithelium. Exposure of the hepatic enzymes may also be high, although substantial intestinal first-pass metabolism of the inducer may limit its access to the hepatic enzymes. Zhang *et al.* (1996) reported that intestinal CYP1A1 was more sensitive to orally administered β-naphthoflavone, whereas induction of hepatic CYP1A1 was more sensitive to intraperitoneally administered β-naphthoflavone. Following systemic administration of an enzyme inducer, however, exposure of the intestinal CYP enzymes may be more limited. Indeed, CYP3A enzymes are most abundant at the tips of the villi, with lower levels found in the crypt cells (Kolars *et al.* 1992, Watkins *et al.* 1997). Consequently, an inducer present in the systemic circulation can only reach these enzymes by diffusion or transport across the intestinal epithelium from the basal to the apical side. The results of the present study show that there is clear induction of intestinal CYP3A activity following i.v. administration of dexamethasone indicating that this inducer has access from the systemic circulation to the CYP3A enzymes at the tips of the enterocyte villi. However, the degree of intestinal CYP3A induction is more pronounced when dexamethasone is administered orally. The inducibility of intestinal CYP3A activity following systemic administration of an enzyme inducer will depend upon the diffusion/transport characteristics of the inducer.

That induction of hepatic CYP3A activity is more pronounced following p.o. than i.v. administration of dexamethasone is not unexpected assuming that dexamethasone is not metabolized to a very high extent during its first pass through the intestinal epithelium to metabolites lacking enzyme induction properties. All dexamethasone absorbed from the gastrointestinal tract and which escapes the first-pass effect to 'inactive' metabolites, i.e. metabolites lacking induction

capacity, arrives in the portal circulation and passes through the liver, whereas following i.v. administration only approximately 25% of the cardiac output passes through the liver. Consequently, concentrations of dexamethasone in the portal circulation, and therefore induction of hepatic enzymes, may be higher following p.o. compared with i.v. administration.

CYP3A1 and CYP3A2 expression in the liver was significantly increased by dexamethasone pretreatment. This finding is consistent with previously published results showing that both hepatic CYP3A enzymes are induced by dexamethasone (Chung *et al*. 1998, Watanabe *et al*. 1998, Wong *et al*. 1999). However, the results related to the induction by dexamethasone of CYP3A enzymes in rat enterocytes are more difficult to interpret. First, the CYP3A1 protein levels in enterocytes did not significantly increase after dexamethasone treatment. These results are not consistent with previously published data demonstrating the inducibility by dexamethasone of CYP3A1 in the rat small intestine (Kolars *et al*. 1992, Schmiedlin-Ren *et al*. 1993). In addition, our results indicate that the intestinal CYP3A2-like protein is different from the hepatic CYP3A2 protein. Indeed, the commercially available CYP3A1 and CYP3A2 antibodies showed specificity for the CYP3A1 and CYP3A2 supersomes. However, the CYP3A2 antibodies reacted with a protein in enterocyte microsomes, which showed a different migration distance in the SDS-PAGE compared with the migration distance of the antibody–CYP3A2 protein complex as revealed in the CYP3A2 supersomes and the liver microsomes. This indicates that the intestinal CYP3A2-like protein is very likely another CYP3A enzyme showing cross-reactivity with the commercial CYP3A2 antibody. Guschin *et al*. (1999) recently demonstrated the presence of a new CYP3A enzyme in rat intestinal microsomes. The gene for this intestinal CYP3A isoenzyme shows 97% identity with rat olfactory *CYP3A9*. Based on their results, Guschin *et al*. suggest that rat intestinal CYP3A differs from CYP3A1 and CYP3A2.

In conclusion, the results of the present study show that i.v. administration of dexamethasone leads to significant induction of both intestinal and hepatic CYP3A activity towards midazolam. Oral administration of dexamethasone, however, is more efficient than i.v. administration inducing CYP3A activity in both these tissues. Hepatic CYP3A1 and CYP3A2 protein levels were increased by dexamethasone pretreatment. Intestinal CYP3A1 protein levels, however, were not affected by dexamethasone pretreatment. In addition, the CYP3A2 antibodies reacted with a protein in the intestinal microsomes, which was different from the hepatic CYP3A2 as demonstrated by immunoblotting. These results support the finding of Gushchin *et al*. (1999) that intestinal CYP3A enzymes in rat differ from hepatic CYP3A1 and CYP3A2.

References

Chung, W. G., Roh, H. K., Kim, H. M. and Cha, Y. N., 1998, Involvement of CYP3A1, 2B1, and 2E1 in C-8 hydroxylation and CYP 1A2 and flavin-containing monooxygenase in *N*-demethylation of caffeine, identified by using inducer treated rat liver microsomes that are characterized with testosterone metabolic patterns. *Chemical and Biological Interactions*, **113**, 1–14.

Eeckhoudt, S. L., Desager, J. P., Horsmans, Y., De Winne, A. J. and Verbeeck, R. K., 1998, Sensitive assay for midazolam and its metabolite 1′-hydroxymidazolam in human plasma by capillary high-performance liquid chromatography. *Journal of Chromatography B*, **710**, 165–171.

Ghosal, A., Sato, R., Thomas, P. E., Bush, E. and Moore, D., 1996, Inhibition and kinetics of cytochrome P4503A activity in microsomes from rat, human, and cDNA-expressed human cytochrome P450. *Drug Metabolism and Disposition*, **24**, 940–947.

Gorski, J. C., Hall, S. D., Jones, D. R., VandenBranden, M. and Wrighton, S. A., 1994, Regioselective biotransformation of midazolam by members of the human cytochrome P450 (CYP3A) subfamily. *Biochemical Pharmacology*, **47**, 1643–1653.

Gushchin, G. V., Gushchin, M. I., Gerber, N. and Boyd, R. T., 1999, A novel cytochrome P450 3A isoenzyme in rat intestinal microsomes. *Biochemical and Biophysical Research Communications*, **255**, 394–398.

Higashikawa, F., Murakawi, T., Kaneda, T. and Takano, M., 1995, *In vivo* and *in vitro* metabolic clearance of midazolam, a cytochrome P450 3A substrate, by the liver under normal and increased enzyme activity in rats. *Journal of Pharmaceutics and Pharmacology*, **51**, 405–410.

Kaminsky, L. S. and Fasco, M. J., 1992, Small intestinal cytochrome P450. *Critical Reviews in Toxicology*, **21**, 407–422.

Keelan, M., Doring, K., Tavernini, M., Wierzbicki, E., Clandinin, M. T. and Thomson, A. B., 1994, Dietary omega 3 fatty acids and cholesterol modify enterocyte microsomal membrane fosfolipids, cholesterol content and phospholipid enzyme activities in diabetic rats. *Lipids*, **29**, 851–858.

Kolars, J. C., Schmiedlin-Ren, P., Dobbins, W. O., Schuetz, J., Wrighton, S. A. and Watkins, P. B., 1992, Heterogeneity of cytochrome P450IIIA expression in rat gut Epithelia. *Gastroenterology*, **102**, 1186–1198.

Krishna, D. R. and Klotz, U., 1994, Extrahepatic metabolism of drugs in humans. *Clinical Pharmacokinetics*, **26**,144–160.

Leclercq, I., Saliez, A., Wallemacq, P. E., Horsmans, Y. and Lambotte L., 1997, The monoethylglycinexylidide test does not correctly evaluate lidocaine metabolism after ischemic liver injury in the rat. *Hepatology*, **26**, 1182–1188.

Lowry, O. H., Rosebrough, N. J., Farr, A. L. and Randall, R. J., 1951, Protein measurement with the Folin phenol reagent. *Journal of Biological Chemistry*, **193**, 265–275.

Lu, A. Y. and West, S. B., 1979, Multiplicity of mammalian microsomal cytochromes P-450. *Pharmacology Reviews*, **31**, 277–295.

Porter, T. D. and Coon, M. J., 1991, Cytochrome P450: multiplicity of isoforms, substrates, and catalytic and regulatory mechanisms. *Journal of Biological Chemistry*, **266**, 13469–13472.

Rendic, S. and Di Carlo, F. J., 1997, Human cytochrome P450 enzymes: a status report summarizing their reactions, substrates, inducers, and inhibitors. *Drug Metabolism Reviews*, **29**, 413–580.

Schmiedlin-Ren, P., Benedict, P. E., Dobbins, W. O., Ghosh, M., Kolars, J. C. and Watkins, P. B., 1993, Cultured adult rat jejunal explants as a model for studying regulation of CYP3A. *Biochemical Pharmacology*, **46**, 905–918.

Telkada, M. B., Pereira, T. M. and Lechner, M.-C., 1992, Effect of dexamethasone and phenobarbital on run-on transcription rate and CYP3A mRNA concentration in rat liver: changes during development. *Archives in Biochemistry and Biophysics*, **298**, 715–725.

Thummel, K. E., O'Shea, D., Paine, M. F., Shen, D. D., Lunze, K. L., Perkins, J. D. and Wilkinson, G. R., 1996, Oral first-pass elimination of midazolam involves both gastro-intestinal and hepatic CYP3A-mediated metabolism. *Clinical Pharmacology and Therapeutics*, **59**, 491–502.

Thummel, K. E. and Wilkinson, G. R., 1998, *In vitro* and *in vivo* drug interactions involving human CYP3A. *Annual Reviews in Pharmacology and Toxicology*, **38**, 389–430.

Watanabe, M., Tateishi, T., Asoh, M., Nakura, H., Tanaka, M., Kumai, T. and Kobayashi, S., 1998, Effects of glucocorticoids on pharmacokinetics and pharmacodynamics of midazolam in rats. *Life Sciences*, **63**, 1685–1692.

Watkins, P. B., Wrighton, S. A., Schuetz, E. G., Molowa, D. T. and Guzelian, P. S., 1987, Identification of glucocorticoid-inducible cytochromes P-450 in the intestinal mucosa of rats and man. *Journal of Clinical Investigation*, **80**, 1029–1036.

Wong, S. G., Lin, E. H. and Marks, G. S., 1999, Cytochrome CYP sources of *N*-alkylprotoporphyrin IX after administration of porphyrogenic xenobiotics to rats. *Drug Metabolism and Disposition*, **27**, 960–965.

Wu, C.-Y., Benet, L. Z., Herbert, M. F., Gupta, S. K., Rowland, M., Gomez, D. Y. and Wacher, V. J., 1995, Differentiation of absorption and first-pass gut and hepatic metabolism in humans: studies with cyclosporin. *Clinical Pharmacology and Therapeutics*, **58**, 492–497.

Zhang, Q.-Y., Wiko, J., Dunbar, D. and Kaminsky, L., 1996, Characterization of rat small intestinal cytochrome P450 composition and inducibility. *Drug Metabolism and Disposition*, **24**, 322–328.

XENOBIOTICA, 2002, VOL. 32, NO. 11, 985–996

Taylor & Francis
healthsciences

Characterization of testosterone metabolism and 7-hydroxycoumarin conjugation by rat and human liver slices after storage in liquid nitrogen for 1 h up to 6 months

C. GRANHALL†, E. FLOBY†, A. NORDMARK‡, A. ORZECHOWSKI†, A. THÖRNE§, G. TYBRING‡ and A.-K. SOHLENIUS-STERNBECK†*

† Research DMPK, AstraZeneca R&D Södertälje, S-151 85 Södertälje, Sweden
‡ Department of Medical Laboratory Sciences, Division of Clinical Pharmacology and Technology, Karolinska Institute, and § Division of Surgery, Centre for Surgical Sciences, Huddinge University Hospital, S-141 86 Huddinge, Sweden

Received 17 April 2002

1. Slices of human and rat liver were cryopreserved in 18% dimethyl sulphoxide (DMSO) and subsequently stored in liquid nitrogen for periods up to as long as 6 months. After thawing, the metabolism of testosterone to hydroxylated products and conjugation of 7-hydroxycoumarin were investigated.

2. Rat liver slices stored in liquid nitrogen for 6 months exhibited rates of formation of 7α-, 6β- 16α- and 2α-hydroxytestosterone, and of androstenedione that did not differ significantly from those observed with fresh slices.

3. No formation of 2α-hydroxytestosterone was detected with slices of human liver. However, in contrast with the rat, human slices produced 2β-hydroxytestosterone. The rates of formation of 7α-, 6β-, 16α- and 2β-hydroxytestosterone and of androstenedione by human liver slices after 6 months of storage in liquid nitrogen were 82, 71, 236, 66 and 92%, respectively, of the corresponding rates by fresh slices.

4. The rates of sulphation and glucuronidation of 7-hydroxycoumarin by slices from rat liver were 97 and 119%, respectively, of the corresponding fresh values after 6 months of storage in liquid nitrogen.

5. 7-Hydroxycoumarin glucuronidation by human liver slices was 53% of the corresponding fresh values after 6 months of storage. However, human slices showed little or no capacity to conjugate 7-hydroxycoumarin with sulphate.

6. It was demonstrated that slices of both human and rat liver can be cryopreserved and stored in liquid nitrogen for at least 6 months without major changes in their rates of metabolism of testosterone to its hydroxylated products and of 7-hydroxycoumarin conjugation. These findings further emphasize that cryopreservation of liver slices can be an effective tool in the use of biological material of limited availability.

Introduction

In recent years, liver slices have found increasing use as an *in vitro* system for studies of drug metabolism. Unlike systems involving hepatocytes or microsomes, cell–cell contacts and the functional acinar architecture are maintained in liver slices, which also contain all the enzyme systems of the cell and physiological concentrations of cofactors (for general reviews, see Ekins 1996, Lerche-Langrand and Toutain 2000). An additional advantage in the use of liver slices is the ease with which they can be prepared and handled.

* Author for correspondence; e-mail: anna-karin.sternbeck@astrazeneca.com

Xenobiotica ISSN 0049–8254 print/ISSN 1366–5928 online © 2002 Taylor & Francis Ltd
http://www.tandf.co.uk/journals
DOI: 10.1080/0049825021000012646

Cryopreservation of tissue slices with as little damage as possible would allow efficient use of biological material of limited availability, including human liver. To this end, thorough characterization of various drug-metabolizing enzyme systems in cryopreserved slices of human and rat liver is desirable. Previous investigations have demonstrated that cryopreservation of liver slices effectively maintains cytochrome P450-dependent catalytic activities (de Kanter *et al.* 1997, 1998, Glöckner *et al.* 1998, Sohlenius-Sternbeck *et al.* 2000). Phase II-conjugating activities are more sensitive to cryopreservation, a problem which, however, can be circumvented by employing 18% (instead of the usual 12%) dimethyl sulphoxide (DMSO) as cryoprotectant (de Graaf *et al.* 2000, Sohlenius-Sternbeck *et al.* 2000). Recently, it has even been demonstrated that 7-ethoxycoumarin *O*-deethylation activity can be induced by β-naphthoflavone in rat liver slices after cryopreservation (Glöckner *et al.* 2001).

To date, no detailed information concerning possible effects of the length of storage of liver slices in liquid nitrogen on the activity of drug-metabolizing enzymes is available. Previous studies have generally been performed on slices thus stored for a period of 1 h up to a few days. In fact, most studies involving cryopreserved liver slices do not even discuss the influence of long-term storage in liquid nitrogen.

The present study investigated the metabolism of testosterone to hydroxylated products and the sulphation and glucuronidation of 7-hydroxycoumarin by slices of rat and human liver cryopreserved in 18% DMSO and subsequently stored in liquid nitrogen for periods from 1 h up to as long as 6 months. The pattern of testosterone hydroxylation by different forms of cytochrome P450 is commonly used to characterize Phase I metabolism in the rat (Arlotto *et al.* 1991). Conversion of testosterone to 6α- and 2α-hydroxytestosterone in rat liver is catalysed by CYP2A1 and CYP2C11, respectively. Both CYP2B1 and CYP2C11 are involved in the formation of 16α-hydroxytestosterone in the same tissue, where formation of 7α-hydroxytestosterone is mediated by CYP2A and androstenedione is formed by CYP2C11 and CYP2B1/2B2. Several forms of rat liver cytochrome P450, including CYP3A, can metabolize testosterone to 6β-hydroxytestestosterone.

The CYP forms involved in the metabolism of testosterone in human liver differ from those in rat (Rendic and Di Carlo 1997). Forms of CYP3A are involved in the formation of 6β-, 16α- and 2β-hydroxytestosterone by human microsomes. Human CYP2D6 is also capable of producing 16α-hydroxytestosterone, whereas CYP2C19 alone converts testosterone to androstenedione (Yamazaki and Shimada 1997).

The activities of the Phase II-conjugating enzymes UDP-glucuronosyltransferase and sulphotransferase are often assayed using 7-hydroxycoumarin as a diagnostic substrate (Walsh *et al.* 1995). We demonstrated previously that these activities can be readily measured in fresh and cryopreserved rat liver slices (Sohlenius-Sternbeck *et al.* 2000).

The present study monitors cytotoxicity on the basis of mitochondrial reduction of AlamarBlue^{TM}, which is a simple one-step approach that has previously been applied primarily to isolated cells (Ahmed *et al.* 1994, Nociari *et al.* 1998).

Materials and methods

Chemicals

Williams' medium E was purchased from Life Technologies AB (Täby, Sweden); testosterone from Janssen, Chimica (Geel, Belgium); testosterone metabolites for qualitative determinations were kindly provided by AstraZeneca R&D Lund (Sweden); 6β-hydroxytestosterone for quantitative determination was from Ultrafine Chemicals (Manchester, UK). Dulbecco's phosphate-buffered saline (without calcium chloride), 7-hydroxycoumarin, Krebs–Henseleit buffer (without calcium chloride) were obtained from Sigma Chemical Co. (St Louis, MO, USA); AlamarBlue^{TM} came from BioSource International, Inc. (Camarillo, CA, USA). All other chemicals were of analytical grade and obtained from common commercial sources.

Tissue culture plates

Falcon tissue culture plates with six or 24 wells were obtained from Labora AB (Johanneshov, Sweden), and 96-well microplates came from Greiner GmbH (Frickenhausen, Germany).

Animals

Male Sprague–Dawley rats (B&K Universal AB, Sollentuna, Sweden), weighing 225–250 g, were maintained under a 12-h light/dark cycle in steel cages with free access to commercial food pellets (Lactamin, Stockholm, Sweden).

Handling of livers

Rat liver. After anaesthetizing the rats with Forene® (isofluran; Abbott Scandinavia AB, Kista, Sweden), the liver was perfused *in situ* with ice-cold Krebs–Henseleit buffer.

Human liver. Human liver samples were obtained from a donor liver bio-bank established at the Division of Clinical Pharmacology, Huddinge University Hospital, Sweden, with the approval of the hospital Ethics Committee. Three of the human liver specimens were obtained by partial hepatectomy of patients with liver tumours. These liver samples were perfused with ice-cold Krebs–Henseleit buffer within 1–1.5 h after removal. Two other samples were obtained from organ donors, whose livers had been perfused *in situ* with ice-cold University of Wisconsin organ preservation solution (DuPont Pharmaceuticals, Wilmington, DE, USA). For a summary of the relevant information, see table 1.

The human liver samples were placed on ice in Krebs–Henseleit buffer for transportation to the laboratory at AstraZeneca in Södertälje.

Preparation of liver slices

Slices from both rat and human liver samples were prepared using the same protocol. A motor-driven drill press (8 mm in diameter) was used to obtain cores of liver tissue. Liver slices were prepared in ice-cold Krebs–Henseleit buffer with a Krumdieck slicer (Krumdieck *et al.* 1980) set at a thickness of 250 µm. The slices thus obtained were stored in ice-cold Krebs–Henseleit buffer until use (within 1 h after preparation).

Cryopreservation of the liver slices

The procedure employed for cryopreservation has been described in detail by Sohlenius-Sternbeck *et al.* (2000). Briefly, slices from both human and rat liver were incubated in Williams' medium E containing 18% DMSO as cryoprotectant at 2 °C for 30 min under an atmosphere of 5% CO_2/95% O_2. The slices were subsequently transferred directly into precooled freezing vials containing 1 ml fresh ice-cold cryopreservation medium (five slices per vial) and the vials were immediately immersed into liquid nitrogen, where they were stored for times from 1 h up to as long as 6 months before thawing and use.

Table 1. Characteristics of the human liver samples.

Sample	Sex of donor	Age of donor (years)	Source
LB13	F	52	partial hepatectomy
HL79	F	56	organ donation
LB14	F	55	partial hepatectomy
LB18	M	65	partial hepatectomy
HL80	M	50	organ donation

Thawing of cryopreserved liver slices

For thawing, the vials were transferred directly from the liquid nitrogen storage tank into a water bath at 37 °C and shaken until partial thawing allowed the frozen medium containing the slices to be removed. The slices were then immediately transferred to 200 ml Williams' medium E that had been precooled at −20 °C for 15 min. Washing was performed in this medium by gentle shaking. In some of the experiments with rat liver slices (those stored for 1 h), this washing was performed in the same medium at approximately 20 °C.

Measurement of drug-metabolizing activities and viability

Before incubation, each slice was pre-incubated for 1 h in 3.2 ml Williams' medium E or Krebs–Henseleit buffer at 37 °C under an atmosphere of 5% CO_2/95% O_2. Enzyme assays were performed using saturating substrate concentrations and conditions of linearity with time and carried out at least in duplicate.

Testosterone metabolism by slices of rat and human liver. These incubations were performed in six-well plates. After pre-incubation in Williams' medium E (as described above), fresh and cryopreserved liver slices were incubated individually with 250 μM testosterone in 3.2 ml Williams' medium E at 37 °C for 30 min. Metabolism was terminated by homogenizing each slice by hand (15 up-and-down strokes in a glass homogenizer in the case of rat liver slices and 30 strokes for human liver slices) in the incubation medium at 2 °C and subsequent freezing of the homogenate thus obtained on ethanol/dry ice. (Before this freezing, an aliquot of each homogenate was removed for protein determination.) After thawing, the homogenate was extracted twice with 3 vols dichloromethane for 10 min. After centrifugation, the organic phase was transferred to a new test tube and evaporated to dryness under a stream of nitrogen. The dried residues were dissolved in 250 μl ethanol:water (30:70 v/v) and 100 μl of these samples were injected onto a HPLC system.

A LiChr°CART column (250 × 4 mm, LiChropher 100, RP-18, 5 μm) equipped with a LiChr°CART (4 × 4 mm) guard column (Merck, Darmstadt, Germany) was used and the compounds were detected at 254 nm using a UV/VIS detector (Spectra-Physics, Stockholm, Sweden). The mobile phases employed consisted of (A) 30% and (B) 60% (v/v) ethanol in water. During the 55-min run, the proportion of B in the mobile phase was increased linearly from 0 to 67% with a flow rate of 0.8 ml min^{-1}. The levels of testosterone metabolites were quantitated by comparison with a standard curve obtained with synthetic 6β–hydroxytestosterone.

Conjugation of 7-hydroxycoumarin by slices of rat and human liver. These incubations were also carried out in six-well plates. After pre-incubation in Krebs–Henseleit buffer (as described above), fresh and cryopreserved liver slices were incubated individually with 25 μM 7-hydroxycoumarin in 2.0 ml Krebs–Henseleit buffer at 37 °C for 60 min. At the end of this incubation period, the medium was removed, passed through 0.22-μm filter and subsequently analysed by HPLC as described by Walsh *et al.* (1995). Previous studies have demonstrated that 7-hydroxycoumarin metabolites are not retained in liver slices (Barr *et al.* 1991a).

Reduction of AlamarBlue™ by slices of rat and human liver. After the pre-incubation in Krebs–Henseleit buffer (as described above), fresh and cryopreserved liver slices were incubated individually in 24-well plates with 0.5 ml 10% AlamarBlue™ solution in Krebs–Henseleit buffer at 37 °C for 15–60 min. Following incubation, 100 μl of the medium was transferred to a 96-well microplate (Greiner GmbH, Frickenhausen, Germany) and the fluorescence was monitored using an excitation wavelength of 545 nm and emission wavelength of 590 nm employing a Spectra Max Gemini plate reader (Molecular Devices, Sunnyvale, CA, USA). In initial experiments, the linearity of the rate of AlamarBlue™ reduction by liver slices could be established for incubations up to 60 min. Incubations of 40 min were thereafter employed throughout this study.

Protein determination

For determination of protein content, each slice was homogenized by hand in Williams' medium E or Krebs–Henseleit buffer (15 up-and-down strokes in a glass homogenizer in the case of rat liver slices and 30 strokes for human liver slices). The protein concentrations were determined according to Bradford (1976) using a protein assay kit (Bio-Rad Laboratories, Richmond, CA, USA) and with bovine serum albumin as the standard.

Statistical analysis

Data are means SDs of the number of experiments indicated. Statistical evaluations of the cryopreserved liver data were performed using the Student's *t*-test. The results of these evaluations are given whenever there is a significant difference from the fresh data.

Results

AlamarBlue™ reduction by slices from rat and human liver

After storage in liquid nitrogen for 1 h, the reduction of AlamarBlue™ by rat liver slices was approximately 140% of the corresponding activity observed with fresh slices (table 2). The level of AlamarBlue™ reduction was studied in slices from the human livers LB18 and HL80. Although there was a large variation in reduction capacity between these two tissue samples, cryopreservation for 1 h had little effect on this reduction.

Testosterone metabolism by slices from rat and human liver

Incubation of fresh and cryopreserved rat liver slices with 250 μm testosterone gave rise to several products. Figure 1 shows two representative HPLC chromatograms obtained after incubation with fresh slices (A) and slices cryopreserved for 2 months (B) with 250 μm testosterone. As can be seen, after 2 months of storage, the rates of formation of 7α-, 6β-, 16α- and 2α-hydroxytestosterone and of androstenedione were approximately the same as with fresh slices. Moreover, storage in liquid nitrogen for as long as 6 months did not alter the formation rates of these same testosterone metabolites (table 3). Similar results were also obtained after storage of rat slices for 1 h (data not shown). The relative rates of formation of 6β-hydroxytestosterone by rat liver slices stored in liquid nitrogen for 1 h or for 2 or 6 months are compared in figure 2.

The corresponding metabolic pattern obtained upon incubation of human liver slices with testosterone differed somewhat from that observed with rat slices, as can be seen from the two representative HPLC chromatograms illustrated in figure 3. The formation rate of 6β-hydroxytestosterone was generally higher in human than in rat slices. In contrast, neither in fresh nor in cryopreserved human slices could formation of 2α-hydroxytestosterone be detected. However, unlike rat liver slices, human slices exhibited readily detectable formation of 2β-hydroxytestosterone. The rate of formation of 16α-hydroxytestosterone was lower in human than in rat liver slices.

The rates of formation of testosterone metabolites by slices from the different human livers varied considerably (table 4). For example, the specific

Table 2. Reduction of AlamarBlue™ by fresh and cryopreserved slices of rat and human liver. The level of fluorescence reflects the extent of AlamarBlue™ reduction.

	AlamarBlue™ reduction by liver slices (fluorescence units mg^{-1} protein)	
Tissue	Fresh	Cryopreserved[b]
Rat liver[a]	1680 ± 740	2360 ± 472
Human liver LB18	650	560
Human liver HL80	5590	5120

[a] Means ± SD of four rat livers.
[b] Stored in liquid nitrogen for 1 h.

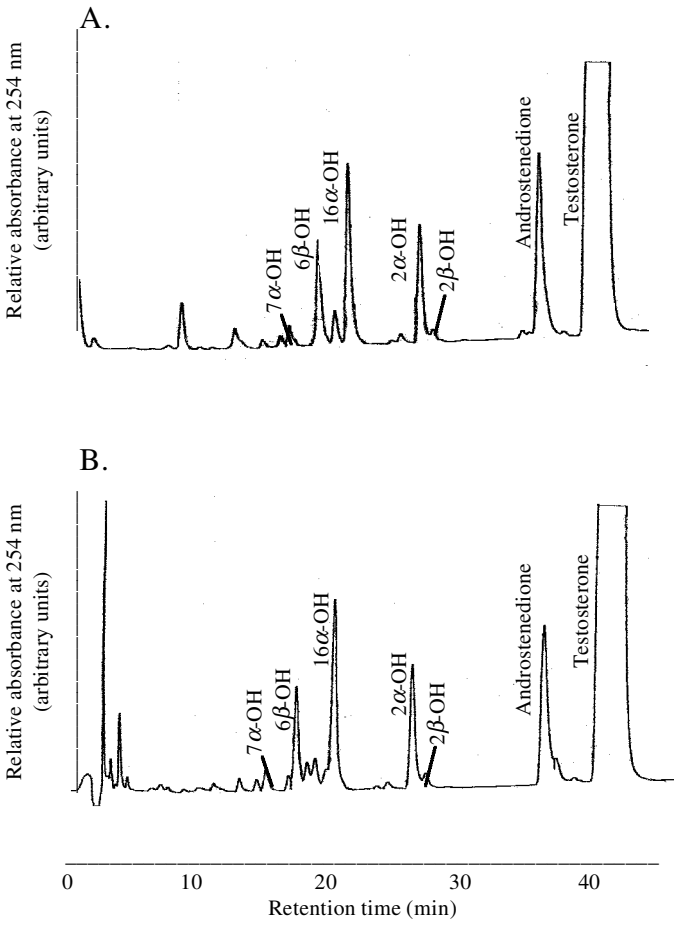


Figure 1. Analysis of the testosterone metabolites produced by (A) fresh rat liver slices and (B) rat liver slices stored in liquid nitrogen for 2 months. The chromatograms were obtained from liver slices with a similar protein concentration and are representative of the results obtained with five separate livers. The identity of each metabolite is indicated above its peak, e.g. 7α-OH = 7α-hydroxytestosterone.

Table 3. Testosterone metabolism by fresh slices of rat liver and by slices stored in liquid nitrogen for 6 months.

	Rate of metabolite formation by rat liver slices (pmol min^{-1} mg^{-1} protein)	
Metabolite	Fresh	Cryopreserved
7α-OH	8.0 ± 3.3	9.8 ± 2.2
6β-OH	39 ± 13	48 ± 13
16α-OH	79 ± 19	102 ± 31
2α-OH	53 ± 15	72 ± 20
Androstenedione	160 ± 59	187 ± 91

Data are means ± SDs of the values obtained with fresh slices from five different livers and with cryopreserved slices from three different livers.

The specific rates of formation of testosterone metabolites were determined by comparison with a standard curve prepared with synthetic 6β-hydroxytestosterone.

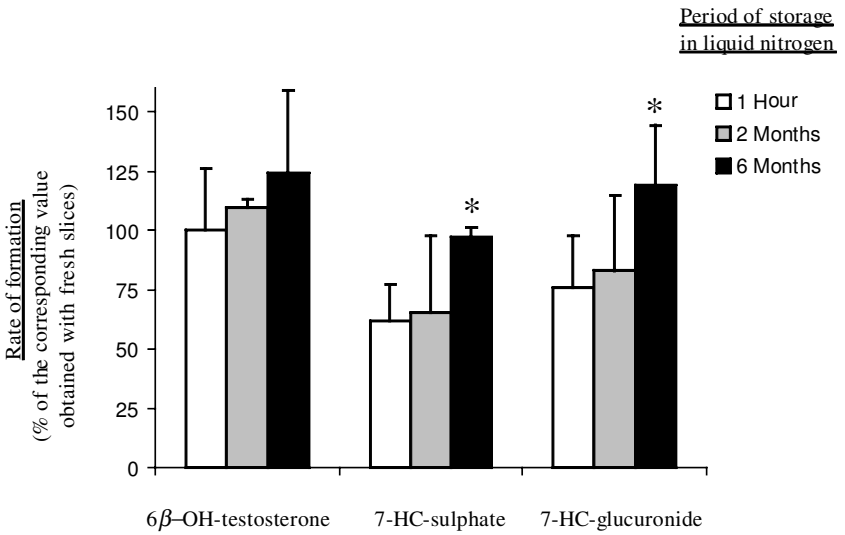


Figure 2. Relative rates of formation of 6β-hydroxytestosterone from testosterone and of the sulphate and glucuronide conjugates of 7-hydroxycoumarin by rat liver slices stored in liquid nitrogen from 1 hour up to as long as 6 months. The specific rate of 6β-hydroxytestosterone formation (determined by comparison with a standard curve prepared with synthetic 6β-hydroxytestosterone) by fresh slices (i.e. the 100% value) is shown in table 3. The specific rates of sulphation and glucuronidation of 7-hydroxycoumarin (estimated from the ratio between the area under the absorption peak for the conjugate and the sum of the areas of all of the peaks) by fresh slices (i.e. the 100% value) were 51 ± 14 and 99 ± 37 pmol min^{-1} mg^{-1} protein, respectively. The data are means $\pm$ SD of the values for three to five separate livers. $^{*}P < 0.05$ compared with the corresponding value for slices stored for 1 h. HC, hydroxycoumarin.

rate of formation of 6β-hydroxytestosterone by fresh slices ranged from 68 to 239 pmol min^{-1} and mg^{-1} protein. Therefore, the rates of metabolite formation by cryopreserved slices were also expressed as the percentage of the corresponding values obtained with fresh slices from the same liver (table 4). The rates of formation of 7α- and 6β-hydroxytestosterone and of androstenedione by human liver slices were not significantly altered after 6 months of storage in liquid nitrogen. In contrast, such storage increased 16α-hydroxytestosterone formation to 236% and decreased 2β-hydroxytestosterone formation to 66% of the corresponding fresh values. Similar results as shown in table 4 were also obtained after storage of human slices for 1 h and 2 months (data not shown). In figure 4, the rates of 6β-hydroxytestosterone formation by human liver slices stored in liquid nitrogen for 1 h or 2 or 6 months are documented.

Conjugation of 7-hydroxycoumarin by slices from rat and human liver

Incubation of rat liver slices with 25 µM 7-hydroxycoumarin resulted in the appearance of both sulphate and glucuronic acid conjugates. The rates of 7-hydroxycoumarin glucuronidation by rat liver slices stored in liquid nitrogen for 1 h or for 2 or 6 months were 76, 83 and 119%, respectively, of the corresponding rate observed with fresh slices (figure 2). After these same storage periods in liquid nitrogen, the rates of sulphation of 7-hydroxycoumarin were 62, 65 and 97% of the

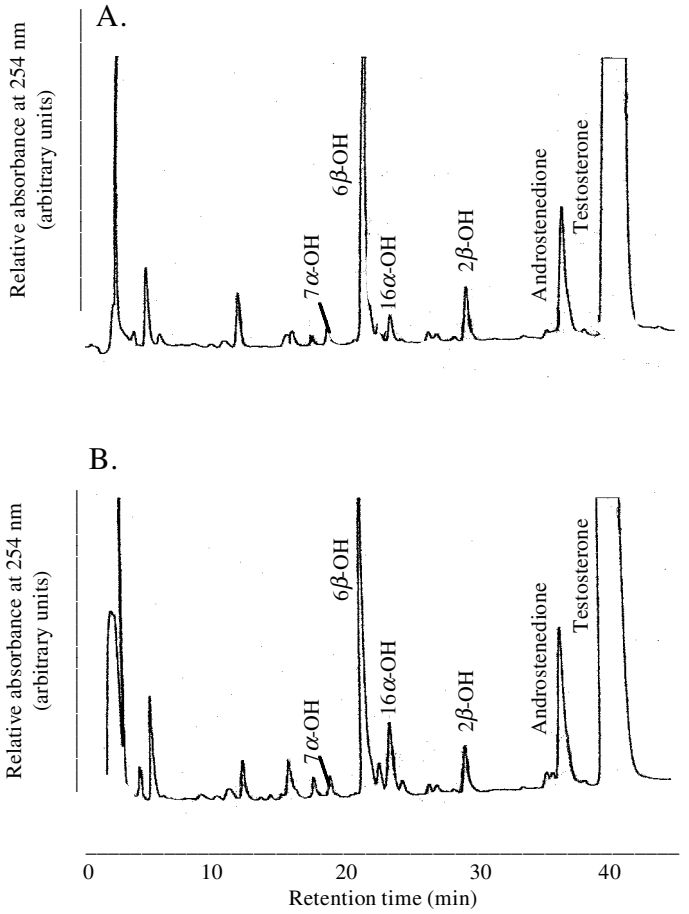


Figure 3. Analysis of the testosterone metabolites produced by (A) fresh human liver slices and (B) human liver slices stored in liquid nitrogen for 2 months. The chromatograms were obtained from liver slices with similar protein concentration and are representative of the findings obtained with four separate livers. The identity of each metabolite is indicated above its peak, e.g. 7α-OH = 7α-hydroxytestosterone.

fresh value. The rates of both these forms of conjugation by rat liver slices stored in liquid nitrogen for 6 months differed significantly from those in slices stored for 1 h (figure 2). Of possible significance in this connection is the fact that the rat slices stored for 6 months were thawed in medium that had been precooled at −20 °C for 15 min, whereas the slices stored for 1 h were thawed at room tempered medium (see the Materials and methods).

In the case of human livers, conjugation of 7-hydroxycoumarin with sulphate was not detected, with the exception of slices from one liver (HL80), which produced low levels of sulphate conjugate both in the fresh state and after cryopreservation (data not shown). After 1 h, 2 or 6 months of storage in liquid nitrogen, the rates of glucuronidation of 7-hydroxycoumarin were 63, 67 and 53%, respectively, of the corresponding value for fresh slices (figure 4).

Table 4. Testosterone metabolism by fresh slices of human liver and by slices stored in liquid nitrogen for 6 months.

Metabolite	Status of the slices	Rate of formation by individual human livers (pmol min^{-1} mg^{-1} protein)				Combined % of the corresponding value for fresh slices[a]
		LB13	HL79	LB14	LB18	
7α-OH	fresh	4.0	7.5	4.9	11.0	82 ± 14
	cryopreserved	3.0	7.7	3.7	8.5	
6β-OH	fresh	68	140	125	239	71 ± 34
	cryopreserved	47	167	69	135	
16α-OH	fresh	69	33	20	23	236 ± 74*
	cryopreserved	107	85	65	47	
2β-OH	fresh	7.4	21	13	26	66 ± 20*
	cryopreserved	5.8	18	5.5	15	
Andro-stenedione	fresh	49	95	74	241	92 ± 31
	cryopreserved	46	127	55	157	

[a] Calculated by comparing the cryopreserved value with the corresponding fresh value and expressed as means ± SDs. The data are means ± SD for values obtained with slices from four different livers. * $p < 0.05$ compared with the corresponding value for fresh slices (i.e. 100%). The specific rates of formation of the testosterone metabolites were determined by comparison with a standard curve prepared with synthetic 6β-hydroxytestosterone.

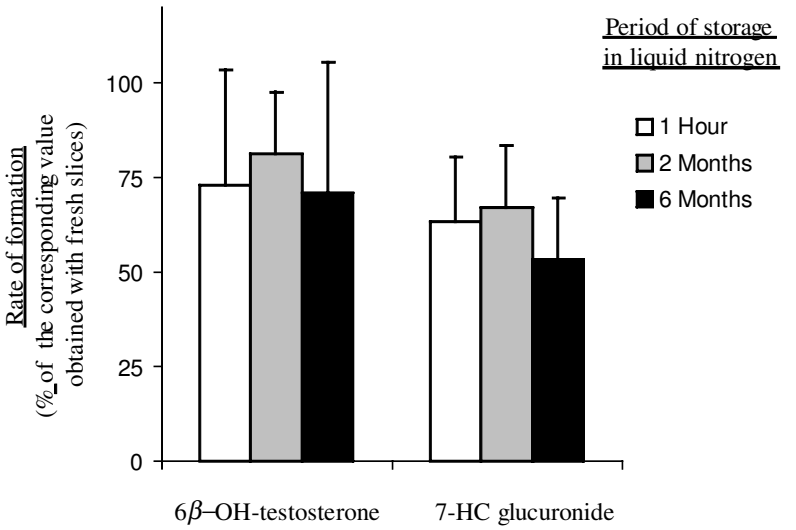


Figure 4. Metabolism of testosterone to 6β-hydroxytestosterone and glucuronidation of 7-hydroxycoumarin by slices of human liver stored in liquid nitrogen for 1 h up to as long as 6 months. The specific rate of 6β-hydroxytestosterone formation (determined by comparison with a standard curve prepared with synthetic 6β-hydroxytestosterone) by fresh slices is shown in table 4. Since the rates of formation of 6β-hydroxytestosterone by slices from the different livers varied considerably, the value for cryopreserved slices is expressed as a percentage of the corresponding value for fresh slices from the same liver. The specific rate of glucuronidation (estimated from the ratio between the area under the absorption peak of the glucuronide and the sum of the areas of the peaks for the glucuronide and unconjugated 7-hydroxycoumarin) by fresh liver slices (i.e. 100%) was 100 ± 26 pmol min^{-1} mg^{-1} protein. The data are means ± SD for values obtained with slices from four different livers.

Discussion

In the present study, the effects of long-term storage of slices of rat and human liver in liquid nitrogen on testosterone metabolism and conjugation of 7-hydroxycoumarin have been characterized. It has previously been demonstrated that cytochrome P450-catalysed activities in slices of human and rat liver can be effectively maintained by cryopreservation (de Kanter *et al*. 1997, 1998, Glöckner *et al*. 1998, Sohlenius-Sternbeck *et al*. 2000). Furthermore, after cryopreservation in 18% DMSO the activities of Phase II-conjugating systems in rat liver slices are retained (de Graaf *et al*. 2000, Sohlenius-Sternbeck *et al*. 2000).

However, to date no investigation has focused on whether long-term storage in liquid nitrogen affects such xenobiotic-metabolizing systems in liver slices. Such information is of considerable practical importance since cryopreserved liver slices are regarded as a reliable *in vitro* system for studies on drug metabolism. Therefore, slices of rat and human liver have been cryopreserved in the current study in 18% DMSO, subsequently stored in liquid nitrogen for periods from 1 h up to as long as 6 months and thereafter examined for alterations in testosterone metabolism and conjugation of 7-hydroxycoumarin.

Reduction of AlamarBlue^{TM}, catalysed by mitochondrial enzymes, was used as an indicator of possible cytotoxicity caused by cryopreservation of the slices. The extent of this reduction varied between the two human livers examined, while being more constant in the case of different rat livers. However, cryopreservation had little effect on AlamarBlue^{TM} reduction by slices from either the rat livers or the two human livers (table 2), which may indicate the absence of cytotoxicity.

Incubation of slices of rat and human liver with testosterone resulted in the formation of several hydroxylated metabolites (figures 1 and 3). Formation of the 6β-hydroxy metabolite of testosterone is frequently used as a measure of CYP3A-catalysed activity in microsomes from these tissues. Indeed, in the human liver this metabolite is produced by CYP3A4/5 (Rendic and Di Carlo 1997). In the case of the rat liver, additional forms of CYP, including CYP1A1, CYP2A2 and CYP2C13, can catalyse this same reaction (Arlotto *et al*. 1991). The rates of formation of 6β-hydroxytestosterone by rat and human slices after storage in liquid nitrogen for as long as 6 months were 123 and 71%, respectively, of the corresponding formation by fresh slices (figures 2 and 4). In addition, storage for as long as 6 months did not alter the rates of formation of other hydroxylated products of testosterone much, except for 16α- and 2β-hydroxytestosterone in the case of human slices (table 4).

The pattern of testosterone metabolism by human liver slices differed somewhat from that observed with rat liver slices (figures 1 and 3). The rate of formation of 6β-hydroxytestosterone is generally higher in the human tissue, whereas formation of 16α-hydroxytestosterone is more rapid in the case of rat. Transformation of testosterone to 2β-hydroxytestosterone occurs to a very small or undetectable extent in rat liver slices, but is readily detected in human liver slices. On the other hand, production of 2α-hydroxytestosterone, catalysed by CYP2C11 in rat liver, cannot be detected with human liver slices. In this context, it has been shown previously that the CYP2C family in human liver does not catalyse 2α-hydroxylation (Yamazaki and Shimada 1997), nor has any other human cytochrome P450 been reported to catalyse this reaction.

The differences in testosterone metabolism by rat and human liver slices observed in the present study are in agreement with findings from

studies on microsomal preparations (Yamazaki and Shimada 1997, Bogaards *et al.* 2000). Thus, liver slices handled as described here appear to be well suited for comparative investigations of xenobiotic metabolism in different species.

Cryopreservation of rat liver slices and subsequent storage in liquid nitrogen for 6 months did not alter the rates of glucuronidation and sulphation of 7-hydroxycoumarin (figure 2). Note that these conjugation reactions are significantly more rapid in rat liver slices stored in liquid nitrogen for 6 months than following storage for 1 h. It seems likely that this difference is a consequence of the slightly different thawing procedures employed. After 1 h of storage of rat liver slices, washing in connection with thawing was performed at room temperature, i.e. approximately 20 °C, whereas after 6 months this washing was performed on ice in a medium that had been precooled at −20 °C for 15 min. Possibly, the DMSO present in the cryopreservation medium affects the cells negatively in this context when thawing is performed at room temperature.

Following cryopreservation of human liver slices and subsequent storage in liquid nitrogen for 6 months, the observed rate of 7-hydroxycoumarin glucuronidation was 53% of the corresponding rate with fresh tissue (figure 4). However, with the exception of one liver, neither of these preparations of slices exhibited sulphation of 7-hydroxycoumarin. De Kanter *et al.* (1998) reported similar observations, detecting 7-hydroxycoumarin sulphation at low levels in fresh slices from three of six human livers. One possible explanation for these findings might be individual differences in the expression of sulphotransferases. The liver slices that produce 7-hydroxycoumarin sulphate came from a donor liver that had been perfused *in situ*, which may also indicate the importance of perfusion before slicing. On the other hand, a second liver perfused in the same manner did not sulphate 7-hydroxycoumarin. There is also a possibility that formation of 7-hydroxycoumarin sulphate by human liver slices requires incubation times >1 h. In fact, Barr *et al.* (1991b) reported sulphate conjugation by fresh human liver slices after incubation with 25 μM 7-hydroxycoumarin for 2 h.

The present study demonstrates that slices of human and rat liver can be cryopreserved and subsequently stored in liquid nitrogen for at least 6 months without major changes in their capacity to metabolize testosterone to hydroxylated products and to conjugate 7-hydroxycoumarin. We thus propose that the successful maintenance of xenobiotic metabolism in cryopreserved slices is dependent more on the conditions employed during the cryopreservation procedure and thawing than on the length of storage in liquid nitrogen. In summary, these findings illustrate further the potential usefulness of cryopreservation of liver slices for achieving efficient utilization of biological material of limited availability.

Acknowledgements

These studies were supported by grants from the Swedish Medical Research Council (3902 and 04496), the National Institute of Health, USA (1R01 GM60548-01A2) and the Karolinska Institute.

References

Ahmed, S. A., Gogal, R. M. and Walsh, J. E., 1994, A new rapid and simple non-radioactive assay to monitor and determine the proliferation of lymphocytes: an alternative to [3H]thymidine incorporation assay. *Journal of Immunological Methods*, **170**, 211–224.

Arlotto, M. P., Trant, J. M. and Estabrook, R. W., 1991, Measurement of steroid hydroxylation reactions by high-performance liquid chromatography as indicator of P450 identity and function. *Methods in Enzymology*, **206**, 454–462.

Barr, J., Weir, A. J., Brendel, K. and Sipes, I. G., 1991a, Liver slices in dynamic organ culture. I. An alternative *in vitro* technique for the study of rat hepatic drug metabolism. *Xenobiotica*, **21**, 331–339.

Barr, J., Weir, A. J., Brendel, K. and Sipes, I. G., 1991b, Liver slices in dynamic organ culture. II. An *in vitro* cellular technique for the study of integrated drug metabolism using human tissue. *Xenobiotica*, **21**, 341–350.

Bogaards, J. J., Bertrand, M., Jackson, P., Oudshoorn, M. J., Weaver, R. J., van Bladeren, P. J. and Walther, B., 2000, Determining the best animal model for human cytochrome P450 activities: a comparison of mouse, rat, rabbit, dog, micropig, monkey and man. *Xenobiotica*, **30**, 1131–1152.

Bradford, M. M., 1976, A rapid and sensitive method for the quantitation of microgram quantities of protein utilizing the principle of protein–dye binding. *Analytical Biochemistry*, **72**, 248–254.

De Graaf, I. A. M., van der Voort, D., Brits, J. H. F. G. and Koster, H. J., 2000, Increased post-thaw viability and phase I and II biotransformation activity in cryopreserved rat liver slices after improvement of a fast-freezing method. *Drug Metabolism and Disposition*, **28**, 1100–1106.

De Kanter, R., Olinga, P., Hof, I., de Jager, M., Verwillegen, W. A., Sloo, M. J., Koster, H. J., Meijer, D. K. and Groothuis, G. M., 1998, A rapid and simple method for cryopreservation of human liver slices. *Xenobiotica*, **28**, 225–234.

De Kanter, R., Olinga, P., Koster, H. J., de Jager, M., Sloo, M. J. H., Meijer, D. K. F. and Groothuis, G. M. M., 1997, A simple method for the cryopreservation of liver slices from man and other species. In L. F. M. van Zutphen and M. Balls (eds), *Animal Alternatives, Welfare and Ethics* (Amsterdam: Elsevier), pp. 851–856.

Ekins, S., 1996, Past, present, and future applications of precision-cut liver slices for *in vitro* xenobiotic metabolism. *Drug Metabolism Reviews*, **28**, 591–623.

Glöckner, R., Rost, M., Pissowotzki, K. and Müller, D., 2001, Monooxygenation, conjugation and other functions in cryopreserved rat liver slices until 24 h after thawing. *Toxicology*, **161**, 103–109.

Glöckner, R., Steinmetzer, P., Drobner, C. and Müller, D., 1998, Application of cryopreserved precision-cut liver slices in pharmacotoxicology — principles, literature data and own investigations with special reference to CYP1A1-mRNA induction. *Experimental and Toxicological Pathology*, **50**, 440–449.

Krumdieck, C. L., dos Santos, J. E. and Ho, K. J., 1980, A new instrument for the rapid preparation of tissue slices. *Analytical Biochemistry*, **104**, 118–123.

Lerche-Langrand, C. and Toutain, H. J., 2000, Precision-cut liver slices: characteristics and use for *in vitro* pharmaco-toxicology. *Toxicology*, **153**, 221–253.

Nociari, M. M., Shalev, A., Benias, P. and Russo, C., 1998, A novel one-step, highly sensitive fluorometric assay to evaluate cell-mediated cytotoxicity. *Journal of Immunological Methods*, **213**, 157–167.

Rendic, S. and Di Carlo, F. J., 1997, Human cytochrome P450 enzymes: a status report summarizing their reactions, substrates, inducers, and inhibitors. *Drug Metabolism Reviews*, **29**, 413–580.

Sohlenius-Sternbeck, A. K., Floby, E., Svedling, M. and Orzechowski, A. 2000, High conservation of both phase I and II drug-metabolizing activities in cryopreserved rat liver slices. *Xenobiotica*, **30**, 891–903.

Walsh, J. S., Patanella, J. E., Halm, K. A. and Facchine, K. L., 1995, An improved HPLC assay for the assessment of liver slice metabolic viability using 7-ethoxycoumarin. *Drug Metabolism and Disposition*, **23**, 869–874.

Yamazaki, H. and Shimada, T., 1997, Progesterone and testosterone hydroxylation by cytochromes P450 2C19, 2C9, and 3A4 in human liver microsomes. *Archives of Biochemistry and Biophysics*, **346**, 161–169.

XENOBIOTICA, 2002, VOL. 32, NO. 11, 997–1006

Taylor & Francis
healthsciences

Comparison of rat and human cytochrome P450 (CYP) sources of *N*-alkylprotoporphyrin IX. Formation after interaction with porphyrinogenic xenobiotics: studies with cDNA-expressed single CYP enzymes

J. T. GAMBLE, K. NAKATSU and G. S. MARKS*

Department of Pharmacology & Toxicology, Faculty of Health Sciences, Queen's University, Kingston, Ontario, Canada K7L 3N6

Received 17 April 2002

1. The porphyrinogenicity of certain xenobiotics is due to mechanism-based inactivation of selected cytochrome P450 (CYP) enzymes, with concurrent formation of *N*-alkylprotoporphyrins (*N*-alkylPPs), which disrupt control of haem biosynthesis. An ambiguity arises when extrapolating results obtained with such porphyrinogenic xenobiotics in animals to humans owing to species' differences in CYP enzymes. The objective was to use cDNA-expressed individual rat CYP enzyme preparations in microsomes prepared from baculovirus-infected insect cells to determine which rat CYP enzymes were the source of *N*-alkylPPs after interaction with three porphyrinogenic xenobiotics and to compare the results with formation of *N*-alkylPPs in individual human CYP enzyme orthologues.

2. A sensitive fluorometric technique was employed to quantitate *N*-alkylPP formation after interaction of individual CYP enzymes with a porphyrinogenic xenobiotic.

3. *N*-alkylPP formation was found following the interaction of three porphyrinogenic xenobiotics with CYP1A2, 2B1, 2C6, 2C11 and 3A2, in amounts ranging from 0.45 to 0.07 nmol *N*-alkylPP $nmol^{-1}$ CYP. The results obtained with rat CYP1A2, 2C6, 2C11 and 3A2 were compared with those previously obtained with the human CYP orthologues 1A2, 2C9 and 3A4.

4. Some results corresponded while others did not, reinforcing a previous recommendation that when dealing with xenobiotics whose porphyrinogenicity depends upon interaction with CYP enzymes resulting in *N*-alkylPP formation, animal experiments should be augmented with studies using human CYP preparations.

Introduction

Mechanism-based inactivation of cytochrome P450 (CYP) involves the biotransformation of xenobiotics to reactive species. In some cases, this is followed by binding of the reactive species or a fragment of the reactive species to one of the four pyrrole nitrogens of the haem moiety of CYP (Marks *et al*. 1988, Ortiz de Montellano and Correia 1996), and after loss of an iron atom from the alkylated haem moiety, a *N*-alkylPP dissociates from the CYP apoprotein. 3-[(Arylthio)-ethyl]sydnone (TTMS) and 3,5-diethoxycarbonyl-1,4-dihydro-2,6-dimethyl-4-ethylpyridine (4-ethylDDC) are porphyrinogenic xenobiotics capable of undergoing mechanism-based inactivation by CYP to form *N*-vinylPP and *N*-ethylPP, respectively. These *N*-alkylPPs can inhibit ferrochelatase (FC) (EC 4.99.1.1) activity in rat and other animal species (Tephly *et al*. 1979, De Matteis *et al*.

* Author for correspondence; e-mail: gsm@post.queensu.ca

Xenobiotica ISSN 0049–8254 print/ISSN 1366–5928 online © 2002 Taylor & Francis Ltd
http://www.tandf.co.uk/journals
DOI: 10.1080/00498502100012637

1980, Ortiz de Montellano and Grab 1986, Sutherland *et al.* 1986, Riddick *et al.* 1990). FC inhibition results in decreased haem production, less control over the rate-controlling enzyme, aminolevulinic acid synthase (ALAS) (EC 2.3.1.37), porphyrin accumulation and porphyria (De Matteis and Marks 1996). The porphyrinogenic xenobiotic, allylisopropylacetamide (AIA) causes mechanism-based inactivation of CYP but the *N*-AIAPP formed does not inhibit FC activity. The porphyrinogenicity of AIA is explained as follows. The dissociation of the *N*-AIAPP from the CYP leaves the apoprotein intact, and it can be reconstituted with a new functional haem molecule to form functional CYP (Bornheim *et al.* 1987). This new CYP in turn can undergo mechanism-based inactivation forming another *N*-AIAPP molecule. Progression of this cycle can lead to depletion of the free haem pool, which in turn allows a rise in the activity of ALAS, the rate-controlling enzyme of the haem biosynthetic pathway and eventually to porphyria (De Matteis *et al.* 1980, Ortiz de Montellano and Mico 1981).

Currently, when a xenobiotic is tested for porphyrinogenicity in animals, it is a problem to relate the results to humans. When a xenobiotic owes its porphyrinogenicity to mechanism-based inactivation of selective CYP enzymes with formation of *N*-alkylPPs, the problem arises, at least in part, from differences in CYP enzymes between humans and animals. For this reason, it is important to determine which CYP enzymes in rats and humans are targets for mechanism-based inactivation, resulting in *N*-alkylPP formation. Evidence has been provided by our laboratory that different CYP enzymes of CYP in rat liver are responsible for the production of *N*-alkylPPs from different xenobiotics (McNamee and Marks 1996, Wong *et al.* 1998, 1999). Thus, CYP3A was shown to be the major source of *N*-vinylPP production following the administration of TTMS, and CYP2C11 was the major source of *N*-ethylPP following 4-ethylDDC administration, and *N*-AIAPP following administration of AIA (table 1). The above studies were carried out *in vivo* in rats and depended on (1) a comparison of the hepatic formation of *N*-alkylPP between female rats that lack CYP3A and CYP2C11 and male rats that possess both enzymes after administration of TTMS, 4-ethylDDC and AIA; and (2) on measurements of hepatic *N*-alkylPP formation after administration of TTMS, 4-ethylDDC and AIA to the male and female rat pretreated with a variety of CYP inducers and/or CYP inhibitors. Because the CYP inducers and inhibitors are not totally selective, some ambiguity is associated with previous conclusions. Moreover, the techniques used in the above studies could detect major CYP

Table 1. Ratio of the *N*-alkylPP formation to the amount of CYP present in Supersomes® possessing cDNA-expressed rat CYP enzymes (1A2, 2B1, 2C6, 2C11 or 3A2) after interaction with porphyrinogenic xenobiotics TTMS, 4-ethylDDC and AIA. Data are expressed in the units as indicated. Each value is the average of the values obtained in two or three experiments (individual values are shown in parentheses).

	Porphyrinogenic drug (nmol *N*-alkylPP nmol^{-1} CYP)		
CYP	TTMS	4-ethylDDC	AIA
1A2	0.13 (0.15, 0.11)	0.24 (0.25, 0.23)	0.067 (0.08, 0.054)
2B1	0.31 (0.24, 0.37)	0.26 (0.25, 0.27)	0.33 (0.40, 0.26)
2C6	0.16 (0.13, 0.18)	0.11 (0.093, 0.13)	0.12 (0.10, 0.13)
2C11	0.067 (0.052, 0.082)	0.13 (0.082, 0.17)	0.28 (0.072, 0.35, 0.42)
3A2	0.45 (0.40, 0.50)	0.099 (0.078, 0.12)	0.065 (0.048, 0.081)

enzymes responsible for *N*-alkylPP formation, but were not sufficiently sensitive to detect involvement of the full range of CYP enzymes.

Recently, a fluorescence technique has been developed in our laboratory that allows detection of *N*-alkylPPs formed following interaction of porphyrinogenic xenobiotics with cDNA-expressed individual CYP enzyme preparations available commercially (Lavigne *et al*. 2002). The first objective of the present study was to use this fluorescence technique and cDNA-expressed individual rat CYP enzyme preparations in microsomes prepared from baculovirus-infected insect cells (Supersomes®) to determine directly which rat CYP enzymes are the source of *N*-alkylPPs after interaction with three porphyrinogenic xenobiotics, namely TTMS, 4-ethylDDC and AIA. By this means, we may be able to detect a larger range of CYP enzymes involved in *N*-alkylPP formation after interaction with porphyrinogenic xenobiotics.

In a recent study, Lavigne *et al*. (2002) used cDNA-expressed individual human CYP enzyme preparations in microsomes prepared from baculovirus-infected insect cells (Supersomes®) to determine which of the major human hepatic CYP enzymes (1A2, 2C9, 3A4 and 2D6) were involved in formation of *N*-alkylPPs after interaction with TTMS, 4-ethylDDC and AIA. The second objective of this study was to compare the formation of N-alkylPPs in individual rat CYP enzymes with the formation of *N*-alkylPPs in the individual human CYP enzyme orthologues. For xenobiotics, which owe their porphyrinogenicity to *N*-alkylPP formation, such information will be of value in extrapolating results obtained with porphyrinogenic xenobiotics in animals to humans (Lavigne *et al*. 2002).

Materials and methods

Source of chemicals

TTMS and 4-ethylDDC were obtained from Colour Your Enzyme (Bath, Ontario, Canada). AIA was a gift from Hoffman-La Roche (Vaudreuil, Quebec, Canada). Solvents were purchased from VWR Canada (Mississauga, Ontario, Canada). NADPH was purchased from Sigma Chemical Co. (St Louis, MO, USA). Supersomes® were purchased from Gentest Corporation (Woburn, MA, USA).

Mechanism-based inactivation of rat CYP enzymes in Supersomes® with porphyrinogenic xenobiotics

Microsomes containing single cDNA-expressed CYP enzymes and NADPH-cytochrome P450 reductase from baculovirus-infected insect cells (Supersomes®) were rapidly thawed in a 37 °C shaking water bath and added to 5-ml Erlenmeyer flasks. The flasks also contained 2.0 mM NADPH and either TTMS (0.5 mM), 4-ethylDDC (1.0 mM) or AIA (10 mM) in a final volume of 1 ml. The sample mixture was then incubated for 30 min at 37 °C in a shaking water bath. For the experiment where TTMS was incubated with Supersomes® containing CYP3A2, 0.5 nmol CYP were used. For all other experiments, the incubation mixture contained the porphyrinogenic xenobiotic, NADPH and 1.0 nmol CYP.

Partial purification and measurement of N*-alkylPP formation in the Supersomes®*

After the incubation period, the sample mixture was combined with 5 vols ice-cold 5% H_2SO_4:methanol (v/v) and stored in the dark at 4 °C for 18 h. This mixture was then filtered, diluted with an equal volume of deionized water and the *N*-alkylPPs were extracted twice by the addition of dichloromethane (DCM) in a separatory funnel. The DCM extract was washed with 5% sodium bicarbonate, and zinc acetate (12 µmol) in 1 ml methanol was added to form the Zn *N*-alkylPP dimethyl ester. The DCM solution was evaporated to dryness under a stream of nitrogen and the Zn *N*-alkylPP dimethyl ester was redissolved in 2.0 ml DCM. The amount of Zn *N*-alkylPP dimethyl ester formed was subsequently estimated via fluorometry using an excitation wavelength of 432 nm and measuring the peak height of the major emission band at 650–660 nm (Lavigne *et al*. 2002).

Results and discussion

Microsomes prepared from baculovirus-infected insect cells (Supersomes®) possessing single cDNA-expressed rat CYP enzymes (3A2, 2C11, 2C6, 2B1 and 1A2) were incubated with TTMS, 4-ethylDDC and AIA, plus NADPH and *N*-alkylPP formation was quantitated using fluorometry. Controls, consisting of the CYP enzyme and NADPH but omitting the porphyrinogenic xenobiotics were run for each isozyme (figure 1). A control consisting of CYP3A2 and TTMS, omitting NADPH, was also examined (figure 1f). The fluorescence detected at 650–660 nm was determined as it was in this range of wavelengths that the major peak of the emission fluorescence spectra of *N*-alkylPPs was detected. This value was subtracted from the peak fluorescence detected from samples containing the CYP enzyme, NADPH and a porphyrinogenic xenobiotic to determine the amount of *N*-alkylPP formed via mechanism-based inactivation of CYP. The data are presented in the text as the average of two or three individual values shown in parentheses.

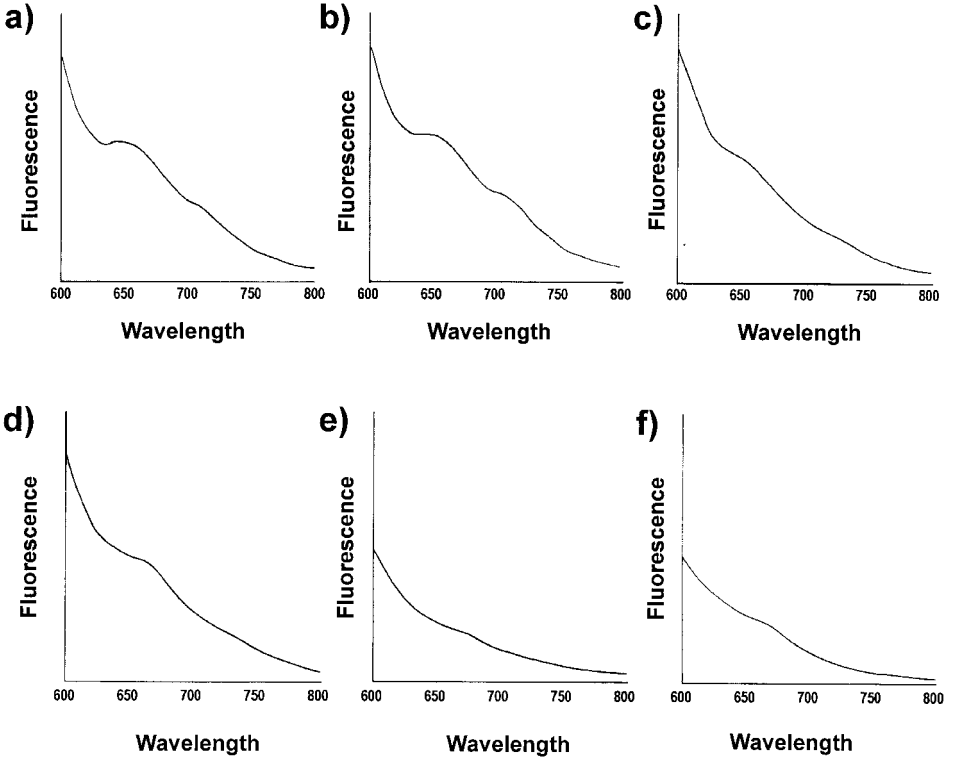


Figure 1. Fluorescence spectra serving as controls resulting from the incubation of NADPH with Supersomes® containing (a) CYP1A2, (b) CYP2B1, (c) CYP2C6, (d) CYP2C11 and (e) CYP3A2, and (f) fluorescence spectrum resulting from the incubation of TTMS with Supersomes® containing CYP3A2. The fluorescence axis has been adjusted automatically to maximize the fluorescence peak heights.

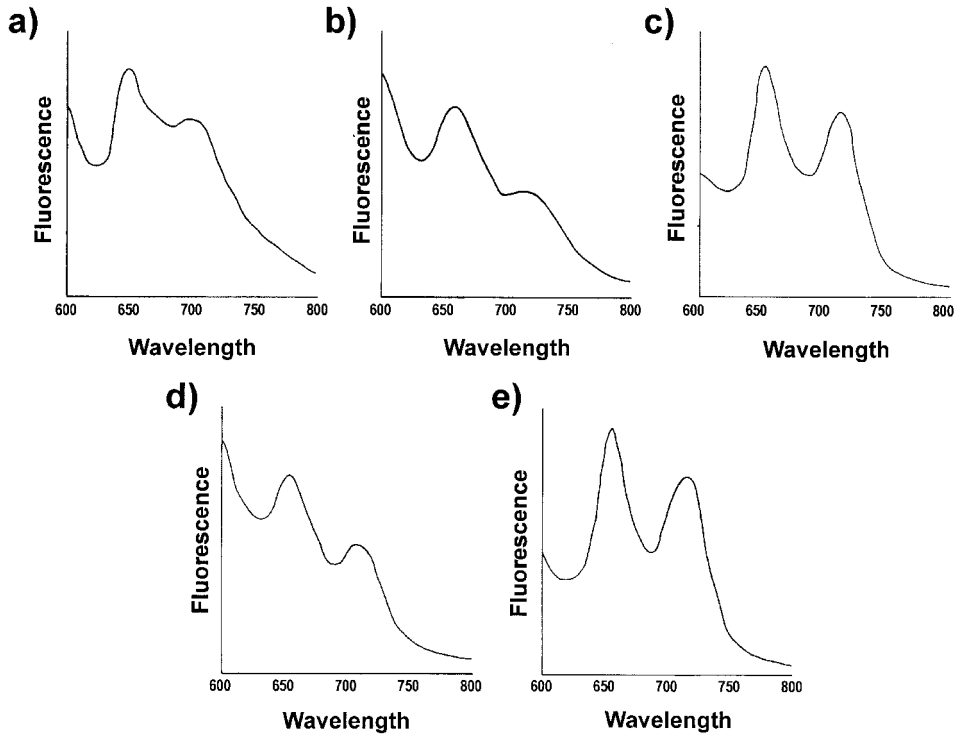


Figure 2. Fluorescence spectra resulting from the incubation of NADPH, TTMS and Supersomes® containing (a) CYP1A2, (b) CYP2B1, (c) CYP2C6, (d) CYP2C11 and (e) CYP3A2. The fluorescence axis has been adjusted automatically to maximize the fluorescence peak heights.

Determination of N*-vinylPP production following interaction of TTMS with Supersomes® containing rat CYP enzymes*

When TTMS (0.5 mM) was incubated *in vitro* with NADPH and Supersomes® containing CYP3A2, 2C11, 2C6, 2B1 and 1A2, varying amounts of *N*-vinylPP formation were observed with each of the CYP enzymes tested (table 1 and figure 2). The highest amount of *N*-vinylPP formation was observed with CYP3A2 (table 1 and figure 2e). In this case, the average ratio of *N*-vinylPP formation to the amount of CYP3A2 present in the Supersomes® (nmol nmol^{-1}) was to be 0.45 (0.40, 0.50). The fact that the highest amount of *N*-vinylPP formed was observed following interaction of CYP3A2 and TTMS corresponds with previous *in vivo* studies (McNamee and Marks 1996) where 75% of hepatic *N*-vinylPP was derived from CYP3A in the DEX-treated rat and 66% of *N*-vinylPP was derived from CYP3A2 in the untreated rat. The amounts of *N*-vinylPP formed after interaction of TTMS with the remaining CYP enzymes tested were (nmol *N*-vinylPP:nmol CYP enzyme): CYP2B1, 0.31 (0.24, 0.37); CYP2C6, 0.16 (0.13, 0.18); CYP1A2, 0.13 (0.15, 0.11); and CYP2C11, 0.067 (0.052, 0.082) (table 1 and figure 2b, c, a, d). The fact that the second highest level of *N*-vinylPP was found after interaction of TTMS with CYP2B1 accords with our previous finding in the PB-induced female and male rat, where it was concluded that CYP2B1/2 are major sources of *N*-vinylPP in the PB-induced rat. The formation of *N*-vinylPP after interaction of TTMS with CYP1A2 and 2C6 was not observed in our previous *in vivo* rat

studies. The finding of a low level of *N*-vinylPP formation after interaction of TTMS with CYP2C11 (0.067 nmol nmol^{-1} CYP) differed from our *in vivo* studies with male and female rats from which it was previously concluded that while CYP3A2 is a major source of *N*-vinylPP formation, CYP2C11 is also a significant source. Thus, in addition to CYP3A2, 2C11 and 2B1, known from our previous *in vivo* studies to be sources of *N*-vinylPP, we now add CYP1A2 and 2C6 as sources of *N*-vinylPP.

Determination of N-ethylPP production following interaction of 4-ethylDDC with Supersomes® containing rat CYP enzymes

When 4-ethylDDC was incubated *in vitro* with NADPH and Supersomes® containing CYP1A2, 2B1, 2C11, 2C6 and 3A2, varying amounts of *N*-ethylPP formation were observed with each of the CYP enzymes tested (table 1 and figure 3). The observation of a high level of *N*-ethylPP formation (0.24 nmol nmol^{-1} CYP) (0.25, 0.23) after interaction of 4-ethylDDC with CYP1A2 (table 1 and figure 3a) is in accordance with the previous observation of CYP1A2 as an important source of *N*-ethylPP formation after 4-ethylDDC administration to the βNF-induced male rat (Wong *et al.* 1998). The formation of *N*-ethylPP after interaction of 4-ethylDDC with CYP2C11 (0.13 nmol nmol^{-1} CYP) (0.082, 0.17) and CYP2C6 (0.11 nmol nmol^{-1} CYP) (0.093, 0.13) (table 1) was anticipated in view of our previous studies in the untreated male and female rat (Wong *et al.*

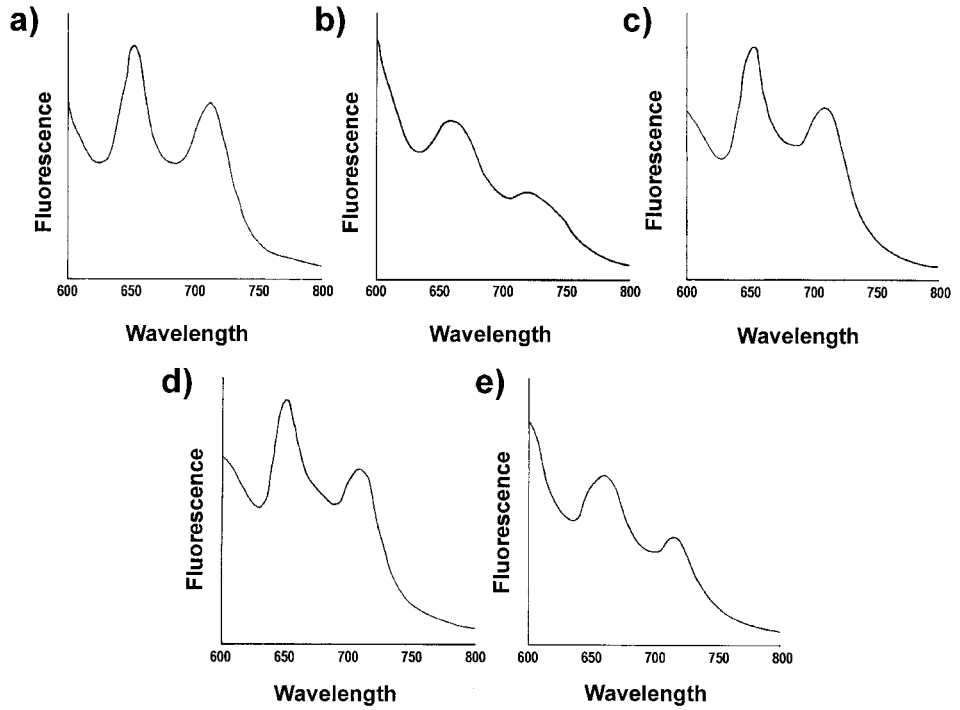


Figure 3. Fluorescence spectra resulting from the incubation of NADPH, 4-ethylDDC and Supersomes® containing (a) CYP1A2, (b) CYP2B1, (c) CYP2C6, (d) CYP2C11 and (e) CYP3A2. The fluorescence axis has been adjusted automatically to maximize the fluorescence peak heights.

1998). In previous studies, CYP2C11 was a major source and CYP2C6 a minor source of *N*-ethylPP. On the other hand, the formation of *N*-ethylPP after interaction of 4-ethylDDC with either CYP2B1 (0.26 nmol nmol^{-1} CYP) (0.25, 0.27) or CYP3A2 (0.099 nmol nmol^{-1} CYP) (0.078, 0.12) (table 1 and figure 3b, e) was not observed in our previous studies. Thus, in addition to CYP1A2, 2C11 and 2C6, known from our previous *in vivo* studies to be sources of *N*-ethylPP, we now add CYP2B1 and 3A2 as sources of *N*-ethylPP.

Determination of N-*AIAPP production following interaction of AIA with Supersomes® containing rat CYP enzymes*

When AIA was incubated *in vitro* with NADPH and Supersomes® containing CYP2B1, 1A2, 2C11, 2C6 and 3A2, varying amounts of *N*-AIAPP were observed with each of the CYP enzymes tested (table 1 and figure 4). The observation of a high level of *N*-AIAPP formation (0.33 nmol nmol^{-1} CYP) (0.40, 0.26) (table 1 and figure 4b) is in accordance with previous findings in this laboratory where CYP2B1 was identified as an important source of *N*-AIAPP formation after AIA administration to the PB-induced female rat. The formation of *N*-AIAPP after interaction of AIA with CYP2C6 (0.12 nmol nmol^{-1} CYP) (0.10, 0.13) and CYP2C11 (0.28 nmol nmol^{-1} CYP) (0.072, 0.35, 0.42) (table 1 and figure 4c, d) was anticipated in view of our previous studies in the male and female rat (Wong *et al*. 1999). The formation of *N*-AIAPP following interaction of AIA with

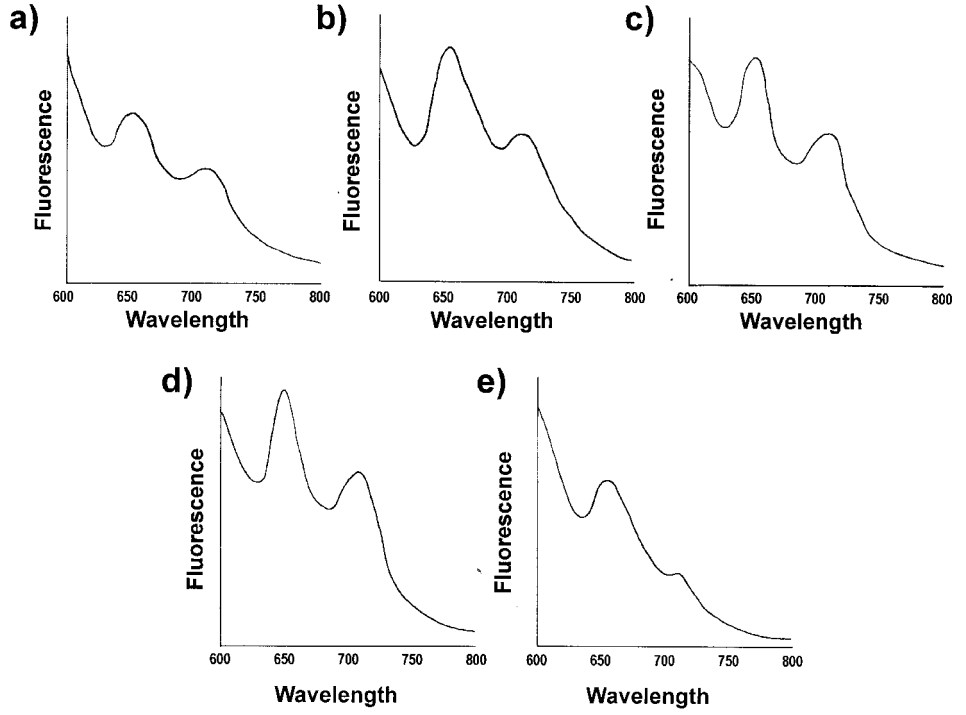


Figure 4. Fluorescence spectra resulting from the incubation of NADPH, AIA and Supersomes® containing (a) CYP1A2, (b) CYP2B1, (c) CYP2C6, (d) CYP2C11 and (e) CYP3A2. The fluorescence axis has been adjusted automatically to maximize the fluorescence peak heights.

CYP1A2 (0.067 nmol nmol^{-1} CYP) (0.08, 0.054) or from CYP3A2 (0.065 nmol nmol^{-1} CYP) (0.048, 0.081) (table 1 and figure 4a, e) was not observed in our previous studies. Thus, in addition to CYP2B1, 2C11 and 2C6 known from our previous *in vivo* studies to be sources of *N*-AIAPP, we now add CYP1A2 and 3A2 as sources of *N*-AIAPP formation.

The advantage of using single CYP expression systems in this study was that the effect of TTMS, 4-ethylDDC and AIA on single CYP enzymes could be observed without the interference of other CYP enzymes. Thus, in contrast to previous *in vivo* studies (Wong *et al.* 1998, 1999), we have determined a more complete range of CYP enzymes capable of forming *N*-alkylPPs. Whereas the major CYP enzymes involved in *N*-alkylPP formation were detected in the *in vivo* studies, other CYP enzymes capable of contributing to *N*-alkylPP formation were detected in the single CYP enzyme studies. It appears that a high conversion ratio (nmol *N*-alkylPP formed nmol^{-1} CYP) for a single CYP enzyme *in vitro* reflects, in most cases, a significant role for that enzyme in the *in vivo* metabolism of the porphyrinogenic xenobiotic, and subsequent mechanism-based inactivation of the CYP enzyme resulting in formation of *N*-alkylPP. Relevant to our studies is the fact that results obtained in single CYP enzyme systems may not reflect the *in vivo* effects that these porphyrinogenic xenobiotics may exert. Differences in the phospholipid environment, the lipid-to-protein ratio and the NADPH-CYP reductase-to-CYP ratio may be different between *in vivo* systems and cDNA-expressed single-CYP enzyme systems (Rodrigues 1999). In addition, *in vivo* porphyrinogenic effects are also dependant on the specific activity and relative abundance of each CYP enzyme in the *in vivo* system. Thus, although each of the CYP enzymes tested can undergo mechanism-based inactivation and form a *N*-alkylPP following interaction with porphyrinogenic xenobiotics, these CYP enzymes may not act in this fashion *in vivo*. It is therefore clear that both single CYP enzyme studies and *in vivo* studies are required to obtain comprehensive information on the mechanisms of action of xenobiotics that owe their porphyrinogenicity to mechanism-based inactivation of CYP enzymes with accompanying formation of *N*-alkylPPs.

In a recent study, Lavigne *et al.* (2002) used single cDNA-expressed human CYP enzymes in microsomes prepared from baculovirus-infected insect cells (Supersomes®) to determine which CYP enzymes were the major sources of *N*-alkylPP formation after interaction with TTMS, 4-ethylDDC and AIA. These *in vitro* results were compared with an *in vivo* study where results obtained with their rat CYP orthologues after administration of TTMS, 4-ethylDDC and AIA to rat. In general, similarities were found between results with human CYP enzymes in Supersomes® and their rat CYP orthologues in rat liver microsomes, although some differences were found.

The second objective of the present study was to compare the formation of *N*-alkylPPs in individual rat CYP enzymes with the formation of *N*-alkylPPs in their individual human CYP orthologues (Lavigne *et al.* 2002). The major human CYP enzyme involved in *N*-vinylPP formation after interaction with TTMS is CYP3A4 (table 2), which corresponds with the fact that the rat CYP orthologue CYP3A2 is the major CYP enzyme responsible for the formation of *N*-vinylPP (table 2). On the other hand, whereas rat CYP1A2, 2C11 and 2C6 are involved in *N*-vinylPP formation, the corresponding human CYP orthologues CYP1A2 and 2C9 are not. The major human CYP enzyme responsible for *N*-ethylPP formation from 4-

Table 2. Comparison of *N*-alkylPP formation between Supersomes® containing single cDNA-expressed human CYP enzymes (1A2, 2C9 or 3A4) Lavigne *et al.* 2002) and single cDNA-expressed rat CYP enzymes (1A2, 2C6, 2C11 or 3A2). Differences in the *N*-alkylPP formation between rat and human CYP orthologues are indicated by boxes. Each value is the average of the values obtained in two or three experiments (individual values shown in parentheses).

	Porphyrinogenic drug (nmol *N*-alkylPP nmol^{-1} CYP)		
CYP	TTMS	4-ethylIDDC	AIA
Rat 1A2	0.13 (0.15, 0.11)	0.24 (0.25, 0.23)	0.067 (0.08, 0.054)
Human 1A2	n.d.	0.60 (0.94, 0.25)	n.d.
Rat 2C6	0.16 (0.13, 0.18)	0.11 (0.093, 0.13)	0.12 (0.10, 0.13)
Human 2C9	n.d.	0.29 (0.39, 0.16)	0.21 (0.26, 0.16)
Rat 2C11	0.067 (0.052, 0.082)	0.13 (0.082, 0.17)	0.28 (0.072, 0.35, 0.42)
Human 2C9	n.d.	0.29 (0.39, 0.16)	0.21 (0.26, 0.16)
Rat 3A2	0.45 (0.40, 0.50)	0.099 (0.078, 0.12)	0.065 (0.048, 0.081)
Human 3A4	0.87 (0.85, 0.89)	n.d.	0.30 (0.28, 0.32)

n.d., Not detected.

ethylDDC is CYP1A2, which corresponded with the finding with the rat CYP1A2 orthologue (table 2). The fact that interaction of human 2C9 with 4-ethylDDC is an important source of *N*-ethylPP formation corresponded with the findings with the rat CYP2C6 and 2C11 orthologues. However, whereas rat CYP3A2 was a source of *N*-ethylPP formation, the human orthologue CYP3A4 was not. Rat CYP2C6, 2C11 and 3A2 were sources of *N*-AIAPP, a result that corresponded with results obtained with the human orthologues CYP2C9 and 3A4. However, whereas rat CYP1A2 was a source of *N*-AIAPP, human CYP1A2 was not.

Lavigne *et al.* (2002) recommended that when dealing with xenobiotics whose porphyrinogenicity depends on the interaction with CYP enzymes resulting in *N*-alkylPP formation, animal experiments should be augmented with studies using cDNA-expressed human CYP enzyme preparations. The finding of the present study where important differences were found between human and rat CYP orthologues (table 2) reinforce the above recommendation.

Acknowledgements

The study was supported by the CIHR.

References

Bornheim, L. M., Underwood, M. C., Caldera, P., Rettie, A. E., Trager, W. F., Wrighton, S. A. and Correia, M. A., 1987, Inactivation of multiple hepatic cytochrome P-450 isozymes in rats by allylisopropylacetamide: mechanistic implications. *Molecular Pharmacology*, **32**, 299–308.

De Matteis, F., Gibbs, A. H., Cantoni, L. and Francis, J., 1980, Substrate-dependent irreversible inactivation of cytochrome P-450: conversion of its haem moiety into modified porphyrins. *Ciba Foundation Symposium*, **76**, 119–139.

De Matteis, F. and Marks, G. S., 1996, Cytochrome P450 and its interactions with the heme biosynthetic pathway. *Canadian Journal of Physiology and Pharmacology*, **74**, 1–8.

Lavigne, J. A., Nakatsu, K. and Marks, G. S., 2002, Identification of human hepatic Cytochrome P450 sources of *N*-alkylprotoporphyrin IX after interaction with porphyrinogenic xenobiotics. *Drug Metabolism and Disposition* **30**, 788–794.

Marks, G. S., McCluskey, S. A., Mackie, J. E., Riddick, D. S. and James, C. A., 1988, Disruption of hepatic heme biosynthesis after interaction of xenobiotics with cytochrome P-450. *FASEB Journal*, **2**, 2774–2783.

McNamee, J. P. and Marks, G. S., 1996, Cytochrome P4503A is the major source of *N*-vinyl-protoporphyrin IX formation after administration of 3-[2-(2,4,6-trimethylphenyl)thioethyl]-4-methylsydnone to untreated and dexamethasone-pretreated rats. *Drug Metabolism and Disposition*, **24**, 872–878.

Ortiz de Montellano, P. R. and Correia, M. A., 1996, Inhibition of cytochrome P450 enzymes. In P. R. Ortiz de Montellano (ed.), *Cytochrome P450: Structure, Mechanism, and Biochemistry* (New York: Plenum), pp. 305–364.

Ortiz de Montellano, P. R. and Grab, L. A., 1986, Inactivation of cytochrome P450 during catalytic oxidation of a 3-[(arylthio)ethyl]sydnone: N-vinyl heme formation via insertion into the Fe-N Bond. *Journal of the American Chemical Society*, **108**, 5584–5589.

Ortiz de Montellano, P. R. and Mico, B. A., 1981, Destruction of cytochrome P-450 by allylisopropylacetamide is a suicidal process. *Archives in Biochemistry and Biophysics*, **206**, 43–50.

Riddick, D. S., Park, S. S., Gelboin, H. V. and Marks, G. S., 1990, Effects of 4-alkyl analogues of 3,5-diethoxycarbonyl-1,4-dihydro-2,4,6-trimethylpyridine on hepatic cytochrome P-450 heme, apoproteins, and catalytic activities following *in vivo* administration to rats. *Molecular Pharmacology*, **37**, 130–136.

Rodrigues, A. D., 1999, Integrated cytochrome P450 reaction phenotyping: attempting to bridge the gap between cDNA-expressed cytochromes P450 and native human liver microsomes. *Biochemical Pharmacology*, **57**, 465–480.

Sutherland, E. P., Marks, G. S., Grab, L. A. and Ortiz de Montellano P. R, 1986, Porphyrinogenic activity and ferrochelatase-inhibitory activity of sydnones in chick embryo liver cells. *FEBS Letters*, **197**, 17–20.

Tephly, T. R., Gibbs, A. H. and De Matteis, F., 1979, Studies on the mechanism of experimental porphyria produced by 3,5-diethoxycarbonyl-1,4-dihydrocollidine. Role of a porphyrin-like inhibitor of protohaem ferro-lyase. *Biochemical Journal*, **180**, 241–244.

Wong, S. G., Kobus, S. M., McNamee, J. P. and Marks, G. S., 1998, Gender differences in *N*-alkyl protoporphyrin IX production in rats after the administration of porphyrinogenic xenobiotics. *Drug Metabolism and Disposition*, **26**, 739–744.

Wong, S. G., Lin, E. H. and Marks, G. S., 1999, Cytochrome CYP sources of *N*-alkylprotoporphyrin IX after administration of porphyrinogenic xenobiotics to rats. *Drug Metabolism and Disposition*, **27**, 960–965.

XENOBIOTICA, 2002, VOL. 32, NO. 11, 1007–1016

Taylor & Francis
healthsciences

Changes in glutathione-redox balance induced by hexachlorocyclohexane and lindane in CHO-K1 cells

A. J. GARCÍA-FERNÁNDEZ§, A. E. BAYOUMI‡, Y. PÉREZ-PERTEJO†, D. ROMERO§, C. ORDÓÑEZ†, R. M. REGUERA†, R. BALAÑA-FOUCE† AND D. ORDÓÑEZ†*

† Dpt. Farmacología y Toxicología (INTOXCAL), Universidad de León, Campus de Vegazana s/n, E-24071 León, Spain
‡ Dpt. Plant Protection, Faculty of Agriculture, University Aim Shams, Cairo, Egypt
§ Dpt. Ciencias Sociosanitarias, Universidad de Murcia, Campus de Espinardo E-30071, Murcia, Spain

Received 19 April 2002

1. The basal cytotoxic effect of the organochlorine pesticides hexachlorocyclohexane and lindane on CHO-K1 cultures was assessed at fractions of their lethal doses as determined by the neutral red incorporation (NRI) assay ($NRI_{6.25}$, $NRI_{12.5}$ and NRI_{25}). The sulphur-redox cycle enzymes glutathione peroxidase, glutathione reductase and glutathione *S*-transferase, and total and oxidized glutathione were evaluated at several points during the standard growth curve of the cultures.

2. After incubation with each compound for 24 h, both glutathione peroxidase and reductase showed a substantial increase at the lowest exposure doses ($NRI_{6.25}$) – more significantly for lindane than for 1,2,3,4,5,6-hexachlorocyclohexane (HCH) – and dropped at higher doses of both compounds. The reduced and oxidized glutathione content was greatly diminished at the lower exposures, whereas the total glutathione content was higher at $NRI_{12.5}$ values.

3. Changes in cell membrane integrity were assessed for a wide range of pesticide concentrations with the lactate dehydrogenase release assay and lipid peroxidation. Membrane leakage and peroxide production were significantly enhanced at concentrations of HCH 50 $\mu g\,ml^{-1}$, although this effect was not significant at lindane concentrations $< 200\,\mu g\,ml^{-1}$.

4. Lipid peroxidation increased with exposure to HCH at concentrations as low as $NRI_{6.25}$, whereas in the case of lindane, this increase was only significant at doses of NRI_{25} and above.

Introduction

Lindane, the γ-isomer of the 1,2,3,4,5,6-hexachlorocyclohexane (HCH), is an effective organochlorine insecticide widely used on fruit and vegetable farming, seed treatment and forestry, as well as for animal health in the treatment of head and body lice and scabies (ATSDR 1992). Unlike HCH isomer mixtures, lindane is widely used for agricultural and clinical purposes in industrialized countries, making the assessment of the possible risks such use involves a concern to be addressed. As in other organochlorine insecticides, the most usual route for human exposure is oral ingestion of food containing the insecticides, although cases of dermal and inhalatory exposures have also been reported (Loffler and van Bavel 2000, Nordt and Chew 2000, Klein *et al.* 2001). Acute and/or chronic responses to

* Author for correspondence; e-mail: dftrbf@isidoro.unileon.es

Xenobiotica ISSN 0049–8254 print/ISSN 1366–5928 online © 2002 Taylor & Francis Ltd
http://www.tandf.co.uk/journals
DOI: 10.1080/00498250210012628

these pesticides include neurotoxicity and the effects on the cardiovascular, gastrointestinal, immune, and muscle and skeletal systems (Videla *et al.* 1990, ATSDR 1992, Arisi *et al.* 1994). Histological and biochemical alterations of the liver such as hypertrophy, steatosis and necrosis (Junqueira *et al.* 1988), and impairment of reproductive function in male animals have been described after chronic exposure (Samanta *et al.* 1999). There is growing evidence that most of these processes may be the result of free-radical intermediates induced by exposure to environmental contaminants (Junqueira *et al.* 1988, Videla *et al.* 1990, Arisi *et al.* 1994, Samanta and Chainy 1997, Samanta *et al.* 1999).

In vivo experimental studies have shown that the HCH and lindane hepatotoxicity may be due to oxidative stress associated with lipid peroxidation (Videla *et al.* 1990, Hassoun *et al.* 1993, Arisi *et al.* 1994, Samanta and Chainy 1995). Similar mechanisms have been reported in reproductive organs such as the testis and placenta as well as in foetuses (Hassoun and Stohs 1996, Chitra *et al.* 2001, Sujatha *et al.* 2001) and the immune system (Koner *et al.* 1998). More controversial reports have likewise been published on effects on cerebral tissue (Arisi *et al.* 1994, Sahoo *et al.* 2000). Agrawal *et al.* (1991) suggested that HCH produces significant changes in the glutathione redox system in rat erythrocytes, leading to oxidative membrane damage, although Junqueira *et al.* (1994) did not observe alterations in pro-oxidant/antioxidant status.

Lipid peroxidation destroys membrane integrity, causing cell dysfunction and ultimately cell death (Zaman and Pardini 1996). Junqueira *et al.* (1988) reported morphological evidence of hepatic cell injury in lindane-treated rats, which appeared to increase with time and be associated with enhanced formation of thiobarbituric acid reactants. Moreover, in one of the rare studies on cultured cells, Verma *et al.* (1992) suggested that the primary action of biologically active HCH isomers is to disrupt the organization of the plasma membrane, affecting cell viability. Hassoun and Stohs (1996) and Hassoun *et al.* (1993), in turn, described increased DNA single-strand breaks in foetal and placental tissues and in the liver, respectively. However, unlike other organic pesticides such as the herbicide paraquat (Palmeira *et al.* 1994), in the substances addressed in the present study the source of the reactive oxygen species (ROS) that have deleterious effects on many cellular processes is not yet known.

The ROS species induced by lindane and HCH may, like the paraquat ROS, be neutralized by the cellular antioxidant system, comprising both mitochondrial Mn-containing and cytosolic Cu- and Zn-containing superoxide dismutases (SODs) (Bagley *et al.* 1986), as well as glutathione peroxidase and glutathione reductase, which are instrumental in maintaining the balance between the reduced and oxidized forms of glutathione (Krall *et al.* 1991). Although superoxide anion radicals can be rapidly removed, the hydroxyl-free-radical (OH), formed by the Fenton reaction, reacts efficiently with polyunsaturated fatty acids and other lipid membrane components, being the source of various deleterious lipid peroxidation species (Samanta and Chainy 1997). Involvement in pathological processes occurs when free-radical production exceeds the tissue free-radical-scavenging capacity (Zaman and Pardini 1996). Despite information on lipid peroxidation induced by HCH and lindane in experimental animals (Hassoun and Stohs 1996, Junqueira *et al.* 1997, Samanta and Chainy 1997), more information about its role in cellular cytotoxicity or its effect on free-radical-scavenging enzymes is necessary.

This study compares the dose–response effects of HCH and lindane on membrane permeability and glutathione content and interconversion in Chinese hamster ovary cells (CHO-K1) in order to ascertain whether ROS are involved in the toxicity of these pesticides in mammalian cells.

Materials and methods

Chemicals

Culture medium Hams' F12, gentamicine sulphate (10 mg ml^{-1}), neutral red dye (NR), reduced and oxidized glutathione (GSSG) and glutathione reductase were from Sigma Chemical Co. (St Louis, MO, USA). Hexachlorocyclohexane isomer mixture and the γ-isomer (lindane) were acquired from Alltech Associates (Deerfield, IL, USA). Foetal calf serum was purchased from Boehringer Mannheim GmbH (Mannheim, Germany). CytoTox 96® LDH-releasing kit was from Promega (Madison, WI, USA). All other reagents were of standard laboratory grade.

Cell culture and media

CHO-K1 cells were obtained from the American Type Culture Collection (ATCC CCL 61); 10^4 cells cm^{-2} were plated in monolayer in 22.1-cm^2 polystyrene tissue culture dishes with Hams' F12 supplemented with 25 mm Hepes buffer (pH 7.4), 10% heat inactivated foetal calf serum and gentamicine (30 µg ml^{-1}) at 37 °C. Cells were counted in an improved Neubauer haemocytometer and viability was determined by exclusion of Trypan blue. Cells were grown to 65% confluence (day 3, mid-log phase) and then pulsed with different concentrations of organochlorine insecticides dissolved in 1% dimethylsulfoxide (DMSO). Control wells were pulsed with a similar volume of DMSO solution. After 24 h, cells were washed with phosphate-buffered saline (PBS) and medium was replaced. Cell extracts were used to determine sulphur-redox species and the enzymes involved in glutathione metabolism.

Determination of cytotoxicity

The cytotoxicities of lindane and HCH were estimated in CHO-K1 cells using the neutral red incorporation (NRI) assay described by Borenfreund and Puemer (1985). Cells were grown up to 65% confluence and then pulsed with different concentrations of lindane and HCH (ranging from 0.1 to 500 µg ml^{-1}). After 24 h, cells were washed and medium replaced with fresh medium, containing 40 µg ml^{-1} NR dye. After 3 h, cells were washed with PBS and fixed with 0.5% formaldehyde and 1% $CaCl_2$ in distilled water. Colour was developed with 0.2 ml 1% acetic acid, 59% ethanol and water. The absorbance at 540 nm of each plate was determined in an automatic ELISA reader and curves were fitted using Sigma Plot (v.2.1, Microsoft®) for non-linear regression using probit/log curves to obtain the concentrations of each insecticide equivalents to their correspondent fractions of NRI ($NRI_{6.25}$, $NRI_{12.5}$, NRI_{25}, NRI_{50}).

Alteration of membrane permeability induced by HCH and lindane insecticides was assessed in CHO-K1 cultures. Membrane status was analysed by measuring the lactate dehydrogenase (LDH) released to the culture medium by CHO-K1 cells exposed to different concentrations of these insecticides in a short period (as short as 4 h). LDH release was spectrophotometrically estimated using the CytoTox 96 kit (Promega), following the manufacturer's manual. One hundred per cent of LDH release was determined adding 1 mg ml^{-1} SDS to control-column wells.

Lipid peroxidation assay

Malondialdehyde (MDA) measurement was used as indicator of lipid peroxidation in CHO-K1 cells after exposure to lindane and HCH. Cells were grown in 24-well plates using medium supplemented with 10% foetal calf serum. After cell adherence was achieved, the medium was replaced with 0.5 ml serum-free medium containing the insecticide at final concentrations ranging from 6.25 to 50 µg ml^{-1}. After 4-h exposure, the medium was collected, centrifuged and 250 µl of the supernatant was transferred to a test tube for the lipid peroxidation assay. The reaction mixture contained 250 µl sample, 100 µl 7% sodium dodecyl sulfate (SDS), 1 ml 0.1 N HCl, 150 µl 1% phosphotungstic acid and 500 µl 0.67% thiobarbituric acid (TBA). The mixture was mixed thoroughly and heated at 95 °C for 60 min in the dark. After cooling in an ice bath, 1 ml *n*-butanol was added, and the mixture was shaken vigorously. After centrifugation at 1200*g* for 10 min, the organic layer was analysed for MDA by spectrofluorometry at 350 nm (ex.) and 590 (em.). MDA standards and blanks (cells exposed to 1% DMSO) were also assayed.

Glutathione content

Intracellular total glutathione was determined spectrophotometrically using the method described by Akerboom and Sies (1981). CHO-K1 monolayers from 22.1-cm^2 polystyrene Petri dishes were harvested from the plastic surface with a trypsin/EDTA solution, washed twice with PBS, pH 7.4, and disrupted by sonication with 1 M cold perchloric acid (PCA) containing 2 mM EDTA. One hundred microlitres of the extracts were neutralized with 70 µl KOH and 70 µl MOPS 0.3 M before measuring glutathione. The protocol for total glutathione determination was as follows: 730 µl 0.1 M potassium phosphate buffer, pH 7.0, containing 1 mM EDTA, 200 µl neutralized cell extracts, 50 µl 4 mg ml^{-1} NADPH dissolved in 0.5% $NaHCO_3$ and 20 µl 1.5 mg ml^{-1} 5,5′-dithiobis(2-nitrobenzoic acid) (Sigma) in 0.5% $NaHCO_3$ were combined to a final volume of 1 ml. Reactions were started with 6 U glutathione reductase and measured at 412 nm for 1 min at 25 °C. Slopes of each determination were interpolated from a calibration curve expressing the total content of glutathione as nmol mg^{-1} total protein.

GSSG was assayed in freshly acidified cell extracts using the method described by Anderson (1985). CHO-K1 cultures were harvested and disrupted as above. PCA-treated extracts were then centrifuged and neutralized with 2 µl 2-vinylpyridine Fluka Chemie (Buchs, Switzerland) and 824 µl 25% triethanolamine. The reaction mixture contained in a 1 ml final volume: 650 µl sodium phosphate buffer, 0.1 M, pH 7.5, that included 6.3 mM EDTA, 50 µl 4 mg ml^{-1} NADPH, 100 µl DTNB 6 mM, 200 µl cell extracts and 1 U glutathione reductase. Similarly to total glutathione, GSSG was estimated by interpolating the slopes of each assay to a standard curve, expressing GSSG content as nmol mg^{-1} total protein.

Enzyme assays

The glutathione reductase mixture contained, in a final volume of 1 ml, 500 µl potassium phosphate buffer, 0.2 M, pH 7.0, with 2 mM EDTA, 50 µl of a 2 mM NADPH solution dissolved in 10 mM HCl-Tris, pH 7.0, 50 µl 20 mM GSSG, 300 µl distilled water and 100 µl freshly isolated cellular extract. The absorbance rate of the reaction mixture at 340 nm was measured after incubation at 30 °C for 1 min. One unit of glutathione reductase activity is defined as the amount of enzyme reducing 1 µmol GSSG min^{-1} mg^{-1} soluble protein.

Total glutathione peroxidase was assayed as described by Wendel (1981). Included in a 1-ml final volume was 500 µl potassium phosphate buffer 0.25 M, pH 7.0, containing 2.5 mM EDTA and 2.5 mM sodium azide, 100 µl 10 mM reduced glutathione, 100 µl 2.5 mM NADPH in 0.1% $NaHCO_3$ solution and 100 µl 2.4 U ml^{-1} freshly prepared glutathione reductase in PBS. One hundred microlitres of cell extracts were added and incubated at 37 °C. The assay was started by adding 100 µl 12 mM *tert*-butyl peroxide (Sigma) and monitoring the absorbance rate at 366 nm during 1 min at 37 °C. One unit of glutathione peroxidase is defined as the amount of enzyme that oxidizes 1 µmol reduced glutathione min^{-1} mg^{-1} soluble protein. Protein was assayed according to Bradford (1976).

Glutathione *S*-transferase was measured spectrophotometrically according to Habig *et al.* (1974). In a 1-ml plastic cuvette, the following reagents were added: 800 µl sodium phosphate buffer, 0.2 M, pH 6.5, 50 µl chlorodinitrobenzoic acid (Sigma) 20 mM dissolved in 95% ethanol, 50 µl reduced glutathione 20 mM, and 100 µl enzymatic extract. Enzymatic activity was assayed at 25 °C for 1 min at 340 nm. One unit of GST activity is defined as the amount of enzyme consuming 1 µmol GSH min^{-1} mg^{-1} protein.

Results

HCH and lindane cytotoxicities were determined using the neutral red incorporation (NRI) assay, which monitors lysosomal cell function. Both organochlorine compounds were added to CHO-K1 cultures during the mid-log phase (day 3) and incubated for 24 h, after which cell viability was analysed by the above technique. The probit/log curves yielded the NRI values shown in table 1. HCH was 2.5–3.4 times more toxic than lindane in CHO-K1 cells. On the grounds of the high reliability of the NRI assay, fractions of the NRI_{50} ($NRI_{6.25}$, $NRI_{12.5}$ and NRI_{25}) were used to determine the biochemical parameters assayed here.

The metabolic effects of HCH and lindane on the sulphur-redox cycle were measured after exposure to the agents for 24 h in the presence of foetal calf serum in the culture medium. Table 2 summarizes total glutathione and GSSG content, determined in the mid-/late log phase after exposure to HCH and lindane. Total glutathione was found to increase significantly ($p < 0.01$) at HCH and lindane concentrations equivalent to their $NRI_{12.5}$, but remained unchanged with respect to control cells at higher and lower concentrations. Unlike total glutathione,

Table 1. Basal cytototoxicities of HCH and lindane on CHO-Kl cells using the neutral red uptake (NRI) method.

	Insecticide concentrations ($\mu g\,ml^{-1}$)				
Insecticide	$NRI_{6.25}$	$NRI_{12.5}$	NRI_{25}	NRI_{50}	r^2
HCH	5.9 ± 0.6	10.5 ± 0.9	46.9 ± 1.1	55.7 ± 1.2	0.97
Lindane	19.4 ± 0.8	33.3 ± 2.2	105.4 ± 1.9	144.1 ± 1.7	0.97

Cells were grown until mid-log phase and were then exposed to different concentrations of HCH and lindane for 24 h. NRI values were calculated by the probit/log approach. Results are the average ± SEM of three independent experiments.

Table 2. Intracellular glutathione (total and oxidized forms) content in 24-h HCH and lindane-treated CHO-Kl cells.

		Glutathione content ($nmol\,mg^{-1}$ protein)		
Insecticide	Glutathione	$NRI_{6.25}$	$NRI_{12.5}$	NRI_{25}
HCH	total	25.82 ± 1.45	40.80 ± 4.90	26.10 ± 1.56
	GSSG	0.18 ± 0.01***	0.22 ± 0.02*	0.26 ± 0.01**
	GSSG/total	0.007	0.0054	0.01
Lindane	total	25.80 ± 2.73	49.22 ± 1.58***	30.77 ± 3.73
	GSSG	0.18 ± 0.03*	0.16 ± 0.01***	0.17 ± 0.04*
	GSSG/total	0.007	0.0032	0.0055

CHO-K1 cultures were grown up to 65% confluence (day 3) and then incubated with fresh medium containing concentrations of HCH and lindane equivalent to its $NRI_{6.25}$, $NRI_{12.5}$ and NRI_{25}. Each value is the average ± SEM of three independent experiments. *** $p \leq 0.001$; ** $p \leq 0.01$; * $p \leq 0.05$ with respect to control $23.48 \pm 0.67\,nmol\,mg^{-1}$ protein (total glutathione) and with respect to 0.32 ± 0.05 (GSSG), respectively, obtained in control cultures.

Table 3. Glutathione peroxidase, reductase and *S*-transferase activities in CHO-Kl cells exposed to different sublethal concentrations of HCH and lindane.

	$NRI_{6.25}$	$NRI_{12.5}$	NRI_{25}
Glutathione peroxidase activity			
HCH	235.96 ± 6.04***	231.10 ± 13.71**	177.56 ± 7.04**
Lindane	686.13 ± 27.41***	324.40 ± 0.12***	321.07 ± 33.91**
Glutathione reductase activity			
HCH	48.07 ± 1.81‡‡	36.03 ± 1.46	33.30 ± 0.26
Lindane	158.86 ± 5.24‡‡‡	59.76 ± 1.41‡‡‡	42.07 ± 5.06
Glutathione *S*-transferase activity			
HCH	38.60 ± 1.67	$30.23 \pm 0.88^{+++}$	$20.56 \pm 1.58^{+++}$
Lindane	39.73 ± 2.63	$22.33 \pm 2.41^{++}$	$51.21 \pm 0.19^{+++}$

Cells were grown until mid-log phase and then equivalent concentrations to their $NRI_{6.25}$, $NRI_{12.5}$ and NRI_{25} were added for 24 h to the cultures. Each value is the average ± SEM of three independent experiments. *** $p \leq 0.001$, ** $p \leq 0.01$ with respect to $129.19 \pm 9.68\,nmol\,min^{-1}\,mg^{-1}$ protein obtained in control cultures. ‡‡‡ $p \leq 0.001$, ‡‡ $p \leq 0.01$ with respect to $34.19 \pm 1.33\,nmol\,min^{-1}\,mg^{-1}$ protein obtained in control cultures. $^{+++}$ $p \leq 0.001$, $^{++}$ $p \leq 0.01$ with respect to $42.05 \pm 1.81\,nmol\,min^{-1}\,mg^{-1}$ protein obtained in control cultures.

GSSG levels showed significant ($p < 0.01$) depletion at HCH and lindane concentrations equivalent to their $NRI_{6.25}$.

Large increases in glutathione peroxidase activities are associated with exposure to HCH and lindane (table 3). Total glutathione peroxidase activity at HCH and lindane concentrations equivalent to their $NRI_{6.25}$ was 1.8- and >5.3 times

Table 4. Membrane permeability assessment using LDH released to culture medium after 4-h HCH and lindane exposed CHO-K1 cells.

	LDH released (%)					
Concentration ($\mu g\,ml^{-1}$)	6.25	12.5	25	50	100	200
HCH	n.d.	n.d.	0.41 ± 0.60	5.06 ± 1.26	31.22 ± 1.07	44.72 ± 0.47
Lindane	n.d.	n.d.	n.d.	0.83 ± 1.03	6.12 ± 0.46	18.15 ± 1.33

CHO-K1 cultures were grown up to 65% confluence (day 3) and then incubated for 24 h with fresh medium containing different concentrations of HCH and lindane insecticides. Incubation media were removed to fresh plates and analysed for LDH content using the CytoTox96® (Promega) assay. Each value represents the average ± SEM of three independent experiments. n.d., Not detected.

higher, respectively, than recorded for the control culture. At higher levels of exposure to HCH, glutathione peroxidase activity remained high. Most significantly, glutathione peroxidase induction persisted in lindane-exposed cells at insecticide concentrations equivalent to the NRI_{25}.

Glutathione reductase remained almost unchanged at pesticides concentrations equivalent to their NRI_{25}, although it did respond to exposure to lindane at the $NRI_{12.5}$ and $NRI_{6.25}$, and to HCH at $NRI_{6.25}$ (table 3). On the contrary, the activity of glutathione *S*-transferase, one of the enzymes involved in Phase II detoxification in mammals, was only induced at the highest concentration of lindane, remaining unchanged or declining at the lowest concentrations of lindane and at all concentrations of HCH (table 3).

Since lipid peroxidation is one of the causes of cell membrane disruption and necrosis in organisms (Chitra *et al.* 2001), membrane permeability and lipid peroxidation were studied in CHO-K1 cells exposed to lindane and HCH. The two compounds induced similar modifications in membrane permeability, as measured by LDH release from the cells, at concentrations equivalent to their $NRI_{6.25}$, $NRI_{12.5}$ and NRI_{25}, releasing significant quantities of LDH into the medium at HCH concentrations $> 25\,\mu g\,ml^{-1}$ and lindane concentrations $> 50\,\mu g\,ml^{-1}$. In any event, LDH release was 2.5–5.0 times higher in cells exposed to HCH than in cells exposed to lindane (table 4).

The reaction of peroxides with thiobarbituric acid is a classical method to measure lipid peroxidation in biological samples (Hiroski *et al.* 1979). Figure 1 shows that both HCH and lindane prompted a significant increase ($p < 0.001$) in peroxides at concentrations equivalent to NRI_{25}. Therefore, owing to the greater toxicity of HCH, lipid peroxidation occurs at lower concentrations than with lindane. In any event, lipid peroxidation followed a pattern similar to the behaviour observed for LDH release (figure 1A, B).

Discussion

Several reports have documented the role of lindane and HCH in producing oxidative stress in experimentally exposed animals (Verma *et al.* 1992, Junqueira *et al.* 1997, Sahoo *et al.* 2000, Sujatha *et al.* 2001). Oxidative stress is thought to be the primary cause of lipid peroxidation (Videla *et al.* 1990, Hassoun *et al.* 1993, Samanta and Chainy 1995), DNA damage (Hassoun and Stohs 1996), morphological alterations in several tissues (Videla *et al.* 1990, Junqueira *et al.* 1997) and, finally, carcinogenic processes (Iscan *et al.* 2002). On the basis of lindane being an

animal liver carcinogen, the US Environmental Protection Agency (1994) has classified this compound as Group B2 (possible human carcinogen of low to medium carcinogenic hazard).

Unlike other pesticides such as the herbicide paraquat, where the source of ROS is well established (Smith *et al*. 1979), in the case of HCH isomers the origin of these active species is not clear. Junqueira *et al*. (1988) reported that the increase in superoxide anion content in rat cells exposed to lindane is time- and dose-dependent. These latter authors suggested that both cytochrome P450 induction and the increase in microsomal generation of superoxide anion occur in parallel with the increase of cellular lipid peroxidation (Junqueira *et al*. 1997).

Several parameters, including sulphur redox-cycle enzymes and total and oxidized glutathione levels, were analysed in the present study to assess the toxicity of NRI_{50} fractions of lindane and HCH isomers in CHO-K1 cells.

Untreated control cells showed high glutathione peroxidase activity during the CHO-Kl mid-log phase, the period of maximum growth rate, with activity declining in the late and stationary phases (Bayoumi *et al*. 2000). Since oxygen consumption in aerobic cells peaks coinciding with maximum ROS production, the role of glutathione peroxidase, together with superoxide dismutase and catalase, are likely related to membrane disruption (Meister and Anderson 1983). Furthermore, glutathione reductase activity was found to peak at 48 h in the subculture, thereby maintaining a high reduced to oxidized glutathione ratio during CHO mid-log phase.

The exposure of mid-log CHO-Kl cultures to NRI_{50} fractions of lindane and HCH for 24 h produced substantial changes in the antioxidant metabolism. Our results show that exposure to these compounds prompted a large increase in total glutathione peroxidase activity. The highest glutathione peroxidase activity (more than fivefold) was found for lindane, the less toxic of the two compounds, with a milder effect on membrane permeabilization. Similar findings have been reported previously for cyclodiene insecticides (Bayoumi *et al*. 2001) and may explain the culture resistance to this compound. The induction of glutathione peroxidase is associated with overexpression of SOD, the enzyme controlling superoxide anion disruption and cell homeostasis. Lee and Ho (1994) reported that CHO cells exhibiting glutathione peroxidase activities 10-fold higher than human HFW fibroblasts are 10 times more resistant to xenobiotics. Warner *et al*. (1993) provided evidence of enhanced resistance to several xenobiotics in a human SOD-transfected CHO cell line. These findings agree with the experiments reported by Cutler (1985) for mammals, which correlated the enzymatic antioxidant defence system with the life span of several organisms.

Owing to high glutathione peroxidase activity and the significant induction of glutathione reductase by the insecticides at the lowest NRI_{50} fraction, it is not unreasonable to find glutathione levels within the normal range. Thus, at the lowest NRI_{50} fraction, total glutathione levels remained unchanged, whereas GSSG concentrations fell significantly. These results may be explained as the antioxidant mechanism response to weak damage induced by the insecticides. However, glutathione peroxidase and glutathione reductase activity declined at the highest concentrations in the series, concurrent with a significant increase in lipid peroxidation which in turn affected plasma membrane integrity and caused LDH leakage (figure 1). Similar findings have been reported for CHO-K1 cells exposed to cyclodiene (Bayoumi *et al*. 2001). In a study on V79 cells, Verma *et al*. (1992)

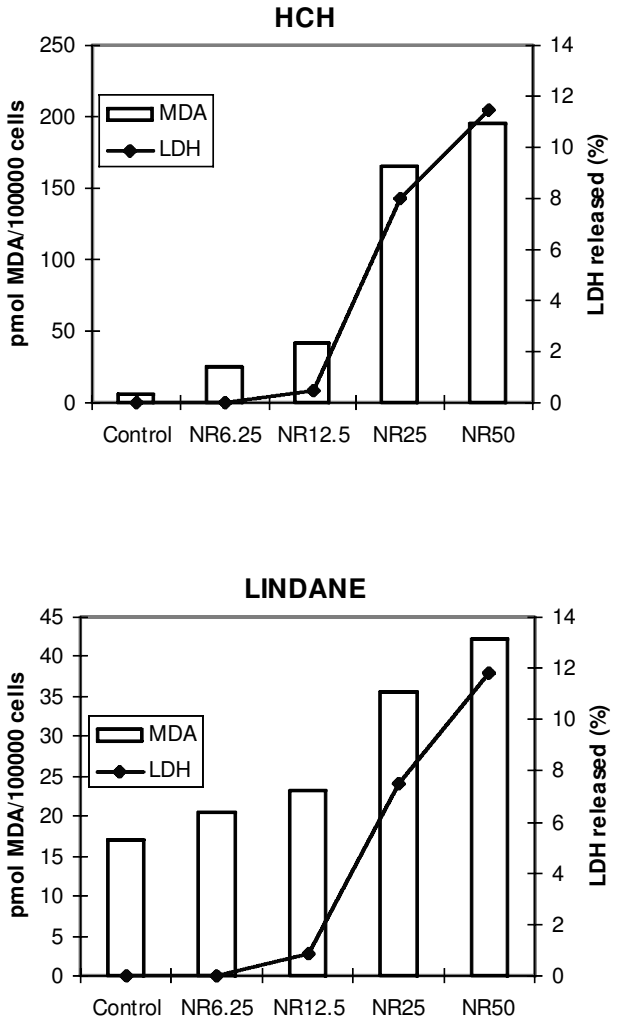


Figure 1. Comparison of plasma membrane integrity using the LDH-releasing assay with lipid peroxidation induced by HCH (A) and lindane (B) after a 4-h exposure. CHO-K1 cultures were grown up to 65% confluence (day 3) and then incubated with fresh medium containing different concentrations of HCH and lindane. Incubation media were removed to fresh plates analysed for LDH content using the CytoTox96® (Promega) assay or the lipid peroxidation using the thiobarbituric method. Each value is the average of three independent experiments. The ordinate scales are different in the two panels.

suggested that HCH isomers disrupted the plasma membrane, affecting cell viability. Bagchi *et al.* (1995) reported that exposing neuractive PC12 cells to various pesticides produced a significant increase in lipid peroxidation and membrane leakage at concentrations as low as 100 nM. These results were similar to findings for rat liver and brain tissue treated with these pesticides, thereby demonstrating that consistency between the pathological events observed *in vitro* and *in vivo*.

The results of the present study suggest that lindane and the HCH isomer mixture induced substantial increases in both total glutathione peroxidase and glutathione reductase activities in CHO-K1 cultures after exposure for 24 h at the

lowest doses ($NRI_{6.25}$) as a defence mechanism against oxidative stress. The release of LDH into the culture medium is indicative of dose–response membrane leakage, which may be the result of lipid peroxidation owing to the oxidative stress induced by these compounds at higher doses (NRI_{25} and higher).

Acknowledgements

This work was supported in part by grants from CICYT IFD 97-0224-CO3-03 and Diputación Provincial de León. A. E. B. held a postgraduate scholarship of Agencia Española de Cooperación Internacional (AECI).

References

Agrawal, D., Sultana, P. and Gupta, G. S., 1991, Oxidative damage and changes in the glutathione redox system in erythrocytes from rats treated with hexachlorocyclohexane. *Food Chemistry Toxicology*, **29**, 459–462.

Akerboom, T. P. M. and Sies, H., 1981, Assay of glutathione, glutathione disulfide and glutathione mixed disulfides in biological samples. *Methods in Enzymology*, **77**, 373–382.

Anderson, M. E., 1985, Determination of glutathione and glutathione disulfide in biological samples. *Methods in Enzymology*, **113**, 548–555.

Arisi, A. C., Simizu, K., Kogake, M., Bainy, A. C., Silva, M. A., Barros, S. B., Boveris, A., Videla, L. A. and Junqueira, V. B., 1994, Brain and liver lipid peroxidation levels following acute and short-term lindane administration in the rat. *Toxicology Letters*, **74**, 61–68.

ATSDR Agency for Toxic Substances and Disease Registry, 1992, *Toxicological Profile for α, β, δ and γ-hexachlorocyclohexane*. Draft (Atlanta: US Public Health Service, US Department of Health and Human Services).

Bagchi, D., Bagchi, M., Hassoun, E. A. and Stohs, S. J., 1995, *In vitro* and *in vivo* generation of reactive oxygen species, DNA damage and lactate dehydrogenase leakage by selected pesticides. *Toxicology*, **104**, 129–140.

Bagley, A. C., Krall, J. and Lynch, R. E., 1986, Superoxide mediates the toxicity of paraquat for Chinese hamster ovary cells. *Proceedings of the National Academy of Sciences, USA*, **83**, 3189–3193.

Bayoumi, A. E., García-Fernández, A. J., Ordóñez, C., Pérez-Pertejo, Y., Cubría, J. C., Reguera, R. M., Balaña-Fouce, R. and Ordóñez, D., 2001, Cyclodiene organochlorine insecticide-induced alterations in the sulfur-redox cycle in CHO-K1 cells. *Comparative Biochemistry and Physiology*, **130[C]**, 315–323.

Bayoumi, A. E., Pérez-Pertejo, Y, Ordóñez, C., Reguera, R. M., Cubría, J. C., Balaña-Fouce, R. and Ordóñez, D., 2000, Alterations on polyamine content and glutathione metabolism induced by different concentrations of paraquat in CHO-K1 cells. *Toxicology in Vitro*, **14**, 211–217.

Borenfreund, E. and Puemer, J. A., 1985, Toxicity determined *in vitro* by morphological alteration and neutral red absorption. *Toxicology Letters*, **24**, 119–124.

Bradford, M., 1976, A rapid sensitive method for quantification of microgram quantities of protein utiIizing the principle of protein–dye binding. *Analytical Biochemistry*, **72**, 248–254.

Chitra, K. C., Sujatha, R., Latchoumycandane, C. and Mathur, P. P., 2001, Effect of lindane on antioxidant enzymes in epididymis and epididymal sperm of adult rats. *Asian Journal of Andrology*, **3**, 205–208.

Cutler, R. G., 1985, Antioxidants and longevity of mammalian species. *Basic Life*, **35**, 15–73.

Habig, W. H., Pabst, M. J. and Jakoby, W. B., 1974, Glutathione *S*-transferase. The first enzymatic step in mercapturic acid formation. *Journal of Biological Chemistry* **249**, 7130–7139.

Hassoun, E. and Stohs, S. J., 1996, TCDD, endrin and lindane induced oxidative stress in fetal and placental tissues of C57BL/6J and DBA/2J mice. *Comparative Biochemistry and Physiology*, **115[C]**, 11–18.

Hassoun, E., Bagchi, M., Bagchi, D. and Stohs, S. J., 1993, Comparative studies on lipid peroxidation and DNA-single strand breaks induced by lindane, DDT, chlordane and endrin in rats. *Comparative Biochemistry and Physiology*, **104[C]**, 427–432.

Hiroski, O., Nobuko, O. and Kunio, Y., 1979, Assay for lipid peroxids in animal tissues by TBA reaction. *Analytical Biochemistry*, **95**, 351–358.

Iscan, M., Coban, T., Cok, I., Bulbul, D., Eke, B. C. and Burgaz, S., 2002, The organochlorine pesticide residues and antioxidant enzyme activities in human breast tumors: is there any association? *Breast Cancer Research and Treatment*, **72**, 173–182.

Junqueira, V. B., Bainy, A. C., Arisi, A. C., Azzalis, L. A., Simizu, K., Pimentel, R., Barros, S. B. and Videla, L. A., 1994, Acute lindane intoxication: a study on lindane tissue concentration and oxidative stress-related parameters in liver and erythrocytes. *Journal of Biochemical Toxicology*, **9**, 9–15.

Junqueira, V. B., Koch, O. R., Arisi, A. C., Fuzaro, A. P., Azzalis, L. A., Barros, S. B., Cravero, A., Farre, S. and Videla, L. A., 1997, Regression of morphological alterations and oxidative stress related parameters after acute lindane-induced hepatotoxicity in rats. *Toxicology*, **117**, 199–205.

Junqueira, V. B., Simizu, K., Van Halsema, L., Koch, O., Barros, S. B. and Videla, L. A., 1988, Lindane-induced oxidative stress. I. Time course of changes in hepatic microsomal parameters antioxidant enzymes, lipid-peroxidative morphological characteristics. *Xenobiotica*, **18**, 1297–1304.

Klein, R. G., Schmezer, P., Amelung, F., Schroeder, H. G., Woeste, W. and Wolf, J., 2001, Carcinogenicity assays of wood dust and wood additives in rats exposed by long-term inhalation. *International Archives of Occupational and Environmental Health*, **74**, 109–118.

Koner, B. C., Banerjee, B. D. and Ray, A., 1998, Organochlorine pesticide-induced oxidative stress and immune suppression in rats. *Indian Journal of Experimental Biology*, **36**, 395–398.

Krall, J., Speranza, M. J. and Lynch, R. E., 1991, Paraquat resistant HeLa cells increased content of glutathione peroxidase. *Archives of Biochemistry and Biophysics*, **286**, 311–315.

Lee, T. C. and Ho, I. C., 1994, Differential cytotoxic effects of arsenic on human and animal cells. *Environmental and Health Perspectives*, **102**, 101–105.

Loffler, G. and van Bavel, B., 2000, Potential pathways and exposure to explain the human body burden of organochlorine compounds: a multivariate statistical analysis of human monitoring in Wurzburg, Germany. *Chemosphere*, **40**, 1075–1082.

Meister, A. and Anderson, M. E., 1983, Glutathione. *Annual Reviews of Biochemistry*, **52**, 711–760.

North, S. P. and Chew, G., 2000, Acute lindane poisoning in three children. *Journal of Emergencies Medical*, **18**, 51–53.

Palmeira, C. M., Moreno, A. J. and Madeira, V. M., 1994, Metabolic alterations in hepatocytes promoted by the herbicides paraquat, dinoseb and 2,4-D. *Archives of Toxicology*, **68**, 24–31.

Sahoo, A., Samanta, L. and Chainy, G. B., 2000, Mediation of oxidative stress in HCH-induced neurotoxicity in rat. *Archives of Environmental Contamination and Toxicology*, **39**, 7–12.

Samanta, L. and Chainy, G. B. N., 1995, Hexachlorocyclohexane-induced changes in lipid peroxidation, superoxide dismutase and catalase activities and glutathione content in chick liver. *Indian Journal of Experimental Biology*, **33**, 131–333.

Samanta, L. and Chainy, G. B. N., 1997, Comparison of hexachlorocyclohexane-induced oxidative stress in the testis of immature and adult rats. *Comparative Biochemistry Physiology*, **118[C]**, 319–327

Samanta, L., Sahoo, A. and Chainy, G. B. N., 1999, Age-related changes in rat testicular oxidative stress parameters by hexachlorocyclohexane. *Archives of Toxicology*, **73**, 96–107.

Smith, L. L., Rose, M. S. and Wyatt, I., 1979, *The Pathology and Biochemistry of Paraquat: Oxygen Free Radicals and Tissue Damage* (London: CIBA Foundation), pp. 321–341.

Sujatha, R., Chitra, K. C., Latchoumycandane, C. and Mathur, P. P., 2001, Effect of lindane on testicular antioxidant system and steridogenic enzymes in adult rats. *Asian Journal of Andrology*, **3**, 135–138.

USEPA US Environmental Protection Agency, 1994, Technical Background Document to Support Rulemaking Pursuant to the Clean Air Act-Section 112(g). Ranking of Pollutants with Respect to Hazard to Human Health. EPA450/3-92-010 (Research Triangle Park: Emissions Standard Division, Office of Air Quality Planning and Standards).

Verma, S. P., Rastogi, A. and Lin, P. S., 1992, Hexachlorocyclohexane pesticides reduce survival and alter plasma membrane structure of Chinese hamster V79 cells. *Archives of Biochemistry and Biophysics*, **298**, 587–593.

Videla, L. A., Barros, S. B. and Junqueira, V. B., 1990, Lindane-induced liver oxidative stress. *Free Radicals in Biology and Medicine*, **9**, 169–179.

Warner, B., Papes, R., Heile, M., Spitz, D. and Wispe, J., 1993, Expression of human Mn SOD in Chinese hamster ovary cells confers protection from oxidant injury. *American Journal of Physiology*, **264**, L598–L605

Wendel, A., 1981, Glutathione peroxidase. *Methods in Enzymology*, **77**, 325–333.

Zaman, K. and Pardini, R. S. 1996, An overview of the relationship between oxidative stress and mercury and arsenic. *Toxic Substance Mechanisms*, **15**, 151–181.

XENOBIOTICA, 2002, VOL. 32, NO. 11, 1017–1031

Taylor & Francis
healthsciences

In vitro biotransformation of 2,6,9-trisubstituted purine-derived cyclin-dependent kinase inhibitor bohemine by mouse liver microsomes

M. RYPKA†, J. VESELÝ†*, Z. CHMELA†, D. RIEGROVÁ†, K. ČERVENKOVÁ†, L. HAVLÍČEK‡, K. LEMR§, J. HANUŠ¶, B. ČERNÝ¶, J. LUKEŠ|| and K. MICHALÍKOVÁ†

† Department of Pathological Physiology, Medical Faculty, Palacký University, Olomouc, Czech Republic
‡ Institute of Nuclear Medicine, Medical Faculty I, Charles University, Prague, Czech Republic
§ Department of Analytical Chemistry, Faculty of Natural Science, Palacký University, Olomouc, Czech Republic
¶ Institute of Experimental Botany, Academy of Science, Prague, Czech Republic
|| Department of Nuclear Medicine, University Hospital in Olomouc, Czech Republic

Received 17 April 2002

1. Biotransformation pathways of the cyclin-dependent kinase inhibitor 6-benzylamino-2-(3-hydroxypropylamino)-9-isopropylpurine (bohemine) by mouse liver microsomes *in vitro* were investigated.

2. Metabolite profiles of [8-^{3}H]-labelled bohemine were established by TLC/^{3}H-autoradiography and enzymatic and MS analyses were used to elucidate the chemical structures of the metabolites. The structures of the main primary metabolites were confirmed by synthesis of authentic compounds.

3. A schema of the primary NADPH-dependent pathways has been proposed involving N^2- and N9-dealkylation, N^6-debenzylation, aromatic hydroxylation, and C2 side chain oxidation of bohemine. Three of the primary metabolites detected, 6-(benzylamino)-2-(3-hydroxypropylamino)purine (M4), 6-amino-2-(3-hydroxypropylamino)-9-isopropylpurine (M5) and 6-(4-hydroxybenzylamino)-2-(3-hydroxypropylamino)-9-isopropylpurine (M6), all retaining their parent primary hydroxyl group, were subsequently shown to be converted, by a liver cytosolic NAD^+-dependent system, into their corresponding carboxylic acids. M6 was subject to microsomal glycosidations requiring UDP-sugar donors. NADPH-dependent conversion of M6 into M5 by microsomes was also demonstrated.

4. Cytochrome P450 (CYP) enzymes-selective inhibitors were used to identify CYPs involved in bohemine biotransformation. The findings suggested that *CYP2a* and *CYP3a* substantially contributed to the NADPH-dependent bohemine transformation *in vitro*.

5. The findings will facilitate experiments designed to dissect enzymatic systems catalysing clearance of C2,C6,N9-trisubstituted purine compounds from mammalian tissues.

Introduction

Recently, several types of selective synthetic inhibitors of cyclin-dependent kinases (CDKs) have been implicated as novel and invaluable reagents for molecular biological, biochemical and morphological studies of the cell cycle (reviewed in Meijer *et al*. 1999, Sielecki *et al*. 2000). The antiproliferative activity of the inhibitors has been well documented both *in vitro* and *in vivo*, a fact that has

* Author for correspondence; e-mail: vesely@tunw.upol.cz

Xenobiotica ISSN 0049–8254 print/ISSN 1366–5928 online © 2002 Taylor & Francis Ltd
http://www.tandf.co.uk/journals
DOI: 10.1080/00498250210012600

encouraged a number of authors to consider the inhibitors as potentially new anticancer drugs (reviewed in Buolamwini 2000, Fischer and Lane 2000). Unlike substances that kill transformed cells, CDK inhibitors seem able to re-establish appropriate mechanisms governing cells' fate. The potential use of the inhibitors is also being investigated in various clinical domains such as nephrology, dermatology and vascular diseases (reviewed in Gray *et al*. 1998, 1999). The survival-promoting, anti-apoptotic activity of the inhibitors on nerve cells seems noteworthy in respect of Alzheimer disease (reviewed in Meijer 2000). Furthermore, these inhibitors have been reported to alter the rhythm of a molluscan circadian pacemaker and inhibit both virus and unicellular parasite cycling (reviewed in Meijer *et al*. 2000, Rosania and Chang 2000).

The first CDK-selective inhibitor derived from purines to be discovered was the 2,6,9-trisubstituted purine olomoucine (Veselý *et al*. 1994). Since then, thousands of new purine analogues have been synthesized, using a solid-phase approach and/or computer-aided drug design combined with a structure-based library strategy. The new compounds have been screened for their activity as well as for different aspects of their cellular effects (Gray *et al*. 1998, 1999, Chang *et al*. 1999, Legraverend *et al*. 1999, Meijer *et al*. 1999, Sausville *et al*. 1999). To date, among the CDK inhibitors, the purines are best understood in terms of their structure–activity relationships (Fischer and Lane 2000, García-Echeverría *et al*. 2000). Nonetheless, the metabolic profile of these inhibitors remains poorly understood.

Chmela *et al*. (2001) studied the metabolism of an olomoucine-type CDK-selective inhibitor, 6-benzylamino-2-(3-hydroxypropylamino)-9-isopropylpurine, designated as bohemine (Sielecki *et al*. 2000), in mouse *in vivo*. Bohemine was metabolized rapidly and was almost exclusively excreted in the form of metabolites. The liver and kidney were the main organs responsible for fast bohemine clearance. The principal Phase I bohemine reaction was bohemine oxidation to a carboxylic acid, which could be catalysed by a cytosolic, 4-methylpyrazole-sensitive, alcohol dehydrogenase. The Phase II-predominant biotransformation route was UDP-glucoside-dependent bohemine β-glucosidation. The third metabolite identified by Chmela *et al*. was bohemine glucuronide.

Generally, among Phase I drug-metabolizing enzymes, microsomal cytochromes P450 (CYPs) are known to exert the most prominent role (reviewed in Rendic 2002), are widely distributed in the tissues of all mammalian species and are most abundant in mammalian liver (Venkatakrishnan *et al*. 2001). It was a challenge to examine the participation of mouse liver microsomes in bohemine metabolism since, surprisingly, the aforementioned *in vivo* study (Chmela *et al*. 2001) failed to reveal any specific individual products of their activity. Some preliminary results of the current study were published as conference abstracts (Chmela *et al*. 1998, Belejová *et al*. 1999, Michalíková *et al*. 1999, Červenková *et al*. 2000).

Materials and methods

Chemicals

2,6-Dichloropurine, 2-amino-6-chloropurine, β-NADPH (N1630), β-glucosidase, EC 3.2.1.21 (G4511), α-glucosidase, EC 3.2.1.20, recombinant form, from *Saccharomyces cerevisiae* (G0660), UDP-glucuronic acid, UDP-glucose, coumarin, 8-methoxypsoralen, troleandomycin and ketoconazole

were purchased from Sigma-Aldrich (St Louis, MO, USA); bovine serum albumin (fraction V) was from Bioveta (Ivanovice n.H., Czech Republic); and Silica gel 60 F_{254} TLC sheets and Silica gel for column chromatography (Kieselgel 60, particle size 40–63 μm) were purchased from Merck (Darmstadt, Germany). All other chemicals and reagents used were of analytical or HPLC grade.

Chemical syntheses

Solvents were evaporated *in vacuo* at $<80\,^{\circ}C$, unless otherwise specified. Melting points (mp) were determined on a Kofler block and were uncorrected.

Bohemine was synthesized as described by Havlíček *et al.* (1997), and its carboxylic derivative 6-benzylamino-2-(2-carboxyethylamino)-9-isopropylpurine and 6-benzylamino-2-(3-hydroxypropylamino)-9-isopropyl [8-^{3}H]purine (=[^{3}H]bohemine) were prepared as described by Chmela *et al.* (2001). The specific activity of the [^{3}H]bohemine was 587 TBq mol^{-1} and its radiochemical purity was at least 98% when checked by TLC on Silikagel 60 F_{254} sheets (Merck) with chloroform–methanol (95:5).

Bohemine metabolite reference compounds were synthesized and labelled by ^{3}H at position 8 of their purine rings following the reaction strategy described previously (Havlíček *et al.* 1997, Otyepka *et al.* 2000, Chmela *et al.* 2001). All synthesized compounds gave a satisfactory element analysis (±0.4%) and their chemical structures were verified by MS and NMR measurements.

2,6-Dichloro-9-isopropylpurine

2,6-Dichloropurine (5.1 g, 27 mmol), potassium carbonate (6.8 g, 49 mmol) and isopropyliodide (5 ml, 50 mmol) were vigorously stirred in DMSO (50 ml) overnight. After evaporation of the volatile components, the product (i.e. the principal spot on TLC) was isolated by means of column chromatography (20% ethylacetate in heptane); yield 65%; mp 150–151 °C. The compound was not labelled by ^{3}H.

^{1}H-NMR (400 MHz, CD_3OD): 1.672 (6H, d, $\mathcal{J}=6.8$, $(CH_3)_2$), 4.932 (1H, m, $CH(CH_3)_2$), 8.673 (1H, s, HC^8). ^{13}C-NMR (100 MHz, CD_3OD): 22.74 Qqd ($\mathcal{J}=128.0$, $\mathcal{J}=4.6$, $\mathcal{J}=4.6$, CH_3), 50.79 Dsep ($\mathcal{J}=143.4$, $\mathcal{J}=4.4$, CH), 132.41 d ($\mathcal{J}=11.6$, C-5), 147.67 Dd ($\mathcal{J}=214.0$, $\mathcal{J}=4.4$, C-8), 152 s, 153.91 s, 154.75 bm.

6-Benzylamino-2-(3-hydroxypropylamino)purine (an M4 spot metabolite reference)

6-Benzylamino-2-chloropurine (0.102 g, 0.39 mmol) prepared according to Hocart *et al.* (1991) and 3-hydroxypropylamine (3 ml) were heated to 160 °C for 2 h. Excess amine was evaporated and the product was crystallized from 1-butanol; yield 67%, mp 201–202 °C. The specific activity of the ^{3}H-labelled M4 spot metabolite reference was 561 TBq mol^{-1}, a its radiochemical purity was at least 98% when checked by TLC on Silikagel 60 F_{254} sheets (Merck) with chloroform–methanol–conc. aqueous ammonia (90:10:0.2) and by HPLC on RP-18 with methanol–water (9:1).

MS (VG7070E): 298 ($M^{+\cdot}$, 55%), 267 (17), 253 (26), 175 (17), 129 (18), 111 (15), 106 (18), 97 (33), 91 (77), 81 (42), 71 (48), 60 (43), 57 (95), 55 (88), 43 (100), 41 (84). ESI-MS (LCQ Finnigan MAT): m/z $[M+1]^+=299$; ESI-MS^2: m/z (%)=91 (47.3), 135 (1.9), 136 (4.6), 150 (5.7), 163 (32.9), 164 (45.2), 165 (23), 175 (3.1), 177 (66.4), 178 (26.5), 189 (51.1), 191 (26.7), 199 (1.3), 200 (1.9), 203 (6.3), 207 (6.3), 208 (55.1), 221 (6.3), 225 (7.6), 239 (1.3), 240 (21.9), 241 (24.3), 253 (96.3), 257 (1.1), 264 (1.0), 281 (100). ^{1}H-NMR (400 MHz, $CDCl_3$): 1.791 (2H, pen, $\mathcal{J}=6.4$, $CH_2CH_2CH_2$), 3.470 (2H, t, $\mathcal{J}=6.5$, CH_2O or CH_2NH), 3.641 (2H, t, $\mathcal{J}=6.3$, CH_2O or CH_2NH), 4.768 (2H, s, CH_2Ph), 7.22–7.42 (5H, m, Ph), 7.684 (1H, s, HC^8).

6-Amino-2-(3-hydroxypropylamino)-9-isopropylpurine (an M5 spot metabolite reference)

2,6-Dichloro-9-isopropylpurine (199 mg, 0.86 mmol) was heated in 15 ml conc. NH_4OH to 85 °C for 9 h. After cooling, the crude product was filtered and rinsed with water. The product (mp 257–259 °C) and 3-hydroxypropylamine (3 ml) were heated in a sealed ampoule to 165–170 °C for 5 h. Excess amine was evaporated, and the residue was crystallized from water; yield 30%, mp 143–144C. Recrystallization was achieved in methanol–diethylether, mp 143–145 °C. The specific activity of the ^{3}H-labelled M5 spot metabolite reference was 545 TBq mol^{-1}, and its radiochemical purity was at least 98% when checked by TLC on Silikagel 60 F_{254} sheets (Merck) with chloroform–methanol–conc. aqueous ammonia (90:10:0.2) and by HPLC on RP-18 with methanol–water (9:1).

MS (VG7070E): 250 ($M^{+\cdot}$, 83%, $C_{11}H_{18}N_6O$; 0.0), 219 (60), 206 (73), 205 (98), 192 (25), 177 (49), 163 (100), 150 (50), 134 (65). ESI-MS (LCQ Finnigan MAT): m/z $[M+1]^+=251$; ESI-MS^2: m/z (%)=151 (1.3), 163 (7.3), 191 (17.4), 205 (8.8), 209 (100), 233 (9.7). ^{1}H-NMR (400 MHz, $CDCl_3$): COSY [1.546 (6H, d, $\mathcal{J}=6.8$, $(CH_3)_2CH$), 4.63 (1H, hept, $\mathcal{J}=6.8$, $(CH_3)_2CH$)], COSY [1.73 (2H, m, $CH_2CH_2CH_2$), 3.59–3.67 (4H, m, $CH_2CH_2CH_2$)], COSY [4.97 (1H, bt, $\mathcal{J}=6.7$, NH), 3.59–3.67], 5.40 (2H, bs, NH_2), 7.57 (1H, s, HC^8).

6-(4-Hydroxybenzylamino)-2-(3-hydroxypropylamino)-9-isopropylpurine (an M6 spot metabolite reference)

2,6-Dichloro-9-isopropylpurine (508 mg, 2.2 mmol), 4-hydroxybenzylamine (406 mg, 3.3 mmol) prepared according to Jones and Pyman (1925), and triethylamine (1 ml) were heated and stirred in 6 ml 1-butanol (115 °C, 2 h). After evaporation of the volatile components, the crude product was isolated by stepwise gradient column chromatography (0, 1, 2, 3, 4% methanol in $CHCl_3$) and crystallized from benzene; yield 95%, mp 100–105 °C. The product (115 mg) and 3-amino-1-propanol (3 ml) were heated in a sealed ampoule to 160 °C for 2 h. Excess amine was evaporated. The final product was isolated by stepwise gradient column chromatography (1, 2, 3, 4% methanol in $CHCl_3$) and crystallized from ethylacetate; yield 50% when calculated on 2,6-dichloro-9-isopropylpurine, mp 169–170 °C. The specific activity of the ^{3}H-labelled M6 spot metabolite reference was 560 TBq mol^{-1}, and its radiochemical purity was at least 98% when checked by TLC on Silikagel 60 F_{254} sheets (Merck) with chloroform–methanol (9:1) and by TLC on aluminium oxide 60 F_{254} neutral sheets (Merck) with toluene–methanol (9:1).

MS (Jeol JMS-D100): 356 ($M^{+\cdot}$, 43%, $C_{18}H_{24}N_6O_2$, +0.3), 250 (46%, $C_{11}H_{18}N_6O$, +1.5), 219 (62%, $C_{10}H_{15}N_6O$, +0.4), 164 (45), 163 (100), 150 (55), 134 (73), 122 (91), 108 (48), 107 (65). ESI-MS (LCQ Finnigan MAT): m/z $[M+1]^+ = 357$; ESI-MS^2: m/z (%) = 209 (5.8), 251 (100), 263 (4.4). ^{1}H-NMR (200 MHz, $CDCl_3$): 1.509 (6H, d, $J = 6.8$, $(CH_3)_2CH$), 1.70 (2H, m, $CH_2CH_2CH_2$), 3.60 (4H, t, $CH_2CH_2CH_2$), 4.60 (3H, m, $CH_2Ph + CH(CH_3)$), 6.71 (2H, d, 7.5, Ph), 7.10 (2H, d, 7.5, Ph), 7.512 (1H, s, HC^8).

6-(3-Hydroxybenzylamino)-2-(3-hydroxypropylamino)-9-isopropylpurine

2,6-Dichloro-9-isopropylpurine (487 mg, 2.11 mmol), 3-hydroxybenzylamine (431 mg, 3.5 mmol) prepared according to Epstein *et al.* (1964), and triethylamine (1 ml) were heated and stirred in 10 ml 1-butanol (115 °C, 2 h). After evaporation of volatile components the crude product was isolated by stepwise gradient column chromatography (0, 1, 2, 3, 4% methanol in $CHCl_3$) and crystallized from $CHCl_3$; yield 95%, mp 217–218 °C. The product (640 mg) and 3-amino-1-propanol (3 ml) were heated in a sealed ampoule to 160 °C for 4 h. Excess amine was evaporated. The final product was isolated by stepwise gradient column chromatography (1, 2, 3, 4% methanol in $CHCl_3$) and crystallized from ethylacetate-diethylether; yield 17% when calculated on 2,6-dichloro-9-isopropylpurine, mp 133–135 °C. The compound was not labelled by ^{3}H.

MS (VG7070E): 356 ($M^{+\cdot}$, 100%, $C_{18}H_{24}N_6O_2$; −0,1), 325 (43), 312 (42), 311 (43), 298 (24), 191 (17), 122 (24), 107 (62). ^{1}H-NMR (400 MHz, $CDCl_3$): 1.562 (6H, d, $J = 6.8$, $+(CH_3)_2CH$), 1.747 (2H, m, $CH_2CH_2CH_2$), 3.65 (4H, m, $CH_2CH_2CH_2$), 4.59 (2H, bd, CH_2Ph), 4.66 (1H, sept, $J = 6.8$, $CH(CH_3)_2$), 5.034 (1H, t, $J = 6.9$, exc. H), 6.4 (1H, bs, exc. H), 6.73–6.82 (3H, m, Ph), 7.06–7.12 (1H, m, Ph), 7.265 (1H, s, HC^8), 7.605 (1H, s, phenolic H). COSY [1.562 d and 4.66 sept], COSY [1.747 m and 3.65 m], COSY [4.59 bd and 6.4 bs], COSY [3.65 m and 5.034 t], COSY [7.09 m and 6.77 m].

6-(2-Hydroxybenzylamino)-2-(3-hydroxypropylamino)-9-isopropylpurine

2,6-Dichloro-9-isopropylpurine (231 mg, 1 mmol), 2-hydroxybenzylamine (185 mg, 1.5 mmol) prepared according to Raiford and Clark (1923) [17] and triethylamine (0.41 ml) were heated and stirred in 10 ml 1-butanol (115 °C, 3 h). After evaporation of the volatile components, the crude product was isolated by column chromatography (4% MeOH in $CHCl_3$) and crystallized from diethylether; yield 95%, mp 170–171 °C. This product (226 mg) and 3-amino-1-propanol (2 ml) were heated in a sealed ampoule to 160 °C for 3 h. Excess amine was evaporated. The residue was purified by stepwise gradient column chromatography (0, 1, 1.5% methanol in $CHCl_3$) and a final syrupy product (125 mg) was obtained; yield 35% when calculated on 2,6-dichloro-9-isopropylpurine. The compound was not labelled by ^{3}H.

MS (VG7070E): 356 ($M^{+\cdot}$, 57%), 325 (6), 312 (8), 298 (7), 250 (69), 219 (65), 206 (71), 205 (100), 177 (37), 163 (72), 150 (37), 134 (50), 108 (38), 106 (28), 78 (53). ^{1}H-NMR (200 MHz, $CDCl_3$): 1.52 (6H, d, $J = 6.6$, $(CH_3)_2CH$), 1.78 (2H, m, $CH_2CH_2CH_2$), 3.66 (4H, m, $CH_2CH_2CH_2$), 4.54–4.60 (2H, bs, CH_2Ph), 4.57 (1H, hept, $J = 6.6$, $(CH_3)CH$), 5.11 (1H, bt, exc. H), 6.53 (1H, bs, exc. H), 6.82–6.93 (2H, m, Ph), 7.17–7.27 (2H, m, Ph), 7.52 (1H, s, HC^8).

2-Amino-6-benzylamino-9-isopropylpurine (an M8 spot metabolite reference)

2-Amino-6-chloropurine (170 mg, 1.4 mmol) and benzylamine (3.8 ml, 35 mmol) were heated with stirring in 3 ml *n*-butanol to 110 °C for 3 h. After cooling, the crude product, 2-amino-6-benzylaminopurine, was filtered. This product (170 mg, yield 51% when calculated on 2-amino-6-chloropurine) was vigorously stirred with powdered potassium carbonate (0.5 g, 3.6 mmol), and isopropyliodide (0.5 ml, 5 mmol) in 5 ml DMSO overnight. After evaporation of the volatile components the final product was purified by column chromatography with 1% methanol in $CHCl_3$ and crystallized from methanol–

diethylether; yield 34% when calculated on 2-amino-6-chloropurine, mp 191–193 °C. The compound was not labelled by ^{3}H.

MS (VG7070E): 282 ($M^{+\cdot}$, 100%, $C_{15}H_{18}N_6$, −0.2), 239 (52), 177 (42), 135 (62%, $C_5H_5N_5$, 0.0), 106 (82), 91 (80). ESI-MS (LCQ Finnigan MAT): m/z $[M+1]^+ = 283$; ESI-MS^2: m/z (%) = 91 (23.5), 150 (2.2), 163 (1.2), 192 (13.7), 205 (2.3), 241 (100). ^{1}H-NMR (400 MHz, $CDCl_3$): 1.54 (6H, d, $\mathcal{J} = 6.8$, $(CH_3)_2CH$), 4.68 (1H, hept, $\mathcal{J} = 6.8$, $(CH_3)_2CH$), 4.68 (2H, bs, NH_2), 4.81 (2H, bd, CH_2), 5.82 (1H, bs, NH), 7.26–7.40 (5H, m, Ph), 7.535 (1H, s, HC^8).

Incubation of bohemine and its metabolites with liver microsomal and cytosolic subcellular fractions

All experiments using animals were authorized by the Institutional Ethical Committee and carried out according to institutional guidelines in compliance with Czech national laws and in agreement with the Declaration of Helsinki. Monitored male NMRI outbred mice of mixed genetic background and of approximately 20–25 g body weight between 5 and 7 weeks of age (VUFB, Konarovice, Czech Republic) were used to obtain subcellular fractions.

The fractions were prepared in 0.25 M sucrose solution by differential centrifugation and their protein content was determined as described by Chmela *et al.* (2001). The microsomes were transferred by repeated centrifugation (100 000*g*, 60 min) into phosphate buffer (0.1 M, pH 7.4) shortly before use. Two sets of microsomal incubations were run in the phosphate buffer: one in the presence of NADPH, the other containing glycosyl donors. The incubations conducted in the presence of glycosyl donors (0.2 ml, final volume) employed 0.4 mg microsomal protein, and either UDP-glucuronic acid (5 mM) or UDP-glucose (5 mM). They were further supplemented with either about 10 kBq ^{3}H-labelled metabolite spot extract or with a newly synthesized, ^{3}H-labelled authentic reference compound (296 kBq; the concentration was adjusted to 5 μm by an addition of the appropriate unlabelled compound) as substrates. The NADPH mixtures (0.2 ml, final volume) employed 0.10 mg microsomal protein, 5 mM NADPH, 5 mM $MgCl_2$ and were supplemented with either 296 kBq [^{3}H]bohemine (3 μM), or about 10 kBq [^{3}H]-labelled metabolite spot extract or with 296 kBq (5 μM) ^{3}H-labelled authentic reference compound. Incubations with mouse liver cytosolic fraction (0.2 mg protein) in the presence of NAD^+ coenzyme (5 mM) were performed as described by Chmela *et al.* (2001) in the above phosphate buffer supplemented with about 10 kBq [^{3}H]-labelled metabolite spot extract, or with 296 kBq (5 μM) ^{3}H-labelled authentic reference compound. Finally, to identify the CYPs involved in the bohemine metabolism, CYP-selective inhibitors were included in the NADPH-containing assays at concentrations indicated in the Results. Each of the mechanism-based inhibitors ketoconazole, 8-methoxypsoralen or troleandomycin were pre-incubated with microsomes in the presence of NADPH at 37 °C for 15 min (Newton *et al.* 1995, Chauret *et al.* 1997, Court *et al.* 1997) before the reaction which was initiated by the addition of radioactive substrate (20 μl). All reactions were allowed to proceed at 37 °C under continuous mixing in open tubes. For the inhibition studies, aliquots removed within an incubation interval between 5 and 20 min were selected after our preliminary tests with mouse liver microsomes revealed a linear reaction during this period.

Extraction of metabolites and TLC analysis

For [^{3}H]-metabolite analysis, incubations were stopped, homogenized and extracted with a ninefold volume of ethanol. The ethanolic extracts (supernatants, 4000*g*, 5 min) were analysed by TLC with subsequent ^{3}H-autoradiography and densitometry. In particular, TLC was routinely run in acidic mobile phase chloroform–methanol–acetic acid 90:10:1 (by vol.; phase A); this phase was used to resolve the most polar spots localized in the vicinity of the origin. Acetic acid was replaced by 1 vol. conc. aqueous ammonia (phase B) to diagnose (by changing TLC mobility of the spots) the acidic/basic character of substances. The spots were visualized by autoradiography, scraped off and extracted to identify metabolite chemical structures that were analysed by means of chemical modification with diazomethane, enzymatic analyses and mass spectroscopy (Chmela *et al.* 2001).

Enzymatic analyses

Incubates of metabolites extracted from TLC spots containing about 10 kBq radioactivity were supplemented either with 0.67 Sigma units β-glucuronidase or 2.5 Sigma units β-glucosidase in a citrate buffer (0.05 M, pH 5.0). The α-glucosidase incubation mixture contained the recombinant enzyme (2.5 Sigma units) in the above phosphate buffer. The mixtures were then incubated in open tubes under continuous gentle mixing at 37 °C. Aliquots were removed at 10, 30 and 120 min. The volumes of incubation mixtures were increased 10–20 times for preparatory purposes.

Spectroscopic methods

Electron ionization mass spectra (MS) of newly synthesized authentic compounds (see above) were recorded on a VG-7070E instrument (EI, ionizing energy 70 eV, 50 or 100 μA, 200 °C, direct inlet; purchased from Vacuum Generators, Manchester, UK) or a Jeol JMS-D100 (EI, 80 eV, 300 μA, 200 °C,

direct inlet; purchased from Japan Electron Optics Laboratory, Tokyo, Japan) with a peak-matching method using perfluorokerosene as a standard [m/z (%, elem. comp., deviation in ppm)]. A soft ionization MS of both the newly synthesized references and metabolites extracted from TLC spots (see the Results) was carried out using an ion-trap mass spectrometer LCQ Finnigan MAT (San Jose, CA, USA). Samples were either standards diluted with 1% acetic acid in ethanol, or ethanolic extracts of TLC spots acidified with acetic acid to the 1% concentration. Samples were introduced with a flow-rate 2 µl min^{-1} to the electrospray interface with source voltage 5.6 kV, sheath gas flow 28 (arbitrary units) and a capillary temperature of 200 °C. The selected ions were fragmented in an ion trap (m/z isolation width 6.0, collision energy 25%). Mass spectra were scanned in full-scan mode as well as in a zoom scan and MS^n. ^{1}H- and ^{13}C-NMR spectra of newly synthesized reference compounds were measured either on a Varian VXR-400 instrument at 400 MHz (^{1}H) or 100 MHz (^{13}C), or on a Varian XL-200 (Palo Alto, CA, USA) at 200 MHz. J were given in Hz.

Results

Metabolite profiles in microsomal incubates supplemented with NADPH

Chmela *et al.* (2001) identified three bohemine metabolites that were designated as M1 (bohemine β-glucuronide), M2 (bohemine β-glucoside) and M3 (bohemine carboxylic acid). The metabolites newly detected in this study were marked according to the same scheme, i.e. M4–M8 as described below. From figure 1 it can be seen that most [^{3}H]bohemine (>85%) was metabolized into its metabolites during a 120-min incubation of the parent compound in mouse liver microsomes supplemented with NADPH. The incubation resulted in a complex metabolite profile. The microsomes gave a spot M3 identical to that described by Chmela *et al.* (2001), which was confirmed as containing a carboxylic acid, 6-benzylamino-2-(2-carboxyethylamino)-9-isopropylpurine. This aside, five addi-

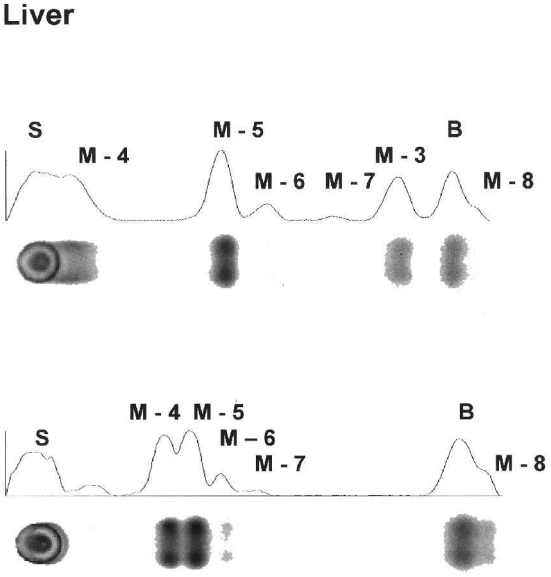


Figure 1. ^{3}H-autoradiographic and densitometric analysis of [^{3}H]bohemine incubation with mouse liver microsomes in the presence of NADPH. The incubation interval was 120 min and incubates were resolved by TLC in chloroform–methanol–acetic acid 90:10:1 (phase A, upper) or in chloroform–methanol–conc. aqueous ammonia 90:10:1 (phase B, bottom). B, bohemine; S, start (origin).

tional distinct spots M4–M8 were detected. M4 and M5 represented the major spots, whereas M6–M8 were minor components (figure 1).

Elucidation of new metabolite structures

The chemical structures of the new metabolites formed in the NADPH-microsomal system (figure 1) were elucidated as follows. A metabolite in a spot M4 extract displayed $m/z = 299$ $[M+1]^+$ and was tentatively identified by MS^n scan as 6-benzylamino-2-(3-hydroxypropylamino)purine, a product of bohemine deisopropylation (table 1). A metabolite detected in an M5 extract exhibited $m/z = 251$ $[M+1]^+$ and was similarly identified as 6-amino-2-(3-hydroxypropylamino)-9-isopropylpurine, a product of bohemine debenzylation (table 1). The chemical structures of both products were confirmed by comparing their TLC characteristics and MS spectra with those of authentic reference compounds (see the Materials and methods) (table 1).

MS^n analysis also suggested that a microsomal metabolite extracted from spot M6 and exhibiting $m/z = 357$ $[M+1]^+$ could be a product of hydroxylation directed to the benzyl ring attached to the N^6-atom of bohemine. This was supported by a reaction with diazomethane (table 1). Subsequently, all three potential positional isomers, i.e. 6-(4-hydroxybenzylamino)-, 6-(3-hydroxybenzylamino)- and 6-(2-hydroxybenzylamino)-2-(3-hydroxypropylamino)-9-isopropylpurine were synthesized. A comparison of their TLC and MS characteristics with

Table 1. Primary products of NADPH-dependent transformation of bohemine: R_F, methylation and spectroscopic data.

Compound	Analytical method	Data
Bohemine[a]	TLC	R_f: 0.63 (phase A), 0.75 (phase B)
M3[a]	TLC	R_f: 0.55 (phase A), 0.01 (phase B)
M4	TLC ESI-MS ESI-MS^2	R_f: 0.07–0.17 (phase A), 0.23 (phase B) m/z $[M+1]^+$: 299 m/z (%): 91 (34), 163 (25), 164 (34), 165 (18), 177 (54), 178 (20), 189 (45), 191 (25), 207 (6), 208 (47), 240 (11), 241 (20), 253 (79), 281 (100)
M5	TLC ESI-MS ESI-MS^2	R_f: 0.26 (phase A), 0.28 (phase B) m/z $[M+1]^+$: 251 m/z (%): 191 (14), 205 (9), 209 (100), 233 (12)
M6	TLC ESI-MS ESI-MS^2 TLC of an M6 methylderivative	R_f: 0.31 (phase A), 0.33 (phase B) m/z $[M+1]^+$: 357 m/z (%): 209 (7), 251 (100) R_f: 0.62 (phase A), 0.75 (phase B)
M7	TLC ESI-MS ESI-MS^2	R_f: 0.41 (phase A), 0.38 (phase B) m/z $[M+1]^+$: 357 m/z (%): 191 (13), 192 (22), 205 (20), 206 (79),235 (63), 247 (8), 315 (100), 339 (41)
M8	TLC ESI-MS ESI-MS^2	R_f: 0.68 (phase A), 0.78 (phase B) m/z $[M+1]^+$: 283 m/z (%): 91 (14), 192 (17), 241 (100)

[a] For the spectroscopic data of bohemine and those of M1 to M3, see Chmela *et al.* (2001). TLC, thin layer chromatography. For the mobile phase A (acidic) and phase B (alkaline), see the Materials and methods. ESI, electrospray ionization.

those of the metabolite revealed that the metabolite in spot M6 was 6-(4-hydroxybenzylamino)-2-(3-hydroxypropylamino)-9-isopropylpurine (see the Materials and methods) (table 1). In detail, MS^n data of 6-(4-hydroxybenzylamino)-2-(3-hydroxypropylamino)-9-isopropylpurine were very alike to those of 6-(2-hydroxybenzylamino)-2-(3-hydroxypropylamino)-9-isopropylpurine. However, these two could easily be differentiated from each other by their distinct TLC mobilities, the latter being chracterized by R_f's = 0.64 (phase A) and 0.75 (B). 6-(3-Hydroxybenzylamino)-2-(3-hydroxypropylamino)-9-isopropylpurine clearly differed from these two isomers by both MS^n and TLC characteristics ($R_f = 0.35$ both in phases A and B).

Spot M8, representing about 5% of the total radioactivity in incubates, was observed with a slightly greater mobility than that of parent bohemine (figure 1). Such migration suggested that a product in M8 was a less polar compound than bohemine. Indeed, MS analysis indicated the presence of a metabolite localized in spot M8 and displaying $m/z = 283$ $[M+1]^+$ (table 1). An MS^n scan suggested a molecular structure of 2-amino-6-benzylamino-9-isopropylpurine, another product of bohemine dealkylation. Again, comparison with an authentic, newly synthesized reference compound corroborated this assumption (see the Materials and methods) (table 1).

Identification of a minor metabolite contained in minor spot M7 and representing $< 3\%$ of the total radioactivity in the incubates (figure 1) was hampered by the small quantities extracted thus far. It was characterized by an MS peak of $M_r \sim 356$ ($m/z = 357$ $[M+1]^+$) suggesting attachment of a hydroxyl group to bohemine. The molecular structure of this metabolite remains to be elucidated (table 1).

Incubation of primary metabolites with formation of secondary metabolites

The primary metabolite spots M3–M6 and M8 were extracted and extracts evaporated to dryness. The dry residues were then re-solved and re-incubated with either mouse liver cytosol or microsomes in the presence of appropriate coenzymes (NAD^+, NADPH) or UDP-glycosyl donors.

First, the NAD^+ coenzyme-supplemented cytosolic fractions generated secondary products M4′–M6′ from the primary M4 to M6 extracts, respectively (table 2). Each of the three secondary products M4′–M6′ could be subsequently modified by a reaction with diazomethane. Notably, diazomethane treatment of M6′ gave two derivatives with mutually different R_f that indicated the presence of two acidic hydroxyl groups in M6′ (table 2). These findings suggested that the secondary products M4′–M6′ could represent carboxylic acids, i.e. 6-(benzylamino)-2-(2-carboxyethylamino)-9-purine, 6-amino-2-(2-carboxyethylamino)-9-isopropylpurine and 6-(4-hydroxybenzylamino)-2-(2-carboxyethyl-amino)-9-isopropylpurine, derived from the primary metabolites M4–M6, respectively. MS^n analysis of M4′–M6′ further supported this deduction (table 2). No new spots appeared when the cytosols were incubated with M3 or M8 extracts.

Second, M6 was converted into M5 by microsomes in the presence of NADPH, as checked by TLC and MS characteristics of the latter (table 1). No secondary products were detected when the primary metabolites M3–M5 and M8 were incubated with microsomes supplemented with NADPH-coenzyme.

Table 2. Secondary products of NAD^+-dependent cytosolic transformation of bohemine primary metabolites: R_f, methylation and spectroscopic data.

Compound	Analytical method	Data
Secondary product M4′	TLC	R_f: 0.05 (phase A), 0.00 (phase B)
	ESI-MS	m/z $[M+1]^+$: 313
	ESI-MS^2	m/z (%): 91 (4), 253 (91), 295 (100)
	TLC of an M4′ methylester	R_f: 0.16 (phase A), 0.44 (phase B)
Secondary product M5′	TLC	R_f: 0.15 (phase A), 0.01 (phase B)
	ESI-MS	m/z $[M+1]^+$: 265
	ESI-MS^2	m/z (%): 205 (100), 223 (17), 247 (20)
	TLC of an M5′ methylester	R_f: 0.48 (phase A), 0.53 (phase B)
Secondary product M6′	TLC	R_f: 0.20 (phase A), 0.00 (phase B)
	ESI-MS	m/z $[M+1]^+$: 371
	ESI-MS^2	m/z (%): 205 (8), 265 (100), 277 (16)
	TLC of a presumed M6′ methylester	R_f: 0.55 (phase A), 0.52 (phase B)
	TLC of a presumed M6′ dimethylderivative	R_f: 0.77 (phase A), 0.87 (phase B)

TLC, thin layer chromatography. For the mobile phase A (acidic) and phase B (alkaline), see the Materials and methods. ESI, electrospray ionization.

Third, in the presence of UDP-glucoside, the microsomes readily produced a new spot from the primary M6 spot extract. A structure of a β-glucoside conjugate with a glucoside moiety attached to the aliphatic hydroxyl of M6 was assigned to this new product. This was based on the origin, sensitivity to β-glucosidase, insensitivity to α-glucosidase, MS data of the assumed aliphatic M6 conjugate, and considering its ability to react with diazomethane that indicated the presence of a free acidic hydroxyl group (presumably the aromatic one) in its molecule (table 3). No new products were identified when M3–M5 or M8 spot extracts were incubated with UDP-glucoside-enriched microsomes.

Fourth, microsomes supplemented with UDP-glucuronic acid produced a new metabolite spot from the primary M6 spot extract. This secondary metabolite of M6 was tentatively identified as M6 monoglucuronide based on its sensitivity to β-glucuronidase and MS^n analysis (table 3). The fact that only one product was detected after this secondary metabolite had been subject to methylation argues for the occupancy of the aromatic hydroxyl on the M6 benzyl ring by the

Table 3. Secondary products of UDP-glucose- and UDP-glucuronic acid-dependent transformations of primary bohemine M6: R_f, methylation and spectroscopic data.

Compound	Analytical method	Data
M6 – UDP-glucose reaction product	TLC	R_f: 0.06 (phase A), 0.02 (phase B)
	ESI-MS	m/z $[M+1]^+$: 519
	ESI-MS^2	m/z (%): 251 (8), 357 (9), 413 (100)
	TLC of a methylderivative of the product	R_f: 0.16 (phase A), 0.09 (phase B)
M6 – UDP-glucuronic acid reaction product	TLC	R_f: 0.00 (phase A), 0.00 (phase B)
	ESI-MS	m/z $[M+1]^+$: 533
	ESI-MS^2	m/z (%): 209 (6), 251 (100), 357 (49)
	TLC of a methylderivative of the product	R_f: 0.12 (phase A), 0.06 (phase B)

TLC, thin layer chromatography. For the mobile phase A (acidic) and phase B (alkaline), see the Materials and methods. ESI, electrospray ionization.

diazomethane-reactive glucuronide moiety. No new metabolites were observed when M3–M5 or M8 extracts were incubated with these microsomes.

To strengthen the main findings on secondary metabolites described, we used [8-^{3}H]-labelled authentic standards of the primary metabolites (see the Materials and methods) and incubated them with either cytosol or microsomes in the presence of the above coenzymes and donors. These incubations gave the same carboxylated and glycosylated secondary products as were found in incubates employing the primary spot extracts, based on their TLC mobility and MS analysis (data not shown; cf. tables 1–3). Surprisingly, we were unable to force M8 to react in any catalytic system used throughout this work.

Effects of selective inhibitors of cytochrome P450 forms

CYP form-selective probes were used, namely coumarin, ketoconazole, 8-methoxypsoralen and troleandomycin. Experiments using these inhibitors at concentrations between 0.2 and 250 μM under linear reaction conditions revealed ketoconazole and 8-methoxypsoralen as potent agents in inhibiting bohemine biotransformation *in vitro* (figure 2). 8-Methoxypsoralen substantially inhibited the formation of spot M4 at concentrations ≥ 5 μM and formation of spots M3 and M5 at concentrations ≥ 25 μM (figure 2). The appearance of M4 was also prevented by coumarin at concentrations > 50 μM. Ketoconazole and troleandomycin preferentially blocked the formation of spots M3 and M5 rather then that of M4, provided the inhibitors were present at concentrations of about ≥ 1 μM (figure 2).

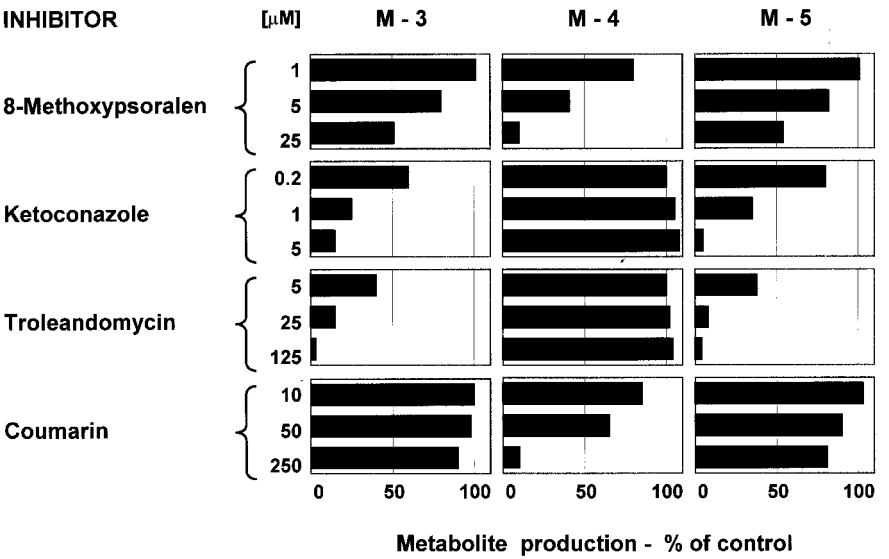


Figure 2. Effects of CYP form-selective chemical inhibitors on bohemine transformation by mouse liver microsomes in the presence of NADPH. Data, which were obtained by TLC resolution and consequent ^{3}H-autoradiographic/densitometric evaluation of the metabolite spots, are the means from triplicate experiments. The amount of each metabolite was compared with that formed in parallel control incubations conducted in the absence of inhibitors, and expressed as a per cent of the corresponding control.

Discussion

Chmela *et al.* (2001) reported that a cytosolic, NAD^+-dependent alcohol dehydrogenase class I could catalyse transformation of bohemine into an acid and that UDP-sugar-dependent enzymatic mechanisms were responsible for bohemine glucoside and glucuronide formation in mice *in vivo*. They were unable to observe any specific individual products indicating participation of the microsomal, NADPH-dependent CYP system in bohemine clearance from the mouse. However, in view of the well-known prominent expression of CYPs in animal tissues, further experimentation was warranted.

The data presented here show that bohemine has been changed into its metabolites during a 120-min incubation of the parent compound in mouse liver microsomes supplemented with NADPH. The proposed primary NADPH-dependent reactions of bohemine in this model have included oxidation (spot M3), hydroxylation (spot M6), two types of dealkylation (spots M4 and M8) and debenzylation (spot M5) (figure 3). Importantly, not only a cytosolic alcohol dehydrogenase, as found by Chmela *et al.* (2001), but also liver microsomes enriched in NADPH, as shown here, have been found to be capable of producing bohemine carboxyl acid, elucidated as a spot M3 metabolite.

Additionally, we have identified several potential secondary pathways mediating primary metabolite biotransformations. First, all the primary metabolites that retained their aliphatic hydroxyl group at the C2 side chain could be oxidized by liver cytosol in an NAD^+-dependent manner to their corresponding acids. This fits well with our previous results showing a substantial role of cytosolic alcohol dehydrogenase in mediating bohemine metabolism (Chmela *et al.* 2001). Second, primary metabolite transformations explored by us have suggested that the spot M6 metabolite is exceptional owing to its predisposition to be modified by both

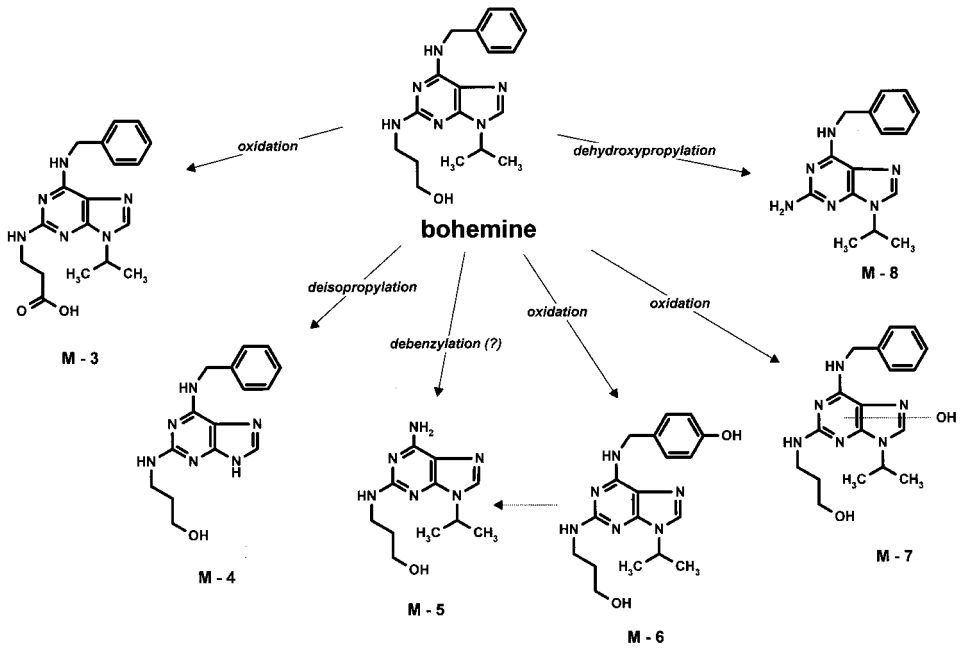


Figure 3. Proposed bohemine primary biotransformation pathways.

type I and type II reactions. Particularly, this primary metabolite could be conjugated with UDP-glucoside. In this context, it is noteworthy that our current findings show that bohemine glucosidation is species specific, in that microsomes from rat, monkey and/or human origin do not support this reaction (Červenková *et al*. 2002). Furthermore, the fact that M6 can serve as a precursor for product M5 is of particular importance since it makes M5 as the primary metabolite uncertain (figure 3).

Molecular structures of both the primary and secondary metabolites and, subsequently, a scheme of bohemine transformation pathways have been proposed based on several types of evidence: (1) TLC mobile phase-dependent monitoring; (2) enzymatic hydrolysis/oxidation (including NAD^+-dependent oxidation); (3) chemical modification (methylation) that can help unmask the presence of an acidic hydroxyl, such as a carboxylic or aromatic one; and (4) MS scanning. Moreover, use of authentic reference compounds has further substantiated our findings concerning primary metabolites M3–M6 and those characterizing M8. We can refer back to known facts concerning bohemine metabolites M2 (the glucoside) and M3 (the acid) that have molecular characteristics established by NMR (Chmela *et al*. 2001). Nevertheless, as our new structural data have not yet been ultimately validated by a direct molecular analysis, we feel obliged to declare here their tentative character.

Several strategies may be followed to gain an insight into which CYPs are responsible for metabolizing bohemine. Numerous investigators have substantiated an inhibition-based approach using CYP-selective probes (Newton *et al*. 1995, Hickman *et al*. 1998). In mouse tissues, 8-methoxypsoralen has been used by Pelkonen *et al*. (1997), Gu *et al*. (1998) and Patten *et al*. (1998) to inhibit mouse *CYP2a* form(s). Furthermore, ketoconazole and troleandomycin, human *CYP3A4*-selective inhibitors, are known to inhibit mouse *CYP3a* form(s) (Gallagher *et al*. 1994, Bourrié *et al*. 1996, Doostzadeh *et al*. 1998a, b, Eagling *et al*. 1998, Boogaards *et al*. 2000, Wilson and LeBlanc 2000, Honda *et al*. 2001, Quintieri *et al*. 2001). In the present study, we inhibited NADPH-dependent bohemine degradation by varying concentrations of chemical inhibitors including 8-methoxypsoralen (*CYP2a*), ketoconazole, troleandomycin (*CYP3a*) and coumarin, a *CYP2A6/2a5* substrate (Boogaards *et al*. 2000, Juvonen *et al*. 2000).

We have observed notable inhibitory effects of 8-methoxypsoralen on M4 formation. This strong inhibitory effect at low concentrations (5 μM) of 8-methoxypsoralen could reasonably be explained by a substantial role of a *CYP2a* form in NADPH-dependent bohemine transformation *in vitro*. A suppressive effect of 25 μM 8-methoxypsoralen on M3 and M5 accumulation probably indicates a loss of selectivity of this inhibitor at high concentrations. Ketoconazole and troleandomycin (at concentrations about 1 μM) each blocked M5 and, partly, M3 formation. These effects presumably suggest a contribution of a ketoconazole/troleandomycin-sensitive *CYP3a* form in bohemine degradation. Thus, at least two mice CYPs, namely *CYP2a* and *CYP3a*, could participate in bohemine transformation. It can be speculated that *CYP2a* mainly catalysed deisopropylation. By contrast, *CYP3a* seemed to be pluripotent and capable in mediating several pathways, e.g. bohemine debenzylation and oxidation. Naturally, these findings do not exclude a possible participation of other CYPs in bohemine metabolism.

Metabolic information obtained from microsomes and cytosols concerns only metabolism at the subcellular level. In spite of the ability of CYP systems to

metabolize bohemine extensively *in vitro*, participation of the microsomal CYP systems in bohemine metabolism *in vivo* may be of a secondary importance, at least in mouse. This follows from the results obtained by Chmela *et al.* (2001). Recently, we obtained data indicating that metabolic pathways contributing to the bohemine transformation also mediate metabolism of other olomoucine-type derivatives such as olomoucine, roscovitine and some others (unpublished data). Hopefully, the present findings will facilitate future experiments designed to dissect enzymatic systems contributing to the clearance of C2,C6,N9-trisubstituted purine compounds from mammalian tissues.

Acknowledgements

The work was supported, in part, by the Ministry of Education, Youth and Sports of the Czech Republic (MSM 153110001, COST B5/B17) and by the Grant Agency of the Czech Republic (301/02/0475/A). The authors thank H. Rozsypalová, S. Snášelová and V. Langerová for excellent technical assistance. They also thank P. Sedmera, M. Kuzma and V. Havlíček, Institute of Microbiology, Academy of Sciences, Czech Republic, for NMR measurements and valuable contribution to the interpretation of MS spectra. Last, but not least, they are indebted to Alexander Oulton and Jarmila Potomková for editorial assistance.

References

Belejová, M., Chmela, Z., Rypka, M., Lemr, K., Lukeš, J., Hanuš, J., Ulrichová, J. and Veselý, J., 1999, Metabolism of synthetic CDK-inhibitors in mammalian cells. Paper presented at the 15th Biological Days, 6–8 September, České Budějovice, Czech Republic; repr. J. Berger (ed.), *Cells* (České Budějovice: KOOP), p. 39.

Boogaards, J. J. P., Bertrand, M., Jackson, P., Oudshoorn, M. J., Weaver, R. J., Van Bladeren, P. J. and Walther, B., 2000, Determining the best animal model for human cytochrome P450 activities: a comparison of mouse, rat, rabbit, dog, micropig, monkey and man. *Xenobiotica*, **30**, 1131–1152.

Bourrié, M., Meunier, V., Berger, Y. and Fabre, G., 1996, Cytochrome P450 isoform inhibitors as a tool for the investigation of metabolic reactions catalyzed by human liver microsomes. *Journal of Pharmacology and Experimental Therapeutics*, **277**, 321–332.

Buolamwini, J. K., 2000, Cell cycle molecular targets in novel anticancer drug discovery. *Current Pharmaceutical Design*, **6**, 379–392.

Červenková, K., Belejová, M., Chmela, Z., Rypka, M., Riegrová, D., Michnová, K., Michalíková, K., Šůrová, I., Brejcha, A., Hanuš, J., Černý, B., Fuksová, K., Havlíček, L., Veselý, J., 2002, In vitro glycosidation potential towards olomoucine-type cyclin-dependent kinase inhibitors in rodent and primate microsomes. *Physiological Research*, accepted for publication.

Červenková, K., Chmela, Z., Rypka, M., Lemr, K., Hanuš, J., Havlíček, L., Belejová, M., Lotková, H., Červinková, Z. and Veselý, J., 2000, Metabolism of cyclin-dependent kinase inhibitor bohemine at the cellular and subcellular levels. Paper presented at the 2nd FEPS Congress, 29 June–4 July 1999, Prague, Czech Republic; abst. *Physiological Research*, **49**, P42.

Chang, Y. T., Gray, N. S., Rosania, G. R., Sutherlin, D. P., Kwon, S., Norman, T. C., Sarohia, R., Leost, M., Meijer, L. and Schultz, P. G., 1999, Synthesis and application of functionally diverse 2,6,9-trisubstituted purine libraries as CDK inhibitors. *Chemistry and Biology*, **6**, 361–375.

Chauret, N., Gauthier, A., Martin, J. and Nicoll-Griffith, D. A., 1997, *In vitro* comparison of cytochrome P450-mediated metabolic activities in human, dog, cat, and horse. *Drug Metabolism and Disposition*, **25**, 1130–1136.

Chmela, Z., Veselý, J., Lemr, K., Hanu, J., Havlíček, L., Rypka, M., Kryštof, V., Ulrichová, J., Walterová, D., Fuksová, K., Lukeš, J., Kolářová, H., Strnad, M. and Lenobel, R., 1998, Metabolism of olomoucine, roscovitine, and bohemine in small laboratory rodents. Paper presented at the 1st International Conference on Inhibitors of Protein Kinases, 15–20 September, Warsaw, Poland; abst. *Cellular and Molecular Biology Letters*, **3**, 280.

Chmela, Z., Veselý, J., Lemr, K., Rypka, M., Hanuš, J., Havlíček, L., Kryštof, V., Michnová, L., Fuksová, K. and Lukeš, J., 2001, *In vivo* metabolism of 2,6,9-trisubstituted purine-derived cyclin-dependent kinase inhibitor bohemine in male mice: glucosidation as the principal metabolic route. *Drug Metabolism and Disposition*, **29**, 326–334.

Court, M. H., Von Moltke, L. L., Shader, R. I. and Greenblatt, D. J., 1997, Biotransformation of chlorzoxazone by hepatic microsomes from humans and ten other mammalian species. *Biopharmaceutics and Drug Disposition*, **18**, 213–226.

Doostzadeh, J., Cotillon, A.-C., Benalychérif, A. and Morfin, R., 1998a, Inhibition studies of dehydroepiandrosterone 7α- and 7βhydroxylation in mouse liver microsomes. *Steroids*, **63**, 608–614.

Doostzadeh, J., Cotillon, A.-C. and Morfin, R., 1998b, Hydroxylation of pregnenolone at the 7 alpha- and beta-positions by mouse liver microsomes. Effects of cytochrome p450 inhibitors and structure-specific inhibition by steroid hormones. *Steroids*, **63**, 383–392.

Eagling, V. A., Tjia, J. F. and Back, D. J., 1998, Differential selectivity of cytochrome P450 inhibitors against probe substrates in human and rat liver microsomes. *British Journal of Clinical Pharmacology*, **45**, 107–114.

Epstein, J., Plapinger, R. E., Michel, H. O., Cable, J. R., Stephani, R. A., Hester, R. J., Billington. C., Jr and List, G. R., 1964, Reactions of isopropyl methylphosphonofluoridate with substituted phenols. I. *Journal of the American Chemical Society*, **86**, 3075–3084.

Fischer, P. M. and Lane, D. P., 2000, Inhibitors of cyclin-dependent kinases as anti-cancer therapeutics. *Current Medicinal Chemistry*, **7**, 1213–1245.

Gallagher, E. P., Wienkers, L. C., Stapleton, P. L., Kunze, K. L. and Eaton, D. L., 1994, Role of human microsomal and human complementary DNA-expressed cytochromes P4501A2 and P4503A4 in the bioactivation of aflatoxin B1. *Cancer Research*, **54**, 101–108.

García-Echeverría, C., Traxler, P. and Evans, D. B., 2000, ATP site-directed competitive and irreversible inhibitors of protein kinases. *Medical Research Reviews*, **20**, 28–57.

Gray, A. S., Wodicka, L., Thunnissen, A.-M. W. H., Norman, T. C., Kwon, S., Espinoza, F. H., Morgan, D. O., Barnes, G., Leclerc, S., Meijer, L., Kim, S.-H., Lockhart, D. J. and Schultz, P. G., 1998, Exploiting chemical libraries, structure, and genomics in the search for kinase inhibitors. *Science*, **281**, 533–538.

Gray, N., Detivaud, L. and Meijer, L., 1999, ATP-site directed inhibitors of cyclin-dependent kinases. *Current Medicinal Chemistry*, **6**, 859–875.

Gu, J., Zhang, Q. Y., Genter, M. B., Lipinskas, T. W., Negishi, M., Nebert, D. W. and Ding, X., 1998, Purification and characterization of heterogously expressed mouse CYP2A5 and CYP2G1: role in metabolic activation of acetaminophen and 2,6-dichlorobenzonitrile in mouse olfactory mucosal microsomes. *Journal of Pharmacology and Experimental Therapeutics*, **285**, 1287–1295.

Havlíček, L., Hanuš, J., Veselý, J., Leclerc, S., Meijer, L., Shaw, G. and Strnad, M., 1997, Cytokinin-derived cyclin dependent kinase inhibitors: synthesis and cdc2 activity of olomoucine and related compounds. *Journal of Medicinal Chemistry*, **40**, 408–412.

Hickman, D., Wang, J. P., Wang, Y. and Unadkat, J. D., 1998, Evaluation of the selectivity of *in vitro* probes and suitability of organic solvents for the measurement of human cytochrome P450 monoxygenase activities. *Drug Metabolism and Disposition*, **26**, 207–215.

Hocart, C. H., Letham, D. S. and Parker, C. W., 1991, Substituted xanthines and cytokinin analogues as inhibitors of cytokinin *N*-glucosylation. *Phytochemistry*, **30**, 2477–2486.

Honda, A., Salen, G., Matsuzaki, Y., Batta, A. K., Xu, G., Leitersdorf, E., Tint, G. S., Erickson, S. K., Tanaka, N. and Shefer, S., 2001, Side chain hydroxylations in bile acid biosynthesis catalyzed by CYP3A are markedly up-regulated in Cyp27–/– mice but not in cerebrotendinous xanthomatosis. *Journal of Biological Chemistry*, **276**, 34579–34585.

Jones, E. C. S. and Pyman, F. L., 1925, The relation between chemical constitution and pungency in acid amides. *Journal of the Chemical Society*, **127**, 2588–2598.

Juvonen, R. O., Gynther, J., Pasanen, M., Alhava, E. and Poso, A., 2000, Pronounced differences in inhibition potency of lactone and non-lactone compounds for mouse and human coumarin 7-hydroxylases (CYP2A5 and CYP2A6). *Xenobiotica*, **30**, 81–92.

Legraverend, M., Ludwig, O., Bisagni, E., Leclerc, S., Meijer, L., Giocanti, N., Sadri, R. and Favaudon, V., 1999, Synthesis and *in vitro* evaluation of novel 2,6,9-trisubstituted purines acting as cyclin-dependent kinase inhibitors. *Bioorganic and Medicinal Chemistry*, **7**, 1281–1293.

Meijer, L., 2000, Cyclin-dependent kinases inhibitors as potential anticancer, antineurodegenerative, antiviral and antiparasitic agents. *Drug Resistance Updates*, **3**, 83–88.

Meijer, L., Leclerc, S. and Leost, M., 1999, Properties and potential applications of chemical inhibitors of cyclin-dependent kinases. *Pharmacology and Therapeutics*, **82**, 279–284.

Michalíková, K., Michnová, L., Belejová, M., Chmela, Z., Rypka, M., Lemr, K., Havlíčk, L., Lukeš, J., Veselý, J. and Ulrichová, J., 1999, Enzyme systems involved in metabolism of purine-related cyclin-dependent kinase inhibitors. Paper presented at the 15th Biological Days, 6–8 September, České Budějovice, Czech Republic; abst. J. Berger (ed.), *Cells* (České Budějovice: KOOP), p. 97.

Newton, D. J., Wang, R. W. and Lu, A. Y. H., 1995, Cytochrome P450 inhibitors. Evaluation of specifities in the *in vitro* metabolism of therapeutic agents by human liver microsomes. *Drug Metabolism and Disposition*, **23**, 154–158.

Otyepka, M., Kryštof, V., Havlíček, L., Iglerová, V., Strnad, M. and Koča, J., 2000, Docking-based development of purine-like inhibitors of cyclin-dependent kinase-2. *Journal of Medicinal Chemistry*, **43**, 2506–2513.

Patten, C. J., Peterson, L. A. and Murphy, S. E., 1998, Evidence for metabolic activation of *Ń*-nitrosonornicotine and *N*-nitrosobenzyl methylamine by rat nasal coumarin hydroxylase. *Drug Metabolism and Disposition*, **26**, 177–180.

Pelkonen, O., Maenpaa, J., Taavitsainen, P., Rautio, A. and Raunio, H., 1998, Inhibition and induction of human cytochrome P450 (CYP) enzymes. *Xenobiotica*, **28**, 1203–1253.

Quintieri, L., Rosato, A., Napoli, E., Sola, F., Geroni, C., Floreani, M. and Zanvello, P., 2000, *In vivo* antitumor activity and host toxicity of methoxymorpholinyl doxorubicin: role of cytochrome P450 3A. *Cancer Research*, **60**, 3232–3238.

Raiford, L. C. and Clark, E. P., 1923, Diacyl derivatives of *ortho*-hydroxybenzylamine. *Journal of the American Chemical Society*, **45**, 1738–1743.

Rendic, S., 2002, Summary of information on human CYP enzymes: human P450 metabolism data. *Drug Metabolism Reviews*, **34**, 83–448.

Rosania, G. R. and Chang, Y.-T., 2000, Targeting hyperproliferative disorders with cyclin-dependent kinase inhibitors. *Expert Opinion on Therapeutic Patents*, **10**, 215–230.

Sausville, E. A., Zaharevitz, D., Gussio, R., Meijer, L., Louarn-Leost, M., Kunick, C., Schultz, R., Lahusen, T., Headlee, D., Stinson, S., Arbuck, S. G. and Senderovicz, A., 1999, Cyclin-dependent kinases: initial approaches to exploit a novel therapeutic target. *Pharmacology and Therapeutics*, **82**, 285–292.

Sielecki, T. M., Boylan, J. F., Beneld, P. A. and Trainor, G. L., 2000, Cyclin-dependent kinase inhibitors: useful targets in cell cycle regulation. *Journal of Medicinal Chemistry*, **43**, 1–18.

Venkatakrishnan, K., Von Moltke, L. L. and Greenblatt, D. J., 2001. Human drug metabolism and the cytochromes P450: application and relevance of *in vitro* models. *Journal of Clinical Pharmacology*, **41**, 1149–1179.

Veselý, J., Havlíček, L., Strnad, M., Blow, J. J., Donella-Deana, A., Pinna, L., Letham, D. S., Kato, J., Detivaud, L., Leclerc, S. and Meijer, L., 1994, Inhibition of cyclin-dependent kinases by purine analogues. *European Journal of Biochemistry*, **224**, 771–786.

Wilson, W. S. and LeBlanc, G. A., 2000, The contribution of hepatic inactivation of testosterone to the lowering of serum testosterone levels by ketoconazole. *Toxicological Sciences*, **54**, 128–137.

XENOBIOTICA, 2002, VOL. 32, NO. 11, 1033–1043

Taylor & Francis
healthsciences

Induction of cytochrome P4501A1 by autoclavable culture medium change in HepG2 cells

Q. FENG, T. KUMAGAI, Y. NAKAMURA, K. UCHIDA and T. OSAWA*

Laboratory of Food and Biodynamics, Graduate School of Bioagricultural Sciences, Nagoya University, Nagoya 464-8601, Japan

Received 7 January 2002

1. Without the addition of xenobiotics, only by changing the culture medium can one induce extensively and transiently cytochrome P4501A1 (CYP1A1) protein and mRNA in human hepatoma HepG2 cells. The induction was aryl hydrocarbon receptor (AhR)-dependent, and was proven by: (1) the medium change activated the AhR, as judged by a electrophoretic mobility shift assay; and (2) the AhR inhibitor α-naphthoflavone inhibited the medium change-mediated induction.

2. Induction of CYP1A1 was related to medium prepared by autoclaving. By screening the ingredients in the medium, the serum had no effect on CYP1A1 induction, whereas both photo-oxidized and autoclaved tryptophan were shown to induce CYP1A1, as indicated by CYP1A1 protein or ethoxyresorufin-*O*-deethylase activity. The autoclaved tryptophan contained in an autoclavable medium was a more potent inducer of CYP1A1 than photo-oxidized tryptophan.

3. The results provide some practical suggestions with experiments related to CYP1A1.

Introduction

Cytochrome P4501A1 (CYP1A1) is a member of the large cytochrome P450 gene family. The CYP1A1 gene product has been implicated in the metabolism and bioactivation of exogenous compounds, mainly polycylic aromatic hydrocarbons (PAHs), many of which, such as 2,3,7,8-tetrachlorodibenzo-*p*-dioxin (TCDD), benzo(*a*)pyrene (B[a]P) and 3-methylcholanthrene (3-MC), also extensively induce this gene expression (Whitlock 1999). The mechanism of induction by PAHs has been intensively studied. Briefly, once a PAH enters the cells, it binds to and activates a cytosolic protein called the aryl hydrocarbon receptor (AhR) and causes the AhR to translocate to the nucleus where the activated AhR heterodimerizes with another protein, the aryl hydrocarbon receptor nuclear translocator (Arnt). The heterodimer then binds to an enhancer sequence, the xenobiotic-responsive element (XRE), acting as a transcription factor and activates the CYP1A1 gene (Whitlock 1999). Besides PAHs, some indole compounds and benzimidazole derivatives can also highly induce CYP1A1 (Jellinck *et al.* 1993, Krusekopf *et al.* 1997). CYP1A1 is generally induced by xenobiotics, but in some situations, it can be activated without any exposure to exogenous ligands. These situations include stress conditions such as hyperoxia (Okamoto *et al.* 1993) and

* Author for correspondence; e-mail: osawat@agr.nagoya-u.ac.jp

Xenobiotica ISSN 0049–8254 print/ISSN 1366–5928 online © 2002 Taylor & Francis Ltd
http://www.tandf.co.uk/journals
DOI: 10.1080/0049825021000012583

hypoxia (Carriere *et al.* 1998), and suspension of the attached cells (Sadek and Allen-Hoffman 1994a, b).

Cultured cells provide a practical model for studying the effects of exogenous compounds on endogenous enzyme regulation. It is usually assumed that the culture medium has little influence on the enzymes to be investigated; hence, exogenous compounds are added to the culture medium and incubated with the cells to investigate the effects of the compounds. However, by accident, we found that CYP1A1 is transiently and highly induced by simply changing the culture medium in human HepG2 hepatoma cells. This finding coincided with two other reports that observed that a medium change could induce ethoxyresorufin-*O*-deethylase (EROD) activity in the rainbow trout liver cell line RTL-W1 (Segner *et al.* 2000) and increased CYP1A1 mRNA in rat hepatocytes (Kocarek *et al.* 1994). However, our investigation went further to confirm that the induction was AhR-dependent and revealed that autoclaved tryptophan in the autoclaveable culture medium contributes to inducing CYP1A1 much more than mildly photo-oxidized tryptophan, which has been reported previously (Kocarek *et al.* 1994, Segner *et al.* 2000).

Materials and methods

Reagents

Autoclavable tissue culture medium powder, Dulbecco's modified Eagle's medium (DMEM), was from Nissui Pharmaceutical Co., Ltd (Tokyo, Japan). The tested medium components such as amino acids, vitamins, inorganic salts and glucose were from Wako Pure Chemical Industries, Ltd (Osaka, Japan). Foetal bovine serum (FBS) was from Sigma Chemical Co. (St Louis, MO, USA).

Cell culture

HepG2 cells were from the Japanese Cancer Research Resources Bank. The cells were cultured in DMEM containing 100 U ml^{-1} penicillin, 100 μg ml^{-1} streptomycin, 588 μg ml^{-1} L-glutamine, 0.16% $NaHCO_3$ and 10% heat-inactivated FBS. Cells were grown at 37 °C in an atmosphere of 95% air and 5% CO_2.

Immunoblotting analysis

After the cells were treated with medium change or certain compounds for the indicated time, they were washed with phosphate-buffered saline (PBS, pH 7.0) and lysed by lysis buffer (50 mM Tris-HCl, pH 7.0, 150 mM NaCl, 1% Triton X-100, 0.5% sodium deoxycholate, 0.1% SDS, 100 μg ml^{-1} phenylmethylsulfonyl fluoride). A 30-μg sample of the cell protein was subjected to 10% sodium dodecylsulfate polyacrylamide gel electrophoresis (SDS-PAGE). For the immunoblots, the proteins were transferred to a nitrocellulose membrane using a semidry blotting technique. After blocking with 5% skimmed milk, the membrane was probed with antiserum for human CYP1A1 (Daiichi Pure Chemicals Co., Tokyo, Japan). This was followed by the addition of horseradish peroxidase conjugated to immunoglobin (Ig) G and the enhanced chemiluminescence (ECL) reagent. The signals were visualized and quantified using the Light Capture System (ATTO Co., Tokyo, Japan).

Reverse transcription polymerase chain reaction (RT-PCR)

The treated cells were washed twice with PBS (pH 7.0) and the total RNA was isolated using ISOGEN reagent (Nippon Gene Co., Tokyo, Japan). The reverse transcription (RT) reaction was performed with 10 μg total RNA and an oligo-(dT) primer using the First-Strand cDNA synthesis kit (Life Technology, Inc., Rockville, MD, USA). Biologica Co. synthesized the polymerase chain reaction (PCR) primers. The primer sequences of CYP1A1 and the PCR reaction were performed according to Guigal *et al.* (2000). As the internal control, the amount of GAPDH mRNA was also measured. The PCR cycles were 25 for CYP1A1 and 36 for Glyceraldehyde-3-phosphate dehyrogenase (GAPDH). The PCR products were analysed by electrophoresis on 1.5% agarose gel and visualized by ethidium bromide staining. The amount of PCR product was also measured using the Light Capture System.

Electrophoretic mobility shift assay (EMSA)

After the medium change for 1 h, nuclear extracts were isolated from the confluent culture of HepG2 cells (Denison *et al.* 1988). Electrophoretic mobility shift assay (EMSA) was performed as according to Burczynski and Penning (2000) with a slight modification. Briefly, synthetic oligonucleotides (Amersham Pharmacia Biotech., Little Chalfont, UK) containing the AhR-binding site of XRE (Burczynski and Penning 2000) were labelled with [α-^{32}P]dATP. The binding reaction was carried out for 30 min at room temperature and contained in a total volume of 15 µl with 5 µg nuclear protein and labelled XRE oligonucleotide (20 000 cpm) in a buffer of a final concentration of 10 mM Hepes-KOH (pH 7.8), 50 mM KCl, 1 mM EDTA (pH 8.0), 5 mM $MgCl_2$, 10% glycerol, 5 mM DTT, 0.7 mM PMSF, 2 µg ml^{-1} aprotinin, 2 µg ml^{-1} pepstatin, 2 µg ml^{-1} leupeptin, 1 mM sodium orthovanadate and 0.1 µg µl^{-1} poly [dIdC] (Amersham Pharmcia Biotech., Little Chalfont, UK). DNA–protein complexes were separated under non-denaturing conditions of 4.5% PAGE using 0.5 × Tris/Borate/EDTA (TBE) as a running buffer. After the gel had dried, the DNA–protein complexes were detected and quantified with a BAS2500 Imaging System (Fuji Film Co., Tokyo, Japan).

Ethoxyresorufin-O-deethylase (EROD) activity assay

The ethoxyresorufin-*O*-deethylase (EROD) activity assay method was modified as according to Kennedy *et al.* (1993). Briefly, HepG2 cells were evenly seeded in 96-well plates and cultured to 90% confluence. After a medium change or treatment with certain compounds, the cells were washed with PBS (pH 7.0). The multiplate was treated with several freeze/thaw cycles to make the cells permeable and then used for the activity assay. A 100-µl final volume of the reaction liquid containing 50 mM Tris buffer (pH 7.2), 1.3 mg ml^{-1} bovine serum albumen (BSA), 5 µM ethoxyresorufin and 1.7 mM NADPH was added to each well. The plate was kept at 37 °C for 15 min, then the reaction was stopped by adding 150 µl ice-cold methanol. After the reaction, the liquids were transferred to a fluorescence plate for 15 min and the plate was then scanned by a Fluorescence Scan II plate reader (Dainippon Pharmacology. Co., Tokyo, Japan) for formed resorufin with a 530-nm excitation filter and a 590-nm emission filter. Each sample occupied four wells (one for control, three for assay detection). The control wells had Tris buffer instead of NADPH.

HPLC analysis

Tryptophan (0.016 g l^{-1}) was autoclaved at 121 °C for 20 min or irradiated with germicidal ultraviolet (UV) light for 6 h at a distance of approximately 40 cm. Tryptophan, autoclaved and UV-oxidized tryptophan were analysed by reversed-phase HPLC (JASCO Co., Tokyo, Japan) equipped with a Develosil ODS-HG-5 column (4.6 × 250 mm; Nomura Chemicals Co., Seto, Japan). The elution of tryptophan from the column was carried out at a flow rate of 0.8 ml min^{-1} using a linear gradient of 0–100% methanol over 60 min. The absorbance of the column eluates was monitored at 254 nm.

Results and discussion

Medium change induces CYP1A1 protein, mRNA and activates AhR transformation

When HepG2 cells were passaged for 3–4 days, the spent medium was removed and changed to fresh culture medium at 3, 6, 9, 12 and 24 h. Cells not subjected to the medium change were used as controls (0 h). Changes in CYP1A1 protein and mRNA after the medium change were measured by immunoblotting and semi-quantitative RT-PCR. Figure 1A, B shows that both CYP1A1 protein and mRNA increased, reached a maximum at about 9 h after the medium change, then decreased and returned to the basal level at 24 h after the medium change. Compared with the induction by PAH, 3-MC and TCDD, the medium change-induced CYP1A1 is a transient phenomenon because the peak of the CYP1A1 protein level induced by 3-MC appeared at 20 h and TCDD at 24 h in HepG2 cells (data not shown). An alternative explanation for the difference in the time course for CYP1A1 induction following exposure to medium and 3-MC or TCDD may be that the compound present in the medium is eliminated more rapidly than either of the other inducers or perhaps that the medium change causes some metabolism in the cells which increases the degradation of CYP1A1. In addition,

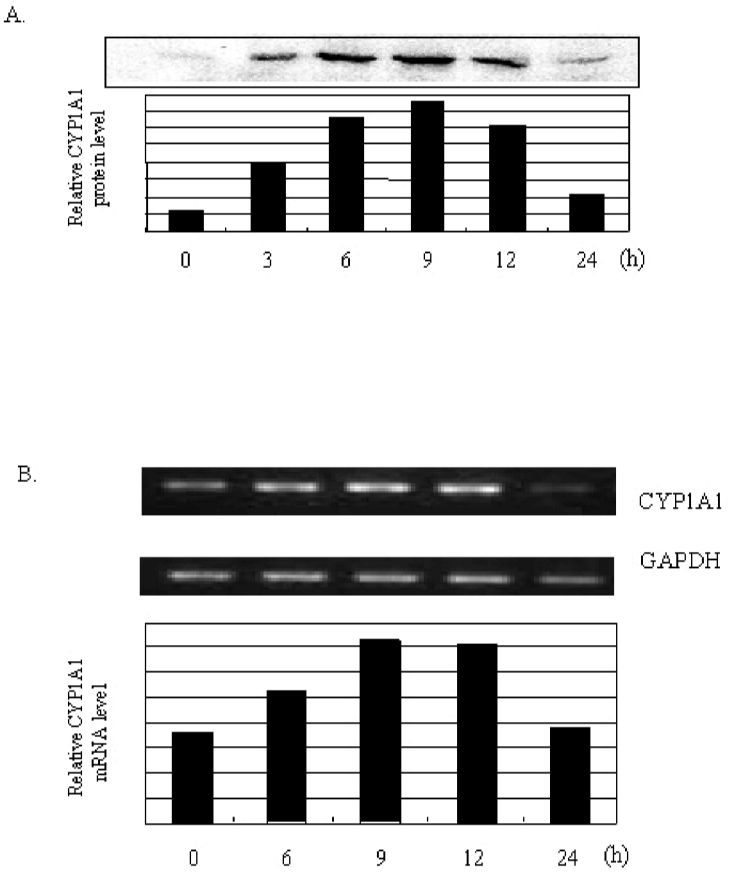


Figure 1. Transient induction of CYP1A1 by medium change in HepG2 cells. Cells were passaged for 4 days. The spent medium was then removed and changed to fresh culture medium for a certain period. Changes in the CYP1A1 protein level (A) and mRNA level (B) after the medium change were analysed by immunoblot and RT-PCR, as described in the Materials and methods. In (A), the bar graph indicates the corresponding bands of the CYP1A1 protein level; in (B), the amount of CYP1A1 mRNA was normalized to the amount of GAPDH mRNA.

the induction of the CYP1A1 level by the medium change was also observed in another cell line: rat liver epithelial cell RL-34 cells (data not shown). Seger *et al.* (2000) observed that EROD activity was increased in the RTL-W1 cell line, and Kocarek *et al.* (1994) reported that CYP1A1 mRNA was induced after the medium change in rat hepatocytes. These results indicate that induction of CYP1A1 by a medium change in the cells could be a universal phenomenon.

However, no attempt was made by these latter authors to investigate if the medium change would cause transformation of the AhR in the cells. In the present study, nuclear extracts were isolated from HepG2 cells incubated with fresh medium for 1 h or no medium change, and the nuclear protein–XRE complex was resolved by EMSA. Figure 2A shows that a gel-shift band was observed when the nuclear extracts prepared from cells with a medium change were incubated with radiolabelled 32-bp oligonucleotide containing XRE specific to AhR and subjected to non-denaturing PAGE. The specificity of the AhR–XRE complex was verified by the ability of a 100-fold excess of unlabelled XRE oligonucleotide

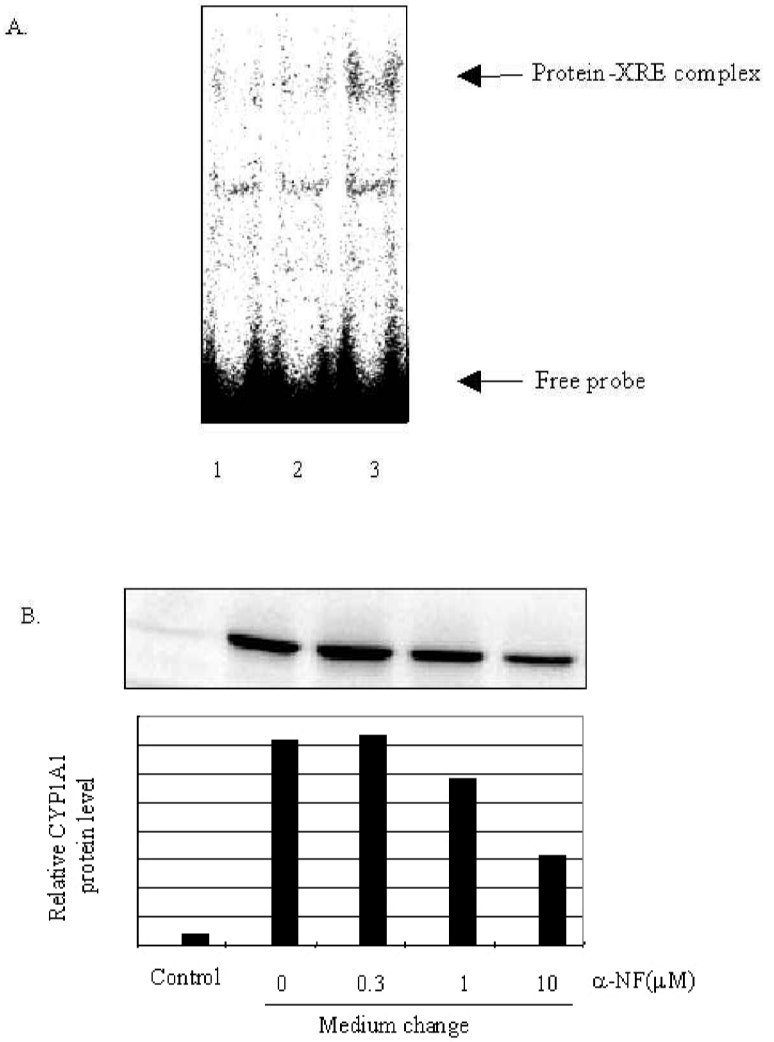


Figure 2. Medium change mediating CYP1A1 induction is AhR-dependent. (A) Medium change activates AhR transformation in the nucleus. Nuclear extracts, prepared from HepG2 cells subjected to medium change for 1 h, were incubated with ^{32}P-labelled XRE oligonucleotide in the absence (lane 3) or presence (lane 2) of a 100-fold excess of unlabelled XRE oligonucleotide as the competitor, the protein–DNA complex was resolved by EMSA, as described in the Materials and methods. Cells without a medium change were used as a control (lane 1). (B) α-NF inhibited CYP1A1 protein induced by the medium change. Cells were changed with the medium containing various concentrations of α-NF for 8 h. Immunoblot analysis was then carried out as described in the Materials and methods. The bar graph indicates the corresponding levels of the CYP1A1 protein.

to compete against the medium change-induced binding of the transformed AhR to ^{32}P-XRE. This implies that the complex was specific for the XRE. This result suggests that the medium change initiates the activation of AhR, resulting in the binding of the Arnt protein and translocation of the liganded AhR complex into the nucleus followed by binding of the activated AhR directly to the core sequences of XRE of the CYP1A1 gene, thereby activating its transcription.

To confirm that AhR plays a role in CYP1A1 induction by a medium change, the AhR antagonist α-naphthoflavone (α-NF) was administered to cells with a fresh medium change. α-NF is a potent AhR inhibitor at low doses, while behaving as an AhR agonist at high doses (Merchant *et al.* 1992, Santostefano *et al.* 1993). α-NF at 10 μM inhibited the medium change-mediated induction of CYP1A1 by about 50% (figure 2B), implying that an antagonist blocked the agonist binding to the AhR to cause induction of CYP1A1. The accumulation of activated AhR in the nucleus and the ability of α-NF to eliminate the increase in CYP1A1 protein when HepG2 cells were subjected to a medium change indicate a role for the AhR pathway in this medium change-mediated induction. Alternatively, this also indicates that there may be some AhR agonists in the medium.

Serum has no effect on CYP1A1 induction

The culture medium is composed of serum, inorganic salts, carbohydrates, amino acids and vitamins. Guigal *et al.* (2000, 2001) reported that serum could induce CYP1A1 in an AhR-independent way in both Caco-2 and HepG2 cells. However, the present results did not prove that the serum could induce CYP1A1. After the HepG2 cells were passaged for 3–4 days, they were changed to a serum-free medium for 24 h. The spent medium was removed and then changed to serum-free medium. This was the same treatment of cells as described in Guigal *et al.* (2000, 2001). Figure 3A shows that the CYP1A1 protein level is induced after

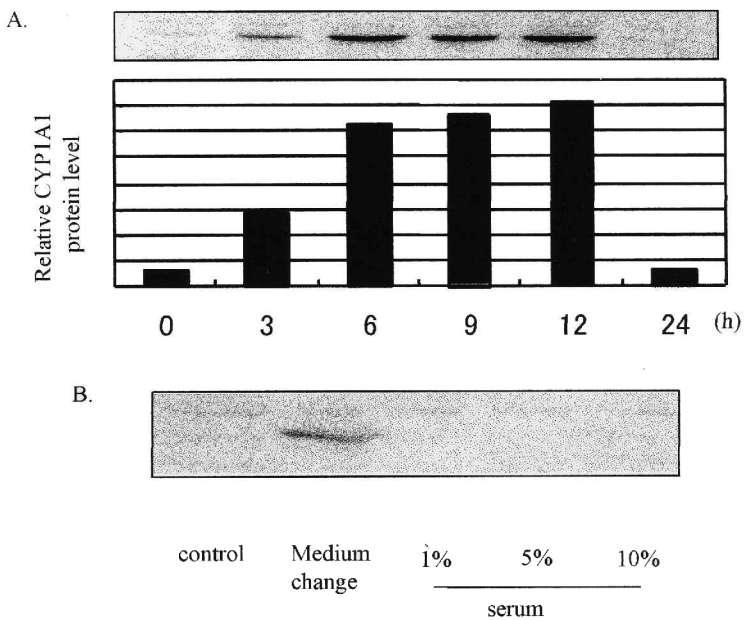


Figure 3. Serum had no effect on CYP1A1 induction. (A) After passage for 4 days, HepG2 cells were starved for 24 h in serum-free medium. They were then changed with serum-free medium at different times. Changes in the CYP1A1 protein were analysed by immunoblot. The bar graph indicates the corresponding bands of CYP1A1 protein. (B) After the HepG2 cells were passaged for 4 days, 1–10% FBS was added to the spent medium. The CYP1A1 protein was then analysed by immunoblot.

the serum-free medium change. Moreover, if 1, 5 or 10% serum was added directly to the non-changed cultured medium for 6 or 9 h, CYP1A1 could not be induced at all (figure 3B). In Guigal *et al.* (2001), the CYP1A1 level did not increase as the serum concentrations increased. It was concluded that this was due to the CYP1A1 reaching a plateau at a certain concentration. The non-dose-dependent effect of serum concentration should be explained by the serum not being the CYP1A1-inducing factor.

Autoclaved tryptophan contained in DMEM is a good CYP1A1 inducer

Since 'Nissui' DMEM is autoclaveable, the autoclaved (instead of filtered) DMEM was mixed with serum, filtered glutamine and antibiotic in the culture medium preparation. Interestingly, EROD activity was induced by the autoclaved medium change as extensively as by 1 μM 3-MC, while the medium prepared by filtration had little effect on EROD activity (figure 4). This suggests that some components would be changed to a CYP1A1 inducer during autoclaving. Therefore, the various autoclaved components contained in the medium were investigated to see if they had the ability to induce EROD activity. HepG2 cells were placed in 96-well plates and cultured for 3 days. They were then incubated separately with various ingredients contained in the medium for 6 h without a medium change. The final concentrations of medium ingredients in the spent medium were the same as those in the fresh medium. By measuring EROD activity, it was found that only autoclaved tryptophan could induce EROD significantly (table 1). Tryptophan, especially the photo-oxidized form, has been reported as being an AhR agonist and it induces CYP1A1 in several cell lines (Rannug *et al.* 1987, Sindhu *et al.* 1996, Heath-Pagliuso *et al.* 1998, Wei *et al.*

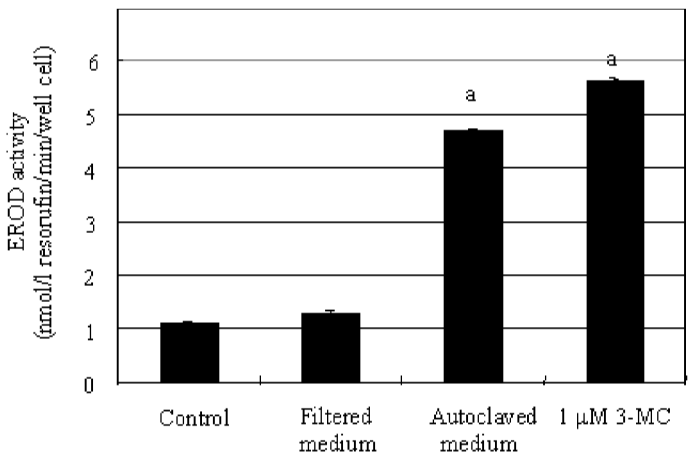


Figure 4. Effect of autoclaved and filtered medium change on EROD activity. Autoclavable 'Nissui' DMEM was subjected to autoclaving (121 °C, 20 min) or filtration and then mixed with serum, glutamin, 10% $NaHCO_3$ and antibiotics. EROD activity was measured in HepG2 cells with autoclaved or filtered medium change for 8 h. For comparison, 1 μM 3-MC was added to the spent medium. Each value represents the mean ± SD, for $n = 3$. Statistical significance was determined by a Student's *t*-test and is expressed as: (a) versus control (without a medium change), $p < 0.005$.

Table 1. Effect of the autoclaved DMEM ingredients on EROD activity.

Treatment	EROD activity	Treatment	EROD activity
Control (H_2O)	0.47 ± 0.0	L-Arg	0.32 ± 0.10
NaCl	0.41 ± 0.02	L-Cys	0.55 ± 0.21
$CaCl_2$	0.43 ± 0.01	Gly	0.34 ± 0.04
$MgSO_4$	0.31 ± 0.01	L-His	0.61 ± 0.08
NaH_2PO_4	0.38 ± 0.01	L-Ile	0.57 ± 0.10
$Fe(NO_3)_3$	0.29 ± 0.01	L-Leu	0.44 ± 0.11
Glucose	0.44 ± 0.03	L-lys	0.62 ± 0.04
Sodium pyrutate	0.51 ± 0.02	L-Met	0.49 ± 0.07
Succinic acid	0.55 ± 0.04	L-Phe	0.49 ± 0.17
Sodium succinate	0.49 ± 0.05	L-Ser	0.51 ± 0.10
Choline	0.35 ± 0.01	L-Thr	0.43 ± 0.05
Nicotinamide	0.42 ± 0.06	L-Trp	6.88 ± 1.35*
Calcium pantothenic	0.33 ± 0.05	L-Tyr	0.47 ± 0.12
Pyridoxal	0.29 ± 0.01	L-Val	0.36 ± 0.06
Riboflavin	0.46 ± 0.11	Phenol red	0.28 ± 0.07
Thiamine	0.35 ± 0.05		
i-Inositol	0.48 ± 0.03		

Various ingredients were prepared at 100-fold medium concentration and added to HepG2 cells, which were cultured in 96-well plates and incubated with various ingredients for 6 h. The final concentration of each compound was the same as those in fresh medium. EROD activity (nmol l^{-1} resorufin min^{-1} well cells) was then measured as detailed in the Materials and methods. Each value is the mean $\pm$ SD ($n = 3$).

Statistical significance was determined by the Student's-*t* test and expressed as: *versus control, $p < 0.001$.

1998, Sindhu and Kikkawa 1999, Yan *et al*. 1999). Photo-oxidized tryptophan can be obtained either by being irradiated by UV light and O_3 (Sindhu *et al*. 1996) or by being illuminated by a lamp or natural light (Kocarek *et al*. 1994, Segner *et al*. 2000).

In the present study, we found that autoclaved tryptophan contributed more to CYP1A1 induction than did mildly photo-oxidized tryptophan that has been thought to be the cause of induction of CYP1A1 mRNA in rat hepatocytes (Kocarek *et al*. 1994) and EROD activity in RTL-W1 cells (Segner *et al*. 2000). Medium prepared by autoclaving and filtration was exposed to room (using) and refrigerator (stock) lighting for about 2 weeks and then compared with freshly prepared medium for the induction of EROD activity. Figure 5A shows that EROD activity in cells changed to medium prepared 2 weeks earlier was higher than that in freshly prepared medium. This is likely attributed to mild photo-oxidized tryptophan in the medium. However, induction by the autoclaved medium change was significantly ($p < 0.005$) extensive than that by the filtered medium, implying that autoclaved tryptophan was largely responsible for the CYP1A1 induction. This result was confirmed by treating the cells with autoclaved tryptophan and natural lighting-illuminated tryptophan for immunoblot analysis (figure 5B).

It has been reported that UV-oxidized tryptophan is a potent CYP1A1 inducer (Sindhu *et al*. 1996). HPLC analysis was carried out by us to determine whether there were similar components in UV-oxidized tryptophan and autoclaved tryptophan. Figure 6 shows that non-oxidized tryptophan eluted as a single peak off

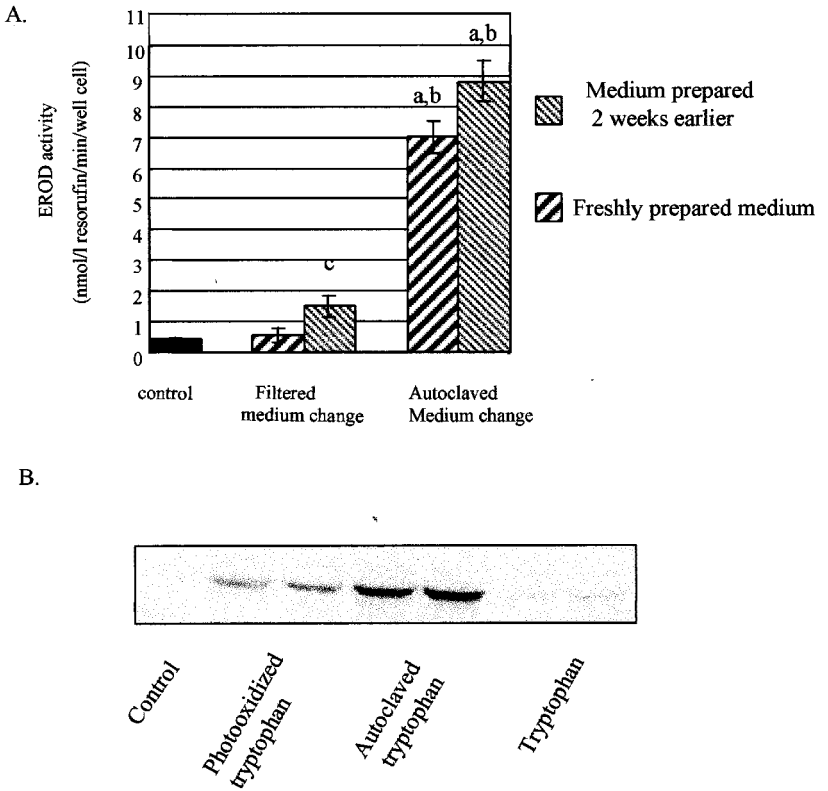


Figure 5. Comparison of mildly photo-oxidized and autoclaved tryptophan on EROD activity. (A) A medium change was performed in HepG2 cells using medium freshly prepared or prepared 2 weeks earlier (2-week spent medium was used in normal light and stored in a refrigerator). After a medium change for 8 h, EROD activity was measured, as described in the Materials and methods. Each value represents the mean ± SD, for $n = 3$. Statistical significance was determined by a Student's t-test and expressed as: (a) versus control (without a medium change), $p < 0.001$; (b) versus filtered medium change, $p < 0.005$; and (c) versus control, $p < 0.05$. (B) Tryptophan illuminated by natural room light or subjected to autoclaving was administered to cells for 8 h without a medium change. CYP1A1 protein level was analysed by immunoblot.

the HPLC column, whereas there was a new peak in UV-oxidized tryptophan and autoclaved tryptophan. This suggests that UV-oxidized tryptophan and autoclaved tryptophan share the similar compound(s) that induces CYP1A1. The precise chemical nature of the compound is unknown, but it may have an indole-like structure which is known to be a ligand of the AhR (Heath-Pagliuso *et al.* 1998, Wei *et al.* 2000).

Our findings not only agree with the previous observation that mild photo-oxidation of tryptophan is responsible for induction of CYP1A1, but also emphasize that autoclaved tryptophan is the major cause of CYP1A1 induction by a medium change. Since the autoclavable powdered culture medium was successfully used for mammalian cells in the 1960s (Yamane *et al.* 1968), autoclavable culture medium powder has been made and sold in some major medium-making chemical companies such as Sigma, Gibco (Invitrogen), Nissui, etc. Moreover, tryptophan is a basic amino acid present in all kinds of medium. Therefore, the autoclaved medium change-mediated CYP1A1 induction could be a common

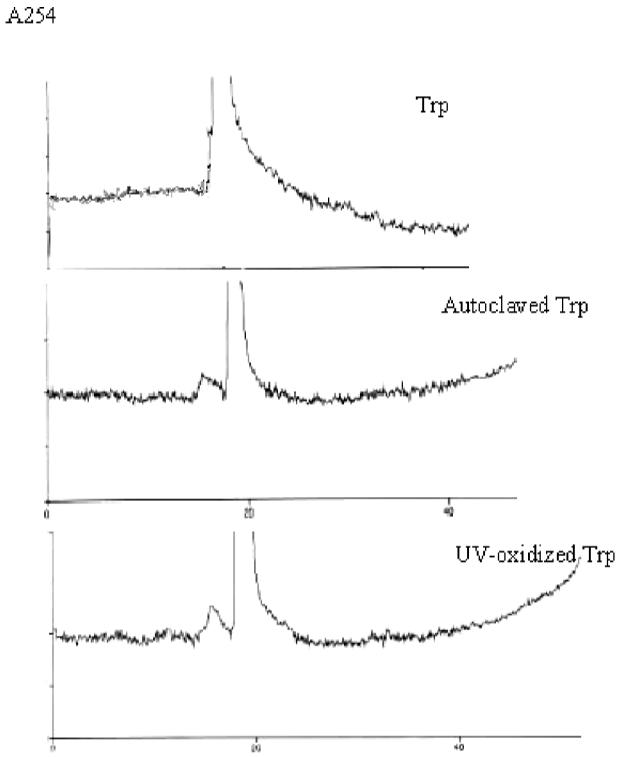


Figure 6. Reversed-phase HPLC separation of tryptophan (A), autoclaved tryptophan (B) and UV-oxidized tryptophan using a C18 analytical column, as described in the Materials and methods. The column elute was monitored at 254 nm.

phenomenon in cell culture experiments. To eliminate the influence of the medium on CYP1A1 induction, xenobiotics administered to cells should be done without changing the medium concurrently, and the culture medium should be prepared by filtration if used for CYP1A1 studies.

References

Burczynski, M. E. and Penning, T. M., 2000, Genotoxic polycyclic aromatic hydrocarbon *ortho*-quinones generated by aldo-keto reductases induce CYP1A1 via nuclear translocation of the aryl hydrocarbon receptor. *Cancer Research*, **60**, 908–915.

Carriere, V., Rodolosse, A., Lacasa, M., Cambier, D., Zweibaum, A. and Rousset, M., 1998, Hypoxia and CYP1A1 induction-dependent regulation of proteins involved in glucose utilization in Caco-2 cells. *American Journal of Physiology*, **274**, G1101–1108.

Denison, M. S., Fisher, J. M. and Whitlock, J. P., Jr, 1988, The DNA recognition site for the dioxin–Ah receptor complex: nucleotide sequence and functional analysis. *Journal of Biological Chemistry*, **263**, 17221–17224.

Guigal, N., Seree, E., Bourgarel-Rey, V. and Barra, Y., 2000, Induction of CYP1A1 by serum independent of AhR pathway. *Biochemical and Biophysical Research Communications*, **267**, 572–576.

Guigal, N., Seree, E., Nguyen, Q. B., Charvet, B., Desobry, A. and Barra, Y., 2001, Serum induces a transcriptional activation of CYP1A1 gene in HepG2 independently of the AhR pathway. *Life Sciences*, **68**, 2141–2150,

Heath-Pagliuso, S., Rogers, W. J., Tullis, K., Seidel, S. D., Cenijn, P. H., Brouwer, A. and Denison, M., 1998, Activation of the Ah receptor by tryptophan and tryptophan metabolites. *Biochemistry*, **37**, 11508–11515.

Jellinck, P. H., Forkert, P. G., Riddick, D. S. and Okey, A. B., Michnovicz, J. J.Bradlow, H. L., 1993, Ah receptor binding properties of indole carbinols and induction of hepatic estradiol hydroxylation. *Biochemical Pharmacology*, **45**, 1129–1136.

Kennedy, S. W., Lorenzen, A., James, C. A. and Collins, B. T., 1993, Ethoxyresorufin-*O*-deethylase and porphyrin analysis in chicken embryo hepatocyte cultures with a fluorescence multiwell plate reader. *Analytical Biochemistry*, **211**, 102–112.

Kocarek, T. A., Schuetz, E. G. and Guzelian, P. S., 1993, Transient induction of cytochrome P450 1A1 mRNA by culture medium component in primary cultures of adult rat hepatocytes. *In Vitro Cellular Development Biology*, **29A**, 62–66.

Krusekopf, S., Kleeberg, U., Hildebrandt, A. G. and Ruckpaul, K., 1997, Effects of benzimidazole derivatives on cytochrome P450 1A1 expression in a human hepatoma cell line. *Xenobiotica*, **27**, 1–9.

Merchant, M., Morrison, V., Santostefano, M. and Safe. S., 1992, Mechanism of action of aryl hydrocarbon receptor antagonists: inhibition of 2,3,7,8-tetrachlorodibenzo-*p*-dioxin-induced CYP1A1 gene expression. *Archives of Biochemistry and Biophysics*, **298**, 389–394.

Okamoto, T., Mitsuhashi, M., Fujita, I., Sindhu, R. K. and Kikkawa, Y., 1993, Induction of cytochrome P450 1A1 and 1A2 by hyperoxia. *Biochemical Biophysical Research Communications*, **197**, 878–885.

Rannug, A., Rannug, U., Rosenkranz, H. S., Winqvist, L., Westerholm, R., Agurell, E. and Grafstrom, A. K., 1987, Certain photooxidized derivatives of tryptophan bind with very high affinity to the Ah receptor and are likely to be endogenous signal substances. *Journal of Biological Chemistry*, **262**, 15422–15427.

Sadek, C. M. and Allen-Hoffmann, B. L., 1994a, Cytochrome P450IA1 is rapidly induced in normal human keratinocytes in the absence of xenobiotics. *Journal of Biological Chemistry*, **269**, 16067–16074.

Sadek, C. M. and Allen-Hoffman, B. L., 1994b, Suspension-mediated induction of hepa 1c1c cyp1a1 expression is dependent on the Ah receptor signal transduction pathway. *Journal of Biological Chemistry*, **269**, 31505–31509.

Santostefano, M., Merchant, M., Arellano, L., Morrison, V., Denison, M. S. and Safe, S., 1993, alpha-Naphthoflavone-induced CYP1A1 gene expression and cytosolic aryl hydrocarbon receptor transformation. *Molecular Pharmacology*, **43**, 200–206.

Segner, H., Behrens, A, Joyce, E. M., Schirmer, K. and Bols, N. C., 2000, Transient induction of 7-ethoxyresorufin-*o*-deethylase (EROD) activity by medium change in the rainbow trout liver cell line, RTL-W1. *Marine Environmental Research*, **50**, 489–493.

Sindhu, R. K. and Kikkawa, Y., 1999, Superinduction of oxidized tryptophan-inducible cytochrome P450 1A1 by cycloheximide in Hepa 1c1c7 cells. *In Vitro and Molecular Toxicology*, **12**, 149–162.

Sindhu, R. K., Reisz-Porszasz, S., Hankinson, O. and Kikkawa, Y., 1996, Induction of cytochrome P450 1A1 by photooxidized tryptophan in Hepa 1c1c cells. *Biochemistry Pharmacology*, **52**, 1883–1893.

Wei, Y. D., Bergander, L., Rannug, U. and Rannug, A., 2000, Regulation of CYP1A1 transcription via the metabolism of the tryptophan-derived 6-formylindolo[3,2-*b*]carbazole. *Archives of Biochemistry and Biophysics*, **383**, 99–107.

Wei, Y. D., Helleberg, H., Rannug, U. and Rannug, A., 1998, Rapid and transient induction of CYP1A1 gene expression in human cells by the tryptophan photoproduct 6-formylindole[3,2]-carbazole. *Chemico-Biological Interactions*, **110**, 39–55.

Whitlock, J. P., 1999, Induction of cytochrome P450 1A1. *Annual Review of Pharmacology and Toxicology*, **39**, 103–125.

Yamane, I., Matsuya, Y. and Jimbo, K., 1968, An autoclavable powdered culture medium for mammalian cells. *Proceedings of the Society for Experimental Biology and Medicine*, **127**, 335–336.

Yan, R., Sindhu, R. K. and Kikkawa, Y., 1999, Effect of ozone-oxidized tryptophan on [Ah]gene battery enzymes in Hepa 1c1c7 cells. *In Vitro and Molecular Toxicology*, **12**, 33–45.

XENOBIOTICA, 2002, VOL. 32, NO. 11, 1045–1052

Taylor & Francis
healthsciences

Disposition of LY333531, a selective protein kinase C β inhibitor, in the Fischer 344 rat and beagle dog

J. L. BURKEY*, K. M. CAMPANALE, D. D. O'BANNON, J. W. CRAMER and N. A. FARID

Lilly Research Laboratories, Division of Eli Lilly and Co., Lilly Corporate Center, Indianapolis, IN 46285, USA

Received 18 April 2002

1. Studies were conducted in the Fischer 344 rat and beagle dog to determine the disposition of LY333531 and its equipotent active *des*-methyl metabolite, LY338522, both potent and selective inhibitors of the β-isozyme of protein kinase C.

2. Male Fischer 344 rats and female beagle dogs received a single 5-mg kg^{-1} oral dose of ^{14}C-LY333531. Urine, faeces, bile and plasma were collected and analysed for ^{14}C, LY333531 and LY338522.

3. LY333531 was eliminated primarily in the faeces (91% by 120 h in rat, 90% by 96 h in dog). Bile contributed the majority of the radioactivity excreted in the faeces in rat (66% in the cannulated bile duct study) and a variable but significant proportion in dog.

4. Pharmacokinetics following a single 5 mg kg^{-1} oral dose of ^{14}C-LY333531 to the male rat produced C_{max} and $AUC_{0\text{-}\infty}$ for LY333531 of 14.7 ng ml^{-1} and 60.8 ng h ml^{-1}, respectively, with a half-life of 2.5 h. LY338522 and total radioactivity showed similar profiles.

5. In the female dog at the same dose, C_{max} and $AUC_{0\text{-}\infty}$ of LY333531 were higher, producing 245 ± 94 ng ml^{-1} and 1419 ± 463 ng h ml^{-1}, respectively, with a half-life of 5.7 h.

6. The data indicate that the disposition of LY333531 is similar in rat and dog.

Introduction

Abnormal activation of the protein kinase C (PKC) system by hyperglycaemia has been implicated in the development of diabetic microvascular complications, including diabetic retinopathy and diabetic macular oedema (Koya and King 1998). LY333531, (*S*)-13-[(monomethylamino)methyl]-10,11,14,15-tetrahydro-4,9:16,21-dimetheno-1*H*,13*H*-dibenzo [*E*,*K*] pyrrolo-[3,4-*H*][1,4,13]oxadiaza-cyclohexadecine-1,3(2*H*)-dione (figure 1), is a potent and specific inhibitor of the β-isozyme of PKC. The IC_{50} of LY333531 is 5 nM for the β-isozyme, which is at least 100-fold lower than for α-, γ- or δ-isoforms of PKC. LY338522, the *N-des*-methyl metabolite of LY333531 (figure 1), was identified in preliminary metabolism studies as the major metabolite of LY333531 and was equipotent with LY333531 in inhibiting PKC β (Eli Lilly, data on file). Thus, total PKC β inhibitory activity is based on the combined plasma concentrations of LY333531 and LY338522. *In vitro* and *in vivo* studies have shown that PKC β is inhibited by LY333531 and LY338522 at concentrations between 10 and 50 nM (Eli Lilly, data on file). The selective inhibition of PKC β has been shown to inhibit diabetes-

* Author for correspondence; e-mail: burkey_jennifer_l@lilly.com

Xenobiotica ISSN 0049–8254 print/ISSN 1366–5928 online © 2002 Taylor & Francis Ltd
http://www.tandf.co.uk/journals
DOI: 10.1080/00498250210012619

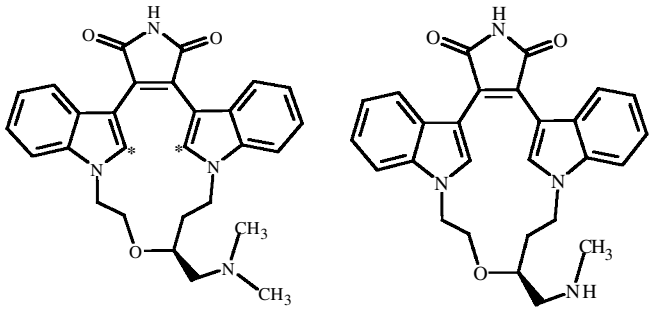


Figure 1. Structure of LY333531 and its *des*-methyl metabolite. *Position of the ^{14}C label.

induced abnormalities in retinal blood flow and intra-ocular neovascularization caused by retinal ischaemia in animals (Danis *et al.* 1998, Kowluru *et al.* 1998). Previous studies using LY333531 have shown efficacy in reversing diabetes-associated microvascular abnormalities induced in diabetic animals (Ishii *et al.* 1996), and diabetes-induced elevations in PKC β activity in the retina and kidneys of diabetic animals were normalized (Kowluru *et al.* 1996).

The disposition of ^{14}C-LY333531 in rat and dog following administration of a single 5-mg kg^{-1} oral dose is reported. The pharmacokinetics of LY533531 and LY338522 in both rat and dog following a single 5 mg kg^{-1} oral dose of LY333531 as the mesylate salt are also discussed.

Materials and methods

Animals and treatments

Rat. Male F344 rats (Harlan Sprague Dawley, Inc., Indianapolis, IN, USA) (elimination studies $n = 4$, pharmacokinetic study $n = 3$/time point) weighed 150–170 g for the elimination studies, 160–200 g for the single-dose pharmacokinetic study and 215–240 g for the bile cannulation study. Animals were identified by tail markings and were housed in either stainless steel or nalgene metabolism cages or in shoebox cages. The rats were fasted overnight before the initiation of the elimination studies and at least 2 h before the initiation of the pharmacokinetic study. Water was provided *ad libitum*. Each animal received a single 5-mg kg^{-1} oral dose of ^{14}C-LY333531 kg^{-1} in a 10% acacia suspension; 23.1 μCi kg^{-1} for the elimination study and 109 μCi kg^{-1} for the bile elimination study. Rats in the pharmacokinetic study received a single 5-mg kg^{-1} oral dose of ^{14}C-LY333531 (53.25 μCi kg^{-1}) in a 10% acacia suspension.

Dog. Female (elimination and pharmacokinetic study, $n = 4$) and male (bile cannulation study, $n = 3$) beagle dogs (Marshall Farms, North Rose, NY, USA) weighed 10–14.3 kg for the elimination and pharmacokinetic studies and 8.9–9.8 kg for the bile cannulation study. The animals were housed in stainless steel metabolism cages, fasted overnight before initiation of the studies and water was provided *ad libitum*. Each animal received a single 5-mg kg^{-1} oral dose of ^{14}C-LY333531 kg^{-1} in a 10% acacia suspension in a capsule, 5.24 μCi kg^{-1} for the elimination and pharmacokinetic studies, and 15 μCi kg^{-1} for the bile elimination study. All animal studies and procedures followed were in accordance with institutional guidelines.

Chemicals. LY333531 and [^{14}C]-LY333531 were synthesized, as the mesylate salt, at Eli Lilly and Company (Indianapolis, IN, USA). The radiochemical purity, determined by high-performance liquid chromatography (HPLC), was 96.5% and the specific activity was 10.35 μCi mg^{-1} salt for the rat and dog elimination studies and for the dog pharmacokinetic study. The radiochemical purity and specific activity were 98.2% and 88.29 μCi mg^{-1} salt for the rat pharmacokinetic and bile cannulation studies, and 99.1% and 37.1 μCi mg^{-1} salt for the cannulated bile duct dog study. LY338522 was synthesized at Eli Lilly and was used to validate the bioanalytical assay.

Sample collection

Rat. Faeces, urine and cage wash samples were collected at 24-h intervals up to 120 h after drug administration during the elimination studies. Plasma and the carcass were collected at 120 h after drug administration. In the bile elimination study, bile samples from the biliary cannula were collected at −20 °C in a refrigerated collection rack at 6-h intervals up to 48 h after drug administration. Urine, faeces and cage wash samples were collected at 24 and 48 h. Samples and carcasses were stored at −70 °C before analysis. In the pharmacokinetic study, blood samples were obtained by cardiac puncture at 0.5, 1, 2, 3, 5, 12, 24, 32, 48 and 72 h after drug administration. Plasma was obtained and stored at −70 °C before analysis.

Dog. Faeces, urine, cage wash and plasma samples were collected at 24-h intervals up to 96 h after drug administration during the elimination studies. Plasma was obtained and stored at −70 °C before analysis. In the bile elimination study, bile samples from the biliary cannula were collected at −20 °C in a refrigerated collection rack at 4–24-h intervals up to 72 h after drug administration. Samples were stored at −70 °C before analysis. In the pharmacokinetic study, blood samples were obtained from the cephalic or jugular veins at 0 (predose), 0.5, 1, 2, 3, 4, 6, 8, 12, 20, 24, 32, 48, 72 and 96 h after drug administration. Plasma was separated and samples were stored at approximately −70 °C before analysis.

Sample analysis

The concentrations of radiocarbon (^{14}C) in the dosing solution, urine, cage wash and plasma samples obtained from both species were determined in three aliquots of each sample by liquid scintillation counting (LSC). Faecal samples were soaked in de-ionized water, shaken vigorously to produce a slurry and three aliquots of each faecal slurry were dried and combusted in a Packard Tricarb Oxidizer 307 (Perkin Elmer Life Sciences Inc., Boston, MA, USA). The resulting $^{14}CO_2$ was trapped within the oxidizer in liquid scintillation fluid and assayed for radioactivity using LSC. Rat carcasses were gently boiled in a beaker containing ethanol and potassium hydroxide until all tissues had dissolved. Aliquots of the resulting digests, with added H_2O_2 (30%), were assayed for radioactivity using LSC. Correction for quenching was accomplished by external standardization. The plasma concentration of radioactivity was calculated as the ng-equivalent of LY333531 ml^{-1}.

The concentrations of LY333531 and LY338522 in plasma were determined by LC/MS/MS methods validated for each species (Brewer *et al*. 1999). Both methods were validated using calibration curves encompassing the lower and upper limit of the assay, validation samples at three concentrations including the lower and upper limit of the assay, and quality-control samples prepared to evaluate the dilution accuracy. A sensitivity (lower limit of quantification) of 0.5 ng ml^{-1} for the dog and of 1 ng ml^{-1} in the rat was established within 20% of nominal. The intra-assay accuracy was established by determining the relative error (RE), and intra-assay precision was established by determining the relative standard deviation (RSD), of the validation samples. Concentrations were determined as follows. Briefly, 300 µl of plasma were extracted using a 7-mm 3-M Empore polystyrenedivylbenzene membrane disk. The disk was washed with 3 ml water, the analytes eluted with 1 ml CH_3CN and then dried under N_2. The sample was reconstituted in 150 µl methanol/50 mm acetonitrile (1:1 v/v) and injected. A 30 × 4.6 mm ABI/Brownlee RP-18, 5 µm, column was used to separate the analytes, using methanol/250 mm acetonitrile (3:1 v/v) as the mobile phase. The flow rate was 1.0 ml min^{-1}. MS/MS detection was accomplished using positive-ion APCI (heated nebulizer interface) and data were collected using selected reaction monitoring (SRM) turbo ion-spray LC/MS/MS. Deuterated (D-6) LY333531 was used as an internal standard and was added before extraction.

Pharmacokinetic analysis

Pharmacokinetic parameters were obtained using the validated Eli Lilly ADME/PTK pharmacokinetic computer software application. Maximum plasma concentration (C_{max}) and the corresponding T_{max} were reported as observed. Concentration–time data for the analytes were plotted on a semilogarithmic scale and the terminal log–linear phase was identified by inspection and used to calculate the half-life ($T_{1/2}$). The area under the curve $AUC_{0\text{-}\tau}$ and $AUC_{0\text{-}\infty}$ were calculated using the linear–logarithmic trapezoidal method.

Results

In rat and dog, faeces was the major route of elimination of the radiocarbon following a single 5-mg kg^{-1} oral dose of ^{14}C-LY333531 as the mesylate salt. Rats eliminated 84.2% ± 2.0% (mean ± SEM, $n = 4$) of the oral dose in the faeces within the first 24 h, and 91.0% ± 3.4% by 120 h (figure 2). Only 1.31% ± 0.18% of the oral dose was recovered in the urine over 120 h. Of the administered oral dose,

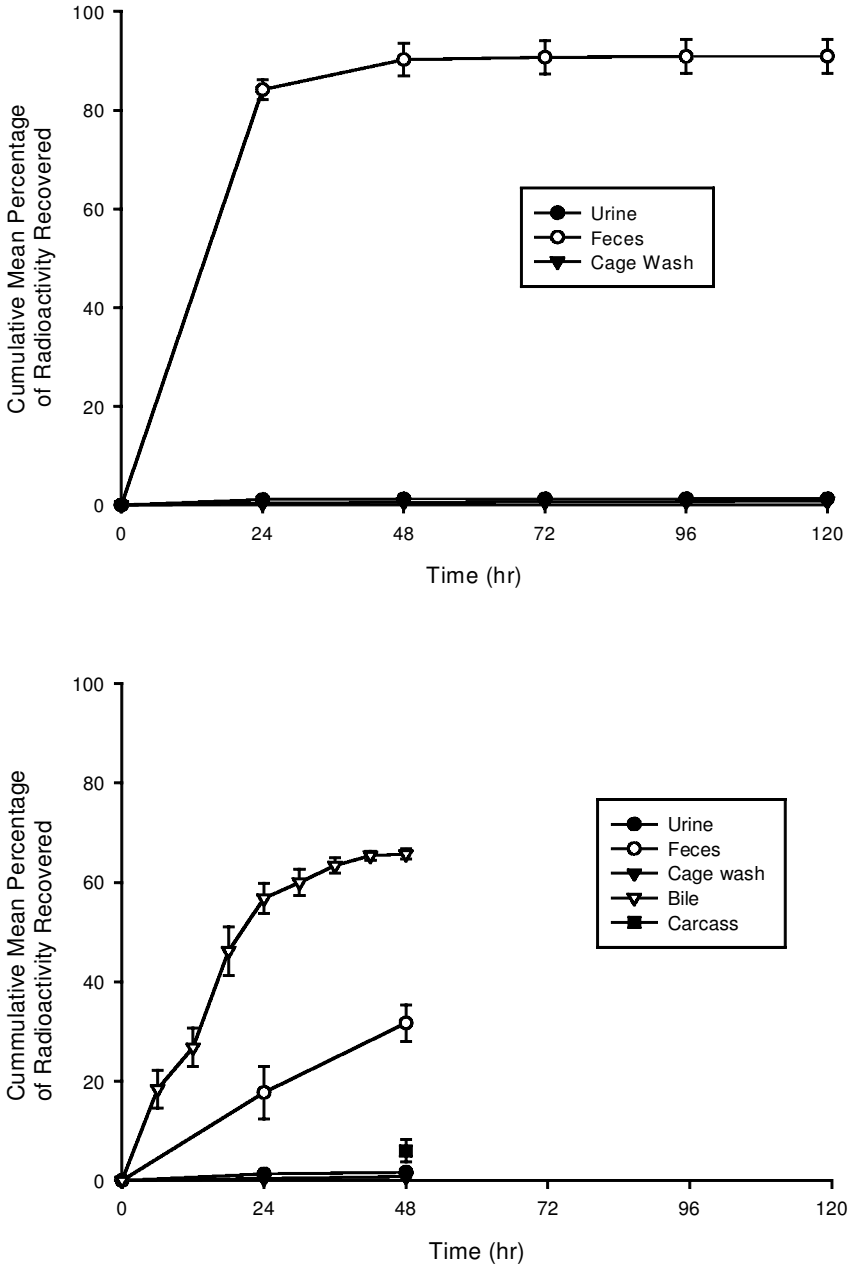


Figure 2. Cumulative mean percentage (± SEM) of the radioactive dose recovered from the Fischer 344 rat ($n = 4$) following a single oral 5 mg kg^{-1} dose of ^{14}C-LY333531 administered as the mesylate salt (elimination study top graph, bile elimination bottom graph).

0.93% ± 0.06% remained in the body. Overall, 94% ± 3.5% of the administered ^{14}C-LY333531 dose was recovered. In the biliary excretion study, rats eliminated 56.8% ± 3.0% (mean ± SEM, $n = 4$) of the dose in the bile within the first 24 h, increasing to 65.7% ± 1.0% by 48 h post-dosing (figure 2). The percentage of the dose excreted in the urine over 48 h, 1.66% ± 0.04%, was comparable with that

obtained in the previous elimination study. Faeces collected during the first day contained 17.7% ± 5.3% of the dose, which increased to 31.7% ± 3.7% of the administered dose by 48 h. Some of the radioactivity present in the faeces in the biliary excretion study could be attributed to unabsorbed drug. The residual radioactivity in the carcass was 6.0% ± 2.3%. The overall recovery rate of the radioactivity was 105.9% ± 3.1%.

Similarly, dogs eliminated 64.5% ± 3.5% (mean ± SEM, $n = 4$) of the ^{14}C dose in the faeces within the first 24 h, increasing to 89.8% ± 1.5% by 96 h (figure 3). Only 1.20% ± 0.07% of the administered dose was recovered in the urine over 96 h, with 91.3% ± 1.6% of the administered ^{14}C-LY333531 dose recovered. A noticeable amount of ^{14}C was obtained between 72 and 96 h post-dose (2.08% ± 0.75%), suggesting that the overall recovery data would have been higher had the collection proceeded beyond 96 h. In the biliary excretion study, there was large variability between animals, with dogs eliminating 1, 6 and 33% of the radioactivity in the bile by 48 h. All dogs excreted minimal radioactivity in the urine and 25–65% of the radioactivity in the faeces in this study, which was consistent with the distribution of elimination seen in the previous elimination study.

The plasma concentrations and pharmacokinetic parameters of radioactivity, LY333531 and LY338522 were determined following a single 5-mg kg^{-1} dose of ^{14}C-LY333531 to both rat and dog. These data are shown in table 1. In rat, the mean (± SEM) maximum plasma radioactivity concentration (C_{max}) was 121 ng-equivalent of LY333531 ml^{-1}, achieved 2 h after dosing (table 1 and figure 4). Plasma concentrations of radioactivity decreased with a $T_{1/2} = 11.0$ h. Radio-

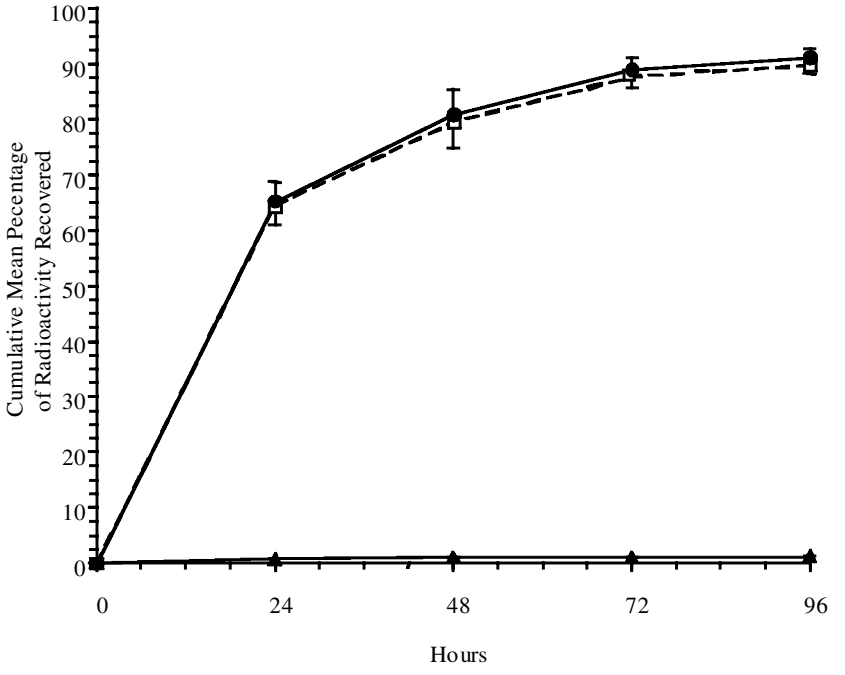


Figure 3. Cumulative mean percentage (± SEM) of the radioactive dose recovered from the faeces (box), urine (triangle), and total (circle) from the beagle dog ($n = 4$) following a single oral 5 mg kg^{-1} dose of ^{14}C-LY333531 administered as the mesylate salt.

Table 1. Mean plasma concentrations and pharmacokinetic parameters of ^{14}C, LY333531 and LY335822 in the male F344 rat and female beagle dog following a single 5 mg kg^{-1} oral dose of ^{14}C-LY333531 administered as the mesylate salt.

	^{14}C-equivalents	LY333531	LY338522
Pharmacokinetic parameter: rat ($n = 3$)			
C_{max} (ng ml^{-1})	121[c]	14.7	46.0
T_{max} (h)	2	2	2
$T_{1/2}$ (h)	11.0	2.5	4.3
AUC (ng h ml^{-1})[a]	688[d]	58.7	235
$AUC_{0-\infty}$ (ng h ml^{-1})	730[d]	60.8	238
Pharmacokinetic parameter: dog ($n = 4$) ($\pm$ SEM)			
C_{max} (ng ml^{-1})	1445 ± 589[c]	245 ± 94	736 ± 338
T_{max} (h)	3.3 ± 0.5	2.3 ± 0.6	3.8 ± 0.3
$T_{1/2}$ (h)	11.1 ± 1.9	5.7 ± 0.6	10.7 ± 0.7
AUC (ng h ml^{-1})[b]	$18\,870 \pm 6740$[d]	1412 ± 463	9013 ± 4140
$AUC_{0-\infty}$ (ng h ml^{-1})	19760 ± 6740[d]	1419 ± 463	9037 ± 4150

[a] AUC were calculated from 0–32, 0–12 and 0–24 h for ^{14}C, LY333531 and LY335822, respectively.

[b] AUC were calculated from 0–48, 0–48 and 0–96 h for ^{14}C, LY333531, and LY335822, respectively.

[c] ng equivalents ml^{-1}.

[d] ng equivalents h ml^{-1}.

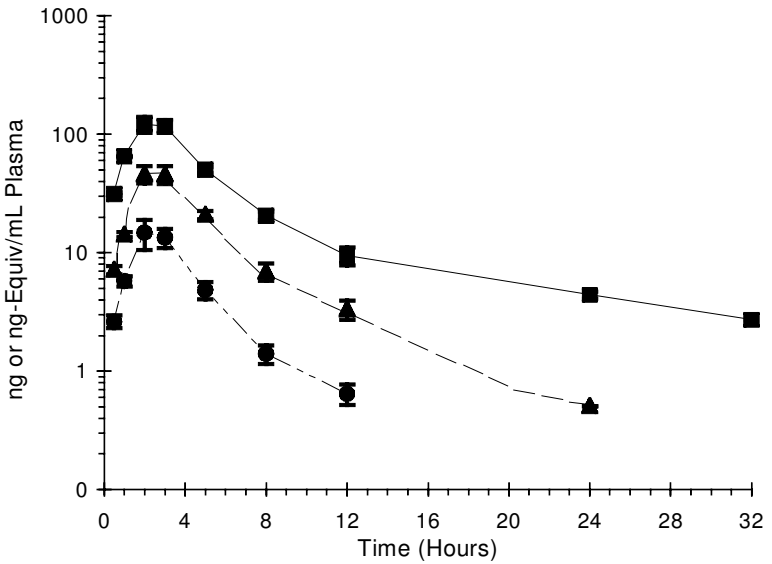


Figure 4. Mean ($\pm$ SEM) plasma concentrations of ^{14}C (boxes), LY333531 (circles) and LY338522 (triangles) following a single 5 mg kg^{-1} oral dose of ^{14}C-LY333531 administered as the mesylate salt to the Fischer 344 rat ($n = 3$).

activity was detected in only one of three rats at 32 h (2.7 ng-equivalent ml^{-1}), and no radioactivity was detected in plasma samples collected at and beyond 48 h post-dose. The mean C_{max} values of LY333531 and LY338522 were 14.7 and 46.0 ng ml^{-1}, respectively; both were attained 2 h after drug administration. LY333531 and LY338522 accounted for approximately 12 and 38%, respectively, of the plasma radioactivity at 2 h after the dose. The $T_{1/2}$ values for LY333531 and

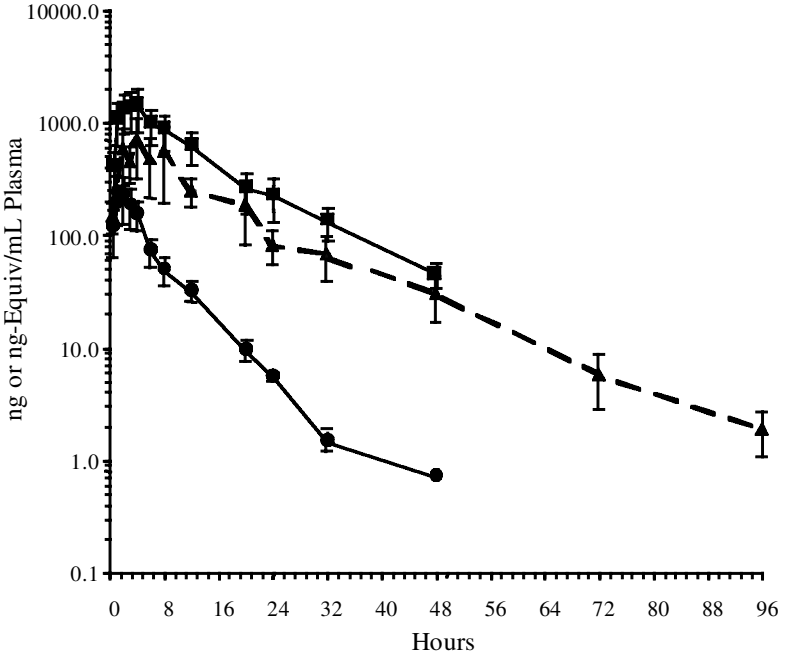


Figure 5. Mean (±SEM) plasma concentrations of ^{14}C (boxes), LY333531 (circles) and LY338522 (triangles) following a single 5 mg kg^{-1} oral dose of ^{14}C-LY333531 administered as the mesylate salt to the beagle dog ($n = 4$).

LY338522 were 2.5 and 4.3 h, respectively. The $AUC_{0\text{-}\infty}$ for radioactivity was 730 ng-equivalent h ml^{-1}, and those for LY333531 and LY338522 were 60.8 and 238 ng h ml^{-1}, respectively. Based on the $AUC_{0\text{-}\infty}$ data, LY333531 and LY338522 accounted for approximately 41% of the radioactivity in the plasma. This corresponds with the percentage of dose eliminated in the bile shown above. In dog, the C_{max} of radioactivity was 1445 ng-equivalent of LY333531 ml^{-1}, achieved approximately 3 h after dosing (table 1 and figure 5). Plasma concentrations of radioactivity decreased with a $T_{1/2} = 11.0$ h, as was seen for rat. No radioactivity was detected in plasma samples collected at and beyond 72 h post-dose. The mean C_{max} values of LY333531 and LY338522 were 245 and 736 ng ml^{-1}, respectively, 2–4 h after drug administration. LY333531 and LY338522 accounted for approximately 13.5 and 37.6%, respectively, of the plasma radioactivity between 2 and 4 h after the dose. The $AUC_{0\text{-}\infty}$ for radioactivity was 19760 ± 6740 ng-equivalent h ml^{-1}, while those for LY333531 and LY338522 were 1419 ± 463 and 9037 ± 4150 ng h ml^{-1}, respectively. Based on the $AUC_{0\text{-}\infty}$ data, LY333531 and LY338522 accounted for approximately half of the radioactivity in the plasma.

Discussion

Plasma concentrations of LY333531 and the active *N-des*-methyl metabolite LY338522 were measurable in all studies, indicating that LY333531 is absorbed following oral administration to rat and dog. Of the absorbed fraction of the dose, the bile is the primary route of elimination for ^{14}C-LY333531 for both species, with approximately 57% of the administered dose eliminated in the bile, and

approximately 97% eliminated in the bile and faeces combined in rat. Some of the radioactivity present in the faeces may be attributed to non-absorbed ^{14}C-LY333531 since approximately one-third of the radioactivity was found in this matrix. Renal elimination of LY333531 is a minor pathway in rat. Similarly, in dog, up to 33% of the administered dose is eliminated in the bile, with the majority of the excreted radioactivity eliminated in the bile and faeces combined. Thus, in both species, the primary route of excretion is faecal, with a substantial biliary component, and urinary excretion is a minor pathway of elimination. The large proportion of radioactivity in the faeces may be the result of limited systemic absorption of LY333531 or possible intestinal metabolism of the compound.

Single-dose pharmacokinetic studies in both species indicate that LY333531 is absorbed and that both parent and metabolite are detectable in the plasma. Together, parent and metabolite accounted for approximately 41% of the radioactivity in plasma for rat, and approximately half of the radioactivity in dog. The greater AUC and longer elimination half-life determined for radioactivity in the plasma for rat indicate the possible presence of other metabolite(s) of LY333531 that may have a longer $T_{1/2}$ than LY333531 or LY338522. The difference in half-life between the radioactivity and the metabolite is not as pronounced in dog, but the greater AUC for total radioactivity also suggests the possible presence of other metabolite(s) of LY333531.

The results show that, in general, the disposition of ^{14}C-LY333531 is comparable in rat and dog.

References

Brewer, E., Vitale, K., Mann, M., Lowes, S., Humphries, D., Li, Q., Garner, C. O. and Henion, J. 1999. Determination of LY333531 and its desmethyl metabolite in plasma from multiple species by API LC/MS/MS. In Proceedings of the 47th American Society for Mass Spectrometry Conference on Mass Spectrometry and Allied Topics. Dallas, TX.

Danis, R. P., Bingaman, D. P., Jirousek, M. R. and Yang, Y., 1998, Inhibition of intraocular neovascularization caused by retinal ischemia in pigs by PKC β inhibition with LY333531. *Investigative Ophthalmology and Visual Science*, **39**, 171–179.

Ishii, H., Jirousek, M. R., Koya, D., Takagi, C., Xia, P., Clermont, A., Bursell, S.-E., Kern, T. S., Ballas, L. M., Heath, W. F., Stramm, L. E., Feener, E. P. and King, G. L., 1996, Amelioration of vascular dysfunctions in diabetic rats by an oral PKC β inhibitor. *Science*, **272**, 728–731.

Kowluru, R., Jirousek, M., Stramm, L., Engerman, R. and Kern, T., 1996, Diabetes-induced disorders of retinal protein kinase C and Na,K-ATPase are inhibited by LY333531. *Diabetes*, **45**(S2), 16A.

Kowluru, R. A., Jirousek, M. R., Stramm, L. E., Farid, N. A., Engerman, R. L. and Kern, T. S., 1998, Abnormalities of retinal metabolism in diabetes or experimental galactosemia. V. Relationship between protein kinase C ATPases. Retinal protein kinase C in diabetes. *Diabetes*, **47**, 464–469.

Koya, D. and King, G. L., 1998, Protein kinase C activation and the development of diabetic complications. *Diabetes* **47**, 859–866.

XENOBIOTICA, 2002, VOL. 32, NO. 11, 1053–1062

Taylor & Francis
healthsciences

Phenotype distribution and gender-related differences of CYP2E1 activity in a Chinese population

XIAO-PING CHEN, XING-MEI HAN, CHANG-HONG JIANG, SONG-LIN HUANG, ZHAO-QIAN LIU, BING ZHU, GAN ZHOU and HONG-HAO ZHOU*

Pharmacogenetics Research Institute, Xiang-Ya School of Medicine, Central South University, Changsha, Hunan 410078, PR China

Received 14 February 2002

1. The aim was to investigate the phenotype distribution characteristic and gender-related differences of CYP2E1 activity in a healthy Chinese population.

2. Two hundred and three healthy Chinese subjects (105 men, 98 women) were enrolled in this study.

3. CYP2E1 activity was determined by plasma 6-hydroxychlorzoxazone-to-chlorzoxazone concentration ratio (CHZ-MR) 4 h after chlorzoxazone dosing. The concentrations of 6-hydroxychlorzoxazone and chlorzoxazone in plasma were detected by reversed-phase HPLC.

4. The results showed an almost 9-fold variation of CYP2E1 activity at a range of from 0.23 to 1.99. The coefficient of variation CY % was demonstrated with skewness and kurtosis of the ratios in the studied population were 44%, 0.96 and 1.10, respectively.

5. CYP2E1 activity was normally distributed in logarithmic form of 6-OH-CHZ/CHZ as evaluated by Kolmogorov–Smirnov test of normality ($p = 0.20$). Probit plots of the CYP2E1 activity index of men shifted to the right as compared with that of women. The mean CHZ-MR in men was significantly higher than that in women (0.76 ± 0.30 versus 0.60 ± 0.28, $p < 0.001$), and this difference still existed when normalized by weight (0.73 ± 0.28 versus 0.66 ± 0.32, $p = 0.016$). Body weight correlated positively with CYP2E1 activity in the total group($r < 0.212$, $p < 0.01$).

Introduction

Ethanol-inducible CYP2E1 is one of the major cytochrome P450 forms in the human liver and constitutive expression of CYP2E1 is localized mainly in the central lobule region of the organ, which contributes to about 7% of the total cytochrome P450 protein in the adult liver (Shimada *et al.* 1994). Minor expression of CYP2E1 protein can also be detected in some extrahepatic tissues such as the lung, kidney, placenta (Vieira *et al.* 1998), brain (Upadhya *et al.* 2000) and peripheral lymphocytes (Raucy *et al.* 1997). CYP2E1 is involved in the metabolism of a number of drugs such as chlorzoxazone (CHZ) (Lucas *et al.* 1999), paracetamol (Manyike *et al.* 2000), trimethadione (Kurata *et al.* 1998) and many halogenated volatile anaesthetics including methoxyflurane, enflurane, isoflurane and sevoflurane (Kharasch and Thummel 1993, Garton *et al.* 1995, Wandel *et al.* 1997, Kharasch *et al.* 1999a). It is also involved in the metabolic activation of procarcinogens such as *N*-nitrosamines, which are found in tobacco smoke and food, and many low molecular weight protoxins, such as ethanol, carbon tetra-

* Author for correspondence; e-mail: hhzhou@public.cs.hn.cn

Xenobiotica ISSN 0049–8254 print/ISSN 1366–5928 online © 2002 Taylor & Francis Ltd
http://www.tandf.co.uk/journals
DOI: 10.1080/00498250210163270

chloride and benzenes (Tanaka *et al*. 2000). CYP2E1 has been postulated to play a role in the pathogenesis of alcohol-induced liver disease (Ingelman-Sundberg *et al*. 1993, Morimoto *et al*. 1993). Furthermore, it has been reported to be responsible for the hepatotoxicity and nephrotoxicity mediated by paracetamol or fluorinated anaesthetic through formation of their respective toxic metabolites (Fuhr 2000, Prescott 2000).

Considerable interindividual variation in CYP2E1 activity has been reported in Caucasians irrespective of whether measured *in vitro* in hepatic microsomes or *in vivo* using the 6-hydroxylation of CHZ as a phenotypic probe (Kim *et al*. 1995, Vesell *et al*. 1995, Carriere *et al*. 1996). Interracial differences in both CYP2E1 protein level and catalytic activity have been described in a study showing that Japanese subjects expressed significantly lower CYP2E1 activity than in Caucasians (Kim *et al*. 1996). *In vivo* CYP2E1 activity is modulated by many factors including obesity, fasting, dietary lipids, diabetes and liver transplantation (Johansson *et al*. 1990, O'Shea *et al*. 1994, Burckart *et al*. 1998, Lucas *et al*. 1998, Le Marchand *et al*. 1999, Boucher *et al*. 2000), as well as several xenobiotics such as isoniazid, disulfram, alcohol and diallyl sulphide (Zand *et al*. 1993, Kharasch *et al*. 1999b, Prescott 2000, Loizou and Cocker 2001). Such modulation in expression influences the toxicity of substrates for CYP2E1 (Prescott 2000). Assessment of CYP2E1 *in vivo* status in man and its distribution characteristic in populations will provide a sound theoretical basis for clinical drug administration and a reasonable explanation for CYP2E1-associated diseases.

In vivo activity of CYP450s can be measured by administration of corresponding probe drugs as reviewed by Streetman *et al*. (2000). CHZ is a skeletal muscle relaxant used for the treatment of painful muscle spasms and it mainly undergoes hydroxylation to form 6-hydroxychlorzoxazone in the liver (Peter *et al*. 1990). Though previous studies have suggested that CYP1A1, CYP1A2 and, possibly, CYP3A are involved in CHZ 6-hydroxylation, particularly at lower serum concentrations (Carrier *et al*. 1993, Ono *et al*. 1995, Gorski *et al*. 1997), Carriere *et al*. (1996) and Lucas *et al*. (1999) demonstrated that rates of CHZ 6-hydroxylation were significantly correlated with the level of immunochemically detected CYP2E1 or its catalytic activity detected by other *in vitro* probes in human liver microsomes, and the CHZ metabolic ratio was not affected by inducers or inhibitors of CYP1A and CYP3A. When the relative contents of CYP2E1, CYP1A and CYP3A in the liver are considered further, it can be deduced that CYP2E1 is the major enzyme involved in CHZ 6-hydroxylation and that the contribution of CYP1A and CYP3A is very minor. Accordingly, CHZ has been proved the only safe and acceptable probe for the determination of CY2E1 *in vivo* activity. Various pharmacokinetics parameters have been proposed to reflect CYP2E1 *in vivo* activity, among which the ratio of single plasma concentrations of 6-OH-CHZ/CHZ measured at 2, 3, 4 and 5 h after oral CHZ dose correlates well with fractional CHZ clearance by 6-hydroxylation and was indicative of CYP2E1 activity (Kim *et al*. 1995, Frye *et al*. 1998). More recently, CYP2E1 has been reported to be expressed in peripheral lymphocytes. Importantly, a positive correlation is observed between CYP2E1 content in lymphocytes and CHZ clearance rates, even under induced states (Raucy *et al*. 1997). Thus, the 6-hydroxylation of chlorzoxazone provides an ideal non-invasive drug for estimating both CYP2E1 hepatic activity and the molecular mechanisms of its regulation under various pathophysiological conditions in man.

In the present study, CYP2E1 activity determined by CHZ 6-hydroxylation was measured in a healthy Chinese population. The aim was to investigate the phenotype distribution characteristics and interindividual variation of CYP2E1 in this population.

Materials and methods

Subjects

The study was approved by the Ethics Committee of Xiang-Ya School of Medicine, Central South University, and performed after informed consent of all subjects. Two hundred and three healthy Chinese volunteers (105 men, 98 women, aged 18–23 years) were recruited. The average weight and body mass index (BMI) of the men and women were 60.3 ± 6.9 kg (range 50–76 kg) and 21.2 ± 2.0 kg m^{-2} (17.5–27.6 kg m^{-2}), 51.4 ± 5.1 kg (43–65 kg) and 20.3 ± 1.5 kg m^{-2} (17.0–24.6 kg m^{-2}), respectively. Each subject was in good health based on medical history, physical examination and laboratory evaluation. None of the subjects were tobacco users or taking any medication. All subjects abstained from alcohol- and caffeine-containing food or drink for at least 1 week before the study.

Chemicals

CHZ tablets were products of Hongqi Pharmaceutical Co. (Shanghai, China). CHZ and 6-OH-CHZ were bought from UltraFine Chemicals (Manchester, UK), phenacetin (used as internal standard) and β-glucoronidase were purchased from Sigma Chemical Co. (St Louis, MO, USA). Methanol and acetonitrile were of hplc grade and other reagents were of AR grade unless indicated.

Experimental protocol

After an overnight fast, all subjects were orally administrated a 200-mg CHZ tablet with about 150 ml water in the morning of the study. A venous blood sample of 5 ml, using EDTA as anticoagulant, was obtained from an arm vein 4 h after drug administration. Plasma was harvested by centrifuging and stored at –20°C before analysis.

Phenotype

Plasma CHZ and 6-OH-CHZ were determined by reversed-phase hplc as reported by Lucas *et al.* (1993) with a modest modification. Plasma (0.5 ml) was added to 1 ml of 0.2 mol l^{-1} sodium acetic acid buffer (pH 4.75) containing 1000 U β-glucuronidase. The sample was vortex-mixed and incubated at 37°C for 4 h. After incubation, 50 µl phenacetin (internal standard, 20 µmol l^{-1}) was added to the sample and extracted with 5 ml ethyl ether. The sample was shaken for 4 min and centrifuged at 2000*g* for 10 min. The upper organic phase was transferred to clean glass tubes and evaporated to dryness under a stream of nitrogen at 37°C. The residue was dissolved in 50 µl mobile phase, and a 20-µl aliquot was injected into the hplc system. The hplc system consisted of a HP 1050 series, a reversed-phase C8 column (4.6 × 150 mm, 5 µm particle size, Hewlett Packard) and a UV detector. The mobile phase was composed of 25 mmol l^{-1} sodium dihydrogen phosphate, acetonitrile and methanol at a ratio of 66:24:10 (v/v/v), and the pH of the eluent was finally adjusted to 3.5 with orthophosphoric acid. The flow rate was 0.7 ml min^{-1} for 0–5 min, and then 1.4 ml min^{-1} afterwards. The UV detector was set at 282 nm for 0–6 min, and then shifted to 264 nm thereafter. The column temperature was maintained at 37°C. The molar concentration ratio of 6-OH-CHZ/CHZ was determined and represents CYP2E1 activity, as discussed above.

Data analysis

Statistic analysis of the data was performed by SPSS 10.0 for Windows. Frequency distribution and probit plots were determined for the phenotype distribution of CYP2E1 activity. The normal distribution of CYP2E1 activity was assessed by the Kolmogorov–Smirnov test. A general linear model was applied to analyse the correlation between CYP2E1 activity and body weight or BMI. CYP2E1 activity (mean SD) differences between men and women were compared using the Mann–Whitney *U*-test. Statistical significance was regarded as $p < 0.05$.

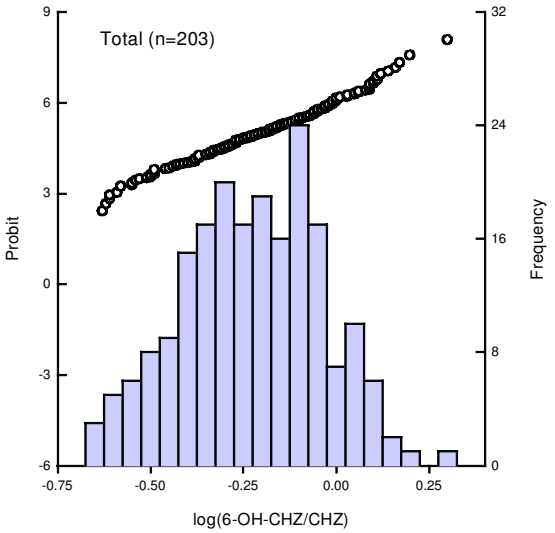


Figure 1. Probit plot and frequency distribution of CYP2E1 activity index in Chinese subjects.

Results

Phenotype distribution of CYP2E1 activity in Chinese subjects

The mean level of CYP2E1 activity was 0.69 0.30 in the 203 subjects. An almost 9-fold variation of CYP2E1 activity was observed over the range 0.23–1.99. The coefficient of variation (CV%), skewness and kurtosis of the ratios were 44%, 0.96 and 1.10, respectively. CYP2E1 activity in the total subjects was not normally distributed as assessed by the Kolmogorov–Smirnov test of normality ($p < 0.001$); however, a normal distribution was indicated after logarithmic transformation of the ratios ($p = 0.20$). In addition, CYP2E1 activity, as indicated by log(6-OH-CHZ/CHZ), appeared to be unimodally distributed in the studied population by visual inspection of the frequency distribution and probit plots (figure 1).

Gender-related differences in CYP2E1 activity

The mean value of 6-OH-CLZ/CLZ in men was significantly higher than that in women (0.78 ± 0.30 versus 0.60 ± 0.28, $p < 0.001$). Figure 3 shows that the probit plot of CYP2E1 activity index in men shifted right as compared with women. Analysis of demographic characteristic shows that both average body weight (60.2 ± 6.7 versus 51.4 ± 5.0 kg, men versus women, $p < 0.001$) and average BMI (21.2 ± 2.0 versus 20.3 ± 1.5 kg m^{-2}, men versus women, $p < 0.001$) in men were significantly greater than that in women (table 1). In view of this, CYP2E1

Table 1. Demographic characteristics of male and female subjects.

	Male	Female	*P* male versus female
n	104	99	
Age (year)	20 ± 1	20 ± 1	
Weight (kg)	60.24 ± 6.73	51.38 ± 5.04	< 0.001
BMI (kg m^{-2})	21.24 ± 2.00	20.33 ± 1.50	< 0.001

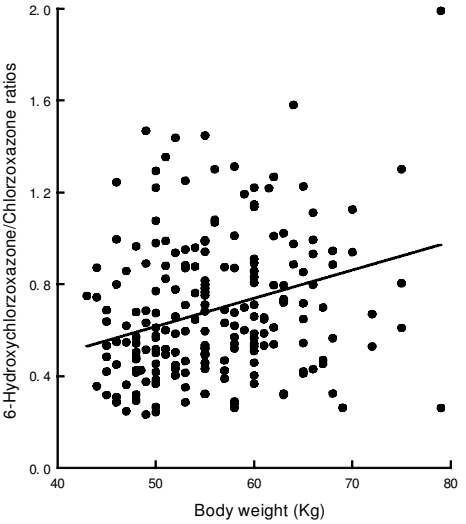


Figure 2. Correlation between body weight and CYP2E1 activity in Chinese subjects ($r < 0.212$, $p < 0.01$, $n = 203$).

activity was further adjusted by body weight, but the gender-related differences in CYP2E1 activity still existed (0.73 ± 0.28 versus 0.66 ± 0.32, men versus women, $p = 0.016$).

Relationship between body weight or BMI with CYP2E1

Correlation analysis showed that there was a significant positive correlation between body weight and CYP2E1 activity in the total subjects group ($r < 0.212$, $p < 0.01$, $n = 203$) as shown in figure 2, but this correlation disappeared when

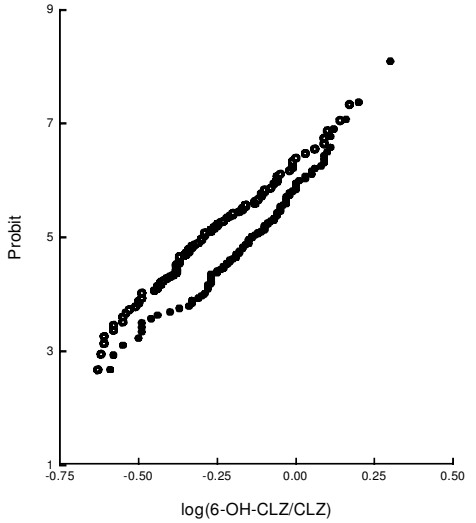


Figure 3. Probit plots of CYP2E1 activity index in men (solid circles) and women (open circles).

analysed as respective subgroups of male and female subjects. No correlation was found between BMI and CYP2E1 activity.

Discussion

Phenotype polymophisms of several drug-metabolizing enzyme has been reported in a Chinese population by our laboratory, such as CYP2C19 and CYP2D6 (Zhou and Liu 2000). However, no data are available about the phenotype distribution characteristics of CYP2E1 in Chinese to date and this study is the first to do so. Our results have shown that CYP2E1 *in vivo* activity is normally distributed in a previously studied population, and an almost 9-fold interindividual variation in CHZ 6-hydroxylation activity is observed. Kim *et al.* (1994, 1995) also reported a unimodal distribution of CYP2E1 activity in Caucasians estimated by both oral clearance of CHZ and the percentage of the administered dose excreted as the 6-hydroxy metabolite in the urine. The distribution fashion of CYP2E1 activity in the current Chinese population is consistent with that in Caucasians. The interindividual difference observed by us was comparable with that reported in Caucasians, which was 2–5-fold (Kim *et al.* 1994, 1995, Vesell *et al.* 1995). However, this variability is far less than that detected based on either immunochemically determined CYP2E1 protein levels or CYP2E1 activity in human liver *in vitro*, which has been reported to be almost 40–50-fold (Shimada *et al.* 1994, Carriere *et al.* 1996). This interindividual difference may not be due to obesity because none of the subjects could be regarded as obese according to their BMIs, which were 17.5–27.6 $kg\,m^{-2}$ in men and 17.0–24.6 $kg\,m^{-2}$ in women.

The interindividual differences play an important role in the formation of inorganic fluoride, the hepatotoxic and nephrotoxic metabolite of fluorinated anaesthetics mediated by CYP2E1 (Wandel *et al.* 1997). In another study where CYP2E1 activity was estimated by the fractional excretion of CHZ, subjects with a rapid fractional excretion have an increased risk of benzene poisoning compared with those with a slow fractional excretion (Rothman *et al.* 1997). Increased CYP2E1 activity has also been postulated to be responsible for increased hepatotoxicity induced by the activate metabolite of paracetamol (Prescott 2000) and for complications of insulin-dependent diabetes mellitus (IDDM) (Hannon-Fletcher *et al.* 2001). It has been speculated that individual susceptibility to CYP2E1-associated adverse drug reaction and chemical toxicity is likely related to the expression level of the CYP2E1 enzyme. Therefore, accurate estimation of the CYP2E1 phenotype distribution in the population becomes increasingly more important in drug therapy and for the prediction of individual risk for putative CYP2E1-related toxicant or disease susceptibility, and a lower level of CYP2E1 would be expected to reduce susceptibility to some chemical-induced carcinogenecity, as occurs in animals.

Our correlation analysis also identified a significantly positive linear relationship between CYP2E1 activity and body weight in total subjects, but this correlation disappeared when analysed as the respective subgroups of male and female subjects. However, the correlation coefficient in the total group is 0.212, indicating that body weight is a minor contributor to CYP2E1 *in vivo* activity, and this is far less than the result of Le Marchand *et al.* (1999) who reported that body weight is a major contributor, about 43%, to the interindividual variability in the oral clearance of CHZ. Of course, it is not known whether the higher degree of

relationship in Hawaii-Japanese reported by Le Marchand *et al.* is caused by the obesity. Thus, CYP2E1 activity is regulated to a small extent by body mass in non-obese individuals, an association may reflect a relationship with liver size.

In the present study, a gender difference in CYP2E1 activity was observed, with men demonstrating significantly higher CYP2E1 activity than women. Gender-related difference in CYP2E1 activity is in agreement with Kim *et al.* (1995) and Lucas *et al.* (1995), who observed a significantly higher clearance of CHZ or basal CYP2E1 activity in non-smoking men compared with non-smoking women. However, no gender difference in CYP2E1 protein level and catalytic activity was found *in vitro* in human liver microsomes (Hunt *et al.* 1990, Shimada *et al.* 1994). In view of the effect of body weight on CYP2E1 activity observed in the current study and that the average weight in men was significantly higher than that in women, the gender difference in the CHZ metabolic ratio was further analysed after weight normalization. However, the difference was still present. In Kim *et al.* (1995) and Le Marchand *et al.* (1999), the gender difference was less striking and not statistically significant after normalization according to body weight, although the trends remained. Our previous results have indicated an intrinsic enzymatic difference in drug metabolism between men and women irrespective of differences in body size and it may have resulted from differences in steroid hormones such as testosterone (Pan *et al.* 1992). It is well known that oesophageal cancer is prevalent in North China and that *N*-nitrosamines in food are one of the causative factors (Lu *et al.* 1991). The incidence of oesophageal cancer in this high-risk region of China was markedly higher in men than in women (Yu *et al.* 1993). Whether these gender differences were partially due to the gender-related difference in CYP2E1 activity and consequent metabolic activation of *N*-nitrosamines and precursors is as yet unknown.

Genetic polymorphisms and individual variation in CYP450s have been intensively studied in populations with different ethnic background in recent years (Han and Zhou 2000, Zhou and Liu 2000). Few frequent functional mutations have been found in exons of *CYP2E1*, indicating the important physiological role of CYP2E1 *in vivo*. Several restriction fragment-length polymorphisms have been detected in the regulative region and introns of *CYP2E1*, among which *CYP2E1*5B* and *CYP2E1*6* genetic polymorphisms have been studied intensively in the last decade (Hayashi *et al.* 1991, Uematsu *et al.* 1991). *CYP2E1*5B* polymorphism has been reported to affect the transcriptional expression of a reporter gene *in vitro* (Hayashi *et al.* 1991). Both these polymorphisms were reported to be associated with a modified risk of susceptibility to several types of cancer, such as lung, nasopharyngeal, oesophageal and gastric (Uematsu *et al.* 1991, Wu *et al.* 1998, Han and Zhou 2000, Tan *et al.* 2000). Le Marchand *et al.* (1999) and Kim *et al.* (1995) have also shown a decreased CYP2E1 activity by the rare alleles *CYP2E1*5B* or *CYP2E1*6*. However, other studies performed on Caucasians (Lucas *et al.* 1995, Carriere *et al.* 1996, Kim *et al.* 1996) demonstrated no associations between these genetic polymorphisms and CYP2E1 activity both *in vivo* and *in vitro*. Because frequencies of these rare alleles are markedly different among populations with different ethnic background, controversial results may occur owing to the limited power of statistic in some studies. *CYP2E1*5B* or *CYP2E1*6* mutations are more frequent in Chinese as have been shown in some case-control studies (Lin *et al.* 1998, Tan *et al.* 2000). Whether these marked interindividual differences in CYP2E1 activity observed herein in a Chinese

population resulted from these genetic polymorphisms is an issue worthy of further investigation.

Acknowledgements

The project was supported by China Medical Board of New York, Grant Nos 99-697 and 01-755, and by the National Nature Science Foundation of China Grant No. 30130210.

References

Boucher, P., Seree, E., Vidon, C., de Souza, A. C., Villard, P. H., Chambon, R., Barra, Y. and Vallon, J. J., 2000, Dietary lipid affect human ethanol-inducible CYP2E1 gene expression *in vivo* in mononuclear cells. *Life Science*, **67**, 1307–1316.

Burckart, G. J., Frye, R. F., Kelly, P., Branch, R. A., Jain, A., Fung, J. J., Starzl, T. E. and Venkataramanan, R., 1998, Induction of CYP2E1 activity in liver transplant patients as measured by chlorzoxazone 6-hydroxylation. *Clinical Pharmacology and Therapeutics*, **63**, 296–302.

Carrier, V., Goasduff, T., Ratanasavanh, D., Morel, F., Gautier, J. C., Guillouzo, A., Beaune, P. and Berthou, F., 1993, Both cytochromes P450 2E1 and 1A1 are involved in the metabolism of chlorzoxazone. *Chemical Research in Toxicology*, **6**, 852–857.

Carriere, V., Berthou, F., Baird, S., Belloe, C., Beaune, P. and de Waziers, I., 1996, Human cytochrome P450 2E1 (CYP2E1): from genotype to phenotype. *Pharmacogenetics*, **6**, 203–211.

Frye, R. F., Adedoyin, A., Mauro, K., Matzke, G. R. and Branch, R. A., 1998, Use of chlorzoxazone as an *in vivo* probe of cytochrome P450 2E1: choice of dose and phenotypic trait measure. *Journal of Clinical Pharmacology*, **38**, 82–89.

Fuhr, U., 2000, Induction of drug metabolising enzymes. *Clinical Pharmacokinetics*, **38**, 493–504.

Garton, K. J., Yuen P., Meinwald, J., Thummel, K. E. and Kharasch, E. D., 1995, Stereoselective metabolism of enflurane by human liver cytochrome P450 2E1. *Drug Metabolism and Disposition*, **23**, 1426–1430.

Gorski, J. C., Jones, D. R., Wrighton, S. A. and Hall, S. D., 1997, Contribution of human CYP3A subfamily members to the 6-hydroxylation of chlorzoxazone. *Xenobiotica*, **27**, 243–256.

Han, X. M. and Zhou, H. H., 2000, Polymorphism of CYP450 and cancer susceptibility. *Acta Pharmacologica Sinica*, **21**, 673–679.

Hannon-Fletcher, M. P., O'Kane, M. J., Moles, K. W., Barnett, Y. A. and Barnett, C. R., 2001, Lymphocyte cytochrome P450-CYP2E1 expression in human IDDM subjects. *Food and Chemical Toxicology*, **39**, 125–132.

Hayashi, S., Wantanabe, J. and Kavajiri, K., 1991, Genetic polymorphisms in the 5′-flanking region change transcriptional regulation of human cytochrome P4502E1 gene. *Journal of Biochemistry*, **110**, 559–565.

Hunt, C. M., Strater, S. and Stave, E. M., 1990, Effect of normal aging on the activity of human hepatic cytochrome P450IIEI. *Biochemical Pharmacology*, **40**, 1666–1669.

Ingelman-Sundberg, M., Johansson, I., Yin, H., Terelius, Y., Eliasson, E., Clot, P. and Albano, E., 1993, Ethanol-inducible cytochrome P4502E1: genetic polymorphism, regulation, and possible role in the etiology of alcohol-induced liver disease. *Alcohol*, **10**, 447–452.

Johansson, I., Lindros, K. O., Eriksson, H. and Ingelman-Sundberg, M., 1990, Transcriptional control of CYP2E1 in the perivenous liver region and during starvation. *Biochemical and Biophysical Research Communications*, **173**, 331–338.

Kharasch, E. D. and Thummel, K. E., 1993, Identification of cytochrome P450 2E1 as the predominant enzyme catalyzing human liver microsomal defluorination of sevoflurane, isoflurane, and methoxyflurane. *Anesthesiology*, **79**, 795–807.

Kharasch, E. D., Hankins, D. C. and Cox, K., 1999a, Clinical isoflurane metabolism by cytochrome P450 2E1. *Anesthesiology*, **90**, 766–771.

Kharasch, E. D., Hankins, D. C., Jubert, C., Thummel, K. E. and Taraday, J. K., 1999b, Lack of single-dose disulfiram effects on cytochrome P-450 2C9, 2C19, 2D6, and 3A4 activities: evidence for specificity toward P-450 2E1. *Drug Metabolism and Disposition*, **27**, 717–723.

Kim, R. B., O'Shea, D. and Wilkinson, G. R., 1995 Interindividual variability of chlorzoxazone 6-hydroxylation in men and women and its relationship to CYP2E1 genetic polymorphism. *Clinical Pharmacology and Therapeutics*, **57**, 645–655.

Kim, R. B., O'Shea, D. and Wilkinson, G. R., 1994, Relationship in healthy subjects between CYP2E1 genetic polymorphisms and the 6-hydroxylation of chlorzoxazone: a putative measure of CYP2E1 activity. *Pharmacogenetics*, **4**, 162–165.

Kim, R. B., Yamazaki, H., Chiba, K., O'Shea, D., Mimura, M., Guengerich, F. P., Ishizaki, T., Shimada, T. and Wilkinson, G. R., 1996, *In vivo* and *in vitro* characterization of CYP2E1 activity in Japanese and Caucasians. *Journal of Pharmacology and Experimental Therapeutics*, **279**, 4–11.

Kurata, N., Nishimura, Y., Iwase, M., Fischer, N. E., Tang, B. K., Inaba, T. and Yasuhara, H., 1998, Trimethadione metabolism by human liver cytochrome P450: evidence for the involvement of CYP2E1. *Xenobiotica*, **28**, 1041–1047.

Le Marchand, L., Wilkinson, G. R. and Wilkens, L. R., 1999, Genetic and dietary predictors of CYP2E1 activity: a phenotyping study in Hawaii Japanese using chlorzoxazone. *Cancer Epidemiology, Biomarkers and Prevention*, **8**, 495–500.

Lin, D. X., Tang, Y. M., Peng, Q., Lu, S. X., Ambrosone, C. B. and Kadlubar, F. F., 1998, Susceptibility to esophageal cancer and genetic polymorphisms in glutathione *S*-transferases T1, P1, and M1 and cytochrome P450 2E1. *Cancer Epidemiology, Biomarkers and Prevention*, **7**, 1013–1018.

Loizou, G. D. and Cocker, J., 2001, The effects of alcohol and diallyl sulphide on CYP2E1 activity in humans: a phenotyping study using chlorzoxazone. *Human and Experimental Toxicology*, 20, 321–327.

Lu, S. H., Chui, S. X., Yang, W. X., Hu, X. N., Guo, L. P. and Li, F. M., 1991, Relevance of *N*-nitrosamines to oesophageal cancer in China. *IARC Scientific Publications*, 105, 11–17.

Lucas, D., Berthou, F., Girre, C., Poitrenaud, F. and Menez, J. F., 1993, High-performance liquid chromatographic determination of chlorzoxazone and 6-hydroxychlorzoxazone in serum: a tool for indirect evaluation of cytochrome P4502E1 activity in humans. *Journal of chromatography*, **622**, 79–86.

Lucas, D., Farez, C., Bardou, L. G., Vaisse, J., Attali, J. R. and Valensi, P., 1998, Cytochrome P450 2E1 activity in diabetic and obese patients as assessed by chlorzoxazone hydroxylation. *Fundamental and Clinical Pharmacology*, **12**, 553–558.

Lucas, D., Ferrara, R., Gonzalez, E., Bodenez, P., Albores, A., Manno, M. and Berthou, F., 1999, Chlorzoxazone, a selective probe for phenotyping CYP2E1 in humans. *Pharmacogenetics*, **9**, 377–388.

Lucas, D., Menez, C., Girre, C., Berthou, F., Bodenez, P., Joannet, I., Hispard, E., Bardou, L. G. and Menez, J. F., 1995, Cytochrome P450 2E1 genotype and chlorzoxazone metabolism in healthy and alcoholic Caucasian subjects. *Pharmacogenetics*, **5**, 298–304.

Manyike, P. T., Kharasch, E. D., Kalhorn, T. F. and Slattery, J. T., 2000, Contribution of CYP2E1 and CYP3A to acetaminophen reactive metabolite formation. *Clinical Pharmacology and Therapeutics*, **67**, 275–282.

Morimoto, M., Hagbjork, A. L., Nanji, A. A., Ingelman-Sundberg, M., Lindros, K. O., Fu, P. C., Albano, E. and French, S. W., 1993, Role of cytochrome P4502E1 in alcoholic liver disease pathogenesis. *Alcohol*, **10**, 459–464.

Ono, S., Hatanaka, T., Hotta, H., Tsutsui, M., Satoh, T. and Gonzalez, F. J., 1995, Chlorzoxazone is metabolized by human CYP1A2 as well as by human CYP2E1. *Pharmacogenetics*, **5**, 143–150.

O'Shea, D., Davis, S. N., Kim, R. B. and Wilkinson, G. R., 1994, Effect of fasting and obesity in humans on the 6-hydroxylation of chlorzoxazone: a putative probe of CYP2E1 activity. *Clinical Pharmacology and Therapeutics*, **56**, 359–367.

Pan, J., Hong, J. Y. and Yang, C. S., 1992, Post-transcriptional regulation of mouse renal cytochrome P450 2E1 by testosterone. *Archives of Biochemistry and Biophysics*, **299**, 110–115.

Peter, R., Bocker, R., Beaune, P. H., Iwasaki, M., Guengerich, F. P. and Yang, C. S., 1990, Hydroxylation of chlorzoxazone as a specific probe for human liver cytochrome P-450IIEI. *Chemical Research in Toxicology*, **3**, 566–573.

Prescott, L. F., 2000, Paracetamol, alcohol and the liver. *British Journal of Clinical Pharmacology*, **49**, 291–301.

Raucy, J. L., Schultz, E. D., Wester, M. R., Arora, S., Johnston, D. E., Omdahl, J. L. and Carpenter, S. P., 1997, Human lymphocyte cytochrome P450 2E1, a putative marker for alcohol-mediated changes in hepatic chlorzoxazone activity. *Drug Metabolism and Disposition*, **25**, 1429–1435.

Rothman, N., Smith, M. T., Hayes, R. B., Traver, R. D., Hoener, B., Campleman, S., Li, G. L., Dosemeci, M., Linet, M., Zhang, L., Xi, L., Wacholder, S., Lu, W., Meyer, K. B., Titenko Holland, N., Stewart, J. T., Yin, S. and Ross, D., 1997, Benzene poisoning, a risk factor for hematological malignancy, is associated with the NQO1 609C → T mutation and rapid fractional excretion of chlorzoxazone. *Cancer Research*, **57**, 2839–2842.

Shimada, T., Yamazaki, H., Mimura, M., Inui, Y. and Guengerich, F. P., 1994, Interindividual variation in human liver cytochrome P-450 enzymes involved in the oxidation of drugs, cardinogens and toxic chemicals: studies with liver microsomes of 30 Japanese and 30 Caucasians. *Journal of Pharmacology and Experimental Therapeutics*, **270**, 414–423.

Streetman, D. S., Bertino, J. S. and Nafziger, A. N., 2000, Phenotype of drug-metabolizing enzymes in adults: a review of *in-vivo* cytochrome P450 phenotype. *Pharmacogenetics*, **10**, 187–216.

Tan, W., Song, N., Wang, G. Q., Liu, Q., Tang, H. J., Kadlubar, F. F. and Lin, D. X., 2000, Impact of genetic polymorphisms in cytochrome P450 2E1 and glutathione *S*-transferases M1, T1, and P1 on susceptibility to esophageal cancer among high-risk individuals in China. *Cancer Epidemiology, Biomarkers and Prevention*, **9**, 551–556.

Tanaka, E., Terada, M. and Misawa, S., 2000, Cytochrome P450 2E1: its clinical and toxicological role. *Journal of Clinical Pharmacy and Therapeutics*, **25**, 165–175.

Uematsu, F., Kikuchi, H. and Motomiya, M., 1991, Association between restriction fragment length polymorphism of human cytochrome P4502E1 and susceptibility to lung cancer. *Japanese Journal of Cancer Research*, **82**, 254–256.

Upadhya, S. C., Tirumalai, P. S., Boyd, M. R., Mori, T. and Ravindranath, V., 2000, Cytochrome P4502E (CYP2E) in brain: constitutive expression, induction by ethanol and localization by fluorescence *in situ* hybridization. *Archives of Biochemistry and Biophysics*, **373**, 23–34.

Vesell, E. S., Seaton, T. D. and A-Rahim, Y. I., 1995, Studies on interindividual variations of CYP2E1 using chlorzaxazone as an *in vivo* probe. *Pharmacogenetics*, **5**, 53–57.

Vieira, I., Pasanen, M., Raunio, H. and Cresteil, T., 1998, Expression of CYP2E1 in human lung and kidney during development and in full-term placenta: a differential methylation of the gene is involved in the regulation process. *Pharmacology and Toxicology*, **83**, 183–187.

Wandel, C., Neff, S., Keppler, G., Bohrer, H., Stockinger, K., Wilkinson, G. R., Wood, M. and Martin, E., 1997, The relationship between cytochrome P4502E1 activity and plasma fluoride levels after sevoflurane anesthesia in humans. *Anesthesia and Analgesia*, **85**, 924–930.

Wu, X., Amos, C. I., Kemp, B. L., Shi, H., Jiang, H., Wan, Y. and Spitz, M. R., 1998, Cytochrome P450 2E1 DraI polymorphisms in lung cancer in minority populations. *Cancer Epidemiology, Biomarkers and Prevention*, **7**, 13–18.

Yu, Y., Taylor, P. R., Li, J. Y., Dawsey, S. M., Wang, G. Q., Guo, W. D., Wang, W., Liu, B. Q., Blot, W. J. and Shen, Q., 1993, Retrospective cohort study of risk-factors for esophageal cancer in Linxian, People's Republic of China. *Cancer Causes and Control*, **4**, 195–202.

Zand, R., Nelson, S. D., Slattery, J. T., Thummel, K. E., Kalhorn, T. F., Adams, S. P. and Wright, J. M., 1993, Inhibition and induction of cytochrome P4502E1-catalyzed oxidation by isoniazid in humans. *Clinical Pharmacology and Therapeutics*, **54**, 142–149.

Zhou, H. H. and Liu, Z. Q., 2000, Ethnic difference in drug metabolism. *Clinical Chemistry and Laboratory Medicine*, **38**, 899–903.

XENOBIOTICA, 2002, VOL. 32, NO. 12, 1063–1077

Taylor & Francis
healthsciences

Quantitative structure–activity relationship (QSAR) and three-dimensional QSAR analysis of a series of xanthates as inhibitors and inactivators of cytochrome P450 2B1

I. LESIGIARSKA†, I. PAJEVA† and S. YANEV‡*

† Centre of Biomedical Engineering and ‡ Department of Drug Toxicology, Institute of Physiology, Bulgarian Academy of Sciences, Acad. G. Bonchev Str., bl.23, 1113 Sofia, Bulgaria

Received 20 February 2002

1. Various xanthates (R-OCS_2) were found to be mechanism-based inactivators of cytochrome P450 2B1 (CYP2B1) and CYP2B6 via formation of reactive metabolites.

2. In the present study, quantitative structure–activity relationships (QSARs) were derived with inhibitory and inactivation potencies of 15 xanthates (R = two to 20 methylene groups, allyl, cyclohexyl or *O*-tricyclo[5.2.1.$0^{2,6}$]dec-9-yl (D609)) against purified, reconstituted rat liver CYP2B1. Factor, regression and comparative molecular field analyses (CoMFA) were used.

3. The compounds formed two groups whose activities depended on different structural features: the first group consisted of compounds with ethyl, propyl, allyl, cyclohexyl and D609 substituents; the second involved compounds with eight to 20 methylene groups.

4. High correlation between the molecular volume and inhibitory potency of the xanthates of the second group was found. The inactivation potency in the first group correlated with the charge of the first carbon atom of R, identifying this atom as a potential target for metabolic attack. A decrease in the inactivation potency with an increase in the size of R was observed in the second group. This finding could be explained by a decreased rate of metabolism of the long alkyl chain compounds and/or by difficulty in binding of the resulting metabolite(s) to the enzyme molecule.

Introduction

Cytochromes P450 (CYPs) are haem-containing enzymes involved in the metabolism of many endogenous and exogenous compounds and are classified into families and subfamilies according to their primary sequence homology. The CYP2 family is the most widespread one in the animal species, consisting of 15 subfamilies (CYP2A to CYP2Q) (Nelson *et al.* 1996). The CYP2B subfamily is expressed at low levels in man, but plays an important role in the metabolism of xenobiotics in rodents and other mammalian species.

Information about the key amino acid residues that take part in substrate metabolism is provided by site-directed mutagenesis studies and by multiple sequence alignments of the enzyme and bacterial CYPs with known crystal structure (CYP102, 101, 108) (He *et al.* 1992, Halpert and He 1993, He *et al.* 1994, 1995, Luo *et al.* 1994, Szklarz *et al.* 1995, Chang *et al.* 1996, Fang *et al.* 1997, Lewis and Lake 1997, Dai *et al.* 1998, Kobayashi *et al.* 1998, Waller *et al.* 1999).

* Author for correspondence; e-mail: tox@bio.bas.bg

Xenobiotica ISSN 0049–8254 print/ISSN 1366–5928 online © 2002 Taylor & Francis Ltd
http://www.tandf.co.uk/journals
DOI: 10.1080/0049825021000012574

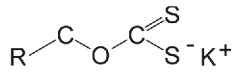
Although the substrates of the CYP2B subfamily have distinct chemical structures, many of them possess high lipophilicity and have non-planar molecular geometries and are often comprised of two aromatic rings and a central tetrahedral carbon atom, which adopts a 'V'-shape or 'butterfly wing' conformation (Lewis *et al*. 1987, Rossi *et al*. 1987). Many CYP2B substrates also possess an alkyl chain, e.g. alkyl benzenes, benzphetamines, aliphatic primary amines and 2,4-dichlorophenoxy *N*-alkyl *N*-methylethylamines (Lewis and Lake 1997). The length of this chain appears to be an important factor for enzyme–substrate interactions (Lewis and Lake 1997). For example, 7-pentoxyresorufin has been shown to be a CYP2B-specific substrate in a homologous series of 7-alkoxyresorofines (Burke *et al*. 1985), while *n*-octylamine exhibits the maximal binding affinity for rabbit CYP2B4 in a series of aliphatic primary amines (Jefcoate *et al*. 1969).

Quantitative structure–activity relationship (QSAR) analysis relies on the assumption that the biological effect of a certain bioactive compound is a function of its chemical structure. The analysis results in mathematical models that describe quantitatively the relationship between chemical structure and biological activity in a series of similar compounds with the same mechanism of action. The models are based on the linear relationship of the free energy ΔG of the investigated process on the compound structural descriptors. ΔG is related to the parameter describing biological activity K (equilibrium constant of binding or inhibition, rate constant of metabolism or distribution) by the logarithmic dependence:

$$\Delta G = -2.303RT \log K.$$

where R is the gas constant (1.987 cal deg^{-1} mol^{-1}) and T is the absolute temperature (310 K). Consequently, the QSAR models use the logarithm of the bioactivity parameters.

Several QSAR studies on CYP2B enzymes have been published. For example, Murray (1989) performed a QSAR analysis of a series of 2- and 10-substituted phenothiazine tranquillizers that revealed the importance of lipophilicity of the 2-position substituent and the negative effect of flexibility of the 10-position substituent for the enzyme inhibition. Lewis *et al*. (1995a) investigated *para*-substituted toluenes and reported that the free energies of binding to CYP2B4 could be well described by combinations of the volume of the solvent-accessible molecular surface and the energy of the highest occupied molecular orbital (HOMO) or the same volume and the average energy of the lowest unoccupied molecular orbital (LUMO) population density of methyl hydrogen atoms, whereas the rate constants for hydroxylation could be described by a two-parameter equation involving the dipole moment and the volume of the solvent-accessible molecular surface. Performing QSAR investigation of a series of alkoxyresofurins, Lewis *et al*. (1995b) established metabolism rate dependence on different parameters of overall molecular shape of the substrates (length and depth). According to the QSAR results of Lewis and Lake (1997) (biological and structural data from Roffey 1993), there is a quadratic dependence of the rate of *N*-demethylation of 2,4-dichlorophenoxy-*N*-alkyl-*N*-methylethylamine compounds on the molecular surface area. In the same paper, a QSAR study of a series of halothanes (biological and structural data from Eldirdiri 1992) was reported demonstrating the importance of the partition coefficient 'oil–water' $\log P$ and the difference between HOMO and LUMO energies for the substrate-binding affinity.



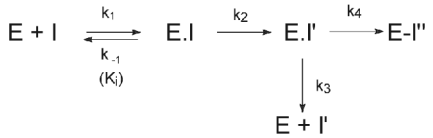


Figure 1. General chemical structure of *n*-alkylxanthates (Yanev *et al*. 1999) and a kinetic scheme of inhibition and inactivation of the CYP enzyme (Waley 1980).

Xanthates (R-OCS_2) are aryl- or alkyl-substituted derivatives of the dithiocarbonic acid and are widely used in industry and analytical chemistry as powerful heavy metal complexing agents. They have been shown to be potent inhibitors and selective mechanism-based inactivators of some mammalian cytochrome CYP isoforms, namely rat CYP2B1 and human CYP2B6 (Yanev *et al*. 1985, Kent *et al*. 1999, Yanev *et al*. 1999, 2000). It has been found that after binding to the enzyme (inhibition of the enzyme), the compounds undergo catalytic conversion to reactive intermediates that covalently bind to the enzyme molecule and cause its inactivation (figure 1) (Kent *et al*. 1999, Yanev *et al*. 2000). Because of the ability of the dithiocarbonate group to form complexes with metal ions, it has been suggested that the binding of xanthates to CYP2B1 and CYP2B6 is, at least partially, due to the formation of complexes with the haem iron (Yanev *et al*. 2000). The chemical structure of the metabolites has not yet been identified. Kent *et al*. (1999) and Yanev *et al*. (2000) suggested that the initial site of metabolism was the first carbon atom of the hydrocarbon chain (figure 1). Inactivation potency is described by the concentration of the compounds that yields half-maximal inactivation (K_I) and the rate constant of inactivation k_{inact}. According to Yanev *et al*. (1999), K_I depends on K_i, k_2, k_3 and k_4, and k_{inact} is a function of k_2, k_3 and k_4 (figure 1).

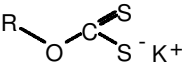
In the present study, QSAR and three-dimensional (3D) QSAR analysis of a series of 15 xanthates with inhibitory and inactivation activities against CYP2B1 has been performed to understand better the mechanism of interactions with the enzyme and to provide information for the synthesis of new, more potent and selective CYP inactivators.

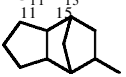
Materials and methods

The compounds used were tested for CYP2B1 inhibitory activity by Yanev *et al*. (1999). Table 1 shows the structural and biological data.

Modelling was done with Sybyl 6.5 molecular modelling software (Tripos Associates, St Louis, MO, USA). Molecular mechanics calculations were performed with Tripos force field (Powell method, no electrostatics, 0.05 kcal mol^{-1} convergence criterion). For quantum chemistry calculations, the semi-empirical method PM3 (Mopac 6.0, Sybyl 6.5) was used. Log*P*'s were calculated with the programme ClogP 1.0 (ClogP 1.0 for Windows, Biobyte Corp. 1995). The factor and regression analyses were performed with Statistica 5.0 (Statistica 5.0 for Windows; StatSoft, Inc. Tulsa, OK, USA 1995). 3D-QSAR was done with comparative molecular field analysis (CoMFA) (Sybyl 6.5).

Table 1. Chemical structures and biological activities of the investigated compounds.



Compound no.	Compound code	R	K_i (μM)	K_I (μM)	k_{inact} (min^{-1})
1	C2	$-CH_2CH_3$	66	27	0.22
2	C3	$-(CH_2)_2CH_3$	21	40	0.21
3	C3iso	$-CH(CH_3)_2$	3.5	5.4	0.05
4	C3allyl	$-CH=CH-CH_3$	26	11	0.07
5	C4	$-(CH_2)_3CH_3$	5	23	0.09
6	D609	$-C_{11}H_{15}$ 	20	15	0.10
7	Cycloh	$-C_6H_{11}$ 	71	16	0.06
8	C5	$-(CH_2)_4CH_3$	7.2	10	0.07
9	C8	$-(CH_2)_7CH_3$	6.4	2.4	0.07
10	C10	$-(CH_2)_9CH_3$	8.2	8.3	0.11
11	C12	$-(CH_2)_{11}CH_3$	5.8	14	0.12
12	C14	$-(CH_2)_{13}CH_3$	3.6	21	0.05
13	C16	$-(CH_2)_{15}CH_3$	3.3	52	0.03
14	C18	$-(CH_2)_{17}CH_3$	3.0	31	0.02
15	C20	$-(CH_2)_{19}CH_3$	2.3	69	0.03

K_i, K_I - the concentrations of the compounds required for half-maximal inhibition and inactivation of CYP2B1 respectively; k_{inact}, rate constant of inactivation.

The X-ray structure of *n*-butylxanthate (C4, table 1) (Cambridge crystallographic data centre, V.5.13, University Chemical Laboratory, Cambridge, UK) served as a starting conformation. Conformational analysis was performed using Sybyl 6.5 Systematic search by rotation of the single bonds rb1, rb2, rb3 and rb4 (figure 2) with an increment of 30°. The oxygen O4 atom was used as an anchor atom and van der Walls radius scale factors were 0.8 for general and 1,4 interactions and 0.65 for hydrogen bond interactions. Two global minimum energy conformations were found (2.24 kcal mol^{-1} after molecular mechanics optimization) with torsions (0, 180, 300, 180°) and (0, 180, 60, 180°), respectively, for rb1, rb2, rb3 and rb4. The two conformations were mirror-like and identical in their structural descriptors (HOMO, LUMO, heat of formation, charges on the atoms) after optimization with PM3. Therefore, the conformation (0, 180, 300, 180°) was chosen for the further analyses that corresponded to the X-ray conformation and also served for building the rest of the compounds in the series. The side chain after C8 in the structures of the compounds with unbranched R was built maximally extended (figure 2). The energetically more preferable 'chair' conformation of the cyclohexane ring was used for compound Cycloh (table 1) and the *trans*-isomeric form for C3allyl (table 1). All structures were first optimized with molecular mechanics and then with PM3.

The reciprocal K_i and K_I ($1/K_i$, $1/K_I$) were used to obtain higher values for the more active analogues. Plotting $\log(1/K_I)$ or $\log(1/K_i)$ against the number of carbon atoms in the xanthates with an *n*-alkyl chain, the free energy increment of inhibition or inactivation that accompanies the addition of one methylene group to the alkyl chain was calculated according the equation:

$$\Delta\Delta G = 2.303RT\Delta \log(1/K_I) \qquad (\text{or } \Delta \log(1/K_i)),$$

where $\Delta \log(1/K_I)$ (or $\Delta \log(1/K_i)$) are the slopes of the lines.

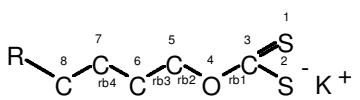


Figure 2. Rotatable bonds of *n*-alkylxanthates used in the systematic conformational search.

To perform CoMFA, the molecules were aligned with Sybyl 6.5 Database Alignment on the dithiocarbonate group because of the suggested identical way of binding to the enzyme through a complex formation with the haem iron. The electrostatic and steric interaction energies were calculated with a sp3 carbon probe atom of $+1$ charge. The grid spacing of 2 Å, column-filtering σ_{min} of 2 kcal mol^{-1}, energetic field cut-off values of 30 kcal mol^{-1}, no electrostatic interactions at bad steric contacts and distance-dependent dielectric constant were used. PLS leave-one-out cross-validated procedure was applied.

Results and discussion

The calculated structural descriptors used in the QSAR analysis are summarized in table 2. The ClogP programme reported 'not valid due to missing data' log P for the compound C3allyl, and 'too big values, unrealistic in nature' for the log P of compounds C12–C20.

The intercorrelation coefficients (R) of the calculated structural descriptors are shown in table 3. The statistically significant coefficients ($p < 0.05$) are shown in **bold**. According to R, the structural descriptors can be divided into two main sets with significant internal correlations between the descriptors: (1) QC, QO, HOMO, LUMO, I_POT, P_MIN; and (2) HEAT_F, MV, MW, ClogP. P_MAX could not be assigned to either set. The descriptors in the first set relate mostly to the electronic nature of the compounds and could influence the electrostatic interactions with the enzyme; those in the second set refer to the volume and size of the compounds and could affect the distribution of the compounds in the lipid environment of the enzyme and the steric interactions.

A number of QSAR models were examined with the measured biological activities and calculated structural descriptors that combined different numbers of compounds and different combinations of structural descriptors. In the first runs, all compounds were included. The best statistically significant models are presented in equations (1–3):

$$\mathrm{Log}(1/K_i) = +0.003(\pm 0.001)\mathrm{MV} + 4.397(\pm 0.224), \quad (1)$$

where $n = 15$, $R^2 = 0.446$, $F = 10.481$, $s = 0.372$.

$$\mathrm{Log}k_{\mathrm{inact}} = -0.002(\pm 0.001)\mathrm{MV} - 0.735(\pm 0.133), \quad (2)$$

where $n = 15$, $R^2 = 0.484$, $F = 12.196$, $s = 0.220$.

$$\mathrm{Log}k_{\mathrm{inact}} = -0.003(\pm 0.001)\mathrm{MV} + 21.594(\pm 7.417)\mathrm{QC} - 0.813(\pm 0.109), \quad (3)$$

where $n = 15$, $R^2 = 0.698$, $F = 13.843$, $s = 0.175$.

Figure 3a shows predicted values by equation (1) versus the observed log(1/K_i). As seen from the plot, the compounds with longer hydrocarbon chains are fairly well described by the model whereas those with smaller substituents are more scattered. This fact suggests that the variations in the volume/size descriptors cannot represent adequately the variations in activity in the whole series, and that the compounds in the series may form groups in which different structural descriptors might correlate with activity.

Figure 3b shows predicted versus observed log k_{inact} corresponding to equation (3). Although this model has the best statistical parameters (possibly due to the two-parametric dependency used; QC alone was not significant), the plot remains relatively scattered with large residuals for some of the compounds.

To investigate the structural homogeneity in the series, the PLS X scores of CoMFA steric and electrostatic fields of 14 compounds were explored (as shown

Table 2. Calculated structural descriptors of the investigated xanthates.

Compound no.	Compound code	QC (e)	QO (e)	HOMO (eV)	LUMO (eV)	I_POT (eV)	P_MIN (eV)	P_MAX (eV)	HEAT_F (kcal)	MV ($Å^3$)	MW	$C \log P$
1	C2	0.016	_0.191	_3.913	3.678	3.913	_96.378	_0.931	_48.49	88.4	121.2	2.11
2	C3	0.012	_0.190	_3.924	3.666	3.924	_96.300	_0.842	_53.31	104.5	135.2	2.63
3	C3iso	_0.006	_0.185	_3.942	3.621	3.942	_94.971	2.678	_54.78	104.1	135.2	2.41
4	C3allyl	_0.004	_0.138	_4.170	3.209	4.170	_91.270	9.356	_31.73	96.9	133.2	1.45*
5	C4	0.012	_0.191	_3.937	3.650	3.937	_96.120	_0.768	_58.89	120.6	149.3	3.16
6	D609	0.005	_0.182	_4.006	3.541	4.006	_94.370	7.852	_52.63	186.8	227.4	4.23
7	Cycloh	_0.002	_0.184	_3.970	3.581	3.970	_94.603	1.966	_62.22	142.1	175.3	3.61
8	C5	0.012	_0.191	_3.944	3.645	3.944	_96.024	_0.261	_64.34	136.7	163.3	3.69
9	C8	0.012	_0.191	_3.954	3.635	3.954	_95.897	3.901	_80.73	184.9	205.4	5.28
10	C10	0.011	_0.191	_3.953	3.633	3.953	_95.969	5.223	_91.58	217.0	233.4	6.34
11	C12	0.011	_0.191	_3.956	3.632	3.956	_95.987	5.649	_102.45	249.2	261.5	7.40**
12	C14	0.010	_0.191	_3.956	3.628	3.956	_95.951	6.104	_113.29	281.2	289.5	8.45**
13	C16	0.011	_0.191	_3.960	3.630	3.960	_95.876	6.720	_124.15	313.4	317.6	9.51**
14	C18	0.011	_0.192	_3.954	3.629	3.954	_96.035	7.058	_134.99	345.5	345.6	10.57**
15	C20	0.011	_0.191	_3.955	3.632	3.955	_96.024	7.186	_145.84	377.7	373.7	11.63**

* Not valid owing to missing data (ClogP 1.0 for Windows, Biobyte Corp. 1995).

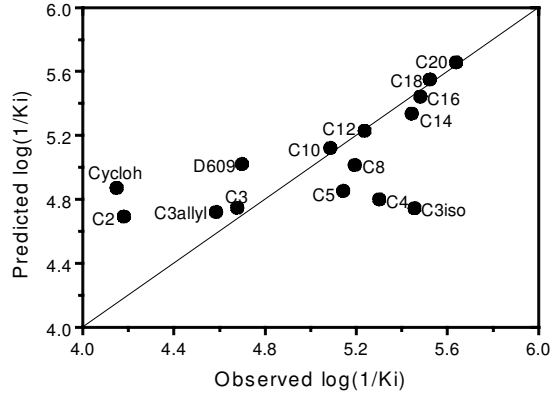
** Too big a value, too unrealistic in nature (ClogP 1.0 for Windows, Biobyte Corp. 1995).

QC, charge of the first carbon atom of the alkyl chain C5 (figure 2); QO, charge of the oxygen atom O4 (figure 2); HOMO, energy of the highest occupied molecular orbital; LUMO, energy of the lowest unoccupied molecular orbital; I_POT, ion potential; P_MIN, minimal electrostatic potential around the molecule; P_MAX, maximal electrostatic potential around the molecule; HEAT_F, heat of formation; MV, van der Waals volume of the molecule; MW, molecular weight; $C \log P$, partition coefficient 'oil–water' of the neutral forms of the corresponding acids ($R–OCS_2H$).

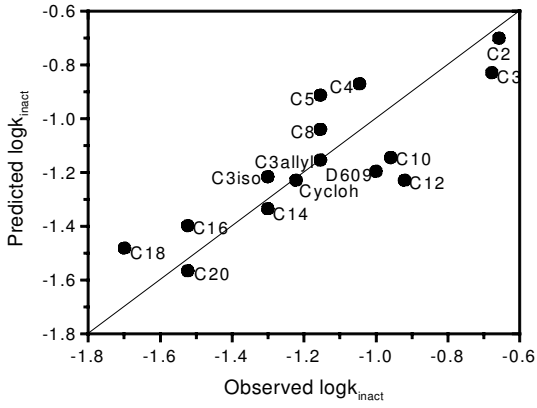
Table 3. Correlation coefficients between the calculated structural descriptors.

	QC	QO	HOMO	LUMO	I_POT	P_MIN	P_MAX	HEAT_F	MV	MW	*C*log*P*
QC	1.00	**_0.65**	**0.59**	**0.63**	**_0.59**	**_0.78**	_0.28	_0.41	0.33	0.31	0.38
QO		1.00	**_0.96**	**_0.99**	**0.96**	**0.96**	0.42	0.48	_0.36	_0.34	_0.42
HOMO			1.00	**0.99**	**_1.00**	**_0.95**	**_0.62**	_0.30	0.14	0.12	0.22
LUMO				1.00	**_0.99**	**_0.97**	**_0.54**	_0.38	0.23	0.21	0.31
I_POT					1.00	**0.95**	**0.62**	0.30	_0.14	_0.12	_0.22
P_MIN						1.00	0.49	0.48	_0.32	_0.30	_0.40
P_MAX							1.00	_0.45	**0.61**	**0.64**	**0.54**
HEAT_F								1.00	**_0.97**	**_0.95**	**_0.99**
MV									1.00	**1.00**	**0.99**
MW										1.00	**0.99**
C log *P*											1.00

For abbreviations, see table 2.
Values in **bold** indicate a significant correlation.



(a)



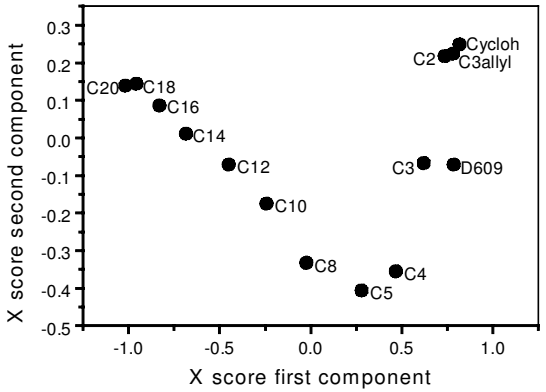
(b)

Figure 3. Predicted versus observed values of (a) $\log(1/K_i)$ by equation (1) and (b) $\log k_{inact}$ by equation (3).

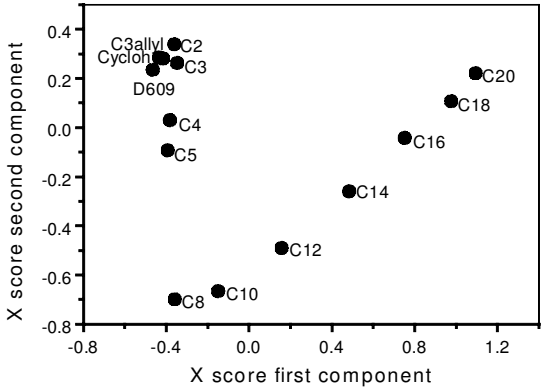
below, C3iso considerably worsened the models.) Figure 4a shows a plot of the X scores of the first versus the second component obtained with PLS analysis of the inhibitory parameter K_i and with CoMFA steric fields ($Q^2 = 0.757$, SEP $= 0.288$, optimal number of components $= 4$). This plot indicates two compound groups: C2, C3, C3allyl, D609 and Cycloh forming one group, C8–C20 (with longer hydrocarbon chains) forming another group. C4 and C5 can be assigned to either group. PLS X scores of the CoMFA steric field model with the inactivation parameter K_I ($Q^2 = 0.490$, SEP $= 0.338$, optimal number of components $= 5$) showed the same grouping of the compounds (figure 4b), but in this case C4 and C5 could be assigned to the first group (with C2, C3, C3allyl, D609 and Cycloh). Although the statistical parameters of the PLS equations with the CoMFA electrostatic fields were slightly worse (as shown below), similar results were obtained with the corresponding PLS X scores (data not shown).

The factor analysis performed on the calculated structural descriptors outlined the similar grouping of the compounds (data not shown).

Similar groups were also identified when plotting the inhibitory parameter K_i versus the number of methylene groups of the compounds with the *n*-alkyl side



(a)



(b)

Figure 4. X scores of the first two PLS components: (a) K_i and CoMFA steric field ($Q^2 = 0.757$, SEP $= 0.288$, optimal number of compounds $= 4$); and (b) K_I and CoMFA steric field ($Q^2 = 0.490$, SEP $= 0.338$, optimal number of compounds $= 5$).

chains only (figure 5). The inhibitory potency increased when the carbon chain length increased until the fourth methylene group (C4) and the free energy increment $\Delta\Delta G = 0.795\,\text{kcal mol}^{-1}$. A further increase in the carbon chain length (until C20) slightly enhanced the inhibitory potency, reflecting in a small $\Delta\Delta G$ ($0.052\,\text{kcal mol}^{-1}$). These results assume that xanthates with five or more methylene groups possess almost equal inhibitory activity. When C2 to C4 or C2 to C5 were considered, no statistically significant linear dependency of $\log(1/K_I)$ on the number of methylene groups was observed. For C8 to C20, a linear dependency with a small negative $\Delta\Delta G$ ($-0.154\,\text{kcal mol}^{-1}$) was observed (data not shown). This fact can be related to the more complex character of the inactivation process, which depends on the binding to the enzyme molecule, the rate of metabolism of the compounds and the binding properties of the active metabolite(s) to the enzyme (Yanev *et al.* 1999, 2000).

Based on the above analyses, a number of QSAR models were also examined on the outlined groups of compounds. Considering that C4 and C5 could be assigned to either group, QSAR models with and without these compounds in the groups

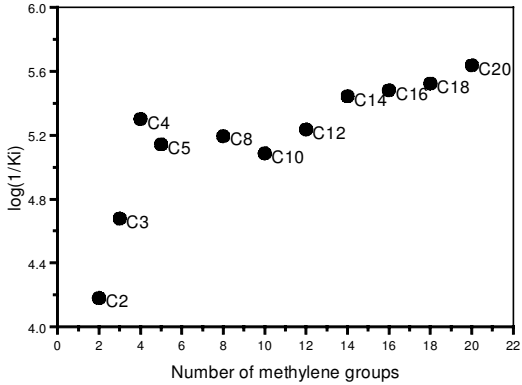


Figure 5. $\mathrm{Log}(1/K_i)$ versus the number of methylene groups in *n*-alkylxanthates.

were investigated. Models with and without C3iso were also attempted for the first group (table 4).

In the first group (C2, C3, C3allyl, D609 and Cycloh), statistically significant correlations between the inhibitory potency K_i and the generated structural descriptors were not obtained. This suggests that the inhibition of the enzyme by the xanthates investigated may be described by structural features different from those included in our investigation. In the same group, significant QSAR models were obtained only with the constants related to the inactivation process (K_I, k_{inact}) and the charge of the first carbon atom of the alkyl chain QC (table 4).

Table 4. QSAR results in the two compound groups.

Compounds	*n*	Activity parameter	Structural descriptor(s)	R^2	*F*	*S*
C2, C3, C3allyl, D609, Cycloh and C3iso	6	$\log(1/K_I)$	QC	0.754	12.260	0.168
C2, C3, C3allyl, D609, Cycloh and C3iso, C4	7	$\log(1/K_I)$	QC	0.755	15.395	0.154
C2, C3, C3allyl, D609, Cycloh and C3iso, C4, C5	8	$\log(1/K_I)$	QC	0.502	6.050	0.209
C2, C3, C3allyl, D609, Cycloh	5	$\log k_{inact}$	QC	0.943	50.068	0.072
C2, C3, C3allyl, D609, Cycloh and C3iso	6	$\log k_{inact}$	QC	0.958	92.365	0.063
C2, C3, C3allyl, D609, Cycloh and C3iso, C4	7	$\log k_{inact}$	QC	0.786	18.386	0.129
C2, C3, C3allyl, D609, Cycloh and C3iso, C4, C5	8	$\log k_{inact}$	QC	0.580	8.277	0.168
C8 to C20	7	$\log(1/K_i)$	MV	0.885	38.426	0.075
C8 to C20 and C5	8	$\log(1/K_i)$	MV	0.853	34.749	0.084
C8 to C20 and C5, C4	9	$\log(1/K_i)$	MV	0.676	14.577	0.116
C8 to C20	7	$\log(1/K_i)$	MV	0.881	37.024	0.189
C8 to C20 and C5	8	$\log(1/K_i)$	MV	0.707	14.538	0.276
C8 to C20 and C5, C4	9	$\log(1/K_i)$	no significant model			
C8 to C20	7	$\log k_{inact}$	MV	0.672	10.223	0.188
C8 to C20 and C5	8	$\log k_{inact}$	MV	0.551	7.350	0.204
C8 to C20 and C5, C4	9	$\log k_{inact}$	MV	0.569	9.226	0.193

n, Number of compounds included in the analysis; R^2, correlation coefficient; *F*, *F*-value; *s*, standard error of estimate.

As seen in table 4, compound C3iso improved the statistical parameters of the K_I models whereas it had no influence on the models with k_{inact} (without C3iso $R^2 = 0.943$, with C3iso $R^2 = 0.958$). The statistical parameters of the models with inactivation potency K_I were comparable when C4 was included in the group, but including C5 gave worse results. The models with k_{inact} were better without C4 and C5. It can be concluded, therefore, that the inactivation potency of compounds C4 and particularly C5 cannot be adequately described by QC.

Some of the QSAR equations in the first group from which valuable information can be obtained are given in equations (4) and (5):

$$\text{Log}(1/K_2) = -29.160(\pm 8.328)\text{QC} + 4.904(\pm 0.075), \quad (4)$$

where $n = 6$, $R^2 = 0.754$, $F = 12.261$, $s = 0.168$ (with C3iso).

$$\text{Log}k_{inact} = +30.088(\pm 3.131)\text{QC} - 1.108(\pm 0.028), \quad (5)$$

where $n = 6$, $R^2 = 0.958$, $F = 92.365$, $s = 0.063$ (with C3iso).

According to these models, the charge of the first carbon atom of the alkyl chain (QC) is important for the inactivation of the enzyme. As the inactivation is mechanism-based (figure 1), it can be assumed that QC influences the rate of metabolism to reactive derivatives or their binding to the enzyme. From the models, the opposite influences of QC on the potency of inactivation (negative coefficient of QC in model 4) and on the rate of inactivation of the enzyme (positive coefficient of QC in model 5) are evident. This is also apparent from figure 6, where $\log(1/K_I)$ and $\log k_{inact}$ of all six compounds (C2, C3, C3iso, C3allyl, D609 and Cycloh) are plotted against QC. Gao and Hansch (1996) reported similar observations and established that the influence of the electronic properties of the CYP substrates in more cases appear to be opposite when related to the formation of the enzyme–substrate complex and to the rate constants of metabolism.

In the second group (C8–C20), significant QSAR models were derived with all biological parameters and MW and MV (models with $C\log P$ were also obtained, but they are not presented here because of the uncertainty in the calculated $C\log P$) (table 2). This is in agreement with the observed linear dependencies of $\log(1/K_i)$ and $\log(1/K_I)$ on the number of methylene groups in the alkyl chain. As MW and MV are strongly intercorrelated ($R = 1.00$), only the models with MV

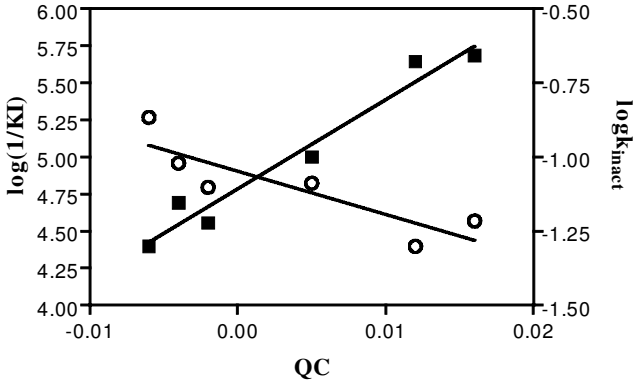


Figure 6. Observed $\log(1/K_I)$ and $\log k_{inact}$ versus QC: ○, $\log(1/K_I)$, $R^2 = 0.754$; ■, $\log k_{inact}$, $R^2 = 0.958$.

are presented (table 4, equations 6–8). Again, involvement of C4 and C5 resulted in models with worse statistical parameters (table 4):

$$\mathrm{Log}(1/K_\mathrm{i}) = +0.003(\pm 0.0004)\mathrm{MV} + 4.605(\pm 0.127), \quad (6)$$

where $n = 7$, $R^2 = 0.885$, $F = 38.426$, $s = 0.075$.

$$\mathrm{Log}(1/K_\mathrm{I}) = -0.007(\pm 0.0011)\mathrm{MV} + 6.645(\pm 0.321), \quad (7)$$

where $n = 7$, $R^2 = 0.881$, $F = 37.024$, $s = 0.189$.

$$\mathrm{Log}\, k_\mathrm{inact} = -0.004(\pm 0.0011)\mathrm{MV} - 0.301(\pm 0.320), \quad (8)$$

where $n = 7$, $R^2 = 0.672$, $F = 10.223$, $s = 0.188$.

Equation (6) confirms the slight increase in inhibitory potency with increasing alkyl chain length of the compounds. As seen from equations (7) and (8), in contrast to the inhibition, the longer alkyl chain may perturb the enzyme inactivation. One possible explanation is that the long chain may decrease the rate of metabolism and/or that the active metabolite(s) remain weakly bound to the enzyme.

In addition to the QSAR, 3D-QSAR analysis was also performed using CoMFA. It should be stated in advance that the number of compounds was very small, so that all compounds were used to derive the 3D-QSAR models and, subsequently, no tests were done to estimate the external predictivity of the models. Thus, 3D-QSAR was performed first to check how it agreed with the QSARs and, second, to extract, if possible, some more information from the available data set. The best CoMFA models obtained are summarized in table 5. The Q^2 with all compounds involved show that these models have moderate predictive properties. The K_i models (nos 1 and 2) had $Q^2 > 0.35$, suggesting that they could predict better than the mean. The statistical parameters were considerably improved when C3iso was excluded (models 4–7). In the first group of compounds, the best model obtained (no. 9) also had moderate predictivity ($Q^2 = 389$, table 5). The K_i models improved when C4 and C5 were included (models 11 and 12, table 5). In contrast, involvement of C4 and C5 resulted in worse models with K_I (model 10, table 5) in accordance with the QSAR results. In the second group of compounds, very good models with K_i and K_I were obtained (nos 13–16, table 5). When C5 was added, the results remained approximately the same (models 18–21, table 5), but the inclusion of C4 resulted in worse models for both K_i and K_I (nos 22–25, table 5).

Figure 7 shows the contour map with coefficient*SD contributions obtained from one of the best models in the first group (no. 12, table 5). More bulky substituents in the regions around the molecules, labelled with black points in figure 7, increase the inhibitory potency of the compounds, whereas the substituents in the grey-labelled regions must be less bulky. Thus, bulky substituents at the unbranched alkyl chain would favour inhibitory potency. Analyses of the coefficient*SD contributions for the models of the second group showed that bulky hydrocarbon chains would increase the inhibitory potency and decrease the inactivation potency (data not shown), which was in accordance with the QSAR results.

The presented study is the first that reports QSAR and 3D-QSAR analyses of xanthates in their interactions with enzymes of the CYP superfamily. As already discussed, the CYP2B QSAR studies of different substrates and inhibitors

Table 5. CoMFA results (models with $Q^2 > 0.3$ only being shown).

Model no.	Compounds	n	Activity parameter	CoMFA field	Q^2	SEP	N_{opt}
1	All	15	$\log(1/K_i)$	electrostatic	0.392	0.390	1
2	All	15	$\log(1/K_i)$	steric	0.378	0.394	1
3	All	15	$\log(1/K_I)$	electrostatic	0.344	0.366	4
4	All without C3iso	14	$\log(1/K_i)$	electrostatic	0.726	0.290	3
5	All without C3iso	14	$\log(1/K_i)$	steric	0.757	0.288	4
6	All without C3iso	14	$\log(1/K_I)$	electrostatic	0.438	0.354	5
7	All without C3iso	14	$\log(1/K_I)$	steric	0.490	0.338	5
8	All without C3iso	14	$\log k_{inact}$	steric	0.353	0.386	5
9	C2, C3, C3allyl, D609, Cycloh	5	$\log(1/K_I)$	steric	0.389	0.349	3
10	C2, C3, C3allyl, D609, Cycloh and C4	6	$\log(1/K_I)$	steric	0.342	0.259	3
11	C2, C3, C3allyl, D609, Cycloh and C4, C5	7	$\log(1/K_i)$	electrostatic	0.357	0.383	1
12	C2, C3, C3allyl, D609, Cycloh and C4, C5	7	$\log(1/K_i)$	steric	0.385	0.375	1
13	C8 to C20	7	$\log(1/K_i)$	electrostatic	0.843	0.138	4
14	C8 to C20	7	$\log(1/K_i)$	steric	0.816	0.095	1
15	C8 to C20	7	$\log(1/K_I)$	electrostatic	0.632	0.368	2
16	C8 to C20	7	$\log(1/K_I)$	steric	0.628	0.374	2
17	C8 to C20	7	$\log k_{inact}$	steric	0.334	0.548	3
18	C8 to C20 and C5	8	$\log(1/K_i)$	electrostatic	0.864	0.140	5
19	C8 to C20 and C5	8	$\log(1/K_i)$	steric	0.841	0.096	2
20	C8 to C20 and C5	8	$\log(1/K_I)$	electrostatic	0.573	0.334	1
21	C8 to C20 and C5	8	$\log(1/K_I)$	steric	0.578	0.343	1
22	C8 to C20 and C4, C5	9	$\log(1/K_i)$	electrostatic	0.721	0.142	4
23	C8 to C20 and C4, C5	9	$\log(1/K_i)$	steric	0.715	0.117	2
24	C8 to C20 and C4, C5	9	$\log(1/K_I)$	electrostatic	0.474	0.407	3
25	C8 to C20 and C4, C5	9	$\log(1/K_I)$	steric	0.430	0.548	5
26	C8 to C20 and C4, C5	9	$\log k_{inact}$	steric	0.328	0.481	4

n, Number of compounds included in the analysis; Q^2, crossvalidated correlation coefficient; SEP, standard error of prediction; N_{opt}, optimal number of components.

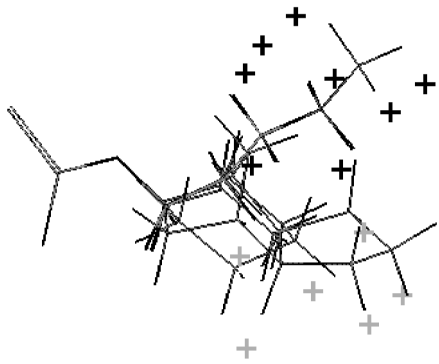


Figure 7. Contour map of the coefficient*SD contributions obtained from model 12 (table 5). Black points label regions where more bulky substituents would increase the inhibitory potency of the compounds, while the substituents in the gray-labelled regions must be less bulky.

reported in the academic literature demonstrate that the size and lipophilicity of the compounds are important for their binding to the enzyme. In the present study, a high correlation between the molecular volume and the inhibitory potency of the xanthate derivatives was also found. The same linear relationship between the alkyl chain length of the substituents and some more general biological (animal toxicity; Zahradnik 1960, Zahradnik *et al.* 1962) and chemical (sorption rate on mineral surface, Szymula *et al.* 1996) activities of different xanthates was also demonstrated.

The electronic characteristics in the published QSAR studies were mainly related to HOMO and LUMO values. Because of the integral nature of these descriptors, their physical interpretation is obscure. Our QSAR results indicate the possible role of the charge of the first carbon atom in the hydrocarbon chain for xanthate metabolism. This is in accordance with previously reported investigations of Kent *et al.* (1999) and Yanev *et al.* (2000) that the oxidative attack of CYP2B1 on the xanthate molecule occurs at this position (by allocation of one or two hydrogen atoms). We also described quantitatively the decreasing inactivation potency with the increasing size of the alkyl chain substituents. This could be related to the decreased rate of metabolism and/or by the difficulty in binding of the resulting metabolite(s) to the enzyme molecule.

The reported QSAR analysis could direct the rational synthesis of new, more potent and selective CYP inactivators. One possible suggestion for a compound that might have high inactivation potency is 5-methylpropylxanthate (figure 1), in which the charge at the first carbon atom of the alkyl chain was calculated as _0.008.

Acknowledgements

The authors thank the National Science Fund of Bulgaria (Grant MU-I-8/98) for financial support.

References

Burke, M. D., Thompson, S., Elcombe, C. R., Halpert, J., Haaparanta, T. and Mayer, R. T., 1985, Ethoxy-, pentoxy- and benzyloxyphenoxazones and homologues: a series of substrates to distinguish between different induced cytochromes P450. *Biochemical Pharmacology*, **34**, 3337–3345.

Chang, Y. T., Stiffelman, O. B. and Loew, G. H., 1996, Computer modeling of 3D structures of cytochrome P450s. *Biochimie*, **78**, 771–779.

Dai, R., Pincus, M. R. and Friedman, F. K., 1998, Molecular modeling of cytochrome P450 2B1: mode of membrane insertion and substrate specificity. *Journal of Protein Chemistry*, **17**, 121–129.

Eldirdiri, N., 1992, Uptake and metabolic effects of some halogenoalkanes. PhD thesis, University of Surrey, Guildford.

Fang, X., Kobayashi, Y. and Halpert, J. R., 1997, Stoichiometry of 7-ethoxycoumarin metabolism by cytochrome P450 2B1 wild-type and five active-site mutants. *FEBS Letters*, 416: 77–80.

Gao, H. and Hansch, C., 1996, QSAR of P450 oxidation: on the value of comparing k_{cat} and K_m with k_{cat}/K_m. *Drug Metabolism Reviews*, **28**, 513–526.

Halpert, J. R. and He, Y. A., 1993, Engineering of cytochrome P450 2B1 specificity. Conversion of an androgen 16 beta-hydroxylase to a 15 alpha-hydroxylase. *Journal of Biological Chemistry*, **268**, 4453–4457.

He, Y. A., Balfour, C. A., Kedzie, K. M. and Halpert, J. R., 1992, Role of residue 478 as a determinant of the substrate specificity of cytochrome P450 2B1. *Biochemistry*, **31**, 9220–9226.

He, Y. A., Luo, Z., Klekotka, P. A., Burnett, V. L. and Halpert, J. R., 1994, Structural determinants of cytochrome P450 2B1 specificity: evidence for five substrate recognition sites. *Biochemistry*, **33**, 4419–4424.

He, Y. Q., He, Y. A. and Halpert, J. R., 1995, *Escherichia coli* expression of site-directed mutants of cytochrome P450 2B1 from six substrate recognition sites: substrate specificity and inhibitor selectivity studies. *Chemical Research and Toxicology*, **8**, 574–579.

Jefcoate, C. R., Gaylor, J. L. and Calabrese, R. L., 1969, Ligand interactions with cytochrome P450. I. Binding of primary amines. *Biochemistry*, **8**, 3455–3463.

Kent, U. M., Yanev, S. and Hollenberg, P., 1999, Mechanism-based inactivation of cytochromes P450 2B1 and P450 2B6 by *n*-propylxanthate. *Chemical Research and Toxicology*, **12**, 317–322.

Kobayashi, Y., Fang, X., Szklarz, G. D. and Halpert, J. R., 1998, Probing the active site of cytochrome P450 2B1: metabolism of 7-alkoxycoumarins by the wild type and five site-directed mutants. *Biochemistry*, **37**, 6679–6688.

Lewis, D. F. V., Ioannides, C. and Parke, D. V., 1987, Structural requirements for substrates of cytochromes P450 and P-448. *Chemico-Biological Interactions*, **64**, 39–60.

Lewis, D. F. V., Ioannides, C. and Parke, D. V., 1995a, A quantitative structure–activity relationship study on a series of 10 *para*-substituted toluenes binding to cytochrome P4502B4 (CYP2B4), and their hydroxylation rates. *Biochemical Pharmacology*, **50**, 619–625.

Lewis, D. F. V. and Lake, B. G., 1997, Molecular modelling of mammalian CYP2B isoforms and their interactions with substrates, inhibitors and redox partners. *Xenobiotica*, **27**, 443–478.

Lewis, D. F. V., Lake, B. G. and Parke, D. V., 1995b, Molecular orbital-generated QSARs in an homologous series of alkoxyresorufins and studies of their interactive docking with cytochromes P450. *Xenobiotica*, **25**, 1355–1369.

Luo, Z., He, Y. A. and Halpert, J. R., 1994, Role of residues 363 and 206 in conversion of cytochrome P450 2B1 from a steroid 16-hydroxylase to a 15 alpha-hydroxylase. *Archives of Biochemistry and Biophysics*, **309**, 52–57.

Murray, M., 1989, Inhibition of hepatic drug metabolism by phenothiazine tranquillizers: quantitative structure–activity relationships and selective inhibition of cytochrome P450 isoform-specific activities. *Chemical Research and Toxicology*, **2**, 240–246.

Nelson, D. R., Koymans, L., Kamataki, T., Stegeman, J. J., Feyereisen, R., Waxman, D. J., Waterman, M. R., Gotoh, O., Coon, M. J., Estabrook, R. W., Gunsalus, I. C. and Nebert, D. W., 1996, P450 superfamily: update on new sequences, gene mapping, accession numbers and nomenclature,. *Pharmacogenetics*, **6**, 1–42.

Roffey, S. J., 1993, Structure–activity relationships in the metabolism of a series of tertiary amines by cytochrome P450. PhD thesis, University of Surrey, Guildford.

Rossi, M., Markovitz, S. and Callahan, T., 1987, Defining the active site of cytochrome P450: the crystal and molecular structure of an inhibitor, SKF-525A. *Carcinogenesis*, **8**, 881–887.

Szklarz, G. D., He, Y. A. and Halpert, J. R., 1995, Site-directed mutagenesis as a tool for molecular modeling of cytochrome P450 2B1. *Biochemistry*, **34**, 14312–14322.

Szymula, M., Koziol, A. E. and Szczypa, J., 1996, Effect of xanthates chain length on decrease of xanthates concentration in solutions in contact with copper sulphides. *International Journal of Mineral Processing*, **46**, 123–135.

Waley, S. G., 1980, Kinetics of suicide substrates. *Biochemical Journal*, **185**, 771–773.

Waller, S. C., He, Y. A., Harlow, G. R., He, Y. Q., Mash, E. A. and Halpert, J. R., 1999, 2,2′,3,3′,6,6′-hexachlorobiphenyl hydroxylation by active site mutants of cytochrome P450 2B1 and 2B11. *Chemical Research in Toxicology*, **12**, 690–699.

Yanev, S., Frank, H., Remmer, H. and Stoytchev, T., 1985, Xanthogenates as 'suicide' substrates of cyt P450. In L. Vereczkey and K. Magyar (eds), *Cytochrome P450 Biochemistry, Biophysics and Induction* (Budapest: Akademia Kiado), pp. 87–90.

Yanev, S., Kent, U. M., Pandova, B. and Hollenberg, P., 1999, Selective mechanism-based inactivation of cytochromes P450 2B1 and P450 2B6 by a series of xanthates. *Drug Metabolism and Disposition*, **27**, 600–604.

Yanev, S., Kent, U. M., Roberts, E. S., Ballou, D. P. and Hollenberg, P. F., 2000, Mechanistic studies of cytochrome P450 2B1 inactivation by xanthates. *Archives of Biochemistry and Biophysics*, **378**, 157–166.

Zahradnik, R., 1960, Reaktionskinetik und eigenschaften von stoffen in homologen reihen nichtaromatischer verbundungen. V. Zerzatzung in sauerem milieu und spektraleigenschaften der alkylxanthogensauren. *Zeitschrift fur Physikalische Chemie*, **213**, 318–337.

Zahradnik, R., Hvatil, M., Vostal, I. and Teisinger, I., 1962, Toxicology of alcohols and potassium salts of alkylxanthogenic acids. *Farmakologia I Toksikologia*, **25**, 618–622. [in Russian]

XENOBIOTICA, 2002, VOL. 32, NO. 12, 1079–1091

Taylor & Francis
healthsciences

Binding of brominated diphenyl ethers to male rat carrier proteins

H. HAKK†*, G. LARSEN†, Å. BERGMAN‡ and U. ÖRN‡

† US Department of Agriculture, Agricultural Research Service, Biosciences Research Laboratory, PO Box 5674-University Station, Fargo, ND 58105, USA
‡ Department of Environmental Chemistry, Stockholm University, SE-106 91 Stockholm, Sweden

Received 7 March 2002

1. Two [^{14}C]-labelled brominated diphenyl ethers, 2,2′,4,4′,5-pentabromodiphenyl ether (BDE-99) and decabromodiphenyl ether (BDE-209), were separately administered to the male Sprague–Dawley rat as a single oral dose (2.2 mg kg^{-1} body weight and 3.0 mg kg^{-1}, respectively).

2. Very low [^{14}C] urine excretion was observed for both congeners (< 1% of the dose), and cumulative biliary excretion was approximately 4% for BDE-99 and 9% for BDE-209.

3. More than 6% of the pooled urine from the BDE-99-treated rat was protein-bound to an 18-kDa protein characterized by sodium dodecyl sulphate-polyacrylamide gel electrophoresis and Western immunoblot analysis as α_{2u}-globulin. Eighteen per cent of the radioactivity from the pooled urine from the BDE-209 treated rat was bound to albumin; no binding to α_{2u}-globulin was detected.

4. In bile, 27–39% of the radioactivity from the BDE-99-dosed rat was bound to an unidentified 79-kDa protein, whereas essentially all (> 87%) of the biliary radioactivity from BDE-209 was bound to the 79-kDa protein. Both parent BDE-99 and -209 and their metabolites were detected by thin layer chromatography in the extracted fraction of this bile protein.

5. By differential centrifugation, the subcellular localization of the ^{14}C derived from each congener in selected tissues was quantified. The cytosolic [^{14}C] from livers of the BDE-209-treated rat was bound to a 14-kDa protein, which was characterized as a fatty acid-binding protein.

Introduction

Decabromodiphenyl ether (BDE-209) is the most highly brominated congener in the polybrominated diphenyl ether (PBDE) family and is the PBDE produced commercially in the highest quantity. The most important end-product use of BDE-209 is as an additive flame retardant in high-impact polystyrene, but it is also used for textiles in automobiles, tents and soft furnishings. 2,2′,4,4′,5-Pentabromodiphenyl ether (BDE-99) is the major component of commercial pentabromodiphenyl ether used in epoxy resins and polyurethane foam. Owing to their extremely low water solubility and vapour pressure, BDE-99 and -209 would be expected to be persistent and to bioaccumulate.

Halogenated aromatic hydrocarbons can bind to endogenous carrier proteins in the urine and bile of rat, either as the parent compound or as metabolites. Toxic (Hakk *et al.* 1998, 1999) and non-toxic dioxins (Larsen *et al.* 1995, Wiener and Larsen 1997) and metabolites of polychlorinated biphenyls (Larsen *et al.* 1990a)

* Author for correspondence; e-mail: hakkh@fargo.ars.usda.gov

Xenobiotica ISSN 0049–8254 print/ISSN 1366–5928 online © 2002 Taylor & Francis Ltd
http://www.tandf.co.uk/journals
DOI: 10.1080/00498250210016345

have been shown to interact in this way. The reason for the binding has not been firmly established, but it may be to facilitate the elimination of these lipophilic xenobiotics. Studies of the binding of carrier proteins with xenobiotics may help in the understanding of the importance of carrier protein systems in the overall pharmacokinetics of xenobiotics. In addition, the binding may interfere with the normal function of these proteins. Therefore, a greater understanding of the toxicity of these substances may be forthcoming.

The purpose of the present study was to administer a single oral dose of either BDE-99 or -209 to the male rat, to quantitate the amount of each PBDE congener excreted in the urine and bile, and to characterize the nature and extent of binding to proteins in these excreta, as well as in selected tissue samples.

Materials and methods

Chemicals

2,2′,4,4′,5-Pentabromo-[^{14}C and ^{12}C]diphenyl ether (BDE-99) was synthesized in-house by the method of Örn *et al.* (1996). The radiolabelled purity of [^{14}C] BDE-99 (>98%; 49 mCi mmol^{-1}) was determined by silica TLC (50:50 hexane:methylene chloride) and HPLC (C18, H_2O:CH_3CN gradient). Chemical purity of [^{12}C] BDE-99 (97%) was determined by ^{1}H-NMR analysis. [UL-^{14}C and ^{12}C]decabromodiphenyl ether (BDE-209) was synthesized from [UL-^{14}C and ^{12}C]2,2′,4,4′-tetrabromodiphenyl ether (Örn *et al.* 1996) via direct bromination with a large excess of bromine in tetrachloromethane and by use of aluminium bromide as a catalyst. Purification was performed by preparative thin layer chromatography (TLC, silica gel) with hexane as the mobile phase. The chemical and radiochemical purity of [UL-^{14}C and ^{12}C] BDE-209 was >98% confirmed by GC/MS. The specific activity of [UL-^{14}C]BDE-209 was 15 mCi mmol^{-1}.

Antibodies

Authentic rat α_{2u}-globulin and rabbit anti-rat α_{2u}-globulin IgG were gifts from Dr Otto Neuhaus, University of South Dakota, Vermillion, SD. Authentic rat albumin was purchased from Sigma Chemical Co. (St Louis, MO, USA) and rabbit anti-rat albumin was purchased from Accurate Chemical and Scientific Corp. (Westbury, NY, USA).

Animal treatment

The radiolabelled [^{14}C]BDE-99 dose was administered orally (2.2 mg/rat in 0.5 ml corn oil; 1.0 μCi/rat) to three male Sprague–Dawley rats (271 ± 21 g; 14.5 μmol kg^{-1}; 'conventional') and five bile duct-cannulated rats (238 ± 11 g; 16.5 μmol kg^{-1}; 'cannulated'). Bile duct cannulation was conducted as reported by Hakk *et al.* (2000). A single dose of radiolabelled [^{14}C]BDE-209 was administered orally (3.0 mg/rat in 0.5 ml Lutrol F127, soya phospholipid and water; 4 μCi/rat) to four conventional male rats (218 ± 5 g; 3.0 μmol kg^{-1}) and four bile duct-cannulated rats (201 ± 6 g; 3.0 μmol kg^{-1}).

All rats were individually housed in stainless steel metabolism cages. Urine and bile were collected at 24-h intervals for 72 h. The rats were anesthetized with halothane and exsanguinated. Gastrointestinal mucosal cells (scraped from the inner wall of the small intestine), kidneys, liver and lungs were removed and stored at −20 °C until analyses could be performed.

Sodium dodecyl sulphate-polyacrylamide gel electrophoresis (SDS-PAGE) and immunological procedures

Protein-binding studies were conducted as described by Larsen *et al.* (1990a). Owing to the low amount of [^{14}C] in urine in both treatment groups, 0–72-h urine collected for all rats was pooled. Bile from cannulated rats was pooled on a daily basis. Urine and bile were chromatographed successively on Sephadex G-75 (G-75; 4.5 × 90 cm) and Sephacryl S-200 (S-200; 2.2 × 85 cm; both Pharmacia Biotech, Piscataway, NJ, USA) gel filtration columns. The columns were eluted with 0.05 M phosphate buffer (pH 7.2). SDS-PAGE using 13% polyacrylamide separating gels was performed as described by Mazel (1971). All electrophoresis materials were purchased from Bio-Rad Laboratories (Richmond, CA, USA). Protein samples (0–72-h urine, or 0–24-, 24–48-, 48–72-h bile) were electrophoretically transferred to a sheet of nitrocellulose (Schleicher & Schuell, Keene, NH, USA; Western blot) by the method of Towbin and Gordon (1984). The Western blots of separated proteins were blocked by incubation for 2 h in Tris–saline–Tween buffer (0.15 M Tris, 0.5 M NaCl, 0.05% Tween 20, pH 7.5), and then incubated for 2 h at room temperature with rabbit anti-rat α_{2u}-globulin (α_{2u}) or rabbit anti-

rat albumin antibodies (1:800 dilution in Tris–saline–Tween buffer). The Western blots were washed three times with Tris–saline–Tween buffer (5 min each) and then incubated with the same buffer containing goat anti-rabbit horseradish peroxidase conjugate antibody (Bio-Rad, 1:3000 dilution) for 1 h at room temperature. The Western blots were washed twice with Tris–saline–Tween buffer (5 min each), once with Tris–saline buffer (0.15 M Tris and 0.5 M NaCl, pH 7.5), and then incubated in colour reagent (25 ml Tris–saline buffer plus 12.5 µl 30% H_2O_2 and 5 ml 3 mg ml^{-1} solution of 4-chloro-1-naphthol). The remainder of the protein-bound fractions from urine and bile was extracted with methylene chloride (3). The combined organic layers were concentrated under a stream of nitrogen and spotted onto silica gel TLC plates (5 × 20 cm; 250 µm thickness; Analtech, Newark, DE, USA). TLC plates were developed in 1:1:2 tetrahydrofuran:ethyl acetate:hexane with BDE-99 and -209 as standards.

Tissue preparation and centrifugation analyses

The small intestine was flushed with saline (0.9% NaCl), opened longitudinally and the intestinal mucosa gently isolated with the edge of a razor blade. Livers, kidneys, intestinal mucosal cells and lungs were homogenized separately in 0.05 M potassium phosphate buffer (pH 7.2) and centrifuged at 10 000*g* for 30 min. The supernatant was decanted and assayed for [^{14}C], and the pellet (membrane fraction) was combusted on a Packard Model 307 tissue oxidizer (Packard, Meridan, CT, USA). The 10 000*g* supernatant (soluble fraction) was recentrifuged at 100 000*g* for 90 min. The supernatant was removed and assayed for [^{14}C] and the pellet (microsomal fraction) was combusted. The 100 000*g* supernatant from BDE-209 dosed rat livers was applied to a G-75 gel filtration column (as described above), and selected protein-bound fractions were subjected to a fatty acid-binding protein (FABP) assay.

Liver protein delipidization and binding assay for fatty acid-binding protein (FABP)

A 45-min delipidization procedure was conducted according to Cham and Knowles (1976). Sample preparation required a 4:1 ratio of sample to Lipidex® (Sigma) solution, which was prepared in a 1.0 ml microcentrifuge tube, and incubated 45 min at 41 °C. The tubes were centrifuged at 14 000*g* for 2 min. The FABP characterization procedure was run in triplicate, as described by Larsen *et al.* (1992). Briefly, 300 µl 10 mM potassium phosphate buffer, pH 7.2, and 300 µl [^{14}C]oleic acid solution (about 10 000 dpm) were added to the blank and control tubes. The sample tube contained 300 µl prepared sample supernatant, which was vortexed and incubated at room temperature for 3 h. A 250-µl volume of water was added to the blanks, and 250 µl 60% solution of Lipidex in 10 mM potassium phosphate buffer was added to the remaining tubes. All samples were vortexed and centrifuged at 14 000*g* for 2 min; 200 µl of the supernatant was assayed for radioactivity. The blank tube supernatant contained 10 000 dpm [^{14}C]oleic acid solution. The control tube supernatants, after assaying, had low amounts of radioactivity because Lipidex bound the free [^{14}C]oleic acid. The presence of FABP was determined by comparing radioactivity in the supernatant of the unknown samples to the controls.

Isoelectric focusing

The isoelectric focusing procedure for an isolated 79 kDa biliary protein used agarose gel (pH 3–10). The anolyte was 0.5 M acetic acid, and the catholyte was 10 M NaOH. The 79 kDa bile protein was loaded onto the gel, which was prefocused for 15 min at 2 watts (W). The conditions for the remainder of the focusing were a 15 min hold at 270 volts (V), followed by a 20-min hold at 810 V, and a 45-min hold at 1000 V. The gel was maintained at 1000 V until the current and wattage decreased, and the bands were resolved. The gel was removed and placed into a fixative solution for 30 min (3.6 g sulfosalicylic acid, 6.0 g trichloroacetic acid, 36 ml methanol, brought up to 100 ml volume with distilled water). The sample was rinsed in a solution of 25 ml ethanol, 9 ml of glacial acetic acid and brought up to 100 ml with distilled water for 10 min. A 50-ml staining solution prepared with 1.0 g Coomassie Brilliant Blue R-250, 250 ml ethanol, 90 ml glacial acetic acid, brought up to 1 litre with distilled water was added for 60 min, discarded and followed by a 50-ml rinse solution (see above) until bands were visible.

Quantification of radioactivity

Urine, bile, tissue supernatants and protein-bound extracts were assayed for radioactivity by counting aliquots in a Packard Model 1900 CA liquid scintillation counter (LSC). Pellets from centrifugation of homogenized tissues were air dried, and aliquots were removed in triplicate, weighed and combusted with a Packard Model 307 tissue oxidizer. Radiolabelled CO_2 was trapped in CARBO-SORB® E, and measured for [^{14}C] in Permafluor scintillator (all Packard) with a LSC. Radiolabelled bands on silica TLC plates were quantitated using a System 2000 Imaging Scanner (Bioscan, Inc., Washington, DC, USA).

Results

Excretion of congeners

Daily excretion of both flame retardants, BDE-99 and -209, via the urine was extremely low in male rats, being $\leq$0.4% of the administered dose (table 1). Cumulative excretion in the urine at 72 h was $<1\%$ of the administered dose for each congener, and excretion via the bile was favoured for both congeners. Over 9% of BDE-209 dose was excreted in rat bile by 72 h, whereas nearly 3% of BDE-99 was excreted in the bile at 72 h (table 1). Six per cent of BDE-209 was eliminated in 0–24-h bile, and it decreased steadily with time. Excretion of BDE-99 in both urine and bile of bile duct-cannulated rats peaked at 24–48 h, suggesting that absorption and/or metabolism was slower for this congener.

Urine

The 0–72-h urine sample from the conventional rat dosed with BDE-99 was chromatographed on a G-75 gel filtration column (figure 1A), and radiolabelled, protein-bound fractions were further chromatographed on an S-200 gel filtration column. Urine from the bile duct-cannulated rat was chromatographed in the same

Table 1. Mean radioactivity excreted in male rat urine and bile following a single oral dose of [^{14}C]-2,2′,4,4′,5-pentabromodiphenyl ether (BDE-99; 2.2 mg kg^{-1} body weight) or [^{14}C]-decabromodiphenyl ether (BDE-209; 3.0 mg kg^{-1} body weight) administered in 0.5 ml peanut oil.

	Per cent of dose			
	Conventional		Bile-duct cannulated	
Excreta	BDE-99 ($n = 3$)	BDE-209 ($n = 4$)	BDE-99 ($n = 5$)	BDE-209 ($n = 4$)
Urine				
0-24 h	0.4	0.019	0.1	0.020
24–48 h	0.3	0.008	0.2	0.020
48–72 h	0.2	0.006	0.05	0.007
Bile				
0–24 h	–	–	0.7	6.0
24–48 h	–	–	1.8	2.5
48–72 h	–	–	1.4	0.7

Table 2. Binding of [^{14}C]-2,2′,4,4′,5-pentabromodiphenyl ether (BDE-99) and/or its metabolites to proteins in rat urine and bile.

		Per cent bound		
Excreta	Per cent unbound	Total	α_{2u}	79 kDa
Urine				
0–72 h Conv	75.5	6.6	6.3	
0-72 h Cann	100	0	–	
Bile				
0–24 h	61.0	28.4		27.0
24–48 h	58.1	34.4		30.0
48–72 h	43.2	46.9		39.4

Data are the mean from three conventional rats and five bile-duct cannulated rats.

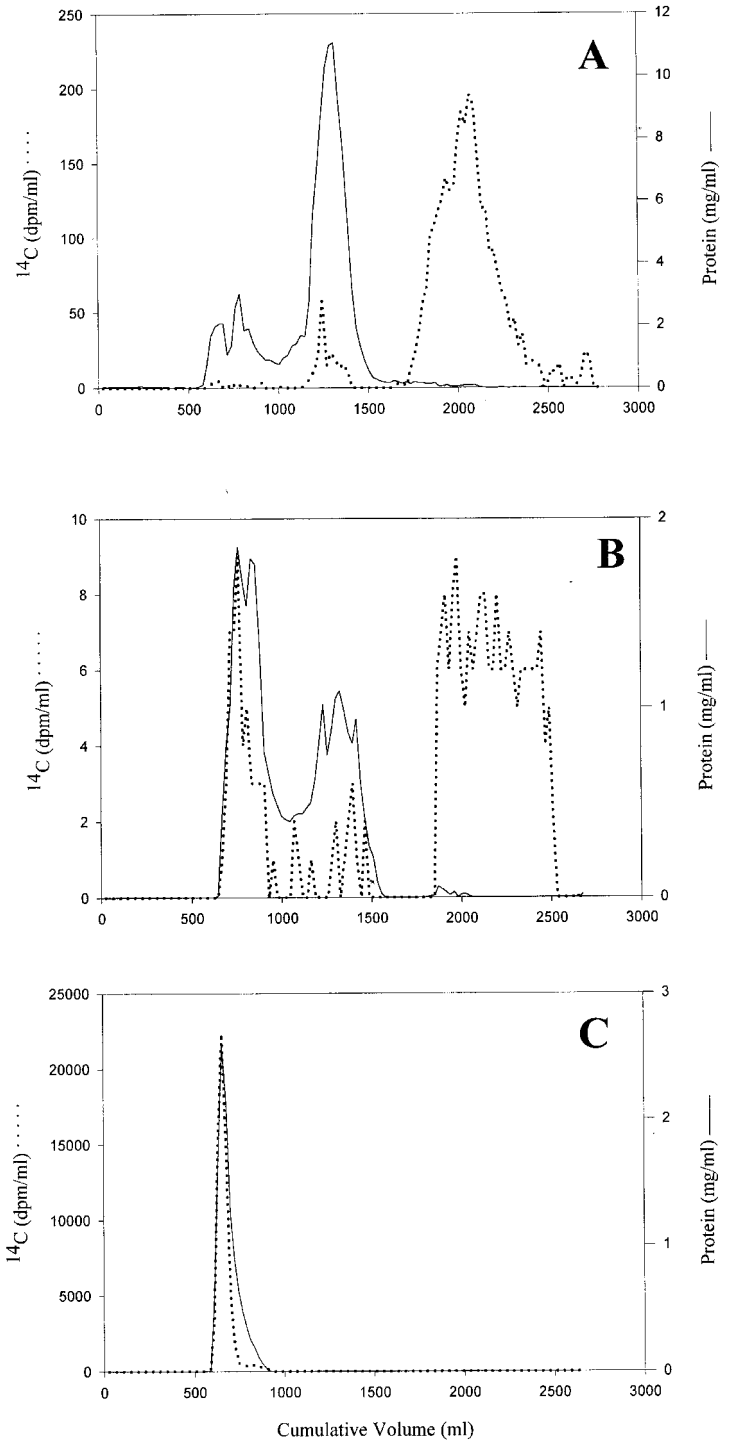


Figure 1. Elution patterns from Sephadex G-75 gel filtration columns in the partial purification of urine protein from the conventional rat dosed with (A) [^{14}C]BDE-99, (B) [^{14}C]BDE-209 or (C) bile protein from the bile duct-cannulated rat dosed with [^{14}C]BDE-99. Fractions were assayed for protein (——) and radioactivity (- - -).

manner. The majority of the BDE-99-derived [^{14}C] in conventional and cannulated rat urine was not associated with protein (75.5 and 100%, respectively; table 2). The protein that associated with BDE-99-derived [^{14}C] in conventional urine samples was an 18-kDa monomeric protein (figure 2A), which was cross-reactive with rabbit anti-rat α_{2u}-globulin (α_{2u}) by Western immunoblot analysis (data not

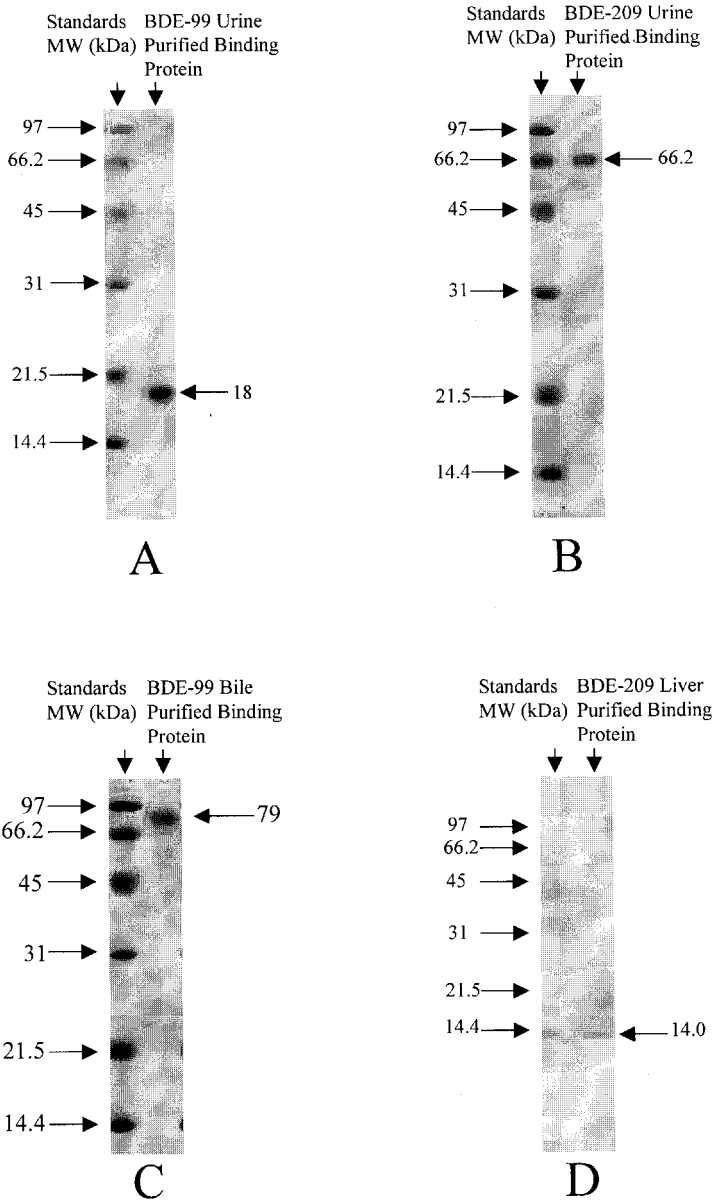


Figure 2. Comparison of the SDS-PAGE of protein standards with (A) α_{2u}-globulin obtained from the protein-bound fractions of BDE-99-dosed conventional rat urine, (B) albumin obtained from the protein-bound fractions of BDE-209-dosed conventional rat urine, (C) an unidentified 79-kDa bile protein obtained from the protein-bound fractions of BDE-99 dosed rat bile, and (D) FABP obtained from soluble 100 000*g* fraction from BDE-209-dosed conventional rat livers.

Table 3. Binding of [^{14}C]-decabromodiphenyl ether (BDE-209) and/or its metabolites to proteins in rat urine and bile.

Excreta	Per cent unbound	Per cent bound		
		Total	Albumin	79 kDa
Urine				
0-72 h Conv	73.4	19.7	18.0	–
0-72 h Cann	18.2	68.3	68.3	–
Bile				
0–24 h	–	97.5		94.4
24–48 h	–	92.0		89.5
48–72 h	–	90.4		87.4

Data are the mean from four conventional and four bile-duct cannulated rats.

shown). The protein-bound radioactivity was not extracted. Therefore, it was not possible to determine the form of the dosed material by TLC.

The pooled 0–72-h urine sample from the conventional rat dosed with BDE-209 was chromatographed on a G-75 column (figure 1B), followed by more refined chromatography achieved with an S-200 column. The majority of the BDE-209-derived [^{14}C] in conventional urine was free of association with protein (73.4% of 0–72-h urine; table 3). The opposite was true of urine from cannulated rats dosed with BDE-209, where 18.2% of the 0–72-h urine was free and 68.3% was protein-bound. In both conventional and cannulated urine samples, the protein that associated with BDE-209-derived [^{14}C] was a 66.2-kDa monomeric protein (figure 2B), which was cross-reactive with rabbit anti-rat albumin by Western immunoblot analysis (data not shown). Forty-three per cent of the protein-bound [^{14}C] from conventional urine (BDE-209) was extractable into methylene chloride, and silica TLC chromatography displayed the presence of two polar metabolites, but no parent BDE-209 (data not shown). Characterization of the two metabolites was not possible owing to insufficient mass.

Bile

The pooled 0–24-h bile sample from BDE-209 rats was chromatographed on a G-75 gel filtration column (figure 1C), and essentially all of the [^{14}C] was protein-bound ($>$97%; table 3). A similar level of protein binding of BDE-209-derived radioactivity was observed with bile obtained at 24–48 or at 48–72 h (table 3). Purification of the protein-bound region on an S-200 column and chromatography on SDS-PAGE with protein MW standards revealed the presence of a 79-kDa protein (figure 2C). The characteristics of the bile protein were that it was monomeric, N-terminal blocked, had an isoelectric point of 5.7 and did not react with antisera directed against rat albumin (data not shown). Extractability of the bound biliary radioactivity from BDE-209 rats ranged from 87 to 100%. Approximately 17% of extractable [^{14}C] from 0–24-h bile was parent compound, and the remainder was metabolites as determined by TLC analyses (data not shown). Owing to insufficient purified mass, metabolite identification was not possible by GC/MS. At 48 and 72 h, no parent BDE-209 was detected in the extractable, protein-bound fraction.

The pooled 0–24-h bile sample from BDE-99 rats chromatographed on a G-75 column revealed that 28% of the biliary [^{14}C] was associated with protein (table 2). The association steadily increased to 47% by 72 h. All BDE-99-derived [^{14}C] was bound to a 79-kDa protein that had the same characteristics as the one isolated in BDE-209-treated rat bile. Extractability of BDE-99-derived radioactivity from rat bile protein ranged from 27 to 85%. Twenty-one per cent of bound, extractable radioactivity in the 0–24-h bile sample was parent compound and the remainder was polar metabolites (data not shown). At 48 and 72 h, only metabolites were observed bound to the 79-kDa protein.

Tissues

The majority of the BDE-99- and -209-derived [^{14}C] from each sampled tissue was associated with the membrane fraction (figure 3). Minor amounts of [^{14}C] were present in the microsomal fraction (0–29% of the tissue ^{14}C) as well as in the soluble fraction (4–24%). In the soluble fraction of livers from BDE-209 dosed rats, the [^{14}C] was bound to a 14-kDa protein (figure 2D), which was characterized as a liver fatty acid-binding protein by the FABP assay (see the Materials and methods; data not shown). No other tissue contained sufficient radioactivity in the soluble fraction following the 100 000*g* centrifugation to perform the gel filtration column chromatography necessary before the FABP assay.

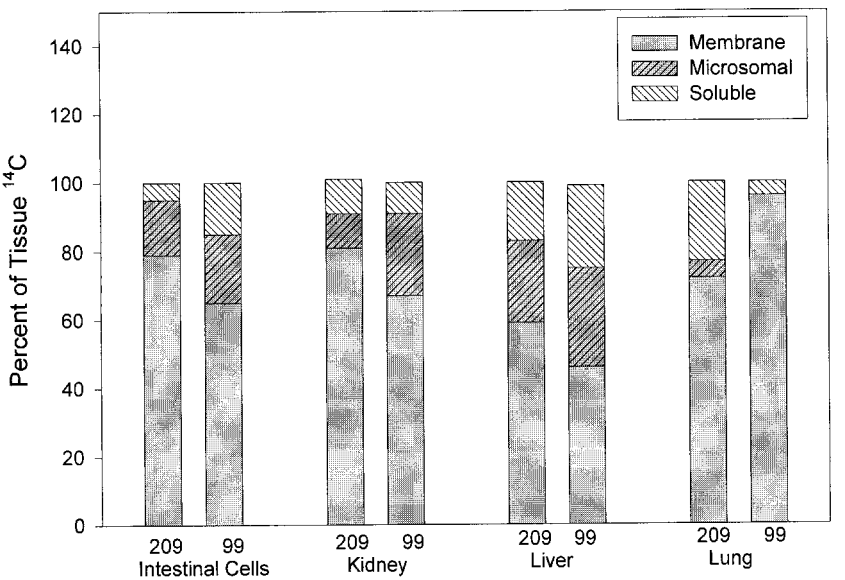


Figure 3. Subcellular localization of [^{14}C]BDE-99 and -209 in selected tissues from the conventional rat obtained by differential centrifugation. The membrane fraction was the 10 000*g* pellet, the soluble fraction was the supernatant from the 100 000*g* centrifugation and the microsomal fraction was the pellet from the 100 000*g* centrifugation. Data were derived from three rats dosed with BDE-99 and four rat dosed with BDE-209.

Discussion

At 72 h, 6% of BDE-99 and 20% of BDE-209 cumulative urinary [^{14}C] were protein-bound. Metabolism of both congeners appeared necessary for excretion by the rat kidneys. Although the protein-bound radioactivity from urine of BDE-99 rats was not extracted, the extractable radioactivity from BDE-209 rats was characterized as metabolites, and the non-extractable radioactivity suggested metabolic activation. Highly polar metabolites were also detected in the unbound fraction of urine for both congeners (data not shown). The urinary [^{14}C] from each congener associated with a different protein, which indicated a selectivity for each binding protein. In conventional BDE-99 rats, the urine-binding protein was identified as α_{2u}-globulin (α_{2u}). Binding to urinary α_{2u} was not detected in BDE-209-dosed rats, instead all the [^{14}C] was bound to albumin. Very different levels of urinary protein binding were observed in cannulated rats between the two congeners. No binding was detected in bile duct-cannulated BDE-99 dosed rats (table 2), whereas the majority of BDE-209-derived [^{14}C] in cannulated rat urine was bound (68%; table 3).

The binding of xenobiotics to urinary proteins has been previously reported. Toxic (Hakk *et al*. 1998, 1999) and non-toxic dioxin metabolites (Wiener 1999) bind to both α_{2u}-globulin and albumin in male rat urine. However, much higher levels are associated with albumin. Methyl sulfonyl metabolites of 2,2′,5,5′-tetrachlorobiphenyl and *m*-dichlorobenzene bind to α_{2u} in rat urine (Larsen *et al*. 1990a, b), but not to albumin.

The sex-dependent α_{2u} is a hepatically synthesized protein under androgenic control (Borghoff *et al*. 1990) that is filtered through the glomeruli filter of the nephron, but 60% can be reabsorbed by the proximal tubules (Neuhaus and Lerseth 1979). The protein constitutes the major urinary protein in mature male rats and accounts for approximately 30% of the total (Roy *et al*. 1966). Apparently, the function of α_{2u} is as a pheromone carrier protein (Shaw *et al*. 1983) and to maintain spermatogenesis (Ekstrom and Hoekstra 1984). α_{2u} belongs to a family of low molecular weight transport proteins, which also includes bovine β-lactoglobulin, mouse major urinary protein (MUP) and human retinol-binding protein. Each protein has an eight-stranded β-barrel secondary structure lined with hydrophobic amino acids that serves as a hydrophobic-binding pocket for ligands (Borghoff *et al*. 1990, Papiz *et al*. 1986, Pervaiz and Brew 1987). Ligand specificity for members of this family is determined by the composition of hydrophobic amino acids in the inner wall of the β-barrel. It is possible that excretion of BDE-99 in female rats or other organisms lacking α_{2u} may be delayed or diverted into other excretion pathways owing to a lack of this carrier protein mechanism.

Albumin is the most abundant plasma protein and has many diverse functions. It serves as a transporter of numerous compounds, including fatty acids (Goodman 1958). It is also capable of associating non-covalently with many small molecules because of six binding domains, each with a different specificity (Kragh-Hansen 1981). High rates of albumin excretion into urine are associated with glomerular dysfunction due to chemical toxicity (Nomiyama *et al*. 1982). The binding of phenolic metabolites of carcinogens to albumin has been used as a dosimeter for carcinogen exposure (El-Bayoumy *et al*. 1994). These previously published results, as well as the data presented here, indicate a degree of selectivity for xenobiotic binding to albumin and suggest that albumin can serve as the preferred excretion vehicle for the clearance of some xenobiotics.

Considerably more of the bile-excreted BDE-209 was protein-bound than the BDE-99 at all time points (>90 versus <47%, respectively; tables 2 and 3). The basis of the association of each congener with the biliary 79-kDa protein may be physiochemical in nature because BDE-209 has a higher octanol:water partition coefficient, i.e. $k_{ow} = 9.97$, than does BDE-99 ($k_{ow} = 6.64$) (WHO/ICPS 1994), and the magnitude of this difference may also extend to the metabolites. Like α_{2u} and albumin in urine, the 79-kDa protein may be necessary to facilitate elimination of the lipophilic BDE-99 and -209 and their metabolites via the bile. Another possibility for the difference in the extent of biliary protein binding observed between these two congeners is that BDE-209 and/or its metabolites may serve as more specific ligands than BDE-99 and/or its metabolites for a binding site on the 79-kDa protein.

Previous studies to characterize rat biliary proteins using two-dimensional gel electrophoresis did not report the detection of a 79-kDa monomeric protein among the 16 proteins observed in hooded rats (Mullock *et al*. 1978). Of these 16 proteins, 13 were immunologically identical to rat serum proteins. Transferrin is the only known rat serum protein with a molecular weight sufficiently near 79 kDa. A monomeric, 76.5-kDa non-haem glycoprotein essential for iron transport in the serum, it is known to be excreted in rat urine (Gordon *et al*. 1997). However, we are not aware of any report of transferrin excretion into bile.

Only a limited number of reports exist on biliary proteins that bind to xenobiotics. Samuels *et al*. (1983) reported that 10% of the bile radioactivity from a dose of the hepatocarcinogenic azo dye 3-methyl-*N*,*N*-dimethyl-4-aminoazobenzene bound to a 50-kDa rat bile protein as phenolic metabolites. Two specific binding sites were indicated following CNBr cleavage and SDS-PAGE because radioactivity was bound to two of the peptide fragments. Non-toxic (Larsen *et al*. 1995, Wiener and Larsen 1997) and toxic (Hakk *et al*. 1998, 1999) dioxins and/or their metabolites have been shown to bind to an unidentified 79-kDa protein in the bile of male Sprague–Dawley rats. In these latter studies, the extent of xenobiotic association with the 79-kDa protein ranged from 7 to 47% of the biliary [^{14}C]. Therefore, the present results with BDE-209 represent the first report of nearly 100% association of an excreted xenobiotic with a bile protein.

The majority of the intracellular [^{14}C] for both congeners localized in the membrane fraction of the selected tissues at 72 h (figure 3), and the amount of tissue [^{14}C] that localized in the microsomal fraction ranged from 0 to 29%. Each PBDE congener partitioned into the microsomes within each tissue to approximately the same extent, i.e. very low in the lung (0 and 5% of tissue [^{14}C] for BDE-99 and -209 rats, respectively; figure 3) and relatively high in the liver (29 and 24%, respectively). The microsomal PBDE congeners may have been subject to cytochrome P450 oxidation, but in a published study no oxidative products were detected in whole extracts of BDE-99 lung or kidney cells by silica gel TLC and GC/MS (Hakk *et al*. 2002). However, the liver extracts from BDE-99 treated rats contained a minor amount of a monohydroxylated metabolite by GC/MS (Hakk *et al*. 2002). No tissue extraction, TLC or mass spectral data were conducted on BDE-209 tissue samples in the present study because of limited quantities of radiolabelled material.

Based on the lipophilicity of both PBDE congeners, the radioactivity detected in the cytosolic fraction of each tissue was probably solubilized by carrier proteins (figure 3). The results from the FABP assay of the soluble fraction of rat liver

suggested that BDE-209 bound to liver FABP (figure 1D). FABP is found in the cytosol of various tissues and is capable of binding to halogenated aromatics (Larsen *et al.* 1991, 1992), although its native function is for the absorption, intracellular transport, compartmentalization and metabolism of free fatty acids and their acyl-SCoA esters (Bass 1988). Other cytosolic proteins also serve to bind xenobiotics, and this can result in tissue accumulation. Lund *et al.* (1988) purified a 13-kDa uteroglobulin-like protein in rat lung cytosol that bound to a methylsulfonyl metabolite of 2,2′,5,5′-tetrachlorobiphenyl. Association of methyl sulfonyl metabolites of 1,3-dichlorobenzene with cytosolic kidney α_{2u}-globulin was concluded as being responsible for the high levels of metabolites present in rat kidney (Kato *et al.* 1986). Finally, cytosolic proteins are also known to be involved in the excretion of xenobiotics. In mice, a methyl sulfonyl metabolite of 2,2′,5,5′-tetrachlorobiphenyl was associated with MUP in urine, but not in the kidney (Larsen *et al.* 1990a).

Some cytosolic carrier proteins can also be involved in a toxicological response following xenobiotic ligand binding. α_{2u} has been shown to be a mediator of nephropathy in male rat kidneys (Swenberg 1994). The condition is characterized by an excessive accumulation of protein droplets packaged in lysosomes in P_2 renal epithelial cells. Lysosomal protein overload occurs, which causes necrosis of individual epithelial cells and the release of cellular debris, and accumulation near the thin loop of Henle. To compensate for the loss, cell proliferation ensues, which occasionally can promote formation of neoplastic lesions (Dietrich and Swenberg 1991). A number of compounds are known to cause the nephropathy and tumours in male rat kidneys: 2,2,4-trimethylpentane (a major component of unleaded gasoline), D-limonene, 1,4-dichlorobenzene, isophorone and hexachloroethane. Mammals that do not synthesize α_{2u} do not show signs of the nephropathy when exposed to these agents. It is not known if homologous human members of the α_{2u} superfamily, i.e. urine protein 1, retinol-binding protein or α_1-acid glycoprotein, bind to these compounds in a similar manner, or whether nephrotoxicity or carcinogenicity mechanisms occur. Likewise, it is unknown whether BDE-99 exposure could lead to nephropathy in rats, despite the demonstrated ability of BDE-99 and/or its metabolites to associate or tightly bind with α_{2u} in the urine of the present study.

Acknowledgements

The high degree of technical assistance was provided by Barbara K. Magelky and Colleen Pfaff is gratefully appreciated. The use of trade, firm or corporation names in this paper is for the information and convenience of the reader. Such use does not constitute an official endorsement or approval by the US Department of Agriculture or the Agricultural Research Service of any product or service to the exclusion of others that may be suitable.

References

Bass, N., 1988, The cellular fatty acid binding proteins: aspects of structure, regulation, and function. *International Review in Cytology*, **3**, 143–184.

Borghoff, S. J., Short, B. G. and Swenberg, J. A., 1990, Biochemical mechanisms and pathobiology of α_{2u}-globulin nephropathy. *Annual Reviews in Pharmacology and Toxicology*, **30**, 349–367.

Cham, B. E. and Knowles, B. R., 1976, A solvent system for delipidation of plasma or serum without protein precipitation. *Journal of Lipid Research*, **17**, 176–181.

Dietrich, D. R. and Swenberg, J. A., 1991, The presence of α_{2u}-globulin is necessary for d-limonene promotion of male rat kidney tumors. *Cancer Research*, **51**, 3512–3521.

Ekstrom, R. C. and Hoekstra, W. G., 1984, Investigation of putative androgen-like activity of α_{2u}-globulin in castrated and estrogen treated male rats. *Proceedings of the Society of Experimental Biology and Medicine*, **175**, 491–496.

El-Bayoumy, K., Johnson, B., Partian, S., Upadhyaya, P. and Hecht, S. S., 1994, *In vivo* binding of 1-nitropyrene to albumin in the rat. *Carcinogenesis*, **15**, 119–123.

Goodman, D. S., 1958, The interaction of human serum albumin with long-chain fatty acid anions. *Journal of the American Chemical Society*, **80**, 3892–3898.

Gordon, S., Tee, R. D. and Newman Taylor, A. J., 1997, Analysis of rat serum allergens. *Journal of Allergy and Clinical Immunology*, **99**, 716–717.

Hakk, H., Feil, V. J. and Larsen, G., 1998, The binding of 2,3,7,8-tetrachlorodibenzo-*p*-dioxin metabolites with rat urinary and biliary carrier proteins. *Organohalogen Compounds*, **37**, 395–399.

Hakk, H., Larsen, G. L., Bergman, Å. and Örn, U., 2000, Metabolism, excretion, and distribution of the flame retardant tetrabromobisphenol-A in conventional and bile-duct cannulated rats. *Xenobiotica*, **30**, 881–890.

Hakk, H., Larsen, G. and Feil, V. J., 1999, The binding of 1,2,3,7,8-pentachlorodibenzo-*p*-dioxin metabolites with rat urinary and biliary carrier proteins. *Organohalogen Compounds*, **40**, 125–128.

Hakk, H., Larsen, G. L. and Klasson-Wehler, E., 2002, Tissue disposition, excretion, and metabolism of 2,2′,4,4′,5-pentabromodiphenyl ether (BDE-99) in the male Sprague–Dawley rat. *Xenobiotica*, **32**, 369–382.

Kato, Y., Kogure, T., Sata, M., Murata, T. and Kimura, R. 1986, Evidence that methylsulfonyl metabolites of *m*-dichlorobenzene are causative substances of induction of hepatic microsomal drug-metabolizing enzymes by the parent compound in rats. *Toxicology and Applied Pharmacology*, **78**, 505–511.

Kragh-Hansen, U., 1981, Molecular aspects of ligand binding to serum albumin. *Pharmacology Reviews*, **33**, 17–51.

Larsen, G. L., Bakke, J. E. and Huwe, J. K., 1990a, Methylsulphone metabolites of *m*-dichlorobenzene as ligands for α_{2u}-globulin in rat kidney and urine. *Xenobiotica*, **20**, 7–17.

Larsen, G. L., Bergman, Å. and Klasson-Wehler, E., 1990b, A methylsulphonyl metabolite of a polychlorinated biphenyl can serve as a ligand for α_{2u}-globulin in rat and major-urinary-protein in mice. *Xenobiotica*, **20**,1343–1352.

Larsen, G. L., Bergman, Å., Klasson-Wehler, E. and Bass, N. M., 1991, A methylsulfonyl metabolite of a polychlorinated biphenyl can serve as a ligand for liver fatty acid binding protein in rat intestinal mucosa. *Chemico-Biological Interactions*, **77**, 315–323.

Larsen, G. L., Huwe, J. K., Bergman, Å., Klasson-Wehler, E. and Hargis, P., 1992, Methylsulfonyl metabolites of xenobiotics can serve as ligands for fatty acid binding proteins in chicken liver and intestinal mucosa. *Chemosphere*, **25**, 1189–1194.

Larsen, G. L., Wiener, C., Hakk, H. and Feil, V. J., 1995, Interaction of 1,2,7,8-tetrachloro-*p*-dioxin metabolites with mammalian carrier proteins. *Organohalogen Compounds*, **25**, 249–251.

Lund, J., Nordlund, L. and Gustafsson, J.-Å., 1988, Partial purification of a binding protein for polychlorinated biphenyls from rat lung cytosol; physiochemical and immunochemical characterization. *Biochemistry*, **27**, 7891–7901.

Mazel, J. V., Jr, 1971, Polyacrylamide gel electrophoresis of viral proteins. *Methods in Virology*, **5**, 179–246.

Mullock, B. M. Dobrota, M. and Hinton, R. H., 1978, Sources of the proteins of rat bile. *Biochimica et Biophysica Acta*, **543**, 479–507.

Neuhaus, O. W. and Lerseth, D. S., 1979, Dietary control of the renal reabsorption and excretion of α_{2u}-globulin. *Kidney International*, **16**, 409–415.

Nomiyama, K., Nomiyama, H. and Yotoriyma, M., 1982, Low-molecular-weight proteins in urine from rabbits given nephrotoxic compounds. *Industrial Health*, **20**, 1–10.

Örn, U., Eriksson, L., Jakobsson, E. and Bergman, Å., 1996, Synthesis and characterization of polybrominated diphenyl ethers-unlabelled and radiolabelled tetra-, penta-, and hexa-bromodiphenyl ethers. *Acta Chimica Scandinavica*, **50**, 802–807.

Papiz, M. Z., Sawyer, L., Eliopoulos, E. E., North, A. C. T., Findlay, J. B., Sivaprasadarao, R., Jones, T. A., Newcomer, M. E., Kraulis, P. J., 1986, The structure of β-lactoglobulin and its similarity to plasma retinol-binding protein. *Nature*, **324**, 383–385.

Pervaiz, S. and Brew, K., 1987, Homology and structure–function correlations between α_1-acid glycoprotein and serum retinol-binding protein and its relatives. *FASEB Journal*, **1**, 209–214.

Roy, A. K., Neuhaus, O. W. and Harmison, C. R., 1966, Preparation and characterization of a sex-dependent rat urinary protein. *Biochimica et Biophysica Acta*, **127**, 72–81.

Samuels, A., Freedman, J. H. and Bhargava, M., 1983, Purification and characterization of a novel abundant protein in rat bile that binds azo dye metabolites and copper. *Biochimica et Biophysica Acta*, **759**, 23–31.

Shaw, P. H., Held, W. A., Hastie, N. D., 1983, The gene family for major urinary proteins: expression in several secretory tissues of the mouse. *Cell*, **32**, 755–761.

Swenberg, J. A., 1994, α_{2u}-Globulin nephropathy: Review of the cellular and molecular mechanisms involved and their implications for human risk assessment. *Environmental Health Perspectives*, **101(suppl. 6)**, 39–44.

Towbin, H. and Gordon, J., 1984, Immunoblotting and dot immuno-binding-current status and outlook. *Journal of Immunological Methods*, **72**, 313–340.

WHOICPS, 1994, Brominated Diphenyl Ethers. Environmental Health Criteria 1762 (Geneva: World Health Organization).

Wiener, C., 1999, Association of dioxins and/or their metabolites with mammalian carrier proteins. Thesis, North Dakota State University, Fargo.

Wiener, C. and Larsen, G. L., 1997, Covalent binding of dioxin metabolites to a 79 kDa protein isolated from bile of rats dosed with either 1,2,7,8-; 1,3,7,8-; or 1,4,7,8-tetrachlorodibenzo-*p*-dioxin. *Organohalogen Compounds*, **34**, 195–198.

XENOBIOTICA, 2002, VOL. 32, NO. 12, 1093–1107

Taylor & Francis
healthsciences

Comparative biotransformation of morphine, codeine and pholcodine in rat hepatocytes: identification of a novel metabolite of pholcodine

M. JAIRAJ†, D. G. WATSON†, M. H. GRANT‡, A. I. GRAY† and G. G. SKELLERN*

† Department of Pharmaceutical Sciences, University of Strathclyde, 27 Taylor Street, Glasgow G4 0NR, UK
‡ Bioengineering Unit, 106 Rottenrow East, Glasgow G4 0NW, UK

Received 25 March 2002

1. Pholcodine (3-morpholinoethylmorphine), a semi-synthetic alkaloid, is widely used as an antitussive agent.

2. Norpholcodine [7,8-didehydro-4,5α-epoxy-3-(2-morpholinoethoxy)morphinan-6α-ol] (NP) and pholcodine-*N*-oxide [1(9a)-dehydro-(4a*R*,5*S*,7a*R*,9c*S*,12*S*)-4a,5,7a,8,9,9a-hexahydro-5-hydroxy-12-methyl-3-morpholinoethoxy-1*H*-8,9,c-(iminoethano)phenanthro[4,5-bcd] furan-12-oxide] (PNOX) were identified in incubations of pholcodine with freshly isolated rat hepatocytes by liquid chromatography/electrospray-mass spectrometry (LC/ESI-MS).

3. Synthesized NP and PNOX were characterized by mass spectrometry and nuclear magnetic resonance (NMR) spectroscopy.

4. *N*-oxidation was the major metabolic pathway for pholcodine, producing a previously unreported metabolite.

5. The metabolism of morphine and codeine was also determined using freshly isolated hepatocytes.

6. For morphine, 3-glucuronidation was the major metabolic pathway, whilst for codeine it was dealkylation (*O*- and *N*-).

7. Neither morphine nor its metabolites were metabolites of pholcodine.

8. This observation supports the hypothesis that the absence of analgesic activity with pholcodine may be due to less *O*-dealkylation *in vivo*.

9. Together with the slow biotransformation of pholcodine ($k_{met} = 0.021\,\mu M\,min^{-1}$) in comparison with morphine ($k_{met} = 0.057\,\mu M\,min^{-1}$) and codeine ($k_{met} = 0.112\,\mu M\,min^{-1}$), the results obtained were consistent with its low addiction potential and suggest that its antitussive efficacy is mediated by the parent drug or one of its metabolites other than morphine.

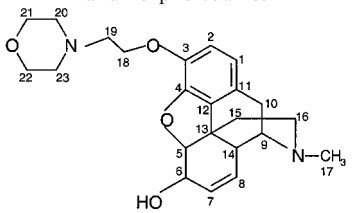
Introduction

Morphine and its analogues, e.g. codeine and pholcodine, are widely used as analgesics and antitussives. The pharmacological effects of many drugs can be attributed wholly or partially to the action of metabolites rather than to a direct action of the drug (Paul *et al*. 1989). Indeed, the main activity of morphine is now associated with its metabolite morphine-6-glucuronide (Paul *et al*. 1989, Gong *et al*. 1991), and as codeine readily undergoes demethylation to morphine (Findlay *et al*. 1986, Pawula *et al*. 1994), it is morphine that is primarily thought to mediate the analgesic activity of codeine.

* Author for correspondence; e-mail: g.g.skellern@strath.ac.uk

Xenobiotica ISSN 0049–8254 print/ISSN 1366–5928 online © 2002 Taylor & Francis Ltd
http://www.tandf.co.uk/journals
DOI: 10.1080/0049825021000017911

Table 1. Structure of pholcodine and NMR chemical shift data of pholcodine, pholcodine-*N*-oxide and norpholcodine.



	Pholcodine		Pholcodine-*N*-oxide		Norpholcodine	
	^{1}H-NMR	^{13}C-NMR	^{1}H-NMR	^{13}C-NMR	^{1}H-NMR	^{13}C-NMR
C-atom	δ_H (ppm)	δ_C (ppm)	δ_H (ppm)	δ_C (ppm)	δ_H (ppm)	δ_C (ppm)
1	6.51 (d)	120.5	6.62 (d)	121.2	6.62 (d)	121.2
2	6.68 (d)	118.1	6.80 (d)	119.3	6.80 (d)	119.2
3	–	142.5	–	142.5	–	142.6
4	–	149.2	–	149.8	–	149.7
5	4.80 (d)	93.3	4.97 (d)	92.8	4.95 (d)	93.3
6	4.17 (m)	68.3	4.27 (m)	67.5	4.31 (d)	68.0
7	5.68 (d)	134.1	5.72 (d)	135.1	5.76 (d)	135.9
8	5.35 (td)	129.6	5.36 (td)	127.5	5.33 (td)	126.5
9	3.31 (dd)	60.2	3.92 (dd)	75.9	3.4 (dd)	53.2
10	3.05 (d)	21.8	3.32 (d)	26.9	3.1 (s)	27.6
	2.39 (d)		2.98 (dd)			
11	–	129.5	–	125.9	–	126.7
12	–	133.0	–	132.6	–	131.2
13	–	44.5	–	42.9	–	44.4
14	2.68 (m)	41.6	3.83 (m)	35.0	2.88 (m)	38.7
15	1.81 (d)	36.6	1.87 (d)	32.1	2.05 (d)	33.7
	2.08 (dt)		2.71 (dt)		2.27 (dt)	
16	2.35 (t)	47.5	3.25 (t)	60.4	3.01 (d)	38.6
	2.72 (dt)		3.38 (dt)		3.34 (dt)	
17	2.58 (s)	43.2	3.44 (s)	58.5	–	–
18	4.15 (ddd)	68.7	4.23 (ddd)	67.7	4.31 (ddd)	68.5
	4.28 (ddd)		4.39 (ddd)		4.43 (ddd)	
19	2.75 (t)	59.2	3.10	58.7	3.05 (t)	58.8
20, 23	2.62 (m)	54.0	2.95	54.7	2.85 (m)	54.9
21, 22	3.71 (t)	67.8	3.82 (t)	66.6	3.78 (t)	67.1
OH-6		–		–		–

s, Singlet; d, doublet; dd, doublet of doublet; ddd, doublet of doublet of doublet; dt, doublet of triplet; td, triplet of doublet; t, triplet; m, multiplet.

Pholcodine (3-morpholinoethylmorphine) (table 1), a semisynthetic alkaloid, is widely used as an antitussive agent. Investigations on its antitussive properties have shown it to be equivalent or superior to codeine (Findlay 1988). Despite its widespread use, there is limited published information on its metabolism and pharmacokinetics. The characterized metabolites of pholcodine include norpholcodine, hydroxy pholcodine, desmorpholinohydroxy pholcodine and a not clearly identified 'oxo pholcodine' (Maurer and Fritz 1990), conjugates with glucuronic acid (Johansen *et al.* 1990, 1992), and, most importantly with regard to its analgesic activity, morphine (Maurer and Fritz 1990, Johansen *et al.* 1992). The bulky morpholinoethyl group in pholcodine (table 1) appears to undergo only limited *O*-dealkylation to morphine, a fact that may contribute to its lack of analgesic activity and the low addiction potential reported (Butz *et al.* 1983). In

addition, this bulky group may also sterically inhibit enzymic conjugation with glucuronic acid at the 6-hydroxy position (Findlay 1988). However, other studies (Findlay *et al*. 1986, Chen *et al*. 1988) report no formation of morphine from pholcodine and an absence of glucuronides. These marked differences, especially regarding the formation of morphine, might be due to the use of non-specific analytical techniques (Chen *et al*. 1988).

The current study therefore aimed to investigate the metabolic fate of pholcodine in freshly isolated rat hepatocytes. Isolated hepatocytes have several advantages over preparations of hepatic microsomes and liver homogenates since the cells possess an intact array of drug-metabolizing enzymes (Aasmundstad *et al*. 1993). Furthermore, isolated cells also express metabolic capacity in a coordinated fashion that is more similar to *in vivo* conditions (Aasmundstad *et al*. 1993).

Materials and methods

Chemicals and reagents

Acetonitrile (HiPerSolv) was purchased from BDH (Poole, Dorset, UK); ammonium formate (98%), 3-chloroperoxybenzoic acid (57–86%), 1-chloro-ethyl-chloroformate, normorphine HCl (NM), morphine HCl (M), morphine-d_3-HCl, codeine HCl (C) and norcodeine HCl (NC) were purchased from Sigma–Aldrich Ltd (Poole, UK); morphine-3-glucuronide (M3G) was purchased from Lipomed AG (Arlesheim, Switzerland). Pholcodine hydrate BP (P) and codeinone were a gift from Macfarlan Smith Ltd (Edinburgh, UK).

Norpholcodine [7,8-didehydro-4,5α-epoxy-3-(2-morpholinoethoxy)morphinan-6α-ol] (NP) was synthesized by published methods for the *N*-demethylation of tertiary amines (Olofson 1984, Pelander *et al*. 1997). In brief, pholcodine hydrate BP (250 mg) was dissolved in dried dichloroethane (60 ml) and the solution cooled to 4°C. 1-Chloroethyl chloroformate (440 µl) was slowly added to this solution and the mixture was stirred for 4 h at 0–4°C. The resulting carbamate intermediate was hydrolysed (50°C for 20 min) in 50 ml methanol. The synthesized norpholcodine was purified with a preparative HPLC system consisting of Gilson 305 and 307 pumps and a Gilson 118 UV-Vis detector (Anachem, Luton, UK). The column used was a ODS-2 LUNA (250 $\times$ 10 mm i.d. 10 µm particle size, Phenomenex, Macclesfield, UK) with the following gradient elution programme. A mixture of acetonitrile 10% (v/v) in ammonium formate buffer (10 mM, pH 8.0) was delivered for 6 min at 5 ml min^{-1} after which time the acetonitrile concentration was increased to 40% (v/v) and maintained for 3 min with a flow rate of 10 ml min^{-1} before decreasing the acetonitrile concentration back to 10% for the final 5 min with a flow rate of 5 ml min^{-1}. The separation was performed at ambient temperature. The fractions containing norpholcodine were mixed with ethanol and then evaporated under vacuum to remove any residual water and ammonium formate. The purified norpholcodine (purity > 90%) was recrystallized from ethanol as the formate salt and identified by mass spectrometry and NMR spectroscopy as described below.

Pholcodine-*N*-oxide [1(9a)-dehydro-(4a*R*,5*S*,7a*R*,9c*S*,12*S*)-4a,5,7a,8,9,9a-hexahydro-5-hydroxy-12-methyl-3-morpholinoethoxy-1*H*-8,9,c-(iminoethano)phenanthro[4,5-bcd]furan-12-oxide] (PNOX) was synthesized using a previously published method for the synthesis of *N*-oxides of morphine analogues by oxidation with *m*-chloroperoxybenzoic acid (Philipson *et al*. 1976). The reaction products were separated by preparative HPLC using the system described above but with isocratic conditions at ambient temperature with a mobile phase consisting of 3% (v/v) acetonitrile in 1 mM ammonium formate buffer, pH 3.5. The fractions containing pholcodine-*N*-oxide were mixed with ethanol and evaporated under vacuum to remove any residual water and ammonium formate. The purified *N*-oxide (purity > 90%) was recrystallized from ethanol and identified by mass spectrometry and NMR spectroscopy as described below.

Preparation of hepatocytes

Studies were performed using suspensions of hepatocytes freshly isolated from male Sprague–Dawley rats (190–250 g). Anaesthesia was induced by intraperitoneal (i.p.) injection of a solution of pentobarbitone sodium (60 mg kg^{-1}, Sagatal®, Rhone Poulenc Rohrer, Dagenham, UK). Hepatocytes were obtained from whole livers by a two-step collagenase perfusion, as reported by Moldeus *et al*. (1978). The initial viability of the hepatocytes was typically > 85%, as determined by trypan blue exclusion. Preliminary experiments indicated that the viability was retained for at least 4 h. Furthermore, incubation of hepatocytes for 4 h with the opiate substrates did not decrease cell viability compared with the control incubations (data not shown).

Incubation conditions

Isolated hepatocytes (2×10^6 viable cells ml^{-1}) were incubated with solutions of pholcodine hydrate, codeine HCl, normorphine HCl or morphine HCl (50 μM in Krebs–Henseleit buffer, pH 7.6, containing 12.5 mM HEPES [*N*-(2-hydroxyethyl) piperazine-*N'*-([2-ethanesulphonic acid)] in rotating 50-ml round-bottomed flasks, for 4 h, at 37°C in an atmosphere of 95% O_2/5% CO_2 (v/v). Samples of the incubation suspension (500 μl) were removed after 5, 10, 15, 20, 30, 60, 90, 120, 180 and 240 min and an equal volume of 0.2% (w/v) NaCl in methanol was added to them to stop the reaction. The sample mixture was ultrasonicated (5 min) and centrifuged (20000*g* for 10 min) after which morphine-d_3-HCl was added (10 μl ml^{-1} of a 2.05 mg ml^{-1} solution in water) before analysis by LC/MS. Control incubations were performed containing only cell suspensions or opiate solutions in Krebs–HEPES buffer and were treated in a similar way to the samples. Sample solutions were stored at −20°C until analysis.

Liquid chromatography

The LC/MS system consisted of a SpectraSYSTEM P4000 gradient pump, a SpectraSYSTEM AS3000 autosampler (equipped with a type 7010-150 Rheodyne injection valve, 20 μl loop) and a SpectraSYSTEM UV6000LP UV-DAD detector (Thermo Separation Products Ltd, Hemel Hempstead, UK). The column, which was at ambient temperature, was a ODS-2 LUNA column (75 × 4.6 mm i.d., 3 μm particle size; Phenomenex, Macclesfield, UK). Analytes in the morphine and pholcodine incubation mixtures were separated isocratically with a mobile phase consisting of 3% (v/v) acetonitrile in 1 mM ammonium formate buffer, pH 3.5, and 15% acetonitrile in 10 mM ammonium formate buffer, pH 6.0, with a flow-rate of 0.4 ml min^{-1}. The injection volume was 20 μl. The following gradient elution programme was used for the separation of analytes in the codeine reaction solutions. A mixture of acetonitrile (3% v/v) in 1 mM ammonium formate buffer, pH 3.5, was delivered for 4 min after which time the acetonitrile concentration was increased to 12% v/v and kept constant for 4 min before restoring it back to 3% v/v for the final 4 min at a flow-rate of 0.4 ml min^{-1}. All of the eluent was introduced into the mass spectrometer source.

LC-MS analyses

The mass spectrometer was an Automass MS (Thermoquest, Hemel Hempstead, UK) equipped with an electrospray source; all samples were analysed in positive electrospray ionization (ESI) mode. The mass spectrometric conditions were optimized every day to produce the highest signal-to-noise ratio. Typical conditions were: temperature 500°C, cone voltage 24 V, corona needle voltage 2450 V. Analytes were quantified using selected ion monitoring: m/z = 286(morphine); 289 (morphine-d_3); 298 (norcodeine); 300 (codeine); 313 (normorphine); 385 (norpholcodine); 400 (pholcodine); 448 (normorphine-3-glucuronide); 416 (pholcodine-*N*-oxide); and 462 (morphine-3-glucuronide). PNOX was monitored at m/z = 416 rather than at the expected molecular ion at m/z = 415, since with the LC/MS conditions described above the ion at m/z = 416 was formed. This was most likely due to the low-resolution settings of the instrument (0.7 mass units at base). Quantification was achieved using morphine-d_3 as an internal standard. The absence of the formation of the 6-dehydrogenated metabolite of codeine, codeinone, was confirmed by comparison with the authentic standard substance. For morphinone no standard was obtainable.

Validation of the LC/MS methods

The validation of the LC/MS methods was performed on 2 days with solutions in a concentration range of 1–30 μM pholcodine, pholcodine-*N*-oxide and norpholcodine, and morphine, morphine-3-glucuronide, normorphine, norcodeine and codeine prepared in the mobile phase containing morphine-d_3. The precision of the methods was determined for analyte solutions of 5 μM by injecting the standard solutions four times on each of the 2 days. To assess recoveries of the substrates in the hepatocyte incubations, individual solutions of 25 μM morphine, codeine and pholcodine were incubated with suspensions of cells in methanol/0.2% (w/v) NaCl mixed with Krebs–HEPES buffer (1:1 v/v). Before the addition of the substrate solutions, the cell suspensions were ultrasonicated to destroy any metabolic capabilities.

MS analysis

High-resolution mass spectra of pholcodine, norpholcodine and pholcodine-*N*-oxide were obtained with a Jeol AX 505 instrument. The samples were inserted via a heated probe into the mass spectrometer and the mode of ionization used was electron impact (EI) at 70 eV.

For PNOX, direct injection ESI-MS analysis was performed on a TSQ 7000 MS/MS instrument (Thermo Finnigan, Hemel Hempstead, UK) equipped with an electrospray source.

Nuclear magnetic resonance spectroscopy

^{1}H- and ^{13}C-NMR spectra, heteronuclear multiple quantum coherence (HMQC) spectra and heteronuclear multiple bond correlation (HMBC) spectra were recorded for norpholcodine and pholcodine-*N*-oxide on a DPX 400 NMR instrument (Bruker, Coventry, UK). ^{1}H- and ^{13}C-NMR spectra were recorded for pholcodine and pholcodine-*N*-oxide on a Jeol Ex 270 instrument (Jeol, Welwyn Garden City, UK). The samples were prepared for analysis by dissolving approximately 10 mg of each compound in 1 ml deuterated methanol.

Data analysis

Rate constants of metabolism (k_{met}) and formation rate constants (k_{form}) were calculated by plotting $\log_{10}$ of the concentration of analyte against time (k = slope * ln 10).

Results

Characterization of the synthesized standard substances

The structural identification of the synthesized norpholcodine and pholcodine-*N*-oxide [1(9a)-dehydro-(4a*R*,5*S*,7a*R*,9c*S*,12*S*)-4a,5,7a,8,9,9a-hexahydro-5-hydroxy-12-methyl-3-morpholinoethoxy-1*H*-8,9,c-(iminoethano)phenanthro[4,5-bcd]furan-12-oxide] was accomplished by detailed NMR spectroscopic and MS analyses. Table 1 shows the ^{1}H and ^{13}C assignments for pholcodine and its two metabolites, pholcodine-*N*-oxide and norpholcodine. The numbering system adopted in table 1 for pholcodine, although being non-systematic, has been widely used (Findlay 1988) and is thus used throughout, replacing the systematic numbering above. Comparison of the ^{1}H- and ^{13}C-NMR spectra for pholcodine and pholcodine-*N*-oxide shows that all the signals due to pholcodine were present in the spectrum of pholcodine-*N*-oxide. Changes of the chemical shift values were observed for the hydrogen and carbon atoms near the nitrogen atom of the morphine group (C-9, C-10, C-14, C-16 and C-17). Similar changes near the *N*-atom are observed for norpholcodine with the prominent signal corresponding to the *N*-CH_3 (C-17) of the morphine group being absent. The hydrogen atoms attached to C-10 appear to be equivalent in norpholcodine, resulting in a single signal (δ_H = 3.1 ppm).

Table 2 shows the mass spectrometric data for pholcodine, pholcodine-*N*-oxide and norpholcodine. Pholcodine and norpholcodine produced the expected molecular ions at m/z = 398 and 384, respectively. However, pholcodine-*N*-oxide readily loses the oxygen atom under the conditions of EI-MS (Midha 1991) and thus does not show a molecular ion at m/z = 414. With ESI-MS it forms a molecular ion with m/z = 415. The main fragmentation ion at m/z = 114 for all three substances was consistent with the loss of the morpholinoethyl group.

Table 2. Mass spectrometric data (m/z values) for pholcodine, pholcodine-*N*-oxide and norpholcodine.

	EI-MS			ESI-MS
	Molecular ion	Base peak	Fragment ions[a]	Principal ion
Pholcodine	398	114	100, 115, 101	400
Pholcodine-*N*-oxide	–	114	398, 115, 133	415[b]
Norpholcodine	384	114	100, 115, 149	385

[a] Abundance >70% of the base peak.
[b] Determined by direct injection with a Thermo Finnigan TSQ 7000 MS instrument.

Validation

No interfering peaks could be detected in the mass chromatograms at the expected retention times of each analyte (figures 1, 3 and 4). Although M3G and NM3G co-elute, they can be easily distinguished by single-ion monitoring (SIM) of their M + H+ ions. The calibration curves (table 3) were linear between 1 and 30 μM for all analytes with a correlation coefficient, r^2, > 0.99 with the exception of norpholcodine ($r^2 = 0.96$) and pholcodine-*N*-oxide ($r^2 = 0.98$). The standard deviations calculated for replicate injections of analyte solutions ($n = 4$, $c = 5$ μM on two different days) ranged between ±0.18 and ±0.8 μM. The absolute recoveries of the opiate substrates that were expressed as peak area ratios (in percentage) of the corresponding concentrations of substrate incubated with dead cell suspensions and incubation buffer were between 88 and 93% (table 3).

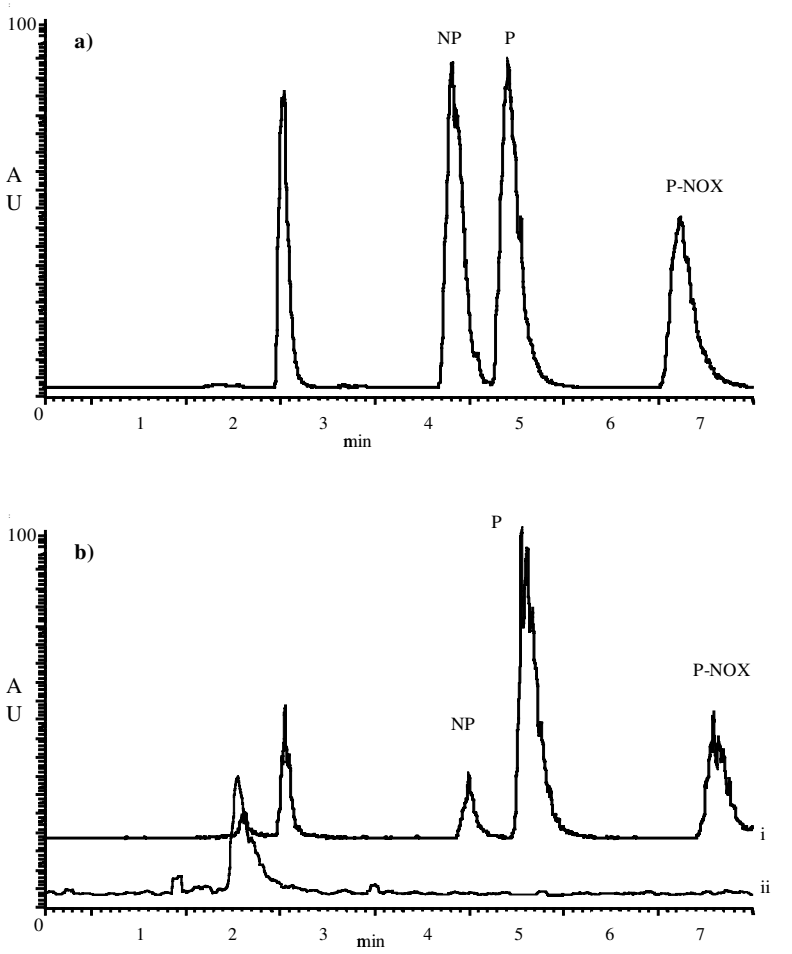


Figure 1. Typical LC/MS traces (SIM mode monitoring ions at $m/z = 385$, 400, 416) of: (a) a standard solution containing 5 μM pholcodine (P), norpholcodine (NP) and pholcodine-*N*-oxide (PNOX) in methanol/0.2% (w/v) NaCl in Krebs–HEPES buffer (1:1); and (b) (i) extract of a 45-min incubation of 50 μM pholcodine with hepatocytes (2×10^6 viable cells ml^{-1}) in Krebs–HEPES buffer; (ii) incubation of hepatocytes (2×10^6 viable cells ml^{-1}) in methanol/0.2% (w/v) NaCl in Krebs–HEPES buffer (1:1).

Table 3. Validation data for the determination of morphine, codeine, pholcodine and their proposed metabolites by LC/MS.

Analyte	Linearity	r^2	Precision (SD)[a]	Recovery (%)[b]
M	$y = 0.02211x + 0.00146$	0.9971	0.11	92
C	$y = 0.03365x + 0.02810$	0.9938	0.10	93
P	$y = 0.59959x + 0.52469$	0.9954	0.08	88
M3G	$y = 0.01044x + 0.00069$	0.9927	0.10	
NM	$y = 0.009625x + 0.00618$	0.9976	0.10	
NC	$y = 0.02077x + 0.01267$	0.9929	0.12	
NP	$y = 0.32709x + 0.68250$	0.9625	0.18	
PNOX	$y = 0.42787x + 0.135141$	0.9819	0.14	

[a] Calculated for replicate injections $(n = 4)$ on two different days for analyte solutions of 5 μM.
[b] Defined as the percentage peak area of the analyte incubated with dead hepatocytes compared with incubation in the buffer.

Pholcodine metabolism

Comparison of the chromatograms of the incubation solutions and a standard mixture containing the synthesized metabolites and pholcodine (figure 1) confirmed the presence of two metabolites, a monoxygenated one (pholcodine-*N*-oxide) and norpholcodine.

By reference to the synthesized standard substances, pholcodine, norpholcodine and pholcodine-*N*-oxide were quantified in the incubation solutions (figure 1) over 4 h (figure 2a). Pholcodine has an overall rate constant for its metabolism of $0.021 \pm 0.0015\,\mu M\ min^{-1}$, with the rate constants for the formation of norpholcodine and pholcodine-*N*-oxide of $0.008 \pm 0.003$and $0.011 \pm 7 \times 10^{-4}\,\mu M\ min^{-1}$, respectively. The concentrations of both metabolites reached a plateau at around 100 min, which suggests that pholcodine-*N*-oxide is not an intermediate in the *N*-demethylation of pholcodine to norpholcodine and that both metabolites are sufficiently hydrophilic to be excreted without any further biotransformation by the hepatocytes.

Normorphine, morphine and codeine metabolism

Normorphine-3-glucuronide (NM3G) was not quantified in the incubation mixtures of morphine and codeine due to the lack of a reference standard. However, when normorphine was incubated on its own with hepatocytes, the rate constant for its biotransformation was $0.009\,\mu M\,min^{-1}$ with NM3G being the only metabolite detected.

Morphine and its metabolites are baseline separated from each other (figure 3). Compared with pholcodine (figure 2a), morphine (figure 2b) has a higher rate of metabolism ($k_{met} = 0.057 \pm 0.004\,\mu M\,min^{-1}$). The maximum concentration of its major metabolite, morphine-3-glucuronide, occurs at 60 min with a rate constant for its formation of $0.056 \pm 0.008\,\mu M\ min^{-1}$, after which it slowly decreases. Interestingly, the maximum concentration of normorphine occurred at 30 min (figure 2b), which corresponds to the disappearance of most of the morphine at this time point. The metabolism of normorphine ($k_{met} = 0.0076 \pm 0.0012\,\mu M\,min^{-1}$) in the morphine incubations after 30 min is considerably slower than in the incubations where normorphine itself is the initial substrate. That its metabolism is slower in

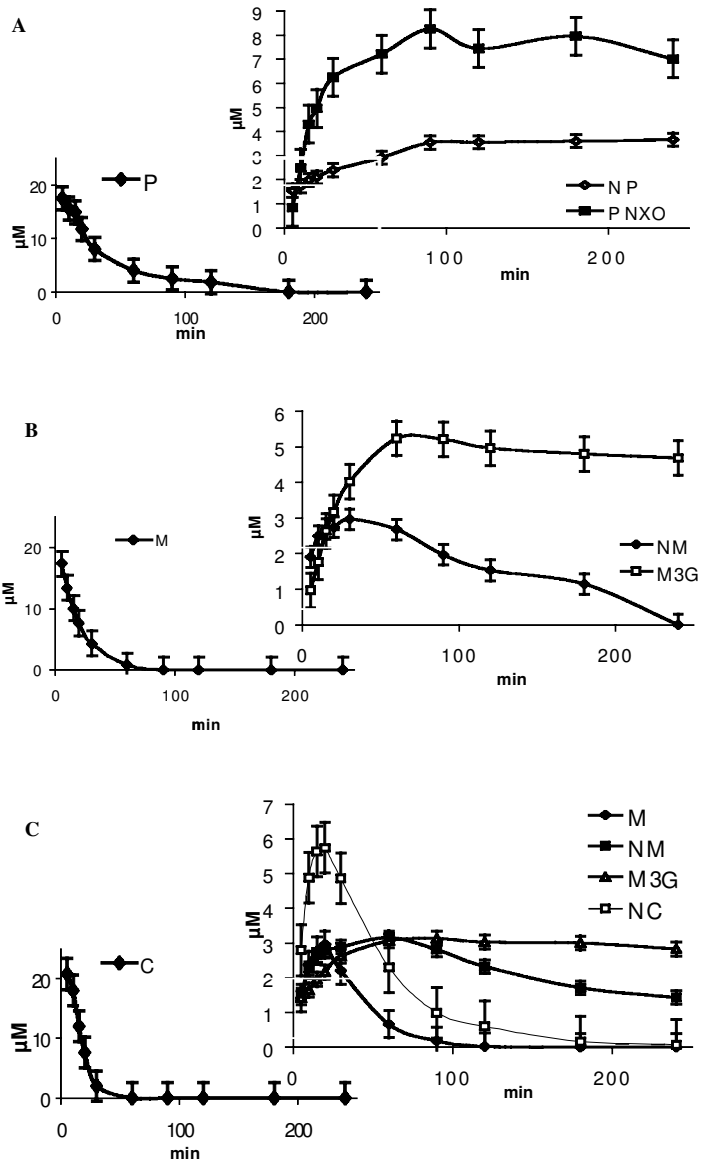


Figure 2. Concentration–time profiles for the disappearance and formation of: (A) pholcodine (P), norpholcodine (NP) and pholcodine-*N*-oxide (PNOX) in incubations of hepatocytes with pholcodine (50 μM; (B) morphine (M), normorphine (NM) and morphine 3-glucuronide (M3G) in incubations of hepatocytes with morphine (50 μM; and (C) codeine (C), morphine (M), normorphine (NM), morphine 3-glucuronide (M3G) and norcodeine (NC) in incubations of hepatocyte with codeine (50 μM). The results are means ± SE of three incubations.

these incubations is most likely due to the competitive glucuronidation between morphine and normorphine.

The separation of codeine and its metabolites can be seen in the extracted ion chromatograms of the standard solution and incubation mixture (figure 4). The rate constant for the metabolism of codeine is $0.112 \pm 0.045\ \mu M\ min^{-1}$ and it is the most rapid of the opiates studied (figure 2c). Initially, codeine is metabolized to

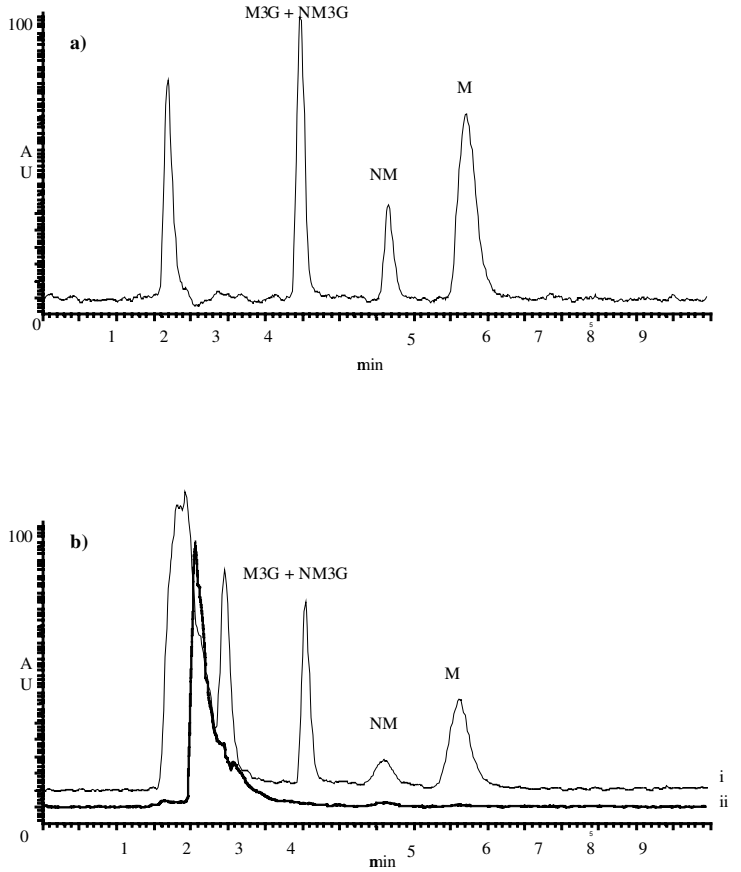


Figure 3. Typical LC/MS traces (SIM mode monitoring ions at $m/z = 286$, 313, 448, 462) of: (a) a standard solution containing 5 μM morphine-3-glucuronide (M3G), normorphine (NM) and morphine (M) methanol/0.2% (w/v) NaCl in Krebs–HEPES buffer (1:1); and (b) (i) extract from a 30-min incubation of 50 μM morphine with hepatocytes (2×0^6 viable cells ml^{-1}) in Krebs–HEPES buffer; (ii) incubation of hepatocytes (2×10^6 viable cells ml^{-1}) methanol/0.2% (w/v) NaCl in Krebs–HEPES buffer (1:1).

morphine and norcodeine with formation rate constants of 0.048 ± 0.004 and 0.045 ± 0.015 μM min^{-1}, respectively. Both products reach a maximum concentration at 20 min, corresponding to the disappearance of most of the codeine at this time point (figure 2c). Thereafter, morphine, which had been formed from codeine, is metabolized ($k_{met} = 0.057 \pm 0.012$ μM min^{-1}) to morphine-3-glucuronide the formation rate constant of which is 0.024 ± 0.006 μM min^{-1}, and normorphine. The overall elimination of morphine correlates very well with the data obtained for the biotransformation of morphine as the initial substrate with the cells, as described above ($k_{met} = 0.057 \pm 0.004$ μM min^{-1}). However, the rate of formation of the morphine-3-glucuronide in the incubations with codeine ($k_{form} = 0.024 \pm 0.006$ μM min^{-1}) is $>50\%$ lower than that for the incubations with morphine. This is most likely a reflection of the complexity of the system. Norcodeine, formed from codeine, is metabolized to normorphine ($k_{met} = 0.029 \pm 0.013$ μM min^{-1}). Thereafter, the normorphine, formed from both morphine and norcodeine, with an overall rate constant of 0.039 ± 0.007 μM

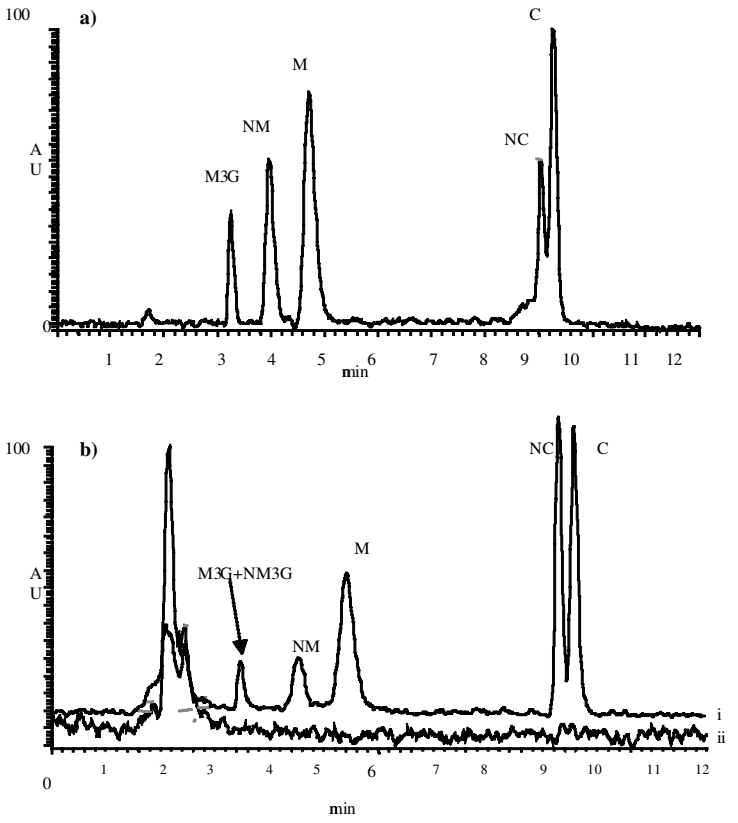


Figure 4. Typical LC/MS traces (SIM mode monitoring ions at $m/z = 286, 313, 448, 462, 300$) of: (a) a standard solution containing 5 μM morphine-3-glucuronide (M3G), normorphine (NM) morphine (M), norcodeine (NC) and codeine (C) in methanol/0.2% (w/v) NaCl in Krebs–HEPES buffer (1:1); and (b) (i) extract from a 20-min incubation of 50 μM codeine with hepatocytes (2×10^6 viable cells ml^{-1}) in Krebs–HEPES buffer; (ii) incubation of hepatocytes (2×10^6 viable cells ml^{-1}) methanol/0.2% (w/v) NaCl in Krebs–HEPES buffer (1:1).

min^{-1}, is metabolized to normorphine-3-glucuronide ($k_{met} = 0.007 \pm 0.0019$ μM min^{-1}). This transformation is slightly slower than for normorphine and morphine when used as initial substrates with cells. The reason for this difference is thought to be replenishment of normorphine by the simultaneous *N*-demethylation of norcodeine.

Discussion

To our knowledge, this is the first study that describes quantitatively the metabolism of morphine, codeine and pholcodine in rat hepatocytes. The metabolites identified for morphine and codeine have been previously reported (Bodd *et al.* 1986, Aasmundstad *et al.* 1993) in similar studies with isolated rat hepatocytes. Moreover, this study confirms previous studies in rat (Aasmundstad *et al.* 1993) and man (Aasmundstad and Storset 1998) showing that 3-glucuronidation is the major metabolic pathway for morphine, followed by *N*-demethylation (figure

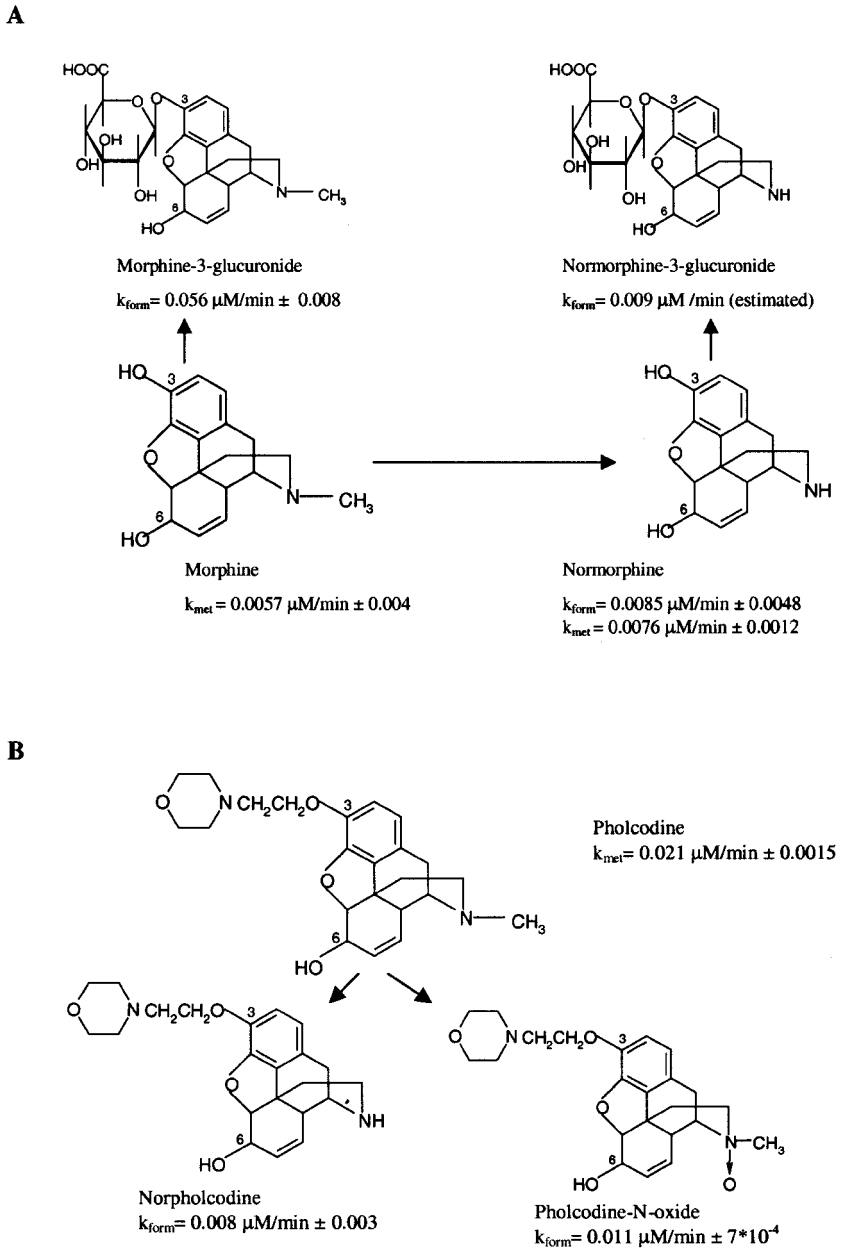


Figure 5. Metabolism and pharmacokinetics of morphine (A) and pholcodine (B) in rat hepatocytes. Rate constants of metabolism (k_{met}) and formation (k_{form}) are means of three incubations $\pm$ SD. The k_{form} of NM3G was estimated from incubations using NM as the initial substrate.

5a). For codeine, *N*- and *O*-demethylation appear to be equivalent metabolic pathways (figure 6).

Two metabolites were identified for pholcodine: norpholcodine and pholcodine-*N*-oxide (figure 5b). Although this is the first report of pholcodine-*N*-oxide being a metabolite of pholcodine, it is possible that it may be the 'oxo pholcodine'

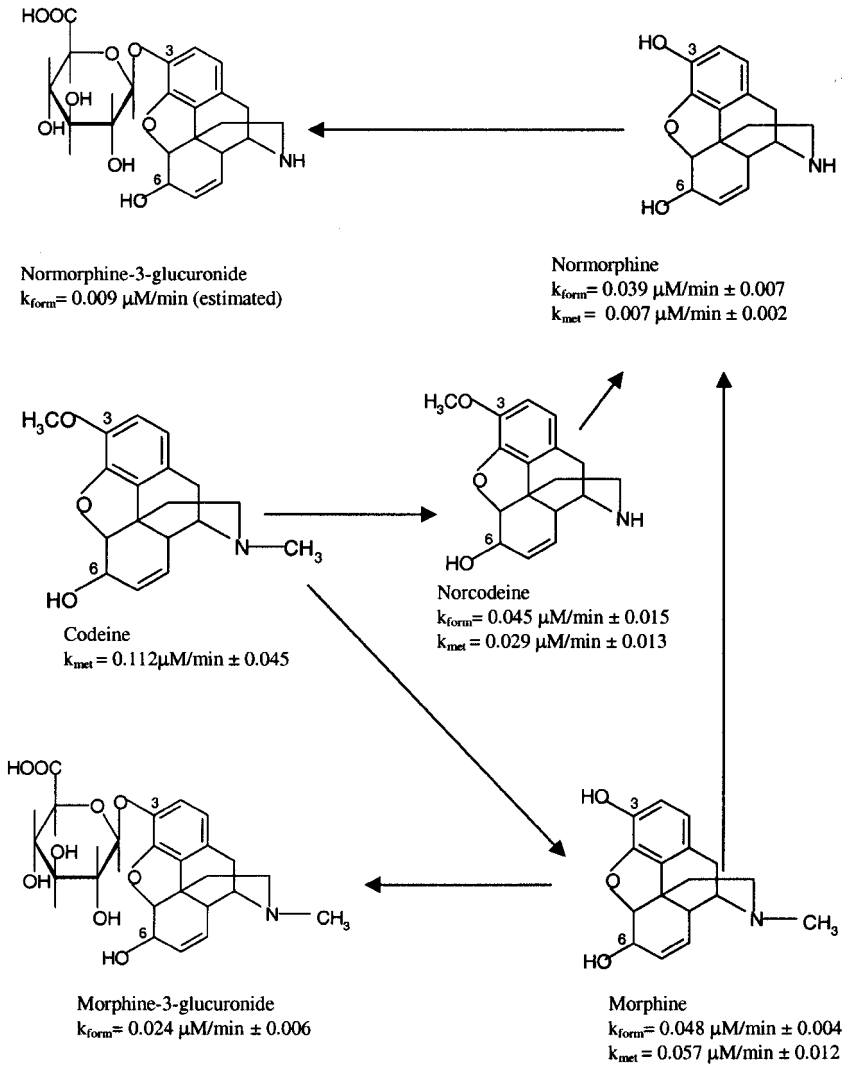


Figure 6. Metabolism and pharmacokinetics of codeine in rat hepatocytes. Rate constants of metabolism (k_{met}) and formation (k_{form}) are means of three incubations ± SD. The k_{form} of NM3G was estimated from incubations using NM as the initial substrate.

reported previously (Maurer and Fritz 1990). Both metabolites are the products of oxidation at the *N*-methyl group of the morphine ring. In the case of the formation of norpholcodine, this oxidative demethylation is cytochrome P450-mediated (Mikus *et al.* 1991, Xu *et al.* 1995). However, the formation of pholcodine-*N*-oxide is more likely to be mediated by a flavin-containing mono-oxygenase (Ziegler 1991), with cytochrome P450, whilst capable of catalysing *N*-oxygenation, making a much smaller contribution to *N*-oxygenation reactions (Seto and Guengerich 1993). The observed formation of pholcodine-*N*-oxide underlines an advantage of using hepatocytes in studying the biotransformation of xenobiotics as the activity of flavin-containing mono-oxygenases can be readily lost in microsomal prepara-

tions due to tissue disruption and unsuitable storage conditions (Cashman 1999), procedural steps that are alleviated with hepatocytes.

The current study demonstrates that rat hepatocytes provide a suitable model for studying the *O*- and *N*-dealkylation of morphine and its analogues, as results analogous to *in vivo* studies (Svensson *et al*. 1995) were obtained. Interestingly, neither morphine nor its metabolites were detected as metabolites of pholcodine. That *O*-dealkylation of pholcodine was not detected is in agreement with a previous study (Butz *et al*. 1983) and supports the hypothesis that the lack of analgesic activity with pholcodine may be due to morphine not being formed *in vivo*. Together with its slow rate of metabolism ($k_{met} = 0.021 \pm 0.0015\,\mu M\ min^{-1}$) in comparison with morphine metabolism ($k_{met} = 0.057\,\mu M\ min^{-1} \pm 0.004$) and codeine metabolism ($k_{met} = 0.112 \pm 0.045\,\mu M\ min^{-1}$), the results for pholcodine are consistent with its low addiction potential (Butz *et al*. 1983) and suggest that its antitussive activity is mediated by the parent drug or one of its metabolites other than morphine.

Neither codeinone, its glutathione adduct or morphinone, which were previously reported for the metabolism of codeine (Ishida *et al*. 1991, Ishida *et al*. 1998), nor morphinone and its glutathione adduct, which were previously reported for the metabolism of morphine (Kumagi *et al*. 1990, Yamano *et al*. 1997), were found in the current study. However, it is important to note that the 6-dehydrogenated metabolites (morphinone and codeinone) in these latter reports were isolated from rat and guinea pig bile. Morphine-6-dehydrogenation was also shown using a 9000*g* liver homogenate supernatant as the enzyme source (Yamano *et al*. 1997). That different experimental models were used may explain why neither morphinone nor codeinone were detected in rat hepatocytes. However, Nagamatsu *et al*. (1986) demonstrated the formation of morphinone and its glutathione conjugate when morphine, at a concentration 10 times greater than that used in this study, was incubated with isolated rat hepatocytes under conditions similar to those used in the present study. At this concentration of morphine, however, cell death occurred after 2 h, whilst in the present study, with a concentration of 50 μM, there was no reduction of cell viability after 4 h compared with control incubations containing no substrate. It is possible that in the latter study the glucuronidation pathway was saturated by the very high substrate concentrations employed, thus inducing 6-dehydrogenation of morphine to morphinone as suggested by Correia *et al*. (1984). In the current study, morphine and codeine were metabolized very rapidly. It is likely that the 6-dehydrogenation pathway is not an important route of metabolism for morphine and codeine. However, with pholcodine the latter is unlikely: glucuronidation did not occur, which would facilitate 6-dehydrogenation to pholcodinone even at the lower concentrations employed in this study. Furthermore, its rate of metabolism was also the slowest of the substrates studied. The absence of pholcodinone in the incubation mixtures is therefore most likely a true reflection of the biotransformation of pholcodine by hepatocytes. However, in view of the aforementioned results and the associated toxicity of the 6-dehydrogenated compounds (Nagamatsu *et al*. 1986), the formation of morphinone, codeinone and pholcodinone *in vivo* should not be excluded and requires further investigation.

Whilst rat hepatocytes would appear to be a useful model system for studying the metabolism of morphine, they are not an ideal model for examining the glucuronidation of opiates as they lack the ability to glucuronidate the 6-hydroxy

group in the opiates. Glucuronidation at this position is mediated in man by UDP-glucuronyltransferase 2B7 (Radominska-Pandya *et al.* 2001). The absence of morphine-6-glucuronidation in rats (Aasmundstad *et al.* 1993) suggests the lack of this enzyme. Previous studies (Johansen *et al.* 1990, 1992) reported the presence of glucuronides of pholcodine in human urine samples. In pholcodine, the 6-hydroxy position is the only available residue liable to glucuronidation. Any differences to previously reported results are therefore most likely the result of the absence of opiate-6-glucuronidation in rats. Guinea pigs have been suggested as a more suitable model for studying the glucuronidation of morphine and its analogues as their glucuronidation pattern resembles closer that of humans (Aasmundstad *et al.* 1993).

Another suitable model is the use of human hepatoma cell lines for studying the glucuronidation of opiates. In a previous study, HepG2 cells were reported to have similar UDP-glucuronyl transferase activities to freshly isolated human adult hepatocytes (Grant *et al.* 1988a). Moreover, the glucuronidation of morphine in HepG2 cells has also been demonstrated (Grant *et al.* 1988b). HepG2 cells will be employed in future studies to examine the glucuronidation of pholcodine.

In conclusion, the use of freshly isolated rat hepatocytes in combination with analysis by LC/MS, as employed in this study, provided a powerful and very reproducible approach in assessing the qualitative and quantitative biotransformation of the opiates morphine, codeine and pholcodine.

References

Aasmundstad, T. A., Ripel, A., Bodd, E., Bjorneboe, A. and Morland, J., 1993, Different biotransformation of morphine in isolated liver cells from guinea pig and rat. *Biochemical Pharmacology*, **46**, 961–968.

Aasmundstad, T. A. and Storset, P., 1998, Influence of ranitidine on the morphine-3-glucuronide to morphine-6-glucuronide ratio after oral administration of morphine in humans. *Human and Experimental Toxicology*, **17**, 347–352.

Bodd, E., Drevon, C. A. and Kveseth, N., 1986, Ethanol inhibition of codeine and morphine metabolism in isolated rat hepatocytes. *Journal of Pharmacology and Experimental Therapeutics*, **237**, 260–264.

Butz, R. F., Jones, E. C., Welch, R. M. and Findlay, J. W. A., 1983, Pharmacokinetics and *O*-dealkylation of morphine-3-alkyl ethers in the rat. A radioimmunoassay study. *Drug Metabolism and Disposition*, **11**, 481–488.

Cashman, J. R., 1999, *In vitro* metabolism: FMO and related oxygenations. In T. F. Woolf (ed.), *Handbook of Drug Metabolism* (New York: Marcel Dekker), pp. 477–506.

Chen, Z. R., Bochner, F. and Somogyi, A., 1988, Pharmacokinetics of pholcodine in healthy volunteers: Single and chronic dosing studies. *British Journal of Clinical Pharmacology*, **26**, 445–453.

Correia, M. A., Wong, J. S., Soliven, E., 1984, Morphine metabolism revisited: I. Metabolic activation to a reactive species in rats. *Chemico-Biological Interactions*, **49**, 255–268.

Findlay, J. W. A., 1988, Pholcodine. *Journal of Clinical Pharmacy and Therapeutics*, **13**, 5–17.

Findlay, J. W. A., Fowle, A. S. E. and Butz, R. F., 1986, Comparative disposition of codeine and pholcodine in man after single oral doses. *British Journal of Clinical Pharmacology*, **22**, 61–71.

Gong, Q. L., Hedner, T., Hedner, J., Bjorkman, R. and Nordberg, G., 1991, Antinociceptive and ventilatory effects of the morphine metabolites: morphine-6-glucuronide and morphine-3-glucuronide. *European Journal of Pharmacology*, **193**, 47–56.

Grant, M. H., Doostdar, H., Maley, M., Melvin, W. T., Engeset, J. and Burke, M. D., 1988b, Glucuronidation in rat and human hepatocyte cultures and in human HEP G2 hepatoma cells. In G. Siest, J. Magdalou and B. Burchell (eds), *Cellular and Molecular Aspects of Glucuronidation* (Paris/John Libbey Eurotext), pp. 129–136.

Grant, M. H., Duthie, S. J., Gray, A. G. and Burke, M. D., 1988a, Mixed function oxidase and UDP-glucuronyltransferase activities in the human Hep G2 hepatoma cell line. *Biochemical Pharmacology*, **37**, 4111–4116.

Ishida, T., Yano, M. and Toki, S., 1991, *In vivo* formation of codeinone and morphinone from codeine: isolation and identification from guinea pig bile. *Drug Metabolism and Disposition*, **19**, 895–899.

Ishida, T., Yano, M. and Toki, S., 1998, *In vivo* formation of codeinone–glutathione adduct: isolation and identification of a new metabolite in the bile of codeine-treated guinea pig. *Journal of Analytical Toxicology*, **22**, 567–572.

Johansen, M., Rasmussen, K. E. and Christophersen, A. S., 1990, Determination of pholcodine and its metabolites in urine by capillary gas chromatography. *Journal of Chromatography-Biomedical Applications*, **532**, 277–284.

Johansen, M., Tonnesen, F. and Rasmussen, K. E., 1992, Column-switching high-performance liquid chromatographic detection of pholcodine and its metabolite in urine with fluorescence and electrochemical detection. *Journal of Chromatography — Biomedical Applications*, **573**, 283–288.

Kumagi, Y., Todaka, T. and Toki, S., 1990, A new metabolic pathway of morphine: *in vivo* and *in vitro* formation of morphinone and morphinone–glutathione adduct in guinea pig. *Journal of Pharmacology and Experimental Therapeutics*, **255**, 504–510.

Maurer, H. H. and Fritz, C. F., 1990, Metabolism of pholcodine in man. *Arzneimittel-Forschung*, **40**, 564–566.

Midha, K. K., Jaworski, T. J., Hawes, E. M., McKay, G., Hubbard, J. W., Aravagiri, M., Marder, S. R., 1991, Radioimunoassay and other methods for the trace analysis of *N*-oxide compounds. In P. Hlavica and L. A. Damani (eds), *N-Oxidation of Drugs* (London: Chapman-Hall), pp. 37–55.

Mikus, G., Somogyi, A. A., Bochner, F. and Eichelbaum, M., 1991, Codeine *O*-demethylation: rat strain differences and the effects of inhibitors. *Biochemical Pharmacology*, **41**, 757–762.

Moldeus, P., Hogberg, J. and Orrenius, S., 1978, Isolation and use of liver cells. *Methods in Enzymology*, 60–71.

Nagamatsu, K., Ohno, Y. and Ikebuchi, H., 1986, Morphine metabolism in isolated rat hepatocytes and its implications for hepatotoxicity. *Biochemical Pharmacology*, **35**, 3543–3548.

Olofson, R. A., Martz, J. T., Senet, J. P., Piteau, M. and Malfroot, T., 1984, A new reagent for the selective, high-yield *N*-dealkylation of tertiary amines: improved syntheses of naltrexone and nalbuphine. *Journal of Organic Chemistry*, **49**, 2081–2082.

Paul, D., Standifer, K. M., Inturrisi, C. E. and Pasternak, G. W., 1989, Pharmacological characterization of morphine-6beta-glucuronide, a very potent morphine metabolite. *Journal of Pharmacology and Experimental Therapeutics*, **251**, 477–483.

Pawula, M., Shaw, P. N. and Barett, D. A., 1994, Determination of codeine and its metabolites in microsomal incubates by high-performance liquid chromatography. *Journal of Chromatography B — Biomedical Applications*, **653**, 106–111.

Pelander, A., Ojanpera, I. and Hase, T. A., 1997, Preparation of *N*-demethylated drug metabolites for analytical purposes using 1-chloroethyl chloroformate. *Forensic Science International*, **85**, 193–198.

Philipson, J. D., Handa, J. S. and El-Dabbas, W., 1976, *N*-oxides of morphine, codeine and thebaine and their occurrence in *Papaver* species. *Phytochemistry*, **15**, 1297–1301.

Radominska-Pandya, A., Little, J. M. and Czernik, P. J., 2001, Human UDP-glucuronosyltransferase 2B7. *Current Drug Metabolism*, **2**, 283–298.

Seto, Y. and Guengerich, F. P., 1993, Partitioning between *N*-dealkylation and *N*-oxygenation in the oxidation of *N*,*N*-dialkylarylamines catalyzed by cytochrome P450 2B1. *Journal of Biological Chemistry*, **268**, 9986–9997.

Svensson, J. O., Yue, Q. Y. and Sawe, J., 1995, Determination of codeine and metabolites in plasma and urine using ion-pair high-performance liquid chromatography. *Journal of Chromatography-Biomedical Applications*, 674, 49–55.

Xu, B. Q., Aasmundstad, T. A., Bjorneboe, A., Christophersen, A. S. and Morland, J., 1995, Ethylmorphine *O*-deethylation in isolated rat hepatocytes. *Biochemical Pharmacology*, **49**, 453–460.

Yamano, S., Takahashi, A., Todaka, T. and Toki, S., 1997, *In vivo* and *in vitro* formation of morphinone from morphine in rat. *Xenobiotica*, **27**, 645–656.

Ziegler, D. M., 1991, Mechanism, multiple forms and substrate specificities of flavin containing monooxygenases. In P. Hlavica and L. A. Damani (eds), *N-Oxidation of Drugs* (London: Chapman-Hall), pp. 59–68.

XENOBIOTICA, 2002, VOL. 32, NO. 12, 1109–1126

Taylor & Francis
healthsciences

Inhibition of the microsomal metabolism of 1,8-cineole in the common brushtail possum (*Trichosurus vulpecula*) by terpenes and other chemicals

G. J. PASS† AND S. MCLEAN*

School of Pharmacy, University of Tasmania, Hobart 7001, Australia

Received 29 May 2002

1. Brushtail possums (*Trichosurus vulpecula*) ingest large amounts of terpenes in their diet of *Eucalyptus* leaf. Previously, we showed that dietary terpenes induce the cytochrome P450 enzymes (CYPs) responsible for their metabolism. The present study examined the effects of various CYP inhibitors on the metabolism of 1,8-cineole, the major dietary terpene, by liver microsomes from the possum and rat.

2. Ketoconazole inhibited the major reactions of terpene-induced microsomes in both species: 9-hydroxylation in the possum and 2-hydroxylation in the rat. This suggests the involvement of CYP3A enzymes, although in the possum there was a lack of the expected inhibition by troleandomycin or activation by α-naphthoflavone, highlighting the differences between species in CYP forms. Diethyldithiocarbamate also inhibited 9-hydroxylation in the possum, indicating that a CYP2E1-like enzyme contributes to this reaction.

3. Three other dietary terpenes were potent competitive inhibitors of 9-hydroxylation in the possum. K_i (μM) (mean $\pm$ SE, $n = 4$) were: α-pinene, 4.4 ± 1.1; limonene, 7.8 ± 2.1; *p*-cymene, 44.3 ± 11.2; cuminyl alcohol (a *p*-cymene metabolite), 6.0 ± 0.8. It appears likely that *p*-cymene acts via its metabolite to inhibit 1,8-cineole metabolism.

4. Inhibitory interactions between dietary terpenes, as well as other plant secondary compounds, may impose a significant constraint on foliage consumption in the common brushtail possum, therefore explaining the obligatory generalist nature of this browsing marsupial and other generalist herbivores.

Introduction

Common brushtail possums (*Trichosurus vulpecula*) are one of four native Australian marsupials that include significant amounts of *Eucalyptus* leaves in their diet. However, they are unable to maintain themselves exclusively on a eucalyptus diet (Hume 1999). *Eucalyptus* leaves contain an array of plant secondary metabolites (PSMs), including terpenes which make up a large proportion of the total PSMs and are considered an important component of the plant's chemical defence against herbivory. Although there is no simple relationship between terpene content and herbivory (Lawler *et al*. 1998, Dearing and Cork 1999), ingestion of large amounts of dietary terpenes presents a toxic challenge which requires a metabolic response. For example, possums browse the leaf of *E. melliodora* which contains terpenes in the following relative proportions: 1,8-cineole (65%), α-pinene (25%), (*S*)-(−)-limonene (8%) and *p*-cymene (2%) (Boland and Brophy 1991). Once

* Author for correspondence. e-mail: Stuart.McLean@utas.edu.au

*Present address: Merck Sharp & Dohme, The Neuroscience Research Centre, Terlings Park, Harlow CM20 2QR, UK.

Xenobiotica ISSN 0049–8254 print/ISSN 1366–5928 online © 2002 Taylor & Francis Ltd
http://www.tandf.co.uk/journals
DOI: 10.1080/0049825021000022294

acclimated to this terpene mixture, possums can ingest as much as 1.8 g kg^{-1} in their diet on a regular daily basis (Pass *et al.* 1999), a dose which is toxic to humans and other animals (Jenner *et al.* 1964, Barnes 1996). Therefore, it appears that possums and other *Eucalyptus* folivores can metabolize dietary terpenes fast enough to prevent their accumulation to toxic levels.

Previously we have reported that ingestion of the four dietary terpenes of *E. melliodora* by brushtail possums significantly induced the activity of some liver cytochrome P450 (CYP) enzymes (Pass *et al.* 1999). We have also demonstrated that the metabolism of the two major dietary terpenes, 1,8-cineole and *p*-cymene, is increased in hepatic microsomes from terpene-treated possums (Pass *et al.* 2001, 2002). As yet, however, the specific CYP enzymes involved in the metabolism of terpenes in the possum are unknown.

The use of chemical inhibitors has been a common approach for determining the contribution of individual CYP enzymes to the metabolism of drugs. Potent inhibitors of specific human CYP forms include ketoconazole, which selectively inhibits CYP3A4 (Maurice *et al.* 1992); sulfaphenazole, which is often used as a probe for CYP2C9/10 (Veronese *et al.* 1993); and 4-methylpyrazole, a CYP2E1 inhibitor (Feierman and Cederbaum 1987). It must be noted that although these inhibitors are often used as probes for identifying specific CYP enzyme activity in humans, many have also been shown to exhibit cross-reactivity with other CYPs when extrapolated to other species (Eagling *et al.* 1998). Nevertheless, they are a good starting point for gaining insight into the drug metabolizing enzymes in different species.

There have been two studies that have used form-specific inhibitors as tools for gaining information on individual CYP isoforms in brushtail possums. Ho *et al.* (1998) investigated the *in vitro* metabolism of quinine and found that midazolam and troleandomycin, both CYP3A substrates and inhibitors in humans, caused substantial inhibition of 3-hydroxyquinine formation. Olkowski *et al.* (1998) reported that the *in vitro* effects of some imidazole inhibitors (ketoconazole, clotrimazole, miconazole and cimetidine) were greater on the activity of common markers of CYPs in possums than in the rat, rabbit, sheep or chicken. However, the demonstration of inhibition did not by itself allow conclusions about the specific forms involved. In addition, variability in the potency of inhibitors was highly variable across species, suggesting differences in the nature of CYPs in the brushtail possum and other mammals.

The aims of the current study were to examine the effects of both form-specific and general inhibitors of human and rat CYP enzymes on the *in vitro* metabolism of 1,8-cineole in liver microsomes from brushtail possums and, to enable direct comparison with the literature, rats. 1,8-Cineole was chosen as substrate because it is the major dietary terpene, and induced as well as untreated liver microsomes were used because wild possums eating their usual food would have their CYP enzymes induced by dietary terpenes (Bolton and Ahokas 1997).

In addition, it has been well established that compounds of similar structure and function can be metabolized by the same CYP forms (Correia 1995). Competition for CYPs is an important mechanism of drug–drug interactions and can result in a drug reaching toxic concentrations after normal doses (Weaver 2001).

We therefore carried out a series of experiments to test the effect of other dietary terpenes on the *in vitro* metabolism of 1,8-cineole in the brushtail possum.

The terpenes chosen were those from *E. melliodora* (*p*-cymene, limonene, α-pinene) as used in the previous study of enzyme induction (Pass *et al.* 1999). The effect of cuminyl alcohol on microsomal 1,8-cineole metabolism was also examined. Cuminyl alcohol is the major metabolite of *p*-cymene in the brushtail possum *in vitro* (Pass *et al.* 2002). There are a number of reports in the literature that the inhibitory effects of some drugs can be attributed to their metabolites (Kharasch *et al.* 1993, Nakajima *et al.* 1999). Therefore, this terpene metabolite was included as a potential inhibitor of 1,8-cineole metabolism.

Materials and methods

Animal treatment

The acquisition and treatment of the brushtail possums and rats and preparation of liver microsomes has been described previously (Pass *et al.* 1999, 2001). Briefly, male possums (weight 4.19 $\pm$ 0.16 kg, mean $\pm$ SE, $n = 8$) were maintained on a diet of fruits and vegetables, to which a mixture of 1,8-cineole (65.4%), α-pinene (24.7%), *p*-cymene (1.8%) and (*S*)-(–)-limonene (8.0%) was added for the terpene-treated group (Pass *et al.* 1999). The terpene mixture comprised 2.13 g per 100 g dry matter for 5 days, increased to 4.26 g per 100 g for the next 5 days. The proportions of terpenes were based on the terpene content of *E. melliodora* leaf (Boland and Brophy 1991), a food for these animals. Animals in the untreated group ($n = 4$) were maintained on the diet without terpenes. On the 10th day, possums were killed and liver microsomes prepared.

Male Hooded Wistar rats (aged 7–8 weeks) were maintained on a standard pellet diet (Pivot Nutrition, Pivot Ltd, Melbourne, Australia) and water *ad libitum*. Induced rats were gavaged with either the terpene mixture in peanut oil (400 mg kg^{-1}, $n = 2$) or an aqueous solution of phenobarbitone (80 mg kg^{-1}, $n = 2$) daily for 6 days. On the seventh day the rats were killed using pentobarbitone (about 325 mg kg^{-1}, i.p.) and liver microsomes prepared.

Inhibition studies

General. The standard selective chemical inhibitors of CYP forms used in this study are summarized in table 1. The terpenes used in the dietary mixture were also studied as potential inhibitors. The effects of inhibitors were measured on the conversion of 1,8-cineole to the major *in vitro* metabolite each animal species: 9-hydroxycineole in the possum and 2-hydroxycineole in the rat (Pass *et al.* 2001). In addition, 9-hydroxycineole formation was also measured in rat microsomes to enable direct comparison with the possum, and two other significant possum metabolites (3- and 7-hydroxycineole) were measured.

In all cases, the putative inhibitor was pre-incubated with possum and rat microsomes before addition of 1,8-cineole. This was done to maximize the effect of the mechanism-based inhibitors: piperonyl butoxide, troleandomycin, diethyldithiocarbamate and cimetidine. Pre-incubation was also performed for the reversible inhibitors (ketoconazole, 4-methylpyrazole, α-naphthoflavone, quinidine, tolbutamide, sulfaphenazole and coumarin) as the mechanism of action of these compounds has never been investigated in the brushtail possum. It is possible that these chemicals are metabolized by possum liver into metabolites that may be more inhibitory than the parent compound. Furthermore, by pre-incubating all inhibitors, the conditions of microsomal incubations were kept constant, therefore eliminating a possible area of variability.

Possum microsomes. Two concentrations of 1,8-cineole were used. The first (10 μM approximated the apparent K_m for 9-hydroxylation in terpene-treated and -untreated possum microsomes as determined previously in these livers (about 10.5 μM; Pass *et al.* 2001) and the second (100 μM was 10 times greater. At 10 μM 1,8-cineole, all of the putative chemical inhibitors were studied over the concentration range of 1–100 μM. At 100 μM 1,8-cineole, the concentration range was increased to 200 μM for diethyldithiocarbamate, 4-methylpyrazole, quinidine, piperonyl butoxide and cimetidine and to 1000 μM for tolbutamide. All inhibitors were screened using microsomes from two terpene-treated and two untreated possums.

4-Methylpyrazole was dissolved in phosphate buffer (0.1 M, pH 7.4) and added to individual incubation vials. Other inhibitors were added in methanol (5–50 μl), which was evaporated under a gentle stream of nitrogen at 30°C, and the residue reconstituted with possum microsomes in phosphate buffer (100 μl containing 0.25 mg protein, 0.1 M, pH 7.4). Control incubations were treated the same way using methanol without inhibitor. The NADPH-generating system (200 μl consisting of 1 mM $NADP^+$, 4 mM isocitric acid, 0.4 IU isocitric dehydrogenase and 8 mM $MgCl_2$) was added and the solution pre-incubated for 5 min at 37°C. The reaction was initiated by the addition of 1,8-cineole in phosphate buffer to make a final volume of 1.0 ml. After 10-min incubation, the reaction was stopped in

Table 1. Inhibitors used in the present study and their specificity for both rat and human CYPs and their mode of action.

Inhibitor	CYPs inhibited/ activated	Mode of inhibition	Reference
Cimetidine*	multiple, CYP2C11	competitive and MI complexation	Winzor *et al.* (1986)
Coumarin	CYP2A6	substrate/competitive	Yun *et al.* (1991)
Diethyldithiocarbamate	CYP2A6, 2E1	irreversible/mechanism-based	Halpert *et al.* (1994)
Ketoconazole	CYP3A (low concentration), multiple at high concentration	competitive	Maurice *et al.* (1992)
4-Methylpyrazole	CYP2E1	competitive	Feierman *et al.* (1987)
α-Naphthoflavone	CYP1A1 (low concentration), known to activate CYP3A at high concentration	competitive	McManus *et al.* (1990)
Piperonyl butoxide	multiple	quasi-irreversible/MI complexation	Franklin (1972)
Quinidine	CYP2D6	competitive	Guengerich *et al.* (1986)
Sulfaphenazole	CYP2C9/10	competitive	Veronese *et al.* (1993)
Tolbutamide	CYP2C8/9	substrate/competitive	Doecke *et al.* (1991)
Troleandomycin*	CYP3A	quasi-irreversible/MI complexation	Chang *et al.* (1994)

*Screened in possum microsomes only.

ice and internal standard (4 μg 2,5-dimethylbenzoic acid in 25 μl H_2O) and acid (5M HCl, 25 μl) were added. After extraction and derivatization (trimethylsilyl), samples were analysed by GC-SIM-MS (Pass *et al.* 2001).

Rat microsomes. The concentration of 1,8-cineole used was 10 μM for all rat microsomal incubations and the putative inhibitors were studied at concentrations commonly used in other studies of this kind (Anderson *et al.* 1993, 1994, Zhang *et al.* 1997, Ho *et al.* 1998). The concentrations of each inhibitor were: α-naphthoflavone, 10 μM; sulfaphenazole, 25 μM; coumarin, 25 μM; ketoconazole, 5 μM; diethyldithiocarbamate, 50 μM; 4-methylpyrazole, 100 μM; quinidine, 25 μM; piperonyl butoxide, 5 μM; and tolbutamide, 10 μM. The incubation conditions were otherwise as described above with the exception of phenobarbitone-treated rat microsomes, which were incubated with 1,8-cineole for only 5 min to ensure linearity over the incubation period. All inhibitors were screened using microsomes from two terpene-treated and two phenobarbitone-treated rats. The activity of uninduced liver microsomes was too low to study inhibition.

Use of terpenes as inhibitors of possum microsomal metabolism

Terpene inhibition of aminopyrine metabolism. Aminopyrine demethylase activity was measured by formaldehyde formation using a substrate concentration of 25 mM (Nash 1953). Each terpene (1,8-cineole, *p*-cymene, limonene or α-pinene) was added in 25 μl ethanol to give a final concentration of 100 μM terpene in 1 ml incubate. Ethanol alone was added to control incubations.

Terpene inhibition of 1,8-cineole metabolism. The terpenes used were *p*-cymene, α-pinene, limonene and cuminyl alcohol (the major *in vitro* metabolite of *p*-cymene (Pass *et al.* 2002). Only the terpene-treated possum microsomes were tested.

The incubation conditions were essentially the same to those described above for the specific inhibitors. Terpene inhibitors (in 5 μl ethanol) were mixed with phosphate buffer containing 1,8-cineole, microsomes (100 μl) were added followed by the NADPH-generating system (200 μl) to start the reaction. The final concentrations of terpene inhibitors in the 1 ml incubation mixtures were 5–100 μM, and the 1,8-cineole concentrations were 10 and 100 μM. After incubation for 10 min at 37°C, the sample was analysed as outlined above.

Identification and quantitation of metabolites

Three metabolites (9-, 3- and 7-hydroxycineole) were isolated from the urine of a possum dosed with 1,8-cineole and used as analytical standards for the analysis of microsomal metabolites by GC-MS using selected ion monitoring (SIM), as described by Pass *et al*. (2001). Further structural data was obtained by NMR analyses, which were kindly performed and interpreted by Dr D. McGuinness. ^{1}H- and ^{13}C-NMR spectra were recorded at ambient temperature. Signals were referenced to solvent residual peaks relative to tetramethylsilane.

Calibration curves were done with each day's analysis and were linear over the appropriate concentration ranges ($r^2 > 0.999$). Reproducibility between days (cv%, $n = 5$) was 2.5, 4.4 and 2.8% for 9-, 3-, and 7-hydroxycineole, respectively. The calibration curve for 3-hydroxycineole was also used for 2-hydroxycineole.

Data and statistical analysis

Data for each inhibitor concentration are expressed as a percentage of the corresponding control metabolite formation. Inhibition > 30% was considered as significant (Liapis *et al*. 2000). The concentration of the inhibitor (IC_{50}) that produced a 50% decrease in the formation of a hydroxycineole metabolite was determined from plots of the percentage decrease versus the natural log of the inhibitor concentration.

For the terpene inhibition studies, although only two 1,8-cineole concentrations were tested, the kinetic inhibition constant (k_i) was estimated and the mechanism of inhibition was elucidated from Dixon plots (1/velocity versus inhibitor concentration) and Cornish–Bowden plots ([substrate]/velocity versus inhibitor concentration) for each terpene inhibitor tested.

All data are means with standard errors (SE). The mean differences between the terpene-treated and -untreated possums over the range of inhibitor concentrations were compared using univariate ANOVA (SPSS 7.5, SPSS, Inc., Chicago, IL. USA).

Results

Metabolites identified

NMR spectra of 9-hydroxycineole confirmed that this metabolite was the same as the possum urinary metabolite of 1,8-cineole which was first reported by Flynn and Southwell (1979) and later identified as racemic 9-hydroxycineole (Carman and Klika 1992). It was not possible to determine the relative proportions of the optical isomers from this study as access to chiral GC was not available. ^{1}H-NMR (400 MHz, CD_2Cl_2): δ 3.53 (d, br, $\mathcal{J}$ = 10.8 Hz, 1H, C9*H*); 3.34 (m, br, 1H, C9*H*); 1.93–2.04 (m, 2H); 1.83 (s, br 1H, O*H*); 1.46–1.71 (m, 7H); 1.21 (s, 3H, 3-CH_3); 1.01 (s, 3H, 1-CH_3). ^{13}C-NMR (100 MHz, CD_2Cl_2): δ 75.9 (C9); 70.4, 69.6 (C1, C8); 32.5, 32.3 (C3, C5); 30.3, 27.6, 24.0 (C2, C4, C6); 23.4, 23.2 (C7, C10).

Comparisons made between the ^{1}H- and ^{13}C-NMR data of the 3-hydroxycineole and reported for a rabbit urinary metabolite of 1,8-cineole (Miyazawa *et al*. 1989) indicated that this metabolite was 3-exo-hydroxycineole. ^{1}H-NMR (200 MHz, $CDCl_3$): δ 4.46 (m, br, 1H, C3H); 1.98–2.20 (m, 2H); 1.40–1.98 (m, 5H); 1.29, 1.21, 1.06 (three s, 9H, C7H_3, C9H_3, C10H_3). ^{13}C-NMR (50 MHz, $CDCl_3$): δ 73.4, 71.1 (C1, C8); 65.4 (C3–OH); 43.0, 40.5, 31.2, 29.1, 28.5, 27.2, 14.8.

The amount of 7-hydroxycineole isolated was insufficient for NMR analysis.

Effects of form-specific inhibitors on 1,8-cineole metabolism

Possum microsomes. 9-Hydroxycineole formation was greater in terpene-treated than in -untreated liver microsomes (figure 1, A), as reported by Pass *et al*. (2001). This difference was preserved in the presence of the form-specific inhibitors at all concentrations used. When the rate of metabolite formation was expressed as a

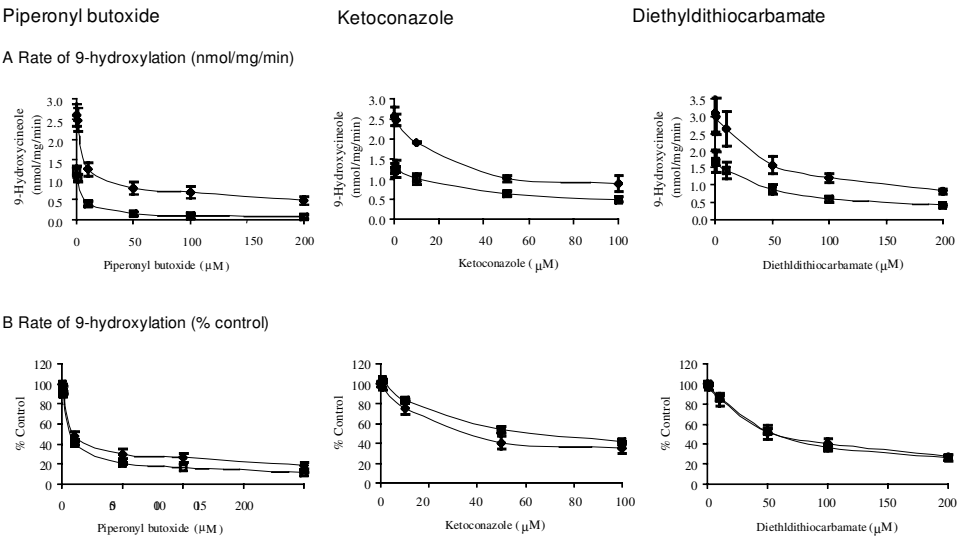


Figure 1. 9-Hydroxycineole formation from 1,8-cineole (100 μM) in the presence of piperonyl butoxide, ketoconazole and diethyldithiocarbamate in liver microsomes from untreated possums (□) and terpene-treated possums (◆). Data are expressed as the mean ± SE of single determinations from two possums in each group.

percentage of that without inhibitor (% control), there were no significant differences in the degree of inhibition between terpene-treated and -untreated microsomes. Figure 1B demonstrates this with the three inhibitors that produced > 30% inhibition of 9-hydroxycineole formation: piperonyl butoxide, ketoconazole and diethyldithiocarbamate.

Piperonyl butoxide was the most potent inhibitor, reducing 9-hydroxycineole formation to 18% control activity at both low and high substrate concentrations. Ketoconazole was the next most potent inhibitor, with 9-hydroxycineole formation reduced to 15% control at low substrate concentration (10 μM and 30% at high substrate concentration (100 μM. Diethyldithiocarbamate also caused substantial inhibition (to 28–48% control at low and high substrate concentrations, respectively) of 9-hydroxycineole formation. The IC_{50} of these inhibitors for the formation of 9-hydroxycineole in possum microsomes are given in table 2. No significant differences were detected in the IC_{50} of these inhibitors between terpene-treated and untreated microsomes.

Ketoconazole inhibited 3- and 7-hydroxylation in terpene-treated possum liver microsomes, but piperonyl butoxide and diethyldithiocarbamate were relatively ineffective (table 2). Similar data (not shown) were obtained with the higher concentration of 1,8-cineole.

Quinidine exhibited moderate inhibition with 9-hydroxycineole formation reduced to around 64% of control activity at both low and high concentrations of 1,8-cineole. Although 4-methylpyrazole and α-naphthoflavone exhibited some inhibition, for both of these inhibitors, the degree of inhibition was not above 30% and was therefore not considered as significant. Troleandomycin, sulfaphenazole, coumarin, cimetidine and tolbutamide had little or no effect on the conversion of 1,8-cineole to 9-hydroxycineole at both substrate concentrations.

Table 2. IC_{50}'s of chemical inhibitors of hydroxylation of 1,8-cineole in possum liver microsomes.

Concentration of 1,8-cineole	Pretreatment of possums	Hydroxylation reaction	IC_{50} (μM) mean + SEM (n) or mean [range] (n), where $n = 2$		
			Ketoconazole	Piperonyl butoxide	Diethyldithio-carbamate
10 μM	untreated	9-	18.0 [11.7–24.3] (2)	5.9 [5.3–6.5] (2)	100.3 ± 12.6 (4)
	terpene-treated*	9-	13.5 [8.3–18.7] (2)	12.0 ± 3.8 (4)	114.7 ± 18.3 (4)
		3-	4.9 [2.5–7.3] (2)	189.0 ± 47.8 (3)	70.7 [12.2–129.1] (2)
		7-	14.6 [6.2–23.0] (2)	50.3 ± 28.6 (3)	186.6 ± 39.4 (3)
100 μM	untreated				
		9-	67.0 [58.6–75.5] (2)	9.5 [9.4–9.6] (2)	52.1 ± 8.2 (4)
	terpene-treated*	9-	34.0 [29.0–38.9] (2)	17.8 ± 5.1 (4)	56.9 ± 9.0 (4)

*IC_{50}'s for 9-hydroxylation by terpene-treated microsomes were not significantly different from those for untreated microsomes.

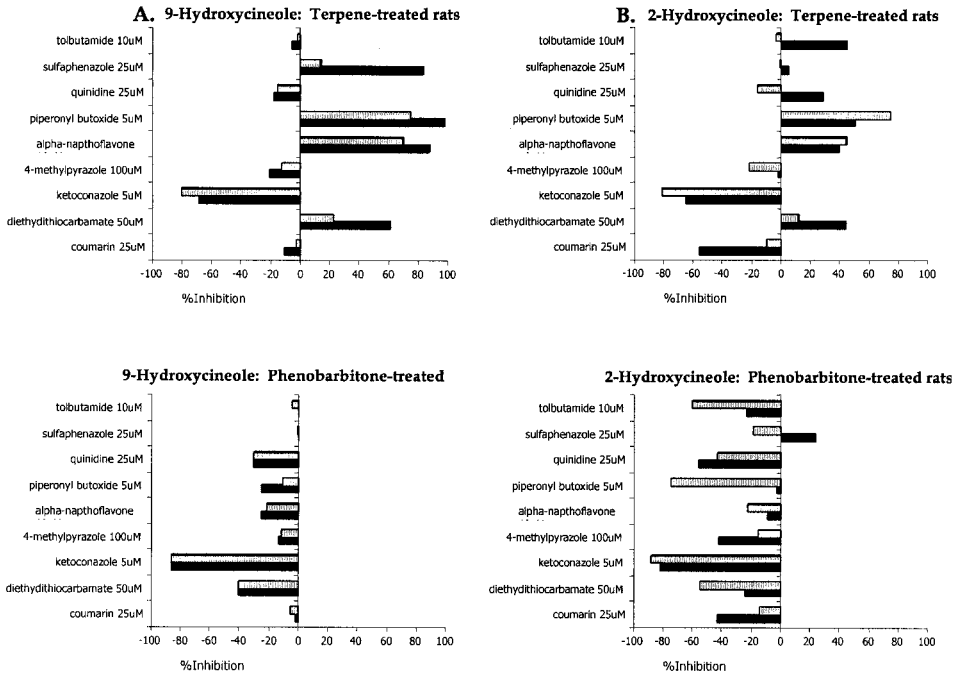


Figure 2. Effect of chemical inhibitors on the formation of (A) 9-hydroxycineole, (B) 2-hydroxycineole and in terpene-treated (upper panels) and phenobarbitone-treated (lower panels) rat liver microsomes. Data from individual rats. Mean $\pm$ SE ($n = 4$) control values (100%) were: for terpene-treated rats, V_{max} 9-OH 0.302 ± 0.052, 2-OH 0.987 ± 0.189 nmol/mg protein/min; and for phenobarbitone-treated rats, V_{max} 9-OH 0.836 ± 0.034, 2-OH 2.960 ± 0.198 nmol/mg protein/min.

Rat microsomes. Figure 2 shows the effects of the form-specific inhibitors on the formation of 9- and 2-hydroxycineole from 1,8-cineole by rat microsomes which had been induced by terpenes or phenobarbitone. Despite variability in effects within and between groups for all inhibitors screened, some general trends are evident. Ketoconazole is a potent inhibitor of 1,8-cineole metabolism in all rat microsomes tested, with the formation of both hydroxymetabolites reduced to around 12–25% control activity (figure 2). For other inhibitors that produced significant effects, these tended to differ between terpene-treated and phenobarbitone-treated microsomes.

In terpene-treated rat microsomes, only ketoconazole was clearly an inhibitor, while α-naphthoflavone and piperonyl butoxide both significantly activated 1,8-cineole metabolism, with the formation of both metabolites being increased by $\geq$50% (figure 2). The data from one rat indicate that diethyldithiocarbamate and sulfaphenazole (9- and 2-hydroxy) and tolbutamide (2-hydroxy) can also cause substantial activation of 1,8-cineole metabolism in these microsomes.

In contrast, little inhibition and no activation were found with the inhibitors screened with phenobarbitone-treated rat microsomes. Ketoconazole was the most effective inhibitor, with the formation of each metabolite being reduced by around 85% (figure 2). However, diethyldithiocarbamate and to a lesser extent, quinidine, also inhibited metabolism. In addition, piperonyl butoxide, 4-methylpyrazole,

Table 3. Effect of terpenes on aminopyrine demethylase activity in possum liver microsomes.

	Possum group			
	Untreated		Terpene-treated	
Treatment†	Activity*	% Control	Activity*	% Control
No terpene (control)	2.355		4.944	
1,8-Cineole	2.469	105	3.948	80
p-Cymene	2.497	106	4.773	96
Limonene	2.497	106	4.574	93
α-Pinene	2.042	87	3.237	65

Data are the mean of triplicate determinations from one terpene-treated and one untreated possum.
* Activity in nmol mg^{-1} microsomal protein min^{-1}.
† 100 μM.
Aminopyrine concentration was 25 mM.

tolbutamide and coumarin were found to exhibit moderate inhibition of 2-hydroxycineole formation.

In data not shown, the same trends were seen for the effects of the inhibitors on 3-hydroxcineole formation in terpene- and phenobarbitone-treated rat liver microsomes.

Effect of terpenes on metabolism by possum microsomes

Aminopyrine metabolism. The effects of the four terpenes (1,8-cineole, *p*-cymene, limonene and α-pinene) on aminopyrine demethylase activity are shown in table 3. α-Pinene had the greatest effect of all terpenes tested, with aminopyrine demethylase activity in terpene-treated microsomes being reduced to 65% control activity, although there was little effect in untreated microsomes.

1,8-Cineole metabolism. Figure 3 shows the effects of four terpenes (*p*-cymene, limonene, α-pinene and cuminyl alcohol) on the metabolism of 10 μM 1,8-cineole to its three major metabolites (9-, 3- and 7-hydroxycineole) in microsomes from terpene-treated possums. All the terpenes were found to inhibit 9-hydroxycineole formation, however there was some variability in the effectiveness of their inhibition of the formation of the other hydroxycineole metabolites. α-Pinene was the most effective inhibitor of the formation of all three hydroxycineole metabolites. At the lower 1,8-cineole concentration (10 μM, the amounts of 9-, 3- and 7-hydroxycineole formed were reduced to 3, 13 and 27% control values, respectively, in the presence of 100 μM α-pinene (figure 3); and at 100 μM substrate concentration to 23, 30 and 35% control amounts (data not shown).

IC_{50}'s for each metabolite at both high and low 1,8-cineole concentrations are shown in table 4. They tended to be lowest for 9-hydroxylation and greatest for 7-hydroxylation, although at the higher 1,8-cineole concentration there was considerable variability between microsomes from individual possums and fewer of the differences were statistically significant.

After α-pinene, limonene and cuminyl alcohol were the next most potent inhibitors of 1,8-cineole metabolism, with both terpenes exhibiting similar degrees

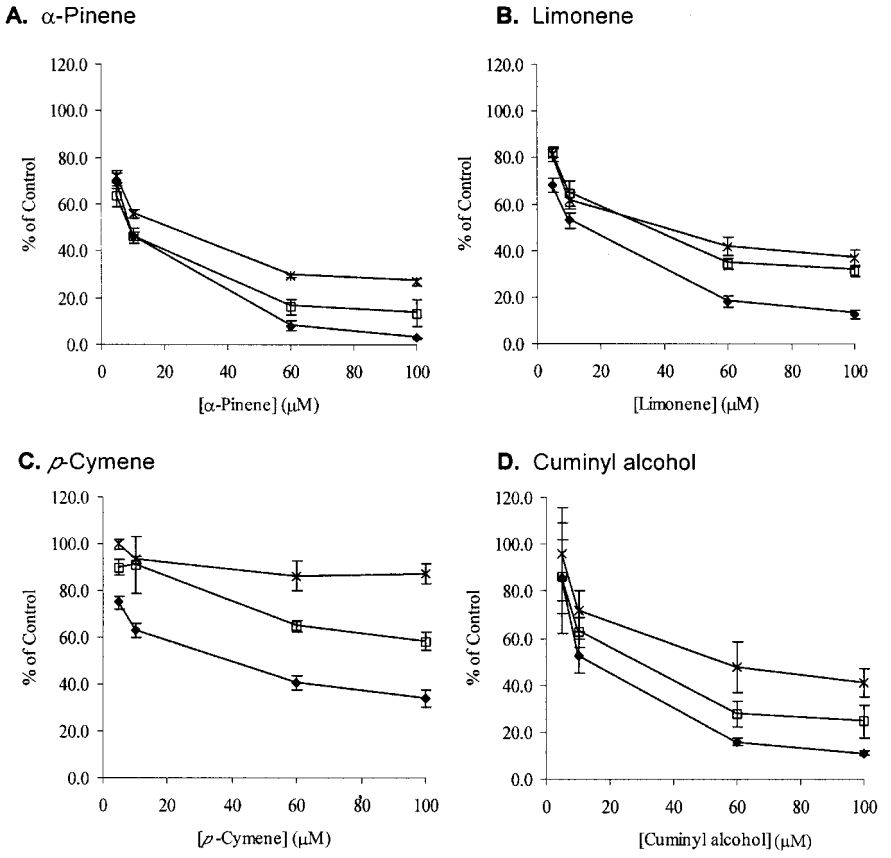


Figure 3. Comparison of 9-hydroxycineole (◆), 3-hydroxycineole (□) and 7-hydroxycineole (*) formation in terpene-treated possum liver microsomes in the presence of α-pinene (A), limonene (B), *p*-cymene (C) and cuminyl alcohol (D). 1,8-cineole = 10 μM, data are expressed as the mean ± SE from four individual possum microsomal incubations. Mean ± SE (n = 4) control values (100%) were: 9-OH 2.542 ± 0.142, 3-OH 1.033 ± 0.155, 7-OH 0.310 ± 0.024 nmol/mg protein/min.

of inhibition and IC_{50}'s (figure 3 and table 4). At both substrate concentrations, the formation of all hydroxycineole metabolites was inhibited to a significant degree (i.e. > 30%). *p*-Cymene was the least inhibitory of all terpenes tested (figure 3 and table 4), although it also produced relatively high levels of inhibition of 9-hydroxycineole formation at the low 1,8-cineole concentration (to 34% control activity). However, it was not as effective at inhibiting the formation of the other two hydroxymetabolites. At the higher substrate concentration, only 9-hydroxycineole was inhibited to a significant level (to 61% control activity).

Dixon plots of the terpene inhibitory data show that the lines of best fit at the two substrate concentrations intersected above the *x*-axis, and Cornish–Bowden plots reveal that the lines of best fit are parallel (figure 4). Table 5 shows the mean calculated K_i's of each terpene for 9-hydroxycineole formation by terpene-treated possum microsomes.

Table 4. IC_{50}'s of terpenes on hydroxycineole formation in possum liver microsomes.

	IC_{50} (μM) mean ± SEM ($n = 4$)											
	α-Pinene			Limonene			Cuminyl alcohol			*p*-Cymene		
Terpene-treated possums	9-OH	3-OH	7-OH	9-OH	3-OH	7-OH	9-OH	3-OH	7-OH	9-OH	3-OH	7-OH
10 μM 1,8-cineole	10.3 ± 0.9	9.1 ± 1.3	17.8 ± 1.1	12.6 ± 1.6	28.3 ± 1.7	38.7 ± 7.4	13.4 ± 4.5	26.2 ± 11.2	57.1 ± 28.7	32.6 ± 6.3	> 235	128.2 ± 45.0
p-value versus 9-OH		0.466	< 0.001		0.034	0.002		0.626	0.119		0.037	0.277
100 μM 1,8-cineole	40.3 ± 12.1	49.3 ± 17.4	63.6 ± 24.1	89.6 ± 9.8	196.2 ± 16.9	252.2 ± 73.9	74.7 ± 5.3	155.9 ± 14.7	180.3 ± 20.5	325.8 ± 81.6	> 500	> 500
p-value versus 9-OH		0.741	0.397		0.122	0.028		0.003	0.001		NI	NI

NI, no inhibition.

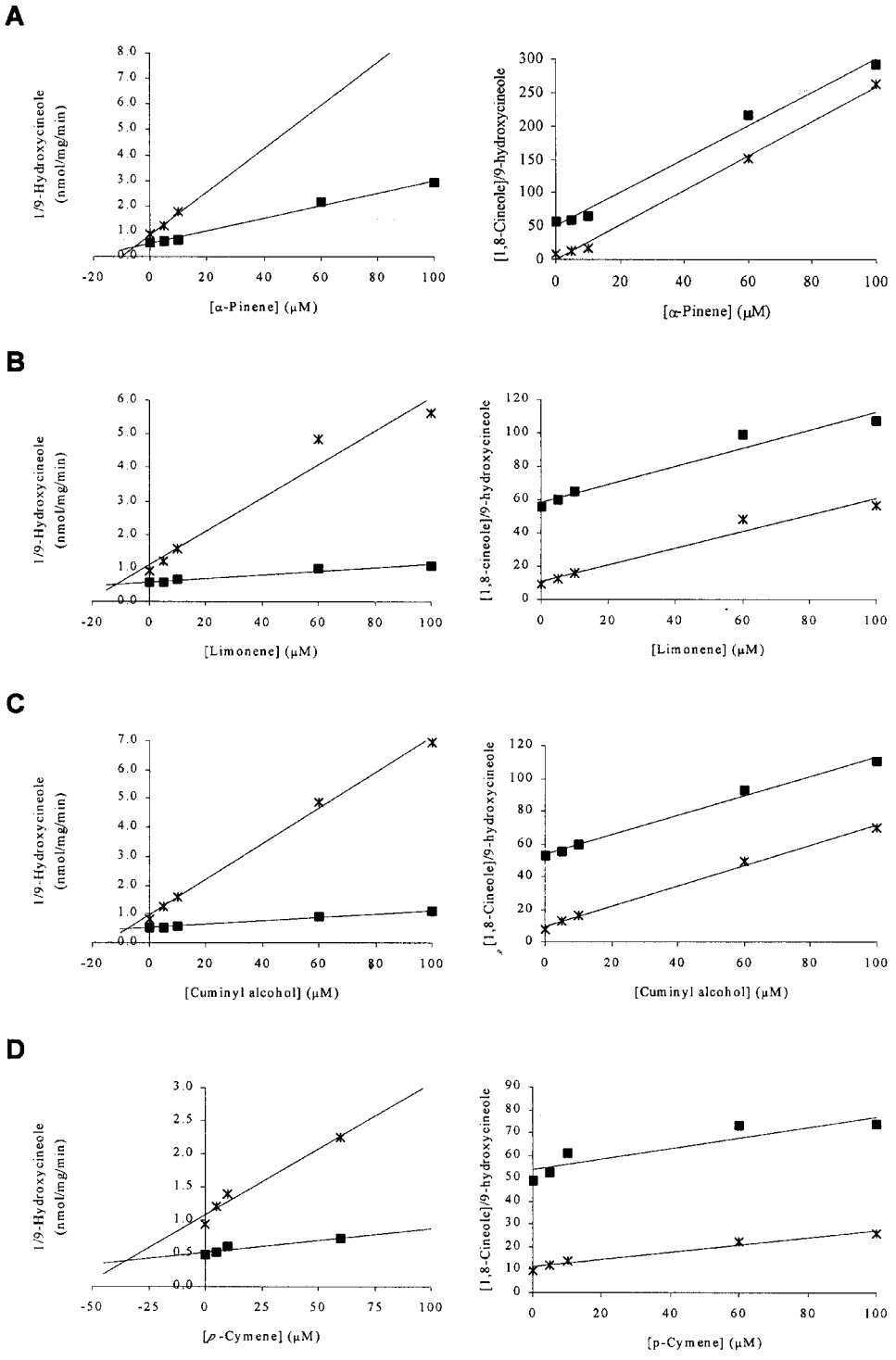


Figure 4. Representative Dixon (left) and Cornish-Bowden (right) plots for α-pinene (A), limonene (B), cuminyl alcohol (C) and *p*-cymene (D) at 10 μM (*) and 100 μM (■) 1,8-cineole. Individual data points are from single determinations in terpene-treated possum 4.

Table 5. K_i's for each terpene on 9-hydroxycineole formation in terpene-induced possum liver microsomes.

	Inhibitor constant (K_i) (μM)			
	α-Pinene	Limonene	Cuminyl alcohol	*p*-Cymene
Mean ± SEM ($n = 4$)	4.4 ± 1.1	7.8 ± 2.1	6.0 ± 0.8	44.3 ± 11.2

Discussion

Our knowledge of the microsomal metabolites of 1,8-cineole can now be updated combining the findings of our group with those of Miyazawa *et al.* (1989, 2001). The major metabolite in human and induced rat microsomes is 2-*exo*-hydroxycineole, whereas in the possum and koala it is 9-hydroxycineole (Pass *et al.* 2001). Each species forms both metabolites. Significant amounts of 3-*exo*-hydroxycineole are also found in the rat, possum and koala and 7-hydroxycineole in the possum and koala (Pass *et al.* 2001). We found that derivatization and GC-MS in SIM mode was necessary to detect and quantitate all the metabolites, which may explain why only 2-hydroxycineole was found by Miyazawa *et al.* (2001).

Ketoconazole was the most effective form-specific inhibitor of 1,8-cineole metabolism in both possum and rat liver microsomes. Formation of all hydroxycineole metabolites was reduced to about 25% of the control value in possum microsomes. Ketoconazole similarly inhibited both 9- and 2-hydroxylation in rat liver microsomes, supporting a recent report (Miyazawa *et al.* 2001) that ketoconazole inhibits 2-hydroxylation of 1,8-cineole in rat and human liver microsomes. This, and other evidence of Miyazawa *et al.*, indicates that CYP3A enzymes catalyse 2-hydroxylation of 1,8-cineole in human and rat liver microsomes.

However, the role of CYP3A-like enzymes in the hydroxylation of 1,8-cineole by possum liver microsomes is less certain. Although ketoconazole is a potent and selective inhibitor of CYP3A4 mediated reactions in humans, with an $IC_{50} < 1$ μM against probe substrates, at higher concentrations other CYP enzymes (CYP2C8/9, CYP2C19 and CYP1A1) are significantly inhibited (Eagling *et al.* 1998, Sai *et al.* 2000). In addition, ketoconazole is far less selective for CYP3A4 in rats, highlighting the differences between species in the activity of CYP enzymes (Eagling *et al.* 1998). The IC_{50}'s for inhibition of 9-hydroxylation in terpene-treated microsomes were relatively high (14–34 μM, table 2); concentrations that may be sufficient to inhibit CYP enzymes in addition to CYP3A forms. The lack of either inhibition by troleandomycin or activation by α-naphthoflavone supports this hypothesis. Troleandomycin has been shown to be a selective inhibitor of CYP3A activity in humans (Chang *et al.* 1994, Sai *et al.* 2000) and α-naphthoflavone has been shown to activate CYP3A mediated activity in humans and rats (Lee *et al.* 1997, Nakajima *et al.* 1999). If 1,8-cineole metabolism were carried out by forms similar to those belonging to the human/rat CYP3A subfamily, it would be reasonable to expect either troleandomycin inhibition or α-naphthoflavone activation, or both. Furthermore, we have previously reported that androstenedione 6β-hydroxylase activity, a marker of CYP3A activity, is low in microsomes from possum liver even after treatment with terpenes (Pass *et al.* 1999).

Piperonyl butoxide also inhibited 9-hydroxylation by terpene-treated possum micosomes but was not effective against 3- or 7-hydroxylation. It is a quasi-irreversible, mechanism-based inhibitor of low specificity (Ortiz de Montellano and Reich 1986) and its inhibitory effect on a reaction indicates that it is catalysed by a CYP enzyme but not the form(s) involved. Diethyldithiocarbamate was also found to exhibit moderate inhibition of 9-hydroxycineole formation. Diethyldithiocarbamate is a mechanism based inhibitor and has often been used as a diagnostic inhibitory probe of CYP2E1 activity (Halpert *et al*. 1994). However, the selectivity of this compound has been put into question with a number of studies reporting that it also inhibits CYP1A1, 1A2, 2A6, 2B6, 2C8, 3A3 and 3A4 (Chang *et al*. 1994, Eagling *et al*. 1998). Nevertheless, the effect of diethyldithiocarbamate does correlate well with the finding that aniline hydroxylase activity, a marker of CYP2E1, was substantially induced by the four terpenes in microsomes from brushtail possums (Pass *et al*. 1999).

The effect of adding chemical inhibitors to microsomal incubations with 1,8-cineole resulted in different levels of inhibition for 9-hydroxylation compared to 7- and 3-hydroxylation. This suggests that these pathways of 1,8-cineole metabolism in the possum may be carried out by different isoforms. The effect of the inhibitors on 1,8-cineole metabolism differed markedly between terpene-treated and phenobarbitone-treated rats, and rat and possum liver microsomes. Significant activation by piperonyl butoxide and α-naphthoflavone (and possibly other substances) was seen in terpene-treated rat microsomes but not in phenobarbitone-treated rat microsomes or possum microsomes. Phenobarbitone is a potent inducer of multiple CYPs in many species. In rats, it is known to induce enzymes belonging to the CYP2A, CYP2B, CYP2C and CYP3A subfamilies (Correia 1995, Lewis 1998). It seems likely that different enzymes are induced and catalyse 1,8-cineole metabolism in the two animal and treatment groups, and that multiple enzymes may be involved in each case.

The lack of inhibitory effect by sulfaphenazole and tolbutamide, both CYP2C family inhibitors, in possum liver microsomes was somewhat surprising as we have previously reported evidence of induction of CYP2C11 and CYP2C6 in possums treated with terpenes (Pass *et al*. 1999). These results suggested that enzymes belonging to the CYP2C subfamily may play a role in terpene metabolism in this species. A recent study by a collaborating group (Liapis *et al*. 2000) reported that tolbutamide hydroxylase activity (a marker for CYP2C8/9) was increased in possum microsomes after terpene treatment. In addition, they reported that 1,8-cineole is a potent competitive inhibitor of the enzyme responsible for tolbutamide hydroxylation.

There are a number of examples where chemicals can be inhibitors of certain enzymes, without being substrates for that particular enzyme. For example, quinidine has been shown to be a relatively selective inhibitor of CYP2D6 in humans, yet it is mainly metabolized by CYP3A4 (Guengerich *et al*. 1986, Schellens *et al*. 1991). It is possible that, in the possum, 1,8-cineole acts to inhibit metabolism by CYP2Cs without itself being a substrate.

The results from this study have provided direct evidence that the metabolism of one dietary terpene can be inhibited by the presence of another in the common brushtail possum. The *in vitro* metabolism of 1,8-cineole (taken as the sum of all metabolites measured) was reduced to 14% control in the presence of α-pinene, another terpene commonly found in *Eucalyptus* leaves. Although α-pinene was the

most potent inhibitor of 1,8-cineole metabolism in possum liver microsomes, cuminyl alcohol, limonene and *p*-cymene also exhibited high levels of inhibition (to 25, 27 and 45% control activities respectively). Although an extensive study into the mechanism of inhibition was not carried out, the evidence indicates that the terpenes act by competitive inhibition. Firstly, the inhibitory effect of all terpenes was more pronounced at low 1,8-cineole concentrations than at high substrate concentrations. Secondly, although only two substrate concentrations were tested, Dixon and Cornish–Bowden plots both suggest competitive inhibition.

The IC_{50}'s and K_i's for α-pinene, limonene and cuminyl alcohol inhibition of 9-hydroxycineole formation were all low and relatively similar to each other while the corresponding values for *p*-cymene were considerably higher. This suggests that, while α-pinene and limonene act directly to inhibit 1,8-cineole metabolism, *p*-cymene acts via its metabolite, cuminyl alcohol.

There have been a number of studies that have investigated the inhibitory effect of 1,8-cineole and limonene on form-specific substrates. Reicks and Crankshaw (1993) reported that limonene moderately inhibits the metabolism of *p*-nitrophenol and ethoxyresorufin in microsomes from phenobarbitone-treated mice, suggesting the involvement of CYP2E1 and CYP1A1 respectively. Similarly, De-Oliveira *et al*. (1999) reported that 1,8-cineole inhibits the metabolism of pentoxyresorufin (CYP2B1), ethoxyresorufin (CYP1A1) and methoxyresorufin (CYP1A2). Although these latter studies concluded that both terpenes may interfere with the metabolism of drugs specific to these enzyme forms, the degree of inhibition observed was not very high. This is in contrast to the present study, where the inhibition by all terpenes except for *p*-cymene reduced 9-hydroxycineole formation by $>84\%$. The degree of inhibition by these terpenes on 1,8-cineole metabolism suggests that, at least in the possum, the CYPs involved in the metabolism of this terpene show little resemblance to the above-mentioned forms.

The apparent form-specific nature of terpene metabolism was further supported by the lack of effect of 1,8-cineole, limonene, *p*-cymene and α-pinene on aminopyrine demethylation. Aminopyrine is commonly used as a marker of multiple CYPs including those belonging to the CYP1A, CYP2B, CYP2C and CYP3A subfamilies (Correia 1995). Although α-pinene produced a slight inhibition (to 65% control), the general lack of effect suggests that, rather than multiple forms, a specific enzyme, most likely one that does not metabolize aminopyrine, is responsible for terpene metabolism.

The current study is the first to report that the *in vitro* metabolism of one terpene is potently inhibited by another and that the mechanism of inhibition is most likely that of a competitive nature. It therefore provides direct evidence to support Freeland and Janzen's (1974) original hypothesis: that PSMs belonging to the same class are metabolized by common detoxification pathways and this may be a major factor contributing to the obligatory generalist nature of many mammalian herbivores. By including a variety of plant foods in their diet, mammalian herbivores avoid saturation of these specific metabolic pathways.

We have now demonstrated that terpenes are both inducers and inhibitors of CYP enzymes, including those which catalyse terpene metabolism. The phenomenon of *in vivo* induction by *in vitro* inhibitors has been observed with many other substances (Weaver 2001). The significance for animals which ingest large amounts of various terpenes and other PSMs in their diet is that, during any feeding session, their capacity to metabolize and so detoxify the many dietary

PSMs will be the resultant of induction (reflecting recent exposure to inducing PSMs) and inhibition (by the PSMs being eaten at the time). The overall picture will be very complex, particularly as it appears that a number of CYPs may be involved which are induced and inhibited independently by different PSMs in a dose-dependent manner, and thus contribute to different extents to PSM metabolism.

Knowledge of interactions between dietary terpenes may help to explain the reasons behind a browsing animal's dietary preferences. Since concentrations of terpenes in *Eucalyptus* leaf are relatively high, brushtail possums may be limited in the amount they can ingest due to the interactions between individual terpenes, resulting in saturation of metabolic pathways.

Acknowledgements

The authors are grateful to the following people for assistance of this study: Dr N. W. Davies (mass spectrometry), Dr I. Stupans (discussions), Mrs S. Brandon (analyses), Dr D. McGuinness (NMR) and Dr R. Boyle (metabolite standards).

References

Anderson, T., Miners, J. O., Veronese, M. E. and Birkett, D. J., 1994, Identification of human liver cytochrome P450 isoforms mediating secondary omeprazole metabolism. *British Journal of Clinical Pharmacology*, **37**, 597–604.

Anderson, T., Miners, J. O., Veronese, M. E., Tassaneeyakul, W., Tassaneeyakul, W., Meyer, U. A. and Birkett, D. J., 1993, Identification of human liver cytochrome P450 isoforms mediating omeprazole metabolism. *British Journal of Clinical Pharmacology*, **36**, 521–530.

Barnes, W., 1996, Eucalyptus oil poisoning in children. *Australian Journal of Emergency Care*, **3**, 15–20.

Boland, K. J. and Brophy, J. J., 1991, *Eucalyptus Leaf Oils: Use, Chemistry, Distillation and Marketing* (Melbourne: Inkata).

Bolton, R. M. and Ahokas, J. T., 1997, Mixed function oxidases in an Australian marsupial, the Brushtail Possum (*Trichosurus vulpecula*). *Archives of Environmental Contamination and Toxicology*, **33**, 83–89.

Carman, R. M. and Klika, K. D., 1992, Partially racemic compounds as brushtail possum urinary metabolites. *Australian Journal of Chemistry*, **45**, 651–657.

Chang, T. K. H., Gonzalez, F. J. and Waxman, K. J., 1994, Evaluation of triacetyloleandomycin, α-napthoflavone and diethyldithiocarbamate as selective chemical probes for inhibition of human cytochromes P450. *Archives of Biochemistry and Biophysics*, **311**, 437–442.

Correia, M. A., 1995, Rat and human liver cytochrome P450s. Substrate and inhibitor specificities and functional markers. In P. R. Ortiz de Montellano (ed.), *Cytochrome P450: Structure, Mechanism and Biochemistry* (New York: Plenum), pp. 607–630.

Dearing, M. D. and Cork, S., 1999, Role of detoxification of plant secondary compounds on diet breadth in a mammalian herbivore, *Trichosurus vulpecula*. *Journal of Chemistry and Ecology*, **25**, 1205–1219.

De-Oliveira, A. C. A. X., Ribeiro-Pinto, L. F. and Paumgartten, F. J. R., 1999, *In vitro* inhibition of CYP2B1 monooxygenase by b-myrcene and other monoterpenoid compounds. *Toxicology Letters*, **92**, 39–46.

Doecke, C. J., Veronese, M. E., Pond, S. M. and Al, e., 1991, Relationship between phenytoin and tolbutamide hydroxylations in human liver microsomes. *British Journal of Clinical Pharmacology*, **31**, 125–130.

Eagling, V. A., Tjia, J. F. and Back, D. J., 1998, Differential selectivity of cytochrome P450 inhibitors against probe substrates in human and rat liver microsomes. *British Journal of Clinical Pharmacology*, **45**, 107–114.

Feierman, D. E. and Cederbaum, A. I., 1987, Increased sensitivity of the microsomal oxidation of ethanol to inhibition by pyrazole and 4-methylpyrazole after chronic ethanol treatment. *Biochemistry and Pharmacology*, **36**, 3277–3283.

Flynn, T. M. and Southwell, I. A., 1979, 1,3-Dimethyl-2-oxabicyclo[2,2,2]-octane-3-methanol and 1,3-dimethyl-2-oxa-bicyclo[2,2,2]octane-3-carboxylic acid, urinary metabolites of 1,8-cineole. *Australian Journal of Chemistry*, **32**, 2093–2095.

Franklin, M. R., 1972, Inhibition of hepatic oxidative xenobiotic metabolism by piperonyl butoxide. *Biochemistry and Pharmacology*, **21**, 3287–3299.

Freeland, W. J. and Janzen, D. H., 1974, Strategies in herbivory by mammals: the role of plant secondary compounds. *American Nature*, **108**, 269–287.

Guengerich, F. P., Muller-Enoch, D. and Blair, I. A., 1986, Oxidation of quinidine by human liver cytochrome P-450. *Molecular Pharmacology*, **30**, 287–295.

Halpert, J. R., Guengerich, F. P., Bend, J. R. and Correia, M. A., 1994, Selective inhibitors of cytochromes P450. *Toxicology and Applied Pharmacology*, **125**, 163–175.

Ho, R.C., Luo, X.X., Macauley, J. S., Grigor, M. R. and Wanwimolruk, S., 1998, *In vitro* hepatic metabolism of CYP3A-mediated drugs quinine and midazolam in the common brushtailed possum (*Trichosurus vulpecula*). *Environmental Toxicology and Chemistry*, **17**, 317–324.

Hume, I. D., 1999, *Marsupial Nutrition* (Cambridge: Cambridge University Press).

Jenner, P. M., Hagan, E. C., Taylor, J. M., Cook, E. L. and Fitzhugh, O. G., 1964, Food flavourings and compounds of related structure. I. Acute oral toxicity. *Food and Cosmetic Toxicology*, **2**, 327–343.

Kharasch, E. D., Thummel, K. E., Mhyre, J. and Lillibridge, J. H., 1993, Single-dose disulfiram inhibition of chlorzoxazone metabolism: a clinical probe for P450 2E1. *Clinical Pharmacology and Therapeutics*, **53**, 643–650.

Lawler, I. R., Foley, W. J., Eschler, B. M., Pass, D. M. and Handasyde, K., 1998, Intraspecific variation in Eucalyptus secondary metabolites determines food intake by folivorous marsupials. *Oecologia*, **116**, 160–169.

Lee, C. A., Manyike, P. T., Thummel, K. E., Nelson, S. D. and Slattery, J., 1997, Mechanism of cytochrome P450 activation by caffeine and 7,8-benzoflavone in rat microsomes. *Drug Metabolism and Disposition*, **25**, 1150–1156.

Lewis, D. F. V., 1998, The CYP2 family: models, mutants and interactions. *Xenobiotica*, **28**, 617–661.

Liapis, P., Pass, G. J. and Stupans, I., 2000, Characterisation of tolbutamide hydroxylase activity in the common brushtail possum (*Trichosurus vulpecula*) and koala (*Phascolarctos cinereus*): inhibition by the *Eucalyptus* terpene 1,8-cineole. *Comparative Biochemistry and Physiology*.

Maurice, M., Pichard, L., Daujat, M. and Al, E., 1992, Effects of imidazole derivatives on cytochromes P450 from human hepatocytes in primary culture. *FASEB Journal*, **6**, 752–758.

McManus, M. E., Burgess, W. M., Veronese, M. E., Huggett, A., Quattrochi, L. C. and Tukey, R. H., 1990, Metabolism of 2-actylaminofluorene and benzo(a)pyrene and activation of food-derived hererocyclic amine mutagens by human cytochromes P450. *Cancer Research*, **50**, 3367–3376.

Miyazawa, M., Kameoka, H., Morinaga, K., Negoro, K. and Mura, N., 1989, Hydroxycineole: Four new metabolites of 1,8-cineole in rabbits. *Journal of Agricultural and Food Chemistry*, **37**, 222–226.

Miyazawa, M., Shindo, M. and Shimada, T., 2001, Oxidation of 1,8-cineole, the monoterpene cyclic ether originated from *Eucalyptus Polybractea*, by cytochrome P450 3A enzymes in rat and human liver microsomes. *Drug Metabolism and Disposition*, **29**, 200–205.

Nakajima, M., Kobayashi, K., Oshima, K., Shimada, N., Tokudome, S., Chiba, K. and Yokoi, T., 1999, Activation of phenacetin *O*-deethylase activity by α-napthoflavone in human liver microsomes. *Xenobiotica*, **29**, 885–898.

Nash, T., 1953, The colormetric estimation of formaldehyde by means of the Hontzsch reaction. *Biochemistry Journal*, **55**, 416–421.

Olkowski, A., Gooneratne, R. and Eason, C., 1998, Inhibition of cytochrome P450 enzymes in the Australian brushtail possum, *Trichosurus vulpecula*: comparison with that of the rat, rabbit, sheep and chicken. *Veterinary and Human Toxicology*, **40**, 208–212.

Ortiz de Montellano, P. R. and Reich, N. O., 1986, Inhibition of cytochrome P-450 enzymes. In P. R. Ortiz de Montellano (ed.), *Cytochrome P450: Structure, Mechanism and Biochemistry* (New York: Plenum).

Pass, G., McLean, S., Stupans, I. and Davies, N., 2002, Microsomal metabolism and enzyme kinetics of the terpene, *p*-cymene, in the common brushtail possum (*Trichosurus vulpecula*), koala (*Phascolarctos cinereus*) and rat. *Xenobiotica*, **32**, 383–397.

Pass, G. J., McLean, S. and Stupans, I., 1999, Induction of xenobiotic metabolising enzymes in the common brushtail possum, *Trichosurus vulpecula*, by *Eucalyptus* terpenes. *Comparative Biochemistry and Physiology*, **124**, 239–246.

Pass, G. J., McLean, S., Stupans, I. and Davies, N., 2001, Microsomal metabolism of the terpene, 1,8-cineole, in the common brushtail possum (*Trichosurus vulpecula*), koala (*Phascolarctos cinereus*), rat and human. *Xenobiotica*, **31**, 205–221.

Reicks, M. M. and Crankshaw, K., 1993, Effects of d-limonene on hepatic microsomal monoxygenase activity and paracetamol-induced glutathione depletion in mouse. *Xenobiotica*, **23**, 809–819.

Sai, Y., Dai, R., Yang, T. J., Krausz, K. W., Gonzalez, F. J., Gelboin, H. V. and Shou, M., 2000, Assessment of specificity of eight chemical inhibitors using cDNA-expressed cytochromes P450. *Xenobiotica*, **30**, 327–343.

Schellens, J. H. M., Ghabrial, H., van der Wart, H. H. F., Bakker, E. N., Wilkinson, G. R. and Breimer, D. D., 1991, Differential effects of quinidine on the disposition of nifedipine, sparteine, and meqpenytoin in humans. *Clinical Pharmacology and Therapeutics*, **50**, 520–528.

Veronese, M. E., Doecke, C. J., Mackenzie, P. I., McManus, M. E., Minors, J. O., Rees, D. L., Gasser, R., Meyer, U. A. and Birkett, D. J., 1993, Site-directed mutation studies of human liver cytochrome P450 isoenzymes in the CYP2C subfamily. *Biochemistry Journal*, **289**, 533–538.

Weaver, R. J., 2001, Assessment of drug–drug interactions: concepts and approaches. *Xenobiotica*, **31**, 499–538.

Winzor, D. J., Ioannoni, B. and Reilly, P. E. B., 1986, The nature of microsomal monooxygenase inhibition by cimetidine. *Biochemistry and Pharmacology*, **35**, 2157–2161.

Yun, C. H., Shimada, T. and Guengerich, R. P., 1991, Purification and characterization of human microsomal cytochrome P450 2A6. *Molecular Pharmacology*, **40**, 679–685.

Zhang, H., Coville, P. F., Walker, R. J., Miners, J. O., Birkett, D. J. and Wanwimolruk, S., 1997, Evidence for involvement of human CYP3A in the 3-hydroxylation of quinine. *British Journal of Clinical Pharmacology*, **43**, 245–252.

XENOBIOTICA, 2002, VOL. 32, NO. 12, 1127–1138

Taylor & Francis
healthsciences

In vivo metabolism of diallyl disulphide in the rat: identification of two new metabolites

E. GERMAIN†, J. AUGER‡, C. GINIES§, M.-H. SIESS† and C. TEYSSIER†¶

† Unité Mixte de Recherche de Toxicologie Alimentaire and §Unité Mixte de Recherche des Arômes, Institut National de Recherche Agronomique, BP 86510, 17 rue Sully, F-21065 Dijon cedex, France
‡ Institut de Recherche sur la Biologie des Insectes, Centre National de Recherche Scientifique, Université F. Rabelais, Parc Grandmont, F-37200 Tours, France

Received 14 March 2002

1. Diallyl disulphide (DADS), a compound formed from the organosulphur compounds present in garlic, is known for its anticarcinogenic effects in animal models.

2. The aim was to identify and analyse the metabolites produced *in vivo* after a single oral administration of 200 mg kg^{-1} DADS to rats. The organic sulphur metabolites present in the stomach, liver, plasma and urine were measured by gas chromatography coupled with mass spectrometry over 15 days.

3. Data indicate that DADS is absorbed and transformed into allyl mercaptan, allyl methyl sulphide, allyl methyl sulphoxide (AMSO) and allyl methyl sulphone ($AMSO_2$), which are detected throughout the excretion period. Overall, the highest amounts of metabolites were measured 48–72 h after the DADS administration. $AMSO_2$ is the most abundant and persistent of these compounds. The levels of all the sulphur compounds rapidly decline within the first week after administration and disappear during the second week. Only AMSO and $AMSO_2$ are significantly excreted in urine.

4. These potential metabolites are thought to be active in the target tissues. Our data warrant further studies to check this hypothesis.

Introduction

Since early times, many beneficial properties have been ascribed to garlic for human health. Recent investigations have provided a scientific basis to these properties and have shown that garlic can interfere with different processes involved in the development of cardiovascular, neoplasic and several other diseases (Reuter 1995, Amagase *et al.* 2001). The reported biological effects have been attributed to the organosulphur compounds present in the bulb or formed after cutting or chopping the bulb.

Among these compounds, diallyl disulphide (DADS) (figure 1), which accounts for 40–60% of the essential oil of garlic, has often been reported to inhibit or reduce chemically induced carcinogenesis in rodents (Le Bon and Siess 2000, Milner 2001). DADS exerts a broad spectrum of effects on several stages involved in the process of carcinogenesis, including modulatory effects on drug-metabolizing enzymes (Yang *et al.* 2001), prevention of genotoxicity (Guyonnet

* Author for correspondence; e-mail: siess@dijon.inra.fr
¶ Present address: Unité Amélioration, génétique et physiologie forestières, Institut National de Recherche Agronomique, Avenue de la Pomme de Pin — Ardon, BP 20619, F-45166 Olivet cedex, France.

Xenobiotica ISSN 0049–8254 print/ISSN 1366–5928 online © 2002 Taylor & Francis Ltd
http://www.tandf.co.uk/journals
DOI: 10.1080/00498250210001790 2

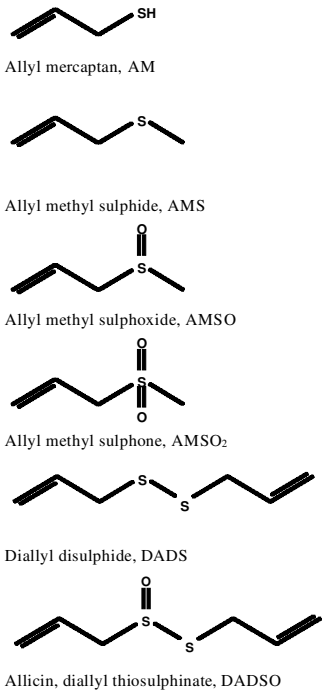


Figure 1. Structure of DADS and its metabolites.

et al. 2001), inhibition of cell proliferation, apoptosis and cell differentiation (Sundaram and Milner 1996, Lea and Ayyala 1997), and an immunostimulating effect (Kuttan 2000). In addition, DADS has also been shown to interact with cholesterol synthesis (Gebhardt and Beck 1996).

Although there is considerable knowledge about the anticarcinogenic effects of DADS, only one study has been dedicated to its *in vivo* metabolism and distribution in rodents. Pushpendran *et al.* (1980) studied the uptake and metabolic fate in mice of labelled DADS given at a sublethal dosage. They reported that DADS was rapidly absorbed, with a maximal concentration in the liver 90 min after i.p. administration. A total of 8% of the radioactivity present in the liver was identified as DADS. In addition, several *ex vivo* and *in vitro* systems have been used to analyse and identify the metabolites of DADS. In a study using an isolated perfused rat liver, DADS appeared to be converted to allylmercaptan (AM) (figure 1) (Egen-Schwind *et al.* 1992a). In primary rat hepatocytes, the metabolites of DADS have been analysed (Sheen *et al.* 1999) and within 120 min the majority of DADS disappeared from the extracellular fluid and was converted to AM and allyl methyl sulphide (AMS) (figure 1). The amount of AM was greater than the amount of AMS. Lawson and Wang (1993) reported that DADS was converted to AM in presence of blood before reaching the liver or other organs. All these results suggest that the metabolism of DADS occurred by way of reduction and methylation. Furthermore, under other experimental conditions, the oxidation of DADS has been reported (Teyssier *et al.* 1999). Previous experiments in our laboratory have demonstrated the oxidation of DADS in allicin in the presence of

human liver microsomes (Teyssier *et al.* 1999). Other naturally occurring organosulphur compounds such as diallyl sulphide (Brady *et al.* 1991) and dipropyl disulphide (Teyssier and Siess 2000) have also been shown to be oxidized. Similarly, Mitchell (1988) pointed out the importance of the *S*-oxidation of sulphides by monooxygenases as a pathway in the biotransformation of several sulphur-containing compounds.

The aim of this current study was to investigate the *in vivo* fate of DADS and its metabolites in rats after a single oral administration. For this purpose, we analysed xenobiotic distribution in various tissues and determined their pharmacokinetic parameters. Special attention was paid to the hypothetical formation of *S*-oxidized metabolites. The study was performed in rats with one oral administration of 200 mg kg^{-1} DADS. At distinct time intervals over 15 days, the concentrations of organosulphur compounds were determined in the stomach, plasma, liver and urine by gas chromatography coupled with mass spectrometry (GC-MS). The data confirmed the presence of AM and AMS as *in vivo* metabolites of DADS. Two new metabolites were detected and identified as allyl methyl sulphoxide (AMSO) and allyl methyl sulphone ($AMSO_2$) (figure 1) by different analytical approaches.

Materials and methods

Chemicals

AM, AMS, sodium metaperiodate, *p*-cymene, nonane and DADS were purchased from Sigma–Aldrich Chemical (Strasbourg, France). DADS was purified by distillation under reduced pressure (95% purity checked by GC-MS), whereas AM (80% purity) and AMS (98% purity) were used as standards without further purification. Allicin (78% purity) was synthesized by the action of metachloroperbenzoic acid on DADS as described by Mondy *et al.* (2001). All other reagents and organic solvents were of HLPC or analytical grades (SDS, Peypin, France). Dichloromethane was distilled before use for the solvent extractions.

Synthesis of AMSO and $AMSO_2$

AMSO and $AMSO_2$ were obtained by oxidation of AMS with sodium metaperiodate in a methanolic solution thawed on ice overnight (Furniss *et al.* 1989). The compounds were extracted before injection into gas chromatography–mass spectrometry (GC-MS) and gas chromatography–Fourier transformed infrared (GC-FTIR) in order to assess their structure. The reaction was total but gave a mixture of AMSO (85%) and $AMSO_2$ (15%) as estimated by GC-MS.

Animals and drug administration

Male 8-week-old Wistar rats ($n = 55$, average weight 350 g) were purchased from Janvier (Le Genest, Saint Isle, France). Rats were housed in individual stainless-wire cages, maintained at 22°C with a 12-h light/12-h dark cycle. They were fed *ad libitum* with standard diet from Harlan France (Ref. 20118S Harlan Gannat, France) and water. The animals were fasted for 18 h before and 6 h after drug administration. DADS, dissolved in corn oil, was orally administered at a dose of 200 mg kg^{-1} body weight. Negative controls were included for seven animals in order to check that no sulphur compounds were detectable in their tissues. After oral administration, animals were maintained separately in metabolic cages. Urine (kept under cold conditions) was collected every 24 h and stored at −20°C until further analysis. Animals were killed by exsanguination under anaesthesia (isoflurane 2.5% in oxygen) 10 ($n = 3$), 20 ($n = 3$), 40 min ($n = 3$), 1 ($n = 3$), 2 ($n = 3$), 6 ($n = 3$), 24 ($n = 3$), 48 ($n = 4$) and 72 h ($n = 3$) after oral dosing and then every 2 days ($n = 3$) during the 12 remaining days of the experiment. Livers and stomachs were removed, weighed and stored at −20°C until further analysis. Blood and urine were immediately centrifuged and were also stored at −20°C before analysis.

Sample preparation

Sample preparation was performed as described by Teyssier and Siess (2000). Briefly, stomachs and livers were homogenized with a high-speed blender in distilled water. A total of 100 µl of an ethanol

solution containing *p*-cymene (0.17 mg ml^{-1}), used as an internal standard (Martin-Lagos *et al.* 1995), was added to the homogenate. After adding 10% w/v trichloroacetic acid 30%, the homogenate was centrifuged and the supernatant extracted three times with dichloromethane. The same protocol without homogenization was used for the plasma samples whereas urine samples were subjected to only the dichloromethane extraction. The extracts were then concentrated by evaporation under a nitrogen stream to a final volume of 500 µl. To this volume, 100 µl nonane dissolved in dichloromethane (0.15 mg ml^{-1}) was added in order to standardize each sample concentration and an aliquot of 2 µl was then injected into the chromatograph under the conditions described below.

GC-MS conditions for DADS, AM, AMS, AMSO and $AMSO_2$ analysis

GC-MS was carried out using a Agilent Technologies (Les Ullis, France) 6890 gas chromatograph coupled to Agilent Technologies 5973 Mass Selective Detector using a capillary DB1701 column (30 m × 0.32 mm i.d., 1 µm film thickness), a splitless injection and an electronic ionization at 70 eV. The oven was programmed from 35°C (2 min) to 220°C at a rate of 5°C min^{-1}. The other conditions were: carrier gas, helium (constant velocity fixed at 35 cm s^{-1}); and temperature of the injection port, 200°C. Peak identifications were based on comparison with retention times and spectra of standards. Each sample was analysed twice. For the first acquisition, GC-MS was used in scan mode from m/z 28–300 amu in order to ascertain the identification of compounds by comparison with standards. For the second acquisition, GC-MS was used in selected ion monitoring (SIM) mode. The quantification of AM, AMS, AMSO, $AMSO_2$ and DADS was achieved by monitoring the ions at m/z 74, 88, 104, 120 and 146, respectively. The purity was continuously checked by the control of the ratio between this quantifying ion and another one, being specific for each compound. Chemical ionization was performed with NH_3 as gas reactant.

GC-MS conditions for allicin analysis

For allicin analysis, we applied the recently developed specific GC-MS method (Mondy *et al.* 2001). Briefly, analyses were carried out on a benchtop Perkin Elmer turbomass system with a split–splitless injector and a fused-silica capillary column (10 m × 0.32 mm) with 4 µm methylsilicon coating. The carrier gas was helium; the oven temperature programme was 5°C min^{-1} from 70 to 250°C. The injection port temperature was 200°C. Total ion chromatograms and mass spectra were recorded in the electron impact ionization mode of 70 eV. The transfer line and source temperature were maintained at 150°C. Peak identifications were based on comparison with retention times and spectra were obtained with pure allicin. These GC-MS conditions allowed the direct detection of allicin and the detection of 3-vinyl[4]-1,2 dithiin and 2-vinyl[4]-1,3 dithiin, two compounds formed from the allicin degradation during GC-process (Mondy *et al.* 2001). The limit of detection of allicin was estimated with a standard solution at 15 ng.

GC-FTIR conditions for AMSO and $AMSO_2$ analysis

AMSO and $AMSO_2$ from dichloromethane extracts were identified by GC-FTIR analysis using a Biorad Digilab FTS 60A spectrometer. This equipment was connected by means of a digilab Tracer® direct-deposition interface to a Hewlett-Packard HP 5890 Series II (Palo Alto, CA, USA) gas chromatograph, which was equipped with a splitless–split injector. GC separation was similar to the above-mentioned method (GC-MS conditions for DADS, AM, AMS, AMSO and $AMSO_2$ analysis).

Quantitative determination of the organosulphur compounds

For each sulphur compound, the sensitivity and linearity of the GC-MS detector used in the SIM mode was calculated from a series of standard solutions dissolved in dichloromethane. The response coefficient (a) was calculated from the curve $y = ax + b$, where y is the adjusted area (with the areas of *p*-cymene and nonane) of the quantified ion and x is the quantity of the compound (ng). The response coefficient of all other compounds was essentially similar, between 1.24 and 4.19, except for $AMSO_2$, which was low (0.32). The lowest correlation coefficient (r^2) was about 0.995. The limits of detection varied depending on the sulphur compounds and were 0.04 ng for DADS, 0.64 ng for AM, 0.04 ng for AMS, 0.03 ng for AMSO and 0.11 ng for $AMSO_2$.

The concentration of each sulphur compound in the biological samples was calculated by the ratio between the area of the sulphur compound and the product of the *p*-cymene area and the nonane area. After excluding every value beneath the linearity region of the detector, the amount of each compound was obtained by integrating its specific response coefficient. Results were given as a mean of three separate experiments (µg g^{-1} organ).

Pharmacokinetic analysis

The non-compartmental method was used to calculate the pharmacokinetic parameters with the Kinetica® software (InnaPhase, Champs sur Marne, France). The area under the plasma concentration–time curve (AUC) was computed using the trapezoidal log–linear method, when $Cn > Cn_1$. The elimination half-life $(t_{1/2})$ was calculated as $t_{1/2} = \ln 2 L_z^{-1}$, where L_z is the elimination rate constant. The plasma clearance (Cl_p) was calculated as $Cl_p = \text{dose AUC}^{-1}$. T_{max} corresponded to the time for which the concentration was maximum (C_{max}).

Results

Identification of volatile metabolites

After DADS administration to rats, the parent molecule was detected in almost all analysed tissues within the first hours (data not shown). In addition, the DADS metabolites such as AM, AMS and two unknown compounds were detected in all the tested organs. Despite the specificity of the method used, neither allicin nor vinyl dithiines were detected. Figure 2 shows a gas chromatogram of the volatile components detected in the stomach. DADS, AM and AMS were identified by comparing their retention times and mass spectra with those of standard compounds. The molecular weights of the two unknown compounds, 104 and 120, were determined by chemical ionization in GC-MS. Owing to the absence of the corresponding standards, their identification was achieved by different approaches summarized in table 1. Based on GC-MS data (figure 3), the intensity of the ion at

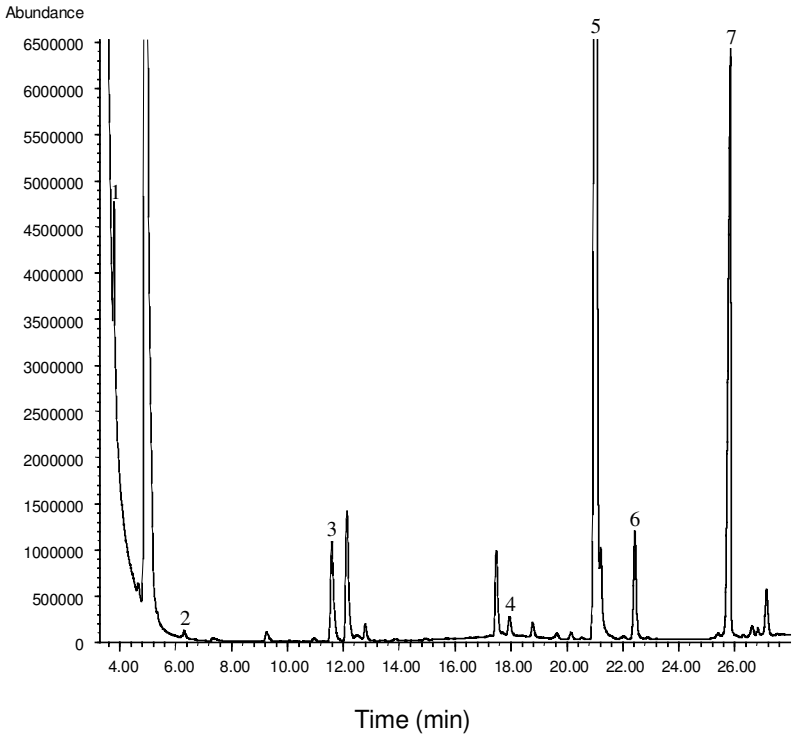


Figure 2. Total ionic current chromatogram of extracted stomach (second day) obtained on GC-MS. Peaks 1, AM; 2, AMS; 3, nonane; 4, *p*-cymene; 5, DADS; 6, AMSO; 7, $AMSO_2$. *Unidentified compounds detected both in extracts originating from control and DADS-treated animals.

Table 1. Chemical characteristics of the AMSO and $AMSO_2$ metabolites.

	MW	CI[a] $(MH)^+$	Isotopic ratio (%)[b]	Formula
AMSO	104	105	106/105 5.95 (5.36) 107/105 4.71 (4.60)	C_4H_8SO
$AMSO^2$	120	121	122/121 5.80 (5.40) 123/121 4.72 (4.80)	$C_4H_8SO_2$

[a] Chemical ionization.

[b] Reported values (relative abundance) correspond to the isotopic ratio of the pseudo-molecular ion $(MH)^+$. The theoretical values are given in parentheses

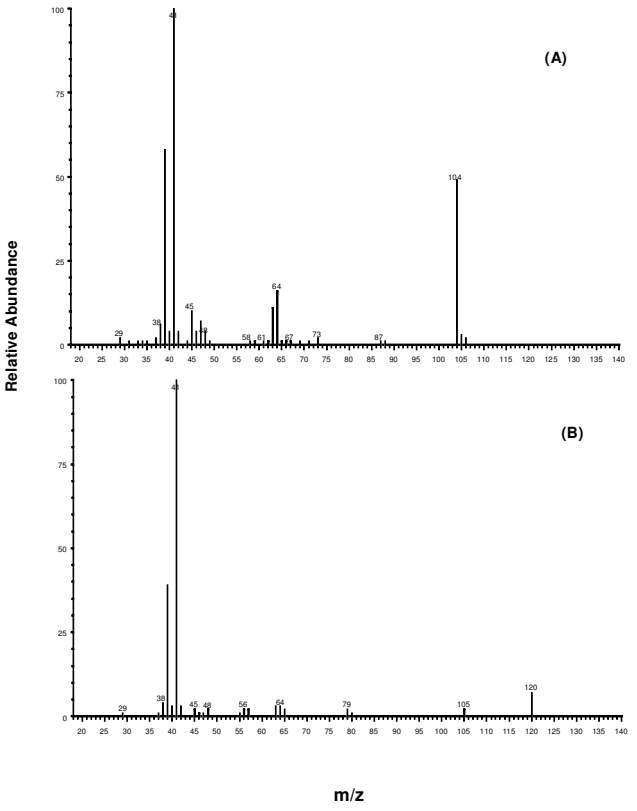


Figure 3. Mass spectra of AMSO (A) and $AMSO_2$ (B).

the m/z ratio of $(M+2)$ indicated the presence of one sulphur atom in each compound. The observed isotopic ratios were in agreement with the calculated ratios for molecules containing one atom of sulphur, four atoms of carbon, eight atoms of hydrogen and one or two atoms of oxygen for the first and the second metabolites, respectively. Since oxidation of sulphur compounds has been reported in the literature (Williams *et al.* 1966, Brady *et al.* 1991, Nickson *et al.* 1995, Teyssier and Siess 2000), we hypothesized that these two unknown metabolites corresponded to AMSO and $AMSO_2$. Subsequently, the chemical synthesis of these compounds was undertaken. Their chemical structures were ascertained by GC-MS and GC-FTIR. Indeed, the infrared spectra showed strong absorption bands for the sulphoxide moiety ($\nu_{S=O} = 998\,cm^{-1}$), for the sulphone moiety

(symmetric stretching $\nu_{SO_2} = 1136\,cm^{-1}$; asymmetric stretching ($\nu_{SO2} = 1289\,cm^{-1}$) and small absorption bands for the allyl chain ($\nu_{C=C} = 1641\,cm^{-1}$; $\nu_{=C_H} = 3088\,cm^{-1}$) (Socrates 1994). Hence, the *in vivo* metabolites were then compared with the synthesized standards and were identified as AMSO and $AMSO_2$.

Metabolite profiles in stomach, liver, plasma and urine

Figure 4 shows the time-dependent tissue concentrations of DADS and its metabolites AM, AMS AMSO and $AMSO_2$ after DADS oral administration. In the stomach, all these compounds were detected with various rates of appearance

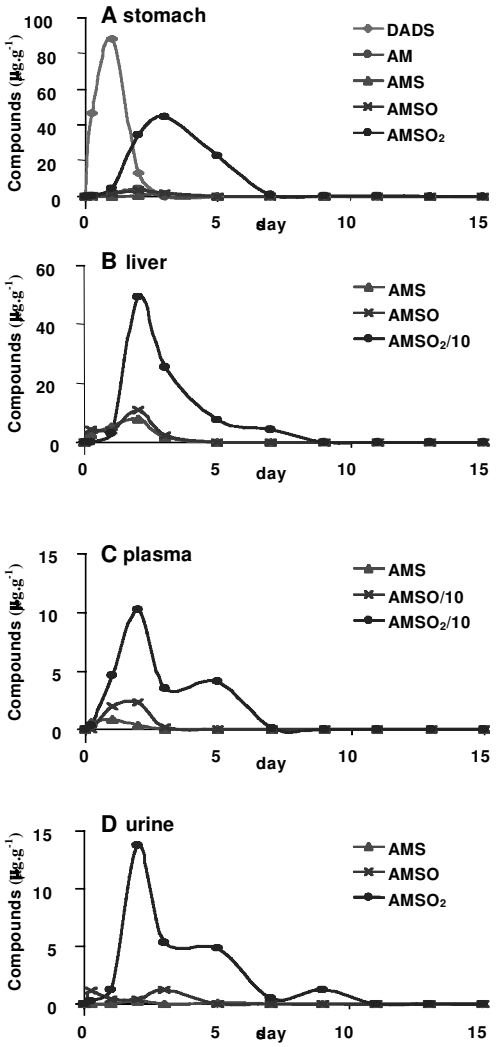


Figure 4. Concentrations of volatile metabolites in the stomach, liver, plasma and urine after one oral administration of DADS to male rats ($200\,mg\,kg^{-1}$). Results are the mean of three separate experiments ($\mu g\,g^{-1}$ organ).

and different concentration–time profiles (figure 4A). The highest levels of DADS were found during the 24 h. Thereafter, it sharply decreased and was not detectable 3 days after oral administration. In contrast, $AMSO_2$ reached a maximal concentration later in the period of follow-up, i.e. on the third day, and was still detectable for 11 days (figure 4A). In the plasma and the liver, $AMSO_2$ was the most abundant and persistent compound. The other compounds were, by rank order: AMSO and then AMS. In plasma, AM was barely detectable and DADS appeared transiently at 20 min after administration (data not shown). $AMSO_2$ concentration reached its maximum on the second day and thereafter decreased, formed a plateau between days 3 and 5 and became undetectable on day 9 (figure 4C). In liver, DADS and AM were detected only during the first hours (data not shown). The levels of $AMSO_2$ increased extensively over the first 2 days (figure 4C). After reaching a maximum, the level of $AMSO_2$ slowly decreased but was still detected 11 days after DADS administration. In urine, neither AM nor DADS were detected (figure 4D). Only trace amounts of AMS were excreted only on the second day, whereas AMSO and $AMSO_2$ were excreted throughout a longer period. The $AMSO_2$ concentration–time profile was similar to the one observed in plasma with its highest level in urine corresponding to 15% of the maximal plasma level (figure 4C, D).

Pharmacokinetic parameters

The plasma concentration–time curve of the metabolites of DADS after oral administration to the rat is shown in figure 5 and the pharmacokinetic parameters are summarized in table 2. In the case of DADS, only C_{max} and T_{max} were determined since the plasma concentrations were too low to enable an accurate determination of other pharmacokinetic parameters. The C_{max} of the metabolites were higher than that of DADS (0.001 mmol l^{-1}) as were plasma T_{max}. Indeed, the

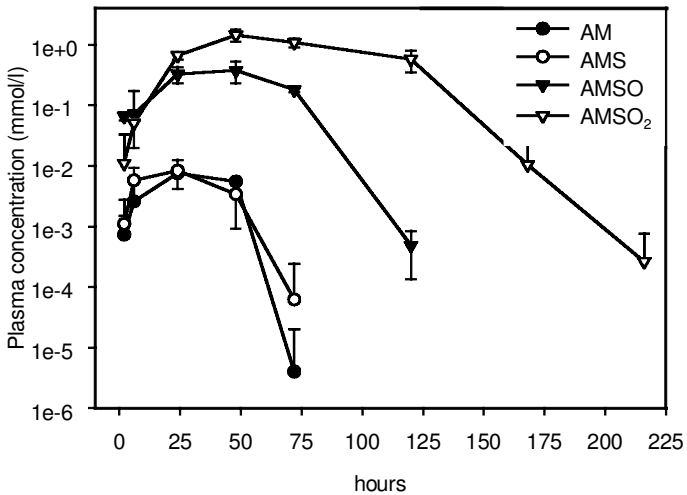


Figure 5. Plasma concentration–time curve of metabolites of DADS after one oral administration of DADS (200 mg kg^{-1}) to male rats. Data are the means of three separate experiments ± SEM. After 75 h for AM and AMS, and after 125 h for AMSO, the measured amounts were beneath the detection limit.

Table 2. Pharmacokinetic parameters of DADS and its metabolites after a single oral administration.

	DADS	AM	AMS	AMSO	$AMSO_2$
$t_{1/2}$(h)	n.d.[a]	4.39	6.78	7.16	8.64
C_{max} (mmol l^{-1})	0.001	0.008	0.008	0.376	1.440
T_{max}(h)	<1[b]	24	24	48	48
AUC total (h mmol l^{-1})	n.d.	0.324	0.328	23.75	116.86
Cl_p($l\,h^{-1}$)	n.d.	1.475	1.455	0.020	0.004

Parameters were calculated from three separate experiments.
[a] Not determined; [b] estimated value.

DADS T_{max} was estimated to be $<$ 1 h whereas this time increased to 24 h for AM and AMS and to 48 h for AMSO and $AMSO_2$. The AUC for AM of 0.324 h mmol l^{-1} increased for the other metabolites until the maximal value of 116.86 h mmol l^{-1} was determined for $AMSO_2$.

Discussion

The present study was carried out to investigate the *in vivo* biotransformation of DADS after oral administration to rats. For this purpose, we applied a quantitative and sensitive GC-MS method suitable for organosulphur compound analysis, which has already been validated (Martin-Lagos *et al.* 1995). We measured not only the amounts of DADS, but also those of AM, AMS, AMSO and $AMSO_2$, which were identified as DADS metabolites in the stomach, plasma, liver and urine. Based upon their plasma concentrations, their pharmacokinetic parameters were determined. We observed large interindividual variations which are particularly representative in the bioavailability (coefficient of variation of DADS, n.d.; AM, 81%; AMS, 32%; AMSO, 38%; $AMSO_2$, 7%). Our results, reported herein, show that DADS is absorbed, but owing to its low plasma concentrations, it was not possible to determine accurately the related pharmacokinetic parameters. However, the uptake of DADS in the liver was observed only during the first 2 h after dosing (data not shown), and DADS was transiently detected in plasma and was totally undetectable in the urine. The DADS levels in the liver and plasma did not exceed 0.5% of the DADS level in the stomach. These data are in accordance with a previous study in humans in which no DADS was detected in the blood and urine after ingestion of raw garlic (Amagase *et al.* 2001). The fact that DADS was hardly detected in any sample could be linked with its metabolism. Indeed, in an experiment in our laboratory using an isolated rat liver perfused with DADS, the apparent $t_{1/2}$ of DADS was estimated as $<$1 h (unpublished data). In spite of the impossibility of assessing the *in vivo* pharmacokinetic parameters of DADS, all these observations taken together strongly suggest that once absorbed, DADS is rapidly and extensively metabolized.

Our data show that DADS is transformed into AM, AMS, AMSO and $AMSO_2$. Among these metabolites, $AMSO_2$ and AMSO are the major and more persistent volatile metabolites found in all assayed tissues. $AMSO_2$ appears to be the final metabolite since no new metabolite was detected when $AMSO_2$ levels decreased. In the same way, Nickson *et al.* (1995) reported that only dipropyl sulphone was detected in the urine of rats after oral ingestion of dipropyl sulphoxide, indicating the absence of subsequent biotransformation of the sul-

phone. AM and AMS were actually detected, but their bioavailabilities (table 2) were lower than those of the *S*-oxidized metabolites (table 2). The rapid elimination of AM and AMS in the breath described by Rosen *et al.* (2001) could explain their moderate amounts and low bioavailability observed in our study. However, an alternative hypothesis is that AMS is the precursor of AMSO and $AMSO_2$. This hypothesis is consistent with the T_{max} of the metabolites which are compatible with sequential DADS transformation into AM to AMS to AMSO and finally to $AMSO_2$ (table 2).

Interestingly, as far as pharmacokinetic profiles were concerned, AMSO and $AMSO_2$ presented similar patterns. In the liver and the plasma, they were characterized by an initial sharp rise during the first 2 days followed by a slow decline lasting 3–9 days suggesting a slow elimination. This phenomenon was unexpected since the overall hydrophilic nature of *S*-oxidized metabolites would favour a rapid and complete urinary excretion. However, owing to the charge separation of sulphur-oxygen linkages in the *S*-oxidized metabolites, it is possible that these metabolites may interact more strongly with proteins and lipids and thereby be retained in the body, delaying their overall excretion. Similar pharmacokinetic results have been described during a study in rats on the bioavailability of vinyldithiins, other transformation products of allicin (Egen-Schwind *et al.* 1992b). These latter compounds are additional transformation products of allicin with elimination half-lives of about 5 h and were detected in many tissues over 24 h, but the maximal serum concentration was observed within the 30 first min after ingestion. In any case, the poor elimination of the sulphone correlates with the persistence of these sulphur compounds in plasma enabling their availability to the organism.

In good agreement with the literature, our study confirms that the liver plays a major role in the *in vivo* fate of DADS not only in terms of metabolism, but also as a storage site. Indeed, the liver was the organ with the highest concentrations of all sulphur compounds (figure 4) and this phenomenon is further highlighted when the organ weight is taken into account. Moreover, the close quantitative and qualitative profiles obtained in the liver, plasma and urine for sulphur compounds strongly suggest that their output from the liver is performed by the plasma, and subsequently to the urine. The well-known poor elimination of sulphone by the kidney before the passing on to urine is also observable in our study by the persistence of these sulphur compounds in plasma.

This study has clearly established the presence of volatile metabolites in several organs after DADS ingestion but the formation of other metabolites cannot be ruled out. In particular, it has been reported that several glutathione conjugates are formed from diallyl sulphide (Jin and Baillie 1997) and dipropyl disulphide (Teyssier and Siess 2000), which could also happen during the DADS metabolic process. Hence, if those conjugates actually exist, it would be of major interest to compare their levels with those of AMSO and $AMSO_2$.

In conclusion, we confirmed that AM and AMS are *in vivo* metabolites of DADS and identified AMSO and $AMSO_2$ as new and predominant metabolites of DADS *in vivo* in rats. Previously, DADS has been assumed to be one of the active components of garlic *in vivo*. Nevertheless, owing to the rapid and extensive hepatic metabolism described herein, there seems to be no systemic bioavailability of DADS after oral administration. Taking into account the time of exposure and quantity of the different metabolites of DADS, the oxidized compounds are

probably involved in the beneficial effects ascribed to garlic. Further studies are needed to assess the biological effects of these metabolites of DADS.

Acknowledgements

The authors thank Etienne Sémon and Joëlle Chevalier for technical assistance. This research was carried out within the framework of the EU Garlic & Health project (QLK1-CT-1999-00498). The authors acknowledge the financial support of the EU.

References

Amagase, H., Petesch, B. L., Matsuura, H., Kasuga, S. and Itakura, Y., 2001, Intake of garlic and its bioactive components. *Journal of Nutrition*, **131**, 955S–962S.

Brady, J. F., Ishizaki, H., Fukuto, J. M., Lin, M. C., Fadel, A., Gapac, J. M. and Yang, C. S., 1991, Inhibition of cytochrome P-450 2E1 by diallyl sulfide and its metabolites. *Chemical Research in Toxicology*, **4**, 642–647.

Egen-Schwind, C., Eckard, R. and Kemper, F. H., 1992a, Metabolism of garlic constituents in the isolated perfused rat liver. *Planta Medica*, **58**, 301–305.

Egen-Schwind, C., Eckard, R., Jekat, F. W. and Winterhoff, H., 1992b, Pharmacokinetics of vinyldithiins, transformation products of allicin. *Planta Medica*, **58**, 8–13.

Furniss, B. S., Hannaford, A. J., Smith, P. W. G. and Tatchell, A. R., 1989, *Vogel's Text Book of Practical Organic Chemistry*, 5th edn (Harlow: Wiley).

Gebhardt, R. and Beck, H., 1996, Differential inhibitory effects of garlic-derived organosulfur compounds on cholesterol biosynthesis in primary rat hepatocyte cultures. *Lipids*, **31**, 1269–1276.

Guyonnet, D., Belloir, C., Suschetet, M., Siess, M. H. and Le Bon, A. M., 2001, Antimutagenic activity of organosulfur compounds from *Allium* is associated with phase II enzyme induction. *Mutation Research*, **495**, 135–145.

Jin, L. and Baillie, T. A., 1997, Metabolism of the chemoprotective agent diallyl sulfide to glutathione conjugates in rats. *Chemical Research in Toxicology*, **10**, 318–327.

Kuttan, G., 2000, Immunomodulatory effect of some naturally occurring sulphur-containing compounds. *Journal of Ethnopharmacology*, **72**, 93–99.

Lawson, L. D. and Wang, Z. J., 1993, Pre-hepatic fate of the organosulfur compounds derived from garlic (*Allium sativum*). *Planta Medica*, **59**, A688–A689.

Le Bon, A. M. and Siess, M. H., 2000, Organosulfur compounds from *Allium* and the chemoprevention of cancer. *Drug Metabolism and Drug Interaction*, **17**, 51–79.

Lea, M. A. and Ayyala, U. S., 1997, Differentiating and growth inhibitory effects of diallyl disulfide on cancer cells. *International Journal of Oncology*, **11**, 181–185.

Martin-Lagos, R. A., Serrano, M. F. and Lopez, M. D. R., 1995, Determination of organic sulphur compounds in garlic extracts by gas chromatography and mass spectrometry. *Food Chemistry*, **53**, 91–93.

Milner, J. A., 2001, A historical perspective on garlic and cancer. *Journal of Nutrition*, **131**, 1027S–1031S.

Mitchell, S. C., 1988, Biological consequences of drug sulphoxidation. *Drug Metabolism and Disposition*, **6**, 245–252.

Mondy, N., Naudin, A., Christides, J. P., Mandon, N. and Auger, J., 2001, Comparison in GC-MS and HPLC in *Allium* volatiles analysis. *Chromatographia*, **53**, S356–S360.

Nickson, R. M., Mitchell, S. C. and Zhang, A. Q., 1995, Fate of dipropyl sulphone in rat. *Xenobiotica*, **25**, 1391–1398.

Pushpendran, C. K., Devasagayam, T. P., Chintalwar, G. J., Banerji, A. and Eapen, J., 1980, The metabolic fate of [^{35}S]-diallyl disulphide in mice. *Experientia*, **36**, 1000–1001.

Reuter, H. D., 1995, *Allium sativum* and *Allium ursinum*: Part 2. Pharmacology and medicinal application. *Phytomedicine*, **2**, 73–91.

Rosen, R. T., Hiserodt, R. D., Fukuda, E. K., Ruiz, R. J., Zhou, Z., Lech, J., Rosen, S. L. and Hartman, T. G., 2001, Determination of allicin, *S*-allylcysteine and volatile metabolites of garlic in breath, plasma or simulated gastric fluids. *Journal of Nutrition*, **131**, 968S–971S.

Sheen, L. Y., Wu, C. C., Lii, C. K. and Tsai, S. J., 1999, Metabolites of diallyl disulfide and diallyl sulfide in primary rat hepatocytes. *Food and Chemical Toxicology*, **37**, 1139–1146.

Socrates, G., 1994, *Infrared Characteristic Group Frequencies. Tables and Charts*, 2nd edn (Chichester: Wiley).

Sundaram, S. G. and Milner, J. A., 1996, Diallyl disulfide induces apoptosis of human colon tumor cells. *Carcinogenesis*, **17**, 669–673.

Teyssier, C., Guenot, L., Suschetet, M. and Siess, M. H., 1999, Metabolism of diallyl disulfide by human liver microsomal cytochromes P-450 and flavin-containing monooxygenases. *Drug Metabolism and Disposition*, **27**, 835–841.

Teyssier, C. and Siess, M. H., 2000, Metabolism of dipropyl disulfide by rat liver phase I and phase II enzymes and by isolated perfused rat liver. *Drug Metabolism and Disposition*, **28**, 648–654.

Williams, K. I., Burstein, S. H. and Layne, D. S., 1966, Metabolism of dimethyl sulfide, dimethyl sulfoxide, and dimethyl sulfone in the rabbit. *Archives of Biochemistry and Biophysics*, **117**, 84–87.

Yang, C. S., Chhabra, S. K., Hong, J. Y. and Smith, T. J., 2001, Mechanisms of inhibition of chemical toxicity and carcinogenesis by diallyl sulfide (DAS) and related compounds from garlic [Review]. *Journal of Nutrition*, **131**, 1041S–1045S.

XENOBIOTICA, 2002, VOL. 32, NO. 12, 1139–1149

Taylor & Francis
healthsciences

Differences in pharmacokinetics and hepatobiliary transport of a novel anti-inflammatory agent between normal and adjuvant arthritis rats

M. ACHIRA, R. TOTSUKA and T. KUME

Discovery Research Laboratory, Tanabe Seiyaku Co., Ltd, 2-2-50 Kawagishi Toda Saitama 335-8505, Japan

Received 27 February 2002

1. The pharmacokinetics, particularly the hepatobiliary transport of T-5557 ((3-methyl-2-oxo-piperadin-3-yl)-acetic acid *N′*-(3-thieophen-2-yl-8-methoxy-quinazolin-1-yl)-hydrazide), a novel anti-inflammatory agent, has been examined in normal and adjuvant arthritis (AA) rats.

2. Following oral administration of T-5557, the absolute bioavailability in AA rats was increased by sixfold compared with normal rats. The extent of binding T-5557 to plasma proteins obtained from AA rats was markedly greater than in normal rats (97.0 versus 88.2%). The biliary clearance in AA rats was significantly lower than that in normal rats (1.186 versus 5.621 ml min^{-1} kg^{-1}), and lower intrinsic biliary clearance was also observed in AA rats (40.33 versus 69.83 ml min^{-1} kg^{-1}).

3. Concomitant administration of T-5557 with quinidine, a potent P-glycoprotein inhibitor, to normal rats caused a significant decrease in the biliary clearance of T-5557 by 37.9%. Moreover, the transport of T-5557 for the apical-to-basal compartment in a Caco-2 cells' monolayer was fourfold lower than that for the opposite direction, and was increased in the presence of quinidine and verapamil.

4. These results suggest that P-glycoprotein is involved in the biliary excretion of T-5557 and the decrease in the transport activity as well as the increase in plasma protein binding caused the elevated plasma concentration and bioavailability of T-5557 in AA rats.

Introduction

Rheumatic diseases are estimated to affect up to 1.1% of the world's population (Harris 1981) and these patients are often treated with steroids, non-steroidal anti-inflammatory drugs (NSAIDs), disease-modifying anti-rheumatic drugs (DMARDs) and/or immunosuppressive drugs. T-5557 (3-methyl-2-oxo-piperadin-3-yl)-acetic acid *N′*-(3-thiophen-2-yl-8-methoxy-quinazolin-1-yl)-hydrazide) (figure 1) has an anti-inflammatory effect on the basis of the inactivation of transcriptional pathways related to nuclear factor-κB (NF-κB), which is thought to play an important role in the inflammatory process. In the development of compounds as anti-rheumatic drugs, adjuvant arthritis (AA) rats have been used as an animal model because they represent a systemic inflammatory disease with bone and cartilage changes similar to those observed in rheumatoid arthritis (Williams *et al*. 1992). The changes in the pharmacokinetics or pharmacological effects in AA rats have been reported, e.g. elevated plasma concentrations of cyclosporine A,

* Author for correspondence; e-mail: m-achira@tanabe.co.jp

Xenobiotica ISSN 0049–8254 print/ISSN 1366–5928 online © 2002 Taylor & Francis Ltd
http://www.tandf.co.uk/journals
DOI: 10.1080/0049825021000017920

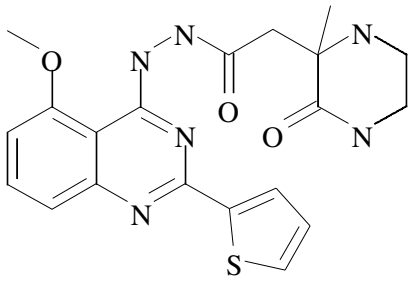


Figure 1. Chemical structure of T-5557.

acebutolol and propranolol (Piquette-Miller and Jamali 1992, 1993, Shibata *et al.* 1993), and prolongation of sleeping time with pentobarbital (Dipasquale *et al.* 1974). The increases of α_1-acid glycoprotein in plasma and the decreases of cytochrome P450 and other hepatic enzymes like UDP-glucuronosyltransferase are well known as being involved in these changes (Bishop *et al.* 1981, Yasuhara *et al.* 1985, Belpaire *et al.* 1989, Toda *et al.* 1994, Meunier and Verbeeck 1999). Buchar and Janku (1985) suggested that AA alters the phospholipid composition of the endoplasmic reticulum in the liver as a result of decreased synthesis of phosphatidylcholine and phosphatidylethanolamine, and that this alteration might lead to an impairment of the function of the microsomal enzymes.

Recently, we confirmed that the hepatobiliary transport of methotrexate and doxorubicin were significantly decreased in AA rats (Achira *et al.* 2000, 2002). Multidrug resistance-associated protein 2 (MRP2) and P-glycoprotein (P-gp) are involved in the hepatobiliary transport of methotrexate and doxorubicin, respectively (Masuda *et al.* 1997, Booth *et al.* 1998), and the expression levels of these transporters are decreased in AA rats (Achira *et al.* 2000). Moreover, in rats treated with lipopolysaccharide (LPS), an animal model for cholestasis, it was reported that the expressions of hepatic P-gp and MRP2 were decreased (Piquette-Miller *et al.* 1998, Nakamura *et al.* 1999). Recently, it has been recognized that the cytokines, such as tumour necrosis factor α (TNFα) and/or interleukin 1 (IL-1) released from activated Kupffer cells, are responsible for the down-regulation of MRP2 in parenchymal hepatocytes (Nakamura *et al.* 1999). Although the mechanism of the down-regulation of these transporters in AA rats is not clear, similar reactions should occur because cytokines such as TNF(and IL-6 in the plasma are elevated in AA rats (Philippe *et al.* 1997).

Thus, the pharmacokinetics of drugs may be altered in AA rats because of the change of metabolism, protein binding and biliary excretion. However, there have been few compounds describing in detail the pharmacokinetic changes in AA rats. In the present study, we have investigated the effect of AA on the pharmacokinetic profile of T-5557, particularly hepatobiliary transport, and confirmed the mechanisms of altered hepatobiliary transport of this compound.

Materials and methods

Chemicals

T-5557 was synthesized at Tanabe Seiyaku Co., with purity > 99.0%. *Mycobacterium butyricum* was purchased from Difco Lab. (Detroit, MI, USA). Verapamil and quinidine were purchased from Sigma Chemical Co. (St Louis, MO, USA). Caco-2 cells were obtained from American Type Culture

Collection (ATCC, Rockville, MD, USA). Transwell® inserts were purchased from Corning-Coaster (Cambridge, MA, USA). All other chemicals were analytical grade.

Animals

Female Lewis rats (8 weeks, approximately 150 g) were purchased from Charles River Japan (Tokyo, Japan) and acclimatized in our laboratory 7 days before experiment. The animals were allowed free access to standard laboratory chow (CE2, Japan Crea, Tokyo, Japan) and water. Rats were gang-housed in rooms with controlled temperature (23°C), humidity (55%) and light cycle (12/12 h). Studies were approved by the Animal Ethics Committee of Tanabe Seiyaku Co., Ltd.

AA was induced by an injection of *M. butyricum* suspended in liquid paraffin (0.5 mg/0.1 ml/animal) into the subplantar region of the right hindpaw. Rats were studied 17–21 days after the adjuvant injection when they had developed swelling of the left hindpaw (secondary inflammation).

Plasma concentrations

For oral administration, a 30 mg kg^{-1} dose (in water) of T-5557 was administered to fasting normal and AA rats via gastric intubation. For intravenous administration, a 3 mg kg^{-1} dose (in isotonic saline) of T-5557 was administered to fed rats via one of the femoral vein under ether anaesthesia. Blood samples (0.3 ml) were taken from the jugular vein at each predetermined time point (5, 15, 30 min, 1, 2, 4 and 8 h after oral administration and 1, 3, 5, 10, 20, 30 min, 1, 2, 4 and 8 h after intravenous administration) using a heparinized syringe and the plasma was separated by centrifugation (3000*g* for 15 min). All samples were stored at −20°C until analysis.

Biliary excretion

Rats were anesthetized with diethyl ether, and a polyethylene tubing (SP10, Natsume, Inc., Tokyo, Japan) was surgically inserted into the common bile duct of each animal and fixed. After the rats had recovered from anaesthesia, aliquots of each dose formulation were injected via femoral vein at a dose of 3 mg kg^{-1} to each rat. The rats were placed individually in Bollman cages (Natsume) after dosing. Bile samples were collected separately in ice-cold glass tubes for 0–1, 1–2, 2–4 and 4–8 h. All samples were stored at −20°C until analysis.

Plasma protein binding

The protein binding of T-5557 in plasma obtained from normal and AA rats was measured by ultracentrifugation at 50 000*g* for 16 h (HIMAC centrifuge SCP85H, Hitachi Koki Co., Ltd, Tokyo, Japan) as described by Gomi *et al.* (1969). Aliquots of the supernatant were sampled as protein-free fractions. Unbound fraction in the plasma was estimated as the ratio of the concentration in protein-free fraction to that before centrifugation. Non-specific binding to the tubes used for ultracentrifugation was negligible.

Effect of quinidine on the biliary excretion

Rats were anaesthetized with diethyl ether and fixed in a supine position on a surface kept at 37°C to maintain normal body temperature. Cannulation (polyethylene tubing, PE50, Becton-Dickinson, Franklin Lake, NJ, USA) was made at a femoral vein for the administration of T-5557, and a bile duct for collecting bile samples. T-5557 was constantly infused via cannula inserted at a femoral vein at a rate of 5 μg/10 μl min^{-1}. The blood and bile samples were collected at 15-min intervals for 90 min as a control phase. After the control-phase study, quinidine was co-infused at a dose of 50 μg/10 μl min^{-1}, and the blood and bile samples were also collected until 180 min as an inhibition phase.

Permeability across Caco-2 cells' monolayer

Transcellular transport studies across a Caco-2 cell monolayer was performed according to the method described by Hunter *et al.* (1993). Caco-2 cells were cultured in Dulbecco's modified Eagle's medium (DMEM) containing 4.5 g l^{-1} glucose, 5% foetal bovine serum (FBS), 0.1 mM non-essential amino acids, 4 mM L-glutamine and antibiotics/antifungal agents in an atmosphere of 95% O_2/5% CO_2. Monolayers of Caco-2 cells formed by incubating the confluent cells for additional 20 days were used for the transcellular transport studies. Each Caco-2 cell monolayer was washed twice with phosphate-buffered saline (PBS) before the pre-incubation for 30 min in DMEM, which contained no FBS. Transcellular transport experiments were initiated by adding T-5557 to the apical or basal side. At 1, 2 and 4 h, aliquots of medium in the receiver side were removed to determine the T-5557 concentration by high-performance liquid chromatography (HPLC). The inhibitor was added to donor side at the same time of T-5557 injection.

High-performance liquid chromatography assay

Concentrations of T-5557 in plasma, bile and Caco-2 cells medium samples were determined by HPLC. An HPLC system (D-7000 Liquid Chromatograph, Hitachi, Tokyo, Japan) was equipped with a variable wavelength UV monitor (L-7400 Hitachi) setting at 290 nm. An ODS column (Mightysil RP-18 (L), 150 $\times$ 4.6 mm i.d., particle size 5 mm; Kanto Chemical, Tokyo, Japan) was used. The mobile phase was a mixture of 10 mM phosphate buffer (pH 6.0) and acetonitrile. A linear gradient of 10–70% acetonitrile over 24 min was used at a flow rate of 1.0 ml min^{-1}. The column temperature was maintained at 40°C.

The plasma samples were deproteinized by adding 1 ml acetonitrile. After centrifugation (10 000*g* for 5 min), supernatant was injected into chromatograph. Bile and Caco-2 cell medium samples were diluted with Hank's balanced salt solution (pH 6.5) and injected directly to the chromatograph. The HPLC method had acceptable accuracy (85–115% of true values) and precision (assay coefficient variations $< 15\%$). Assay specificity was indicated by the absence of interfering chromatographic peaks in plasma and bile samples. Limit of quantification was 30 ng ml^{-1}.

Data analysis

Plasma concentration profiles following oral and bolus intravenous administration were fitted to moment (model-independent) analysis using a non-linear least-squares regression computer program, WinNonlin (Pharsight, Mountain View, CA, USA). Hepatobiliary transport was analysed using a method described by Kato *et al.* (2000). Biliary clearance (CL_{bile}) was obtained from:

$$CL_{bile} = (\text{total amount in the bile})/AUC, \quad (1)$$

where AUC is the area under the plasma concentration profile.

$CL_{bile,int}$ was calculated using equation (2) for a well-stirred model:

$$CL_{bile,int} = CL_{bile} \times Q/(f_p \times (Q - CL_{\text{bile}}/R_b)), \quad (2)$$

where R_b, Q and f_p are the blood-to-plasma concentration ratio, the hepatic blood flow rate (58.8 ml min^{-1} kg^{-1}) (Lin *et al.* 1982) and the unbound fraction in plasma, respectively.

Total body clearance (CL_{tot}) and biliary clearance (CL_{bile}) at steady-state following continuous infusion were calculated using equations (3) and (4), respectively:

$$CL_{tot} = I_0/C_{ss}$$

$$CL_{bile} = V_{\text{bile}}/C_{ss}, \quad (4)$$

where I_0, C_{ss} and V_{bile} are the constant infusion rate (= 5 μg min^{-1}), the plasma concentration at a steady-state and the biliary excretion velocity of T-5557, respectively.

The permeability of T-5557 across the Caco-2 cells' monolayer (P_{app}) was calculated using:

$$P_{app} = dA/dt/S/C_0, \quad (5)$$

where S, C_0 and A are the surface area of the Caco-2 cells' monolayer, the initial concentration of T-5557 in the donor side and the amount of T-5557 transferred to the receiver side, respectively.

Statistical analysis

The results are means $\pm$ SD. A Student's t-test determined the significance of differences between normal and AA rats.

Results

Mean plasma concentration–time curves of T-5557 following oral and intravenous administration to normal and AA rats are shown in figures 2A and B, respectively. Plasma concentrations of T-5557 in AA rats were five- to 10-fold higher than those in normal rats following oral and intravenous administration. The pharmacokinetic parameters derived from both groups of rats are shown in table 1. Following intravenous administration, the elimination of T-5557 from plasma was tri-exponential, with terminal half-lives of 0.79 and 1.26 h for normal and AA rats, respectively. In AA rats, the terminal half-life of T-5557 was prolonged. C_0 and AUC in AA rats were much higher than those in normal rats, giving total clearances (CL_{tot}) of 17.84 and 2.81 ml min^{-1} kg^{-1} in normal and

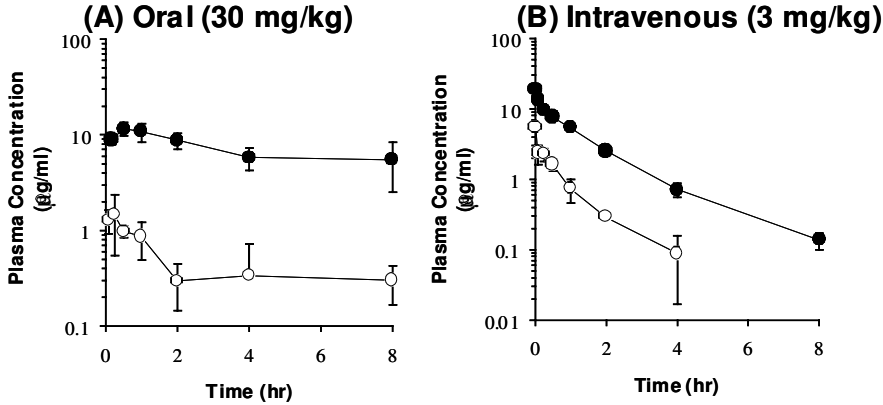


Figure 2. Plasma concentration of T-5557 following oral (A) and intravenous (B) administration to normal and adjuvant arthritis (AA) rats. Data are the mean $\pm$ SD $(n = 3)$; ○, normal rats; ●, AA rats.

Table 1. Pharmacokinetic parameters of T-5557 in normal and adjuvant arthritis (AA) rats.

Parameter	Normal	AA
Oral administration	(30 mg kg^{-1})	(30 mg kg^{-1})
C_{max} (μg ml^{-1})	1.58 $\pm$ 0.75	11.60 $\pm$ 1.84[a]
$AUC_{0-\infty}$ (μg h ml^{-1})	1.94 $\pm$ 0.50	77.35 $\pm$ 3.15[a]
CL_{oral} (ml min^{1} kg^{-1})	283 $\pm$ 74	6.47 $\pm$ 0.26[a]
MRT (h)	1.51 $\pm$ 0.38	7.21 $\pm$ 1.53[a]
Bioavailability (%)	6.89 $\pm$ 1.65	43.44 $\pm$ 0.25[a]
Intravenous administration	(3 mg kg^{-1})	(3 mg kg^{-1})
C_0 (μg ml^{-1})	6.88 $\pm$ 0.08	21.13 $\pm$ 1.84[a]
$t_{1/2\lambda}$ (h)	0.79 $\pm$ 0.29	1.26 $\pm$ 0.07[b]
$AUC_{0-\infty}$ (μg h ml^{-1})	2.82 $\pm$ 0.24	17.81 $\pm$ 0.77[a]
$V_{d,ss}$ (l kg^{-1})	1.11 $\pm$ 0.39	0.25 $\pm$ 0.01[a]
CL_{tot} (ml min^{-1} kg^{-1})	17.84 $\pm$ 1.45	2.81 $\pm$ 0.12[a]
MRT (h)	1.02 $\pm$ 0.30	1.50 $\pm$ 0.08

Data are means $\pm$ SD $(n = 3)$; [a,b] significant difference from normal rats at $p < 0.01$ and < 0.05, respectively.

C_{max}, maximum concentration; AUC, area under the plasma concentration curve; CL_{oral}, oral clearance; MRT, mean resident time; C_0, concentration at time 0; $V_{d,ss}$, distribution volume at a steady-state; CL_{tot} total clearance.

AA rats, respectively. The volume of distribution ($V_{d,ss}$) in AA rats was extremely low (0.25 l kg^{-1}), as compared with normal rats (1.11 l kg^{-1}).

Following oral administration of T-5557, the C_{max} and AUC in AA rats were markedly higher than those in normal rats. Based on the comparison of AUC following oral and intravenous dosing, the bioavailability in normal and AA rats were estimated as 6.89 and 43.44%, respectively.

It is well known that the inflammatory disease process changes the binding ratios of some drugs to plasma protein, so we investigated the effect of AA on the plasma protein binding of T-5557 (table 2). The plasma protein binding of T-5557 in AA rats was increased significantly to 97.0% compared with approximately 90% in normal rat plasma.

Table 2. Plasma protein binding of T-5557 in normal and adjuvant arthritis (AA) rats.

Concentration ($\mu g\,ml^{-1}$)	Normal (%)	AA (%)
3	91.1 ± 0.32	–
30	88.2 ± 0.71	97.0 ± 0.06[a]

Data are means $\pm$ SD ($n = 3$); – not tested; [a] Significant difference from normal rats at $p < 0.01$.

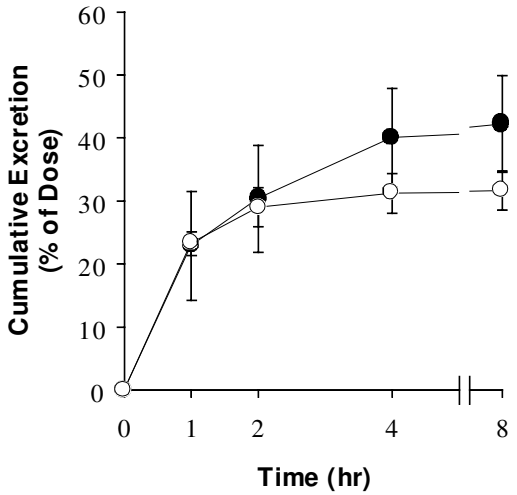


Figure 3. Cumulative biliary excretion of T-5557 following intravenous administration to normal and adjuvant arthritis (AA) rats. Data are the mean $\pm$SD ($n = 3$); ○, normal rats; ●, AA rats.

Table 3. Biliary clearance (CL_{bile}) and intrinsic biliary clearance ($CL_{bile,int}$) of T-5557 in normal and adjuvant arthritis (AA) rats.

	Normal	AA
CL_{bile} ($ml\,min^{-1}\,kg^{-1}$)	5.621 ± 0.543	1.185 ± 0.215[a]
$CL_{bile,int}$ ($ml\,min^{-1}\,kg^{-1}$)	69.83 ± 6.106	40.33 ± 7.157[a]

Data are means $\pm$ SD ($n = 3$); [a] significant difference from normal rats at $p = 0.01$.

The cumulative excretion of T-5557 into bile following intravenous administration ($3\,mg\,kg^{-1}$) to bile duct-cannulated normal and AA rats are shown in figure 3. Within 8 h, 31.65 ± 3.06 and 42.22 ± 7.65% of the dose were excreted as unchanged drug in the bile following intravenous administration of T-5557 to normal and AA rats, respectively. The biliary clearance (CL_{bile}) and its intrinsic clearance ($CL_{bile,int}$) estimated by using equations (1) and (2) are shown in table 3. Although a significant difference in the cumulative excretion of T-5557 into bile was not observed between normal and AA rats, CL_{bile} and $CL_{bile,int}$ in AA rats were significantly lower than those in normal rats.

To examine the possible involvement of active transporters in the hepatobiliary transport of T-5557, the effect of quinidine, a potent P-gp inhibitor (Su and

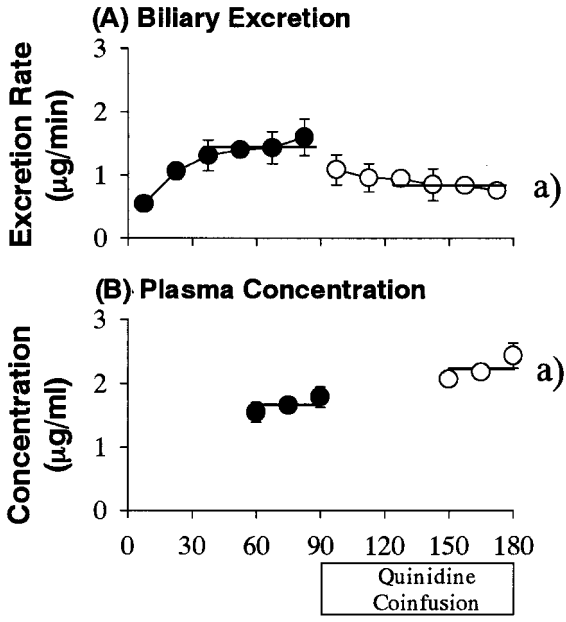


Figure 4. Biliary excretion rate (A) and plasma concentration (B) of T-5557 following continuous infusion of T-5557 to normal rats. Data are the mean ± SD ($n = 3$); ●, absence of quinidine; ○, presence of quinidine; [a]significant difference from the absence of quinidine at $p < 0.05$.

Table 4. Effect of quinidine on the total clearance (CL_{tot}) and biliary clearance (CL_{bile}) of T-5557 in normal rats.

	Quinidine absence	Quinidine presence
CL_{tot} (ml min^{-1} kg^{-1})	13.4 ± 0.51	9.86 ± 0.23[a]
CL_{bile} (ml min^{-1} kg^{-1})	4.09 ± 0.84	1.55 ± 0.12[a]

Data are means ± SD ($n = 3$); [a] significant difference from the absence of quinidine at $p < 0.01$.

Huang 1996), on the biliary excretion of T-5557 in rats was investigated. The time courses of biliary excretion rate and plasma concentration of T-5557 before and after co-administration of quinidine are shown in figure 4. The biliary excretion rate of T-5557 reached steady-state within 60 min after infusion, and quinidine inhibited the biliary excretion of T-5557. CL_{tot} and CL_{bile} were significantly decreased to 73.3 and 44.3% in the presence of quinidine, respectively (table 4).

Figure 5 shows the transcellular transport of T-5557 across Caco-2 cell monolayers and was linear up to 4 h (data not shown). The apparent permeability coefficient (P_{app}) for the basal-to-apical compartment (30.6×10^{-6} cm s^{-1}) was fourfold higher than that in the opposite direction (7.40×10^{-6} cm s^{-1}) (figure 5A). The apical-to-basal flux (absorptive direction) was significantly increased in the presence of 100 μM verapamil and quinidine (figure 5B), suggesting that T-5557 was a good P-gp substrate.

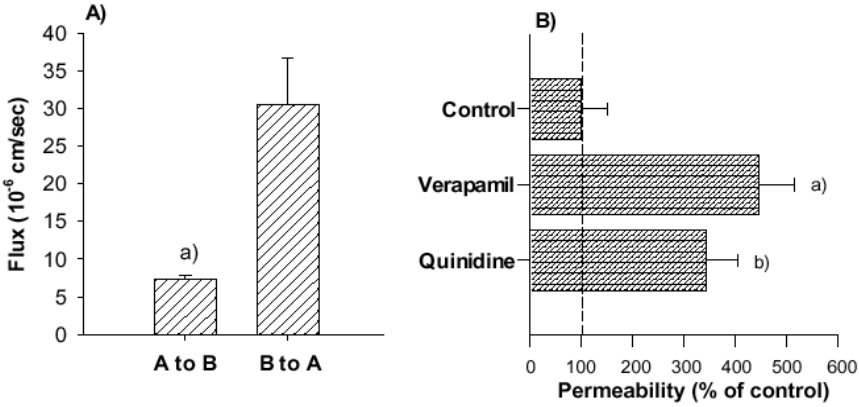


Figure 5. Permeability of T-5557 across Caco-2 cells' monolayers. (A) Direction of T-5557 across Caco-2 cells' monolayers, [a]significant difference from the permeability across basal-to-apical compartment at $p < 0.01$; A to B, apical-to-basal; B to A, basal-to-apical. (B) Effects of P-gp inhibitors on the permeability of T-5557 across apical-to-basal compartment in Caco-2 cells' monolayers, [a,b]significant difference from control at $p < 0.01$ and $p < 0.05$, respectively. Data are the mean SD from three determinations.

Discussion

AA rats are often used as an animal model for rheumatoid arthritis. We have previously reported that the transport activity and expression level of transporter protein in canalicular membrane such as P-gp and multidrug resistance-associated protein 2 (MRP2) were changed in AA rats (Achira *et al.* 2000, 2002). These transporters in addition to plasma protein binding and metabolism play important roles in the determination of pharmacokinetics of drugs, and the altered activity of these transporters may cause the change of pharmacokinetics and pharmacological effects. In the current study, we have investigated the effect of AA on the pharmacokinetics T-5557, which is currently being developed for the treatment of rheumatoid arthritis and in particular hepatobiliary transport.

Marked increases in the plasma concentration of unchanged T-5557 following oral and intravenous administration were observed in AA rats. Both the total clearance (CL_{tot}) and distribution volume ($V_{d,ss}$) of T-5557 in AA rats were significantly lower than those in normal rats (table 1). As plasma protein binding has often an effect on these parameters, it was suggested that the difference in the plasma protein-binding ratio of T-5557 was responsible for the change of pharmacokinetics of T-5557 in AA rats. In fact, the plasma protein binding ratio of T-5557 in AA rats was 97.0% and significantly higher than that in normal rats (88.2–91.1%) (table 2), indicating that the unbound plasma fraction in normal rats was three- to fourfold higher than that in AA rats. Not only albumin, but also α_1-acid glycoprotein which might increase depending on the inflammation, was expected to bind to T-5557. It has been reported that the oral clearance of drugs in AA rats is significantly decreased due to the increased level of α_1-acid glycoprotein (Bishop *et al.* 1981). Moreover, in Croon disease patients, this more serious disease condition (i.e. the increased level of α_1-acid glycoprotein) causes the more increased plasma concentration of propranolol (Schneider *et al.* 1979). In addition to plasma protein binding, hepatic metabolic activity was changed in inflammation disease (Schneider *et al.* 1979, Piquette-Miller and Jamali 1992, 1993). Although

the piperidine ring was oxidized in liver microsomes prepared from normal rats (data not shown), the extent of metabolism was very low. Thus, T-5557 was metabolically stable in the liver microsomes and the contribution of metabolism by cytochrome P450 must be relatively low in normal rats as well as AA rats, though the involvement of other metabolic enzymes on the metabolism of T-5557 are still unclear.

We investigated the hepatobiliary transport of T-5557 following intravenous administration (figure 3 and table 3). Although the biliary excretion of T-5557 in AA rats tended to be higher than that in normal rats, no significant difference was observed. Because there was a fivefold difference on the values for AUC, biliary clearance in AA rats was significantly lower compared with that in normal rats. There was no difference in hepatic blood flow rate between normal and AA rats (Achira *et al*. 2002), and the intrinsic biliary clearance estimated by considering plasma protein binding and hepatic blood flow rate in AA rats was also lower than that in normal rats. These results suggest that the decreased biliary clearance was due to not only the increase of plasma protein binding, but also a decrease in biliary excretion. We have previously reported the down-regulation of hepatic P-gp and MRP2 in AA rats (Achira *et al*. 2000, 2002), we therefore examined whether T-5557 is a substrate for these transporters. The biliary clearance of T-5557 in normal rats was significantly lowered by quinidine, which is a potent P-gp inhibitor (table 4). Moreover, the permeability of T-5557 across Caco-2 cell monolayer was unidirectional, and the permeability of T-5557 across the apical-to-basal compartment was increased in the presence of quinidine and verapamil, the latter also being a potent P-gp inhibitor (figure 5). These results suggest that T-5557 was excreted into the bile via P-gp and the reduction of the expression of hepatic P-gp protein causes the significant decrease in the biliary excretion of T-5557 in AA rats.

Although the mechanism of down-regulation of P-gp in AA rats has not fully been clarified, cytokines such as tumour necrosis factor α(TNFα) and interleukin 6 (IL-6) may be involved because their levels are elevated in AA rat plasma (Philippe *et al*. 1997). Additionally, it has also been reported that TNF(causes the down-regulation of P-gp in human carcinoma cells (Borsellino *et al*. 1994, Varga *et al*. 1996).

The difference in plasma concentration between normal and AA rats following oral administration was larger than that following intravenous administration, and the bioavailability of T-5557 in AA rats was substantially increased compared with that in normal rats (43.44 versus 6.89%). Because total clearance and biliary clearance were much lower than hepatic blood flow even in normal rats, the contribution of hepatic first-pass elimination (metabolic and biliary) to the bioavailability must be low. Thus, it is suggested that the intestinal absorption is also altered in AA rats. P-gp, which essentially functions as an absorption barrier, is also localized in epithelial cells in the intestine (Terao *et al*. 1996). The intestinal P-gp, however, would have no effect on the altered intestinal absorption in AA rats, because we previously reported that the activity of intestinal P-gp was not altered in AA rats (Achira *et al*. 2000). Other factors are very likely to be involved in the altered intestinal absorption in AA rats. The mean absorption time ($MAT = MRT_{p.o.} - MRT_{i.v.}$, where MRT is mean resident time) in AA rats was significantly longer than that in normal rats, suggesting that other factors such as

the intestinal motility may affect bioavailability in AA rats. Further work is needed to interpret the elevation of bioavailability in AA rats.

In conclusion, AA rats are a useful animal model for rheumatoid arthritis, but the change of the P-gp activity as well as plasma protein binding and hepatic metabolism must be considered in future studies. Although there is no information available on the expression and activity of P-gp in patients with rheumatoid arthritis, our results suggest that altered drug pharmacokinetics are a possibility.

References

Achira, M., Totsuka, R., Fujimura, H. and Kume, T., 2002, Tissue-specific regulation of P-glycoprotein in adjuvant arthritis rats. *European Journal of Pharmaceutical Science*, **16**, 29–36.

Achira, M., Totsuka, R., Fujimura, H. and Kume, T.Yoshikawa, M., 2000, Effect of adjuvant arthritis on the activity of the P-glycoprotein in the liver. Paper presented at the Annual Meeting of Japanese Society for the Study of Xenobiotics.

Belpaire, F. M., Smet, F. De, Chindavijak, B., Fraeyman, N. and Bogaert, M. G., 1989, Effect of turpentine-induced inflammation on the disposition kinetics of propranolol, metoprolol and antipyrine in the rat. *Fundamental of Clinical Pharmacology*, **3**, 79–88.

Bishop, H., Schneider, R. E. and Welling, P., 1981, Plasma propranolol concentrations in rats with adjuvant-induced arthritis. *Biopharmakinetics and Drug Disposition*, **2**, 291–297.

Booth, C. L., Brouwer, K. R. and Brouwer, K. L. R., 1998, Effect of multidrug resistance modulators on the hepatobiliary disposition of doxorubicin in the isolated perfused rat liver. *Cancer Research*, **58**, 3641–3648.

Borsellino, N., Crescimanno, M., Flandina, C., Flugy, A. and D'Alessandro, N., 1994, Combined activity of interleukin-1alpha or TNF-alpha and doxorubicin on multidrug resistant cell lines: evidence that TNF and DXR have synergistic antitumor and differentiation-inducing effects. *Anticancer Research*, **14**, 2643–2548.

Buchar, E. and Janku, I., 1985, The effect of adjuvant-induced arthritis on rat liver microsomal phospholipid metabolism. *Methods and Findings in Experimental and Clinical Pharmacology*, **7**, 469–472.

Dipasquale, G., Welaj, P. and Rassaert, C. L., 1974, Prolonged pentobarbital sleeping time in adjuvant-induced polyarthritic rats. *Research Communications in Chemical Pathology and Pharmacology*, **9**, 253–264.

Gomi, J., Aoyagi, T., Oana, M., Mitsuno, Y., Kawai, T., Yamada, Y. and Yamada, Y., 1969, Studies on flucloxacillin binding rate and capacity to horse serum protein. *Chemotherapy*, **17**, 1363–1366.

Harris, E. D., 1981, Rheumatoid arthritis; the clinical spectrum. In *Textbook of Rheumatology* (Philadelphia: W. B. Saunders), pp. 928–963.

Hunter, J., Hirst, B. H. and Simmons, N. L., 1993, Drug absorption limited by P-glycoprotein-mediated secretory drug transport in human intestinal epithelial Caco-2 cell layers. *Pharmacology Research*, **10**, 743–742.

Kato, Y., Yamazaki, M. and Sugiyama, Y., 2000, Biliary excretion. In *Sohgo Seizaigaku* (Tokyo: Nanzando), pp. 112–128.

Lin, J. H. Sugiyama, Y., Awazu, S. and Hanano, M., 1982, *In vitro* and *in vivo* evaluation of the tissue-to-blood partition coefficient for physiological pharmacokinetic models. *Journal of Pharmacokinetics and Biopharmacology*, **10**, 637–647.

Masuda, M., Iizuka, Y., Yamazaki, M., Nishigaki, R., Kato, Y., Ni'inuma, K., Suzuki, H. and Sugiyama, Y., 1997, Methotrexate is excreted into the bile by canalicular multispecific organic anion transporter in rats. *Cancer Research*, **57**, 3506–3510.

Meunier, C. J. and Verbeeck, R. K., 1999, Glucuronidation of *R*- and *S*-ketoprofen, acetoaminophen, and diflunisal by liver microsomes of adjuvant-induced arthritic rats. *Drug Metabolism and Disposition*, **27**, 26–31.

Nakamura, J., Nishida, T., Hayashi, K., Kawada, N., Ueshima, S., Sugiyama, Y., Ito, T., Sobue, K. and Matsuda, H., 1999, Kupffer cell-mediated down regulation of rat hepatic cMOAT/MRP2 gene expression. *Biochemical and Biophysical Research Communications*, **255**, 143–149.

Philippe, L., Gegout-Pottie, P., Guingamp, C., Bordji, K., Terlain, B., Netter, P. and Gillet, P., 1997, Relations between functional, inflammatory, and degenerative parameters during adjuvant arthritis in rats. *American Journal of Physiology*, **273**, R1550–R1556.

Piquette-Miller, M. and Jamali, F., 1992, Effect of adjuvant arthritis on the disposition of acebutolol enantiomer in rats. *Agent Actions*, **37**, 290–296.

Piquette-Miller, M. and Jamali, F., 1993, Selective effect of adjuvant arthritis on the disposition of propranolol enantiomer in rats detected using a stereospecific HPLC assay. *Pharmacology Research*, **19**, 294–299.

Piquette-Miller, M., Pak, A., Kim, H., Anart, R. and Shanhzamanti, A., 1998, Decreased expression and activity of P-glycoprotein in rat liver during acute inflammation. *Pharmacology Research*, **15**, 706–711.

Schneider, R. E, Bishop, H. and Hawkins, C. F., 1979, Plasma propranolol concentrations and the erythrocyte sedimentation rate. *British Journal of Clinical Pharmacology*, **8**, 43–47.

Shibata, N., Shimakawa, H., Minouchi, T. and Yamaji, A., 1993, Pharmacokinetics of cyclosporin A after intravenous administration to rats in various disease states. *Biology and Pharmacology Bulletin*, **16**, 1130–1135.

Su, S. F. and Huang, J. D., 1996, Inhibition of the intestinal digoxin absorption and exsorption by quinidine. *Drug Metabolism and Disposition*, **24**, 142–147.

Terao, T., Hisanaga, E., Sai, Y., Tamai, I. and Tsuji, A., 1996, Active secretion of drugs from the small intestinal epithelium in rats by P-glycoprotein functioning as an absorption barrier. *Journal of Pharmaceutics and Pharmacology*, **48**, 1083–1089.

Toda, A., Ishii, N., Kihara, T., Nagamatsu, A. and Shimeno, H., 1994, Effects of adjuvant-induced arthritis on hepatic drug metabolism in rats. *Xenobiotica*, **26**, 603–611.

Varga, A., Nugel, H., Baehr, R., Marx, U., Hevér, A., Nacsa, J., Ocsovszky, I. and Molnar, J., 1996, Reversal of multidrug resistance by amitriptyline *in vitro*. *Anticancer Research*, **16**, 209–212.

Williams, R. O., Feldmann, M. and Maini, R. N., 1992, Anti-tumor necrosis factor ameliorates joint disease in murine collagen-induced arthritis. *Proceedings of the National Academy of Sciences, USA*, **89**, 9784–9788.

Yasuhara, M., Fujiwara, J., Kitade, S., Katayama, H., Okumura, K. and Hori, R., 1985, Effect of altered plasma protein on pharmacokinetics and pharmacodynamics of propranolol in rats after surgery. *Journal of Pharmacology and Experimental Therapeutics*, **235**, 513–520.

XENOBIOTICA, 2002, VOL. 32, NO. 12, 1151–1160

Taylor & Francis
healthsciences

Decreased hepatobiliary transport of methotrexate in adjuvant arthritis rats

M. ACHIRA, R. TOTSUKA, H. FUJIMURA and T. KUME

Discovery Research Laboratory, Tanabe Seiyaku Co., Ltd, 2-2-50 Kawagishi Toda Saitama 335-8505, Japan

Received 27 February 2002

1. We investigated the difference in hepatobiliary transport of methotrexate in normal and adjuvant arthritis (AA) rats and substantiated the expression level of multidrug resistance-associated protein 2 (MRP2) in the liver.

2. Biliary clearance of methotrexate in normal and AA rats was calculated from plasma concentrations and biliary excretion following intravenous infusion and hepatic uptake clearance was estimated from an integration plot using methotrexate concentrations in plasma and liver.

3. Biliary clearance of methotrexate in AA rats was $2.30 \pm 0.23\,ml\,min^{-1}\,kg^{-1}$ (mean SD) and significantly lower than in normal rats ($8.42 \pm 0.81\,ml\,min^{-1}\,kg^{-1}$). The uptake clearance of methotrexate in AA rats was also lower than in normal rats (0.138 versus $0.278\,ml\,min^{-1}\,g\,liver^{-1}$).

4. MRP2 in the liver was detected by fluorescein isothiocyanate-labelled antibody and visualized using a confocal laser microscope system. The expression level of MRP2 in AA rats was very low compared with normal rats, indicating a down-regulation in AA rats.

5. In conclusion, biliary clearance of methotrexate was decreased due to the lower activities in both uptake and canalicular secretion, suggesting that several active transporters in the liver, including MRP2, are down-regulated in AA rats.

Introduction

Rheumatic diseases are estimated to affect up to 1.1% of the world's population (Harris 1981) and patients are often treated with non-steroidal anti-inflammatory drugs (NSAIDs), disease-modifying anti-rheumatic drugs (DMARDs) and/or immunosuppressive drugs. Adjuvant arthritis (AA) rats have been used as an animal model for rheumatoid arthritis because they represent a systemic inflammatory disease with bone and cartilage changes similar to those observed in rheumatoid arthritis (Williams *et al.* 1992). The changes in the pharmacokinetics or pharmacological effects in AA rats have been reported, e.g. elevated plasma concentration of cyclosporine A, acebutolol and propranolol (Piquette-Miller and Jamali 1992, 1993, Shibata *et al.* 1993), and prolongation of sleeping time with pentobarbital (Dipasquale *et al.* 1974). Changes in the levels of albumin and α_1-acid glycoprotein in plasma and in the activities of cytochrome P450 and other hepatic enzymes such as UDP-glucuronosyltransferase are involved in these changes (Bishop *et al.* 1981, Yasuhara *et al.* 1985, Belpaire *et al.* 1989, Toda *et al.* 1994, Meunier and Verbeeck 1999). Buchar and Janku (1985) suggested that AA alters the phospholipid composition of the endoplasmic reticulum in the liver as a result of decreased synthesis of phosphatidylcholine and phosphatidylethanol-

* Author for correspondence; e-mail: m-achira@tanabe.co.jp

Xenobiotica ISSN 0049–8254 print/ISSN 1366–5928 online © 2002 Taylor & Francis Ltd
http://www.tandf.co.uk/journals
DOI: 10.1080/0049825021000017939

amine, and that this alteration may lead to an impairment of the function of the microsomal enzymes. Altered plasma protein binding and metabolism have been the main focus in the studies on changes of pharmacokinetics in AA rats to date.

In addition to hepatic metabolism, urinary and biliary excretion are the major pathways involved in the removal of xenobiotics. Recently, it was reported that carrier-mediated transport contributes to hepatic uptake, biliary excretion and urinary excretion (He *et al*. 1991, Masuda *et al*. 1997, Booth *et al*. 1998). In particular, active transport mechanisms have been shown to be responsible for the biliary excretion of anticancer drugs and organic anions including glutathione and glucuronic acid conjugates. However, little has been reported about the effects of AA on the activity and expression of active transport mechanisms.

Methotrexate is commonly used as a DMARD in rheumatoid arthritis and 72% of the dose is excreted into the bile of male rats (Masuda *et al*. 1997). Active transporters are involved in the hepatic uptake of methotrexate and these transporters are ATP- and/or Na+-dependent (Honscha and Petzinger 1999). On the other hand, the secretion of methotrexate on the bile canalicular membrane is greatly reduced in Eisai hyperbilirubinemic rats, which have a hereditary deficiency in multidrug resistance-associated protein 2 (MRP2) (Masuda *et al*. 1997). Saturable kinetics with ATP-dependence were found in its uptake by canalicular membrane vesicles obtained from Sprague–Dawley rats but not from Eisai hyperbilirubinemic rats (Masuda *et al*. 1997). Thus, MRP2 seems to be predominantly involved in methotrexate secretion at the bile canalicular membrane.

In the current study, we have investigated the effects of AA on the pharmacokinetics of methotrexate, especially hepatobiliary transport of methotrexate *in vivo*, and substantiated the expression level of MRP2 using immunohistochemical methods.

Materials and methods

Chemicals and reagents

Methotrexate was purchased from Sigma Chemical Co. (St Louis, MO, USA). *Mycobacterium butyricum* was purchased from Difco Lab. (Detroit, MI, USA). M_2III-6, an anti-MRP2 antibody and fluorescein isothiocyanate-labelled anti-mouse IgG antibody (rat adsorbed) were purchased from Kamiya Biomedical Co. (Tokyo, Japan) and Vector Laboratory, Inc. (Burlingame, CA, USA), respectively. M_2III-6 reacts with an internal epitope of human and rat MRP2 and the immunogen is a bacterial fusion protein of MRP2 containing the 202-amino acid C-terminal end of the protein. Other reagents used were of analytical grade.

Animals

Female Lewis rats (8 weeks, about 120–150 g body weight) were purchased from Charles River Japan (Tokyo, Japan). The animals were allowed free access to standard laboratory chow (CE2, Japan Crea, Tokyo, Japan) and water. Studies were approved by the Animal Ethics Committee of Tanabe Seiyaku Co., Ltd.

AA was induced by an injection of *M. butyricum* suspended in liquid paraffin (5 mg ml^{-1}) into the subplantar region of right hindpaw at a dose of 0.1 ml/rat.

Biliary excretion in constant rate intravenous infusion

Rats were lightly anesthetized with ether, and the right femoral vein and bile duct were cannulated with polyethylene tubing (PE50 and PE10, respectively, Becton-Dickinson, Franklin Lake, NJ, USA). The rats received methotrexate by continuous intravenous infusion at a rate of 10 nmol min^{-1} via the right femoral vein for 120 min. The blood and bile samples were collected at 15-min intervals for 120 min. At the end of the infusion, the rats were exsanguinated by bleeding from the carotid artery.

The abdomen was opened immediately and the liver rapidly excised and homogenized to determine its methotrexate concentration.

Hepatic uptake clearance

Following intravenous bolus administration of methotrexate at a dose of 6.6 μmol kg^{-1}, blood samples were collected at 1, 2, 2.5, 3 and 5 min. The rats were killed at the designated times and the liver excised and homogenized to measure its methotrexate concentration. When the hepatic uptake is measured within a short period, during which the efflux and/or elimination of methotrexate from the liver are negligible, the hepatic uptake at time t is proportional to AUC_{0-t}. By dividing $C_{H,t}$ and AUC_{0-t} by $C_{p,t}$, CL_{uptake} was obtained from the slope of the plot of $C_{H,t}/C_{p,t}$ (i.e. liver/plasma concentration ratio at time t, in ml g^{-1} liver) versus $AUC_{0-t}/C_{p,t}$ (Murata *et al.* 1998).

Protein binding

Protein binding in plasma, determined by an ultrafiltration method, was determined as described by Lin *et al.* (1982). After removing the liver from normal and AA rats, liver homogenates (10, 20, 30 and 40% w/v) were prepared in Hank's balanced buffer solution (pH 7.4). Protein binding in each homogenate samples was determined by ultrafiltration and extrapolated to the value in 100% homogenate.

HPLC assay

Concentrations of methotrexate in plasma, bile and liver homogenate samples were determined by high-performance liquid chromatography as described by Masuda *et al.* (1997) with slight modifications. A high-performance liquid chromatograph (D-7000 Liquid Chromatograph; Hitachi, Tokyo, Japan) was equipped with a variable wavelength UV monitor (L-7400 Hitachi) set at 303 nm. An ODS column (Symmetry C18, 250 × 4.6 mm i.d., particle size 5 μm; Waters, Milford, MA, USA) was used, and the mobile phase was a mixture of acetonitrile and 20 mM ammonium acetate, 7:93 (v/v). The flow rate was 1.0 ml min^{-1}.

Samples were deproteinized by adding 1 M $HClO_4$ containing aminopterin (2.1 nmol) as an internal standard. After centrifugation (10 000*g* for 5 min), supernatant was injected into chromatograph. The HPLC method had acceptable accuracy (85–115% of true values) and precision (assay coefficient variations < 15%). Assay specificity was indicated by the absence of interfering chromatographic peaks in plasma, bile and liver homogenate samples. The limit of quantification was 0.22 nmol ml^{-1} or nmol g liver^{-1}.

Immunodetection

Rats were exsanguinated by bleeding from the carotid artery; the livers were then excised and embedded in cryoprotectant medium (Tissue-Tek O.C.T. Compound, Miles, Inc., West Haven, CT, USA) on dry ice for immunohistochemistry.

After blocking with skimmed milk (Block Ace, Dainippon Pharmaceutical, Osaka, Japan) for 30 min, the cryocut sections of livers were incubated with anti-MRP2 (M_2III-6) antibody at 4°C overnight, followed by fluorescein isothiocyanate labelled anti-mouse IgG antibody for 2 h at room temperature. Confocal imaging was performed using a Leica TCS-NT confocal scanning microscope.

Data analysis

For continuous infusion, the total body clearance (CL_{tot}) and biliary clearance ($CL_{bile,p}$) were obtained from the following equations, respectively:

$$CL_{\mathrm{tot}} = \mathrm{dose}/C_{\mathrm{p,ss}} \quad (1)$$

$$CL_{\mathrm{bile,p}} = V_{\mathrm{bile,ss}}/C_{\mathrm{p,ss}}, \quad (2)$$

where $C_{p,ss}$ and $V_{bile,ss}$ are the plasma concentration and biliary excretion velocity at steady-state.

$CL_{bile,int,all}$ was calculated using equation (3) for a well-stirred model:

$$CL_{bile,int,all} = CL_{bile,p} \times Q/(f_p \times (Q - \mathrm{CL}_{\mathrm{bile,p}}/R_b)), \quad (3)$$

where Q and R_b are the hepatic blood flow rate and blood-to-plasma concentration ratio $(= 1.0)$, respectively.

$CL_{bile,int}$ was calculated as follows:

$$CL_{bile,int} = V_{\mathrm{bile,ss}}/(C_{\mathrm{H,ss}} \times f_{\mathrm{H}}). \quad (4)$$

PS_{inf} was calculated using equation (5) for a well-stirred model:

$$PS_{inf} = CL_{uptake} \times Q/(f_{\mathrm{p}} \times (Q - \mathrm{CL}_{\mathrm{uptake}}/R_b)). \quad (5)$$

Statistical analysis

Results are means $\pm$ SD A Student's *t*-test determined the significance of differences between normal and AA rats.

Results

Rats developed swelling of the left hindpaw (secondary inflammation) approximately 17–21 days after adjuvant injection (data not shown) and were used as AA rats. The plasma concentration–time profile curves of methotrexate in normal and AA rats following continuous intravenous infusion at a constant rate are shown in figure 1A. The plasma concentration of methotrexate reached steady-state at approximately 75 min after the initiation of the intravenous infusion in both groups of rats. The mean plasma concentration at a steady-state in AA rats was twofold higher than that observed in normal rats.

The methotrexate concentration in the liver at the end of continuous infusion in AA and normal rats are shown in figure 1B and there was no significant difference in AA rats.

The biliary excretion velocities of methotrexate in normal and AA rats following continuous infusion are shown in figure 1C and also reached steady-state at approximately 75 min after the initiation of the infusion, corresponding to the time profile of the plasma concentrations. The mean biliary excretion velocity in normal rats was 0.818 ± 0.036 nmol min^{-1} g liver^{-1} (about 6 nmol min^{-1}/rat) at steady-state. By comparison, the mean biliary excretion velocity in AA rats was markedly lower (0.363 ± 0.047 nmol min^{-1} g^{-1} liver). The total clearance (CL_{tot}) and biliary clearance defined in terms of plasma concentration ($CL_{bile,p}$) in AA rats were two- and fourfold lower than those found in normal rats, respectively (table 1).

The unbound fraction ratio of methotrexate to plasma and liver protein are shown in table 2. The unbound fraction of methotrexate to the plasma of AA rats was significantly lower than that of normal rats. The ratio of bound methotrexate concentration to unbound methotrexate concentration in the liver homogenate increased proportionally with protein concentration and was extrapolated to the value in the 100% homogenate to calculate the unbound fraction ratio to liver protein. There was no significant difference in the unbound fraction of metho-

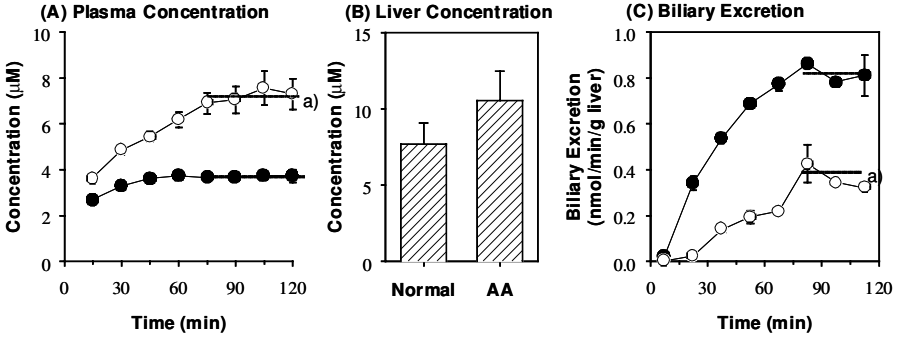


Figure 1. Plasma concentration (A), hepatic concentration at the end of the infusion (B) and biliary excretion velocity (C) of methotrexate following continuous infusion at a constant rate (10 nmol_min^{-1}) to normal and AA rats. Data are the mean $\pm$ SD ($n = 3$); ●, normal rats; ○, AA rats. [a]Significant difference from normal rats ($p < 0.01$).

Table 1. Total clearance (CL_{tot}) and biliary clearance ($CL_{biel,p}$) following continuous infusion at a constant rate to normal and AA rats.

	Normal rats	AA rats	p
CL_{tot} (ml min^{-1} kg^{-1})	18.4 ± 0.68	10.0 ± 0.80	< 0.01
$CL_{bile,p}$ (ml min^{-1} kg^{-1})	8.42 ± 0.81	2.30 ± 0.23	< 0.01

Data are the mean $\pm$ SD $(n = 3)$. CL_{tot} and $CL_{bile,p}$ were calculated as described in the Materials and methods.

Table 2. Unbound fraction ratios of methotrexate to plasma and liver proteins in normal and AA rats.

	Normal rats	AA rats	p
Plasma	0.624 ± 0.046	0.452 ± 0.016	< 0.01
Liver protein	0.077 ± 0.004	0.100 ± 0.021	ns

Data are the mean $\pm$ SD $(n = 3)$. ns, No significant difference

Table 3. Pharmacokinetic parameters for the hepatobiliary transport of methotrexate in normal and AA rats.

	Normal rats	AA rats	p
$CL_{bile,int,all}$ (ml min g $liver^{-1}$)	0.402 ± 0.060	0.098 ± 0.007	< 0.01
$CL_{bile,int}$ (ml min g $liver^{-1}$)	1.461 ± 0.354	0.323 ± 0.058	< 0.01
CL_{uptake} (ml min g $liver^{-1}$)	0.278	0.138	
PS_{inf} (ml min g $liver^{-1}$)	0.522	0.280	

Data for $CL_{bile,int,all}$ and $CL_{bile,int}$ are the mean $\pm$ SD $(n = 3)$. CL_{uptake} and PS_{inf} were calculated as described in the Materials and methods.

trexate to the liver protein between AA and normal rats. Overall intrinsic biliary clearance ($CL_{bile,int,all}$) and intrinsic biliary clearance ($CL_{bile,int}$) in normal and AA rats calculated by using both unbound fraction ratios and hepatic blood flow rate are shown in table 3. Both $CL_{bile,int,all}$ and $CL_{bile,int}$ in AA rats were significantly lower than those values found in normal rats.

It has been reported that MRP2 is involved in the excretion of methotrexate at the canalicular membrane (Masuda *et al.* 1997). Because $CL_{bile,int}$ was markedly decreased in AA rats (table 3), we investigated the expression level of MRP2 using an *in situ* immunostaining method (figure 2A). In normal rat liver, the hepatocelluar biliary domain clearly showed positive staining for MRP2 and was decreased in AA rat liver. The mean staining intensity for MRP2 in the AA rat liver was twofold lower than that found in the normal rat liver (figure 2B), corresponding to the reduction of $CL_{bile,int}$ in the *in vivo* study.

Functional changes in the hepatic uptake of methotrexate (MTX) in AA rats were also investigated by applying an integration plot method as described in the Materials and methods. As shown in figure 3, the slopes of the integration plots were linear up to 6 and 15 min for normal and AA rats, respectively. The hepatic uptake clearance (CL_{uptake}) and intrinsic hepatic uptake clearance (PS_{inf}) estimated from the initial slopes are shown in table 3. CL_{uptake} and PS_{inf} in AA rats were twofold lower than those found in normal rats.

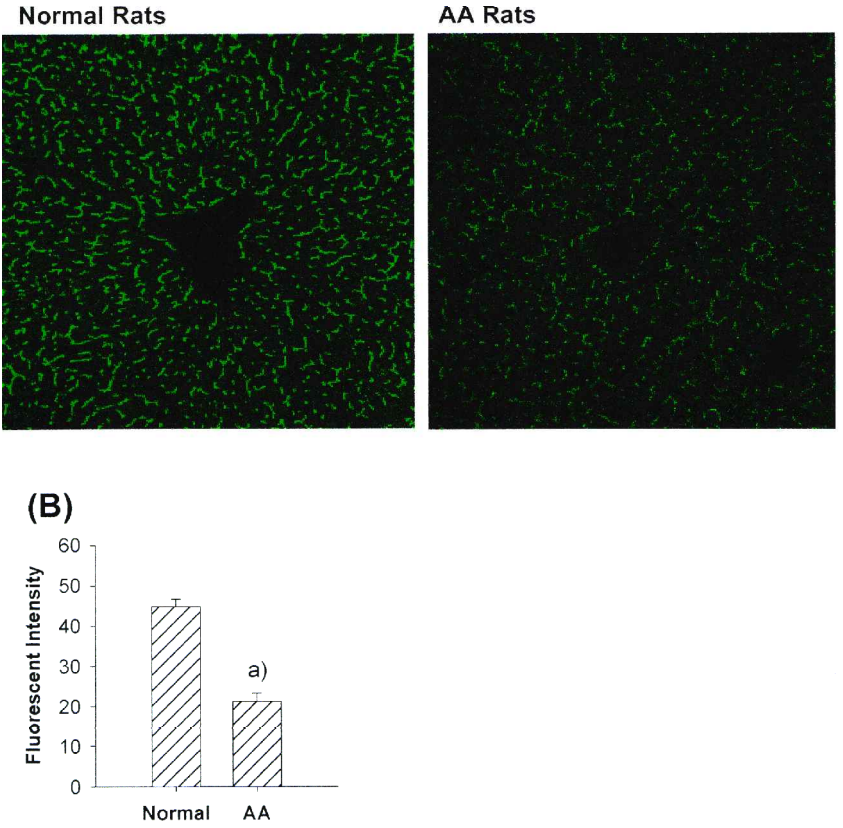


Figure 2. (A) Immunohistochemical detection of frozen liver sections from normal and AA rats with anti-MRP2; (B) fluorescent intensity with anti-MRP2 of frozen liver sections from normal and AA rats. Fluorescent intensity data are represented as the mean with SD $(n = 3)$.

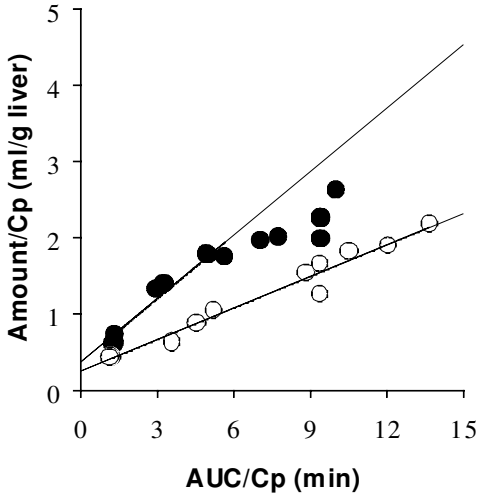


Figure 3. Integration plot of hepatic uptake of methotrexate in normal and AA rats; ●, normal rats; ○, AA rats.

Discussion

Methotrexate is often administered to rheumatoid arthritis patients as a disease-modifying anti-rheumatic drug (DMARD). Because plasma concentrations of some drugs are altered in patients with Crohn's disease, an inflammatory disease (Schneider *et al*. 1979) and AA rats (Piquette-Miller and Jamali 1992, 1993, Shibata *et al*. 1993), we investigated the effect of arthritis on the pharmacokinetics of methotrexate using AA rats. Methotrexate is mainly eliminated by excretion into the bile in rats (Masuda *et al*. 1997) and therefore biliary excretion should regulate the disposition of methotrexate.

We compared the biliary excretion of methotrexate between normal and AA rats. Following continuous intravenous infusion, the plasma concentration of methotrexate at steady-state was twofold higher in AA rats compared with that in normal rats (figure 1A), and the biliary clearance defined in terms of the plasma concentration ($CL_{bile,p}$) in AA rats was fourfold lower than that in normal rats (table 1). It was likely that decreased biliary clearance in AA rats caused a rise in concentration. Although the plasma protein binding was significantly lower in AA rats (table 2), the approximately 80% decrease in overall biliary intrinsic clearance ($CL_{bile,int,all}$) resulted in lowering overall biliary excretion (table 3). $CL_{bile,p}$ in normal rats was 45.8% of CL_{tot} and this value was lower than that reported by Masuda *et al*. (1997). There may be a gender difference in the biliary excretion of methotrexate because the data reported previously were obtained from male rats, whereas we used female rats in the current study. There was no detectable difference in the hepatic blood flow rate between AA and normal rats (65 ± 6 versus 58 ± 4 ml min^{-1} kg^{-1}). Masuda *et al*. (1997) reported that MRP2 is involved in the excretion of methotrexate at the canalicular membrane. Our results from the immunohistochemical study indicated that the expression level of MRP2 was markedly decreased in AA rat liver, and it therefore seems reasonable to suggest that this transporter plays an important role in the hepatobiliary transport of methotrexate. Urinary bilirubin concentration in AA rats was twofold higher than that in normal rats (Toda *et al*. 1996). The decreased expression level of MRP2 may be involved in the increased urinary bilirubin concentration, because bilirubin is excreted into the bile via MRP2. In rats treated with lipopolysaccharide (LPS), an animal model of cholestasis, the expression of MRP2 is also decreased (Vos *et al*. 1998). It has been reported that the level of MRP2 in parenchymal hetatocytes is decreased when normal parenchymal hepatocytes are co-cultured with Kupffer cells prepared from the rats treated with LPS (Vos *et al*. 1998). Moreover, the inflammation-promoting cytokines such as tumour necrosis factor-α (TNFα), interleukin 1 (IL-1) and/or IL-6 released from activated Kupffer cells causes down-regulation of MRP2 in parenchymal hepatocytes (Nakamura *et al*. 1999). Although the mechanism associated with the development of arthritis and down-regulation of the expression level of MRP-2 in AA rats has not yet been clarified, TNFα and IL-6 levels in plasma are elevated in AA rats (Philippe *et al*. 1997). These results suggest that cytokines are also involved in the down-regulation of MRP2 in AA rats.

Active transporters are also involved in the hepatic uptake of methotrexate (Honscha and Petzinger 1999), although they have not yet been identified. We investigated the effect of AA on the hepatic uptake of methotrexate. Hepatic uptake clearance (CL_{uptake}) and intrinsic clearance (PS_{inf}) were significantly decreased in AA rats (table 3), suggesting the involvement of down-regulated

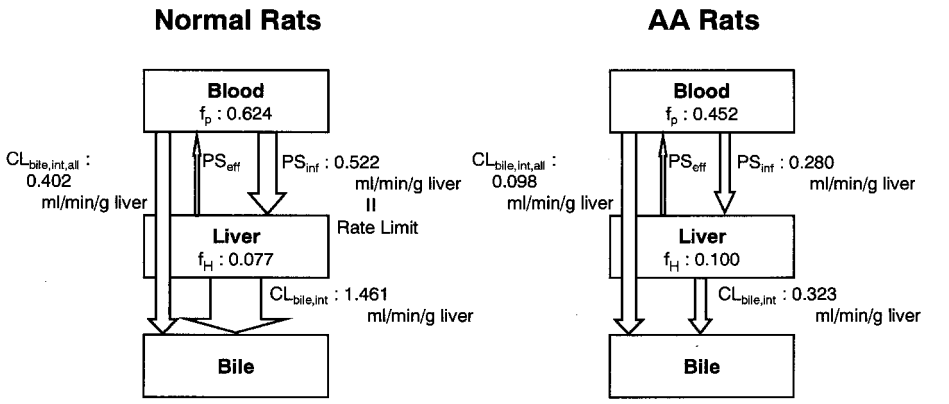


Figure 4. Summary of pharmacokinetic parameters for hepatobiliary transport of methotrexate in normal and AA rats.

transporters in the hepatic uptake process. However, the decreased level in the hepatic uptake process was minor compared with that found in MRP2. Cytokines such as TNFα, IL-1 and/or IL-6 might be also involved in the down-regulation of the active transporters in the hepatic uptake of methotrexate. Vos *et al.* (1998) reported altered mRNA levels of some active transporters in LPS-treated rat liver. The *mdr1b* mRNA was increased whereas *Bsep* mRNA was decreased and *mdr1a* and *mdr2* mRNA did not change in the LPS-treated rat liver. Thus, some transporters were up-regulated, while others were down-regulated or unchanged in the LPS-treated rat liver. In AA rats, similar changes in the levels and/or activities of transporters may be altered.

The parameters for the hepatobiliary transport estimated by continuous intravenous infusion and integration plot method are summarized in figure 4. In normal rats, intrinsic hepatic uptake clearance (PS_{inf}) was lower compared with the intrinsic biliary clearance ($CL_{bile,int}$), whereas PS_{inf} was comparable with $CL_{bile,int}$ in AA rats. The overall biliary intrinsic clearance ($CL_{bile,int,all}$) is represented as the following equation in the hybrid model of hepatobiliary transport:

$$CL_{bile,int,all} = PS_{inf} \times CL_{bile,int} / (PS_{eff} + CL_{bile,int}), \quad (6)$$

where PS_{eff} is the efflux clearance through the sinusoidal membrane defined in terms of the hepatic concentration.

Equation (6) clearly shows that $CL_{bile,int,all}$ becomes equal to PS_{inf} when $CL_{bile,int}$ is much greater than PS_{eff}. On the other hand, when PS_{eff} is equal to PS_{inf} and is much greater than $CL_{bile,int}$, $CL_{bile,int,all}$ becomes equal to $CL_{bile,int}$. In the case of methotrexate in normal rats, $CL_{bile,int}$ might be much greater than PS_{eff} because $CL_{bile,int}$ was greater than PS_{inf} and, moreover, PS_{inf} might be much greater (five- to 10-fold) (Honscha and Petzinger 1999) than PS_{eff} due to the involvement of active transporters in hepatic uptake in normal rats. As described above, equation (6) yields equation (7) in the case of methotrexate in normal rats:

$$CL_{bile,int,all} = PS_{inf}. \quad (7)$$

According to equation (7), the hepatic uptake process is rate limiting in biliary excretion of methotrexate. Overall, biliary intrinsic clearance ($CL_{bile,int,all}$) is comparable with the uptake intrinsic clearance (PS_{inf}) in normal rats (figure 4).

In AA rats, on the other hand, PS_{eff} might not be negligible as compared with $CL_{bile,int}$ because of a marked decrease of $CL_{bile,int}$. Both $CL_{bile,int}$ and PS_{inf} influence $CL_{bile,int,all}$ in AA rats as shown in equation (6), suggesting that decreased biliary excretion clearance ($CL_{bile,p}$) in AA rats is due to the decreased hepatic uptake of methotrexate and decreased secretion of methotrexate at the canalicular membrane.

The changes in plasma protein binding, metabolism by cytochrome P450 and conjugation in AA rats have previously been reported (Bishop *et al*. 1981, Yasuhara *et al*. 1985, Belpaire *et al*. 1989, Toda *et al*. 1994, Meunier and Verbeeck 1999). In the current study, we confirmed that the changes in the activity and expression level of active transporters are related to both the hepatic uptake and excretion processes. These changes may cause the different disposition of compounds, which are excreted into bile via MRP2. The changes in drug disposition in disease states should be considered in the clinical situation, although it has been reported that methotrexate is mainly excreted into urine in human (Tracy *et al*. 1994). The findings here are of value in the use of animal models in the development of new medicine, and consideration of the pharmacological and/or toxicological effects in clinical use.

References

Belpaire, M. F., De Smet, F., Chindavijak, B., Fraeyman, N. and Bogaert, G. M., 1989, Effect of turpentine-induced inflammation on the disposition kinetics of propranolol, metoprolol and antipyrine in the rat. *Fundamentals in Clinical Pharmacology*, **3**, 79–88.

Bishop, H., Schneider, E. R. and Welling, P., 1981, Plasma propranolol concentrations in rats with adjuvant-induced arthritis. *Biopharmacology and Drug Disposition*, **2**, 291–297.

Booth, L. C., Brouwer, R. K. and Brouwer, L. R. K., 1998, Effect of multidrug resistance modulators on the hepatobiliary disposition of doxorubicin in the isolated perfused rat liver. *Cancer Research*, **58**, 3641–3648.

Buchar, E. and Janku, I., 1985, The effect of adjuvant-induced arthritis on rat liver microsomal phospholipid metabolism. *Methods and Findings in Experimental and Clinical Pharmacology*, **7**, 469–472.

Dipasquale, G., Welaj, P. and Rassaert, L. C., 1974, Prolonged pentobarbital sleeping time in adjuvant-induced polyarthritic rats. *Research Communications in Chemical Pathology and Pharmacology*, **9**, 253–264.

Harris, E. D., 1981, Rheumatoid arthritis; the clinical spectrum. In *Textbook of Rheumatology* (Philadelphia: W. B. Saunders), pp. 928–963.

He, L. Y., Tanigawara, Y., Yasuhara, M. and Hori, R., 1991, Effect of folinic acid on tissue residence and excretion of methotrexate in rats. *Drug Metabolism and Disposition*, **19**, 729–734.

Honscha, W. and Petzinger, E., 1999, Characterization of the bile acid sensitive methotrexate carrier of rat liver cells. *Naunyn-Schmiedeberg's Archives in Pharmacology*, **359**, 411–419.

Lin, J. H., Sugiyama, Y., Awazu, S. and Hanano, M., 1982, In vitro and in vivo evaluation of the tissue-to-blood partition coefficient for physiological pharmacokinetic models. *Journal in Pharmacokinetics and Biopharmacology*, **10**, 637–647.

Masuda, M., I'izuka, Y., Yamazaki, M., Nishigaki, R., Kato, Y., Ni'inuma, K., Suzuki, H. and Sugiyama, Y., 1997, Methotrexate is excreted into the bile by canalicular multispecific organic anion transporter in rats. *Cancer Research*, **57**, 3506–3510.

Meunier, J. C. and Verbeeck, K. R., 1999, Glucuronidation of *R*- and *S*-ketoprofen, acetoaminophen, and diflunisal by liver microsomes of adjuvant-induced arthritic rats. *Drug Metabolism and Disposition*, **27**, 26–31.

Murata, M., Tamai, I., Sai, Y., Nagata, O., Kato, H., Sugiyama, Y. and Tsuji, A., 1998, Hepatobiliary transport kinetics of HSR-903, a new quinolone antibacterial agent. *Drug Metabolism and Disposition*, **26**, 1113–1119.

Nakamura, J., Nishida, T., Hayashi, K., Kawada, N., Ueshima, S., Sugiyama, Y., Ito, T., Sobue, K. and Matsuda, H., 1999, Kupffer cell-mediated down regulation of rat hepatic CMOAT/MRP2 gene expression. *Biochemistry and Biophysics Research Communications*, **255**, 143–149.

Philippe, L., Gegout-Pottie, P., Guingamp, C., Bordji, K., Terlain, B., Netter, P. and Gillet, P., 1997, Relations between functional, inflammatory, and degenerative parameters during adjuvant arthritis in rats. *American Journal of Physiology*, **273**, R1550–R1556.

Piquette-Miller, M. and Jamali, F. 1992, Effect of adjuvant arthritis on the disposition of acebutolol enantiomer in rats. *Agent Actions*, **37**, 290–296.

Piquette-Miller, M. and Jamali, F., 1993, Selective effect of adjuvant arthritis on the disposition of propranolol enantiomer in rats detected using a stereospecific HPLC assay. *Pharmaceutical Research*, **19**, 294–299.

Schneider, R. E., Bishop, H. and Hawkins, C. F., 1979, Plasma propranolol concentrations and the erythrocyte sedimentation rate. *British Journal of Clinical Pharmacology*, **8**, 43–47.

Shibata, N., Shimakawa, H., Minouchi, T. and Yamaji, A., 1993, Pharmacokinetics of cyclosporin A after intravenous administration to rats in various disease states. *Biological and Pharmacological Bulletin*, **16**, 1130–1135.

Toda, A., Ishii, N., Kihara, T., Nagamatsu, A. and Shimeno, H., 1994, Effects of adjuvant-induced arthritis on hepatic drug metabolism in rats. *Xenobiotica*, **24**, 603–611.

Toda, A., Kihara, T., Ono, N., Nagamasu, A. and Shimeno, H., 1996, Liver haem metabolism in adjuvant-induced arthritis rats. *Xenobiotica*, **26**, 415–423.

Tracy, T. S., Worster, T., Bradley, J. D., Greene, P. K. and Brater, D. C., 1994, Methotrexate disposition following concomitant administration of ketoprofen, piroxicam and flurbiprofen in patients with rheumatoid arthritis. *British Journal of Clinical Pharmacology*, **37**,453–456.

Vos, T. A., Hooived, G. J. E., Koning, H., Childs, S., Meijer, D. K. F., Moshage, H., Jansen, P. L. M. and Müller, M., 1998, Up-regulation of the multidrug resistance genes, mrp1 and mdr1b, and down-regulation of the organic anion transporter, mrp2, and the bile salt transporter, spgp, in endotoxemic rat liver. *Hepatology*, **28**, 1637–1644.

Williams, R. O., Feldmann, M. and Maini, N. R., 1992, Anti-tumor necrosis factor ameliorates joint disease in murine collagen-induced arthritis. *Proceedings of the National Academy of Sciences, USA*, **89**, 9784–9788.

Yasuhara, M., Fujiwara, J., Kitade, S., Katayama, H., Okumura, K. and Hori, R., 1985, Effect of altered plasma protein on pharmacokinetics and pharmacodynamics of propranolol in rats after surgery. *Journal of Pharmacology and Experimental Therapeutics*, 235, 513–520.

XENOBIOTICA, 2002, VOL. 32, NO. 12, 1161–1172

Taylor & Francis
healthsciences

Studies on the metabolic fate of M17055, a novel diuretic (6). Assessment for drug–drug interactions of M17055 in metabolism, distribution and excretion

H. NAKAJIMA*, T. NAKANISHI, H. NABA, K. NAKAI, S. MATSUMOTO, K. NAGASAWA, K. IDA, T. OGIHARA and N. OHZAWA

Drug Metabolism and Pharmacokinetics Laboratory, Research Center, Mochida Pharmaceutical Co., Ltd, 722 Jimba-aza-Uenohara, Gotemba Shizuoka 412-8524, Japan

Received 19 June 2002

1. The potential of M17055, a novel diuretic candidate, to affect the activities of human CYP enzymes, alter the plasma unbound fraction and compete with concomitant drugs in renal secretion as part of an assessment for drug–drug interactions in metabolism, distribution and excretion was investigated.

2. The effects of M17055 on the activities of human CYP1A2, CYP2E1, CYP2C9, CYP2C19, CYP2D6 and CYP3A4 were considered negligible at clinically relevant concentrations.

3. The majority of M17055 (99%) was bound to human plasma proteins, but it is unlikely to alter the binding of other clinically relevant drugs.

4. The renal clearance of M17055 (corrected for the plasma unbound fraction in male rats) substantially exceeded the glomerular filtration rate and was markedly reduced by treatment with probenecid, suggesting that the renal excretion of M17055 is controlled predominantly by an active secretion mechanism.

5. The results show that M17055 is unlikely to cause or undergo significant pharmacokinetic interactions with concomitant drugs in metabolism and distribution. However, when it is administered simultaneously with certain organic anions, drug–drug interactions during kidney excretion may be possible.

Introduction

M17055, 7-chloro-2,3-dihydro-1-(2-methylbenzoyl)-4(1H)-quinolinone 4-oxime-*O*-sulfonic acid potassium salt was discovered as a novel diuretic derivative of quinolinone oxime sulfonic acid (Shinkawa *et al*. 1992a) and has a potent diuretic activity when administered to rats, mice and dogs (Shinkawa *et al*. 1992b). The mechanism of action is reported to be that M17055 acts not only on the thick ascending limb of the loop of Henle, but also on the distal segments via the inhibition of electrogenic Na+ transport (Shinkawa *et al*. 1993).

Studies on the pharmacokinetics and disposition of this drug candidate have been conducted in the course of preclinical evaluation (Nakajima *et al*. 2001a–c, 2002a, b), and with relevance to drug–drug interactions, we reported that (1) the majority of M17055 (94–97%) binds to plasma proteins in rats and dogs; (2) the

* Author for correspondence; e-mail: h-naka@mochida.co.jp

Xenobiotica ISSN 0049–8254 print/ISSN 1366–5928 online © 2002 Taylor & Francis Ltd
http://www.tandf.co.uk/journals
DOI: 10.1080/0049825021000035317

metabolism of M17055 in man is catalysed mainly by CYP3A4 and CYP2C9; and (3) the renal clearance of free M17055 in rats substantially exceeds the glomerular filtration rate.

Drug–drug interactions can arise during absorption, distribution, metabolism and excretion (European Agency for the Evaluation of Medical Products 1997). An inhibition of cytochrome P450 (CYP) enzymes is the predominant cause of drug–drug interaction in metabolism. High protein binding may cause the displacement of the drug from plasma proteins and is the most common mechanism in altered distribution. The active secretion process, suggested in the renal excretion of M17055, may also cause the competitive inhibition of the renal clearance of drugs.

The present study investigated the effects of M17055 on the activities of CYP enzymes, the potential to displace concomitant drug from plasma proteins and the competition for renal clearance in order to assess the potential of this drug candidate to cause or undergo drug–drug interactions in metabolism, distribution and excretion. The interaction of M17055 with other drugs during absorption is negligible because M17055 has been developed for intravenous injection.

Materials and methods

Chemicals

17055 (chemical purity > 99%) and [^{14}C]M17055 (radiochemical purity > 97%) were supplied by the Pharmaceutical Laboratory of the Mochida Pharmaceutical Co., Ltd (Shizuoka, Japan) and Amersham International (Amersham, UK), respectively, as described in Nakajima *et al.* (2001a). The chemical structure of [^{14}C]M17055 is shown in figure 1. β-Nicotinamide adenine dinucleotide phosphate (β-NADP+), human serum albumin (HSA, essentially free of fatty acid and globulin), α_1-acid glycoprotein (α_1-AGP), digitoxin, warfarin, diclofenac, theophylline, probenecid and urethane were purchased from Sigma Chemical Co. (St Louis, MO, USA). Glucose 6-phosphate (G6P) and glucose 6-phosphate dehydrogenase (G6PDH) were purchased from Oriental Yeast, Co., Ltd (Tokyo, Japan). Phenobarbital, aminopyrine, furosemide, diazepam and tolbutamide were purchased from Wako Pure Chemicals (Tokyo, Japan). Radiolabelled compounds used in the competitive binding study were: [^{3}H]digitoxin, [^{3}H]diazepam and [^{3}H]inulin from Daiichi Pure Chemicals Co., Ltd (Tokyo, Japan), [^{3}H]theophylline from Moravek Biochemicals, Inc. (La Brea CA, USA), [^{14}C]warfarin from Amersham. Glibenclamide and fluconazole were extracted and purified from Euglucon^{TM} (Yamanouchi Pharmaceutical Co., Ltd, Tokyo, Japan) and Diflucan^{TM} (Pfizer Pharmaceuticals, Inc., Tokyo, Japan), respectively. Specific marker substrates, their metabolites, positive controls and internal standards for high-performance liquid chromatographic (HPLC) analyses used in the inhibition study against cytochrome P450 forms are summarized in table 1. Other reagents and solvents used are commercially available products of analytical grade or chromatographic grade.

Test systems

Five male Wistar rats of 13–14 weeks of age from Japan SLC, Inc. (Shizuoka, Japan) were used for the renal clearance study. The animals were kept in the animal room at constant temperature (23 $\pm$ 2°C) and humidity (55 $\pm$ 15%), with 12 h of light per day and were allowed access to water and given a commercially available diet, CE-2 (Clea Japan, Tokyo, Japan). Normal human plasma was obtained

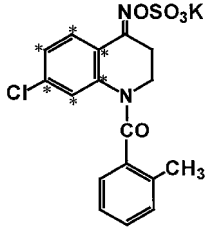


Figure 1. Chemical structure of [^{14}C]M17055. *Labelled positions.

Table 1. Reagents used for the *in vitro* inhibition of human CYPs by M17055.

Cytochrome P450	Reagent	Use	Supplier
CYP1A2	phenacetin	marker substrate	Sigma Chemical Co. (St. Louis, MO, USA)
	4-acetamidephenpol	authentic metabolite	Sigma
	p-anisamide	internal standard for HPLC	Nakarai Tesque, Inc. (Kyoto, Japan)
	furafylline	specific inhibitor	Research Biochemical, Inc. (Natik, MA, USA)
CYP2E1	chlorzoxazone	marker substrate	Research Biochemical
	6-hydroxychlorzoxazone	authentic metabolite	Research Biochemical
	diethyldithiocarbamic acid	specific inhibitor	Aldrich Chemical (Milwaukee, WI, USA)
CYP2C9	tolbutamide	marker substrate	Sigma
	3-hydroxytolbutamide	authentic metabolite	Research Biochemical
	sulfaphenazole	specific inhibitor	Meiji Yakuhin Co. (Tokyo, Japan)
CYP2C19	*S*-mephenytoin	marker substrate	Sumika Chemical Analysis Service Ltd (Osaka, Japan)
	4′-hydroxy *S*-mephenytoin	authentic metabolite	Research Biochemical
	phenobarbital	internal standard for HPLC	Wako Pure Chemical Industries Ltd (Osaka, Japan)
	omeprazole	specific inhibitor	Extracted and purified from Omepral™
CYP2D6	bufuralol	marker substrate	Gentest Corp. (Woburn, MA, USA)
	1′-hydroxybufuralol	authentic metabolite	Gentest Corp.
	quinidine	specific inhibitor	Sigma
CYP3A4	testosterone	marker substrate	Nakarai Tesque
	6β-hydroxytestosterone	authentic metabolite	Sumika Chemical Analysis Service
	ketoconazole	specific inhibitor	Sigma

from healthy male volunteers with their informed consent and was pooled before use. Human Pooled Hepatosomes (Lot Nos HBI 14–17, 19–21) purchased from Human Biologics, Inc. (Scottsdale, AZ, USA) were the source of human liver microsomes.

Effects on the activities of human CYP enzymes

The activities of phenacetin *O*-deethylation (CYP1A2), chlorzoxazone 6-hydroxylation (CYP2E1), tolbutamide methylhydroxylation (CYP2C9), *S*-mephenytoin 4′-hydroxylation (CYP2C19), bufuralol 1′-hydroxylation (CYP2D6) and testosterone 6β-hydroxylation (CYP3A4) were assayed as the probes of major human P450 activities using HPLC analysis (table 2) (Newton *et al*. 1995, Ono *et al*. 1996). Human microsomal protein in the NADPH-generating system (containing 10 mM G6P, 1 mM β-NADP$^+$, 1.4 U ml^{-1} G6PDH, 6 mM $MgCl_2$, 1 mM EDTA) was incubated at 37°C with specific marker substrates in the absence or presence of M17055 or diagnostic inhibitors at a final concentration of 100 M. Generated metabolites were extracted with ethyl acetate, reconstituted in the mobile phase and subjected to HPLC analysis. Analyses were performed with an HPLC system (Millipore Corp., Bedford, MA, USA) consisting of a 600s system controller, a 616 pump, a 717+ autosampler and a 486 UV detector (or a Jasco (Tokyo, Japan) 820-FP fluorescence detector) equipped with a Millennium integrator at a flow rate of 1.0 ml min^{-1}. The Jasco Tri-Rotar-VI HPLC system (Japan Spectroscopic Co. Ltd, Tokyo, Japan) was also used for part of the study. Details of the assay conditions and the analytical methods are summarized in table 2. If the activity in the presence of M17055 showed a significantly lower or higher level than that in the negative control, then another assay was performed with a lower concentration range.

The inhibitors against the activities of each CYP used as positive controls were furafylline (for CYP1A2) (Newton *et al*. 1995, Bourrie *et al*. 1996), sulfaphenazole (for CYP2C9) (Newton *et al*. 1995, Bourrie *et al*. 1996, Ono *et al*. 1996, Ko *et al*. 1997), omeprazole (for CYP2C19) (Ko *et al*. 1997), quinidine (for CYP2D6) (Newton *et al*. 1995, Bourrie *et al*. 1996, Ono *et al*. 1996), diethyldithiocarbamate (DDC, for CYP2E1) (Newton *et al*. 1995, Ono *et al*. 1996) and ketoconazole (for CYP3A4) (Newton *et al*. 1995, Bourrie *et al*. 1996). All substrates and inhibitors were dissolved in methanol and added to the incubation mixture (final methanol concentration within 1% of the total volume).

Characteristics of protein binding in human plasma

Determination of binding protein. Protein binding of [^{14}C]M17055 was determined by using an ultrafiltration method. Human plasma or a phosphate-buffered solution (pH 7.4) of HSA (concentration 40 mg ml^{-1}) or α_1-acid glycoprotein (concentration 1 mg ml^{-1}), which were added to a known amount of drug, was incubated at 37°C for 30 min. Aliquots of the incubation mixture were then introduced into the reservoir of the ultrafiltration kit (Centrifree MPS-3, Millipore) and centrifuged at 1700*g* for 15 min. The plasma before filtration and the corresponding filtrate were used for the measurement of radioactivity or HPLC analysis to determine the protein-bound fraction.

Displacement by drugs. [^{3}H]Diazepam, [^{3}H]digitoxin, [^{3}H]theophylline, [^{14}C]warfarin and tolbutamide were dissolved in ethanol and added (1% in the incubation mixture) to blank human plasma to make up final concentrations of 3, 0.04, 30, 5 and 50 μg ml^{-1}, respectively. Then, after M17055 was added to the plasma (final concentration 2 μg ml^{-1}), the mixture was treated as described above.

[^{14}C]M17055 was added to another blank human plasma to make up the final concentration of 1 μg ml^{-1}. The ethanol solution (1% in the incubation mixture) of digitoxin, diazepam, warfarin, theophylline, fluconazole, diclofenac, glibenclamide, tolbutamide and furosemide was then added at final concentrations of 0.05, 5, 10, 40, 40, 1, 1, 100 and 10 μg ml^{-1}, respectively. The concentration of each drug was set by referring to the maximum plasma concentration in clinical use. The mixture was treated as described above.

Quantitative analysis of drugs. Concentrations of [^{14}C]M17055, [^{3}H]diazepam, [^{3}H]digitoxin, [^{3}H]theophylline and [^{14}C]warfarin in plasma or filtrate were determined by measuring the radioactivity in each sample using an LS-6000TA (Beckman, Instrument, Inc., Fullerton, CA, USA) liquid scintillation counting system.

The concentration of tolbutamide in the filtrate was measured by directly injecting it into the HPLC. A 600s system controller, a 616 pump, a UV970 detector (Japan Spectroscopic) and a 717+ autosampler, equipped with a Millennium integrator (Millipore) were used for the determination of tolbutamide in the filtrate. Analyses were performed on a Capcell pack C18SG120 (4.6 $\times$ 250 mm; Shizeido, Tokyo, Japan) column at 1.0 ml min^{-1} using isocratic elution with 20% acetonitrile/80% 20 mM phosphate buffer (pH 7.0). The detection wavelength and column temperature were set at 227 nm and 35°C, respectively.

Table 2. Assay conditions and analytical methods for in vitro inhibition of human CYPs.

CYP	Substrate	Concentration of substrate (μM)	Concentration of protein (mg ml^{-1})	Incubation time (min)	HPLC condition		
					Column	Mobile phase	Detection
CYP1A2	phenacetin O-deethylation	100	0.2	20	Develosil ODS HG-5 (4.6 ± 150 mm)	acetonitrile–50 mM acetate buffer pH 3.5 (7.5:92.5)	UV 254 nm
CYP2E1	chlorzoxazone 6-hydroxylation	500	0.1	30	Inertsil ODS-3 (4.6 ± 250 mm)	acetonitrile–50 mM acetate buffer pH 3.5 (20:80)	UV 287 nm
CYP2C9	tolbutamide methylhydroxylation	500	0.2	60	Develosil ODS HG-5 (4.6 ± 150 mm)	acetonitrile–10 mM phosphate buffer pH 5 (20:80)	UV 230 nm
CYP2C19	*S*-mephenytoin 4′-hydroxylation	200	0.2	60	Develosil ODS HG-5 (4.6 ± 150 mm)	acetonitrile–10 mM phosphate buffer pH 7 (15:85)	UV 204 nm
CYP2D6	bufuralol 1′-hydroxylation	100	0.05	30	Develosil ODS HG-5 (4.6 ± 150 mm)	acetonitrile–10 mM phosphate buffer pH 7.4 (20:80)	FL Ex: 252nm, Em: 302nm
CYP3A4	teststerone 6β-hydroxylation	200	0.05	30	Develosil ODS HG-5 (4.6 ± 150 mm)	H_2O–methanol–acetonitrile (66:30:4)	UV 254 nm

Competition for renal clearance in the rat

Experimental procedure. The examination of renal clearance was performed by using the steady-state infusion method (Arita *et al*. 1969). Both ureters of five male rats were cannulated under urethane anaesthesia for urine collection. [^{3}H]inulin, dissolved in saline, was infused into the femoral vein at a dose-rate of 0.25 μg h^{-1}. After 2 h of infusion, urine was collected every 10 min for three times (triplicate samples from one animal). Blood samples were taken from the jugular vein at the mid-point of each urine collection period and centrifuged at 1700*g* for 15 min to generate the plasma samples. Subsequently, M17055 dissolved in saline was infused into the femoral vein at a dose-rate of 50 μg h^{-1}. After 2 h of M17055 infusion, urine and plasma samples were obtained in the same way as described above. Finally, M17055 and probenecid were simultaneously infused at dose-rates of 50 μg h^{-1} and 20 mg h^{-1}, respectively. After 2 h of M17055 and probenecid infusion, urine and plasma samples were obtained in the same way. After the final sampling of urine, blood was withdrawn from the jugular vein for the determination of free plasma fractions.

Determination of [^{3}H]inulin and M17055 in plasma and urine. The concentrations of [^{3}H]inulin in plasma and urine were determined by measuring the radioactivity in each sample using an LS-6000TA (Beckman) liquid scintillation counting system. The concentrations of M17055 in plasma and urine were determined by HPLC analysis as described in Nakajima *et al*. (2002b).

Pharmacokinetic analysis of renal clearance. The renal clearance (CL_r) and total body clearance (CL_{tot}) were calculated by using the following equations. The derived renal clearance of [^{3}H]inulin was expressed as the glomerular filtration rate (GFR). The non-renal clearance (CL_{nr}) was calculated by subtracting CL_r from CL_{tot}:

$$CL_r = \frac{U \times V}{P \times W}, \quad CL_{tot} = \frac{I}{P},$$

where P is the plasma concentration, U is the concentration in urine, V is the urinary volume excreted per minute, W is the body weight and I is the infusion rate of M17055.

Results

Influence of M17055 on human CYPs

The effects of M17055 on the activities of the major CYP forms are shown in table 3 compared with those of specific inhibitors. The activities of human CYP1A2, CYP2E1, CYP2C19, CYP3A4 were not affected by the addition of M17055 at a concentration of 100 μM. Since M17055 inhibited CYP2C9 activity by 68% and enhanced CYP2D6 activity by 94% at 100 μM, the effects on these two enzymes were examined further at a lower concentration range. The results

Table 3. Effects of M17055 and diagonistic inhibitors on CYPs.

Selective reaction	Drug	Activity (% of control)[a]
Phenacetin *O*-deethylation (CYP1A2 activity)	M17055	97
	furafylline	12
Chlorzoxazone 6-hydroxylation (CYP2E1 activity)	M17055	98
	DDC	14
Tolbutamide methyl hydroxylation (CYP2C9 activity)	M17055	32
	sulfaphenazole	14
S-mephenytoin 4-hydroxylation (CYP2C19 activity)	M17055	92
	omeprazole	25
Bufuralol 1′-hydroxylation (CYP2D6 activity)	M17055	194
	quinidine	24
Testosterone 6β-hydroxylation (CYP3A4 activity)	M17055	107
	ketoconazole	4

[a] Each value was derived from mean activity of triplicate assay.
Concentrations of M17055 and diagnostic inhibitors were 100 μM.

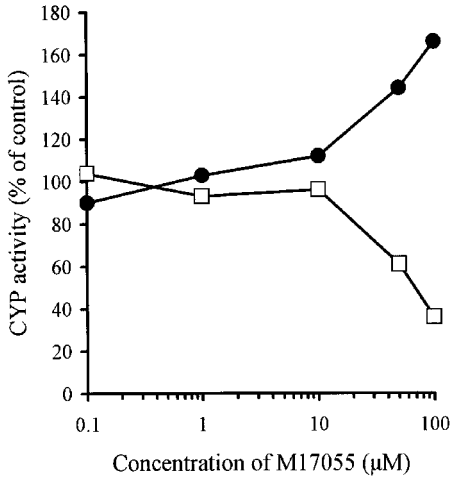


Figure 2. Effects of M17055 on the activities of tolbutamide methyl hydroxylation (CYP2C9 activity) and bufuralol 1′-hydroxylation (CYP2D6 activity) in human liver microsomes. Open squares and closed circles denote the tolbutamide methyl hydroxylation and bufuralol 1′-hydroxylation, respectively. Data were derived from triplicate determinations.

showed that the effects on the activities of both forms seemed to be slightly below 10 μM (figure 2).

Characteristics of protein binding in human plasma

Determination of binding protein. The binding of [^{14}C]M17055 to human plasma, HSA and α_1-AGP is shown in table 4. The *in-vitro* protein binding of [^{14}C]M17055 to human plasma was very high with 99.22% of the radioactivity bound, which was almost equal to that for HSA. In contrast, the binding of [^{14}C]M17055 to α_1-AGP was low with 18.33% of the radioactivity bound.

Displacement of M17055 binding by drugs. The plasma protein binding of [^{3}H]diazepam, [^{3}H]digitoxin, [^{3}H]theophylline, [^{14}C]warfarin and tolbutamide in the presence or absence of M17055 are shown in table 5. The protein binding of any drug tested was not affected by the addition of M17055 at 2 μg ml^{-1}.

Table 4. Binding of [^{14}C]M17055[a] to human plasma protein, human serum albumin (HSA) and human α_1-acid glycoprotein (α_1-AGP).

	Protein binding (%)
Human plasma	99.22 ± 0.01
HSA[b]	99.48 ± 0.02
α_1-AGP[b]	18.33 ± 0.71

Data are the mean ± SD of three samples.
[a] Concentration of [^{14}C]M17055 was 1 μg ml^{-1}.
[b] Concentration of HSA and α_1-AGP was 40 and 1 mg ml^{-1} respectively.

Table 5. Effects of M17055 on the binding of [^{3}H]diazepam, [^{3}H]digitoxin, [^{3}H]theophylline, [^{14}C]warfarin and tolbutamide to human plasma protein.[a]

Drug	Concentration of drug ($\mu g\,ml^{-1}$)	Protein binding of drug (%)	
		Control (without M17055)	With M17055
[^{3}H]diazepam	3	98.41 ± 0.04	98.42 ± 0.01
[^{3}H]digitoxin	0.04	98.02 ± 0.08	98.02 ± 0.03
[^{3}H]theophylline	30	56.66 ± 0.40	57.09 ± 0.30
[^{14}C]warfarin	5	99.17 ± 0.01	99.16 ± 0.03
Tolbutamide	50	97.17 ± 0.02	97.15 ± 0.02

Each value represents the mean $\pm$ SD of three samples.
[a] Concentration of M17055 was $2\,\mu g\,ml^{-1}$.

Table 6. Effects of digitoxin, diazepam, warfarin, theophylline, fluconazole, diclofenac, glibenclamide, tolbutamide and furosemide on the binding of [^{14}C]M17055[a] to human plasma proteins.

Drug	Concentration of drug ($\mu g\,ml^{-1}$)	Protein binding of [^{14}C]M17055 (%)
Control (without drug)	–	98.75 ± 0.02
Digitoxin	0.05	98.73 ± 0.02
Diazepam	5	98.73 ± 0.04
Warfarin	10	98.75 ± 0.04
Theophylline	40	98.72 ± 0.03
Fluconazole	40	98.76 ± 0.01
Diclofenac	1	98.75 ± 0.02
Glibenclamide	1	98.77 ± 0.02
Tolbutamide	100	98.48 ± 0.04
Furosemide	10	98.90 ± 0.04

Each value represents the mean $\pm$ S.D. of three samples.
[a] Concentration of [^{14}C]M17055 was $1\,\mu g\,ml^{-1}$.

The plasma protein binding of [^{14}C]M17055 in the presence or absence of digitoxin, diazepam, warfarin, theophylline, fluconazole, diclofenac, glibenclamide, tolbutamide and furosemide are shown in table 6. Again, the *in-vitro* plasma protein binding of [^{14}C]M17055 was not affected by the additions of digitoxin, diazepam, warfarin, theophylline, fluconazole, diclofenac, glibenclamide and furosemide, and was only slightly affected by the addition of tolbutamide.

Competition for renal clearance

The derived parameters for renal function and clearance of M17055 in male rats before and after treatment with probenecid are shown in table 7.

The GFR before and after probenecid treatment showed similar values, whereas the CL_r of M17055 was markedly reduced with probenecid treatment. $CL_{r,u}$, which expresses the renal clearance of the plasma unbound fraction of M17055, substantially exceeded the GFR in the absence of probenecid. $CL_{r,u}$ of M17055 in the presence of probenecid was approximately equal to the GFR.

Discussion

When M17055 was incubated with marker substrates of human CYPs, the activities of CYP1A2, CYP2E1, CYP2C19 and CYP3A4 were not affected by the addition of M17055 at a concentration of 100 μM, which is about 40 times higher

Table 7. Renal function and clearance of M17055 before and after probenecid infusion in male rats.

Administration	GFR ($ml\,min^{-1}\,kg^{-1}$)	CL_{tot} ($ml\,min^{-1}\,kg^{-1}$)	CL_r ($ml\,min^{-1}\,kg^{-1}$)	CL_{nr} ($ml\,min^{-1}\,kg^{-1}$)	$CL_{r,u}$[a] ($ml\,min^{-1}\,kg^{-1}$)	Clearance ratio ($CL_{r,u}/GFR$)
M17055 infusion	6.82 ± 0.27	34.16 ± 2.66	6.40 ± 0.57	27.76 ± 2.16	194 ± 17	28.5
M17055 with probenecid infusion	6.09 ± 0.44	16.43 ± 1.40	0.85 ± 0.10	15.58 ± 1.42	7.7 ± 0.9	1.3

[a] $CL_{r,u}$; renal clearance of plasma unbound fraction of M17055.
Each value represents the mean $\pm$ SD of five animals.
M17055 and probenecid were infused at $50\,\mu g\,h^{-1}$ and $20\,mg\,h^{-1}$ respectively.
The mean plasma unbound fraction of M17055 without and with probenecid were 3.3 and 11.0%, respectively.

than the maximum plasma concentration of M17055 in humans ($< 1\,\mu g\,ml^{-1} = 2.3\,M$). Although M17055 inhibited CYP2C9 activity by 68% at 100 μM, the inhibitory effect was low below 10 μM. Similarly, the enhancement of CYP2D6 activity by M17055, which was observed at high concentrations, seemed to be negligible below 10 μM. These results suggest that M17055 is unlikely to cause drug–drug interaction by interfering with the activity of these CYP forms at a clinically relevant concentration. The activation of CYP2D6 with M17055 at high concentration is potentially very interesting observation. However, the mechanism of this phenomenon has not been clarified at this time.

Another issue is the possibility that other co-administered drugs may inhibit the metabolism of M17055. However, the alteration in the pharmacokinetic profile of M17055 caused by concomitant administration of CYP inhibitors is considered to be small, because M17055 is eliminated via multiple pathways: most of the dose (58.9–71.6%) is excreted as unchanged drug into the urine in a clinical Phase I trial (unpublished data) and a small fraction would be cleared by the two hepatic CYPs (CYP3A4 and CYP2C9) (Nakajima *et al.* 2002a).

The results of the *in-vitro* binding study suggest that HSA is the dominant protein that binds M17055. In comparison with other loop diuretics, the free plasma fraction of M17055 is somewhat lower than those of furosemide and piretanide (Elliott *et al.* 1982, Andreasen *et al.* 1983), but similar to that of torasemide (Knauf and Mutschler 1998).

Drugs binding to class I (warfarin site), class II (benzodiazepine site) and class III (digoxin site) binding sites (Fehske *et al.* 1981) were chosen for investigation in competitive binding studies. The results showed that the *in-vitro* plasma protein binding of [^{14}C]M17055 was not affected by the addition of all drugs tested except for tolbutamide. The free plasma fraction of M17055, which was increased by tolbutamide and was estimated to be 22% at most, would not cause a significant alteration in clinical use. In addition, protein binding of [^{3}H]diazepam, [^{3}H]digitoxin, [^{3}H]theophylline, [^{14}C]warfarin and tolbutamide was not affected by the addition of M17055. Thus, it appears that a significant displacement of M17055 and these representative drugs is unlikely to occur on the binding sites of HSA.

Many organic anions including some loop diuretics are known to be excreted into urine not only via glomerular filtration, but also by an active secretory mechanism in the kidney (Weiner *et al.* 1959, Bidiville and Roch-Ramel 1986, Brater *et al.* 1987, Dixey *et al.* 1988, Zeeuw *et al.* 1988, Tanaka *et al.* 1991, Terashita *et al.* 1995). In the renal clearance study using male rats, the GFR before and after probenecid treatment showed similar values, suggesting that it was not affected by probenecid. In contrast, the $CL_{r,u}$, which substantially exceeded the GFR, was reduced to a value nearly equal to the GFR by probenecid. The excretion of drugs via the nephron is well known to be controlled mainly by three factors, i.e. glomerular filtration, active secretion and passive reabsorption. Generally, polar and ionized substances are considered to undergo little passive reabsorption (Bonate *et al.* 1998). Considering the pK_a of M17055 (i.e. 2.39), most M17055 is ionized at physiological pH, suggesting that passive reabsorption of M17055 is unlikely to occur. Thus, like other loop diuretics, the renal excretion of M17055 is considered to be controlled predominantly by an active secretion mechanism.

Recently, many forms of the organic anion transporter (OAT/oatp) family have been identified and characterized (Abe *et al*. 2001). For instance, OAT1 was assumed to cause an interaction between methotrexate and non-steroidal anti-inflammatory drugs (NSAIDs) (Uwai *et al*. 2000a), and also thiazide diuretics, loop diuretics and acetazolamide (Uwai *et al*. 2000b). This information strongly suggests that the OAT/oatp family may contribute to the active tubular secretion of M17055.

In conclusion, M17055 is considered unlikely to cause or undergo significant pharmacokinetic interactions with co-administered drugs in metabolism and distribution. However, care should be taken when M17055 is administered simultaneously with certain organic anions, such as probenecid, *p*-aminohippurate and NSAIDs (Andreasen *et al*. 1980, Bidiville and Roch-Ramel 1986, Brater *et al*. 1987, Dixey *et al*. 1988).

References

Abe, T., Unno, M., Onogawa, T. and Tokui, T., 2001, Molecular identification of organic anion transporter oatp/LST family. *Tanpakushitsu Kakusan Koso*, **46**, 612–620.

Andreasen, F., Hansen, U., Husted, S. E. and Jansen, J. A., 1983, The pharmacokinetics of frusemide are influenced by age. *British Journal of Clinical Pharmacology*, **16**, 391–397.

Andreasen, F., Sigurd, B. and Steiness, E., 1980, Effect of probenecid on excretion and natriuretic action of furosemide. *European Journal of Clinical Pharmacology*, **18**, 489–495.

Arita, T., Hori, R., Owada, E. and Takahashi, K., 1969, Transformation and excretion of drugs in biological systems. I. Renal excretion mechanisms of sulfonamides (1). *Chemical and Pharmaceutical Bulletin*, **17**, 2526–2532.

Bidiville, J. and Roch-Ramel, F., 1986, Competition of organic anions for furosemide and *p*-aminohippurate secretion in the rabbit. *Journal of Pharmacology and Experimental Therapeutics*, **237**, 636–643.

Bonate, P. L., Reith, K. and Weir, S., 1998, Drug interactions at the renal level. *Clinical Pharmacokinetics*, **34**, 375–404.

Bourrie, M., Meunier, V., Berger, Y. and Fabre, G., 1996, Cytochrome P450 isoform inhibitors as a tool for the investigation of metabolic reactions catalyzed by human liver microsomes. *Journal of Pharmacology and Experimental Therapeutics*, **277**, 321–332.

Brater, D. C., Leinfelder, J. and Anderson, S. A., 1987, Clinical pharmacology of torasemide, a new loop diuretic. *Clinical Pharmacology and Therapeutics*, **42**, 187–192.

Dixey, J. J., Noormohamed, F. H., Pawa, J. S., Lant, A. F. and Brewerton, D. A., 1988, The influence of nonsteroidal anti-inflammatory drugs and probenecid on the renal response to and kinetics of piretanide in man. *Clinical Pharmacology and Therapeutics*, **44**, 531–539.

Elliott, H. L., Ansari, A. F., Campbell, B. C. and Lawrence, J. R., 1982, Protein binding of piretanide in normal and uraemic serum. *European Journal of Clinical Pharmacology*, **21**, 311–313.

Fehske, K. J., Muller, W. E. and Wollert, U., 1981, The location of drug binding sites in human serum albumin. *Biochemical Pharmacology*, **30**, 687–692.

Knauf, H. and Mutschler, E., 1998, Clinical Pharmacokinetics and pharmacodynamics of torasemide. *Clinical Pharmacokinetics*, **34**, 1–24.

Ko, J.-W., Sukhova, N., Thacker, D., Chen, P. and Flockhart, D. A., 1997, Evaluation of omeprazole and lansoprazole as inhibitors of cytochrome P450 isoforms. *Drug Metabolism and Disposition*, **25**, 853–862.

Nakajima, H., Naba, H., Nakanishi, T., Nakai, K., Watanabe, T., Ida, K. and Ohzawa, N., 2002b, Studies on the metabolic fate of M17055, a novel diuretic (5): pharmacokinetics and pharmacodynamics of unchanged drug in rat and dog after intravenous administration of M17055. *Drug Metabolism and Pharmacokinetics*, **17**, 214–220.

Nakajima, H., Nakanishi, T., Naba, H., Ida, K. and Ohzawa, N., 2001b, Studies on the metabolic fate of M17055, a novel diuretic (2): tissue distribution and transfer of radioactivity into fetus and milk in rat after a single intravenous administration of [^{14}C]M17055. *Xenobiotic Metabolism and Disposition*, **16**, 314–324.

Nakajima, H., Nakanishi, T., Naba, H., Ida, K. and Ohzawa, N., 2001c, Studies on the metabolic fate of M17055, a novel diuretic (3): plasma concentration, distribution and excretion of radioactivity in male rats after repeated daily intravenous administration of [^{14}C]M17055. *Xenobiotic Metabolism and Disposition*, **16**, 325–332.

Nakajima, H., Nakanishi, T., Naba, H., Tanaka, H., Ida, K., Ogihara, T. and Ohzawa, N., 2001a, Studies on the metabolic fate of M17055, a novel diuretic (1): plasma concentration and excretion of radioactivity in rat and dog after a single intravenous administration of [^{14}C]M17055. *Xenobiotic Metabolism and Disposition*, **16**, 304–313.

Nakajima, H., Nakanishi, T., Nakai, K., Matsumoto, S., Ida, K., Ogihara, T. and Ohzawa, N., 2002a, Studies on the metabolic fate of M17055, a novel diuretic (4): species difference in metabolic pathway and identification of human CYP isoform responsible for the metabolism of M17055. *Drug Metabolism and Pharmacokinetics*, **17**, 60–74.

Newton, D. J., Wang, R. W. and Lu, A. Y. H., 1995, Cytochrome P450 inhibitors: Evaluation of specificities in the *in vitro* metabolism of therapeutic agents by human liver microsomes. *Drug Metabolism and Disposition*, **23**, 154–158.

Ono, S., Hatanaka, T., Hotta, H., Satoh, T., Gonzalez, F. J. and Tsutsui, M., 1996, Specificity of substrate and inhibitor probes for cytochrome P450s: evaluation of *in vitro* metabolism using cDNA-expressed human P450s and human liver microsomes. *Xenobiotica*, **26**, 681–693.

Shinkawa, T., Nakajima. H., Nishijima, K., Yamasaki, F., Kato, K., Ohzawa, N. and Mizota, M., 1992a, A novel quinolinone diuretic, M12285, and its activation mechanism through sulfate conjugation. *European Journal of Pharmacology*, **219**, 217–224.

Shinkawa, T., Yamasaki, F., Kikuchi, A., Nakakuki, M., Nishijima, K., Uemura, A., Mizota, M. and Orita, Y., 1992b, Pharmacological properties of the novel highly potent diuretic 7-chloro-2,3-dihydro-1-(2-methylbenzoyl)-4(1H)-quinolinone 4-oxime-*O*-sulfonic acid potassium salt. *Arzneimittel-Forschung/Drug Research*, **42**, 1466–1472.

Shinkawa, T., Yamasaki, F., Notsu, T., Nakakuki, M., Nishijima, K., Yoshitomi, K., and Imai, M., 1993, Loop and distal actions of a novel diuretic, M17055. *European Journal of Pharmacology*, **238**, 317–325.

Tanaka, Y., Deguchi. Y., Ishii, I. and Terai, T., 1991, Sex differences in excretion of zenarestat in rat. *Xenobiotica*, **21**, 1119–1125.

Terashita, S., Sawamoto, T., Deguchi, S., Tokuma, Y. and Hata, T., 1995, Sex-dependent and independent renal excretion of nilvadipine metabolites in rat: evidence for a sex-dependent active secretion in kidney. *Xenobiotica*, **25**, 37–47.

The European Agency for the Evaluation of Medical Products, Committee for Proprietary Medical Products, 1997, *Note for Guidance on the Investigation of Drug Interactions*, pp. 3–7.

Uwai, Y., Saito, H., Hashimoto, Y. and Inui, K., 2000b, Interaction and transport of thiazide diuretics, loop diuretics, and acetazolamide via rat renal organic anion transporter rOAT1. *Journal of Pharmacology and Experimental Therapeutics*, **295**, 261–265.

Uwai, Y., Saito, H. and Inui, K., 2000a, Interaction between methotrexate and nonsteroidal anti-inflammatory drugs in organic anion transporter. *European Journal of Pharmacology*, **409**, 31–36.

Weiner, I. M., Washington, J. A. and Mudge, G. H., 1959, Studies on the renal excretion of salicylate in the dog. *Bulletin of the Johns Hopkins Hospital*, **105**, 284–297.

Zeeuw, D., Jacobson, H. R. and Brater, D. C., 1988, Indomethacin secretion in the isolated perfused proximal straight rabbit tubule. *Journal of Clinical Investigation*, **81**, 1585–1592.

XENOBIOTICA, 2002, VOL. 32, NO. 12, 1173–1183

Taylor & Francis
healthsciences

PCBs alter gene expression of nuclear transcription factors and other heart-specific genes in cultures of primary cardiomyocytes: possible implications for cardiotoxicity

J. BORLAK* and T. THUM

Fraunhofer Institute of Toxicology and Aerosol Research, Center for Drug Research and Medical Biotechnology, Nicolai-Fuchs-Str. 1, D-30625 Hannover, Germany

Received 8 May 2002

1. Polychlorinated biphenyls (PCBs) are well-known environmental pollutants that bioaccumulate mainly in the fatty tissue of animals and humans. Although contamination occurs primarily via the food chain, waste combustion leads to airborne PCBs. From epidemiological studies, there is substantial evidence that cardiovascular disease is linked to air pollution, but little is known about the underlying molecular events.

2. We investigated the effects of Aroclor 1254, a complex mixture of >80 PCB isomers and congeners, on the expression of nuclear transcription factors (GATA-4, Nkx-2.5, MEF-2c, OCT-1) and of downstream target genes (atrial and brain natriuretic peptide, alpha- and beta-myosin heavy chain, alpha-cardiac and alpha-skeletal actin), which play an important role in cardiac biology.

3. We treated cultures of primary cardiomyocytes of adult rats with Aroclor 1254 (10.0 μM) and found significant induction of the transcription factor genes GATA-4 and MEF-2c and of genes regulated by these factors, i.e. atrial natriuretic peptide, brain-type natriuretic peptide, alpha- and beta-myosin heavy chain, and skeletal alpha actin.

4. We have shown PCBs to modulate expression of genes coding for programmes of cellular differentiation and stress (e.g. atrial natriuretic peptide, brain-type natriuretic peptide) and these alterations may be important in the increase of cardiovascular disease in polluted areas.

Introduction

Polychlorinated biphenyls (PCBs) are well-known environmental pollutants and bioaccumulate mainly in the fatty tissue of animals and humans (Cogliano 1998). PCB contamination occurs primarily via the food chain, but waste combustion leads to airborne PCBs (Launhardt and Thoma 2000) and thus to an alternative route of incorporation via inhalation. There is substantial epidemiological evidence that air pollution in urban and industrial regions is an important risk factor for developing cardiovascular diseases (Haug *et al.* 2001) and PCBs have been linked to endothelial dysfunction, arteriosclerosis and cardiotoxicity (Toborek *et al.* 1995, Heid 2001). The molecular events underlying this phenomenon are largely undefined. Certain PCBs and other polynuclear aromatic hydrocarbons have the ability to activate the aryl-hydrocarbon receptor (Ahr) and this nuclear receptor forms a heterodimer that interacts with DNA via the

* Author for correspondence; e-mail: borlak@ita.fhg.de

Xenobiotica ISSN 0049–8254 print/ISSN 1366–5928 online © 2002 Taylor & Francis Ltd
http://www.tandf.co.uk/journals
DOI: 10.1080/0049825021000022311

dioxin-responsive element (DRE) to drive gene transcription of Ah-responsive genes (Reyes *et al.* 1992, Nebert *et al.* 2000, Borlak and Thum 2001, Safe 2001).

In the current study, we have investigated the effects of Aroclor 1254, a complex mixture of >80 PCB isomers and congeners, on the expression of transcription factors important in cardiovascular biology (GATA-4, Nkx-2.5, MEF-2c, OCT-1), all of which have established DNA consensus binding sites in the promoter regions of the investigated downstream target genes (atrial and brain natriuretic peptide – ANP and BNP – alpha- and beta-myosin heavy chain, alpha-cardiac and alpha-skeletal actin; Lee *et al.* 1997, Lakich *et al.* 1998, Sepulveda *et al.* 1998, Charron *et al.* 1999) to further our understanding on the molecular events that are maybe linked to cardiotoxicity.

Here, we test our hypothesis whether treatment of cultures of primary adult cardiomyocytes with Aroclor 1254 would lead to changes in gene expression and thus have studied transcriptional activation of a selected group of genes coding for cellular differentiation, cytoskeleton and cellular stress (e.g. ANP, BNP). The rational for gene selection was based on their proven role and importance in heart muscle cell biology (Schwartz *et al.* 1993, Yoshimura *et al.* 1993, Lowes *et al.* 1997, Nakao *et al.* 1997, Thum and Borlak 2001).

We used the cytoprotective agent butanedione monoxime (BDM) in the isolation and cultivation buffer to maintain highly differentiated cardiomyocytes during culture (Thum and Borlak 2001a, b). We have correlated expression of transcription factor (TF) genes and of genes regulated by these factors to obtain additional information on PCB and, in part, Ah-receptor-driven gene expression, and we have measured CYP1A1 gene expression and enzyme activity as an established endpoint for activation of this particular nuclear receptor.

Overall, this study focuses on gene expression of transcription factors and downstream target genes after exposure of cultures of cardiomyocytes with PCBs.

Materials and methods

Animals

All animal procedures described here were approved by the local authorities and the investigation conforms with the *Guide for the Care and Use of Laboratory Animals* published by the US National Institutes of Health (NIH Publication No. 85-23, revd 1996). Male Sprague–Dawley rats weighing 200 ± 40 g were obtained from Charles River (Sulzfeld, Germany). Food (1324N, Altromin, Germany) and water was given *ad libitum*.

Anesthesia. Rats were anaesthetized with ketamin (anaesthetic) and xylazin hydrochloride (muscle relaxant) with 0.1 ml ketamin per 100 g body weight and 0.05 ml xylazin hydrochloride per 100 g body weight. In addition, 2000 international units heparin were given intraperitoneally before surgery.

Isolation and cultivation of cardiomyocytes of adult rats

The isolation was done as described by Thum and Borlak (2000a, b). In brief, the thorax was opened by surgical procedures and the aorta ascendens anatomically prepared. The heart was perfused *in situ* with the washing solution (Joklik medium – Biochrom, Berlin, Germany – 500 μM EDTA and 15 mM BDM – Fluka, Deisenhofen, Germany – for 1 min). Then, the digestion solution (Joklik medium with 15 mM BDM, 1% bovine serum albumin, 20 μM calcium chloride, 1 mg ml^{-1} collagenase II; Worthington, Freehold, USA) was pumped through the rat heart to obtain cardiomyocytes. The cell yield was determined with the Neubauer's counting chamber (Hecht, Sondheim, Germany) and cardiomyocytes were cultured with Joklik medium with 5% foetal calf serum at 37°C at 5% CO_2 for 1 day before starting the experiment. Based on phase-contrast light microscopy, the purity was >95% and further improved by preplating cell suspension on plastic flasks for 2 h (Chajek *et al.* 1977). Myocytes were cultured for up to 3 days in the presence of Aroclor 1254 (10.0 μM; dissolved in dimethylsulfoxide) and controls received the

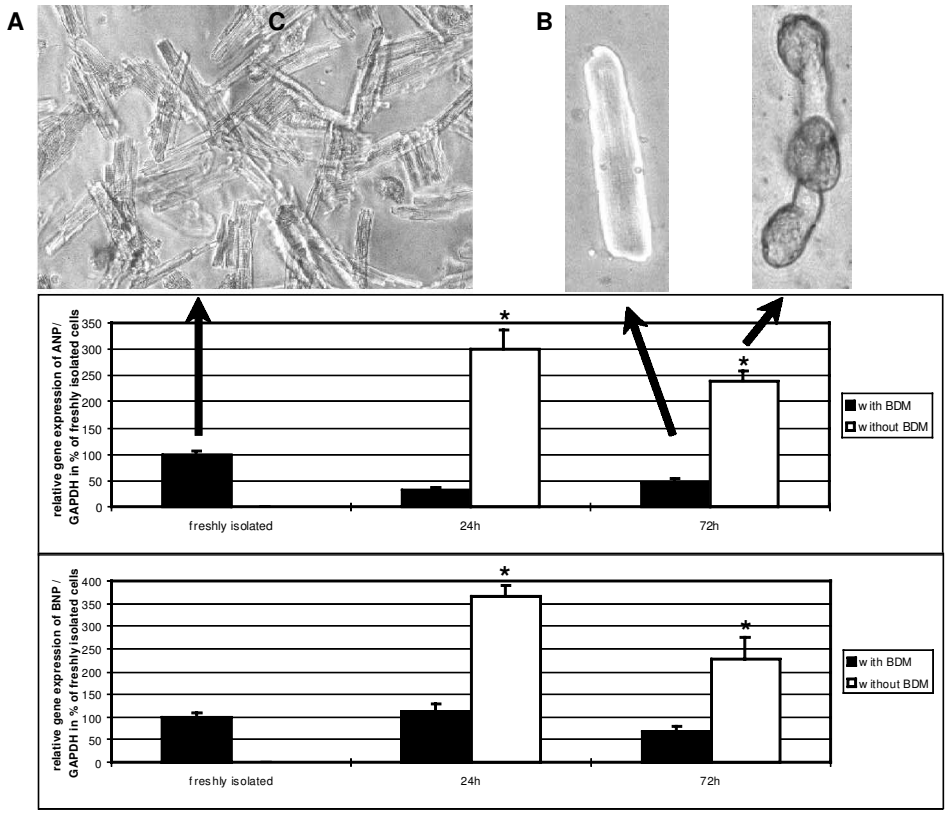


Figure 1. Cultured cardiomyocytes by the phase-contrast microscope: (a) freshly isolated and healthy cardiomyocytes; (b) day 3 in culture with BDM; (c) day 3 in culture without BDM. The relative gene expression of ANP/GAPDH (upper) and BNP/GAPDH (lower) of cultured cardiomyocytes in the presence or absence of BDM is shown. Data are the mean $\pm$ SD of $n = 3$ determinations ($* p < 0.05$).

vehicle only (e.g. DMSO). The DMSO concentration was 2.8 µl ml^{-1} medium, which accounts for < 0.3 v/v%. Healthy isolated and cultivated cardiomyocytes are shown in figure 1. In addition, cells were cultivated in the presence and absence of the protective agent BDM, which prevented cardiomyocytes from cellular dedifferentiation (Thum and Borlak 2001).

Gene expression studies

RNA and cDNA. RNA was isolated from cardiomyocytes shortly after isolation and after 1 and 3 days of culture using the SV total RNA Isolation System (Promega, Mannheim, Germany) according to the manufacturer's recommendation. The quality of isolated RNA was checked using a 1.0% agarose gel. A total of 4 µg total RNA from each sample was used for reverse transcription. RNA and random-primer (Roche, Mannheim, Germany) were preheated for 10 min at 70°C. Then 1 $\times$ RT-AMV (reverse transcriptase-avian myeloblastosis virus) buffer, 0.4 mM dNTPs, 40 U RNAse inhibitor (Stratagene, Amsterdam, the Netherlands), 20 U AMV-RT (Promega) were added and diethyl pyrocarbonate (Sigma, Deisenhofen, Germany) treated water was added to a final volume of 20 µl. Then, reverse transcription was carried out for 60 min at 42°C and stopped by heating to 95°C for 5 min. The resulting cDNA was frozen at $-$20°C until further experimentation.

Thermocycler RT-PCR. For the PCR amplification of cDNA, a 25-µl reaction mixture was prepared containing 10$_\times$ polymerase reaction buffer (100 mM Tris-HCl, 500 mM KCl), 1.5 mM $MgCl_2$, 0.4 mM dNTPs (Roche, Mannheim, Germany), 400 nM concentration of the 3′- and 5′-specific primer (synthesized by Gibco, Karlsruhe, Germany), 1 U TAQ-polymerase (Roche) and 1 µl cDNA.

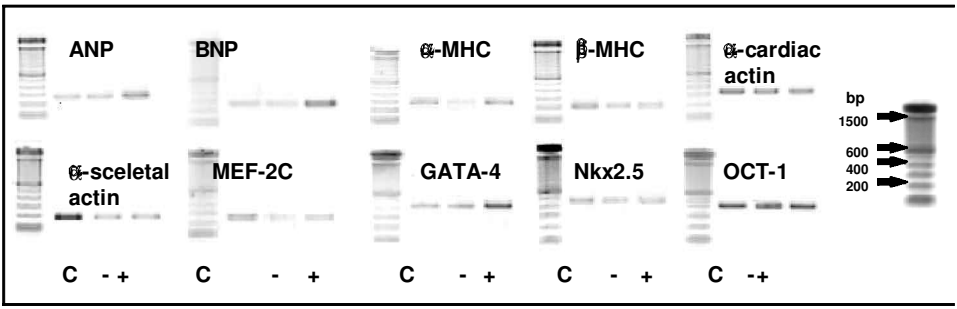


Figure 2. mRNA expression of genes ANP, BNP, α-MHC, β-MHC, α-cardiac actin, α-skeletal actin and the transcription factors GATA-4, MEF-2c, Nkx-2.5 and OCT-1 in cultures of cardiomyocytes. C, control; $_+$ and ($_-$), cultivated in the presence (absence) of 10 μM Aroclor 1254.

PCR reactions were carried out in a thermal cycler (Biometra) using melting, annealing and extension cycling conditions as described in table 1. PCR products were separated using a 1.8% agarose gel and stained with ethidium bromide and photographed on a transilluminator (figure 2).

Real-time semiquantitative RT-PCR. cDNA was diluted 1:10 with nuclease-free water and 1 μl of the diluted cDNA was added to the Lightcycler-Mastermix (0.4 μM of specific primer, 3 mM $MgCl_2$ and 2 μl Master-SYBR-Green; Roche). Water was added to a final reaction volume of 20 μl. All reactions were done on a Lightcycler.

The PCR reaction was completed after 35–45 cycles and at the end of each extension phase fluorescence was measured and used for quantitative purposes. A melting point analysis was carried out by heating the amplicon from 65 to 95°C and a characteristic melting point curve was obtained for each product (data not shown).

In addition, a serial dilution experiment was carried out with cDNA produced from cardiomyocyte total RNA using a 1:10 dilution regimen to estimate the mRNA expression levels of genes. Control samples contained water instead of cDNA and it should be noted that oligonucleotide dimers were produced in the PCR cocktail, but they could easily be distinguished by the melting point analysis. Expression levels were given as the ratio of the gene of interest (numerator) versus the GAPDH (denominator).

EROD assay. This assay was done essentially as described by Grant *et al.* (1987). Control cells and cells treated with Aroclor 1254 were incubated with 2 μM 7-ethoxyresorufin and 10 μM dicumarol (Sigma) and the supernatants were removed from the cultures at time points of 0, 1, 2 and 4 h. A total of 500 μl glycine buffer (1.6 M glycine, 1.3 M NaOH, pH 10.3) was added to 500 μl of the samples and subsequent fluorometric analysis was carried out on a spectrofluorophotometer (RF-1501, Schimadzu). In addition, aliquots were incubated at 37°C with 100 U ml^{-1} β-glucuronidase (not sulfatase-free; Sigma) overnight to assess the product release of β-glucuronide conjugates. The fluorometric analysis of the resultant product resorufin was done at an excitation wavelength of 530 nm and an emission wavelength of 585 nm. The calibration of the system was done with appropriate standards at a concentration range of up to 100 nM.

Statistical analysis

Results are the mean $\pm$ SD. The Wilcoxon signed-rank test was used where control and treatment dishes were studied in parallel and, consequently, the treated dishes and corresponding controls were paired in a given experiment. Differences were considered significant at $p < 0.05$.

Results

Cell culture

On average about $11.9 \pm 0.3 \times 10^6$ cells/heart could be isolated, the viability rate being $92.7 \pm 1.8\%$ based on rod-shaped morphology of cardiomyocytes determined by phase-contrast light microscopy. Based on phase-contrast light microscopy, the purity of cultures was >95%. Freshly isolated cardiomyocytes

Table 1. Oligonucleotides used in gene expression studies.

Ascession no.	Gene	Forward primer (5′-3′ sequence)	Reverse primer (5′-3′ sequence)	Product length (bp)	PCR conditions
M60731	*ANP*	GCCGGTAGAAGATGAGGTCA	GGGCTCCAATCCTGTCAATC	269	1
M25297	*BNP*	TCTGCTCCTGCTTTTCCTTA	GAACTATGTGCCATCTTGGA	258	1
X15938	*α-MHC*	GGAAGAGCGAGCGGCGCATCAAGG	CTGCTGGACAGGTTATTCCTCA	304	2
X15939	*β-MHC*	GCCAACACCAACCTGTCCAAGTTC	TTCAAAGGCTCCAGGTCTCAGGGC	202	2
X80130	*cardiac α-actin*	ACTCCTATGTAGGTGACGAGGC	GACGTTATGAGTCACACCGTCG	337	3
V01218	*skeletal α-actin*	ATCTCACGTTCAGCTGTGGTCA	ACCACCGGCATCGTGTTGGAT	182	3
AA955670	*MEF2c*	CCGATGCAGACGATTCAGTAG	GTGTCACACCAGGAGACATAC	260	4
L22761	*GATA4*	AGCAAGGACTAGGCACCTCTAGC	ATAGCCAGGCTTTGGTACATCGC	410	4
AF006664	*Nkx2.5*	CACGCCCTTCTCAGTCAAAGAC	AGGTACCGCTGTTGCTTGAAGC	461	4
U17013	*Oct-1*	CAATTGCAACAGCTTCAGCAGC	CATAGCAAGCCCAACATCACC	407	4
X02231	*GAPDH*	GGCCAAGGTCATCCATGA	TCAGTGAGCCCAGGATG	353	4

PCR conditions: 1: 30 s at 94°C, 30 s at 60°C, 30 s at 72°C, 29 cycles; 2: 60 s at 94°C, 60 s at 65°C, 90 s at 72°C, 28 cycles; 3: 60 s at 94°C, 60 s at 55°C, 60 s at 72°C, 29 cycles; 4: 45 s at 94°C, 45 s at 58°C, 60 s at 72°C, 28 cycles. All programmes are initiated with a 2-min denaturation step and stopped with a final 7-min elongation step.

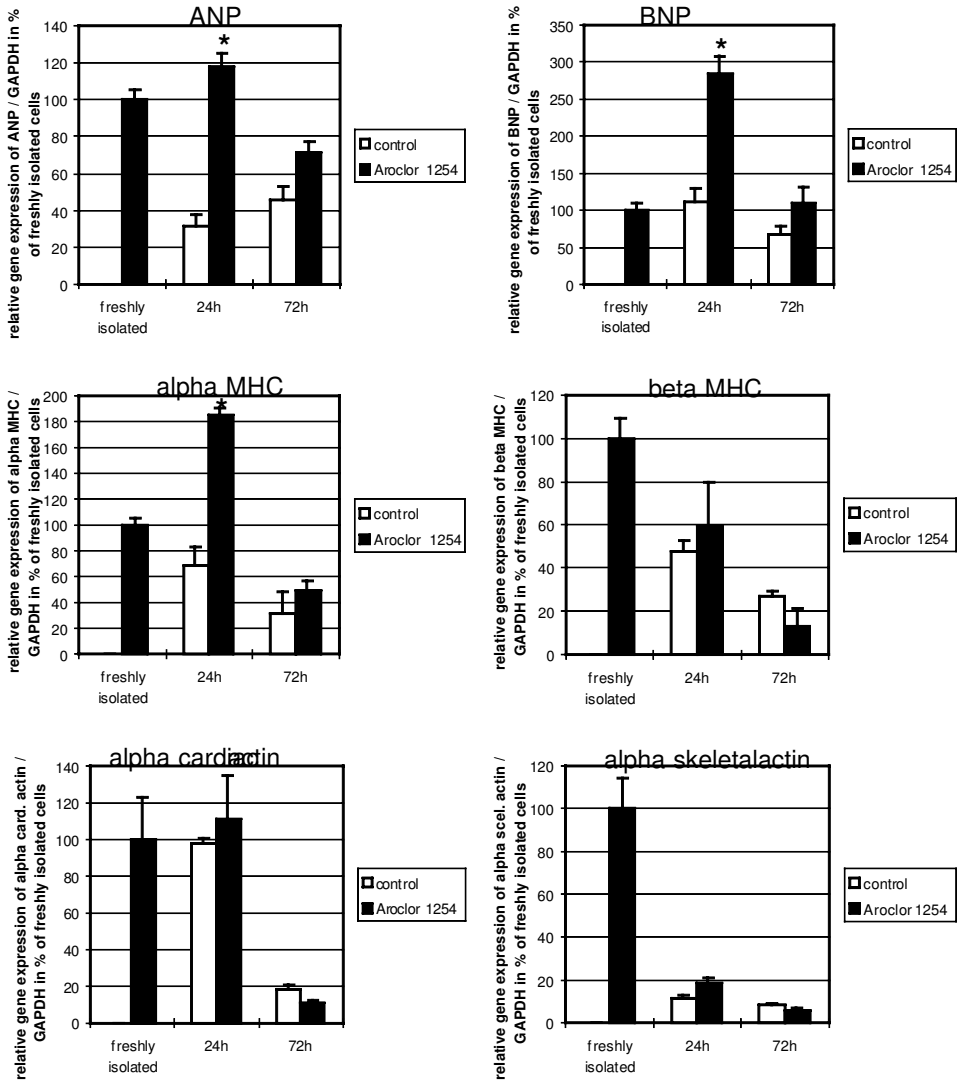


Figure 3. Semiquantitative real-time PCR of transcription factors and target genes in cultures of cardiomyocytes. The results obtained with freshly isolated cells were set to 100%. The relative expressions of MEF-2c, GATA-4, Nkx-2.5, OCT-1, ANP, BNP, α-MHC, β-MHC, α-cardiac actin and α-skeletal actin are shown. Cells were treated with 10 μM Aroclor 1254 or with vehicle (DMSO) only. Data are the mean $\pm$ SD of three individual cell culture experiments with about 2 million cells per culture dish. $*p < 0.05$.

were rod shaped and had well-defined cross-striations (figure 1a). At the end of the cultivation period (day 3) cardiomyocytes developed cytoskeletal defects with loss of rod shape morphology (figure 1c). This could be prevented when the cytoprotective agent BDM (15 mM) was added to the culture medium (figure 1b).

Furthermore, cardiomyocyte cultures expressed significant increased mRNA levels of the stress markers ANP (eightfold) and BNP (fourfold) if not treated with BDM (figure 1) and therefore all studies were done with BDM-treated cardio-

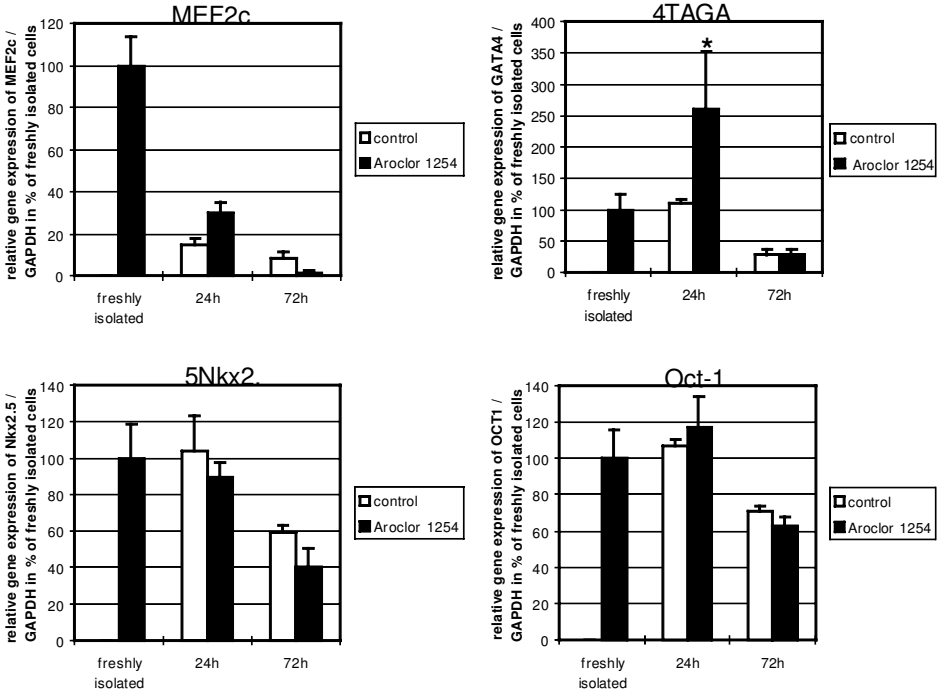


Figure 3. *Continued.*

myocyte cultures. The cytoprotective effect of BDM during isolation and cultivation was reviewed by Thum and Borlak (2001b).

Effects of Aroclor 1254

Based on phase-contrast light microscopy, no visible cellular dedifferentiation was obvious when cardiomyocytes were cultured with media containing BDM (figure 1b). Treatment of cultures with Aroclor 1254 resulted in three-, four- and threefold increases in expression of ANP, BNP and alpha-myosin heavy chain (MHC) (figures 2 and 3a). The gene expression of MEF-2c and GATA-4 was also increased two- and threefold, whereas the expression of beta-MHC, alpha-skeletal actin, alpha-cardiac actin, Nkx-2.5, OCT-1 and the housekeeping gene GAPDH was unchanged (figure 3b). The effects of Aroclor 1254 treatment were maximal 24 h post-treatment and declined thereafter.

We also investigated gene expression of CYP1A1 in BDM containing and Aroclor 1254-treated cardiomyocyte cultures, as well as in untreated controls and observed fourfold increases in CYP1A1 mRNA expression upon Aroclor 1254 treatment, 24 h post-dosing (figure 4a).

Ethoxyresorufin-O-deethylase activity assay

7-Ethoxyresorufin is a substrate for CYP1A1 and we showed a dose- and time-dependent increase in CYP1A1 activity (figure 4b). The fivefold increase in

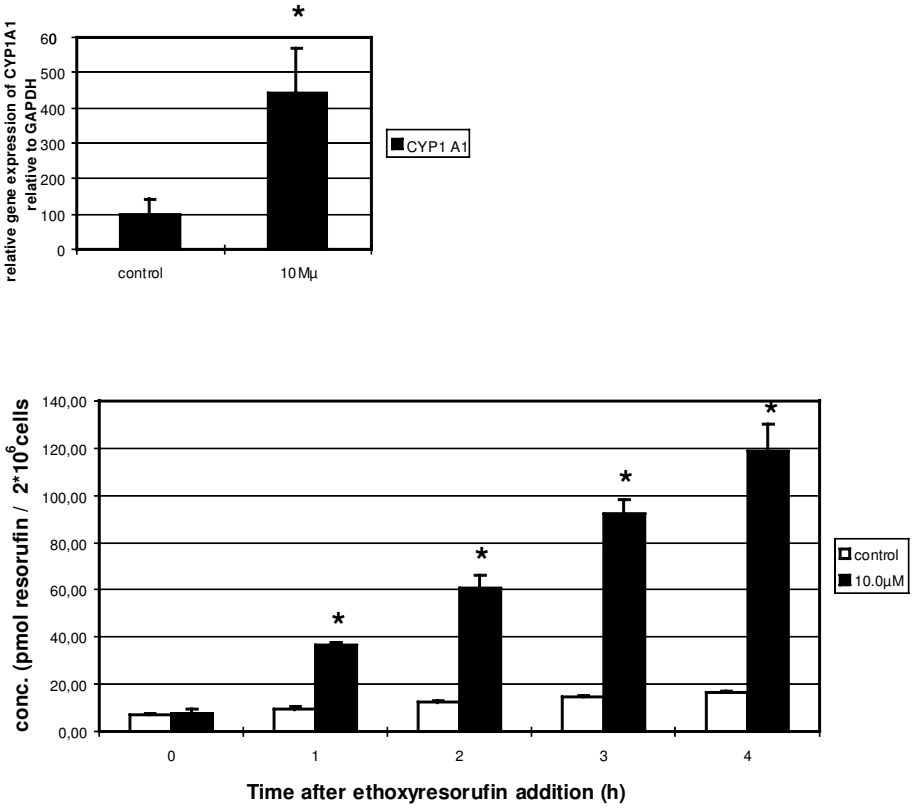


Figure 4. Gene expression (a) and enzyme activity (b) of CYP1A1 in cultures of adult cardiomyocytes upon 24-h treatment with Aroclor 1254 (10 μM). Data are the mean $\pm$ SD of $n = 3$ determinations (* $p < 0.05$).

CYP1A1 enzyme activity agrees well with the increased CYP1A1 mRNA expression described above. Furthermore, we did not observe the production of resorufin-glucuronoides, as judged by beta-glucuronidase digestion of culture media (data not shown).

Ahr-ARNT binding sites in promoters of responsive genes

Table 2 shows cognate recognition sites for Ahr-ARNT binding in the promoters of ANP, BNP, alpha-MHC and beta-MHC. Unfortunately, no promoter sequence information was available for the other genes investigated (see MatInspector V2.2 of the TRANSFAC 4.0 database at http://transfac.gbf.de/TRANSFAC/index.html for details). As shown in table 2, no simple correlation can be made between Ah-ARNT binding sites and increased gene expression, i.e. the presence of more than one recognition site and spatial separation, but nonetheless there appears to be a relationship between the predicted Ah-ARNT promoter interaction and the transcriptional activation of these genes. The presence of binding sites does not necessarily lead to transcriptional activation and,

Table 2. Ahr-ARNT binding sites in promotors of responsive genes.

Gene	Promoter (accession no.)	Ahr-ARNT-binding site (5′-TNGCGTG-3′) (core binding site in capital letters)	Region in promotor (bp)
ANP	AJ250806	gtgtgtgcgCGTGtgc	687–703
BNP	U02972	gagtggttgCGTGagc	1859–1875
		agcagctcgCGTGcac	2503–2519
Alpha-MHC	K01464	ctcattccgCGTGcct	560–576
		ggagtttagCGTGggg	621–637
Beta-MHC	X16291	agcagtgtgCGTGtgc	1393–1408
		gtgtgtgcgCGTGtgt	1441–1456
		ttgtgcatgCGTGcgc	1454–1469
Alpha-skeletal actin	none found		
Alpha-cardiac actin	none found		
Nkx2.5	none found		
GATA-4	none found		
MEF2c	none found		
Oct-1	none found		

indeed, we showed that the beta-MHC promoter potentially contained three Ahr-ARNT-responsive elements, but gene expression was unchanged in our study.

Discussion

We have investigated the effects of Aroclor 1254 on the gene expression of cardiomyocyte-specific transcription factors and of others that play an important role in cardiac biology. We have also confirmed activation of the Ah receptor by examining CYP1A1 gene expression and enzyme activity and have shown PCBs to activate this particular receptor in cultures of cardiomyocytes (Thum and Borlak 2000a). We obtained detailed DNA sequence information for the promoters of ANP, BNP alpha-MHC and beta-MHC of the rat genome (table 2), but were unable to identify DNA sequence information for any of the other promoters investigated by us (for further details see Entrez from the National Center for Biotechnological Information; http://www.ncbi.nlm.nih.gov). We propose altered expression of TFs and genes regulated by these factors to be, at least in part, under the control of the Ah receptor. We have provided experimental evidence that PCBs regulate expression of genes' coding for cardiac function and this could help in the interpretation of recent epidemiological findings which link occurrence of cardiac disease to heavily polluted areas (Haug *et al*. 2001). We have used CYP1A1 gene expression and enzyme activity as an endpoint to demonstrate activation of the Ah-nuclear receptor and propose increased expression of ANP and BNP to be the result of an interaction of this receptor with the response elements in the promoters of these genes (table 2; MatInspector V2.2 of the TRANSFAC 4.0 database). From table 2 it is obvious that no simple correlation can be made between potential Ahr binding sites and induction of TF gene expression. Therefore, the presence of binding sites does not necessarily lead to transcriptional activation and, indeed, beta-MHC may contain three Ahr-ARNT-responsive elements, but was basically unchanged in our gene expression study. In addition, although binding of the Ah-ARNT to the responsive elements is an important

event in the transcriptional activation of responsive genes, there is also networking and recruitment/cooperation of additional TFs.

We have shown previously that the myosin ATPase inhibitor BDM reduces ANP and BNP gene expression in cultures of cardiomyocytes (Thum and Borlak 2001), but in strong contrast, treatment of cultures with Aroclor 1254 induced ANP and BNP gene expression and thus counteracted the alleviating effects of BDM. We view these data as a stress response to Aroclor 1254 treatment and demonstrate the importance of the Ah-receptor in the transcriptional activation of ANP and BNP. Our experimental data support the link between binding sites of Ah-ARNT and transcriptional activation in heart muscle cells. By using matched controls, we were able to study the effects of Aroclor 1254 on the expression of the here reported genes, but wish to point out that BDM may alter the response to Aroclor 1254 treatment in non-BDM-containing culture media of cardiomyocytes.

Cellular stress and metabolic deregulation of cardiomyocytes fosters the expression of the 28 amino acid polypeptide ANP and the BNP. These peptides are mainly secreted in atrial and ventricular tissue to produce decreased blood pressure by vasodilatation and natriuresis, all of which are upregulated in the heart in response to hypertrophic signals or cardiotoxicity (Yoshimura *et al*. 1993, Lowes *et al*. 1997, Rahman *et al*. 2001). These peptides are considered to be good diagnostic markers for the onset of human heart failure as well as for congenital heart disease (Schwartz *et al*. 1993, Nakao *et al*. 1997, Thum and Borlak 2001). There is also a good correlation between gene expression of ANP and BNP and its protein translation (de Bold *et al*. 1996).

The few reports linking halogenated hydrocarbons to cardiotoxicity are those of Heid *et al*. (2001) and Walker and Catron (2000), who reported cardiotoxicity on the basis of increased heart weights of chick embryos (*Gallus gallus*) and diagnosed dilated cardiomyopathy. The formation of the avian Ahr-ARNT–DNA binding complex in chicken hepatoma cells would suggest induction of cardiotoxicity via an avian Ah-receptor signalling pathway. We extend the findings of Walker and Catron (2000) and confirm elevated ANP levels in response to PCBs in cultures of rat cardiomyocytes. We propose cardiotoxicity induced by halogenated hydrocarbons to be linked to altered gene expression of heart-specific transcription factors and genes regulated by these factors and suggest Ahr-ARNT to play a role in the transcriptional activation of heart specific genes.

References

Borlak, J. and Thum, T., 2001, Induction of nuclear transcription factors, cytochrome P450 monooxygenases, and glutathione *S*-transferase alpha gene expression in Aroclor 1254-treated rat hepatocyte cultures. *Biochemical Pharmacology*, **61**, 145–153.

Chajek, T., Stein, O. and Stein, Y., 1977, Rat heart in culture as a tool to elucidate the cellular origin of lipoprotein lipase. *Biochimica et Biophysica Acta*, **488**, 104–144.

Charron, F., Paradis, P., Bonchain, O., Nemer, G. and Nemer, M., 1999, Cooperative interaction between GATA-4 and GATA-6 regulates myocardial gene expression. *Molecular and Cellular Biology*, **19**, 4355–4365.

Cogliano, V. J., 1998, Assessing the cancer risk from environmental PCBs. *Environmental Health Perspectives*, **106**, 317–323.

De Bold, A. J., Bruneau, B. G. and de Bold, M. L., 1996, Mechanical and neuroendocrine regulation of the endocrine heart. *Cardiovascular Research*, **31**, 7–18.

Grant, M. H., Burke, M. D., Hawksworth, G. M., Duthie, S. J., Engeset, J. and Petrie, J. C., 1987, Human adult hepatocytes in primary monolayer culture. Maintenance of mixed function oxidase and conjugation pathways of drug metabolism. *Biochemical Pharmacology*, **36**, 2311–2316.

Haug, T., Sostrand, P., Lovik, M. and Langard, S., 2001, Public health and air pollution. *Lancet*, **357**, 70–71.

Heid, S. E., Walker, M. K. and Swanson, H. I., 2001, Correlation of cardiotoxicity mediated by halogenated aromatic hydrocarbons to aryl hydrocarbon receptor activation. *Toxicology Science*, **61**, 187–196.

Lakich, M. M., Diagana, T. T., North, D. L. and Whalen, R. G., 1998, MEF-2 and Oct-1 bind to two homologous promoter sequence elements and participate in the expression of a skeletal muscle-specific gene. *Journal of Biological Chemistry*, **273**, 15217–15226.

Launhardt, T. and Thoma, H., 2000, Investigation on organic pollutants from a domestic heating system using various solid biofuels. *Chemosphere*, **40**, 1149–1157.

Lee, Y., Nadal, G. B., Mahdavi, V. and Izumo, S., 1998, Myocyte-specific enhancer factor 2 and thyroid hormone receptor associate and synergistically activate the alpha-cardiac myosin heavy-chain gene. *Molecular and Cellular Biology*, **17**, 2745–2755.

Lowes, B. D., Minobe, W., Abraham, W. T., Rizeq, M. N., Bohlmeyer, T. J., Quaife, R. A., Roden, R. L., Dutcher, D. L., Robertson, A. D., Voelkel, N. F., Badesch, D. B., Nakao, K., Monobe, W., Roden, R., Bristow, M. R. and Leinwand, L. A., 1997, Myosin heavy chain gene expression in human heart failure. *Journal of Clinical Investigation* 100, 2362–2370.

Nebert, D. W., Roe, A. L., Dieter, M. Z., Solis, W. A., Yang, Y. and Dalton, T. P., 2000, Role of the aromatic hydrocarbon receptor and [Ah] gene battery in the oxidative stress response, cell cycle control, and apoptosis. *Biochemical Pharmacology*, **59**, 65–85.

Rahman, A., Alam, M., Rao, S., Cai, L., Clark, L. T., Shafiq, S. and Siddiqui, M. A., 2001, Differential effects of doxorubicin on atrial natriuretic peptide expression *in vivo* and *in vitro*. *Biology Research*, **34**, 195–206.

Reyes, H., Reisz-Porszasz, S. and Hankinson, O., 1992, Identification of the Ah receptor nuclear translocator protein (ARNT) as a component of the DNA binding form of the Ah receptor. *Science*, **256**, 1193–1195.

Safe, S., 2001, Molecular biology of the Ah receptor and its role in carcinogenesis. *Toxicology Letters*, **120**, 1–7.

Schwartz, K., Chassagne, C. and Boheler, K. R., 1993, The molecular biology of heart failure. *Journal of the American College of Cardiology*, **22**, 30A–33A.

Sepulveda, J. L., Belaguli, N., Nigam, V., Chen, C. Y., Nemer, M. and Schwartz, R. J., 1998, GATA-4 and Nkx-2.5 coactivate Nkx-2 DNA binding targets: role for regulating early cardiac gene expression. *Molecular and Cellular Biology*, **18**, 3405–3415.

Thum, T. and Borlak, J., 2000a, Cytochrome P450 mono-oxygenase gene expression and protein activity in cultures of adult cardiomyocytes of the rat. *British Journal of Pharmacology*, **130**, 1745–1752.

Thum, T. and Borlak, J., 2000b, Isolation and cultivation of Ca^{2+} tolerant cardiomyocytes from the adult rat: improvements and applications. *Xenobiotica*, **30**, 1063–1077.

Thum, T. and Borlak, J., 2001a, Reprogramming of gene expression in cultured cardiomyocytes and in explanted hearts by the myosin ATPase inhibitor butanedione monoxime. *Transplantation*, **71**, 543–552.

Thum, T. and Borlak, J., 2001b, Butanedione monooxime increases the viability and yield of adult cardiomyocytes in primary cultures. *Cardiovascular Toxicology*, **1**, 61–72.

Toborek, M., Barger, S. W., Mattson, M. P., Espandiari, P., Robertson, L. W. and Hennig, B., 1995, Exposure to polychlorinated biphenyls causes endothelial cell dysfunction. *Journal of Biochemistry and Toxicology*, **10**, 219–226.

Walker, M. K. and Catron, T. F., 2000, Characterization of cardiotoxicity induced by 2,3,7,8-tetrachlorodibenzo-*p*-dioxin and related chemicals during early chick embryo development. *Toxicology and Applied Pharmacology*, **167**, 210–221.

Yoshimura, M., Yasue, H., Okumura, K., Ogawa, H., Jougasaki, M., Mukoyama, M., Nakao, K. and Imura, H., 1993, Different secretion patterns of atrial natriuretic peptide and brain natriuretic peptide in patients with congestive heart failure. *Circulation*, **87**, 464–469.